Q
1
S3
ser. A
v. 75
1972
ubj.
ndex
cience
n/c

Physics Abstracts

164

Science Abstracts Series A
July–December 1972

Subject Index part A

U. of ILL. LIBRARY
MAY 9 1973
CHICAGO CIRCLE

inspec
The Institution of Electrical Engineers

Physics Abstracts

Volume 75, part 2 July–December 1972

Subject Index part A

Physics Abstracts is published every two weeks by the Institution of Electrical Engineers in association with the American Institute of Physics. Twice-yearly subject and author indexes covering the period January–June and July–December are included in the subscription. Printed by Unwin Brothers Limited, Old Woking, Surrey, England. Second class postage paid in New York, NY 10001, USA.

© 1972: THE INSTITUTION OF ELECTRICAL ENGINEERS

CONTENTS

Title page i
Contents list and explanation ii
Subject index S 901

Six-monthly indexes

Cumulative indexes to Science Abstracts are published twice a year covering the period January-June and July-December. They comprise Author and Subject indexes and some specialised or 'small' indexes.

Author index

This lists in alphabetical order all authors of papers abstracted in the abstracts journal during the six months covered by the index, together with the title of the paper. Where there are co-authors of a paper the title of the paper is given only under the name of the first author. The serial number of the paper in the abstracts journal is in the form 2-12345, ie 1972—abstract no. 12345.

'Small' indexes

These are specialised indexes which allow the user to find quickly particular types of information which might be difficult to find using the subject or author indexes.

Bibliography index

In this index reference is made to articles which contain a significant list of references or bibliography on the subjects listed.

Book index

This gives details of books received and abstracted by the abstracts journal.

Patent and Report indexes

These give details of those reports or patents which have been abstracted in the abstracts journal during the past six months.

Conference index

This index lists conferences for which published proceedings have been received and abstracted. Reference is given to the individual papers and their serial numbers in the abstracts journal.

Subject index

The subject index provides an alphabetical subject key to the articles included in the abstracts journal. Some general guidance on its use is given below:

1. Look in the index for the name of the specific subject in which you are interested. In most cases this name will be a heading in the index and you will find relevant articles listed under it.

2. Occasionally you will be directed from the subject heading chosen to a different heading under which the relevant or additional articles are listed.

3. If you do not find the subject heading you first choose, try a more general heading.

4. If you have difficulty at any stage in determining the appropriate heading, consult the Classified List of Headings on the yellow pages at the end of the index. This gives for each broad subject area the headings used in the subject index. Choose the most appropriate and look them up in the index.

5. Each entry under the heading relates to an article appearing in the abstracts journal and gives the serial number of that article in the journal preceded by the last digit of the current year, eg 2—12345: ie Abstract number 12345 in the abstracts journal for 1972.

Subject Index

4π counters *see Counters*
Abacs *see Nomograms*
Aberrations, optical
see also Electron lenses; Ion optics; Optical instrument testing; Optics/geometrical; Particle optics
— 2—73161
achromatic Fourier transformation 2—42225
astigmatism and surface striae 2—70053
astigmatism correction in grating spectrographs 2—73679
astronomical images, due to atmospheric turbulence, restoration by optical array technique 2—85074
astronomical Ritchey-Chretien telescopes, and extending field of view 2—58567
astronomical telescope, aberrations due to temperature deformations and convective fluxes, interferometric investigations 2—48821
asymmetric quadrupole lenses, third order geometric aberrations 2—63281
atmospherically degraded satellite images, restoration 2—79308
chromatic, correction method 2—70002
chromatic, of reconstructed holographic image, compensation by dispersive lens 2—42133
chromation in magnification, nonisoplanar transmission functions 2—66806
circular dichroism, analogue computing system for gaussian and lorentizian simulation 2—45782
colour correction of systems operating in visible light 2—59257
concentric systems, third-order aberrations, object plane positions 2—59259
condenser systems, dispositive plane, light intensity distribution calc. 2—59217
corrected lens, as function of defocussing and pupil position 2—45777
correction of optical elements by selective deposition by Glacier process 2—79395
deformational, telescope main mirror, holographic correction 2—59251
Delano diagram, application to optical design 2—79402
and design, tutorial 2—42179
and design, tutorial 2—52447
design, tutorial 2—59248
design and fibre optics 2—63372
design considerations, tutorial 2—59211
design problems, tutorial 2—49410
distortion, astigmatism and coma in electron optics, quadrupole, hexapole and octipole lenses as correctors 2—63282
double monochromators, compensation for coma and anamorphic effect 2—55773
double-meniscus astrograph, lateral chromatic aberration 2—48828
edge image characteristics of systems with electron optical brightness intensifiers 2—82576
electostatic prism spectrometer with quadrupole lenses 2—49632
electron, field aberrations in electrostatic single axially-symmetrical lenses 2—76452
electron, optimization of antisymmetric quadrupole rel. to aperture and chromatic aberrations 2—79062
electron, spherical aberration correction in electron microprobe by non axially symmetric elements 2—81560
electron, third order of axially symmetric lenses 2—59091
electron gun, field emission, for 75-100 kV electron microscopy 2—69878
electron gun problems of computation and design 2—76454
electron lens, immersion, spherical and chromatic aberration, magnification depend. 2—49321
electron lens, spherical aberration rel. to coma, function of object and position 2—59089
electron lens, spherical and chromatic correction 2—59080
electron magnetic lenses, asymptotic aberration coefficients 2—79060
electron microscope, displaced aperture dark field images by an aberration correction technique 2—79053
electron microscope, effect of spherical aberration and defocussing 2—79124
electron microscope, ultimate resolution 2—82448
electron microscope image resolution, object scattering effects 2—79006
electron microscopes, image resolution 2—82449
electron microscopical installation, resolution improvements 2—79028
electron microscopy, space charge correction of spherical aberration 2—79075
electron optical, correction in two stage magnetic deflection system 2—79061
electron optical magnification system, new aspects in design 2—79074
electron optics, minimum spherical aberration of coma free magnetic round lenses 2—79059
electron optics systems, book 2—66715
electron quadrupole lenses, third order coeffs. 2—79058

Aberrations, optical continued
electron ring shaped objective lenses, correction of spherical aberration by two round lenses 2—79051
enlarger, condenser type, design 2—66829
extremely wide angle, lenses, design 2—59216
eye, diffusive properties of rotation 2—78675
Fraunhofer holograms, wavelength dependent distortion 2—63358
Fresnel zone plate spectrometer with central stop 2—59283
holograms, side band, with electrons, compensation 2—45764
illumination distrib. produced by system in arbitrary plane, computer program 2—59258
illumination systems tutorial paper 2—66800
instrument design 2—73626
lenses, design, tutorial 2—42178
lenses, two surfaces with object at infinity 2—59214
mirror design 2—70037
monochromatic, effect of spherical spectacle lenses 2—78676
monochromator, Czerny-Turner, without intermediate slit, aberration coma free 2—79438
off-axis beams, triplet lens system for correcting, design fabrication and testing 2—79426
optical design and aberrations, part XXVIII 2—69999
particle, multipole elements for corrections 2—73520
particle spectrometers, trajectories in toroidal condenser to third order approx. 2—76447
plane symmetric systems, coeff. determ. 2—73627
primary, of two-lens systems of reversed Ramsden and reversed Huygenian types 2—63373
quadratic approximation, optical systems design 2—45803
relativity and aberration of components of double stars 2—73024
sagittal ray correction method for reduction of primary aberration 2—55729
spectrograph, two-mirror, plane-grating, central ray and spherical aberrations 2—42271
spherical, 5 electrode quadrupole-octupole triplet lens 2—78999
spherical, of magnetic lenses, calc. 2—41924
spherical, partially coherent diffraction at circular aperture 2—45794
summing of optical system aberrations caused by decentring 2—59215
symmetrical three-aperture electrostatic lens 2—66717
system design, teaching 2—73630
system design, teaching 2—76506
systems design, tutorial 2—49411
systems design, tutorial 2—59218
systems design, tutorial 2—63382
systems design, tutorial 2—45775
systems design, tutorial 2—52446
systems without symmetries, Lagrangian aberration coeffs. 2—79297
total aberration formula, skew rays optical aberration 2—76505
unusual image distortion, use of spline aspheric surfaces 2—79403
visual, of large pupil systems 2—66801
Wadsworth mounting, three-dimensional theory 2—63389
wide field imaging with aberration minimised JEM-100B electron microscope 2—79071
zonal coma of semi-aplanat reflecting microscope, error in theory 2—82570
zone plates, third order and chromatic 2—59227
zoom lenses, optical design and aberrations, tutorial series 2—52448

Abrasion
see also Hardness; Wear
diamond, abrasion resist. during polishing and grinding, microscopic cleavage mechanism 2—74868
fibre composite, brittle matrix, abrasion resist. 2—53968
glass, optical, relation between abrasion, micro indentation hardness and maximum fracture velocity, expts. 2—56550
surface deformation and destruction, statistical structural model 2—43746
surface shape, microscopic probability model 2—47562
wear testers, for cast iron, obs. 2—50792
Al_2O_3, subsurface damage due to, examination using transmission electron microscopy 2—80870
$BaTiO_3$, surface domain reorientation, X-ray diffraction exam. 2—80544
Bi-Ag eutectic alloy, surface damage after polishing, e. microscope study 2—67898
Ga, surface struct. rel. to plastic deform. by unidirectional abrasion and rolling 2—83856
MoS_2, abrasiveness, role of impurities 2—47552
TiB_2 coatings characteriz. 2—51460

Absorption
see also Alpha-particles; Beta-rays; Cosmic rays; Electrons; Gamma-rays; Hyperons; Mesons; Neutrons and antineutrons; Protons and antiprotons; and also Sorption; X-ray absorption
cone wall, of external radiant power, radiant cooling 2—55569
elastic waves, in saturated porous media, calc. using Frenkel-Biot theory 2—82343
elastic waves, in solid granules, effect of grain size 2—84204
gas bubble rising in water 2—46907
of gas into turbulent liquid 2—50298

Absorption continued
- gases of different solubility in laminar gas and liquid flow 2—50290
- glasses containing La and Ce, radiation and optical stability 2—70071
- glow discharges, transition and line shapes, meas. method 2—70080
- seismic waves on moon, duration, scattering and attenuation 2—73072
- semiconductor, effect on exciton luminesc. 2—78129
- semiconductor, effect on recomb. luminesc. 2—78128
- single gas into sheared liquid film interface with and without chemical reaction 2—67749
- single line Mossbauer effect, optimum absorber thickness, in presence of strong nonresonant absorption 2—59684
- solar radiation by cloud layers, Monte Carlo calc. 2—48486
- H_2O, of CO_2 2—67816
- Nb, of H, solubility 2—50542
- W, of Ag, field emission microscope obs. 2—60690
- W, of O_2, M_2 CO, SIMS, EID, flash filament obs., binding states 2—47170

acoustic waves
- *see also Noise abatement; Transmission/acoustic waves*
- acoustic linings, optimization in presence of wall shear layers 2—71077
- in acoustically lined circular ducts, in fluid flow 2—58913
- active compensation multichannel systems for bounded structs. 2—45468
- aeronautical absorbent materials, resonant structures 2—45510
- air duct, active sound absorbers 2—73433
- atmospheric absorption at 20°C in frequency range 100 Hz-1 MHz 2—75616
- atmospheric absorption of sound, energy transfer mechanisms 2—44739
- attenuation, frequency range 500 to 10000 Hz, Lake Superior experiment 2—44663
- attenuation, high-frequency sound, in deep Pacific Ocean, pressure depend. 2—44662
- attenuation coeff. of plane coherent waves in turbulent medium 2—41721
- attenuation due to spin-phonon interactions in a conc. paramag. crystal, $S={}^{1}/_{2}$ 2—64846
- baffles, for noise abatement in corridors 2—41809
- blast wave attenuation by atm. 2—65811
- computer program for det. in porous material lined cylindrical ducts 2—41730
- conducting medium, short wave obs. by electrons 2—43977
- critical region phenomena, intermediate and h.f. dispersion 2—54027
- cylindrical and annular ducts, refraction and attenuation 2—58917
- damping coefficients in loudspeaker-excited closed cylindrical tube 2—55529
- diffuse sound field, reverberation time formulae 2—63115
- displacive and mag. order-disorder phase transition phenomena 2—54026
- ducts lined with nonisotropic materials 2—41729
- ducts with anisotropic lining, silencers 2—76376
- electrolyte solutions, Rayleigh and Brillouin scattering studies 2—43360
- erythrocytes, macromolecular interaction 2—48878
- F-1 acoustic liner, little improvement in combustion stability 2—52234
- facade walls, insulation from external noise with balconies and loggias 2—63137
- ferromagnetic insulators, acoustic attenuation and frequency shift for 2 magnon-one phonon processes 2—80907
- fibrous structures, influence of microstructure on oblique-incidence behavior 2—41724
- field measurement by reflection technique 2—41723
- gas of Maxwell molecules, absorption coefficient and phase velocity 2—41707
- hearing protectors in industrial noise, variation with noise spectra and with people 2—73217
- human blood, at 1 to 10 MHz 2—82363
- impedance of perforated plate liners with two frequency excitation 2—41728
- insulation, lightweight concrete walls, effect of air flow resistance 2—41725
- liquid, coeff. calc. using rigid sphere equation of state 2—46918
- liquid thermal relaxation times using improved rigid sphere equation of state rel. to sound absorption 2—56499
- material within cavity of timber stud/plasterboard partition, effect on sound transmission 2—41726
- measurement, using correlation technique 2—69737
- molecular collisions, rot. energy transfer meas. 2—64209
- muffler element performance and effects of high intensity sound 2—41727
- in multicomponent fluid systems near critical point 2—67574
- noise, steady state measurements 2—41818
- nonlinear attenuation, parametric array 2—41742
- oil-damped resonance absorber for underwater sound 2—55527
- Pacific Ocean, horizontal underwater paths 2—55530
- panel struct., directional props. of sound insulation 2—45547
- panels, correlate method of obs. 2—76369
- parametric acoustic array, analytical model using shock waves 2—76373
- partition walls, influence of structural stiffness, attenuation 2—41827
- plate with damping layer, transmission loss 2—45509
- polyurethane expanded foam, mechanical and acoustic properties 2—69727
- polyurethane foam, highly absorbing sample, measurements in reverberation room 2—63114
- porous absorbers, quasihomogeneous absorber theory rel. to Rayleigh theory 2—55528
- porous fibrous absorbents, oblique incidence behaviour 2—69736
- porous materials, oblique incidence, waveguide meas. 2—69738
- reduction index measurements, effects of laboratory designs and mounting conditions 2—78924
- resonant system props. 2—45516
- rigid and rough tubes with turbulent air flow 2—52233
- rigid sphere, coeff. due to thermal and viscous losses 2—55435
- sea surface as random filter 2—57838
- sea water, classical theory 2—51536

Absorption continued

acoustic waves continued
- sea water, empirical equation for acoustic impedance 2—48423
- seawater, sound absorption, multistate dissociation 2—48434
- semiconductors, and amplification 2—51029
- sound in mag. field at low temp., meas. 2—61092
- suspensions and emulsions, sound attenuation 2—43395
- $Bi_{12}GeO_{20}$, surface wave attenuation, frequency and temp. depend. 2—51024
- $Bi_{12}GeO_{20}$, surface wave propag., 200-2000 MHz loss mechanism 2—61094
- CoO, coefficients at room temp. 2—43971
- Cu hypersonic attenuation and nonlinearity constant D, temp. depend. 2—47744
- n-GaAs, attenuation, rel. to acoustoelec. current oscill. 2—51040
- Gd, magnetoelastic depend of attenuation, 13 kOe max., 270-320 K 2—44260
- H_2, isotopic, rotational relaxation effects 2—46858
- $LiNbO_3$, rotated Y cuts, leaky wave attenuation 2—51025
- MnO, coefficients at room temp. 2—43971
- NiO, coefficients at room temp. 2—43971
- $5PbO.3GeO_2$, ferroelec. material, acousto-optical figure of merit, acoustic attenuation 2—64849
- SiC, fracture energy relation, thermal shock behaviour, acoustic damping 2—60890
- TeO_2, attenuation coeffs. rel. to acousto-optic device applic. 2—51027
- YIG garnet, magnetoelasticity, domain wall motion 2—61097

acoustic waves, ultrasonic
- *see also Nuclear acoustic resonance*
- — 2—72462
- acetic acid/acetone mixtures, H bond formation causing ultrasonic relaxation, two state model 2—43322
- alcohols, compressional study through pseudo-Gruneisen parameters 2—83789
- alkali halide, phonon absorp., relax. theory 2—68233
- anharmonic metal, attenuation in collision free regime 2—43966
- anharmonic metal, attenuation in collision-dominated regime 2—43965
- aqueous acetic acid solution, u.s. absorption from 15-85 MHz 2—74542
- aqueous solutions of DNA, relaxation frequencies 2—80116
- attenuation, CW technique for obs. 2—58914
- attenuation and modulus meas. in wires at elevated temp. and ultrasonic thermometry 2—49189
- attenuation dependence on pressure in perfect crystal 2—73072
- attenuation meas., beam divergence effect 2—73434
- p-azoxyanisole liquid crystals as function of orientation and temp. 2—50334
- p-azoxyphenetole liquid crystals as function orientation and temp. 2—50334
- benzene, attenuation meas. in 600-900 MHz range using Brillouin scattering techniques 2—71198
- benzene-cyclohexane system on saturation line 2—71199
- chemical relaxation studies, resonance technique 2—76372
- cryostat for investigations of massive solids from 0.32 to 2.2°K 2—61093
- ferromagnet, rel. to dynamic effects of domain struct. 2—61488
- flexural wave attenuation in tube for liquid level detection 2—49168
- flint, u.s. attenuation 10-70 MHz 2—70025
- fluids of non-uniformity of acoustical fields 2—82365
- halobenzenes, 20—96°C, hypersonic freq. 2—77429
- iron, cast, during solidification 2—71669
- isopaustic glasses, u.s. delay lines 2—78928
- liquid crystal, study of hypersonic waves at cholesteric-isotropic transition 2—80454
- liquid crystals, cholesteric nematic transition, ultrasonic pulse-echo attenuation meas. 2—80456
- MBBA liquid crystals as function of orientation and temp. 2—50334
- methane binary mixtures with He, Ar, Xe, meas. of rotational relaxation times 2—64219
- N-p- methoxybenzylidine-p-butylaniline nematic liquid crystal, temp. dependence of attenuation 2—46953
- microwave surface wave attenuation due to gas loading 2—51009
- momentary contact method with pressure coupling for hot specimens rel. to u.s. attenuation in steel at 1200°C 2—74978
- polymer solutions, 9-900 MHz, 20°C, effect of conc., meas. 2—46954
- polymer solutions, ultrasound attenuation, frequency behaviour 2—56503
- polymethylmethacrylate, temp. dependence of u.s. absorption in conc. solns. in 9 to 900 MHz range 2—60472
- polystyrene, temp. dependence of u.s. absorption in conc. solns. in 9 to 900 MHz range 2—60472
- polystyrene solns., relax. freqs. 2—80114
- polyvinyl acetate solution in toluene dielectric dispersion 2—83376
- primary alcohols, evaluated from relaxation time and relaxing compressibility 2—74541
- pulse echo system for obs. in megahertz region 2—55526
- relaxation spectra of coupled chemical reactions, interpretation within theory of irreversible thermodynamics 2—54532
- Rochelle salt, attenuation and ferroelectric anomalies 2—74988
- semiconductor, C_{6v} class cryst., piezoelec. interaction of transverse u.s. waves with charge carriers 2—54030
- space charge effects on attenuation symmetry of u.s. amplification by piezoelectric semiconductors 2—51031
- spin echoes, generation and detection 2—44312
- steel, cast, during solidification 2—71669
- superconductor, dirty two-band, mixed state coeffs. near H_{c2} 2—47871
- surface, and applications 2—43973
- water, excess absorption evaluated from relaxation time and relaxing compressibility 2—74541
- water, open packed state mole fraction, adiabatic volume viscosities, press. depend., u.s. absorpt. obs. 2—60447
- Ag, attenuation, Gruneisen mode and const., phonon viscosity and thermoelastic effects 2—68234
- Al, electron-phonon interaction const. determ. in normal and supercond. states 2—81049
- Ar-N_2 mixtures, kinetic interpret. of relaxational absorpt. 2—71116

Absorption continued
acoustic waves, ultrasonic continued
Au-47.5 at.%Cd alloy, attenuation in cubic-orthothombic phase transform. region 2—77643
Au, attenuation, Gruneisen mode and const., phonon viscosity and thermoelastic effects 2—68234
Au films, temp. depend. meas. by pulse-echo method 2—77780
CS_2-organic liquid binary mixtures 2—46951
CdS, non-electronic attenuation of longit. waves 2—43974
CdS, role of hopping conductivity 2—71733
$Ce(NO_3)_3$, aqueous solution at 25°C, relaxation obs. 2—53427
Cu, attenuation, Gruneisen mode and const., phonon viscosity and thermoelastic effects 2—68234
D_2O, structural absorption and adiabatic volume viscosity 2—56500
$GdAlO_3$, obs. of u.s. attenuation in high magnetic field, spin wave interactions 2—54348
o-H_2, rot. relax., 170-300K 2—80909
Ho, paramag. phase, quadratic field depend. of attenuation coeff. 2—68522
InSb, degenerate, attenuation variation of 9 GHz u.s. waves 2—64845
$KMnF_3$, attenuation decrease below canting transition due to magnetoelastic propag. 2—54356
$xK_2O(1-x)SiO_2$ glass, u.s. vel. and absorpt., meas. apparatus, 0—300K 2—74983
$La(NO_3)_3$, aqueous solution at 25°C, relaxation obs. 2—53427
$LiNbO_3$, hypersonic attenuation, 2620 MHz, temp. depend., 77-300 K 2—57050
$LiNbO_3$, X-cut, microwave phonon attenuation, hypersonic attenuation obs., temp. effects 2—68225
NaCl, dislocation- phonon interaction, 70-300K, attenuation study 2—83975
$NaClO_3$, excitation of ^{23}Na n.m.r. 2—78166
Nb, supercond., longitudinal absorpt., 2-band character 2—68347
Nb, superconducting, meas. of longitudinal ultrasonic attenuation, evidence against multiple energy gaps 2—75070
Ni, 5-134MHz, mag. contribution 2—77782
Pb film, supercond., attenuation at 9.4 GHz 2—61229
$Pr(NO_3)_3$, aqueous solution at 25°C, relaxation obs. 2—53427
$RbMnF_3$, attenuation near Neel temp., antiferromagnetic resonance 2—43975
Sb_2S_3, and vel. 2—80914
Se, molten, relaxational ultrasonic attenuation 2—43353
p-Si, attenuation stress depend., bound hole model 2—54031
Sn, superconducting, effect of strain 2—51106
$SrTiO_3$, degenerate semicond., effects of longitudinal mag. field 2—71731
TiO_2, rutile, temp dependent attenuation for 3GHz and 9GHz waves 2—51028
$Y_3Fe_5O_{12}$ garnet, ultrasound absorpt. in vicinity of mag. phase transition 2—71735
$Yb(NO_3)_3$, aqueous solution at 25°C, relaxation obs. 2—53427

electromagnetic waves
see also Spectra (radiofrequency subheadings)
acrylates, max. in mm. region 2—60491
atmosphere, extinction of e.m. energy in 8-12 μm window by particulate matter 2—65772
atmospheric impurity gases O_3, CO, N_2O 2—48518
attenuation compensation analysis rel. to radar meas. of rain rate 2—75501
clouds, i.r. absorption off tropical east-coast Australia 2—65764
D-region, rel. to solar proton during PCA events 2—48575
dilute medium, absorpt. coeff. freq. shift rel. dielec. const. 2—66658
Earth-crust waveguide, e.l.f. 2—45616
Earth-crust waveguide, u.l.f. modes 2—45617
Earth-crust waveguide from e.l.f. to v.l.f. 2—52334
Einstein-de Sitter cosmology with plasma coupled to radiation at relativistic temperature 2—68998
Einstein-de Sitter cosmology with plasma coupled to radiation at non-relativistic temperature 2—68997
hot spot generation in lossy multilayer spheres, differential temp. rise obs. 2—49203
human body in resonance region, rel. to admittance and radiation efficiency meas. in 30 to 70 MHz 2—49227
interstellar, research development (1900-30 period) 2—81842
ionosphere, 2.0, 2.5, 3.0 MHz frequencies, seasonal anomaly 2—78395
ionosphere, attenuation surfaces in vicinity of cross-over level and whistler propagation 2—72858
ionosphere, cosmic radio noise absorption, riometry 2—84902
ionosphere, obs. by radio astronomic polarization method 2—48567
ionosphere, radiowave absorption on 1.725 MHz and winter anomaly during sunspot minimum 2—54891
ionosphere, worldwide morphology 2—84905
ionospheric D- and E-regions, absorption at 2.2 MHz over Haringhata 2—65968
ionospheric v.l.f. and e.l.f. waves in whistler mode, variation in absorption with solar activity and latitude 2—72855
ketones, aliphatic, in benzene, of microwaves, dielec. absorpt. and props. 2—60509
laser beam in water and atmospheric media 2—69955
lower nighttime ionosphere, indication of ionization processes 2—48579
metal films in magnetic field, microwave absorption peaks due to Doppler-shifted cyclotron resonances 2—80941
microwave absorption heated samples, dynamic high-temp. complex permittivity meas. 2—49237
microwave absorption in lower atmosphere of Venus 2—48780
microwave absorption in polar liquid, Brownian motion 2—49209
millimeter waveguide line attenuation, meas. by shuttle pulse method and pulse single reflection method 2—63192
plasma, absorption of extraordinary wave 2—70907
plasma, in hybrid resonance region 2—46736
plasma, linear transformation and absorption of e.m. waves 2—56352
polar liquid, microwave radiation 2—55604
rain, meas. at 10 GHz using ADA 2—54865
rain, on slant-path at 10 GHz, radar-derived statistics 2—54867
rectangular waveguide loaded with dielectric slab in H-plane 2—59001
in snowfall at centimetre and millimetre wavelengths 2—51628

Absorption continued
electromagnetic waves continued
submillimetre wavelengths, air pressure effect 2—55602
tropospheric slant path, at 11.75 and 17 GHz, in UK 2—72811
v.l.f./e.l.f., transpolar propagation, laboratory simulation 2—65942
water, dielectric absorption around 70 MHz, meas. of total impedance and phase angle 2—74552
Ar and Kr laser lights in water 2—76512
BaF_2, low temp. plasma produced radiational defects 2—71452
CO compressed gas, meas. of microwave absorption of 9.75 GHz using resonant cavity technique 2—53339
Er, mag. reson., microwave absorpt., 24 GHz and 100 GHz 2—65318
Ge:Sb, monochromatic submillimeter, photocond. 2—81180
Ge microwave absorpt., by electron-hole drops 2—57209
H, interstellar, self absorption in large region toward galactic centre 2—44885
H_2, of microwaves, at high press., Uranus atmos. obs. 2—55150
InSb, hot electron absorp. of mm. and sub mm. waves 2—78119
InSe single crystals reflection and absorption in the i.r. region 2—81395
$MnAu_2$, mag. reson., microwave absorpt. obs. 2—65318
N_2O compressed gas, meas. of microwave absorption at 9.75 GHz using resonant cavity technique 2—53339
$NaNO_2$, ferroelec., modulation of millimeter wave absorp. by polariz. reversal 2—48212
O plasma, 50-70 MHz 2—74368
Pb-Ir superconducting wire, microwave absorpt., rel. to mag. field and temp., 9.2 GHz 2—84306
Si microwave absorpt., by electron-hole drops 2—57209
Tb, ferromag. reson. at 24 GHz, microwave absorpt. obs. 2—65318

light
see also Atmospheric optics; Densitometry; Films, solid/optical properties; Filters, optical; Optical constants; Pleochroism; Spectra; Transmission/light
— 2—68427
— 2—68653
$A^2B^4C_2^5$ type semiconductors lowest conduction band minima 2—80983
acetic acid, O—H overtone bands and pot. energy curves 2—56211
acetonitrile-chloroform mixtures, complex form., solid phase 2—60042
aerosol attenuation of visible and i.r. radiation rel. to air humidity 2—81660
aerosols, atmospheric, from 0.2 to 40 μm real and imaginary values 2—65773
aerosols in atmos., radiative props. of atmospheric windows 2—65793
alkali borate glasses, Ni^{2+}-containing, anomalies, ligand field approach 2—75303
alkali halide crystal, high symmetry exciton 2—68308
alkali halide phosphors, lineshpaes of C-bands by method of moments 2—57346
alkali halides, $Co(CN)_6^{3-}$ doped, vibr. and electronic props. 2—54413
alkali halides, coloured, spin-orbit effects in F- and K-bands 2—51335
alkali halides, F-centre band, spin mixing and circular dichroism, electron spin memory 2—53750
alkali halides, rare earth doped, Z-centres, optical absorpt. and e.p.r. at 77K 2—71526
alkali halides, reson. of electronic polaron 2—72313
alkali metals, interband absorpt., plasmon sidebands 2—51334
alkali metals, phonon effects 2—61628
alkali silicate glass, Er^{3+} sites, low temp. spectroscopy study 2—54429
alkaline earth fluorides, point defects vibr. spectra, i.r. absorpt. obs. 2—71724
alkyl benzenes, pulsed radiolysis, spectra of transitory species 2—57435
alloy, virtual bound state, model 2—65245
alloyed semiconductor, absorption coeff. in $\omega > Eq$ region in presence of resonant scattering 2—72316
o-, m-, p-aminobenzaldehydes, vibr. assignments 2—56214
m- aminobenzotrifluoride, fund. vibr. assignment 2—56215
amorphous, intrinsic behaviour, electronic and vibronic contribs., review 2—72293
amorphous system, theory 2—61622
analogue computing system for gaussian and lorentzian simulation 2—45782
aniline derivatives, u.v. absorpt., temp. effect, conform. change 2—68812
anthracene, auto-association of frozen solns., absorption spectra 2—54557
anthracene crystals and molecules in solution, two-photon absorption spectra meas. using dye lasers 2—72354
antiferrodielectric, effective electrodipole transitions, optical and spin excited states 2—72290
antiferromagnetic insulator, magnon induced sidebands in optical transitions 2—54408
aromatic molecules adsorbed on MgO surface, photoactivation by u.v. radiation, electronic absorption spectra 2—78206
atmosphere, i.r. attenuation, aerosol extinction contrib. 2—81647
atmosphere, realistic calc. 2—62271
atmosphere absorption profile, determ. by scatt. independent method 2—81645
atmospheric aerosol constituents 2—57946
atmospheric aerosols, and scattering 2—65780
atmospheric aerosols, sunlight absorption coefficients, measurement methods 2—51617
atmospheric mols., absorpt. cross sections, 100-600 Å 2—80057
atmospheric transparency in u.v. 2—75608
atmospheric water vapour measurement, absorption hygrometry technique, models 2—84864
atomic, criterion for overlapping spectral lines 2—52903
atomic two-level system, theory of saturated- absorption line shapes 2—70569
ATR spectroscopy, use in surface chemistry 2—65360
azines, triplet-triplet and singlet-singlet absorpt. band intensities, electronic transitions 2—77138

Absorption continued
light continued
azolidones, i.r. absorpt. spectra rel. to H bonding and mol struct. 2−56216
BDPA film, organic free radical, vapour deposited 2−56598
bee photoreceptor 2−62886
benzene, i.r. dispersion study of absolute integrated absorption intensity 2−64464
benzene, liquid, meas. of absorption spectra in u.v. region in room temp. to freezing point range 2−71208
benzene, pure and isotropic mixed crystals, absorption spectroscopic study of isotope effects intermolecular interactions 2−81357
benzoyloxyimino-4 tetrahydroquinazolines and hexahydropyrimidines, vibr. band obs. 2−53049
benzylamine, near u.v. absorption spectrum 2−74286
bleachable absorber-laser amplifier-detector combination, wide-angle low-noise laser receiver 2−45755
borazine, gaseous, 2000Å absorpt. system, vibronic analysis, electronic transition 2−80090
boundary conditions in exciton absorption region 2−65244
α-brass, optical transitions 2−44362
β-carotene, 5000-25000Å 2−72072
β-carotene film, solid, gas adsorption effect on absorpt. spectra 2−57355
chalcogenide glass, evidence for states in band gap 2−61334
chalcogenide glass, parasitic absorpt. bands elimination 2−54411
1-chloronaphthalene, liquid, complete polarization study of two-photon absorption 2−43371
chlorostyrenes, i.r. absorpt. bands, vibr. assignment 2−56225
colour centre behaviour and band modes in semiconductors and insulators 2−54448
colouring of Martian surface rel. to laboratory studies $(C_3O_2)n$ polymer 2−78542
complex molecules in solid solutions, with two-photon excitation, dichroism of two-photon light absorption 2−42837
crystal, at 10.6 μ via ionic dipole-dipole interactions 2−57320
crystal, excitonic region, review 2−72317
crystal surface, i.r., rel. to surface phonons and gas surface interactions 2−50522
cu Cu-Pd alloy, disordered and ordered band struct. 2−84237
detergent solutions, dye aggregation 2−78202
diamond, first-principles energy-band calc. 2−84464
diamond, irradiated, N impurity effects on annealing obs. 2−71453
1,4-diazabicyclo (2.2.2) octane and methyl analogue, struct. effects on photophys. processes 2−81512
dielectric film, sputtered and evap., optical props. as function of deposition conditions 2−48131
2,3-difluoroaniline, u.v. spectra, vapour phase 2−77100
4-N-dimethylaminopyridine, EPA solution, flash photolysis, triplet-triplet absorption 2−74548
dimethyloxalate, electronic states 2−42980
diode, light emitting, efficiency, carrier diffusion length, absorpt., auto-photovoltaic meas. 2−61451
diphenyl crystal, rel. to luminesc. and electron excitation energy migration 2−72425
diphenylamine, two-photon fluorescence patterns, absorption cross sections and picosecond relaxation times 2−43379
disordered force constant systems, effect of disorder on absorption determ. from single particle Green's function 2−43958
disperse systems, effect on dependence of relaxation coefficients on particle size 2−53461
dispose systems, link with solid state spectra through weak absorption 2−53460
DNA hypochromism, sequence depend. using Hartree calcs. 2−80118
DPPH film, organic free radical, vapour deposited 2−56598
Drosophila melanogaster visual screening pigments in situ absorption spectra 2−69472
dye laser, triplet state, rel. to chem. quenching 2−63334
E1 sum rule, rel. to orbital g-factor change due to exchange currents 2−63757
electron-photon interaction, anomalous, quantum transport in strong elec. fields 2−61147
ethylene-vinyl acetate copolymers, liquid lattice type absorption for far i.r. and millimetre waves 2−53437
exchange interaction meas. technique 2−61730
exciton lines, at high exciton conc., theory 2−71807
F-centres, higher absorp. bands, calc., review 2−56746
f.c.c. cryst., antiferromag., by magnons 2−61550
feldspar, force field obs. 2−43955
ferroelectric, interband absorpt., in quasi-classical random field, theory 2−48166
films, extinction coeff. det. 2−59224
filter multilayer, tandem arrays, radiant transmittance, attenuation optimization 2−79382
filters, for contrast enhancement of light sources 2−55763
fluoromethane, solid, i.r. spectra, vibr. modes 2−57356
fluorophlogopite, Ti and V impurities, spectra and e.p.r., levels of Ti^{2+} and Ti^{3+} ions 2−84562
formic acid, O−H overtone bands and pot. energy curves 2−56211
fulminic acid, u.v. absorpt. spectrum, gas phase, ground-excited state transition 2−80098
furazan, u.v. absorpt., non-planar state obs. and barrier to planarity 2−70768
in galaxies, statistical evaluation 2−72978
garnet, almandine, optical absorpt spectra of Fe, cubic field approx. 2−72328
gas meas. of effective absorption coeff. using wide bandwidths and a number of path lengths 2−43270
gas-dust medium, meas. of shock relaxation time by attenuation technique 2−46834
germanium (IV)-mandelic acid coordinated cpds., i.r. spectra 2−83332
glass:Nd, effect of phase separation 2−57372
glass, exponential absorp. edge, theory review 2−78078
glass, photochromic, containing AgCl, effects of heat treatment, u.v. irrad. and CuO additive 2−78065
glass fibre, effect on light propag. 2−42242

Absorption continued
light continued
glasses and melts, systems $Co(PO_3)_2$-$NaPO_3$ and $Co(PO_3)_2$-KPO_3, spectra, effect of comp., temp., and wavelength on molar absorption coeff. 2−84481
glasses containing Pr combined with Cr, spectral properties 2−75286
graphite, from energy band struct. 2−84234
group III-V semiconductor, core levels detn. 2−65240
heart conditions by photometry using whole blood 2−45023
hemoprotein derivatives, circular dichroism in visible region, nonlinear iron-ligand bonds 2−64197
heterocyclic five membered ring compounds, solns. i.r. spectra 2−83284
hexamethylbenzene, absorption spectra, vibronic bands 2−51351
ice, trapped electron, optical absorption spectra 2−75295
III-V compounds, dominant second order dipole moment contribution two two-phonon sidebands in i.r. absorption 2−75284
indirect many-photon transitions, in quantizing mag. field, in Ge- and GaP-type crysts. 2−71920
interband absorption, in quasi-classical random field, theory 2−48166
intermolecular complexes, mol. crysts., absorpt. spectra, bibliography 2−48159
interstellar, UBV photometry of Maffei 1 and 2 2−55016
iodide, charge-transfer- to-solvent absorpt. bands in far-u.v. 2−56505
ionic crystals multistage formation of irradiation-induced F-centres 2−78087
ionic solid, exponential absorp. edge, theory review 2−78078
ions, vacuum u.v. absorption meas. using new continuum light source 2−77001
i.r., by atmospheric aerosol substances 2−65777
laminar specimen of translucent and photoluminescent material 2−57343
laser beam intensity attenuation by turbulent absorbing media, analyses 2−49389
laser pulse, short duration, peak intensity and energy content estimation using saturable absorbers 2−66775
laser pulse propagation in molecular absorber and minimizing of heating effects applic. to atmosphere 2−84860
lightning channel 2−65796
low loss optical glasses, laser measurement 2−63407
macromolecules in solution, transient light scattering 2−50378
magnetically ordered crystal, i.r. spectra, morphic effects 2−72359
many-photon absorpt. in crystals and their applications, review 2−75282
$Me^{II}Me^{VI}O_4$:U single crystals with scheelite structure, Me^{II}=Ca, Sr, Ba, Me^{VI}=Mo, W, absorption and luminescence spectra 2−68676
measurement, by disturbance of total internal refl., accuracy 2−45781
metal clad dielec. waveguide, mode selective props., attenuation, phase consts. 2−78964
metal film, quantum size effect 2−72314
methane, 3.39 μm transition, laser freq. and wavelength meas., speed of light 2−78758
methane, laser radiation absorption behind shock wave front 2−64396
methane, transient saturated molecular absorption 2−43274
m-, p- methoxyphenyl thioethers, u.v. spectra, steric interactions 2−56247
methyl cyanide and isocyanide in solid Ar, matrix isolation studies 2−56246
methyl group stretching and bending vibrs., substituent effect on i.r. intensities 2−56245
methyl iodide, ν_4 band, spectroscopic consts. detn. 2−60077
mica, thermally modulated absorption of Fe^{2+} ions 2−61637
mineral, spectra meas. at high shock press., apparatus design 2−61828
minor atmospheric constituents near 8 cm^{-1} 2−51585
molecular, crystals, temp. depend. of absorpt. bands intensities of spectra at Fermi resonance 2−81373
molecular cryst., impurity one-phonon spectra, mirror symmetry breakdown 2−65271
molecular crystal with 2 exciton state regions, absorption spectrum 2−72310
molecules, two-photon absorption cross section meas. 2−41952
molecules in solution organic dye two-photon absorption profile, apparatus 2−66734
moving particle, emission and absorption, relativistic kinetic temperatures 2−66474
multiphoton absorption cross sections, exptl., determ. of correction factor for distrib. of laser intensity 2−49990
naphthalene vapour, vacuum u.v. absorption spectrum, Rydberg series assigned 2−80064
α-naphthol in pure and mixed crysts., electronic singlet-singlet spectra 2−65395
negative, by dense ionized gas 2−70910
nonlinear, and optical breakdown of liquid laser attenuators 2−42119
nonlinearity in coefficient, spectrometric determ. 2−63427
O_2 and O_3 in atmosphere, of solar radiation in 2150 Å region 2−65766
olivine, thermally modulated absorption of Fe^{2+} ions 2−61637
optically inhomogeneous layer, exact solutions for inverse boundary-value problem 2−59223
organic dye solutions in far anti-Stokes region, correspondence with fluorescence spectra 2−74546
organic laser dyes, changes caused by photobleaching 2−69928
organic liquids, inverse Raman effect 2−71206
oxalic acid, electronic states 2−42980
oxide glass, alkali metal cation vibrs., far i.r. spectra study 2−71284
paraffins, liq., two-phonon absorpt. processes 2−74550
paramagnetic crystal, one-phonon absorpt. by impurity ions, intensity calc. 2−51331
particulate suspensions, interpretation of Kubelka-Munk coefficients 2−49426
permalloy, film, on CaF_2, optical absorpt., polarization anisotropy rel. to thickness and orientation 2−57324
phenanthrene, polarized absorpt. edge and exciton-photon interaction 2−44386
phonon-photon interactions in solids, review 2−72318

Absorption continued
light continued
phthalocyanine solns., absorpt. from excited singlet states 2—84677
phthalocyanine solns., characterization of generation region of ruby lasers 2—49379
in plane parallel turbid media, equivalence of Kubelka-Munk and Chandrasekhar approaches 2—49416
PMMA, γ-irrad., absorpt. spectrum, optical density increment, u.v. filter 2—72357
polar liquids, far-i.r. and microwave absorpt., theory 2—77434
poly(methyl methacrylate), radiation produced free radicals 2—84671
polyatomic mols., absorpt. and luminesc. relationship in four-level system of electronic states 2—64087
polymethine cyanide dye, saturable props. rel. to variable ultrafast photographic shutter 2—49405
polystyrene, isotactic, crystallization from solution , i.r. spectra 2—43456
polystyrene latexes, multiple scattering, determ. of coeffs. of scattering and absorption 2—43400
powder, Kubelka-Munk diffuse reflectance remission function rel. to fund. optical parameters 2—79329
propionitrile-chloroform mixtures, complex form., solid phase 2—60042
pyrimidine crystals, spectra at 4.2K 2—44412
quartz, rel. to electrolysis in air and vacuum 2—74802
quartz, synthetic, loss at 1.06 μ, related to fibre optic appl. 2—48136
racemic mixtures, polarization dependence of multipole absorption probability rel. to optical activity 2—49994
rare earth β-diketonate complexes, i.r. absorpt., vibr. modes 2—46577
rare earth metal garnet, containing Fe ion 2—75305
rare earth metal halides, variation of i.r. absorption spectra with nature and structure 2—78083
rare earth oxide systems, far-i.r. spectra, phonon excitation 2—51346
Rayleigh approx., and emission cross sections of nonspherical particles 2—64477
Renner systems, semiclassical approximation of absorpt. and luminesc. bands due to crystal imperfections 2—81393
Renner-type system, with strong vibr. coupling, band shape determ. 2—65248
Rhodamine 6G, excited band obs. 2—60484
rhodamine 6G, two-photon fluorescence patterns, absorption cross sections and picosecond relaxation times 2—43379
ruby, h.p. spectra below elastic limit 2—61630
saturable absorber, picosecond and subpicosecond light pulse generation using Nd:glass laser 2—42104
scattering media, light beam attenuation, exponential low limits, scatt. indicatrix 2—56527
sea water, axially symmetric submarine daylight field 2—65607
seawater, beam attenuation coeff. rel. to axially symmetric light field 2—57892
semiconductor, amorphous, absorp. edge pressure effects rel. to bond struct. 2—61333
semiconductor, amorphous, absorption edge temp. depend. 2—75293
semiconductor, amorphous, Urbach tail in optical absorpt. edge 2—68641
semiconductor, degenerate, free carrier absorp., quantum theory 2—51329
semiconductor, direct gap, exciton absorpt. meas. method 2—44373
semiconductor, disordered, optical absorp. edge, effective impurity model 2—61169
semiconductor, disordered, theory of electroabsorption 2—51330
semiconductor, electronic transitions, opt. consts. evaluation, review 2—72291
semiconductor, exponential absorp. edge, theory review 2—78078
semiconductor, group II-VI cpds., radiation induced and growth defect obs. 2—47372
semiconductor, heavily doped, absorp. edge at low temp. 2—65247
semiconductor, II-IV-V_2 and I-III-VI_2, i.r. transmission cut-off 2—78058
semiconductor, incompletely ordered, exciton light absorpt. 2—78094
semiconductor, many photon absorpt. by carriers, inc. electron-phonon interaction 2—84521
semiconductor, nonparabolic band, free carrier light absorp. theory 2—75285
semiconductor, photomagnetoelec. circulating current study, mag. flux rel. to absorpt. 2—68483
semiconductor, plasmon-assisted i.r. absorpt., cyclotron resonance harmonics 2—54409
semiconductor, polar, exciton-phonon interactions, Urbach's rule 2—44369
semiconductor, two-photon interband transition in arbitrary elec. field 2—61623
semiconductor, with band extrema at Brillouin zone centre, interband optical transitions 2—65250
semiconductor, with nipi superstruct., critical and electrical props. 2—65237
semiconductor film/solid surface, as substrate thermal transients meas. technique 2—58972
semiconductors, II-VI, deep Cu impurity, dynamical Jahn-Teller interaction 2—80954
silicate glass, ligand field spectra of Ni^{2+} and struct. 2—50409
small polaron, in high electric fields 2—57344
soda glass:Tb^{3+} 2—57374
solar broadband irradiance attenuation in ocean 2—62019
solar cells, honeycomb absorbers on collecting base surface, absorption efficiency 2—41909
solids, optical versus thermal transitions at high pressure 2—51328
solvated electrons, absorpt. spectrum resolution, band shapes 2—67831
spectrometer, pseudo-double beam atomic absorption, capable of compensating for nonspecific absorption 2—59287
spinels, II-IV, i.r. absorpt. spectra, ionic ordering 2—72342
in stratified Rayleigh atmosphere, numerical model 2—73078
TCNQ complexes, with quinolinium and triethylammonium, i.r. spectra, vibronic effects 2—81387
tetrolaldehyde, internal rot. effects on band contours 2—80093

Absorption continued
light continued
thiazanes, i.r. absorpt. spectra rel. to H-bonding and mol. struct. 2—56261
thin film multilayer system, transmittance performance evaluation using computer 2—59222
thin film waveguides 2—63416
thiourea, ferroelec. and paraelec. phases, i.r. 2—75309
three-photon phenomena for randomly oriented molecules, polarization dependence 2—67441
toluqinone single cryst., excitonic and zero-field splittings of first triplet state 2—78209
transition metals optical absorption, a model calc. 2—84498
trapped electrons in spherical pots., photodetachment spectra 2—53435
triaryl 1,3,5-trivinylbenzene derivatives, i.r. spectral band obs. 2—83333
trifluorochloroethylene, absorption saturation and optical strength for CO_2 laser pulses 2—67523
triglycine sulphate, forbidden band, width determ. 2—77932
triphenylamine light-induced conversion to excited triplet state of 11,12-dihydrocarbazole 2—57431
triphenylmethane, exciton splitting in electronic spectra 2—81523
turbid medium, radiative transfer theory, efficient stream distributions 2—79356
two photon absorption by a crystal in elec. field 2—65243
two-photon, by excitons, elec. field effect 2—65221
two-photon abs. coeff. in crystals, polarization dependence, calc. 2—78060
two-zone molecular crystal and absorption band spectra 2—72315
Urbach rule, unified mechanism 2—54430
vapour with hidden alignment in magnetic field, meas. of relaxation constant 2—42741
vibronic spectra of absorption and luminescence, distortion of mirror symmetry 2—78108
1-vinylpyrene and poly(1-vinylpyrene), photophys. processes 2—65400
visual photoreceptors, light absorpt. rel. to anomalous dispersion 2—82062
vivianite, thermally modulated absorption of Fe^{2+} ions 2—61637
water, meas. in vacuum u.v. 2—50361
water vapour absorption meas. using single frequency CO laser 2—82519
p-xylene, relative intensities of vibr.-struct. lines in absorpt. spectrum 2—67525
$[PtCl_4]^{2-}$ type planar square complexes, absorpt. band lineshape, electron-vibr. interaction 2—80054
Ag particles in glass matrix, particle size effects 2—54412
$AgBr:Ti^{3+}$, V^{3+}, Cr^{3+}, charge transfer spectra 2—51333
AgBr, chemical sensitization by doping, obs. of electronic mechanism 2—81545
$AgCl:Ti^{3+}$, V^{3+}, Cr^{3+}, charge transfer spectra 2—51333
$AgGaS_2(Se_2)$, band struct. study 2—75276
Ag_2S epitaxial thin films, meas. at room and liquid nitrogen temps. 2—53567
Al, absorpt. peak temp. shift 2—54414
Al, far-u.v. spectra, discrete features identification 2—67388
Al film, struct. change effects on opt. absorpt. 2—54415
AlAs epitaxial layer, on GaAs, rel. to semicond. props. 2—71881
Al_2O_3, ruby, energy levels of Cr^{3+} pairs 2—68633
$Al_2O_3CR_2O_3$ system, colour changes rel. to sub-solidus phases 2—53983
Ar-Xe solid solution, 8-10.5eV, rel. to exciton studies 2—68634
Ar, absorption coeff. of spectral lines in wall stabilized arc at atmos. press. 2—70575
Ar I, relative transition probabilities, absorpt. determ. 2—70582
$As_xIn_{1-x}SeI$ vitreous compounds, $x=1.00$, 0.95, 0.90, 0.80, i.r. absorption, determ. of energy structure 2—78095
As_2S_3 crystals, massive and thin film, self-absorption edges, effect of temperature and polarization 2—84479
As_2Se_3, vitreous, i.r., effects of group III A element dopant 2—61300
As_2Se_3, vitreous and crystalline, modulation spectroscopy, electron energy spectrum obs. 2—61631
As_2Se_3 film, crystalline and amorphous, ion bombardment effects 2—60646
$3As_2Se_3.2Sb_2Se_3$, films, amorphous, band struct. obs. 2—54186
AsTeI glass, rel. to electronic transport props. 2—61296
Au-Cr(V) alloy systems, band struct. obs. 2—44371
Au black deposit, i.r., rel. to prep. conditions 2—57347
B, far-u.v. spectra, discrete features identification 2—67388
BN, from energy band struct. 2—84234
$B_3N_3H_6$, symmetry-forbidden ${}^1A_2'$-${}^1A_1'$ transition analysis 2—70684
BP, bandgap obs. 2—50567
$BaBr_2$, F-centre spectra 2—51336
$Ba(Ce_{1-x}Ta_x)O_3$, and electronic transition at $Ta^{4+}(5d^1)$ 2—75203
$BaCl_2$, F-centre spectra 2—51336
BaF_2, high temp., colour centres 2—77597
BaF_2, low temp. plasma produced radiational defects obs. 2—71452
BaF_2 colour centre interconversion induced by electron irradiation 2—77598
BaFCl, X-irrad. and additively coloured, F-centres 2—64680
BaO, free carrier absorption in near i.r. due to F, F^+ centres 2—74803
$Ba_2ZnGe_2O_7:Nd^{3+}$, absorpt. and fluorescence spectra, Nd^{3+} stimulated emission and laser action 2—61705
Be, far-u.v. spectra, discrete features identification 2—67388
Be film, on dielec. substrate, elec. resist., supercond. transition temp., absorpt. spectra 2—72323
BiOI, BiOBr, BiOCl, fundamental absorp. edge, band struct. effects on laminarity 2—75287
C, far-u.v. spectra, discrete features identification 2—67388
C black, tinting strength 2—75281
C film, amorphous 2—61302
CO, adsorbed on Au, i.r. refl.-absorpt. spectra study 2—60676
CO, chemisorbed layer on W, vibr. freq. refl.-absorption i.r. spectra 2—47154
CO laser radiation, intracavity water vapour cell to meas. absorptive losses, applic. to atmospheric transmission 2—82518
CO_2, 9.33 and 10.18 μm transitions, laser freq. and wavelength meas., speed of light 2—78758

- **Absorption** continued
  - **light** continued
    - CO_2, press.- induced absorpt., ν_1 band, density and temp. depend. of intensity, crit. phenomena 2−56158
    - CO_2 continuous spectrum, calculation of absorption coeffs. oven temp. range 20000-100000°K 2−70692
    - CS_2, u.v. absorpt. near N_2 laser wavelengths, excited states population 2−80014
    - CaF_2:La,Ce, uncoloured and X-irrad., charge transfer processes 2−65253
    - CaF_2, absorp. band growth on proton irrad. 2−71454
    - CaF_2, absorp. superposition due to $\langle 100\rangle$ and $\langle 110\rangle$ oriented F_2-centres 2−53751
    - CaF_2, colour centre interconversion induced by electron irradiation, changes in adsorption spectrum 2−77598
    - CaF_2, coloured, zero-phonon lines 2−53752
    - CaF_2, high temp., colour centres 2−77597
    - CaF_2, ionicity, rel. to dispersion and absorpt. energies 2−44374
    - CaF_2, low symmetry complexes involving hydride ions paired with rare earth ions 2−47434
    - CaF_2, low temp. plasma produced radiational defects obs. 2−71452
    - CaF_2, optical absorption following intense γ- irradiation 2−84529
    - $CaF_2.3Ca_3(PO_4)_2:Nd^{3+}$, M-, N-, P_1- and P_2-centres 2−64681
    - CaO, F^+ and F-centres, temp. depend. 2−84537
    - CaO, F^+ and F′ bands 2−71523
    - CaO, Jahn-Teller coupling in excited level of F^+ centre, uniaxial stress effects 2−68635
    - CaO, neutron irrad., $F_a{}^+$ centre obs. 2−71522
    - CaS phosphor, activator and co-activator absorp. spectra 2−48239
    - $CaTiO_3:La_2O_3$, lattice distorted, colour obs. 2−74724
    - CaX_2 in e.u.v. 25 to 72 eV 2−42882
    - $CdCl_2$ crystals, impurity ion spectra at 5 eV 2−84475
    - $CdCr_2S_4$, red shift peak, mag. F′ centre model 2−80712
    - $CdF_2:Er^{3+}$, C_{2v} local-site symmetry 2−78164
    - $CdF_2:Er^{3+}$, i.r. transitions, Stark dissoc. by cryst. field 2−65305
    - CdF_2, of Er^{3+}, ion site obs. 2−54416
    - CdO microcrystals, coupled surface phonon-surface plasmon modes, i.r. 2−84263
    - CdS, exciton-impurity complex, anomalous intensity 2−72324
    - CdS, induced by strong excitation 2−78097
    - CdS, rel. to optical modulation due to moving acoustic domains 2−54418
    - CdS, single crystal, spectrum rel. to exciton band shape at 4.2K 2−80999
    - CdS, spectra, at 4.2K, localized exciton struct. 2−51366
    - CdS, two-phonon sidebands in i.r. absorption due to third order potential 2−75284
    - CdS film, optical absorpt. edges, rel. to pot. barriers at microcryst. boundaries 2−65256
    - CdS_xSe_{1-x}, by free carriers 2−75288
    - CdSe:S, local impurity and lattice vibrs., Fermi reson., absorpt. spectra obs. 2−80895
    - CdSe, exciton bound to ionized centre magneto optical obs. 2−68636
    - CdSe, exciton scatt. by dislocations 2−81007
    - $CdSe_xTe_{1-x}$, absorp. edge obs., energy band struct. detn. 2−84517
    - $CdSiP_2$, i.r., characterization 2−80599
    - CdTe, absorpt. spectra, direct exciton transitions 2−65255
    - p-CdTe, exciton mechanism, rel. to photosensitivity 2−48217
    - CdTe, resonant excitons 2−61200
    - Ce, optical absorpt. spectra, 4d-4f transition, 4d level binding energy 2−75301
    - Cl_2, cryst., i.r.-active intermol. translational band intensities, intermole. bonding obs. 2−74967
    - Cs thin films, 0.3 to 0.9 μ region 2−68597
    - CsBr:K, non-cubic Ag- centres in mixed crystals 2−44370
    - CsBr, cation impurity, i.r. spectra 2−61635
    - CsBr, electric field effects on F-band 2−51347
    - CsBr, X-irrad. at cryogenic temps., I-, α-, H, H′ and V_4 centres 2−68038
    - $CsCl:K^+$ (Rb^+), impurity-induced i.r. absorpt. calcs., lattice dynamical model 2−54419
    - CsCl, U band shape from first electronic transition of H- and D-substitutional impurities 2−47446
    - CsCl(Br)(I), vibr. absorpt. spectrum of $NO_2{}^-$ and $NO_3{}^-$ 2−77769
    - $CsCrCl_3$, single crystal polarized absorption spectra, ligand field interpretation 2−81363
    - $CsI:PO_4{}^{3-}(SiO_4{}^{4-})$, i.r. 2−54424
    - $CsI:SO^{2-}{}_4$, $CrO^{2-}{}_4$, $SeO^{2-}{}_4$, i.r. absorpt. by impurity anions 2−78086
    - $CsMgCl_3:CsCrCl_3$, single crystal polarized absorption spectra, ligand field interpretation 2−81363
    - Cs_2UBr_6, Zeeman effect of vibronic transitions 2−84528
    - $Cs_2ZrB_6:Re^{47}$, vibr. mode energies of ground state 2−57370
    - $Cs_2ZrCl_6:Ir^{4+}$, absorption spectra 2−57342
    - $Cs_2ZrCl_6:U^{4+}$, Zeeman effect of vibronic transitions 2−84528
    - Cs_2ZrCl_6, high resolution spectra analysis 2−75289
    - Cu-Ni alloys, props. of optical spectra rel. to pure Cu 2−81330
    - CuCl, electrolytic coloration study 2−83985
    - CuCl, u.v., confirmation of calc. band struct. 2−71793
    - CuCl crystals fine struct. of excitonic lines 2−80985
    - CuCl(Br), 3-30 eV 2−72326
    - CuI, low temp. reflection spectra, excitonic transitions and levels 2−72302
    - γ-CuI thin film, piezo-optical effect at 77K in fundamental absorption band region 2−48172
    - $CuInTe_2$, 295K and 77K, 0.6−5.7 eV, rel. to band struct. determ. 2−78098
    - CuNi dilute alloy, meas. at 4K, effect of virtual-bound-state 2−51337
    - Cu_2O, 1s exciton state in green series 2−72327
    - Cu_2O, i.r., normally forbidden transitions obs. 2−61636
    - Cu_2O, near i.r., rel. to band scheme 2−54420
    - $Cu_{2-x}S$, 400-1200 nm 2−78085
    - DCN, liquid and crystalline, i.r. spectra 2−57351
    - D_2pellet, laser irrad., parametric instabilities of plasma 2−67679
    - $DyVO_4$, uniaxial stress effects on absorp. spectra 2−51338
    - Er^{3+} glass, stimulated emission cross section, relative gain coeff., absorpt. and fluorescence spectra obs. 2−75323
    - Er^{3+} in phosphate and borate glasses, spectra, cryst. field effects, luminesc. efficiency 2−75307
    - Er^{3+} ions in silicate glass, photoinduced absorption spectra 2−75291
    - $Er_2O_2S:Er^{3+}$, energy levels and crystal field splittings, spectra obs. 2−51339
    - EuO:Gd, rel. to exchange-induced imperfection ionization 2−68598
    - EuO film, transparent, prep. by oxid. of Eu film 2−64568
    - Eu_3SiO_5, absorpt. edge shifts rel. to Curie temp. 2−48173
    - Fe-Au alloy, intraband absorpt., anomalous temp. depend. 2−81388
    - Fe^{2+} in micas, vivianite and olivine, thermally modulated spectra 2−61637
    - $FeBO_3$, i.r. absorpt. spectra 2−75292
    - Fe_xO-MnO solid solns., absorpt. edge, cryst. field transitions 2−48174
    - GaAs:Mg-Li, i.r. absorpt. due to pair defects, absorpt. cross section 2−81360
    - GaAs-GaP, i.r. lattice absorpt., thermodynamic props. detn. 2−57074
    - GaAs, 5 MeV proton irrad. 2−48177
    - GaAs, electron and neutron irrad., i.r. absorpt. 2−72332
    - GaAs, eletron, and neutron irrad., i.r. absorpt. band obs. 2−48180
    - GaAs, exciton absorpt. meas. method 2−44373
    - GaAs, exciton struct. of fundamental absorpt. edge and oscillatory magnetoabsorpt. 2−72331
    - GaAs, i.r. lattice absorpt., thermodynamic props. detn. 2−57074
    - GaAs, impurity electroabsorption 2−65258
    - GaAs, impurity induced i.r. absorpt., calc. by Green's function technique 2−61639
    - GaAs, many-photon absorp., carrier generation obs. 2−84519
    - GaAs, near band edge optical absorpt. rel. to excitons 2−84516
    - GaAs, resolved free-excition transitions 2−84259
    - p-GaAs, saturation intensity at 10.6 μm 2−79227
    - GaAs exciton-phonon coupling obs. 2−61642
    - GaAs(P), ionicity, rel. to dispersion and absorpt. energies 2−44374
    - $Ga_{1-x}In_xN$, fundamental absorpt. edge and energy gap 2−72329
    - GaN, fundamental absorpt. edge and energy gap 2−72329
    - GaP:N, i.r., localized vibr. modes due to N isotopes 2−68639
    - GaP:O p-n junction, deep double electron O trap transitions, photocapacitance obs. 2−75013
    - GaP, i.r. lattice absorpt., thermodynamic props. detn. 2−57074
    - GaP, laminar specimen obs. technique 2−57343
    - GaSb, excitonic effects in Landau transitions at E_1 edges 2−68404
    - GaSe, anisotropy near band edge 2−48178
    - GaSe, exciton absorpt. peak shift and phase change induced by hydrostatic press. 2−72330
    - GaSe single crystal, anomalous light dispersion in exciton line 2−78099
    - GaTe forbidden band width and exciton binding energy detn. 2−75294
    - $GdAlO_3$:Er, Zeeman spectra, Er^{3+}-Gd^{3+} exchange interaction obs. 2−57349
    - $GdCl_3$, single-ion-induced absorpt. lineshapes, magnon and exciton states dispersion 2−48181
    - $Gd(OH)_3$, single-ion-induced absorpt. lineshapes, magnon and exciton states dispersion 2−48181
    - Ge:As, far i.r., impurity conc. and compensation effects 2−68642
    - Ge:Sn heavily doped, temp. and concentration effects, direct and indirect transitions 2−77911
    - Ge, acceptors, Zeeman effect, group theoretical study 2−84264
    - Ge, electroabsorpt. edge, exciton effects 2−48189
    - Ge, far i.r., exciton and electron-hole drop obs. 2−78100
    - n-Ge, modulation by non-equilib. optical phonons in pulsed elec. fields 2−78069
    - p-Ge, photon-induced hopping on acceptors, theory 2−47923
    - Ge, quadratic Zeeman splitting of donor lines 2−57350
    - p-Ge, saturation intensity at 10.6 μm 2−79227
    - $Ge_{1-x}Si_x$, wavelength modulated, indirect phononless optical transitions obs. 2−68640
    - Ge_xTe_{1-x} alloy, amorphous, band struct. obs. 2−77904
    - H_2, collision-induced absorpt. near $\lambda=1$ mm 2−77084
    - H_2, solid, ortho, absorpt. spectra rel. to libron-libron interactions 2−74975
    - HCN, liquid and crystalline, i.r. spectra 2−57351
    - HD, vac. u.v., Rydberg states and ionization energy 2−50038
    - H_2O vapour absorpt. lines, atm., using tunable i.r. laser spectroscopy 2−84843
    - ^2H solid target, wavelength dependence of laser light absorption 2−43176
    - He-Ar mixtures, collision-induced, absorpt. near $\lambda=1$ mm 2−77084
    - He, relative absorpt. of 3889 and 10830 Å lines 2−59949
    - Hg vapour, absorpt. coeff. meas. in reson. region 2−46428
    - HgSe, HgSe-HgS solid solution, rel. to energy band struct. 2−84522
    - n-HgTe, pure, i.r. and magnetooptical absorp. 2−78101
    - Ho, u.v. spectrum classification 2−52920
    - In-Te system, film, band gap determ. for In_2Te_3 phase 2−60662
    - In film, ellipsometry obs. rel. to electronic struct. 2−72334
    - n-InAs, compensated, absorpt. edge obs. 2−75297
    - $InBO_3$, i.r. absorpt. spectra 2−75292
    - InN, fundamental absorpt. edge and energy gap 2−72329
    - In_2S vapour, thermodynamic functions, electronic and i.r. spectra, heats of sublimation and formation, 273-2000 K 2−74485
    - InSb:Zn,Ge, far i.r., energy levels of shallow acceptors detn. 2−75296
    - InSb, excitonic effects in Landau transitions at E_1 edges 2−68404
    - n-InSb, far i.r., impurity band and shallow donors obs. 2−81389
    - p-InSb, i.r. absorpt. rel. to hole and plasma currents 2−72335
    - InSe, 300K and 70K, 2.3 to 3.0 eV, hyperbolic excitons 2−81398
    - InSe, exciton-phonon interaction, absorption edge obs. 2−84518
    - In_2Se_3 film, flash evaporated, optical gap detn. 2−56593
    - $In_2Se_{3x}Te_{3(1-x)}$ single crystal, optical props. detn. 2−54422
    - Ir, absorpt. coeff. meas. in range 15-0.302 μm at 77 and 295 K 2−81359
    - K, anomalous i.r. absorpt. and collective oscills. in small metal particles 2−65210
    - K, coeff determ. in 4-10.7 eV photon energy range 2−68593
    - KBr:Na, F_b centres 2−64682
    - $KBr:PO_4{}^{3-}(SiO_4{}^{4-})$, i.r. 2−54424
    - $KBr:SH^-(SD^-)$, i.r., expt. and interpretation 2−84491
    - KBr, analysis of R_2 absorp. struct. 2−51342
    - KBr, colour centre, transient form., pulsed electron beam 2−53753

Absorption continued

- **light** continued
  - KBr, effect of melting on multiphonon i.r. spectra 2−68220
  - KBr(Cl)(F)(I), ionicity, rel. to dispersion and absorpt. energies 2−44374
  - KCL, H-centre prod. by u.v. photodestruction of U_2-centres, optical and e.s.r. obs. 2−77599
  - KCl:Ag, obs. of colour centre form. 2−80713
  - KCl:Br-, with low Br- conc., 77K 2−65259
  - KCl:Ca, Sr, X-irradiated, thermal annealing of defects, absorp. bands obs. 2−50696
  - $KCl:Co(CN)_6^{3-}$, vibr. and electronic props. 2−54413
  - $KCl:Li^+$, reorientation motions of H_a-centre 2−43648
  - KCl:Na, F_b centres 2−64682
  - KCl:Na, non-cubic Ag- centres in mixed crystals 2−44370
  - $KCl:Na^+$, X-ray irrad., hole centres, conversion and struct., optical absorpt. 2−84523
  - KCl:NaCl, symmetry of far i.r. resonant-pair mode 2−84507
  - KCl:Pb, rapidly grown from melt, impurity depend. 2−50649
  - $KCl:SH^-(SD^-)$, i.r., expt. and interpretation 2−84491
  - $KCl:SO_4^{2-}$, anion vacancy trapping, i.r. study 2−43620
  - KCl:Sr, X-ray induced defects, thermal annealing effects 2−64684
  - KCl:Tl, electron pulse irrad., rel. to colour centre formation 2−71524
  - KCl:Tl, room temperature absorption and thermal glow 2−75333
  - KCl, analysis of R_2 absorp. struct. 2−51342
  - KCl, F-centre colouring, γ-ray induced, strain effects 2−71528
  - KCl, γ-irrad. at liq. N_2 temp., hardening, H_a band obs. 2−53754
  - KCl crystals, charges during flash light excitation, spectrophotometric investigation 2−43649
  - $KI:SH^-(SD^-)$, i.r., expt. and interpretation 2−84491
  - KI-SH-, phonon sideband struct. in i.r. absorpt. spectrum 2−48185
  - $KMgF_3$-$KMnF_3$ mixed crysts., electron irrad., single defect involving F-centre, prod. mechanism 2−68040
  - KN_3, i.r. spectra, selection rules and internal ± internal and internal ± external mode absorpts. 2−72336
  - KN_3, u.v. irrad., defect identification 2−75299
  - $KTa_xNb_{1-x}O_3$, conduction band edge splitting 2−54425
  - $KTa_xNb_{1-x}O_3$, absorpt. edge splitting, paraelec. and ferroelec. phases 2−48184
  - $KTaO_3$, Urbach's tail behaviour, unified mechanism 2−54430
  - La, optical absorpt. spectra, 4d→4f transition, 4d level binding energy 2−75301
  - $LaAlO_3:Nd^{3+}$ laser crystal, absorp. spectra 2−75302
  - $La_{2.97}In_{1.94}Ga_{3.09}O_{12}$, coeff. 2−75300
  - Li films, structure causing absorption bands 2−65260
  - Li^- ion, continuous absorpt. coeff. rel. to temp. and wavelength 2−70583
  - LiF:Mg, thermoluminescence variation with impurity distribution 2−84552
  - LiF, analysis of R_2 absorp. struct. 2−51342
  - LiF, assignments of two-phonon i.r. spectrum 2−61645
  - LiF, effect of melting on multiphonon i.r. spectra 2−68220
  - LiF, isotope-induced one-phonon i.r. absorpt. 2−78103
  - LiF i.r. absorpt. and refl., breathing shell model 2−78102
  - LiF;Ti thermoluminescence variation with impurity distribution 2−84552
  - $LiIO_3$, α and β forms compared 2−81326
  - $LiNbO_3$ spontaneous parameteric scattering, idler absorption and dispersion 2−44337
  - Li_2O-B_2O_3-GeO_2 glass, i.r. spectra rel. to struct. 2−47059
  - $LiTaO_3:Cu^{2+}$, rel. to optical generation of intense picosec. electrical pulses 2−45768
  - $LiTaO_3$, self-induced thermal effects on light extinction 2−72254
  - $LiTmF_4:Ho^{3+}$, optical absorpt., emission and excitation spectra 2−81418
  - Lu I, u.v. region line series 2−56100
  - Mg, far-u.v. spectra, discrete features identification 2−67388
  - Mg_2, matrix-isolated, absorpt. peaks 3540-3700, absence of optical pumping 2−80041
  - MgF_2:CO(Mn)(Ni), impurity-ion spin-forbidden absorpt. enhancement by colour centres 2−78104
  - MgO, ionicity, rel. to dispersion and absorpt. energies 2−44374
  - MgO, MeV Ne^+ irrad., F-type centre prod., absorpt. band obs. 2−68042
  - MgO, radiation-induced $[Na]^0$ centres 2−43651
  - MgO, V_{oh} centre obs. 2−54426
  - MgO film, 0.22-8μ 2−79369
  - n-MgTe, interband magnetoabsorpt., $\Gamma_6 \to \Gamma_8$, transmission obs. at 4.4K 2−68644
  - $(Mn, Fe)_3O_4$, i.r. spectra and cation distrib. 2−61648
  - MnF_2, magnon sideband intensity 2−61647
  - MnF_2, temp. depend. oscill. strengths 2−54428
  - MnF_2, two-magnon absorpt., spin-flop transition effects 2−54358
  - MnF_2, two exciton transition, temp. depend. intensity calc. 2−61654
  - MnF_2, zero field circular dichroism, uniaxial stress depend. 2−44376
  - $MnKH(SO_4)_2.2H_2O$, Zeeman decomp. of visible absorpt. lines 2−54427
  - MoS_2, composite exciton absorpt. spectrum, optical phonon effects 2−44377
  - MoS_2, layer semicond., magneto-optical interband absorp., energy band model 2−81333
  - $MoSe_2$, i.r. absorpt. spectra, transverse optic lattice vibr. freq. 2−78105
  - $MoTe_2$, composite exciton absorpt. spectrum, optical phonon effects 2−44377
  - N, far-u.v. spectra, discrete features identification 2−67388
  - N_2, new Rydberg bands 2−42915
  - NO, i.r. vibr.-rot. spectrum, nucl. hyperfine splitting 2−64143
  - Na, anomalous i.r. absorpt. and collective oscills. in small metal particles 2−65210
  - Na atom, forward resonance scatt. in case of strong absorption 2−56101
  - Na in upper atmosphere, abundance det. 2−65831
  - $NaCl:Ag^+$, far i.r., expt. and calc. 2−84508
  - $NaCl:Co(CN)_6^{3-}$, vibr. and electronic props. 2−54413
  - NaCl:Tl, X-irrad., rel. to traps responsible for 360 and 390 K glow peaks 2−54476
  - NaCl. effect of melting on multiphonon i.r. spectra 2−68220

Absorption continued

- **light** continued
  - NaCl, F→X-centre conversion, lattice and disloc. mechanism 2−50698
  - NaCl, γ-irrad., plastic deform. effect on F-aggregate colour centres 2−53755
  - NaCl crystals containing colour centres, flow stress spectroscopy 2−81396
  - NaF:Eu crystals grown by Czochralski method, luminescence, absorption and excitation spectra 2−68686
  - $NaF:Ni^{2+}$, visible and i.r. 300K and 80K 2−84490
  - NaF, M centre optical props. 2−51343
  - NaI, adsorbed O effects 2−81399
  - $NaMnF_3$, spectra at 300K and 80K, vibration frequency determination 2−65262
  - $NaNO_3$, optical props. in vacuum u.v. region 2−84487
  - Na_2O-SiO_2 glass, i.r. spectra, pressure depend. 2−53782
  - $NdCrO_3$, optical spectroscopy 2−84512
  - Nd_2O_2S, Nd^{3+} ion spectra and crystal field parameters 2−65263
  - NdP_5O_{14}, laser material 2−73587
  - Ne absorption tube in alternating magnetic field in laser cavity as frequency standard 2−78757
  - Ne discharge in hollow cathode, effect of nonlinear absorption at 0.63 m wavelength 2−83641
  - Ni, i.r. resonance, exchange energy detn. 2−65264
  - Ni film, on CaF_2, rel. to thickness and orientation 2−57324
  - $NiBr_2(Cl_2)$, electronic spectra, cryst. field parameters, phonon and magnon sidebands 2−51345
  - NiS_2, energy gap obs. 2−81020
  - NiS_2, semiconducting, and conductivity obs., rel. to band model 2−68417
  - O_2, fine struct. parameters of $B_3\Sigma_u^-$ state 2−64150
  - O_3^- and O_4^- anions in Ar matrix, spectrum and struct. 2−56191
  - $PbBr_2$ thin film, optical constants and absorption spectra, 2-10 eV 2−57321
  - $PbCl_2$, optical consts. and exciton states 2−68625
  - PbI_2, band structure and absorp. edge 2−68418
  - PbI_2 thin film, influence of nature of substrate and preparation conditions on exciton spectrum 2−48188
  - PbO film, absorp. edge and acceptor levels detn. 2−57352
  - PbS photosensitive layers, prepared by different methods 2−61652
  - PbSe, band struct., absorp. edge and intraband transition region obs. 2−81402
  - Pt, 0.265-7 μ, 295 and 77K, rel. to band struct. 2−81358
  - RbBr:OH, as function of applied pressure, paraelastic alignment obs. 2−61596
  - RbCl:Na, F_b centres 2−64682
  - RbCl, vibr. absorpt. spectrum of NO_2^- and NO_3^- 2−77769
  - RbI:OH, as function of applied pressure, paraelastic alignment obs. 2−61596
  - $RbMnF_3$, 3900 Å region, exciton, magnon and phonon struct. 2−65266
  - $RbMnF_3$, temp. depend. oscill. strengths 2−54428
  - $RbMnF_3$, two exciton transition, temp. depend. intensity calc. 2−61654
  - ReO_3, 0.11-2.8 eV, rel. to band struct. 2−84499
  - SF_6, saturation behaviour at high pressure and laser intensity 2−74277
  - $SO^{35}Cl^{37}Cl$, rot. and centrifugal distortion consts. 2−60032
  - Sb_2S_3 film, single cryst., band edge detn. 2−81390
  - SbSBr, i.r., rel. to band gap determ. 2−72346
  - SbSI, electro-optic effects on absorp. edge 2−81379
  - Sb_2Se_3 film, amorphous, optical props. 2−61323
  - Sb_3Se_3 film, amorphous 2−53576
  - Se, amorphous, i.r. absorpt. obs. of ring-chain-struct. 2−78088
  - Se, monoclinic, excitons and direct gap obs. 2−68648
  - Se film, crystalline and amorphous, ion bombardment effects 2−60646
  - Se_xTe_{1-x}, synchrotron radiation, d level spin orbit splitting obs. 2−81401
  - Si:Au, near i.r. region 2−72348
  - n-Si:Li, irrad. induced defects and impurity effects 2−47385
  - Si:P, far i.r., due to transition to cond. band edge region 2−72347
  - Si:P(As) radiation-induced infrared absorption bands, piezospectroscopic studies 2−68650
  - Si, acceptors, Zeeman effect, group theoretical study 2−84264
  - Si, electroabsorpt. edge, exciton effects 2−48189
  - Si, far-u.v. spectra, discrete features identification 2−67388
  - p-Si, i.r. absorpt. by free carriers 2−48190
  - Si, i.r. spectra, O and C impurities detn. 2−71502
  - Si, ion irrad., divacancy formation and annealing, i.r. study 2−71457
  - Si, ion irradiated, apparent damage induced absorp., scatt. from defect zones 2−48158
  - Si, irrad. with 400 eV ions, increase in i.r. absorption 2−47081
  - Si, neutron irrad., divacancy obs. 2−48194
  - Si, neutron irrad. damage, piezospectroscopic obs. 2−48193
  - Si, neutron irrad. induced defect clusters, edge absorpt. obs. 2−47389
  - Si, quadratic Zeeman splitting of donor lines 2−57350
  - p-Si, saturation intensity at 10.6 μm 2−79227
  - Si, surface oxide layer influence 2−51325
  - Si film, amorphous, rel. to band struct. 2−61655
  - n-Si i.r. free carrier absorpt. consts. 2−81408
  - SiC, 6H electroabsorption due to indirect excitons 2−81331
  - α-SiC, i.r. absorpt. spectra due to electron transitions in deep impurity centres 2−78106
  - α-SiC, neutron and alpha-particle irrad. effects 2−48294
  - SiC 6H cryst., absorption edge struct. at 9K 2−68649
  - SiO_2, vitreous, lattice vibrational spectra, pressure densification effects, i.r. obs. 2−74971
  - SiO_2 film, r.f. sputtered, i.r. effect of substrate temp. 2−83865
  - SiO_2 film, thermally grown, struct., i.r. study 2−53579
  - SiO_2 thermally grown film, i.r. absorpt. meas. 2−71999
  - SiO_x film, r.f. sputtered in Ar-O_2, i.r. spectra, O_2 conc. effects 2−60667
  - SmS, rel. to semicond.-metal transition 2−80994
  - SmS, SmSe, SmTe, amorphous semicond., rel. to energy band struct. 2−61657
  - SmSe, press. depend. of absorpt. edge 2−75098

- **Absorption** continued
  - **light** continued
    - SmSe film, absorpt. spectra, resolution using mag. circular dichroism 2−81324
    - SmTe, press. depend. of absorpt. edge 2−75098
    - SmTe film, absorpt. spectra, resolution using mag. circular dischroism 2−81324
    - $SrAlF_5$, pure and Eu^{2+}-doped, characterization 2−60726
    - $SrB_2Si_2O_8:Eu^{2+}$ excitation spectrum 2−81420
    - $SrCl_2$, mag. circular dichroism on F-centre absorpt. band, $g_{orbital}$ factor 2−74805
    - $SrCl_2$, U-centres obs. 2−71531
    - SrF_2:La,Ce, uncoloured and X-irrad., charge transfer processes 2−65253
    - SrF_2, absorp. superposition due to ⟨100⟩ and ⟨110⟩ oriented F_2-centres 2−53751
    - SrF_2, coloured, zero-phonon lines 2−53752
    - SrF_2, high temp., colour centres 2−77597
    - SrF_2, low temp. plasma produced radiational defects obs. 2−71452
    - SrF_2 colour centre interconversion induced by electron irradiation 2−77598
    - SrO, radiation-induced $[Na]^0$ centres 2−43651
    - $SrTiO_3$, differential spectra and band struct. 2−72307
    - $SrTiO_3$, fundamental absorpt. edge, 6-300K 2−78107
    - $SrTiO_3$, Urbach's tail behaviour, unified mechanism 2−54430
    - $SrTiO_3$, wavelength modulated, rel. to phase transition 2−51348
    - Te, amorphous, tight binding model calc. of optical props. 2−61658
    - Te, thermomodulation, rel. to indirect transitions 2−65242
    - Te glass systems, rel. to chemical binding and physical props. 2−60599
    - TeS, gaseous, electronic spectrum, rot. struct. of bands 2−64158
    - tertiary butyl chloride, absorption spectra, concentration dependence, obs. 2−50088
    - TiC-TiN solid solution, 0.6-5.5 eV, band struct. determ. 2−51080
    - TiO_2 amorphous film, room temp. 2−72068
    - Ti(0001) single crystal, and polycrystalline, obs. as function of temp. 2−44341
    - TlBr(Cl), ionicity, rel. to dispersion and absorpt. energies 2−44374
    - TlCl, X-point direct exciton, magnetoabsorp. obs. 2−72352
    - $TlInSe_2$:Cu,Sn, cryst. and film, photosensitivity, optical absorpt., dark cond., forbidden band width 2−57197
    - $Tl_2SeAs_2Te_3$ chalcogenide semiconductor, liquid and glassy, struct. obs. 2−60420
    - Tm^{3+} in phosphate and borate glasses, spectra, cryst. field effects, luminesc. efficiency 2−75307
    - $TmVO_4$, Jahn-Teller induced magnon sidebands 2−81377
    - $TvVO_4$, cooperative Jahn-Teller transition obs. 2−65269
    - V^{3+} complexes, trigonally distorted octahedral, lattice-ion interactions in the ligand field theory 2−81205
    - V_2O_3, absorpt. and refl. spectra in metal-semicond. transition 2−81407
    - W, n and k dispersion, interband transitions 2−72353
    - W(110) single crystal and polycrystalline, obs. as function of temp. 2−44341
    - Xe, solid, vacuum u.v. absorpt., temp. depend. 2−81371
    - Y-Fe garnet, effect of magnetic ordering on optical absorption spectrum 2−81392
    - $Y_3Al_5O_{12}$:Pr(Tb)(Eu)(Yb) colour centre investigation during γ-irradiation 2−80714
    - YIG:Si, photoinduced dichroism, model 2−72260
    - YIG(Si), rel. to reversible photoelectromagnetic effects microscopic theory 2−54259
    - $Y_2O_2S:Er^{3+}$, energy levels and crystal field splittings, spectra obs. 2−51339
    - $Y_2SiO_5:Nd^{3+}$, 4.2, 77 and 290K 2−78123
    - Zn film, on dielec. substrate, elec. resist., supercond. transition temp., absorpt. spectra 2−72323
    - $ZnAs_2$, edge absorp., band struct. detn. 2−51326
    - $ZnGeP_2$, i.r., characterization 2−80599
    - ZnO:Cu film, amorphous, band struct. and impurity state energy spectrum 2−68421
    - ZnO, two-phonon sidebands in i.r. absorption due to third order potential 2−75284
    - ZnO differential absorption spectra on adsorption of molecules of donor-acceptor type 2−68651
    - ZnO film, Burstein-Moss effect obs. 2−51350
    - ZnP_2, edge absorp., band struct. detn. 2−51326
    - $ZnS:Mn^{2+}$, fine struct. of 21500 cm^{-1} band, uniaxial stress effects 2−84506
    - ZnS, many-photon absorp., carrier generation obs. 2−84519
    - ZnS, two photon photocond. 2−61450
    - ZnS differential absorption spectra on adsorption of molecules of donor-acceptor type 2−68651
    - $ZnSe:Cr^{2+}$, Jahn-Teller splitting obs. 2−65270
    - ZnSe, electron irrad., vacancy obs. 2−47366
    - ZnSe, ionicity, rel. to dispersion and absorpt. energies 2−44374
    - ZnSe, many-photon absorp., carrier generation obs. 2−84519
    - ZnSe differential absorption spectra on adsorption of molecules of donor-acceptor type 2−68651
    - ZnTe, resonant excitons 2−61200
    - ZnTe, visible region to 15μm, due to acceptor levels 2−57353
    - ZrO_2, stable white pigment, for space environment 2−44799
- **Abundance ratio** *see Elements/relative abundances; Isotopes/relative abundances*
- **Acceleration** *see Dynamics; Kinematics*
- **Acceleration measurement**
  - *see also Velocity measurement*
  - — 2−61945
  - — 2−61904
  - accelerometer, wide band horizontal, with preliminary Earth normal mode and seismic band 2−48975
  - accelerometer for low-level building vibrs. 2−45467
  - accelerometer instrument correction, strong motion accelerograms 2−48384
  - accelerometers, automated precision calibration system 2−45219
  - integrating and double integrating accelerometers 2−45222
  - kinematics transducers calibration by interferometric method 2−73634
  - lunar acceleration contour maps from gravitational coefficients 2−44917
- **Acceleration measurement** continued
  - shock-induced flow in Ar, acceleration measurements 2−53297
- **Accelerators** *see Particle accelerators*
- **Accommodation coefficient** *see Gases; Kinetic theory/gases; Surface phenomena*
- **Accumulators** *see Electric cells*
- **Acids, inorganic** *see individual compounds, and Hydrogen compounds*
- **Acids, organic** *see Organic compounds*
- **Acoustic amplification in solids** *see Acoustoelectric effects*
- **Acoustic analysis**
  - Aeolian sound under water, ocean current passing test cable 2−76377
  - air duct, active sound absorbers 2−73433
  - benzene mono- and disubstituted derivatives, sound propagation rel. to H bonding analysis 2−56502
  - complex shaped enclosures, natural modes and frequencies 2−73451
  - emission, generic discussion 2−49134
  - image method for calc. of sound pressure levels within rectangular room 2−55558
  - long narrow rectangular baffled piston, radiation impedance 2−73424
  - marine sediments, and geotechnical obs. 2−57834
  - modified ray theory, convergence zone caustic 2−73426
  - monochromatic point source, field in randomly inhomogeneous medium 2−69720
  - noise field models, particle velocity components, spatial correlation fns. 2−69776
  - parametric array, analytical model using shock waves 2−76373
  - pressure in nearfield of circular baffled piston, method for high speed calc. 2−41698
  - propagation in circular duct, continuously varying cross sectional area 2−73430
  - rectangular ducts, sound propagation 2−73429
  - rigid movable sphere, motion when struck by plane or spherical acoustical waves 2−73402
  - shape recognition 2−45506
  - sound field of sources in motion 2−73422
  - submarine biological objects, acoustic characteristics of fish species 2−69763
  - surface wave filters 2−49144
  - turbulent flow over rigid half plane, sound radiation 2−74311
  - underwater acoustic communication channel, model capacity 2−49157
- **Acoustic emission** *see Acoustic waves*
- **Acoustic field** *see Acoustic radiators; Acoustics; Intensity measurement/acoustics*
- **Acoustic generators**
  - *see also Musical instruments*
  - Aeolian sound under water, ocean current passing test cable 2−76377
  - axial flow machines, applic. of linear acoustic theory 2−69730
  - clackers, energy pathway 2−41753
  - closed resonance tube, sound generated by piston 2−73440
  - combustion noise in burning fuel-air mixtures 2−55534
  - dielectric transducers, u.s. waves 2−55535
  - electro-spark pressure source in water, optimum depth for seismoacoustic investigations 2−44572
  - e.m. generation of ultrasound in hot metals 2−69751
  - flames, oscillating, probe measurements 2−82356
  - heated channels 2−58920
  - impulse response of baffled rectangular piston 2−41752
  - in head localization of sound source rel. to headphones and loudspeakers 2−55540
  - infrasound, instrumentation for 2-20 Hz region 2−69768
  - l.f. sound, natural sources and propagation 2−75617
  - Rijke tube, generation using two heating coils 2−58922
  - stress wave emission on material deformation 2−69745
  - surface wave steering by nonlinear mixing 2−80903
  - transient sources in idealized jet 2−55536
  - turbulent MHD, Lighthill theory 2−53170
  - ultrasonic, magnetically tunable with laminated Fe core 2−49132
  - ultrasonic pulses, transducer with intermediate layer of quarter wavelength, transient response analysis 2−41769
  - ultrasonic second harmonic generation in resonant nonlinear elastic solids 2−41750
  - underwater, APPRES 2−69748
  - underwater, boomer class of seismic sources 2−57661
  - u.s., parametric, based on acoustic waveguide with liq. 2−58923
- **Acoustic impedance**
  - caps and rings on oblate spheroidal baffles 2−41722
  - cholesteric liquid crystals, ultrasonic 2−43350
  - cider bottle, reactance and decay of free oscillations 2−63124
  - guinea pig middle ear, effects of middle ear muscles 2−45097
  - holes in wall of flow ducts 2−78922
  - human body surface, impedance rel. to stethoscopes and auscultation 2−52228
  - impulse response model for input impedance of interdigital surface wave transducer 2−49141
  - long narrow rectangular baffled piston, freq. dependence 2−73424
  - measurement at high intensities, standing wave tube 2−69728
  - multiple spheres, interactions effects 2−55538
  - mutual, between circular and arbitrary shaped pistons 2−41696
  - nonlinear, perforated plates, parametric dependence 2−69729
  - panels, correlate method of obs. 2−76369
  - rectangular piston in baffle plate 2−52227
  - transforming wave systems, spatially varying density or elasticity 2−41765
  - transmission lines, effective density of viscoelastic material 2−55525
- **Acoustic mode, crystals** *see Crystals/lattice mechanics*
- **Acoustic paramagnetic resonance**
  - *see also Ferroacoustic resonance*
  - — 2−72495
  - absorption of ultrasound by conduction electrons 2−81464
  - dielectric with paramagnetic ions, theory of higher order transitions 2−51400
  - ferromagnet, magnetoacoustic instability during biharmonic pumping 2−84559
  - low temp. ultrasonic techniques review 2−82349

- **Acoustic paramagnetic resonance** continued
  - ruby, Fe^{2+} ion obs. and cross relax. processes 2−51285
  - u.s., dewar insert for microwave X-band spectrometer 2−63203
  - MgO:Fe^{2+}, higher order transitions 2−51406
  - $NaNO_3$, n.m.r. of ^{23}Na, intensity variations under u.s. stimulating quadrupole transitions 2−81483
  - TiO_2:Cr, γ-irradiated, Cr^{3+} spin-phonon coupling constants detn. 2−51408
- **Acoustic radiators**
  - *see also Doppler effect*
  - Al rod, axial velocity profiles and acoustical fields 2−41694
  - bowed stringed instruments, directional characteristics, effect on orchestral sound in concert halls 2−45521
  - complete sound field within hollow cylinder, reconstruction using Pohlman cell in acoustic holography 2−69977
  - continuous end fire line array, close-form soln. for acoustic field 2−41702
  - cylindrical fluid duct, hard-walled, radiation field produced by unbaffled vibrating rod 2−55533
  - cylindrical shell, statistical properties of radiation field 2−69721
  - field created by radially oscillating cylindrical emitter in elastic medium 2−61890
  - field from source of arbitrary directivity, coherent reflection by rough sea surface 2−57837
  - field scattered by rigid sphere, separation and anal. 2−58916
  - free-free beams, radiation by resonance 2−55537
  - high speed fans, tone noise from rotor/stator interactions 2−82355
  - horn theory and acoustic phonograph 2−41766
  - horns, generalized theory of propagation 2−41764
  - horns, impedance transforming wave systems 2−41765
  - loudspeaker, underwater, small size, high efficiency 2−41770
  - loudspeaker cones, paper, scanned holography 2−55541
  - loudspeaker diaphragm, dynamic behaviour, holographic obs. 2−45519
  - loudspeaker horn theory, impedance concept 2−41762
  - loudspeaker horns, for sound reproduction, historical review 2−41763
  - machine noise, sound field near array of noise sources 2−41813
  - models and computer analysis 2−76374
  - moving multiple sources in free-space 2−66620
  - moving rigid bodies, multipole expansion of sound radiation 2−58921
  - multiple spheres, interaction of spheres effects of sound field and acoustic impedance 2−55538
  - multipole expansion of sound radiation from moving rigid bodies 2−41695
  - nearfield calibration arrays of arbitrary configuration, design 2−41699
  - noise radiation by plane arrays of incoherent sources 2−73449
  - nonlinear transmitting array, for sonar 2−41782
  - parametric array, difference frequency, using exact description of primary sound field 2−41747
  - parametric array, nonlinear attenuation 2−41742
  - parametric source, conversion efficiency 2−41744
  - parametric source design, model 2−41745
  - parametric sources, farfield interactions 2−41746
  - parametric transmitting array, high intensity primary wave effects 2−41743
  - parametric transmitting arrays, review 2−41741
  - plate, infinite, excited, sound radiation 2−45517
  - point source radiation, rough surface shadowing, theory 2−55518
  - point source simulation in h.f. acoustical system 2−52242
  - pressure impulse over arbitrary surface, response, visualizing and calculating 2−41739
  - pulsed planar straight-edged, sound field 2−41738
  - quartz disc, u.s. pattern visualization by optical illumination in direction of propagation 2−55547
  - ray intensity field calc. at point using ray sweep-out method 2−58909
  - rectangular, pulsed, farfield 2−55542
  - rectangular piston radiation impedance functions, tables 2−45502
  - reverberation sound field, effective modal density for finite sized sources 2−41799
  - single rotor siren for wideband noise generation 2−69747
  - spectrum meas. in field of extended source 2−41700
  - theory of horns, brass instrument design 2−41775
  - time depend. flow coupled to inhomogeneous solid surface 2−77320
  - transducer array on finite cylinder, radiation 2−41697
  - two spheroids, acoustic field 2−55519
  - ultrasonic, using standing wave formation 2−49133
  - u.s., focusing, effiecency index 2−69746
  - u.s. field meas. by liquid surface relief method 2−63110
  - vibrating composite circular and annular membranes 2−66584
  - v.s., bolt clamped electrostrictive torsional vibrator 2−69725
- **Acoustic receivers**
  - *see also Microphones*
  - degree of coherence of sound incident at different angles in reverberant chamber 2−52246
  - directivity of sonar receiving arrays, nonomnidirectional case 2−41701
  - dynamic response of suspended underwater hydrophone systems 2−41754
  - horns, conical and sinusoidal, soundtraps 2−41773
  - one path ultrasonic fluid flowmeter using electroacoustic feedback 2−55549
  - parametric, underwater performance for spherically spreading pump and plane wave signal 2−41748
  - parametric receiving arrays, theory for array performance 2−41749
  - pressure gradient hydrophones, wide range calibration system 2−45518
  - surface wave compressive receiver 2−49161
- **Acoustic resonators**
  - absorbing and insulation props. of reson. systems 2−45516
  - diffusion flame, production of sound 2−52240
  - fluid mechanics phenomena produced by the non- stationarity of singluar charge losses in pipes 2−56278
  - pressure transient response spectra of double resonator 2−41751
  - $LiGaO_2$, electromech. coupling factor and reson. freq. 2−51206
- **Acoustic streaming**
  - effect on convective heat transfer from vibrating cylinder 2−41861
  - gases, heat balance, thermally driven oscillations 2−80358
  - particulate aerosol, sonic agglomeration 2−43407
  - viscous fluid in circular duct, secondary flow induced by transverse resonant acoustic field 2−67590
  - He II, emission of white noise during cavitation 2−56464
- **Acoustic transducers** *see Transducers*
- **Acoustic wave amplification**
  - *see also Acoustoelectric effects*
  - drift field induced carrier inhomogeneities in low conductivity accumulation layer surface wave amplifiers 2−51030
  - glass-semiconductor-$LiNbO_3$ structures, acoustoelectric dispersive surface wave amplification 2−49129
  - ideal gas with unimolecular reactions 2−75369
  - monolithic amplifiers with $Bi_{12}GeO_{20}$ substrates, gains 2−52238
  - piezosemiconductor, effect on polarization on ultra-sound amplification 2−84202
  - piezosemiconductor, narrow propagating domains of acoustic flux, prod. method 2−43978
  - pressure transient response spectra of double acoustic resonator 2−41751
  - semiconductor, and electron temp. 2−51121
  - semiconductor, piezoelectric, effect of weak inhomogeneity in carrier density 2−74984
  - semiconductors, and absorption 2−51029
  - solid, random field, discrete levels sound amplification nonlinearity 2−68236
  - space charge effects on attenuation symmetry of u.s. amplification by piezoelectric semiconductors 2−51031
  - surface, CdS plate-fluid layer-$LiNbO_3$ structure 2−49130
  - surface, layered structures, numerical solutions for free surface wave and monolithic amplifiers 2−49128
  - u.s., by interaction with electrons, elec. field effects 2−77776
  - U.S devices, h.f., review in book 2−57046
  - CdS-water-$LiNbO_3$ surface wave convoluter, output, enhancement 2−80904
  - CdS, piezoelec. semicond., amplification threshold field nonmonotonic cond. depend., 5-120 MHz 2−77783
  - GaAs, piezoelectrically amplified, abrupt decrease in gain at quantum limit 2−51033
  - GaAs, surface shear wave mode characts., bulk wave theory incl. trapping effects 2−68241
  - n-GaAs, u.s., generation and detection 2−77774
  - GaAs magnetic enhancement of acoustoelectric gain, obs. by Brillouin scattering 2−51034
  - n-InSb, gain parameter meas. 2−68243
  - inInSb, in crossed elec. and mag. fields at 77K 2−68238
  - n-InSb, time and spatial distrib. of amplified acoustic flux 2−68242
  - n-InSb, u.s., generation and detection 2−77774
  - InSb microwave radiation, acoustoelectric amplification 2−54159
  - $LiNbO_3$ with CdSe film, surface state effect 2−84201
  - in n-GaAs, ultrasonic injected coherent shear waves under small, large signal conditions 2−64847
- **Acoustic wave propagation**
  - *see also Absorption/acoustic waves; Acoustic wave amplification; Dispersion/acoustic; Doppler effect; Helium/liquid, sound propagation; Shock waves; Velocity/acoustic waves*
  - absorption coefficient, field measurement by reflection technique 2−41723
  - acoustic field, Monte Carlo analysis 2−41689
  - acoustic transmission into basin with bigradient sound speed profile 2−44654
  - acoustic-gravity waveforms in laterally inhomogeneous media, large scale meteorological influences 2−54809
  - air duct, active sound absorbers 2−73433
  - air ducts, multiply connected cross sections, cutoff freqs. 2−73428
  - amplitude and phase fluctuations of field in waveguide with rough wall 2−41688
  - anharmonic metal, collision free regime 2−43966
  - anharmonic metal, collision-dominated regime 2−43965
  - Arctic SOFAR propagation, effect of ice layer 2−41787
  - atmosphere, upper, possible existence of infrasonic waves 2−72815
  - in attenuating duct, utility of Galerkin method for shear flow analysis 2−69723
  - attenuation in ducts with anisotropic lining, silencers 2−76376
  - axial flow machines, applic. of linear acoustic theory 2−69730
  - biological tissues, thermal effects of acoustic waves 2−66271
  - bone density, separated animal tibias, acoustic resonance frequency 2−81998
  - bounded media, statistical props., wave propag. const. 2−58910
  - channel with horizontal and vertical sound-speed gradients, reflected/refracted ray propagation 2−57841
  - circular duct, continuously varying cross sectional area 2−73430
  - circular plane piston acoustic field in limits of short wavelength or large radius 2−73421
  - continuous isotropic medium, fluctuation from Lagrangian measure function 2−41736
  - continuous isotropic medium, sound fluctuation 2−41720
  - convolution of signals by surface wave nonlinearities, detection 2−71739
  - curved waveguides, thin film, scalar potential function 2−49122
  - cylindrical and annular ducts, refraction and attenuation 2−58917
  - decay modes in exterior of reflecting body 2−82359
  - dielectric crystal, adiabaticity 2−61086
  - in duct shear layers, soln. for initial sound pressure profiles 2−58911
  - elastic cylindrical shell surrounded by thermo-viscous media 2−66621
  - elastic waveguide, tunnel effect 2−52231
  - emission angles, determination for depth dependent propagation speeds 2−45507
  - ferromagnet, freq. shift at low temps. in mag. field 2−74985
  - fibrous materials, stacked cylinder model 2−69726
  - finite amplitude entropic waves, mechanism 2−41712
  - finite amplitude waves in flexible tubes 2−41718
  - fluid wedge, field due to point source 2−41716
  - focusing of finite amplitude cylindrical and spherical waves in viscous and heat conducting medium 2−41710

Acoustic wave propagation continued
- gas of Maxwell molecules kinetic theory 2−41707
- geometric spreading loss, invariance with changes in ray parametrization 2−55524
- glass, birefringence under strong uniaxial compression 2−54028
- helical surface waves on cylindrical bodies from non-contacting electrodynamic transducers 2−78913
- higher alkanes, meas. of acoustic nonlinearity parameter 2−71197
- homogeneous isotropic media, finite element coupling matrices 2−69722
- horn theory and acoustic phonograph 2−41766
- horns, impedance transforming wave systems 2−41765
- human blood, absorption at 1 to 10 MHz 2−82363
- infra-sonic propagation expt. to determ. wind and temperature fluctuations in atmospheric boundary shears 2−54816
- interaction with gas phase reactions 2−75369
- ionized gases nonisothermal 2−66618
- isotropic media, study by stochastic Eulerian-Lagrangian procedure 2−82353
- l/f. in lined duct, model 2−69731
- Lamb modes, symmetric high order, pure longitudinal displacement 2−69733
- level and phase fluctuations for randomly inhomogeneous medium 2−69734
- l.f. sound propagation in offshore shelf zone under conditions of varying depth 2−72719
- in loudspeaker horns, generalized theory 2−41764
- modal spectra in hard walled cylindrical ducts 2−41804
- models and computer analysis 2−76374
- modified ray theory, convergence zone caustic 2−73426
- monatomic gas binary mixtures, calc. from plane wave solns. of coupled linearized Boltzmann eqns. 2−50272
- moving multiple sources in free-space 2−66620
- in multicomponent fluid systems near critical point 2−67574
- multilayered liquid solid half space with liquid bottom, integral soln. 2−41690
- multilevel system, theory of spectrophone effect 2−80410
- N-waves, focusing by spherical mirror 2−41711
- noise signature of aircraft in level flight, over hydrophone in sea 2−73423
- nonlinear impedance, perforated plates, parametric dependence 2−69729
- nonlinearity 2−41717
- normal-mode generation with vertical array of projectors in shallow water 2−44660
- North American Basin, convergence zone propagation 2−44657
- ocean, in uniformly moving ocean channel with depth-dependent sound speed 2−57839
- ocean, ray propagation in channel with depth variable sound speed and current 2−62029
- oceanographic applications, velocity profiles in geometrical acoustics 2−44653
- one dimensional nonlinear wave, in dissipative gas 2−52229
- Pacific Ocean, horizontal underwater paths, absorption 2−55530
- parameterless intensity formula, from Eikonal eqn. 2−41715
- piezo-semiconductors, waveguide effect of surface domains 2−54029
- piezoelectric crystals, nonlinear parameters 2−61087
- in plate structures, response analysis using finite element method 2−41703
- polymethyl methacrylate, epoxy formulations, u.s. dispersion, acoustic characterization 2−80905
- polyolefins, variation in velocity rel. to deformation 2−80750
- porous media, theory 2−55522
- pulsed rectangular acoustic radiator, farfield 2−55542
- random medium, nonlinear theory 2−41708
- ray acoustics, intensity differential eqn. 2−73425
- Rayleigh waves excitation on unphased interdigital structure 2−69732
- rectangular ducts, with gradients of mean flow and temp. 2−73429
- reflecting body, modes of decay in exterior 2−82359
- refracting medium, reflection obs. 2−55531
- relaxing fluids, Eulerian equations of motion 2−43256
- scattering from fluid-inversed elastic bodies, numerical solution 2−66622
- shallow water, normal mode amplitude functions 2−77428
- shallow water ray tracing, nonlinear velocity profiles 2−73432
- shear discontinuity between hot and cold regions, transmission and reflection 2−78921
- solid, random field, discrete levels sound amplification nonlinearity 2−68236
- solid waveguides, dispersion relations in normal modes 2−66624
- sonic boom, policy considerations 2−76379
- sound transmission in a duct with flow 2−66619
- spatial coherence and structure of propagating medium 2−55377
- stochastic transients, power moments spectra 2−58912
- superdense plasma, superluminal sound propagation 2−70874
- surface, and appl. 2−43973
- surface wave convolution in piezoelectric materials, nonlinear interaction 2−51001
- surface wave interactions, nonlinear 2−69735
- surface wave propagation, guided by ridges calc. by finite element technique 2−76335
- surface wave propagation in monolayers of soluble polymers using Moire fringes 2−73445
- surface wave steering by nonlinear mixing 2−80903
- surface waves in layered media on sapphire substrates 2−51000
- switching and steering of surface waves by nonlinear mixing in anisotropic media 2−51005
- theory of horns, brass instrument design 2−41775
- in time dependent channels, multipath c.w. and repeated pulse 2−55523
- torsional waveguides, with steps, analysis by infinite matrix method 2−69724
- transmission lines, impedance properties 2−55525
- turbulence effect on weak shock waves 2−66633
- two-dimensional impulsive waves in linear acoustic medium, integration of describing equations 2−73427
- underwater, losses predicted by modified ray theory 2−41714

Acoustic wave propagation continued
- underwater sound, integral soln. of sound field in interbedded liq.-solid half space 2−82366
- from vibrating plates, with density and stiffnesss discontinuities 2−45450
- viscoelastic solid, deformed, sinusoidal small amplitude waves 2−41705
- Voigt fluid, viscoelastic 2−60468
- water, deep and shallow geometries, spatial coherence 2−44655
- in waveguide filled with gas mixture with transverse concentration gradient 2−41719
- Webster horn equation and stepped duct, matched asymptotic expansion methods 2−41706
- West Greenland Sea, acoustic meas. 2−44656
- Al, acoustic shock pulse generation, nonlinear elastic behaviour obs. 2−64842
- Al, attenuation and velocity of circularly polarized u.s. shear waves in a magnetic field 2−47789
- Al, e.m. wave transmission, helicon waves, Gantmakher- Kaner excitations, sound waves, quantum effects 2−57135
- $BaTiO_3$ plate, dispersion curves of flexural modes 2−84205
- BeO, surface and bulk characteristics 2−51042
- $Bi_{12}GeO_{20}$, acoustic surface wave propag., 200-2000 MHz loss mechanism 2−61094
- $Bi_{12}GeO_{20}$, nonlinear surface wave generation 2−51007
- $Bi_{12}GeO_{20}$, propagation of Bleustein-mode piezoelectric surface wave 2−61095
- Ca-Bi-V ferrite rods, excitation of longit. acoustic waves 2−43968
- $CaWO_4$, adiabatic eleastic stiffness moduli, u.s. pulse superposition meas., 15-300K 2−84037
- CdS-$LiNbO_3$, convolution and correlation by nonlinear interactions between sonic induced space charge and field waves 2−51015
- CdS, wave mixing and amplitude dependent phase velocity 2−51032
- CdS plate, dispersion curves of flexural modes 2−84205
- Cs vapour, acoustic radiation from shock front 2−71115
- Ge, n-type, effect of higher energy states on acoustic attenuation 2−74987
- $LiNbO_3$, nonlinear interac. of hypersonic waves along [001] axis in an acoustic resonator 2−71734
- $LiNbO_3$, nonlinear surface wave generation 2−51007
- $LiNbO_3$, propagation of Rayleigh-mode piezoelectric surface wave 2−61095
- $LiNbO_3$, surface wave device, shear wave probing using laser beam 2−68232
- Pb(Ti, Zr)O_3 plate, dispersion curves of flexural modes 2−84205
- $PbTiO_3$ plate, dispersion curves of flexural modes 2−84205
- Pb(Zr,Ti)O_3-Si-$LiNbO_3$, convolution and correlation by nonlinear interactions between sonic induced space charge and field waves 2−51015
- Sb, attenuation and velocity of circularly polarized u.s. shear waves in a magnetic field 2−47789
- Si-$LiNbO_3$, convolution and correlation by nonlinear interactions between sonic induced space charge and field waves 2−51015
- Si-PZT coupled system, acoustic surface wave convolution by 14.5 MHz Bleustein-Gulyaev waves 2−71742
- SiO_2, birefringence under strong uniaxial compression 2−54028
- Sn, attenuation and velocity of circularly polarized u.s. shear waves in a magnetic field 2−47789
- ZnO film, d.c. triode sputtered, u.s. surface elastic waves, coupling factor phase velocity, propag. loss 2−80560
- ZnO plate, dispersion curves of flexural modes 2−84205

ultrasonic
- in aminoacid solutions, velocity measurement using conventional flow detector 2−60467
- benzene-cyclohexane system, acoustical properties on saturation line 2−71199
- bonding materials, for u.s. delay line, high temp. characs. 2−77777
- crystal dislocations, resistance to motion, meas. method 2−68030
- cylindrical layered ferrite-metal medium, independent propagation of magnetostatic surface waves 2−81285
- fast reactions, ultrasonic and relaxation spectroscopy, expression for C_p/C_v 2−81499
- ferroelectric crysts., hypersonic waves, nonlinear effects, slowly varying amplitudes method 2−77775
- fractional harmonic generation, in resonant wave system 2−58919
- freezing-in phenomenon of standing waves in concentration gradients, optical Philpot-Svensson method 2−78917
- guided waves in symmetric fluid-solid systems, normal modes 2−49123
- homogeneous fluid, 'freezing effect' 2−43349
- liquid crystal, attenuation and velocity changes of hypersonic waves at cholesteric-isotropic transition 2−80454
- metallic glass. softening of long-wavelength transverse phonons 2−54021
- N-p-methoxybenzylidine-p-butylaniline nematic liquid crystal, temp. dependence of anisotropic propagation 2−46953
- multilayered medium, n.d.t. technique 2−69762
- nonpiezoelectric conductor, u.s. generation by deform. interaction with carriers 2−64841
- piezoelectric crystal, charge storage of acoustic r.f. signals 2−61085
- piezoelectric semiconductor, second harmonic generation in mag. field 2−68239
- piezosemiconductor, second harmonic generation 2−51039
- polystyrene in alcohol suspensions, ultrasonic relaxation 2−53462
- real-time u.s. kinoform, wide band modulation of light 2−73623
- relaxation and light scattering in liquids 2−50356
- Rochelle salt, attenuation and ferroelectric anomalies 2−74988
- semiconductor, piezoelectric, effect of weak inhomogeneity in carrier density 2−74984
- semimetal, e.m. excitation in moderately strong mag. fields 2−71727
- shear wave excitation by interdigital transducer operated at surface-wave centre freq. 2−51008
- solids, generation by dielectric transducer 2−55535
- sonoluminescence of liquids, effect of dissolved salts and reducing agents 2−71210
- steel spheres, lunar seismic signals 2−44927
- surface acoustic wave correlation echo, generation from coupling to charge carriers 2−57045

Acoustic wave propagation continued
ultrasonic continued
surface wave delay line, suppression of spurious triple transit signals 2−57044
surface wave guidance by $(\Delta v/v)$ guidance structures 2−51010
surface wave steering and switching by nonlinear mixing in anisotropic media 2−51011
water, turbulent free jet flow, amplitude modulation of ultrasound 2−74494
wedge waves, parametric interaction 2−66626
Au, quantum oscill. of u.s. attenuation 2−51037
Bi, e.m. generation of shear and longit. waves 2−43967
Bi, electromagnetic generation of shear and longitudinal u.s. waves 2−71729
$CaMoO_4$, rel. to elastic consts. determ. 2−77773
$CaWO_4$, rel. to elastic consts. determ. 2−77773
CdS, dispersion, role of hopping conductivity 2−71733
Cu, noncollinear surface wave interactions 2−51004
$DyVO_4$, obs. of elastic consts. anomalous behaviour at Jahn-Teller induced phase transition 2−84038
He, solid h.c.p. crystal, elastic constants detn., pulse time of flight obs. 2−43972
Ho-50%Tb, elastic consts. and u.s. attenuation, anomalous effects, antiferromag. spiral spin state 2−64843
In films, e.m. generation of transverse acoustic waves, supercond. parameters 2−71866
K, electromagnetic generation and attenuation of u.s. shear waves 2−71729
KBr-KI solid solution single crystals, elastic constants and Debye temp. temp. depend. detn. 2−71550
KD_2PO_4, u.s. stress wave interaction with domain walls 2−71740
$LiIO_3$, elastic surface wave props. and device applics. 2−77778
$LiNbO_3$, acoustic convolution and correl., nonlinearity parameters 2−51014
$LiNbO_3$, shear wave excitation by interdigital transducer operated at surface-wave centre freq. 2−51008
$LiNbO_3$, Y cut, parameter-periodic coupling of volume modes 2−51003
$LiNbO_3$ with semiconductor layer, surface wave convolution 2−47741
Pb, damping of crystal imperfection motion, meas. method. 2−68030
$Pb(Zr, Ti)O_3$, shock induced electromech. conversion, additives influence 2−84359
Rh, amplitude depend. shear wave attenuation near T_c 2−47745
Se amorphous, Young's, rigidity moduli, 0-60°C 2−57051
$SrMoO_4$, rel. to elastic consts. determ. 2−77773
Tb, magnetic fields effects and temperature dependence 2−51036
$TbVO_4$ obs. of elastic consts. anomalous behaviour at Jahn-Teller induced phase transition 2−84038
YIG, ferroacoustic surface wave resonance 2−51035
ZnO/Al_2O_3, heteroepitaxial layer structure, surface props. rel. to delay line fabrication and behaviour 2−68235

Acoustic waves
see also Diffraction; Interference, etc.; Elastic waves; Shock waves; Ultrasonics
aerothermal amplification in tubes 2−41740
analysis and synthesis on basis of sound microunits 2−52239
atmospheric, ray tracing, three-dimensional, using hybrid computer 2−81653
averaged sound pressure in reverberation chamber, rotating vane effect 2−41693
Bragg imaging of ultrasonic waves, nonlinearity 2−41788
bulk wave transducer, thin film mosaic 2−49135
contact-free stimulation of waves in steel plates 2−78914
continuous end fire line array, close-form soln. for acoustic field 2−41702
cross correlograms, effects of dispersion 2−55517
detection of sampled signals 2−41772
excitation of surface acoustic waveguides using wedge transducers 2−49131
fatigue, high-temperature, monitoring using acoustic emission 2−56872
head waves formation, investigation using X-ray flash tube 2−85181
Helmholtz waves, lower atmosphere, obs. with acoustic sounder 2−78382
impact of spherical tool against sonic transmission line 2−55446
initially distorted sinusoidal, weak shock solution, boundary conditions 2−41709
interdigital transducers, impedance and capacity for Rayleigh and SV modes 2−49151
ion, nonlinear, Kortweg-de Vries eqn. derivation including ion Landau damping 2−70940
ion, radially propagating in Hg positive column, microwave scatt. obs. 2−74387
ion acoustic and electron plasma waves excitation by h.f. electric field 2−67684
ion acoustic waves in plasma, mode coupling 2−67682
ion acoustic waves in plasma, stationary solitary, snoidal and sinusoidal 2−74390
ion-acoustic collisionless shocks in Q-machine 2−77272
ionospheric response to v.l.f. ion-acoustic waves rel. to sudden geomagnetic storms 2−83614
l.f. mechanical filters 2−49150
longitudinal mode losses in short rocket nozzles 2−55516
Love wave, surface excitation 2−63111
metal, excitation by relativistic electron beams 2−57089
music analysis for performer in real time by computer driven c.r.t. 2−41780
non acoustic instability in collisionless shocks 2−77299
non-destructive testing of stressed materials, meas. of internal noise 2−60927
nondestructive monitoring for optimization of in-service performance tests 2−60924
nondestructive testing for brazed metal to ceramic bond 2−74833
optical det. of nonlinearity parameter of water 2−43351
particle counter, evaluation 2−51597
phase, optical recording, for meas. turbulent props. of fluids 2−60123

Acoustic waves continued
plasma, interaction 2−46772
pressure in nearfield of circular baffled piston, method for high speed calc. 2−41698
ray acoustic and Fermat's principle in moving inhomogeneous medium 2−45504
ray theory for inhomogeneous moving medium 2−45503
shock pulses for meas. of stress-strain relationships in solids, application to Al 2−43777
single vapour bubble round pulse, origin, and nucleate boiling of liquids 2−60554
solid state laser array control applications 2−66760
spatial correlation of reverberant sound fields by k-transform technique 2−41687
spectrum meas. in field of extended source 2−41700
spherical, transient interaction with spherical elastic shell, Cesaro mean appl. 2−66614
statistics of sound power radiation in reverberant room 2−41691
steels, mild, acoustic emission and energy transfer during crack propag., instrum. for detectn. 2−69767
surface, annular piezoelectric, transversely isotropic substrate, boundary value soln. 2−63112
surface, grating array transducer 2−49153
surface, hybrid junction interdigital transducers 2−49154
surface, in nonpiezoelectric conductors 2−51002
surface, long time delays 2−49162
surface, on impedance bodies of resolution 2−52226
surface, phase shifter, electronically variable 2−49124
surface, ridge waveguides 2−49121
surface in solids 2−51029
surface probe, electrostatic, waveform distortion meas. 2−49170
surface wave components incorporating multistrip coupler 2−49172
surface wave sequence generator/correlator, switchable 2−49126
surface wave transducers, apodized wideband, wavefront distortion meas. by electric probe 2−49138
surface waveguides and components, properties and applications 2−49120
thermoacoustic fatigue testing of space shuttle thermal protection panels 2−56873
transformation from acoustic waves by piezoelectric plate 2−65070
ultrasonic in methanol, thermal excitation by laser beams interference 2−41737
ultrasonic second harmonic generation in resonant nonlinear elastic solids and elastic constants det. 2−41750
underwater, detection by microwave radiation, obs. 2−48425
u.s. wave prod. by activated flame plasma 2−83531
visualization by acoustic stroboscopy 2−78927
Al alloys, acoustic emission and energy transfer during crack propag., instrum. for detectn. 2−69767
$Bi_{12}GeO_{20}$, surface wave devices, fabrication techniques 2−51013
C fibre-epoxy composite, acoustic emission during continuous tensile cycling 2−56986
Pb, sound excitation by electrons, positrons and photons 2−61089
ZnO film surface acoustic wave transducers, coupling constants and film thickness 2−49152

effects
see also Chemical effects of radiations/acoustic waves
arterial morphology, focussed ultrasound effect 2−51919
benzene vapour, u.s. excited shift in u.v. absorption band, sound velocity dispersion curve obs. 2−56218
biological tissues, heating 2−66271
cavitation bubble implosion pressure pulses and cavitation damage 2−56469
cavitation velocity in stationary wave 2−56463
disorganization and disruption of mammalian and amoeboid cells by acoustic microstreaming 2−66267
elastic conical shell, fastened in screen, effect of sound press. wave 2−69712
e.m. waves amplitude modulation by acoustic waves in dispersive plasma 2−80251
flame combustion 2−52285
interaction with coherent light beam, phase fluctuations 2−73435
jet, turbulent, sound influence, vortex generation 2−46842
light diffraction by adjacent parallel u.s. waves with arbitrary frequencies 2−55738
light diffraction by waves consisting of fundamental tone and first n−1 harmonics 2−63398
liquid, forced oscillations of gas bubbles 2−64423
muffler element performance, effects of high-intensity sound 2−73448
nonmagnetized plasma, ion heating via turbulent ion acoustic waves 2−53178
optical Bragg diffraction by standing ultrasonic waves with application to optical demultiplexing 2−49421
panel arrays, vibr. characts. 2−69715
paramagnet, perturbed γ-γ angular correl. eff. of spin-lattice relaxation and ultrasound 2−72241
on photographic emulsions, u.s. radiation, mechanism 2−70094
plates and shells, statistics of acoustically induced vibrs. 2−45465
response of infinite strip to fluctuating pressure fields 2−41565
rigid sphere in gas, response to pulse 2−64384
sonic boom damage to large windows 2−55564
steel, mech. props. and fine struct., u.s. vibr. effects 2−53877
steel, mild high energy, u.s. waves, effect on structure and hardness 2−77673
steel, u.s. cavitation erosion mechanism 2−71606
surface wave excitation on bubbles, thresholds 2−43307
thermally driven gas oscillations, heat balance, acoustic streaming 2−80358
u.s. exposure thresholds for cavitation in cells and tissues 2−66266
viscous fluids in circular duct, secondary flow induced by transverse resonant acoustic field 2−67590
water, sound pressure due to source in air 2−43348
water surface waves, spatial resonance phenomena 2−43295
CdS, acoustoelectric instability, scattering of light by sound 2−71728
Fe-Zn system ultrasonic strain, effect on diffusion growth of various phases 2−43655
Fe, cast, u.s. cavitation erosion mechanism 2−71606
$MgZn_2$, deformed by u.s. vibrs., dislocation behaviour 2−64666

- **Acoustic waves continued**
  - **effects continued**
    - NaCl, u.s. cavitation erosion mechanism 2—71606
- **Acoustical laboratories**
  - anechoic chamber, Nat. Bureau of Standards, wedge design 2—82352
  - automated environmental control 2—69770
  - polyurethane foam, highly absorbing sample, measurements in reverberation room 2—63114
  - reduction index measurements, effects of laboratory designs and mounting conditions 2—78924
  - synthetic sound fields, spatial distrib. of directions 2—52247
- **Acoustical measurement**
  - *see also Interferometry/acoustic waves; and under separate subjects e.g. Intensity measurement/acoustics*
  - absorption, porous materials, oblique incidence, waveguide meas. 2—69738
  - absorption coefficient, using correlation technique 2—69737
  - air ducts, multiply connected cross sections, cutoff freqs. 2—73428
  - attenuation meas., beam divergence effect 2—73434
  - closed resonance tube, sound generated by piston 2—73440
  - computer programming requirements 2—58908
  - crystal surface orientation meas. by u.s. beam displacement 2—56604
  - detection and location of noise source in dispersive medium 2—55554
  - emission, meas. device for use with metals and alloys 2—80783
  - fishing sonar with advanced design 2—69764
  - flint glass acoustic vibration determ. by Bragg diffraction 2—66839
  - fluids, influence of non-uniformity of acoustical fields 2—82365
  - hearing aids, time constant of compression, comparison measurements 2—45142
  - impedance, at high intensities, standing wave tube 2—69728
  - infrasonic acoustic bridge 2—69766
  - infrasonic detector, based on L-R-C acoustic circuit 2—69766
  - infrasonic noise, field meas. 2—52224
  - infrasound, instrumentation for 2-20 Hz region 2—69768
  - jets perturbed by screens, near field pressure and hot wire meas. 2—41820
  - joints, diffusion bonded, rel. to pulse echo, testing technique 2—43766
  - large machine noise, nearfield measurements and sound power 2—41814
  - machine noise, as installed measurements 2—41817
  - machine noise, measurement errors, ISO recommendation 2—41815
  - machine noise, measurement standards 2—41812
  - mechanical equipment, noise source identification, real time analogue digital signal analyzer 2—69772
  - musical instruments, duration of initial transients in tone of C octave series 2—41774
  - noise, in-ear meas., individual's exposure 2—45082
  - noise, steady state measurements, of power and absorption 2—41818
  - noise, very low levels, method using principle of energy addition 2—66630
  - noise in semireverberant rooms, steady state reference sound sources 2—41816
  - noise level generated by grille in an airflow 2—45529
  - noise pollution, measurement procedures for regulation and monitoring 2—78929
  - noise rating assessment and dB(A) levels, computer compression 2—63133
  - nonlinearity parameters of liquefied N_2, O_2 and methane, temp. depend. 2—56501
  - piezoelectric semiconductors, impurity diffusion coefficients, ultrasonic meas. method 2—50691
  - pitch of short sinusoidal pulses as function of initial phase 2—55515
  - polyurethane foam, highly absorbing sample, measurements in reverberation room 2—63114
  - portable sound analyzer and recording system 2—55550
  - pulsed r.f. fields, absolute calibrator 2—49171
  - rapidly varying hydraulic flow rates by ultrasonic waves 2—46890
  - reverberation time measurement in open plan offices 2—58931
  - sound field probing, Bragg diffraction method 2—45525
  - sound signals, level and dynamic range, indicating instruments 2—66629
  - standard unit of sound pressure, in pneumatic medium 2—55369
  - submarine biological objects, acoustic characteristics of fish species 2—69763
  - universal measuring apparatus system 2—82361
  - u.s., multiple crystal folder 2—82360
  - u.s. power meas. by calorimetric meas., effects of thermal parameters 2—52245
  - u.s. pulse echo investigation of ~~solids~~, electronic equipment 2—73499
  - u.s. vel. and absorpt. of solids, meas. apparatus 2—74983
  - u.s. welding equipment, microinch displacement monitoring 2—69755
  - vehicle noise, roadside large-display sound- level meter 2—45527
  - water-drop impacts, electro-acoustic meas. of drop size, shape and velocity 2—63129
  - weak waves, by capacitance transducer 2—41793
- **Acoustics**
  - *see also Acoustic resonators; Architectural acoustics; Atmospheric acoustics; Hearing; Noise/acoustic; Sound reproduction; Speech; Ultrasonics; Vibrations*
  - applications and role in society 2—41686
  - array subject to constraint, signal-to-noise ratio, adaptive nonlinear optimization 2—55544
  - bone density, separated animal tibias, acoustic resonance spectra 2—81998
  - conference, 83rd meeting Acoustical Society of America, (New York, April 1972) 2—41683
  - delay lines, precisely controlled, time delay trimming using thin film overlays 2—51006
  - diagnostic techniques, applic. in nuclear reactor operation and development 2—63974
  - duct flow, conference, Southampton, Jan 1972 2—55539
  - echolocating bats, horizontal angle resolution 2—48930
  - echolocating bats, horizontal angle resolution 2—48930
  - emission as non-destructive testing tool 2—58926
  - foundations, basic mathematics, book 2—41682
- **Acoustics continued**
  - holographic imaging, for medical diagnosis 2—76089
  - holography, current and potential appls. 2—82536
  - holography applications, conference (Los Angeles, Feb. 1972) 2—82534
  - holography Pohlman cell applic. to reconstructing complete sound fields in hollow cylinders 2—69977
  - holography with scanned linear detector array and electronically stimulated reference wave 2—76368
  - hyperbolic horn, four-pole parameters 2—41768
  - imaging sensor, piezoelectric transducer array, characts. 2—63127
  - impulse precision sound level meter, limitations in use 2—41800
  - Korotkov sound processor, automated blood pressure measuring system 2—51885
  - macrosonics, ultrasonic and macrosonic motors 2—41783
  - metal working processes, sonically assisted 2—41784
  - n.d.t. of adhesive bonded metal-to-metal joints 2—47674
  - nonlinear, singular perturbation methods 2—41684
  - nonlinear flows, spherically symmetric, nearfield in unbounded ideal gas 2—43266
  - nonlinearities origin, two-category classif. 2—45505
  - oceanographic, intensity range relations 2—72715
  - oceanographic, intensity range relations 2—72715
  - pulse echo system for ultrasonic velocity and attenuation obs. 2—55526
  - pulsed r.f. fields, absolute calibrator 2—49171
  - relationship to physics 2—41685
  - sea surface in Block Island Sound, remote sensing by underwater acoustics 2—57886
  - solid, random field, discrete levels sound amplification nonlinearity 2—68236
  - sound beam visualization utilizing Raman-Nath diffr. of light 2—78991
  - surface wave convoluters and correlators, nonlinearity parameters 2—49167
  - surface wave pulse compression filters, corrections for diffraction effects 2—49158
  - techniques for obs. Earth's upper mantle 2—57450
  - time varying power spectra, optimum window length 2—55520
  - Al alloys, acoustic emission due to low level periodic stress 2—51012
  - CdS, piezoelec. semicond., amplification threshold field nonmonotonic cond. depend., 5-120 MHz 2—77783
  - **musical**
    - *see also Musical instruments*
    - brass instrument design, theory of horns 2—41775
    - flute and clarinet spectra, amplitude distortion 2—63125
    - sharp and soft initial sound in music rel. to delayed architectural reflections 2—55559
    - sound studios, digital control meas. for automation 2—58928
    - transients, piecewise periodic analysis 2—82350
    - tuning forks' eigenfrequencies, numerical determination 2—69698
- **Acousto-optical effects**
  - acoustic wave visualization by acoustic stroboscopy 2—78927
  - acoustooptic diffraction grating modulators, design theory 2—79221
  - acoustooptic laser beam deflector, performance, optical analysis 2—79220
  - Bragg deflection of He:Ne laser beam using high acoustic power levels from n-GaAs ultrasonics amplifier 2—64847
  - Bragg imaging of ultrasonic waves, nonlinearity 2—41788
  - deflector, 600 MHz bandwidth, use as delay line and light scanner 2—51296
  - diffraction by progressive supersonic waves, oblique incidence case, Raman-Nath eqns. 2—66822
  - dye laser electronic tuning using acousto-optic filter 2—82481
  - Gunn oscillator-piezoelectric structures, deflection 2—84458
  - light diffraction by acoustic waves consisting of fundamental tone and first n—1 harmonics 2—63398
  - liquid crystal, nematic, acoustic modulation of light 2—59241
  - modulator, developments 2—73657
  - modulators and deflectors 2—55709
  - moving media, dispersion analysis 2—42214
  - multilevel system, theory of spectrophone effect 2—80410
  - optical properties of isotropic half-space with surface wave 2—70024
  - photochromic film, acoustic wave mapping and holography 2—55548
  - pulsed Bragg diffraction method of ultrasonic visualization 2—49164
  - surface wave deflection of optical guided wave and coupling in thin films 2—49431
  - transducer deflector, high capacity composite 2—69753
  - ultrasonic waves thermal excitation in methanol by laser beams interference 2—41737
  - u.s. imaging by Bragg diffr., acoustic phase conservation 2—49447
  - u.s. interference pattern visualization by optical illumination in direction of propagation 2—55547
  - u.s. light modulation and det. of photoelastic constants in flints 2—70025
  - As_2Se_3 vitreous, appl. in i.r. modulator 2—84459
  - CO_2, vibrational relaxation time in inert gas mixtures, meas. using acousto-optical effect 2—59995
  - CdS, optical modulation by acoustic phonon flux 2—61088
  - La flint glass, Bragg diffraction rel. to acousto-optic applications 2—66839
  - $LiNbO_3$, acousto-optical deflector, thinning by ion etching 2—63417
  - $LiNbO_3$, obs. of triply phase matched five wave acoustooptic interaction 2—44349
  - $LiNbO_3$, triply phase-matched 5 wave acousto-optic interaction 2—48139
  - NaCl laser beam optical probing for sound intensity distribution 2—51026
  - Pb Mo acousto-optic deflector 2—79419
  - $5PbO.3GeO_2$, ferroelec. material, acousto-optical figure of merit, acoustic attenuation 2—64849
  - TeO_2, characteriz. for devices, acoustic attenuation coeffs. 2—51027
  - TeO_2, light deflector with 1000 spot capacity and 40 microsecond retrace time 2—51016
  - TeO_2 single crystal 2—77779
  - Tl_3AsS_4, optoacoustic figure of merit and acoustic losses 2—61597
  - Tl_3AsS_4 acousto-optic crystal, props. 2—76530
  - Tl_3AsS_4 single crystal, properties 2—48137
- **Acoustoelasticity** *see Elasticity*

Acoustoelectric effects
see also Acoustic wave amplification
- acoustic surface-wave filters 2−58924
- conducting crystals, e.m. wave scatt. by sound, electron conc. wave contrib. 2−54396
- conducting medium, dimensional quantization condition 2−43977
- convolution of signals by surface wave nonlinearities, detection 2−71739
- dimensional quantization condition in conducting medium 2−43977
- drift field induced carrier inhomogeneities in low conductivity accumulation layer surface wave amplifiers 2−51030
- electron drag related, review of developments 2−51029
- group III-V cpds., semicond., review 2−77774
- in head localization of sound source rel. to headphones and loudspeakers 2−55540
- microwave surface wave attenuation due to gas loading 2−51009
- piezo-semiconductors, waveguide effect of surface domains 2−54029
- piezoelectric, stimulated sound scatt. by elec. field oscills. 2−74981
- piezoelectric semiconductor, moving domain nucleation 2−68237
- piezosemiconductor, effects at large sound intensities 2−61098
- piezosemiconductor, fluctuating elec. field and Franz-Keldysh effect inside domains 2−54033
- piezosemiconductor, narrow propagating domains of acoustic flux, prod. method 2−43978
- piezosemiconductor, u.s. second harmonic generation 2−51039
- Rochelle salt, attenuation and ferroelectric anomalies 2−74988
- semiconductor, C_{6v} class cryst., piezoelec. interaction of transverse u.s. waves with charge carriers 2−54030
- semiconductor, carrier trapping effects 2−47746
- semiconductor, elastomagnetic waves, coupled e.m. and lattice oscills. 2−64848
- semiconductors, piezoelectric, volume negative differential cond. at large acoustic intensities 2−80915
- space charge effects on attenuation symmetry of u.s. amplification by piezoelectric semiconductors 2−51031
- surface acoustoelectric current in semiconductors 2−68240
- surface wave guidance by $(\Delta v/v)$ guidance structures 2−51010
- surface wave steering and switching by nonlinear mixing in anisotropic media 2−51011
- surface wave steering by nonlinear mixing 2−80903
- three phonon processes in acoustoelectric interaction 2−84181
- transducer array, for acoustic holography 2−69765
- u.s. amplification by interaction with electrons, elec. field effects 2−77776
- U.S devices, h.f., review in book 2−57046
- CdS-water-$LiNbO_3$ surface wave convoluter, output, enhancement 2−80904
- CdS, Brillouin scatt. from longit. acoustoelec. domains 2−43974
- CdS, current and field at large acoustic flux intensities 2−80915
- CdS, multistep current saturation 2−75078
- CdS, photoconducting, theory and expt. 2−54171
- CdS acoustoelectric instability, scattering of light by sound 2−71728
- CdS high-field domains, propagation characteristics 2−61099
- CdS photoconductor, transverse surface wave depth penetration 2−84206
- CdSe, photoconducting, effects of traps 2−61100
- n-GaAs:O, piezoelectric stiffening of active bulk modes and increase in velocity of 30 MHz shear wave 2−51204
- GaAs, acoustic amplification, surface shear wave mode characts., bulk wave theory incl. trapping effects 2−68241
- n-GaAs, acoustoelec. current oscill., temp. depend. 2−51040
- GaAs, acoustoelec. domains, elec. and optical props. 2−80912
- GaAs, origin and properties of domains 2−54034
- GaAs, piezoelectric amplification of acoustic waves abrupt decrease in gain at quantum limit 2−51033
- n-GaAs, review 2−77774
- GaAs magnetic enhancement of acoustoelectric gain, obs. by Brillouin scattering 2−51034
- Ge, quadrupole and octupole electron phonon coupling 2−61101
- n-InSb, gain parameter meas. 2−68243
- n-InSb, magnetoacoustoelectric effect, acoustoelec. domain form. and instabilities 2−64850
- InSb, origin and properties of domains 2−54034
- n-InSb, quenching of sound amplification and e.m. wave radiation by holes 2−71929
- n-InSb, review .2−77774
- n-InSb, time and spatial distrib. of amplitude acoustic flux 2−68242
- InSb microwave radiation, acoustoelectric amplification 2−54159
- KD_2PO_4, u.s. stress wave interaction with domain walls 2−71740
- $LiNbO_3$-Si layered structure, transverse effect obs. using capacity probes 2−51038
- $LiNbO_3$, acoustic convolution and correl., nonlinearity parameters 2−51014
- $LiNbO_3$, shear wave excitation by interdigital transducer operated at its surface-wave centre freq. 2−51008
- $LiNbO_3$ single crystal delay line 2−71741
- $LiNbO_3$ with CdSe film, surface state effect on surface wave amplification 2−84201
- n-GaAs, ultrasonic amplification of injected coherent shear waves, small, large signal conditions 2−64847
- SbSI, paraelec. region, rel. to illumination effects on V-I characts. 2−81163
- Se-Te alloy, acoustoelec. phenomena relating to two carriers 2−80908
- Se-Te alloy, u.s. amplification, room temp. 2−51041
- Si-PZT coupled system, acoustic surface wave convolution by 14.5 MHz Bleustein-Gulyaev waves 2−71742
- Si, quadrupole and octupole electron phonon coupling 2−61101
- p-Si, u.s. attenuation stress depend., bound hole model 2−54031
- Te:Sb, single crystal 2−71828
- Te, acoustomagnetoelectric effect 2−74986
- n-ZnO, oscills. 2−61332
- ZnO device, resistivity, threshold field, current oscills., current oscills., uniaxial press. effect 2−63119

Acoustomagnetic effects *see Magnetoacoustic effects*

Actinide compounds
see also the compounds of the individual elements
- magnetic properties of actinide Halide compounds 2−68505

Actinide compounds continued
- transition metal- actinide alloys, mag. susceptibility interpret., narrow band reson. model 2−54286

Actinides
see also the individual elements
- actinides, elec. dipole polarisabilities 2−59917
- atom, relative energies of lowest levels of f^qds^2, f^qds^2, $f^{q+1}s^2$ electron configurations 2−49950
- atomic vapours, energy differences between electron configs. 2−46440
- contamination by wounds, determ. of therapeutic procedure 2−55235
- detection and analysis of actinide contaminants in ^{239}Pu reactor fuel 2−74179
- fission product yields predicted by extrapolation of existing data 2−46355
- impurities in 3d ferromag. hosts, hyperfine field data 2−68588
- ions, effect of core polarization on f-f interactions 2−52929
- ions in single crysts., two-photon absorpt. and stimulated emission 2−48225
- irradiated nuclear fuel, analysis for actinides and burn-up determ. 2−74183
- magnetism, hybridized 6d and 5f virtual-bound-states model 2−68516
- nuclear targets, electrodeposition methods of prep. for cross section obs. and accelerator bombardment 2−73919
- systematics in relative energies of f-electron configurations 2−79937
- target fabrication, sample assay 2−57440
- targets for fission cross-section obs. and accelerator bombardments, electrodeposition methods of prep. 2−49618
- Th/U fuel elements with known irradiation data, actinide composition studies 2−75403

Actinium
- atom, iterative numerical method 2−64010
- metallic radius determ. 2−79857
- ^{227}Ac fuel in thermionic converter 2−49292
- ^{227}Ac fueled thermionic generator 2−49262

Actinium compounds
No entries

Actinometry *see Photometry*

Activation analysis *see Chemical analysis/by nuclear reactions*

Active nitrogen *see Nitrogen*

Active oxygen *see Oxygen*

Adhesion
- adhesive wear, sliding model 2−68110
- bimetallic surface, adhesion bonding in terms of electronic struct. of combined metals 2−74652
- blood platelets to glass, effect of shear rate, model anal. 2−55215
- ceramic-metal reaction welding, microscopic and macroscopic obs. 2−64785
- ceramic-metal systems, chem. bonding 2−50861
- crack stability of adhesive layer 2−55458
- elastic peel films, mechanics, elastic and elastic-plastic behaviour 2−71666
- honeycomb sandwich structures, adhesive layer, elastic vibrations 2−50927
- metal-to-metal joints, non-destructive testing, acoustic emission and radiography 2−47674
- particles, effect of flattening 2−74560
- polymer-solid, breakdown rel. to radio emission parameters 2−52314
- polymers, stability criteria for study of thermoresistant structural adhesives · 2−57006
- polymers as adhesives binders and hermetic sealers, investigation of moisture effects by electrical methods 2−53979
- powder, cohesivity, effect of temp. and press. 2−43880
- powdered metals, e. microscopy study of contact zones 2−64789
- stresses in bonded materials with perpendicular crack at interface 2−60901
- superalloy, powder, elec. discharge activated press. sintering, composite struct. bonding 2−53938
- tensile stage for meas. during scanning electron microscope obs. 2−82440
- Van der Waals atrraction, role of surface plasmons 2−51088
- Al/resin/Al sandwich bar, complex dynamic modulus 2−80742
- Al film, to polymer substrate, scratching method meas. 2−43476
- C fibres, adhesion to organic matrices 2−84101
- Co alloys, metallurgical structure and properties 2−71667
- Pb, on SiO, sticking coeff., effect of water vapour 2−64572
- TaN film, to ceramic, effect of substrate surface chem. 2−57005

Adiabatic demagnetization *see Magnetic cooling*

Adion *see Adsorption*

ADP (ammonium dihydrogen phosphate) *see Nitrogen compounds/ammonium compounds*

Adsorbed layers
- — 2−67876
- adatom capture, rel. to vapour deposition 2−50475
- adatom position in surface from fluoresc., adsorbed atoms determ. 2−77488
- adsorbate covered surface, field emitted electron energy distribs. 2−48013
- alkali metal, nonmetallic to metallic transition 2−83870
- atoms adsorbed on W substrate, backscattering cross sections for K-shell ionization by electron impact 2−79919
- chemisorbed atoms on metals, pseudopot. for calc. of transition rates 2−43492
- chemisorption, struct. types, LEED obs. 2−56600
- cyanine dye, monolayer on AgBr, spectral sensitization 2−81551
- 1,1′- diethyl-2,2′-cyanine, adsorbed on Ag halide emulsion grains, J-aggregates props. 2−81027
- dye, sensitizing and desensitizing, on AgCl photographic coatings, photocurrents 2−81183
- dye aggregates on AgBr, struct. and spectra 2−80557
- at electrode-ionic solution interphase, calc. of dielectric coefficients 2−48335
- electronic structure of adsorbed atoms on metal substrate, inhomogeneous charge distribution 2−53589

Adsorbed layers continued
- equation of state in approximated fugacity expansions 2−53584
- gas, on metal film, demetallization phenomenon 2−47150
- ice film on cooled surface, microstruct. rel. to deposition rate, elec. field, vacuum breakdown 2−83866
- internal diffusion coeff. calcs. for arbitrary isotherms 2−47143
- layer formation on metal surfaces by anodic reaction within an electrolyte solution, thermodynamics 2−68781
- metal surfaces covered by electropositive adsorbates, thermodynamic analysis 2−53588
- metallic, plasmon excitations 2−47826
- methane, on graphite, film formation stages 2−47152
- methane, on graphite, spin-lattice and spin-spin relax. 2−67925
- methane, on MgO, microdynamics, n.m.r. relax. obs. 2−83875
- monolayer, partially ionized, surface press., from Vrij's formula 2−47144
- monolayers, physically adsorbed, recent exptl. and theoretical developments 2−43490
- monolayers, surface diffusion, theory and exptl. obs. 2−71179
- monomolecular films on Hg, review 2−74645
- monomolecular layer formation by spreading copper stearate soln. 2−71177
- myristic acid monolayers, surface diffusion, theory and exptl. obs. 2−71179
- naphthalene on metal-substituted type-X zeolites, luminesc. and adsorption characts. 2−80585
- organic groups chemisorbed on silica, i.r. spectral study 2−84643
- rare gas, on graphite, film formation stages 2−47152
- sodium oleate, preadsorbed on minerals, effect on N_2, Kr and H_2O adsorption 2−47155
- stearic acid, monolayers, surface diffusion, theory and exptl. obs. 2−71179
- surface-active molecules on kaolin, i.r. spectroscopic study of effect on structure 2−84642
- thermal disorder of adatoms, 1-dimens. model, LEED pattern calc. 2−60672
- thick, rel. to heterogeneous nucleation 2−64577
- thin films formed at metal-electrolyte interfaces, determ. of potential barriers and eqns. of tunnelling limiting current 2−57426
- water, on collagen, effect on elec. props. 2−47908
- water on zeolite, molar heat, 90-300K 2−60694
- Al monolayer, struct. determ. by Tucker-Duke energy averaging method 2−47149
- Ar, on Al or Sn film, depression of supercond. transition temp. 2−61228
- Ar monolayer, binding energy of ^{3}He and ^{4}He, low temp. 2−43493
- Ar substrate, mobility of adsorbed He atoms near 2K 2−67920
- Ba disordered layer, on Ni(001), specular electron refl. 0-30eV 2−60681
- C, on W, K shell total electron impact ionization cross sections, Auger spectra 2−64579
- CO, chemisorbed on Ir-Pt alloy, i.r. spectra 2−68645
- CO, on Au, i.r. refl.-absorpt. spectra study 2−60676
- CO_2, on W, binding states, condensation kinetics, decomp. 2−77513
- CS_2- on MgO, e.p.r. obs. 2−72494
- Cd, vacuum evap., selective condensation on macroinhomogeneous surface 2−74628
- Cos- on MgO, e.p.r. obs. 2−72494
- Cs-Rb mixtures on graphite, vapour press. 2−53592
- Cs, on W, work function rel. to surface struct. 2−68487
- Cs disordered layer, on Ni(001), specular electron refl., 0-30eV 2−60681
- Cu, of S ions, phase transitions in two dimensional layer 2−50535
- D_2 on W, field emitted electrons energy distrib. as function of coverage 2−48016
- Ge on W, electronic props., field emission obs. 2−71349
- H, on TiC_x and NbC_x, surface recomb. rel. to carbide work function 2−50549
- H_2, on W, field emitted electrons energy distrib. as function of coverage 2−48016
- H_2, ortho -para conversion on paramag. surfaces 2−43496
- H_2 on ferromagnetic catalyst, ortho-para conversion, surface magnetization orientation effect 2−71342
- H_2O on silica, freezing process, n.m.r. obs. 2−53596
- H_2O on silica, self-diffusion obs. 2−60686
- He, submonolayer on Ar and Ne, two phase model 2−80581
- He monolayer adsorbed on surface of Ar crystal, calcs. of heat of absorption and band widths 2−43490
- He monolayer behaviour in mobile limit 2−77457
- He on Ar, correlation energy 2−74644
- ^{3}He monolayer film adsorbed on graphite, motional narrowing in NMR 2−64578
- ^{3}He monolayer form. and struct., n.m.r. obs. 2−80509
- ^{4}He, submonolayer on Cu and Ar and Ne monolayers on Cu, low temp. specific heat 2−80580
- ^{4}He adsorbed on graphite, flow 2−74575
- ^{4}He film, superfluid, quartz microbalance obs. 2−64497
- Hg excited atoms and molecules, interaction, on ZnO 2−47175
- K, on Ni (001), specular electron refl. 2−50544
- K, on W(100), surface plasmon losses, energy loss spectra obs. 2−64903
- K disordered layer, on Ni(001), specular electron refl., 0-30eV 2−60681
- N, on W, K shell total electron impact ionization cross sections, Auger spectra 2−64579
- Na, on Ni (001), specular electron refl. 2−50544
- Na, on W, K shell total electron impact ionization cross sections, Auger spectra 2−64579
- Na disordered layer, on Ni(001), specular electron refl., 0-30eV 2−60681
- Ne, on Al or Sn film, depression of supercond. transition temp. 2−61228
- Ne, on Ar coated grafoil, two phase systems obs. 2−80582
- Ne, on Ge, mol. beam scatt., survival rel. to coverage 2−47159
- O/ZnO sensitizing action of chlorophyll to corono discharge 2−44176
- O, Ni, thermal disorder, LEED pattern interpretation 2−60672
- O, on Ni, He^+ backscatt. and LEED study 2−50543
- O, on W, K shell total electron impact ionization cross sections, Auger spectra 2−64579

Adsorbed layers continued
- O_2-, on Ag, e.p.r. obs. 2−50531
- O_2, on NaI, effect on X-ray, u.v. and visible spectra 2−81399
- O_2 on NiO and CuO, species characterization by X-ray photoelectron spectroscopy 2−77516
- O_2^- chemisorbed on thermally activated MgO powders, e.s.r. obs., 2−56602
- OH, on quartz, refl. spectra obs. 2−48163
- P, on Si, Auger electron signals as function of coverage 2−47080
- Pb, on Ni, low index surfaces, LEED obs. 2−60682
- Pb, on SiO, sticking coeff., effect of water vapour 2−64572
- Pb monatomic film on W(100) surface, struct., LEED obs. 2−77511
- Rb, on W(100), surface plasmon losses, energy loss spectra obs. 2−64903
- Rh surface self-diffusion on Rh, low temp. 2−64555
- W, surface self-diffusion rel. to C adsorpt., field emission obs. 2−64582

Adsorption
- *see also Chemical analysis/adsorption; Chromatography; Films; Heat of adsorption; Sorption*
- adatom position in surface from fluoresc., adsorbed atoms determ. 2−77488
- anthracene crystal, adsorbed dye soln., sensitized photoconduction and delayed fluorescence 2−81169
- aromatic molecules adsorbed on MgO surface, photoactivation by u.v. radiation 2−78206
- benzene, adsorbed on gel, n.m.r. 2−46614
- Burnett-isochoric coupled data, applic. to adsorbing gases 2−67868
- calorimetry, twin heat conduction calorimeter design 2−52302
- carbon blacks, surface oxygen complexes, effect on selective adsorption of non electrolytes from mixtures 2−64552
- carbon tetrachloride-He system, autoadsorption rel. to surface tension, 1-71 atm., room temp. 2−64453
- β-carotene film, solid, gas adsorption effect on absorpt. spectra 2−57355
- cell, of virus, kinetics 2−73167
- charcoal, simultaneous adsorpt. of benzene and cyclohexane 2−68779
- composite isotherm resolution using 'ternary phase diag.' approach 2−53586
- cubic tight binding solid, anisotropic oscill. indirect interact. between adatom pairs 2−47146
- diamond powder, oxygen chemisorption, kinetics 2−65374
- dyes on gelatin coatings 2−70092
- fugacity expansions, convergence and first-order approx. 2−53584
- gas-surface interactions, computation of scattering kernels, boundary-value problem 2−49042
- gases, at solid interface in fluidized beds 2−80163
- glass, of ^{18}F, time depend. curve 2−83877
- glass of Xe, isotherms at various temp. meas. 2−50529
- graphite, isotropic nuclear and 'Poco', of oxygen, reactivity obs. 2−59843
- graphite, of CO and H_2 in high vac. range 2−43494
- graphite, of oxygen complexes, surface polarity obs. 2−64550
- graphite, of Xe, LEED study 2−50533
- graphite, or rare gases or CH_4, film formation states 2−47152
- graphitized carbon, of normal liq. paraffins, quasicryst. layer form. 2−50532
- ice, of H, at 4.2K 2−50539
- ice and solid CO, of H, interstellar 2−55076
- kaolinite rods, elastic consts. from adsorptive length changes 2−77641
- kinetics in case of rectangular adsorption isotherm 2−83879
- Knudsen gas, rarefied, equilib. state, effect of adsorbing surfaces 2−50263
- liquid mixtures on solids, excess props. and temp. coeffs. using Gibbsian thermodynamics 2−53583
- manganese oxides, of chemically nonequivalent O atoms (ions) 2−47167
- metal, adsorbate-covered, electron field emission, effect of lattice potential 2−61457
- metal, effects on hydrogen permeation 2−77608
- metal, needle-like microcrysts., effect on strength, ion emission microscope obs. 2−80729
- metal, of alkali atoms, theory of work function changes 2−48007
- metal film, supercond. transition temp. change due to noble gas adsorption 2−47856
- metal surfaces, dipole cross depolarization effects 2−50521
- methane, adsorbed on gel, n.m.r. 2−46614
- minerals, of N_2, Kr, and H_2O vapour, hydrophilic character determ. 2−47155
- molecular in thin film optical waveguides and absorption 2−63416
- multicomponent solutions, Gibbs equation, nonelectrolyte and neutral salts 2−83873
- multicomponent solutions, Gibbs equation, organic ions 2−83874
- multicomponent systems, differential rates, simplex method study 2−47141
- multilayer, on heterogeneous surfaces, graphical estimation method 2−83876
- nylon 66 fibres, of polyacrylic acids, model compounds and vapours, rel. to textile size applic. 2−60696
- nylon 66 powder, of polyacrylic acids and model compounds, rel. to textile size applic. 2−60695
- organic semiconductors, gas reactions, photoelectric detection method 2−72570
- of polyelectrolyte macromolecules on flat interface, approx. theory for low potentials 2−61793
- pore structure analysis, t-method, applic. to circularly cylindrical pores 2−53975
- pore structure analysis, t-method, applic. to slit- shaped pores 2−50925
- porous glass, of hydrocarbons, counterdiffusion 2−60685
- porous material, mech. effects of adsorption, field theory 2−60670
- porous material, of N_2 gas at liq. N_2 temps. 2−50541
- pressure effects on magnetron press. gauge on satellite O VI-15 2−58148
- pseudocapacity depend. on potential for Temkin isotherm case 2−47142

Adsorption continued
pyrolytic graphite basal plane, reaction with modulated O_2 beam, study of surface chemistry 2−51447
quantum gas, physical adsorption in subomonolayer region, significant structure theory 2−67917
rough surface, isotherms 2−67919
semiconductor film, single crystal, electrical conductivity and adsorption, combined meas. 2−71932
on semiconductors, physisorption 2−47147
silica gel, of electron pair donors, H bonding 2−77515
solid surfaces, conference, Boston Mass., USA, Oct. (1971) 2−47070
of solute from dilute liquid solution, derivation of virial equation 2−53585
solution, rel. to mol. clustering and segregation 2−60439
stepwise adsorption isotherms applied to study of surface phases 2−77518
surface area meas. using N adsorption and Harkins and Jura isotherm 2−58686
surface phonons and gas surface interactions 2−50522
synthetic sodium-containing adsorbants, of NH_3, temp. and press. depend. 2−47160
tetrahydrofuran, of $Hg(CN)_2$, rel. to addition cpd. formation 2−60706
thermokinetic, computer soln. 2−53587
three-dimensional treatment of inhomogeneous solid-fluid systems using equations of state for homogeneous systems 2−43489
on three-phase system, of surface active agent 2−71173
transition metal, of alkali metal, atomic theory of work function variation 2−71343
transition metal on transition metal, tight binding model 2−50527
uranium oxides, of chemically nonequivalent O atoms (ions) 2−47167
vanadium oxides, of chemically nonequivalent O atoms (ions) 2−47167
zeolite, of ethane and ethylene, effects of size, charge and conc. of exchange cation 2−74646
zeolite, of water, molar heat, 90-300K 2−60694
zeolite surfaces, low-temperature emission excited by electron impact, rel. to adsorption and energy of surface states 2−77973
zeolites, noncooled, vacuum tests, trapping and pumping props. 2−76131
ZnSe, differential absorption spectrum on adsorption of molecules of donor-acceptor type 2−68651
Ag, of O_2, e.p.r. obs. 2−50531
Ag, of oxygen, slow irreversible processes, work function depend., LEED pattern changes 2−60675
Ag halide, of gelatin and photographic stabilizers 2−80584
Ag halides, of 1,1′-diethyl-2,2′-cyanine, J-aggregates props. 2−81027
Al, adsorption of Cl, Auger spectrosc., ellipsometry and surface potl. meas. of clean films 2−71345
Al, adsorption of water, detn. by meas. of work function 2−71346
Al, of O_2, work function changes obs. 2−77517
Al of ^{18}F, time depend. curve 2−83877
Al superconducting films, of molecular oxygen, density of states change 2−51111
γ-Al_2O_3, specific surface area meas. 2−64548
Ar, of H, at 4.2K 2−50539
Ar on porous Ag, onset of Henry's Law 2−60674
Au, adsorption of water, detn. by meas. of work function 2−71347
BiI_3, effect on photocond., dark cond. and thermionic work function 2−47993
C, microporous polymer, of CO_2, applic. of potential theory 2−53591
C, of H and H_2, rel. to work function variation 2−60677
C, porous, of liquids, high resoln. n.m.r. obs. 2−53594
C, thermal accommodation coeffs. for gases, Royal Aircraft Establishment review 2−43903
C blacks, using precision microgravimetric system 2−53593
C fibre, microporosity determ. 2−53952
C on (111) face of Ir, effect on surface ionization of CsCl 2−64543
CO, of CO, change in work function 2−71348
CO_2, on W, binding states, condensation kinetics, decomp. 2−77513
CaX synthetic zeolites, preferred rotation of adsorbed ClO_2 molecules 2−80579
Cd, stepwise adsorption isotherms of SF_6 2−77518
Cs on W(100) surface, work function 2−83878
Cu-Ni alloy, of CO and O_2 2−50536
Cu, Ar plated Cu, heats of adsorp, and adsorp. isotherms for Ne 2−47157
Cu, of CO and H_2, weak adsorp. obs. 2−50537
Cu (100) surface, CO weak adsorp., structure and binding 2−50538
Cu film, of Xe, roughness and surface potential 2−50556
CuO, of O_2, adsorbed species characterization by X-ray photoelectron spectroscopy 2−77516
Fe, of CO, change in work function 2−71348
Fe film, of Xe, roughness and surface potential 2−50556
GaAs of Cs, ESCA obs. and photoyield 2−53595
p-Ge, influence of adsorption of sIo molecs. on field emission 2−72076
Ge, of Cd, heat of adsorption, mol. beam technique 2−50534
Ge clean surface, of CH_3OH and CH_3SH 2−56601
Ge single crystal, of Cd, by mol. beam technique, rel. to nucleation 2−47158
H-metal interaction, piezoelectrical quartz crystal micro-balance 2−74643
H, on (111) face of Ge single crystals 2−80583
H_2O-He system, autoadsorption rel. to surface tension, 1-71 atm., room temp. 2−64453
He monolayer formation on graphite, densities at completion 2−71253
Hg, of gases, monomolecular films, review 2−74645
KBr, molecular CO^{2-}_3 centre formation, i.r. spectra obs. 2−71350
KCl, molecular CO^{2-}_3 centre formation, i.r. spectra obs. 2−71350
LiF(001), of H_2O, effect on dislocation mobility 2−43627
MgO, charge transfer in adsorption of chlorine and oxygen obs. of ESR signal 2−47139
Mn, of CO, change in work function 2−71348
Mo, of alkali metals, LEED and Auger spectroscopy obs. 2−50540

Adsorption continued
Mo, of O_2, atomic and electronic processes 2−74649
Mo, of O_2, Auger spectrum chem. shift 2−51223
NH_4ClO_4, of water or NH_5, rel. to proton transfer cond. 2−84361
Na film, of Xe, roughness and surface potential 2−50556
NaCl(001), of H_2O, effect on dislocation mobility 2−43627
NaX synthetic zeolites, preferred rotation of adsorbed ClO_2 molecules 2−80579
NaX zeolites, of H_2O, proton magnetic relaxation meas. used to determ. structure and dynamic properties of adsorbed phases 2−54515
Nb, of H, and absorption 2−50542
Nb crystal surface, of Cs and Ba simultaneously, work function and thermal stability obs. 2−67923
Nb polycrystalline wire, of H_2, u.h.v. technique 2−47161
$NbSe_2$, Auger electron spectroscopy investig. of adsorption anisotropy 2−60687
Ne, of H, at 4.2K 2−50539
Ni, of CO, preferential orientation, extended Huckel calc. 2−50546
Ni, of Hg, alloy formation 2−77489
Ni, of O, S, Se, surface reconstruction, Madelung potential 2−47162
Ni crystal face, of benzene and cyclohexane, LEED and mass spectrometer obs. 2−50545
Ni film, of H_2, effect on saturation magnetization 2−48094
Ni film, of H under ultra-high vacuum conditions, meas. of desorption spectrum 2−53590
Ni film, of Xe, surface potential, photoelec. emission obs. 2−47163
NiO, of O_2, adsorbed species characterization by X-ray photoelectron spectroscopy 2−77516
Ni(110), N or S adsorbate-covered, electron energy loss spectra, elastic scatt. 2−84222
O on (111) face of Ge single crystals 2−80583
$POCl_3$, effect on oxidation of graphite 2−68783
Pt/Al_2O_3 catalyst, butene adsorption, high resolution n.m.r. obs. 2−60683
Pt, chemisorpt. of H_2, adsorpt. and desorpt. kinetics 2−77514
Pt, interaction with O_2, thermodynamic props. of volatile products, obs. method 2−65378
Pt, interactions with O_2 2−51450
Pt, of Ba, field emission microscope work function obs. 2−67924
Pt, of H, promoted evap., field ion microscopy obs. 2−50548
Pt, of noble gases, accommodation coeffs., 80-450K 2−56603
Pt film, cond. rel. to temp., 77-573 K, adsorpt. effects 2−64917
Re, interactions with O_2 2−51450
Si, of O_2, comments on expts. 2−47165
Si, of O_2 2−47164
Si (111), of O_2, localized vibrations, low energy electron spectroscopy obs. 2−50987
Si (111) surface, of Ni molecular beam in u.h.v. obs. using mass spectrometer 2−50499
Si clean surface, of CH_3OH and CH_3SH 2−56601
Si substrate, impurity adsorption, effect on epitaxial layers 2−74647
SiO_2, of CO_2, e.s.r. obs., E′, dangling bonds 2−71352
SiO_2, of CO_2, u.h.v. studies 2−71353
SiO_2, of polystyrenes, competitive effects 2−60684
SiO_2, of water, effect of surface acidity, n.m.r. and DTA studies 2−53597
ThO_2, effect of fluoride adsorp. on hot-pressed density 2−74648
Ti-Ni-H, intermetallic phase and absorption of hydrogen 2−71354
Ti, of Cs, ellipsometry, Auger spectra and surface pot. difference obs. 2−50550
Ti, photoemission energy level meas. of sorbed gases 2−47166
Ti of ^{18}F, time depend. curve 2−83877
TiO_2, doped and undoped, frequency dependence of conductivity and adsorption of CO 2−77906
TiO_2, of water, and desorption 2−60688
$TiTe_2$, Auger electron spectroscopy investig. of adsorption anisotropy 2−60687
W-He energy accommodation coeffs., one-phonon inelastic scattering 2−50528
W, (211) and (110) planes, of Cl, field emission study 2−60693
W, cathode, O_2 pumping effect 2−48943
W, cathode, O_2 pumping effect 2−48943
W, decay of surface state obs. in photoemission due to gas adsorption 2−75197
W, lifetime, of O_2, as function of coverage 2−47171
W, of CO, on (210) surface, binding states and work function 2−60692
W, of Cd, heat of adsorption, mol. beam technique 2−50534
W, of Cs, ellipsometry, Auger spectra and surface pot. difference obs. 2−50550
W, of Cs and O, double layer form., LEED and work function obs. 2−47169
W, of methane, field ion microscopy obs. 2−64583
W, of N, surface crystallographic effects 2−47168
W, of N_2O, binding states, LEED obs. 2−64581
W, of O, low coverage at 78K, field ion microscopy 2−64584
W, of O_2, atomic and electronic processes 2−74649
W, of O_2, thermionic electron emission and work function obs. 2−47172
W, of O and Cs, and O-Cs co-adsorption, rel. to work function 2−54266
W, polycrystalline, of D_2 and ethylene 2−44484
W, polycrystalline equilibrium Cs adsorption measurement, ellipsometry technique 2−63232
W, pure O_2, Cs vapour/O_2 mixtures, work function changes due to, analytical model 2−63231
W, sensitivity of surface state obs. in photoemission to adsorption of hydrogen 2−75198
W, surface self-diffusion rel. to C adsorpt., field emission obs. 2−64582
W (100) face, of methane, ethane and propane 2−74642
W (100) surface, adsorption state of hydrogen 2−50555
W (110), polarizability of W adatoms, field ion microscope obs. 2−60689
W crystal face, of ethylene, flash desorption obs. 2−50552
W crystal surface, of Cs and Ba simultaneously, work function and thermal stability obs. 2−67923
W single crystal plane, of O, field emission microscope obs. 2−64580

Adsorption continued
- W surface, alkalis, rare gases and H_2 adsorbate structure 2–50554
- W surface of O, inhibition of reactions with H 2–71344
- W(112) single crystal, effect of O adsorption on scattering of He and Ar atoms 2–67894
- Xe, solid, of He and Ne, energy spectrum calculation method 2–43499
- Xe crystal edges and vertices, of Ar atom 2–47174
- Y, of O_2, Auger spectrum chem. shift 2–51223
- Zn, stepwise adsorption isotherms of SF_6 2–77518
- ZnO, differential absorption spectrum on adsorption of molecules of donor-acceptor type 2–68651
- ZnO, differential absorption spectrum on adsorption of molecules of donor-acceptor type 2–68651
- ZnS, differential absorption spectrum on adsorption of molecules of donor-acceptor type 2–68651
- ZnSe, differential absorption spectrum on adsorption of molecules of donor-acceptor type 2–68651

Aerials *see Electromagnetic waves/radiators*

Aerodynamics
- *see also Flow/gases; Jets; Shock waves; Supersonic flow; Turbulence*
- 83681
- ablation surface pattern, effect of nose blunting, exposure time and initial temp., cross hatching 2–46816
- absolute flow near impeller inlet of centrifugal turbomachine 2–80381
- aeroelastic stability of flat anisotropic sandwich-type plates 2–49073
- aeroelasticity, trends and achievements 2–50254
- aerofoils, flow around leading edge 2–77362
- aerosound, source theory 2–46840
- aerospace sciences progress, theory and experimental techniques, book 2–81748
- aerospace vehicle design, small scall wind shear definition 2–44798
- air jet as acoustic lens or waveguide 2–45508
- air-natural gas jet, characteristics for combustion in transitional flow region 2–53317
- aircraft and missiles, three-dimensional flow separations 2–56422
- aircraft wake vortices, acoustic ray deflection 2–56430
- airfoil, nearwake props. leading to generation of vortex shedding sound 2–46844
- airfoil, thin highly cambered, section data in compressible flow 2–67728
- airfoil stall and stall flutter 2–67725
- airfoils, surface evaluation, holographic contouring 2–82537
- arc jet material ablation studies, channel test device 2–53313
- architectural, periodic flow phenomena 2–80207
- artificial satellites, aerodynamic forces, drag and lift, theoretical determination 2–62419
- atmospheric boundary layers 2–68899
- atmospheric drag cross section solar cell arrays, nodal regression, solar declination 2–83677
- atmospheric re-entry, numerical treatment 2–53320
- axially symmetric bodies, laminar, transition and turbulent heat transfer to leeward side 2–53306
- axisymmetric bodies at small angles of attack, boundary layers 2–50243
- axisymmetric jets and wakes, implicit finite difference soln. 2–60325
- blunt bodies, supersonic nonequilibrium flow 2–83678
- blunt bodies, transonic region, shock waves 2–77329
- blunt body flows, effects of nonequilibrium dissociation 2–77361
- blunt body heat transfer, effects of slip 2–60359
- bluntness of nose shape, effect on pitching moment of bodies of revolution 2–53325
- boundary turbulence, application of Reichardt model 2–53304
- boundary value problem, variational soln. and error bound 2–77340
- buffet phenomena applic. of miniature pressure transducers 2–46827
- buoyancy, three-dimensional, shape- preserving convective elements, numerical simulation 2–48447
- burner, flat-flame, motion of gases in open flame 2–58970
- Chapman-Jouguet detonation, self-similar blast waves 2–80392
- circular arc using profiles with critical asymptotic Mach number 2–60349
- compressed gas volume expansion, two-dimensional unsteady problem 2–77325
- compressible turbulent boundary layer heat transfer to rough surfaces in pressure gradient 2–56425
- compressible unsteady boundary layer eqns., 3D soln. 2–83680
- computing methods 2–82284
- conference, Israel, 1972, aviation and astronautics 2–50253
- conical nose shape effects on drag and static stability at Mach 10 2–43251
- continuous media, stability conditions for basic stationary motion 2–67722
- coordinate perturbation and multiple scale techniques 2–50249
- cylindrical flare bodies, bundary layer effects, in supersonic flow 2–77359
- delta wing, symmetrically deformed influence of vortices on aerodynamic characteristics in supersonic flow 2–50261
- delta wings with trailing edge spoilers, rarified hypersonic flow 2–71091
- detonation, blast wave and finite kinetic rate models, review 2–80378
- diamond shock pattern, decay 2–77355
- diffusers for centrifugal turbomachines, gas flow studies 2–43243
- diffusion gas mixture, propagation of weak oblique shock 2–43241
- direction-insensitive static head sensor, wind-induced pressure in ambient air stream 2–82131
- discrete tone radiation from supersonic jet 2–46841
- downwash eval. on rectangular wings 2–64379
- downwash integral eval. by subsonic lifting-surface method 2–67715
- drag of cylinder with air blowing in air stream 2–71074
- dust collection efficiency for power law bodies in hypersonic flight 2–60351
- exhaust plume/boundary layer interactions at supersonic speeds 2–56423

Aerodynamics continued
- explosions and shock waves, conference (Marseille, France, Sept. 1971) 2–80375
- film cooling effectiveness and skin friction in hypersonic turbulent flow 2–83666
- flames, laminar diffusion formed by jet emanating from narrow extended slit 2–53303
- flap turbulent heating, skin friction and pressure data from hypersonic shock tunnel 2–53314
- flat plate boundary-layer transition in supersonic wind tunnels 2–43248
- flight mechanics, transformation of derivatives 2–53322
- flight on great circle, lateral dynamics and stability 2–43244
- flight test base pressure data results at hypersonic Mach numbers in turbulent flow 2–43247
- flow noise, cross correl. method 2–45533
- flow over mountains, three-dimensional effects 2–84814
- flow past annular aerofoils, survace vorticity theory 2–67577
- flying vehicles, rotationally symmetric, direct methods for investigation of stability and transient motion 2–50255
- focused supersonic booms in turning flight, elimination 2–74479
- frictional heating and surface temp. due to flow over plate 2–64366
- galloping and vortex excitation of rectangular block in uniform flow 2–53316
- gas-dust medium, shock relaxation 2–46834
- heating, supersonic flow, oil flow patterns, space shuttle vehicles 2–83679
- heating effects on sounding rockets 2–53309
- heating of a shell in supersonic turbulent flow 2–60368
- high lift, augmentor wing research 2–77318
- high temp., i.r. diagnostic techniques 2–82562
- hypersonic bodies, maximum drag for reentry vehicles 2–60360
- hypersonic flow, internal, inviscid, about unyawed cones, closed form solutions 2–56428
- hypersonic low-density cone drag 2–56421
- hypersonic nose and loading edge shapes, minimum energy 2–43250
- hypersonic projectile wake, electron density fluctuation meas. 2–60352
- hypersonic separated region, effects of transverse outflow 2–46814
- hypersonic wake, vel. field determ. by ion probe pairs 2–74477
- hypersonic wake in ballistic apparatus, conductivity measurement 2–74480
- ideal gas behaviour, sound amplified by unimolecular reactions 2–75369
- incompressible thin wing flow, vortex lattice numerical solution, accuracy 2–53271
- industrial, compact wind tunnel, adaptations 2–64381
- industrial, compact windtunnel design and construction 2–67716
- industrial, wind tunnel applics. 2–80384
- inviscid fluid flow, design of axisymmetric convergent cones with plane sonic outlets 2–50244
- inviscid nonuniform freestreams, supersonic flow, blunt cones, wakes 2–83675
- inviscid supersonic flow, over blunt delta wing, space shuttle reentry 2–71093
- jet, turbulent, sound influence, vortex generation 2–46842
- jet noise, generalized theory 2–55552
- jet noise, simple pressure source model 2–56429
- jet noise, theory using method of matched inner and outer expansions 2–77326
- jet penetration into airstream using swept back injectors at angle of attack 2–71085
- laminar, transitional and turbulent boundary-layer profiles on wedge at local Mach numbers 6.5 and 20 2–71103
- laminar boundary layer equations from differential- difference method 2–80398
- laminar boundary layer on rotating round-nosed blade 2–43062
- laminar coaxial jets, recirculating cells 2–83667
- laser instrumentation in test facilities 2–46848
- lifting aerofoils and slender bodies, transonic flows 2–71092
- lifting line theory for wire in nonuniform motion 2–77324
- lifting surface theory in subsonic flow, exptal. checking 2–71097
- liquid sheets, instability 2–67779
- local skin friction evaluation 2–53299
- Mach 3 windtunnel, design criteria 2–77360
- meteor flight and explosion 2–81900
- meteorological ballon shelters, wind tunnel investigation of shape 2–75517
- minimum drag in free-molecular flow, determination of optimum non-slender bodies of revolution 2–53122
- motion of rigid sphere responding to passage of acoustic pulse 2–64384
- mountain ranges, mathematical model for calculating non-linear effects on lee side 2–72784
- multidimensional gas, time dependent finite difference analysis 2–74478
- multitube multishroud supersonic jet noise suppressor 2–43233
- noise from circular jets 2–64387
- noise generated by air flow through circular nozzles 2–46845
- noise of obstacle placed in stream 2–46846
- non-steady flow direction generation and obs. 2–46847
- nonaxial symmetric bodies, in subsonic and supersonic flow 2–53327
- nonequilibrium radiative, pointed bodies 2–43253
- nonlinear, rolling re-entry vehicle 2–78422
- nonlinear actuator disk theory, propeller streamlines 2–53326
- nonlinear wave interactions 2–80405
- numerical methods for 3 dimens. layers 2–53266
- ogive-cylinder bodies at high angles of attack, side forces in transonic flow 2–64383
- one-dimensional, unsteady, nonequilibrium dissociative, simple waves 2–46809
- one-dimensional problems, boundary conditions 2–62970
- optimal atmospheric entry trajectories 2–53310
- optimal reentry control problem, perturbation technique 2–60350
- oscillating aerofoil section, aerodynamic force by Mach-Zehnder interferometer 2–77358
- plane aerofoil, lift forces in incompressible potential flow 2–53328
- plug nozzle installed on underwing nozzle, installation effects 2–67729

Aerodynamics continued
plume induced boundary layer separation in rocket engines 2−53308
pressure and temperature behind blunt bodies in supersonic flow with supply of inert and reacting gases to base region 2−60332
pressure fluctuation, interaction between shock wave and turbulent boundary layer 2−43257
profile and cascade of profiles calc. for given velocity distrib. as function of potential 2−71098
radial laminar flow of compressible fluid between two coaxial discs 2−50260
radiation props. of semi infinite vortex sheet 2−77320
rain, erosion model, effect on supersonic flight 2−43252
re-entry electrical phenomena simulation using hotshot wind tunnel 2−72931
re-entry vehicle dynamic stability, effect of lagging pitching moment 2−66027
re-entry vehicles, optimal three dimensional motion 2−77331
rectangular block, gas flow patterns and aerodynamic characteristics 2−50262
relaxing fluids, Eulerian equations of motion for wave propagation 2−43256
review of work at National Physical Laboratory, 1917-70 period 2−67720
rotating body, slender, aeroelastic equations 2−50257
sea ice cover, air drag coefficients and roughness length 2−65566
semispan stol jet transport wing, static longit. characts. 2−67730
separated flow noise, wall press. spectra and r.m.s. levels 2−45532
sharp cones at angle of attack, hypersonic characteristics 2−53307
shock tube, contact surface 2−50252
shock wave acceleration in gas with density gradient 2−64386
shock wave turbulent boundary layer interaction on blunted compression surface 2−53315
shock waves, oblique, partly dispersed, reflection from plane wall 2−78933
shocks converging spherical and cylindrical, zero temp. gradient in rear flow field 2−52257
skin friction sensor development 2−60362
slender wing in uniform stream, vortices over leading edge 2−77332
slotted wind tunnel interference parameter calculation 2−64378
small disturbance eqns., flow field analysis using numerical soln. 2−71104
smoke trail motion through fluids with constant vel. shear 2−65833
sonic boom, far-field, non-asymptotic effects 2−53318
sonic boom, UK research review 2−45534
sonic boom of hypersonic vehicles 2−46813
sonic boom signatures by bicharacteristic method 2−83668
sonic flow around wing profiles, numerical calculation 2−74476
sonic flow round wing profile, calc. 2−53300
sounding rocket, dynamics of ascending flight 2−80400
sounding rockets, nonlinear aerodynamic characteristics 2−53312
space shuttle, optimal transition from entry to cruising flight 2−53311
space vehicle entry simulation, arc-heated duct facilities for turbulent flow 2−66028
sphere drag in laminar flow, employing subsonic wind tunnel 2−67719
spherical balloon wind sensors 2−57933
spiral curve control, with neutral and manoeuvre points as limiting positions of the indifference point 2−64375
stol wing propulsion system, pot. flow soln. 2−67726
streamlines, in dissociative nonequilibrium flow, normals and binormals 2−43236
structure of boundary layer over flat plate with diffusion flame 2−83659
subsonic and supersonic static characts. of bulbous base cones 2−71105
subsonic static characts. of slender wing configs. using mag. suspension and balance system 2−67727
subsonic turbulent jets, pressure fluctuations 2−60347
subsonic wind tunnels, displacement correction and limits of operation 2−67724
super critical aircraft wing design, computer aided 2−71099
supersonic air ejectors, performance and noise characts. 2−46843
supersonic flow, holographic interferometer and fringe analyser, use in wind tunnel 2−46836
supersonic flow around thin shaped tail group edges 2−71096
supersonic plane symmetrical gaseous mol. beam, vel. distrib. and Mach no. 2−53302
supersonic surface jet, hypersonic flow interaction with axial symmetry 2−56424
supersonic transport, materials testing using simulated flight-by-flight loading 2−60952
supersonic uplift flow, drag on aeroplanes with three pointed edges 2−67723
swirling flow in combustion systems 2−80376
switching for., sign behaviour in elliptic coast trajectories 2−53321
thin wing, Baranoff's analytical form of kernal of Possio's integral eqn. 2−53323
three dimensional lifting flow 2−56427
throttling of two-dimens. nozzle flows 2−60357
towed vehicle system in coordinated turn by towing vehicle 2−43245
transient axisymmetric thermoelastic problem, two-temperature theory rel. to aerodynamic heating stresses of of solid isotropic sphere 2−45433
transient flow field produced by secondary injection, numerical solution 2−43255
transonic airfoil with asymptotic crit. Mach no., numerical analysis 2−60348
tube, cryogenic pump calc. 2−82078
tube vehicle systems, thrust and power requirements 2−43246
turbofans, mixed and unmixed, transient characteristics and steady state off design operation 2−53324
turbulent air, meas., three component dynamic wind tunnel balance design 2−46829
turbulent flow, complex and non-self-similar 2−77321
turbulent flow in aircraft design 2−60353
turbulent flow through porous tube with suction, friction factors 2−60338
turbulent flux near ground, field obs. 2−78354
two-stream propulsive systems 2−50256

Aerodynamics continued
underexpanded exhaust plumes, flowfield interactions 2−43232
unified area rule for hypersonic and supersonic using bodies 2−71094
unsteady loadings caused by trailing edge control surface motions 2−71106
variational solutions using stepwise constant functions, linear equations 2−43249
viscous interaction over concave and convex surfaces at hypersonic speeds 2−77357
viscous three dimensional flow, numerical soln., application to hypersonic leading edge 2−46835
vortex core structure 2−64382
vortex filament with axial flow, motion 2−60361
vortex induced wing loads 2−71073
vortex wake system, motion through stratified atmosphere 2−81670
VTOL aircraft, jet impingement, flow field meas. 2−83664
wake density fluctuations meas. using pulsed laser holographic interferometer 2−46833
wave patterns near sonic line in non-homentropic flow 2−60355
wave rider at low Reynolds number 2−43254
wind tunnel, NOR hypervelocity, boundary layer in nozzle 2−67731
wind tunnel, NOR hypervelocity, design 2−71100
wind tunnel, V/STOL, design 2−71101
wind tunnel corrections using three dimensional model meas. 2−56432
wind tunnel instrumentation, problems due to high power and temp., techniques 2−83685
wind tunnel interference in dynamic measurements 2−60354
wind tunnel magnus testing of canted fin of self rotating configuration 2−71095
wind tunnel model trajectory simulation system, digital computer applic. to closed loop control 2−46849
wind tunnel models, applic. of miniature pressure transducers 2−46828
wind tunnel models design for aeroelastic studies in transonic flow 2−46838
wind tunnel stability testing using five component oscillating balance 2−45215
wind tunnel wall interference reduction by streamwise porosity distrib. 2−46812
wing-body interaction, flow field 2−80401
wings with blunt trailing edge, base drag reduction method 2−60356
yawed flat plate, turbulent boundary layer 2−53319
H_2 with decreasing density, strong shock propagation 2−60358

Aeronomy *see Atmosphere; Meteorology*

Aerosols
see also Foams
— 2−67786
— 2−71276
— 2−71279
aerosols and atmospheric chemistry, Kendall award symposium, Los Angeles, (1971) 2−46993
air contamination by radioactive particles, estimation methods 2−58012
air pollution mapping, Q-switched ruby laser radar 2−78350
airborne particles, diffusional separation 2−80496
alveolar deposition, algebraical model 2−69234
aspiration study by photographing particle tracks under flash illumination 2−43404
atmosphere, interaction with outgoing terrestral radiation 2−65653
atmosphere, i.r. attenuation, aerosol extinction contrib. 2−81647
atmosphere, i.r. radiation transfer profiles 2−65755
atmosphere, Pasadena, chemical elements, calc. based on source contribs. 2−51587
atmosphere, sea ice open channels as ion sources 2−81669
atmosphere, simulated, effects of humidity and water droplet clouds on light scattering 2−57991
atmosphere, suspended particulates, size distribution 2−65677
atmosphere, tropical, long-wave radiative transfer model 2−65654
atmosphere-ocean system, effects of aerosol variation on radiance 2−57990
atmospheric, Aitken nucleus characteristics correlation with mass concentration 2−78347
atmospheric, characterization and monitoring by fluorescence 2−81692
atmospheric, condensational growth and particle size distrib. 2−48461
atmospheric, continuous sampling device for electron microscopy 2−57945
atmospheric, det. of water soluble matter 2−44694
atmospheric, effect on flux of i.r. radiation 2−62129
atmospheric, effect on radiance and colour of twilight sky light 2−81690
atmospheric, effects on sunlight 2−81689
atmospheric, height distribution det. by lidar 2−57949
atmospheric, i.r. absorption 2−65777
atmospheric, irregular particle scattering 2−62254
atmospheric, light absorption, radiative props. of atmospheric windows 2−65793
atmospheric, light scattering from measured aerosol size distributons, six component log gaussian model 2−81688
atmospheric, meas. of complex refr. index 2−62252
atmospheric, optical attenuation coefficient, vertical profile 2−57996
atmospheric, optical constants of constituents 2−57946
atmospheric, optical spatial filtering for detection of particular shape 2−48462
atmospheric, particle size distrib., photometric obs. 2−75538
atmospheric, particles rel. to humidity, extinction coeff. for visible light 2−84818
atmospheric, particulate layers erfect on i.r. transfer 2−62130
atmospheric, refractive index and absorption 2−65773
atmospheric, scatt. and absorbing props. 2−65780
atmospheric, scattering of e.m. radiation 2−62267
atmospheric, single particle light scattering obs. 2−72802
atmospheric, size-altitude distrib., light scatt. obs. 2−65778
atmospheric, trace material obs. program in atmosphere 2−62152
atmospheric, water and ice nucleating effectiveness 2−51613

Aerosols continued
atmospheric aerosol light scattering from extinction measurements at remote clean air locations 2−51621
atmospheric aerosols, climatic effects rel. to direct solar radiation heating 2−65767
atmospheric aerosols, sunlight absorption coefficients, measurement methods 2−51617
atmospheric aerosols rel. to hemispheric long-wave irradiance incident at Earth's surface 2−65448
atmospheric dust, Mauna Loa meas. of global trends 2−62147
atmospheric haze, brown colour from atmospheric aerosol and NO$_2$ content 2−62264
atmospheric pollutants, remote sensing by light scattering 2−81693
atmospheric pollution aerosol monitoring by scatter of Ar-ion laser beam, interferometry 2−51600
atmospheric pollution drift deduced from electrical conductivity of atmosphere 2−62154
atmospheric turbidity meas. w. laser radar 2−62272
atmospheric turbidity rel. to aerosols above McCall glacier 2−62273
atomization of liquids, with ultrasonics 2−80495
attenuation of visible and i.r. radiation rel. to air humidity 2−81660
beam focusing and spectrometry 2−85158
bipolarly charged, coagulation and dispersion 2−80492
bronchial tree, diffusion deposition of small-sized particles 2−85123
charged drop, oscillations, relaxation and damping, EHD stability 2−80227
charging theories, comments 2−50385
cloud seeding, complexing of AgI-NaI systems 2−62247
cloud seeding, particle size distrib. determ. method 2−62246
coacervate formation by aerosol OT with NaCl 2−74570
coalescence theory, scalar transport equation, family of exact solutions 2−57970
coalescence theory, scalar transport equation, moments and kernels 2−57969
dibutyl phthalate, kinetics of growth in flow reactor, exptl. 2−50386
dibutyl phthalate, kinetics of growth in flow reactor, theory 2−50387
Differential II, an instrument for measuring light scatt. of individual particles 2−47000
drop removal, design of rotary impaction filters with tapered filaments 2−43402
dust, particle size distrib. determ. by gravimetric sedimentation method 2−78754
dusty gas, flow past body 2−53278
electrically suspended water droplets, wind correction to evaporation rate and Rayleigh instabilities 2−56531
evaporation, in low temp. flame photometry 2−48358
exploded wire generator, evaluation for use in inhalation obs. 2−85160
filter collection efficiency, as fm. of particle size and velocity 2−56530
finite-difference cloud droplet collection equation, critique and reply 2−68904
fog modification at several temps. using physico-chemical methods 2−72796
gas to aerosol conversions, classification of physical nature 2−43406
gas-solid suspension, mean for characts. 2−67711
gas-solids suspensions, turbulent pipe flow, particle slip velocity 2−53284
generation, kinetics of growth in flow reactor, exptl. 2−50386
generation, kinetics of growth in flow reactor, theory 2−50387
glass particles in turbulent air flow, suspension trajectories, velocity of particles 2−76395
ice forming, downward transport from stratosphere 2−62165
ice nuclei, size distribution det. 2−60529
ice nuclei smoke particles, method of generating for weather modification 2−62099
ion annihilation by aerosol particles in the atmosphere up to 60 km. altitude 2−65953
ion induced nucleation phenomenon, role of small clusters 2−83812
isotropic spherical particles, light scattering function calc. 2−50383
Jupiter atm., distrib. determ. from satellite eclipse obs. 2−75877
latex, detection of emulsifier particles using procedure of shadowing electron microscope grids 2−71249
latex particles size distribution meas. usinf electron microscopy 2−43405
light scattering, chemical composition, at atmospheric humidity, adsorption 2−83815
liquid and solid suspensions, acoustic dispersion and velocity 2−74569
Los Angeles smog, comparison of calculated and measured light scattering 2−51623
Los Angeles smog, dynamics, physical mechanisms 2−51590
Los Angeles smog, inadvertent weather modification, Los Angeles smog 2−51572
Los Angeles smog, light scatt., comparison to light extinction by NO$_2$ 2−51625
Los Angeles smog, light scatt., correlation with size distrib. and vol. concentration 2−51624
Los Angeles smog, particle size distrib., Minnesota aerosol analyzing system obs. 2−51588
Lovelace particle separator, design and performance 2−64483
lower troposphere, wind velocity by Doppler optical radar 2−78359
Mars, atmospheric aerosol emission and transmission effects on i.r. spectra 2−78547
mass transfer rates from spherical particle boundary-layer injection suction considerations, variational analysis 2−77397
mass transfer with radial axial diffusion in laminar flow in narrow rectangular channel 2−53269
Mie scatt. by three polydispersions, atmos. aerosol. models 2−65779
mono-dispersed drops, production by vibration- atomization 2−71246
multichannel particle counter, choice design and performance 2−82075
optical and dynamical properties, review 2−46998
optical particle counters, coincidence and cross- channel sensitivity 2−43403
organic, production by X-rays 2−46999

Aerosols continued
particle counter, response curve rel. to optical system aperture 2−67852
particle counter, self contained automatic portable apparatus 2−67850
particle detection and size det. using open cavity of He-Ne gas laser 2−56528
particle diffusive growth, kinetic equation 2−71248
particle size distrib., determ. using Boltzmann's charge distrib. law 2−71244
particle size distrib., multistage sampler data determination 2−53465
particle size distrib., self-preserving, for Brownian coagulation in free-molecule regime 2−50384
particle size obs., for cloud seeding 2−60528
particle size spectrometer, electro-optical technique, meas. from aircraft 2−82579
particulate, acoustic streaming, agglomeration 2−43407
Pasadena smog, aerometric factors affecting evolution 2−51573
Pasadena smog, carbonate and noncarbonate carbon content 2−51603
Pasadena smog, chemical states of N and S, photoelectron spectroscopy obs. 2−51602
Pasadena smog, particle mass and size distrib., Minnesota aerosol analyzing system obs. 2−51589
photochemical, mass concentration rel. to light scattering 2−48511
pollution, inorganic analysis, by neutron and gamma ray spectrometry 2−48360
polydisperse, submicron, size distribution determ. by response matrix method 2−74568
polydisperse spray detonations, reaction zone characteristics 2−80489
polymer solutions, atomization and drop size using grooved-core nozzle 2−50377
production and transplant optimization for introduction of analytic materials into plasmas 2−84692
radioactive, estimation of risk from inhalation and appropriate protection measures 2−55242
radioactive, technique for use in U mines 2−84819
rotary impaction filter efficiency, droplet removal, fast flowing air stream 2−67849
sampler, chemical and disperse phase analysis 2−53463
satellite droplets formed by liquid atomization by rotating disk 2−60404
size distribution, informational entropy appl. 2−67851
size distribution, vertical flux, wind erosion, atmospheric soil particles, jet impactors 2−84827
size distribution from spectral attenuation meas. 2−56529
smog and synthetic smog, comparison of i.r. spectra 2−51620
smog in Los Angeles, measurement techniques 2−75532
sodium-colled fast reactor SNR300, behaviour under hypothetical accident 2−49877
solution nebulization device and d.c. arc for multicomponent plasma obs. 2−64300
specific radioactivity measurements rel. to particle size of labelled aerosols 2−53464
spectral impactor, size distribution meas. 2−64488
spiral centrifuge, distrib. analysis of aerodynamic size and mass of aerosol particles 2−50382
stratospheric, size and composition obs. 2−62156
stratospheric levels 12-25 km 2−81687
suspended particulates in air, evaluation of methods of meas. 2−71245
transmission efficiency of aerosol sampling lines rel. to deposition 2−60526
transport in naturally convected boundary layer 2−67786
transverse migration of particles, in turbulent flow 2−74571
tropospheric, lidar obs. 2−57942
tropospheric distribution 2−62281
turbulence charact. by laser Doppler vel. meter 2−69540
upper atmosphere, rocket mounted laser radar obs. 2−54878
urban, St. Louis, Mo., Lidar obs. 2−62145
urban aerosols in atmosphere, extinction and lidar backscatter measurements 2−51622
urban air pollution aerosol model, spectral absorption and extinction coefficients 2−62265
water droplets, capture by plane stellate crystalline obstacles 2−71247
water droplets, interactons with positive corona streamers, atmospheric significance 2−64489
water-affected fraction of natural 1.5-9 μ diam. aerosol particles 2−75598
Ag-NaI-H$_2$O, cloud interactions, parcel model 2−60527
AgCl, scavenging by falling water droplet, particle size effect 2−75599
B particle nonequilibrium effects, air augmented combusting ducted flows 2−70836
^{51}Cr labelled iron oxide particles, inhalation 2−48891
NaCl, formed by condensation, density distrib. 2−60530
Pb, ageing, numerical model simulating coagulation and sedimentation 2−64487
Pb$^+$ ion gas-phase hydration, mass spectrometric obs. 2−80493
^{237}Pu labelled iron oxide particles, inhalation 2−45048
Ra-A, filtration of 0.001 μ particles by wire screens 2−85159
RaA airborne atoms, collection on wire gauze 2−69344

Afterglow *see Discharges, electric*

Ageing
— 2−68027
aerosols, Brownian coagulation, self-preserving particle size distrib. 2−50384
alloy, supersaturated solid soln. decomp., review 2−43928
alloys, with different volume disparity between precip. phase and matrix, X-ray diffr. 2−71634
Co-Ni-Cr-Ti alloy, quench-ageing behaviour, 700-900°C 2−68138
ferroelectric ceramic, transparent, grain size and porosity effects 2−57244
fish, age visual pigments and crystalline lens of rudd 2−69473
metal tritide film, bubble form. and rupture 2−43478
nimonic alloy, solid soln. decomp. and volume change 2−50805
plastic, ABS, light ageing behaviour, test method 2−50793
plastics, testing of, colorimetric aspects 2−47671

Ageing continued
polyethylene, ageing under natural atmos. condit. i.r. spectroscopy study 2—64800
solid solution composition changes from lattice parameters 2—61027
stainless steel, electron contrast in ferritic phase 2—80873
steel, austenitic, strengthening, optimal conditions 2—53876
steel, austenitic, strengthening due to VC precip. 2—47636
steel, by u.s. vibr., effect on mech. props. and microstruct. 2—53877
steel, ductile-brittle transition, deform. mode influence 2—43694
steel, fracture behaviour rel. to dislocation substruct. 2—47413
steel, high carbon, workhardened, hardness and resistivity obs. 2—47597
steel, low-C, dynamic strain aged, work softening 2—80837
steel, low-C martensitic 2—50834
steel, maraging, effect on plane strain fracture toughness 2—60979
steel, maraging with 18%Ni, flow behaviour 2—84068
steel, martensitic stainless, phase transforms. and mech. props. 2—53989
steel, press. vessel material, time-depend. embrittlement phenomena 2—59849
steel, quenched, quench-aged, fatigue behaviour rel. to microstruct. instability 2—50768
steel, strain-ageing resistance 2—43800
thermoluminescence, studies, quartz 2—84720
Ti-Mo binary alloys, phase separation processes in beta phase during aging 2—80816
Zircaloy-2, irrad. and temp. effect on tensile and creep props. 2—43802
Al-Ag alloy, pre-precip., elec. resist. and Hall coeff. variations 2—77692
Al-Ag alloy, precipitation process study 2—84133
Al-1.2 wt%Mg_2Si alloy, two-step ageing behaviour 2—64765
Al-Ag alloys, supercond., pre-precip. state props. 2—64944
Al-Cu alloys, quenched-in defect elimination mechanism 2—84149
Al-Mg-Li alloy, 01420, rel. to phase comp. changes 2—47594
Al-Mg-Si-Cu-Mn-Fe alloy, kinetics, temp.-time ranges 2—50802
Al-Mg-Si alloy, strengthening rel. to age hardening, thermally activated dislocation motion 2—56717
Al-Mg-Si alloy, structure of metastable precipitates 2—56909
Al-Mg-Si alloys, quenched-in defect elimination mechanism 2—84149
Al-9%Mg alloy, effects of additional elements on clustering and precip. 2—50801
Al-(N at.%) Mg, N=10, 8, alloy, age hardening and related properties 2—47612
Al-Mg_2Si alloy, rel. to preageing 2—50822
Al-Ni-Cu-Ti alloy, age hardening, precip. 2—53878
Al-Zn-Mg-Mn alloy, strength rel. to rest between quenching and ageing, effect of additions 2—50803
Al-Zn-Mg alloy, after quenching and cold work, resistometric obs. 2—71632
Al-Zn-Mg alloy, precipitate free zone, elec. microscope obs. 2—56902
Al-Zn alloy, and formation of GP zones, elec. resistivity obs. 2—50800
Al, water-quenched, yield stress, strain ageing effect 2—50799
Al alloy, AL9V, rel. to small additions of transition metals 2—47595
Al alloy, multiphase, metallographic investigation of grain boundary sliding 2—80820
AlCu alloy, (Al 4 WT %), structure changes during ageing studied by the channeling technique 2—80827
Al4%Cu alloy, effects of additional elements 56910 2—56910
As_2S_3/Ag system, effects on photochemical transf. rate 2—57433
Au-Co alloys, nucl. spin entropy changes during ageing 2—43798
$BaTiO_3$, dynamic fatigue, ageing of switching props. 2—72031
$CoFe_2O_4$-Co_3O_4 alloy, quenched, aged, saturation magnetization, intrinsic coercive force, rel. to microstruct. 2—81233
Cu:O wire, cold worked, press. induced thermal activation, tensile strength 2—43781
Cu-Be-Ag alloys, structural states in decomposition process, e. diffr., e. micro. and microhardness exam. 2—80782
Cu-Ni:Mn, Cr, Al, struct. and props. with ageing and hardening 2—83954
Cu-(30 wt.%)Ni-0.3 wt.%)Be alloy, age hardening precipitate phases, struct. and morphology 2—50934
Cu-Zr-Cr, alloy, precip. processes specific heat and resistivity obs. 2—50933
Cu-1 at.%Fe alloy, precip. of Fe during ageing, Mossbauer obs 2—77724
Cu films in storage, ageing effects on substruct. and mech. props. 2—83863
Cu(15.1 at.%)Sn alloy, β_1 phase stabilization mechanism 2—47684
Fe-0.3% Nb, dynamic strain ageing47598 2—47598
Fe-C alloy, quench ageing and reversion 2—56903
Fe-C alloy, recovery of internal friction after strain ageing 2—47481
Fe-C alloy, strain ageing, internal friction obs. 2—56904
Fe-N alloy, quench ageing and reversion 2—56903
Fe-N alloy, strain ageing, internal friction obs. 2—56904
Fe-Nb-Al bearing steel, dynamic strain ageing 2—47598
Fe-Ni-C alloy, martensitic, microplastic deform. and isothermal transform. 2—43808
Fe-Ni-C alloy, martensitic, effect on microplastic deform. 2—43807
Fe-Ni-Mn martensitic alloys, reversion behaviour 2—77747
Fe-Ni-Nb-C alloy, precip. reaction 2—47596
Fe-Ni alloy, Mossbauer obs. of atom redistrib. 2—60981
Fe-Ti-Si alloy, precipitation and yield stress 2—43806
Fe, strain ageing, stress-assisted diffusion to dislocations, theory 2—43652
Fe, strain ageing and formation of Cottrell atmospheres 2—71624
Fe, strengthening mech., dynamic strain ageing, dislocation struct. 2—56911
Ge, mosaic structure during testing, X-ray and e. microscope exam. 2—71475
Mg-(10.8 wt%)Y alloy, ductility and high strength 2—47588
Mo alloy, precip. of Ti and Zr carbides, strengthening 2—47643
Ni-Be alloy, texture variation 2—50806
Ni-40%Cr alloy, age hardening, effects of Al and Ti64767 2—64767
Ni-base heat- resistant alloys, carbide transformations during long-time ageing 2—71673
Ni, texture variation 2—50806

Ageing continued
Ni_2V alloy, ordering transformation for wide range of subcritical temps. 2—74938
Pb-Ag system, softening mechanism and kinetics 2—43860
Pb aerosol, numerical model simulating coagulation and sedimentation 2—64487
Ti-Mo alloy, ω-phase precip., rel. to resist. anomalies 2—84297
Ti-Mo base β-alloy, rel. to tensile props. and microstruct. 2—50807
U alloy, effects on microstruct., ion etching and scanning electron microscope obs. 2—56578
V-N system, V_3N precip., electron microscope obs. 2—50978
ZnS:Cu, Cl, changes in brightness wave during ageing 2—65316
Zr-(2at.%)Cr-(0.16at.%)Fe alloy, precip. reactions rel. to corrosion resist. 2—53919
Zr-(1.5wt.%)Cr-(0.1wt.%)Fe tubing, heat-treated and hydrided 2—53918
Zr-Nb alloy, rel. to supercond. transition temp. 2—51107
Zr alloys, high-strength, development 2—53920
Zr and Zr-O alloy, internal friction and electron microscope obs. 2—47599

Air
see also Atmosphere
20 kW plasma torch induction and applications 2—46757
— 2—67786
a.c. arc constricted horiz. column motion due to buoyancy 2—71051
a.c. corona inception voltage of gaps in nonuniform fields, calc. 2—71048
acetylene-air flames, impingement heat transfer rates 2—52288
air and H_2 turbulent streams, optical method for concentration measurement 2—67704
air-sea interaction, state-of-art 2—61840
air-sea interaction studies in Davis Strait 2—62121
air-sea interface, unified model for heat and gas exchange 2—62069
air-water concurrent flow on flat plate, enhancement of heat transfer by waves 2—56494
air-water two-phase flow, horizontal, pressure as stochastic parameter 2—43096
air-water-glass bead three phase flow system, exptl. investigation of hold-up 2—67605
alpha particle energy loss and stopping power 2—56433
ambient medium for photopotential of CdS 2—68482
atmospheric pressure, streamer propagation, mathematical model for computer simulation 2—64359
breakdown at uniform fields, conditions for transition from Townsend to streamer mechanism 2—64353
breakdown characteristics at 50 Hz at high temp. 2—74437
breakdown induced by CO_2 laser, numerical solutions 2—46801
breakdown induced by pulsed CO_2 TEA lasers 2—46800
breakdown voltage estimation using empirical semi-empirical methods, pressures up to 7 atmospheres 2—56392
clean air turbulence, remote i.r. detection 2—84866
clear air, turbulence, global dynamics, statistical self-similarity theory 2—68898
clear air turbulence, automated forecasting 2—72750
clear air turbulence, generation by nonlinear waves 2—54831
condensation, transient heat and mass transfer controlled 2—77466
convection, developing laminar free, between vertical flat plates with asymmetric heating 2—76402
corona point discharge at atmospheric pressure, obs. of small ion clusters 2—53259
d.c. breakdown voltage, effect of particles and fibers 2—71032
density variations, upper atmosphere, obs. of orbital periods of satellites 2—65819
discharge, long gap, investigation of leader channel by probe electrode 2—70992
discharge and partial discharges, air gap between dielectrics, space and time picture 2—74426
dry, sparking potentials in crossed electric and magnetic fields 2—74445
dry and humid, elec. breakdown due to large number of electrons 2—83709
electric parameters meas., associating biological effects 2—58003
electrode in organic systems, feasibility for electrochem. energy conversion 2—84652
electron temperature and relaxation phenomena behind shock waves 2—54542
electron velocity distribution function in r.f. discharges 2—77262
entrainment in breaking waves 2—57924
excitation of atmospheric gases by low energy proton bombardment 2—84792
flow, nonequilibrium, mass spectrometric anal. at high temps. and pressures 2—48354
flow across mountain barrier, numerical shallow fluid model with variable grid 2—48478
flow in square channel with partially heated sides, temp. field 2—53336
flow in thunderstorm weak echo regions, obs. using slowfall chaff 2—75565
flow over sudden change of surface roughness, numerical computation 2—48480
flow resistance meas. in porous layers 2—56405
flowrate measurement, pitot traverses, comparison for accuracy with orifice plates 2—74471
gaps, long, 50 Hz breakdown characteristics 2—74438
gaps, long, impulse breakdown 2—74435
glass particles in turbulent air flow, suspension trajectories, velocity of particles 2—76395
glow discharge, obs. near i.r. emission spectrum 2—46798
heat exchanger, flow characts. in box plenum chamber 2—71088
heat transfer in two-dimensional stagnation point flows of binary mixtures 2—45576
heat transfer to transpired turbulent boundary layer 2—45577
high-wavenumber temp. and velocity spectra over tidal mud flat 2—81662
impulse surface discharge rel. to applied voltage and specific capacitance, obs. 2—71017
interferometric meas. of convection in rectangular air filled cavities 2—76400
ionization extrapolated ranges and energy losses of N, Na and Ar ions 2—79917

Air continued
ionized, MHD, unsteady free convection flow past infinite vertical plate, variable suction 2−83526
i.r. dispersion meas. 2−60376
i.r. emission, absorpt. coeffs., 6000-8500K 2−73240
jet, as mixing device, theory 2−83693
jet with natural gas, aerodynamical characteristics for combustion in transitional flow region 2−53317
jets, incompressible, turbulent, three dimensional issuing tangentially to and flowing along curved wall, mean velocities 2−71083
liquid, thermal cond., 100-150K, 10-500 bar, calc. 2−71190
luminescence decay time, excited by α-particles 2−50057
optical breakdown in presence of elec. discharge 2−50232
photoionization, by extreme u.v. radiation of laser produced plasma 2−53242
plasma, electrical conductivity and total radiant power 8000 to 12500 K 2−71061
pollution, detection of pollutant gases by CO and CO_2 lasers 2−81668
propane-air mixture, turbulent flow, burning stability 2−67702
Rayleigh convection, roll diameter dependence and effect on heat flux 2−60370
remote sensing of ambient air quality and gaseous pollutant flow 2−84870
spark breakdown phenomena at h.v. 2−56394
subsonic turbulent jets, pressure fluctuations 2−60347
supersonic flow, wave resistance of thin spindle 2−83645
supersonic free jets, velocity and temperature 2−77352
temporal growth of ionization in long uniform field gaps 2−71029
thermodynamic and transport props., sea level to 300000 ft. 2−72760
turbulence, small-scale structure, temp. obs. 2−77323
turbulence intensity and time-mean velocity distributions in low Reynolds number pipe flows 2−46832
turbulent channel flow, contraction effect 2−60345
turbulent flow in plain tube, heat and mass transfer 2−76397
turbulent flow through porous tube with suction, friction factors 2−60338
turbulent wakes, temp. fluctuations, measurement by probe 2−77330
ultra-cold neutron attenuation 2−67084
velocity obs. using reverse flow sensing hot wire anemometer 2−67707
water flow, air entrained, under reduced ambient pressure 2−77404
air/H_2 combustion, shock-induced 2−83651
Air-SF_6 mixtures, pressure dependence of resonance fluorescence lifetimes 2−42932
H_2 and air-methanol mixtures, thermal explosion, boundary of flame propagation region 2−75378

Airglow
see also Atmospheric spectra; Aurora; Sky brightness, Twilight; Zodiacal light
continuum, determ. of photochemical processes responsible for emission 2−65887
dayglow, rocket meas. of low energy electrons and optical emissions 2−84882
dayglow rocket photometry, tilting filter meas. 2−81646
daytime and nighttime, observation from manned spacecraft 2−75624
electron-water vapour interaction effects 2−53019
equatorial u.v. airglow, azimuth angle dependence from rocket observations 2−72833
intensity and polarization, measurements made during 1965 total solar eclipse 2−72832
night, intensity ratio bet. (5,1) and (9,4) bands of OH emission 2−72836
night sky continuum, obs. in range 4100-8200 Å 2−68942
nightglow, 5577 photometric observations 2−48545
nightglow, 6300Å line intensity, correlation with F-region parameters 2−65890
nightglow, 6300 Å emission, variation and decay 2−48544
nightglow, O I5577 A, and lunar semidiurnal variation 2−65891
nightglow, OH rot. temp. 2−54882
nightglow, OI (6300 Å), equatorial anomaly 2−62340
nightglow, OI (6300 Å), low latitude phenomena 2−62339
noctilucent clouds, summary of occurrences in 1971 over western Europe 2−58017
OSO-5 dim light monitor 2−72943
predawn enhancement, at 6300 Å, ionospheric electron density 2−48542
predawn enhancement, photoelectrons from magnetically conjugate point 2−48541
predawn enhancement of 6300 Å emission 2−62360
terrestrial tropical u.v. dayglow, application of atomic collision processes 2−44941
u.v. spectra of day airglow, polar aurora, tropical airglow, interpretation using cross sections for electron excitation of O, N 2−67397
wavelength 6300 Å, relations with F-region parameters 2−48543
MgI and MgII dayglow, near u.v. 2−65884
NI 5200 Å observations at Arecibo using Hadamard photometer 2−72834
NI allowed transitions, high excitations 2−48547
O 5577 Å emission intensity, nocturnal and semiannual variations 2−65889
O emission at 6300 Å, during geomagnetic storms 2−48540
O λ6300 and λ5577 profiles, det. of neutral temp. in ionospheric F_2 and E-regions 2−65973
O nightglow emission at 5577 Angstroms during 1958-67 period above Ashkhabad 2−84881
O nighttime 6300 Angstroms airglow emission at magnetic equator rel. to ionospheric anomaly 2−84880
OH airglow at 2.2 μ rel. to possibility of ground- based observations of zodiacal light 2−65886
OH nightglow emissions, spectrophotometric study 2−48546
OI 5577 Å observations at Toronto using Hadamard photometer 2−72834
OI 6300 Angstroms emission, predawn enhancement above Abastumani 2−84883
OI (6300 Å) emission, global mapping 2−62337
OI (6300 Å) emission, post sunset enhancement 2−62342

Airglow continued
OI (6300 Å) emission, pre-dawn enhancement 2−62341
OI allowed transitions, high excitations 2−48547

Albedo *see Cosmic rays; Earth; Neutrons and antineutrons/reflection; Nuclear reactors, fission*

Alfven waves *see Magnetohydrodynamic waves*

Algebra
C*-algebra methods and their application 2−58756
C* theory, nonequilibrium statistical mechanics, dynamics of open and mechanically driven systems 2−58784
calculus of variations 2−45428
CAR, number operator states 2−52041
CAR, purification of factor states 2−82159
coherent states for arbitrary Lie group 2−41508
computer program solutions, impact on physics 2−82279
correspondence between points on curve, symmetry condition 2−58700
finite-dimensional real algebra of linear operators generated by physical filters 2−82157
functional analysis methods for stat. mech. of infinite systems 2−58796
G-factorial states in C* algebras 2−82155
incidence eqn. $AA^t = PA$, theorem proof 2−82168
infinite systems of linear equations, solved by method of successive refinements 2−73290
isomorphism between para-Fermi algebra and 0(n,n+1) algebra 2−55374
Lie, automorphisms 2−48978
Lie, finite dimensional real, integrability of representations 2−78764
Lie algebra applic. to Coulomb problem, book 2−63017
Lie algebra common to dual models, current algebra, dynamical groups, gauge groups 2−45854
Lie algebras, classification of semisimple algebras up to rank 6 2−82165
modularity of decision effects, symmetry of physical probability 2−82158
monotonic product sequences, matrix transformations 2−52043
vonNeumann, rel. to nonrelativistic time-dependent theory of single channel scattering 2−41517
of observables, construction in classical field theory 2−82151
Pade approximation, mathematical features and physical applications 2−73291
Poisson bracket, defining eqn. 2−41457
pseudo-orthogonal, range of validity of Gell-Mann formula 2−42313
quaternion determinant with non-commuting elements 2−76172
statistical mechanics and quantum field theory, algebraic methods 2−45336
trace inequalities 2−45231
von Neumann, noncommutative probability 2−41486
von Neumann, trace inequalities 2−48979
weight diagrams and Lie algebra 2−62972

Algol *see Calculating apparatus/digital computer programmes*

Algorithms *see Calculation*

Alignment *see Mechanical measurement*

Aliphatic compounds *see Organic compounds*

Alkali metal compounds
see also the compounds of the individual metals
alkali borate and silicate glasses, n.m.r. obs. of ^{7}Li ionic motion 2−64690
alkali feldspars, Na-K mixing, polymorphism 2−53675
alloys, liq., Knight shift and Pauli susceptibilities 2−72515
ammonia solns., solvation model 2−84614
borate glass, e.s.r. spectrum, hole and electron centres, obs. 2−54489
borate glasses, Ni^{2+}-containing, absorpt. anomalies, ligand field approach 2−75303
chlorates, ^{35}Cl n.q.r. 2−44464
diatomic molecules, hetero-and homonuclear, theoretical ground state and excited state potential energy 2−42906
glass, mixed alkali effect, electrodynamic interaction 2−53524
glass, molten, of mixed alkali $PbSiO_3$, viscosity meas. 2−77416
group IA-VB compounds, photoelectric emission, electronic struct. 2−72088
halides, extrapolation of elastic props. to high pressure 2−65575
metaborates, interpretation of mass spectra 2−59889
metavanadates, cryst. growth and characteriz. 2−47261
nitrates, molten, and binary mixtures, electrical conductivity 2−46979
oxide glass, alkali metal cation vibrs., far i.r. spectra study 2−71284
ozonides, Raman spectra, O_2^- and O_3^- ion props., solid-solid transition effects 2−81354
silicate glass, γ-irrad., thermolum. 2−81410
silicate glass, Brillouin scatt. 2−57365
silicate glass, Er^{3+} sites, absorpt. study 2−54429
sulphates, coherent neutron scatt. amplitudes from powders 2−53654
superoxides, Raman spectra, O_2^- and O_3^- ions props., solid-solid transition effects 2−81354
trialkali-Sb photocathodes technology 2−44196

halides
see also the compounds of the individual metals
absorption and emission bands of F, F_{a1}, F_{a2}, U centres, temp. dependence of peak position 2−75298
alkali halide crystals, nonactivated, luminescence centres formation in very strong electric fields 2−84542
aquoluminescence from γ-irradiated crysts., effect of isothermal annealing 2−43376
azides, X-ray photoelectron spectra, core and valence electronic levels 2−67466
borate glass, e.s.r. spectrum, hole and electron centres, and halogen atom obs. 2−54489
bromides, gradient-elastic tensor, n.m.r. acoustic saturation study 2−44457
chlorides, dissociation rates and mechanism 2−60021
coherent neutron scatt. amplitudes from powders 2−53654
colour centres, extended Mollwo- Ivey relation 2−60824
colour centres, models, review 2−71519
complex impurity centres model with cations in anion sites 2−47441

Alkali metal compounds continued
  halides continued
    cryst., u.v. and electron irradiation effects, decoration techniques 2−80607
    crystal growth, large single crysts., using interconvertible unit 2−56610
    crystal growth from solution, nucleation, dissolved O_2 and H ion conc. effect 2−74674
    crystals, electrons trapped in edge dislocations 2−81200
    defect pairs, intrinsic and extrinsic, Maxwell-Boltzmann distrib. 2−83971
    dielectric consts., l.f., press. and temp. derivatives 2−51188
    diffusion coeff. of self- trapped holes and migration to thallium centres 2−68709
    dissociation mechanism 2−60020
    doped with CrO_4^{2-} optical and i.r. vibrational absorption spectra used to study defects in host crystal 2−48171
    elastic property changes under pressure, u.s. meas. method 2−68060
    electric polarization of crystals by inertial forces 2−54238
    electron density anisotropy and effective charge 2−54100
    electronic polarons, correl. formulae 2−51086
    electrons trapped in edge dislocations 2−81200
    epitaxial growth of Te at 100°C 2−47120
    e.s.r. of irrad. paramag. centres 2−81467
    F-centre, relaxed excited state, dynamical Jahn-Teller effect 2−43647
    F-centre absorpt. band, spin mixing and circular dichroism, electron spin memory 2−53750
    F-centres, excited, emission mechanisms 2−80709
    F-centres, optical pumping cycle dynamics, relaxed-excited state detection 2−53749
    F-centres, X-ray scatt., quantum theory 2−47444
    film, charact. energy losses by slow electrons 2−81532
    fluorescence spectra, obs., Cu doped, Mollwo-Ivey relations 2−61712
    fluorides, Raman spectra, phonon modes 2−48196
    fluorides and chlorides, Hartree- Fock band struct. 2−61172
    Frenkel defect, lattice statics and deformation dipole model 2−60789
    gases and solids, connection between ion-atom potentials and repulsive potentials 2−42773
    Gruneisen constant at absolute zero 2−61113
    high symmetry exciton 2−68308
    hydroxide-doped, tunnelling levels, low temp. thermal cond. obs. 2−71758
    impurity motions from Stark modulated microwave spectra 2−70739
    ionic crysts., NaCl type struct., hardness anisotropy 2−56836
    ionic radii, effect of pressure 2−76124
    ionic stabilization energy and Coulombic attraction in molecules 2−53030
    ionisarion pot. meas by X-ray photoelectron spectroscopy 2−83259
    lattice dynamics, high press. and temp. props. 2−61072
    lattice dynamics, resonant phonon modes of Ag^+ and Au^+ 2−54018
    lattice dynamics of B-2 type crysts. 2−50993
    limiting optical frequency calculation, temp. variation 2−72311
    liquid, interionic distance estimation 2−43320
    local and gap modes due to substitutional impurity 2−47731
    luminescence, fast recomb. transition lifetimes 2−54450
    molecule, nucl. quadrupole coupling consts. 2−59989
    molecule, potential energy curves 2−77076
    neutron irrad., transient dislocation-point defect interaction effects 2−43634
    optical absorption, reson. of electronic polaron 2−72313
    overlap repulsion, modified logarithmic form 2−43502
    phosphor, lineshapes of C-bands by method of moments 2−57346
    photoconductivity spectra due to lattice distortion produced by edge disloc. 2−74777
    photoelectric emission, electronic struct. 2−72088
    point defect form. mechanism and struct. 2−80702
    rare earth doped, Z-centres, optical absorpt. and e.p.r. at 77K 2−71526
    reflectance, synchrotron radiation 2−47789
    rigid lattice band mass of electron, Feynman's polaron theory 2−61202
    Rittner's potential function, modified form 2−42904
    scintillators, impurity activated, response curves 2−55913
    second sound velocities 2−61091
    spin-orbit effects in F^- and K-bands 2−51335
    sputtering, positive ion ejection patterns 2−44008
    Stark effect of M- and N-centres 2−61624
    surface optical modes, reflection obs. 2−51344
    thermoreflectance spectra at room temp. 2−44363
    U-centre, localized freq., method of moments 2−50984
    u.s. waves, phonon absorp., relax. theory 2−68233
    vapour, u.v. absorption cross sections, potential curve and excited state radiative lifetime determination 2−70738
    vapour pressures and enthalpies of vaporization, detn. 2−77473
    weighting coeffs. in approx. of Debye temp. in cubic crystals 2−74991
    X-ray diffuse scattering, higher anharmonic contribs. 2−61059
    $Co(CN)_6^{3-}$ doped, vibr. and electronic props. 2−54413
    KBr, quenching of cathodoluminescence as a function of colour centres, at 90 and 300 K 2−68704
    KCl, quenching of cathodoluminescence as a function of colour centres, at 90 and 300 K 2−68704
    KI, diffusion coeff. of self-trapped holes and migration to thallium centres 2−68709
    KI, quenching of cathodoluminescence as a function of colour centres, at 90 and 300 K 2−68704
    N_2O, matrix isolated i.r. spectrum, temp. depend. 2−74269
    NaI, diffusion coeff. of self-trapped holes and migration to thallium centres 2−68709
    Ni^{2+} doped, optical spectra 2−44379
    RbI, diffusion coeff. of self-trapped holes and migration to thallium centres 2−68709
Alkali metals
  see also the individual metals
  adsorbed layers, nonmetallic to metallic transition 2−83870
  adsorption on metal, theory of work function changes 2−48007
  adsorption on Mo, LEED and Auger spectroscopy obs. 2−50540
Alkali metals continued
  adsorption on transition metal, atomic theory of work function variation 2−71343
  alloys, u.v. bandpass filter 2−66846
  anisotropic transport scattering times, calc. 2−75014
  atom, $6^2P_{1/2}$-$6^2P_{3/2}$ excitation transfer induced in noble gas collisions 2−74231
  atom, collisional excitation of H 2−67426
  atom, electron scatt., spin polarization and differential cross sections 2−83183
  atom, transition probabilities between hyperfine levels 2−56088
  atoms, analytic multipole polarizabilities of ground and excited states, Coulomb approximation 2−46403
  atoms, ang. distrib. and spin orientation of photoelectrons 2−56107
  atoms, calc. of absorption line profiles and satellite bands caused by inert gas perturbing atom 2−70568
  atoms, excited $^2P_{3/2}$ state, nuclear spin in optical pumping with D_2-light 2−74227
  atoms, ground-state, fine and hyperfine structure in laser saturation spectroscopy 2−46411
  atoms, quadratic hyperfine pressure shift in inert gas atmospheres 2−77013
  binding energy, pseudopotential calc. 2−77832
  binding energy and compressibility, empty core model pot. calc. 2−64586
  binding energy in pseudo-ion approx. 2−83883
  boiling, temp. inversion in tubes under annular flow 2−64514
  cohesive energies and bulk properties, calc. 2−83884
  crystal, centred cubic, mean square displacement of atoms, simple calc. 2−57037
  crystals, quantum mechanical study 2−64585
  dense vapours, semiconductor model of electrical conductivity 2−54183
  diatomic molecules, hetero- and homonuclear, theoretical ground state and excited state potential energy 2−42906
  diatomic molecules, SCF calcs. using Pariser- Parr-Pople type method of Pohl 2−80049
  duality, theorem and high-field linear magnetoresistance, geometrical effects 2−81031
  elastic constants, 2nd and 3rd order, calc. using pseudopotential methods 2−60836
  elastic constants, pressure derivatives calculation 2−60839
  electrical resist., pseudopot. calc. 2−75052
  electron collision cross sections for momentum transfer at low energies 2−83186
  equation of state, Gruneisen parameters, and temp. effects, calc. 2−74997
  excited atom collisions with unexcited atoms, inert gas atoms or molecules, transfer of excitation between fine-structure levels 2−42776
  Hall const. temp. depend. rel. to electron-phonon interaction anisotropy 2−57104
  ion beam irradiation of W, secondary emission of W^+ 2−48031
  ion-atom system, charge transfer at large internuclear distances 2−79915
  Knight shift and Pauli susceptibilities 2−72515
  liquid, determ. of pseudo-Gruneisen parameters 2−74540
  liquid, electron spectrum, calc. by cell method 2−83797
  liquid, self-diffusion, temp. depend. 2−67817
  liquid, significant liquid-structure theory of viscosity and self-diffusion 2−56489
  liquid, significant structure theory of surface tension 2−50346
  liquid, struct. factor rel. to entropy of melting 2−64434
  metal, neutral atom model, ion-electron-ion interaction 2−68271
  metal-NH_2 solns., transport props. in the non-metal-metal transition range 2−80484
  model pseudopotential and energy wave number characteristics 2−75024
  molten, interionic interaction and thermodynamic potl., analysis 2−84650
  optical absorpt., phonon effects 2−61628
  optical props. and interband transitions, review 2−72292
  plasmon sidebands in interband absorpt. 2−51334
  screw dislocation energy, band struct. energy contrib. 2−50669
  self-consistent screening calculation 2−77830
  spin and orbital susceptibilities of nearly free electrons in spatially varying field 2−61493
  spin-lattice relaxation of conduction electrons, improved average nuclear contact density 2−54372
  surface energy, rel. to bulk density of lattice energy 2−77493
  thermal resistivity, high temp., and electron-phonon interaction 2−68258
  vapour, adsorbate structure, on W surface 2−50554
  vapour, magnetic resonance, optical detection using D_1 and D_2 radiation simultaneously 2−56443
  vapour magnetometer, optically pumped, effect of nonresonant r.f. field 2−59066
Alkaline earth compounds
  see also the compounds of the individual metals
  chlorates, ^{35}Cl n.q.r. 2−44464
  fluorides, e.p.r., linear elec. field effects for Ce^{3+}-F^- tetragonal sites 2−48285
  fluorides, l.f. dielec. consts., temp. and press. derivatives 2−51189
  fluorides, point defects vibr. spectra, thermal cond., i.r. absorpt., Raman scatt. obs. 2−71724
  fluorites with tripositive rare earth ions, possible existence of separate cubic symmetry 2−80705
  halide crystals, vibronic spectra exam. 2−71705
  ionic crysts., NaCl type struct., hardness anisotropy 2−56836
  nitrates, molten, and binary mixtures, electrical conductivity 2−46979
  oxide:Ce^{3+}, cubic site symmetry from e.p.r. obs. 2−54491
  BaO-ZrO_2-SiO_2, excitation and emission spectra 2−75320
  CaO-ZrO_2-SiO_2, excitation and emission spectra 2−75320
  SrF_2:Ge^{3+}, possible existence of separate cubic symmetry 2−80705
  SrO-ZrO_2-SiO_2, excitation and emission spectra 2−75320
Alkaline earth metals
  see also the individual metals
  model pseudopotential and energy wave number characteristics 2−75024
  photocathode, energy structure 2−44195

Allotropes *see Phase transformations; Polymorphism*

Alloys
see also Ageing; Crystal structure, atomic/alloys; Heat treatment/alloys; Solid solutions; Steel; and under alloys or compounds of the named elements. Alloys such as Au_3Cu, Au-Cu, Au-Cu-Zn are indexed under compounds of the named elements, i.e. Gold compounds, Copper alloys, Zinc compounds in these examples
79NM, influence of thermomagnetic treatment on mag. props. 2−72048
800, low-cycle fatigue and stress relaxation at elevated temps. 2−60947
ageing, different volume disparity between precip. phase and matrix, X-ray obs. 2−71634
ageing, supersaturated solid soln. decomp., review 2−43928
AK-4 alloy, strengthening and roughness of rubbing surfaces, effect on wear and bearing capacity 2−60916
alkalis, u.v. bandpass filter 2−66846
amorphous, electronic struct., clustering effects 2−61170
amorphous and liquid, microsegregation, X-ray diffr. 2−60570
B-2 type, thermodynamics and lattice disorder 2−43819
b.c.c., interstitials influence on ordering and magnetiz. 2−43818
binary, config. entropy of mixing 2−43820
binary, diffusion of hydrogen, struct. influence 2−77611
binary, disordered, band struct. Fermi surface energy gaps 2−77826
binary, disordered, cluster effects 2−68270
binary, disordered, CPA, off-diag. randomness 2−61163
binary, disordered, electronic struct., single band model 2−61161
binary, disordered, vacancy equilibrium conc. calc. 2−53688
binary, electronic states localization lengths in one dimensional disordered potential chains 2−61136
binary, heat of soln. at infinite dilution, pseudopotential perturbation method 2−56495
binary, interdiffusion coeffs. determ. by electron microprobe analysis 2−80719
binary, localized states 2−84252
binary, molten, surface electric charge, rel. to thermodynamic props. 2−56515
binary, one dimensional disordered system, localization lengths 2−61176
binary, solidification, dendritic coarsening, model 2−50818
binary, vaporization, condensation and solidification diagrams 2−53509
binary equil. diagram, isothermal reaction stage influence on cpd. growth by diffusion 2−64686
binary one-dimens., phase transitions 2−50980
binary ordered, with tertiary impurity elements, electron energy spectrum 2−44023
C16-type structure, stability and competitive structs. 2−50851
C16-type structure, supercond. transition temp. 2−51104
C16-type structures, lattice parameters, rel. to band struct., theory 2−43573
C16-type structures, prep. and X-ray study 2−43572
carburized W-Re alloys, work function in 1600-1800 K range 2−54267
casting characteristics and solidification morphology 2−64770
cermet, B2Zh, prep. and mech. characterization 2−77720
cermet hard alloys based on Ni-containing titanium carbonitrides 2−68152
coating of materials, use of composite powders, new developments 2−61010
coatings, high temp., deposition from fused salts and by ion plating 2−50860
coherent phase formation, and mech. props., review 2−57007
coherent potential approximation, applic. 2−61141
commercial, method for correlating creep and rupture strengths 2−47607
commercial, thermal conductivity Lorentz number and Smith Palmer equation 2−54042
creep, high temp., monograph 2−60871
data compilation, NBS Permuted Materials Index 2−68155
diffuse Laue-scatt. and prepeaks in partial struct. factors 2−53391
diffusion coeff. determ. method using soln. treatments and metallography 2−56748
diffusion mechanisms, review 2−68044
diffusion numerical calc. of redistribution of interstitial solute in thermal gradient 2−77601
dilute, electronic struct. of hydrogen 2−77822
dilute, low temp. cond., Green function calc. 2−61219
dilute, nearly mag., magnetiz. 2−44218
dilute, resist. temp. depend. rel. to spin fluctuations 2−57148
dilute binary, solute redistrib. in melt, conc. and temp. gradient effects 2−47260
dilute quantum crystal, theory of vibrations 2−43948
dislocations, passing, equil. configs. on parallel slip planes 2−50665
disordered, concentrated strong scattering, elec. resist., temp. depend 2−44049
disordered, CPA generalizations and cluster effects 2−44022
disordered, self-consistent cluster theory 2−44024
disordered, ternary, single band Hamiltonian description 2−80966
disordered, X-ray spectra, interpretation of exptl. data 2−61671
disordered, X-ray spectra intensity, Green's function method 2−51359
disordered binary, many site interactions and correlations 2−61138
disordered binary, pair effects, multiple-scatt. formulation 2−75011
disorfered, electronic density of states, CPA method 2−61160
dispersed particles, size stability in diffuse interface limit 2−43816
dissociated dislocations, analysis of electron micrograph images 2−80624
domains, interface geometry, contrast effects, electron microscope and diffr. obs. 2−56718
ductile fracture prediction under discrete loading 2−43728
electron charge transfer and electrochemical effects, theory 2−64884
electron microprobe analysis, correction for absorption and atomic number 2−65417
electron microscopy, electrolytic jet thinning apparatus, specimen holder design 2−67959
eutectic solidification, thermodynamics 2−47035
eutectics containing compound phases, thermodynamics and morphology 2−47600

Alloys continued
eutectoid decomp., lamellar eutectoid growth, stepwise growth model 2−50814
fatigue, design for use in gas turbines 2−56882
fatigue testing of heat resistant alloys at elevated temperatures and aeronautical applic. 2−56870
f.c.c., dil., vacancy jump. freq. ratio, determ. by electromigration 2−83995
f.c.c., interstitials influence on ordering and magnetiz. 2−43817
f.c.c. ternary, atomic ordering, theory 2−43571
ferromagnetic, anomalous Hall effect, phonon scatt. effects 2−81223
ferromagnetic, coherent potential approximation, application 2−61500
ferromagnetic, disordered, magnetiz.-temp. curves, influence of conc. statistical fluctuations 2−61512
ferromagnetic, polycrystalline, elastic waves interactions with magnetic fields 2−43673
fracture resistance physical and technological significance 2−71580
grain and particle size distrib. analysis, review 2−50817
grain boundary precipitate coarsening, cumulative size distrib. function 2−47604
grain boundary structure and segregation, conf., London, England [Nov 1971] 2−47606
hard metal, fracture surfaces, crack path, electron microscope replica obs. 2−50773
Heisenberg ferromagnet, CPA approx. with random off-diagonal elements 2−78004
high temperature, long cylindrical shell, creep collapse under external pressure at elevated temp. 2−76329
high-coherence, magnetic after effect 2−68552
used in HTR, high temperature behaviour in He coolant gas and impurities42673 2−42673
Incoloy 800 high cycle fatigue properties at elevated temperatures 2−60951
Inconel 718, surface integrity effect on fatigue at elevated temps. 2−60944
Inconel alloy, X-750, fracture and creep-fatigue behaviour 2−56860
intermetallic compound, atomic vol. variation, pseudopotential theory 2−64774
interstitial, role of impurities in low temp. softening 2−47495
lattice defect form. under radioactive irrad., review 2−47362
light, s.c.c., microstruct. effects 2−56826
liquid, binary, cluster model 2−46917
liquid, dil., mag. susceptibility, quasi-atomic model 2−53454
liquid, electronic struct., clustering effects 2−61170
liquid, electrotransport, rel. to amorphous semiconductors 2−60455
liquid, nucl., quadrupole relaxation, ionic motion contrib. 2−43316
liquid, speed of sound calc. using perturbation and pseudopotential theories 2−46952
long range order and segregation, high voltage electron metallography 2−56632
low stacking fault energy, interaction between quenching defects and dislocations 2−64662
magnetic, dil., spin reson. theory 2−78160
materials choosing for power and industrial applic., conf., Saclay, France (June 1970) 2−60971
mictomagnetic, mag. struct. model 2−65166
noble metal-noble metal, electronic struct., reflectance obs. 2−61174
nondestructive crack detection method using liquid crysts. 2−43760
nonferrous, elastic waves interactions with magnetic fields 2−43673
nonideal axial ratios, analysis for close-packed hexagonal structures 2−71396
optical props. and electronic transitions, review 2−72292
ordered, AuCu-type, breaking through of dislocations across domain boundaries, activation energy 2−56692
ordered, channelling of foreign ions 2−44003
ordering, stat. theory, lattice distortions 2−43812
particle coarsening processes, cumulative distrib. functions 2−47603
partly ordered, channelling 2−44004
pitting, intergranular corrosion and stress-corrosion cracking, significance of protection potential 2−68787
pitting potential, electrochemical obs. 2−54546
Portevin-Le Chatelier effect, and density and activation entropy of moving dislocations 2−80748
quenched, transients in annealing of vacancies 2−80842
reactor core materials characteriz. 2−59862
refractory carbide/liquid metal contact interactions 2−68190
Rene 80, Inconel 718, surface integrity effect on fatigue at elevated temps. 2−60944
Rene 95, Inconel 718, surface integrity effect on fatigue at elevated temps. 2−60944
rolled plate, anisotropy of fatigue limit 2−74872
semiconducting, binary disordered, two band model in CPA 2−61162
semiconductor, substitutional, nonexistence of localized tail states 2−64996
short range ordering, rel. to long range interatomic interactions 2−50819
sintered, containing ZrC_x and HfC_x, effects of protective atmos. 2−77721
solid solution hardening in body centred cubic alloys, theory 2−77691
solid solutions, B2 and $L1_2$ superstruct., superdislocation-antiphase boundary interactions 2−47416
solid solutions, B2 and $L1_2$ superstruct., superdislocations and antiphase boundaries 2−47417
solidification, growth morphology, in-situ radiographic obs. 2−47605
solidification rate rel. to thermal contact resist. 2−74586
sound emission, impact forces, meas. device 2−80783
spring material mechanical strength under atmospheric ambient 2−43748
structural materials, irradiation induced volumetric swelling caused by void formation 2−74758
substitutional, averaged electronic resolvent, approx. 2−64885
substitutional, calc. of vacancy characts. 2−71462
substitutional, calc. of vacancy characts. 2−71464
substitutional, calc. of vacancy characts. 2−71463

Alloys continued
substitutional, electronic relaxation calc. using single band model 2-47790
substitutional, off-diagonal randomness, theory 2-44027
superalloy, powder, elec. discharge activated press. sintering, composite struct. bonding 2-53938
superalloys, chemical analysis of conjugate phases 2-77681
superalloys, precipitation hardened, study of submicroscopic particles using extraction replica electron microscopy 2-80817
superalloys, thermal fatigue behaviour, effect of metallurgical variables 2-56879
superconducting, type II, structure and compositions of materials 2-75071
superconducting, with paramag. impurity and local states in gap, crit. field, order parameter, sp. ht. 2-71857
superconducting mag., localized bound state and impurity band props. 2-77873
surface reconstruction due to chemisorption 2-50524
surface roughness factor determ. method 2-47067
ternary, b.c.c., Snoek effect, rel. to substitutional solute atom pairing 2-43672
ternary, monovariant solidification, and zone melting 2-47601
ternary, solidification behaviour, microsegregation and precip. mechanism 2-56915
ternary, thermodynamic props., prediction from binary alloy data 2-43814
thermal expansion, tabulation of quadratic function coefficients 2-71639
thermal microstresses of multiphase alloy, direct x-ray photography method 2-53884
ultrasonic production of alloys otherwise difficult to make 2-50820
unidirectional solidification, review 2-80850
virtual bound state, optical absorp. models 2-65245
Waspaloy sheet, sensitivity of creep-rupture properties to sharp-edged notches in temp. range 1000-1400°F 2-47609
waves, finite amplitude in rods, subject to impact loading, Bell's parabolic law study 2-58901
weakly magnetic, influence of heterogeneities on magnetic isotherms 2-65150
weld metal, toughness below 0°C, effect of metallurgically conditioned inhomogeneities 2-74890
YuNDK24, Fe atoms, exam. by nuclear γ reson. after thermomagnetic treatment 2-84471
Au-Ga, metallurgical properties, contact characteristics 2-84069
Bi, apertures for Cu K_α X-ray experiments 2-85184
Co, ticonal annealed at 800°C electron microscope exam. of struct. 2-80781
CoCrMo total joint replacement, wear products in body 2-69292
Cr-Au alloy pressure transducers, influence of high pressure H_2 on resistance, compared with manganin 2-76122
CsCl-phases, thermodynamics and lattice disorder 2-80843
Mo base, properties under He high temperature conditions 2-42674
Pb-In-Sn superconducting wire, magnetic properties, flux flow voltages 2-81037
Pd 24% Ag-H foils, electron microscope examination 2-56948
PdRhNi, spin fluctuation resistivity 2-64916
Ti-Gd alloy, thermal conductivity and electrical resistivity 2-64866
Zr-alloy reactor pressure tubes rel. to tube irradiation programme 2-76953

Alnico alloys *see Nickel alloys*

Alpha decay *see Nuclear decay theory, Radioactivity/decay periods; Radioactivity/decay schemes*

Alpha-particle model *see Nucleus/models*

Alpha-particle spectra
see also Nuclear decay theory
spectroscopy, using Th daughter products, applic. to nuclear chemistry teaching 2-62931
^{160}Dy(n,α), energy spectra $E_n=18$ MeV, knock-on mechanism 2-67298
^{162}Dy(n,α), energy spectra $E_n=18$ MeV, knock-on mechanism 2-67298
^{164}Dy(n,α), energy spectra $E_n=18$ MeV, knock-on mechanism 2-67298
^{155}Gd(n,α), determ. of distrib. of total alpha-particle widths of neutron resonances 2-67297
^{177}Hf(n,α), determ. of distrib. of total alpha-particle widths of neutron resonances 2-67297
^{240}Pu, alpha particle emission energy meas. 2-76823
^{147}Sm(n,α), determ. of distrib. of total alpha-particle widths of neutron resonances 2-67297
^{86}Sr(^{3}He, $\alpha\gamma$)^{85}Sr, 17 MeV meas. of $\alpha\gamma$ coincidences, mean lives of low lying levels in ^{85}Sr deduced 2-42514
^{232}U, alpha particle emission energy meas. 2-76823
^{236}U, specific activity determination 2-46206

Alpha-particle spectrometers
analysis of irradiated reactor fuels, properties of operating reactors 2-76925
gas multiple scattering effect on solid angle subtended by circular aperture 2-70285
surface barrier detector for monitoring 2-59627
n- GaAs surface barrier diodes, high purity 2-49628
Ge counter, γ-compensated, as α and β particle spectrometer 2-52696
Ge(Li), dead layer effects 2-49663
He recoil 2-73932
PbI_2, crystal growth and detection props. 2-46037
PbO, crystal growth and detection props. 2-46037
Si(Li) dead layer effects 2-49663

Alpha-particles
see also Cosmic rays/alpha-particles and helium nuclei; Radioactivity
anomalous straggling in Al 2-49911
from Cracow U-120 cyclotron, properties determination from ion optics principles 2-55945
internal structure, effect on nuclear α-cluster model 2-70357
plasma probing for current distribution 2-46763
shell model wave function and binding energy 2-46109
stopping power of Be, Al, Cu, Mo, Ta, Au at 28 MeV 2-54099

Alpha-particles continued
Au, channelling 1.8 MeV α-particles in planar directions, continuum potentials deduced 2-44006
C, π- absorption from rest, obs. of α spectrum, p spectrum and secondary particles 2-63902
GaAs, surface studies by Rutherford scatt. and channelling 2-64553
W thick target, energy loss of scatt. particles 2-80928
absorption
air, residual energy and stopping power, obs. 2-56433
hydrocarbons, influence of mol. binding on stopping power in gas and solid 2-64869
CO_2, residual energy and stopping power, obs. 2-56433
He, residual energy and stopping power, obs. 2-56433
angular distribution
cosmic ray primary produced in nuclear emulsion 2-49608
elastic scattering on nuclei at 166 MeV, determ. of differential cross sections, neutron radii 2-63904
(α,α) scattering amplitude determ. including angular-momentum matching of absorbed partial waves 2-49821
^{11}B(p,^{4}He)^{8}Be, distrib. for first 2 states, c. of m. 20-160° 2-46255
^{11}B(p, α)^{8}Be*, 2.9 MeV, detector arrangement 2-74086
^{9}Be(p,^{4}He)^{6}Li, distrib. for first 3 states, c. of m. 20-160° 2-46255
^{12}C, alpha-gamma ang. correlation studies 2-70477
^{12}C(^{7}Li,α)^{15}N, 28-38 MeV, triton transfer, excited states of ^{15}N 2-70481
^{12}C(d,d')^{12}C $\rightarrow {}^8$Be + α, 9.6 MeV, meas. of angular correlation function of (d,α) coincidences, comparison with theory 2-49832
^{252}Cf fission, long range α-particle emission 2-83037
^{252}Cp, spontaneous fission, α-particle emission 2-49851
^{65}Cu(t, α), $E_t=12$ MeV, excitation of ^{64}Ni, level struct. 2-76878
^{19}F(d,α)^{17}O, 3 MeV, meas. of α-particle angular distribs. 2-67151
^{7}Li(d,α)^{5}He reaction, rel. to spin and parity assignment of levels of ^{9}Be 2-74111
^{24}Mg(α,α), meas. of differential cross sections between 27 and 28 MeV, optical-model and Hauser Feshbach analysis 2-49824
^{24}Mg(α,α)^{24}Mg, 20-23 MeV, compound nucleus effects in elastic scatt. 2-46303
^{26}Mg(α,α), meas. of differential cross sections between 22 and 28 MeV, optical-model and Hauser Feshbach analysis 2-49824
^{20}Ne(^{3}He, ^{4}He)^{19}Ne, 18 MeV, meas. of excitation energies of states in ^{19}Ne, angular distrib. of ^{4}He 2-63780
^{58}Ni, alpha- gamma ang. correlation studies 2-70477
^{239}Pu, subthermal-, thermal-, and reson.-neutron fission, long-range α-particle emission 2-83032
^{224}Ra α decay, study of hyperfine interactions when implanted in Fe, Al, Cd, Bi, α-γ correlation meas. 2-81341
^{220}Rn α decay, study of hyperfine interactions when implanted in Fe, Al, Cd, Bi, α-γ correlation meas. 2-81341
^{28}Si(α,α,γ)^{28}Si, 10-18 MeV, angular correlation studies for excitation of 1.78 MeV 2^+ state 2-63787
^{28}Si(α,α), meas. of differential cross sections between 22 and 28 MeV, optical-model and Hauser Feshbach analysis 2-49824
^{227}Th decay, α-γ coincidence and directional correlation studies 2-63852
^{227}Th $\rightarrow {}^{223}$Ra decay, α-γ coincidence and directional correlation studies 2-49776
^{238}U fission, long range α-particle emission 2-83037
Zn(α,α'), A=68, 70, 31 MeV 2-42581
detection, measurement
see also Alpha-particle spectrometers; Dosimetry; Particle detectors; Radioactivity measurement
1,12-benzyperylene fluorescent thin films 2-73939
cellulose triacetate as track imaging detector of alpha-particles 2-82827
liquid scintillation, for environmental and medical research 2-70297
sodium salicylate fluorescent thin films 2-73939
He recoil spectrometer 2-73932
LiF thermoluminescent dosimeter response 2-85135
Si drift detector, effective thickness of dead layer 2-42467
effects
see also Nuclear reactions and scattering due to/alpha-particles
atmosphere, small ion production 2-51586
atomic Coulomb excitation by heavy charged particles 2-79911
fluorite, thermoluminesc. 2-51379
quartz, thermoluminesc. 2-51379
thin target, fast particle damage production, theory 2-50636
Al, irrad., low-temp. sp. ht. obs. of He bubble form. 2-50644
Al foil, irrad., growth of very small He bubbles 2-80688
Al_2O_3, Al Kβ X-ray spectra, molecular struct. obs. 2-81381
CO_2 laser, performance in presence of alpha-particle source 2-52415
CaF_2:Mn, CaF_2:Tb thermoluminesc. 2-51379
CsI:Tl, α-particle irrad., scintillation yield orientational depend. 2-81434
CsI:Tl, scintillation growth times 2-73938
$CuSo_4$:Mn thermoluminesc. 2-51379
^{151}Eu, Mossbauer effect after Coulomb excitation with 3.3 MeV α-particles 2-84473
GaP, electron-hole pair form. by irrad. with α-particles, form. energy 2-71808
α-SiC, irrad. effects on e.p.r. and i.r. absorpt. 2-48294
Ti, bombarded, X-ray Kα and Kβ spectra 2-57368
Ti, X-ray de-excitation 2-57367
interactions
$\alpha\gamma \rightarrow p\pi^-$(ppn) cross section around Δ(1236) 2-79493
scattering
gas atoms near counter, effect on solid angle subtended by circular aperture 2-70285
inverse problem, connection between parametrized phase-shift and optical-potential models 2-73747
Rutherford scattering, model 2-47770
Si amorphous films, density detn. by backscattering of 2500 keV alpha parts. 2-80559

Altimeters *see Length measurement*

Aluminium
— 2-67388
— 2-72272
— 2-57380
acoustic shock pulse generation, nonlinear elastic behaviour obs. 2-64842

Aluminium continued
- adsorbed monolayer, struct. determ. by Tucker-Duke energy averaging method 2−47149
- adsorption of Cl, Auger spectrosc., ellipsometry and surface potl. meas. of clean films 2−71345
- adsorption of O_2, work function changes obs. 2−77517
- adsorption of water, detn. by meas. of work function 2−71346
- alloys, meas. of mechanical properties at high shear- strain rates 2−53821
- alpha-irradiated, low-temp. sp. ht. obs. of He bubble form. 2−50644
- anomalous straggling of α-particles 2−49911
- appearance potential spectra, correlation with soft X-ray absorp. 2−81378
- application as impact energy absorber 2−66632
- application in particle accelerator construction 2−67102
- atom, electron-bremsstrahlung cross-section meas. at incident energy 0.2 MeV, photon energies 0.02-0.2 MeV 2−70613
- atom, h.f.s. in ground multiplets, mag. dipole radial parameters 2−70576
- atom, ioniz. of L-shell, by inelastic collisions of fast particles 2−64026
- Auger spectra 2−71313
- axial velocity profiles and acoustical fields of cylindrical rod 2−41694
- bar, elastic strain waves on centre line, resulting from impact, expt. and numerical obs. 2−66605
- Brillouin scattering of light by long wavelength acoustic phonons 2−54438
- Burgers vectors determ. using g.b = 2 contrast in electron microscope 2−60792
- cast morphology, anodic oxidation etching study 2−47602
- cavitation in liquid oxygen, plastic deformation in metal surface layers 2−71306
- characteristic energy loss, for low energy electrons 2−51091
- chemical reaction with bismuth oxide ceramics rel. to use in nuclear fuels 2−83064
- coating on U-Nb alloy, effect on stress corrosion cracking 2−53911
- combustion propagation in cylindrical specimens 2−61785
- complex dynamic modulus of Al/resin/Al sandwich bar 2−80742
- composite, B(C) fibre reinforced, fatigue 2−56976
- compressed by shock wave X-ray Debyegram recording 2−84045
- Compton profile, symmetry, 59.54 keV γ-rays 2−71764
- cover on ceramic BeO during γ- and X-ray irradiation, effect on TSEE response 2−68491
- creep, high temp.-low stress, directional diffusion vs. dislocation process mechanisms 2−50755
- creep, study by differential method of temp. variation at const. rate 2−80731
- creep tests in tension and compression, elec. resist. 2−50754
- critical strains, Bloch waves electron microscope study 2−80629
- crystal growth, from the melt, nucleation by Tl cpds. 2−47098
- crystal growth in macrosonic fields, dislocation structures 2−50590
- crystallization, convective cooling of articles obtained from melt by Stepanov method 2−47574
- crystals, dislocation accumulation and plastic deformation under stress 2−80696
- cylinder, surface plasma waves, optical refl. study 2−61210
- decarburizing of cast Fe with graphite, struct. effects 2−43837
- deformation, corners in yield surface under biaxial zig zag loading 2−43686
- deformed, dislocation loop struct. rel. to deform. method 2−77574
- deformed by rolling, positron interaction with defects 2−71460
- deposition on Nb, LEED and Auger spectroscopy obs., 22-1200°C 2−50484
- di-directional solidification and dendritic growth 2−50823
- diffusion, review 2−83992
- diffusion of Co, 400-640°C 2−64691
- diffusion of Ga, 100−310°C, solid solubility, X-ray diffr. obs. 2−74810
- diffusion of Mg, Fe, Cu, Zn, Ge and Ag, interpreted rel. to oscill. form of inter-ion potential 2−64691
- dislocation configuration, as result of thermal treatment 2−47411
- dislocation loop formation during electron irrad., microstruct. depend. 2−53733
- dislocation loop size and density, rel. to solute-vacancy binding energy in alloys 2−74762
- dislocation mobility and damping const., phonon-dislocation interactions 2−50671
- dislocation multiplication mechanism 2−80679
- dislocation substruct. form., strain rate role 2−47499
- dislocations, multiplication mechanism, near surface, Lang X-ray obs. 2−43635
- doping of diamond, elec. resistivity obs. 2−68396
- ductility rel. to strain rate, −196 to 400°C 2−74834
- effective and economic use of special characteristics, conf., Zurich, Switzerland, Sept (1972) 2−60973
- elastic constants, 2nd and 3rd order, calc. using pseudopotential methods 2−60836
- elastic constants, high pressure effects, meas. using torsional oscillatory method 2−68061
- electrical cond, meas. by inductive method 2−49239
- electrical resist. due to interstitials, pseudopotential method 2−57152
- electrical resist. temp. coeff. rel. to equilib. vacancies 2−77856
- electron, irrad. induced pt. defect clustering, high- voltage electron microscopy 2−56682
- electron backscattering, spectral ang. distrib. meas. 2−84218
- electron beam deposition, sublimation energies 2−60644
- electron beam straggling, calc. of range for energies up to 30 MeV 2−68266
- electron diffraction, Kikuchi band and abnormal absorpt., exchange effects, calc. 2−64631
- electron displacement damage, high-voltage electron microscopy 2−56683
- electron irradiated, stage III recovery obs. 2−43805
- electron microscope exam., crit. stress effect on contrast 2−67983
- electron momentum distribution, from Doppler-broadened annihilation lineshapes 2−71782
- electron-phonon interaction const. determ. in normal and supercond. states by u.s. attenuation 2−81049

Aluminium continued
- e.m. wave transmission, helicon waves, Gantmakher- Kaner excitations, sound waves, quantum effects 2−57135
- embrittlement by molten Ga 2−43721
- excitation in Lewis Rayleigh N_2 afterglow 2−77011
- exo-emission, threshold illumination intensity 2−44189
- fatigue, slip struct. and crack growth 2−47519
- fatigue deformation, cross slip, elec. microscope obs. 2−77686
- Fermi, surface rel. to alloying 2−77826
- Fermi surface, third zone, uniaxial compression effects 2−71790
- Fermi surface press. depend. 2−61180
- Fermi surface rel. to magnetostriction and stress 2−68286
- film, ang. distrib. meas. of secondary electrons 2−44213
- film, electromigration, effect of oxygen 2−50703
- film, epitaxial growth on NaCl and KBr substrates 2−77501
- film, evap., optical constants in e.u.v. 2−48133
- film, laser beam hole ('bit') creation, physical processes 2−69989
- film, normal-state cond. and supercond. transition temp., electrostatic charging effects 2−71845
- film, on KCl, epitaxy rel. to nucleation 2−67905
- film, oxidation, LEED obs. 2−51445
- film, photoelec. emission due to nonradiative surface plasma waves 2−44200
- film, resist., thermal cond., and integrated radiating power 2−74999
- film, struct. change effects on opt. absorpt. 2−54415
- film, supercond. transition temp. depression by noble gas overlayers 2−61228
- film, thickness det., comparison of multiple beam Fizeau interferometry, photoelectric shearing interferometry and stylus instrument methods 2−47118
- film, transmission, reflection, and absorption of high current density electron pulses 2−84223
- film, vacuum evaporated into polymer, adhesion mechanism 2−43476
- film, with interlayered transition metals, effect on ^{27}Al n.m.r. 2−68743
- film on Si, ion channelling 2−54094
- film thickness control, automatic apparatus for preparation of MIM interference filters 2−70029
- films, electron multiwave scattering at 70 keV, scatt. intensity detn. 2−71451
- flow stress meas. using torsional split Hopkinson bar 2−68124
- foil, α-irrad., growth of very small He bubbles 2−80688
- foil, direct-recording electronograph in study of objects giving increased background 2−53639
- foil, h-pit production by hydrating and annealing 2−74616
- foil, mosaic block misorientation during creep, X-ray obs. 2−74848
- foil, recrystn., effect of small alloying additions 2−47578
- foil, X-ray scatt. from surface rel. to polishing 2−74617
- foil sample thickness obs. in X-ray transmission texture photography 2−41447
- form factors, Harrison's pseudopotential 2−64877
- grain boundaries, coincidence-ledge-dislocation model, supporting evidence 2−47426
- grain boundaries, resistivity changes in deformed samples 2−53744
- grating, interaction radiation of moving electron 2−73526
- heat radiation, influence of surface roughness 2−55574
- heat transfer to boiling He 2−66362
- heavily deformed, conditions of formation of recrystn. nuclei 2−56901
- helicon resons., audio freq., magnetoresist., Hall coeff. 2−57136
- high purity, deformation props., review 2−68076
- high speed impact and induced shock waves, theoretical model 2−41836
- hot rolling, determ. of roll forces 2−53881
- hyperfine field, in Fe matrix, spin echo obs. 2−72229
- hyperfine interactions of implanted ^{220}Rn and ^{224}Ra study by α-γ correlations 2−81341
- integranular flow study, role of inperfections 2−43643
- interface with water, u.s. refl., surface wave creation 2−64851
- intergranular corrosion in HCl, symmetrical flexion boundaries 2−72561
- internal friction, comparison of values for neutron-irradiated and annealed specimens 2−60850
- internal friction, effect of tempering 2−77699
- internal friction of workhardened and irrad. crysts. 2−43669
- internal photoemission, struct. on high energy side of KL$_{23}$M Auger peak 2−44212
- ion implantation profile of ^{85}Kr, calc. 2−74795
- K-shell ionization cross sections by ^{20}Ne and ^{22}Ne bombardment, isotope effect 2−74216
- Kikuchi patterns, displaced lines 2−53636
- Knoop hardness anisotropy 2−43738
- laser shock-induced microstructure and mech. prop. changes in 7075 Al 2−68075
- LEED, expt. and theoretical rotation diagrams 2−50433
- LEED from {001} surface, expt. and theory 2−50428
- LEED intensities, quantum field theory calc. for (100) and (111) faces 2−74712
- LEED intensity, temp. depend., Debye temp. calc. 2−60624
- LEED on (001) surface 2−64549
- LEED rotation diagram for (100) face, calc. 2−74618
- LEED spectra, calc. for {111} and {110} surfaces 2−83857
- linear dimensions variation under γ-ray irrad. 2−43607
- liquid, diffusion in Fe(steel)/Al system 2−80715
- liquid, ion-ion pot. calc. from diffr. data 2−50315
- liquid, meas. of structure factor by neutron diffraction techniques 2−64435
- liquid, optical consts. 2−43359
- liquid, struct. factor, X-ray diffr. apparatus 2−74516
- liquid, struct. factor rel. to entropy of melting 2−64434
- low dislocation density crystal, anomalous X-ray transmission due to subtopographic defect clusters 2−47395
- mim structure, electrical pulse regime and switching study 2−77917
- neutron irrad., pt. defect clustering, low temp. electron microscope obs. 2−60783
- neutron irrad., void annealing 2−53705
- neutron irrad., void distrib., struct. imperfections in fluence 2−53736

Aluminium continued
- n.m.r. obs. in solid and liquid, room temp.-1100°C 2−54503
- non-isoaxial bicrystal, tensile deformation, effect of tilt boundaries 2−50740
- non-isoaxial bicrystal, tensile deformation, effect of twist boundaries 2−50741
- optical absorpt. peak temp. shift 2−54414
- optical constants ε_1 and ε_2, absolute values 2−48134
- oxidation, growth of α-Al_2O_3 whiskers 2−74637
- oxidation influence on lubricated friction of steel 2−53844
- oxidation of ribbons, thermal spectral radiation 2−61629
- oxide formation mechanism rel. to nucleation and electrochemical transport processes 2−68798
- photoelectric determination of electron attenuation length 2−44201
- photoelectric emission, two-photon photoelec. effect 2−48021
- plane shock structs., strain rate functions 2−60800
- plasma, laser produced, IV spectra, line identification 2−74212
- plastic deformation, dislocation dynamics, high voltage electron microscopy 2−56785
- plastically deformed, dislocation arrangement in surface layer, electron microscope obs. 2−43465
- plastically deformed, evidence of glide on {110} plane 2−50760
- plastically deformed, mobile dislocation density and velocity 2−43690
- plastically deformed, mobile dislocation density and velocity 2−43689
- plastically deformed by lateral rolling, dislocation struct. and fracture 2−74837
- point defects produced by quenching and electron irrad., annealing 2−60785
- polycrystalline, recovery of mech. props. after severe rolling 2−71633
- positron and dislocation binding 2−83977
- positron deformation potential, estimate from positron trapping rate by vacancies 2−80675
- positron lifetimes and trapping probabilities at vacancies and dislocations 2−44010
- powder, sintering, effect of oxide film 2−43888
- pressure vessels, porosity formation 2−62896
- programme toughened single crystal, crit. sliding stress, temp. depend. 2−71582
- projectile penetration forces 2−53803
- protective properties of anodic oxide films on Al and its alloys 2−53886
- quenched, annealing kinetics of point defects, resist. and magnetoresist. study 2−80680
- radiation damage induced by high energy electron channelling 2−53713
- radiation generated during rapid deform. and rupture tribolum. 2−54482
- recrystallization, electron microscope obs. 2−80859
- recrystallization nuclei formed by Rowland transform. 2−43822
- recrystallized monocrystals, appl. to X-ray optics and spectroscopy 2−64611
- reflection grating, surface plasmon resonance effect in holography 2−59197
- rolled sheet, rolling and annealing texture of outer layer 2−64756
- rolling texture and deformation banding, single crystal 2−56788
- sheet specimen, coarse-grained, influence of hydrostatic pressure soaking on structural change X-ray study 2−84127
- shock wave compression, X-ray diffr. obs. in single crystals 2−56646
- shock waves, and temp. derivation along Hugoniot curves, appl. of fourth-order anharmonic theory 2−84188
- single crystal, influence of anodic coating on slip 2−71576
- single crystals, possibility of use of oscillating film spectrometer for detn. of dislocation density homogeneity 2−77582
- single crystals, substruct. changes during high-temp. deform. in creep 2−84078
- slowing down spectra of secondary electrons 2−75006
- sound velocity, influence of dHvA effect 2−51018
- spherical shell, fluid filled, dynamic loading 2−73363
- stacking fault energy rel. to n-value 2−53737
- steel strand reinforced, thermal and elec. cond. 2−53946
- stopping power for 28 MeV α-particles 2−54099
- stopping power for protons and deuterons at same velocity 2−54098
- stopping powers for 30-90 MeV ^{238}U ions 2−47773
- strain ageing in specimens quenched from 650°C 2−50799
- stress effect on resist./strain relation 2−64700
- stress strain relationship meas. by acoustic shock pulses 2−43777
- sub-grain boundary migration 2−80824
- substructural strengthening, effect of dislocations 2−50763
- super-pure, hydrostatically extruded, substruct. and flow stress detn. 2−74876
- superconducting film, density of states change due to adsorbed molecular oxygen 2−51111
- superconducting film, thermodynamic fluctuations in resistive transition 2−71858
- surface, (100), LEED, elastic and inelastic scatt., bulk and surface plasmon excitation 2−50434
- surface, (100), LEED intensity profiles 2−50436
- surface, cleaned and oxidized, secondary ion yield 2−61471
- surface, impact effects, impingement erosion 2−68113
- surface, LEED obs., 40-80 eV 2−50437
- surface, sputter deposition and sputter removal of Mo, Auger spectroscopy 2−50520
- surface adsorption of ^{19}F, time depend curve 2−83877
- surface plasmon dispersion, inelastic LEED obs. 2−51090
- surface prep. by electrolytic etching and polishing apparatus 2−50431
- surface struct., kinematic LEED intensities extraction from averaged data 2−43462
- target, micrometeoroid simulation, Fe microparticles from Van de Graaff accelerator 2−66187
- thermal vibr. freqs., X-ray scatt. obs. 2−61073
- thin films, hillock growth 2−77506
- tube, steel wire reinforced, bursting under biaxial tension stresses 2−71661
- tubes, wound with steel wire, bursting strength and toughness 2−71660
- u.s. shear wave, circularly polarized, attenuation and vel. in magnetic field 2−47789
- u.v. refl. rel. to LiF and MgF_2 films overcoating 2−79370
- volume coefficient of expansion of metals, use of hydrostatic microbalance 2−80785
- wires, cyclic textures 2−77700
- X-ray emission spectra, satellites, rel. to double ionization theory 2−72381
- X-ray L emission band, short-wave satellites 2−51361
- X-ray photoemission, internal, valence-electron excitation 2−54276
- yield surfaces at elevated temps. 2−71563
- Al/α-Al_2O_3 composite, mech. props. 2−53947
- Al/Cu/Al films, electromigration obs. by transmission electron microscopy 2−64879
- Al/Fe system, diffusion, barrier effect of intermediate Ag layers 2−47461
- Al-Al_2O_3-Pb junction, impurity assisted tunnelling, 4.2-148 K 2−44140
- Al-Al_2O_3 granular films, superconducting, sp. ht. obs., T_c enhancement 2−77878
- Al-Ar^+ collisions from 25 to 200 keV, noncharacteristic X-ray bands 2−56116
- Al-B composite, deform. and failure under transverse loading 2−84110
- Al-Ge, contact, slow states activation energy, barrier height temp. depend 2−75135
- Al-Ir abundance association in L chondrites 2−73099
- Al-Mg, interdiffusion, 325-425°C 2−64692
- Al-Si contacts, electromigration failure 2−50706
- Al-SiO_2-Si, m.o.s., transport props. in inversion region, 123-573 K 2−47954
- Al-SiO_2-Si, m.o.s. system, effect of bias-temp. treatments 2−84345
- Al-Zn(4at%), fatigue hardening 2−80840
- Al-borosilicate glass-Al thin film sandwich, elec. cond. props., negative resist., electroforming and electron emission 2−71989
- Al, angular distrib. of inelastically reflected electrons 2−80551
- Al, multilayer film structures, internal stresses, X-ray and Newton's rings obs. 2−43475
- Al III, elec. quadrupole transitions, multiplet strengths 2−56102
- Al polycrystalline films, on NaCl substrate, effect of annealing 2−80566
- ^{26}Al, content of Aouelloul crater glass rel. to Zli sandstone 2−65584
- Ar^+ ion bombardment, transmission sputtering and recoil implantation 2−54090
- CdS:Al, field quenching, influence of doping 2−54170
- Cu-Al crystals, internal oxidation, comments 2−65377
- GaP: Zn, Al, photolum. and electrolum., 1.7 to 2.3eV 2−75321
- H content determination using an omegatron partial-pressure gauge 2−53866
- in Ni alloy, effect on phase transforms. 2−43925
- Ti/Al chem. diffusion couple, Al_3Ti growth and solubility limits 2−53757
- ^{235}U fission fragment range 2−61125
- ZnS:Al,Co^{2+}, grown from melt, struct. rel. to Al additions, Co^{2+} spectra obs. 2−77559
- ZnS:Cu, Al, Br film, temp. depend. of electrolum. and thermal quenching 2−84533
- ZnTe:Al, high temp. elec. props., self-compensation model 2−51128

Aluminium alloys
- *see also Aluminium compounds*
- acoustic emission and energy transfer during crack propag., instrum. for detectn. 2−69767
- acoustic emission due to low level periodic stress 2−51012
- AL9V, ageing, rel. to small additions of transition metals 2−47595
- Al-Ni alloy, influence of short-range order on elec. and mag. resist. 2−71423
- combustion propagation in cylindrical specimens 2−61785
- constructional materials, life, effect of low level of service load range 2−43750
- crack growth rate obs. in fatigue, special gauges for det. 2−60934
- α-Cu-Al, stacking fault energy, electron microscope obs. 2−50682
- dilute, Al-3d-transition metal, temp. depend. of charge perturbation, n.m.r. study 2−44452
- dilute, deformation props., review 2−68076
- dilute, reson. and charge neutrality, semiphenomenological model 2−71783
- dilute, with transition metal impurities, temp. depend. of charge perturbation 2−48304
- dilute magnetic, semiphenomenological model for reson. and charge neutrality 2−68291
- effective and economic use of special characteristics, conf., Zurich, Switzerland, Sept (1972) 2−60973
- fatigue damage at high temperature 2−80808
- fatigue-crack front straightness in K_{Ic} testing 2−71591
- foil, recrystn., effect of small alloying additions 2−47578
- fracture toughness and stress corrosion cracking of hand forgings 2−60906
- fracture toughness and stress corrosion cracking of hand forgings 2−60905
- hot dip Al coated stainless steel, alloy layer struct. and composition 2−56937
- hot formability criteria 2−80852
- hot rolling, determ. of roll forces 2−53881
- liquid, with Cr or Mn impurity, susceptibility near nonmag.-mag. transition 2−80486
- microstructure and topography analysis by electron emission microscopy 2−80875
- multiphase, microstructure and grain boundary sliding, metallographic investigation 2−80820
- multiphase, strengthening by dislocation substructures 2−56706
- β-Nb-Al-Si alloys, superconducting critical temp. detn. 2−71869
- nimonic, ageing, solid soln. decomp. and volume change 2−50805
- pitting, intergranular corrosion and stress corrosion cracking, significance of protection potential 2−68787
- plastic deformation resistance, evaluation of irregularity 2−53802
- precipitation process study of Al-Ag alloy 2−84133
- pressure-vessel alloys, tensile, creep and stress-rupture tests 2−77671

Aluminium alloys continued
pressurization of solidifying sphere 2−47039
protective properties of anodic oxide films on Al and its alloys 2−53886
rapid cooling by laser melt quenching 2−56897
resistance, 'temperature increment' for temp. correction of resistance meas. 2−44051
resistivity, low temp., deviations from Matthiesen's rule 2−64910
SAP-1 plate, fine struct. and recrystn. 2−53870
shear creep fracture prediction, complex stress creep characts. 2−53813
superstrength, by continuous cyclic thermomech. treatment 2−47614
surface prep. by electrolytic etching and polishing apparatus 2−50431
thermal cond., 10-300 K 2−47760
tubes, production by cold extrusion, technical problems and factors influencing extrusion pressure 2−68157
two-phase, dislocation struct. on plastic deformation 2−56789
ultrasonic plane waves scattering, computer simulation 2−51023
X-ray stress measurement in NS.5 alloy, effect of preferred orientation 2−71643
β-Ag-Al, splat quenched, martensitic transform 2−71672
Ag-Zn-Al, transition from internal to external oxidation 2−48331
Al-3d transition metal dil. alloys, validity of Kondo model 2−81029
Al-Ag, Al-Zn type alloys, GP zone composition by relative intensitives of diffuse effects 2−68035
Al-Ag, pre-precip., elec. resist. and Hall coeff. variations 2−77692
Al-Ag, supercond., pre-precip. state props. 2−64944
Al-1.2 wt%Mg_2Si, two-step ageing behaviour 64765 2−64765
Al-Ag, thermal expansion, 10-300K 2−43992
Al-Ag system, discontinuous precipitation reactions and ternary component influence 2−71674
Al-Al_2O_3, ball-milled, mech. strength 2−53887
Al-Au, dilute, Mathiessens rule deviation due to scatt. processes 2−80969
Al-Au, electronic struct., soft X-ray emission obs. 2−68671
Al-B, determ. of B content, Boreal array 2−63976
Al-29 at.%Zn, spinodal decomp., metastable rhombohedral form., elastic anisotropy effects56923 2−56923
Al-2.5 wt.%Mg neutron irrad., transmutation produced Mg_2Si precip.56922 2−56922
Al-Cr dilute alloys impurity resistivity, temp. dependence 2−84278
Al-Cr solution, highly supersaturated, range extension in equilibrium diagram when cooled 2−43824
Al-Cu-Fe-Co-Ni-Ti YuNDK42T8, homogeneizing rel. to phase comp., mech. and mag. props. 2−47688
Al-Cu-Mg-Mn-Fe-Si-Ni-Zr-Ti, D16T, recryst. and uncryst. struct., fracture under static and cyclic conditions 2−47527
Al-Cu-Mg-Mn, mosaic angle and dislocation density, tensile deform. depend. 2−80772
Al-Cu-Mg-Ni, forged after quenching, recovery treatment, creep strain mechanisms 2−43804
Al-Cu-Mg, eutectic, microstruct., orientation relationships 2−74893
Al-Cu-Mg oversaturated solid soln. state, mech. props. rel. to strain rate and temp. 2−56547
Al-Cu-Mn, heat treatment, homogenization, precip. 2−43786
Al-Cu-Mn, spinodal, interphase interfaces, interfacial dislocations 2−56719
Al-(4 wt.%)Cu, Guinier-Preston zone form. 2−43825
Al-Cu, b.c.c., superplasticity 2−50745
Al-Cu, cast morphology, anodic oxidation etching study 2−47602
10at.%Al-Cu, deformed, neutron irrad., dislocation strain fields, low temp. lattice thermal cond. obs. 2−71498
Al-Cu, di-directional solidification and dendritic growth 2−50823
Al-Cu, Frank loop nucleation on screw dislocations 2−50670
Al-Cu, melting, application of Lindemann's rule 2−74582
Al-Cu, quenched-in defect elimination mechanism 2−84149
Al-(4.5wt.%)Cu alloy, late stage of solidification, two-dimensional flow of liquid 2−47038
Al-Cu film, precip., G.P. zone form., rel. to bulk alloy props. 2−47099
Al-Cu intergranular precipitates identification by double diffraction using transmission electron microscopy 2−80615
Al-Cu system, drops, supercooling and spheroidizing, Cu conc. effects 2−43441
Al-4%Cu, ageing, effects of additional elements 2−56910
Al-4%Cu, vacancy-Ge binding energy 2−50824
Al-4%Cu alloy, influence of precipitates on cavity formation for irrad. by fast neutrons 2−67984
Al-Fe-Ni, martensite transform, effect of disperse particles 2−50942
Al-9.5 wt.%Mg:Ti,Zr,Mo,B, mech. props., fracture toughness, cracking, effect of alloy in additions 2−47546
Al-Fe, microhardness rel. to precip. of Fe and annealing out of lattice defects 2−50828
Al-Fe, struct., mech. and elec. props., precip. of Fe 2−50827
Al-(0.5 wt.%)Fe, creep, high temp.-low stress, directional diffusion vs. dislocation process mechanisms 2−50755
Al-Fe(Co)(Cr), liq., resist., conc. depend., 1650°C 2−46980
Al-Ge, rapidly solidified, constitution and microstruct. 2−43929
Al-Ge, vacancy-solute binding energies 2−74763
Al-Ge alloys, microstruct. and metastable phases, detn. 2−71675
Al-Li, behaviour of neutron irradiation produced gas atoms observed by ^3H autoradiography 2−44009
Al-Li, neutron irrad., inerg gas bubble effects on mech. props. 2−43688
Al-Mg-Li, 01420 alloy, ageing, phase comp. changes 2−47594
Al-Mg-Si-Cu-Mn-Fe, AK6, ageing, temp.-time ranges 2−50802
Al-Mg-Si, extrusion temp. effects on toughness 2−60974
Al-Mg-Si, quenched-in defect elimination mechanism 2−84149
Al-Mg-Si, struct. of metastable precip. formed during ageing 2−56909
Al-Mg-Si strength rel. to dislocation motion and GP zones 2−56717
Al-Mg-Zn, decomposition, phase transform., influence of Zn 2−43911
Al-Mg-Zn, soln. softening effect of Zn additions at high temps. 2−47613
Al-(3 at.%)Mg, high temp. deformation, lattice rotation, dislocation dragging 2−74835
Al-Mg, band struct., Fermi surface, energy gaps 2−77826
Al-Mg, β, γ phases, atomic structure 2−71642

Aluminium alloys continued
Al-Mg, high temp. creep mechanism 2−68089
Al-Mg, intergranular corrosion susceptibility 2−71646
Al-Mg, kinetics of isothermal coalescence of dispersed phase 2−47611
Al-Mg, Portevin-Le Chatelier effect, role of vacancies 2−47490
Al-Mg, slip struct. and crack growth during fatigue 2−47519
Al-Mg, stress corrosion cracking, effect of Cu and Zr addition 2−50775
Al-Mg alloy, dislocation network form. during hot deform. 2−56712
Al-Mg alloys, viscous glide in solid solution, dislocation climb and Newtonian viscous deformation mechanisms 2−64718
Al-Mg and Al-Mg-Zn, preprecip. zone obs. 2−53885
Al-Mg single crystals, infl. of strain rate and temp. on Portevin-Le Chatelier effect 2−71560
Al-9%Mg, effects of additional elements on clustering and precip. during ageing 2−50801
Al-(N at.%) Mg, N=10, 8, age hardening and related properties 2−47612
Al-Mg(Cu), solute-vacancy binding energy, determ. from quenched-in defect conc. 2−74762
Al-Mg_2Si supersaturated solid soln., precip. clustering mechanism 2−50822
Al-Mn-Ag, high coercivity, struct. of ferromag. precip. 2−43821
Al-Mn, dil., high temp. impurity resist. 2−44050
Al-Mn, dil., neutron scatt. by spin fluctuations 2−61473
Al-Mn, structural features of a plane strip obtained directly from melt by Stepanov method 2−50821
Al-Mn dilute alloys impurity resistivity, temp. dependence 2−84278
Al-Mn solid solution, high supersaturated, range extension in equilibrium diagram when cooled 2−43824
Al-Mo, binary phase diagram, obs. 2−50955
Al-Nb supercond., heat treatments rel. to transition temp. 2−47589
Al-Ni-Cu-Ti, age hardening, precip. 2−53878
Al-Si, dil., film, Si precip., resist. study 2−50825
Al-Si, solidification in shell mould, and effects of additional elements 2−84134
Al-Ti-Zr-N film, sputtered, struct., elec. resist. props. 2−47130
Al-(1.7 at.%) Zn, vacancy-impurity binding energy, positron-annihilation study 2−53727
Al-Zn-Mg-Cu-Mn forging alloy, fracture toughness rel. to microstructure 2−53826
Al-Zn-Mg-Cu, tensile deform. and high-temp. creep rel. to microstruct. 2−56800
Al-Zn-Mg-Cu alloy, fatigue behaviour of bolted joints 2−71622
Al-Zn-Mg-Mn, strength rel. to rest between quenching and ageing, effect of additions 2−50803
Al-Zn-Mg, ageing process after quenching and cold work, resistometric obs. 2−71632
Al-Zn-Mg, extrusion temp. effects on toughness 2−60974
Al-Zn-Mg, stress corrosion crack paths 2−43732
Al-Zn-Mg alloy, solute distrib. using electron probe analyzer EMMA-4 2−56924
Al-Zn-Mg precipitate free zone, elec. microscope obs. 2−56902
Al-Zn, (Cu), (Ag), effects of coherency strain fields on dislocation struct. 2−56702
Al-Zn, ageing and formation of GP zones, elec. resistivity obs. 2−50800
Al-Zn, Seebeck coeff., comp. depend., 400°C 2−81162
Al-Zn liq., Zn activity at 1053K, comp. depend., Krupkowski's eqn. 2−56498
Al-Zn solid solution, miscibility gap, resist. study 2−50826
Al-6.8Zn, diffusion, and effects of Ag, Si, or Mg 2−56753
Al-1% Mg, creep deformation, electron microscopic obs. 2−80753
Al-1% Mo-1% Ti-8% V, accelerated stress-corrosion cracking in presence of hydrogen recombination poison 2−68107
6Al-4V-Ti, surface embrittlement charact. during diffusion bonding 2−68160
Al-6Cu, DTD 5014 (RR58), L65, 2024-T 81, heat effects on fatigue of structural elements 2−60949
Al-5 at.%Mg solid soln., steady state creep, dislocation mechanism, 570-800K56801 2−56801
Al alloy strip with steel rod inserts, transverse tensile properties 2−64701
Al alloys, eutectic, microstructures for unidirectional solidification 2−67985
Al alloys in thick sections, fatigue-crack propagation characteristics 2−71592
AlCr, impurity resistivity 2−68337
AlCu, (Al 4 wt %), structure changes during ageing studied by the channeling tecynique 2−80827
Al1-5% Mg, serrated flow study −50 to 150°C 2−43706
AlMn, impurity resistivity, 4-200K 2−68337
$AlMn_{0.0014}$, mag. scatt. of neutrons from dissolved Mn atoms 2−61474
Al_3Ti growth in Ti/Al chem. diffusion couple 2−53757
Au-Al, α-phase dil., band struct., refl. study, 1.1-11.5 eV 2−75278
$CeAl_x$, n.m.r. and magnetic susceptibilities 2−84594
Co-Al, liq., interatomic interaction energy, viscosity study 2−71155
Co-Al, near equiatomic, positron annihilation relative probability, conc. depend. 2−77804
Co-Mn-Al system, decomp. studies 2−64816
Cu-7.5 at.%Al, deformed in tension, dislocations, etch pit obs. 2−64664
Cu-Al-Fe bronze, superplastically deformed, textures and anisotropic flow 2−43831
Cu-Al-Ni, damping characts. and causes 2−80776
Cu-Al-Ni, martensite memory, shape recovery effect 2−50935
Cu-Al-Ni, shape memory effect 2−80844
Cu-Al-Ni(Mn), martensitic transform., interphase boundary shifting 2−43910
Cu-Al, additives influence on stacking fault energy 2−77665
Cu-Al, Cu-rich, microstruct. and microhardness 2−71678
Cu-Al, cyclic fatigue damage, thermal cond. meas. 2−50672
Cu-Al, equation of states determ. 2−56929
Cu-Al, exo-electron emission, interdependence with annealing processes 2−48011
Cu-Al, exoemission kinetics and hardness depend. on strain or elongation 2−74836

Aluminium alloys continued
- Cu-Al, liq., with Mn and Fe impurities, cond.-electron spin polarization 2−53455
- Cu-Al, neutron irrad., lattice thermal cond. 2−51060
- Cu-Al, plastically deformed, conc. heterogeneities on stacking faults 2−50681
- Cu-Al, quantitative microanalysis, applic. of Monte Carlo calcs. 2−68830
- Cu-Al alloy, α-phase, Fermi surface, comparison of optical and positron annihilation obs. 2−64888
- Cu-Al alloys, mechanical properties and ductility as a function of temperatures 2−64776
- Cu-Al system, $Cu_3Al_{2\|}$(h) and CuAl(r), cryst. struct. 2−74730
- Cu-Al tempered martensite, long period superlattice phases 2−43914
- Cu-16%Al, sigmoidal transient creep, internal stress and disloc. struct. 2−53816
- Cu-Al(10 wt%), high fluence neutron irrad. damage, electron microscope obs. 2−80686
- Cu-Zn-Al, solubility of As 2−47619
- α-Cu-16 at.%Al, spherical single crysts., struct. anomalies 2−71429
- Fe-Al-C, martensite cryst. struct. change, −196 to 20°C 2−80766
- Fe-Al-C alloys, influence of ordering and martensitic transformations during quenching 2−84073
- Fe-Al-Ni-Co-Ti, prod. by Magnicol process, reaction mechanisms 2−43834
- Fe-Al, diffuse X-ray scatt. and temp. depend. of sp. ht. 2−56654
- Fe-Al, magnetic anisotropy 2−54319
- Fe-Al, quantitative microanalysis, applic. of Monte Carlo calcs. 2−68830
- Fe-Al dil. alloy, ave.-moment-internal field variations 2−78008
- Fe-Al system, β-solid solns., order-disorder processes, sp.ht. obs. 2−54002
- Fe-Co(Ni)-Ti-Al, solid soln. decomp. 2−56933
- Fe-Cr-Al, potentiodynamic curves as function of tensile stress 2−44488
- Fe-Ni-Al-Cu, struct. and mag. props., alloying additive effects 2−43845
- Fe-Ni-Al, martensitic transformation, effect of dispersion particles 2−57015
- Fe-12.3 at.%-Al, Mossbauer determination of short-range order, heat treatment and cold rolling effects 2−51311
- Fe_3(Al,Ge), influence of Ge on struct. changes, nuclear γ-reson., X-ray diffract. and dilatometric analyses 2−80779
- Fe_3Al, compression induced mag. anisotropy and superlattice dislocations 2−61516
- $La_{1-x}Gd_xAl_s$, nuclear spin lattice relax. 2−54370
- Li-Al solid solution, electronic props., Green function calc. 2−75029
- Mn-Al-Ge, hysteresis, domain structure and nucleation centres 2−68550
- Mn-Al, mag. props., effect of $\varepsilon\rightarrow\tau$ transform. 2−57280
- Mn-Al, τ phase, microstruct. 2−50838
- Nb-Al-Ge system, phase equilib. and supercond. props. 2−43936
- Nb-Al system, diffusion in $NbAl_3$, Nb_2Al and Nb_3Al phases 2−74815
- Nb_3Al, supercond. critical current variation, a.c. current obs. 2−61240
- Ni-Al-W, γ' matrix, fatigue fracture 2−43716
- Ni-Al, flow-stress recovery 2−74888
- Ni-Al, high temp. deformed, flow-stress recovery 2−74889
- Ni-Al system, lattice parameters and density of β-NiAl and δ-Ni_2Al_3 phases 2−43938
- Ni-Al system, vacancy filling on high temp. compression 2−43939
- Ni-Ta-Al system, Ni_3Al-Ni_3Ta eutectic, directional solidification growth 2−47644
- Ni_3(Al,Ti), Ni-rich γ'-phase, solidification behaviour and γ-precip. 2−53904
- β-NiAl, ordered b.c.c. alloy, creep, transmission electron microscope obs. 2−56807
- Ni_3Al, hardness, effect of Cr, Ti or W alloying 2−43740
- Ni_2(AlTi), Ni_2(AlNb), ordered ternary b.c.c. alloys, creep, transmission electron microscope obs. 2−56807
- Re-Al-B system, phase equilib., X-ray study 2−64822
- Si_3N_4-AlN-Al_2O_3 system, solid solution, X-ray diffr. obs. 2−43823
- Ti-Al-Mo-V alloy, fatigue fracture behaviour in dry Ar environments 2−84118
- Ti-Al-Mo-Zr, ductility, influence of β-phase 2−50746
- Ti-Al-V, mill-annealed, fatigue crack growth, temp. effects 2−60904
- Ti-Al-V brazed foils, scanning e. microscope metallographic study 2−68158
- Ti-Al, cold-worked, X-ray diffr. study 2−80860
- Ti-V-Al-O solid solutions, charact. temp. and elasticity modulus 2−50844
- Ti(13 wt.%)V-(11 wt.%)Cr-(3 wt.%)Al beta alloy, mech. prop.-fracture-microstruct. relns. 56950 2−56950
- V-Al, struct. and props., comp. depend. 2−53912
- V-Ga-Al, A15 struct., superconducting crit. temp. and current density 2−57168
- V-Ge-Al, Knight shift meas. 2−57398
- Yb-Al system eutectic transformations 2−80797
- $YbAl_2$, $YbAl_3$ magnetic susceptibility and expansion coefficient 2−81218
- Zn-Al alloy, solute distrib. using electron probe analyzer EMMA-4 2−56924
- Zn-Al alloys, strain-rate depend. of deform. mechanism and texture form. 2−84011
- Zn-Al eutectic alloy, room-temp. deform. characts. rel. to superplasticity 2−43701
- Zr-Al, dil., ordering and stacking faults 2−47354

Aluminium compounds
- *see also Aluminium alloys; Ruby*
- Al oxide-Nb metal seals, by solder glass in system CaO-Al_2O_4-SiO_2-MgO 2−66377
- β-alumina, ($NaAl_{11}O_{17}$) solid electrolyte, use in anisotropic electrochem. conc. cell 2−61799
- alumina, zero point of charge, temp. depend. 2−72567
- alumina from vapour-deposited powders, reactive hot pressing 2−68171

Aluminium compounds continued
- aluminas, polycrystalline, influence of texture on mechanical props. 2−68093
- aluminium alloy (2618-T6), fatigue testing at elevated temperatures and aeronautical application 2−56870
- alumino silicate refractory fibre, props. and applicatons 2−56953
- aluminosilicate, Li^+ ion gun 2−59116
- BORSIC aluminium fibre-matrix interfacial region, exam. 2−64546
- ceramic, corundum base, elec. cond. rel. to sintering 2−53927
- ceramic, corundum based, thermal stability rel. to microstruct. 2−56959
- glass-Al_2O_3 two-phase composite, verification of fracture theory 2−74860
- mullite, press.-sintered, mech. props., porosity depend. 2−50722
- mullite, press.-sintering kinetics and mechanism 2−50874
- mullite, stoichiometric, synthesis and mech. props. 2−50873
- pseudoboehmites in dil. nitrate electrolytes, point of zero charge 2−75390
- pyrophyllite, mech. props., effect of firing temp. 2−50890
- sapphire, melt growth of single cryst. ribbons, use as substrates 2−60719
- sapphire, relationship between laser induced surface damage and surface plasmas 2−60266
- sapphire, self focusing threshold enhancement with elliptical beams 2−61578
- sapphire, substrate, transport props., electron injection by internal photoemission 2−81110
- sapphire filament growth, void-free at rates up to 3 cm/min, effect of using W growth orifices 2−60720
- sapphire filaments, high temp. testing of strength 2−60956
- X-ray spectra, band type and crystal struct. influence on Al Kα-satellite 2−51360
- YAG laser, Ge photodiode detecting head 2−66761
- zeolite, Y-type, e.p.r. study of Cu^{2+} pairs 2−75343
- zunyite, structural changes on heating 2−75451
- $[Al(ha)_6]Br:Ti^{3+}$, luminesc., $^2E\rightarrow{}^2T_2$ transition mechanism 2−65302
- Al:Al_2O_3, dispersion hardened, prep. of thin foils for transmission electron microscopy 2−80549
- Al-Al_2O_3-Pb junction, impurity assisted tunnelling, 4.2-148 K 2−44140
- Al-Ga-In-P system, props. with view to use in injection laser 2−42096
- 97.4%Al-Mg alloy, fatigue crack dependence, temperature dependence 2−56866
- Al-Si-N-O, new ceramic materials 2−60990
- Al-Si-O glass, prep. and processing, i.r. spectra, crystn. products, mineral species form. 2−56557
- Al-Zn alloys, morphology and crystal structure of a precipitate, Y-phase, exam. 2−67986
- Al-Zn alloys, X-ray central diffusion study of Guinier Preston zones after quenching 2−64632
- (Al, Cu), ion emission, secondary, influence of asymmetrical correlations 2−68502
- (Al, O), ion emission, secondary, influence of asymmetrical correlations 2−68502
- $(Al,Cr)(ur)_6(ClO_4)_3$ low-temp. polarized absorption spectra, determ. of cubic and trigonal parameters 2−51289
- $(Al,Si)(N,O)_4$ tetrahedral structure 2−60997
- $(Al,Ti)(ur)_6X_3$, X=Cl, Br, I, low-temp. polarized absorption spectra, determ. of cubic and trigonal parameters 2−51289
- Al complex, AlX_3-dimethyl sulphoxide coordination compound (X=Cl, Br), vibrational spectra 2−52992
- AlAs, cryst. growth, vapour phase 2−43511
- AlAs, energy bands, relativistic APW calc. 2−81014
- AlAs epitaxial layer, on GaAs, elec. props. and optical absorp. 2−71881
- $AlBr_3(CH_3)_2O$, force field compared with the derivatives $(CH_3)_2O$ and $AlBr_4^-$ 2−42869
- $AlCl_3$-Ar collision processes, molec. orbital study 2−59990
- Al_2Cl_6, normal coordinate anal. and thermodynamic props. 2−42945
- $AlCl_3(CH_3)_2O$, force field compared with the derivatives $(CH_3)_2O$ and $AlCl_4^-$ 2−42869
- AlF_2, heat of formation, reaction $2AlF(g)\rightleftharpoons Al(g)+AlF_2(g)$ 2−72543
- $Al_2Fe_3(SiO_4)_3$, almandite, garnet, elec. field gradient, internal mag. field, Mossbauer obs. 2−54388
- $Al_2Fe_3(SiO_4)_3$, almandite, garnet, mag. struct., cryst. struct. 2−54349
- $Al_xGa_{1-x}As$-GaAs-$Al_xGa_{1-x}As$ heterojunction laser, radiation spectral distrib. and polarization 2−63342
- AlGaAs-GaAs heterojunctions, band filling process 2−47941
- $Al_xGa_{1-x}As$-GaAs heterojunction, prep. by multiple layer liq. phase epitaxy 2−50482
- $Al_xGa_{1-x}As$-GaAs n-p heterojunction, current flow during electrolum. 2−72438
- $Al_xGa_{1-x}As$, $0.16\leqslant x\leqslant 0.58$, photolum. spectra, 1.6-300K 2−61683
- $Al_xGa_{1-x}As$ heterojunction, electroluminescence characs. 2−81431
- $Al_xGa_{1-x}As$ solid solns., in heterostructs., optical and electronic channelling rel. to comp. 2−63341
- AlGaAsP, solution growth, stimulated emission, luminescence, laser operation 2−45747
- AlGaAsP solid soln., prep., use in heterojunction lasers, forbidden band rel. to comp. 2−63343
- $Al_yGa_{1-y}As_xSb_{1-x}$-$GaAs_xSb_{1-x}$ double heterojunction laser, prep. and emission spectra 2−59184
- AlH in solar sunspot spectrum, 4900-6441 Angstrom range 2−62743
- AlI_3, continuum radiation from discharges 2−74421
- $Al_{1-x}In_xP$, cryst. growth, vapour phase 2−43511
- $AlMgBO_4$, vibrational spectra, interpretation by factor group approx., calc. of force constants for BO_4 group 2−70728
- Al_2MgO_4 lattice dynamics, elastic properties, seismic velocity and density profiles 2−72636
- $Al_2(MoO_4)_3$-Rb_2MoO_4 solid soln., phase diagram 2−57033
- AlN:Eu,Mn, radical recomb. luminesc. and photoluminesc. 2−57371
- AlN:Mn, spectrum of luminescence centres 2−75319
- AlN-Al_2O_3-Mo cermet, prep., microstruct., hardness, strength, density 2−43869
- AlN-Y_2O_3, sintered, with fibrous struct., textural determ. 2−47666
- AlN, band struct. calc. 2−71925

Aluminium compounds continued
AlN, emission spectrum, rotational analyses and isotopic studies 2−42868
AlN, i.r. cathodoluminescence, 110-353 K, Huang-Rhys factor determ. 2−75336
AlN, in m.i.s. struct., deposition and props. 2−54225
AlN, precip. in low-C low-alloy steel 2−50833
AlN ceramic, thermal cond., characteriz. 2−50864
AlN_x, preparation by reactive r.f. sputtering 2−77507
$Al_2(NH_4)_2(SO_4)_4.24H_2O$, cryst. growth 2−47202
α-Al_2O_3:Fe, α-Al_2O_3, Ti and α-Al_2O_3(Fe,Ti), polarized and high resolution UV, visible and IR spectra, e.s.r. spectra 2−78082
Al_2O_3:Ti, precip. hardening kinetics 2−50872
$Al_2O_3:Ti^{3+}$, corundum, e.p.r. g-value calc., Jahn-Teller theory 2−65331
Al_2O_3:V, before and after γ-irrad., phonon scatt., thermal cond. study 2−68214
$Al_2O_3:V^{3+}$, ground state study using phonon generation in Sn 2−47735
$Al_3O_3:V^{3+}$, phonon scatt, using superconducting tunnel junction source obs. 2−47732
Al_2O_3/Al ribbon system, thermal spectral radiation 2−61629
$Al_2O_3/ZrO_2/Y_2O_3$ eutectic, directionally solidified, mech. props. 2−47526
$Al_2O_3/ZrO_2/Y_2O_3$ system eutectics, strength 2−47525
Al_2O_3-Al alloy, ball-milled, mech. strength 2−53887
9 Al_2O_3-AlN, periodic antiphase domain struct. 2−50618
Al_2O_3-CaO-Fe_2O_3, phase comp. analysis by X-ray diffr. 2−74725
Al_2O_3-CaO-SiO_2 melt, dynamic viscosity, effect of CO_2, 1400−1700°C 2−74527
Al_2O_3-CaO.Al_2O_3-CaF_2 solid soln., phase diagram 2−57029
Al_2O_3-CoO neutron dosimeter, high temperature 2−49684
Al_2O_3-Cr_2O_3-P_2O_5 coating, radiative capacity rel. to struct., 600-2000K 2−57087
Al_2O_3-Cr_2O_3 and Al_2O_3-Cr_2O_3-Fe_2O_3 systems, orientation of modulated structs. 2−50853
Al_2O_3-Cr_2O_3 phase diagram and ideal soln. behaviour 2−50852
Al_2O_3-Cr_2O_3 system, sub-solidus phase equilibria 2−53983
Al_2O_3-CuO solid soln., form. of $CuAl_2O_4$ phase at 890°C, stability 2−74899
Al_2O_3-Cu_2O solid soln., form. of $Cu_2Al_2O_4$ phase at 930°C, stability 2−74899
Al_2O_3-Fe_2O_3 solid solns., impurity ion effects on spin relax. time of ferric ions 2−54368
Al_2O_3-Fe_2O_3 solid solution, mag. interactions , e.p.r. study 2−75351
Al_2O_3-Mo cemets, thermophysical characteristics in range 500-1300°K 2−43999
Al_2O_3-$Ni(NO_3)_2.6H_2O$ system, effect of heating in oxidizing and reducing media 2−60992
Al_2O_3-P_2O_5-Cr_2O_3 ceramic coating on steel, props. 2−56960
Al_2O_3-PbO-YF_3 crystallization of YAG and det. of stability range 2−74692
Al_2O_3-SiO_2-CaO glass, stratification, liquation, opalescence 2−56564
Al_2O_3-SiO_2-R_xO glass, struct. state of Al ion, complex stability 2−56556
Al_2O_3-SiO_2-TiO_2-Li_2O-MgO, glass-ceramic, crystn., microstruct., indentation hardness 2−80535
Al_2O_3-TiO_2 ceramic, sprayed layers, thermal. cond. 2−44000
Al_2O_3-Y_2O_3 system, noncrystalline film prep. by sputtering 2−47114
Al_2O_3-1% CoO as neutron dosimeter at high temps., prep. 2−73949
1Al_2O_3-nSiO_2, isopaustic glasses, u.s. delay lines 2−78928
Al_2O_3-solids, exoelectronic properties, use in TSEE dosimetry 2−68490
AlO, spectral isotopic method for determ. of oxygen using laser torch as light source 2−84701
AlO $^2\Sigma^+ - x^2\Sigma^2$ band system, calc. of Franck-Condon factors and r centroids using RKR potentials 2−70679
AlO band system, Morse Franck-Condon factors and r-centroids 2−67467
Al_2O_3, ^{17}O enriched, growth by floating zone technique in image furnace 2−74686
Al_2O_3, 0-1000°C dielec. props. 2−72012
Al_2O_3, absorption spectra and reln. between thermoluminescence and thermobleaching 2−71521
Al_2O_3, alumina, coupled solute solid soln. softening with MgO and TiO_2 2−47653
Al_2O_3, alumina, grain boundary grooving on single cryst. surfaces 2−50432
Al_2O_3, alumina, high temp. creep, and grain boundary sliding 2−50753
β-Al_2O_3, alumina, hot pressing, strength and fracture 2−50875
Al_2O_3, alumina, phosphate bonded, strength props., elec. microscope obs. 2−77662
Al_2O_3, alumina, thermodynamic props., condensed phase near melting point 2−54044
Al_2O_3, α-phase polycrystalline, e.p.r. study γ, n in-pile radiation of effects 2−80667
Al_2O_3, C continuous fibre-reinforced, mech. props. 2−50919
Al_2O_3, C discontinuous fibre-reinforced, fabrication and mech. props. 2−50918
Al_2O_3, ceramic, microstruct. rel. to deform. processes 2−60993
Al_2O_3, ceramic to metal seal for thermionic fuel elements 2−53928
α-Al_2O_3, cleavage on {1011} planes, elec. microscope and X-ray obs. 2−74657
Al_2O_3, corundum, atmospheric aerosol constituent, optical consts. 2−57946
Al_2O_3, corundum, cryst. growth, thermodynamic anal. 2−47204
α-Al_2O_3, corundum, enthalpy, heat of fusion, and melting point 2−53490
Al_2O_3, corundum, high temp. creep, microstruct. changes 2−71574
α-Al_2O_3, corundum, Verneuil grown cryst., cryst. axis orientation 2−60701
Al_2O_3, crystn. of amorphous anodic film by heating in vac., morphology 2−83861
α-Al_2O_3, deformation memory 2−71566
Al_2O_3, dielectric breakdown, 300 to 1200°K, mechanisms 2−65056
Al_2O_3, effect on immiscibility temp. of Na_2O-SiO_2 glass 2−53539
Al_2O_3, elec. cond. meas. above 1600°C in air 2−47921

Aluminium compounds continued
Al_2O_3, electrostatic charging after contact with metals 2−72005
Al_2O_3, elemental anal. using neutron capture X-rays 2−44513
Al_2O_3, escape depth of X-ray excited electrons and Auger electrons 2−51224
Al_2O_3, fast neutron irradiation, thermionic reactor design 2−53707
Al_2O_3, fine grained, rate controlled sintering 2−77660
α-Al_2O_3, forbidden e.s.r. transitions of Fe^{3+} 2−78158
Al_2O_3, friction and wear, fund. review 2−47554
Al_2O_3, grain boundary enhanced diffusion 2−50705
Al_2O_3, high temp. strength improvement by surface prestressing 2−50870
Al_2O_3, in m.i.m. struct., photosensitive tunnelling conductance 2−54222
Al_2O_3, in m.i.m. struct., space charge dependence of barrier height on insulator thickness 2−51185
Al_2O_3, ion bombarded, electron yield 2−51228
Al_2O_3, LEED, (0001) surface structure detn. 2−67897
Al_2O_3, leucosapphire, breakdown by mode-locked laser radiation, i.r. 2−79251
Al_2O_3, light scatt. by elastic waves and rot. of polarisation plane 2−72358
Al_2O_3, liq., covalent bonding correl. with phys. props. 2−43338
Al_2O_3, molecular struct. effects in Al Kβ X-ray spectra in proton and alpha particle excitation 2−81381
Al_2O_3, molten, elec. cond. 2500-2000 K 2−56516
Al_2O_3, molten, surface tension, density, volume change on melting 2−80465
β-Al_2O_3, Na, K, Rb, and Na-K substituted, rel. to mech. behaviour 2−56770
α-Al_2O_3, plastic deform., 1650-2000°C, thermoactive nature 2−53804
Al_2O_3, plastic deformation in hot-pressing 2−77735
Al_2O_3, polycrystalline, stress corrosion in moist air and toluene, time-dependent failure characteristics 2−84039
α-Al_2O_3, polymorphic transform. under electron irrad., thermodifferential analysis 2−47681
Al_2O_3, porous compact, grain growth, electron microscope obs. 2−43905
Al_2O_3, porous polycrystalline, compressive creep 2−47513
Al_2O_3, positron lifetime spectra, temp. depend. 2−75003
Al_2O_3, powder, initial sintering rel. to surface diffusion, neck growth obs. 2−43887
Al_2O_3, rapid sintering by glow-discharge apparatus 2−80804
Al_2O_3, ruby, energy levels of Cr^{3+} ions 2−68633
Al_2O_3, sapphire, dislocation tangle formation, X-ray obs. 2−80703
Al_2O_3, sapphire, fracture and strength 2−50774
Al_2O_3, sapphire, grain boundary migration 2−50704
Al_2O_3, sapphire, strength, temp. depend. 2−50762
Al_2O_3, sapphire, temperature field, effect of optical characteristics 2−68256
Al_2O_3, sapphire filament, fracture strength in tension 2−50917
Al_2O_3, sapphire filament, growth and microstruct. 2−50916
Al_2O_3, sapphire filaments, strength enhancement due to continuous flame polishing 2−80867
Al_2O_3, single and polycryst., ionic and electronic cond. 2−47978
Al_2O_3, sintered, radiative and lattice thermal cond. simultaneous meas. 2−51052
Al_2O_3, sintering, surface area and pore-size distrib. obs. 2−50866
Al_2O_3, sintering kinetics, effect of iron oxide 2−50865
γ-Al_2O_3, specific surface area meas. 2−64548
α-Al_2O_3, spreading critical surface energy, from liq. metal wetting obs. 2−80558
Al_2O_3, static and cyclic fatigue behaviour 2−50766
Al_2O_3, strength, biaxial flexure tests 2−60919
Al_2O_3, subsurface damage due to abrasion, examination using transmission electron microscopy 2−80870
α-Al_2O_3, surface finishing by flame polishing, annealing techniques 2−80865
α-Al_2O_3, tab growth, vapour−liquid−solid phase mechanism 2−43508
α-Al_2O_3, thermal expansion, 100 to 800K 2−51047
Al_2O_3, thermal grooving and growth kinetics 2−80545
Al_2O_3, translucent alumina prep. and characteriz. 2−50863
Al_2O_3, transmission e. microscopy obs. of subsurface damage caused by mech. polishing and grinding 2−71418
Al_2O_3, viscosity and loss angle of Young's modulus calc. 2−84055
α-Al_2O_3, whisker growth during Al oxidation 2−74637
Al_2O_3 (99 + %), ceramic, white spots characteristic 2−84064
Al_2O_3 additions in Nb, effect on supercond. behaviour 2−44077
α-Al_2O_3 alumina, (0001) surface, structure, LEED obs. 2−50435
Al_2O_3 amorphous anodic films, partial model for structure from X-ray scattering data 2−47100
Al_2O_3 and Al_2O_3/B fibre composites, high temp. bearing characts. 2−47558
Al_2O_3 based refractories, stress-strain behaviour in torsion test 2−43687
Al_2O_3 bicrysts., porosity distrib. and pore growth on grain boundaries 2−60991
Al_2O_3 ceramic, fine grain, Cr_2O_3 additions effect on struct. and props. 2−50867
Al_2O_3 ceramic, internal friction, temp. depend. 2−71553
Al_2O_3 ceramic, strengthened by surface compression, thermal stress fracture 2−50871
Al_2O_3 ceramic insulator, swelling in neutron irradiation 2−53706
Al_2O_3 ceramics, high temp. strength 2−50868
Al_2O_3 ceramics, microwave machining and piercing characteristics 2−53867
Al_2O_3 ceramics, quenched, residual stress determ. from mirror dimens. 2−50869
Al_2O_3 coatings on BeO, neutron irrad. effect on protective behaviow and crack form. 2−43870
α-Al_2O_3 filament reinforced Al composite, mech. props. 2−53947
Al_2O_3 film, anodic, breakdown by impact ionization 2−57235
Al_2O_3 film, electron beam produced, electrostatic potential effects 2−60645
Al_2O_3 film, growth by plasma anodization 2−43477
Al_2O_3 film, in m.i.m. struct., transients, capacitance variation with temp. 2−57219

Aluminium compounds continued
  Al_2O_3 film, plasma and gas plasma deposited, struct. determ. 2−64563
  Al_2O_3 film, step and ramp voltage breakdown tests 2−72024
  Al_2O_3 film, struct. and props., effect of chem. vapour deposition temp. 2−50483
  Al_2O_3 film annealing effect on MAS charact. 2−71997
  Al_2O_3 films on glycerol as specimen support film for atomic resolution electron microscopy 2−43556
  α-Al_2O_3 formation, in presence of AlF_3 2−47704
  Al_2O_3 particle growth in Ni ceramic, matrix density effects 2−68169
  Al_2O_3 particles, radioactive props., high temp. 2−78183
  Al_2O_3 particles in flames, i.r. emission and temperature measurements 2−73468
  Al_2O_3 powder, thermal diffusivity and cond. simultaneous meas. by flash method 2−43996
  Al_2O_3 protective coating on W filaments in composite 2−53967
  Al_2O_3 seals, fast-neutron irradiation effect 2−63227
  α-Al_2O_3 single crystals, flat bars, flame polishing, problems, limitations 2−80866
  Al_2O_3 thermoluminescence emission band at 4100 Å suitability as radiation detector 2−57376
  Al_2O_3 whiskers of fibres, poor efficiency in reinforcing Ni for high temp. use 2−47668
  αAl_2O_3 X-ray detn. in alumina crystallites 2−56647
  Al_3O_3, crystal growth, from the flux systems PbO-V_2O_5 and Bi_2O-V_2O_5 2−50589
  $AlOF_2$, heat of formation, reaction 1$AlOF_2$(g) 2−72543
  α-$Al(OH)_3$, hydrogen atom positions and hydrogen bonds prediction 2−47312
  $AlPO_4$, partial volume determination, influence of composition for solid solution glass ceramics 2−56562
  AlSb, amorphous, phonon density of states, Raman scatt. obs. 2−61664
  AlSb, elastic consts. 2−77626
  AlSb, i.r. dispersion of second order electric susceptibilities 2−61581
  AlSb band struct., critical point detn., wavelength modulation derivative spectroscopy obs. 2−48160
  $Al_2(SiO_3)_3$, room-temp. strengths for various biaxial stress states 2−77677
  Al_2SiO_5, high and low pressure polymorphs, rel. to thermal conductivity 2−65582
  $Al_xSi_yO_z$, in m.a.o.s. struct., polarization effect causing instability 2−65044
  Ba-mica/Al_2O_3 composite, fabrication and props. 2−56977
  CaO-Al_2O_3-SiO_2 glasses, i.r. spectra, struct. study 2−47057
  $Ce_{0.25}(Y,La)_{9.75}Al_2$, inelastic neutron scatt. determination of cryst. field levels of Ce^{3+}, susceptibility calc. 2−72105
  CoO-Al_2O_3-SiO_2 glass system, low field mag. suscept. 2−65178
  Cu-Al-alloys, microstructures and mechanical props. of phases after quenching and isothermal treatment 2−60932
  Fe-Al-Cr alloys, effect of zirconium on mech. props. and oxidation resistance 2−60935
  $Ga_xAl_{1-x}As$-GaAs p-n heterojunction, field effect of GaAs photolum. 2−72399
  $Ga_xAl_{1-x}As$, optical electron-nuclear reson. 2−61695
  GaAs-AlAs, solid solution heterojunction injection laser, 7400-9000 Å range 2−73596
  $(La,Gd)Al_2$, dilute system, n.q.r. and relax. obs., ordering onset 2−68754
  Li_2O-Al_2O_3-SiO_2 glass-ceramic, strength and microstruct. 2−53931
  $MgAl_2O_4$-Al_2O_3 system, liquidus- solidus determ. 2−50971
  MgO-Al_2O_3 system, noncrystalline film prep. by sputtering 2−47114
  MgO-SiO_2-Al_2O_3, pressure sintered specimens, phase composition and dielectric constants 2−57226
  $MgO.Al_2O_3.SiO_2$ glass-ceramic, ZrO_2-nucleated, phase transitions 2−47691
  Na-β-Al_2O_3 phases formation and area of existence 2−84066
  Na_2O-Al_2O_3-SiO_2, glass, X-ray diffraction study 2−60585
  Na_2O-B_2O_3-Al_2O_3, nabal glass, self-diffusion of Na ions and interdiffusion coeffs. 2−60832
  PbO-Al_2O_3-SiO_2-B_2O_3 glass, between metal electrodes, memory effect 2−71915
  Pt/Al_2O_3 catalyst, butene adsorption, high resolution n.m.r. obs. 2−60683
  SiO_2-Al_2O_3-Na_2O-K_2O-CaO-MgO glass, viscosity-temp. relations 2−67883
  SiO_2-Al_2O_3 glass, crystallization, DTA, elec. microscope and X-diffr. obs. 2−53542
  SiO_2-B_2O_3-Na_2O-Al_2O_3 system, comp. fluctuation and phase decomp. 2−53543
  SiO_2-CaO-MgO-Na_2O-AlF_3:Dy^{3+} glass system, luminesc., effect of heat treatment 2−48228
  $SrAlF_5$, pure and Eu^{2+}-doped, cryst. growth and characterization 2−60726
  ZnO/Al_2O_3, heteroepitaxial layer structure, surface acoustic props. rel. to delay line behaviour 2−68235
  ZnO-Al_2O_3-SiO_2 glass-ceramics, dielec. props. and effects of adding (CaO, SrO, BaO) 2−65045

Americium
  in Ap star HD 25354, spectral obs. 2−72994
  biological damage, interactions with cells and tissues 2−78659
  in nuclear fuels determ. during reprocessing 2−74178
  nuclear targets, electrodeposition methods of prep. for cross section obs. and accelerator bombardment 2−73919
  targets, prep. techniques 2−73912
  whole body counting, γ-rays, Anger camera 2−78663
  Am^{4+} ions in cubic site, J-mixing effect on g-values of Γ_7 ground state 2−48119
  ^{241}Am radiology, bone mineral content, in vivo measurement 2−69313

Americium compounds
  AmI_2, crystal structure and magnetic susceptibility 2−80643
  AmO_2, thermal cond., self-irrad. effects 2−54078
  AmOI, X-ray diffraction determ. of lattice constants 2−80643

Ammonia *see Nitrogen compounds/ammonia*

Ammonium compounds *see Nitrogen compounds/ammonium compounds*

Amorphous state
  see also Vitreous state
  chalcogenide alloy film, sputtered, thermally stimulated Ar release study 2−43472
  chalcogenide films, Seebeck coeff. 2−61442
  chalcogenide threshold and memory devices, preswitching props., forming and switching 2−77920
  coherent scattering in random-network model 2−64521
  copolymers, amorphous blocks cast from soln., domain struct. 2−83848
  density of states, upper and lower bounds, from Tchebycheffs inequality 2−68283
  diamagnetic susceptibility enhancement of disordered or highly compensated crystalline semiconductors 2−81206
  disordered systems, correlation phenomena 2−64815
  electrical cond., carrier flow through localized and extended states 2−77882
  electron microscopy 2−83937
  electron scattering, transition matrix approach 2−83936
  electronic Green's function, density of states 2−71786
  electronic structure, Anderson model 2−61166
  ferromagnet, free energy lower bound 2−78006
  ferromagnet, ground state instability and long-wavelength spin wave form. 2−48043
  ferromagnet, susceptibility and Curie temp. rel. to spin fluctuations 2−57277
  ferromagnets, conditions for existence, const. coupling approx. 2−81274
  film, chalcogenide, dielec. const., elec. cond., struct. features 2−61309
  film, chalcogenide, grown by vapour deposition, contribs. to growth temp. 2−64564
  film, chalcogenide, pre- and postswitching characts. 2−61310
  group III-V compounds, static electronic dielectric constant 2−51300
  hard sphere aggregates prep. on computer 2−53514
  high field conductivity 2−54168
  imaging, by structural alteration 2−60568
  ion irrad., range profiles, damage distribs. 2−47776
  microsegregation in binary systems, X-ray diffr. 2−60570
  noncrystalline solids, molecular dynamics, ENDOR and ELDOR obs. 2−65353
  optical properties, interband transitions, review 2−72293
  optical properties and X-ray diffraction 2−61622
  phenol formaldehyde resin, thermal degraded, a.c. and d.c. cond. 2−47903
  polymer, cell model partition function for thermodynamic calc. 2−43457
  polymer films amorphous and crystalline, electrical conductivity in strong electric fields 2−84340
  polymers, creep recovery, influence of volume change 2−56809
  polyvinylchloride, drawn samples, molec. orientation determ. by broad line p.m.r. 2−51417
  rhodamine 6G film, carrier trapping, thermostimulated cond. study 2−54180
  rubber, amorphous sodium-butadiene and butadiene-nitrile, stress and electrical conductivity study 2−60873
  rubber, styrene-butadiene, molecular orientation during stretching 2−56549
  scanning high energy electron diffraction, review 2−74710
  semiconductor, avalanche ionization, Shockley hot-electron model 2−61287
  semiconductor, conducting filament rel. to electrotransport in liquid alloys 2−60455
  semiconductor, conf., Ann Arbor, USA, Aug. (1971) 2−61258
  semiconductor, conf., Ann Arbor, USA, Aug. (1971) 2−61259
  semiconductor, conf., Warsaw, Poland, July (1972) 2−68384
  semiconductor, diamag. enhancement of susceptibility, mechanisms 2−44219
  semiconductor, disordered, problems arising from energy spectrum and change carrier kinetics theory 2−68391
  semiconductor, elec. instabilities of mixed electronic and thermal origin, theory 2−61285
  semiconductor, electronic struct., LCAO calc. 2−68414
  semiconductor, electrothermal switching, models 2−61284
  semiconductor, field dependent mobility, model 2−61286
  semiconductor, ion implantation induced lattice disorder 2−47367
  semiconductor, localized state density energy depend. determ. using field effect 2−47911
  semiconductor, lone pair, refr. index press depend. 2−68594
  semiconductor, long range order, short range order and energy gaps 2−61158
  semiconductor, metal-insulator phase transitions, science and technology 2−57205
  semiconductor, organic, elec. cond., press. depend., random field model 2−44108
  semiconductor, photocond. response characts., obs. with photocond. ccts. 2−84375
  semiconductor, radiation stability, effects of microstruct. 2−60567
  semiconductor, reversible elec. and optical memory effects, rel. to phase transition 2−57185
  semiconductor, reversible optical effects, laser induced 2−60569
  semiconductor, structural models 2−60566
  semiconductor, theory and band models 2−47879
  semiconductor, tight-binding model 2−84275
  semiconductor, trap levels, thermally stimulated capacitor discharge study 2−54188
  semiconductor, trapping mechanism, cavity perturbation study 2−61443
  semiconductor, Urbach tail in optical absorpt. edge 2−68641
  semiconductor, with globular inhomogeneities, interglobular electronic transport 2−68390
  semiconductor film, ohmic and non-ohmic cond. 2−61289
  semiconductor with undulatorily-graded band edges, props., prediction 2−61282
  semiconductors, band struct. calcs., short survey 2−81012
  semiconductors, struct. modelling 2−67881
  structure, determ. by extended X-ray absorpt. fine struct. method 2−71283

Amorphous state continued
- tetrahedrally bonded solid, band struct., tight- binding Hamiltonian 2−84274
- transition element oxide glasses, amorphous antiferromagnets, absence of ordering 2−81301
- transition metal film, deposition and annealing, resist. study 2 77499
- 4d transition metals, vapour deposited, electron microscope obs. 2−60594
- vibrational properties, frequency spectrum moment method 2−50981
- Al_2O_3, crystn. of amorphous anodic film by heating in vac. 2−83861
- Al_2O_3 anodic films, partial model for structure from X-ray scattering data 2−47100
- As-Te-Ge, cryst. layer form., effect of water during heat treatment 2−60571
- As, different forms 2−60572
- As_2S_3, photoelastic consts. freq. depend., one-oscillator model 2−54383
- As_2S_3 and As_4S_4 films, a.c. cond., temp. depend. 2−68392
- As_2S_3 glassy state, n.q.r. obs. 2−84605
- $As_2S_3(Se_3)$, refl. spectra, vibr. modes 2−61614
- $As_xSb_{2-x}Se_3$, threshold and memory switching 2−77883
- As_2Se_3, a.c. cond., 30Hz-10.3GHz, −180-500°C 2−81070
- As_2Se_3 film, a.c. cond., temp. depend. 2−68392
- As_2Se_3 film, charge transport, photocond. and dark current obs. 2−68393
- As_2Se_3 film, memory switching rel. to thickness 2−81072
- $As_2Se_3(Te_3)$ film, trap-limited processes 2−61325
- C, band struct., from X-ray photoelectron spectra, amorphization effects 2−57262
- C, ion irrad., nuclear ion-atom interactions, Z_1 oscills., non-evidence 2−47780
- C, lampblack, graphitization 2−56995
- C, microstructure, high-resoln. electron microscopy obs. 2−53532
- C black, paracryst. distortions 2−53974
- C film, elec. and optical props. and struct. 2−61302
- C film, graphitization by light pulses 2−61030
- C film, graphitization under light pulse irrad. 2−57002
- C products, graphitization effects on neutron irrad. induced dimensional changes 2−56996
- C pyrolytic, fluidized-bed, mech. rel. to struct. props. 2−56768
- Cd film, supercond. energy gap and transition temp. 2−54134
- CdS film, in m.i.m. struct., electroforming and elec. cond. props. 2−64978
- Fe_xGd_y alloy films, mag. props. 2−44275
- GaAs, thermoelec. power, cond., hopping cond., annealing effects 2−61312
- Ge-Se-Te-As system, composition and physical props. 2−60573
- Ge-Te phases, structural differences 2−60577
- Ge, atomic arrangement, computer simulation 2−60574
- Ge, band struct. rel. to struct. 2−68436
- Ge, dark-field electron microscope obs. 2−60593
- Ge, different forms 2−60572
- Ge, diffr. props., consistency with continuous random network model 2−64618
- n-Ge, disordered region prod. by 28 MeV electrons 2−47931
- Ge, electron tunnelling, phonon density of states 2−44125
- Ge, Fourier analysis of EXAFS 2−60576
- Ge, irrad. induced damaged region form. 2−47384
- Ge, struct. extended X-ray absorpt. fine struct. determ. 2−71283
- Ge, temp. dependence of elec. conductivity 2−47924
- Ge, thermoelec. power, cond., hopping cond., annealing effects 2−61312
- Ge, unannealed, residual cond. at 77K 2−47926
- Ge film, anisotropic elec. props. 2−68430
- Ge film, crystalline transform. rel. to thickness and environment 2−67882
- Ge film, microcrystallite struct. 2−43479
- Ge film, ohmic and non-ohmic cond. 2−61289
- Ge film, secondary electron emission spectrum obs. of electron states and disorder 2−61353
- Ge film, small angle X-ray scatt. obs. 2−60661
- Ge film, struct. rel. to angle of evaporation 2−71330
- GeO_2, Fourier analysis of EXAFS 2−60576
- GeO_2, struct., extended X-ray absorpt. fine struct. determ. 2−71283
- GeSe, Fourier analysis of EXAFS 2−60576
- GeSe, struct., extended X-ray absorpt. fine struct. determ. 2−71283
- Ge_xSe_{1-x} alloy film, radial distrib., elec. diffr. obs. 2−60659
- $Ge_{0.17}T_{0.83}$, neutron and X-ray diffr. radial distrib. functions 2−56548
- $GeTe_2$ film, local order and microstructure 2−60660
- Ge_xTe_{1-x} alloy, structure and bonding, X-ray obs. 2−60575
- Mo-Zr, Mo-Ru alloys, vapour deposited, electron microscope obs. 2−60594
- Nb-Zr, Nb-Mo alloys, vapour deposited, electron microscope obs. 2−60594
- Sb, Raman spectra 2−68665
- $Sb_{1-x}Se_x$ film, photocond. spectral response rel. to comp. 2−81167
- Se, compressed, crystn., photocurrent and thermally stimulated current obs. 2−64533
- Se, crystn., effect of alternating elec. field 2−60565
- Se, diamag. mag. susceptibility, 40-300K 2−77988
- Se, different forms 2−60578
- Se, i.r. absorpt. obs. of ring-chain-struct. 2−78088
- Se, kinematics of deep trapping 2−61344
- Se, layers, photo-effect 2−84374
- Se, structure of three forms 2−43451
- Se, u.s. propagation, vel., Young's, rigidity moduli, 0-60°C 2−57051
- Se, valence band density of states, vacuum photoemission study 2−84258
- Se film, a.c. cond., temp. depend. 2−68392
- Se film, one- and two-carrier space-charge-limited currents 2−75097
- 19 at.%Si-Te alloy, struct. 2−53515
- Si, amorphous layer prod. by ion bombardment 2−71456
- Si, atomic arrangement, computer simulation 2−60574
- Si, band struct. rel. to struct. 2−68436

Amorphous state continued
- Si, characteriz. as function of decreasing spin conc., e.p.r. obs. 2−78162
- Si, cryst. polytypes, electronic struct., pseudopot. and tight binding models 2−71946
- Si, dark-field electron microscope obs. 2−60593
- Si, electron tunnelling through oxide barrier 2−61359
- Si, irrad. induced damaged region form. 2−47384
- Si film, density determ. by backscattering of 2500 keV alpha particles 2−80559
- Si film, elec. cond., 77-300K, annealing effects 2−61360
- Si film, localized state distrib., field effect study 2−68437
- Si film, microcrystallite struct. 2−43479
- α-SiC, residual lattice disorder due to ion bombardment 2−47391
- SiO, trap levels, thermally stimulated capacitor discharge study 2−54188
- SiO_2 film, pyrolytic, struct., electron diffr. obs. 2−80571
- SnTe, Raman spectra 2−68665
- Te films, localized states, photoemission quantum yield 2−68422
- TeO_2, electronic bonding of Cu^{2+} e.p.r. and optical spectra obs. 2−72501
- TiO film, sputtered, dielec. props., equiv. elec. cct. 2−47970
- TiO_2 film, photocond. and photolum., room temp. 2−72068
- Tl-Te alloy, film, cond., band struct. model 2−61328
- WO_3, ion bombardment-induced amorphization and mean damage rates determ. 2−77576
- ZnS film, in m.i.m. structs., electroforming and elec. cond. props. 2−64978
- ZrO_2, radiation induced thermal effects 2−64522

Amplifiers
- amplifying tract of spherical ion trappers, calibration system 2−85061
- compensation, for catheter manometer systems 2−51896
- conductive mode, for scanning electron microscope 2−55639
- d.c., fast, with autoranging over six decades 2−49241
- d.c., with current output, frequency characteristics 2−59035
- electrometer, for radiotherapy depth dose scanning system 2−69302
- and filter system for telluric signals 2−81627
- invivo preamplifiers for Si detectors, medical and biological applications 2−51938
- ionisation vacuum gauge meter, stabilised amplifier and picoamperemeter 2−78699
- laser, driven by cw oscillator, gain saturation 2−41966
- linear for high resolution nuclear pulse analysis 2−63710
- longitudinal stress pulse amplification in elastic bars with intermediate tapered region 2−41678
- low noise, for semiconductor X-ray detectors 2−52702
- low noise preamplifier for high count rates 2−49687
- magnetron amplifier frequency multiplying properties 2−59105
- metal-$SiO_2(TiO_2)$-Si-$SiO_2(TiO_2)$-metal structures, of light signals 2−45694
- molecular amplifiers, influence of relaxation on amplification 2−41963
- nuclear, low noise, pulse shaping, noise analysis 2−42474
- parametric, for mechanical vibrations 2−55480
- photodiode-operational as relative-energy monitor for pulse laser systems 2−52441
- photoelectronic channel, output signal variation stability 2−82804
- photovaristor modulator for pyrometric instruments 2−69846
- plasma current multiplier for a.c. or d.c. current amplification 2−70921
- preamplifier-dual discriminator, in proportional counter hodoscopes 2−49640
- pulse, for photon counting 2−59124
- pulse storage system, studying properties of laser photons 2−42110
- quartz crystal, uniaxial plane-parallel, finite thickness, effect of two-element metal arrays 2−63177
- rhodamine B doped polyurethane film ring laser, light amplification and coupling 2−42055
- seismic, phase characteristics with high-pass and low-pass filters 2−44566
- sterically hindered pulse in isotropic medium 2−73539
- video preamplifiers, noise model 2−66685
- waveguide gas lasers 2−41987
- CO_2 TEA, oscillator amplifier laser, 2 GW peak power generation 2−41994
- CO_2 TEA laser fluorescence and gain measurement 2−41995
- KH_2PO_4, parametric light amplification and oscillation, with mode locked pump 2−42052
- $LiIO_3$, elastic surface wave props. and device applics. 2−77778
- Nd-glass thin film waveguide for amplification at 1.06 microns 2−42057
- $POCl_3$:$ZrCl_4$:Nd^{3+} liquid laser, amplification of mode locked trains 2−59167
- Xe filled proportional counters, gas amplification factor 2−63697

Analogue computer applications *see Computer applications*

Analogue computers *see Calculating apparatus/analogue apparatus*

Analysis *see Chemical analysis; Statistical analysis*

Anechoic rooms *see Acoustical laboratories*

Anelasticity *see Internal friction*

Anemometers
- cup, response to fluctuating wind speeds 2−75576
- cylindrical probes, factors influencing heat transfer 2−58949
- dynamics, error analysis 2−75573
- flow measurement, conference, Harwell, England (1971) 2−83508
- heated films and wires for flow angle and shear stress meas. 2−46686
- hot film, forced heat transfer in two-dimensional unsteady flow 2−80431
- hot film, turbulence in open channel flow 2−77386
- hot wire, adaptation to meas. turbulent boundary layer fluctuations 2−53274
- hot wire, calibration for obs. of small gas velocities 2−67717
- hot wire, construction for hypersonic turbulent flow 2−64373
- hot wire, determ. of dependence of signal on angle of yaw, support orientation and wire length to diameter ratio 2−64369
- hot wire, filaments in air stream, aeroelastic behaviour 2−55498
- hot wire, free and forced convection in steady flow 2−80173
- hot wire, linearization circuits 2−53281

Anemometers continued
hot wire, meas. of nonbuoyant vortex ring 2−77250
hot wire, meas. of vortices and unsteady flow 2−77242
hot wire, reverse flow sensing 2−67707
hot wire, spatial calibration properties in longitudinal and transverse waves 2−60341
hot wire, turbulence measurements in water 2−77385
hot wire, turbulence obs., in nonisothermal flow 2−43081
hot-wire, airborne, optimal choice of parameters for obs. of small scale atmos. turbulence 2−44680
hot-wire, normal and inclined, calibration technique 2−43089
hot-wire, temperature sensitive feedback, criteria for operating point 2−44669
hot-wire filaments, aeroelastic instability 2−80406
laser, Doppler difference method, automatic data processing system 2−84789
laser, measuring individual realizations for turbulence meas. 2−80182
laser, supersonic wind tunnel measurements 2−83682
laser, tracer behaviour in turbulent flow 2−43054
laser Doppler anemometer, flow meas. in strong swirl 2−83511
optical, volumetric flow measurement of liquids and gases 2−83512
paired-Gill. algorithm for reducing errors based on response function 2−44679
pressure-sphere anemometer, improved design 2−44673
reed switch anemometer, housing design 2−65709
suspension wire probe, turbulence in open channel flow 2−77386
thermoanemometer, temp. compensation method 2−71080
turbulent intermittent boundary layers on porous plate, meas. 2−83445
United States Midwest tornado wind records, geometrical analysis 2−75577
vertical wind measuring instrument 2−62109
X-array hot wire, effect of wire length and separation on meas. errors 2−64367

Angle measurement
contact angle, soap film stabilised with ionic surfactant, impurity effects 2−60410
methods of counting and interpolating interference fringes rel. to length and angle measurement 2−76155
microwave transhorizon propagation, angle and Doppler spectrum obs. 2−54869
optical angular displacement meter, accuracy analysis 2−63404
optical circular table 800 2−55753
optical electronic goniometers, modulation characteristics 2−55359
optical surfaces parallelism using c.w. gas laser 2−82532
optoelectronic sensor, errors from atmospheric turbulence 2−58690
space vehicle orientation, using inertial sensors 2−54973

Angular distribution *see Gamma-rays/angular distribution; Neutrons and antineutrons/angular distribution; Protons and antiprotons/angular distibution*

Angular momentum theory *see Quantum theory*

Angular velocity measurement
see also Stroboscopes
compensation methods for assigning small linear and angular speeds 2−76160

Anisotropy, magnetic *see Magnetic anisotropy*

Annealing
β Ti-V alloys, thermal etching and dislocations 2−80546
alkali halides, γ-irrad., isothermal annealing effect on aquoluminescence 2−43376
alloys, quenched, transients in annealing of vacancies 2−80842
austenitic stainless steels, solution, annealed, intergranular corrosion tests based on potentiokinetic polarization curves 2−68791
brass, work hardened, strength and struct. development, recrystn. 2−43789
bubble garnets, magnetiz. reversal 2−51253
carbons irradiated by neutrons, electronic props. change 2−68137
chalcogenide glass, threshold and memory types, cond., DTA, and X-ray studies 2−71917
diamond, irradiated, effects of N impurity 2−71453
diamond graphitization at zero pressure and at high pressure 2−47677
electric wire arrangement for thermocouples, temp. control and obs. 2−45603
fission tracks in mica and volcanic glass, stability rel. to water effects 2−67097
glass fibre, aluminoborosilicate, effect on B coordination number 2−64528
graphite, artificial, neutron irrad. damage and effects on thermal conductivity 2−54073
graphite, neutron irrad. defect struct., single cryst. 2−53709
graphite, pyrolytic, electron irrad., recovery, resist. study 2−80659
graphitisation of carbon products, infl. on dimensional variations of n irradiation 2−68175
graphitization of diamonds, obs. of electroluminescence 2−84546
isothermal, for $Pb_{1-x}Sn_xTe$, $Pb_{1-y}Sn_ySe$ thin films, effects on carrier concentration, mobility 2−64999
metal, dislocation loops and tetrahedra 2−53698
metal, secondary defects annealing behaviour 2−43619
metal recrystallization and transition bands 2−68135
naphthalene crystals, X-ray irradiated, effect on colour centres and e.s.r. spectrum 2−80711
neutron damage, in Si n-channel junction of f.e.t. 2−51181
nichrome, resistive thin film, evaporated from liquid phase by electron beam gun 2−71332
nickel zinc ferrites, hot-pressed, flame-sprayed, permeability, temperature coefficient changes 2−84430
nylon 66 fibres, drawn, effect of high-temperature annealing on structure and morphology 2−74602
organic glasses, influence of annealing on thermal behaviour in glass transition region 2−71744
Permalloy films, mag. anisotropy depend. 2−61525
plastic, laser irrad., stimulated Brillouin scatt. obs. 2−68668
polyethylene, oriented, struct. effect of annealing under high press. 2−83395
polymer, amorphous, effect on morphology 2−60610
polymer, effect on morphological struct. 2−60611

Annealing continued
postirradiation, swelling prediction rel. to pore migration by surface diffusion 2−53548
radiation defect accumulation and annealing kinetics, testing apparatus 2−84062
radiation defects, in crystals, vacancy-impurity complex, annealing kinetics 2−80693
stainless steel, ferritic sheet, texture development 2−77701
stainless steel, type 304, passivity, effect of plastic deformation 2−78195
steel, 304L stainless, vacuum, in-situ surface characterization by proton induced X-rays 2−50832
steel, high temp. fracture, influence of annealing twins 2−56833
steel, hyper-eutectoid, graphitization, effect of Ca and Ba, 550-700°C 2−47583
steel, impact fatigue effects on microstructure 2−80809
steel, low carbon, influence of vacuum annealing on dislocation structure and hydrogen saturation 2−60958
steel, low-alloy and low-C, irrad., radiation and anneal-hardening 2−80681
steel, sheet, cold rolled, annealed, grain growth, X-ray obs. 2−47621
steel, stainless, Cr depletion of surface by vacuum annealing 2−47075
steel surface oxidation during annealing, obs. 2−67899
steel wire, annealing struct. of heavily drawn pearlite 2−64760
stress relieving, welded joints, crack formation 2−64759
supersaturated constituents, migration to surface sinks 2−80720
titanomagnetites, effect on exchange anisotropy 2−72927
Zircaloy-2, irrad. and temp. effect on tensile and creep props. 2−43802
n-Ge, electron irrad., low temp., diffusion limited recovery 2−47378
Ag, ion irrad. induced damage 2−47368
Ag, γ-irrad., recrystn., internal friction obs. 2−64758
Ag, recrystalliz., annealing peak obs. 2−47577
Ag, work hardened, anelastic phenomena at low temp. 2−60848
Ag film, hillock and island form, by surface diffusion mechanism 2−67896
Ag film, on mica, oriented recrystallization 2−47097
Ag film, single crystal prep. and characterization 2−56586
Al-Fe, of lattice defects 2−50827
Al-Fe alloy, microhardness rel. to precip. of Fe and annealing out of lattice defects 2−50828
Al-(1.8 wt.%)Mn alloy, decomp. products 2−47615
Al, defects produced by quenching and electron irrad. 2−60785
Al, neutron irrad., of voids 2−53705
Al, quenched, annealing kinetics of point defects, resist. and magnetoresist. study 2−80680
Al film, struct. change effects on opt. absorpt. 2−54415
Al foil, electron irradiated, isochronal, stage III recovery obs. 2−43805
Al sheet, rolling and annealing texture of outer layer 2−64756
As_2Se_3 film, crystalline and amorphous, rel. to ion bombardment effects 2−60646
$As_2Se_3-xAs_2Te_3$, amorphous, effect on elec. cond., Hall effect, and thermopower 2−77893
Au, ion irrad. induced damage 2−47368
Au, plastically deformed after quenching, resist. recovery 2−56790
Au, quenched, stacking fault tetrahedra growth and annealing 2−77590
Au films, rel. to low temp. migration of Cr, backscatt. obs. 2−56754
Au thin films obtained by sputtering, changes of electrical and structural properties changes during annealing process 2−60647
$BaTiO_3$, surface domain reorientation, X-ray diffraction exam. 2−80544
Be, elec. resist, laser irrad. and annealing effects 2−81036
C, isotropic pyrolytic, formed below 1500° C. effects and mechanism 2−61022
C, neutron irrad., changes in electronic props. 2−57000
C, pyrolytic, neutron-irrad. 2−56993
C film, amorphous, graphitization by light pulses 2−61030
C low density, effect on thermal diffusivity obs. 2−54076
Cd, with Sb or Bi impurity, pore formation 2−71665
CdS platelets, electron irradiated, luminescence properties 2−68703
CdSb, evaporation of Cd atoms, effect on elec. props. 2−47890
CdSe films, influence of Se vapour annealing on electrical conductivity 2−44094
p-CdTe, annealing effect on conductivity and photoconductivity, obs. 2−61263
Co film, effect on n.m.r. 2−81471
Cr, deformed at 77, 213 and 293K, recovery 2−53805
Cs_2CO_3, proton irradiated, production of radioactive Sb and Te, annealing effects 2−68817
Cs_2CrO_4, proton irradiated, production of radioactive Sb and Te, annealing effects 2−68817
$CsNO_3$, proton irradiated, production of radioactive Sb and Te, annealing effects 2−68817
Cs_2SO_4, proton irradiated, production of radioactive Sb and Te, annealing effects 2−68817
Cu-Al alloy, exo-electron emission, interdependence with annealing processes 2−48011
Cu-C alloy, prep. by vac. deposition, rel. to microstruct. 2−56928
Cu-Cr alloy, internal friction and Young's modulus, after isochronal annealing 2−77633
Cu-Ni alloy, surface composition, Auger spectroscopy obs. 2−50440
Cu-(30 wt.%)Zn alloy, relax. of diffused Zn during short-range-ordering 2−77705
Cu, ion irrad. induced damage 2−47368
Cu, Mo fibre reinforced, internal friction obs. 2−56987
Cu, neutron irrad., effect on positron annihilation 2−75004
Cu, plastically deformed, positron annihilation, annealing temp. depend. 2−54123
Cu film, electroplated and vapour deposited, struct. rel. to annealing 2−77497
Cu foil recrystallization in a high voltage electron microscope 2−80825
Cu_2O, elec. conductivity, relationship in samples annealed at various temp. to activation energy 2−75092
Cu_2O, influence on near i.r. photocond. 2−47994

Annealing continued
  Cu_2O, recrystn. and grain growth kinetics 2−43788
  ^{163}Dy, grain growth 2−74667
  ^{170}Er, grain growth 2−74667
  Fe-Ni, ferromagnetic resonance line width, effect of Ni content after quenching or annealing 2−72174
  Fe-Ta alloy, at 700°C, initial softening 2−57020
  Fe-12.3 at.%-Al, Mossbauer determination of effect on short-range order 2−51311
  Fe, cast, precip. of spheroidal graphite 2−47584
  Fe, fast neutron irrad. at 77K, anneal hardening 2−80689
  α-Fe, irrad., radiation- and anneal-hardening 2−80681
  Fe plates, in dry H_2 atmosphere, effects on magnetic properties 2−81271
  p-GaAs:C ion implanted, carrier conc. and Hall mobility obs. 2−64986
  n-GaAs:S ion implanted, carrier conc. and Hall mobility obs. 2−64986
  n-GaAs:Si ion implanted, carrier conc. and Hall mobility obs. 2−64986
  GaAs:Si(Te), electron irrad., recovery stage obs. 2−47917
  GaAs-Cu, supersaturated solid solution, decomposition, dependence of Cu concentration on annealing time and temperature 2−83836
  GaAs, amorphous, thermoelec. power, cond., hopping cond., annealing effects 2−61312
  GaAs, ion implantation lattice disorder, low temp. channelling obs. 2−47373
  GaAs, strain induced phonon line broadening observed by surface reflection Raman scattering 2−83858
  GaP, 40 keV Te implantation damage and annealing 2−80706
  Ge, amorphous, thermoelec. power, cond., hopping cond., annealing effects 2−61312
  Ge, defects, formation and annealing during bombardment with Kr ions 2−71461
  n-Ge, disordered region prod. by 28 MeV electrons 2−47931
  n-Ge, electron irrad., annealing kinetics 2−47380
  p-Ge, electron irrad., conductivity obs. of defects 2−47377
  n-Ge, electron irrad., impurity depend. 2−47376
  n-Ge, electron irrad., impurity depend. of annealing, vacancy-interstitial pair effects 2−47379
  Ge, film, deposition and annealing parameters, influence on strain sensitivity 2−77709
  Ge, ion bombardment induced disorder 2−43466
  Ge, isothermal, migration energy of quenched-in defects, detn. 2−71536
  p-Ge, low temp. elec. irrad., Hall coeff. and cond. obs. 2−47381
  p-Ge, low temp. electron irrad., 220K defect, resistivity and Hall obs. 2−47928
  Ge, low temp. irrad., defect models, review 2−47375
  p-Ge, neutron irrad. effects, 77K 2−47930
  Ge, radiation defects 2−47383
  $Ge_{15}Te_{80}As_5$ semiconducting glasses, thermally induced surface and bulk electrical effects 2−68401
  HfB_2ZrN alloy, effect on microhardness and resist. 2−47638
  InSb, ion bombardment induced disorder 2−43466
  KBr, colour centre decay rel. to molecular $CO^{2-}{}_3$ centre formation, i.r. spectra obs. 2−71350
  KCl:Ca, Sr, X- irradiated, thermal annealing of defects 2−50696
  KCl:Sr, X-ray induced defects., absorp. and luminesc. obs. 2−64684
  KCl, colour centre decay rel. to molecular $CO^{2-}{}_3$ centre formation, i.r. spectra obs. 2−71350
  $KMgF_3$-$KMnF_3$ mixed crysts., electron irrad., single defect involving F-centre, prod. mechanism 2−68040
  LiF, rel. to disloc. loops and radiation colloids, elec. microscope obs. 2−74760
  Mg-(10.8 wt.%)Y alloy, ductility and high strength 2−47588
  Mg, neutron irrad., struct. damage and annealing 2−80683
  Mg, plane strain extrusions, texture control and yield anisotropy 2−80848
  MgO, hot-pressed, effect on elastic props. 2−50888
  MgO, hot-pressed, strength and fracture reln. to annealing rates 2−71589
  MgO, plastically deformed, pipe diffusion prod. of prismatic dislocation loops after annealing 2−64689
  MgO, self climb of dislocation loops 2−80672
  Mo, before and after neutron irradiation, physical mechanical properties 2−53730
  Mo, deformed, Young's modulus and Poisson ratio, annealing time and temp. depend. 2−84054
  Mo, neutron irrad., void formation during annealing, electron microscope obs. 2−77575
  Mo, room temp. ductility and intergranular cracking after annealing 2−53875
  Mo alloy TZM, sintered compact production, solid state reactions 2−56906
  MoS_2 layer struct., contact annealing effect on Hall data 2−54177
  NH_4NO_3 and ND_4NO_3, influence of sample listing on transition temps. of II→III, II→IV and IV⇄III transitions 2−50946
  $Na_2O.2SiO_2$ glass, annealing atmosphere effects on Na diffusion 2−53767
  Nb-O solid soln., form. of Nb_4O during decomp., annealing effects, 500-700°C 2−53902
  Nb-Zr-Ti alloy, supercond., struct. after low temp. annealing 2−50842
  Nb, cold-worked or neutron irrad., recovery, resist. study 2−64766
  Ni-Cr alloys, effect on mag. props. 2−44256
  Ni-Fe, f.c.c., domain struct. after different annealing treatments, Kerr effect obs. 2−78016
  Ni-Fe (50-50) alloy, mag. annealing effects 2−81241
  Ni-Fe alloy, sheets, heavily rolled, annealing textures, recryst. mechanism 2−74886
  Ni-P chemically deposited films, structure and elec. conductivity 2−77510
  Ni, condensate prod. by laser irrad. 2−53726
  Ni, electrolytic, changes in internal energy 2−43784
  Ni, electron irradiated, rel. to ferromag. after effect at 55K 2−78026
  Ni ceramic, refractory oxide particle growth, matrix density effects 2−68169

Annealing continued
  Pb-Sb(8 to 17%) alloy, influence of annealing temp. on thermal expansion 2−43995
  Pb, with Ag impurity, pore formation 2−71665
  $Pb_{1-x}Sn_xTe$ alloy, crystals grown by Bridgman technique, carrier conc. variation 2−53618
  PtSi film on single crystal Si substrate, thermal stability 2−71334
  SF_4, low temperature films, vibrational spectra and transitions 2−44381
  Se film, crystalline and amorphous, rel. to ion bombardment effects 2−60646
  p-Si:B, Li-compensation influence on irrad. defect form. 2−47390
  Si:In, ion implanted, photoelectromag. effect rel. to dose and annealing 2−72077
  Si:Li, electron irrad., luminesc., annealing and Li impurity effects 2−48229
  Si:P, implanted, resist. and Hall effect study 2−77594
  Si-Si_3N_4-SiO_2-Si structure, effect on elec. characts. 2−71984
  Si, amorphous film, dark-field electron microscope obs. 2−60593
  Si, amorphous film, dark-field electron microscope obs. 2−60593
  Si, effect on electronic properties of surfaces and atomic structure 2−72095
  Si, electron irrad., effect on recomb. luminesc. 2−48231
  p-Si, electron irrad., Hall coeff. and cond. study 2−71944
  n-Si, fast electron irrad., rel. to vacancy capture and transfer between defect complexes 2−80694
  Si, ion bombardment induced disorder 2−43466
  Si, ion irrad., divacancy formation and annealing, i.r. absorpt. study 2−71457
  Si, P-implanted, resist. and electron microscope study 2−64678
  Si films, amorphous, effect on elec. cond., 77-300K 2−61360
  α-SiC, residual lattice disorder due to ion bombardment 2−47391
  SiO_2 layers on Si, ion implant and annealing effects, ir abs. and ellipsometric meas. 2−74791
  SiO_2 on Ge, deposition and post-deposition treatments, interface C-U characts. 2−61402
  n-Si;Li, irrad., Li-defect interaction obs. 2−48293
  ^{154}Sm, grain growth 2−74667
  α-Sn, electron irrad., atomic displacement process evidence 2−53722
  α-Sn, electron irrad., damage production and thermal annealing, resist. study 2−80682
  Te, electron irrad. damage 2−47392
  TiN-VN particles, and nitriding effects on phase comp. 2−68202
  U, recrystallization after annealing and cold rolling at room temp. 2−68141
  UO_2 pellets, grain growth, long term obs. under annealing 2−49898
  V, condensate prod. by laser irrad. 2−53726
  V, neutron irrad., anneal and radiation hardening, tensile props. 2−80665
  V foil, quenched, vacancy detects, electron microscope obs. 2−71472
  W:K,Si,Al wire, incandescent lamp filament, working and process annealing 2−47590
  W, before and after neutron irradiation, physical mechanical properties 2−53730
  W foil, rolling and annealing textures 2−43796
  Yb films, f.c.c.-h.c.p. transform. 2−50952
  ZnSe, cathodolum., isochronal annealing characts. 2−61723
  ZrO_2, calcia stabilized, thermal stress induced microstruct. modifications 2−50901

Annihilation of electrons *see Electron pairs/annihilation*

Anodes
  see also Cathodes; Electrochemistry/electrodes
  adjustment, effect in low pressure discharges in transverse mag. field 2−74416
  in arc, electric, transpiration cooled, temp. determ. 2−83634
  conical, in X-ray tubes, construction and application 2−58674
  effect of changing surface on breakdown of Hg vapour 2−74436
  metallic, surface layer formation in electrolyte solution thermodynamics 2−68781
  spot, calc. of current density 2−74417
  CdS(Se), electron injection 2−61797
  Cs thermionic diode, diffused electronic and ionic current 2−45659
  Hg/Zn, in HgO/Zn cell, electrochemical reactions 2−84655
  ZnO, electron injection 2−61797

Anodic films *see Electrochemistry; Films, solid*

Antennas *see Electromagnetic waves/radiators*

Antiferroelectric materials
  see also Ferroelectric materials
  critical, phenomena, equation of state 2−84360
  $CsH_3(SeO_3)_2$, neutron struct. anal. 2−71428
  KH_2PO_4, molecular dynamics study and ferroelec.-antiferroelec. transitions by NMR and dielec. relax. 2−72032
  $NH_4H_2AsO_4$, EPR and ENDOR 2−68734
  $(NH_4)_2H_3IO_6$, n.m.r. level crossing expt. 2−61749
  $NH_4H_2PO_4$ long-wavelength polarization fluctuations 2−78113
  $Pb_{1-3x/2}La_xZr_{0.65}Ti_{0.35}O_3$, ferroelec. to antiferroelec. transition 2−57245
  $PbZnO_3$, internal electric field gradient by perturbed angular correlations 2−81156
  $SrTiO_3$, antiferrodistortive transition, fluctuation phenomena, e.p.r. obs. 2−84574
  $V_{0.95}Cr_{0.05}O_2$, orthorhombic, antiferroelec. displacements of cations 2−43592

Antiferromagnetic resonance
  biaxial antiferromagnet, coupled spin waves and magnon-magnon resonances 2−72457
  easy axis anisotropic crysts., freq. shift phenomena 2−81482
  magnetic impurity atom located between magnetic sublattices, effects 2−72458
  uniaxial magnet, linewidth phenomena, relax. mechanisms 2−81443
  $CoCl_2.6H_2O$, partially deuterated, sublattice coupling 2−54350
  CoF_2, 0 to 250 kOe, in [001] direction 2−68725
  CoF_2, orientational depend. 2−72460
  $CsMnF_3$, Neel pt. phenomena 2−68726
  EuTe, critical phenomena near Neel temp. 2−61728
  $FeBO_3$, above Neel temp., reson. absorpt. line obs. 2−72461

Antiferromagnetic resonance continued
$FeBO_3$, antiferromagnetic resonance in an ordered state, induced by external magnetic field over the Neel temp. 2−84558
$FeBO_3$, high-frequency obs. 2−72459
$GdAlO_3$, antiferroacoustic resonance and magnetoelastic coupling 2−72462
$KMnF_3$, canted antiferromagnet 2−84556
$LiCuCl_3.2H_2O$, crit. paramag. linewidth obs. 2−68727
Mg-Mn alloy, transition from e.p.r. 2−44438
MnF_2, fundamental relax. mechanisms, linewidth obs. 2−51398
MnF_2, linewidth phenomena, relax. mechanisms 2−81443
MnO, l.f. branch obs. 2−72463
NiO, l.f. branch obs. 2−72463
$RbMnF_3$, u.s. attenuation near Neel temp. 2−43975

Antiferromagnetism
see also Exchange interactions; Magnetic properties of substances/antiferromagnetic; Metamagnetism
antiferromagnetic-ferromag. transform., mag. moment oscill., mag. dipole radiation 2−78007
canted ferrimagnet, intrinsic biquadratic exchange and sublattice magnetizations 2−54346
chain, XY model in adiabatic approx., thermodynamic props. and magnetostruction 2−84439
critical neutron scatt., spin fluctuations 2−54361
critical spin dynamics, symmetry and conservation laws 2−54308
dimerized one quarter filled band Hubbard chain, antiferromag. semicond. behaviour 2−61177
domain structure in tilted mag. field 2−81306
easy plane anisotropy, additional absorpt. and parallel pumping 2−81308
e.p.r. linewidth, near crit. point in antiferromagnets with dipolar interaction 2−75341
e.p.r. linewidth and zero field relaxation time, crit. point anomalies 2−78159
exchange parameters, indirect of two-sublattice antiferromagnets 2−81299
f.c.c. type-2 ordering, stability and exchange constant calc. 2−61549
film, spin wave spectrum, calc. 2−81289
Heisenberg, bound spin waves 2−44234
Heisenberg chains, impure linear, spin correls. 2−48048
Heisenberg diluted system, transition temp. depend. 2−48046
Heisenberg magnet, two-dimens., with nearly continuous symmetry, low temp. behaviour 2−44288
Heisenberg magnet, two-magnon Raman scatt. at finite temp. 2−54431
Heisenberg magnet at infinite temp., two-time spin-pair correl. function 2−61548
Heisenberg model, insufficiency for polynuclear clusters 2−44294
Heisenberg model, linear chain, short range order effect on anisotropy 2−44295
Heisenberg model, principal susceptibilities, spin wave theory 2−65172
Hubbard model, cluster approach 2−44287
Hubbard model, disordered four point, thermodynamic properties 2−81300
Hubbard model, ground state energy 2−54291
Hubbard model, one-dimens., susceptibility at zero temp. 2−54303
insulator, phase transitions influence on light scatt. spectrum 2−54399
interacting electron model, ground state degeneracy 2−58806
Ising chains, finite, effects of a magnetic field 2−75235
Ising spin systems, property of zeros of partition function 2−44283
Ising-model metamagnet, high-temperature expansions study 2−54302
itinerant model, for transition metal alloys 2−44286
Kondo problem, renormalization-group techniques 2−81259
linear Heisenberg chain, study on basis of Fermi representation 2−81298
magnon localization, rel. to impurity conc. 2−44284
magnon model, Goldstone theorem 2−75236
magnon parametric instability due to three-magnon processes 2−48050
magnon scatt. in Raman scatt., four-magnon excitation 2−54433
metal-nonmetal transition, two-band model in Hartree-Fock approx. 2−57307
non-Heisenberg magnet, exchange interaction effects 2−72133
one dimensional spin chain, instability in mag. field 2−65173
one-band model, const.-coupled, with finite site number, exact eigenvalues 2−54305
one-band model, spin waves in spin density wave ground state 2−68563
phase transition in uniaxial magnet of finite dimensions 2−72208
phase transitions, model studies 2−58798
polaron, self-trapped, T=0 K, theory 2−71812
quasi isotropic layer-type magnets, zero-pt. spin deviation effects on perpendicular susceptibility 2−51275
s-d exchange model of weak ferromagnetism 2−81257
semiconductor, canted, s-d model, magnetization curve 2−81309
slow e.m. wave propagation, near transition to ferromag. phase 2−54347
specific heat anomalies due to simultaneous effects of exchange and mag. fields, low temp. 2−57308
spin lattice systems interacting through arbitrarily many-body and indefinitely-long-range interactions 2−54298
spin systems with mixed ferro- and antiferromag. coupling, crit. temps. 2−65131
spin wave and exciton density of states 2−51276
spin wave theory, two sublattice model, algebraic realization 2−44237
spin waves and generalized susceptibilities for classical models 2−44269
spin waves theory and coherent potl. approx. applic. to mag. excitations 2−78044
split band antiferromagnetic state, Hubbard model, correlation effects 2−57117
superantiferromagnetism, lattice model 2−72206
superconductivity in s-d exchange model, effect of localized magnetic moment 2−47840
superexchange models based on factorization of orbital matrix elements 2−48103

Antiferromagnetism continued
superexchange ordering of degenerate orbitals and mag. structure of crysts. with Jahn-Teller ions 2−68565
transition element oxide glasses, amorphous antiferromagnets, absence of ordering 2−81301
transition from nonuniform to uniform state, in an inclined field 2−72210
two-dimensional magnet, phase transition 2−68566
two-dimensional magnet, spin-wave spectrum, temp. depend. 2−44240
Cr, spin wave theory 2−61555
$FeTiO_3$, Mossbauer spectra below Neel temp. 2−57330

Antimony
amorphous and cryst., Raman spectra 2−68665
determination, in Sn-Pb alloy, atomic absorp. spectroscopy obs. 2−78218
diatomic molecule, vibrational and rotational analysis of B→X system 2−50068
diffusion, in Ge, influence of In concentration gradient 2−71516
diffusion in Bi-Te unitcrystals as function composition 2−68051
diffusion in Pb, temp. depend., 188-315°C 2−77617
diffusion in Si, enhancement by proton irrad., dose rate effects 2−80707
diffusion in Si epitaxial film, temp. and dislocation density depend. 2−74816
electron diffusion through shock wave front 2−71771
etch pit orientation determination 2−47187
impurity in Ge, absorption and movement of melted zone in the solid phase 2−83892
in pig iron, neutron activation analysis, spectral method 2−78215
liquid, diffusion of Tl 2−46945
liquid, effective interionic pair potentials, calc. from structural diffraction data 2−50312
macroblock formation in crystals grown from melt, estimation of transverse dimensions 2−50683
Mossbauer effect of ^{119}Sb, ^{119}Sn valence state obs. 2−54392
polymorphic transitions, press.-induced, and supercond. phase 2−44058
powder, Raman effect 2−81383
radioactive Sb produced in Cs compounds by 660 MeV p irradiation 2−68817
single crystal piezoreflectance obs. and rel. to optical interband transitions 2−65213
thermal expansion, coeffs., anisotropy, 2-30K, 55-90K, and at 283K, Gruneisen parameters 2−77784
u.s. shear wave, circularly polarized, attenuation and vel. in magnetic field 2−47789
Young's modulus and Poisson's ratio, orientation depend. 2−74821
Cd, Sb-doped, pore formation on annealing 2−71665
GaP:Sb, recomb. radiation involving isoelectronic centres 2−72407
Ge:Sb, electron irrad., phonon scatt. and induced energy levels, thermal cond. obs. 2−47766
Ge:Sb, heavily doped, temp. depend. of resist. 2−71940
Ge:Sb, photocond., monochromatic submillimeter radiation 2−81180
Sb-Cs photocathode study using scanning electron diffraction system 2−75195
Sb VII, e.u.v. spectra, energy levels 2−64001
$Sb_4 \rightleftharpoons 2Sb_2$, heat of reaction, and heat of sublimation of Sb_3 2−72554
Si:Sb, cond. band, deform. potential const. from piezospectroscopy of donors 2−68438
Si:Sb, ground state wavefunctions of shallow donor electrons, Fermi contact consts. 2−71950
Si-Sb compressed composite, obs. of neutron energies in range 13-15 MeV 2−59633

Antimony compounds
— 2−72233
group V_2VI_3 semiconductor, Mossbauer effect of ^{121}Sb and ^{125}Te nuclei 2−75274
group V double and triple chalcogens, n.q.r. of ^{75}As, ^{79}Br, ^{81}Br, ^{127}Sb, ^{123}Sb, ^{127}I, ^{209}Bi 2−48311
group V-VI-Vii semiconductor, Mossbauer effect of ^{121}Sb and ^{125}Te nuclei 2−75274
$As_xSb_{2-x}Se_3$, amorphous and crysts., threshold and memory switching 2−77883
$3As_2Se_3.2Sb_2Se_3$ films, amorphous, elec. props., band struct. 2−54187
$3As_2Se_3.2Sb_2Se_3$ films, amorphous, band. struct., optical props. 2−54186
$1-xAs_2Se_3.xSb_2Se_3$ semiconductor system, devitrification characs. 2−71286
Bi-Sb alloy, 5-100% Sb, Mossbauer effect of ^{121}Sb, 80K 2−81345
Bi-Sb alloy, antimony concentration, radiactivation determination 2−81554
Bi-Sb alloy, band edge parameters, calc. 2−75027
Bi-Sb alloy, for magneto-thermoelec. and thermomag. cooling, props. 2−75161
Bi-Sb alloy, thermomag. props., rel. to device appl. 2−59064
Bi-Sb alloy, transport effects, effects of Ag, In and Pt addition 2−71896
Bi-Sb alloys, pressure-temp.-comp. diagrams 2−68192
Bi-Sb low-concentration alloy, band structure study using cyclotron resonance 2−47807
BiSb alloy, interband breakdown, voltage instabilities in electron-hole plasma 2−81095
$Bi_{88}Sb_{12}$, mag. susceptibility, effects of SN and Te impurities 2−72109
$Bi_{92}Sb_{08}$, dc-pumped, line narrowing of microwave radiation caused by nuclear electric quadrupole transition in ^{209}Bi 2−44403
$Ce_xY_{1-x}Sb$, $Ce_xLa_{1-x}Sb$, antiferromagnetically ordered, Neel temp. dependence on lattice constants 2−72212
Co-Ni-Sb system, intermetallic cpds., X-ray diffr. study 2−43940
Cu-Sb alloy near 20 at.% Sb, long period superstruct. with hexagonal symmetry 2−71430
Fe-Ga-Sb and Fe-Sb systems, constitution and mag. props. 2−64821
Fe-Sb alloy, molten, paramag props. 2−80488
Ga-Sb system, solid and liq., constitution and mag. props. 2−64820
Ge-Sb system, struct. and alloy chem. of metastable GeSb 2−47329
Hg-Sb amalgam, dil., viscosity, comp. depend., 0-100°C 2−64451

Antimony compounds continued
In_2Se_3-Sb_2Te_3 system, phase diagram, intermediate cpd. formation 2−61048
Mg-Sb amorphous alloy, exciton screening 2−78115
MnSb-(Sb,Bi) and MnSb-(Sb,Sn) eutectics, morphology, growth rate effects 2−47641
Ni-Sb system, intermetallic cpds., X-ray diffr. study 2−43940
Pb-Sb alloy, precip. mechanism, hardness, resist. and microscopy studies 2−80858
Rh-Mn-Sb system, Cl_b type alloy, mag. props. and cryst. struct. 2−65156
Sb-As(Ge) alloy, etch pit orientation determ. 2−47187
Sb-Bi alloy system, cryst. growth rate, diffusional supercooling theory 2−53613
Sb-Bi alloys, band struct., magnetoreflection obs. 2−54405
Sb-Bi solid soln., thermomagnetogalvanic props. 2−54245
Sb-Ge-I-S glass system, glass forming regions 2−80533
Sb-Se-I-R-H_2O system, R=solvent=HI, HCl, Na_2Se, hydrothermal crystn. process, 300-450°C 2−74682
Sb-Se system, phase separation 2−60591
Sb-Sn-Zn system, heats of mixing, 650°C 2−43336
Sb-Sn alloy, liq., determ. of interdiffusion coeffs. 2−53415
Sb-Sn alloy, peritectic crystn., pore form. 2−53906
Sb complex, methyltrichloro(acetylacetonato)antimony(V), molecular structure 2−42935
Sb_2Ae_3 film, amorphous, prep. and optical props. 2−53576
2 $SbCl_3$ with naphthalene, nuclear quadrupole resonance, temp. dependence of resonance frequencies 2−84587
$SbCl_6^-$, force constants determ. from frequency data using general valence, orbital valence and Urey- Bradley force fields 2−42934
$SbCl_3(Br_3)$, molecular vibr. freq., isotope effects 2−80022
SbF_5, gas phase Raman spectrum, evidence for trigonal bipyramidal shape of monomeric species 2−50067
SbI_3, $SbI_3.3S_8$, Mossbauer effects, of ^{129}I, bond character 2−78071
$SbNbO_4$, hydrothermal growth and ferroelec. props. 2−72037
Sb_2O_3, valentinite and senarmontite polymorphs, crystalliz. under hydrothermal cond. 2−74683
Sb_2S_3, electrical conductivity, temp. dependence, change of colour 2−54160
Sb_2S_3, enthalpy and entropy of vaporization 2−74595
Sb_2S_3, liquid, switching effect 2−60503
Sb_2S_3, liquid semiconductor, switching, thermal breakdown mechanism 2−81096
Sb_2S_3, u.s. absorpt. and vel. 2−80914
Sb_2S_3 film, single cryst., optical absorp. edge obs. 2−81390
SbSBr, i.r. transmission, indirect transitions and band gap determ. 2−72346
SbSI:Sb_2S_3, prep., spontaneous polarization, dielec. permittivity, photocurrent, dark current rel. to phase transition, −50-50°C 2−75143
SbSI, boson echos obs. 2−65071
SbSI, critical light scatt. phenomena 2−61612
SbSI, effect on absorp. edge, electro-optic effects on absorp. edge 2−81379
SbSI, far i.r. reflectivity, complex dielec. const. deriv., soft mode in paraelec. phase 2−61619
SbSI, ferroelec., electrostriction, piezoelectricity, and elasticity 2−54240
SbSI, ferroelec., p-T phase diagram rel. to critical point 2−72038
SbSI, ferroelec. semicond., photoelec. e.m.f., temp. depend. 2−72078
SbSI, ferroelec. semicond., influence of nonequilib. carriers on domain struct. 2−72036
SbSI, ferroelec. semicond., photoluminescence of single crystals 2−72443
SbSI, ferroelectric, one dimensional mech. stress effect on phase transition, permittivity obs. 2−75155
SbSI, paraelec. region, voltage-current characts., illumination effects 2−81163
SbSI, phase transition, illum. and rate of coding depend. 2−47986
SbSI, Seignette semicond., thermal currents induced by light 2−72039
SbSI, semicond. ferroelec., trapping levels, thermally stimulated photocurrents obs. 2−75154
$Sb_2S_3(Te_3)$, Mossbauer effect of ^{119}Sb, ^{119}Sn valence state obs. 2−54392
Sb_2Se_3-As_2Se_3 glass, e.s.r. and X-ray studies 2−61734
Sb_2Se_3-SbI_3 system, phase diagram 2−43942
$Sb_{1-x}Se_x$ film, amorphous, photocond. spectral response rel. to comp. 2−81167
Sb_2Se_3, amorphous, density of states at quasi-Fermi level from photocond. 2−81167
Sb_2Se_3, electron energy states for amorphous and cryst. material 2−68627
Sb_2Se_3, polycryst., threshold and memory switching 2−77883
Sb_2Se_3, Sb_2Se_3-Bi_2S_3 alloy, switching behaviour 2−75096
Sb_2Se_3, semicond. liq., Hall effect 2−60498
Sb_2Se_3 film, amorphous, optical and transport props. 2−61323
SbSi, naturally polarized crysts., photodomain effect on illumination 2−77940
Sb_2Te_3-Bi_2Te_3, efficiency criterion for thermogenerators 2−75158
Sn-Sb alloy, unidirectional solidification, uniaxed crystal origin 2−74882
Sn-Sb alloys, liq., interdiffusion coeffs. 2−50349
SnO_2-SbSI, dielec.semicond. junc., memory and switching effects 2−61366
Te-Se-Sb glass, memory type, thermal effects 2−71917
$TlSbS_2$, thin films on NaCl, determ. of cryst. struct. 2−80564
U-Sb alloys, liq., thermodynamic props., 1130°C 2−56497
Antineutrinos *see Neutrinos and antineutrinos*
Antineutrons *see Neutrons and antineutrons*
Antinucleons *see Nucleons and antinucleons*
Antiparticles *see corresponding particle*
Antiphase domains *see Alloys; Crystal structure/microstructure; Solids/structure*
Antiprotons *see Protons and antiprotons*
Antireflection coatings *see Films, solid/optical properties*
Apodization *see Optical images*
Apparatus *see Cosmic rays/apparatus; Instruments; Ionosphere measuring apparatus; Laboratory apparatus and technique; Radioactivity measurement/apparatus; Vacuum apparatus; X-ray crystallography/apparatus. Further entries describing apparatus for specific purposes are included under the headings of the appropriate subjects*
Appearance potential *see Ionization potential*
Architectural acoustics
see also Echo; Noise abatement; Reverberation; Transmission/acoustic waves
absorption coefficient, field measurement by reflection technique 2−41723
airborne sound insulation in buildings, standardization of measuring techniques 2−52251
Blossom Music Centre, design and performance 2−41829
complex shaped enclosures, natural modes and frequencies 2−73451
concert halls, recording studios, acoustic modelling techniques 2−82348
curved partition sound transmission props. 2−45548
facade walls, insulation from external noise with balconies and loggias 2−63137
hall, large, scale model studies 2−45550
hall, light-construction, sound propag., reverberation and refl. 2−45552
hall, one-dimens., model obs. 2−45555
high rise buildings, noise due to external air flows 2−63136
image method for calc. of sound pressure levels within rectangular room 2−55558
impulse response of room, audibility of small changes 2−52250
industrial room models, noise propag. 2−45546
interference pattern method for meas. reflection from uneven surfaces 2−69740
landscaped office, sound masking obs. 2−41832
landscaped office ceilings, performance of various configurations for speech attenuation 2−41834
lecture room audio equipment 2−45544
New NHK Hall Japan, computer aided design of shape, calculation of acoustical conditions using scale model 2−82357
noise in study offices, meas. for improving acoustic comfort 2−45556
office landscape ceilings, specifications 2−41833
open plan offices, reverberation time measurement, equipment 2−58931
open-air theatre, multiple echo reflectors 2−45551
panel, influence of measuring facility on measured sound insulating property 2−63131
panel struct., directional props. of sound insulation 2−45547
parallelepipedic auditoria, optimal sound distrib. 2−45559
partition walls, porous absorber materials, influence of structural stiffness, attenuation on sound insulating efficiency 2−41827
prefabricated sound absorbing modules 2−45558
reduction index and boundary conditions for wall between rectangular rooms 2−55556
reduction index and boundary conditions for wall between rectangular rooms 2−55557
resonator with impedance wall 2−69777
reverberant hall, electroacoustic equipment influence on speech intelligibility 2−45557
reverberation curves simulation in rectangular rooms with diffuse sound field 2−55555
rooms, obs. using vibrations of strings and thin plates, warble-tone excitation 2−78910
rooms with interconnecting services, obs. of sound transmission using statistical energy anal. 2−41830
sharp and soft initial sound in music rel. to delayed architectural reflections 2−55559
sound studios, digital control meas. for automation 2−58928
synagogue design requirements 2−41828
for TV and radio studios, book45545 2−45545
wall opening, directivity pattern of sound radiation 2−45549
wall-recovering for controlling acoustic quality in domestic apartments 2−45553
Arcs, electric
a.c., current chopping during extinction 2−74452
a.c., design of cylindrical arc 2−60322
a.c., wall stabilized, current zero behaviour 2−71056
a.c., wall stabilized, current zero behaviour 2−71057
air plasma, electrical conductivity and total radiant power 8000 to 12500 K 2−71061
anode, porous, transpiration cooled, temp. determ. 2−83634
anodic spot, growth kinetics 2−60319
atmospheric, a.c. constricted horiz. column motion due to buoyancy 2−71051
auroral, stable, red, obs. from OV1-10 2−65896
cascaded, electron temp. and density meas. using scattered laser light 2−53260
cathode erosion, displacement of arc support points 2−80367
cathode sheath, thermal reignition 2−74450
cathode sleeve, double arc phenomena 2−56400
cathodic contact erosion due to gas breakdown arcs 2−43223
charged particle loss processes in arc plasma 2−67681
cold cathode, model of cathode phenomena, dynamic field emission 2−71059
constant press. axial flow, local convection effects 2−74351
convection dominated, temperature profile 2−71062
current-voltage characteristics, approx. solution of Elenbaas-Heller equation 2−64362
d.c., disc stabilized, and solution nebulization device, for multicomponent plasma obs. 2−64300
d.c., free-burning, up to 2160A, plasma velocity distrib. meas. 2−60320
deformation and cut-off model for arc in transverse magnetic field 2−60321
diameter in air blast interrupter nozzle at 45000 A 2−71053
discharge growth on polluted insulating surfaces, theor. anal. 2−83635
electron temperature, current dependence and shape of volt-ampere characteristic 2−53263
gas fed, hollow cathode, theoretical evaluation 2−74453
graphite, electrode temps. and reignition characts. 2−50236

Arcs, electric continued
- high current, free burning 2−71054
- high current, in narrow tube, spectral obs. 2−74414
- high current, Schlieren techniques 2−64360
- high-current, diffusion model of near-cathode region 2−74448
- high-current discharge for optical pumping of continuous-wave lasers based on ionic crystals 2−55703
- hollow cathode arc discharges as dense plasma source 2−74384
- hollow cathode discharge, metastable atom production rel. to glow discharge 2−74211
- i.r. laser heating of dense electric arc plasma 2−43148
- jet material ablation studies, channel test device 2−53313
- lamps, high intensity, selection for particular application and construction 2−76538
- low voltage, effect of sheaths on I-V characteristics 2−71052
- metal chloride molecular discharges, thermodynamic and kinetic considerations 2−64354
- MEVARC, sready-state and post-arc spatial temp. distrib. obs. 2−71060
- modelling based on Mayr and Cassie equations 2−64361
- Penning source, formation position of ions, dependence on mag. field 2−53262
- plasma, anode flowing, with external axial anodic mag. field 2−71002
- plasma, d.c., column, frequency-rotation function, in approx. by rigid conductor 2−60221
- plasma, d.c., Na diffusion, obs. using intensity distrib. of emitted light 2−60211
- plasma, d.c., rise time to stationary state 2−60222
- plasma, effect of reaction energies on radial temperature distribution 2−53261
- plasma, electron density alteration effect on temp. distribution 2−46726
- plasma, in curved discharge tube, computer simulation 2−53173
- plasma arc, magnetized, h.f oscills., obs. using h.f. Stark effect 2−70942
- plasma characteristics, chemical reaction effects 2−50237
- plasma sprayed coating, variables influencing characteristics, review 2−53562
- power arcing, contact materials in switching devices 2−74454
- pulsed plasma arc lamps, transmittance measurements 2−83643
- pulsed vacuum, energy distributions of ions from anode plasma 2−46803
- quartz Hg lamp, far i.r. emission 2−55766
- recovery strength, influence of stability 2−60323
- refractory electrode region recovery, effect of arc gas 2−74451
- research at Culham laboratory 2−74446
- retrograde motion of cathode spot and heat conduction 2−71003
- spectrochemical trace analysis in arc plasmas, use of external magnetic fields 2−51477
- spot welding, electrode fault-free life 2−69479
- square wave power pulses, transient parameter calculation 2−67696
- stable, short time burning, calc. of current density in anode spot 2−74417
- stationary atomic distribution in column with axial plasma injection 2−74447
- stationary cathodic arcing in vacuum 2−43221
- in steady, laminar, longitudinal flow 2−71055
- thermionic converters, arc mode, influence of collector material work funct. 2−49281
- thermionic emission converter, arc mode, nonequilibrium electron distrib. funct. 2−49275
- thermionic emission converter, transient pressures, during ignition and quenching 2−52377
- in thyratron, arc pot. obs. in H pulse discharges 2−56399
- Townsend-Huxley propagation in E × B direction 2−74455
- trace element analysis in arc plasma, spectral line intensity depend. on magnetic field 2−48356
- triggered vacuum gap for initiating arcs in vacuum 2−43222
- vacuum, cathode region, gasdynamics problems 2−77309
- weld pool stability, study using gas-liq. interface analysis 2−43224
- welding, conduction, acoustic vibrations effect 2−71050
- welding, heat content and size distrib. of electrode metal droplets 2−69483
- welding, square wave current pulses 2−69480
- Xe 50 KW short arc lamp in elliptical collector 2−76540
- He, atmospheric, determ. of thermal conditions in asymptotic region by spectroscopy and using equilibrium flow model 2−77317
- N_2, atmospheric, determ. of thermal conditions in asymptotic region by spectroscopy and using equilibrium flow model 2−77317
- Ar, atmospheric cascade, electric field intensity and wall heat transfer meas. 2−46804
- Ar, cw breakdown using 10.6 μm laser radiation 2−60313
- Ar, high pressure, column electric fields 2−71063
- Ar, non local thermodynamic equilibrium, electron densities $<5 \times 10^{16}$ cm^{-3} 2−77306
- Ar arc lamp 400 KW for solar simulation 2−78414
- Ar discharge, investigation at 950 atm. 2−67662
- Ar discharge tube, d.c. constricted horiz. column motion due to buoyancy 2−71051
- Ar luminescent-arc discharge, meas. of OH rotational temperature 2−43210
- Ar plasma, near thermodynamic equilibrium, stationary and relaxational props. 2−60223
- Ar plasma, stabilized, cylindrical, emission line profile 2−64307
- Ar + H_2, plasma, stabilized, cylindrical, emission line profile 2−64307
- C, d.c., in air, in ext. mag. field, electron temp. from line intensities 2−50238
- C, d.c., line intensity, effect of mag. field, 230-790 Oe 2−49943
- C, high current, electron temp., Thompson scatt. obs. 2−64363
- Cs, low voltage discharge, excitation and ionization processes 2−53265
- Cs, low voltage discharge, Maxwellization of precathode electron distrib. fn. 2−53264
- Cs, thermionic converter, low vapour pressures, arc mode 2−52376
- Cs thermionic convertor, ion loss and electron temp. 2−80369
- Cs thermionic diode, ignited mode, charge influence of V-I characteristics 2−52378
- Cu, d.c., line intensity, effect of mag. field, 230-790 Oe 2−49943

Arcs, electric continued
- Cu, free burning with 1-15A current, atom population and electron concentration 2−71064
- Cu alloy, point-to-plane Uni-Arc excitation, effect of extraneous materials 2−56398
- Cu electrodes, current density and behaviour of cathode spots 2−71058
- D_2 lamp, recalibration of spectral radiance in near u.v. 2−79450
- H_2, rotating helical, arc diameter 2−74449
- He, atmospheric cascade, electric field intensity and wall heat transfer meas. 2−46804
- He, atmospheric pressure, spectroscopic intensity measurement 2−43225
- He plasma with superposition of h.v. pulse, interaction giving 2 to 40 GHz radiation 2−50212
- Hg-Ar, cathode spaces, influence of cathode qualities 2−60324
- Hg axially uniform column, arc chopping 2−70995
- Kr lamps, influence of gas pressure on pumping efficiency of cw garnet laser 2−42072
- N, cylindrical, radiative energy balance 2−67697
- N_2, atmospheric cascade, electric field intensity and wall heat transfer meas. 2−46804
- N_2 plasma, disequilibrium effects 2−70898
- Na vapour, high pressure, radial temp. distribution 2−71065
- SF_6, gas-blasted in nozzle, voltage distribution 2−71066
- SF_6 gas flow, temp. profile around arc column 2−71049
- SF6 decomposition, current interruption, gas circuit breakers 2−74489
- Xe arc lamp, stability tests 2−45813
- Xe lamps, influence of gas pressure on pumping efficiency of cw garnet laser 2−42072
- Xe radiation source, short arc, high reliability and power for solar simulation 2−76535

Area measurement
- γ-Al_2O_3, specific surface area meas. 2−64548
- N adsorption and use of Harkins and Jura isotherm 2−58686

Area measurement, porous substances *see Surface measurement*

Argon
- 4W laser, photocoagulation therapy; retinal diseases, design and construction, clinical results 2−82018
- — 2−67435
- absorbed He atom mobility near 2K 2−67920
- absorption coeff. of spectral lines in wall stabilized arc at atmos. press. 2−70575
- adsorption, on Xe crystal edges and vertices 2−47174
- adsorption of H at 4.2K 2−50539
- adsorption of He monolayer, calc. of heat of adsorption and band widths 2−43490
- afterglow, benzene $^1B_{2u} \to {}^1A_{1g}$ emission obs. 2−70747
- afterglow plasma, diffusion cooling 2−56336
- afterglow plasma, magnetic field errors in supported spherator 2−50205
- arc, atm. cascade, electric field intensity and wall heat transfer meas. 2−46804
- arc, non local thermodynamic equilibrium, electron densities $<5 \times 10^{16}$ cm^{-3} 2−77306
- arc discharge, investigation at 950 atm. 2−67662
- arc lamp 400 KW for solar simulation 2−78414
- arc plasma effect of reaction energies on radial temperature distribution 2−53261
- atom, Auger electron spectroscopy, comparison of exptl. and theoretical intensities, condition for non-isotropic emission 2−42756
- atom, autoioniz. by slow electron impact 2−74229
- atom, collision with ^{7}Li, absolute total scattering cross sections, derivation of interatomic potential 2−49968
- atom, collision with $AlCl_3$, molec. orbital study 2−59990
- atom, collision with H^+ at 5 eV, interatomic potential determination by inversion of elastic differential cross section data 2−59930
- atom, collisions with H^+ at 4 keV, probability ratio for neutralization of H^+ to H(2p) or H(1s) 2−42802
- atom, densities of generalized oscillator strengths 2−52912
- atom, elastic scatt. of H^+, excited states 2−64051
- atom, elastic scattering of Au^0, 5-90 eV, determ. of interaction potential 2−56114
- atom, electron impact cross sections 2−49962
- atom, electron impact excitation function from threshold to 200 eV for formation of metastable states 2−70640
- atom, electron impact ioniz., slow electron obs. 2−64033
- atom, ionization cross sections for high-energy electrons and positrons 2−70598
- atom, ionization in slow collisions with He and He^+, meas. of energy spectra and angular distribs. of ejected electron 2−56119
- atom, metastable, deexcitation in collisions with gases, cross sections 2−64054
- atom, metastable, dissoc. collision with H_2O, rotational excitation of $OH(A^2\Sigma^+, v'=0)$ 2−64215
- atom, outer s shell role in single ioniz. by electron impact 2−67399
- atom, relative transition probabilities meas. by optical absorption 2−64012
- atom, resonance absorption and fluorescence 2−52933
- atom, scattering of K^+, 150-2350 eV, effective total cross section meas. 2−67415
- atom, small angle electron impact spectra, optical sums 2−70612
- atom scattering of inert gas and period II element ions in 8-25 keV range, comparison of exptl. and theoretical interatomic potentials 2−56118
- atom-electron impact ionization, double and triple differential cross-sections 2−74246
- atomic beam, scatt. from W surface 2−47084
- atomic collisions with N_2 and O_2, Lennard-Jones potentials determ. 2−56272
- atoms, collisions with Mg atoms causing broadening and shift of Mg spectral lines 2−70588
- atoms, multi-level initial ionization behind strong shocks and average atom-atom cross sections for excitation and ionization 2−67398
- binary mixture with methane, ultrasonic absorption meas. of rotational relaxation time 2−64219
- breakdown, by 0.35μ picosecond laser pulse 2−60314
- breakdown, laser-induced, electron cascade theory 2−60312
- breakdown at low pressure, study using Townsend theory 2−71037

Argon continued
- Burnett apparatus for accurate determination of gas compressibility and second virial coefficients 2−56439
- collisions with H^-, He^-, determ. electron detachment cross sections, 4-30 keV 2−77017
- compressed, complete spectrum of collision-induced light scattering analysed using Michelson interferometer 2−80408
- crystal, ideal tensile and shear strengths computer calc. 2−77630
- crystal, stability and mode of fracture of highly stressed ideal crystal 2−77631
- crystal data application to testing Kihara intermolecular potential 2−70811
- diffusion, in B_2O_3 glass, mass spectrometery obs. 2−53758
- diffusion in rocks, det. of source material for ultramafic minerals 2−65583
- dilute gas viscosity coeffs. and second virial coeffs. using various interatomic potential models 2−64393
- discharge, hollow cathode, electron density obs. 2−70988
- discharge, hollow cathode, electron temp. and density profiles 2−77307
- discharge, hollow cathode, excitation mechanisms, electron and ion temp. and density 2−77308
- discharge, motion of ionization front in microwave e.m. field 2−60238
- discharge, noise temperature variation with mount style, meas. at 147 MHz 2−60304
- discharge, pulsed, in cylindrical magnetron diode, spectral obs. 2−71007
- discharge, radial distrib. of temp. and density of charged particles 2−50228
- discharge, self excited striations in tube of varying diameter 2−71012
- discharge tube d.c. arc constricted horiz. column motion due to buoyancy 2−71051
- elastic scattering for slow positrons 2−70644
- energy loss and straggling of 6.05 and 8.78 MeV α-particles, meas. using Si surface barrier detector 2−79626
- fluid around critical point, density fluctuations in microscopic volumes 2−56539
- freejet plasma, nonequilibrium effects, shock wave duration 2−70900
- gas, cw breakdown using 10.6 μm laser radiation 2−60313
- gas, electron momentum transfer cross section from Boltzmann eqn. 2−83708
- gas, intermolecular potential energy functions determ. from viscosity meas. by new iterative method 2−64206
- gas, pulsed with 10.6 μm laser radiation, gas breakdown thresholds 2−83707
- gas discharge, low pressure type, properties 2−71011
- gas laser second harmonic generation, 5145 Å 2−49358
- gaseous and liquid behaviour, prediction from adapted van der Waals eqn. of state 2−71109
- high gain neutral laser lines in pulsed discharge 2−41979
- high pressure arcs, high pressure, column electric fields 2−71063
- ideal tensile strength, relationship to surf. energy, expt. 2−64721
- ion bombardment of Al films, transmission sputtering and recoil implantation 2−54090
- ion ring laser, meas. of mode-competition discriminant 2−59141
- ionization by electron impact, efficiency curves 2−59921
- ionized, steady state electron mean energy between parallel plates 2−43201
- ions, 5-30 keV, correlated successive collisions on Cu, Ge, Si, ion scatt. processes 2−47775
- ions, irrad. of semicond., cond., noncond. targets, secondary ion emission 2−48029
- ions, irrad. of Si surface, damage, change in optical consts., ellipsometric obs. 2−47081
- ions, multiply ionized, laser oscill. in Z-pinch discharge 2−49352
- ions, range-energy relations in Ar, N_2, O_2 and air, 0.3-1.0 MeV 2−79917
- ions, scatt., multiple, by C and Ge foils 2−47781
- ions, scatt. from solid surface, surface analysis technique 2−47072
- isotope separation factor between liq. and vapour 2−80521
- laser, 4880 Å output, scintillation obs. using ground- aircraft path 2−81682
- laser, c.w., characteristics 2−49357
- laser, c.w., metal tube plasma container 2−63321
- laser, electron temp., meas. using Al double probe system 2−74349
- laser, frequency stabilization 2−41990
- laser, molecular-beam-stabilized, 5145 Å 2−79185
- laser, oscill. quenching model, collisional and deexcitation processes 2−59143
- laser, single frequency, with absorbing film, spectral characteristics 2−42036
- laser lights attenuation charact. in water 2−76512
- light distortion, freq. dependence 2−50273
- liquefied, maximum coefficient of heat transfer 2−83788
- liquid, bulk viscosity, temp. depend. 2−74526
- liquid, dynamics from first moments of coherent neutron scattering function 2−46922
- liquid, electronic detection of ionizing particles, spark chamber 2−73955
- liquid, Kerr effect induced by fluctuational statistical processes 2−46955
- liquid, memory effects and dynamical correlations 2−60416
- liquid, neutron scatt., coherent- and incoherent-scatt. laws 2−67798
- liquid, next-neighbour distribs. 2−64432
- liquid, struct., radial distrib. function anal. 2−83764
- liquid, transport coeffs., derived from mol. mechanical model 2−71187
- liquid, velocity autocorrel., memory function 2−64433
- liquid, v.p. rel. to surface tension and surface curvature 2−46943
- liquid doped with ethylene, absorption spectra 2−46603
- low pressure discharge, self excited running layers and noise phenomena 2−43209
- luminescent-arc discharge, meas. of OH rotational temperature 2−43210
- lunar atmosphere, density and flux distrib. 2−66156
- metastable atoms, time-of-flight technique for detection 2−79878
- MHD plasma in Cs seed, stability 2−80262

Argon continued
- molecular beam, produced by multichannel source, speed distrib. meas. 2−50018
- molecular cluster fragmentation, detection with time-of-flight mass spectrometry 2−42870
- monolayer, binding energy of ^3He and ^4He, low temp. 2−43493
- multiwire chamber filled with Ar-ethylbromide mixture 2−70291
- non-ideal reference system, virial expansion, chain approximations, applic. 2−55436
- optical breakdown, formation of non-stationary radiation driven detonation 2−80377
- overlayer on Al or Sn film, depression supercond. transition temp. 2−61228
- partially ionized, heat transfer in laminar flow in pressure of transverse mag. field 2−53298
- photo-ion drift vel., diffusion coeffs. and temps. 2−64339
- photoionization by X-rays, relative abundances of multiply charged ions 2−53245
- physical adsorption on porous Ag, onset of Henry's Law 2−60674
- plasma, backscattering of electrons, Monte Marlo simulation 2−70892
- plasma, collisionless, nonlinear coupling of ion acoustic waves 2−80319
- plasma, continuous radiation, h.p. 2−43117
- plasma, continuous radiation, influence of lowering of ioniz. energy 2−70911
- plasma, dynamics of inverse pinch 2−56358
- plasma, e.f. waves, mode-coupling 2−70958
- plasma, electrical conductivity using average-gradient and tuned-circuit-Q method 2−56386
- plasma, electron thermal conductivity temperature dependence 2−60263
- plasma, electron-neutral collision freq. near Ramsauer minimum 2−74354
- plasma, Faraday ring currents in low-pressure ring-shaped duct with radial mag. field 2−60219
- plasma, flowing, anode heat transfer at elevated temp. 2−67626
- plasma, high pressure, radiation capacity det. 2−64260
- plasma, high-pressure thermal, use as high-radiance standard 2−46713
- plasma, laser perturbed, transient light emissions 2−80231
- plasma, LTE rel. to critical electron density 2−67632
- plasma, propagation of non-axisymmetric Alfven waves 2−53231
- plasma, pulsed, containing 1-2% H_2, spectra, plasma temp., particle conc.49941 2−49941
- plasma, seeded free jet, anomalous excitation of N_2 2−42916
- plasma, stabilized arc, cylindrical, emission line profile 2−64307
- plasma, thermal excitation functions of intense spectral lines in three different regions of spectrum 2−52911
- plasma, with polydispersed Ti, thermophysical processes, investigation 2−46762
- plasma diagnostics using i.r. technique 2−82562
- plasma discharge, flowing, radial and axial characteristics 2−70896
- plasma discharge, high current, pulsed, electron density obs. in early stages 2−60261
- plasma in low-voltage spark discharge, space and time distribution of temperature 2−70881
- plasma jet, radial temp. distrib. meas. 2−46767
- plasma low density, hypersonic, effect of angle of incidence on probe response 2−77285
- plasma stabilized arc, near thermodynamic equilibrium, stationary and relaxational props. 2−60223
- plasma temp. meas. in arc discharge 2−58971
- pressure and temperature behind blunt bodies in supersonic flow with supply of inert gases to base region 2−60332
- radioactive dating, K-Ar, origin of Hawaiian Ridge 2−57725
- radiogenic, excess in metamorphic amphibotes and biotites in Norwegian Caledonides 2−44601
- r.f. break down potential at high pressure and under magnetic field 2−71036
- scattering of Ar and He atoms from a W(112) single crystal, effect of O adsorption 2−67894
- scattering of H atoms, absolute total cross sections, interatomic forces 2−67424
- shock-heated, ionization relax. time calc. 2−70978
- shock-induced flow acceleration measurements 2−53297
- slightly ionized, electron energy distrib. and swarm parameters 2−70891
- small-angle scattering of range of elements, meas. of inelastic energy losses 2−64045
- solar overabundance, accelerated by solar flares 2−76001
- solid, adsorption of He, correlation energy 2−74644
- solid, elastic const. calcs. using Monte Carlo procedure 2−68062
- solid, elastic consts., Monte Carlo calc. 2−84058
- solid, elastic consts., stimulated Brillouin scatt. obs. 2−68231
- solid, energy bands, Hartree-Fock approx. 2−84272
- solid, specific heat, anharmonic corrections at high temp. 2−68247
- solid, static lattice energies, PV relation, at T=0K 2−80889
- solid, substituted, mol. oxygen luminesc. and excitation spectra at 4.2K 2−48215
- spallogenic gas in Weston chondrite 2−73098
- spark of Townsend mechanism, effect of cathode 2−71047
- spectra by proton bombardment 2−74235
- spectral line shapes and transition probabilities 2−70080
- thermal cond., 800-2000K meas. 2−71112
- third virial coeff. and nonadditivity 2−60367
- third virial coeff. calc. at low temps. 2−56440
- third virial coefficients 2−74482
- threshold conditions at superhigh-pressure produced by Q-switched lasers 2−64355
- Townsend discharge, electron energy distribs., expt. 2−43211
- Townsend discharge, electron energy distributions 2−70987
- viscosity, temp. depend. of coeffs. on saturation line of liq. and vapour phases at const. density 2−71170
- viscosity and thermal conductivity coeffs. calc. using modified Enskog theory over wide temp. and density range 2−64227
- X-ray $L_{2,3}$ emission spectrum, satellite spectrum 2−74214
- Z pinch Ar discharge electron density gradients meas. using modified Jamin interferometer 2−66771
- Ar/He, transmission through activated C adsorbent 2−43242

Argon continued
- Ar^+/He^+ simultaneous ion heating in linear turbulent-heating expts., mass dependence 2−80288
- Ar/K radioactive dating, rift volcanics in S. Kenya 2−61993
- Ar-Ar collisions, production of electrons, energy distribution 2−76993
- Ar-Ar pairs, retarded van der Waals pot. 2−67412
- Ar^{2+}-Ar collisions, 2-8 keV, meas. of cross sections, competition between single and double electron transfer processes 2−79870
- Ar-CO gas mixture vibrational relaxation rate in nozzle flow 2−80142
- Ar-H_2 plasma, blast waves generation, by pulsed electric discharges 2−74360
- Ar-He discharge, cataphoresis separation of constituents 2−77313
- Ar-He mixture, glow discharge spectroscopic measurements of cataphoresis 2−71022
- Ar-Hg-Ne discharge, probe measurements in positive column 2−74425
- Ar-Hg and Ar-Hg-N_2 discharges, electrodeless, r.f., electrical characterisics 2−71014
- Ar-Hg discharge, voltage frequency influence on instantaneous densities of excited Hg atoms and electronic energies 2−74424
- Ar-K plasma, heat flow meas. to electrodes 2−60209
- Ar-K plasma generator, nonequilibrium effects, obs. 2−59048
- Ar-K^+ collision, scatt. cross section, ion inelastic energy loss and u.v. emission 2−79925
- Ar-N binary mixtures, Percus-Yevick theory of radial distribution fns., thermodynamic props. and vapour-liquid equilibrium 2−67552
- Ar-N_2, −CO mixtures, heteronuclear associative ionization, formation of ArN_2^+, $ArCO^+$, Ar_2^+ following 30 eV electron impact 2−51430
- Ar-N_2, rotational excitation of rigid rotor, classical results 2−50125
- Ar-N_2 collision, comparison of generalized phase shift with classical trajectory calcs. of rotational inelasticity 2−43032
- Ar-N_2 mixtures, u.s. absorpt., kinetic interpret. 2−71116
- Ar-N_2 plasma in low power MHD generator, spectroscopic temp. detn. 2−46716
- Ar-N_2 system, rot. relax. time, classical trajectory calcs. 2−77165
- Ar-N_2 system, rot. relax. time, GPS calc. 2−77164
- Ar-Na gas-liquid system, influence of gas on nucleation in sinusoidal pressure field 2−46893
- Ar-O_2 mixture, excitation by low energy proton bombardment rel. to atmospheric gases 2−84792
- Ar-O_2 mixture, spectra by proton bombardment 2−74235
- Ar-O_2 system, solid, lattice mechanics, Raman spectra and luminesc. sideband obs. 2−75310
- Ar-Pt system, thermal cond., accommodation effect 2−67734
- Ar-Xe laser, energy transfer as excitation mechanism 2−41988
- Ar-methane-Kr and Ar-methane-H_2 mixtures, mean ionization energy 2−60290
- Ar electron capture collisions with H(2s), cross section meas. 2−56123
- Ar I, relative transition probabilities, optical absorpt. determ. 2−70582
- Ar I isoelectronic sequence, Hartree Fock predictions of ^1P term in p^5d configurations 2−46422
- Ar I lines, Stark widening of h.f. electrodeless discharge 2−46423
- Ar I spectral line halfwidths in wall-stabilized cascade arc 2−67387
- Ar II-Ar VIII, excited lifetimes, beam foil spectra radiative decay times 2−79873
- Ar II, transition branching ratios 2−83194
- Ar I(II) radiative lifetimes meas. in electron tube using oscillograph method of delayed coincidences 2−77006
- Ar singly ionized, specific refractivity 2−79903
- Ar solid-Ar^+ collisions, 25 to 200 keV, noncharacteristic X-ray bands 2−56116
- Ar VIII, Na-like, collisional-rate coeff. meas. in plasmas 2−46450
- Ar XII-XVI lines in e.u.v. spectra of solar flares 2−58546
- Ar XVII, lifetime of 2^1S_0 state 2−42809
- Ar^+, angular and temp. depend. of Cu sputtering 2−51064
- Ar^+, angular distributions in electron impact ionization 2−56108
- Ar^+, effect of reson. on vibr. distrib. in charge transfer reactions with HCl and HBr 2−51424
- Ar^+ beam interacting with surface, obs. of mass spectrum 2−79849
- Ar^+ ion beam, optical spectra Zeeman splitting 2−70577
- Ar^+ ion laser, properties of emission spectrum 2−41989
- Ar^+ laser plasma, population inversion, collisional radiative calc. 2−79197
- Ar^+ plasma, shock generated, interaction with transverse mag. field 2−77268
- Ar^{18+}, accelerated to 1.17×10^{10} eV, Princeton synchrotron accelerator 2−79701
- Ar_2, experiment potential curve, comparison with optimised calculations 2−56142
- Ar_2, spectroscopic dissociation energy for ground state 2−50022
- Ar_2, Van der Waals dimers, Raman spectra 2−80050
- Ar_2^+ afterglow dissociative recomb. at elevated temp. 2−83262
- Ar_3, binding energies, calc. for Lennard-Jones 12-6 pair potentials 2−60023
- Ar(II), calc. of transition probabilities and lifetimes for radiative transitions using multi-configuration model 2−64004
- $^{15}Ar^+$, highly excited, metastable autoionizing states, electronic energies and electron emission lifetimes 2−42749
- ^{37}Ar in expired air after low level neutron irradiation as measure of total body Ca content 2−69365
- $^{40}Ar/^{36}Ar$ ratio and Ar excess in submarine basalts rel. to Earth-atmosphere evolution model 2−72689
- $^{40}Ar^{40}/^{39}Ar$ stepwise degassing technique, reappraisal 2−57806
- ^{41}Ar, environmental significance of release from Lowell Technological Institute reactor 2−59875
- Ar + Ar intermolecular potentials from differential scattering cross-sections 2−42782
- Ar + CsI collisions, vibrational energy transfer, ballistic mechanism 2−67536
- Ar + N_2 high-frequency discharge, cross sections for excitation of $N_2(C^3\Pi u)$ 2−43041
- Ar + $OH(A^2\Sigma^+)$, near resonant vibration-rotation energy transfer calc. of cross sections and rate consts. using IOS and DW approx. 2−70818
- Ar_2^*, temp. dependence of vacuum u.v. emission spectra in gas and liquid phases 2−70680

Argon continued
- Ba-Ar collisions, excitation of metastable levels of Ba behind shock waves 2−79932
- Cd-Ar vapour, phase-matched, vacuum u.v. radiation generation 2−79904
- GaAs:Ar ion implanted, radiation damage, elec. microscope obs. 2−60821
- H_2-Ar and D_2-Ar systems, conc. depend. of binary diffusion coeffs., 300K 2−64399
- H_2 in Ar, multiple quantum transition effects on dissociation constant 2−50035
- H^+ + Ar, total differential cross-section, energy depend. 2−79858
- $H_2 + Ar^+$ reaction, spin-orbit states of Ar^+ 2−81498
- H(2s)-Ar, 20-120 keV charge-changing collisions, meas. of absolute cross sections and electron capture cross sections 2−70638
- He-Ar gaseous mixtures, sound dispersion as test for linearized Boltzmann eqns. 2−60375
- He-Ar mixtures, collision induced- absorpt. near $\lambda = 1$ mm 2−77084
- He-Ar system, conc. depend. of diffusion coeff. at 300 K and 1 atm. press. 2−71121
- He-Ne colour TV laser display system wide screen and high definition, NHK Model 101C, 525 line 2−82506
- He + Ar collisions, chemi-ionization cross sections 2−64080
- Hg-Ar arc discharges, cathode spaces, influence of cathode qualities 2−60324
- Hg-Ar discharge, l.p., mass spectrometric analysis of Hg_2^+ form. in positive column 2−83640
- I + Ar→IAr, equilibrium constant 2−80009
- K/Ar data rel. to origin of feldspar megacrysts in alkali basalt 2−54729
- K-Ar ages of zenoliths from Tahiti 2−57808
- K^+ − Ar scatt., potentials derivation from intermediate and strong field mobility data 2−79912
- N_2-Ar mixture, viscosity, 25 to 500°C 2−80419
- N_2 + Ar system, three-body recomb. and dissoc., Monte Carlo trajectory calcs. 2−64108
- Ne-Ar pairs, retarded van der Waals pot. 2−67412
- Si-Ar^{++} collisions, K X-ray yields of Si, double-scattering mechanism 2−42786
- Tl-Ar collisions, excitation of metastable levels of Tl behind shock waves 2−79932

Argon compounds
- Ar:OF_2, Raman spectra 2−51466
- Ar-Kr(Xe) film, struct., 6K to sublimation temp., electron diffr. obs. 2−80573
- Ar-Xe solid solution, absorpt., 8-10.5 eV, rel. to exciton studies 2−68634
- ArH^+, energy curves, ground and excited state calcs. 2−64051
- Rb-Ar, Van der Waals molecules, action of r.f. field 2−56194

Aromatic compounds *see Organic compounds*

Arsenic
- amorphous state, different forms 2−60572
- crystallographic axes, assignment, etch pit study 2−47186
- diffusion in Si, from arsenosilicate glass source, 1000-1200°C 2−83980
- diffusion in Si, props. of SiO_2:As and Ge/SiO_2:As diffusion sources 2−83979
- diffusion into Si by evacuated capsule method 2−71518
- etch pit orientation determination 2−47187
- high pressure superconducting phase 2−44058
- single crystals, modulated piezoreflectance 2−75262
- solubility in Cu-Zn and Cu-Zn-Al 2−47619
- thermal expansion, coeffs., anisotropy, 2-30K, 55-90K, and at 283K, Gruneisen parameters 2−77784
- Young's modulus and Poisson's ratio, orientation depend. 2−74821
- As(111) crystal, evaporating molecule speed and spatial distributions 2−67879
- Co:As, hyperfine mag. fields at As, rel. to host mag. moments 2−78018
- Fe:As, hyperfine mag. fields at As, rel. to host mag. moments 2−78018
- in Fe-1%C alloy, effect on tempering stages 2−50796
- Ge:As, far i.r. absorpt., impurity conc. and compensation effects 2−68642
- Ge:As, heavily doped, temp. depend. of resist. 2−71940
- n-Ge:As, resist. decrease due to donor spin reson. 2−81106
- Ni:As, hyperfine mag. fields at As, rel. to host mag. moments 2−78018
- Se: As, film, vacuum evap., transport props., time resolved drift technique 2−44104
- Si:As, cond. band deform. potential const. from piezospectroscopy of donors 2−68438
- Si:As, diffusion by using emulsion type doped oxide 2−71517
- Si:As, ground state wavefunctions of shallow donor electrons, Fermi contact consts. 2−71950
- Si:As, He ion min. backscatt. yield variation obs. 2−60820
- Si:As, impurity distrib., determ. by He ion channeling obs. 2−60818

Arsenic compounds
- — 2−60573
- — 2−61242
- arsenate minerals and rocks, visible and near i.r. spectra 2−72672
- binary arsenosilicate glass film, diffusion source, thermal stresses 2−71325
- binary arsenosilicate glass film, vapour deposition for diffusion source 2−71324
- group V double and triple chalcogens, n.q.r. of ^{75}As, ^{79}Br, ^{81}Br, ^{127}Sb, ^{123}Sb, ^{127}I, ^{209}Bi 2−48311
- pyroarsenates (As_2O_7 systems), normal coordinate analysis 2−77079
- As-Ge solid soln., absorpt. and scatt. of X-rays by cluster defects and dislocation loops 2−77584
- As-S-Ge glass film, laser induced refractive index changes 2−61583
- As-S-Te, vitreous semicond., γ-ray induced cond. 2−54252
- As-S glass, mechanism of hologram formation 2−59204
- As-Sb alloy, etch pit orientation determ. 2−47187
- As-Se-Ge-Sn glass, Mossbauer effect, isomeric shift, quadrupole splitting, phase diagram 2−75267
- As-Se-Ge glass film, amorphous to crystalline state conversion by light irradiation 2−75077
- As-Se-Te, vitreous semicond., γ-ray induced cond. 2−54252

Arsenic compounds continued
As-Se amorphous layers, carrier lifetime determ. 2−81088
As-Se glass, Ag doped, elec. props. 2−64975
As-Si-Ge-Te glass, comp. vs. glass transition temp 2−60597
As-Te-Ge-Se glass switching device, small signal behaviour 2−61376
As-Te-Ge-Si glass, thermal breakdown 2−61298
As-Te-Ge, amorphous, cryst. layer form., effect of water during heat treatment 2−60571
As-Te, memory glass system, glass forming regions, transition temps., melt crystn. temps. 2−80805
As-Tl-X glass, (x=chalcogen), e.p.r., fine struct. 2−72476
As-V(Cr)(Mn)(Fe)(Co)(Ni) dilute liquid alloy, susceptibility 2−80485
As complex, Menshutkin's type, n.q.r. freq. shifts nature 2−83274
AsF spectrum, near vacuum u.v. and near i.r. vibr. and rot. analysis, transitions 2−56154
AsF_3, ambiguities in harmonic force fields 2−50063
AsI_3, $AsI_3.3S_8$, Mossbauer effects, of ^{129}I, bond character 2−78071
$As_xIn_{1-x}SeI$ vitreous compounds, x=1.00, 0.95, 0.90, 0.80, i.r. absorption, determ. of energy structure 2−78095
AsO radical, rot. analysis of $C^2\Delta$ and $D^2\Sigma^-$ states, C-state perturbations 2−74255
As_2S_3/Ag system, photochem. transformation rate temp. depend., ht. treatment and ageing effects 2−57433
AsS, $A/^2\pi_{3/2}-X^2\pi_{3/2}$ band system, vibrational analysis and rotational constants 2−77080
AsS, refl. spectra, 100-800 nm, at 77K and 293K 2−75277
As_2S_3, amorphous, photoelastic consts., freq. depend., one-oscillator model 2−54383
As_2S_3, amorphous, refl. spectra, vibr. modes 2−61614
As_2S_3, n.q.r., cryst. and amorphous state studies 2−84605
As_2S_3, refl. spectra, 100-800 nm, at 77K and 293K 2−75277
As_2S_3, vitreous, local struct. order, ^{75}As n.q.r. obs. 2−57404
As_2S_3, vitreous, localized state distrib., Fermi level analysis from transient photocond. obs. 2−47913
As_2S_3, vitreous, Raman scatt., vibrational states density detn. 2−61663
As_2S_3, vitreous, vibration spectra, computer generated 2−74966
As_2S_3 and As_4S_4 amorphous films, a.c. cond., temp. depend. 2−68392
As_2S_3 crystals, massive and thin film, self-absorption edges, effect of temperature and polarization 2−84479
As_2S_3 film, amorphous, thermally stimulated cond. 2−57189
As_4S_4 film, amorphous, thermally stimulated cond. 2−57189
β As_4S_4 nuclear quadrupole resonance of ^{75}As 2−84595
AsSI and AsSeI, vitreous and molten, temp. depend. of density, mag. susceptibility and forbidden band width 2−84393
$As_2S_3(Se_3)$ cryst., photodecomp. 2−51463
$As_2S_3(Se_3)(Te_3)$, amorphous, trapping mechanism, cavity perturbation study 2−61443
$As_xSb_{2-x}Se_3$, amorphous and crysts., threshold and memory switching 2−77883
As_2Se_3-$As_2Te_3(Tl_2Se)(Sb_2Se_3)(As_2S_3)$ glass, e.s.r. and X-ray studies 2−61734
As_2Se_3, amorphous, a.c. cond, 30Hz-10.3GHz, −180-500°C 2−81070
As_2Se_3, amorphous, refl. spectra, vibr. modes 2−61614
As_2Se_3, amorphous film, optical const. determination from reflectivity spectra 2−61620
α-As_2Se_3, crystal growth, vapour transport method 2−43510
As_2Se_3, glassy, high field cond. 2−68394
As_2Se_3, liquid semiconductor, switching, thermal breakdown mechanism 2−81096
As_2Se_3, refl. spectra, 100-800 nm, at 77K and 293K 2−75277
As_2Se_3, vitreous, effects of group III A dopant on physical props. 2−61300
As_2Se_3, vitreous, low temp. mag. susceptibility 2−54293
As_2Se_3, vitreous, polymeric struct. and energy spectrum 2−60590
As_2Se_3, vitreous, recombination centre nature 2−61686
As_2Se_3, vitreous, vibration spectra, computer generated 2−74966
As_2Se_3, vitreous and cryst., combination scatt. spectra, 5-1000 cm^{-1}, 100-300 K 2−84524
As_2Se_3, vitreous and crystalline, electron energy spectrum, modulation spectroscopy obs. 2−61631
As_2Se_3, vitreous and monocryst., recomb. radiation mechanism 2−54451
As_2Se_3 amorphous film, a.c. cond., temp. depend. 2−68392
As_2Se_3 film, amorphous, charge transport, photocond. and dark current obs. 2−68393
As_2Se_3 film, amorphous, grown by vapour deposition, contribs. to growth temp. 2−64564
As_2Se_3 film, amorphous, memory switching rel. to thickness 2−81072
As_2Se_3 film, amorphous, thermally stimulated cond. 2−57189
As_2Se_3 film, crystalline and amorphous, ion bombardment effects 2−60646
As_2Se_3 films, amorphous, dark discharges 2−49458
As_2Se_3 glass, high field conductivity 2−51134
As_2Se_3 layers, carrier lifetime determ. 2−81088
As_2Se_3 vitreous, acousto-optical props., appl. in i.r. modulator 2−84459
$AsSe_{1.5}Sn_{0.28}$, pyroceramic, semicond., elec. cond. mechanism, 285-385K 2−75089
$As_2Se_3(Te_3)$ amorphous film, trap-limited processes 2−61325
$As_2Se_3-xAs_2Te_3$, amorphous, elec. cond., Hall effect, and thermopower 2−77893
$2As_2Se_3.As_2Te_3$, amorphous, minor switching and r.f. oscillations 2−61275
$3As_2Se_3.2Sb_2Se_3$ films, amorphous, band. struct., optical props. 2−54186
$3As_2Se_3.2Sb_2Se_3$ films, amorphous, elec. props., band struct. 2−54187
$1-xAs_2Se_3.xSb_2Se_3$ semiconductor system, devitrification characs. 2−71286
As_2Te_3-As_2Se_3 glass, elec., thermal and structural props. 2−61299
As_2Te_3-As_2Se_3 glass, microstruct. a.d. and d.c. cond. 2−60589
As_2Te_3-As_2Se_3 glass, switching rel. to comp. and thermal treatment 2−61295
As_2Te_3-$GaAs(Ga_2Te_3)$ system, phase diagram 2−47713

Arsenic compounds continued
As_2Te_3-Si glass, electronically assisted thermal breakdown 2−61276
As_2Te_3-Tl_2Se, vitreous, photocond kinetics, photoresponse 2−72067
As_2Te_3, polycryst., threshold and memory switching 2−77883
As_2Te_3, refl. spectra, 100-800 nm, at 77K and 293K 2−75277
As_2Te_3 film, amorphous, a.c. cond. rel. to localized tail states 2−61288
As_2Te_3 glassy, electronic props. 2−61297
As_2Te_3 glassy, switching characts., cond. exponential temp. depend. 2−81073
$As_{38}Te_{55}Ge_4Si_3$, amorphous, minor switching and r.f. oscillations 2−61275
AsTeI glass, electronic transport props. 2−61296
As_2Te_2Se, amorphous semicond., thermalization in energy band tails 2−61685
As_xSey glasses, e.s.r., spin conc. and signal intensity 2−65332
Cd-Si-As system, glass-forming region determ. by differential thermal analysis 2−74599
Co-As dilute system, internal hyperfine mag. field determ. 2−44321
Cu-As-Se compositions, voltage controlled switching 2−67886
Cu-As system, phases, struct., homogeneity rangers 2−74731
Fe-1%C-0.5%As alloy, anomalous precip., resistivity, internal friction and elec. microscope obs. 2−50940
Ga-As-Te system, GaAs-Te polythermal section determ. 2−61047
Ga-As-Zn system, GaAs-Zn polythermal section determ. 2−61046
Ge-As-Se-Pd(Cd) glass, microstruct. and immiscibility temp. 2−56561
Ge-As-Se glass chalcogenide system, atomic distribution and coordination numbers 2−56559
Ge-Te-As glass, high current density path shape 2−57193
$Ge_xAs_{40-x}S_{60}$ glasses and liquids, heat capacity 2−51045
$Ge_{16}As_{35}Te_{28}S_{21}$, amorphous, semiconductor- metal contact, photovoltaic effect and space charge capacitance 2−61374
glass, As-S, As-S-I, As-S-Tl viscosity in transition region 2−84049
Ni-As dilute system, internal hyperfine mag. field determ. 2−44321
Se-As glasses, thermal characteristics near glass transformation point 2−61104
Si-As-Te, amorphous semicond., energy gap depend. on glass transition and softening temp. 2−61346
Si-As-Te amorphous semiconductor, relation between band gap and density 2−65003
Sn-Bi-As system, Sn_4As_3-Bi-SnAs subsystem, phase equilib. 2−74942
Te-As-Ge-S glass films, four-element quantitative analysis 2−72593
Te-As-Ge-Si, amorphous, trapping mechanism, cavity perturbation study 2−61443
Te-As-Ge amorphous alloy, negative differential capacitance 2−64961
Te-As-Si-Ge film, amorphous, a.c. cond. rel. to localized tail states 2−61288
Te-As system, vapour press. of Te_2, As_4, and As_2 over molten As_2Te_3 2−47046
Te-Ge-As glass, u.s. velocity, hydrostatic press. effects 2−47742
$Te_{60}As_{25}Ge_{13}M_x$, M=S, Se, chalcogenide glass, interdepend. between, switching memory and thermal behaviour 2−47901
$Tl_2Se.As_2Te_3$, amorphous, Hall coeff. and magnetoresistance 2−61331

Assistors *see Conductivity, electrical; Semiconducting devices*

Association
N-methylaniline, dissolved, low temp. i.r. study of self-association by H bonds 2−54540

gases
constants rel. to virial coefficients, rigorous expression 2−43261
equation of state derivation 2−46856
statistical theory, for system with many molecular species 2−46850
Ba^{2+}, meas. of termolecular association rate constants with Ar, O_2, N_2, CO, CO_2, N_2O, H_2O in flowing afterglow 2−48316
Ca^{2+}, meas. of termolecular association rate constant, with Ar, O_2, N_2, CO, CO_2 N_2O, H_2O in flowing afterglow 2−48316
Mg^{2+}, meas. of termolecular association rate constant, with Ar, O_2, N_2, CO, CO_2, N_2O, H_2O in flowing afterglow 2−48316
N_2, nonequilibrium dissociation, effects on blunt body flows 2−77361

liquids
see also Colloids
alcohols in n-heptane soln., from dielec. dispersion obs. 2−84611
anthracene, auto-association of frozen solns,., fluorescence 2−54558
anthracene, auto-association of frozen solns., absorption spectra 2−54557
benzene-nitroalkane solns., from Rayleigh scatt. and depolarization obs. 2−64444
tetracene in soln., auto-associated species identification 2−81520

Astatine
No entries

Astatine compounds
No entries

Asteroids
amino acid abundance 2−57729
Bamberga, visible and i.r. photometric obs. 2−78493
bolometric Bond albedo and size determ. from photometric models 2−78492
Eunomia, period of rotation 2−48784
1620 Geographos, shape, laboratory studies 62715 2−62715
Icarus and unidentified minor planet, Maksutov telescope photographs 2−48782
Iris, visible and i.r. photometric obs. 2−78493
Kirkwood gap located at 1:2 resonance with Jupiter, evolution of orbits 2−62457
light curve, simulation 2−48783
mass and dynamics, statistics 2−75917
meteorite origin hypotheses rel. to asteroid parent body break-up 2−78514
meteoritic source, possibility 2−58531
observations made at Crimean astrophysical laboratory 2−69168
observations made at Hradec Kralove observatory 2−69167

Asteroids continued
occultations of stars 2−48768
occultations of stars by planets, satellites and asteroids, predictions and observations 2−78515
orbit corrections of 161 minor planets 2−69166
2 Pallas, photometric parameters 2−51834
positions during 1970 2−73091
precise obs. of 1 Ceres, 3 Juno, 11 Parthenope, 18 Melpomene, 39 Laetitia, 40 Harmonia, 433 Eros at Sydney 2−75918
probes, trajectory considerations, flight modes 2−58522
reflection spectra and composition 2−62714
rotational properties of different groups 2−75857
shape, orientation of rotation axis, photometric observations 2−58517
rel. to solar system origin and evolution, space mission 2−51835
space missions to comets and asteroids rel. to understanding of solar system 2−78411
surface composition from spectral reflectivities obs. in 0.3 to 1.1 range 2−81909
topography, models for static loading and creep deformation 2−78491
1685 Toro, capture resonance by Earth 58518 2−58518
Toro, capture resonance by the Earth 2−69169
1685 Toro, improved orbit with resonances with three planets 2−58516
Vesta, bolometric Bond albedo and size determ. from photometric models 2−78492
Vesta, visible and i.r. photometric obs. 2−78493
Vesta and others, reflection spectrum 2−62713
Astigmatism *see Aberrations, optical*
Astronautics *see Space research*
Astronomical instruments
see also Radioastronomy; Telescopes/astronomical
Apollo fine sun sensor electrooptical system 2−81960
band-width synthesis interferometer, operation and obs. 2−58388
Bergedorf Perth meridian circle with digitalized photoelectric micrometers 2−62809
book on new techniques 2−58562
buffer unit for increasing time resolution of multichannel scaler, for digital signal averaging 2−45012
camera, electronic, for photometric meas. binaries 2−44876
Carnac alignments of megalithic stones, 1970-1 research work 2−81966
Cerro Tololo data acquisition system 2−45011
Cerro-Calan Observatory meridian circle, value of screw of ocular micrometer 2−51874
Cherenkov detector in high energy astronomical observatory cosmic ray experiment 2−49605
chopper improvement for use in i.r. photometry 2−85067
clock drives for telescopes and cameras, invertor circuits and motors 2−45006
computer control system, portable, primarily for photopolarimeters 2−45007
computer controlled spectrometers at McDonald Observatory 2−45010
computer system for Hale observatory 2−45008
30-inch coude spectrograph, instrumental profile 2−51876
Coude spectrograph, Kitt Peak, calibration curves for various emulsions 2−76041
coude spectrograph system 2−58573
Culgoora radioheliograph, multiple frequency operation 2−69186
Danjon's astrolabe, contrib. to stellar proper motions study 2−66069
Danjon prism astrolabe, meas. of longitude differences between two astronomical stations at Irkutsk 2−73154
data acquisition system for photoelectric photometry 2−55326
data system for rapid scanner 2−76050
digicon, use with telescopes 2−58574
direct electronography, review 2−66243
double-meniscus astrograph, lateral chromatic aberration 2−48828
e.u.v. and X-ray spectroheliograph 2−78578
GALAXY-machine meas. of Schmidt plate for precise stellar positions 2−45001
grating spectroheliograph for observing solar MgII and CaII resonance lines 2−45014
high energy observatory, conceptual definition 2−48831
image splitter prism for photographic photometry 2−48830
interface for small computer allowing variable star data to be recorded 2−62481
interferential filters, Lyot-Ohman, tuning results 2−51875
i.r. diffractional spectrometer, estimates of efficiency 2−45821
i.r. Fourier transform interferometer with 500-5000 cm^{-1} bandwidth 2−62818
i.r. radiometer, Mariner orbiter mission (1971) 2−85076
i.r. stellar interferometer, heterodyne detectors 2−81975
limb illumination, photoelectric system of automatic guiding of measuring machines 2−48829
Meridian Circle graduation, Brun's method for error determ. 2−73164
meteorites, radiolocation instruments 2−69173
MF-4 microphotometer, program control system for two- coordinate frame motion 2−45798
Michelson interferometers, applics. 2−62812
mirrors, reflection factor determination using a portable device, construction principles 2−45774
modulation collimator, variable spacing for X-ray astronomy 2−73053
moon's first observatory, Apollo 16 2−45002
multichannel solar spectrometer at Sacramento Peak Observatory 2−76051
Nimbus limb radiometer electrooptical system 2−81960
OSO for 1 arc sec obs. of quiet sun 2−58541
photoelectric stellar spectrophotometer with pressure scanned Fabry-Perot etalon and echelle grating 2−73162
photometer, synchronous, 3-colour, with sampling circuits 2−45799
photometer and polarimeter, automatic photoelectric, with fast digital recording system 2−45005
photometers, 'Irtran-1' reflection filter for 20μ atmospheric window 2−73163
polarimeter, photon counting, design and fabrication 2−76048
portable night sky photometer 2−69199
Astronomical instruments continued
Pulkovo meridian circle division errors from observations of AGK3R and FK4 stars 2−48826
Pulkovo ZTL-180 tube, ocular micrometer screw rotation value, observations of wide scale pairs 2−48827
radiointerferometry signal processing with positive constraint 2−55198
188cm reflector, Coude spectrograph, high resolution scanning equipment 2−48824
refractional anomalies in the ZTL-180 tube, thermoresistors measurements 2−48816
scintillation counters, det. of cosmic ray induced radioactivity 2−62816
Skylab multispectral scanner electrooptical system 2−81960
solar image system at 1.65 μ using 64 element array of PbS detectors 2−81961
solar oblateness measurement, nonimaging technique 2−75939
solar probe, HELIOS, design and development 2−48789
sounding rockets, uses, applics. and future 2−81971
spectrograph camera designs 2−58575
spectrophotometer for use at Cassegrain focus of telescopes, teaching equipment 2−78635
stellar interferometer 2−69200
stellar photometer, with Cassegrainian optical system for 1300-2000 Å region 2−69050
three channel SEC vidicon system for photometric obs. of solar corona 2−76024
Toepfer meridian circle, contact micrometer screw rotation effects from observations of stellar right ascensions 2−51873
TV photometer, low light system 2−85070
UBV photometry at Bologna astronomical observatory 2−51869
unitized multiplex for processing photographic images of planetary objects 2−78634
u.v. detector, response to solar radiation rel. to altitude 2−81962
u.v. sky scan telescope in TD1 satellite 2−58261
vidicon system, rocket borne, for e.u.v. obs. of Sun 2−44990
X-ray polarimeter, Thompson scattering, design 2−51795
He-D_3 spectroheliograms, distrib. of photospheric mag. field 2−73103

Astronomical observations
see also Radioastronomy
1973 Handbook of British Astronomical Association, ephemerides 2−85073
Abell 2199 cluster of galaxies, static properties of 170 objects 2−69030
absolute flux meas. and error in standard star Vega 2−81974
absolute radio brightness temperatures in Southern Sky 2−69115
AFU-75 camera, observations of satellite Pageos 2−62817
al-Biruni's solar data, det. of terrestrial and lunar accelerations 2−65427
asteroids, orbit corrections 2−69166
ASTRA project, air pollution obs. 2−58563
astroclimate of eastern Pamir Mountains, rel. to possible observing site 2−48813
astroclimate of four positions in middle Asia rel. to stellar image quality 2−48814
Astrographic Catalogue (Carte du Ciel), definitive plate constants for four zones 2−66239
astrometry, effect of error in plate reduction 2−58259
astronomical ephemerides, program for modern aberration coefficients 2−69194
atmospheric aerosol light scattering from extinction measurements at remote clean air locations 2−51621
atmospheric deterioration studies by astronomical techniques, symposium 2−51570
atmospheric extinction observations for 1955-1972 at Flagstaff U.S. Naval Observatory 2−54861
atmospheric monochromatic extinction from UBV photometry of stars 2−54864
atmospheric pollution meas. and environmental investigations rel. to astronomical observations at Mt. Hopkins Observatory 2−54859
atmospheric seeing conditions on Mt. Wilson rel. to Agassiz Station, interferometric study 2−68909
B2 catalogue, 408 MHz observations 2−78480
baseline determination problems in 21-cm. H line observations 2−55193
Bennett's comet, Steinberg Institute Observatory, (1969) 2−69170
book on new techniques 2−58562
4C catalogue, obs. at 408 MHz in the declination range 20° to 0° 2−48740
4C radiosources, identification of 59 objects with galaxies 2−81786
catalogue of lunar crater diameters, depths and morphologies, the System of Lunar Craters, revision 2−44918
catalogue of lunar occultation diffraction patterns for single and double stars 2−75701
catalogue of spectral classifications, radial velocities and u.b.v. photometry of stars in LMC 2−62548
celestial light sources, low intensity, surface photometry from space vehicle 2−45003
celestial nuclear γ-ray monitoring from OSO-7 2−58438
conference, (E. Lansing, Mich., USA, Aug. 1972) 2−75656
constant of aberration and short-period terms of nutation from Pulkovo polar tube observations 2−51722
continuum radiation at 820 MHz between declinations -7° and +85° 2−62606
coordinate dets. of stars and artificial satellites by wide angle ballistic camera installed in aeroplane 2−51865
cosmic ray meas. by Intercosmos 3, PG-1 apparatus 2−81650
Culgoora solar magnetograph, image motion due to vibr. 2−85071
daylight observations of comets, Venus and Mercury when close to the Sun 2−48781
diffraction limited resolution obtained with large telescopes, autocorrelation methods 2−66238
double stars, photographic meas. of separations and position angles of 111 objects 2−66107
double-stars, list of 271 objects with equal components, spectral evidence of binary nature 2−55061
dwarf K- and M-type stars in Southern Hemisphere, spectral classification of 624 objects 2−69076

Astronomical observations continued
  Earth's orbital velocity, determination from stellar radial velocity 2−44938
  Earth Moon system, evidence for existence of non gravitational forces 2−58477
  ephemerides for Jan. and Feb. 1973, tables 2−81964
  errors of Southern Reference Star program 2−48817
  extragalactic distance determ. using classical Cepheids 2−69095
  FK4 catalogue, stellar proper motions rel. to galactic rotation constants 2−69021
  FK4 system, right ascension by meridian observation with the Dollen method 2−69052
  flux densities, accurate, at 5009 MHz, 1007 sources 2−75803
  flux densities, positions and structure of 424 intense radio sources at 1400 MHz 2−69120
  for u.v. camera, operated from Moon by Apollo 16 crew 2−75699
  galactic H II regions, radio emission at 1400 MHz from 130 areas 2−58252
  Galactic spiral structure determ. 2−51703
  galaxies, Zwicky catalogue, brightness distributions 2−58226
  galaxies microwave radiation obs. rel. to maser mechanism 2−69016
  Galaxy, Cepheus extension of Perseus spiral arm from 1500 stellar observations 2−78445
  Galaxy and the distance scale, Woolley symposium, Herstmonceaux, Aug (1972) 2−69015
  gravitational mass, theory and detection, binary stars 2−66037
  gravitational radiation, positive signature for recognition 2−76042
  high-velocity interstellar H I up to high galactic latitudes, survey 2−58355
  IDS catalogue, proper motions of possible double and multiple systems 2−48718
  image aberrations due to atmospheric turbulence, removal by optical array technique 2−85074
  image deterioration of extraterrestrial objects due to atmospheric turbulence effects on refractive index 2−81677
  interferometry, effects of irregular propagation media 2−58560
  international ultraviolet explorer, payload 2−62421
  i.r., solar spectrum, Arizona NASA atlas, 21492-25583 Å 2−69182
  i.r., solar spectrum, Arizona NASA atlas, 25583-30920 Å 2−69183
  i.r. solar spectrum, Arizona NASA atlas, 12187- 17731 Å 2−69179
  i.r. solar spectrum, Arizona NASA atlas, 19374-20930 Å 2−69181
  i.r. solar spectrum, Arizona NASA atlas, 4 m spectrometer 2−69180
  i.r. solar spectrum, Arizona-NASA atlas, 1.4 μ H_2O band 2−69178
  JOSO 71 site testing program at Tenerife, results 2−51868
  Jupiter's Red Spot, isodensity and photometric profiles for 1971 2−69149
  KSZ stars, re-reduction of 107 additional objects in northern sky galaxy areas 2−48681
  Large Magellanic Cloud, topography of 1830 variable stars 2−75691
  Large Magellanic Cloud UBV photoelectric photometry of 160 O-B supergiants 2−62546
  latitude obs. for 1935.0-1947.0 at Muzusawa, Kitab, Gaithersburg and Ukiah 2−44514
  latitude obs. using Danjon astrolabe at Paris observatory, (1956.5 to 1970.8) 2−44515
  latitude observations, effect of refractional anomalies in the ZTL-180 tube 2−48816
  latitude observations rel. to declination errors in various star catalogues 2−51724
  latitude observations with prismatic astrolabe at Pulkovo Observatory 2−51723
  limiting magnitudes of visual observations of stars 2−48677
  limiting stellar magnitudes in observations with visual telescopes 2−48678
  longitude differences between two astronomical stations at Irkutsk 2−73154
  lunar and planetary positions using 13-inch photographic equatorial refractor 2−66163
  lunar eclipses, umbral contact moments, accuracy determinations 2−58446
  lunar laser ranging expt. 2−44930
  lunar occultation, near-ellpitic bright stars 2−85063
  RRLyrae-type stars, motions and absolute magnitudes for 65 objects 2−78466
  Lyrids meteor shower 1969, radiant position and meteor characteristics, visual and telescopic observations of 4377 meteors 2−58527
  Magellanic clouds and distance scale 2−69038
  map of galactic centre region, high resolution and sensitivity at 15.5 GHz 2−75818
  Martian craters, circularity 2−85039
  Mercury, perihelion advance, radar determ., general relativity confirmed 2−51824
  Mertz shadowgram reconstruction for X-ray source astronomy 2−66129
  minor planets, Crimean astrophysical laboratory 2−69168
  minor planets, Hradec Kralove observatory 2−69167
  national observatory, 1971 almanac 2−73155
  NGC 6866, open cluster, catalogue of proper motions for 2036 stars 2−48720
  night errors, refraction anomalies or variable systematic instrumental errors 2−66240
  NRAO interferometric position accuracies for point radiosources 2−58391
  OB faint stars, search technique 2−76039
  OB stars in Norma, UBV and Hβ photometry of 99 objects 2−69075
  observation reduction, HI regions, linear polarization antenna radiation patterns 2−85060
  observatory sites, meteorological conditions and optical turbulence 2−51867
  occultations of stars by planets, satellites and asteroids, predictions and observations 2−78515
  open star clusters and HI regions, open cluster, catalogue and identification 2−44878
  optical identifications of radiosources in the B2 catalogue 2−62607
  optical positions of 48 QSOs rel. to AGK3 and SAO stellar positions 2−69116
  optical survey of southern galaxies with bright nuclei 2−58222
  orientation of astrophotographs and reduction of double stars measurements 2−51864
  phase errors in interferometry, identification and removal 2−66241

Astronomical observations continued
  photoelectric meridian circle of Bergedorf/Perth 2−62809
  photographic image calibration with 45° second surface reflector plate 2−75700
  photographic zenith tube obs. rel. to N. American-Eurasian plate motions 2−75424
  photometry UBV, van Wijk sequence obs. in Large Magellanic Cloud 2−69033
  planet detection, trans-Pluto, from observations of comets 2−69139
  planetary diameter meas. using double image micrometry, application to Venus 2−75916
  planetary nebulae, spatial spectroscopic diagnostic using synthetic approach 2−69041
  planetary nebulae, spatial spectroscopic diagnostics, analytical approach using inverse integral equations 2−72982
  planetary nebulae catalogue, radio observations of total fluxes, morphology and spectra 2−44845
  point source, confusion error on flux estimate 2−62810
  psychological influences on solar observation 2−69197
  Pulkovo catalogues of declinations $Pu_{50}F$ and $Pu_{50}Z$ 2−51721
  Pulkovo meridian circle division errors from observations of AGK3R and FK4 stars 2−48826
  pulsars, new method based on detection of v.l.f. e.m. radiation associated with period 2−73041
  radial velocity meas. using the coude spectrograph 2−69078
  radiosources at 408 MHz, positions and flux densities 2−58411
  reference catalogue system influence on coords. of stars det. in zonal meridian obs. 2−51866
  refractional and circumzenithal Talcott pairs, observations with ZTL-180 tube 2−48682
  right ascension, corrections to FK4 catalogue, meridian circle observations 2−48680
  rocket techniques, review of past 25 yrs. 2−62811
  SC-type stars, image-tube spectrograms of 51 stars 2−78463
  β Scorpii, occultation on 1971, May 13-14, by Jupiter and its satellite Io 44879 2−44879
  β Scorpii, transit of Jupiter's system across the multiple star 44874 2−44874
  seeing power of telescope in thermally turbulent atmos. 2−73160
  solar activity, yellow coronal line at Lomnicky Stit 2−73109
  solar activity macrostructure distribution using photographic method 2−69191
  solar and lunar photographic degradation by atm., resolution enhancement by computer processing 2−76040
  solar corona, polarization photography 2−58561
  solar flares, matched patrol telescope systems 2−78614
  solar images, dependence of quietness and sharpness 2−73111
  solar right ascension, systematic errors in astronomical ephemerides 2−48788
  solar small scale visible features, application of interferometry 2−55164
  solar soft X-radiation photometry with broad band detectors for signal-energy conversion function 2−73117
  space borne instruments and problems they will help to solve 2−55195
  spectral resolution enhancement technique 2−85059
  spectrophotometric study of weak CN and strong line stars 2−55057
  star catalogue, application of obs. of Moon to improvement of zero-points 2−76044
  star catalogue corrections from satellite obs. 2−62479
  star fields, absolute calibration of objective prism plates for computer reduction 2−75698
  stars, right ascension observations rel. to the Toepfer meridian circle, contact micrometer screw rotation effects 2−51873
  stellar absolute declinations from measured differences of zenith distances 2−48815
  stellar images, statistical analysis of form variations, large-scale TV images 2−48676
  stellar optical energy meas., using Hewlett Packard 3721A correlator. 2−69196
  stellar parallax, first measurements 2−69521
  stellar radial velocity evaluations using standard wavelengths in Fe spectrum 2−48687
  stellar radial velocity tables with heliocentric reductions 2−48686
  sun coronal lines, 5303Å and 6374Å, reduced intensities 2−73110
  supergiant stars, results of observations 2−62482
  Talcott star pairs, working ephemerides for latitudes 0-15 degrees N 2−76046
  time and latitude bulletins of Tokyo astronomical observatory 2−48812
  time and latitude observations for July 1971, Tokyo Astronomical Observatory 2−44814
  Tokyo Astronomical Observatory, time and latitude bulletins 2−75697
  from Tokyo observatory 78632 2−78632
  Tokyo time and latitude bulletins for 1971, October 2−78631
  Tokyo time and latitude bulletins for 1971, September 2−78630
  trigonometric parallaxes, errors 2−69055
  TV cameras, advantages over photographic plates 2−51870
  TV microphotometry of photographic stellar images 2−76045
  UBV, integrated magnitudes, colours, bright galaxies 2−84956
  Upgren's G5-G7 unclassified stars, spectra rel. to densities of G-type dwarfs 2−81820
  u.v. astronomy programme 2−44857
  u.v. sky scan, TD1 satellite telescope 2−58261
  very long baseline interferometry, mapping of radiosources 2−58564
  VRO radiosources extended observations at 750, 1400 and 2700 Mhz for 494 objects 2−81866
  $Me_{50}1(\delta)$ declination catalogue rel. to FK4 and N30 catalogues 2−48679

Astronomical spectra
  see also Atmospheric spectra; Cosmic radiations, radio-frequency; Stars/spectra; Sun/spectra; and other individual astronomical bodies
  Anon 0947 + 31, bright u.v. knots, H II regions 2−84962
  Anon 1242 + 28, bright u.v. knots, H II regions 2−84962
  asteroids, reflection, composition inferred 2−62714
  asteroids, surface composition from spectral reflectivities obs. in 0.3 to 1.1 range 2−81909
  average interstellar radiation density calc, 1250-4250Å 2−75796

Astronomical spectra continued
3C391, radiosource, continuum spectrum effect of interstellar gas 2−58390
3C 120, Seyfert galaxy, optical spectrum 2−58203
CGCG 1622+4112 extremely compact galaxy 2−55018
Coal Sack, southern, formaldehyde absorption 2−69042
Coude spectrogram calibration at Kitt Peak 2−76041
Crab Nebula, interstellar reddening det. from obs. of S II lines 2−58247
Cyg A, radio-galaxy, emission-line spectrum 2−66060
Cyg X-3 radio outburst 2−85023
extragalactic radiosources, flux densities meas. at 111.5 to 606 MHz 2−69125
extragalactic rings 2−58207
galaxies in rich clusters, blue emission-line 2−84961
galaxies southern, with bright nuclei 2−58222
gaseous nebulae, obs. of radio recombination lines 2−75694
gaseous nebulae recombination spectra, pressure broadening of radio recombination lines 2−75693
Giacobinid meteor spectra from 1946 shower rel. to chemical compositions 2−78570
giant planets, determination of H_2/He mixing ratio 2−62693
H II southern regions, H 109α recombination line and continuum obs. 2−69045
Hoffman i.r. sources, OH emission 2−81870
interstellar extinction laws in spiral arms and field regions 2−84980
Jovian atmosphere absorption bands, obs. using Galilean satellite eclipse obs. 2−58490
Jovian visible clouds, structure determ. from methane and H_2 quadrupole lines 2−75875
Jupiter, ^{13}C methane identification and ^{12}C/^{13}C ratio 2−75883
Jupiter, emission between 1200 and 1950 Å 2−75879
Jupiter, H_2 quadrupole lines, level of formation 2−75874
Jupiter, in 3200 to 11200Å region 2−75880
Jupiter, i.r. spectrum and radiative props. of clouds 2−75884
Jupiter, isolated 5μ source obs. 2−75881
Jupiter, NH_3 variations over disk, spectrophotometric obs. at 1.5 μ window 2−75876
Jupiter, quadrupole H_2 absorption 2−75872
Jupiter atmosphere, obs. of singly deuterated methane in 4- to 5-micron spectrum 2−51826
Jupiter decimetre flux density, long-term variations 2−69147
low energy cross sections for transitions between highly excited states, application to interstellar radio recombination lines 2−46405
lunar reflectance ratios, computer generated colour image display 2−66877
lunar surface, spectrozonal map 2−73070
lunar surface comp. mapping using mid-i.r. spectroscopic remote sensing 2−58463
M31, Wing-Ford band at 9910 Å as population indicator 2−58217
M51, UBV photoelectric obs. 2−58215
M81, photometric obs. 2−58214
M 81, photoelectric study 2−66055
Markarian 231, absorption-line Seyfert galaxy 2−66057
Markarian galaxies 2−58205
Markarian galaxies 2−58189
Mars, between 8 and 13 microns 2−62702
Mars, circular polarization spectrum 2−81910
Mars, photometric props., effect of surface roughness 2−44951
Mars, photometry and topography 2−44950
Mars, Syrtis Major blue clearing phenomenon 2−44952
Martian dust storms, CO_2 absorption obs. at 10500 Å 2−81918
Martian i.r. emission spectra, 5-50 μ range 2−75897
molecular u.v. photoabsorption cross sections, critical review 2−42838
molecules in interstellar space, detection and meas. 2−75799
Moon, between 8 and 13 microns 2−62702
moon, effect of soil glasses 2−58464
nebulae, Z-dependence of level intervals in $2s^22p^2$, $2s^22p^3$ and $2s^22p^4$ 2−73114
NGC 1068, Seyfert galaxy, emission line profiles 2−58219
NGC 1068 and 1566 Seyfert galaxies, comparison 2−44842
NGC 2261 cometary nebula, spectrophotometry 2−58237
NGC 3115 and 4472, absorption features in spectra, radial variations in strength 2−51709
NGC 6572, intermediate nebula, i.r. spectrum 2−58249
noctilucent clouds, spectral intensity obs. 2−65822
Nova Cephei 1971, spectrophotometry 2−62572
Nova Delphini 1967, non spherical nebular ejecta 2−62573
Nova Serpentis 1970, infrared spectrum 2−78454
Nova Serpentis 1970, non spherical nebular ejecta 2−62573
Nova Vulpeculae 1968(i), non spherical nebular ejecta 2−62573
open clusters, slit spectra, UBV photometry 2−84955
Orion A, recombination line obs. at Ku band 2−69048
PHL 957, quasar, absorption line profiles 2−58373
photoelectric meas. of 6284 Å diffuse interstellar line 2−58367
planetary absorption line profiles and equivalent widths in spectra from two model atmospheres 2−81930
planetary atm., analytic scattering diagrams for computation 2−44936
planetary atm., cloudy, spectral line formulation , application to Jupiter and Venus 2−62710
planetary nebulae, C IV emission line polarization 2−48669
planetary nebulae, C IV emission spectrum with different excitation conditions 2−48668
planetary nebulae i.r. spectra prediction 2−51716
plasma, astrophysical, atomic spectra 2−75703
plasma spectral intensities and their interpretation 2−74370
profiles of diffuse interstellar lines 2−48728
pulsar dynamic spectrum, interstellar inhomogeneities effect 2−58370
pulsars, H I emission lines at 21 cm 2−48744
quasar redshift and distance 2−69118
quasars, composite spectrum, redshift 2−75820
quasars, excitation of CII line 2−44889
radio galaxies, luminosity-spectral index relationship 2−78481
radio recombination line observations, critical review of available data 2−48737
radiosources, compact, extragalactic, nonthermal, BL Lac type 2−51788

Astronomical spectra continued
radiosources, obs. at 2.7 and 5 GHz 2−75806
radiosources with flat spectra, cosmological implications 2−48751
raindrop size spectra, det. of parameters affecting shape 2−65751
red shift interpret. 2−54993
resolution enhancement technique 2−85059
Saturn, i.r. spectrum rel. to Titan's spectrum 2−81906
Saturn, quadrupole H_2 absorption 2−75872
Sco X-1, less prominent features in optical spectrum 2−58305
FH Serpentis 1970, nova 2−58330
solar flares, 1971, January and September, composition and energy spectra of heavy nuclei, 0.5 to 40 MeV per nucleon 2−58556
supernova in NGC 5253, extragalactic Ca II absorption lines 2−73015
supernova in NGC 5253, interstellar lines 2−81828
supernovae, type I 2−73011
Titan i.r. spectrum, methane bands rel. to Saturn's spectrum 2−81906
Ton 1530, quasar, absorption lines 2−58372
Uranus, in 8060-8360Å region, pressure induced absorptions 2−75913
u.v. absorption in continuous spectrum of Jupiter and Saturn, time variations 2−75869
Venus, microwave spectrum in 18.5-24.0 GHz range 2−62712
Vesta and other asteroids, reflection 2−62713
W33, formaldehyde absorption 2−81869
W3, W49, W51, recombination line obs. at Ku band 2−69048
W 44 supernova remnant, formaldehyde absorption 2−84983
IZw 129, compact galaxy, intwnal kinematics 2−51704
IIZw 70, compact galaxy, internal kinematics 2−51704
^{13}C methane and ^{12}C/^{13}C in Jovian atm. 2−66170
CaI interstellar lines, photoelectric obs. and CaI/CaII ratio 2−78474
H II region, Sharpless 266, i.r. photometry 2−48673
H_2, Lyman band absorptions, equivalent widths 2−56170
H_2 mol., highly excited electronic levels, radio band 2−48732
H_γ spectral lines, influence of shock waves 2−58314
HI regions, u.v. absorption-line spectra, charge exchange reaction effects 2−58243
Hα, Hβ lines, night sky emission, local and galactic contributions 2−62338
He line spectra in gaseous nebulae, level populations 2−48672
N II 6584/Hα line intensity ratio of planetary nebulae in Small Magellanic Cloud 2−44844
O_2 emission in night glow of Martian atmosphere, height of emitting layer 2−55145
OH in interstellar medium, amplified spontaneous emission 2−55075
SIII forbidden lines in diffuse nebulae spectra 2−58242
TiO, α-system, perturbations 2−50070
Astronomical telescopes *see Radioastronomy; Telescopes/astronomical*
Astronomy and astrophysics
see also Cosmology; Infrared astronomy; Radioastronomy
1973 Handbook of British Astronomical Association, ephemerides 2−85073
AFCRL bibliography for Solar System, 1971, first quarter 2−75842
AFCRL bibliography for Solar System, 1971, second quarter 2−75843
American Astronomical Society 137th meeting (April 1972) 2−58152
ASTRA project, air pollution obs. 2−58563
ASTRA project, conference, (Seattle, April 1972) 2−58153
astronautics, conference (Konstanz, Germany 1970) 2−44815
Bode's law and missing planet 2−81928
Carnac alignments of megalithic stones, 1970-1 research work 2−81966
charged particle mass rot. around axis, relative equil. 2−72946
comet astronomy in the USSR, review 2−75919
computer program applications 2−84932
computing methods 2−82284
conference, (E. Lansing, Mich., USA, Aug. 1972) 2−75656
conference, Astronomical Society of Australia, Adelaide, (Dec. 1971) 2−62430
conference, Jerusalem, Israel (May 1972) 2−70340
cosmic rays composition and origin in galaxy of radiation with energies $>10^{15}$ eV 2−62449
dense objects, theories, review 2−62622
dynamic astronomy, meeting (College Park, USA, March 1972) 2−58166
early hadron universe implications of Hagedorn's exponentially increasing mass spectrum for baryons on temperature maximum 2−81767
e.m. and gravitational radiation by sources moving with velocity greater than light in vacuum 2−48642
equilibrium and stability of rotating gaseous systems in magnetohydrodynamics 2−48641
George Ellery Hale, astronomical history, book 2−84946
globular clusters and the distance scale 2−75780
gravitational field, axially symmetric and the Kerr metric 2−82199
gravitational plasmas, non-Markovian time evolution, weakly oscillatory relax. process. 2−68999
hierarchical universe, Yukawa range and cosmological constant 2−58155
high energy, conference (San Juan, Puerto Rico, Dec 1971) 2−62620
high-energy e.m. phenomena rel. to astrophysics 2−78442
IAU constants, reevaluation from space tracking data 2−58441
ill conditioned linear equations, solution method 2−69195
inner bremsstrahlung, X-ray background, steady state universe 2−58434
i.r. and submillimeter background radiation 2−62616
Killing fields of stationary axisymmetric universe, extremal properties of rotating stars in general relativity 2−44851
kinematic dynamo equations, Lagrangians and variational principles 2−56315
lepton nonconservation, consequences in nuclear astrophysics 2−46066
magnetic field generation in large bodies, solar dynamo 2−58542
non-Newtonian gravity, astrophysical test for dilaton theory 2−78796

Astronomy and astrophysics continued

- nucleosynthetic chronologies rel. to ^{146}Sm and p-process nucleosynthesis 2−51686
- orbiting astronomical observatory using 20 Ah Ni-Cd cell 2−85075
- particle acceleration by mag. dipole radiation 2−55936
- plasma phenomena in high energy astrophysics 2−78432
- problems of current interest 2−82086
- radiating particle anomalous motion in strong fields 2−55403
- radiative transfer in line frequencies, approximate soln. 2−75702
- rapid cosmic processes, morphology 2−81749
- rare astronomical phenomena 2−62429
- Rayleigh-Taylor instability, in composite medium 2−67676
- research development in interstellar absorption during 1900-30 period 2−81842
- right ascension derivation from differential obs. with meridian circles and $\Delta\alpha_\alpha$ in FK$_4$ system 2−55194
- solar neutrino problem, discrepancy between astrophysical predictions and terrestial exptl. obs. 2−44979
- solar physics, conference (College Park, Md., USA, April 1972) 2−75935
- stellar evolution endpoints, discussion of various possibilities and relation to phenomena of high energy astrophysics 2−78460
- supergiant stars, colloquium (Trieste, Italy, Sept. 1971) 2−58262
- teaching nonscience students, topical approach 2−78715
- time measures, universal and ephemeris time 2−62431
- uniform model universe, interacting matter and blackbody radiation 2−58154
- uniformly expanding atmosphere, soln. of transport eqn. in vel. field 2−72947
- universal dimensionless formulae for spherical media 2−78712
- universal e.m. background radiation 2−69001
- x.u.v. survey from rocket altitudes 2−58165
- H atoms, collisional excitation and ionization rates rel. to classical and quantum mechanical formulae 2−49977

Atmosphere

- *see also Air; Electromagnetic wave propagation/atmosphere; Ionosphere*
- absorption of solar protons, solar proton event, Nov. 18, (1968) 2−58123
- absorption of sunlight, application of i.r. heterodyne radiometer 2−58549
- aerosol, particle size distrib., photometric obs. 2−75538
- air mass transformation experiment, East China Sea 2−62164
- balancing and damping of gravitational oscillations for forecast models including orography 2−51571
- barotropic current, mountains, coriolis parameter 2−84783
- barotropic planetary boundary layer, universal profiles 2−51567
- boundary layer description, review 2−65694
- CAT, generation by nonlinear waves 2−54831
- clear air scatter layers, meteorological structure meas. by ultra high resolution radar 2−75540
- cosmic rays, effects on neutron component, regression analysis 2−70275
- dew point of gases containing low conc. H$_2$SO$_4$ 2−75536
- diffusion, crosswind shear effects 2−57961
- diffusion and air pollution control 2−62090
- Earth-atmosphere evolution model rel. to Ar excess in submarine basalts 2−72689
- Earth-atmosphere-ocean system, intransitive model 2−44518
- effective emissivity under clear skies, contrib. of H$_2$O, CO$_2$ and O$_3$ 2−51616
- energy spectra, scale representation in terms of degree of Legendre polynomial expansion 2−62182
- evolution, prediction of runaway greenhouse effect 2−73083
- excitation wave propagation following light flash 2−48477
- Fourier truncation and linear digital filtering compared 2−78342
- gamma quanta, generation by cosmic rays, collective interactions 2−73887
- geostrophic turbulence, resolution implications 2−78363
- gravitational potential, effect on geoid 2−54801
- line thermals, lab. study 2−57936
- Martian, O$_2$ emission in night glow, height of emitting layer 2−55145
- mesoscale tropical convection intensity, remote sensing using geostationary satellite 2−44726
- model, homogeneous and inhomogeneous, synthetic absorption profiles 2−66165
- molecular absorption cross sections, photodissociation 2−48548
- with molecular anisotropy, soln. of auxilliary equation of radiative transfer 2−62690
- neutral and stably stratified surface layers, dispersion of matter 2−78369
- numerical models, vertical structure, Laguerre polynomials 2−65649
- O$_2$ and O$_3$ absorption of solar radiation in 2150 Å region 2−65766
- ocean-atmosphere system, albedo calc. from cloudiness data 2−51581
- particle diffusive growth, kinetic equation 2−71248
- penetration of density interface by heavy vortex rings 2−77214
- plane-laminated medium, cumulative distribution of dielectric constant 2−75486
- potential gradient, influence of point discharge current and precipitation on vertical profile 2−65783
- predictability, spatial variations, errors 2−78340
- predictability function for prediction of state given initial imprecisely known state 2−78343
- prediction models, filtered-equation, pressure-coordinate, numerical model 2−44678
- radar wave propagation and sea evaporation effects 2−65629
- radiation, determ. of total outgoing intensity of earth-atmosphere system 2−54810
- radiation balance mapping 2−48506
- radiative equilibrium, effect of various physical factors 2−62262
- re-entry vehicle dynamics, effects on atmospheric data in PAET project 2−75528
- realistic, radiative transfer 2−65754
- remote i.r. imaging instruments, limits operating between 2, 5 and 18 μ 2−44697
- remote probing, statistical methods 2−44683
- remote sensing, conference (Colorado Springs, June 1971) 2−44682
- remote sensing, i.r. and multispectral 2−44577

Atmosphere continued

- remote sensing systems, applic. of Monte Carlo method 2−44751
- resistance law in diabatic Ekman layer, baroclinicity effects 2−51568
- Rossby and pure rotational waves 2−78362
- scalar fields, linear prediction analysis 2−72749
- scale interactions in tropics during northern summer 2−62168
- sea-atmosphere interaction, conference, Ft. Lauderdale, Fla., USA, (Dec. 1971) 2−65637
- solar, upper bound of longitudinal MHD wave frequency 2−74347
- spectra, mm wavelength, by obs. of solar radiation at sea level 2−54852
- steepening of long internal waves in stratified fluid influenced by vertical density profile curvature 2−53148
- stratospheric and tropospheric region, chemistry studied by atomic collision processes 2−44941
- sunrise and sunset, effects on processes in Sun-Earth space 2−65763
- thermal radiation field, spectral angular and height distribution 2−72798
- total incident global radiation under cloudless conditions for high relief areas 2−57988
- turbulence, rel. to air traffic control, laser beam detection 2−78337
- turbulence in dynamic models 2−75555
- turbulence investigated by optical wave, criterion for choice of exposure time 2−81678
- turbulent boundary layer over sloping underlying surface 2−72785
- vertical number density profile of atmospheric gases from stellar occultation data 2−84839
- wave packet propagation in baroclinic shear flow 2−62094
- whistler mode reflection coeff., wave interference effect for model lower ionospheres 2−58072
- zonal kinetic energy balance and effects of Earth's rotation 2−51569
- He gas, instantaneous point source diffusion, within turbulent boundary layer 2−72780

composition

- absorption by minor atmospheric constituents near 8 cm^{-1} 2−51585
- aeronomical balloon obs. 2−72769
- aerosol, Aitken nucleus characteristics correlation with mass concentration 2−78347
- aerosol, continuous sampling device for electron microscopy 2−57945
- aerosol, heterogeneous nucleation effects on cloud and precipitation formation 2−51613
- aerosol, upper atmosphere, rocket mounted laser radar obs. 2−54878
- aerosol, urban, St. Louis, Mo., Lidar obs. 2−62145
- aerosol constituents, optical constants 2−57946
- aerosol height distribution det. by lidar 2−57949
- aerosol models, Mie scatt. by three polydispersions 2−65779
- aerosol particles, condensational growth and particle size distrib. 2−48461
- aerosol particles, det. of water soluble matter 2−44694
- aerosol particles rel. to humidity, extinction coeff. for visible light 2−84818
- aerosol substances, i.r. absorption 2−65777
- aerosols, polydisperse, submicron, size distribution determ. by response matrix method 2−74568
- aerosols and atmospheric chemistry, Kendall award symposium, Los Angeles, (1971) 2−46993
- air pollution, monitoring, state of the art 2−81694
- air pollution, project ASTRA 2−58563
- air pollution mapping, Q-switched ruby laser radar 2−78350
- air pollution meteorology rel. to pollution control 2−75489
- aircraft pollutants rel. to radiation budget of stratosphere 2−65663
- Aitken and cloud nuclei production by urban area of St. Louis 2−65726
- Aitken nuclei, vertical distribution downwind of urban pollution sources 2−48466
- Aitken nuclei and small ions, vertical distrib. up to 6 km 2−51594
- atmospheric, trace material obs. program in atmosphere 2−62152
- atmospheric haze, brown colour from atmospheric aerosol and NO$_2$ content 2−62264
- background contamination, estimation from chemical composition of precipitation 2−54832
- bent over plumes, wet rel. to dry, theory 2−51593
- C, soot, particulate borne, long distance transport in Sweden Sept-Dec 1969 2−72766
- changes between summer and winter rel. to electron density distrib. 2−51649
- cloud condensation nuclei concentration, isothermal determination method 2−62233
- cometary, Tago-Sato-Kosaka and Bennett comets, water in atmosphere 2−58521
- comparitive chloride concentrations, Mauna Loa Observatory and Hilo, Hawaii 2−65673
- correlation interferometry and spectroscopy for aerospace monitoring of earth resource and pollution 2−62159
- deterioration studies by astronomical techniques, symposium 2−51570
- dispersion and chemical reactions in air pollution 2−48454
- dust influx above 30 km, laser radar obs. 2−48470
- electrostatic precipitators, particle charging time 2−62142
- equilibrium layers, epithermal neutrons, energy spectrum 2−48455
- fine structure monitoring, propagation effects using side scatter 2−44695
- gas scavenging by rain 2−72789
- gas trace detection spectroscopy 2−65664
- Hawaii, sources of atmospheric particulate matter 2−54825
- Hawaiian atm. proportions of organic and inorganic particulate matter 2−62153
- heavy metal distribution in vicinity of industrial complex 2−65674
- ice nucleus and chloride particle concentrations at Mauna Loa Observatory 2−65672
- ionosphere 220 to 4360 km, vertical space probe meas. 2−54873
- ions, small and large, density fluctuons 2−48436
- i.r. laser system for long path air pollution monitoring 2−62150
- isokinetic sampler for det. of particulate matter, for use on aircraft 2−57943
- Los Angeles, pollutant monitoring data, time series analysis and forecast 2−57944
- Los Angeles smog, dynamics, physical mechanisms 2−51590
- Los Angeles smog, inadvertent weather modification 2−51572

Atmosphere continued
  composition continued
    Los Angeles smog, size distrib., Minnesota aerosol analysing system obs. 2−51588
    mass spectrometer experiment during Planetary Atmosphere Experiments Test 2−75533
    mesosphere, neutral comp. meas. in ALADDIN I program 2−57952
    mesosphere, positive ion composition obs. during summer at high latitude 2−65829
    mesospheric O_3 abundance, seasonal changes inferred from twilight $O_2(^1\Delta_g)$ emission 2−57951
    methane concentration between 44 and 62 kms altitude 2−65667
    minor components stationary diffusion at night allowing for recombination 2−72773
    monitoring during SiC single crystal growth 2−60704
    neutral density, temp. and press. profiles meas., ALADDIN program 2−57953
    neutral ultrafine particles and small ions, derived from gaseous impurities, formulation and props. 2−51586
    neutrons, large area detector for search in 2-100 MeV range 2−72818
    nighttime number density of O_2 and O_3 from stellar occultation data 2−58034
    noctilucent clouds, heavy metal particles, possible solar origin 2−65888
    overlap emissivity of CO_2 and H_2O 2−57947
    ozone total content correl. with ionospheric D-region radio wave 2−78399
    particles, acoustical counter evaluation 2−51597
    particles, formation and chemical reactions 2−48460
    particles, i.r. spectra monitoring method 2−68885
    particles, optical spatial filtering for detection of shape 2−48462
    Pasadena aerosol, chemical elements, calc. based on source contribs. 2−51587
    Pasadena smog, aerometric factors affecting evolution 2−51573
    Pasadena smog, carbonate and noncarbonate carbon content 2−51603
    Pasadena smog, chemical states of N and S, photoelectron spectroscopy obs. 2−51602
    Pasadena smog, particle mass and size distrib., Minnesota aerosol analyzing system obs. 2−51589
    photochemical model, radiation structure effects 2−65757
    photochemically produced aerosols, mass concentration rel. to light scattering 2−48511
    photochemistry of lower troposphere, steady state model 2−54823
    pollutants conc. rel. to averaging time, statistical principles 2−68887
    pollution, conference (Las Cruces, USA, Dec 1971) 2−62146
    pollution, gaseous, effects on physical props. 2−48471
    pollution, pulsed Raman spectroscopy, applic. of N_2 TEA u.v. laser 2−42025
    pollution, urban technology, conference, San Francisco (1972) 2−82029
    pollution aerosol monitoring by scatter of Ar-ion laser beam, interferometry 2−51600
    pollution control and atmospheric diffusion 2−62090
    pollution effects on cloud condensation nuclei, obs. at Los Angeles 2−65713
    pollution levels in industrial and urban areas of Japan 2−75535
    pollution meas. and environmental investigations rel. to astronomical observations at MT. Hopkins Observatory 2−54859
    pollution monitoring and remote sensing spectrometry 2−75604
    pollution monitoring using on-line computer 2−62091
    pollution studies, using tunable semiconductor laser 2−65675
    pollutions, technical means of reduction 2−75537
    production of cloud nucleates by urban industrialized complex and colloidal stability of clouds 2−65725
    proton pitch-angle distributions in 100-300 keV range, satellite observations 2−65821
    pullutants, remote sensing by light scattering 2−81693
    radiation belt particle-flux limits measured in synchronous orbit 2−65931
    remote sensing of ambient air quality and gaseous pollutant flow 2−84870
    remote sensing of Earth resources and environment, seminar (Palo Alto, USA, Nov. 1971) 2−84767
    S, particulate borne, long distance transport in Sweden Sept-Dec 1969 2−72766
    S budget over N. Europe, emission and deposition 2−54824
    seawater evaporation, migration of chemical components from ocean to atmosphere, ratios 2−62151
    shock layer radiometry of re-entry vehicle in PAET project 2−75534
    sky particulate carrier from light scatt. obs. 2−65778
    smog in Los Angeles, measurement techniques 2−75532
    stratosphere, aerosols, size and composition obs. 2−62156
    stratosphere, air density distribution 2−57938
    stratosphere and mesosphere, model of minor components 2−62155
    stratospheric aerosol levels, 12-25 km 2−81687
    stratospheric water vapour content meas. 2−65665
    surveillance of molecules and intensity studies in terrestrial atmosphere 2−51599
    suspended particulates, evaluation of methods of meas. 2−71245
    suspended particulates, size distribution 2−65677
    thermosphere, equatorial, neutral comp. 2−58033
    thermosphere, longitudinal variations indicating magnetic control of polar heat input 2−65827
    thermosphere, lower, neutral comp. meas. in ALADDIN I program 2−57952
    thermosphere, mass spectrometry and incoherent scatter sounding 2−65824
    thermosphere, minor constituents meas. by mass spectra 2−62295
    thermosphere, molecular O_2 densities from Ariel 3 measurements 2−51631
    thermosphere, neutral composition above Fort Churchill 2−65828
    thermosphere, positive ion composition obs. during summer at high latitude 2−65829
    thermosphere, theoretical and empirical approaches 2−58031
    thermosphere explorer program 2−58032
    thermospheric O_2 abundance variation, 6300Å twilight airglow obs. 2−58055
    total pollution system monitoring concept 2−65407
    trace constituents quantitative meas. by Raman scattering 2−57941

Atmosphere continued
  composition continued
    trace gas analysis, conc. of pollutants 2−54818
    troposphere, clustering of ions 2−62157
    tropospheric aerosols, lidar obs. 2−57942
    tunable dye lidar technique for meas. of atmospheric constituents 2−84868
    upper, det. using linear water cooled ablating-wall flashlamp pumped dye laser 2−73580
    upper, study from stellar occultations 2−54877
    upper atmosphere, distributions of minor neutral constituents, theoretical model, boundary conditions 2−72819
    urban air pollution aerosol model, spectral absorption and extinction coefficients 2−62265
    urban area source pollutants, numerical modelling, advection and diffusion, numerical modelling 2−51605
    v.h.f. and l.f. night recordings (1969-71) 2−75613
    water vapour absorption rel. to surface temperature determinations from satellite radiometric measurements 2−54821
    B exchange between sea and atmosphere 2−57851
    CO, ^{222}Rn and methane conc. correl. with airborne continental dust 2−62158
    CO, atmospheric, trace material obs. program in atmosphere 2−62152
    CO content and seasonal variations in atmosphere 2−81659
    CO mixing ratio decrease at tropopause 2−65670
    CO_2, atmospheric, trace material obs. program in atmosphere 2−62152
    CO_2, atmospheric, varying partial pressure, effect on biological carbon cycle 2−48838
    CO_2, rate of increase, model 2−68886
    CO_2 15 micron band emission using Nimbus 4 selective chopper radiometer 2−65660
    CO_2 and dust monitoring at Mauna Loa 2−62147
    H densities at exobase 2−65832
    HNO_3 vapour in stratosphere 2−51596
    He, thermosphere, longitudinal variations indicating magnetic control of polar heat input 2−65827
    He I density, 10830Å obs. in tropical latitudes 2−65823
    ^3He balance and thermal loss of atmosphere during 1947-68 period 2−78433
    N and NO content variations at 100-250 km height, rel. to solar activity 2−48528
    N_2, thermosphere, longitudinal variations indicating magnetic control of polar heat input 2−65827
    N_2^+, flux in higher atm. at middle latitudes 2−48526
    NO, mesospheric concentration during PCA 2−65666
    NO_2 concentrations, fluorescence obs. 2−81692
    NO_2 photometric measurements using Fabry-Perot filters 2−54827
    Na abundance in upper atmosphere and stratospheric warmings 2−78385
    Na abundances in upper atmosphere, absorption meas. 2−65831
    Na layer, daytime laser radar obs. 2−81703
    O, thermosphere, longitudinal variations indicating magnetic control of polar heat input 2−65827
    O atmospheric concentrations from OI 5577 Å line emission at auroral zone latitude 2−84890
    O concentration, semiannual variations 2−48529
    O concentrations from incoherent- scatter and satellite-drag data 2−65826
    O density in thermosphere, meas. with rocket-borne open-source mass spectrometers 2−68929
    O layer in upper atmos., estimates of height and concentration 2−48527
    O^+, dependence of calculated production rates on solar activity 2−48464
    O_2 concentration, vertical profile, 2-wavelength lidar method 2−62135
    O_2 concentration in 70-95 km region 2−48463
    O_3, atmospheric, trace material obs. program in atmosphere 2−62152
    O_3, biological evolution, possibility of ineffective O_3 screen 2−78348
    O_3, data, lunar influences 2−48469
    O_3, dust and natural radioactivity in urban atmosphere 2−62144
    O_3, power spectrum analysis during summer season, periodicities 2−51598
    O_3, total content and distribution obs. using satellite 2−48456
    O_3 concentrations rel. to aeronomic chemistry of atmosphere 2−84837
    O_3 content, Dobson spectrophotometer, modification 2−75539
    O_3 content, Dobson spectrophotometer and filter ozonometer obs. 2−48468
    O_3 content and dust measurements using multi-colour extinction measurements 2−54858
    O_3 content det. using satellite horizon obs. in 1042 cm^{-1} band 2−48458
    O_3 content during solar proton event 2−84803
    O_3 content from Nimbus 4 IRIS spectral data, elimination of cloud effects 2−65662
    O_3 distrib., troposphere, measurements aboard airliners 2−57950
    O_3 measurements, 1969, April, May and June 2−78351
    O_3 vertical sounding with Nimbus IV i.r. spectrometer expt. 2−48452
    OH, meas. of small relative concentrations using high-power frequency-controlled dye laser 2−42109
    OH concentration, resonance fluorescence obs. using dye laser 2−72765
    Rn, steady-state turbulent diffusion 2−65669
    ^{22}Rn daughter ions, relative concentrations 2−65668
    ^{222}Rn, vertical distrib. up to 6 km 2−51594
    S, effects on crop yields 2−78301
    SF_6 detection, test of airborne gas chomatograph 2−48467
    SO_2 clustering to NO^+ 2−61762
    SO_2 distribution over Hungary, obs. 2−54819
    SO_2 emission estimated from airborne meas. 2−62143
    SO_2 pollutants, detection using current tunable $Pb_{1-x}Sn_xTe$ diode lasers 2−57940
    $^{35}SO_2$, determ. of average concentration in air, method based on selective absorption in oxidant soln. 2−58013

Atmosphere continued
humidity
see also Humidity
aerosol attenuation of visible and i.r. radiation rel. to air humidity 2−81660
aerosol height distribution det. by lidar 2−57949
altitudes above radiosonde hygristor cutoff region, radiometric method for data retrieval 2−48465
over Black Sea, fluctuations at height of 5 m 72768 2−72768
chemical composition, light scattering, aerosols, adsorption 2−83815
cloud data, ground-based, for mesoscale analysis 2−65661
dew point curves and dirunal temp., use in short-range forecasting 2−72763
effect on discharge processes of negative a.c. corona 2−71044
evaporation meas. by pulsation method, humidity sensor 2−54822
Gauhati Airport, upper air mean dry bulb and dew point temp. profiles 2−72757
ice nuclei, time lag in activation 2−57973
light scattering at different RH by atmos. aerosols 2−65780
low lying haze, short term effect on temp. regime 2−72770
lower stratospheric water vapour concentrations, radiometric obs. of variability 2−54826
measurement, absorption hygrometry techniques, models 2−84864
moisture and temperature limits of equilibrium evapotranspiration model 2−57948
New York, vertical moisture content 2−75526
Northern India, dry line, cumulonimbus convection 2−68905
nucleating ability and size of AgI particles 2−48459
potential evaporation, Penman's and Ivanov's methods 2−65676
potential evapotranspiration, calc. by various methods 2−62149
radio telemetering system for meteorological investigations 2−75520
effects on refractive index and density fluctuations over ocean 2−81676
saturated, stably-stratified shear layer, stability 2−62169
synoptic-scale moisture using Nimbus 4 THIR 6.9 micrometer obs. 2−62257
thermal radio emission in submm. wave range as method of obs. 2−48457
troposphere, effect on radiowave range error parameter 2−54868
troposphere, fluctuations in water vapour content, from microwave observations of celestrial radiosources 2−51591
turbulent heat and mass transfer from large-body of water, effect of atm0s. relative humidity 2−57891
vertical profile determination from ground-based passive probing measurements of atmosphereic absorption 2−44693
vertical sounding with Nimbus IV i.r. spectrometer expt. 2−48452
vertical water vapour flux, airborne measurements 2−78349
water vapour profiles, cloud free regions, winds, temperature, microwaves, isentropic analysis 2−83834
ionization *see Atmospheric electricity; Ionization, atmosphere; Ionosphere*
movements
see also Wind
— 2−72788
— 2−72758
advection and diffusion of urban area source pollutants, numerical modelling 2−51605
aerosol pollution, oceanic drift, determ. from elec. conductivity meas. 2−62154
ageostrophic effects on baroclinic instability 2−78361
air flow across mountain barrier, numerical shallow fluid model with variable grid 2−48478
air flow over sudden change of surface roughness, numerical computation 2−48480
air props., sea level to 300000 ft., viscosity, Prandtl no. 2−72760
air trajectories, det. from tetroon flights in planetary boundary layers 2−57965
airflow pattern and droplet trajectories about electrostatic cloud droplet probe 2−57981
amplifying baroclinic waves evolution, pressure area development 2−57954
angular momentum exchange in rotating fluid 2−80430
Arecibo, large nighttime gravity wave 2−65687
atmospheric diffusion equation, tensor form, numerical solution 2−72781
atmospheric gravity waves, perturbation profiles in ionospheric F-region 2−65987
atmospheric surface layer, turbulent diffusion 2−62092
atmospheric type boundary layers with large Reynolds number 2−43235
balance eqn., use for computation of geopotential in tropics 2−62179
baroclinic annulus waves at large Taylor numbers 2−62093
baroclinic instability, post bifurcation stage, finite-amplitude analysis 2−44710
barotropic zonal current, stability properties of nongeostrophic disturbances 2−57959
Benard convection with black and mirror boundaries, radiative stabilization 2−68890
boundary layer, mixed convection over heated horizontal plane 2−80391
boundary layers, aerodynamic characteristics 2−68899
buoyancy, three-dimensional, shape- preserving convective elements, numerical simulation 2−48447
buoyant thermals, dynamics with radiative cooling 2−65657
CAT, detect using lidar 2−81649
causing e.m. wave distortions, h.f. plane wave filter function for folded path 2−75609
circulation, autumnal build-up, cloud bands associated with tropical storms 2−44725
circulation, correlation with macrostructure of interplanetary medium 2−44704
circulation, during last ice age 2−75521
circulation, effect on solar obs. 2−73111
circulation, in snow conditions, dual Doppler radar obs. 2−75552
circulation, orographic induced, radar obs. 2−75553
circulation, test of 26 month cycle hypothesis from monthly number of days with meridional circulation in Europe 2−54577
circulation interaction with Pacific polar front 2−54771
clean air turbulence, remote i.r. detection 2−84866

Atmosphere continued
movements continued
clear air, turbulence, global dynamics, statistical self-similarity theory 2−68898
clear air convection, radar reflectivity and refractive index spectra 2−75614
clear air convective fields, radar and drone aircraft measurements 2−75554
clear air echoes, coexistent waves and turbulence, near marine inversion 2−75546
clear air layer in lower troposphere, study using Doppler radar 2−54834
clear air turbulence, air motion meas. using high-power Doppler radar 2−78366
clear air turbulence, life cycle by mesoscale analysis 2−75544
clear air turbulence, radar and radiosonde measurements 2−75545
cloud motion meas. from geostationary satellite spin scan camera pictures 2−65716
cloud motion vectors, computation of kinematic properties 2−65693
coastal frontogenesis 2−65698
conditions for emergence within F_2-layer at sunrise 2−84909
convective flow, self preserving, energy deficiencies 2−44689
convective instability, friction term formulation 2−78357
convective plumes of cool air 2−65704
cyclone, intermediate scale, numerical simulation of development in moist model atm. 2−84793
cyclone development off N.E. Greenland 2−54837
diabatic processes and generation of available potential energy, multilayer calc. 2−65681
diffusion coeffs. from ALADDIN TMA releases 2−58019
diffusion eqn. for expanding gas cloud in const. shear flow 2−72821
diffusion of particulate and gaseous material in 10-100 km range 2−51592
Doppler spectra, X-band, hailstones, depolarization 2−84830
downward transport of ice-forming aerosols from stratosphere 2−62165
dust storms, radiation fluxes during 2−48505
E-region ionosphere dispersion, Antarctic obs. 2−62370
easterly wave development in tropical Atlantic, satellite study of air disturbance 2−54833
equations of motion, numerical approximations, sources of error 2−81671
equatorial stratospheric waves induced by diabatic heat sources 2−84802
evaporating cloud layer, radar observations of undulance 2−75596
exosphere, mean rot. speed near 550 km, Explorer 24 meas. 2−58052
flow over mountains, three-dimensional effects 2−84814
flow round a storm, study of flow past smooth and rough cylinders as model 2−62185
flow system instabilities associated with clear air turbulence 2−72782
free convection similarity, flows with and without shear 2−78358
frontal motions, instability, fluid mechanics 2−84799
frontogenesis, quasi-geostrophic versus non-geostrophic 2−44675
frontogenesis models, mathematical formulation and solution 2−44676
general circulation, one-dimensional radiation model compared with Mintz-Arakawa model 2−68907
general circulation model, six-layer, new initialization technique for NCAR 2−65683
geostrophic drag, heat and mass transfer coefficients for the diabatic Ekman layer 2−57957
Global Radio Meteor Wind Studies Project 2−58036
global scale circulation cells in tropics with 40-50 day period 2−84800
gravity wave perturbation models 2−72822
gravity wave phenomena accompanying cyclogenesis on East Coast 2−65697
gravity waves, effect on ionospheric parameters determined during vertical sounding 2−72877
gravity waves, frequency spectra, from ionospheric electron content 2−57983
gravity waves, internal standing, breaking mechanism, in atmos. and ocean 2−72776
gravity waves, rel. to dynamics of atmos. 2−72777
gravity waves, supersonic cooling region during solar eclipse 2−84835
gravity waves from tropospheric winds, jet streams, weather fronts and thunderstorms 2−57955
heat island formation, numerical expt. 2−75527
horizontal motions, energy spectrum of synoptical processes 2−48472
hydrodynamic barrier flow rel. to weather forecasting 2−65635
hydromagnetic waves launched by expanding metallic sphere 2−65686
inertia in ocean and atmosphere and long-range forecasting 2−62123
inflection point instability mechanism 2−78360
inter-tropical convergence zone, seasonal variations, interacting atmosphere and ocean model 2−72734
internal gravity wave, self destructing 2−78355
internal gravity wave spectra, wave number dependence 2−65690
internal gravity waves, nonlinear model of break-up due to exponential growth w height 2−65689
internal gravity waves and turbulence, ALADDIN I obs. 2−58038
inversion, strong, low-level subsidence, diagnosis 2−62127
ionospheric micropulsations from finite source, ground signal rel. to Pc 1 disturbances 2−65960
ionospheric propagation of oblique hydromagnetic plane waves at micropulsation frequencies 2−65959
jet streams over India in winter 2−65685
jet-stream model with thermodynamic parameter of cloud convection 2−81656
Kelvin Helmholtz billows in upper tropospheric jet stream, radar Doppler meas. 2−75541
kinetic energy spectrum of large scale atmospheric flow, power law 2−84844
kinetic energy spectrum power laws using spherical harmonic functions 2−75558

- **Atmosphere** continued
  - **movements** continued
    - Lake effect storms, mesoscale numerical model 2−84794
    - Lake Michigan, effect of cold water on atmospheric circulation 2−65691
    - Lamb waves in presence of realistic temp. and dissipation distribs. 2−65688
    - large cooling tower plumes, rise and condensation 2−75556
    - large scale processes, influence of Earths surface 2−48440
    - large-scale flow and dynamic parameters, prediction of precipitation 2−65715
    - laser anemometer, Doppler difference method, automatic data processing system 2−84789
    - lower troposphere, aerosol motion and wind velocity by Doppler optical radar 2−78359
    - macroscale-mesoscale numerical model and intense mesoscale baroclinic development 2−62161
    - magnetosphere, barium ion cloud expt., analysis of optical data obtained by NASA 2−62299
    - magnetospheric compressional wave propagation to the ground 2−68935
    - magnetospheric connection, effect of polar cap elec. fields 2−65962
    - magnetospheric convection obs. from Ba cloud motions 2−62298
    - magnetospheric plasma velocity, nucleation of artificially deposited Ba ion cloud striation 2−62301
    - maintenance of axisymmetric part of flow 2−51608
    - mean rotational speed determinations from orbit of Cosmos 307 rocket (1969-94b) 2−54989
    - mesoscale convection processes 2−72738
    - mesoscale quasi-geostrophic vertical motions associated with squall line 2−62174
    - mesosphere and stratosphere, temp. changes and circulation changes in winter 2−62133
    - minor components stationary diffusion at night allowing for recombination 2−72773
    - momentum and heat transports, non-geostrophic baroclinic stability 2−58481
    - momentum transfer from ambient magnetospheric to seeded Ba plasma, NASA/MPE cloud expt. 2−62300
    - monsoons of southern Asia, review 2−48485
    - morning glory, atmospheric hydraulic jump in Gulf of Carpentaria 2−51604
    - motion with radiative dissipation, linear harmonic analysis 2−68891
    - mountainous terrain, potential analysis 2−44690
    - Navier-Stokes eqns., solns. for hydrocyclone with central air column 2−83454
    - neutral, importance of nonlinear term in equation of motion 2−48474
    - neutral wind motions from Ba ion cloud releases, observational problems 2−72820
    - night time inversion, dynamic stability of coupled wave-turbulence system in parallel shear flow 2−68892
    - Northern Hemisphere general circulation rel. to drought in northeast Brazil 2−84849
    - numerical circulation model, use of satellite radiance meas. 2−62134
    - Pasquill stability classes, turbulence intensity and stability ratio measurements 2−65692
    - passive scalar dispersion in non-uniform turbulent flow, Wiener-Hermite expansion 2−56325
    - Pc 1 hydromagnetic wave propagation across North America 2−68936
    - penetrating convection, model 2−48451
    - persistent, intense, clear air turbulence in upper level frontal zone 2−57966
    - planetary boundary layers, neutral and unstable, numerical investigations 2−44672
    - plasmasphere, convection penetration 2−58048
    - plasmasphere bulge interpret. as due to short- duration gusts 2−58051
    - plasmasphere-plasmapause dynamics 2−58046
    - point explosion in arbitrary atm. 2−84817
    - polar thermospheric winds, convection electric fields in ionospheric model 2−65855
    - pollutants propagation over large distances rel. to vertical diffusivity with time and height 2−81661
    - precipitation patterns, modelling, mesoscale rain areas, cells 2−84823
    - predictability with aid without random external forces 2−62163
    - prediction, long-term 2−62162
    - premonsoon squall lines, Gauhati Airport, radar obs. 2−62167
    - pressure gradient effects on flow 2−78341
    - quasi-biennial cycle of tropical stratosphere 2−84798
    - quasi-geostrophic flow, generalized potential vorticity equation 2−57857
    - radiative transfer in atmosphere-ocean system, Monte Carlo calcs. of the flux 2−65627
    - radiative transfer in atmosphere-ocean system, Monte Carlo calcs. of radiance 2−65628
    - radiative-dynamical model for static stability of rotating atmospheres 2−58480
    - rain drop size distribution determ. by radar, errors rel. to vertical air motion 2−75592
    - rising plume, viscous dissipation contribution to atmospheric temp. 2−62137
    - Rossby wave motion, barotropic instability 2−48473
    - Saharan air outbreaks over northern equatorial Atlantic 2−54829
    - saturated, stably-stratified shear layer, stability 2−62169
    - seeded convective storms, ice form. mechanism 2−84856
    - south coast of England, sea breeze front 2−54838
    - Southern Ocean cyclones, available sensible heating, generation by sensible heating 2−65695
    - springtime anomalous atmospheric circulation rel. to prediction of summer rainfall and temp. for England and Wales 2−75518
    - stable stratification, mechanism of blocking 2−67710
    - stagnation periods, simulation of wind conditions 2−75557
    - stationary barotropic flow crossing a meridional mountain barrier 2−54835
    - STORMFURY project, numerical expts. on artificial heating of eyewall 2−62187
    - storms and depressions, movement in Bay of Bengal 2−62166

- **Atmosphere** continued
  - **movements** continued
    - stratified Eikman boundary layer instability and internal gravity wave generation 2−57958
    - stratosphere, half-yearly temperature wave obs. 2−62140
    - stratospheric air detection at Earth's surface 2−65809
    - stratospheric circulation patterns, large scale 2−72778
    - surface layer turbulence, cospectral similarity 2−68895
    - surface layer turbulence, over water, velocity and temp. fluctuations 2−68903
    - surface layer turbulence, spectral characteristics 2−65696
    - surface layer turbulence over water, instrumentation 2−68902
    - synoptic scale flow, influence of mesoscale latent heat 2−65679
    - synoptic-scale motion, two-layer numerical model of orography 2−65680
    - temperature wave propagation in non-grey radiative fluid 2−65656
    - theory of linear oscillations of dissipative atmosphere 2−84838
    - thermal convection in polytropic atmosphere rel. to structure of thermics 2−68881
    - thermal influence on stability of motion 2−62170
    - thermosphere, one- and three-dimens. model obs. 2−58039
    - thermosphere dynamics, boundary conditions problem 2−84804
    - thermosphere energy source, convection elec. fields 2−58041
    - thermospheric winds role in F_2 layer maintenance 2−58093
    - three-layer atmosphere model with isentropic stratosphere, instability 2−84845
    - tornadic storms, radio noise obs. 2−84813
    - tornado, effects of ground roughness, laboratory simulation 2−48482
    - tornado dynamics, obs. using lab. model 2−84809
    - Tornado funnel, force field required to maintain dynamics and shape 2−62186
    - transfer velocity of pressure fluctuations near ground surface 2−68882
    - travelling ionospheric disturbances, theory and expt. 2−72873
    - tropical cyclones, as origin of longitudinal microseismic waves 2−61888
    - tropical disturbance, radiative interactions 2−65762
    - tropical disturbances, balance model in conditionally unstable atmosphere 2−57956
    - tropical storm development conditions 2−62188
    - tropical stratosphere, deduced from satellite tracking of horizontally floating balloons 2−72779
    - tropical stratosphere air motions, from satellite-tracked horizontal floating balloons 2−57962
    - tropical wave disturbances, empirical orthogonal functions time series, frequency domain, Rossby-gravity waves 2−84821
    - tropics, general circulation, numerical simulation expts. 2−84797
    - troposphere, extreme highs, indices of energetic solar events 2−62125
    - troposphere, turbulent kinetic energy 2−72775
    - tropospheric wave motions with baroclinic basic flow in equatorial latitudes 2−84847
    - turbulence, Doppler radar observations at vertical incidence 2−75550
    - turbulence, filtering, radar pulse volume 2−75549
    - turbulence, filtering of radar pulse volume measurements 2−75551
    - turbulence, hybrid analogue data acquisition system 2−78353
    - turbulence, incoherent radar meas. 2−75542
    - turbulence, intermittent, energy budget 2−44702
    - turbulence, intermittent, phase angle considerations in modelling 2−48479
    - turbulence, near ground level, determ. from optical spherical wave propag. 2−81684
    - turbulence, predictability calc. ω test field model 2−65682
    - turbulence, sensing based on wave mechanics theory 2−44705
    - turbulence, small scale, optimal choice of parameters of airborne hot-wire anemometer for obs. 2−44680
    - turbulence, temp. gradients 2−44703
    - turbulence and dispersion parameters, direct determination 2−44701
    - turbulence effect on wind and temp. profiles 2−62172
    - turbulence intensity within canopies with simple and complex roughness elements 2−72772
    - turbulence resolution by line-of-sight microwave propagation expt. 2−68897
    - turbulence structure function, radar measurements 2−75548
    - turbulence structure of surface layer, modelling 2−62160
    - turbulent, predictability 2−84795
    - turbulent boundary layer flow over surface distorted by water waves 2−84717
    - turbulent clear air, veloc. field meas., by Doppler radar 2−75543
    - turbulent Ekman boundary layer, laboratory study 2−54828
    - turbulent elements in atmosphere, size distribution using solar scintillation meas. 2−62171
    - turbulent flow, effects of evaporation on stability, and radiation on temp. fluctuations 2−44699
    - turbulent flux near ground, field measurements 2−78354
    - turbulent fluxes over snow 2−72737
    - turbulent kinetic energy, dissipation, aircaft measurements 2−68896
    - turbulent transports, near ground, on-site data analysis 2−78352
    - two-dimensional turbulence, numerical simulation studies, models of statistically steady turbulence 2−68893
    - unstable baroclinic waves, limit cycles 2−44709
    - upper atm. superrotation theories, review 2−75620
    - upper atmosphere wind speed and direction, air density and temperatures up to 95 km, simultaneous meas. using chaff cloud sensors 2−54876
    - upper tropospheric frontogenesis, non-Boussinesq effects 2−68894
    - urban area, two-dimensional numerical simulation of warm, rough flow 2−75574
    - velocity fluctuations over tidal mud flat 2−81662
    - vertical circulation of troposphere, radiation induced, magnitude and character 2−68889
    - vertical turbulent diffusion coefficient variations above flat ground 2−72759
    - vertical velocity distrib. in westerly disturbance determ. by numerical soln. of diabatic quasi-geostrophic omega eqn. 2−62131
    - vertical velocity profile including orographic effects, geopotential calculation model 2−81655
    - vertical wind structure, effect on aspects of convective activity at Bombay 2−62178

Atmosphere continued
movements continued
vertically propagating planetary waves, effect of i.r. radiative transfer and frictional dissipation 2−65684
v.l.f. disturbances assoc. with solar X-ray bursts 2−73119
v.l.f. field, computation of height dependence 2−72806
vortex street phenomena, Lin parameter, obs. above Canary islands 2−44698
vortices, columnar, concentrated, structure and dynamics 2−80156
vortices, tropical cyclones, dynamics 2−78367
vortices leeward of islands, velocity field 2−48481
vorticity balance at 200 mb in tropics during northern Summer 2−84801
vorticity flow, nonuniform turbulent streams 2−72774
Wangara, west wind belts, vertical propagation of angular momentum 2−65712
wave disturbances, cross spectrum analysis empirical orthogonal functions, frequency domain, time series 2−84820
wave momentum flux rel. to GARP weather forecasting 2−65678
waves, interaction with ionosphere 2−44671
waves in equatorial stratosphere generated by tropospheric heat sources 2−48448
weak cyclones and tropical waves, satellite obs., intensity evaluation 2−57960
wind computation by forced adjustment to height field 2−44714
wind erosion, soil particles, aerosol size distribution, vertical flux 2−84827
wind field, adjustment to geopotential data in primitive equations model 2−84796
wind patterns, model calcs. 2−58040
wind profile development above locally adjusted sea surface 2−44707
wind waves and swell, differential low of hydrometeorological characteristics distrib. 2−44636
windfield in northern hemisphere, zonal harmonic analysis, rel. to geostrophic flow pattern 2−48476
zonal circulation in equatorial region, baroclinic model 2−81654
zonal winds in upper atmosphere from orbit analysis of Cosmos 316 (1969-108A) 2−51632
He cloud diffusion, neutral turbulent boundary layer, simulated point-source, downstream cross sections, statistical parameters, concentration 2−84825
Rn, steady-state turbulent diffusion 2−65669
SF_6 as gas-air tracer 2−62095

precipitation
see also Ice; Rain; Snow
air bubble in hailstones 2−78371
Aitken and cloud nuclei production by urban area of St. Louis 2−65726
Alberta hailstorms, aircraft seeding using pyrotechnic flare system 2−65746
Arctic ionosphere auroral precipitation patterns, airborne observations 2−84907
areal coverage in N.W. Utah, probability prediction 2−57976
artificially induced, cloud seeding with organic substances 2−65753
aurora, ^{4}He flux precip. meas. 2−65910
auroral electrons, twin payload obs. 2−62344
as auroral hisslers generation mechanism 2−65918
auroral latitudes, energetic heavy ion obs. during mag. storm 2−65911
auroral oval, polar rain 2−65913
auroral zone, field-aligned electron precip., morphology 2−65908
backscatter obs. at 1.8 cm with polarization diversity radar 2−75579
British Isles, westerly type rainfall and atmospheric mean sea level pressure 2−54842
chemical composition and estimate of atmospheric background contamination 2−54832
cloud condensation nuclei, air pollution effects, obs. at Los Angeles 2−65713
cloud seeding, electrostatic techniques 2−62191
cloud seeding, system for direct detection of effects 2−65734
cloud seeding materials, target area persistence 2−65732
cloud seeding simulation in mountain cumuli numerical model 2−65735
clouds 2−84836
colloidal stability of clouds and production of nucleates by urban industrialised complex 2−65725
continental convective clouds randomized seeding 2−62216
convective cloud development in Texas 2−62215
convective shower cells, radar obs. in alpine regions 2−65782
cosmogenic radionuclide scavenging 2−62237
deposited snow, measurement of specific surface 2−75441
detection by acoustic echo sounding 2−62234
distribution rel. to wind direction, source areas of positive anomalies 2−62200
drizzle drops, effect of fluctuations in vertical acceleration on coalescence growth 2−48491
droplet growth, heat conduction constraint 2−43301
electrons, in radiation belts, ang. distrib. and energy spectra 2−65938
formation, atmospheric aerosols as heterogeneous nuclei 2−51613
formation of two dimensional ice embryos on basal and prismatic faces of ice crystal 2−48497
formation of water droplets and ice crystals in deep cloud cover 2−68875
freezing of water drops by contact with CuS particles 2−48499
frontogenesis, quasi-geostrophic versus non-geostrophic 2−44675
frontogenesis models, mathematical formulation and solution 2−44676
gas scavenging by rain 2−72789
ground clutter effects on Z-v_{rms} relationship for statiform rain at vertical incidence 2−75595
groundwater fluctuations in Delhi in relation to rainfall, mass-scale study 2−62261
growing water drop rel. to diffusion-kinetic approach 2−56471
hail formation in steady convective cloud 2−72792
hail growth by stochastic collection in cumulus model 2−44719
hail rel. to organized updrafts at thunderstorm bases 2−65748
hail seeding, simple technique for determining location of AgI particles 2−65747

Atmosphere continued
precipitation continued
hail suppression in Texas 2−62217
hail suppression program, seeding technique 2−62196
hailstorms, multi-cell, structure and motion 2−48503
hailstorms, severely sheared storms, structure and motion 2−48504
hailstorsms, supercell, structure and motion 2−48502
ice embryos, high temperature contact nucleation, supercooled water, organic chemicals 2−84828
ice particle growth from vapour and cloud drop accretion 2−54849
ice particles in clouds over Pacific Northwest, techniques for collection and automatic counting 2−54850
ice phase from orographic clouds, numerical model 2−65730
influence on vertical profile of potential gradient 2−65783
internal circulation for drops falling at terminal velocity in air 2−64414
laser radiation in turbulent weak drizzle, intensity fluctuations spectra 2−75607
loss cone electron fluxes during strong precip. events 2−65835
monsoon period in S.W. India, rainfall and floods 2−62230
National Hail Research Experiment, NOAA objectives 2−65736
natural and AgI freezing nuclei, behaviour during repeated freezing 2−48500
operational hydrology, use of radar data from D/RADEX 2−75581
orographic, natural efficiency 2−65729
patterns, storms, mesoscale rain areas, cells, modelling 2−84823
Peninsular Spain rainfall obs. 2−65752
prediction from large-scale flow and dynamic parameters 2−65715
primitive equation multilayer model for forecasting in N.E. coastal sections of USA 2−44724
radar and raingauge meas. of precipitation in Welsh hilly region 2−75589
radar echo from precipitation, spectrum shape at 3.2 centimetre wavelength 2−81658
radar echo intensity and modified coeff. for weather radar eqn. 2−75508
radar evaluation of artificial precipitation enhancement using computer 2−75585
radar meas., accuracy of estimates of surface precipitation 2−65750
radar meteorology in Soviet Union during 1970, review 2−75488
radar obs. of anisotropy of media 2−62238
radar obs. of variation of precipitation echoes with respect to their aerial coverage at Gauhati airport 2−62228
radar raingauge system for accurate precipitation measurements 2−75594
radiation meas. w. SIRS-B, precipitable water 2−62258
radioactivity and fall-out, relationship to precipitation 2−62282
rain modification evaluation by rain cell approach 2−65728
rain shower formation by AgI seeding, related calculations 2−65749
raindrop size rel. to drop impaction 2−65714
rainfall and runoff data, conceptual anal. with hybrid computer 2−78302
rainfall anomalies in randomized seeding project 2−62222
rainfall augmentation via warm rain process 2−62205
rainfall rate-attenuation relationship, variability 2−75597
rainfall rate-radar reflectivity relationships for individual storms 2−48494
rainfall-runoff regression with logarithmic transforms and zero's in data 2−78375
runoff producing rainfall, stochastic model for summer type storms 2−62119
runoff volumes from small urban watersheds 2−57824
Santa Barbara aerial seeding program (1971-72) 2−65641
satellite data rel. to precipitation estimates for hydrologic applications 2−84869
scavenging by falling water droplet, particle size effect 2−75599
seedability and horizontal dimension of convective events 2−62212
from seeded convective storms, Ag fallout patterns 2−62220
seeding potential and thermodynamic characteristics of central Sierra snowstorms 2−65731
serially correlated normally distributed rainfall durations generation 2−57982
stratiform precipitation structure rel. to bright double band radar observations 2−75587
supercooled cloud droplets and ice particles, airborne obs. of distribs. 2−54848
T in daily rainfall, Rhodesia, indicator of airmass source 2−72795
terminal velocities of ice crystals in air, equivalent metal disk models 2−57972
thunderstorms, efficiency in high plains 2−62176
thunderstorms in northeastern Colorado, radar climatology 2−65702
urban areas effects 2−65724
urban weather modifications, integrated cloud physics approach 2−54846
water aerosol droplets, capture by plane stellate crystalline obstacles 2−71247
water-affected fraction of natural 1.5-9 μ diam. aerosol particles 2−75598
weather modification, a review 2−62104
western France, ground seeding for hail prevention, economic efficiency 2−62218
winter orographic, radar obs. of small scale structure 2−75582
wintertime, project Snowman evaluation 2−62199
wintertime orographic randomized seeding project 2−62201
^{18}O and deuterium content, model 2−62240

radiation belts
cross L diffusion of belt particles, preservation of second adiabatic invariant 2−65927
differential energy spectra of electrons in inner and outer belts, ionizing radiation at 200-300 km 2−48557
DR-currents and middle lattitude red arcs, dynamics during magnetic storm 2−48558
dynamical model of belt in self-consistent magnetic field 2−62349
electron, formation of slot between inner and outer belts 2−62350
electron precip., ang. distrib. and energy spectra 2−65938
electron spectra of inner belt in 0.13−15 MeV range 2−72844
electrons, inner and outer zone, formation of quiet time electron slot 2−72830
geomagnetic field distortions rel. to radiation belt particles 2−62382

Atmosphere continued
radiation belts continued
geomagneticall trapped electrons, effect on geomagnetic storms 2−78406
geomagnetically captured protons, energies > 350 MeV, generation by atmospheric and non adiabaticity 2−54886
geomagnetically trapped alpha particles, time variations of intensity 2−65937
geomagnetically trapped protons, differential energy spectrum 2−65930
high latitude boundary of stably trapped radiation zone on day-side of magnetosphere 2−44746
inner, composition of fast charged particles 2−51640
inner, trapped alpha particle flux distrib. 2−65935
inner proton belt, effect of secular mag. variation 2−65926
inner zone, decay lifetimes of electrons generated by Starfish nuclear explosion 2−72846
low energy electron fluxes variation with direction of interplanetary mag. field and geomagnetic activity 2−65858
low energy trapped protons, changes in distribution associated with magnetic storm 2−65924
magnetosheath particle precipitation, effects on dayside ionosphere 2−58073
nuclear explosion effects, hard radiation meas. 2−51639
outer, strong pitch angle scattering of energetic electrons in presence of electrostatic waves 2−65929
outer zone, behaviour during magnetospheric substorms 2−81709
partial ring current, field asymmetry 2−48559
particle-flux limits measured in synchronous orbit 2−65931
proton spectra of inner belt, long-term variations 2−72843
protons, effect of solar neutron burst 2−62348
protons, satellite instrument for obs. in energy range 0.1 MeV to 6 MeV 2−65923
protons in ring current diffusion by turbulent electrostatic oscillations 2−68940
ring current, decaying, as source of large scale magentospheric electric fields 2−78386
ring current effect on F-region disturbance 2−72896
ring current effects, magnetospheric electron density profiles 2−54880
ring current growth rel. to growth rate of main phase field 2−72845
solutions representing dipole field immersed in plasma 2−43130
Starfish nucl. explosion electron decay time limits 2−65934
trapped alpha particle intensity and $j\alpha/jp$ ratio meas. during geomag. storm 2−65936
trapped and precipitated protons, in magnetic storm of March 8, 1970 2−48556
trapped particle redistribution, correlation with interplanetary magnetic field fluctuations 2−65925
trapped particles, response to collapsing dipole 2−68957
trapping boundary, behaviour of low energy particles during substorms 2−81711
trapping boundary and field-line motion during geomag. storms 2−65932
Van Allen, proton shielding of space vehicles 2−85065
whistler instability in anisotropic plasma, simulation 2−60283
whistler-mode waves, v.l.f., in slot region 2−65868
C, N, O, geomagnetically trapped 2−65933
radioactivity
see also Fallout
— 2−72795
aerosols, nuclepore and golden membrane filters for meas. 2−84819
automated atmospheric Rn sampling system, critique 2−62283
biosphere, book 2−73177
contamination by gases and aerosol particles, estimation methods 2−58012
fallout, conference (Mishima, Japan, Nov. 1971) 2−62284
fallout, secular effects in atmospheric electricity 2−65805
fallout in rain, Melbourne, (1958-1970) 2−72814
fission fragments localization from high- altitude nuclear explosion 2−51630
gross β-radiation, measurement 2−62290
ground level monitoring and indicator of tropospheric and stratospheric sources 2−65806
interhemispheric transport of radioactive debris, role of Indian monsoons 2−65807
liquid scintillation α-particle detection applics. 2−70297
low level contamination near nuclear power station, use of tacky cloth collectors 2−58010
Mediterranean and Atlantic Ocean near water atmospheric layers 2−54820
monitoring for air contamination with personal air samplers 2−58011
natural, diurnal variations in air borne dust 2−62287
nuclear fallout and release from nuclear power stations, γ-spectroscopic obs. 2−72690
nuclear power stations, health physics aspects of environmental monitoring in event of accidental release of radioactivity 2−55226
nuclear reactors in Canada, releases of radioactivity and heat 2−62292
population exposure from planned or accidental releases of radioactivity to environment, estimation method 2−55298
and precipitation, relationship investigated 2−62282
Starfish nuclear explosion, decay lifetimes of artificial electrons 2−72846
stratospheric air detection at Earth's surface 2−65809
urban atmosphere, meas. 2−62144
α-activity in air near ground, meas. method and results 2−84850
^{14}C, lightweight molecular sieve stratospheric sampler 2−65804
^{14}C environmental contamination due to nuclear power stations 2−54871
^{141}Ce-^{144}Ce, isotopic activity ratios in rainwater 2−62289
^{38}Cl, ^{39}Cl, model for in-cloud scavenging 2−65808
^{3}H contamination, thermoluminescence dosimetry obs. 2−62291
^{24}Na, model for in-cloud scavenging 2−65808
^{63}Ni contamination, thermoluminescent dosimetry obs. 2−62291
^{210}Pb, in area of Roumania with increased natural background, meas. of absorption levels in population 2−58633
^{147}Pm contamination, thermoluminescence dosimetry obs. 2−62291
Ra daughters det. by α- spectrometric extrapolation method 2−75615

Atmosphere continued
radioactivity continued
Rn daughters, analysis methods, comparison using computer simulation 2−62288
Rn(A = 220, 222) activity and potential alpha energy in different air atmospheres 2−56078
^{222}Rn, ^{220}Rn and daughters, concentration in air in radon-spa dependence on meteorological variables 2−58014
^{222}Rn and daughter ions, vertical profiles in air layer adjacent to ground 2−54870
^{222}Rn and daughters, captive balloon measurements 2−68923
^{222}Rn daughter ions, numerical study of diffusion in fair weather and thunderstorms 2−62184
^{103}Ru-^{106}Ru, isotopic activity ratios in rainwater 2−62289
$^{35}SO_2$, determ. of average concentration in air, method based on selective absorption in oxident soln. 2−58013
^{90}Sr and ^{89}Sr fallout from Chinese nuclear tests 2−62285
^{90}Sr fallout, bearing on weather conditions 2−62286
^{238}U, in area of Roumania with increased natural background, meas. of absorption levels in population 2−58633
structure
cloud vortices, southern hemisphere, surface pressure anomaly patterns, classification schemes, models 2−84822
Planetary Atmosphere Experiments Test Project, terrestrial atmospheric structure meas. 2−75855
storms, modelling, precipitation patterns, mesoscale rain areas, cells 2−84823
stratified Ekman boundary layer, inflection point instability 2−78356
surface boundary layer, stratification, wind profile 2−84782
waves, planetary-scale, travelling components estimated 2−62120
temperature
— 2−62292
aerosol effect on flux of i.r. radiation 2−62129
aerosol interaction with outgoing terrestral radiation 2−65653
ALADDIN TMA release meas. 2−58019
anomalies of monthly mean, prediction 2−54812
Arcasonde-1A temperatures, magnitudes and uncertainties of corrections 2−65818
atmospheric aerosols, climatic effects rel. to direct solar radiation heating 2−65767
Baffin Island, increased glacierization and climatic cooling trend 2−51527
Baltic coastal region, temp. variations, internal Kelvin waves 2−72758
Benard convetion with black and mirror boundaries, radiative stabilization 2−68890
buoyant thermals, dynamics with radiative cooling 2−65657
cometary, Tago-Sato-Kosaka and Bennett comets 2−58521
convective field in clean air, plume theory 2−44686
deviations from International Standard, effect on barometric altimeters 2−48638
diabatic processes and generation of available potential energy, multilayer calc. 2−65681
diffusion model for thermospheric density-temperature phase delay 2−65816
diurnal temperature variations with height over sea 2−62136
equatorial stratosphere, diurnal variation 2−68883
e.u.v. heating of atmosphere, annual and sub-annual effects rel. to density variations 2−84841
exospheric temperature, semiannual change 2−68938
fluctuations, in atmospheric boundary shears, meas. by infra-sonic wave propagation expt. 2−54816
forecasting temp. for gas and electricity industries 2−75531
Gauhati Airport, upper air mean dry bulb and dew point temp. profiles 2−72757
gradients associated with turbulence 2−44703
greenhouse effect on ambient air temperature distribution 2−72756
heat island formation, numerical expt. 2−75527
height distribution for neutral atmosphere, MR12 rocket probe meas. 2−54874
high-wavenumber, turbulent temp. fluctuations over tidal mud flat 2−81662
homogeneous, above basement layer, radiant heat exchange 2−48444
inversion, strong, low-level subsidence, diagnosis 2−62127
ion temperature errors in retarding potential analyzers, grid-plane potential 2−68927
i.r. cooling rate over S. Norway, Rodgers' method 2−54813
irregular variations between 50 and 200 km 2−72764
limb radiance obs., improved algorithm for inversion 2−62250
limb radiance obs., radiative response of atmos. 2−62249
lower thermosphere, variation with latitude 2−72817
macroscale-mesoscale numerical model and intense mesoscale baroclinic development 2−62161
mesoscale latent heat, influence on synoptic scale flow 2−65679
mesosphere, vertical temp. struct., effects of latent heat release in troposphere 2−72761
mesosphere and stratosphere, temp. changes and circulation changes in winter 2−62133
microthermal fluctuations, detm. of astronomical seeing and telescope modulation transfer function 2−73160
motion with radiative dissipation, linear harmonic analysis 2−68891
mountainous terrain, potential analysis 2−44690
neutral-particle wake method for satellite-borne temperature measurements 2−68925
Nibmus 4 i.r. spectroscopy, calibrated thermal emission spectra 2−65765
nocturnal profiles for Edmonton, Alberta 2−48450
palaeotemperature data, cyclic temperature oscillations from 0-20300 yr. BP 2−51583
particulate layers effect on i.r. transfer 2−62130
potential energy in atmosphere, theoretical calculation 2−57989
profile derived from satellite radiation meas. simulation of effect of varying atmospheric statistics 2−62138
profile det. using Raman backscatter 2−44691
profiles, microwave emission, atmosphere O_2 angular scan, multi spectral measurements, radiometers 2−84826
profiles, real-time retrieval from satellite obs. for dynamic forecasting 2−48449

Atmosphere continued
temperature continued
radiative heating, effect of changing CO_2 concentration 2−72800
radiative transfer, conf., August 1972, Colorado 2−62248
radio telemetering system for meteorological investigations 2−75520
radiometer, 60 GHz, for outside air temp. 2−62141
radiometer system for ground-based temperature measurement of upper atmosphere 2−68928
effects on refractive index and density fluctuations over ocean 2−81676
remote sensing of temp. profiles, optimization of spectral intervals 2−78339
satellite i.r. spectrometer data, insertion into forecasts 2−62139
satellite radiance meas., insertion into numerical circulation model 2−62134
sensors, airborne, anal. of time responses 2−55815
SKUA rocket sonde temp. sensor, corrections 2−44692
snowmelt flood discharge in mountainous catchment, northern Iran 2−68856
solar eclipse, 1970, March 7, atmospheric pressure and temperature changes during totality 2−57937
solar EUV heating, annual and subannual effects, comparison with density obs. 2−58028
solar EUV heating, annual and subannual effects, harmonic analysis 2−58027
stability in lower atmosphere, radar meas. 2−75547
stratification, fine structure 2−48445
stratosphere, half-yearly temperature wave obs. 2−62140
stratospheric structure from limb radiance profiles 2−62128
stratospheric temp. and height distribs. from Nimbus III radiation data 2−68884
stratospheric warmings and Na abundance in upper atmosphere 2−78385
stratospheric winds and winter warmings in Southern Hemisphere 2−65711
structure coeff., vertical profiles, turbulence obs. 2−81683
summer temp. and rainfall prediction for England and Wales from springtime anomalous atmospheric circulation 2−75518
thermal sounding from satellites problems 2−48453
thermistor for use in atmos. boundary layer, radiation shield 2−51579
thermosphere, diurnal variations of temp. and density, influence of vertical motions 2−65820
thermosphere, global mean temp. maintenance by EUV flux absorpt. 2−58026
thermosphere, measurements in polar zone 2−48523
thermosphere, neutral particle temp. meas. from San Marco III 2−58020
thermosphere, tidal temp. oscillations from incoherent scatter obs. 2−58024
thermosphere explorer program 2−58032
transmittance effects, in 4.3 μm and 15 μm bands of CO_2 2−65771
tropical, long-wave radiative transfer model 2−65654
turbulence effect on wind and temp. profiles 2−62172
turbulent flow, effects of evaporation on stability, and radiation on temp. fluctuations 2−44699
upper, meas. of rotational temperature using electron beam 2−48524
upper atmosphere, monitoring using expanded synoptic network of infrasound recorders 2−44743
upper atmosphere wind speed and direction, air density and temperatures up to 95 km, simultaneous meas. using chaff cloud sensors 2−54876
upper regions, obs. using homodyne detection 2−72816
urban area, wind computation 2−75572
urban growth area, micrometeorological observations, urban heat island 2−44685
urban heat island, effect on winds in Ekman layer over St. Louis 2−75665
urban heat island, numerical model 2−75525
urban meas., tower networks 2−75516
variation, lidar absorption method 2−62135
vertical profile det. from microwave emission meas. of O_2 2−65658
vertical profiles in boundary layer, radiometric obs. 2−51584
vertical sounding with Nimbus IV i.r. spectrometer expt. 2−48452
warm core and coreless witners in polar regions, generation conditions 2−54805
wave propagation in non-grey radiative fluid 2−65656
wavenumber-frequency spectra in free atmosphere 2−44687
winds, isentropic analysis, microwave, water vapour, cloud free regions 2−84834
winter rainfall and temp. for England and Wales, foreshadowing 2−44681
zenith brightness temp. at 2.66 GHz 2−84810

thermodynamics
air props., sea level to 300000 ft., enthalpy, compressibility, sp.ht., thermal cond. 2−72760
atmospheric radiative heating rel. to BOMEX core experiment 2−65444
basin cooling in winter, radiation from snow covered mountains 2−75530
convective activity at Bombay, effect of vertical wind structure 2−62178
energy balance from scatt. and absorpt. obs. of atmos. aerosols 2−65780
energy budget, deconvolution of wide-field radiative meas. from satellites 2−65447
energy budget rel. to mean annual global radiation budget, satellite measurements 2−65445
equation balance, hyperbolic case 2−54814
equatorial tropospheric waves, induced by diabatic heat sources 2−78346
equivalent potential temperature and static energy, comparison 2−44688
geostrophic drag, heat and mass transfer coefficients for the diabatic Ekman layer 2−57957
global radiation and energy budget, historical review 2−61864
gravity waves, supersonic cooling region during solar eclipse 2−84835
heating, charged particle energy sources, geomag. control 2−58021

Atmosphere continued
thermodynamics continued
i.r. contribution to energy budget of southern hemisphere up to tropopause 2−65655
jet-stream model with thermodynamic parameter of cloud convection 2−81656
latent heat of condensation, and sensible heat effects on vertical velocity distrib. in westerly disturbance 2−62131
latent heat release, intensity variations, numerical model 2−48448
latent heat release, vertical distrib. and mechanism of conditional instability of second kind 2−48446
local free convection, similarity and budgets, of shear stress and heat flux 2−84816
outgoing i.r. flux meas. from SIRS radiance measurements 2−65446
radiation budget, effect of contrail sheets of ice spheres 2−62148
radiation budget of stratosphere rel. to transport aircraft pollutants 2−65663
radiative transfer eqn., general relaxation method for inverse solution 2−62132
at sea surface, comparison of total static energy classification with energy flux classification 2−54815
shock induced, dynamics of low density heated fluid element, model of gravitational thermals 2−50259
stability, heat and momentum fluxes, during dry unstable conditions 2−75529
stagnation temperature-temperature difference for in natural convection flow 2−62137
thermal convection in polytropic atmosphere rel. to structure of thermics 2−68881
thermal pollution, general circulation model, possible climatic changes 2−75524
thermosphere, lower, quiet day Joule heating rate 2−58023
thermosphere, neutral heating efficiency 2−58025
thermosphere, one- and three-dimens. model obs. 2−58039
thermosphere energy source, convection elec. fields 2−58041
thermospheric heating and energetics 2−58022
tropical Atlantic air masses, thermodynamic properties 2−57939
troposphere, latent heat release, effect on vertical temp. struct. in mesosphere 2−72761
variables, tidal variation 45-60 km up 2−62189

upper
see also Magnetosphere
Arcasonde-1A temperatures, magnitudes and uncertainties of corrections 2−65818
atom, metastable ^{1}D, deactivation in upper atmospheric conditions 2−65814
auroal particles, origin, props. 2−68943
auroral ionosphere mode, electron density height profile 2−81723
composition det. using linear water cooled ablating-wall flashlamp pumped dye laser 2−73580
dayside polar cusp boundaries, magnetospheric observations of plasma waves 2−65853
density and temperature meas. using rocket- borne electron gun 2−48524
density scale height and mean rotational speed determinations from orbit of Cosmos 307 rocket (1969-94b) 2−54989
diffusion eqn. for expanding gas cloud in const. shear flow 2−72821
electron density and temperature profiles in height range 80-170 km 2−54875
electron-density profiles deduced from plasmapause whistlers 2−68939
energy releases during geomag. disturbances 2−81717
equatorial electrojet, radiowave propagation effects 2−65919
equatorial electrojet and solar flux effects on diurnal development of total electron content of equatorial anomaly 2−65921
equatorial electrojet instability analysis 2−58070
e.u.v. heating of atmosphere, annual and sub-annual effects rel. to density variations 2−84841
excess radiation intensity variations, 200-350 km altitude 2−75619
exosphere, calc. of H distribution 2−75621
exosphere, mean rot. speed near 550 km, Explorer 24 meas. 2−58052
exospheric temperature, semiannual change 2−68938
geomagnetically trapped protons in inner Van Allen zone, differential energy spectrum 2−65930
Global Radio Meteor Wind Studies Project 2−58036
gravity wave perturbation models 2−72822
heating, charged particle energy sources, geomag. control 2−58021
high latitude density, inferred from low altitude satellite drag data 2−65815
infrasonic waves, possible survival 2−72815
internal gravity waves and turbulence, ALADDIN I obs. 2−58038
loss cone electron fluxes during strong precip. events 2−65835
magnetosheath electron precipitation rel. to dayside auroral-oval plasma density and conductivity 2−65854
magnetosphere, three dimensional, analytical model with defined magnetopause 2−65813
mapping of electric field Sq current into lower atmosphere 2−68956
minor neutral constituents, height distributions, theoretical model, boundary conditions 2−72819
model development, specified solar flux and boundary conditions 2−81697
Na layer, daytime laser radar obs. 2−81703
neutral, height distributions of composition, temp., electron density and temp. 2−54874
neutral atmosphere, radio meteor method of observing winds and turbulence 2−48522
neutral density meas. near 400 km using Ogo 6 microphone density gauge 2−68924
neutral-particle wake method for satellite-borne temperature measurements 2−68925
nighttime number density of O_2 and O_3 from stellar occultation data 2−58034
noctilucent clouds, in daytime, circumpolar particulate layers near summer mesopause 2−84885
noctilucent clouds, Russian observations in 1969-70 period 2−58053
noctilucent clouds, spectral intensity obs. 2−65822
observatory, design, location and operation 2−62293

Atmosphere continued
upper continued
photoelectron flux at 560 km altitude, latitude variation 2−65845
plasmapause, Cerenkov instability and v.l.f. emissions 2−72827
plasmapause, irregular structure of thermal ion plasma, Ogo 3 and Pc 1 obs. 2−65838
polar cap particle flux variations, two-satellite observations 2−68937
polar electrojets, easterly and westerly, intensity variations in universal time 2−72842
polar thermospheric winds, convection electric fields in ionospheric model 2−65855
positive ions, spiral electron multiplier operation characts. 2−66724
proton pitch-angle distributions in 100-300 keV range, satellite observations 2−65821
protonosphere, ioniz. flux into F-region, rel. to nighttime maintenance 2−58094
Q-switched ruby laser radar, atmospheric backscatter 2−51638
radiometer system for ground-based temperature measurement 2−68928
seasonal changes in flux at synchronous altitudes 2−48531
soft particle fluxes near equator, charact. spectrograms 2−65834
solar EUV heating, annual and subannual effects, comparison with density obs. 2−58028
solar EUV heating, annual and subannual effects, harmonic analysis 2−58027
solar e.u.v. heating in upper atmosphere, annual and sub-annual effects 2−84840
superrotation, theories, review 2−75620
temperature obs. using homodyne detection 2−72816
temperatures, diffusion coeffs. and densities from ALADDIN TMA releases 2−58019
thermosphere, chem. release obs. from high flying aircraft 2−58035
thermosphere, daytime neutral wind measurements 2−84886
thermosphere, equatorial, neutral comp. 2−58033
thermosphere, global mean temp. maintenance by EUV flux absorpt. 2−58026
thermosphere, lower, neutral comp. meas. in ALADDIN I program 2−57952
thermosphere, lower, quiet day Joule heating rate 2−58023
thermosphere, minor constituents meas. by mass spectra 2−62295
thermosphere, neutral composition above Fort Churchill 2−65828
thermosphere, neutral heating efficiency 2−58025
thermosphere, neutral particle temp. meas. from San Marco III 2−58020
thermosphere, one- and three-dimens. model obs. 2−58039
thermosphere, photodissociation rates of O_2 2−65830
thermosphere, positive ion composition obs. during summer at high latitude 2−65829
thermosphere, quenching of vibr. excited N_2 by CO_2 2−58029
thermosphere, tidal temp. oscillations from incoherent scatter obs. 2−58024
thermosphere dynamics, heat input and eigenfunctions 2−81699
thermosphere dynamics, planetary waves 2−81701
thermosphere dynamics, tidal waves 2−81700
thermosphere energy source, convection elec. fields 2−58041
thermosphere explorer program 2−58032
thermospheric comp., theoretical and empirical approaches 2−58031
thermospheric composition, longitudinal variations indicating magnetic control of polar heat input 2−65827
thermospheric density, annual and semiannual variations 2−48525
thermospheric dynamics, obs. using travelling ionospheric disturbances 2−65958
thermospheric heating and energetics 2−58022
thermospheric model, satellite orbital decay densities, incoherent scatter temps. 2−81702
thermospheric O_2 abundance variation, 6300Å twilight airglow obs. 2−58055
thermospheric winds from exptl. density data 2−58042
thin film atomic oxygen sensors 2−65403
tunable dye lidar technique for meas. of atmospheric constituents 2−84868
turbulent mixing, thermal effects of buoyancy forces 2−48530
vertical scatter distribution, observed twilight intensity 2−72835
wind and density obs. using v.h.f. radar 2−75618
wind and temp. monitoring using expanded synoptic network of infrasound recorders 2−44743
wind patterns, model calcs. 2−58040
wind speed and direction, air density and temperatures up to 95 km, simultaneous meas. using chaff cloud sensors 2−54876
winds, study by analysis of orbital changes of Cosmos 316 (1969-108 A) satellite 2−84927
winds obtained by radar meteor trails and chem. release methods, comparison 2−58037
winds of constant vel. shear, motion of smoke trails 2−65833
zonal winds from orbit analysis of Cosmos 316 (1969-108A) 2−51632
Ba ion cloud releases, analysis of observational problems 2−72820
FeO chemiluminescence and resonance fluorescence on release of $Fe(CO)_5$ 2−65825
H and He distributions, transport mechanisms 2−78383
H Lyman-α absorption rel. to pressure, density and scale height 2−65817
He I density, 10830Å obs. in tropical latitudes 2−65823
Li atom emission spectrum, chem. reactions 2−58030
N and NO content variations at 100-250 km height, rel. to solar activity 2−48528
Na abundance and stratospheric warmings 2−78385
Na abundances, absorption meas. 2−65831
O concentration, semiannual variations 2−48529
O concentrations from incoherent- scatter and satellite-drag data 2−65826
O layer, estimates of height and concentration 2−48527
O_2 concentration in 70-95 km region 2−48463
$O_2(^1\Delta_g)$ altitude profile at night 2−72837
Thermospheric winds and ioniz. into protonosphere, role in F2 layer maintenance 2−58093

Atmospheric acoustics
absorption of sound, energy transfer mechanisms 2−44739

Atmospheric acoustics continued
absorption of sound in air at 20°C in frequency range 100 Hz-1 MHz 2−75616
acoustic-gravity waves, obs. using Hg tiltmeter 2−65810
airblast overpressure decay at long ranges 2−65812
blast wave attenuation 2−65811
Helmholtz waves, lower atmosphere, obs. with acoustic sounder 2−78382
infrasonic wave propag. in upper atmosphere 2−72815
l.f. sound, natural sources and propagation 2−75617
line-of-sight probing of atmospheric turbulence 2−54872
longitudinal compression waves, ray tracing program using Haselgrove's eqns. 2−84857
lower troposphere acoustic sounder experiments 2−48521
microbaroms and temp. and wind of upper atmosphere 2−44743
natural infrasound of 6-9Hz 2−58016
radio acoustic sounding, atmospheric parameter remote meas. 2−57929
ray tracing, three-dimensional, using hybrid computer 2−81653
reflection from stably stratified atmosphere 2−44742
scattering of acoustic waves in turbulence 2−44705
sonic boom focus 2−58015
sonic boom propagation, nonlinear theory 2−41708
thunder signature, phenomenological model obs. using computer 2−44741
turbojet exhaust noise, propagation at shear discontinuity between hot and cold regions 2−78921
vortical sound, statistical characteristics over ocean 2−44740
WKB approximation, turning points and meas. of phase vel. 2−57840

Atmospheric disturbances *see Atmosphere/movements; Thunderstorms*

Atmospheric duct *see Electromagnetic wave propagation*

Atmospheric electricity
see also Atmosphere/radioactivity; Atmospherics; Aurora; Electromagnetic wave propagation/atmosphere; Ionization, atmosphere; Lightning; Thunderstorms
— 2−72810
aeronomical balloon obs. 2−72769
air ionization principles, rel. to human biological behaviour 2−58591
air-earth current, diurnal variation at Kyoto, Japan 2−78379
Alouette 2 satellite meas. of atmospheric v.l.f. and e.l.f. noises 2−81667
AU and AL indices on international quiet days and geomagnetic field variations at high latitudes 2−48602
aurora, parallel elec. field obs. 2−65913
auroral electrojet effects, lab. simulation 2−58071
auroral electrojets, long term variations 2−65922
auroral electron energy spectra variations during auroral substorms 2−84876
auroral electron fluxes from N_2 positive and N_2^+ band systems 2−54884
auroral energy spectra rel. to precipitating electrons 2−65914
Birkeland currents intensification due to elec. fields 2−65904
charge of small (1-40 μ) particles, effects of weather 2−78380
charge screening layers around electrified clouds 2−65742
charges and fields, numerical modelling 2−65781
conductivity monitoring for determ. of drift of atmospheric pollution 2−62154
current pot. grad. daily variations, e.m. induction by equitorial electrojet, Zaria, Nigeria 2−65998
current systems of weak geomagnetic disturbances at polar caps 2−84923
dawn and dusk conductivity gradients effects on equatorial electrojet 2−54885
electric cloud modelling 2−58005
electric fields at high latitude 2−72866
electric fog effect and forecasting 2−51582
electrode effect of boundary layer over sea, time-dependent model 2−65785
electrojet, equatorial, airborne meas. of magnetic effects in ocean areas 2−54913
electrojet, nonlinear theory of cross field instability 2−65920
electrojet region, equatorial, e.m. induction, magneto-telluric relations 2−62386
electron cyclotron and Langmuir frequency ratio in magnetosphere 2−72841
equatorial electrojet, geomagnetic variation studies in Ethiopia 2−57792
equatorial electrojet, radiowave propagation effects 2−65919
equatorial electrojet and solar flux effects on diurnal development of total electron content of equatorial anomaly 2−65921
equatorial electrojet current system rel. to ionospheric processes 2−84791
equatorial electrojet instability analysis 2−58070
field during tropical thunderstorms 2−65784
field in dynamo region, deduced from magnetic field variations due to substorm 2−48601
field variations during substorms, OGO 6 obs. 2−81714
high latitudes, elec. fields and zonal currents induced by merging of field lines 2−62351
ionization in air traffic control laboratory, personnel performance 2−75612
ionosphere, effective height integrated conductivity 2−65949
ionospheric and magnetospheric elec. fields, meas. techniques and props. 2−72878
ionospheric electric field pot. distrib., world-wide meas. 2−65963
ionospheric electric fields, horizontal, air electric meas. 2−54890
ionospheric fields, and ionization drift in F_2 regions 2−84911
ionospheric fields during pulsating auroras 2−48572
l.f. e.m. noise model 2−68916
LHR hiss rel. to magnetospheric and auroral activity 2−68953
lightning, electric field recovery, response of conducting atmosphere to field charge 2−68919
lightning return strokes, electric field risetimes 2−68917
low energy electrons and optical emission in dayglow and aurora, rocket measurements 2−84882
low-energy electron precipitation rel. to visible auroral arc 2−68949
lower troposphere, potential gradient and air earth current, influence of solar activity 2−44735

Atmospheric electricity continued
- magnetic DP-2 vars., equivalent current system 2−72911
- magnetosphere, induced by radial penetration of hot plasma 2−65862
- magnetosphere, three dimensional, analytical model with defined magnetopause 2−65813
- magnetosphere, whistler wave amplification, pitch angle and energy diffusion coefficients 2−48516
- magnetospheric convection electric fields in high latitudes, satellite measurements 2−75626
- magnetospheric elec. fields model 2−65879
- magnetospheric electric fields, decaying ring current as origin 2−78386
- magnetospheric fields deduced from drifting whistler paths 2−65859
- mapping of electric field Sq current into lower atmosphere 2−68956
- measurement using aircraft borne cylindrical field meas. 2−58004
- mechanical transfer currents 2−65786
- nuclear explosion, electric field effects, obs. 2−62277
- Peruvian electrojet, lunar variations using E-region electron-drift measurements 2−68955
- photoelectron flux at 560 km altitude, latitude variation 2−65845
- photoelectron flux in lower ionosphere in 3-50 eV range, effect of 1970, March 7 solar eclipse 2−65948
- point discharge current, influence on vertical profile of potential gradient 2−65783
- polar cusp, electric fields and electron fluxes 2−54895
- potential gradient, diurnal variations and field station for obs. 2−58002
- potential gradient changes, radioactive fallout 2−65805
- precipitation current, change after sudden change of electric field in tropical thunderstorm 2−65784
- proton motion due to electric field in magnetosphere as explanation of frequency drift of PDP type geomagnetic pulsations 2−48599
- radio noise meas. rel. to lightning flashes in India 2−84790
- raindrop charge size meas. in warm rain 2−65740
- ring current effect on F-region disturbance 2−72896
- ring current effects, magnetospheric electron density profiles 2−54880
- sea ice open channels as ion sources 2−81669
- sferics pulse frequency rel. to solar chromospheric flare activity 2−65797
- Sq currents, north south asymmetry, study using ionospheric dynamo model 2−58114
- thundercloud, calc. of electric field in ionosphere and magnetosphere 2−62347
- thunderstorm, electrical shielding layer around charged clouds 2−84812
- tornado, 1955 Blackwell, Oklahoma, sferic rate azimuth profile 2−78368
- v.l.f. auroral hiss rel. to precipitating low-energy electrons 2−68952
- v.l.f. emission during substorms 2−81747
- v.l.f. field, computation of height dependence 2−72806
- westward travelling surge, associated mag. effects 2−68888
- whistler precursors, trigger delay 2−68918
- whistler propag. at low latitudes 2−84884

Atmospheric optics
- *see also Airglow; Sky brightness; Sunlight; Twilight*
- — 2−72801
- — 2−70009
- absorption coeffs., realistic calc. 2−62271
- absorption hygrometry, water vapour measurement technique 2−84864
- absorption of i.r. radiation by gases at high temps. and pressures 2−48509
- absorption profile, determ. by scatt. independent method 2−81645
- aerial photography, automatic exposure control rel. to seeing conditions 2−82602
- aerosol, optical constants of constituents 2−57946
- aerosol attenuation coefficient, vertical profile 2−57996
- aerosol attenuation of visible and i.r. radiation rel. to air humidity 2−81660
- aerosol effects on hemispheric long-wave irradiance incident at Earth's surface 2−65448
- aerosol light scattering from extinction measurements at remote clean air locations 2−51621
- aerosol variation effects on radiance in atmosphere ocean system 2−57990
- aerosols, light scattering, chemical composition, atmospheric humidity, adsorption 2−83815
- aerosols, meas. of complex refr. index 2−62252
- aerosols, single particle light scattering obs. 2−72802
- aerosols characterization and monitoring by fluorescence 2−81692
- aerosols effects on sunlight 2−81689
- air pollution mapping, Q-switched ruby laser radar 2−78350
- airborne fly ash, complex index of refraction, laser radar and collection of particles 2−78376
- albedo of surfaces, as fn. of solar zenith angle 2−75485
- amplitude scintillations in turbulent atmosphere 2−65775
- angle-of-arrival fluctuations of spherical wave propagated near ground level 2−81684
- anomalous transparency effect, due to scattering by molecular portion of atmos. 2−62268
- arc phenomena obs. 2−84788
- astronomical image aberrations due to turbulence, removal by optical array technique 2−85074
- atmospheric dispersion of telescope images, automatic compensation 2−48825
- atmospheric turbidity rel. to aerosols above McCall glacier 2−62273
- aureole, scattering of e.m. radiation from polydisperse medium 2−62267
- automated solar seeing measurements 2−78581
- beam shape effects on phase fluctuations of e.m. propagation in turbulent medium 2−44728
- beam spreading in turbulent medium, calc. by modified von Karman spectrum 2−49415
- cirrus cloud layers, light scattering 2−62253
- cloud emissivity, variation in i.r. 2−65738
- cloud field height determ. by ground photometric survey using two spherical mirrors 2−84852

Atmospheric optics continued
- cloud microstructure determ. by spectrometer 2−48492
- clouds, angular transmittance props. 2−57977
- clouds, backscattering, first and second order, illuminated by lidar beam 2−51610
- coherence meas. of laser beams at 10.6 and 0.63μ 2−81674
- cosmic X-ray det. using atmospheric fluorescence as ground-based method 2−44902
- day sky brightness phase function rel. to optical thickness of atmosphere 2−62274
- dayglow rocket photometry, tilting filter meas. 2−81646
- daylight, spectral irradiance for air mass 2 2−72799
- degraded light beam obs., averaging times 2−81686
- degraded satellite images, restoration 2−79308
- depolarization of visible light from H_2O clouds for monostatic Lidar 2−78377
- electro-optical systems design conference 1971 West 2−82473
- e.m. distortions produced by turbulence, h.f. plane wave filter function for folded path 2−75609
- extinction and lidar backscatter measurements rel. to urban aerosols 2−51622
- extinction coeff. calc., model atmospheres 2−57993
- extinction measurements and deterioration studies by astronomical techniques, symposium 2−51570
- extinction measurements for monitoring O_3 content and dust 2−54858
- extinction observations for 1955-1972 at Flagstaff, U.S. Naval Observatory 2−54861
- fluctuations of submillimeter waves in turbulent atmosphere 2−51629
- focused irradiance fluctuations beyond layer of turbulence 2−54856
- fog element length, horizontal transmittance discontinuities 2−75602
- fourth statistical moment of scalar wave propagating in random medium 2−59219
- Gaussian light beams fluctuating properties in turbulence from viewpoint of mode conversion 2−46859
- green flash, 1971 observations 2−72803
- halo phenomena, frontal rain 2−84853
- haze, brown colour from atmospheric aerosol and NO_2 content 2−62264
- haze layers, influence on remotely sensed surface props. 2−62269
- ice crystal haloes, photographs taken in Antarctica 2−68913
- image deterioration of extraterrestrial objects due to turbulence effects on refractive index 2−81677
- instrument for scattered light obs., energetic calibration 2−48513
- interferometric investigation of phase fluctuations 2−72740
- i.r., transmission in 10-12 μm window 2−68912
- i.r. attenuation, aerosol extinction contrib. 2−81647
- i.r. laser radiation, 10.6, 0.63 μm, attenuation coefficients in snow, rain, drizzle 2−75611
- i.r. transmittance, universal representations for applic. to nonhomogeneous paths 2−62270
- i.r. u.v., visible and X-ray transmission, aeronomical balloon obs. 2−72769
- irradiance fluctuations in transmission through atmosphere 2−51619
- Kirchhoff-Fresnel diffraction in turbulent atmosphere 2−45791
- laser beam, spot dancing, obs. 2−54800
- laser beam broadening in turbulent atmosphere along sloping traces of propagation 2−45756
- laser beam in water and atmospheric media 2−69955
- laser beam propagated in turbulent atmosphere 2−57995
- laser beam propagation, effects of atmospheric turbulence 2−84861
- laser beam propagation. Maxwell's eqn. 2−59190
- laser beam propagation through atmosphere 2−42155
- laser beam propagation through turbulent atmosphere, spot dancing 2−76500
- laser beam scintillation in Earth to space propagation path 2−51618
- laser beam wander phenomenon in turbulent lower atmosphere 2−84862
- laser beams self induced thermal lens effects on imaging or tracking systems viewing along same path, image quality degradation 2−49391
- laser pulse propagation in molecular absorber and minimizing of heating effects 2−84860
- laser radar transmission 2−62281
- laser radiation, 10.6 μm, attenuation in artificial, real fog 2−72804
- laser radiation in turbulent weak drizzle, intensity fluctuations spectra 2−75607
- laser range meas., accuracy of atmospheric corrections 2−54857
- lidar probing of troposphere, comments 2−62266
- lidar study of O_2 vertical concentration profile 2−62135
- light beam gravity centre floating, correlation meas. 2−48435
- light beam in turbulent atmosphere, meas. illumination and intensity fluctuations 2−49413
- light detection and ranging, remote atmospheric probe 2−54802
- light scattering, albedo and luminance of planet surface 2−48766
- light scattering, upper atmosphere aerosol, rocket mounted laser radar obs. 2−54878
- light scattering and size-altitude distrib. of atmos. aerosols 2−65778
- light scattering by ice clouds in visible and i.r. regions 2−58000
- line of sight, cloud free, photogrammetrically 2−75610
- Los Angeles, transfer of near u.v. through smog 2−57992
- Los Angeles smog, comparison of calculated and measured light scattering 2−51623
- Los Angeles smog, light scatt., comparison to light extinction by NO_2 2−51625
- Los Angeles smog, light scatt., correlation with size distrib. and vol. concentration 2−51624
- matrix-operator theory for Rayleigh and maritime haze phase functions 2−76235
- Mie scatt. by three polydispersions, atmos. aerosol. models 2−65779
- Milne problem for polarized radiation with nonconservative Rayleigh scattering 2−52459
- mock suns and moons, 1971 observations 2−72803
- monochromatic extinction from UBV photometry of stars 2−54864
- multiple scattering obs. in synthetic foggy atmosphere 2−64478
- multiwavelength scintillation phenomena and turbulence characteristics 2−65774
- nephelometer, balloon-borne, for high altitude meas. of light scatt. 2−72805

Atmospheric optics continued
noncoherent scattering problem, probabilistic formulation 2−57994
ocean colour determination through scattering atm. 2−65587
ocean remote spectroscopy from high altitude, effect of atmospheric backscatter on reflection spectra 2−84774
optical transfer function, turbulent atmosphere, averaging time depend. 2−57997
particulate extinction in near i.r. spectrum of sun 2−57999
phase difference spectra for 20.6 μ laser beam 2−81673
phase fluctuations meas. with strioscopic appliance 2−48512
photoelectron spectra of atmospheric molecules including N_2, O_2 and CO_2 at 304 Å 2−80058
plane light wave in turbulent medium, amplitude-phase fluctuations 2−48507
pollution meas. and environmental investigations rel. to astronomical observations at MT. Hopkins Observatory 2−54859
pollution studies, using tunable semiconductor laser 2−65675
predawn airglow enhancement, photoelectrons from magnetically conjugate point 2−48541
Project ASTRA, collection of world-wide extinction data, seasonal variations 2−54863
propagation in an inhomogeneous atmosphere, experiments at Emerson Lake 2−68915
radiance and colour of twilight sky light effect of aerosols 2−81690
radiation compensation method for submillimetre radio telescopes 2−58565
radiative transfer, conf., August 1972, Colorado 2−62248
radiometry at 350 and 700 microns, extinction measurements 2−78527
rainbow, colour and intensity, inhomogeneities 2−44733
Raman scattering for quantitative meas. of trace constituents 2−57941
refraction during total solar eclipse from Fresnel patterns 2−58001
refractive index and density fluctuations over ocean, effects of temp. and humidity 2−81676
refractive index of natural aerosols from 0.2 to 40 μm 2−65773
refractive index structure, remote sensing using ultrahigh resolution radar 2−44696
refractive index structure coefficients and turbulence profiles in troposphere 2−65776
Salt Lake Valley, surface wind flow during low visibility-ventilation episode 2−75575
Saskatoon halo display, unusual arc obs. 2−62343
scanner extinction measurements, departures from Rayleigh scattering 2−54860
scattering data using large laser radar equipment 2−84867
scattering for point isotropic light sources in model atm. 2−81691
scattering from measured aerosol size distributions, six component log gaussian model 2−81688
scattering layer, scanning f.m.-CW radar sounder for obs. 2−84842
scattering of line radiation, source function 2−41551
scintillation, laser beam meas. from 1.5 to 10.5 km altitude 2−81672
scintillation, turbulence profile correlation with stellar obs. 2−81683
scintillation obs. using ground-aircraft path 2−81682
scintillation of sources of finite angular dimensions 2−81651
scintillation of spherical and plane waves, turbulence model 2−81680
scintillation of upward directed laser beams, wave front curvature and beam waist effects 2−81681
seeing conditions on Mt. Wilson rel. to Agassiz Station, interferometric study 2−68909
self induced transparency in NH_3 at 10 μ, extrapolation to CO_2 laser radiation atmospheric propagation 2−43268
slant path scintillation in planetary boundary layer of laser beam 2−81675
smog aerosol, i.r. spectra, comparison with synthetic smog 2−51620
smoke plume transmittance, remote obs. using ruby lidar system 2−68910
solar radiation absorption by atm. dust, effect of cloud scattering 2−84806
solar telescopes, modulation transfer fn., atmospheric turbulence 2−76049
spatially bounded light beam propagation in turbulent atmosphere, influence of initial diameter on beam axis intensity 2−44730
spatially-bounded light beams, correlation function of axial displacements in turbulent medium 2−44729
spectral transparency, visible and i.r. region, apparatus and technique 2−54855
spectrometry, pollution monitoring and remote sensing 2−75604
spectroscopical sounding of clouds 2−44731
stratified Rayleigh atmosphere, sunlight absorption, numerical model 2−73078
stratosphere, characteristics of Mie scatterers, inversion technique for obs. 2−65768
stratospheric aerosol levels, 12-25 km 2−81687
sunlight absorption by atmospheric aerosols, coefficient measurement methods 2−51617
surface layer attenuation coefficient, laser beam location method 2−57998
target edge response viewed through atmospheric turbulence over water 2−81648
temporal spectra of phase difference fluctuations 2−81685
terrestrial scintillation, meteorological influences 2−78378
transmission functions, calc. over inhomogeneous paths 2−65769
transmission in 0.76 microns O_2 band 2−44732
transmission in i.r. region, two beam spectrophotometer obs. 2−48508
transmission on, Curtis-Godson approx. for non- homogeneous atm. 2−84805
transmittance, dependence on temp., water vapour and O_3 distrib. 2−65771
transparency in u.v. 2−75608
transparency measurements, worldwide variations in 1902-50 period 2−54862
turbidity meas. w. laser radar 2−62272
twilight, circular polarization of scattered light 2−68911
twilight sky, atmospheric scattering rel. to meas. of light polarization 2−81657

Atmospheric optics continued
twilight sky optical properties, effect of Orionid 1970 meteor shower 2−84781
u.l.f. and v.l.f. spectra, probability distrib. of noise intensity overshoots 2−72809
urban air pollution aerosol model, spectral absorption and extinction coefficients 2−62265
vertical number density profile of atmospheric gases from stellar occultation data 2−84839
vertical transparency, obs. using artificial i.r. source 2−48510
visibility, extinction coeff. of aerosol particles rel. to humidity 2−84818
visibility, mass concentration anomaly in photochemical aerosols 2−48511
visibility needed for astronomical obs. 2−62275
visibility obs. in Los Angeles, air pollution effects on cloud condensation nuclei 2−65713
visibility observations in low-temperature fog, urban growth effects over airports 2−44717
visibility rel. to gaseous pollution 2−48471
water vapour absorption meas. using single frequency CO laser 2−82519
windows, radiative props. 2−65793
Ba ion cloud in magnetosphere, Portuguese obs. of related luminous phenomena 2−72831
CO laser radiation intracavity water vapour cell to meas. absorptive losses 2−82518
CO_2 spectra, radiative transfer obs. 2−65770
He-Ne laser, wavelength changes, correction to laser interferometer 2−69957

Atmospheric pressure and density
air density variation, obs. of orbital periods of satellites 2−65819
airblast overpressure decay at long ranges 2−65812
ALADDIN TMA release meas. 2−58019
amplifying baroclinic waves evolution, pressure area development 2−57954
British Isles, westerly type rainfall and atmospheric mean sea level pressure 2−54842
constituent density determ. by lidar 2−62135
Cyprus, extreme weather conditions during April (1971) 2−54806
density variations at 140 km. from precise satellite radar tracking data 2−68926
diffusion model for thermospheric density-temperature phase delay 2−65816
electron beam meas. of density using bremsstrahlung 2−58018
fluctuations, effect on geyser activity 2−65572
gradient effects on flow 2−78341
ground-level pressure fluctuations, large scale meteorological influences 2−54809
high latitude density, inferred from low altitude satellite drag data 2−65815
irregular variations between 50 and 200 km 2−72764
lower boundary layer, measurement of static pressure fluctuations, instrumentation 2−72755
magnetospheric electron-density profiles deduced from plasmapause whistlers 2−68939
magnetron press. gauge on O VI-15, adsorption/desorption press. effects 2−58148
microbaroms, origin rel. to that of microseisms 2−57612
microbaroms obs. at Boulder, Colorado, meas. of azimuth of arrival and amplitude 2−54817
micrographic signals from presumed atmospheric explosions 2−57633
microscale pressure fluctuations, within lower atmospheric boundary layer 2−44700
microseisms from small closed basins and inland seas rel. to atmospheric pressure 2−44541
neutral density meas. near 400 km using Ogo 6 microphone density gauge 2−68924
pressure level determ. by two-satellite microwave occultation method 2−84858
radio telemetering system for meteorological investigations 2−75520
satellite radiance meas., insertion into numerical circulation model 2−62134
sea level, derived from simulated obs. of satellite radar-radiometer data 2−57963
sea level pressure and surface wind fields, adjustment by variational matching 2−65705
sea-level pressure distrib., response to solar corpuscular radiation 2−84811
Siberian Anticyclone, November 1967 to April 1968, periodicity in average daily strength 2−84851
solar eclipse, 1970, March 7, atmospheric pressure and temperature changes during totality 2−57937
stratified Ekman boundary layer, inflection point instability 2−78356
stratosphere, air density distribution 2−57938
thermosphere, diurnal variations of temp. and density, influence of vertical motions 2−65820
thermospheric density, annual and semiannual variations 2−48525
thickness calc. from satellite radiance meas. 2−62256
transfer velocity of pressure fluctuations near ground surface 2−68882
upper, meas. of density using electron beam 2−48524
upper atmos., v.h.f. radar obs. 2−75618
upper atmosphere, density scale height and mean rotational speed determinations from orbit of Cosmos 307 rocket (1969-94b) 2−54989
upper atmosphere, distributions of minor neutral constituents, theoretical model, boundary conditions 2−72819
upper atmosphere wind speed and direction, air density and temperatures up to 95 km, simultaneous meas. using chaff cloud sensors 2−54876
variations related to internal gravity waves 2−72762
zonal harmonic standing waves in Southern Hemisphere 2−65659
H Lyman-α absorption rel. to pressure, density and scale height of upper atmosphere 2−65817
O density in thermosphere, meas. with rocket-borne open-source mass spectrometers 2−68929

Atmospheric spectra
  see also Atmospheric optics
  — 2—65660
  absorption coeffs., realistic calc. 2—62271
  absorption hygrometry, atmospheric water vapour measurement, models 2—84864
  air, i.r. emission, absorpt. coeffs., 6000-8500K 2—73240
  attenuation of 4.3 mm waves by atmospheric water and O_2 2—68914
  aurora, backscattering irregularities, spatial correl. of optical and radar data 2—58068
  aurora, between 2000 and 3000 Å, using fast scanning spectrometer 2—48554
  aurora, Doppler radar signatures 2—58069
  aurora, IBC$\simeq$3, averaged spectra, 7000-9000 Å, relative intensities 2—75625
  aurora, intensity meas. of primary electrons during intense breakup 2—58065
  aurora, intensity ratios of emission features 2—48552
  aurora, low intensity red arcs, scanning photometry 2—48551
  aurora, magnetic bay accompanied, rocket meas. of keV electron spectra 2—58064
  aurora, space-time regularities, electron fluxes, luminesc., review 2—68944
  aurora, type-A red, low energy electron meas. 2—58063
  aurora, u.v., N_2, N I and O I lines 2—65897
  auroral arc OI and NI emission spectra 2—72839
  auroral emission, vacuum u.v. meas., luminosity profiles 2—58062
  auroral energy spectra rel. to precipitating electrons 2—65914
  auroral spectroscopy and excitation processes, review 2—48553
  auroral zone, 1.2 μ O_2 i.r. band intensity 2—58067
  cometary, Tago-Sato-Kosaka and Bennett comets 2—58521
  daylight, spectral irradiance at Pretoria 2—62263
  differential energy spectra of electrons in inner and outer belts, ionizing radiation at 200-300 km 2—48557
  electron spectra of inner radiation belt in 0.13—15 MeV range 2—72844
  emission, determ. hemispheric reflectance of plane water surface for clear sky and overcast sky 2—54853
  equilibrium layers, epithermal neutrons, energy spectrum 2—48455
  excess radiation intensity variations, 200-350 km altitude 2—75619
  excitation of atmospheric gases by low energy proton bombardment 2—84792
  gas trace detection spectroscopy 2—65664
  gravity waves, frequency spectra, from ionospheric electron content 2—57983
  i.r. absorption, at high temps. and pressures 2—48509
  i.r. radiation meas. from satellites for estimation of extratropical cyclone parameters 2—54840
  i.r. spectroscopy, surveillance of molecules and intensity studies in terrestrial atmosphere 2—51599
  Jupiter, computation of transmission profiles in v_4 band of methane 2—48769
  kinetic energy spectrum power laws using spherical harmonic functions 2—75558
  light scattering by ice clouds in visible and i.r. regions 2—58000
  lightning channel, optical absorption 2—65796
  mm wavelength, by obs. of solar radiation at sea level 2—54852
  molecular u.v. photoabsorption cross sections, critical review 2—42838
  Nibmus 4 i.r. spectroscopy, calibrated thermal emission spectra 2—65765
  nightglow, 6300 Å emission, variation and decay 2—48544
  nightglow, OH rot. temp. 2—54882
  overlap emissivity of CO_2 and H_2O 2—57947
  particulate extinction in near i.r. spectrum of sun 2—57999
  planetary gases, theoretical studies on line widths 2—53105
  plasmapause, obs. of optical emissions 2—62326
  pollution aerosol monitoring by spectral distribution of scatter of Ar-ion laser beam 2—51600
  proton spectra of inner radiation belt, long-term variations 2—72843
  radiative properties of particulates composed of SiO_2, $CaCO_3$, H_2O, in spectral interval 500-1500 cm^{-1} 2—54854
  radio aurora, caused by plasma instabilities 2—48555
  radio refractive index spectra, clear air convection 2—75614
  stratified Rayleigh atmosphere, absorption lines, numerical model 2—73078
  stratosphere, emission obs., anal. for features produced by sources outside the Earth's atmosphere 2—44734
  submillimeter isotropic background limits 2—44734
  surface layer turbulence, cospectral similarity 2—68895
  surface layer turbulence, spectral characteristics 2—65696
  thermosphere explorer program 2—58032
  transmission measurements in 0.35 to 1.6 μm spectral range, world-wide variations in 1902-50 period 2—54862
  urban air pollution aerosol model, spectral absorption and extinction coefficients 2—62265
  u.v. of day airglow, polar aurora, tropical airglow, interpretation using cross sections for electron excitation of O, N 2—67397
  water vapour absorption rel. to surface temperature determinations from satellite radiometric measurements 2—54821
  CO_2, radiative transfer obs. 2—65770
  H_2O vapour, absorpt. lines, using tunable i.r. laser spectroscopy 2—84843
  Hα, Hβ lines, night sky emission, local and galactic contributions 2—62338
  He and He^+ emission from magnetosphere, e.u.v. resonance radiation 2—68934
  Li atom emission spectrum, chem. reactions 2—58030
  N_2 i.r. emission spectra in auroral excitation conditions 2—84873
  N_2 spectrum in i.r. range 6500-11500 Angstroms rel. to auroral spectra 2—84874
  NI allowed transitions in airglow and aurora 2—48547
  NO_2, search for telluric lines in spectrum of star α Virginis (Spica) 2—51601
  NO_2 photometric measurements using Fabry-Perot filters 2—54827
  Na D-line emission from the atmosphere, solar eclipse effects 2—65885
  O 5577 Å emission intensity, nocturnal and semiannual variations 2—65889
  O atom excitation to S^1 state during aurora borealis 2—44745

Atmospheric spectra continued
  O nightglow emission at 5577 Angstroms during 1958-67 period above Ashkhabad 2—84881
  O nighttime 6300 Angstroms airglow emission at magnetic equator rel. to ionospheric anomaly 2—84880
  O_2 excitation cross sections and intensity ratios in auroral conditions 2—84872
  O_3 9.6 μm band in Nimbus 4 IRIS spectral data, elimination of cloud effects 2—65662
  $O_2(^1\Delta_g)$ twilight emission, altitude profile 2—58054
  OI 5577 Å line emission at auroral zone latitude rel. to O concentrations 2—84890
  OI 6300 Angstroms airglow emission, predawn enhancement above Abastumani 2—84883
  OI allowed transitions in airglow and aurora 2—48547

Atmospherics
  Alouette 2 satellite meas. of atmospheric v.l.f. and e.l.f. noises 2—81667
  auroral hisslers generation mechanism 2—65918
  dispersive auroral hiss, m.f. whistler mode 2—68954
  e.l.f., Schumann resonance frequency, day-to-day variation, rel. to solar activity 2—58006
  e.l.f. hiss, Ogo 4 satellite observations 2—65928
  international lightning counter, construction, aims and results 2—62280
  ion, cyclotron whistlers, p and He, satellite obs. over 400 km, 100-500 Hz. 2—72849
  l.f. electromagnetic noise model 2—68916
  LHR hiss rel. to magnetospheric and auroral activity 2—68953
  line type angel echo, formation, X-band radar obs. 2—62276
  magnetosphere, upper-hybrid reson. noise obs. by IMP-6 AC-elec. fields exp. 2—65869
  magnetospheric v.l.f. emissions, summary 2—81707
  particles trapped by whistler wave, detrapping by second wave 2—69860
  pc 1 hydromagnetic whistler diurnal effects rel. to early afternoon source model 2—84922
  plasmapause whistlers and deduced magnetospheric electron-density profiles 2—68939
  pulsating aurora, v.l.f., daytime chorus, post breakup phase of polar substorms 2—72915
  quasimonochromatic whistler mode wave packets, shape evoluution and interactions 2—84891
  quasiperiodic v.l.f. emissions, hydromagnetic modulations, relation to micropulsations 2—72921
  radar echo distributions rel. to Arizona summer thunderstorm regime 2—65700
  radio noise characteristics of auroral ionosphere 2—72840
  radio noise meas. rel. to lightning flashes in India 2—84790
  rain drop size distributions model, time-dependent 2—57930
  sferics pulse frequency rel. to solar chromospheric flare activity 2—65797
  sudden decreases at 5 kHz; 1962-69 review 2—48515
  thunderstorm recorder for storms within a 200 km. radius 2—65710
  tornadic storms, radio noise obs. 2—84813
  u.h.f. lightning receiver, direction finding apparatus 2—65799
  v.l.f. and e.l.f. noises, Alouette 2 satellite meas. 2—72830
  v.l.f. atmospherics, comparison of broad and narrowband counters 2—65798
  v.l.f. emission during substorms 2—81747
  v.l.f. emission in geomag. tail 2—81715
  v.l.f. field variations in polar region, diurnal and seasonal patterns 2—48517
  v.l.f. hiss and plasma phenomena in polar magnetosphere 2—65839
  v.l.f. hiss onset impulsive character, rel. to auroral substorm phase 2—65917
  v.l.f. magnetospheric emissions, naturally occurring and triggered 2—81706
  v.l.f. radio noise rel. to visible auroral arc emissions 2—65916
  v.l.f. Wait and Walters model, surface impedance concept 2—58009
  whistler dispersion and electron density variation during one solar cycle in magnetosphere 2—44744
  whistler instability in anisotropic plasma, simulation 2—60283
  whistler mode signals from v.l.f. transmitter in Australia 2—78396
  whistler obs. of plasmasphere-plasmapause dynamics 2—58046
  whistler precursors, trigger delay 2—68918
  whistler propag. at low latitudes 2—84884
  whistler turbulence, computer simulation 2—65867
  whistler-mode wave refraction by large-scale gradients in middle-latitude ionosphere 2—84893
  whistler-mode waves, v.l.f., radiation belt slot region 2—65868
  whistlers, drifting paths used for detection of magnetospheric electric fields 2—65859
  whistlers, e.l.f. hiss and discrete emissions in plasmapause during large mag. storm 2—65850
  whistlers, monthly and diurnal occurrences in conjugated regions, comparison with gyroelec. echoes 2—84896

Atomic beams
  see also Particle velocity analysis
  beam foil technique, rel. to atomic lifetime study 2—52932
  beam-foil spectroscopy, modulated decays, zero-field oscillation obs. 2—59895
  deflection and broadening by recoils due to photon absorption or emission 2—70619
  elastic scatt. from solid surface with Yakawa-type interaction law 2—74239
  equilibrium charge distributions of light ions in He, meas. with position sensitive open electron multiplier 2—52698
  excited state mass energy analyser, excited state populations of atomic beams 2—67417
  focusing atomic beam magnetic resonance apparatus, construction 2—69842
  focusing atomic beam magnetic resonance apparatus optimum design 2—69843
  frequency shifts, due to Ramsey type interrogation 2—64056
  injection into D-T mirror fusion power system 2—64262
  ion source, compact polarized, atomic beam aspects 2—66725
  ionization, using high power electron bombardment system 2—63271
  metal vapour, production of constant stream by control of electron emission 2—67890

Atomic beams continued
scattering by W surface, effect of surface composition and cryst. orientation 2−47084
scattering by well defined surfaces 2−50422
spin exchange, with free trapped electron, rel. to spin polariz. detection and r.f. spectroscopy 2−79898
stimulated absorpt. or emission of photons 2−45700
Ar metastable atoms, time-of-flight technique for transit time distribution 2−79878
Ba, plasma production from photoionisation metastable states 2−83197
Ba, slow electron beam excited, spectrometry with high resolving power 2−63426
Cs, three-quantum photoionization 2−70604
D, charge fractions and excited atom populations of 8 to 100 keV beams from solid films of C, Mg, Nb, Au 2−49981
H, interaction with Ne, Ar and ice surfaces at 4.2K 2−50539
H, thermal energy range, prodn. by microwave discharge 2−67427
H atom injector for fast atom bunches 2−53204
He, metastable, elec. field effect 2−83215
He, scatt. by Ag surface 2−50430
He, scatt. by LiF, one-phonon transitions 2−50451
He elastic scatt. from LiF solid surface, Yukawa-type interaction 2−74239
K, reaction with methyl iodide in crossed beams, energy dependence 2−68771
K + molecule, atomic beam, reaction cross- sections meas. 2−51433
Mg isotope, light source, theory and experimental verification 2−64057
NII, mean lives of excited levels, beam foil study 2−64020
Na, deflection by radiation pressure of cw dye laser light 2−73624
Ne metastable atoms, time-of-flight technique for transit time distribution 2−79878
Ne scatt. from (001) LiF surface, systematic trials study 2−74241
Ne scattering from LiF surface, Lennard-Jones potential calc. 2−74240
Ne$^+$ scattering from C foil, foil lifetime, charge state distributions and beam scattering 2−52825
O, system for obs. of mass spectrometer response in upper atmos. 2−64058
T polarized, elastic scattering of low energy electrons in crossed beam 2−46459

Atomic clocks *see Time measurement*
Atomic frequency standards *see Time measurement*
Atomic mass and weight
see also Isotopes; Mass spectra
trans uranium elements 2−64055
Cr mass determination of all stable isotopes 2−46470
Fe mass determination of all stable isotopes 2−46470
Mn mass determination of all stable isotopes 2−46470
Ti mass determination of all stable isotopes 2−46470
V mass determination of all stable isotopes 2−46470
Atomic orbitals *see Atoms/structure; Orbital calculation methods*
Atomic scattering factors *see Crystal structure, atomic; X-ray crystallography; X-ray scattering*
Atomic spectra *see Spectra/atoms*
Atoms
see also Atoms, mesic and muonic; Collision processes/atoms; Elements; Nucleus; Polarisability; Positronium
actinides, elec. dipole polarisabilities 2−59917
analytic multipole polarizabilities of ground and excited states, Coulomb approximation 2−46403
antiprotonic, strong interaction effects 2−79966
Bohr model classical derivation from Rutherford model 2−58742
book, introduction to atomic physics 2−83203
bremsstrahlung generated in thick plane absorbing target, attenuation characts. 2−64000
current developments and applications 2−82110
damped two-level, quantum theory 2−42708
decay, fast electron gun from tetrode nuvistor for delayed coincidence study 2−45682
decaying two-level atom, interaction with linearly polarized oscillating field 2−79879
dipole polarizabilities, coupled multiconfig. SCF method 2−64005
dynamic polarizability estimate using Tchebycheff theory and moment technique 2−74192
energy flow from atomic dipole in classical electrodynamics 2−59891
European Phys. Soc. conf., Wiesbaden, Germany (Oct. 1972) 2−76139
field ionization in mass spectrometer chamber, ion current and ion distrib. 2−49921
Green function techniques, reviews 2−49919
ground state binding energies and bound free cross sections in pulsar atmospheres 2−58407
hydrogen-like, calc. of frequency-dependent dipole and quadrupole polarizability using method of Steiner 2−70632
hydrogenic, multiphoton ionization, using non-perturbation method 2−79951
information retrieval of atomic codes, computer code 2−67378
interactions between atoms, long-range electrostatic and electromagnetic 2−42771
London van der Waals forces, unretarded, derivation from classical electrodynamics with classical e.m. zero-point radiation 2−46464
major problems of contemporary physics 2−42309
matter-antimatter rearrangement and annihilation cross sections 2−62433
metastable, time-of-flight technique for detection 2−79878
metastable one-electron, interaction with e.m. radiation, calc. for second-order radiative processes 2−46488
model Hamiltonian, rel. to building up of many- electron ground states 2−59892
nonlinear oscillator interaction with radiation field 2−64006
on-line data bank for conversational retrieval 2−42723
optical properties second-order estimate using Tchebycheff theory and moment technique 2−74192
photoelectron spectra, chemical effects on linewidths 2−70597
physics, recent advances, book 2−49914
physics course on modified Keller plan 2−78719

Atoms continued
polarisability, relation with interaction energy for a quantum mech. system 2−76979
rare earth metals, elec. dipole polarisabilities 2−59917
reduced rotation matrix elements, subprogram for calc. 2−66452
repulsive potentials 2−67379
retarded interatomic dispersion energy, derivation of multipole expansion from quantum electrodynamics 2−49935
retarded interatomic dispersion energy, multipole expansion, long and short range behaviour 2−79888
retarded interatomic dispersion energy, multipole expansion, spherical-tensor formalism 2−79887
retarded interatomic pot. energy, multipole expansion, induction energy for degenerate ground states 2−79889
spin-coupled wave functions, review of general theory 2−49918
spontaneous emission theory, Wigner- Weisskopf, rotating wave and ladder approxs. 2−74209
static hyperfine interactions at free atoms 2−70560
superradiance, radiative decay solutions 2−73260
systems with closed core plus two electrons, detachment potentials calc. method 2−46421
two level atom in arbitrarily strong sinusoidal field, Liouville eqn. soln. 2−66736
two-electron system, dipolar polarizabilities, variational calc. 2−46471
two-level, spatially extended system, interacting with e.m. field, eigensolns. 2−42717
two-level, ultrashort optical pulse propagation, method of characteristics 2−41943
Van der Waals forces for systems involving non-spherical atoms 2−63998
van der Waals interactions between rare gas atoms in a dense classical fluid 2−74234
variational bounds for imaginary frequency polarizability and dispersion interaction constant 2−52943
variational wavefunctions, relativistic connection 2−70557
X-ray fluorescence, intermediate state proximity effects 2−70563
$Z \leqslant 18$, method for determ. of total binding energies and their derivatives 2−56094
Ar-Ar pairs, retarded van der Waals pot. 2−67412
Cs, two level spin-system, nondiagonal magnetic resonance 2−56110
H-H, long-range interaction 2−42813
H-He, pairs, retarded van der Waals pot. 2−67412
H-inert gas dispersion prices, improved rigorous bounds 2−42801
H, production of spin polarized atoms in Xe-H$^+$ collisions, three-state calcs. 2−79918
He-He pairs, retarded van der Waals pot. 2−67412
He, ground state wavefunctions calc. 2−83211
He isoelectronic sequence, coherent atomic scatt. factor for ground state 2−64071
Hg vapour, nucl. spin relax., solid surface influences 2−42731
Li, model potential calc. of electron affinity 2−42752
Ne-Ar pairs, retarded van der Waals pot. 2−67412
Ne-Ne pairs, retarded van der Waals pot. 2−67412
Ne, interatomic potential of Siska used to calc. bulk gas properties 2−46863
Ne, multipole long range interaction coeffs. 2−64023
Ni K-shell and beta-decay, summing-energy spectrum meas. 2−46186
O and O$^-$, calc. of electron affinity using symmetry-adapted pair correlations 2−42709
Rb-Ar, Rb-Kr, Van der Waals molecules, action of r.f. field 2−56194
Rb vapour, self-defocusing of laser light by adiabatic following 2−70608

electron scattering
— 2−67431
alkali metal atoms, spin polarisation and differential cross sections 2−83183
alkali metals, collision cross sections for momentum transfer at low energies 2−83186
amplitudes and spin polarizations, electron energies 100 to 1500 eV, solution at Dirac equation 2−52940
Born's wave version treatment of electron capture 2−83170
bremsstrahlung, 180-2000 keV interactions with various atoms 2−64041
broadening of spectral lines, long-range and short-range potentials 2−42839
computer methods and software packages 2−42764
conference, physics of electronic and atomic collisions, Amsterdam (1971) 2−42772
double-continuum Coulomb wave function, asymptotic expansions 2−76973
effective potentials and variational formulations for positron and electron scatt. 2−67423
eikonal theory at intermediate energies 2−42758
elastic, of 100 to 150 keV electrons, ang. depend. 2−59926
electron microscope imaging of heavy atoms patterns in monomolecular layers 2−80639
experiment-computer system, on-line operation 2−42781
few-electron corrections of stat. exchange pot. in low-energy scatt. 2−79856
film, electron elastic plural scatt. by atoms, intensity-angular distribs. 2−84220
generalized-random-phase-approximation optical potential exact and semiempirical analysis 2−79916
Glauber approximation for estimation of cross sections 2−42779
Glauber type eikonal approximation for 'angle' trajectories 2−79876
imaging of single atoms in scanning microscopy 2−79162
inelastic, study of electron spin polarization 2−42763
inelastic collisions of fast electrons studied in Bethe theory 2−42780
inert gas-positron collisions below inelastic threshold, determ. of elastic and annihilation cross sections 2−74233
inner shell ionization, bremsstrahlung production, at 140 keV 2−42760
inner-shell electron excitation by photons and fast electrons 2−42747
inner-shell excitation by electron bombardment, study of mechanisms involved 2−42745

- **Atoms** continued
  - **electron scattering** continued
    - intermediate energies, optimized pseudostates and collective modes 2−67406
    - inverse bremsstrahlung absorpt. in large radiation fields, Born approx. 2−59925
    - ionisation, secondary-electron-production cross sections 2−76963
    - ionization, differential cross-sections 2−56108
    - ionization, electron-impact double and triple differential cross sections 2−74246
    - ionization cross section, determ. polarization of characteristic X radiation 2−76975
    - ionization cross-sections, velocity distrib. of bound electron in classical impulse approx. of binary encounter theory 2−67395
    - ionosphere, ionization cross sections, secondary electron distributions 2−78389
    - ions, multiply charged, trapped in hollow electron beam, meas. of electron impact ionization cross section 2−70609
    - K-shell ionization of atoms adsorbed on W substrate, backscattering cross sections 2−79919
    - line radiation excitation, polarization variation with scattering angle 2−46457
    - low energy cross sections for transitions between highly excited states, application to interstellar radio recombination lines 2−46405
    - multichannel scattering study of optimized minimum-norm and optimized anomaly-free variational methods 2−76994
    - polarized orbital approximations, review 2−64039
    - positrons, single-quantum annihilations by screened K- and L-shell electrons 2−76981
    - potential scattering, minimum-variance method 2−79913
    - pseudo-state expansion applications 2−42762
    - pseudo-state expansions, study of close- coupling approx., minimum principle, correlation methods, Born approx. 2−42761
    - quantum electrodynamics of scattering phenomena involving bound states 2−55794
    - Ramsauer effect, demonstration 2−67407
    - rare gas, 0-12 eV, failure of exchange potentials to satisfy data 2−73332
    - rare gases, Fermi press. shift and scatt. lengths 2−64038
    - separable approximation for correlation function, intermediate energy 2−42759
    - spin exchange, with free trapped electron, rel. to spin polariz. detection and r.f. spectroscopy 2−79898
    - Stark broadening, one-electron approximation 2−42757
    - stopping cross-section at nonrelativistic velocities, three-parameter formula 2−76992
    - structure and excitation determ. using fast general-purpose computer programs 2−42765
    - transport coeff. meas. for obtaining cross sections 2−64397
    - vacancy cascades created, meas. of atomic spectra and lifetimes 2−42722
    - Ag, absolute total cross section from K-shell ionization by electron impact, 30-140 keV 2−46458
    - Ag, K-shell ionization, absolute cross-sections 2−79931
    - Al, bremsstrahlung cross-section meas. at incident energy 0.2 MeV, photon energies 0.02-0.2 MeV 2−70613
    - Ar, autoioniz. by slow electron impact 2−74229
    - Ar, effect on freq. depend. of light distortion 2−50273
    - Ar, elastic scattering cross sections for slow positrons 2−70644
    - Ar, electron impact excitation function from threshold to 200 eV for formation of metastable states 2−70640
    - Ar, impact cross sections 2−49962
    - Ar, impact ioniz., slow electron obs. 2−64033
    - Ar, ioniz. by electron impact, efficiency curves 2−59921
    - Ar, small angle impact spectra, optical sums 2−70612
    - Ar ionization, electron-impact, double and triple differential cross-sections 2−74246
    - Au, absolute total cross section for K-shell ionization by electron impact, 90-140 keV 2−46458
    - Au, bremsstrahlung cross-section meas. at incident energy 0.2 MeV, photon energies 0.02-0.2 MeV 2−70613
    - B, electron impact ionization, calc. for $1s^22s^22p$ configuration 2−46451
    - Be, electron-impact double excitation cross sections calc. in Born-Oppenheimer approx. 2−70607
    - Bi, positron elastic scattering, 100, 200 keV, differential cross sections 2−79877
    - C, K and L shells, 9 keV, coincident measurement of quasifree scattering 2−70614
    - C atom K-shell X-ray fluorescence, effect of molecular environment 2−49995
    - C II, electron impact ionization, calc. for $1s^22s^22p$ configuration 2−46451
    - C V in D plasma, meas. of depopulation of $2^3P_{0,1,2}$ triplet levels 2−79961
    - CIII, collision strengths for transitions, distorted wave and close coupling calculation 2−76970
    - Ca, electron-impact double excitation cross sections calc. in Born-Oppenheimer approx. 2−70607
    - Ca^+ reson. lines, electron impact broadening 2−59914
    - Cd in He-Cd glow discharge 2−71024
    - Cs, elastic, differential cross-section calc., excitation threshold to 5eV 2−79883
    - Cu, absolute total cross section for K-shell ionization by electron impact, 20-135 keV 2−46458
    - Cu, bremsstrahlung cross-section meas. at incident energy 0.2 MeV, photon energies 0.02-0.2 MeV 2−70613
    - Cu, K-shell ionization, absolute cross-sections 2−79931
    - F VIII in D plasma, meas. of depopulation of $2^3P_{0,1,2}$ triplet levels 2−79961
    - H, application of quasiminimum principle to calcs. of variational lower bounds 2−49979
    - H, complex coordinate space calculations for position and width of lowest ^1S resonance 2−70636
    - H, coupled channels with square well potentials, Fredholm-Pade approx. 2−76205
    - H, cross sections, correl. approx. modification 2−67422
    - H, effective potentials nd variational formulations for positron and electron scatt. 2−67423

- **Atoms** continued
  - **electron scattering** continued
    - H, elastic, variational principles for multichannel Feshbach equations 2−52898
    - H, elastic differential cross sections, off-shell Coulomb T matrix 2−42797
    - H, elastic phase shifts comput. 2−64065
    - H, elastic positron scatt., calc. with Kohn variational method 2−46479
    - H, elastic scattering of e±, method of T-matrix extrapolation from complex energies 2−42799
    - H, elastic scattering of positions, optical potential method calc. 2−46421
    - H, electron impact cross-sections, representation for ionization and excitation 2−64063
    - H, energies >30 eV, Glauber approximation for estimation of cross sections 2−42779
    - H, excitation by electron and positron impact calc. in eikonal approx. 2−52944
    - H, four-channel approx. approach 2−83212
    - H, Glauber type eikonal approximation for ‘angle’ trajectories 2−79876
    - H, inelastic collisions, adiabatical approx. 2−64064
    - H, inelastic cross sections calc., adiabatic approx. 2−46481
    - H, low-energy, pseudo-state expansion applications 2−42762
    - H, positron elastic scatt., inclusion of long range effects via pseudostate expansion 2−42798
    - H, positron elastic scattering, test of approximate methods, positronium formation 2−42800
    - H, positron pickup, treated by theory of sequential projections and quasiminimum principal 2−42803
    - H, Stark broadening, one-electron approximation 2−42757
    - H, threshold behaviour of ionization internal function calc. using classical three body computer programme 2−56122
    - H, virial theorem generalization 2−64066
    - H excitation of $n=2$ levels, eikonal theory at intermediate energies 2−42758
    - H in plasma, time evolution operator in semiclassical theory of Stark-broadening 2−42793
    - H plasma line electron broadening, boundary of quasistatic region 2−77022
    - H^-, autoionization, projection-operator approximation in inelastic scattering region 2−77019
    - H_2 Fredholm optical potential calc. of elastic phase shifts 2−46480
    - He^+-He^{2+}-e plasmas, calc. of collisional-radiative volume recombination and ionization coefficients 2−50193
    - He, $1^1S \rightarrow 4^1D$ transition, excited by inelastically scattered electrons, absolute differential cross sections 2−74247
    - He, 44 71.48 Å line, plasma broadened, distant electron collisions effects 2−67429
    - He, application of various forms of second Born approximation to collisions in range 200-500 eV 2−56132
    - He, autoionization, projection-operator approximation in inelastic scattering region 2−77019
    - He, effective potentials and variational formulations for positron and electron scatt. 2−67423
    - He, electron impact excitation functions from threshold to 200 eV for formation of metastable states 2−70640
    - He, electron impact excitation of 2^1S state, 26.5-83 eV, calc. of Glauber cross sections 2−70642
    - He, electron impact excitation, high energy limit, differential cross sections 2−59950
    - He, excitation of autoionized $^3P^{(-)}$ states and resonance inoization, Fano’s theory 2−79953
    - He, impact ioniz., slow electron obs. 2−64033
    - He, inelastic collisions, adiabatical approx. 2−64064
    - He, inelastic cross sections calc., adiabatic approx. 2−46481
    - He, ionization, electron-impact, double and triple differential cross-sections 2−74246
    - He, positron collisions, total cross sections meas. 2−64078
    - He, positron elastic scattering, annihilation and positronium formation 2−42800
    - He, positron scattering, swarm- and beam-technique meas. of positron annihilation, ortho-positronium quenching, cross sections 2−42812
    - He, reson. ioniz. by fast electrons 2−67432
    - He, second Born scatt. amplitude considerations 2−64077
    - He, simultaneous excitation and ionization, calc. of cross sections and nuclear charge dependence 2−79954
    - He, simultaneous excitation and ionization of 4^2P and 4^2S states by electron impact, meas. of relative cross sections 2−64076
    - He, total cross sections of positrons, 15 to 23 eV 2−59951
    - He, vac. u.v. meas. of electron impact excitation 2−49983
    - He elastic reson. energy 2−74230
    - He electron impact excitation, broad P-wave reson. obs. 2−64075
    - He in He-Cd glow discharge 2−71024
    - He($s=1$), He^+($s=1/2$), electron polarization by exchange scattering 2−59952
    - Hg, differential and total cross sections for elastic and inelastic scattering at 6.703 eV 2−79881
    - Hg, excitation of 6^1P_1 and $6p'\ ^3P_1$ states, cross-section meas. 2−42732
    - Hg, inelastic, study of electron spin polarization caused by excitation of 6^1P_1 and $6p^3P_1$ states 2−42763
    - Hg, spin polarization and ang. distrib. 2−42789
    - K, differential and direct differential elastic scattering cross-sections 2−64040
    - K, elastic, differential cross-section calc., excitation threshold to 5eV 2−79883
    - K, polarized atoms, differential cross-sections for elastic scatt. of low energy electrons 2−46459
    - Kr, elastic reson. energy 2−74230
    - Kr, oscillator strengths for multiple ioniz. in outer and first inner shells 2−79891
    - Li, elastic, differential cross-section calc., excitation threshold to 5eV 2−79883
    - Li, electron-impact double excitation cross sections calc. in Born-Oppenheimer approx. 2−70607
    - Mg, electron-impact double excitation cross sections calc. in Born-Oppenheimer approx. 2−70607
    - Mg^+ reson. lines, electron impact broadening 2−59914

Atoms continued
electron scattering continued
N, absolute cross section for electron impact excitation, application of results to atmospheric spectra 2−67397
N III, electron impact ionization, calc. for $1s^22s^22p$ configuration 2−46451
N VI in D plasma, meas. of depopulation of $2^3P_{0,1,2}$ triplet levels 2−79961
Na, elastic, differential cross-section calc., excitation threshold to 5eV 2−79883
Na, four state exchange close coupling eqns. 2−64042
Na, low energy electron scatt., 0.5-20 eV, cross-section meas. 2−64022
Na excitation of D lines meas. from threshold to 1000 eV, determ. cross section, polarization 2−49959
Ne, differential and total cross sections for elastic and inelastic scattering at 2.104 eV 2−79881
Ne, elastic scattering at 150 eV, absolute differential cross sections 2−59935
Ne, impact ioniz., slow electron obs. 2−64033
Ne, reson. energy, bound-state calc. 2−59927
Ne, simultaneous ionization and excitation 2−42754
Ne, simultaneous ionization and excitation by electron impact 2−49960
Ne elastic reson. energy 2−74230
Ne IX in D plasma, meas. of depopulation of $2^3P_{0,1,2}$ triplet levels 2−79961
Ne(^1S), determ. of elastic, inelastic and total intensities for fast electrons, importance of electronic correlations 2−79882
O, absolute cross section for electron impact excitation, application of results to atmospheric spectra 2−67397
O, close-coupling calculations 2−42766
O, cross section calcs. using polarized orbital close coupling theory 2−64043
O IV electron impact ionization, calc. for $1s^22s^22p$ configuration 2−46451
O VII in D plasma, meas. of depopulation of $2^3P_{0,1,2}$ triplet levels 2−79961
Rb, spin-exchange optical pumping expts., determ. of temperature dependence of cross sections 2−70615
Se, positron elastic scattering, 100, 200 keV, differential cross, sections 2−79877
Si XII, excitation cross sections for 2s-np, ns-n'd, 2p-nd, 3s-np transitions calc. by Coulomb-Born method 2−56109
Xe, effect on freq. depend. of light distortion 2−50273
Xe, elastic reson. energy 2−74230
Xe, elastic scattering cross sections for slow positrons 2−70644
Xe, oscillator strengths for multiple ioniz. in outer and first inner shells 2−79891
excitation
see also Auger effect
2S atom production by dissociative excitation of D_2 2−42889 — 2−67417
actinide ions, effect of core polarization on f-f interaction calc. by perturbed-function approach 2−52929
alkali, $^2P_{3/2}$ state, collisional relaxation, nuclear spin in optical pumping with D_2-light 2−74227
alkali excited atom collisions with unexcited alkali atoms, inert gas atoms or molecules, transfer of excitation between fine-structure levels 2−42776
atom-atom-photon collisions, excitation mechanisms 2−83174
Born's wave version treatment aspects of electron scattering 2−83170
Brillouin's theorem for intershell correlations in HF method 2−70596
collision processes, spin exchange without internal energy change 2−59928
collision with fast charged particle, spectral line shift due to forced transitions 2−52905
collisional depolarization of excited states, effective lifetime rel. to correlated photons in cascade 2−74226
Coulomb excitation by heavy charged particles 2−79911
ejection of electrons by protons, character of interference of resonances with continuum in spectra 2−70618
electron impact, line radiation polarization variation with scattering angle 2−46457
electron impact excitation of characteristic X radiation, polarization determ. 2−76975
energy, self-consistent relativistic OPW calc. 2−81015
fluorescence lifetimes, device for det. based on phase-shift techniques 2−55366
fluorescence yields in K, L, and M shells, review of exptl. and theoretical techniques 2−42755
Hanle effect rel. to coherence effects 2−59912
heavy ion-atom collisions, high resolution X-ray spectrometry study of excitation and deexcitation processes 2−42777
inner-shell, by ion-atom collisions at keV energies, study of mechanisms for symmetric and asymmetric collisions 2−42746
inner-shell, comparison between photon, electron, proton, heavy ion production, study of mechanisms 2−42745
inner-shell deexcitation mechanisms, X-ray emission, Auger electron emission 2−42745
inner-shell electron excitation by photons and fast electrons 2−42747
inner-shell ionization, test of invariance of ionization- energy threshold value with ejection energy 2−52930
interaction of radiation with atoms subject to collisions with perturbation atoms, quantum mechanical transport eqn. 2−46449
ionization cross sections for electron and positrons, 0.1-2.7 MeV 2−70598
ionosphere, ionization cross sections, secondary electron distributions 2−78389
K-shell internal ioniz. probability, accompanying β decay, direct collisions contrib. 2−59919
K-shell ioniz. by high energy electrons 2−52928
L-shell excitation in asymmetric atomic collisions, extension of electron-promotion model 2−49966
laser saturated atomic reson. fluoresc. non-quenching collisions influence 2−83199
level crossing, two-level system, integration of Schrodinger eqn. 2−79862

Atoms continued
excitation continued
level crossing and effect of re-encounters 2−79863
lifetime measurement, beam-foil technique 2−52932
lifetime studies, using beam-foil light source 2−63994
light absorption by vapor with hidden alignment in magnetic field, meas. of relaxation constant 2−42741
light atoms, excitation energies calc. by decoupled Hartree-Fock method 2−52904
metastable atom production in hollow cathode arc-discharge, rel. to glow discharge 2−74211
metastables, production and detection 2−64050
modulated decays, zero-field oscillation obs. in beam-foil spectroscopy 2−59895
multilevel atom excited states, lifetime meas. by photon correlation method 2−42743
multiphonon ioniz., circular versus linear polarization 2−56105
multiphoton ioniz., high-order, polarization effects 2−79906
multiphoton ioniz. by circularly and linearly polarized light 2−83182
negative ions produced by surface ionization, mass spectra 2−79851
one-electron ions 2−52949
photoionization by low-energy photons in intense laser fields 2−52927
plasma level populations, distribution function 2−77269
population inversion in X-ray region in ion-atom collisions, amplifier design 2−82084
radiative decays, optical waveforms, single photon techniques for precision obs. 2−49339
rare-earth ions, effect of core polarization on f-f interaction calc. by perturbed-function approach 2−52929
resonance excitation diffusion, stimulated emission effect 2−59903
Sn I, multipole radiation excitation 2−46441
spin-flip resonance, theoretical refinements 2−46447
statistical formulation of response to external disturbance 2−70600
superluminal motion in inverted media 2−82608
three particle system stationary states 2−74210
two level atom, incoherent source model 2−79895
two-level atom, modified Bloch equations at optical frequencies 2−67396
two-level system, scattering of intense light studied using Green's function 2−49938
two-level system, spontaneous emission analysis in rot. wave approx. 2−82461
two-level system, spontaneous emission analysis in rot. wave approx. 2−82460
two-level system in intense multimode radiation field, excited states population 2−66730
two-photon ionization, analysis using Laplace transformation theory 2−64029
universal function for ionization by structureless charged particles of arbitrary mass and charge 2−52925
unlike atoms, excitation exchange, rel. to collective radiative processes 2−79926
X-ray fluoresc. yields, Auger and Coster-Kronig transition probabilities, review 2−79923
Z=23-83, K-shell ionization cross sections for 2.04 MeV electrons 2−74204
Z between 4 and 54, nonrelativistic K-shell Auger rates and matrix elements 2−49961
B, K-shell fluorescence yields with synchrotron radiation 2−77012
Be, K-shell fluorescence yields with synchrotron radiation 2−77012
C, K-shell fluorescence yeilds with synchrotron radiation 2−77012
Al, ioniz. of L-shell, by inelastic collisions of fast particles 2−64026
Al in Lewis Rayleigh N_2 afterglow 2−77011
Ar-N_2, −CO mixtures, heteronuclear associative ionization, formation of ArN_2^+, $ArCO^+$, Ar_2^+ following 30 eV electron impact 2−51430
Ar-Xe laser, energy transfer as excitation mechanism 2−41988
Ar, behind strong shocks, average atom-atom cross sections 2−67398
Ar, electron impact excitation function from threshold to 200 eV for formation of metastable states 2−70640
Ar, electron impact ioniz., slow electron obs. 2−64033
Ar, outer s shell role in single ioniz. by electron impact 2−67399
Ar, resonance absorption and fluorescence 2−52933
Ar deexcitation in collisions with gases, cross sections 2−64054
Ar II-Ar VIII, excited lifetimes, beam foil spectra radiative decay times 2−79873
ArH^+, energy curves, ground and excited state calcs. 2−64051
$^{15}Ar^+$, metastable autoionizing states, electronic energies and electron emission lifetimes 2−42749
$Ar+H^+$ elastic scatt., excited states 2−64051
Ba atomic beam, by slow electron beams, spectrometry with high resolving power 2−63426
Ba^+, meas. of absolute cross section for single ionization by electron impact in 10-1000 eV range 2−70601
Be, ^1S excited state, total energy by density matrix study 2−79872
Be, electron-impact double excitation cross sections calc. in Born-Oppenheimer approx. 2−70607
C, 1s-hole state, chemical effects on lifetime 2−70602
C, polyatomic negative ions, surface ionization 2−79928
C, population inversion in recombining plasma flow 2−46452
C V in D plasma, meas. of depopulation of $2^3P_{0,1,2}$ triplet levels by electron collisions 2−79961
Ca, electron-impact double excitation cross sections calc. in Born-Oppenheimer approx. 2−70607
^{45}Ca in solid Xe, β-decay, optical excitation of the daughter atoms Sc. 2−84244
Cd, 5^3P_1 state, colliding with inert gas atoms, meas. of relaxation constants 2−42783
Cd, magnetic depolarization of fluorescence lines, Hanle effect 2−79860
CdI vapour, reson. obs. in absorpt. spectrum at 30 Å 2−76996
Cl fast ion beams, beam-foil excitation, metastable X-ray emitters 2−42788
$^{14}Cl^+$ metastable autoionizing states, electronic energies and electron emission lifetimes 2−42749
Cs, electronic excitation transfer by atomic collisions, expt. 2−64030
Cs, optical pumping, effect of transverse pumping 2−70605
Cs, photoioniz. cross sections 2−59922

Atoms continued
excitation continued
Cu in Lewis Rayleigh N_2 afterglow 2−77011
D, excited atoms population of 8 to 100 keV beams from solid films of C, Mg, Nb, Au 2−49981
Dy^{2+} effect of core polarization on f-f interaction calc. by perturbed-function approach 2−52929
Er^{3+} effect of core polarization on f-f interaction calc. by perturbed-function approach 2−52929
F VIII in D plasma, meas. of depopulation of $2^3P_{0,1,2}$ triplet levels by electron collisions 2−79961
F + HF collisions, temp. dependence of vibrational energy transfer probability, 300 to 1500K 2−43037
Fe I, Fe II resonance transitions, radiative lifetimes, applic. to Fe abundance det. in sun and QSO PHL 938 2−58547
Fe I, total photoioniz. cross section contribs. 2−67400
Fe I ionization and excitation equilibrium in solar atmosphere 2−66230
Fe I ionization and excitation equilibrium in solar atmosphere 2−58559
^{155}Gd, half-life obs. using two dimensional analyzer and computer, γ-γ coincidence method 2−59715
H^+-H collisions, differential cross-section for H(n=2) direct excitation 2−46482
H-, position of lowest D autoionization states calc. using Feshbach's Q-operator formalism 2−49982
H, by gravitational wave, semiclassical treatment 2−77021
H, collisional excitation and ionization rates rel. to classical and quantum mechanical formulae in astrophysical calculations 2−49977
H, electron capture into $n=3,4$ states by H^+, H_2^+ impact, cross sections 2−70637
H, electron impact cross-sections, representation for ionization and excitation 2−64063
H, electron scattering, complex coordinate space calculations for position and width of lowest ^1S resonance 2−70636
H, ground and first excited states of excitons in mag. field 2−64060
H, in collisions with alkali metal atoms 2−67426
H, interaction with intense laser radiation, time- dependent approach 2−79955
H, lowest excitation energy, in mag. field 10^8-10^{11} gauss 2−67419
H, multiphoton ionization in presence of intense e.m. field 2−49978
H, one dimens., repulsive core term in coulomb pot., energy levels in strong mag. field 2−59940
H, positive column plasma, population density and local thermal equlib. of excited atoms 2−43128
H, two-quantum photon-plasmon $2S_{1/2}-1S_{1/2}$ transition 2−79962
H beam-foil excited, obs. of fine structure interference effects in Lyman β radiation 2−64062
H excitation of n=2 levels, eikonal theory at intermediate energies 2−42758
H isoelectronic sequences, electron impact, interpolation formulae 2−74244
H plasma, expanding, population inversion of excited atomic levels 2−46709
H plasma, population inversion 2−49973
H(2S) metastable atoms produced in dissociative excitation of H_2, meas. of time-of-flight spectrum 2−46551
H(2p) vacuum u.v. excitation by electron impact on H_2, polarization free meas. of Lyman α radiation 2−80120
H(2s), formation by dissociation of H_2^+, meas. of angular distribs. 2−70816
He-He for collisions, influence of metastable atoms 2−42814
He, $1^1S \rightarrow 4^1D$ transition, excited by inelastically scattered electrons, absolute differential cross sections 2−74247
He, angular distrib. of differential cross sections and cross sections for simultaneous ionization and excitation 2−70639
He, beam-foil excited, 40 keV, meas. of relative level populations 2−52955
He, collisional ioniz. by slow electrons 2−64074
He, electron impact, broad P-wave reson. obs. 2−64075
He, electron impact, excitation of autoionized $^3P^-$ states and resonance ionization, Fano's theory 2−79953
He, electron impact excit. to metastable states, Born-Oppenheimer approx. 2−46490
He, electron impact excitation functions for singlet and triplet levels 2−67431
He, electron impact excitation functions from threshold to 200eV for formation of metastable states 2−70640
He, electron impact excitation, high energy limit, differential cross sections 2−59950
He, electron impact excitation of 2^1S state, 26.5-83 eV, calc. of Glauber cross sections 2−70642
He, electron impact ioniz., slow electron obs. 2−64033
He, fast proton impact, Born cross-sections 2−79949
He, formation of $(1s2p)^{1,3}P$ state, $He^+(2p)$ and He^{2+} in inelastic collision with He^+ 1-3 keV 2−56133
He, metastable atom creation by electro-ion recomb., in postlum. of discharge 2−64345
He, multiphoton ioniz. from excited states 2−46492
He, Penning-ionizing collisions, excited-ion lifetimes 2−67433
He, position of lowest D autoionization states calc. using Feshbach's Q-operator formalism 2−49982
He, reson. ioniz. by fast electrons 2−67432
He, simultaneous excitation and ionization by electron impact, calc. of cross sections and nuclear charge dependence 2−79954
He, simultaneous excitation and ionization of 4^2P and 4^2S states by electron impact, meas. of relative cross sections 2−64076
He, singlet + triplet mixing in n=3 states excited by proton impact 2−56130
He, triplet metastable, reson. multiphoton ioniz. 2−46491
He, vac. u.v. meas. of electron impact excitation 2−49983
He deexcitation in collisions with gases, cross sections 2−64054
He gas, excitation transfer meas. using p beam 2−42819
He I, energies and lifetimes of doubly excited states meas. using beam-foil technique 2−52954
He isoelectronic sequence, dynamic polarizabilities and mean excitation potentials 2−77026
He isoelectronic sequence, electron impact, interpolation formulae 2−74244

Atoms continued
excitation continued
He isoelectronic sequence, oscillator strength for allowed nd-n′f transitions 2−56125
He isoelectronic sequence, upper and lower bounds of excited states 2−64073
He triplet metastable, 5 photon ionization probability light intensity depend. 2−74248
He triplet metastable, resonance multiphonon ionisation 2−42811
He +, intensity decay curves, cascade-induced alignment changes 2−42753
He^+, lifetime of $2^2S_{1/2}$ state 2−70641
He^+, lifetime of 2S state 2−67430
^{3}He discharge optically pumped, detection of orientation of $^3He^+$ by absorption of 10830A line of ^{4}He 2−74245
$He + h\nu = He^+(n=2) + e$, simultaneous ionization and excitation, 100-200 eV, meas. of cross section ratio 2−56131
Hg, 6^3P levels, in Ar-Hg discharge, voltage frequency influence on instantaneous densities 2−74424
Hg, excitation of 6^1P_1 and $6p'$ $^3P_1$ states, cross-section meas. 2−42732
Hg vapour, selective refl., crossing effect between Zeeman sublevels of isotopes 2−79900
I, decay rates, using time-depend. gain meas. of photochem. laser 2−52440
I ions, charge states 2^+ to 18^+, meas. of charge-changing cross sections in H and O, 5-25 MeV 2−70623
K vapour, multiphoton resonant processes under laser irradiation 2−42750
K vapour, three-photon excitation using dye laser beam 2−74215
Kr^+-Kr collisions, inelastic energy losses in electron transitions 2−64034
Kr, Hanle effect meas. of lifetimes of excited states 2−42751
Kr, outer s shell role in single ioniz. by electron impact 2−67399
Li, beam-foil excited, 40 keV, meas. of relative level populations 2−52955
Li, electron-impact double excitation cross sections calc. in Born-Oppenheimer approx. 2−70607
Li, K-shell fluorescence yields with synchrotrons radiation 2−77012
Li, three-electron S state, Hylleraas-type wave functions 2−76991
Li I, doubly excited states, energies and lifetimes 2−42735
Li II, obs. of transition between doubly excited state using beam-foil technique 2−52954
Li isoelectronic sequence electron impact, interpolation formulae 2−74244
Li^+, intensity decay curves, cascade-induced alignment changes 2−42753
Mg, electron-impact double excitation cross sections calc. in Born-Oppenheimer approx. 2−70607
N, 1s-hole state, chemical effects on lifetime 2−70602
N, absolute cross section for electron impact excitation, application of results to atmospheric spectra 2−67397
N, beam-foil lifetime meas. of excited levels 2−79890
N, doubly ionized by slow proton impact, Auger spectra, intense satellite lines 2−83195
N VI in D plasma, meas. of depopulation of $2^3P_{0,1,2}$ triplet levels by electron collisions 2−79961
NII, mean lives of excited levels, beam foil study 2−64020
Na, atomic resonance by tunable dye laser 2−59920
Na D-line radiation excited in collisions of atoms with vibrationally excited H_2, D_2, N_2 2−70627
Na electron excitation of D lines meas. from threshold to 1000 eV, determ. cross section, polarization 2−49959
Ne-Br_2 mixtures, r.f. discharge spectrum, excitation mechanisms 2−71018
Ne^+-Ne collisions, inelastic energy losses in electron transitions 2−64034
Ne, absolute cross sections for excitation by impact of 20-180 keV H^+, H_2^+, He 2−70628
Ne, cascade effects in 2p level life time meas. 2−64032
Ne, electron impact excitation, 42-51 eV obs. of autoionizing $2s^22p^43s3l$ states and related Ne^- resonances 2−67402
Ne, electron impact ioniz., slow electron obs. 2−64033
Ne, excitation of 2p-3s lines in He-Ne mixture 2−42742
Ne, optical pumping with laser beam nonlinear effects in weak magnetic field 2−46453
Ne, outer s shell role in single ioniz. by electron impact 2−67399
Ne, simultaneous ionization and excitation by electron impact 2−42754
Ne, simultaneous ionization and excitation by electron impact 2−49960
Ne atom-ion asymmetric collisions, electron promotion model 2−79899
Ne deexcitation in collisions with gases, cross sections 2−64054
Ne IX in D plasma, meas. of depopulation of $2^3P_{0,1,2}$ triplet levels by electron collisions 2−79961
Ne isoelectronic sequence electron impact, interpolation formulae 2−74244
Ne isoelectronic series, energies of excited- state terms 2−74221
Ne metastable state 2−67629
NeVII, mean life meas., oscillator strengths detn. 2−64017
O^+-Ne close-encounter collisions, 50-200 keV, study of inner shell excitations 2−79914
O, 1s-hole state, chemical effects on lifetime 2−70602
O, absolute cross section for electron impact excitation, application of results to atmospheric spectra 2−67397
O, auroral, ^1S-level excitation by delayed processes 2−81705
O, electron impact excitation cross sections, ionospheric models 2−81724
O atom excitation to S^1 state during aurora borealis 2−44745
O VII in D plasma, meas. of depopulation of $2^3P_{0,1,2}$ triplet levels by electron collisions 2−79961
$O(^1D)$ collisional quenching by N_2 2−67416
OI $(^5S^0)$, dissociative excitation, absolute cross sections and radiative lifetime 2−56106
$O(2^1D_2)$, electronically excited, kinetic study by time-resolved atomic absorption spectroscopy in vacuum u.v. 2−83168
Pb metastable and excited states, cross section for collisional quenching depolarization of alignment by inert gases 2−42785

Atoms continued
excitation continued
$Pb(6^1D_2)$ electronically excited, atomic absorption spectroscopy using attenuation of resonance radiation 2−79859
Pr^{3+} effect of core polarization on f-f interaction calc. by perturbed-function approach 2−52929
Pu^{3+} effect of core polarization on f-f interaction calc. by perturbed-function approach 2−52929
Rb, $6^2P_{1/2}$-$6^2P_{3/2}$ excitation transfer induced in noble gas collisions 2−74231
Rb, optical pumping, optical detection system 2−77008
Rb, S and D states, cascade r.f. spectroscopy, anomalous D-state hyperfine structure 2−70606
Se, forbidden transitions in the ground configuration 2−74224
SiXii, electron excitation cross sections for 2s-np ns-n′d, 2p-nd, 3s-np transitions calc. by Coulomb-Born method 2−56109
Sn, inner-shell ioniz. cross sections calc. 2−52936
Te, in He or Ne buffer gas, charge transfer and cw laser action 2−56098
Xe, by collisions with metastable Kr atoms 2−59936
Xe, high current relativistic electron beam excitation, vacuum u.v. stimulated emission obs. 2−70584
Xe, outer s shell role in single ioniz. by electron impact 2−67399
ZnI, Hanle effect obs. of $4s4p^3P_1$ and $4s5s^3S_1$ levels 2−74232
magnetic moment
see also Gyromagnetic ratio
rare earth metals, diamag. susceptibilities 2−59918
BaI, obs. of new band system in 4481-4300 Å region, study of electronic transitions, vibrational analysis 2−70685
Cs, hyperfine structure coupling const. determ. from magnetic dipole transition in optical double resonance expt. in magnetic field 2−52916
Cs, optically oriented, transverse relaxation time 2−83191
He, ratio for 2^3S, ^4He level and fundamental ^3He level 2−56127
TeI, investigation of hyperfine structure of ^{125}Te in $5p^36s$ $^5S_2$ level by optical double resonance and level crossing spectroscopy 2−76998
structure
see also Hartree-Fock method; Russell-Saunders coupling; Nucleus; Spectra/atoms
actinide metal vapours, energy differences between electron configs. 2−46440
actinides, relative energies of lowest levels of f^qds^2, f^qds^2, $f^{q+1}s^2$ electron configurations 2−49950
actinides systematics in relative energies of f-electron configurations 2−79937
antisymmetric terms eval. for LS-coupled equivalent electrons 2−77000
bibliography on energy levels and spectra, Jul 1968 to Jun 1971 2−83206
book, development of present day concepts, based on course for arts students 2−62954
book, rigorous quantum mechanical results 2−83204
bound and continuum state problems 2−77003
bound electron g-factor, nuclear mass. correction 2−67386
bound state systems, integral eqn. approach, energy values 2−70630
bound state wavefunctions, asymptotic behaviour, derivation of upper bound 2−70562
bound states of one and two particle systems, variational trial functions 2−59937
bound-state calcs. use of regional wavefunctions 2−49937
Brillouin's theorem for intershell correlations in HF method 2−70596
Brueckner orbitals determ. by iterative procedure 2−50006
Brueckner-Goldstone many-body perturbation theory, use of multiple basis sets 2−46445
closed shell system, many-body Green's functions 2−59913
complex atoms, bound wave functions 2−76974
complex electronic configurations, scheme for using non-orthogonal radial orbitals 2−42711
computer applications to calc. of bound state energies and eigenfunctions of atoms with two or more electrons 2−83171
computing methods for determ. correlated wave functions 2−42860
configuration interaction rel. to method of electron correl. factors 2−79854
continuous spectrum of one and two particle systems, variational trial functions 2−59938
core-electron binding energies from orbital energies 2−79861
correlation models, Hartree-Fock functions and correlation splitting model 2−49933
correlation models, radial and ang. correlation $1s^2$ and $1s1s^1$ configurations 2−49931
correlation models, variational calculations for configurations containing several terms 2−49932
correlation theory, symmetry methods 2−59911
Coulomb correlation effects and the exchange correlation energy, atomic and band struct. calc. 2−61157
d-shell computational tools and calculations bibliography 2−49924
decoupled Hartree-Fock calculations for atoms with orthogonalized orbitals 2−52904
effective magnetic operations for inequivalent electrons 2−79936
electron densities, percentage contour maps, teaching demonstration 2−48958
electron spin-spin contact interaction in many-electron atoms 2−59905
electron velocity in atoms, Compton effect demonstration for students 2−78722
electronic wavefunctions, Serber-type spin eigenfunctions in terms of spin-adapted antisymmetrized products 2−74195
electrostatic interaction between p^4l and p^4l', matrix element calculation 2−56093
energy levels, calculation for light atoms 2−62940
energy levels, demonstration by Frank-Hertz experiment using oscilloscope 2−82096
energy levels in modified quantum statistical potentials 2−59881
excited levels, weak h.f.s. meas. by magnetic depolarization 2−59902
excited stationary states, isolated atom energy spectra, three particle system 2−74210
extended method of calculation, general theory 2−42712

Atoms continued
structure continued
f^n configuration, complete electron spin-spin contact interaction 2−46407
Feynman diagrams with simple denominators, summation in perturbation series 2−67381
fine structure cross sections from reactance matrices, FORTRAN IV program 2−52942
first-row atoms, B to Ne, ground state orbital approx. using cusped gaussian wave functions 2−49916
fundamental state energy level calcs. for Z-2 or Z-3 ionized systems 2−63993
fundamental states of Z-p times ionized atoms, degeneration 2−79853
g electron, position in periodic table of first appearance 2−56090
Gaussian atomic orbitals, property- optimized 2−46401
geminals, diagrammatical method based on second quantization formalism, Wick's theorem, Feynman-like diagrams 2−56081
geminals, diagrammatical method calc. of overlap and energy mean value expressions for wavefunctions 2−52894
ground state, effect of Pauli-forbidden intermediate states and operator identities 2−64003
ground state, reduced partitioning procedure for configuration interaction studies 2−42703
ground state spin rearrangement in strong mag. field 2−67383
ground states, quadrupole shielding and antishielding factors 2−76982
Hartree approx., variational principles for single-particle expectation values 2−66450
Hartree- Fock eqns, iterative numerical method 2−64010
Hartree-Fock calc. for energy interactions in $3d^n4s^0$ and $3d^n4s^2$ configuration excited states of transition elements 2−76965
Hartree-Fock calculation for p^n excited states, B to Br atoms 2−76964
Hartree-Fock eqn., full correl. 2−59910
Hartree-Fock valence shell orbitals, optimization of transferability 2−70564
heavy atom, configuration-space Hamiltonian constructed from QED, correction to Briet interaction 2−42719
heavy atoms and positive ions, semiempirical model for electrons 2−70570
highly ionized, hyperfine interactions of excited nuclei 2−52906
hydrogenlike, calc. of energy levels in magnetic field by new method 2−70634
ionic core, energy levels of optical electron, calc. using perturbation theory 2−46420
ionized, energy levels of fund. states, theor. schemes construct. 2−70561
isoelectronic series of light atoms, perturbation calc. of oscillator strengths 2−76999
K-shell electrons, exchange and correlation potentials 2−42710
Kepler problem, free fall zero angular momentum soln. in presence of mag. moment 2−70567
l-shell, of heavy atoms, effective nuclear charges 2−46404
lanthanides, systematics in relative energies of f-electron configurations 2−79937
level population determ. using flame atomic absorption spectroscopy 2−49939
many electron problem 2−49936
many-electron theory in exactly solvable model 2−52907
many-electron wavefunction, probabilistic interpretation of cluster function series development 2−70554
many-electron wavefunctions expanded in spin-adapted antisymmetrized products, expectation values 2−74194
mesic atom energy levels, nuclear polarization corrections 2−52958
multiconfiguration self-consistent field theory for localized orbitals, derivation of variational equations 2−52908
n-electron problem and matrices representing symmetric groups 2−52896
N-electron systems, evaluation of matrix elements for one-body spin-dependent operators 2−59896
natural orbitals, properties and uses, review 2−59880
non-compact groups and harmonic oscillator 2−59909
odd excited configurations $4f^{12}(5d+6s)6p$ and $4f^{13}7s$ 2−46443
one electron radial wave functions, obs. using computer produced movies 2−79934
one-electron energies, relativistic corrections to universal pot. 2−79852
one-electron ions, population of levels 2−52949
with open 2p subshells, correlation effects on hyperfine-structure expectation values 2−70571
oscillator strength calculations in frozen core HF approx. length and velocity formulae 2−46408
pair correlation energies from analysis of semiempirical values of correl. energies 2−59897
periodic table, n+1 filling rule and focussing potentials 2−79927
pionic and kaonic, static quadrupole hyperfine structure 2−49713
polarized core approx. for calcs. 2−70565
positronium, fine-structure interval of ground state 2−79964
pseudopotential SCF calculations 2−59904
rare earth, relative energies of lowest levels of f^qps^2, f^qds^2, $f^{q+1}s^2$ electron configurations 2−49950
rare earth metal vapours, energy differences between electron configs. 2−46440
rare earth metals, nucl. mag. shielding consts. 2−59918
rare-earth ions in crystal matrices, moments of radial function distributions, dependence on calc. method 2−65199
relativistic atomic energies, fine structure splitting 2−42713
Rydberg-state calcs. using generalized-random- phase-approximation optical potential 2−79916
second order energies, exact evaluations of partial sums for ground and singly excited states 2−46412
second row atoms, use of cusped gaussian wave functions 2−49917
shadowing of nuclear charge in relation to electron grouping of atom 2−63992
shell theory, three-electron scalar interactions rel. to $4f^n$ config. 2−59908
shells, selection rules 2−49940
simultaneous eigenfunctions of $\mathfrak{L}^2$ and $\mathfrak{S}^2$ by direct diagonalization, spin-adapted antisymmetrized products formalism 2−74196

Atoms continued
- **structure** continued
  - superheavy atoms, electronic structure 2-67385
  - term splittings, electron affinities, Bethe-Goldstone calculations based on configurational excitations 2-76983
  - transition density matrices, suggested calculations 2-59882
  - transition metals, approximate analytical wavefunctions 2-49930
  - transition metals, central-field models for open shells, SCF calcs. 2-64025
  - tunable wavelength spectroscopy, high-resolution techniques 2-55777
  - two particle correlations, evaluation of an integral 2-59898
  - two-electron, simple radially correlated ground state wavefunction 2-46472
  - two-electron, upper and lower bounds to eigenvalues 2-42807
  - two-electron ions, application of commutator techniques in perturbation theory 2-69593
  - two-electron ions, fine struct. singlet-triplet correction 2-83210
  - two-electron system, cusp conditions in extended SCF methods 2-59939
  - two-electron systems, cusp-satisfying orbitals effect on electron densities at nucleus 2-83208
  - two-level system, representation as linear oscillator 2-49927
  - virtual orbitals in Hartree-Fock method 2-64070
  - wavefunctions, explicitly correlated, partially antisymmetric 2-42701
  - Z^{-1} expansion, nuclear magnetic shielding constant and X-ray form factor for 2-, 3- and 4-electron atoms and ions 2-46460
  - Z-5 times ionized atoms, fund. states 2-74207
  - Z-expansion coeffs., number of electrons depend. 2-64002
  - K^--mesic levels energy shifts and widths 2-46494
  - Ac, metallic radius determ. 2-79857
  - Ar, densities of generalized oscillator strengths 2-52912
  - Ar XVII, lifetime of 2^1S_0 state 2-42809
  - BaI, auto-ionization resonance structures, high resolution photometry 2-79943
  - Be, ^1S excited state, total energy by density matrix study 2-79872
  - Be, accurate ground-state wave-function, geminal energy analysis 2-76989
  - Be, ground state, full correl. in Hartree-Fock theory 2-59910
  - Be, many-body Green's functions natural orbitals, total ground state energies 2-59913
  - Be, second-order Rayleigh-Schroedinger perturbation energy for ground state 2-64072
  - Be, use of cusped gaussian wave functions 2-49916
  - Be I, configuration-interaction calcs. on 2sns ^1S and 2p3p $^{3,1}P$ series 2-70578
  - Bi I, radiative lifetimes of excited levels belonging to $6p^27s$ and $6p^26d$ configurations by Hanle method 2-49942
  - C 2p3p, term dependence of Hartree-Fock results 2-56092
  - C correlation energy, dipole polarizability and long range interaction calc. using many-body perturbation theory 2-52914
  - C^{2+}, bound wave functions 2-76974
  - CI, even parity levels, frozen cores approximation 2-42726
  - ^{13}C, hyperfine structure in $sp^3(^5S)$ state 2-42725
  - Ca 3d4d, term dependence of Hartree-Fock results 2-56092
  - Ce^{3+}, analytical SCF wavefunctions for ground and some excited states, calc. of oscillator strengths for optical transitions 2-52915
  - Cl II, new wavelengths and energy levels 2-79946
  - Cs-Rb, difference of atomic electric dipole moments meas. using optically pumped atomic light modulation oscillators 2-46424
  - Cs, 7 $^2P_{1/2}$ hyperfine structure, core polarization, optical double resonance obs. 2-74213
  - CsI, investigation of $np^2P_{3/2}$ level sequence by level crossing spectroscopy 2-79920
  - Cu, valence states produced by ion-sputtering reduction, X-ray photoelectron spectroscopic obs. 2-57263
  - Cu^{2+}, analytical SCF wavefunctions for ground and some excited states, calc. of oscillator strengths for optical transitions 2-52915
  - D, hyperfine structure, $\alpha m/M$ correction 2-66902
  - Er, relative isotope shifts in u.v. region, determ. of coeff. of nuclear deformation and internal quadrupole moment 2-49947
  - F^-, stability of self-consistent symmetries 2-76986
  - Fe, valence states produced by ion-sputtering reduction, X-ray photoelectron spectroscopic obs. 2-57263
  - Fe group elements, ions analytic wave functions consisting of 2 Slater type orbitals 2-83205
  - Fe in $3d^64s^2$ and unstable Fe^+ $3d^7$ states, produced by decay of ^{57}Co in Xe 2-46426
  - Ga, Ga^+, lifetime meas. by beam-foil technique 2-42730
  - H-, autoionization states, computation using Feshback formalism 2-46487
  - H, bound states, rel. to four-dimens. harmonic oscillator 2-42792
  - H, electronic energy levels 2-45206
  - H, energy levels and wave functions by momentum representation treatment 2-56120
  - H, excited state wavefunctions, comparison of Messmer and Rayleigh-Ritz- variational methods 2-59942
  - H, frequency dependent properties, generalized eigenvalue equation approach 2-56121
  - H, ground-state energy, u.v. convergence of e.m. correction 2-42795
  - H, integral eqn. approach, energy values 2-70630
  - H, radial-angular factorized, 'natural' group scheme and selection rules 2-59944
  - H, S-like energy spectrum, analytic treatment of Coulomb potential in path integral formalism 2-46473
  - H bound state radial functions used to construct basis for unitary representation of algebra O(2,3) 2-42791
  - H^-, energies and wavefunctions of ground state calc. using least squares method 2-56129
  - H^-, influence of electron correlation on one-particle electron density and solid expectation values 2-52950
  - H^-, proof that 2 $^{1,3}S$ states are not bound 2-42807
  - He, 2 ^3P fine-structure splittings 2-52951
  - He, and He-like ions, ^1S ground states, algebraic 1 matrices and radial momentum distribs. from Hylleraas-type wavefunctions 2-52953
  - He, autoionization states, computation using Feshbach formalism 2-46487
  - He, beam-foil excited, 40 keV, meas. of relative level populations 2-52955
  - He, energies and wavefunctions for unbound $2s^2$ 1S and $2p^2$ ^1S states and ground and excited bound states calc. using least squares method 2-56129
  - He, excited states, virtual orbital approach 2-64070
  - He, Feshbach-type $^{1,3}P^3$ autoionization states, applic. of multiconfiguration energy bound method 2-46486
  - He, fine-struct. splittings, nucl.-motion corrections 2-77020
  - He, influence of electron correlation on one-particle electron density and radial expectation values 2-52950
  - He, integral eqn. approach, energy values 2-70630
  - He, many-body Green's functions, natural orbitals, total ground state energies 2-59913
  - He, nsms ^1S states with orthogonal orbitals, theorem on Hartree-Fock eqns. 2-56128
  - He, polarized core approx. for calcs. 2-70565
  - He, second-order Rayleigh-Schroedinger perturbation energy for ground state 2-64072
  - He 1s2s, term dependence of Hartree-Fock results 2-56092
  - He ground state, effect of Pauli-forbidden intermediate states and operator identities 2-64003
  - He isoelectronic sequence, dynamic polarizabilities and mean excitation potentials 2-77026
  - He isoelectronic sequence, upper and lower bounds of excited states 2-64073
  - He to Kr, Hartree Fock values of energies, interaction constants and atomic properties for ion and neutral atom groundstates 2-49923
  - ^3He, relativistic contribution to the hyperfine interval of metastable triplet state 2-42808
  - ^3He, weak hyperfine struct. interaction consts., determ. by mag. depolarization 2-59902
  - ^{193}Hg 3.5h, h.f.s. and isotope shift, by new Zeeman-scanned optical pumping method 2-46429
  - ^{199}Hg isotope, hyperfine struct. for (6s, 6d) configuration 2-56095
  - I-, accurate analytical wave functions 2-42733
  - $InIn^+$ lifetime meas. by beam-foil technique 2-42730
  - Kr, use of cusped gaussian wave functions 2-49917
  - Li, 2^2P state, electron correlations and quadrupole hyperfine structure 2-70587
  - Li, accurate perturbative calc. based on Hartree H_0 2-46432
  - Li, beam-foil excited, 40 keV, meas. of relative level populations 2-52955
  - Li, intermediate Hamiltonians 2-52923
  - Li^+, influence of electron correlation on one-particle electron density and radial expectation values 2-52950
  - Li^+, oscillator orbitals in CI calculations 2-59883
  - Li_1Li^-, approximate natural orbitals for groundstates, electron affinity 2-46433
  - Lu I, theoretical study of odd configurations $5d6s6p + 6s^27p + 5f6s^2 + 5d^26p$ 2-64018
  - Lu IV $4f^{13}6s$, $4f^{13}6p$, $4f^{13}5d$ configurations and effective magnetic operations for inequivalent electrons 2-79936
  - Mg IV spectrum analysis, radial integrals and level assignments, 90-2100 Å 2-59899
  - N, electronic struct., correl. energy 2-64021
  - N, fine-structure density shift 2-79964
  - Na, electronic energy levels 2-45206
  - Na III, 2500-1300 Å, $2p^43s$, 3d, 3p and 4s configurations 2-83196
  - Na III, level system location from obs. spectrum 2-79921
  - Nd^{3+}, analytical SCF wavefunctions for ground and some excited states, calc. of oscillator strengths for optical transitions 2-52915
  - Ne- compound atom, ground state parameter eval. 2-52924
  - Ne, correlation energy calc. using linked cluster many body perturbation theory 2-67484
  - Ne, stability of self-consistent symmetries 2-76986
  - Ne isoelectronic series, energies of excited- state terms 2-74221
  - Ne transition probabilities and collision induced transitions in excited levels 2-63995
  - Ni II, odd configurations, theoretical investigation 2-79874
  - ^{61}Ni, hyperfine structure of $3d^84s^{23}F_2$ metastable state 2-46438
  - O, atom, lifetime of $2p^33s^5S$ metastable state 2-42737
  - O II, 3p and 3p′ level radiative lifetimes 2-76985
  - O^-, stability of self-consistent symmetries 2-76986
  - O^{7+}, hyperfine interaction of $^{18}O[2+]$ at 1.98 MeV 2-52906
  - Pr^{3+}, analytical SCF wavefunctions for ground and some excited states, calc. of oscillator strength for optical transitions 2-52915
  - Sc III, level structure from obs. spectra 2-79922
  - Sr III energy-level system determ. from spectra obs. in 9800-350 Å range 2-76997
  - TeI, investigation of hyperfine structure of ^{125}Te in $5p^36s$ $^5S_2$ level by optical double resonance and level crossing spectroscopy 2-76998
  - Tl, Tl^+, lifetime meas. by beam-foil technique 2-42730
  - Tm, I, $4f^{13}5d6s$ and $4f^{12}6s^26p$ config., theory 2-56104
  - Tm II, electronic configurations $4f^{12}(5d+6s)^2+4f^{13}6p$ 2-46442
  - Tm^{n+}, n=2,3, calc. of analytical SCF wave functions for ground and excited states, free-ion energy levels, spin-orbit coupling consts. 2-46444
  - ^{169}Tm, K-shell perturbations caused by static nuclear quadrupole moment 2-42738
  - YIV, energy level determ. from spectrum anal. in 300 to 5200 Å range 2-79948
  - Yb III $4f^{13}6s$, $4f^{13}6p$, $4f^{13}5d$ configurations and effective magnetic operations for inequivalent electrons 2-79936

Atoms, mesic and muonic
- exotic, determination of polarizabilities of nuclei and elementary particles 2-67439
- isomer shifts of gamma transitions in ^{153}Eu 2-59714
- levels, nuclear polarization corrections 2-52958
- muonic, μ^- depolarization in aliphatic hydrocarbons, molec. wt. and temp. dependence 2-64083
- muonic, expts. in meson factories 2-82640
- muonic, higher-order vacuum polarization corrections 2-52959
- muonic atom in matter, hyperfine splitting freq. 2-70649
- muonic transfer from proton to deuteron, rate meas. 2-59960
- muonic-atom energy levels, weak interaction corrections 2-49510
- orbits with small and large overlap, use to test quantum electrodynamics and elementary particle and nuclear properties 2-77027

Atoms, mesic and muonic continued

- pionic and kaonic, static quadrupole hyperfine structure 2−49713
- polarization shifts 2−79963
- review of exotic atoms 2−70650
- K^--mesic levels energy shifts and widths 2−46494
- $K_L^0 \to \nu\pi\mu$ where π and μ form a mesic atom, probability calc. 2−64085
- μ^- depolarization in monomers and polymers 2−64084
- ^{209}Bi, isomer shift analyzed in terms of single particle or hole coupled to core vibrations 2−70579
- ^{153}Eu, theoretical investigation of muonic and Mossbauer isomer shifts 2−42526
- Hg, muonic, energies of 5g to 4f X-rays, quantum-electrodynamical corrections 2−59962
- Ne, pionic, strong interaction effects in 2p-1s transition 2−59964
- ^{206}Pb muonic atom, analysis of muonic X-rays in terms of equivalent radius 2−59963
- ^{207}Pb isomer shift analyzed in terms of single particle or hole coupled to core vibrations 2−70579
- ^{208}Pb muonic, energies and relative intensities of transitions to and from 2s level 2−42823
- ^{203}Tl, muon X-rays, nucl. γ-rays and μ-capture γ-rays analysis 2−59961
- ^{203}Tl, muonic, energies of 5g to 4f X-rays, quantum- electrodynamical corrections 2−59962
- ^{205}Tl, muon X-rays, nucl. γ-rays and μ-capture γ-rays analysis 2−59961

Attenuation *see Absorption*

Auger effect

- anticoincidence installation for internal counting counter 2−82814
- atom, $4 \leqslant Z \leqslant 54$, nonrelativistic K-shell rates and matrix elements 2−49961
- atomic, electron spectroscopy, applic. to surface chemistry 2−48357
- atomic inner-shell deexcitation mechanism, combination with X-ray emission 2−42745
- atomic radiationless transition probabilities, review 2−79923
- atoms, Auger lines in X-ray photoelectron spectrometry 2−52937
- atoms, photoionization, angular distribution of electrons 2−52939
- atoms electron spectroscopy, comparison of exptl. and theoretical intensities, condition for non-isotropic emission 2−42756
- Auger electron spectroscopy, general topics 2−57264
- Auger emission, kinematic theory, dynamic theory 2−48010
- ceramic substrate, effect of surface chem. on TaN adhesion 2−57005
- electron emission spectroscopy for detection of K, L, and M shell atomic fluorescence yields 2−42755
- electron spectrometer using concentric hemispheres, design and construction 2−74610
- electron spectrometry, low energy, book 2−41925
- electron spectroscopy, review in relation to vacuum technique 2−59924
- electron spectrum intensity used to determ. total electron impact cross-sections for excitation of inner-shell 2−42747
- energy meas. of Auger lines from solid surfaces using cylindrical analysis 2−84382
- film nucleation and growth obs. with LEED-Auger instrument 2−74624
- fracture surfaces spectrographic analysis 2−47541
- Hartree Fock Slater model nonrelativistic, Auger and X-ray transition probabilities 2−64008
- inert gases, correlation effects in Auger spectrum 2−46456
- KLL-Auger transition absolute probabilities, $30 \leqslant Z \leqslant 94$ 2−67404
- laser, X-ray, soft, rel. to ionization, inversion, stimulated emission and Auger effect 2−79209
- LEED-AES system, electrods and circuits 2−74612
- light elements, LMM Auger transitions vs. LLM transition 2−48015
- limitations and present state-of-art 2−71409
- metal, dynamical screening effects, spectral determ. 2−44211
- metal surface, contaminated, spatial distrib. of H_2 obs. 2−50526
- mica, Auger emission, relative intensities of lines 2−72081
- molecules, application of Auger electron spectroscopy to structure determ. 2−42756
- principles and applications, review 2−77481
- secondary electron spectra, from ion bombarded solid targets 2−51229
- secondary emission analogue for improved spectroscopy with retarding potential analyzers 2−59923
- spectrometer combined with LEED system 2−76739
- spectroscopy, comparison of X-ray and electron impact ionization 2−61467
- spectroscopy for det. of element profiles across oxide films 2−56580
- spectroscopy in emission electron microscope 2−81196
- steel, stainless, types 316 and 304, Mo surface conc., electron spectroscopy obs. 2−50442
- substrate design incorporating single crystal disc for use in ultra high vacuum 2−60617
- surface analysis, Auger electron spectroscopy rel. to appearance pot. spectroscopy 2−47071
- surface and interface obs. in mats. science using electron spectroscopy 2−56571
- surface impurities, bulk to surface equilib., Auger spectroscopy obs. 2−50465
- Z=12 to 21, electronic correls. effect on KLL lines 2−52938
- Z=35-85, calc. of Auger group rates and fluorescence yields for vacancy in 3p or 3d shell using nonrelativistic HFS model 2−70572
- zeolite, cation-exchanged, Mossbauer effect of Fe^0-atoms 2−54390
- Ag, adsorption of oxygen studies 2−60675
- Ag, and Ag on Be, quantitative spectroscopy and electron ranges 2−71304
- Ag, fine struct. in secondary electron spectrum 2−54280
- Al, adsorption of Cl, Auger spectrosc., ellipsometry and surface potl. meas. of clean films 2−71345
- Al, internal photoemission, struct. on high energy side of $KL_{23}M$ Auger peak 2−44212
- Al, spectra obs. 2−71313
- Al, sputter deposition and sputter removal of W, spectroscopy 2−50520
- Al_2O_3, escape depth of X-ray excited electrons and Auger electrons 2−51224

Auger effect continued

- Ar, electron spectroscopy, comparison of exptl. and theoretical intensities, conditions for non-isotropic emission 2−42756
- Au, escape depth of X-ray excited electrons and Auger electrons 2−51224
- Au, sputter deposition and sputter removal of W, spectroscopy 2−50520
- Be, and Be on Ag, quantitative spectroscopy and electron ranges 2−71304
- C, adlayer on W, K shell total electron impact ionization cross sections, Auger spectra 2−64579
- CO, electron and Auger electron spectroscopy, review in relation to vacuum technique 2−59924
- Cr surface, appearance potential spectrum, L_3/L_2 intensity ratio 2−51230
- Cu-Ni alloy, Auger spectroscopy obs. 2−50536
- Cu-Ni alloy, surface composition after annealing and sputtering, Auger spectroscopy obs. 2−50440
- Cu, and Cu on Ag, quantitative spectroscopy and electron ranges 2−71304
- Cu, Auger spectra, LMM, fine struct., L-S coupling interpretation 2−61453
- Cu, high-resolution meas. of Auger transitions, valence band density of states 2−81193
- Cu, sputter deposition and sputter removal of W, spectroscopy 2−50520
- Cu surface, phase transitions in two dimensional adsorbed layer of S ions obs. 2−50535
- Cu surface angular dependence of Auger electron emission 2−84388
- Fe-2.89%Si (100) face, surface composition rel. to photoelec. work function 2−61463
- GaAs, (110)-surface 2−76739
- p-GaAs, Auger recomb. of excess carriers, spin split off band effect 2−81067
- GaAs, surface stoichiometry and structure, surface vacancy model, Auger spectroscopy obs. 2−50445
- GaP, surface stoichiometry and structure, surface vacancy model, Auger spectroscopy obs. 2−50445
- GaS, surface electronic props. detn. 2−65106
- p-GaSb, Auger recomb. of excess carriers, spin split off band effect 2−81067
- GaSe, surface electronic props. detn. 2−65106
- GaSe, surface struct., surface states, Auger spectroscopy obs. 2−48024
- GaTe, surface electronic props. detn. 2−65106
- He, ang. anisotropy of Auger electrons 2−67432
- p-InAs, Auger recomb. of excess carriers, spin split off band effect 2−81067
- InAs, surface struct. obs. 2−50449
- p-InP, Auger recomb. of excess carriers, spin split off band effect 2−81067
- KCl spectra using spectrometer with concentric hemispheres 2−74610
- Li, Auger spectra, relative intensities, determ. and interpret. 2−65111
- LiH, surface struct., contamination, Auger spectroscopy obs. 2−47078
- Mg, spectra obs. 2−71313
- MgO, high resolution Auger electron spectra meas. with new Auger spectrometer 2−77972
- MgO spectra using spectrometer with concentric hemispheres 2−74610
- Mo, adsorption of alkali metals, Auger spectroscopy obs. 2−50540
- Mo, chem. shift on adsorption of O_2 2−51223
- Mo surface, proton and electron excited, surface composition detn. 2−50453
- N, adlayer on W, K shell total electron impact ionization cross sections, Auger spectra 2−64579
- N atom, doubly ionized by slow proton impact, Auger spectra, intense satellite lines 2−83195
- N_2, application of Auger electron spectroscopy to structure determ. 2−42756
- N_2^{2+}, prod. from N_2 by 430 eV electrons, cross sectional increase 2−83404
- Na, adlayer on W, K shell total electron impact ionization cross sections, Auger spectra 2−64579
- Na, Auger spectra, relative intensities, determ. and interpret. 2−65111
- Nb, deposition of Al, LEED and Auger spectroscopy obs., 22-1200°C 2−50484
- $NbSe_2$, Auger electron spectroscopy investig. of adsorption anisotropy 2−60687
- Ni, high-resolution meas. of Auger transitions, valence band density of states 2−81193
- Ni(001), impurity segregation, electron spectroscopy obs. 2−53554
- O, adlayer on W, K shell total electron impact ionization cross sections, Auger spectra 2−64579
- Pt(110), CO catalytic oxidation, Auger spectroscopy obs. 2−51443
- S, electron and Auger electron spectroscopy, review in relation to vacuum technique 2−59924
- Si-Au, mixed phase formation at interface, Auger electron spectroscopy, 100-300C 2−74619
- Si, amorphous, electronic structure obs. 2−61454
- Si, Auger electron signals of P surface impurity as function of coverage 2−47080
- Si, cleaning in H_2O_2 soln., electron spectroscopy obs. 2−53555
- Si, intrinsic, Auger electron spectroscopy analysis of photoemission processes as a function of caesium coverage 2−72082
- Si, surface Auger electron spectroscopy and electron impact desorpt. combined studies 2−64556
- n-Si (111) surface, structure obs. 2−50464
- Si_3N_4 film, detection of silicon oxynitride layers on surface by Auger elec. emission 2−50506
- $TiTe_2$, Auger electron spectroscopy investig. of adsorption anisotropy 2−60687
- U surface, chem. shifts in Auger transitions 2−67901
- V, surface chem. comp., chem. shift and peak intensity anal. 2−51480
- $VO_{0.92}$, surface chem. comp., chem. shift and peak intensity anal. 2−51480

Auger effect continued
VO$_2$, surface chem. comp., chem. shift and peak intensity anal. 2−51480
V_2O_3, surface chem. comp., chem. shift and peak intensity anal. 2−51480
W, sputter deposition and sputter removal of W, spectroscopy 2−50520
W surface, Cs adsorption obs. 2−50550
Xe (111) surface, thermal scatt. obs. 2−50470
Y, chem. shift on adsorption of O$_2$ 2−51223
Zn, Auger spectra, LMM, fine struct., L-S coupling interpretation 2−61453
Zr, L X-ray emission spectrum interpret. 2−64037

Auger showers *see Cosmic rays/showers and bursts*

Aurora
see also Airglow; Atmospheric spectra
1970, March 8, observations at Kerguelen and Sogra 2−84879
1970, March 8 storm, study of perturbations in midnight sector 2−84878
1970, March 8-9 arc event, OI and NI emission spectra 2−72839
arc, effects on ionospheric electron density 2−81725
Arctic ionosphere auroral precipitation patterns, airborne observations 2−84907
AU and AL indices on international quiet days and geomagnetic field variations at high latitudes 2−48602
auroal particles, origin, props. 2−68943
backscattering irregularities, spatial correl. of optical and radar data 2−58068
belt ionospheric currents, Harang discontinuities 2−68947
Birkeland currents intensification due to elec. fields 2−65904
chemical excitation of $O_2(^1\Delta_g)$ and $O_2(^1\Sigma_g)$ 2−58060
conjugate points, relative motion during substorms 2−65899
current system, formation under action of charged particle flux interactions and ionization 2−48549
D and E layers electron density, incoherent scatter radar obs. 2−81735
dayside auroral particle precipitation mechanism, mid-latitude v.l.f. emissions 2−48538
Doppler radar signatures 2−58069
electrojet current motions, effect on mag. field, plasma two stream instability 2−68948
electrojet effects, lab. simulation 2−58071
electrojet polarization, idealized model 2−65901
electrojets, long term variations 2−65922
electron and proton induced processes, fluoresc. efficiencies 2−58061
electron auroral morphology, substorms and magnetospheric processes 2−84875
electron differential energy spectrum, interchange between acceleration and thermalization processes 2−65907
electron energy spectra variations during auroral substorms 2−84876
electron precip., field-aligned, morphology 2−65908
electron precipitation, magnetic field aligned 2−65892
electron temp. vertical gradients in ionospheric topside 2−62358
electron-water vapour interaction effects 2−53019
electrons, precipitated and backscattered, twin payload obs. 2−62344
emission, vacuum u.v. meas., luminosity profiles 2−58062
energy spectra rel. to precipitating electrons 2−65914
expanding auroral bulge during substorm, airborne photography 2−48550
flickering, colour TV film analysis 2−58058
geomagnetic storm of 1970, March 8, development peculiarities rel. to solar wind, magnetosphere and aurora 2−84917
heating, bulge obs. in neutral N_2 atmosphere 2−58057
high latitude, classification, polar graphs, grouping model 2−68946
hiss, dispersive, m.f. whistler mode 2−68954
hisslers generation mechanism 2−65918
IBC$\simeq$3, averaged spectra, 7000-9000 Å, relative intensities 2−75625
incoherent scatter measurements, 1290 MHz aurural zone radar, Chatanika, Alaska 2−72884
infrasonic wave generation mechanism 2−65898
intensity meas. at conjugate pts. 2−58059
intensity ratios of emission features 2−48552
ionosphere model, electron density height profile 2−81723
LHR hiss rel. to magnetospheric and auroral activity 2−68953
low energy electrons and optical emission rocket measurements 2−84882
low energy ion composition measurements, H^+ and He^{++} 2−68950
low intensity red arcs, scanning photometry 2−48551
magnetic bay accompanied, rocket meas. of keV electron spectra 2−58064
midday, equatorward motion during substorms 2−65893
midday and polar cap, characts., satellite and airborne all-sky data 2−68945
midday auroras at South Pole during magnetospheric substorms 2−65900
molecular absorption cross sections, photodissociation 2−48548
morphology, quiet, growth, expansive and recovery phases 2−81716
oval, field aligned currents mechanism 2−65912
oval, polar cap particle fluxes 2−65913
oval geographical position determ. technique 2−65906
patch formation, during substorm, in midday sector 2−66008
periodically varying radio aurora from 48 MHz radar records 2−84877
photometric observations at geomagnetically conjugate points 2−72838
plasma instability and dumping of particles 2−54883
polar, interpretation of u.v. spectra using cross sections for electron excitation of O, N 2−67397
positive ion comp., mass spectrometric obs. 2−58066
precipitating energetic heavy ion obs. during mag. storm 2−65911
proton pitch-angle distributions in 100-300 keV range, satellite observations 2−65821
protons, satellite instrument for obs. in energy range 0.1 MeV to 6 MeV 2−65923
protons and alpha particles, energy and pitch angle distribs., current sheet acceleration model 2−65909

Aurora continued
pulsating, daytime chorus, post breakup phase of polar substorms 2−72915
pulsating, effective lifetime of O(^{1}S) atoms 2−81704
pulsating, electric fields in ionosphere 2−48572
quiet arcs., rel. to electrodynamic coupling between ionosphere and magnetosphere 2−65905
radio, at high altitudes controlling factors, Greenland, 1957-1959 igy period 2−68951
radio, caused by plasma instabilities 2−48555
radio, vertical gradients in theory 2−65915
radio aurora, periodically varying 2−62345
radio auroral aspect sensitivity and plasma two stream instability 2−68948
radio noise characteristics of auroral ionosphere 2−72840
red arcs, altitudes of 6300, 5577, and 9278 A emissions 2−65902
red arcs, middle lattitude, and belts of DR-currents, dynamics during magneic storms 2−48558
Saskatoon halo display, unusual arc obs. 2−62343
simulation possibilities 2−65894
soft electron zone, effects of dipole tilt, interplanetary field and substorms 2−65903
solar activity effects 2−66226
space-time regularities, electron fluxes, luminesc., review 2−68944
spectra, between 2000 and 3000 Å, using fast scanning spectrometer 2−48554
spectral intensity meas. of primary electrons during intense breakup 2−58065
spectroscopy and excitation processes, review 2−48553
stable red arcs, obs. from OV1-10 2−65896
striations, pulsations and substorm activity on v.h.f. radar records 2−62346
sub-auroral plasma trough morphology 2−58056
substorm adiabatic processes 2−65871
TV techniques appl. for data acquisition in auroral and ionospheric research 2−84892
type-A red, low energy electron meas. 2−58063
u.v. spectrum, N_2, N I and O I lines 2−65897
visible auroral arc rel. to low-energy electron precipitation 2−68949
v.l.f. auroral hiss rel. to precipitating low-energy electrons 2−68952
v.l.f. hiss and plasma phenomena in polar magnetosphere 2−65839
v.l.f. hiss onset impulsive character, rel. to substorm phase 2−65917
v.l.f. radio noise rel. to visible auroral arc emissions 2−65916
X-ray and visible bursts, simultaneous, balloon obs. 2−65895
^{4}He flux precip. meas. 2−65910
N_2 afterglow, O_2 and temp. effect on first positive bands 2−77304
N_2 i.r. emission spectra in auroral excitation conditions 2−84873
N_2 positive and N_2^+ band systems rel. to energy spectra of auroral electrons 2−54884
N_2 spectrum in i.r. range 6500-11500 Angstroms rel. to auroral spectra 2−84874
NI allowed transitions, high excitations 2−48547
O ^{1}S-level excitation by delayed processes 2−81705
O atom excitation to S^1 state during aurora borealis 2−44745
O_2 excitation cross sections and intensity ratios in auroral conditions 2−84872
O_2 i.r. band spectra, 1.27 μ 2−58067
OI allowed transitions, high excitations 2−48547
O^{1}S atoms in pulsating aurora, method for estimating indirect process in production 2−84888

Austenite *see Iron alloys; Steel*

Autoionization *see Ionization*

Avogadro's number *see Constants*

Axicons *see Lenses*

Backscattering *see Scattering, particles; and under 'scattering' subheadings of the appropriate particles*

Backward wave oscillations *see Electromagnetic oscillations; Electron tubes*

Balances
balance microcalorimeter for gas-solid reactions in fluorine chemistry 2−52305
continuous conveyor scales, analysis of weighing systems 2−55362
current, temperarure rise in coil former due to resistance in windings and corrections 2−41896
current balance, classroom expt. 2−48962
derived thermograph from thermobalance and recorder 2−63159
Faraday, for static mag. susceptibility obs. at low temps. 2−73512
hydrostatic weighing, density obs. to 10^{-4} 2−58691
magnetic, for determ. of ferrite phase in austenitic stainless steel 2−44245
magnetic susceptibility, sapphire filaments as hang down supports 2−45673
microgravimetric system for precision adsorption studies 2−53593
quartz, meas. of 10^{-12} g/s mass variations 2−52035
quartz crystal microbalance, techniques for chem. reaction studies 2−41450
quartz spring microbalance, ultrahigh vacuum, evaporation rate and vapour pressure 2−85175
strain gauge suspension 2−66407
strain gauged, oscillating, five component, dynamic characteristics 2−45215
thermobalance up to 1800°C in air 2−73283
thermogravimetric apparatus for pressures up to 70 atoms. 2−61759
three component dynamic wind tunnel, for turbulent air flow meas. 2−46829
time variations of weight, automatic recording balance for thermogravimetric meas. 2−69529
torsion, calibration with conducting loop 2−66018
torsion, effect of convection and nonequilibrium flow on motion 2−72605
torsion, relative deflection meas. in 10^{-9} sensitivity range 2−82184
vibrating quartz balance, very sensitive, appl. to gas-solid interactions 2−69538
weight meas., chemical analyses 2−57441

Ballistics
see also Impact
Coriolis deflection in gravitational field of rotating Earth 2−73270
fragmentation, acceleration phase 2−66491
hypervelocity, laser optical system 2−82578

Ballistics continued
Mount Etna and Stromboli geologic and photoballistic obs. 2−81567
projectile range, effect of rotation of Earth 2−73276
projectiles, teaching expt. using spring-gun portion of ballistic pendulum 2−78733
testing of eye protector lens materials 2−48926
testing of eye protector lens materials 2−48926
trajectory det. from shock arrival times 2−45352

Band theory of solids *see Crystal electron states/band structure; Solids/theory*

Bardeen-Cooper-Schrieffer theory *see BCS theory*

Barium
abundance concentrations at oceanographic stations Geosec I and III 2−75468
abundance profiles in Pacific and Mediterranean sea water 2−75467
abundance profiles in southwest Pacific from Geosecs III station near Tonga 2−75466
adsorption, on Pt, field emission microscope work function obs. 2−67924
adsorption, on W and Nb simultaneously with Ba, work function and thermal stability obs. 2−67923
artificial cloud growth in highly conducting medium 2−65950
artificial cloud in ionosphere, electron density increase in E-layer 2−68969
atom, collisional reaction with O_2, laser-induced fluorescence meas. of product internal state distribution 2−61770
atom, oscillator strengths for resonance transitions 2−79875
atomic beam, production from Ba in metastable states 2−83197
atomic beam excitation by slow-electron beams, spectrometry with high resolving power 2−63426
cloud experiments rel. to mechanism of photoionization and radiative transfer problem in freely expanding gaseous clouds 2−46791
cloud motions in magnetosphere 2−62298
cloud release at five earth radii 2−62296
cloud released in magnetosphere, mag. field meas. 2−62297
disordered overlayers, on Ni(001), specular electron refl. 2−60681
flame spectrometric determ. in presence of excess Co using phototransition as detection devices 2−68486
ion cloud expt. in magnetosphere, analysis of optical data obtained by NASA 2−62299
ion cloud in magnetosphere, Portuguese obs. of related luminous phenomena 2−72831
ion cloud released at 31000 km, analysis of resonance scattering of solar radiation 2−62303
ion cloud striations, acceleration to ambient magnetospheric plasma velocity 2−62301
oxidation kinetics, photoemission spectra of chemisorbed levels 2−51446
plasma, laser-generated, spectral line parameters 2−67643
plasma released in magnetosphere, instability mechanism for formation of striations 2−62302
seeded plasma, momentum transfer from ambient magnetospheric plasma, NASA/MPE cloud expt. 2−62300
thermal expansion, 1.5-30K, 55-90K and room temp. 2−74993
Ba-Cs filled thermionic converter, optimization 2−49283
Ba-Cs filled thermionic converter, current voltage characteristics 2−49286
Ba-Cs filled thermionic converter, influence of magnetic pressure 2−49282
Ba-Cs filled thermionic converter, ignited mode 2−49285
Ba-Ne collisions, excitation of metastable levels of Tl behind shock waves 2−79932
Ba-W_{110} system, temperature dependence of work function 2−75186
Ba I, auto-ionization resonance structures, high resolution photometry 2−79943
Ba II- and R-type stars, UBVRI photometry and spectra 2−81844
Ba ion cloud releases, analysis of observational problems 2−72820
Ba^+, meas. of absolute cross section for single ionization by electron impact in 10-1000 eV range 2−70601
Ba^{2+}, meas. of termolecular association rate constants with Ar, O_2, N_2, CO, CO_2, N_2O, H_2O in flowing afterglow 2−48316
$Ba + Cl_2 \rightarrow BaCl + Cl$ crossed beam reactions, primitive product ang. distrib. 2−81493
$Ba + HI \rightarrow BaI + H$, meas. of angular distrib. of product, determ. of threshold kinetics energy limits on D_0° 2−81494
$Ba + NO_2 \rightarrow BaO + NO$ crossed beam reactions, primitive product ang. distribs. 2−81493
$CsCl{:}Ba^{2+}$, ionic cond., 250-500°C 2−54232
$CsCl{:}Ba^{2+}$, self-diffusion, 360-460°C 2−74813

Barium compounds
borate glasses, struct. changes, e.p.r. 2−54496
Ba-mica/Al_2O_3 composite, fabrication and props. 2−56977
Ba formates, formation and surf props. of electron emissive coatings 2−65365
Ba silicates, phase relations 2−54006
$BaAl_2SiO_8$-$SrAl_2SiO_8$ solid soln., isomorphism, phase diagram 2−54009
$Ba_2B_5O_9Br(Cl)$, cryst. struct. 2−53657
$BaBr_2$, F-centre, optical absorp. and e.s.r. spectra obs. 2−51336
$BaCO_3$ diffusion screens for u.v. radiation 2−45823
$BaCaAlF_7{:}Eu^{2+}$, three polymorphs, luminesc. 2−72420
$BaCaKNb_5O_{15}$, crystallographic, dielec. and nonlinear optical properties 2−75251
Ba_2CaMO_6 ordered perovskites, M = Mo, Te, W, meas. of vibrational spectra, assignment of internal vibrations 2−81370
$BaCaNaNb_5O_{15}$, crystallographic, dielec. and nonlinear optical properties 2−75251
$BaCl_2$, F-centre, optical absorp. and e.s.r. spectra obs. 2−51336
$Ba(ClO_4)_2.3H_2O/Ba(MnO_4)_2.3H_2O$ mixed crystal, effect of uniaxial pressure on absorption spectra, confirmation of red band system of MnO_4^- as $^1T_1 \leftarrow {}^1A_1$ 2−81372
$BaCl_2.2H_2O$, i.r. spectra of H_2O in crystals 2−48170
$Ba_5Co_2(Cu_2)Ti_3Fe_{12}O_{31}$, magnetiz. and anisotropic props., rel. to microwave applic. 2−44273
$BaCoF_4$, two-dimensional antiferromagnet, mag. struct. 2−72211
$BaCo_xTi_xFe_{12-x}O_{19}$, mag. struct. 2−48102
$BaF_2{:}Er$, spin lattice relax. of ^{19}F in laboratory frame and rot. frame 2−68582

Barium compounds continued
$BaF_2{:}Eu^{2+}$, diffusion vanishing spin-lattice relax. of ^{19}F 2−44315
$BaF_2{:}Sm^{2+}$, one phonon sideband fluoresc. theory 2−65304
$BaF_2{:}Yb^{3+}$-Ho^{3+}, anti-Stokes luminescence, spectrum and excitation energy dependence 2−61688
BaF_2-P_2O_5-LaF_3, R = Ba, Mg, triangular diagrams, crystn. and vitrification regions 2−57035
BaF_2-SrF_2, solid solution, theoretical study 2−64772
BaF_2-TiO_2 system, $BaTi_{1-x}{}^{4+}Ti_x{}^{3+}O_{3-x}F_x$ formation and props. 2−47705
BaF_2, colour centres, high temp. absorpt. study 2−77597
BaF_2, e.p.t., linear elec. field effects for Ce^{3+}-F^- tetragonal sites 2−48285
BaF_2, elastic wave damping, effective anharmonicity consts. 2−80913
BaF_2, force fields, contrib. of three-body overlap effects 2−77765
BaF_2, l.f. dielec. consts., temp. and press. derivatives 2−51189
BaF_2, Raman spectra, lattice dynamics 2−57040
BaF_2, trigonal Gd^{3+} e.s.r. centres produced by hydrolysis reaction 2−84582
BaF_2, two-electron U-centres, point-ion models 2−83987
BaF_2 colour centre interconversion induced by electron irradiation 2−77598
BaFCl, crystal growth, modified Kyropoulos method 2−43523
BaFCl, X-irrad. and additively coloured, F-centres 2−64680
$BaF_{12}O_{13}$, grinding and thermal treatment effects 2−54342
BaF_2O_4, high temp. enthalpy and specific heat 2−54049
$Ba(Fe_{0.35}Al_{0.65})_2O_4$, disordered solid solution, blocking temps. of mag. random clusters from Mossbauer spectra 2−57309
$BaFe_{12}O_{19}$, deform. texture 2−56962
$BaFe_{12}O_{19}$, high temp. enthalpy and specific heat 2−54049
$BaFe_{12}O_{19}$, saturation magnetization, reduced temp. depend. by As or P substitution 2−78019
$BaFe_{12}O_{19}$, sintering kinetics 2−77738
$BaFe_2S_3$, cryst. struct., cryst. chem. 2−60750
Ba_2FeS_3, cryst. struct., cryst. chem. 2−60750
$Ba_6Fe_8S_{15}$, cryst. struct., cryst. chem. 2−60750
$BaFe_2Se_3$, cryst. struct., cryst. chem. 2−60750
Ba_2FeSe_3, cryst. struct., cryst. chem. 2−60750
$Ba_8Fe_2Se_7$, cryst. struct., cryst. chem. 2−60750
$BaFe_{12-x}Ti_xZn_xO_{19}$ ferrite, mag. props., Ti-Zn cation distrib. effects 2−72195
Ba_2FeUO_6, susceptibility and magnetization saturation 2−68570
$BaGeO_3$-$Ca(Ba)GeO_3$ solid solutions, struct., i.r. spectra study 2−65251
BaI, produced in Ba + HI reaction, determ. of lower bound for D_0° 2−81494
$Ba_2KNb_5O_{15}$, Ta-substitution influence on crystallographic and dielec. props. 2−47315
$Ba_2LiNb_5O_{15}$, cryst. growth, Czochralski method 2−60721
Ba_2LnMoO_6, paramag. susceptibility, rel. to Mo valence state determ. 2−72112
$Ba_\alpha(MO)_{0.133}MO_3(M = Nb, W)$, structural evolution as a function of α 2−83958
Ba_2MReO_6, (M = Mn,Re,Co,Ni), perovskites, synthesis and characteriz. 2−50876
$BaMe^{VI}O_4{:}U$, single crystals with sheelite structure, Me^{VI} = Mo, W luminescence and absorption spectra between 300K and 4.2K 2−68676
$Ba_2MgGe_2O_7{:}Eu^{3+}$, Tb^{3+}, Nd^{3+}, crystal and glass matrices, luminesc. props. 2−72423
$Ba_{2.96}MgSi_2O_8{:}Eu^{2+}$, luminescent props., prep. depend. 2−84550
Ba_2MgWO_6 ordered perovskite, meas. of vibrational spectra, assignment of internal vibrations 2−81370
$Ba(NO_3)_2$, precip. in KNO_3, solid soln. form. 2−56942
$Ba_2NaNb_5O_{15}$, crystallographic, dielec. and nonlinear optical props. 2−75251
$Ba_2NaNb_5O_{15}$, far-i.r. dispersion, room temp. reflectivity spectrum analysis 2−68622
$Ba_2NaNb_5O_{15}$, fluorescence, tunable, stimulated parametric, induced by picosecond pump pulses 2−69889
$Ba_2NaNb_5O_{15}$, Gd, substituted, thermal expansion 2−51048
$Ba_2NaNb_5O_{15}$, temp. of phase synchronization for two wave freq. addition 2−48128
$Ba_2NaNb_5O_{15}$ ceramic, sintering behaviour, scanning elec. microscope obs. 2−53929
$BaNb_2O_6$-$NaNbO_3$-$BaTiO_3$ system, tungsten bronze field, lattice parameters and Curie point 2−72034
$BaO{:}Ce^{3+}$, cubic sites, EPR investigations, g values 2−54491
BaO-B_2O_3-Fe_2O_3, glass elec. and mag. props., microstruct. effects 2−65113
BaO-B_2O_3-Fe_2O_3 glass, microstruct., ultrastruct., mag. props. 2−56558
BaO-B_2O_3 glass, stratification effects on comp. depend. of elasticity modulus 2−47478
BaO-Dy_2O_3 solid soln., phase diagram 2−54005
BaO-Y_2O_3 solid soln., phase diagram 2−54005
BaO-Yb_2O_3 solid soln., phase diagram 2−54005
BaO-ZrO_2-SiO_2, excitation and emission spectra 2−75320
$3BaO$-$5SiO_2$ glass, controlled spherulitic crystallization, 800-950°C 2−80530
BaO, microwave rotational transition in short lived state obs. 2−67468
BaO powder, recomb. luminesc., 103-423 K 2−61687
$3BaO.5SiO_2$ glass-ceramic, mechanical props. 2−53930
$BaPrO_3$ and $BaTbO_3$, neutron diffr. and mag. susceptibility meas., mag. props. detn. 2−81217
$BaSO_4{:}MnO_4{}^{2-}$, polarized optical absorption and e.s.r. spectra, crystal field transition e-t_2 assignment 2−48274
$BaSO_4$-$SrSO_4$, solid solution, theoretical study 2−64772
$BaSO_4$, crystal growth from silica gels 2−43519
$BaSO_4$, precipitation kinetics and mechanisms 2−51420
X BaSe-$Ge_{1.5}As_{0.5}Se_3$, pseudobinary system, glass formation 2−80531
$BaSrKNb_5O_{15}$, crystallographic, dielec. and nonlinear optical properties 2−75251
$BaSrNaNb_5O_{15}$, crystallographic, dielec. and nonlinear optical props. 2−75251
$Ba_{0.5}Sr_{0.5}Nb_2O_6$, absolute signs of second harmonic generation coeffs. 2−44332

Barium compounds continued
$Ba_{0.5}Sr_{0.5}Nb_2O_6$, cryst. growth rate variation with supersaturation in fluxed melts 2−47255
$Ba_4SrNb_{10}O_{30}$, solidification structs. 2−47654
$Ba_xSr_{1-x}Nb_2O_6$, semicond., high 1/f noise anomaly 2−47888
$Ba_xSr_{1-x}ZrO_3$ dielectrics, high-permittivity temp.-stable, low microwave loss 2−51190
Ba_2TaCoO_6, cryst. struct. and mag. props. 2−47316
$BaTiO_3$, surface potential variation, observation with scanning electron microscope 2−81157
$BaTiO_3$ plate, dispersion curves of flexural modes 2−84205
$BaTiO_3$ surface domain reorientation prod. by abrasion and annealing, X-ray diffraction exam. 2−80544
$Ba_2(UMg)O_6$-$Ba_2(U_{2/3}Fe_{4/3})O_6$ solid soln., prep. and struct. 2−56648
$Ba_3(VO_4)_2$, vibrational spectra 2−44382
$BaY_2F_8:Er^{3+}$, laser emission in the visible 2−61704
$Ba_2Zn_2Fe_{12}O_{22}$ crystal, grown by seeding, density and distribution of dislocations 2−68026
$Ba_3Zn_2Fe_{24}O_{41}$, hexagonal, anisotropy, comparison with $BaMg_2Fe_{12}O_{22}$ 2−72451
$Ba_2ZnGe_2O_7:Nd^{3+}$, absorpt. and fluorescence spectra, Nd^{3+} stimulated emission and laser action 2−61705
PbF_2-BaF_2, solid solutions, theoretical study 2−64772
PbO-BaO-GeO_2 structure and properties 2−53540
$PbSO_4$-$BaSO_4$, solid solutions, theoretical study 2−64772
barium titanate
see also Ferroelectric materials/barium titanate
dielectric const. changes after electron or gamma irrad., X-ray study 2−65047
distortion of cry. lattice and effect of admixed nickel 2−71406
electron diffraction, OOl systematic reflections 2−84367
film on Si by r.f. sputtering 2−75148
films, discrete vacuum evaporation method for ferroelectric behaviour, study of comp. and structure 2−83894
permittivity, influence of amplitude of free vibrations 2−81154
Raman cross sections, temp. dependence 2−84514
Raman scatt. line shape of soft E polariton mode 2−78112
surface domain reorientation prod. by abrasion and annealing, X-ray diffr. exam. 2−72364
surface potential variation, scanning electron microscope obs. 2−75203
vibrational amplitudes and Debye- Waller factors from elastic consts. and Raman freqs. 2−50983
(Ba, Pb)TiO_3 ceramic, light emission by surface microplasma new Curie temp. 2−65303
$Ba_{1-x}Sr_xTiO_3$, mobility, gravimetric determ. 2−81086
$BaTiO_3:F$, prep. by precip. from $TiCl_4$ and $Ba(NO_3)_2$ aq. solns. 2−74675
$BaTiO_3$-$BaGeO_3$ system phase equilibria 2−84105
$BaTiO_3$-Bi_2O_3, La doped composite ceramic, two-step anomalous resistivity increase 2−68395
$BaTiO_3$, conducting crystals, temp. depend. of carrier mobility 2−81100
Barkhausen effect *see Magnetization process*
Barnett effect *see Gyromagnetic effect*
Baryons
see also Hyperons; Nucleons and antinucleons
— 2−63649
baryon-antibaryon pairs and quarks, production, modified peripheral model 2−82711
classification from asymptotic algebraic realization of SU(3), determ. of D/F ratio and $g_a(0)$ 2−52629
conjugation symmetry of baryon number 2−76701
early universe implications of Hagedorn's exponentially increasing mass spectrum for baryon on temperature maximum 2−81767
e.m. mass differences, deep-inelastic contribution 2−76705
e.m. structure function meas. using NAL and ISR 2−73812
excited states, infinite-component wave eqns. and mass splittings within SU(3) and SU(2) multiplets 2−52630
isobars in superdense neutron star matter, energy shifts 2−58313
ladder U(6,6) symmetry, classification and mass formulae 2−45990
leptonic decays, determ. of masses, coupling consts., weak decay consts. in effective Lagrangian model 2−76703
mass, empirical formula relating baryon and meson masses 2−67041
mass splitting D/F ratio linked to lepton-nucleon scattering by sum rule 2−70153
matrix elements, octet dominance, explanation for vanishing of neutron charge radius 2−67059
meson-nucleon backward scattering extrapolations to baryon pole, rel. to coupling constant 2−76702
neutral, calculation of masses from beta decay of neutron using Heisenberg uncertainty principle 2−67042
non-local field, use in construction of mesons 2−79463
number, nonexistence for black holes 2−55385
octet baryon nonleptonic decay mode in current-current quark model 2−76723
octet r.m.s. tensor mass radii 2−73767
Reggeized baryon exchange, residue functions eliminating all parity doublets 2−79605
slopes of linear trajectories in GMO mass formula and $(mass)^2$ hypothesis 2−49587
spin 3/2, medium strong mass splittings in fifth interaction 2−70204
state mixing, model based on exchange degeneracy of pseudoscalar meson-baryon scatt. 2−63648
two-body baryon model construct. 2−76704
N*(1450) production in $pn \to pp\pi^-$ reaction at 5.9 GeV/c 2−70257
$p\pi^+\pi^-$, 1500 and 1700 MeV enhancements in pp reaction at 19 GeV/c 2−49599
interactions
effective-Lagrangian model of strong interactions with spin-one and spin-zero mesons 2−76703
meson-baryon hypercharge exchange reactions, differential cross-sections by new interference model 2−55868
pressure-density relation, applic. of relativistic quantum many-body theory 2−66447
SU(3) predictions or cross sections, introduction of angular momentum barrier penetration coeffs. 2−59556

Baryons continued
resonances
D_{13}, F_{15} states in $\gamma p \to K^+ \Lambda$ evidence for 2−52646
decay rates, qualitative breaking of SU(3) 2−76726
decays involving two partial waves, test for basic violation of $SU(6)_w$ 2−63642
electroproduction on nucleons, form factors 2−55881
exotic exchange reactions, insertion of total widths of baryon resonances into leading terms of Veneziano model 2−66961
meson-baryon resonances, high energy forward scattering, duality and SU(3) 2−42404
missing parity partners on trajecories difference in mechanism for N(938) and P_{33} resonance 2−63671
nucleon, possible existence of I=5/2 resonances 2−82785
parameters from partial-wave amplitudes 2−63636
production in $\pi N \to V + N'$ reactions model of higher baryon couplings 2−45983
production in single-pion photoproduction processes, e.m. decay widths in model of higher baryon couplings 2−45955
proton Compton effect, differential cross section meas. of Δ(1236) resonance region 2−63653
Regge trajectory correlations 2−59591
Roper, low mass due to SU(6) force 2−76616
spectroscopy, SU(3) and quark model predictions 2−59431
spin assignment and equal-phase assumption 2−63669
spin distribution function in dual resonance model 2−42358
three-nucleon system, low energy 2−42424
two-body baryon model construct. 2−76704
Δ, method for estimating total cross section of resonance on nucleons from final state Δ production on nuclei 2−42425
Δ,Δ production in $pn\pi^+\pi^-$ final state in pd reaction at 5.55 GeV/c 2−63663
Δ (1238) production in final state with K° in 3.4 GeV/c K-d interactions 2−67011
Δ^- (1236) production in K^-d interactions at 5.5 GeV/c 2−59515
Δ^{++} in $\pi^+ p \to \omega\Delta^{++}$ at 2.67 and 2.30 BeV/c, differential cross sections, decay density matrix elements 2−45987
Δ^{++} production in $K^-p \to pK^0\pi^+\pi^-\pi^-(\pi^0)$ reactions at 10 GeV/c 2−73808
$\Delta\Delta \to p\pi^-p\pi^+$, from pp, angular correlation theory 2−45863
Δ(1230) prod. in final state of pn reaction 2−52638
Δ(1231), prod. in K^+p interactions 2−73809
Δ(1236), dispersion relations and data on reactions $\gamma n \rightleftharpoons p\pi^-$ in this region 2−42324
Δ(1236), electromagnetic struct. study via deuteron photo- and electrodisintegration 2−82784
Δ(1236), radiation from mag. dipole moment, πp scatt. obs. 2−76685
Δ(1236) dominance in π-nucleus scatt., Coulomb flux corrections and total cross sections 2−67314
Δ(1236) isobars, possible study method for e.m. interactions 2−46017
Δ(1236) production in π^+p interactions for single pion production 2−42390
Δ(1236) production reactions, application of Regge-pole model 2−73856
$\Delta^{++}(1236)$, from $K^-p \to K^-\pi^-\Delta^{++}(1236)$ at 8.25 GeV/c 2−55847
Δ(1238 $|T_z|=3/2$ production in pp interactions at 6.6 GeV/c 2−67062
Δ(1955), in 7+/2 multiplet 2−42422
Δ(2850) prod. in $pp \to pp\pi^+\pi^-X^0$ 2−63654
$\gamma p \to K^+\Lambda$ photoproduction below 2.2 GeV c.m. energy, analysis of resonance contribs., radiative widths, stray baryonic states 2−82673
NN(1970), quantum numbers, total width, partial width 2−59592
N_α' reduced coupling to πΔ in $\pi N \to \pi\Delta$ reaction 2−59534
N*, production by high-energy neutrinos and electrons calc. in harmonic-oscillator quark model 2−52647
N*, production in high energy pp collisions, calc. using modified shell-model wave functions 2−49600
N*, scattering and photoproduction formalism, review 2−46016
$N^{*3/2}$ partial widths and branching ratios, calc. from $\pi^+p \to K^+\Sigma^+$ process 2−70268
N_{33}^*, effective range formulae, energy bands 2−49602
$N^{**} \to N^*\gamma$, sum rules for isovector e.m. transition moments, derivation using combined back and forward dispersion relations 2−49601
N*-(1236), prod. in K-n interac., 4.91 GeV/c 2−42372
$N^{*0}(1236)$ production in π-$p \to p\pi^+\pi$-π- at 20 GeV/c 2−45963
$N^{*++}(1236)$ production in π-$p \to p\pi^+\pi$-π- at 20 GeV/c 2−45963
N*(1688) production in pp collisions at 5.5 GeV/c, U(6,6)⊗O(3,1) peripheral absorption model study 2−55882
N(1512), obs. in $\pi^\pm$ p total cross section, 0.4-0.9 GeV/c 2−63611
N(1990), 7+/2 multiplet obs. 2−42422
$p\pi$- from interaction of 25-30 GeV/c neutrons with C 2−63670
$p\pi^-$ mass enhancement in $K^+n \to K^+N^{*0} \to K^+\pi^-p$ at 12 GeV/c 2−82742
πΔ, static model for elastic scattering, possible improvements 2−42399
$\pi\Delta \to \omega\Delta$, dual amplitudes and relations between coupling consts. 2−76684
πΔΔ (p-wave) coupling to πΔ in $\pi N \to \pi\Delta$ reaction 2−59534
πN resonance, dynamics, review 2−46015
πN systems prod. in pp inelastic scatt. at 6.6 GeV/c, isotopic spin $^1._2$ and $^3._2$ cross-sections 2−76710
Σ-(1197) production in π-p and π-K^+ at 2.45 GeV 2−42403
Σ(1385) production in π-p and π-K+ at 2.45 GeV 2−42403
Σ(1385)π decay mode of D_{03} resonances, relation to SU(3) 2−42426
Σ(2080) with $J^P=3/2^+$, studied by partial wave analysis of $K^-n \to \pi^-\Lambda$ reaction, 1.9-2.2 GeV 2−52600
Y* spectroscopy, review of theory and expt. 2−52648
Y^*_1 (2030), resonance parameters, formation in K-$n \to \pi^0\Sigma$- reactions 2−59516
Y*(1385), produced in K^-p interactions, meas. of mass, width and branching ratios 2−66994
$Y_1^*(1385)^0$ produced in π^-p interactions at 1.69 GeV/c, meas. of mass, width, spin, parity of resonance 2−46018
$Y_0^*(1405)$ produced in π^-p interactions at 1.69 GeV/c, meas. of mass, width, spin, parity of resonance 2−46018
$Y^{*+}(1385)$, two-step decay in reaction $K^-p \to \pi^-Y^{*+}(1385)$ 2−70211

Baryons continued
- **resonances** continued
  - Z^* exotic resonance predicted by Argand diagrams in K^+p scatt. 2−70212
  - N^* electroproduction in quark model 2−42423
  - N^* K^+p interactions in bubble chamber 2−45941
- **scattering**
  - baryon-baryon, meson-baryon and meson-meson scattering, unified treatment in Veneziano model 2−70190
  - meson baryon, elastic, σ-term in any (8,8) model of chiral symmetry 2−45928
  - meson-baryon, backward amplitudes and average radius of interaction on duality basis 2−66997
  - meson-baryon, multiple scatt. model, duality breaking effects 2−63572
  - meson-baryon, partial wave relations from fixed-u dispersion relations 2−59505
  - meson-baryon, problem of sigma terms 2−45929
  - meson-baryon, pseudoscalar, exchange degeneracy rel. to baryon state mixing model 2−63648
  - meson-baryon, strangeness-exchange interactions at high energy 2−76650
  - meson-baryon, SU(3)×SU(3) model with broken chiral symmetry 2−73774
  - meson-baryon resonances, duality and SU(3) 2−42404
  - pseudoscalar meson-baryon, calc. of s- and p-wave lengths 2−63573
  - $\pi\Delta \to \omega\Delta$, dual amplitudes and relations between coupling consts. 2−76684

Barysphere *see Earth*

Batteries *see Electric cells*

Bauschinger effect *see Deformation*

Bayard-Alpert gauges *see Vacuum gauges*

Bays *see Earth/magnetic field; Magnetic storms*

BCS theory
- cycle analysis of diagrams generated by Hamiltonians 2−58746
- generalized BCS theory, comparison with Hartree Fock Bogoliubov approx. 2−46072
- isolated flux line core, gap parameter $T \geqslant 0.7\ T_c$, BCS value 2−75069
- superconducting critical phenomena, functional integral method 2−68351
- superconducting neutron star matter, thermodynamic crit. field 2−73008
- superconductor, struct. of Cooper pairs 2−61232
- superfluidity, applic. to neutron stars 2−48703
- Nb, ultrasonic evidence against multiple energy gaps 2−75070

Bells *see Musical instruments*

Bending
- *see also Stress analysis; Torsion*
- — 2−66536
- aluminas, polycrystalline, influence of texture on mechanical props. 2−68093
- anisotropic cylindrical shells, stress and deformations 2−45374
- anisotropic rectangular plates, double Fourier series soln. of maximum deflection and bending moments 2−69669
- battened columns, out of plane buckling 2−69651
- beam and shell deflection, numerical soln. of boundary value problem 2−82314
- beam cantilever, Saint-Venant bending, closed form elasticity solns. 2−66505
- buckling, clamped circular arches subjected to point load 2−58873
- buckling, Euler method in static stability, follower problem 2−52183
- buckling, numerical analyses of compound branching 2−52180
- buckling, of orthotropic skew plates, formulation using Ritz variational method 2−49090
- buckling, prestressed circular plate 2−78886
- buckling, truss-type corrugated-core sandwich panels in compression 2−52142
- buckling and flutter of plates, due to action of flowing medium 2−41566
- buckling loads of tapered inelastic columns, improved bounds 2−66523
- buckling of beams and plates on two unattached foundations 2−66534
- buckling of elastic systems, stability theory 2−76242
- buckling of infinite sheet with one-sided constraint 2−45386
- buckling of rigid thick walled spherical shells under hydrostatic pressure 2−78897
- buckling of shallow spherical caps and truncated hemispheres under axisymmetric loads 2−41574
- circular annulus, depression due to load uniformly distributed 2−52156
- circular hollow beam problems 2−66549
- circular plate on elastic sheet 2−66501
- composite materials, glass fibre reinforced, laminated elastic moduli and strength 2−84123
- crack in elastic plate, part-through surface, elastic analysis 2−45378
- cracks subjected to, stress intensity factor evaluation, numerical technique 2−66504
- creep buckling of plates and shells 2−76318
- critical buckling load and deflection of beams, det. by three unknowns method 2−41580
- critical buckling loads of anisotropic shallow shells 2−41659
- curved strip, optimum thickness variation 2−58840
- cylindrical beams, orthotropic and almost, Saint-Venant problem 2−49063
- cylindrical shell subject to local load, precise theory 2−78890
- cylingrical specimens, method of forming axially symmetric surface cracks 2−50785
- deflection of simply-supported transversely loaded orthotropic sandwich plates 2−76310
- displacement constraints, invariant imbedding and optimum beam design 2−52147
- elastic-plastic buckling, variational method 2−78891
- elasto-plastic plates, finite element analysis 2−76254
- electrostrictive dielectric plate, pure bending 2−65068
- endurance testing unit for thin flat samples 2−56853
- Euler-Bernoulli, on elastic foundations, dynamical problem, perturbation soln. 2−66498

Bending continued
- fatigue, low-cycle, machine for testing 2−64740
- finite, of a compressible anisotropic rectangular block into a hyperbolic shell, exact solution 2−55455
- finite deflections of uniform beams using Euler-Bernoulli law of bending 2−52145
- finite elastic-plastic deflections in circular plates, numerical analysis 2−41629
- girders, thin walled and various cross-sections, stability to central compression 2−63071
- glass, slag, bending strength, softening temp., conc. depend. 2−56814
- inhomogeneous bodies 2−66541
- initial postbuckling behaviour of optimally designed columns and plates 2−76287
- laminated fibre-reinforced plates, plane strain bending 2−66543
- linearly viscoelastic shallow spherical shell, large deflections 2−66566
- magnetoelastic buckling of beams and thin plates of magnetically soft material 2−66554
- metal, meas. of elastic moduli and internal friction between 20 and 800°C 2−64749
- microhardness tester attachment for meas. of deformation of wire in coiling 2−82129
- multilayered sandwich plates, analysis by finite strip method 2−58889
- multimode buckling, postcritical behaviour of discrete conservative systems 2−76243
- natural bending frequency rel. to rotational frequency in rotating cantilever beam 2−66594
- nonlinear theory of arches with transverse shear deformation and rotary inertia 2−73372
- oval cylindrical shell, buckling and initial postbuckling 2−76290
- pipe bends, multi-mitred, subject to internal pressure and external loading, stress and flexibility factors 2−66530
- plate, analysis by quadratic programming 2−76316
- plate bending, triangular finite element analysis 2−52164
- plate bending problem, applic. of dual analysis principle 2−52167
- plate bending problem, local solution approach in finite element methods 2−52166
- plates, convergence of finite element solutions represented by nonconforming basis 2−69658
- plates, laminated orthotropic layers, analysis by finite element displacement 2−68057
- plates, rectangular, of linearly varying thickness, general equation of middle surface 2−58856
- plates of arbitrary planform, analysis using triangular, rectangular finite elements based on hybrid formulation 2−66495
- polypropylene sandwich mouldings, deflection during bending, stress function solns. 2−43663
- postbuckling anal. of magnetoelastic beam 2−45381
- prismatic plate assemblies, computation of initial buckling stresses 2−41588
- rectangular beam, computer calc. of optimal parameters for oblique bending 2−82303
- rectangular plate with mixed edge conditions, eigenvalue problems 2−66516
- rotating fatigue test, press-fitted shafts under two-step pulsating load 2−69639
- shallow circular arches, effect of initial imperfections on buckling load 2−66556
- shallow hyperbolic paraboloidal shells, analysis using finite Fourier transformations 2−73375
- shallow notched bar, as in Charpy test, slip line field solutions 2−41632
- shells, finite element model, from discrete Kirchhoff hypothesis 2−73367
- shells of revolution without bending under uniform axial loading rel. to composite materials 2−58845
- simply supported plate clamped around central circular hole 2−45396
- simply supported skew plates under combined loading, stability 2−45391
- skew plates of variable rigidity 2−66547
- snap-through buckling, elastic-plastic shells of revolution, finite element large deflection anal. 2−78875
- steatite materials, effect of modifying agents on strength 2−53933
- steel, annealed mild, effect of upper yield stress 2−43685
- steel, austenitic, surface slip lines and incipient cracks, during reverse bending 2−53837
- steel, carbon strain energy during rotatory bending fatigue, effect of pearlite patches 2−84125
- steel, effect of cyclic bending on strength and plasticity 2−84080
- steel, fatigue behaviour under reverse bending 2−50769
- steel, low-C, bending fatigue tests, Wohler curves, slip lines, cracks 2−50979
- steel, low-C, fracture rel. to microstruct., embrittlement, bend tests 2−56823
- steel, shear behaviour in heavy forming apparatus 2−53823
- stress analysis, photo-rheological method 2−82318
- stresses, around elliptic hole in cylindrical shell 2−45365
- strips, measurement of residual stresses effect of paint coatings 2−80788
- systems with coincident buckling loads influence of imperfections 2−55452
- thick rectangular plates and laminates, flexure with temp. variation across thickness 2−52196
- thin circular plate of variable thickness, buckling under uniform compression 2−63066
- thin elastic plate in bipolar coordinates, circular plate with eccentric circular hole 2−69671
- thin elastic plate in bipolar coordinates, solution of biharmonic equation 2−69670
- thin plates, annular segment finite element 2−76315
- thin section material, low cycle fatigue bend test method 2−47570
- transverse, thin plates, Dugdale mathematical model 2−52163
- uniformly loaded circular plate with mixed boundary conditions 2−58839
- unit for determining the elastic limit in pure bending under the action of surface and corrosion active media 2−85156

Bending continued
variable rectangular profile shell, influence of end plate and bulkhead 2−78876
vibrating combined cylindrical shell, bending moment 2−76346
waves, bending, diffr. and scatt. by mass impedance loadings of plane plate 2−63099
AlN-Al_2O_3-Mo cermet, ultimate bending strength 2−43869
n-CdTe, bending producing 60° dislocations, effect on conductivity and photoconductivity 2−61264
Fe-Ni superalloys, bend fatigue testing at elevated temperatures 2−56884
$GaAs_xP_{1-x}$, epitaxial growth on GaAs substrate, anisotropic bending 2−80567
$Ga_xIn_{1-x}As$, epitaxial growth on GaAs substrate, anisotropic bending 2−80567
Ni-base superalloy, dispersion strengthened, rotating bending fatigue tests 2−56883
TiC-Ni-Mo alloy, cermet, bending strength, Mo alloying effects 2−47534
W, sintered, bending resist., porosity influence 2−84145

Bending of light *see Gravitation; Light*

Berkelium
nuclear targets, electrodeposition methods of prep. for cross section obs. and accelerator bombardment 2−73919

Berkelium compounds
$BkCl_3$, low temp. absorption spectra, obs. 2−64116

Beryllium
— 2−67388
atom, electron-impact double excitation cross sections calc. in Born Oppenheimer approx. 2−70607
atom, ground state, full correl. in Hartree-Fock theory 2−59910
atom, ground-state wave-function, geminal energy analysis 2−76989
atom, K-shell ionization by protons and heavy ions 2−83179
atom, many-body Green's functions, orbitals, ioniz. pots., ground state energies 2−59913
atom, second-order Rayleigh-Schroedinger perturbation energy for ground state 2−64072
Auger spectroscopy, quantitative, and electron ranges 2−71304
cyclotron resonance, and mag. surface levels 2−84257
deformation obs. by synergy of TEM, selected area X-ray topography and line profile analysis 2−56791
electrical resistance, laser irrad. and annealing effects 2−81036
electromigration of C 2−43657
electron momentum distribution, from Doppler-broadened annihilation lineshapes 2−71782
film, condensed on glass, amorphous to cryst. transition temp. 2−43474
film, crit. thickness, Hall const. determ. 2−56587
film, on dielec. substrate, elec. resist., supercond. transition temp., absorpt. spectra 2−72323
film, structure effect on secondary electron emission 2−57265
friction stress temp. depend. for basal dislocations, 300-500K 2−64753
ground and ^1S excited state, total energy by density matrix study 2−79872
Hartree-Fock calculation, of electron states 2−80978
interstellar, production by cosmic rays 2−84970
interstellar possible production by low energy cosmic rays 2−62593
K-shell fluorescence yields by synchrotron radiation 2−77012
LEED intensities from (0001) surface 2−50438
LEED intensities from cleaved surface 2−60625
melting enthalpy 2−53491
microplastic deformation resistance, effect of thermocyclic treatment 2−53871
monocrystals, growth by Czochralski technique, obs. of cryst. perfection 2−47262
negative cond. electron contrib. to field gradient 2−68277
neutron diffusion length, depend. on temp. 2−76898
neutron pulse non-exponential decay at low temperature 2−56030
neutron source Be, D^+, attenuation in tissue equivalent 2−69322
plastic deformation anisotropy after programmed loading 2−80775
plastic yielding, high pressure effects 2−68081
pulsed neutron techniques, pseudo mode decay, anal. by inelastic scatt. expansion 2−83046
quantum oscillation waveforms, of transport props. rel. to $\partial M/\partial H$ oscillations 2−80963
rocks, US geological survey standard, content 2−61817
secondary electron spectra, ion-bombardment, Auger electrons and surface plasmon characteristic losses 2−51229
stopping power for 28 MeV α-particles 2−54099
target, dosimetry of neutron fields produced by d bombardment 2−67320
Be-Cu electron multiplier dynodes, cleaning and activation 2−82793
Be-Pu source, neutron spectrum det. using multisphere spectrometer 2−59878
Be I, configuration-interaction calcs. on 2sns ^1S and 2p3p $^{3,1}P$ series 2−70578
Be III, term system 2−42806
^7Be concentrations in Atlantic Geosecs II water column rel. to oceanic circulation 2−75475
p-Si:Be, hole transport, piezoresist. gauge factor 2−54198
^{235}U fission fragment range 2−61125

Beryllium compounds
bronze, precipitation hardening, cold worked, press. induced thermal activation 2−43781
oxyacetate, spin-lattice relax. of dipole-dipole reservoir and slow motion, n.m.r. obs. 2−72525
Be-Cu alloy, dilute, Fermi surface, electron scatt., de Haas-van Alphen and residual resist. obs. 2−71791
Be-Fe alloy, dilute, Fermi surface, electron scatt., de Haas-van Alphen and residual resist. obs. 2−71791
Be-(1 wt.%)Fe alloy, precip., Mossbauer obs.50931 2−50931
Be-Ni alloy, dilute, Fermi surface, electron scatt., de Haas-van Alphen and residual resist. obs. 2−71791
$Be_2Al_2Si_6O_{18}$, beryl, anharmonicity of i.r. vibration modes, reflectivity obs. 2−51317
BeB_2H_8, BeB_2D_8, BeB_2HD_7, i.r. and Raman spectra, frequency assignment and structure determination 2−52994

Beryllium compounds continued
$BeCl_2$, BeF_2, electronic structure and conformation, CNDO approx. 2−46529
$Be_2(Cr_{1-x}Mn_x)$, $Be_2(Mn_{1-x}Fe_x)$ specific heat meas. at 1-4 Kelvin 2−57059
BeF_2, vitreous, polycrystalline and molten, Raman spectra to 630°C, i.r. spectrum of vitreous at 25°C 2−48197
BeF_2 melt, structure and motion, molecular dynamics calc. 2−74515
BeH_2, comparison of resonance, perfect pairing and MO wavefunctions 2−52995
BeH_2, strongly orthogonal geminal wavefunctions for lowest singlet states 2−70686
BeH(D) λ doubling variation with rot. quantum no. 2−83261
$Be^{2+}He_2$ ion-induced dipole clusters, stability against dissoc., binding mechanism 2−80001
BeI, electronic spectrum of first excited state 2−42872
BeO:Si for environmental and personnel dosimetry in tropical countries 2−85133
BeO, alumina-coated, neutron irrad. effect on coating protective behaviour 2−43870
BeO, bromellite, growth from Li_2MoO_4-MoO_3 flux 2−77529
BeO, crystallographic transition study using DTA 2−64808
BeO, dependence of TSEE on various oxide and silicate admixtures after high temperature pretreatment 2−68493
BeO, dielectric breakdown, 300 to 1200°K, mechanisms 2−65056
BeO, dislocation etchant consisting of HCl 2−53600
BeO, electron irrad., F^+ centre, e.p.r. obs. 2−47366
BeO, hot-pressing 2−74914
BeO, irrad., V_1 centre, hyperfine parameters, ENDOR obs. 2−54498
BeO, γ-irrad. induced effects, e.s.r. obs. 2−44445
BeO, physical properties and electrical conductivity after neutron irradiation 2−52881
BeO, plastic deform. in single and polycrystalline mat. under high press. 2−68082
BeO, powder, glass-sealed, densification by hot isostatic pressing 2−53940
BeO, radiative lifetimes of excited vibrational states 2−46528
BeO, role of Si activator in exoelectron emission 2−59635
BeO, Stark shift of nuclear spin levels of ^9Be, n.m.r. obs. 2−44453
BeO, thermodynamic properties in solid and liquid phases 2−56496
BeO, vibrational amplitudes and Debye-Waller factors from elastic consts. and Raman freqs. 2−50983
BeO ceramic, chemically, thermally and radiation-induced changes in TSEE characteristics 2−68492
BeO ceramic, effect of different absorbing materials during γ- and X-ray irradiation on TSEE response 2−68491
BeO for microacoustoelectronic applications, characterisation 2−51042
BeO low-Z activated, use as high sensitivity radiation detector in TSEE dosimetry 2−67089
BeO powder, direct-recording electronograph in study of objects giving increased background 2−53639
BeO powder, initial stage sintering mechanism 2−47662
Be_2SiO_4:Cr_2O_3, e.s.r. of Cr^{5+}, 77K and 4.2K, 9.5GHz 2−72477
Be_2SiO_4, phenacite, growth from Li_2MoO_4-MoO_3 flux 2−77529
Cu-Be-Ag alloys, structural states in decomposition process, e. diffr., e. micro. and microhardness exam. 2−80782
Cu-Be-Ag and Cu-Be-Ti, decomposition of solid solns., phase transformations 2−68194
Cu-Be alloy, extra spots in electron diffr. pattern, obs. during G.P. zone formation 2−77578
Cu-Be alloy evaporation, mass spectrometer control 2−73233
Cu-(30 wt.%)Ni-0.3 wt.%)Be alloy, cryst. struct. and morphology of age hardening precipitate phases 2−50934
KF-BeF_2 glass, stratification effects on comp. depend. of elasticity modulus 2−47478
Ni-Be alloy, deform., recrystn., and ageing, texture variation 2−50806
Ni-Be alloy, deform., recrystn., and ageing, texture variation 2−50806
Ni-Be alloy, extra spots in electron diffr. pattern, obs. during G.P. zone formation 2−77578

Bessel functions *see Functions*

Beta-decay theory
see also Nuclear decay theory
asymmetry calc. in terms of polarization, Gorter-Rose method 2−82920
auto-ionization, L-shell model 2−46181
delayed neutron emission, β-strength functions and gross properties 2−49855
delayed neutron emissions, applic. of gross theory of β-decay 2−46352
Fermi decays, e.m. corrections 2−67192
impulse approximation, limitation on use 2−74047
induced-tensor and second-order-forbidden terms 2−46183
K-shell internal ioniz. probability, contrib. from direct collisions . 2−59919
mirror nuclei, meson exchange corrections to β decay 2−42414
neutron, application of model of Tanikawa et al in μ^-p resonances and duality in weak processes 2−70265
odd, non-axial, β-transitions calcs. 2−55973
probability of K-shell internal ionization calc. using theory of Stephas and Crasemann 2−70566
recoil effects in allowed decay 2−42541
semi-leptonic weak interactions in nuclei, analysis using electron scattering on basic, application to ^{16}O 2−76831
T invariance tests in allowed nuclear β decays 2−46182
vector coupling const., rel. to work interactions 2−59395
$^{10}C \rightarrow {}^{10}B$(2155 keV) β branch strength 2−46185
^{64}Ga ground state, isospin impurity 2−79771
^{203}Hg, nuclear matrix elements in first-forbidden beta-decay 2−46204
^{115}Xe and neighbouring region, shell-model calc. of β^+ strength 2−82922

Beta-ray spectra
see also Nuclear decay theory
data-handling system, multi-purpose 2−52667
^aSb, A=110-114, product and decay consts. of γ transition, β-γ, γ-γ coincidence meas., β spectra and point meas. 2−46191

Beta-ray spectra continued
^{198}Au beta spectral shape, precision analysis 2−67198
^{252}Cf, fission products, and associated inner bremsstrahlung radiation 2−59806
^{20}F β-emission, production by capture of polarized neutrons in MgF_2, static electric quadrupole interaction 2−75356
^{3}H, decay investigations 2−67193
^{3}H, meas. using magnetic spectrometer, determ. of upper limit for electron-antineutrino rest mass 2−73751
$^{147}Pm_2O_3$, thick cylindrical sources, bremsstrahlung 2−67191
^{90}Sr-$^{90}YTiO_3$, thick cylindrical sources, bremsstrahlung 2−67191
^{204}Tl, β-decay, internal bremsstrahlung spectral distrib. 2−42549
$^{204}Tl_2O_3$, thick cylindrical sources, bremsstrahlung 2−67191
^{206}Tl β-decay, meas. of spectral shape and nuclear matrix elements 2−63851
^{170}Tm decay, first forbidden beta matrix elements 2−42548
^{90}Y, internal bremsstrahlung spectrum, contrib. of detour transitions 2−42542
Zn, A=73, 74, decay characteristics 2−79746
conversion electrons
coincidence apparatus for β-e and β-γ meas. 2−52697
excited nuclear decay, in-beam studies, applic. to proton excitation studies 2−70417
internal, role in Gd-exposure neutron imaging 2−59638
$^{240}Am \rightarrow ^{240}Pu$ electron capture decay, meas. of γ-ray and conversion electron spectra, determ. of conversion coeffs. and multipolarities 2−79770
$Ba_2Bi^{5+}Bi^{3+}O_6$, phase transition, dielectric const. and loss obs. 2−75150
$^{137}Ba^{m}$ K-conversion lines meas. with Si(Li)-β-spectrometer in 4π geometry 2−63689
^{138}Ba, γ-ray and conversion electron spectra, spin-parity assignments 2−46155
$^{198}Bi \rightarrow ^{198}Pb$, $^{200}Bi \rightarrow ^{200}Pb$, γ-ray and conversion electron spectra 2−46174
$^{205}Bi \rightarrow ^{205}Pb$ decay, level scheme of ^{205}Pb 2−82928
^{206}Bi decay, study of level structure of ^{206}Pb 2−70413
^{133}Cs, exptl. study 2−70422
^{135}Cs, ^{137}Cs, ^{139}Cs, γ-ray and conversion electron spectra, spin-parity assignments 2−46155
$^{59}Fe \rightarrow ^{59}Co$ β-decay, determ. of coincident intensity ratio for γ-rays and X-rays from K-electron conversion 2−79769
^{154}Gd, exptl. study 2−70422
^{156}Gd, conversion electron intensities and γ-ray intensities obtained 2−46162
$^{113}In^{m}$ K-conversion lines meas. with Si(Li)-β-spectrometer in 4π geometry 2−63689
^{92}Mo + p in-beam spectroscopy 2−82913
^{101}Pb, intensities, conversion coefficients 2−49770
^{203}Po, decay, transition multipolarities 2−49774
^{205}Po, decay, transition multipolarities 2−49774
^{75}Se, coeffs. of low level transitions, using ^{75}As(p,n) 2−52752
^{181}Ta, exptl. study 2−70422
^{154}Tb, decay scheme determ. 2−52784
$^{235}U(n,\gamma)^{236}U$, conversion electron spectrum, level struct. of ^{236}U 2−67309
^{133}Xe, ^{135}Xe, ^{136}Xe, γ-ray and conversion electron spectra, spin-parity assignments 2−46155
^{96}Zr(p,p′e), rel. to meas. of first excited state lifetime of ^{96}Zr 2−59704

Beta-ray spectrometers
azimuth-dependent magnetic fields with Fe-free coils 2−79674
electrostatic for 1 to 50 keV, design 2−63690
electrostatic prism type with quadrupole lenses 2−49632
focussing and selection, geometrical ray tracing for astigmatic sector spectrograph 2−52673
large angle scattering, using Si surface barrier detector for 20 to 50 keV electrons 2−79679
magnetic, compact, for in-beam meas. of internal conversion coefficients 2−73929
magnetic, review 2−79670
magnetic prism, theory, aberrations, design and characteristics 2−73930
retarding potential diff. and retarded energy, variations in scattering cross sections 2−67074
scintillation counter, plastic, spectrum meas. 2−55915
semiconductor Si(Li), with mag. trochoidal electron transporter 2−59607
Ge counter, γ-compensated, as α and β particle spectrometer 2−52696
Ge(Li), dead layer effects 2−49663
^{63}Ni, disintegration rate by 4π counting 2−79672
with Si detector, superconducting magnet and liquid helium cryostat 2−52680
Si(Li), dead layer effects 2−49663
4π-Si(Li), reproduction of monoenergetic electron lines using coincidence method 2−63689

Beta-rays
see also Electrons
sources, thick cylindrical, bremsstrahlung 2−67191
$^{147}Pm_2O_3$, thick cylindrical sources, bremsstrahlung 2−67191
^{90}Sr-$^{90}YTiO_3$, thick cylindrical sources, bremsstrahlung 2−67191
$^{204}Tl_2O_3$, thick cylindrical sources, bremsstrahlung 2−67191
absorption
see also Electrons/absorption
Au foil, correction factors for self-absorption 2−76956
angular distribution
detection, measurement
see also Beta-ray spectrometers; Dosimetry; Particle detectors; Radioactivity measurement
extrapolated range, generalized semiempirical equations 2−70281
low-background β counter layout and operation 2−82813
effects
see also Electron beams/effects; Nuclear reactions and scattering due to/ electrons
dosimetry phosphors, 6, thermally stimulated exoelectron emission and thermoluminescence 2−82821
fluorite, thermoluminesc. 2−51379
quartz, thermoluminesc. 2−51379

Beta-rays continued
effects continued
CaF_2:Mn, CaF_2:Tb, thermoluminesc. 2−51379
$CaSo_4$:Mn, thermoluminesc. 2−51379
polarization
^{148}Pm decay, β-γ circular polarization correl. 2−42547
scattering
see also Electrons/scattering
No entries
Betatrons *see Particle accelerators/betatrons*
Bethe-Salpeter equation
bound-state solutions derived with ladder approx. 2−45991
covariant, calc. of quantum electrodynamical corrections to fine structure splitting of He 2−42810
field correlation function to discrete scattering medium 2−55593
hadron dynamics interpret., composite theory 2−52576
infinite-component solutions 2−70119
non-zero mass system description 2−59358
particles of spin $\leqslant 1$, two particle bound states, extension of BS eqn. for H atom 2−66902
quark bound states, particle exchanges 2−63554
relativistic quark models 2−52566
spinor eqns., partial-wave analysis for single particle exchange 2−73724
rel.to spontaneous violation of dilatation invariance in relativistic theories 2−59365
T-matrix approximation scheme, crossing and unitarity 2−63454
vibrational Pade solution 2−73709
Wick-Cutkosky model, Regge poles for large coupling constants 2−59350
(d, p), reaction study 2−83012
N form factors, asymptotic behaviour, solution of eqn. 2−79606
π form factor 2−63601
Bethe-Uhlenbeck equations *see Statistical mechanics*
Bevatrón *see Particle accelerators*
Binary stars *see Multiple stars*
Binding energy
see also Bonds; Lattice energy; Nuclear forces
— 2−63767
— 2−67117
adenine, 1s binding energy calc. for C and N atoms using perturbational model 2−77156
alkali metal halides, X-ray photoelectron spectral determ. of binding energy, comparison with point charge model 2−83259
alpha-cluster model effect of internal structure of α particle 2−70357
atomic core-electron binding energies from orbital energies 2−79861
atoms, test of invariance of ionization-energy threshold value with ejection energy 2−52930
atoms with $Z \leqslant 18$, method for determ. of total binding energies and their derivatives 2−56094
benzenes, fluorinated, X-ray photoelectron spectra, binding energy shifts 2−83289
core level binding energy shifts for C, N, O.and S containing mols. 2−83224
core renormalization, Coulomb energy differences 2−82847
diatomic molecule, critical binding 2−46498
double-closed-shell nuclei, Hartree-Fock calcs. using modified delta interaction 2−63747
from electron spectra, low energy 2−41925
even-even nuclei, symmetry energy 2−79729
furan, 1s binding energy for C atom 2−77156
ground state, of s-d shell nuclei, calc. using Strutinsky model 2−82875
halomethanes, K-shell electron binding energy and n.m.r. chem. shifts correl. 2−56235
hypernuclei, light, applic. of Garvey-Kelson mass formulas 2−46115
mE-Oh (Me-Cr, Mn, Fe, Co, Ni, Cu, Zn) molecule calc. using semi-empirical LCAO-MO method 2−42867
metal, nearly-free-electron, calc. using struct.-independ.-formalism 2−47801
metal, pseudo-ion approx. 2−83883
metal, single-atomic, in liquid state 2−71152
mirror nuclei residual n-p interaction derived from binding energy data 2−63731
molecule, small, core-level binding-energy shifts, relax. correction 2−67459
N-methylphenazinium 7,7,8,8-tetracyanoquinodimethanide, Ewald's method calc. 2−67931
neutron rich light nuclei, calc. of stable isotopes 2−82841
nitroso rubbers, determ. by ESCA 2−83350
nuclear, distrib. in ground state, binary clustering 2−83038
nuclear, retardation, nonlocal potential development 2−82856
nuclear, sufficient conditions for saturation 2−46079
nuclei, Hartree-Fock approximation, ^{16}O considered 2−42490
nucleus, continuum effects in Strutinsky calculations of shell corrections 2−52724
organic donor-acceptor crystals, electrostatic binding energy by Ewald's method and charge transfer in lattices 2−67928
positronium atom in NaCl type ionic crysts. 2−77793
positronium molecule 2−64111
pyridine, 1s binding energy for N atom 2−77156
pyrrole, 1s binding energy calc. for C and N atoms using perturbational model 2−77156
semiconductor, exciton bound to neutral impurities complex binding energy and stability 2−77835
semiconductor, exciton complexes binding energies, exciton neutral donor complex 2−80970
solute-vacancy interaction energies, measurement methods, review 2−68019
statistical or liquid drop expressions, shell correction calc. by Strutinsky's method 2−52727
superheavy nuclei, using Hartree-Fock calculations 2−63838
three and four nucleon systems, tensor forces 2−52732
three body quantum mechanical problem, approximate solutions 2−52081
three nucleon bound state, convergence of generalized spherical harmonic emphasis 2−63765
three-body break-up, application of method of moments 2−73748

Binding energy continued
  three-nucleon bound state from Faddeev equations with realistic potential 2−63763
  tri-nucleon systems, effect of $\Delta(1236)$ resonance 2−49712
  Wurster's blue perchlorate, electrostatic binding energy using Ewald's method 2−67927
  Λ, for p-shell hypernuclei, shell-model analysis 2−63760
  pn bound state and mass of nucleon quark 2−73840
  Al-Ge, vacancy-solute binding energies 2−74763
  Al-(1.7 at.%) Zn, vacancy-impurity, positron- annihilation study 2−53727
  Ar crystal data application to testing Kihara intermolecular potential 2−70811
  Ar monolayer, of ^{3}He and ^{4}He, low temp. 2−43493
  Ar_3, calc. for Lennard-Jones 12-6 pair potentials 2−60023
  C, 1s electron 2−70602
  CO_2, adsorbed in W, binding states 2−77513
  ^{40}Ca, Hartree-Fock calculations with Feshbach-Lomon potential 2−73995
  ^{48}Ca, Hartree-Fock calculations with Feshbach-Lomon potential 2−73995
  Cl^-, hydrated binding energy calc. by ab initio, semi-empirical MO and classical methods 2−50030
  F^-, hydrated, binding energy calc. by ab initio semi-empirical MO and classical methods 2−50030
  H atom, in mag. field 10^{8}-10^{11} gauss 2−67419
  H_2, calc. by contracted gaussian type function 2−83243
  H_2^+, charge shifts in formation of covalent bonds 2−80034
  ^{3}H, D-state probability, using Riihimaki potential 2−67142
  ^{3}H, Faddeev approach with two-body local interactions 2−73994
  ^{3}H, ground state with realistic interactions 2−76777
  ^{3}H, low energy three nucleon parameters and short-range repulsion 2−46080
  ^{3}H, off-shell variation of binding energy for exactly phase-equivalent separable potentials 2−55956
  ^{3}H, reaction matrix approach 2−59687
  ^{3}H, Reid potential calc., of binding energy admixture probabilities and charge form factor 2−76779
  He liquid, of two-roton bound states 2−83828
  He on graphite, first few atoms of second layer 2−71253
  ^{4}He, Hartree-Fock calculations with Feshbach-Lomon potential 2−73995
  ^{4}He, modified shell model wave function and binding energy 2−46109
  ^{4}He, reaction matrix approach 2−59687
  ^{4}He photodisintegration cross-sections 2−83003
  Kr_3, calc. for Lennard-Jones 12-6 pair potentials 2−60023
  Li complex, Li^+-H_2O, Hartree-Fock calculation 2−60010
  Li^+, hydrated binding energy calc. by ab initio, semiempirical MO and classical methods 2−50030
  ${}^{3}_{\Lambda}$H and ΛN potential, Λp scatterin data 2−82876
  ${}^{4}_{\Lambda}$H, effects of Λ-Σ coupling 2−74002
  ${}^{4}_{\Lambda}$H and ΛN potential, Λp scattering data 2−82876
  ${}^{4}_{\Lambda}$He, effects of Λ-Σ coupling 2−74002
  ${}^{4}_{\Lambda}$He and ΛN potential, Λp scattering data 2−82876
  ${}^{5}_{\Lambda}$He, effects of Λ-Σ coupling 2−74002
  N, 1s electron 2−70602
  Na^+, hydrated binding energy calc. by ab initio, semi-empirical MO and classical methods 2−50030
  Ne_3, calc. for Lennard-Jones 12-6 pair potentials 2−60023
  O, 1s electron 2−70602
  O_2, pot. curves for lowest three states, CI treatments 2−80012
  O_2^-, optimized valence configurations method for binding energy of ground state, determ. of electron affinity of O_2 2−50019
  ^{16}O, first 0^+ excited state, α-particle model 2−73998
  ^{16}O, Hartree-Fock calculations with Feshbach-Lomon potential 2−73995
  ^{16}O, off-shell effects in binding energy calcs. for set of phase-shift equivalent potentials 2−70376
  ^{16}O calc. using generalized method of harmonic polynomials 2−79727
  Pb, from electron-ion interaction pseudopot. model 2−77812
  Pu atomic electron binding energies 2−46179
  Si, due to K electrons, Compton profile obs. 2−83882
  SiC, 6H exciton electroabsorption, exciton binding energy from optical transition spectrum 2−81331
  SiO_2-Al_2O_3-R_xO glass, struct. state of Al ion, complex stability 2−56556
  Xe_3, calc. for Lennard-Jones 12-6 pair potentials 2−60023
Binding energy, solid state *see Bonds; Lattice energy; Solids*
Bingham plastics and solids *see Rheology*
Biographies
  Bose, S.N., co-founder of quantum statistics 2−62916
  Burgers, W.G. 2−66392
  Burgers, W.G. 2−66393
  Faraday as natural philosopher, book 2−41427
  Luis Enrique Erro, dedication of lunar crater 2−73062
  Verneuil, Dr. A. V. L. 2−45203
Biological effects of radiations
  accident simulation with phantom, real neutron dose compared to badge meas. 2−52893
  arterial morphology, focussed ultrasound effect 2−51919
  body organs, model for estimating space proton dose 2−58590
  bone contamination by β emitters ^{89}Sr, ^{90}Sr, calc. of local and average doses 2−55265
  broadcast radiation, existing and safe levels 2−78647
  cat's visual pathways, X-ray effects on interaction of flash evoked cortical potentials 2−45179
  cats, evoked tactile and auditory central nervous system responses after 915 MHz microwave irradiation 2−51923
  cell population, radiation effects, kinetic analysis 2−69328
  cell survival curves, damage and recovery 2−69327
  cells, mammalian, in vivo and in vitro, X-ray irrad., lethal damage expression 2−62851
  cells, radiobiology problems 2−73181
  cellular response, computer generated model 2−69326
  children, gonad doses at X-ray examinations 2−69335
  chimpanzees, chronic exposure to impusive noise, bheavioral effects 2−45154

Biological effects of radiations continued
  Chinese hamsters, 2430 MHz microwave irradiation, cytogenetic effect 2−51925
  CHLF hamster cells resistance to 1.5 MHz ultrasonic radiation 2−48873
  chromosome aberration induction rel. to ultrasound intensity 2−48867
  chromosome damage by ultrasound at diagnostic power and frequency ranges 2−48870
  chromosome damage in Chinese hamster cells following high intensity pulsed ultrasound irradiation 2−48869
  chromosome damaging effects of ultrasound on human blood cells 2−48871
  chromosomes, of Nagasaki citizens exposed to A-bomb fallout 2−62846
  chromosomes, X-ray irrad. electron microscope obs. 2−62853
  diagnostic radioisotopes procedures, obs. of radiation doses to children 2−69244
  diagnostic ultrasound, teratogenic effects 2−73203
  disorganization and disruption of mammalian and amoeboid cells by acoustic microstreaming 2−66267
  DNA, in mice leukemic cells, effect on replication 2−62852
  DNA single-strand breaks produced by γ-ray after treatment with 2, 4-dinitrophenol 2−66272
  dose-rate effects rel. to use of Cathetron ^{60}Co after-loading unit 2−69331
  e.l.f. from SANGUINE submarine communication system 2−76080
  e.m. radiation, on vision during welding 2−69461
  e.m. waves, human health effects rel. to Canadian legislation 2−51920
  energy deposition produced by fast neutron irradiation in equivalent-tissue volumes 2−73182
  environmental radiation due to nucl. power prod., population dose 2−70548
  enzyme activity of cell enzymes, h.f. e.m. waves 2−48834
  eye, carotid angiography, X-ray doses 2−69334
  fallout, u.v. and X-rays, conference (Mishima, Japan, Nov. 1971) 2−62284
  foetal bone, radioactive contamination 2−62844
  foetus and placenta, supervoltage and intracavitary radiotherapy 2−48860
  fractional cell survival rel. to depth of tissues exposed to high energy ions 2−69330
  genetic effects of low and high-energy radiation 2−62845
  genetically significant radiation dose determ. from brain scintigraphy 2−73187
  gynecologic radiation therapy, dose distrib. by meas. and computer 2−69411
  health hazard expt., 1-12 GHz, with human volunteers 2−55229
  health physics problems of instant contamination, 2nd European congress on radiation protection, Budapest (3-5 May 1972) 2−55219
  HELA cell survival at ultra high dose-rates of high energy electrons 2−69339
  h.f. irradiation, differential power meas. technique 2−52002
  human blood coagulation processes, effects of 2450 MHz microwave radiation 2−58586
  internal contamination by radionuclides, control of radiological hazards 2−55220
  lens change in rabbit, X-ray and proton induced 2−78673
  lens opacification in mice, dose dependence of fast neutron RBE 2−78671
  lesion formation by high intensity ultrasound, relation of temperature 2−51917
  light, medical significance and effects 2−82067
  linear accel., 35 MeV, A-bomb radiation simulation 2−59648
  living organisms, book 2−73177
  low illumination effects on galvanic skin response 2−73230
  lymphocytes, chromosome aberrations, ultrasonic irradiation 2−48868
  mammalian cell survival, post-irradiation hypoxia 2−69333
  mammalian cells, transient change in radioresistivity due to pre-irradiation culture conditions 2−62850
  mating pattern of male mice 2−69230
  medical radiobiology, modification of radiation response 2−69325
  mice, tumorigenesis, immunocompetence, relative potency of X-rays and γ-rays 2−62854
  microwave irradiation and bone marrow function 2−69338
  microwave radiation effects and standards criteria 2−48874
  microwaves, cutaneous perception pain threshold 2−55228
  microwaves, potential hazards, safety standards 2−82025
  microwaves, reactions of white blood cell systems 2−82028
  mouse, mammary carcinoma, effect on blood vessels 2−62847
  negative pions and muons use in therapeutic and diagnostic medicine 2−76084
  neutron beam dosimetry, obs. using CaF_2:Mn and ^{7}LiF thermoluminescent dosimeters 2−69382
  neutron radiation on human body, expt. with tissue equivalent substance 2−55239
  neutrons, cancer therapy T(d,n) gas target source 2−69340
  neutrons produced by d bombardment of Be 2−67320
  nitella flexilis cells X-ray effects on membrane potential, membrane resistance and action potential 2−66268
  nonionizing effects on tissues 2−48875
  nonionizing e.m. waves, lower r.f. through optical spectrum 2−45038
  perception of pulse-modulated u.h.f. electromagnetic energy, psychophysical obs. 2−51954
  phospholipid membrane, $^{22}Na^+$ effects 2−58587
  photocoagulation of eye tissue, for therapy 2−48876
  progress of biology and health physics division 2−82032
  protein film, contaminative behaviour of $PuCl_4$ 2−78648
  rabbit brain, change in specific gravity after high doses of X-rays 2−62849
  rabbit eye lens opacities after 2.45 GHz irradiation 2−51926
  radiation biophysics, topicality 2−55203
  radiation protection criteria and recommendations 2−76082
  radiation therapy at AAPM radiological physics center 2−69324
  radiation therapy at AAPM radiological physics center 2−69324
  radiation therapy facility at NAL 2−69320
  radiodiagnosis, analysis of risks 2−48881

Biological effects of radiations continued
radioisotopic power source, accident analysis 2−55218
radionuclides, medically applied, effect on radioresistance of red blood cells, determ. of dose dependence 2−55237
rat, morphological changes in cortical medullary thymocytes 2−62848
rat femurs, effects of X-rays on mechanical properties 2−69228
rats, general activity depression and recovery after 2450 MHz microwave irradiation 2−51922
rats, thermoregulatory and metabolic functions after 2450 MHz microwave irradiation 2−51921
regenerating rat liver, hydrolytic enzyme activation 2−66270
retinal lesions caused by microwave exposure 2−69460
salivary gland growth in rat, local X-radiation 2−76078
sheep, acute β-irradiation, blood changes 2−66269
skin, permissible exposure tested using relationship between absorbed dose, mithotical activity, chromosome aberrations 2−55230
sound pressure levels from stereo components, damage risk 2−66292
thorotrast cases in Czechoslovakia, study of radiotoxicological effects 2−55238
thymocytes, effect of sulphydryl protecting and blocking agents on radiosensitivity 2−69332
tissue equivalent, attenuation of neutron beam 2−69322
tissue equivalent gas, ionization distrib. obs. 2−51918
tissues, thermal effects of acoustic waves 2−66271
transuranium elements, interactions with cells and tissues 2−78659
transuranium elements, U.S. Transuranium Registry data and autopsy findings 2−69245
tumor sensitivity, synergistic effect, hyperthermia 2−69329
tumour blood flow, meas. by ^{133}Xe clearance rel. to capillary 2−62863
u.h.f. pulse-modulated e.m. energy, animal perception and avoidance obs. 2−51924
ultrasound of low magaHertz frequencies, production of haemorrhagic injury and paraplegia in rat spinal cord 2−48872
underground uranium miners in USA, dose-effect relationship of radiation and induction of lung cancer 2−55240
u.s., therapeutical intensities, breakdown of calculi 2−69343
u.s. exposure thresholds for cavitation in cells and tissues 2−66266
u.v. effects on RNA phage MS2 2−62823
u.v. effects on RNA synthesis 2−62824
Vicia faba roots, 1.5 MHz ultrasound effects on growth 2−48833
X-rays, mitotic activity of subependymal plate of rats 2−55227
X-rays and pulsed γ-neutron radiation, brain blood flow, vascular resistance, blood pressure and heart rate obs. in monkeys 2−69316
π^- beams, radiotherapy, biomedical facilities 2−69341
π^- beams, radiotherapy, Los Alamos Meson Physics Facility 2−69342
^{241}Am, dose-effect curves for bone and lung tumours 2−55281
^{241}Am, estimation of permissible radiation dose to gonads and foetus 2−55280
^{241}Am sealed sources, accidental contamination during handling 2−55234
Ar 4W laser, photocoagulation therapy; retinal diseases, design and construction, clinical results 2−82018
BaF$_2$-YF$_3$ system, phase relations 2−74922
^{60}Co, γ-ray irradiation of malignant lymphopathies, dose distribution 2−69412
^{60}Co medical therapy, process control by electronic calculator 2−82027
^{132}Cs, comparative behaviour in males and females following oral administration 2−55292
^{137}Cs, absorption through skin, influence of decontamination treatment on degree of internal contamination 2−55236
^{131}I, estimation of permissible radiation dose to gonads and foetus 2−55280
^{192}Ir sealed sources, accidental contamination during handling 2−55234
^{192}Ir wire, contamination hazard in handling 2−69319
^{237}Np, dose- effect curves for bone and lung tumours 2−55281
^{210}Po, kinetics of metabolism in body after radionuclide intake through skin and determ. of contamination levels 2−55283
^{238}Pu sealed, for cardiac pacemakers 2−51905
^{239}Pu, dose-effect curves for bone and lung tumours 2−55281
^{239}Pu late phase lung clearance, in vivo det. 2−58588
Ra daughters, lung cancer risk in relation to long-term exposure 2−55231
^{224}Ra, ^{226}Ra, kinetics and decay products in mice, dose-effect relation 2−55279
^{226}Ra, late effects induced in mice, meas. of total activities, determ. of death causes 2−55232
^{222}Rn and daughter products, dependence of chromosomal aberrations in peripheral blood lymphocytes on inhaled internal dose 2−55272
^{222}Rn inhalation in rats, meas. of lung burden of ^{210}Po, ^{210}Pb short-lived daughters 24 hours after ending exposure 2−55287
^{222}Rn short-lived daughters, 'lung-model' concept and lung cancer incidence in miners used for assessment of MPAI-value 2−55270
^{222}Rn short-lived daughters, incidence of lung cancer amongst miners and determ. of maximum permissible doses 2−55271
^{85}Sr, absorption through skin, influence of decontamination treatment on degree of internal contamination 2−55236
^{90}Sr, estimation of permissible radiation dose to gonads and foetus 2−55280
^{90}Sr sealed sources, accidental contamination during handling 2−55234
T$_2$O, estimation of permissible radiation dose to gonads and foetus 2−55280
^{95}Zr, absorption through skin, influence of decontamination treatment on degree of internal contamination 2−55236

Biological technique and instruments
absolute organ activity scanning with positron emitting radionuclides 2−69286
acoustical holographic imaging for diagnosis 2−76089
acoustical pattern recognition of knee joint diseases 2−45047
actinides, contamination by wounds, determ. of therapeutic procedure 2−55235
action potential and temp. obs. in human voluntary muscle, simultaneous recording 2−48852
albedo-type personnel neutron dosimeter 2−73208
Anger camera, optimizing window for ^{99m}Tc 2−48857

Biological technique and instruments continued
Anger gamma camera system, improvement of intrinsic resolution 2−63707
annular collimator for scanners 2−69288
aorta, in vivo meas. of press./vol. characts., balloon pulsation system 2−62830
arterial flow monitoring, u.s. Doppler probe 2−69367
arterial volume determ. using aortic characteristics 2−73172
artificial heart, development prospects in France, DELPHI technique 2−51913
artificial heart pacemaker, ^{238}Pu energy source, investigation of radiation dose incurred 2−51949
artificial hearts, radioisotope powered, USAEC programme 2−51915
auditory evoked potential in man, review 2−62875
autofluoroscope brain imaging rel. to rectilinear scanning and neuroradiologic exam. 2−73193
automatic biochemical analyser 2−78216
automatic scanning speed modulator for radioisotope scanners 2−69287
autoradiography, techniques and applics. 2−76072
bidirectional analogue processing of radioisotope scan data 2−45031
bioelectrode systems, interface design 2−85085
biological systems, obs. of surface reactions by ellipsometry, review 2−69203
bioluminescence phenomena, new biotelemetric method 2−85112
biophysics and bioengineering, book 2−81987
biopotential meter, meas. of electrical activity of nerve cells 2−69240
biotelemetry, conference (Nijmegen, Netherlands, May 1971) 2−82003
biotelemetry system, operating in 1 to 7 channels 2−82006
biotelemetry systems and techniques, conference (Pretoria, S. Africa Dec. 1972) 2−73179
blood and tissue gas meas. by mass spectroscopy, membrane 2−51892
blood cells, volume histograms obs. using pulse height analyser 2−69279
blood flow acceleration and peak velocity in aortic arch, transcutaneous meas. 2−48889
blood flow measurement 2−78645
blood pressure monitor, miniaturised 2−58584
blood velocity profiles, real-time obs. using u.s. multigated pulsed Doppler velocimeter 2−69311
blood vessel imaging using ultrasound 2−69310
bone densitometer using transmitted and scattered γ-rays 2−69222
brain scintigraphy, genetically significant radiation dose determ. 2−73187
breast cancer diagnosis, thermography 2−62868
breast tumour detection by radioactive phosphors 2−62867
cameras for single and serial exposures from X-ray image intensifiers, medical applications 2−73202
capacitance meter for artificial lipid bilayer membranes 2−82422
cardiac catheter electrode, very flexible, development 2−51898
cardiac evaluation from radioisotope dynamics 2−73194
cardiac pacemaker, ^{3}H nuclear battery using electron-voltaic effect 2−51908
cardiac pacemakers, application of Gipsie radioisotopic generator 2−51906
cardiac pacemakers, nuclear batteries thermoelements fabrication techniques 2−51907
cardiovascular data, multichannel telemetry 2−82016
catheter semiconductor radiation detector 2−51937
caval blood in lungs, selective distrib. meas. 2−73197
cell discrimination by ultrasonic probing 2−51880
cinedensigraphic equipment, technical principles 2−69352
cineradiography, eval. and selection of optimum factors 2−69253
cisternography with chelated complex of ^{99m}Tc 2−66258
clinical linear electron accelerator, Mitsubishi model ML-15M II, for cancer treatment 2−69236
colour television microscopy 2−58613
combined liver-lung scanning, subdiaphragmatic abscess 2−58610
compensation amplifier for catheter manometer systems 2−51896
contact probe for skin temp. obs. 2−69233
control system for radiation doses during Co therapy 2−69337
cyclotron, selection of size 2−69272
dark field electron microscopy of biological macromolecular complexes 2−82001
deep body temp. monitoring technique 2−69277
depth dose calorimeter, for high intensity, l.v., flash X-ray machines 2−66285
device for protection of testicles in X-ray examination 2−73185
devices displayed at 1972 Physics Exhibition 2−58581
diagnostic photography, review 2−76075
diagnostic radioisotopes procedures, obs. of radiation doses to children 2−69244
diagnostic ultrasonic moving target indicator systems 2−51931
diagnostic X-ray tubes, voltage meas. using K-characteristic fluorescence 2−66279
dielectric meas. 20 to 500 kHz, three-terminal bridge 2−55206
diffusion deposition of small-sized particles in bronchial tree 2−85123
discharge frequency and pattern of human motor units during voluntary contraction of muscle 2−55208
discriminant analysis of visually encoded e.e.g. data 2−45026
display of three dimensional u.s. data for medical diagnosis using computer 2−66273
display systems, performance obs. for radionuclide imaging 2−69282
distributed sources in human phantom, whole body efficiency calcs. 2−58614
dose-reducing fluoroscopy system 2−73184
dosimetry, radiopharmaceutical pediatric, diagnostic procedures and radiation, protection 2−69379
dosimetry system using TDL for obs. during radiotherapy 2−69400
dye dilution technique for measuring cardiac output, analysis system 2−69265
dynamic scintigraphy, hepatic phagocytic, metabolic and blood flow evaluation 2−48884
dynamic scintillation scanning on canine osteosarcomas 2−69227

Biological technique and instruments continued
- dynamic vascular scintiphotography of liver, ^{75}Se and ^{67}Ga as imaging agents 2−58609
- earphone coupling system for acute physiological obs. 2−82054
- e.c.g., radiotelemetering 2−82015
- e.c.g. signal transmission over radio or telephone links 2−45042
- e.c.g. telemeter, remotely operated, chronic implantation in rats 2−85110
- e.e.g., recording system for space flight 2−76057
- e.e.g., suppressed motor behaviour during sleep and waking in cat 2−66254
- e.e.g. and clinical change after bilateral and unilateral electroconvulsive therapy 2−62837
- e.e.g. future technology, conference (Minneapolis USA Sept. 1972) 2−76055
- e.e.g. techniques, future developments 2−76060
- e.e.g. technology, future trends in diagnostics 2−76059
- e.e.g. technology, technician training methods 2−76058
- e.e.g. technology trends, computer applications 2−76056
- e.e.g. telemetering and neuronal spike activity in rabbit 2−85105
- eeg telemetry system, long-term 2−85104
- effect of antianginal drugs on coronary blood flow 2−76061
- e.k.g., storage telemetry, Holter Monitor 2−82012
- electrical impedance plethysmography, workable vol. and flow concepts of bio-segments 2−69238
- electrn diffraction reconstruction of three-dimensional objects 2−81980
- electro-oculography, for oculomotor imbalance investigation 2−51941
- electro-optical Fourier transforms of leukocytes 2−51884
- electrodes for bioelectric event obs., book 2−55216
- electrolytic iodination of human serum albumin at alkaline pH 2−55213
- electrometer amplifier system for radiotherapy depth dose scanning system 2−69302
- electromyographic obs. of articulatory movements for bilabials in normal and cleft palate speakers 2−45059
- electron beam anal. of thick tissue samples 2−69299
- electron beam therapy technique, megavolt 2−69318
- electron microscopy, simulation of shadow width distributions for protein molecules 2−79099
- electron microscopy by electrostatic phase plate of biological specimens 2−66265
- electron microscopy rapid processing techniques 2−45043
- electronic accessories, medical diagnostics and therapy, survey 2−81978
- electronystagmography instrumentation 2−69458
- electrophoresis of particles and cells, det. from Doppler shift of scattered laser light 2−79385
- electroretinogram, components 2−51940
- electrorheocardiotelemetric device, cardiac contraction 2−82014
- e.m.g. from smooth musculature in unrestrained animals by telemetering 2−85103
- e.m.g. indwelling wire electrodes, histological response of rat skeletal muscle 2−55211
- energy dispersive analysis of biological thin sections in electron microscope 2−82002
- epochal ratemeter for neurophysiological studies 2−76063
- evoked potential analysis by complex demodulation 2−55209
- experiments system 2−85090
- extra-corporeal irradiators for radiation therapy, development 2−69242
- farmer dosemeter, design of thimble chamber 2−45049
- fetal monitoring, radiotelemetry system 2−82017
- fibre optic catheter for obs. of blood pressure and O_2 2−51897
- filter with continuously adjustable hole size 2−85088
- flow chamber for conc. step expts. with epithelial membranes 2−69206
- flow fluorimeter obs. of cell states 2−69280
- flow measurement, n.m.r. technique, velocity distribution fn. 2−83757
- flowmeters in anaesthetic machines, prevention of inaccuracies due to electrostatic charges 2−69281
- fluorescein derivative uptake in traumatised rat muscle, potential use as scanning agent 2−69300
- fluorescence emission methods, recent developments 2−81995
- f.m. telemetry transmitters, registration of biopotentials 2−85111
- freeze dryer with improved standards of biological safety, design and construction 2−78638
- freeze etching technique for biological specimens for electron microscope obs. 2−45022
- freeze-etching technique, temperature, vacuum and fracturing considerations in electron microscopy 2−79100
- Fresnel zone plate, use in gamma-ray imaging 2−73196
- Fresnel zone plate imaging 2−58583
- gait analysis after prosthetic replacement of hip joint 2−69256
- gait analysis with neurologically induced varus foot loading 2−69258
- gait biomechanics after arthrodesis in lower limb 2−69255
- gait patterns before and after intertrochanteric osteotomy in osteoarthritis of hip 2−69257
- gamma camera, anal. and correction of spatial distortions 2−48855
- gamma imager, fully automated 2−69283
- gamma ray camera-computer systems, maximum frame rates 2−78652
- gamma-ray imaging for diagnosis, imaging cosmetics 2−76077
- genetic damage, heritable, screening for environmental agents 2−62864
- Harrington distraction rods in patients with idiopathic scoliosis, intravital wireless telemetry of axial forces 2−69260
- health and medical physics procedures following nuclear reactor accident 2−73175
- heart rate monitoring, using piezoelectric transducer and tape recorder 2−82013
- heart rate variation obs. using tape recorder and mini-computer 2−69247
- heart tissue cultures, chronotropic responses 2−76062
- helical scanning, computerized, location of radionuclides in human body 2−76099
- h.f. irradiation, differential power meas. technique 2−52002

Biological technique and instruments continued
- high resistivity thermoluminescent dosimeter, operational evaluation 2−85081
- high resolution microscopy of biological systems in high pressure chamber 2−85086
- histological response of rat skeletal muscle to e.m.g. fine wire electrodes, insulation significance 2−55212
- Hodgkin's disease, isotope scanning using ^{67}Ga citrate 2−55246
- holographic interference microscopy of biological cells 2−62827
- human scalp recorded somatosensory evoked response, initial positive potential 2−62836
- hybrid computer for generating exponentially weighted RR-interval histogram 2−69248
- imaging system for diagnostic radiography using pulse compression techniques 2−51930
- implantable artificial organs, energy requirements, nuclear energy sources 2−51914
- implantable biologic force transducer 2−51894
- implantable pacemakers using Pu, Pm isotopes, safety criteria, test results 2−51927
- implantable radio telemetrical meas. device, body temp. and serum albumin turnover in rabbit 2−85108
- in vivo counting of transuranium isotopes in human body, detector calibration by phantoms 2−58616
- inhalation obs., evaluation of exploded wire aerosol generator 2−85160
- inspiration- expiration scintiphotographs, det. of intrinsic or extrinsic nature of liver defects 2−66259
- instantaneous ratemeter for cardiac rate obs. and rate change obs. 2−69278
- intra-modality selective attention and evoked cortical potentials to randomly presented patterns 2−62834
- intracranial pressure obs. with modified pressure transducer 2−69296
- intracranial pressure wave detection with ultrasound 2−69304
- intrauterine dosimeter 2−76093
- intravascular pressure transducer, materials for construction 2−69225
- ionization chamber in water phantom, control by direct connection to digital computer 2−69384
- i.r. radiation, therapeutic diagnostic applications, review 2−85131
- i.r. thermography, appls. 2−76076
- isodose scanner, computerized 2−69355
- isotope imaging and counting, comparison of scintillation and semiconductor detectors 2−49643
- Janus irradiation facility, neutron spectrum map using proton recoil proportional counters 2−62842
- keratin fibre surfaces, scanning electron microscope examination 2−82442
- large-volume liquid scintillation whole body counting control of extremal sources of variation 2−69378
- laser beam applications, book 2−73178
- laser flying spot scanner, for use in automated fluorescence microscopy 2−66264
- LET-spectra det. for gamma-neutron radiation with low efficiency counters 2−58622
- life detection on Mars, computer-controlled analytical instrumentation of Viking spacecraft 2−54977
- life detection on Mars, soil gas chromatography/mass spectrometry by Viking spacecraft 2−55147
- linear accelerator, 4 MeV, reliability record and safety features 2−67105
- lip and tongue pressure patterns during syllable production 2−45057
- liquid scintillation α-particle detection applics. 2−70297
- liver investigation in nuclear medicine 2−69363
- liver volume determ. by u.s. scanning 2−69348
- lung mechanical parameter anal., on-line laboratory computer program 2−69249
- lung scanning, ^{113m}In albumin aggregates 2−55251
- lung tomography, using X-rays 2−45045
- mammalian cell identification, differential light scatt. 2−66244
- materials for cardiovascular implants, electrochemical methods for selection and eval. 2−69226
- medical electronics, reliability 2−85079
- medical heavy ion beams, composition 2−69321
- medical physics and engineering, conference, Gothenburg, Sweden (1972) 2−69231
- micro-electrode suspension for intracellular recording from moving tissue 2−48835
- microscopy, phase-contrast and interference-contrast, for living cells in gynaecology 2−58612
- microscopy of living tissue, colour contrast methods 2−76054
- microtensiometer for obs. of perilymph 2−45036
- microtron, accelerator for radiation therapy 2−69276
- microwave field perturbation by animals and apparatus 2−52004
- mineral content of bone, measuring sites and methods 2−69262
- mobile telemetric equipment for e.c.g. and respiratory frequency data transmission 2−82010
- model diagnostic system, dependence on photon energy and exposure of X-ray pattern from phantom 2−69383
- molecular beam microscopy 2−67464
- motor nerve conduction and delay value obs. in leprosy polyneuritis patients 2−62839
- motor nerve conduction dispersion in Charcot-Marie-Tooth-Hoffmann disease and Steinert syndrome 2−62840
- moving table technique for irradiation of large irregular fields 2−69275
- multichannel e.m. flowmeter telemetry system 2−82008
- multichannel miniaturized f.m./a.m. telemetering system 2−82009
- multiple gate pulse Doppler flowmeter for spatial velocity profiles in blood vessels 2−51934
- muscle blood flow and capillary permeability using ^{133}Xe and ^{77}Br 2−69359
- muscle phosphorylases a and b, electron micrograph analysis by optical diffraction and filtering 2−79145
- myocardial imaging with $^{13}NH_3$, feasibility 2−45030
- myocardium, normal and infected, ultrasonic techniques for differentiation 2−51889
- needle type solid state detectors for in vivo meas. of tracer activity 2−66275

Biological technique and instruments continued
needle-shaped semiconductor detectors, regional distribution and transport of labelled compounds 2-66276
neurological recording, signal distortion by a.c. electrode polarization 2-51895
neutron activation analysis rel. to bone Ca content 2-69364
neutron activation analysis rel. to human placenta and filter effects 2-69443
neutron production by electron accelerators 2-45035
neutron radioactivation analysis in vivo of Ca, P, N and Cl in rat's organism 2-54575
neutron therapy, techniques and safety precautions 2-69259
n.m.r. blood flowmeter for pulsatile flow, analysis 2-81981
n.m.r. studies of rate phenomena, molecular structure 2-81988
noninvasive pressure pulse recorder, clinical applications 2-69264
normal gait, biomechanical study on walk-ways 2-69254
nuclear devices, safety analysis 2-51911
nuclear medicine, diagnostic image quality using scintillation and semiconductor detectors 2-49645
Nuclear- Chicago Pho/Gamma III camera, inexpensive remote start switch 2-76066
nucleonic instrumentation in medicine 2-76092
ophthalmology, average visual evoked potentials 2-62835
optical system for continuous monitoring of haemolysis in flow system 2-51883
pacemakers, ^{238}Pu demand, statistical analysis 2-51912
pacemakers, design and fabrication of Pu 238 sources 2-51910
pacemakers, radiation protection, plutonium 238, biological dose 2-51948
pacemakers, safety aspects, radiation protection 2-51928
pancreas scanning after ten years' experience 2-76086
patient identification and disease categorization using discriminant and cluster analyses 2-69361
peripheral joint imaging, variations in normal children 2-58582
photocoagulation of eye tissue, for therapy 2-48876
photoelectric plethysmography in periphery and haemoglobin O_2 conc., meas. device 2-62831
photography, capabilities in terms of human-performance 2-76070
photography, conference (Newton, Mass., USA, July 1972) 2-76068
photography, lighting, posing and background requirements 2-76069
photography of live white blood cells 2-62832
photon absorptiometry, meas. of bone turnover 2-73195
photoscanning, daignosis of splenic infarction 2-66280
placental scanning and soft tissue radiography 2-48859
plethysmography, venous occlusion, temp. dependence of pressure change 2-45034
Pod, propulsion mechanism 2-50283
polyaminopolyalkylphosphonic acids as effective ligands for binding and eliminating U and fission products from body 2-55258
polymethylmethacrylate, Monte Carlo simulation of energy dissipation of electron beam 2-62826
polythene catheters, heparinization method 2-69291
positron camera, MGH, medical use with, short-lived cyclotron produced radionuclides 2-69444
positron camera, multicrystal for use with radionuclides 2-55248
potentiated H-reflexes in healthy and hemiplegic subjects 2-62838
pressure waves for breaking up kidney stones 2-51890
programmable four channel radio telemetry system 2-82005
prosthetic gait anal., asymmetry and speed dependence of gait patterns 2-69261
pulsatile flow simulator design and applics. 2-51900
radiation and isotope applics., book 2-73177
Radiation Control for Health and Safety Act of 1968, regulatory programs development 2-48879
radiation protection in diagnostic radiology 2-69336
radiation therapy, diagnostic u.s. applics. 2-69303
radioactive tracer method with compensation for activity decay for monitoring of rate of hemodialysis 2-51887
radiodiagnostics, image intensifiers and photography 2-70070
radiographic intensifier with improved picture quality 2-62909
radiography air gap technique, effect on detail and contrast 2-69250
radioisotope angiography of spinal cord for diagnosis 2-66282
radioisotope metabolism of Na, Cs, Ca, Sr, I, procedures for calc. of metabolic constants in compartment models 2-55222
radioisotope powered cardiac pacemakers, legal and administrative problems in Italy 2-51916
radioisotopic cardiac pacemaker, ^{238}Pu fuel, Bi_2Te_3 thermocouples 2-51888
radionuclide imaging, rel. to display performance 2-69282
radionuclide imaging, three dimensional, using detection of cascading γ-rays in coincidence at 90° 2-69284
radionuclides for evaluation of pancreas and exocrine function 2-76085
radiopharmaceuticals and radiation protection 2-73186
radiotherapy, physical props. of high energy beams 2-69274
radiotherapy calcs., applic. of simple empirical formulae 2-69407
radiotherapy dosage calculator 2-69408
radiotherapy linear accelerator, history, principles and developments 2-69273
rapid scan microspectrophotometer, for monitoring intracellular pigment kinetics 2-48866
rapid sequence imaging device for use with gamma camera 2-69289
red blood cells, automatic washing machine 2-85120
renal localization technique, renal scan prior to biopsy 2-66256
respiratory mechanics, phase method of calculation using digital computer 2-66247
respiratory rate monitoring, patent 2-85095
respiratory rate monitoring, patent 2-85095
retinophot, fluorescence colour photography of fundus oculi 2-45830
review paper given to practising doctors 2-85091
r.f. surgical brain probe, heat transfer analysis 2-51899
ribosome microcrystals, optical diffraction from electron micrographs 2-82000
rodent phantom models, u.h.f. cavity exposure chamber, dosimetry 2-52003
scanning electron microscopy 2-76074
scanning-be whole-body counter, design and evaluation 2-85080

Biological technique and instruments continued
scintigraphy, dot counting 2-66263
scintillation camera, field uniformity distortion using pinhole collimator 2-48856
scintillation counter for X-ray tube kilovoltage, radiation exposure rates and γ-emission contamination obs. 2-63700
secondary standard, therapy- level X-ray exposure meter 2-76149
secondary standard instrument for protection level dose rates 2-69243
sequential scintigraphy with γ-camera, use in children with renal diseases 2-69298
simultaneous recording of temp. and action potentials in human voluntary muscles 2-55210
skeletal health, computer assessment, scanning of radiographic image 2-69375
skeletal muscle vascular resistance, analogue computer calculation 2-82023
specially collimated scintillation detector, reduction of extrathyroidal neck radioactivity 2-76095
specimen preparation with freeze-drying technique for electron microscopy 2-79098
spectrophotometer design, three-dimensional optical diffusion theory 2-45824
spectrophotometry of nucleotides in cerebral tissue, spleen and liver 2-75410
stereostaxic apparatus for use on small animals 2-48837
structure determination, neutron diffraction 2-81994
surface electromyography, paint-on electrodes 2-45037
synchronization of cardiac pacemaker with repetitive stimulation of carotid sinus nerve, in dog 2-76052
syringe radiation shield for short lived radionuclides 2-48861
telemetering of restrained small animals normal activity-rest cycle 2-85118
telemetric obs. of local blood flow by heat conduction probes 2-82007
Telemetric technique for meas. of muscle tension in consious, unrestrained animals 2-85107
telemetric transmission of ergonomical and time study data, work load of radar controllers 2-85116
telemetric transmission of work load factors in ergononics research, multidimensional coding 2-85115
telemetry, meas. of body temp., e.c.g., e.e.g., in rat 2-85114
telemetry, meas. of variation of human intracranial pressure 2-85106
telemetry, multichannel, body temp, e.c.g., e.e.g., in rat 2-85113
telemetry, noise and artefact avoidance 2-85100
telemetry, transmission of e.c.g and e.m.g. under strenuous working conditions 2-85102
telemetry for physiological data collection during exercise 2-82004
telemetry of biomechanical forces during exercise 2-85101
telemetry of cardiovascular parameters of fighter aircraft pilots 2-85117
telemetry of respiratory air flow 2-85098
telemetry systems, implanted, single and multichannel 2-85109
teleradiology, remote interpretation of roentgenograms 2-76091
teletherapy, optimization by regression methods 2-69410
television retinoscopy, teaching and research tool 2-45172
thermoelectric isotope battery for pacemakers 2-76064
thermography, liquid crystal, techniques and applics. 2-76071
thermography as screening test for breast cancer 2-69354
thermoluminescent dosimeters, response to fast neutrons 2-85082
thermoluminescent dosimeters, TLD-700, response to protons and α-particles 2-81979
thermoluminescent dosimetry for dose meas. in hands of nuclear medicine technicians 2-73207
thin cut tomographic motions, modulation transfer fn. 2-69353
three dimensional location, using planar X-ray system 2-62960
three-channel telemetry system for e.e.g. and e.c.g. 2-85097
thyrometer for obs. of laryngeal control of speech 2-45056
time domain technique for meas. of dielectric props. of biological substances 2-81985
tomographic and section imaging devices, quantification of depth effect 2-45032
tomographic scintillation camera, performance and reliability 2-69285
tomography, variable depth display, holographic methods 2-69371
total body Ca from meas. of ^{37}Ar in expired air after low level neutron irradiation 2-69365
total body water det. using D_2 and photo-disintegration assay 2-69269
Total Organ Kinetic Imaging Monitor, positron mode, design and applications 2-69362
tracer expts. and biological half-time 2-73174
tracer kinetic data, optimization procedures 2-48885
transcutaneous aortovelography and cardiovascular information 2-69357
transcutaneous aortovelography for blood velocity obs. in aortic arch 2-69312
transducers, biological and engineering constraints, applics. 2-73180
transmission electron microscopy, appl. to pulmonary pathophysiologic obs. 2-76073
transmission u.s. soft tissue visualization 2-69307
transmission-emission scanning in diagnosis of pericardial effusion 2-58606
tumour blood flow, meas. by ^{133}Xe clearance rel. to capillary 2-62863
tumour cells in cerebrospinal fluid by fluorescence microscopy with acridine orange 2-55256
tumour temp., monitoring using implanted thermistors to det. optimum therapy for breast cancer 2-69241
tympanometry in normal and pathalogical ears 2-69452
ultrasonic, broad-band technique 2-45046
ultrasonic arteriography using phase locked echo tracking for meas. of arterial diameter changes 2-51932
ultrasonic B scan examination difficulties 2-76083
ultrasonic Doppler probe for studying foetal cardiac activity 2-51939
ultrasonic imaging, with good lateral resolution, for medical diagnosis 2-51935

Biological technique and instruments continued
- ultrasonic liver scanning, A- scan obs. of normal and cirrhosis liver 2−45033
- ultrasonic pulsed Doppler velocity detector, evaluation 2−51933
- ultrasonic spirometer for chronic respiratory monitoring 2−55247
- ultrasonic systems for diagnostic visualization 2−69239
- ultrasonic technique, broad-band, human skull bone, impedances 2−48890
- ultrasound as alternative to X-rays for examination during pregnancy 2−73203
- unidirectional scanning, advantages 2−66261
- u.s. B-scanning in differentiation of Baker's cyst and thrombophlebitis 2−78636
- u.s. cross sectional echography, diagnosis 2−76371
- u.s. Doppler blood flow indicator and u.s. B-scanner for blood vessel imaging 2−69310
- u.s. Doppler blood flowmeter, theory 2−85092
- u.s. echo ranging applics. to oral mucosa 2−51945
- u.s. encephalographic system, patent 2−85093
- u.s. intracardiac scanner, circular array cathetertip 2−45044
- u.s. laminography of laryngeal tumours 2−69306
- u.s. pulse echo visualization for clinical diagnosis 2−51942
- u.s. rotational fast scanner applic. to diagnosis 2−51943
- u.s. scanner for two- dimensional instantaneous obs. of moving cardiac structures 2−69308
- u.s. scanning system for heart obs. 2−69309
- u.v. radiation, therapeutic diagnostic applications, review 2−85131
- variable baseline scanner 2−78653
- vertebral bone mineral mass determ. by transmission obs. 2−69263
- video kymography, diagnostic method 2−69351
- visual evoked cortical response to patterns, pattern dimension and contrast density effects 2−62833
- vocal fold movement obs. using ultrasound 2−69305
- volume flow meas. with CW Doppler u.s. flowmeter 2−51901
- well counter adaption for measuring cardiac output 2−73200
- whole body counter efficiency calc. for distributed sources in human phantom 2−66278
- whole body counting, γ-rays, Anger camera 2−78663
- whole-body counter measuring device for assessment of low energy photon emitters in man 2−55261
- whole-body counter with high sensitivity, clinical applications 2−69420
- whole-body counters and thyroid monitor for meas. of internal contamination by γ emitters 2−58629
- whole-body counting, phantom for simulation of subject size and shape 2−69378
- windowless p-n junction for β emitter meas. in vivo and in vitro 2−78655
- wire spark chamber γ-ray imaging system 2−69290
- X-ray camera, diagnostic applics. 2−48853
- X-ray diffraction spectrograph automatic 2−55201
- X-ray radiography, calc. object pattern rel. to image intensity distrib. 2−69252
- X-ray screen, applics., image intensity improvement 2−62843
- X-ray system performance, method for testing presented 2−62906
- X-ray visualization and memorization device 2−76744
- BaO, F, F^+ centres obs. at 77 K 2−74803
- ^{11}C, production with 3 MeV Van de Graaff 2−70646
- Ca det. in humans, using neutron activation anal. 2−48854
- CaF_2 dosimeter in sunburn range 2−85136
- CdTe, miniature medical probe 2−69271
- CdTe probes, efficiency, resolution and absorption 2−51891
- ^{252}Cf therapeutic sources, absorbed dose and linear energy transfer distributions 2−45039
- ^{60}Co radiation therapy, determ. of treatment time using computer 2−69317
- ^{60}Co teletherapy apparatus, rotational type 2−69349
- ^{51}Cr labelled iron oxide particles, inhalation 2−48891
- D-T neutron generator, for fast neutron therapy 2−69246
- ^{52}Fe, ^{127}Cs and ^{129}Cs production 2−69270
- ^{67}Ga, ^{111}In and ^{75}Se in tumours, Ge(Li) detector for simultaneous meas. 2−73206
- ^{67}Ga for tumour localization 2−69297
- Ge(Li), coaxial, gamma ray camera for medical use, computerised display 2−51936
- ^{131}I-triolein absorption test for fat balance obs. 2−45029
- ^{131}I-triolein excretion test for steatorrhoea using unabsorbed radioactive marker 2−69267
- ^{131}I rose bengal imaging, differential diagnosis of jaundiced patients 2−58611
- ^{131}I take-up, determ. of normal amount 2−66257
- ^{131}I therapy and whole-body scanning in thyroid carcinoma 2−48883
- ^{111}In, ^{67}Ga and ^{75}Se in tumours, Ge(Li) detector for simultaneous meas. 2−73206
- ^{43}K and ^{129}Cs myocardial uptake and clearance characteristics 2−66260
- ^{43}K production for therapy 2−73173
- ^{140}La, contamination of monkeys by inhalation exposure, DTPA treatment 2−55259
- LiF teflon rod dosemeters, calibration for internal β-ray dosimetry 2−45050
- ^{7}LiF, dosimeter, changes in gamma sensitivity 2−85084
- N ion beam at 3.9 GeV, meas. of physical and radiobiological parameters 2−69425
- $Na_2{}^{75}Se$ disappearance rate in rat's eye, comparison of meas. with CdTe and Si(Li) probes 2−51992
- O_2 availability, in tunnel of Corti, Meas. by microelectrode 2−66307
- O_2 consumption during exercise radiotelemetry obs. 2−85099
- pO_2 telemetry system for obs. during exercise 2−82011
- ^{32}P content in breast cancer, surface detection of diurnal variation 2−69266
- ^{203}Pb, carrier-free, for tracer obs. 2−69268
- Pu content in biological samples, separation and anal. 2−62045
- Pu excretion equation evaluation, simplified method 2−62860
- Pu systematic burden, manual and computer evaluation 2−78664
- ^{237}Pu labelled iron oxide particles, inhalation 2−45048
- ^{238}Pu nuclear fuel, artificial heart appl. 2−51909
- ^{239}Pu, in vivo meas. in man, comparison of different counting equipments 2−58617
- ^{224}Ra, ^{226}Ra, analysis of γ spectra in non-equilibrium with decay products, application to retention in mice 2−58615
- ^{222}Rn and daughters, detection of α-decay particles by triacetate cellulose foils for exposure evaluation 2−58618
- ^{75}Se- selenomethionine uptake for diagnosis of hepatoma 2−66281
- ^{75}Se, ^{67}Ga and ^{111}In in tumours, Ge(Li) detector for simultaneous meas. 2−73206
- Si detectors and preamplifiers medical and biological applications 2−51938
- Si low-noise planar detectors with room temp. applic. 2−79654
- Si rubber membranes as supporting medium for cells for electron microscopy 2−79097
- Si(Li) detector, X-ray fluorescence spectrometry applied to environmental and biological analysis 2−51482
- Si(Li) detectors for β and γ meas. in superficial and deep parts of living tissue 2−55252
- Si(Li) semiconductor probe for semi-microscanning device 2−55250
- ^{89}Sr and ^{90}Sr determination by liquid scintillation beta spectroscopy 2−85083
- Tc^{99m} generator for medical diagnosis 2−62859
- $^{99}Tc^{m}$ thyroidal uptake, meas. by profile scanning 2−73191
- ^{99m}Tc thyroidal uptake, area and profile scanning 2−69360
- Xe, liquid, gamma emitting radioisotope camera 2−55249
- ^{90}Y determination by liquid scintillation beta spectroscopy 2−85083

Biology
- *see also Medical science; Physiology; Zoology*
- carbon cycle, effect of variable CO_2 atmospheric partial pressure 2−48838
- laser beam applications and fundamentals 2−69961
- muscle phosphorylases a and b, electron micrograph analysis by optical diffraction and filtering 2−79145
- psychological correlates digital simulation for transform model of human visual system 2−85155
- statistical analysis with MATLAN matrix language 2−82274

Biophysics
- — 2−69234
- — 2−62025
- acceleration effects on organisms using zero g and hyper-g 2−45025
- arterial constitutive relations, finite deformation theory of elasticity 2−55199
- arterial flow model, laminar flow in tubes with constriction 2−74335
- artificial mastoids, threshold values for audiometric bone conduction calibration 2−82056
- automated blood pressure measuring system, Korotkov sound processor 2−51885
- bacteria, laser meas. of chemotactic response 2−58577
- and bioengineering, book 2−81987
- biological cavitation, book 2−71140
- biological structure analysis of atomic and molecular level, role of computers in collection and pouring of data 2−83340
- biological systems, obs. of surface reactions by ellipsometry, review 2−69203
- biology and health physics division Atomic Energy Canada, progress 2−85132
- biology rel. to atmospheric electricity 2−58591
- bioluminescence, in marine teleost Porichthys notatus 2−55202
- bioluminescence obs., data acquisition system 2−52005
- biotelemetry, conference (Nijmegen, Netherlands, May 1971) 2−82003
- blood, flow in artificial arteries 2−43284
- blood circulation, biomechanics, numerical studies 2−78644
- blood flow, laminar, time dependent, effect of high molecular weight additive 2−48850
- blood flow control system to vascular bed of awake baboon, occlusion cuff system 2−85128
- blood flow in small curved glass tubes 2−48849
- blood flow measurement, review of technique and instruments 2−78645
- blood tests, sedimentation rate, technical aspects 2−69223
- blood vessel wave propagation, application of prestressed shell theories 2−82338
- bone, cortical, as solid-liquid composite, mechanical props. 2−69220
- bone densitometer using transmitted and scattered γ-rays 2−69222
- bone density, separated animal tibias, acoustic resonance frequency 2−81998
- bovine serum albumin, cryst., Raman spectra, water content depend. 2−60092
- carbon cycle, effect of variable CO_2 atmospheric partial pressure 2−48838
- cell colonies, synchrony loss, applic. of Gibbs ensemble formalism 2−69620
- cell cycle, regulation of energy flow and control 2−55205
- cell discrimination by ultrasonic probing 2−51880
- cell functional morphology, electron autoradiography 2−81999
- cell population, radiation effects, kinetic analysis 2−69328
- cell processes studied with microautoradiography 2−73165
- cells, mammalian, in vivo and in vitro, X-ray irrad., lethal damage expression 2−62851
- cells, virus adsorption kinetics 2−73167
- circulation model, computerised, pulse curve oscillations 2−69213
- collapsible tubes, steady pressure-flow characteristics 2−46698
- constant magnetic field, effects on biological systems 2−69229
- contaminant retention by organism, random sequence treatment 2−48877
- cooperative and dynamic crit. phenomena 2−58579
- coronary circulation in conscious dog with cardiac neural ablation 2−85121
- cortical evoked potential from visual stimulus 2−62878
- dark field electron microscopy of biological macromolecular complexes 2−82001
- Deep Sea Drilling Project, biostratigraphy 2−62066
- dielectric properties of materials 2−48839
- diffusion, moving-boundary problem for oxygen in absorbing medium 2−83997
- DNA, in mice leukemic cells, effect on replication 2−62852
- dog gracilis muscle, blood-tissue transport of ^{42}K, ^{86}Rb and ^{22}Na 2−62822

- **Biophysics** continued
  - dog Piirkinje system, extracellular potentials, rel. to intercellular action potentials 2–62819
  - dog Purkinje fibres, electrophysiological props., effects of blood perfusion 2–62821
  - drosophila, transient and receptro potentials in electroretinogram 2–85153
  - dynamic scintillation scanning on canine osteosarcomas 2–69227
  - e.e.g. findings in hyperthyroidism 2–45019
  - elasticity of pulmonary alveolar microvascular sheet of cat 2–51877
  - elasticity of pulmonary alveolar sheet of cat 2–51878
  - electric interaction in striated muscle contraction 2–45015
  - electrical activity from single and multi units from pituitary stalk of sheep 2–45021
  - electro-optical Fourier transforms of leukocytes 2–51884
  - electron beam anal. of thick tissue samples 2–69299
  - electrophysiology, fluid mosaic model for excitable membranes 2–69237
  - energetics of development and maintenance of isometric tension by mammalian fast and slow muscles 2–66248
  - energy dispersive analysis of biological thin sections in electron microscope 2–82002
  - enzyme activity of cell enzymes, effect of h.f. e.m. waves 2–48834
  - enzyme amplifier systems triggered by white noise 2–76053
  - erythocyte, Stokes problem soln. 2–60173
  - erythrocytes, sound absorption, macromolecular interaction 2–48878
  - evoked activity of single units and neural populations in cats hippocampus 2–45020
  - femur, determ. of individual load and diagram of forces at proximal part 2–69218
  - fluorescein derivative uptake in traumatised rat muscle, potential use as scanning agent 2–69300
  - freeze etching technique for biological specimens for electron microscope obs. 2–45022
  - generation of biocompatible material, biolization, hypothetical process 2–69224
  - heart tissue cultures, chronotropic responses 2–76062
  - heart valves flow patterns, numerical solution of Navier-Stokes equations 2–85126
  - heat of evaporation of sweat, thermodynamic considerations 2–66246
  - human being rel. to light atmospheric ions 2–58585
  - human body, equal comfort contours for whole body vertical, pulsed sinusoidal vibrations, 4 to 80 Hz 2–73169
  - human body-mechanical vibratory system analysis 2–62865
  - human intervertebral disk in pre compression, stress distribution 2–55217
  - human lung tissue, computer method for counting number of alveoli per unit area 2–81983
  - human placental barrier, intracellular transport of Ca 2–69210
  - human spinal column, mechanical impedance relations 2–69221
  - human visual evoked response, ensemble characteristics, periodic and random stimulation 2–81982
  - in vivo tissue transfer fns., crosscorrelation techniques 2–69214
  - inhalation obs., evaluation of exploded wire aerosol generator 2–85160
  - integrated human thermal system, optimal control at unsteady state condition 2–69216
  - ionic diffusion through excitable membranes, theory, obs. using equivalent electrical circuit 2–48843
  - kinetic equations, asymptotically stable, stability theory 2–54534
  - left ventricular model, ejection cycle, parameter estimates 2–69212
  - light absorption and scattering factors in whole blood 2–45023
  - light scattering from E. coli cells, angular dependence and cell models 2–45017
  - liquid crystal, role in animate systems 2–53392
  - liquid crystalline biological materials, viscoelastic props. in vicinity of isotropic-cholesteric phase transition 2–51881
  - living plant cell walls, sample preparation for scanning electron microscopy 2–78641
  - low illumination effects on galvanic skin response 2–73230
  - lubrication of weight bearing joints 2–69219
  - macromolecule study, interactive display generation program 2–69204
  - macromolecules, quasielastic light scattering 2–81991
  - macromolecules, struct. aspects in biological roles, review 2–83383
  - magnetic susceptibility studies, appls., review 2–52381
  - magnetomyography, mag. fields around human body produced by skeletal muscles 2–69201
  - materials for cardiovascular implants, electrochemical methods for selection and eval. 2–69226
  - materials for intravascular pressure transducer 2–69225
  - median nerve afferent action potential recorded at wrist 2–81984
  - membrane water transport across, study technique 2–69207
  - membranes, plasticity, nonstatic model 2–81989
  - mice, bioelectric activity in immobilized muscle 2–81997
  - mice, tumorigenesis, immunocompetence, relative potency of X-rays and γ-rays 2–62854
  - microwave power symposium, Ottawa (1972) 2–49199
  - molecular structure, computer graphics representation 2–81993
  - monkey optic tract fibers maintained activity and lateral geniculate nucleus cells 2–52000
  - mouse, mammary carcinoma, effect on blood vessels 2–62847
  - multichannel miniaturized f.m./a.m. telemetering system 2–82009
  - multiple schlerosis, correlation between muscle strength and peripheral nerve conduction 2–55200
  - multiplication of living organisms, mathematical models 2–95078
  - muscle induced ejection flows, model 2–48832
  - muscular contraction, phenomenological eqns. of biological motility 2–73170
  - myocardial mechanics, force velocity relation, sliding filament theory 2–69211
  - myocardium, contractile state, thermodynamic characterization 2–62820
  - mysids, energy equivalents of body mass, respiration and calorific value 2–78639
  - nerve axons, signal transmission mechanisms 2–81992
  - network thermodynamics, biological systems 2–48836
  - neural masses, dynamics, linear analysis 2–81990
- **Biophysics** continued
  - n.m.r. studies of rate phenomena, molecular structure 2–81988
  - nuclear power stations, radiological safety for general public, health physics aspects 2–55226
  - occipital spikes rel. to visual evoked responses in photosensitive epilepsy 2–45027
  - organisms, physiological and metabolic changes in constant electrostatic field 2–48851
  - periodicities, stochastic processes, geophysics meteorology 2–52084
  - Pinus radiata, sample preparation for light microscopy 2–78640
  - pituitary adrenal system, cybernetic aspects 2–69217
  - polymeric mats., biomedical props. rel. to spatial gradients and applics. 2–61026
  - primary hemostasis, convective transport theory anal. 2–48846
  - protein and α-tocopherol membranes photovoltaic e.m.f. 2–85089
  - psychophysical curves and meas. of thresholds 2–69208
  - quantitative physical biology, key problems 2–45016
  - radiation, topicality 2–55203
  - radiation effect on mating pattern of male mice 2–69230
  - radiobiology problems 2–73181
  - rat femurs, effects of X-rays on mechanical properties 2–69228
  - red blood cell segregation and sedimentation in u.s. standing waves 2–81986
  - regulation of conditioned tracking motor defensive reflexes in dogs 2–69209
  - respiratory mechanics, phase method of calculation using digital computer 2–66247
  - review paper given to practising doctors 2–85091
  - rhythmic after activity to flashes, rel. to background alpha preceding and following photic stimuli 2–45018
  - scanning electron microscopy, sample preparation 2–78642
  - scanning microinterferometer, laser illuminated, for det. of dry mass of living cells 2–45785
  - seroalbumin polysaccharide complexes, u.s. spectrometric study of formation 2–73171
  - skeletal muscle dynamics, fatigue, stochastic model 2–69215
  - specific mechanical impedance of skin, probe effects 2–66245
  - spontaneous brain activity as background noise to visual evoked response 2–66311
  - squid, light evoked responses from extra-ocular photoreceptors 2–48931
  - squid, light evoked responses from extra-ocular photoreceptors 2–48931
  - squid giant axon, propagated subthreshold oscillatory response and classical electronic response 2–55204
  - sterilization probability for small particles, entering Martian atmosphere 2–62701
  - synchronization of cardiac pacemaker with repetitive stimulation of carotid sinus nerve, in dog 2–76052
  - technique to rapidly advance microelectrodes into biological cells 2–58578
  - telemetric obs. of local blood flow by heat conduction probes 2–82007
  - tetrahymena culture systems, bioconvective fluid instabilities 2–77451
  - thrombus formation on intra-arterial heart and valve prostheses 2–48847
  - thymocytes, effect of sulphydryl protecting and blocking agents on radiosensitivity 2–69332
  - tissue microscopy, colour contrast methods 2–76054
  - tissue preparation for light and electron microscopy 2–78643
  - tissues, peak osmotic water displacement induced by gases 2–45024
  - underwater bioluminograph for meas. of bioluminescence potentials of luminous organisms 2–54749
  - u.v. effects on RNA phage MS2 2–62823
  - u.v. effects on RNA synthesis 2–62824
  - vegetable pigments in soln. and chloroplastic media, reson. Raman spectra 2–81977
  - vertebral bone mineral mass determ. by transmission obs. 2–69263
  - visually evoked cortical potential, photopic and scotopic contribution 2–85143
  - wave velocity in proximal aorta 2–66249
  - wet biological materials, high voltage electron microscope obs. 2–73168
  - X-ray diffraction and kinetics of ordering of lipids in E.coli membranes, use of new detector 2–66251
  - Young's modulus of muscle during development of rigor mortis 2–66252
  - ^{137}Cs, ^{133}Cs, distrib. of radioactive and stable isotropes to human body 2–55224
  - LiBr shortened glycerinated muscle fibres, electron microscope obs. 2–62825
  - O_2 absorption rate into blood under turbulent conditions 2–73166
  - ^{239}Pu, determ. of quantity in living human organism from rate of elimination 2–55301
  - Si rubber membranes as supporting medium for cells for electron microscopy 2–79097
- **Biot-Savart law** *see Electromagnetism*
- **Birefringence** *see Double refraction*
- **Bismuth**
  - Alfven wave amplitudes and carrier relax. times 2–51092
  - Alfven-waves damping in single crystals 2–68316
  - alloys, apertures for Cu K_α X-ray experiments 2–85184
  - amorphous state, Hall effect 2–75048
  - atom, positron scattering, 100, 200 keV, diff. cross-sections 2–79877
  - band edge parameters, calc. 2–75027
  - band structure, determ. of cyclotron effective masses of carriers, mass parameters of electron pockets 2–47807
  - bulk, nonextremal Fermi-surface orbits 2–77827
  - bulk, nonextremal Fermi-surface orbits 2–77828
  - density of states, relativistic effects, mass velocity and Darwin terms 2–84242
  - diamagnetism of free and Bloch electrons, many-body effects 2–68518
  - dislocation delineation, temp. effect 2–56707
  - dispersion relation for holes, from band structure changes under hydrostatic pressure 2–61223
  - droplets, crystallization and nucleation 2–71382

Bismuth continued
elastic stiffness constants, room temp. to m.p., u.s. determ. 2−74822
electron diffusion through shock wave front 2−71771
e.m. generation of u.s. waves 2−43967
etch pit orientation determination 2−47187
film, charact. electron energy loss spectra 2−44044
film, condensed on glass, amorphous to cryst. transition temp. 2−43474
film, crit. thickness, Hall const. determ. 2−56587
film, disordered, supercond. transition temp. and normal state cond., effects of surface charge 2−44070
film, in picosecond holography using Nd:glass laser 2−55714
film, i.r. holograms using pulsed high power lasers 2−55713
film, magnetoresistance as function of thickness 2−84332
film, significance of electric field on growth 2−60634
film, supercond. transition temp. change due to noble gas adsorption 2−47856
film, thermo-e.m.f. rel. to struct. 2−81161
film thermoelectric figure of merit 2−55642
grain boundaries, high temp. behaviour, heterophase dislocation theory 2−56733
graphite-Bi mixture obs. on neutron diffusion lengths 2−49861
hyperfine interactions of implanted ^{220}Rn and ^{224}Ra study by α-γ correlations 2−81341
liquid, density obs. between m.p. and 600°C 2−43339
liquid, diffusion of Tl 2−46945
liquid, effective interionic pair potentials, calc. from structural diffraction data 2−50312
liquid, optical consts. 2−43359
liquid, struct. factor, X-ray diffr. apparatus 2−74516
liquid, u.s. velocity, theory and expt. 2−80469
liquid-solid interface, damping of oscillations by magnetic field 2−71303
magnetoacoustic effects, anisotropic deformation potential for electrons, holes, ultrasonic determination 2−61096
magnetoresistivity and thermoelectric power, frozen-in defects 2−68336
magnetoresistivity coeffs. electron and hole transport, low field galvanomag. tensors, 77-300K 2−84233
magnetoresistivity tensor components, at intermediate mag. fields, 77 K 2−75053
melting curve maxima phenomenological relationship between solid and liquid phases 2−74581
phonon drag thermomag. at low temps. 2−54244
polycrystalline, Hall voltage and magnetoresistance obs. by sum frequency method in belt apparatus 2−57267
polymorph III modification at 42 kbar and 20°C, volume change 2−74925
polymorphic transitions, press.-induced, and supercond. phase 2−44058
polymorphic transitions under pressure, strain gauge obs. of volume changes 2−47678
powder, Raman effect 2−81383
radiation generated during rapid deform. and rupture tribolum. 2−54482
radiative lifetimes 2−63997
resonance electrostatic meas. of temp. depend. of elastic constants 2−71545
second sound, diffusion propagation of heat pulses 2−47762
single crystal piezoreflectance obs. and rel. to optical interband transitions 2−65213
specific heat below 30 K 2−68249
superconductivity, in high pressure phases up to 30 kbar 2−68357
superheating, anomaly between small particles and bulk 2−77467
surface tension, 239°C 2−56577
thermal expansion, coeffs., anisotropy, 2-30K, 55-90K, and at 283K, Gruneisen parameters 2−77784
thermomagnetic properties, rel. to device appl. 2−59064
thermopower, low temp., sample dimens. influence 2−47992
thin films, permittivity meas. 2−47975
twin boundary movement during cycling 2−83970
u.s. waves, shear and longitudinal, electromagnetic generation 2−71729
vacuum evaporation, selective condensation on macroinhomogeneous surface 2−74628
whisker, deform. twinning, nucleation and propag. stresses 2−47424
whiskers, resist. oscills. in mag. field at 4.2 K 2−68338
Young's modulus and Poisson's ratio, orientation depend. 2−74821
Bi:Sn, magnetoacoustic oscills. 2−54032
Bi:Sn, magnetoacoustic oscillations, with mag. field orthogonal to sound propagation 2−71738
Bi:Te, effect of high hydrostatic pressures on heavy conduction electron band 2−81102
Bi:Te deposits, optical and electrical props. 2−75255
Bi-Cd binary system, pressure effect on eutectic temp. 2−76124
Bi-Cs layers, photoemission properties 2−65102
Bi-Pb-Hg liquid metal systems, effectiveness of boiling separation 2−74594
Bi-Sn, magnetoacoustic oscills. with mag. field orthogonal to sound propag. direct., fields to 100 kG 2−84203
Bi I, radiative lifetimes of excited levels belonging to $6p^27s$ and $6p^26d$ configurations by Hanle method 2−49942
Bi_3, heat of sublimation, third law anal. 2−72554
Bi^{3+}, activator in CaS:Bi, Pd, thermoluminesc. 2−54475
Cd, Bi-doped, pore formation on annealing 2−71665
GaP:Bi, luminesc., kinetics due to bound excitons, 77.3K 2−65292
GaP:N(Bi), exciton binding to impurities, uniaxial stress effects 2−75108
$LaGaO_3$:Bi^{3+}, luminesc. props. 2−48245
Ni: ^{206}Bi, mag. hyperfine field at Bi 2−81251
Si:B, impurity lattice location, He^+ ion channelling obs. 2−60819

Bismuth compounds
— 2−67467
ceramics, use in nuclear reactors, interactions with aluminium and magnesium 2−83064
group V double and triple chalcogens, n.q.r. of ^{75}As, ^{79}Br, ^{81}Br, ^{127}Sb, ^{123}Sb, ^{127}I, ^{209}Bi 2−48311
oxyhalides, i.r. spectra, vibrs. assignments 2−57348
pyrochlores, $Bi_2M_2O_7$, (M=Ru,Ir,Os), struct. and props. 2−60987

Bismuth compounds continued
Woods alloy, thermodynamic props., calorimetric obs. 2−57056
BI_3, Mossbauer effects, of ^{129}I, bond character 2−78071
Bi-Ag eutectic alloy, surface damage after polishing, e. microscope study 2−67898
Bi-Cd, eutectic, unidirectional solidification 2−43442
Bi-Cd eutectic, cellular solidification, plane front-cell transition 2−43443
Bi-In alloy, thermodynamic props., calorimetric obs. 2−57056
Bi-In(Sn)(Tl) alloys, induced high press. phases, X-ray and specific volume studies 2−74926
Bi-Ln-Th soln., Ln=La, Eu, Nd, mutual solubilities, 350-700°C 2−67809
Bi-Pb alloy, supercond. under high press., supercond. transition 2−47868
Bi-Pb alloy, thermal expansion meas. in room temp.-100°C range, applicability of rule of mixtures 2−60975
Bi-Pb alloy, thermodynamic props., calorimetric obs. 2−57056
Bi-Sb alloy, 5-100% Sb, Mossbauer effect of ^{121}Sb, 80K 2−81345
Bi-Sb alloy, antimony concentration, radiactivation determination 2−81554
Bi-Sb alloy, band edge parameters, calc. 2−75027
Bi-Sb alloy, for magneto-thermoelec. and thermomag. cooling, props. 2−75161
Bi-Sb alloy, transport effects, effects of Ag, In and Pt addition 2−71896
Bi-Sb alloy, transport effects, effects of Ag, In and Pt addition 2−71896
Bi-Sb alloy system, cryst. growth rate, diffusional supercooling theory 2−53613
Bi-Sb alloys, pressure-temp.-comp. diagrams 2−68192
Bi-Sb low-concentration alloy, band structure study using cyclotron resonance 2−47807
Bi-Sb solid soln., thermomagnetogalvanic props. 2−54245
Bi-Sb(Ag) alloy, thermomag. props., rel. to device appl. 2−59064
Bi-Se system, phase separation 2−60591
Bi-Sn alloy, thermal expansion meas. in room temp.-100°C range, applicability of rule of mixtures 2−60975
Bi-Sn(Pb)-Zn system, activity coeffs., calc. 2−43827
Bi-Te unit crystals, determ. Sb diffusion rate on function of composition 2−68051
Bi-Zn, liquid binary alloys, absolute thermoelectromotive force 2−56518
Bi-Zn alloys density obs. between m.p. and 600°C 2−43339
Bi-Zn(Ag) eutectic alloy, morphology, electron diffr. obs. 2−60976
BiCl, rotational analysis of A-X band system 2−50024
$BiCl_3$, n.q.r. of ^{209}Bi, temp. and press. depend. 2−78177
$BiCl_3$ cryst. and mol. struct. 2−77553
$BiFeO_3$, lattice parameters, thermal expansion, elec. Curie temp. 2−47317
$Bi_{12}GeO_{20}$, acoustic surface wave propag., 200-2000 MHz loss mechanism 2−61094
$Bi_{12}GeO_{20}$, acoustic wave velocity meas. change caused by thin conducting film 2−51017
$Bi_{12}GeO_{20}$, cryst. growth, Czochralski method, diameter control, laser appl. 2−60715
$Bi_{12}GeO_{20}$, elastic, piezoelectric and dielectric constants 2−51203
$Bi_{12}GeO_{20}$, nonlinear surface wave generation 2−51007
$Bi_{12}GeO_{20}$, propagation of Bleustein-mode piezoelectric surface wave 2−61095
$Bi_{12}GeO_{20}$, Rayleigh wave electromech. coupling const., acoustic wave vel. obs. 2−43969
$Bi_{12}GeO_{20}$, surface wave attenuation, frequency and temp. depend. 2−51024
$Bi_{12}GeO_{20}$, surface wave devices, fabrication techniques 2−51013
$Bi_{12}GeO_{20}$ switching and steering of surface waves by nonlinear mixing in anisotropic media 2−51005
$Bi_4Ge_3(Si_3)O_{12}$ electro-optic crysts., quadrupole coupling consts. 2−84604
BiI_3-Bi solutions, semicond. behaviour 2−64472
BiI_3, localized states and electron-hole processes, photopolariz. and photoluminesc. obs. 2−61706
BiI_3, non isothermal relax. of photoelectret state 2−57247
$Bi_2Mg_3(NO_3)_{12}.24\ H_2O$, e.p.r. of Gd^{3+} in single crystals below 40G 2−51405
Bi_2O_3-B_2O_3 stratification effects on comp. depend. of elasticity modulus 2−47478
Bi_2O_3-V_2O_5 flux system, for oxide crystal growth 2−50589
Bi_2O_3, amorphous and polycrystalline film prep. by cathode reactive sputtering 2−80594
Bi_2O_3, as grain boundary element in La doped $BaTiO_3$ ceramics, resistivity temperature characteristic anomaly at transitions 2−84366
Bi_2O_3, transform. deform. 2−50932
Bi_2O_3 sintered containing SrO, CaO, La_2O_3 ion conduction meas. 2−61418
BiOBr, photoemission, determ. of optical transitions and Fermi level 2−81197
BiOCl, photoemission, determ. of optical transitions and Fermi level 2−81197
BiOI, BiOCl, BiOI, fundamental absorpt. edge, band struct. and effects of laminarity 2−75287
BiOI, photoemission, determ. of optical transitions and Fermi level 2−81197
Bi_2S_3:Pb, capture level parameters, thermo-stimulated cond. study 2−71923
n-Bi_2S_3, Hall coeff. temp. depend. 2−44092
$Bi_{1-x}Sb_x$:Cd(In)(Sn), elec. props., (x=0-0.2), 180-420K 2−61301
BiSb, narrow band emission, nuclear electrical quadrupole radiative transitions 2−78118
BiSb alloy, interband breakdown, voltage instabilities in electron-hole plasma 2−81095
$Bi_{88}Sb_{12}$, mag. susceptibility, effects of SN and Te impurities 2−72109
$Bi_{92}Sb_{08}$, dc-pumped, line narrowing of microwave radiation caused by nuclear electric quadrupole transition in ^{209}Bi 2−44403
Bi_2Se_3-Bi_2Te_2S solid soln., phase diagram 2−57028
p-Bi_2Se_3, Hall and cond. mobilities, carrier compensation, galvanomag. effects, 4.2-300K 2−81076
BiSeI, band struct., elec. cond. 77−460 K, thermo e.m.f. 300−400 K 2−80997

Bismuth compounds continued
$Bi_{12}SiO_{20}$ electro-optic image modulator for optical processing 2−79416
$Bi_{12}SiO_{20}$ electro-optic image modulator, sensitivity and resolution 2−79417
$Bi_2Sn_2O_7$, flux growth and single cryst. X-ray diffr. 2−60717
Bi_2Te_3-Bi_2Se_3(Sb_2Te_3), efficiency criterion for thermogenerators 2−75158
Bi_2Te_3-GeTe solid soln., Hall carrier conc., elec. cond., thermal e.m.f., thermal cond., struct., hardness 2−74903
BiTe, diffusion of Cd and In, effect of distrib. of diffusing element, thermal e.m.f. and orientation relative to basal plane, creation of p-n junctions 2−83991
BiTe and BiSe, single-crystal plates, electrical conductivity, thermal e.m.f. and carrier conc., etching method for dislocations 2−84322
p-Bi_2Te_3, low- and high-field galvanomag. props. 2−51135
Bi_2Te_3, performance as solar thermoelectric generator material 2−59058
p-Bi_2Te_3, second valence band, magneto-Seebeck and Shubnikov-de Haas obs. 2−61339
p-Bi_2Te_3, valence band struct., Shubnikov-de Haas oscills. of magnetoresist. 2−77805
p-Bi_2Te_3, valence bands, saturation and quantum oscill. in magneto-Seebeck effect obs. 2−81159
Bi_2Te_3 and alloys, for Peltier cooling, thermoelec. props., review 2−75160
$Bi_8Te_7S_5$, single crystal film, Hall eff. meas. and detn. of carrier mobility 2−77851
$Bi_8Te_7S_5$ layered material, thickness distrib. in cleaved single cryst. films 2−47103
Bi_2Te_2Se, 7.5 MeV proton irrad. induced disorder, X-ray obs. 2−64653
$Bi_2Te_{3-x}Se_x$, temp. depend. of electron effective mass and mobility 2−81099
$Bi_4Ti_3O_{12}$, structure det. from X-ray data and neutron powder diffraction 2−71425
$Bi_xTi_yO_z$, hydrothermal crystn. and nonlinear optical props. 2−47231
Bi_2WO_6, growth, cryst. struct. and dielec. props. 2−47263
Bi−GeTe solid soln., regions of existence at 250, 400, 500 and 600°C 2−53888
Ca-Bi-V ferrite rods, excitation of longit. acoustic waves 2−43968
Cu-Bi, grain boundary fragility and segregation 2−53830
Hg-Bi amalgam, dil., viscosity, comp. depend., 0-100°C 2−64451
In-Bi alloys, liq., longit. spin relax. of ^{115}In 2−50370
In-Bi alloys, supercond., flux flow state props. 2−44074
In-Bi liquid alloy equi-atomic, transport props. 2−46939
In_5Bi_3 phase, thermodynamic props. 2−71687
Li-Bi liquid alloy, solubility of Nd and Th 2−43334
Mg-Bi amorphous alloy, exciton screening 2−78115
Mn-Bi alloy, hysteresis, domain structure and nucleation centres 2−68550
Mn-Bi films, intermediate cpds., polarization microscope images 2−57301
MnBi film, prep., props., domain struct. 2−44263
MnBi film, struct. and orientation, electron microscope and diffr. obs. 2−47119
MnSb-(Sb,Bi) eutectic, morphology, growth rate effects 2−47641
Pb-Bi-Sn eutectic, superplasticity 2−80839
Pb-Bi, liquid binary alloys, absolute thermoelectromotive force 2−56518
Pb-Bi alloy, neutron scattering law determ. 2−80931
Pb-Bi alloys, nonequilib. freezing, quantitative predic. by classical eqn. 2−47032
Pb-Bi peritectic alloy, heat of solidification, calc. 2−43444
$Pb_{0.9}Bi_{0.1}$ alloy, strong coupling superconductor, crit. mag. field temp. variation 2−68356
Sb-Bi alloys, band struct., magnetoreflection obs. 2−54405
Sb_2Se_3-Bi_2S_3 alloy, switching behaviour 2−75096
Sn-Bi-As system, Sn_4As_3-Bi-SnAs subsystem, phase equilib. 2−74942
Zn-Bi alloy, surface tension, 860-920K 2−43341
Zn-Sn-Cd-Bi liquid quaternary solution, thermodynamic props., e.m.f. method 2−71186
ZnO-Bi_2O_3 ceramic, elec. props. 2−57198

Bitter patterns *see Domains*

Bitumen *see Materials*

Bloch walls *see Ferromagnetism; Domains*

Blood
abnormal pulmonary circulatory dynamics, simulation 2−48862
acoustic wave absorption at 1 to 10 MHz 2−82363
aortic diameter pulsatile variations, u.s. meas. 2−51944
aortic flow disturbances, in vivo study 2−48842
arterial branching in models using flow birefringence 2−66250
arterial flow model, laminar flow in tubes with constriction 2−74335
arterial flow monitoring, u.s. Doppler probe 2−69367
arterial morphology, focussed ultrasound effect 2−51919
arterial stenoses models, flow, geometry influence 2−51904
arterial velocity profiles direct numerical calc. 2−48845
arterial volume determ. using aortic characteristics 2−73172
blood bank computerized management information system 2−82031
cardiac output meas. using dye dilution technique, analysis system 2−69265
caval, selective distrib. in lungs 2−73197
cells, volume histograms obs. using pulse height analyser 2−69279
cerebral blood flow, sympathetic control in dogs 2−85122
cerebral circulation, digital dynamic radionuclide studies, automatic analysis 2−76094
circulation, biomechanics, numerical studies 2−78644
coagulation processes, effects of 2450 MHz microwave radiation 2−58586
collateral flow, inaccuracy of retrograde flow and peripheral coronary pressure methods of obs. 2−48844
coronary circulation in conscious dog with cardiac neural ablation 2−85121
diffusion of oxygen, protein conc. effect 2−51886
dog Purkinje fibres, electrophysiological props., effects of blood perfusion 2−62821

Blood continued
extra-corporeal irradiators for radiation therapy, development 2−69242
flow, laminar, time dependent, effect of high molecular weight additive 2−48850
flow, pulmonary, alveolar 2−51879
flow, subendocardial distrib., effect of antianginal drugs 2−76061
flow acceleration and peak velocity in aortic arch, transcutaneous meas. 2−48889
flow characteristics in mild arterial stenosis 2−51882
flow control system to vascular bed of awake baboon, occlusion cuff system 2−85128
flow dynamics at aortic bifurcation 2−48841
flow evaluation in liver using dynamic scintigraphy 2−48884
flow in arterials, effects of continuous obstruction 2−48848
flow in artificial arteries 2−43284
flow in capillaries, analysis 2−48840
flow in renal vascular and tubular compartments, digital simulation 2−51903
flow in small curved glass tubes 2−48849
flow meas. by forced heat transfer from hot film 2−80431
flow measurement, n.m.r. technique, velocity distribution fn. 2−83757
flow measurement, review of technique and instruments 2−78645
flow obs. using e.m. telemetry 2−82008
flowing, platelet diffusion, effect of hematocrit and shear rate 2−55214
flowing, platelet diffusion and adhesion to glass, model anal. 2−55215
gas bubble nucleation rate 2−45028
haemoglobin, O_2 conc., meas. device 2−62831
haemolysis in flow system, optical technique for continuous monitoring 2−51883
heart valves flow patterns, numerical solution of Navier-Stokes equations 2−85126
hepatic flow measurement, removal efficiency of dyes 2−58607
hepatic mass lesions, blood pool scanning 2−58608
light absorption and scattering factors in whole blood 2−45023
live white cells, photography 2−62832
mass spectroscopy meas., membrane 2−51892
microcell automatic analyzer 2−51929
muscle blood flow and capillary permeability using ^{133}Xe and ^{77}Br 2−69359
n.m.r. flowmeter for pulsatile flow, analysis 2−81981
peripheral leukocytes automated classification by pattern recognition 2−69202
portal circulation evaluation using scintillation camera 2−73199
pressure and flow in brain, effect of X-rays and pulsed γ-neutron radiation in monkeys 2−69316
pressure and O_2 content., fibre optic catheter for obs. 2−51897
pressure measuring system, automated, Korotkov sound processor 2−51885
pressure monitor, miniaturised 2−58584
primary hemostasis, convective transport theory anal. 2−48846
pulsatile flow in arteries, nonlinear anal. 2−82024
pulsatile flow simulator design and applics. 2−51900
radioactive tracer method with compensation for activity decay for monitoring of rate of hemodialysis 2−51887
radionuclides, medically applied, effect on radioresistance of red blood cells, determ. of dose dependence 2−55237
red cell rotation model, verification using holography 2−85096
red cell structure, effect on deformability, anomalous flow behaviour, review 2−69205
red cells, segregation and sedimentation in u.s. standing waves 2−81986
regional organ flow, radioisotope technique, mathematical model 2−78637
reindeer, cryorheology 2−77419
sampling, Vacutainer, attachment for Coulter counter S 2−69235
sheep, changes following acute β-radiation of skin 2−66269
telemetric obs. of local blood flow by heat conduction probes 2−82007
tests, sedimentation rate, technical aspects 2−69223
transcutaneous aortovelography for blood velocity obs. in aortic arch 2−69312
tumour blood flow, meas. by ^{133}Xe clearance rel. to capillary 2−62863
u.s. detection of bubbles with Doppler flow transducers 2−66277
u.s. Doppler flowmeter, theory 2−85092
u.s. Doppler technique for imaging blood vessels 2−62828
velocity profiles, real-time obs. using u.s. multigated pulsed Doppler velocimeter 2−69311
vessel imaging using ultrasound 2−69310
vessel wave propagation, application of prestressed shell theories 2−82338
volume flow meas. with CW Doppler u.s. flowmeter 2−51901
wave velocity in proximal aorta 2−66249
white blood cell systems, microwaves effects 2−82028
^{115m}Cd, retention and elimination in man, meas. of radioactivity in whole blood, red blood cells and plasma 2−55285
Cs^+ ion transport of red blood cells of rats, comparison with K^+ by kinetic tracer model 2−55257
K^+ ion transport of red blood cells of rats, comparison with Cs^+ by kinetic tracer model 2−55257
O_2 absorption rate into blood under turbulent conditions 2−73166
U miners, investigation of immunoglobin levels in blood serum after high exposure to ionizing radiation 2−55296

Boiling
see also Distillation
acetone, heat transfer to liquid drops from small diameter channel in film boiling temp. range 2−53379
alkali metals, temp. inversion in tubes under annular flow 2−64514
channel, thermohydrodynamic stability, D marking method, computer calc. 2−56454
diaphasic resistance variations 2−53504
ethyl alcohol, overheating, nuclear reactor coolants 2−42686
explosive, coolants for reactors 2−42686
fluid flow and heat transfer, conference (Lucas Heights, Australia Aug. 1971) 2−43077
freon, overheating, nuclear reactor coolants 2−42686

Boiling continued
freon-113 on nonisothermal surface, meas. of local heat transfer 2−64516
Hg, vapour pressure, ebulliometric meas. and variations with temp. 2−67877
methanol, heat transfer to liquid drops from small diameter channel in film boiling temp. range 2−53379
nuclear reactor, nucleate and film boiling, heat transfer mechanisms 2−53510
nucleate, heat transfer function tested by temp. control feedback system 2−53506
nucleate heat flux, varying levels of subcooling and acceleration 2−47043
nucleation models 2−53503
under quenching conditions, effect of effusivity and thermal resistance of solid surface 2−60555
rod surface, effect of transition regime on propagation of temp. oscillations 2−64513
from small cylinders in water and organic liquids, identification of heat removal modes 2−77472
steady, laminar, natural convection film on vertical surface, stability analysis 2−43448
surface, thermoacoustic effects 2−60554
water, heat transfer to liquid drops from small diameter channel in film boiling temp. range 2−53379
water, nucleate conditions at artificially active nuclei 2−50405
water, overheating, nuclear reactor coolants 2−42686
water and glycerol-water mixture, heat transfer in 2−60556
water vapour bubble motion in annular channel 2−74592
water-Freon 113 system, interfacial boiling, direct contact heat transfer in stratified flow 2−50285
$CdFe_2O_4$, specific saturation magnetization depend. on time of boiling 2−84432
$EuCl_2$, normal boiling pt. calc. 2−64515
He, heat transfer from Al surfaces 2−66362
He I, pool boiling, thermosiphon boiling, rel. to refrigerant applic. 2−64491
Hg-Bi-Pg liquid metal systems, effectiveness of boiling separation 2−74594
K, forced convective boiling, controlling heat transfer and fluid flow mechanisms 2−71280
N_2 liq. film, heat transfer in plug stage, expt. 2−56546
N_2O_4, nucleate, criterial equation 2−45586
$N_2O_4.2NO_2$ nucleate boiling, stability of superheated liquid phase of dissociated N_2O_4 2−47044

Boiling point
water, contact angle rel. to drop size at b.p. for 50-760 Torr 2−77474
$InBr_2$, heterogeneous equilib. 750-1050 K, enthalpy, entropy of evaporation, boiling point 2−74593

Bolometers
horizon sensor for geostationary satellite 2−44808
integral normal radiating power meas. between 600 and 1500 K 2−63143
semiconductor on quartz substrate, time and mechanical stress stability 2−55571
superconducting tunnel junction, for heat-pulse determ. of acoustic wave dispersion in InSb 2−80911
thin layers, properties of the layer, selection and research properties 2−82377
Ge:Ga, construction and performance 2−41847
InSb, hot electron, props. for submm. astronomy 2−73158

Boltzmann equation
see also Transport processes
aerosol, particle size distrib., determ. using Boltzmann's charge distrib. law 2−71244
BGK linearized, finite element analysis 2−58766
binary gas mixture, asymptotic theory for steady source expansion 2−71108
chemical relaxation as transport process 2−48315
derivation, simplified 2−73492
droplet growth in nucleation, kinetic theory 2−60551
eigendistributions of linear Boltzmann operator in modal approx. 2−76217
exponential asymptotic stability props. of total equilibrium 2−63023
fermion statistics 2−73339
first order ordinary linear systems, solution of boundary value problem, neutron transport eqn. 2−83042
gaseous mixtures, exptl. test of linearized eqns. using sound dispersion 2−60375
gases, mixtures, chem. reacting, transport processes 2−48320
group III to V semiconductors, solution 2−54162
hard-sphere gas, thermal fluctuations 2−76224
heat conduction differential equation, modification when temperature changes within mean free path 2−58958
hydrodynamics, foundations, views of Predvoditelev 2−67548
limiting properties of solutions 2−69603
linear, internal limits in weakly nonlinear region 2−78837
Master eqn. soln for K interacting with π, $l\nu$ pairs, and Onsager relation 2−73799
molecules, rigid ovaloid, generalization of collision processes 2−43028
neutron transport, elementary solutions including anisotropic scattering 2−63944
neutron transport, in-reactor, regular and adjoint time moments 2−70505
neutron transport reaction rate error estimation using functional analysis technique 2−70501
neutron wave propagation, eigenfunctions expansion method, pseudo mode calc. 2−52837
nonlinear, solution by discrete velocity method 2−52082
plasma, non-Lorentzian, transport coeffs. 2−80241
Poisson Boltzmann eqn. analytical scheme giving approximate solution 2−49026
rarefied gases, exact solution of temperature slip problem 2−50270
relativistic, for fluids near equilibrium, supplementary conditions 2−49024
semiconductor, hot electron effects calc. 2−54193
semiconductor, solved using high field carrier distrib. function 2−61292
semiconductors, carrier waves with velocity distributions 2−84324

Boltzmann equation continued
time correlation functions 2−45284
time-dependent transport equation, new approach to solution 2−66454
transport equation for electron current and thermionic emission 2−64878
wind-tree model with overlapping scatterers, abnormal diffusion 2−52114
Ar gas, electron momentum transfer cross section from Boltzmann eqn. 2−83708
K elec. conductivity calc., electron-phonon scatt., soln. of Boltzmann eqn. 2−71830

Bonding of materials *see Adhesion*

Bonds
see also Binding energy; Lattice energy; Molecules
— 2−71359
— 2−67970
acetic acid/acetone mixtures, H bond formation causing ultrasonic relaxation, two state model 2−43322
acetonitrile, in trialkylphosphines and CCl_4, H bonding, spectral study 2−46647
acrylonitrile-styrene copolymers, acrylonitrile-acrylonitrile bond 2−67528
adsorption on metal surfaces, dipoles cross depolarization effects 2−50521
alcohol-tetraalkylphosphorus salt, spectroscopic study of H-bond strength 2−53044
alcohols, hydrogen bonds, ionization potential and proton- acceptor props. 2−50076
alkali halide molecule, ionic stabilization energy and Coulombic attraction 2−53030
alkali metal, binding energy, empty core model pot. calc. 2−64586
alkali metals, binding energy, pseudopotential calc. 2−77832
alkali metals, cohesive energy calc. 2−83884
alkanes, bond energies, Del Re parameters 2−67505
alkanes and derivatives, polarization tensor study 2−70736
alkyl halides, bond energies, Del Re parameters 2−67505
all-valence-electron molecular orbital theory, bond order-bond length relationship 2−46513
alloy, short range ordering rel. to long range interatomic interactions 2−50819
amines, primary H bonding effect on stretching frequencies 2−83266
anatase, molecular charge distribs. K X-ray emission obs. 2−67930
anorthite, Si-O and Al-O bond length parameters analysis 2−61850
average valency V materials, trends in ionicity 2−83887
azolidones, i.r. absorpt. spectra rel. to H bonding and mol struct. 2−56216
benzenes, substituted, bond lengths and angles in first excited state 2−50084
bicrystal, epitaxial, interface struct., effect of misfit, bonding and cryst. dimens. 2−56690
bicyclo[1.1.0]butane, ab initio SCF calculations 2−42963
bicyclo[1.1.0]pentane, ab initio SCF calculations 2−42963
bimetallic surface, adhesion bonding in terms of electronic struct. of combined metals 2−74652
binary cpds., nearest-neighbour distance rel. to quantum and atomic nos. and valence 2−47178
breaking H bond, directions of normal vibrations of protons 2−67458
buckling, finite, of fibre reinforced columns 2−41570
butyl hydroperoxides, H bonding, effect of solvent, i.r. spectra study 2−46964
cantharidine, X-ray diffraction study, molecular bond lengths and conformation 2−68010
carboxylic acids, alkoxy substituted, intramol. hydrogen bonding effect on i.r. bands 2−67510
ceramic-metal reaction welding, microscopic study 2−64785
chlorobenzol-n-butanol system, microwave absorpt. and complexing 2−67810
circulator rings coupled first bending vibrations, effect of transverse shear and rotary inertia 2−45560
composite, Ni/Al_2O_3, reinforcement/matrix bond failure 2−47668
conjugated hydrocarbons, Huckel MO π resonance energies, σ structure 2−53068
conjugated mols., complementarity condition and bond orders 2−70672
coumarins, H-bonding effects on excited $\pi\pi^*$ and $n\pi^*$ states 2−60057
covalent, formation im molecules, charge shifts 2−80034
cubic tight binding solid, anisotropic oscill. indirect interact. between adatom pairs 2−47146
cumene hydroperoxides, H bonding, effect of solvent, i.r. spectra study 2−46964
cycloalkanes, ring strain effects on stretching vibrations of methylene group 2−42972
cyclohexanol, crystalline, dielec. relax. below glass temp. by rotation of OH bond 2−81144
cyclohexyl hydroperoxide, in bases, H bonding, from i.v. spectra 2−46601
cyclopentadienylberyllium chloride, microwave spectrum analysis 2−70763
B-decachlorocarboranes, H bonding, i.r. spectr. study 2−46602
diatomic oxides and sulfides, gaseous, bond energies and force constants, stabilities 2−64107
3,4-dimethylenecyclobutene, valence shell calculations of bond populations 2−60063
dimethylselenone, strength and nature of valence bonds 2−77143
dimethylselenoxide, strength and nature of valence bonds 2−77142
DNA, simultaneous motion of protons in hydrogen bonds, Schrodinger eqn. soln. 2−70799
DNA base pairs, proton transitions in H bonds 2−80115
elements, atomic coordination valency 2−80591
elements, nearest-neighbour distance rel. to quantum and atomic nos. and valence 2−47178
formic anhydride, bond lengths and valency angles, electron diffraction investigation 2−60070
glass, n.m.r. obs. 2−54500
graphite, interstitial atoms in interlayers 2−56605
group II-IV-V_2 compound, ionicity and effective charges 2−60699
hemoprotein derivatives, circular dichroism in visible region, nonlinear iron-ligand bonds 2−64197

Bonds continued
homoallylic H-H coupling constants, conformational dependence 2−42856
hydrates of ions Li^+, Na^+, Be^{2+}, F^-, Cl^-, calc. by CNDO/2 method, determ. of H bond strength 2−50053
hydrogen, MO theory, calcs. on dimers containing NH_2OH, H_2O, HOF, and H_2O 2−67491
hydrogen bond stability, charge transfer influence 2−70671
hydrogen bonding, dependence on groups taking part 2−74280
hydrogen bonds, depend. on groups taking part 2−74280
hydrogen bonds, extremely high polarizability 2−56147
hydrogen bonds in pyrrole-pyridine system 2−43007
hydroxyapatites, OH ions i.r. spectra, stretching and librational modes, H-bonding 2−61650
α-(0-hydroxyphenyl)-N-phenylnitrone, evidence for intramolec. H-bonding from dipole moment meas. 2−64179
ice, low entropy form obtained from a linear step growth model 2−83906
imidazole free radical, ENDOR determ. of hyperfine tensors for protons of hydrogen bonds 2−65394
iminoxyl radicals, spin density propag. via bonds 2−80110
inorganic cryst., prediction of hydrogen bonds 2−47312
intramolecular hydrogen bond effects on mol. dipole moments 2−77127
ion in dielectric medium, SCF Dirac-Slater calcs. 2−53403
ion-neutral system, bonding energies 2−67532
isotropically substituted molecules, effect of inaccurate assignments, by least squares method 2−46500
laminated Reissner plates, bonded by thin adhesive layer 2−41649
liquids, H bonded, review of i.r. and Raman spectroscopy relating to structure properties 2−43315
localized molecular orbital, symmetry in self-consistent field theory 2−59979
metal, close-packed, relation between cohesive energy and Debye temp. 2−60697
metal, cohesive force conjugate to uniform expansion 2−67929
metal-C, rel. to C content of metals 2−56917
methanol, in trialkylphosphines and CCL_4, H bonding, spectral study 2−46647
2-methoxyethanol, intramolec. H bond, determination from microwave spectrum 2−50098
methyl-substituted chloroaluminate ions, i.r. and Raman spectra, determ. of bonding and structure 2−77117
N-methylaniline, dissolved, low temp. i.r. study of self-association by H bonds 2−54540
methylphenylsilanes, hyperconjugation of S-H bonds, spectra obs. 2−50111
micas, H bonding from i.r. spectra study in OH vibr. region 2−48168
molecular shapes models, prediction of bond angles and bond lengths 2−50016
monoalkylbenzenes, conformational analysis 2−42953
monohalides, group III, character of molecular orbital 2−80027
$NaHF_2$, neutron diffraction data refined, location of H, thermal motion and F-F distance 2−77087
network model for mols. and solids 2−71773
network model of molecules and solids 2−77520
noble metals, cohesive props., rel. to equation of state 2−68063
nylon 6 fibres, bond rupture, reaction rate model of fracture 2−74854
orbital dependence of electronegativity, a basic problem 2−47176
organic donor-acceptor crystals, electrostatic binding energy by Ewald's method and charge transfer in lattices 2−67928
organophosphorus esters, n.m.r. spectra, peak doubling, H bonding 2−70788
oxamides and thio-oxamides, hydrogen bonding obs. 2−56252
oxides, perovskite struct., interatomic distances calc. based on deform. lengths of bonds 2−74720
oxyhaemoglobin and haem derivatives, SCC-EH-MO calc. on bonding and electric field gradient 2−60098
2(2′-oxyphenyl)-benztriazole derivatives, intermol. hydrogen bond form. 2−83334
peptide, SCF calculations of glycine and glycylglycine 2−56233
peptides, ab initio studies of H bonding, mutual orientation of peptide planes 2−46634
phenol-triethylamine complexes, H-bond polarity, effect of permittivity of medium 2−46621
phenysilane, hyperconjugation of Si-H bonds, spectra obs. 2−50111
polymer crystal, π-electron spectrum, effect of stochastic bond defects 2−47812
polymers, effect of form of inelastic deformation on hydrogen bonds 2−80119
polymers, radiation-induced rupture of stressed bonds caused by interaction with thermal electrons 2−47517
potassium hydrogen di-trifluoracetate, deuteron quadrupole coupling const. relationship 2−72528
purine aqueous solutions, i.r. spectra study of formation of strong polarizable H bonds with increasing protonation 2−50112
pyridinium-pyridine system, H-bonded, extended Huckel calculation 2−70789
random buckling behaviour, axially loaded cylindrical shells 2−41587
rare earth transition metal cpds., $CaCu_5$ type, valence bond form. 2−50559
refractory carbides, nitrides and borides, NASA research 2−64801
resonance integral-bond length relationship 2−50009
rutile, molecular charge distribs. K X-ray emission obs. 2−67930
salicyl aldehyde, structure of H bond from microwave spectra 2−43008
saturated molecules, Fourier component analysis of internal rotation potential functions 2−56208
semiconductor, diamond-type, phonon induced quadrupole potential 2−71772
semiconductor, non-crystalline, bond theory approach 2−57173
semiconductor glass, rel. to mag. susceptibility 2−61480
semiconductors, cubic, stress dependence of the Raman frequencies and elastic constants 2−84497
semiconductors, rel. to band structure, survey 2−81012
silica gel, absorpt. of electron pair donors, H bonding 2−77515

Bonds continued
silicate glass, rel. to effect of synthesis conditions on crystn. 2−64530
single, polarizability, Stark effect on nuclear quadrupole resonance 2−52984
steroids, influence of ring unsaturated position and delta eight double bond on mesophase 2−80458
styrene-butadiene rubber mixture, electron microprobe study of chemical bond 2−64536
ternary refractory carbide, rel. to thermodynamic props. 2−71652
thermoplastics, amorphous, hydrogen bonding influence on stress crazing and cracking 2−60908
thiazanes, i.r. absorpt. spectra rel. to H-bonding and mol. struct. 2−56261
thioamides, heterocyclic H-bonding formation of cyclic dimers 2−83318
thioamides 2−43011
three-bond fragments, proton spin-spin coupling, Dirac vector model and variational treatments 2−77050
transition metal difluorides, covalency parameters 2−77057
transition metal hydrides, review 2−77731
transition metal nitrides, rel. to microhardness, thermal expansion and elastic props. 2−61112
1,2,4-triazole free radical, determ. of hyperfine tensors for protons of hydrogen bonds 2−65394
triglycinefluoroberylate cryst., H_2 bonds and energies from l.f. Raman spectra 2−51357
triglycinesulphate cryst., H_2 bonds and energies from l.f. Raman spectra 2−51357
trimethyl(phenylethynyl)-silane, ^{13}C Fourier transform n.m.r. study, detection of ^{19}Si-^{13}C spin-spin coupling, bonding 2−83312
triterpenes, influence of ring unsaturated position and delta eight double bond on mesophase 2−80458
valence bond waefunctions, density matrices for 4 × 4 square planar net 2−52099
valence bond wavefunctions, reduced density matrices 2−49028
Van der Waals atrraction, role of surface plasmons 2−51088
water, H-band rupture mechanism of temp. effects on structure and kinetics 2−60417
water, near i.r. studies of structure in mixed solvent systems 2−50316
water-like particles in two dimensions, statistical mechanics of one-component systems 2−80449
Wurster's blue perchlorate, electrostatic binding energy using Ewald's method 2−67927
wurtzite type crystal, spontaneous distortion from tetrahedral struct., rel. to electron bonding 2−67981
XY_4 and XY_3 type mols., orbital valency force field, approx. to general valence force fields 2−70663
Ag, total energy, pseudopot. theory, applic. to binding energy 2−61137
AgBr crystals, outer shell overlap integrals 2−50558
AgCl crystals, outer shell overlap integrals 2−50558
AgF crystals, outer shell overlap integrals 2−50558
6Al-4V-Ti, surface embrittlement charact. during diffusion bonding 2−68160
Al, energy and struct. calcs., effect of statistical exchange approx. on pseudopotential calcs. 2−80960
Al compound, influence on X-ray K-satellite of Al 2−51360
Al_2O_3, alumina, phosphate bonded, strength props., elec. microscope obs. 2−77662
Al_2O_3, liq., covalent bonding correl. with phys. props. 2−43338
Al_2O_3, molecular struct. effects in Al $K\beta$ X-ray spectra in proton and alpha particle excitation 2−81381
AsIn, $AsI_3.3S_8$, determ. by Mossbauer effect of ^{129}I 2−78071
As_2S_3, vitreous, pyramidal apex bond angle distrib., n.q.r. obs. 2−57404
AsSI and AsSeI, vitreous and molten, chemical bond during transitions 2−84393
As_2Se_3 film, crystalline and amorphous, ion bombardment effects 2−60646
Au, total energy, pseudopot. theory, applic. to binding energy 2−61137
$B_{10}H_{14}$, bonding props. and valence structures, SCF study 2−64115
B_2H_6, B_4H_{10} B_5H_{11}, B_6H_{10} unique preferred localized valence structures 2−50023
B_2O_3, orders and indices from electron population analysis 2−70683
B_2O_3 glass, hydrostatically compacted, X-ray scatt., electron radial distrib. obs. 2−53527
$BaCl_2.2H_2O$, i.r. spectra, H bonds in H_2O 2−48170
BeB_2H_8, BeB_2D_8, BeB_2HD_7, determination from i.r. and Raman spectra 2−52994
Bi_3, determ. by Mossbauer effect of ^{129}I 2−78071
C-C in organic compounds, bond character 2−83287
C-F, partial double-bond character in CH_3F, CH_2 F_2 and CHF_3 2−43000
C-P, in methylenephosphorane, ab initio LCAO-MO-SCF calculations 2−56240
C, glassy, struct. 2−53529
C, glassy fibres, derived from phenolic resin, mech. props. 2−84100
CH radical, ab initio valence bond treatment 2−50025
CaF_2, ionicity, rel. to dispersion and absorpt. energies 2−44374
$Ca^{181}HfO_3$, perovskite-type, covalent bonding effects rel. to nuclear quadrupole interactions 2−72244
CdCN in Ar matrix, e.p.r. 2−50072
$CdCu_{1.5}Ga_{0.5}$, Laves phases, enthalpies of soln. and formation detn. 2−47692
CdTe, covalence character of chemical bonds, determination from mag. susceptibility meas. 2−61482
Ce film, core level binding energies, X-ray photoelectron spectra study 2−72096
Cl tetrahedral oxy-compounds, force constants and regularities of chemical bonding 2−70725
Cl_2, cryst., i.r.-active intermol. translational band intensities, intermol. bonding obs. 2−74967
^{35}Cl with B, C, N, P, and S, n.q.r. study 2−64112
Co compounds, chemical bonding study using X-ray photoelectron spectroscopy 2−53002
Co film, two-layer, bonding energy determ. 2−57298

Bonds continued
- Co(II) complexes with N,N′-ethylenebis(acetylacetoneimine), i.r. spectra, normal coordinate analysis 2—70695
- $Co(PO_3)_2$, molten, density measurements relation to bonding and coordination 2—84034
- Cr carbides, nitrides and borides, atomic interactions 2—48206
- Cr compounds, chemical bonding study using X-ray photoelectron spectroscopy 2—53002
- $CsPO_3$, molten, density measurements relating to bonding and coordination 2—84034
- $Cs_2[CuCl_4]^{2-}$, covalency and excited 4p states effects on 3d ground states of Cu^{2+} 2—84578
- Cu, charge density form factor, X-ray scatt. determ. 2—84251
- Cu, total energy, pseudopot. theory, applic. to binding energy 2—61137
- Cu (100) surface, CO weak adsorp., structure and binding 2—50538
- Cu alloys, influence on partial free enthalpy of formation of solid solns. and filling of 4s band Cu 2—80811
- Cu^{2+} tetragonal complexes, covalency effects in anisotropic h.f.s. 2—84580
- CuCl and CuBr, anomalous thermal expansion with i.r. spectroscopy 2—43993
- Cu(I) and (II) complexes with sulphur ligands, K- absorpt. edge shift depend. 2—56167
- Cu(II) complex, bond properties determ. using modified Pariser-Pole-Pople method 2—67471
- Cu(II) complexes, chromophore trans- CuN_2S_2, covalent bonding, e.s.r. and electronic spectra 2—46539
- Cu_3MX_4 (M=V,Nb,Ta; X=S,Se) 2—42888
- $D_3Co(CN)_6$, hydrogen bonds, total energy of ground state of system 2—42895
- EuTe, Eu_3Te_4, Eu_4Te_7, Eu_3Te_7, Mossbauer spectra, sublattice covalent bonding, isomer shift, internal mag. field at Te nuclei 2—54389
- F^--F^- interionic potential, computation using Hartree-Fock and semiempirical methods 2—74651
- Fe complexes, nitroprussides, bond strength between Fe atom and ligands obtained from ^{57}Fe Mossbauer effect 2—44352
- Fe compounds, chemical bonding study using X-ray photoelectron spectroscopy 2—53002
- GaAs, chem. shift in binding energies of Zn and Cd 2—65001
- GaAs, layer compound, chemical bonding rel. to empirical pseudopotential calc. 2—81016
- GaAs(P), ionicity, rel. to dispersion and absorpt. energies 2—44374
- GaP, chem. shift in binding energies of Zn and Cd 2—65001
- Ge covalent-metallic phase transition under pressure, theory 2—83886
- Ge III, polymorphs, distorted tetrahedral bonding, Raman scattering from phonons 2—72372
- Ge III band structure 2—80980
- Ge surface, dangling bonds, field ion microscopy at 80K 2—64554
- GeH_2Br and GeHBr, i.r. spectra obs. 2—61804
- Ge_xS_{1-x} alloys, covalent bonding 2—53536
- Ge_xTe_{1-x} alloy, amorphous, random covalent struct. model 2—60575
- H-bonded arsenates, EPR and ENDOR studies 2—68734
- H-bonded solvents, lattice models 2—41526
- H, polarizable, i.r. investig. for pKa depend. for aqueous solns. of protonated amines 2—68652
- H, role in formation of OH radicals from water of crystallization 2—81495
- H metallic phase, influence of expression for dielectric function in structure calcs. 2—77521
- $HBr.4H_2O$, solid and liquids, H-bonds, Raman and i.r. spectra 2—43314
- $H_3Co(CN)_6$, hydrogen bonds, total energy of ground state of system 2—42895
- HF-HCN dimer, H-bonding and structure, prediction by ab initio molecular orbital methods 2—80005
- H_2O, electrooptical parameters, H bond distortion 2—46548
- H_2O bond angle change effect on stretching frequencies 2—83266
- Hf_2S, metalic bonding, Brewer Engel correl. 2—47180
- ^{181}Hf cpds., ABO_3-type, perovskite-type, covalent bonding effects rel. to nuclear quadrupole interactions 2—72244
- HgCN in Ar matrix, e.p.r. 2—50072
- KBr(Cl)(F)(I), ionicity, rel. to dispersion and absorpt. energies 2—44374
- K_2CrO_4 struct. redeterm., effect of electrostatic crystal forces on observed bond lengths 2—77550
- KD_2PO_4, monoclinic, P-O bond lengths, X-ray determ. 2—64640
- $K_4Fe(CN)_6.3H_2O$, ferroelec., crystal chemistry of hydrogen bonds rel. to twinning and polymorphism, p.m.r. obs. 2—74655
- KHF_2, neutron diffraction data refined, location of H, thermal motion and F-F distance 2—77087
- KI:Tl covalency, overlap calcs. absorption spectra 2—61643
- K_2MnF_4, planar antiferromagnet, isotropic nature of Mn-F bond 2—54510
- β-K_2SO_4 struct. redeterm., effect of electrostatic crystal forces on observed bond lengths 2—77550
- KrF_2, ionic and covalent behaviour 2—83251
- La film, core level binding energies, X-ray photoelectron spectra study 2—72096
- $LiH_3(SeO_3)_2$, ferroelec., thermal expansion rel to band arrangement, -150 to +25°C 2—68253
- Li_2O-B_2O_3-GeO_2 glass, rules for struct. 2—47059
- Mg-Cu-Ni, Mg-Zn-Ni, Laves phases, enthalpies of soln. and formation detn. 2—47692
- Mg, energy and struct. calcs., effect of statistical exchange approx. on pseudopotential calcs. 2—80960
- MgCuGa, Laves phases, enthalpies of soln. and formation detn. 2—47692
- MgO:V^{3+}, covalency from model for effect of strains on e.p.r. spectrum 2—72495
- MgO, ionicity, rel. to dispersion and absorpt. energies 2—44374
- Mn compounds, chemical bonding study using X-ray photoelectron spectroscopy 2—53002
- $MoO_3.2H_2O$, role of hydrogen atoms in bonding, X-ray diffraction study 2—43583
- MoS_2, rigid layer lattice vibrations and van der Waals bonding 2—84194
- NH_3 ions, substituted, ^{14}N n.q.r. studies 2—42914
- NH_4Br:Cu^{2+}, covalency, core polarization 2—78154

Bonds continued
- NH_4HF_2, neutron diffraction data refined, location of H, thermal motion and F-F distance 2—77087
- NH_3...H-OH mol., hydrogen bonding 2—67475
- NO in X_3NO compounds, LCAO MO CNDO/2 study 2—42866
- N_4S_4, and $N_4S_4F_4$, electron delocalization, CNDO/2 calculation 2—77089
- Na, metallic, cohesive energy, Kohn-Sham self-consistent calc. 2—60698
- $Na_2B_4O_6(OH)_2.3h_2O$, kernite, charge distribution from analysis of X-ray data 2—50560
- tris-$Nd_2(SO_4)_3$, diffuse reflectance spectrum, meas. of bonding and screening parameters 2—61617
- Ni, rel. to preferential orientation of CO adsorption 2—50546
- Ni, with chemisorbed O, S, Se, orbital electron energy spectra 2—48328
- $Ni(C_5H_5)NO$, SCF-MO calculations 2—50064
- $Ni(CN)_4^{2-}$, SCF-MO calculations 2—50064
- $Ni_{1.2}Fe_{1.7}Sb_{0.1}O_4$, supertransferre d hyperfine fields and covalency at diamag. cations 2—48150
- Ni(II) complexes with N,N′-ethylenebis(acetylacetoneimine), i.r. spectra, normal coordinate analysis 2—70695
- Np, covalent model for nature of 5f bonding 2—84396
- OH groups, dependence of torsional vibration frequency on H bond energy 2—42857
- P tetrahedral oxy-compounds, force constants and regularities of chemical bonding 2—70725
- PH_5, MO calc. for idealized geometries of D_{3h}, C_{4v} and C_s symmetries 2—53035
- PH_5, nonempirical MO calc., intramolecular ligand exchange in phosphoranes 2—53033
- $(PNX_2)_3$ (X=halogen), gas phase electron diffraction determination of bond lengths and angles 2—53036
- PO in X_3PO compounds, LCAO MO CNDO/2 study 2—42866
- P_4O_{10} SCF calculations 2—60030
- P_4O_6, SCF calculations 2—60030
- $Pb^{181}HfO_3$, perovskite-type, covalent bonding effects rel. to nuclear quadrupole interactions 2—72244
- PbSe monocryst., heat treated, covalent, from mag. suscept. meas. 2—48035
- Pd(II) complexes with N,N′-ethylenebis(acetylacetoneimine), i.r. spectra, normal coordinate analysis 2—70695
- Pu, covalent model for nature of 5f bonding 2—84396
- S tetrahedral oxy-compounds, force constants and regularities of chemical bonding 2—70725
- SF_4, intermolecular bond strength 2—44381
- SbI_3, $SbI_3.3S_8$, determ. by Mossbauer effect of ^{129}I 2—78071
- Sc diatomic intermetallic, bond energies from dissociation energies of Sc monoaurides 2—50557
- Se film, crystalline and amorphous, ion bombardment effects 2—60646
- SeF_4, axial and equatorial bridging interactions 2—83265
- Si/Cs-O, neg.-electron-affinity surface obs., photoemission obs. 2—81185
- Si, bonding electron distrib., rel. to forbidden (442) refl. temp. depend. 2—83885
- Si, due to K electrons, Compton profile obs. 2—83882
- Si, hybridization of atomic orbitals at structural defects by tetrahedral bond rupture 2—81005
- Si and cpds., mol. orbital model interpret. of X-ray spectra 2—48210
- Si covalent-metallic phase transition under pressure, theory 2—83886
- Si III, polymorphs, distorted tetrahedral bonding, Raman scattering from phonons 2—72372
- Si III band structure 2—80980
- Si tetrahedral oxy-compounds, force constants and regularities of chemical bonding 2—70725
- SiC, self-bonded, texture and strength detn. to 1300°C in air and to 1750°C in argon 2—71393
- SiO_2, bond breaking, model 2—80656
- SiO_2, e.s.r. obs. of E'_s, dangling bonds and CO_2^- adsorbed radicals 2—71352
- SiO_2, noncryst., rel. to defect struct. 2—60596
- SiO_x, non crystalline, optical and bonding model 2—61656
- SiO_xN_y, non crystalline, optical and bonding model 2—61656
- Sm-Sn system, relative stability of intermetallics 2—47573
- Sm ionic, semicond. and metallic cpds., covalency effects on Mossbauer isomer shifts 2—48154
- Sn covalent-metallic phase transition under pressure, theory 2—83886
- Sn halides, pi bonding effects on relationship between Mulliken electronegativities and ^{119}Sn Mossbauer shifts 2—44359
- $Sn^{181}HfO_3$, perovskite-type, covalent bonding effects rel. to nuclear quadrupole interactions 2—72244
- Sr vanadates, strength of interatomic bonds, polarity 2—43589
- $Sr^{181}HfO_3$, perovskite-type, covalent bonding effects rel. to nuclear quadrupole interactions 2—72244
- Ta_2P, metallic bonding, Brewer-Engel correl. 2—47180
- Ta_2S, metallic bonding, Brewer-Engel correl. 2—47180
- Te glass system, rel. to glass formation 2—60599
- Te hexahalides, 5p shell holes rel. to ^{125}Te Mossbauer isomer shifts 2—61608
- TeF_4, axial and equatorial bridging interactions 2—83265
- TeO_2, amorphous and cryst., electronic bonding of Cu^{2+} 2—72501
- Ti carbides, nitrides and borides, atomic interactions 2—48206
- Ti_4O_7, metal-insulator transitions, charge localization 2—44087
- TiS, rel. to thermal expansion, 25-1300°C 2—54062
- TlBr(Cl), ionicity, rel. to dispersion and absorpt. energies 2—44374
- U, covalent model for nature of 5f bonding 2—84396
- V carbides, nitrides and borides, atomic interactions 2—48206
- V^{3+} complexes, trigonally distorted octahedral, lattice-ion interactions in the ligand field theory 2—81205
- V_4O_7, metal-insulation transitions, charge localization 2—44087
- W, (210) surface, CO adsorption, binding states 2—60692
- W, chemisorption states of CO, thermal desorp. spectra obs. 2—47173
- W surface, alkalis, rare gases and H_2 adsorbate structure 2—50554
- XeO_4, valence stretching force consts. and bonding determ. from i.r. and Raman spectra 2—80023
- Y diatomic intermetallic, bond energies from dissociation energies of Sc monoaurides 2—50557

Bonds continued
- Y film, core level binding energies, X-ray photoelectron spectra study 2—72096
- Yb-Sn system, relative stability of intermetallics 2—47573
- ZnSe, ionicity, rel. to dispersion and absorpt. energies 2—44374

Bone *see Materials*

Bootstrapping
- coupling parameter sum rule, unitarization of dual models and bootstrap 2—55834
- diffraction dissociation, inclusive bootstrap constraints 2—59475
- finite energy sum rules bootstrap rel. to generalized interference model 2—73792
- hadronic internal symmetry groups deform. of nature from duality, absence of exotic resonances, quark diagrams 2—76637
- hadronic mass spectrum, analytical soln. 2—66991
- hadronic matter, ultradense, properties 2—55828
- inclusive bootstrap, deduced by diagonalization of inclusive sum rules 2—66992
- inclusive single-particle spectra calc. using thermodynamic model 2—79549
- inelastic hadronic processes, threshold enhancements and statistical bootstrap 2—70189
- intermediate-energy dynamics based on average nonlinear duality, calcs. of Pomeranchuk residue at $t=0$ 2—66986
- multiperipheral bootstrap model, exptl. consequences 2—79541
- multiperipheral model, self-consistent diffraction 2—59502
- multiperipheral model, statistical generalization of one-dimensional version 2—70197
- Odorico's bootstrap extension for ω-φ mixing and photon interactions 2—73836
- partial bootstrap model for hadron structure and parton-parton interaction 2—66950
- Pomeranchuk singularity, diffractive-multiperipheral model, relation to inclusive expts. 2—45907
- Regge exchange amplitude, ρ-P cut, partial bootstrap and phenomenological pole 2—59496
- Regge trajectories, indefinitely rising, bootstrap mechanism 2—45905
- spin 0-spin 0 and spin $^1{}_{.2}$-spin 0 amplitudes, summing of partial wave series 2—76825
- statistical model, inclusive distribution in dual resonance 2—70175
- statistical model, modification of Fermi model for high energy hadron collisions, expts. on NN annihilation ar rest. 2—82703
- statistical model for hadrons, new statistical treatments of hadron interactions, analogies with nuclei 2—82702
- strong bootstrap model, rel. to thermodynamic inclusive single particle spectra 2—82706
- K*, bootstrap calculation using effective-potential method 2—45989
- Kπ phase shifts, duality structure 2—59543
- π spectra energy depend., fireball model 2—82751
- $\pi\pi$ phase shifts, duality structure 2—59543
- $\pi\pi$ scattering models, review 2—45978

Bordoni effect *see Acoustic wave propagation/ultrasonic; Damping; Internal friction*

Boron
- anomalous diffusion, in Si 2—50694
- atom, electron impact ionization, calc. for $1s^22s^22p$ configuration 2—46451
- atom, far-u.v. absorpt. spectra analysis 2—67388
- atom, h.f.s. in ground multiplets, mag. dipole radial parameters 2—70576
- atomic projectile interaction with Hg, pot. cross sections 2—77015
- chemical analysis in aqueous and solid samples, activation analysis by Cherenkov counting of 22 ms ^{12}B 2—51488
- content determ. in B-Al alloy samples, Boreal array 2—63976
- control rods of ^{10}B-stainless steel, effect of B concentration gradient on thermal reactor performance 2—76948
- diamond:B, e.p.r. of free and bound holes 2—81458
- diffusion, in Si, effect of mask edges 2—54205
- diffusion, in Si, from doped oxide layers 2—64677
- diffusion, in Si, using B_2H_6-CO_2 system 2—43645
- diffusion, in Si-SiO_2 system 2—68037
- diffusion, in SiC, distrib., elec. cond. and p-n junc. obs. 2—74797
- diffusion coeffs. in Si 2—56745
- diffusion in Si, from localized surface source 2—56739
- diffusion in Si, induced defect struct., X-ray diffraction topography 2—77567
- diffusion in Si, Si-B phase influence 2—77523
- doping of diamond, elec. resistivity obs. 2—68396
- epoxy composite, stress wave dispersion 2—47743
- exchange between sea and atmosphere 2—57851
- fibre reinforced Al composite, fatigue 2—56976
- fibre/Al_2O_3 composite, high temp. bearing characts. 2—47558
- filament, chem. vap. deposited on C monofilament, compatibility problems 2—53956
- filaments embedded in Al alloy, initial yield surface 2—66507
- glass, refractive index control by selective applic. of neutron irradiation 2—59226
- implantation in Si, channelling and anomalous diffusion effects on charge carrier distrib. 2—47432
- implantation profile in Si, calc. 2—74795
- impurity conc. profile determ. techniques 2—71505
- interstellar, production by cosmic rays 2—84970
- interstellar possible production by low energy cosmic rays 2—62593
- ions, implantation and channelling on Si, computer simulation 2—47439
- isotope separation, ion exchange process 2—64082
- K-shell fluorescence yield by synchrotron radiation 2—77012
- low concentration diffusion in Si, under sealed tube conditions 2—74792
- magnetic susceptibility 2—77987
- monograph, covering modern use 2—65358
- Mossbauer effect of ^{57}Co and ^{57}Fe in β-rhombohedral phase 2—61603
- neutron activation analysis using (n, α) reaction 2—84686
- neutron filter for nondestructive activation anal. 2—72598
- predeposition into Si 2—71503
- quantitive det. in various matrices using nuclear track technique 2—48364
- rhombohedral, $\alpha \to \beta$ transform., electron diffr. study 2—47680

Boron continued
- rhombohedral, β-phase, carrier mobility in intrinsic cond. region 2—75090
- in steel, segregation 2—47623
- tracer technique for determ. material movement 2—65421
- W substrate, adsorbate induced work function changes 2—72084
- water, borated, neutron collision rate calc. 2—70501
- Al-9.5 wt.%Mg:B alloy, mech. props., fracture toughness, cracking effect of alloy in additions 2—47546
- B-Al composite, deform. and failure under transverse loading 2—84110
- B-epoxy laminated composite plates, holographic stress analysis 2—78895
- in Ge, g-factors, Zeeman effect obs. 2—54402
- in Mo, effect on struct. and mech. props. 2—56943
- Si:B, diffusion by using emulsion type doped oxide 2—71517
- Si:B, implantation profiles determ. by secondary ion mass spectrometry 2—74794
- Si:B, ion implanted, conc. distrib. by (n,^{4}He) nuclear reaction 2—56743
- Si:B, ion microprobe analysis of implanted ion distribs. 2—64674
- Si:B, lateral spread of implanted ions, obs. by junction delineation 2—71508
- Si:B, shear deform. pot. consts. of B acceptors ground state, piezospectroscopy obs. 2—75306
- Si:B implanted, photocond. obs. 2—44126
- Si:B impurity enhanced diffusion 2—50693
- ZnS:B, luminesc., 400-800 nm, 110, 295 and 430K 2—75322

Boron compounds
- binary alloys, phase diagram, review 2—50957
- borate glass, He migration 2—53759
- borate glasses, non-destructive method for ceric/cerous ratio determ. 2—48362
- borate minerals and rocks, visible and near i.r spectra 2—72672
- borides, high temp. coatings, deposition from fused salts and by ion plating 2—50860
- borosilicate films, current-voltage characts. 2—47950
- BORSIC aluminium fibre-matrix interfacial region, exam. 2—64546
- chemistry conference in Prague 21-25 June 1971 2—51421
- epoxy composites, irrad. in nuclear reactor, strength 2—80801
- glasses, refractive index variation with hydrostatic press. up to 7 kbar, prep. history and structure 2—68595
- monograph, covering modern use 2—65358
- Ag_2O-B_2O_3 glass system, n.m.r., B sites obs. 2—65342
- B:Fe, crystallographic positions of Fe, isomer shifts, Mossbauer obs. 2—51305
- B-Al alloys, determ. of B content, Boreal array 2—63976
- B-Hf-Nb alloy, phase equilibria, at 1400°C, X-ray obs. 2—43912
- B-SiC alloy, phase composition rel. to press., 50-60 kbar 2—53996
- B-Ta-Cr alloy, phase equilibria, at 1400°C, X-ray obs. 2—43912
- BAs, prep. from gas phase 2—74669
- BAs, thermal decomp., mass spectrometry, X-ray and DTA studies 2—48321
- $B_{48}B_2C_2$, tetragonal phase, prep. and cryst. struct. 2—74723
- $B_{48}B_2N_2$, tetragonal phase, prep. and cryst. struct. 2—74723
- BC neutron absorber rods, modelling of swelling and gas release 2—52861
- B_4C, neutron irrad. damage, electron microscope obs. 2—47369
- B_4C, neutron radiation induced defects, transmission e. microscope obs. 2—67355
- B_4C, thermal reactor irradiated, empirical He release 2—76954
- B_4C irradiation-induced dimensional change 2—76949
- B_4C irradiation in fast neutron spectra, meas. of pellet density, swelling, gas release, thermal conductivity 2—83116
- B_4C neutron absorber in fast and thermal reactors, swelling gas release and structural integrity 2—83115
- BCl_3, i.r. double resonance, relaxation obs. 2—46526
- B_2Cl_4 vapour, obs. of torsional mode in Raman spectrum excited by Kr laser 2—52993
- BF, molecular vibration effect on apparent bond lengths 2—56136
- BF_3, ambiguities in harmonic force fields 2—50063
- BF_3, fluorescence surrounding CO_2 laser induced sparks 2—74440
- BF_3, nucl. spin relax. obs. of spin-rot. interaction 2—56200
- BF_3 i.r. spectra, obs. of l-type resonances in Q branches of ν_4 bands, determ. of cubic potential consts. 2—70682
- BF_3 tubes, correction factors for neutron monitoring 2—59636
- BH, calc. of force constants by Hellmann-Feynman theorem 2—80055
- BH, computation of force constants and dipole moment derivatives using Hartree-Fock 2—50052
- BH, self-consistent procedures for generalized valence bond wavefunctions 2—53012
- BH_2, ab initio calcs. including electron correl. of lowest states 2—80011
- BH_2, structure of transition dipole moment 2—80025
- BH_n series, generalized valence bond approach 2—59991
- $B_{10}H_{14}$, SCF study 2—64115
- B_2H_6, B_2D_6, potential function for ring puckering vibration 2—74256
- B_2H_6, B_4H_{10} B_5H_{11}, B_6H_{10} unique preferred localized valence structures 2—50023
- B_2H_6, molec. properties from minimum basis set and extended Slater orbital wave functions 2—64114
- B_2H_6 Slater basis set difference density maps, minimum and expanded, comparison 2—77088
- B_2H_h, X-ray diffr. two-centre formalisms in least-squares refinement 2—83913
- n-B_9H_{15}, resolution enhancement in partially relaxed Fourier transform ^{11}B n.m.r. 2—56521
- $B_{10}H_{10}D_4$, $B_{10}H_4D_{10}$, ^{2}H n.m.r., quadrupole coupling constants 2—44461
- BH_3NH_3, SCF calcs. of internal rotation barrier and its derivatives 2—42873
- BH_3.CO, electronic structure and conformation 2—46527
- BN, band struct. and optical props., pseudopotential calc. 2—61345
- BN, compact specimens, thermal cond., 100-1000 K 2—47761
- BN, cubic, cryst. growth, pertinent phase equilib. in Li-B-N system 2—50970
- BN, energy spectrum and cryst. fine struct., X-ray studies 2—75026
- BN, hexagonal, energy band calcs. using tight-binding approx. 2—68287

Boron compounds continued
BN, hexagonal, paramag. centres, thermolum., thermally stimulated currents, e.p.r. 2−74804
BN, hexagonal, rigidity and limiting strength, comparative estimates 2−47475
BN, hexagonal, thermolum. and e.s.r., paramag. centre identification 2−72430
BN, hexagonal to cubic transform., synthesis at high press. 2−83903
BN, variational calc. of $A^3\pi$ excited state configuration using McWeeny's SCF method 2−70681
BN energy band struct., tight binding approx., optical absorpt. 2−84234
B_xN, tetragonal, derived from icosahedral frameworks 2−50572
$(BNH_2)_x$, mean-square amplitude of vibration detn. 2−80021
$B_3N_3H_6$, symmetry-forbidden ${}^1A_2'$-${}^1A_1'$ transition analysis 2−70684
B_2O_3-BaO-Fe_2O_3 glass, microstruct., ultrastruct., mag. props. 2−56558
B_2O_3-GeO_2 glass, n.m.r. of ${}^{11}B$ 2−54506
B_2O_3-Li_2O-H_2O system borate hydrates, cryst. chem., equil. 2−47181
B_2O_3-MgO, phase relations determined by quenching 2−74936
B_2O_3-MgO system, phase relation obs. using thermobalance 2−73283
B_2O_3-Na_2O(BaO)(Bi_2O_3) glasses, stratification effects on comp. depend. of elasticity modulus 2−47478
B_2O_3-P_2O_5-Cs_2O glass, struct., e.p.r. obs. of Cu(II) paramag. centres 2−48291
BO_2, fluorescent band enhancement, chemiluminescent reaction of O with triethyl boron 2−44475
BO_2^-, in KBr, KCl crystal, molecular force constants meas. 2−42871
B_2O_3, apex angle in C_{2v}-'V' struct. 2−70683
B_2O_3, glass-forming, He migration 2−50707
B_2O_3 glass, diffusion of Ar and Ne, mass spectrometry obs. 2−53758
B_2O_3 glass, hydrostatically compacted, X-ray scatt., electron radial distrib. obs. 2−53527
B_2O_3 glass, n.m.r. powder pattern, graphic analysis in the presence of quadrupole interactions 2−48300
B_2O_3 glasses, photo- and X-ray luminescence, obs. of luminescent centres 2−84547
BP-P system, h.p. phase equil. 2−50956
BP, band struct. and optical props., pseudopotential calc. 2−61345
BP, growth by closed tube chem. transport method 2−74670
BP, heat of formation, calc. from heat of reaction $9BCl_3.PCl_5$(s) 2−48330
BP, single cryst. synthesis 2−50567
BP layers, vapour growth using open and closed tube processes 2−50486
B_xP, tetragonal, derived from icosahedral frameworks 2−50572
BS, e.s.r. at 4K, g tensors, hyperfine structure const. 2−80030
${}^{10}BF_3$, interference effects for spin-lattice and spin-spin relaxation 2−72506
${}^{10}BF_3$ neutron detector, end window, multifilament use with time-of-flight spectrometer 2−59612
$Ba_2KNb_5O_{15}$, crystallographic, dielec. and nonlinear optical props. 2−75251
BaO-B_2O_3-Fe_2O_3 glass, elec. and mag. props., microstruct. effects 2−65113
Cr-Ni-B system, isothermal section at 800°C 2−61044
CrB, thermal emission properties, obs. 2−44191
Er-B system, phase diagram and props. 2−50964
Fe-B-metal melts, mag. behaviour 2−72138
Fe-Mn-B-C alloy, struct. and strength 2−56941
Fe_2O_3-B_2O_3, phase relations rel. to applic. to $FeBO_3$ crystal growth 2−50594
Gd-B system, phase behaviour 2−50969
MgO-B_2O_3, system, phase relations, quenching method 2−57031
Na_2O-B_2O_3-Al_2O_3, nabal glass, self-diffusion of Na ions and interdiffusion coeffs. 2−60832
Na_2O-B_2O_3 system, glassy and crystalline compounds, n.m.r. spectra, structural obs. 2−48301
Ni-B electrolytic coatings, particle distrib., heat treatment effects 2−77730
Ni-B thin films, electrical conductivity 2−77860
PbO-Al_2O_3-SiO_2-B_2O_3 glass, between metal electrodes, memory effect 2−71915
Re-Al(Si)-B systems, phase equilib., X-ray study 2−64822
SiO_2-B_2O_3-Na_2O-Al_2O_3 system, comp. fluctuation and phase decomp. 2−53543

Borrmann effect *see X-ray diffraction*

Bose gas *see Quantum fluids/boson systems*

Bosons
see also Gravitons; Internal bosons; Photons; Quantum fluids/boson systems; Statistical mechanics/quantum
dually charged particles and dual invariance, classical description 2−52539
Goldstone, of broken scale invariance, ε(700) meson 2−45982
Goldstone, rel. to realisation of scale and chiral SU(3) × SU(3) invariance 2−59386
missing mass spectrum rel. to internal hadron struct. 2−55829
non-uniform broadening of spectral lines, effect on formation process of boson avalanches 2−66906
one boson exchange potential in Λp interaction 2−82783
pair creation in alternating external field 2−42318
scalar, trilinear coupling in small mass limit, S-matrix and field-theoretical arguments 2−59387
spectroscopy, review of current exptl. problems 2−76647
spin zero, finite quantum electrodynamics 2−66901
spinless boson creation and annihilation operators, tensorial character 2−59909
two-level magnetic system damped by interaction with bosons, transverse susceptibility 2−49022
urfermion represent. of boson creation and annihilation 2−79470
weak scalar, production and decay in very high energy cosmic ray interactions, muon ang. distribution 2−70278
NN elastic scattering, one-boson exchange model with amplitudes constructed from Veneziano functions 2−45994

Boundary layers
— 2−67786

Boundary layers continued
air, heat transfer to transpired turbulent layer 2−45577
air over heated horizontal plane, mixed convection 2−80391
air-water interface, thermal boundary layer, temp. difference 2−65625
atmosphere, vorticity flow, temperature stratification 2−72774
atmosphere over sea, time-dependent model of electrode effect 2−65785
atmosphereic stratified Ekman boundary layer instability and internal gravity wave generation 2−57958
atmospheric, aerodynamic characteristics 2−68899
atmospheric, description, review 2−65694
atmospheric, He gas, instantaneous point source diffusion 2−72780
atmospheric, stability, heat and momentum fluxes, during dry unstable conditions 2−75529
atmospheric, static pressure fluctuation measurement, instrumentation 2−72755
atmospheric, vortex streets wind tunnel simulation 2−72771
atmospheric ${}^{222}Rn$ and daughter ions, vertical profile 2−54870
atmospheric geostrophic drag, heat and mass transfer coefficients for the diabatic Ekman layer 2−57957
atmospheric planetary, slant path scintillation of laser beam 2−81675
atmospheric surface layer, turbulent diffusion 2−62092
atmospheric surface winds, adaptation of marine model 2−65699
atmospheric turbulent Ekman boundary layer, laboratory study 2−54828
atmospheric type boundary layers with large Reynolds number 2−43235
atmospheric vortices, tropical cyclones, dynamics 2−78367
axial flow turbomachines, annulus wall boundary layer development 2−77351
axisymmetric bodies at small angles of attack 2−50243
axisymmetric turbulent boundary layers in zero pressure-gradient flows 2−46691
Benard convetion with black and mirror boundaries, radiative stabilization 2−68890
benzoic acid/water, mass transfer coeffs. on flat plate by parallel channel flow and turbulence promoter 2−67601
binary diffusion of jet embedded in boundary layer 2−71072
boundary layer eqn., solns., appl. for non-zero wall vel. 2−83458
Boussinesq fluid, temperature adjustment process via buoyancy-induced meridional circulation 2−67742
centrifugal chamber, flow calc. 2−71126
characteristcs in liquids, determ. by solution of solid-method 2−80426
coastal upwelling layers in wind-driven ocean 2−78237
compressible, stability at subsonic velocities 2−64247
compressible turbulent heat transfer to rough surfaces in pressure gradient 2−56425
compressible unsteady boundary layer eqns., 3D soln. 2−83680
continuum gas flows over heated sphere, kinetic effects 2−80403
convection on vertical plate with blowing and suction 2−45591
cylindrical flare bodies, in supersonic flow 2−77359
deformation of velocity profile in turbulent boundary layer in water and oil 2−74492
development in flow in inlet region of a channel, effect of injection 2−64229
displacement thickness across isothermal laminar axial flow in annulus with rotating inner cylinder 2−43075
Ekmans non-linear boundary layer in deep sea, theory 2−51538
exhaust plume interactions at supersonic speeds 2−56423
flat plate boundary-layer transition in supersonic wind tunnels 2−43248
flow, laminar, three dimensional, calc. 2−43066
flow across gas dynamic discontinuity vorticity and current density jump 2−83644
flow and heat transfer on flat plate normal to two-dimensional laminar jet from nozzle of finite height 2−77224
flow behaviour in pre-separation zone of laminar boundary layer, effect of free-stream variables and wall temperature 2−60146
flow development, travelling shock waves 2−80211
flow in diffusers for centrifugal turbomachines 2−80383
flow in ducts, numerical predictions 2−70843
flow of fluid film on flat plate at zero incidence receiving a single free jet 2−43070
flow of laminar, incompressible jet along a parabola 2−46900
flow on circular cylinder moving in fluid at rest 2−83477
flow over flat plate in entrance region, variational method, hybrid computer soln. 2−67572
flow past circular cylinder, incompressible laminar boundary layers, curvature and displacement speed effects 2−74331
flow past magnetized plate, mag. field oscillations effects 2−83530
flow past spheres at very high Reynolds numbers, laminar to turbulent transition 2−67750
flow through contractions, numerical model 2−77377
flows, hydrodynamics stability analysis 2−77208
flows, inverse problem, numerical computation 2−67576
fluid, micropolar, unsteady boundary layer flow along an infinite plate 2−80165
free shear layers, instability considerations 2−80198
ground-atmosphere thermal boundary layer structure, transient variation 2−66175
growth, on hemisphere on infinite plane 2−43283
headpieces conically converging, input angle and length effect on flow coefficient 2−83446
heat transfer, improved Lighthill analysis 2−45574
heat transfer with dissipation, surface curvature effects for large Prandtl no. 2−76219
heated ellipsoid of revolution, steady laminar free convection boundary layer 2−56286
high mass transfer rates, variational analysis from spherical particle boundary-layer injection suction considerations 2−77397
highly accelerated, reversion from turbulent to laminar flow 2−77191
hypersonic boundary-layer transition obs. using hot wire anemometry 2−60328
hypersonic laminar, of ideal dissociating gas, analysis of structure for frozen and equilibrium flows 2−67698
hypersonic model flow with strong shock waves 2−83686

Boundary layers continued
- hypersonic transitional boundary layers, space-time correlation meas. 2−60329
- hypersonic turbulent boundary layers structure 2−50247
- hypersonic unsteady compressible boundary layer depend. on Prandtl number 2−56416
- near impeller inlet of centrifugal turbomachine, absolute flow obs. 2−80381
- incompressible flow, instabilities in limiting laminar layers 2−43069
- incompressible unsteady, at flat plates and cylinders 2−83475
- integration of boundary layer eqns. through region of reverse flow 2−43219
- interaction with shock waves, effects of transition 2−43053
- ion acceleration at plasma boundaries, soln. of Poisson's equation 2−77263
- ion in plasma, on probes 2−56338
- jet, axisymmetric free laminar, power-law fluid, solution of boundary layer equations 2−60170
- Knudsen layer over solid, kinetics of evaporation 2−77465
- lake coastal, for finite vertical Ekman numbers 2−57909
- Lake Ontario, coastal boundary layer in summer-fall regime 2−65622
- laminar, along infinite porous plate, in presence of transverse magnetic field 2−60204
- laminar, developed within unsteady expansion and compression waves 2−46808
- laminar, on rotating sphere 2−80185
- laminar, separated, mass flow rate and mean density obs. 2−46820
- laminar, separation obs. in water tunnel using Schlieren technique 2−67760
- laminar, simple quadrature method for computing 2−74315
- laminar, stability on concave wall in presence of mag. field 2−80221
- laminar, with continuous or local injection and variable wall temp., analytical soln. 2−83688
- laminar, with large injections, eqn. soln. 2−83471
- laminar boundary layer equations from differential- difference method 2−80398
- laminar boundary layer on rotating round-nosed blade 2−43062
- laminar compressible unsteady, numerical calculations 2−46673
- laminar flat plate, nonequilibrium, dissociating, integral method 2−46819
- laminar flow past bluff body with separated wake 2−46675
- laminar hypersonic interacting layers, subcrit. branching in strong interaction regime 2−83691
- laminar in model for turbulent heat transfer to non-Newtonian liquids 2−50297
- laminar mixing of two uniform parallel semi-infinite streams 2−77227
- laminar thermal boundary layers on continuous surfaces, heat transfer characteristics 2−41849
- laminar transitional and turbulent flow, compressible nonadiabatic boundary layers calc. 2−70861
- laminar two-phase flow over flat plate, Karman- Pohlhausen approx. 2−46822
- laminar without pressure gradient, computation of skin friction and adiabatic wall temperature 2−53129
- laminer and turbulent flow theory of small disturbances 2−77187
- laplace's equations and elasticity theory application 2−82309
- laser interferometer, boundary layer study in fluids 2−59228
- longitudinal vortices growth with time along concave walls 2−43059
- magnetic, along curved interface between two opposing fluid streams carrying oppositely directed mag. fields 2−80225
- MHD, flow meas., laser Doppler velocimeter 2−80217
- MHD, interaction with weak shock waves 2−50174
- MHD, laminar, during blowing and suction 2−67614
- mixing layer, solns. by Blasius diff. eqn. 2−46656
- molecular gas radiation, effect of nongray self- absorption by cold boundary layers 2−77367
- momentum transfer between rotating cylinders, narrow fluid gap problem 2−46692
- napthalene/air, mass transfer coeffs. on flat plate by parallel channel flow and turbulence promoter 2−67601
- naturally convected, aerosol transport 2−67786
- near wake of a slender body, decay rate of turbulence 2−56411
- near-wall collateral flow in three-dimensional turbulent boundary layers 2−43063
- non-Newtonian power-low fluids, boundary layer with arbitrary pressure gradients 2−60147
- non-stationary axially symmetric motion of incompressible fluid, time-periodic solns. 2−64241
- in nozzle of hypervelocity wind tunnel 2−67731
- numerical methods for 3 dimens. layers 2−53266
- obstacle in nonuniform motion, solution of three-dimensional laminar boundary layer equation 2−53133
- Oseen solution, modified, extension for laminar viscous flow past a semi-infinite plate 2−83452
- parabolic flow, response of heat transfer from moving flat plate 2−55581
- paradichlor benzene/air and ammonia/air, mass transfer coeffs. on flat plate by parallel channel flow and turbulence promoter 2−67601
- partial differential equations, method of solution 2−53119
- plane-parallel symmetric, form. during sudden occurrence of motion 2−67584
- planetary, air trajectories, det. from tetroon flights 2−57965
- planetary, barotropic, universal profiles 2−51567
- planetary, convective baroclinic, wind field structure 2−51609
- planetary, diurnal wind variation 2−78365
- planetary, eddy viscosity, baroclinicity 2−84786
- planetary, neutral and unstable, numerical investigations 2−44672
- planetary, radiometric obs. of vertical temp. profiles 2−51584
- planetary, steady neutral, forced by horizontally non uniform flow 2−62642
- planetary atmospheres, baroclinic effects on resistance law 2−84784
- plasma cord, displacement with longitudinal current 2−70883
- plume induced boundary layer separation in rocket engines 2−53308
- polyacrylamide aqueous soln., pulsation velocity in turbulent boundary layers 2−74491

Boundary layers continued
- porous convection, variational problem 2−67820
- power-law non-Newtonian fluid on slender cylinder 2−67566
- pressure gradient effects on profiles in wind tunnel 2−83662
- real gases, laminar flow on flat plate, local heat transfer 2−60369
- Reynolds stress near wall in turbulent boundary layer flow 2−77260
- rough and smooth wall layers, statistical props. of turbulence 2−77180
- second order effects, for large injection or suction 2−77182
- separation on slender cone at angle of attack 2−56409
- separation patterns over inclined body of revolution 2−77215
- separation process, incompressible flow past parabola at angle of attack 2−46690
- sharp-cone equations, solution in plane of symmetry 2−67560
- ship hydrodynamics, theoretical models, review 2−77379
- shock tubes, conical, boundary layer closure 2−55561
- side-wall, in rotating axial flow 2−83460
- slightly viscous fluids, evaluation of iterated parameters for boundary vorticity 2−53135
- slow-moving, equations of motion in rotating fluids 2−53142
- solutions, boundary layer props., capillary osmosis 2−46902
- space shuttles, aerodynamic heating, surface oil flow patterns 2−83679
- stability for gas flow over porous surface 2−64377
- stagnation point viscous flow modification by thin plate 2−46668
- stratified, rotating, stability problem, applic. of shooting method 2−67575
- streaminf fluid, deformation of free surface when a flat plate floating on it is suddenly stopped 2−83453
- subsonic and supersonic flow past wavy wall 2−56408
- supersonic, turbulent in adverse pressure gradient 2−46806
- supersonic nozzle, turbulent boundary layer meas. with and without wall cooling 2−53287
- supersonic turbulent, in adverse pressure gradient, data analysis 2−56426
- surface, wind profile 2−84782
- surface reactions in flowing layer 2−68769
- surface waves on water with depths less than boundary layer thickness 2−74503
- suspension of particles, convective diffusion for case of Stokes flow of fluid 2−64481
- Sweet's mechanism for mag. flux destruction 2−67612
- terrestrial mantle, upper, temp. gradient in boundary layer 2−57493
- Texas coastline, surface roughness and internal boundary layer 2−65708
- thermal convection in horizontal fluid layer, volumetric energy sources 2−80429
- thermal laminar with arbitrary surface temp. distrib., exact solutions 2−60150
- thermodynamic theory for uni-phase, -component fluids 2−82382
- thick, generation to simulate shear and turbulence props. of Earth's wind boundary layer in wind tunnel 2−80384
- thin layer approx. for mass transfer from bubble in non-Newtonian fluid 2−53376
- three dimensional disturbances in boundary layer along concave wall 2−74495
- three dimensional with heat transfer, iterative calculation 2−53275
- three phase media, motion in round cylindrical tube 2−43072
- three-dimensional stagnation point flows, heat and mass transfer from foreign gas injection 2−64370
- three-dimensional turbulent, low-speed, flow characts. 2−70859
- trade-wind profile and shearing stress on tropical windward coast 2−44706
- transformation of eqns. for compressible layers, Stewartson type 2−80194
- transition, turbulence and pressure gradient effects 2−50152
- transition from laminar to turbulence at supersonic velocities over parabolic wing 2−64376
- transition induced by two dimensional roughness element 2−50157
- transition layer effects in gyrotropic and nongyrotropic media 2−69820
- transpired turbulent velocity and shear stress distrib. 2−46688
- turbulence fluid near wall, stat. analysis by conditional sampling 2−83430
- turbulent, 3-dimensional, calc. by explicit finite-difference scheme 2−46661
- turbulent, air flow over sudden change of surface roughness, numerical computation 2−48480
- turbulent, along curved surfaces, flow characts. 2−67602
- turbulent, analysis for incompressible axial flow past a long cylinder 2−46689
- turbulent, anomalies in anemometer obs. 2−80406
- turbulent, application of Reichardt model 2−53304
- turbulent, at low Reynolds number 2−60126
- turbulent, calc. 2−74305
- turbulent, discontinuity in wall temp. and concentration, heat and mass transfer 2−53274
- turbulent, effects of injection through porous surface 2−74458
- turbulent, flow, effects of strong axial pressure gradients 2−83481
- turbulent, flow along circular cylinder, mean velocity profile 2−70835
- turbulent, flow separation, model 2−43084
- turbulent, free boundary obs. 2−83433
- turbulent, friction in gas saturated liquid 2−53375
- turbulent, highly nonequilibrium, velocity and shear stress obs. and calc. 2−80214
- turbulent, in supersonic nozzles 2−71071
- turbulent, incompressible shear stress distrib., in air flow 2−60333
- turbulent, influence of uniformly sheared free stream 2−77353
- turbulent, interaction with shock wave on blunted compression surface 2−53315
- turbulent, interactions of shock wave, pressure fluctuation 2−43257
- turbulent, intermittent nature 2−77183
- turbulent, intermittent phenomena, theory and analog computer obs. 2−43079
- turbulent, intermittent structure of wall region 2−77181
- turbulent, large Reynolds number, asymptotic expansion of eqns. of motion 2−74330
- turbulent, nonlinear panel response, vibration of flexible elastic plate 2−71090

Boundary layers continued
- turbulent, on porous plate, meas. in aerodynamic tunnel 2−83445
- turbulent, on yawed flat plate 2−53319
- turbulent, response to step change in surface roughness, rough-to-smooth 2−50248
- turbulent, separation in strong adverse pressure gradients with injection through porous flat plate 2−74317
- turbulent, separation influenced by blowing 2−46810
- turbulent, supersonic, impact probe displacement 2−46815
- turbulent, supersonic, incipient separation, heat transfer 2−71070
- turbulent, three dimensional, hodograph models for cross flow velocity components 2−67587
- turbulent, three dimensional, wall jet growth 2−77200
- turbulent, three-dimens., behind yawed separation bubbles, flow props. 2−67699
- turbulent, time scales and correlations 2−64403
- turbulent, two dimensional, in increasingly adverse pressure gradients 2−43086
- turbulent, uniform mass transfer including low Reynolds numbers 2−43064
- turbulent, wake hypothesis 2−43083
- turbulent, with foreign gas injection, compressible, numerical soln. 2−67718
- turbulent, with heat transfer and press. gradient using compressibility transform., flow characts. 2−70862
- turbulent, with heat transfer and press. gradient using compressibility transform., flow characts. 2−70864
- turbulent and laminar, development on circular cylinder, separation bubbles 2−80437
- turbulent compressible, calculation method with heat transfer 2−43061
- turbulent flow, memory effect due to axial variation of meas. velocity gradient 2−77185
- turbulent flow model 2−77190
- turbulent flow over surface distorted by water waves 2−84717
- turbulent meas. of Reynolds shear stress fluctuations 2−64385
- turbulent on flat plate, wall heat flux obs. 2−43082
- turbulent over sloping underlying surface 2−72785
- turbulent pressure excitation, response of finite periodic beam 2−76358
- turbulent shear flow, conditional sampling 2−70860
- turbulent shear stress, calculation method 2−67588
- turbulent swirling flame flow, inverse solution method 2−46671
- turbulent with mass transfer, data survey 2−43055
- turbulent with positive pressure gradient and injection 2−74328
- two dimensional, in free stream which oscillates without reversing 2−80172
- two-dimensional turbulent jet attachment on plane wall 2−83689
- in unsteady Falkner-Skan flow, transient response rel. to pressure gradient 2−53144
- unsteady flow in convergent channel 2−60137
- unsteady growth and formation of regular components in random field of turbulent fluctuations 2−74327
- velocity distrib. over flat plate with diffusion flame 2−83659
- vertical cylinder, pure and simultaneous heat and mass transfer 2−53270
- viscous liquid, boundary layer equations for impulsive flow past semi-infinite flat plate 2−46873
- viscous sublayer, intermittent character, with interpretation of probability density measures 2−83432
- wakes, definition by vortex sheets 2−77239
- walls axisymmetric stagnation point flow with uniform suction, porous, impermeable walls 2−83447
- water, mech. and thermal props., temp. depend. 2−67739
- weather forecasts using eight-level boundary layer physical-numerical model 2−65634
- wedge, laminar, transitional and turbulent profiles at local Mach numbers 6.5 and 20 2−71103
- weirs and flumes, flow measurement 2−83756
- wind stress parameterization, geostrophic drag coefficient variation, cross isobar angle variation 2−84785
- winds in Ekman layer over St. Louis 2−75665
- yaw characteristics of Preston tubes 2−43042
- Au, transmission of struct. information 2−77494
- Hg, partially ionized, growth in shock tube flow 2−64389
- O_2 gas flow condensation 2−77354

Bragg reflection *see X-ray crystallography*

Brass *see Copper alloys*

Bravais lattice *see Crystal structure, atomic*

Breakdown, electric
- *see also Discharges, electric; Electric strength*
- air, temporal growth of ionization in long uniform field gaps 2−71029
- condensed media, nanosecond, unit for optical and electrical characteristics obs. 2−77316
- in crosslinked polyethylene cables, treeing phenomena 2−57237
- high vacuum, breakdown, field emission 2−48942
- high vacuum, breakdown, field emission 2−48942
- laser triggered, effects of spark gap geometry and laser components 2−71034
- long air gaps under positive linearly rising voltages, predischarge phenomena 2−77315
- between parallel plate electrodes in vacuum 2−43218
- pattern of Marx generators 2−71026
- plasma in microwave cavity excited by quadrupole mode 2−74371
- predischarge negative currents, under variable pressure, obs. 2−60308
- rod-plane gaps under positive switching impulses 2−74431
- spark, mechanism in N_2, O_2, SF_6 2−60318
- spark gap, point-plate, flashover voltage, obs. 2−60315
- sphere, rod gaps under short, long waveform impulse voltages, humidity effects 2−74433
- streamers, guidance by laser induced rarefaction channels 2−80362
- thresholds for CO_2 laser produced plasma in magnetic field 2−43134
- vacuum, due to microparticle impact, charge acquisition and reversal effects 2−83638
- vacuum, effect of nonmetallic inclusions in cathodes 2−64356
- vacuum, field emission measurements and breakdown 2−44188

Breakdown, electric continued
- vacuum, macroparticle detachment of electrode surface at pulsed voltage 2−62898
- vacuum gap, elec. characts., prebreakdown current, breakdown voltage, 4-300K 2−63294
- vacuum gap, pulse breakdown, velocity of expansion of cathode flare plasma 2−83636
- vacuum gap conditioning, by sparks and ion bombardment 2−67694
- vacuum insulation between plane parallel metal electrodes 2−64357
- vacuum insulation in accelerator tubes, leakage current development 2−70323
- p-nGe, secondary breakdown formation 2−71962
- N_2, temporal growth of ionization in long uniform field gaps 2−71029
- SF_6, compressed, and prebreakdown dark current 2−71035

gases
- air, at uniform fields, conditions for transition from Townsend to streamer mechanism 2−64353
- air, dry and humid, due to large number of excess electrons 2−83709
- air, minimum breakdown voltage estimation using empirical, semi-empirical methods, up to 7 atmospheres 2−56392
- air, optical strength under laser irrad. 2−50232
- air, static-breakdown voltage measurements at h.v. 2−56394
- air at atmos. pressure, effect of particles and fibers on d.c. breakdown voltages 2−71032
- air at high temps., 50 Hz and d.c. breakdown 2−74437
- air breakdown induced by CO_2 laser, numerical solutions 2−46801
- air gaps, long, 50 Hz breakdown characteristics 2−74438
- air gaps, long, as found in u.h.v. transmission systems 2−74435
- air-gaps, prebreakdown current meas. 2−43216
- breakdown induced by pulsed CO_2 TEA lasers 2−46800
- cathodic contact erosion due to gas breakdown arcs 2−43223
- computer simulation 2−53257
- current oscillations in subnormal glow discharges 2−74427
- diffusion controlled, in rectangular microwave cavity 2−80412
- diffusion-controlled, in microwave cavity excited in TM_{0n0} mode 2−50231
- diode, high-current field-emission plasma instabilities 2−49325
- divergent field gaps, effect of charged particles 2−71041
- electron density of laser produced plasma, interferometric holography 2−83559
- epoxy resin chamber for high voltage breakdown studies in high vacuum 2−53256
- exo-electron emission meas. 2−56390
- gas mixtures, nearly uniform field, breakdown characteristics 2−56391
- h.f. discharges, in supersonic flow 2−74418
- high pressure, field emission mechanisms 2−67695
- h.v. Z-pinch, formative phase analysis of low pressure gases 2−67650
- inductive ring discharge, behaviour 2−53249
- ionization processes 2−46802
- large spheregaps, analysis of volt-time characteristics by integration method 2−71031
- laser induced, method of obs. density distribs. in high pressure gas jet 2−46823
- laser-induced, electron cascade theory 2−60312
- l.p. gaps 2−80416
- pre-breakdown phenomena in long positive point/plane gaps 2−74434
- pre-breakdown phenomena of discharges between heated W electrodes 2−71028
- re-ignition, influence of metastable states 2−43217
- spark chamber gap, phenomenological model of development 2−70315
- streamer propagation in divergent electric fields 2−74412
- vacuum spark gap triggered by electron beam 2−71027
- Ar, at low pressure, study using Townsend theory 2−71037
- Ar, by 0.35μ picosecond laser pulse 2−60314
- Ar, cw breakdown using 10.6 μm laser radiation 2−60313
- Ar, high pressure, under magnetic field, r.f. break down potential 2−71036
- Ar, threshold conditions at superhigh-pressure produced by Q-switched lasers 2−64355
- CO_2, optical strength under laser irrad. 2−50232
- H_2, due to large number of excess electrons 2−83709
- H_2, re-ignition, influence of metastable states 2−43217
- He, pressurized, obs. 2−50233
- Hg vapour, between hemispherical electrodes 2−71030
- Hg vapour, effect of changing electrodes at low density 2−74436
- Mo controlled electrode surfaces, prebreakdown current 2−80370
- N_2, due to large number of excess electrons 2−83709
- N_2, ionizing gas breakdown waves in strong fields 2−80414
- N_2, re-ignition, influence of metastable states 2−43217
- N_2, spark breakdown at high pressure 2−71043
- N_2 by 0.35μ picosecond laser pulse 2−60314
- N_2 minimum breakdown voltage estimation using empirical, semi-empirical methods, up to 7 atmospheres 2−56392
- N_2O at high voltages, mechanisms 2−71038
- Ne, in cells with external electrodes, a.c. breakdown 2−50234
- Ne, re-ignition, influence of metastable states 2−43217
- O_2, due to large number of excess electrons 2−83709
- SF_6, compressed, a.c. breakdown, calculation of spherical particle motion in. 2−56393
- SF_6, compressed, surface flashover on solid insulation 2−71040
- SF_6, d.c. breakdown at e.h.v., coaxial systems, similarity law 2−74432
- SF_6, edge breakdown between uniform field electrodes 2−71033
- SF_6, electrode surface conditions and dust particle effects 2−74439
- SF_6, electron diffusion and drift 2−43202
- SF_6, pressure dependent electron attachment process 2−71039
- SF_6 static-breakdown voltage measurements at h.v. 2−56394

liquids
- condensed matter motion, electric spark in dielectric liquid, X-ray flash investigation 2−46876
- dielectric, and conduction, book contrib. 2−46978
- dielectric liquid breakdown, elimination using diffusion electrodes 2−77444
- dielectrics, rel. to vapour bubble formation 2−56509
- n-hexane, electrically stressed, prebreakdown processes 2−60490

- **Breakdown, electric** continued
  - **liquids** continued
    - light pulse emission before breakdown 2−43382
    - oil, prebreakdown cond. pulses, autocorrel. pulses 2−43383
    - He, pressurized, obs. 2−50233
  - **solids**
    - book contrib. 2−47959
    - breakdown properties, electrical and thermal, book contribs. 2−47959
    - cavity formation and damage during breakdown of ionic crystals 2−72022
    - critical field strength 2−75146
    - glass, chalcogenide, film, thick and thin, switching temp. depend., onset of breakdown 2−77895
    - glass, laser-induced destruction of surface and interior 2−79256
    - insulators, irreversible local breakdown and electric stress, reln. 2−68466
    - Mylar thin films negative resistance charact. 2−57203
    - polyethylene insulators, treeing, voltage and temp. dependence obs. 2−72023
    - polymer films, elec. and optical breakdown stimulation 2−47980
    - polymer films, internal struct. of single hole breakdown 2−47981
    - polymethylmethacrylate insulators, treeing, voltage and temp. dependence obs. 2−72023
    - polythene, irreversible local breakdown and electric stress, reln. 2−68466
    - quartz, breakdown field, dielectric dispersion analysis 2−61421
    - semiconductor, amorphous, avalanche ionization, Shockley hot-electron model 2−61287
    - semiconductor, amorphous, elec. instabilities of mixed electronic and thermal origin, theory 2−61285
    - semiconductor, switching phenomenon, contrib. of lateral thermal instability 2−61283
    - semiconductor devices, breakdown voltage measurement instrumentation 2−82423
    - transparent dielectrics, by mode-locked laser radiation, i.r. 2−79251
    - Al_2O_3 300 to 1200°K, mechanisms 2−65056
    - Al_2O_3 film, anodic, impact ionization 2−57235
    - Al_2O_3 film, step and ramp voltage breakdown tests 2−72024
    - As-Te-Ge-Si glass, thermal breakdown 2−61298
    - As_2Te_3-Si glass system, electronically assisted thermal breakdown 2−61276
    - $BaTiO_3$, laser irrad., breakdown threshold at Curie temp. 2−79252
    - BeO 300 to 1200°K, mechanisms 2−65056
    - BiSb alloy, interband breakdown, voltage instabilities in electron-hole plasma 2−81095
    - GaAs:Si p-n junction, reverse branch of I-V characts. and breakdown 2−71959
    - GaAs, interfacial defect role, device manuf. considerations 2−54215
    - Ge, p-n junc., microplasma turn-on voltage, illumination effect 2−75124
    - Ge p-n junction, avalanche breakdown mechanism 2−71963
    - Ge p-n junction, IV characts. of microplasma 2−75125
    - $LiNbO_3$, laser irrad., surface damage, ferroelec. props. effects 2−79252
    - $LiTaO_3$, laser irrad., breakdown threshold at Curie temp. 2−79252
    - NaCl, laser induced breakdown 2−54376
    - NaCl, polarity effect 2−72021
    - Si, avalanche breakdown, statistical theory based on Boltzmann transport equation, scattering mechanisms 2−54202
    - Si hyperabrupt p-n junction 2−84347
    - SiO_2, in Al-SiO_2-Si struct., IV characs., breakdown, and switching 2−71996
    - SiO_2, thermally grown film, rel. to oxidation temp. and atmosphere 2−71999
    - SiO_2 film, on Si, current instability and dielec. breakdown 2−47955
    - SiO_2 film, prep. by oxygen bombardment of Si, dielectric strength 2−51176
    - VO_2 threshold switching device, capacitance discharge 2−54211
- **Breaking strength** *see Mechanical strength*
- **Breeders** *see Nuclear reactors, fission*
- **Bremsstrahlung**
  - *see also Electrons/radiation; Gamma-ray spectra; Gamma-rays; X-ray spectra/emission; X-rays*
  - atomic and molecular production by electron scattering 2−42760
  - atomic-field bremsstrahlung by electrons, screening and second Born corrections 2−83193
  - betatron, applications to physical research 2−46234
  - black hole, accretion of interstellar gas causing ion-electron and electron-electron 2−75661
  - charge falling in strong gravitational field, relativistic treatment 2−78797
  - coherent, of high-energy electrons passing through crystal, reduction of coherence area 2−54096
  - cross section in nuclear fields formula including high-order Coulomb correction 2−42328
  - dose albedos of intermediate energy bremsstrahlung on reactor shielding materials 2−76958
  - electron, cross-section meas. at short-wavelength limit for metal targets 2−44361
  - electron, from hot plasma in strong mag. field, rel. to X-ray pulsars 2−78478
  - electron, in atmospheric density meas. expt. 2−58018
  - electron bremsstrahlung, 180-2000 keV interactions with various atoms 2−64041
  - electron-electron, 180-2000 keV, absence of evidence 2−64041
  - electron-nucleus, ion-ion correlation effects 2−49785
  - electrons, nonrelativistic, in single crystal, origin of oriented maxima in spectrum 2−80932
  - extragalactic X-ray sources, thermal bremsstrahlung and inverse Compton models 2−75835
  - fast electron and photon transport in matter, Monte Carlo simulation 2−80926
  - free-free, plasma electron vel. distribution determination from polarization 2−56332
  - free-free radiation from relativistic plasma with anisotropic electron energy distribution 2−67622
  - gamma-ray shielding parameters determ. with bremsstrahlung radiation 2−83156
- **Bremsstrahlung** continued
  - inclusive photon yields from high-energy bremsstrahlung on H target 2−76595
  - inhomogeneous absorber, photon-electron conversion during bremsstrahlung irradiation 2−44018
  - inverse, multiphoton ionization of gases at high pressures 2−43199
  - inverse absorpt. in large radiation fields during binary collisions, Born approx. 2−59925
  - neutron star, inner bremsstrahlung rel. to v.h.f. gravitational radiation 2−73007
  - nucleon-nucleon Burentt-Kroll soft-proton theorem applic. 2−82855
  - pair production by collision of laser beam with bremsstrahlung beam 2−66904
  - penetration in extended media, calculation by computer 2−47777
  - photo neutron mean energies conversion to monochromatic photo neutron mean energies 2−63682
  - photon differential albedo measurement 2−76959
  - photon emission rate from Maxwellian plasma to det. electron temp. 2−46764
  - photoneutron data from monochromatic γ excitation calc. using bremsstrahlung photoneutron data 2−70432
  - in plasma, inverse 2−43147
  - plasma instability, induced by electron streaming 2−67680
  - potential scattering, soft photon theorem 2−59412
  - programming system for multi-parameter experiments 2−78861
  - proton, suprathermal, cross-section 2−69008
  - proton-proton bremsstrahlung calcs. at unequal angles in coplanar geometry 2−76769
  - relativistic, as source of γ-ray background flux 2−62626
  - scanning electron microscopy of metals, Lilienfeld radiation 2−79131
  - source of u.h.f. emissions in lightning discharges 2−65801
  - spectra, electron irrad. diamond 2−49499
  - straggling of moderately relativistic electrons due to inelastic scattering and bremsstrahlung 2−68266
  - superconducting tunnel junction phonon bremsstrahlung, modulation 2−47732
  - in thick plane absorbing target, attenuation characts. 2−64000
  - two counter geometry factor for bremsstrahlung expts. 2−49616
  - two-photon process, influence of polarization of electrons and γ-quanta 2−70149
  - Z-pinch, high pressure confinement, losses 2−83600
  - (p,p) scattering, calc. of couble differential bremsstrahlung cross section in forward direction at 51.8 MeV 2−49789
  - from β-decay of ^{235}U, ^{239}Pu fission fragments produced by thermal neutrons 2−63843
  - e beams, 10 keV-100 MeV, yield calc. in 59 elements, 55 compounds and soft tissue 2−54095
  - μ pair bremsstrahlung process in electron collisions 2−82684
  - n production from P by high energy beam 2−55980
  - np non-coplanar bremsstrahlung obs. at 200 and 130 MeV, application to N-N interaction off-shell energy properties 2−79718
  - pp, double differential cross-section for production meas. 2−45996
  - pp low energy scattering, cross-section 2−73851
  - pp scattering, cross section calcs. including relativistic corrections to Pauli-Schroedinger eqn. 2−67054
  - Al, electron-bremsstrahlung cross-section meas. at incident energy 0.2 MeV, photon energies 0.02-0.2 MeV 2−70613
  - Au, electron-bremsstrahlung cross-section meas. at incident energy 0.2 MeV, photon energies 0.02-0.2 MeV 2−70613
  - ^{262}Cf, fission products, associated inner bremsstrahlung radiation 2−59806
  - ^{137}Cs, internal bremsstrahlung spectrum of unique β-transition 2−82932
  - Cu, electron-bremsstrahlung cross-section meas. at incident energy 0.2 MeV, photon energies 0.02-0.2 MeV 2−70613
  - H-He plasma, absorption coefficients of i.r. radiation 2−46744
  - He gas discharge, X-ray production in strong electric field 2−80368
  - $^4He(\alpha, \alpha\gamma)^4He$, meas. of bremsstrahlung cross section 12.5-19.0 MeV 2−74105
  - N_2 gas discharge, X-ray production in strong electric field 2−80368
  - $^{147}Pm_2O_3$, thick cylindrical beta source, determ. 2−67191
  - ^{90}Sr-$^{90}YTiO_3$, thick cylindrical beta source, determ. 2−67191
  - ^{204}Tl, β-decay, internal bremsstrahlung spectral distrib. 2−42549
  - $^{204}Tl_2O_3$, thick cylindrical beta source, determ. 2−67191
  - W thick target, calc. of bremsstrahlung spectra produced by electrons using thin-target formulas 2−42739
  - ^{90}Y, internal bremsstrahlung spectrum, contrib. of detour transitions 2−42542
- **Brightness**
  - *see also Illumination*
  - 500 kV electron microscope gun, from 200-500 kV accel. volt. 2−55660
  - 3 58, supernova remnant, obs. at 2.8 cm 2−75757
  - atmosphere, satellite radiance meas., insertion into numerical circulation model 2−62134
  - electroluminescent capacitor, brightness, temp. depend. 2−72435
  - IC 443, supernova remnant, obs. at 2.8 cm 2−75757
  - lamp, straight tubular gas-discharge, effect of bulb on brightness distrib. 2−43208
  - laser, amplified systems, far field brightness 2−79224
  - Mach bands meas. by compensation method 2−69464
  - meteors, maximum brightness and ablation coefficient 2−75923
  - microwave brightness temp. of natural sea ice and salt water ice 2−84777
  - Moon, far i.r. brightness lens for sunlit surface 2−73066
  - Moon, intensity and colour variations across surface, high resolution scans 2−78520
  - quasar 3C 273, brightness distribution and polarization of A and B components 2−73043
  - reference, effects on slit diaphragm photometer errors 2−73648
  - solar brightness-temperature contour maps at 3.3 mm wavelength, temperature depressions 2−78596
  - spectral brightness outside instrumental range, statistical estimation 2−76547
  - Venus, radar image and brightness map of surface 2−78504
  - visual, electrical filter model lateral facilitation and inhibitory feedback 2−66346
  - w28, supernova remnant, obs. at 2.8 cm. 2−75757
  - w44, supernova remnant, obs. at 2.8 cm. 2−75757

Brightness continued
- water, disturbed surface, i.r., statistical characts. 2−48418
- ZnS:Cu, Cl, changes in brightness wave during ageing 2−65316

Brillouin scattering *see Scattering/light, Brillouin spectra*

Brillouin zones
- C16-type compounds and pseudobinary alloys, rel. to supercond. props. 2−51104
- group II-IV-V_2 chalcopyrite crysts., assignment of E_1 transitions 2−81384
- semiconductor, with band extrema at centre, interband optical transitions 2−65250
- sums on cubic lattices, evaluation 2−57115
- GaAs, [110] surface Brillouin zone, intrinsic localized states, calc. 2−65007
- HfC, secular equation, soln. 2−57126
- InP, [110] surface Brillouin zone, intrinsic localized states, calc. 2−65007
- MgF_2, energies of high symmetry pts. 2−54109
- $MoTe_2$, optical consts. complex structure, assignment 2−48162
- Ni, ferromagnetic, tight binding method energy band calc. 2−47810
- PbTe, electronic charge density 2−44121
- Sb-Bi alloys, band struct., magnetoreflection obs. 2−54405
- TaC, secular equation, soln. 2−57126
- Ti alloys, rel. to exponential temp. depend. of resist. 2−54129
- TiC, secular equation, soln. 2−57126
- Zr alloys, rel. to exponential temp. depend. of resist. 2−54129

Brittleness
- *see also Mechanical strength*
- brittle body fracture by explosion, anal. 2−69782
- brittle materials, crack propag. rel. to nonrecoverable elastic energy, Griffith criteria 2−71595
- ceramic, strength, review 2−47520
- ceramic substrate, biaxial flexure test method 2−60919
- cold straightening effects on welded joints 2−71628
- fatigue failure probability determination 2−60994
- fracture faces, interpretation in physics and geology 2−47540
- fracture in compression 2−84018
- fracture initiation under triaxial stress conditions, Gibbs free energy 2−84016
- fracture of brittle bodies, by impact, fracture mech. study 2−69642
- fragility testing, simple economical method 2−56856
- graphite, fatigue failure probability determ. 2−60994
- hydrogen embrittlement, stress corrosion cracking, catalytic dissociation as primary process 2−84020
- ice, columnar-grained, failure processes 2−64732
- material, tensile testing, application of point loaded discs and blocks 2−66526
- metal, arising from action of liquid metal, diffusional theory 2−71594
- metal, b.c.c., ductile-brittle transition, theory 2−43720
- metal, brittle fracture, ductile-brittle transition 2−43730
- metal, brittle fracture surface energy from phonon freqs. 2−60902
- metal, role of impurities and cryst. struct. 2−43719
- metal, shock spallation, appl. of phonon theory of brittle fracture 2−80747
- oceanic basalt, brittle fracture 2−61971
- quartz, static fatigue, earthquake phenomena 2−65499
- radiation induced embrittlement by neutron reaction-produced He in structural mats. at high temps. 2−68100
- radiation involved brittle fracture in structural materials 2−68099
- reactor fuel particles, irrad. induced 2−43772
- rock deformation, volume changes at high pressure 2−62006
- rock-joint deformation, modelling 2−72668
- rocks, effect of stress gradient on brittle fracture initiation 2−72667
- rocks, statistical theory of polyaxial compressive strength 2−72670
- rupture tests, method of forming axially symmetric surface cracks 2−50785
- Solenhofen limestone, effects of strain rate changes on strength and ductility 2−62007
- steel, brittle fracture, effect of grain boundary form 2−80765
- steel, brittle fracture resist., tempering temp. effects 2−53838
- steel, brittle fracture susceptibility, effect of V alloying 2−53896
- steel, ductile-brittle transition, deform. mode influence 2−43694
- steel, ductile-brittle transition, theory 2−43720
- steel, ductile-to-brittle transition, influence of cold rolling and heat treatment 2−80777
- steel, ferritic, irrad. embrittlement 2−43854
- steel, hydrogen embrittlement, mechanistic model 2−77653
- steel, low C, effect of microstructure on embrittlement 2−84158
- steel, low carbon, microstructure and embrittlement 2−43783
- steel, low-alloy, cold brittleness, effect of Ce addition 2−53831
- steel, low-alloy, temper-brittle fracture and grain boundary segregation 2−47624
- steel, low-C, fracture rel. to microstruct., embrittlement, bend tests 2−56823
- steel, pearlite, struct. effects 2−43724
- steel, press. vessel material, time-depend. embrittlement phenomena 2−59849
- steel, quenched, tempered, resist. to plastic deform. and cold brittle failure 2−47502
- steel, sintered, for fuel element jackets, processing and mech. characterization 2−76951
- steel, structural, single crystal temper brittleness 2−60982
- steel, temper brittleness, role of cryst. distortions 2−43792
- thermoplastics, long term strength, ductile failure, brittle failure 2−43718
- transition metal, H embrittlement, theory 2−77654
- transition metals, b.c.c., cold brittleness 2−43726
- welded pressure vessels, loading capacity, stressed at high temps. 2−64771
- Al, embrittlement by molten Ga 2−43721
- Al_2O_3, biaxial flexure tests 2−60919
- Al_2O_3, polycrystalline, stress corrosion in moist air and toluene, time-dependent failure characteristics 2−84039
- Al_2O_3, static and cyclic fatigue behaviour 2−50766
- Co alloys, metallurgical structure and properties 2−71667
- Cr, ductile-brittle transition, effect of rare-earth metals 2−43691
- Cr, high-purity phase obs. 2−47531
- Cu-Bi alloy, grain boundary fragility and segregation 2−53830
- Cu-Cr alloy, embrittlement, under elevated temp. stress 2−43722

Brittleness continued
- Cu, stress pulse damping in region of propagating brittle crack 2−60801
- Cu_6Sn_5 fibres, brittle fracture surface morphologies 2−80744
- Fe-Co-V alloy, tensile tests, and plastic deform. 2−60868
- Fe-Cr steel, embrittlement at 475°C, ordering, decomp. of ferrite 2−47634
- Fe-Ni-C alloy, quenching and hydrogenation effects 2−43723
- Fe-Ni-Si alloy, temper brittleness development, grain boundary adsorption of P, internal friction study 2−80767
- Fe-Ni and Fe-Ni-C martensitic alloys, hydrogen embrittlement 2−64731
- Fe, influence of N_2 on ductile-brittle transition point 2−47629
- Fe, zone-refined, hydrogen embrittlement 2−43725
- Mo alloy, ductile-to-brittle transition, rel. to struct. changes during deform. 2−50839
- Ni-ThO_2, dispersion-strengthening effects on hydrogen susceptibility 2−74862
- W:K,Si,Al wire, incandescent lamp filament, working and process annealing 2−47590
- Zr-(2.5 wt.%) Nb press. tubes, heat-treated, embrittlement 2−50770

Bromine
- atomic stopping cross sections of α particles by application of Bragg additive rule to molecular stopping cross sections 2−70820
- methylbromide + ^{80}Br, H and halogen displacement factors; survival probability of products 2−84664
- molecular cryst., harmonic freqs. of vibr., harmonic intermol. pot. 2−81349
- molecule, collisional reaction with methyl radical, molec. beam study 2−61779
- molecule, outer vibr. turning pts. near dissoc. in B($^3\Pi_{0u}{}^+$) state 2−77082
- molecule, thermal decomp. in inert gas, diffusion theory approach 2−80059
- AgBrI:Br^-, NH_3, cryst. morphology rel. to impurities 2−80648
- Br_2-Ne mixtures, r.f. discharge spectrum, excitation mechanisms 2−71018
- Br I, e.u.v. spectra, energy levels 2−64001
- Br_2, dissociation in presence of CO_2, shock tube investigation 2−67469
- Br_2 vapour, reson. Raman effect in absorpt. continuum, excitation freq. influence on line intensity 2−52996
- $Br_2{}^{79}$ and $Br_2{}^{81}$ hyperfine structure near 6328 Angstroms by laser saturated absorption spectroscopy 2−46554
- ^{77}Br used to determine capillary permeability in anterior tibial muscle 2−69359
- $Br_2 + H$, energy distribution among reaction products 2−65370
- DBr-Br_2 system, hot atom reactions rates 2−72549
- HBr-Br_2 system, hot atom reaction rates 2−72549
- KCl:Br-, with low Br- conc., optical absorpt., 77K 2−65259
- KCl:Br, $BrCl^- - V_k$ centre, e.s.r. 2−81461
- ZnS:Cu, Al, Br film, temp. depend. of electrolum. and thermal quenching 2−84533

Bromine compounds
- graphite-Br intercalation compound, Fermi surface, Shubnikov-de Haas oscill. obs. 2−68288
- halogenosilane bis-pyridine and o-phenanthroline complexes, vibr. spectra, normal coord. analysis, struct. 2−77081
- $BrNSF_2$ vibrational spectra, tentative assignment, band shape and G-matrix element calcs. 2−70697
- BrO, electron resonance spectra in $J=5/2$ rotational levels 2−46530
- $BrO_3{}^-$, vibrational spectra and force constants 2−59996

Brownian motion
- aerosol, Brownian coagulation 2−46998
- aerosols, Brownian coagulation, self-preserving particle size distrib. 2−50384
- autocorrelation functions for particle 2−58778
- Brownian particles, sedimentation rate, diffusion coeff., holographic interferometry 2−45767
- demonstration 2−66400
- dilute suspensions, rheological properties in presence of rotary Brownian motion and external couples 2−50375
- diophantine property of trajectories 2−82271
- gelatin gels, diffusion of water, interfacial contact resist. 2−60533
- generalized Langevin eqn. for projections of n-dimensional Gaussian-Markov processes 2−66456
- Indian ink particles, in water and $FeCl_3$ aq. soln., in uniform mag. field 2−67846
- inertial effects in motion driven by hydrodynamic fluctuations 2−70827
- liquids, finite step rotational Brownian motion, generalization to anisotropic rotators 2−60414
- luminescence decay law in liquids, effect of Brownian motion on transfer of excitation energy 2−53439
- macromolecular system, rot. motion and polarized fluoresc. 2−60091
- microwave absorption in polar liquid 2−49209
- N-interacting particles, extension of Einstein diffusion relation 2−66465
- plasma-electron beam interaction, collective oscillatory motion, Brownian motion model 2−67628
- real symmetric matrices class, eigenvalue distrib. 2−58791
- role in control of detrital remanent magnetization 2−74564
- Schrodinger-Langevin eqn. for Brownian particle interacting with thermal environment 2−82220
- seeded convective storms, ice form. mechanism 2−84856
- suspension of nearly spherical particles, rheology 2−83813

Brush discharges *see Corona, electric discharge*

Bubble chambers
- Big European pictures meas. with Hough Powell device 2−76749
- correction for loss of charged Σ decays 2−55930
- deuterium, background due to tritium decay 2−79682
- heavy liquid, momentum estimation at position beam and γ rays produced in instructions 2−52704
- heavy liquid, with mag. field, determ. of fraction of π^--p interactions 2−70313
- Mirabel, for Serpukhov acceleration, design and construct. 2−55929
- Mirabelle, new liquid H chamber, use with Serpukov accelerator 2−76746

Bubble chambers continued
- particle track visualization, optical image recognition applications 2−79684
- pattern recognition of tracks, computerised 2−79688
- photogram transmission system, LSI most-memory in digital data 2−55932
- review of current expts. and proposals for future expts. 2−76748
- track images matching using computer program 2−55931
- u.s., development 2−67099
- H_2, 75 cm, characteristics 2−63716

Bubbles
- *see also Foams*
- aeration, control factors 2−77400
- air, in hailstones 2−78371
- air bubbles in water, acoustic scattering strength meas. 2−74511
- air entrained water flows, under reduced ambient pressure 2−77404
- air entrainment in breaking waves 2−57924
- air in water, shock excited pulsations 2−80438
- base wake, structure in swirling flow 2−80157
- behaviour in gas-solid fluidized beds, theory for initial bubble formation 2−50145
- in blood, detection by Doppler flow transducers 2−66277
- boundary layer separation patterns over inclined body of revolution 2−77215
- captive, surface and interfacial tensions, from profile 2−67789
- cascade reactor, unidirectional flow of gas and liquid, flow studies 2−67783
- cavitation, collapse and rebound, extreme cases 2−77402
- cavitation, interaction mechanism with particles of solid and liquid phases 2−64415
- cavitation bubble implosion pressure pulses and cavitation damage 2−56469
- collapse adjacent to rigid wall, flexible wall and second bubble 2−67792
- collapse and rebound, laser induced cavitation 2−43289
- collapse of nearly spherical cavity in liquid, nonlinear effects 2−46911
- column, effect of liquid flow on axial mixing of liquid 2−67762
- columns, relative gas content, dynamic meas. by X-ray absorpt. 2−64420
- condensing, collapse in compressible liquids 2−43298
- convective heat transfer enhancement to water containing bubbles 2−60464
- dielectric liquids, rel. to breakdown 2−56509
- diffusion at moving boundary 2−64421
- difluorochloromethane, evaporation, influence of pressure 2−73244
- dynamics of vapour cavities and gas filled bubbles 2−43304
- expanding, velocity effects in acoustic scattering underwater explosions 2−52237
- expansion of underwater cylindrical gas bubble, differential equation approximation 2−43306
- fission gas, in solids, re-solution, asymptotic behaviour 2−53690
- flowing, turbulence characteristics 2−80440
- fluid, mutually migrating mixture dynamics 2−67785
- in fluidized beds, gas transfer to dense phase 2−80163
- in fluidized beds, slug flow regime 2−77401
- formation, from orifice in two dimensional fluidized bed 2−77403
- formation in Al, K, or Si doped W rods, identification of impurities 2−80792
- friction in gas saturated liquid, turbulent boundary layers 2−53375
- gas in liquid, acoustically forced oscillations 2−64423
- glass melts, bubble formation 2−64531
- in glass melts, formation and removal 2−56551
- growth and collapse in narrow tubes with nonuniform initial temp. profiles 2−67787
- growth of spherical bubble controlled by heat diffusion, approximate soln. including convective flow 2−83729
- hemispherical on heated wall, thermocapillary flow 2−50303
- inert gas, in irrad. Al-Li alloys, effects on mech. props. 2−43688
- inert gas in solids, computer simulation of precipitation kinetics 2−64424
- isothermal motion through a rotating liquid 2−46912
- liquid, high speed photography of laser-induced breakdown 2−56470
- liquid-air ejector system system, horizontal, momentum transfer 2−67781
- liquid-bubble mixtures, shock wave propagation and relaxation effects 2−77453
- in liquids, conjugate flow theory 2−67709
- mass transfer following entrance into liquid 2−43299
- mass transfer from single gas bubble 2−46907
- mass transfer rates from spherical particle boundary-layer injection suction considerations, variational analysis 2−77397
- menisci, axisymmetric, tables of profiles 2−60413
- motion in slit channels in liquids of varying viscosity 2−64422
- non-Newtonian fluid, low Reynolds number, mass transfer using this boundary layer approx. 2−53376
- non-Newtonian liqs., mass transfer, power law model 2−53374
- nonspherical, dynamics and oscillations 2−43305
- nucleation in liquids, applic. to gases dissolved in blood 2−45028
- organic dye solution, formation by emission from Xe impulse lamp 2−53378
- pointed, in slow viscous flow 2−80494
- polyphase flow, conference (San Francisco March 1972) 2−67603
- rising velocity in vertical columns of biological suspensions 2−83825
- semi-batch packed bubble column, mass transfer and liquid mixing 2−74508
- separation, prediction on circular cylinder 2−80437
- separation bubble upstream of flow past circular disk 2−50291
- separation from horizontal surface, kinetics 2−67791
- single vapour bubble round pulse, origin, and nucleate boiling of liquids 2−60554
- size, produced by dissolved gas coming out of solution on pipe walls in flowing systems 2−50306
- in solid, nucleation, diffusion 2−50632
- spatial distrib. in freely bubbling fluidized beds 2−83503
- spherical, with internal circulation 2−83730
- spheroidal gas bubble rising in water, effect of periodic nature of drag, vortex structure 2−80425

Bubbles continued
- stability while undergoing non-spherical oscillations 2−53372
- steady state turbulent flow of liquids with bubbles asymptotic theory applics. 2−43310
- Stokes flow in and around fluid sphere in presence of another sphere or plane boundary 2−80164
- submerged orifices, regimes of bubbling and jetting 2−60399
- surface tension computations in the stretched regions of bubble surfaces 2−64454
- surface waves and subharmonics, thresholds for acoustic excitation 2−43307
- turbulent flow, method of limited expansions 2−56462
- turbulent flow, of liquids with bubbling, method of limited expansions 2−56462
- underwater, planar, cylindrical and spherical, expansion and contraction 2−77405
- vapour, growing, heat and mass transfer 2−53377
- vapour, kinetic and thermal expansion 2−46909
- vapour, thermal equilibrium, effects of liquid motion induced by phase change and thermocapillarity 2−77399
- in viscoelastic material, gas bubble behaviour in creep process 2−50699
- water, nonspherical vapour bubbles, dynamics 2−77407
- water, nonsteady fow at high speeds 2−77371
- water vapour, motion in annular channel 2−74592
- CaO-CaF_2 system liquidus line determ. by the capillary method 2−84683
- H_2 bubble apparatus for water flow velocity measurements 2−71135
- He, form. in α-irrad., Al 2−50644
- Na bond disruption by gas bubbles in fast breeder reactor 2−49888
- Na single bubble growth in fast breeder reactor coolant, safety factors 2−74143
- O_2, isothermal motion through rotating annuli of distilled water and glycerine 2−46912
- UO_2, fission gas bubbles, nucleation and evolution, math. treatment 2−67358
- W, increase in high temperature strength due to, mechanism 2−71581

Burgers vector *see Crystal imperfections/dislocations*

Cadmium
- adsorption and nucleation, on Ge single cryst., by mol. beam technique 2−47158
- adsorption and nucleation on W and Ge, mol. beam technique 2−50534
- adsorption of SF_6, stepwise isotherms 2−77518
- alloys, diamagnetism, types and magnitudes of structures 2−81203
- arc lamp for deep ocean water light source 2−49442
- atom, 5 $^3P_2$ state, colliding with inert gas atoms, meas. of relaxation constants 2−42783
- atom, L-shell photoelec. cross sections of gamma-rays 2−76967
- atom, magnetic depolarization of fluorescence lines, Hanle effect 2−79860
- clusters, electronic props., mol. orbital calc. 2−81026
- coating on U-Nb alloy, effect on stress corrosion cracking 2−53911
- density of Bi- or Sb-doped specimens, annealing effects 2−71665
- diffusion in Ag, 375-650°C, near-surface effects 2−68049
- diffusion in BiTe, effect of distrib. of diffusing element, thermal e.m.f. and orientation relative to basal plane, creation of p-n junctions 2−83991
- diffusion of Ag, tracer diffusion 2−56755
- distribution in N. Atlantic deep sea sediments 2−81618
- electron transmission, det. of lattice potentials 2−83942
- Fermi surface topology rel. to hydrostatic press., magnetoacoustic meas. 2−77806
- film, disordered, supercond. energy gap and transition temp. 2−54134
- hyperfine interactions of implanted ^{220}Rn and ^{224}Ra study by α-γ correlations 2−81341
- impurity diffusion in single crysts. 2−43658
- ion implantation in GaAs, residual bombardment disorder and atom location 2−60813
- lattice dynamics, third order elastic consts., and thermal expansion 2−84182
- liquid, u.s. velocity, theory and expt. 2−80469
- liquisol quenching, effect on lattice parameters and vacancy conc. 2−77572
- neutron filter for nondestructive activation anal. 2−72598
- neutron monitor, correction faults for 9 and 10 inch spheres 2−59636
- porous electrodes, passivation in KOH solution 2−84656
- positron angular distributions using wavefunctions with proper crystal symmetry 2−80942
- powder, Raman effect 2−81383
- relative isotope shift, (112-114)/(110-112) of 4416Å spectral line 2−64016
- self-diffusion in CdS, radiotracer study 2−83993
- specific heat below 30 K 2−68249
- thermal conductivity, Ziman-Baym theory calc. 2−51058
- vacuum evaporation, selective condensation on macroinhomogeneous surface 2−74628
- whiskers, vapour growth in various atmospheres 2−47134
- AgCl:Cd, crysts., nuclear particle track detectors, development and props. 2−79687
- $Bi_{1-x}Sb_x$:Cd, elec. props., (x=0-0.2), 180-420K 2−61301
- Cd-Ar vapour, phase-matched, vacuum u.v. radiation generation 2−79904
- Cd-Bi binary system, pressure effect on eutectic temp. 2−76124
- Cd-He, gas mixture, glow discharge, laser action in Crookes region 2−79196
- Cd-He gas mixture glow discharge, distribution functions and kinetic coeffs. 2−71024
- Cd-He lasers using recirculation geometry 2−59157
- Cd-He mixture, glow discharge, electron distrib. fns. 2−74429
- Cd-Pb amalgam electrode, standard cell, reduced temp. coeff. 2−82118
- Cd-Se rectifier, I-V and C-V characts., rel. to existence of CdSe interface layer 2−54219
- Cd ion charge transfer excited laser, cathode glow discharge in transverse hollow cathode structure 2−79205
- CdI vapour, reson. obs. in absorpt. spectrum at 30 Å 2−76996

Cadmium continued
CdII vapour ion laser, exptl. and theoretical studies including spectroscopic data 2−52422
$Cd(^3P_0) + NH_3 \rightarrow CdNH_3^*$ reaction kinetics, rate constant, excimer formation 2−81514
in GaAs(P), chem. shift in binding energies of Zn and Cd. 2−65001
GaN:Cd, acceptor site location and new emission band obs. 2−72398
He-Cd laser, 4416 Å, excitation mechanism, and operation parameters 2−79181
He-Cd laser, determ. of wavelength for centre of Lamb dip 2−66754
He-Cd laser, pumping mechanism and plasma parameters 2−76474
He-Cd laser generating at 4416 Å 2−45749
He-Cd vapour-ion laser, CW, developments, review 2−42021
He-Cd vapour laser, role of thermal energy-charge exchange 2−42019
Hg-Cd sensitized fluoresc., amplitude modulation 2−64014
inInSb, distrib. coeff., conc. depend. 2−47438
InSb junction, Cd diffused, I-V characts. and magnetotunnelling 2−54216
$NaCl:Cd^{2+}$, dissolution of precipitates study 2−83844
inNaCl, vacancy-impurity complex, slow motion press. effects, n.m.r. study 2−72514
n-Si, Cd-compensated, current oscills. 2−71949

Cadmium compounds
$CdGeAs_2$ and $CdGeP_2$ energy level changes for polymorphic transitions 2−80947
CdSe photoconductive films, field quenching 2−77964
p-Cu_2Se-n-CdSe hterojunctions, Zener breakdown by tunnelling electrons 2−68442
Ag-Cd, alloy, stress corrosion sensitivity in $FeCl_3$ and $Fe_2(SO_4)_3$ solns. 2−64733
β-Ag-Cd alloy, operative slip systems 2−60874
Ag-Cd alloys, solubility of hydrogen, rel. to Fermi level position and clustering 2−77716
Ag-Cd dilute alloy, Righi-Leduc and Hall coeff., 2.5-120 K 2−75050
Cd-Ag alloy, application of Lindemann's rule for melting 2−74582
Cd-Ag alloy, impurity scatt., electron lifetimes, Fermi surface, de Haas-van Alphen meas. 2−61148
47.5 at.%Cd-Au alloy, elastic and enelastic props. near cubic-orthorhombic phase transform. 2−77643
Cd-Bi, eutectic, unidirectional solidification 2−43442
Cd-Bi eutectic, cellular solidification, plane front-cell transition 2−43443
Cd-Cu alloy, weakening resist. rel. to deform., heating time and temp. 2−50764
Cd-Cu system, liq., elec. resist. 2−46981
Cd-Ge-As-Se glass, microstruct. and immiscibility temp. 2−56561
Cd-Hg alloy, 0-14 at.% Hg, room temp. Hall effect 2−77855
Cd-Hg alloy, thermodynamic props., calorimetric obs. 2−57056
Cd-Hg alloys, diamagnetism, susceptibility curves 2−81203
Cd-In, binary systems, electrotransport and elec. resist. detn. for density of states at Fermi level 2−80476
Cd-In system, liq., elec. resist. 2−46981
Cd-Mg alloy, poison rod, burn-up, expt. and theory 2−49879
Cd-Mg alloys, diamagnetism, susceptibility curves 2−81203
Cd-Pb-Sn alloy, eutectic morphology, unidirectional solidification microstruct. 2−74895
Cd-Si-As system, glass-forming region determ. by differential thermal analysis 2−74599
Cd-Sn-Zn system, activity coeffs., calc. 2−43827
Cd-Tl, binary systems, electrotransport and elec. resist. detn. for density of states at Fermi level 2−80476
Cd-Zn alloy, microsegregation of Cd during growth, partition coefficient 2−47648
Cd-Zn system, liq., elec. resist. 2−46981
Cd Te, halogen doped, gamma ray detector 2−55920
Cd_3As_2-NiAs eutectic, Nernst effect and thermal radiation detector fig. of merit 2−54246
Cd_3As_2-NiAs eutectic, thermomag. props., rel. to device appl. 2−59064
Cd_3As_2-2CdTe system, phase diagram 2−47708
$CdAs_2$ glass, i.r. spectra in range 2 to 25 mk 2−61627
$CdBr_2$-Pb crystals, temp. depend. of recombinat. luminesc. and photocond. 2−72049
$CdBr_2$(Pb,Mn), recombination interact. of luminescence centres, 90-400 K 2−84544
CdCN, e.p.r. and chemical bonding 2−50072
$CdCl_2:Co^{2+}$, obs. of vibrational-electronic coupling in high resolution spectrum of spin forbidden band 2−81356
$CdCl_2$, adiabatic compressibility and sound propag. speed, reln. to molec. struct. 2−72564
$CdCl_2$ crystals, impurity ion spectra at 5 eV, optical and epr, radiation effects 2−84475
$CdCl_2$(Pb,Mn) + ρε∞ΔμβΣυατΣΔυ Συτερα∞τ; Δφ λ→μΣυεσ∞ευ∞ε ∞ευτρεσ +)':[" K 2−84544
$CdCr_2S_4$, red shift peak in absorpt. band, mag. F′ centre model 2−80712
n-$CdCr_2Se_4$:Ga, h.f. cond., freq. dispersion, Curie pt. phenomena 2−44095
$CdCr_2Se_4$, ferromag. reson., 4.2-293K 2−68722
$CdCr_2Se_4$, ferromag. reson. anisotropy 2−54487
$CdCr_2Se_4$, mag. permeability rel. to illum., photoferromag. effect 2−54324
$CdCr_2Se_4$ film, deposition and mag. props. 2−60649
$CdCu_{1.5}Ga_{0.5}$, Laves phases, enthalpies of soln. and formation detn. 2−47692
$CdEr_2S_4(Se_4)$, crystallographic and mag. props. 2−72113
$CdF_2:Er^{3+}$, correlated e.p.r. and optical study 2−78164
$CdF_2:Er^{3+}$, i.r. transitions, Stark dissoc. by cryst. field 2−65305
$CdF_2:Er^{3+}$ i.r. quantum counter, noise effects 2−59631
$CdF_2:Gd^{3+}$, second order spin-lattice coeffs., temp. depend., e.p.r. obs. 2−80890
$CdF_2:Mn^{2+}$, obs. of hyperfine and superhyperfine splittings in e.p.r. spectra 2−48276
$CdF_2:Na^+(Ag^+)(Li^+)(La^{3+})(In^{3+})(Gd^{3+})$, ionic thermocurrents, temp. depend. 2−81089
CdF_2, absorpt. and fluoresc. of Er^{3+}, ion site obs. 2−54416
CdF_2, absorption spectra of Co^{2+}, V^{3+} and Cr^{3+} impurities 2−54417

Cadmium compounds continued
CdF_2, high purity, semiconducting photoconductivity spectrum interpreted in terms of band structure 2−84378
CdF_2, surface optical modes, reflection obs. 2−51344
CdF_2, thermal defect order, mobility and complex form., ionic cond. mechanism 2−51194
CdF_2, two-electron U-centres, point-ion models 2−83987
CdFOH, ^{19}F and ^1H n.m.r. 2−84591
$Cd_3Fe_{2-x}M_xGe_xGe_3O_{12}$, $M = Al^{3+}, Ga^{3+}, Cr^{3+}, Sc^{3+}, In^{3+}$, Mossbauer study of lattice 2−72278
$CdFe_2O_4$, specific saturation magnetization depend. on pH of soln., time of boiling and Si 2−84432
$CdGeAs_2$, $CdGeP_2$, glass, i.r. spectra in range 2 to 25 mk 2−61627
$CdGeAs_2$, liq., elec. cond., thermopower 2−60496
$CdGeAs_2(P_2)$, i.r. birefr. and optical activity 2−72261
Cd_2GeO_4, rhombic cell parameters and struct. detn. by oscillating crystal method 2−71426
$Cd_2(Ge_2O_6)$, hydrothermal synthesis and cryst. struct. 2−74687
$CdGeP_2$, $CdGeAs_2$, sphalerite-chalcopyrite transition, struct. of phases, microhardness 2−57025
$CdGeP_2$, crystal lattice disorder, effects on vibr. spectrum and optical states 2−72299
$CdGeP_2$ zone recrystallised, optical props. and energy zone calc. 2−80595
$CdGeP_{2x}As_{2-x}$, prep., struct., hardness and m.p. 2−47616
$CdGe_xSi_{1-x}P_2$, prep., struct., hardness and m.p. 2−47616
$Cd_{0.20}Hg_{0.80}Te$, photocond. oscillations in a magnetic field and photomagnetic effects 2−75169
$Cd_xHg_{1-x}Te$ mixed crysts., reststrahlen spectra, transverse optical modes 2−44366
$CdHo_2S_4(Se_4)$, crystallographic and mag. props. 2−72113
CdI, polytypes, phase transform. 250−280°C 2−77745
CdI_2, growth characts., stacking faults distrib. and stability, polytypism 2−74781
CdI_2 crystals, room temp. effect on dislocations, X-ray diffr. obs. 3-4 yrs after growth 2−68027
CdI_2 polytypes, occurrence of Zhdanov numbers 1,2, and 3 2−83945
CdI_2 polytypes, twelve-layered, cryst. struct. 2−43577
$CdIn_2S_4$:Cr, cryst. growth, vapour transport method 2−71369
$CdIn_2S_4$, intrinsic and Co^{2+} doped, effect of S vacancies 2−68735
$CdIn_2S_4$ single crystal, photocurrent oscillations 2−75170
$CdK_2(SO_4)_2 2H_2O$ crystal struct. determ. 2−77545
$CdLu_2S_4$, crystallographic and mag. props. 2−72113
Cd_3Mg, two-phase region, morphology, habit planes and orientation relns., metallographic obs. 2−61042
$Cd(NO_3)_2$, precip. in KNO_3, solid soln. form. 2−56942
CdO, dissociation and form. equilib. const. from saturation v.p. temp. depend. 2−75371
CdO, electron concentration determ. using T activity 2−71934
CdO, X-ray induced electron emission, core electron energy levels detn. 2−48019
CdO film, transparent electrode for CdS 2−54209
CdO microcrystals, coupled surface phonon-surface plasmon modes, i.r. absorpt. 2−84263
CdO(c), heat capacity, drop calorimetry and diff. scanning calorimetry 2−54047
Cd_3P_2-2CdSe system, phase diagram 2−47708
CdP_2, cathodolum. and photolum., recomb. mechanisms 2−72394
CdP_2 glass, i.r. spectra in range 2 to 25 mk 2−61627
Cd_2P_3Br, cryst. struct., synthesis 2−60754
Cd_2P_3Cl, cryst. struct., synthesis 2−60754
Cd_2P_3I, cryst. struct., synthesis 2−60754
$Cd_2Pb_{1-x}Se$ alloy, Hall coeff., Hall mobility, thermoelec. power, optical energy gap, 77-450 K 2−64977
CdS, acoustoelectronic effects at large acoustic intensities 2−80915
CdS, polymorphic transform. under electron irrad., thermodifferential analysis 2−47681
CdS resonance Raman scattering by turnable dye laser 2−84486
CdS semiconductors, dipole active exciton absorption, nonlinearity 2−44333
$CdSO_4$, 'acid' standard cell, e.m.f.-temp. coeff., 15° to 40°C 2−82130
$CdS_{1-x}Se_x$:Mn, Mn^{2+} conc., e.p.r. determ. 2−72481
CdS_xSe_{1-x}, graded band gap crysts., tunable laser emission by two photon excitation 2−69948
CdS_xSe_{1-x} selective photoresistors for visible region 2−44172
CdS_xSe_{1-x}, free carrier optical absorption 2−75288
CdS_xSe_{1-x} mixed crystal, study of lattice dynamics, phonon-phonon interactions by Raman spectra 2−51353
CdSb:Ag, electrical conductivity for pressed powders, detn. 2−64906
CdSb:Te, elec. cond. and Hall const., 78-293K 2−61307
CdSb, Debye charact. temp. det. from elastic modulus 2−64854
CdSb, elec. props., effect of evaporation of Cd atoms 2−47890
p- CdSb, photoelectric props., conductivity anisotropy effects 2−57257
CdSe:Ag, impurity levels 2−51151
CdSe:Cu, a.c. photocond. in negative photocond. region 2−65081
CdSe:S, local impurity and lattice vibrs., Fermi reson., absorpt. spectra obs. 2−80895
$CdSe:Ti^{2+}$ ligand hyperfine interaction of Ti^{2+} on sites with trigonal symmetry C_{3v} 2−80977
CdSe-CdS film photoresistor, role of activating powder 2−65096
CdSe-CdS mixed crystals, reson. Raman effect 2−72365
X CdSe-$Ge_{1.5}As_{0.5}Se_3$, pseudobinary system, glass formation 2−80531
CdSe-Se n-p heterojunction, diffusion potential determ. 2−47942
CdSe-SiO_x, electron transport study in space charge layer of vacuum-deposited film 2−77852
CdSe, absolute signs of second harmonic generation coeffs. 2−44332
CdSe, bound exciton to ionized centre, magneto-optical obs. 2−68636
CdSe, conductivity changes, O_2 chemisorption induced 2−47886
CdSe, cryst. growth, static sublimation method 2−47217
CdSe, eff. of real growth on elec. and photoelec. props. 2−71419
CdSe, elec. behaviour between room temp. and 600C 2−61305
CdSe, elec. field distrib., subjected to 0-600 V applied voltages 2−64960

Cadmium compounds continued
CdSe, electron energy loss spectra, rel. to interband transitions, bulk and surface plasmons 2–68318
CdSe, emission spectra under laser excitation, exciton interactions, exciton molecules formation 2–77840
CdSe, exciton-ionized donor complex, binding energy, theory and expt. 2–84266
CdSe, exciton photoluminesc., picosec. and nanosec. spectroscopy obs. 2–72421
CdSe, exciton scatt. by dislocations, absorpt. study 2–81007
CdSe, high temp. defect equilib., elec. transport props. 2–44096
CdSe, hole photoemission into S, 2.11 to 3.54 eV 2–84265
CdSe, homogeneity regions by mass-spectrometry, solubility of Cd and Se 2–83837
CdSe, impure, multiphoton luminesc. satellites in strong e.m. field 2–61679
CdSe, kinetics of high pressure polymorphic transitions from wurtzite to rock salt structure 2–61031
n-CdSe, magnetophonon spectroscopy study 2–68385
CdSe, memory and photocond., 77 and 300K 2–75168
CdSe, photocond., undamped oscillations 2–54253
CdSe, photoconducting, effect of traps on acoustoelec. props. 2–61100
CdSe, pumped by $CaF_2:Dy^{2+}$, parametric generation 3.37-7.86μ 2–69937
CdSe, room temp. hole and electron drift velocity, time of flight obs. 2–61306
CdSe, single crystals, l.f. noise, obs. 2–51136
CdSe, singly resonant i.r. parametric oscillator 2–69903
CdSe, solid-gas phase equilibria and thermodynamic props. 2–71368
CdSe, spontaneous and stimulated luminescence by high-density excitations in 77 to 300 K range 2–44406
CdSe, spontaneous and stimulated emission, 2-100K, exciton interactions 2–68677
CdSe, temp. quenching of photocond., thermoelec. skin effect in presence of shallow levels 2–81171
CdSe, thin film transducer, operation characteristics and anomalous behaviour 2–77922
CdSe, vapour growth, donor and acceptor identification 2–50573
CdSe, X-ray induced electron emission, core electron energy levels detn. 2–48019
CdSe anode, electron injection 2–61797
CdSe film, a.c. photocond. on excitation with intensity-modulated light, trapping levels 2–57255
CdSe film, elec. props. rel. to substrate temp., 25-200°C 2–64980
CdSe film, epitaxial, struct., composition and elec. props. 2–56582
CdSe film, epitaxial growth under isothermal conditions 2–47106
CdSe film, O_2 and N_2 effects on Hall and field effect mobilities 2–57191
CdSe film, photoelectronic props. 2–51212
CdSe film, residual gas analysis during vapour deposition 2–78697
CdSe film, struct. and photoelec. props. 2–57253
CdSe film on $LiNbO_3$, surface states effect on surface wave amplification 2–84201
CdSe films, energy spectrum and nature of trapping centres detn. by induced impurity photocond. method 2–71501
CdSe films, influence of Se vapour annealing on electrical conductivity 2–44094
CdSe i.r. parametric oscillator, pumped by Q-switched Nd:YAG laser 2–42061
CdSe laser crystal, electron excited, photocurrent and light emission obs. 2–77965
CdSe parametric oscillator, pumped with tunable dye laser 2–42053
CdSe powders, Cu, Cl_2 impurities, negative resistance behaviour, effects of light intensity, frequency variations 2–71919
CdSe resonant interaction of LO phonon and donor electron 2–68278
CdSe vacuum evaporated films structure on mica, NaCl, PbSe substrates, electron microscopy, electron diffraction techniques 2–71327
$CdSe_xS_{1-x}:Mn^{2+}$, hyperfine interaction const., temp. and comp. depend., e.p.r. study 2–81456
$CdSe_{1-x}S_x$ film, transmission, 7000-21000 cm^{-1}, band gap calc. 2–61633
$CdSe_xTe_{1-x}$, exciton reflection spectra and absorp. edge obs. 2–84517
$CdSe_xTe_{1-x}$, n-type solid soln. photoelec. props. and recombination diagram 2–72061
$CdSiAs_2$, i.r. birefr. and optical activity 2–72261
$CdSiAs_2$, polarized reflectance spectra 2–61626
$CdSi_xGe_{1-x}As$, glassy, photocond. and elec. cond., rel. to band struct. determ. 2–61448
$CdSiP_2$, cryst. growth and struct., optical props. and energy gap 2–80599
$CdSiP_2$, i.r. transmission cut-off 2–78058
$CdSnAs_2$, $CdSnP_2$, band structure, electroreflectance spectra obs. 2–81404
$CdSnAs_2$, $CdSnP_2$, polarized reflectance spectra 2–61626
$CdSnAs_2$, sphalerite-chalcopyrite transition, struct. of phases, microhardness 2–57025
n-Cd_2SnO_4, optical and elec. props. 2–51137
$CdSnP_2$:Ag(Cu), spontaneous- and stimulated- emission spectra 2–51365
$CdSnP_2$, current controlled negative resist. due to Gunn effect 2–61304
$CdSnP_2$, photocunductivity spectra in extrinsic (impurity) range, and effects of doping 2–57256
CdTe:Fe^{2+}, phonon conductivity 2–64864
CdTe:In, Cu, high temp. cond., impurity effects 2–61303
CdTe:In, self-compensation calc. assuming Cd vacancies and impurity-vacancy complexes 2–47889
CdTe:Li, self-compensation and interaction of Li with defects 2–75107
CdTe-CdSe, system, phase diagram, rel. to cryst. growth technique selection 2–47702
CdTe, absolute signs of second harmonic generation coeffs. 2–44332
CdTe, absorpt. spectra, direct exciton transitions 2–65255
p-CdTe, annealing effect on conductivity and photoconductivity, obs. 2–61263

Cadmium compounds continued
n-CdTe, bending producing 60° dislocations, effect on conductivity and photoconductivity 2–61264
CdTe, biomedical, efficiency, resolution and absorption 2–51891
CdTe, compensation by intrinsic point defects, elec. cond. obs. 2–84334
CdTe, diffusion of Cu from evaporated and chemically plated Cu layers, He ion backscatt. obs. 2–64676
CdTe, electroabsorpt., light quanta with energy less than forbidden bandwidth 2–78059
CdTe, electrochem. preparation 2–75384
CdTe, electron energy loss spectra, rel. to interband transitions, bulk and surface plasmons 2–68318
CdTe, electron radiation damage and cathodolum. edge emission 2–48254
CdTe, epitaxial growth, on CdS, closed-tube chem. transport technique 2–77498
CdTe, growth from soln. melts, elec. props. 2–74677
CdTe, high temp. defect equilib., elec. transport props. 2–44096
CdTe, hole transport, taking into account polar scatt., Monte Carlo study 2–64968
CdTe, i.r. absorpt. spectra, shallow donor impurity transitions, polaron Zeeman effect 2–61634
CdTe, ion implantation doping 2–74790
CdTe, kinetics of high pressure polymorphic transitions from zinc-blende to rock salt structure 2–61031
CdTe, mag. susceptibility of defects, 4.2-290K 2–77980
CdTe, miniature medical probe 2–69271
CdTe, naturally doped p-n structs. 2–84349
CdTe, optical grade cryst. prod. by directional solidification 2–50607
CdTe, phase equil. considerations in prep. and props. 2–50593
CdTe, photoplastic behaviour 2–50742
CdTe, Poole-Frenkel effect of holes 2–44119
CdTe, radiation effects, carrier conc., Hall mobility, photocond. 2–47892
CdTe, resonant exciton absorpt. structures 2–61200
CdTe, spontaneous luminescence and lum. spectra detn. 2–72417
CdTe, susceptibility meas. determination of covalence character of chemical bonds 2–61482
CdTe, thermal cond. and phonon scatt. by Fe^{2+} impurities 2–84213
CdTe, thermal neutron damage, photolum. and elec. resist. 2–48219
CdTe, X-ray induced electron emission, core electron energy levels detn. 2–48019
CdTe detectors, ion-implanted contacts 2–49670
CdTe epitaxial film, optimum growth conditions 2–47105
CdTe film, a.c. photocond. on excitation with intensity-modulated light, trapping levels 2–57255
CdTe film, epitaxial growth under isothermal conditions 2–47106
p-CdTe film, photolum. and photocond. 2–48217
CdTe film, with anomalously high photovolt., photomag. effect 2–75178
CdTe layers and solar cells 2–41907
CdTe preparation for nuclear detectors 2–49668
CdTe room-temperature radiation detector possibilities 2–52692
$Cd_{2.8}Zn_{0.2}As$, high mobility, scattering, galvanomagnetic effects study 2–81090
Cu_2S-CdTe film heterojunction, photovoltaic effect 2–81123
p-Ge-n-CdS_xSe_{1-x} epitaxial heterojunction, prep., struct. and elec. props. 2–77924
Hg-Cd amalgam, dil., viscosity comp. depend., 0-100°C 2–64451
$Hg_{1-x}Cd_xTe$, sweep out of minority carrier holes 2–54255
$Hg_{1-x}Cd_xTe$ alloy, cryst. growth using Te as solvent 2–47271
In-Cd alloy, quadrupole interactions of 247- keV state of ^{111}Cd, perturbed ang. correl. studies 2–75246
In-Cd alloy, type II superconductivity and mag. hysteresis 2–71863
In-Cd dilute alloy, pressure and strain derivatives of supercond. transition temp., Fermi surface topology effects 2–71859
Mg-Cd alloys, supercond. transition temp., electronic sp. ht., Debye temp. 2–47859
MgTe-CdTe mixed crystals, lattice vibrs., Raman spectra study 2–71714
Na-Cd dilute alloy, liq., compressibility determ. 2–77415
Se-CdSe heterojuncton, electrolum. 2–54481
Si-CdSe, p-n heterojunctions vacuum deposition preparation and properties 2–77925
Sn-Cd dilute alloy, lattice thermal cond. and Matthiessen's rule deviations 2–84295
$Tl_2Cd_2(SO_4)_3$ ferroelectric Langbeinite, optical and dielectric props. 2–51199
$Y_3Cd_4Zn_7$ crystallographic system, lattice parameter and space group determ. 2–80644
Zn-Cd-Te, system, phase diagram, rel. to cryst. growth technique selection 2–47702
Zn-Cd dilute alloy, dendrite growth and morphology 2–43488
Zn-0.1%Cd, single crystal, deformed, slip lines, elec. microscope obs. 2–47421
Zn-Sn-Cd-Bi liquid quaternary solution, thermodynamic props., e.m.f. method 2–71186
$Zn_xCd_{1-x}Te$ solid solution, phonon freq. detn. from reflection spectra 2–72308
ZnS-CdS:Er^{3+} mixed fluorescent compounds, spectroscopic investigation 2–84545
ZnSe-CdTe system, miscibility 2–77464

cadmium sulphide
— 2–68256
— 2–61690
acoustic wave attenuation, non-electronic lattice losses 2–43974
acoustic wave mixing and amplitude dependent phase velocity 2–51032
acoustoelectric instability, scattering of light by sound 2–71728
acoustoelectronic effects at large acoustic intensities 2–72079
anode, electron injection 2–61797
auto-photoemission, spectral investig. under pulsed and const. voltage condits. 2–72090
boson echos 2–65071
bound exciton lines, strain splitting 2–68678
bound-to-bound emission at 510 nm 2–61691
cathodoluminescence, donor-acceptor pair emission, electron irrad. damage effects 2–54478

Cadmium compounds continued
cadmium sulphide continued
cathodoluminescence, electron beam microprobe exam. of crystal structure defects 2−53745
conductivity changes, O$_2$ chemisorption induced 2−47886
core electron energy levels, X-ray induced electron emission obs. 2−48019
crystal growth, donor and acceptor identification 2−50573
crystallites, Raman scattering from surface modes 2−75311
cyclotron resonance of piezoelectric polarons, far i.r. 2−71924
deconvoluted spectra and higher resolution for Auger electron spectroscopy 2−72082
donor-acceptor luminesc., temp. depend. 2−48261
donor-acceptor pair radiation, phonic recurrence 2−72395
electron beam pumping, production of super radiant light sources 2−79215
electron concentration determ. using T activity 2−71934
electron energy loss spectra, rel. to interband transitions, bulk and surface plasmons 2−68318
electron irradiated, stage III$_R$ recovery, activation energy 2−71455
electron-phonon interactions and current stabilization 2−47891
epitaxial film, optimum growth conditions 2−47105
evaporated layers, thinning for transmission electron microscopy 2−67962
exciton photoluminescence, picosec. and nanosec. spectroscopy obs. 2−72421
exciton-exciton emission line shift 2−44407
exciton-impurity complex, optical absorp. anomalous intensity 2−72324
film, a.c. photocond. on excitation with intensity-modulated light, trapping levels 2−57255
film, amorphous, in m.i.m. structs., electroforming and elec. cond. props. 2−64978
film, c-axis orientation modification, evaporation by reflection 2−50487
film, electron mobility and scatt. rel. to grain boundaries and surfaces 2−61149
film, electron scatt. by stacking faults rel. to elec. props. 2−61150
film, epitaxial, struct., composition and elec. props. 2−56582
film, epitaxial growth under isothermal conditions 2−47106
film, Hall mobility, thickness depend., effects of Cu impurity 2−77894
film, liquid phase epitaxial growth 2−47104
film, optical absorpt. edges, rel. to pot. barriers at microcryst. boundaries 2−65256
film, photocond., prolonged relax. of dark current after illumination 2−81173
film, photocond. with gain in through thickness operation 2−44173
film, photoelectret state formation and temp. depend. 2−77939
film, photorectification in longitudinal quasi unipolar photocond. with non uniform illumination 2−81172
film, polarized memory device, photovoltage obs. 2−61381
film, sputter deposition and photocond. 2−53571
film growth by evaporation, inclined orientation 2−71370
films, evaporated in vacuum, crystal structure 2−77508
films produced by r.f. sputtering of CdS powder in Ar effects of sputtering conditions on photoconductive characteristics 2−68479
gamma detector using sintered CdS 2−42469
hexagonal, Gd^{3+} centres at sites of axial symmetry, e.p.r. obs. 2−65333
h.f. domain propagation, two-dimensional charact. 2−51156
high-field domains, propagation characteristics 2−61099
hole photoemission into S, 2.11 to 3.54 eV 2−84265
hot electron mobility 2−84276
induced optical absorption by strong excitation 2−78097
kinetics of high pressure polymorphic transitions from wurtzite to rock salt structure 2−61031
laser, electron beam pumped, photon loss and gain 2−42077
luminescence, 2.0 eV band, donor-acceptor recomb. model 2−84539
luminescence, fast electron excitation, phonon assisted exciton recombination 2−48240
luminescence, obs. 2−54479
luminescence spectra fine struct., localized exciton struct., at 4.2K 2−51366
m.i.s.m. and m.s.i.m. structures, electron emission 2−57218
mobility, maximum absorpt. freq. eval. expression 2−57176
m.o.s. system, amplification of pulse photoelectric current 2−44146
multistep current saturation 2−75078
neutron activated, X-ray detector 2−42466
optical absorption spectra, rel. to optical modulation due to moving acoustic domains 2−54418
optical cavity, total internal refl. and Fabry-Perot configs., electrolum. spectra, laser action 2−81413
optical modulation by acoustic phonon flux 2−61088
optical waveguide, fabrication by Se diffusion 2−66842
phosphor, microwave photocond. and luminesc. 2−51213
photocell with non-linear characteristics, obs. of relative spectral sensitivity 2−42463
photoconducting, acoustoelec. current, theory and expt. 2−54171
photoconducting props., prep. by reactive sputtering 2−65082
photoconductivity, effects of 10 MeV electron irradiation 2−57254
photoconductivity, temp. quenching, thermoelec. skin effect in presence of shallow levels 2−81171
a.c. photoconductivity in single crystal with insulated barriers 2−68478
photoconductivity spectrum, anisotropy 2−72060
photon drag effect, electron- phonon interaction, generated elec. field 2−68274
photopotential, surface, effect of ambient kerosene instead of air 2−68482
photoresistor, FSK-type, response to low-intensity modulated radiation 2−61452
photosensitive material, Ag, Cu, and In impurities, spectral characts. 2−72059
photosensitivity, luminesc. intensity, rel. to donor-acceptor photothermal dissociation 2−72393
photosensitivity rel. to elec. field 2−75167
piezoemission, free exciton obs. 2−78143
plate, dispersion curves of flexural modes 2−84205

Cadmium compounds continued
cadmium sulphide continued
platelets, drift meas., Schottky contact effects 2−77884
platelets, electron irradiated, radiation damage effects on luminescence at low temperatures 2−68703
Poisson and transport equations, high field domain solns. 2−54167
polariton emission 2−48218
polytypic growth of single crystals 2−60769
powder, electroluminesc. brightness, effect of nonstoichiometric deviations 2−61716
Raman scatt., electron spin-flip, 70-100 KG at 4.2K 2−68658
Raman scattering from lattice vibs., resonant cancellation 2−68657
recombination luminesc. rel. to absorption, recomb. and field mechanisms 2−78128
relaxation oscillations, induced by laser irrad. 2−64979
resonant interaction of LO phonon and donor electron 2−68278
self-diffusion of Cd, radiotracer study 2−83993
single crystal films, epitaxial growth 2−53572
solar cells, thin films, state of the art and space applications 2−59059
sound amplification threshold field nonmonotonic cond. depend., 5-120 MHz 2−77783
spin-flip Raman scatt., theory 2−57359
spin-flip Raman scatt. anomaly 2−57358
spin-flip Raman scattering, linewidths and two-electron processes 2−84501
spin-flip scattering from free and bound electrons 2−44389
spontaneous and stimulated emission, 2-100K, exciton interactions 2−68677
surface, (0001), (00) LEED beam intensity at normal incidence 2−71308
thermal cond., pulsed region cathodolum. obs. 2−54077
thermal neutron damage, photolum. and elec. resist. 2−48219
transducer deposition, parameters controlling device usefulness 2−67906
transverse surface wave depth penetration in photoconducting CdS 2−84206
trapping levels, slow, optically pumped differential absorption apparatus 2−68427
two-phonon sidebands in i.r. absorption due to third-order potential 2−75284
u.s. absorption and dispersion, role of hopping conductivity 2−71733
valence band energy levels, Γ-point, from emission spectra due to A- and B-band excitons 2−68289
Al-CdS-In thin film struct., memory effect, switching characts. 2−44139
CdS:Ag(Al), field quenching, influence of doping 2−54170
CdS:Co^{2+}, lattice thermal cond., phonon-reson. scatt. 2−47763
CdS:Co^{2+}, spin-lattice relax., Orbach process Debye temp. 2−54367
CdS:Cu, trapping parameters, photocond. response, i.r. quenching, photochem. effects 2−65000
CdS:Cu powder phosphors, a.c. electroluminesc. characts. 2−44420
CdS:Cu powder phosphors, d.c. electroluminesc. characts. 2−44419
CdS:In laser, spin flip, visible, operation at liq. He temps. 2−66768
CdS:Ti^{2+}, ligand hyperfine interaction on sites with trigonal symmetry C_{3v} 2−80977
CdS:Yb^{3+}, emission spectrum at 10 K, before and after e irrad. 2−75339
CdS:Yb^{3+}, mechanisms effecting optical spectra of 4f^{13} ions 2−61625
CdS-Au, study of anode hole injection 2−84346
CdS-CdSe film photoresistor, role of activating powder 2−65096
CdS-Cu$_2$S, photovoltaic cell, props., doping effects 2−65092
CdS-Cu$_{2-x}$Te heterojunction photoelements, spectral response curves and current-voltage characteristics 2−44184
CdS-LiNbO$_3$, convolution and correlation by nonlinear interactions between sonic induced space charge and field waves 2−51015
CdS, retaining metastable phases by quenching under pressure 2−84152
n-CdS, thin compound semicond., sorption-induced conductivity changes 2−77886
CdS films, shift in lux-ampere and I-V characts. due to photoelectret effect 2−81170
CdS$_{1-x}$Se$_x$:Mn, Mn^{2+} conc., e.p.r. determ. 2−72481
CdS$_{1-x}$Se$_x$:Mn^{2+}, hyperfine interaction const., temp. and comp. depend., e.p.r. study 2−81456
CdS$_{1-x}$Se$_x$, reson. Raman effect 2−72365
CdS$_x$Se$_{1-x}$ film, transmission, 7000-21000 cm^{-1}, band gap calc. 2−61633
CdS$_{1-x}$Zn$_x$S:Mn, Mn^{2+}conc., e.p.r. determ. 2−72481
n-CdS−p-Cu$_2$S film heterojunction, rectification, photosensitivity and tunnelling 2−71955
Cd$_{1-x}$Zn$_x$S:Mn^{2+}, hyperfine interaction const., temp. and comp. depend., e.p.r. study 2−81456
Cd$_x$Zn$_{1-x}$S film, prep. and comp. depend. of energy gap and resist. 2−54169
Cu$_2$S-CdS heterojunction, prep. and photoelectronic props. 2−72056
Cu$_2$S-CdS heterojunction, photocapacitance effects 2−51221
Cu$_x$S-CdS photovoltaic cell, model 2−54261
GaAs-CdS heterojunction, isotypic, prep. and photosensitive props. 2−71956
Se-CdS heterojunction, electrolum. 2−54481
(Zn, Cd)S:Ag, Ni, fluorescence, efficiency curves, investigation of Klasens' simple thermal quenching theory 2−48250
Zn$_x$Cd$_{1-x}$S:Cu, cl temp. and i.r. quenching of luminescence and photocond. 2−84543
Zn$_{1-x}$Cd$_x$S, melt-grown single crysts., struct. 2−64646
ZnS-CdS, evaporated layers, mosaic heterojunction photo-emf 2−77970

Caesium
acoustic radiation from shock front 2−71115
adsorbed on W, LEED and work function obs. 2−47169
adsorption, on W and Nb simultaneously with Ba, work function and thermal stability obs. 2−67923
adsorption and O-Cs co-adsorption of W single crystal surface rel. to work function change 2−54266
adsorption on GaAs, ESCA obs. and photoyield 2−53595
adsorption on Mo, LEED and Auger spectroscopy obs. 2−50540

Caesium continued
adsorption on W, atomic theory of work function variation 2−71343
adsorption on W(100) surface, work function 2−83878
adsorption on W and Ti, ellipsometry, Auger spectra and surface pot. difference obs. 2−50550
arc mode theory, assumptions, parameters 2−63249
arc mode thermionic converter, low vapour pressures 2−52376
atom, 7 $^2P_{1/2}$ hyperfine structure, core polarization, optical double resonance obs. 2−74213
atom, cascade-decoupling meas. of excited S-state hyperfine structures 2−52922
atom, determ. of g_j factor in $7^2P_{3/2}$ state by optical double resonance in strong magnetic field 2−52916
atom, elastic electron scatt., differential cross-section calc. 2−79883
atom, excited-state photoioniz. cross sections 2−59922
atom, optically pumped, influence of modulation of crossbeam on amplitude of r.f. field 2−52934
atom, oriented $6^2P_{1/2}$, m_j mixing in collisions with inert atoms 2−46468
atom, reactive collision cross section with I_2 2−70738
atom, Stark effect investigation of third excited $^2P_{3/2}$ levels in first spectrum, tensor polarizability determ. 2−70591
atom, three-quantum photoionization 2−70604
atomic level population determ. using flame atomic absorption spectroscopy 2−49939
atomic time scales, generation dissemination stability and accuracy 2−78749
atoms, optical pumping, effect of transverse pumping 2−70605
atoms, two level spin-system, nondiagonal magnetic resonance 2−56110
desorption of submonolayer from Ge(100) substrate 2−67921
discharge, cold cathod pulsed, current maxima 2−74422
discharge, resonance radiation effects on plasma 2−70908
discharge tube, ionization in nuclear reactor 2−53252
disordered overlayers, on Ni(001), specular electron refl. 2−60681
film, adsorbed on W, work function rel. to surface struct. 2−68487
film, photoemission, 3.7-21.2eV 2−54277
ion beam, neutral atom rate meas. 2−53207
ionized vapour, electron density determ. from spectral line mixing 2−46792
lattice vibration based on Toya's electron-phonon interaction 2−64834
lattice vibrations, anharmonicity estimation from X-ray interference intensity coeff. 2−54017
liquid, determ. of pseudo-Gruneisen parameters 2−74540
liquid, elec. resist. and electron collapse 2−46982
liquid, electron spectrum, calc. by cell method 2−83797
liquid, self-diffusion, calc. 2−67817
low voltage arc discharge, excitation and ionization processes 2−53265
low voltage arc discharge, Maxwellization of precathode electron distrib. fn. 2−53264
optical constants in liquid and solid, 0.3 to 2.5 μ region, dependence on temp. 2−68596
optically oriented, transverse relaxation time 2−83191
photoemissive yield from caesiated semiconductors, model 2−61460
plane aparallel diode, I-V characteristics 2−49287
plasma, collisional, space pot. oscills., hot-probe meas. 2−67677
plasma, dense strongly nonideal, elec. cond., 1000- 10000 K and 130-350 atm. 2−80292
plasma, forbidden line transitions, thermionic diode 2−60237
plasma, ion temps. determ. using probe with cold collector grid 2−74356
plasma, partially ionized, impedance determ. 2−56343
plasma, prod. by reson. absorpt., contrib. of dissociative recomb. 2−67666
plasma, pulsed X-ray obs. of shock waves 2−64297
plasma, reson. absorpt. produced, radial distrib. of electron density 2−46727
plasma, s.h.f. emission 2−67641
plasma, stationary supersonic flow in magnetic de Laval nozzle, characteristics 2−50203
plasma, thermodynamic props. 2−56328
plasma, W cathode electron emission rel. to temp. and current density 2−75191
plasma diode, collisionless, current oscillations 2−63220
plasma in thermionic convertor, electron temp. effect on electron density 2−63244
resonant charge exchange cross sections at low energies in Q-machines 2−56115
specific heat, elec. and thermal resistivities calc. according to Sharma-Joshi model 2−47749
supercritical state, cond. nature 2−60500
thermionic arc convertor, ion loss and electron temp. 2−80369
thermionic converter, discharge modes, polarization and interferometric investigations 2−49288
thermionic converter, nonequilibrium relaxation phenomena, near emitter region 2−49276
thermionic diode, diffused electronic and ionic currents through grid type anode 2−45659
thermionic diode, ignited mode, charge influence of V-I characteristics 2−52378
thermionic diode, model improvements 2−49277
thermoelectric power rel. to Fermi surface shape and sample dimens. effects 2−68296
thin films, electrical resistance from 0.3 to 0.9 μ region 2−68597
thin films, optical properties, 0.3 to 0.9 μ region 2−68597
vapour, charge-exchange process for production of 2.5 keV metastable H atoms 2−56124
vapour, gas laser, phase matched, generation of u.v. radiation 2−42027
vapour, photoionization by method of space charge amplification 2−70603
vapour, study of electron spin polarization 2−42763
vapour, thermodynamic properties 2−50264
vapour, two step photoionization 2−64036
vapour cells, wall coated, preparation 2−69517
vapour Q-switches for synchronizing mode-locked laser pulse trains with external events 2−73546
vapour source, for Cs-graphite thermionic converter 2−52372

Caesium continued
work fn. determ., Cs covered surfaces, with plane parallel Cs diode, physical basis 2−61456
work fn. determ., Cs covered surfaces, with plane parallel Cs diode, technology 2−61455
Ar MHD plasma instability 2−80262
$CaMoO_4$, photoluminescent props. 2−72441
$Ca_5(PO_4)_3Cl:Mn^{2+}$, e.p.r. obs., site substitution by Mn, field parameters 2−72479
Cs-Ba filled thermionic converter, current voltage characteristics 2−49286
Cs-Ba filled thermionic converter, ignited mode 2−49285
Cs-Ba filled thermionic converter, optimization 2−49283
Cs-Ba filled thermionic converter, influence of magnetic pressure 2−49282
Cs-Bi layers, photoemission props. 2−65102
Cs-He plasma, oscillations and stability in mag. field 2−60267
Cs-NH_3 solutions, velocity of 10 MHz waves on function of temp. and metal concentration, structural changes 2−43352
Cs-O layers, on GaAs and $InAs_{0.4}P_{0.6}$ cathodes, thickness rel. to photoemission 2−75194
Cs-O_2 sources in systems for thermionic converters 2−63222
Cs-Rb differential Stark shift investigated using optically pumped atomic light modulation oscillators 2−46424
Cs-Rb mixtures sorbed on graphite, vapour press. 2−53592
Cs, cylindrical converter, I-V characteristics 2−52375
Cs, thermionic energy convertors, probe measurements, space craft power source 2−54991
Cs^+, desorption from W, mol. beam study 2−60691
Cs^+ ion transport of red blood cells of rats, comparison with K^+ by kinetic tracer model 2−55257
Cs^+ ions, free, n.m.r. involving photoionization, optical pumping and charge exchange 2−79897
CsI, investigation of $np^2P_{3/2}$ level sequence by level crossing spectroscopy 2−79920
^{127}Cs, ^{129}Cs production for medical use 2−69270
^{129}Cs, myocardial uptake and clearance characteristics rel. to ^{43}K 2−66260
^{133}Cs, phase destruction detection of ground state hyperfine transitions and population inversion with GaAs lasers 2−70599
$^{133}Cs^+$ ion, free, n.m.r. freq. shift due to charge exchange with Cs atom 2−79896
^{137}Cs, seawater content, of fallout origin 2−62043
^{137}Cs accumulation in coastal sediments 2−62044
^{137}Cs fallout in reservoir sediment 2−57802
^{137}Cs fuel elements apparatus for studying radial migration of radioactive products 2−52847
Cs + CH_3I, rotational polarization of reaction products and reprojection of angular momentum in molecular beam expts. 2−65367
Cs + HBr, rotational polarization of reaction products and reprojection of angular momentum in molecular beam expts. 2−65367
Cs + HI, rotational polarization of reaction products and reprojection of angular momentum in molecular beam expts. 2−65367
He-Cs gas plasma MHD, two-dimensional calc. of ionization fluctuations 2−80265
K-Cs collisions, broadening of principal series lines 2−56117
La:Ce, skew scattering of electrons, Hall effect obs. 2−75055
Sb-Cs photocathode study using scanning electron diffraction system 2−75195

Caesium compounds
— 2−72214
alums, interpretation of Ti^{3+} e.s.r. spectra 2−81445
borate glass, n.m.r. powder patterns, graphic analysis in the presence of quadrupole interactions 2−48300
$CaWO_4:Tb^{3+}$ or Er^{3+}, compensation of the excess charge during activation of scheelites with rare-earth ions 2−72480
Cs-K alloy, Ashcroft's empty core model 2−74898
Cs-K alloys, molten, electric transport, electrical resistance and density of electron states 2−60497
Cs-K(Rb) alloy, heat of soln., pseudo alloy atom model 2−74897
Cs-Na alloys, molten electric transport, electrical resistance and density of electron states 2−60497
Cs-Rb alloy, Ashcroft's empty core model 2−74898
$CsAlF_6$, mag. susceptibility, temp. depend., 300-700K 2−72110
$CsBO_2$, evaporation, mass spectrometric obs. 2−64512
$CsBe_2(BO_3)F_2$, synthesis and physicochemical props. 2−47210
$CsBe_2F_5$, pentafluorodiberyllate, structure determination by X-ray and neutron diffraction 2−56653
CsBr:K, non-cubic Ag- centres in mixed crystals 2−44370
CsBr, cation impurity, i.r. absorp. obs. 2−61635
CsBr, CsBr:Tl, CsBr:In, luminesc. crystals, exciton and hole migration 2−48242
CsBr, electric field effects on F-band 2−51347
CsBr, lattice dynamics 2−50993
CsBr, photoemission and photostimulated emission rel. to image storage targets 2−48023
CsBr, X-irrad. at cryogenic temps., I-, α-, H, H' and V_4 centres 2−68038
CsBr(Cl)(I), coherent neutron scatt. amplitudes from powders 2−53654
Cs_2CO_3 proton irradiation, 660 MeV production of radioactive Sb and Te, annealing effects 2−68817
$CsCl:Ba^{2+}$, ionic cond., 250-500°C 2−54232
$CsCl:K^+(Rb^+)$, impurity-induced i.r. absorpt. calcs., lattice dynamical model 2−54419
CsCl, $B2 \rightleftharpoons B1$ phase transition kinetics 2−53984
CsCl, elastic props. based on interatomic force model 2−68854
CsCl, in sulfolane-water mixtures, conductance at 35°C 2−78199
CsCl, lattice dynamics 2−50993
CsCl, phonon-dispersion, neutron spectrometer study and shell model anal. 2−84192
CsCl, photoemission and photostimulated emission rel. to image storage targets 2−48023
CsCl, pure and Ba^{2+}-doped, self-diffusion, 360-460°C 2−74813
CsCl, surface ionization on Ir film, effect of C adsorption on Ir (111) face 2−64543
CsCl, U band shape from first electronic transition of H- and D-substitutional impurities 2−47446
CsCl B2 type struct., transform. twinning, inhomogeneous shear model, reply to comments 2−64810

Caesium compounds continued
CsCl B2 type struct., transform. twinning, inhomogeneous shear model, comments 2–61032
CsCl m.p. and phase transform., effects of KCl and NaCl additions 2–43932
CsCl(Br)(I), vibr. absorpt. spectrum of NO_2^- and NO_3^- 2–77769
$CsCoCl_3$, mag. struct. 2–72213
$CsCoCl_3$, one-dimens. mag., Mossbauer obs. 2–72160
$CsCrCl_3$, crystal structure, Jahn-Teller distortion 2–81363
Cs_xCrF_3, cryst. struct. 2–60760
Cs_2CrO_4, proton irradiation, 660 MeV production of radioactive Sb and Te, annealing effects 2–68817
$CsCr(SO_4)_2.12H_2O/D_2O$, Cr^{3+} spectroscopy 2–54400
$CsCuCl_3$, one- dimens. mag., Mossbauer obs. 2–72160
CsF, phonon dispersion relations, neutron scatt. study 2–64840
CsF, Raman spectra, phonon modes 2–48196
CsF scatt. by electrons, cross sections 2–64214
$CsFeF_4$, ferroelastic effect, spontaneous lattice strain 2–71571
$CsFeF_4$, planar antiferromagnet, X-ray diffr., suscept., and Mossbauer obs. 2–65180
Cs_2GeF_6, press.-induced phase transform. 2–71677
CsH_2AsO_4, ferroelec. phase transition dynamics, spin-lattice relax. meas. by double reson. 2–84450
γ-$CsHCO_3$, cryst. struct. 2–43579
$CsH_3(SeO_3)_2$, neutron struct. anal. 2–71428
Cs_2HfCl_6, e.s.r. of Yb^{3+} in octahedral cryst. field 2–72482
CsHg, free paramanetic van der Waal molecule produced 2–67545
CsI:Na, mechanism of thermally stimulated afterglow in 60-90 K range 2–72431
CsI:PO_4^{3-}(SiO_4^{4-}), i.r. absorpt. 2–54424
CsI:$SO^{2-}{}_4$, $CrO^{2-}{}_4$, $SeO^{2-}{}_4$, i.r. absorpt. by impurity anions 2–78086
CsI:Tl, α-particle irrad., scintillation yield orientational depend. 2–81434
CsI:Tl, α and γ scintillation growth times 2–73938
CsI:Tl single crystal, influence of channelling on scintillation efficiency 2–72396
CsI, defect spatial decoration, methods and mechanism 2–80695
CsI, lattice dynamics 2–50993
CsI, quadrupole h.f.s. on rot. transition, ^{127}I coupling consts. 2–53003
CsI, relaxed state of self-trapped exciton 2–65291
CsI, secondary slip generated by point load 2–74849
CsI, thermal dissociation rate meas. 2–70738
CsI, Xe diffusion and calc. of activation energies 2–74812
$CsICl_4$, lattice parameters, normal modes of vibr. 2–71427
CsI(Na), nature of luminescence centres, hypothesis based on properties of CsI crystals 2–68679
CsI(Tl)-NaI(Tl) scintillation detector, thin layer, low background, for soft protons 2–59622
CsI + Ar collisions, vibrational and rotational energy transfer, ballistic mechanism 2–67536
$CsMgBr_3$:Ni polarized spectra, near i.r. and visible, ligand field model interpretation 2–84483
$CsMgCl_3$:Ni polarized spectra, near i.r. and visible, ligand field model interpretation 2–84483
$CsMnBr_3$, cryst. struct. 2–43578
$CsMnBr_3$, crystal growth and perfection 2–47224
$CsMnCl_3.2H_2O$, mag. anisotropy, short range order effect 2–44295
$CsMnF_3$, antiferromag. and nucl. mag. reson. freq. shift phenomena 2–81482
$CsMnF_3$, antiferromag. and paramag. reson. linewidths near Neel temp. 2–68726
$CsMnF_3$, perovskite, polarised i.r. refl. spectra, phonon dielec. dispersion 2–51319
$CsNO_2$, phase diagrams, cryst. struct., to 40 kbar 2–74951
$CsNO_3$, molten, interdiffusion coeff. of Ag^+ 2–65383
$CsNO_3$, proton irradiation, 660 MeV production of radioactive Sb and Te, annealing effects 2–68817
$CsNiBr_3$ polarized spectra, near i.r. and visible, ligand field model interpretation 2–84483
$CsNiCl_3$, n.m.r. of ^{35}Cl and ^{133}Cs, determ. of mag. props. and struct. 2–72215
$CsNiCl_3$, one-dimens. antiferromag., spin-wave approach 2–54352
$CsNiCl_3$, one-dimens. mag., Mossbauer obs. 2–72160
$CsNiCl_3$ polarized spectra, near i.r. and visible, ligand field model interpretation 2–84483
$CsNiF_3$, one-dimens. mag. behaviour 2–44241
$CsNiF_3$, three dimensional mag. struct., neutron diffr. obs. 2–61556
Cs_2O-B_2O_3-P_2O_5 glass, struct., e.p.r. obs. of Cu(II) paramag. centres 2–48291
Cs_2O-Cs soln., as source of Cs and O_2, in thermionic converters 2–49280
CsO_2, magnetic properties, obs. of structural and magnetic transitions 2–65116
$CsO_{2(3)}$, Raman spectra, O_2^- and O_3^- ion props., solid-solid transition effects 2–81354
$CsPO_3$, molten, meas. of density in temp. range 800-1050°C, relation to bonding and coordination 2–84034
$CsPbCl_3$, cubic-tetragonal transition temp., press. depend. 2–71676
$CsPbCl_3$, far i.r. refl. spectra, Kramers- Kronig analysis, optical lattice vibrs. 2–72300
$CsPr(MoO_4)_2$, crystal struct. and thermal stability 2–74729
Cs_2PtCl_6, n.q.r., spin-lattice relax., rotary lattice mode freq. 2–77748
Cs_2SO_4, coherent neutron scatt. amplitudes from powders 2–53654
Cs_2SO_4, proton irradiation, 660 MeV production of radioactive Sb and Te, annealing effects 2–68817
Cs_2SO_4, sound velocity, 1046 to 1156°C 2–71194
$Cs_2SO_4.Cr_2(SO_4)_3.24H_2O$ alum., paramag. spin-lattice relax. times of Cr^{3+} 2–84444
Cs_3Sb, photoemission, integral sensitivity 2–65103
Cs_2UBr_6, force constants, lattice dynamics 2–74968
Cs_2UBr_6, Zeeman effect of vibronic transitions 2–84528
$Cs_2UO_2F_4.H_2O$, crystalline structure from X-ray studies 2–56652
Cs_2ZrB_6:Re^{47}, sharp- line luminesc., vibr. mode energies 2–57370
Cs_2ZrCl_6:Ir^{4+}, high resolution MCD, and absorption spectra 2–57342
Cs_2ZrCl_6:U^{4+}, Zeeman effect of vibronic transitions 2–84528

Caesium compounds continued
Cs_2ZrCl_2, high resolution absorpt. and mag. circular dischroism spectra analysis 2–75289
Cs_2ZrCl_6, press.-induced phase transform. 2–71677
$Cs_2[CuCl_4]^{2-}$, covalency and excited 4p states effects on 3d ground states of Cu^{2+} 2–84578
$CuCs_2(SO_4)_2.6H_2O$, electron spin- lattice relax. of Zeeman and interaction systems 2–68580
K-Cs alloy, pseudopotential theory and Vegard's rule 2–67992
K-Cs alloys, liq., elec. resist., temp. depend. 2–64471
K_2CsSb photocathode, thermionic emission 2–61459
$Li_2SO_4-Cs_2SO_4$ system, phase diagram 2–80527
Na-Cs alloys, liq., elec. resist., temp. depend. 2–64471

Calcium
in 56 Arietis spectrum, variations 44860 2–44860
atom, 3d4d, term dependence of Hartree-Fock results 2–56092
atom, collisions with atmospheric ions, meas. of charge transfer cross-section for formation of Ca^+, 1-500 eV 2–79865
atom, electron-impact double excitation cross sections calc. in Born Oppenheimer approx. 2–70607
atom, Hartree-Fock eqns, iterative numerical method 2–64010
atom, oscillator strengths for resonance transitions 2–79875
atoms, matrix isolated, absorption spectrum 2–49944
bone Ca content from neutron activation analysis 2–69364
diffusion, in fluorapatite 2–77609
in divines of Murchison and Vigarano meteorites 2–51840
film, photoelec. props., elec. field influence 2–81188
human content, det. using neutron activation anal. 2–48854
intracellular transport across human placental barrier 2–69210
K-line luminosities and calibration of G-K type giant stars 2–69082
K-line observations of binary stars rel. to Fe/H abundance ratio 2–73036
neutron radioactivation analysis in vivo of Ca, P, N and Cl in rat's organism 2–54575
optical constants ε_1 and ε_2, absolute values 2–48134
piezoresistance, temp. and uniaxial stress dependence obs. 2–71840
radiative-neutron-capture gamma-ray analysis by linear combination technique 2–54574
solar abundance, collision broadening of Ca I and Ca II lines 2–75948
solar Ca II K_{2v} spectral features in non-magnetic regions, temporal behaviour 2–55170
solar continuum, near H and K lines of Ca^+ 2–58548
spectral line intensities, effect of HCl, H_3PO_4 and $AlCl_3$ in arc and flame 2–51478
total body Ca content from meas. of ^{37}Ar in expired air after low level neutron irradiation 2–69365
tropical Atlantic, distribution 2–54763
Ca/H abundance ratio in solar corona from observations of Ca XV lines 2–55159
Ca-ammonia solution relaxation times and Overhauser enhancements for protons obs. 2–46988
Ca II, H and K emissions, disk chromosphere spectroscopy 2–76019
Ca II, interstellar line in supernova spectrum in NGC 5253 2–81828
Ca II, Stark broadening and shift of lines 2–60245
Ca II absorption lines, extragalactic in spectra of supernova in NGC 5253 2–73015
Ca II interstellar lines in southern sky, comparison with 21 cm absorption line 2–75795
Ca II K-line and Hα solar chromospheric short-lived brightening event 2–78612
Ca II K-line profiles in quiet sun 2–73113
Ca II line profiles in plages, chromosphere and sunspots 2–75947
Ca K line obs. in chromospheric and coronal networks, correlation between intensity fields 2–76021
Ca XIV-XVIII lines in e.u.v. spectra of solar flares 2–58546
Ca XIX in solar flares, calc. of wavelengths in X-ray region 2–85050
Ca^+, measurement and calculation of Stark broadening parameters for resonance lines 2–42727
Ca^+, reson. lines, electron impact broadening 2–59914
Ca^+ in $Ca_5(PO_4)_3F$, crystal field parameters 2–78161
Ca^{2+}, effect on dynamic props. of muscle proteins, quasielastic light scatt. study 2–70798
Ca^{2+}, meas. of termolecular association rate constants with Ar, O_2, N_2, CO, CO_2, N_2O in flowing afterglow 2–48316
CaI, photoionization, absolute absorption cross-sections at 1886.5, 1765.1 Å 2–76971
CaI interstellar lines, photoelectric obs. and CaI/CaII ratio 2–78474
CaII K line, model chromosphere of Procyon 2–75712
CaII K line in solar spectrum, intensity fluctuations rel. to contribution functions 2–48792
CaII solar resonance lines, observations using a compact grating spectroheliograph 2–45014
CaII→FeI resonance, T-Tauri stars 2–75744
Ca + HI→CaI + H, meas. of angular distrib. of product, determ. of threshold kinetic energy limits on $D_0°$ 2–81494
KCl:Ca^{2+}, positron annihilation, temp. and mag. field effects 2–77850
$Na°/Ca^+$ ratio in interstellar medium, model of clouds 2–75785
O^{5+}-Ca collisions, observation of Kα hypersatellites 2–64046
YIG:Si^{4+},Ca^{2+} magnetostriction rel. to mag. field inclination to crystallographic axes at 4.2K, 77K and room temp. obs. 2–84437

Calcium compounds
anorthite, Si-O and Al-O bond length parameters analysis 2–61850
calcia-stabilized ZrO_2, fracture toughness 2–50777
calcia-stabilized ZrO_2, thermal stress induced microstruct. modifications 2–50901
chlorapatite, hydrothermal growth 2–47234
dicalcium lead propionate, spin-lattice relax. near crit. point 2–65196
fluorite, natural X-ray topographic obs. 2–80669
formates, formation and surface props. of electron emissive coatings 2–65365
halides, absorption in e.u.v. 25 to 72 eV 2–42882
Plaster of Paris, fracture of triangular plates due to contact explosive pressure 2–53793
spodiosite analogues, i.r. and Raman spectra 2–51318
Ca-Bi-V ferrite rods, excitation of longit. acoustic waves 2–43968
Ca-Fe olivines, X-ray diffraction study 2–47325

Calcium compounds continued
$Ca-NH_3$ solution, Hall coeff. and elec. cond., 203-243K 2−46984
$CaAl_{12-x}Fe_xO_{19}$ solid soln., $x \leqslant 4.8$, e.s.r. and Mossbauer obs., ferric ion positions 2−75268
$Ca_3Al_2(SiO_4)_3:Fe^{3+}$, optical spectra calc. 2−72295
$Ca_2B_5O_9Br(Cl)$, cryst. struct. 2−53657
$Ca_2B_6O_{11}.5H_2O$, colemanite, temp. depend. of switching rate 2−72041
$CaCO_3:Fe^{3+}$, spin-lattice relax. obs. 2−65177
$CaCO_3$, a.c. polarographic det. of Mn 2−48353
$CaCO_3$, calcite, atmospheric aerosol constituent, optical consts. 2−57946
$CaCO_3$, calcite, habit rel. to growth soln. comp. 2−74676
$CaCO_3$, calcite, twinning boundaries, thermal shift after annealing 2−77573
$CaCO_3$, calcite,crystal growth, travelling solvent zone melting 2−50591
$CaCO_3$, elemental anal., using neutron capture γ-rays 2−44513
$CaCO_3$, generalized Gruneisen parameters and thermal expansion 2−74996
$CaCO_3$, Madelung parameters and electrostatic energies for calcite, aragonite and vaterite and charge distrib. on $CO_3{}^{2-}$ ion 2−43500
$CaCO_3$, monocryst., elastic consts., u.s. obs. 2−80727
$CaCO_3$, optical strength and damage caused by laser radiation 2−72273
$CaCO_3$, photoelastic tensor elements, Brillouin scatt. study 2−78114
$CaCO_3$, rare earth doped, X-ray excited optical fluorescence 2−61707
$CaCO_3$, synthetic calcite, dislocations, X-ray obs. 2−47412
$CaCO_3$ atmospheric particulates, radiative properties in spectral interval 500-1500 cm^{-1} 2−54854
$CaCO_3$ powders, failure props. 2−43889
$Ca_3Cr(GeO_4)_3$, mag. struct. and space group determ. 2−72145
$Ca_3(CrO_4)_2$, X-ray charact. of crystal parameters 2−53658
CaF_2, crystal perfection, dependence on growth technique 2−47396
CaF_2, ENDOR spectrum of U^{3+}-F^- 2−84607
$CaF_2.3Ca_3(PO_4)_2:Nd^{3+}$, local compensation of Nd^{3+} ionic charge 2−64681
$Ca_3Fe_2(SiO_4)_3:Fe^{3+}$, optical spectra calc. 2−72295
$CaGeO_3$-$Sr(Ba)GeO_3$ solid solutions, struct., i.r. spectra study 2−65251
CaH_2-LaH_3 system, dissoc. press. and thermodynamic props. 2−50958
CaH in solar sunspot spectrum, 4900- 6441 Angstrom range 2−62743
$Ca(H_2AsO_4)_2$, cryst. struct., neutron diffr. obs. 2−67988
$Ca(HClO_4)_2$, NH_4ClO_4 and metal mixture systems, rate of combustion 2−61784
$CaHPO_4.2H_2O$, brushite, growth, by diffusion in silica gel and in solution 2−47233
CaI_2:K, Pb, Mn, fluorescence, investigation using 365 nm u.v. irradiation 2−51387
CaI, produced in Ca + HI reaction, determ.of lower bound for $D_0{}^\circ$ 2−81494
CaLa silicate oxyapatite:Nd crystalline laser materials, pulsed and Q-switched characteristics 2−42060
$CaLaSi(PO_4)_2CaF_2$:Nd 2−49380
$Ca_{2-x}Ln_xMnO_4$ solid soln., Ln = Pr, Nd, Sm, Eu, Gd struct. 2−60753
$CaMe^{VI}O_4$:U, single crystals with scheelite structure, Me^{VI} = Mo, W luminescence and absorption spectra between 300K and 4.2K 2−68676
$CaMg(CO_3)_2$, monocryst., elastic consts., u.s. obs. 2−80727
$Ca_3Mg[SiO_4]_2$, merwinite, at. arrangement 2−78219
$CaMoO_4$, elastic consts., u.s. determ. 2−77773
$Ca(NO_3)_2$, precip. in KNO_3, solid soln. form. 2−56942
$Ca(NO_3)_2.4H_2O$, molten, hypersonic vel. dispersion obs. by Brillouin spectroscopy 2−77427
$CaNb_2O_6$:Nd, cryst. growth and laser operation 2−50592
$CaO:Ce^{3+}$, cubic sites, EPR investigations, g values 2−54491
$CaO:Fe^{3+}$, e.p.r. obs. 2−48275
$CaO:Gd^{3+}$, spin-lattice coeffs. calc. 2−51286
$CaO:Li^+,Na^+$, e.p.r. of Mn^{4+} ions, spin Hamiltonian parameters detn. 2−51402
$CaO:Mn^{2+}(Fe^{3+})$, spin-lattice coeffs., relativistic cryst. field contrib. 2−65203
CaO-Al_2O_3-Fe_2O_3, phase comp. analysis by X-ray diffr. 2−74725
CaO-Al_2O_3-SiO_2 glasses, i.r. spectra, struct. study 2−47057
CaO-Al_2O_3-SiO_2 melt, dynamic viscosity, effect of CO_2, 1400-1700°C 2−74527
CaO-CaF_2 system liquidus line determ. by the capillary method 2−84683
CaO-FeO-Fe_2O_3, synthesis and physico-chem. props. 2−43871
CaO-Na_2O-MgO-SiO_2 glass, phase equilib. in glass forming region 2−57023
CaO-Nb_2O_5-TiO_2-SiO_2 system, liquidus temps. 2−43436
CaO-SiO_2-Al_2O_3 glass, stratification, liquation, opalescence 2−56564
CaO-ZrO_2-SiO_2 2−75320
CaO-ZrO_2 ceramic, struct., thermomech. props. 2−43876
CaO, effect on elec. resist. of ZrO_2 2−53936
CaO, elastic consts., temp. depend. 2−74823
CaO, excited state of F-centres, paramagnetic resonance 2−44437
CaO, F^+ and F-centres, absorpt. and emission, temp. depend. 2−84537
CaO, F^+ and F' centres 2−71523
CaO, Gruneisen parameter and thermal expansion 2−47756
CaO, Jahn-Teller coupling in excited level of F^+ centre, uniaxial stress effects 2−68635
CaO, neutron irrad., $F_a{}^+$ centre, absorp. and emission band obs. 2−71522
CaO, phonon dispersion, three body force shell model 2−68216
CaO, rare earth doped, X-ray excited optical fluorescence 2−61707
CaO in Bi_2O_3, ion conduction obs. 2−61418
$Ca(OCl)_2.2Ca(OH)_2$, i.r. and Raman spectra, obs. of fundamental vibration of ClO^- anion, determ. of force constant and bond length 2−57341
$Ca(OCl)_2.4H_2O$, i.r. and Raman spectra, obs. of fundamental vibration of ClO^- anion, determ. of force constant and bond length 2−57341
$Ca(OH)_2:Mn^{2+}$, e.p.r., 4.2−800 K, vibronic effects 2−78163

Calcium compounds continued
CaOH in stellar atmospheres of M-dwarf stars 2−75729
$CaO.Al_2O_3$-Al_2O_3-CaF_2, solid soln., phase diagram 2−57029
$CaO.Al_2O_3.CaF_2$ glasses, coordination numbers from i.r. spectral data 2−64587
$2CaO.Fe_2O_3$, subst. of Mn for Fe ions, study by X-ray diffr., mag. and Mossbauer effect meas. 2−43644
$3CaO.SiO_2$:Cr, struct. rel. to reactivity 2−80877
$CaO.2Al_2O_3$: Nd^{3+}, stimulated cross section 2−54452
$Ca_5(PO_4)_3Cl$, chlorapatite, synthetic, monoclinic struct. 2−53656
$Ca_5(PO_4)_3F:Nd^{3+}$, e.p.r. obs. crystal field at Ca^+ position 2−78161
$Ca_3Pd_2H_4$, prep., struct., and elec. resist. 2−47347
$CaRuO_3$, orthorhombic perovskites, metallic elec. props. of single crystals 2−84291
CaS:Bi:Fe phosphors, emission characteristics, role of S^{2-} and Cl^- determ. by Fe^{3+} impurity 2−65311
CaS:Bi, Pd phosphors, thermoluminescence 2−54475
$CaS:Fe^{3+}$, e.p.r. obs. 2−48275
CaS phosphor, activator and co-activator emission characts. 2−48239
CaS phosphors, self activated emission, study of trap depths and nature of trapping centres 2−54473
$CaSO_4$:Dy phosphor, thermoluminescent for thermal neutron dosimetry 2−83160
$CaSO_4$:Dy phosphor for meas. of u.v. irradiances 2−82561
$CaSO_4$:Dy thermoluminescence dosimeters for environmental monitoring 2−79675
$CaSO_4$:Mn response to n, γ irradiation 2−83161
$CaSO_4$:Mn thermoluminescence, dose relationship, energy response and rate dependence from 8 keV-30 MeV 2−68701
$CaSO_4$:Tm, thermolum. dosimeter characts. as personnel monitor 2−70552
$CaSO_4$:Tm phosphor for meas. of u.v. irradiances 2−82561
$CaSO_4$:Tm phosphor powder use for fast neutron dosimetry 2−78666
$CaSO_4$:Tm thermoluminescent dosimeter construction and characts. 2−55923
$CaSO_4$, neutron dosimetry, using thermoluminescence 2−69345
$CaSO_4$, plaster of paris, P, S and Rayleigh waves 2−41674
$CaSO_4.2H_2O$, gypsum, atmospheric aerosol constituent, optical consts. 2−57946
$CaS_2O_6.4H_2O$, second harmonic generation 2−75248
$CaSe:Fe^{3+}$, e.p.r. obs. 2−48275
$CaSiO_3$-$NdSiO_5$ system, phase equilib. 2−47707
Ca_3SiO_5, hydrated, pore structure, temp. effects 2−71664
$CaSo_4$:Mn, relative thermoluminesc. effects of α- and β-radiation 2−51379
$CaSo_42H_2O$, symmetry of SO_4 ion 2−64635
Ca_3TeO_6, elementary cell data 2−43576
$CaTiO_3$, effect of La_2O_3 on lattice distortion 2−74724
$CaTiO_3$, photochromic crystals, erase-mode optical recording characteristics 2−63422
$Ca_3(VO_4)_2$, $Ca_2V_6O_{17}$, growth from $Ca(NO_3)_2$-K_3VO_4-H_2O system, pH effects 2−47232
$CaWO_4:Eu^{2+}$, e.p.r., elec. field effect 2−48287
$CaWO_4$-Nd laser, active Q switching technique for high power in single longitudinal mode 2−63337
$CaWO_4$, adiabatic eleastic stiffness moduli, u.s. pulse superposition meas., 15-300K 2−84037
$CaWO_4$, elastic consts., u.s. determ. 2−77773
$CaWO_4$ following low temp. X-irradiation, photoconductivity 2−81175
$CaWO_4$ scintillator, optical meas. in far u.v. 2−52689
$Ca_3WO_5Cl_2$, orthorhombic, crystallographic data 2−47318
CaX synthetic zeolites, preferred rotation of adsorbed ClO_2 molecules 2−80579
$Ca(Zr,Ti)O_3$ dielectrics, high-permittivity temp.-stable, low microwave loss 2−51190
$CaZrO_3$-$CaHfO_3$ system solid solns., lattice parameters 2−43575
$CaZrTiO_5$, zirkelite, lunar U-bearing phase 2−44909
$Ca_2[AsO_4B(OH)_4]$, vibrational spectra, interpretation by factor group approx. calc. of force constants for BO_4 group 2−70728
PbO-CaO-GeO_2 glass, structure and properties 2−53540
SiO_2-Al_2O_3-Na_2O-K_2O-CaO-MgO glass, viscosity-temp. relations 2−67883
SiO_2-CaO-MgO-Na_2O-$AlF_3:Dy^{3+}$ glass syst., luminesc., effect of heat treatment 2−48228
zeophyllite, crystal struct. determ. 2−77547
ZrO_2.CaO solid electrolyte, ion transport number 2−65054

calcium fluoride
anisotropic thermal conduction at low temperatures, boundary limited phonon mean free path 2−68260
centres of C_{4v} symmetry containing trivalent rare earth-interstititał hydride in pairs, rel. to u.v. irrad 2−83984
colour centre interconversion induced by electron irradiation 2−77598
colour centres, high temp. absorpt. study 2−77597
crystal growth, oxygen impurity removal, using COF_2 scavenger 2−50568
defect struct., containing excess anions, neutron diffuse scatt. 2−77570
defects, low temp. plasma produced radiational defects 2−71452
dielectric consts., l.f., temp. and press. derivatives 2−51189
dosimeters, thermoluminescent, preparation and props. 2−82824
elastic wave damping, effective anharmonicity consts. 2−80913
e.p.r., linear elec. field effects for Ce^{3+}-F^- tetragonal sites 2−48285
F_2-centres, ⟨100⟩ and ⟨110⟩ oriented, spectral obs. 2−53751
F-centres, zero-phonon line obs. 2−53752
film, spectral emission by polaritons, 400-1100 cm^{-1} 2−65252
fluorite structure, Gruneisen parameters an interatomic forces 2−51050
force fields, contrib. of three-body overlap effects 2−77765
friction and wear, fund. review 2−47554
intrinsic radiational defect formation, mechanisms 2−56680
ionicity, dispersion, and optical spectra 2−44374
lattice dynamics, neutron scatt. anal. 2−71723
low symmetry complexes involving hydride ions paired with rare earth ions 2−47434
natural and Dy doped phosphor, thermoluminescent for thermal neutron dosimetry 2−83160

Calcium compounds continued
calcium fluoride continued
neutron dosimetry, using thermoluminescence 2−69345
optical absorption bands and e.s.r. props. following intense γ-irradiation 2−84529
photochromic, erase-mode optical recording characteristics 2−63422
photochromic, La doped, application as recording medium for holographic interferometry 2−66789
powder, sintering activity, effect of calcination 2−61004
powder phosphor, characteristics for thermally stimulated exoelectron emission dosimetry 2−67091
pressed fused disc for X-ray fluorescence meas. on U minerals 2−65586
proton irrad., elec. cond. 300-800K, anion vacancy cond. mechanism 2−57230
proton irrad. density change and absorption band growth 2−71454
Raman spectra, lattice dynamics 2−57040
rare earth doped, interstitial dipole relax., thermal depolarization obs. 2−60790
sintering, effect of additives, comments 2−77723
sintering, effect of additives, reply to comments 2−80876
stimulated emission from rare earth and actinide ions 2−48225
surface optical modes, reflection obs. 2−51344
thermoluminescence dosimeter characts. as personnel monitor 2−70552
thermoluminescence due to Gd^{3+}, hole activation energies, 4.2 to 600K 2−57377
thermoluminescence under exposure to u.v. light 2−68700
thermoluminescent dosimeter for meas. natural background radiation 2−42698
two-electron U-centres, point-ion models 2−83987
u.v. dosimeter in sunburn range 2−85136
vibrational amplitudes and Debye- Waller factors from elastic consts. and Raman freqs. 2−50983
CaF$_2$:Ce^{3+}, paramag. relax. due to flux jumping, nonequilib. spin distribs. 2−72231
CaF$_2$:Dy, scintillating phosphor in radioactive reference lights, transient temp. dependence 2−49443
CaF$_2$:Dy dosimetry of 80 kVp X-rays 2−55925
CaF$_2$:Dy thermoluminescence dosimeter meas. of background radiation in USA 2−84859
CaF$_2$:Dy^{3+}, magnetic circular dichroism rel. to detection of giant spin relaxation times 2−44313
CaF$_2$:Dy^{3+}, spin lattice relax. rate rel. to temp. 2−84198
CaF$_2$:Er^{3+}, two photon excitation by Nd laser wavelength depend. 2−48216
CaF$_2$:Eu^{2+}, electronic interactions in 4f^6 5d config. 2−72237
CaF$_2$:Gd very small specimens, precision density meas. 2−47473
CaF$_2$:Gd^{3+}, second order spin-lattice coeffs., temp. depend., e.p.r. obs. 2−80890
CaF$_2$:Gd^{3+}, spin-lattice coeffs. calc. 2−51286
CaF$_2$:H-, local modes studied with intense CO$_2$ laser 2−61632
CaF$_2$:Ho^{3+} two photon excitation by Nd laser wavelength depend. 2−48216
CaF$_2$:La,Ce, uncoloured and X-irrad., optical absorpt., charge transfer processes 2−65253
CaF$_2$:Mn, CaF$_2$:Tb, relative thermoluminesc. effects of α- and β-radiation 2−51379
CaF$_2$:Mn, scintillating phosphor in radioactive reference lights, transient temp. dependence 2−49443
CaF$_2$:Mn, thermoluminescence and thermally stimulated exoelectron emission, trapping centres 2−68699
CaF$_2$:Mn response to n, γ irradiation 2−83161
CaF$_2$:Mn thermoluminescence dosimeters, influence of size on ^{60}Co γ-ray dosimetry in extended media 2−67088
CaF$_2$:Mn thermoluminescent γ-dosimeter, sensitivity to neutrons 2−82820
CaF$_2$:Na, conc. and mobility of F ion vacancies, elec. conductivity obs. 2−47979
CaF$_2$:Nd$_2$O$_3$ (NdOF), optical spectra of Nd^{3+}, Stark effect obs. 2−61702
CaF$_2$:O, meas. of ^{19}F dynamic polarization, e.p.r. investigation 2−51295
CaF$_2$:Pr^{3+}, energy levels of tetragonally sited Pr^{3+} 2−80989
CaF$_2$:Pr^{3+}, linear dichroism due to stress induced mixing of electronic states of anisotropic centres 2−84462
CaF$_2$:Tb^{3+}, photo- and X-ray luminescence, obs. of luminescent centres 2−84547
CaF$_2$:Tm^{2+}, Kramers doublets with hyperfine coupling, meas. 2−78048
CaF$_2$:Tm^{2+}, mechanisms effecting optical spectra of 4f^{13} ions 2−61625
CaF$_2$:Tu^{2+} crystal, Stark structure of ground state of Tu^{2+} 2−61611
CaF$_2$-Nd^{3+}. energy level shifts at oxygen^2 compensated Nd sites 2−84229
CaF$_3$-YF$_3$:Er^{3+}, spectroscopic study of stimulated radiation 2−61689
CaF$_2$ plates, plug cutting 2−45182
Calculating apparatus
see also Fourier analysis; X-ray crystallography/calculation apparatus
A/D conversion/computer interface 2−52666
analogue to digital conversion for oil prospecting 2−84754
application in radiation therapy, process control by electronic calculator 2−82027
digital integrator for gas chromatography 2−65409
digitization of information on oscilloscope photographs 2−48934
digitization of information on oscilloscope photographs 2−48934
electrooptical data processor, u.s. light diffractors, high speed printer 2−76116
MEGAHPOL, fast online noncomputer multiparameter data reduction system, nuclear applications 2−73952
memory materials and devices, conference (Princeton, 1 May, 1972) 2−69478
programmable calculator for data acquisition and processing in thermal tests 2−63148
zoom lens, depth-of-focus calculator 2−52449
analogue apparatus
see also Nomograms
hybrid analogue data acquisition system, for atmospheric turbulence 2−78353

Calculating apparatus continued
analogue apparatus continued
nuclear reactor reactivity, time-variant, on-line determination using process computer 2−52886
optical data processor, patent 2−69996
pattern velocity computers, for wind velocity obs. 2−57968
digital computer programmes
− 2−67965
aerosol particle size det. by comparison of broadened X-ray diffraction profiles with standard lines 2−60528
ALGOL program for determ. of multiple parameters of arbitrary spin particles 2−42315
algorithm for automatic sorting of signals in shift reagent spectra 2−83218
algorithm for flow between rot. coaxial disks 2−56292
algorithm for Stokes problem, applic. to erythocyte 2−60173
algorithm for Stokes problem 2−56311
algorithmic language for intensity meas. 2−43569
arbitrarily loaded shells of revolution, geometrically nonlinear analysis, in FORTRAN IV 2−66562
astronomical ephemerides, program for modern aberration coefficients 2−69194
atomic codes, dynamic information theory, computer code 2−67378
atomic fine structure cross sections from reactance matrices, FORTRAN IV program 2−52942
for automatic anal. of Ge(Li) γ-ray spectra 2−82082
beam-columns, transverse vibration calc. 2−66599
BEHAVE-2 code, modelling of oxide fuel struct. evolution 2−52858
Bessel functions, FORTRAN subroutine for calculating $j_l(\rho)$, $J_{l+1/2}(\rho)$ and derivatives 2−41459
cavity distortions in massive liquid due to inertial effects, numerical soln. of differential eqn. on MINSK-22 2−83745
charged particle beams, simulation 2−79696
classical motion of two particles, ASA FORTRAN program 2−52127
classical relative motion of two particles, ASA FORTRAN program 2−52126
classical three body programme for eH collisions ionization threshold law 2−56122
code KSPACE for space time reactor kinetics 2−76934
colour rendering of light sources investigation 2−45802
COMETHE code, prediction of oxide fuel pin behaviour 2−52859
coolant heat transfer, multichannel calc., lumped model 2−83080
Coulomb function, FORTRAN IV subroutine, numerical accuracy 2−45237
crystal struct. soln. by Patterson heavy atom technique, FORTRAN programs 2−73267
crystallographic analysis using aspherical atomic scattering factor, in FORTRAN 2−77543
crystallography, for symmetrified plane wave calc. 2−60747
dilute gas, collision integrals, FORTRAN IV program adapted to run on IBM computers 2−53340
elastic stability of hyperboloidal shell of revolution 2−66550
electron beams and bremsstrahlung, penetration in extended media 2−47777
electron-atom collisions, computer methods and software packages 2−42764
electron-atom collisions, structure and excitation determ. using fast general-purpose computer programs 2−42765
ellipsometer data analysis with small programmable desk calculator 2−42208
energy loss of charged particles, FORTRAN-4 computer program 2−64870
estrogenic steroids, structure elucidation from computer interpretation of mass spectra 2−84685
FISP, for generating fission product inventories for nuclear fuel 2−76955
fitting theoretical expressions to statistical distributions, computer program suite 2−66483
fluids physical properties data base system 2−74309
Fortran IV program for statistical error calc. of electron probe microanalysis 2−82083
FORTRAN packages and routines, set of documentation conventions 2−52117
Fourier analysis, discovery approach, use of computer as calculational aid 2−78734
fuel rod behaviour analysis using CYGRO-F computer code 2−76946
for gamma spectra attributions and neutron activation analysis 2−82859
gaseous discharge growth in space-charge distorted fields 2−67689
GASVIP and VIPAL, det. of natural frequencies and initial buckling stresses of prismatic plate assemblies 2−41588
geodesy, pseudoinverse of sparse matrices, algorithm 2−54605
high energy physics data analysis, software strategies 2−46029
image processing in nuclear medicine 2−82810
International Ice Patrol, processing of digital data logger STD tapes 2−57883
ion-bombarded targets, damage distributions calc. 2−79678
ionosphere propagation of e.m. waves, 2 dimen' tracing, computer program 2−65944
iterative calc. of mass flow and pressure in pipe systems 2−64232
iterative determ. of analytic continuation of scattering amplitudes, application to pp forward amplitude 2−59396
Knoop indentation testing, resolved shear stress distrib. calcs., computer program 2−60941
macromolecule study, interactive display generation program 2−69204
macromolecules, programmes for analysis of normal vibrations 2−43017
magnetic coil, high field, for stress calcs. 2−73519
Martian topographic contour map generation 2−81911
matrix method of vibrational analysis of framed structures 2−76355
MCCOY and SIMLA, for one-dimensional unsteady compressible fluid 2−70865
modelling of swelling and gas release in neutron absorber rods 2−52861
modular ray trace program, Fortran program 2−79345
molecular moment of inertia derivatives with respect to internal coords., calc. using general machine algorithm 2−52961

- **Calculating apparatus** continued
  - **digital computer programmes** continued
    - molecular structure modelling 2—79990
    - molecular structure radial distribution curves 2—77154
    - molecular vibrations, mean amplitudes and correction coeffs., computation method 2—67444
    - molecular vibrations, normal coordinate analysis 2—70665
    - molecules, asymmetric top, Coriolis perturbations 2—46508
    - molecules, periodic potential functions for internal rotation 2—64095
    - Monte Carlo program, response of NaI counter to monoenergetic γ-rays 2—79651
    - Monte Carlo treatment of thermal neutron scattering 2—63943
    - Mossbauer scattering spectra, computer simulation, FORTRAN program 2—68609
    - multicentre quantum chem. integrals and matrix elements, computation method 2—79848
    - multigroup-transport- burnup program NEUTRA for determ. of flux density in MTR fuel elements 2—76914
    - multilayer media, impact and contact stress analysis in classical electricity theory, computer calcs. 2—82304
    - neutron absorption in spherical and cylindrical sources, computer code calculation 2—42600
    - neutron activation prediction program system 2—63947
    - neutron induced energy release, computer program NERMA 2—42599
    - neutron spectrometer resolution function 2—80609
    - Newman-Penrose eqns., extension of asymptotic solns. using algebraic programming system FORMAC 2—76195
    - NMR, computer assistance in spectral analysis 2—52345
    - n.m.r. spectra plotting 2—52344
    - nuclear bremsstrahlung measurements, multi-parameter experiments 2—78861
    - nuclear fuel temp. and heat flux distrib., computer program THISTLE 2—83149
    - nuclear reaction DWBA analysis 2—70480
    - nucleon elastic scattering from targets with spin 2—67215
    - for numerical integration of Thompson scattering from coronal streamer models 2—76026
    - for numerical solution of induction logging problem in inhomogeneous media 2—78261
    - on-line, for calc. of lung mechanical parameters 2—69249
    - one-dimensional transport code for reactor fuel studies 2—83127
    - optical potential calc. of absorption and elastic cross sections, FORTRAN program 2—52078
    - optical system in arbitrary plane, illumination distrib. calc. 2—59258
    - optimization problems, review of methods for solution 2—52116
    - partial pressure, calc. from total press. curve 2—43449
    - particle accelerator, interactive beam design program with Monte Carlo capabilities 2—82831
    - photoionization cross section for low-Z element, calc. using program of Brysk and Zerby 2—77010
    - physical chemistry programs for laboratory expts., classroom problems 2—82101
    - physical properties computer accessed data bank development 2—75362
    - plane stress analysis of elastic plate structures by finite element method 2—73384
    - plasma minimum-B mirror devices, stable equilibria computation, computer program 2—67652
    - polyatomic molecules, complex program for treatment of i.r. spectra 2—52968
    - polymer conformation, simulation program 2—70801
    - for pore struct. analysis 2—47145
    - positron lifetime spectra analysis using FORTRAN program 2—52561
    - pressurized water reactor one-point 4-group algorithm for computing nuclear fuel depletion 2—63956
    - procedure for application of Gringberg's soln. to engineering design of MHD duct 2—67613
    - Raman-infrared generalized program for prolate symmetric top mols. 2—70662
    - REACTION, for multicomponent geological system studies 2—61847
    - reduced rotation matrix elements, subprogram for calc. 2—66452
    - reduction of objective prism plates of star fields, absolute calibration 2—75698
    - relativistic kinematics of three body reaction 2—74054
    - RKVI program for determ. of fuel rod vibration characteristics in parallel flow 2—63973
    - s-channel transformation matrices for helicity and invariant amplitudes for γN→0-B calc. using REDUCE language 2—55812
    - sampling programme for control of persons working with open radioactive materials 2—52889
    - satellite drag-free orbits, long-term development study using computer program PROD 2—68992
    - SCHROD, numerical soln. of radial Schrodinger eqn. 2—66442
    - Schroedinger eqn., finite difference method for one-dimensional eigenvalues, computer program 2—66443
    - search algorithms for determ. topological properties of molecules 2—52960
    - smooth contour plotting of single-valued arbitrary three-dimensional surface, FORTRAN subroutine CONTOR 2—82282
    - sound absorption in porous material lined cylindrical ducts 2—41730
    - space vehicle mission analysis and Trajectory Simulation, gravity model 2—54990
    - spectra absorption for calc. position and optical density of each band 2—46418
    - spectral analysis by iterative deconvolution, FORTRAN computer program 2—63054
    - staggered-net scheme for numerical simulation of open channel surges and bores 2—43277
    - statically loaded plane frames, nonlinear analysis 2—66535
    - stress-rupture data, relative abilities of time- temperature parameters to correlate and extrapolate data 2—47608
    - structure factor simulation and one-dimens. electron density calc. 2—73268
    - super critical aircraft wing design, computer aided 2—71099
    - superconducting phonon spectra, determ. by computer from tunnelling effect 2—81056
    - suspension, Coulter counter instrument settings, calc. 2—50380
- **Calculating apparatus** continued
  - **digital computer programmes** continued
    - swelling and creep of irradiated metals, theory based computer code, application to in-pile behaviour of steel 2—76939
    - THAPA, for activation analysis 2—84689
    - theta pinch discharge, investigation of relation between compression, relaxation and end losses by two-dimensional m.h.d. computer programme 2—43160
    - track detection program for Hough Powell device 2—76747
    - transmission electron diffr. pattern generation 2—43549
    - turbulence measurement, in two-phase region of hydraulic jump 2—64235
    - two-electron integrals in LCAO-MO calculations, economic storage and processing method 2—52979
    - unfolding electron energy profiles 2—73345
    - worldwide cloud cover distribution data program 2—81696
    - X-ray diffraction line deviation as measure of Scherrer eqn. broadening, curve fitting 2—77542
    - X-ray diffraction profile correction and calcs. before Fourier analysis 2—47303
    - X-ray line broadening analysis, background separation 2—74714
    - yield stress radiation damage function of Fe, determ. using SAND II code for data analysis 2—79840
    - ^{75}As, low-lying negative parity states, core-excitation calculations, least squares iteration program 2—70396
    - ^{13}C(^{3}He,n)^{15}O reaction at 5.5 and 6.2 MeV analysed with DWBA code DWUCK and Hauser-Feshlach-Moldauer code MANDY 2—46316
    - ^{89}Sr and ^{90}Sr determination by liquid scintillation beta spectroscopy 2—85083
    - ^{90}Y determination by liquid scintillation beta spectroscopy 2—85083
  - **digital computers**
    - astronomical photographic degradation by atm., resolution enhancement by computer processing 2—76040
    - bubble chamber transmission system, LSI most-memory in digital data 2—55932
    - mini-computer, time shared, inexpensive system for spectroscopy 2—70086
    - data acquisition system for astronomical photoelectric photometry 2—55326
    - data-handling system, multi-purpose 2—52667
    - gas flow through entrance region of cooled tube, heat transfer at v. high temp. 2—46818
    - geophysics, automatic contouring using bicubic functions 2—78239
    - graphical plotting on line printer using high density plotting symbols 2—66485
    - hybrid, for generating exponentially weighted RR-interval histogram 2—69248
    - incremental integration with serial-parallel processing for differential equations 2—82283
    - ionization chamber in water phantom, control by direct connection to digital computer 2—69384
    - phase equilibria and complex reaction problem calculation 2—74580
    - scientific research in Europe 2—82087
    - slotted wind tunnel interference parameter calculation 2—64378
    - spin-lattice relaxation time meas. with saturation recovery method using on-line computer 2—66672
- **Calculation**
  - *see also Graphs; Nomograms*
  - — 2—59022
  - — 2—66402
  - accuracy of complex finite elements 2—41553
  - adiabatic kinetics model parameters, variational estimation 2—83103
  - algorithm for linear energy transfer analysis 2—45051
  - algorithm for profiling common depth surface from multiple reflections of seismic waves 2—44567
  - analytical method for calc. of redistribution of interstitial solute in thermal gradient 2—77601
  - applied mathematics, computing methods 2—82284
  - approximate Z-transform technique, transient anal. of lumped and distributed parameter systems 2—55440
  - approximation techniques for the design of geometries for γ radiation scattering 2—79847
  - baroclinic quasi-geostrophic model, numerical scheme 2—57932
  - beam and shell deflection, numerical soln. of boundary value problem 2—82314
  - blood circulation, biomechanics, numerical studies 2—78644
  - boundary layer, three dimensional with heat transfer, iterative calculation 2—53275
  - boundary layers in ducts, numerical predictions 2—70843
  - boundary value problems in optically thick media, Lie series treatment 2—83112
  - boundary-initial-value problems, semidiscrete approx. 2—63053
  - Brillouin zone sums on cubic lattices, evaluation 2—57115
  - buckling, numerical analyses of compound branching 2—52180
  - capillarity, volume-area relationship 2—83721
  - circular plate post buckling analysis, finite element 2—73357
  - computation time reduction possibilities when programming fuel injection process on digital computer 2—58818
  - countercurrent flow systems, method for numerical determination of transients 2—60142
  - cubic spline interpolation applic. to reaction rate determ. 2—68767
  - diatomic molecules, vibrational-rotational states, optimised calc. 2—56142
  - diffraction grating, triangular, with 100° apex angle 2—63386
  - diffusion, numerical soln. of problem 2—66481
  - discrete numerical approach dynamics 2—80218
  - double integration of e.p.r. spectra in presence of base line drift, numerical method 2—52341
  - dropwise condensation, numerical simulation 2—77471
  - dynamics, variational analysis, finite element method 2—77211
  - elastic hollow sphere, axially symmetric deformation, soln. of boundary value problem 2—82329
  - elastic plates anal. of vibrational modes, finite element method 2—82341
  - elastic rotating discs, stress analysis and optimum design, using dynamic programming 2—73373
  - elastic spherical shells, numerical soln. of deformation problems 2—58861
  - elastic systems, automatic computation 2—41614
  - elastodynamic tensile fault 2—72610

Calculation continued
- electron gun computation and design problems 2−76454
- electron lens analysis by computer, real and virtual cardinal points, aperture and aberration constants 2−76453
- electronic wavefunctions, Serber-type spin eigenfunctions in terms of spin-adapted antisymmetrized products 2−74195
- energy modal synthesis appl. to fast reactor burnup anal. 2−83043
- epithermal, in reactor lattices, spherical harmonics treatment 2−76901
- explicit discrete mechanics using difference equations, with applics. 2−73348
- extinction theorems in theory of e.m. scattering 2−78979
- Falkner-Skan flow, unsteady, finite difference method of solution 2−53144
- film thickness, maximum uniformity, algorithms for experimental parameters optimization 2−50478
- finite difference numerical solutions to Navier-Stokes eqns. for liquid film flow in entry region 2−67793
- finite element analysis of linearized BGK Boltzmann equation 2−58766
- finite element Galerkin method soln. of multi-dimensional neutron transport eqn. 2−76896
- finite element method calc., comparison with expt., dynamic stability problem 2−69631
- finite element method in stress analysis 2−69662
- finite element soln. for large elastic deformation, discontinuous fields 2−76274
- finite element solution of electrokinetic and hydrodynamic coupled flow 2−74310
- finite-difference equations, use of nonuniform grids 2−82281
- finite-element method, perturbation errors 2−66484
- flat membranes, large deflection analysis, numerical methods 2−73346
- flow, plane steady around profile situated between straight parallel lines 2−64230
- flow between converging flat plates, numerical analysis 2−67777
- flow through contractions, numerical model 2−77377
- force constants, implication methods 2−67450
- geophysical e.m. induction, finite element method of solution 2−54705
- gradually and spatially varied flows, numerical integrations 2−77243
- Harris instability with collisions, numerical simulation 2−70968
- Hartree-Fock equations, iterative solution with improved stability 2−83181
- heart valves flow patterns, numerical solution of Navier-Stokes equations 2−85126
- heat conduction dual analysis, by finite element method 2−73464
- heat eqn. soln. using Chebyshev series 2−58957
- heat transfer multi-region problems, improved point-matching techniques. 2−52269
- hybrid displacement method for buckling of thin elastic plate 2−82311
- hydrodynamics, free-surface, initial value techniques 2−56467
- hyperbolic differential equations, second-order difference method 2−69716
- incremental method, thermal cond. of organic liqs., molecular structure depend. 2−80468
- infinite elastic thick plate, load symmetrical to axis of revolution and middle plane, stress analysis 2−78887
- initial value method for Ambarzumian integral equation 2−41550
- invariant difference methods application to gas dynamics 2−77334
- ionosphere, numerical integration method, chemical and charge balance conservation 2−81721
- iteration method for calc. of vibrational frequency increments of polyatomic molecules 2−77047
- iterative deconvolution procedure for spectra analysis 2−70073
- iterative method for Hartree- Fock eqns. for atoms 2−64010
- lateral shearing interferograms evaluation 2−79351
- lateral shearing interferometry data reduction, application to turbulent medium 2−79352
- least squares estimation rel. to satellite tracking 2−41554
- least squares method, applic. to anal. of decay curves 2−63842
- least squares methods for evaluation of osmotic pressure data 2−43343
- light scattering on spherical particles, computer calculations 2−63396
- linear dynamical problems in continuum mechanics with random loads 2−76244
- linear fracture thermodynamics of solids, convolution inverse variational principles applics. 2−55466
- liquids, significant structure, numerical methods 2−56475
- microwave open resonator with spherical mirrors, variational calc. of resonant freq. to test beam-wave theory 2−58984
- minimality props. of local pot. 2−63052
- mixed finite element methods, applic. to stress concentration problems of cylindrical shells with circular cutout or crack 2−73355
- molecular quantum mechanical calc., integral transformations 2−56146
- molecular transmission probability of complex systems 2−82268
- moving boundary problem with variable diffusivity, soln. using method of successive approximations 2−49045
- multidimensional gas dynamics, boundaries characteristics, in time dependent finite difference analysis 2−74478
- natural convection, between parallel vertical plates, numerical analysis 2−52281
- natural convection in porous medium between two concentric cylinders, numerical analysis 2−69800
- Navier-Stokes eqns., numerical soln. 2−67558
- Navier-Stokes eqns., two-dimensional unsteady compressible, numerical scheme 2−56291
- necking in circular cylindrical bar, numerical study 2−52148
- neutron multigroup diffusion eqn., comparison of finite element and finite difference approxs. for numerical soln. 2−76900
- neutron transport, first flight collision probability for finite cylinder 2−83045
- neutron transport discrete ordinate eqn., effect of singularities on approximation in S_n methods 2−79825
- neutron transport discrete ordinate eqn. equivalent to P_l approx. 2−79824

Calculation continued
- neutron transport eqn., spherical harmonic solns. from discrete ordinate codes 2−76899
- Newton-Raphson analysis of temp. dependence of nuclear quadrupole resonance frequencies 2−70675
- non-Newtonian fluids, two-dimensional flow in channel with rectangular cavities, finite difference scheme 2−67563
- non-Newtonian fluids, under complex rheological conditions, modelling 2−82302
- nonlinear buckling of cylindrical shells, numerical soln. 2−73360
- nonlinear heat eqn., uniform convergence of finite difference scheme 2−69796
- nonlinear optimization methods, comparison of four 2−55439
- nonlinear parametric interactions, instabilities, numerical study 2−78780
- nonlinear vibration of rotating cantilever blades treated by Ritz averaging process 2−78865
- nuclear fission reactors adaptive control models 2−59817
- nuclear fission reactors control system design and modelling 2−59813
- nuclear reactor control rod motion transients, computational model 2−83106
- numerical, by finite element method, for lake circulation around island 2−74493
- numerical, finite difference method for two-dimensional flow 2−74332
- numerical, finite element model for shells by discrete Kirchhoff hypothesis 2−73367
- numerical, limitations on hexahedron finite elements with derivative degrees of freedom 2−73369
- numerical, of vibration problems by isoparametric shell elements 2−73397
- numerical, reduced integration and isoparametric elements 2−73370
- numerical approximations, eqns. of atm. motion, sources of error 2−81671
- numerical filters, truncating and weighting functions 2−41555
- numerical integration methods for CIE chromaticity coordinates computation 2−73651
- numerical iterative procedure, for elasto-plastic stress analysis 2−73388
- numerical soln. of strain energy function and boundary value problems in finite elasticity 2−73381
- numerical solution of dispersion equation, bi-Maxellian plasma, Newton's method 2−80330
- numerical solution using Runge-Kutta method 2−84535
- numerically integrated stiffness matrices 2−73368
- optimization problems, review of methods for solution 2−52116
- partial differential eqns. soln., use of fast Fourier transforms 2−55442
- percolation of fluid through porous dam, numerical treatment of singularity in free boundary problem 2−83469
- physical data, math. struct. analysis 2−58819
- plane strain consolidation in saturated clays, finite element method 2−76314
- plasma, particle-in-cell model, elec. resist., computer simulation, review 2−80256
- plasma, two-dimensional heat flow at toroidal inclusion 2−53177
- plasma echoes, numerical simulation 2−70954
- plasma phenomenon, fusion, numerical simulation, review 2−80254
- plasma physics computational models, comparison, including super-particle, water-bag 2−80255
- plasticity, constrained minimisation problems 2−76331
- plate bending, convergence of finite element solutions represented by non-conforming basis 2−69658
- plate bending analysis by quadratic programming 2−76316
- plates, elastic-plastic and eccentrically stiffened, finite element analyses 2−66561
- plates on a two parameter foundation model, finite element analysis 2−73359
- pulse propagation, numerical Laplace transform inversion of function 2−82313
- quadrature method for computing laminar boundary layers 2−74315
- resonant states in atomic collisions, determ. of wavefunctions and energies using finite-difference boundary value method 2−70616
- rotating circular plates with peripheral edge slots, stability control analysis by finite element procedure 2−76357
- scattering, momentum-space eqns., peaked potentials, numerical aspects 2−55421
- Schrodinger eqn., numerical soln. 2−55415
- Schrodinger eqn., one-dimensional, new method for rapid numerical solution 2−82234
- seismic data, optical processing, description 2−72622
- shock computations, self-adjusting hybrid schemes 2−55560
- simultaneous eigenfunctions of $\mathfrak{L}^2$ and $\mathfrak{S}^2$ by direct diagonalization 2−74196
- small parameter expansion method, reactor power response determ. to sinusoidal reactivity input 2−83067
- solid state, neutron, theoretical, nuclear, maths. and computation, progress report of Atomic Energy of Canada 2−62910
- sonic flow around wing profiles, numerical calculation 2−74476
- statically loaded plane frames, nonlinear analysis 2−66535
- statistical mechanics, numerical expts. on equilibrium and non-equilibrium properties 2−82245
- stress analysis of thin plates, annular segment finite element 2−76315
- stresses in cantilever plates, numerical methods 2−73362
- structural mechanics, boundary value problems, integral equation method of solution 2−58826
- structural mechanics boundary value problems, integral equation method of solution 2−58825
- switched Shuman filters, for numerical calculation of shock waves 2−45561
- symmetrical bending of circular plates, finite element method 2−73358
- synthetic seismograms obtained by eikonal method, series developments convergence 2−84711
- tensor diffusion equation, atmospheric, numerical solution 2−72781
- thermal expansion, 1.5-30K, 55-90K and room temp. 2−74993
- thermionic convertors, simplification 2−63245

Calculation continued
- thin shells analysis with doubly curved quadrilateral finite elements 2−73361
- three dimensional density reconstruction from series of two dimensional projections 2−49047
- Tokamaks, neoclassical transport theory in banana/plateau regimes 2−70919
- transient free-surface flow in porous media by finite element method 2−53359
- Troesch's two-point boundary value problem, solution by combination of techniques 2−83553
- tuning forks' eigenfrequencies, numerical determination 2−69698
- turbulent boundary layer, 3-dimensional, calc. by explicit finite-difference scheme 2−46661
- turbulent two dimensional separation, numerical experiment 2−70839
- two-overlapping-group transport computational method for thermal neutron problems 2−83054
- upwind difference scheme for solution of transport problems 2−58811
- variational acceleration on technique for iterative solution of two group neutron diffusion equations 2−59809
- variational principle for irreversible phenomena 2−76239
- vibratory systems with collision, numerical calculation for transient responses 2−82291
- viscous fluid motion past impulsively started semi-infinite flat plate, numerical soln. 2−83459
- Vlasov equation, difference scheme for numerical solution 2−53176
- wave propagation, transient linear, in shells, analysis by finite difference method 2−63109
- Ca surface abundance in high velocity A-stars, from Ca II 3933 Angstrom line 2−48702
- H_2^+, finite-difference soln. of united atom, one centre expansion of molecular wavefunctions 2−80048
- O_2, radiative transfer, 100 to 1000 K, Planck mean absorption coeff. 2−76391
- U enrichment, calc. of flow rate in cascade separator 2−83082

Calculus *see Differential equations; Integrals; Mathematics*

Californium
- nuclear targets, electrodeposition methods of prep. for cross section obs. and accelerator bombardment 2−73919
- whole body counting, γ-rays, Anger camera 2−78663
- ^{252}Cf, as neutron source 2−82795
- ^{252}Cf medical neutron source, ion chamber dosimetry 2−69441
- ^{252}Cf neutron activation, mineral analysis on ocean floor 2−65522
- ^{252}Cf spontaneous fission neutron source for medical implant therapy, dose tables and modified distribution system 2−69442
- ^{252}Cf therapeutic sources, absorbed dose and linear energy transfer distributions 2−45039

Californium compounds
- $CfCl_3$ low temp. absorption spectra, obs. 2−64116

Calorimeters
- adiabatic, construction details 2−76406
- adiabatic, for in-pile meas. of absorbed dose in nuclear reactors, status, export from Hungary 2−63977
- automatic adiabatic, polymer sp.ht and enthalpy meas. in temp. range −180 to +270°C 2−63165
- balance microcalorimeter for gas-solid reactions in fluorine chemistry 2−52305
- circulating, flowmeter applic. 2−80388
- in critical assemblies, for heat release meas. 2−42680
- depth dose, for high intensity, l.v., flash X-ray machines 2−66285
- flow microcalorimeter, rapid response high sensitivity 2−45605
- heat flow, for in-pile meas. of absorbed dose in nuclear reactors, status, export from Hungary 2−63977
- heat-loss-compensated, for absorbed dose obs. in graphite 2−67366
- ionization in hodoscopic system for study of interactions in 1 MeV region 2−82805
- isoperibol, for energy obs. of high power laser pulses 2−73474
- isothermal, design using thermal bridge principle 2−82386
- laser cone, spectral response 2−73473
- lasers, high power c.w., total energy measurement 2−78937
- liquid flow, pumping systems 2−83736
- metal rod, gas dumping, meas. of gamma-heat in nuclear reactor core 2−83079
- microcalorimeter, portable, for meas. of characts. of X-ray beams 2−85180
- microcalorimeter, vacuum adiabatic, for 12-300K use 2−66655
- microcalorimeter design, linearity errors 2−82374
- miniaturized microcalorimeter with resistance against fluoridizing agents 2−55592
- Nernst calorimeter, modified design 2−41869
- precise drop heat capacity, design for small samples 2−52303
- radiation dosimetry in WR-1 nuclear reactor 2−46396
- reaction calorimeter, design and appl. 2−48314
- reference, for laser energy meas. 2−49395
- shock tube, for dissoc. energy determ. of mol. F_2 2−83253
- spark, for investigation of formation mechanism of groups of penetrating particles 2−73878
- thermal analysis calorimeter and liq. Woods alloy soln. calorimeter 2−57056
- thin foil, high speed thermal anal. 2−63164
- twin heat conduction, for gas and liquid adsorption studies 2−52302
- vacuum adiabatic, for specific heat studies in critical liquid mixtures 2−49191
- X-ray, array, development 2−63708
- X-ray fluence and front surface dose, simultaneous obs. 2−58672

Calorimetry
- *see also Heat of adsorption, etc; Specific heat*
- adiabatic scanning, high speed thermal anal. 2−63164
- cholesteryl esters, differential scanning calorimeter meas. of temps. and heat of transition 2−80452
- direct calorimetric analysis, temp. and heat of reaction determ. 2−54522
- Evanohm heater wire, resistance- temperature ratios at low temps. 2−66654
- gamma heating, calorimetric determ. in material testing reactor ESSOR 2−83065

Calorimetry continued
- gauge for delineating convective and radiative wall heat flux 2−41850
- glass, enthalpy meas. and calc. of sp. ht. 2−74992
- grain boundary energy measurement, appl. to Cu alloys 2−83967
- heat pipes, plasma jet, stagnation point 2−43164
- in-pile, for meas. of absorbed dose in nuclear reactors, status, export from Hungary 2−63977
- metal, liq., equilib. thermodynamic states, enthalpy meas. technique 2−46949
- microcalorimetry methods for heats of mixing 2−77426
- new developments in chemical research and instrumentation 2−82380
- non-destructive burn-up determ. for spent fuel elements using heat output 2−74181
- optical power meas. of pulsed lasers 2−79232
- polyethylenes, chlorinated, differential scanning calorimetry 2−50400
- precision microcalorimetry, pulsed current control and measurement system 2−45604
- specific heat meas. at low temps. 2−41868
- thermal fluxmeter response distortion 2−82375
- ultrasonic power meas. by calorimetric meas., effects of thermal parameters 2−52245
- work hardening process obs., differential calorimetry applied to arbitrary real castings 2−47576
- ^{241}Am, half-life determ. from metal sample using adiabatic microcalorimetric method 2−52789
- CO_2, N flow-type adiabatic, isobaric sp. ht. of carbon dioxide with nitrogen impurity at supercritical pressures 2−83712
- Pu/U oxides reactor fuel, determ. of Pu content by calorimetry 2−74164

Cameras
- aerial, focussing, using modulation measurement 2−63447
- AFU-75 camera, observations of satellite Pageos 2−62817
- Albionflex, design and generation 2−76555
- Anger, optimizing window for ^{99m}Tc 2−48857
- Anger gamma system, improvement of intrinsic resolution 2−63707
- cine, rotating prism, analysis of operation and calc. of maximum framing speed 2−52513
- Cranz-Schardin, high-speed for dynamic photomechanics 2−63448
- Debyye-Scherrer and Guinier-de Wolff diffraction cameras, integrating 2−83925
- electron diffraction, UEG-150, high voltage, accelerating voltage up to 150 kV 2−59085
- electronic, with storage tube for high-speed cinematography 2−73697
- electronic for photometric meas. of close visual binary stars 2−44876
- electronic multiband camera film viewer with 1000 TV-line resolution 2−82601
- film advance in camera of airborne thermal scanner 2−70091
- gamma, anal. and correction of spatial distortions 2−48855
- gamma, as diagnostic instruments 2−73192
- gamma emitting radioisotope camera using liquid Xe for medical use 2−55249
- gamma ray camera-computer systems, maximum frame rates 2−78652
- gamma ray pin hole camera, wide angle 2−67069
- image converter control by giant pulse laser 2−73672
- intensified electron bombarded Si tube, performance in low light level TV systems 2−42290
- Kerr cell shutter with ten picosecond time resolution, application to particle accelerators 2−42291
- lens screen, high speed, using turbine driven disc 2−52514
- liquid crystal, for visual obs. of laser modes 2−52421
- microelectronics, photomask production facility 2−66880
- multiband cameras for space missions, review of recent developments 2−82600
- nuclear track visualization RFK-5 photographic camera used in start-stop mode 2−70312
- Nuclear-Chicago Pho/Gamma III scintillation camera, inexpensive remote start switch 2−76066
- objective-prism of very low dispersion, spectral classification of close star groups 2−75749
- optical adaption to image intensifier 2−73674
- photogrammetric, in stereophotography in track devices, correction of external orientation elements 2−59639
- photogrammetric systems, imaging characteristics 2−59337
- pinhole, efficiency comparison for photographically recording of X-ray smalll angle scattering 2−73690
- Polaroid, sequential exposures at 1.5 second intervals, one step colour photography 2−66876
- positron, MGH, medical use with, short-lived cyclotron produced radionuclides 2−69444
- positron, multicrystal, for use with radionuclides, medical application 2−55248
- precession, alignment fixtures 2−64608
- rotating mirror, high-speed, simultaneous operation as streak and framing camera matched with laser light 2−52510
- scintillation, field uniformity distortion using pinhole collimator 2−48856
- scintillation, tomographic, performance and reliability 2−69285
- self threading microfilm camera and processor system 2−59330
- shutters, comprehensive testing of dynamic characteristics 2−70097
- single and serial exposures from X-ray image intensifiers, medical applications 2−73202
- solid state array, review 2−42289
- spectrograph, designs 2−58575
- stray light, quantitative determination 2−59327
- Supper and Stoe precession, consid. of optimum precession angle 2−64607
- ultra high speed, functioning principles, description of framing and 'total activity' camera 2−52511
- view-finder, exp. determ. of optimum diopter value 2−63446
- Viking lander system, for Mars remote exploration 2−85077
- wafer image intensifier 2−59275
- Weissenberg, high temp. furnace 2−76119
- X-ray, high-pressure, diffraction pattern recording w. two film cassette 2−66872
- X-ray, medical diagnostic applics. 2−48853

Cameras continued
X-ray, monitor for recording small angle scattering 2−55894
X-ray topography, low cost ω axis and linear slide 2−66390
Ge(Li), coaxial, gamma ray camera for medical use, computerised display 2−51936

Candoluminescence *see Luminescence*

Capillarity
see also Bubbles; Drops; Films/liquid; Foams; Surface tension
contact angles, solid-liquid, in saturated system or controlled atmosphere, obs. rel. to temp. 2−43342
diffusive pressure effect in capillary for all ranges of Knudesn number 2−83717
distilled water, capillary wicking in quartz sand and cylindrical glass capillaries in magnetic fields 2−60402
jet, inviscid cylindrical, electric current effect on capillary instability 2−60401
Laplace theory, from application of second gradient theory to mechanics of fluids 2−56280
liquid gravity waves, flow over wavy bottom 2−77374
mass transfer analytical problems 2−83720
meniscus, vel. profiles for plate withdrawal, Navier-Stokes eqns. 2−60383
Oldroyd rate type fluid, Bagley end correction factor and die swell 2−67600
plasma, capillary, radiation and conductivity 2−70895
polybutadienes, narrow distribution, flow rate through capillaries 2−60394
polyethylene, high density, melt rheology 2−83371
polyisoprenes, narrow distribution, flow rate through capillaries 2−60394
polypropylene melt, end corrections in capillary flow with positive exit pressure 2−64408
polypropylene melt, rel. to mol. wt. capillary flow props. 2−46885
polystyrene, sheared, flow in capillaries, concept of molecular migration 2−50293
porous finite capillary body of arbitrary geometry, temperature and moisture distributions 2−66649
porous partitions, capillary osmosis 2−46902
thermocapillary flows near hemispherical bubble on heated wall 2−50303
thermodynamics of electrocapillary phenomena and thin films 2−43344
viscometer, for volatile liquids 2−43297
viscous gas flow through capillaries at large pressure differences 2−83672
volume-area relationship, math. derivation 2−83721
waves, interac. with gravity waves, Fokker-Planck type eqn. 2−50304
Young and Laplace eqns., review 2−46903
CaO-CaF$_2$ system liquidus line determ. by the capillary method 2−84683
D$_2$O, at boiling point, contact angles on Cu and polytetrafluoroethylene surfaces, 10-770 torr 2−74533
Hg, expression for capillary depression 2−60403

Capture cross-sections *see Nuclear reactions and scattering and subheadings*

Caratheodory's principle *see Thermodynamics*

Carbon
see also Diamonds; Graphite
— 2−67388
activated adsorbent, transmission of Ar/He 2−43242
adlayer on W, K shell total electron impact ionization cross sections, Auger spectra 2−64579
adsorbed on W, effect on surface self-diffusion, field emission obs. 2−64582
adsorption of H and H$_2$, rel. to work function variation 2−60677
adsorption on Ir(111) face, effect on surface ionization of CsCl 2−64543
amorphous, ion irrad., nuclear ion-atom interactions, Z$_1$ oscills., non-evidence 2−47780
arc, high current, electron temp. detn., Thompson scatt. obs. 2−64363
atom, 1s-hole state, chemical effects on lifetime 2−70602
atom, 2p3p, term dependence of Hartree-Fock results 2−56092
atom, ^{13}C hyperfine structure in sp^3(^{5}S) state 2−42725
atom, electron quasifree scattering at 9 keV from K and L shells 2−70614
atom, in reactions of active nitrogen with org. gases 2−61767
atom, K-shell X-ray fluorescence, effect of molecular environment 2−49995
atom, pulsed stimulated emission 2−79194
atom correlation energy, dipole polarizability and long range interaction calc. using many-body perturbation theory 2−52914
atom K-shell ionization by fast protons 0.3-2.0 MeV 2−42748
atomic dipole polarizabilities, coupled multiconfig. SCF method 2−64005
atoms, population inversion in recombining plasma flow 2−46452
atoms adsorbed on W substrate, backscattering cross sections for K-shell ionization by electron impact 2−79919
band struct. from X-ray photoelectron spectra, amorphization effects 2−57262
biological C-cycle, effect of variable CO$_2$ atmospheric partial pressure 2−48838
black, paramcryst. distortions 2−53974
black, tinting strength 2−75281
black family, P33, e.p.r., 4.2-300 K, phenom. model 2−57390
blacks, adsorption obs. using precision microgravimetric system 2−53593
blacks, surface oxygen complexes, effect on selective adsorption of non electrolytes from mixtures 2−64552
charcoal, simultaneous adsorption of benzene and cyclohexane 2−68779
chemisorption, on W, K shell ionization by electron impact 2−50553
columnar growth, electron diffraction analysis 2−80603
composite, c-metal, high strength, evaluation as sliding material 2−61019
composite, chem. vap. deposited felt and filament wound, flight-tested, phys. props. 2−61017

Carbon continued
composite, chem. vap. deposited felts, compressed, mech. props. 2−61018
composite, fibre reinforced, thermal insulation 2−56984
composite, fibre reinforced resin matrix, elastic props., u.s. obs. 2−53964
composite, filament wound cylinders, CVD C infiltrated, mech. props. 2−56985
composite, graphite matrix, microstruct. effects on mech. props. 2−61015
composite, PHS, effect of variation in precursor resin on struct. and mech. props. 2−53958
composites, mech. and nondestructive props. 2−61016
conference, Bethleham, USA, June (1971) 2−53943
diffusion in α-Fe, press. effect 2−43660
diffusion in disordered V$_6$C$_5$ 2−60834
diffusion in Fe, effective radii of diffusing particles, diffusion mechanisms 2−50709
diffusion in Fe, solid and liq. states 2−43661
diffusion in Fe-C-i-j-...-n multicomponent solid solution, thermodynamic interpretation 2−43662
diffusion in Fe-Ni along austenite/ferrite phase boundary 2−68052
diffusion in steel, Ni martensite, effect of dislocations 2−56758
diffusion in ternary solid solns., conc. curve. at interface 2−47454
electromigration in polycrystalline Be 2−43657
electron diffraction patterns from C fibres, interpretation by optical analogue techniques 2−80613
electrotransport in Gd 2−80716
fibre, (hk) interferences, linewidth, effects of preferred orientation 2−53627
fibre, appl. for carrier injection in anthracene electrolum. diodes 2−75338
fibre, diamagnetism rel. to tensile modulus and structure depend. 2−57270
fibre, electron microscopy 2−53950
fibre, fast neutron irrad. effects on mech. props. 2−56992
fibre, mech. and crystallographic props., S impurity effects 2−50913
fibre, microporosity 2−53952
fibre, monofilament substrate for chem. vap. deposited B composites 2−53956
fibre, neutron irrad. effect on mech. props. 2−43708
fibre, neutron irrad. effects on elec., mag. and thermal props. 2−56998
fibre, PAN-based, fine struct. 2−53948
fibre, preferred lattice orientations, three-dimensional crystallinity 2−53973
fibre, produced from lignin and PVA, voids, X-ray obs. 2−47667
fibre, rel. to composite material technology 2−47663
fibre, struct., neutron irrad. effects 2−56991
fibre, surface props. 2−53951
fibre, tensile strength, fast neutron irrad. effects 2−80830
fibre, thermal expansion, room temp. −1800°C 2−53953
fibre, thermal expansion anisotropy effects on struct. and mech. strength 2−54054
fibre, unidirectionally reinforced plastic, shear strength and modulus 2−74921
fibre, X-ray preferred orientation obs. 2−53949
fibre and composites, u.s. elastic consts. 2−50723
fibre micromechanics rel. to chem. vap. deposited C composites 2−53955
fibre reinforced Al composite, fatigue 2−56976
fibre reinforced glass, fracture energy 2−84104
fibre reinforced Ni composite, prep., thermal expansion, high temp. deformation characts. 2−74919
fibre strength and Griffith equation 2−53944
fibre wettability meas. 2−64802
fibre-reinforced ceramics and glass, continuous fibres, mech. props. 2−50919
fibre-reinforced ceramics and glass, discontinuous fibres, fabrication and props. 2−50918
fibres, adhesion to organic matrices 2−84101
fibres, elec. resistivity and diamag. susceptibility, meas. 2−68331
fibres, field emission source 2−72086
fibres, gas chromatographic obs. of surface reactivity 2−60623
fibres, glassy, derived from phenolic resin, mech. props. 2−84100
fibres, in composite materials, book 2−43904
fibres, ion beam thinning for t.e.m. 2−79104
fibres, property changes during fast neutron irradiation 2−53965
fibres, radiation effects on mech. props. based on 'sheath' and 'core' model of fibre structure 2−64702
fibres, strengthening by fast neutron irradiation 2−71662
fibres, thinned, low energy electron diffr. 2−64634
fibres, two dimensional lattice orientation and three dimensional crystallinity 2−68177
fibrous structures, pyrolytic C infiltration 2−53957
film, amorphous, elec. and optical props., and struct 2−61302
film, amorphous, graphitization by light pulses 2−61030
film, deposition and diamond-like props. characterization 2−56588
film, evaporation production technique 2−49625
film, graphitization under light pulse irrad. 2−57002
film, on Al, Zr, or steel reactor material, thickness determ. 2−44509
film prep. using plasma jet in vacuo 2−83889
film production using evaporation method 2−74629
films, turbostratic, optical spectra, effects of thermal treatment, comparison with graphite 2−78080
foil, multiple scatt. of H, He, Li, Ne, Ar and Kr ions, 100-1000 keV 2−47781
foil, scattering of Ne$^+$ beam, foil lifetime charge state distribution and beam scattering 2−52825
foil cover on ^{252}Cf source, effect on fission fragment energy loss and spectrum parameter changes 2−42445
glass like, thermal shock and crack propagation 2−56822
glassy, electrode, molecular sieve, blacks, and fibres, present and future applications 2−68172
glassy, optical consts., 0-82 eV, refl. meas. 2−61584
glassy, pore struct. 2−47056
glassy, struct. 2−53529
glassy, struct. X-ray obs. 2−53531

Carbon continued
glassy, thermal expansion to 2300°C 2–54056
glassy, X-ray small-angle scatt. obs. 2–53530
glassy and pyrolytic, activation energies for creep 2–53815
glassy electrode in coulostatic analysis 2–72587
glassy monofilament, prep. and props. 2–56982
graphitisation and irradiation with neutrons, electronic props. change 2–68137
graphitisation of carbon products, infl. on dimensional variations of n irradiation 2–68175
graphitized film, anisotropy of g-value 2–78153
impurity in metal foils, assay by meas. of proton energy spectra 2–50389
intensity ratios of 002 and 004 diffraction lines, comparison for various carbons 2–64633
interstellar, abundance det. from u.v. stellar spectra 2–58359
interstitial in α-Fe, atomic relax., modified lattice statics approach 2–60784
ions, 0.5-2 MeV, stopping powers in Cr, Fe, Co, Ni, Cu, Zn 2–47782
ions, irrad. of Si for prod. of SiC heterostruct. films 2–50504
isotropic, poorly crystalline, dimensional charges induced by neutron irradiation 2–76916
isotropic poorly crystalline and C-Si alloys, dimensional changes and creep during neutron irradiation 2–76917
isotruxene carbons, formation and microstruct. from X-ray exam. 2–61023
Jupiter, ^{13}C methane identification and ^{12}C/^{13}C ratio 2–75883
K-shell fluorescence yield by synchrotron radiation 2–77012
laser beam irrad., chaoite formation in craters 2–56574
line spectra, d.c. arc, effect of mag. field on intensity, 230-790 Oe 2–49943
low density, thermal diffusivity obs., annealing and environment effects 2–54076
lunar and terrestrial basalt composition 2–58457
lunar samples from Apollo 11, 12 and 14, total C content and abundances 2–78513
massive stars, C burning, advanced evolution 2–66087
massive stars, He burning, advanced evolution, ^{12}C nucleosynthesis 2–66086
microporous polymer, adsorption of CO$_2$, applic. of potential theory 2–53591
microscopy at high resolution, sample prep., technique improvement 2–53637
microstructure, high-resoln. electron microscopy obs. 2–53532
molecular crystal model 2–56649
molecule, SCF-MO-CI calc. using atomic basis of contracted Gaussian lobe functions 2–64120
multiphase system, galvanomag. effects 2–57112
multiple scattering, anomalous z_1 depend. of interaction potential 2–77794
neutron irrad. at high-temp., mech. interactions among crystallites 2–56679
neutron irrad. poorly crystn. isotropic mat., dimensional changes 2–56767
neutron irradiated, thermal annealing, changes in electronic props. 2–57000
non-crystalline, relation between specific heat and Curie temp. mag. susceptibility 2–65123
innuclear fuels, chemical anal. 2–74176
in nuclear fuels, chemical analysis techniques 2–74168
nuclei, geomagnetically trapped 2–65933
Orion Nebula, 85α recombination line survey 2–81797
Pasadena smog, chemical composition 2–51603
photon absorption cross sections, 250-1000MeV 2–72272
polyatomic negative ions, surface ionization 2–79928
polymorphism, chaoite formation, and new form obs. 2–56650
porous, adsorption of liquids, high resoln. n.m.r. obs. 2–53594
porous, multiple X-ray small-angle scatt. 2–53978
products, graphitization effects on neutron irrad. induced dimensional changes 2–56996
pyrocarbon, thermal diffusivity and conductivity fast neutron irrad. effects 2–54046
pyrocarbon coated reactor fuels, anisotropy determination using scanning electron microscope 2–74145
pyrocarbon coating, neutron irrad. effects on mech. props. 2–56771
pyrocarbons, lattice thermal expansion perpendic. to layer planes, depend. on struct. props. 2–68252
pyrolytic, γ-irrad. stress-graphitized, dynamic mech. props. 2–53775
pyrolytic, (hk) interferences linewidth, effects of preferred orientation 2–53627
pyrolytic, anisotropic neg. and posit. magnetoresistance 2–57111
pyrolytic, fluidized-bed, mech. rel. to struct. props. 2–56768
pyrolytic, highly graphitized, microstruct., X-ray obs. 2–60752
pyrolytic, impregnation with graphite, neutron irrad. stability 2–56997
pyrolytic, isotropic, formed below 1500° C, annealing effects and mechanism 2–61022
pyrolytic, lattice thermal expansion perpendicular to layer planes, depend. on struct. props. 2–61108
pyrolytic, neutron-irrad., annealing 2–56993
pyrolytic, neutron-irrad., thermal conductivity 2–57082
pyrolytic, preferred orientation 2–60751
recombination lines, partially ionized interstellar cloud, microwave observations 2–81807
removal from Mo by heating in H$_2$ atmos. 2–64763
resistance thermometer, time response and thermal diffusivity 2–49184
resistor thermometer, method of reducing effective magnetoresistance 2–52295
review of work at Royal Aircraft Establishment 2–43903
self-diffusion in dolomite, obs. using isotopic exchange 2–68855
slip system, effects of crystal anisotropy and cryst. struct. 2–71577
smectic liquid crystal, magnetic instabilities 2–60433
soft carbons, sp. ht. obs., low temp., rel. to heat treatment 2–54045
soft pregraphitic, Hall coeff. depend. on heat treatment and doping 2–44113
solar atmosphere, density dependent ionization balance 2–66231
solar overabundance, accelerated by solar flares 2–76001

Carbon continued
soot, particulate borne, long distance transport in Sweden Sept.-Dec. 1969 2–72766
specific heat, 0.5-5 K, effect of heat treatments at 600- 1600°C 2–57061
specific heat, strong mag. field obs., 1.3 to 4.3 K 2–43980
star of 0.8 $M_{\odot}$, 50% C^{12}, evolution and secular stability 55033 2–55033
in steel, diffusion layer, distrib. by local spectral anal. 2–47435
steels, weldability to Cr-Ni steel, gas pressure process 2–68146
stopping powers for 30-90 MeV ^{238}U ions 2–47773
structure, defect theory 2–53729
surface impurity on Th, bulk to surface equilib. 2–50465
thermometer, cryogenic, interpolation routines for calibration 2–52294
three dimensional structure synthesis, at one atmosphere in graphite fibres 2–56979
Van der Waals forces for systems involving non-spherical atoms 2–63998
vitreous and common, bulk resistivity and temp. coeff. 2–71827
vitreous C electrode material, electrochemical evidence for structure 2–84649
work function, variation with adsorption of H and H$_2$ 2–60677
X-ray diffraction intensity effective temperature factor 2–53655
C-Ar$^+$ collisions from 25 to 200 keV, noncharacteristic X-ray bands 2–56116
C-C composite, fluted core, 3D reinforced, fabrication and mech. props. 2–53961
C-C composite, mech. props. rel. to ‘moulded carbon’ process 2–53962
C-C composite, phys. and mech. props. of mats. fabricated by wet winding endless fibres with pitch 2–53959
C-C unidirectional composites, fibre-matrix interactions 2–56978
C, lampblack, graphitization 2–56995
C fibre-epoxy composite, acoustic emission during continuous tensile cycling 2–56986
C fibre reinforced plastic beams, dynamic moduli and loss factors 2–47487
C fibres electron diffraction studies, lattice fringes rel. to defects and diffraction geometry 2–80634
C I, 5052.16 Å, solar photospheric fluctuations, radial veloc. coherence and phase spectra 2–75950
C I, C II and C III, interstellar, ionization structure 2–81829
C I, interstellar, effect of radiation pressure round stars, galactic evolution 2–48730
C I 2478 line, Stark half-width estimation 2–59916
C I reson. lines in far-u.v. spectrum of Venus 2–58515
C II, electron impact ionization, calc. for $1s^22s^22p$ configuration 2–46451
C II, vacuum u.v. absorption meas. using new continuum light source 2–77001
C II and C III solar u.v. line anal., statistical equilibrium and radiative transfer equations 2–51847
C IV, in planetary nebulae, emission lines, polarization 2–48669
C IV, in planetary nebulae, emission spectrum with different excitation conditions 2–48668
C V in D plasma, meas. of depopulation of $2^3P_{0,1,2}$ triplet levels by electron collisions 2–79961
C$^-$ formation from CO by electron impact 2–83415
C$^+$, reactive collision with O$_2$ and N$_2$ at 3 to 100 eV, calculated cross sections for mass transfer, molecular and dissociative charge exchange reactions 2–48322
C$^+$ reactions with ethane, ethylene and acetylene, behaviour of cross section as function of incident energy, 2-100 eV 2–57416
C$_2$ in sunspot umbras spectrum 2–73140
C$_2$ lines in sunspot spectra 2–73139
C$_2^-$ radical, search for in solar and HD 201626 spectra 2–44861
C^{2+}, bound wave functions 2–76974
C^{5+}, Lamb shift studied via motional electric field quenching of $2^2S_{1/2}$ state 2–70633
CI, even parity levels, frozen cores approximation 2–42726
CII line excitation in quasars 2–44889
CIII, electron scattering, collision strengths for transitions, distorted wave and close coupling calculations 2–76970
CIII λ5696 line of recomb. spectrum of stars 2–85009
CIV doublet in Ton 1530 quasar absorption spectra 2–58372
CO$_2$, near-resonant energy transfer to (00°1) vibr. level due to Hf collisions 2–53101
^{11}C, in vivo metabolism meas. 2–69388
^{11}C, use in clinical research 2–69387
^{12}C/^{13}C abundance ratio in SgR A and SgrB2 and absorption spectrum of ^{13}C isotope of formaldehyde 2–48671
^{12}C/^{13}C interstellar ratio in CH$^+$ molecules towards various stars 2–48731
^{12}C/^{13}C interstellar ratio, obs. at 4232 Å 2–73039
^{13}C profiles in CO$_2$ total content in seawater at Geosecs II in North Atlantic Ocean 2–75470
^{14}C, counting together with T, optimization 2–59615
^{14}C, lightweight molecular sieve stratospheric sampler 2–65804
^{14}C energy spectra, comparison of chemiluminescence 2–59605
^{14}C in lunar rock depth profile 2–85035
^{14}C labelled organic vapours, self-diffusion through polymer membrane obs. using radio tracer technique 2–71180
^{14}C self supported target preparation techniques 2–49624
^{14}C tektites 2–66189
^{14}C thin self-supporting nuclear target, preparation 2–73921
C$^+$ + N$_2$, K vacancy production probability depend. on relative Z numbers 2–74304
C$^+$ + NH$_3$ K vacancy production probability depend. on relative Z numbers 2–74304
C248α transition in W51 radio source 2–75815
Ir(111)-C film emitter with two-dimensional phase transitions, props. 2–65100
Lu-C system, vaporization investigations in temp. range 2100 to 2600K 2–64518
MgO-c inclusions, polycryst., creep, four point bending obs. 2–56805
Mo:C film, supercond. transition temp., struct. 2–57169
Mo:C film, supercond. transition temp. effect of C coating 2–54145

Carbon continued
in Ni alloy, effect on phase transforms. 2−43925
O ions, radiative lifetimes for u.v. transitions by pulse decay method 2−46413
Si:C, low temp. electron irrad. damage, i.r. absorp. obs. 2−48191
Si:Ge, O, C, low temp. electron irrad. damage, i.r. obs. 2−48192
inSi, i.r. and activation analysis 2−71502
in U-Mo alloy, effect on stress corrosion cracking in humid air 2−53839
^{235}U fission fragment range 2−61125
ZnO:Cu film, amorphous, band struct. and impurity state energy spectrum 2−68421
ZrC_x/C composite, vapour deposition by iodide process 2−50922

Carbon compounds
see also Organic compounds
− 2−65660
$(C_2NO_2H_5)_3H_2SO_4$, triglycine sulfate, second order ferroelec. transitions, calorimetric exam. 2−77951
absorption cross sections between 100 and 600 Å 2−80057
carbides, high temp. coatings, deposition from fused salts and by ion plating 2−50860
carbides, noncrystalline film prep. by sputtering 2−47114
carbides, wetting by liq. metals, relative surface energies 2−50427
carbonates, Pasadena smog, chemical composition 2−51603
CO, totally inverted vibr. population rel. to laser applic. 2−61777
composite fetl, neutron irrad., thermal expansion, 20-1000°C 2−54055
fuel cells, high temperature, hydrocarbon conversion 2−49257
graphite-Br intercalation compound, Fermi surface, Shubnikov-de Haas oscill. obs. 2−68288
molecular beam, scatt. from W surface 2−47084
9Ni-4Co-0.30C, fracture mechanics of crack growth at elevated temperatures 2−56867
organometallic complex, rel. to prep. under pressure of glassy C precursor 2−61014
polyatomic negative ions, surface ionization 2−79928
precursor, spheroidal isotropic, pressure carboniz. of divinyl-benzene 2−56983
triglycine sulphate, field effect and Hall mobility of Te and PbTe 2−77814
triglycine sulphate, structural inhibition of ferroelec. switching, X-irrad. field treatment 2−77952
$[C_nO_n]^{-2}$ dianions, geometry and electronic struct., u.v. spectrum 2−70689
Ar-CO mixtures, heteronuclear associative ionization, formation $ArCO^+$ following 30 eV electron impact 2−51430
C-Fe film on Al, Zr, or steel reactor material, thickness determ. 2−44509
C-Si alloys, co-deposited, high-fluence irrad.-induced dimens. changes 2−53776
C_2, molecule, Franck-Condon factors of Morse oscillator when $\Delta S>0$ 2−60017
CCl_4, electronic structure, dipole moments, n.m.r. and n.q.r. constants 2−83324
CCl_4 liquid, interactions of the radiation with conduction, analysis based on spectroscopic information 2−43346
CF_4 collisional de-excitation of vibrationally excited 2,4-dimethylpentyl-2*(-d_1*) 2−46648
CH, CI calcs. of potential curves for low lying excited electronic states $a^4\Sigma^-$, $A^2\Delta$, $B^2\Sigma^-$, determ. spectroscopic consts. 2−56160
CH, diatomic, calc. of Hartree-Fock photoionization cross section using many body perturbation theory 2−80018
CH, excited states, Rydberg and valence shell character as functions of internuclear distance 2−50056
CH, interstellar abundance discussed with reference to Franck-Condon factor measurements 2−44887
CH, Rydberg levels, calc. and comparison with expt. 2−53001
CH, upper limits of rotational states studied using potential energy functions of Morse and Hulburt-Hirschfelder 2−46543
CH radical, ab initio valence bond treatment 2−50025
CH^+, interstellar, interferometric obs. 2−75798
CH^+, upper limits of rotational states studied using potential energy functions of Morse and Hulburt-Hirschfelder 2−46543
CH^+ interstellar abundance discussed with reference to Franck-Condon factor measurements 2−44887
CH_2, structure of transition dipole moment 2−80025
CH_4 and C_2H_6 in size-fractionated lunar fines in Apollo 12 and 14 samples 2−55121
$CH(^2\Pi)$, pulse radiolytically produced, reaction with methane, kinetics of ethylene production 2−48347
CN, $a^2\Pi$ and $B^2\Sigma$ rotational states, level crossing 2−67449
CN, calc. of Franck-Condon factors and R centroids for $B^2\Sigma\rightarrow A^2\Pi$ band system, validity of Morse potential 2−46535
CN, galactic, radial band strength gradients near nuclei of galaxies 2−51708
CN, in M supergiants, 8 colour narrow band i.r. photometry 2−62552
CN, interstellar, detection of 1.32 mm background radiation in spectrum of Ophiuchi 2−48736
CN, true pot. energy curves, Morse r-centroids and Franck-Condon factors for $E^2\Sigma^+$-$X^2\Sigma^+$ band system 2−42880
CN bands, intensity variation with temp. in N_2 + methylene chloride chemiluminescent reaction 2−83240
CN in solar sunspot spectrum, 4900- 6441 Angstrom range 2−62743
CN radical, level anticrossing 2−42878
CN red band system, shock tube determ. of electronic transition moment 2−77083
CN stars in solar neighbourhood, rel. to radial composition gradient in galactic disk 2−58181
CN^- in RbCl, dielec. susceptibility 2−51192
CNO, unstable β-emitters, low energy solar positrons 2−66214
CO_2:^{4}He, 300 to 600 K, vibrational relaxation times of 00°1 levels 2−42881
CO_2:N_2:H_2O c.w. gas dynamic laser, unstable resonator calculations 2−82483
CO_2:N_2, 300 to 600 K, vibrational relaxation times of 00°1 levels 2−42881
CO_2/O_2 mixing ratio in Martian atmosphere from photoelectric spectra 2−78550
CO-CO_2 laser, sealed, room temp. operation at 5 or 10μ 2−49364

Carbon compounds continued
CO-CO_2 system, vibr. energy transfer, shock tube study 2−77166
CO-COS collisions meas. of vibrational energy transfer on test of harmonic oscillator model 2−80140
CO_2-H-, halide mixtures, vibration-to-vibration energy transfer 2−43036
CO_2-H_2 mixtures, simultaneous vibr.-translation, vibr.-rot. and rot.-translation exchanges 2−53099
CO-He-N_2-O_2 laser, CW operation in some CO lines below 5.0 μ 2−45726
CO_2-He-N_2 TEA laser, double discharge trigger circuit 2−79199
CO_2-He laser, chemical, pulsed, output pulse obs., pumping mechanism 2−73561
CO_2-N_2-H_2O arc-driven supersonic laser operating in gas-dynamic mode, numerical analysis 2−49359
CO_2-N_2-He deexcited plasma, quantitative emission spectroscopy 2−79206
CO_2-N_2-He laser discharges, high-pressure, uniform glow, afterglow gain meas. 2−42003
CO_2-N_2 collisions, line broadening of CO_2 using laser source spectroscopy, application of Anderson Tsao and Curnutte theory 2−79993
CO_2-N_2 mixing laser, CW gasdynamic thermally excited and selectively pumped 2−63322
CO_2-N_2(CO) system, vibr. energy transfer, shock tube study 2−77166
CO_2-N_2-^{3}He laser, high press., preionized in a reactor, performance 2−69916
CO_2-N_2O mixtures, competitive photolysis, 1633 Å 2−65389
CO-O_2 gas mixtures ionization 2−60288
CO_2-Pt system, thermal cond., accommodation effect 2−67734
CO, adsorbed on Au, i.r. refl.-absorpt. spectra study 2−60676
CO, adsorbed on W, electron stimulated desorption 2−47153
CO, adsorp. on Ni, preferential orientation, extended Huckel calc. 2−50546
CO, adsorpt, on Fe, Co, Mn, change in work functions 2−71348
CO, adsorption and dissociation on W surface, field emission microscope obs. 2−71355
CO, adsorption on graphite in high vac. range 2−43494
CO, atmospheric conc. correl. with airborne continental dust 2−62158
CO, C^- and O^- production by dissociative resonance electron capture 2−83415
CO, C X-ray emission spectra, obs. by grazing incidence grating spectrometer 2−74260
CO, CN, cool supergiant stars, model atmospheres, compositions 2−66074
CO, CO-Ar, CO-N_2 gas mixtures, vibrational relaxation rate in nozzle flow 2−80142
CO, catalytic oxidation on Pt surfaces 2−78185
CO, chemisorbed on Ir-Pt alloy, i.r. spectra 2−68645
CO, chemisorbed on W, vibr. freq. refl.-absorption i.r. spectra 2−47154
CO, chemisorption on Cu, weak adsorp. obs. 2−50537
CO, chemisorption on CuO, catalytic activity rel. to semicond. 2−75093
CO, chemisorption on W, thermal desorp. spectra quantitative analysis 2−47173
CO, collisional excitation, interstellar clouds 2−66115
CO, core excited resonances, electron transmission spectroscopic investigation 2−46547
CO, $\Delta v=1$ transitions, relative Einstein A coefficients 2−46531
CO, electron and Auger electron spectroscopy, review in reln. to vacuum technique 2−59924
CO, electron impact excitation of vacuum u.v. radiation, threshold studies 2−80141
CO, field desroption from W, in FIM, image gas enhancement 2−60673
CO, forced convective flow laser 2−69920
CO, fundamental i.r. spectra, solar photosphere structure 2−76003
CO, half-widths of lines in fundamental and first overtone bands broadened by CO_2 and air calc. using Anderson-Tsao-Curnutte theory 2−53105
CO, i.r . absorption coeffs. 2−56156
CO, i.r. fluoresc., Hg*-sensitized, vibr. distrib. in electronic-vibr. energy transfer 2−59988
CO, i.r. vibr.-rot. spectra, approx. calcs. of abs. coeff., 300 and 1200 K 2−46534
CO, intensity meas. of $d^3\Delta\rightarrow a^3\Pi$ emission system, determ. of relative electronic transition moments 2−80035
CO, isolated in solid Ne and Ar matrices, laser excited vibrational fluorescence 2−59994
CO, laminar flow with radiative interaction 2−43229
CO, Martian airglow, u.v. spectral obs. 2−66178
CO, matrix-isolated, i.r. obs. at cryogenic temps., interactions 2−68638
CO, photoelectron spectra, search for core electron satellites 2−42876
CO, solar, calc. of vibration-rotation line profiles and equivalent widths 2−73147
CO, solid and liq., charge transport processes 2−77820
CO, sorbed on Ti surface, photoemission energy level meas. 2−47166
CO, spectrum of $a^3\Pi$ state at 5 to 1000 MHz, fine structure, dipole moment and perturbation analysis 2−50026
CO, threshold electron impact spectrum, reson. struct. 2−70687
CO, vibr. excitation by O + Cs reaction, chem. laser studies 2−72552
CO, vibr. relax. near 100K using discharge laser 2−80128
CO, vibrational-rotational band, total band absorptance and absorption coefficient 2−56140
CO, vibrational matrix elements of quadrupole moment functions 2−64129
CO, weak adsorp. on Cu, strcuture and binding 2−50538
CO $(A^1\Pi)$ cross sections from photodissociative excitation of CO_2 2−56163
CO $(a^3\Pi)$ quenching by $O(^3P)$, rate coeffs. 2−64213
CO A $^1\Pi$ state, zero-field level crossing spectrosopy, obs. of fluorescence of resolved rotational features 2−70691
CO adsorption on Cu-Ni alloy 2−50536

Carbon compounds continued
CO and CO_2 Raman scattering cross sections and depolarization ratio 2-53026
CO and CS molecular lines in interstellar spectrum of Ophiuchi, equivalent width measurements and calculations 2-55072
CO atmospheric, trace material obs. program in atmosphere 2-62152
CO atmospheric pollution in Los Angeles 2-57944
CO catalytic oxidation, on Pt(110) surface, Auger spectroscopy obs. 2-51443
CO chemical laser, arc excited flowing, performance 2-41993
CO compressed gas, meas. of microwave absorption of 9.75 GHz using resonant cavity technique 2-53339
CO configuration interaction wavefunctions and dipole moment calc. 2-74258
CO content and seasonal variations in atmosphere 2-81659
CO cooling effect in atmospheres of red giant stars 2-75709
CO desorption and adsorption on W, SIMS, EID, flash-filament obs. 2-47170
CO electron impact threshold excitation spectrum meas. using trapped-electron method, structure identification 2-80146
CO electron scattering, study of resonance phenomena associated with 10.04 eV Feshbach resonance 2-80147
CO formed in O_2 + acetylene reaction, vibrational population distrib. 2-46532
CO fourth positive chemilum. excitation and quenching due to reactions involving C_2O 2-84628
CO gas, influence on Mo photoemission 2-51227
CO high pressure electrically excited laser, transient oscillator analysis 2-69921
CO laser, c.w. chemical type, R-branch emission, vibr. levels inversion ratios increase 2-73560
CO laser, chemical, flowing, arc excited 2-73559
CO laser, chemical, transverse-flow transverse-pulsed 2-45727
CO laser, electric-discharge gas- dynamic, operating parameters 2-45720
CO laser, frequency gain profile obs. using tunable semiconductor laser 2-45718
CO laser, gain line shape measurement using tunable semicond. laser 2-45728
CO laser, high-gain double-discharge, pulsed and spectral output characts. 2-69913
CO laser, high pressure, electrically excited 2-45743
CO laser, line selection for high atmospheric transmission by intercavity water vapor cell 2-42001
CO laser, potential scaling to large scale high power operation 2-82480
CO laser, sealed-off, Lamb dip evolution obs. 2-45719
CO laser lines quenching by self absorpt. 2-69912
CO lasers, detection of air pollution 2-81668
CO line in high photosphere, thermal oscill. 2-66224
CO lines in interstellar spectrum of ξ Persei 2-81836
CO luminescence, energy dependence of collisional deactivation cross section 2-46646
CO mixing ratio decrease at tropopause 2-65670
CO mol., Born-Oppenheimer approx. breakdown 2-56151
CO molecule, Franck-Condon factors of Morse oscillator when $\Delta S>0$ 2-60017
CO molecule, vibration to vibration energy transfer in N_2-CO 2-67489
CO multiquantum vibrational-energy, evaluation of S-matrix elements 2-70809
CO oxidation in shock waves, catalytic effect of $Fe(CO)_5$ 2-57417
CO photoionization by soft X-rays, meas. of total and relative abundances of thermal energy ions and dissociation cross sections 2-80024
CO population by active nitrogen, rate coeffs. 2-70718
CO positive band system in far-u.v. spectrum of Venus 2-58515
CO quantum yield in CO_2 photolysis at 1470Å and 1500 to 1670Å 2-69141
CO singlet and triplet state excitation by active N_2 2-70717
CO solid, spectra of trapped atoms, importance of intermolecular interactions of excited species 2-78096
CO TEA laser, laser action at 4.96-5.61 μm at 77K 2-79187
CO vibrational relaxation, transient stimulated Raman scatt. obs. 2-56150
CO^+, comet tail system, electronic transition moment 2-50029
CO^+, electronic transition moments for A→X, B→X, B→A transitions, abs. absorption cross sections 2-52998
CO^+, emission produced by A→X transitions, meas. of lifetimes, cross section for excitation of comet-tails 2-46563
CO^+, radiative lifetimes of $A^2\Pi$ state 2-74259
CO^+ reactions, with H_2, CO_2, CH_4, N_2O, SO_2, O_2, C_2H_2, COS, NO and rate constants 2-51434
$CO^{2-}{}_3$ centre, in KCl and KBr, i.r. spectra obs. 2-71350
CO_2, ^{18}O enriched, high resolution study of near i.r. bands 2-70693
CO_2, 300 to 600 K, vibrational relaxation times of 00°1 levels 2-42881
CO_2, adsorbed on W, binding states, condensation kinetics, decomp. 2-77513
CO_2, adsorption-desorption from SiO_2, u.h.v. studies 2-71353
CO_2, adsorption on microporous polymer C, applic. of potential theory 2-53591
CO_2, adsorption on SiO_2, e.s.r. obs., E′, dangling bonds 2-71352
CO_2, alpha particle energy loss and stopping power 2-56433
CO_2, atmospheric, effect on radiative equilibrium 2-62262
CO_2, atmospheric, trace material obs. program in atmosphere 2-62152
CO_2, atmospheric, varying partial pressure, effect on biological carbon cycle 2-48838
CO_2, atmospheric concentration, radiative heating 2-72800
CO_2, atmospheric pressure laser, optically pumped 2-55689
CO_2, bubble formation and removal in glass melts 2-56551
CO_2, CO laser, transverse excitation in gas dynamically cooled mixtures 2-49362
CO_2, chemical analysis by metastable ion detection 2-65402
CO_2, decomposition on W(100) surface, flush desorp. mass spectrometry obs. 2-50551
CO_2, dissociative excitation of $CO(A^1\pi)$ system by electron impact 2-56164

Carbon compounds continued
CO_2, distrib. on Martian surface for 1971 opposition 2-81912
CO_2, Earth limb radiance profiles from thermal emission 2-62128
CO_2, electron impact dissociation, meas. of lifetime of a $^3\Pi$ state of CO 2-50028
CO_2, electron impact dissociation, production of $CO(a^3\Pi)$ and other metastable fragments 2-64117
CO_2, eqn. of state from triplet point to critical point, droplet 2-67869
CO_2, filled for exhalation radiometry of ^{14}C- 2-58619
CO_2, flow through stainless steel tubes, heat transfer 2-43228
CO_2, gaseous, γ radiolysis at high densities 2-61814
CO_2, general quartic force field, calc. using Parr-Brown anharmonic potential function 2-52999
CO_2, heat transfer at supercritical pressure 2-64394
CO_2, high pressure pulsed chemical transfer laser 2-59154
CO_2, i.r. absorption coeffs. 2-56156
CO_2, i.r. spectral emissivity data, comparison with total emissivity charts 2-83702
CO_2, i.r. vibr.-rot. spectra, approx. calcs. of abs. coeff., 300 and 1200 K 2-46534
CO_2, in atmosphere, rate of increase, model 2-68886
CO_2, in seawater, effect on sound velocity 2-65605
CO_2, intermol. interaction pot., with CO_2, N_2, O_2, CO 2-46643
CO_2, laser, electrically excited, electron energy conversion to optical energy 2-59151
CO_2, laser, matrix type, TEA, gain characts. 2-63323
CO_2, laser, photon-drag detector using p-Te 2-79170
CO_2, laser, transversely excited, cavity dumping 2-59149
CO_2, laser action, transverse, press. to 6 ‘atm’, peak power, optimum press 2-66745
CO_2, laser source spectroscopy obs. of 00^01-$(10^00$-$02^00)_1$ band 2-74257
CO_2, lattice parameter of solid at −190°C 2-50619
CO_2, liquid, thermodynamic relations 2-69789
CO_2, Mars atmosphere, discrete white clouds, diurnal and seasonal behaviour 2-69152
CO_2, Martian dust storms, absorption obs. at 10500 Å 2-81918
CO_2, mass spectrometric study of dissociative electron attachment 2-42883
CO_2, metastable anions 2-42875
CO_2, method for single frequency laser action from vibrational- rotational transition 2-66743
CO_2, microwave discharge, spectroscopic and photometric study 2-77303
CO_2, mode-locked TEA, single pulse selection 2-73562
CO_2, N isobaric sp. ht. with nitrogen impurity at supercritical pressures, flow-type adiabatic calorimetry 2-83712
CO_2, optical breakdown in presence of elec. discharge 2-50232
CO_2, outgassing role in evolving Martian atmosphere 2-58507
CO_2, partial ioniz. cross sections by electrons (25-600 eV) 2-70979
CO_2, photodissociative excitation, $CO(A^1\Pi)$ cross sections 2-56163
CO_2, press.- induced absorpt., ν_1 band, density and temp. depend. of intensity, crit. phenomena 2-56158
CO_2, pulsed transversly excited, gain, spatial and temmporal depend. 2-49363
CO_2, quenching of vibr. excited N_2 in thermosphere 2-58029
CO_2, semi-empirical analysis of electronic spectra and molecular structure 2-42891
CO_2, shock-heated, laser absorption meas. of vibrational relaxation of bending mode 2-56161
CO_2, shock tube investigation of Br_2 dissociation in presence of 2-67469
CO_2, solid, electronic excitation in extreme u.v. 2-44365
CO_2, solid, symmetry of vibrs., group theoretical study 2-43953
CO_2, solid and cold fog seeding at Oslo Airport 2-72793
CO_2, sorbed on Ti surface, photoemission energy level meas. 2-47166
CO_2, spectra, atmospheric radiative transfer 2-65770
CO_2, stimulated Raman scatt., time meas. for vibr.-trans. energy transfer 2-64118
CO_2, TEA laser, heating of small θ-pinch plasma 2-83606
CO_2, thermal relaxation of vibration, period determ. by impact tube method 2-83398
CO_2, total content in seawater at Geosecs II in North Atlantic Ocean 2-75470
CO_2, translational spectra due to overlap moments induced by collisions with He 2-50129
CO_2, u.v. photolysis, optical emission from $O(^1D)$ and $O_2(b^1\Sigma_g)$ 2-61801
CO_2, vibrational relaxation time in inert gas mixtures, meas. using acousto-optical effect 2-59995
CO_2, viscosity and second virial coeff., m-6-8 pot. analysis 2-77370
CO_2 7820 Å band in atmosphere of Venus, temperature distributions from reflected sunlight 2-62711
CO_2 absorption in pure water 2-67816
CO_2 and H_2O ice layers in Martian polar cap. rel. to theory of formation 2-81931
CO_2 and vibrationally excited N_2, high velocity mixing 2-83661
CO_2 atmosphere, meas. of collision-broadened line shape parameters for HCl and HF 2-42879
CO_2 band spectroscopic Venus observations during 1971 superior conjunction 2-78565
CO_2 Burnett apparatus for accurate determination of gas compressibility and second virial coefficients 2-56439
CO_2 charged asthenosphere, model 2-57705
CO_2 clouds in atmosphere of Venus, variability and lateral inhomogeneity 2-78563
CO_2 clusters, model for electron impact ionization cross sections including energy losses inside cluster 2-80150
CO_2 continuous spectrum, calculation of absorption coeffs. oven temp. range 20000-100000°K 2-70692
CO_2 diffusion laser, interaction kinetics of diffusion mixing of CO_2 and N_2 2-73565
CO_2 dissociative electron capture, production of O^- 2-80026
CO_2 distrib. on Mars, ground-based obs. 2-62705
CO_2 electric discharge convection lasers, model and experiment 2-45716
CO_2 electron impact dissociation, production of $CO(a^3\pi)$ and other metastable fragments 2-42884

Carbon compounds continued
CO_2 from aircraft rel. to pollutant effects on radiation budget of stratosphere 2−65663
CO_2 gas-dynamic laser system, gain and power output calculations 2−59145
CO_2 gas, absorption into turbulent distilled water 2−50298
CO_2 gas dynamic laser, importance of nozzle geometry 2−66748
CO_2 gas dynamic RASTA high power laser, design and performance 2−76480
CO_2 gas for reactor cooling, comparison with He cooling 2−56032
CO_2 gas laser, cutting of various materials, techniques, advantages and disadvantages 2−82497
CO_2 gas laser, with N_2 and He mixtures, temp. meas. from R-branch bands of N_2 2−46769
CO_2 glow discharge, electron energy distrib., new probe technique 2−64348
CO_2 helical TEA laser, line structure 2−42000
CO_2 high power laser, gas circulation regime at optimized partial pressure for CO_2-N_2-He mixture 2−45731
CO_2 in atm., Mauna Loa meas. of global trends 2−62147
CO_2 in atmosphere of Venus, 8710 Å line profile meas. rel. to atmospheric models 2−78560
CO_2 in caves, gaseous subterranean diffusion and air circulation 2−48412
CO_2 in lower atm. of Venus, radio obs. 2−75914
CO_2 laser, active gas cell for Q-modulation 2−76481
CO_2 laser, cathode glow discharge in transverse hollow cathode structure 2−79205
CO_2 laser, closed cycle d.c. elec. discharge convection, r.f. augmentation 2−55690
CO_2 laser, commercial air cooled, LG-17 type, construction and characteristics 2−41998
CO_2 laser, competition effects on spatial coherence 2−55688
CO_2 laser, continuous operation at atmospheric pressure 2−42002
CO_2 laser, employing dielec. waveguide discharge tube 2−45729
CO_2 laser, freq. and wavelength meas. 2−78758
CO_2 laser, gas-dynamic, by detonation of solid explosive 2−45722
CO_2 laser, harmonic generator 2−82505
CO_2 laser, high-pressure, gas-dynamic performance 2−45723
CO_2 laser, high c.w. power, thermal effects and molecular dissociation 2−76473
CO_2 laser, high power, hole burning 2−69910
CO_2 laser, high press., pulsed, gas breakdown, ionization by rad., operating press. limit 2−69919
CO_2 laser, initiated by cold cathode glow discharge electron gun 2−69915
CO_2 laser, inverted Lamb dip in spectroscopy and laser stabilisation 2−63326
CO_2 laser, magneto Raman scattering, obs. 2−45730
CO_2 laser, mode-locked, pulse duration meas. using optical bridge 2−73563
CO_2 laser, mode selective output-coupling apertures 2−73564
CO_2 laser, monochromatic TEA, 10μ operation 2−52418
CO_2 laser, optical investigation of plasma composition and mechanims of laser action for various systems 2−49361
CO_2 laser, optically pumped using transverse-discharge HBr laser 2−42006
CO_2 laser, passive Q-switching near 9.2μ using difluorodichloromethane 2−45725
CO_2 laser, performance in presence of alpha-particle source 2−52415
CO_2 laser, plasmotron excitation by plasma jet injection 2−69917
CO_2 laser, pulse discharge development and generation process 2−45717
CO_2 laser, pulsed, fast response thin film wattmeter for power obs. 2−63325
CO_2 laser, pulsed, gas dynamic eqns. and vibr. relax. rate eqns. 2−69911
CO_2 laser, Q-switched, vibr.-rot. line content 2−59144
CO_2 laser, Q-switched, with variable pulse delay 2−66746
CO_2 laser, Q-switched by rotating mirror, Doppler effect mechanism 2−59150
CO_2 laser, r.f. preionization in transversely excited supersonic flow 2−59146
CO_2 laser, Rogowski-type TEA, design, construction and operational parameters 2−63324
CO_2 laser, single-mode, Doppler Q-switching by rot. mirror 2−69914
CO_2 laser, spectrum generated at reduced pressure of working mixture 2−73566
CO_2 laser, TEA, GW range in 50 nS pulses, modular construction 2−76476
CO_2 laser, TEA, high power, high energy 2−42005
CO_2 laser, TEA, pulsed volume, single transverse mode operation using unstable resonator 2−69918
CO_2 laser, TEA, uniform discharge excitation method 2−66744
CO_2 laser, transversely excited, simple longitudinal mode operation 2−59148
CO_2 laser, transversely excited atmospheric pressure, comparison of excitation methods 2−52412
CO_2 laser discharges, afterglow, power decay meas. 2−42004
CO_2 laser electric discharge convection, flow conditioning 2−59152
CO_2 laser induced sparks in molecular gases, obs. of surrounding fluorescence 2−74440
CO_2 laser LG 1061 with 100 W 2−59153
CO_2 laser media, parametric studies of electron beam controlled discharge 2−41996
CO_2 laser pulse time modulation Q-switch, patent 2−69931
CO_2 laser radar, 10.6 μ, parametric obs. 2−55681
CO_2 lasers, detection of air pollution 2−81668
CO_2 lasers, for study of resonance in $CaF_2:H^-$ 2−61632
CO_2 lasers, high power, review 2−52419
CO_2 lasers, high power 2−69907
CO_2 liquid, heat transfer at supercritical pressure and temp. heads up to 850°C 2−60463
CO_2 long pulse laser, excitation by short pulse longit. electron beam 2−55682
CO_2 lower laser level relax. saturation 2−59992
CO_2 MHD laser, ionization instabilities and discharge characteristics 2−79207

Carbon compounds continued
CO_2 molecular absorptions, laser freq. and wavelength meas., speed of light 2−78758
CO_2 molecular velocity distribution effect on the shape of spectral line wings 2−64119
CO_2 photoelectron spectra at 304 Å 2−80058
CO_2 photoionization by soft X-rays, meas. of total and relative abundances of thermal energy ions and dissociation cross sections 2−80024
CO_2 photolysis at 1460Å and 1500 to 1670Å, CO quantum yield 2−69141
CO_2 planetary atmospheres, aeronomy of Mars and Venus 2−73075
CO_2 plasma, atmospheric pressure, 6500 to 9500 K, emission capacity in visible spectral range 2−43155
CO_2 polyatomic mixtures, laser excited, vibrational relaxation 2−43035
CO_2 ring laser, high power, hybrid injection locking, frequency stabilization 2−45724
CO_2 self-mode-locked atmospheric pressure laser, construction and operation 2−59147
CO_2 solid, librational modes, application of quantum lattice dynamics formalism 2−71709
CO_2 solid (ν_1, $2\nu_2$) vibron-phonon infrared absorption band in temp. range 88-160 K 2−81347
CO_2 TEA-laser with high output pulses 2−42009
CO_2 TEA, oscillator amplifier laser, 2 GW peak power generation 2−41994
CO_2 TEA amplifier, fluorescence and gain measurement 2−41995
CO_2 TEA laser, cavity-dumped, short pulses 2−42008
CO_2 TEA laser, high voltage and pressure 2−41984
CO_2 TEA laser, input power, gain and output 2−66747
CO_2 TEA laser, medium diagnostics, interferometric obs. 2−49365
CO_2 TEA laser, output energy depend. on excitation current pulse width 2−42007
CO_2 TEA laser, volume excited, unstable resonator configuration for mode selectivity 2−41991
CO_2 thermospheres of Mars and Venus, large- scale circulation effects 2−58508
CO_2 transversely pulsed discharge, effect of discharge driving capacitance on small signal gain 2−79190
CO_2 unstable confocal ring resonator laser 2−41992
CO_2 variations in atmosphere of Venus during 1971 superior conjunction, spectroscopic observations 2−78562
CO_2 Venus atmosphere, Venera entry probes and Mariner flyby 2−69164
CO_2 waveguide gas laser, characts. 2−59136
CO_2^+, Martian airglow, u.v. spectral obs. 2−66178
CO_2^+, photoelectron spectroscopy det. of branching ratios 2−50032
CO_2^+, predissoc., photoelectron- photoion coincidence spectroscopy and photoion kinetic energy analysis 2−67470
CO_2^+, relative intensity meas. on Fox-Duffendack-Barker ($A^2\Pi_u$-$X^2\Pi_g$) and u.v. doublet ($B^2\Sigma_u^+$-$X^2\Pi_g$) band systems 2−56162
CO_3^{2-} in complex structs. with bridge coord., plane vibr. freqs. 2−70690
$CO \rightarrow CO^+$ system, electronic transition moments for $A \leftarrow X$ $B \leftarrow X$ transitions, abs. absorption cross sections 2−52998
C_3O_2, Martian atmosphere, minor constituents, Mariner borne i.r. spectrometer 2−69156
CO($A^1\Pi$) system dissociative excitation by electron impact of CO_2 2−56164
COF_2, molecular g-values from Zeeman effect 2−70739
COS- on MgO, e.p.r. obs. 2−72494
COS, centrifugal distortion and anharmonic potential constants 2−52997
COS, Martian atmosphere, minor constituents, Mariner borne i.r. spectrometer 2−69156
COS + CO_2, shock heated mixtures, vibrational energy transfer processes 2−53100
CO_2 − DF vibrational de-excitation on the basis of vibration-to-rotation energy transfer, 300-2000K 2−83406
CO_2 − HF vibrational de-excitation on the basis of vibration-to-rotation energy transfer, 300-2000K 2−83406
CO + CO collisions, vibrational transition probabilities, temp. dependence below 300K 2−60117
CO + CO collisions, vibrational energy transfer 2−46642
CO + CO_2, N_2O, COS, shock-heated mixtures, vibrational energy transfer processes 2−53100
$CO_2 + N_2O$ collisions, vibr.-translation and vibr.-vibr. exchanges 2−43034
$CO_2 + N_2$ + He, active medium in tuned prismatic resonator, selective properties 2−52411
$CO + O(^3P) \rightarrow CO_2$ rate coeffs., meas., 250-370K 2−51438
CO_2^-. energy curves of $^2A_1$ and $^2B_1$, states 2−42874
CO($a^3\Pi$), lifetime meas. following electron impact dissociation of CO_2 2−50028
CO($a^3\Pi$), production by electron impact dissociation of CO_2 2−64117
(C_3O_2)n polymer production in Martian atmosphere and colouring of surface, laboratory studies 2−78542
C_5PO_3-Co$(PO_3)_2$ solid soln., phase diagrams, invariant points 2−74950
CS_2-O_2 chem. laser, c.w. overtone bands 2−49360
CS_2-organic liquid binary mixtures, u.s. absorpt. 2−46951
CS, Hanle effect measurement of the lifetime of the $A^1\Pi$ vibration-rotation levels 2−42885
CS, new symmetry assignment to k state from LCAO MO SCF calcs. 2−70688
CS and CS^+ thermochemistry 2−72544
CS lines in interstellar spectrum of ξ Persei 2−81836
CS_2- on MgO, e.p.r. obs. 2−72494
CS_2, calc, of parallel component of shielding tensor and relationship to ^{13}C chemical shift 2−53000
CS_2, general quartic force field, calc. using Parr-Brown anharmonic potential function 2−52999
CS_2, MO LCAO-CNDO calc. of electronic structure, comparison with X-ray spectra 2−60034
CS_2, nonlinear U(u) Hugoniot below 15kb 2−53390
CS_2, u.h.f. Kerr effect detection and obs. at 9227.12 MHz 2−74544
CS_2, u.v. absorpt. near N_2 laser wavelengths, excited states population 2−80014

- **Carbon compounds** continued
  - CS_2 fine structure of ultrasoft X-ray absorption spectra of S in 160-210 eV range 2−42939
  - CS_2 liquid, effects of intermolecular interactions on Raman spectrum 2−71205
  - CS_2 second harmonic laser light scattering 2−43357
  - CS_2 stimulated scattering in wing of Rayleigh line with psec. extinction 2−81375
  - C_3S_2, visible and near u.v. spectra, vibrational analysis 2−42877
  - C_3S_2 Raman spectra, assignment of bonds to components of first overtone, crystalline structure study 2−51354
  - $CSCl_2$, vibrational intensities from i.r. spectra 2−46533
  - CSF_2, vibrational intensities from i.r. spectra 2−46533
  - CS_2-O_2 CW chem. laser, reactions producing vibrationally excited CO 2−79202
  - CW crystals in cobalt, kinetics of growth 2−64590
  - $^{12}C^{14}N$ and $^{13}C^{14}N$ radicals in spectra of three carbon stars 2−75735
  - $^{12}C^{32}S$, $^{12}C^{34}S$, $^{13}C^{32}S$, $^{12}C^{33}S$, interstellar, isotopic abundance ratio and CS optical depth 2−75791
  - $^{13}C^{16}O$, $^{12}C^{18}O$ molecules, weak angstrom bands obs. 2−56157
  - $CaCO_3$ emission polarization 2−72692
  - Co-C interstitial solid solution, sat. magnetiz. and high field suscept. 2−81249
  - Co-C solid solution, X-ray study 2−50830
  - Co-C system, Curie temp. depend. on C conc., thermodynamic evaluation 2−44246
  - Co-Cr-C solid soln., activity and solubility of C 950-1200°C, precip., space equilib. diagram 2−56925
  - Co, adsorption on W(210), binding states and work function 2−60692
  - Co, molecular vibration effect on apparent bond lengths 2−56136
  - Cu-C alloy, prep. by vac. deposition, microstruct. 2−56928
  - Fe-Al-C alloy, martensite cryst. struct. change, −196 to 20°C 2−80766
  - Fe-C-W alloy, precipitation of eutectic carbide, and microsegregation obs. 2−74929
  - Fe-C-i-j-...-n multicomponent solid solution, C diffusion coeff., thermodynamic interpretation 2−43662
  - Fe-1%C-0.5%As, anomalous precip., resistivity, internal friction and elec. microscope obs. 50940 2−50940
  - Fe-C, baikovite, a new struct., produced by ultra rapid heating and cooling by laser beam 2−47630
  - Fe-C alloy, quench ageing and reversion 2−56903
  - Fe-C alloy, recovery of internal friction after strain ageing 2−47481
  - Fe-C alloy, strain ageing, internal friction obs. 2−56904
  - Fe-C system, diffusion of impurities, theory 2−50708
  - Fe-1%C alloy, effect of As and Sn on tempering stages 2−50796
  - Fe-Cr-C system, (Fe,Cr)-$(Cr,Fe)_7C_3$ composite, growth and props. 2−50920
  - Fe-Mn-C alloy, long period stacking order structure formed by thermal cycling 2−67990
  - Fe-Mn-C alloy, martensitic transformations and temp.-conc. boundaries 2−71683
  - Fe-Mn-C alloy, orientation relationship of the (225) martensitic transform. 2−74928
  - Fe-MoC, quenched and tempered, microstruct., field ion microscopy obs. 2−47581
  - Fe-N alloy, strain ageing, internal friction obs. 2−56904
  - Fe-Ni-C-Mo-Cr alloy, tempering, effect on struct. and mech. props. 2−43853
  - Fe-Ni-C, alloy, phase transform., martensite to austenite, rel. to heating rate 2−53985
  - Fe-Ni-C alloy, deform.-induced martensitic reaction, kinetics 2−80833
  - Fe-Ni-C alloy, deform. martensite formation, effect on mech. props. 2−71684
  - Fe-Ni-C alloy, isothermal and athermal, deform. induced martensitic transform. 2−71685
  - Fe-Ni-C alloy, martensite, surface plastic deform., X-ray obs. 2−80769
  - Fe-Ni-C alloy, martensitic microplastic deform. and isothermal transform. 2−43807
  - Fe-Ni-C alloy, martensitic, microplastic deform. and isothermal transform. 2−43808
  - Fe-Ni-C alloy, tempering, effect on struct. and mech. props 2−43853
  - Fe-Ni-C martensitic alloys, delayed fracture formation during cathodic charging under static stress 2−64731
  - Fe-Ni-Nb-C alloy, ageing, 700 and 800°C 2−47596
  - Fe-Sn-C system, formation and stability range of ternary cpds. 2−43933
  - Fe-V-C steel, fibrous vanadium carbide occurrences after thermal or continuous cooling transformation 2−61033
  - Fe-V-C system, phase diagram, pseudo-binary section at 0.5 wt-%V 2−47711
  - $^2HF-CO_2$ chemical transfer laser, model predictions and exptal. results 2−42016
  - $He/N_2/CO_2$ gas mixture, atmospheric pressure uniform d.c. discharge using gas additives 2−43214
  - $He-CO_2$ mixture, atmospheric pressure discharge 2−60305
  - $He-CO_2$ system, binary diffusion coeffs. conc. depend. 2−67737
  - $He(2^3S)+CO\rightarrow(CO^+)^*+He+e[C^*+O+He]$, excitation transfer and Penning ionization reactions, determ. rate constants for production of excited products 2−54535
  - Hg^*-CO collisions, electronic-vibrational energy transfer 2−80144
  - N_2-CO transfer laser, low temp., energy exchange processes 2−69924
  - Ni-C interstitial solid solution, sat. magnetiz. and high field suscept. 2−81249
  - $O^+ + CO\rightarrow CO^+ + O$, apparent charge transfer reaction, meas. of cross section from threshold to 100 eV 2−80133
  - $O+CS\rightarrow CO^\dagger+S$, chem. laser studies of initial vibr. distrib. of CO 2−72552
  - SiC system, phase relations, X-ray obs. 2−50972
  - U-Pu-W-C system, phase relations 2−54011
  - (U-Pu)C, two-phase mixed carbides, quantitative analysis by X-rays 2−64626
  - $(U-Pu)_2C_3$, two-phase mixed carbides, quantitative analysis by X-rays 2−64626
  - UO_2-C-N_2 reaction kinetics, 1695°C, carbonitride form. 2−54537

- **Carbon compounds** continued
  - V-C alloys, ordering effects in struct. obs. comp. depend. 2−71378
  - WC-Co cemented carbide, internal friction recovery obs. 2−68070
  - WC-Co hard metals, mixed milling effect on sintering, electron microscope investigation 2−56899
  - Y-Ce alloys, n.m.r. meas. 2−65350
- **Carbon tetrachloride (CCl_4)** *see Organic compounds*
- **Carcinotrons** *see Electromagnetic oscillations; Electron tubes*
- **Carrier density** *see Crystal electron states; Electron density*
- **Carrier mobility** *see Crystal electron states/transport processes; Semiconducting materials; Semiconductors*
- **Carrier scattering** *see Crystal electron states/transport processes; Semiconducting materials; Semiconductors*
- **Catalysis**
  - *see also Reaction kinetics*
  - benzene flash desorption and decomp. from clean or contaminated W polycryst. 2−84624
  - diamond synthesis, metallic catalysts, influence of alloying elements 2−68782
  - dissociation as primary process in hydrogen embrittlement and stress corrosion cracking 2−84020
  - orbital symmetry rules for surface sites prediction 2−51441
  - Shell 405 catalysts for N_2H_4 thrusters, decomposition storage 2−84632
  - silver halide crystal, development, redox potential, filamentary silver 2−84673
  - solid surfaces, conference, Boston Mass., USA, Oct. (1971) 2−47070
  - CO oxidation, on Pt(110) surface, Auger spectroscopy obs. 2−51443
  - CO oxidation in presence of $Fe(CO)_5$ in shock waves 2−57417
  - CuO, semiconduction rel. to catalytic activity 2−75093
  - DF, vibr. relax., catalytic efficiencies of NO 2−77163
  - H_2 on ferromagnetic catalyst, ortho-para conversion, surface magnetization orientation effect 2−71342
  - HF, vibr. relax., catalytic efficiencies of NO, H_2O, D_2O and HCl 2−77163
  - NiO, magnetocatalytic effects at Neel pt. 2−44480
  - Pt/Al_2O_3 catalyst, butene adsorption, high resolution n.m.r. obs. 2−60683
  - Pt surface, oxidation of CO 2−78185
- **Cataphoresis** *see Electrophoresis*
- **Cathode-ray oscillographs** *see Electrical measurement*
- **Cathode-ray tubes** *see Electron tubes*
- **Cathode rays** *see Electron beams*
- **Cathodes**
  - *see also Anodes; Electron emission*
  - — 2−75185
  - cermetelectrodes, bare and covered surfaces, local thermionic emission 2−54273
  - cold cathode arcs, model of cathode phenomena, dynamic field emission 2−71059
  - contact erosion due to gas breakdown arcs 2−43223
  - effect of changing surface on breakdown of Hg vapour 2−74436
  - electron gun assembly, with inert replaceable filament 2−45683
  - erosion, arc discharge, displacement of arc support points 2−80367
  - heat conduction and retrograde motion of cathode spot in arcs 2−71003
  - hollow, gas fed, arcs, theoretical evaluation 2−74453
  - hollow, in magnetic field, photoemission rel. to discharge glow in He 2−43215
  - hot, effects of fluctuating microfields on emission characteristics 2−63293
  - material, effect on sparking voltage in Townsend discharge 2−71047
  - metal, nonlinear effect due to optical field emission 2−44193
  - metal, nonlinearity of photoelec. emission, optical field emission effects 2−48020
  - microtron injector, loss measurement 2−79702
  - m.i.m. structures, surface roughness effect on electron distrib. 2−47948
  - nonmetallic inclusions, effect on vacuum breakdown 2−64356
  - oxide, effect of axial mag. field on Boltzmann temp. 2−59103
  - photocathode, using alkaline earth metals, energy structure 2−44195
  - photocathode sensitivity enhancement by multiple internal total reflection 2−44197
  - photomultiplier, distrib. of relative sensitivity 2−49682
  - razor blades, in high-current field-emission diodes 2−49325
  - region of 15 mm positive point-plane gap in air, spectral obs. in 3000-4000 Å region 2−74415
  - region of vacuum arc discharge, gasdynamics problems 2−77309
  - sheath, a.c. arc, thermal reignition 2−74450
  - spaces, influence of cathode qualities on Hg-Ar arc discharges 2−60324
  - spectral sources, hollow, use in absorption spectrophotometry 2−76544
  - spike, field emission from a regular array of spikes 2−48014
  - thermionic converters, high melting point electrode materials 2−54272
  - transmission secondary electron emitters resolution rel. to backscatter of electrons 2−81184
  - transverse hollow cathode gas and metal vapour lasers 2−79205
  - trialkali photocathode, thermionic emission 2−61459
  - trialkali-Sb photocathodes technology 2−44196
  - vacuum gap conditioning, by sparks and ion bombardment 2−67694
  - $Al-Al_2O_3-Al$ tunnel, cold emission distrib. 2−81125
  - CaSi system, temp. vs. comp. and press. vs. temp. diagrams, correl. 2−71699
  - CrB, thermionic emission, obs. 2−44191
  - GaAs-(AlGa)As heterojunction structure, factors affecting extended operation 2−48012
  - GaAs, negative electron affinity, photoemission rel. to Cs-O layers thickness 2−75194
  - GaAs photocathodes, Cs adsorption effect 2−53595
  - Ge, field-emission, preparation technique 2−82433
  - HgO, in HgO/Zn cell, electrochemical reactions 2−84655
  - $InAs_{0.4}P_{0.6}$/Cs-O i.r. photocathode, wavelength depend. of Cs-O optimum thickness 2−68498
  - $InAs_{0.4}P_{0.6}$, negative electron affinity, photoemission rel. to Cs-O layers thickness 2−75194

Cathodes continued
Ir, ThO_2 coated, as electron emitter for electron bombarded semiconductor devices 2−65099
K_2CsSb photocathode, thermionic emission 2−61459
LaB_6, electron gun, brightness and energy distrib. 2−73525
LaB_6 rod cathode low power heater 2−62888
Mo, flashing effect, surface atom migration, field ion microscopy 2−53557
Mo, monocrystal, electrical characteristics, thermionic converter 2−54275
Pt cermet cathodes, electron microscope study of thermal activation 2−81506
Sb-Cs photocathode study using scanning electron diffraction system 2−75195
Si, field-emission, preparation technique 2−82433
Si field photocathode, emission on illumination from reverse side 2−44209
Si single crystal, thermionic emission anisotropy obs. 2−65101
W, flashing effect, surface atom migration, field ion microscopy 2−53557
W, in Cs plasma, electron emission rel. to temp. and current density 2−75191
W, monocrystal, electrical characteristics, thermionic converter 2−54275
W, pumping effect, of O_2, rel. to ionization gauges and mass spectrometers 2−48943
W, pumping effect, of O_2, rel. to ionization gauges and mass spectrometers 2−48943
W electrostatic lens, surface temp. det. in electrostatic field of immersion objective 2−41923
W locally heated, in electron gun 2−79026

oxide
NiO, true work function, A constant, normal energy distribution 2−44192

Cathodoluminescence
diamond, changes caused by deformation, electron microscopy obs. 2−81428
information storage, elec. irrad. defect inhibition of cathodoluminescence 2−57379
P-15 phosphor, meas. of decay time by delayed coincidence technique 2−48260
phosphor, absolute radiative efficiency 2−72432
AlN, i.r. cathodoluminescence, 110-353 K, Huang-Rhys factor determ. 2−75336
CdP_2, recomb. radiation, 63-300K 2−72394
$CdS:Yb^{3+}$, emission spectrum at 10 K, before and after e irrad. 2−75339
CdS, donor-acceptor luminesc., temp. depend. 2−48261
CdS, donor-acceptor pair emission, electron irrad. damage effects 2−54478
CdS, electron beam microprobe exam. of crystal structure defects 2−53745
CdS, pulsed region, thermal cond. obs. 2−54077
CdS platelets, radiation damage effects at low temps. 2−68703
CsI:Tl, α-particle irrad., scintillation yield orientational depend. 2−81434
p-GaAs, electron beam excited, internal quantum efficiency, effect of beam voltage increase 2−72433
GaAs epitaxial film, carrier mobility effects 2−72434
GaAs targets, luminescence obs. 2−54479
GaP-ZnSe alloy, cond. hopping contrib., ionized impurity scatt., electrolum. and cathodolum. 2−81415
KBr, quenching of cathodoluminescence as a function of colour centres, at 90 and 300 K 2−68704
KCl:KI films, slow electron impact, luminescence excitation and characteristic energy losses 2−81417
KCl, quenching of cathodoluminescence as a function of colour centres, at 90 and 300 K 2−68704
KI, quenching of cathodoluminescence as a function of colour centres, at 90 and 300 K 2−68704
KI films, slow electron impact, luminescence excitation and characteristic energy losses 2−81417
Si, γ-irrad., vibronic spectra, temp. depend. 2−48262
$Y_2O_2S:Eu^{3+}$, sensitization by Pr^{3+} and Tb^{3+} 2−51371
ZnS:Cu phosphor particles with nonluminescent coatings, cathode-ray efficiency, voltage depend. 2−51383
ZnS, rel. to S atom displacement by electron irrad. 2−48263
ZnSe, electron irrad., Se atom displacement 2−61723
$ZnSe_xTe_{1-x}$ p-n junction diodes, struct., props., electron microscope and cathodolum. obs., 77-300K 2−81118
$Zn_2SiO_4:Mn^{2+}$, willemite, electron microprobe obs. 2−51382
ZnTe, due to donor to double-acceptor recomb. 2−54480
ZnTe, electron irrad., threshold energy for Te displacement detn. 2−68018

Causality *see Physics fundamentals*

Cavitation
see also Vortices
acoustic cavitation at 10 kHz 2−56464
bubble implosion pressure pulses and cavitation damage 2−56469
bubbles, collapse and rebound, extreme cases 2−77402
bubbles, produced by dissolved gas coming out of solution on pipe walls in flowing systems 2−50306
collapse of one-dimensional cavities in compressible liquids 2−71139
condensing bubbles in compressible liquids 2−43298
critical, flow-limiting, for moving system 2−67774
damage in flow system, dimensional anal. 2−67776
diaphasic resistance variations 2−53504
dimensional perturbation calc. of contraction coeff. 2−46894
erosion, determination of resistance of materials by magnetostrictive vibratory method 2−76115
erosion focuses, primary and secondary, structure of cavitation zones 2−60390
erosion testing and cutting, using simple cavitating nozzle 2−77388
flow about supercavitating lifting hydrofoils, second- order results 2−46895
formation during creep testing, t.e.m. obs. 2−80871
hydroacoustical noise spectra 2−43287

Cavitation continued
hydrodynamic marine systems, erosion due to prevention, cure 2−77387
infinite cavity flow, theory of optimum shapes, minimum drag profiles 2−80175
interaction mechanism between cavitation bubbles and particles of solid and liquid phases 2−64415
laser induced, bubble collapse and rebound 2−43289
liquid, acoustic cavitation at 10 kHz 2−56464
liquid, high speed photography of laser-induced breakdown 2−56470
liquid explosives, low velocity detonation mechanism 2−83723
liquid flow over step, applic. of cavitation schemes 2−60391
liquids, nucleation models 2−53503
in loaded hydraulic cylinder with step inputs 2−77389
nonlinear effects in collapse of nearly spherical cavity in liquid 2−46911
polyphase flow, conference (San Francisco March 1972) 2−67603
practical concepts and testing, book 2−71140
pressure distrib., effect of nuclei size 2−67773
rotating disc, damage 2−77390
ship hydrodynamics, theoretical models, review 2−77379
supercavitating hydrofoils with rounded noses 2−67775
turbopump inducers for rocket engines, internal streamliner flow analysis 2−43288
u.s., review 2−78925
u.s. exposure thresholds in cells and tissues 2−66266
velocity in acoustic stationary wave 2−56463
volume effects on cavitation mechanism and stability 2−80424
water, effects of surface tension on threshold 2−43290
water, nonsteady fow at high speeds 2−77371
Al single crystals, cavitation in liquid oxygen, plastic deformation in metal surface layers 2−71306
Cu-Zn(40%) microduplex, metallographic study 2−80738
He I, acoustic cavitation at 10 kHz 2−56464
He II, acoustic cavitation at 10 kHz 2−56464
He II, light scattering by ultrasonic cavitation 2−43427
He superfluid, vortices and turbulence as nucleation mechanism 2−43426
Na-Ar liquid gas system, influence of gas on nucleation in sinusoidal pressure field 2−46893
Zn single crystals, cavitation in liquid oxygen, plastic deformation in metal surface layers 2−71306

Cavity resonators *see Acoustic resonators; Electromagnetic oscillations*

Celestial mechanics
— 2−72937
area-preserving mapping, stability 2−62455
artificial satellite motion, tidal effects 2−84933
astronomical ephemerides 2−66044
attitude libration interaction with orbital motion of rigid body in near Keplerian orbit of low eccentricity 2−44832
axial rotation, viscous friction effects 2−55006
bipolar moments integral 2−72968
Brown's lunar theory, different methods of derivation of differentials 2−84938
capture resonance of asteroid 1685 Toro by the Earth 2−69169
cascade dynamics, simulation of collective motion 2−81779
circular motion with nonuniform velocity 2−81772
circular orbits det., multiple solutions 2−51698
close binary systems, effect of viscous friction on precession and nutation 2−75663
collapsing galaxy, variations of stellar orbits 2−81784
collision singularity in perturbed N-body problem 2−62454
comet and asteroid probes, trajectory considerations 2−58522
comet Finsler (1937 V), definitive orbit allowing for five major planet perturbations 2−58519
cometary orbits rel. to interstellar gravitational perturbations 2−69171
comets, long-period, planetary perturbations of orbits, dependence on inclination 2−75920
comets, perturbation by planets and stars close to solar system 2−81783
comets, short period, effect of multiple encounters with Jupiter and Saturn on orbits 2−58523
conference, Tokyo, Japan (1972) 2−81771
critical inclinations and eccentricities in N-planet problems 2−85033
Delauney elements, canonical generalization 2−58173
differential eqns. of motion, power series solns., transforms. applic. 2−62453
disk like stellar systems, constant models 2−81774
distant Earth satellite resonant motion rel. to Moon and Sun, laser ranging and geodetic applications 2−81760
dynamic astronomy, meeting (College Park, USA, March 1972) 2−58166
dynamic space, curvature and ergodicity Riemannian geometry 2−81778
Earth and lunar orbiters, higher order analysis of drag-free satellites 2−78423
Earth-to-Moon trajectory, asymptotic matching in restricted three-body problem 2−48655
equinoctial orbit elements for two-body problem 2−62452
faint M stars near N galactic pole, proper motions 2−55030
finite two body problem, common and individual rotation 2−81780
flat galaxy, speed distribution function 2−81773
formula manipulation system TRIGMAN precompiler 2−58171
four and five body systems, dynamics, equations of motion, stability 2−58260
Galaxy, approximate form of third integral 2−81801
general three body problem, numerical integration 2−81777
generalized Kepler motion, motor integrals 2−84936
gravitational constant, possible anisotropy effects on celestial orbits 2−81755
Hansen's planetary theory, computer implementation 2−62694
Ideal Resonance Problem, comparison of global and classical solutions 2−72963
Ideal Resonance Problem, normality condition derived from first-order solution 2−81753
infinitely small body, stability of motion in gravitational field of Earth and Sun, radiation pressure effects 2−69012
interplanetary objects, statistics of masses and dynamics 2−75917

Celestial mechanics continued
interplanetary trajectories, approximation by Chebyshev series 2−44831
interplanetary trajectories by quasilinearization with Chebyshev series 2−58167
Kallisto satellite, influence of Halileys satellites of Jupiter on motion 2−58491
Kepler's eqn., exact closed form soln. 2−58174
Keplerian motion, numerical stabilization of the differential equations 2−72965
lunar motion, errors, numerical methods, lasers, Doppler effect 2−84939
lunar orbital, laser ranging data, trial solns. 2−58449
lunar theory, numerical isolation of flaws 2−81923
χ Lupi, double lined binary Hg star, orbital elements44852 2−44852
mean motions of bodies, close commensurability, perturbation function expansions 2−69011
motion of ecliptic determ. for reciprocal planetary masses 2−81904
n-body problem with variable gravitational constant, dynamical consequences 2−81769
Newton's law of gravitation, closed orbits 2−48985
non-conservative systems, nonlinear oscillations 2−48658
numerical artificial satellite theory using Picard iteration process 2−58149
orbital clustering, due to elastic and inelastic scattering 2−58177
orbital elements soln. and derivation for Moon and planets 2−62645
orbits, optimal spatial one-impulse transfer from hyperbolic to circular 2−51697
orbits in vicinity of 1:2 Kirkwood gap, evolution 2−62457
origin of short-period meteor orbits rel. to perturbations of Jupiter 2−58525
perturbation theory, book 2−72969
perturbation theory, book 2−69013
perturbation theory, Lindelof's method 2−81782
planar three-body problem, regularization of binary collisions 2−81758
planets, perihelion motion from new gravitational theory 2−62977
planets beyond Pluto, orbit determination from comet obs. 2−69139
point mass past large mass of prolate ellipsoid of revolution, motion 2−55451
pole of the ecliptic, position from improved values of reciprocal planetary masses 2−58172
potential development of smooth, dense rotating body rel. to planets 2−81757
regularization of conservative central fields 2−66045
regularization of Ideal Resonance Problem 2−44834
relativistic runaway problem of binary system with primary mass loss 2−72967
resonances in rotations of celestial bodies and Cassini's laws 2−78498
resonant stellar orbits in spiral galaxies 2−75684
restricted four body problem, sphere of interaction 2−68996
restricted three body problem, periodic librations 2−58168
restricted three body problem, two-parameter survey of periodic orbits 2−72964
restricted three-body problem periodic perturbation of libration points 2−78427
review, present and future 2−81785
review of celestial mechanics in twentieth century 2−78443
satellite motion about its centre of gravity, effect of terrestrial magnetic field 2−72938
satellite perturbed motion rel. to solar radiation pressure effects 2−84935
satellites, reference loci applied to four-body dynamics 2−78431
single close encounters in three-body problem rel. to planetary problem 2−81759
single collision periodic orbits 2−72962
spectroscopic visual binary in ADS 14893 triple system, orbital elements 2−75779
spherical fluid model of celestial body, e.m. field and internal motions 2−48657
spherical systems of galaxies, predominant motions, instability 2−58199
spherically symmetric system of revolving masses, collective oscillations 2−62456
stability of motions of body of resolution in Newtonian field studied by Lyapunov methods 2−58176
star-Sun-comet system using restricted hyperbolic three-body problem 2−85032
stationary motions of triaxial body and stabilities 2−66047
stellar encounters, new treatment in computation of N-body systems 2−58170
stellar proper motions, contrib. of Danjon's astrolabe to study 2−66069
symbolic programming rel. to computation of general normalized inclination functions 2−81754
symplectic mappings, parametric stability 2−81781
three bodies, three dimensional restricted problem, periodic solutions 2−51696
three body problem, collision and regularisation 2−81775
three body problem, hyperbolic-elliptic motion 2−81776
three body problem, improved criteria for hyperbolic elliptic motion 2−66046
three body restricted problem, periodic orbits of collision 2−49054
three dimensional restricted three body problem, nonlinear stability problem 2−72966
three-body problem, class of high energy close approach trajectories 2−48659
three-body problem, new form of differential equations of relative motion of planets 2−81756
three-body problem with nonstationary Newton-Hooke interaction, motions in universe 2−75664
1685Toro asteroid, capture resonance by Earth 2−58518
translatory-rotary motion of rigid bodies, first integrals of generalized problem 2−81751
triaxial rigid satellite in precessing elliptic orbit, effects of gravity-gradient torque on rotational motion 2−81752
triple gravitational systems, evolution, termination of binary 2−58175
triple star systems, stability criteria 2−58169

Celestial mechanics continued
triple systems, binary formation 2−51775
two point boundary value problems using perturbation method, intermediate matching technique 2−44833
Cell model *see Liquids, theory*
Centrifuges
high-speed rotating devices 2−58828
isotope separation, plasma centrifuge 2−70648
spiral, aerosol particle, distrib. analysis of aerodynamic size and mass 2−50382
U enrichment, gas centrifuge method 2−70530
Ceramics
8/65/35 PLZT fine grained ferroelec. ceramic, dielec. and optical fatigue effects 2−77953
alloy, B2Zh, prep. and mech. characterization 2−77720
alumino silicate refractory fibre, props. and applicatons 2−56953
aluminosilicate, thermomechanically strengthened, thermal-stress fracture 2−50738
automatic TV image analyzer, application 2−56957
bismuth oxide, use in nuclear reactors 2−83064
brittle, strength, review 2−47520
carbides, wetting by liq. metals, relative surface energies 2−50427
CC $MgAl_2O_4$ polycryst., prep. and characteriz. 2−50887
ceramic-metal reaction welding, microscopic and macroscopic obs. 2−64785
ceramic-metal systems, interfacial phenomena, chem. bonding 2−50861
ceramic-metal systems, ion tunnelling 2−51183
ceramics, texture with ref. to mech. props. 2−67949
cermet, Fe-based, antifriction props. rel. to sintering in various protective atmospheres 2−77727
cermet, Fe-based, effects of protective sintering atmos. on physiomech. props. 2−68166
cermet, sintering, in container with melting closure 2−50882
cermet, yield limit change regularities in compaction rolling 2−68126
cermet hard alloys based on Ni-containing titanium carbonitrides 2−68152
cermet. ZHGp1.5D2.5, effects of cooling after sintering on struct. and mech. properties 2−77722
cermets, fatigue testing at elevated temperatures and aeronautical application 2−56870
cermets, thin film, strain gauge factor study 2−77710
chemically reacted matrix, for fibre reinforced composites 2−56972
composite, C continuous fibre-reinforced, mech. props. 2−50919
composite, C discontinuous fibre-reinforced, fabrication and props. 2−50918
composite, glass-crystal two-phase, fracture, theory 2−74860
composites with alumina matrix, impact strength and dynamic loading 2−80758
conference, Washington, USA, (May 1972) 2−47650
corundum base, elec. cond. rel. to sintering 2−53927
corundum based, thermal stability rel. to microstruct. 2−56959
crack propag., subcritical growth and fracture energy 2−50857
crystalline, precipitation 2−84063
diamond-metal system, compaction during liq.-phase sintering 2−80829
dielectric, high-permittivity temp.-stable, low microwave loss 2−51190
direct calorimetric analysis, temp. and heat of reaction determ. 2−54522
electrolyte in high-temp. fuel cell, conversion of cheap fuels 2−59041
electron microscope study, high-voltage, of texture by Harwell 1 MV microscope 2−71412
electron multiplier, design and performance 2−49679
ferrite memory cores, elastic constants 2−84431
ferroceramics, microstruct., domain struct. 2−53925
ferroelectric, transparent, elec. and optical props., grain size and porosity effects 2−57244
ferroic, coupled props. 2−57238
fracture energy meas., notched beam test 2−50858
fracture topography of polycrysts., mirror obs. 2−50855
friction and wear, fund. review 2−47554
friction and wear characts. 2−47555
friction and wear characts. of material coupled with surface-hardened metallic alloy 2−47556
glass, fluor-richterite composition of high mechanical strength, microstructure determ. 2−77704
glass, high quartz solid solution, fine grained crystallization rel. to nucleating agents 2−50411
glass, lithium silicate, fracture energy as function of struct. 2−50886
glass, workability, thermal and dielec. props. 2−43868
−glass capacitance thermometer, performance in 0.007 to 0.040 K range 2−66371
glass-ceramic, Nd^{3+} doped, lasing threshold and efficiency 2−73589
glass-ceramic, viscosity changes during nucleation and crystallization 2−53923
glass-ceramic capacitance thermometer for obs. in 1.7 to 300K range 2−76404
glass-ceramics, elemental analysis, using scanning elec. microscope 2−60579
grain size, very fine, X-ray beam diffracted power obs. 2−56958
graphite, Cu plated, cermet on Fe base, sintering 2−53863
graphite, fatigue failure probability 2−53827
high quartz solid solution glass-ceramics, influence of composition on density 2−56562
homogenous systems, A_uX_v-B_uY_v type, ideal soln. behaviour 2−50852
hot stage microscope applications 2−56838
liquid metal-ceramic systems, critical surface energy of spreading 2−50425
machining, surface finishing techniques, effects, symposium, Gaithersburg (1972) 2−80864
magnesia, polycrystalline, deformation in compression, 1100-1750°C 2−68167
metal-ceramic materials, technique for determ. of plasticity and strength 2−68161
metallized ceramic heat sink, thermal cond. obs. 2−76118

Ceramics continued
mica glass-ceramics, microstruct. and mech. props. 2–60999
microstructures, sequence and effects 2–67948
modulated struct. orientation in rhombohedral system 2–50853
mullite, press.-sintered, mech. props., porosity depend. 2–50722
mullite, press.-sintering kinetics and mechanism 2–50874
mullite, stoichiometric, synthesis and mech. props. 2–50873
mullite, Young's modulus rel. to porosity 2–43906
nonlinearities, effect on design of sonar and industrial transducers 2–49156
nuclear materials, application of linear analysis to study of porosity using Cahn-Fullman relation 2–74147
nuclear reactor fuel material in fast reactor environment 2–56058
oxide fuel pin behaviour, COMETHE code 2–52859
oxide fuel struct. evolution, modelling using BEHAVE-2 code 2–52858
$Pb_xLa_{1-x}(Zr, Ti)O_3$ ceramics for selectively erasable image storage and display 2–79454
piezoceramic bimorph, infinitely extended, mixed boundary value problem 2–72043
plastic deform., dislocation motion role 2–47493
PLZT ceramics, crystal structure and enhanced ordering of ferroelec. domains 2–80760
porous, polymer impregnated, strength rel. to temp. 2–43899
portland cement paste, microstruct. effects on deform. and fracture 2–60995
powder, binderless granulation mechanism and sphere growth 2–47660
preparation by calcining of fusible clays 2–64784
pyrophyllite, mech. props., effect of firing temp. 2–50890
reactor fuel, 90% dense, fabrication for irrad. testing 2–53924
reactor fuel, irrad., neutron radiography obs. 2–52856
reactor fuel performance models, review 2–52857
refractory oxide, oxide filament reinforced, characs. 2–56973
scanning electron microscope applications 2–56956
scanning electron microscope-probe analyser combination, use 2–71414
seals fast-neutron irradiation effect 2–63227
sintered, metal fibre reinforced, manufacture, applications, props. 2–43866
sintering, rel. to wetting phenomena 2–43867
sintering kinetics, at const. heating rate, equation 2–47652
sintering under isostatic press. 2–50859
solid/liquid phase interactions, wetting study 2–43464
steatite, mech. props., effect of firing temp. 2–50890
steatite materials, sintered, effect of modifying agents on struct. and electromech. props. 2–53933
strength, microstruct. influence, review 2–47521
strength testing methods comparison 2–47563
strength/grain size effects 2–68092
strengthened by surface compression, thermal stress fracture 2–50871
stress corrosion failure under dynamic loading conditions 2–50771
substrate, effect of surface chemistry on adhesion of TaN 2–57005
substrates, strength, biaxial flexure tests 2–60919
surface texture examination by reflective replica technique 2–80869
tensile creep testing apparatus using simple knife edge universal joints 2–47568
textural studies by electron probe microanalysis 2–71411
texture and phases in spark plugs, e. probe anal. and X-ray diffr. study 2–71390
textured studies by scanning electron microscopy, examples of use 2–71413
thermal conductivity, high temp. obs. 2–77734
thermometers, capacitance, glass-ceramic, low temp., equations 2–49187
tile bodies, effect of polymer impregnation on physical and mech. props. 2–80759
transducers, under mechanical load, meas. of clamped capacitance and electromechanical coupling coeffs. 2–52241
transition metal carbides and nitrides, (Gp IV and V), nonstoichiometry rel. to order-disorder changes 2–61029
transmission electron microscope examination 2–56954
transmission electron microscope obs., at high voltage 2–56631
transparent, cryst., optical applications, prep. 2–60988
volume diffusion controlled pore shrinkage during final stage sintering 2–50854
wetting angle, statistical interpretation 2–60970
wustite, fracture energy invariance with grain size 2–50880
yttralox, characteriz. as laser material 2–49381
Yttralox, Th-doped, processing 2–50900
Al-Si-N-O, new ceramic materials 2–60990
AlN-Al_2O_3-Mo cermet, prep., microstruct., hardness, strength, density 2–43869
Al_2O_3-Mo cemets, thermophysical characteristics in range 500-1300°K 2–43999
Al_2O_3-P_2O_5-Cr_2O_3, coating on steel, props. 2–56960
Al_2O_3-TiO_2, sprayed layers, thermal cond. 2–44000
Al_2O_3, alumina, coupled solute solid soln. softening with MgO and TiO_2 2–47653
Al_2O_3, alumina, high temp. creep, and grain boundary sliding 2–50753
β-Al_2O_3, alumina, hot pressing, strength and fracture 2–50875
Al_2O_3, alumina, phosphate bonded, strength props., elec. microscope obs. 2–77662
Al_2O_3, ceramic, microstruct. rel. to deform. processes 2–60993
Al_2O_3, ceramic to metal seal for thermionic fuel elements 2–53928
Al_2O_3, corundum, high temp. creep, microstruct. changes 2–71574
Al_2O_3, fine grain, Cr_2O_3 additions effect on struct. and props. 2–50867
Al_2O_3, fine grained, rate controlled sintering 2–77660
Al_2O_3, high temp. strength 2–50868
Al_2O_3, high temp. strength improvement by surface prestressing 2–50870
Al_2O_3, internal friction, temp. depend. 2–71553
Al_2O_3, quenched, residual stress determ. from mirror dimens. 2–50869
Al_2O_3, sintering, surface area and pore-size distrib. obs. 2–50866
Al_2O_3, sintering kinetics, effect of iron oxide 2–50865
Al_2O_3, static and cyclic fatigue behaviour 2–50766

Ceramics continued
Al_2O_3, strength, biaxial flexure tests 2–60919
Al_2O_3, strengthened by surface compression, thermal stress fracture 2–50871
Al_2O_3, subsurface damage due to abrasion, examination using transmission electron microscopy 2–80870
α-Al_2O_3, surface finishing by flame polishing, annealing techniques 2–80865
Al_2O_3, translucent alumina prep. and characteriz. 2–50863
Al_2O_3 (99+%), white spots characteristic 2–84064
Al_2O_3 and Al_2O_3/B fibre composites, high temp. bearing characts. 2–47558
Al_2O_3 bicrysts., porosity distrib. and pore growth on grain boundaries 2–60991
Al_2O_3 ceramics, microwave machining and piercing characteristics 2–53867
Al_2O_3 for electronic device substrates, surface analysis, characterization techniques 2–80868
Al_2O_3 insulators for thermionic reactors, neutron induced swelling as function of neutron energy 2–63228
α-Al_2O_3 single crystals, flat bars, flame polishing, problems, limitations 2–80866
Al_2O_3 whiskers of fibres, poor efficiency in reinforcing Ni for high temp. use 2–47668
Aln, thermal cond., characteriz. 2–50864
$AsSe_{1.5}Sn_{0.28}$, pyroceramic, semicond., elec. cond. mechanism, 285-385K 2–75089
Au-SiO film, cermet, struct., elec. props., rel. to deposition condition 2–64976
(b,La)(Zr,Ti)O_3, cold pressing and low temp. sintering 2–50892
BC neutron absorber rods, modelling of swelling and gas release 2–52861
BN, compact specimens, thermal cond., 100-1000 K 2–47761
Ba-mica/Al_2O_3 composite, fabrication and props. 2–56977
$BaFe_{12}O_{19}$, deform. texture 2–56962
$Ba_2NaNb_5O_{15}$, Gd, substituted, thermal expansion 2–51048
$Ba_2NaNb_5O_{15}$, sintering behaviour, scanning elec. microscope obs. 2–53929
3BaO.5SiO_2 glass-ceramic, mechanical props. 2–53930
$BaTiO_3$-Bi_2O_3, La doped composite ceramic, two-step anomalous resistivity increase 2–68395
$BaTiO_3$, dielec. props., sintering parameter effects 2–57241
$BaTiO_3$, La doped, Bi_2O_3 as grain boundary element, resistivity temperature characteristic anomaly at transitions 2–84366
BeO powder, initial stage sintering mechanism 2–47662
CaO-ZrO_2, struct., thermomech. props. 2–43876
CeO_2, sintering, effect of TiO_2 addition on grain growth 2–47655
$CoAl_2O_4$, porosity effect on elastic moduli 2–50729
CoO-MgO solid solns., porosity effect on elastic moduli 2–50729
Cr-Si-Fe-W films, electron microscope study of laser produced holes 2–80780
Cr-SiO films, electron microscope study of laser produced holes 2–80780
Fe cermet, highly porous, thermophysical properties 2–71651
Fe cermets, thermal stability of sulphides of some metals 2–68164
Fe_2O_3, experimental sintering kinetics, approx. equation 2–47652
Gd_2O_3:Eu^{3+} transparent phosphor, prep. and optical props. 2–72409
HfC, hot pressing for high temp. bearing applications, NASA research 2–64801
HfN-ZrB_2 cutting tool materials characteriz. 2–50883
HfN, hot pressing for high temp. bearing applications, NASA research 2–64801
$LiAl_5O_8$, transparent, prod. by hot-pressing 2–43873
$Li_{0.5}Fe_{2.5}O_4$, mag. props., synthesis conditions influence 2–44277
Li_2O-Al_2O_3-SiO_2 glass-ceramic, strength and microstruct. 2–53931
$MgAl_2O_4$ spinel, densification kinetics 2–50889
MgF_2, X-ray structural study of texture of KO-1 optical ceramic 2–70042
MgO-Li_2O-Al_2O_3-SiO_2-TiO_2, glass-ceramic, crystn., microstruct., indentation hardness 2–80535
MgO-SiO_2-Al_2O_3, pressure sintered specimens, phase composition and dielectric constants 2–57226
MgO, hot-pressed, annealing effect on elastic props. 2–50888
MgO, sintering, surface area and pore-size distrib. obs. 2–50866
MgO refractories, effect of stress on grain growth 2–74915
MgO.Al_2O_3.SiO_2 glass-ceramic, ZrO_2-nucleated, phase transitions 2–47691
Mo-Cu-Co cermet contact, elec. erosion characts. working surface struct., rel. to Co content 2–47659
Na-β-Al_2O_3 phases formation and area of existence 2–84066
Ni/SiO_2 cermet films, granular, microstruct. 2–50498
Ni, refractory oxide particle growth, matrix density effects 2–68169
Ni cermet, highly porous, gas permeability 2–56965
NiO, experimental sintering kinetics, approx. equation 2–47652
NiO, high temp. transport props. 2–84314
(Pb,La)(Hf,Ti)O_3, hot-pressed, material and electrooptic props. 2–56966
(Pb,La)(Zr,Ti)O_3, electrooptic, fabrication by atm. sintering 2–56967
(Pb,La)(Zr,Ti)O_3, phase boundary and defect struct. 2–56968
$Pb_{1-x}La_x(Zr_yTi_z)_{1-x/4}O_3$ ceramic, radial mode coupling factors det. with large Poissons ratio variations 2–51195
$PbMg_{1/3}Nb_{2/3}O_3$-$PbTiO_3$-$PbZrO_3$ solid solution, hot-pressed, electrooptic props. 2–57328
$Pb(Mn_xNb_{1-x})O_3$ perovskites, synthesis and characteriz. 2–50893
PbO-P(As)(V)$_2O_5$ systems, cpds., synthesis and crystallography 2–74741
Pb(Ti,Zr)O_3, cold pressing and low temp. sintering 2–50892
Pb(Ti,Zr)O_3 system, intrinsic nonstoichiometry 2–50894
$PbTiO_3$-$Pb(Cd_{0.5}W_{0.5})O_3$, electromechanical props. 2–64788
$Pb(Zn_{0.33}Nb_{0.67})O_3$ electrooptical props. rel. to sintering conditions 2–65223
Pb(Zr, Ti)O_3, shock induced electromech. conversion, additives influence 2–84359
Pb(Zr,Ti)O_3, microstruct., role of Fe_2O_3 2–50895
Pb(Zr,Ti)O_3 type, static dielec. const. and dissipation factor, nonlinear field depend. 2–72035
$PbZr_{0.5}Ti_{0.5}O_3$, single-phase, intrinsic nonstoichiometry 2–50896
Pt cermet cathodes, electron microscope study of thermal activation 2–81506

Ceramics continued
^{238}PuO$_2$ fuel fabrication by hot pressing 2−53932
(Si,Al)(N,O)$_4$ tetrahedral structure 2−60997
SiC ceramic, resistance to dynamic fatigue at room temp. in air 2−80761
Si$_3$N$_4$, high density, fatigue behaviour, 250-1200°C 2−60897
Si$_3$N$_4$, hot pressed, fracture energy at high temps. 2−60907
Si$_3$N$_4$, hot pressed, high temp. strength 2−60884
Si$_3$N$_4$, hot pressed, strength fracture energy, microstruct. relationships 2−60883
SmC$_x$, chem., metallographic and X-ray characterization 2−71653
TaC neutron absorber rods, modelling of swelling and gas release 2−52861
ThN-ThO$_2$-Th system, phase behaviour 2−50977
ThO$_2$:Y$_2$O$_3$, high optical quality, powder prep. and processing technique 2−77736
ThO$_2$ powder compacts, desintering 2−50898
TiC-Ni-Mo cermet alloy, hardness, bending strength, wear resist. 2−47534
UC$_x$, high temp. deform., proportional limit 2−53809
UO$_2$-Mo cermet, finely-dispersed, creep rate and particle growth 2−71650
UO$_2$-PuO$_2$, mixed fuel, control and behaviour of O/M, offgas and moisture during fabrication 2−53934
UO$_2$-PuO$_2$ mixed fuel, plastic flow and stress relax. 2−53808
UO$_2$ fuel, bubble re-soln. and creep 2−52862
Uo$_2$-PuO$_2$ mixed fuels, advanced characteriz. 2−52870
W-Y$_2$O$_3$ two-phase system, black-body radiation and elec. resist. 2−43875
WC-Co cermets, plasticity, slip, grain boundary sliding 2−47505
zirconia, phase analysis by X-ray analysis, matrix method, polymorph technique 2−80879
ZnO-Al$_2$O$_3$-SiO$_2$ glass-ceramics, dielec. props. and effects of adding (CaO, SrO, BaO) 2−65045
ZnO-Bi$_2$O$_3$, elec. props. and microstruct. 2−57198
ZnO, experimental sintering kinetics, approx. equation 2−47652
ZnO powder, particle size distrib. data processing, computer appl. 2−53942
ZrO$_2$-6 mol%CaO, castable, elec. cond., 900-1700K 53936 2−53936
ZrO$_2$, calcia-stabilized, destabilization by ZrB$_2$ 2−50902
ZrO$_2$, calcia-stabilized, fracture toughness 2−50777
ZrO$_2$, calcia stabilized, thermal stress induced microstruct. modifications 2−50901

Cerenkov radiation *see Cherenkov radiation*

Cerium
in borate glasses, non-destructive method for ceric/cerous ratio determ. 2−48362
electronic energy bands for α- and γ-phases 2−44031
film, core level binding energies, X-ray photoelectron spectra study 2−72096
isotopes, arc and spark spectra, ^{140}Ce-^{142}Ce shifts 2−79893
isotopes, arc and spark spectra, isotope shifts 2−79892
optical absorpt. spectra, 4d→4f transition, 4d level binding energy 2−75301
oxidation, u.v. photoelectron spectroscopy obs. 2−72557
phase transformation, $\gamma \rightleftarrows \alpha$, critical point determ. 2−57009
phase transition, $\alpha-\gamma$, mean field approx. 2−57119
phase transition, α-α', model 2−84309
series 100 glasses, spectral analysis, monitoring of radiation resistance 2−63981
in steel, low-alloy, effect on mech. props. and brittle fracture 2−53831
steel, spectral analysis of residual content 2−54572
in superalloy, for control of residual S 2−47637
thermal cond., high temp., Lorenz no. 2−51059
thick target, energy loss of scatt. protons 2−80928
CW crystals in cobalt, kinetics of growth 2−64590
CaF$_2$:Ce^{3+}, paramag. relax. due to flux jumping, nonequilib. spin distribs. 2−72231
CaF$_2$:La,Ce, uncoloured and X-irrad., optical absorpt., charge transfer processes 2−65253
Ce^{3+}-F$^-$ tetragonal sites in alkaline earth fluorides, e.p.r. 2−48285
α-Ce, exchange-enhanced, resist. temp. and press. depend., spin-fluctuation resist. 2−81219
β-Ce, low temp. heat capacity and mag. ordering 2−47748
Ce^{3+}, analyical SCF wavefunctions for ground and some excited states, calc. of oscillator strengths for optical transitions 2−52915
Ce^{3+}, codopant effect on Gd^{3+} e.p.r. spectrum in SrF$_2$ 2−61737
Ce^{3+}, crystal field levels in Ce$_{0.25}$(Y,La)$_{0.75}$Al$_2$, determination by inelastic neutron scatt. 2−72105
Ce^{3+}, cubic site symmetry in alkaline earth oxides, e.p.r. obs. 2−54491
Ce^{3+}, impurity in NaF:Eu^{3+}(Sm^{3+}), effect on luminescence 2−65295
Ce^{3+} in crystalline cerium dipicolinate, measurement of g-values and g-axes 2−72487
Ce^{3+} in SrF$_2$ possible existence of separate cubic symmmetry 2−80705
CeI and CeII, infrared spectra between 0.8 and 2.4 μm 2−76969
^{141}Ce-^{144}Ce, isotopic activity ratios in rainwater 2−62289
^{144}Ce, seawater content, of fallout origin 2−62043
in Cr, O-enriched, solubility 2−43830
La$_2$Mg$_3$(NO$_3$)$_2$.24H$_2$O:Ce^{3+},Pr^{3+}, spin-phonon interaction, e.p.r. obs. 2−44316
SrF$_2$:La,Ce, uncoloured and X-irrad., optical absorpt., charge transfer processes 2−65253
UO$_2$-PuO$_2$ mixed fuel, thermal creep, 1300-1700°C 2−53818

Cerium compounds
alloy, γ phase stability rel. to mag. ordering 2−68571
binary alloys, isomorphic transform. theory, metastable constitution diagram 2−50959
binary alloys, isomorphic transform. theory, stable constitution diagram 2−50960
ethyl sulphate, heat capacity, demagnetiz. and susceptibility meas. below 1K 2−68551
ethyl sulphate, low temp. calorimetry 2−44229
mischmetal-Co permanent magnets, development 2−84406
Ce-Th(Pu)(Ln) alloy, isomorphic transforms 2−50959
β-Ce-Y alloys, low temp. heat capacity and mag. ordering 2−47748

Cerium compounds continued
CeAg$_2$Si, prep. and cryst. struct. 2−74735
CeAl$_2$, CeAl$_3$, resistance minimum of Kondo-type numerical soln. for self-energy of conduction electrons 2−75054
CeAl$_2$, resistivity under pressure, Kondo effect and Ce crystalline field variations 2−77857
CeAl$_x$, n.m.r. and magnetic susceptibilities 2−84594
CeB$_2$, exchange interactoon and fluctuation effects 2−54339
CeB$_6$, nonstoichiometry 2−47183
CeBi, mag. struct. 2−44291
Ce$_2$(CO$_3$)$_3$.6H$_2$O, standard heats of form. 2−43335
CeCl$_3$, n.q.r., hydrostatic press. coeffs., soft sphere model 2−54519
CeCo$_5$, permanent mag. 2−52385
Ce$_2$(Co$_{1-x}$Fe$_x$)$_{17}$, lattice consts. 2−50626
CeF$_3$ film, evap., a.c. elec. props. 2−44153
Ce$_2$Fe$_{17}$, ferromag.-helimag. transition 2−54325
Ce$_{1-x}$Gd$_x$Ru$_2$ alloys, supercond. and normal, magnetiz. curves 2−44073
Ce$_{1-x}$Gd$_x$(Tb$_x$)Ru$_2$, mag. ordering and supercond. coexistence 2−43981
CeH$_{2\pm x}$ system, nonstoichiometric, defect struct. and ordering 2−77755
CeH$_x$, metal-semicond. transition 2−77899
Ce$_x$La$_{1-x}$Pd$_3$ alloy, Kondo effect, elec. resistivity and heat capacity 2−51098
CeMg$_2$(NO$_3$)$_6$, powder, Johnson noise temp. rel. to 16Hz mag. temp., 2-20 mK 2−71897
Ce$_2$Mg$_3$(NO$_3$)$_{12}$.24H$_2$O, ^{14}N n.m.r. 2−48305
Ce$_2$Mg$_3$(NO$_3$)$_{12}$.24H$_2$O, caloric and mag. obs. 2−68523
Ce$_2$Mg$_3$(NO$_3$)$_{12}$.24H$_2$O, diluted, adiabatic demagnetiz. 2−45185
Ce$_2$Mg$_3$(NO$_3$)$_{12}$.24H$_2$O, paramag. relax at liq. He temps. 2−68736
Ce$_2$Mg$_3$(NO$_3$).24H$_2$O, temp. scale to 1.6 mK 2−45187
Ce$_2$(MoO$_4$)$_3$, cryst. struct. 2−74736
Ce(NO$_3$)$_3$, aqueous solution at 25°C, u.s. relaxation 2−53427
CeNi$_2$, CeCo$_2$, electronic specific heats 2−57064
CeO$_2$:Gd^{3+}, spin-lattice coeffs. calc. 2−51286
CeO$_2$-ZrO$_2$-Y$_2$O$_3$ solid solns., electronic behaviour 2−47893
Ce$_2$O$_3$-ZrO$_2$, phase relation by quenching between 1350 and 1900°C 2−74935
CeO$_2$, far-i.r. spectra, phonon excitation 2−51346
CeO$_2$, oxygen sorption, e.s.r. study 2−47156
CeO$_2$, sintering, effect of TiO$_2$ addition on grain growth 2−47655
CeO$_2$, thermal conductivity in range 300-1200°C 2−61116
CeO$_2$, u.v. irrad. paramag. hole centres, e.s.r. obs. 2−65322
CeO$_2$ in silicate glasses, radiation and optical stability 2−70071
CeRh$_x$Pd$_x$ alloys electronic state, magnetic susceptibility and lattice spacings 2−81317
CeRu$_2$:Gd^{3+}, supercond. transition temp. rel. to Gd^{3+} conc. 2−84302
CeRu$_2$, CeRu$_{2-x}$Pt$_x$, superconductors, low temp. ht. capacity 2−77879
CeRu$_2$(Os$_2$), struct., high press. effects 2−71689
CeS, prep. from CeO$_2$, Ce$_2$S$_3$ and coke 2−47656
Ce$_x$S$_y$, heats of atomization, from mass spectrometric studies 2−72545
CeS(Se)(Te), energy spectrum of carriers, group theoretical calc. 2−80948
CeSb, mag. struct. 2−44292
Ce$_2$Se$_3$-GeS$_2$ system, phase diagram, intermediate cpd. formation 2−61043
Ce$_3$Se$_4$, thermal and elec. cond., thermal e.m.f., 80−680 K, complex cond. band 2−80918
Ce$_2$Si$_2$O$_7$, prep. and luminescent props. 2−48220
CeSn$_3$, absence of magnetic ordering from n.m.r. obs. 2−84588
Ce$_{0.25}$(Y,La)$_{9.75}$Al$_2$, inelastic neutron scatt. determination of cryst. field levels of Ce^{3+}, susceptibility calc. 2−72105
Ce$_x$Y$_{1-x}$Al$_2$, elec. resistivity and mag. susceptibility, 4.2-300K 2−64912
Ce$_x$Y$_{1-x}$Sb, Ce$_x$La$_{1-x}$Sb, antiferromagnetically ordered, Neel temp. dependence on lattice constants 2−72212
Ce$_x$La$_{1-x}$ Sb, crystal field splitting of Ce^{3+}, magnetiz. obs. 2−61570
Ce$_x$Y$_{1-x}$ Sb, crystal field splitting of Ce^{3+}, neutron scatt. and magnetiz. obs. 2−61570
Co-Cu-Fe-Ce permanent magnet prep. by directional solidification 2−43787
Co-Cu-Fe-Ce permanent magnet, sintered, prep. and props. 2−50910
La-Ce dil. alloys, supercond., temp.-depend. pair breaking 2−54144
La$_{1-x-y}$Ce$_x$Tb$_y$PO$_4$, fluoresc. quantum efficiency 2−48246
Na$_3$[Ce(C$_7$H$_3$NO$_4$)$_3$].15H$_2$O, mag. and thermometric props. in 2-20 mK range 2−82079
PrF$_4$, thermal decomp., elec. deflection study 2−51431
Th-Ce alloy, phase transition critical region, elec. resistivity obs. 2−50951
ThCe, supercond transition temp., 0-20 kbar press. 2−47870
Ti-Ce-S system, struct. and phase equilib. 2−43943
Y-Ce alloy, Kondo effect under press. 2−71839

Cermets *see Ceramics; Metals*

Change of state *see Boiling; Condensation; Freezing; Melting; Phase transformations; Sublimation; Vaporization*

Channelling
alkali halides, proton dechannelling obs. of incident beam damage 2−43606
alloy, ordered, of foreign ions 2−44003
alloy, partly ordered, disordering effects 2−44004
anisotropic scatt. of fast and heavy particles, theory using 3D model of crystal 2−71768
Bloch waves, extended Lindhard's theory 2−60737
continuum potential from planar channelling 2−44006
crystalline solid, of high energy He$^+$ ions 2−77791
cubic crystal, electron channelling pattern geometry computer simulation 2−68267
electron, crystallog. orientation patterns in scanning electron microscopy 2−56637
electron, crystallog. orientation patterns in scanning electron microscopy 2−56638
electron channelling pattern, scanning electron microscopy of surfaces 2−47074

Channelling continued
electron microscope channelling patterns, meas. of image contrast changes 2−83944
electron microscopy, selected area channelling patterns, rocking angle and working distance effects 2−53642
electron microscopy, selected area channelling patterns from 1μ specimen areas 2−53643
flux peaking effect, double and multiple peaks 2−44005
goniometer for implantation and channelling exprts. 2−74788
ions, heavy, abnormal stopping power in low velocity region, from Firsovs theory 2−68268
laser induced, guidance of electrical breakdown streamer 2−80362
lattice disorder profiles determ. by nucl. backscatt. 2−53689
particle beam interaction with crystal structure channelling and shadow theories 2−84225
pattern recording using radioactive recoil atoms 2−54088
patterns recorded with heavy radioactive ions 2−61121
pinhole channelling patterns and applic. to cryst. defect studies 2−43605
radiation damage induced by channelling effect of high energy electrons 2−43604
scanning electron microscope, multiple inelastic scattering 2−80936
scattering theory for channelled ions, determ. of thermal vibration of impurity atom 2−80897
scintillation efficiency for random and heavy channelled ions at intermed. vels., track-account theory 2−70316
steel, stainless, damage induced by high energy electron chanelling 2−53713
stopping power, position depend., for protons and ions 2−44014
Ag, 21.6 MeV I ions, axial channelling phenomenon 2−44007
Ag, hyperchannelling of ^{127}I and ^{4}He ions 2−47778
Al, damage induced by high energy electron channelling 2−53713
AlCu alloy, (Al 4 WT %), structure changes during ageing studied by the channeling technique 2−80827
$Al_xGa_{1-x}As$ solid solns., in heterostructs., optical and electronic channelling rel. to comp. 2−63341
Au, 1.8 MeV α-particles in planar directions, continuum potentials deduced 2−44006
Au, beam foil spectroscopy, search for channelling effect 2−80930
Au, effects on transmission of MeV H_2^+ ions through thin single crystals 2−44011
Au, hyperchannelling of ^{127}I and ^{4}He ions 2−47778
Au films, as self-supporting targets 2−71326
$BaTiO_3$, proton channelling, above and below ferroelec. Curie temp. 2−65059
CsI:Tl single crystal, influence of channelling on scintillation efficiency 2−72396
Cu, foil, heavy ion irrad., rel. to defect prod. 2−43608
GaAs, ion implantation lattice disorder obs. 2−47373
GaAs, of α-particles, surface studies 2−64553
Ge, dechanneling of 0.3-1.5 MeV protons, Lindhard's multiple scatt. 2−47788
Ge electronic scattering in planar dechannelling, protons and deuterons 2−61128
He$^+$, backscattering and channelling effects in crystalline solids 2−84224
KCl-KBr, mixed cryst., proton dechannelling, lattice distortion effects 2−47785
KCl, effect on diffusion of ion- implanted ^{85}Kr 2−68053
KCl, pattern recording using radioactive recoil atoms 2−54088
NaCl, ion beam induced damage, backscatt. obs. 2−43611
Nb, location of interstitial D sites by deuteron channelling 2−60811
Ni, foil, of deuterons, polarization 2−47784
Si:As, He ion min. backscatt. yield variation obs. 2−60820
Si:As, of He ions, impurity distrib. determ. 2−60818
Si:B, impurity lattice location, He$^+$ ion channelling obs. 2−60819
Si:B, ion implanted lattice disorder distributions, channelling effect analysis 2−68036
Si-Ge alloy, He$^+$ ions, rel. to atomic displacements 2−47388
Si, channel-to-random transition meas. on single crystal overlaid with amorphous layer 2−61127
Si, dechannelling of 0.3-1.5 MeV protons, Lindhard's multiple scatt. 2−47788
Si, dechannelling of 7.15 MeV He ions 2−61120
Si, electronic scattering in planar dechannelling, protons and deuterons 2−61128
Si, energy spectra of back-scattered protons, variations 2−54093
Si, He$^+$ ions, rel. to atomic displacements 2−47388
Si, ion-implanted, radiation damage under channelling conditions 2−68017
Si, ion implantation damage and impurity location study 2−71511
Si, of B ions, implantation, computer simulation 2−47439
Si, of implanted B and P, effect on charge carrier distrib. 2−47432
Si and SiO_2, pattern recording using radioactive recoil atoms 2−54088
Si overlaid with Al and Au films, yield profiles, dechannelling 2−54094
W, foil, of Au ions 2−43616
W, foil, of Au ions 2−43616
W surface, of 275 keV He$^+$ ions, and low angle scatt. 2−80929

Characteristic temperature *see Specific heat*

Charcoal *see Carbon*

Charge *see Electric charge*

Charge carriers *see Crystal electron states; Semiconducting materials; Semiconductors*

Charge compensation
CaF_2, ENDOR spectrum of U^{3+}-F- 2−84607
SrF_2, ENDOR spectrum of U^{3+}-F- 2−84607

Charge exchange
— 2−68774
— 2−68774
πN scattering charge-exchange at 6 GeV/c, structure of partial wave amplitudes 2−59533
(anthracene)-$(CH_2)_n$-(N, N-dimethylaniline) systems, intramol. electron donor-acceptor interactions 2−60047
alcohol ions, formed by charge exchange in in-line tandem mass spectrometer 2−64168
alkane ions, formed by charge exchange in in-line tandem mass spectrometer 2−64168

Charge exchange continued
N- aralkylpyridinium ions, conformational influences on intramolecular charge transfer transition 2−42955
charge transfer in the mass spectrometer 2−46400
charged particle transport by stream of gas or steam 2−60295
collisions of fast nuclei with one electron systems 2−59946
cross-sections of negative halide ions in range 300-3000 eV 2−64052
dipoles cross depolarization during adsorption on metal surfaces 2−50521
electron capture cross-sections, calc. by approximation procedures, book 2−63986
electron transfer reactions in solution, generalized mobility theory 2−84648
fast heavy ions, charge states and charge changing cross sections for penetration through gaseous and solid media, review 2−60294
hadron scatt., charge and hypercharge exchange reactions 2−55841
hydrocarbons CH_n^+, reactions with gas targets at 40-140 keV 2−64218
interplanetary neutral H and solar wind protons, charge exchange collisions 2−55157
ion-atom collisions, one-electron model 2−83177
ionosphere, topside F-region, ioniz. loss interpret., rel. to nighttime maintenance 2−58098
ketone, ions, formed by charge exchange ion in-line tandem mass spectrometer, dissociation 2−64168
meson-baryon reactions with t-dependent residues, differentaial cross sections 2−52574
methane-CH_4^+ charge exchange cross-section 2−67542
near resonant charge transfer processes at thermal energies application to interstellar matter 2−58353
nuclear analogue state excitation by double charge exchange of pions, nuclear medium corrections 2−74103
nuclear reactions, unbound residual states, microscopic form factors 2−49778
projectile ion thermal energy charge transfer reactions to methane, reson. effects 2−80132
rare gas ion thermal energy charge transfer reactions to methane, ethane, propane and silane 2−83399
thermal energy, role in rare gas-metal vapour lasers 2−42019
vector-meson production with hypercharge exchange, study of $K^-p\rightarrow(\omega,\varphi)\Lambda$ and $\pi^-p\rightarrow K^{*0}\Lambda$ reactions 2−82743
(p,n) reaction, energy depend., coupled-channel calcs. 2−59759
K-p differential cross sections, evidence for tachyonic resonances 2−63546
K^-p scattering, cross section at 1.8 GeV/c 2−59521
$K^-p\rightarrow K^0n$, cross section difference with $K^+n\rightarrow K^0p$, Regge analysis 2−76658
$K^\pm p$ elastic scatt., s-channel helicity amplitudes without pomeron 2−59520
np scatt., 8 to 29 GeV/c, differential cross sections 2−55879
pd scatt., production of high energy polarized neutrons 2−70264
pn processes, fixed poles, unitarity and duality 2−79533
πN forward scatt. finite energy sum rules and Regge cuts 2−59537
πN polarization and violation of Pomeranchuk theorem 2−45976
πN scatt., dual geometrical model 2−67031
πN scatt., relativistic Regge-cut model for invariant functions 2−76667
πN scattering, fixed-t dispersion relations and polarization 2−63624
πN scattering, strong suppression of Regge-Regge cuts 2−59493
π-p differential cross sections, evidence for tachyonic resonances 2−63546
π-p$\rightarrow n\pi^0$ meas. of differential cross section at 317, 452, 491 MeV/c using $n\gamma$ coincidence method 2−63617
π^-p elastic scatt., s-channel helicity amplitudes without pomeron 2−59520
π^-p reactions, kinematic variable 2−79595
$\pi^-p\rightarrow\pi^0n$, charge exchange differential cross sections at 3.67 and 4.83 GeV/c and intermediate momentum transfers 2−63619
$\pi^-p\rightarrow\pi^0n$, momentum dependence of differential cross section at 180° in 1.8-6.0 GeV/c range 2−82758
$\pi^+\pi^-\rightarrow\pi^0\pi^0$ charge exchange reaction, cross-section obtained from $\pi^-p\rightarrow\pi^0\pi^0n$ and $\pi^+n\rightarrow\pi^0\pi^0p$ 2−82764
Ag vapour, high-current hollow cathode discharge, effect on radiation 2−74423
Au vapour, high-current hollow cathode discharge, effect on radiation 2−74423
$Cl_2+NO_2\rightarrow Cl^-+NO_2Cl$, thermal energy rate consts. 2−68774
Cs, resonant, cross sections at low energies in Q-machines 2−56115
Cs vapour, charge-exchange process for production of 2.5 keV metastable H atoms 2−56124
Cs$^+$, free ions, rel. to n.m.r. 2−79897
^{133}Cs$^+$ ion, free, n.m.r. freq. shift due to charge exchange with Cs atom 2−79896
Cu vapour, high-current hollow cathode discharge, effect on radiation 2−74423
Ge p-n junction, γ-ray detector, space charge region polarization, impurity centre charge exchange 2−65026
H, collision with proton, Coulomb T matrix calc. 2−46483
H, electron capture into $n=3,4$ states by H$^+$, H_2^+ impact, cross sections 2−70637
H_2^+ discharge charge-exchange analysis of cathode dark-space data 2−67693
HBr, effect of resonance on vibr. distrib. charge transfer reactions with Kr$^+$ and Ar$^+$ 2−51424
HCl, effect of resonance on vibr. distrib. charge transfer reactions with Kr$^+$ and Ar$^+$ 2−51424
$H^++H(1s)\rightarrow H(1s)+H^+$, charge transfer scatt. at high energies 2−77023
He$^+$ + He collisions, very-small-angle charge exchange, technique for studying structure 2−42818
He(s=1), He$^+$(s=1/2), electron polarization by exchange scattering 2−59952
Li$^+$-He, oscillation of charge exchange cross section 2−64053
Li$^+$ + He, elastic and inelastic scattering 2−42790
$NO_2^-+Cl_2\rightarrow Cl_2^-+NO_2$, thermal energy rate consts. 2−68774
N_2+C^+ reactive collisions, 3 to 100 eV, molecular dissociative charge exchange cross sections 2−48322
Ne gas, reaction rate constant for $Ne^++2Ne\rightarrow Ne_2^++Ne$ 2−43226
O_2+C^+ reactive collisions, 3 to 100 eV, molecular and dissociative charge exchange cross section 2−48322

Charge exchange continued
(p,n) charge exchange reaction, qualitative studies of angular distribution 2−46253
$SH^- + Cl_2 \rightarrow Cl_2^- + SH$, thermal energy rate consts. 2−68774
Te in He or Ne buffer gas, excitation and cw laser action 2−56098
VV charge transfer spectra 2−83268
$Xe\text{-}H^+$ collisions, three-state calcs. of spin polarization 2−79918

Chelates *see Molecules; Organic compounds. For inorganic chelates see under metal compound headings*

Chemical analysis
see also Electron probe analysis; Spectrochemical analysis
Apollo 16 lunar soil 68501, trace element geochemistry 2−75851
binary gas mixtures, fast-response probe 2−56401
cellulose acetate, H detection by neutron radiography 2−65408
continuous flow, Cenco UNMF system 2−68823
data treatment system, computerised 2−84699
delayed fission neutron spectrometry applic. to nucl. materials assay 2−67361
differential thermal analysis, interpretation of anomalous peak shape 2−57438
electron energy spectroscopy in i.r. region 2−81565
electron spectroscopy, e.s. energy analyser 2−68829
fast reactor fuel burn-up measurement methods, review 2−74188
fast reactor fuels burn-up determ. by Mo complex equilibria 2−79837
gas, reacting and high temp., kinetic studies 2−71107
geochemistry, use of ion microanalyzer 2−44504
Girgenti meteorite, mineralogical and chemical analysis of L-chondrite 2−75928
glass, glass-ceramics, using scanning electron microscope 2−60579
glass, oxide content, by physical methods, computer calcs. 2−44500
glass, physical analysis of small changes in composition 2−44499
illite, microstructure and chemical comp. 2−84710
ion scattering, spectroscopic tool for study of outermost atomic layer of solid surface 2−50416
irradiated nuclear fuel, analysis for actinides and burn-up determ. 2−74183
irradiated nuclear fuels, determ. of fission products by isotopic dilution 2−75400
luminescent soln., dimer conc. and equilib. const. determ. from photolum. 2−81503
lunar and terrestrial materials, ESCA study 2−48761
lunar basaltic rocks and minerals, Mg + Fe comp., rel. to parental liq. comp. 2−62676
lunar clastic materials, Apollo 14 samples, comp. characts. 2−58459
lunar glass spherule comparison with microtektites 2−62670
lunar igneous rocks, Apollo 15 samples, rare earth element analysis 2−62669
lunar regolith, noble gas variations with depth 2−58461
lunar soils, Apollo 14 and 15 samples, inorg. gas release obs. 2−62672
mine air, using cross section ionization 2−68821
nuclear fuel cycle, analytical methods, review 2−74161
nuclear fuel cycle, reference materials for accurate determ. of U, Pu and Th 2−74160
nuclear fuels, U, Pu, C, O_2, S determ. for quality control and characterization 2−74176
nuclear fuels for HIGCR, techniques for control and evaluation 2−74168
nuclear reactor fuel, chemical analysis service of JEN for purification 2−83077
nuclear samples, mass assay by physical methods 2−75397
nuclear samples, using titration, complexometry, coulometry 2−75406
partial pressure of oxygen, determ. using ZnO thin film sensor 2−41454
photoelectron spectroscopy, applications 2−53862
photoemission electron microscopy, analytical methods 2−56636
pollution aerosols, by neutron and gamma ray spectrometry 2−48360
reactor fuel materials, statistically designed program for sampling and chemical analysis 2−74156
reactor fuel pins, irrad., tritium meas. techniques 2−42663
residual gas analyzer data acquisition system 2−58649
rock systems, Fe^{2+}-Fe^0-Si relations 2−61848
samples for nuclear measurements, using counting 2−57440
samples for nuclear measurements using physical methods 2−57439
seawater, for NH_3, automated methods 2−72708
semiconductor cpds., departures from stoichiometry determ. 2−43503
steel, H content determ., diffusion kinetics method 2−64780
superalloy, conjugate phases detn. 2−77681
thin film atomic oxygen sensors 2−65403
total pollution system monitoring concept 2−65407
ultracentrifuge, alignment of schlieren and interence optical systems 2−61819
by weight meas., reliability 2−57441
Be content of US geological survey standard rocks 2−61817
^{13}C characteristic n.m.r. chemical shifts in organic compounds 2−56209
Fe rich minerals, Cu and Zn det., radioisotope detector-radiator assembly 2−61821
LiF:Mg thermal-activation analysis study of impurity hardening 2−71491
Mn crusts of Atlantis Fracture Zone 2−61983
Np concentration determ. in irradiated fuel reprocessing solutions 2−74180
Pu/U oxide fabrication process, sampling and analysis 2−74157
Pu/U oxide fuels, gravimetric methods of studying O/metal ratio 2−74152
Pu/U oxides, comparison of thermogravimetric and direct meas. of O/heavy metal atom ratios 2−74154
Pu/U oxides, comparison of oxygen analysis and thermodynamicmetric methods for determ. of O/metal ratios 2−74153
Pu, titration errors 2−74166
Pu fuels, irradiated, determ. of Pu, Am, Cm and Pu valency in reprocessing 2−74178
PuO_2-UO_2 fuels, analysis techniques for process control, quality assurance and post-irradiation examination 2−74170
PuO_2, reference specimens for determ. of impurities in reactor fuels 2−74158

Chemical analysis continued
SO_3 concentration in flue gases, chemical anal. method, automatic 2−78214
SmC_x characterization 2−71653
Th/U fuel elements with known irradiation data, actinide composition studies 2−75403
U/Pu oxide fuel, reference material for chemical specification analysis 2−74159
U oxides reactor fuels, O/U ratio determ. methods, review and comparisons 2−74155
UC_2-ThC_2, UO_2-ThO_2 coated fuels for GCR, techniques 2−74169
UO_2-PuO_2 nuclear fuels, techniques 2−74171
UO_2 unirradiated nuclear fuel, analytical methods for determ. of total U and impurities 2−74162

adsorption
see also Chromatography
adiabatic adsorption column, analysis, adsorption in high temperature range 2−68780
aerosols, humidity, lightscattering adsorption 2−83815
transformer insulation, gaseous decomposition products, gas chromatography applications 2−68828

by mass spectrometry
see also Mass spectrometers/applications
Apollo lunar module exhaust gas 2−58145
aurora, positive ion comp. obs. 2−58066
computer aided solid mass spectral analysis 2−84688
computer interpretation of high resolution spectra of complex molecules 2−84685
computer pattern recognition, low resolution spectra 2−81559
dimer formation in noneffusive expansions, causing errors 2−68825
estrogenic steroids, structure elucidation by computer 2−84685
insulating materials, new technique using ion microanalyzer 2−84687
ion probe mass spectrometer for multielement analysis of Na corrosion and mass transfer in nuclear reactors 2−83118
ionization technique 2−54566
i.r. laser induced chemical reactions 2−44501
laser induced chem. reaction studies using modulated beam technique 2−81490
life detection on Mars, soil gas chromatography/mass spectrometry by Viking spacecraft 2−55147
Mars, K-Ar age determination 2−62706
methane $^{13}C/^{12}C$ ratio detn. 2−48355
mixed oxide nuclear fuels, burn-up and isotopic distribution meas. 2−75401
nitroethylene, negative ion formation, obs. 2−57432
nonequilibrium air flows at high temps. and pressures 2−48354
nuclear sample assay, isotope dilution 2−75406
oil-paper insulation systems, gaseous decomposition products 2−68824
post-irradiation analysis of nuclear fuels for burn-up and heavy isotope content 2−75402
reactor fuel, filling and fission gas meas. 2−42668
reactor fuel burn-up determ. by gamma and mass spectrometric methods 2−75408
reactor fuel particles, coated, gas content determ. 2−42664
spark-source, semi-automatic system for operation of electrical detection 2−84700
thermosphere, minor constituents meas. 2−62295
trace metal determ. with probe and ion current integration 2−49985
AlF_2 and $AlOF_2$, gaseous molecules, heats of formation determ. 2−72543
Au traces concentration by spark source mass spectroscopy 2−61823
BAs, thermal decomp. study 2−48321
Bi_3, heat of sublimation determ. 2−72554
C fibre, outgassing, residual impurities 2−50913
CdSe, homogeneity regions, solubility of Cd and Se 2−83837
CeF_4, thermal decomp. products study 2−51431
Ce_xS_y, heats of atomization determ. 2−72545
GaAs, laser induced evaporation analysis of ions in vapour 2−75409
GaP laser induced evaporation analysis of ions in vapour 2−75409
$Ge + SiO \rightleftharpoons GeO + Si$, heat of reaction determ. 2−72548
H_2O vapour on lunar surface, Apollo 14 SIDE analysis 2−58468
PrF_4, thermal decomp. products study 2−51431
Pt traces concentrations by spark source mass spectroscopy 2−61823
Sb_2S_3, enthalpy and entropy of vaporization determ. 2−74595
$Sb_4 \rightleftharpoons 2Sb_2$, heat of reaction determ. 2−72554
TbF_4, thermal decomp. products study 2−51431
U and Pu, automatic analysis in solutions 2−75411
UF_6, spark source mass spectrometric anal. of trace elements 2−74172
UO_2 reactor fuel, burn-up meas. from mass spectrometry of stable fission-product Nd 2−74182

by nuclear reactions
activation analysis, DT neutron production rates 2−65422
activation analysis, self- consistent deciphering of spectra 2−72594
biological specimens, radiochemical separation scheme for quantitative determination of 45 elements using neutron activities 2−51489
computer code for searching attributions, use in neutron activation analysis 2−82859
geological materials, neutron capture gamma ray studies 2−61846
glass, soda lime silicate, neutron activation analysis 2−60580
isotope hydrology in Latin America 2−61822
lunar soil samples, L16/O78, nondestructive neutron activation analysis of Si and O_2 abundances 2−85043
medical neutron activation analysis rel. to human placenta and filter effects 2−69443
neutron activation, flow rate determ. 2−83518
neutron activation anal. of flowing solutions, optimal measuring conditions 2−72596
neutron activation analysis, apparatus for, gamma spectroscopy 2−51490
neutron activation analysis applic. to nondestructive techniques for neutron absorpt. and fission rates meas. 2−56040
neutron activation analysis logging in mineral exploration programmes 2−57805
neutron activation analysis of wear of friction material 2−47551
neutron activation obs. of dopant profiles in Si 2−56738
neutron radioactivation analysis in vivo of Ca, P, N and Cl in rat's organism 2−54575

Chemical analysis continued
  by nuclear reactions continued
    nondestructive neutron activation anal., choice of filters 2–72598
    pig iron, antimony content neutron activation analysis, spectral method 2–78215
    radiative-neutron-capture gamma-ray analysis by linear combination technique 2–54574
    radioactivation analysis for elemental, isotopic analysis 2–65419
    resonance activation integrals of nuclides of interest in neutron activation analysis 2–70451
    rotating target for radiational analysis of specimens cooled to liquid nitrogen temps., by elastic scattering 2–72597
    semiconductor, B impurity conc. profile determ. using ^{10}B(n, ^{4}He)^{7}Li 2–71505
    semiconductor, impurity solubility, autoradiographic variant of activation analysis 2–72595
    surface layers, analysis by elastic backscattering 2–80923
    surface regions, nuclear densities isotopic tracing, by charged particle beam 2–80556
    THAPA, program for activation analysis 2–84689
    (n, α), determ. of B, Li content of various mats. 2–84686
    B-Al alloys, determ. of B content, Boreal array 2–63976
    B, quantitative det. in various matrices, using nuclear track technique 2–48364
    B content determ. using (n, α) reaction 2–84686
    Be, determ. in ores by neutron activation, high sensitivity instrument 2–65423
    Bi-Sb alloy, antimony concentration, neutron-activation analysis 2–81554
    Ca in humans, det. using neutron activation anal. 2–48854
    ^{252}Cf neutron activation, mineral analysis on ocean floor 2–65522
    Li, quantitative det. in various matrices, using nuclear track technique 2–48364
    Li content determ. using (n, α) reaction 2–84686
    N, quantitative det. in various matrices, using nuclear track technique 2–48364
    NaI(Tl) shielded Ge(Li) detector system for activation analysis, applic. to geological material 2–72599
    Nb, photoactivation analysis in ores 2–65424
    O and C assay in metal foils by meas. of proton energy spectra 2–50389
    O_2 content of lunar sample by neutron activation anal. 2–69138
    ^{16}O(d,p)^{17}O, stoichiometric analysis of evaporated silica thin films 2–61835
    Si:Ag, deep impurity determ., neutralization analysis 2–61363
    Si, ^{3}He activation technique, O and C impurities detn. 2–71502
    ^{28}Si(d,p)^{29}O, stoichiometric analysis of evaporated silica thin films 2–61835
    Ta, photoactivation analysis in ores 2–65424
    Te-As-Ge-S glass films, four-element quantitative analysis 2–72593
    Th, quantitative det. in various matrices, using nuclear track technique 2–48364
    U, quantitative det. in various matrices, using nuclear track technique 2–48364
    U assay in rocks using ^{140}La line 2–84690
    ^{182}W(N, γ)^{183}W rapid determ. of tungsten in rocks 2–61834
    Zr alloy fuel element sheaths, F combination, proton activation analysis 2–52876
  electrochemical
    coulometric titrator with feedback controlled electrolysis current 2–65404
    coulostatic analysis with glassy C electrode 2–72587
    polarographic obs. of friction of film on inclined plane 2–83728
    polarographic technique for U determ. in nuclear fuels 2–74169
    polarography, nuclear sample assay 2–75406
    sequential ion exchange separation in mixed oxide nuclear fuels, burn-up and isotopic distribution meas. 2–75401
    signal generator for voltammetric techniques 2–65405
    Ag in various stages of oxidation, paste electrodes 2–65384
    Fe and Cr simultaneous estimation in stainless steel by polarographic method 2–48352
    Mn in $CaCO_3$, a.c. polarographic det. 2–48353
    O_2, CO_2 metastable ions detection, discharge glow 2–65402
  radioactive
    see also Radiochemistry
    activation, microtron as neutron source 2–52708
    chondrites, H-group, distribution of Ni, Ga, Ge and Ir in metal and silicate portions, neutron activation 2–62719
    chondrites, volatile trace elements by neutron activation analysis 2–62722
    elemental, using neutron capture γ-rays from mixtures and geological samples 2–44513
    fission fragment ranges in U-Al alloys, UO_2, U_3O_8 2–83028
    high temperature reactor fuel cycle, burn-up determ. 2–74184
    post-irradiation analysis of nuclear fuels for burn-up and heavy isotope content 2–75402
    radio-liquid chromatograph for simultaneous recording of light absorbance and radioactivity 2–65420
    semiconductor electron concentration determ. using T activity 2–71934
    semiconductor surface contamination, obs. 2–53748
    B determ. in aqueous and solid samples, activation analysis by Cerenkov counting of 22 ms ^{12}B 2–51488
    ^{3}H in thin-layer chromatograms, det. using luminous Zn compounds 2–61832
    ^{3}H in two-dimensional chromatograms, automatic scintillation scanning unit 2–61831
    Pu/U oxides reactor fuel, determ. of Pu content by calorimetry 2–74164
    ^{239}Pu reactor fuel, detection and analysis of actinide contaminants 2–74179
    ^{222}Rn, determ. of concentration in hot spring water using scintillation chamber 2–61833
    U content determ., delayed neutron counting method 2–44512
  X-ray
    see also X-ray examination of materials
    apparatus with monochromatized X-ray source, for ESCA 2–57261
    applications of recrystallized Al monocrystals 2–64611

Chemical analysis continued
  X-ray continued
    bronze, ancient, rapid non-destructive analysis by X-ray fluorescence 2–44505
    carbide mixtures, VC with Mn_6C and VC with Cr_7C_3 2–44506
    electron microscope attachment, EMMA 2–61829
    electron probe microanalysis, statistical error calc. using Castaing's First approximation 2–82083
    electron spectroscopy using monochromatized X-rays 2–54573
    elemental, sensitivity, rel. to target backings, α-excited X-ray fluorescence 2–44507
    fluorescence, theory of double concentration method for liquid and solid solutions 2–51487
    fluorescence, using solid solution specimens, influence of quality of primary radiation 2–51486
    fluorescence, using solid solution specimens, influence of quality of primary radiation 2–51485
    fluorescence spectrometers for trace element 2–48951
    fluorescence spectrometers for trace element 2–48951
    fluorescence spectrometry by pulsed excitation 2–51483
    glass, batch and raw materials, computer controlled fluorescence 2–64525
    glass, problems with automatic X-ray spectrograph 2–64523
    glass, raw material analysis, by fluorescence spectroscopy 2–64524
    high spatial resolution analysis, electron probe 2–81564
    milliprobe for small lunar single crystals 2–51481
    mushketovite, ion content determ. by local anal. 2–51246
    sample preparation variables in spectrochemical analysis 2–65416
    semiconductor detector X-ray fluorescence spectrometry applied to environmental and biological analysis 2–51482
    spectral analysis, reduction of matrix influences by means of braking continuum 2–51484
    spectrometer, single axis 2-crystal for fluorescent X-ray analysis 2–44508
    BAs, thermal decomp. study 2–48321
    $CdFe_2O_4$, presence of Si which influences mag. behaviour 2–84432
    Mn-Mg-Fe ferrite film, flash evaporated, chem. comp., X-ray fluoresc. obs. 2–71331
    Pb, in paint, X-ray fluorescence instruments 2–65418
    Te-As-Ge-S glass films, four-element quantitative analysis 2–72593
    U and Pu, automatic analysis in solutions 2–75411
    U and Pu determ. in reprocessing of Rapsodie fuel using X-ray fluorescence 2–74173
    UO_2 and UO_2/PuO_2 nuclear fuels, X-ray spectrometric obs. of impurities 2–74167
Chemical effects of radiations
    see also Nuclear reactions and scattering/chemical effects; Photochemistry
    acetylene dicarboxylic acid dihydrate crystal, e.s.r. free radicals 2–75348
    analysis of irradiated reactor fuels, isotopic dilution, α and γ spectrometry, properties of operating reactors 2–76925
    aqueous solutions, identification of H_3O radical 2–72583
    t-butyl chloride γ-irradiated, e.s.r. evidence for planarity of t-butyl radical 2–74288
    cellulose triacetate, γ- or u.v. irradiated, e.s.r. obs. of radicals formed 2–44494
    cryptocyanine Q-swithces for ruby laser, photochemical decomposition due to light source 2–49378
    cyanoacetohydrazide, X-irradiated, obs. of e.s.r. spectrum of RNHNH type radical 2–81530
    graphitisation of carbon products, infl. on dimensional variations of n irradiation 2–68175
    nitroglycerine in inert gases, u.v. radiation, determ. of aspects which cause explosion 2–81486
    phenylphosphinic acid and salts, X-irradiation, e.s.r. spectrum study of radical formation 2–72584
    poly-4-methylpentone-1, irradiated, e.s.r. of radical pairs 2–75395
    succinic acid, radical isomerization following conformational change 2–81528
    thyamine, radiation abstraction of H atoms, analysis by e.s.r. spectroscopy 2–72585
    trifluoroacetamide, X-irradiated, analysis of internal rotation of CF_2CONH_2 radical obs. in e.s.r. spectrum 2–81526
    trimethyl phosphite, γ-irradiated, e.s.r. spectrum of radicals 2–81534
    triphenylamine in alkane solvent, viscosity dependent ion recombination rate following electron pulse irradiation 2–46968
    $Ca_3Fe_{2-x}M_xGe_3O_{12}$, $M = Al^{3+}$, Ga^{3+}, Cr^{3+}, Sc^{3+}, In^{3+}, Mossbauer study of lattice 2–72278
    ^{60}Co γ-rays, effect on luminescence of Tb^{3+} ions in crystals and glasses 2–84547
  acoustic waves
    ultrasonically induced chemical reactions 2–51475
  ionizing radiations
    adamantane, free radicals in high energy irrad., e.s.r. obs. 2–54562
    L-alanine, unstable radical CH_3CHR, temp. dependence of ESR spectrum 2–68818
    alkyl benzenes, pulsed radiolysis, spectra of transitory species 2–57435
    amino acids, γ-irrad., effect of cryst. struct. on stability, yield, and shape of e.s.r. spectra 2–81536
    bromomethane, pulse radiolysis, electron disappearance 2–61816
    chloromethane, pulse radiolysis, electron dissappearance 2–61816
    Cyanoacetylurea, X and gamma irradiated, radical formation 2–51473
    cyclohexane solns., psec. pulse radiolysis 2–81519
    cystine dihydrochloride, e.s.r. centre formation by monochromatic u.v. radiation 2–61811
    dielectric liquids, scavenging probability in gamma radiolysis, applic. of Laplace transform method in ion neutralization theory 2–44493
    digital recording of fast phenomena in pulse radiolysis 2–72582
    dimethyl sulphoxide, pulse radiolysis, transient species 2–68819
    dipeptides, γ-irrad, effect of cryst. struct. on stability, yield, and shape of e.s.r. spectra 2–81536
    DL-serine, X-ray irradiated, 153 to 340K, free radicals by ESR and ENDOR 2–75350
    ethanol, glassy, effect of dipole reorientation on trapped electron spectra, semicontinuum model 2–44495

Chemical effects of radiations continued
ionizing radiations continued
ethanol, pressure effects on reaction rates of solvated electrons 2−61812
ethanol, semicontinuum model applied to pressure effects 2−61807
ethanol glass, electron trapping and solvation at 4 K, optical absorption and e.s.r. meas. 2−61810
ethyl bromide and chloride, pulse radiolysis, electron disappearance 2−61816
graphite/CO_2 excitation of CO, 225-375°C 2−57434
I_0 subtraction unit for use with pulsed or d.c. light sources, application to pulse radiolysis 2−45801
lead acetate hydrate, X-irradiated, Pb^+ and Pb^{2+} identification, e.p.r. 2−75347
malonamide, X and gamma irradiated, radical formation 2−51473
methanol, solvated electron spectra, semicontinuum model applied to pressure effects 2−61807
neopentane-d_{12}-alkane mixtures, gas phase pulse radiolysis 2−68820
nitroethylene, negative ion formation, mass spectrometric study 2−57432
organic electronic spectra of trapped electrons 2−81516
picosecond pulse radiolysis, reaction rates of electrons 2−65401
poly(methyl methacrylate), radiation produced free radicals 2−84671
polyvinylalcohol films irradiated by ^{60}Co γ-rays, trapped radicals in u.v. and visible absorption spectra 2−57437
pulse radiolysis study of hydrated-electron reactions not controlled by diffusion 2−78210
radiolysis of water, study of 'dry' electrons 2−61813
rare earth metal ions, electron transfer reactions and oxidation potential in aqueous soln., pulse radiolysis study 2−61815
trapping of H atoms and electrons in acid glass 2−81535
$CH(^2\Pi)$, pulse radiolytically produced, reaction with methane, kinetics of ethylene production 2−48347
CO_2, gaseous, γ radiolysis at high densities 2−61814
D_2O crystals, pulse radiolysis at -150°C optical absorption spectrum of trapped electrons, visible and i.r. 2−48348
K_2CrO_4 irradiated at ambiant temp., e.s.r. spectroscopy study of paramagnetic centres 2−48280
$5(NH_4)_2O.12WO_3.5H_2O$, polycrystalline, paramagnetic centres formed by γ irradiation 2−48349
Pu- HNO_3 solns., radiolytic generation of H_2 and O_2 during storage 2−48350

Chemical equilibrium *see Chemical reactions*

Chemical exchanges *see Exchanges, chemical*

Chemical kinetics *see Reaction kinetics*

Chemical reactions
see also Chemiluminescence; Chemisorption; Exchanges, chemical; Heat of formation; Heat of reaction; Oxidation; Photochemistry; Photochromism; Polymerization; Reaction kinetics
— 2−70317
absorption coupled, mass transfer coeff. 2−83495
acetylene, formation of metastable triplet state in Hg photosensitized reaction, obs. of biacetyl emission 2−51467
acetylene, photoionization products, rate coeffs. for reactions 2−51435
aeronomic ion-neutral molecule reactions rel. to direct ionospheric measurements 2−83397
alkali ion hydration 2−68772
alkyl radical reaction products, chem. induced dynamic nucl. polarization 2−81540
alloy, binary, isothermal reaction stage influence on cpd. growth by diffusion 2−64686
apparatus for obs. of chemical reactions involving changes in conductivity 2−66373
association, formation of large interstellar molecules 2−44884
in atmosphere, dispersion effects and air pollution 2−48454
atmospheric particles, formation and reactions 2−48460
atom-heteronuclear diatom system, exact quantum reactive cross sections for three dimensional angle dependent model 2−44469
atom-molecule collision, optical model for vibrational relaxation 2−65362
aurora, excitation of $O_2(^1\Delta_g)$ and $O_2(^1\Sigma_g)$ 2−58060
balance microcalorimeter for gas-solid reactions in fluorine chemistry 2−52305
benzoyl peroxide, reaction with diphenyl amine and tetraphenyl hydrazine, reaction rate consts., chemilum. 2−78191
bimolecular, study of chemical relaxation as transport process 2−48315
boundary layers, flowing, surface reactions 2−68769
branched, quantum mech. model calc. 2−65366
ceramic-metal systems, interfacial phenomena 2−50861
chemical equilibrium, thermodynamic treatment 2−44465
chemiluminescent, kinetics obs. using fibre optics 2−48319
classical trajectory method of computer simulation 2−44471
concerted, correl. diagrams using orbital symmetry from exact wavefunctions 2−72539
crossed molecular beams, reactive scattering of atoms and molecules 2−44470
in developing laminar and turbulent duct flow 2−83658
diabatic transition state theory and temp. concept. 2−68762
diatomic gas in shock front and wake, relaxation equations for vibrational and rotational energy including transport processes and chemical reactions 2−52966
diatomic mols., thermal decomp. in inert gas, diffusion theory approach 2−80059
dichloroethane, chem. activated, vibr. energy transfer probabilities, collisional deactivation 2−83409
dichloroethane-d_0 and -d_4, chem. activated, cascade deactivation and nonequil. kinetic isotope effects 2−83408
differential thermal analysis, interpretation of anomalous peak shape 2−57438
dimer and cluster formation in free jets 2−84626
electric arc, effects on arc plasma characteristics 2−50237
electrochemical, proposed use of electrode potential control of ZnO green luminescence as probe 2−61717
environmental, obs. using high voltage electron microscopy 2−56642
ethane-methyl radical decomposition and recombination reactions, theoretical critical configuration 2−57420

Chemical reactions continued
ethylene, photoionization products, rate coeffs. for reactions 2−51435
exoergic, product static distrib. and temp. concept 2−68761
fast, ultrasonic and relaxation spectroscopy, expression for C_p/C_v 2−81499
fusion reactors, blanket chemistry 2−63953
gas mixture, equilibrium distribution of chemical constituents 2−54525
gas mixtures, chem. reacting, transport processes 2−48320
gases nonhomogeneous, equations of transfer 2−68765
geological systems, multicomponent, REACTION program 2−61847
graphite, surface study of gases prod. by thermal decomposition from acidic surface oxides 2−64551
graphite composite, Pyrostrand, erosion resistance in reactive environments 2−53960
graphites, nuclear, reaction of hydrogen 2−59842
halide ion hydration 2−68772
halogenated molecule-nitroxide radical interaction, ^{13}C constant shift and MO studies 2−51440
high temp. kinetic obs., tubular fast flow reactor 2−48318
hot-atom substitution products, decomposition, RRKM theory, methyl isocyanide paradox 2−51428
in HTR reactor, oxidation of graphite by water, He gas quality control, gas circuit purification42675 2−42675
hydrocarbon negative ions, CNDO calculations and reactions 2−64184
ideal gas, interaction with acoustic waves 2−75369
inelastic and reactive collisions, semiclassical transition probabilities, classically inaccessible transitions 2−70617
ion source, for studying low energy ion mol. reactions 2−82458
ion-molecule, surface crossing model 2−81498
i.r. laser induced, mass spectrometric obs. 2−44501
irreversible thermodynamics, rel. to interpretation of u.s. relaxation spectra 2−54532
isomerization, examination of underlying stochastic process 2−51426
Markov chain and ordinary differential equation models, comparison 2−75364
mass transfer, coupling with membrane transport processes 2−56493
mechanism obs. using electron microscope with gas reaction stage 2−65363
methane, photoionization products, rate coeffs. for reactions 2−51435
methane-d_4 + silane ion molecule reactions, hydride ion transfer and isotope effects 2−68778
methyl radical + $Cl_2(Br_2)$, collisional, molec. beam study 2−61779
models for non-equilibrium phase transitions 2−51422
molecular, nonlinear boundary value problem, variational solution and error bounds 2−72537
molecular collision dynamics, classical S-matrix theory 2−72551
molecular collisions, characterization of product energy distribs., information and entropy deficiency 2−54529
molecular collisions, induced electronic excitation, model 2−61766
near resonant charge transfer processes at thermal energies application to interstellar matter 2−58353
organic groups chemisorbed on silica, i.r. spectral study 2−84643
organic semiconductors with gases, photoelectric detection method 2−72570
plasma, steady state nonisothermal low pressure, statistical model 2−57411
polymer fluorination, free radical formation detected by e.s.r. 2−61771
polymer transformations, conf., Bratislava, Czechoslovakia (1971) 2−54533
polystyryl radicals, chain length dependence of coupling reactions 2−72556
quantitative chem. laser studies of reaction energy partitioning, F atom sources 2−68807
quartz crystal microbalance, techniques for chem. reaction studies 2−41450
quasistatistical complexes, collisional reactions 2−51427
rare earth tetraborides, thermal stability 2−53995
reaction products, internal state distribution meas. using laser- induced fluorescence 2−61770
reactors with axial diffusion, variational solution of nonlinear boundary value problem 2−84633
relaxation, u.s. cavity resonator technique 2−76372
seeding aerosols, complexing of AgI-NaI systems 2−62247
selective laser photochem. reactions using predissoc. of mols. 2−68803
spiropentane, energy nonrandomized decomposition initiated by recoil T substitution reactions 2−81533
stars, rate, infleunce of excited states of target nuclei in vicinity 2−62507
thermodynamic concentration fluctuations by fluorescence correlation spectroscopy 2−72540
thermosphere, chem. release obs. from high flying aircraft 2−58035
thioformaldehyde, pyrolysis products of dimethyldisulphide, photoelectron spectrum 2−72538
three body rearrangements in reactive scattering, application of τ operator formalism 2−44467
three-dimensional, natural bifurcation coordinates 2−75363
triethyl boron with O, chemiluminescent fluorescent enhancement of BO_2 band 2−44475
troposphere, clustering of ions 2−62157
two species isothermal reactions in homogeneous turbulence 2−83426
ultrasonically induced 2−51475
unimolecular, expression for activation energy valid for all pressure regions 2−68768
unimolecular, stochastic model and RRKM theory 2−84634
urea, changes in bond length and angles on protonation 2−60089
World Ocean, constituents of chemical balance 2−62051
$X_2 + M \rightleftharpoons 2X + M$ dissociation, thermal 2−83235
$N_2O + e^- \rightarrow N_2 + O^-$, dissociative attachment rate constant, regeneration of electrons 2−74270
AG halides, photographic process, initial chem. development reaction 2−81547

Chemical reactions continued
AgBr, sol, conversion to AgI; kinetics, turbidimetric obs. 2-81542
α-Al_2O_3, whisker formation, role of water 2-74638
BAs, thermal decomp., mass spectrometry, X-ray and DTA studies 2-48321
$B_{10}H_{14}$, static reactivity indices, SCF study 2-64115
Ba formates, formation and surf. props. of electron emissive coatings 2-65365
BaF_2, hydrolysis effects on Gd^{3+} e.s.r. centres 2-84582
$Ba + HI \rightarrow BaI + H$, meas. of angular distrib. of product, determ. of threshold kinetic energy limits on D_0° 2-81494
$Ba + O_2 \rightarrow BaO_2$, collisional, internal state distribution of reaction products, laser-induced fluorescence meas. method 2-61770
$Bi_2O_3 + Al(Mg)$, rel. to use in nuclear fuels 2-83064
$^{80}Br + CH_3Br$, H and halogen, displacement factors, survival probability of products 2-84664
C, glassy fibres, derived from phenolic resin, pyrolysis mechanisms for mech. props. 2-84100
C fibres, reactivity, heat treatment effects 2-53951
C^+, reactive collisions with O_2 and N_2, 3 to 100 eV, calculated cross sections for mass transfer, molecular and dissociative charge exchange reactions 2-48322
$CF_3 + NH_3$, Arrhenius parameters, kinetic isotope effects and tunneling corrections 2-81496
$CH_3 + NH_3$, Arrhenius parameters, kinetic isotope effects and tunneling corrections 2-81496
CO^+, with H_2, CO_2, CH_4, N_2O, SO_2, O_2, C_2H_2, COS, NO and rate constants 2-51434
CS and CS^+ thermochemistry 2-72544
Ca formates, formation and surf. props. of electron emissive coatings 2-65365
$3CaO.SiO_2$:Cr, struct. rel. to reactivity 2-80877
$Ca + HI \rightarrow CaI + H$, meas. of angular distrib. of product, determ. of threshold kinetic energy limits on D_0° 2-81494
CeF_4, thermal decomp., elec. deflection study 2-51431
$Ce_2S_3 + CeO_2 + 2C \rightarrow 3CeS + 2CO$, optimum conditions for CeS prep. 2-47656
$^{38}Cl + CH_3Cl$, H and halogen displacement factors, survival probability of products 2-84664
Cl + HI(DI), exoergic, product static distrib. and temp. concept 2-68761
$Cl + IBr \rightarrow ClI + Br$ or $\rightarrow I + ClBr$, quantum mech. model calc. 2-65366
$Cs + I_2$, reactive collision cross section meas. 2-70738
Cu-Be-Ag and Cu-Be-Ti, decomposition of solid solns., phase transformations 2-68194
Cu wire, reactions during degassing ultrahigh vacuum 2-60679
CuO, thermal e.m.f. temp. depend. during dissociation, 960-1330K 2-57251
DBr-Br_2 system, hot atom reaction rates 2-72549
DI + Cl, energy distribution among reaction products 2-65369
$D + Cl_2$, energy distribution among reaction products 2-65370
$D + H_2 \rightarrow HD + H$, cross-section 2-61773
$D + H_2 \rightarrow HD + H$, quantum cross section 2-61772
$F + H_2 \rightarrow FH + H$, potential energy surface including electron correlation, refined linear surface 2-78189
$F_2 + H_2$ mixture excited by short electrical discharge, population of HF vibration-rotation levels, pulse laser investigation 2-66750
$F + H_2(D_2)$, energy distribution among reaction products 2-65368
$F + H_2(D_2)$, exoergic, product static distrib. and temp. concept 2-68761
$Fe + O_2$, fast flow reactor for kinetic obs. 2-48318
$Ge/H_2O/H_2$ system, etching rate, average reaction enthalpy, 950-1200K 2-74661
Ge, sulphidization, effect on surface recomb. 2-71938
$H_2:SF_6$, chemical efficiency of HF production 2-79191
$H_2/O_2/N_2$ flames, radical recomb. reactions, HO_2 participation 2-65373
$H_2/O_2/N_2$ flames, with Cr and K additives, electron attachment and negative ion form. 2-72555
H_2-H collisions, saddle point on H_3 potential surfaces 2-51429
H_2-metal reactions, rate at reaction measurement 2-78190
between H_2, H, H-, H^+, $H^+{}_2$, $H^+{}_3$ and electrons in dark interstellar clouds 2-75786
H_2, reactive collisions with ions, effect of reactant internal energy on spectator stripping 2-44472
H_2 pyrolysis on W filaments, atomization, e.s.r. obs. 2-72550
HBr-Br_2 system, hot atom reaction rates 2-72549
$HD + {}^{18}F$, classical dynamics of hot-atom reactions 2-81497
H_2S-Eu_2O_3 reaction at high temps., form. of EuS crysts. 2-50569
HY + X (X = Cl, Br; Y = Br, I), energy distribution among reaction products 2-65369
H + formaldehyde, abs. rate constant, investigation using formaldehyde photolysis 2-54539
$H_2 + Ar^+$, spin-orbit states of Ar^+, surface crossing model 2-81498
$H_2 + D \rightarrow HD + H$, molec. beam study 2-72546
$H + H_2$ linear collisions, classical S-matrix theory 2-72551
$H + H_2$ planar, hindered rotor states, natural bifurcation coordinates 2-75372
$H + H_2$ vibr. excitation process, rate const. 2-67537
$H_2 + H_2$ system, vibr. nonequil. effects 2-84627
$H_2 + O$ on Cu single crystal 2-54531
$H + O_2 \rightleftharpoons OH + O$ correlation diagram, calc. of ground and excited states of HOO 2-50040
$H + X_2(X = Cl_2Br)$, energy distribution among reaction products 2-65370
He + Ar collisions, chemi-ionization cross sections 2-64080
$He + H_2{}^+ \rightarrow HeH^+ + H$, reaction cross-section enhancement by vibrational excitation of $H_2{}^+$ 2-81500
$I + Ar \rightarrow IAr$, equilibrium constant 2-80009
$K_2CO_3 + 2PbSiO_3$ subsolidus reaction, kinetics and mechanism 2-60996
$K_2CO_3 + 2(4PbO.SiO_2)$, kinetics and mechanism 2-50884
KCl:Ba, solid soln. two temperature regions of decomposition 2-80526
K + molecule, atomic beam, reaction cross- sections meas. 2-51433
$K + CH_3I \rightarrow KI + CH_3$, translational energy depend., reaction cross-section 2-51432
$K + I_2$, exoergic, product static distrib. and temp. concept 2-68761
$K + O_2$, in Ar matrix, Raman spectra of products 2-61776

Chemical reactions continued
K + methyl iodide → KI + methyl radical, interpretation of product ang. and energy distribution using direct interaction model 2-57412
Li processes in upper atmosphere 2-58030
$Li_6W_2O_9$, peritectoid decomp. 2-54007
Mo_2C-$Fe_{(l)}$, contact interactions 2-77728
$N_2{}^+$ with H_2, CO_2, CH_4, N_2O, SO_2, O_2, C_2H_2, COS, NO and rate constants 2-51434
NH_3-N_2O population inversion in exothermal decomposition reactions on shock 2-73553
N_2H_4 catalysts, decomposition, storage 2-84632
$NH_3 + HCl$ system, potential energy curves for proton motion, extended Huckel calculation 2-43040
N_2O molecular beam, reactive scatt. from clean and C covered Pt(100) surface 2-50547
$NOCl + H_2$, vibr. energy distrib. of HCl mols. 2-53005
$NO^+ + H_2O$, in photoioniz. mass spectrometer 2-68775
$N_2O^+ + N_2O \rightarrow NO^+N + N_2O$, $N_2O^+ + N_2O \rightarrow O^+ + N_2 + N_2O$, mass spectrometric study 2-51436
N + CN + organic gas, C atoms obs. 2-61767
N + NO, production of $O(^1D)$ 2-51437
$Na + O_2$, fast flow reactor for kinetic obs. 2-48318
$Na + O_2$, in Ar matrix, Raman spectra of products 2-61776
O_2-H_2O system, formation and decomposition of water cluster ions 2-57414
O_2-S, on Ni surface, LEED obs. 2-78184
O + triethyl boron, chemiluminescent, fluorescent enhancement of BO_2 band 2-44475
O atoms with ethylene and propylene, products obs. in high-intensity mol. beams 2-68763
$O(^1D) + O_3 \rightarrow 2O_2\dagger$, $2O(^3P) + O_2$ energy distribution of products, ozone u.v. photolysis 2-84668
$O(^3P) + CO \rightarrow CO_2$, rate coeffs., meas., 250-370K 2-51438
$O + CS \rightarrow CO\dagger + S$, chem. laser studies of initial vibr. distrib. of CO 2-72552
O + acetylene, totally inverted vibr. population of CO 2-61777
O_2 + acetylene → CO, vibrationally excited, population distrib. 2-46532
Pb^+ ion gas-phase hydration, mass spectrometric obs. 2-80493
PrF_4, thermal decomp., elec. deflection study 2-51431
Pt-Si contacts, solid-solid reactions 2-50715
Pt, interaction with O_2, thermodynamic props. of volatile products, obs. method 2-65378
PuO_2 chlorination in melts of alkali metal chlorides, valent states 2-68776
$Rb + CH_3I \rightarrow RbI + CH_3$, 6-atom potential determ. using Monte Carlo trajectory methods, prediction of cross sections in 0-2 eV range 2-72553
$RhC_{(2)}$, heats of atomization determ. by high temp. mass spectrometry 2-84623
SO_2 clustering to NO^+ 2-61762
Si (111) crystal surface reaction with bromine studies using He^+ and Ne^+ ion scattering 2-50416
$SiH_4 + H(CH_3)$, intermediate SiH_5 radical obs. 2-57415
SiO_2, Si_3N_4 and SiC, interactions with metals at phase boundaries, thermodynamic analysis 2-84093
Sn-Pb alloy, solder, interaction with NO_2, corrosion, humidity effects 2-65382
Sr formates, formation and surf. props. of electron emissive coatings 2-65365
SrF_2, hydrolysis effects on Gd^{3+} e.s.r. centres 2-84582
$Sr + HI \rightarrow SrI + H$, meas. of angular distrib. of product, determ. of threshold kinetic energy limits on D_0° 2-81494
TbF_4, thermal decomp., elec. deflection study 2-51431
$TeI_4 \rightarrow TeI_2 + I_2$, and sublimation, 300-900 K 2-54526
$3Te + 4HNO_3 \rightarrow 4NO + 3TeO_2 + 2H_2O$, crystn. of TeO_2, rel. to conditions 2-56612
TiC_2, heats of atomization determ. by high temp. mass spectrometry 2-84623
Tl + Se, reactivity of equimolar mixtures, 132-180°C 2-53771
$2UC_2 \rightleftharpoons U_2C_3 + C$, contamination effects 2-46384
UO_2-C-N_2 reaction kinetics, 1695°C, carbonitride form. 2-54537
$U + O_2 \rightarrow UO_2{}^+ + e$ chemi-ionization, determ. probability of occurrence 2-68766
$U^+ + O_2(N_2) \rightarrow UO^+ + O$, determ. of reaction rate from thermal energy to 5 eV using drift mobility-tube-mass spectrometer 2-68766
W + H, inhibition by O adsorption on W surface 2-71344
ZrC-C composites, vapour deposition by the chloride process 2-80793

Chemical shift
acetone-d_5, D shifts meas. by ^1H-$\{^2H\}$ INDOR 2-42947
acetoxime, ^{13}C n.m.r., solvent and isotope effects 2-64165
acetylene, effects of deuterium substitution 2-77096
allene, ^{13}C n.m.r. shifts 2-77102
amino acid, proton mag. resonance 2-46989
benzene, solid, anisotropic nucl. spin relax. of ^{13}C 2-81310
1,3-butadiene oriented in nematic mesophase p.m.r. 2-60053
cyano group long-range shielding effects 2-77098
cyclopropylidene cycloalkanes chemical shift in ^{13}C n.m.r. 2-42975
1,2:5,6-di-O-isopropylidene-α-D-allofuranose-3d, D shifts meas. by ^1H-$\{^2H\}$ INDOR 2-42947
dimethyl phosphite, neat and in dilute soln., effect of deuterium substitution on $^1J(^{31}P$-$H)$ 2-80104
dimethylphosphoryl halides, ^1H n.m.r. spectra 2-46616
dimethylsulphoxide-d_5, D shifts meas. by ^1H-$\{^2H\}$ INDOR 2-42947
dipolar solutes in benzene and fluorinated benzene, n.m.r. study of solvent induced shift effects on ^1H and ^{19}F 2-83311
DNA bases, shifts of inner-shell electrons, CNDO/2 calcs. charge redistrib. effect 2-83345
ethylene, ^{13}C n.m.r. shifts 2-77102
halogenated molecule-nitroxide radical interaction, ^{13}C contact shift and MO studies 2-51440
halomethanes, K-shell electron binding energy and n.m.r. chem. shifts correl. 2-56235
hexafluorobenzene, n.m.r. study of gas to infinite dilution chemical shifts 2-74291
hydrocarbons, ^{13}C shifts determ. from INDO perturbation calc. of magnetic shielding consts. 2-64162
lanthanide ions in solution, pseudocontact contribution to n.m.r. shifts 2-80481

Chemical shift continued
metal complexes, polar and nonpolar in benzene and hexafluorobenzene, p.m.r. study of solvent induced shifts 2−83264
metals, X-ray absorption edges, effective nuclear charge 2−74208
molecules containing sulphur, n.m.r., electronic struct. investig. 2−83290
monomethylphosphoryl halides, ^{1}H n.m.r. spectra 2−46616
Mossbauer spectra, determination of explicit value 2−61598
nicotinamide, its cations and related compounds, ^{13}C chemical shifts determ. from n.m.r. investigation 2−83309
organomercury compounds, heteronuclear double magnetic resonance studies of ^{199}Hg nuclear shielding consts. 2−57403
polyatomic mols., mol. orbital theories of n.m.r. shifts 2−67461
pseudo-contact, effect of molecular magnetic multipoles 2−64101
pyridine, its cations and related compounds, ^{13}C chemical shifts determ. from n.m.r. investigation 2−83309
pyridines, monosubstituted, ^{14}N n.m.r. 2−56257
rare spins in solids, high resolution n.m.r. 2−81479
11-cis-retinal, p.m.r. shifts, PCILO calculation 2−77153
review, literature from July 1969 to July 1971 2−52342
shift reagent spectra, automatic sorting of signals 2−83218
silver trifluoroacetate, ^{19}F shielding tensors of trifluoromethyl group 2−68751
trifluoroethane and trifluoroethane-d_3, ^{19}F n.m.r. shifts in gas phase 2−83308
trifluoromethyl group, shifts of individual fluorines 2−77113
water dimer, hydrogen-bond n.m.r. shift 2−60003
^{13}C, of methylcyclohexanes, cyclohexanols, D-glucose, rel. to C electron densities 2−42948
^{13}C absolute determ. from $\sigma\|$ for CS_2 2−53000
^{13}C in organic compounds, characteristic n.m.r. shifts 2−56209
^{13}C n.m.r., calc. using mol. orbital theory 2−77102
$CaWO_4:Nd^{3+}$, photon echoes, generation, detection, mag. field and temp. depend. 2−72251
Cu salts, n.m.r. shifts of ^{63}Cu 2−44455
D shifts meas. by $^{1}H\{^{2}H\}$ INDOR 2−42947
^{19}F n.m.r. in ZnFOH, CdFOH and HgFOH 2−84591
FeS, antiferromagnetic, Mossbauer studies at 300K, 650K 2−81344
^{57}Fe, calibration of Mossbauer isomer shift 2−46137
GaAs, binding energies of Zn and Cd 2−65001
GaP, binding energies of Zn and Cd 2−65001
HCl, parameters of proton shielding function determ. from temperature dependence meas. of proton chemical shift 2−80046
$K_3Co(CN)_6$, n.m.r. of ^{59}Co 2−65345
$K_3Co(CN)_6$, n.m.r. of ^{59}Co 2−54509
$Mn(CO)_5$-X_3M adducts, single crystal ^{55}Mn broad-line n.m.r., anisotropic chem. shift tensor 2−68747
$Mn_2(CO)_{10}$ single crystal, anisotropic shift in broadline n.m.r. spectrum 2−57397
Mo, of Auger spectra on adsorption of O_2 2−51223
PBr_3, gas phase and solvent, ^{31}P n.m.r. studies 2−46575
$P_2Se_3-As_2Se_3$ semiconductor glasses, pseudobinary section, n.m.r. of ^{31}P, dependence on comp. 2−84584
$Re_2(CO)_{10}$ single crystal, anisotropic shift in broadline n.m.r. spectrum 2−57397
$ReMn(CO)_{10}$ single crystal, anisotropic shift in broadline n.m.r. spectrum 2−57397
Se, anisotropic shift in n.m.r. 2−44459
U surface, shifts in Auger transitions 2−67901
V, Auger electron spectroscopy of surface chemical composition 2−51480
$VO_{0.92}$, Auger electron spectroscopy of surface chemical composition 2−51480
VO_2, Auger electron spectroscopy of surface chemical composition 2−51480
V_2O_3, Auger electron spectroscopy of surface chemical composition 2−51480
Y, of Auger spectra on adsorption of O_2 2−51223

Chemical structure
see also Bonds
electron absorption spectra at u.v. and visible range for computer search system 2−79969
excitable membranes, dipole model and cooperative behaviour 2−60459
moon, internal constitution, models 2−62677
organic, by molecular spectroscopy on computer 2−79968
polyester resins, unsaturated, crosslinked with styrene, structure, Raman spectroscopy 2−44482
polymeric mats., spatial gradients rel. to chem. props. and applics. 2−61026
polyvinyl chloride, struct. characterization using laser-excited Raman spectroscopy 2−83343
sodium phosphate glasses, rel. to heat of solution 2−74598
stearate multilayers 2−46633
Cu_3MX_4 (M=V,Nb,Ta; X=S,Se) 2−42888
rare earth elements, polymolybdates, $Ln_2O_3.4MoO_3$ type, classification into four structural groups 2−83838

Chemical technology
chemical engineering, equipment design and automation (conference Prague, Sept. 1972) 2−83483
flow measurement, n.m.r. technique, velocity distribution fn. 2−83757
laminar nonisothermal contracted flow in chem. engineering processes, theoretical analysis 2−83423
mass transfer in fluidized beds of wetted spherical particles 2−83497
missile propulsion project engineering for chemical engineers 2−44793
pattern recognition applied to interpretation of chemical data 2−78182

Chemiluminescence
alkali halides, γ-irrad., aquoluminesc. on dissolution 2−43376
3-aminobenzaldehyde, in aprotic solvent, on ozonization 2−54538
benzoyl peroxide, during reaction with diphenyl amine and tetraphenyl hydrazine 2−78191
charged particle emission from surface during heterogeneous chem. reaction of atom recomb. 2−48269
dioxane based scintillation fluid 2−52687
kinetics obs. using fibre optics 2−48319

Chemiluminescence continued
liquid scintillation counters, efficiency, cost data 2−76730
luminol, induced by internal irrad. 2−48325
luminol oxidation in liquid phase and NO/O gas phase, absolute quantum yields 2−65372
naphthalene adsorbed on metal-substituted type-X zeolites 2−80585
photoelectrochemical image conversion, i.r. to visible 2−42254
reacting system, thermodynamic concentration fluctuations by fluorescence correlation spectroscopy 2−72540
triethyl boron + O reaction, fluorescent enhancement of BO_2 band 2−44475
turbulent flame struct. applic. 2−61780
two-body radiative recombination of atoms, rel. to resonance scattering 2−67409
CO fourth positive chemilum. excitation and quenching due to reactions involving C_2O 2−84628
^{14}C energy spectra comparison with phosphorescence 2−59605
DF, quenching, vibr. energy transfer to CO_2 and HF 2−65371
FeO, after release of $Fe(CO)_5$ in upper atmosphere 2−65825
HF, quenching, vibr. energy transfer to CO_2 and HF 2−65371
^{3}H energy spectra comparison with phosphorescence 2−59605
NO/O gas phase and luminol oxidations liquid phase, absolute quantum yields 2−65372
$NO+O\rightarrow NO_2+h\nu$, air-afterglow reaction mechanism 2−68773
$N+O_2\rightarrow NO+O$ reaction, overtone photon efficiency 2−57409
N_2 + methylene chloride, intensity variations of CN bands with temp. 2−83240
Na excitation by active N_2, interferometric obs. of D-line profiles 2−81492
O + triethyl boron reaction, fluorescent enhancement of BO_2 band 2−44475
O + acetylene reaction, i.r. chemilum., rel. to CO laser applic. 2−61777
TiO, electronic, emission spectrum 2−77068
ZnO, adsorbed gas depend. 2−78121

Chemisorption
Ag, activated chemisorption and oxygen coverage 2−78192
alloy, surface reconstruction due to chemisorption 2−50524
Au, adsorption of water, detn. by meas. of work function 2−71347
benzene flash desorption and decomp. from clean or contaminated W polycryst. 2−84624
diamond powder, oxygen chemisorption, kinetics 2−65374
electrode, of org. cpds. in double layer 2−84646
gas, chemisorbed, thermal desorption kinetics, review 2−67918
graphite, isotropic nuclear and 'Poco', of oxygen, reactivity obs. 2−59843
metal, of atoms, theory, review 2−48329
metal, of gas, thermodynamic and struct. aspects 2−50530
metal film, associated demetallization phenomenon 2−47150
metal surfaces, layer formation by anodic reaction within an electrolyte solution, thermodynamics 2−68781
methyl iodide fixation by silver zeolites 2−84640
molecular orbital approach, LCAO band struct. and molecular unit cell 2−50525
orbital symmetry rules for surface sites prediction 2−51441
semiconductor, amorphous, contact and surface photovoltage obs. 2−77969
silica gel, absorpt. of electron pair donors, H bonding 2−77515
soda lime glass, rel. to slow environment sensitive crack growth 2−64729
solid surfaces, conference, Boston Mass., USA, Oct. (1971) 2−47070
structure types, LEED obs. 2−56600
Ag, of O_2, e.p.r. obs. 2−50531
Ag, of O_2, rel. to surface struct. LEED and secondary electron spectroscopy 2−51442
Ag, of oxygen, slow irreversible processes, work function depend., LEED pattern changes 2−60675
Al, of O_2, work function changes obs. 2−77517
Ba, oxidation kinetics photoemission spectra of chemisorbed levels 2−51446
C, of O_2, effects on X-ray photoelectron spectra 2−57262
CdS, of O_2, conductivity changes 2−47886
n-CdS, thin compound semicond., sorption-induced conductivity changes 2−77886
CdSe, of O_2, conductivity changes 2−47886
Cu, of CO and H_2, weak adsorp. obs. 2−50537
Cu, of oxygen on (110) and (100) faces, electron diffr. obs. 2−60678
Cu of H_2 and O_2, obs. of reaction mechanism of H_2-O_2 reaction 2−54531
CuO, of CO, catalytic activity rel. to semicond. 2−75093
Ge, of nitrobenzene, effect on surface recomb. 2−71938
HBr on PbO layers, examination 2−75377
Ir-Pt alloy, chemisorbed CO, i.r. spectra 2−68645
MgO powders, thermally activated, O_2^- ion e.s.r. obs. 2−56602
Mo, of H, interaction with H beam 2−50461
Ni, of CO, energy detn., extended Huckel calc. 2−50546
Ni, of Hg, alloy formation 2−77489
Ni, of O, S, Se, local bonding structs., electron orbital energy spectra 2−48328
Ni, reactions of O_2 and S on surface 2−78184
Ni (111) plane, flash desorption spectroscopy study of H_2 adsorption 2−80568
NiO, magnetocatalytic effects at Neel pt. 2−44480
O on W(100) surface, work function 2−83878
PbI_2, of O_2, conductivity changes 2−47886
Pt, interactions with O_2 2−51450
Pt, of H, interaction with H beam 2−50461
Pt, of H_2, adsorpt. and desorpt. kinetics 2−77514
Re, interactions with O_2 2−51450
Rh, of methane, activation mechanism 2−80577
Si(111) surface, chemisorbed O_2, electron bombardment surface ion desorption study 2−71351
Sn-Pb alloy, solder, interaction with NO_2, corrosion, humidity effects 2−65382
Sr, oxidation kinetics photoemission spectra of chemisorbed levels 2−51446
W, adsorption and dissoc. of CO, field emission microscope obs. 2−71355

Chemisorption continued

- W, Cs sticking coeff., surface oxygen contamination effects 2−50550
- W, flash and electron stimulated desorption of CO on (100) planes 2−71356
- W, of CO, thermal desorp. spectra quantitative analysis 2−47173
- W, of CO, vibr. freq. refl.-absorption i.r. spectra 2−47154
- W, of N_2O, binding states, LEED obs. 2−64581
- W, of O, mass spectrometric obs. of desorption 2−48327
- W, polycrystalline, mixed adsorption of D_2 and ethylene 2−44484
- W of C, N and O, K shell ionization by electron impact 2−50553
- ZnO, luminesc. depend. on adsorbed gases 2−78121
- ZnO, of H_2, i.r. studies of isotope effects 2−65375

Cherenkov radiation

- *see also Counters/Cherenkov; Electrons/radiation*
- as auroral hisslers generation mechanism 2−65918
- charge in magnetoplasma, energy loss 2−46725
- charge moving in isotropic transparent medium in field of intense e.m. wave 2−78775
- charged paticle creation, e.m. field and rate of increase of field energy 2−63260
- dielectric media, alternating electric field 2−69822
- dispersion relation for radiation of moving test particle in magnetoplasma 2−80250
- EAS, 10^{11}-10^{12} eV, Monte Carlo calc. of time dependence of isophotes and multiple pulses in Cherenkov light 2−52657
- EAS, analysis of geometry effects in detection of Cherenkov light 2−52656
- EAS, determ. of relation of shower size to primary energy 2−73870
- EAS, form of radiation pulses at large distances from shower axis 2−73871
- EAS, meas. of rise time, width and shape of Cherenkov pulses 2−52655
- extensive air showers, γ-ray point source search by registration of Cherenkov light 2−51801
- MHD wave generation by moving charged particles 2−83525
- neutron induced, in mag. field, spectral distrib. intensity, theory 2−49500
- neutron induced, interac. with diff. polariz. 2−49501
- particle detector, metal, using generation of, for ultrahigh energy particles 2−73941
- plasma, spontaneous emission in presence of finite amplitude wave 2−64311
- plasma osc. generation by beam-plasma interaction, light emission 2−70945
- propagation in sinusoidally space-time periodic media 2−52318
- pulsar CP 1133, Cherenkov light registration from extensive air showers 2−51791
- in space-time periodic media, and transition radiation 2−66657
- tachyon monopoles, searches in photoproduction reactions at 1 MeV, detection by emitted Cherenkov radiation 2−82638
- bytachyons, Lorentz-invariant formulation 2−69559
- tachyons 2−55408
- uniformly moving charged particle in random inhomogeneous medium, Cherenkov and transient radiation 2−52312
- Vavilov-Cerenkov effect, in medium with wave phase velocity exceeding velocity of light 2−78776
- Vavilov-Cherenkov radiation, charged particle motion along optic axis of transparent uniaxial crystal 2−76416
- Ca-Si system, phase equilib., existence of silicides 2−71700
- ^{32}P electrons, applic. to detection of eye lesions 2−69459

Chirality

- — 2−70219
- — 2−63532
- (8,8) chiral symmetry model, dimensionality of δ 2−49481
- (8, 8) chiral symmetry breaking parameter determ. from spectral-function sum rule 2−63484
- book, chiral dynamics 2−82667
- chiral Lagrangian models, minimal coupling and nonlinearization in presence of e.m. interaction 2−45864
- chiral SU(2)⊗SU(2) symmetry, nonuniqueness of effective Lagrangian, $\pi\pi$ and πN interactions 2−45845
- chiral symmetry breaking model for πN scatt. 2−45929
- Lagrangian from scalar curvatures 2−42301
- liquid crystals, induced circular dichroism method of determ. for cholesteric mesophase 2−80460
- nonlinear realizations of chiral algebras and Lagrangians, rel. to SU(n) theory 2−76561
- nucleon structure and chiral symmetry 2−76707
- ps. meson, photoproduction, scale dimension of chiral symmetry breaking Hamiltonian 2−49540
- quark-gluon model, chiral symmetry realization 2−45897
- quartet scheme of hadrons in chiral U(4)xU(4) 2−45896
- spontaneous breaking of chiral SU(3) × SU(3) symmetry of hadrons 2−66952
- SU(2) × SU(2) dynamics, invariant functional formulation 2−70127
- SU(3) × SU(3), canonical second rank tensor 2−42311
- SU(3) × SU(3), non-linear chiral dynamics, violated Lagrangian 2−63573
- SU(3) × SU(3) invariance, scale and chiral, realisation with Goldstone bosons and broken SU(3) coupling constants 2−59386
- SU(3) × SU(3) mass breaking, effect of 'weighted' linear transforms 2−49480
- SU(3) × SU(3) spontaneous breaking, mass relations and particle mixings 2−66910
- SU(3) × SU(3) symmetry best of (3,3) breaking via σ term of KN scattering 2−63598
- SU(3) × SU(3) symmetry breaking and mass-dispersion relations 2−66911
- SU(3) σ model of $0^{\pm}$ fields, effects of adding $1^{\pm}$ gauge fields, chiral and scale symmetry breaking 2−79469
- SU(n) × SU(n) chiral interaction and localizability for $n \geqslant 3$ 2−79474
- symmetry, and CP violation 2−55804
- symmetry, in single-meson production processes 2−63612
- symmetry, relation to current algebra and PCAC, approach to strong interactions 2−63489
- symmetry breaking, meson nucleon sigma terms, theoretical estimate 2−63571
- symmetry breaking, W-parity, octet dominance 2−73739
- symmetry breaking and dual pion model 2−73813

Chirality continued

- trensors which transform according to (1,8) representation of SU(3) × SU(3), commutators with axial charges 2−76585
- W-parity, octet dominance and breaking of chiral symmetry 2−66909
- weak processes, leptonic and semileptonic, lepton-number and chirality nonconservation 2−45865
- A_1 isomultiplet, dynamic chiral symmetry and cancellation of divergences in mass differences 2−52628
- $\eta \rightarrow 2\gamma$, approach using scheme of chiral u(4)xu(4) symmetry 2−66996
- $\eta' \rightarrow \eta\pi\pi$, breaking of chiral symmetry 2−55866
- $\eta' \rightarrow \eta\pi\pi$, calc. of decay rate with chiral and dilatational symmetry breaking 2−52591
- $K \rightarrow \pi\pi\mu(e)\nu$, form factor deviation from chiral symmetry value, light cone corrections 2−63582
- KN scattering, chiral symmetry braking 2−49554
- ν scattering, current algebra sum rules and scale dimension of chiral symmetry breaking Hamiltonian 2−55818
- π isomultiplet, dynamic chiral symmetry and cancellation of divergences in mass differences 2−52628
- $\pi^+ p \rightarrow \rho^0{}_{1236}{}^{++}$, near threshold, chiral SU(2) × SU(2) dynamics 2−67025
- $\pi\pi$ scatt., chiral invariance and effective range expansion 2−79587
- ρ isomultiplet, dynamic chiral symmetry and cancellation of divergences in mass differences 2−52628

Chlorine

- — 2−68774
- — 2−68774
- — 2−68774
- adsorption of W, field emission study 2−60693
- adsorption on MgO, obs. of ESR signal, charge transfer effects 2−47139
- atmosphere, ice nucleus and chloride particle concentrations at Mauna Loa Observatory 2−65672
- atmospheric chloride concentrations, comparison between Mauna Loa Observatory and Hilo, Hawaii 2−65673
- atom, pulsed stimulated emission 2−79194
- atomic, metastable autoionizing states in sodiumlike Cl^{6+} 2−49945
- atomic stopping cross sections of α particles by application of Bragg additive rule to molecular stopping cross sections 2−70820
- diffusion, in RbCl, tracer and sectioning technique 2−47471
- ion beams, metastable X-ray emitters produced in beam-foil excitation 2−42788
- liquid, n.m.r. and n.q.r. studies 2−72507
- liquid, Raman spectra, fund. vibr. freqs. 2−43369
- molecular collisions, vibrational transition probabilities, temp. dependence below 300K 2−60117
- molecular cryst., harmonic freqs. of vibr., harmonic intermol. pot. 2−81349
- molecule, collisional reaction with methyl radical, molec. beam study 2−61779
- molecule, outer vibr. turning pts. near dissoc. in $B(^3\Pi_{0_u}{}^+)$ state 2−77082
- molecule, thermal decomp. in inert gas, diffusion theory approach 2−80059
- molecules, self induced transparency, in pure Cl_2 and mixtures with Ar and He 2−46534
- neutron radioactivation analysis in vivo of Ca, P, N and Cl in adult rat 2−54575
- solid, i.r.-active intermol. translational band intensities, intermol. bonding obs. 2−74967
- solid, n.m.r. and n.q.r. studies 2−72507
- $Ba + Cl_2 \rightarrow BaCl + Cl$ crossed beam reactions, primitive product ang. distrib. 2−81493
- in CdSe-CdS film photoresistor, activating role 2−65096
- Cl_2-Kr mixtures, shock tube heated, electron affinity continuum 2−53243
- Cl_2-Kr mixtures, shock tube heated, dissoc. relax. times 2−53244
- Cl-, in NaCl, X-ray Kβ emission and K absorp. spectra obs. 2−65288
- Cl II, new wavelengths and energy levels in spectrum 2−79946
- Cl^-, heat of hydration, SCF Dirac-Slater calcs. 2−53403
- Cl^-, hydrated binding energy calc. by ab initio, semi-empirical MO and classical methods 2−50030
- Cl^- content of rain, rel. to electrical conductivity 2−65741
- Cl_2, H_2, O_2, subsonic flow, photochemical initiation of combustion 2−84660
- $^{14}Cl^+$, highly excited, metastable autoionizing states, electronic energies and electron emission lifetimes 2−42749
- ^{35}Cl, solar abundance from i.r. umbral spectrum 2−55163
- ^{38}Cl, ^{39}Cl, cosmogenic radionuclides, model for in-cloud scavenging 2−65808
- $^{38}Cl + CH_3Cl$, H and halogen displacement factors, survival probability of products 2−84664
- Cl + DI, energy distribution among reaction products 2−65369
- $Cl_2 + H$, $Cl_2 + D_2$, energy distribution among reaction products 2−65370
- Cl + HI(DI) reaction, exoergic, product state distrib. and temp. concept 2−68761
- $Cl + IBr \rightarrow ClI + Br$ or $\rightarrow I + ClBr$, quantum mech. model calc. 2−65366
- Li/Cl secondary cell with inorganic electrolyte 2−66689
- Na/Cl secondary cell with inorganic electrolyte 2−66689
- Se: Cl, film, vacuum evap., transport time resolved drift technique 2−44104
- $Zn_xCd_{1-x}S$:Cu, Cl temp. and i.r. quenching of luminescence and photocond. 2−84543
- ZnS:Ag,Mn,Cl phosphors, mechanism of activator interactions 2−84551
- ZnS:Cl, quenching of photolum. by elec. field 2−72416
- ZnS:Cl film, photovolt, polarity reversal by excess Zn 2−51222
- ZnS:Cu, Pb, Cl film, temp. depend. of electrolum. and thermal quenching 2−84533
- ZrC-C composites, vapour deposition by the chloride process 2−80793

Chlorine compounds

- alkali chlorides, dissociation rates and mechanism 2−60021
- halogenosilane bis-pyridine and o-phenanthroline complexes, vibr. spectra, normal coord. analysis, struct. 2−77081

Chlorine compounds continued
tetrahedral oxy-compounds, force constants and regularities of chemical bonding 2—70725
ClCN, general quartic force field, calc. using Parr-Brown anharmonic potential function 2—52999
Cl_2CNCl, i.r. and Raman spectra 2—70694
ClCO, ClOO radicals, e.s.r. spectra, g-factor and h.f.s. tensors and nuclear quadrupole coupling constants 2—50031
Cl_2CS fluorescence, laser excited $^1(\pi^*\text{-}n)$ eigenstates 2—83282
ClNCO, microwave spectrum and struct. 2—56165
$ClNSF_2$ vibrational spectra, tentative assignment, band shape and G-matrix element calcs. 2—70697
ClO_2, $^2A_2 \leftarrow {}^2B_1$ transition, Zeeman effect 2—77064
ClO_2, crystal structure from i.r. and Raman spectra 2—77561
ClO_2 adsorbed on CaX and NaX synthetic zeolites, preferred rotation 2—80579
ClO_3^-, vibrational spectra and force constants 2—59996
ClOF, localized orbital calc. of bonding 2—67498
ClO_2F_3, LCAO MO SCF calcs., configuration 2—80000
ClO_3F, force constant calculations 2—64121
ClO_3F electronic structure, exptl. and theoretical study 2—46587
^{35}Cl n.q.r. in various compounds, study of bonding with B, C, N, P, and S 2—64112
^{35}ClF, hyperfine structure constants in J=1, J=2 rotational states using molecular beam electric resonance spectroscopy 2—74261

Chondrites *see Meteorites*

Chromatic aberration *see Aberrations, optical*

Chromatography
see also Adsorption; Chemical analysis/adsorption
digital integrator for gas chromatography 2—65409
gas, correlation techniques applic., with environmental pollution meas. applic. 2—75396
gas, investigation of pore formation in weld deposits made from low alloyed steel welding rods 2—50809
gas, mass spectrometer for, RM-50GC model 2—42704
gas, obs. of surface reactivity of C fibres 2—60623
gas analysis, transformer insulation decomposition products 2—68828
gas chromatograph, airborne, for atmospheric anal. 2—48467
gas chromatograph, portable, self-contained, design and fabrication 2—75398
gas samples injection apparatus under vacuum 2—61820
gel permeation, mean molecular weight, thermal degradation, monodisperse polystyrene 2—78186
gel permeation, molec. structure determination of high pressure polyethylene 2—67530
life detection on Mars, soil gas chromatography/mass spectrometry by Viking spacecraft 2—55147
liquid, developments and applics., review 2—44498
multichannel statistical optimiser use 2—78217
nucleotides, spectrophotometry of very small volumes using TLC method 2—75410
polyethylene, high density, melt rheology 2—83371
polymers, randomly crosslinked, with Schulz- Zimm primary distributions, gel permeation chromatography analysis 2—61818
purification applications 2—54565
radio-liquid chromatograph for simultaneous recording of light absorbance and radioactivity 2—65420
sampling valve for gas chromatography, high temps. and pressures 2—44497
thin layer, apparatus, review of trends 2—68822
H_2 isotopic molecules, gas separation and quantitative det. 2—52956
^3H in thin-layer chromatograms, det. using luminous Zn compounds 2—61832
^3H in two-dimensional chromatograms, automatic scintillation scanning unit 2—61831
PuO_2-UO_2 fuels, determ. of non-metallic specification impurities 2—74177
U determination by liquid phase method 2—74165

Chromium
alloying addition to WC-Co cemented carbides, effect on structure 2—43864
antiferromagnetic, Q-switch and polarization domains, obs. with neutron diffraction topography 2—65179
antiferromagnetic transition first-order 2—57119
antiferromagnetism, itinerant, 2 band model 2—44289
atom, highly-ionized, far u.v. spectra, rel. to solar lines 2—83189
atomic central-field models for open shells, SCF calcs. 2—64025
atomic scatt. factor, determ. by vanishing Kikuchi line electron diffr. method 2—74750
bombarded by C, N and O ions, 0.5-2 MeV, stopping power 2—47782
cold-worked, recovery, resist. study 2—53805
dendrites, galvanostatiscally obtained from CrO_3-H_2SO_4- dimethylsuphoxide-H_2O solution 2—47135
diffusion in GaAs, 800-1100°C 2—60829
diffusion in Mo, bulk and boundary diffusion 2—53766
diffusion in NiO, temp. depend. 2—50713
ductile-brittle transition, effect of rare earth metals 2—43691
electrical and thermal cond., 20 to 1200°C 2—47769
electrodeposited, internal stresses 2—64565
excitonic phase, thermoelec. power calc. 2—65077
film, amorphous, deposition and annealing, resist. study 2—77499
film, condensation on NaCl 2—50488
film, sputtered, supercond. props. rel. to deposition conditions 2—81045
free energies, interfacial meas. 2—80795
grain-size dependences of the failure mode and ductility transition temperatures 2—68098
impurity in Ge(Li) detector, trap parameters 2—46045
Invar effect 2—57269
magnetic generalized spin susceptibility, interband contribs., Lindhard expression 2—61554
magnetic struct. intensity, temp. hysteresis, sign change 2—54328
magnetic transition manifestations in thermal cond. and Lorenz functions 2—57311
magnon-phonon interaction 2—48109
mechanical props. of high-purity phase 2—47531
migration, low temp. in Au films, backscatt. obs. 2—56754

Chromium continued
neutron displacement cross sections, based on Lindhard model 2—83053
plastic yielding, high pressure effects 2—68081
in ruby, doping during hydrothermal growth 2—47230
solar overabundance, accelerated by solar flares 2—76001
solar photospheric abundance det. from spectrum synthesis 2—58554
solubility of Ce, Pr, and Nd in O-enriched Cr 2—43830
specific heat, 280-330K, antiferromag.-paramag. transition 2—75238
spin wave theory 2—61555
surface, (100), Debye-Waller factor and thermal exp. coeff., LEED obs. 2—50992
surface, cleaned and oxidized, secondary ion yield 2—61471
surface, soft X-ray and Auger appearance pot. spectra, L_3/L_2 intensity ratio 2—51230
surface atom mean square displacements, theory 2—61075
target, prep. of self-supporting metallic foils using electrodeposition 2—73920
targets, isotopic, self-supporting foil, preparation by electrodeposition 2—49619
tensile failure, crack propagation and nucleation 2—84041
thin oxide formation in aqueous electrolyte solutions passing anodic current, reaction kinetics 2—68784
$3CaO.SiO_2$:Cr, struct. rel. to reactivity 2—80877
$CdIn_2S_4$:Cr, cryst. growth, vapour transport method 2—71369
Cr:Fe, elec. conductivity 0.3-300K, and high temp. Neel points in different magnetic field intensities 2—68567
Cr-NbC, pseudobinary, phase equilib., phase diagram 2—68199
Cr-Ni steels, weldability to C steels, gas pressure process 2—68146
2-$^1/_4$ Cr-1 Mo steel, effect of carbon content on high temperature properties 2—60880
Cr and Fe simultaneous estimation in stainless steel by polarographic method 2—48352
Cr I, 5051.91 Å, solar photospheric fluctuations, radial veloc. coherence and phase spectra 2—75950
Cr^+, in MgO, e.p.r. obs. 2—75346
Cr^{2+}, in ZnSe, Jahn-Teller splitting, optical absorp. spectrum obs. 2—65270
Cr^{2+} in MgO, ground state obs. from thermal cond. meas. 2—72238
Cr^{3+}, in AgCl and AgBr, charge transfer spectra 2—51333
Cr^{3+}, in γ-irradiated TiO_2, spin-phonon coupling constants detn., acoustic paramag. resonance obs. 2—51408
Cr^{3+}, in MgO, anharmonic interact. on spin-lattice relax. 2—65195
Cr^{3+}, in $ZnWO_4$, temp. variation of e.p.r. line splitting by external electric field 2—72473
Cr^{3+}, spin-lattice relax. field effect obs., Van Vleck theory 2—65193
Cr^{3+} e.p.r. in $ND_4Al(SO_4)_2.12D_2O$ 2—84576
Cr^{3+} exchange coupled pairs in $YAlO_3$, optical spectrum 2—72415
Cr^{3+} impurity in Al_2O_3-Fe_2O_3 system, effects on spin relax. time of ferric ions 2—54368
Cr^{3+} in CdF_2, optical absorption bands due to photoionization 2—54417
Cr^{3+} in $LiNbO_3$ and $LiTaO_3$, optical excitation, dipole moments and macroscopic polarization 2—48138
Cr^{3+} in MgO, phonon sideband of R line 2—48187
Cr^{3+} in MgO, Raman relax. modifications due to substitutional effects 2—48114
Cr^{3+} ion pair, in ruby, energy levels 2—68633
Cr^{5+}, in Be_2SiO_4, e.s.r., 77K and 4.2K, 9.5GHz 2—72477
^{51}Cr bulk diffusion in α-Zr 2—67357
G^{3+} in SnO_2, e.p.r. 2—48309
GaAs:Cr, deep levels and radiative recomb., photolum. and photocond. study 2—71927
GaAs:Cr, instability of recomb. radiation and photocurrent 2—84540
GaAs:Cr p-i-n diode, nonadditive photocond. under combined excitation conditions 2—72080
in $H_2/O_2/N_2$ flames, electron attachment and negative ion form. 2—72555
$KMgF_3$:$^{53}Cr^+$, ENDOR of $^{53}Cr^+$, hyperfine const., covalency depend. 2—68753
in Ni_3Al, effect on hardness 2—43740
TiO_2:Li,V,Cr,Mn,Fe, transition metal impurity levels, esr determ. 2—44117
Tm:Cr:$YAlO_3$, laser, four-level operation at 2.35 microns 2—42075
YIG:Cr^{3+},Cu^{2+} garnet, hyperfine interactions of Cr^{3+} and Cu^{2+} ions, n.m.r. obs. at 4.2 K 2—72504
$ZnWO_4$:Cr^{3+}, impurity conc. determ., e.s.r. and optical emission studies 2—78157

Chromium compounds
alloy, dil., ordering wave-vector, model 2—84441
alloy, excitonic phase, thermoelec. power calc. 2—65077
alloy, mag. transition manifestations in thermal cond. and Lorenz functions 2—57311
alloy, ternary, nonferromagnetic Invar alloy, Elinvar characs. 2—77981
chemical bonding study using X-ray photoelectron spectroscopy 2—53002
Co-Ni-Cr-Ti alloy, quench-ageing behaviour, 700-900°C 2—68138
complexes, polar and nonpolar in benzene and hexafluorobenzene, p.m.r. study of solvent induced shifts 2—83264
$Cr_2S_2Te_x$, $0<x\leqslant 1$, magnetization, susceptibility, ordering of vacancies, 80-800K 2—54343
$^1/_2$Cr-Mo-V steels, high-strain fatigue properties 2—60948
dilute liquid alloy, Cr in Cu, CuZn, Zn, ZnGa, Ga, GaGe, GeAs, As, mag. susceptibility 2—80485
$Fe_{36}Cr_{22-x}Ti_x$, χ-phase alloy, $8<x<10$, inversion domain obs. 2—64637
Hastelloy-X, neutron irrad., void form. and swelling resist. 2—53721
Incoloy-800, neutron irrad., void form. and swelling resist. 2—53721
Inconel-625, neutron irrad., void form. and swelling resist. 2—53721
nichrome, film, prod. by multiple sublimation, vacuum system, props. 2—47121
nichrome, Mo or W reinforced, filament-matrix interface struct. 2—53966
nichrome, W filament reinforced, microstruct. 2—53970
nichrome, W filament reinforced, struct. and props. 2—53967
nichrome thin films, sintering 2—68151

Chromium compounds continued
- Nimonic 90, tensile creep under transient stresses, elevated temp. 2−71575
- nimonic alloy, ageing, solid sln. decomp. and volume change 2−50805
- refractories, atomic interactions 2−48206
- Al-Cr dilute alloys impurity resistivity, temp. dependence 2−84278
- Al-Cr liquid alloy, resist., conc. depend., 1650°C 2−46980
- Al-Cr solution, highly supersaturated, range extension in equilibrium diagram when cooled 2−43824
- $(Al,Cr)(ur)_6(ClO_4)_3$ low-temp. polarized absorption spectra, determ. of cubic and trigonal parameters 2−51289
- AlCr, impurity resistivity 2−68337
- Al_2O_3-Cr_2O_3 and Al_2O_3-Cr_2O_3-Fe_2O_3 systems, orientation of modulated structs. 2−50853
- Al_2O_3-Cr_2O_3 phase diagram and ideal soln. behaviour 2−50852
- Au-Cr alloy pressure transducers, influence of high pressure H_2 on resistance, compared with manganin 2−76122
- Au-Cr alloy systems, optical absorpt., band struct. 2−44371
- $Ca_3Cr(GeO_4)_3$, mag. struct. and space group determ. 2−72145
- $CdCr_2S_4$:Fe^{2+}, anisotropy of tetrahedral Fe^{2+} ions 2−72161
- $CdCr_2Se_4$ film, deposition and mag. props. 2−60649
- Co-Cr-C alloy, effect of $Cr_{23}C_6$ precip. on strengthening 2−57011
- Co-Cr alloys, effect of scale porosity, second- phase oxides and doping on oxidation 2−75379
- Co-Cr dilute alloy, n.m.r. and nuclear relaxation study of satellite lines 2−44454
- Co-10%Cr, thermal stability and corrosion of Al coatings after heat treatments 2−60959
- Co, Cr-$Cr_{7-x}Co_xC_3$, monovariant eutectic, faceted-nonfaceted, strongly coupled growth 2−57010
- Cr/H system, form. and decomp. equil. 2−77715
- Cr-B system, phase diagram 2−50957
- Cr-Co-C solid soln., activity and solubility of C 950-1200°C, precip., space equilib. diagram 2−56925
- Cr-Cu alloy, f.c.c.-b.c.c. interphase boundary dislocation structs. 2−56734
- Cr-Cu alloy, weakening resist. rel. to deform., heating time and temp. 2−50764
- Cr-Fe-Mn alloy, α-γ phase equilib., effect of transition metal additions 2−47687
- Cr-Fe alloy, Hall effect, magnetoresist., $T\leqslant 4.2K$ 2−47836
- Cr-Ga alloy, phase diagram, intermetallic cpds. 2−64817
- Cr-I system, phase diagram and phase identification 2−71701
- Cr-Mo-Si system constitution diagram 2−50961
- Cr-Mo-V steels, constitution diagrams for service lifetimes 2−60838
- Cr-Ni-B system, isothermal section at 800°C 2−61044
- Cr-Ni, Cr-Pd, Cr-Pt, structure of $K_{\beta 5}$ emission band 2−72378
- Cr-Ni alloy, hydrogenated, elec. resist. rel. to mag. field, localized moments 2−81034
- Cr-Ni alloy, tensile strength, stress rupture, hardness, alloying additions effect 2−74856
- Cr-Ni steels, austenitic, stabilisation of resistance to intercrystalline corrosion 2−65380
- Cr-Re dil. alloys, single cryst., mag. struct., neutron diffr. exam. 2−61553
- Cr-Ru alloy, absolute thermoelec. power, 350-1000K 2−68476
- Cr-Si-Fe-W ceramic film, electron microscope study of laser produced hole 2−80780
- Cr-SiO ceramic film, electron microscope study of laser produced hole 2−80780
- Cr-Ta-B alloy, phase equilibria, at 1400°C, X-ray obs. 2−43912
- Cr-Ti compounds phase transformations 2−80798
- Cr-V alloy system, melting equil. diagram 2−47709
- Cr-W alloy, dilute, phonon freqs. and widths rel. to force const. changes 2−68223
- Cr-1.6%W alloy, phonon freqs., neutron scatt. obs. 2−74973
- $2^1/_4$Cr-1Mo ferritic steel high cycle fatigue properties at elevated temperatures 2−60951
- Cr complex, $[Cr_3O(CH_2COO)_6(H_2O)_3]^+$, insufficiency of Heisenberg model 2−44294
- Cr complex, di-μ-hydroxotetraglycinatodichromium(III), structural and magnetic characterization 2−80645
- Cr complex, hexacarbonyl X-ray photoelectron spectra, multiple peak structure 2−46538
- Cr complexes, Cr(III) dimethylsulfoxide compounds, low temp. luminescence and vibrational spectra 2−51375
- Cr complexes, tris sulphur chelates chromium (III), luminescence and electronic absorption spectra 2−65306
- Cr III complexes, polarized crystal spectra, comparison with theoretical investigation of electronic spectra of trigonally distorted complexes 2−44372
- CrB, thermionic emission, obs. 2−44191
- CrB_2, electronic spectra, MOLKAO method calc. 2−71792
- CrB_x, thermionic emission, rel. to electronic struct. 2−48017
- $CrBr_3$, three-dimens. magnetization struct., Faraday effect obs. 2−78013
- Cr_7C_3, mixture with VC, X-ray analysis 2−44506
- $Cr(CH_3NH_3)(SO_4)_2.12H_2O$ paramagnetic salt temperature scale for 0.9 to 18 K range 2−55586
- $CrCl_2.3AlCl_3$, chem. transport of $CrCl_2$, $CrCl_2$ prep. method 2−65361
- CrCoMo alloy, total joint replacement, wear products in body 2−69292
- $(Cr_{0.8}Fe_{0.2})(OH)_3$, thermal conversion to $(Cr_{0.8}Fe_{0.2})O_3$, Mossbauer parameters variation 2−72547
- $CrFeTi_2O_7$, cryst. struct. 2−74727
- CrH_x, electrodeposited, f.c.c., h.c.p.→b.c.c. transform., heating time and temp. effects 2−47682
- CrH_x, electrodeposited from chromic acid soln., struct., lattice consts., deposition conditions 2−47320
- Cr(III) cpds. in soln., spin-lattice relax. 2−77447
- Cr(III) thiacyanate complex in dimethyl-sulfoxide, phosphorescence spectra 77-150 K 2−83269
- Cr(III) triethylenediamine chloride, vibr. spectra analysis 2−72325
- $Cr(III)S_6$ trigonal systems, electronic structures and MCD spectra 2−59997
- $Cr_xMn_{1-x}Sb$, internal mag. fields, n.m.r. obs. 2−54513
- $Cr_2(MoO_4)$-Li_2MoO_4 solid soln., phase diagram 2−57033
- CrN_x, hexagonal, magnetic and Mossbauer obs. 2−54331

Chromium compounds continued
- Cr_2O_3-Al_2O_3-P_2O_5, coating, radiative capacity rel. to struct., 600-2000K 2−57087
- Cr_2O_3-Al_2O_3-P_2O_5 ceramic coating on steel, props. 2−56960
- Cr_2O_3-Al_2O_3 system, sub-solidus phase equilibria 2−53983
- Cr_2O_3-Si_3N_4 refractories, thermal resistance, oxidizability, sintering, porosity and impact strength 2−68162
- Cr_2O_3-TiO_2 system, rutile struct. solid soln., interdiffusion and solubility limits 2−47618
- Cr_2O_3-Ti_2O_3 solid solution, mag. ordering, diffr. and e.s.r. obs. 2−48104
- Cr_2O_3-V_2O_3 mixtures, powder pattern detn. of Cr_2O_3 and V_2O_3 2−74728
- Cr_2O_3-V_2O_3 solid solution, mag. ordering, diffr. and e.s.r. obs. 2−48104
- CrO_2, phonon spectra rel. to VO_2, Raman spectra obs. 2−65277
- $CrO_4{}^{2-}$, resonance Raman spectra, analysis of ν_1 breathing mode 2−50054
- $CrO_4{}^{2-}$, ground states, SCF-MO calcs. and X-ray spectroscopy 2−77095
- $CrO_4{}^{2-}$, valence region X-ray photoelectron spectra, energy spread of ioniz. pots. 2−80004
- Cr_2O_3, crystal growth, from the flux systems PbO-V_2O_5 and Bi_2O_3-V_2O_5 2−50589
- Cr_2O_3, e.p.r. spectra below Neel temp. 2−54492
- Cr_2O_3, molten, surface tension, density, volume change on melting 2−80465
- Cr_2O_3, wavelength modulated reflectivity, rel. to absorp. of other Cr^{3+} containing insulators 2−65257
- Cr_2O_3 effect on sintering of Al_2O_3 2−50866
- Cr_2O_3 effect on struct. and props. of Al_2O_3 ceramic 2−50867
- Cr_2O_3 magnetic tape, pulse recording and FM applications, thermoremanent duplication 2−66701
- CrP_4, cryst. struct., synthesis, props. 2−53659
- $Cr_2(SO_4)_3$, $(CH_3NH_3)_2SO_4$, $24H_2O$, sp. ht. and susceptibility and above crit. temp. 2−48105
- CrSe film, vacuum deposited, struct. 2−67907
- $CrSi_2$-$MgSi_{1.72}$ solid soln., prep., thermal e.m.f., elec. and thermal cond. 2−74905
- CrSi, $CrSi_2$, Cr_3Si, Cr_5S_3, isobaric-isotherm. potl., entropy and heat of formation detn. by meas. galvanic e.m.f. 2−68246
- CrSi, elec. cond., thermal e.m.f. and Hall coeff. detn. 2−77797
- $CrSi_2$, formation on Si from Cr film 2−43861
- $CrSi_2$, thermoelec. props., cryst. growth 2−84370
- CrTe, mag. props. and lattice parameters detn., 67-400K 2−72148
- CrTe film, vacuum deposited, struct. 2−67907
- CrTe thin film, ferromag. reson. 2−57387
- $Cr_{1-x}Te$, magnetic anisotropy with $x=0.077$ 2−84415
- CrV steels, free energy changes and boundary segregation of Sn and Sb 2−71309
- $Cr_3\square Te_4$, Curie temp., press. effect 2−54336
- $Cr_7\square Te_8$, Curie temp., press. effect 2−54336
- $Cr(ur)_6I_3$, ${}^4A_2\rightarrow{}^2E$ transition, spin-orbit interaction and Jahn-Teller distortion effects in calc. of vibronic spectra 2−51291
- $Cr(ur)_6I_3$ and deuterated complex, luminescence low temp. spectra, obs. of ${}^2E$ level splitting, zero-phonon transitions 2−51290
- $Cr(ur)_6I_3$ low-temp. polarized absorption spectra, determ. of cubic and trigonal parameters 2−51289
- $CsCr(SO_4)_2.12H_2O/D_2O$, Cr^{3+} spectroscopy 2−54400
- CsI:$CrO^{2-}{}_4$, i.r. absorpt. 2−78086
- $Cs_2SO_4.Cr_2(SO_4)_3.24H_2O$ alum., paramag. spin-lattice relax. times of Cr^{3+} 2−84444
- Cu-Cr, Cu-Zr-Cr, alloys, precip. size effect on recrystalliz. temp. 2−56927
- Cu-Cr alloy, dispersoid struct. precipitated by tempering 2−43832
- Cu-Cr alloy, embrittlement, under elevated temp. stress 2−43722
- Cu-Cr alloy, internal friction and Young's modulus, after isochronal annealing 2−77633
- Cu-(0.6 at.%)Cr alloy, precip.-hardening, neutron irrad. effect 2−43833
- Cu-Zr-Cr alloy, precip. processes, specific heat and resistivity obs. 2−50933
- Fe-Al-Cr effect of zirconium on mechanical props. and oxidation resistance 2−60935
- Fe-Cr-Al alloy, potentiodynamic curves as function of tensile stress 2−44488
- Fe-Cr-Co system, phase boundary $\alpha+\gamma/\gamma$ determ. 2−84164
- Fe-Cr-Mn system, phase boundary $\alpha+\gamma/\gamma$ determ. 2−84164
- Fe-Cr-N alloy system, microstructure revealing nitride phase 2−53894
- Fe-Cr-Ni, plastic deform., low temp. 2−43693
- Fe-Cr-Ni system, phase boundary $\alpha+\gamma/\gamma$ determ. 2−84164
- Fe-Cr alloys, sp. ht. and thermopower near mag. crit. pts. 2−57290
- Fe-Cr dil. alloy, Mossbauer effect, lattice disturbance produced by solute 2−44354
- Fe-Cr system, computed low temp. phase equilib. 2−50966
- Fe-Cr σ-phase, atomic distrib. and mag. props., Mossbauer obs. 2−44253
- Fe-Cr(8%) alloy, martensite substruct., quenching and tempering temp. effects, rel. to strengthening 2−84071
- Fe-Ni-C-Mo-Cr alloy, tempering, effect on struct. and mech. props. 2−43853
- (Fe,Cr)-$(Cr,Fe)_7C_3$ composite, growth and props. 2−50920
- Fe(16 wt.%)Cr alloy, electromigration of Fe and Co 47460 2−47460
- Ge-Cr film, amorphous, hopping cond. 2−61313
- $(M,Cr)(ur)_6(ClO_4)_3$, M = Al, Ga, low temp. spectra, obs. of ${}^2E$ level splitting, zero-phonon transitions 2−51290
- $(M,Cr)(ur)_6I_3$, M = Al,Ga, low temp. spectra, obs. of ${}^2E$ level splitting, zero-phonon transitions 2−51290
- MgO-Cr_2O_3-CuO(Cu_2O) system, phase diagram 2−43931
- 2 $MgO.5SiO_2.2Al_2O_3.nCr_2O_3$ glass due to Cr_2O_3 additions, e.s.r. obs. 2−83850
- $Mn_{1-x}Cr_xSb$ films, ferromag. reson. 2−72450
- Mo-Cr-alloyed or unalloyed case hardened steel, residual stresses in carbonized layers for different thermal treatments 2−56931
- Ni-Cr-Mo alloy, porous material, physicomech., hydraulic, and corrosion props. 2−53977
- Ni-Cr-Nb-W-Mo alloy, struct. and phase comp. 2−43941
- Ni-Cr-Ti alloys, strengthening by precip. of intermetallic phases 2−43859

Chromium compounds continued
- Ni-Cr alloys, mag. props. temp. depend., deform. and annealing influence 2−44256
- Ni-Cr base alloys, filament reinforced, mech. props. 2−56988
- Ni-Cr lamellar composite alloy, fatigue deformation, crack propag., fracture energy 2−56821
- Ni-Cr steels, effect of Cu additive on tempering 2−60957
- Ni-Cr system, heat of disordering of Ni_2Cr 2−50954
- Ni-40%Cr alloy, effects of Al and Ti on age hardening 2−64767
- Ni-Fe-Cr based alloy, γ'-hardened, electron irrad., void swelling 2−80684
- Ni_3Cr alloy, oxidation effects on mag. props. 2−54338
- Pr-Cr_2O_3 glasses, absorption spectra 2−75286
- Si-$CrSi_2$, $CrSi_2$ fibres in Si matrix, anisotropy columnar structs., resist. anisotropy 2−74920
- Ti-Cr alloy, fracture modes, effect of ω phase 2−47547
- TiO_2-Cr_2O_3 system, solid solubility of $Ti_2Cr_2O_7$ 2−47719
- TiO_2-Cr_2O_3 system, solid solns. and cryst. shear struct., electron microscope obs. 2−47406
- Ti(13 wt.%)V-(11 wt.%)Cr-(3 wt.%)Al beta alloy, mech. prop.-fracture-microstruct. relns. 56950 2−56950
- V-Cr alloy, struct. and props., comp. depend. 2−53912
- $V_{1-x}Cr_xBe_2$, n.m.r. and mag. props. 2−72520
- Zn-Cr alloy, dilute, elec. resist., $T<0.1K$ 2−68342
- Zn-Cr dilute alloy, Kondo effect and localized spin fluctuations 2−64918
- Zn-Cr Kondo alloys, supercond. below 0.1K 2−44082
- Zr-(2at.%)Cr-(0.16at.%)Fe alloy, precip. reactions rel. to corrosion resist. 2−53919
- Zr-(1.5wt.%)Cr-(0.1wt.%)Fe tubing, hydrided, mech. props. and struct. 2−53918
- Zr-Cr-Fe alloy, correl. of microstruct. with properties 2−53922

Chromosphere
- 1964-6 chromosphere observations in Hα light 2−78622
- cell points intensity variations in quiet regions 2−76012
- chromosphere-corona transition region, structure and energy balance 2−44998
- chromospheric and coronal networks, correlation between intensity fields 2−76021
- continuum emission obs. at 7 March 1970 total eclipse 2−66233
- continuum obs. at eclipse and model of low chromosphere 2−66232
- current dissipation rel. to energy of solar flares 2−62800
- e.u.v. spectroheliograms, temp. gradient and electron density maps 2−76022
- features, rel. to photospheric magnetic fields 2−66234
- fine structures, high resolution spectroscopy 2−76018
- flare activity rel. to atmospheric electrical elements in lower troposphere 2−65797
- flare knots, motion of details 2−51860
- flares, motion rel. to magnetic field 2−51861
- force-free mag. field, non-linearity of dynamical behaviour 2−78582
- inhomogeneities, quiet Sun brightness distribs. at millimeter wavelengths 2−85053
- ion-sound current instability, turbulent resistivity 2−78616
- line formation, mean depth in a magnetic field 2−73112
- magnetic field, practical representation 2−76023
- magnetic field network, effect on spatial structure of corona 2−78604
- magnetic fields, electrical currents and Lorentz forces 2−76010
- magnetism, force free field configurations 2−76014
- metallic abundances as function of height 2−55191
- microturbulence and line profiles, generated by acoustic waves 2−76016
- multidimensional transfer problems, interpolation functions, accuracy and stability 2−58558
- network, EUV obs. 2−66235
- oscillation in Hα plage 2−78606
- photosphere-chromosphere transition region, brightness temperature minimum 2−62802
- Procyon, one component model 2−75712
- radio emission, source of slowly varying component at cm. and mm. wavelengths 2−76020
- rotation rate of material across disc from EUV spectroheliograms 2−78583
- short-lived brightening observed in Hα and Ca II K-line 2−78612
- spectral analysis of highly inhomogeneous chromospheric flares, radiation dilution 2−62797
- spectral line profiles, relation to intensity gradients 2−48809
- spectral line profiles of chromospheric H lines on the disk 2−48810
- stars, Wolf-Rayet, chromospheric heating by radiation driven sound waves 2−69062
- sunspot area, east west asymmetry, faculae 2−55179
- superrotation, height gradient 2−76013
- transition region with corona, review of physical properties 2−73148
- upper, high resolution obs. at 3.71 and 11.1 cms 2−75983
- C, O_2, Ne density dependent ionization balance 2−66231
- Ca II, H and K emissions, time resolution observations 2−76019
- Ca II K-line profiles in quiet sun 2−73113
- Ca II K_{2v} spectral features in non-magnetic regions, temporal behaviour 2−55170
- Ca II line profiles in plages, chromosphere and sunspots 2−75947
- Dy II identification 2−66200
- Fe I ionization and excitation equilibrium 2−66230
- H_α flares rel. to chromospheric response to downward propagating shock waves 2−78620
- H_α mottles 2−66201
- He I and H lines intensity ratio in prominence 2−66229
- He_{II}4686 intensity 2−73144

Chronographs *see Time measurement*

Cinematography
- *see also Cameras*
- 16 mm film production techniques, positive/negative/reversal systems 2−42286
- anamorphic lens attachments for wide-screen systems 2−52509
- automated 16 mm projector equipment, development 2−55780
- electronic cameras and other devices 2−73697
- frequency contrast functions, comparison of experimental and calculated values 2−52496

Cinematography continued
- Fuji CVR, new audio-visual system using single-8 film cartridges 2−52495
- holographic developments 2−69967
- incandescent printing lamps, luminous flux variations 2−66874
- lens screen camera, high speed, using turbine driven disc 2−52514
- light sources, colour rendering index 2−82596
- photographic materials, black and white, light sensitivity 2−66873
- prism cameras, analysis of operation and calc. of maximum framing speed 2−52513
- projection screens, description 2−66875
- rifled picture screens, optical parameters 2−76554
- scientific developments 2−52494
- obs. of shrinkage of metalloceramic materials during sintering 2−63450
- sound effects equipment, Rotophone CR-4E 2−66628
- step printer for 16 mm film, pulse controlled 2−70089
- synchronous sound film, editing considerations 2−66860
- time lapse and sequence, obs. of geologic processes at Athabasca Glacier 2−57813
- white light, high speed obs. of compressional waves in corona during solar eclipse 2−76033
- Ag sound tracks, in colour reversal film 2−76551

Circuits
- *see also Amplifiers; Counting circuits; Oscillators*
- − 2−59022
- accelerator tank, energy stabilization 2−59654
- amplitude modulation, impedance pneumograph output, gain stabilised, patent 2−85095
- automatic balanced bridge for e.p.r. spectrometer 2−66665
- control for laser pump lamp power supply 2−45648
- corona stabilizer for Van de Graaf accelerators 2−76754
- cryogenic liquid level indicator 2−41898
- current pulse generator for n.m.r. self-diffusion obs. by pulsed gradient technique 2−73502
- for dead time correction in pulse height anal. 2−70309
- decision system, fully automatic, for digital compensation of impedance bridges 2−45644
- decision system for digital compensation of impedance bridges, optimization using phase control circuit 2−45645
- device for det. fluorescence lifetimes based on phase-shift technique 2−55366
- digital demonstration units as teaching aids 2−82099
- digital electronic interface between multichannel analyzer and tape transport 2−79655
- direct registration of electron densities measured interferometrically 2−67658
- 1/H drive, for use with superconducting solenoid magnet system 2−45650
- drive mechanism for exptal. apparatus in vacuum system 2−58666
- dual input networks, all-pass characteristics 2−59034
- dual parameter pulse height analyser, 128 × 128 channel, computer controlled, for solid state laser tests 2−73584
- dynamometer wattmeter for power loss obs. in Si iron 2−73501
- elements for thin-film integrated optics 2−79413
- equivalent cct. for TiO film dielec. props. 2−47970
- equivalent electrical circuit for longitudinal vibrations in electromechanically excited bar 2−78916
- fast Marx generators, spark gap overvoltages and breakdown patterns 2−71026
- feedback, for torsional magnetic balance 2−76439
- h.v. pulse generator for spark chambers in space 2−55933
- h.v. source with digital control for dielectric obs. 2−66682
- h.v. sweep and controlled magnetic lens current supplies for electron microprobe 2−66718
- hydraulic measuring bridge, theory 2−45649
- I_0 subtraction unit for use with pulsed or d.c. light sources, application to pulse radiolysis 2−45801
- inductive store for 20MJ, construction and operation 2−59021
- integrated, coherent optical techniques for filtering of defects 2−42103
- integrated, surface wave filters 2−49112
- interlock protection, for vacuum system 2−48945
- interlock protection, for vacuum system 2−48945
- LEED-AES system, electrodes and circuits 2−74612
- linear capacitance micrometer, output voltage proportional to displacement 2−62959
- linearization of output of hot wire anemometer 2−53281
- for medical diagnostics and therapy, survey 2−81978
- memory, minimum voltage, microphotometer digital readout system 2−52353
- n.m.r. spectrometer electromagnet current stabilizer 2−76424
- nonlinear elements, transient behaviour of energy transport networks 2−73498
- nuclear amplifiers, low noise, pulse shaping, noise analysis 2−42474
- nuclear reactor control system, effect of noise currents 2−42636
- for on-line evaluation of noise, applic. to atmospheric turbulence and seeing conditions 2−45633
- optical thickness gauge for semiconductors 2−67902
- parallel LC containing real inductor with non-zero resistance, laboratory expt. 2−78728
- phase selective detector system, applic. to electrochemical photoeffect obs. 2−59032
- printed circuit boards, thermal analysis method 2−52354
- production of h.v. step 2−66683
- pulse amplifier and discriminator for photon counting 2−59124
- pulse delay generator, counter accessory 2−55892
- pulse generator for obs. of nanosecond breakdown of condensed media 2−77316
- pulse generator with exponentially decreasing repetition rate suitable for time marking 2−55640
- pulse phase-locked system dynamics 2−82500
- pulse shape, discriminator, semiconductor gamma ray spectrometer, isotope determination, Compton scattering suppression 2−82796
- pulse shaper with differentiation at input 2−82803
- pulse stabilization, transit time, spark gaps, streamer chamber 2−82826
- ratio, for plotting dose distribution in radiation field of 8 MV linear accelerator 2−59653

Circuits continued
- repetitive multiloop resistive, solution by finite- difference equations 2−62942
- r.f. regulator for Saturne synchrotron's 20 MeV proton linac injector 2−49701
- semiconductor, in d.c. circuit, self-oscill. due to recombinational instability 2−49231
- signal generator for voltammetric techniques 2−65405
- simulation of radiated heat exchange 2−52263
- square root function generator using binary rate divider 2−41899
- superconducting thin film Dayem bridge, I-V charact. near transition temp. 2−71844
- supply unit for h.f. film deposition 2−78696
- surge generator, for physics research, analogue computer analysis 2−78987
- for tagging analog-digital conversion address for multispectral scaling 2−70310
- theory applied to infrasonic detectors 2−69766
- timing system for coincidence and nuclear lifetime obs. with Ge(Li) detector 2−49662
- transistor physics and circuit properties, book 2−84356
- transistorized pulser for r.f. ion sources 2−49332
- transmission line, for reliable spark gap operation 2−66684
- trigger, for double-discharge TEA lasers 2−79199
- two channel boxcar analogue integrator for pulsed n.m.r. relaxation time meas. 2−52343
- two port, analogy with linear optical systems 2−79367
- underdamped LCR, for l.f. electrical oscillations 2−73265
- u.s. pulse echo investigation of solids, electronic equipment 2−73499
- for vacuum pumping system 2−78697
- Wien filter, double-focusing, as full-image energy analyzer for electron microscope 2−79077
- X-ray tube anode current stabilizer using a triac 2−45652

Clathrates *see Molecules; Organic compounds*

Clay
- clays, yield and failure 2−76268
- compressibility rel. to sands 2−62017
- controlled humidity generator for X-ray struct. determ. of clay minerals 2−56623
- Debye-Huckel theory, appl. to clay minerals 2−83809
- dielectric properties, meas. method eliminating contact pheomena 2−72009
- flow behaviour of clay-H_2O suspensions 2−83816
- flow peculiarities 2−83820
- fusible, ceramic prep. by calcining 2−64784
- illite, microstructure and chemical comp. 2−84710
- kaolinite, Egyptian, radiation effects on surface structure 2−53550
- kaolinite rods, elastic consts. from adsorptive length changes 2−77641
- palygorskite colloid soln., stability, transient elec. light scatt. obs. 2−74567
- progressive failure of clay slopes, growth of slip surfaces 2−78238
- quick clays, Rosenqvist theory, liquid crystal dispersant 2−60517

Cleavage
- crystal orientation by cleavage plane reflected laser beam 2−74656
- diamond, abrasion resist. during polishing and grinding, microscopic cleavage mechanism 2−74868
- feldspar, axial growth of inclined en echelon cleavage cracks during compression 2−61972
- ice, columnar-grained, cracking 2−64732
- microcline, shock deform. struct. 2−61843
- steel, low carbon, microstructure and embrittlement 2−43783
- steel, low-carbon, facets on fractured surface with relatively high propag. rate 2−84126
- α-Al_2O_3, {1011} planes, elec. microscope and X-ray obs. 2−74657
- GaAs, strain induced phonon line broadening observed by surface reflection Raman scattering 2−83858
- guanidinium aluminium sulphate hexahydrate, optical and interferom. studies of cleavages and etch patterns 2−64670
- KCl single crystal, dependence on cooling velocity 2−84122
- $KNbO_3$, ferroelectric domain investigations using pseudocubic {001} cleavage planes 2−61429
- MgO, plastic deform. during cleavage fracture 2−71570
- NaCl, electrical processes occurring at moment of cleavage 2−74659
- NaCl selective dissolution, complexes responsible for etching 2−74658
- W single crystal, {110} in ⟨110⟩ axis 2−56606

Clebsch-Gordan coefficients *see Field theory, quantum; Nucleus/theory; Quantum theory*

Climatology *see Meteorology*

Clock paradox *see Relativity*

Clocks *see Time measurement*

Cloud chambers
- automated analysis of tracks, counting individual droplets 2−67098
- interactions, 25-10000 GeV, studied with multiplate cloud chamber using Monte Carlo simulations for energy calibration 2−42436
- ^{4}He interaction with π^+, exp. apparatus 2−52703

Clouds
- *see also Nucleation*
- airflow pattern and droplet trajectories about electrostatic droplet probe 2−57981
- Aitken and cloud nuclei production by urban area of St. Louis 2−65726
- Alberta hailstorms, aircraft seeding using pyrotechnic flare system 2−65746
- angular transmittance props. 2−57977
- anomalous ice concentration, and freezing of rain drops with different solutes 2−54843
- Arctic stratus, physical properties 2−57987
- Arizona cloud-seeding experiment, re-evaluation 2−62239
- atmospheric line of sight, cloud free, photogrammetrically 2−75610
- automated tracking, by precisely aligned digital ATS pictures 2−48438
- backscattering, first and second order, illuminated by lidar beam 2−51610
- ball lightning, new theory, seed for linear lightning 2−65802
- bands, broad and extensive, associated with tropical atoms, autumnal build-up of planetary circulation 2−44725

Clouds continued
- cap, natural, ice crystal conc., nucleation obs. 2−48488
- charged, electrical shielding layer around, role in thunderstorm electricity 2−84812
- circulation, orographic induced, radar obs. 2−75553
- cirrus clouds and climate 2−78374
- cirrus layers, light scattering 2−62253
- clearance and visibility standards 2−68879
- cloud motion vectors, computation of kinematic properties 2−65693
- clusters, over tropical north Atlantic Ocean, satellite study 2−65718
- coalescence theory, scalar transport equation, family of exact solutions 2−57970
- coalescence theory, scalar transport equation, moments and kernels 2−57969
- colloidal stability and production of cloud nucleates by urban industrialised complex 2−65725
- condensation nuclei, air pollution effects, obs. at Los Angeles 2−65713
- condensation nuclei, rel. to inadvertent weather modification in Los Angeles smog 2−51572
- condensation nuclei concentration, isothermal determination method 2−62233
- condensation nuclei counter, for automatic meas., patent 2−72797
- condensation nucleus counter, automatic 2−51580
- continental convective, randomized seeding 2−62216
- convection, North Sea coast, low sea surface temps. 2−54830
- convective, numerically simulated, micro- and macro-structures 2−48490
- convective, seeding effects, project Cloud Catcher 2−62210
- convective development in Texas 2−62215
- convective development model 2−62213
- cover estimate from satellites, effect of sensor spatial resolution, simulation study 2−48495
- cumulonimbus, breaking billows 2−84854
- cumulonimbus anvil growth data rel. to thunderstorm circulation and severe local storms 2−84846
- cumulonimbus convection, dry line of Northern India 2−68905
- cumulonimbus effects on airborne 30-mm radar at long ranges 2−81664
- cumulonimbus mesoscale system, construction of composite maps 2−62244
- cumulonimbus protruding into stratosphere 2−75606
- cumulus, ice whiskers, nuclei and crystal concentrations 2−84855
- cumulus, ice-phase seeding potential for modification, model 2−48493
- cumulus, model of hygroscopic seeding 2−62204
- cumulus, numerical model, simulation, of salt seeding 2−62206
- cumulus, seeded, three dimensional growth rate obs. 2−75580
- cumulus, seeding during 1971 south Florida drought 2−62225
- cumulus, warm, modification expt., seeding using encapsulated urea 2−62207
- cumulus entrainment and one-dimensional models 2−44723
- cumulus model, hail growth by stochastic collection 2−44719
- detection by acoustic echo sounding 2−62234
- diffuse reflectivity from cloudy planetary atmospheres, lab. simulation 2−44933
- drop size distribution in Florida summer showers, simultaneous radar reflectivity and rainfall data 2−62214
- droplet distrib. ice crystal concentration, vertical velocity, temperature, in-cloud measurements 2−54851
- droplet or ice particle formation on aerosol particles, temp. and humidity conditions 2−51612
- droplets, effect on solar radiation absorption by atm. dust 2−84806
- dynamic seeding expt. in Florida 2−62221
- electric, modelling 2−58005
- electric, modelling 2−65781
- electric field recovery, after lightning, response of conducting atmosphere to field charge 2−68919
- electrified, charge screening layers 2−65742
- emissivity, variation in i.r. 2−65738
- evaporating cloud layer, radar observations of undulance 2−75596
- evaporation accelerating the ice phase in supercooled water 2−62236
- expanding gas, in const. shear flow, diffusion eqn. 2−72821
- finite-difference cloud droplet collection equation, critique and reply 2−68904
- forecasting of cloud ceiling from forecast winds 2−65717
- formation, atmospheric aerosols as heterogeneous nuclei 2−51613
- formation process in moist air by non-adiabatic thermal convection, one-dimensional model 2−44721
- giant cumulonimbus, potential vertical extent 2−57980
- glaciation, thermodynamics 2−62211
- gravitational coagulation of droplets, numerical simulation 2−65739
- ground survey using two spherical mirrors, determ. of height of cloud field 2−84852
- hail bearing, numerical model 2−84807
- hail formation in steady convective cloud 2−72792
- hail-model, size distrib. and accumulation zones 2−84808
- heterogeneous nucleation of ice clouds rel. to AgI-bearing smoke activity curves 2−57971
- hurricane rainband, modification numerical simulation 2−62224
- ice condensation nuclei rel. to numerical estimates of humidity in membrane-filter ice nucleus chamber 2−65671
- ice forming activity of γ irradiated AgI particles 2−48498
- ice nuclei, rate of soln. in water drops, nucleation 2−75600
- ice particle growth in atmosphere from vapour and cloud drop accretion 2−54849
- ice particles in clouds over Pacific Northwest, techniques for collection and automatic counting 2−54850
- ice phase seeding, cumulus clouds 2−84833
- intertropical convergence zone, position fluctuations 2−44720
- i.r. absorption off tropical east-coast Australia 2−65764
- i.r. radiation transfer profiles 2−65755
- jet-stream model with thermodynamic parameter of cloud convection 2−81656
- laboratory, drop size distribution obs. 2−57978
- large scale systems in tropical Pacific time-spectral characteristics 2−48487
- laser beam attenuation 2−57998
- light depolarization from H_2O clouds for monostatic Lidar 2−78377
- light scattering by ice clouds in visible and i.r. regions 2−58000

Clouds continued
liquid water content Obs., conventional devices rel. to integrated optical devices 2–57975
mesoscale tropical convection intensity, remote sensing using geostationary satellite 2–44726
microstructure, det. by optical cloud particle spectrometer 2–48492
molecular, near galactic centre, kinematics 2–58180
motion, and registering landmarks from satellite data by computer 2–48439
motion meas. from geostationary satellite spin scan camera pictures 2–65716
multiple contrail streamers from cirrus clouds observed by radar 2–75588
multispectral identification technique using satellite meas. 2–65758
nacreous clouds rel. to low pressure water vapour condensation and growth of ice 2–53498
natural, nuclei size det. by means of Nucleopore filters 2–48489
Nimbus 4 IRIS spectral data for O_3, elimination of cloud effects 2–65662
noctilucent, in daytime, circumpolar particulate layers near summer mesopause 2–84885
noctilucent, Russian observations in 1969-70 period 2–58053
noctilucent, solar activity effects 2–66226
noctilucent, spectral intensity obs. 2–65822
noctilucent, summary of occurrences in 1971 over western Europe 2–58017
noctilucent clouds, heavy metal particles, possible solar origin 2–65888
nuclear debris cloud, temporal charges in horizontal diffusion parameters 2–65745
nucleating ability and size of AgI particles 2–48459
nuclei, vertical distribution downwind of urban pollution sources 2–48466
nuclei from September 1970-August 1971, automated obs. in Australia 2–78373
numerical model, use in project Cloud Catcher 2–62209
orographic, conc. of crystal fragments det. from continuous formvar replicas 2–65733
orographic, numerical model of ice phase precipitation 2–65730
patterns, anal. of 500 mb level in tropics 2–62231
photoionization and radiative transfer problem in freely expanding gaseous clouds rel. to Ba cloud experiments 2–46791
photons effective path length 2–72791
precipitating convective, numerical simulation formation of long-lasting cloud 2–84815
precipitation, study of physical conditions inside clouds 2–84836
radar reflectivity factors in cloud model rel. to analyzed radar returns 2–75586
radiational cooling computations including latent load 2–44722
rain drop spectra determination at base from ground spectra 2–72794
rain modification evaluation by rain cell approach 2–65728
raindrop size, distribution at 12000 feet, electro- optical technique 2–84863
rainfall anomalies in randomized seeding project 2–62222
Santa Barbara aerial seeding program (1971-72) 2–65641
sea surface temp. remote sensing from NOAA-I satellite, effects of percentage and height of cloud cover 2–57888
seedability and horizontal dimension of convective events 2–62212
seeded convective clouds, radar echoes, height, temperature, NaCl, AgI 2–84829
seeding, AgI as contact or sublimation nucleus, electron microscope obs. 2–62190
seeding, AgI ice nucleation mechanisms 2–62192
seeding, AgI particle solubility in NaI and KI solutions 2–51595
seeding, convective growth, computer model 2–75601
seeding, descent of negative thermal energy, applic. to hurricane energy control 2–62223
seeding, dynamic calibration of airborne ice nuclei generator 2–62193
seeding, electrostatic precipitation techniques 2–62191
seeding, ground based solution burner, for ice nuclei generation 2–62100
seeding, hail suppression program, AgI-NaI compared to AgI-NH_4I 2–62194
seeding, pyrotechnic devices, rain stimulation and hail suppression programs 2–62195
seeding, single area expt. 2–51614
seeding, system for direct detection of effects 2–65734
seeding aerosol particle size distrib. determ. method 2–62246
seeding aerosols, complexing of AgI-NaI systems 2–62247
seeding expt., project Hailstop, supercell and multicellular hailstorms 2–62219
seeding expt., randomized winter orographic 2–62198
seeding expts., analysis of effects and benefits 2–62202
seeding expts. in Arizona, program anal. 2–62203
seeding materials, target area persistence 2–65732
seeding potential and thermodynamic characteristics of central Sierra snowstorms 2–65731
seeding simulation in mountain cumuli numerical model 2–65735
seeding with organic substances 2–65753
semi-transparent, radiative transfer props. in thermal i.r. 2–65737
simulated atmospheric aerosols, effects on light scattering 2–57991
small droplets, collisions, gas kinetic effects 2–78370
small water droplets, collision efficiency 2–68906
solar radiation reflection and absorption 2–48486
spectral albedo 1-6 μm 2–72790
spectroscopical sounding 2–44731
stratiform, dynamics 2–51611
supercooled droplets and ice particles, airborne obs. of distribs. 2–54848
supersaturation in simple models 2–48496
temperature and structure obs. by i.r. radiometry 2–44727
temperature measurement of individual droplets in cloud of drops 2–67784
thermal diffusion chambers, computation of steady-state supersaturations 2–62235
thermodynamics of freezing of small solution droplets containing insoluble particles 2–54841
top height meas. by radar 2–75583
top temp. and altitude det. using i.r. images 2–48501

Clouds continued
tracer chemical injection into storm systems, deposition patterns 2–65727
tracking, winds, temperature, water vapour, geosynchronous satellites 2–84834
troposphere, water vapour fluctuations, troposphere, fluctuations in water vapour content, from microwave observations of celestial radiosources 2–51591
upper tropospheric frontogenesis, non-Boussinesq effects 2–68894
urban weather modifications, integrated cloud physics approach 2–54846
Venezuela, top distrib., radar obs. 2–62243
warm convective, modification by hygroscopic and hygrophilic materials 2–62208
water aerosol droplets, capture by plane stellate crystalline obstacles 2–71247
water droplet and ice crystal formation in deep cloud cover 2–68875
water vapour prediction from mesoscale analysis of ground-based data 2–65661
water vapour transfer processes rel. to ice cryst. form. on AgI particles 2–84856
water-affected fraction of natural 1.5-9 μ diam. aerosol particles 2–75598
wintertime, project Snowman evaluation 2–62199
worldwide cloud cover distribution data, computer program 2–81696
AgI seeding, rain shower formation 2–65749
Ba artificial cloud growth in ionosphere 2–65950
Ba ion cloud in magnetosphere, Portuguese obs. of related luminous phenomena 2–72831
Ba ion cloud releases, analysis of observational problems 2–72820
^{38}Cl, ^{39}Cl content, model for in-cloud scavenging 2–65808
^{24}Na content, model for in-cloud scavenging 2–65808
Clusius-Dickel columns *see Isotope separation*
Coal
No entries
Cobalt
β-phase, structure and orientation of electrolytically deposited films 2–53561
adsorption of CO, change in work function 2–71348
atom, highly-ionized, far u.v. spectra, rel. to solar lines 2–83189
atom, K X-rays produced by heavy ions, energy shifts and relative intensities 2–64013
atomic central-field models for open shells, SCF calcs. 2–64025
bombarded by C, N and O ions, 0.5-2 MeV, stopping power 2–47782
contact charge density of conduction electrons for ^{57}Fe in Co metal, internal conversion meas. 2–51307
deformation of single crystals, review 2–84008
density at elevated temperatures exptl. results in liquid and solid phases 2–64505
diffusion along grain boundaries in W 2–47472
diffusion in Ag, 375-650°C, near-surface effects 2–68049
diffusion in Al, 400-640°C 2–64691
diffusion in GaAs, 800-1100°C 2–60829
diffusion in n-GaAs, temp. depend. 2–47463
domain wall movement retardation, due to interaction with dislocations 2–68540
dosimetry, compensation for large irregular ^{60}Co fields in radiation therapy 2–69395
dosimetry of radioisotopes in Man 2–62870
effective magnetic field on ^{67}Zn 2–84404
ferromagnetic, domain width thickness depend., theory 2–65145
film, 2000 Å, n.m.r. level inversion of ^{59}Co 2–68744
film, amorphous, deposition and annealing, resist. study 2–77499
film, electrodeposited with [0001] axis of preferred orientation, dependence of magnetic properties on texture perfection 2–54327
film, evaporated at oblique incidence, mag. contrib. of columnar grains 2–72184
film, in Al-Al_2O_3-Co supercond. junc., electron spin polariz. detn. 2–64958
film, meas. of longitudinal Faraday effect 2–54379
film, n.m.r., effect of constitution and temp. 2–81471
film, two-layer, bonding energy determ. 2–57298
film epitaxial growth and mag. domain config. 2–61524
fine particles, ferromag. reson., 4-300K, 10-47GHz 2–57386
fracture, large grain size specimens, 3 kbar range pressure effects 2–68097
h.c.p., band struct. and mag. props. calc. 2–61181
impurity in Ge(Li) detector, trap parameters 2–46045
Kerr effect meas. for increasing accuracy of magneto-opt. parameters 2–84461
magnesium ferroaluminate: Co, formation from metal hydroxides 2–47239
magnetic after-effect of hydrogen 2–78029
magnetic anisotropy consts. temp. depend. 2–54321
magnetic domains, electron microscope study 2–44262
magnetic permeability calc. from optical spectra 2–65155
magnetic saturation, determination using Stern-Gerlach experiment with neutrons 2–54326
magnetization process, h.v. electron microscopy 2–84402
particles, preparation and magnetic properties 2–75218
porous, dry wear behaviour, rubbed against mild steel 2–60911
precipitates, coherent, in a Cu foil, diffraction contrast 2–80671
resonance lines, intensities using different spectral lamps 2–52492
self-diffusion in Co-Ni-Fe alloy, Fe content effects 2–43659
single crystal, thermoelectric power obs. at low temp. 2–65078
solar overabundance, accelerated by solar flares 2–76001
solute in liq. Sn, thermoelec. power 2–71227
thermotransport in liq. Ag, heat of transport 2–53414
two-dimensional ferromagnetic domain walls, electron images 2–51247
whiskers martensitic transformations, constitution and dislocation structure 2–71340
$CdIn_2S_4:Co^{2+}$, e.p.r., effect of S vacancies 2–68735
Co:As, hyperfine mag. fields at As, rel. to host mag. moments 2–78018
Co:^{42}Ca, hyperfine fields, perturbed angular correlation studies, g-factor of 3.19 MeV 6^+ state in ^{42}Ca 2–72243
Co-NbC, pseudobinary, phase equilib., phase diagram 2–68199

Cobalt continued
β-Co, diffusion of O and Si, 1000-1300°C, internal oxidation studies 2−74811
Co I, hyperfine structure and hyperfine broadening 2−79940
Co XVII, multiplet strengths for electric quadrupole transitions calc. using HF orbital wave functions 2−42728
Co^{2+}, in ZnSe, ligand hyperfine struct., molecular orbital approx. Calc. 2−51294
Co^{2+}, spin-lattice relaxation and time constant meas. in $ZnWO_4$ 2−81311
Co^{2+} in CdF_2, optical absorption bands 2−54417
Co^{2+} in CdS, lattice thermal cond., phonon-reson. scatt. 2−47763
Co^{2+} in CdS, spin-lattice relax., Orbach process Debye temp. 2−54367
Co^{2+} in MgF_2, impurity-ion spin-frbidden absorpt. enhancement by colour centres 2−78104
Co^{2+} substitution in $RbMnF_3$, effect on e.p.r. linewidth and g-values 2−48292
^{60}Co, absorption and retention in man, det. by whole body counting 2−62841
^{60}Co, γ-ray irradiation of malignant lymphopathies, dose distribution 2−69412
^{60}Co, teletherapy, skin doses 2−69417
^{60}Co, ultra-fast diffusion in α-Zr 2−64697
^{60}Co accumulation in coastal sediments 2−62044
^{60}Co Cathetron after-loading unit rel. to dose-rate effects 2−69331
^{60}Co dosimetry, computer calculation of dose for irregularly shaped fields 2−69434
^{60}Co radiation therapy, process control by electronic calculator 2−82027
^{60}Co teletherapy apparatus, rotational type 2−69349
^{60}Co teletherapy two dimensional dose distributions with coplanar beams 2−78665
InSb:Co, Mossbauer effect of ^{57}Co 2−65235
Si:Au, Ag, Co, trapped minority carrier thermal emission rates, meas. technique 2−71784
Ta + Co, Laves phases and thermodynamic props., solid-electrolyte galvanic cell studies 2−77424
WC-Co composite, microstruct. interpretation of stress-strain behaviour 2−47670
$Y_3Fe_5O_{12}$:Co^{2+}, Mn^{3+}, anisotropy and magnetostriction consts. rel. to Co^{2+} and Mn^{3+} ion substitutions 2−75233
ZnS:Al,Co^{2+}, grown from melt, struct. rel. to Al additions, Co^{2+} spectra obs. 2−77559

Cobalt compounds
alloy, h.c.p.→f.c.c. transform, enthalpy, transform. temp. 2−43913
alloy, high hot strength, mech. props., microstruct. 2−50831
alloy, WI-52 cast high-temp., microstructure 2−47617
alloys, metallurgical structure and properties 2−71667
antiferromagnetic reson., 0 to 250 kOe, in [001] direction 2−68725
chemical bonding study using X-ray photoelectron spectroscopy 2−53002
$Co_xMg_{1-x}O$, single crystal film, epitaxial growth method 2−60650
Co-base superalloys, thermal fatigue crack propagation under strain-temperature cycles 2−56868
cobalt superalloy, FSX 414, thermal fatigue crack propagation testing 2−56878
crystalline ceramics, precipitation 2−84063
dilute liquid alloy, Co in Cu, CuZn, Zn, ZnGa, Ga, GaGe, GeAs, As, mag. susceptibility 2−80485
dispersion, Co in MC (M = refractory metal), prep. 2−74896
ferrite, cation reordering, temp. depend. of cond. time variation obs. 2−75145
microwave field visualization, $CoCl_2$ solution water evaporation 2−55605
mischmetal-Co permanent magnets, development 2−84406
9Ni-4Co-0.30C, fracture mechanics of crack growth at elevated temperatures 2−56867
phthalocyanine, fluoresc. and photocond. 2−72426
rare earth Co compounds, with $CaCu_5$ struct., stability 2−80796
rare earth cobaltides, Co atom paramagnetic moments 2−72116
rare earth intermetallics, 2-17 type, mag. characteriz. 2−61510
superalloys, powder metallurgy 2−43828
Vanadium Permendur, dimens. stability 2−43994
Al-Co liquid alloy, resist., conc. depend., 1650°C 2−46980
Au-Co alloys, nucl. spin entropy changes during ageing 2−43798
Au-Co dilute alloys, deviation from Matthiessen's rule, 0.5-60 K 2−77854
Co-Al alloy, disintegration of solid solution under hardening and cooling 2−60977
Co-Al alloy, liq., interatomic interaction energy, viscosity study 2−71155
Co-Al alloy, near equiatomic, positron annihilation relative probability, conc. depend. 2−77804
Co-As dilute system, internal hyperfine mag. field determ. 2−44321
Co-C interstitial solid solution, sat. magnetiz. and high field suscept. 2−81249
Co-C solid solution, X-ray study 2−50830
Co-C system, Curie temp. depend. on C conc., thermodynamic evaluation 2−44246
Co-Cr-C alloy, effect of $Cr_{23}C_6$ precip. on strengthening 2−57011
Co-Cr-C solid soln., activity and solubility of C 950-1200°C, precip., space equilib. diagram 2−56925
Co-Cr alloys, effect of scale porosity, second- phase oxides and doping on oxidation 2−75379
Co-Cr dilute alloy, n.m.r. and nuclear relaxation study of satellite lines 2−44454
Co-10%Cr, thermal stability and corrosion of Al coatings after heat treatments 2−60959
Co-Cu-Fe-Ce permanent magnet prep. by directional solidification 2−43787
Co-Cu-Fe-Ce permanent magnet, sintered, prep. and props. 2−50910
2 at.%Co-Cu alloy, superparamag. relax. time rel. to Co precip. particle size 2−48067
Co-Fe/Fe-Ni alloy, layers, permeability, intrinsic magnetization, coercivity, remanence 2−61536
Co-Fe-V alloy, ordered and disordered, recovery behaviour 2−50804

Cobalt compounds continued
Co-Fe, structure and orientation of electrolytically deposited films 2−53561
Co-Fe (8 at.% Fe) alloys, anisotropic magnetization and magnetic anis. 2−81255
Co-Fe alloy, Hall effect, magnetoresist., $T \leqslant 4.2K$ 2−47836
Co-MC dispersion, M = refractory metal, prep. 2−74896
Co-Mn-Al system, decomp. studies 2−64816
Co-Mn dilute alloy, n.m.r. and nuclear relaxation study of satellite lines 2−44454
Co-Ni-Fe alloy, ^{60}Co self-diffusion, Fe content effects 2−43659
Co-Ni-Sb system, intermetallic cpds., X-ray diffr. study 2−43940
Co-Ni-Ti-Al-Cu-Fe alloy, YuNDK42T8, homogenizing rel. to phase comp., mech. and mag. props. 2−47688
Co-Ni-Ti system, decomp. and formation of modulated struct. in coherent phase zone of stability 2−57030
Co-P film, electroless deposited, growth and struct. 2−53566
Co-P film, mag. hysteresis characts. rel. to heat treatment conditions 2−48091
Co-Pr-Sm alloys, 10000 Oe B-coercive force magnet, props. optimization 2−44247
Co-Pt alloy, electrodeposited, mag. props., dispersity, struct. 2−44268
Co-S solid solution, thermodynamic props. 2−50837
Co-Se(Te) system, nonstoichiometric phases, thermodynamic props. 2−43829
Co-Sm permanent magnet alloy, sintering mechanisms 2−57289
Co-Ti alloy, solid soln. decomp. 2−56933
σ-Co-V, n.m.r. of ^{51}V, quadrupole satellite intensity variation 2−72519
Co-V dilute alloy, n.m.r. and nuclear relaxation study of satellite lines 2−44454
Co-(31.8 wt.%)W alloy, excess vacancy conc. effect on grain boundary diffusion 2−47455
Co-base alloys, microstruct. obs. of phase transformations, photoemission e. micro. obs. 2−68193
Co-base composite materials, superalloys with fibres obtained by direct solidification, props. 2−64793
Co, Cr-$Cr_{7-x}Co_xC_3$, monovariant eutectic, faceted-nonfaceted, strongly coupled growth 2−57010
Co complex, $[Co(NH_3)_6][CuBr_3Cl_2]$, mag. susceptibility, 4.2-292K 2−81296
Co complex, $[Co(phen)_3](ClO_4)_2.2H_2O$, spin triplet states of Fe(II) in Mossbauer spectra 2−68806
Co complex, acetylacetonate, u.v. and visible spectra calc. using MO LCAO method 2−83326
Co complex, diarsine complexes, Mossbauer absorption spectra, after effects of electron capture decay 2−65232
Co complex, diarsine complexes, Mossbauer emission spectra, after effects of electron capture decay 2−65233
Co complex, trisethylenediamine cobalt(III) thiophosphate, i.r. spectra 2−46537
$CoAl_2O_4$, porosity effect on elastic moduli 2−50729
CoB, resist., thermal cond., and thermo-e.m.f., 100-1200°C 2−51099
CoB_x, rel. to elec. resist., 300-1200K 2−51100
Co_3B, electron structure, Co X-ray K-emission obs. 2−72379
$Co_3B_7O_{13}I$, ferroelec. transition temp., hydrostatic press. depend. 2−47984
$CoBr_2.6H_2O$, mag. phase transitions 2−44293
$Co(CN)_5{}^{3-}$, low spin square-pyramidal, SCCC calc. of orbital energy levels 2−46536
$Co(CN)_6{}^{3-}$ in alkali halides, vibr. and electronic props. 2−54413
$CoCO_3$, antiferromag., rhombohedral, spontaneous mag. moment along trigonal axis 2−68572
$CoCO_3$, antiferromag. and nucl. mag. reson. freq. shift phenomena 2−81482
$CoCl_2$, adiabatic compressibility and sound propag. speed, reln. to molec. struct. 2−72564
$CoCl_2$, X-ray Kβ emission and K absorpt. spectra 2−65287
$CoCl_2[(NH_2)CS]_4$, paramag.-antiferromag. and antiferromag.-spin flop phase boundaries, thermal cond. study 2−81302
$CoCl_2.2H_2O$, relax. phenomena of metamagnetic transition, a.c. suscept. obs. 2−57310
$CoCl_2.6H_2O$, antiferromag. spin wave theory 2−54351
$CoCl_2.6H_2O$, mag. phase transitions 2−44293
$CoCl_2.6H_2O$, oriented ^{54}Mn, γ radiation pattern change, obs. by spin flop transition 2−61552
$CoCl_2.6H_2O$, partially deuterated, sublattice coupling, antiferromag. reson. obs. 2−54350
$CoCl_2.6H_2O$, proton spin-lattice relax. time, 1.12−4.18 K 2−78050
CoCrMo alloy, total joint replacement, wear products in body 2−69292
$CoCr_2S_4$, cryst. growth, by chem. vapour transport 2−71371
CoF_2, antiferromag. reson., orientational depend. 2−72460
CoF_2, covalency parameters 2−77057
CoF_2, oxygen scavenger for CaF_2 crystal growth 2−50568
CoF_2, Raman spectra from high lying electronic excitations 2−44390
$CoF_2.5HF.6H_2O$, study of internal motion by meas. of temperature dependence of n.m.r. linewidth and second moments 2−65343
$Co_{0.91}Fe_{0.09}$, f.c.c., temp. dependence of mag. moment distrib. 2−65165
$Co_2Fe(CN)_5NO.2H_2O$, i.r. spectra, cryst. chem. 2−78081
$CoFe_2O_4$-Co_3O_4 alloy, quenched, aged, saturation magnetization, intrinsic coercive force, rel. to microstruct. 2−81233
$CoFe_2O_4$ films, monocryst., domain struct. and mag. polarity reversal 2−61523
$Co_{1-x}Fe_xSi$ solid solution, ferromag. props. 2−48068
Co(II) complex, paramag. shift of n.m.r. line due to outersphere coordination of solvent molecules 2−80106
Co(II) complexes with N,N′-ethylenebis(acetylacetoneimine), i.r. spectra, normal coordinate analysis 2−70695
Co(III), complexes, cis-$[Co(en)_2Cl_2]Cl.H_2O$ and cis-$[Co(en)_2Cl_2]NO_3$, ^{59}Co n.q.r. 2−75358
Co(III) dithiocarbamates: Mn^{3+}, e.s.r. spectra 2−48281
Co(III) triethylenediamine chloride, vibr. spectra analysis 2−72325
CoMnSb, cryst. struct., rel. to $C1_b$ type 2−74726
$Co_{1-x}Mn_xSi$ solid solution, paramag. props. 2−48068
Co_2MnSn, Heusler ferromag. alloy, atomic and mag. struct. 2−48075

Cobalt compounds continued
- $Co_4Mn(Ta)_2O_9$, magnetoelectric effect and Neel temp. determ. 2−54359
- $Co_xNi_{1-x}Fe_2O_4$ ferrite, magnetostriction and mag. parameters, temp. variation 2−72196
- CoO-Al_2O_3-SiO_2 glass system, low field mag. suscept. 2−65178
- CoO-Al_2O_3 and CoO-MgO neutron dosimeters, high temp. 2−49684
- CoO-MgO solid solns., porosity effect on elastic moduli 2−50729
- CoO-NiO solid solution, cryst. growth, for neutron monochromator appl. 2−47205
- CoO, band strcut., refl. and thermorefl. study 2−84505
- CoO, elastic constants and acoustic absorption coefficients 2−43971
- CoO, paramag., phonon dispersion relations, three body force shell model 2−68222
- CoO, positron lifetime spectra, rel. to cond. and nonstoichiometry 2−71825
- CoO, pure and Li-doped, final stage densification kinetics 2−50879
- CoO, sintering, comp. depend. 2−50878
- $(CoO)_{1.4}.P_2O_5$, glasses, antiferromag. interactions 2−75237
- CoP_2, high-press. synthesis and props. 2−83899
- $Co(PO_3)_2$-C_5PO_3, phase diagrams, invariant points solid soln. 2−74950
- $Co(PO_3)_2$-KPO_3 system, glasses and melts, absorption spectra and volume properties of melts 2−84481
- $Co(PO_3)_2$-$NaPO_3$, phase diagrams, invariant points solid soln. 2−74950
- $Co(PO_3)_2$-$NaPO_3$ system, glasses and melts, absorption spectra and volume properties of melts 2−84481
- $Co_2P_2O_7$, crystal struct. determ. 2−77552
- $Co(Po_3)_2$, molten, meas. of density in temp. range 1100-1200°C, relation to bonding and coordination 2−84034
- CoS_2 powder, ferromag. reson. line width, freq. depend. 2−72452
- Co_3S_4, n.m.r. of Co^{3+}, apparent hyperfine field 2−81475
- CoSi, near-stoichiometric, sp.ht., mag. susceptibility and n.m.r. 2−68521
- Co_2Si, solidification characts. 2−43924
- Co_5Sm magnet alloy, mag. moment and hysteresis props. 2−51254
- Co_3Sn_2, superlattice struct. 2−47319
- Co_2TiO_4, i.r. absorpt. spectra, ionic ordering 2−72342
- Co_2TiSn, Heusler alloy, ferromag. props. 2−51255
- Co_2VSn, Heusler alloy, ferromag. props. 2−51255
- $CoWO_4$, flux growth 2−60717
- $Co_xZn_{1-x}Fe_2O_4$, ferrite, Fe^{3+} spin fluctuations mag. hyperfine splitting, relax. effects, Mossbauer spectra 2−81287
- Cu-Co alloy, effect of coherency strain field on disloc. struct. 2−56702
- Cu-Co alloy, liquid, density, max. bubble pressure method 2−56488
- Cu-Co alloy f.c.c. single crystals, effect of coherent precip. on work-hardening 2−50798
- Cu-Co dilute system, n.m.r. and double resonance studies of electron spin density near Co atom, obs. of satellite lines 2−75204
- $DyCo_2$, Co atom paramagnetic moments 2−72116
- $ErCo_2$, Co atom paramagnetic moments 2−72116
- Fe-Al-Ni-Co-Ti alloy, prod. by Magnicol process, reaction mechanisms 2−43834
- Fe-Co/LiF/Fe film system, quasistatic mag. reversals 2−84408
- Fe-Co-C, struct. and strength 2−56941
- Fe-Co-Ni alloy, coherent potential approx. calc. 2−71794
- Fe-Co-Ni alloy powder, highly disperse, effect of electrolytic prep. variables on mag. props. 2−68543
- Fe-Co-Ti-Al alloy, solid soln. decomp. 2−56933
- Fe-Co-V, alloy, plastic deform. and brittleness 2−60868
- Fe-Co, equiatomic alloys, magnetic anisotropy energetics, order determ. 2−61507
- Fe-Co alloy, metamagnetic character, rel. to temp. depend. of mag. props. 2−51258
- Fe-Co alloy, ordering effects on electronic struct. 2−44249
- Fe-Co dilute alloy, hyperfine fields, ^{57}Fe n.m.r. study 2−65344
- Fe-Co very dilute alloy, 25 mK, spin-lattice relax. of ^{60}Co, field depend. 2−72232
- Fe-Cr-Co system, phase boundary $\alpha+\gamma/\gamma$ determ. 2−84164
- Fe-Ni-Co alloys, cumulative thermal cycling behaviour, 300°C/hr. 2−60960
- Fe-Ni-Co alloys, dilatometric study of vol. exp. for fcc to bcc transformations 2−65146
- $(Fe,Co)_2Mo_3O_8$, Mossbauer effect 2−75270
- FeCo-(2 wt.%)V alloy, crack propagation and nucleation in ductile fracture 2−53835
- $Fe^{60}Co$, single- passage resonance obs. by β-emission and spin-lattice relax. meas. 2−72508
- $(Fe_{1-x}Co_x)Si$ solid solns., moment form., n.m.r. obs. 2−44223
- FeSi-CoSi system, itinerant ferromag., ^{59}Co n.m.r. obs. 2−61745
- $GdCo_2$, Co atom paramagnetic moments 2−72116
- $HoCo_2$, Co atom paramagnetic moments 2−72116
- $Mg_{1-y}Co_yFe_2O_4$, mag. anisotropy, ferromag. reson. study 2−81283
- Mo-Cu-Co cermet contact, elec. erosion characts. working surface struct., rel. to Co content 2−47659
- Ni-Co-Zn ferrite, h.f. magnetic props., temp. depend. 2−68723
- Ni-Co, alloy, f.c.c., dislocation bands produced by electrolytic hydrogen charging 2−56713
- Ni-Co, coarse grained polycrystalline, Co self-diffusion at low temp. 2−47450
- Ni-Co alloy, thermo e.m.f. and Nernst-Ettingshausen effect, temp. depend. 2−72051
- Ni-Co alloys, diffn. of Co at temps. up to 1000°C 2−71538
- Ni-Co alloys, exchange consts. and saturation magnetiz. 2−44265
- Ni-Co alloys, magnetic structure during electrodeposition in presence of magnetic field 2−77995
- Ni-Zn-Co ferrite film, anisotropy induced by thermomagnetic treatment 2−81228
- Ni_xO-Co_xO system, interdiffusion 2−50714
- Pd-Co, dil. alloys, mag. ordering obs. 2−81246
- Pt-Co dil. alloys, nucl. sp. ht., low temp. 2−43986
- Pt-Co dilute alloy, disappearance of giant mag. moments 2−81211
- Sm-Co alloys, comp. effect on mag. props. 2−51262
- $(Sm_{1-x}Pr_x)Co_5$, $0<x<1$, alloys, saturation magnetization, anisotropy field, coercive force 2−68510

Cobalt compounds continued
- TaC-Co alloy, oversaturated, microstruct. and reaction behaviour 2−64775
- $TbCo_2$, Co atom paramagnetic moments 2−72116
- TiC-Co alloy, oversaturated, microstruct. and reaction behaviour 2−64775
- WC-Co alloy, oversaturated, microstruct. and reaction behaviour 2−64775
- WC-Co cemented carbide, internal friction recovery obs. 2−68070
- WC-Co cemented carbides, effects of Cr and Ni additions on structure 2−43864
- WC-Co cermets, plasticity, slip, grain boundary sliding 2−47505
- WC-Co hard metal, X-ray stress meas. at carbide phase 2−74910
- WC-Co hard metals, mixed milling effect on sintering, electron microscope investigation 2−56899
- Y-Co-Ni pseudobinary compounds, magnetization minima 2−75223
- Y-Co-Ni(Fe) system, $CaCu_5$-type phase stability 2−43944
- $ZnSO_4.7H_2O-NiSO_4.7H_2O-CoSO_4.7H_2O$, isomorphous relationships, distribution coeff. 2−74959
- Zr-Co alloy system, paramagnetic behaviour in non stoichiometric composition of the Laves phase compound 2−81220

Cochlea *see Ear*

Coherence *see Electromagnetic waves; Lasers; Light/coherence; Masers*

Cohesive energy *see Bonds; Solids*

Coincidence circuits *see Counting circuits*

Cold working
see also Plastic deformation; Slip; Work hardening
- – 2−56920
- cermet, yield limit change regularities 2−68126
- metal, f.c.c., simulation of rolling texture development 2−43813
- metal, nucleation of new grains in recrystallization 2−68134
- metal wire, pressure induced thermal activated processes, tensile strengths 2−43781
- metals, strengthening, under variable stress 2−53812
- pyrofoil tape, production and characterisation for reactor use 2−56050
- rolling, preparation of stable isotope targets 2−49620
- stainless steel, 20% cold-worked Type 316, fatigue-crack growth at elevated temps. 2−84141
- stainless steel, ferritic sheet, texture development 2−77701
- stainless steel, type 304, passivity, effect of plastic deformation 2−78195
- steel, ductile-brittle transition, deform. mode influence 2−43694
- steel, sheet, cold rolled, annealed, grain growth, X-ray obs. 2−47621
- steel, stainless, irrad., cold work effects on void form. 2−50646
- steel, stainless, ridging phenomenon in sheets 2−68131
- steel, strength and ductile-brittle transition, effect of cold rolling and heat treatment 2−80777
- straightening effects on welded joints 2−71628
- swaged and drawn, deform. textures 2−53868
- Ag, rolling texture form. mechanism 2−60972
- Al-Zn-Mg alloy, resistometric obs. of ageing 2−71632
- Al, high purity and dil. alloys, review 2−68076
- Al, recrystn. nuclei formed by Rowland transform. 2−43822
- Cr, deformed at 77, 213, and 293K, recovery resist. study 2−53805
- Cu-Ga alloy, cold-worked, defects, X-ray obs. 2−80861
- Cu, cold worked at 200-300°C, creep and recovery 2−84163
- Cu, texture transition mechanism during rolling, X-ray obs. 2−47323
- Cu and Cu-Zn alloys, development of texture 2−80849
- Fe-Co-V alloy, ordered and disordered, recovery behaviour 2−50804
- Fe-12.3 at.%-Al, Mossbauer determination of cold-rolling effect on short-range order 2−51311
- Mn-Cu-Mo alloy, cold worked, heat treated, Young's modulus, rigidity, hardness, thermal expansion 2−47476
- Mn-Cu-W alloy, cold worked, heat treated, Young's modulus, rigidity, hardness, thermal expansion 2−47477
- Nb-H system, H-dislocation interaction, cold work peak study 2−80841
- Nb, cold-worked, annealing, resist. study 2−64766
- $Pb(Ti,Zr)O_3$ and $(Pb,La)(Zr,Ti)O_3$, cold pressing and low temp. sintering 2−50892
- Ti-Al alloy, cold-worked, X-ray diffr. study 2−80860
- W foil, rolling and annealing textures 2−43796
- Zr, fault elimination by cold rolling, determ. by meas. elec. resist. 2−43797

Collections of physical data
Only comprehensive works of reference are listed here
- alloys and engineering materials, thermal expansion, tabulation of quadratic function coeffs. 2−71639
- astronomy, right ascension system derivation from differential obs. with meridian circles and $\Delta\alpha_\alpha$ in FK_4 system 2−55194
- atomic spectra, L X-ray transition probabilities 2−46406
- coherent neutron scattering amplitudes 2−53645
- cosmic ray data gathered by NM-64 neutron monitor, barometer corrected and uncorrected data 2−42430
- crystal struct. analysis, mean squared atomic scatt. factors for all atoms, tables 2−53624
- diatomic mol. ground state dissoc. energies 2−56152
- diatomic molecules, compilation of measured lifetimes 2−46502
- electron affinities of atoms and mols. 2−64035
- electron beam energy loss and bremsstrahlung in 59 elements and 55 compounds, calc. 2−54095
- high energy physics, total cross sections and cone slope 2−82699
- light pressure efficiency factor for spherical particles of graphite and metallic materials 2−45772
- menisci, axisymmetric, tables of profiles 2−60413
- molecular dissociation in single heavy particle collisions, book 2−83419
- Mossbauer isotopes 2−63759
- nuclear energy levels, A=18, 19, 20 2−59686
- nuclear reactions, ang. distribution coeff. for (gamma, particle) and (particle, gamma) reactions 2−52795
- nucleons, expansion coefficients of many-body matrix elements of two-body interaction 2−52721
- photodetachment cross-sections for atoms and mols. 2−64035

Collections of physical data continued
- photon attenuation coefficient, meas. from 10 eV to 100 GeV 2—46243
- Pulkovo catalogues of declinations Pu$_{50}$F and Pu$_{50}$Z 2—51721
- secondary-electron-production cross sections 2—76963
- spectral atlas 2—64164
- N IV, V, VI, VII, atomic energy levels and multiplet tables 2—46434

Collective model *see Nucleus/models*

Collision processes
- *see also Atoms/electron scattering; Charge exchange; Elementary particles; Field theory, quantum/interactions; Ionization; Nuclear forces; Nuclear reactions and scattering; Scattering, particles; and under the individual particles*
- in celestial mechanics, collision singularitiy in perturbed N-body problem 2—62454
- celestial mechanics, three body problem 2—81775
- chain collisions, velocity, momentum and energy transmission 2—55444
- classical binary encounter approximation, derivation from Born approximation 2—41515
- dipole coupling potential, Harris-Nesbet method 2—66449
- eikonal approximation for coupled equations for multichannel scattering 2—52944
- gas of hard spheres, three-particle collision integrals 2—46851
- gas-solid interactions, development of very sensitive vibrating quartz balance 2—69538
- interplanetary neutral H and solar wind protons, charge exchange collisions 2—55157
- ionosphere D-region, frequency meas. partial reflection method 2—51651
- in liquids, generalized Rice-Allnatt theory for transport processes 2—74524
- low energy particle surface collisions, surface comp. determ. 2—84636
- metallic solids, high speed collisions, wave phenomena 2—76252
- reactive mixture, reciprocal relations in relativistic kinetic gas theory 2—64392
- rearrangement, multichannel Feshbach eqns., variational principles 2—52898
- three body and three dimensional calc. reactive scattering, exact quantum mechanical 2—79867
- three body break-up processes, Kohn variational principle 2—41516
- transport collision integrals $\Omega^{(l,s)*}$, empirical equations for calc. in Lennard-Jones (12-6) potential 2—58812
- vibratory systems, numerical calculation for transient responses 2—82291
- virial theorem generalization 2—64066
- **atoms**
  - aeronomy, application of collision processes to phenomena in atmospheres of planets 2—44941
  - alkali excited atoms with unexcited alkali atoms, inert gas atoms or molecules, transfer of excitation between fine-structure levels 2—42776
  - alkali metals, calc. of absorption line profiles and satellite bands caused by inert gas perturbing atom 2—70568
  - alkali-ion-alkali-atom system, charge transfer at large internuclear distances 2—79915
  - alkalies in inert gas atmospheres, quadratic hyperfine pressure shift 2—77013
  - angular momentum transfer in theory of angular distributions 2—49965
  - anharmonic oscillator-atom, vibrational excitation cross-sections 2—80124
  - associative ionization in slow collisions between atoms 2—83180
  - asymmetric, extension of electron- promotion model 2—49966
  - atom-atom, Drawin formula for ionization 2—46466
  - atom-atom photon atomic excitation mechanism 2—83174
  - atom-atom scattering and radiative processes, applic. of molec. wave functions, review 2—50007
  - atom-diatom, conservation rule for total cross section 2—53098
  - atom-diatom, Faddeev eqns., spin-depend. atomic pair interactions 2—67410
  - atom-diatomic molecule scattering, Lennard- Jones potentials determ. 2—56272
  - atom-diatomic oscillator, influence of attractive forces on quantum mechanical transition probabilities 2—77169
  - atom-heteronuclear diatom system, exact quantum reactive cross sections for three dimensional angle dependent model 2—44469
  - atom-ion, excitation transfer, spin exchange collisions without internal energy change 2—59928
  - atom-molecule, electron loss cross sections 2—64216
  - atom-molecule, low energy and involving several nuclear degrees of freedom, electronic transitions 2—46640
  - atom-molecule, reactive, optical model for vibrational relaxation 2—65362
  - atom-photon, effect of screening in atomic field on pair production at intermediate and high energies 2—83201
  - atom-rigid rotor diatom, Neumann series solution 2—83413
  - book 2—64049
  - Born lineshift integral, second order, closed form 2—79855
  - bremsstrahlung by electrons, screening and second Born corrections 2—83193
  - broadening of spectral lines, long-range and short-range potentials 2—42839
  - CC Ar, scattering of inert gas and period II element ions in 8-25 keV range, comparison of exptl. and theoretical interatomic potentials 2—56118
  - charge exchange, of fast nuclei with one electron systems 2—59946
  - with charged particle, fast moving, spectral line shift due to forced transitions 2—52905
  - collinear atom-oscillator collision, semiclassical approx., average over thermal vibrational distribution 2—79869
  - collisional depolarization of excited states, effective lifetime rel. to correlated photons in cascade 2—74226
  - conference, physics of electronic and atomic collisions, Amsterdam (1971) 2—42772
  - conference, Split, Yugoslavia (1972) 2—60291
  - Coulomb excitation by heavy charged particles 2—79911
  - Coulomb T matrix, dispersion relation off-shell 2—76972
  - curve crossing with variable interaction potential 2—46463

Collision processes continued
- **atoms** continued
  - detailed balancing in time-dependent impact parameter method, coupled state approx. 2—83172
  - ejection of electrons by protons, character of interference of resonances with continuum in spectra 2—70618
  - elastic and inelastic scattering, implications for electron microscopy 2—83207
  - elastic influence on broadening of spectral lines in a gas 2—83418
  - elastic scattering in Born's treatment of excitation, wave version 2—83170
  - electron capture cross sections by protons and deuterons 2—67411
  - electron capture cross-sections, calc. by approximation procedures, book 2—63986
  - electron harpooning, quantum effects 2—80153
  - excitation transfer, spin exchange collisions without internal energy change 2—59928
  - excited atoms, with molecules, multipole-multipole quenching cross section 2—42767
  - experiment-computer system, on-line operation 2—42781
  - Faddeev equations, applications at low and high energies 2—42778
  - fine structure cross sections from reactance matrices, FORTRAN IV program 2—52942
  - Glaubet approximation for estimation of cross sections · 2—42779
  - heavy ion collisions and formation of superheavy molecules 2—60112
  - heavy ion-atom collisions, total cross section meas. for characteristic X-ray production 2—42777
  - heavy ions, solution of Dirac equation for strong external fields 2—42769
  - heavy particle collisions, exchange matrix elements, differential eqns. soln. 2—64044
  - highly excited atom, reaction with molecule, 82, theory 2—80145
  - hot-atom reactions in dilute heat gas, time dependent theory 2—48317
  - hydrogen-like, dipole approx. of nonrelativistic cross section for Compton scattering by K-shell electrons 2—70611
  - hydrogen-like, nonrelativistic Compton- like scattering of photons by K-shell electrons 2—70610
  - inelastic, between structureless atom and harmonic model molecule, exact classical treatment of vibration- translation energy transfer 2—50127
  - inelastic, classical picture and semiclassical formulation for derivation of eqns. 2—56111
  - inelastic, semiclassical theory, momentum-space formulation derivation of classical trajectory equations 2—52945
  - inelastic and reactive collisions, semiclassical transition probabilities, classically inaccessible transitions 2—70617
  - inelastic and reactive scattering, effective separable approx. for multichannel Green's functions 2—46639
  - inelastic atom-surface scattering, quantum theory 2—46465
  - inelastic collisions of fast charged particles studied in Bethe theory 2—42780
  - inelastic energy losses, precision obs. 2—64047
  - inert gas, constant acceleration approx. in collision-induced absorption 2—53096
  - inert gas atoms and ions with inert gas structure, repulsive interactions in 0.1-10 eV 2—42773
  - inert gas ions, collision-induced ioniz., ion kinetic energy spectra 2—83175
  - inert gases, mixed interaction, test for Munn potential 2—67414
  - inert gases, proton impact double ioniz. 2—83176
  - inner shell ioniz. by violent ion-atom collisions at moderate nucl. vels. 2—77014
  - inner-shell excitation by proton and heavy ion bombardment, study of mechanisms involved 2—42745
  - interaction of radiation with atoms subject to collisions with perturbation atoms, quantum mechanical transport eqn. 2—46449
  - interactions, relativistic, and long-range 3-body, error bounds 2—76968
  - ion streams, thermalization, beyond plasmapause 2—65946
  - ion-atom, charge exchange one-electron model 2—83177
  - ion-atom, inner shell ionization, X-ray production, review 2—83198
  - ion-atom, inverted populations in X-ray region, amplifier design 2—82084
  - ion-atom, radiation electron capture 2—77016
  - ion-atom at keV energies, inner-shell excitations, study of mechanisms for symmetric and asymmetric collisions 2—42746
  - ion-atom cross sections at 200-3000 eV, exptal. apparatus for obs. 2—64048
  - ion-atom potentials derivation from intermediate and strong field mobility data 2—79912
  - ion-dipole collisions, computer plotter studies of vibrational effects, classical tunnelling 2—46467
  - ion-molecule collisions, K vacancy production, depend on relative Z of colliding atoms 2—74304
  - ionization, relation between angular distribution of secondary electrons for photon and charged particle impact 2—52931
  - ionization probability for atom crossing metal/vacuum surface 2—48032
  - ions, collision processes with H$_2$, effect of reactant internal energy on spectator stripping 2—44472
  - ions, optically pumped, cross sections for depolarizing collisions, charge exchange, formation of molecules 2—77009
  - K-Cs, broadening of principal series lines 2—56117
  - K-shell ioniz. by high energy electrons 2—52928
  - K-shell ionization by protons, impact parameter dependence of angular distribution of scattered fragments 2—79909
  - laser spectroscopy applics., high precision techniques 2—77004
  - long range retarded dipole forces, exptl. detection feasibility 2—67408
  - long-range curve crossings, impact parameter treatment 2—74303
  - metal surface, secondary electron ejection by metastable atoms, energy and ang. distribution 2—48026
  - metastable atoms, production and detection 2—64050
  - Mg, with 21 MeV O ions, obs. of 1s-2p transitions 2—46469
  - multichannel scattering study of optimized minimum-norm and optimized anomaly-free variational methods 2—76994

Collision processes continued
atoms continued
muonium in inert gas atmospheres, quadratic hyperfine pressure shift 2−77013
noble gases, pot. parameters of interaction 2−60375
non-adiabatic theory, advantages over alternative formulations 2−42774
noncolinear collisions with diatomic molecules, inelastic vibrational transitions 2−70810
nonradiating excited complexes, props. 2−67531
optical potential calc. of absorption and elastic cross sections, computer program 2−52078
optically pumped vapour, relaxation of electronic spin polarization by collisions with cell wall 2−76995
particle rearrangement with a few open channels, treated by theory of sequential projections and quasiminimum principle 2−42803
photodetachment, cross-sections and electron affinities 2−64035
photodisintegration products, angular distrib. and parity-unfavoured transitions 2−79908
potential curve crossing problem, general theory and model for close crossings 2−56112
potential scattering, minimum-variance method 2−79913
pressure broadening as example of relaxation using cumulant expansions 2−76987
pseudo-state expansions, study of close- coupling approx., minimum principle, correlation methods, Born approx. 2−42761
quantum electrodynamics of scattering phenomena involving bound states 2−55794
rare gas electronic energy transfer 2−79868
resonant, two-body, vel. depend. of forward scatt. amplitude 2−52941
resonant states determ. using finite-difference boundary value method 2−70616
scattering, Fredholm-Pade approximation for problems involving pair of coupled channels with square well potentials 2−76205
scattering, interference phenomena, review of calc. methods 2−56113
scattering, low energy, by r^{-3} potential 2−49963
scattering T-matrix, eikonal expansion 2−70621
single electron capture from two electron systems by fast positive ions 2−59958
slow ion-atom, structure of total cross-sections for diabatic processes 2−42775
small-energy-transfer collisions in dominant long-ranged forces, theory 2−70817
soft sphere atom lattice, first approximation for normal incidence 2−55437
solid surface, atomic He scattering and diffraction 2−67889
solid surface, scatt. from with Yukawa-type interaction law 2−74239
T-matrix extrapolation methods for calc. of cross sections 2−42799
three-atom rearrangement processes, $A+BC\rightarrow AB+C$, open-channel projectors 2−80151
transition probabilities using Landau-Zener model 2−49967
two-body radiative recombination, rel. to resonance scattering 2−67409
Van der Waals forces for systems involving non-spherical atoms 2−63998
Van der Waals potential between halogen and inert gas atoms 2−80123
X-ray generation by proton and heavy-ion bombardment 2−49964
Ag, incoherent γ-ray scatt. by K-shell electrons 2−59931
Al-Ar ion, 25 to 200 keV, noncharacteristic X-ray bands 2−56116
Al, ioniz. of L-shell, by inelastic collisions of fast particles 2−64026
Ar-AlCl$_3$, molec. orbital study 2−59990
Ar-Ar, production of electrons, energy distribution 2−76993
Ar^{2+}-Ar, 2-8 keV, meas. of cross sections, competition between single and double electron transfer processes 2−79870
Ar-H$^+$, spectra, dependence on proton energy 2−74235
Ar-N$_2$, comparison of generalized phase shift with classical trajectory calcs. of rotational inelasticity 2−43032
Ar-N$_2$, rotational excitation of rigid rotor, classical results 2−50125
Ar-O$_2$, probability of excitation of vibrs. and dissociation 2−83416
Ar-O$_2$ hot gas, rates of vibr. and dissoc. excitation 2−83417
(ar, O$_2$) mixture-H$^+$, spectra, dependence on proton energy 2−74235
Ar, behind strong shocks, average atom-atom cross sections for excitation and ionization 2−67398
Ar, compressed, complete spectrum of collision-induced light scattering analysed using Michelson interferometer 2−80408
Ar, energy loss and straggling of 6.05 and 8.78 MeV α-particles, meas. using Si surface barrier detector 2−79626
Ar, ionization processes in slow collisions with He and He$^+$ 100eV-5000eV 2−56119
Ar, metastable, dissoc. collision with H$_2$O, rotational excitation of OH($A^2\Sigma^+$, $v'=0$) 2−64215
Ar, small-angle scattering of range of elements, meas. of inelastic energy losses 2−64045
Ar, with H$^+$ at 4 keV, probability ratio for neutralization of H$^+$ to H(2p) or H(1s) 2−42802
Ar deexcitation in collisions with gases, cross sections 2−64054
Ar ions, meas. of range-energy relations in Ar, N$_2$, O$_2$ and air, 0.3-1.0 MeV 2−79917
Ar solid-iron, 25 to 200 keV, noncharacteristic X-ray bands 2−56116
Ar VIII, Na-like, collisional-rate coeff. meas. in plasmas 2−46450
Ar + Ar intermolecular potentials from differential cross-sections 2−42782
Ar + CsI, vibrational and rotational energy transfer, ballistic mechanism 2−67536
Ar + H$^+$, 5 eV, interatomic potential determination by inversion of elastic differential cross section data 2−59930
Ar + H$^+$ elastic scatt., excited states 2−64051
Ar + OH($A^2\Sigma^+$), near resonant vibration-rotation energy transfer calc. of cross sections and rate consts. using IOS and DW approx. 2−70818
Au^0-Ar, velocity dependence of total elastic cross section, 5-90 eV, determ. of interaction potential 2−56114
Au, L X-ray production by 0.5-3.0 MeV protons, relativistic effects 2−52913
Ba-Ar, excitation of metastable levels of Ba behind shock waves 2−79932

Collision processes continued
atoms continued
Ba-Ne, excitation of metastable levels of Ba behind shock waves 2−79932
Ba + O$_2$ → BaO$_2$, internal state distribution of reaction products, laser-induced fluorescence meas. method 2−61770
Be, K-shell ionization by protons and heavy ions 2−83179
Br-, decay and charge exchange cross sections in 300-3000 eV range 2−64052
Br, calc. of stopping cross sections of α particles by application of Bragg additive rule to molecular stopping cross sections 2−70820
C-Ar ion, 25 to 200 keV, noncharacteristic X-ray bands 2−56116
C, K-shell ionization by fast protons 0.3-2.0 MeV 2−42748
C$^+$, with O$_2$ and N$_2$, 3 to 100 eV, calculated cross sections for mass transfer, molecular and dissociative charge exchange reactions 2−48322
CO$_2$-Hf, near-resonant energy transfer to (00°1) vibr. level 2−53101
Ca collisions with atmospheric ions, meas. of charge transfer cross-section for formation Ca$^+$, 1-500 eV 2−79865
Cd, 5^3P_1 state, colliding with inert gas atoms, meas. of relaxation constants 2−42783
Cl-, decay and charge exchange cross sections in 300-3000 eV range 2−64052
Cl, calc. of stopping cross sections of α particles by application of Bragg additive rule to molecular stopping cross sections 2−70820
Cs, electronic excitation transfer by atomic collisions, expt. 2−64030
Cs, emission profiles of resonance lines broadened by collisions with inert gases, extreme-wing line broadening, adiabatic potentials 2−70622
Cs, oriented $6^2P_{1/2}$, m_j mixing in collisions with inert atoms 2−46468
Cs, resonant charge exchange cross sections at low energies in Q-machines 2−56115
Cs$^+$, free ions, n.m.r. involving photoionization, optical pumping and charge exchange 2−79897
^{133}Cs$^+$ ion, free, n.m.r. freq. shift due to charge exchange with Cs atom 2−79896
Cs + I$_2$, reaction cross section meas. 2−70738
Cs* + Cs associative ionization processes, analysis of ions in terms of potential energy waves 2−70603
D + H$_2$ → HD + H, molec. beam study 2−72546
F-, decay and charge exchange cross sections in 300-3000 eV range 2−64052
F, calc. of stopping cross sections of α particles by application of Bragg additive rule to molecular stopping cross sections 2−70820
F + HF collisions, temp. dependence of vibrational energy transfer probability, 300 to 1500K 2−43037
Fe collision with atmospheric ions, meas. of charge transfer cross sections for formation of Fe ions, 2-500 eV 2−79866
H-H, spin-change frequency shifts 2−42770
H$^+$-H, differential cross-section for H($n=2$) direct excitation 2−46482
H$^+$-H, high-energy, pseudo-state expansion applications 2−42762
H$^+$-H$_2$ collisions, vibrational excitation, 15-1000 eV, semiclassical theory 2−80152
H$^+$-H$_2$ vibrational excitation, application of theory for small- energy-transfer collisions in dominant long-ranged forces 2−70817
H-H$_2$ collinear collisions, reaction probabilities and high energy trajectories 2−50130
H$_2$-H collisions, saddle point on H$_3$ potential surfaces 2−51429
H$^-$-He, angular distribution of autodetached electrons 2−77024
H$^+$-He, differential scattering cross-sections, calculation and measurement at 8.826 hartrees 2−46484
H-Hg elastic scatt., orbiting resons., rel. to vibr.-rot. levels obs. of diatomic mol. 2−77018
H-rare gas scatt., absolute total cross sections, interatomic forces 2−67424
H, 2.5 keV metastable, produced by charge-exchange process in Cs vapour, absolute detection and collisional destruction 2−56124
H, charge exchange collision with proton, Coulomb T matrix calc. 2−46483
H, electron capture into $n=3,4$ states by H$^+$, H$_2^+$ impact, cross sections 2−70637
H, non-additive effects in first-order interaction energy 2−49980
H, positron pickup, treated by theory of sequential projections and quasiminimum principal 2−42803
H, proton scatt. four-channel approx. approach 2−83212
H, with inert-gas atoms and diatomic molecules, coincidence studies of elementary processes 2−42804
H atom-H mol. collisions, saddle point on H$_3$ potential surfaces 2−51429
H$^-$, proton-ion electron capture collisions 2−64067
H$^-$, with inert-gas atoms and diatomic molecules, coincidence studies of elementary processes 2−42804
H$^-$ electron detachment cross sections in H, He, Ar, 4-30 keV 2−77017
H$^+$, absolute differential ion and charge transfer scattering cross sections for collisions with He, Ne, Ar, Kr, 500-5000 eV 2−46485
H$^+$, with He, Ne, Ar and H$_2$ at 4 keV, probability ratio for neutralization of H$^+$ to H(2p) or H(1s) 2−42802
H$^+$, with inert-gas atoms and diatomic molecules, coincidence studies of elementary processes 2−42804
H$^+$ + Ar, total differential cross- section, energy depend. 2−79858
H- + H$^+$ → H(n,l) + H$^+$ + e, electron detachment by charged particle collision 2−59947
H + H, polarization interaction in ground and first excited state 2−67425
H + H interaction, higher multipole coeffs. determ. from dynamic multipole polarizabilities 2−59945
H + H$_2$ linear collisions, classical S-matrix theory 2−72551
H + H$_2$ linear reactive collisions below the classical threshold complex-valued classical trajectories determ. from S-matrix theory 2−44474
H + H$_2$ vibr. excitation process, rate const. 2−67537
H + H$_2$(N$_2$)(O$_2$), electron loss cross sections 2−64216
H$^+$ + H(1s) → H(1s) + H$^+$, charge transfer scatt. at high energies 2−77023
H$^+$ + He, metastable H ang. distrib. 2−64069
H$^+$ + Kr total differential cross-section, energy depend. 2−79858
H + alkali metal, excitation processes 2−67426

Collision processes continued

- **atoms** continued
  - H^+ + noble gas, differential cross sections, 500-3000 eV 2−64068
  - H(2s)-Ar, 20-120 keV charge-changing collisions, meas. of absolute cross sections and electron capture cross sections 2−70638
  - H(2s)-He, 20-120 keV charge-changing collisions, meas. of absolute cross sections and electron capture cross sections 2−70638
  - H(2s)-N_2, 20-120 keV charge-changing collisions, meas. of absolute cross sections and electron capture cross section 2−70638
  - H(2s) with Ar, N_2, O_2, meas. of cross section for electron capture in 1.4-8 keV range 2−56123
  - He-Ar mixtures, collision induced- absorpt. near $\lambda = 1$ mm 2−77084
  - He-Cd laser, 4416 Å, excitation mechanism, and operation parameters 2−79181
  - He-D_2, He-HT quantum mechanical scatt., comparison of systems 2−60115
  - He-H_2, meas. of absolute integral total cross sections and interaction potential 2−70814
  - He-H_2, total scattering cross section of thermal energies 2−64212
  - He-HD, low-energy, rotational transitions in HD 2−46644
  - He^+-He^{2+}-e plasmas, calc. of collisional-radiative volume recombination and ionization coefficients 2−50193
  - He-He, excitation, influence of metastable atoms 2−42814
  - He-He, intermolecular potential determ. from energy depend. of cross section 2−64079
  - He-He fast collisions, electron loss cross sections 2−70645
  - He^+-He, meas. of differential cross section for excitation of inelastic processes in energy range 1-3keV 2−56133
  - He^+-He collisions, formation of doubly charged ions 2−59954
  - He-I_2, inelastic non-reactive energy transfer, calc. and analysis of probabilities and cross sections 2−60116
  - He-ion, 10 to 75 keV, outer shell excitations 2−74238
  - He, collisional ioniz. by slow electrons 2−64074
  - He, electron impact excit. to metastable states, Born-Oppenheimer approx. 2−46490
  - He, electron impact ionization, energy and ang. distrib. of secondary electrons 2−64031
  - He, fast proton impact excitation, Born cross-sections 2−79949
  - He, Penning-ionizing collisions, excited-ion lifetimes 2−67433
  - He, singlet + triplet mixing in $n = 3$ states excited by proton impact 2−56130
  - He, with CO_2, N_2, methane, ethane, translational spectra due to collision-induced overlap moments 2−50129
  - He, with H^+ at 4 keV, probability ratio for neutralization of H^+ to H(2p) or H(1s) 2−42802
  - He deexcitation in collisions with gases, cross sections 2−64054
  - He gas, excitation transfer meas. using p beam 2−42819
  - He ionization by H^+ impact 2−42817
  - He ionization by proton impact 2−59955
  - He plasma, influence on collisional- radiative ionization and recombination coeffs. 2−67630
  - He thermal atoms, scattering from Hg film deposited on LiF substrate 2−56573
  - He^- electron detachment cross sections in H, He, Ar, 4-30 keV 2−77017
  - He^+, absolute differential ion and charge transfer scattering cross sections for collisions with He, Ne, Ar, Kr, 500-5000 eV 2−46485
  - He^+ inelastic scattering on Ne atoms differential cross sections 2−59956
  - ^3He-^3He cross- section meas., 1.5-2.1K 2−67437
  - $^3He + {^3He}$ interaction pots. from low-energy scatt. cross-section meas. 2−67434
  - ^4He-^4He cross-section meas. 1.5-2.1K 2−67437
  - $^4He + {^4He}$ interaction pots. from low-energy scatt. cross-section meas. 2−67434
  - ^4He + He interaction pot. from low energy total cross section meas. 2−59953
  - He + Ar, metastable, chemi-ionization cross sections 2−64080
  - $He^+ + H_2$, low-energy, optical excitation and polarization 2−67436
  - He + He scatt., long range retarded dipole forces, exptl. detection feasibility 2−67408
  - He^+ + He, inelastic, time-of-flight analysis of neutral products 2−70807
  - He^+ + He, very-small-angle charge exchange, technique for studying structure 2−42818
  - He + Ne, broadening of mag. reson. line of Ne laser obs. 2−64024
  - He* + Ar ioniz. total cross sections, semiempirical calcs. 2−67435
  - Hg-Ar discharge, l.p., mass spectrometric analysis of Hg_2^+ form. in positive column 2−83640
  - Hg, self broadening of Hanle signals, backscattered light obs. 2−59932
  - Hg interatomic pots. with light projectiles 2−77015
  - Hg(6^3P_1), spin-orbit relaxation in presence of various gases 2−46461
  - Hr meson slow collisions, muonium form 2−83217
  - I-, decay and chrage exchange cross sections in 300-3000 eV range 2−64052
  - I, calc. of stopping cross sections of α particles by application of Bragg additive rule to molecular stopping cross sections 2−70820
  - I ion-Au, Th, U collisions, 10 to 60 MeV, X-ray spectra of temporarily formed superheavy quasiatoms 2−74236
  - I ions, charge states 2^+ to 18^+, meas. of charge-changing cross sections in H and O, 5-25 MeV 2−70623
  - I recombination to I_2 in Ar, using flash photolysis 2−80009
  - In spectral lines temperature effects in pressure broadening in flames 2−67413
  - K^+-Ar, scatt. cross section, ion inelastic energy loss and u.v. emission 2−79925
  - K^+-He(Ne,Ar) scattering, 150-2350 eV, effective total cross section meas. 2−67415
  - K-K, broadening of principal series lines 2−56117
  - K-O_2, spin exchange scatt. obs. 2−67541
  - K, superthermal, angular scattering by I_2 2−42787
  - K scattering by inert gases, meas. of total cross sections 2−83192
  - K scattering from methane, meas. of velocity dependence and total cross section, study of glory undulations 2−70821
  - K^+ ions elastic scatt. from diatomic mols., 150-4000 eV 2−80149
  - $K^+ -$ Ar scatt., potentials derivation from intermediate and strong field mobility data 2−79912
  - K + molecule, atomic beam, reaction cross- sections meas. 2−51433

Collision processes continued

- **atoms** continued
  - K + methyl iodide → KI + methyl radical, interpretation of product ang. and energy distribution using direct interaction model 2−57412
  - Kr^+-Kr, charge transfer cross section and effect of initial J-states in ions 2−70624
  - Kr^+-Kr, inelastic energy losses in electron transitions 2−64034
  - Kr, alignment depolarization cross- sections due to collisions 2−42751
  - Kr, electron impact ionization, energy and ang. distrib. of secondary electrons 2−64031
  - Kr, ionization processes in slow collision with He and He^+ 100eV-5000eV 2−56119
  - Kr ions, three body concersion to mol. ions 2−83188
  - Kr^+ + Kr, charge transfer and fine struct. transitions 2−46462
  - $Kr^{**} + CCl_4 \rightarrow Kr^+ + CCl_3 + Cl^-$, rate const. prediction 2−80145
  - Li^+-He, oscillation of charge exchange cross section 2−64053
  - Li^+, vibrational excitation of H_2, quantum mechanical studies 2−77171
  - LiF surface-gas atom potentials 2−50450
  - ^7Li + Ar, absolute total scattering cross sections, derivation of interatomic potential 2−49968
  - $Li^+ + H_2$ collisions, model potential for vibrational excitation of H_2 2−43038
  - Li^+ + He, elastic and inelastic scattering, charge exchange channels 2−42790
  - Li^+ + He, elastic and inelastic scattering 2−42815
  - Li^+ + He, elastic and inelastic scattering, rotational coupling 2−42816
  - Li^+ + He, elastic scattering cross sections, repulsive potential derivation 2−59934
  - $Li + Na^+$ asymmetric nonresonant charge transfer, theoretical description by two-state approx. 2−70626
  - $Li + Na^+ \rightarrow Li^+ + Na$, nonresonant charge-transfer, multistate mol. wave-function approach 2−76980
  - Li^+ + Na asymmetric nonresonant charge transfer, theoretical description by two-state approx. 2−70626
  - Mg and Ar, broadening and shift of lines by van der Waals interaction 2−70588
  - N atoms and ions, electron capture and losses in air, N_2 and O_2 2−70620
  - N ions, meas. of range-energy relation in N_2 and air, 0.3-2.0 MeV 2−79917
  - $NO^+ + O^-$, mutual neutralization rates, ionospheric D-region 2−65969
  - $N + N_2$ exchange reaction, exptl. investigation 2−54528
  - Na-He, broadening of D_2 line at high temp. 2−74237
  - Na-He, broadening of D lines and relaxation of resonance levels of Na 2−42784
  - Na-He, depolarization cross-sections for D lines 2−83169
  - Na-He, depolarization cross- sections of D lines 2−59957
  - Na, optically orientated, with buffer gas atom, spin exchange 2−79901
  - Na D-doublet, temperature dependence of quenching cross section by N_2 and H_2O in flames of 1500-2500K 2−46454
  - Na ions, meas. of range-energy relations in air, 0.3-2.0 MeV 2−79917
  - Na scattering from methane, methanol, methyl chloride, trimethylmethane, study of glory undulations 2−70821
  - Na with vibrationally excited H_2, D_2, N_2, excitation of Na D-line 2−70627
  - $Na^+ + O^-$, mutual neutralization rates, ionospheric D-region 2−65969
  - Ne^+-N_2, vibrational distribution of $N_2^+ B^2\Sigma$ products 2−56273
  - Ne-Ne^+, inelastic, ab initio H.F. calcs. for Ne_2, Ne_2^+, Ne_2^{++} systems for different interatomic distances 2−49969
  - Ne^+-Ne, inelastic energy losses in electron transitions 2−64034
  - Ne-ion, 10 to 75 keV, outer shell excitations 2−74238
  - Ne, absolute cross sections for excitation by impact of 20-180 keV H^+, H_2^+, He 2−70628
  - Ne, cross sections for 2p levels at 870K 2−42768
  - Ne, ionization processes in slow collision with He and He^+ 100eV-5000eV 2−56119
  - Ne, polarization of light emitted on de-excitation under H ion impact 2−42736
  - Ne, scattering of inert gas and period II element ions in 8-25 keV range, comparison of exptl. and theoretical interatomic potentials 2−56118
  - Ne, small-angle scattering of range of elements, meas. of inelastic energy losses 2−64045
  - Ne, transition probabilities and collision induced transitions in excited levels 2−63995
  - Ne, with H^+ at 4 keV, probability ratio for neutralization of H^+ to H(2p) or H(1s) 2−42802
  - Ne atom-ion asymmetric collisions, electron promotion model 2−79899
  - Ne atomic beam scatt. from (001) LiF surface, systematic trials study 2−74241
  - Ne atomic beam scatt. from LiF surface, Lennard-Jones potential calc. 2−74240
  - Ne deexcitation in collisions with gases, cross sections 2−64054
  - O^{5+}-Ca, observation of Kα hypersatellites 2−64046
  - O^+-Ne close-encounter collisions, 50-200 keV, study of inner shell excitations 2−79914
  - O, ground and excited states, collision integrals 2−83184
  - O, metastable ^1D, deactivation in upper atmospheric conditions 2−65814
  - O, quenching of ^1D state by N_2 and vibrational relaxation of N_2 in collisions with O(^3P) 2−67416
  - O atoms and ions, electron capture and losses in air, N_2 and O_2 2−70620
  - O ions, with atoms with $13 \leqslant Z \leqslant 79$ at 7.510 40 MeV, characteristic X-ray production 2−70629
  - O(^1S), quenching by O(^3P) 2−49970
  - O(^1S) deactivation by CO_2, O_2, N_2, Ar, temp. depend. 2−79871
  - $O^+ + CO \rightarrow CO^+ + O$, apparent charge transfer reaction, meas. of cross section from threshold to 100 eV 2−80133
  - $O^- + O_2$ reaction rates 2−53248
  - p + H- → H(nl) + H recombinations in slow collisions 2−59948

Collision processes continued
atoms continued
Pb metastable and excited states, cross section for collisional quenching depolarization of alignment by inert gases 2−42785
Rb-Ar, 100 torr, displacement of 7947 Å line of Rb 2−59933
Rb-He, 100 torr, displacement of 7947 Å line of Rb 2−59933
Rb-Kr, 100 torr, displacement of 7947 Å line of Rb 2−59933
Rb-N_2, 100 torr, displacement of 7947 line of Rb 2−59933
Rb-Ne, 100 torr, displacement of 7947 Å line of Rb 2−59933
Rb + noble gas, $6^2P_{1/2}$-$6^2P_{3/2}$ excitation transfer, sensitized fluoresc. obs. 2−74231
Si-Ar ion, 25 to 200 keV, noncharacteristic X-ray bands 2−56116
Si-Ar^{++}, K X-ray yields of Si, double-scattering mechanism 2−42786
Sm, incoherent γ-ray scatt. by K-shell electrons 2−59931
Ta, incoherent γ-ray scatt. by K-shell electrons 2−59931
Tl-Ar, excitation of metastable levels of Tl behind shock waves 2−79932
Tl-He, effect of He on resonance broadening of $7^2S_{1/2}$ state studied by level-crossing spectroscopy 2−49955
Tl-Ne, excitation of metastable levels of Tl behind shock waves 2−79932
Tl-Tl, resonance broadening of $7^2S_{1/2}$ state studied by level-crossing spectroscopy 2−49955
Tl, theory of self-broadening and Tl*-Tl-foreign gas collisions 2−49956
U ions, charge states in emergent beams from solid foils, 29.2 - 45.7 MeV 2−49971
W(112) single crysts., He and Ar atom scatt., effect of O adsorption 2−67894
Xe-H^+ charge exchange collisions, 15 eV, three-state calcs. of spin polarization 2−79918
Xe^+-Xe, charge transfer cross section and effect of initial J-states in ions 2−70624
Xe, excitation by metastable Kr atoms 2−59936
Xe, ionization processes in slow collisions with he and He^+ 100eV-5000eV 2−56119
Xe ions, three-body conversion to mol. ions 2−83188
Xe^+ $^2P_{3/2}$ and $^2P_{1/2}$ ions, in Xe and O_2, charge transfer cross section 2−70625
Xe^+ + Xe, charge transfer and fine struct., transitions 2−46462
ZnI with hydrogen, nitrogen and rare gases, $4s4p^3P_1$ and $4s5s^3S_1$ level obs. 2−74232
molecules
see also Molecules/electron scattering
aeronomic ion-neutral molecule reactions rel. to direct ionospheric measurements 2−83397
angular momentum transfer in theory of angular distributions 2−49965
anharmonic oscillator-atom, vibrational excitation cross-sections 2−80124
Appleton-Hartree equation generalization of collision frequency theories 2−82400
asymmetric molecules, quantum mechanical scattering, interaction potential 2−53097
atmospheric ions, collisions with Ca, meas. of charge transfer cross-section for formation Ca^+, 1-500 eV 2−79865
atmospheric ions, collisions with Fe, meas. of charge transfer cross sections for formation of Fe ions, 2-500 eV 2−79866
atom-diatomic molecule scattering, Lennard- Jones potentials determ. 2−56272
atom-heteronuclear diatom system, exact quantum reactive cross sections for three dimensional angle dependent model 2−44469
atom-molecule, electron loss cross sections 2−64216
atom-molecule, low energy and involving several nuclear degrees of freedom, electronic transitions 2−46640
atom-molecule, reactive, optical model for vibrational relaxation 2−65362
atom-rigid rotor diatom, Neumann series solution 2−83413
benzene excitation with metastable Ar atoms produced in low power microwave discharge 2−70747
3,4-benzophenanthrene, interaction between excited molecules in solution rel. to bimolec. fluorescence quenching 2−56506
Born lineshift integral, second order, closed form 2−79855
n-butyl-α-naphthalenide$^-$ + n-butyl-α-naphthyl → exchange, comparison with intramol. collisions 2−56236
n-butyl-α-naphthalenide$^-$ + n-butyl-α-naphthyl → exchange, rel. to intramol. collisions 2−53067
charge transfer in the mass spectrometer 2−46400
classically forbidden processes, analytic continuation of classical mechanics 2−43029
collisional depolarization of excited states, effective lifetime rel. to correlated photons in cascade 2−74226
complex molecules in solution, structure and formation constant, determination from dielec. polarisation meas. 2−60486
conservation rule for total cross section 2−53098
constant acceleration approx. in collision-induced absorption 2−53096
coronene, interaction between excited molecules in solution rel. to bimolec. fluorescence quenching 2−56506
crossed molecular beam apparatus for meas. of differential elastic or reactive cross section, determ. of intermolecular potentials 2−64211
cyclobutanone ($^1A_2$, predissociation of and collisional energy transfer from vibronically selected species 2−48343
cyclopentadiene, negative ion-molecule proton transfer and proton plus H transfer reactions 2−46986
diamagnetic diatomic, evaluation of kinetic theory collision integrals 2−53095
diatomic, perturbed by linear mols. with high moment of inertia, rotational spectral line breadth 2−50011
diatomic, rotational excitation, effect of generalized phase shift expansion terms on classical limit of gas transport coefficients 2−43030
diatomic, vibrational and rotational excitation within an electronic transition induced by positive ion or electron impact 2−42865
diatomic, vibrational energy transfer process 2−50123
diatomic, with H°, H^+, H^-, coincidence studies of elementary processes 2−42804
diatomic molecules, noncolinear collisions with atoms, inelastic vibrational transitions 2−70810

Collision processes continued
molecules continued
diatomic mols., electronic-vibr. energy transfer, vibr. distrib., i.r. fluoresc., Hg*-sensitized 2−59988
diatomic mols., matrix elements near pseudocrossing of pot. energy curves 2−83411
diatomic mols., vibr. transition probabilities calc. method 2−80122
diatomic oscillator-atom, influence of attractive forces on quantum mechanical transition probabilities 2−77169
dichloroethane, chem. activated, vibr. energy transfer probabilities, collisional deactivation 2−83409
dichloroethane-d_0 and -d_4, chem. activated, cascade deactivation and nonequil. kinetic isotope effects 2−83408
2,4-dimethylpentyl-2*(-d_1*) vibrationally excited collisional de-excitation by H_2, D_2, CF_4 2−46648
dipole-dipole collisions, evidence for neutral collision complexes, computer-graphics studies 2−67533
dissociation in single heavy particle collisions, book 2−83419
drift tube, variable length, ionic reaction meas. 2−60292
elastic induction interaction, calc. through fifth-order perturbation theory, applic. to HF + HF collision 2−50126
elastic influence on broadening of spectral lines in a gas 2−83418
elastic scattering cross section determ. by laser spectroscopy method 2−83414
electron capture cross-sections, calc. by approximation procedures, book 2−63986
electron harpooning, quantum effects 2−80153
electron-molecule interactions in photoelectron spectroscopy 2−83402
energy transfer from excited donor molecule to acceptor molecule in solution, Forster- Dexter theory 2−53093
equations of transfer in chemically reacting nonhomogeneous gases 2−68765
ethane + He, translational spectra due to collision-induced overlap moments 2−50129
ethanol, ethanol-d_1, ethanol-He, microwave double resonance studies of collision-induced transitions 2−60118
ethylene oxide, collision broadening of rot. lines by polar mols. 2−77115
with excited atoms, multipole- multipole quenching cross section 2−42767
fluoranthene, interaction between excited molecules in solution rel. to bimolec. fluorescence quenching 2−56506
gas-surface interactions, computation of scattering kernels, boundary-value problem 2−49042
gases, transport collision integral evaluation using rigid core model 2−60363
generalized Enskog method, theory 2−84639
glory extrema in total scattering cross-section 2−49017
glory undulations in scattering cross sections, physical interpretation 2−67534
ground state collisions with excited alkali atoms, transfer of excitation between fine-structure levels 2−42776
halogen-carbon compounds, meas. of stopping cross sections of α particles, 0.3-2.0 MeV 2−70820
halogenated molecule-nitroxide radical interaction, ^{13}C constant shift and MO studies 2−51440
high-energy head-on collisions, energy transfer to diatomic mol. 2−80148
highly excited atom, reaction with molecule, 82, theory 2−80145
hydrocarbon 40 keV $CH^+ \rightarrow C^+ + H$, $C + H^+C^+ + H^+ + e$, fragment kinetic energy meas. 2−70772
hydrocarbons $CH_n{}^+$, reactions with gas targets at 40-140 keV 2−64218
hydrocarbons collisional rotational transitions 2−74301
hydrocarbons of form $CH_n{}^+$, n = 2, 3, 4, 5, dissociation, kinetic energy of H^+, $H_2{}^+$, $H_3{}^+$ fragments 2−70771
hydrogen halides, compressed foreign gas effect on intensity of vibration-rotation spectra 2−74263
inelastic, between structureless atom and harmonic model molecule, exact classical treatment of vibration- translation energy transfer 2−50127
inelastic, glory occurrence nonmonotonic temp. dependence of collision rates 2−43025
inelastic and reactive collisions, semiclassical transition probabilities, classically inaccessible transitions 2−70617
inelastic and reactive scattering, effective separable approx. for multichannel Green's functions 2−46639
inelastic collisions of fast charged particles studied in Bethe theory 2−42780
intersystem crossing, relax. phenomena 2−60110
ion formation as result of triple collisions 2−56271
ion-dipole collisions, computer plotter studies of vibrational effects, classical tunnelling 2−46467
ion-molecular reactions, mechanism, relative cross-section rel. to collision ion energy 2−50122
ion-molecule, freq. in gases determined by phase coherent pulsed ion cyclotron resonance 2−43027
ion-molecule, inelastic, time-of-flight analysis of neutral products 2−70807
ion-molecule, nonreactive collision rate constants by ICR spectra 2−80143
ion-molecule collisions, K vacancy production, depend on relative Z of colliding atoms 2−74304
ion-molecule reaction studies with quadrupole ion storage trap 2−83405
ionization, relation between angular distribution of secondary electrons for photon and charged particle impact 2−52931
ketone energy transfer to rare earth ions, mechanism 2−60482
laser spectroscopy applics., high precision techniques 2−77004
linear mols., effective intermol. potentials 2−64208
liquid, binary collision model of vibrational relaxation 2−53388
liquid, collision frequency computation using cell model and exact formula 2−53389
long range force vibr. energy transfer and off-reson. transfer 2−64207
long-range curve crossings, impact parameter treatment 2−74303
low energy ion-molecule scattering apparatus 2−63302
metastable molecules, production and detection 2−64050

Collision processes continued
molecules continued
methane, methane-d_4, in liquid Ar solutions, system dynamics investigation via collision induced far i.r. spectra 2−43372
methane, scattering of Na, K, meas. of velocity dependence and total cross sections, study of glory undulations 2−70821
methane, studies on collision-broadened rotational lines in ν_4-fundamental 2−42999
methane + He, translational spectra due to collision-induced overlap moments 2−50129
methane binary mixtures with He, Ar, Xe, ultrasonic absorption meas. of rotational relaxation 2−64219
methane-CH_4^+ charge exchange cross-section 2−67542
methanol, scattering of Na, meas. of velocity dependence and total cross sections, study of glory undulations 2−70821
methanol-potassium bromide vibrationally excited, inelastic scatt. 2−64220
methyl bromide, broadening of 0,0→1,0 rotational line by polar molecules 2−42996
methyl bromide, collision broadening of o,o rh 1 o rot. lines 2−83303
methyl chloride, scattering of Na, meas. of velocity dependence and total cross section, study of glory undulations 2−70821
methyl iodide, reactive scattering of Rb, determ. of potential and cross sections 2−72553
methyl iodide + K → KI + methyl radical, interpretation of product ang. and energy distribution using direct interaction model 2−57412
methyl radical + $Cl_2(Br_2)$, molec. beam study of reaction 2−61779
mixture, linearized collision operator, modelling theory 2−56435
molecular randomicity propagation 2−58780
molecule-atom systems, vibrational excitation of diatomic Morse-oscillator 2−70806
motion in liquids, use of generalized Langevin eqn. 2−66456
multiquantum vibrational-energy exchange, evaluation of S-matrix elements 2−70809
NA, excited collision-induced tor. and vibr. transfer laser-induced fluoresc. obs. 2−83412
nonpolar-polar gas mixtures, calc. of collision integrals required for evaluation of transport properties 2−80413
nonradiating excited complexes, props. 2−67531
optically active mols., discrimination energy calc. 2−80127
organic, in gas phase, meas. of radiationless triplet-triplet energy transfer 2−53094
photodetachment, cross-sections and electron affinities 2−64035
planetary atms., collision integrals 2−62692
polynuclear hydrocarbons, quenching of triplet excited states by O_2, possible effects of magnetic fields 2−50124
potential curve crossing problem, general theory and model for close crossings 2−56112
predissociation by rot. and long-range interactions 2−77041
projectile ion thermal energy charge transfer reactions to methane, reson. effects 2−80132
quantum electrodynamics of scattering phenomena involving bound states 2−55794
radiative processes, applic. of molec. wave functions, review 2−50007
rare gas ion thermal energy charge transfer reactions to methane, ethane, propane and silane 2−83399
rare gas molecule-atom collisions, electronic energy transfer 2−79868
reactive, characterization of product energy distribs., information and entropy deficiency 2−54529
reactive, quasistatistical complexes 2−51427
reactive collisions, induced electronic excitation, model 2−61766
rearrangement processes, general form for projector onto open channels, study of three-atom processes 2−80151
reversible energy transfer, analysis of transient and steady-state kinetics 2−50128
rigid ovaloid, Boltzmann equation, generalization 2−43028
rotational absorption spectrum of linear molecules in nonpolar buffer gas, collisional broadening 2−67535
rotational energy exchange, multipole interaction effects 2−50269
rotational energy transfer, acoustic meas. 2−64209
rotational motion of dipole molecule in fluid undergoing frequent collisions 2−74307
rotational transitions induced, rates calc. 2−74301
rotationally inelastic, exponential approxs. 2−56270
scattering of gas molecules in Knudsen cell, determ. of absolute total cross section 2−71068
semiclassical theory for low- energy inelastic or reactive scattering 2−80152
small-energy-transfer collisions in dominant long-ranged forces, theory 2−70817
spherical top mols., collision-modulated spin-rot. interaction, nucl. spin relax. obs. 2−56199
superheavy, solution of Dirac equation for strong external fields 2−42769
symmetric top mols., collision-modulated spin-rot. interaction, nucl. spin relax. obs. 2−56200
symmetrical top angular relaxation, finite collision rough sphere model for resistance in bath of atoms 2−70808
three-body recomb. dynamics via reson. complex mechanism 2−80130
trimethylmethane, scattering of Na, meas. of velocity dependence and total cross sections, study of glory undulations 2−70821
vibration-rotation Hamiltonian for 2 molecule collisions 2−46641
water vapour, saturated and superheated, neutron inelastic scatt. 2−67539
$AlCl_3$-Ar, molec. orbital study 2−59990
Ar-N_2, comparison of generalized phase shift with classical trajectory calcs. of rotational inelasticity 2−43032
Ar-N_2 system, rot. relax. time, classical trajectory calcs. 2−77165
Ar-N_2 system, rot. relax. time, GPS calc. 2−77164
Ba + O_2 → BaO_2, internal state distribution of reaction products, laser-induced fluorescence meas. method 2−61770
Br_2, long-range interaction energy, Pade approx., rel. to Rydberg-Klein-Rees curve of B state 2−77082
CO-CO_2, calc. of half-widths of CO lines broadened by CO_2 and air using Anderson-Tsao-Curnutte theory 2−53105
CO_2-CO system, vibr. energy transfer, shock tube study 2−77166

Collision processes continued
molecules continued
CO-COS meas. of vibrational energy transfer on test of harmonic oscillator model 2−80140
CO_2-H-, halide mixtures, vibration-to-vibration energy transfer 2−43036
CO_2-H_2 mixtures, simultaneous vibr.-translation, vibr.-rot. and rot.-translation exchanges 2−53099
CO_2-Hf, near-resonant energy transfer to (00°1) vibr. level 2−53101
CO_2-N_2, line broadening of CO_2 using laser source spectroscopy, application of Anderson Tsao and Curnutte theory 2−79993
CO_2-N_2 system, vibr. energy transfer, shock tube study 2−77166
CO, C^- and O^- production by dissociative resonance electron capture 2−83415
CO, electronic-vibr. energy transfer, vibr. distrib., i.r. fluoresc., Hg*-sensitized 2−59988
CO ($a^3\Pi$) quenching by O(^{3}P), rate coeffs. 2−64213
CO collisional energy transfer of electronic and vibr. energy 2−56159
CO luminescence, energy dependence of collisional deactivation cross section 2−46646
CO population by active nitrogen, rate coeffs. 2−70718
CO singlet and triplet state excitation by active N_2 2−70717
CO_2, dissociative excitation of CO($A^1\pi$) system by electron impact 2−56164
CO_2, thermal relaxation of vibration, period determ. by impact tube method 2−83398
CO_2 laser, spectrum generated at reduced pressure of working mixture 2−73566
CO_2 polyatomic mixtures, laser excited, vibrational relaxation 2−43035
CO_2 − DF vibrational de-excitation on the basis of vibration-to-rotation energy transfer, 300-2000K 2−83406
CO_2 − HF vibrational de-excitation on the basis of vibration-to-rotation energy transfer, 300-2000K 2−83406
CO + CO, vibrational energy transfer 2−46642
CO + CO, vibrational energy transfer 2−46642
CO + CO, vibrational transition probabilities, temp. dependence below 300K 2−60117
CO + CO_2, N_2O, COS, shock-heated mixtures, vibrational energy transfer processes 2−53100
CO_2 + He, translational spectra due to collision-induced overlap moments 2−50129
CO_2 + N_2O vibr.-translation and vibr.-vibr. exchanges 2−43034
Cl_2, long-range interaction energy, Pade approx., rel. to Rydberg-Klein-Rees curve of B state 2−77082
Cl_2 + Cl_2, vibrational transition probabilities, temp. dependence below 300K 2−60117
CsI + Ar, vibrational and rotational energy transfer, ballistic mechanism 2−67536
Cs + CH_3I, rotational polarization of reaction products and reprojection of angular momentum in molecular beam expts. 2−65367
Cs + HBr, rotational polarization of reaction products and reprojection of angular momentum in molecular beam expts. 2−65367
Cs + HI, rotational polarization of reaction products and reprojection of angular momentum in molecular beam expts. 2−65367
D_2-He, quantum mechanical scatt., comparison with He-HT system 2−60115
D_2-He collisionally induced vibration, effect of rotational motion 2−80139
D_2-Ne Van der Waals complexes in collision-induced fund. bands of deuterium, spectra 2−64127
D_2-Ne(N_2)(Ar) systems, conc. depend. of binary diffusion coeffs., 300K 2−64399
D_2, effects on Raman line profiles 2−43039
D_2, HD, HCl, H_2 mixtures, relaxation times, energy transfer study 2−80134
D_2, vibrationally excited, collisions with Na atoms, excitation of D-line radiation 2−70627
D_2 considered as Morse oscillator DWBA theory for collisional dissociation with Ar, He 2−43033
DF, vibr. relax., catalytic efficiencies of NO 2−77163
D + H_2 → HD + H, cross-section 2−61773
D + H_2 → HD + H, quantum cross section 2−61772
H^+-H_2 vibrational excitation, application of theory for small- energy-transfer collisions in dominant long-ranged forces 2−70817
H-H_2 collinear collisions, reaction probabilities and high energy trajectories 2−50130
H_2-H^+ vibrational excitation, 15-1000 eV, semiclassical theory 2−80152
H_2-He collisionally induced vibration, effect of rotational motion 2−80139
H_2-He^+, low-energy, optical excitation and polarization 2−67436
H_2-He(Ne) mixtures, collision broadening of depolarized Rayleigh and Raman line 2−70700
H_2-Ne van der Waals complexes in collision-induced fund. bands of hydrogen spectra 2−64127
H_2-Ne(N_2)(Ar) systems, conc. depend. of binary diffusion coeffs., 300K 2−64399
H_2^+-atom superelastic collisions, vibrational excitation of H_2^+ 2−70815
H_2-inert gas binary mixtures, construction from collision to proton spin lattice relaxation times 165-265K range 2−46645
H_2^+-molecule superelastic collisions, vibrational excitation of H_2^+ 2−70815
H_2, effects on Raman line profiles 2−43039
H_2, reactive collisions with ions, effect of reactant internal energy on spectator stripping 2−44472
H_2, vibrationally excited, collisions with Na atoms, excitation of D-line radiation 2−70627
H_2, with H^+ at 4 keV, probability ratio for neutralization of H^+ to H(2p) or H(1s) 2−42802
H_2 considered as Morse oscillator, DWBA theory for collisional dissociation with Ar, He 2−43033
H_2 vibrational excitation by Li^+, quantum mechanical studies 2−77171
H_2^+ dissociation by impact On He, Ar, H_2, N_2 at 4-12 keV, meas. of cross sections for angular distribs. of H(2s) 2−70816
$\mu^+ + H_2 \rightarrow H^+ + \mu H$, differential cross section 2−67481
$\mu^+ + H_2 \rightarrow \mu H + H^+$, total cross- section 2−67482

Collision processes continued
- **molecules** continued
  - HBr, effect of resonance on vibr. distrib. charge transfer reactions with Kr^+ and Ar^+ 2−51424
  - HBr, vibr.-vibr. energy transfer and collisional pumping 2−80129
  - HCl-HCl and DCl-DCl, evidence for neutral collision complexes, computer-graphics studies 2−67533
  - HCl, effect of resonance on vibr. distrib. charge transfer reactions with Kr^+ and Ar^+ 2−51424
  - HCl, vibrational fluorescence, vibrational energy transfer from molecule to molecule 2−83256
  - HCl in CO_2 atmosphere, line shape parameters 2−42879
  - HD-He, low-energy, rotational transitions in HD 2−46644
  - $HD^* + HD(He)$, collision-broadened cross-sections from peak-absorbancy meas. 2−67479
  - HF, vib.-vib. energy transfer time. vib. fluorescence obs. 2−60005
  - HF, vibr. relax., catalytic efficiencies of NO, H_2O, D_2O and HCl 2−77163
  - HF in CO_2 atmosphere, line shape parameters 2−42879
  - HF + F collisions, temp. dependence of vibrational energy transfer probability, 300 to 1500K 2−43037
  - H_2-^4He system, thermal diffusion factor and quantum collision integrals, effect of inelastic collisions 2−56449
  - H_2O-atom, classical rotational excitation probabilities of H_2O 2−80136
  - H_2O, kinetic energy of dissociation 2−80028
  - H_2O quenching of Na D-doublet in flames of 1500-2500 K, temp. dependence of cross sections 2−46454
  - H_2O vapour, absorption lines in ν_1-band, collisional narrowing 2−79992
  - H_2S, kinetic energy of dissociation 2−80028
  - HT-He, quantum mechanical scatt., comparison with He-D_2 system 2−60115
  - $H_2 + D_2 \rightarrow 2HD$ four-centre exchange reaction ab initio calcs. of orbitals, contragradience and reaction surface 2−48323
  - $H_2 + D \rightarrow HD + H$, molec. beam study 2−72546
  - $H + H_2$ linear collisions, classical S-matrix theory 2−72551
  - $H + H_2$ linear reactive collisions below the classical threshold complex-valued classical trajectories determ. from S-matrix theory 2−44474
  - $H + H_2$ vibr. excitation process, rate const. 2−67537
  - $H_2 + H_2$, structure of linear symmetric molecule H_4 2−50039
  - $H_2 + H_2$ reactive vibr. nonequil. effects 2−84627
  - $H + H_2(N_2)(O_2)$, electron loss cross sections 2−64216
  - $H_2 + Li^+$ collisions, model potential for vibrational excitation of H_2 2−43038
  - H(2s)-N_2, 20-120 keV charge-changing collisions, meas. of absolute cross sections and electron capture cross section 2−70638
  - He-H_2, meas. of absolute integral total cross sections and interaction potential 2−70814
  - He-H_2, total scattering cross section of thermal energies 2−64212
  - He-I_2, inelastic non-reactive energy transfer, calc. and analysis of probabilities and cross sections 2−60116
  - He_2, crossed beam differential elastic scatt. rel. to meas. of attractive well 2−50133
  - $He(2^3S) + CO$, excitation transfer and Penning ionization reactions 2−54535
  - $He_2(3p^3\pi)$, quenching of excited states 2−46552
  - Hg^*-CO, electronic-vibrational energy transfer 2−80144
  - I_2-He mixture, interaction of dissoc. and vibr. relax. behind shock wave 2−77168
  - I_2, angular scattering of superthermal K atoms 2−42787
  - $I_2 + Cs$, reaction cross section meas. 2−70738
  - $I_2 + H_2$, dynamics of mol. and atomic exchange reaction 2−51423
  - K-O_2, spin exchange scatt. obs. 2−67541
  - K^+ ions elastic scatt. from diatomic mols., 150-4000 eV 2−80149
  - K + HBr, rotational polarization of reaction products and reprojection of angular momentum in molecular beam expts. 2−65367
  - $Kr^{**} + CCl_4 \rightarrow Kr^+ + CCl_3 + Cl^-$, rate const. prediction 2−80145
  - N_2-Ar, rotational excitation of rigid rotor, classical results 2−50125
  - N_2-Ar mixtures, rel. to relaxational absorpt. of sound 2−71116
  - N_2-CO vibration to vibration energy transfer, laser excited fluorescence obs. 2−67489
  - N_2-Na vibrational relaxation times in rapid expansion interpretation of Na line-reversal meas. 2−53102
  - N_2, energy loss and range-energy relations for N ions and Ar ions, 0.3-2.0 MeV 2−79917
  - N_2, in high-frequency $Ar + N_2$ discharge, effective cross sections for excitation of $C^3\Pi u$ state 2−43041
  - N_2, quenching of $O(^1D)$ and vibrational relaxation in collision with $O(^3P)$ atoms 2−67416
  - N_2, rate constants for deactivation of $B^3\Pi_g$ and $A'^1\Sigma_u^-$ states 2−80125
  - N_2, vibrationally excited, collisions with Na atoms, excitation of D-line radiation 2−70627
  - N_2 afterglow, O_2 and temp. effect on first positive bands 2−77304
  - N_2 luminescence, energy dependence of collisional deactivation cross section 2−46646
  - N_2 quenching of NaD-doublet in flames of 1500-2500 K, temp. dependence of cross sections 2−46454
  - $N_2(A^3\Sigma_u^+)$ metastable, production of $N_2(C^3\Pi_u)$ and $N_2(C'^3\Pi_u)$ by mutual collisions 2−50132
  - NH_3 spectral lines, collision-broadened by hydrogen, shapes and widths 2−67493
  - $NH_2(A^2A_1)$ produced by photolysis, collisional deactivation 2−50060
  - NO, Penning ionization by $Ar(^3P_1)$ 2−53041
  - NO_2, collisionally induced excitation, radiative lifetime 2−80015
  - N_2O, air broadened absorption lines, calc. of rotational half-widths using Anderson-Tsao-Curnutte theory 2−53105
  - N_2O, collisional broadening of absorption lines 2−80056
  - N_2O, thermal relaxation of vibration, period determ. by impact tube method 2−83398
  - N_2O band intensities and half-width of N-broadened lines rotational lines in ν_3 fundamental meas. near 4.5 μ 2−42923
  - $N_2O^+ + N_2O \rightarrow NO^+N + N_2O$, $N_2O^+ + N_2O \rightarrow O^+ + N_2 + N_2O$, mass spectrometric study 2−51436
  - $N_2 + C^+$, 3 to 100 eV, calculated cross sections for mass transfer, molecular and dissociative charge exchange reactions 2−48322
  - $N_2 + He$, translational spectra due to collision-induced overlap moments 2−50129
  - $N + N_2$ exchange reaction, exptl. investigation 2−54528
  - $N_2 + N_2$, vibrational transition probabilities, temp. dependence below 300K 2−60117
  - $N_2 + O_2(HCl)$, vibr.-vibr. energy exchange 2−83407
  - N_2^*, vibrationally excited, quenching by O, determ. of rate coeff. 2−83400
  - Na_2, with inert gases, h_2, HD, D_2, N_2, CH_4, meas. of asymmetries in cross section for rotational transitions in $B^1\Pi_g$, state 2−56274
  - NaLi, fluoresc. obs., heat-pipe oven applic. 2−49453
  - Ne^+-N_2, vibrational distribution of $N_2{}^+B^2\Sigma$ products 2−56273
  - O_2-Ar, probability of excitation of vibrs. and dissociation 2−83416
  - O_2-Ar collision, hot gas, rates of vibr. and dissoc. excitation 2−83417
  - O_2-Ar compressed mixtures, meas. of microwave absorption in 48-81 GHz region using Fabry-Perot interferometer 2−74273
  - $O_2{}^+$-He, vibrational excitation of diatomic Morse-oscillator 2−70806
  - O_2-N_2 compressed mixtures, meas. of microwave absorption in 48-81 GHz region using Fabry-Perot interferometer 2−74273
  - $O^+ (^4S) + N_{2(v)}(^1\Sigma)$ crossed molecular beams, cross section for formation of NO^+ 2−54530
  - O_2, electronic energy transfer from $^{32}O_2(a^1\Delta_g)$ to $^{36}O_2(X^3S_g$-), meas. of rate constant 2−53103
  - O_2, energy loss and range-energy relations for Ar ions, 0.3-1.0 MeV 2−79917
  - O_2, impact line shift in 0.762 μ band 2−77092
  - O_2, transitions causing airglow continuum 2−65887
  - O_2 ion-pair production of O^+ and O^- by $He(2^12^3S)$ metastables 2−83260
  - O_2 luminescence, energy dependence of collisional deactivation cross section 2−46646
  - $OH(A^2\Sigma^+) + Ar$, near resonant vibration-rotation energy transfer calc. of cross sections and rate consts. using IOS and DW approx. 2−70818
  - $O_2 + C^+$, 3 to 100 eV, calculated cross sections for mass transfer, molecular and dissociative charge exchange reactions 2−48322
  - $O^+ + CO \rightarrow CO^+ + O$, apparent charge transfer reaction, meas. of cross section from threshold to 100 eV 2−80133
  - $O^- + O_2$ reaction rates 2−53248
  - $O_2{}^+ + O^-$, mutual neutralization rates, ionospheric D-region 2−65969
  - $O_2 + O_2$, vibrational transition probabilities, temp. dependence below 300K 2−60117
  - $O_2{}^\dagger + O(^3P)$ vibrational energy transfer, O_3 photolysis 2−51465
  - $O_2 + Xe^+ \rightarrow Xe + O_2{}^+$, charge transfer cross sections of $^2P_{3/2}$ and $^2P_{1/2}$ ions 2−70625
  - $O_2{}^+(b^4\Sigma^-{}_g)$ collisional deactivation rates for O_2 and N_2 2−77172
  - $O_2(^1\delta_g)$, Penning ionization by $Ar(^3P_1)$ 2−53041
  - Pt (100) surface, clean and C covered, N_2O molecular beam reactive scatt. obs. 2−50547

Collision processes, plasma *see Plasma/collision processes*

Colloids
- *see also Electrophoresis; Emulsions; Gels; Sols; Thixotropy*
- blood, primary hemostasis, convective transort theory anal. 2−48846
- colloidal dispersions, viscoplastic deposit formation in turbulent pipe flow 2−83826
- detergent solutions, dye-aggregation 2−78202
- electrical double layer, Esin-Markov coefficient 2−60524
- electrical double layer round spherical particle, functional representation of properties 2−60525
- electrokinetic movement of suspended colloids in flowing medium, expt. obs. 2−71127
- electron density of particles in colloidal suspensions, X-ray study under different collimation conditions 2−71285
- electrophoretic deposition, kinetics studies 2−68793
- gravitational deposition from laminar channel flow 2−83814
- heterocoagulation in mixed dispersions, effects of size, conc., surface potential 2−71243
- latex particles in electrolyte, evidence for Kirkwood-Alder transition 2−67874
- micelle solns., electron excitation energy transfer and conc. phenomena 2−60523
- palygorskite soln., stability, transient elec. light scatt. obs. 2−74567
- pseudoboehmites in dil. nitrate electrolytes, point of zero charge 2−75390
- turbulent flow study using optical dispersion by colloids 2−77216
- KCl, F-centres, thermal transform. with colloids, dislocation induced precip. 2−71525
- Pd particles, struct. depend. on electrolytic deposition parameters 2−83818
- TiO_2 hydrosol, optical properties, turbidity and refractive index 2−74574

Colorimeters *see Colorimetry*

Colorimetry
- *see also Spectrochemical analysis; Spectrophotometry*
- CIE chromaticity coordinates computation using numerical integration methods 2−73651
- colour coordinates, connection with substractive colour coordinates 2−66825
- colour distance determ. between two arbitrary colours, geodesics, in colour 3 space 2−79361
- instrumentation systems, review 2−70028
- light sources, colour rendering investigation 2−45802
- lunar and planetary space missions 2−81938
- measuring methods 2−79363
- photographic light sources, colour rendering index 2−82596
- plastics ageing testing applic. 2−47671
- polarization effects on reflectance factor meas. 2−70010
- precision measurement and calibration 2−82560
- receptor set correction 2−52462
- SPEKOL, selected ordinate method 2−79362
- subjective effects 2−82063
- subjective measuring system for industrial measurements 2−63400
- trichromator, numerical control 2−70027
- UBV, bright galaxies, integrated magnitude 2−84956

- **Colorimetry** continued
  - white light colour rendering capability and luminosity obs. 2−73652
- **Colour**
  - *see also Photography/colour*
  - Cepheids in small magellanic cloud, influence of metal lines 2−81823
  - contrast methods in microscopy of living tissue 2−76054
  - diamonds, Ni inclusions, determ. of Curie points for different coloured diamonds 2−81213
  - dichroic filter props. 2−70064
  - distance determ. between two arbitrary colours, geodesics, in colour 3 space 2−79361
  - fluorophlogopite crystals, Ti and V impurities, explained by valence states and coordinations of Ti and V in mica structure 2−84562
  - glasses containing Pr combined with Cr, spectral properties 2−75286
  - Martian surface rel. to laboratory studies $(C_3O_2)n$ polymer 2−78542
  - Moon, intensity and colour variations across surface, high resolution scans 2−78520
  - optical systems operating in visible light, colour correction 2−59257
  - red highway flares, luminous power spectrum 2−59270
  - sensation, subjective effects 2−82063
  - thermoindicators of melting, coloured, for monitoring heat regimes 2−82381
  - tinted ophthalmic lenses, function, evaluation and evaluation 2−62881
  - twilight sky, effect of aerosols 2−81690
  - white light colour rendering capability and luminosity obs. 2−73652
  - C black, tinting strength 2−75281
  - $(NO)_2$ dimer, origin of blue colour in liquid and solid 2−67495
  - Ni films, exptl. obs. and mechanisms 2−59243
- **Colour centres**
  - *see also F-centres*
  - alkali halide, method of moments for U-centre localised freq. 2−50984
  - alkali halide, Stark effect of M- and N-centres 2−61624
  - alkali halide phosphors, lineshpaes of C-bands by method of moments 2−57346
  - alkali halides, γ-irrad., aquoluminesc., energy levels of trapped electrons 2−43376
  - alkali halides, extended Mollwo-Ivey relation 2−60824
  - alkali halides, F_{a1}, F_{a2}, U centres, temp. dependence of peak position of absorption and emission bands 2−75298
  - alkali halides, fast recomb. luminesc. transition lifetimes 2−54450
  - alkali halides, models, review 2−71519
  - alkali halides, rare earth doped, Z-centres, optical absorpt. and e.p.r. at 77K 2−71526
  - alkali halides, spin-orbit effects in K-bands 2−51335
  - borophosphate glasses, X-irrad., e.p.r. obs. 2−44444
  - decoloration, effects, thermal excitation function 2−50695
  - electronic structure, theoretical developments, review 2−56746
  - glass, nontransparent quartz, investigation by e.p.r. and elec. cond. meas., importance of melting temp. and atmosphere and impurity ions Ti^{3+} in formation 2−84482
  - ice, KF and NH_4F doped and irradiated, role of F- in increased colouring 2−60823
  - ionic crystals, two-electron U-centres, point-ion models 2−83987
  - naphthalene crystals, X-ray irradiated, annealing behaviour and e.s.r. spectrum 2−80711
  - paraelectric crysts., ENDOR of A-centre electrons, elec. field effects 2−78176
  - photoluminescence, comments on theory of concentrational depolarization 2−78146
  - quartz, radiation-induced diffusion of alkali ions and protons and formation of colour centres 2−71532
  - quartz, rel. to electrolysis in air and vacuum, i.r. spectra obs. 2−74802
  - radiophotoluminescent glass dosimeters, formation kinetics 2−67092
  - U-centre behaviour and band modes in semiconductors and insulators 2−54448
  - Al_2O_3, absorption spectra and reln. between thermoluminescence and thermobleaching 2−71521
  - BN, hexagonal, paramag. centres, thermolum., thermally stimulated currents, e.p.r. 2−74804
  - BaF_2, high temp. absorpt. spectrum 2−77597
  - BaF_2 colour centre interconversion induced by electron irradiation 2−77598
  - BeO, irrad., V_1 centre, hyperfine parameters, ENDOR obs. 2−54498
  - CaF_2, colour centre interconversion induced by electron irradiation, changes in adsorption spectrum 2−77598
  - CaF_2, high temp. absorpt. spectrum 2−77597
  - CaF_2 centres of C_{4v} symmetry containing trivalent rare earth-interstitial hydride in pairs, rel. to u.v. irrad. 2−83984
  - $CaF_2.3Ca_3(PO_4)_2:Nd^{3+}$, absorpt. coeffs. 2−64681
  - $CdBr_2(Pb,Mn)$, recombination interact. of luminescence centres, 90-400 K 2−84544
  - $CdCl_2$ crystals, determ. of impurity ions spectra rel. to 5 eV band 2−84475
  - $CdCl_2(Pb,Mn)$, recombination interact. of luminescence centres, 90-400 K 2−84544
  - CeO_2, u.v. irrad. paramag. hole centres, e.s.r. obs. 2−65322
  - CsBr:K, non-cubic Ag- centres in mixed crystals 2−44370
  - CsBr, X-irrad. at cryogenic temps., I-, α-, H, H′ and V_4 centres 2−68038
  - CsCl, U band shape from first electronic transition of H- and D-substitutional impurities 2−47446
  - CsI, relaxed state of self-trapped exciton 2−65291
  - CuCl, electrolytic coloration, absorpt. spectra study 2−83985
  - KBr-KCl mixed crystal, with and without colour centres, spectra 2−74801
  - $KBr-K_2O-B_2O_3$ glass, X-irrad., e.p.r. obs. of Br^0 2−81463
  - KBr, analysis of R_2 absorp. struct. 2−51342
  - KBr, computation of electronic structure of colour centres and electronic polarization fields 2−71520
  - KBr, fast recomb. luminesc. transition lifetimes 2−54450
  - KBr, quenching of cathodoluminescence as a function of colour centres, at 90 and 300 K 2−68704
  - KBr, scanning electron microscope observation 2−80708
  - KBr, transient form., pulsed electron beam 2−53753
- **Colour centres** continued
  - KBr crystals, u.v. irrad. and colour centre prod. from exciton decay 2−71527
  - KCL, H-centre prod. by u.v. photodestruction of U_2-centres, optical and e.s.r. obs. 2−77599
  - KCl:Ag, form. by X-ray irrad., e.p.r. and optical obs. 2−80713
  - KCl:Br, $BrCl^- - V_k$ centre, e.s.r. 2−81461
  - KCl:$(Li^+,Br-)$, $H_a(Li^+)$-type BrCl- centre, e.p.r. obs. 2−60825
  - KCl:$(Li^+,I-)$, $H_a(Li^+)$-type ICl- centre e.p.r. obs. 2−60825
  - KCl:Li^+, reorientation motions of H_a-centre 2−43648
  - KCl:Na, non-cubic Ag- centres in mixed crystals 2−44370
  - KCl:Na^+, X-ray irrad., hole centres, conversion and struct., optical absorpt. 2−84523
  - KCl:Pb^{2+}, electrolytically coloured, T-centre struct. 2−64679
  - KCl:Sr, X-irrad., thermal annealing, absorpt. and luminesc. obs. 2−64684
  - KCl:Tl, electron pulse irrad., absorpt. study 2−71524
  - $KCl-K_2O-B_2O_3$ glass, X-irrad., e.p.r. obs. of Cl^0 2−81463
  - KCl, analysis of R_2 absorp. struct. 2−51342
  - KCl, computation of electronic structure of colour centres and electronic polarization fields 2−71520
  - KCl, decay on annealing rel. to molecular $CO^{2-}{}_3$ centre formation, i.r. spectra obs. 2−71350
  - KCl, diffusion coeff. of self-trapped holes and migration to thallium centres 2−68709
  - KCl, γ-irrad. at liq. N_2 temp., hardening, H_a band obs. 2−53754
  - KCl, magnetic amplification of positronium effect 2−68039
  - KCl, positron capture, tempering effect 2−54092
  - KCl, quenching of cathodoluminescence as a function of colour centres, at 90 and 300 K 2−68704
  - KCl, scanning electron microscope observation 2−80708
  - KCl crystals, absorption band spectra obs. of quasimetallic centres 2−72338
  - KCl(Br)(I), Ag^- centres, polarization and decay time of luminesc. 2−80710
  - KI:K, additively coloured, colloidal absorption bands 2−47448
  - KI, diffusion coeff. of self-trapped holes and migration to thallium centres 2−68709
  - KI, fast recomb. luminesc. transition lifetimes 2−54450
  - KI, quenching of cathodoluminescence as a function of colour centres, at 90 and 300 K 2−68704
  - KN_3, u.v. irrad., absorpt. bands identification 2−75299
  - $KX-K_2O-B_2O_3$ glass, $(X=F,I,O)$, X-irrad., e.p.r. obs. 2−81463
  - LiF, analysis of R_2 absorp. struct. 2−51342
  - LiF, R-centre states in the region of F and M bands 2−47445
  - LiF, scanning electron microscope observation 2−80708
  - LiF, X-irrad., 340 nm centres, formation and effect on thermoluminesc. 2−43650
  - M centre triplet state, quadrupole interactions, ENDOR obs. 2−72533
  - MgF_2:CO(Mn)(Ni), impurity-ion spin-forbidden absorpt. enhancement by colour centres 2−78104
  - MgF_2, H-centres, radiation damage process 2−56747
  - MgO, radiation-induced $[Na]^0$ centres 2−43651
  - MgO, V_{oh} centre obs. from absorpt. at 2.21 eV 2−54426
  - MgO, V_1 paramag. centre 2−64685
  - MgO surface, $V_{oh}{}^*$ trapped hole centre obs. by e.p.r. 2−81447
  - $Na_8Al_6Si_6O_{24}X_2$ sodalite $(X=Cl, Br, I)$, cathodochromism, elucidation of damage mechanism by ESCA 2−47447
  - NaCl:Sr^{2+}. Z_1 generation, kinetics 2−84515
  - NaCl-KCl mixed crystal, with and without colour centres, spectra 2−74801
  - NaCl, computation of electronic structure of colour centres and electronic polarization fields 2−71520
  - NaCl, F→X-centre conversion, lattice and disloc. mechanism 2−50698
  - NaCl, fast recomb. luminesc. transition lifetimes 2−54450
  - NaCl, scanning electron microscope observation 2−80708
  - NaCl, thermal decoloration, mutual dependence of ε and p_0 in thermal excitation function 2−50697
  - NaCl, thermolum. rel. to alkali stoichiometric excess, glow peak due to F' centres, 77 K 2−81423
  - $NaClO_3$, ClO_3 centres formed by low temp. X-irradiation, e.s.r. study 2−51407
  - NaF, M centre, optical props. and reorientation 2−51343
  - NaI, diffusion coeff. of self-trapped holes and migration to thallium centres 2−68709
  - $PbBr_2(Cl_2)$, u.v. irrad., e.p.r. and luminesc. obs. of centres 2−44448
  - RbI:K, additively coloured, collisional absorption bands 2−47448
  - RbI, diffusion coeff. of self-trapped holes and migration to thallium centres 2−68709
  - Si, hyperfine structure of the e.s.r. spectrum of A centre 2−81005
  - $SrCl_2$, U- and U_2-centres, absorpt. spectra and e.p.r. 2−71531
  - SrF_2, high temp. absorpt. spectrum 2−77597
  - SrF_2 colour centre interconversion induced by electron irradiation 2−77598
  - SrO, radiation-induced $[Na]^0$ centres 2−43651
  - $Y_3Al_5O_{12}$:Eu(Yb), reduction to Eu^{2+} and Yb^{2+} during irradiation, recombination and thermoluminescence on heating 2−80714
  - $Y_3Al_5O_{12}:Pr^{3+}(Tb^{3+})$, absorpt. of γ-irradiated crystals, recombination and thermoluminescence on heating 2−80714
- **Colour photography** *see Photography/colour*
- **Colour vision**
  - anomaloscope, transformation of arbitrary data to CIE system of specifications 2−66347
  - chromatic adaptation of orientation and size specific visual processes in Man 2−69470
  - colour contrast borders, visibility 2−62885
  - colour interval perception, Mansell renotations spacing in MacAdam geodesic diagram 2−82060
  - colour shift obs., with and without chromatic adaptation 2−51988
  - discrimination abilities, tests 2−82068
  - discrimination in frog, retinal ganglion cell interaction 2−78683
  - Drosophila melanogaster visual screening pigments in situ absorption spectra 2−69472
  - fly absorption spectrum of rhabdomere 2−66358
  - goldfish, optic nerve fibres, rod and cone input 2−66352
  - human subjective colour perception, crosscorrelation theory 2−69471

Colour vision continued
late receptor potential generation, excitatory-inhibitory phenomenon in vision 2−69476
line element in zone fluctuation model 2−66350
line element in zone fluctuation model 2−66349
mammals with all cone retinas, visual capacities 2−82072
mesopic region, differential sensibility and black light density 2−78682
motion after effect, colour sensitivity 2−66327
ocular fundus reflectometer 2−66312
oil droplets in passerine birds, distribution localization and absorption characts. 2−69475
organisation at central forea in humans 2−85152
parafoveal spectral sensitivity, neural functioning 2−66348
photoreceptors, light absorpt. rel. to anomalous dispersion 2−82062
pigeon eye, elec. responses to wavelength changes of stimulating light 2−51990
precision measurement and calibration colorimetry 2−82560
Prevost-Fetchner-Benham effect 2−45177
primate photoreceptors selective chromatic adaptation 2−51989
rate, photoptic system, electroretinographic investigation 2−66353
saturation scales for surface colours 2−82070
sensitivity in region of chromatic borders 2−85147
small targets, psychophysical measurement and functional model 2−78681
spectral sensitivity, effect of intense spectral light 2−66351
stereoscopic phenomenon, effect of pupil size variations 2−51991
tests comparison superiority of Farnsworth Lantern 2−73232
tetrachromatic matches 2−45178
transition effects at colour border 2−82071
trichromator, numerical control 2−70027

Columbium *see Niobium*

Coma *see Aberrations, optical*

Combustion
see also Explosions; Flames; Heat of combustion; Reaction kinetics
acoustic conductivity of burning surface of mixed solid fuel 2−44479
air-natural gas jet, aerodynamical characteristics in transitional flow region 2−53317
analysis of each engine cycle by computer 2−58940
blast wave propagation in combustible gas 2−80380
convectively controlled burning, response to nonlinear disturbances 2−84620
damping of precessing vortex cores in swirl generators 2−83427
detonation velocity in iso-atomic gas mixtures 2−83649
droplets in super-critical conditions and gas pockets, model 2−81487
energy transfer in confined combustions and detonations 2−84618
exothermic hypersonic flows about blunt projectiles, periodicity 2−83650
flame autostabilization in combustion chamber of liq. rocket engine 2−52287
flames, effects of acoustic waves 2−52285
flow in cylindrical tube, laminar combustion stability 2−56284
front, velocity and existence in relativistic MHD 2−60179
fuel droplets in shock heated oxygen, study of autoignition process 2−83724
of fuels in metal oxide during reduction of metal ores, mechanism 2−44478
gases, ionization nonequilibrium phenomena, calc. 2−80261
heat loss by radiation, calorimetric meas. 2−58965
instabilities in reaction zones of detonation waves 2−83646
internal combustion engines, thermodynamic cycles and efficiency 2−58939
i.r. band model technique for diagnostics 2−44477
kinetic, in laminar gas stream, stationary processes 2−84635
monodisperse spray deflagration, burning velocity distrib. 2−84619
noise generation in burning fuel-air mixtures 2−55534
nonlinear heat transfer problems, analytic solns. 2−56329
nuclear metal, burning curve ignition; theory 2−46383
particle characteristics from its dimensions, error in statistical method 2−61786
plasma, elec. conductivity meas., apparatus 2−80259
powders in gas stream, mathematical model 2−61782
propane, heat release in multistage reaction 2−58146
range pair counting method application to oxidation in combustion chamber exhaust gases 2−57421
reacting liquid sprays, in-line holography 2−83755
recording combustion curves when operating with an FES-1 steelometer 2−84682
solid propellant in semiclosed volume, transient processes 2−61783
in supersonic streams, degree cf combustion calc. methods 2−61788
systems, gasdynamics of swirling flow 2−80376
turbulent processes, acoustic noise generated by, analytical results 2−69774
turbulent swirling boundary layer flow, inverse solution method 2−46671
Al alloys, propagation, physical 2−61785
B particle nonequilibrium effects, air augmented combusting ducted flows 2−70836
$H_2/O_2/N_2$ mixtures, self-inflammation rates 2−81488
H_2/air and H_2/O_2, shock-induced 2−83651
H_2, O_2, Cl_2, in subsonic flow, photochemical initiation 2−84660
NH_4ClO_4, $Ca(HClO_4)_2$ and metal mixture systems, rate of combustion 2−61784
Pu, expt. confirmation of burning curve ignition theory 2−46383
U, expt. confirmation of burning curve ignition theory 2−46383

Comets
Bennett, 1969i, direct i.r. obs. of thermal radiation from nucleus 2−51836
Bennett's, observations at Steinberg Institute Observatory, (1969) 2−69170
Bennett 1969i, photographs 2−73095
Bradfield 1972f, obs. and photographs 2−73092
comet astronomy in the USSR, review 2−75919
dynamics, perturbation by planets and stars close to solar system 2−81783
exploration, utilization of Jupiter swingby trajectories 2−54975
Finsler (1937 V), definitive orbit allowing for five major planet perturbations 2−58519
formation, solar nebula studies 2−78494

Comets continued
formation, structure, and composition, review 2−44966
Giacobini Zinner, meteor shower prediction, October (1972) 2−58528
Halley's, perturbations of orbit over last 28 revolutions 2−58520
Halleys, effect of trans-Plutonian planet 2−44937
Ikeya-Seki (1967n) photographic positions and Leyden reduction procedure 2−44965
long-period, planetary perturbations of orbits, dependence on inclination 2−75920
mass and dynamics, statistics 2−75917
material composition 2−62716
motion of comets with near-parabolic and short period orbits 2−73093
natural oscillations of type-I comet tails rel. to solar wind fluctuations 2−81937
Olbers, effect of trans-Plutonian planet 2−44937
orbits rel. to interstellar gravitational perturbations 2−69171
P/Encke, probe trajectory 2−58522
periodic with large aphelions, use in trans-Pluto planet detection 2−69139
Pons-Brooks, effect of trans-Plutonian planet 2−44937
probes, trajectory considerations, flight modes 2−58522
research reviewed, structure and history of solar system 2−58524
Seki-Lines, isophotometric maps of dust tail 2−75921
short period, effect of multiple encounters with Jupiter and Saturn on orbits 2−58523
short-period meteor orbits rel. to parent comet and perturbations of planets 2−58525
solar activity effects 2−66226
space missions to comets and asteroids rel. to understanding of solar system 2−78411
star-Sun-comet system using restricted hyperbolic three-body problem 2−85032
sungrazing comets, daylight observations when close to the Sun 2−48781
Tago-Sato-Kosaka, radiation, elliptical polarization search 2−75724
Tago-Sato-Kosaka and Bennett, water in atmosphere 2−58521
type I oscillations of tails 2−73094
unmanned exploration employing nuclear reactor power systems 2−66032
H_2O, effects of electron-water vapour interactions 2−53019

Communications, optical *see Laser beams/applications*

Compasses
No entries

Complementarity *see Physics fundamentals; Quantum theory*

Composite materials
asbestos filled PVC, mechanical props., anisotropy 2−77668
bone, as solid-liquid composite, mechanical props. 2−69220
BORSIC aluminium fibre-matrix interfacial region, exam. 2−64546
buckling analysis of multilayered orthotropic elements 2−69682
carbon phenolic, two dimensionally reinforced, re-entry material, characterization 2−56980
ceramic, C continuous fibre-reinforced, mech. props. 2−50919
ceramic, C discontinuous fibre-reinforced, fabrication and props. 2−50918
ceramic composites with alumina matrix, impact strength and dynamic loading 2−80758
ceramic-metal systems, ion tunnelling 2−51183
composite fuel annular bodies, fracture and elastic props. 2−71588
composite porous fibre material, strength rel. to porosity 2−43707
concrete, steel reinforced, conf., Adelaide, Australia, Sep (1971) 2−61013
discontinuous fibre, matrix stress conc. factor rel. to modulus ratio 2−61012
dispersion relations and elastic props., variational methods 2−66604
elastic, multi-continuum theory 2−71655
elastic behaviour of multilayered bidirectional composites 2−69664
elastic composite laminates vibration in cylindrical landing, exact solution 2−66493
elastic moduli, effective uniqueness 2−66546
electron diffraction patterns from C fibres, interpretation by optical analogue techniques 2−80613
epoxy matrix with graphite particles on fatigue damage indicator 2−53971
fabrication by unidirectional solidification 2−80850
failure criteria of concrete rel. to incremental constitutive laws 2−58864
fatigue crack damage, vibr. testing 2−60921
fibre, brittle matrix, strength, thermal shock resist., impact and abrasion resist. 2−53968
fibre composite, containing discont. fibres, theory for steady state creep 2−47510
fibre reinforced, chemically reacted ceramic matrix props. 2−56972
fibre reinforced, elastic waves 2−43673
fibre reinforced, elimination of coupling effects 2−74917
fibre reinforced, fracture toughness 2−77667
fibre reinforced, strength, review 2−61009
fibre reinforced, u.s. elastic consts. 2−50723
fibre-reinforced, graphite/epoxy, compressive fatigue 2−61021
fibre-reinforced, shrinkage stresses near discontinuity 2−71659
fibre-reinforced, state-of-the-art 2−47663
fibre-reinforced, stress boundary value problem for plane strain deform. 2−58868
fibre-reinforced metal, resist., calc. 2−50915
fibres, in metal matrix, precise alignment and uniform distrib. 2−77666
fibres, longitudinal tensile failures 2−64745
fibrous, plastic flow and fracture obs. 2−43898
fibrous metallic, thermophysical characs. 2−54070
filament reinforced, multiple fracture 2−56975
filament reinforced materials, plastic limit behaviour and failure 2−84086
filament wound pressure vessels, quality control, nondestructive testing 2−64791
filament wound rings, orthotropic photoelastic analysis of residual stresses 2−41601
glass, C continuous fibre-reinforced, mech. props. 2−50919

Composite materials continued
glass, C discontinuous fibre-reinforced, fabrication and props. 2−50918
glass fibre, high modulus, prep. and crystn. kinetics 2−43902
glass fibre reinforced, laminated, tensile and bending strength 2−84123
glass fibre reinforced nylon 6, dynamic viscoelasticity temp. depend., two-phase blend system model applic. 2−71556
glass fibre reinforced plastic beams, dynamic moduli and loss factors 2−47487
glass fibre/polyester resin, cracking and debonding on water uptake 2−61020
glass reinforced plastics, debonding and cracking under tensile and fatigue loading 2−64725
glass reinforced plastics, stress distribs., debonding, stress concentrators effects, microdamage effects 2−64724
glass-crystal two-phase, fracture, theory 2−74860
glass-reinforced plastics, behaviour in water under high stress 2−84083
gradient, review 2−50914
graphite, pyrolytic, ribbon reinforcement production and mech. props. 2−56999
graphite, Pyrostrand, fabrication, struct., mech. and thermal props. 2−53960
graphite$-$ZrC_x($-$Zr) systems, durability props. rel. to comp. and struct. 2−77741
graphite fibre, reinforcement for struct. applic. in nuclear reactors 2−56992
graphite-epoxy composites, radiation effects on mech. props. 2−64795
graphite/SiC, thermal expansion, 300 to 800 K 2−54057
hemispherical laminar, thermal expansion, 300 to 800 K 2−54057
hyperelastic media, laminated, control vol. approach to propagating shock front 2−47486
laminar debounded, torsion 2−50912
laminated, thermally induced stress waves 2−47665
laminated arch under mech. and thermal action, elastoplastic behaviour 2−76324
laminated fibre-reinforced plates, plane strain bending 2−66543
magnetostrictive phase, piezoelec. phase, magnetoelec. prod. prop. 2−47664
mechanical props. and structure, review 2−43901
metal, strengthening by explosive incorp. of strong wires 2−61011
metal fibre/refractory oxide matrix, growth and characterization 2−56990
metal matrix, radiography, review 2−43768
metal-matrix, mech. strength and thermal stability, development 2−43900
nichrome, W filament reinforced, microstruct. 2−53970
nichrome, W filament reinforced, struct. and props. 2−53967
nichrome, W or Mo reinforced, filament-matrix interface struct. 2−53966
off-eutectic composite growth, transient composition changes, calc. 2−60548
organic matrix, thermally degrading, thermal expansion, theory 2−53963
oriented, prep. from solid phase by directional eutectoid demixing and oriented cellular separation 2−74918
photoelastic tensor, calc. 2−61593
plastic, C-fibre reinforced, interlaminar-shear fatigue props. 2−71656
plastic, fibre reinforced, stress distrib. in brittle matrix surrounding woven or crimped fibres 2−71657
plastic, unidirectional C-fibre reinforced, shear strength and modulus 2−74921
polyester, glass fibre-reinforced, fracture energy determ. 2−50780
polyester, glass- or C-fibre reinforced, work of fracture 2−74863
polyester resin, steel wire reinforced, fracture toughness 2−47528
polyethylene filled with randomly oriented glass fibres 2−77690
polystyrene-poly(2,6-dimethylphenylene oxide) freeze dried blends, viscoelastic response, rheological compatibility 2−83353
powder metallurgy of high-temp. materials, conference, Tyrol, Austria, June 1971 2−53937
powders, use for coatings, new developments 2−61010
pressed metal-fibrous mats., radial thrust calc. 2−68150
PVC-filler composites, influence of fillers on dynamic mechanical props. 2−64792
re-entry materials, carbon, thermal props. 2−56981
refractory oxide, oxide filament reinforced, characs. 2−56973
resin, fibre-reinforced, metal incorporation using organometallics 2−50923
rocks, effective elastic modulus calc. 2−56974
shells of revolution without bending under uniform axial loading rel. to composite materials 2−58845
steel, bonded 2-layer plate, ballistic props. 2−60980
steel, multilayer, strength rel. to soft steel percentage 2−53824
strength, interfacial shear and tensile, Auger electron spectroscopy 2−56571
stress analysis of layered material, continuum model 2−66533
superalloy, powder, elec. discharge activated press. sintering, composite struct. bonding 2−53938
superconducting, filamentary, for pulsed magnets 2−63257
superconducting multifilamentary composites, degradation and losses 2−64935
superconductor, stability 2−44057
synthetic fibres, properties and applic. 2−77702
thermally stable macro-composite structures 2−64794
tridimensional textiles for strengthening, physical properties 2−71658
viscoelastic theory of time-hardening media 2−77706
Al/α-Al_2O_3, mech. props. 2−53947
Al/B(C) fibre, fatigue 2−56976
Al-B, deform. and failure under transverse loading 2−84110
Al, steel reinforced, thermal and elec. cond. 2−53946
Al alloy strip with steel rod inserts, transverse tensile properties 2−64701
Al alloys, eutectic, microstructures for unidirectional solidification 2−67985
Al tube, steel wire reinforced, bursting under biaxial tension stresses 2−71661

Composite materials continued
Al tube, wound with steel wire, bursting strength and toughness 2−71660
Al_2O_3/B fibre, high temp. bearing characts. 2−47558
Al_2O_3, ceramic to metal seal for thermionic fuel elements 2−53928
B-epoxy, fibre reinforced, stress waves dispersion 2−47743
B epoxy composites, irrad. in nuclear reactor, strength 2−80801
B filaments embedded in Al alloy, initial yield surface 2−66507
Ba-mica/Al_2O_3, fabrication and props. 2−56977
C-C, mech. and nondestructive props. 2−61016
C-C, mech. props. rel. to 'moulded carbon' process 2−53962
C-C, phys. and mech. props. of mats. fabricated by wet winding endless fibres with pitch 2−53959
C-C composites unidirectionally reinforced with carbon and graphite fibres, exam. of props. 2−68176
C-C fluted core, 3D reinforced, fabrication and mech. props. 2−53961
C-C unidirectional, fibre-matrix interactions 2−56978
C-graphite matrix, microstruct. effects on mech. props. 2−61015
C-metal, high strength, evaluation as sliding material 2−61019
C, chem. vap. deposited felt and filament wound, flight tested, phys. props. 2−61017
C, chem. vap. deposited felts, compressed, mech. props. 2−61018
C, fibre reinforced resin matrix, elastic props., u.s. obs. 2−53964
C, glassy fibres, derived from phenolic resin, mech. props. 2−84100
C, PHS, effect of variation in precursor resin on struct. and mech. props. 2−53958
C felt, neutron irrad., thermal expansion, 20-1000°C 2−54055
C fibre-epoxy composite, acoustic emission during continuous tensile cycling 2−56986
C fibre-reinforced, electron microscope obs. 2−53951
C fibre, reinforcement for struct. applic. in nuclear reactors 2−56992
C fibre materials, book 2−43904
C fibre monofilament substrate/chem. vap. deposited B, compability problems 2−53956
C fibre reinforced, thermal insulation 2−56984
C fibre reinforced, X-ray preferred orientation obs. 2−53949
C fibre reinforced chem. vap. deposited C composites, micromechanics 2−53955
C fibre reinforced glass, fracture energy 2−84104
C fibre reinforced plastic beams, dynamic moduli and loss factors 2−47487
C fibre resin composites, Royal Aircraft Establishment review 2−43903
C fibres, adhesion to organic matrices 2−84101
C fibres, property changes during fast neutron irradiation 2−53965
C fibres, strengthening by fast neutron irradiation 2−71662
C fibres, two dimensional lattice orientation and three dimensional crystallinity 2−68177
C fibres electron diffraction studies, lattice fringes rel. to defects and diffraction geometry 2−80634
C filament wound cylinders, CVD C infiltrated, mech. props. 2−56985
C precursor, spheroidal isotropic, pressure carboniz. of divinyl-benzene 2−56983
Cu-W, continuous-fibre metal-matrix, fracture surface energy det. 2−55475
Cu, Mo fibre reinforced, rolling and annealing characts., internal friction obs. 2−56987
(Fe,Cr)-(Cr,Fe)$_7$C$_3$ eutectic, growth and props. 2−50920
Mg systems, fuel cladding, corrosion in CO_2 2−57424
Nb_3Sn, multifilamentary composite in ductile matrix, supercond. props. 2−51113
NbTi filaments of round composite superconductors, anisotropy of critical current density 2−71870
Ni-Cr base alloys, filament reinforced, mech. props. 2−56988
Ni-(5wt.%)Fe-(5wt.%)W, powder composite, fracture micromechanism obs. 2−56947
Ni-base, superalloys with fibres obtained by direct solidification, props. 2−64793
Ni, Al_2O_3 whisker or fibre reinforcement, poor efficiency 2−47668
Ni, C fibre reinforced, prep., thermal expansion, high temp. deformation characts. 2−74919
Pb-Sn eutectic alloy reinforced by stainless steel fibres, tensile strength 2−77742
Pb containing P bronze, fibre composite, steady state creep meas. 2−47515
Si-$CrSi_2$, $CrSi_2$ fibres in Si matrix, anisotropy columnar structs., resist. anisotropy 2−74920
Si-Sb compressed composite, obs. of neutron energies in range 13-15 MeV 2−59633
SiC/W layer, thermal cond. and diffusivity 2−47768
SiC base composites, impact strengths, 72-2400°F 2−60885
Si_3N_4 base composites, impact strengths, 72-2400°F 2−60885
Sn-Pb alloy stainless steel fibre reinforced, fracture behaviour 2−50921
$TiC_{1-x}N_x$ in Ni binder, cermet hard alloy, prep. and props. 2−53945
UO_2/W, unidirectional solidification behaviour 2−47669
UO_2/W system, eutectic structs., influence of growth parameters 2−53969
W-HfO_2, thermal shock resistance 2−56989
WC-Co, microstruct. interpretation of stress-strain behaviour 2−47670
ZnO/Al_2O_3, heteroepitaxial layer struct., surface acoustic props. rel. to delay line behaviour 2−68235
ZrC_x/C, vapour deposition by iodide process 2−50922
ZrC-C composites, vapour deposition by the chloride process 2−80793
ZrO_2-W, growth by unidirectional solidification of eutectic melt 2−64796
ZrO_2, thermal shock resistance 2−56989

Composite particles
see also Alpha-particles; Deuterons; Helium-3; Tritons
parton, calculation, field theoretic. 2−82616
relativistic wave functions 2−63007
vector, with small energy, asymptotic scattering formula 2−46019
^{8}He production in K^- interactions on emulsion nuclei 2−79792

Compressibility
see also High-pressure phenomena and effects
— 2—58781
alkali metal, empty core model pot. calc. 2—64586
rel. to anharmonicity estimation, using X-ray interference intensity coeff. 2—54017
bone, considered as solid-liquid composite 2—69220
buckling of shells with cutouts 2—52146
diamond-metal system, compaction during liq.-phase sintering 2—80829
diatomic molecular crystal, calc. using lattice vibr. model 2—43960
elastic solids, nearly incompressible, theory of small deformations 2—52170
electron gas, formulation 2—47825
electron liquid in metallic density range 2—54117
elemental solid, static method in piston cylinder apparatus to 45 kb 2—50739
elements, atomic coordination valency 2—80591
fluids, real, eqns. of state, compressibility factors 2—53108
graphite single crystal, X-ray diffr. during shock wave compression 2—56646
human intervertebral disk in pre compression, stress distribution 2—55217
ionic cryst., Szigeti relation 2—43952
isotropic plastic solids, geometric instabilities under uniaxial compression 2—66513
metal, liquid, statistical mechanical perturbation theory 2—80461
metal, nearly-free-electron, calc. using struct.-independ.-formalism 2—47801
metallic system, dynamic compressibility curve determ. from eqn. of state of constituents 2—60861
particle size distribution, effect on packing props. in high silica 'roseki' refractories 2—64786
Poisson coefficient for thinly layered medium 2—60862
polytetrafluorethylene, shock compression, acoustic velocity behind stress wave front 2—77781
rare earth monochalcogenides, up to 300 kbar, high press. X-ray diffr. obs. 2—68297
rigid plastic material with entrapped viscous lubricant on platen face, plane strain 2—55467
sands rel. to clays 2—62017
shock wave propagation in compressible medium, hydrodynamic theory and scheme for incompressibility 2—82370
silica glass, anomalous properties, interpretation 2—67884
spherical shell compressed between rigid plates, axisymmetric post-buckling and nonsymmetric buckling 2—45376
ternary refractory carbide, rel. to thermodynamic props. 2—71652
unit-compressibility line for deriv. of eqn. of state 2—53330
Al single crystal, X-ray diffr. during shock wave compression 2—56646
GaAs-GaP alloy, i.r. lattice absorpt. obs. 2—57074
GaAs, i.r. lattice absorpt. obs. 2—57074
GaP, i.r. lattice absorpt. obs. 2—57074
H, solid, at high density 2—43501
He, solid h.c.p. crystal, from elastic consts. by sound propagation 2—43972
He monolayer formation on graphite, compressibilities at completion 2—71253
^{4}He, near critical point, temp. depend. 2—80505
Kr, solid, elastic constants detn. 2—50725
LiF single crystal, X-ray diffr. during shock wave compression 2—56646
Na, metallic, Kohn-Sham self-consistent calc. 2—60698
NaCl, dynamic compression porosity effect 2—53800
$Te_{15}Ge_3As_2$ glass, calc. from u.s. velocity 2—47742
W, explosive compaction of powders by direct method, survey 2—61008
$ZrSiO_4$, anisotropy, X-ray obs. 2—54064
gases
— 2—67870
adiabatic compression unit, investigation of parameters 2—56402
Burnett apparatus for accurate determination 2—56439
classic particle in 1-D box, compression heating 2—62948
dense gases, calc. 2—80386
ethyl esters of some carboxylic acids, adiabatic compressibility 2—74486
methane, unit-compressibility line for deriv. of eqn. of state 2—53330
rarefaction effects, high altitude rocket plumes 2—44790
turbulent boundary layer calc. with foreign gas injection 2—67718
liquids
alcohols, compressional study through pseudo-Gruneisen parameters 2—83789
benzene plus cyclohexane, dilution piezometer meas. at 298.15K 2—67823
collapse of condensing bubble 2—43298
condensed matter formed by electric spark in dielectric, X-ray flash investigation 2—46876
electrolyte soln., conc. depend., ion-dipole free energy 2—50342
from isobaric ensemble formalism in Monte Carlo calcs. 2—64428
metal, statistical mech. perturbation treatment 2—71350
nonlinear response to laser pulses, effect of steric effects and compressibility, rel. to diameters of self- trapped filaments 2—71200
spherical shell, translatory motion under the effect of spherical wave in compressible liquid 2—71122
water under negative pressure, vapour pressure and bulk modulus 2—83734
$CdCl_2$, adiabatic compressibility and sound propag. speed, reln. to molec. struct. 2—72564
$CoCl_2$, adiabatic compressibility and sound propag. speed, reln. to molec. struct. 2—72564
^{4}He, isothermal compressibility, rel. to light scatt. intensity peak near λ line 2—50391
Kr liquid 145-240 K sound velocity adiabatic compressibility and specific heats 2—83790
Mg from interforce functions temp., range 50 to 150°C, X-ray 2—67802
$MgCl_2$, adiabatic compressibility and sound propag. speed, reln. to molec. struct. 2—72564
Na alloy, density and sound velocity studies 2—77415

Compressibility continued
liquids continued
Ne, adiabatic and isothermal, determ. from sound velocity measurements 2—46950
$NiCl_2$, adiabatic compressibility and sound propag. speed, reln. to molec. struct. 2—72564
Rb, calc. using sound velocity data at high pressures 2—71195

Compressive strength *see Mechanical strength/compressive*

Compton effect
3-channel helicity conservation, a critical test 2—79491
Compton forward scatt. amplitudes, sum rules 2—79498
electron scattering, Regge behaviour of amplitude and tests of complex scaling 2—59426
electron velocity in atoms, Compton effect demonstration for students 2—78722
extragalactic X-ray sources, Compton scattering of electrons and photons rel. to extended and compact sources 2—51798
extragalactic X-ray sources, thermal bremsstrahlung and inverse Compton models 2—75835
fast electron and photon transport in matter, Monte Carlo simulation 2—80926
fixed poles in scatt. amplitudes, rel. to bound-state nature of phys. nucleon 2—66928
forward scattering, kinematics of coupling of Regge poles to photons 2—63605
high intensity scattering, origin of wavelength shift, semiclassical treatment 2—55814
hydrogen-bonded glasses, Compton electrons generated by pulse radiolysis, Frohlich polaron model for trapping 2—44040
hydrogen-like atom, nonrelativistic Compton-like scattering of photons by K-shell electrons 2—70610
hydrogen-like atoms, dipole approx. of nonrelativistic cross section for Compton scattering by K-shell electron 2—70611
imaging of light waves by electron microscope and stimulated Compton scattering 2—82451
inverse, as energy loss mechanism in CTR 2—83100
iso-vector 0^+ meson, 'near universality' of functions in dual reson. model 2—66970
laser photons scattered by electrons 2—52435
lepton-hadron scatt., virtual, duality, scaling and fixed poles 2—63506
metal, momentum density of cond. electrons, theory 2—84255
on nucleons, fixed pole in virtual Compton effect amplitude 2—45873
photon-lepton scatt., fourth-order Compton amplitude in Weinberg model, Drell-Hearn sum rule 2—59408
plasma, Stokes line generation during laser irrad. 2—74369
proton, differential cross section meas. in $\Delta(1236)$ resonance region 2—63653
radiation from relativistic particles in rarefied plasma, depression of power spectrum 2—80228
relativistic derivation for non-stationary electron case 2—45874
scattering, analysis of finite-energy sum rules using Regge-pole model including cuts 2—63494
scattering, calc. of spectral forms for invariant amplitudes to order e^4 2—76597
scattering, corrections to vector meson dominance, estimation using light cone expansion 2—42326
scattering, light core approach to fixed poles 2—59409
scattering breakdown of vector-meson dominance in parton model for photon process 2—66923
scattering centre motion effects 2—42325
scattering sum rules, photonlike particles in dual resonance model 2—59469
scattering suppression, semiconductor gamma ray spectrometer, guard scintillator, pulse shape discriminator, isotope determination 2—82796
spectrometer, construction with Si(Li) and Ge(Li) detection for obs. of lower energy γ-rays in complex spectra 2—79642
stimulated, harmonic generation due to electron retardation in presence of intensive light wave 2—66796
vector meson photoproduction, and nucleon Compton scatt. amplitude, quark model 2—55865
virtual Compton amplitude and fixed-pole 2—52552
X- and gamma-ray spectrometry, improvement of accuracy by summing 2—59632
X-ray scattering, use in studying properties of solids 2—82114
X-ray sources, scattering by thermal electrons 2—73040
$e\gamma$ scattering, polarized target, calc. of differential cross section to order e^6 and left-right asymmetry 2—76598
ep scattering sum rule connecting resonance region of virtual Compton amplitude to deep inelastic region 2—70161
e^-p, virtual scatt. of forward direction, scaling limit 2—63510
γp scatt., forward, cross section analysis 2—52553
n-Compton scattering, evaluation of $J=0$ fixed pole 2—76721
π scattering, low-energy theorem and threshold identity arguments for fixed pole 2—76671
Ag, photometry of scattered X-rays, Compton effect scatt. power 2—68213
Al, symmetry of profile, 59.54 keV γ-rays 2—71764
Li, momentum density of cond. electrons, determ. 2—84255
LiF X-ray Raman spectrum, peaks superimposed on Compton distrib. 2—72386
MnO, Compton profiles, electron momentum distrib. 2—78116
Na, momentum density of cond. electrons, determ. 2—84255
Sc, Compton profiles, electron momentum distrib. 2—78116
Si, obs. of K electron binding effect 2—83882
TiB and TiB_2, Compton profiles, electron momentum distrib. 2—48211
TiO, Compton profiles, scatt. factors, determ. of electron state 2—68628
V, electron momentum distrib. obs. 2—51081
V, polycrystalline, profile interpret. by renormalized-free-atom model, and electron momentum distrib. 2—68670

Computation *see Calculation*

Computer applications
— 2—67572
γ and α spectra analysis and interpretation 2—63702
acoustic laboratory, automated environmental control 2—69770

Computer applications continued
acoustic measurements, programming requirements 2–58908
acoustic noise evaluation in Algol-60 2–58930
acoustic noise on-line evaluation 2–58929
aerospace, conference, Las Vegas, Nev., USA (1971) 2–48636
air and water pollution monitoring using on-line computer 2–62091
algebraic techniques, use of computer programs impact on physics 2–82279
amorphous hard sphere aggregates prep. 2–53514
analogue computing system for gaussian and lorentzian simulation of absorption, circular dichroism and e.s.r. spectra 2–45782
analogue expt. to determ. effect of turbulence spectrum band-width on nonlinear characteristics of filament vibrations 2–73405
Anger gamma camera system, improvement of intrinsic resolution 2–63707
anharmonic crystal interacting with ideal gas, dynamical study using computer expts. 2–58787
anisotropic tapered elements stress analysis using displacement models, FORTRAN IV subroutines 2–58849
arc plasma in curved discharge tube, computer-simulation 2–53173
architectural acoustics of New-NHK Hall in Japan, design of shape 2–82357
astronomical ephemerides, program for modern aberration coefficients 2–69194
astronomical instruments control system, portable, primarily for photopolarimeters 2–45007
astronomical optical telescopes, data acquisition, control 2–85069
astronomical telescope and dome control 2–58562
astronomical telescope automation with on line data processing 2–45013
astrophysics, computer program applications 2–84932
astrophysics data system for rapid scanner 2–76050
atmospheric acoustic waves, ray tracing using hybrid computer 2–81653
atmospheric longitudinal compression waves, ray tracing program using Haselgrove's eqns. 2–84857
atmospheric stagnation periods, simulation of wind conditions 2–75557
atomic and molecular physics, on-line data bank for conversational retrieval 2–42723
atomic collision processes, experiment-computer system, on-line operation 2–42781
atomic one electron radial wave functions, obs. using computer produced movies 2–79934
atomic structure calcs. impact of computers 2–83172
auroral oval geographical position determ. technique 2–65906
automated multiple specimens holder for X-ray powder diffractometer 2–83926
automatic comparator for U spectral obs. between 19080 and 30261 cm^{-1} 2–79944
automatic indexing by trial-and-error, method of X-ray powder patterns 2–64600
averaging time determ. for atmospherically degraded light beams 2–81686
Barringer INPUT data, digital processing 2–54723
b.c.c. lattice, screw dislocation; motion under stress at 0 K, computer simulation 2–71484
biology, skeletal muscle vascular resistance, analogue computer calculation 2–82023
biomedical on-line computing, AAMI Conf., Los Angeles, March (1971) 2–62861
blood bank computerized management information system 2–82031
boiling channel, l.f. stability, D marking method, computer calc. 2–56454
bubble chamber tracks, pattern recognition, computerised 2–79688
buffered data resolving system, dead-time losses 2–79644
calculations on radio emission from extensive air showers 2–46024
Camac system controller 2–78688
cantilevered columns under periodic loads, stability and non-stationary vibration digital simulation 2–69705
carrier conc. in semicond. structures in transient conditions, two dimensional model 2–54210
celestial mechanics, precompiler for the formula manipulation system TRIGMAN 2–58171
celestial mechanics, symbolic programming rel. to computation of general normalized inclination functions 2–81754
cellular response to radiation, computer generated model 2–69326
cerebral circulation, digital dynamic radionuclide studies, automatic analysis 2–76094
Cerro Tololo data acquisition system 2–45011
charged particle beams, simulation 2–79696
chemical structure search by molecular spectroscopy 2–79968
chromatography, multichannel statistical optimiser use 2–78217
chronic respiratory monitoring using ultrasonic spirometer 2–55247
closed loop control of wind tunnel model trajectory simulation system 2–46849
cloud seeding, convective growth, model using Project Whitetop data 2–75601
clouds motion meas. from ATS pictures 2–48438
coastline under hurricane action, computer simulation 2–57875
colour photography, mask characts. in photomechanical process 2–63445
computer enhancement of high resolution electron micrographs with weak periodic information, computer enhancement 2–79143
conductor material, temp. distrib. in d.c. heated conductors, calc. 2–57054
conference, physics of electronic and atomic collisions, Amsterdam (1971) 2–42772
control of electron microprobe analyzer 2–66718
control of thermal ionization mass spectrometer 2–63987
countercurrent flow systems, method for numerical determination of transients 2–60142
creep data acquisition system, applications to reactor component design 2–83120
cryogenic plant design, BWR eqn. of state development and use 2–76121
crystal growth, Czochralski method, computer controlled with i.r. TV system 2–47258
crystal surface structure and growth kinetics, simulation 2–50564
crystallisers, dynamic and steady-state, simulation 2–64596

Computer applications continued
crystallographic computation, mol. model generation and fitting 2–53647
crystallography, absorption programs, checking method for crystal absorption 2–64628
crystallography, calc. and control equipment 2–60748
crystallography, program checking, I.U.C. commission tests 2–67965
crystals of arbitrary symmetry and orientation, stereographic projection 2–43533
cubic crystal, crystal face growth kinetics, computer simulation 2–60703
cumulus clouds, model of hygroscopic seeding 2–62204
data acquisition and control system for 46 m radio telescope 2–45009
data acquisition system for spectrophotofluorometer 2–82584
data processing for weather radar 2–75506
data reduction in technique of three dimensional location, using planar X-ray systems 2–62960
data treatment system, gas chromatography, mass and infra-red spectral analysis 2–84699
defectoscopy, quantitative, simulation 2–60745
density matrix values in configuration space, computer method 2–52897
design of power transfer system for inductively coupled oceanographic sensors 2–72725
dielectric layers with imposed spectral characts., control and preparation 2–63418
dielectric props. of high or low loss materials, short-circuited waveguide meas., computer program 2–49236
differential refractometry with numerical reading 2–55731
diffraction method of controlling amplitude variations in computer generated holograms 2–79271
digital simulation of blood flow in renal vascular and tubular compartments 2–51903
digital spectral analysis, applic. to diagnostics of plasma fluctuations 2–70926
digitized weather radar data, computer processing techniques 2–75500
dipole-dipole collisions, evidence for neutral collision complexes, computer-graphics studies 2–67533
disk galaxy studies, construction of static self-consistent model 2–58229
dispersive syst., colliding jets, motion of solid particles, computer anal. 2–56310
display of three dimensional u.s. data for medical diagnosis 2–66273
domains, cylindrical dimens. in presence of wall coercivity and wall energy anisotropy computer studies 2–81232
dosimetry in radiotherapy using PDP8/I computer 2–69394
dual parameter pulse height analyser, 128 × 128 channel, computer controlled, for solid state laser tests 2–73584
Earth resources technology satellites, digital image processing techniques 2–81624
e.e.g. technology trends 2–76056
elastic-plastic-creep solutions for ratchetting 2–56895
elastodynamic near-field of finite propagating tensile fault, computer generated waveform plots 2–72610
electric arc, analogue modelling 2–64361
electromagnetic induction 2–62925
electron absorption spectra at u.v. and visible range for computer search system 2–79969
electron beam, relativistic, mag. focusing by mirror mag. field, computer simulation 2–79012
electron channelling pattern geometry, computer simulation in cubic crystal 2–68267
electron lens analysis, real and virtual cardinal points, aperture and aberration constants 2–76453
electron microscope images, crystal containing plate shaped crystal, and crystal lattice 2–53641
electron microscope ring diffraction patterns analysis 2–79153
electron microscopy, automation of structural analysis of images 2–71417
electron microscopy, simulation of shadow width distributions for protein molecules 2–79099
electron probe microanalysis 2–58823
electron trajectories in arbitrary static e.m. fields, elimination of integration truncation errors 2–73528
electron-atom collisions, computer methods and software packages 2–42764
elementary particle, machine recognition of patterns 2–82637
e.m. radiation properties of smooth arbitrary shaped conducting bodies near external source, numerical analysis 2–63202
e.m. wave propagation in hollow conducting waveguides of arbitrary cross section, solution of nonlinear integral eigenvalue equation 2–63198
engine cycle instantaneous combustion analysis 2–58940
epitaxial electrodeposition simulation, two dimensional nucleation effect on electrocrystalliz. rate 2–71320
e.p.r. spectra, comparison with expt. for Tb^{4+} e.p.r. in TbO_2 2–54494
e.s.r. spectra, recording in digital form by remote computer 2–59010
estuaries, shallow barricaded, variable-boundary tidal circulation model 2–57873
experimental data processing, systematic SEDAP software package 2–78863
experiments for school science course, analog simulation 2–78742
extrusion of polymer melts, computer aided rheology measurements and processing 2–64400
eye, perimetry, information theoretic basis for computer control of automated perimetry 2–85142
fast breeder reactor, steam generator vessel pressures resulting from sodium-water reaction, computer analysis using SWEAR code 2–46377
fast reactor control rods, performance modelling 2–76950
fatigue failure obs. of materials under broad band random vibrations 2–77707
ferrite, spinel struct., magnetostriction consts. estimated 2–78036
ferromagnetic disordered alloy, magnetiz.- temp. curves, influence statistical fluctuations of conc., calc. 2–61512
film generation, for teaching aids in solid- state physics 2–78729

Computer applications continued
flow between converging flat plates, numerical analysis 2–67777
fluid dynamics, computer implementation using IBM system/360 operating system 2–43043
fluid mechanics simulation of various flow types 2–83440
fluids physical properties data base system 2–74309
forecasting of F_2 layer parameters 2–84912
Fourier analysis, signal processing technique to obtain Kerr effect M-H loops 2–48064
Fourier spectroscopy, digital data handling of spectra 2–52485
Fourier transform spectroscopy, high resolution 2–63429
frequency-time analysis of oscillations rel. to seismic waves using computer procedure 2–84703
galactic spiral structure, development and application of computer models, obs. of density waves 2–78444
rel. to galactic spiral structure 2–51703
gamma camera, anal. and correction of spatial distortions 2–48855
gamma ray camera, coaxial Ge(Li) for medical use, computerised display 2–51936
gamma ray camera-computer systems, maximum frame rates 2–78652
gamma-ray spectra analysis 2–61564
gas behaviour det. in cryogenic turbines and low temp. machines 2–52006
gas electrical breakdown simulation 2–53257
gas permeability of metals under non- isothermal conditions, calc. 2–60826
gases, average pressure measurement 2–53268
gases, polyatomic, program to predict phys. props. from mol. struct. 2–83698
geodesy, weighting function approach to surface modelling 2–54609
geoelectric sounding curves, multilayer, computer processing and representation 2–44562
geology, nonuniform density of data points in three variable closed array 2–81594
geophysics, balanced computer systems 2–54587
geophysics, influence of computers on development of various fields 2–84712
geophysics, mini-system for computer controlled field systems and office playback systems 2–54588
glass, chem. analysis, oxide content, by physical methods, computer calcs. 2–44500
glass analysis batch and raw materials, computer controlled X-ray fluorescence 2–64525
grain boundaries, entropy, Einstein cryst. model and Morse pot., computer calcs. 2–56727
grain boundary structs. and energies, computer calcs. 2–56725
gravitational waves, detector coincidences, computer analyses, local disturbance elimination 2–82202
gravity and magnetics, 1964-71, data processing and interpretation methods 2–78242
gravity data, standard format-prerequisite to routine computer applications 2–57476
gravity waves, Stokes expansion 2–77197
Hale observatory 2–45008
heart rate variation obs. using tape recorder and mini-computer 2–69247
Heisenberg ferromagnet simulation 2–81272
helical scanning, location of radionuclides in human body 2–76099
heuristic value of computers in physics 2–82280
hexagonal grid work of straight elastic rods, soln., digital computer application 2–45371
hologram imagery, aberrations analysis 2–52439
holograms, recording methods and noise charact. 2–82498
holographic automatic surface mapping, tracking and measurement 2–79275
hull structure design, finite element method for stress concentration 2–73371
human auditory system modelling 2–76105
human lung tissue, computer method for counting number of alveoli per unit area 2–81983
hydrodynamics, numerical solution of cylindrical shock problem, computer oriented 2–67557
iceberg trajectory computation, comparison with observations 2–57881
image filtering with fast Fourier transformation 2–79142
image method for calc. of sound pressure levels within rectangular room 2–55558
incompressibel turbulent flow, resolution of split flows at thick bodies, numerical method for computer solution 2–64231
incompressible fluid, laminar flow in conduit computer-oriented solution 2–46684
industrial research and development 2–82088
inert gas bubbles in solids, computer simulation of precipitation kinetics 2–64424
interactive computer graphics system in spark chamber events display 2–48936
interactive computer graphics system in spark chamber events display 2–48936
interface for small computer allowing variable star data to be recorded 2–62481
interferograms analysis 2–79353
intersecting, stacking faults, intersecting, electron diffraction contrast, intersecting overlapping stacking faults, computer simulation method display 2–80625
ion-dipole collisions, computer plotter studies of vibrational effects, classical tunnelling 2–46467
ionosphere, gravity wave induced irregularities, receiver drift expt. simulation 2–62364
ionosphere D-region, diurnal models, transient conditions, photochemical computer code 2–81731
ionosphere F region, seasonal anomaly, simulation 2–78402
ionosphere incoherent scatter sounder, design optimization 2–78392
ionosphere propagation of e.m. waves, 2 dimen' tracing, computer program 2–65944
ionospheric modelling, synthesis of Jicamarca magnetic storm data 2–72916
i.r. spectrometry, developments and digital computer control 2–70075
isodose scanner 2–69355

Computer applications continued
isotope separation on-line facility at Buenos Aires IALE project 2–52957
iterative calc. of mass flow and pressure in pipe systems 2–64232
Jahn-Teller effect, dynamical, numerical analysis 2–78056
Josephson junction, subharmonic steps in V-I curves on microwave irrad. analog computer studies 2–81046
junctions, diffused, capacitance, C^{-3} vs. U intercept with U axis, computer calcs. 2–81115
K giant stars, metal abundances from synthetic stellar spectra 2–69083
kaon decay, charge asymmetry meas. system 2–52690
kinoform filter generation for image production 2–79313
Knudsen cell orifices, conical, divergent particulate fluxes, computer simulation 2–50136
laser anemometer, Doppler difference method, automatic data processing system 2–84789
laser beams, thermal blooming, computer simulation 2–82521
laser Raman spectroscopy of matrix isolated species, time averaging 2–66850
laser resonators, transverse modes, diffractive calculations 2–82471
LATREP lattice code accuracy 2–46244
lens assembly system, mini computer controlled 2–79399
lens design packages 2–70001
lens design system, LASL, improved speed 2–79405
life detection on Mars, computer-controlled analytical instrumentation of Viking spacecraft 2–54977
light scattering function calculation, for isotropic spherical particles 2–50383
liquid scintillation counting, external standard channel ratio quench correction, computer aided calibration 2–59618
liver tumour detection with ^{67}Ga-citrate and scintillation camera, computer scintigraphy 2–73198
Lorentz micrograph simulation in electron microscopy 2–79135
lunar regolith evolution mechanisms from impact experiments and computer simulations 2–81943
lunar spectral reflectance ratios, computer generation colour image display 2–66877
magnetic coils, high field, uniform current density, stress calcs., computer program 2–73519
magnetic field in conducting ferromagnetic plates, analogue computer study 2–73509
magnetic phase transitions, dynamics, determ. by computer simulation 2–78948
magnetometer, for measuring remanent magnetism of rock and mud samples 2–54958
magnetospheric elec. fields model 2–65879
magnetospheric processes simulation 2–65867
magnetostriction curves calc. 2–81244
marine exploration, GULFREX computer systems 2–54798
mass spectra, low resolution, pattern recognition anal. 2–81559
mass spectra of solids, automated analysis 2–84688
mass spectrometer, quadrupole ion entrance masking 2–42707
mass spectrometer, spark-source, semi- automatic system for operation of electrical detection 2–84700
mass spectrometry 2–59887
material integrity of mechanical structures by computer interpretation of vibration analysis 2–60925
materials testing, automation using process control computer 2–58822
matrix displacement analysis of shells and plates including transverse shear effects 2–52137
mechanical test data analysis 2–58821
metal, hexagonal, dislocations, undissociated, computer simulation of images 2–43632
meteorological rocket data processor and results from 7 March 1970 solar eclipse 2–65648
meteorology, computerized radar system with real- time display 2–75503
meteorology, diurnal temperature and dew point tables production 2–72763
meteorology, impact of computers 2–84787
meteorology, impact of computers 2–84787
meteorology, using splitting up techniques 2–81695
MICRETE 4, basic theory 2–46359
micropulsations, spectral and polarization analysis, computer assisted, of obs. by ATS-1 2–62391
model calcs. of systematic errors in e/m expt. with cathode ray tube 2–78730
model of circularly polarized plasma waves in homogeneous plasma 2–43181
model of initial Ba ion cloud expansion in magnetosphere 2–62305
modelling of thunder for acoustic obs. 2–44741
modulus of elasticity calc. 2–53785
molecular and atomic structure calculations using computing methods 2–42860
molecular dynamics, simulation 2–46638
molecular dynamics of dilute gases, computer experiments 2–83704
molecular structure, computer graphics representation 2–81993
molecule structural representations algorithm 2–64103
molecules structure and properties from spectra, automation 2–79967
monitoring, automatic readout, film information, optical scanning 2–82566
Monte Carlo method for obs. of kinetics of homogeneous condensation 2–43445
Mossbauer spectra of complex structures, data processing by computer 2–61600
mountainous region, elec. field intensity, computation 2–48519
multi-terminal interactive graphics system for visual inspection of particle tracks 2–79683
multichannel neutron recording system 2–70296
multicomponent vapour-liquid equilibrium data computation 2–74589
music analysis for performer in real time by computer driven c.r.t. 2–41780
neutron capture gamma ray spectra, satellite data acquisition 2–78862

Computer applications continued
- neutron scattering, Monte Carlo evaluation of multiple scatt. and resolution effects in double differential cross section meas. 2−56024
- n.m.r. spectra, spin-1 nuclei perturbed by quadrupole coupling, calculation method 2−73490
- n.m.r. spectra of AB spin system, quantum mechanical calc. using analogue computer 2−66668
- n.m.r. spin-lattice relaxation times, automatic determination 2−55633
- non-linear effects in electroluminescent cell obs. 2−63420
- nonlinear buckling of cylindrical shells, differential eqns. soln. 2−73360
- nonspherical vapour bubbles, in water, finite element soln. 2−77407
- nonsteady state diffusionless phase transition in a binary system, comput. simulation 2−71671
- nuclear bremsstrahlung measurements, multi-parameter experiments 2−78861
- nuclear fission, algorithm for calc. of specific activity of products 2−83027
- nuclear fuel core exit, COBRA-II subchannel analysis 2−76929
- nuclear fuel rod assembly, forced flow mixing model, COBRA-II, COBRA-III B analysis 2−76931
- nuclear medicine, computer analysis 2−69323
- nuclear potential-energy surfaces and half-lives of heavy and superheavy elements 2−82843
- nuclear reactor, critical time step approach to Monte Carlo reliability calculation 2−56038
- nuclear reactor core neutron flux distribution, on-line computer control 2−59814
- nuclear reactor period, algorithms for precise meas. for use with real-time computer 2−74140
- nuclear reactor piping system, obs. of dynamic response to multi-inputs 2−70540
- nuclear reactor WR-1 flux density calculation by codes 2−83159
- nuclear research experimental data processing 2−79706
- numerical methods and computational problems in MHD 2−80267
- objective analysis of sea level winds and pressures derived from simulated obs. of satellite radar-radiometer data 2−57963
- ocean currents simulation rel. to two fluid media model 2−78320
- ocean wave data management 2−75484
- oceanography, collection and processing of data from instrumental measurements 2−62047
- oceanography collection and processing of data from instrumental measurements 2−62047
- offshore refraction, field and data processing techniques 2−54665
- on-line data aquisition and analysis of spark chamber expt. 2−76741
- on-line meas. of burn-up of irrad. fuel 2−42630
- one-dimensional Schrodinger equation 2−73274
- optical design, application of Delano diagram 2−79402
- optical design, curvilinear bicubic spline fit interpolation scheme 2−79404
- optical elements interferometric testing, computer generated holograms 2−82572
- optical surfaces, ionic polishing, control applications 2−79434
- optical system of computer output microfilm 2−59295
- optimal vibration mode det. for turbine disk 2−41651
- Orr-Sommerfeld problems, numerical solution 2−46667
- osmotic pressure data, numerical treatment 2−43343
- partial differential eqns., solutions with hybrid computers 2−69628
- particle accelerating reverse beam plant, computer- aided control 2−52707
- particle accelerator beam flatness 2−67103
- particle orbits in cyclotrons, design study 2−76753
- particle pulse counting expts., PDP-8/E for on-line data 2−67071
- particle size measurements, data processing for ZnO 2−53942
- partition and thermodynamic functions determination, hybrid method 2−73334
- pattern recognition applied to interpretation of chemical data 2−78182
- pattern velocity computers, for wind velocity obs. 2−57968
- pearlite electron diffraction patterns, orientation determinations 2−68188
- pendulum simulation by analogue computer 2−73347
- perceived noisiness, study of Doppler shift effects, computer analysis of data 2−66631
- permanent magnet design 2−73516
- phase conditions of excitation of secondary electron resonance in three-electrode system 2−59107
- photon correlation spectroscopy using digital PDP-9 computer 2−79443
- physical metallurgy, computational techniques, conf., Leeds, England, Jan. (1971) 2−58820
- physics education 2−58679
- physics research 2−41422
- physics teaching, digital computer applications in A-level course 2−41442
- physics teaching 2−41441
- piezoelectric surface wave calc. 2−81130
- planetary atm., analytic scattering diagrams for computation of synthetic spectra 2−44936
- planetary nebulae, calcs. on ejection of material from white dwarf 2−72980
- plasma, asymptotic behaviour of electrostatic current-driven cross-field instability 2−83633
- plasma focus expt. rel. to two-dimensional MHD code 2−83584
- plasma loss-cone flute instabilities, single, resonant, nonlinear stabilization 2−70966
- plasma pumped by e.m. wave, nonlinear instability of Bernstein modes 2−70965
- plasma simulation, particle-in-cell model 2−80256
- plasma simulation, study of nonlinear and turbulent phenomena 2−83532
- plasmas, counterstreaming magnetized, laminar interaction simulation 2−43125
- plasticity, constrained minimisation problems 2−76331
- point charges, teaching paper, computer plotting of equipotential lines 2−78744
- polarity cross correlation noise analysis 2−73904

Computer applications continued
- pole figures, computer plotting using CDC 6600 and SC 4020 from X-ray crystal data 2−67978
- polyatomic molecule vibrations, automization of symmetry calculations 2−64097
- program control system, CARONTE modular system, status, applications, future developments 2−83071
- pulse control and data collection in n.m.r. Fourier spectroscopy 2−45627
- quantum mechanics, eigenvalues, computer- generated film 2−73272
- radar data remoting and recording system SCEPTRE for distributing CAPPI maps 2−75414
- radar evaluation of artificial precipitation enhancement using computer 2−75585
- radio interferometer at K_u-band incorporating PDP-8 computer for real-time data analysis 2−55197
- radio signals from Venera-7 spacecraft during descent to surface of Venus, digital computer analysis 2−73088
- radioastronomy and cosmic ray air shower arrays 2−81976
- radiometer, dual-channel polarizing, high-precision computer controlled, atmospheric use 2−62260
- rainfall and runoff data, conceptual anal. with hybrid computer 2−78302
- Raman spectra, overlapping band separation, depolarization ratio determ. 2−66849
- random eigenvalue problems in structural analysis, computerized Monte Carlo simulation 2−45356
- rare earth compounds, A_3B, A_2B and AB types, prediction of existence 2−74597
- reactor fuel element, electronic processing system for data from post-irradiation examination 2−52885
- reactor shield design 2−42694
- real-time anal. of flare-associated photospheric magnetic fields 2−75980
- reconstruction of holograms 2−69982
- rectangular beam, computer calc. of optimal parameters for oblique bending 2−82303
- reduction of objective prism plates of star fields, absolute calibration 2−75698
- reflectometer, automated, for u.h.v. obs. 2−79409
- respiratory mechanics, phase method of calculation using digital computer 2−66247
- restoration of optical holograms 2−69981
- satellite data processing, for cloud motion and landmark registration 2−48439
- scanning electron microscope AUTOSCAN 2−79016
- scanning spectroradiometer applying computer analysis of spectral data 2−42258
- Schrodinger eqn., one-dimensional, soln. by resistance network 2−73319
- Schrodinger equation, radial, program for numerical soln. 2−66442
- sea surface temp. nonuniformity data processing system 2−44644
- seismic and velocity data in Australia, computer mapping 2−57497
- seismic data, computer-designed wavelet Wiener filters 2−54623
- seismic data, saturation velocity analysis, computer picking 2−57673
- seismic data interpretation using interactive computer graphics 2−54649
- seismic data plotting system, high-speed, computer controlled 2−54648
- seismic data processing by general reflection point method using digital computer 2−84734
- seismic processing hardware design, vendor and user responsibility 2−54650
- seismic reflection data, automatic X^2- T^2 velocity analysis 2−57674
- seismic reflection picking in time, moveout and dip space, automated 2−54662
- seismic reflections, optimum stacking weights det. 2−54663
- seismic refraction modelling 2−54657
- seismic wavelet process, computer program 2−54661
- semiconductor, simulation of transient space-charge flow under ionizing radiation 2−71954
- service life prediction in a fatigue creep environment 2−60953
- simulation method for det. best analysis methods for Rn-daughter activity in air 2−62288
- simulation of anomalous absorption effects on image contrast of stacking faults in wedge shape crystals 2−43551
- simulation of atomic displacement cascades in metals 2−53700
- simulation of basilar membrane, bandpass noise stimulation 2−82041
- simulation of beam-plasma instability in finite length system 2−80321
- simulation of cochlear microphonic potential augmentation during intercochlear perfusion 2−45167
- simulation of data from airborne γ-ray spectrometer 2−65440
- simulation of dynamic vibration neutralizer with motion limiting stops, theory 2−66589
- simulation of hologram transmission using random phase reference 2−73606
- simulation of ion-acoustic wave and pseudowave generation in collisionless plasma 2−80320
- simulation of ion-sound plasma instability 2−53234
- simulation of linear unbiased restoration of degraded images at low light levels 2−79304
- simulation of mol. dynamics in vicinity of melting pt. 2−56540
- simulation of multilevel systems, e.p.r. and stationary ENDOR dynamics, stat. diff. of populations 2−84572
- simulation of packing of equal and unequal spheres in two and three dimensions 2−78838
- simulation of Peterson-Bogert model of cochlear partition 2−48880
- simulation of plasma heating by electric field induced instabilities 2−64334
- simulation of plasma waves and instabilities, role of trapped particles 2−80316
- simulation of reactive collisions using classical trajectory method 2−44471
- simulation of reverberation curves in rectangular rooms with diffuse sound field 2−55555

- **Computer applications** continued
  - simulation of r.f. confinement of plasmas in open-ended toroidal quadrupole 2−53199
  - simulation of scavenger competition effect on hot atom reactions 2−72542
  - simulation of sputtering of b.c.c. lattice 2−71763
  - simulation of superconducting ring cct. inductively L-C coupled 2−71844
  - simulation of three point bending test, non-linear fracture mechanics 2−43758
  - simulation of turbulent energy production in boundary layers, intermittent phenomena obs. 2−43079
  - simulation of void nucleation and growth in metals 2−53699
  - simultaneous eigenfunctions of $\mathfrak{L}^2$ and $\mathfrak{S}^2$ by direct diagonalization 2−74196
  - slotted disk velocity selectors, for molecular beams, design 2−59986
  - Solar corona study, mathematical technique for separation into electronic and dust scattered components 2−73153
  - solid iron spectrograph, on-line data recording and analysis 2−42428
  - sonar signal processing, off-line digital techniques 2−57901
  - sound wave radiation analysis 2−76374
  - space-time patterns in seismicity of western USA, obs. using interactive computer-generated graphics display technique 2−57583
  - speaker verification, implementation of on-line scheme 2−48897
  - spectra analysis by deconvolution 2−70073
  - spectrometers at McDonald observatory; control 2−45010
  - spectrophotometry, CIE colour and solar energy transmittance and reflectance values, automatic computation 2−63431
  - spectroscopic measurements, data processing 2−76545
  - spectroscopy, time-shared mini-computer, low cost 2−70086
  - speech, basic frequency determ. 2−66288
  - speech analysis and recognition, using zero crossing information 2−58635
  - speech analysis technique 2−55304
  - speech formant parameters of vocal tract, digital computer determination 2−73213
  - stability of selective gray in subtractive colour photography, simulation 2−59311
  - statistical analysis with MATLAN language 2−82274
  - steel tempering, Ostwald ripening obs., grouping errors in data analysis 2−60942
  - stellar rotation and simulation of intensity interferometer 2−58270
  - stellar systems, dynamical evolution, application of direct integration 2−78471
  - stereo mensuration system for extracting 3D data from stereo film chips 2−59342
  - stray magnetic fields in cylindrical coils determ. with desk calculator 2−76407
  - stress analysis of thin plates, annular segment finite element 2−76315
  - structure analysis of atomic and molecular level, role of computers in collection and pouting of data 2−83340
  - study of galactic spiral arm formation 2−81792
  - subnuclear particle track visualization, optical image recognition 2−79684
  - surface distribution of elements, analyzing system using electron probe microanalyzer 2−65412
  - surface tension computations in the stretched regions of bubble surfaces 2−64454
  - surface topography during ion bombardment, computer simulation 2−60619
  - surge generator, for physics research, analogue computer analysis 2−78987
  - synchrotron magnet with Fe yoke, saturation and error fields 2−73518
  - teaching physical sciences, computer based methods 2−41440
  - telemetric transmission of work load factors in ergononics research, multidimensional coding 2−85115
  - temperature obs. from self radiation 2−58973
  - temperature stress distrib. calc. for strain hardening material due to uniform heat source 2−45384
  - thermal conductivity, relaxation time analysis 2−71756
  - thermal scattering power for X-ray scattering by a molecular crystal (H.M.T.), calculation 2−53632
  - thermokinetics of adsorption 2−53587
  - thin film deposition, calc. of R and T for coating different from $\lambda_0/4$ 2−80602
  - thin film multilayer system, optical performance evaluation using computer 2−59222
  - three parameter nuclear coincidence data collection and magnetic recording system 2−76735
  - time series analysis applications, developments 2−42598
  - Total Organ Kinetic Imaging Monitor, positron mode, design and applications 2−69362
  - track images matching from three views in bubble chamber 2−55931
  - transmission line, e.m. wave propagation, analysis in transient regime 2−82406
  - transport processes of liquids under high shearing forces, computer simulation 2−60442
  - transport processes simulation, review 2−82253
  - turbulence measurements in nonisothermal flow 2−43081
  - vapour deposition simulation 2−50476
  - velocity distrib. determ. in impact tube method for meas. of period of thermal relaxation of vibration of polyatomic mols. 2−83398
  - vibrations of dynamic system with dry friction, analogue computer 2−82287
  - virial coeffs. from exp. (p,v,t) data, calc. 2−56438
  - vision nerve cell expt. 2−85090
  - visual spectrum anal. 2−55768
  - vocal tract X-rays anal. using interactive computer graphics 2−69449
  - VSA gravity meter system, development and tests 2−65436
  - water table aquifer, two-dimens., Boussinesq eqn., computer simulation 2−67764
  - wave front meas. system for display of surface quality and lens performance 2−79398
  - waves, simulation 2−62947
  - weather data radar system of IAS 2−75504
  - weather forecasting, application of computer derived synoptic maps 2−62122

- **Computer applications** continued
  - weather forecasting and analysis, conference, Portland, Ore., USA (1972) 2−62097
  - weather forecasting using computer time-sharing 2−72736
  - weather radar photographs analysis 2−75505
  - well logging data anal. 2−84748
  - whistler instability in anisotropic plasma, simulation 2−60283
  - X-ray absorption edge, X-ray fluorescence and X-ray diffraction anal. 2−64606
  - X-ray line broadening analysis, background separation, computerized iterative technique 2−74714
  - X-ray powder diffractometer, computer controlled, on-line data processing 2−64609
  - Zubov's vertical winter circulation scheme, computer analysis 2−62055
  - Al alloys, ultrasonic plane waves scattering, computer simulation 2−51023
  - As_2S_3, vitreous, vibrational spectra generated 2−74966
  - As_2Se_3, vitreous, vibrational spectra generated 2−74966
  - $BaTiO_3$, lattice vibr., monatomic linear chain, double min. potential, computer simulation 2−54019
  - CO_2:N_2:H_2O c.w. gas dynamic laser, unstable resonator calculations 2−82483
  - ^{60}Co dosimetry, computer calculation of dose for irregularly shaped fields 2−69434
  - ^{60}Co radiation therapy, determ. of treatment time 2−69317
  - Cs plasma, calc. of thermodynamic props. 2−56328
  - Cu, edge and screw dislocations, Schockley partials separation, computer simulation 2−60802
  - CuO film, optical const. determ., computerized technique 2−48135
  - F^--F^- interionic potential, computation using Hartree-Fock and semiempirical methods 2−74651
  - α-Fe, edge dislocation, elastic field, computer simulation 2−56710
  - α-Fe, edge dislocations, core characts., computer simulation 2−60803
  - GaAs bulk element, static negative resistance due to geometrical effect, computer analysis 2−84320
  - ^{155}Gd, half-life obs. using two dimensional analyzer and computer, γ-γ coincidence method 2−59715
  - Ge, amorphous, atomic arrangement, computer simulation 2−60574
  - Ge, vacancy equilibrium configuration calc. 2−71467
  - Ge(Li) γ-ray spectra automatic anal. on small computers 2−82082
  - H_2+F_2 pulsed laser simulation 2−41978
  - KCl ionic melt, microstructure calcs. 2−43319
  - MgF_2, valence band struct. by tight-binding method, computation 2−61186
  - Mg_2SiO_4 polymorphs, observed and hypothetical, crystal structure simulation 2−47335
  - Ni isotopes, proton elastic scattering, phase analysis using computer 2−67214
  - Si, amorphous, atomic arrangement, computer simulation 2−60574
  - Si, implantation of B ions, channelling, depth distrib., computer simulation 2−47439
  - Si, vacancy equilibrium configuration calc. 2−71467
  - Si crystal, brittle-fracture and crack propag., atomistic computer simulation 2−84036
  - UO_2-PuO_2 fuel, temp. calc., use of GAPCON and HYBRID-SINTER programs 2−52854
- **Computer memories** *see Calculating apparatus/digital computers; Magnetic devices; Storage devices; Superconducting devices*
- **Computer programs** *see Calculating apparatus/digital computer programmes*
- **Computers** *see Calculating apparatus*
- **Concrete**
  - composite, conf., Adelaide, Australia, Sep (1971) 2−61013
  - composite steel concrete beams with welded stud shear connectors, behaviour under sinusoidal bending deformation 2−58836
  - creep, nonlinear analysis of two-dimensional problems 2−66557
  - failure criteria of concrete rel. to incremental constitutive laws 2−58864
  - pressure vessel, cylindrical, prestressing by wedge winding method 2−76933
  - radiation shielding, suitability of two types for neutron and γ shielding 2−79846
  - reactor shielding, meas. of dose albedos of intermediate energy bremsstrahlung 2−76958
  - reactor vessel, pre-stressed, ultimate anal. 2−70520
  - reinforced vessels, for nuclear power reactors, present status and future trends 2−46388
- **Condensation**
  - *see also Drops; Fog*
  - alloy, binary, phase diagram 2−53509
  - annular flow heat transfer in horizontal tubes, prediction of mean Nusselt number 2−83444
  - atmospheric, large cooling tower plumes, rise and condensation 2−75556
  - atmospheric aerosol particles, condensational growth and particle size distrib. 2−48461
  - binary mixture, transient heat and mass transfer controlled 2−77466
  - cloud and ice condensation nuclei, numerical estimates of humidity 2−65671
  - cloud condensation nuclei, air pollution effects, obs. at Los Angeles 2−65713
  - cloud condensation nuclei concentration, isothermal determination method 2−62233
  - clouds, nuclei counter, for automatic meas., patent 2−72797
  - clouds, precipitation 2−84836
  - droplet or ice particle formation on aerosol particles, temp. and humidity conditions 2−51612
  - drops, heat transfer, numerical simulation 2−77471
  - F-ensemble calculation 2−45321
  - film, of pure and binary vapours at forward stagnation point of horizontal cylinder 2−77410
  - film of binary vapours, effects of forced flow and variable properties 2−77411
  - film-type, over-all coefficient of heat transfer between vapour and cooling water 2−43446
  - fluid flow and heat transfer, conference (Lucas Heights, Australia Aug. 1971) 2−43077

Condensation continued
Freon 11, heat transfer, finned tubes 2−82248
gas flow in supersonic nozzles and jets, nonequilibrium condensation 2−60331
homogeneous, Monte Carlo method for obs. of kinetics 2−43445
laminar film, on porous horizontal plate with large suction 2−60552
laminar film, vapour shear boundary condition 2−53501
laminar flowing vapour with arbitrary pressure gradients 2−47042
low pressure water vapour condensation and growth of ice on cold metal 2−53498
nucleation theory, thermodynamics of cluster formation 2−43435
nucleus growth, microdynamics, liq. phase ordering time depend. 2−56540
one-dimensional EHD flow with variable mobility coeff. 2−83528
perfect boson gas, Einstein condensation 2−45327
plasma, two-dimens., canonical partition function stability 2−46715
polar molecules, exhibiting an electric double layer at liquid surface, correction to class. homogeneous nucl. theory 2−50403
precipitation of clouds 2−84836
solar nebula, formation of chondrites 2−58443
steam, heat transfer under stratified flow conditions, empirical correlation 2−83670
vapour, simultaneous condensation and freezing on horizontal plate 2−67878
vapour bubble, thermal equilibrium, effects of liquid motion induced by condensation and evaporation 2−77399
water, props. of clathrate-like cluster structures, theory 2−50404
water drop, stationary, in superheated vapour 2−53500
water vapour heterogeneous nucleation 2−47047
Bi, vacuum evap., selective condensation on macroinhomogeneous surface 2−74628
CO_2, on W(100) surface, rel. to decomposition 2−50551
Cd, vacuum evap., selective condensation on macroinhomogeneous surface 2−74628
H_2O, cluster nucleation and growth, Rayleigh scatt. obs. 2−64511
Hg, applic. of modified dropwise condensation theory 2−52899
In film, on Si substrate, mass spectrometer obs. 2−47117
O_2 gas flow condensation in boundary layer 2−77354
Sf_6, liquid-vapour coexistence curve, interferometric obs. 2−74591
Si (111) surface, of Ni molecular beam in u.h.v. obs. using mass spectrometer 2−50499

Condensation of gases *see Liquefaction, gases*

Conduction, electrical *see Conductivity, electrical*

Conduction, heat *see Heat conduction*

Conduction, ionic, solids *see Ionic conduction, solids*

Conduction bands *see Crystal electron states/band structure*

Conduction electron scattering *see Crystal electron states/transport processes*

Conductivity, electrical
see also Ionic conduction, solids; Kondo effect; Semiconducting materials; Semiconductors; Skin effect; Superconducting materials; Superconductivity
alkali metal plasma, rel. to electron collision cross sections determ. 2−83186
combustion gases, nonequilibrium phenomena, calc. 2−80261
Dhanbad, quartz reefs, resistivity profiles 2−68850
4,4′-di-n-heptyloxyazoxybenzene, nematic phase, anomalous alignment due to elec. fields 2−77412
Earth, conductive structure in N.W. USA and S.W. Canada, determination from geomagnetic variation data 2−54706
Earth, conductive structure in S. Central Australia, magnetometer array study 2−54917
Earth, deep electrical soundings of crust- upper mantle in South Africa 2−54707
Earth, geomagnetic variation studies in Ethiopia 2−57792
Earth, magnetic and telluric field obs. in Azores 2−54708
Earth, magnetotelluric method, transfer fns. 2−57788
Earth, under Great Plains region of USA, derivation from fluctuation geomagnetic field properties 2−57791
Earth conductive structure, rel. to magnetometer array study of daily geomagnetic variation 2−54916
Earth resistivity, magnetotelluric obs. of lateral changes beneath Iceland 2−57793
EKG system, in vivo tissue transfer fns., crosscorrelation techniques 2−69214
fluidised beds, liquid solid, local porosity fluctuations, study by elec. conductance meas. 2−77178
high vacuum, breakdown, field emission 2−48942
high vacuum, breakdown, field emission 2−48942
ionosphere, dawn and dusk conductivity gradients effects on equatorial electrojet 2−54885
ionosphere, effective height integrated conductivity 2−65949
liquid crystal, nematic with negative dielec. anisotropy, cond. regime 2−60494
magnetospheric plasma 2−51636
Martian ionosphere, h.f., cond. calc. 2−51828
membranes, preselective, ion and water movements, equilib. props. 2−60460
metallic surface roughness, conduction losses 2−53547
MHD flow, two-dimensional, calc. 2−80260
ohm, state primary standard of unit of electric resistance 2−58682
plasma, in combustion MHD generator, obs. 2−80257
plasma, nonideal, low temp., compression and metallization 2−64295
plasma, Ruhr coal combustion, obs. 2−80259
plasma, stratified, with tensor cond., elec. field periodic struct. 2−83542
plasma, three-dimensional magnetized equil., rel. to transverse diffusion coeffs. 2−56333
plasma, turbulent resistivity in low β perpendicular MHD shock waves 2−53187
plasma, weakly nonideal, in shock tube 2−60220
plasma of combustion products, and turbulence 2−64265
plasma resistance, anomalous, rel. to Bernstein modes buildup 2−56342
random system, universal depend. on density near dielec.-metal-transition 2−54101
Red Sea hot brines, electrical resistivity probings of marine sediments 2−72729

Conductivity, electrical continued
relativistic magnetohydrodynamics, infinite conductivity 2−74345
resistivity, general expression derived using projection techniques with Liouville equation 2−55423
salt systems binary and ternary, simultaneous recording of electrical conductivity and DTA 2−78179
soil, along power transmission lines 2−61985
tertilium charge, during detonations induced by shock waves 2−63139
trotilium charge, during detonations induced by shock waves 2−63139
Z-pinch, high pressure confinement, losses 2−83600
Al-Mn dilute alloys impurity resistivity, temp. dependence 2−84278
Ar plasma, average-gradient and tuned-circuit- Q method 2−56386
Cs, supercritical state, rel. to struct. 2−60500
Cs plasma, dense strongly nonideal, 1000-10000K and 130-350 atm. 2−80292
Hg, crit. fluid, metal-nonmetal transition, influence on thermoelec. power 2−60377
Hg, supercritical state, rel. to struct. 2−60500
Kr pulsed discharge, as function of discharge conditions 2−43212
Ne plasma in Tokamak, electrical resistivity 2−64266
Xe discharge, pulsed, rel. to current density 2−60302
Xe discharge plasma 2−56341

gases
air, meas. data associating biological effects 2−58003
gas flow, in molecular flow range, dynamic method of obs. 2−46817
Ar electrodeless discharge 2−50228
CuCl with point defects associated with impurities, absorpton spectra and e.p.r. 2−75290
Hg vapour, metal-insulator transition range of densities 2−60378
Kr electrodeless discharge 2−50228
Kr pulsed discharge, as function of discharge conditions 2−43212
Xe electrodeless discharge 2−50228

liquids
— 2−68259
aniline-cyclohexane opalescent mixture, r.f. cond. 2−71230
benzene-phenol mixture, applied voltage, comp. and temp. depend. 2−60508
charge transmission through dielectric interfaces, application to liquid He 2−43413
critical points meas. of liquid metals 2−83804
dielectric, conduction and breakdown, book contrib. 2−46978
hexane, charge carriers apparent mobilities 2−74556
hydrocarbon 2−56511
isobutyric acid-water solns., supercrit. 2−53453
liquid cryst., nematic, orientation behaviour, elec. and optical behaviour 2−80444
metal, elec. resist. expression 2−60492
metal, electron transport rel. to hard-sphere interference functions, temp. dependence 2−67796
metal, resist. near crit. point, calc. ·2−67838
metal, temp. depend. and electronic struct. 2−67842
metal, temp. depend. of resist., pseudopotential calc. 2−80478
metal, transition and noble elec. resist., nearly free electron model, muffin tin potential 2−56514
metal-ammonia solns., density depend. 2−54101
metal-NHz solns., transport props. in the non-metal-metal transition range 2−80484
metals, liquid, detn. by pseudopotential method, accuracy of integral 2−80477
nematic liquid crystal, transient response caused by low freq. voltage pulse 2−53398
nitrobenzene-n-hexane opalescent mixture, r.f. cond. 2−71230
polystyrene lattices, surface conductance, comparison of theory and expt. 2−60521
rain water, rel. to Cl^- content 2−65741
seawater, conversion to salinity with digital temp.-salinity probe 2−54769
semiconductor, rel. to heat transfer mechanisms 2−81094
water, electrical probe characteristics, isothermal plasma model 2−74554
water, resistivity under irradiation, applic. in dosimetry 2−69402
water-polyvinyl alcohol mixtures, conductance meas., internal viscosity estimation 2−50345
Ag-Zn, temp. depend. in range, melting pt. to 1100°C 2−71826
Ag_2Te, at m.p. and to 1500 K 2−60495
Al-Fe(Co)(Cr) alloy, conc. depend., 1650°C 2−46980
Al_2O_3, 2500-2000 K 2−56516
Al_2O_3, correl. with covalent bonding 2−43338
As_2Se_3, switching, thermal breakdown mechanism 2−81096
BiI_3-Bi solutions, semicond. behaviour 2−64472
Ca-NH_3, solution, 203-243K 2−46984
Cd-Cu(In)(Zn) systems, resist., nearly free electron theory 2−46981
Cd-In, binary systems, electrotransport and elec. resist. detn. for density of states at Fermi level 2−80476
Cd-Tl, binary systems, electrotransport and elec. resist. detn. for density of states at Fermi level 2−80476
$CdGeAs_2$, and thermopower 2−60496
Cs-K melts, resistance obs. 2−60497
Cs, resist. and electron collapse 2−46982
Cu_x-Sn_{1-x} alloy, resistivity computation, comparison with exptl. data 2−43387
Cu-Zn, temp. depend. in range, melting pt. to 1100°C 2−71826
Cu_2S-CuCl melt, ionic and electronic 2−46983
Fe, Earth's core, calc. of resistivity 2−54674
FeS-$FeCl_2$ melt, ionic and electronic 2−46983
Ga, thermal cond. from Lorenz number and elec. cond. 2−71188
$GeSe_2$, switching, thermal breakdown mechanism 2−81096
He II, negative charge carriers 2−47024
Hg-K melt, conc. depend. 2−56517
Hg, density depend., metal- nonmetal transition 2−60499
Hg, Lorenz number and thermal cond., meas. by modified Kohlrausch method 2−71189
Hg, supercrit., density depend. 2−54101
In-Hg amalgam, diluted, near metal-nonmetal transition of pure Hg 2−53451
In-Te alloy, molten, cond. and temp. depend. 2−77446
$In_2Se(Te)$, molten, temp. depend. 2−67837

Conductivity, electrical continued
  liquids continued
    $In_2Te_{0.5}Se_{0.5}$, molten, temp. depend. 2—67837
    InTlSe(Te), molten, temp. depend. 2—67837
    K-Cs alloys, resist., temp. depend. 2—64471
    K-NH_3, solution, 203-243K 2—46984
    KCl, aqueous solution, high pressure cell for obs. 2—48940
    KCl, aqueous solution, high pressure cell for obs. 2—48940
    Li-NH_3, solution, 203-243K 2—46984
    $LiNO_3$-KNO_3, mixtures, temp. dependence 2—53452
    Mg-Sn alloy, Faber- Ziman theory, partial interference functions 2—83799
    Mo, temp. dependence near melting point 2—57066
    N_2O_4, ioniz. enthalpy determ. 2—84612
    Na-Cs alloys, resist. temp. depend. 2—64471
    Na-Cs melts, resistance obs. 2—60497
    Na-Hg melt, conc. depend. 2—56517
    Na, Lorenz function, 40 to 360K 2—57086
    $Na_xV_2O_5$, n-type semicond. and ionic cond. props. 2—83795
    Ne, liquid, negative carrier mobility rel. to localized electrons 2—46916
    Ni complexes, trimethylphosphines Ni(II) in solution 2—77091
    Pb, elec. resist. and thermoelec. power temp depend., models 2—60501
    Pb, temp. depend., freezing point to 800°C 2—43388
    Pb from electron-ion pseudopot. model 2—77812
    Rb-NH_3 solutions, electrodeless method 2—71226
    Rb, resistivity calc. from liquid structure factors 2—71195
    Sb_2S_3, switching, thermal breakdown mechanism 2—81096
    Sb_2S_3, switching effect 2—60503
    Se-Te alloy, switching phenomena 2—60504
    Se-Te melt, electronic transport behaviour, switching, optical gap 2—60502
    Se, switching, thermal breakdown mechanism 2—81096
    Se, switching and anomalous magnetoresistance 2—60505
    Se, switching effect 2—60503
    Se, switching phenomena 2—60504
    Te, liquid, rel. to n.m.r. obs. 2—71237
    TeI_4-Te solutions, semicond. behaviour 2—64472
    V_2O_5-Na_2O-Fe_2O_3 system, n-type semicond. and ionic cond. props. 2—83796
    V_2O_r, temp. and oxygen partial press. depend. n-type semicond. 2—83794
    W, determ. by pulse heating method 2—74584
    W, temp. dependence near melting point 2—57066
    Zn-Pb alloy, resist. at 500°C rel. to Ziman-Ashcroft-Langreth theory 2—60507
    Zn-Sn alloy, resist. at 500°C rel. to Ziman-Ashcroft-Langreth theory 2—60507
  liquids, electrolytic
    see also Chemical analysis/electrochemical; Ion velocity/electrolytic
    Debye-Huckel theory, appl. to clay minerals 2—83809
    isobutyric acid-water mixture near critical point, temperature dependence of resistance 2—80525
    molten salts, frequency and temperature dependence activation energies and pre-exponential factors computed 2—43385
    nitrates, molten, and binary mixtures, meas. using capillary cell 2—46979
    water, cell flowmeter based on variations in electrical resistances for meas. of turbulent velocity fluctuation 2—71137
    CO, drift mobility of ions 2—77820
    CsCl, in sulfolane-water mixtures, study at 35°C 2—78199
    Cu coatings rel. to acidic bath composition 2—84647
    K_2SO_4, aqueous soln. resist. in electrolytic cell, geom. parameters depend. 2—78200
    LiCl, in sulfolane-water mixtures, study at 35°C 2—78199
    N_2, drift mobility of ions 2—77820
    $Na_xV_2O_5$, ionic cond. props. 2—83795
    O_2, drift mobility of ions 2—77820
    RbCl, in sulfolane-water mixtures, study at 35°C 2—78199
    V_2O_5- Na_2O-Fe_2O_3 system, ionic cond. props. 2—83796
  measurement
    apparent resistivity calc. for laterally inhomogeneous semi-infinite conducting half-plane 2—57783
    audio frequencies, elimination of contact phenomena 2—72009
    audio frequency magnetotellurics application to mineral exploration 2—57800
    conducting media impedance by waveguide probe, effects of e.m. wave front curvilinearity 2—49240
    cylindrical shells, by inductive method 2—76430
    Geodyne model underwater sensor unit 2—72720
    geology, airborne resistivity mapping using E-PHASE 2—54727
    glass, nontransparent quartz, investigation of colour changes and formation of centres 2—84482
    guard ring method, air gap conductance 2—47921
    hermetic cell for obs. of melted salts, design 2—71222
    high-temps., fast system 2—52299
    hypersonic wake in ballistic apparatus, downstream decay of electron density 2—74480
    low conductivity materials, techniques for obs. at high pressure 2—59030
    lunar surface mag. meas. and interior properties 2—55128
    marine frequency soundings, apparent resistivity curves in wave zone 2—72700
    massive conductors, direct field distribution calc. 2—45643
    metal, liq., equilib. thermodynamic states, at high temp. and press. 2—46949
    metallic cylinder, by inductive method 2—76429
    metallic cylinders, inductive method 2—49239
    moon, disribution meas. by Apollo 15 subsatellite 2—55129
    moon, radial profile, from surface mag. fields meas. 2—55130
    m.o.s. transistor drain-source conductance in saturated current region 2—63211
    nonlinear, in boreholes, observation of effects 2—54703
    plasma, Ruhr coal combustion, apparatus 2—80259
    profiled crystals, contactless method for meas. of volume distribution of resistivity 2—51159
    profiled single crystals, instrument for meas. of specific resistivity with automatic compensation for geometrical factors 2—51158
    semiconductor, contactless method 2—47922

Conductivity, electrical continued
  measurement continued
    semiconductor, spreading resistance correction factor calc. 2—51162
    semiconductors, at high temperatures 2—44123
    solid, simultaneous obs. of thermophysical props. of elec. cond. materials at high temp. 2—57078
    specific resistivity, van der Pauŵ's theorem extension to anisotropic media 2—44047
    thermally stimulated currents and voltages, theory for linear nonisothermal effects 2—45632
    thermoelectric materials, rapid meas. of temperature dependence of thermal e.m.f. and electrical conductivity 2—52351
    transconductance and variation, method for m.o.s.t. using differential amplifier 2—63210
    upper mantle conductivity structure in Nigeria 2—57782
    Ag_2S, molten, comp. and temp. depend., change of sign of temp. coeff. with increasing S conc. 2—83798
    Cu, as fn. of molar heat content, meas. by pulse method 2—64914
    Cu, low temp. dependence, undergraduate expt. 2—73262
    Ge in powerful electric fields by contactless method 2—61350
    Ge resistivity by spreading resistance technique 2—54194
    N plasma, transport processes 2—56335
    Pb, as fn. of molar heat content, meas. by pulse method 2—64914
  solids
    — 2—72154
    — 2—71831
    — 2—68382
    σ and π electron interactions in free electron model, revised integrals for 3-dimensions 2—77813
    Al-Ni alloy, influence of short-range order on elec. and mag. resist. 2—71423
    alkali metals, resist., pseudopot. calc. 2—75052
    alloy, commercial, rel. to thermal cond. and Lorenz number 2—54042
    alloy, concentrated strong scatt. disordered, temp. depend. 2—44049
    alloy, dil., electron-phonon scatt. contrib., Green function calc. 2—61219
    alloy, dil. mag., resist. in s-d model 2—51274
    alloy, dilute, resist. temp. depend. rel. to spin fluctuations 2—57148
    amorphous, carrier flow through localized and extended states 2—77882
    amorphous, high field conductivity 2—54168
    amorphous chalcogenide threshold and memory devices, preswitching props., forming and switching 2—77920
    anthracene, freq. depend. cond. in single cryst. with monopolar injection 2—64993
    anthraquinone-pyrometallic anhydride polymer, dielec. relax., permittivity, a.c. and d.c. cond. 2—81143
    antiferromagnetic alloy, effect of spin orbit interaction 2—57295
    antistatic agent film, on plastic, surface cond. recovery 2—65073
    p-benzoquinone, conduction mechanism, molecular orbital energies 2—75015
    borosilicate films, current-voltage characts. 2—47950
    bronze powder, spherical particles, rel. to sintering kinetics determ. 2—43890
    carbon, vitreous and common, bulk resistivity and temp. coeff. 2—71827
    carbons irradiated by neutrons and annealed, props. changes 2—68137
    β-carotene, temp., appl. potential, and appl. field depend. 2—72072
    ceramic, corundum base, rel. to sintering 2—53927
    chalcogenide, amorphous film, thermally stimulated cond. 2—57189
    chalcogenide, film, on SnO_2 coated glass, polarized memory effect 2—64971
    chalcogenide glass, physical mechanisms, review 2—61267
    chalcogenide glass, threshold and memory types, thermal effects 2—71917
    chalcogenide glasses, resist. changes in surface region 2—54190
    chalcogenide-glass switches, preswitching behaviour in terms of space charge injection mechanism 2—68379
    p-chloranil, conduction mechanism, molecular orbital energies 2—75015
    clay, meas. method eliminating contact phenomena 2—72009
    cochlear membrane, resistance obs. analysis 2—48898
    Coles alloys, temp. depend. of resist. due to localized spin fluctuations 2—75056
    collagen, effect of adsorbed water 2—47908
    composite, fibre-reinforced, calc. 2—50915
    conductor material, temp. distrib. in d.c. heated conductors, calc. 2—57054
    Cr and alloys, excitonic phase, calc. 2—65077
    crosslinked epoxy polymers effect, of free volume 2—57233
    crystals, thermally stimulated current and voltage obs. 2—72004
    cylindrical conductor, heat radiating, energy dissipation 2—49233
    Dar Zarrouk curves and differential resistivity soundings 2—57502
    d.c. hopping conduction, percolation treatment 2—68273
    diamond, heavily doped with B, Al and Ti, impurity band props. 2—68396
    dielectric, conduction phenomena, book contrib. 2—47958
    dielectric film, Poole-Frenkel pre-exponential factor 2—57217
    dielectrics, inorganic, for reactor use, radiation induced changes 2—52851
    diphenylpolyene film, temp. depend. 2—84338
    disordered systems, semiconductor model of conductivity in dense metallic vapours 2—54183
    double exchange ferromagnet, quantum theory 2—54295
    Dykes of Dhanbad, resistivity profiles 2—57780
    Earth, depth of investigation of direct current methods 2—78292
    Earth, determ. from secular geomag. field variations data 2—72686
    Earth, inverse problem of geomagnetic induction 2—65563
    Earth, resistivity sounding data, linear filter method interpretation 2—72633
    Earth, resistivity sounding on three-dimensional transitional model 2—72625
    Earth, square array resistivity meas., effects of anisotropy 2—72623
    Earth, Wenner three-electrode and dipole-dipole d.c. resistivity methods, investigation depth 2—72629
    Earth valleys with elliptic cross-section, resistivity meas. 2—72630

Conductivity, electrical continued
solids continued
electrical insulation and dielectric phenomena, conference, Williamsburg (1971) 2−57222
electron traps, thermally stimulated conductivity, alternating current method 2−75113
electron-impurity system, freq. dependent relax. times 2−51068
electron-phonon system, elec. current in strong mag. field at low temp. 2−57100
electronic Green functions calc. using nonorthogonal basis functions, crystal applic. 2−61131
Evanohm heater wire, resistance- temperature ratios at low temps. 2−66654
excitonic phase, mag. and non-mag. impurities, calc. 2−65077
Fe_2SiO_4, olivine and spinel forms, pressure-induced increase rel. to red shift in absorption spectra 2−54421
ferromagnet, metallic, resist. behaviour in crit. region 2−57279
ferromagnetic alloy, effect of spin orbit interaction 2−57295
ferromagnetic metal, anisotropy, two-zone model of electron scatt. 2−71833
ferromagnets, influence of domain boundaries 2−72147
fibrous metallic composite, thermophysical characs. 2−54070
film, chalcogenide, amorphous, dielec. const., elec. cond., struct. features 2−61309
film, chalcogenide, amorphous, pre- and postswitching characts. 2−61310
film, chalcogenide, noncrystn., threshold and memory switching at low temps. 2−61308
film, chalcogenide glass, amorphous, switching behaviour 2−81071
film, metal, discontinuous, elec. props. rel. to strain 2−64908
films, metallic semiconducting and dielectric, review 2−64907
films grown by evaporation in elec. field, effect on resistance 2−71341
free charge permanent distribution rel. to relaxation time 2−49197
frequency dependent conductivity in electron-impurity system, calc. 2−71780
n-GaAs, anisotropy of the submillimeter conductivity of warm carriers 2−84330
galvanomagnetic phenomena, longitudinal, in thin wires, oscillations of resistances 2−68328
p-Ge, electron irrad., defect prod. and annealing obs. 2−47377
n-Ge, nonstationary elec. cond., momentum relax. time 2−68435
Gilsocarbon, neutron irrad. effects rel. to high temp. reactor design 2−52871
glass, a.c. conductivity, atomic and electronic hopping 2−47881
glass, chalcogenide, film, thick and thin, switching temp. depend., onset of breakdown 2−77895
glass, chalcogenide, i.r. cond., 10^9-10^{13}Hz 2−61638
glass, chalcogenide, threshold switching, time delay 2−61273
glass, chalcogenide, threshold switching mechanisms 2−61272
glass, oxyfluorphosphate, alkali free, elec. resist. 250-500°C 2−57192
glass, switching, lateral expansion of conducting channel 2−61274
glass chalcogenide, switching behaviour between Ge electrodes, firing 2−81074
glass films, thermally switching, pulse response of cond. channel 2−51129
graphite, electrothermal, rel. to crystallite size 2−57001
graphite, I-V characts., in transverse mag. field, multiple kink effect 2−44093
graphite, nuclear, high fluence neutron irrad. behaviour, two-phase model 2−56048
graphite, porosity effects 2−50926
graphite, pyrolytic, low temp. electron irrad. damage and recovery, resist. study 2−80659
graphite, pyrolytic, meas. over wide temp. range 2−84208
graphite from isotruxene carbons 2−61023
group II-VI compound film, epitaxial, specific resistance and mobility 2−56582
hopping cond., freq. depend. 2−61270
hopping impurity conduction, Hall effect 2−57178
Icelandic basalt, resistivity measurements 2−65562
in inorganic glasses, empirical relation with dielectric polarization 2−57188
insulating solids 2−57186
insulator, film, in m.i.m. struct., d.c. conduction mechanisms, thermally stimulated current analysis 2−61394
insulator, thermal switching behaviour 2−61268
Io, conductivity rel. to structure 2−75868
linear conducting chains, review 2−61140
longitudinal optical phonon, coupled with Stark ladder electron, current charact. 2−68276
lunar interior, det. from magnetic field obs. 2−51810
lunar profile and nonuniqueness of e.m. data inversion 2−75850
lunar samples from Apollo mission 2−66158
lunar surface rocks 2−51819
macroscopic, from Bether-Salpeter eqn. 2−77834
magnesium phthalocyanine film, impurity level energies from photoemission and cond. obs. 2−81028
manganin pressure transducers, influence of high pressure H_2 on electrical resistance, compared with Au-Cr alloy 2−76122
many-phonon system, contrib. of hydrodynamic excitations 2−71775
marine sediments, electrical resistivity meas. system for porosity determination 2−75481
Matthiessen's rule, deviations from, review and critical evaluation 2−71753
Matthiessen's rule deviations for resist. 2−44048
metal, f.c.c., irrad., elec. resist. of defects 2−75045
metal, influence of point defects at high temp. 2−54040
metal, Lorenz function at high temperatures 2−54124
metal, Matthiessen's rule deviations due to phonon spectrum changes 2−75046
metal, normal and supercond., mag. field induced surface state contrib. to h.f. surface cond. 2−51083
metal, polyvalent, effect of Fermi surface shape on ideal resist. 2−75044
metal, refractory, high temp. measurement 2−57077
metal, resist. change in gas, rel. to diffusion coeff. determ. 2−47452
metal, r.f. size effect 2−57384

Conductivity, electrical continued
solids continued
metal filled supercond. multifilamentary braids, pulsed field losses 2−61253
metal film, discontinuous, non-ohmic behaviour 2−57150
metal film, elastoresist., relax. phenomena 2−56765
metal film, epitaxial, on alkali halides, cryst. orientation influence 2−53565
metal film, longitudinal and transverse strain coeff. of resistance 2−61218
metal film, surface impedance under anomalous skin effect conditions 2−51096
metal film, with adsorbed gas layer, demetallization phenomenon 2−47150
metal oxides, classification 2−57106
metal-insulator phase transitions, science and technology 2−57205
metal-insulator transition, Hubbard model, cluster approach 2−44287
metal-$PbTiO_3$-metal, Seebeck effect 2−44169
metal-semicond. contact, semicond. base region, overheating mechanism rel. to negative resist. 2−65035
metal-ZnTe-metal device, switching and memory props. 2−44142
metal/SiO_2 cermet film, produced by recoil atom implant 2−53578
metallic conductors, optical cond., phenomenological model 2−75253
metals, electrical resist. var. with temp. reln. to interstitials and vacancies 2−68329
p-methoxybenzylidene-p-butylaniline liquid crystals, variation in electric and magnetic fields 2−46985
mica, surface conduction and surf. Hall coeff. dependence on temp. and mag. field 2−80541
microwave-induced anisotropy, for semiconductors in quantizing magnetic field 2−71893
m.i.m. structure, space charge limited to electrode limited current transition theory 2−47949
Moon, exptal. det. 2−62664
Moon models, compatibility with Apollo 12 magnetometer data 2−51803
multiphase mixtures, composition dependence of flux propagations 2−75252
Mylar, pulsed X-ray irrad. induced 2−65091
Mylar thin films negative resistance charact. 2−57203
n-p-i structs., current-voltage characts., S and N type negative resist. regions 2−65022
naphthalene compressed pellets, 1 kc/s to 100 Mc/s 2−61415
α-naphthylamine compressed pellets, 1 kc/s to 100 Mc/s 2−61415
negative differential mobility elements, linearized equation for current flow 2−84319
non-crystalline materials, theory, review 2−61143
non-degenerate single-valley semiconductors, a.c. and d.c. conductivities 2−66454
noncrystalline system, min. metallic cond., calc. 2−77888
nonstationary current transfer at switch off 2−47976
olivine, conductivity meas. rel. to temperature profile of lunar interior 2−66142
olivine, det. up to 1200°C and 7.5 kb 2−65580
olivine, lunar, rel. to temp. profile 2−51806
one-dimensional conductors, temp. dependence 2−47831
ore-zone excited by current carrying cable, induction anomaly 2−57781
organic material, d.c. cond. mechanism 2−47904
organic materials, mechanism, carrier mobility study 2−47905
Pd, 77-300K, effect of paramagnons 2−61226
phenol, formaldehyde resin, thermal degraded, a.c. and d.c. cond. 2−47903
photo-semiconductors, high resistivity, meas. of dark current using electron beam contact 2−75166
poly N-vinylcarbazole, investigation of trap structure by thermally stimulated currents 2−54182
polyethylene, film, I doped, form of current transients 2−64994
polyethylene, temp. depend., rel. to crystn. 2−71290
polyethylene terephthalate, electret, thermally stimulated current obs. 2−65076
polyfluoroethylene, filler content influence 2−47553
polymer, electron irrad., temp. and electron dose effects 2−84316
polymer films, use as dielectric layers in m.i.m. structures 2−83859
polymer films amorphous and crystalline, electrical conductivity in strong electric fields 2−84340
polymer resistance meas. rel. to humidity effect 2−57223
polymers, and mol. mechanisms 2−57143
polymers, radiation-induced, relationship with radiation-induced creep 2−47517
polymers, semiconducting, Co chelate, of dihydroxyquinones, meas. of elec. resist. 2−80815
polymers, thermally stimulated current and voltage obs. 2−72004
polyphenylacetylene, also ESR absorption 2−51127
polystyrene films, passage of transient currents along surface 2−72001
polytetrafluoroethylene, pulsed X-ray irrad. induced 2−65091
polythene 2−65091
polyvinyl fluoride, thermally stimulated conductivity 2−64995
powder, effect of temp. and press. 2−43880
precious metal pyrochlores, semicond. and metallic 2−60987
PVC, charged with carbon black, negative differential resist. 2−81064
rare earth hydrides, electronic props. review 2−77899
rare earth metals, resist., mag. crit. scatt. role 2−57271
rare earth metals, resist. due to short range spin correls. 2−57272
residual, frozen-in, model 2−57101
resistivity of semiconductor single crystals, apparatus for automatic obs. 2−61349
rhodamine 6G amorphous film, carrier trapping, thermostimulated cond. study 2−54180
rocks, mountain, seismoactive areas, electrical resistivity variation 2−65561
Ru, elec. resistance anisotropy at low temps. 2−68333
sandstone, universal formulae 2−62015
sandstones, Indian, resistivity obs. under dry and saturated conditions 2−75460
selenides, mol. transform. rel. to elec. resist. 2−47900

Conductivity, electrical continued
solids continued
semiconducting crystals, meas. by four-probe method 2−54191
semiconducting glass, endotherm in switch-on process 2−64964
semiconducting glass, endotherm in switch-on process 2−64965
semiconducting single crystal, monitoring of uniformity by meas. of specific resistivity 2−51160
semiconducting thin films, theory for high electric field 2−64558
semiconductor, amorphous, charge controlled switching effect 2−61271
semiconductor, amorphous, elec. instabilities of mixed electronic and thermal origin, theory 2−61285
semiconductor, amorphous, electrothermal switching, models 2−61284
semiconductor, amorphous, reversible elec. and optical memory effects 2−57185
semiconductor, amorphous, with undulatorily graded band edges, prediction 2−61282
semiconductor, amorphous organic, press. depend., random field model 2−44108
semiconductor, C_{6v} class cryst., piezoelec. interaction of transverse u.s. waves with charge carriers 2−54030
semiconductor, compensated, metal-nonmetal transition, theory 2−68412
semiconductor, due to variable range hopping in nonuniform density of states 2−81104
semiconductor, many-valley, n-type effects of light pumping on conductivity 2−57204
semiconductor, microwave cond., in heating fields and in presence of electron-hole interaction 2−75084
semiconductor, n-type, thermally produced current-voltage characts. 2−71891
semiconductor, narrow band, current rel. to elec. field 2−77891
semiconductor, pulsed electron beam excited, β-conductive signal 2−71887
semiconductor, strongly doped, model interpret. 2−77880
semiconductor, superlattice struct., transport props., h.f. cond., e.m. wave amplification 2−64974
semiconductor, switching phenomenon, contrib. of lateral thermal instability 2−61283
semiconductor, thermal-switching, static I-V characts., calc. for cylindrical symmetry 2−54207
semiconductor, transient space charge limited current on voltage removal 2−84336
semiconductor device, switching, thermal current-voltage characts., temp., elec. field, current density distribs. 2−71953
semiconductor film, amorphous, ohmic and non-ohmic cond. 2−61289
semiconductor film, single crystal, electrical conductivity and adsorption, combined meas. 2−71932
semiconductor film 2−44089
semiconductor glass, cond. mechanism, model 2−61335
semiconductor multilayer film, rel. to thermoelec. props. 2−51054
semiconductor plate, in mag. field, anisotropy 2−75087
semiconductor thin bar, β-conductive signal, effect of surface recomb. velocity 2−51130
semiconductor with non-standard zone, in alternating mag. filed, theory 2−84318
semiconductors, heat treatment and props. of doping element 2−84321
semiconductors, multi-valley. discontinuities in V/I characts. 2−71895
semiconductors, vol. negative differential cond. assoc. with acoustoelectric effect 2−80915
semiconductors with nonparabolic bands, conditions for negative differential resistance 2−81101
solar cell, Si, series resistance methods of determ. 2−66692
space charge limited current, with coulombic trapping, trap filled limit 2−57183
spinal ferrite, temp. and composition depend. 2−48100
spinel ferrite, time variation 2−47882
stearic acid films, high-field transient behaviour 2−77950
steel, high carbon, workhardened, ageing and recovery obs. 2−47597
stilbene, in weak and strong elec. fields 2−77901
superconductors condensed on cold substrates, film, surface resistance meas. 2−64924
TCNQ complex, thermally assisted hopping mechanism 2−68409
TCNQ complexes, hopping cond. 2−44109
TCNQ salts, role of disorder 2−64920
tetracene films, investigation high and low conductivity stable states and switching 2−54181
thermally-stimulated current obs. for non-luminescent dosimetry applic. 2−70308
thin specimen, resistivity measurement using electrical-contact four-electrode transducer, measurement errors 2−45642
transition metal film, amorphous, deposition and annealing resist. study 2−77499
transition metal germanide, temp. depend. 2−57175
transition metal monoxides, rel. to positron lifetime spectra 2−71825
transition metal nitrides, hot pressing, sintering, elec. resist. 2−47661
transition metals, resist., 20 to 1200°C 2−47769
triethylammonium(tetracyanoquinodimethan)$_2$ (TEA(TCNQ)$_2$, anisotropy 2−75016
triethylammonium-(TCNQ)$_2$, 77-355K, and metal-insulator transition 2−68410
trisiloxane film, electron beam polymerized 2−47909
Zircaloy-2 anodic oxide, in m.i.m. struct., pre-breakdown electrical switching 2−47951
Ag-Au-Cu alloy, residual resist. meas. 2−75051
Ag-Au alloy, calc. using coherent pseudopotential model 2−75025
Ag-Au alloy, effects of pressure 2−51097
Ag-Au alloy, residual resist. meas. 2−75051
Ag-Mn dilute alloys, low temp. resistivity 2−44214
Ag, bulk, cond. electron mean free path determ. from size effect of thin films 2−75012
Ag, epitaxial films, temp. coefficient of resistance 2−61221
Ag, film, size effect on strain coefficient of resistance 2−57151
Ag, phonon drag effects 2−64909

Conductivity, electrical continued
solids continued
Ag, proton, deuteron and He-ion damage obs. 2−50643
Ag film on mica, modulation of conductance due to changing interface, metallic field effect 2−75047
Ag Hall and Righi-Leduc coeffs., 4-125 K, Weidemann-Franz law 2−61224
AgBr, chemical sensitization by doping, obs. of electronic mechanism 2−81545
Ag_2S epitaxial thin films, variation of resistance with temperature 2−53567
Ag_2Se thin films, variation of resistance with temperature 2−53570
n-Ag_2Te, Lorenz number, electron scatt. inelasticity obs. 2−84337
Al-1.2 wt%Mg_2Si alloy, two-step ageing study 2−64765
Al-Ag alloy, preprecip. study 2−77692
Al-Al_2O_3-Al, eff. of reactor radiation 2−81114
Al-Al_2O_3-Au in m.i.m. structure, thermally stimulated currents 2−77928
Al-Au alloy, dilute, Mathiessens rule deviation due to scatt. processes 2−80969
Al-Cr dilute alloys impurity resistivity, temp. dependence 2−84278
Al-Fe alloy, rapidly solidified 2−50827
Al-9%Mg alloy, rel. to effects of additional elements on clustering and precip. during ageing 2−50801
Al-Mn dil. alloys, high temp. impurity resist. 2−44050
Al-Si dilute alloy film, Si precip., resist. study 2−50825
Al-SiO_x/B_2O_3-Al, m.i.m. struct., current-voltage characts. 2−47950
Al-SiO_x-Al eff. of reactor radiation 2−81114
Al-Zn-Mg alloy, ageing process after quenching and cold work, resistometric obs. 2−71632
Al-Zn alloy, GP zones obs. 2−50800
Al-Zn solid solution, miscibility gap, resist. study 2−50826
Al-based dilute alloy, reson. and charge neutrality, semiphenomenological model 2−71783
Al-borosilicate glass-Al thin film sandwich, elec. cond. props., negative resist., electroforming and electron emission 2−71989
Al, deformed, changes in vicinity of grain boundaries 2−53744
Al, during creep tests 2−50754
Al, elec. resist. due to interstitials, pseudopotential method 2−57152
Al, quenched, annealing kinetics of point defects 2−80680
Al, resist. temp. coeff. rel. to equilib. vacancies 2−77856
Al, steel-reinforced, rel. to struct. 2−53946
Al, stress effect on resist./strain relation 2−64700
Al alloy, low temp., deviations from Matthiesen's rule 2−64910
Al alloys, 'temperature increment' for temp. correction of resistance meas. 2−44051
Al film, electrostatic charging effects 2−71845
Al film, temp. coeff. 2−74999
AlCr, impurity resistivity 2−68337
AlMn, impurity resistivity, 4-200K 2−68337
Al_2O_3, meas. above 1600°C in air 2−47921
Al_2O_3, single and polycryst., high temp. 2−47978
As-Se glass, Ag doped, d.c. cond. and pressure depend. 2−64975
As-Te-Ge-Se glass switching device, small signal behaviour 2−61376
As-Te-Ge-Si glass, thermal breakdown 2−61298
As_2S_4 and As_4S_4 amorphous films, a.c. cond., temp. depend. 2−68392
$As_xSb_{2-x}Se_3$, amorphous and crysts., threshold and memory switching 2−77883
As_2Se_3, amorphous, a.c. cond, 30Hz-10.3GHz, −180-500°C 2−81070
As_2Se_3, glassy, high field cond. 2−68394
As_2Se_3 amorphous films, a.c. cond., temp. depend. 2−68392
As_2Se_3 film, amorphous, charge transport, photocond. and dark current obs. 2−68393
As_2Se_3 film, amorphous, memory switching rel. to thickness 2−81072
As_2Se_3 glass, high field, Poole Frenkel, space charge limited and self heating models 2−51134
As_2Se_3 vitreous, effects of group III A element dopant 2−61300
$AsSe_{1.5}Sn_{0.28}$, pyroceramic, semicond., elec. cond. mechanism, 285-385K 2−75089
$As_2Se_3(Te_3)$ film, amorphous, trap-limited processes 2−61325
$As_2Se_3-xAs_2Te_3$, amorphous, as func. of temp. and subsequent annealing 2−77893
$3As_2Se_3.2Sb_2Se_3$ films, amorphous, temp., field, and illumination depend. 2−54187
As_2Te_3-As_2Se_3 glass, cond. and switching 2−61299
As_2Te_3-As_2Se_3 glass, microstruct. a.c. and d.c. cond. 2−60589
As_2Te_3-As_2Se_3 glass, switching rel. to comp. and thermal treatment 2−61295
As_2Te_3, glassy, rel. to electronic props. 2−61297
As_2Te_3, polycryst., threshold and memory switching 2−77883
As_2Te_3 film, amorphous, a.c. cond. rel. to localized tail states 2−61288
As_2Te_3 glassy, switching characts., cond. exponential temp. depend. 2−81073
$As_{38}Te_{55}Ge_4Si_3$, $2As_2Se_3.As_2Te_3$, amorphous, minor switching and r.f. oscillations 2−61275
Au:Cu, impurity-vacancy binding energy, equilib. resistivity obs. 2−71465
Au-Fe(Mn)(Co)(Ni)(Ti) dilute alloys, deviation from Matthiessen's rule, 0.5-60 K 2−77854
Au-Pd alloy, short-range order formation, resistivity obs. 2−74894
Au-SiO cermet film post-deposition resistance increase, obs. 2−61222
Au-SiO film, cermet, struct., elec. props., rel. to deposition condition 2−64976
Au-Ti dil. alloys, weak resist. minimum 2−44052
Au, bulk, cond. electron mean free path determ. from size effect of thin films 2−75012
Au, Hall and Righi-Leduc coeffs., 4-125 K, Weidemann-Franz law 2−61224
Au, plastically deformed after quenching, resist. recovery 2−56790
Au, proton, deuteron and He-ion damage obs. 2−50643
Au contact resistance on NiO 2−61370
Au film, discontinuous, on soda-lime substrate, resist. rel. to ion drift in substrate 2−47833
Au film post-deposition resistance increase, obs. 2−61222

Conductivity, electrical continued
solids continued
$Ba(Ce_{1-x}Ta_x)O_3$, and valency transfer from (Ce^{4+}-Ta^{4+}) to (Ce^{3+}-Ta^{5+}) with increasing temp. 2−75203
$BaTiO_3$-Bi_2O_3, La doped composite ceramic, two-step anomalous resistivity increase 2−68395
$BaTiO_3$, meas. in ferroelectric and paraelectric phases 2−81100
$BaTiO_3$ ceramics, La doped, Bi_2O_3 as grain boundary element, resistivity temperature characteristic anomaly at transitions 2−84366
$BaTiO_3$ reduced single crystal and Y doped, phase transition effects on d.c. conductivity 2−68468
Be-transition metal alloys, Fermi surface, electron scatt., residual resist. 2−71791
Be, laser irrad. and annealing effects 2−81036
Be film, on dielec. substrate, elec. resist., supercond. transition temp., absorpt. spectra 2−72323
BiI_3, effect of adsorption 2−47993
Bi_2S_3:Pb, capture level parameters, thermo-stimulated cond. study 2−71923
$Bi_{1-x}Sb_x$:Cd(In)(Sn), ($x=0$-0.2), 180-420K 2−61301
BiSe and BiTe, single crystal plates, comparison with polycrystalline specimens 2−84322
BiSeI, band struct. determ., 77−460 K 2−80997
C, lampblack, rel. to graphitization obs. 2−56995
C, vitreous and common, bulk resistivity and temp. coeff. 2−71827
C fibres, elec. resistivity, 77-300 K, meas. 2−68331
C fibres, neutron irrad. effects 2−56998
C film, amorphous, change on graphitization by light pulses 2−61030
C film, amorphous, temp. depend. 2−61302
C glassy monofilament, prep. and props. 2−56982
CaF_2, proton irrad., elec cond. 300-800K, anion vacancy cond. mechanism 2−57230
$Ca_3Pd_2H_4$ characterization 2−47347
$Ca_3(VO_4)_2$, $Ca_2V_6O_{17}$ formation study, in $Ca(NO_3)_2$-K_3VO_4-H_2O system 2−47232
n-$CdCr_2Se_4$:Ga, h.f. cond., freq. dispersion, Curie pt. phenomena 2−44095
CdS:Ag(Al), field quenching, influence of doping 2−54170
CdS, hopping cond., role in u.s. absorption and dispersion 2−71733
CdS, O_2 chemisorption induced changes 2−47886
CdS, piezoelec. semicond., sound amplification threshold field non-monotonic cond. depend., 5-120 MHz 2−77783
n-CdS, thin compound semicond., sorption-induced conductivity changes 2−77886
CdS film, amorphous, in m.i.m. structs. 2−64978
CdS film, spectral response and Hall mobility, thickness depend., effects of Cu impurity 2−77894
CdS(Te), resist. changes due to thermal neutron damage 2−48219
CdSb:Ag powders, influence of grain size, sintering temp. and time and protective atmos. 2−64906
CdSb:Te, with low Te content, 78-293K 2−61307
CdSb, effect of evaporation of Cd atoms 2−47890
CdSe-SiO_x, electron transport study in space charge layer of vacuum-deposited film 2−77852
CdSe, elec. behaviour between room temp. and 600C 2−61305
CdSe, memory and photocond., 77 and 300K 2−75168
CdSe, O_2 chemisorption induced changes 2−47886
CdSe film, thermally stimulated, and space charge limited, rel. to photoelec. props. 2−51212
CdSe films vacuum deposited, Hall mobility 2−83868
CdSe powder containing Cu, Cl_2 impurities, negative resistance behaviour, variation of threshold voltage with light intensity, frequency 2−71919
CdSe thin films, influence of Se vapour annealing 2−44094
CdSe(Te), high temp. defect. equilib., elec. transport props. 2−44096
$CdSi_xGe_{1-x}As$, glassy, temp. depend., rel. to band struct. determ. 2−61448
n-Cd_2SnO_4 amorphous films 2−51137
$CdSnP_2$, current controlled negative resist. due to Gunn effect 2−61304
CdTe:In, Cu, high temp., impurity effects 2−61303
CdTe:Li, rel. to self-compensation and interaction of Li with defects 2−75107
p-CdTe, annealing effect on conductivity and photoconductivity, obs. 2−61263
CdTe, compensation by intrinsic point defects, elec. cond. obs. 2−84334
CdTe, growth from soln. melts, elec. props. 2−74677
$Cd_xZn_{1-x}S$ film, comp. depend. 2−54169
α-Ce, exchange-enhanced, resist. temp. and press. depend., spin-fluctuation resist. 2−81219
$CeAl_2$, resistivity under pressure, Kondo effect and Ce crystalline field variations 2−77857
CeH_x, metal-semicond. transition 2−77899
$Ce_xLa_{1-x}Pd_3$ alloy, Kondo effect 2−51098
CeO_2-ZrO_2-Y_2O_3 solid solns., electronic behaviour 2−47893
Ce_3Se_4, 80−680 K, complex cond. band 2−80918
$Ce_xY_{1-x}Al_2$, resistivity, 4.2-300K 2−64912
CoB, temp.depend., 100-1200°C 2−51099
CoB_x, 300-1200K 2−51100
Cr:Fe, 0.3-300K, low temp. maxima 2−68567
Cr, deformed at 77, 213, and 293K, recovery resist. study 2−53805
CrSi, elec. cond., thermal e.m.f. and Hall coeff. detn. 2−77797
$CrSi_2$ thermoelectric props. and crystal growth 2−84370
Cs calc. using lattice dynamical model of Sharma and Joshi 2−47749
Cs thin films, resistance from 0.3 to 0.9 μ region 2−68597
CsCl, B2⇌B1 phase transition kinetics study 2−53984
Cu-Au alloy, resistivity, temp. dependence 2−75049
Cu-Cu_3Au alloy, Debye temp., elastic moduli, comp. and temp. depend. 2−47752
Cu-Ni-Mn, dilute alloy, magnetoresist., Z-100K, Kondo effect 2−47835
Cu-Ni-Mn alloy, order-disorder transform study 2−54001
Cu-Ni(Cr) alloy, Kondo effect 2−64913
Cu-Pd alloys, influence of domain size and ordering on mech. props. and elec. resist. 2−68506
Cu-Zn-Mn system, rel. to phase diagram detn. 2−50963
Cu-Zr-Cr alloy, rel. to precip. processes 2−50933

Conductivity, electrical continued
solids continued
Cu-based dilute alloy, reson. and charge neutrality, semiphenomenological model 2−71783
Cu, commercial electrorefined wire, metallurgical factors effects 2−47579
Cu, during creep tests 2−50754
Cu, Hall and Righi-Leduc coeffs., 4-125 K, Weidemann-Franz law 2−61224
Cu, low temp. dependence, undergraduate expt. 2−73262
Cu, neutron irrad., impurity atom effect on recovery, elec. resistivity obs. 2−60964
Cu, polycrystalline, resistivity changes during tensile deformation 2−47834
Cu, residual resistivity, high-temp. oxidation influence 2−71832
Cu, surface stress, strain produced by He bubbles, elec. resistivity obs. 2−43678
Cu film, props. thermoelec., resist., cond. electron m.f.p. 2−68477
$CuCr_2Se_4$, temp. depend., 100-650K 2−81091
CuO, semiconduction rel. to catalytic activity 2−75093
Cu_2O, thermal activation energies, rel. to prep. conditions, −40-250°C 2−71898
Cu_2O relationship in samples annealed at various temp. to activation energy 2−75092
Cu_2O thermal behaviour, role of defects, review 2−75091
Cu_xS, differential thermal analysis of the Cu-S system, 30-500°C 2−84138
Cu_2Te-Ag_2Te system, comp. and temp. dependence 2−84323
Dy-Nd alloys, spin disorder resist. 2−51237
Eu, electronic thermal resist., critical divergence at Neel point 2−57124
$Eu_{1-x}Gd_xO$, metal-nonmetal transition 2−71899
EuO:Gd, bidirectional threshold and memory type switching 2−81081
EuO, insulator-metal transition and bound mag. polarons 2−80975
n-EuS, 140 kOe, negative magnetoresist. obs. 2−47895
EuS, slightly Eu rich, high-temp. resistivity 2−75094
Fe-1%C-0.5%As alloy, anomalous precip. obs.50940 2−50940
Fe-1%C alloy, rel. to effect of As and Sn on tempering stages 2−50796
Fe-Mn alloy, b.c.c., shock deformed, recovery 2−56912
Fe-Ni alloy, magnon scattering processes 2−65142
55Fe-45P_2O_5 glass, a.c. and d.c. characteristics, correlation with structure 2−81142
Fe, Mg olivines, electrical conductivity in solid solutions rel. to planetary mantles 2−84292
Fe, plastically deformed, defects, resist. study 2−80740
FeB_x, 300-1200K 2−51100
α-Fe_2O_3, d.c. cond., O_2 partial press. depend., 950-1422°C 2−51138
FeSi, elec. cond., thermal e.m.f. and Hall coeff. detn. 2−77797
$Fe_{1-x}Ti_{1+x}$, resist. minimum, magnetization and sp. ht. study 2−44252
Fe_2Ti, elec. resist. thermo-hysteresis rel. to martensitic transform., 4.2−1200K 2−71834
FeV_2Te_4, resist., metallic cond. 2−60757
GaAs-GaAlAs layered structs., current-voltage characts., transport props. 2−68399
GaAs, amorphous, field depend. 2−77896
GaAs, amorphous, hopping and intrinsic, influence of annealing 2−61312
GaAs, current instability rel. to mag. field, negative resist 2−64984
p-GaAs, effect of pressure, 10000 kg/cm² 2−44099
n-GaAs, electron irrad., annealing behaviour 2−47918
GaAs, electron irrad., asymmetric damage regions obs. 2−74759
GaAs, electron mobility meas. 2−64969
n-GaAs, heavily-doped, temp. depend. 2−61342
GaAs, heavily doped, band tail states, localization study 2−71922
n-GaAs, hot electrons heated by high microwave fields 2−77897
n-GaAs, mag. field effect on impurity cond. 2−81085
GaAs, n- and p-type, electron irrad., defect levels determ. 2−80992
GaAs, neutron irrad., resistivity temp. depend. 2−51157
GaAs, split, negative differential cond., i.r. emission 2−61311
GaAs, undoped, point defect conc. effects on temp. depend. 2−71905
n-GaAs bulk element, uniform cross-section, doping inhomogeneity, static electric field distribution 2−84315
GaAs epitaxial layer, origin of high resistance region at substrate interface 2−71883
$GaInS_3$, thermally stimulated cond., dark current, capture levels 2−75162
$Ga_{2x}In_{2(1-x)}S_3$, thermostimulated cond. 100-350K 2−84317
GaP p-n-p-n green light emitting diode, negative resist. 2−72436
n-GaSb, resist., temp. and mag. field depend., cond. band parameter obs. 2−57206
Gd-Th alloys, resist., mag. ordering effects 2−84294
Gd, effect of press., 77-400K 2−77858
Gd, resist. anomaly near Curie pt. 2−57291
A-Gd_2S_3, resistivity of crystals grown from gaseous phase, temp. dependence 2−53607
$GdTiO_3$, resist., 77-1500 K 2−57144
Ge:Au diode, fabrication, double injection negative differential resist. 2−71974
Ge:Cu $P^+-\pi-N^+$ structures, negative resistance and magnetic sensitivity 2−75130
Ge:Mn, nonlinear IV characts., exclusion and charge exchange between impurity levels 2−75115
n-Ge:P(As), resist. decrease due to donor spin reson. 2−81106
Ge:Sb(P)(As), heavily doped, temp. depend. of resist. 2−71940
Ge-Cr film, amorphous, hopping cond. 2−61313
Ge-Se glass, microphase separation effect on semicond. behaviour 2−60592
Ge-Si heterojunction, pulse characts. 2−71961
Ge-Te-As glass, high current density path shape 2−57193
p-Ge-n-CdS_xSe_{1-x} epitaxial heterojunction 2−77924
p-Ge, 220K defect, resistivity obs. 2−47928
n-Ge, absolute negative cond., current instability, Erlbach effect 2−68433
Ge, amorphous, hopping and intrinsic, influence of annealing 2−61312

Conductivity, electrical continued
  solids continued
    Ge, amorphous, resistivity as function of hydrostatic pressure and temp. 2−61352
    Ge, amorphous, temp. dependence 2−47924
    Ge, amorphous, unannealed, residual cond. at 77K 2−47926
    n-Ge, below 1K, anomalous temp. depend. 2−57210
    n-Ge, cond. relax., rel. to elec. field depend. of energy relax. time 2−65010
    Ge, density depend. 2−54101
    n-Ge, disordered region prod. by 28 MeV electrons 2−47931
    Ge, electron irrad., 8.5MeV, high field domain instability 2−57208
    Ge, electron irrad., asymmetric damage regions obs. 2−74759
    Ge, electron irrad., change in length and elec. resist. 2−68016
    Ge, heavily doped, 0.02-300K, cond. mechanism 2−81109
    Ge, in contact with electrolyte, shunting effect, pot. distrib. 2−65016
    Ge, longitudinal and transverse specimens, meas. of distrib. of resistivity by single probe method 2−51163
    p-Ge, low temp. elec. irrad., point defect annealing 2−47381
    n-Ge, neg. diff. cond. obs. of hot electron instabilities 2−77912
    n-Ge, negative absolute resist. 2−71937
    p-Ge, neutron irrad. effects, 77K 2−47930
    Ge, pulsed elec. field, minority carrier mobility, influence of majority carriers 2−75114
    n-Ge, resist. rel. to donor spin reson., spin energy transfer model, 4K 2−68434
    Ge, time depend., surface orientation effects 2−71935
    Ge cylindrical crystal, contactless method for measurement of volume distribution of resistivity 2−51159
    Ge film, amorphous, anisotropy in resist. 2−68430
    Ge film, amorphous, effects of substrate temp. 2−64987
    Ge film, amorphous, ohmic and non-ohmic cond. 2−61289
    Ge film, thickness depend. 2−54192
    Ge surface, charge relax., contact potential and surface cond. study 2−81105
    Ge surface, rel. to reaction with O_2 2−50448
    GeO, layers, defective, hopping cond., elec. cond., 77-453 K, 20-100 MHz 2−54173
    $GeTe$-Bi_2Te_3 solid soln. 2−74903
    Ge_xTe_{1-x} alloy, amorphous, rel. to band struct. detn. 2−77904
    $Ge_{15}Te_{80}As_5$ semiconducting glasses, thermally induced surface and bulk electrical effects 2−68401
    Hf, explained by electron scattering mechanisms 2−81035
    HfB_2-ZrN alloy, conc. depend. 2−47638
    HfO_2, 1600-1900K 2−54233
    Hg, ideal resitivity at low temps. 2−57153
    Hg, Lorenz number and thermal cond., meas. by modified Kohlrausch method 2−71189
    p-$Hg_{1-x}Cd_xTe$, carrier freeze-out and acceptor energies obs. 2−57194
    Hg_3Te_3-In_2Te_3 alloys, cond. types of h.p. phases 2−54175
    HgTe, in high mag. field, 4.2, 77 and 300 K 2−64988
    HgTe films, temp. dependence, and of Hall coeff. 2−54174
    In, cylindrical, r.f. size effect 2−44053
    InBi, effect of thermal cycling 2−51101
    InBr(I), resist., I-V characts. 2−64638
    InP, high resistance, Cu, Fe or Cr doped, synthesis and meas. of this prop. 2−83895
    In_2S_3, thermostimulated cond., 100-350K 2−84317
    n-InSb, anisotropic complex small signal cond. of hot electrons at 84K and 134 GHz 2−61318
    InSb, changes on heat treatment, field effect obs. 2−64989
    InSb, negative differential mobility rel. to contact effect on microwave emission 2−47897
    n-InSb, nonlinear transport props. of hot electrons in strong mag. field 2−47896
    n-InSb, resistivity and carrier distrib., hot electron cyclotron resonance obs. 2−77845
    n-InSb, transport coeffs. at high temp., degeneracy and screening effects 2−68378
    InSe, flash evaporated thin films, eff. of thermal treatment on props. 2−77853
    In_2Se_3, flash evaporated thin films, eff. of thermal treatment on props. 2−77853
    In_2Se_3 film, flash evaporated, resistivity rel. to structure 2−56593
    $IrB_{1.1}$, temp. depend. 2−47657
    $Ir(CO_3)Br$, organometallic, thermoelec. analysis 2−72055
    K, r.f. size effect, calc. 2−71835
    K, resist., temp. and volume depend., 20K-m.p. 2−84296
    K, resistivity, contribution of Umklapp processes 2−84293
    K complex, $K_2Pt(CN)_4Br_{0.3}.xH_2O$, temp. depend. 2−44110
    K elec. conductivity calc., electron-phonon scatt., soln. of Boltzmann eqn. 2−71830
    $K_{0.3}MoO_3$, blue phase, semicnd. to metal transition 2−61151
    KNO_3, bicond. phenomena 2−61319
    K_2O-SiO_2 glass, as function of thermal history 2−54229
    $K_2Pt(CN)_4Br_{0.3} \times 2.3H_2O_2$, $2.3H_2O_2$, one-dimensional conductivity, defect effects 2−68339
    $K_2Pt(CN)_4Br_{0.30}.3H_2O$, one-dimens. cond. as two-dimens. problem 2−51142
    $K_2Pt(CN)_4Cl_{0.3}.xH_2O$, organometalllic thermoelec. analysis 2−72055
    $KTaO_3$, three terminal meas. and rel. to point defect models 2−47967
    $LaAl_2$, resistivity under pressure, Kondo effect and Ce crystalline field variations 2−77857
    La_2Te_3-La_3Te_4 system, meas. suggests semiconducting nature of La_3Te_4 2−80919
    La_3Te_4, 80−680 K, complex cond. band 2−80918
    $LaTiO_3$, resist., 77-1500 K 2−57144
    Li, resistivity, contribution of Umklapp processes 2−84293
    Li_2O-Fe_2O_3-SiO_2 system, dispersion, composition depend. 2−54333
    Lu-H(D) system, resist. obs. of α-phase characts. 2−77749
    MgF_2, hot pressed, temp. depend. 2−47898
    n-Mg_2Ge, temp. depend. and cond. mechanism 2−51143
    MgO-Fe_2O_3-CaO-Al_2O_3-SiO_2, charges caused by phase transformations during heating 2−83839
    MgO, 800-1300°C 2−81065
    MgO crysts. growth by chem. vapour deposition 2−47223

Conductivity, electrical continued
  solids continued
    $MgSi_{1.72}$-$CrSi_2$ solid soln., 20-1050°C 2−74905
    $MgSi_{1.72}$-Ge solid soln., 20-1050°C 2−74905
    Mg_2Sn pressure dependence of electrical resistance 2−84326
    α-Mn, residual resist. press. depend. 2−54357
    Mn phosphate glass, rel. to mag. props. and structure obs. 2−57292
    MnAs, phase boundary motion at coupled lattice- and spin-disorder transition, resist. study 2−78021
    $Mn_xHg_{1-x}Te$ films, vacuum deposited 2−71885
    α-MnS from sulphurization of Mn in H_2S-H_2 gas mixtures at 550° to 711°C, obs. 2−75079
    MnSi, elec. cond., thermal e.m.f. and Hall coeff. detn. 2−77797
    Mo, electron irrad. at 4.2K, stage I recovery 2−53718
    Mo, film, size effect 2−81030
    Mo, temp. dependence near melting point 2−57066
    Mo, up to 2600K 2−54130
    MoO_3, ion bombardment enhanced cond. 2−68408
    MoO_3, ion impact effects 2−60779
    MoO_3 film, a.c. elec. props. and I-V characts. under d.c. bias 2−68454
    MoS_2 layer structures, a.c. conductivity in high and low frequency limit 2−81062
    NH_4ClO_4, proton transfer cond. 2−84361
    Na-Sn silicate glasses, effect of Sn content 2−47055
    Na, 35°C-m.p. 2−84211
    Na, Lorenz function, 40 to 360K 2−57086
    Na, resist., temp. and volume depend., 50K-m.p. 2−84296
    Na, resistivity, contribution of Umklapp processes 2−84293
    NaCl, doped with Bi^{3+} coordinately bound on O 2−51191
    NaCl, NaCl:Ca, γ-irrad., d.c. obs., room temp. −70°C, electronic and ionic contribs. 2−57231
    α'-$NaV_2O_{5-x}F_x$, $0 \leqslant x \leqslant 1$, d electron distrib. on V atoms, from elec. and mag. props. 2−75080
    Nb, above 2650K, pulse heating method 2−53487
    Nb, cold-worked or irrad., stage III recovery study 2−47404
    Nb, cold-worked or neutron irrad., recovery, resist. study 2−64766
    Nb, high purity, resistivity from 20°K to fusion temperature 2−81032
    Nb polycrystalline wire, rel. to H_2 adsorp., clustering model 2−47161
    Nb_2O_5, ion impact effects 2−60779
    Nb_2O_5 film, amorphous, switching states 2−61320
    $NbSe_2$, resist. anisotropy with press. 2−51116
    $NdCo_2$, dissolved hydrogen effect on resist. 2−48040
    Nd_2O_3, p- and n-type behaviour rel. to press. 2−44103
    Nd_3S_4, 80−680 K, complex cond. band 2−80918
    Ni-B thin films obtained by oxidation-reduction in liquid phase 2−77860
    Ni-Cr alloy, hydrogenated, elec. resist. rel. to mag. field, localized moments 2−81034
    Ni-Cu, elec. resist. near Curie point, resist. anomaly 2−61225
    Ni-Fe-Nb alloy, and magnetic characts. 2−57293
    Ni-Fe-W high permeability alloy 2−48076
    Ni-P chemically deposited films, relation with structure 2−77510
    Ni-Pd-P-base amorphous alloy containing Fe, resistivity-temperature relationship, $T^{-1/2}$ singularity 2−44215
    Ni, electrical resistivity due to dislocations, at low temps. 2−81033
    Ni, electron-irrad., low temp. recovery 2−64655
    Ni, Ni:Sn, plastically deformed, deviations from Matthiesen's rule 2−71837
    Ni, porous, transport props. depend. on porosity 2−77740
    Ni, recovery after 300 kbar shock wave loading 2−56794
    NiB, temp. depend., 100-1200°C 2−51099
    NiB_x, 300-1200K 2−51100
    Ni_3Cr alloy, oxidation effects 2−54338
    $Ni_3(Mn,Co)$ and $Ni_3(Mn,Fe)$ alloys, electron and hole mobility obs. 2−47837
    $Ni_{0.6}Mn_{2.4}O_4$, elec.-field-depend. cond. for hopping-type charge transport 2−81082
    NiO, high temp. cond. mechanism 2−84314
    NiS, 80−400 K, semicond.-semimetal transition 2−81097
    NiS_2, semicond., temp. depend. 2−81020
    NiS_2, semiconducting, and opt. absorpt. meas. rel. to band model 2−68417
    NiS + NiO physical mixtures, electrical conduction rel. to planetary mantles 2−84292
    NiTi, non-stoichiometric phase, comp. and temp. depend. 2−74885
    Ni + NiO physical mixtures, electrical conduction rel. to planetary mantles 2−84292
    Pb-Sb alloy, precip. mechanism study 2−80858
    Pb, from electron-ion interaction pseudopot. model 2−77812
    Pb, intermediate state, isotropic and anisotopic galvanomag. props. 2−47866
    $PbBr_2$, elec. cond. in cell arrangement, space charge effects, elec. polarization 2−61420
    $PbBr_2$, electronic cond., hole cond., elec. polarization 2−61419
    $PbBr_2$, pure and doped, hole cond., defect chem. 2−61322
    $PbCrO_3$, perovskite, struct., elec. resist., mag. susceptibility 77-550K 2−61321
    PbI_2, O_2 chemisorption induced changes 2−47886
    PbO-Al_2O_3-SiO_2-B_2O_3 glass, between metal electrodes, rel. to memory effect 2−71915
    PbO-RO-GeO_2, R = Mg, Ca, Sr, Ba, glass, rel. to structure 2−53540
    PbO, autocompensated photoconductor, inversion of the sign of conductivity 2−44175
    PbS layers, determ. of photocond. mechanism 2−81166
    PbSe epitaxial films on NaCl substrate, effects of ambient gas uptake 2−65008
    n-PbSe(Te), hot-electron cond., velocity-field characts., 77 and 4.2K 2−68407
    n-$Pb_{1-x}Sn_xTe$, hot-electron cond., velocity-field characts., 77 and 4.2K 2−68407
    p-PbTe-PbSe alloys, temp. depend. 2−75164
    $PbTiO_3$, conversion to semicond. state by doping resist. positive temp. coeff. 2−81098
    Pd-Co(Fe)(Mn) dil. alloys, mag. ordering obs. 2−81246
    Pd-rare earth intermetallic compounds, anomalous resistivity effects 2−51102
    Pd_5B_2, Pd_3B, synthesis and specific resistance 2−72054

Conductivity, electrical continued
- **solids** continued
  - PdRhNi alloy, spin fluctuation resistivity 2−64916
  - polyazophenylenes, semiconducting 2−44118
  - Pr:Fe, 0.3-300K, low temp. maxima 2−68567
  - Pr, temp. depend., anomaly near Neel point 2−51281
  - $PrCo_2$, dissolved hydrogen effect on resist. 2−48040
  - Pt/SiO cermet films, resist. in a.c. 2−75095
  - Pt, film, discontinuous, current noise 2−68340
  - Pt, proton, deuteron and He-ion damage obs. 2−50643
  - Pt, vacancy conc. rel. to press., quenching effects, excess resist. obs. 2−60788
  - Pt film, rel. to temp., 77- 573 K, adsorpt. effects 2−64917
  - PtSi on single crystal Si substrate, thermal stability, sheet resistivity meas. 2−71334
  - quinolinium $(TCNQ)_2^-$, temp. depend. 2−44110
  - Rb, resistivity, contribution of Umklapp processes 2−84293
  - RuO_2, room temp. 1300K 2−57145
  - RuO_2 film 1-5 μm thick 2−47123
  - Sb_2S_3, temp. dependence, and change of colour 2−54160
  - SbSI:Sb_2S_3, prep., spontaneous polarization, dielec. permittivity, photocurrent, dark current rel. to phase transition, −50-50°C 2−75143
  - SbSI, Seignette semicond., thermal currents induced by light 2−72039
  - Sb_2Se_3-SbI_3 system, 300 to 500K 2−43942
  - Sb_2Se_3, polycryst., threshold and memory switching 2−77883
  - Sb_2Se_3, Sb_2Se_3-Bi_2S_3 alloy, switching behaviour 2−75096
  - Sb_2Se_3 film, amorphous, transport props. 2−61323
  - Sc film, size effect 2−81030
  - Sc_2O_3 film, a.c., hopping model 2−61324
  - Se, amorphous, threshold and memory switching effects 2−57196
  - Se, compressed, thermally stimulated current obs. of crystn. 2−64533
  - Se, field effect rel. to temp., field mobility, surface cond. 2−71933
  - Se, non-crystalline, impurity effects 2−61326
  - Se amorphous films, a.c. cond., temp. depend 2−68392
  - Se film, rolling texture determ. 2−64574
  - Se film, vitreous, trap-limited processes 2−61325
  - Si:Au, thermally-stimulated current from deep-lying trapping levels 2−68149
  - p^+-n Si:Au diode, current filament behaviour in mag. field 2−71975
  - p-Si:Be, resist., temp. and doping depend. 2−54198
  - n-Si:Li, irrad. induced defects and impurity effects 2−47385
  - Si:Na(K), impurity atomic radius effects 2−71948
  - Si:P, heavily doped, temp. depend. of resist. 2−71940
  - Si:P, implanted, annealing characts. 2−77594
  - Si:P, intermediate region of impurity cond., effect of e.s.r. of donor electrons 2−72498
  - n-Si:P, stress depend., 4.2, 77 and 300K 2−71945
  - Si-$CrSi_2$, $CrSi_2$ fibres in Si matrix, anisotropy columnar structs., resist. anisotropy 2−74920
  - Si-SiO_2-metal, m.o.s., potentials and d.c. rel. to oxide thickness and interface states 2−61406
  - Si, amorphous, field depend. 2−77896
  - Si, amorphous, tunnelling cond. 2−61359
  - Si, anisotropy and hot electron effects, 1-300 K 2−84342
  - n-Si, Cd-compensated, current oscills. 2−71949
  - n-Si, cond. relax., rel. to elec. field depend. of energy relax. time 2−65010
  - n-Si, due to stress induced electric fields 2−44127
  - Si, electron irrad., asymmetric damage regions obs. 2−74759
  - Si, electron irrad., liquid He temp., a.c. hopping cond. obs. 2−47936
  - p-Si, electron irrad. effects 2−54201
  - p-Si, electron irrad. effects 2−71944
  - Si, grown by pedestal technique using electron beam heating, radial variation 2−43512
  - n-Si, hot electron cond., mag. field strength depend. 2−65018
  - Si, γ-ray and neutron irrad. induced defect obs. 2−47937
  - n-Si, neg. diff. cond. obs. of hot electron instabilities 2−77912
  - Si, P-implanted, annealing characts. 2−64678
  - n-Si, resist. rel. to donor spin reson., spin energy transfer model, 4K 2−68434
  - Si, spreading resistance, contact resistance temp. depend. 2−51161
  - n-Si, weak cond. anisotropy in static mag. field, e.m. propag. obs. 2−84343
  - Si film, amorphous, 77-300K, annealing effects 2−61360
  - Si film, amorphous, effects of thermal neutron irrad. 2−60666
  - Si film, amorphous, rel to localized state distrib. determ. 2−68437
  - Si film, gas doped during deposition 2−50690
  - Si film and bulk, electron irrad., defect prod., resist. change 2−80655
  - n-Si inversion layer, rel. to two dimensional impurity states 2−51170
  - Si junction, thermally diffused, avalanche multiplication rel. to dislocation lines 2−65027
  - n-Si proton bombardment induced shallow donors, elec. props. 2−61355
  - SiC:B, impurity distrib. obs. 2−74797
  - SiO_2:Au ion implanted, carrier transport rel. to floating gate devices 2−68458
  - SiO_2, in Al-SiO_2-Si struct., IV characs., breakdown, and switching 2−71996
  - SiO_2 film, on Si, Fowler-Nordheim tunnelling 2−47955
  - Sm-Sn system intermetallics, correl. with electronic struct. 2−47573
  - Sm, elec. resist., thermoelec. power, anomalous behaviour, 300-1000K 2−54128
  - SmS, semicond.-metal transition, optical consts. and energy levels study 2−80994
  - Sn-Cd dilute alloy, Matthiessen's rule deviations, 4.2-80K 2−84295
  - α-Sn, electron irrad., atomic displacement process evidence 2−53722
  - Sn, skin effect, anamolous, d.c. cond., m.f.p., reflectivity factor 2−68341
  - Sn film, quantrum oscill. amplitude, temp. depend. 2−71838
  - Sn film, quantum size effect oscillatory depend. on thickness 2−57164
  - SnS_2, a.c. conductivity meas., −100°C to 120°C 2−84290
  - SnTe, polycrystalline film, specific resistance, temp. depend. 2−71916

Conductivity, electrical continued
- **solids** continued
  - $SrPd_2H$ characterization 2−47347
  - Sr_2PdH_4 characterization 2−47347
  - Ta-H system, resist. rel. to solute conc. 2−80857
  - Ta-10%W alloy, pulse heating obs., 1500-3200K 2−57069
  - TaS_2, 1S and 2S polymorphs, temp. depend. 2−47226
  - Tb, effect of press., 77-400K 2−77858
  - Te-As-Si-Ge film, amorphous, a.c. cond. rel. to localized tail states 2−61288
  - Te, electron irrad. damage obs. 2−47392
  - Te film, on glass, temp. depend., below 300 K 2−75099
  - Te film, thermoelectric power, Hall and Seebeck coeffs., resistivity 2−54249
  - Te glass systems, activation energy rel. to chemical aspects 2−60599
  - $Te_{60}As_{25}Ge_{13}M_x$, M=S, Se, chalcogenide glass, interdepend. between, switching memory and thermal behaviour 2−47901
  - Th-Ce alloy, rel. to phase transition critical region 2−50951
  - ThO_2 and solid solns., rel. to solid electrolyte applic. 2−65053
  - $(ThO_2)_{1-x}(YO_{1.5})_x$ solid soln., electronic contrib. to mixed conductivity 2−75100
  - Ti-Au film, conductor stripes, electromigration damage rel. to pulsed d.c. powering 2−80940
  - Ti-Gd alloy 2−64866
  - Ti-Mo alloy, anomalous resist, rel. to microstruct. 2−84297
  - Ti-TiO_2-Au film diode, I-V characts., negative resist. 2−61390
  - Ti-Zr-Al-N film, sputtered, resist., struct. 2−47130
  - Ti, explained by electron scattering mechanisms 2−81035
  - Ti alloys, exponential temp. depend. 2−54129
  - TiC, changes in microhardness, lattice parameters, electrical resistance following neutron irradiation 2−52848
  - TiO-MnO alloy, synthesis and props. 2−74908
  - TiO_2, doped and undoped, frequency dependence of conductivity and adsorption of CO 2−77906
  - TiO_2, ion impact effects 2−60779
  - TiO_2, rutile, powder in lightly pressed tablets, 300-1300K 2−77821
  - $Ti_xTa_{1-x}S_2$ $(0.1 \leqslant x \leqslant 0.9)$ solutions, resistivity 2−61266
  - Tl-Te alloy, amorphous film, comp. and temp. depend. 2−61328
  - $TlBiTe_2$ and TlTe, temp. depend. of resist. 2−51144
  - $TlInSe_2$:Cu,Sn, cryst. and film, photosensitivity, optical absorpt., dark cond., forbidden band width 2−57197
  - $Tl_2SeAs_2Te_3$ glass, switching rel. to radiation emission 2−64981
  - Tl_2Te single crystal, temp. depend., semicond. props. 2−64990
  - UC_{1-x}, estimation of resistivity increase due to C deficients 2−43874
  - $UC_{1-x}N_x$, $O \leqslant x \leqslant 1$, meas. of resistivity and absolute Seebeck coeff. 2−44105
  - $U(C_{1-x}N_x)$, rel. to electronic props. 2−57268
  - V-Ti(Cr)(Sn)(Al) alloy, comp. depend. 2−53912
  - VC_x, order-disorder transitions study 2−54004
  - $V_{1-x}Cr_x)_3Si$, ternary alloys, physical props. and electron struct. and elec. resistivity 2−68514
  - $V_{1-x}Nb_xO_2$, metal-insulator transition, theory 2−75103
  - $V_{1-x}Nb_xO_2$, metal-insulator transition study 2−75101
  - V_2O_5-P_2O_5 glass, rel. to comp. 2−60601
  - VO_2 switching device, influence of high-conducting bubble 2−54208
  - VO_x, 80-1400K 2−64991
  - V_2O_3, VO_2, V_2O_5 films, prep. by pyrolysis, temp. depend. of resistance 2−44106
  - V_2O_5, ion bombardment enhanced cond. 2−68408
  - V_2O_5, ion impact effects 2−60779
  - V_2O_5 bronzes, electrical conductivity in solid and liquid state 2−84339
  - V_nO_{2n-1} (n=3,4 ..., 8) single cryst., temp. depend., meas. 2−43509
  - W-Mo alloy, high temp., conc. depend. 2−54130
  - W-SiO_2:C-Au tunnel cathode, using amorphous dielectric, threshold emission and elec. switching 2−81122
  - W-Y_2O_3 two-phase system, 1100-3200°K 2−43875
  - W, above 3600 K, determ. by pulse heating method 2−74584
  - W, sintered, porosity influence 2−84145
  - W, stress induced growth irradiated at low temp. 2−60781
  - W, temp. dependence near melting point 2−57066
  - W, up to 3000K 2−54130
  - WO_3-P_4O_{10}-V_2O_5, and mag. resonance obs. 2−54495
  - WO_3, temp. depend., four probe method and reflected microwave current obs. 2−71914
  - WSe_2-$NbSe_2$ alloy, and antifriction props., comp. depend. 2−68115
  - Y-Ce alloy, decrease in elec. resist. under press. 2−71839
  - Y film, size effect 2−81030
  - YIG-Si, thermally induced negative resistance 2−51145
  - Yb-Sn system intermetallics, correl. with electronic struct. 2−47573
  - $YbMnO_3$-$YbCrO_3$, $YbMnO_3$-$TbFeO_3$, solid solutions, and mag. props. 2−51235
  - Zn-Cr alloy, dilute, elec. resist., $T < 0.1K$ 2−68342
  - Zn-M dilute alloy, M=Mn, Cr, Fe, Kondo effect and localized spin fluctuations 2−64918
  - Zn-Mn alloy, dilute, elec. resist., $T < 0.1K$ 2−68342
  - Zn, anisotropy in the phonon limited resistivity 2−64919
  - Zn film, on dielec. substrate, elec. resist., supercond. transition temp., absorpt. spectra 2−72323
  - $Zn_xMFe_{2-x}O_{4-x}F_x$, M=Ni, Co, ferrite, synthesis, magnetization, hopping cond. 2−75234
  - ZnO:Cu film, amorphous, band struct. and impurity state energy spectrum detn. 2−68421
  - ZnO-Bi_2O_3 ceramic, cond. mechanism 2−57198
  - ZnO, piezoelec. semicond., grown by chemical transport method 2−43516
  - ZnO, study of interactions in adsorbed layers 2−47175
  - ZnO acoustoelectric device, high and low field resistivity, uniaxial press. effect 2−63119
  - ZnS:Cu, surface, volume, and contact components of current 2−71918
  - ZnS film, amorphous, in m.i.m. structs. 2−64978
  - ZnS single crystal, homogeneous, and u.v. electroluminescence 2−68712
  - $ZnS_{1-x}Se_x$, stimulated cond. with persistent memory 2−75104
  - ZnTe:Al, high temp. elec. props., self-compensation model 2−51128
  - ZnTe, high temp. defect. equilib., elec. transport props. 2−44096

Conductivity, electrical continued
solids continued
Zr, explained by electron scattering mechanisms 2−81035
Zr alloys, exponential temp. depend. 2−54129
ZrC_x fibres, physical and mech. props. detn. 2−68178
ZrO_2-Yb_2P_3 and ZrO_2-Yb_2O_3-Y_2O_3 solid solutions 2−47721
ZrO_2-6 mol%CaO, castable, 900-1700K 2−53936
ZrO_2, 1600-1900K 2−54233
ZrO_2, nonstoichiometric, thermodynamic props. determ. 2−43506

Conductivity, thermal
see also Heat conduction
binary mixture, asymptotic behaviour of Green Kubo integrands 2−74308
contact resistance rig 2−66644
fluid, dil. or moderately thick, kinetic equation 2−67551
fluids, Kubo integrands, low-frequency behaviour of transport coefficients 2−43048
hollow cylinder, nonstationary optimal temp. regimes 2−63152
hollow cylinders, thermal characts. in contact planes 2−69794
infinite plate, inverse problem 2−41863
Kapitiza, phonon attenuation effects, acoustic mismatch model 2−67853
Kapitza resist., phonon absorpt. 2−54072
Kapitza resistance, effect of low energy vibr. modes 2−51053
Kapitza resistance, transfer hamiltonian approach 2−56533
laminar heat transfer with axial conduction, error in paper by Chia-Jung Hsu, 1967 2−66639
liquid crystals, effect of mag. field 2−80463
lunar surface layer, calc. 2−48763
mean heat cond. for nonhomogeneous media, phenomenological definitions 2−69797
metal-superfluid He interface, low temp. anomalies 2−54065
multilayered shells, equations 2−66643
nonlinear rigid conductor, material response function as Cauchy problem soln. 2−82272
nonlinear viscoelastic fluid flow 2−67599
nuclear fuel, oxide, porosity effects 2−52852
nuclear materials, measurement methods 2−49903
optical waveguide, temperature difference reduction in shielding pipes 2−76511
p-anisylidene p-aminophenylacetate, nematic, ordering influence of interface 2−80467
plasma, electron thermal conductivity in Tokamak system 2−53203
plasma, heavy component contribution in partially ionized gases 2−43122
plasma, laser produced, heat cond., Fourier's theory, applicability 2−80245
plasma, resistive with flow, toroidally confined, effects on containment 2−46756
pressure vessel internal loose-fill insulant 2−69498
reactor thermal insulation systems for He cooled HTR, waffle plate concept 2−42620
Soret driven instability in fluid 2−64222
thermal resistance meas. of solid deposits on surface of working structures 2−69799
thermophysical properties at high temperatures, conf., Turin, June (1972) 2−54035
turbulent and heat transfer in turbulent flow 2−77219
two-phase systems, model 2−53459
unsteady cond. for cylinder and parallelepiped, three dimens., anal. 2−55582
Z-pinch, high pressure confinement, losses 2−83600
Ar, calc. of coeffs. using modified Enskog theory over wide range of temperature and mass density 2−64227
Ar plasma, temperature dependence 2−60263
Cu, Kapitza, to solid and liq. ^{4}He at 1.9 K, rel. to Khalatnikov model 2−67854
p-H_2, calc. of coeffs. using modified Enskog theory over wide range of temperature and mass density 2−64227
He/Cu interface, Kapitza resist., Rayleigh waves influence 2−47764
He/metallic layer/He bath system, energy flux calc. 2−47010
He/metallic layer/He bath system, energy flux eval. 2−53474
He/solid interface, Kapitza resist. 2−47008
^{3}He solid interface, Kapitza resist., single- particle vs zero-sound couplings 2−47006
Kr plasma, temperature dependence 2−60263
N_2 plasma, 5000-18000 K 2−74350
O atoms, collision integrals 2−83184
O_2, calc. of coeffs. using modified Enskog theory over wide range of temperature and mass density 2−64227
Xe plasma, temperature dependence 2−60263

gases
air, Rayleigh convection, roll diameter dependence and effect on heat flux 2−60370
correlation formula, transport processes 2−50275
diethyl ether-methyl chloride mixtures meas. by hot-wire method in 80-200°C range, comparison with theory 2−53337
methyl acetate, exp. meas. at various temps. and pressures 2−60373
mixtures, expression in terms of props. of pure components 2−53341
multicomponent system of polyatomic molecules, rotational coeff. 2−50280
multipole interaction effects on rotational energy exchange in molecular collisions 2−50269
polyatomic, frequency dependence, two-temp. hydrodynamic theory 2−60371
rarefied gases, nonlinear conduction 2−83700
velocity-correlation functions in two and three dimensions, low density limit 2−53329
Ar, 800-2000K meas. 2−71112
Ar electrodeless discharge 2−50228
D_2, compressed, coupling with thermal relax., rel. to Rayleigh-Brillouin scatt. 2−56171
H, meas. in range 1 to 10^5K 2−50276
H_2, compressed, coupling with thermal relax., rel. to Rayleigh- Brillouin scatt. 2−56171
HD, compressed, coupling with thermal relax., rel. to Rayleigh- Brillouin scatt. 2−56171
Kr, 800- 2000K meas. 2−71112
Kr electrodeless discharge 2−50228

Conductivity, thermal continued
gases continued
N_2, 800-2000K meas. 2−71112
Pt-O_2(CO_2)(Ar)(SO_2) system, accommodation effect 2−67734
SF_6, frequency dependence, two-temp. hydrodynamic theory 2−60371
Xe electrodeless discharge 2−50228

liquids
air, 100-150K, 10-500 bar, calc. 2−71190
alloy, solidification rate rel. to thermal contact resist. 2−74586
p-azoxyanisole, nematic liquid crystal, interfacial effect 2−50323
p,p′-azoxyanisole liquid crystals, in magnetic fields 2−67828
Boussinesq fluid, temperature adjustment process via buoyancy-induced meridional circulation 2−67742
correlation formula, transport processes 2−50275
glass, flowing, energy transport in cylindrical channels 2−56552
metal, above and below melting point, laser pulse technique 2−54041
metal, laser flash method for thermal diffusivity determ. 2−53423
methyl acetate, exp. meas. at various temps. and pressures 2−60373
organic, molecular structure depend., Debye model incremental method 2−80468
potential parts determ. for 6-12 Lennard Jones potential, using generalized Rice Allnatt theory 2−74524
seawater, depth survey equipment 2−72727
semiconducting melts, band struct. 2−60466
semiconductor, heat transfer mechanisms 2−81094
silicone oil, Rayleigh convection, roll diameter dependence and effect on heat flux 2−60370
single-component system, derived from mol. mechanical model 2−71187
water, Rayleigh convection, roll diameter dependence and effect on heat flux 2−60370
water-ethanol liq. layer, heated from below, temp. field oscills. due to thermal diffusion 2−67821
CCl_4 interaction of thermal radiation with conduction, analysis, based on spectroscopic information 2−43346
Ce, high temp. obs. 2−51059
Ga, from Lorenz number and elec. cond. 2−71188
GaSe, and of solid 2−64865
Hg, det. by laser flash technique at elevated temps. 2−46946
Hg, Lorenz number and thermal cond., meas. by modified Kohlrausch method 2−71189
In, Lorenz no. 2−43347
InSe, and of solid 2−64865
Na, Lorenz function, 40 to 360K 2−57086
Pb, Lorenz no. 2−43347
Se, and of solid 2−64865

measurement
apparatus for metal studies, sensitivity and precision 2−54067
coefficient experimental study for electrical coils 2−78949
convective conductance meter, design and evaluation 2−51051
cylindrical hot wire gauge range extension to atmospheric pressure by natural convection 2−45195
detector, square wave operation 2−63149
diffusivity, determ. by phase shift method using discs and nonuniform irrad. 2−52273
diffusivity, in transient region, by short signal method 2−76218
enstatite, anisotropic lattice thermal conductivity as function of pressure and temperature 2−54619
equipment for dielectrics obs. 2−71755
frequency method for det. of thermal diffusivity coeff. 2−63150
heat flux gradient determ., using radiation from sample tube 2−69798
heat pulse methods, apparatus, 20-300°C 2−55573
high temperature techniques 2−71616
high-temperature gases, apparatus for 800-2000K 2−71112
laser flash method, for thermal diffusivity determ. of liq. metals 2−53423
laser flash technique, applic. to liq. metals 2−46946
lunar heat flow experiment, Apollo 15 mission 2−55135
metal and semiconductor, thermic non-stationary regime 2−47758
needle probe method for obs. of igneous rocks 2−44592
porous materials, high temp. method 2−54074
powders using probe and bridge circuit 2−64863
pulse method, radial cond. effects, boundary heat losses 2−78938
pulse method of meas. 2−63163
radiative and lattice cond., simultaneous meas. technique 2−51052
solid, direct heating methods for high-temp. thermophysical props. 2−54068
solid, simultaneous obs. of thermophysical props. of elec. cond. materials at high-temp. 2−57078
solid, small regular specimen, diffusivity 2−78935
solid, small very thin specimens, diffusivity 2−78936
solid material, hot wire method 2−51055
solids, high temp., periodic heating technique 2−57077
thermal diffusivity, calculation, sine wave modulation method, modifications of Cowan's eqns. 2−61114
of thermoelectric materials in small specimens 2−52276
transient method, by continuous heating 2−41862
transient region meas. method for materials in contact 2−78832
transient simultaneous measuring method for wet porous materials near f.p. 2−74989
N plasma, transport processes 2−56335

solids
– 2−71775
adhesive compounds, meas. of thermal resistance 2−58971
alkali halides, hydroxide-doped, tunnelling levels, low temp. 2−71758
alkaline earth fluorides, point defects vibr. spectra, cond. obs. 2−71724
alloy, commercial, Lorenz number and Smith Palmer equation 2−54042
alloy, solidification rate rel. to thermal contact resist. 2−74586
anisotropic relax. of cryst. momentum transport in Umklapp-dominated regime 2−43997
antiferromagnetic alloy, effect of spin orbit interaction 2−57295
bone, low temp., phonon mean free path, hydroxyapatite crystallite struct. 2−61115

Conductivity, thermal continued
- **solids** continued
  - boronated graphite, irradiation induced increase in thermal expansion and decrease in conductivity 2−76949
  - breakdown, rel. to elec. breakdown, book contrib. 2−47959
  - Callaway model, generalization to include polarizations 2−77788
  - cathodes and retrograde motion of cathode spot in arcs 2−71003
  - ceramics, high temp. obs. 2−77734
  - complementary variational principle, application to conductivity of lattice 2−77785
  - conductor material, temp. distrib. in d.c. heated conductors, calc. 2−57054
  - copper formate, low dimensional antiferromagnet 2−51062
  - copper formate tetrahydrate, antiferromagnet, magnon contrib. 2−72226
  - Cr and alloys, excitonic phase, calc. 2−65077
  - cubic crysts., determ. of elastic wave damping anharmonicity consts. 2−80913
  - cylinder, hollow, unsteady cond., three dimens. problem, anal. 2−55582
  - dielectric thin layers and plates, thermal cond. and Poiseuille flow of phonons 2−61058
  - dilute quantum crystal alloys, mass-defect induced changes 2−43948
  - electron-phonon system, heat flow in strong mag. field at low temp. 2−57100
  - excitonic phase, mag. and non-mag. impurities, calc. 2−65077
  - ferromagnetic alloy, effect of spin orbit interaction 2−57295
  - ferromagnetic insulator, critical dynamics 2−57288
  - fibrous metallic composite, thermophysical characs. 2−54070
  - glass, phonon scatt., low temp., elec. and mag. field depend. 2−51056
  - glass, simultaneous meas. of diffusivity and cond. by flash method 2−43996
  - granular material, simultaneous meas. of diffusivity and cond. by flash method 2−43996
  - graphics, pyrolytic, high temp. thermal diffusivity 2−54066
  - graphite, artificial, neutron irrad. effects 2−54073
  - graphite, electrothermal, rel. to crystallite size 2−57001
  - graphite, neutron irrad., 50- 1000°C 2−54075
  - graphite, nuclear, high fluence neutron irrad. behaviour, two-phase model 2−56048
  - graphite, polycrystn., effect of B doping 2−57084
  - graphite, porosity effects 2−50926
  - graphite, porous, high temp. meas. 2−54074
  - graphite, pyrolytic, and diffusivity above 1500 K 2−57083
  - graphite, pyrolytic, highly oriented, high dose fast neutron effects 2−57072
  - graphite, pyrolytic, meas. over wide temp. range, electronic component and characteristic temperatures 2−84208
  - graphite, thermal diffusivity, 650-2700K 2−54082
  - graphite composite, Pyrostrand, rel. to fabrication and struct. 2−53960
  - graphite nuclear reactor core, calc. of thermal resistance between hexagonally arrayed channels 2−42651
  - igneous rocks, estimation from mineral and chemical composition 2−44593
  - igneous rocks, needle probe method 2−44592
  - insulating crystal with paramagnetic impurities, changes due to spin-phonon modes 2−71706
  - insulators and structural materials, inc. diffusivity obs. 2−57080
  - interface, nonelectronic cond. at low temp. 2−43998
  - lunar fines, Apollo 12 samples 2−51811
  - lunar rocks, breccias and fines from Apollo missions 2−62661
  - Matthiessen's rule, deviations from, review and critical evaluation 2−71753
  - metal, above and below melting point, laser pulse technique 2−54041
  - metal, Lorenz function at high temperatures 2−54124
  - metal, low temp. cond. calc. and phonon spectrum 2−71754
  - metal, meas. accuracy 2−54067
  - metal, monovalent, high-temp. thermal resistivity and electron-phonon interaction 2−68258
  - metal, refractory, high temp. measurement 2−57077
  - metallized ceramic heat sink 2−76118
  - $MgSi_{1.72}$-Ge solid soln., at room temp. 2−74905
  - multiphase mixtures, composition dependence of flux propagations 2−75252
  - mylar, between 0.05 and 0.5K 2−47759
  - nonmetallic refractory compound, high temp. electrical insulator material 2−57079
  - n.q.r. spectroscopy 2−81477
  - parallelepiped, finite, unsteady cond., three dimens. problem, anal. 2−55582
  - polyfluoroethylene, filler content influence 2−47553
  - polymer with inorg. chain mols., self-lubricating heat-resisting antifriction props. 2−43745
  - polystyrene, foamed, rel. to struct. 2−43412
  - pyrocarbon, 25-1100C, fast neutron irrad. effects 2−54046
  - pyroelectric detectors voltage response rel. to thermal diffusivity 2−81135
  - quartz-sand layers in N. Atlantic basin, heat flow obs. 2−65553
  - radiation heated bodies, heat transfer characts. 2−63146
  - radiative and lattice cond., simultaneous meas. technique 2−51052
  - rare earth dodecaborides 2−47838
  - rare earth garnets, LnAlG and LnGaG, phonon cond. 2−77786
  - rare earth metals, mag. transition manifestations, Lorenz functions 2−57311
  - re-entry materials, carbon, thermal props. 2−56981
  - refractory bricks, hot wire method 2−51055
  - relaxation time analysis using computer 2−71756
  - ribbed surfaces, effect on heat transfer performance 2−45579
  - Rochelle salt, thermal phonon scatt. by polarization fluctuations 2−44001
  - rod surface, effect of boiling transition regime on propagation of temp. oscillations 2−64513
  - ruby rod, Cr^{2+} conc. determ. and correl. with laser output 2−59169
  - semiconductor, II-VI, 3-300K 2−84213
  - semiconductor multilayer film, rel. to thermoelec. props. 2−51054
  - semiconductor planar structures 2−51125

Conductivity, thermal continued
- **solids** continued
  - semitransparent materials, cond. and diffusivity at high temps. 2−54069
  - silica, vitreous, hot wire method 2−51055
  - steel, stainless, thermal diffusivity, thickness effects 2−57085
  - steel laminate stacks, surface texture effects 2−49180
  - superconductor, dirty, transport props. of transition metals near upper critical point 2−77876
  - superconductor, dirty two-band, mixed state coeffs. near H_{c2} 2−47871
  - superconductor, thin film, mag. field depend. 2−68344
  - teflon, 0.17 to 4.0 K, dislocation scattering 2−71762
  - temperature propagation and thermal diffusivity, transmission line analogy 2−57081
  - thin plate, thermal diffusivity sine wave modulation method, modifications of Cowan's eqns. 2−61114
  - thin samples, parallel flow sandwich technique using Peltier effect 2−68257
  - transition metal, superconducting, with non-mag. impurities, two-band model 2−71874
  - transition metals, phonon contrib., 20 to 1200°C 2−47769
  - transition metals 2−71757
  - triglycine selenate, temp. depend., deuteration effects 2−72042
  - triglycine sulphate, near Curie point 2−44002
  - triglycine sulphate, temp. depend., deuteration effects 2−72042
  - two-phase system, effective consts. estimation method 2−54071
  - wet porous materials near f.p., transient simultaneous measuring method 2−74989
  - wires, thermokinetic potentials, curent-affinity relations, nonequilibrium thermodynamics 2−49031
  - Zircaloy-2, thermal diffusivity, thickness effects 2−57085
  - Ag-Au(Cd)(In) dilute alloy, evaluation from Righi-Leduc coeff. 2−75050
  - Ag, Hall and Righi-Leduc coeffs., 4-125 K, Weidemann-Franz law 2−61224
  - $AgCl:Ni^{2+}$, relaxation time approx. analysis 2−51057
  - AgCl, pure and doped, transverse phonon contrib. 2−77789
  - n-Ag_2Te, Lorenz number, electron scatt. inelasticity obs. 2−84337
  - Al, steel-reinforced, rel. to struct. 2−53946
  - Al alloy, 10-300 K 2−47760
  - Al film, determ. from temp. distrib. studies 2−74999
  - AlN ceramic characteriz. 2−50864
  - Al_2O_3:V, before and after γ-irrad., phonon scatt. study 2−68214
  - Al_2O_3-Mo cermets, in range 500-1300°K 2−43999
  - Al_2O_3-TiO_2 ceramic, sprayed layers 2−44000
  - Al_2O_3-TiO_2 ceramic, sprayed layers 2−44000
  - Al_2O_3, sintered, radiative and lattice cond. simultaneous meas. 2−51052
  - Al_2O_3 powder, simultaneous meas. of diffusivity and cond. by flash method 2−43996
  - Al_2SiO_5 high and low pressure, polymorphs, rel. to density 2−65582
  - AmO_2, self-irrad. effects 2−54078
  - Au, Hall and Righi-Leduc coeffs., 4-125 K, Weidemann-Franz law 2−61224
  - BN, compact, 100-1000 K 2−47761
  - Be, quantum oscillation waveforms rel. to $\partial M/\partial H$ oscillations 2−80963
  - Bi, diffusive propagation of heat pulses, second sound 2−47762
  - Bi_2Te_3 and alloys, for Peltier cooling, review 2−75160
  - C, low density, diffusivity obs., annealing and environment effects 2−54076
  - C, pyrolytic, neutron-irrad. 2−57082
  - C, resistance thermometer, time response and thermal diffusivity 2−49184
  - C composite, chem. vap. deposited felt and filament wound, flight-tested, phys. props. 2−61017
  - C fibre reinforced composite, insulating 2−56984
  - C materials at high temps., modulated electron beam technique 2−84210
  - CaF_2 single crystals, at low temperatures, anisotropy 2−68260
  - Cd, Ziman-Baym theory calc. 2−51058
  - $CdS:Co^{2+}$, lattice cond., phonon-reson. scatt. 2−47763
  - CdS, pulsed region cathodolum. obs. 2−54077
  - $CdTe:Fe^{2+}$, phonon conductivity 2−64864
  - Ce, high temp., Lorenz no. 2−51059
  - CeO_2, in range 300-1200°C 2−61116
  - Ce_3Se_4, thermal and elec. cond., thermal e.m.f., 80−680 K, complex cond. band 2−80918
  - CoB, temp. depend., 100-1200°C 2−51099
  - $CoCl_2[(NH_2)Cs]_4$, 0.35-20K, in mag. fields up to 20 kG 2−81302
  - Cr and alloys, mag. transition manifestations Lorenz functions 2−57311
  - Cs calc. using lattice dynamical model of Sharma and Joshi 2−47749
  - Cu-Al alloy, neutron irrad. effects on lattice cond. 2−51060
  - Cu-Al alloys, cyclic fatigue damage obs. 2−50672
  - Cu-10at.%Al alloy, deformed, neutron irrad., dislocation strain fields, low temp. lattice thermal cond. obs. 2−71498
  - Cu-7at.%Ge alloy, deformed, neutron irrad., dislocation strain fields, low temp. lattice thermal cond. obs. 2−71498
  - Cu, Hall and Righi-Leduc coeffs., 4-125 K, Weidemann-Franz law 2−61224
  - Cu, mechanism importance in nuclear refrigeration, by adiabatic demagnetization 2−66364
  - $CuK_2(Rb_2)Cl_4.2H_2O$, critical dynamics 2−57288
  - Eu, electronic thermal resist., critical divergence at Neel point 2−57124
  - Fe-Ni alloy, magnon heat conduction 2−65142
  - Fe_2SiO_4 high and low pressure, polymorphs, rel. to density 2−65582
  - GaSb, heavily doped, phonon scatt. 2−47765
  - GaSe, and of liquid 2−64865
  - Ge:Sb, electron irrad., phonon scatt. and induced energy levels 2−47766
  - n-Ge, magnetocond., electron-phonon scatt., doping effects 2−81084
  - Ge, three phonon resist., second upper bound 2−71759
  - Ge, Ziman limit of thermal resist. due to three-phonon scatt. 2−75000
  - GeO_2 high and low pressure polymorphs, rel. to density 2−65582
  - GeTe-Bi_2Te_3 solid soln. 2−74903

Conductivity, thermal continued
- **solids** continued
  - He, anisotropy, Umklapp thermal relax. time tensor 2−74579
  - He, anisotropy 2−56536
  - ^{3}He-^{4}He mixtures, phase separation region 2−47027
  - ^{4}He, temp. pulse propag. in diffusive, second sound and ballistic regions 2−71268
  - Hf, meas. at high temps., explained by electron scattering mechanisms 2−81035
  - Hf, thermal diffusivity, thickness effects 2−57085
  - Hg, Lorenz number and thermal cond., meas. by modified Kohlrausch method 2−71189
  - In-Mn, superconducting thin films with paramagnetic impurities, electronic transport 2−68352
  - In, superconducting film, electronic thermal conductivity 2−68352
  - n-InSb, transport coeffs. at high temp., degeneracy and screening effects 2−68378
  - InSe, and of liquid 2−64865
  - K, low-temp. resist., electron- phonon umklapp processes 2−51061
  - KCl, temp. depend., role of longitudinal and transverse phonons 2−84214
  - $KCuF_3$, low dimensional antiferromagnet 2−51062
  - $KCuF_3$, one dimensional antiferromagnet, anomalous thermal cond. 2−71760
  - $KMnF_3$, antiferromagnet, anomalous thermal cond. 2−71761
  - La_2Te_3-La_3Te_4 system, meas. and effect of defects, semiconducting nature of La_2Te_4 2−80919
  - La_3Te_4, thermal and elec. cond., thermal e.m.f., 80−680 K, complex cond. band 2−80918
  - LiF deformed crystals along [110] axis, 0.04 to 0.8°K, dynamic scattering of slow transverse phonons due to mobile dislocation 2−68218
  - MgO:Fe^{2+}, phonon conductivity 2−64864
  - MgO, ground state of Cr^{2+} obs. 2−72238
  - $MgSi_{1.72}$-$CrSi_2$ solid soln., at room temp. 2−74905
  - Mo, rel. to superconductivity 2−47832
  - Mo, up to 2600K 2−54130
  - Na, 35°C-m.p. 2−84211
  - Na, Lorenz function, 40 to 360K 2−57086
  - NaCl, temp. depend., role of longitudinal and transverse phonons 2−84214
  - NaF, low temp., obs. of intrinsic anharmonic phonon-phonon interactions 2−68228
  - $NaNO_3$:Ca, near critical point, obs. 2−60542
  - $NaNO_3$, critical parameters 2−57052
  - Nb/Cu metal interface, thermal conductance measurements between 1.4 and 5°K 2−54141
  - Nb, supercond., phonon scatt. 2−47767
  - Nd_3S_4, thermal and elec. cond., thermal e.m.f., 80−680 K, complex cond. band 2−80918
  - Ni, porous, transport props. depend. on porosity 2−77740
  - NiB, temp. depend., 100-1200°C 2−51099
  - NiS, 80−400 K, semicond.-semimetal transition 2−81097
  - Pb-In alloy, supercond., temp. and mag. field depend. 2−47867
  - Pb-In alloy superconducting film, electronic 2−81042
  - Pb-In alloys, superconductivity, temp. and mag. field depend. 2−71872
  - PbSe(Te), temp. depend. of separate components 2−68259
  - p-PbTe-PbSe alloys, temp. depend. 2−75164
  - PuO_2, self-irrad. effects 2−54078
  - $Pu_xU_{1-x}O_2$, 673-1273K 2−54079
  - Re, 1200-2500K 2−54080
  - Se-As glaases, obs. near glass transformation point 2−61104
  - Se, and of liquid 2−64865
  - Si, neutron irrad., phonon boundary scatt. obs. 2−80917
  - Si diode, mesa type, reversely biased, effect of p-n junction size on thermal resistance 2−71967
  - Si single crystals, low temperatures, anisotropy 2−68260
  - SiC/W layer composites characteriz. 2−47768
  - SiC, polycryst., effects of crystallite size 2−56774
  - SiO_2, vitreous, phonon scatt., low temp., elec. and mag. field depend. 2−51056
  - Sn-Cd dilute alloy, 4.2-80K, lattice cond. 2−84295
  - ThO_2, thermal diffusivity, 900-2550°C 2−54081
  - $Th_{1-x}U_xO_2$, thermal diffusivity, 650-2700K 2−54082
  - Ti-Gd alloy 2−64866
  - Ti, meas. at high temps., explained by electron scattering mechanisms 2−81035
  - UO_2-Zircaloy-2 contacts for nuclear reactors 2−42655
  - UO_2, thermal diffusivity, 750-2700°C 2−54081
  - UO_2, thermal diffusivity, 625-2700K 2−54082
  - $VO_{0.79}$-$VO_{1.29}$, between 100 and 1000°K 2−64867
  - W-Mo alloy, high temp. 2−54130
  - W, sintered, porosity influence 2−84145
  - W, up to 3000K 2−54130
  - Zr, meas. at high temps., explained by electron scattering mechanisms 2−81035
  - ZrC, between 2100 and 3400 K 2−61117
  - ZrC_x fibres, physical and mech. props. detn. 2−68178

Confinement of plasma *see Plasma/confinement*

Constants
- 2e/h, a.c. Josephson effect, calibration as voltage standard 2−78746
- 2e/h, as-maintained voltage standards, international comparisons 2−78748
- 2e/h measurement, a.c. Josephson effect, Weston cell voltage standard 2−78747
- coupling, variation with time 2−59658
- fine struct., determ. using aether theory 2−82203
- fundamental, constant value 2−82136
- h/m, meas. using rotating supercond. rings to 500 ppm 2−71844
- Lifshitz-Van der Waals constant calcs. from optical states 2−53457
- solar constant and air mass zero solar spectral irradiance specifications 2−78580
- solar constant and solar spectral irradiance, radiation scales 2−78579
- speed of light, laser freq. and wavelength meas. 2−78758

Contact angle *see Capillarity; Surface tension; Wetting*

Contacts, electrical
- bulk 1/f noise, exptl. evidence for existence 2−47938

Contacts, electrical continued
- Fowler universal photoemission curve, operational equivalent 2−72087
- insulators, electrostatic charging after contact with metals 2−72005
- metal-semicond. contact, semicond. base region, overheating mechanism rel. to negative resist. 2−65035
- metal-semiconductor, surface elec. field, determ. by differential electroabsorpt. 2−65036
- polymers-Hg, electric field effect 2−57236
- potential difference meas., u.h.v. guarded Kelvin probe 2−45647
- semiconductor, amorphous chalcogenide, low resistance contacts 2−75121
- semiconductor-metal, current transport, unified approach 2−51175
- superconducting weak link point contacts, thermal effects 2−47874
- Al-Ge, slow states activation energy, barrier height temp. depend 2−75135
- Au-Ga alloys, characteristics, metallurgical properties 2−84069
- CdO film, transparent electrode for CdS 2−54209
- CdSe-electrolyte blocking contact, photosensitivity and noise 2−72079
- GaAs-electrolyte contact, differential capacitance, Mott-Schottky relation 2−51174
- n-GaSb-Pb, tunnelling spectroscopy and band struct., press. effects 2−84351
- In_2O_3/SnO_2 film, transparent electrode for CdS 2−54209
- InSb, effect on microwave emission 2−47897
- MoS_2 film, sputtered, slip ring lubricant 2−56596
- Nb-Zr alloys, superconducting point contacts, static and microwave properties 2−81054
- Nb, superconducting point contacts, static and microwave properties 2−81054
- Si-Si, symmetrical, thermal effects 2−61379
- Si, spreading resistance measurement, temp. depend. of contact resistance 2−51161
- Sn, superconducting point contacts, static and microwave properties 2−81054
- ZnTe, ohmic, specific contact resistance measurement 2−64962

Continuous creation hypothesis *see Cosmology*

Convection
- — 2−71280
- — 2−60176
- aerosol transport in naturally convected boundary layers 2−67786
- arc, temp. profile 2−71062
- astronomical telescope, optical aberrations due to temperature deformations and convective fluxes, interferometric investigations 2−48821
- in Atlantic Ocean, evidence for lateral movement 2−78325
- atmosphere, cold plumes 2−65704
- atmosphere, influence of convective heat release on synoptic scale flow 2−65679
- atmosphere, mesoscale processes 2−72738
- atmosphere, seedability and horizontal dimension of convective events 2−62212
- atmosphere, similarity, flows with and without shear 2−78358
- atmospheric, intensity obs., remote sensing using geostationary satellite 2−44726
- atmospheric jet-stream model with thermodynamic parameter of cloud convection 2−81656
- atmospheric thermics rel. to thermal convection in polytropic atmosphere 2−68881
- atmospheric zonal circulation in equatorial region, baroclinic model 2−81654
- Benard, with black and mirror boundaries, radiative stabilization 2−68890
- bifurcation in internally heated fluid layers 2−80180
- boiling from small cylinders in water and organic liquids, identification of heat removal modes 2−77472
- boundary layer on a vertical plate, blowing and suction 2−45591
- in boxes, determ. of critical Rayleigh numbers 2−66647
- cabbeling instability under oceanic conditions 2−57919
- celestial body, internal motions of spherical fluid model 2−75715
- clean air, plume theory 2−44686
- clear air convective fields, radar and drone aircraft measurements 2−75554
- cloud formation process in moist air by non-adiabatic thermal convection, one-dimensional model 2−44721
- clouds, development in Texas 2−62215
- clouds, North Sea coast, low sea surface temps. 2−54830
- clouds, successive development model 2−62213
- conductance meter, design and evaluation 2−51051
- conjugate free, from horizontal conducting circular cylinders 2−58959
- continuum gas flows, thermostress and concentration stress convection 2−80403
- cumulus cloud top obs., Venezuela 2−62243
- current dependence in electrolytically heated fluid layers 2−49182
- density convection currents, relative to loss of dust in particle-size distribution measurement 2−78754
- developing laminar free, between vertical flat plates with asymmetric heating 2−76402
- dielectrophoretic Poiseuille flow, overstability in thin annulus 2−64404
- with dissipation, surface curvature effects for large Prandtl no. 2−76219
- dynamo, hydromagnetic, convection driven 2−73504
- Earth, shallow mantle, one-dimensional 2−65450
- Earth, thermal convection within mantle, linear stability problem 2−78248
- Earth's mantle, convective heat transport with strongly temp. variable viscosity 2−57492
- earth's mantle hotspot tendency to cluster 90° from relative rot. poles 2−57494
- Earth mantle and polar ice sheets, critical Rayleigh number 2−51517
- electric arc, const. press. axial flow, local convection effects 2−74351
- electro-winning cell, decrease in mass-transfer rate obs. due to opposing convective flows 2−46868
- electroconvection, insulating liq. purity depend. 2−52278
- electroconvection of dielectric fluids under alternating electric field 2−53151

Convection continued
finite amplitude, effect of magnetic field, application to solar convective layer 2–58961
finite amplitude in self gravitating fluid sphere 2–41864
flow in box of porous material saturated with fluid 2–56308
fluid mixture, stagnation point flow effect on entropy variation rate 2–80162
forced, elec. field influence on heat and mass transfer 2–52282
forced, from sphere immersed in stream of inviscid fluid at small Peclet number 2–45596
forced, heat transfer to liquids, influence of property variation 2–55577
forced and free, heat transfer from vertical thin needles in uniform stream 2–80179
forced convection, solution of solids to determine diffusion parameters in liquids 2–80426
forced droplet evaporation with finite vaporization kinetics and liquid heat transfer 2–77398
forced-free, rel. to development of laminar flow in isothermal vertical tube, vertical tube, numerical analysis of gravity effect 2–53138
free, from longitudinally vibrating vertical plate, effect of oscillations 2–45593
free, three-dimensional, near two-dimensional isothermal surface 2–46672
free, with radiation, investigation in absorbing emitting and scattering medium 2–45582
free and forced, fine hot wire in steady flow 2–80173
free and forced through vertical noncircular ducts 2–60135
fully developed laminar free, between vertical plates heated asymmetrically 2–56287
gas, compressible, deep atmosphere, penetrating convection modes 2–48451
gas motion about strongly heated bodies 2–77346
glass, flowing, energy transport in cylindrical channels 2–56552
growth of spherical bubble controlled by heat diffusion, approximate soln. including convective flow 2–83729
heat, from vibrating cylinder, effect of acoustic streaming 2–41861
heat transfer from flames, soln. of conservation eqns. 2–76401
heat transfer from hot air to wetted ribbed tube, solution using enthalpy difference 2–69801
heat transfer from rotating disc 2–73465
heat transfer from vertical plates to conducting fluid in magnetic field 2–60181
heat transfer of MHD jet flow near wall 2–60200
heated ellipsoid of revolution, steady laminar free convection boundary layer 2–56286
holographic recorder for transient and high speed events 2–76494
horizontal fluid layer with volumetric energy sources 2–80429
hydrodynamic free convection flow, $P_m = 1$ near flat plate 2–53157
hydromagnetic free convection in electrically conducting nonmagnetic fluid flowing past flat plate 2–53150
instabilities in unsteady flow or configurations 2–56300
instability in fluid layer, light scatt. obs. 2–46660
instability in hydrodynamically coupld vertical channels 2–77221
interaction in cylinder heated from botton side and free surfaces 2–76399
interferometric meas. of convection in rectangular air filled cavities 2–76400
ionospheric wind fields, vertical motion domination 2–58077
laminar forced, in curved pipes with uniform wall temp. 2–52280
laminar free, from nonisothermal plate in temp. stratified medium 2–45592
layered, in density stratified fluid, physical and numerical experiments 2–66646
liquid, local natural convection mass transfer, electrochemical technique obs. 2–50288
liquid flow, at bottom of system with axial mixer and radial baffles 2–83752
liquid layer placed in time-periodic external forces 2–67822
liquids, elastico-viscous, free flow past infinite porous plate 2–46881
low gravity environment, demonstration of convection driven by surface tension 2–58954
magnetosphere, effect of polar cap elec. fields 2–65962
magnetospheric, obs. from Ba cloud motions 2–62298
magnetospheric convection electric fields, high latitude satellite obs. 2–75626
Marangoni at liquid-liquid interface, effect of heats of solution 2–77381
melt, convective instability rel. to stratified impurity distribution during crystallisation 2–53610
melt, setting, calc. of thermal convection 2–60547
in MHD channel flow between conducting walls 43108 2–43108
mixed, air over heated horizontal plane 2–80391
model using strong alternating electric field gradient in dielectric liquid 2–52279
natural, between parallel vertical plates, numerical analysis 2–52281
natural, effects in inclined cells 2–41866
natural, in confined medium, theory and expt. 2–55583
natural, promotion or restriction in industrial problems 2–58962
ocean, free convection onset in upper layer 2–72713
plane-parallel flow in vertical slot, oscillatory instability 2–83472
plasma, rotating 2–70967
plasmasphere, time scale interpret. 2–58048
polar ice sheets, relation to empirical flow laws of ice 2–48410
polar thermospheric winds, convection electric fields in ionospheric model 2–65855
porous layer, bounds derivation 2–67820
porous medium between two concentric cylinders numerical analysis 2–69800
post-main sequence stellar evolution, semi-convective mixing 2–58277
Rayleigh, roll diameter dependence and effect on heat flux 2–60370
Rayleigh-Benard, dynamics and stable flows 2–77205
Reynolds flux, relation with Danckwerts surface renewal theory 2–45595
rotation of stars rel. to transition from shallow to deep convection zones 2–81824
sea, stratified bay, three-dimensional circulation under variable wind-stress 2–44633

Convection continued
sea surface layer film and droplet formation 2–78323
sea water currents, role in freezing 2–65601
seafloor spreading, thermal aspects 2–62087
self preserving flow, energy deficiencies 2–44689
self propagating, MHD in ferromagnetic liquids 2–53160
in shallow atmosphere, convective instability, friction term formulation 2–78357
solar zone model, derivation of temperature profile from finite-amplitude convection theory 2–62741
Soret driven instability in fluid 2–64222
sphere, heat transfer in l.f. subsonic stream 2–53305
sphere slowly rotating in viscous incompressible fluid, steady state forced convection 2–64228
sphere with blow, effects on temp. field 2–77345
stability of horizontal two component fluid with positive vertical temp. gradient 2–70831
stability of radially bounded rotating fluid heated from below 2–64224
steady, in porous medium 2–55584
stellar and planetary atmospheres, hydrodynamic motions in stratified convective zones 2–78455
stellar convection envelope response to tidal variations of gravitation field 2–85008
supercritical fluid, effect of diameter of heated wire on free convective heat transfer 2–41865
suspension of particles, convective diffusion for case of Stokes flow of fluid 2–64481
thermal, effects of rotation, application to solar convection 2–58960
thermal, in pulsating flows, effect of velocity pulsations on heat transfer 2–60166
thermoconvective instability, completely confined regions 2–52283
thermohaline, fluids, oblique gradients effects 2–77212
thermohaline, numerical simulation 2–57916
thermosphere energy source, convection elec. fields 2–58041
torsion balance, effect on motion 2–72605
transfer, from internally heated slab, cylinder or sphere, exact steady state solutions 2–52284
transient laminar free, between vertical plates including entrance effects 2–45589
transient processes, onset near suddenly heated horizontal wire 2–45594
turbulent flow heat transfer of liquid in tube 2–60461
two-dimensional flow with conduction and convection, convergence and accuracy of finite difference schemes 2–60153
unsteady free convective flow, past infinite vertical porous plate with constant suction, viscous dissipation effects 2–46869
unsteady-state temperature distrib. in convecting fin of constant area 2–63154
upwind difference scheme for solution of transport problems 2–58811
water, flow, laminar, mixed convection 2–53343
water containing bubbles, heat transfer enhancement 2–60464
$CuSO_4$ liquid electrolyte horizontal layer exhibiting concentration polarization, hydrodynamic stability w.r.t. natural convection 2–48338
He I, force convection boiling and heat transfer, rel. to refrigerant applic. 2–64491
N_2O_4, liquid, heat exchange at precritical and supercritical pressures 2–46947

Conversion electrons *see Beta-ray spectra/conversion electrons; Gamma-rays/internal conversion*

Cooling
see also Joule-Thomson effect; Low-temperature production; Magnetic cooling; Supercooling
atmosphere, i.r. cooling rate over S. Norway, Rodgers' method 2–54813
buoyant thermals, dynamics with radiative cooling 2–65657
clouds, radiational computations including latent load 2–44722
desorption, below 12 K using ^{4}He desorbed from synthetic zeolite 2–52009
diabatic, airflow over arbitrary mountain ridge 2–78364
electron diffraction pattern of beam-sensitive specimens, cooling effects 2–79140
evaporative, body of water 2–77475
FFTF reactor, coolant system 2–63966
heated sylinder, applic. of Gegenbauer (ultraspherical) polynomial to diff. eqns. 2–82242
heated wire, unsteady surface cooling rate, response of temp. distribution 2–52292
hypersonic turbulent flow, film cooling effectiveness 2–83666
liquid film for protecting solid surface in hot gas streams, correlation with mass transfer data 2–67795
liquid N_2 system for solid state lasers 2–63339
lunar surface, post-sunset behaviour 2–51804
MHD convertor cryogenically 2–69848
nuclear reactor, by He and CO_2, comparison 2–56032
nuclear reactor active zone, temp distrib. obs. 2–42637
nuclear reactor fuel rod bundle-geometries, variation of heat transfer 2–74146
nuclear reactor fuel rod in vertical coolant tube, hydrodynamics, vibration and wear obs. 2–52844
nuclear reactors, heat transfer 2–49883
nuclear reactors, secondary cct. components steady and testing 2–63958
p-n junction thermoelement, effect of switching layer resistance on transient cooling 2–65079
parametrized i.r., numerical model of, upper tropospheric cold core cyclones 2–68900
polypropylene, effects of cooling rate from melt on struct., strength and fracture 2–56908
pulsars and superfluid neutron stars 2–66127
radiant, cone wall absorption of external radiant power 2–55569
reactors, water cooled and gas cooled, relative merits with view to future use in UK 2–59828
salt systems binary and ternary, simultaneous recording of electrical conductivity and DTA 2–78179
sea surface, evaporation, radiation and heat transfer 2–65593
sodium phosphate melt, condensed, vitrifaction, effect of cooling rates 2–77479

Cooling continued
  solenoid with water cooling 2−59071
  steel, hot-worked austenitic and ferritic, recrystn. during continuous cooling 2−53873
  stellar atmospheres, radiation field effects 2−58268
  Ti alloy VT14, phase transf. during heating and cooling 2−68201
  vtrifaction of condensed sodium phosphate melts, effect of cooling rates 2−77479
  Al, convective cooling of articles obtained from melt by Stepanov method 2−47574
  CO cooling effect in atmospheres of red giant stars 2−75709
  Co-Al alloy, disintegration of solid solution under hardening and cooling 2−60977
  Fe-Ni-C alloy, rel. to deform. induced martensitic transform. 2−71685
  ^{3}He, by Pomeranchuk effect, cryostat construct. 2−45191
  ^{3}He refrigerator, 200 mW recirculating 2−52008
  KCl single crystal and steel, dependence of natural cleavage and grain size on cooling velocity 2−84122
  Na cooled fast breeder reactor, heat transfer problems 2−52843
  Ni_2V alloy, ordering transformation for wide range of subcritical temps. 2−74938
  Xe, afterglow plasma, electron temp. lowering by diffusion cooling 2−70882
  Zn-Ti alloys, effect of cooling rate on as cast microstructure 2−80818
Copper
  adsorption, of Ni, on Cu surface and Ar plated Cu 2−47157
  adsorption of H_2 and O_2 on surface, obs. of reaction mechanism of H_2-O_2 reaction 2−54531
  angular dependence of Auger electron emission 2−84388
  anisotropic cubic crystals, elastic displacement field of point defects 2−80697
  anode, with V, Cr and Fe secondary anodes, K_α emission, primary and secondary excitation 2−61673
  arc, free burning with 1-15A current, atom population and electron concentration 2−71064
  arcs, current density and behaviour of cathode spots 2−71058
  atom, absolute total cross section for K-shell ionization by electron impact, 20-135 keV 2−46458
  atom, electron-bremsstrahlung cross-section meas. at incident energy 0.2 MeV, photon energies 0.02-0.2 MeV 2−70613
  atom, K-shell ionization by electron impact, absolute cross- sections 2−79931
  Auger spectra, LMM, fine struct., L-S coupling interpretation 2−61453
  Auger spectroscopy, quantitative, and electron ranges 2−71304
  Auger transitions, high-resolution meas., valence band density of states 2−81193
  band structure, crit. point detn., wavelength mod. derivative spectroscopy obs. 2−48160
  band structure, critical point determ., wavelength modulation derivative spectroscopy obs. 2−48160
  bimetallic wire with Nb-Zr-Ti alloy, strong pulsed magnetic field in solenoid 2−63255
  bombarded by C, N and O ions, 0.5-2 MeV, stopping power 2−47782
  Burgers vector rel. to external geometry at initial deform. stage 2−50673
  charge density form factor, X-ray scatt. determ. 2−84251
  chemisorption, weak adsorp. of CO and H_2 2−50537
  chemisorption of oxygen on (110) and (100) faces, electron diffr. obs. 2−60678
  coatings' hardness and conductivity 2−84647
  cold rolled, development of texture 2−80849
  contact potential, compressionally induced change 2−75187
  correlated successive collisions of 5-30 keV Ar ions, ion scatt. processes 2−47775
  creep, 400-800°C, stochastic model 2−68090
  creep, study by differential method of temp. variation at const. rate 2−80731
  creep and recovery of cold worked Cu at 200-300°C 2−84163
  creep deformation under bending stress 2−80836
  creep fracture of cylindrical bars under pure torque 2−64754
  creep tests in tension and compression, elec. resist. 2−50754
  critical strains, Bloch waves electron microscope study 2−80629
  crystal, dislocation free, growth by Czochralski method 2−67942
  crystal growth, dislocation free, by Czochralski method 2−47264
  crystal growth, horizontal Bridgman method 2−60722
  crystals, dislocation accumulation and plastic deformation under stress 2−80696
  Cu:Mn giant e.s.r. transmission through one-sided and two-sided ion implanted Cu foil 2−84569
  deformation, corners in yield surface under biaxial zig zag loading 2−43686
  deformation potentials for shear-strain, determ. of strain-induced shifts of energy levels 2−80976
  dendrites, habit and morphology, crystn. mode effects 2−47136
  density changes of solid and molten state at elevated temps. 2−64699
  desorption, of H_2, spatial distrib. obs. 2−50526
  determination, in Sn-Pb alloy, atomic absorp. spectroscopy obs. 2−78218
  diffusion, in CdTe from evaporated and chemically plated Cu layers, He ion backscatt. obs. 2−64676
  diffusion, in Pu 2−71539
  diffusion, of Zn, residual activity method 2−47457
  diffusion in Al, interpreted using oscill. form of inter-ion potential 2−64691
  diffusion in Pb, 0 to 56 kbars 2−47470
  diffusion in Pb, evidence for two simultaneous mechanisms 2−84001
  diffusion of Au, comp. profiles near grain boundaries, electron diffr. obs. 2−56757
  diffusion of Nb by an electrical-resistance method 2−53762
  diffusion of Ni, 600 and 900°C 2−53761
  diffusion of Pt, 750-1075°C 2−56756
  dipole interactions and diffusion of μ^+ meson 2−57090
  dislocation damping study by stress pulse method 2−60801
  dislocation line tension, effects of elastic anisotropy 2−74772
  dumbbell interstitials, reorientation in deformed crystals 2−50655
  durability, influence of air, oxygen or vacuum 2−60912
Copper continued
  dynamic strengthening singularities under infl. of shock waves 2−84075
  edge and screw dislocation, Schockley partials separation, computer simulation 2−60802
  Ekco mineral analyser, radio-isotopic X-ray fluorescence 2−81643
  elastic constants, high pressure effects, meas. using torsional oscillatory method 2−68061
  electrical cond, meas. by inductive method 2−49239
  electrical conductivity at low temp., undergraduate expt. 2−73262
  electrical conductivity of commercial electrorefined wire, metallurgical factors effects 2−47579
  electrical resistance, as fn. of molar heat content, meas. by pulse method 2−64914
  electrical resistivity of polycrystalline sample, changes during tensile deformation 2−47834
  electrodeposited, morphology, current density and substrate orientation effects 2−48340
  electrodes, pulsed ablation accelerator plasma, electron density measurement 2−80297
  electrolytic deposition, cathodic impedance study 2−48339
  electrolytic purification and single cryst. prep. 2−72565
  electrolytic refining, behaviour of $(NH_2)_3CS$ 2−75389
  electron, irrad. induced pt. defect clustering, high- voltage electron microscopy 2−56682
  electron backscattering, spectral ang. distrib. meas. 2−84218
  electron emission from (001) and (011) faces, H ion induced 2−75199
  electron irradiated, lattice parameter and resistivity changes 2−60777
  electron microscope exam., crit. stress effect on contrast 2−67983
  electron momentum distribution, from Doppler-broadened annihilation lineshapes 2−71782
  electron relax. time, magnetoacoustic determ. electron relaxation time, magnetoacoustic determ. 2−77818
  electron relaxation time, magnetoacoustic determ. 2−77819
  electron scatt. by dislocations, de Haas-van Alphen effect obs. 2−61214
  electron-phonon renormalization, anisotropy 2−84256
  electronic wavefunctions, rapid calculation 2−75018
  e.m. wave transmission, helium propag., Gantmakher-Kaner oscill. 2−61211
  energy bands, Fong-Cohen pseudopotentials 2−84271
  epitaxial electrodeposit, defect obs. 2−47107
  epitaxial electrodeposition, computer simulation 2−71320
  equation of state, based on elastic and cohesive props. 2−68063
  excitation in Lewis Rayleigh N_2 afterglow 2−77011
  fatigue cracking, effects of grain and twin boundaries, slip mode behaviour 2−71598
  fatigue hardening, influence of point-defect clusters 2−53724
  Fermi surface, de Haas-van Alphen meas., infinite field phases 2−61182
  Fermi surface, phase shift parametrization 2−44030
  Fermi surface orbits, integral calc. method 2−44028
  film, condensed in presence of residual gases, oxidation 2−71328
  film, Debye characteristic temp. 2−61102
  film, deposition on cold substrate, fibre texture formation 2−50480
  film, electroplated and vapour deposited, struct. rel. to annealing 2−77497
  film, epitaxial, microstruct., orientation and imperfections 2−67909
  film, facuum-deposited, substruct., deposition rate effects 2−50489
  film, far-i.r. transmission, surface plasma oscillation obs. 2−54401
  film, lattice consts. of small nuclei, rel. to surface stress 2−60655
  film, r.f. sputtered, film thickness distrib. 2−60651
  film, thermoelec., resist., cond. electron m.f.p. 2−68477
  film, Xe adsorp., roughness and surface potential 2−50556
  film growth kinetics near melting point 2−60652
  films, Hall coeff. detn. and existence of size effect 2−77985
  films in storage, ageing effects on substruct. and mech. props. 2−83863
  foil, heavy ion irrad., rad. damage, electron microscope obs. 2−43608
  freezing point determ. 2−53496
  gaseous, spectra rel to matrix isolated atoms in Ar matrix 2−52902
  grain boundaries, coincidence-ledge-dislocation model, supporting evidence 2−47426
  growth of twin free crystals by secondary recrystn. and zone refining 2−47580
  Hall and Righi-Leduc coeffs., 4-125 K, Weidemann- Franz law 2−61224
  hardness, scratch and indentation meas. 2−53841
  heat capacity between 300 and 900 K 2−57065
  high purity, recrystn., polygonization 2−68136
  hypersonic attenuation and nonlinearity constant D, temp. depend. 2−47744
  interace with liq. He, Kapitza resist., Rayleigh waves influence 2−47764
  ion, influence of ethanol on first hydration shell, e.s.r. obs. 2−64123
  ion range of energetic Xe 2−61126
  K_α X-ray experiments, apertures, Bi alloys 2−85184
  Kapitza cond. with solid and liq. ^{4}He, at 1.9 K 2−67854
  LEED from {001} surface, expt. and theory 2−50428
  line spectra, d.c. arc, effect of mag. field on intensity, 230-790 Oe 2−49943
  linear dimensions variation under γ-ray irrad. 2−43607
  liquid, optical consts. 2−43359
  liquid, wetting of carbides, relative surface energies 2−50427
  liquid, wetting of TaC 2−43468
  liquid, with Mn and Fe impurities, cond.-electron spin polarization obs. 2−53455
  magnetic surface levels and electron-phonon scatt. rate determ. 2−68290
  in marine suspension, microquantities det. 2−54768
  melting line determ. 2−80518
  mineral deposits, relation to tectonic features 2−57724
  neutron irrad. temp. effect on defect aggregate size 2−53711
  neutron irradiated, cleared channels, correl. with surface slip steps 2−50761
  neutron irradiated, impurity atom effect on recovery, elec. resistivity obs. 2−60964

Copper continued
neutron irradiated, void formation, fluence effects 2—80687
neutron irradiation damage, high fluence, electron microscope obs. 2—80686
n.m.r., fast magic-angle rot. technique 2—81480
n.m.r. thermometer, pulsed, construction and use 2—49185
noncollinear ultrasonic surface wave interactions 2—51004
nuclear refrigeration, by adiabatic demagnetization 2—66364
nuclear spin-lattice relax. of Zeeman and spin-spin systems, 1 to 17 mK 2—68581
optical props. and interband transitions, review 2—72292
oxidation, internal, at low pressures, comments 2—65376
oxidation, nucleation and growth of oxide, Rheads scheme 2—51449
oxidation and corrosion, protection by reactively sputtered Si_3N_4 film 2—43481
oxide nucleation on (001) face, off angle effect 2—64566
permeation of hydrogen, surface effects 2—77608
phase picture production by metallographic examination with ZnSe coating 2—56918
phonon dispersion curve, psuedopotential calc. 2—57039
photoelectric emission, two-photon photoelec. effect 2—48021
piezoreflectance, a.c. modulated, symmetry breaking effects of shear stress 2—47789
pitting, intergranular corrosion and stress-corrosion cracking, significance of protection potential 2—68787
plastic flow, grain topography in early stage 2—47500
plastically deformed, exo-emission rel. to surface struct. 2—77975
plastically deformed, positron annihilation, annealing temp. depend. 2—54123
plastically deformed, specific dislocation energy determ. 2—53734
plastically deformed at 77K, neutron irrad. effects on struct. and mech. props. 2—83968
plated graphite cermet, on Fe base sintering 2—53863
polycrystalline, recovery of mech. props. after severe rolling 2—71633
polycrystalline, strain hardened, thermally activated deform. mechanisms 2—77679
porous, shock response, Hugoniot elastic limits, model 2—61024
positron angular distributions using wavefunctions with proper crystal symmetry 2—80942
positron annihilation, solid and liq. state 2—75004
positron annihilation ang. correl., plastic deform. influence 2—51063
positron annihilation radiation, angular correl. 2—80968
powder, drying, effect of temp. and ambient 2—80828
powder, particle size distrib. determ. 2—43891
powder, vibr. packing, inertial loading effect 2—50911
powder, X-ray diffr., intensity rel. to granularity 2—74700
programme toughened single crystal, crit. sliding stress, temp. depend. 2—71582
proton reactions with, use in cyclotron beam monitors 2—70334
pure elimination by hydrostatic pressures and density increase at 20 kbar 2—71626
radiation damage, atomic displacement cascades, computer simulation 2—53700
radiation damage, nature and annealing characts. 2—47368
radiation generated during rapid deform. and rupture tribolum. 2—54482
ranges and range straggling of ^{150}Sm 2—68269
recrystallization in a high voltage electron microscope 2—80825
recrystallization kinetics of tough-pitch copper 2—71623
residual resistivity, high-temp. oxidation influence 2—71832
resonance lines, intensities using different spectral lamps 2—52492
shock waves, and temp. derivation along Hugoniot curves, appl. of fourth-order anharmonic theory 2—84188
single cryst., depend. of deform.-resist. on rate and temp. of prev. loading 2—84010
single crystal, initial disloc. density effects on disloc. multiplication and work hardening characs. 2—64665
single crystals, mech. twinning during elongation or torsion at 78 K and room temp. 2—74783
sintering, effects of hydrostatic pressure on removal of internal porosity 2—68130
sintering of powder by electrolytic heating 2—74891
slowing down spectra of secondary electrons 2—75006
solubility, of O_2, single cryst. obs., 350-1000°C 2—56926
solubility and diffusion in Ge, temp. depend. 2—77613
specific heat, high purity sample, 2-1357K 2—54048
specific heat 1-30 K, effect. of temp. scale differences on anal. of heat capacity data 2—47751
sputtering, Ar^+ and Ne^+, angular and temp. depend. of sputtering 2—51064
sputtering, energy spectrum 2—47783
stacking fault energy rel. to n-value 2—53737
stopping power for 25-250 keV H ions 2—47774
stopping power for 28 MeV α-particles 2—54099
stopping power for protons and deuterons at same velocity 2—54098
strain rate effect on hardening on single crystals deformed in tension 2—84160
superficial autodiffusion 2—71535
surface, (001) and (111), (00) LEED beam intensity at normal incidence 2—71308
surface, (100), CO weak adsorp., structure and binding 2—50538
surface, cleaned and oxidized, secondary ion yield 2—61471
surface, punched-out dislocation rosettes 2—50439
surface, sputter deposition and sputter removal of Mo, Auger spectroscopy 2—50520
surface, two dimensional adsorbed layer of S ions, phase transitions 2—50535
surface, wetting angle of D_2O at boiling point, 10-770 Torr 2—74533
surface diffusion of Ag on (100), (111) and (110) planes 2—60626
surface stress, strain produced by He bubbles, elec. resistivity obs. 2—43678
target, micrometeoroid simulation, Fe microparticles from Van de Graaff accelerator 2—66187
texture transition mechanism during rolling, X-ray obs. 2—47323
thermal phonons in symmetry zones of Fermi surface, scattering of quasiparticle excitations 2—44020
thermal resistivity, high temp., and electron-phonon interaction 2—68258

Copper continued
thermoelectric power rel. to Fermi surface shape and sample dimens. effects 2—68296
total energy, pseudopot. theory 2—61137
trichites, orientation and degree of perfection 2—47321
u.s. attenuation, Gruneisen mode and const., phonon viscosity and thermoelastic effects 2—68234
valence band density of states, X-ray photoemission spectroscopy obs. 2—65104
valence states produced by ion-sputtering reduction, X-ray photoelectron spectroscopic obs. 2—57263
vapour, high-current hollow cathode discharge, radiation, effect of reson. and recomb. 2—74423
vapour laser, effective generation of visible band, with high ave. power 2—82475
void growth on grain boundaries, rel. to creep 2—50685
whiskers, ductility determ. 2—56810
whiskers, growth by halide reduction, and defect struct. 2—80570
whiskers, vacancy formation 2—47397
wire, degassing in ultrahigh vacuum 2—60679
wire, recrystallization, cold worked, press. induced thermal activation 2—43781
wire specimens, plastic deformation and static lattice distortion, X-ray diffraction determinations 2—53890
X-ray fluorescence anal. in Fe-rich minerals radioisotope detector-radiator assembly 2—61821
yield behaviour, effect of disloc. density and cryst. size effects 2—56792
Al/Cu/Al films, electromigration obs. by transmission electron microscopy 2—64879
inAl-Mg alloy, effect on stress corrosion cracking 2—50775
Au:Cu, impurity-vacancy binding energy, equilib. resistivity obs. 2—71465
CdS:Cu, photosensitive material, spectral characts. 2—72059
CdS:Cu, trapping parameters, photocond. response, i.r. quenching, photochem. effects 2—65000
in CdSe-CdS film photoresistor, activating role 2—65096
CdTe:In, Cu, high temp. cond., impurity effects 2—61303
Cu:S, Bragg peaks, temp. effects 2—71310
Cu/W composite, fibre reinforced, resist. 2—50915
Cu-Al crystals, internal oxidation, comments 2—65377
Cu-Au bimetallic film, interdiffusion, X-ray obs. 2—60828
Cu-Au foils, quantitative microanalysis with combined electron microscope-microanalyser (EMMA-3) 2—81561
Cu-Be electron multiplier dynodes, cleaning and activation 2—82793
Cu-Ni junction, e.m.f. generated by shock wave propag. 2—75010
Cu-Ni solid solution, X-ray determ. of composition profiles and diffusion generated substructure 2—74696
Cu-W composite, continuous-fibre metal-matrix, fracture surface energy det. 2—55475
Cu-constantan junction, e.m.f. generated by shock wave propag. 2—75010
Cu-constantan thermocouple, magnetic field effects on Seebeck effect 2—63162
Cu-constantan thermocouple in linear direct reading thermometer 2—73469
Cu angular distrib. of inelastically reflected electrons 2—80551
Cu I spectral lines, oscillator strengths 2—64011
Cu single crystals, mech. twinning during elongation or torsion at 78 K and room temp. 2—74783
Cu^{2-} centres, in Ge, hot electron capture 2—71936
Cu^{2+}, analytical SCF wavefunctions for ground and some excited states, calc. of oscillator strengths for optical transitions 2—52915
Cu^{2+}, e.s.r. in ZnO, doping and temp. depend. 2—65328
Cu^{2+}, in $LiTaO_3$, optical generation of intense picosec. electrical pulses 2—45768
Cu^{2+}, in semiconductors, II-VI, e.s.r. and optical spectra, dynamical Jahn-Teller interaction 2—80954
Cu^{2+}, in triglycine fluoroberylate, e.p.r. spectra, applic. of rhombic spin Hamiltonian formalism 2—51410
Cu^{2+}, in tryglycine fluoroberylate, spin Hamiltonian parameter and hyperfine struct. 2—51409
Cu^{2+} aggregates in triglycine fluoroberylate, e.p.r. spectrum 2—84575
Cu^{2+} in amorphous and cryst., TeO_2, electronic bonding 2—72501
Cu^{2+} in distorted T_d symmetry, covalency and excited 4p states effects on 3d ground states 2—84578
Cu^{2+} in NH_4Br, e.p.r., covalency, core polarization 2—78154
Cu^{2+} pairs in Y-type zeolite, e.p.r. study 2—75343
^{63}Cu crystals, sp. ht., anharmonicity manifestations in comparison with phonon model 2—64855
GaAs:Cu, behaviour in strong elec. field 2—71904
GaAs:Cu, elec. props., impurity centre form., conditions and mechanism 2—64985
n-GaAs:Cu film, epitaxial, carrier mobility, impurity effects, scatt. by space charge centres 2—64983
in GaAs, supersaturated solid solution, differences in laws of decomposition 2—83836
p-GaP:Cu,O, bound exciton luminesc., emission and excitation spectra 2—78131
Ge:Cu, donor compensation density determ. by Hall and mobility analysis 2—51166
Ge:Cu, heated by h.f. elec. field., hot electron recomb., electron capture 2—64972
Ge:Cu, recomb. cross section for holes at singly ionized impurity 2—51215
p-Ge:Cu thermalization time of hot photoexcited holes 2—51214
He migration and release after implantation 2—50639
KI:Cu, anomalous transmission spectra, 300-450 nm 2—72337
KI:Cu, antiresonance phenomena in transmission spectra 2—54423
MgO, plastic yielding, high pressure effects 2—68081
Mo fibre reinforced composite, rolling and annealing characts., internal friction obs. 2—56987
NaCl:Cu, one electron energy levels, charge consistent extended Huckel approach 2—77831
NaCl:Cu, X-ray coloured, Cu activated thermolum., 300-510K 2—78122
in Nb-Sn sinter material, supercond., effect on screening behaviour 2—75061
$PbBr_2:Cu^+$, defects, ionic cond. and dielec. loss study 2—47402

Copper continued
- $PbMoO_3$:Cu, Gd, site occupancies of dopant and trace impurity 2−68739
- $TlInSe_2$:Cu,Sn, cryst. and film, forbidden band width, elec. and photoelec., props. 2−57197
- YIG:Cr^{3+},Cu^{2+} garnet, hyperfine interactions of Cr^{3+} and Cu^{2+} ions, n.m.r. obs. at 4.2 K 2−72504
- $Zn_xCd_{1-x}S$:Cu, Cl temp. and i.r. quenching of luminescence and photocond. 2−84543
- ZnS:Cu, Al, Br, film temp. depend. of electrolum. and thermal quenching 2−84533
- ZnS:Cu, Pb, Cl, film, temp. depend. of electrolum and thermal quenching 2−84533
- ZnS:Cu, surface, volume, and contact components of current 2−71918
- ZnS-Cu crystallites, electroluminesc., influence of milling 2−51390
- in ZnS, effects on electroluminesc. 2−51394

Copper alloys
- *see also Copper compounds*
- – 2−71430
- binary, liquid, density, max. bubble pressure method 2−56488
- brass, annealing after work hardening 2−43789
- α-brass, containing SiO_2 particles, dislocation generation during plastic deform. 2−56708
- brass, elec. cond. meas. by inductive method 2−49239
- brass, extrusion behaviour rel. to solidification texture 2−43809
- brass, fatigue, high power ultrasonics 2−50794
- brass, fatigue cracking, effects of grain and twin boundaries, slip mode behaviour 2−71598
- brass, fatigue stability tests, sensitivity estimates for asymmetrical loading cycles from strain diagrams 2−56840
- α-brass, Fermi surface, positron annihilation study 2−80955
- brass, magnetic susceptibility obs. using SQUID 2−52384
- brass, O_2 content, spectrochemical determination, effect of heat 2−72590
- α-brass, optical transitions 2−44362
- α-brass, Portevin-le Chatelier effect and vacancies production during cyclic stressing 2−74827
- α-brass, Portevin-le Chatelier effect and vacancies production during cyclic straining 2−74828
- α-brass, recrystn. texture, X-ray obs. 2−68139
- β-brass, stress corrosion cracking obs. by optical microscopy 2−84132
- α-brass, stress corrosion sensitivity in $FeCl_3$ and $Fe_2(SO_4)_3$ solns. 2−64733
- α + β brass, superplasticity 2−64714
- α-brass, tarnish films and stress corrosion cracking, theory 2−64734
- brass, u.s. fatigue inhibition 2−50767
- β-brass obs. of anomaly in thermopower near order-disorder transition 2−84371
- brass polycrystals doped with zinc, meas. of amplitude independent internal friction 2−64706
- β- brass type, lattice vibrs. rel. to martensite struct. 2−56930
- β- brass type alloys, quenched, structure and microstructure review 2−84106
- bronze, ancient, rapid non-destructive analysis by X-ray fluorescence 2−44505
- bronze powder, spherical particles, sintering kinetics 2−43890
- Co-Ni-Cr-Ti alloy, quench-ageing behaviour, 700-900°C 2−68138
- cold worked, X-ray line profile analysis, instrumental broadening correction 2−64636
- constantan-Cu thermocouple, magnetic field effects on Seebeck effect 2−63162
- constantan-Fe(Ni) junction, e.m.f. generated by shock wave propag. 2−75010
- contamination by oxided nonmetallic inclusions, scale for point evaluation 2−84684
- α-Cu-Al, stacking fault energy, electron microscope obs. 2−50682
- Cu-Cu_3Au, Debye temp., elastic moduli, elec. resist., temp. depend., 4.2-293K 2−47752
- dilute, elec. field gradients 2−51413
- dilute, Kondo model validity 2−81029
- dilute, reson. and charge neutrality, semiphenomenological model 2−71783
- dilute magnetic, semiphenomenological model for reson. and charge neutrality 2−68291
- grain boundary energy measurement, isothermal calorimetry method 2−83967
- hot formability criteria 2−80852
- hot strength, in presence of secondary phases 2−84135
- intermetallic compounds, mechanical properties, obs. 2−50782
- Kondo systems, exchange splitting of electron spins 2−77848
- solution hardening, stress equivalence 2−80834
- stacking fault energy rel. to n-value 2−53737
- Uni-Arc, point-to-plane excitation, effect of extraneous materials 2−56398
- Ag-Au-Cu, sp. ht. and residual resist. 2−75051
- Ag-Cu, 7.5 wt% Cu, discontinuous precip. kinetics, 200-500°C 2−80856
- Ag-Cu alloy, rapid cooling by laser melt quenching 2−56897
- Al-Cu-Mg-Mn, mosaic angle and dislocation density, tensile deform. depend. 2−80772
- Al-Cu-Mg-Ni, forged after quenching, recovery treatment, creep strain mechanisms 2−43804
- Al-(4 wt.%)Cu, Guinier-Preston zone form. 2−43825
- Al-Cu, cast morphology, anodic oxidation etching study 2−47602
- Al-Cu, di-directional solidification and dendritic growth 2−50823
- Al-Cu, liq., Cr or Mn impurity, susceptibility near nonmag.-mag. transition 2−80486
- Al-Cu, quenched-in defect elimination mechanism 2−84149
- Al-Cu, solute-vacancy binding energy, determ. from quenched-in defect conc. 2−74762
- Al-(4.5wt.%)Cu alloy, late stage of solidification, two-dimensional flow of liquid 2−47038
- Al-Cu alloy, effect of coherency strain field on disloc. struct. 2−56702
- Al-Cu system, drops, supercooling and spheroidizing, Cu conc. effects 2−43441
- Al-4%Cu, ageing, effects of additional elements 2−56910

Copper alloys continued
- Al-4%Cu, vacancy-Ge binding energy 2−50824
- Al-4%Cu alloy, influence of precipitates on cavity formation for irrad. by fast neutrons 67984 2−67984
- Al-Zn-Mg-Cu-Mn forging alloy, fracture toughness rel. to microstructure 2−53826
- Al-Zn-Mg-Cu alloy, fatigue behaviour of bolted joints 2−71622
- AlCu, (Al 4 wt %), structure changes during ageing studied by the channeling tecynique 2−80827
- Au-Cu, Zener relax., internal friction obs. 2−60852
- Au-Cu ordered alloys, dislocation mechanisms of twinning 2−68033
- $AuCu_3$, effect of ordering on lattice heat capacities 2−57060
- Be-Cu evaporation, mass spectrometer control 2−73233
- Cd-Cu system, liq., elec. resist. 2−46981
- Co-Cu-Fe-Ce permanent magnet prep. by directional solidification 2−43787
- Co-Cu-Fe-Ce permanent magnet, sintered, prep. and props. 2−50910
- Cu:O, ageing, cold worked, press. induced thermal activation 2−43781
- Cu-Ag, electronic struct., reflectance obs. 2−61174
- Cu-Ag, eutectic, freezing and melting point determ. 2−53486
- Cu-Ag, weakening resist. rel. to deform., heating time and temp. 2−50764
- Cu-Al-Fe bronze, superplastically deformed, textures and anisotropic flow 2−43831
- Cu-Al-Mg-Mn-Fe-Si-Ni-Zr-Ti, D16T, recryst. and uncryst. struct., fracture under static and cyclic conditions 2−47527
- Cu-Al-Mg-Si-Mn-Fe, AK6, ageing, temp.-time ranges 2−50802
- Cu-Al-Mg, eutectic, microstruct., orientation relationships 2−74893
- Cu-Al-Mg oversaturated solid soln. state, mech. props. rel. to strain rate and temp. 2−56547
- Cu-Al-Mn heat treatment, homogenization, precip. 2−43786
- Cu-Al-Ni, damping characts. and causes 2−80776
- Cu-Al-Ni, martensite memory, shape recovery effect 2−50935
- Cu-Al-Ni, shape memory effect 2−80844
- Cu-Al-Ni(Mn), martensitic transform., interphase boundary shifting 2−43910
- Cu-Al-Zn-Mg, tensile deform. and high-temp. creep rel. to microstruct. 2−56800
- Cu-Al-alloys, microstructures and mechanical props. of phases after quenching and isothermal treatment 2−60932
- Cu-Al, additives influence on stacking fault energy 2−77665
- Cu-Al, b.c.c., superplasticity 2−50745
- Cu-Al, Cu-rich, microstruct. and microhardness 2−71678
- Cu-Al, cyclic fatigue damage, thermal cond. meas. 2−50672
- Cu-Al, equation of states determ. 2−56929
- Cu-Al, exo-electron emission, interdependence with annealing processes 2−48011
- Cu-Al, exoemission kinetics and hardness depend. on strain or elongation 2−74836
- Cu-Al, Frank loop nucleation on screw dislocations 2−50670
- Cu-Al, liq., with Mn and Fe impurities, cond.-electron spin polarization 2−53455
- Cu-Al, melting, application of Lindemann's rule 2−74582
- Cu-Al, neutron irrad., lattice thermal cond. 2−51060
- Cu-Al, plastically deformed, conc. heterogeneities on stacking faults 2−50681
- Cu-Al, quantitative microanalysis, applic. of Monte Carlo calcs. 2−68830
- Cu-Al alloy, α-phase, Fermi surface, comparison of optical and positron annihilation obs. 2−64888
- Cu-Al alloys, mechanical properties and ductility as a function of temperatures 2−64776
- Cu-Al film, precip., G.P. zone form., rel. to bulk alloy props. 2−47099
- Cu-Al intergranular precipitates identification by double diffraction using transmission electron microscopy 2−80615
- Cu-Al system, $Cu_3Al_{2\|}$(h) and CuAl(r), cryst. struct. 2−74730
- Cu-Al tempered martensite, long period superlattice phases 2−43914
- Cu-10at.%Al, deformed, neutron irrad., dislocation strain fields, low. temp. lattice thermal cond. obs. 2−71498
- Cu-16%Al, sigmoidal transient creep, internal stress and disloc. struct. 2−53816
- Cu-Al(10 wt%), high fluence neutron irrad. damage, electron microscope obs. 2−80686
- Cu-As-Se compositions, voltage controlled switching 2−67886
- (Cu-Au)-Fe, dil., mag. susceptibility 2−61483
- Cu-Au, diffused, comp. profiles near grain boundaries, electron diffr. obs. 2−56757
- Cu-Au, elastic consts., press. depend. up to 7 kbar 2−74824
- Cu-Au, electronic struct., reflectance obs. 2−61174
- α-Cu-Au, low temp. sp. ht., conc. depend. 2−51044
- Cu-Au, melting, strain energy effects 2−53492
- Cu-Au alloy, electrical resistivity, temp. dependence 2−75049
- Cu-Au alloys, side bands of fundamental reflections and diffuse superstructure lines, detection 2−64614
- Cu-Au disordered alloys, correlation phenomena 2−64815
- Cu-Au film, epitaxial growth by r.f. sputtering, microstruct. 2−67908
- Cu-Au of Au, misfit dislocation behaviour 2−71497
- Cu-Au system, superdislocations in Cu_3Au, electron microscope obs. 2−80666
- Cu-Be-Ag alloys, structural states in decomposition process, e. diffr., e. micro. and microhardness exam. 2−80782
- Cu-Be-Ag and Cu-Be-Ti, decomposition of solid solns., phase transformations 2−68194
- Cu-Be, extra spots in electron diffr. pattern, obs. during G.P. zone formation 2−77578
- Cu-Be, Fermi surface, electron scatt., de Haas-van Alphen and residual resist. obs. 2−71791
- Cu-Bi, grain boundary fragility and segregation 2−53830
- Cu-C, prep. by vac. deposition, microstruct. 2−56928
- Cu-Cd, weakening resist. rel. to deform., heating time and temp. 2−50764
- Cu-Co, effects of coherency strain fields on dislocation struct. 2−56702
- Cu-Co alloy f.c.c. single crystals, effect of coherent precip. on work-hardening 2−50798

Copper alloys continued
Cu-Co foil, diffraction contrast from coherent Co precipitates 2−80671
Cu-Cr, dispersoid struct. precipitated by tempering 2−43832
Cu-Cr, embrittlement, under elevated temp. stress 2−43722
Cu-Cr, f.c.c.-b.c.c. interphase boundary dislocation structs. 2−56734
Cu-Cr, internal friction and Young's modulus, after isochronal annealing 2−77633
Cu-Cr, precip. size effect on recrystalliz. temp. 2−56927
Cu-Cr, weakening resist. rel. to deform., heating time and temp. 2−50764
Cu-(0.6 at.%)Cr, precip.-hardening, neutron irrad. effect43833 2−43833
Cu-Fe-Co-Ni-Ti-Al YuNDK42T8, homogenizing rel. to phase comp., mech. and mag. props. 2−47688
Cu-Fe, dil., paramag. susceptibility, 1.7-300K 2−61483
Cu-Fe, dispersion strengthening model, slip dislocation precipitate interaction 2−50744
Cu-Fe, distrib. of nearest neighbour atoms, Mossbauer obs. 2−74900
Cu-Ga, cold-worked, defects, X-ray obs. 2−80861
Cu-Ga system, determ. of partial free enthalpy of formation and intermetallic phases, thermodynamic investigation 2−80811
Cu-Ge, dil., vacancy-impurity complexes and positron annihilation 2−47398
Cu-Ge, liquid, struct., X-ray diffr. interference functions 2−83774
Cu-Ge solid soln. single crysts., growth and characteriz. 2−53614
Cu-Ge solid solution, cryst. growth, for neutron monochromator appl. 2−47205
Cu-Ge system, determ. of partial free enthalpy of formation and intermetallic phases, thermodynamic investigation 2−80811
Cu-7at.%Ge, deformed, neutron irrad., dislocation strain fields, low temp. lattice thermal cond. obs. 2−71498
Cu-In, de Haas-van Alphen oscills. amplitude reduction by signal dephasing by strain fields round impurities 2−77846
Cu-In, liquid, struct., X-ray diffr. interference functions, 700°C 2−83775
Cu-In system, determ. of partial free enthalpy of formation and intermetallic phases, thermodynamic investigation 2−80811
Cu-Mg, weakening resist. rel. to deform., heating time and temp. 2−50764
Cu-Mg(Mo)(W) solid solns., binding energy of dislocations to impurities, internal friction obs. 2−43630
Cu-Mn-Al, spinodal, interphase interfaces, interfacial dislocations 2−56719
Cu-Mn-Mo, cold worked, heat treated, Young's modulus, rigidity, hardness, thermal expansion 2−47476
Cu-Mn-W, cold worked, heat treated, Young's modulus, rigidity, hardness, thermal expansion 2−47477
Cu-Mn, dil., neck effect in ang. correl. of positron annihilation 2−44046
Cu-Mn, dil., thin film, e.s.r. study 2−44446
Cu-Mn, short range ordering, diffuse scattering peak between {100}, {110} positions 2−71644
Cu-Mn, thermo-e.m.f., 4.2-250K 2−57250
Cu-Mo-Co cermet contact, elec. erosion characts. working surface struct., rel. to Co content 2−47659
Cu-Ni:^{57}Fe, Mossbauer doublets, time-differential perturbed angular correlations 2−72275
Cu-Ni:Mn, Cr, Al, struct. and props. with ageing and hardening 2−83954
Cu-(3o wt.%)Ni-0.3 wt.%)Be, cryst. struct. and morphology of age hardening precipitate phases 2−50934
Cu-Ni-Al-Ti, age hardening, precip. 2−53878
Cu-Ni-Fe, intergranular fracture on spinodal decomp., mechanism 2−57012
Cu-Ni-Fe, spinodal, interphase interfaces, interfacial dislocations 2−56719
Cu-Ni-Mg alloys eutectic mixtures constitution 2−84103
Cu-Ni-Mn, dilute soln., resist., magnetoresist., Z-100K, Kondo effect 2−47835
Cu-Ni-Mn, order-disorder transform., resist. and thermopower study 2−54001
Cu-Ni, adsorption of CO and O_2 2−50536
Cu-Ni, d-band filling, X-ray spectra 2−47809
Cu-Ni, dil., vacancy-impurity complexes and positron annihilation 2−47398
Cu-Ni, elec. resist. behaviour in crit. region 2−57279
Cu-Ni, elec. resist. near Curie point, resist. anomaly 2−61225
Cu-40 at.% Ni, sp. ht. below 3K, effect of clusters and quenching 2−61103
Cu-Ni, film, growth, struct., epitaxial temp. rel. to comp. 2−60654
Cu-Ni, grown by Bridgmans method, microstruct. 2−47322
Cu-Ni, neutron irrad., void formation, fluence effects 2−80687
Cu-Ni, optical properties in visible and ultraviolet spectral regions 2−81330
Cu-Ni, surface composition after annealing and sputtering, Auger spectroscopy obs. 2−50440
Cu-Ni, susceptibility in high intensity fields 2−65151
Cu-Ni, thermoelec. power rel. to Fermi surface shape and sample dimens. 2−68296
Cu-Ni film, soft X-ray absorpt., band struct. interpretation 2−65286
Cu-Ni plates for relay thin leaf springs, surface structure, mechanical properties 2−80862
Cu-Ni(Cr), resistivity and magnetoresistance, Kondo effect 2−64913
Cu-P system, constitution diagram determ. 2−61045
Cu-(7wt.%)P superplastic behaviour 2−74838
Cu-Pd, disordered and ordered, band struct. optical absorpt. study 2−84237
Cu-Pd alloys, influence of domain size and ordering on mech. props. and elec. resist. 2−68506
Cu-Se, extension of equilibrium diagram 2−64812
Cu-Si single crystal, tensile deformation 2−50743
Cu-Sn, α-phase, low temp. electronic sp. ht. 2−43982
Cu-Sn, electrolytically deposited on steel 08kp 2−47683
Cu-Sn, liq., optical consts. 2−43359
Cu-Sn, martensitic transform., interphase boundary shifting 2−43910

Copper alloys continued
Cu-Sn alloys, unidirectionally solidified, columnar dendrite structure 2−74641
Cu-Sn γ phase decomposition at lower temps. 2−71679
Cu-Sn system, determ. of partial free enthalpy of formation and intermetallic phases, thermodynamic investigation 2−80811
Cu-Sn system, electrodeposited, phase diagram 2−84085
Cu_x-Sn_{1-x} alloy, resistivity and thermopower computation, comparison with exptl. data 2−43387
Cu-V(Cr)(Mn)(Fe)(Co)(Ni), dil. liq., mag. susceptibility 2−80485
Cu-Zn-Mn system, phase diagram 2−50963
Cu-(30 wt.%)Zn, relax. of diffused Zn during short-range-ordering 2−77705
Cu-Zn, b.c.c., superplasticity 2−50745
Cu-Zn, dil., vacancy-impurity complexes and positron annihilation 2−47398
Cu-Zn, electrical conductivity, temp. depend. in range, melting pt. to 1100°C 2−71826
Cu-Zn, electrometric characterization of tarnish films 2−77717
Cu-Zn, martensite memory, shape recovery effect 2−50935
Cu-Zn, melting, application of Lindemann's rule 2−74582
Cu-Zn (10 wt.%) and Cu-Zn, (30 wt.%) development of texture 2−80849
Cu-Zn alloys, with tarnish film in stress corrosion environments, electrometric study 2−68785
Cu-Zn and Cu-Zn-Al, solubility of As 2−47619
Cu-Zn solid solution, Zn diffusion, residual activity method 2−47457
Cu-Zn system, deform. influence on diffusion processes during electron irrad. 2−47456
Cu-Zn(40%) microduplex, metallographic study of superplasticity and cavitation 2−80738
Cu-Zr-Cr, precip. processes, specific heat and resistivity obs. 2−50933
Cu-Zr-Cr, precip. size effect on recrystalliz. temp. 2−56927
Cu-Zr, dil. alloys., softening resistance mechanism 2−56709
Cu-Zr, precip. size effect on recrystalliz. temp. 2−56927
Cu-Zr, weakening resist. rel. to deform., heating time and temp. 2−50764
α-Cu-16 at.%Al, spherical single crysts., struct. anomalies 2−71429
Cu-2 at.%Co, superparamag. relax. time rel. to Co precip. particle size 2−48067
Cu-7.5 at.%Al, deformed in tension, dislocations, etch pit obs. 2−64664
Cu base solid solution, grain boundary strengthening 2−53891
$CuAgTe_2$, synthesis and struct. detn. 2−71431
CuAu, Cu_3Au, effect of ordering on optical properties, reflectance measurements 2−72303
Cu_3Au, flow stress temp. depend. 2−43692
Cu_3Au, free vacancy no. determ. in fission-neutron displacement cascade 2−53712
Cu_3Au, low temp. electronic sp. ht., ordering influence 2−47750
$Cu_{80}Au_{20}$, model of structure periodically modulated in three dimensions 2−50615
Cuat.%Fe, precip. of Fe during ageing, Mossbauer obs. 2−77724
$Cu_{64}In_{36}$, phase bundles and homogeneity detn. 2−71680
CuNi, dilute, optical absorptivity meas. at 4K, virtual-bound-state obs. 2−51337
Cu(15.1 at.%)Sn alloy, β_1 phase stabilization mechanism47684 2−47684
Cu_6Sn_5 fibres, brittle fracture surface morphologies 2−80744
Cu_2Te-Ag_2Te systems, elec. and galvanomag. props., influence of defects, compensation hopping cond. and scattering of carriers 2−84323
CuZn-V(Cr)(Mn)(Fe)(Co)(Ni), dil. liq., mag. susceptibility 2−80485
CuZn, elastic moduli, antiphase boundary and long-range order effects 2−47416
CuZn, superdislocations and antiphase boundaries 2−47417
Fe-Cu-O system, equilib. phase diagram detn. 2−64818
Fe-Ni-Al-Cu, struct. and mag. props., alloying additive effects 2−43845
Ni-Cu-Mn, mag. props. 2−78025
Ni-Cu, ferromag., density of states 2−54110
Ni-Cu, X-ray appearance pot. spectra, density of states 2−61674
Ni-Cu alloys single crystals, magnetostriction constants by optical lever method 2−65159
Ti-Ni-Cu homogeneity range by electron microprobe X-ray analysis 2−43858
$YbCu_{6.5}$, cryst. struct. determ. 2−43594

Copper compounds
see also Copper alloys
— 2−72511
p-Cu_2Se-n-CdSe hterojunctions, Zener breakdown by tunnelling electrons 2−68442
ferrite, cation reordering, temp. depend. of cond. time variation obs. 2−75145
formate tetrahydrate, thermal cond., magnon contrib. 2−72226
halides, lattice props., calc. using ionic Rydberg function 2−47727
n.m.r. chem. shifts in cuprous salts 2−44455
phthalocyanine, fluoresc. and photocond. 2−72426
Tutton salts, spin system dynamics obs. 2−84445
X-ray photoelectron spectroscopy of compounds and complexes, study of satellite lines 2−80047
Au-Cu-V dil. alloys, thermopower and resistivity obs, Kondo temp. determ. 2−71831
CU(II) complexes, six-coordinated, determ. of vibrational degrees of freedom associated with dynamic Jahn-Teller effect 2−53004
n-CdS−p-Cu_2S film heterojunction, rectification, photosensitivity and tunnelling 2−71955
Cu-As system, phases, struct., homogeneity rangers 2−74731
Cu-Co dilute system, n.m.r. and double resonance studies of electron spin density near Co atom, obs. of satellite lines 2−75204
Cu-$CuSO_4$ unpolarizable electrodes, battery operated electrograph for Earth's induced field 2−57790
Cu-P-O system phase relations 2−50962
Cu (II), (III) complexes involving oxygen ligands, meas. of edge-shift and edge-width of K-absorption of Cu 2−56166
Cu complex, copper hydroxyquinolinate, host lattice effects on e.p.r. and optical spectra 2−81455

Copper compounds continued

- Cu complex, copper picolinate, host lattice effects on e.p.r. and optical spectra 2–81455
- Cu complex, Cu(II) croconate trihydrate, mag. susceptibility, 3-292 K 2–72106
- Cu complexes, Cu(II) bis(dithiocarbamate) and Cu(II) bis(diselenocarbamate), anisotropic hyperfine coupling tensors 2–59999
- Cu^{2+} complex ion, tetragonal, ligand contribution to spin-spin anisotropic hyperfine interaction 2–56168
- Cu^{2+} complexes, magnetic circular dichroism spectra of vibronically allowed d-d transitions 2–64124
- Cu^{2+} tetragonal complexes, covalency effects in anisotropic h.f.s. 2–84580
- $CuAlS_2(Se_2)$, i.r. transmission cut-off 2–78058
- CuBr, X-ray K emission bands, valence electron obs. 2–68672
- CuCl, bi-exciton formation, theory 2–75037
- CuCl, conduction band, orthogonalized plane wave calc. 2–71793
- CuCl, electrolytic coloration, absorpt. spectra study 2–83985
- CuCl, Frenkel defects, equilib. conc. perturbation by microwave pulse, ionic cond. change 2–80698
- CuCl, gaseous mols., dissociation energy 2–83255
- CuCl, $K\beta$ emission and K absorpt. of Cl, rel. to band struct. 2–75315
- CuCl, molten, Hall effect 2–67839
- CuCl, Raman spectra and interpretation 2–65278
- CuCl, second harmonic generation and two-photon luminesc. in exciton region 2–54453
- CuCl, valence bands, X-ray photoelectron study 2–44204
- CuCl and CuBr, anomalous thermal expansion with i.r. spectroscopy 2–43993
- CuCl crystals fine struct. of excitonic lines 2–80985
- CuCl with point defects associated with impurities, absorption spectra and e.p.r. 2–75290
- $CuCl_2$ cathode in organic electrolyte batteries with high energy densities 2–66688
- Cu_2Cl_2 gaseous mols., dissociation energy 2–83255
- CuCl(Br), absorpt. spectra, 3-30 eV 2–72326
- CuCl(Br)(I) layer, on Ag or Cu, light sensitivity spectra 2–77966
- $Cu(ClO_4)_2$ solutions in methanol and water, temp. and magnetic field dependence of electron and nuclear spin relaxation 2–81452
- $CuCl_2.2H_2O$, exchange interactions, antisymmetric, rel. to spin-spin relax. 2–68579
- $CuCl_2.2H_2O$, proton spin-lattice relax. time, 1.12–4.18 K 2–78050
- $CuCo_3.Cu(OH)_2$, vibr. freqs. assignment method 2–42886
- $CuCr_2Se_4$, galvanomag. props., 100-650K 2–81091
- $CuCs_2(SO_4)_2.6H_2O$, electron spin- lattice relax. of Zeeman and interaction systems 2–68580
- $Cu_2Fe(CN)_5NO.2H_2O$, i.r. spectra, cryst. chem. 2–78081
- $Cu_{0.5}Fe_{2.5}O_{4\|x}$, spinel ferrite, neutron-diffraction study, with and without mag. field 2–61543
- $Cu_xFe_yO_z$, nonstoichiometry and defect struct., O vacancies 2–74764
- $CuFe_2O_4-CuGa_2O_4$ system, phase diagram 2–71702
- Cu_2FeSnS_4, antiferromag. ordering, Mossbauer obs. 2–75239
- $CuGa_{1-x}In_xS_2$, soln. growth using In solvent 2–74679
- $CuGaS_2$, soln. growth using In solvent 2–74679
- $CuGaS_2(Se_2)$, i.r. transmission cut-off 2–78058
- CuH, dissociation energy and potential energy curves 2–59998
- CuI, crystalliz. under hydrothermal condits. 2–71420
- CuI, emission under high density excitation 2–72397
- CuI, low temp. reflection spectra, excitonic transitions and levels 2–72302
- Cu(I) and (II) complexes with sulphur ligands, K-absorpt. edge shift 2–56167
- α-CuI solid electrolyte, ionic cond. and permittivity, 2-40 GHz 2–83989
- γ-CuI thin film, piezo-optical effect at 77K in fundamental absorption band region 2–48172
- Cu(II) ammine complexes, tetragonal, electronic spectra, symmetry-restricted covalence effects 2–80017
- Cu(II) bis(di-n-butyldiselenocarbamate):Ni e.p.r. spectra of single crystal, polycrystalline sample, frozen soln. 2–48277
- Cu(II) complex, bis- diethyldithiophosphate, hyperfine couplings of ^{33}S 2–81446
- Cu(II) complex, bis(O,O′-di-iso-propyl-dithiophosphato) copper(II), s.h.f. splitting, e.p.r. 2–81510
- Cu(II) complex, diammine-(o-phthalato) Cu(II), e.s.r. study 2–65335
- Cu(II) complex, hydroxyquinolinate, in phthalimide crysts., ^{17}O h.f.s. in e.s.r. spectra 2–80071
- Cu(II) complex, interpretation of u.v. spectrum using modified Pariser-Pople method 2–67471
- Cu(II) complex of tetraethylthiuramdisulphide, single crystal e.s.r. study, determ. of Cu sites 2–72483
- Cu(II) complexes, chromophore trans- CuN_2S_2, covalent bonding, e.s.r. and electronic spectra 2–46539
- Cu(II) complexes, meas. of mean magnetic susceptibilities and anisotropies in temperature range 300K to 68K 2–54285
- Cu(II) complexes, tetrameric, $Cu_4OX_6L_4$, $X=Cl$, $L=(C_6H_5)_3PO$ and $X=Br$, $L=(C_6H_5)_3PO$ or C_5H_5N, magnetic susceptibility 2–51233
- Cu(II) zeolites, meas. of enhancement of proton resonance line on saturation of e.p.r. at liquid He temp. 2–54517
- $CuInSe_2$, transitions from Cu of levels in valence band 2–80974
- $CuInTe_2$, band struct., refl., absorpt. and theoretical studies 2–78098
- $CuK_2Cl_4.2H_2O$, critical dynamics of thermal cond. 2–57288
- $CuLiCl_3.2H_2O$, mag. phase transitions 2–44293
- $CuLi(PO_3)_3$, space group, lattice parameters 2–67989
- $CuMX_4$ ($M=V,Nb,Ta;X=S,Se$), i.r. and Raman spectra 2–42888
- $Cu_4Mn_2Te_4$, cryst. struct., mag. props. and Seebeck coeff. 2–84442
- $Cu(NH_4)_2Br_4.2H_2O$, uniaxial ferromag., low temp. magnetiz. 2–61514
- $Cu(NH_4)_2Cl_4$, mag. susceptibility and transition, 1.1 to 300K 2–65152
- $Cu(NH_3)_4SO_4.NH_3$, exchange integral variation with lattice spacing, sp. ht. obs. 2–54353
- $Cu(NO_3)_2$, paramag. relax., mag. field and conc. depend. 2–54365
- $Cu(NO_3)_2.2^1/_2H_2O$, differential susceptibility, energy levels and relaxation effects 2–48106
- $CuNa_2(PO_3)_4$ crystal struct. determ. 2–77546

Copper compounds continued

- $CuO-Al_2O_3$ solid soln., form. of $CuAl_2O_4$ phase at 890°C, stability 2–74899
- $Cu_2O-Al_2O_3$ solid soln., form. of $Cu_2Al_2O_4$ phase at 930°c, stability 2–74899
- $CuO-SeO_2$ system phases, e.p.r. spectrum and mag. props. 2–84573
- CuO, absorpt of O_2, adsorbed species characterization by X-ray photoelectron spectroscopy 2–77516
- CuO, CNDO-II approx SCF molecular orbital method, levels calc. 2–83252
- CuO, semiconduction rel. to catalytic activity 2–75093
- CuO, sensitizer effect in photochromic glass containing AgCl 2–78065
- CuO, single cryst. prep. by sublimation 2–74678
- CuO, thermal e.m.f. temp. depend. during dissociation, 960-1330K 2–57251
- CuO film, optical consts. wavelength depend., 450-800 mμ thickness 2–48135
- Cu_2O, 1s exciton state in green series 2–72327
- Cu_2O, bi-exciton formation, theory 2–75037
- Cu_2O, elec. cond., thermal activation energies, rel. to prep. conditions, −40-250°C 2–71898
- Cu_2O, elec. conductivity, relationship in samples annealed at various temp. to activation energy 2–75092
- Cu_2O, electric field effects on excitons, electroreflectance obs. 2–51320
- Cu_2O, electrical conduction, thermal behaviour, role of defects, review 2–75091
- Cu_2O, exciton luminesc., effect of absorpt., surface annihilation of excitons 2–78129
- Cu_2O, exciton luminesc. spectra, ortho- and para-exciton interactions, optical phonon freq. 2–57133
- Cu_2O, $\Gamma^+{}_5$ exciton quadrupole transition rel. to static elec. field, Stark splitting 2–81406
- Cu_2O, light scatt. and i.r. absorp., normally forbidden transitions obs. 2–61636
- Cu_2O, near i.r. absorpt. and photocond., band scheme interpretation 2–54420
- Cu_2O, near i.r. photocond., influence of annealing 2–47994
- Cu_2O, photocond., spectral depend., oscills., up to 180 K 2–77963
- Cu_2O, recrystn. and grain growth kinetics 2–43788
- Cu_2O, resonant Raman scatt. near 1S exciton level 2–54434
- Cu_xO_y, nonstoichiometry and defect struct., O vacancies 2–74764
- Cu_3PSe_4, cryst. struct. 2–77562
- $CuRb_2Br_4.2H_2O$, uniaxial ferromag., low temp. magnetiz. 2–61514
- $CuRb_2Cl_4.2H_2O$, critical dynamics of thermal cond. 2–57288
- Cu_2S-CdS, photovoltaic cell, props., doping effects 2–65092
- Cu_2S-CdS heterojunction, photocapacitance effects 2–51221
- Cu_2S-CdS heterojunction, prep. and photoelectronic props. 2–72056
- Cu_xS-CdS photovoltaic cell, model 2–54261
- $Cu_2S-CdTe$ film heterojunction, photovoltaic effect 2–81123
- $Cu_2S-CuCl$ melt, electrical and structural props. 2–46983
- CuS mol., rot. consts. of (0,0) band in A-system 2–42887
- CuS semiconducting film, supercond. transition temp. obs. 2–51112
- $Cu_{2-x}S$, refl. and absorpt., 400-1200 nm 2–78085
- $Cu_{2-x}S$ film, on NaCl, deposition and phase struct. 2–60653
- Cu_xS, differential thermal analysis of the Cu-S system, 30-500°C 2–84138
- $CuSO_4$, moisture content detn., n.m.r obs. 2–48303
- $CuSO_4$, triboluminesc. intensity obs. rel. to elastic const. detn. 2–51396
- $CuSO_4$ aqueous and hydrated solid, obs. of water isotope effects 2–47324
- $CuSO_4$ electrolytic aqueous solutions with concentration polarization, exptl. determ. of critical Rayleigh number 2–48338
- $CuSO_4$ solutions rel. to tarnish film on Cu-Zn alloys 2–68785
- $Cu_2S(Se)(Te)(Te_xS_{1-x})$, efficiency criterion for thermogenerators 2–75158
- Cu_2Se, $\alpha\to\beta$ phase transform 2–64811
- CuTe, band structure, reflection spectra obs. 2–72301
- CuTe, liquid, structure, total neutron scatt. patterns obs. 2–60421
- Cu_2Te, carrier effective mass, reflection spectra obs. 2–84520
- Cu_xTe, thermal e.m.f., electronic and ionic cond. at 400°C, composition 2–54247
- Cu(II) complexes in aqueous solutions, pressure, temp. and conc. effects 2–46960
- Ga_2Te_3-Cu system, phase diagram and elec. props. 2–47715
- In_2Te_3-Cu system, phase diagram and elec. props. 2–47715
- $KCuF_3$, stacking disorder, X-ray diffr. obs. 2–77569
- Li/CuF_2 secondary cell with inorganic electrolyte 2–66689
- Mg-Cu-Ni alloy, Laves phases, enthalpies of soln. and formation detn. 2–47692
- $MgO-Cr_2O_3-CuO(Cu_2O)$ system, phase diagram 2–43931
- $Zn_{1-x}Cu_xCr_2Se_4$, magnetization and susceptibility, 4.2-900 K 2–44311
- $Zn_xCu_{(1-x)}Fe_x\,Mn_{(2-x)}O_4$, X-ray determ. of lattice parameters, assignment of crednerite and gahnite symmetries 2–60768

Corbino effect *see Current, electrical*

Coriolis forces *see Dynamics*

Cornea *see Eye*

Corona, electric discharge

see also Breakdown, electric

- a.c., from twisted conductors and thin wires 2–74442
- air at high temps., 50 Hz and d.c. breakdown 2–74437
- air gaps, long, 50 Hz breakdown characteristics 2–74438
- air gaps in nonuniform fields, a.c. inception voltage calc. 2–71048
- audible, reduction on a.c. transmission lines 2–71001
- d.c., electric field measurements by e.s. fluxmeter 2–74444
- d.c. transmission line, effects of wind, loss on monopolar lines 2–74441
- field strength obs. cylindrical electrostatic fluxmeter 2–45646
- h.f., space charge in initial stages, photoelectric investigation 2–74443
- impulse, divergent field gaps, effect of charged particles 2–71041
- negative a.c., effects of humidity on discharge processes 2–71044
- organic insulating materials, partial discharge 2–71006
- point discharge in air at atmospheric pressure, obs. of small ion clusters 2–53259

Corona, electric discharge continued
- power transmission lines, equivalent parameters 2−60317
- stabilizer for Van de Graaf accelerators 2−76754
- water droplets, interactions with positive corona streamers, atmospheric significance 2−64489
- F gas, voltage-current characts., 100 torr to 1 atm, obs. 2−71013
- H, between concentric hemispheres, positive ion species determ. 2−43220
- O_2, ion form. mechanism 2−83637

Corona, solar *see Sun/corona*

Coronagraphs *see Sun/corona*

Corpuscular streams *see Cosmic rays; Sun/radiation, corpuscular*

Correspondence principle *see Quantum theory*

Corrosion
- alloy, light, s.c.c., microstruct. effects 2−56826
- alloy, pitting potential, electrochemical obs. 2−54546
- arrays of heated horizontal cylinders 2−45590
- austenitic stainless steels, intergranular, sensitized or solution-annealed, potentiokinetic polarization 2−68791
- austenitic stainless steels, susceptibility to stress corrosion cracking, evaluation by chemical, electrochemical methods 2−68104
- β-brass, stress corrosion cracking obs. by optical microscopy 2−84132
- α-brass, stress corrosion sensitivity in $FeCl_3$ and $Fe_2(SO_4)_3$ solns. 2−64733
- α-brass, tarnish films and stress corrosion cracking, theory 2−64734
- brittle materials, stress corrosion failure under dynamic loading conditions 2−50771
- electron microscope determ, applic. of high voltage metallography 2−56632
- glass, automatic analysis techniques 2−65379
- glass, crack tip profile and stress corrosion 2−53521
- hydrodynamic marine systems, cavitation erosion, prevention, cure 2−77387
- INCO 713C, thermal stability and corrosion of Al coatings after heat treatments 2−60959
- International Society of Electrochemistry, 23rd meeting, Stockholm (1972) 2−68792
- metal, stress corrosion crack propagation, film rupture mechanism 2−43727
- metal-environment systems, stress-corrosion cracking, study using transient straining electrodes 2−68103
- metals, effect of deformation, autoclave for obs. 2−66375
- metals and alloys, pitting, intergranular corrosion and stress corrosion cracking, protection potential 2−68787
- nondestructive crack detection method using liquid crysts. 2−43760
- nuclear reactor core, with Zr alloy cladding 2−49892
- pitting, sensitized ferritic stainless steel 2−78193
- plastic, crack tip profile and stress corrosion 2−53521
- plastic solids, stress corrosion cracking, role of H environment 2−77654
- refractory meterials, wetting effects 2−43867
- silicate glass, binary, surface structure 2−53541
- stainless steel, intergranular corrosion by potentiodynamic polarization 2−68788
- stainless steel, type AISI 304, accelerated intergranular stress corrosion cracking tests using potentiostatic polarization 2−68105
- stainless steel cladding for fast reactor fuel elements 2−59846
- steel, 18% Cr ferritic stainless, stress corrosion cracking 2−74901
- steel, austenitic Cr-Ni, intergranular corrosion susceptibility 2−71646
- steel, austenitic stainless, in acid agressive media 2−68790
- steel, austenitic stainless, stress corrosion cracking under pulsating load 2−53836
- steel, austenitic stainless, stress corrosion testing, mech. behaviour 2−50765
- steel, high-alloy, suppression of pitting, in phase analysis 2−57423
- steel, inoxidizable, passivation film study rel. to stress corrosion cracking 2−54547
- steel, stainless, 18-10, electrochemical study for compounds which inhibit stress corrosion 2−65381
- steel, stainless, 19Cr-9Ni, effects of alloying elements on stress corrosion cracking 2−77656
- steel, stainless, melted by different methods, O impurity effects 2−53899
- steel, stainless, type 304, pitting susceptibility rel. to electronic props. of oxide films 2−57422
- steel under caustic stress, electrochemical studies 2−68789
- stress corrosion cracking, capillary model, test using pressure effects 2−74857
- stress corrosion cracking, hydrogen embrittlement, catalytic dissociation as primary process 2−84020
- stress cracking, cathodic protection, hydrogen permeation 2−78194
- unit for determining the elastic limit in pure bending under the action of surface and corrosion active media 2−85156
- water corrosion in nuclear installations 2−59845
- Zircaloy-2, dispersion strengthened with yttria 2−53917
- Zircaloy-2, in steam-water mixture under reactor radiations 2−51456
- Ag-Cd(Zn) alloys, stress corrosion sensitivity in $FeCl_3$ and $Fe_2(SO_4)_3$ solns. 2−64733
- Al-Mg alloy, intergranular corrosion susceptibility 2−71646
- Al-Mg alloy, stress corrosion cracking, effect of Cu and Zr addition 2−50775
- Al-Zn-Mg alloy, stress corrosion crack paths 2−43732
- Al, intergranular corrosion in HCl, symmetrical flexion boundaries 2−72561
- Al alloy hand forgings, fracture toughness and stress corrosion cracking 2−60905
- Al alloy hand forgings, fracture toughness and stress corrosion cracking 2−60906
- Al_2O_3 coatings on BeO, neutron irrad. effect on protective behaviow and crack form. 2−43870
- C film, resist. to HF attack, diamond-like props. characterization 2−56588
- Co-base composite materials, superalloys with fibres obtained by directed solidification, properties 2−64793
- Co10%Cr alloy, thermal stability and corrosion of Al coatings, after heat treatments60959 2−60959

Corrosion continued
- Cr-Ni steels, austenitic, stabilisation of resistance to intercrystalline corrosion 2−65380
- Cu-Zn alloys, tarnish film formation, electrometric study 2−68785
- Cu-Zn alloys, tarnish films, electrometric characterization 2−77717
- Cu, protected by Si_3N_4 reactively sputtered film 2−43481
- Fe-Cr-Al alloy, potentiodynamic curves as function of tensile stress 2−44488
- Fe film, corrosion products in $NaNO_2$, internal conversion electrons, Mossbauer study 2−72281
- Mg alloys, and radiation damage resistance 2−60778
- Mg composites, in CO_2, rel. to use as fuel cladding 2−57424
- Na, flowing, nonisothermal, ^{60}Co transport processes, corrosion and deposition rates 2−67344
- Na reactor coolant corrosion and mass transfer analysis using ion probe mass spectrometer 2−83118
- Ni-Cr-Mo alloy, porous material, stability in HNO_3 and HCl 2−53977
- Ni-Mo alloy, porous material, stability in HNO_3 and HCl 2−53977
- Ni-base composite materials, superalloys with fibres obtained by directed solidification, properties 2−64793
- Ni alloys, suppression of pitting in phase analysis 2−57423
- Sn-Pb alloy, solder, interaction with NO_2, humidity effects 2−65382
- steel, austenitic stainless, microstructure determ. of oxide film 2−81505
- TZM alloy, arc casted, corrosion resist. 2−53825
- Ti-8% Al-1% Mo-1%V, accelerated stress-corrosion cracking in presence of hydrogen recombination poison 2−68107
- Ti alloys, crack growth criteria in stress corrosion cracking for thin materials 2−71600
- U-Mo alloy, stress corrosion cracking in humid aid, C content effects 2−53839
- U-Nb alloy, stress corrosion cracking, metallic protective coating 2−53911
- Zr-Cr-Fe alloy, resistance, correlation with microstruct. 2−53922
- Zr-(2at.%)Cr-(0.16at.%)Fe alloy, precip. reactions rel. to corrosion resist. 2−53919
- Zr-(2.5 wt.%) Nb press. tubing, hydriding, orientation and effect on tensile props. 2−50849
- Zr, neutron irrad. effects on aqueous oxidation, 290°C 2−44486
- Zr alloy, stress corrosion cracking in Hg, fracture surface study 2−43737
- Zr alloys, behaviour in org. coolants for reactor applic. 2−51454
- Zr alloys, high-strength, characteriz. for press. tubes 2−53921
- Zr alloys, high-strength, corrosion resist. 2−53920
- Zr alloys, in-flux corrosion in pressurized water loop 2−51455
- Zr alloys, resist. in steam, 400 to 500°C 2−51457

Cosmic dust *see Interplanetary matter; Interstellar matter; Meteorites*

Cosmic noise *see Cosmic radiations, radiofrequency*

Cosmic radiations, radiofrequency
see also Quasars; Pulsars; Radioastronomy; Radiosources; Sun/radiation, radiofrequency
- 21-cm. observations of high velocity HI regions rel. to continuum jets near galactic centre 2−55008
- absolute radio brightness temperatures in Southern Sky 2−69115
- background at 3.3mm., small scale anisotropy 2−58164
- 3C 391, supernova remnant, nature of low frequency absorption at 31.4 GHz 2−55085
- closed line as explanation of 3 K isotropic black body background radiation 2−84942
- Cygnus X-3, outburst of radio emission rel. to possible superrova precursor 2−73056
- e.l.f. hiss, Ogo 4 satellite observations 2−65928
- extragalactic, polarization structure 2−58402
- extragalactic radiosources, emission mechanisms 2−48754
- Faraday depolarization of extragalactic radio sources 2−73042
- flux densities, accurate, at 5009 MHz, 1007 sources 2−75803
- galactic, modulation by interplanetary mag. field 2−62458
- galactic, solar modulation, Compton-Getting coeff. implications 2−62459
- galactic background continuum at 15 GHz, thermal and nonthermal components 2−58187
- galactic background radiation spectrum between 0.2 and 2.6 MHz 2−75675
- galactic disk, continuum radio structure 2−69023
- i.r. sources associated with W3 2−58417
- Jupiter, radio emission at 102 MHz and measure of brightness temperature 2−81936
- Jupiter, sporadic decameter radio emission from extensive air showers 2−81932
- Jupiter IV, Callisto, thermal radio-emission rel. to thick icy surface layer 2−75870
- LHR hiss rel. to magnetospheric and auroral activity 2−68953
- M31 (Andromeda galaxy) and halo, radio observations in v.h.f. range 2−81787
- M82, peculiar exploding galaxy, millimetre observations, loop stability 2−55011
- noise absorption at 24.6 MHz, effect of magnetic activity at low latitudes 2−54935
- planetary temperature meas. at 350 and 700 microns 2−78527
- polarization radio sources, meas. at 9.55 mm wavelength 2−55082
- power law deviations of discrete 30-300 MHz sources, explanation 2−85017
- pulsar radio intensity fluctuations and subpulse structure 2−78484
- radio noise characteristics of auroral ionosphere 2−72840
- radio pulses rel. to gravitational waves from the Galactic Centre 2−58369
- radio recombination line observations, critical review of available data 2−48737
- recombination line emission from galactic ridge, excess H II regions 2−66123
- solar modulation parameter changes from 1965 to 1970, neutron multiplicity monitor meas. 2−62460
- submillimetre background radiation, limit on energy density 2−75822
- synchro-Compton radiation, polarisation 2−72983
- troposphere, fluctuations in water vapour content, from microwave observations of celestrial radiosources 2−51591
- universal background radiation 2−69001
- v.l.f. radio noise rel. to visible auroral arc emissions 2−65916

Cosmic radiations, radiofrequency continued
H radio recombination line data rel. to non-LTE theory 2–69113
HI 21-cm. line observations, low emission regions and baseline determination problems 2–55193
OH maser sources, search for departure of radiation from Gaussian statistics 2–73048

Cosmic rays
acceleration, effect of pulsars, theory rel. to obs. 2–51693
acceleration in supernova remnants 2–62568
age estimation using ^{10}Be isotope as clock 2–82961
balloon applics. in detection 2–70272
dose equivalent in United States, population distribution with respect to elevation 2–57803
energetic particles at very low altitudes near geomagnetic equator 2–44775
galactic, correlation analysis in space and on the Earth 2–51694
galactic, nonlinear interaction with interplanetary magnetic fields and solar wind 2–48653
galactic, radial gradient over solar cycle 2–75636
high energy, consequences of scaling 2–52649
idealized model for radial gradient of modulated cosmic rays in interplanetary medium 2–66191
intensity, N-S anomalies 2–66014
intensity relationship to solar activity indices 2–48805
magnetic mirrors in space, cosmic rays and magnetic storms 2–55888
new event interpret. and weak decay processes 2–52651
radiation exposure in manned spaceflight 2–51947
solar, acceleration, rel. to microwave type IV radio bursts 2–85025
solar, cutoff rigidity during polar cap absorption event at commencement of geomagnetic disturbance 2–48802
solar semi-diurnal variation, pitch angle distribution hypothesis 2–78441
solar semi-diurnal variation, three dimensional anisotropy 2–78440
TeV range, new processes 2–49603
transport in solar corona rel. to photospheric granular cell boundaries 2–44984
ultra-high-energy, possible generalization of relativistic theory 2–46023
Z>75, propagation, r-process source 2–62447
X-particle interpret. rel. to O(4) symmetry 2–55844

absorption
solar protons, in Earth's atmosphere, solar proton event, Nov. 18, (1968) 2–58123

alpha-particles and helium nuclei
see also Quasars; Radioastronomy; Sun/radiation r.f.
anti α-particles, search for in primary radiation 2–63673
aurora, low energy ion composition measurements 2–68950
radial gradients and anisotropy vector, numerical calculations 2–55002

apparatus
see also Particle detectors
albedo neutron fluxes in near Earth space, equipment for meas. 2–46021
Betasonde density data at high altitudes 2–73863
Cherenkov detector in high energy astronomical observatory 2–49605
emulsion pile, large volume for primary radiation 10^{12}-10^{13} eV 2–73861
four array hodoscopic counter, graphite target, spark chamber and 4-layer emulsion stack 2–73899
40 m^2 hodoscopic assembly with Geiger-Mueller counter for underground meas. of muon component in EAS 2–73876
Intercosmos-3 meas with PG-1 apparatus 2–81650
ionization calorimeter for investigation of ultrahigh energy muons 2–73862
meteorological correction coefficients, zenith angle depend. 2–63674
p-methoxy benzylidene p-n butylaniline, liq. cryst., nematic-isotropic liq. phase transition, sp. ht. obs. 2–74523
muon telescope calibration 2–70270
muonic spatial and temporal distribs. in EAS, design, construction and use of apparatus 2–42429
neutron spectrograph using recording channels with different τ 2–46022
NM64 neutron monitor, multiple neutron distribs. rel. to gate time width 2–52650
proportional counter hodoscopes, using low power preamplifier dual discriminator 2–49640
scintillation counter telescope for detection of 1/3e and 2/3e charged quarks at 2750 m altitude 2–76728
scintillation counter telescope for detection of 4/3e charged diquarks at 2750 m altitude 2–76729
scintillator counting rate depend. on area for sea-level cosmic rays 2–73865
shower counters, correction of light attenuation 2–73864
solar flare gamma ray meas. between 50 and 500 MeV from satellite 2–73142
solid iron spectrograph, for muons charge ratio and vertical spectrum, computer applic. 2–42428
spark chamber telescope for underground meas. of muon component in EAS 2–73876
spectrographs, lateral multiple-scattering muon distributions 2–49604
TeV range, detection of interactions 2–49603
thin polypropylene window propotional counter for soft X-ray obs. 2–70271
X-ray camera array for meas. of e-p showers and γ bremsstrahlung produced by μ in lead 2–73894
X-ray det. using atmospheric fluorescence as ground-based method 2–44902

composition
antinuclei content in primary rays, upper limit 2–48654
chemical, effect of spallation processes in space 2–63677
chemical composition 2–49606
diquarks with charge 4/3e, search at 2750 m altitude using scintillation counter telescope 2–76729
galactic and solar flare, identification with solid dielec. track detectors 2–63714

Cosmic rays continued
composition continued
primary, in galaxy, with energy $>10^{15}$ eV 2–62449
primary particles, high energy, rel. to shower development 2–79627
pulsar-accelerated, energy spectrum and composition 2–66043
quarks with electric charge 1/3e and 2/3e, search at 2750 m altitude using scintillation counter telescope 2–76728
relative abundances of extremely heavy cosmic rays, meas. 2–67064
solar flare accelerated particles, in $6 \leqslant Z \leqslant 26$ charge range 2–78601
He, solar, relative abundance 2–75971
Li to Fe nuclei at high energies, charge composition 2–63676

deuterons
No entries

effects and interactions
see also Nuclear reactions and scattering due to/cosmic rays
10^{11}-10^{12} eV with light nuclei, multiplicity depend. on energy 2–73885
10^{14} eV, in atmosphere, production of families of γ-quanta 2–73890
– 2–66043
150 Kg chondrite of Keyes, Oklahoma, depth variations in cosmic ray spallation produced noble gases 2–58534
chondrites, recently fallen, noble gas analysis, ages 2–58535
coherent particle production due to 20-600 GeV protons 2–73898
collective interactions, nucleons in heavy nuclei 2–59593
dense targets, hadronic scaling 2–67063
e.m. showers generated by muons in heavy substances, fluctuations in spatial distrib. of particle number 2–73879
Glauber and optical models compared for high energy N-nuclear interactions 2–73892
heavy primary, interactions in emulsions, meas. of interaction lengths of emitted secondary particles, anomalous behaviour 2–79629
high energy, scattering 2–62448
induction of radioactivity in scintillation detectors 2–62816
interactions, E>1 TeV, new processes and detection 2–49603
interstellar medium, production of D_2, ^{3}He, Li, Be and B 2–84970
l.f. radio emission from extensive air showers 2–49609
man, radiation dose from galactic cosmic rays 2–58595
Monte Carlo simulation at high and ultrahigh energies 2–73893
multifireball theory of multiple production, similarity considerations 2–73891
multiple particle generation processes >200 GeV 2–73886
multiple production of secondary particles, meas. of angular distrib. for t-cut phase volume 2–70277
particle interaction with nuclei, multiplicity depend. on energy of primary 2–74057
quarks, relativistic charge $^{2}{}_{.3}$e, search 2–59600
sea-level studios, lossrate curves, energy spectra 2–70273
secondary γ-spectrum, 0.2-5 GeV, 0-16 km in earth's atmos., meas. 2–51660
secondary particle ang. distrib. obs. on showers, 200-500 GeV 2–73897
single-particle spectra, comparison at accelerator and cosmic-ray energies, evidence for clustering 2–63549
solar and galactic cosmic rays, interaction with Moon 2–66149
visual perception of accelerated N nuclei interacting with human retina 2–76112
γ-quanta, high energy, generation in atmosphere, collective interactions 2–73887
γ quanta families 120, 250 TeV due to interactions at $E_0 \sim 10^{15}$ eV 2–73884
γ rays above 10^{12} eV, produced in interactions of very energetic primaries with universal black body radiation 2–69009
μ in lead, production of e-p showers and γ bremsstrahlung, determ. of energy spectrum and angular distrib. 2–73894
μ interactions with Fe meas. of cascades with energies $\geqslant 1$ GeV using ionization calorimeter 2–73895
π secondary, due to cosmic rays $>10^{12}$ eV, ang. distrib. and multiplicity 2–73899
π° production by high energy cosmic ray π and N (>1 TeV) 2–73888
Al-N, A-π interactions, 100-300 GeV 2–73896
B production in interstellar space 2–62593
Be production in interstellar space 2–62593
C-N, C-π interactions, 100 to 300 GeV 2–73896
C-N high energy interaction, cf. of Glauber and optical model calculations of multi-particle production 2–73892
^{57}Fe-N high energy interaction, cf. of Glauber and optical model calculations of multi-particle production 2–73892
Li production in interstellar space 2–62593
LiH, target for 150-550 GeV cosmic ray nucleons, multiplicity of particles generated 2–74070
Pb, cosmic ray hadron interaction, 3-30 TeV 2–73889
^{208}Pb-N high energy interaction, cf. of Glauber and optical model calculations of multi-particle production 2–73892

electrons
data from OGO5 satellite (from March 1968) 2–55005
EAS, electron space distrib. function calc. 2–82789
in EAS at mountain altitudes 73875 2–73875
electron-photon cascades, review of Janossy's expts. 2–79628
electron-photon showers caused by 50-400 MeV electrons and γ-quanta in Pb 2–67065
energy spectrum in 1 to 25 GeV range, balloon observations 2–63679
galactic, equilibrium energy spectrum 2–78426
interaction with relict radiation, attenuation length for high-energy γ rays 2–55004
interplanetary electron component, 200 keV, source models 2–81929
interplanetary electron component from 18 keV to 1.8 MeV during solar quiet time 2–78496
interplanetary temporal variations of 3 to 12 MeV electrons 2–66192
production of knock-on electron and electron pairs in e.m. interactions of high energy cosmic ray muons 2–55885
quiet-time electron increases as measure of outer Solar System conditions 2–75933
quiet-time electron increases rel. to outer solar system modulating mechanism 2–66193
in showers generated by muons in heavy substances, fluctuations in spatial distrib. of particle number 2–73879
spatial distrib. function near axis of cascade shower 2–73880

Cosmic rays continued
electrons continued
spectra of number of electrons in showers with energies >5 GeV, determ. of primary radiation spectrum 2−73866
e-γ shower development in liquid Xe by 1600 MeV γ-quanta, cascade curves and fluctuation of mean characteristics 2−79633
eγ cascades, Monte Carlo simulations in multiplate cloud chambers 2−42436

jets *see Cosmic rays/showers and bursts*

mesons
interactions, 25-10000 GeV, multiplate cloud chamber using Monte Carlo simulation for energy calibration 2−42436
interactions, analysis, sea-level obs. 2−70273
limiting fragmentation description of high energy cascade in atmosphere 2−79631
nucleon-meson cascades high energy, in thick targets, Monte-Carlo calcs. and comparison with expt. 2−79630
photographic emulsion, primary energy determ. 2−73957
surface intensity in London, atmospheric effects 2−70276
temperature coeffs., rel. to diurnal variation 2−58124
π diffusion model for momentum spectrum of muons at sea level 2−67066

muons
absolute vertical intensity at sea level for muons with momentum above 0.88 GeV/c 2−52652
angular distribution, in zenith angle range 0-65° and energy 200-500 GeV 2−73858
angular distribution, production and decay of weak scalar bosons in very high energy interactions 2−70278
cascades of energies >0.37 eV, energy spectrum and angular distrib. 2−73877
charge ratio and vertical spectrum meas., solid iron spectrograph with computer 2−42428
charge ratio in 10-300 GeV/c range, improved meas. 2−42434
EAS, mean muon density and relative response of muon and Cherenkov detectors 2−82787
EAS, number dependence on shower size 2−73882
in EAS, underground meas. of component near axis using 40 m^2 hodoscopic assembly or spark chamber telescope 73876 2−73876
in EAS and tridents, formation mechanism for bursts, investigation by spark calorimeter method 2−73878
in EAS at mountain altitudes, calcs. using 2-fireball isobaric model 73875 2−73875
in EAS at sea level, comparison of theoretical and exptl. data on spatial distribs. 2−73873
EAS component obs. form Haverah Park array 2−52659
e.m. interactions at high energy, meas. of production of knock-on electrons and electron pairs 2−55885
energy spectrum and angular distrib. for energies 2-10 TeV, underground measurements 2−73894
energy spectrum at great depths, produced by neutrinos 2−42437
generation and interactions, energies $\geqslant 10^{12}$ eV 2−46028
horizontal fluxes in water, influence of single scattering processes 2−67067
hourly rates connected for atmospheric temp. and press. 2−42431
ionization calorimeter for investigation of ultrahigh energy muons 2−73862
jet, abnormally low muon conc. 2−52653
lateral multiple scattering distributions, spectrographs 2−49604
limiting fragmentation and charge ratio 2−46027
limiting fragmentation description of high energy cascade in atmosphere 2−79631
local prod. underground, stopping rate meas. 2−82788
momentum spectrum at sea level meas. for near vertical incidence in 5-1200 GeV/c range 2−67066
monitor data, corrected hourly rates 2−82790
radioisotope prod. by stopped negative muons 2−82953
sea level absolute vertical integral intensities 2−59596
sea level intensities relation to primary nucleon intensity as test of scale invariance in particle production 2−49607
shower generation in heavy substances, determ. fluctuations in spatial distributions of number of particles 2−73879
shower studies and use of neon flash-tubes and solid iron magnets 2−79628
showers, muon spectrum 2−73883
spectra of number of muons in showers with energies >5 GeV, determ. of primary radiation spectrum 2−73866
stopping particles underground 2−59594
stopping-muon flux, underground meas. 2−59599
telescope calibration 2−70270
underground component, conventional explanation 2−42432
$\mu\mu$- pairs, possible bounds on production in super-high-energy hadron-hadron collisions 2−63537
EAS, muonic component, spatial and temporal distribution 2−42429
Fe, multiple scattering in 10 to 70 GeV/c range 2−73859

neutrinos
expanding universe, gravitational influence of homogeneous neutrino sea 2−68994
four-component hypermass eqn. from quarternion mass generalization, application to unstable neutrinos 2−78791
neutrino absorption rel. to cosmological models with continuous creation 2−84943
neutrino absorption rel. to cosmological models without continuous creation 2−84944
shower studies and use of neon flash-tubes and solid iron magnets 2−79628
solar, flux calc. of effect of dilaton theory of gravity 2−79632
solar neutrino emission rel. to nuclear physics and theoretical solar structure and evolution 2−58553
solar reactions, resonant energy depend. of ^{3}He + ^{3}He 2−82990

neutrons
albedo neutron fluxes in near Earth space, equipment for meas. 2−46021
atmospheric effects on neutron component, regression analysis 2−70275
barometer corrected and uncorrected cosmic ray data gathered by NM-64 neutron monitor 2−42430
cascade through atmosphere, comparison with model for $pp \rightarrow nX$ based on one-pion exchange 2−63681

Cosmic rays continued
neutrons continued
collective interactions, nucleons in heavy nuclei 2−59593
detection, balloon and satellite expts., Max-Planck Inst. 2−51692
EAS, calc. of number of low energy nucleons in showers of given number of particles 2−73874
hourly data using NM64 monitor, uncorrected and barometer corrected 2−59595
IGY monitor data, Jan to Dec 1959 at Deep River, Canada 2−59597
IGY neutron monitor data 2−42438
intensity spectrum at top of atmosphere, relation to sea level muon intensity as test of scale invariance 2−49607
interactions, analysis, sea-level obs. 2−70273
limiting fragmentation description of high energy cascade in atmosphere 2−79631
limiting fragmentation description of high energy cascade in atmosphere 2−79631
monitor data from Canadian stations 2−63680
nucleon-meson cascades high energy, in thick targets, Monte-Carlo calcs. and comparison with expt. 2−79630
primary ray modulation of attenuation coeff. 2−73867
sea level flux determ., using knock-on protons 2−42433
sea level meas. 2−70279
temperature coeffs., rel. to diurnal variation 2−58124
C, inelastic interac. with cosmic nucleons, 760-7600 GeV 2−42558

nucleons
No entries

origin
extragalactic cosmic rays and production of light elements, diffusion coefficients 2−55003
galactic origin, determ. of anisotropy above 10^{17} eV 2−44829
magnetic white dwarf theory 2−69007
metagalactic origin of primary component of cosmic rays rel. to gamma radiation flux from Magellanic Clouds 2−72959
polarization of EAS emission at 6 MHz as test of theories 2−70274
primary, in galaxy, with energy $>10^{15}$ eV 2−62449
pulsar physics, book 2−73050
sources of cosmic X-ray, gamma-ray and particles, book 2−44830
ultra high energy 2−72960
urbaryon model use to explain cosmic ray cut-off 2−73868
γ rays, review 2−69010

photons
No entries

primary
No entries

protons
120, 250 TeV families due to interactions at $E_0 \sim 10^{15}$ eV 2−73884
− 2−66043
anti α-particle search 2−63673
antinuclei content, upper limit 2−48654
aurora, low energy ion composition measurements 2−68950
chemical compos. det. form radio emission obs. 2−46024
chondrites, ^{3}He production rate by solar protons 2−62721
coherent particle production, energy depend, 20-600 GeV 2−73898
composition and origin in galaxy of radiation with energies $>10^{15}$ eV 2−62449
EAS, antimatter and ball lightning theories 2−81666
electron energy spectrum in 1 to 25 GeV range, balloon observations 2−63679
electron-photon cascades, review of Janossy's expts. 2−79628
electron-photon showers caused by 50-400 MeV electrons and γ-quanta in Pb 2−67065
emulsion-nuclei interactions with p at 22.6 GeV/c, velocity distrib. of secondary π meson 2−76840
energetic solar particles, observations during solar cosmic ray events 2−85054
energy, relation to EAS size determ. by meas. of Cherenkov radiation 2−73870
energy spectrum and composition at energies 5×10^{13}- 5×10^{15} eV 2−73866
gamma rays, absence of fluctuations in ground level background 2−63675
gamma rays, source for high energy point sources, Cygnus region 2−73061
gamma rays from galactic centre 2−62451
gamma rays from galactic centre 2−62451
gamma-rays, diffuse, obs. in 30-50 MeV region 2−51800
gamma-rays above 60 MeV in Northern Hemisphere, extraterrestrial, balloon search 2−73060
generation by atmospheric and non adiabaticity losses, energies >350 MeV 2−54886
heavy, interactions in emulsion, meas. of interaction lengths of emitted secondary particles, anomalous behaviour 2−79629
high energy, detection, balloon and satellite expts., Max-Planck Inst. 2−51692
high energy, total energy spectrum problems, comp. 2−79627
interaction in air, upper limit 2−52653
interaction with relict radiation, attenuation length for high-energy γ rays 2−55004
interactions, investigation of properties between 100 and 1000 GeV 2−55876
ionospheric detection of cosmic X-ray phenomena 2−68968
limiting fragmentation description of high energy cascade in atmosphere 2−79631
limiting fragmentation description of high energy cascade in atmosphere 2−79631
in lower atmosphere, 0-16 km in height, secondary spectrum, 0.2-5 GeV 2−51660
lunar photon albedo from galactic and solar proton bombardment 2−66148
metagalactic γ-rays from relativistic bremsstrahlung interactions 2−62634
metagalactic opacity to photons of 10^{17} eV 2−84940
metagalactic origin of primary component of cosmic rays rel. to gamma radiation flux from Magellanic Clouds 2−72959
multiply charged particles, nuclear disintegrations produced in nuclear emulsions 2−49608
neutron component, regression analysis of atmospheric effects 2−70275

Cosmic rays continued
protons continued
nucleonic component, modulation by primary rays of attenuation coeff. 2−73867
Orion Nebula, λ4686 He II line intensity, reln. to cosmic ray flux 2−69043
power spectrum of neutrino sea in Universe 2−72951
primary, proton-nucleus inelastic cross sections behaviour, 10^2 to 10^5 GeV 2−63678
primary above 10^{12} eV, produced in interactions of very energetic primaries with universal black body radiation 2−69009
proton-nucleus inelastic cross sections behaviour, 10^2 to 10^5 GeV 2−63678
radial gradients and anisotropy vector, numerical calculations 2−55002
γ-ray obs. above 250 MeV 2−62628
relative abundances of extremely heavy cosmic rays, meas. 2−67064
restricted diffusion model of propagation 2−81761
review of γ astronomy, cosmic-ray sources and production and propagation in interstellar and intergalactic space 2−69010
secondary, due to cosmic rays $>10^{12}$ eV, ang. distrib. and multiplicity 2−73899
secondary, production in pp collisions in simulation of EAS 2−52658
secondary spectrum, 0.2-5 GeV, 0-16 km in earth's atmos., meas. 2−51660
selection mechanism, overabundance of heavy elements 2−75662
solar, >75 GeV, above vertical geomagnetic cutoff 2−55175
solar, absorpt. in Earth's atmosphere, solar proton event, Nov. 18, (1968) 2−58123
solar flare gamma ray meas. between 50 and 500 MeV from satellite 2−73142
solar particle entry anomalies, magnetospheric models 2−65865
solar protons, interaction with Moon 2−66149
solar spectrum, integral production multiplicities for computing 2−73131
solar wind, collisionless protons, comparison of kinetic and hydrodynamic descriptions 2−62785
suprathermal bremsstrahlung, cross-section 2−69008
trajectories in galaxy, determ. of anisotropy of cosmic rays above 10^{17} eV 2−44829
trapped and precipitated, in magnetic storm of March 8, 1970 2−48556
u.h. energy non-existence of cut-off due to thermal radiation, choice of absolute reference system 2−72960
X-ray background, observations of diffuse component 2−51695
e-γ shower development in liquid Xe by 1600 MeV γ-quanta, cascade curves and fluctuation of mean characteristics 2−79633
eγ cascades, Monte Carlo simulations in multiplate cloud chambers 2−42436
γ rays above 10^{12} eV, produced in interactions of very energetic primaries with universal black body radiation 2−69009
pp collisions in EAS, simulation model 2−52658

showers and bursts
air shower, non-existence of cut-off at 10^{20}eV 2−72960
air showers, review of quark searches 2−59598
arrays, computer applications 2−81976
cascade, e.m. in atmosphere, 3-dimensional theory of development 2−73881
charged secondaries in multiparticle processes, asymmetry parameter 2−46026
counters, correction of light attenuation 2−73864
dust grain origin 2−55886
EAS, 10^{11}-10^{12} eV, Monte Carlo calc. of time dependence of isophotes and multiple pulses in Cherenkov light 2−52657
EAS, age parameter depend. on penetrating component density 2−42435
EAS, analysis of geometry effects in detection of Cherenkov light 2−52656
EAS, angular distributions meas. at zenith angles $>60°$ 2−73872
EAS, calc. of number of low energy nucleons in showers of given number of particles 2−73874
EAS, Cherenkov radiation and relation of shower size to primary energy 2−73870
EAS, directions of arrival compared with predicted anisotropy of galactic cosmic rays 2−44829
EAS, electron space distrib. function calc. 2−82789
EAS, features of muon and electron components at mountain altitudes 2−73875
EAS, form of Cherenkov radiation pulses at large distances from shower axis 2−73871
EAS, formation mechanism for μ bursts, investigation by spark calorimeter method 2−73878
EAS, meas. of rise time, width and shape of Cherenkov pulses 2−52655
EAS, muon studies 2−82787
EAS, muons $\geqslant 150$ GeV 2−73882
EAS, obs. at 6 MHz of radio pulses 2−62450
EAS, size spectra at sea level for $N=10^7$-10^9 2−73869
EAS, spectra of associated muons with energies $\geqslant 0.5$ TeV in central regions 2−73866
EAS, underground meas. of muon component near axis using 40 m^2 hodoscopic assembly or spark chamber telescope 2−73876
EAS at sea level, investigation of characteristics by classic methods and radio emission method 2−73873
EAS caused by primary cosmic rays, antimatter and ball lightning theories 2−81666
EAS emission, polarization at 6 MHz 2−70274
EAS rel. to scintillation counting rate 2−73865
EAS with medium-strong interaction, improved simulation 2−52658
electron showers in Pb, investigation at high primary energies 2−55887
electron-photon cascades, penetrating showers and EAS, review of Janossy's expts. 2−79628
electron-photon showers caused by 50-400 MeV electrons and γ-quanta in Pb 2−67065
e.m. cascades, theory of longitudinal development 2−52654
e.m. showers generated by muons in heavy substances, fluctuations in spatial distrib. of particle number 2−73879

Cosmic rays continued
showers and bursts continued
extensive air showers, γ-ray point source search by registration of Cherenkov light 2−51801
extensive air showers, radio emission obs. 2−46024
formation mechanism for bursts investigation by spark calorimeter method 2−73878
hadron cascades, Monte Carlo simulations in multiplate cloud chambers 2−42436
interaction of electrons and photons with relict radiation, attenuation length for high-energy γ rays 2−55004
jet, ang. istrib., particle content depend., rel. to upper limit of interaction distance 2−52653
Jupiter, sporadic decameter radio emission from extensive air showers 2−81932
l.f. radio emission, improvement to theory 2−49609
limiting fragmentation description of high energy cascade in atmosphere 2−79631
muon spectrum 2−73883
nucleon-meson cascades high energy, in thick targets, Monte-Carlo calcs. and comparison with expt. 2−79630
primary comp. rel. to shower development 2−79627
production of knock-on electron and electron pairs in e.m. interactions of high energy cosmic ray muons 2−55885
pulsar CP 1133, Cherenkov light registration from extensive air showers 2−51791
quarks among delayed shower particles at 70 m w.e. underground 2−46025
secondary particle ang. distrib. obs. on showers, 200-500 GeV 2−73897
Tokyo large air shower event, lower primary energy result 2−52660
e-γ shower development in liquid Xe by 1600 MeV γ-quanta, cascade curves and fluctuation of mean characteristics 2−79633
e spatial distrib. function near axis of cascade shower 2−73880
eγ cascades, Monte Carlo Simulations in multiplate cloud chambers 2−42436
μ cascades of energies >0.37 eV, energy spectrum and angular distrib. 2−73877
μ component in extensive air showers, Haverah Park array obs. 2−52659
N cascade through atmosphere comparison with model for $pp \rightarrow nX$ based on one-pion exchange 2−63681
EAS, muonic component, spatial and temporal distribution 2−42429

variations
air plasma, 8000 to 12500 K 2−71061
anisotropies, theory and search for 2−72961
constancy obs. using ^{36}Cl prod. from high energy protons 2−59753
corotation effect on ray intensity 2−82786
density gradient perpendicular to ecliptic plane 2−48605
diurnal effect, Oct. 1965 - June 1966, equatorial anisotropy and interplanetary mag. field 2−62396
diurnal effect, Oct. 1965-June 1966, method of analysis and stat. distrib. 2−62395
diurnal intensity variation during Forbush decreases between 2 and 20 GV, diffusion processes 2−73860
diurnal variation characts. from neutron and meson data, temp. effects 2−58124
diurnal vectors, neutron and muon monitor 2−44759
Forbush decrease, March 1966, and discontinuous struct. of interplanetary medium 2−62393
Forbush decreases in spaces 2−62394
galactic, solar activity effects 2−66226
geomagnetic cutoffs at high altitudes, 28 to 250 MeV 2−66015
meteorological correction coefficients, zenith angle depend. 2−63674
muon flux at sea level, intensity meas. 2−59596
North-South anisotropy and radial gradient in vicinity of earth 2−62397
solar, diurnal anisotropy, limiting primary rigidity rel. to coronal green line intensity 2−62744
solar flare characteristics and magnitude of solar cosmic ray increase 2−75969
solar proton wind, anisotropy, thermal, due to binary encounters 2−73128
transient north-south anisotropies in cosmic ray intensity 2−48606
ultrasonic attenuation meas., beam divergence effect 2−73434

X-rays
atmospheric X-ray contribution, altitude depend., 0.1-1 MeV 2−81742
background radiation, significance of small scale isotropy 2−62623
det. using atmospheric fluorescence as ground-based method 2−44902
diffuse, 30-250 KeV, OSO-5 obs. 2−62627
diffuse, low energy, origin, galactic component 2−51797
diffuse soft, spatial distribution 2−62446
extraterrestrial background, observations of diffuse component 2−51695
intensity and spectrum of diffuse background 2−52661
ionospheric detection of cosmic X-ray phenomena 2−68968
soft, in energy range 0.2 to 10 keV obs. of Sgr region 2−85010
thin polypropylene window propotional counter for soft X-ray obs. 2−70271
transition radiation from passage of relativistic charged particles through interstellar grains as source 2−48726
universal background, and thermal emission from neutron stars 2−55884
universal background radiation 2−69001
upper limit on flux associated with gravitational radiation 2−44826

Cosmogony *see Cosmology*

Cosmology
see also Elements, origin
— 2−58728
anisotropic, galaxy formation 2−69014
anisotropic Euclidean homogeneous, perturbations 2−72956
antimatter particles, expt. work, state-of-the-art 2−63481
atomic matter-antimatter rearrangement and annihilation cross sections 2−62433
Bianchi cosmologies, diagonal 2−66428

Cosmology continued
- Bianchi-type expanding universe in Brans-Dicke cosmology 2-81766
- black holes and temporal ordering 2-81764
- Brans-Dicke, e.m. wave dispersion 2-62437
- Brans-Dicke, Faraday rot. 2-62436
- Brans-Dicke, Hamiltonian approach to dynamics of expanding homogeneous universes 2-58160
- Brans-Dicke theory, gravitation, fast rotating solar core, general relativity 2-78430
- chaotic universe, origin of cosmic microwave background radiation 2-51689
- closed anisotropic models of universe 2-78425
- closed line as explanation of 3 K isotropic black body background radiation 2-84942
- closed rotating, containing matter described by kinetic theory, entropy production in collision time approx. 2-48648
- closed universe, electrodynamic Green function in 2-69562
- composition data variable stars in Magellanic Clouds 2-66103
- conformally flat axisymmetric models 2-62441
- conformally invariant theory relationship 2-76176
- cosmic neutrino absorption rel. to cosmological models with continuous creation 2-84943
- cosmic neutrino absorption rel. to cosmological models without continuous creation 2-84944
- cosmic objects and phenomena, frequency distribution w.r. to importance as monotonically decreasing function 2-44818
- cosmogony of solar system, nebular hypothesis of Isaac Orr, historical aspects 2-81926
- cosmological spatial homogeneity criteria 2-66427
- coupling constants, variation with time 2-59658
- covariant chronogeometrical space time model and extreme distance 2-44816
- curved space bounds on time variation 2-58157
- distance redshift relation for universes with no intergalactic medium 2-75658
- Earth movement relative to microwave background 2-48656
- Einstein and Teilhard de Chardin, science and synthesis 2-69519
- Einstein equation for space filled with matter, exact solutions 2-51688
- Einstein-de Sitter, with plasma coupled to radiation at non-relativistic temperature, e.m. waves absorption 2-68997
- Einstein-de Sitter, with plasma coupled to radiation at relativistic temperature 2-68998
- evolution of radio sources of large angular extent 2-69124
- evolution of uniform models containing both radiation and matter 2-81768
- expanding hot universe, evolution and galaxy formation 2-51712
- expanding universe, damping of adiabatic perturbations 2-72954
- expanding universe, gravitational influence of homogeneous neutrino sea 2-68994
- expanding universe, proton-neutron concentration ratio at stages preceding element formation 2-51691
- expanding universe, thermal instability, rel. to galaxy formation 2-51714
- expanding universe and its thermodynamics 2-44817
- expansion of the universe, review paper 2-62442
- Faraday rotation by intergalactic magnetic field and steady state and Einstein-de Sitter cosmologies 2-54999
- Friedman universe, redshift magnitude relations 2-69003
- Friedmanian perfect-fluid, for Deser scalar-tensor theory 2-72950
- Friedmann's model, non-homologous expansion 2-48650
- Friedmann models, zero pressure, exact expressions in terms of Jacobian Elliptic Functions 2-66039
- galaxy distances rel. to expanding universe, Hubble constant and Friedmann time 2-69039
- galaxy formation from prieval universal turbulence 2-62465
- general relativity, exptl. tests using radar and radio waves 2-76198
- generalized Taub solution 2-78428
- gravitational collapse, white holes and particle creation 2-78438
- gravitational collapse and black holes, review 2-78437
- gravitational waves galactic radiation and effects on calculated lifetime of universe 2-81765
- hadron era, physical conditions and evolution 2-54997
- hierarchical universe, Yukawa range and cosmological constant 2-58155
- homogeneous universes, stability 2-48645
- hot universe, non-existence of cosmic-ray cut-off around 10^{20}eV, choice of absolute reference system 2-72960
- hot universe with small density perturbations, model 2-75679
- irreversibility, its origin, time anisotropy, thermodynamic foundations of natural sciences 2-54995
- irrotational dust cosmologies, quantum models for lowest-order velocity-dominated solution 2-55402
- lepton nonconservation consequences 2-46066
- Lyttleton-Bondi theory, metric of an astronomical object 2-75660
- macroscopic rotators, quantization 2-75657
- magnetic, qualitative phase plane analysis of anisotropic model 2-51685
- magnitude-redshift relation in Brans-Dicke cosmology 2-75659
- many-body forces and the effect of the matter distrib. in the universe on the gravitational constant 2-58156
- mass difference of muon and electron, possible cosmological origin 2-76606
- matter at extremely high temp. and pressure 2-62912
- matter-antimatter annihilation in universe and γ-ray background spectrum 2-69004
- matter-antimatter asymmetry and joining of two semiclosed worlds 2-62440
- matter-antimatter hydrodynamics, coalescence effect 2-44820
- metagalactic background radiation, red shift losses and evolutionary effects 2-48649
- MHD universes of Godel type 2-51684
- missing mass, possibility of solid H_2 grains supplying this 2-75667
- momenta description by pseudotensor technique in various universes 2-69002
- neutrino sea, interaction with nuclei, phenomenological causal model of nuclear decay 2-78434
- nonrelativistic kinematics, Hooke's symmetries, relation to Galilei group 2-54996

Cosmology continued
- nucleosynthesis and formation of superheavy elements 2-84947
- nucleosynthesis theory and formation of elements up to Fe group 2-72949
- observational, role of radio galaxies and quasars 2-75804
- Olber's paradox rel. to evolutionary cosmology 2-72948
- Omnes model, annihilation, γ-ray spectrum 2-62434
- particle counts in relativistic revolutionary cosmos 2-48988
- perturbation in expanding universe of free particles 2-62432
- planetary evolution from dust 2-69144
- power spectrum of neutrino sea in Universe 2-72951
- proto-galaxy formation, from gravitational instability in expanding universe 2-51713
- quarks as indicators of cosmological models 2-51683
- quasars, cosmological redshift rel. to obs. of Faraday depolarization 2-73042
- quasars, geometrical interpretation of luminosity distributions rel. to separate big bang 2-55079
- quasars, summary of arguments for and against cosmological redshift 2-81877
- rapid cosmic processes, in astrophysics, morphology 2-81749
- relativistic, non-zero pressure 2-84931
- relativistic perfect fluid, Einstein field equations, spherically symmetric solns. 2-56277
- Robertson-Walker and Friedmann cosmologies 2-72952
- rotational perturbations in anisotropic cosmology 2-81770
- scalar-tensor, classical tests 2-81750
- Schwarzschild interior soln., conformally flat system 2-78429
- solar system origin, secular rotation 2-85038
- spherical rotating layers, gravitational field in linear approximation 2-76190
- static Robertson-Walker models, solns. of generalized field eqns. 2-69000
- stellar matter, black hole and expanding universe 2-66042
- surface-of-resolution model, connection to real universe 2-66038
- symmetry problems and epochs rel. to Universe evolution 2-62435
- Taub-Kazner metric generalization in scalar-tensor gravitation theory 2-78435
- Treder gravitational theory, cosmological solution 2-48644
- uniform model universe, interacting matter and blackbody radiation 2-58154
- universal dimensionless formulae for spherical media 2-78712
- universe, disk and ring structures 2-48651
- universe, expansion, neutrino rest mass 2-72953
- universe, expansion-induced backscatt. of e.m. waves 2-55392
- universe, gravitation and Mach's principle concepts applic. 2-58736
- Universe, hot model, role of intergalactic mag. fields 2-66049
- Universe, initial state ordered or chaotic 2-48646
- universe, magnetic field structures 2-51690
- Universe, non-singular, spin effect 2-44819
- Universe, origin of elements, book 2-55000
- universe, uniformly expanding, Mach's principle 2-58735
- Universe with small scale condensations, equations 2-62438
- weak interactions, cosmological time dependence 2-73299
- He abundance in primordial matter 2-48647

Cosmotron *see Particle accelerators*

Costa Ribeiro effect *see Dielectric phenomena; Phase transformations*

Cotton-Mouton effect *see Magneto-optical effects*

Cottrell atmosphere *see Crystal imperfections/dislocations*

Couette flow *see Flow; Hydrodynamics*

Counters
- *see also Ionization chambers*
- aerosol particles, multichannel, choice design and performance 2-82075
- cloud condensation nuclei, for automatic meas., patent 2-72797
- displayed at 1972 Physics Exhibition 2-55899
- with electric sensing zone, for particles in electrolyte 2-44489
- four array hodoscopic counter for cosmic ray detection 2-73899
- gamma sensitive probe for high temp. industrial applications 2-67083
- light nuclei production from p-nucleus interaction, experimental set up for study 2-55889
- low noise preamplifier for high count rates 2-49687
- multichannel, photons, luminescence decay meas. 2-78127
- neutron counter efficiency, gas radiat. iostropic flux 2-82799
- parallel plate available counter telescope for (n, α) reactions 2-70453
- parallel plate avalanche counter telescope for (n, α) reactions 2-70307
- particle, Coulter principle operation, patent 2-73947
- photocounting receiver performance for detection of multimode laser or scattered radiation 2-41948
- photoelectric, for nuclei concentration determ. 2-62117
- photon, pulse amplifier and discriminator 2-59124
- photoresistor dosimetric characteristics, γ-ray detectors 2-82800
- phototubes, testing device, design, for long-term stability 2-55896
- radiation protection instrumentation and applics. 2-70545
- scanning-be whole-body counter, design and evaluation 2-85080
- shadow-shield whole-body counter calibration for use in psychiatric hospital 2-69422
- shower, correction of light attenuation 2-73864
- solid angle subtended by circular cylinder 2-55893
- transition, for detection of radiation from ultrarelativistic charged particles 2-73946
- two counter geometry factor for bremsstrahlung expts. 2-49616
- whole body counting systems, performance and applications 2-69419
- whole-body counter with high sensitivity, clinical applications 2-69420
- whole-body radioactivity monitor, effect of deposited Rn daughter products on background count rate 2-69421
- X-ray, monitor for recording small angle scattering 2-55894
- $CdF_2:Er^{3+}$ i.r. quantum counter, noise effects 2-59631
- T, gas counting tube 2-70306

accessories
- *see also Counting circuits*
- A/D conversion/computer interface 2-52666
- anticoincidence installation for internal counting counter 2-82814

Counters continued
accessories continued
data-handling system, multi-purpose, beta- and gamma-ray spectra 2−52667
digital corrector for multichannel counting of short- and medium-lived nucleides 2−70284
PDP-8/E for on-line data from pulse counting experiments 2−67071
pulse delay generator 2−55892
random pulse sampler 2−73945
shift register delays for random asynchronous data input 2−70283
Cherenkov
applications, teaching paper 2−82105
calibration by light oscillator 2−59624
cosmic ray detection in high energy astronomical observatory 2−49605
gas, with large aperture for distinguishing between pions kaons and protons 2−76742
metal, ferro- or nonferromagnetic, radiation generation for meas. ultrahigh energy particles 2−73941
monochromatic method for meas. of 665 MeV proton energy by Vavilov Cherenkov radiation 2−73940
plastic threshold Cherenkov detector with wavelength shifter and quencher 2−70298
plastic threshold with wavelength shifter and quencher 2−55916
powder, for high energy particles 2−42460
solar flare gamma ray meas. between 50 and 500 MeV from satellite 2−73142
in transition counter for detection of radiation from ultrarelativistic charged particles 2−73946
crystal
arc, welding, acoustic vibrations effect 2−71050
Ge(Li) detectors, method for controlling surface properties 2−59625
LiF detector, thermoluminescent, for neutron and gamma radiation 2−52691
LiI(Eu) detector, meas. of fast- and thermal neutron fluxes 2−42461
NaI(Tl) detectors in symmetrical two-crystal Compton polarimeter for γ-rays 2−79641
NaI(Tl) for in vivo meas. of ^{239}Pu in man 2−58617
Geiger
beta ray calibration at protection levels 2−42449
intrinsic γ detection efficiencies for cylindrical G-M tubes by Monte Carlo methods 2−73933
noise effects after filling a counter, mechanism 2−63694
open counter design for metal surface study by exo-emission method 2−44187
open window G.M., use with proportional counter for thermally, stimulated exoelectron emission meas. 2−67090
CO_2, filled for exhalation radiometry of ^{14}C 2−58619
operation technique
see also Counting circuits
alpha-particle scattering by gas, effect on solid angle subtended by circular aperture 2−70285
reaction yield dependence on type of slit 2−79650
β-e and β-γ coincidence apparatus, internal conversion electron meas. 2−52697
UO_2 deposit thickness, effect on fission fragment double kinetic energy meas. 2−55895
proportional
$^{10}BF_3$, end-window, multifilament for neutrons, use with time-of-flight spectrometer 2−59612
bifilar helical multiwire chamber, for position sensitive detection of minimum ionizing particles 2−79652
butane-propane flow, use with open window G.M. counter for thermally stimulated exoelectron emission meas. 2−67090
circuit for processing signals from chambers, thick film hybrid form 2−52684
cosmic soft X-rays, thin polypropylene window counter 2−70271
energy resolution, gas multiplication factor 2−82798
gas, for localisation of ionizing radiation 2−73935
gas-filled proportional counter photon camera for impact location 2−49638
high resolution fast neutron spectrometry 2−67075
hodoscopes, using low power preamplifier dual discriminator 2−49640
hybrid chamber, proportional chamber with gated spark readout 2−55904
for in vivo meas. of ^{239}Pu in man, comparison with crystal counters 2−58617
in-flight pion beam flux monitor 2−55908
interference tube filled with pentane for T det. in gas phase 2−55906
large dynamical device for charged particle identification 2−63695
low background, for ^{3}H dating 2−52685
luminous radiations in proportional counters, meas. using photomultiplier 2−46033
mkltiwire chamber design as part of split field spectrometer at CERN intersecting storage rings 2−76740
multi-wire proportional chamber for nuclear medicine applications 2−49639
multifilament proportional counter, use in meas. nuclear reaction cross sections 2−70455
multiwire, for muon identification 2−73934
multiwire, large area, replacement for plastic scintillators 2−59611
multiwire, short resolution time and insensitive to magnetic fields 2−46042
multiwire, utilisation for multichannel Mossbauer spectrometry 2−42446
multiwire chamber performance 2−59608
multiwire chamber systems, for use in large gap magnetic spectrometer 2−79666
multiwire chambers, construction and props. 2−42451
multiwire chambers, h.v. digital read-out 2−42452
multiwire chambers for use in π^-−e expt., and beam monitoring 2−42450
multiwire chambers for X-ray transition radiation detection, use for relativistic particle separation 2−67081
multiwire proportional chamber readout, coaxial and pointed circuit delay lines 2−49636
multiwire with integral readout delay line 2−79660

Counters continued
proportional continued
multiwre structures rel. to recent progress in large detector systems 2−49637
neutron multiplicity counter, superheavy element search 2−52683
noise effects after filling a counter, mechanism 2−63694
nuclide activity, movable insulator 2−82797
particle coordinate determination 2−59610
particle identification for position sensitive counter 2−63696
position sensitive, for X-ray crystallography 2−80611
proton recoil, used for neutron spectrum map of Janus-irradiation facility 2−62842
resistive-wire position sensitive transmission counter for detection of heavy ions in focal plane of magnetic spectrometer 2−79640
response versus Linear Energy Transfer 2−59609
sealed Ti window, for $^1/_2$ keV X-rays detection 2−55905
selective triggering system for small angle π-p scattering at 40 and 50 GeV 2−79669
self pressure regulating, for space applics. 2−42453
thermally stimulated exo-electron detection 2−67079
thin, gas-filled, fluctuations in energy loss of 66 and 100 MeV protons 2−49634
wire counters using chamber with new gas mixture 2−49635
X-ray meas., astronomical applications 2−70292
Ar-ethylbromide mixture in multiwire chamber 2−70291
CO_2 filling, detection efficiency variations, background variations, elimination 2−55898
^{4}He, Monte Carlo calc. of α-particle recoil spectra for incident neutrons 2−42454
T content meas. of water samples using gas proportional counter 2−82808
Xe filled, gas amplification factor 2−63697
Xe gas proportional scintillation counter, improved low energy resolution 2−59619
scintillation
alkali halide, impurity activated, response curves 2−55913
alpha-particle, for environmental and medical research 2−70297
automatic scanning unit for 2-dimensional chromatograms with ^{3}H 2−61831
1,12-benzperylene thin films for α particle detection 2−73939
beta ray spectrum meas., plastic detector 2−55915
Bonner sphere, effects of scattered neutrons on calibration 2−79638
charge asymmetry meas. system for kaon decay 2−52690
circuits and systems, (conference, Washington USA, March 1972) 2−49644
combined, directional properties shielding effects 2−70295
cosmic ray detector, det. of induced radioactivity 2−62816
counting characteristics, noise, temperature, fluorescence signal to noise ratio 2−82801
counting rate depend. on area for sea-level cosmic rays 2−73865
curved channel multipliers, origin of background counting rate 2−63699
cylindrical, directional props. 2−55910
cylindrical, with sleeve-type lead screening, suitability of screening for determ. directional detection properties 2−59874
detector for (n,γ) cross section meas. 2−55911
dioxane based fluid, chemiluminescence 2−52687
electron diffraction unit, with counting system for small angle diffr. by gases 2−64133
guard, semiconductor gamma ray spectrometer, isotope determination, pulse shape discriminator, Compton scattering suppression 2−82796
hodoscopes, polarimeter and spark chambers as apparatus for spin rotation meas. at high energies of π-p scattering 2−73901
inert gas, design and development 2−82825
isotope imaging and counting, comparison of scintillation and semiconductor detectors 2−49643
large-volume liquid whole body counters, accuracy in low level measurements 2−69378
light response and pulse shape discrimination of NE 232 for electrons and deuterons 2−55914
liquid, counting vials materials, comparison 2−52688
liquid, efficiency, cost data 2−76730
liquid, external standard channel ratio quench correction, computer aided calibration 2−59618
liquid assay of ^{3}H-labelled protein in rabbit lens 2−42457
liver tumour detection with ^{67}Ga-citrate and scintillation camera, computer scintigraphy 2−73198
MEGAHPOL, fast online noncomputer multiparameter data reduction system for readout of 100 counters 2−73952
Mossbauer spectra, recording by current method 2−59620
Naton 136 plastic scintillator, C recoil produced by neutrons 2−63701
NE 230 and NE 231 liquid scintillators, response to deuterons and protons 2−79653
NE-102 plastic scintillator, response to 3.5, 5.8 and 10.5 MeV protons rel. to electrons 2−79663
NE-228 liquid scintillator, response to 3.5, 5.8 and 10.5 MeV protons rel. to electrons 2−79663
neutron recording, multichannel system using computer 2−70296
nuclear medicine, diagnostic image quality using scintillation and semiconductor detectors 2−49645
Nuclear-Chicago Pho/Gamma III scintillation camera, inexpensive remote start switch 2−76066
optimization of counting of samples with double radioactive labelling 2−59615
organic, absolute efficiency meas. for neutrons of 30 to 150 MeV 2−63698
organic, det. of bias setting 2−49648
phototubes, testing device, design, for long-term stability 2−55896
plastic, polyvinyltoluene, effects of degradation by u.v. light 2−76731
polymethylmethacrylate, deuterated 2−59617
precision time measurements, using pulse height analyzer 2−49685
pulse shape discrimination in NE 211 2−79661
reflector surfaces for light collection in rectangular scintillation detectors 2−82807
sample analysis, patent 2−59623
scintillation camera and portal circulation evaluation in medicine 2−73199

Counters continued
  scintillation continued
    sodium salicylate thin films for α particle detection 2−73939
    spark chamber combination, 1.5 m spectrometer, high aperture ratio 2−59621
    specially collimated scintillation detector, reduction of extrathyroidal neck radioactivity 2−76095
    stabilization by light output control of pulsed light source 2−82575
    thin plastic scintillators sandwich of various diameters for low background β-scintillation meas. 2−42459
    tomographic camera, performance and reliability 2−69285
    in transition counter for detection of radiation from ultrarelativistic charged particles 2−73946
    well counter adaption for measuring cardiac output 2−73200
    white oil based, efficiency obs. 2−55912
    X-ray tube kilovoltage, radiation exposure rates and γ-emission contamination obs. 2−63700
    ^{14}C and tritium energy spectra, comparison of chemiluminescence and phosphorescence 2−59605
    CaF$_2$ thermoluminescent, for meas. natural background radiation 2−42698
    CaWO$_4$, optical meas. in far u.v. 2−52689
    CsI:Tl, α and γ scintillation growth times 2−73938
    CsI(Tl)-NaI(Tl), thin layer, low background, for soft protons 2−59622
    Li-glass scintillator tip for detection of secondary electrons in electron microscopes, long life 2−82430
    Li, neutron detection sensitivity 2−55909
    NaI/Tl detector of whole body counter, efficiency calc. for distributed sources in human phantom 2−66278
    NaI detectors, response functions for γ-rays 2−79668
    NaI(Tl), 6″ × 4″, empirical formulae for calc. of full energy peak efficiency 2−42458
    NaI(Tl) cryst., elongated, errors in γ spectra meas. 2−42456
    NaI(Tl) good-geometry large volume detector, response function to γ-ray cascade 2−79665
    NaI(Tl) shielded Ge(Li) detector system for activation analysis, applic. to geological material 2−72599
    TlCl(Be,I) scintillator as a total absorption shower cascade detector 2−49646
    TlCl(I,Be) scintillation crystals, response to energetic ionizing radiation 2−49649
    Xe, dependence of deexcitation time of slow component on pressure 2−59616
    Xe gas proportional scintillation counter, improved low energy resolution 2−59619
    Zn luminous compounds as ^{3}H det. in thin-layer chromatograms 2−61832
  semiconductor
    alpha monitor using surface barrier detector 2−59627
    amplifiers, low noise, for X-ray detectors 2−52702
    catheter radiation detector for medical use 2−51937
    charged particle position sensing preserving energy resolution 2−49647
    circuits and systems, (conference, Washington USA, March 1972) 2−49644
    Compton polarimeters, relative peak efficiencies 2−76743
    computer analysis and interpretation of γ and α spectra 2−63702
    gamma X-ray and nuclear radiation detection 2−46043
    heavy ion detector, over biased thin surface barrier detectors 2−63705
    i.r. detector parameter uniformity in alloy semiconductors 2−52274
    isotope imaging and counting, comparison of scintillation and semiconductor detectors 2−49643
    ladder, signal processing system 2−49631
    large dynamical device for charged particle identification 2−63695
    linear ratemeter 2−70300
    liquif N$_2$ level indicator, thermistors 2−85164
    m.o.s. capacitors, time-resolved X-ray detection 2−49669
    n-p(n-i-p) detectors, space charge layer polarization during irrad. 2−65023
    needle type solid state detectors for in vivo meas. of tracer activity 2−66275
    needle-shaped detectors, regional distribution and transport of labelled compounds 2−66276
    new applications, review 2−55917
    nuclear medicine, diagnostic image quality using scintillation and semiconductor detectors 2−49645
    particle spectroscopy in 80 MeV range 2−49626
    proton recoil, detection efficiency and response function, axial symmetry to point neutron source 2−55921
    pulse height spectrum shape analysis 2−49675
    short lined isotopes, transporting device, mass spectrometers 2−83164
    soft γ and X-ray spectrometry, review 2−70287
    surface barrier, preparation method 2−49651
    surface barrier particle detectors, technique for fabrication 2−82812
    telescope for detection of light recoiling nuclei in coherent elastic scattering expts. at high energy 2−46058
    windowless p-n junction for β emitter meas. in vivo and in vitro 2−78655
    X-ray, in Kratky X-ray small angle scattering camera 2−59626
    X-ray detectors, efficiency calibration for range 3-200 eV 2−46053
    Cd Te, halogen doped, gamma ray detector 2−55920
    CdS, neutron activated, for X-rays 2−42466
    CdS photocell with non-linear characteristics, obs. of relative spectral sensitivity 2−42463
    CdTe, ion-implanted contacts 2−49670
    CdTe, preparation by travelling heater method 2−49668
    CdTe biomedical probes, efficiency, resolution and absorption 2−51891
    CdTe for meas. of disappearance rate of Na$_2{}^{75}$Se in rat's eye, comparison with Si(Li) probe 2−51992
    CdTe room-temperature detector possibilities 2−52692
    GaAs, for γ-rays, crystal growth and material quality obs. 2−46052
    GaAs, in vivo β-ray detector for biomedical applications 2−49667
    GaAs room-temperature detector possibilities 2−52692
    n-GaAs spectral response, liquid phase epitaxial, interface effects 2−49658
    Ge(-i), timing props. of ORTEC model 2−42462

Counters continued
  semiconductor continued
    Ge, coaxial and planar, space charge effects on fields and charge collection 2−49661
    Ge, coaxial γ-ray detectors, efficiency instability problem 2−49671
    Ge, effect of Si and O impurities, smooth pits and trapping 2−49652
    Ge, high-purity detectors, characteristics analysis and obs. 2−52695
    Ge, high purity, operating temp. limitations 2−49656
    Ge, high purity, p type grooving for fabrication 2−49654
    Ge, high resolution, using radiation defect compensation 2−82815
    Ge, ion-implanted, high purity 2−46047
    Ge, γ-compensated, as α and β particle spectrometer 2−52696
    Ge, p-n junction, γ-ray detector, space charge region polarization, impurity centre charge exchange 2−65026
    Ge, performance improvement 2−49660
    Ge, quality control of p-type and intrinsic Ge monocrystals 2−46044
    Ge, rise time gated leading edge trigger for improved timing of monoenergetic gamma rays 2−63703
    Ge evaluation by pulse meas. on guard ring radiation detectors 2−49653
    Ge high purity, ion implantation and glow discharge methods for contacts 2−49655
    Ge high volume detector, characteristics 2−79662
    Ge very pure, γ-ray detector 2−52694
    Ge(Li), absolute γ-ray efficiencies for thermal neutron capture studies 2−67256
    Ge(Li), fission track dosimeter monitoring of neutron flux incident 2−74191
    Ge(Li), for detection and energy det. of high energy protons 2−46055
    Ge(Li), pulse shape from gamma photon 2−42465
    Ge(Li), reactivation technique, using reverse bias clean up 2−49664
    Ge(Li), side entry and thin contact types, dead layer effects for α- and β-particles 2−49663
    Ge(Li), timing system for coincidence and nuclear lifetime obs. 2−49662
    Ge(Li), trap parameters of Ag, Co, Cr and Te impurities 2−46045
    Ge(Li), with highly compensated intrinsic regions 2−46050
    Ge(Li) coaxial detector, local efficiency variations 2−70301
    Ge(Li) coaxial detectors used as spectrometer, pulse shape analysis 2−46054
    Ge(Li) detector, fast neutron flux meas. 2−63704
    Ge(Li) detector, timing system 2−73942
    Ge(Li) detectors in symmetrical two-crystal Compton polarimeter for γ-rays 2−79641
    Ge(Li) diodes, trapping parameters, chemical impurities effect 2−49666
    Ge(Li) for meas. of total internal conversion coefficients 2−73982
    Ge(Li) γ-ray detectors, evaluation procedures 2−55919
    Ge(Li) photon detector, efficiency det. using ^{226}Ra source 2−42464
    Ge(Li) well-type, semitoroidal configuration, performance 2−46046
    Ge(Li)γ-ray detector for college laboratories, nonsensitive area determ. 2−62929
    H atom concentration measurements using semiconductor detectors 2−52693
    HgI$_2$ room-temperature detector possibilities 2−52692
    NaI(Tl) thin crystals, Monte Carlo calc. of pulse height response to protons of energy less than 100 keV 2−49686
    Si, coaxial, tissue equivalent, for in-vivo dosimetry 2−46049
    Si, high-purity detectors, characteristics analysis 2−52695
    Si, invivo, medical and biological applications 2−51938
    Si, ion-implanted, characteristic properties for alpha particles and electrons 2−49672
    Si, obs. of average energy per electron-hole pair generation between 5 and 320K 2−70299
    Si, p + n, low noise oxide passivated, fabrication and electrical props. 2−46048
    Si, pn, diffused, energy resolution, charge collection from entrance windows 2−49665
    Si, simple multicounter system 2−55918
    Si detector with partially depleted surface barrier for meas. of low-energy β-nucleide radioactivity 2−49673
    Si drift, effective thickness of dead layer 2−42467
    Si low-noise planar detectors with room temp. applic. 2−79654
    Si photocell with non-linear characteristics, obs. of relative spectral sensitivity 2−42463
    Si photodiodes for fast neutrons, properties 2−46057
    Si phototransistor with non-linear characteristics, obs. of relative spectral sensitivity 2−42463
    Si surface barrier, radiation damage effects from 2 MeV protons 2−46056
    Si surface barrier, temp. response, used in clinical dosimetry 2−69399
    Si surface barrier detector, electron beam monitor 2−63723
    Si surface barrier detector, low-cost fabrication for laboratory use, characteristic 2−78731
    Si surface barrier detectors, derivation of fast time marking signals 2−46051
    Si(Li), beta-ray spectrometer with mag. trochoidal electron transporter 2−59607
    Si(Li), dead-time corrections for X-ray intensity obs. 2−73943
    Si(Li), escape peaks and internal fluorescence in X-ray spectra 2−67082
    Si(Li), Ge(Li) detectors used in construction of Compton spectrometer for obs. of lower energy γ-rays in complex spectra 2−79642
    Si(Li), miniaturized, for β and γ meas. in superficial and deep parts of living tissue 2−55252
    Si(Li), radiation-damaged, i.r. response meas. 2−49657
    Si(Li), radiation damage by thermal neutrons 2−76732
    Si(Li), timing behaviour, comparison of methods for det. 2−49674
    Si(Li) detector, X-ray fluorescence spectrometry applied to environmental and biological analysis 2−51482
    Si(Li) detector meas. of X-ray peak intensities by integration over fixed energy range 2−82809
    Si(Li) detectors, radiation damage effects of electrons, protons and neutrons 2−49659
    Si(Li) for meas. of disappearance rate of Na$_2{}^{75}$Se in rat's eye, comparison with CdTe probe 2−51992
    Si(Li) semiconductor probe for semi-microscanning device 2−55250

Counters continued
semiconductor continued
Si(Li) semictor adaptation for X-ray diffractometer 2−47298
Si(Li) side entry and thin contact types, dead layer effects for α- and β-particles 2−49663
Si(Li) X-ray detection systems, pulse pile-up rejection 2−73944

spark
on-line data aquisition and analysis of spark chamber expt. 2−76741
triggered spark gap with rotating Sparkonite electrodes 2−79643

statistical analysis
coincidence count correction, optical and resistive pulse counters 2−73915
cosmic ray spectrographs, lateral multiple-scattering muon distributions 2−49604
differential cross section for scattering of non-parallel non-uniform beam 2−52668
random events, Poisson distributed, errors 2−49615
resonance spectra fitting by linear combination of Lorentzian and Gaussian profiles 2−52662
NaI, Monte Carlo program for evaluating response to monoenergetic γ-rays 2−79651

Counting circuits
angular correlation meas. of positron annihilation gamma-ray pairs, continuous scanning method using multiple channel analyser 2−42447
anticoincidence gate 2−63711
anticoincidence network for nanosecond range 2−59637
decaying radioactive source, device for maintaining constant detector counting rate 2−79647
digital corrector for multichannel counting of short- and medium-lived nucleides 2−70284
fast-slow coincidence, using Ge(Li) detector, excited state lifetime obs. in 300 nsec range 2−70311
five-channel strobed coincidence unit 2−42475
frequency marker generator 2−63215
multispectral scaling module 2−70310
pileup rejector in quantitative pulse spectrometry 2−79657
pulse counting apparatus for particle beam 2−82811
pulse height analyser, fast single channel, for precision timing with scintillation counters 2−49685
pulse height analyser for obs. of volume histograms of blood cells 2−69279
pulse height analyser test method using pseudorandom noise signal 2−52701
pulse height spectroscopy, lifetime correction 2−59606
pulse rate dependent noise and counting losses in active processor with fast recovery 2−70303
pulse shaper with universal logic of operation 2−73953
random pulse sampler 2−73945
rise time gated leading edge trigger for improved timing of monoenergetic gamma rays for Ge detectors 2−63703
scintillation pulse shape obs. with linear gate and integrator 2−42473
source follower linearization of diode pump integrator 2−49688
thick film hybrid form, processing signals from multiwire proportional chambers 2−52684
three parameter nuclear coincidence data collection and magnetic recording system 2−76735
timing system for Ge(Li) detector 2−73942
tunnel diode comparator, fast recovery, high input impedance 2−73951
X-ray, used in electron microprobe anal., source and nature of dead-time 2−63706

CPT conservation
− 2−70208
beta-asymmetry, calc. in terms of polarization, Gorter-Rose method 2−82920
C-even resonance production in ee colliding beams 2−82693
CP invariance violation in leptonic processes 2−73760
CP symmetry in $K^\circ \to \pi\mu\nu$ decay 2−45940
CP violation, and chiral symmetry 2−55804
CP violation, schizon model, application to $K^0_s \to \mu\mu$ decay 2−79557
CP violation, weak hadron interactions, review of exptl. studies 2−49525
CP violation in K_l decay to $\mu^+\mu^-$ 2−73800
CP violation in weak interactions 2−59393
CP violation search in $K^\pm \to 3\pi$ decay by comparison of Dalitz-plot distrib. for τ^+ and τ^- decays 2−52598
CP-invariance violating K-systems, higher order weak interaction theory 2−73801
CP-violating gauge interactions, derivation of Lagrangian 2−63453
CPT breaking, effects on $K_l \to 2\mu$ decay 2−45938
field theory, transformation properties under broken symmetry 2−45850
identical particles with crossing, invariance of $A + B \to A + B$ reaction 2−55803
kaons, mass distribs., CPT invariance of CT- noninvariant and CP-invariance theories 2−67000
massive and massless vector particles, current conservation, Lorentz condition, weak gauge invariance 2−70248
microscopic causality and reversibility rel. to neutral K decays 2−82734
p violation, meson and baryon, explanation in terms of dynamic interpretation of mass formulae 2−63649
parity violating analyzing power for p-p scatt. 2−82772
parity-nonconserving $\Delta S = 0$ nonleptonic processes in presence of second class currents 2−82656
in parton dual reson. model 2−59478
relativistic wave equations for particles of arbitrary spin, Poincare and CPT invariance 2−45848
renormalizable model of weak and e.m. interactions with CP violation 2−79489
scattering, four-fermion amplitude free from kinematical singularities 2−59399
symmetry relation for elastic neutrino reactions on neutrons and protons 2−52557
T invariance tests in allowed nuclear β decays 2−46182
T reversal for unstable particles 2−66908
T reversal invariance, exptl. test in $np \to \gamma d$ reaction 2−46007
time reversal, exptl. information 2−52541

CPT conservation continued
time reversal, validity tests, optimization 2−63750
time-reversal invariance conditions on phase of ρ-ω mixing 2−45986
violating model of weak interactions 2−63490
weak interactions in particle physics, 1965-72 2−63491
$\eta \to \pi^+\pi^-\gamma$ decay, charge asymmetry, C-invariance 2−59506
$\eta \to \pi^+\pi^-\pi^0$ decay, charge asymmetry, C-invariance 2−59507
K interacting with π, $l\nu$ pairs, and Onsager relation 2−73799
K^0 decay, limits on variance g CP-, T-, CPT symmetry 2−76651
K^0 weak decay amplitudes, unitarity and CPT properties in S-matrix approach 2−70215
$K^0 \to \pi^+\pi^-\gamma$, experimental test of CP non-invariance 2−79561
$K^0 \to \pi^+\pi^-\pi^0$, ratios of CP-violating K^0_s and K^0_l amplitudes and CP-conserving K^0_s and K^0_l amplitudes 2−67003
$K^\pm \to \pi^+\pi^- e^\pm \nu_e$, discrete symmetries test 2−67001
$K \to \mu^+\mu^-$, lower bound for CP nonconservation 2−73803
$K \to \pi\pi$, $K \to \pi\pi\pi$, difference in interference formulas for CPT or T invariance 2−82738
$K \to \pi\pi$, $K \to \pi\pi\pi$ difference in interference formulas for CPT or T invariance 2−82738
$K_s \to 2\gamma$ rate calc. on CP invariance basis 2−59512
$K_s \to \mu\mu$, 2π-2μ interaction, CP noninvariance, decay widths 2−59509
$K^0_{l,s} \to \pi^0\pi^0$, reevaluation of relative decay rate and CP violation 2−76653
$K_l \to \mu^+\mu^-$, possible CPT violation 2−59511
$K_l \to \mu\mu$, test for possible class of CP invariant solutions 2−63579
$K^0 \to \pi\pi$, nonlocal effects, violation of CP, T, and CPT invariance 2−70214

Cracks
− 2−60857
alloy, ductile fracture prediction under discrete loading 2−43728
alloy, hard metal, fracture surfaces, crack path electron microscope replica obs. 2−50773
alloy, light, s.c.c., microstruct. effects 2−56826
aluminosilicate ceramic, thermomechanically strengthened, thermal-stress fracture 2−50738
austenitic stainless steels, susceptibility to stress corrosion cracking, evaluation by chemical, electrochemical methods 2−68104
axial, in pressurized circular cylindrical shell, perturbation solutions of stresses 2−82307
bimetallic orthotropic media, elastic interaction of screw dislocation with interface micro crack 2−76279
brass, fatigue cracking, effects of grain and twin boundaries, slip mode behaviour 2−71598
β-brass, stress corrosion cracking obs. by optical microscopy 2−84132
α-brass, stress corrosion sensitivity in $FeCl_3$ and $Fe_2(SO_4)_3$ solns. 2−64733
α-brass, tarnish films and stress corrosion cracking, theory 2−64734
brittle body with disc-like crack, limiting equil. under force and temp. fields 2−45403
brittle fracture in compression 2−84018
brittle fracture initiation triaxial stress conditions, Gibbs free energy 2−84016
brittle materials, crack propag. rel. to nonrecoverable elastic energy, Griffith criteria 2−71595
brittle materials, stress corrosion failure under dynamic loading conditions 2−50771
brittle materials under compressive forces, limiting strength problem 2−80736
ceramic, subcritical crack growth and fracture energy 2−50857
Chelmsford granite, cylindrical specimens, growth rate obs. 2−75456
circular, propagation for tension and torsion 2−60900
circular cylinder containing symmetric array of edge cracks, analysis under torsion 2−66538
circumferential and axial, stress analysis at tip 2−45365
coatings, high-temp., nondestructive testing technique 2−43763
cobalt superalloy, FSX 414, thermal fatigue crack propagation testing 2−56878
collinear equal, periodic array, constrained 2−41583
compliance K-calibration for a pressurized thick wall cylinder with radial crack 2−69644
composite, C discontinuous fibre reinforced ceramics and glass 2−50918
composite, fatigue crack damage, vibr. testing 2−60921
composite, fibre-reinforced, graphite/epoxy, compressive fatigue 2−61021
composite, fibre-reinforced, shrinkage stresses rel. to matrix cracking 2−71659
composite, glass-crystal two-phase, theory 2−74860
composite materials, fibrous and laminates review 2−43901
concrete creep, nonlinear analysis of two-dimensional problems 2−66557
continuous testing apparatus for crack detection using water-washable penetrants 2−56857
crack tip stress singularity calc., geometrical-optic method of caustics 2−52161
cracked anisotropic finite elements, Lekhnitskii-Savin complex stress function approach 2−76285
cracking stress of glass fibre reinforced inorganic cement, use of fracture mechanics 2−64726
creep rupture, applic. of wedge-crack growth theory for hot torsion 2−68095
critical opening, effect of temp. 2−56824
crystalline solids, pore growth and mechanism during plastic deform. 2−80653
cylindrical shell, stress concentration problems, applic. of mixed finite element methods 2−73355
cylindrical specimens, method of forming axially summetric surface cracks 2−50785
deformation zones at crack tips, interferometric obs. 2−60903
delayed, in steel welding, restraint stress effect 2−77711
depth measurement using u.s. surface waves 2−71614
diamond, atomistic study of structure 2−56831
diffraction of tension stress wave and fracture 2−69654
disc with diametral crack, stress state 2−45404
dislocation analysis under varying applied stresses 2−50772

Cracks continued
- dislocation behaviour and contrast effects 2—56701
- Earth's interior, stress concentration and rupture propagation for semi-infinite longitudinal-shear cracks 2—61939
- elastic, parallel, noncoplanar, interaction, narrow spacing case 2—43731
- elastic material strips under plane extension, propag. problem 2—45407
- in elastic plate, part-through surface, tensile stretching and bending 2—45378
- elastic solid subjected to general loading, constant rate of extension 2—55470
- elastic solid subjected to general loading, non-uniform rate of extension 2—55471
- elastostatic stresses and displacement near tip, finite deformation analysis 2—77639
- electron microscope obs., applic. of high voltage fractography 2—56825
- electron microscope obs., applic. of high voltage metallography 2—56632
- elliptic notch with collinear cracks at tip, stress intensity factor during longit. shear 2—73392
- energy release rates and stress-intensity factors, by finite-element method 2—66531
- extension force, normal anisotropic elastic body 2—41612
- fatigue, instrument for recording time of initiation 2—71610
- fatigue crack initiation and propagation, review 2—60892
- fatigue crack propag., kinetic theory, activation energy estimation 2—73391
- fatigue crack propagation analysis 2—77655
- fatigue failure at elevated temperatures, effect of material props. 2—60893
- fatigue fractures, in zone of stress concentrators 2—80787
- fatigue limit definition 2—53832
- fatigue-crack front straightness in K_{Ic} testing 2—71591
- fatigue-crack growth under cyclic loads, theory 2—69643
- fatigue-crack initiation from flaws using fracture mechanics theory 2—69649
- fatigue-crack propagation in metals and polymers, review 2—64728
- feldspar, axial growth of inclined en echelon cleavage cracks during compression 2—61972
- finite, in plane extension, impact response 2—45366
- foils, in situ investigation in high-voltage electron microscope 2—80853
- formation in heat affected zones of welded joints during heat treatment 2—71596
- fretting fatigue, effects of contact pressure and hardness 2—43712
- glass, crack tip profile, static fatigue and stress corrosion 2—53521
- glass, laser irrad., microcracks, electron microscope obs. 2—60588
- glass, propagation, effect of aqueous, solns. 2—64730
- glass, subcritical crack growth and fracture energy 2—50857
- glass ceramic, lithium silicate, fracture energy as function of struct. 2—50886
- glass fibre/polyester resin composite, cracking and debonding on water uptake 2—61020
- glass reinforced plastics, debonding and cracking under tensile and fatigue loading 2—64725
- graphite, stress intensity factor at onset of rapid propag. 2—56828
- Griffith, coplanar, in infinite elastic medium, diffraction of elastic waves 2—41671
- Griffith, two coplanar, thermal stress in two-dimensional infinite elastic medium 2—58882
- ground, effect of earthquakes 2—78279
- growth, energy storage before, focal mechanism 2—65529
- growth in A286 at 1100°F effects of frequency and environment 2—56861
- hydrogen-induced propagation, decohesion theory testing 2—74859
- ice, columnar-grained, cracking activity during compressive creep 2—64732
- Inco 713C alloy, low cycle fatigue tests and crack propagation rate at 1400F 2—56885
- infinite plate with crack along circular arc, mixed boundary value problem of elasticity 2—52172
- infinite transversely isotropic medium, coplanar cracks 2—78879
- initiation and propagation analysis using finite element methods 2—52165
- longitudinal-shear, seismic source time function of propagation 2—65493
- low-cycle fatigue cracking, prediction method including biaxial stress and notch effects 2—56888
- lunar glass, interferometric evidence for low temp. shock 2—55124
- metal, b.c.c., brittle fracture, theory 2—43720
- metal, ductile fracture prediction under discrete loading 2—43728
- metal, fractography by crack replication 2—47545
- metal, stress corrosion crack propagation, film rupture mechanism 2—43727
- metal subjected to variable amplitude cyclic loading, crack growth predictions 2—47542
- metal-environment systems, stress-corrosion cracking, study using transient straining electrodes 2—68103
- metals and alloys, stress corrosion cracking, significance of protection potential 2—68787
- mica glass-ceramics, propag. rel. to microstruct. 2—60999
- model, nonlinear defect, to explain generation 2—84047
- 9Ni-4Co-0.30C, fracture mechanics of crack growth at elevated temperatures 2—56867
- nickel silvers, fire-cracking mechanism 2—43794
- nickel superalloy, Rene' 77, thermal fatigue crack propagation testing 2—56878
- nondestructive crack detection method using liquid crysts. 2—43760
- notch root radius effects on fatigue crack propagation and initiation 2—69648
- notched parts with compressive mean load, fatigue crack growth 2—47543
- nucleation and growth, rel. to high temperature low cycle fatigue 2—77682
- nucleation and growth of fatigue cracks from root of a notch 2—56817
- oil and water simultaneous flow through cracked porous medium of small inclination, finger-imbibition phenomenon 2—53358

Cracks continued
- opening displacement and fatigue crack growth rate 2—84019
- oxide fuel pin behaviour, COMETHE code 2—52859
- oxide fuel struct. evolution, modelling using BEHAVE-2 code 2—52858
- parabolic, on infinite elastic plate, mixed boundary value problem 2—41617
- pastes and polymers, deform. through shear strength limit 2—68085
- penny shaped, between two bonded dissimilar materials, stress intensity factors 2—45390
- penny shaped, sudden twisting, stress analysis 2—66510
- penny shaped at elastic half-space rigid foundation interface, effect of shear, stress field 2—73387
- penny-shaped, on interface, stress analysis 2—66542
- perspex, complex stress intensity factors at bifurcated cracks 2—71597
- perspex strips, interaction between two collinear assymetric cracks 2—68109
- photoelastic detn. of mixed mode stress intensity factors 2—69650
- plastic, crack tip profile, static fatigue and stress corrosion 2—53521
- plastic deformation at stably growing crack tip 2—84014
- plastic solids, stress corrosion cracking, role of H environment 2—77654
- plexiglass plate cracks, interferometric determination of opening and edge sliding mode stress-intensity factors 2—47544
- polycaprolactam, stressed, mechanism of submicrocrack generation 2—74858
- polyethylene, crack growth under tensile creep conditions 2—47548
- polyethylene, stressed, mechanism of submicrocrack generation 2—74858
- polyethylene insulators, treeing breakdown, voltage and temp. dependence obs. 2—72023
- polyethylene terephthalate, stressed, crack propag. in presence of org. liqs. 2—50781
- polymer, under load, submicroscopic crack formation, X-ray scatt. obs. 2—68108
- polymethyl methacrylate, internal flaws, crack nuclei density 2—64537
- polymethylmethacrylate insulators, treeing breakdown, voltage and temp. dependence obs. 2—72023
- polypropylene, stressed, mechanism of submicrocrack generation 2—74858
- polystyrene, crazing in sample containing two rubber balls, model for ABS plastics 2—60909
- polystyrene, low-angle X-ray scattering from crazes and fracture surfaces 2—74855
- polyvinyl chloride, fatigue crack propag. mechanism, comparison with polypropylene and ABS blend polymer 2—71601
- post yield fracture mechanics, crack model for high and low strength materials 2—64727
- propagating in infinite medium, exact solution for elastic displacements, seismological applications 2—61940
- propagation, Cranz-Schardin camera for obs. 2—63448
- propagation rel. to fatigue mechanism, scanning electron microscope obs. 2—56787
- PVC, stress cracking and crazing in hexane and hexane/toluene environments 2—50779
- quartz, static fatigue, earthquake phenomena 2—65499
- quartzite, static fatigue and creep mechanism 2—60898
- radial, emanating from pin loaded hole, strain energy release 2—84017
- radial, in a circular ring, elastic anal. and comparison to internally pressurized cylinders 2—69647
- radial, in a circular ring, elastic analysis and modified mapping-collocation technique 2—69646
- radial in finite rotating discs, stress intensity factors 2—58844
- reactor fuel, irrad., neutron radiography obs. 2—52856
- rectangular plate, orthotropic, centrally placed crack, stress intensity factors 2—66525
- reflected-shadow method for constrained zone study of cracks in birefringent media 2—68101
- reinforced materials, rheo-mobility effects in creep instability 2—49059
- rock, brittle, anal. of associated stresses 2—75457
- rock deformation, volume changes at high pressure 2—62006
- rock discs and rings loaded in diametral compression, controlled failure 2—62011
- rocks, effect of stress gradient on brittle fracture initiation 2—72667
- rocks, time dependent growth, creep 2—65576
- rubber, yielding due to crazing 2—43710
- rubber components, tearing energy detn. 2—68102
- ruby, stream paterns, microscopic examination and associated microcracks 2—71424
- running crack arrest in elastic plates for transverse loading 2—69645
- sea ice, due to surface tension, source of underice noise 2—65578
- shear, longitudinal, propagation and parameters of seismic sources 2—57561
- shell, closed, cylindrical, with crack, determ. of stressed state 2—69641
- slip plane decohesion in notched specimens 2—60950
- soda lime glass, slow environment sensitive growth 2—64729
- solid soln., crack propag. rate 2—43729
- stability in adhesive layer 2—55458
- stainless steel, 20% cold-worked Type 316, fatigue- crack growth at elevated temps. 2—84141
- stainless steel, type AISI 304, accelerated intergranular stress corrosion cracking tests using potentiostatic polarization 2—68105
- steel, 18% Cr ferritic stainless, stress corrosion cracking 2—74901
- steel, 1%C, fatigue crack propagation, stress intensity and microstruct. effects 2—71645
- steel, alloys, fracture mechanics of crack growth at elevated temperatures 2—56867
- steel, austenitic, surface slip lines and incipient cracks, during reverse bending 2—53837
- steel, austenitic, type 316, grain-boundary and intergranular cracking, relation to boron content 2—60872
- steel, austenitic stainless, rel. to stress corrosion testing, mech. behaviour 2—50765
- steel, austenitic stainless, stress corrosion cracking under pulsating load 2—53836

Cracks continued
steel, brittle fracture, theory 2−43720
steel, crack propag. resist., tempering temp. effects 2−53838
steel, effects due to stress fields around inclusions 2−47491
steel, estimating work done in development 2−53834
steel, fatigue-crack growth, effects of oxygen, water-vapour and hydrogen 2−68067
steel, high strength, growth in H_2 and H_2S gas environments 2−71599
steel, high temp. fracture, influence of annealing twins 2−56833
steel, inoxidizable, passivation film study rel. to stress corrosion cracking 2−54547
steel, low-C, bending fatigue tests, Wohler curves, slip lines 2−50979
steel, low-carbon, topography charge on fatigue fractured surface with crack propagation rate 2−84126
steel, maraging weldments, sustained load failures 2−71590
steel, martensitic, tempered, initiation and propag., plastic replication and electron microscope obs. 2−43734
steel, mild, fatigue cracking, initiation, growth, rel. to thickness 2−53833
steel, quenched, aged, cooled, dislocation substruct. rel. to microcrack 2−47413
steel, stainless, 19Cr-9Ni, effects of alloying elements on stress corrosion cracking 2−77656
steel, stainless, in situ investigation in high-voltage electron microscope 2−80853
steel, stainless austenitic 25%Ni 20%Cr, rel. to tertiary creep processes 2−47514
steel, stainless weldments, type 304, fatigue crack growth at elevated temperatures 2−56865
steel, stresses at start and finish 2−56832
steel, structural, propag. direction rel. to inclusion orientation 2−43713
steel castings, flaw formation 2−68149
steel in caustic environment, electrochemical study 2−68789
steel in hydrogen atmosphere or vacuum, low-cycle fatigue 2−60891
steel press. vessel, biaxially stressed, crack tolerating factor 2−50835
steels, austenitic, fatigue crack growth at high temperatures for types 304, 316, 321 and 348 2−56864
steels, mild, acoustic emission and energy transfer during crack propag., instrum. for detectn. 2−69767
steels ferritic, fatigue crack growth, threshold at 300°C 2−56863
straight, on infinite elastic plate, mixed boundary value problem 2−41617
stress corrosion, cathodic protection, hydrogen permeation 2−78194
stress corrosion cracking, capillary model, test using pressure effects 2−74857
stress corrosion cracking, hydrogen embrittlement, catalytic dissociation as primary process 2−84020
stress intensity factor of crack originating at edge of circular hole 2−82336
stress intensity factor under conditions of tension, torsion, flexure, evaluation by numerical technique 2−66504
stress wave emission, review 2−69745
stresses in bonded materials with perpendicular crack at interface 2−60901
suddenly expanding in elastic solid, obs. of initial wave front 2−66612
surface, infinite solid, stress intensity factors 2−45379
tensile crack formation rel. to tectonic energy release 2−72659
thermoelastic stress distribs. in vicinity of external crack in infinite medium 2−82308
thermoplastics, amorphous, hydrogen bonding influence on stress crazing and cracking 2−60908
viscoelastic media, variational principle applied to theory 2−63088
welded joints, formation in stress relieving annealing 2−64759
welded pressure vessels, loading capacity, stressed at high temps. 2−64771
Zircaloy-2, containing ZrH_x, fatigue fracture 2−47649
Ag-Cd(Zn) alloys, stress corrosion sensitivity in $FeCl_3$ and $Fe_2(SO_4)_3$ solns. 2−64733
Ag, in situ investigation in high-voltage electron microscope 2−80853
Al-Cu-Mg-Ni, forged after quenching, rel. to creep strain mechanisms 2−43804
97.4%Al-Mg alloy, fatigue crack dependence, temperature dependence 2−56866
Al-Mg alloy, slip struct. and crack growth during fatigue 2−47519
Al-Mg alloy, stress corrosion cracking, effect of Cu and Zr addition 2−50775
Al-9.5 wt.%Mg:Ti,Zr,Mo,B alloy, susceptibility, nucleation and development, rel. to alloy additions 2−47546
Al-Zn-Mg alloy, stress corrosion crack paths 2−43732
Al, slip struct. and crack growth during fatigue 2−47519
Al alloy, shear creep fracture prediction, complex stress creep characts. 2−53813
Al alloy hand forgings, fracture toughness and stress corrosion cracking 2−60906
Al alloy hand forgings, fracture toughness and stress corrosion cracking 2−60905
Al alloys, acoustic emission and energy transfer during crack propag., instrum. for detectn. 2−69767
Al alloys, acoustic emission due to low level periodic stress 2−51012
Al alloys, growth rate in fatigue, special gauges for det. 2−60934
Al alloys in thick sections, fatigue-crack propagation characteristics 2−71592
Al tube, steel wire reinforced, bursting under biaxial tension stresses 2−71661
Al tube, wound with steel wire, bursting strength and toughness 2−71660
Al_2O_3, polycrystalline, stress corrosion in moist air and toluene, time-dependent failure characteristics 2−84039
Al_2O_3, sapphire, subsurface damage effect on crack initiation and propag. 2−50762
Al_2O_3 coatings on BeO, neutron irrad. effect on protective behaviow and crack form. 2−43870
C, glass like, thermal shock and crack propagation 2−56822

Cracks continued
C, glassy fibres, derived from phenolic resin, mech. props. 2−84100
C fibre reinforced glass, fracture energy 2−84104
0.55%C steel, propagation under varying load conditions 2−43733
CaO-ZrO_2 ceramic, thermally stressed 2−43876
Co-base superalloys, thermal fatigue crack propagation under strain-temperature cycles 2−56868
Cr, coarse-grain melted, failure by crack propagation 2−68098
Cr, polycrystalline tensile failure, crack propagation and nucleation 2−84041
Cu-Al alloys, mechanical properties and ductility as a function of temperatures 2−64776
Cu-Zn alloys, intergranular stress corrosion cracking 2−77717
Cu, fatigue cracking, effects of grain and twin boudaries, slip mode behaviour 2−71598
Cu, stress pulse damping in region of propagating brittle crack 2−60801
Cu_6Sn_5 fibres, brittle fracture surface morphologies 2−80744
FeCo-(2wt%)V alloy, crack propagation and nucleation in ductile fracture53835 2−53835
Ge, atomistic study of structure 2−56831
LiF, spark discharge induced damage 2−68013
Mn-Zn ferrite cores, reduction by calcination prior to sintering 2−68163
Nb-H foil, microcracks, transmission electron microscope obs. 2−68106
Nb, rel. to oxide wedge formation and stress effects on oxid. process 2−43736
Ni-Cr lamellar composite alloy, fatigue deformation, crack propag., fracture energy 2−56821
Ni-base superalloys, thermal fatigue crack propagation under strain-temperature cycles 2−56868
Si, atomistic study of structure 2−56831
Si crystal, brittle-fracture and crack propag., atomistic computer simulation 2−84036
Ti-Al-V alloy, mill-annealed, fatigue crack growth, temp. effects 2−60904
Ti-8% Al-1% Mo-1%V, accelerated stress-corrosion cracking in presence of hydrogen recombination poison 2−68107
Ti alloys, crack growth criteria in stress corrosion cracking for thin materials 2−71600
U-Mo alloy, stress corrosion cracking in humid aid, C content effects 2−53839
U-Nb alloy, stress corrosion cracking, metallic protective coating 2−53911
UC-UC_2 and UC_2 phases, microcracks due to U_2C_3 formation 2−47720
W, coarse-grain melted, failure by crack propagation 2−68098
WC-(25 wt.%)Co alloy, surface finish effects 2−43717
ZnS epitaxial film, on GaAs, microcrack formation 2−71339
Zr-(2.5 wt.%) Nb press. tubes, heat-treated, embrittlement 2−50770
Zr-(2.5wt.%)Nb press. tubes, irrad. effects 2−53913
α-Zr, unloading effects on propag. 2−50778
Zr alloy, stress corrosion cracking in Hg, fracture surface study 2−43737
Zr containing refractories, products obtained on calcining $ZrO_2 + CeO_2 + Cr_2O_3$ mixture remain crack free on high rate of heating 2−84095
ZrO_2, calcia-stabilized, fracture toughness 2−50777

Cranking model *see Nucleus/theory*

Creation of electron pairs *see Electron pairs*

Creep
see also Slip
absolute capacitance microcreep and dimensional stability measuring system 2−71620
albite, microstructure and dislocation distrib. obs. 2−81623
alloys, commercial, method for correlating creep and rupture strengths 2−47607
amorphous polymers, recovery, influence of volume change 2−56809
apparatus, high vacuum and rarefied atmos. 2−60918
automated strain measurements using AIMA-5-1 testing machine 2−53859
bar, prismatic, in steady creep, bounds for torsional stiffness 2−45421
belting, power-transmission, uniaxial tensile creep meas. 2−43702
buckling of plates and shells 2−76318
butyl rubber, temp. and extension time depend. of creep recovery 2−71555
cavity formation during testing, t.e.m. obs. 2−80871
cement, hardened paste, short time creep recovery 2−80755
composite materials, fibrous and laminates review 2−43901
concrete, nonlinear analysis of two-dimensional problems 2−66557
core restraint system design effects of irradiation creep and swelling on structural materials 2−83124
creep buckling analysis incorporating elastic deformation and time-hardening creep 2−58863
creep collapse of a cylindrical shell, effect of time-varying external pressure 2−41575
cyclic stress and derivation of a formula for failure in creep fracture 2−56862
data acquisition system, application to reactor component design 2−83120
deformation, mathematical model for low stress 2−64717
deformation, transition theory, spherical shells considered 2−52132
deformation kinetics criteria of low cyclic creep fatigue at high temps. 2−56886
deformation of asteroids and major planets satellites 2−78491
deformation under hydrostatic pressure 2−68088
delay time, surface layer stress relax. time 2−71573
diffusion creep, grain boundary sliding contrib. to axial strain 2−47509
diffusional, atomistic aspects, dislocations 2−56729
diffusional, grain boundary dislocation climb sources, interface reaction control conditions 2−50752
diffusional, grain boundary sliding 2−56730
dislocation mechanisms, review 2−53811
dislocation pile-ups, kinetics of changes 2−50661

Creep continued
ductility exhaustion model for prediction of thermal fatigue and creep interaction 2−60896
Earth and planets law which accounts for damping 2−58482
fast reactor, sub-assemblies, voidage-induced bowing, importance of irradiation and thermal creep 2−59831
fatigue, high temperature phenomenological mechanisms 2−56818
fault, California, rel. to geomag. obs. 2−65560
fault, tectonic stress release 2−57728
fibre composite, containing discont. fibres, theory for steady state creep 2−47510
fracture, due to diffusional growth of grain boundary voids 2−47523
fracture, secondary, influence on fatigue failure at elevated temperatures 2−60893
gases, thermal transpiration expts. on inert gases 2−74484
geological massif, effect on stress concentration round supported elliptical tunnel 2−44590
graph analytic method of evaluation of relationship with stress relaxation 2−64743
graphite, high temp. neutron irrad. expt. in Dragon reactor 2−56802
graphite, isotropic, effect on elastic modulus, cryst. orientation, and density 2−56963
graphite, nuclear, nat. graphite filler, neutron irrad. behaviour rel. to comp. 2−56049
graphite, Poco, at high temp. 2−56803
graphite, POCO grade HPD-1, at high temperatures, comparison with polycrystalline graphites 2−77625
hollow circular disk with heated stamps on external surface, stress relief 2−66558
ice, columnar-grained, cracking activity during compressive creep 2−64732
Inconel alloy, X-750, fracture and creep-fatigue behaviour 2−56860
irradiated specimens, meas. by neutron radiography 2−71621
irradiated specimens, measurement by neutron radiography 2−82593
kinetics, dislocation glide and viscous bowing, modified Orowan eqn. 2−56694
long cylindrical shell, creep collapse under external pressure at elevated temp. 2−76329
low alloy steel, creep rupture strength, microstruct. depend. 2−77685
low stress deformation, mathematical model 2−64717
low-cycle creep fatigue testing, method and equipment 2−56874
machine for testing neutron effects in nuclear reactor 2−46391
metal, full creep process, model 2−47507
metal, in tension, under hydrostatic press., time depend. 2−80728
metal, Nabarro-Herring creep rate reduction by oxide dispersions 2−47512
metal, reversed creep deformation behaviour 2−77629
metal, strain-hardened, plastic flow theory 2−43684
metal fatigue in liquid metal reactor component design 2−56893
metal foils, apparatus for testing 2−56852
metal forming processes, tensile creep 2−76262
metallic, complete description of process 2−52187
metals, strengthening, under variable stress 2−53812
metals and alloys, high temp., monograph 2−60871
metals under fast-neutron irradiation interrelation between swelling and irradiation creep 2−76941
method of testing metal in thin wall parts 2−68120
Nimonic 90, tensile creep under transient stresses, elevated temp. 2−71575
nonlinear law, combined strain- and time-hardening 2−49077
nonlinear viscoelastic solid, single integral constitutive law 2−76332
nuclear fuels and structural materials, radiation induced, effect on performance 2−46387
nylon 6 monofilament, model for deform. and fracture from creep and birefringence obs. 2−84021
nylon 6 monofilament, model for deform. and fracture from creep and birefringence obs. 2−84022
nylon-epoxide adhesive 2−47673
omphacite, microstructure and dislocation distrib. obs. 2−81623
Orowan eqn., modified, form for internal stress due to dislocation interactions 2−74847
Permalloy, film, rel. to thickness 2−56806
plates, circular, flat, rel. to geometry changes during deform. 2−66555
poly-n-butylmethacrylate, tensile creep, effects of equilibrium vapour sorption 2−50758
polycarbonate, yield locus det. 2−43778
polyethylene, crack growth under tensile creep conditions 2−47548
polyethylene, stress level and temp. effect 2−47518
polyethylene terephthalate, non-linear viscoelastic behaviour 2−56777
polymer, combined tension-torsion testing 2−71619
polymers, radiation-induced, relationship with radiation-induced electric conductivity 2−47517
polymers, stand for testing 2−71611
polymethylmethacrylate, tensile creep behaviour and fracture mechanics, liquid environment 2−53819
powder metallurgy of high-temp. materials, conference, Tyrol, Austria, June 1971 2−53937
pressure vessels, internal pressure effects 2−69497
primary recovery creep, physical basis 2−47508
pyrofoil tape, production and characterisation for reactor use 2−56050
quartzite, axial crack growth mechanism 2−60898
radiation-enhanced, implications in fast reactor design 2−49900
rate, rel. to void growth on grain boundaries 2−50685
reactor materials, obs. and effects 2−70538
recording apparatus, for teaching use 2−52027
recovery-creep model with effective and internal stress evaluation 2−68087
recovery-work hardening theory 2−56799
recrystallization, dynamic 2−68133
resistance and rate in specimens with soft interlayers 2−68086
resistance wire strain gauges, method for testing creep 2−82126
rocks, after partial melting under low stresses 2−57764
rocks, high-temp. rheology 2−57823
rocks, time dependent crack growth 2−65576
rods with initial deflection rheo-mobility effects in creep instability 2−49059

Creep continued
rubber, amorphous sodium-butadiene and butadiene-nitrile, stress effect study 2−60873
rubber, cross-linked by dicumyl peroxide, exptl. obs. of creep modulus 2−50757
rupture, applic. of wedge-crack growth theory for hot torsion 2−68095
rupture of structures, failure times 2−69655
San Andreas fault, water level fluctuations 2−57635
service life prediction in a fatigue creep environment 2−60953
shell, steady-state creep pot. construct. 2−76330
shells of revolution, finite-element method of analysis 2−82317
Solenhofen limestone, testing at constant stress and constant force 2−62008
stainless, type 304, ratchetting, parametric study for design curves and design rules 2−56895
stainless steel, annealed type 316, effect of fast reactor radiation on creep behaviour 2−83123
stainless steel, types 304, 316 estimates of creep-fatigue interaction in irradiated and unirradiated samples 2−83121
stainless steel cladding for fast reactor fuel elements, irradiation creep 2−59846
steady state and transient, relation between stress sensitivity parameters 2−77634
steel, 11% Cr, tensile and compressive creep at constant stress 2−68091
steel, 11% Cr, tensile creep under transient stresses, elevated temp. 2−71575
steel, austenitic, obs. 2−56920
steel, austenitic, rel. to shape and dimens. of particles 2−50656
steel, austenitic, type 316, creep-rupture behaviour relative to boron content 2−60872
steel, austenitic stainless, effect of loading at high temp. 2−60946
steel, characteristics at ambient temp. 2−64747
steel, Kh18N10T, fine structure changes for degree of deformation in creep 2−83956
steel, stabilized recovery-induced substruct., formation for improved creep resistivity 2−56913
steel, stainless, characteriz. for fast breeder reactors 2−50648
steel, stainless austenitic 25%Ni 20%Cr, tetiary creep processes 2−47514
steel, stainless types 304, 316 time-dependent deformation behaviour, elevated temp. design criteria 2−83119
steel, type 304 stainless, prediction of in-pile behaviour using SCIM, theory based computer code 2−76939
steel tube, stainless, type 304L, in-reactor creep 2−46382
strainrange partitioning approach for creep fatigue analysis 2−56889
structural, motion in continuum bodies 2−49058
structural materials, irradiation effects 2−74757
structures, relationship between plastic and creep deformation 2−76261
superconductor, creep strain delay at transition temp. 2−74846
superplasticity mechanism, metallographic obs. 2−56786
surface energy, zero creep condition, grain boundary term 2−56569
tensile, testing apparatus for ceramic materials using simple knife edge universal joints 2−47568
testing method, effect of error on statistical spread 2−53847
theory taking into account anisotropic hardening 2−52140
transient and steady state, relations between exptl. parameters 2−47511
transition theory, applic. to spherical shells 2−52132
vibration, machine for testing, constructional foam plastics 2−56847
viscoelastic material, gas bubble behaviour in creep process 2−50699
Waspaloy sheet, sensitivity of creep-rupture properties to sharp-edged notches in temp. range 1000-1400°F 2−47609
Zircaloy-2, irrad. and temp. effect 2−43802
Ag-GaO$_x$, alloy, dispersion strengthened 2−53814
Al-Cu-Mg-Ni, forged after quenching, recovery treatment, creep strain mechanisms 2−43804
Al-Li alloys, neutron irrad., inert gas bubble effects 2−43688
Al-Mg alloy, high temp. mechanism 2−68089
Al-Mg alloys, viscous glide in solid solution, dislocation climb and Newtonian viscous deformation mechanisms 2−64718
Al-Zn-Mg-Cu alloy, tensile deform. and high temp. creep rel. to microstruct. 2−56800
Al-1% Mg, deformation, electron microscopic obs. 2−80753
Al-5 at.%Mg solid soln., steady state, dislocation mechanism, 570-800K 2−56801
Al, Al-0.5 wt.%)Fe alloy, high temp.-low stres, directional diffusion vs. dislocation process mechanisms 2−50755
Al, elec. resist. during creep tests 2−50754
Al, high purity, and dil. alloys, review 2−68076
Al, study of differential method of temp. variation at const. rate 2−80731
Al alloy, multiphase, creep tested under stress, study of microstructure 2−80820
Al alloy, shear creep fracture prediction, complex stress creep characts. 2−53813
Al foil, block misorientation, X-ray study 2−74848
Al pressure-vessel alloys, tensile, creep and stress-rupture tests 2−77671
Al single crystals, substruct. changes during high-temp. deform. in creep 2−84078
Al_2O_3, alumina, high temp. creep, and grain boundary sliding 2−50753
Al_2O_3, corundum, high temp., microstruct. changes 2−71574
Al_2O_3, porous polycrystalline, compressive creep 2−47513
$BaFe_{12}O_{19}$, creep, deform. texture 2−56962
C, glassy and pyrolytic, activation energies 2−53815
C, neutron irrad. at high-temp., mech. interactions among crystallites 2−56679
C and C-Si alloys, effect of neutron irradiation 2−76917
C fibre monofilament substrate, rel. to B chem. vap. deposition 2−53956
Co-base composite materials, superalloys with fibres obtained by directed solidification, properties 2−64793
Cr-Mo-V creep resisting steels, constitution diagrams for service lifetimes 2−60838

- **Creep** continued
  - Cr-Mo-V steels, resisting props. constitution diagrams for service lifetimes 2−60838
  - Cu-16%Al alloy, sigmoidal transient, internal stress and disloc.. struct. 2−53816
  - Cu-Cr alloy, embrittlement, under elevated temp. stress 2−43722
  - Cu, 400-800°C, stochastic model 2−68090
  - Cu, cold worked at 200-300°C, creep and recovery 2−84163
  - Cu, creep deform. under bending stress 2−80836
  - Cu, creep fracture of cylindrical bars under pure torque 2−64754
  - Cu, elec. resist. during creep tests 2−50754
  - Cu, rel. to void growth on grain boundaries 2−50685
  - Cu, study by differential method of temp. variation at const. rate 2−80731
  - Fe-Al-Cr alloys, effect of zirconium 2−60935
  - Fe-Mo solid solution, creep type, variation with applied stress 2−43703
  - Fe, high parity and Swedish pure, creep testing during thermal cycling 2−56881
  - α-Fe, high temp., dislocation struct. and stresses 2−43637
  - α-Fe single crystal, high temp. creep and substructures 2−56804
  - Fe_2O_3, density changes and pore distribution during heat treatment 2−68140
  - Ge, creep, and stress effects 2−84040
  - Ge, mosaic structure during testing, X-ray and e. microscope exam. 2−71475
  - InBi, hot hardness and indentation creep 2−71602
  - Mg-Zr alloy, creep resist. on diffusion of Ni 2−47467
  - MgO-C inclusions, polycryst., four point bending obs. 2−56805
  - MgO-$MgAl_2O_4$ system eutectic struct. 2−47658
  - MgO, compression creep at high temps. 2−74845
  - MgO, influence of inclusions 2−56964
  - Mo, at high temp. and high stress 2−53817
  - Mo powder, hot pressing with and without addition of oxides 2−77694
  - Mo single crystals, stress anal. for high temp.-creep and slip 2−84012
  - NaCl, at high temps., compression tests, stress dependence, creep mechanism 2−77651
  - NaCl at high temp., creep substructure., tilt walls around parallelipipedic blocks 2−77579
  - Ni-base composite materials, superalloys with fibres obtained by directed solidification, properties 2−64793
  - Ni, porous, kinetics, in acid and neutral media 2−43704
  - Ni powder, hot pressing with and without addition of oxides 2−77694
  - Ni_3Al-Ni_3Ta eutectic, high temp. 2−47644
  - β-NiAl, ordered b.c.c. alloy, transmission electron microscope obs. 2−56807
  - $Ni_2(AlTi)$, $Ni_2(AlNb)$, ordered ternary b.c.c. alloys, transmission electron microscope obs. 2−56807
  - Pb-Sn alloy, superplastically deformed, const. stress creep and strain rate tensile tests 2−47504
  - Pb containing P bronze, fibre composite, steady state rate meas. 2−47515
  - Si, deform. behaviour, $T>850$°C 2−56808
  - $SrZrO_3$, behaviour, 1160-1275°C 2−43705
  - Ti alloys, comparison with theoretical investigation of plastic deformation peculiarities in planar stress state 2−43698
  - TiB_2, rel. to effect of particle size on sintering kinetics 2−61006
  - TiC-Nb cermet, rel. to hot pressing kinetics 2−56914
  - U, superplastic behaviour under tensile stress and temp. cycles 2−47516
  - UO_2-Mo cermet, finely-dispersed, creep rate and particle growth 2−71650
  - UO_2-PuO_2 mixed fuel, thermal creep, 1300-1700°C 2−53818
  - UO_2 fuel, radiation enhanced creep 2−52862
  - UO_2 single crystal, influence of stoichiometry on compression creep 2−67350
  - W-Re-ThO_2 alloy, 1800-2200°C 2−64719
  - W powder, hot pressing with and without addition of oxides 2−77694
  - W wire, from powder metallurgical, pure, doped and thoriated material, high temp. creep behaviour 2−61007
  - WC-Nb cermet, rel. to hot pressing kinetics 2−56914
  - Zn superplastic behaviour under tensile stress and temp. cycles 2−47516
  - Zr, rel. to vacancy formation energy 2−53728
  - Zr alloys, anisotropic creep behaviour under fast neutron flux 2−50756
  - Zr alloys, anisotropy of secondary in-reactor creep, relation to texture 2−67349
  - Zr alloys, high-strength, characteriz. for press. tubes 2−53921
  - ZrC-NbC, solid solution, compression, temp. range 2600-3150 K 2−84033
  - ZrC_x fibres, physical and mech. props. detn. 2−68178
- **Critical constants, thermal**
  - binary mixture, hydrostatic effect near critical point 2−60537
  - characteristic temperatures of matter on the saturation line 2−71270
  - continuously variable critical exponents, exact solutions 2−60540
  - fluid turbulent heat transfer near pseudo-critical temp. in supercritical pressure 2−74320
  - improved state eqn. effect in vicinity of critical point 2−80522
  - steam, coexistence curve, specific heat and compressibility near critical point 2−67870
  - thermodynamic method for obtaining equalities 2−49033
  - two-species model, idealized properties 2−78946
  - ^3He-^4He mixture, second sound velocity and superfluid density near tricritical point 2−74578
  - ^3He and ^3He-^4He mixtures, obs. of critical point phenomena 2−64493
  - $NaNO_3$:Ca, specific heat, diffusivity and conductivity near transition point 2−60542
  - Ne, critical temperature and constant volume specific heat 2−71113
- **Critical mixtures** *see Solutions*
- **Critical opalescence** *see Phase transformations; Solutions*
- **Crowdions** *see Crystal imperfections/interstitials*
- **Cryogenics** *see Cryostats; Low-temperature/phenomena; Low-temperature production; Low-temperature technique*
- **Cryopumping** *see Vacuum pumps; Vacuum technique*
- **Cryoscopy** *see Freezing; Low-temperature production; Low temperature technique*
- **Cryostats**
  - BWR eqn. of state development and applic. for c.-a.d. of cryogenic plant 2−76121
  - bypass valve for liquid He transfer 2−58657
  - cryomagnetic assembly for neutron diffraction studies 2−66372
  - desorption cooling below 12 K using ^4He desorbed from synthetic zeolite 2−52009
  - e.p.r., liquid He cooling of samples, 4.2-100 K 2−76425
  - level indicators of liquid He and N_2, circuits described 2−41898
  - metal, KG series 2−66370
  - neutron diffraction, 1-300K 2−73245
  - nuclear target orientation using cryogenic apparatus of ^3He refrigerator and solenoid superconducting magnet 2−76736
  - optical, with controlled cooling in range 5 to 260K 2−55329
  - optical cryostat for two-beam spectrophotometers 2−73682
  - with optimization of low pressure condensation cryopumping, for investigation of H_2 saturated vapour pressure deviation from Clausius Clapeyron law 2−45190
  - Pomeranchuk effect, cooling of ^3He 2−45191
  - for semiconductor device props. meas., 77 to 300 K 2−85169
  - super high vacuum, with self contained pump 2−66367
  - for superconducting lenses of 400 kV electron microscope 2−63291
  - ultrasound absorption of massive solids from 0.32 to 2.2°K 2−61093
  - variable temp., for far i.r. obs. at high pressures 2−69489
  - with warm horizontal apertures 2−66369
  - He, for X-ray analysis of single crysts. 2−43546
  - He, liquid, level sensor, operating conditions for NbTi filaments 2−66368
  - He liquid, automatic level regulator 2−69488
- **Cryotrons** *see Superconducting devices*
- **Crystal chemistry**
  - chlorates, alkali and alkaline earth, cation electronegativity difference effect on ^{35}Cl n.q.r. 2−44464
  - d orbitals, 5 equivalent, packing of molecules in crystal 2−74193
  - group IV elements, oxides, metals and nonmetals 2−71360
  - group IV elements 2−71360
  - hydrogen containing compounds, neutron diffr. obs., review 2−74653
  - kenotetrahedral spinel and rutile types, Madelung number rel. to anion parameter 2−67926
  - oxide fuels, irrad., oxygen distrib. 2−52869
  - Pauling third rule amendment rel. to Mg_2SiO_4 polymorphism 2−47335
  - rare earth hexaborides, nonstoichiometry 2−47183
  - semiconductor cpds., departures from stoichiometry determ. by chemico-analytical methods 2−43503
  - semiconductor II-VI cpds., deviations from stoichiometry 2−50657
  - semiconductors diamond-like 2−54158
  - titanomagnetite, Mossbauer determination of cation distribution, geological significance 2−54965
  - transition metal carbides and nitrides, (Gp IV and V), nonstoichiometry rel. to order-disorder changes 2−61029
  - transition metal phosphides and arsenides, MM'P and MM'As, metallic interactions, struct. evolution 2−71361
  - B_2O_3-Li_2O-H_2O system borate hydrates 2−47181
  - Ba_2FeS_3, and cryst. struct. 2−60750
  - $Ba_6Fe_8S_{15}$, and cryst. struct. 2−60750
  - $BaFe_2Se_3$, and cryst. struct. 2−60750
  - $BaFe_2Se_3$, and cryst. struct. 2−60750
  - Ba_2FeSe_3, and cryst. struct. 2−60750
  - $Ba_3Fe_3Se_7$, and cryst. struct. 2−60750
  - $Ba_2KNb_5O_{15}$, Ta-substituted, quadratic tungsten oxygenated bronze struct. 2−47315
  - Ba_2LnMoO_6, valence state of Mo, mag. susceptibility study 2−72112
  - Ca-Fe olivines, X-ray diffraction study 2−47325
  - $Ca_3Fe_{2-x}M_xGe_3O_{12}$, $M=Al^{3+}$, Ga^{3+}, Cr^{3+}, Sc^{3+}, In^{3+}, Mossbauer study of lattice 2−72278
  - $CaO.Al_2O_3.CaF_2$ glasses, coordination numbers from i.r. spectral data 2−64587
  - $Cd_3Fe_{2-x}M_xGe_3O_{12}$, $M=Al^{3+}$, Ga^{3+}, Cr^{3+}, Sc^{3+}, In^{3+}, Mossbauer study of lattice 2−72278
  - $Co_2Fe(CN)_5NO.2H_2O$, i.r. spectra obs. 2−78081
  - $CsCr(SO_4)_2.12H_2O/D_2O$, Cr^{3+} spectroscopy 2−54400
  - $Cu_2Fe(CN)_5NO.2H_2O$, i.r. spectra obs. 2−78081
  - Eu-Fe-O system, rel. to cpd. formation 2−47710
  - Eu-W-O, subsolidus phase relations and cryst. chem., phase diagram 2−74952
  - Eu_2TiO_4, rel. to mag. props. 2−51249
  - $Eu_3Ti_2O_7$, rel. to mag. props. 2−51249
  - $Fe_3(CN)_5NO.2H_2O$, i.r. spectra obs. 2−78081
  - Ge-Sb system, metastable GeSb phase 2−47329
  - $In_{6.6}Ca_{3.1}S_{13}$, and cryst. struct. 2−60758
  - $K_5(UO_2)F_9$, struct. of binucl. $(UO_2)_2F_9^{5-}$ ion 2−83953
  - $Na_2B_4O_6(OH)_2.3h_2O$, kernite, charge distribution from analysis of X-ray data 2−50560
  - γ-Na_2BeF_4, high-temp. X-ray diffr. obs. 2−61109
  - $Na_{2x}Sr_{1-x}Pb(OH)_6$, nonstoichiometric 2−71437
  - $Ni_2Fe(CN)_5NO.2H_2O$, i.r. spectra obs. 2−78081
  - $Ni_{1-x}S$:O(Se), rel. to mag. susceptibility conc. depend. 2−44255
  - NiS, stoichiometry effect on metal-to- transition 2−51280
  - $PbBr_2$, pure and doped, hole cond., defect chem. 2−61322
  - $PbZr_{0.5}Ti_{0.5}O_3$, single-phase, intrinsic nonstoichiometry 2−50896
  - Sn halides, electronegativity correlations with ^{119}Sn Mossbauer shift 2−44360
  - Sn halides, Mulliken electronegativities rel. to ^{119}Sn Mossbauer shifts 2−44359
  - $Sr_2KNb_5O_{15}$, Ta-substituted, quadratic tungsten oxygenated bronze struct. 2−47315
  - Ti_4O_7, metal-insulation transitions, charge localization 2−44087
  - $(U,Pu)O_{2-x}$fuel irrad., oxygen redistrib. 2−52868
  - V_4O_7 metal-insulation transitions, charge localization 2−44087
  - $Zn_2Fe(CN)_5NO.2H_2O$, i.r. spectra obs. 2−78081
  - ZrO_2, nonstoichiometric, microscopic thermodynamic props., rel. to macroscopic props. 2−43506
  - $Zr_2Si_2Se_2$, nonstoichiometry, X-ray obs. 2−43505

Crystal classes *see Crystal structure, atomic; Crystallography*
Crystal cleavage *see Cleavage*
Crystal counters *see Counters/crystal*
Crystal electron states
see also Colour centres; Helicons; Pseudopotential methods
actinide metals, hybridized 6d and 5f virtual-bound-states model rel. to magnetism 2−68516
alkali halide, electron density anisotropy and effective charge 2−54100
alkali metal, liq., calc. by cell method 2−83797
aromatic ion radical crystals, electrostatic energy calc. 2−51073
bifluctuons, possible existence near critical point 2−64904
Bloch electron, oscillation in constant electric field 2−64874
Bloch electron in mag. field, invariance group represent. 2−61132
bound eigenstates of electron in exponential cosine screened Coulomb potential 2−69597
close-packed lattices, density of states of simple excitations 2−57094
computer generated films for motion of electron in periodic potentials 2−78729
conducting crystals, e.m. wave scatt. by sound, electron conc. wave contrib. 2−54396
dielectric wedge, electrostatic edge modes 2−84363
disordered system, functional equation of self-energy 2−61133
electronic Green functions calc. using nonorthogonal basis functions 2−61131
epitaxial substrate carrier meas. by i.r. interference envelope technique 2−82567
exact boson representation of spin operators, thermodynamical function evaluation 2−64882
Fermi fluid model of s-d electrons, rule of sums 2−80944
ferromagnetic complex lattice, bound state energy, using boson Hamiltonian 2−51245
graphite, interlayer force, Thomas-Fermi calc. 2−77823
ionic crystal, F-centre electronic wave functions 2−84247
lattice electron behaviour in a uniform magnetic field 2−84231
localization lengths in one dimensional disordered potential chains 2−61136
metal, neutral atom model, ion-electron-ion interaction 2−68271
metal, quantum waves in strong mag. field, theory 2−81008
metal particle, minute, enhancement of electronic polarizability 2−72006
molecular cryst., intermol. electronic relax. pathways, determ. by photon echoes 2−68696
molecular cryst., valence struct. from X-ray diffr. data 2−64610
nonequilibrium, superconductors, photoexcitation of quasiparticles 2−77868
nonlinear response of electrons to X-rays 2−61576
nuclei plus electrons system, magnetism, numerical analyses 2−54284
periodic lattice, dielec. function, self-consistent calc. 2−54116
photoelectron spectroscopy, review 2−68495
radial equation in 3 dimensions, appl. of soln. to one-dimens. Schrodinger eqn. for arbitrary potential 2−84273
rare earth ions in cryst. field, optical transitions, interference effects 2−84494
rare earth metal, single electron energies, many electron effects, renormalized atom scheme 2−64875
semiconductor, indirect interaction of nuclear spins through electrons in valence zones of semicond. 2−76760
semiconductor, quantum theory introduction, book 2−47876
semiconductors, dielectric screening 2−61217
semimetal, quantum waves in strong mag. field, theory 2−81008
semipolar crysts. of NaCl-type, normalization integrals allowing for perturbations in ψ and ψ^* 2−57097
small aggregates, molecular orbital theory applic. 2−77796
solid state physics, an overview 2−57093
spin polarized case, local exchange-correlation potential 2−57266
spin-phonon interaction, ground state 2−68272
structure with two point defect types, quantum states and energy spectrum 2−80998
symmetric Anderson model, fourth order ground state energy 2−64876
symmetry labelling, orientation depend. 2−61134
TCNQ ditoluolchromium complex, electronic states localised characts., n.m.r. 2−72529
virtual electronic levels, review 2−59982
Wannier functions, generalized symmetrical, props. 2−64889
Ag, clusters, electronic props., mol. orbital calcs. 2−81026
Ag, total energy, pseudopot. theory 2−61137
Ag halides, physics and chem., conf., Montreal, Canada, Aug. (1972) 2−81541
As_2S_3, amorphous, photoelastic consts. freq. depend., one-oscillator model 2−54383
Au, total energy, pseudopot. theory 2−61137
Be atoms in small aggregates, Hartree-Fock calculation of electron states 2−80978
Bi density of states, relativistic effects, mass velocity and Darwin terms 2−84242
Cd, clusters, electronic props., mol. orbital calcs. 2−81026
Cu, total energy, pseudopot. theory 2−61137
Fe, atomic magnetic moment dependence on the lattice parameter 2−81256
HfH_x, electron-nuclear interactions, rel. to spin-lattice relax. 2−78047
K, anomalous i.r. absorpt. and collective oscills. in small metal particles 2−65210
Li atoms in small aggregates, Hartree-Fock calculation of electron states 2−80978
LiCl, possibility of regeneration of wave functions of localized electrons for F-centres 2−68041
Na, nuclear contact densities for electrons 2−61569
α'-$NaV_2O_{5-x}F_x$, $0 \leqslant x \leqslant 1$, d electron distrib. on V atoms, from elec. and mag. props. 2−75080
Pb, clusters, electronic props., mol. orbital calcs. 2−81026
Pb density of states, relativistic effects, mass velocity and Darwin terms 2−84242
Si, electron momentum distrib., Compton profile obs. 2−57128
TiO, Compton profiles, scatt. factors, determ. of electron state 2−68628
Tih_x, electron-nuclear interactions, rel. to spin-lattice relax. 2−78047

Crystal electron states continued
Tl density of states, relativistic effects, mass velocity and Darwin terms 2−84242
V, renormalized-free-atom model, and electron momentum distrib. 2−68670
V_3Au, supercond. transition temp. rel. to ordering, rel. to phonons and electronic density of states 2−84308
$(V_{1-x}Cr_x)_3Si$, ternary alloys, physical props. and electron struct. 2−68514
V_nO_{2n+1}, (n=3,4), electronic localization of d electrons 2−84239
ZnO thermal control coating pigment, u.v. irrad., vacancy level, e.s.r. study 2−81460
ZnS, effects on extinction of luminescence by electric field 2−75331
ZrH_x, electron-nuclear interactions, rel. to spin-lattice relax. 2−78047

band structure
see also Brillouin zones; Crystal field theory
$A^2B^4C_2^5$ type semiconductors lowest conduction band minima 2−80983
$A^{II}B^{IV}C^V_2$, polymorphic transitions and changes of the forbidden zone width 2−80947
AlGaAs-GaAs heterojunctions, filling process 2−47941
alkali fluorides and chlorides, Hartree-Fock band struct. 2−61172
alkali metal, self-consistent screening calc. 2−77830
alkali metals, cohesive energies and bulk properties, band calc. 2−83884
alloy, binary disordered, CPA, off-diag. randomness 2−61163
alloy, binary disordered, electronic struct., single band model 2−61161
alloy, binary ordered, with tertiary impurity elements, electron energy spectrum 2−44023
alloy, disordered, CPA generalizations and cluster effects 2−44022
alloy, disordered, density of states, CPA method 2−61160
alloy, disordered, self-consistent cluster theory 2−44024
alloy, disordered binary, pair effects, multiple-scatt. formulation 2−75011
alloy, disordered ternary, single band Hamiltonian description 2−80966
alloy, liquid and amorphous, electronic structure, clustering effects 2−61170
alloy, substitutional, averaged electronic resolvent, approx. 2−64885
alloy, substitutional, randomness, theory 2−44027
alloy, virtual bound state, rel. to optical absorp. models 2−65245
alloyed semiconductor, absorption coeff. in $\omega > Eq$ region in presence of resonant scattering 2−72316
alloys, coherent pseudopotential model, appl. to Ag-Au system 2−75025
amorphous, interband transitions, intrinsic opt. props., review 2−72293
amorphous solid, density of states, upper and lower bounds, from Tchebycheffs inequality 2−68283
amorphous solid, tetrahedrally bonded, tight-binding Hamiltonian 2−84274
amorphous system, electronic Green's function, density of states 2−71786
augmented plane wave method, linearized form 2−44021
band splitting, intinerent electron magnetization at low temps. 2−78005
basis function method for energy band calculations 2−80991
b.c.c. lattice, LCAO wave functions and energies 2−64873
bimetallic surface, adhesion bonding in terms of electronic struct. of combined metals 2−74652
binary alloy, localized states 2−84252
binary cpds., nearest-neighbour distance rel. to quantum and atomic nos. and valence 2−47178
bridge and layer compounds, microscopic model, comparison of maximum superconducting transition temperatures 2−44054
Brillouin zone sums on cubic lattices, evaluation 2−57115
C16-type structures, rel. to lattice parameters 2−43573
carbon tetrafluoride, solid, conduction band data from vacuum u.v. spectroscopy of Wannier impurity states 2−49957
chalcogenide glass, states in the gap, expt. evidence 2−61334
charge transfer systems, excitation by coherent light, effect of nonuniform broadening on energy migration processes 2−54443
chemisorption, molecular orbital approach, LCAO band struct. and molecular unit cell 2−50525
computation using tight binding augmented plane wave, Green's function, orthogonalized plane wave and pseudopotential methods 2−84227
Coulomb correlation effects and the exchange correlation energy 2−61157
cubic crystal, Green's function method, KKR formulation, struct. consts. 2−54107
d-band metals, clean and cesiated samples, photoemission meas., construction of empirical band structures 2−84386
degenerate band models, absence of complete ferromagnetism 2−72127
degenerate Fermi systems, threshold anomaly 2−54432
diamond, optical absorpt. first-principles energy-band calc. 2−84464
1,4-dibromonapthalene, triplet exciton state band structure, properties of real linear chain 2−47820
dimerized one quarter filled band Hubbard chain, antiferromag. semicond. behaviour 2−61177
disordered crystal, impurity band formation, fluctuation effects 2−61165
disordered lattice, localization of electrons, Anderson's probabilistic approach 2−64880
disordered system, Anderson model 2−61166
disordered system, cluster scatt. and multiple scatt. formalism 2−47800
disordered system, electron wave function localization 2−61168
disordered system, nonexistence of localized tail states 2−64996
disordered system, one electron metal-insulator transition, Anderson model 2−61167
disordered systems, semiconductor model of conductivity in dense metallic vapours, number density of electrons 2−54183

Crystal electron states continued
band structure continued
disordered systems, stat. electron-hole correls., interband transitions 2−51072
distorted chain with random impurity distrib., density of states 2−54104
doubly degenerate band, electron correlation 2−84425
DPPH-benzene, band model application 2−68299
Dyson equation, spurious structure from approximations, electron spectral properties 2−80943
elements, nearest-neighbour distance rel. to quantum and atomic nos. and valence 2−47178
ferroelectric, interband absorpt., in quasi-classical random field, theory 2−48166
ferromagnet, model with narrow s-band, temp. depend. of magnetization 2−65140
ferromagnetic metal, elementary spin excitations 2−44238
ferromagnetic transition elements, fermion theory of 3d band 2−76232
finite crystal, Stark ladder existence 2−68281
fluorophlogopite, Ti and V impurities, e.p.r. and optical absorption spectra meas., colour explained by valence states 2−84562
furan quinone pigments, DFC and DF, photoinjection and photoemission, energy levels 2−54256
generalized Wannier function symmetry 2−61173
graphite, calcs. 2−57121
graphite, calcs. using tight-binding approx. 2−68287
graphite, mag. energy levels from magnetoreflection spectrum at high fields 2−57340
graphite, magnetoelectric props., pressure effects, energy level and carrier scattering models 2−57110
graphite, perturbed electronic density of states 2−57123
graphite, pyrolytic, c-axis conduction mechanism from galvanomagnetic obs. 2−57109
graphite, pyrolytic, meas. of thermal and electrical properties, width of forbidden zone 2−84208
graphite, rel. to effect of struct. imperfections on galvanomagnetic props. 2−57190
graphite, secondary electron emission study 2−51150
graphite, tunnelling spectroscopy, state density near Fermi level 2−57122
graphite tight binding approx., optical absorpt. 2−84234
group I-III-VI_2 cpds., s-d hybridization of valence bands 2−44112
group II-IV-V_2 compound, polarized reflectance spectra obs. 2−61626
group IIB-VIA semiconductor compounds, X-ray induced electron emission, core electron energy levels detn. 2−48019
Group III-V cpds., observed structure due to K and L-emission bands 2−65285
group III-V semiconductor, core levels detn. 2−65240
group III-V semiconductor, X-ray photoemission, outermost core d and p electrons obs. 2−81195
group IIIb hydrides, empirically derived band diagrams 2−77833
group IV-VI chalcogenide, transverse Nernst-Ettingshausen effect obs., effect of hydrostatic compression 2−75159
group VI chalcogenides, layer semicond. spectra obs. 2−81334
groups III-V compounds, amorphous, static electronic dielectric constant 2−51300
Hall effect in Hubbard model, low-field regime calcs. 2−77903
h.c.p. metals, Kohn-Rostoker determinant method 2−80959
Heisenberg ferromagnetic alloys, CPA approx. with random off-diagonal elements 2−78004
heterojunction, graded, electronic props., one band one dimens. model 2−68441
Hubbard model, cluster approach 2−44287
Hubbard model, correlation effects 2−57117
Hubbard model, ground state energy 2−54291
indirect many-photon transitions, in quantizing mag. field, in Ge- and GaP-type crysts. 2−71920
InSb, optical nonlinearity dispersion near band gap 2−48127
insulator, electronic correlation, field-theoretic model 2−68411
interband absorption, in quasi-classical random field, theory 2−48166
interzone transitions in b.c.c. pentavalent metals, detn. of freq. and intensities 2−80946
linear conducting chains, review 2−61140
localized correl. onset in narrow s band 2−61154
magnetic conductor influence on skew scatt. w.r.t anomalous Hall effect 2−47791
magnetic metal-nonmetal transition, two-band model in Hartree-Fock approx. 2−57307
magnetism in metallic fine particles, effect of discrete energy levels 2−81215
magneto-optical obs. of electronic transitions, review 2−72294
many-level susceptibility system, quantum state population equations, soln. by elec. modelling 2−77825
metal, band struct. energy contrib. to energy of screw disloc. 2−50669
metal, Doppler-broadened annihilation radiation spectra, electron effective mass 2−61216
metal, dynamical screening effects in Auger spectrum 2−44211
metal, electronic struct. correl. with stacking fault energy 2−43730
metal, electronic transitions from opt. behaviour, review 2−72292
metal, local model potentials, limitations and applics. 2−44026
metal, model pseudopotential and energy wave number characts. 2−75024
metal, momentum density of cond. electrons, rel. to X-ray Compton profile 2−84255
metal, nearly-free-electron, calc. using struct.-independ.-formalism 2−47801
metal, rigid neutral atom density, selfconsistent calc., auxiliary neutral atom model 2−71787
metal oxides, rel. to elec. cond., characts. 2−57106
metal systems, data compilation, NBS Permuted Materials Index 2−68155
metal-insulator phase transitions, model 2−57119
metal-insulator phase transitions, role of phonons 2−57120
metal-insulator phase transitions, science and technology 2−57205
metal-insulator transition, Hubbard model, correlation effects 2−57117

Crystal electron states continued
band structure continued
metal-insulator transition, vacuum polarization and force between two excitons 2−47818
metal-nonmetal transition, Hubbard model, thermodynamic props. 2−80965
metallic fine particles, electronic properties 2−61178
metals, electronic structure 2−61155
metals, theory of photoluminescence in two-band model 2−72439
m.i.m. tunnel junction, non-parabolic E-k relation, effect on VI characs. 2−51184
mixed group III-V semiconductor, X-gap, nonlinear depend. on composition 2−61337
modulated reflectance obs., review 2−72298
molecular crystal with 2 exciton state regions, absorption spectrum 2−72310
molecular crystals, substitutionally disordered, density of excited electronic states, coherent potential approximation 2−48157
Mott transition, plasma oscillations 2−80987
Mott transition, theory and applic. to transition metal oxides 2−57113
Mott transition in quasi-one-dimensional disordered systems 2−84238
muffin tin potentials, canonical density matrix 2−51071
muffin-tin potentials, non-spherically symmetric, KKR and APW methods 2−77811
narrow s-band, spectral moments for Hubbard model 2−75023
tris-$Nd_2(SO_4)_3$, diffuse reflectance spectrum, determ. of electronic energy states 2−61617
network model, energy states and dispersion waves 2−71773
network models, derivation of difference eqn., study of energy spectrum and dispersion curves 2−77520
Ni:H, hydrogenated, thermo-e.m.f., 3d band shape 2−72052
noble metal, critical point detn., wavelength modulation derivative spectroscopy obs. 2−48160
noble metal-noble metal alloy, reflectance obs. 2−61174
one dimensional disordered system, localization lengths 2−61176
one-dimensional disordered systems, density of electronic states 2−75017
optical cooling of conduction electrons on illumination with strong light 2−81004
organic solid, density of states in bandgap 2−47916
paramagnetic resonance absorption of ultrasound by conduction electrons 2−81464
phenanthrene, energy of free electron conduction band, flash photoconducwivity determination 2−44177
photoelectric emission obs., book contrib. 2−72088
photoemissive yield, phonon energy loss effects, band-theoretic model 2−61460
polyacetylene, INDO, MINDO/2 orbital calcs. of band structure and charge distrib. 2−44035
polyethylene, INDO, MINDO/2 orbital calcs. of band structure and charge distrib. 2−44035
polyglycine, INDO, MINDO/2 orbital calcs. of band structure and charge distrib. 2−44035
polymer, effect of stochastic bond defects 2−47812
polymer, energy band derivatives computation 2−57129
polymer films amorphous and crystalline, electrical conductivity in strong electric fields 2−84340
polyvinyl chloride films, model for transport of photoinjected electrons 2−72074
precious metal pyrochlores, rel. to elec. and mag. props. 2−60987
quantum size effect, band theory 2−75020
quinolinium $(TCNQ)_2^{-}$, electron localization 2−44110
rare earth, heavy, energy band theory derived from group theory 2−57114
rare earth dodecaborides, electronic spectra 2−47838
rare earth metal chalcogenides, electronic, struct., rel. to thermophysical props., Mie Gruneisen interatomic pot. model 2−57053
rare earth metals and alloys, 4f state distrib 2−48209
rare earth monochalcogenides, press. induced electronic collapse and struct. changes 2−68297
rare earth monochalcogenides, press. induced transforms. 2−50948
relativistic pseudopotential method 2−61175
Renner systems, absorpt. and luminesc. bands due to crystal imperfections 2−81393
s-band models, absence of complete ferromagnetism 2−72126
Schrodinger equation soln. at band edge in one-dimens. crystal 2−75019
semi-infinite cryst., one electron wavefunction in mixed represent 2−71770
semiconducting disordered binary alloy, two band model in CPA 2−61162
semiconducting melts, thermal cond. obs. 2−60466
semiconductor, $A^{I}B^{III}C^{VI}_2$, rel. to galvanomag. and thermomag. effects 2−71886
semiconductor, AB type, ave. band gap rel. to third moment of imaginary part of dielectric const. 2−68461
semiconductor, amorphous, absorp. edge temp. depend. rel. to valence band 2−75293
semiconductor, amorphous, electronic struct., LCAO calc. 2−68414
semiconductor, amorphous, long range order, short range order and energy gaps 2−61158
semiconductor, amorphous, optical props., pressure effect obs. 2−61333
semiconductor, amorphous, props. prediction from model 2−61282
semiconductor, amorphous, rel. to field dependent mobility, model 2−61286
semiconductor, amorphous, rel. to optical properties 2−61573
semiconductor, amorphous, tight-binding model 2−84275
semiconductor, amorphous tetrahedrally bonded, density of states theory 2−61159
semiconductor, characterization for light source applic. 2−68439
semiconductor, cond. due to variable range hopping in nonuniform density of states 2−81104
semiconductor, conf., Warsaw, Poland, July (1972) 2−68384
semiconductor, covalent with tipological disorder, LCAO energies and wave functions 2−57096
semiconductor, critical point detn., wavelength modulation derivative spectroscopy obs. 2−48160

Crystal electron states continued
- **band structure** continued
  - semiconductor, cubic, correlation with Debye temperature 2−51147
  - semiconductor, disordered, discrete levels in band gap 2−77802
  - semiconductor, disordered, optical absorp. edge, effective impurity model 2−61169
  - semiconductor, disordered, problems arising from energy spectrum and change carrier kinetics theory 2−68391
  - semiconductor, disordered, theory of electroabsorption 2−51330
  - semiconductor, electronic transitions, opt. consts. evaluation, review 2−72291
  - semiconductor, heavily doped, temp. effects on two-band model for neg. magnetoresistance 2−64970
  - semiconductor, III-V, band gap, temp. depend., calc. 2−68415
  - semiconductor, instability due to forbidden band thermal deform. 2−54185
  - semiconductor, linear and nonlinear cond. calc. using energy band models 2−51039
  - semiconductor, magnetic, survey 2−84226
  - semiconductor, magnetooptical transitions, plasmon assisted, cyclotron reson., lineshape calcs. 2−68320
  - semiconductor, magnetophonon spectroscopy study 2−68385
  - semiconductor, model for covalent semicond. with topological disorder 2−51149
  - semiconductor, multiphoton interband transitions, electron-hole pair multiphoton excitation probability 2−77837
  - semiconductor, nonparabolic band, free carrier light absorp. theory 2−75285
  - semiconductor, nonparabolic energy bands, mag. susceptibility calc. 2−71928
  - semiconductor, polar, in quantizing mag. field, rel. to transport props. 2−64967
  - semiconductor, pseudopotential method calc. 2−81013
  - semiconductor, trapping centres, defect related luminesc., two centre model 2−61680
  - semiconductor, two-photon interband transition in arbitrary elec. field 2−61623
  - semiconductor, with band extrema at Brillouin zone centre, interband optical transitions 2−65250
  - semiconductor, with nipi superstructure 2−61336
  - semiconductor glass, perturbed bands, model 2−61335
  - semiconductor substitutional alloy, nonexistence of localized tail states 2−64996
  - semiconductors, energy states, occupancy probability, recombination rate theory 2−47875
  - semiconductors, impure, band tail investigations 2−61338
  - semiconductors, nonparabolic bands, transport props. in strong elec. and mag. fields 2−81101
  - semiconductors, survey of calc. methods, results, binding and transport props. 2−81012
  - semimetal, group V, magneto-optical transitions, energy band struct. model 2−68285
  - semimetal, interband interactions, effect on critical temp. of supercond. transition temp. 2−71842
  - semimetal, intraband and interband scattering of excitonic insulator in mag. field 2−81003
  - semimetal, monotonic behaviour in strong mag. fields 2−44025
  - strongly disordered materials, tight binding expansions 2−61164
  - superconducting A15 cpds., anomalies interpret. 2−77877
  - superconductor, dirty, two-band model rel. to thermal conductivity in transition metals near upper critical field 2−77876
  - superconductor, elemental, energy gap anisotropy 2−54137
  - superconductor, gap, equilib. value, rel. to weak alternating fields 2−57157
  - superconductor, two band, transition temp. and energy gaps rel. to Fermi surface topology change under press. 2−75068
  - superconductor, with strong electron-phonon coupling, rel. to transition temp. 2−57158
  - TCNQ complexes, quasi-one-dimensional disordered systems, Mott transition, susceptibility obs. 2−84238
  - ternary group III-V semiconductor, energy gap and composition from surface photovoltage obs. 2−51220
  - thermodynamics of crystals, book 2−43950
  - tight-binding bands, density of states and electronic struct. detn. considering local at. environment 2−80956
  - transition metal, electronic wavefunction calc. 2−75018
  - transition metal, ferromag., magnetostriction, band model using spin-orbit term 2−48082
  - transition metal, supercond. with non-mag. impurities, rel. to specific heat calc. 2−44061
  - transition metal alloys, dil., two-band model interpret. of Kondo effect 2−61145
  - transition metal borides, of IVA-VIA metals, rel. to thermionic emission 2−48017
  - transition metal chalcogenides, TX_2 type, with pyrite marcasite, arsenopyrite structs., energy bands 2−61189
  - transition metal cpds., binary, Mott insulation breakdown, Mott transition 2−57099
  - transition metal dichalcogenide layers, rel. to layer-layer interactions 2−44378
  - transition metal hydrides, energy band calcs., model obs. 2−61187
  - transition metal on transition metal surfaces, X-ray appearance pot. obs. 2−47816
  - transition metal- actinide alloys, mag. susceptibility interpret., narrow band reson. model 2−54286
  - transition metals optical absorption, a model calc. 2−84498
  - triethylammonium-$(TCNQ)_2$, metal-insulator transition, applicability of band model 2−68410
  - triglycine sulphate, forbidden band, width determ. 2−77932
  - X-ray photoelectron spectroscopy 2−75193
  - zincblende crystal, excitation energy, self-consistent relativistic OPW calc. 2−81015
  - zincblende semiconductor, temp. depend., empirical pseudopot. method using calculated Debye-Waller factors 2−84199
  - Ag, cond. electron optical mass 2−44029
  - Ag, density of states determ. from thermodynamic studies of solid solns. in galvanic cells 2−64887
  - Ag, direct transitions as origins of peaks in secondary electron spectrum 2−54280

Crystal electron states continued
- **band structure** continued
  - Ag, valence band density of states, X-ray photoemission spectroscopy obs. 2−65104
  - Ag evaporated film, interband transitions, piezorefl. and piezotransmission studies 2−81366
  - Ag film, energy gap, rel. to induced supercond. 2−44072
  - Ag film, rel. to dielectric const. changes, piezoreflectivity obs. 2−54382
  - Ag halide, depend. on lattice const. and halogen 2−64886
  - Ag halides, optical transitions, localized electron states, self-bound and impurity trapped excitons 2−81025
  - $AgGaS_2(Se_2)$, electrorefl. and absorpt. studies 2−75276
  - AgPd system, density of states, X-ray photoemission obs. 2−61179
  - Al-Au alloy, electronic struct., soft X-ray emission obs. 2−68671
  - Al-Mg alloy, electronic struct. 2−77826
  - Al, positron deformation potential estimated 2−80675
  - Al, valence-electron excitation by internal X-ray photoemission 2−54276
  - Al superconducting film, density of states change due to adsorbed molecular oxygen 2−51111
  - AlAs, relativistic APW calc. 2−81014
  - $Al_xGa_{1-x}As$, photolum., band to band transitions, band gap 2−61683
  - AlGaAsP solid soln., forbidden band rel. to comp., use in lasers 2−63343
  - AlN:Mn, electron-phonon levels of Mn luminescence centres 2−75319
  - AlN, non-local model potential calc. 2−71925
  - Al_2O_3:V^{3+}, ground state study using phonon generation in Sn 2−47735
  - Ar, Hartree-Fock approx, 2−84272
  - $As_xIn_{1-x}SeI$ vitreous compounds, $x=1.00$, 0.95, 0.90, 0.80, i.r. absorption, determ. of energy structure 2−78095
  - As_2S_3, massive and thin film, self-absorption edges, forbidden band width meas. and type of transition 2−84479
  - As_2S_3, vitreous, localized state distrib., Fermi level analysis from transient photocond. obs. 2−47913
  - AsSI and AsSeI, vitreous and molten, temperature dependence of forbidden band optical width, structure and chemical bond changes in transition 2−84393
  - As_2Se_3, vitreous, polymeric struct. and energy spectrum 2−60590
  - As_2Se_3, vitreous and crystalline, electron energy spectrum, modulation spectroscopy obs. 2−61631
  - As_2Se_3, vitreous and monocryst., rel. to recomb. radiation 2−54451
  - $As_2Se_3(Te_3)$ film, amorphous, rel. to trap-limited processes 2−61325
  - $3As_2Se_3.2SB_2Se_3$ films, amorphous. cond. obs. interpret. 2−54187
  - $3As_2Se_3.2Sb_2Se_3$ films, transmittance and absorpt. obs. 2−54186
  - As_2Te_3, glassy, from elec. and optical props. 2−61297
  - As_2Te_3 film, amorphous, a.c. cond. rel. to localized tail states 2−61288
  - As_2Te_2Se, amorphous semicond., thermalization in energy band tails 2−61685
  - Au-Al, α-phase dil. alloy, refl. study, 1.1-11.5 eV 2−75278
  - Au-Cr(V) alloy systems, absorpt. spectra obs. of interband transition 2−44371
  - Au, d-band structure from photoemission energy distrib. 2−44202
  - Au, high-resolution X-ray photoemission spectrum of valence bands 2−44203
  - Au, refl. study, 1.1-11.5 eV 2−75278
  - Au, rel. to u.v. photoemission spectra computer simulation 2−48022
  - Au, relation of primary photoemission spectra 2−61462
  - $AuAl_2(Ga_2)(In_2)$, density of states and anomalous Knight shift 2−47806
  - β-B, rhombohedral, density of states rel. to transport phenomena 2−75090
  - BN, hexagonal, calcs. using tight-binding approx. 2−68287
  - BN, pseudopotential calc. 2−61345
  - BN, tight binding approx., optical absorpt. 2−84234
  - BN, X-ray emission study 2−75026
  - BP, bandgap obs. 2−50567
  - BP, pseudopotential calc. 2−61345
  - $Be_2(Cr_{1-x}Mn_x)$, $Be_2(Mn_{1-x}Fe_x)$ d electronic character and specific heat meas. at 1-4 K 2−57059
  - Bi:Te effect of high hydrostatic pressures on heavy conduction electron band 2−81102
  - Bi-Sb alloy, band edge parameters, calc. 2−75027
  - Bi-Sb low-concentration alloy, determ. of cyclotron effective masses of carriers, mass parameters of electron pockets 2−47807
  - Bi, band edge parameters, calc. 2−75027
  - Bi, changes under hydrostatic pressure, rel. to hole dispersion relation 2−61223
  - Bi, determ. of cyclotron effective masses of carriers, mass parameters of electron pockets 2−47807
  - Bi, magnetoacoustic effects 2−61096
  - Bi single crystal piezoreflectance obs. and rel. to optical interband transitions 2−65213
  - BiOI, BiOBr, BiOCl, fundamental absorp. edge, laminarity effects 2−75287
  - BiSeI, from elec. cond. 77−460 K, thermo e.m.f. 300−400 K 2−80997
  - p-Bi_2Te_3, second valence band, magneto-Seebeck and Shubnikov-de Haas obs. 2−61339
  - p-Bi_2Te_3, valence band, Shubnikov-de Haas oscills. of magnetoresist. 2−77805
  - p-Bi_2Te_3, valence band ellipsoids 2−51135
  - p-Bi_2Te_3, valence bands, saturation and quantum oscill. in magneto-Seebeck effect obs. 2−81159
  - $Bi_2Te_{3-x}Se_x$, temp. depend. of electron effective mass and mobility 2−81099
  - C, from X-ray photoelectron spectra, amorphization effects 2−57262
  - C, soft pregraphitic, Hall coeff. obs. and dependence on heat treatment and doping 2−44113
  - C film, amorphous, change on graphitization by light pulses 2−61030
  - C film, amorphous, optical and elec. props. study 2−61302
  - CaF_2, rel. to ionicity and absorpt. 2−44374
  - Cd film, disordered, supercond. energy gap 2−54134
  - $CdCl_2$:Co^{2+}, obs. of vibrational-electronic coupling in high resolution spectrum of spin forbidden band 2−81356

Crystal electron states continued
band structure continued
CdF_2, high purity, semiconducting, information from photoconductivity spectrum 2−84378
$CdGeP_2$, zone crystallised energy zone calc. by pseudopotential method 2−80595
CdP_2, interband transitions, photolum. and cathodolum. study 2−72394
$Cd_xPb_{1-x}Se$ alloy, Hall coeff., Hall mobility, thermoelec. power, optical energy gap, 77-450 K 2−64977
CdS, electron energy loss spectra, rel. to interband transitions, bulk and surface plasmons 2−68318
CdS, valence band energy levels, Γ-point, from emission spectra due to A- and B-band excitons 2−68289
CdS crystal, auto-photoemission, spectral investig. under pulsed and const. voltage condits. 2−72090
CdS single crystal, form of exciton absorption bands at 4.2K 2−80999
CdS(Se) anodes, rel. to electron injection behaviour 2−61797
CdS_xSe_{1-x}, optical transmission study 2−61633
CdSe, electron energy loss spectra, rel. to interband transitions, bulk and surface plasmons 2−68318
$CdSe_xTe_{1-x}$, absorp. edge obs. 2−84517
$CdSi_xGe_{1-x}As$, glassy, photocond. and elec. cond. study 2−61448
$CdSiP_2$, energy gap, optical props. study 2−80599
$CdSnAs_2$, $CdSnP_2$, electroreflectance spectra obs. 2−81404
n-Cd_2SnO_4, optical band gap, effective mass 2−51137
CdTe, electron energy loss spectra, rel. to interband transitions, bulk and surface plasmons 2−68318
$Cd_xZn_{1-x}S$ film, energy gap, comp. depend. 2−54169
Ce, α- and γ-phases energy bands, APW calcs. 2−44031
Ce, optical absorpt. spectra, 4d-4f transition, 4d level binding energy 2−75301
CeH_x, metal-semicond. transition 2−77899
CeS(Se)(Te), energy spectrum of carriers, group theoretical calc. 2−80948
Ce_3Se_4, complex cond. band, thermal and elec. cond., thermo e.m.f., 80−680 K 2−80918
Co, h.c.p., density of states, calc. 2−61181
Co containing ^{57}Fe, contact charge density of conduction electrons 2−51307
Co_3B, electron struct., Co X-ray K-emission obs. 2−72379
CoB_x., rel. to elec. resist., 300-1200K 2−51100
$CoCl_2$, rel. to X-ray spectra interpretation 2−65287
CoO, refl. and thermorefl. study 2−84505
Cr, magnetic generalized spin susceptibility, interband contribs., Lindhard expression 2−61554
Cr itinerant antiferromagnetism, 2 band model 2−44289
CrB_2, electronic spectra, MOLKAO method calc. 2−71792
CrSi, energetic electron band and parameter calc. for normal and narrow band models 2−77797
Cs film, rel. to photoemission, 3.7-21.2eV 2−54277
Cu-Ni alloy film, soft X-ray absorpt., interpretation 2−65286
Cu-Ni alloys, d-band filling, X-ray spectra 2−47809
Cu-Ni alloys, to explain optical properties in visible and ultraviolet spectral regions 2−81330
Cu-Pd alloy, disordered and ordered, optical absorpt. study 2−84237
Cu, charge density form factor, X-ray scatt. determ. 2−84251
Cu, deformation potentials, determ. of strain-induced shifts of energy levels 2−80976
Cu, electronic wavefunction calc. 2−75018
Cu, Fong-Cohen pseudopotentials 2−84271
Cu, high-resolution meas. of Auger transitions, valence band density of states 2−81193
Cu, positron annihilation radiation, angular correl. 2−80968
Cu, valence band density of states, X-ray photoemission spectroscopy obs. 2−65104
Cu, valence states produced by ion-sputtering reduction, X-ray photoelectron spectroscopic obs. 2−57263
Cu alloys, effect of bonding on filling of 4s band and density of state of conduction band 2−80811
CuAu, Cu_3Au, effects of ordering, reflectance obs. 2−72303
CuBr, X-ray K emission bands, valence electron obs. 2−68672
CuCl, conduction band, orthogonalized plane wave calc. 2−71793
CuCl, Kβ emission and K absorpt. spectra study 2−75315
CuCl, valence bands, X-ray photoelectron study 2−44204
CuCl(Br), rel. to absorpt. spectra, 3-30 eV 2−72326
CuI, low temp. reflection spectra, excitonic transitions and levels 2−72302
$CuInSe_2$, transitions from Cu of levels in valence band 2−80974
$CuInTe_2$, refl. and absorpt. studies 2−78098
Cu_2O, rel. to near i.r. absorpt. and photocond. 2−54420
$Cu_{2-x}S$, rel. to absorpt. coeff., 400-1200 nm 2−78085
CuTe, reflection spectra obs. 2−72301
D_2:Xe, vacuum u.v. spectroscopic study of Wannier states, conduction band investigation 2−51341
D_2, adsorbed on W, electron field emission obs. 2−48016
EO, EuO:Gd, p-band excitations and dopant effect, investigation using high-resolution photo-emission meas. 2−68497
EuO, doped, metal-semiconductor transition 2−77842
EuS, slightly Eu rich, systematics of conduction in band tail 2−75094
Fe-Au alloy, intraband absorpt., anomalous temp. depend. 2−81388
Fe-Co-Ni alloy, coherent potential approx. calc. 2−71794
Fe-Co alloys, ordering effects on electron asphericity 2−44249
Fe, Armco, plastic deform. influence 2−75028
Fe, b.c.c., electronic wavefunction calc. 2−75018
Fe, valence states produced by ion-sputtering reduction, X-ray photoelectron spectroscopic obs. 2−57263
$FeAs_2$, diamag. semicond., band gap, band model 2−61340
FeB_x., rel. to elec. resist., 300-1200K 2−51100
Fe_3C, electron struct., Fe X-ray K-emission obs. 2−72379
$FeCl_2$, rel. to X-ray spectra interpretation 2−65287
$(Fe_{0.64}Mn_{0.36})_3C$, electron struct., Mn X-ray K-emission obs. 2−72379
Fe_3O_4, magnetite, metal-insulator transition, Verwey temp. 2−57125
Fe_3O_4, one-electron energy levels 2−68292
FeRh, first-order antiferromag.-ferromag. transition, electronic struct. changes 2−84438
$FeSb_2$, band gap, band model 2−61340

Crystal electron states continued
band structure continued
FeSi, energetic electron band and parameter calc. for normal and narrow band models 2−77797
Ga, supercond. energy gap, cryst. orientation depend., tunnel junc. obs. 2−68358
$Ga_{1-x}Al_xAs$, indirect gap semicond., direct band recombination, electroluminesc. obs. 2−75337
n-$Ga_{1-x}Al_xAs$, metal-semicond. surface barrier struct., energy band diagram 2−75134
n-GaAs:Ge film, epitaxial, degenerate, forbidden gap, traps 2−44114
GaAs:Sn exciton energy level structure from photoluminescence props. analysis 2−44427
GaAs-Cu, supersaturated solid solution, decomposition, hole concentration dependence on temperature 2−83836
GaAs, absorpt. edge rel. to Brillouin scattering, fast TA phonon cross section 2−61670
p-GaAs, effect of pressure, 10000 kg/cm² 2−44099
GaAs, eletron, and neutron irrad., i.r. absorpt. band obs. 2−48180
GaAs, energy gap temp. depend. 2−80964
n-GaAs, epitaxial, Hall coeff. and mobility 300-800 K, valley energy separation 2−68398
n-GaAs, heavily-doped, gradual mobility transition in band tails 2−61342
GaAs, intrinsic surface states, photoemission densities 2−44207
GaAs, rel. to dielec. function calc. 2−84262
GaAs, rel. to mag. susceptibility calc. 2−71928
GaAs, undoped, point defect conc. effects on energy spectrum 2−71905
GaAs, valence-band densities, X-ray photoemission valence-band spectra 2−81192
GaAs, valence band, synchrotron radiation photoemission spectroscopy obs. 2−81194
GaAs, X-ray K emission bands, valence electron obs. 2−68672
GaAs, X-ray photoemission study 2−84387
GaAs(P), rel. to ionicity and absorpt. 2−44374
$Ga_{1-x}In_xN$, absorpt. study 2−72329
$Ga_xIn_{1-x}P$ alloy, electroreflectance obs. 2−61641
$GaInS_3$, thermally stimulated cond., dark current, capture levels 2−75162
GaN, absorpt. study 2−72329
GaN, non-local model potential calc. 2−71925
GaP, rel. to wavelength modulated refl. spectra 2−61616
GaP, X-ray photoemission study 2−84387
GaS, direct interband transitions, low energy photoemission spectra 2−51225
β-Ga_2S_3, rel. to photolum. and photocond. 2−84532
GaSb:Te, lightly doped, band gap, photolum. study 2−72402
GaSb:Te(Zn)(Te + Zn), heavily doped, photolum. study 2−72403
GaSb/Cs-O, photoemissivity yield, energy distrib. 2−44205
n-GaSb-Pb contact, tunnelling spectroscopy and band struct. press. effects 2−84351
n-GaSb, cond. band parameters from high-temp. transport meas. 2−57206
n-GaSb, conduction band minima energy separation temp. depend., p-n junc. tunnelling current obs. 2−75109
GaSb, interband optical transitions, photoelectromag. effect study 2−68484
GaSb, Landau levels at saddle point, diffr. reflectivity in mag. field obs. 2−71795
GaSb, Landau transition at E_1 edges, excitonic effects 2−68404
GaSb, variation of energy bands with hydrostatic pressure 2−61393
GaSe, interband Faraday effect 2−72262
GaSe, layer compound, empirical pseudopotential method 2−81016
GaSe, optical consts. anisotropy near band edge 2−48178
GaSe, pseudopot. calcs. 2−61341
GaSe study by reflection spectra, hyperbolic excitons 2−84480
GaTe, forbidden band width, optical absorp. obs. 2−75294
$GdGa_xCu_{1-x}$, cond. electron conc., rel. to mag. order 2−78020
$GdIn_xAg_{1-x}$, cond. electron conc., rel. to mag. order 2−78020
GdS, magnetic coupling and band structure, electron photoemission studies 2−72139
A-Gd_2S_3, forbidden gap thermal width, crystals grown from gaseous phase 2−53607
$GdZn_xAg_{1-x}$, cond. electron conc., rel. to mag. order 2−78020
Ge-Au films, quench-condensed, supercond. energy gap, tunnelling obs. 2−51115
Ge, absorption edge under pressure, high resolution meas. 2−48182
Ge, adsorbed layer on W, field emission obs. 2−71349
Ge, amorphous, electronic spectrum, variational LCAO method 2−61184
Ge, amorphous, photoelectron energy distrib. curve obs. 2−61464
Ge, amorphous, the case for sharp band edges 2−61183
Ge, amorphous and crystalline, photoelectron and secondary electron emission obs. 2−77977
Ge, amorphous film, intraband excitation in valence band 2−80934
Ge, electromodulation study of forbidden indirect transitions 2−72333
Ge, electroreflectance of heavily doped n- and p-type near direct energy gap 2−51321
Ge, emission band, two electron band-to-band transitions, excitation intensity 2−61699
Ge, i.r. Faraday effect, hot electron transfer between equivalent valleys obs. 2−78067
Ge, intrinsic surface states, photoemission densities 2−44207
Ge, metal-insulator transition, d.c. and microwave photocond. obs. 2−77829
Ge, photoelectromag. effect, oscillatory spectral distrib., rel. to direct interband transitions 2−65093
Ge, rel. to dielec. function calc. 2−84262
Ge, tetrahedrally bonded and amorphous, rel. to struct. 2−68436
Ge, using generalized symmetrical Wannier functions 2−64889
Ge, valence-band densities, X-ray photoemission valence-band spectra 2−81192
Ge, valence band, synchrotron radiation photoemission spectroscopy obs. 2−81194
Ge, X-ray K emission bands, valence electron obs. 2−68672
Ge, X-ray photoelectron spectra of valence bands 2−81191

Crystal electron states continued
band structure continued
Ge amorphous, obs. of electron tunnelling between metal electrodes, determ. tunnelling phonon density of states 2−44125
Ge amorphous and crystalline polytypes, electronic struct. calc. 2−68431
Ge film, amorphous, secondary electron emission spectrum obs. 2−61353
Ge III band structure 2−80980
Ge polytype, density of states and optical props. 2−61185
$GeS_2(Se_2)(Te_2)$, calc. from refl., 1-12.5 eV 2−48161
GeS(Te), calc. from refl., 1-12.5 eV 2−48161
$Ge_{1-x}Si_x$, indirect phononless optical transitions, wavelength modulated absorp. obs. 2−68640
GeTe, amorphous and polycryst., photoemission and reflectivity obs. 2−61465
Ge_xTe_{1-x} alloy, amorphous, optical and electrical obs. 2−77904
H_2:Xe, vacuum u.v. spectroscopic study of Wannier states, conduction band investigation 2−51341
H_2, adsorbed on W, electron field emission obs. 2−48016
H_2, metal-insulator transition 2−68282
He, solid, high pressure conversion to conducting phase, calc. 2−68293
HfC, calc. using strong-bond method 2−57126
Hg-Xe layer, insulator-metal transition, Wannier exciton disappearance, u.v. spectra obs. 2−51079
Hg, pseudopot. calcs. 2−64890
HgSe, HgSe-HgS solid solution, optical absorption obs. 2−84522
HgSe, $\Lambda_3-\Lambda_1$ transition, electrorefl. 2−68624
Hg_3Te_3-In_2Te_3 alloys, h.p. phase obs. 2−54175
HgTe, deform. potentials, Shubnikov-de Haas effect study 2−68402
HgTe, magnetoabsorpt. of i.r. and submillimetric waves rel. to mag. field, band struct. 2−68294
n-HgTe, pure, optical absorp. obs. 2−78101
In-Te system, film, In_2Te_3 phase, optical study 2−60662
In, rel. to Righi-Leduc effect, 3.5-8K 2−75163
In film, optical absorption, ellipsometry obs. 2−72334
n-InAs, compensated, absorpt. edge obs. 2−75297
InAs, X-ray photoemission study 2−84387
$In_xGa_{1-x}P$ ternary phase diagram and band gap energy obs. 2−74949
InN, absorpt. study 2−72329
InP, electron transfer 2−61315
InP, excitonic recomb. and photocond. study 2−72410
InP, free and bound electron transitions to acceptors, 1.3776 eV emission 2−72411
n-InP, photon replicas in the induced luminescence spectra under the conditions of two photon excitation 2−81429
n-InP, rel. to velocity-field charact. calc. 2−71912
InP, rel. to wavelength modulated refl. spectra 2−61616
n-InSb, cond. band model calc. of nonlinear optical susceptibility 2−51299
InSb, deformation potentials, from Shubnikov-de Haas measurements 2−68416
n-InSb, electric field modulated laser cyclotron resonance, impurity and cond. electron resonance obs. 2−81021
InSb, forbidden gap pressure coeff. under uniaxial deform. 2−84284
n-InSb, impurity band and shallow donors, far i.r. absorp. obs. 2−81389
InSb, Landau levels at saddle point, diff. reflectivity in mag. field obs. 2−71795
InSb, Landau transitions at E_1 edges, excitonic effects 2−68404
n-InSb, nonparabolicity rel. to microwave self-focusing 2−68591
n-InSb, uniaxial stress effect on magnetophonon effect 2−44115
InSb, X-ray photoemission study 2−84387
InSb wave function, direct meas. from Knight shift in extreme quantum limit 2−68746
n-InSe, rel. to photocond. 2−72063
InSe, study by reflection spectra, hyperbolic excitons 2−84480
In_2Te, calc. from refl., 1-12.5 eV 2−48161
IrB_{11}, rel. to elec. props. 2−47657
K complex, $K_2Pt(CN)_4Br_{0.3}.xH_2O$, electron localization 2−44110
KBr, optical gap assignment from multiphoton conductivity 2−65084
KBr(Cl)(F)(I), rel. to ionicity and absorpt. 2−44374
$K_{0.3}MoO_3$, blue phase, semicond. to metal transition, excitonic insulator 2−61151
KN_3, i.r. spectra, selection rules and internal ± internal and internal ± external mode absorpts. 2−72336
$KTa_xNb_{1-x}O_3$, conduction band edge splitting, absorpt. study 2−54425
$KTa_xNb_{1-x}O_3$, absorpt. edge splitting, paraelec. and ferroelec. phases 2−48184
La, optical absorpt. spectra, 4d→4f transition, 4d level binding energy 2−75301
$LaSn_3$ type compounds, impossibility of simple metal description 2−44032
La_3Te_4, complex cond. band, thermal and elec. cond., thermo e.m.f., 80−680 K 2−80918
Li-Mg(Al) solid solution, Green function calc. 2−75029
Li, metallic, rigid neutral atom density, selfconsistent calc., auxiliary neutral atom model 2−71787
Li, momentum density of cond. electrons, rel. to X-ray Compton profile 2−84255
Li, rapidly convergent pseudopotentials 2−75030
LiF, Ar-ion bombarded, excited particle velocity spectrum obs. 2−48030
LiH, forbidden band width, contact pot. difference meas. 2−57127
LiH, self-consistent local orbitals 2−75031
Mg, X-ray spectra, K-series X-ray valence band line, many body effects 2−68673
MgF_2, valence band energies 2−54109
MgF_2, valence band struct. by tight-binding method, computation 2−61186
n-Mg_2Ge, cond. band minima, symmetry 2−51143
MgO, rel. to ionicity and absorpt. 2−44374
$Mg_xPb_{1-x}Se$ alloy, Hall coeff., Hall mobility, thermoelec. power, optical energy gap, 77-450 K 2−64977
MgS, self-consistent local orbitals 2−75031
Mg_2Sn pressure dependence of electrical resistance 2−84326

Crystal electron states continued
band structure continued
n-MgTe, interband magnetoabsorpt., $\Gamma_6\rightarrow\Gamma_8$, transmission obs. at 4.4K 2−68644
$MnCl_2$, rel. to X-ray spectra interpretation 2−65287
MnO, refl. and thermorefl. study 2−84505
MnSi, energetic electron band and parameter calc. for normal and narrow band models 2−77797
Mo, position annihilation two-photon ang. correl. 2−71824
Mo, superconducting, experimental obs. discussed in terms of band models 2−47832
MoO_3 film, donor band and Schottky barrier obs. using dielectric relax. currents 2−68453
MoS_2, layer- type 2H-polytype, LCAO calcs. 2−47914
MoS_2, layer semicond., magneto-optical interband absorp., energy band model 2−81333
n-GaAs, electroreflectance spectrum, 1.2-5.3 eV photon energy range 2−68619
Na-NH_3, density of states, Mott g ratios, self consistence, significance in MNM transition 2−44033
Na, metallic, rigid neutral atom density, selfconsistent calc., auxiliary neutral atom model 2−71787
Na, momentum density of cond. electrons, rel. to X-ray Compton profile 2−84255
NaCl, Ar-ion bombarded, excited particle velocity spectrum obs. 2−48030
NaCl, rel. to X-ray absorpt. and emission spectra 2−72380
NaCl, X-ray Kβ emission and K absorption spectra obs. 2−65288
NaF, convergence of reciprocal-lattice expansions and self-consistent energy bands 2−84269
NaI:Tl, rel. to recomb. luminesc., 80-300K 2−75334
$NaNO_3$, optical props. in vacuum u.v. region 2−84487
Nb, Fong-Cohen pseudopotentials 2−84271
Nb, supercond., 2-band spectrum, rel. to u.s. absorpt. interpretation 2−68347
Nb, superconducting, meas. of longitudinal ultrasonic attenuation, evidence against multiple energy gaps 2−75070
Nb_3Al, density of states variation, supercond. crit. temp. variation 2−47860
$Nb_3Al_xGe_{1-x}$, density of states variation, supercond. crit. temp. variation 2−47860
NbC_{1-x}, determ. from supercond. transition temp. 2−81055
NbN, pseudopotential calc. 2−84253
Nb_3Sn, band models and effective Fermi temp. 2−51117
Nd_3S_4, complex cond. band, thermal and elec. cond., thermo e.m.f., 80−680 K 2−80918
Ne, self-consistent local orbitals 2−75031
Ni-Fe system, Ni_3Fe ordered alloy, 4-s band, perturbation calc. 2−71801
Ni-Mn system, Ni_3Mn ordered alloy, 4-s band, perturbation calc. 2−71801
Ni-Mo alloy, Kerr and magnetooptical effect study of electronic structure 2−72265
Ni, band model for photoelectron energy distrib. above and below Curie temp. 2−65108
Ni, d-band struct. calcs. of electron spin polarization in field emission 2−44190
Ni, ferromagnetic, tight binding method energy band calc. 2−47810
Ni, high-resolution meas. of Auger transitions, valence band density of states 2−81193
Ni, Kerr and magnetooptical effect study of electronic structure 2−72265
Ni, valence band density of states, X-ray photoemission spectroscopy obs. 2−65104
Ni (111) surface, changes rel. to characteristic energy loss in Curie temp. region 2−51267
Ni alloys, binary, optical obs. of indirect transitions from ground-state to impurity bands 2−71796
$Ni_3Al(Ga)$, band model approach to weak itinerant ferromag. 2−81245
NiB_x, rel. to elec. resist., 300-1200K 2−51100
Ni_3B, electron struct., Ni X-ray K-emission obs. 2−72379
$NiCl_2$, rel. to X-ray spectra interpretation 2−65287
Ni_3Fe, Kerr and magnetooptical effect study of electronic structure 2−72265
NiH_x, energy band calcs., model obs. 2−61187
NiO, refl. and thermorefl. study 2−84505
NiO, thermoreflectance, band transition assignment 2−44368
NiS, hexagonal, heat capacity and metal-nonmetal transition 2−47754
NiS, metal- to-semimetal transition, stoichiometry and impurity effects 2−51280
NiS_2, energy gap, absorption spectra obs. 2−81020
NiS_2, semiconducting, opt. absorpt. and elec. conductivity obs. 2−68417
Np compounds, hybridized band model for magnetic properties 2−84396
Pb, superconducting energy gap, photocurrent temperature dependence due to, 2.5 to 12°K 2−68354
PbI_2, rel. to refl. study of band edge excitons 2−68626
PbI_2, tight binding method computation 2−68418
PbO film, optical absorp. edge detn. 2−57352
PbSe, absorp. edge and intraband transition region obs. 2−81402
PbSe n and p type anisotropy of cyclotron and spin mass 2−80984
$Pb_{1-y}Sn_ySe$ thin films, optical energy gap 2−64999
$Pb_{1-x}Sn_xTe$, i.r. plasma refl. study 2−84504
$Pb_{1-x}Sn_xTe$, reflectivity spectra obs. 2−48164
$Pb_{1-x}Sn_xTe$ thin films, optical energy gap 2−64999
PbTe, electronic charge density 2−44121
Pd, density of states, pseudopot. calcs. 2−47811
Pd to Xe, evolution of core states from energy bands in 4d5s5p region, X-ray photoemission studies 2−64891
Pd_5B_2, Pd_3B, rel. to specific resistance and thermal e.m.f. 2−72054
PdH_x, energy band calcs., model obs. 2−61187
$PdTe_2$, calc. from refl., 1-12.5 eV 2−48161
Pr, combined basis function energy band calculations 2−80991
Pt, absorpt. and refr. study, 0.265-7 μ 2−81358
Pu compounds, hybridized band model for magnetic properties 2−84396
Rb film, rel. to photoemission, 3.7-21.2eV 2−54277

Crystal electron states continued
band structure continued
ReO_3, density of states by X-ray photoelectron spectroscopy 2−54111
ReO_3, rel. to absorpt., 0.11-2.8 eV 2−84499
S, from hole photoemission from CdS(Se), HgS and Se into S 2−84265
Sb-Bi alloys, magnetoreflection obs. 2−54405
Sb single crystal piezoreflectance obs. and rel. to optical interband transitions 2−65213
Sb_2S_3 film, single cryst., optical absorp. edge obs. 2−81390
SbSBr, i.r. transmission, indirect transitions and band gap determ. 2−72346
Sb_2Se_3, amorphous, density of states at quasi-Fermi level from photocond. 2−81167
Sb_2Se_3, reflectance and X-ray photoelectron spectra for amorphous and cryst. material 2−68627
Sb_2Se_3 film, amorphous, optical and transport props. obs. 2−61323
Sb_2Se_3 film, amorphous, optical energy gap 2−53576
ScN, epitaxial, optical band gap 2−50503
Se-Te melt, electronic transport behaviour, switching, optical gap 2−60502
Se, amorphous, valence band density of states, vacuum photoemission study 2−84258
Se, effects of cryst. disorder on electronic struct., photoemission obs. 2−61466
Se, monoclinic, direct gap, optical absorp. obs. 2−68648
Se film, vitreous, rel. to trap-limited processes 2−61325
Se_xTe_{1-x}, synchrotron radiation absorp., d level spin orbit splitting obs. 2−81401
Si:P, absorpt. due to transitions to cond. band edge region 2−72347
Si:P(As) radiation-induced infrared absorption bands 2−68650
Si-As-Te, amorphous semicond., energy gap depend. on glass transition and softening temp. 2−61346
Si-As-Te amorphous semiconductor, relation between band gap and density 2−65003
Si, 2 electron transitions at liquid He temp., emission line obs. 2−51370
Si, amorphous, cryst. polytypes, electronic struct., pseudopot. and tight binding models 2−71946
Si, amorphous, electron emission obs. 2−61454
Si, amorphous, photoelectron energy distrib. curve obs. 2−61464
Si, amorphous, the case for sharp band edges 2−61183
Si, band edge position under uniaxial pressure, Schottky barrier obs. 2−51167
Si, cond. band. deform. potential const. from piezospectroscopy of donors 2−68438
p-Si, i.r. absorpt. by free carriers, overlapping valence band struct. 2−48190
Si, intrinsic surface states, photoemission densities 2−44207
Si, muffin tin potential calc. in open struct. 2−75032
Si, n-type, surface states, energy distribution of photoemitted electrons 2−44208
Si, tetrahedrally bonded and amorphous, rel. to struct. 2−68436
Si, valence band, synchrotron radiation photoemission spectroscopy obs. 2−81194
Si, X-ray photoelectron spectra of valence bands 2−81191
p-Si (001) inversion layer, optical transitions between surface subbands 2−47997
Si (100), photoemission obs., band bending profiles 2−72082
Si amorphous, inferred from tunnelling cond. 2−61359
Si and cpds., mol. orbital model interpret. of X-ray spectra 2−48210
Si emission band, two electron band-to-band transitions, excitation intensity 2−61699
Si film, amorphous, localized state distrib., field effect study 2−68437
Si film, amorphous, optical absorp. and photocond. spectra obs. 2−61655
Si hole, drift velocity rel. to band struct., elec. field effects, at 5K 2−81107
Si III, band structure 2−80980
p-Si inversion layer, piezoresistance and mobility obs. 2−51171
n-Si inversion layers, self-consistent calcs. 2−47934
Si polytype, density of states and optical props. 2−61185
SiC, 6H exciton electroabsorption, spin-orbit and crystal-field splitting in exciton ground state 2−81331
3C-SiC, pseudopotential calc. 2−61345
n-SiC, Raman scatt. from electronic transitions 2−51356
SiP_2, det. from reflectance spectra 2−72306
Sm, ionic, semicond. and metallic cpds., Mossbauer isomer shifts, electronic density changes 2−48154
Sm monochalcogenides and monopnictides, press. effects 2−47915
SmS-SmSe system, metal-insulator behaviour 2−61190
SmS, rel. to semicond.-metal transition 2−80994
SmS, SmSe, SmTe, amorphous, optical absorption obs. 2−61657
SnO_2, calcs. using KKR method 2−54189
SnS_2, pseudopotential calc. 2−44116
SnS(Se)(Te), calc. from refl., 1-12.5 eV 2−48161
$SrTiO_3$, differential optical spectra obs. 2−72307
$SrTiO_3$, optical transitions 2−78107
$SrTiO_3$, self- consistent-field tight-binding calc. 2−61191
Ta-Nb alloys, superconducting, bare-band struct. density of states at Fermi surface 2−71875
TaC, calc. using strong-bond method 2−57126
TaC_{1-x}, determ. from supercond. transition temp. 2−81055
TaS_2, 1S and 2S polymorphs, model, consistency with cond. data 2−47226
TaS_2, two dimensional Van Hove singularity, reflectivity obs. 2−81380
Te-As-Si-Ge film, amorphous, a.c. cond. rel. to localized tail states 2−61288
Te, amorphous, rel. to tight binding model calc. of optical props. 2−61658
Te, effects of cryst. disorder on electronic struct., photoemission obs. 2−61466
Te, k.p perturbation theory calc. 2−81018
Te, Landau levels in the valence band for mag. field at arbitrary angle, calc. 2−71797
Te, mag. susceptibility anisotropy of holes, calc. 2−81214
Te, thermomodulation of optical parameters obs. 2−65242

Crystal electron states continued
band structure continued
Te, valence band Landau levels, cyclotron resonance obs. 2−81017
Te, valence band Landau levels, cyclotron resonance obs. 2−81019
Te, valence band structure and transitions between Landau levels determ., cyclotron resonance obs. 2−68321
Te valence band structure from Shubnikov-de Haas expts. 2−84245
Ti-Nb alloy, X-ray spectral study 2−44402
Ti, Ar-ion bombarded, excited particle velocity spectrum obs. 2−48030
Ti alloys, rel. to exponential temp. depend. of resist. 2−54129
TiB and TiB_2, Compton profiles, electron momentum distrib. 2−48211
TiB_2, electronic spectra, MOLKAO method calc. 2−71792
TiC-TiN solid solution, optical dispersion and absorpt. study 2−51080
TiC, calc. using strong-bond method 2−57126
TiFe, X-ray emission study 2−75316
TiN_x, calc. from X-ray spectra 2−48195
TiNi, X-ray emission study 2−75316
TiO_2 amorphous film, rel. to photocond. 2−72068
TiS_2, calc. by semi-empirical tight binding method 2−84232
$TiSe_2$, calc. by semi-empirical tight binding method 2−84232
TiTe, calc. by semi-empirical tight binding method 2−84232
Tl-Te alloy, amorphous film, model 2−61328
Tl-Te liquid, semicond., Hall mobility, electronic struct., two band model 2−60506
TlBr, rel. to optical consts. detn. by electron energy loss spectra 2−61129
TlBr(Cl), cyclotron reson. of electrons and holes 2−47830
TlBr(Cl), rel. to ionicity and absorpt. 2−44374
TlCl, rel. to optical consts. detn. by electron energy loss spectra 2−61129
TlCl, rel. to X-ray emission spectrum assignment 2−72383
TlCl, valence and conduction band calc., Heine-Abarenkov model 2−75034
TlI, rel. to optical consts. detn. by electron energy loss spectra 2−61129
$TlInSe_2$:Cu,Sn, cryst. and film, forbidden band width, elec. and photoelec., props. 2−57197
U compounds, hybridized band model for magnetic properties 2−84396
V, electron momentum distrib., Compton profile obs. 2−51081
V, valence electron charge density, asphericity 2−80990
VB_2, electronic spectra, MOLKAO method calc. 2−71792
VC, calc. by quasi-self-consistent APW method, determ. of energy eigenvalues and density-of-states histogram 2−51082
VO_2, metal-insulator transition and phonon softening 2−51152
VO_2, semicond.-metal transition, rel. to struct. of $V_{0.95}Cr_{0.05}O_2$ 2−43592
VO_x, localized states, elec. props. study 2−64991
V_2O_3, below Fermi level, X-ray photoelectron spectra obs. 2−61193
V_2O_3, model for metal-insulator transiton 2−72225
Vo_x, $1<x<1.3$, charge carrier freeze-out effects 2−65004
W, optical absorp., interband transitions 2−72353
Xe solid, photocond., energy gap, at 135 K 2−72069
YCu(Zn) intermetallics, APW calcs. 2−54112
Zn, h.c.p., non-relativistic electronic band struct., Korringa-Kohn-Rostoker method 2−68298
Zn film, disordered, supercond. energy gap 2−54134
$ZnAs_2$, edge absorp., reflection and photocond. obs. 2−51326
$Zn_xCd_{1-x}Te$, reflectivity spectra obs. 2−78093
$ZnGeP_2$, energy gap, optical props. study 2−80599
$Zn_xHg_{1-x}Te$ solid soln., light-hole band rel. to transport phenomena 2−64992
ZnO:Cu film, amorphous, optical absorp. and elec. cond. obs. 2−68421
ZnO, photoemission study 2−75196
ZnO, Zeeman splitting of anomalous shallow bound states 2−51349
ZnO anodes, rel. to electron injection behaviour 2−61797
ZnP_2, edge absorp., reflection and photocond. obs. 2−51326
ZnS:Cl, rel. to quenching of photolum. by elec. field 2−72416
ZnS:Mn films, energy level scheme from reflectivity and transmission meas. 2−71799
ZnS, interband transitions, electron energy loss spectra study 2−75111
ZnS electroluminescent p-n junction, electronic behaviour obs. 2−68711
ZnS single crystal, homogeneous, wide-gap semiconductor, rel. to u.v. electroluminesc. 2−68712
$ZnS_{1-x}Se_x$ mixed crystals, optical reflectivity at room temp. and 2.5 to 9.5 eV range 2−54407
ZnSe, interband transitions, electron energy loss spectra study 2−75111
ZnSe, rel. to dielec. function calc. 2−84262
ZnSe, rel. to ionicity and absorpt. 2−44374
ZnSe, self-consistent local orbitals 2−75031
ZnSe, valence-band densities, X-ray photoemission valence-band spectra 2−81192
ZnSe, X-ray K emission bands, valence electron obs. 2−68672
$ZnSe_xTe_{1-x}$, refl. study, 2.0-6.6 eV 2−84500
$ZnSnAs_2$, $ZnSnP_2$, electroreflectance spectra obs. 2−81404
ZnTe, interband transitions, electron energy loss spectra study 2−75111
Zr alloys, rel. to exponential temp. depend. of resist. 2−54129

excitons
− 2−61718
absorption and emission lines, at high exciton conc., theory 2−71807
alkali halide crystal, high symmetry exciton 2−68308
anthracene, carrier-exciton interactions, delayed fluoresc. quenching 2−65308
anthracene, excitonic sounding method for measuring charge density gradient 2−47907
anthracene, singlet exciton collision fluorescence decay following laser stimulation 2−78144
anthracene, steady-state concentration, under light reabsorption conditions 2−61715
anthracene, surface states, luminescence 2−54461
anthracene, triplet and trapped holes, evolution of space charge limited current 2−75105

Crystal electron states continued
excitons continued
anthracene, triplet exciton annihilation fluorescence changes induced by neutron radiation damage 2−84553
anthracene crystal, photoconduction by surface quenching of excitons, generation of free charge carriers 2−81169
anthracene single crystal, intensity of fluorescence depend. on triplet exciton generation, decay and surface quenching 2−81427
antiferrodielectric, effective electrodipole transitions, optical and spin excited states 2−72290
antiferromagnet, density of states singularities 2−51276
benzene, liquid and solid, optical generation of charge carriers via excitons 2−57259
benzene and hexadeuterobenzene impurity, absorption spectra and exciton-phonon interaction 2−71717
benzene crystal, density of state calc., effect of ^{13}C impurity 2−80950
benzene single crystal, assignment of i.r. active exciton components 2−51316
benzol crystal with impurities, low-temperature spectral investigations of formation of local exciton states 2−54464
benzophenone, mutual annihilation velocity constants for triplet excitons following pulsed laser excitation 2−54463
benzyl mutual annihilation velocity constants for triplet exciton following pulsed laser excitation 2−54463
bi-exciton formation, theory 2−75037
biexciton bound state contrib. to nonlinear polarizability 2−84197
biexciton theory, spectrum analysis 2−47817
boundary conditions in exciton absorption region 2−65244
chlorophyll charge transfer complexes, character of e.p.r. signal 2−48298
complex, exciton-ionized donor, binding energy determ., interparticle-coordinates method 2−84266
complexes, interaction potential and polarizability effect 2−61198
coupled molecular aggregates, exciton theory of excited electronic states 2−68301
1,4dibromo-naphthalene, e.s.r. of triplet excitons, optical detection 2−81522
1,4-dibromonaphthalene, triplet exciton diffusion 2−48252
1,4-dibromonapthalene, triplet exciton state band structure, properties of real linear chain 2−47820
dichlorobenzophenone crystal, optical and electric field effects in singlet and triplet states 2−44385
diffusion constants of triplet states, modification of Avakian-Merrifield method 2−68800
diphenyl, migration of triplet excitons and nonlinear effects 2−54474
diphenyl crystal, rel. to luminesc. and electron excitation energy migration 2−72425
electron gas, two-band model, magnetic and excitonic instabilities 2−64881
electron-hole-phonon quasiparticle bound states in strong mag. fields 2−68302
rel. to electroreflectance line-shape analysis 2−78090
elementary excitations, book 2−71806
ferroelectric phase transitions by exciton-phonon interactions 2−81153
ferromagnet, singlet ground state, soft modes 2−51244
fluoranthene, fluorescence quenching due to exciton-exciton interaction, determ. of rate const. and exciton migration rate 2−81426
fluorobenzene, exciton states characts., spectroscopic obs. 2−77807
Frenkel theory, exchange, interactions, local field effects 2−77834
GaAs, near band-edge optical absorpt., rel. to excitons 2−84516
group VI chalcogenides, layer semicond. spectra obs. 2−81334
high density, many electron-hole system theory, optical and transport property model 2−77839
incoherent quenching on lattices, time dependent excitation function 2−45290
instability, in tight binding approximation 2−71805
insulating crystal, magnetic side bands induced by zero point motion 2−81376
intermediately bound exciton states, calc. by integral equation method 2−68309
ionic crystals, fine structure of spectra, exciton echo method 2−54395
ionic crystals, isotropic fine struct. of excitonic lines 2−80985
KI:Tl, total emission spectra and energy transfer from excitons to activator 2−61710
mag. ordering effect on exciton-phonon process compared to absorption in Y-Fe garnets 2−81392
many exciton system, optical response 2−65249
metal-insulator boundary, surface exciton spectra, image forces 2−77921
metal-insulator transition, vacuum polarization and force between two excitons 2−47818
α-methylnaphthalene, liquid, specular reflection spectrum, obs. of excitons 2−80474
molecular cryst., biexciton spectra 2−57338
molecular cryst., exciton interactions between substitutional impurities 2−71803
molecular cryst., excitonic polarons, band narrowing and band shifts 2−44039
molecular crystal, determination of general coupling parameters from classical theory of stimulated Stokes generation 2−51315
molecular crystal, excitation spectra of charge-transfer complexes 2−68631
molecular crystal, exciton induced contact limited photocurrent, field depend. 2−77968
molecular crystal, in contact with ferromagnet, triplet excitons 2−77838
molecular crystal with 2 exciton state regions, absorption spectrum 2−72310
molecular crystal-metal interface, dissociation, photocurrent obs. 2−51085
molecular crystals, effect of resonance interaction and exciton-phonon coupling on absorpt. band intensities 2−81373
molecular crystals, electron-vibrational spectra, review 2−57345
molecular crystals, fine structure of spectra, exciton echo method 2−54395
molecular crystals, high exciton conc. effects, bibliography 2−48159

Crystal electron states continued
excitons continued
molecular crystals, single exciton decay into triplet excitons 2−71811
molecular crystals, singlet spectrum coupling to 2-particle excitations 2−51327
molecular crystals, substitutionally disordered, band structure and density of state 2−48157
molecular crystals, triplet-triplet fission of singlet excitons 2−51084
molecular crysts., dilute mixed, multicomponent cluster states, Frenkel excitons 2−84228
naphthalene, impurity centre conc. and distrib., exciton scatt. theory calc. 2−81436
naphthalene, migration of excitation energy between impurity molecules studied by polarization method 2−54465
naphthalene, Raman spectra, exciton splittings, heavily doped isotopic mixed crystal method 2−57362
naphthalene, triplet exciton diffusion 2−48252
naphthalene isotopic mixed crystals, Raman phonon spectra, exciton model and amalgamation limit 2−57363
naphthalene with indol impurity, spectra of local excitons 2−54466
optical orientation of excitons in crystals with wurtzite struct., influence of mag. field and deformation 2−71804
organic crystal, doped, exciton diffusion theory rel. to luminesc. emmission 2−75325
paramagnet, van Vleck, excitation spectrum 2−61479
phenanthrene, polarized absorpt. edge and exciton-photon interaction 2−44386
phonon- impurity centre-exciton bound states, theory of dielec. modes 2−68303
phonon-exciton boundary state calc. 2−64831
and photons and polaritons, review 2−72317
polariton mode propagation in bounded media 2−68307
polaritons, giant, nonlinear theory of exciton-photon coupling 2−84241
pyrene, Davydov splitting of first triplet state 2−61660
pyrene, exciton-exciton annihilation, luminesc. quenching 2−44409
pyrene crystal, calc. of Davydov splitting 2−51352
pyrene-d-10, temperature dependent saturation meas. in photo-excited triplet state 2−84567
semi-metals, excitonic phase, investigation using strong electron-phonon interaction term 2−64897
semiconductor, complexes binding energies, exciton neutral donor complex 2−80970
semiconductor, conf., Warsaw, Poland, July (1972) 2−68384
semiconductor, degenerate bands, direct exciton energy levels 2−61199
semiconductor, direct gap, exciton absorpt. meas. method 2−44373
semiconductor, effective mass eqn. for Wannier exciton examined rel to electroreflectance 2−72320
semiconductor, electroreflectance line shapes, local-field effects, contact exciton effects 2−68618
semiconductor, exchange interaction in bound excitons 2−81009
semiconductor, exciton luminesc., effect of absorpt., surface annihilation of excitons 2−78129
semiconductor, impurity spin states-bound exciton interaction, rel. to spin-flip Raman scatt. 2−57359
semiconductor, in quantizing mag. field, electron-hole pair multiphoton excitation probability 2−77837
semiconductor, incompletely ordered, exciton light absorpt. 2−78094
semiconductor, isotropic, biexciton binding energy 2−57132
semiconductor, non-equilib. charge carrier condensation and recomb. radiation 2−54184
semiconductor, p-type, recomb. of excitons bound to deep neutral donors and acceptors 2−68682
semiconductor, polar, electron-hole interaction, effective mass eqn., optical phonon effects 2−68306
semiconductor, polar, electron-hole interaction, optical phonon interactions 2−68305
semiconductor, polar, exciton-phonon interactions, Urbach's rule 2−44369
semiconductor, with degenerate bands, 2p-exciton states, calc. 2−84261
semiconductor bound to neutral impurities complex binding energy and stability 2−77835
semimental, excitonic-insulator phase, interband scattering 2−81003
semimetal, e.m. response in mixed phase 2−64898
singlet-exciton energy transfer, generalized random walk model 2−84270
spatially dispersive medium, polarization, generalized extinction theory 2−68304
spin effects in two- particle equation 2−47819
trans-stilbene, triplet exciton diffusion 2−48252
TCNQ salts, e.s.r. dipolar split line obs. 2−61742
tetracene, e.p.r. of triplet excitons, spin polarization and singlet exciton fission role 2−81448
tetracene, e.p.r. of triplet excitons, spin polarization and singlet exciton fission role 2−81449
tetracene, fluoresc. decay and singlet fission 2−54472
tetracene, rel. to anomalous temp. depend. of photovoltaic current 2−72075
1,2,4,5-tetracyanobenzene- durene complex, fluorescence quenching due to exciton-exciton interaction, determ. of rate const. and exciton migration rate 2−81426
thermoelectric power, calc. for excitonic phase 2−65077
toluqinone single cryst., excitonic and zero-field splittings of first triplet state 2−78209
triplet exciton spin systems, Heisenberg exchange 2−68729
triplet excitons, coupled coherent and incoherent motion, effect on e.s.r. lineshape 2−65320
two-photon absorption, elec. field effect 2−65221
uniaxial cryst., surface polarization waves and surface e.m. waves 2−77836
Wannier intermediate states, atomic jump processes 2−71802
Ag halides, optical transitions, localized electron states, self-bound and impurity trapped excitons 2−81025
AgCl:I-, decay mechanism of bound exciton, luminesc., 4.2-80K 2−72392
AgI, absorption spectrum detn. 2−68310

Crystal electron states continued
excitons continued
AgI, optical constants of thin films in exciton band region, meas. 2−65209
$Al_xGa_{1-x}As$, photolum., free and bound exciton recomb. 2−61683
Ar-Xe solid solution, 8-10.5eV absorpt. study 2−68634
BaO powder, thermal dissoc., rel. to recomb. luminesc., 103-423 K 2−61687
CH_3I, mol. cryst., exciton spectrum in presence of Fermi reson., exciton absorpt. 2−68311
CO, optical spectra of trapped atoms, obs. of crystal-shape dependence of dipole excitons, exciton-vibron, exciton-phonon coupling 2−78096
CdP_2, rel. to radiative recomb. mechanisms 2−72394
CdS, exciton-exciton emission line shift 2−44407
CdS, exciton-impurity complex, optical absorp. anomalous intensity 2−72324
CdS, exciton photoluminesc., picosec. and nanosec. spectroscopy obs. 2−72421
CdS, fast electron excitation, phonon assisted exciton recombination 2−48240
CdS, form of absorption bands of single crystals at 4.2K 2−80999
CdS, luminesc. spectra fine struct., localized exciton struct., at 4.2K 2−51366
CdS, photocond., effects of 10 MeV electron irradiation 2−57254
CdS, piezoemission obs. of free excitons 2−78143
CdS, rel. to optical modulation due to moving acoustic domains 2−54418
CdS, resonance Raman scattering by turnable dye laser
CdS, strain splitting of bound excitons 2−68678
CdS, valence band energy levels, Γ-point, from emission spectra due to A- and B-band excitons 2−68289
CdS platelets, luminescence, radiation damage effects at low temps. 2−68703
CdS polariton emission 2−48218
CdS rel. to induced optical absorption by strong excitation 2−78097
CdS semiconductors, dipole active exciton absorption, nonlinearity 2−44333
CdS(Se), spontaneous and stimulated emission, exciton interactions 2−68677
CdSe, emission spectra under laser excitation, exciton interactions, exciton molecules formation 2−77840
CdSe, exciton bound to ionized centre, magneto-optical obs. 2−68636
CdSe, exciton photoluminesc., picosec. and nanosec. spectroscopy obs. 2−72421
CdSe, exciton scatt. by dislocations, absorpt. study 2−81007
$CdSe_xTe_{1-x}$, reflection spectra obs. 2−84517
CdTe, absorpt. spectra, direct exciton transitions 2−65255
CdTe, resonance absorption structures 2−61200
p-CdTe film, rel. to photosensitivity 2−48217
Cr and alloys, excitonic phase, thermoelec. power calc. 2−65077
CsBr, CsBr:Tl, CsBr:In, luminesc. crystals, exciton and hole migration 2−48242
CsI, relaxed state of self-trapped exciton 2−65291
CuCl, second harmonic generation and two-photon luminesc. in exciton region 2−54453
CuCl(Br)(I) layer, on Ag or Cu, rel. to light sensitivity spectra 2−77966
CuI, low temp. reflection spectra, excitonic transitions and levels 2−72302
CuI, rel. to emission under high density excitation 2−72397
γ-CuI thin film, piezo-optical effect at 77K in fundamental absorption band region 2−48172
Cu_2O, 1s exciton state in green series 2−72327
Cu_2O, electric field effects, electroreflectance obs. 2−51320
Cu_2O, exciton luminesc. spectra, ortho- and para-exciton interactions, optical phonon freq. 2−57133
Cu_2O, Γ^+_5 exciton quadrupole transition rel. to static elec. field, Stark splitting 2−81406
Cu_2O, resonant Raman scatt. near 1S exciton level 2−54434
D_2:Xe, vacuum u.v. study of Wannier states, obs. of host isotope effect on linewidth 2−51341
D_2:Xe, vacuum u.v. study of Wannier states, obs. of host isotope effect on linewidth 2−51341
n-$Ga_{1-x}Al_xAs$ epitaxial film, edge photoluminesce, free exciton annihilation contrib. 2−81432
GaAs:Sn, energy level structure from photoluminescence props. analysis 2−44427
GaAs, absorpt. spectrum, resolved free-exciton transitions 2−84259
GaAs, bound exciton photoluminesc. spectra 2−57373
GaAs, elec. field induced interference effects at ground exciton level 2−78084
GaAs, exciton-exciton and electron-exciton interactions in highly excited material 2−78132
GaAs, exciton-phonon coupling, optical absorp. obs. 2−61642
GaAs, exciton absorpt. meas. method 2−44373
GaAs, exciton struct. of fundamental absorpt. edge and oscillatory magnetoabsorpt. 2−72331
GaAs, radiative recomb. of screened excitons 2−72408
GaAs polariton (n=1 exciton) transmittance and reflectance, temp. depend. 2−81400
$GaAs_{1-x}P_x$, p- and n-type, direct and indirect gap, rel. to photoluminesc. spectra 2−84538
GaP:Bi, luminesc., kinetics due to bound excitons, 77.3K 2−65292
p-GaP:Cu,O, bound exciton luminesc., emission and excitation spectra 2−78131
GaP:N, null field splitting of B-line 2−61692
GaP:N, Zeeman effect on bound exciton-complex 2−61693
GaP:N(Bi), binding to impurities, uniaxial stress effects 2−75108
GaP, electron-hole pair form. by irrad. with α-particles, form. energy 2−71808
GaSb:Te, lightly doped, exciton luminesc. peaks 2−72402
GaSb, Landau levels at saddle point, exciton model 2−71795
GaSb, piezoemission, stress effects on bound exciton lines 2−48179
p-GaSb, undoped, photocond. and photoluminesc. obs. 2−61708
GaSe, exciton absorpt. peak shift and phase change induced by hydrostatic press. 2−72330
GaSe, Faraday effect in exciton absorpt. region 2−72263

Crystal electron states continued
excitons continued
GaSe, linear electro-opt. eff. at room temp., photon energy 1.25-1.96eV 2−72270
GaSe, luminesc. of free and bound excitons, 4.2 and 1.8K 2−72406
GaSe crystals, hyperbolic, study by reflection spectra 2−84480
GaSe single crystal, anomalous dispersion study by Rozhdestvenskii hook method 2−78099
GaTe, binding energy, optical absorp. obs. 2−75294
$GdCl_3$, optical exciton dispersion and effect on single-ion-induced absorpt. lineshapes 2−48181
$Gd(OH)_3$, optical exciton dispersion and effect on single-ion-induced absorpt. lineshapes 2−48181
Ge, condensation, ground state energy calc. using improved RPA approx. 2−71809
Ge, condensed electron-hole state, temp. depend. props. 2−68683
Ge, electroabsorpt. edge, exciton effects 2−48189
Ge, electron-hole drops 2−68432
Ge, exciton and electron-hole drop absorp., far i.r. obs. 2−78100
Ge, indirect exciton ground state, exciton line broadening by elec. field 2−77841
Ge, microwave absorpt., by electron-hole drops 2−57209
Ge, pure and doped, radiative recomb. during electron-hole condensation 2−78133
Ge, radiative recomb. of biexcitons 2−78134
Ge, rel. to effect of electron- phonon interaction on radiative recomb., 2-77K 2−68684
Ge single crystals, bound exciton luminesc. 2−68692
H_2:Xe, vacuum u.v. study of Wannier states, obs. of host isotope effect on linewidths 2−51341
Hg-Xe layer, insulator-metal transition, Wannier exciton disappearance, u.v. spectra obs. 2−51079
HgI_2 single crystal, tetragonal, luminesc., temp. depend. 2−84541
InP, bound exciton photoluminesc. spectra 2−57373
InP, free and bound exciton decay 2−72410
InP, photoluminesc. of bound excitons 2−68685
InP, photoluminesc. of excitons bound to neutral acceptors, strain effects 2−48223
InP, photoluminescence spectra of excitons bound to group II acceptors 2−84279
InSb, Landau levels at saddle point, exciton model 2−71795
InSb exciton-hole plasma prod. by laser irrad., two-photon absorpt., direct recomb., 77K 2−80972
InSe, absorpt., 300K and 70K, 2.3 to 3.0 eV, hyperbolic excitons 2−81398
InSe, exciton-phonon interaction, absorption edge obs. 2−84518
InSe crystals, hyperbolic, study by reflection spectra 2−84480
K magnetoplasma, anomalous resistivity 2−70897
KBr:Tl, formation of H centres by ionisation of In^+ and Tl^+ centres 2−81001
KBr, self trapped, transient form., pulsed electron beam 2−53753
KBr crystals, u.v. irrad. and colour center prod. from exciton decay 2−71527
KBr evaporated films, optical absorption spectra 1700-2500 Å, obs. of fine structure in exciton bands 2−44375
KCl:In(Tl) formation of H centres by ionisation of In^+ and Tl^+ centres 2−81001
KCl:Tl, rel. to luminesc. excitation spectra 2−48244
KI:Cu, CuI exciton band rel. to antiresonance phenomena in transmission spectra 2−54423
KI evaporated films, optical absorption spectra 1700-2500 Å, obs. of fine structure in exciton bands 2−44375
$K_{0.3}MoO_3$, blue phase, semicond. to metal transition, excitonic insulator 2−61151
Mg-Bi amorphous alloy, exciton screening 2−78115
Mg-Sb amorphous alloy, exciton screening 2−78115
MnF_2, oscill. strength, exciton-magnon transitions 2−54428
MnF_2, two exciton transition, temp. depend. intensity calc. 2−61654
MoS_2, composite exciton absorpt. spectrum, optical phonon effects 2−44377
$MoTe_2$, composite exciton absorpt. spectrum, optical phonon effects 2−44377
NaBr evaporated films, optical absorption spectra 1700-2500 Å, obs. of fine structure in exciton bands 2−44375
NaCl, core exciton, X-ray K absorption spectra obs. 2−65288
NaI evaporated films, optical absorption spectra 1700-2500 Å, obs. of fine structure in exciton bands 2−44375
$PbBr_2$ thin film, spectral dependence of optical constants, 'cation-exciton' model 2−57321
$PbCl_2$, obs. of Fano effect in exciton spectrum 2−68647
$PbCl_2$, refl. spectrum behaviour 2−68625
PbI_2, anomaly due to cationic nature of exciton 2−51324
PbI_2, band edge excitons, refl. study 2−68626
PbI_2, optical absorp. spectra rel. to band struct. calc. 2−68418
PbI_2 thin film, influence of nature of substrate and preparation conditions on exciton spectrum 2−48188
Pr, f.c.c., singlet-ground-state ferromagnet, neutron scatt. obs. 2−72152
Pr, f.c.c., singlet-ground-states ferromagnet, crystal field levels, theory 2−72153
Pr, mag. exciton excitation spectra, crystal field effects 2−75205
Pr_3Tl, singlet-ground-state ferromagnet, crystal field levels, theory 2−72153
Pr_3Tl, singlet-ground-state ferromagnet, neutron scatt. obs. 2−72152
RbI, Rydberg series up to n=4 of Γ_1 exciton, thermoreflectance spectra at 90K 2−44363
RbI evaporated films, optical absorption spectra 1700-2500 Å, obs. of fine structure in exciton bands 2−44375
$RbMnF_3$, exciton struct. of absorp. spectra in 3900 Å region 2−65266
$RbMnF_3$, oscill. strength, exciton-magnon transitions 2−54428
$RbMnF_3$, two exciton transition, temp. depend. intensity calc. 2−61654
Se, monoclinic, Mott-Wannier excitons, optical absorp. obs. 2−68648
Si, core excitons, X-ray absorption spectra 2−81385
Si, electroabsorpt. edge, exciton effects 2−48189
Si, low field electroabsorpt., split-off exciton and phonon-depend. lineshape 2−72349

Crystal electron states continued
 excitons continued
  Si, pure and doped, radiative recomb. during electron-hole condensation 2−78133
  Si, recomb. luminesc. from excitons, 20-77K 2−78138
  Si condensation, ground state energy calc. using improved RPA approx. 2−71809
  Si microwave absorpt., by electron-hole drops 2−57209
  SiC:H(D), implanted, recomb. radiation of excitons and vibr. spectrum 2−68688
  SiC, 6H electroabsorption due to indirect excitons 2−81331
  SiC, luminesc., Zeeman splittings, bound excitons 2−48227
  Te, binding energy, k.p perturbation theory calc. 2−81018
  TlCl, X-point direct exciton, magnetoabsorp. obs. 2−72352
  $TmVO_4$, Jahn-Teller induced magnon sidebands 2−81377
  WSe_2, exciton mechanism for superconductivity and nonequilibrium systems of excited excitons 2−71868
  WSe_2, line shape of electroreflectance spectra 2−84510
  WSe_2, optical response in excitonic region 2−44383
  WSe_2, transmission spectra obs. 2−81403
  $Zn_xCd_{1-x}Te$, luminesc. reson. Raman scatt., exciton transition 2−54437
  ZnO, resonance Raman scattering by turnable dye laser 2−84486
  ZnS, piezoreflectance, exciton states exchange splitting by stacking faults 2−81391
  ZnS crystals, exciton state excitation, spectroscopic investig. 2−71810
  ZnSe, exciton-donor complex, binding energies 2−51372
  ZnTe, resonant absorption structures 2−61200
 Fermi level
  alloy, dil. mag., rel. to electron energy renormalization in s-d model 2−51274
  alloy, rel. to electron charge transfer and electrochem. effects 2−64884
  energy, Fermi, of 29 elements, from Doppler broadening of positron annihilation radiation 2−68324
  metal/hydrogen systems, rel. to non-ideal soln. behaviour 2−77716
  Schottky diode, cond. mechanism, diffusion and thermionic emission theories, quasi-Fermi levels 2−75128
  semiconductor, compensated, rel. to metal-nonmetal transition 2−68412
  semiconductor, surface space charge, Fermi level near band edges, Raman scatt. obs. 2−47919
  semiconductor inversion layer, rel. to magneto-cond. 2−68387
  Al alloy, dil., semiphenomenological model for reson. and charge neutrality 2−68291
  As_2S_3, vitreous, localized state distrib., Fermi level analysis from transient photocond. obs. 2−47913
  As_2Se_3, trap density at Fermi level and high field cond. 2−68394
  Au-Cr(V) alloy systems, absorpt. spectra obs. of interband transition 2−44371
  Au-Sn alloy, rel. to Mossbauer effect 2−51308
  BiOBr, from photoemission meas. 2−81197
  BiOCl, from photoemission meas. 2−81197
  BiOI, from photoemission meas. 2−81197
  CoB, rel. to resist. and thermo-e.m.f. 2−51099
  Cs-K melts, density of electron states 2−60497
  Cu-Sn alloys, α-phase, low temp. electronic sp. ht. 2−43982
  Cu alloy, dil., semiphenomenological model for reson. and charge neutrality 2−68291
  GaAs, amorphous, hopping at Fermi level 2−61312
  n-GaAs, heavily-doped, temp. depend. 2−61342
  GaAs laser, injection, increase in lasing region 2−79212
  GaAs occupied intrinsic surface states below Fermi level 2−44207
  $Ga_{1-x}Te_x$ alloy, liq., density of states at Fermi level, n.m.r. obs. 2−60512
  Ge_x-Si_{1-x} mixed crystals, rel. to photoelectric emission obs. 2−72092
  Ge, amorphous, hopping at Fermi level 2−61312
  Ge, electroreflectance, cond. band minima change 2−51321
  Ge, occupied intrinsic surface states below Fermi level 2−44207
  Ge_xTe_{1-x} alloy, amorphous, optical and electrical obs. 2−77904
  K, rel. to r.f. size effect calc. 2−71835
  Mo, changes Fermi sea depth due to exposure to CO, N_2 and O_2, photoemission obs. 2−51227
  Na-Cs melts, density of electron states 2−60497
  Ni-Cu alloys, ferromag., density of states 2−54110
  Ni-Cu alloys, X-ray appearance pot. spectra, density of states 2−61674
  NiB, rel. to elec., thermal, and mag. props. 2−51099
  NiO, temp. insensitivity, thermionic emission obs. 2−44192
  Se-Te melt, electronic transport behaviour, localization near Fermi level 2−60502
  Si/Pt interface-state density, transitions below Pt Fermi level 2−44128
  Si, amorphous, density of states 2−47952
  Si, γ-ray and neutron irrad. effects 2−47937
  Si, n-type, surface states below Fermi energy 2−44208
  Si, occupied intrinsic surface states below Fermi level 2−44207
  Si, rel. to cluster model for fast neutron radiation damage 2−48282
  Si amorphous, inferred from tunnelling cond. 2−61359
  Si film, amorphous, rel. to localized state densities 2−68437
  Ti alloys, rel. to exponential temp. depend. of resist. 2−54129
  $Tl_{1-x}Te_x$ alloy, liq., density of states at Fermi level, n.m.r. obs. 2−60512
  V_2O_3, band struct. below Fermi level, X-ray photoelectron spectra obs. 2−61193
  YCu(Zn) intermetallics, APW calcs. 2−54112
  Zr alloys, rel. to exponential temp. depend. of resist. 2−54129
 Fermi surface
  alkali metals, rel. to anisotropic transport scatt. times 2−75014
  APW interpolation scheme, consequences of matrix element conservation 2−64883
  α-brass, positron annihilation study 2−80955
  compressed matter, electron-lattice interaction energy, cryst. struct. depend. term 2−71788
  de Haas-van Alphen areas and cyclotron masses, integral calc. method 2−44028
  graphite-Br intercalation compound, Shubnikov-de Haas oscill. obs. 2−68288

Crystal electron states continued
 Fermi surface continued
  magnetoacoustic attenuation, deformation potential theory 2−71737
  metal, angular correlations of annihilation photons, description of method 2−61171
  metal, helicon dispersion relation 2−57384
  metal, parametrization 2−54103
  metal, point meas. of Fermi vels. by time-of-flight method 2−51075
  metal, polyvalent, effect on ideal resist. 2−75044
  metal, rel. to effect of anomalous field penetration on capacitance 2−80953
  metals, high pressure effects, reviews 2−57118
  metals, surfaces of constant energy 2−61155
  noble metals, rel. to elastic consts. and equation of state determ. 2−68063
  rare earth metals, anisotropy, rel. to elec. resist. due to short range spin correls. 2−57272
  Ru, Hall constant and anisotropy of elec. resistance at low temps., interpretation 2−68333
  space groups, tabulation and procedure to determine point symmetry of positions in Brillouin zone 2−47798
  superconductor, A15 cpds., detection by inelastic neutron scatt. 2−43951
  superconductor, two band, transition temp. and energy gaps rel. to Fermi surface topology change under press. 2−75068
  transition metal, paramagnetostriction, oscillatory magnetostriction, rel. to Fermi surface 2−54290
  transition metal, supercond. with non-mag. impurities, d-band Fermi surface rel. to specific heat calc. 2−44061
  Ag, de Haas-van Alphen meas., infinite field phase 2−61182
  Ag, orbits, integral calc. method 2−44028
  Ag, phase shift parametrization 2−44030
  Ag, shape rel. to thermoelec. power 2−68296
  Ag alloy, impurity scatt., de Haas-van Alphen meas. 2−61148
  Al-Mg alloy, Fermi surface rel. to alloying 2−77826
  Al, press. depend. 2−61180
  Al, rel. to magnetostriction and stress 2−68286
  Al, third zone, uniaxial compression effects 2−71790
  Al alloy, rel. to low temp. resistivity, deviations from Matthiesen's rule 2−64910
  Au, de Haas-van Alphen meas., infinite field phase 2−61182
  Au, phase shift parametrization 2−44030
  Au, rel. to quantum oscill. of u.s. attenuation 2−51037
  Au, shape rel. to thermoelec. power 2−68296
  Au, uniaxial stress effects, de Haas-van Alphen obs. 2−54108
  $AuGa_2$, hydrostatic press. and Pd doping effect 2−51078
  Be-transition metal alloy, and electron scatt. 2−71791
  Bi, bulk, non extremal Fermi-surface orbits 2−77827
  Bi, bulk nonextremal Fermi-surface orbits 2−77828
  Bi, model for obs. of quenching effects on thermoelectric power and magnetoresistivity 2−68336
  p-Bi_2Te_3, effective mass tensor, relax. time anisotropy obs. 2−51135
  Cd-In, binary systems, electrotransport and elec. resist. detn. for density of states at Fermi level 2−80476
  Cd-Tl, binary systems, electrotransport and elec. resist. detn. for density of states at Fermi level 2−80476
  Cd, topology rel. to hydrostatic press., magnetoacoustic meas. 2−77806
  Co, h.c.p., topology, calc. 2−61181
  Cr, rel. to generalized spin susceptibility 2−61554
  Cs, shape rel. to thermoelec. power 2−68296
  Cu-Al alloy, α-phase, comparison of optical and positron annihilation obs. 2−64888
  Cu-Ni alloy, shape rel. to thermoelec. power 2−68296
  Cu-Sb alloy, near 20 at.% Sb, rel. to stabilization of long period superstruct. 2−71430
  Cu, anisotropy of quasiparticle scatt. rate 2−84256
  Cu, de Haas-van Alphen meas., infinite field phase 2−61182
  Cu, electron-phonon scatt. rate determ. and localized electron groups location 2−68290
  Cu, orbits, integral calc. method 2−44028
  Cu, phase shift parametrization 2−44030
  Cu, positron annihilation radiation, angular correl. 2−80968
  Cu, scattering of quasiparticle excitations by thermal phonons in symmetry zones of Fermi surface 2−44020
  Cu, shape rel. to thermoelec. power 2−68296
  CuNi dilute alloy, virtual-bound-state below Fermi energy and optical absorptivity 2−51337
  Ga, Gantmakher-Kaner effect 2−47797
  Ga, rel. to supercond. energy gap, cryst. orientation depend., tunnel junc. obs. 2−68358
  Ga, retardation effects in cyclotron reson. 2−51094
  Ga, temp. variation rel. to high field n.m.r. spectral obs. of e.f.g. tensor 2−57396
  Hf, effect on kinetic properties and electron scattering mechanisms at high temperatures 2−81035
  Hg, pseudopot. calcs. 2−64890
  In-Cd dilute alloy, topology effects on pressure and strain derivatives of supercond. transition temp. 2−71859
  Ir, dHvA obs. 2−61215
  IrO_2, Graebner model rel. to high-field magnetoresistance obs. 2−68295
  K, shape rel. to thermoelec. power 2−68296
  Li, electron dispersion law, spectrum and related charact. near Fermi surface 2−80945
  Li, electron dispersion law, spectrum and related charact. near Fermi surface 2−80945
  $Li(NH_3)_4$, topology relative to magnetic susceptibility below 88.8 K 2−43389
  Mg, hydrostatic press. effects 2−84250
  Nb-mO alloys, rel. to elastic consts. temp. depend. 2−47479
  NbN, pseudopotential calc. 2−84253
  $NbSe_2$, 2H-type, model studies 2−65002
  Ni-Fe system, Ni_3Fe ordered alloy, perturbation calc. 2−71801
  Ni-Mn system, Ni_3Mn ordered alloy, perturbation calc. 2−71801
  Ni, ferromagnetic, tight binding method energy band calc. 2−47810
  Pb, press. depend. 2−44034
  Rb, shape rel. to thermoelec. power 2−68296
  ReO_3, density of states by X-ray photoelectron spectroscopy 2−54111

Crystal electron states continued
Fermi surface continued
Ru, rel. to galvanomagnetic props. 2−51103
Si:As, P, Sb, ground state wavefunctions of shallow donor electrons, Fermi contact consts. 2−71950
Sn, white, Fermi surface cross sections stress derivatives 2−75033
SnTe, de Haas-van Alphen and Shubnikov-de Haas study 2−68420
Tc superconductor magnetic properties, effect of anisotropy of velocity on Fermi surface 2−71864
Ti, effect on kinetic properties and electron scattering mechanisms at high temperatures 2−81035
TiO$_2$, complex impedance and surface Fermi level 2−77906
Tl, in basal plane, r.f. size effect technique 2−71798
Zn, rel. to mag. surface states 2−84254
Zn, stress depend., torque and magnetostriction obs. 2−61194
Zn, topology obs. from stress depend. of oscillatory magnetostriction 2−81204
Zr, effect on kinetic properties and electron scattering mechanisms at high temperatures 2−81035
Zr, rel. to de Haas-van Alphen effect 2−84249
Zr, transverse magnetoresist. study 2−84248
impurity states and effects
see also Electron traps
— 2−80950
— 2−61690
— 2−72498
— 2−72499
alkali silicate glass, γ-irrad., rel. to thermolum. 2−81410
alloy, binary ordered, with tertiary impurity elements, electron energy spectrum 2−44023
alloy, dil., ioniz. probability for crossing atom 2−48032
alloy, dil. mag., electron energy renormalization and resist. in s-d model 2−51274
alloy, dilute, resist. temp. depend. rel. to spin fluctuations 2−57148
alloy, virtual bound state, rel. to optical absorp. models 2−65245
amorphous, effects on light absorpt. 2−72293
Anderson model, conduction electron interaction with mag. impurity 2−71789
Anderson model, localized mag. moments in transition metals and alloys 2−68515
Anderson model, partial cancellation in electron-hole and electron-electron correlation 2−47795
Anderson model, symmetric, partial cancellation in electron-hole and electron-electron correl. 2−47804
Anderson model, t-matrix approach 2−48033
Anderson model applic. to supercond. 2−57159
anomalous charge oscill. around resonant scatt. impurities, theory 2−81029
anthracene single crystal irradiated by electron beam, hole trap 2−51126
atmosphere, aeronomical balloon obs. 2−72769
band modes in semiconductors and insulators, colour centre behaviour 2−54448
carbon tetrafluoride, solid, vacuum u.v. spectroscopy of Wannier impurity states, conduction band data 2−49957
Coles alloys, temp. depend. of resist. due to localized spin fluctuations 2−75056
complex, exciton-ionized donor, binding energy determ., interparticle-coordinates method 2−84266
cross-relaxation, in spectrally inhomogeneous system, equations 2−64899
crossed diagram contribution to electron self-energy due to impurity scattering in magnetic field 2−44019
d.c. hopping conduction, percolation treatment 2−68273
de Haas-van Alphen oscills. amplitude reduction by signal dephasing by strain fields round impurities 2−77846
diamond:B, e.p.r. of free and bound holes 2−81458
diamond, heavily doped with B, Al and Ti, resistivity and impurity band props. 2−68396
diamond, LCAO-MO treatment of vacancy 2−47808
diamond like solid, electronic states of the neutral vacancy 2−47805
dielectric film, Poole-Frenkel pre-exponential factor 2−57217
diode, semicond.-insulator-semicond., rel. to freq. depend. complex admittance 2−61385
diphenyl: benzophenone, generation of triplet excitons in transmission of triplet excitation from impurity to matrix 2−54474
disordered crystal, impurity band formation, fluctuation effects 2−61165
disordered system, electron localization 2−47803
disordered system, extended states 2−51077
disordered system, impurity band, rel. to one electron metal-insulator transition 2−61167
disordered system, localized states 2−51076
disordered system, localized states density 2−51070
disordered system, three-dimens., degree of localization 2−47799
distorted chain with random impurity distrib., density of states 2−54104
donor-acceptor emission energy shift on varying the excitation intensity 2−72388
donor-acceptor pair recomb. emission, random distrib. effects, unified treatment 2−78124
Dyson equation, spurious structure from approximations, electron spectral properties 2−80943
electron irrad., phonon scatt. and induced energy levels, thermal cond. obs. 2−47766
electron traps, thermally stimulated conductivity, alternating current method 2−75113
electron-impurity system, freq. dependent relax. times 2−51068
electrons interacting with paramagnetic impurities, kinetic equations 2−77816
excitation transfer between electronic levels of impurity centres 2−78126
excitonic phase, mag. and non-mag. impurities, thermoelec. power calc. 2−65077
ferromagnet, deformed cubic, Heisenberg model, localized impurity states 2−81273
ferromagnet, point-gauge symmetry and localized impurity problem 2−54304
film, chalcogenide glass, high field effects, Poole-Frenkel emission 2−44097

Crystal electron states continued
impurity states and effects continued
fluorides, MeF$_2$:Ce^{3+}(II), optical properties, of quasi-tetragonal Ce centres 2−61646
Forster-Dexter-Galanin theory of inductive resonance energy transfer, applicability criteria 2−78125
frequency dependent relaxation time in electron-impurity system, calc. 2−71780
GaAs:Te, heavily-doped, nature of defects, photolum. and internal friction study 2−71926
n-Ge, γ-ray irrad., recombination parameters 2−47929
gradients of perturbation in effective-mass theory 2−68284
graphite, galvonomagnetic props., rel. to struct imperfections 2−57190
graphite, neutron irrad., localized paramag. centre, anomalous Schottky anomaly, sp. ht. obs. 2−57063
graphite, perturbed electronic density of states 2−57123
group II-VI semiconductor, excited state laser spectroscopy 2−64997
group III-V semiconductor, excited state laser spectroscopy 2−64997
heavily doped cryst., electronic Green's function self energy 2−61156
hopping impurity conduction, Hall effect 2−57178
impurity centres, double, possible existence near critical point 2−64904
impurity centres, two-level, binary interaction, excitation transfer, spectral theory 2−80996
impurity conduction, continuous time random walk model of hopping transport 2−61280
impurity conduction, percolation treatment of d.c hopping 2−61278
junction, supercond.-insulator-supercond., barrier region tunnelling, paramag. impurity effects 2−61256
local states, iterative procedure 2−77824
magnesium phthalocyanine film, impurity level energies from photoemission and cond. obs. 2−81028
magnetic impurity, symmetric Anderson model and Mattis' model 2−75021
metal, electronic struct. of hydrogen 2−77822
metal, impurity config. of ionic and partly ionic impurities 2−71777
metal (h.c.p.):^{57}Fe electric field gradients 2−80986
metal oxides, rel. to elec. cond., characts. 2−57106
methanol glass at 77K, matrix ENDOR linewidth of trapped electrons 2−57402
2-methyltetrahydrofuran glass at 77K, matrix ENDOR linewidth of trapped electrons 2−57402
m.i.s. structure, defect effects on C-V characts. 2−61396
m.i.s.i.m. structs., props. rel. to electron capture and liberation by surface traps 2−65037
naphthalene, impurity centre conc. and distrib., exciton scatt. theory calc. 2−81436
naphthalene, migration of excitation energy between impurity molecules studied by polarization method 2−54465
network model, energy states and dispersion waves 2−71773
one-dimensional system, soluble, absence of decay and eigenvector localization 2−54105
p-n junction, diffused, with deep impurity centres, struct. and capacitance 2−75122
pair photoluminescence, peak energy, excitation intensity depend. 2−75318
phonon- impurity centre-exciton bound states, theory of dielec. modes 2−68303
phosphors with two capture levels, rel. to thermolum. 2−65313
photoconductivity, theory and obs. rel. to multi-level impurities 2−54251
plasmon energy loss shifts rel. to specimen contamination 2−80935
polyethylene doped with I, h.f. Gunn domains 2−57202
polymer, Poole- Frenkel effect, rel. to photocurrent nonlinear field depend. 2−48004
quantum electron- impurity transport, quasiparticle formulation 2−84240
radioactive impurities, effects of relax. and r.f. field 2−75244
rhodamine 6G amorphous film, carrier trapping, thermostimulated cond. study 2−54180
s-triazine isotopic mixed crystal, variable trap problem 2−75043
Schottky barrier, capacitance rel. to freq., deep level impurity effects 2−44138
semiconductor, A^{III}B^{V} compounds, nonlinear quadratic polarizability due to shallow impurity levels 2−64998
semiconductor, amorphous, localized state density, energy depend. determ. using field effect 2−47911
semiconductor, amorphous, trap levels, thermally stimulated capacitor dscharge study 2−54188
semiconductor, amorphous, trapping mechanism, cavity perturbation study 2−61443
semiconductor, characterization for light source applic. 2−68439
semiconductor, compensated, rel. to metal-nonmetal transition 2−68412
semiconductor, compensated, thermal current instability 2−75088
semiconductor, conf., Warsaw, Poland, July (1972) 2−68384
semiconductor, config. interaction in donor-acceptor pairs 2−84260
semiconductor, degenerate, free carrier absorp., quantum theory 2−51329
semiconductor, diffused, electrostatic field gradient theory 2−61261
semiconductor, diffusivity-mobility ratio, in high mag. field, doping depend. 2−57181
semiconductor, doped, localization of electrons, Anderson's probabilistic approach 2−64880
semiconductor, exciton bound to neutral impurities complex binding energy and stability 2−77835
semiconductor, heavily doped, localization of band tail states, elec. cond. study 2−71922
semiconductor, heavily doped, temp. effects on two-band model for neg. magnetoresistance 2−64970
semiconductor, high-resist. compensated, impurity photocond. kinetics 2−72058
semiconductor, III-V, transition metal doped, anomalous props. 2−68405
semiconductor, impurity band density of states, tight binding approx. 2−68413

Crystal electron states continued
impurity states and effects continued
semiconductor, impurity level activation energy, Hall effect determ. 2—80958
semiconductor, impurity profile, limitation of pulsed capacitance obs. 2—71506
semiconductor, incompletely ordered, rel. to exciton light absorpt. 2—78094
semiconductor, isoelectronic traps, effect on laser transitions, indirect gap materials 2—79217
semiconductor, kq representation 2—77902
semiconductor, laser beam self-focusing mechanism, by energy depend. carrier scatt. 2—59179
semiconductor, low temp. impurity scatt., transport coeffs. determs. 2—47885
semiconductor, many-valley, n-type, rel. to effects of light pumping on cond. 2—57204
semiconductor, n-type, heavily doped, model 2—61347
semiconductor, n-type, quantum transport theory inc. higher order scattering effects 2—47887
semiconductor, p-type, recomb. of excitons bound to deep neutral donors and acceptors 2—68682
semiconductor, spin states-bound exciton interaction, rel. to spin-flip Raman scatt. 2—57359
semiconductor, spin susceptibility of impurity band electrons, correl. effects 2—68520
semiconductor, trapping centres, defect related luminesc., two centre model 2—61680
semiconductor, with deep impurities, double injection 2—77923
semiconductor, with H-like local centres, multiphoton luminesc. satellites in strong e.m. field 2—61679
semiconductor carrier distribution determ., p-n junction C-V characteristic method with feedback 2—68440
semiconductor cyclotron resonance linewidth in quantum limit 2—51148
semiconductor film, impurity conc. determ. 2—71931
semiconductor II-VI cpds., donor and acceptor identification 2—50573
semiconductor surface contamination, obs. 2—53748
semiconductors, heat treatment and properties of doping element 2—84321
sensibilized luminescence, energy transfer from hot donor to acceptor 2—51363
slow vibrational relaxation, effect on Stokes shifted luminesc. and energy transfer 2—51374
spatial charge displaced by impurity scattering, T-matrix approach 2—51074
Stark effect, method of average moments 2—65246
substitional alloys, electronic relaxation calc. using single band model 2—47790
superconducting mag. alloys, localized bound state and impurity band props. 2—77873
superconductor, dirty, thermal conductivity in transition metals near upper critical field 2—77876
superconductor, effect on transition temp. calc. 2—57156
superconductor with dil. mag. impurities, Bogoliubov eqns. 2—71854
thermal ionization of deep centers in the space charge of semicond. 2—71921
transition metal, supercond. with non-mag. impurities, specific heat calc. 2—44061
transition metal, superconducting, with non-mag. impurities, thermal conductivity, two-band model 2—71874
trapped minority carrier thermal emission rates, meas. technique 2—71784
tunnelling, general theory and appl. to static impurity case 2—68275
tunnelling, impurity-assisted, microscopic theory 2—47794
two-electron theory of non-interacting surface and impurity states 2—44036
Ag-Au-Cu alloy, electron-impurity interaction, rel. to sp. ht. 2—75051
Ag-Au alloy, electron-impurity interaction, rel. to sp. ht. 2—75051
Ag alloy, impurity scatt., electron lifetimes, Fermi surface, de Haas-van Alphen meas. 2—61148
Ag halides, thermolum. and photocond., trap levels, meas. apparatus and technique 2—79389
AgBr, chemical sensitization by doping, electronic mechanisms 2—81545
AgBr, positron lifetime, illumination effects, at 300 and 77 K 2—77808
AgBr + AgCl(5%):$C^{5+}(N^{5+})(O^{6+})(S^{6+})$, high energy implantations, electronic environment of defects studied by obs. of positron annihilation photons 2—71507
AgCl:$C^{5+}(N^{5+})(O^{6+})(S^{6+})$, high energy implantation, electronic environment of defects studied by obs. of positron annihilation photons 2—71507
AgCl, positron lifetime, illumination effects, at 300 and 77 K 2—77808
Al-Al_2O_3-Pb junction, impurity assisted tunnelling, 4.2-148 K 2—44140
Al-Au alloy, dilute, Mathiessens rule deviation due to scatt. processes 2—80969
Al-Cr dilute alloys impurity resistivity, temp. dependence 2—84278
Al-Mn dil. alloys, high temp. impurity resist. 2—44050
Al-Mn dilute alloys impurity resistivity, temp. dependence 2—84278
Al-based dilute alloy, reson. and charge neutrality, semiphenomenological model 2—71783
Al, elec. resist. due to interstitials, pseudopotential method 2—57152
Al, temp. depend. of charge perturbation around 3d-transition metal impurities 2—44452
Al alloy, dil., semiphenomenological model for reson. and charge neutrality 2—68291
AlGaAs-GaAs heterojunctions, band filling process 2—47941
Al_2O_3, ruby, energy levels of Cr^{3+} pairs 2—68633
As_2S_3, vitreous, localized state distrib., Fermi level analysis from transient photocond. obs. 2—47913
As_2Se_3 glass, high field cond., Poole Frenkel model 2—51134
$3As_2Se_3.2Sb_2Se_3$ films, amorphous, trap level location 2—54187
$AuGa_2$, Pd doping effect on Fermi surface 2—51078
$BaTiO_3$:Y phase transition effects on d.c. conductivity 2—68468

Crystal electron states continued
impurity states and effects continued
Be-transition metal alloys, electron scatt. 2—71791
Bi:Sn, magnetoacoustic oscills. 2—54032
Bi:Te deposits, optical and electrical props. 2—75255
Bi, frozen-in defects, quenching effects on thermoelectric power and magnetoresistivity 2—68336
BiI_3, localized states and electron-hole processes, photopolariz. and photoluminesc. obs. 2—61706
Bi_2S_3:Pb, capture level parameters, thermo-stimulated cond. study 2—71923
$Bi_{1-x}Sb_x$:Cd(In)(Sn), rel. to elec. props., 180-420K 2—61301
$Bi_2Te_{3-x}Se_x$, temp. depend. of electron effective mass and mobility, influence of impurity scattering 2—81099
C, turbostratic film, free carrier conc., electron traps, spectral determ. 2—78080
CaF_2:Mn, trapping centres from thermoluminescence and thermally stimulated exoelectron emission 2—68699
CaF_2-Nd^{3+}, energy level shifts at oxygen^2 compensated Nd sites 2—94229
CaS phosphors, self activated emission, study of trap depths and nature of trapping centres 2—54473
$CdCl_2$:Co^{2+}, obs. of vibrational-electronic coupling in high resolution spectrum of spin forbidden band 2—81356
$CdIn_2S_4$, intrinsic and Co^{2+} doped, effect of S vacancies 2—68735
CdP_2, rel. to radiative recomb. mechanisms 2—72394
CdS:Ag(Al), field quenching, influence of doping 2—54170
CdS:Cu, trapping parameters, photocond. response, i.r. quenching, photochem. effects 2—65000
CdS, acceptor-donor recomb. emission at 510 nm 2—61691
CdS, donor-acceptor luminesc., temp. depend. 2—48261
CdS, doped, 2.0 eV luminesc. band, donor-acceptor recomb. model 2—84539
CdS, exciton-impurity complex, optical absorp. anomalous intensity 2—72324
CdS, temp. quenching of photocond., themoelec. skin effect in presence of shallow levels 2—81171
CdS, with Ag, Cu and In impurities, photocond., spectral sensitivity curves 2—72059
CdS film, electron mobility and scatt. rel. to grain boundaries and surfaces 2—61149
CdS hot electron mobility 2—84276
$CdS_{1-x}Se_x$:Mn, e.p.r. study 2—72481
CdSe:Ag, thermal stimulus current 2—51151
CdSe, elec. active defect conc., elec. behaviour between room temp. and 600C 2—61305
CdSe, temp. quenching of photocond., thermoelec. skin effect in presence of shallow levels 2—81171
CdSe films, energy spectrum and nature of trapping centres detn. by induced impurity photocond. method 2—71501
CdSe films, energy spectrum and nature of trapping centres detn. by induced impurity photocond. method 2—71501
CdSe powder, Cu, Cl_2 impurities, negative resistance behaviour 2—71919
n-Cd_2SnO_4, vacancies as donor states 2—51137
$CdSnP_2$, photocunductivity spectra in extrinsic (impurity) range, and effects of doping 2—57256
CdTe:In, Cu, high temp. cond., impurity effects 2—61303
CdTe:In, self-compensation calc. assuming Cd vacancies and impurity-vacancy complexes 2—47889
CdTe:Li, self-compensation and interaction of Li with defects 2—75107
CdTe, compensation by intrinsic point defects, elec. cond. obs. 2—84334
CdTe, i.r. absorpt. spectra, shallow donor impurity transitions, polaron Zeeman effect 2—61634
CdTe, ion implantation doping 2—74790
CdTe, Poole-Frenkel effect of holes 2—44119
p-CdTe film, rel. to photolum. and photosensitivity 2—48217
$Cd_{1-x}Zn_xS$:Mn, e.p.r. study 2—72481
Cds, cathodolum., donor-acceptor pair emission, electron irrad. damage effects 2—54478
Cr and alloys, excitonic phase, thermoelec. power calc. 2—65077
CsBr, CsBr:Tl, CsBr:In, luminesc. crystals, exciton and hole migration 2—48242
Cu-Mn dil. alloys, neck effect in ang. correl. of positron annihilation 2—44046
Cu-based dilute alloy, reson. and charge neutrality, semiphenomenological model 2—71783
Cu, electron scatt. by dislocations, de Haas-van Alphen effect, obs. 2—61214
Cu alloy, dil., semiphenomenological model for reson. and charge neutrality 2—68291
CuCl(Br)(I) layer, on Ag or Cu, rel. to light sensitivity spectra 2—77966
CuNi dilute alloys, virtual-bound-state determ. from Anderson model analysis of absorptivity spectra 2—51337
Cu_2O, defect levels, rel. to near i.r. absorpt. and photocond. 2—54420
Cu_2Te-Ag_2Te systems, elec. and galvanomag. props., influence of defects, compensation hopping cond. and scattering of carriers 2—84323
D_2:Xe, vacuum u.v. study of Wannier states, obs. of host isotope effect on linewidth 2—51341
EuO:Gd, dopant effect on band structure, investigation using high-resolution photo-emission meas. 2—68497
EuO:Gd, doping mechanisms, determination from dopant effects on plasma and lattice vibrations 2—68397
EuO:Gd, exchange-induced imperfection ionization, investigation using optical absorption and Faraday rotation 2—68598
EuO, doped, metal-semiconductor transition 2—77842
$Ga_{1-x}Al_xAs$:Si layers, Al conc. effect on amphoteric behaviour of Si 2—51153
GaAs:Cr, deep levels and radiative recomb., photolum. and photocond. study 2—71927
GaAs:Cu, behaviour in strong elec. field 2—71904
GaAs:Cu, elec. props., impurity centre form., conditions and mechanism 2—64985
n-GaAs:Cu film, epitaxial, carrier mobility, impurity effects, scatt. by space charge centres 2—64983

Crystal electron states continued
impurity states and effects continued
n-GaAs:Ge film, epitaxial, degenerate, forbidden gap, traps 2−44114
GaAs:Se, donor self-compensation 2−75110
GaAs:Si, boatgrown and pulled, B impurity, i.r. local mode absorption spectra, comparison 2−61640
GaAs:Si p-n junction, reverse branch of I-V characts. and breakdown 2−71959
GaAs:Sn exciton energy level structure from photoluminescence props. analysis 2−44427
GaAs:Zn(Si)(Te), impurity effects on dislocation velocity 2−68028
GaAs-Pb Schottky barrier tunnel junction, zero-bias anomaly, irrad. effects 2−71960
GaAs, chem. shift in binding energies of Zn and Cd 2−65001
GaAs, epitaxial, rel. to photolum., 8250-8450Å 2−61694
GaAs, heat treated, acceptor centres, Hall effect and photoluminesc. obs. 2−61343
n-GaAs, heavily-doped, gradual mobility transition in band tails 2−61342
n-GaAs, heavily doped, band-to-band recomb., quantum efficiency, lifetime, rel. to impurity conc. 2−61697
GaAs, heavily doped, localization of band tail states, elec. cond. study 2−71922
GaAs, impurity electroabsorption 2−65258
GaAs, impurity induced i.r. absorpt., calc. by Green's function technique 2−61639
n-GaAs, mag. field effect on impurity cond. 2−81085
GaAs, n- and p-type, electron irrad., defect levels, Hall effect and resist. study 2−80992
GaAs, photothermal ionization of shallow donors, photocond. obs. 2−81177
GaAs, rel. to many-photon absorp., carrier generation obs. 2−84519
GaAs epitaxial film, doping level and impurity distrib., substrate orientation effects 2−47436
p-GaAs epitaxial layer, gas transport deposition, orientation effects on doping level 2−71387
GaAs LPE-grown, luminesc., shallow acceptor identification 2−54454
GaAs$_{1-x}$P$_x$:SeTe, donor self- compensation 2−75110
GaAs$_{1-x}$P$_x$:Zn, direct gap, acceptor levels rel. to photoluminesc. spectra 2−84538
GaN:Zn(Cd), luminescence, acceptor site location and new emission band obs. 2−72398
GaP:Bi, luminesc., kinetics due to bound excitons, 77.3K 2−65292
GaP:Ge, e.p.r., linewidth and g-value 2−72484
GaP:N(Bi), exciton binding to impurities, uniaxial stress effects 2−75108
GaP:O p-n junction, deep double electron O trap transitions, photocapacitance obs. 2−75013
GaP:Sn, strain-depend. e.p.r. and spin-valley coupling of donors 2−84570
in-GaP:Te,Zn,O, mean electron conc., electrolum., influence of Te content 2−57381
p-GaP:Zn,O, donor electron capture cross sections, rel. to quantum efficiency limits 2−68681
GaP:Zn,O, luminesc. time response rel. to multiple trapping at Zn-O impurity centres, 4-120K 2−61696
p-GaP:Zn,O, photolum. efficiency and kinetics of Zn-O complex formation 2−51368
GaP, chem. shift in binding energies of Zn and Cd 2−65001
GaP, electrically active background impurities, energy conc. and distrib. determ. by thermal release of space charge 2−80939
GaP, light emitting properties, radiative transitions 2−61724
GaP, pair photolum., peak energy, excitation intensity depend. 2−75318
p-GaP(Zn,O), p-GaP(N), minority carrier lifetime, luminesc. decay time obs. 2−48221
GaSb:Te, lightly doped, photolum. at high excitation levels 2−72402
GaSb:Te,Zn, thermal e.m.f. rel. to carrier conc., 300K 2−54248
GaSb:Te(Zn)(Te+Zn), heavily doped, photolum. at high excitation levels 2−72403
GaSb, piezoemission, stress effects on impurity lines 2−48179
p-GaSb, undoped, acceptor states, photocond. and photoluminesc. obs. 2−61708
Ga$_2$Te$_3$, semicond., radiation stability as result of stoichiometric vacancies 2−71906
Ge:As, far i.r. absorpt., impurity conc. and compensation effects 2−68642
p-Ge:Au, photocond., electron capture coeff., excess free carrier distrib., surface recomb. effects 2−81164
Ge:Cu, donor compensation density determ. by Hall and mobility analysis 2−51166
Ge:Cu, heated by h.f. elec. field., hot electron recomb., electron capture 2−64972
Ge:Cu, recomb. cross section for holes at singly ionized impurity 2−51215
Ge:Mn, nonlinear IV characts., exclusion and charge exchange between impurity levels 2−75115
Ge:Ni, electron and hole capture rates, photomagnetoelec. and photocond. studies 2−75171
n-Ge:P(As), resist. decrease due to donor spin reson. 2−81106
Ge:Sb(P)(As), heavily doped, temp. depend. of resist. 2−71940
Ge, acceptors, Zeeman effect, group theoretical study 2−84264
Ge, donor excited states, Zeeman effect, photocond. spectra obs. 2−75172
Ge, dopant influences on dislocation velocity and electron trapping 2−50674
n-Ge, effect of ionized impurity scattering on Faraday rotation 2−51302
Ge, heavily doped, 0.02-300K, cond. mechanism 2−81109
Ge, hopping cond. rel. to temp., doping, uniaxial compression 2−65013
Ge, hot electron capture by Cu^{2-} centres 2−71936
n-Ge, hot electron charact., high-field scatt. mech. 2−61354
n-Ge, impurity breakdown, size effects, at 4.2K 2−65014
p-Ge, impurity scatt. of warm holes 2−44124
Ge, γ-irrad., donor-vacancy complexes, prod. kinetics and energy spectrum 2−47382

Crystal electron states continued
impurity states and effects continued
Ge, γ-irrad., O-free, divacancy-donor complexes 2−71943
n-Ge, phonon-assisted, tunnelling, impurity dependence 2−54195
p-Ge, photon-induced hopping on acceptors, theory 2−47923
Ge, quadratic Zeeman splitting of donor lines 2−57350
Ge, scatt. of holes by neutral acceptors 2−71941
n-Ge, thermal magnetocond., electron- phonon scatt., doping effects 2−81084
n-Ge microwave Faraday effect, multiple reflections and lattice and impurity scatt. effects 2−75257
Ge p-n junction, γ-ray detector, space charge region polarization, impurity centre charge exchange 2−65026
Ge p-n junction, microplasma turn-on delay time rel. to trapping levels, 77K 2−65025
Ge single crystal, exciton-impurity complex, luminesc. 2−68692
Ge(Li) diodes, trapping parameters, chemical impurities effect 2−49666
p-Hg$_{1-x}$Cd$_x$Te, carrier freeze-out and acceptor energies determ. 2−57194
HgTe, rel. to galvanomag. props. in high mag. field, 4.2, 77 and 300 K 2−64988
n-InAs, compensated, absorpt. edge obs. 2−75297
n-InAs, heavily doped, impact ionization, elec. field depend. 2−81087
InP, doped with Cu, Fe or Cr, prep. and props. 2−83895
InP, free and bound electron transitions to acceptors, 1.3776 eV emission 2−72411
InP, group IV doped, donor and acceptor levels 2−47272
InP, photoluminescence spectra of excitons bound to group II acceptors 2−84279
InSb:Fe, crystallisation features rel. to dopant, hole and acceptor distribution 2−53604
p-InSb:Ge, electrical instability in presence of elec. field 2−71884
InSb:Te, Zn, carrier distrib., thermal e.m.f., degree of compensation 2−44101
InSb:Zn,Ge, energy levels of shallow acceptors, far i.r. absorp. obs. 2−75296
n-InSb, electric field modulated laser cyclotron resonance, impurity and cond. electron resonance obs. 2−81021
n-InSb, electron-hole pair distrib., impact ionization phenomena, mag. field effects 2−61317
n-InSb, heavily doped, impact ionization, elec. field depend. 2−81087
n-InSb, impurity band and shallow donors, far i.r. absorp. obs. 2−81389
InSb, n-type, electronic structure study by a microwave beat method 2−84246
n-InSb, recomb. radiation from impact-ionized shallow donors 2−68707
InSb density of states in impurity bands 2−80961
In$_2$Te$_3$, semicond., radiation stability as result of stoichiometric vacancies 2−71906
IrB$_{1.1}$, rel. to elec. props. 2−47657
KCl:Na$^+$, X-ray irrad., hole centres, conversion and struct., optical absorpt. 2−84523
KCl crystal, with a divalent activator, localized one-electron states 2−84287
KI:Tl, recomb. and capture probabilities of F-centre electrons 2−84285
La:Ce, skew scattering of electrons, Hall effect obs. 2−75055
Li-Mg(Al) solid solution, Green function calc. 2−75029
LiF X-irrad., capture levels, rel. to thermolum. 2−65313
Mo$_{1-x}$M$_x$Ga$_4$, M=Nb, Ru, Mn, Fe, Co, exchange field on conduction electron spins due to paramagnetic impurities 2−77862
MoO$_3$ film, donor band and Schottky barrier obs. using dielectric relax. currents 2−68453
NaCl:Cu, one electron energy levels, charge consistent extended Huckel approach 2−77831
NaCl, NaCl:Ca, γ-irrad., d.c. conductivity obs., room temp. −70°C, electronic and ionic contribs., shallow traps 2−57231
NaOH ice glass at 77K, matric ENDOR linewidth of trapped electrons 2−57402
Nb-Sn sinter material, supercond., screening behaviour on addition of Cu, Ag or Au 2−75061
Pb-Mn superconducting film, conduction electron-mag. impurity interaction rel. to tunnelling conductance 2−71851
PbBr$_2$:Fe, Cu hole cond., hole trapping at Fe^{2+} and Cu$^+$ centres 2−61322
PbO film, acceptor levels, optical absorp. 2−57352
PbS(Se)(Te), charge dislocation-acceptor interaction, effect on mech. props. 2−50784
PbTe:In, donor level above the bottom of the cond. band 2−84281
PbTiO$_3$, conversion to semicond. state by doping resist. positive temp. coeff. 2−81098
Pd alloyed with nonmag. impurities, magnetoresist., carrier scatt. 2−61152
Se: Cl, As film, vacuum evap., transport props., time resolved drift technique 2−44104
Se, non- crystalline, impurity effects on elec. props. 2−61326
Si:Ag deep level props., photoconductivity decay and thermally stimulated current obs. 2−61363
Si:Al, ground state energies from pseudopot. method 2−61357
Si:As, P, Sb, ground state wavefunctions of shallow donor electrons, Fermi contact consts. 2−71950
Si:Au, m.o.s. capacitance meas. of Au levels 2−61362
Si:Au diode, thermally-stimulated current from deep-lying trapping levels 2−68419
Si:B, ground-state energies from pseudopot. method 2−61357
Si:B, shear deform. pot. consts. of B acceptors ground state, piezospectroscopy obs. 2−75306
Si:B implanted, photocond. obs. 2−44126
Si:B impurity enhanced diffusion 2−50693
Si:Ga, ground state energies from pseudopot. method 2−61357
Si:In, ground state energies from pseudopot. method 2−61357
Si:K, doped surface layers, donor props. and diffusion 2−65019
Si:Na(K), elec. props., impurity atomic radius effects 2−71948
Si:Ni, photocond., thermal and field quenching by impurity electron capture 2−65088
Si:P, absorpt. due to transitions to cond. band edge region 2−72347

Crystal electron states continued
impurity states and effects continued
Si:P, electron drag rel. to impurity centre photoionization, photo-e.m.f. 2-65089
Si:P, heavily doped, temp. depend. of resist. 2-71940
Si:P, implanted, carrier density and mobility, depth distrib. 2-80993
n-Si:P, rel. to piezoresist. and piezo-Hall effect, 4.2, 77, and 300K 2-71945
Si:P impurity enhanced diffusion 2-50693
Si:P quadratic Zeeman effect of donor lines in photoexcitation spectrum, transverse effective mass 2-81348
Si:S, deep donor levels, pressure depend. 2-80962
Si:Zn, many-band pseudopotential calc. of photoioniz. 2-61357
n-Si:Zn, photoelectronic props. of Zn centres, Zn^{2-} energy level, centre density 2-61449
Si-SiO_2 interface, ion implanted, deep energy level detn. by m.o.s. technique 2-80938
Si, acceptors, Zeeman effect, group theoretical study 2-84264
Si, BCl_3, diffused p-n junction formation, minority charge carrier diffusion length obs. 2-44133
n-Si, Cd-compensated, current oscills. 2-71949
Si, cond. band. deform. potential const. from piezospectroscopy of donors 2-68438
Si, cyclotron reson. of electrons generated by impurity excitation with CO_2 laser 2-71947
Si, dopant influences on dislocation velocity and electron trapping 2-50674
p-Si, electron irrad., hole emission rates, activation energy and annealing of defects 2-54199
n-Si, fast electron irrad., vacancy capture and transfer between defect complexes 2-80694
Si, free hot carrier impact ionization obs. 2-54203
Si, ground state wave functions for shallow donor electrons 2-61361
Si, group V and VI donor states, multivalley effective mass approx. 2-54204
n-Si, heavy doping effects on elastic consts. under uniaxial stress 2-68066
Si, hybridization of atomic orbitals at structural defects 2-81005
p-Si, impurity scatt. of warm holes 2-44124
Si, isolated vacancy, elec. struct., many electron molecular orbital method 2-47935
Si, Mg donor levels, excitation spectra 2-72351
Si, p-n diode, γ-irrad., impurity effects, photovolt. effect obs. 2-61358
Si, quadratic Zeeman splitting of donor lines 2-57350
Si diode, p^+-n and n^+-p, with Au impurity in base, barrier capacitance 2-71979
n-Si inversion layer, two dimensional impurity states 2-51170
Si pn junction, proton irrad., deep centre spatial distrib. from capacitance meas. 2-68443
n-Si proton bombardment induced shallow donors, elec. props. 2-61355
Si wafer, surface defect generation on reoxidation in H_2O vapour during B diffusion 2-64672
α-SiC, i.r. absorpt. spectra due to electron transitions in deep impurity centres 2-78106
SiO, amorphous, trap levels, thermally stimulated capacitor discharge study 2-54188
$SrTiO_3$, rel. to fundamental absorpt. edge, 6-300K 2-78107
Ta-Ta_2O_5-Au, m.i.m. devices, electron energy distrib. for Schottky/Poole-Frenkel conduction 2-68456
Te, acceptor ground state under hydrostatic pressure, variational calc. 2-61192
Te film, polycryst., on mica, elec. transport props. 2-61330
Te films, amorphous, localized states, photoemission quantum yield 2-68422
$(ThO_2)_{1-x}(YO_{1.5})_x$ solid soln., scatt. centre nature rel. to electronic contrib. to mixed conductivity 2-75100
TiO_2:Fe^{3+}, hole trapping by surface ferric acceptor states, Mossbauer obs. 2-84236
TiO_2:Li,V,Cr,Mn,Fe, transition metal impurity levels, esr determ. 2-44117
TiO_2, reduced, bound polaron hopping and mag. impurity effects 2-47902
V^{3+} complexes, trigonally distorted octahedral, lattice-ion interactions in the ligand field theory 2-81205
VO_x, localized states, elec. props. study 2-64991
Xe:^{45}Ca β-decay, optical excitation of the daughter atoms Sc. 2-84244
Y-Ce alloy, Kondo effect under press. 2-71839
YF_3: Yb, Ho, diffusion and transfer of optical excitation 2-61714
$ZnCd_{1-}S$, steeply graded, formation by diffusional doping and luminescence 2-72444
$Zn_2In_2S_5$ single crystal, local levels, rel. to photocond. relax. 2-75175
ZnO:Cu film, amorphous, energy spectrum, optical absorp. and elec. cond. obs. 2-68421
(ZnO-MgO):Fe,O photoconductor transient effect, shallow trap obs. 2-84377
ZnO, differential absorption spectrum on adsorption of molecules of donor-acceptor type 2-68651
ZnS:B, rel. to luminesc., 400-800 nm, 110, 295 and 430K 2-75322
ZnS:Cu, green luminesc., recombination by tunnelling, donor-acceptor model 2-48236
ZnS:Cu, rel. to surface, volume and contact components of current 2-71918
ZnS:Mn^{2+}, ^4E level, uniaxial stress effects, absorpt. study 2-84506
ZnS-Cu,Co,Cl, differences between optical and thermal depths of electron traps 2-51395
ZnS, differential absorption spectrum on adsorption of molecules of donor-acceptor type 2-68651
ZnS, rel. to many-photon absorp., carrier generation obs. 2-84519
ZnS single crystal, homogeneous, wide-gap semiconductor, rel. to u.v. electroluminesc. 2-68712
$ZnS_{1-x}Se_x$, thermoluminesc. rel. to stimulated cond. with persistent memory 2-75104
ZnSe:Ag, thermal stimulus current 2-51151
ZnSe, differential absorption spectrum on adsorption of molecules of donor-acceptor type 2-68651
ZnSe, optical props. of subsitutional donors 2-51372
ZnSe, pair photolum., peak energy, excitation intensity depend. 2-75318
ZnSe, rel. to many-photon absorp., carrier generation obs. 2-84519
ZnTe, absorpt. due to acceptor levels 2-57353
ZnTe, double-acceptor cathodolum. 2-54480
ZnTe Schottky barrier, admittance spectroscopy of deep impurity levels 2-61391

plasma
alkali metals, interband absorpt., plasmon sidebands 2-51334
Auger emission, Auger electron interaction with surface plasmon 2-48010
collective excitations, fast-electron spectroscopy, quantized formulation 2-68313
degenerate, Landau damping 2-54119
degenerate Fermi gas, high density, high freq. conductivity 2-57105
dielectric film, surface phonons and electron energy losses, metal contact influence 2-47829
dielectric layer, magnetic field effect on plasma-wave dispersion 2-61208
electron gas, degenerate, quasi-particle and plasmaron properties 2-68315
electron irrad., longit. e.m. wave excitation 2-71817
electron-plasmon interaction 2-77795
elementary excitations, book 2-71806
e.m. waves in inclined mag. field, Drude theory, one-band model 2-64901
insulator, electronic correlation, field-theoretic model 2-68411
magneto-optical obs. of collective excitations, review 2-72294
many-body problems at metal- semicond. junctions, surface plasmons and e-e screened interac. 2-75119
metal, electron gas, passage of a positron, energy loss 2-80967
metal, irrad., void clusters, plasmon interaction 2-80677
metal, localized modes of excitation in vicinity of an impurity 2-64902
metal, magnetoplasma surface waves, dispersion relations 2-61206
metal, magnetoplasma surface waves 2-44042
metal, plasmon dispersion relation for electron liquid 2-54117
metal, plasmon theory of surface energy 2-64893
metal, positron vertex renormalization of effective electron-positron interaction 2-54115
metal, positron-plasmon interaction 2-57142
metal, surface plasmons, collective mode excitation in electron and ion-solid scatt., theory 2-51087
metal, two-band, acoustic plasmon phenomena 2-71814
metal films, surface plasmon excitation by transmission of fast electrons 2-47828
metallic films, free and adsorbed, plasmon excitations 2-47826
metals, charging effects in surface plasmon 2-68317
Mott transition, plasma oscillations 2-80987
permittivity, including effects of diffusion 2-75039
photoconductor, plasma injection, basis of new photocond. mode 2-54250
plasma echo from electron phonon interactions in ionic crystal 2-44041
plasma propag. and dispersion in periodic lattices 2-77803
plasmon energy loss shifts rel. to specimen contamination 2-80935
plasmons, multistream medium, nonlinear interactions 2-82223
semiconductor, compensated, thermal current instability 2-75088
semiconductor, degenerate, magnetoplasma surface waves 2-44042
semiconductor, degenerate , scatt. by plasmons rel. to free carrier absorp., quantum theory 2-51329
semiconductor, electron-hole plasma, eddy currents in oscill. mag. field 2-80995
semiconductor, electron-hole plasma, surface generation of current carriers during Θ pinch 2-61294
semiconductor, electron-plasmon coupling, cyclotron resonance harmonics 2-54409
semiconductor, e.m. wave propagation and eigenoscillations, band struct. and elec. field effects 2-77892
semiconductor, magnetoactive plasma, overheat instability of drifting waves, theory 2-61293
semiconductor, magnetooptical transitions, plasmon assisted, cyclontron reson., lineshape calcs. 2-68320
semiconductor, optically induced plasma wave instabilities 2-61209
semiconductor, polar, magnetoplasmon surface waves, retardation effects 2-68377
semiconductor, Raman scatt. from coupled LO-phonon-plasmon modes, theory 2-68663
semiconductor, rel. to stimulated emission 2-61681
semiconductor, surface magnetoplasmons, theory 2-47920
semiconductor p^+nn^+ junctions, trapped plasma mode, obs. 2-47940
semiconductors, recombination by excitation of plasmons 2-81083
solids, surface plasmons, microscopic theory 2-84277
static dielec. const. in presence of strong e.m. wave 2-77843
surface plasmon, secondary electron spectra obs. from ion bombarded solid targets 2-51229
surface plasmon dispersion, electron short range correl. effects 2-61205
surface plasmon dispersion reln. determ. using electron microscopy 2-56635
surface plasmon radiation, scanning electron microscopy of metals, Lilienfeld radiation 2-79131
surface plasmon resonance effect in holography 2-59197
surface plasmons, role in Van der Waals attraction 2-51088
surface plasmons and optical phonons coupling in semi-infinite medium 2-47827
surface plasmons on metal, angular dependence and polarization of light emitted due to roughness 2-75040
transition metal, surface energy, plasmon theory 2-64894
uniaxial conducting crystal, in magnetic field, e.m. wave propagation and coupled cyclotron-plasma resonance 2-84280
van der Waals between cond. mols. 2-47824
Ag, plasmon gains in secondary electron spectrum 2-54280
Ag, spherical particles, radiative decay of surface plasmons 2-51332
Ag, surface plasmon excitation by subwaves produced by gratings 2-64905
Ag cylinder, surface plasma waves, optical refl. study 2-61210

Crystal electron states continued
plasma continued
Ag evaporated film, piezorefl. and piezotransmission studies 2−81366
Al, detection of characteristic energy losses for low energy electrons 2−51091
Al, e.m. wave transmission, helicon waves, Gantmakher- Kaner excitations, sound waves, quantum effects 2−57135
Al, surface plasmon dispersion, inelastic LEED 2−51090
Al (100) surface, LEED, elastic and inelastic scatt., bulk and surface plasmon excitation 2−50434
Al cylinder, surface plasma waves, optical refl. study 2−61210
Al film, photoelec. emission due to nonradiative surface plasma waves 2−44200
Au, electron energy loss spectra, surface plasmon excitation 2−44043
Bi, Alfven wave amplitude and carrier relax. times 2−51092
Bi films, charact. electron energy loss spectra 2−44044
Bi single crystals, Alfven wave damping from effective charge-carrier relaxation times obs. 2−68316
BiSb alloy, voltage instabilities in electron-hole plasma 2−81095
CdO microcrystals, coupled surface phonon-surface plasmon modes, i.r. absorpt. 2−84263
CdS, electron energy loss spectra, rel. to interband transitions, bulk and surface plasmons 2−68318
CdSe, electron energy loss spectra, rel. to interband transitions, bulk and surface plasmons 2−68318
CdTe, electron energy loss spectra, rel. to interband transitions, bulk and surface plasmons 2−68318
Cu, e.m. wave transmission, helium propag., Gantmakher-Kaner oscill. 2−61211
Cu films, far-i.r. transmission, surface plasma oscillation obs. 2−54401
EuO:Gd, plasma resonance, dopant effects 2−68397
GaAs, high purity, plasmaron coupling rel. to mag. field shift of stimulated emission 2−61698
GaAs, rel. to radiative recomb. of screened excitons 2−72408
Ge, electron-hole plasma conductivity, plasma density depend. 2−61212
Ge, screw instability in strong mag. fields 2−77844
Ge p-n junction, bistable state of microplasmas 2−71963
Ge p-n junction, microplasma turn-on delay time rel. to trapping levels, 77K 2−65025
$HgS_{0.2}Se_{0.8}$ solid soln., plasma i.r. reflection at 100 and 300K 2−54404
n-InSb, critical fluctuations, l.f. current noise, 4.5-12K 2−68319
n-InSb, electron-hole plasma form. rel. to current and voltage instabilities 2−57137
InSb, electron-hole plasma in mag. field, carrier wave growth 2−61316
p-InSb, i.r. absorpt. rel. to hole and plasma currents 2−72335
n-InSb, large amplitude current and voltage oscills. 2−57180
n-InSb, plasma echo oscillations 2−57195
n-InSb, quenching of sound amplification and e.m. wave radiation by holes 2−71929
n-InSb, surface plasmon-phonon interaction 2−71930
InSb exciton-hole plasma prod. by laser irrad., two-photon absorpt., direct recomb., 77K 2−80972
n-InSb mixed plasmon-phonon surface modes 2−81006
K, on W(100), surface plasmon losses, energy loss spectra obs. 2−64903
K, optical props. and surface plasmon states 2−71819
Mg, electron emission, secondary, Auger satellite rel. to plasmon absorpt. and double ionization processes 2−77971
Mo, plasma satellites in secondary electron spectrum 2−72099
Na, optical props. and surface plasmon states 2−71819
Ni (100) surface, plasmon angular profiles, LEED obs. 2−51093
Pt film, surface and volume plasmons, for u.v. reflectance obs. 2−61653
Rb, on W(100), surface plasmon losses, energy loss spectra obs. 2−64903
Si, amorphous, secondary electron emission obs. rel. to electronic struct. 2−61454
Si, radiative two-electron transitions in the electron-hole plasma 2−78139
Si p-n junction, microplasma optical interactions 2−65021
SiC, Raman scatt. from coupled LO-phonon-plasmon modes 2−68663
TlBr, rel. to optical consts. detn. by electron energy loss spectra 2−61129
TlCl, rel. to optical consts. detn. by electron energy loss spectra 2−61129
TlI, rel. to optical consts. detn. by electron energy loss spectra 2−61129
V_2O_3, refl. spectra, plasma freq., free carrier effective mass 2−81407
W (110) surface, plasmon angular profiles, LEED obs. 2−51093
ZnS, electron energy loss spectra study 2−75111
ZnSe, electron energy loss spectra study 2−75111
ZnTe, electron energy loss spectra study 2−75111

polarons
— 2−61204
alkali halides, optical absorption, reson. of electronic polaron 2−72313
anthracene, electrons and holes interaction 2−80982
antiferromagnetic polaron, self-trapped, T=0 K, theory 2−71812
benzene, liquid, polaron like states, charge carrier propagation 2−51146
condensed matter theory, intermediate coupling and dispersion relation 2−47822
conductions from band to hopping types, Hall effect 2−84230
disordered material, small polaron hopping and lattice relaxation 2−61144
enery spectrum of bound polaron 2−61203
Feynman theory, improvement 2−61202
hydrogen-bonded glasses, Frohlich polaron model for Compton electron trapping 2−44040
insulating solids 2−57186
ionic crystal, surface polarons, binding energy and ground state wave function 2−84267

Crystal electron states continued
polarons continued
model for photodetachment spectra of trapped electrons in spherical pots. 2−53435
molecular cryst., excitonic polarons, band narrowing and band shifts 2−44039
naphthalene electrons and holes interactions 2−80982
nonmetal, correl. formulae 2−51086
organic solid, polaron effects in the nearly atomic limit of the Hubbard model 2−61204
piezoelectric, simultaneous strong and weak coupling 2−84268
semiconductor, cubic, Hall mobility calc. 2−68383
semiconductor, paramagnetic, magnetic polaron props. 2−47880
semiconductors, ionic, ground state energy for polaron bound to Coulomb potential 2−47821
small polaron absorption, in high elec. fields 2−57344
spinel ferrites, difference between Hall and drift mobility values in framework of Hall theory of small polaron 2−75083
transport properties, acoustic phonon coupling case, theory 2−61201
weakly coupled optical, energy-momentum relation 2−64900
$BaTiO_3$, ferroelectric ordering effects on formation 2−68468
$BaTiO_3$, temp. depend. of carrier mobility explained on small polaron model 2−81100
CO, rel. to temp. depend. of carrier mobility 2−77820
CdS, cyclotron reson. of piezoelec. polarons, far i.r. 2−71924
CdTe, i.r. absorpt. spectra, shallow donor impurity transitions, polaron Zeeman effect 2−61634
EuO, insulator-metal transition and bound mag. polarons 2−80975
Fe_3O_4, high temp. polaronic semicond. i.r. reflectivity obs. 2−61265
N_2, rel. to temp. depend. of carrier mobility 2−77820
NaI, V_k polaron, temp. dependence of jump frequency and diffusion constant 2−71813
$Na_xV_2O_5$, liq., elec. cond. mechanism 2−83795
NiO, bound polaron hopping 2−47899
O_2, rel. to temp. depend. of carrier mobility 2−77820
RbI, V_k polaron, temp. dependence of jump frequency and diffusion constant 2−71813
TiO_2, polaron mass calc. using Hall mobility obs. 2−57174
TiO_2, reduced, bound polaron hopping and mag. impurity effects 2−47902
TlBr(Cl), polaron effective mass 2−47830
V_2O_5-Na_2O-Fe_2O_3 system, liq., elec. cond. mechanism 2−83796
YIG(Si), reversible photoelectromagnetic effects, polaronic charge transfer theory 2−54259

surface
adsorbate covered surface, field emitted electron energy distribs. 2−48013
anthracene, exciton states, luminescence 2−54461
anthracene, reflection and luminescence spectra, evidence for surface states 2−44408
anthracene carrier trapping, involving transient photoinjection current 2−57200
appearance potential spectroscopy 2−81361
Auger emission, kinematic theory, dynamic theory 2−48010
bimetallic surface, adhesion bonding in terms of electronic struct. of combined metals 2−74652
Cambridge surface states, tunnelling and electron field emission theory 2−47814
chalcogenide glasses, cond. skin form. mechanism 2−54190
cubic lattices, electronic surface states calc. 2−47815
cubic tight binding solid, anisotropic oscill. indirect interact. between adatom pairs 2−47146
dielectric film, surface phonons and electron energy losses, metal contact influence 2−47829
dielectric layer, magnetic field effect on plasma-wave dispersion 2−61208
1,1′- diethyl-2,2′-cyanine, adsorbed on Ag halide emulsion grains, J-aggregates props. 2−81027
diode, semicond.-insulator-semicond., rel. to freq. depend. complex admittance 2−61385
film, semicond., transport coeffs. rel. to surface states, Hall and Seebeck coeffs. 2−47884
film, thermally stimulated exo-emission obs. 2−48008
film, two-dimensional energy bands, also bulk states 2−44037
finite one-dimensional model crystal potential calculation 2−72320
ionic crystal, surface polarons, binding energy and ground state wave function 2−84267
ionization probability for atom crossing metal/vacuum surface 2−48032
layered structs., h.f. surface wave amplification, rel. to carrier density, drift vel. 2−65006
LEED, as probe of electronic excitations of surface regions 2−50420
LEED intensity profiles rel. to spin-polarization, atomic core scatt., surface barrier struct. 2−77483
metal, b.c.c., from nearly free electron model 2−57130
metal, charges embedded in surface, self-consistent screening 2−47813
metal, image pot., static point charge interaction energy 2−61195
metal, interaction of conduction electrons 2−68327
metal, magnetoplasma surface waves, dispersion relations 2−61206
metal, nearly free electron, exact and approx. calc. 2−61197
metal, nearly free-electron, analytical calc. 2−61196
metal, normal and supercond., mag. field induced, contrib. to h.f. surface cond. 2−51083
metal, scatt. of ions, dynamic screening effects 2−64892
metal, Shockley states, model 2−71800
metal films, surface plasmon excitation by transmission of fast electrons 2−47828
metal films on alkali halides, electron surface scatt. influence on cryst. orientation 2−53565
metal-insulator boundary, surface exciton spectra, image forces 2−77921
m.i.s. devices, interface states, effect of ambient annealing 2−61397
m.i.s. struct., surface-state density determ. by photovoltage meas. 2−44144
m.i.s. structure, surface-state density determ. by photovoltage meas. 2−44143
m.i.s.i.m. structs., props. rel. to electron capture and liberation by surface traps 2−65037

Crystal electron states continued
- **surface** continued
  - m.o.s., state density at Si/SiO_2 interface 2−61403
  - m.o.s. capacitor for fast states obs. 2−68457
  - photoemission obs. technique 2−48018
  - polymer, insulating, rel. to polarization 2−47971
  - quantum mechanics of infinite chain of atoms 2−84286
  - self-consistent calcs. incorporating 3D nature of lattice potential 2−68300
  - semi-infinite cryst., one electron wavefunction in mixed represent 2−71770
  - semi-infinite medium coupling between surface plasmons and surface optical phonons 2−47827
  - semiconductor, compound, surface state models rel. to chemisorption induced conductivity changes 2−47886
  - semiconductor, degenerate, accumulation layer, surface bound state energy, mag. field effects 2−51124
  - semiconductor, Hubbard model, correlation with e.p.r. data 2−51154
  - semiconductor, polar, magnetoplasmon surface waves, retardation effects 2−68377
  - semiconductor, rel. to surface magnetovoltaic effect in Hall effect measurements 2−68424
  - semiconductor, surface space charge, Fermi level near band edges, Raman scatt. obs. 2−47919
  - semiconductor anomalous magnetoresistance, freq. response and effective carrier lifetime 2−65005
  - semiconductor surface quantization in inversion and accumulation layers 2−51123
  - semiconductor thin bar, β-conductive signal, effect of surface recomb. velocity 2−51130
  - semiconductors 2−75112
  - solid surfaces, conference, Boston Mass., USA, Oct. (1971) 2−47070
  - superconductor, type I, surface excitations in static magnetic field, energy spectrum and density of states 2−61236
  - surface plasmon dispersion, electron short range correl. effects 2−61205
  - tetracene, rel. to anomalous temp. depend. of photovoltaic current 2−72075
  - thin film, calc. of surface states with δ-function array model potential 2−75036
  - transition metal on transition metal surfaces, band struct., X-ray appearance pot. obs. 2−47816
  - transition metal surface, electronic density of states 2−75035
  - two-electron theory of non-interacting surface and impurity states 2−44036
  - zeolite surfaces, low-temperature emission excited by electron impact, rel. to adsorption and energy of surface states 2−77973
  - Ag, surface plasmon excitation by subwaves produced by gratings 2−64905
  - Ag cylinder, surface plasma waves, optical refl. study 2−61210
  - Ag halide, spectral sensitization by trapping of dye mobile positive holes 2−81552
  - Al-pyrolytic SiO_2-Si system, effect of heat treatment on density of fast surface states 2−77915
  - Al cylinder, surface plasma waves, optical refl. study 2−61210
  - Au, electron energy loss spectra, surface plasmon excitation 2−44043
  - Au film, thermoelec. power. rel. to surface scatt., Matthiessen's rule 2−64895
  - Be, mag. surface levels 2−84257
  - Bi whiskers, rel. to resist. oscills. in mag. field at 4.2 K 2−68338
  - CdO microcrystals, coupled surface phonon-surface plasmon modes, i.r. absorpt. 2−84263
  - CdS, electron energy loss spectra, rel. to interband transitions, bulk and surface plasmons 2−68318
  - CdSe, electron energy loss spectra, rel. to interband transitions, bulk and surface plasmons 2−68318
  - CdTe, electron energy loss spectra, rel. to interband transitions, bulk and surface plasmons 2−68318
  - Cr, soft X-ray and Auger appearance pot. spectra, L_3/L_2 intensity ratio 2−51230
  - Cs_3Sb, zone bending rel. to photocurrent obs. 2−65103
  - Cu films, far-i.r. transmission, surface plasma oscillation obs. 2−54401
  - D_2, adsorbed on W, electron field emission 2−48016
  - n-$Ga_{1-x}Al_xAs$, metal- semicond. surface barrier struct., rel. to energy band diagram 2−75134
  - GaAs, 1/f noise due to free surface 2−81079
  - GaAs, [110] surface Brillouin zone, intrinsic localized states, calc. 2−65007
  - GaAs, synchrotron radiation photoemission spectroscopy obs. 2−81194
  - GaAs interface, n-type, small-signal admittance meas. 2−65039
  - n-GaP, metal-semicond. barrier obs. 2−84352
  - GaS, surface electronic props. detn. 2−65106
  - GaSe, surface electronic props. detn. 2−65106
  - GaSe, surface struct., surface states LEED, photoemission, Auger spectroscopy obs. 2−48024
  - GaTe, surface electronic props. detn. 2−65106
  - Ge, density of states, Green function calc. 2−51164
  - Ge, photocond. for wide range of band bending near surface 2−72062
  - n-Ge, slow state relax., point contact diode, microwave e.m.f., contact potential pressure depend. obs. 2−84283
  - Ge, surface recomb., effects of chemisorption and sulphidization 2−71938
  - Ge, synchrotron radiation photoemission spectroscopy obs. 2−81194
  - H_2, adsorbed on W, electron field emission obs. 2−48016
  - $Hg_{1-x}Cd_xTe$, n-p junction, absence of surface effects 2−57194
  - InP, [110] surface Brillouin zone, intrinsic localized states, calc. 2−65007
  - InSb, surface photocond., effect of light and X-rays, at 77K 2−47996
  - n-InSb, surface plasmon-phonon interaction 2−71930
  - n-InSb mixed plasmon-phonon surface modes 2−81006
  - Li, optical consts., 2-3.8 eV, meas. by excitation of nonradiative surface plasmons 2−75256
  - Li film, two-dimensional energy bands, also bulk states 2−44037

Crystal electron states continued
- **surface** continued
  - MgO, V_{oh}* trapped hole centre obs. by e.p.r. 2−81447
  - Mo, positron annihilation study 2−54114
  - Se, amorphous, surface trapping effects 2−61344
  - Se, field effect rel. to temp., field mobility, surface cond. 2−71933
  - Si:K, doped surface layers, donor props. and diffusion 2−65019
  - Si/Cs-O negative-electron- affinity surfaces, photoemission meas. 2−81185
  - Si/Pt interface-state density, photoelectric measurement 2−44128
  - Si-Si_3N_4-SiO_2-Si structure, rel. to elec. characts. 2−71984
  - Si-SiO_2-metal, m.o.s., potentials and d.c. rel. to oxide thickness and interface states 2−61406
  - Si-SiO_2 capacitor, frequency response of interface states 2−61404
  - Si-SiO_2 interface, distrib., m.o.s. characs. obs. 2−47956
  - Si-SiO_2 interface, fixed charge behaviour, rel. to growth conditions 2−54227
  - Si-SiO_2 interface, scatt. of conduction electrons by surface oxide charge 2−72000
  - Si-SiO_2 system, m.o.s. tunnel structure, interface states obs. 2−68459
  - Si, density distrib. rel. to diffusion induced disloc. near junc. formed by P diffusion 2−44038
  - Si, interface states in Al-AlN-Si struct. 2−54225
  - Si, inversion layers, transport processes 2−75117
  - Si, p-type, role of surface states in auto-photoelectric emission 2−44199
  - Si, photocond. for wide range of band bending near surface 2−72062
  - Si, photovoltage, photocond., photocarrier surface trapping effects 2−65086
  - Si, photovoltage, photocond., under different bulk and surface recomb. characts. 2−65087
  - Si, rel. to photocond. obs. 2−47932
  - Si, rel. to surface struct., surface cond., LEED 2−77800
  - Si, spin-depend. recomb. of photocreated excess carriers 2−51217
  - Si, surface impedance, due to generation of unbalanced charge carriers 2−54200
  - Si, synchrotron radiation photoemission spectroscopy obs. 2−81194
  - Si, three parameter local pseudopot. method calc. 2−57131
  - Si films on sapphire, prop. determ. using m.o.s. Hall technique 2−51169
  - n-Si inversion layer, two dimensional impurity states 2−51170
  - n-Si inversion layers, self-consistent calcs. 2−47934
  - Si wafer, surface defect generation on reoxidation in H_2O vapour during B diffusion 2−64672
  - Si(III) surface, relation between atomic struct. and electronic props. 2−72095
  - Si_3N_4-GaAs interface, deposition and surface state density obs. 2−65040
  - Si_3N_4-GaAs interface, m.i.s. cond. study 2−77919
  - SiO_2/Si interface, surface-state density, obs. 2−65041
  - SiO_2-GaAs interface, deposition and surface state density obs. 2−65040
  - Te-SiO, interface states, flat band voltage temp. depend. in m.i.s. struct. obs. 2−77930
  - TiO_2:Fe^{3+}, hole trapping by surface ferric acceptor states, Mossbauer obs. 2−84236
  - W, interband transitions at (110) surface 2−64896
  - W, obs. of photoemission from surface state 2−75198
  - W obs. of photoemission from surface state 2−75197
  - YIG, surface nonlinearities, obs. 2−51270
  - Zn, mag. surface states 2−84254
  - ZnO, (0001) surface, field emission and surface states 2−54271
  - ZnO, photovoltage inversion effect, surface states continuous spectrum 2−48000
- **transport processes**
  - — 2−71775
  - — 2−72498
  - — 2−71945
  - σ and π electron interactions in free electron model, revised integrals for 3-dimensions 2−77813
  - alkali metals, anisotropic transport scatt. times 2−75014
  - alloy, dilute, resist. temp. depend. rel. to spin fluctuations 2−57148
  - alloy, disordered binary, pair effects, multiple-scatt. formulation 2−75011
  - alloy, liquid and amorphous, from electronic struct. detn. using clustering effects 2−61170
  - amorphous, elec. cond., carrier flow through localized and extended states 2−77882
  - amorphous materials, high field conductivity 2−54168
  - anisotropy and spin effects of electrons and holes on phonon instability in a magnetic field 2−84180
  - anthracene, carrier-exciton interactions, delayed fluoresc. quenching 2−65308
  - anthracene, deuterated, isotope effect in carrier mobility 2−47906
  - anthracene, excitonic sounding method for measuring charge density gradient 2−47907
  - anthracene, transient photoinjection current meas. 2−57200
  - anthracene crystal, adsorbed dye soln., hole injection by surface quenching of excitons 2−81169
  - benzene, solid and liquid, electron and hole mobilities 2−51146
  - bimetallic junction, e.m.f. generated by shock wave propag. 2−75010
  - Boltzmann eqn. validity for systems with electron-phonon and impurity scatt. 2−44048
  - bulk 1/f noise, exptl. evidence for existence 2−47938
  - capillary plasma 2−70895
  - β-carotene, cond. modes 2−72072
  - chalcogenide amorphous films, Seebeck coeff. 2−61442
  - chalcogenide glass, physical mechanisms, review 2−61267
  - charge carrier and acoustic and optical polar phonon symmetric contributions 2−47792
  - charged carrier, thermal stimulation depolarisation, degree of recombination 2−77815
  - charges in media with dielectric function 2−57103
  - p-chloranil, conduction mechanism, molecular orbital energies 2−75015
  - conduction electron, relax. times and spin props. de Haas-van Alphen effect applic. 2−77847
  - conductivity, residual, frozen-in, model 2−57101

Crystal electron states continued
transport processes continued
crossed diagram contribution to electron self-energy due to impurity scattering in magnetic field 2−44019
d.c. hopping conductivity, percolation treatment 2−61278
degenerate Fermi gas, high density, high freq. conductivity 2−57105
dielectric, maximum absorpt. freq. eval. expression 2−57176
diode, light emitting, efficiency, carrier diffusion length, absorpt., auto-photovoltaic meas. 2−61451
discrete lattices, non-steady-state diffusion currents in large elec. fields 2−51066
disordered system, Hall coeff. in narrow band, random phase model 2−75008
disordered system, hopping conductivity theory 2−61279
drift mobility detn. using Shockley-Haynes pulse method 2−68380
electrical insulation and dielectric phenomena, conference, Williamsburg (1971) 2−57222
electron field emission rel. to multiple particle tunnelling 2−77976
electron heating, field free, expressions for vel., pressure and temp. 2−51089
electron relaxation time, magnetoacoustic determ. 2−77819
electron relaxation time, magnetoacoustic determ. 2−77818
electron-electron interactions continuously variable in range $2.1>r_s>0.9$ 2−57134
electron-impurity system, freq. dependent relax. times 2−51068
electron-phonon system, in strong mag. field at low temp. 2−57100
electrons interacting with paramagnetic impurities, kinetic equations 2−77816
equations for many-body systems, thermodynamic Green's function methods 2−71779
EuO, ferromag. semicond., Redfield technique detn. of Hall mobility of photoelectrons 2−81060
excitonic phase, thermoelec. power calc. 2−65077
ferromagnetic metal, anomalous Hall effect, contrib. of electron-electron collisions 2−57147
ferromagnetic metal, cond. anisotropy, two-zone model of electron scatt. 2−71833
film, chalcogenide glass, high field effects, Poole-Frenkel emission 2−44097
film, electron mobility, space quantization effects 2−81078
film, metal, Halperns theory of size effects rel. to m.f.p. method 2−57149
film, semicond., transport coeffs. rel. to surface states, Hall and Seebeck coeffs. 2−47884
furan-quinone pigment, DFC, charge transport props. 2−51219
n-GaAs, anisotropy of the submillimeter conductivity of warm carriers 2−84330
n-Ge, nonstationary elec. cond., momentum relax. time 2−68435
graphite, anisotropic electronic correlations 2−57108
graphite, magnetoelectric props., pressure effects, energy level and carrier scattering models 2−57110
graphite, minority and majority carrier location and identification 2−57107
graphite, phonon drag rel. to thermoelectric and thermomagnetic effects 2−57249
graphite, phonon drag thermoelec., low temp., rel. to struct. imperfection 2−44170
graphite, phonon- drag thermoelectricity rel. to structural imperfections 2−57248
graphite, pyrolytic, c-axis conduction mechanism from galvanomagnetic obs. 2−57109
graphite, rel. to effect of struct. imperfections on galvanomagnetic props. 2−57190
graphite, thermomagnetic effects, coupled Boltzmann eqn. 2−54243
graphite very thin crysts., total carrier density behaviour from galvanomag. effects 2−54102
group III to V semiconductors, solution of equation 2−54162
group IV-VI chalcogenide, transverse Nernst-Ettingshausen effect obs., effect of hydrostatic compression 2−75159
Hall effect in Hubbard model, low-field regime calcs. 2−77903
heterojunction, graded, electronic props., one band one dimens. model 2−68441
hopping cond., a.c., linearized rate eqns. Green matrix formulation 2−61142
hopping conduction, correlation effects, multi-electron transition 2−61281
hopping impurity conduction, Hall effect 2−57178
hopping transport, continuous time random walk model, applic. to impurity cond. 2−61280
hot electron population inversion, in crossed elec. and mag. fields, theory 2−75007
insulating solids 2−57186
localized states, size near mobility edge 2−51067
longitudinal optical phonon, coupled with Stark ladder electron, current charact. 2−68276
magnetoplasma, collisional part of a.c. conductivity 2−70876
metal, conduction electrons at zero temp., influence of mag. field on correlation function 2−77798
metal, electron gas, passage of a positron, energy loss 2−80967
metal, electron mean free path detn. 2−71829
metal, Lorenz function at high temperatures 2−54124
metal, monovalent, electronic transport coeffs., using model struct. factor 2−61139
metal, monovalent, high-temp. thermal resistivity and electron-phonon interaction 2−68258
metal, nearly mag., high temp. paramagnon modifications 2−71781
metal, one-dimens., random disorder effect on interrupted strand model 2−47802
metal, simple, homogeneous dynamical conductivity, jellium model 2−61220
metal, under external electric fields, magnetic fields and temp. gradients 2−47793
metal-polymer- Si structures, carrier injection and trapping phenomena 2−71991
metal/hydrogen systems, conf., Julich, Germany (Mar 1972) 2−77713
metals, electron momentum distrib., from Doppler-broadened annihilation lineshapes 2−71782
metals, liquid, specific elec. resist., detn. by pseudopotl. methods, accuracy of integral 2−80477

Crystal electron states continued
transport processes continued
m.i.m. structure, space charge limited to electrode limited current transition theory 2−47949
minority carrier lifetime meas. by photocond. method 2−75179
mobility and surface acoustoelectric current 2−68240
molecular crysts., local elec. field and charge-carrier mobilities 2−81129
Mylar thin films negative resistance charact. 2−57203
nearly free electrons, in mag. field, generalized Wannier functions 2−61146
non-crystalline materials, theory of conduction, review 2−61143
nonpiezoelectric conductor, u.s. generation by deform. interaction with carriers 2−64841
organic materials, carrier drift mobility meas. 2−47905
organic semiconductors with narrow conduction band, soln. of kinetic eqn. 2−81011
organic semiconductors with narrow conductivity zones, electron-phonon interaction 2−77810
organic solids, geminate recombination of charge carriers 2−57187
p^+np^+ structs., current transport mechanism, thermionic injection, space charge limited currents 2−61377
p-n avalanche diode, analytical determ. of small-signal impedance 2−68444
polaron conduction, acoustic phonon coupling case, theory 2−61201
poly (N-vinyl carbazole) film, transient space charge perturbed current 2−57229
polyethylene doped with I, h.f. Gunn domains 2−57202
polyvinyl chloride films, energy-band model for mobility of photoinjected electrons 2−72074
powder luminophore, rel. to elec. field effect on phosphoresc. and luminesc. 2−48214
quantum electron- impurity transport, quasiparticle formulation 2−84240
rare earth dodecaborides, carrier mobility 2−47838
sapphire, substrate, transport props., electron injection by internal photoemission 2−81110
Schottky diode, cond. mechanism, diffusion and thermionic emission theories, quasi-Fermi levels 2−75128
semiconducting compounds, groups III-V and II-VI, negative differential mobility 2−44088
semiconducting melts, thermal cond., band struct. 2−60466
semiconductor, $A^IB^{III}C^{VI}_2$, rel. to band struct. 2−71886
semiconductor, ambipolar diffusion noise spectrum, mag. field effects 2−61269
semiconductor, amorphous, avalanche ionization, Shockley hot-electron model 2−61287
semiconductor, amorphous, field dependent mobility, model 2−61286
semiconductor, amorphous, Hall cond., random phase model 2−61277
semiconductor, amorphous, with globular inhomogeneities, interglobular electronic transport 2−68390
semiconductor, C_{6v} class cryst., piezoelec. interaction of transverse u.s. waves with charge carriers 2−54030
semiconductor, carrier diffusion, effect of h.f. electric field 2−84335
semiconductor, compensated, thermal current instability 2−75088
semiconductor, cond. due to variable range hopping in nonuniform density of states 2−81104
semiconductor, conf., Warsaw, Poland, July (1972) 2−68384
semiconductor, cubic, polaron Hall mobility calc. 2−68383
semiconductor, diffusivity-mobility ratio, in high mag. field, doping depend. 2−57181
semiconductor, disordered, problems arising from energy spectrum and change carrier kinetics theory 2−68391
semiconductor, doped, space-time distribution of excess carriers and their space charge 2−54163
semiconductor, electron diffusion, in high electric fields 2−57177
semiconductor, electron temp. determ. 2−51121
semiconductor, e.m. wave propagation and eigenoscillations, band struct. and elec. field effects 2−77892
semiconductor, extrinsic, nondegenerate, with high cond. electron concs., thermodynamic and kinetic props. 2−77890
semiconductor, high field carrier distrib. function 2−61292
semiconductor, hot carrier instabilities, in strong mag. field 2−75106
semiconductor, hot electron cyclotron resonance, recomb. effects on line profile 2−84282
semiconductor, hot electron distrib. func. and energy losses on interacting with optical phonons 2−71894
semiconductor, hot electron effects, calc. method 2−54193
semiconductor, hot electron population inversion in crossed electric and mag. fields 2−77817
semiconductor, hot electrons in quantizing magnetic fields, review 2−57182
semiconductor, III-V, hot electron magnetophonon reson., theory 2−68386
semiconductor, III-V, transition metal doped, anomalous temp. depend. 2−68405
semiconductor, impact ionization, energy conservation considerations 2−75081
semiconductor, instability due to forbidden band thermal deform. 2−54185
semiconductor, linear and nonlinear cond. calc. using energy band models 2−51039
semiconductor, low mobility, current produced by high elec. field, Poole-Frenkel cond. mechanism 2−77887
semiconductor, low temp. impurity scatt., transport coeffs. determs. 2−47885
semiconductor, magnetic, magnon drag effect 2−54165
semiconductor, magnetophonon spectroscopy study 2−68385
semiconductor, magnetoresistance in strong electric fields 2−75086
semiconductor, many valley cubic, conduction anisotropies detn. 2−68382
semiconductor, microwave cond., in heating fields and in presence of electron-hole interaction 2−75084
semiconductor, n-type, quantum transport theory inc. higher order scattering effects 2−47887
semiconductor, narrow band, current rel. to elec. field 2−77891

Crystal electron states continued
transport processes continued
semiconductor, non-equilib. charge carrier condensation and recomb. radiation 2−54184
semiconductor, optically pumped, instability in strong mag. field 2−71889
semiconductor, p-type, recomb. of excitons bound to deep neutral donors and acceptors 2−68682
semiconductor, Poisson and transport equations, high field domain solns. 2−54167
semiconductor, polar, hole transport, Monte Carlo study 2−64968
semiconductor, polar, in quantizing mag. field, electron momentum distrib. function 2−64967
semiconductor, rel. to stimulated emission 2−61681
semiconductor, supercond., rel. to state mixing between bands due to e.m. field 2−77872
semiconductor, superlattice struct., transport props., h.f. cond., e.m. wave amplification 2−64974
semiconductor, surface transport in inversion and accumulation layers 2−51123
semiconductor, transient space charge limited current on voltage removal 2−84336
semiconductor anomalous magnetoresistance due to surface effect, effective carrier lifetime 2−65005
semiconductor epitaxial layer, rel. to steady state surface photovolt., interpretation 2−75177
semiconductor film, carrier conc. 2−71931
semiconductor film, kinetics of small charge currents and carrier lifetime determ., rel. to photocurrent 2−81088
semiconductor film, rel. to magnetoresist. and Hall effect calc. 2−71892
semiconductor glass, cond. mechanism, model 2−61335
semiconductor inversion layer, quantum galvanomagnetic effects 2−68387
semiconductor multilayer film, rel. to thermoelec. props. 2−51054
semiconductor with hot electrons, nL criterion of elec. domain, charge density 2−51133
semiconductor-metal contact, current transport, unified approach 2−51175
semiconductors, carrier waves with velocity distributions 2−84324
semiconductors, cubic, nonpolar- lattice scattering effect on Ohmic conductivity of holes 2−51131
semiconductors, effect of injected space-charge on equivalent Llewellyn-Peterson equations 2−75082
semiconductors, rel. to band structure, survey 2−81012
semiconductors, under external electric fields, magnetic fields and temperature gradients 2−47912
semiconductors and insulators, amorphous, statistics, recomb. processes and photocond. 2−61290
semiconductors with nonparabolic bands in strong electric and magnetic fields 2−81101
semimetal, monotonic behaviour in strong mag. fields 2−44025
$Si-SiO_2$ interface, e. scatt. by surf. oxide charges and lattice vibrat. 2−71317
single-site theory of transport in systems with randomly distributed scatterers 2−80979
solid and disordered system, Hall resistivity expression using nonequilib. statistical operator 2−71776
spin dependent effects 2−71778
spinel ferrites, difference between Hall and drift mobility values in framework of Hall theory of small polaron 2−75083
steel oxide layers, semiconduction rel. to substrate pitting susceptibility 2−57422
superconductor, dirty, thermal conductivity in transition metals near upper critical field 2−77876
superconductor, in slowly varying elec. field, thermodynamic Green's function methods 2−71779
TCNQ complex, elec. cond., thermally assisted hopping mechanism 2−68409
TCNQ complexes, hopping cond. 2−44109
tetracene crystals, temp. depend. of charge carrier mobility 2−81075
thin film transistors, polarizability of bias-temperature drifted species 2−47946
transition metal cpds., binary, Mott insulation breakdown, Mott transition 2−57099
transport and quantization of Bloch oscillations in strong elec. fields 2−61147
triethylammonium(tetracyanoquinodimethan)$_2$ TEA(TCNQ)$_2$, elec. cond., anisotropy 2−75016
triethylammonium- (TCNQ)$_2$, mobility, 77K, 2−68410
triglycine sulphate, field effect and Hall mobility of Te and PbTe 2−77814
van der Waals between cond. mols. 2−47824
Ag-naphthalene-Ag structures, electronic conduction in dark 2−57199
Ag, bulk, cond. electron mean free path determ. from size effect of thin films 2−75012
Ag, elec. resist., evidence of phonon drag 2−64909
Ag film, electron-electron interaction, rel. to induced supercond. 2−44072
AgBr, photocarrier mobility, electron-lattice interaction effects 2−81181
AgCl, photocarrier mobility, electron-lattice interaction effects 2−81181
AgF, photocarrier mobility, electron-lattice interaction effects 2−81181
Ag_2Te, at m.p. and to 1500 K 2−60495
n-Ag_2Te, Lorenz number, electron scatt. inelasticity obs. 2−84337
Al/Cu/Al films, electromigration obs. by transmission electron microscopy 2−64879
$Al-Al_2O_3-Al$, m.i.m., current density in thermionic and thermionic field emission regions 2−61395
Al-Au alloy, dilute, Mathiessens rule deviation due to scatt. processes 2−80969
Al-Ge, contact, slow states activation energy, barrier height temp. depend 2−75135
$Al-SiO_2-Si$, m.o.s., transport props. in inversion region, 123-573 K 2−47954
Al film with interlayered transition metals, effect on spin density of conduction electrons 2−68743

Crystal electron states continued
transport processes continued
$Al_xGa_{1-x}As$, photolum., distant donor-acceptor pair recomb. 2−61683
As_2Se_3, amorphous, a.c. cond. mechanism, 30Hz to 10.3GHz, −180-500°C 2−81070
As_2Se_3 film, amorphous, charge transport, photocond. and dark current obs. 2−68393
$AsSe_{1.5}Sn_{0.28}$, pyroceramic, semicond., elec. cond. mechanism, 285-385K 2−75089
$As_2Se_3(Te_3)$ film, amorphous, trap-limited processes 2−61325
$3As_2Se_3.2Sb_2Se_3$ films, amorphous, from cond. and spectral response obs. 2−54187
$3As_2Se_3.2Sb_2Se_3$ films, relax. time for free carriers, mobility 2−54186
AsTeI glass, electronic transport model 2−61296
Au-Fe(Mn)(Co)(Ni)(Ti) dilute alloys, rel. to deviation from Matthiessen's rule, 0.5-60 K 2−77854
Au, bulk, cond. electron mean free path determ. from size effect of thin films 2−75012
β-B, rhombohedral, carrier mobility in intrinsic cond. region 2−75090
BaO powder, recomb. luminesc., 103-423 K 2−61687
$Ba_{1-x}Sr_xTiO_3$, mobility, gravimetric determ. 2−81086
$BaTiO_3$, conducting crystals, temp. depend. of carrier mobility 2−81100
Be, negative cond. electron contrib. to field gradient 2−68277
Be, quantum oscillation waveforms rel. to $\partial M/\partial H$ oscillations 2−80963
p-benzoquinone, conduction mechanism, molecular orbital energies 2−75015
Bi:Te deposits, relaxation time of carriers 2−75255
Bi, Alfven wave amplitude and carrier relax. times 2−51092
Bi, magnetoresist. tensor components, at intermediate mag. fields, 77 K 2−75053
Bi, magnetoresistivity coeffs, electron and hole transport, low field galvanomag. tensors, 77-300K 2−84233
Bi, phonon drag thermomag. at low temps. 2−54244
$Bi_{1-x}Sb_x$:Cd(In)(Sn), rel. to elec. props., 180-240K 2−61301
BiSe and BiTe, single crystal plates, carrier conc. 2−84322
p-Bi_2Se_3, Hall and cond. mobilities, carrier compensation, galvanomag. effects, 4.2-300K 2−81076
p-Bi_2Te_3, relax. time anisotropy 2−51135
$Bi_8Te_7S_5$, single crystal film, Hall eff. meas. and detn. of carrier mobility 2−77851
$Bi_2Te_{3-x}Se_x$, temp. depend. of electron effective mass and mobility 2−81099
C, neutron irradiated, thermal annealing, changes in electronic props. 2−57000
CO, drift mobility 2−77820
Cd-In, binary systems, electrotransport and elec. resist. detn. for density of states at Fermi level 2−80476
Cd-Tl, binary systems, electrotransport and elec. resist. detn. for density of states at Fermi level 2−80476
$Cd_xPb_{1-x}Se$ alloy, Hall coeff., Hall mobility, thermoelec. power, optical energy gap, 77-450 K 2−64977
CdS, photosensitivity, luminesc. intensity, rel. to donor-acceptor photothermal dissociation 2−72393
CdS film, electron mobility and scatt. rel. to grain boundaries and surfaces 2−61149
CdS film, electron scatt. by stacking faults rel. to elec. props. 2−61150
CdS hot electron mobility, phonon and impurity atom scattering 2−84276
CdS hot electron mobility 2−84276
CdS platelets, drift meas., Schottky contact effects 2−77884
CdS(Se), hole photoemission into S, 2.11 to 3.54 eV 2−84265
CdS(Se), spontaneous and stimulated emission, exciton interactions 2−68677
$CdSe-SiO_x$, electron transport study in space charge layer of vacuum-deposited film 2−77852
CdSe, room temp. hole and electron drift velocity, time of flight obs. 2−61306
CdSe film, elec. props. rel. to substrate temp., 25-200°C 2−64980
CdSe films vacuum deposited, Hall mobility 2−83868
CdSe(Te), high temp. defect equilib. 2−44096
n-Cd_2SnO_4, charge-carrier mobility 2−51137
CdTe:In, self-compensation calc. assuming Cd vacancies and impurity-vacancy complexes 2−47889
CdTe, growth from soln. melts, elec. props. 2−74677
CdTe, radiation effects, carrier conc., Hall mobility 2−47892
$Cd_{2.8}Zn_{0.2}As_2$, high mobility, scattering processes 2−81090
Cr and alloys, excitonic phase, thermoelec. power calc. 2−65077
$CrSi_2$ thermoelectric props. and crystal growth 2−84370
Cu, electron relax. time, magnetoacoustic determ. 2−77818
Cu, electron relax. time, magnetoacoustic determ. 2−77819
Cu, electron scatt. by dislocations, de Haas-van Alphen effect obs. 2−61214
Cu, scattering of quasiparticle excitations by thermal phonons in symmetry zones of Fermi surface 2−44020
Cu film, thermoelec., resist., cond. electron m.f.p. 2−68477
$CuCr_2Se_4$, scattering mechanism, galvanomag. props. study 2−81091
Cu_2Te-Ag_2Te system, comp. and temp. dependence of carrier conc., influence of defects, compensation trapping cond., and scattering of carriers 2−84323
Cu_2Te, carrier effective mass, reflection spectra obs. 2−84520
Cu_xTe, thermal e.m.f., electronic and ionic cond. at 400°C, composition 2−54247
Eu, electronic thermal resist., critical divergence at Neel point 2−57124
EuS, slightly Eu rich, systematics of conduction in band tail 2−75094
p-GaAs:C ion implanted, carrier conc. and Hall mobility obs. 2−64986
GaAs:Cr, radiative recomb., photolum. study 2−71927
GaAs:Cu, behaviour in strong elec. field 2−71904
n-GaAs:Cu film, epitaxial, carrier mobility, impurity effects, scatt. by space charge centres 2−64983

Crystal electron states continued
transport processes continued
n-GaAs:S ion implanted, carrier conc. and Hall mobility obs. 2−64986
n-GaAs:Si ion implanted, carrier conc. and Hall mobility obs. 2−64986
GaAs:Si(Te), electron irrad., carrier removal, mobility changes, annealing characts. 2−47917
GaAs-GaAlAs layered structs., current-voltage characts., transport props. 2−68399
GaAs-Pb Schottky barrier tunnel junction, zero-bias anomaly, irrad. effects 2−71960
GaAs, amorphous, hopping at Fermi level 2−61312
n-GaAs, carrier conc., rel. to impurity distrib. coeff. anisotropy 2−47437
GaAs, current instability rel. to mag. field, negative resist 2−64984
n- GaAs, effective electron mass. pressure depend. 2−44098
GaAs, electrolum. diode, electron diffusion length, internal quantum efficiency, temp. depend. 2−61725
n-GaAs, electron drift velocity, Monte Carlo calc. 2−71901
n-GaAs, electron drift velocity, rel. to acoustoelec. current oscill. 2−51040
GaAs, electron transfer and velocity-field characts., mag. field effect 2−44100
GaAs, electron velocity field characs. 2−54172
n-GaAs, epitaxial, Hall coeff. and mobility 300-800 K, valley energy separation 2−68398
GaAs, epitaxial, microwave meas. of velocity-elec. field charact. 2−51140
GaAs, epitaxial, rel. to photolum., 8250-8450Å 2−61694
GaAs, epitaxial layers, influence of gas phase comp. 2−83893
n-GaAs, heavily-doped, gradual mobility transition in band tails 2−61342
GaAs, hot electron props., rel. to Gunn effect bulk instabilities 2−57184
n-GaAs, hot electrons heated by high microwave fields 2−77897
n-GaAs, γ-irrad. effects on current instabilities caused by recomb. centres 2−81092
GaAs, layer compound, effective masses, empirical pseudopotential calc. 2−81016
n-GaAs, low field galvanomag. transport, Boltzmann eqn. soln. in mag. field, 77-300K 2−71902
GaAs, neutron irrad., tunnel assisted hopping via defect energy levels 2−51157
GaAs, photoluminesc., nonequilib. carriers strong interaction, 77K 2−68680
n-GaAs, surface barrier diode, hole diffusion length 2−61387
n-GaAs bulk element, uniform cross-section, doping inhomogeneity, static electric field distribution 2−84315
GaAs dielectric-surface-loaded elements, high field domain propagation 2−51141
GaAs electron density ratio in valleys, elec. field depend. in presence of Gunn effect 2−81093
GaAs epitaxial film, carrier mobility depend. of cathodolum. 2−72434
GaAs epitaxial film, carrier mobility and conc., substrate orientation effects 2−47436
GaAs epitaxial films, carrier conc. and Hall mobility 2−53573
GaAs epitaxial layers, free carrier conc. and mobility 2−50492
n- GaAs Gunn oscillators, hot electron microwave mobility 2−51139
n-GaAs involving electron-heating effect by microwave field, rel. to frequency tripler 2−71903
n-Ga$_x$In$_{1-x}$As alloy, effective mass compositional depend., sub mm. cyclotron resonance obs. 2−64982
p-GaP:Zn,O, donor electron capture cross sections, rel. to quantum efficiency limits 2−68681
GaP-ZnSe alloy, cond. hopping contrib., ionized impurity scatt., electrolum. and cathodolum. 2−81415
GaP, electron mobility theoretical calc. 2−77889
GaP, hole effective masses, cyclotron resonance obs. 2−75041
p-GaP(Zn,O), p-GaP(N), minority carrier lifetime, luminesc. decay time obs. 2−48221
β-Ga$_2$S$_3$, photolum. and photocond. studies 2−84532
GaSb:Te,Zn, thermal e.m.f. rel. to carrier conc., 300K 2−54248
p-GaSb, doped, heavy/light hole mobility ratio 2−81063
n-GaSb, electron mobility temp. depend. 2−57206
GaSe, radiative recomb., under two-photon excitation 2−72405
Ge:Cu, carrier conc. and mobility, donor compensation density determ. 2−51166
Ge:Cu, recomb. cross section for holes at singly ionized impurity 2−51215
p-Ge:Cu thermalization time of hot photoexcited holes 2−51214
Ge:Mn, nonlinear IV characts., exclusion and charge exchange between impurity levels 2−75115
Ge:Ni, electron and hole capture rates, photomagnetoelec. and photocond. studies 2−75171
n-Ge, absolute negative cond., current instability, Erlbach effect 2−68433
Ge, amorphous, hopping at Fermi level 2−61312
Ge, amorphous, transport model 2−61352
n-Ge, cyclon reson. study 2−71942
Ge, electron bombarded, pair-prod. energy for free carriers 2−61351
Ge, electron irrad., 8.5MeV, high field domain instability 2−57208
Ge, electron mobility theoretical calc. 2−77889
N-Ge, even and odd Hall effect in strong electric fields 2−81108
Ge, excess minority carriers generated by pulsed electron beam, diffusion length 2−51165
Ge, galvanomagneto-recombination effect kinetics rel. to elec. and mag. fields 2−65015
Ge, heavily doped, 0.02-300K, cond. mechanism 2−81109
Ge, hopping cond. rel. to temp., doping, uniaxial compression 2−65013
Ge, hot electron capture by Cu^{2-} centres 2−71936
n-Ge, hot electron charact., high-field scatt. mech. 2−61354
n-Ge, hot electron effects, calc. method 2−54193
n-Ge, hot electron instabilities, Monte Carlo calc. and neg. diff. cond. obs. 2−77912
p-Ge, impurity scatt. of warm holes 2−44124
n-Ge, γ-ray irrad., recombination parameters 2−47929
n-Ge, laser generated carrier mobility, transient behaviour 2−47925

Crystal electron states continued
transport processes continued
Ge, magneto-microwave free-carrier absorpt. in Faraday config. 2−68605
n-Ge, mobilities due to lattice and impurity scatt. from microwave Faraday effect 2−75257
Ge, n-type, infrared birefringence on hot electrons 2−81328
n-Ge, negative absolute resist. due to intervalley electron transfer 2−71937
n-Ge, phenomenological energy relax. time, elec. field depend., 77K 2−65010
p-Ge, photon-induced hopping on acceptors, theory 2−47923
Ge, pulsed elec. field, minority carrier mobility, influence of majority carriers 2−75114
Ge, radiative recomb., 2-77K, effect of electron-phonon interaction 2−68684
n-Ge, resist. rel. to donor spin reson., spin energy transfer model, 4K 2−68434
Ge, scatt. of holes by neutral acceptors 2−71941
n-Ge, scattering mechanisms, rel. to resist. anomalies below 1K 2−57210
Ge, Surface excitation by Nd laser pulse, surface transport props. obs. 2−84379
Ge, surface recomb., effects of chemisorption and sulphidization 2−71938
Ge, thermophotoelec. effect due to hot carriers, 300 and 77K 2−72057
Ge amorphous, obs. of electron tunnelling between metal electrodes, determ. tunnelling phonon density of states 2−44125
Ge minority hole mobility, on interaction with electrons, high microwave field effects 2−75116
GeO, layers, defective, hopping cond., elec. cond., 77-453 K, 20-100 MHz 2−54173
GeTe- Bi$_2$Te solid soln., Hall carrier conc., elec. cond. 2−74903
He, solid, electron mobility, pressure effects 2−43431
Hf, electron scattering mechanisms at high temps. rel. to kinetic properties 2−81035
p-Hg$_{1-x}$Cd$_x$Te, carrier freeze-out and acceptor energies determ. 2−57194
Hg$_{1-x}$Cd$_x$Te, sweep out of minority carrier holes 2−54255
HgS, hole photoemission into S, 2.11 to 3.54 eV 2−84265
Hg$_3$Te$_3$-Ge$_2$Te$_3$ alloy, near semimetal-semicond. transition at high press. 2−68406
HgTe, Hall coeff. and self-conc. of carriers 2−61314
n-HgTe, pure, effect mass and g-factor for cond. electrons, magnetooptical absorp. obs. 2−78101
In-Mn alloy, superconducting film, electronic thermal conductivity 2−68352
In, rel. to Righi- Leduc effect, 3.5-8K 2−75163
In, superconducting film, electronic thermal conductivity 2−68352
n-InAs, heavily doped, impact ionization, elec. field depend. 2−81087
n-InAs, rel. to temp. effects on photolum., 77-200K 2−72412
InP, electron transfer 2−61315
InP, high resistance, Cu, Fe or Cr doped, meas. of carrier concentration 2−83895
InP, rel. to photoluminesc. of bound excitons 2−68685
n-InP, velocity-field charact., calc. 2−71912
InSb:Te, Zn, current carrier distrib. 2−44101
n-InSb, anisotropic complex small signal cond. of hot electrons at 84K and 134 GHz 2−61318
InSb, changes on heat treatment, field effect and elec. cond. obs. 2−64989
n-InSb, coeffs. at high temp., degeneracy and screening effects 2−68378
n-InSb, electric field modulated laser cyclotron resonance, impurity and cond. electron resonance obs. 2−81021
n-InSb, electron-hole plasma form. rel. to current and voltage instabilities 2−57137
InSb, electron-hole plasma in mag. field, carrier wave growth 2−61316
n-InSb, electron energy dissipation in high mag. fields, phonon heating effects 2−77898
InSb, electron lifetimes, dHvA effect obs. 2−71909
n-InSb, heavily doped, impact ionization, elec. field depend. 2−81087
InSb, hot electron absorp. of mm. and sub mm. waves 2−78119
p-InSb, i.r. absorpt. rel. to hole and plasma currents 2−72335
InSb, impact ionized excess carriers recomb., direct lifetime obs. at 77 K 2−71910
InSb, magnetophonon mass change in drifting hot carriers 2−68389
InSb, n-type, effective mass of conduction electrons det. from magnetophonon effect, undergad. expt. 2−65009
n-InSb, nonlinear, hot electron cyclotron resonance obs. 2−77845
n-InSb, nonlinear transport props. of hot electrons in strong mag. field 2−47896
n-InSb, quenching of sound amplification and e.m. wave radiation by holes 2−71929
InSb, recomb. rate rel. to elec. field, drifted Maxwellians approx. 2−81077
n-InSb film, transport phenomena, 20-100 K and 300-500 K 2−71911
InSb films, thickness dependence of electron mobility, model based on surface accumulation layer 2−68403
n-InSe, rapid recomb. centres, during laser beam excitation 2−72063
K, r.f. size effect, calc. 2−71835
KCl, gamma- irradiated, high temp. dependence of electron Hall mobility 2−44174
KCl, high-field current transients, electron hopping and localized levels 2−68425
KI:Tl, recomb. and capture probabilities of F-centre electrons 2−84285
K$_{0.3}$MoO$_3$, blue phase, semicond. to metal transition, elec. cond. 2−61151
K$_2$Pt(CN)$_4$Br$_{0.30}$.3H$_2$O, one-dimens. cond. as two-dimens. problem 2−51142
La:Ce, skew scattering of electrons, Hall effect obs. 2−75055
Li, electron-electron interaction, conduction e.s.r. study 2−48288
LiFe$_2$F$_6$, electron hopping obs. by Mossbauer effect, 350-700K 2−71913

Crystal electron states continued
transport processes continued
$Li(NH_3)_4$, carrier mobility, Hall effect, magnetoresist., thermoelec. power obs. 2−47894
MgF_2 film, elec. props., thermally assisted hopping mechanism, Poole-Frenkel cond. 2−68279
n-Mg_2Ge, cond. and scatt. mechanism 2−51143
$Mg_xPb_{1-x}Se$ alloy, Hall coeff., Hall mobility, thermoelec. power, optical energy gap, 77-450 K 2−64977
MnO Compton profiles, electron momentum distrib. 2−78116
Mo, electron and hole, free path lengths 2−47796
MoS_2 layer struct., contact annealing effect on Hall data 2−54177
n-GaAs, light and heavy hole transitions, interference 2−68619
N2, drift mobility 2−77820
Na-NH_3, density of states, Mott g ratios, self consistence, significance in MNM transition 2−44033
Na, electron-electron interaction, conduction e.s.r. study 2−48288
NaI:Tl, recomb. luminesc. of crysts. excited in A-band by activator absorpt. 2−75334
Ni ferrites, iron rich, Hall mobility measurements, room temp. to 600°C, activated hopping process 2−81069
$Ni_3(Mn,Co)$ and $Ni_3(Mn,Fe)$ alloys, electron and hole mobility obs. 2−47837
$Ni_{0.6}Mn_{2.4}O_4$, elec.-field-depend. cond. for hopping-type charge transport 2−81082
NiO, bound polaron hopping 2−47899
NiO, mobility 1200-1800K 2−84314
NiO, photoexcited charge carrier drift and lifetime 2−68280
O_2, drift mobility 2−77820
$PbBr_2$, pure and doped, hole cond., defect chem. 2−61322
PbO-SiO_2 glass, hopping cond., photoemission obs. 2−44206
PbS layers, photocond. mechanism, elec. cond. and Hall effect obs. 2−81166
PbS(Se)(Te), carrier conc. effect on mech. props. 2−50784
N-PbSe, elec. effective mass and relaxation time, reflectivity and magnetoreflectivity obs. 2−61651
PbSe (Te), thermal cond., electron component, temp. depend. 2−68259
n-PbSe(Te), hot-electron cond., velocity-field characts., 77 and 4.2K 2−68407
$Pb_{1-x}Sn_xTe$, free carrier effects, optical consts. 2−48165
n-$Pb_{1-x}Sn_xTe$, hot-electron cond., velocity-field characts., 77 and 4.2K 2−68407
PbTe, free carrier effects, optical consts. 2−48165
p-PbTe, high field transport, current-field curves, mixed scatt. by phonons 2−81068
p-PbTe, room temp. props., scattering mechanisms, relative importance 2−54161
Pr, rel. to resist. anomaly near Neel temp. 2−51281
Sb_2Se_3 film, amorphous, rel. to band struct. 2−61323
Sc Compton profiles, electron momentum distrib. 2−78116
ScN, epitaxial, mobility obs. 2−50503
Se: Cl, As film, vacuum evap., transport props., time resolved drift technique 2−44104
Se-CdSe p-n heterojunction, diffusion potential determ. 2−47942
Se-Te alloy, acoustoelec. phenomena relating to two carriers 2−80908
Se-Te melt, electronic transport behaviour, switching, optical gap 2−60502
Se, current flow in Cd-Se rectifier diode 2−54219
Se, field effect rel. to temp., field mobility, surface cond. 2−71933
Se, hole photoemission into S, 2.11-3.54 eV 2−84265
Se, vitreous, hole drift mobility 2−61327
Se amorphous film, one- and two-carrier space-charge-limited currents 2−75097
Se film, vitreous, trap-limited processes 2−61325
p-Si:Be, hole mobility, temp. and doping depend. 2−54198
Si:Na(K), impurity atomic radius effects 2−71948
Si:P, electron drag rel. to impurity centre photoionization, photo-e.m.f. 2−65089
Si:P, implanted, carrier density and mobility, depth distrib. 2−80993
Si:P, phonon and electric field influence on extrinsic photocond. 2−81179
Si-SiO_2 interface, scatt. of conduction electrons by surface oxide charge 2−72000
Si, anisotropy and hot electron effects, 1-300 K 2−84342
Si, avalanche breakdown, statistical theory based on Boltzmann transport equation, scattering mechanisms 2−54202
Si, charge carrier distrib. rel. to implanted B and P channelling and diffusion 2−47432
n-Si, elasto- electronic effects 2−65020
Si, electron bombarded, pair-prod. energy for free carriers 2−61351
Si, electron mobility theoretical calc. 2−77889
Si, high resistivity, space-charge-limited minority hole flow 2−75118
n-Si, hot electron instabilities, Monte Carlo calc. and neg. diff. cond. obs. 2−77912
p-Si, i.r. absorpt. by free carriers 2−48190
p-Si, impurity scatt. of warm holes 2−44124
Si, m.i.s., inversion layer, hole field effect mobility rel. to dielec. charge 2−71992
Si, optically homogeneous, free carrier conc., refl. determ. 2−54406
Si, p-n, meas. by electron beam microprobe 2−44133
n-Si, phenomenological energy relax. time, elec. field depend., 77K 2−65010
n-Si, resist. rel. to donor spin reson., spin energy transfer model, 4K 2−68434
Si, surface impedance, due to generation of unbalanced charge carriers 2−54200
Si, surface inversion layers 2−75117
n-Si, transverse magnetoresist., mag. field strength depend. 2−65018
p-Si (001) inversion layer, electron mobility in surface subbands 2−47997
Si film, amorphous, rel to localized state distrib. determ. 2−68437
Si film, epitaxial film, nonequilibrium carrier lifetime, photoelectric obs. 2−84331
Si films on sapphire, prop. determ. using m.o.s. Hall technique 2−51169

Crystal electron states continued
transport processes continued
Si hole, drift velocity rel. to band struct., elec. field effects, at 5K 2−81107
n-Si i.r. free carrier absorpt. consts. 2−81408
p-Si inversion layer, mobility obs. of band structure 2−51171
n-Si inversion layer, transport props. rel. to two dimensional impurity states 2−51170
Si n-channel m.o.s.f.e.t., electron mobility, electron surfon interact. calc. 2−51172
Si oxidized surface, orientation effects on electron and hole transport props. 2−51173
Si power devices, diodes and thyristors, carrier lifetimes, meas. 2−71977
SiC:H(D), implanted, recomb. radiation of excitons and vibr. spectrum 2−68688
SiO_2, thin layer on Si, hot electron energy losses, photoemission obs. 2−81061
Sn-Ge alloy, Shubnikov-de Haas oscills. rel. to carrier heating in cond. band 2−81080
Sn, skin effect, anamolous, d.c. cond., m.f.p., reflectivity factor 2−68341
SnS_2, hopping conduction, a.c. conductivity meas., −100°C to 120°C 2−84290
SnTe, carrier conc., rel. to Fermi surface studies 2−68420
SnTe, free carrier effects, optical consts. 2−48165
$SrTiO_3$, mobility, gravimetric determ. 2−81086
Ta-Ta_2O_5-Au, m.i.m. devices, electron energy distrib. for Schottky/Poole-Frenkel conduction 2−68456
Te, liquid, rel. to n.m.r. obs. 2−71237
Te film, polycryst. on mica 2−61330
Te film, thermoelectric power, Hall and Seebeck coeffs., resistivity 2−54249
Te films on uhv-cleaved TGS, aftereffects in field eff. at large gate charges 2−77900
$(ThO_2)_{1-x}(YO_{1.5})_x$ solid soln., electronic contrib. to mixed conductivity 2−75100
Ti-Au film, conductor stripes, electromigration damage rel. to pulsed d.c. powering 2−80940
Ti, electron scattering mechanisms at high temps. rel. to kinetic properties 2−81035
TiO_2, reduced, bound polaron hopping and mag. impurity effects 2−47902
$TlBiTe_2$ and TlTe, mobility temp. depend. 2−51144
TlBr, cyclotron reson., electron and hole resons., carrier mobilities 6.5-14K 2−68322
$V_{2-x}Cr_xO_3$, domain form. during Mott metal-insulator transition, geometry and crystallography 2−71785
V_2O_3, refl. spectra, plasma freq., free carrier effective mass 2−81407
Vo_x, $1<x<1.3$, charge carrier freeze-out effects 2−65004
Zn, anisotropy in the phonon limited resistivity 2−64919
$Zn_xHg_{1-x}Te$ solid soln., light-hole band rel. to transport phenomena 2−64992
$Zn_xMFe_{2-x}O_{4-x}F_x$, M = Ni, Co, ferrite, synthesis, magnetization, hopping cond. 2−75234
ZnS:Cu, rel. to surface, volume, and contact components of current 2−71918
ZnS electroluminescent p-n junction, electronic behaviour obs. 2−68711
ZnSe, time of flight mobility, and trapping 2−44107
ZnTe:Al, high temp. defect equilib. 2−44096
Zr, electron scattering mechanisms at high temps. rel. to kinetic properties 2−81035

Crystal energy *see Bonds; Crystals; Solids/structure*

Crystal field theory
see also Hyperfine field interactions
5f complexes, crystal field splittings 2−51288
10Dq calc., ave.-of-config. interpret. in NiF_6^{4-}, self-consistent-field electronic excitation energies 2−72240
10Dq calc., ave.-of-config. interpret. in NiF_6^{4-} 2−72239
adiabatic rapid passage, radiation damping, Bloch eqns. 2−81318
alkali borate glasses, Ni^{2+}-containing, absorpt. anomalies, ligand field approach 2−75303
alkali bromides, gradient-elastic tensor, n.m.r. acoustic saturation study 2−44457
alkali silicate glass, Er^{3+} sites, absorpt. study 2−54429
average valency V materials, trends in ionicity 2−83887
clathrates of $Ni(4\text{-methylpyridine})_4(NCS)_2$ complex study of splitting of out-of-plane CH vibration band by i.r. spectroscopy 2−53053
cobaltocene, electronic structure and dynamic Jahn-Teller effect from e.p.r. and optical studies 2−56226
cubic antiferrodielectric, admixture of $^4T_{1g}$ state to $^6A_{1g}(^6S)$ state of Mn^{2+} 2−65202
dielectrics, consistent many-electron theory 2−81322
europium benzoylacetonate, e.p.r. of Gd^{3+}, cryst. field symmetry 2−81469
fluoride, hexagonal, of type ABF_3 2−51287
glass:Eu^{3+}, emission spectra comp. and temp. depend., effective cryst. field props. 2−78130
harmonic field parameters of paramagnetic s = 1 system temp. dependence, application of theory to dipolar systems 2−65119
ion-lattice interaction of noncentral ions in cubic crystals 2−72236
lanthanum ethyl sulphate:Dy^{3+}, crystal field energy levels and Zeeman spectra 2−80951
lanthanum ethylsulphate:Gd^{3+} zero-field splitting at high and low fields, e.p.r. obs. 2−51405
ligand fields and continuous groups 2−78815
low symmetry crysts., localization of Mn^{2+} 2−84288
magnet system with singlet ground state, excitations, pseudospin formalism 2−72233
molecular cryst., exciton interactions between substitutional impurities 2−71803
molecular crystals, excited-state dipole moments, polarizabilities and local fields 2−81136
nickel sodium triacetylacetonate-dioxane-benzene 2−65122
paramagnet, van Vleck, excitation spectrum 2−61479
paramagnetic crystals, ion-phonon interactions, review 2−48117
paramagnetic ions, $S=1/2$, $I\geqslant 1/2$, and $I=1/2$, $S\geqslant 1/2$ 2−84400

Crystal field theory continued
- paramagnetic ions in axial fields, magnetothermodynamic props. 2-44220
- rare earth, heavy, lattice sums and ionic enhancement potentials 2-61566
- rare earth chalcogenides, exchange interaction problems 2-54373
- rare earth double nitrate, satellite lines, field perturbation energy 2-72345
- rare earth double nitrate, satellite lines, Zeeman effect, field perturbation energy 2-72344
- rare earth double nitrate, satellite lines from non-Kramers distorted trigonal lattice, calcs. 2-72343
- rare earth ions in cryst. field, optical transitions, interference effects 2-84494
- rare earth ions in metals, metal props. rel. to cryst. elec. field splitting 2-57315
- rare earth ions is combined mag. and hexagonal cryst. fields, energy levels and moments 2-72117
- rare earth transition metal cpds., $CaCu_5$ type, valence bond form. 2-50559
- rare-earth ions in crystal matrices, moments of radial function distributions, dependence on calc. method 2-65199
- rhombic spin Hamiltonian formalism with $S=2$ 2-51410
- ruby, h.p. absorpt. spectra below elastic limit 2-61630
- samarium ethylsulphate:Gd^{3+} zero-field splitting at high and low fields, e.p.r. obs. 2-51405
- silicate glass, ligand field spectra of Ni^{2+} and struct. 2-50409
- spin-orbit coupling in ions in crystals, tensor operator formulation 2-65201
- spin-orbit effects in F^- and K-bands 2-51335
- spinel structure compounds, off centre ions, model for local distortions 2-80646
- symmetry of molecular triplet states, detection of deviation by phosphorescence microwave double resonance spectroscopy 2-50010
- thulium ethyl sulphate, splitting of $p_{3/2}$ core levels of Tm^{3+} 2-44318
- toluqinone single cryst., excitonic and zero-field splittings of first triplet state 2-78209
- transition metal complexes, trigonally distorted, theoretical investigation of electronic spectra of d^1, d^3, d^8, d^9 complexes 2-44372
- ytterbium ethylsulphate, rel. to magnetic and thermal props. 2-51241
- yttrium ethyl sulphate:Yb^{3+}, phonon field contrib. to g shift 2-68586
- zero-field splitting of d^5 ion complexes, spin Hamiltonian parameters 2-84289
- $(Al,Cr)(ur)_6(ClO_4)_3$ low-temp. polarized absorption spectra, determ. of cubic and trigonal parameters 2-51289
- $(Al,Ti)(ur)_6X_3$, $X=Cl$, Br, I, low-temp. polarized absorption spectra, determ. of cubic and trigonal parameters 2-51289
- α-Al_2O_3, forbidden e.s.r. transitions of Fe^{3+} 2-78158
- Am^{4+} ions in cubic site, J-mixing effect on g-values of Γ_7 ground state 2-48119
- $Ba(Ce_{1-x}Ta_x)O_3$, ion pair valency at high and low temps., structure, mag. and electrical obs. 2-75203
- BaF_2, e.p.r., linear elec. field effects for Ce^{3+}-F^- tetragonal sites 2-48285
- Ba_2FeUO_6, electronic config. of U^V, mag. props. study 2-68570
- $BaO:Ce^{3+}$, cubic site symmetry from e.p.r. obs. 2-54491
- $BaSO_4:MnO_4^{2-}$, polarized optical absorption and e.s.r. spectra, crystal field transition e-t_2 assignment 2-48274
- $Bi_2Mg_3(NO_3)_{12}.24H_2O:Gd^{3+}$, zero-field splitting at high and low fields, e.p.r. obs. 2-51405
- Ca^+ in $Ca_5(PO_4)_3F$, crystal field parameters 2-78161
- $CaF_2:Eu^{2+}$, electronic interactions in $4f^6$ 5d config. 2-72237
- $CaF_2:Pr^{3+}$, energy levels of tetragonally sited Pr^{3+} 2-80989
- $CaF_2:Tu^{2+}$ crystal, crystal field parameters by MO LCAO method 2-61611
- CaF_2, e.p.r., linear elec. field effects for Ce^{3+}-F^- tetragonal sites 2-48285
- CaF_2, e.s.r. of Mn^{2+}, spin Hamiltonian parameters 2-54497
- $CaO:Ce^{3+}$, cubic site symmetry from e.p.r. obs. 2-54491
- $CaO:Fe^{2+}$, energy of first excited electronic levels 2-72478
- $CaO:Mn^{2+}(Fe^{3+})$, spin-lattice coeffs., relativistic cryst. field contrib. 2-65203
- $Ca_5(PO_4)_3Cl:Mn^{2+}$, e.p.r. obs., site substitution by Mn, field parameters 2-72479
- $CdCr_2S_4:Fe^{2+}$, anisotropy of tetrahedral Fe^{2+}ions 2-72161
- $CdF_2:Er^{3+}$, i.r. transitions, Stark dissoc. by cryst. field 2-65305
- CdF_2, absorpt. and fluoresc. of Er^{3+}, ion site obs. 2-54416
- CdF_2, absorption spectra of Co^{2+}, V^{3+} and Cr^{3+} impurities 2-54417
- CdF_2 e.s.r. of Mn^{2+}, spin Hamiltonian parameters 2-54497
- $CeAl_2$, Ce crystalline field, resistivity under pressure obs. 2-77857
- $CeRh_xPd_x$ alloys electronic state, magnetic susceptibility and lattice spacings 2-81317
- $Ce_{0.25}(Y,La)_{9.75}Al_2$, inelastic neutron scatt. determination of cryst. field levels of Ce^{3+}, susceptibility calc. 2-72105
- Cr complex, di-μ-hydroxotetraglycinatodichromium(III), e.p.r. spectrum, zero-field splitting, domination by Zeeman interaction 2-80645
- $Cr(III)S_6$ trigonal systems, electronic structures and MCD spectra 2-59997
- $Cr(ur)_6I_3$, ${}^4A_2 \rightarrow {}^2E$ transition, spin-orbit interaction and Jahn-Teller distortion effects in calc. of vibronic spectra 2-51291
- $Cr(ur)_6I_3$, and deuterated complex, luminescence spectra, obs. of ${}^2E$ level splitting, zero-phonon transitions 2-51290
- $Cr(ur)_6I_3$ low-temp. polarized absorption spectra, determ. of cubic and trigonal parameters 2-51289
- CsBr:K, non-cubic Ag- centres in mixed crystals 2-44370
- $CsCrCl_3$, single crystal polarized absorption spectra, ligand field interpretation 2-81363
- $CsCr(SO_4)_2.12H_2O/D_2O$, Cr^{3+} spectroscopy, trigonal field splitting 2-54400
- Cs_2HfCl_6, e.s.r. of Yb^{3+} in octahedral cryst. field 2-72482
- $CsMgBr_3$:Ni polarized spectra, near i.r. and visible, ligand field model interpretation 2-84483
- $CsMgCl_3:CsCrCl_3$, single crystal polarized absorption spectra, ligand field interpretation 2-81363
- $CsMgCl_3$:Ni polarized spectra, near i.r. and visible, ligand field model interpretation 2-84483

Crystal field theory continued
- $CsNiBr_3$ polarized spectra, near i.r. and visible, ligand field model interpretation 2-84483
- $CsNiCl_3$ polarized spectra, near i.r. and visible, ligand field model interpretation 2-84483
- Cs_2ZrCl_2, high resolution absorpt. and mag. circular dischroism spectra analysis 2-75289
- $Cs_2[CuCl_4]^{2-}$, covalency and excited 4p states effects on 3d ground states of Cu^{2+} 2-84578
- Cu(II) ammine complexes, tetragonal, electronic spectra, symmetry-restricted covalence effects 2-80017
- Cu(II) complexes, tetrameric, $CU_4OX_6L_4$, $X=Cl$, $L=(C_6H_5)_3PO$ and $X=Br$, $L=(C_6H_5)_3PO$ or C_5H_5N exchange and spin coupling obs. 2-51233
- Cu(II) complexes orbital and spin-orit coupling constants in magnetic susceptibilities and anisotropies for D_{2h} symmetry 2-54285
- $CuInSe_2$, tetragonal field, rel. to transitions from Cu of levels in valence band 2-80974
- ErGa garnet, metamagnetism obs. 2-61557
- $Er_2O_3:Er^{3+}$, electronic excitation, far i.r. and optical spectrosc. obs. 2-81369
- EuF_2, electronic interactions in $4f^6$ 5d config. 2-72237
- $(Fe,M)_2Mo_3O_8$, ($M=Mg$, Zn, Mn, Co, Ni), Mossbauer spectra interpretation 2-75270
- Fe group ion in a tetrahedral field mixing of 3d and excited orbitals, effect on orbital momentum and spin-orbit coupling coeff. 2-80981
- Fe^{2+}, level splitting, effect of configuration interaction 2-51293
- $FeCO_3$, splitting of orbital states of Fe^{2+} ion 2-44297
- FeF_2, magnon-phonon interactions, coupling, spin Hamiltonian 2-80886
- Fe(II) complexes of 2-methyl-1, 10-phenanthroline, ${}^5T_2$-${}^1A_1$, transition, Mossbauer obs. 2-51306
- Fe(III) complexes, magnetic circular dichroism of d-d transition, ligand field theory analysis 2-48176
- $Fe(KSO_4)_2.6H_2O$, ligand field energy pattern 2-54292
- Fe_2MoO_4, spinel, X-ray and neutron diffraction studies 2-84414
- $Fe(NH_4SO_4)_2.6H_2O$, ligand field energy pattern 2-54292
- Fe_xO-MnO solid solns., absorpt. edge, cryst. field transitions 2-48174
- $Fe_{3-x}Sc_xO_4$, electronic struct. of ions 2-48207
- GaP:N, null field splitting of B-line 2-61692
- Gd^{3+}, in zircon struct., ground state splitting, ligand contribs. to quadrupole components 2-84235
- Ge III band structure 2-80980
- IFe, Mossbauer expt., meas. of magnetic moment of 57.6 keV state of ${}^{127}I$, and hyperfine field 2-49747
- $KCl:Co(CN)_6^{3-}$, i.r. spectra, level splitting 2-54413
- $KCl:Co(CN)_6^{3-}$ doped, i.r. spectra, level splitting 2-54413
- KCl-Na, non-cubic Ag- centres in mixed crystals 2-44370
- $KMnCl_3.2H_2O$, mol. field theory for calc. anisotropy and exchange fields 2-68574
- $KNiF_3$, semiempirical LCAO-MO treatment of $[NiF_6]^{4-}$ cluster 2-65200
- K_2ReCl_6, Re X-ray L_{III} absorption discontinuity, crystal field splitting 2-61676
- $KReO_4$, Re X-ray L_{III} absorption discontinuity, crystal field splitting 2-61676
- La complex, lanthanide (III) tropolonates, crystal field effects in i.r. spectra 2-61644
- $LaAl_2$, Ce crystalline field, resistivity under pressure obs. 2-77857
- $LaCl_3:Pm^{3+}$, parameters from absorption spectrum in 12000 to 28000 cm^{-1} range 2-81405
- $LiCuCl_3.2H_2O$, mol. field theory for calc. anisotropy and exchange fields 2-68574
- $LiF:Mn^{2+}$, low-field X-band e.p.r. transitions 2-72492
- $LiNbO_3$: Fe^{3+}, Hamiltonian parameters detn., e.p.r.obs. 2-65324
- $LiNbO_3:Mn^{2+}$ ferroelectric, e.s.r. studies of crystal field parameters 2-81451
- $LiYF_4:Er^{3+}$, crystal field parameters verified 2-51240
- $(M,Cr)(ur)_6(ClO_4)_3$, $M=Al$, Ga luminescence spectra, obs. of ${}^2E$ level splitting, zero-phonon transitions 2-51290
- $(M,Cr)(ur)_6I_3$, $M=Al$, Ga, luminescence spectra, obs. of ${}^2E$ level splitting, zero-phonon transitions 2-51290
- ML_4 complexes, tetrahedral, tetragonally distorted, splitting of d^2-configuration in strong ligand fields of D_{2d} symmetry 2-80937
- $MgO:Mn^{2+}(Fe^{3+})$, spin-lattice coeffs., relativistic cryst. field contrib. 2-65203
- Mg_2SiO_4, localization of Mn^{2+} 2-84288
- Mn^{3+} complexes, octahedral, paramagnetic susceptibilities for all crystal field strengths 2-61484
- $(NH_4)_2$ $SnCl_6$, cryst. field hindering of ammonium ion, low temp. spin-lattice relax. 2-84447
- NH_4Cl, cryst. field hindering of ammonium ion, low temp. spin-lattice relax. 2-84447
- $NH_4Cl(Br)(I)$, ordered low temp. phases 2-74937
- $NaCl:Co(CN)_6^{3-}$, i.r. spectra, level splitting 2-54413
- NbN, bulk and films, spin-orbit scatt. 2-54146
- $NdAlO_3$, Raman scatt. by localized electronic excitations and cryst. field model 2-72371
- $NdCrO_3$, ground state splitting of opt. transition 2-84512
- Nd_2O_2S, Nd^{3+} ion parameters, optical absorp. obs. 2-65263
- NdP, NdAs, NdSb, crystalline electric field levels detn., neutron spectroscopy obs. 2-68585
- Ni complex, high-spin NiN_3O_2 chromophore, polarized single-cryst. electronic spectrum 2-57337
- $NiBr_2(Cl_2)$, electronic absorpt. spectra parameters 2-51345
- NiF_6^{4-}, ave.-of-config. calc. of self-consistent- field electronic excitation energies 2-72240
- NiF_6^{4-}, ave.-of-config. interpret. rel. to 10Dq calc. 2-72239
- NiO, mag. insulator, rel. to exchange interactions 2-68564
- $NiSO_4.6H_2O$ optical activity, calc. of rotatory strengths and dipole strengths associated with electronic transitions 2-57325
- Pb halides, energy level splitting, effective Hamiltonian theory 2-44319
- $PbCl_2$, optical consts. and exciton states 2-68625
- $PbMoO_4$:Cu, Gd site occupancies of dopant and trace impurity 2-68739
- Pr, f.c.c., singlet-ground-state ferromagnet, mag. excitons 2-72153
- Pr, mag. props., double time Green's func. calc. 2-75205

Crystal field theory continued
Pr^{3+}, electronic shielding in crysts., variational and outward integration calc. 2−81319
Pr_3Tl, singlet-ground-state ferromagnet, mag. excitons 2−72153
Pr_3X-La_3X system, singlet ground state obs. 2−61244
$Pr_2Zn_{3c}Mg_{3(1-c)}(NO_3)_{12}.24H_2O$, satellite lines, Zeeman effect, field perturbation 2−72344
$Pr_2Zn_{3c}Mg_{3(1-c)}(NO_3)_{12}.24H_2O$, satellite lines, field perturbation energy 2−72345
Pu^{3+} ions in cubic site, J-mixing effect on g-values of Γ_7 ground state 2−48119
$RbNiF_3$, crystal field pot. acting on Ni^{2+}, calc. 2−51287
$RbNiF_3$, of magnetic anisotropy 2−61546
Sb, Sb_2Te_3, Sb_2S_3, ^{119}Sn valence state after ^{119}Sb decay, Mossbauer obs. 2−54392
Si III, band structure 2−80980
SiC, 6H exciton electroabsorption, crystal- field splitting in exciton ground state 2−81331
$SrCl_2$:Cm^{3+}, e.p.r. investigations of zero-field splittings 2−44449
$SrCl_2$, e.p.r. of Ag^{2+}, conform. instability in hexagonal sites 2−84579
SrF_2:$Cm^{3+}(Am^{2+})$, e.p.r. investigations of zero-field splittings 2−44449
SrF_6:Tm^{2+}, crystal field splitting and g values within $(TmF_8)^{6-}$ cluster framework 2−78054
SrF_2, e.p.r., linear elec. field effects for Ce^{3+}-F^- tetragonal sites 2−48285
$SrMoO_4$:Er^{3+}, crystal field parameters verified 2−51240
SrO:Ce^{3+}, cubic site symmetry from e.p.r. obs. 2−54491
Tb_2O_3, effect of crystal field on direction of magnetic moments of ions in low site symmetry 2−65186
ThO_2:Cm^{3+}, e.p.r. investigations of zero-field splittings 2−44449
ThO_2, e.s.r. absorpt. spectrum of monovalent iron 2−48296
TiO_2, anatase, e.p.r., g-tensor for Ti(III), parametric obs. 2−61739
TlN_3:Mn^{2+}, e.s.r., spin Hamiltonian parameters, temp. depend. 2−72502
Tm^{3+}, electronic shielding in crysts., variational and outward integration calc. 2−81319
TmSb, effects in mag. form factor 2−81254
V^{2+} ion, double chlorides, Ligand field theory 2−61567
V^{3+} complexes, trigonally distorted octahedral, lattice-ion interactions in the ligand field theory 2−81205
Xe:^{45}Ca β-decay, optical excitation of the daughter atoms Sc. 2−84244
$YAlO_3$, optical spectrum of exchange coupled Cr^{3+} pairs 2−72415
YIG, electrostatic forces, elec. field gradient, mol. orbitals construct. 2−68615
$YbPd_3$, rel. to mag. props., Mossbauer obs. 2−54393
Zn complex, 2,6-pyridinedicarboxylate, Cu-doped, e.p.r. obs. 2−78155

Crystal fields *see Crystals/internal fields*

Crystal imperfections
see also Colour centres; Grain boundaries; Stacking faults
alkali halide crystals, nonactivated, luminescence centres formation in very strong electric fields 2−84542
alkali halides: CrO_4^{2-}, optical and i.r. vibrational absorption spectra used to study defects in the host crystal 2−48171
alkali halides, proton dechannelling obs. of incident beam damage 2−43606
alloy, low stacking fault energy, interaction between quenching defects and dislocations 2−64662
anisotropic cubic, elastic displacment field of point defects 2−80697
anodic oxide film formed on Ti, effect of formation electrolyte on no. of imperfections 2−50518
anthracene crystal growth from melt, effect on defects concentrations 2−83904
bicrystal, epitaxial, interface struct., effect of misfit, bonding and cryst. dimens. 2−56690
brass, u.s. fatigue inhibition 2−50767
cavities, defocusing contrast in electron microscope 2−83930
crystal, deformed, resonant absorption of X-rays 2−84474
damage production in thin targets, fast particles of low charge, theory 2−50636
defects, complex, in ionic crystals, equilibrium concentrations, calc. 2−64671
defects, crystal lattice, diffusional relaxation, in the fields of local lattice disturbances 2−84000
defects, diffraction contrast micrographs, transmission and reflection 2−80621
diamond, fast electron irrad. damage 2−60775
diamond, radiation damage, effect of N impurity on annealing 2−71453
diamond, radiation damage, review 2−47371
diffractometric analysis of fine structure, limits 2−74697
diffusion, effect of trapping on annihilation 2−56678
diffusion mechanisms in metals and alloys, point defect behaviour, review 2−68044
disclination, wedge, elastic interactions 2−50658
disclinations, general kinematic equations 2−74780
disclinations and plastic distortion 2−76263
dislocations, relation between continuous and discrete 2−76267
displacement field produced by localized defects, asymptotic behaviour 2−43618
electron irradiation defects, information storage by inhibited cathodoluminescence 2−57379
electron microscope defect contrast, weak beams at 1 MV 2−80632
extraneous inclusions, formation kinetics of isometric form. 2−68015
field-ion image contrast across interfaces, geometrical theory 2−43622
GaAs:Te, heavily-doped, nature of defects, photolum. and internal friction study 2−71926
garnet, bubble domain, epitaxial film, effect of substrate defects 2−47092
gas bubbles, voids, nucleation, diffusion 2−50632
glass fibre, effect on light propag. 2−42242
graphite, artificial, neutron irrad. damage and effects on thermal conductivity 2−54073

Crystal imperfections continued
graphite, electron displacement damage, high-voltage electron microscopy 2−56683
graphite, electron irrad. damage, electron microscope obs. 2−53710
graphite, neutron irrad., rel. to thermal cond. 2−54075
graphite, neutron irrad. at high-temp., mech. interactions among crystallites 2−56679
graphite, neutron irrad. damage, dose rate effects 2−53708
graphite, neutron irrad. defect struct., single cryst. 2−53709
graphite, phonon- drag thermoelectricity rel. to structural imperfections 2−57248
graphite, pyrolytic, meas. of thermal and electrical properties, mean size of defect free region 2−84208
growth defects characteriz. by X-ray topography 2−47216
inclusion identification by vapour phase deposited interference layers 2−56737
inhomogeneities, beam scanning examination 2−80605
insulating layers, obs. using elec. field induced light scatt. in liq. cryst. 2−77918
interphase interfaces, strain fields, steps, electron diffr. contrast 2−56625
ionic crystal, defective, positron centres 2−71823
irradiated material, void stability 2−50650
isotropic defect in anharmonic crystal, local oscillations 2−71473
lattice disorder profiles determ. by nucl. backscatt. 2−53689
lattice dynamics, of defect crystal with singular defect submatrix 2−61066
linear defects, inelastic neutron scatt. cross sections calc. 2−50997
macroblock formation in crystals grown from melt, estimation of transverse dimensions 2−50683
metal, atomic displacement cascades, computer simulation 2−53700
metal, f.c.c., point detect-extended disloc. interaction, elastic modulus effect calc. 2−50652
metal, field emission microscopy, defects produced by method of exam. 2−56567
metal, irrad., explanation of voids 2−80690
metal, irrad., explanation of voids 2−80691
metal, irrad., void clusters, plasmon interaction 2−80677
metal, irrad., void formation 2−47361
metal, irrad., void growth 2−53697
metal, irradiated, voids, review 2−50635
metal, neutron damage simulation by ion bombardment, void form. 2−53693
metal, neutron damage simulation by ion bombardment, void form. 2−53692
metal, neutron irrad., displacement cascade, primary recoil energy depend., review 2−53691
metal, neutron irrad., void form. 2−50641
metal, point defect stability, low-energy-recoil event and vibr. behaviour 2−53723
metal, point defects, effects on elec. resist. temp. depend. 2−68329
metal, points defects and specific heat at high temp. 2−54040
metal, positron trapping obs. of defects, error sources 2−80676
metal, pure and impure, irrad., void form., temp. effect 2−50642
metal, quenched or irrad., void form. mechanisms 2−53696
metal, radiation- induced void form. 2−50638
metal, radiation-induced voids, conf., Albany, USA [June 1971] 2−50637
metal, review 2−68012
metal, shock wave effects, and mech. props. 2−68073
metal, swelling data analysis using displacement rates from Lindhard model 2−52880
metal, void and point defect agglomerate studies using h.v. electron microscopy 2−53695
metal, void nucleation and growth, computer simulation 2−53699
metallic materials, neutron irrad., void form. and growth, theory 2−53701
metallic materials, void nucleation during high-energy irrad. 2−53703
metals, voids, gas containing, thermodynamics 2−50633
metals and alloys, lattice defect form. under radioactive irrad., review 2−47362
nondestructive testing, helical Rayleigh waves, excitation and reception on rods by contactless electrodynamic transducers 2−50634
nuclear reactor structural mat., swelling under neutron irrad., electron microscope obs. 2−59868
phonon spectra of crystal with imperfections of stacking fault type 2−68209
point and line defects, effect on nuclear quadrupole spin-lattice relax. 2−51284
point defect dragging with strong dislocation interaction producing internal friction 2−64704
point defect interaction with grain boundaries, review 2−68032
point defects, migration to surface sinks 2−80720
point defects, stress-assisted diffusion to dislocations, eigenfunction expansion description 2−43652
point defects, study using electron beams and decoration method 2−80604
point defects and disc inhomogeneity, elastic interaction in hexagonal crystal 2−64658
point defects in ionic crystals and limitations of analogy with electrolyte solutions 2−64657
polyoxymethylene, dielec. absorption, analysis of anisotropy due to defects 2−61417
positron trapping, response rel. to trap features 2−71459
precise measurements, using X-ray and γ-ray diffraction techniques 2−47297
radiation damage, conf., Sydney, Australia [Feb. 1972] 2−43603
radiation damage, including swelling, in fissile materials, book 2−70539
radiation damage, pinhole channelling patterns 2−43605
radiation damage induced by channelling effect of high energy electrons 2−43604
radiation damage study by Mossbauer effect 2−50631
radiation-induced defect clusters, transmission electron microscopy 2−50640
radiation-induced void growth, applied stress effects 2−53704
rare-earth oxides, temp. spikes following Coulomb excitation 2−71719

Crystal imperfections continued
reactor cladding and struct. materials, irrad. induced void form. 2—49901
Renner type semiclassical approximation of absorpt. and luminesc. bands 2—81393
resonance vibrational states of crystal with point defects, influence of small perturbations 2—74761
ruby, influence on e.p.r. line shapes 2—72468
ruby boules, quality estimation from e.p.r. line widths 2—54493
rutile, point defect effects on dielec. props. 2—61412
scanning electron microscope backscattered electron contrast, dynamical theory 2—56628
scanning electron microscope obs. using diffraction contrast, theory and practice 2—43562
scanning electron microscopy, elastic waves 2—80623
semiconductor, group II-VI cpds., radiation damage 2—47366
semiconductor, group II-VI cpds., radiation induced and growth defect obs. 2—47372
semiconductor, group III-V cpds., radiation damage, review 2—47365
semiconductor, ion implantation induced lattice disorder 2—47367
semiconductor, lattice damage prod. by ion implantation 2—47374
semiconductor, radiation effects, conf. Albany, (1970) 2—47877
semiconductor, radiation effects, conf. opening address Albany, (1970) 2—47878
semiconductor cpds., departures from stoichiometry determ. by chemico-analytical methods 2—43503
semiconductor II-VI cpds., deviations from stoichiometry 2—50657
semiconductors, and strain 2—75076
semiconductors micro and macrostructures 2—61257
shear, random grouping of anion vacancies model 2—50653
Si, transmission electron diffraction, contrast reversal of Kikuchi bands 2—83921
steel, lattice microdistortions, role in temper brittleness 2—43792
steel, plastically deformed, rel. to austenite form. 2—57014
steel, press. vessel type, radiation sensitivity, effect of impurities 2—53895
steel, rel. to martensite ordering temp. 2—57026
steel, stainless, damage induced by high energy electron chanelling 2—53713
steel, stainless, deuteron generated void form., in-reactor damage simulation 2—53714
steel, stainless, irrad., cold work effects on void form. 2—50646
steel, stainless, irrad., fluence and temp. depend. of void form. 2—50647
steel, stainless, proton irrad., swelling, displacement damage depend. 2—53716
steel, stainless, proton- and nickel-irrad., void form. 2—53715
steel, stainless, suppression of void form. 2—50648
steel, stainless, void form. on quenching 2—53717
steel, stainless, void nucleation and growth during fast neutron irrad. 2—50645
steel, stainless, void nucleation and growth obs. using h.v. electron microscope irrad. 2—53694
strong materials, role in mech. props., book 2—60878
structure with two point defect types, quantum states and energy spectrum 2—80998
surface flaw detection using oblique angle illumination 2—50415
swelling in fast-neutron-irrad. materials, theory 2—53702
tetraphenyl tin and isomorphs, etching and X-ray obs. 2—53731
topaz, electron beam damage obs. 2—60776
transmission electron microscopy contrast, strong beam to weak beam conditions 2—80631
triglycine sulphate single crystal, effect of growth rate on defect struct. 2—47987
twist disclination loop elastic behaviour near free surface 2—50664
two phase materials, circular disclination, elastic fields, interface effects 2—76272
vacuum decoration method, study of growth processes and defect structure 2—80538
void growth and nucleation in irradiated materials 2—47360
void growth on grain boundaries, rel. to creep 2—50685
volume defects, electron energy loss spectra, use for analysis 2—80654
X-ray diffraction applications, review 2—64744
X-ray topographic photography using conical cassette 2—43545
n-Ge, electron irrad., low temp. annealing 2—47378
, Mo, electron irrad., rel. to stage I recovery process 2—53718
Ag, proton, deuteron, and He-ion damage, energy depend. 2—50643
Ag dendrites on amorphous substrates, disclinations 2—53582
Ag halides, physics and chem., conf., Montreal, Canada, Aug. (1972) 2—81541
AgBr, positron annihilation at extended defects 2—81024
AgCl, positron annihilation at extended defects 2—81024
Al-Fe, microstruct., annealing out of lattice defects 2—50827
Al-Fe alloy, microhardness rel. to precip. of Fe and annealing out of lattice defects 2—50828
Al, α-irrad., low-temp. sp. ht. obs. of He bubble form. 2—50644
Al, deformed by rolling, positron interaction with defects 2—71460
Al, electron displacement damage high-voltage electron microscopy 2—56683
Al, γ-ray irrad. induced point defects, correl. with thermal expansion 2—43607
Al, low disloc. density crystal, anomalous X-ray transmission due to subtropographic defect clusters 2—47395
Al, neutron irrad., void annealing 2—53705
Al, neutron irrad., void distrib., struct. imperfections in fluence 2—53736
Al, quenched, annealing kinetics of point defects, resist. and magnetoresist. study 2—80680
Al, workhardened and irrad., point defect migration 2—43669
Al alloys, spherical defects, ultrasonic plane waves scattering, computer simulation 2—51023
Al damage induced by high energy electron channelling 2—53713
AmO_2, thermal cond., self-irrad. effects 2—54078
Au, proton, deuteron, and He-ion damage, energy depend. 2—50643
B_4C, neutron radiation induced defects, transmission e. microscope obs. 2—67355
$BaTiO_3$, point defect effects on ferroelec. props. 2—61412

Crystal imperfections continued
Be, monocrystals, growth by Czochralski technique, obs. of cryst. perfection 2—47262
BeO, γ-irrad. induced effects, e.s.r. obs. 2—44445
Bi, rel. to movement of twin boundaries during cycling 2—83970
Bi_2Te_2Se, 7.5 MeV proton irrad. induced disorder, X-ray obs. 2—64653
C-C composites, effect on mech. props. nondestructive testing 2—61016
C-graphite matrix composites, effect on mech. props. 2—61015
C, defect theory of struct. 2—53729
C, neutron irrad. at high-temp., mech. interactions among crystallites 2—56679
C, pyrolytic, high graphitized, X-ray obs. 2—60752
$CaCO_3$, calcite, twinning boundaries, thermal shift after annealing 2—77573
CaF_2, mechanism of intrinsic radiational defect formation 2—56680
CdS, electron irrad. defects, effects on photocond. 2—57254
CdS platelets, radiation damage effects at low temps. 2—68703
CdTe, compensation by intrinsic point defects, elec. cond. obs. 2—84334
CdTe, mag. susceptibility of defects, 4.2-290K 2—77980
CsI, defect spatial decoration, methods and mechanism 2—80695
CsI(Na), nature of luminescence centres, hypothesis based on properties of CsI crystals 2—68679
Cu-Al(10 wt%), high fluence neutron irrad., electron microscope obs. 2—80686
Cu-Ga alloy, cold-worked, X-ray obs. 2—80861
Cu-Ni alloy, neutron irrad., void formation, fluence effects 2—80687
Cu-40 at.% Ni alloy, sp. ht. below 3K, effect of clusters and quenching 61103 2—61103
Cu, elastic displacement field of point defects 2—80697
Cu, electron irrad., lattice parameter and resistivity changes 2—60777
Cu, high fluence neutron irrad., electron microscope obs. 2—80686
Cu, γ-ray irrad. induced point defects, correl. with thermal expansion 2—43607
Cu, neutron irrad., void formation, fluence effects 2—80687
Cu, neutron irradiated, cleared channels, correl. with surface slip steps 2—50761
Cu, point defect clusters, effect on fatigue hardening 2—53724
Cu, polycrystalline, point defects rel. to elec. resistivity changes during tensile deformation 2—47834
Cu, void growth on grain boundaries, rel. to creep 2—50685
Cu film, epitaxial 2—67909
Cu whiskers, grown by halide reduction 2—80570
Fe_2O_3-TiO_2 solid soln., crystallographic shear struct., planar boundaries 2—74768
FeO, point defects, thermodynamic analysis, migration processes 2—56684
GaAs:Mg-Li, i.r. absorpt. due to pair defects, absorpt. cross section 2—81360
GaAs, electron irrad., asymmetric damage regions, elec. props. obs. 2—74759
GaAs, epitaxially grown, plane defect at interface, X-ray obs. 2—71488
GaAs, ion implantation lattice disorder, low temp. channelling obs. 2—47373
GaAs, undoped, point defect conc. effects 2—71905
p-GaAs epitaxial layer, gas transport deposition, orientation effects on defect conc. 2—71387
GaP, 40 keV Te implantation damage and annealing 2—80706
Ge:Li, electron irrad., Hall effect and minority carrier diffusion length obs. 2—47927
Ge, amorphous film, void structure and optical sum rules 2—78063
Ge, defects, formation and annealing during bombardment with Kr ions 2—71461
Ge, electron and γ-irrad., Mossbauer type photoluminesc. spectra obs. 2—48243
p-Ge, electron irrad., annealing and conductivity obs. 2—47377
n-Ge, electron irrad., annealing kinetics 2—47380
n-Ge, electron irrad., impurity depend. of low temp. annealing 2—47376
p-Ge, low temp. elec. irrad., point defect annealing 2—47381
p-Ge, low temp. electron irrad., 220K defect, resistivity and Hall obs. 2—47928
Ge, low temp. irrad. and annealing, review 2—47375
p-Ge, radiation defect annihilation centre, photocond. obs. 2—83978
Ge, radiation defect form. and annealing 2—47383
HgO, i.r. absorption, reln. to colour and structure changes 2—68643
InSb single crystals, growth of ‘star’ defects and effect of seeding on clustering 2—71476
KCl:Pb, rapidly grown from melt, thermal stress defect model 2—50649
KCl-KBr solid solutions positronium formation 2—80988
KCl, association energies of intrinsic and extrinsic defect pairs 2—80651
KCl, diffusion of ion- implanted ^{85}Kr, effects of radiation damage 2—68053
KCl pure single crystals, extent of perfection 2—60822
$K_2Pt(CN)_4Br_{0.3} \times 2.3H_2O$, defect effects on one-dimensional metallic conductivity 2—68339
$KTaO_3$, point defect models 2—47967
LiF, neutron irrad., X-ray obs. 2—80660
LiF, proton irrad., surface damage monitoring using (p,α) reaction 2—43610
LiF, spark discharge induced damage 2—68013
Mg, neutron irrad., distortion and swelling, effects of alloying additions 2—60778
Mg, neutron irrad., struct. damage and annealing 2—80683
$MgAl_2O_4$ spinel, cation disorder, e.s.r.obs. 2—65325
MgF_2, annealing of defects, effect on temp. depend. of elec. cond. 2—47898
MgO, microcavities, volume determ. by tracer method 2—43623
MnO, point defects, thermodynamic analysis, migration processes 2—56684
Mo, ion irrad., surface damage, LEED obs. 2—50468
Mo, ion irrad., void lattice obs. 2—53720
Mo, irrad., void stability 2—50650

Crystal imperfections continued

- Mo, γ-ray irrad. induced point defects, correl. with thermal expansion 2−43607
- Mo, neutron irrad., void formation during annealing, electron microscope obs. 2−77575
- Mo, neutron irrad., void form. and ordering, alloying and purity effects 2−53719
- Mo, void lattice theory, lattice spacing 2−56685
- NaCl, creep at high temp., creep substruct., tilt walls around parallelipipedic blocks 2−77579
- NaCl, ion beam induced damage, backscatt. obs. 2−43611
- NaCl, quenched, X-irrad., cry. lattice defects and near surface props. 2−71477
- NaCl whiskers inelastic phenomena 2−80575
- Nb, deformed, angle and wave depend. of X-ray diffr. linewidth 2−43625
- Nb, neutron irrad., void form. and ordering, alloying and purity effects 2−53719
- Nb, supercond., critical current rel. to radiation induced defects 2−81053
- Ni-Fe-Cr based alloy, γ'-hardened, electron irrad., void swelling 2−80684
- Ni, deformed, angle and wave depend. of X-ray diffr. linewidth 2−43625
- Ni, electron irrad., void form., effect of injected gas atoms 2−43613
- Ni, electron irrad. damage, recovery, resist. and mag. after-effect study 2−64655
- Ni, neutron irrad., void formation, fluence effects 2−80687
- Ni, ultrasonically treated, positron annihilation obs. 2−43612
- Ni alloys, neutron irrad., void form. and swelling resist. 2−53721
- Ni and alloys, void nucleation and growth obs. using h.v. electron microscope irrad. 2−53694
- NiO, rel. to high temp. transport props. 2−84314
- Pb-Sb alloy, point defects rel. to precip. mechanism 2−80858
- $(Pb,La)(Zr,Ti)O_3$, phase boundary and defect struct. 2−56968
- $PbBr_2$, pure and doped, hole cond., defect chem. 2−61322
- PbSe defects, obs. using hydrostatic weighing 2−58691
- $Pb(Ti,Zr)O_3$ system, intrinsic nonstoichiometry 2−50894
- Pt, proton, deuteron, and He-ion damage, energy depend. 2−50643
- PuO_2, thermal cond., self-irrad. effects 2−54078
- $RbMnF_3$ antiferromagnet, magnetoelastic theory of ^{19}F nuclear acoustic resonance and lattice imperfection 2−51412
- ReO_2, rel. to polymorphic transform. mechanism 2−47695
- Si:B, ion implanted lattice disorder distributions, channelling effect analysis 2−68036
- Si:C, low temp. electron irrad. damage, i.r. absorp. obs. 2−48191
- Si:Ge, O, C, low temp. electron irrad. damage, i.r. obs. 2−48192
- Si:O, lattice damage due to ion implantation, e.p.r. obs. 2−60780
- Si-ge alloy, He$^+$ irrad., atomic displacements, Rutherford scatt. obs. 2−47388
- Si, defects, identification of chem. constituents 2−77913
- Si, electron beam irradiation induced defects, electron microscope examination 2−64656
- Si, electron irrad., asymmetric damage regions, elec. props. obs. 2−74759
- p-Si, electron irrad., hole emission rates, activation energy and annealing of defects 2−54199
- Si, electron irrad., liquid He temp., a.c. hopping cond. obs. 2−47936
- Si, fast neutron radiation damage, e.p.r. obs. 2−48282
- Si, He$^+$ irrad., atomic displacements, Rutherford scatt. obs. 2−47388
- Si, hybridization of atomic orbitals at structural defects 2−81005
- Si, implantation damage and impurity location, channelling obs. 2−71511
- Si, ion-implanted, radiation damage under channelling conditions 2−68017
- Si, ion irradiated, apparent damage induced optical absorp., scatt. from defect zones 2−48158
- Si, irradiation damage, comcepts and correlations 2−47387
- Si, lattice defects, comparative study of X-ray topographic methods 2−47405
- Si, lattice distortions due to scratching 2−43626
- Si, neutron irrad., piezospectroscopic obs. 2−48193
- Si, neutron irrad. damage, Mossbauer effect obs. 2−48153
- Si, small spherical voids, electron diffr. contrast profile, calc. 2−77571
- Si crystals, high-resistive floating-zone, striations revealed by preferential etching 2−74787
- Si film and bulk, electron irrad., defect prod., resist. change 2−80655
- Si planar diode, elec. props. rel. to lattice defects, X-ray obs. 2−47944
- α-SiC, influence of struct. defects on elec. props. and luminescence 2−71774
- α-SiC, residual lattice disorder due to ion bombardment 2−47391
- SiC, transmission electron microscope obs. 2−47423
- SiO_2, point defect prod., model 2−80656
- SiO_2 film, dielec., defects, local junction form 2−71964
- α-Sn, electron irrad., atomic displacement process evidence 2−53722
- α-Sn, electron irrad., damage production and thermal annealing, resist. study 2−80682
- SnSe film, epitaxial on KCl, boundary struct., rotational Moire method obs. 2−74635
- Te, electron irrad. damage obs. 2−47392
- TiO_2:Fe^{3+} spin- lattice relaxation mechanism 2−81459
- TiO_2-Cr_2O_3 system, solid solns. and cryst. shear struct., electron microscope obs. 2−47406
- U alloy, ion etched, scanning electron microscope obs. 2−56578
- UO_2 fuel rod, irrad., pore movement kinetics 2−52873
- U_3Si, irradiated, effect of electropolishing on voids 2−67354
- V, neutron irrad., void form. and ordering, alloying and purity effects 2−53719
- VO short range ordering of defects, electron diffraction study 2−80701
- W-doped with Al, K or Si, rods, bubble-forming impurities, identification 2−80792
- W, ion irrad., surface damage, LEED obs. 2−50468
- $W_xNb_{1-x}Se$, influence on layer struct. 2−60767

Crystal imperfections continued

- WO_3, ion bombardment-induced amorphization and mean damage rates determ. 2−77576
- YAG:Nd, crystal growth, boule defects, and Nd distrib. obs. 2−47246
- ZnO thermal control coating pigment, u.v. irrad., e.s.r. of defects 2−81460
- ZnS single crystals, stacking faults, polytypic growth, electron microscope study 2−60769
- ZnTe, threshold energy for Te displacement, cathodoluminesc. obs. 2−68018
- Zr, elimination by cold rolling, determ. by meas. elec. resist. 2−43797
- ZrO_2, nonstoichiometric, microscopic thermodynamic props., rel. to macroscopic props. 2−43506
- ZrO_2, Y_2O_3-stabilized, current blackening effects, defect struct. obs., e.s.r. spectra 2−61740

dislocations

- — 2−56591
- β Ti-V alloys, correlation with thermal-etch pits and facets 2−80546
- accumulation in stress fields, initial stage of plastic deformation 2−80696
- admixture distribution in crystals during growth 2−50663
- albite, distrib. obs. in plastically deformed sample 2−81623
- alkali halide, lattice distortion produced by edge disloc., photoconductivity spectra obs. 2−74777
- alkali halide crystals, electrons trapped in edge dislocations 2−81200
- alkali halide crysts., u.v. and electron irradiation effects, decoration techniques 2−80607
- alkali halides, transient dislocation-point defect interaction effects, neutron irrad. induced 2−43634
- alloy, AuCu-ype, breaking through of dislocations across domain boundaries, activation energy 2−56692
- alloy, equil. configs. of passing dislocations on parallel slip planes 2−50665
- alloy, low stacking fault energy, interaction between quenching defects and dislocations 2−64662
- alloy, two-phase, struct., effects of coherency strain fields 2−56702
- alloys, body centred cubic, theory of solid solution hardening 2−77691
- alloys, dissociated dislocations, analysis of electron micrograph images 2−80624
- anisotropic six-dimensional formalism, isotropic limiting behaviour 2−50668
- anisotropic theory, isotropic limiting behaviour of six dimensional formalism 2−61727
- barrier form. in dislocation network 2−56699
- b.c.c. anisotropic crysts., networks and reactions, anisotropic elasticity theory 2−56716
- b.c.c. lattice, accommodation of deform. twins by screw dislocations 2−74782
- b.c.c. lattice, screw dislocation; motion under stress at 0 K, computer simulation 2−71484
- b.c.c. metals, distrib. rel. to work hardening 2−60799
- bibliography of work by Burgers (1925-1969) 2−62917
- Borman topographic study, geometrical conditions influence 2−43631
- boundary defects, sliding, diffusional creep, atomistic aspects 2−56729
- boundary models, free volume concept 2−56724
- α-brass, containing SiO_2 particles, dislocation generation during plastic deform. 2−56708
- α- brass, near tarnish film, rel. to stress corrosion cracking 2−64734
- $\alpha+\beta$ brass, rel. to superplastic props. 2−64714
- Burgers vectors, determ. by x-ray interferometry 2−77581
- carbonate crystals, natural rhombohedral, growth defects study by X-ray transmission topography 2−53732
- cell stresses 2−56698
- ceramic, role in plastic deform. 2−47493
- chemical diffusion, phenomenological theory 2−74808
- continuously distributed aggregate, equilib. config. from energy principle 2−74771
- crack lamellae analysis under varying applied stresses 2−50772
- cracks, circular, propagation for tension and torsion 2−60900
- creep, disloc. mechanisms, review 2−53811
- creep, recovery-work hardening theory 2−56799
- creep kinetics, dislocation glide and viscous bowing, modified Orowan eqn. 2−56694
- crystalline solids, pore growth and mechanism during plastic deform. 2−80653
- cubic crysts., screw dislocation motion at finite temp. under const. stress 2−60793
- damping of motion, u.s. meas. method 2−68030
- deformation, dynamic, ideal viscoplasticity, dislocation flux idealization 2−49076
- deformed crystal, screw dislocation, critical shear 2−50659
- density, as limiting factor on crystal growth rate from melt 2−53611
- diamond, plastically deformed, rel. to intersecting twins 2−80692
- diamond cubic lattice, splitting 2−68022
- diffusion, effect of trapping on annihilation 2−56678
- diffusional creep, grain boundary climb for vacancy sources, interface reaction control conditions 2−50752
- dilational strain and strain probability distribution in dislocated materials 2−60794
- disc inhomogeneity as disloc. loop model, elastic interaction with defects in hexagonal crystal 2−64658
- disclination loop behaviour analogy 2−50664
- and disclinations, relation between continuous and discrete 2−76267
- dislocation first contribution to the flow stress 2−83974
- dislocation loops, small perfect, characterisation by transmission electron microscopy 2−80674
- dislocation loops, small perfect, characterization by transmission electron microscopy 2−80673
- domain boundary displacement under deformation, effect of dislocations 2−72143
- domain wall interaction, retardation of movement 2−68540
- eccentric growth, effect of radial temp. grad. on mean density 2−47252
- elastic cylinder, Somigliani type dislocations 2−52159
- elastic Green's function, Debye cutoff 2−64663

- **Crystal imperfections** continued
  - **dislocations** continued
    - electron microscope diffraction contrasts, theor. comput. for obs. of groups of two dislocations 2-67960
    - electron microscopy, transmission, weak beam and 500 KV voltage techniques 2-56700
    - electron microscopy, weak beam method 2-80630
    - epitaxial island alignment rel. to misfit dislocations, misfit strain 2-56697
    - epitaxial islands, equilib. elastic strains, misfit dislocations, size dependence 2-56696
    - epitaxial overgrowths of finite thickness, misfit dislocation energy 2-60798
    - f.c.c. crystal, two-dimens., model, interaction of edge dislocations 2-80652
    - α-Fe and low C steels, effect of deformation temp. on changes of the mech. props. 2-84159
    - ferromagnet, rel. to energy loss during mag. reversal 2-72144
    - film/substrate interface, misfit dislocations, image contrast 2-71483
    - fluorite, natural X-ray topographic obs. 2-80669
    - grain boundaries, coincidence-ledge-dislocation model, supporting evidence 2-47426
    - grain boundary and internal boundary types, behaviour and contrast effects 2-56701
    - grain boundary heterophase dislocation theory, high temp. behaviour 2-56733
    - graphite, interstit. type loop formation on electron irrad. 2-53710
    - group $A^{II}B^{VI}$ cpds., ion etched, scanning electron microscope obs. 2-64540
    - group dynamics, general solutions, n-body problem 2-56704
    - group dynamics, similarity solutions, continuum approx. 2-56705
    - group dynamics, similarity solutions, n-body problem 2-56703
    - growing crystal, succession of structural defects 2-53603
    - hardening, statistical problem, motion and pinning 2-68125
    - hexagonal cryst., anisotropic elasticity of prismatic loop 2-47408
    - hexagonal cryst., elliptical dislocations loops pileups, elastic energy, tip stress 2-60791
    - hydrostatic pressure effects 2-60797
    - ice, plastic deformation, associated activation volume 2-64698
    - ice i_h, effect on dielectric relaxation spectra 2-72013
    - impurity diffusion and effect of stresses on dislocations 2-71481
    - interaction, elastic, between non-parallel slip planes 2-71479
    - interaction between pile ups, rel. to strain hardening 2-50666
    - interaction with grain boundaries, review 2-68032
    - in interface, between two isotropic phases, stress fields and strain energies 2-80668
    - interphase interfaces, strain fields, epitaxial dislocations, steps, electron diffr. contrast 2-56625
    - kinematics rel. to disclinations 2-74780
    - $L1_2$ superstructure, motion resistance caused by short range order 2-47409
    - line defect, dislocation and disclination contents 2-74774
    - line forces, line force dipoles, displacement fields, anisotropic elastic solns. 2-56695
    - liquid crystal, smectic mesophase, screw dislocations 2-74519
    - Luders band growth, rate-determininng process 2-74775
    - martensitic particle, rel. to growth path 2-43907
    - metal, anisotropic, density determ. from second moments of oscillation 2-43628
    - metal, annealing of loops and tetrahedra, rel. to void growth 2-53698
    - metal, band struct. energy contrib. to energy of screw disloc. 2-50669
    - metal, b.c.c., dislocation struct. form. and strengthening mechanisms 2-43629
    - metal, b.c.c., rel. to brittle fracture 2-43720
    - metal, close packed, Burgers vectors determ. using g.b=2 contrast in electron microscope 2-60792
    - metal, cubic, lattice statics of vacancy-screw disloc. interact. 2-56687
    - metal, eigen-frequency of extended disloc. 2-60796
    - metal, f.c.c., hexagonal Frank loop energy 2-50667
    - metal, f.c.c., point detect-extended disloc. interaction, elastic modulus effect calc. 2-50652
    - metal, grain boundary ordered struct., boundary dislocations, transmission electron microscopy 2-53651
    - metal, h.c.p. and f.c.c., atomic stacking order, dislocation theory 2-47422
    - metal, irrad., interstitial dislocation loop form. 2-53696
    - metal, order struct. and dislocations in bubble-raft grain boundary 2-53741
    - metal, review 2-68012
    - metal, role in brittleness 2-43719
    - metal, strain-hardened, plastic flow theory 2-43684
    - metals, deformed polycrystalline sheet, influence of hydrostatic pressure soaking on structural changes, X-ray study 2-84127
    - metals, dislocation line tension, effects of elastic anisotropy 2-74772
    - metals, growth in macrosonic fields, structures 2-50590
    - metals, hexagonal, undissociated, computer simulation of images 2-43632
    - metals, large angle specimen tilting device and stereoscopic obs. 2-82438
    - metals, review of substructure strengthening and mechanical-thermal treatment 2-84099
    - metals under fast-neutron irradiation interrelation between swelling and irradiation creep 2-76941
    - Mo-Ti(0.5%) alloy, transmission e. microscopy obs. of void superlattice after n. irradiation 2-64667
    - mobility, rel. to surface energy, in cryst. with high Peierls barrier 2-71482
    - model, nonlinear defect, to explain generation of cracks 2-84047
    - molecular crystals, effect of dislocations on diffusion mobility 2-80722
    - motion, activation area 2-47407
    - motion, general theory and appl. to one-dimens. lattice 2-80657
    - motion, one-dimens., through cryst. with random barrier height and spacing 2-77587

- **Crystal imperfections** continued
  - **dislocations** continued
    - motion, through random array of thermally activatable obstacles 2-71485
    - motion in a crystal, two dimensional lattice and Lorentz force 2-83972
    - motion through a dislocation array, model 2-71486
    - nematic and cholesteric liquid crystals, irregularities on dislocation lines 2-64430
    - nickel silvers, fire-cracking mechanism 2-43794
    - olivine, dislocation mechanisms rel. to upper mantle flow 2-65533
    - omphacite, distrib. obs. in plastically deformed sample 2-81623
    - Orowan creep eqn., modified, form for internal stress due to dislocation interactions 2-74847
    - Patterson functions, systematic analysis on basis of crystal symmetry, interaction peak relations 2-74695
    - Peierls edge dislocation model, variational principle formulated for size of edge dislocation 2-43633
    - Peierls force, calc. including distortion due to displacement normal to slip plane 2-74773
    - Peierls Nabarro model, dislocation splitting 2-74770
    - Peierls Nabarro model of planar dislocation cores in b.c.c. crystals 2-71480
    - pile-ups, rel. to oscill. internal stresses and Lomer-Cottrell dislocations 2-77580
    - plane pile-up, kinetics 2-50661
    - plastic behaviour of single crystals under high pressure 2-68080
    - plastic deformation, dynamics, high voltage electron microscope obs. 2-56785
    - plastic distortion and disclinations, semi-microscopic 2-76263
    - point defect dragging with strong dislocation interaction producing internal friction 2-64704
    - polyethylene, crysts., slip traces, dislocation motion 2-83847
    - polyethylene, direct obs. of screw dislocations 2-43640
    - Portevin-Le Chatelier effect, and density and activation entropy of moving dislocations 2-80748
    - powders, loosely packed and cold pressed, role in sintering 2-61002
    - quantitative analysis of dislocation distribution, correspondence 2-68025
    - quantitative analysis of dislocation distributions, comments 2-68024
    - quantitative defectoscopy, and computer-simulation of images 2-60745
    - quartz, synthetic, plasticity stages of single crysts. 2-56797
    - quasidislocations in magnetoelasticity 2-61519
    - radiation induced, on ion implantation, effects on solid 2-50631
    - radiation-induced defect clusters, transmission electron microscopy 2-50640
    - scanning electron microscope backscattered electron contrast, dynamical theory 2-56628
    - screw, in presence of orthogonal edge dislocation, shape calc. 2-60795
    - screw, isolated, moving, interac. with circ. cylindrical rigid inclusion 2-50662
    - self-strained bodies, volume dilatation, Zener formula applied to dislocation dipoles and configurations 2-50660
    - slightly compressible materials, finite deforms., screw dislocations governing eqns. 2-78881
    - solid solutions, B2 and $L1_2$ superstruct., superdislocation-antiphase boundary interactions 2-47416
    - solid solutions, B2 and $L1_2$ superstruct., superdislocations and antiphase boundaries 2-47417
    - stainless steel, electron contrast in ferritic phase 2-80873
    - steel, annealed low carbon, model for delayed yielding phenomenon 2-80813
    - steel, austenitic stainless, rel. to stress corrosion testing, mech. behaviour 2-50765
    - steel, austenitic stainless fast neutron induced swelling 2-63969
    - steel, conc. rel. to hot pressing conditions 2-43793
    - steel, dislocation-additive interaction during tempering 2-43790
    - steel, high Ni, austenite stabilization rel. to reverse transformation 2-74930
    - steel, Kh18N10T, fine structure changes for degree of deformation in creep 2-83956
    - steel, low C, changes of dislocation arrangement during fatigue process 2-84162
    - steel, low-alloy and low-C, neutron irrad., rel. to hardening 2-80681
    - steel, low-C, dynamic strain aged, rel. to work softening 2-80837
    - steel, low-C low-alloy, fine struct. and phase comp. at elevated temps. 2-53898
    - steel, mild, effect of high energy ultrasonic waves 2-77673
    - steel, mild, rel. to Bauschinger effect and discontinuous yielding 2-64716
    - steel, mild, rel. to strain hardening 2-80814
    - steel, Ni martensite, effect on C diffusion 2-56758
    - steel, pearlite, struct. effects on strength and brittleness 2-43724
    - steel, quenched, quench-aged, fatigue behaviour rel. to microstruct. instability 2-50768
    - steel, rel. to brittle fracture 2-43720
    - steel, rel. to effect of V alloying on brittle fracture 2-53896
    - steel, rel. to fracture, nucleation of cleavage microcracks 2-47413
    - steel, stainless, AISI 304 and 316, substructure correlation with elevated temperature low cycle fatigue 2-56819
    - steel, stainless, dislocation dipole, electron microscope obs. 2-80666
    - steel, stainless, loop nucleation and growth during fast neutron irrad. 2-50645
    - steel transformer, dislocation density, X-ray diffraction technique 2-43636
    - straight screw, exact solution for interaction with void 2-56693
    - stress-assisted diffusion to dislocations, eigenfunction expansion description 2-43652
    - structure and props. of grain boundaries and interfaces, conference, Yorktown Heights, N.Y., USA, Aug (1971) 2-56722
    - superconductor, type-II, interaction with fluxoids 2-44064
    - superconductor, unpinning rel. to creep strain delay at transition temp. 2-74846
    - superdislocation and dislocation dipole, electron microscope obs. using systematic reflections 2-80666
    - superdislocation of double Frank and Read source 2-74776

Crystal imperfections continued
  dislocations continued
    surface, phonon scatt., rel. to Kapitza resist. 2−54072
    teflon, thermal conductivity, 0.17 to 4.0 K, dislocation scattering 2−71762
    thermal unpinning rel. to Hasiguti peaks of internal friction 2−68023
    thiourea, grown by evaporation, defect struct., X-ray topography obs. 2−74769
    twinning, dislocation model 2−47410
    Udimet 500, substruct. rel. to low cycle fatigue 2−56820
    Udimet 710, nickel-base superalloy, effect of mean stress on high-cycle fatigue at 1000°F 2−60950
    X-ray anomalous transmission for crystals containing dislocations 2−71496
    X-ray topographic photography using conical cassette 2−43545
    zinc blende structure, like-sign asymmetric disloc. 2−71478
    Zircaloy-4, deform. mechanism 2−50747
    Zircaloy-4, neutron irrad., deform. parameters, 300°C 2−50749
    Ag-Sn alloys, density variation with comp. 2−50678
    Ag, dislocation etchants, use of H_2CrO_4 2−71363
    Ag, grain boundary self-diffusion, correl. effects 2−56752
    Ag, network development rel. to recrystalliz. on annealing 2−47577
    Ag, radiation damage, nature and annealing characts. 2−47368
    Ag alloys, rel. to stress equivalence of soln. hardening 2−80834
    Ag on NaCl surface, decoration with anthraquinone, information microstructure 2−71305
    Ag single crystal films, preparation and charact. 2−74627
    Ag whiskers, mechanism of dissolution 2−50517
    AgCl, polycryst., dislocation dynamics, thermally, activated deform., flow stress, 77-400K 2−77589
    AgCl, pure and doped, density obtained from phonon scatt. strengths 2−77789
    Al-5 at.%Mg solid soln., steady state creep, dislocation mechanism, 570-800K56801 2−56801
    Al-Cu-Mg-Mn alloy, dislocation density, tensile deform. depend. 2−80772
    Al-Cu-Mg-Ni, forged after quenching, rel. to creep strain mechanisms 2−43804
    Al-Cu alloy, Frank loop nucleation on screw dislocations 2−50670
    Al-Li alloys, neutron irrad., inert gas bubble effects 2−43688
    Al-Mg-Si alloy, strength rel. to dislocation motion and GP zones 2−56717
    Al-Mg alloy, network form. during hot deform. 2−56712
    Al-Mg alloy, rel. to high temp. creep mechanism 2−68089
    Al-Mg alloys, viscous glide in solid solution, dislocation climb and Newtonian viscous deformation mechanisms 2−64718
    Al-(3 at.%)Mg alloy, high temp. deformation, lattice rotation 2−74835
    Al-Mg(Cu) alloy, rel. to solute-vacancy binding energy determ. 2−74762
    Al, 7075, laser shock-induced microstructure changes 2−68075
    Al, Al-0.5 wt.%)Fe alloy, high temp.-low stres, directional diffusion vs. dislocation process mechanisms50755 2−50755
    Al, deformed, struct. of loops rel. to deform. method 2−77574
    Al, dislocation multiplication mechanism 2−80679
    Al, dynamics on plastic deformation, high voltage electron microscope obs. 2−56785
    Al, influence on substruct. strengthening 2−50763
    Al, loop formation during electron irrad., microstruct. depend. 2−53733
    Al, mobility and damping const., phonon-dislocation interactions 2−50671
    Al, multiplication mechanism, near surface, Lang X-ray obs. 2−43635
    Al, neutron irrad., influence on void form. 2−53736
    Al, neutron irradiation effects as distance between pinning points rel. to internal friction 2−60850
    Al, plane shock structs., strain rate functions 2−60800
    Al, plastically deformed, mobile dislocation density and velocity 2−43689
    Al, plastically deformed, mobile dislocation density and velocity 2−43690
    Al, plastically deformed, surface layer, electron microscope obs. 2−43465
    Al, plastically deformed by lateral rolling 2−74837
    Al, positron and dislocation binding 2−83977
    Al, positron lifetimes and trapping probabilities at dislocations 2−44010
    Al, rel. to effect of deform. and ageing on yield stress 2−50799
    Al, rel. to linear magnetoresistivity 2−57136
    Al, strain rate role in dislocation substruct. form. 2−47499
    Al, workhardened and irrad. rearrangement of dislocations 2−43669
    Al alloy, two-phase, struct. on plastic deform. 2−56789
    Al alloys, multiphase, strengthening by dislocation substructures 2−56706
    Al crystal, configuration as function of thermal treatment 2−47411
    Al single crystals, possibility of use of oscillating film spectrometer for detn. of dislocation density homogeneity 2−77582
    AlAs epitaxial layer, on GaAs, disloc. densities 2−71881
    Al_2O_3, alumina, high temp. creep mechanism 2−50753
    α-Al_2O_3, rel. to plastic deform., 1650-2000°C 2−53804
    Al_2O_3, sapphire, dislocation tangle formation, X-ray obs. 2−80703
    Al_2O_3 ceramic, glide and climb, rel. to deform. processes 2−60993
    Au-Cu ordered alloys, dislocation mechanisms of twinning 2−68033
    Au, bicrystals, grain boundary dislocation behaviour, electron microscope obs. 2−56732
    Au, radiation damage, nature and annealing characts. 2−47368
    Au, Shockley, separation meas. determ. of stacking fault energy 2−77591
    Au bicrystal, ion irrad., g.b. disloc. climb, elec. microscope obs. 2−56731
    Au film, bicryst., electron diffr. by grain boundary dislocation networks 2−77593
    α-Fe-Sn, solid-soln., precip. of FeSn 2−80812
    $Ba_2Zn_2Fe_{12}O_{22}$, grown by seeding, density and distribution of dislocations 2−68026
    Be-(1 wt.%)Fe alloy, role in initial precip. stages on thermal treatment 50931 2−50931
    Be, substruct. on deform., obs. by synergy of TEM, selected area X-ray topography and line pofile analysis 2−56791

Crystal imperfections continued
  dislocations continued
    Be, temp. depend. of friction stress for basal dislocations, 300-500K 2−64753
    BeO, etchant consisting of HCl 2−53600
    Bi, delineation, temp. effect 2−56707
    BiTe, single crystal plate, revealed by etching method 2−84322
    $CaCO_3$, calcite, habit rel. to growth soln. comp. 2−74676
    $CaCO_3$, synthetic calcite, X-ray obs. 2−47412
    CaF_2, density, dependence of growth technique 2−47396
    CdI_2 crystals, room temp. effect, X-ray diffr. obs. 3-4 yrs after growth 2−68027
    CdSe, exciton scatt. by dislocations, absorpt. study 2−81007
    n-CdTe, bending producing 60° dislocations, effect on conductivity and photoconductivity 2−61264
    CdTe, photoplastic behaviour 2−50742
    Co domain wall interaction, retardation of movement 2−68540
    Co whiskers, martensitic transformations, constitution and dislocation structure 2−71340
    CsI, rel. to secondary slip generated by point load 2−74849
    Cu-7.5 at.%Al alloy, deformed in tension, etch pit studies 2−64664
    Cu-Al alloys, cyclic fatigue damage, thermal cond. meas. 2−50672
    Cu-Al alloys, neutron irrad. defect-phonon scatt., lattice thermal cond. 2−51060
    Cu-10at.%Al alloy, deformed, neutron irrad., dislocation strain fields, low temp. lattice thermal cond. obs. 2−71498
    Cu-16%Al alloy, rel. to sigmoidal transient creep 2−53816
    Cu-Al(10wt%), high fluence neutron irrad., electron microscope obs. 2−80686
    Cu-Au alloy, diffusion of Au, misfit dislocation behaviour 2−71497
    Cu-Au system, superdislocations in Cu_3Au, electron microscope obs. 2−80666
    Cu-CR alloy, f.c.c.-b.c.c. interphase boundary dislocation structs. 2−56734
    Cu-Co alloy f.c.c. single crystals, rel. to effect of coherent precip. on work-hardening 2−50798
    Cu-Cr alloy, rel. to internal friction, after isochronal annealing 2−77633
    Cu-Mg(Mo)(W) solid solns., binding energy of dislocations to impurities, internal friction obs. 2−43630
    Cu-Mn-Al alloy, interphase interfaces, interfacial dislocations 2−56719
    Cu-Ni-Fe alloy, interphase interfaces, interfacial dislocations 2−56719
    Cu-Zr, dil. alloys., softening resistance mechanism 2−56709
    Cu, Burgers vector rel. to external geometry at initial deform. stage 2−50673
    Cu, damping in single crystals, study by stress pulse method 2−60801
    Cu, deformed, disloc. induced reorientation of dumbbell interstitials 2−50655
    Cu, dislocation free crystal, growth, dislocation generation mechanisms 2−67942
    Cu, edge and screw dislocations, Schockley partials separation, computer simulation 2−60802
    Cu, epitaxial electrodeposit 2−47107
    Cu, high fluence neutron irrad., electron microscope obs. 2−80686
    Cu, influence on positron annihilation ang. correl. 2−51063
    Cu, initial disloc. density effects on disloc. multiplication and work hardening characs. 2−64665
    Cu, plastically deformed, rel. to positron annihilation 2−54123
    Cu, plastically deformed, rel. to exo-emission 2−77975
    Cu, plastically deformed, specific dislocation energy determ. 2−53734
    Cu, polycrystalline, rel. to elec. resistivity changes during tensile deformation 2−47834
    Cu, polycrystalline, strain hardened, thermally activated deform. mechanisms 2−77679
    Cu, radiation damage, nature and annealing characts. 2−47368
    Cu, rel. to fatigue hardening 2−53724
    Cu, single crystals, deformed in tension, effect of strain rate upon hardening 2−84160
    Cu alloys, rel. to stress equivalence of soln. hardening 2−80834
    Cu base solid solution, rel. to grain boundary strengthening 2−53891
    Cu film, vacuum-deposited, electron microscope obs. 2−50489
    Cu single crystal, density effect in yield behaviour 2−56792
    Cu surface, punched-out rosettes 2−50439
    Cu trichites, Kossel diagram obs. 2−47321
    Cu whiskers, grown by halide reduction 2−80570
    Cu7at.%Ge alloy, deformed, neutron irrad., dislocation strain fields, low temp. lattice thermal cond. obs. 2−71498
    Fe-Au alloy, rel. to precip. 2−43851
    Fe-C alloy, recovery of internal friction after strain ageing 2−47481
    Fe-Co-V alloy, ordered and disordered, recovery behaviour 2−50804
    Fe-Cr(8%) alloy, martensite, quenching and tempering temp. effects, rel. to strengthening 2−84071
    Fe-Cu alloy, dispersion strengthening model, slip dislocation precipitate interaction 2−50744
    Fe-Mn alloy, b.c.c., shock deformed, disloc. climb rel. to recovery 2−56912
    Fe-Mo alloy, rel. to precip. 2−43851
    Fe-Ni-Nb-C alloy, rel. to ageing behaviour 2−47596
    Fe-Ni alloy, hardening at high strain rates, dislocation substruct changes 2−47593
    Fe-Ni alloy, mobile, strain rate sensitivity and density 2−56711
    Fe-Si, dynamics on plastic deformation, high voltage electron microscope obs. 2−56785
    α-Fe, cube edge dislocations, strain displacement field, linear elastic Volterra soln. 2−77568
    Fe, dynamics on plastic deformation, high voltage electron microscope obs. 2−56785
    α-Fe, edge, core characts., computer simulation 2−60803
    α-Fe, edge dislocation, elastic field, computer simulation 2−56710
    Fe, fast neutron irrad. at 77K, rel. to softening and anneal hardening 2−80689
    Fe, H-dislocation interaction 2−53735
    α-Fe, high temp. creep struct. 2−43637
    α-Fe, neutron irrad., rel. to radiation- and anneal-hardening 2−80681
    α-Fe, plastically deformed, nature of debris loops 2−74778

Crystal imperfections continued
dislocations continued
Fe, plastically deformed, resist. study 2–80740
Fe, strain ageing and formation of Cottrell atmospheres 2–71624
Fe, strengthening mech., dynamic strain ageing, dislocation struct. 2–56911
Fe b.c.c., four-fold dislocation node formation 2–77583
Fe domain wall interaction, retardation of movement 2–68540
Fe foil, extended in electron microscope, rel. to cell formation 2–71487
Fe foils, electrocrystn. structures 2–83862
α-Fe single crystal, rel. to high temp. creep 2–56804
Fe$_3$Al, compression induced mag. anisotropy and superlattice dislocations 2–61516
GaAs:Te, Se and S, effect of doping on struct. 2–71432
GaAs:Zn(Si)(Te), impurity effects on dislocation velocity 2–68028
GaAs, dislocation structure formation during Czochralski growth, temp. profile and thermal stress effects 2–53615
GaAs, epitaxially grown, X-ray obs. 2–71488
GaAs, glide arrays, high voltage electron microscope obs., device manuf. considerations 2–54215
GaAs, selective photoetching obs. 2–71364
GaAs, X-ray obs. in single crysts. and epitaxial layers 2–74767
GaAs Gunn diode, degradation by dislocations induced during thermocompression bonding 2–68446
GaAs$_{1-x}$P$_x$, compositionally graded cryst., like-sign asymmetric disloc. 2–71478
GaAs$_{1-x}$P$_x$ epitaxial layer, on GaAs, surface struct., cross-hatch pattern due to misfit disloc. array 2–47110
GaP, growth defects, etch pit obs. 2–50595
Gd thin single crystal films, dislocation loops formed during electron microscopy 2–71489
Ge-As solid soln., absorpt. and scatt. of X-rays by cluster defects and dislocation loops 2–77584
Ge, creep, and stress effects 2–84040
Ge, doping influence on double kink nucleation rate model 2–50674
Ge, etched pits on (111), (110) and (001) surfaces, changes in forms based on corresponding dislocation 2–50446
Ge, rel. to internal friction at low temps., 2–68068
Ge, vel. of screw and 60° dislocations, stress and temp. depend. 2–47415
Ge film, rel. to thickness depend. of elec. cond. and Hall effect 2–54192
Ge single crystals, structure from growth parameters 2–47414
guanidinium aluminium sulphate hexahydrate, optical and interferom. studies of cleavages and etch patterns 2–64670
HfS$_2$, nearly perfect crysts., grown by vapour transport, X-ray obs. 2–50577
In$_{1-x}$Ga$_x$P, compositionally graded cryst., like-sign asymmetric disloc. 2–71478
InSb, needing dislocations related to solid dopant inclusions, X-ray investigation 2–50675
Ir, and alloys, field ion microscopy, geometrical contrast theory analysis 2–77592
KCl-KBr solid solution, rel. to internal stress at Luders band front 2–84043
KCl-NaCl solid solns., dislocations as centres of phase nucleation 2–43921
KCl, Czochralski grown, functional dependence of dislocation formation 2–53616
KCl, F-centres, thermal transform. with colloids, dislocation induced precip. 2–71525
KCl, rel. to surface polygonization by electron bombardment and illumination 2–50457
KCl crystals, effect of γ-irradiation on critical resolved shear stress 2–47492
KCl whiskers, slightly deformed, etch pit study 2–71490
KMnF$_3$, determ. by etch pit form. technique 2–53605
K$_2$SO$_4$.Al$_2$(SO$_4$)$_3$.24H$_2$O, etching obs. with ethanolic tartaric acid solns. 2–74662
K$_2$SiF$_6$.Na$_2$SiF$_6$, occurrence, prep., cryst. data 2–74734
LiF:Mg thermal-activation analysis study of impurity hardening 2–71491
LiF, (100) surface, disloc. etch pit morphology rel. to Cu(II) complex in etchant 2–56608
LiF, (100) surface, disloc. etch pit morphology, effect of anions in etchant 2–56609
LiF, deformed crystals, mobile dislocations, dynamic scattering of slow transverse phonons, 0.04 to 0.8°K 2–68218
LiF, loops, elec. microscope obs. 2–74760
LiF bicrystal, interaction of stress waves with a boundary 2–84061
LiF single crystals containing cavities hydrostatic pressure influence on microstructure 2–83973
LiF$_4$, disloc. displacement mechanism during formation of small disloc. layer at cryst. surface 2–71492
LiF(001), mobility, effects of H$_2$O adsorption 2–43627
Mg/MoS$_2$ film/substrate system, curvilinear dislocations 2–80554
Mg, neutron irrad., rel. to damage production and annealing 2–80683
Mg, pyramidal slip, dislocation configs. 2–47420
Mg alloys, rel. to stress equivalence of soln. hardening 2–80834
MgO, plastically deformed, pipe diffusion prod. of prismatic dislocation loops after annealing 2–64689
MgO, rel. to plastic deform. during cleavage fracture 2–71570
MgO, self climb of dislocation loops 2–80672
MgZn$_2$, deformed by u.s. vibrs. 2–64666
Mo-34%Re, deform. struct. obs. 2–43624
Mo-35%Re alloy, rel. to nucleation and growth of deform. twins 2–56720
Mo-34%Re alloy, superconducting, effect of disloc. tangles on props. 57167 2–57167
Mo, microdeform. under dynamic loading, temp. and impurities influence 2–43696
Mo, single crystals, influence of surf. states and Ti coatings on dislocat. struct. 2–83969
NaCl, creep at high temps., compression tests, stress dependence, creep mechanism 2–77651
NaCl, dislocation-phonon interaction, 70-300K 2–83975

Crystal imperfections continued
dislocations continued
NaCl, generation, grain boundary mechanism, expt. obs. in single and polycrystalline mat. 2–68029
NaCl, kinetics of dislocation, influence of placing dislocations at starting positions 2–71493
NaCl, mech. props. and disloc. struct. in single slip 2–71579
NaCl, neutron irrad. induced dislocation pinning points 2–43638
NaCl, plastically deformed, X-ray and electron microscope obs. 2–53807
NaCl, rel. to F→X-centre conversion 2–50698
NaCl, rel. to surface polygonization by electron bombardment and illumination 2–50457
NaCl crystals containing colour centres, flow stress spectroscopy 2–81396
NaClO$_3$, rel. to cryst. growth rate from soln. 2–47240
NaCl(001), mobility, effects of H$_2$O adsorption 2–43627
NaF, impurity content, etching obs. 2–67934
NaF, internal friction, vibr. depend., dislocation- point defect interaction, 4.2-295 K 2–71554
NaF, mech. props. and disloc. struct. in single slip 2–71579
Nb-40% Ti, alloy, supercond., mag. irreversibility and microstruct. 2–47855
Nb-H system, H-dislocation interaction, cold work peak study 2–80841
Nb-N, interstitial soln., mech. props. depend. on conc. and temp. 2–84009
Nb-N alloy, nitride precip., prismatic loop generation 2–53994
Nb-O, interstitial soln., mech. props. depend. on conc. and temp. 2–84009
Nb-Zr-Ti alloy, supercond. rel. to intermediate phase precip. 2–50842
Nb, stressed, dislocation struct. form. mechanism 2–71494
Nb, supercond., surface pinning by defects, expt. evidence 2–77866
NbH$_x$, α-peak interpret., acoustical loss mechanism, kink generation on dislocations 2–77645
NbTe$_2$, config. and domain struct. 2–60804
Ni-Al alloy, dislocation struct. changes rel. to flow-stress recovery 2–74888
Ni-Al alloy, high temp. deformed, rel. to flow-stress recovery 2–74889
Ni-Co, coarse grained polycrystalline, sub-boundary formation rel. to Co self-diffusion at low temp. 2–47450
Ni-Co alloy, f.c.c., dislocation bands produced by electrolytic hydrogen charging 2–56713
Ni-Cr-Ti alloys, density determ. during precip. strengthening 2–43859
Ni-Cr lamellar composite alloy, struct. during fatigue deformation 2–56821
Ni-Fe, powder compact, struct. charact. 2–56946
Ni, containing H, internal friction, effect of relax. and trapping of dislocations 2–53792
Ni, deformed, disloc. induced reorientation of dumbbell interstitials 2–50655
Ni, electrical resistivity due to dislocations, at low temps. 2–81033
Ni, generation from grain boundaries during premacroyield deform 2–47418
Ni, point defect interactions with dislocations, high-voltage electron microscopy 2–56686
Ni, porous, rel. to creep kinetics 2–43704
Ni, powder compact, struct. charact. 2–56946
Ni, rel. to mag. domain struct. after plastic deform. 2–44244
Ni and alloys fast neutron induced swelling 2–63969
Ni coatings, electrolytically obtained, transmission electron microscopy 2–50519
Ni domain wall interaction, retardation of movement 2–68540
Ni film on NaCl substrate, effect of annealing on dislocation struct. 2–80565
Ni stacking fault propagation from a coherent twin boundary 2–80670
Ni$_3$Al-Ni$_3$Nb eutectic alloy, misfit disloc. at interface between two ordered lattices, elec. diffr. obs. 2–71647
Ni$_4$Mo, internal friction study 2–43670
Pb, damping of motion, u.s. meas. method 2–68030
PbS(Se)(Te), charge dislocation-acceptor interaction, effect on mech. props. 2–50784
δ-Pu, Young's modulus, elastic limit, dislocation interstitial interaction, meas. apparatus, 4-300 K 2–80739
RbMnF$_3$, determ. by etch pit form. technique 2–53605
Se, trigonal crystals, transmission e. microscopy obs. of dislocations after chem. polishing 2–64668
Se, vapour grown single cryst., disloc. networks, X-ray topography obs. 2–50676
Si, defect struct. induced by localized B diffusion, X-ray diffraction topography 2–77567
Si, doping influence on double kink nucleation rate model 2–50674
Si, epitaxial film, lattice resolution e. microscopy obs. of struct. of twin boundaries, faults and dislocats. 2–74779
Si, etch for (100) planes 2–71495
Si, etch pits shapes rel. to mech. stress 2–80553
Si, grown by pedestal technique using electron beam heating, disloc. density detn. 2–43512
Si, hydrostatic press. effect, X-ray obs. 2–47419
Si, moving, obs. by X-ray topography 2–77585
Si, rel. to diffusion of Au at 1000°C 2–60833
Si, surface state density distrib. rel. to diffusion induced disloc. near junc. formed by P diffusion 2–44038
Si, thermally oxidized, X-ray topographic study of small dislocation loops 2–64669
Si, velocities of screw and 60° dislocations 2–80678
Si, X-ray topography, high resolution video display 2–83922
Si epitaxial film, dislocation density, effect on Sb diffusion 2–74816
Si junction, thermally diffused, avalanche multiplication rel. to dislocation lines 2–65027
Si wafer, device-processed, due to thermal oxidation 2–51179
Si wafer, surface defect generation on reoxidation in H$_2$O vapour during B diffusion 2–64672
SiC, transmission electron microscope obs. 2–47423
SiC 2H, mechanisms for low temp. phase transformations 2–71695

Crystal imperfections continued
- **dislocations** continued
  - Si_3N_4, transmission high-voltage electron microscope obs. 2−60998
  - Si_3N_4 film, chemical vapour deposited on Si, generation rel. to stress 2−68031
  - SiO_2, on planar struct., X-ray and i.r. study 2−47124
  - Sn, dislocation generation at single cryst. surface, X-ray obs. 2−47083
  - $SnS_2(Se_2)$, nearly perfect crysts., grown by vapour transport, X-ray obs. 2−50577
  - Ta, deform. mechanism, orientation depend., 4.2-450K 2−50679
  - TaC_{1-x} splitting and C-diffusion-assisted glide in plastic deformation 2−60869
  - Te, piezoelec. semicond. 2−60805
  - Te vapour grown whiskers, disloc. struct. 2−67915
  - Ti-Al alloy, cold-worked, X-ray diffr. study 2−80860
  - Ti, low dislocation density, X-ray characterization 2−77526
  - Ti, rel. to validity of modified Gilman's equation for stress relax. 2−80832
  - Ti, struct. rel. to strength 2−56714
  - Ti martensite, effect of Si, Zr, Al and Mo on struct. and strength 2−64723
  - TiS_2, nearly perfect crysts., grown by vapour transport, X-ray obs. 2−50577
  - U, β phase, microstress behaviour during quenching, dislocation impurity network, relaxation 2−77659
  - V, neutron irrad., dislocation channelling and loops 2−80665
  - V internal stress, during stress relax., rel. to dislocation generation and immobilization 2−43680
  - VC_x:B, struct. and precip., electron microscope obs. 2−61038
  - V_2O_5, X-ray diffr. obs. 2−56691
  - W, foil, 60 kev Au ion irrad., dislocation loop prod. 2−43615
  - W, foil, Au ion irrad., vacancy-type dislocation loop prod. 2−43616
  - W, foil, Au ion irrad., vacancy-type dislocation loop, prod. 2−43616
  - W, rel. to asymmetry of slip 2−56811
  - W powder, role in sintering, effects of sinter activators 2−50899
  - WC-Co cemented carbide, config. and role in internal friction recovery 2−68070
  - $Y_2Fe_5O_{12}$, grown from soln., dislocation density rel. to conditions 2−56715
  - Zn, grown by Bridgeman method, dislocation formation 2−77586
  - Zn, stretched, activated vol. rel. to deformation rate 2−43700
  - Zn single crystals, dislocation structure of the boundary blocks 2−60806
  - ZnS epitaxial film, on GaAs 2−71339
  - ZnSe, dislocation etch bits 2−50677
  - Zr, neutron irrad., dislocation loops characteriz. 2−43639
  - Zr and Zr-O alloy, rel. to strain-ageing mechanism 2−47599
  - ZrS_2, nearly perfect crysts., grown by vapour transport, X-ray obs. 2−50577
  - α-Zr. grain size depend. of deform. behaviour 2−50748
- **impurities**
  - alkali halide, complex impurity centres model with cations in anion sites 2−47441
  - alkali halides, hydroxide-doped, tunnelling levels, low temp. 2−71758
  - alkali halides, local and gap modes due to substitutional impurity 2−47731
  - alkali halides, Maxwell-Boltzmann distrib. of intrinsic and extrinsic defect pairs 2−83971
  - alkali halides, resonant phonon modes of Ag^+ and Au^+ 2−54018
  - alkali halides, tunnelling motions of impurities from Stark modulated microwave spectra 2−70739
  - α-amino acids, e.p.r. of VO^{2+} ions 2−84566
  - anodic sectioning technique for distrib. and diffusion profile obs. 2−60817
  - Cu:Mn giant e.s.r. transmission through one-sided and two-sided ion implanted Cu foil 2−84569
  - de Haas-van Alphen oscills. amplitude reduction by signal dephasing by strain fields round impurities 2−77846
  - diamond type cryst., diffusion, impurity correl. factors 2−60827
  - diamonds, Ni inclusions, determ. of Curie points for different coloured diamonds 2−81213
  - diatomic linear lattice, local and gap modes due to substitutional impurity 2−74963
  - diffusion, from thin layer into semi-infinite medium, conc. depend. diffusion coeff. 2−71513
  - diffusion coefficients in piezoelectric semiconductors, ultrasonic meas. 2−50691
  - F-centre radiative decay, contrib. of random impurities 2−74800
  - film, surface oxide, electromech., photomech. and conc. effects 2−51155
  - fluoranthene, purity determined by spectral depend. of fluorescence lifetime 2−84536
  - fluorophlogopite, Ti and V impurities, e.p.r. and optical absorption spectra, levels of Ti^{2+} and Ti^{3+} ions 2−84562
  - forsterite, flux grown, impurity conc. detn. 2−47265
  - glass, nontransparent quartz, colour centre formation, importance of impurity ions Ti^{3+} 2−84482
  - graphite, halogen dopant-stacking fault interactions 2−53738
  - graphite, polycrystn., effect of B doping on thermal conductivity 2−57084
  - graphite, pyrolytic, highly oriented, B impurity effects on high dose fast neutron irrad. 2−57072
  - group III-V semiconductor, doping by group II metalorganic 2−47091
  - ice, KF and NH_4F doped and irradiated, role of F- in increased colouring 2−60823
  - ice I_h, effect of HF doping on dielectric relaxation spectra 2−72013
  - implantation profiles determ. by secondary ion mass spectrometry 2−74794
  - impurity luminescence, polarization, rel. to nuclear spin 2−44405
  - inclusion, rigid, circ. cylindrical, interac. with moving screw disloc. 2−50662
  - interstitial alloy, role in low temp. softening 2−47495
  - ionic crystals with paraelectric dipolar impurities, dipolar entropy and heat capacity 2−57221
  - low symmetry crystals, site assignment of Fe^{3+} 2−44439

Crystal imperfections continued
- **impurities** continued
  - melt growth, crystn. front fluctuation influence on impurity entry 2−43522
  - metal, effect on grain boundary velocity 2−43785
  - metal, He migration and release after implantation 2−50639
  - metal, role in brittleness 2−43719
  - micro-impurity conc. determ. by phys. methods, review 2−43646
  - model, nonlinear defect, to explain generation of cracks 2−84047
  - molecular cryst., exciton interactions between substitutional impurities 2−71803
  - Mossbauer spectra of impurity atoms in crystals, correlation influence in diffusion 2−65228
  - naphthalene, spherical single cryst., polarization luminesc. rel. to impurity molecule orientation 2−75328
  - noble gas ions entrapment in UO_2 2−60815
  - polar crystals, optical rectification by impurities 2−44327
  - polyethylene doped with I, h.f. Gunn domains 2−57202
  - quartz glass, effect on crystn. rates, 1350-1550°C 2−64529
  - radiation defects, vacancy-impurity complex, kinetics of formation and annealing 2−80693
  - radioactive, radiation characs. 2−61568
  - ruby, G doping during hydrothermal growth 2−47230
  - semiconductor, autoradiographic variant of activation analysis for impurity solubility determ. 2−72595
  - semiconductor, B impurity profiling, techniques 2−71505
  - semiconductor, conc. profiles and site distrib. determ. using i.r. localized vibr. modes 2−47433
  - semiconductor, distrib., soln. of Poisson's equation 2−60816
  - semiconductor, II-VI, Cu impurity, e.s.r. and optical spectra, dynamical Jahn-Teller interaction 2−80954
  - semiconductor, impurity profile, limitation of pulsed capacitance obs. 2−71506
  - semiconductor, ion implantation, radiation effects, conf. opening address Albany, (1970) 2−47878
  - semiconductor, profiles, capacitance- voltage meas. 2−64673
  - semiconductor, two-stage diffusion, layer parameters calc. allowing for evaporation 2−71512
  - semiconductors, ionic doping 2−60812
  - silica, mobilities of OH^- + Na^+, Ca^{2+} and Al^{3+} 2−64696
  - steel, austenitic, creep, rel. to shape and dimens. of particles 2−50656
  - steel, elastic stresses around nonmetallic inclusions 2−53725
  - steel, impact props, rel. to FeO type inclusions 2−47530
  - steel, press. vessel type, effect on radiation sensitivity 2−53895
  - stratified distribution, formation during crystallisation rel. to convective instability in melt 2−53610
  - surface impurities, bulk to surface equilib., Auger spectroscopy obs. 2−50465
  - thermal vibr. amplitude, method for determ. using channelling effect 2−80897
  - transistor, p-type impurity distribs., anomalous base regions 2−71504
  - triglycine sulphate, L-alanine doped, induced growth anisotropy 2−53608
  - Zircaloy-2, interaction with radiation damage defects 2−43802
  - Ag halides, photochemically dyed photochemical properties 2−75392
  - AgBr, interaction with vacancies, diffusion mechanism 2−80699
  - AgBrI:Br^-, NH_3, influence on cryst. morphology 2−80648
  - (AgBr + AgCl (5%)):$C^{5+}(N^{5+})(O^{6+})(S^{6+})$ high energy implantations, Doppler broadening of positron annihilation photons 2−71507
  - AgCl:$C^{5+}(N^{5+})(O^{6+})(S^{6+})$ high energy implantations, Doppler broadening of positron annihilation photons 2−71507
  - AgCl, interaction with vacancies, diffusion mechanism 2−80699
  - Al, neutron irrad., influence on void form. 2−53736
  - α-Al_2O_3:Fe, α-Al_2O_3, Ti and α-Al_2O_3(Fe,Ti), polarized and high resolution UV, visible and IR spectra, e.s.r. spectra 2−78082
  - Au:Cu, impurity-vacancy binding energy, equilib. resistivity obs. 2−71465
  - C fibre, mech. and crystallographic props., S impurity effects 2−50913
  - CaF_2, coloured, zero-phonon line obs. 2−53752
  - CaF_2, low symmetry complexes involving hydride ions paired with rare earth ions 2−47434
  - $2CaO.Fe_2O_3$, subst. of Mn for Fe ions, study by X-ray diffr., mag. and Mossbauer effect meas. 2−43644
  - CdS, thermal diffusion of Ag, Cu and In, photosensitive material produced 2−72059
  - CdTe:In, Cd vacancies and impurity vacancy complexes rel. to self-compensation calc. 2−47889
  - CdTe, ion implantation doping 2−74790
  - Co effective mag. field on ^{67}Zn 2−84404
  - CsCl, U band shape from first electronic transition of H- and D- substitutional impurities 2−47446
  - Cu-Ge(Ni)(Zn) dil. alloys, vacancy-impurity complexes and positron annihilation 2−47398
  - Cu-Mg(Mo)(W) solid solns., binding energy of dislocations to impurities, internal friction obs. 2−43630
  - CuF_2, oxygen impurity removal during growth using CoF_2 scavenger 2−50568
  - Fe-C system, diffusion of impurities, theory 2−50708
  - Fe-Ni-Si alloy, temper brittleness development, grain boundary adsorption of P, internal friction study 2−80767
  - Fe, cast, melt solidification, nodular graphite formation, additive effects 2−74881
  - Fe, effective mag. field on ^{67}Zn 2−84404
  - α-Fe, Mn diffusion, 778.3-901°C, alloying element effects 2−83994
  - Fe, single crystal, deformation at 77K, conc. effects 2−64713
  - GaAs:Ar, Te ion implanted, radiation damage, elec. microscope obs. 2−60821
  - GaAs:Cu, elec. props., impurity centre form., conditions and mechanism 2−64985
  - GaAs:Si, amphoteric impurity distrib. equilib. calc. 2−83981
  - GaAs:Sn, N^+ layer formation by Sn diffusion 2−71515
  - GaAs-Cu, supersaturated solid solution, interaction with Cu atoms during decomposition 2−83836
  - GaAs, epitaxial, growth morphology obs. by sequential changes in doping level 2−47113

Crystal imperfections continued
impurities continued
GaAs, epitaxial conc. profile determ. by Schottky-barrier diode differential capacitance meas. 2—83905
GaAs, epitaxial growth, anisotropy obs. using abrupt changes in doping level 2—47112
GaAs, growth, impurity incorporation, effect of surface space charge layer 2—47428
n-GaAs, impurity distrib. coeff. anisotropy, elec. props. study 2—47437
GaAs, impurity induced i.r. absorpt., calc. by Green's function technique 2—61639
GaAs, obs. in single crystals grown by Bridgeman method 2—60724
GaAs, Si-rich inclusins, high voltage electron microscope obs. device manuf. considerations 2—54215
GaAs epitaxial film, doping level and impurity distrib., substrate orientation effects 2—47436
GaP, melt-grown, S-pit correl. 2—50595
GaSb:Te, segregation coeff. of Te 2—74798
GaSb, diffusion of Zn, temp. and cond. depend., radioactive tracer obs. 2—74799
Gd, purification by electrotransport 2—80716
Ge-As solid soln., absorpt. and scatt. of X-rays by cluster defects and dislocation loops 2—77584
Ge, diffusion enhancement by light ion implantation 2—60814
Ge, diffusion of Sb, influence of In concentration gradient 2—71516
Ge, γ-irrad., donor-vacancy complexes, prod. kinetics and energy spectrum 2—47382
Ge single crystal, rel. to adsorp. and nucleation of Cd 2—47158
InP, group IV doping during cryst. growth by liq. encapsulation 2—47272
InSb:Fe, crystallisation features rel. to dopant, hole and acceptor distribution 2—53604
InSb, doped, growth rate depend. of impurity distrib. 2—47209
InSb, needing dislocations related to solid dopant inclusions, X-ray investigation 2—50675
InSb, showing facet effect, distrib. of Te, Zn, and Cd, conc. depend. 2—47438
Ir, ion implanted, field ion microscope obs. 2—56741
Ir, ion implanted, field ion microscope obs. 2—56740
KCl:Eu^{2+}(Yb^{2+}) (Sm^{2+}), impurity-vacancy dipole relax. and aggregation, and X-ray effects 2—83982
KCl:Na, impurity, effect on radiation damage, colorability 2—77595
KCl:NaCl, symmetry of far i.r. resonant-pair mode 2—84507
KCl:Pb, rapidly grown from melt, thermal stress defect model 2—50649
KCl:Pb^{2+}, grown from soln., inhomogeneous impurity distrib., spectrophotometric obs. 2—74796
KCl:SO$_4^{2-}$, anion vacancy trapping, i.r. study 2—43620
KCl, influence of OH$^-$ ions on water mol. diffusion 2—60831
KCl doped single crystals, extent of perfection 2—60822
KCl(Br)(I), Ag$^-$ centres, polarization and decay time of luminesc. 2—80710
KCl(I), local and gap modes due to substitutional impurity 2—47731
La and Y ethylsulphates: ^{166}Er $\gamma\gamma$ cascade, crystal orientation effect 2—78053
LiF:Mg, impurity associations decomp., light scatt. obs. 2—83983
LiNbO$_3$ and LiTaO$_3$ with Cr^{3+} impurities, optical excitation, dipole moments and macroscopic polarization 2—48138
MgO:V optical absorption and magnetic circular dichroism of impurity 2—68646
Mo, neutron irrad., rel. to void formation during annealing 2—77575
Mo, struct. and mech. props., effect of B 2—56943
NaAlSi$_3$O$_8$:Fe^{3+}, site assignment of Fe^{3+} based on fourth-order spin Hamiltonian constants 2—44439
NaBr(Cl), local and gap modes due to substitutional impurity 2—47731
NaCl, vacancy bound to divalent impurity, slow motion, pressure effects, in n.m.r. study 2—72514
NaF, content of dislocations and grain waves, etching obs. 2—67934
Nb-H system, H-dislocation interaction, cold work peak study 2—80841
in Nb, cold-worked or irrad., role in recovery 2—47404
Nb, location of interstitial D sites by deuteron channelling 2—60811
Ni, containing H, internal friction, effect of relax. and trapping of dislocations 2—53792
Ni, effective mag. field on ^{67}Zn 2—84404
NiS, effect on metal-to- transition 2—51280
PbBr$_2$, impurity-vacancy complexes, ionic cond. and dielec. loss study 2—47402
PbCl$_2$, impurity-vacancy complexes, ionic cond. and dielec. loss study 2—47402
PbMoO$_4$:Cu, Gd site occupancies of dopant and trace impurity 2—68739
δ-Pu, Young's modulus, elastic limit, dislocation interstitial interaction, meas. apparatus, 4-300 K 2—80739
RbBr, reorientation rates of OH- defects, calc. from phonon spectra 2—61080
Se, non-crystalline, impurity effects on struct. 2—61326
Si:As, diffusion by using emulsion type doped oxide 2—71517
Si:As, distrib., determ. by He ion channeling obs. 2—60818
Si:As, evacuated capsule method, appl. to microwave transistor 2—71518
Si:As, He ion min. backscatt. yield variation obs. 2—60820
Si:B, diffusion by using emulsion type doped oxide 2—71517
Si:B, diffusion from doped oxide layers 2—64677
Si:B, impurity lattice location, He$^+$ ion channelling obs. 2—60819
Si:B, ion implanted, conc. distrib. by (n,^{4}He) nuclear reaction 2—56743
Si:B, ion microprobe analysis of implanted ion distribs. 2—64674
Si:B, lateral spread of implanted ions, obs. by junction delineation 2—71508
p-Si:B, Li-compensation influence on irrad. defect form. 2—47390
Si:B, low temp. B diffusion using B$_2$H$_6$-CO$_2$ system 2—43645
Si:B, P, anomalous diffusion 2—50694
Si:B, Si-B phase influence on B surface conc. 2—77523
Si:In, ion implanted, photoelectromag. effect rel. to dose and annealing 2—72077
n-Si:Li, effects on radiation induced defects 2—47385
n-Si:Li, irrad., Li-defect interactions, e.p.r. obs. 2—48293

Crystal imperfections continued
impurities continued
Si:P, diffused, impurity profile kink form. mechanism 2—56742
Si:P, epitaxial, doping during growth 2—47431
Si:P, Knoop hardness and hardness anisotropy, impurity conc. effects 2—71604
Si-SiO$_2$ system, B diffusion 2—68037
Si, behavior of Li in drift and precipitation obs. 2—50692
Si, coeffs. for B diffusion 2—56745
p,n Si, conc. meas. by mercury probe 2—71509
Si, concentrations, lattice locations of As, Sb, Au diffused impurities, He-ion backscattering technique 2—64675
Si, defect struct. induced by localized B diffusion, X-ray diffraction topography 2—77567
Si, diffusion enhancement by light ion implantation 2—60814
Si, diffusion of As, from arsenosilicate glass source, 1000-1200°C 2—83980
Si, dopant profile obs. using neutron activation anal. 2—56738
Si, doping, during whisker growth by gas transport 2—47430
Si, doping inhomogeneities, obs. by electroreflectance 2—71510
Si, electron irrad., Li effect on recomb. luminesc. 2—48231
Si, implantation damage and impurity location, channelling obs. 2—71511
Si, implantation of B ions, channelling, depth distrib., computer simulation 2—47439
Si, low conc. diffusion of P and B under sealed tube conditions 2—74792
Si, O and C detn., i.r. and activation analysis 2—71502
Si, predeposition of B 2—71503
Si, thermally oxidized, effect on stacking fault generation 2—60809
Si B impurity profiling, techniques 2—71505
Si diffusion of As props. of SiO$_2$-As and Ge/SiO$_2$:As diffusion sources 2—83979
Si film, epitaxial, gas doping 2—50690
Si p-n junction, reactor irrad., broadening of Zn and Ga impurity profiles 2—84355
SiC, autoradiographic variant of activation analysis for impurity solubility determ. 2—72595
SiC, diffusion of B, distributions, elec. cond. and p-n junc. obs. 2—74797
SnO$_2$:Ni, e.p.r. of Fe^{3+} centre 2—84564
SrF$_2$:Dy, Tb, Nd, axial distrib. of impurities, neutron activation analysis 2—56744
SrF$_2$, coloured, zero-phonon line obs. 2—53752
Ta-W-Hf alloy, tensile props., effects of O contamination 2—43862
Ta$_2$N film resistor, relative nitrogen doping level by Seebeck effect 2—74793
U-Mo alloy, stress corrosion cracking in humid air, C content effects 2—53839
UO$_2$, lenticular pore migration, impurity effects 2—74150
ZnO:Li(Na)(Cu)(In)(Mn), vapour phase cryst. growth 2—50580
ZnS, melt grown hexagonal, stabilization by donor impurity doping 2—47279
ZnWO$_4$:Cr^{3+}, impurity conc. determ., e.s.r. and optical emission studies 2—78157
ZnWO$_4$, effect of struct. charact. on penetration of Cr and Gd impurities 2—71542
Zr-H(O) dil. alloys, internal friction peak obs. 2—50737

interstitials
alkali halide, Frenkel defect, lattice statics and deformation dipole model 2—60789
alloy, b.c.c., influence on ordering and magnetiz. 2—43818
alloy, f.c.c., influence on ordering and magnetiz. 2—43817
alloy, role of impurities in low temp. softening 2—47495
alloy, ternary, b.c.c., Snoek effect, rel. to substitutional solute atom pairing 2—43672
annealing, cold-worked or irradiated solids, theory 2—43652
annihilation rate, recomb. with vacancies 2—56681
b.c.c. lattice, rel. to void stability 2—50650
Debye solid, diffusion of light interstitials, temp. depend. 2—43653
displacement damage by energetic atoms, collision theory 2—74765
graphite, h.v. electron microscope damage 2—47370
graphite, interlayer props., effect of interstitial atoms, simple model 2—56605
graphite, pyrolytic, low temp. electron irrad. damage and recovery, resist. study 2—80659
graphite, self-diffusion, interstitials as diffusing defect 2—53760
ionic cryst., defect form. mechanism and struct. 2—80702
lattice dynamics, response function, interactions 2—77759
metal, f.c.c., irrad., elec. resist. of defects 2—75045
metal, He migration and release after implantation 2—50639
metal, irrad., interstitial dislocation loop form. 2—53696
metal, stability, low-energy-recoil events and vibr. behaviour 2—53723
metal irradiated, void growth, interstitial and vacancy conc. rate theory eqns. 2—80661
metallic materials, effect on void nucleation during high-energy irrad. 2—53703
metals, deformed polycrystalline sheet, influence of hydrostatic pressure soaking on structural changes, X-ray study 2—84127
metals, polycrystalline and monocrystalline, differences in plastic deformation, interpretation on model of lattice defects mobility 2—84046
model, nonlinear defect, to explain generation of cracks 2—84047
radiation induced, review 2—77577
radiation-induced defect clusters, transmission electron microscopy 2—50640
steel, ε-carbide phase form. and struct. 2—43844
steel, rel. to effect of V alloying on brittle fracture 2—53896
transition metal hydrides, interstitial atom interaction role in solid soln. form. 2—77733
vacancy and interstitial supersaturations, chemical stress concept 2—56688
Ag, neutron irrad., Frankel defects, influence of internal friction and bulk modulus 2—77642
Ag, radiation damage, nature and annealing characts. 2—47368
Ag halides, space charge due to Frenkel defects at surface 2—81022
AgCl, Frenkel defects, equilibr. conc. perturbation by microwave pulse, ionic cond. change 2—80698
AgCl, rel. to ionic cond. 2—68050

Crystal imperfections continued
interstitials continued
Al, annealing of defects produced by quenching and electron irrad. 2−60785
Al, elec. resist. due to interstitials, pseudopotential method 2−57152
Al, electron irrad. induced pt. defects clustering, high-voltage electron microscopy 2−56682
Al, neutron irrad., pt. defect clustering, electron microscope obs. 2−60783
Au-Pb system, interstitial dissolution and compound formation 2−43826
Au, radiation damage, nature and annealing characts. 2−47368
CaF_2, rare earth doped, interstitial dipole relax., thermal depolarization obs. 2−60790
$Ca(Y)F_2$, containing excess anions, defect struct., neutron diffuse scatt. 2−77570
CdF_2, thermal defect order, mobility and complex form., ionic cond. mechanism 2−51194
$CeH_{2\pm x}$ system, nonstoichiometric, defect struct. and ordering 2−77755
Co-C solid solution, interstitial character, X-ray determ. 2−50830
CsBr, X-irrad. at cryogenic temps., I-, α-, H, H′ and V_4 centres 2−68038
Cu, deformed, reorientation of dumbbell interstitials 2−50655
Cu, electron irrad. induced pt. defects clustering, high-voltage electron microscopy 2−56682
Cu, neutron irrad. temp. effect on defect aggregate size 2−53711
Cu, radiation damage, nature and annealing characts. 2−47368
CuCl, Frenkel defects, equilib. conc. perturbation by microwave pulse, ionic cond. change 2−80698
α-Fe:C, atomic relaxations, modified lattice statics calc. 2−60784
Fe-C alloy, recovery of internal friction after strain ageing 2−47481
Fe-Mo alloys, nitrided, substitutional interstitial G.P. zones 2−80826
Fe-V-N alloy, defect model explaining abnormal Snoek peak 2−47482
Fe, fast neutron irrad. at 77K, rel. to softening and anneal hardening 2−80689
Fe, H-dislocation interaction 2−53735
α-Fe, influence on self-diffusion coeffs. 2−47462
α-Fe, plastically deformed, nature of debris loops 2−74778
GaAs, rel. to anomalous diffusion profile of Zn 2−47464
Ge:P, electron irrad., bombardment induced interstitial P, e.p.r. obs. 2−48279
n-Ge, electron irrad., impurity depend. of annealing, vacancy-interstitial pair effects 2−47379
Ge, interstitial diffusion of Li, press. depend. 2−47442
Ge, investigation by non-irrad. techniques 2−47399
Ge, rel. to solubility and diffusion of Cu 2−77613
Hf-O system, near $Hfo_{1/6}$, rel. to order-disorder transform. 2−68205
KBr, X-ray scatt. from displacement field 2−60787
KBr crystals, u.v. irrad. and colour centre prod. from exciton decay 2−71527
KCl:Ca, Sr, X- irradiated, thermal annealing of defects 2−50696
KCl:Li^+, reorientation motions of H_a-centre 2−43648
KCl(Br), halogen atoms ionisation of In^{2+} and Tl^{2+} centres 2−81001
Mg, neutron irrad., pt. defect clustering, electron microscope obs. 2−60783
$Mg_yU_{1-y}O_{2-x}$, structural analysis, O non-stoichiometry assigned to interstitial O 2−47336
Mo, irrad., rel. to void stability 2−50650
Mo, neutron irrad., stress induced ordering of stage I defects 2−64654
in Nb, cold-worked or irrad., role in recovery 2−47404
Nb, cold-worked or neutron irrad., effect on low temp. recovery 2−64766
Nb, location of interstitial D sites by deuteron channelling 2−60811
Nb, O and N Snoek peaks, grain size effect 2−50736
Ni, deformed, reorientation of dumbbell interstitials 2−50655
Ni, neutron irrad., pt. defect clustering, electron microscope obs. 2−60783
Ni, point defect interactions with dislocations, high-voltage electron microscopy 2−56686
Sc_2O_3-MgO solid soln., defectivity, cation vacancies and interstitial anions 2−74906
n-Si:Li, irrad., Li-defect interactions, e.p.r. obs. 2−48293
Si, fast neutron irrad., number of Frenkel defects, calc. 2−71458
Si, investigation by non-irrad. techniques 2−47399
$SrCl_2$:K^+(Na^+), Frenkel defect form. and activation energies 2−47969
Ta-N, effects on asymmetry of yield stress 2−74844
Ta, proton motion, temp. depend. 2−43653
Ti, dislocation structure effects in interstitial solute hardening 2−56714
α-Ti, rel. to ^{63}Ni ultra-fast diffusion 2−64697
TlCl, pulse n.m.r. investigation of vacancy and interstitial diffusion 2−71471
V-Ti alloy, scavenging of interstitials, internal friction study 2−50845
V, neutron irrad., activation volume rel. to dose and strain, interstitial impurity precip. 2−80663
$VC_x(O_x)(N_x)$, cryst. growth by floating zone technique 2−47277
Zr-H(O) dil. alloys, internal friction peak obs. 2−50737
Zr-O α solid solution, O atom arrangement, neutron and X-ray diffr. obs. 2−71443
Zr-O system, near $ZrO_{1/3}$, rel. to order-disorder transform. 2−68205
α-Zr, rel. to ultra-fast diffusion of ^{59}Fe, ^{60}Co and ^{63}Ni 2−64697

vacancies
alkali halides, Maxwell-Boltzmann distrib. of intrinsic and extrinsic defect pairs 2−83971
alloy, disordered binary, equilibrium conc. calc. 2−53688
alloy, f.c.c., dil., vacancy jump freq. ratio, determ. by electromigration 2−83995
alloy, substitutional, calc. of characteristics 2−71464
alloy, substitutional, calc. of characteristics 2−71462
alloy, substitutional, calc. of characteristics 2−71463
alloys, quenched, transients in annealing of vacancies 2−80842
anion, random grouping, crystallographic shear 2−50653
annealing, cold-worked or irradiated solids, theory 2−43652
annihilation rate, recomb. with interstitials 2−56681

Crystal imperfections continued
vacancies continued
b.c.c. lattice, rel. to void stability 2−50650
α-brass, production during cyclic stressing and Portevin-le Chatelier effect 2−74827
α-brass, vacancies production during cyclic straining and Portevin-le Chatelier effect 2−74828
rel. to chemical diffusion, phenomenological theory 2−74808
crystal lattice and chemical potential regarding vacancy diffusion eqn. 2−74807
diamond, irradiated, theory of defects 2−47364
diamond, localized levels, LCAO- MO treatment 2−47808
diamond like solid, electronic states of the neutral vacancy 2−47805
diffusion mechanisms in anomalous metals, review 2−68044
diffusional creep, grain boundary dislocation climb sources, interface reaction control conditions 2−50752
GaAs:Te, heavily-doped, nature of defects, photolum. and internal friction study 2−71926
graphite, pyrolytic, low temp. electron irrad. damage and recovery, resist. study 2−80659
hard sphere and rigid disc solid, concentration, cell cluster technique 2−50654
interstitials and vacancy supersaturations, chemical stress concept 2−56688
ionic cryst., defect form. mechanism and struct. 2−80702
lanthanide sesquichalcogenides, Th_3P_4 struct., tetragonal struct. model for cationic vacancy ordering 2−74743
metal, aggregation under quenching or irrad. conditions 2−53696
metal, cubic, lattice statics of vacancy-screw disloc. interact. 2−56687
metal, f.c.c., hexagonal Frank loop energy 2−50667
metal, f.c.c., irrad., elec. resist. of defects 2−75045
metal, formation energy, determ. from temp. depend. positron annihilation 2−56689
metal, growth and supersaturation, rel. to void growth 2−53698
metal, point defect clusters, secondary defects, review 2−43619
metal, positron trapping rate, temp. depend. 2−80675
metal, quenched, coagulation of excess vacancies, statistical mech. study 2−80658
metal, solute segregation generated by vacancy currents around growing voids 2−53697
metal, stability, low-energy-recoil events and vibr. behaviour 2−53723
metal, vacancy annihilation in oxidation reactions in gases 2−53756
metal irradiated, void growth, interstitial and vacancy conc. rate theory eqns. 2−80661
metallic materials, effect on void nucleation during high-energy irrad. 2−53703
metals, deformed polycrystalline sheet, influence of hydrostatic pressure soaking on structural changes, X-ray study 2−84127
metals, polycrystalline and monocrystalline, differences in plastic deformation, interpretation on model of lattice defects mobility 2−84046
metals and alloys, irradiation induced volumetric swelling caused by void formation 2−74758
model, nonlinear defect, to explain generation of cracks 2−84047
motion and clustering under pressure 2−68020
in precipitation kinetics 2−68187
pyrrhotite, domain structure formation rel. to structural vacancy ordering 2−68021
radiation defects, vacancy-impurity complex, kinetics of formation and annealing 2−80693
radiation-induced defect clusters, transmission electron microscopy 2−50640
reactor materials, void formation studies, use of simulation with accelerators 2−76922
semiconductor, ion implantation induced lattice disorder 2−47367
solid solns., dilute b.c.c., calc. of partial correlation factors 2−80717
solute-vacancy interaction energies, measurement methods, review 2−68019
solute-vacancy interaction energies, measurement methods, review 2−68019
steel, stainless, vacancy loop prod. on quenching 2−53717
stress relief mechanism, at incoherent particles during coarsening 2−53798
voids, nucleation in irradiated stainless steel 2−71466
Ag, grain boundary self-diffusion, isotope effects, correl. effects, vacancy model 2−56752
Ag, γ-irrad., role in recrystn. 2−64758
AgBr, impurity ions and vacancies interaction, diffusion mechanism 2−80699
AgCl, impurity ions and vacancies interaction, diffusion mechanism 2−80699
Al-Cu alloys, quenched-in defect elimination mechanism 2−84149
Al-4%Cu alloy, vacancy-Ge binding energy 2−50824
Al-Ge alloy, vacancy-solute binding energies 2−74763
Al-Mg-Si alloys, quenched-in defect elimination mechanism 2−84149
Al-Mg alloy, role in Portevin-Le Chatelier effect 2−47490
Al-(N at.%) Mg, N = 10, 8, role in age hardening and plastic deformation 2−47612
Al-Mg(Cu) alloy, solute-vacancy binding energy, determ. from quenched-in defect conc. 2−74762
Al-(1.7 at.%) Zn, vacancy- impurity binding energy, positron-annihilation study 2−53727
Al, annealing of defects produced by quenching and electron irrad. 2−60785
Al, effects on subsequent dislocation loop formation during electron irrad. 2−53733
Al, elec. resist. temp. coeff. rel. to equil. vacancies 2−77856
Al, electron irrad. induced pt. defects clustering, high-voltage electron microscopy 2−56682
Al, neutron irrad., pt. defect clustering, electron microscope obs. 2−60783
Al, neutron irrad., vacancy trapping by voids 2−53705
Al, positron lifetimes and trapping probabilities at vacancies 2−44010
Al, rel. to creep mechanism 2−50754
Al, rel. to effect of deform. and ageing on yield stress 2−50799

Crystal imperfections continued
vacancies continued
Al crystal, form. and migration rel. to disloc. config. as result of thermal treatment 2−47411
Al foil, electron irradiated, migration rel. to stage III recovery 2−43805
Al1-5% Mg, and activation energy for serration flow 2−43706
Au:Cu, impurity-vacancy binding energy, equilib. resistivity obs. 2−71465
Au, plastically deformed after quenching, rel. to resist. recovery 2−56790
Au, quenching velocity influence on clusters, elec. microscope obs. 2−71630
CaF_2:Na, conc. and mobility of F ion vacancies, elec. conductivity obs. 2−47979
CaF_2, anion vacancy density, dependence on growth technique 2−47396
Cd, vacancy conc., effect of liquisol quenching 2−77572
CdF_2:Na^+ $(Ag^+)(Li^+)(La^{3+})(In^{3+})(Ge^{3+})$, rel. to ionic thermocurrents 2−81089
$CdIn_2S_4$, intrinsic and Co^{2+} doped, e.p.r., effect of S vacancies 2−68735
CdTe:In, Cd vacancies and impurity vacancy complexes rel. to self-compensation calc. 2−47889
CdTe, electron radiation damage and cathodolum. edge emission 2−48254
Co-(31.8 wt.%)W alloy, excess vacancy conc. effect on grain boundary diffusion 2−47455
$Cr_2S_2Te_x$, $0<x\leqslant 1$, ordering, mag. props., 80-800K 2−54343
CsCl:Ba^{2+}, migration and enthalpy, ionic cond. study 2−54232
CsCl, pure and Ba^{2+} doped, rel. to self-diffusion 2−74813
Cu-Ge(Ni)(Zn) dil. alloys, vacancy-impurity complexes and positron annihilation 2−47398
Cu, electron irrad. induced pt. defects clustering, high- voltage electron microscopy 2−56682
Cu, foil, heavy ion irrad., rad. damage, vacancy-type defect prod. 2−43608
Cu, influence on positron annihilation ang. correl. 2−51063
Cu, neutron irrad. temp. effect on defect aggregate size 2−53711
Cu, polycrystalline, strain hardened, thermally activated deform. mechanisms 2−77679
Cu, rel. to creep mechanism 2−50754
Cu, whiskers, formation 2−47397
Cu_3Au, free vacancy no. determ. in fission-neutron displacement cascade 2−53712
$Cu_xFe_yO_z$, nonstoichiometry and defect struct., O vacancies 2−74764
Cu_2O, defect levels, rel. to near i.r. absorpt. and photocond. 2−54420
Cu_xO_y nonstoichiometry and defect struct., O vacancies 2−74764
D_2 self-diffusion mechanism 2−43656
Fe-Au alloy, rel. to precip. 2−43851
Fe-Mn alloy, b.c.c., shock deformed, vac. migration rel. to recovery 2−56912
Fe-Mo alloy, rel. to precip. 2−43851
α-Fe, plastically deformed, nature of debris loops 2−74778
α-Fe, pure and alloyed, rel. to Mn diffusion, 778.3-901°C 2−83994
α-Fe, rel. to self-diffusion 2−47462
α-Fe, single vacancy atomic relaxations, modified lattice statics calc. 2−60784
γ-Fe_2O_3, distrib. over tetrahedral and octahedral sites 2−60786
GaAs, surface stoichiometry and struct., surface vacancy model 2−50445
GaP, surface stoichiometry and struct., surface vacancy model 2−50445
Ga_2Te_3, semicond., stoichiometric vacancies and radiation stability 2−71906
n-Ge, electron irrad., impurity depend. of annealing, vacancy-interstitial pair effects 2−47379
Ge, equilibrium configuration, computer calc. 2−71467
Ge, estimation of true formation energy 2−47400
Ge, investigation by non-irrad. techniques 2−47399
Ge, γ-irrad., donor-vacancy complexes, prod. kinetics and energy spectrum 2−47382
Ge, γ-irrad., O-free, divacancy-donor complexes 2−71943
Ge, migration energy of quenched-in defects, specimen size effect 2−71536
Ge, mobility and conc., high-temp. behaviour 2−64659
Ge, rel. to solubility and diffusion of Cu 2−77613
H_2, self-diffusion mechanism 2−43656
HfO_2, rel. to elec. cond., 1600-1900K 2−54233
In_2Te_3, semicond., stoichiometric vacancies and radiation stability 2−71906
KBr, X-ray scatt. from displacement field 2−60787
KBr(Cl), cation vacancy motion, Schottky defect form. 2−44154
KCl:$Eu^{2+}(Yb^{2+})(Sm^{2+})$, impurity-vacancy dipole relax. and aggregation, and X-ray effects 2−83982
KCl:Pb, polarized luminesc. and dipolar relax. of Pb-vacancy complexes 2−72424
KCl:SO_4^{2-}, anion vacancy trapping, i.r. absorpt. study 2−43620
KCl:Tl, thermal glow traps responsible single negative ion vacancies 2−75333
La_2Te_3-La_3Te_4 system, effect on thermal cond. of crystal lattice 2−80919
LiF:Mg^{2+}, thermoluminesc. depend. on state of aggregation of Mg^{2+} vacancy pairs 2−44416
Mg, neutron irrad., pt. defect clustering, electron microscope obs. 2−60783
MgO, cation vacancy, self diffusion up to 2350C 2−56761
MgO, Schottky defect, energy of formation 2−64660
Mo, effects of voids on angular correlation of positron annihilation photons 2−71468
Mo, irrad., rel. to void stability 2−50650
Mo, neutron irrad., rel. to void formation during annealing 2−77575
Mo, neutron irrad., stress induced ordering of stage I defects 2−64654
Mo, neutron irradiated, correlation of void size and positron annihilation characteristics 2−71469
Mo, rel. to boundary diffusion of Cr 2−53766
NH_3, self-diffusion due to vacancies 2−47451
NaBr(Cl), cation vacancy motion, Schottky defect form. 2−44154

Crystal imperfections continued
vacancies continued
NaCl:Pb, polarized luminesc. and dipolar relax. of Pb-vacancy complexes 2−72424
NaCl, vacancy bound to divalent impurity, slow motion, pressure effects, in n.m.r. study 2−72514
NbC_{1-x}, vacancy short range order, electron diffr. obs. 2−83965
NbC_x, rel. to surface recomb. of H atoms 2−50549
Ne, high purity crystalline, equilibrium vacancy formation self-diffusion 2−71470
Ni-Al system, vacancy filling on high temp. compression 2−43939
Ni-Al system phase fields 2−43938
Ni, clusters after quenching, electron microscope obs. 2−64661
Ni, condensate prod. by laser irrad. 2−53726
Ni, neutron irrad., pt. defect clustering, electron microscope obs. 2−60783
Ni, point defect interactions with dislocations, high-voltage electron microscopy 2−56686
$Ni_{1-x}S$:O(Se), conc. and distrib. rel. to mag. susceptibility conc. depend. 2−44255
Pb, p-type, obs. using hydrostatic weighing 2−58691
$PbBr_2$, pure and Cu^+-doped, ionic cond. and dielec. loss study 2−47402
$PbBr_2$, pure and Tl^+-doped, enthalpy and entropy of form., ionic cond. study 2−47401
$PbCl_2$, pure and K^+-doped, ionic cond. and dielec. loss study 2−47402
Pt, conc. rel. to press., quenching effects, excess resist. obs. 2−60788
Sc_2O_3-MgO solid soln., defectivity, cation vacancies and interstitial anions 2−74906
Si:P, implanted, rel. to annealing characts. 2−77594
Si, elec. struct., many electron molecular orbital method 2−47935
Si, electron irrad., divacancy obs. rel. to recomb. luminesc. 2−48230
p-Si, electron irrad., low temp. photocond. due to divacancy 2−47999
Si, equilibrium configuration, computer calc. 2−71467
n-Si, fast electron irrad., capture and transfer between defect complexes 2−80694
Si, investigation by non-irrad. techniques 2−47399
Si, ion irrad., divacancy formation and annealing, i.r. absorpt. study 2−71457
Si, irradiated, multiple vacancy centres, e.p.r. obs. 2−48283
Si, irradiated, theory of defects 2−47364
Si, γ-ray and neutron irrad. induced defect obs. 2−47937
Si, mobility and conc., high-temp. behaviour 2−64659
Si, neutron irrad., divacancy obs. 2−48194
Si, neutron irrad. induced defect clusters, edge absorpt. obs. 2−47389
$SrTiO_3$, doubly ionized oxygen vacancy obs. 2−47403
TaC_{1-x}, vacancy short range order, calc. 2−83966
TiC_{1-x}, vacancy short range order, electron diffr. obs. 2−83965
TiC_x, rel. to surface recomb. of H atoms 2−50549
TiN_{1-x}, vacancy short range order, calc. 2−83966
$TiNi_{1-x}$, vacancy short range order electron diffr. obs. 2−83965
TlCl, pulse n.m.r. investigation of vacancy and interstitial diffusion 2−71471
U, β phase, microstress behaviour during quenching, effect of pore form. 2−77659
UC_{1-x}, estimation of electrical resistivity increase due to C deficients 2−43874
V, condensate prod. by laser irrad. 2−53726
V foil, quenched, vacancy detects, electron microscope obs. 2−71472
VC_{1-x}, vacancy short range order, calc. 2−83966
VC_x, influence of vacancy ordering on thermophysical props. 2−54004
V_6C_5, superlattice, C vacancy ordered distrib. 2−43621
VN_{1-x}, vacancy short range order, electron diffr. obs. 2−83965
W, foil, Au ion irrad., vacancy-type dislocation loop prod. 2−43616
W, foil, Au ion irrad., vacancy-type dislocation loop, prod. 2−43616
W, high temp. equilibrium conc., from thermal expansion obs. 2−68255
W, ion irrad., He entrapment at vacancies 2−50651
W powder, role in sintering, effects of sinter activators 2−50899
Zn, activated, self-diffusion coefficients and thermal coeff. of expansion 2−68048
ZnS:Cu phosphors, effect of traps and vacancies on thermoluminescence 2−75335
ZnSe, electron irrad., e.p.r. obs. 2−47366
Zr, form. energy, quenching obs. 2−53728
ZrO_2, rel. to elec. cond., 1600- 1900K 2−54233
$ZrTe_2$, nonstoichiometric phase, struct., homogeneous phase limit 2−60772

Crystal morphology
βTi-V alloys, orientation of facets of thermal- etch pits 2−80546
alloy solidification, growth morphology, in-situ radiographic obs. 2−47605
athermal martensitic morphology, arrow-like formations 2−67980
crystal class 6m2, standard choice of axes for elastic and piezoelec. props. 2−68474
diamond, origin of features 2−74654
equilibrium form. determ., review 2−47189
eutectics containing compound phases, correl. with thermodynamics 2−47600
ilmenites, from Mare Tranquillitatis, morphology, electron microscope obs. 2−44905
isotactic polystyrene from isotactic-atactic blends, effect of noncrystallizable components on morphology 2−71294
marine deposits, Mg content and crystal habits in ancient carbonates 2−54754
martensite crystal habit, phenomenological theory 2−68183
martensitic transformation, concept of habit plane and phenomenological theories 2−68196
mercuric cyanide.tetrahydrofuran addition compound, development of {111} habit 2−60706
metallic solid/liquid interface micromorphology, electron microscopy obs. 2−47194

Crystal morphology continued
- microstructure and inhomogeneities, quantitative examination 2—80605
- using new medium resolution scanning electron microscope 2—66720
- nylon 66 fibres, drawn, effect of high-temperature annealing on structure and morphology 2—74602
- oxalic acid, growth, habit rel. to solution supersaturation 2—74685
- poly(4-methylpentene-1), formation of curved crystals 2—80529
- poly(ethyleneterephthalate) multiple endotherm melting behaviour due to recrystallization, relation to morphology 2—71291
- poly(vinylidene chloride), effect of heat treatment on morphology and structure powder 2—71293
- polyacrylonitrile, effect of heat treatment on morphology and structure of crystals powders and fibres 2—71293
- polyethylene films formed by evaporation and deposition in vacuum 2—50516
- polymer, annealing and temp. effect 2—60611
- polymer, influence on mech. props. 2—60860
- polymer, linear high, extended chain cryst. habits 2—60609
- polymer, symposium, Prague, Czechoslovakia, (Aug-Sep 1971) 2—60608
- polytetrafluoroethylene, cyclic loading effect 2—60870
- polytetrafluoroethylene, emulsion-grade, electron diffraction studies of ribbons and rods 2—71295
- rubber, natural, at high pressures 2—60603
- Saran, effect of heat treatment on morphology and structure of powder 2—71293
- unified approach to habit and crystal growth analysis 2—47195
- Ag filaments, grown from Ag compound, scanning elec. microscope obs. 2—47133
- AgBrI:Br^-, NH_3, ion purity effects 2—80648
- β-AgI crystal shapes rel. to ice nucleation properties 2—64589
- $AgNO_3$, cryst. growth morphology at polymorphic transforms. 2—50945
- Al-Cu alloy, cast morphology, anodic oxidation etching study 2—47602
- Al-Zn alloys, morphology and crystal structure of a precipitate, Y-phase, exam. 2—67986
- Al, cast morphology, anodic oxidation etching study 2—47602
- Al_2O_3 crystals, form from amorphous film by heating 2—83861
- α-Fe-Sn effect of third alloy component 2—80812
- BP, microscope obs. 2—50567
- $BaSO_4$ single crystal, grown from silica gels 2—43519
- Bi-Zn(Ag) eutectic alloy, electron diffr. obs. 2—60976
- $CaCO_3$, calcite, habit rel. to growth soln. comp. 2—74676
- Cd-Pb-Sn alloy, eutectic morphology, unidirectional solidification microstruct. 2—74895
- Cd_3Mg, two-phase region, and orientation relns., metallographic obs. 2—61042
- Cu-(30 wt.%)Ni-(0.3 wt.%)Be alloy, and cryst. struct. of precipitate phases assoc. with age hardening 2—50934
- Cu-Sn alloys, unidirectionally solidified, columnar dendrite structure 2—74641
- Cu, Burgers vector rel. to external geometry at initial deform. stage 2—50673
- Cu, electrodeposited, current density and substrate orientation effects 2—48340
- Cu dendrites, crystn. mode effects 2—47136
- Cu single crystals, mech. twinning during elongation or torsion at 78 K and room temp. 2—74783
- Cu_6Sn_5 fibres, brittle fracture surface morphologies 2—80744
- Fe-30 wt.% Ni, surface martensite obs. 2—68196
- Fe-Ni alloy, martensite comp. depend. 2—80771
- Fe alloys, martensitic structures, classification based on morphological criteria 2—83955
- Fe whiskers, growth morphologies lattice twists 2—80561
- Fe_3C, growth texture 2—43872
- GaAs, epitaxial, selective growth 2—50493
- GaAs, grown from gas phase 2—56656
- GaP, melt grown, cellular growth morphology 2—47268
- GaSe, vapour grown single crysts. 2—50574
- p-Ge-n-CdS_xSe_{1-x} epitaxial heterojunction 2—77924
- Ge ribbon crystals grown by Stepanov method 2—47328
- $GeSe_{(2)}$(Te), vapour-grown crysts. 2—50575
- α-HIO_3, rel. to growth from aqueous solution 2—43520
- $Hg(CN)_2$, grown through slow decomp. of tetrahydrofuran solvate crystal to the air 2—47208
- InBi, effect of thermal cycling 2—51101
- InSb whiskers, grown by gas transport 2—75366
- KNO_3, cryst. growth morphology at polymorphic transforms. 2—50945
- MnSb-(Sb,Bi) and MnSb-(Sb,Sn) eutectics, growth rate effects 2—47641
- NH_4NO_3, cryst. growth morphology at polymorphic transforms. 2—50945
- $PbMoO_4$, sign of Z-axis detn., etch config. and Schaefer-Bergmann diffr. obs. 2—43568
- SiC whiskers, twin morphology 2—53581
- $SrSO_4$ single crystal, grown from silica gels 2—43519
- Te vapour grown whiskers 2—67915
- Ti martensite, effect of Si, Zr, Al and Mo on struct. and strength 2—64723
- TiO_2, rutile, dissolution forms of single crystal spheres 2—47197
- W film, chem. vapour deposition, substrate temp. and gas press. effects 2—47131
- $Y_3Al_5O_{12}:SiO_2$ garnet, grown from melt, habit modification by doping 2—74751
- $Y_3Fe_5O_{12}:SiO_2$ garnet, grown from melt, habit modification by doping 2—74751
- $Y_3Ge_5O_{12}:SiO_2$ garnet, grown from melt, habit modification by doping 2—74751
- Zn-Cd dilute alloy, dendrite growth and morphology 2—43488
- ZnO, physico-chem. conditions influence during growth 2—43514
- ZnO single crystal, hydrothermal growth rate and morphology 2—47247
- $ZnSO_4.7H_2O-NiSO_4.7H_2O-CoSO_4.7H_2O$, isomorphous relationships, distribution coeff. 2—74959

Crystal properties
- cellulose and similar fibrous materials, dielectric constant and crystallinity 2—61408
- independent tensor components, number determ. for cryst. with n-fold symmetry axes 2—83915
- metal, bulk moduli calc. from methods of homogeneous deofrm. and long waves 2—47177
- noncentrosymmetrical crystals, symmetrical properties analysis, with applic. to third order tensors 2—68473

Crystal structure
- *see also Magnetic structure; Polymorphism*
- cellulose, cryst. state, effect of moisture 2—83962
- compressed matter, electron-lattice interaction energy, cryst. struct. depend. term 2—71788
- geometrical description 2—74766
- glass structure, crystallite hypothesis 2—80532
- ice, proton distribution, Kirkwood correlation factor 2—80642
- inclined steps, measurement by reflection electron microscopy 2—60740
- mean squared atomic scatt. factors for all atoms, tables 2—53624
- naphthalene equilibrium form facts, appearance of nonsingular surfaces 2—50561
- poly-N-methyllaurolactam, fully methylated nylon 12, crystallinity 2—83846
- shape and orientation, absorption corrections, checking method 2—64628
- solid state physics, an overview 2—57093
- stereographic projection by computer of crystals of arbitrary symmetry and orientation 2—43533
- transition metal germanides, group IV-VI, microhardness, rel. to atomic volume change, structural loosening 2—74866
- X-ray topography, transmission and reflection methods 2—60730
- Al-4%Cu alloy, influence of precipitates on cavity formation for irrad. by fast neutrons 2—67984
- Al-Zn alloys, morphology and crystal structure of a precipitate, Y-phase, exam. 2—67986
- α-Al_2O_3, corundum, Verneuil grown cryst., cryst. axis orientation 2—60701
- $CsLn(MoO_4)_2$, synthesis, crystalliz. and polymorph. transformation 2—71392
- Cu, grain topography in early stage of plastic flow 2—47500
- Cu dendrites, crystn. mode effects on habit and morphology 2—47136
- Cu trichites, orientation and degree of perfection 2—47321
- Fe-Co-C, rel. to strength, martensite flow stress 2—56941
- Fe-Mn-(B)-C, rel. to strength, martensite flow stress 2—56941
- Fe alloys, martensitic structures, classification based on morphological criteria 2—83955
- NdP_5O_{14}, laser material 2—73587
- rare earth elements, polymolybdates, $Ln_2O_3.4MoO_3$ type, classification into four structural groups 2—83838
- YAG:Nd garnet, grown by Czochralski method, cryst. perfection rel. to melt comp. and rot. speed 2—67945

- **microstructure**
  - *see also Grain boundaries; X-ray examination of materials/microstructure*
  - (hk) interferences linewidth, effects of preferred orientation 2—53627
  - alloy, coherent phase formation, and mech. props., review 2—57007
  - alloy, dispersed particles, size stability in diffuse interface limit 2—43816
  - alloy, grain boundary precip. coarsening, cumulative size distrib. function 2—47604
  - alloy, light, s.c.c., microstruct. effects 2—56826
  - alloy, particle coarsening, cumulative distrib. functions 2—47603
  - alloy, two-phase, effects of coherency strain fields on dislocations struct. 2—56702
  - alloys containing ZrC_x and HfC_x, effects of protective atmos. during sintering 2—77721
  - aluminas, polycrystalline, influence of texture on mechanical props. 2—68093
  - austenite-ferrite mixture, determ. of relative phase vol. by X-ray diffr. 2—71641
  - beam scanning examination 2—80605
  - bicrystal, epitaxial, interface struct., effect of misfit, bonding and cryst. dimens. 2—56690
  - bone, hydroxyapatite crystallite struct. from low temp. thermal cond. meas. 2—61115
  - β- brass type alloys, quenched, structure and microstructure 2—84106
  - carbon phenolic, two dimensionally reinforced, re-entry material, characterization 2—56980
  - ceramic, influence on strength 2—47521
  - ceramic alloy B2Zh, prep. and mech. characterization 2—77720
  - ceramic matrix, chemically reacted, for fibre reinforced composites 2—56972
  - ceramics, electron microscope study, high-voltage, of texture by Harwell 1MV microscope 2—71412
  - ceramics, sequence and effects 2—67948
  - ceramics, textural studies by electron probe microanalysis 2—71411
  - ceramics, texture with ref. to mech. props. 2—67949
  - cermet steel, dynamic hot pressing, thermal treatment effects 2—84146
  - cermet. ZHGp1.5D2.5, effects of cooling after sintering on struct. and mech. properties 2—77722
  - co-existing phases, volume fraction, X-ray detn. 2—56645
  - composite, C continuous fibre reinforced ceramics and glass 2—50919
  - composite, C discontinuous fibre reinforced ceramics and glass 2—50918
  - composite, Ni-Cr base alloy, Mo alloy or W filament reinforced 2—56988
  - composite, nichrome, W filament reinforced 2—53967
  - composite, nichrome, W filament reinforced 2—53970
  - composite, nichrome, W or Mo reinforced, filament-matrix interface 2—53966
  - copolymers, amorphous blocks cast from soln., domain struct. 2—83848
  - crystalline interfaces struct., 0-lattice theory 2—56616
  - diamond, framesite, plastic deform. structs. 2—50877

Crystal structure continued
microstructure continued
diffraction contrast from coherent precipitates in elastically-anisotropic materials 2—80671
diffractometric analysis of fine structure, limits 2—74697
domains, interface geometry, contrast effects, electron microscope and diffr. obs. 2—56718
domains, one-dimensional antiphase, interpretation with non-integral half period 2—53625
electron probe analysis, grain orientation effects on X-ray production 2—83943
f.c.c. microcrystallites, spherical, geometry and stability 2—53598
$Fe_{36}Cr_{22-x}Ti_x$, χ-phase alloy, $8<x<10$, inversion domain obs. 2—64637
ferrous metals, phases, Mossbauer spectroscopy 2—51312
film, rel. to anisotropy of elastic deform. 2—80730
fine grained steel, effect of welding conditions on mechanical properties 2—50808
fine structure, determination from integral width of diffraction lines 2—56618
flaws, inherent, effect of microstruct. on stress to propagate at room temp. 2—68096
glass, fluor-richterite comp., high strength polycryst. material 2—47651
glass ceramic, fluor-richlerite composition of high mechanical strength, struct. determ. 2—77704
grain form, stability in growth from melt in presence of dopants 2—47249
grain size, very fine, X-ray beam diffracted power obs. 2—56958
grain size rel. to spot dimensions on X-ray diffraction photograph 2—71402
grained solid, grains/unit volume, determ. from theory of stochastic processes 2—43877
graphite, artificial, anisotropic and isotropic, struct. distrib. 2—53972
graphite, bulk effects on sublimation characts. 2—60560
graphite, isotropic, cryst. orientation, influence of creep strain 2—56963
graphite, pyrolytic, rel. to thermal conductivity and diffusivity above 1500 K 2—57083
graphite, pyrolytic siliconated, fracture surface, electron microscope obs. 2—74861
graphite fibre, three dimensional carbon structures 2—56979
Guinier Preston zone, size effect on X-ray diffusion near Bragg spots 2—47300
illite, microstructure and chemical comp. 2—84710
INCO 713C, thermal stability and corrosion of Al coatings after heat treatments 2—60959
interphase interfaces, strain fields, epitaxial dislocations, steps, electron diffr. contrast 2—56625
Kossel line method, using divergent X-ray beam 2—43536
low alloy steel, creep rupture strength, microstruct. depend. 2—77685
low angle electron scattering of films with anisotropic distribution of crystallites 2—80640
lunar and terrestrial calcic plagioclases, electron microscope obs. 2—66162
macroblock formation in crystals grown from melt, estimation of transverse dimensions 2—50683
metal, b.c.c., grain diameter, rel. to brittle fracture 2—43720
metal, cold-worked, nucleation of new grains in recrystallization 2—68134
metal, f.c.c., simulation of rolling texture development 2—43813
metal, grain boundary ordered struct., boundary dislocations, transmission electron microscopy 2—53651
metal, polygonized struct., conditions of formation of recrystn. nuclei 2—56901
metal, shock wave effects, and mech. props. 2—68073
metal orientation and recrystallization 2—68135
metal systems, grain and particle size distrib. analysis, review 2—50817
metal/SiO_2 cermet film, produced by recoil atom implantation 2—53578
metals, deformed polycrystalline, influence of hydrostatic pressure soaking, X-ray study 2—84127
metals, polycrystalline and monocrystalline sheet specimens, changes in misorientation during plastic deformation, X-ray study 2—84046
microcline, shock deform. struct. 2—61843
microcrystals in polycrystalline object, investigation of form 2—60741
mullite, press.-sintering kinetics and mechanism 2—50874
mullite, stoichiometric ceramic compact 2—50873
nuclear fuel, irrad. ceramic oxide, microstruct. charact. 2—59869
nylon polymer, preferred orientation 2—60751
oxide fuel struct. evolution, modelling using BEHAVE-2 code 2—52858
phase comp. analysis by X-ray diffr., verification of Ordway elemental phase analysis theory 2—74725
pole figures, theoretical model 2—67947
polycrystal structure, compared with foam struct. 2—47313
polycrystalline single phase material, polygons, no. of sides, mathematical proof 2—47292
polyethylene, crystallite size, nitration effects 2—60612
polyethylene terephthalate, fiber texture sample crystallite orientation distribution, test of refinement procedure 2—80534
polypropylene, drawn and annealed, determ. of crystallite size from breadth of equatorial X-ray reflections 2—71288
polypropylene, effects of cooling rate from melt 2—56908
polypropylene, quenched and annealed samples, wide-angle X-ray scattering in neck region 2—71572
portland cement paste, effects on deform. and fracture 2—60995
pressed parts, produced by dynamic pressing 2—53879
PVA, uniaxially stretched film, mechanical anisotropy 2—83365
pyrophyllite, firing temp. depend. 2—50890
pyroxene, lunar and terrestrial minerals, cooling effects, precip., dendritic growth, domains 2—62689
quartz, structural defects, obs. 2—69718
quartz, synthetic, Dauphine microtwins 2—68003
quartz in prograde metamorphic sequence, preferred orientation 2—57766

Crystal structure continued
microstructure continued
rare earth Co compounds, with $CaCu_5$ struct., stability 2—80796
andrecrystallization, dynamic 2—68133
reflection intensities of point electron diffraction patterns in det. of crystal structures 2—80641
refractories, optical and elec. microscope obs. 2—56955
refractory carbide cemented alloys, carbide grain shape 2—53889
ruby, stream paterns, microscopic examination and associated microcracks 2—71424
SAP-1 plate, fine struct. and recrystn. 2—53870
scapolite, antiphase domain structure 2—62014
solid solutions, B2 and $L1_2$ superstruct., superdislocation-antiphase boundary interactions 2—47416
solid solutions, B2 and $L1_2$ superstruct., superdislocations and antiphase boundaries 2—47417
stainless, managing, high-strength, struct., props., optimum comp. 2—60881
stainless steel, annealed type 316, irradiation induced microstructure development 2—83123
stainless steel, ferritic sheet, texture development 2—77701
steatite, firing temp. depend. 2—50890
steel, 1%C, fatigue crack propagation, microstruct. effect 2—71645
steel, $\alpha\rightarrow\gamma$ transform., singularities, rel. to initial state 2—80764
steel, ausformed by extrusion, form. of struct. 2—47327
steel, austenitic, effect of deform. temp. during thermomech. treatment 2—80770
steel, austenitic, grain coarsening temp., hot rolling effects 2—47582
steel, austenitic, stainless, microstructure determ. of oxide film due to corrosion 2—81505
steel, carbon, volume fraction of retained austenite, X-ray obs. 2—56645
steel, cast struct., effect of induced fluid flow 2—47620
steel, cementite, Ostwald ripening, alloying additions effects 2—50936
steel, effect of heat treatment temp. 2—53842
steel, effect of rare earth alloying 2—53900
steel, En 24, soln. between microstructure and fracture toughness 2—71586
steel, fully heat treated low alloy, effects of sulphide morphology as impact properties 2—56908
steel, grain diameter, rel. to brittle fracture 2—43720
steel, high-C martensitic, singularities 2—56934
steel, high-carbon Mn type, lattice orientation of α-martensite 2—43843
steel, high-speed W-Mo, effects of Co 2—53992
steel, hot-worked austenitic and ferritic, recrystn. during continuous cooling 2—53873
steel, hypereutectoid, low carbon martensite struct., prod. by heat treatment 2—47585
steel, impact fatigue effects 2—80809
steel, Kh18N10T, fine structure changes for degree of deformation in creep 2—83956
steel, low C, effect of microstructure on embrittlement 2—84158
steel, low carbon, microstructure and embrittlement 2—43783
steel, low-C, effect of grain size on tensile props. 2—43695
steel, low-C, fracture rel. to microstruct., embrittlement, bend tests 2—56823
steel, low-C, hot-rolled, quenched, transformation effects 2—57017
steel, low-C low-alloy, fine struct. and phase comp. at elevated temps. 2—53898
steel, low-C low-alloy pipe, formation of abnormal struct. 2—53897
steel, martensitic, effect of lath boundary precip. on fracture toughness 2—57018
steel, martensitic, field ion microscope obs. 2—64779
steel, mild, dissolved oxygen influence 2—47628
steel, mild, effect of high energy ultrasonic waves 2—77673
steel, mild, spark machined and mechanically sectioned, deform. layers 2—74879
steel, MnS inclusion size, effect of solidification rate and S content 2—43852
steel, mosaic struct. rel. to hot pressing conditions 2—43793
steel, Ni martensite, C segregation on dislocations 2—56758
steel, nitrided by ion bombardment 2—56935
steel, phase transforms. during laser beam heating, effect of original struct. 2—53990
steel, plastically deformed, austenite form., kinetics and morphology 2—57014
steel, prep. by powder metallurgy, rel. to sintering conditions 2—43892
steel, press. vessel type, rel. to impurity effects on radiation sensitivity 2—53895
steel, quenched, quench-aged, fatigue behaviour rel. to microstruct. instability 2—50768
steel, sheet, cold rolled, annealed, grain growth, X-ray obs. 2—47621
steel, sintered, for fuel element jackets, processing and mech. characterization 2—76951
steel, stabilized recovery-induced substruct., formation for improved creep resistivity 2—56913
steel, stainless, characteriz. for fast breeder reactors 2—50648
steel, stainless, effect of explosive load 2—43836
steel, stainless, high-tensile, containing Be 2—77672
steel, stainless, melted by different methods, O impurity effects 2—53899
steel, stainless, rel. to ridging phenomenon in cold rolled and annealed sheets 2—68131
steel, structural, austenite grain growth 2—53988
steel, structural, effect of C, Mn and Si on austenite content 2—74875
steel, technical, electronic grain-size analyser 2—60969
steel, transform. of austenite 2—47690
steel, u.s. vibr. effects 2—53877
steel targets, effect on ballistic behaviour 2—60980
steels, carbon, dynamic strengthening singularities under infl. of shock waves 2—84075
steels, stainless, phase state determ. method at rolling temps. 2—84091
structure and props. of grain boundaries and interfaces, conference, Yorktown Heights, N.Y., USA, Aug (1971) 2—56722
subgrain formation 2—80763

Crystal structure continued
- **microstructure** continued
  - substrate role in det. crystallinity of organic thin films 2—77533
  - superalloys, precipitation hardened, study using extraction replica electron microscopy 2—80817
  - thin films, URS-501M diffractometer, vacuum attachment 2—62907
  - topaz, thermal and electron beam induced breakdown 2—60776
  - transformer steel, e. micro and e. diffr. exam. of disperse nonmetallic phase 2—84074
  - transition metal cpds. characterization 2—50571
  - transition zone obs., contrast improvement using ZnSe vapour phase deposition 2—43780
  - triglycine sulphate, electron microscope examination of fine structure of irradiated crystals 2—65067
  - weld metal, toughness below 0°C, effect of metallurgically conditioned inhomogeneities 2—74890
  - wustite, fracture energy invariance with grain size 2—50880
  - X-ray diffraction applications, review 2—64744
  - Yttralox ceramic characteriz. as laser material 2—49381
  - Zircaloy tubing, effect of oxygen and fabrication variables 2—53915
  - Zircaloy-2, radial orientation of hydride, thermal cycling effect 2—53914
  - Zircaloy-4, neutron irrad., deform. parameters, 300°C 2—50749
  - Zircaloy-4 tubing, yield loci, effect of texture variations 2—50850
  - zirconia ceramics, phase analysis by X-ray analysis, matrix method, polymorph technique 2—80879
  - Ag-15% Ge alloy, splat-cooled, martensitic transformation of structure 2—56921
  - Ag, rolling texture form. mechanism 2—60972
  - Ag on NaCl surface, decoration with anthraquinone, information microstructure 2—71305
  - Al-Ag, Al-Zn type alloys, GP zone composition by relative intensitives of diffuse effects 2—68035
  - Al-Cu-Mg-Mn alloy, mosaic angle, tensile deform. depend. 2—80772
  - Al-Cu-Mg alloy, eutectic, orientation relationships 2—74893
  - Al-Cu alloy, cast morphology, anodic oxidation etching study 2—47602
  - Al-Cu alloy, film, precip., G.P. zone form., rel. to bulk alloy props. 2—47099
  - Al-Cu alloy, Frank loop nucleation on screw dislocations 2—50670
  - Al-(4 wt.%)Cu alloy, Guinier-Preston zone form. 2—43825
  - Al-Fe alloy, rapidly solidified 2—50827
  - Al-Ge alloys, rapidly solidified 2—43929
  - Al-Mg-Li alloy, 01420, ageing, phase comp. changes 2—47594
  - Al-Mg-Si alloy, strength rel. to dislocation motion and GP zones 2—56717
  - Al-Mg-Si alloy, structure of metastable precipitates formed during ageing 2—56909
  - Al-Mn alloy, structural features of a plane strip obtained directly from melt by Stepanov method 2—50821
  - Al-Zn-Mg-Cu-Mn forging alloy, rel. to fracture toughness 2—53826
  - Al-Zn-Mg-Cu alloy, rel. to tensile deform. and high temp. creep 2—56800
  - Al-Zn-Mg alloy, precip. free zones, rel. to stress corrosion crack paths 2—43732
  - Al-Zn-Mg alloy, precipitate free zone, elec. microscope obs. 2—56902
  - Al-Zn alloy, and formation of GP zones, elec. resistivity obs. 2—50800
  - Al-6.8%Zn alloy, GP zones rel. to diffusion, and effects of Ag, Si, or Mg 2—56753
  - Al-based material, rel. to hot formability criteria 2—80852
  - Al-1.2 wt%Mg_2Si alloy, Guinier-Preston zone formation, rel. to two-step ageing 2—64765
  - Al, 7075, laser shock-induced microstructure changes 2—68075
  - Al, cast morphology, anodic oxidation etching study 2—47602
  - Al, conditions of formation of recrystn. nuclei 2—56901
  - Al, effect of dislocations on substruct. strengthening 2—50763
  - Al, effects on subsequent dislocation loop formation during electron irrad. 2—53733
  - Al, embrittlement, intercryst. penetration by liq. Ga 2—43721
  - Al, integranular flow, effect on grain boundaries, role of imperfections 2—43643
  - Al, plane shock structs., strain rate functions 2—60800
  - Al, recrystn. nuclei formed by Rowland transform. 2—43822
  - Al, super-pure, hydrostatically extruded, substruct. and flow stress detn. 2—74876
  - Al alloy, multiphase, metallographic investigation of grain boundary sliding 2—80820
  - Al alloy, NS.5, effect of preferred orientation on X-ray stress meas. 2—71643
  - Al alloys, analysis of microstructure and topography by electron emission microscopy 2—80875
  - Al alloys, eutectic, microstructures for unidirectional solidification 2—67985
  - Al alloys, fatigue damage at high temps. 2—80808
  - Al single crystal, rolling texture development and deformation banding tendency 2—56788
  - Al single crystals, substruct. changes during high-temp. deform. in creep 2—84078
  - Al wires, cyclic textures 2—77700
  - AlCu alloy, (Al 4 WT %), structure changes during ageing studied by the channeling technique 2—80827
  - $AlN-Al_2O_3-Mo$ cermet, prep. and props. 2—43869
  - $AlN-Y_2O_3$, sintered, with fibrous struct., textural determ. 2—47666
  - Al_2O_3:Ti, precipitate morphology 2—50872
  - 9 Al_2O_3-AlN, periodic antiphase domain struct. 2—50618
  - $Al_2O_3-Cr_2O_3-P_2O_5$ coating, radiative capacity rel. to struct., 600-2000K 2—57087
  - $Al_2O_3-ZrO_2-SiO_2$ fused grain refractories, rebonded, characteriz. 2—53926
  - Al_2O_3, corundum, change on high temp. creep 2—71574
  - Al_2O_3, sapphire filament, melt grown 2—50916
  - Al_2O_3, thermal grooving and growth kinetics 2—80545
  - αAl_2O_3, X-ray detn. in alumina crystallites 2—56647
  - Al_2O_3 ceramic, fine grain, Cr_2O_3 additions effect 2—50867
  - Al_2O_3 ceramic, rel. to deform. processes 2—60993
  - Al_2O_3 film, plasma and gas plasma deposited 2—64563

Crystal structure continued
- **microstructure** continued
  - Au film, large angle rotation boundaries, electron micrographs 2—56736
  - B_4C, neutron radiation induced defects, transmission e. microscope obs. 2—67355
  - B_4C neutron absorber in fast and thermal reactors, swelling gas release and structural integrity 2—83115
  - $BaFe_{12}O_{19}$, deform. texture 2—56962
  - $Ba_2NaNb_5O_{15}$ ceramic, sintering behaviour, scanning elec. microscope obs. 2—53929
  - $3BaO.5SiO_2$ glass-ceramic, rel. to mechanical props. 2—53930
  - $Ba_4SrNb_{10}O_{30}$, solidification structs. 2—47654
  - $BaTiO_3$ single crystal film, domains and domain walls, elec. microscope obs. 2—68469
  - BeO, during densification, rel. to sintering mechanism 2—47662
  - Bi-Zn(Ag) eutectic alloy, electron diffr. obs. 2—60976
  - C-C composites, effect on mech. props. nondestructive testing 2—61016
  - C-graphite matrix composites, effect on mech. props. 2—61015
  - C, pyrolytic, effects on lattice, thermal expansion perpendicular to layer planes 2—61108
  - C, pyrolytic, high graphitized, X-ray obs. 2—60752
  - C, pyrolytic, preferred orientation 2—60751
  - C fibre, preferred orientation rel. to thermal expansion, room temp. —1800°C 2—53953
  - C fibre, S impurity effects 2—50913
  - C fibres, two dimensional lattice orientation and three dimensional crystallinity 2—68177
  - C PHS composite, PHS, effect of variation in precursor resin on struct. and mech. props. 2—53958
  - $Ca_xFe_yO_z$ nonstoichiometry and defect struct., O vacancies 2—74764
  - $CaO-ZrO_2$ ceramic, and thermomech. props. 2—43876
  - $3CaO.SiO_2$:Cr, struct. rel. to reactivity 2—80877
  - Cd-Ge-As-Se glass, rel. to immiscibility temp. determ. 2—56561
  - Cd-Pb-Sn alloy, eutectic morphology, unidirectional solidification microstruct. 2—74895
  - Cd_3Mg, two-phase region, morphology, habit planes and orientation relns., metallographic obs. 2—61042
  - CeO_2, effect of TiO_2 addition on grain growth 2—47655
  - $Ce_2Se_3-GeS_2$ system, rel. to phase diagram determ. 2—61043
  - Co-Al alloy, disintegration on cooling and work hardening, platelet formation and orientation 2—60977
  - Co-10%Cr alloy, thermal stability and corrosion of Al coatings after heat treatments60959 2—60959
  - Co-Cu-Fe-Ce permanent magnet, sintered 2—50910
  - Co-Mn-Al system, decomp. studies 2—64816
  - Co-base alloys, microstruct. obs. of phase transformations, photoemission e. micro. obs. 2—68193
  - Co-base composite materials, superalloys with fibres obtained by directed solidification, properties 2—64793
  - Co alloy, dispersion hardened 2—50831
  - Co alloy, WI-52 cast high-temp. mat. 2—47617
  - Co film, evaporated at oblique incidence, mag. contrib. of columnar grains 2—72184
  - $CoFe_2O_4-Co_3O_4$ alloy, quenched, aged, saturation magnetization, intrinsic coercive force, rel. to microstruct. 2—81233
  - CrH_x, electrodeposited, f.c.c., h.c.p.→b.c.c. transform., domain size changes 2—47682
  - Cu-Al-Fe bronze, superplastically deformed 2—43831
  - Cu-Al-Ni alloy, rel. to shape memory effect 2—80844
  - Cu-Al-alloys, microstructures and mechanical props. of phases after quenching and isothermal treatment 2—60932
  - Cu-Al alloy, rel. to superplasticity 2—50745
  - Cu-Al alloy, two-phase struct. 2—71678
  - Cu-Be-Ag alloys, structural states in decomposition process, e. diffr., e. micro. and microhardness exam. 2—80782
  - Cu-Be alloy, G.P. zone formation, extra spots in electron diffr. pattern 2—77578
  - Cu-C alloy, prep. by vac. deposition changes on annealing 2—56928
  - Cu-Cr alloy, effect of precip. size on recrystalliz. temp. 2—56927
  - Cu-(30 wt.%)Ni-(0.3 wt.%)Be alloy, and morphology of precipitate phases assoc. with age hardening 2—50934
  - Cu-Ni-Mg alloys eutectic mixtures constitution 2—84103
  - Cu-Ni alloy, grown by Bridgman's method, selective oxidation obs. 2—47322
  - Cu-P system, rel. to constitution diagram 2—61045
  - Cu-Zn alloy, rel. to superplasticity 2—50745
  - Cu-Zn(40%) microduplex, metallographic study of superplasticity and cavitation 2—80738
  - Cu-Zr-Cr alloy, effect of precip. size on recrystalliz. temp. 2—56927
  - Cu-Zr, dil. alloys., softening resistance mechanism 2—56709
  - Cu-Zr alloy, effect of precip. size on recrystalliz. temp. 2—56927
  - Cu-based material, rel. to hot formability criteria 2—80852
  - Cu, deformed at 77K, neutron irrad. effects 2—83968
  - Cu, dynamic strengthening singularities under infl. of shock waves 2—84075
  - Cu, Ni diffusion-generated substruct. 2—53761
  - Cu, texture transition mechanism during rolling, X-ray obs. 2—47323
  - Cu, wire specimens, plastic deformation and static lattice distortion 2—53890
  - Cu and Cu-Zu alloys, development of texture 2—80849
  - Cu film, deposition on cold substrate, fibre texture formation 2—50480
  - Cu film, epitaxial, microstruct. and orientation 2—67909
  - Cu film, vacuum-deposited, electron microscope obs. 2—50489
  - Cu films in storage, ageing effects on substruct. and mech. props. 2—83863
  - Cu_2O, recrystn. and grain growth kinetics 2—43788
  - Cu_xO_y nonstoichiometry and defect struct., O vacancies 2—74764
  - $Dy_2O_3WO_3$ solid soln., of phases 2—57013
  - Fe-Al-Ni-Co-Ti alloy, columnar struct., prod. by Magnicol process, reaction mechanisms 2—43834
  - Fe-Au alloy, G.P. zone form., precip. mechanism 2—43851
  - Fe-Cr-N alloy system, microstructure revealing nitride phase 2—53894
  - Fe-Cr(8%) alloy, martensite, quenching and tempering temp. effects, rel. to strengthening 2—84071

Crystal structure continued
microstructure continued
Fe-Mn alloy, field ion microscopy exam. comparing orientation to ferrite α and iron nitride 2−64777
Fe-Mo-C alloy, quenched and tempered, microstruct., field ion microscopy obs. 2−47581
Fe-Mo alloy, G.P. zone form., precip. mechanism 2−43851
Fe-Mo alloys, nitrided, substitutional interstitial G.P. zones 2−80826
Fe-Ni-C-Mo-Cr alloy, effect of tempering 2−43853
Fe-Ni-C alloy, effect of tempering 2−43853
Fe-Ni alloy, invar, areas of Fe conc., positron annihilation obs. 2−80524
Fe-Ni alloy, martensite comp. depend. 2−80771
Fe-Si, domain width, sample thickness and cryst. orientation depend. 2−48061
Fe-Si, influence on mech. props. 2−80778
Fe-V-C steel, fibrous vanadium carbide occurrences after thermal or continuous cooling transformation 2−61033
Fe, Armco, grain size depend. of tensile strength 2−43846
Fe, cast, ion beam thinning, graphite/pearlite interface, electron microscopy 2−74877
Fe, cast, melt solidification, nodular graphite formation, additive effects 2−74881
Fe, cast, spheroidal graphite, segragations rel. to microstruct. 2−50836
Fe, cast, with graphite, decarburizing, effect of S, Al, or Mg 2−43837
Fe, dynamic strengthening singularities under infl. of shock waves 2−84075
α-Fe, high temp. creep struct. 2−43637
α-Fe, neutron irradiated, elec. microscope obs. 2−60965
Fe film monocrystalline, inter-domain boundaries 2−61533
Fe foil, extended in electron microscope, cell formation obs. 2−71487
Fe single crystal, H induced plastic strain, divergent X-ray beam obs. 2−64715
α-Fe single crystal, rel. to high temp. creep 2−56804
Fe single crystal plates, tensile strength, surface orientation depend. 2−71583
Fe$_3$C, growth texture 2−43872
Fe$_2$O$_3$-TiO$_2$ solid soln., crystallographic shear struct., planar boundaries 2−74768
Fe$_2$O$_3$ and Fe$_3$O$_4$, morphological and struct. changes during reduction 2−50881
Ga single crystal, containing additions, substructure, X-ray obs. 2−71474
Ga$_2$O$_3$-TiO$_2$ solid soln., crystallographic shear struct., planar boundaries 2−74768
Gd$_2$(MoO$_4$)$_3$ diffracted light obs. from domain wall 2−84467
Ge-Si heteroepitaxial structure, u.h.v. evaporated 2−56591
Ge, mosaic structure during testing, X-ray and e. microscope exam. 2−71475
Ge, profiled crystals, surface relief, photogoniography 2−47076
Ge, surface orientation effects on elec. cond. and work function 2−71935
α-GeTe, domain struct., twin and interface boundary interface types 2−72150
GeTe$_2$ film, amorphous, elec. diffr. and microscopy obs. 2−60660
GeTe−Bi solid soln., regions of existence at 250, 400, 500 and 600°C 2−53888
HfN-ZrB$_2$ cutting tool materials characteriz. 2−50883
In, rolled, influence of twinning on texture 2−80774
InP, high resistance, Cu, Fe or Cr doped, phase composition and microstructure 2−83895
In$_2$Se$_3$-Sb$_2$Te$_3$ system, rel. to phase diagram determ. 2−61048
KCl single crystal and steel, dependence of natural cleavage and grain size on cooling velocity 2−84122
K$_2$Si$_2$Pb$_2$O$_7$, product of K$_2$CO$_2$ + 2PbSiO$_3$ subsolidus reaction 2−60996
LiF single crystals containing cavities hydrostatic pressure influence on microstructure 2−83973
LiIO$_3$, α and β forms, anisotropy difference compared from optical properties 2−81326
Li$_2$O-Al$_2$O$_3$-SiO$_2$ glass-ceramic, effect of heat treatment 2−53931
Mg, plane strain extrusions, texture control and yield anisotropy 2−80848
MgF$_2$, hot pressed influence on temp. depend. of elec. cond. 2−47898
MgO-MgAl$_2$O$_4$ system, solidification struct. 2−47658
MgO, influence of inclusions on grain growth 2−56964
MgO, thermal grooving and growth kinetics 2−80545
mischmetal-Mg alloys, dilute, metallographic study of phase transformations 2−80794
Mn-Al alloy, τ phase 2−50838
Mn-Ga alloy, rel. to internal friction 2−50735
MnSb-(Sb,Bi) and MnSb-(Sb,Sn) eutectics, growth rate effects 2−47641
Mo-Hf, internal nitriding, high-temp. props. 2−60968
Mo-34%Re, deform. struct., twin and disloc. microstruct. 43624 2−43624
Mo-Ru alloy, high purity as-cast 2−50840
Mo-Ti alloy, effect of deform. rate and temp. 2−47503
Mo, before and after neutron irradiation, physical mechanical properties 2−53730
Mo, effect of B addition 2−56943
Mo, room temp. ductility and intergranular cracking, after annealing 2−53875
Mo alloy, cellular struct. development during hydroextrusion 2−47642
NaCl, creep at high temp., creep substruct., tilt walls around parallelipipedic blocks 2−77579
Nb-H system, low temp., rel. to diffusivity determ. by Gorsky effect 2−80847
Nb-Zr-Ti alloy, supercond. after cold deform. and low temp. annealing 2−50842
Nb-(40 wt.%)Zr alloy, metallurgical variables influence on supercond.47861 2−47861
Nb, grain size effect on O and N Snoek peaks 2−50736

Crystal structure continued
microstructure continued
NbC, hot working and strength improvement, NASA research 2−64801
NbTe$_2$, domain structure and dislocation config. 2−60804
Ni/SiO$_2$ cermet films, granular grain size 2−50498
Ni-Be alloy, deform., recrystn., and ageing, texture variation 2−50806
Ni-Be alloy, G.P. zone formation, extra spots in electron diffr. pattern 2−77578
Ni-Cr-Nb-W-Mo alloy, struct. and phase comp. 2−43941
Ni-Cr-Ti alloys, Guinier-Preston zone form., during precip. strengthening 2−43859
Ni-Fe-Mo alloys, thin strips, magnetic properties and texture 2−68509
Ni-Fe alloy, sheets, heavily rolled, annealing textures, recryst. mechanism 2−74886
Ni-Fe film, crystallite size, effect on ripple spectrum 2−81279
Ni-base composite materials, superalloys with fibres obtained by directed solidification, properties 2−64793
Ni, deform., recrystn., and ageing, texture variation 2−50806
Ni, dynamic strengthening singularities under infl. of shock waves 2−84075
Ni, textures produced by deform. and primary and secondary recrystn. 2−84070
Ni, work hardened in tension, secondary recrystn. 2−60986
Ni, work hardened in tension, double texture, twinned growth influence 2−60985
Ni alloys, dispersion hardened, role of grain size and shape in strengthening 2−71648
Ni ceramic, refractory oxide particle growth, matrix density effects 2−68169
Ni films, intrinsic stress obs. by optical interference method 2−77649
Ni$_3$Al-Ni$_3$Nb eutectic alloy, interface between two ordered lattices, elec. diffr. obs. 2−71647
Ni$_3$Al-Ni$_3$Ta eutectic 2−47644
NiAl$_2$O$_4$, growth on sapphire, orientation relations 2−71333
Ni$_4$Mo, antiphase domains, internal friction study 2−43670
Ni$_3$Nb phase in Inconel 718 2−77678
Pb-Bi-Sn eutectic, rel. to superplastic props. 2−80839
Pb-Ge-As-Se glass, rel. to immiscibility temp. determ. 2−56561
Pb(Zr,Ti)O$_3$ ceramic, role of Fe$_2$O$_3$ 2−50895
Se film, rolling texture, X-ray and elec. resist. study 2−64574
Si monocrystal, H$_2^+$ ion bombarded, bicrystal formation, X-ray obs. 2−47386
SiC, self-bonded, texture and strength detn. to 1300°C in air and to 1750°C in argon 2−71393
SiC polycryst., effect of crystallite size on physical props. 2−56774
Si$_3$N$_4$, ceramic, hot pressed, strength fracture energy, microstruct. relationships 2−60883
Si$_3$N$_4$, transmission high-voltage electron microscope obs. 2−60998
SiO film, electron diffr., radial distrib. analysis 2−53577
Sn-Pb(Zn, Sb) alloys, unidirectional solidification, equiaxed crystal origin 2−74882
Sn ingot, unidirectional solidification, uniaxed crystal origin 2−74882
SrTiO$_3$, uniaxially stressed, domain struct. at 2K 2−61433
TaC-Co alloy, oversaturated, microstruct. and reaction behaviour 2−64775
Te-Ge-As system, rel. to superconductivity 2−61242
Ti-Al-Mo-Zr alloy, ductility, influence of β-phase 2−50746
Ti-Cr alloy, fracture modes, effect of ω phase 2−47547
Ti-Mo, base β-alloy, ageing characs. and tensile props. 2−50807
Ti-Mo alloy, ω-phase precip., rel. to resist. anomalies 2−84297
Ti-(13 wt.%)V-(11 wt.%)Cr-(3 wt.%)Al, mech. property-fracture-microstruct. reins. 2−56950
Ti, dislocation struct. effects in strain-, grain size− and interstitial solute hardening 2−56714
Ti, dynamic strengthening singularities under infl. of shock waves 2−84075
α-Ti, recrystallized, grain size distrib. 2−56898
Ti alloy, effect of gas saturation 2−53909
Ti alloy, rel. to superplasticity 2−50745
TiC-Co alloy, oversaturated, microstruct. and reaction behaviour 2−64775
TiC-Mo$_2$C-Ni alloy, rupture strength and hardness rel. to microstruct. 2−47538
TiC, changes obs. following neutron irradiation 2−52848
TiC, hot working and strength improvement, NASA research 2−64801
U-Pu-W-C alloys, phase boundaries 2−54011
(U,Pu)O$_2$ fuel pin, porosity and actinide redistrib., grain growth and desintering 2−56043
(U,Pu)O$_2$ microspheres and pellets, sol-gel derived, optical and electron microscopy, electron microprobe analysis, α autoradiography 2−47610
U, β phase, microstress bheaviour as function of number of quenching cycles 2−77659
U alloy, ion etched, scanning electron microscope obs. 2−56578
UO$_2$/W composite, after controlled solidification 2−47669
UO$_2$ fuel rod, irrad., pore movement kinetics 2−52873
UO$_2$ pellets, grain growth, long term obs. under annealing 2−49898
U$_3$Si, irradiated, effect of electropolishing on voids 2−67354
V, neutron irrad., microstruct. changes 2−80665
W-HfO$_2$ composite, rel. to thermal shock resistance 2−56989
W-ZrO$_2$ composite, rel. to thermal shock resistance 2−56989
W, before and after neutron irradiation, physical mechanical properties 2−53730
W, damping of elastic oscillations, orientation depend. 2−43671
W, swaged and drawn, deform. textures 2−53868
W coating, deposited from the gaseous phase, grain size 2−84092
W filament, rel. to appl. to composite reinforcement 2−53970
W foil, rolling and annealing textures 2−43796
W sintered powder, grain size coarsening, effects of sinter activators 2−50899
W wire, drawn, micropore pinning effect on grain boundary motion during recrystn. 2−47647
WC-Co alloy, oversaturated, microstruct. and reaction behaviour 2−64775

Crystal structure continued
microstructure continued
WC-Co cemented carbides, effects of Cr and Ni additions 2−43864
WC-Co composite, microstruct. interpretation of stress-strain behaviour 2−47670
29 at.% Zn-Al alloy, spinodal decomp., metastable rhombohedral form., elastic anisotropy effects 56923 2−56923
Zn-Al alloys, strain-rate depend. of deform. mechanism 2−84011
Zn-Al eutectic alloy, cold-rolled, rel. to superplastic deform. characts. 2−43701
Zn-Ti alloys, effect of cooling rate and composition 2−80818
ZnO-Bi$_2$O$_3$ ceramic, rel. to elec. props. 2−57198
Zr-(1.5wt.%)Cr-(0.1wt.%)Fe tubing, heat-treated and hydrided 2−53918
Zr-Cr-Fe alloy, correlation with mech. props. and corrosion resistance 2−53922
Zr-(2.5 wt.%) Nb press. tubing, hydriding, orientation and effect on tensile props. 2−50849
Zr-Nb alloy, rel. to supercond. transition temp. 2−51107
Zr-(2.5 wt%)Nb press, tubes, texture development 50848 2−50848
Zr alloy tubing, method for determining pole figure 2−67979
Zr alloys, anisotropy of secondary in-reactor creep, relation to texture 2−67349
Zr and Zircaloy tubular materials, texture and anisotropy rel. to plastic deform. 2−53916
ZrC-NbC, solid solution, grain size and creep meas. in compression, temp. range 2600-3150 K 2−84033
ZrO$_2$, calcia stabilized, thermal stress induced microstruct. modifications 2−50901
ZrO$_2$, martensitic transform. struct. 2−50953
α-Zr. grain size depend. of deform. behaviour 2−50748
Crystal structure, atomic
see also Crystal electron states; Crystals / lattice mechanics; Electron diffraction crystallography; Neutron diffraction crystallography; Space groups; X-ray crystallography
cation-cation distances and analysis of cation coordination polyhedra 2−71395
cell parameter determination from Debye photographs, choice of reflections 2−71421
compound with unknown chemical formula, crystal struct. detn. 2−60731
coprime multiplicities of space-group point-positions 2−56614
cosine seminvariants formulas for cos($\varphi + \varphi$) 2−67950
crystallographic computation, mol. model generation and fitting 2−53647
cubic harmonics as linear combinations of spherical harmonics 2−82180
decoration and electron beam determ. 2−80604
defects, diffraction contrast micrographs, transmission and reflection 2−80621
diffraction studies of form factors, desirability of absolute scale 2−77535
direct phasing, Σ_2-relation 2−56615
eenantiomorph. discrimination via calculated cosine invariants 2−67966
experimental investig. methods using neutron and X-ray scattering 2−74706
generalised tangent formula, usefulness 2−83918
group theoretical classification pf repeating representations in quantum-mechanical problems with point-group symmetry 2−83928
ion scattering, angular distributions 2−75005
lattice complexes, invariant and quasi-invariant, data presentation 2−47291
lattice parameter meas. technique 2−47295
lattice parameters, indexing of Kossel X-ray recording 2−47296
magnetic crystals, optical gyrotropy or symmetry property 2−60729
model of structure periodically modulated in three dimensions 2−50615
molecular packing analysis, based on minimization of cryst. lattice energy 2−83880
multiformula procedure for single soln. approach to phase problem 2−43531
network models, derivation of difference eqn., study of energy spectrum and dispersion curves 2−77520
O$_r^3$ type crystals, symmetry types associated with phase transitions of second kind 2−47701
Patterson functions, systematic analysis on basis of crystal symmetry, interaction peak relations 2−74695
point groups, integrity bases 2−71394
polymorphic transitions of the elements and system of structural types 2−71397
refinement by least squares method with constraints 2−50617
Shubrikov point groups and ferroelasticity 2−84006
singular matrix representations, reln. to group representations 2−78771
space group, P2$_1$2$_1$2$_1$, one-dimens. phases expression 2−67951
structural relations between racemic and optically active cryst. structures 2−53626
structure factor detn. of single crystals with high secondary extinction 2−77534
structure factors, probabilistic connection between one phase invariant and moduli 2−83908
two dimensional images, contrast features 2−80627
variances and covariances of the anisotropic temperature parameters, derivation 2−56644
X-ray diffractometer data, optimization for min. average variance in electron density 2−83916
Fe$_3$O$_4$-Fe$_2$TiO$_4$, lattice parameter calc. 2−56655
HgCr$_2$Se$_4$, spinel structure formation, X-ray diffract. study 2−77563
KIO$_3$, crystal struct. exam. and vibrat. struct. detn. by i.r. spectroscopy and n.q.r. 2−71435
Ti martensite, effect of Si, Zr, Al and Mo on struct. and strength 2−64723
alloys
B-2 type phase, disorder, rel. to thermodynamics 2−43819
b.c.c., ordering, insterstitials influence 2−43818
binary, influence on hydrogen diffusion 2−77611
β- brass type alloys, quenched, structure and microstructure 2−84106
C16-type, stability and competitive structs. 2−50851

Crystal structure, atomic continued
alloys continued
C16-type structures, rel. to band struct., theory 2−43573
C16-type structures, X-ray obs. 2−43572
f.c.c., ordering, interstitials influence 2−43817
f.c.c. ternary, theory of ordering 2−43571
invars, neutron diffraction study of crystal structure 2−68002
lattice parameter method for investig. of solid solution precipitation 2−61027
martensite, with abnormal axial ratio 2−68186
martensite-austenite lattices, orientation relationships, application of statistical methods 2−43532
ordering, stat. theory, lattice distortions 2−43812
rare earth-Co Laves phase, LnCo$_2$ 2−81276
rare earth-Ni Laves phase, LnNi$_2$ 2−81277
solid soln., defective MA$_x$B$_y$ type, ordering, cluster model 2−74892
solid solution, X-ray diff. and model of rigid atoms in closed-packed arrangement 2−77768
3dtransition metals, magnetization effect on lattice constants 2−53660
Ag-Mn-Al, high coercivity, struct. of ferromag. precip. 2−43821
Al polycrystalline films, on NaCl substrate, effect of annealing 2−80566
Au-Pb system, intermetallic cpds. 2−43826
Au-Pd alloy, short-range order formation, resistivity obs. 2−74894
CeRh$_x$Pd$_x$ alloys electronic state, magnetic susceptibility and lattice spacings 2−81317
Co-C solid solution, X-ray study 2−50830
Co-Fe, electrolytically deposited films 2−53561
Co-Ni-Sb system, intermetallic cpds., X-ray diffr. study 2−43940
Co$_2$MnSn, Heusler ferromag. alloy 2−48075
Co$_3$Sn$_2$, superlattice struct. 2−47319
Cu-Al system, Cu$_3$Al$_{2\parallel}$(h) and CuAl(r) 2−74730
Cu-Al tempered martensite, long period superlattice phases 2−43914
Cu-Mn short range ordering, diffuse neutron scattering peak between {100}, {110} positions 2−71644
Cu-Ni:Mn, Cr, Al, struct. and props. with ageing and hardening 2−83954
Cu-Sb, near 20 at.% Sb, long period superstruct. with hexagonal symmetry 2−71430
α-Cu-16 at.%Al, spherical single crysts., struct. anomalies 2−71429
Cu$_{80}$Au$_{20}$, model of structure periodically modulated in three dimensions 2−50615
Dy-Nd, lattice parameters, ordering 2−51237
Er-B system phases, lattice parameters 2−50964
Fe-Al-C alloys, influence of ordering and martensitic transformations during quenching 2−84073
Fe-Al alloy, diffuse X-ray scatt. and temp. depend. of sp. ht. 2−56654
Fe-C, baikovite, a new struct., produced by ultra rapid heating and cooling by laser beam 2−47630
Fe-Co, ordering effects on electronic struct. 2−44249
Fe-Co equiatomic alloys, order from magnetic anisotropy energy considerations 2−61507
Fe-Cr σ-phase, Mossbauer obs. 2−44253
Fe-Ga alloys, magnetic props. and Mossbauer investigations 2−84416
Fe-Mn-C, long period stacking order structure formed by thermal cycling 2−67990
Fe-Ni-Al-Cu, lattice parameters, alloying additive effects 2−43845
Fe-Ni quenched alloys, short-range order detn. in first and second coord. spheres from n. scatt. 2−81199
Fe-Si, lattice parameter, ordering, conc. depend. 2−74818
Fe-Si solid solns., b.c.c., ordered atomic configs. 2−47326
Fe-V σ-phase, Mossbauer obs. 2−44253
Fe-12.3 at.%-Al, Mossbauer determination of short-range order, heat treatment and cold rolling effects 2−51311
Fe$_3$(Al,Ge), influence of Ge on struct. changes, nuclear γ-reson., X-ray diffract. and dilatometric analyses 2−80779
Gd-B system phases, lattice parameters 2−50969
Ge-Sb system, metastable GeSb phase 2−47329
GeTe-Bi$_2$Te$_3$ solid soln., cell dimensions, atoms per unit cell 2−74903
K-Cs, K-rb, pseudopotential theory and Vegard's rule 2−67992
Mg-Zn-misch metal alloy, distrib. of rare earth metals in phases 2−50624
MgIn intermetallic compound, struct energy, pseudopot. and perturbation theory calc. 2−50623
Mn$_3$Pd$_5$ phase, crystal and magnetic struct. 2−83960
Ni-Al system, lattice parameter increase due to vacancy filling on high temp. compression 2−43939
Ni-Al system, lattice parameters of β-NiAl and δ-Ni$_2$Al phases 2−43938
Ni-Sb system, intermetallic cpds., X-ray diffr. study 2−43940
Ni$_3$Fe, long range order parameter 2−60984
Ni$_2$MnSb, Ni$_2$MnSn, Heusler ferromag. alloys 2−48075
Ni$_3$Nb phase in Inconel 718 2−77678
Rh-Mn-Sb system, Cl$_b$ type, lattice parameters and mag. props. 2−65156
Sm-Sn system, relative stability of intermetallics 2−47573
Sn-W bronze, space group, unit cell dimensions 2−71441
Tb-Sc, Vegard's law applicability 2−68576
Tc-40 at% Mo, 4.2-298 K 80647 2−80647
ThN-ThO$_2$-Th system, phase behaviour 2−50977
Ti-Ce-S system, struct. and phase equilib. 2−43943
Ti-22at.%Nb, ω-phase, electron diffr. obs. 2−53908
Ti b.c.c. solid solutions, struct. and decomp. 2−68204
Ti base, ω phase struct. symmetry 2−47349
TiO-MnO alloy, synthesis, lattice dimensions, atoms per unit cell 2−74908
V-C alloys, ordering effects, comp. depend. 2−71378
V-N system, V$_3$N phase, electron microscope obs. 2−50978
V-Ti (Cr)(Sn)(Al), lattice parameter, comp. depend. 2−53912
Y$_3$Cd$_4$Zn$_7$ crystallographic system, lattice parameter and space group determ. 2−80644
YCo$_5$-YFe$_5$, lattice parameters, comp. depend. 2−43944
YCo$_5$-YNi$_5$, lattice parameters, comp. depend. 2−43944
YCo$_2$, Laves phase 2−81276
YNi$_2$, Laves phase 2−81277
Yb-Sn system, relative stability of intermetallics 2−47573

Crystal structure, atomic continued
alloys continued
$YbAl_2$, $YbAl_3$ magnetic susceptibility and expansion coefficient 2−81218
$YbCu_{6.5}$, X-ray obs. 2−43594
Zr-Al dilute alloy, ordering and stacking faults 2−47354
Zr-O α solid solution, neutron and X-ray diffr. obs. 2−71443
Zr b.c.c. solid solutions, struct. and decomp. 2−68204
Zr base, ω phase struct. symmetry 2−47349
ZrC-NbC, solid solution, lattice const. and creep meas. in compression, temp. range 2600-3150 K 2−84033
ZrC-W solid soln., interactions, isothermal sections struct. at 2200 and 2600°C 2−74911

elements
C fibre, interlayer spacing, S impurity effects 2−50913
diamond, fast electron irrad., lattice parameter charges 2−60775
graphite, pyrolytic low density, Royal Aircraft Establishment review 2−43903
graphite single crystal, X-ray diffr. during shock wave compression 2−56646
metal, cohesive force conjugate to uniform expansion 2−67929
metal, electron effects on cryst. struct. formation 2−67982
metal, h.c.p. and f.c.c., atomic stacking order, dislocation theory 2−47422
metal, rel. to entropy and heat of fusion 2−64506
noble gas ion probe technique for surf. anal. and struct. exam. 2−71297
rare-earth related forms of coordination polyhedra from icosahedron 2−84094
refractory metals, zone decorations in field evaporated surface 2−53551
Al single crystal, X-ray diffr. during shock wave compression 2−56646
As, assignment of axes, etch pit study 2−47186
As, high press. supercond. phase, lattice consts. 2−44058
Bi, high press. supercond. phase, lattice consts. 2−44058
C, vari forms, comparison of intensity ratios of 002 and 004 diffraction lines 2−64633
C fibres, size effects on radial distribution analysis, influence of atomic bonding 2−64630
C film, lattice const., diamond-like props. characterization 2−56588
Cd, lattice parameters, effect of liquisol quenching 2−77572
Cr, atomic scatt. factor, determ. by vanishing Kikuchi line electron diffr. method 2−74750
Cu, electron irrad., lattice parameter and resistivity changes 2−60777
D_2 cubic phase, orientational order parameter, 0.4-4K 2−60755
Fe whiskers, growth morphologies lattice twists 2−80561
γ-Ga, space group, unit cell, lattice consts. 2−53661
Gd, lattice const. anomaly in c-direction in Curie pt. vicinity 2−57291
Ge covalent-metallic phase transition under pressure, theory 2−83886
H metallic phase, influence of expression for dielectric function in structure calcs. 2−77521
^{4}He, h.c.p., crystallographic angles 2−53663
Na, metallic, equilib. lattice const., Kohn-Sham self-consistent calc. 2−60698
Nb, bond lengths from X-ray K-absorpt. fine struct. 2−68674
Ni, Kikuchi band defect and excess regions calc. 2−60763
Rh, imaging of atoms with convention electron microscope 2−56665
S high pressure, phases I and III, indexing powder patterns 2−53679
Sb, high press. supercond. phase, lattice consts. 2−44058
Si, lattice parameters rel. to thermal expansion, X-ray obs. 2−47757
Si covalent-metallic phase transition under pressure, theory 2−83886
Sn covalent-metallic phase transition under pressure, theory 2−83886
Tc, 4.2-298 K 2−80647
Te, h.p. phase 2−47348
V, atomic scatt. factor, determ. by vanishing Kikuchi line electron diffr. method 2−74750

inorganic compounds
$A^{II}A^{III}B^{IV}B^{V}O_7$ compounds, synthesis and props. from solid-phase reactions 2−71391
AB_2O_6 phases tri-PbO_2 α type struct. 2−83950
Al-Ni alloy, influence of short-range order on elec. and mag. resist. 2−71423
alkali feldspars, Na-K mixing, polymorphism 2−53675
alkali metal metavanadates 2−47261
alkaline earth fluorides, doped with tripositive rare earth ions, existence of separate cubic phase 2−80705
average valency V materials, trends in ionicity 2−83887
C16-type, stability and competitive structs. 2−50851
C16-type structures, rel. to band struct., theory 2−43573
C16-type structures, X-ray obs. 2−43572
celites, determination from i.r. spectra 2−65254
chlorates, alkali and alkaline earth, lattice dimension effect on ^{35}Cl n.q.r. 2−44464
cookeite, in petalite, struct. determ. 2−81628
2,3-dihydro-1,4-benzoxazepin-5(4H)-ones, X-ray powder patterns 2−56672
$Gd_2O_3.GeO_2$, $Gd_2O_3.2GeO_2$, from phase diagram of Gd_2O_3-GeO_2 determ. of lattice parameter 2−84097
glass, alkali borate, containing nickel oxide, spectrophotometric studies rel. to struct. 2−67885
hydrogen atom positions and hydrogen bonds prediction 2−47312
lanthanide sesquichalcogenides, Th_3P_4 struct., tetragonal struct. model for cationic vacancy ordering 2−74743
merwinite, $Ca_3Mg[SiO_4]_2$ 2−78219
metals and alloys, nonideal axial ratios, analysis for close-packed hexagonal structures 2−71396
micas, OH group, effect of Fe subst. for Mg, i.r. spectra study 2−48168
$NaCsCr_2O_7$ crystal struct. determ. 2−77551
niobates, $ABCNb_2O_{15}$, A=Ca, Sr, Ba; B=Ca, Sr, Ba, C=Na, K 2−75251
oxides, perovskite struct., interatomic distances calc. based on deform. lengths of bonds 2−74720

Crystal structure, atomic continued
inorganic compounds continued
plagioclase, at. scatt. factor satellite intensities, reciprocal space distrib. 2−53678
PLZT ceramics, crystal structure and enhanced ordering of ferroelec. domains 2−80760
polyamides, chain-folded lamellar crystals, X-ray diffraction study. 2−47359
precious metal pyrochlores, semicond. and metallic 2−60987
pyrochlore, $A_2B_2O_7$ type, parameter x detn. by geometric analysis of ion contacts 2−74721
rare earth aluminates and orthochromites, i.r. spectra correls. 2−84489
rare earth compounds, $LnAg_2Si$ 2−74735
rare earth compounds, $LnRu_2$ and $LnOs_2$, high press. effects 2−71689
rare earth compounds with zircon struct., temp. dependence of lattice parameters 2−84215
rare earth dihalides and oxybromides 2−47333
rare earth fluorozirconates, $LnZrF_7$ 2−43581
rare earth intermetallics, $R_2(Co_{1-x}Fe_x)_{17}$ type, lattice consts. 2−50626
rare earth metal halides, variation of i.r. absorption spectra with nature and structure 2−78083
rare earth molybdates, Ln_2MoO_6 type, prep. and cryst. struct. 2−74737
rare earth silicates, apatite type struct., synthesis, cation distrib. 2−74742
rare earth silicides, 20-1200°C 2−68005
rare earth sulphides, L_2S_3 type, β-form 2−47345
rare earth sulphotelluride solid solns., high temp. homogeneity regions 2−53905
rare earth tetraborides, lattice consts. 2−81293
rare earth tetraborides, lattice parameters 2−43524
rare earth titanates, $Ln_2Ti_2O_7$ type 2−47344
reference list, materials studied by anomalous X-ray scatt. 2−60749
semiconducting materials, i.r. transmission microscopy using high resolution video display 2−71399
sphalerite, e. microdiffraction exam. of microscopic impurity inclusions 2−71408
spinel structure compounds, off centre ions, model for local distortions 2−80646
spodiosite analogues, i.r. and Raman spectra 2−51318
Staurolite, Fe^{2+} site distribution, Mossbauer spectrum 2−48143
tantalates with potassium tungstate bronze structures, cry. lattice parameters 2−71422
transition metal hydrides, review 2−77731
transition metal phosphides and arsenides, MM'P and MM'As, metallic interactions, struct. evolution 2−71361
wolframites, determination from i.r. spectra 2−65254
wurtzite type crystal, spontaneous distortion from tetrahedral struct. 2−67981
Wyrouboff's hydrated double sulphates 2−77545
$[Ag_4Te][ClO_4]_2$, space group, unit cell dimens. 2−53653
Ag complex, $[C_5H_5NH]Ag_5I_6$, −30-125°C 2−43574
δ-$AgFeO_2$, hexagonal phase 2−53652
AgI-NaI-H_2O system, hydrous phase structs. 2−47314
Ag_7NO_{11}, precise determ. of R factor and position of NO_3^- from diffractometer data 2−77557
Ag_2Se, polymorphic transitions, X-ray obs. 2−64809
Ag_3TlTe_2, electron diffraction obs. 2−74722
Al compound, influence on X-ray K-satellite of Al 2−51360
$Al_2Fe_3(SiO_4)_3$, almandite, garnet, and mag. struct. 2−54349
AmI_2, X-ray diffraction determ. of lattice constants 2−80643
AmOI, X-ray diffraction determ. of lattice constants 2−80643
As_2S_3, n.q.r. obs., comparison with amorphous state 2−84605
AsSI and AsSeI, vitreous and molten, near-order structure during transitions 2−84393
$B_{48}B_2C_2$, tetragonal phase 2−74723
$B_{48}B_2N_2$, tetragonal phase 2−74723
BN, wurtzite-like, fine struct., X-ray determ. 2−75026
B_xN, tetragonal, derived from icosahedral frameworks 2−50572
B_xP, tetragonal, derived from icosahedral frameworks 2−50572
$Ba(Ce_{1-x}Ta_x)O_3$, ion pair valency at high and low temps., structure, mag. and electrical obs. 2−75203
BaFCl, grown by modified Kyropoulos method, lattice parameters detn. 2−43523
$BaFe_2S_3$, and cryst. chem. 2−60750
Ba_2FeS_3, and cryst. chem. 2−60750
$Ba_6Fe_8S_{15}$, and cryst. chem. 2−60750
$BaFe_2Se_3$, and cryst. chem. 2−60750
Ba_2FeSe_3, and cryst. chem. 2−60750
$Ba_3Fe_3Se_7$, and cryst. chem. 2−60750
$Ba_2KNb_5O_{15}$, Ta-substituted, quadratic tungsten oxygenated bronze struct. 2−47315
$Ba_\alpha(MO)_{0.133}MO_3(M=Nb,W)$, structural evolution as a function of α 2−83958
Ba_2MReO_6, (M=Mn,Re,Co,Ni), perovskites, characteriz. 2−50876
$Ba_2NaNb_5O_{15}$, characterization, vibr. props. 2−72364
$BaNaP_3O_9$, space group. cell constants 2−67987
Ba_2TaCoO_6, perovskite cpd. 2−47316
$Ba_2(UMg)O_6$-$Ba_2(U_{2/3}F_{4/3})O_6$ solid soln., and prep. 2−56648
$BiCl_3$, and mol. struct. 2−77553
$BiFeO_3$, lattice parameters, temp. depend. 2−47317
$Bi_2Sn_2O_7$, single cryst. X-ray diffr. 2−60717
$Bi_4Ti_3O_{12}$, X-ray photographs, X-ray diffractometer data and neutron powder diffraction exam. 2−71425
Bi_2WO_6, lattice parameters 2−47263
CO_2, lattice parameter of solid at −190°C 2−50619
C_3S_2 Raman spectra, assignment of bonds to components of first overtone, crystalline structure study 2−51354
$CaAl_{12-x}Fe_xO_{19}$ solid soln., $x \leqslant 4.8$, e.s.r. and Mossbauer obs., ferric ion positions 2−75268
$Ca_2B_5O_9Br(Cl)$ type halogenoborates 2−53657
$Ca_3(CrO_4)_2$, X-ray charact. parameters 2−53658
$CaGeO_3$-$Sr(Ba)GeO_3$ solid solutions, i.r. spectra study 2−65251
$Ca(H_2AsO_4)_2$, neutron diffr. obs. 2−67988
$Ca_{2-x}Ln_xMnO_4$ solid soln., Ln=Pr, Nd, Sm, Eu, Gd 2−60753
$2CaO.Mn_xFe_{2-x}O_3$ $(0 \leqslant x \leqslant 0.5)$, temp. depend. of lattice parameter 2−43644

Crystal structure, atomic continued
inorganic compounds continued
$Ca_5(PO_4)_3Cl$, chlorapatite, synthetic, monoclinic struct. 2−53656
$Ca_3Pd_2H_4$, X-ray diffr. obs. 2−47347
$CaSo_42H_2O$, symmetry of SO_4 ion 2−64635
Ca_3TeO_6, elementary cell data 2−43576
$CaTiO_3$, effect of La_2O_3 on lattice distortion 2−74724
$Ca_3WO_5Cl_2$, orthorhombic, crystallographic data 2−47318
$CaZrO_3$-$CaHfO_3$ system solid solns., lattice parameters 2−43575
$CdEr_2S_4(Se_4)$, X-ray obs. 2−72113
CdFOH, n.m.r. data 2−84591
Cd_2GeO_4, rhombic cell parameters and struct. detn. by oscillating crystal method 2−71426
$Cd_2(Ge_2O_6)$, from hydrothermal synthesis, X-ray obs. 2−74687
$CdGeP_2$, $CdGeAs_2$, sphalerite-chalcopyrite transition, struct. of phases, microhardness 2−57025
$CdGeP_{2x}As_{2-2x}$, lattice parameters, comp. depend. 2−47616
$CdGe_xSi_{1-x}P_2$, lattice parameters, comp. depend. 2−47616
$CdHo_2S_4(Se_4)$, X-ray obs. 2−72113
CdI_2 polytypes, occurrence of Zhdanov numbers 1,2, and 3 2−83945
CdI_2 polytypes, twelve-layered 2−43577
$CdK_2(SO_4)_22H_2O$ 2−77545
$CdLu_2S_4$, X-ray obs. 2−72113
Cd_2P_3Br, and synthesis 2−60754
Cd_2P_3Cl, and synthesis 2−60754
Cd_2P_3I, and synthesis 2−60754
CdS, electron irrad. induced defects, activation energy 2−71455
CdSe vacuum evaporated films structure on mica, NaCl, PbSe substrates, electron microscopy, electron diffraction techniques 2−71327
$CdSiP_2$, characterization 2−80599
$CdSnAs_2$, sphalerite-chalcopyrite transition, struct. of phases, microhardness 2−57025
$Ce_2(MoO_4)_3$, cell dimensions, space group 2−74736
$Ce_2Si_2O_7$, lattice parameters 2−48220
$Ce_xY_{1-x}Sb$, $Ce_xLa_{1-x}Sb$ solid solutions. antiferromagnetically ordered, lattice constant dependence of Neel temp. 2−72212
ClO_2, from i.r. and Raman spectra 2−77561
β-Co, electrolytically deposited films 2−53561
CoMnSb, cryst. struct., rel. to C1_b type 2−74726
$Co_2P_2O_7$ 2−77552
Cr complex, di-μ-hydroxotetraglycinatodichromium(III), structural characterization 2−80645
$CrFeTi_2O_7$, space group, lattice parameters 2−74727
CrH_x, electrodeposited from chromic acid soln., struct., lattice consts., deposition conditions 2−47320
Cr_3NiB_6 and $Cr_2Ni_3B_6$, X-ray obs. 2−61044
CrP_4, and synthesis and props. 2−53659
CrTe, lattice parameter anomalies near Curie temp. 2−72148
$CsBe_2(BO_3)F_2$, symmetry 2−47210
$CsBe_2F_5$, pentafluorodiberyllate, structure determination by X-ray and neutron diffraction 2−56653
$CsCrCl_3$, Jahn-Teller distortion 2−81363
Cs_xCrF_3, prep. and characts. 2−60760
$CsFeF_4$, planar antiferromagnet, X-ray diffr. obs. 2−65180
Cs^2GeF_6, high press. phase, lattice consts. 2−71677
$\gamma CsHCO_3$, x-ray diffr. obs. 2−43579
$CsICl_4$, lattice parameters 2−71427
$CsMnBr_3$ 2−43578
$CsNO_2$, space group, lattice consts., phase diagram, to 40 kbar 2−74951
$CsPr(MoO_4)_2$, X-ray diffraction and thermal stability obs. 2−74729
$Cs_2UO_2F_4.H_2O$, crystalline structure from X-ray studies 2−56652
Cs_2ZrCl_6, high press. phase, lattice consts. 2−71677
Cu-As system, phases, struct., homogeneity rangers 2−74731
Cu-Au alloys, side bands of fundamental reflections and diffuse superstructure lines, detection 2−64614
$CuH_2SO_4.5H_2O$ isotope effects in structure, fractionation of O 2−47324
$CuLi(PO_3)_3$, space group, lattice parameters 2−67989
$Cu_4Mn_2Te_4$, X-ray obs. 2−84442
$CuNa_2(PO_3)_4$ 2−77546
Cu_3PSe_4 2−77562
Cu_2Se, α- and β-phases, rel. to transforms. 2−64811
$DgVO_4$, refined 2−60756
ErC_2, 297-2K, neutron diffr. obs. 2−72217
Eu chelates, comparison of Mossbauer resonant intensities used to determine structure differences 2−48142
$EuLnAlO_4$, (Ln=La, Ce, Pr, Nd, Sm, Eu, Gd) 2−56664
Eu_3NbO_7 2−47346
Fe-Ni films, thermal evaporation prepn., detn. of lattice parameters and mag. props., 0-100% Ni 2−77496
55Fe-$45P_2O_5$ glass, a.c. and d.c. characteristics, correlation with structure 2−81142
Fe complexes, nitroprussides, Mossbauer spectra study of molecular structure 2−44352
Fe_2MoO_4, spinel, X-ray and neutron diffraction studies 2−84414
Fe_2O_3, produced from α-, β-, γ- and δ-FeOOH, X-ray obs. 2−81292
Fe_xO, wustite, lattice parameters, at high temps. 2−43580
FeOOH, α-, β-, γ-, and δ- modifications, X-ray obs. 2−81292
γ-FeOOH, lepidocrocite, at temp. of conversion to α-Fe_2O_3, hematite 2−57287
$Fe_{1.8}Sb$, antiferromagnetism, Mossbauer effect meas. 2−84440
FeV_2Te_4, and elec. and mag. props. 2−60757
Fe_2WO_6, lattice parameters, space group 2−83950
GaAs:Te, Se and S, effect of doping on struct. 2−71432
GaAs, amorphous, e. micro. exam of struct. and short-range order 2−71433
Gd_3NbO_7 2−47346
Ge-As-Se glass chalcogenide system, atomic distribution and coordination numbers 2−56559
Ge, Laue case of X-ray diffraction in nearly perfect crystals, 111 and 440 reflections 2−71403
HFC-Re system, meas. of lattice const. by X-ray, thermal and microhardness methods 2−84096
$H_2Te_2O_6$, single crysts. 2−74747
Hf, refinement from ^{19}F n.m.r. data 2−71434
HfB_2-ZrN system, cell dimensions 2−47638
$Hf_3Cu_4Si_2(Ge_2)$, c/a ratio 2−43597
HgFOH, n.m.r. data 2−84591

Crystal structure, atomic continued
inorganic compounds continued
$Hg(OH)NO_3$ 2−47331
$Hg(SCN)_2$, solution by Patterson method 2−50620
$Hg_3Tl_4As_8Sb_2S_{20}$, vrbaite 2−53664
$Ho_3Fe_5O_{12}$ garnet, cell parameters, X-ray powder data 2−74745
HoPtSn and related intermetallics 2−50621
$HoVO_4$, refined 2−60756
InBr(I) 2−64638
$In_{6.6}Ca_{3.1}S_{13}$, and cryst. chem. 2−60758
$IrCr_3N$, perovskite-type 2−60759
K complex, dipotassium cis-hexacyanobutenediide, packing features, anion electronic structure 2−53667
$KBe_2(BO_3)F_2$, symmetry 2−47210
KCl-KBr, mixed cryst., lattice distortion rel. to proton dechannelling 2−47785
$KClO_3$ II, lattice constants, meas. using powder diffraction 2−47332
K_xCrF_3, prep. and characts. 2−60760
K_2CrO_4 struct. redeterm., effect of electrostatic crystal forces on observed bond lengths 2−77550
KD_2PO_4, monoclinic, X-ray obs. 2−64640
KD_2PO_4, soln. grown, neutron diffr. obs. 2−60712
$KFe(CrO_4).2H_2O$, space group, lattice parameters 2−67991
K_xFeF_3, weak ferromagnet 2−48071
$K_{0.2}FeF_{2.8}O_{0.2}$, weak ferromagnet 2−48071
$K_2Ge(IO_3)_6$ 2−77549
$K_2H(IO_3)_2Cl$, X-ray obs. 2−53665
$K_3Hg(NO_2)_4$ NO_3, parameters determ. by neutron diffraction 2−64639
KIO_3, symmetry props. rel. to use as nonlinear optical material 2−74733
$KIO_3.HIO_3$, determination by three-dimensional X-ray diffraction and neutron powder diffraction 2−53666
$KMnF_3$, superstructure arising from phase transition 2−74933
$KMnLn_3F_{12}$ and $KMYb_3F_{12}$(M=Mg, Zn, Ni, Co) 2−50622
$K_3P_3O_9$, and prep. 2−53668
K_2PO_3F, space groups and lattice parameters 2−83951
$K_{1-x}Rb_xI$, lattice parameters, comp. depend. 2−54289
β-K_2SO_4 struct. redeterm., effect of electrostatic crystal forces on observed bond lengths 2−77550
$K_2SiF_6.Na_2SiF_6$, occurrence, prep., cryst. data 2−74734
$K_5(UO_2)F_9$, struct. of binucl. $(UO_2)_2F_9{}^{5-}$ ion 2−83953
$K_2Zn_2Mo_3O_{12}$, monoclinic 2−77555
$K_5[Au_5(CN)_{10}I_2].2H_2O$ 2−77544
$La_2(MoO_4)_3$, cell dimensions, space group 2−74736
$LaTaO_4$, space group, lattice parameters, X-ray obs. 2−53669
$La_2Ti_2O_7$, single cryst. X-ray diffr. 2−60717
$LiAlSiO_4$, beta eucryptite, high temp. form structural relation to high quartz 2−56659
$(LiAlSiO_4)$, β-eucryptite, structural relationship between low temp. form and low quartz 2−56658
β-$LiAlSiO_4$, eurocryptite, thermal expansion of lattice consts., 20-1100°C 2−54060
Li_2BeF_4, interpretation in terms of Born-Mayer-Huggins model 2−77564
LiF single crystal, X-ray diffr. during shock wave compression 2−56646
$Li_{0.5}Fe_{2.5-x}Al_xO_4$, lattice const., comp. depend. 2−47334
Li(H,D) system, lattice consts., isotopic comp. depend. 2−43582
$LiHC_2O_4.H_2O$, X-ray diffraction study of isotope effect and structure 2−56657
$LiMn(PO_3)_3$, crystallographic data 2−64641
$Li_2Mn(PO_3)_4$, crystallographic data 2−64641
$LiO_2(5-2t)Fe_2O_3tCr_2O_3$ ferrite, influence of heat treatment 2−57021
Li_2TiO_3, X-ray diffract. exam. 2−71425
$Li_6W_2O_9$, cubic 2−54007
$Li_2Zn_2Mo_3O_{12}$, orthorhombic 2−77555
Mg-Mn ferrites, electronic struct. of Mn and Fe ions 2−47182
MgB_4 2−60762
$Mg_{0.5}Fe_{0.5}Ti_2O_5$, armalcolite, X-ray study, comparison with lunar rock sample 2−44928
$6MgO.As_2O_5$, Mn activated phosphor, flux grown crystals 2−43525
$MgSiF_6.6H_2O$, phase transition at 25°C, of low temp. form 2−67996
Mg_2SiO_4 polymorphs, observed and hypothetical, computer-simulated 2−47335
$Mg_yU_{1-y}O_{2-x}$, structural analysis by X-ray and electron microscope meas. 2−47336
Mn-Fe-Ti-O system ferrites, lattice parameter 2−44254
Mn_2As, high press. form., Fe_2 P-type struct. 2−53670
$MnK_2(SO_4)_22H_2O$ 2−77545
$Mn_2(PO_4)Cl$, X-ray obs. 2−67997
$Mn_2(PO_4)F$, X-ray obs. 2−67998
Mo ternary sulphides, crystallographic instability 2−71691
$MoBr_3$, space group and lattice parameters 2−47337
$MoO_3.2H_2O$, crystal structure from X-ray diffractometer data 2−56660
$MoO_3.2H_2O$, X-ray diffraction study, localization and refinement of H atom positions 2−43583
MoP_4, and synthesis and props. 2−53659
MoS_2 intercalation compound, electron microscope and diffr. obs. 2−64643
$MoS_2(Se_2)(Te_2)$, grown by vapour transport 2−60707
NH_4BF_4, at 140K 2−60765
$(N_2H_5)_3CrF_6$, structure determination from X-ray 3-D film data 2−56661
β-$NH_4Fe(CrO_4)_2$, space group, lattice parameters 2−68000
$(NH_4)_2HPO_4$, crystal structure by X-ray examination 2−56662
NH_4HSO_4, room temp. non-ferroelec. phase, applic. of constrained refinement techniques 2−67999
$NH_4NH_2SO_3$, space group, unit cell dimens. 2−53671
NH_4NO_3, phase IV 2−43584
$(NH_4)_3P_3O_9$, and prep. 2−53668
$(NH_4)_2PO_3F.H_2O$, $(NH_4)_2PO_3F$ and $NH_4Li.PO_3F$, space groups and lattice parameters 2−83951
$(NH_4)_2PO_3F.H_2O$, crystal structure from X-ray studies 2−56663
N_2O, parameter detn. of nonvalence interaction curve at 0°K 2−71440
Na-Ta-O-F, pseudoquaternary, struct. of new phases 2−53674

Crystal structure, atomic continued
  inorganic compounds continued
    Na montmorillonite, isolation monocrystalline particles, selected area electron diffraction patterns 2−68001
    $NaBe_2(BO_3)F_2$, symmetry 2−47210
    γ-Na_2BeF_4, struct. refinements, thermal expansion of tetrahedral bonds 2−61109
    β-$Na_2Cr_2O_7$ 2−43585
    $Na_2Ga(NH_2)_5$, lattice parameters 2−47340
    $NaICl_4.2H_2O$, rel. to n.q.r. 2−84590
    $NaIn(WO_4)_2$, cell parameters, space group 2−43586
    $Na_2LiBe_2F_7$, X-ray obs. 2−71438
    $Na_2M(SeO_4)_2.2H_2O$, M=Mg, Mn, Fe, Co, Ni, Cu, Zn, Cd 2−53673
    $NaNO_3$, crystal struct., order-disorder transforms, neutron diffraction obs., 20-290°C 2−77758
    $NaNbO_3$-$BaTiO_3$-$BaNb_2O_6$ system, tungsten bronze field 2−72034
    $NaNbO_3$, 480-575°C, rel. to soft phonon modes 2−80649
    β-$Na_2O.3B_2O_3$ 2−47338
    $Na_4P_2O_7$, 22°C 2−77565
    $Na_3PO_3CO_2.6H_2O$, systematic error differences between two refined sets of position coordinates 2−77554
    $NaRbCr_2O_7$ crystal struct. determ. 2−77551
    $Na_2S_2O_4$, powder diffr. diagram 2−53672
    $Na_{2x}Sr_{1-x}Pb(OH)_6$, nonstoichiometric 2−71437
    $NaTh_2(PO_4)_3$, rel. to ferroelec. props. 2−54237
    $Na_2Zn[PO_4](OH)$, X-ray anal. 2−71439
    $Na_2ZrSiO_5{:}Eu^{3+}$, phosphor 2−72414
    Nb compounds, bond lengths, from X-ray K-absorpt. fine struct. 2−68674
    $Nb(O, F)_x$, cryst. shear struct. 2−47352
    $NbSe_2$, 2H polytype 2−47339
    $NbSe_2$, lattice parameters, rel. to supercond. transition temp., 1.5-6.5 kbar 2−68346
    $NbSe_2$ intercalation compound, electron microscope and diffr. obs. 2−64643
    $Nd(BO_2)_3$. unit cell dimensions, space group, X-ray analysis 2−74738
    $Nd_2Co_{1.7}$ intermetallic, lattice parameters 2−47341
    $Nd_2(MoO_4)_3$, cell dimensions, space group 2−74736
    Ni-Te-Fe-O system, spinel solid solution, effect of lattice parameter on solubility 2−83840
    $NiCl_2.2H_2O$, crystallographic phase transition at 230±20K 2−84143
    $NiCr_xMn_{2-x}O_4$, spinel, atomic and cation distrib., lattice distortion 2−74740
    $NpPd_3$, cubic and hexagonal phases, unit-cell and X-ray powder data 2−64644
    $POBr_3$, isolated in low-temperature matrix 2−44380
    $PbCrO_3$, perovskite, struct., elec. resist., mag. susceptibility 77-550K 2−61321
    PbI_2, lattice parameters meas. by X-ray method in temp. range 25-114°C, evaluation of coeffs. of thermal expansion 2−61110
    $Pb(Mg_{1/3}Nb_{2/3})O_3$ rel. to formation processes in the solid state reaction 2−77560
    $PbMnO_2OH$, quenselite 2−53677
    PbO-$P(As)(V)_2O_5$ systems, and synthesis of cpds. 2−74741
    $PbSnS_3$ phase in SnS_2-PbS system 2−77556
    $PbTiP_2O_6$, single cryst. X-ray diffr. 2−60717
    Pd complex, Pd(II)-bis-biguanide perchlorate, preliminary data 2−50625
    $PdCr_3N$, perovskite-type 2−60759
    Pr oxides, higher 2−47243
    $Pr_2Co_{1.7}$ intermetallic, lattice parameters 2−47341
    $Pr_2(MoO_4)_3$, cell dimensions, space group 2−74736
    Pt complex, bis(triphenylphosphine)(ethylene)platinum 2−43587
    $PtCr_3N$, perovskite-type 2−60759
    $RbBe_2(BO_3)F_2$, symmetry 2−47210
    Rb_2BeF_4-Na_2BeF_4, phase diagram, struct. of phases 2−74957
    $RbBiS_2$, X-ray obs. 2−47342
    $RbBiSe_2$, X-ray obs. 2−47342
    Rb_2CoCl_4 2−83957
    Rb_xCrF_3, prep. and characts. 2−60760
    $RbICl_2$, vibr. spectra, cryst. symmetry 2−75313
    α-$RbIO_3$ 2−77548
    $Rb_3Mn_2Cl_7$ 2−83957
    $RbNO_2$, space group, lattice consts., phase diagram, to 40 kbar 2−74951
    Rb_2PO_3F, space groups and lattice parameters 2−83951
    Rb_2SiF_6, high press. phase, lattice consts. 2−71677
    $Rb_3UO_2F_5$, X-ray examination of powder and twinned crystal crystal samples 2−47343
    $Rb_2UO_2F_4.H_2O$, space group, lattice parameters 2−68004
    $RhCr_3N$, perovskite-type 2−60759
    SCl_2, vibrational spectra, determination of crystal system 2−77059
    SF_4, low temperature 2−44381
    Sb complex, methyltrichloro(acetylacetonato)antimony(V) 2−42935
    Sc ferrite, rel. to spectral props. 2−54440
    Se complex, Se(II) diethyl dithiocarbamate, three-dimensional X-ray investigation 2−56666
    Si, epitaxial film, lattice resolution e. microscopy obs. of struct. of twin boundaries, faults and dislocats. 2−74779
    SiO_2 thin films 2−74623
    SmC_x, X-ray characterization 2−71653
    $Sm_3Fe_5O_{12}$, garnet, cell parameters, X-ray powder data 2−74745
    Sm_3NbO_7 2−47346
    $SnBs_3$, supercond. 2−68371
    $SnCl_2.2H_2O$ and $2D_2O$, anomalous sp ht at phase transition due to glassy cryst. state 2−84212
    $SnCr_3N$, perovskite-type 2−60759
    SnF_2, monoclinic, space group 2−47245
    $SnNbSe_3$, supercond. 2−68371
    SnO_2-TiO_2 mixed crystals, exsolution obs. 2−74746
    Sn_2PO_4Cl, lattice parameters, space group, powder data 2−43588
    SnS_2-Na_2S system phases 2−83952
    $SnTaS_3$, supercond. 2−68371
    Sr vanadates, bonding 2−43589
    $SrF_2{:}Ge^{3+}$, Gd^{3+} or Ce^{3+}, existence of separate cubic phase 2−80705
    $SrGeO_3$-$BaGeO_3$ solid solution, i.r. spectra study 2−65251
    $Sr_2KNb_5O_{15}$, Ta-substituted, quadratic tungsten oxygenated bronze struct. 2−47315

Crystal structure, atomic continued
  inorganic compounds continued
    $Sr_{2-x}K_{1\|x}Nb_5O_{15-x}F_x$, ferroelec. tungsten bronze struct. 2−51198
    $SrLiTa_2O_6F$, pyrochlore struct., X-ray obs. 2−74689
    $SrLnAlO_4$, (Ln=La, Ce, Pr, Nd, Sm, Eu, Gd) 2−56664
    $Sr_\alpha(MO)_\beta MO_3$(M=Ta,W and Nb,W), structural evolution as a function of α 2−83958
    $SrO.2Al_2O_3$, refined struct. 2−68007
    $SrO.xB_2O_3$, n.m.r. of ^{11}B, struct. 2−54504
    $SrPd_2H$, X-ray diffr. obs. 2−47347
    Sr_2PdH_4, X-ray diffr. obs. 2−47347
    $SrSi_2$, space group, cryst. class O(432) 2−68006
    $SrUO_4$, X-ray examination using Hagg-Guinier camera, analogy with $BaUO_4$, calc. of interatomic distances 2−77558
    β-Ta_2H, ordering 2−54003
    TaS_2, 1S and 2S polymorphs 2−47226
    TaS_2 organo intercalation compounds, electron microscope examination of lattice and superconductivity 2−53676
    $TaSe_2$, grown by vapour transport 2−60707
    Tb oxides, higher 2−47243
    $TbAsO_4$, crystallographic distortion at $T<26K$, transition, X-ray diffr. obs. 2−84142
    $Tb_{0.167}Fe_{0.633}Al_{0.20}$, Th_6Mn_{23} struct. type, X-ray powder diffr. obs. 2−64645
    $TbVO_4$, refined 2−60756
    Te_4O_9 single crysts. 2−74747
    α-$TeVO_4$, and synthesis and polymorphism 2−74748
    ThCN, by X-ray and neutron powder diffr. 2−53681
    $ThSiO_4$, atomic positions 2−68008
    $ThSiO_4$, lattice constants 2−43590
    Ti-Ni-H, intermetallic phase and absorption of hydrogen 2−71354
    $TlBiTe_2$ and TlTe 2−51144
    Tl_2CrO_4, X-ray obs. 2−60766
    TlH_2PO_4, lattice parameters 2−53682
    Tl_2XO_4, X=Se, Cr, Mo, and thermal props. 2−53680
    $Tn_xMn_{1-x}O$, $0.07\leqslant x\leqslant 0.9$, mag. props., mag. susceptibility, struct., 100-1000 K 2−54364
    $TvbSe_2$, organo intercalation compounds, electron microscope examination of lattice and superconductivity 2−53676
    UNCl, Patterson function calc. 2−74749
    U_3Se_5, unit cell, space group, interatomic distances 2−53683
    V_6C_5, superlattice, C vacancy ordered distrib. 2−43621
    $V_{0.95}Cr_{0.05}O_2$, orthorhombic phase 2−43592
    V_2MoO_8, cryst. shear struct. 2−47352
    V_4O_7 2−47350
    VO_2, twinned crystal transformation to tetragonal phase, X-ray obs. 2−47698
    $VOPO_4$, β allotropic form obs. 2−50627
    V_7S_8, monoclinic 2−43591
    $VSO_4.xH_2O$, lattice parameters 2−50628
    V_7Se_8, monoclinic 2−43591
    W, contrast patterns produced by self-interstitial ions in field ion microscope images 2−64625
    $W_xNb_{1-x}Se$, lattice parameters, comp. depend. 2−60767
    WO_x and $(W, M)O_x$, (M=V, Nb, Ta, Mo), cryst. shear struct. 2−47352
    $WSe_2(Te_2)$, grown by vapour transport 2−60707
    $W_{1-x}Ta_xSe_2$, cell dimens. 2−43593
    $(W_{0.2}V_{0.8})_3O_7$, space group and lattice parameters 2−47351
    YD_3, neutron and X-ray diffr. obs. 2−74752
    YIG, Ca-Si substituted, flux grown crystals, unit cell dimensions 2−47278
    YIG, nonmag. ion substituted, polycryst., lattice consts. 2−61547
    $Y_3[Si_3O_{10}](OH)$, talenite, X-ray obs. 2−71442
    YbFe garnet, Ca-Si substituted, flux grown crystals, unit cell dimensions 2−47278
    $YbVO_4$, refined 2−60756
    zeophyllite 2−77547
    $Zn_{1-x}Cd_xS$, melt-grown single crysts. 2−64646
    $Zn_xCd_{1-x}Se$ solid solution, rel. to phonons, Raman scatt. obs. 2−64837
    $Zn_xCu_{(1-x)}Fe_x Mn_{(2-x)}O_4$, X-ray determ. of lattice parameters, assignment of crednerite and gahnite symmetries 2−60768
    ZnFOH, n.m.r. data 2−84591
    $ZnGa_2O_4$, spinel, oxygen parameter determ. 2−47353
    $ZnGeAs_2$, $ZnGeP_2$, sphalerite-chalcopyrite transition, struct. of phases, microhardness 2−57025
    $ZnGeP_2$, characterization 2−80599
    $Zn_{1.685}In_{2.21}S_5$, $Zn_{4.37}In_{2.42}S_8$, $Zn_{6.18}In_{2.58}S_{10}$, space group, cell dimens. 2−60771
    $ZnS{:}Al,Co^{2+}$, grown from melt, struct. rel. to Al additions, Co^{2+} spectra obs. 2−77559
    $ZnSO_3.2H_2O$, X-ray single crystal analysis solution from Patterson and Fourier synthesis 2−60770
    ZnSe, grown from vapour phase under controlled partial press. 2−64594
    $ZnSiAs_2$, sphalerite-chalcopyrite transition, struct. of phases, microhardness 2−57025
    $ZnSnAs_2$, $ZnSnP_2$, sphalerite-chalcopyrite transition, struct. of phases, microhardness 2−57025
    Zr containing refractories, influence of Cr_2O_3 content on lattice parameter 2−84095
    $ZrCr_xO_y$, lattice spacing rel. to O content 2−56671
    $Zr_3Cu_4Si_2(Ge_2)$, c/a ratio 2−43597
    Zr_2Ni_7 2−43596
    ZrO_2-Y_2O_3 system, tetragonal-cubic transform., lattice parameters of two phases by X-ray examination 2−84098
    ZrO_2-Yb_2P_3 and ZrO_2-Yb_2O_3-Y_2O_3 solid solutions 2−47721
    Zr_9S_2 2−43595
    $Zr_2Si_2Se_2$, rel. to nonstoichiometry 2−43505
    $ZrTe_2$, nonstoichiometric phase, struct., homogeneous phase limit 2−60772

  organic compounds
    β-(pyrazolyl-3)-L-alanine 2−47358
    α-amino acids, sites of VO^{2+} ion impurities 2−84566
    ammonium oxalate hydrate, rel. to elastic consts. 2−84005
    amylose triacetate 2−83346
    [14]annulene, three-dimensional X-ray study 2−64647
    anthrone, refinement of crystal structure 2−77566
    bis(2-imino-4-amino-4-methyl-pentane)nickel II bromide 2−71445

Crystal structure, atomic continued
organic compounds continued
bis(picolinato)bis(allylthiourea)Cu(II), X-ray analysis and Patterson-Fourier and least-squares methods 2−71446
bis(picolinato)bis(thiourea)Cu(II), X-ray analysis and Patterson-Fourier and least-squares methods 2−71446
caesium methanesulphonate, meas. of Raman and i.r. spectra, correlation with structure 2−72375
cantharidine, X-ray diffraction study, molecular bond lengths and conformation 2−68010
cellulose, crystalline models, conformational terminology 2−43022
cellulose, precipitated, crystal morphology 2−83349
cyclobutane, solid II, mol. packing from spectra and pot. energy calcs. 2−71447
diazoaminobenzene(β modification) 2−71444
4,4′-dibromo- diphenyl ether, n.q.r. study and temp. variation of the frequencies 2−64650
2-dichloromethyl-4-(4-bromobenzyl)-5-(4-bromophenyl)-6-hydroxypyrimidine, X-ray obs. 2−64649
2-dichloromethyl-4- (4-chlorobenzyl)-5-(4-chlorophenyl)-6-hydroxypyrimidine, X-ray obs. 2−64648
diepoxy-cyclohexane 2−43598
diethyl ether, and mol. struct. at 128K 2−68011
2,4-diisopropyl-3-methylthiazolium bromide, structure determinations for the geometry of the thiazolium ring 2−56668
2.5- dimethyl-2, 5-hexamediol tetrahydrate, water-hydrocarbon layer structure 2−50629
estradiol-urea complex., struct. determ. by two-dimens. struct. invariants 2−53686
ethylenediamine, trans conformation obs. 2−43599
glycine silver(I) nitrate, ferroelec. 2−47356
hypotaurocyamine 2−43600
ionic compound, $A^{3+}C^{1+}X_2^{2-}$, theoretical determ. 2−74718
iron(II)formate-magnesium formate system, mixed crystn., Mossbauer obs. 2−56673
light-atom struct., absolute configs. and $\Delta f''$ values determ. 2−47355
mercury picramate, cryst. data, orthorhombic cell dimens. 2−74754
methyl chloroform, crystal and mol. structure at −60° and −145°C 2−53685
N-methyl-4-brom-benzamide, X-ray obs. 2−64651
molecular crysts. 2−48159
m-nitroaniline, rel. to linear electro-optic props. 2−72271
norbornadiene, norbornylene and norbornane, plastic crysts. 2−43601
nylon, solution- grown crystals, combined wide-angle and low-angle X-ray diffraction patterns 2−50630
orthophenylene diamine dihydrochloride, X-ray investigation 2−71449
pentachloronitrobenzene, molecular packing, partial structure determination 2−53684
poly(4-methylpentene-1), formation of curved crystals 2−80529
poly 2,6- dimethylphenylene oxide, unit cell dimensions of single crystals 2−60774
polyethylene, interatomic distances determination from radial distribution function 2−64605
polyethylene, oriented, struct. effect of annealing under high press. 2−83395
polyglycine I, model 2−53687
polypropylene, crystn. on solid surfaces, electron-microscopic study 2−83392
polystyrene structure changes by u.v. rad., reln. to polydispersity of polymer 2−64652
potassium biphthalate, lattice consts. and space group 2−47357
reference list, materials studied by anomalous X-ray scatt. 2−60749
rubidium trihydroselenite, struct. detn. using diffraction data 2−71450
silicate with complex cation, $4[Cu(NH_2CH_2CH_2NH_2)_2]. Si_8O_{20}. 38H_2O$ 2−74753
sodium methanesulphonate, meas. of Raman and i.r. spectra, correlation with structure 2−72375
sodium oxalate, monohydrate, by method of rhombs 2−74755
tetra-acetylethane, neutron diffraction determ. 2−43602
tetramethylammonium cadmium chloride crystal structure using X-ray analysis 2−56651
1,2,3-trichloro-4,5,6-trimethylbenzene, order-disorder orientation change structure determination at 298K from X-ray data 2−56674
1,2,3-trichloro- 4,5,6-trimethylbenzene, order-disorder orientation change, structure determination at 173K from X-ray data 2−56675
2,3,4-trimethylthiazolium bromide, structure determinations for the geometry of the thiazolium ring 2−56668
6α-fluorocortisol, struct. determ. by two- dimens. struct. invariants 2−53686
Ni hexamethylenedithiocarbamate with M-S bonds, X-ray struct. study 2−71448
Crystal symmetry *see Crystallography; Crystal structure, atomic*
Crystallites *see Crystal structure/microstructure*
Crystallization
see also Crystals/growth; Dendrites; Nucleation
agitated vessel crystallizers, slip velocities 2−47202
chalcogenide glass, threshold and memory types, cond., DTA, and X-ray studies 2−71917
chloroprene rubber, study by dielectric method 2−53544
cholesteryl derivatives, crystal nucleation in supercooled mesomorphic phases 2−77414
crystallisers, dynamic and steady-state computer simulation 2−64596
elastomers, effect on strength and toughness at low temperatures 2−60886
epitaxial electrodeposition, two dimensional nucleation effect on electrocrystalliz. rate 2−71320
ferrite, hexagonal, flux-pulling crystalliz. with heterogeneous seeds 2−71379
fractional, in ternary systems, distribution of isomorphous salts between aqueous, solid phases 2−50582
glass, fluor-richterite comp., treatment for obtaining high strength polycryst. material 2−47651
glass, heat treated, frozen elastic stresses 2−56784
glass, oxide systems, crystn. kinetics rel. to fibre prep. 2−43902
glass, pyroxene type, effect of Cr_2O_3 content 2−53533
Crystallization continued
glass-ceramic, fine grain struct. rel. to mixed oxide nucleating agents 2−50411
glass-ceramic, viscosity changes 2−53923
ice, hoar crystals forming on cooling pipes, X-ray Laue examination 2−74732
ice, recrystallization under mechanical strain 2−74691
isotactic polystyrene from isotactic-atactic blends, effect of noncrystallizable components on crystallization kinetics 2−71294
isotactic polystyrene from isotactic-atactic blends, spherulitic growth rate 2−71294
large cryst. prod. by continuous ripening in stirrer tank 2−47201
magnesium highpolyphosphate glass, and thermal props. 2−83851
magnetite, from high Fe glasses 2−54329
neutron matter 2−55049
nucleation, mol. phenomena study by computer simulation 2−47192
nucleation and growth for crystallization operation, method of complete segregation 2−74690
nylon 6, 6-6, 12 rate by depolarized light intensity method 2−56566
nylon 6, crystallization from melt, X-ray diffraction study of α and γ forms 2−74605
α- phenyl o- cresol, growth rate vs. temp. 2−50606
poly(ethylene oxide) of high mol. wt. fractions from dil. soln. in ethanol 2−64538
poly(ethylene terephthalate), growth rate of spherulites 2−64595
poly(ethylene terephthalate), light scattering study of spherulite evolution from rodlike nuclei 2−64535
poly(ethyleneterephthalate) multiple endotherm melting behaviour due to recrystallization, relation to morphology 2−71291
polychloroprene, gel fracture rate, crystallinity effects 2−47483
polychloroprene-rubber, recrystalliz. and reorganization processes, calorimetric obs. 2−71289
polyethylene, at high press., kinetic model 2−83358
polyethylene, elec. cond. study 2−71290
polyethylene, high pressure 2−50414
polyethylene crystallization at high temp. and pressure, birefringence obs. 2−47064
polyethylene oxide fractions, crystallization isotherms 2−74601
polyethylene terephthalate, rate by depolarized light intensity method 2−56566
polyethylene terephthalate, study of spherulite growth 2−43455
polymer, mol. phenomena study by computer simulation 2−47192
polymer, single cryst. form. from soln. 2−60710
polymer crystallization in temperature gradient field with controlled crystal growth, method of study 2−74603
polymer crystals, a non-equilibrium theory of molecular wt. fractionation 2−81501
polymers, method for studying influence of temperature-gradient field, controlled crystal growth 2−74603
polymers, quartz dilatometer applic. to obs. of Avrami parameters 2−56565
polypropylene, effects of pre-melting conditions 2−47066
polypropylene on solid surfaces, electron-microscopic study 2−83392
polystyrene, isotactic, i.r. spectra 2−43456
quartz glass, tubular and bulk specimens, 1350-1550°C 2−64529
recrystallization apparatus, small-scale 2−43526
rubber, natural, at high pressures 2−60603
Seoni meteorite, chondrite composition and evidence of recrystallization 2−75927
silicate glass, effect of synthesis conditions 2−64530
sodium phosphate melt, condensed, vitrifaction, effect of cooling rates 2−77479
steel, low alloy, recrystallization during repeated deformation cycle 2−64778
stirred vessel cooling crystallizer, secondary nucleation 2−47281
supercooled water, nucleus formation 2−74588
tetraborate, binary, from binary borate glass melt 2−53612
two dimensional, by field emission microscopy 2−53622
vtrifaction of condensed sodium phosphate melts, effect of cooling rates 2−77479
Al-Si-O glass, prep. and processing, i.r. spectra, crystn. products, mineral species form. 2−56557
Al, convective cooling of articles obtained by Stepanov method 2−47574
Al_2O_3, crystn. of amorphous anodic film by heating in vac. 2−83861
Au film, on amorphous C, oriented crystn. mechanism, rel. to interaction forces at interface 2−77502
$Ba(NO_3)_2$, rates of growth in aqueous solutions and kinetics of crystallization 2−71376
$3BaO$-$5SiO_2$ glass, controlled spherulitic crystallization, 800-950°C 2−80530
Bi droplets, crystallization and nucleation 2−71382
$Bi_xTi_yO_z$, hydrothermal crystn. 2−47231
CaO-CaF_2 system liquidus line determ. by the capillary method 2−84683
CaO-FeO-Fe_2O_3, synthesis and physico-chem. props. 2−43871
$Cd_2(Ge_2O_6)$, hydrothermal synthesis and cryst. struct. 2−74687
$CdGeP_2$ zone recrystallised, optical props. and energy zone calc. 2−80595
Co, Cr-$Cr_{7-x}Co_xC_3$, monovariant eutectic, faceted-nonfaceted, strongly coupled growth 2−57010
$CsLn(MoO_4)_2$, synthesis, crystalliz. and polymorph. transformation 2−71392
Cu, tough-pitch, kinetics of recrystallization 2−71623
CuI, crystalliz. under hydrothermal condits. 2−71420
Fe alloys, grain growth, second max. and nonuniformity after deform. 2−83961
Fe foils, electrocrystn. structures 2−83862
Fe(II) salt solutions, frozen at normal pressure 2−78178
Ge-Se-Te-As system, amorphous bulk and thin film 2−60573
Ge-Te non-crystalline phases, as structure probe 2−60577
Ge film, amorphous, crystalline transform. rel. to thickness and environment 2−67882
Ge film, amorphous, metal contact induced 2−56590
a-Ge film, elec. microscope obs. 2−60658
GeO_2 and $Si_{1-x}Ge_xO_2$, recrystn. in hydrothermal fluoride solns. 2−47285

Crystallization continued
$Ge_{15}Te_{80}As_5$ semiconducting glasses, rel. to thermally induced surface and bulk electrical effects 2–68401
Hg droplets, crystallization and nucleation 2–71382
InSe film, under elec. bombardment, elec. microscope obs. 2–56594
KBr solution, containing Pb^{2+}, internal evolution of heat 2–47236
$Li_2B_4O_7$, temp. depend. of growth rate from melt 2–53617
Li_2O-MgO-Al_2O_3-SiO_2 glass F addition effects 2–47058
LiO_2-Sc_2O_3-SiO_2-H_2O, hydrothermal crystallization 2–71383
Li_2O-SiO_2 glass, phase separation and crystn., X-ray obs. 2–56560
Li_4SiO_4-Zn_2SiO_4-Mg_2SiO_4-SiO_2 glass, phase equilibria and crystallization 2–64520
$Mg_{0.5}Fe_{0.5}Ti_2O_5$, armalcolite, growth from glass initially having composition of lunar rock sample 2–44928
2 MgO.5SiO_2.2Al_2O_3.nCr_2O_3 glass due to Cr_2O_3 additions, e.s.r. obs. 2–83850
$NaClO_3$, collision breeding of cryst. nuclei 2–50608
$NaClO_3$ seeded solns., secondary nucleation 2–47283
$Na_2Ga(NH_2)_5$, prep. and characteriz. 2–47340
$Na_2HPO_4.12H_2O$, rates of growth in aqueous solutions and kinetics of crystallization 2–71376
Na_2ZnGeO_4, solubility and crystn. kinetics under hydrothermal conditions 2–47242
Ni alloys, grain growth, second max. and nonuniformity after deform. 2–83961
P_2O_5-LaF_3-RF_2, R=Ba, Mg, triangular diagrams, crystn. and vitrification regions 2–57035
PbS film on semiconductor substrate, crystallization from aqueous solution 2–80562
PbSe film on semiconductor substrate, crystallization from aqueous solution 2–80562
Sb-Se-I-R-H_2O system, R=solvent=HI, HCl, Na_2Se, hydrothermal crystn. process, 300-450°C 2–74682
Sb-Sn alloy, peritectic, pore form. 2–53906
Sb_2O_3, valentinite and senarmontite polymorphs, crystalliz. under hydrothermal cond. 2–74683
Se, amorphous, effect of alternating electric field 2–60565
Se, compressed, photocurrent and thermally stimulated current obs. 2–64533
Se, in quinoline, pyridine, diethyl amine, thermal effects 2–53619
Si film, amorphous, metal contact induced 2–56590
SiO_2-Al_2O_3 glass, DTA, elec. microscope and X-diffr. obs. 2–53542
SiO_2-CaO-MgO-Na_2O-AlF_3:Dy^{3+} glass syst., mode of crystall., from luminescence study 2–48228
SiO_2 and $Si_{1-x}Ge_xO_2$, recrystn. in hydrothermal fluoride solns. 2–47285
$SrLiTa_2O_6F$, single cryst. synthesis and crystal struct. 2–74689
Te-Ge based memory glass film, thermal crystn. 2–47128
Te based glass film, sputtered, thermal crystalliz. 2–60668
$Te_{85}Ge_{15}$, $Te_{81}Ge_{15}Sb_4$, $Te_{81}Ge_{15}As_4$ glasses, electron microscope obs. 2–60598
TeO_2, by $3Te + 4HNO_3 \rightarrow 4NO + 3TeO_2 + 2H_2O$ reaction 2–56612
TiO_2, recrystn. in hydrothermal fluoride solns. 2–47285
TiO_2 film, by electron beam irradiation 2–47129
U, recrystallization after annealing and cold rolling at room temp. 2–68141
$VSO_4.xH_2O$, prep. and struct. 2–50628
W, stress induced growth irradiated at low temp. 2–60781
YAG from PbO-YF_3-Al_2O_3 melts, det. of stability range for YAG 2–74692
Zn-Ti alloys, effect of cooling rate on $TiZn_{15}$ crystn. 2–80818
ZnO, from vapour phase, influence of multicomponent conc. 2–43515
ZnO, morphology, physico-chem. conditions influence 2–43514
ZrO_2, amorphous, radiation induced 2–64522

Crystallography
see also Electron diffraction crystallography; Isomorphism; Metallography; Neutron diffraction crystallography; X-ray crystallography
absorption correction algorithm, improvement by analytical method 2–67972
alkali metals, quantum mechanical study 2–64585
compound with unknown chemical formula, crystal struct. detn. 2–60731
computer applications 2–60748
computer program checking, I.U.C. commission tests 2–67965
crystal struct. analysis, mean squared atomic scatt. factors for all atoms, tables 2–53624
crystal surface orientation meas. by u.s. beam displacement 2–56604
crystals, shape, orientation and computer absorption programs, checking method 2–64628
discrepancy factors in struct. analysis 2–67971
dynamical theory of diffraction, equivalence of Darwin and Ewald-Laue methods 2–47294
elastic coefficients, higher order, calcs. for 32 crystal classes, group theoret. method 2–68058
enantiomorph discrimination via calculated cosine invariances 2–67966
f.c.c. microcrystallites, spherical, geometry and stability 2–53598
group concepts applied to simple organic structures 2–67974
lattice complexes, invariant and quasi-invariant, data presentation 2–47291
magnetic crystals, optical gyrotropy or symmetry property 2–60729
metals, hexagonal struct. orientation determ. by etch pit method 2–83923
method of ascent in symmetry, applic. to lattice vibrs. 2–57038
method of ascent in symmetry, applic. to mol. vibrs. 2–56145
molecular arrangement classification using theory of space groups 2–67952
phase determination, applic. of weighted phase sum formulas 2–53646
phase-determ. from resonant X-quantum diffr. 2–67976
polymorphic transitions of the elements and system of structural types 2–71397
radial distrib. function, resolution improvement of interatomic distances in poorly crystallised cpds. 2–64605
retigraph, with pure precession motion 2–53631
rhombohedral crystals, A7 struct. type, assignment of axes 2–47186
semimetal, A7 struct. type, etch pit orientation study 2–47187

Crystallography continued
shadow effect in 3-dimens. crystal model rel. to channelling 2–71768
single-crystal diffractometry, counting time optimization, background counting and slewing times 2–67968
stereographic projection, closed circuit TV teaching aid 2–66397
structural relations and possible transformation mechanisms rel. to topological variation of crystal coordination 2–53599
van der Waals radii, derivation from known cryst. struct. 2–67970
variances and covariances of the anisotropic temperature parameters, derivation 2–56644

Crystals
see also Lattice energy; Liquid crystals
cavity formation and damage during breakdown of ionic crystals 2–72022
clathrate, mol. rot. transitions, damping and laser action 2–54446
dissolution velocity in water 2–74650
electro-optic coeffs. meas. by interferometric method 2–63397
hindered rotation, in various fields of cubic symmetry, Devonshire model 2–60564
hollow, needle like, Me_2X_3 type, growth from vapour 2–74668
light absorption by two-zone molecular crystal and absorption band spectra 2–72315
molecular, elastic props. calc. by method of atom-atom potentials 2–71548
molecular, irradiated, study of diffusion processes using recombination of free radicals 2–80722
molecular, reorientation and correlation functions 2–48302
neopentane, plastic crysts., mol. rot. motion 2–53513
plastic, cyclopentol, solid, unusual dielectric behaviour and molecular motion, dielectric and visual studies 2–57224
weighting coeffs. in approx. of Debye temp. in cubic crystals 2–74991

electron states *see Crystal electron states*

etching
β Ti-V alloys, thermal-etch pits and connection with dislocations 2–80546
alkali halide crystals, nonactivated, luminescence centres formation in very strong electric fields 2–84542
alums, with ethanolic tartaric acid solns. 2–74662
anodic oxidation etching technique, for Al and Al-Cu alloy cast morphology determ. 2–47602
graphite, highly oriented pyrolytic, effects of oxidation on basal and edge surfaces 2–56572
graphite, pitting by atomic and mol. H_2, O_2 and N_2 2–53553
ion impact sputtering, solid state device manuf. 2–43458
metal fibre/refractory oxide matrix, composites, growth and characterization 2–56990
metals, hexagonal struct., orientation determ. by etch pit methpd 2–83923
particle detector, solid states, prolonged etching factor rel. to track detection 2–46031
phlogopite, annealing effect on etching figures of tracks produced by ^{252}Cf disintegration 2–71362
photo-etching techniques for semiconductor devices 2–71301
porosity networks, determ. of infiltration of epoxy mixture 2–80819
rhombohedral crystals, A7 struct. type, rel. to assignment of axes 2–47186
semiconductor amorphous film rel. to morphology obs. by scanning electron microscopy 2–44129
semimetal, A7 struct. type, etch pit orientation 2–47187
structure, of $A^{II}B^{VI}$ compounds, scanning electron microscope examination 2–64540
tetraphenyl tin and isomorphs, defect struct. determ. 2–53731
Ag, dislocation etchants, use of H_2CrO_4 2–71363
Ag on NaCl surface, decoration with anthraquinone, information microstructure 2–71305
Al, modified etchant comp. 2–47185
Al, surface prep. by electrolytic etching and polishing, apparatus 2–50431
Al_2O_3 film, plasma and gas plasma deposited, struct. determ. 2–64563
BeO, dislocation etchant consisting of HCl 2–53600
Bi, dislocation delineation, temp. effect 2–56707
BiTe, single crystal plate, method for revealing dislocations 2–84322
Cu-7.5 at.%Al alloy, deformed in tension, dislocations, etch pit obs.64664 2–64664
GaAs-Cu, supersaturated solid solution, behaviour in decomposition 2–83836
GaAs, anisotropic behaviour of etchants 2–74660
GaAs, etched surface morphology, elec. microscope obs. 2–56575
GaAs, polishing by gaseous etching 2–83853
GaAs, selective photoetching, surface photovoltaic effect 2–71364
GaAs, strain induced phonon line broadening observed by surface reflection Raman scattering 2–83858
GaAs using Br_2-CH_3OH system 2–71311
GaN, electrolytic etching, device fabrication 2–71365
GaP, melt-grown, dislocation and saucer etch pits 2–50595
GaP electrodes, selective etching and anodic dissolution 2–75386
GaP electroluminescent diode, preferential etching, scanning elec. microscope obs. 2–71972
Ge/H_2O/H_2 system, thermodynamics, average reaction enthalpy, transport rate, 950-1200K 2–74661
Ge, etched surface, kinetics of development of first-order network 2–50447
Ge, gas phase etching with water vapour 2–67933
Ge, symmetry and form of etched pits on (111), (110) and (001) surfaces 2–50446
guanidinium aluminium sulphate hexahydrate, optical and interferom. studies of cleavages and etch patterns 2–64670
HI-H_2 vapour etch for low temp. Si epitaxial manufacturing 2–83852
InSb, anodic dissolution potentials and activation energies in HCl 2–71366
InSb, thermal etch pattern form. during diffusion 2–47440
KCl whiskers, slightly deformed, etch pit distrib. 2–71490
KD_2PO_4, in solns. containing acetate ions 2–60712
$KMnF_3$, dislocation density determ. 2–53605

- **Crystals** continued
  - **etching** continued
    - $KNbO_3$, ferroelectric domain investigations using pseudocubic {001} cleavage planes 2−61429
    - LiF, (100) surface, disloc. etch pit morphology, effect of anions in etchant 2−56609
    - LiF, (100) surface, disloc. etch pit morphology rel. to Cu(II) complex in etchant 2−56608
    - LiF single crystals containing cavities hydrostatic pressure influence on microstructure 2−83973
    - NaCl, cleavage, selective dissolution, complexes responsible for etching 2−74658
    - NaF, by acetic acid, impurity sensitive, neg. etching action cause 2−67934
    - $NiFe_2O_4$ films, effect on ferromag. reson. modes 2−44431
    - Pb-Bi solid solutions 2−56607
    - $PbMoO_4$, sign of Z-axis detn., etch config. obs. 2−43568
    - $RbMnF_3$, dislocation density determ. 2−53605
    - Si-Ge alloy oxide layer etched away, reoxidation, production of MOS transistors 2−75132
    - Si, dislocation etch for (100) planes 2−71495
    - Si, dislocation etch pits shapes rel. to mech. stress 2−80553
    - Si, with water-amine solution 2−71316
    - Ti alloy, etching behaviour 2−50687
    - Ti alloy, grain boundary etching, grain surface etching 2−50686
    - U alloy, ion sputtering and scanning electron microscopy 2−56578
    - W, polycrystalline, crystal orientation distribution determination, colour etching process 2−64545
    - ZnSe, dislocation etch bits 2−50677
    - ZrO_2, hydrothermal growth and etching in HF 2−50588
  - **excitons** *see Crystal electron states/excitons*
  - **faces**
    - *see also Cleavage*
    - liquid crystals, restricted-orientation model 2−83772
    - naphthalene equilibrium form facts, appearance of nonsingular surfaces 2−50561
    - surface faceting, size determ. by rel. between surface tension and curvature 2−80550
    - topaz, surface structures of prism faces, development and growth mechanism 2−60702
    - β-AgI crystal shapes rel. to ice nucleation properties 2−64589
    - CaF_2, proton irrad., density change and absorption band growth 2−71454
    - KH_2PO_4-type crystal, optimum cut for transversal modulation 2−61592
    - TiO_2, rutile, dissolution forms of single crystal spheres 2−47197
  - **growth**
    - *see also Crystal morphology; Crystallization; Epitaxy; Zone melting and refining*
    - accelerated crucible rot., stirring technique in high temp. soln. growth 2−47228
    - admixtures, distribution in crystals during dislocation growth 2−50663
    - agitated vessel crystallizers, slip velocities 2−47202
    - alkali halides, from solution, nucleation, dissolved O_2 and H ion conc. effect 2−74674
    - alkali halides, large single crysts., using interconvertible unit 2−56610
    - alkali metal metavanadates, melt growth and characteriz. 2−47261
    - alloy, dil. binary, solute redistrib. in melt, conc. and temp. gradient effects 2−47260
    - ammonium oxalates, from aq. soln. oxalates, cryst. growth from aq. soln. 2−60714
    - amylose triacetate, single crystal growth, morphological features 2−83346
    - anthracene crystals, effect of environment on defect concs. 2−83904
    - apatites, for use as laser hosts 2−42063
    - apparatus for growth from small volumes of soln. 2−43518
    - from aqueous solution of high thermal stability, expts. 2−60709
    - birefringent polymer films on substrates for integrated optics 2−80592
    - from boiling solns., new technique 2−67938
    - boundary problems, solution for control of parameters for restivity, Hall effect, charge carrier lifetime 2−50563
    - carbonate crystals, natural rhombohedral, growth defects study by X-ray transmission topography 2−53732
    - chemical transport reactions in closed volume, theory 2−47214
    - chlorapatite, hydrothermal growth 2−47234
    - coesite, metastable growth in highly strained quartz 2−65579
    - compact gel-growth technique 2−50566
    - conference, Marseille, France [July 1971] 2−47188
    - crystal-melt interface simulation, monoatomic system, hard sphere static model 2−47200
    - crystallization operation, method of complete segregation 2−74690
    - cubic, crystal face growth kinetics, computer simulation 2−60703
    - Czochralski method, computer controlled with i.r. TV system 2−47258
    - Czochralski method, diameter control using laser beam 2−60715
    - Czochralski method, improved cryst. diameter control by crucible base cooling 2−67940
    - Czochralski method, temp. distrib. in growing crystal 2−47256
    - Czochralski method, TV system for controlling crystal dia. 2−47257
    - Czochralski technique, melt mixing investigation during off-centre and group processes 2−53609
    - dendritic, in flowing liquid metal in magnetic field 2−64576
    - dielectric thin films, review of techniques 2−60638
    - diffusion method, mathematical model 2−60708
    - diffusion zone process, from soln. 2−71375
    - disclinations, relation between continuous and discrete 2−74689
    - eccentric, effect of temp. conditions 2−47252
    - edge-defined film-fed growth 2−47254
    - equilibrium form. determ., review 2−47189
    - evaporation model, review 2−47215
    - f.c.c. crystal, (110) cryst.-vapour (melt) interface, surface struct. and diffusion 2−50426
    - ferrite, hexagonal, flux-pulling crystalliz. with heterogeneous seeds 2−71379
    - ferrite and garnet crysts. for bubble domain memories 2−47199
    - fibres, using CO_2 laser as heat source 2−74664
    - flame fusion process, mathematical model 2−47203
- **Crystals** continued
  - **growth** continued
    - flow reactor for chem. vapour deposition props. rel. to gas flow pattern and mass tranfer 2−83896
    - fluxed melts, growth rate variation with supersaturation 2−47255
    - formation of two dimensional ice embryos on basal and prismatic faces of ice crystal 2−48497
    - forsterite, improvements in flux method 2−47265
    - furnace, for Bridgman-Stockbarger and fluxed melt methods, at high gas press. 2−60716
    - grain form stability in presence of dopants 2−47249
    - group II-VI cpds., vapour growth 2−50573
    - heat pipe technology, appl. to cryst. growth 2−50562
    - hollow, needle like, Me_2X_3 type, growth from vapour 2−74668
    - holographic microscopy studies 2−47193
    - homogeneous substituted crystals, optimum conditions, theory 2−47198
    - horizontal zone refiner for crystal growth of group V-VI compounds 2−67941
    - hydrodynamics and convection influences, review 2−47191
    - hydrothermal growth apparatus 2−47235
    - ice, from caphour phase study of abrupt habit changes as function of temperature 2−54847
    - ice, from the vapour in an electric field 2−47221
    - ice, in atmosphere from vapour and cloud drop accretion 2−54849
    - ice, low entropy form obtained from a linear step growth model 2−83906
    - imperfections characteriz. by X-ray topography 2−47216
    - impurity striation formation, effects of thermal oscillations in melt 2−47028
    - interconvertible unit, low power clockwork mechanism 2−56610
    - 2- iododibenzoyl peroxides, conservative twinning, topotaxy 2−77525
    - kinetics, computer simulation 2−50564
    - large cryst. prod. by continuous ripening in stirrer tank 2−47201
    - in liquid columns, effect of high curvature 2−47250
    - magnesium ferroaluminate: Co, formation from metal hydroxides 2−47239
    - from meet, stratified impurity distribution rel. to convective instability in melt 2−53610
    - from melt, conditions for formation of macroblocks 2−50683
    - from melt, factors determining maximum growth rates 2−53611
    - melt growth, crystn. front fluctuation influence on impurity entry 2−43522
    - mercuric cyanide, tetrahydrofuran addition compound, growth mechanism 2−60706
    - metal, dislocation structures in macrosonic fields 2−50590
    - metallic solid/liquid interface micromorphology, electron microscopy obs. 2−47194
    - movies, survey 2−50565
    - mutual crystal orientation terminology 2−83888
    - oxalic acid, habit rel. to solution supersaturation 2−74685
    - oxide, from the flux systems $PbO\text{-}V_2O_5$ and $Bi_2O_3\text{-}V_2O_5$ 2−50589
    - poly(ethylene terephthalate), growth rate of spherulites 2−64595
    - poly 2,6-dimethylphenylene oxide, single crystal growth from solution 2−60774
    - poly γ-benzyl L-glutamate, growth stages in epitaxial crystallisation 2−60605
    - polydisperse crystal suspensions obeying McCabe's ΔL law, growth calc. 2−77524
    - polypropylene, irradiated formation of γ-form crystals from melt 2−60614
    - polypropylene, transcrystalline growth at an internal surface 2−74608
    - potassium oxalates, from aq. soln. oxalates, cryst. growth from aq. soln. 2−60714
    - pressure balancing, technique for suppressing dissoc. during melt growth 2−47259
    - profile curves, influence of surface tension gradient in liquid columns 2−47251
    - pyrrhotite, use of deformed greigite as seed cryst. 2−60723
    - quartz, hydro-thermal growth in Japan 2−74663
    - radiation influence 2−74665
    - rare earth chromate, $RCrO_3$ (R=Lu,Yb) 2−60717
    - rare earth hydroxides, hydrothermal growth 2−47244
    - rare earth manganates, RMn_2O_5 (R=Er to Sm, and Y) $RMnO_3$ (R=Er to Gd), flux method 2−60717
    - rare earth metal isotopes, of large single crysts. 2−47225
    - rare earth orthoferrites, techniques 2−50601
    - rare earth phosphate, RPO_4 (R=Yb to Gd), flux method 2−60717
    - rare earth tetraborides, from flux 2−43524
    - rare gases on graphite, molecular beam system and specimen holder for t.e.m. obs. 2−79113
    - refractory oxides, bicrystals, growth by floating zone method 2−83898
    - review of future studies 2−47190
    - Rochelle salt, grown from soln. size distribution 2−67939
    - ruby, Cr doping during isothermal growth 2−47230
    - sapphire, melt growth of single cryst. ribbons, use as substrates 2−60719
    - sapphire filament, void-free, at rates up to 3 cm/min, effect of using W growth orifices 2−60720
    - semiconductor, bibliography 2−71880
    - semiconductor pseudobinary alloy, by diffusional freezing and soln. zoning 2−47702
    - semiconductors, temp. profile calc. for complex shapes 2−53602
    - snow, growth mechanisms 2−47207
    - solid state recrystn., large cryst. prep. 2−47284
    - solid-liquid growth fronts, solute distrib., contrib. to interfacial undercooling 2−43517
    - from solution, by controlled displacement and liq. phase epitaxy 2−47229
    - from solution, movement of solvent inclusions by centrifugation 2−47465
    - from solution, single cryst. prep. by gradual addition of reactant 2−47238
    - step motion on surfaces under electric fields 2−74613
    - structural defect succession, theoretical treatment 2−53603
    - from supercooled liquid, approx. growth rate estimation 2−56540

Crystals continued
growth continued
surface nucleation growth theory, transient nucleation significance 2−43507
topaz, prism face growth mechanism from surface structure studies 2−60702
topotaxy, templates and twinning 2−77525
transition metal cpds., prep. and characteriz. 2−50571
transition metal oxide solid solns., chem. vapour transport 2−50587
triglycerine sulphate, effect of growth rate on defect struct. and dielec. props. 2−47987
triglycine sulphate, L-alanine doped, induced growth anisotropy 2−53608
two-dimensional nucleus, shape stability 2−47280
unified approach to habit and crystal growth analysis 2−47195
vacuum decoration method, study of growth processes and defect structure 2−80538
Verneuil biography 2−45203
Verneuil furnace, oxidation-reduction potential of environment, thermodynamic calc. 2−60705
zero gravity conditions, floating liquid zone stability 2−47196
Ag, epitaxial growth on substrates, various modes 2−77530
Ag, fibrous growth using solid-state ionics technique 2−80601
Al, from the melt, nucleation by Ti cpds. 2−47098
AlAs, from vap. phase 2−43511
AlGaAsP, liquid epitaxy, stimulated emission, luminescence 2−45747
$Al_{1-x}In_xP$, from vap. phase 2−43511
Al_2O_3, ^{17}O enriched, growth by floating zone technique in image furnace 2−74686
Al_2O_3, corundum, thermodynamic anal. 2−47204
α-Al_2O_3, corundum, Verneuil grown cryst., cryst. axis orientation 2−60701
Al_2O_3, sapphire filament, continuous melt growth 2−50916
α-Al_2O_3, tab growth, vapour−liquid−solid phase mechanism 2−43508
Al_3O_3, sapphire filament, growth conditions rel. to strength 2−50917
$Al_2O_3Cr_2O_3$ system, solubility limit determ. 2−53983
α-As_2Se_3, vapour transport method 2−43510
Au, epitaxial growth on substrates, various modes 2−77530
AuX_2, X=Al, Ga and In, equipment and parameters 2−50600
BAs, prep. from gas phase 2−74669
BN, cubic, pertinent phase equilib. in Li-B-N system 2−50970
B_xN, tetragonal, derived from icosahedral frameworks 2−50572
BP, by closed tube chem. transport method 2−74670
BP, single cryst. synthesis 2−50567
B_xP, tetragonal, derived from icosahedral frameworks 2−50572
BaFCl, modified Kyropoulos method 2−43523
$Ba_2LiNb_5O_{15}$, Czochralski method 2−60721
$Ba(NO_3)_2$, rates of growth in aqueous solutions and kinetics of crystallization 2−71376
$BaSO_4$, from silica gels 2−43519
$BaSO_4$, precipitation kinetics and mechanisms 2−51420
$Ba_{0.5}Sr_{0.5}Nb_2O_6$, growth rate variation with supersaturation in fluxed melts 2−47255
$Ba_{1-x}Sr_xTiO_3$, flux-growth rel. to dielectric props., 4.2-600K 2−47966
$BaTiO_3$:F, prep. by precip. from $TiCl_4$ and $Ba(NO_3)_2$ aq. solns. 2−74675
Be, monocryst., by Czochralski technique, obs. of cryst. perfection 2−47262
BeO, bromellite, from Li_2MoO_4-MoO_3 flux 2−77529
Be_2SiO_4, phenacite, from Li_2MoO_4-MoO_3 flux 2−77529
Bi-Sb alloy system, cryst. growth rate, diffusional supercooling theory 2−53613
$Bi_2Sn_2O_4$, flux method 2−60717
Bi_2WO_6, Czochralski method 2−47263
C columnar growth, electron diffraction analysis 2−80603
CW crystals in cobalt, kinetics of growth 2−64590
$CaCO_3$, calcite, travelling solvent zone melting 2−50591
CaF_2, oxygen impurity removal using CoF_2 scavenger 2−50568
CaF_2, perfection, dependence of growth technique 2−47396
$CaHPO_4.2H_2O$, brushite, by diffusion in silica gel and in solution 2−47233
$CaNb_2O_6$:Nd, pulling by Czochralski method 2−50592
$Ca_3(VO_4)_2$, $Ca_2V_6O_{17}$, from $Ca(NO_3)_2$-K_3VO_4-H_2O system, pH effects 2−47232
$Cd_2(Ge_2O_6)$, hydrothermal synthesis and cryst. struct. 2−74687
CdI_2, growth characts., stacking faults distrib. and stability, polytypism 2−74781
$CdIn_2S_4$:Cr, vapour transport method 2−71369
CdSe, eff. of real growth on elec. and photoelec. props. 2−71419
CdSe, static sublimation method 2−47217
$CdSiP_2$, solution growth method in Sn bath 2−80599
CdTe, from soln. melts, elec. props. 2−74677
CdTe, optical grade cryst. prod. by directional solidification 2−50607
CdTe, phase equil. considerations 2−50593
CdTe preparation for nuclear detectors 2−49668
$CoCr_2S_4$, by chem. vapour transport 2−71371
CoO-NiO solid solution, for neutron monochromator appl. 2−47205
CoP_2, high-press. synthesis and props. 2−83899
$CoWO_4$, flux method 2−60717
Cr dendrites, galvanostatically obtained from CrO_3-H_2SO_4-dimethylsulphoxide-H_2O solution 2−47135
$CrSi_2$ thermoelectric props. and crystal growth 2−84370
$CsBe_2(BO_3)F_2$, synthesis and physicochemical props. 2−47210
$CsMnBr_3$, Bridgman technique, and mosaic spread of neutron diffr. 2−47224
Cu-Ge solid solution, for neutron monochromator appl. 2−47205
Cu-Ge solid. soln. single crysts., and characteriz. 2−53614
Cu, dislocation free, by Czochralski method 2−47264
Cu, dislocation free, growth by Czochralski method 2−67942
Cu, electrodeposited, morphology current density and substrate orientation effects 2−48340
Cu, growth of twin free crystals by secondary recrystn. and zone refining 2−47580
Cu, oriented single crysts., horizontal Bridgman method 2−60722

Crystals continued
growth continued
Cu dendrites, crystn. mode effects on habit and morphology 2−47136
Cu thin film, growth kinetics near melting point 2−60652
Cu whiskers, by halide reduction 2−80570
$CuGa_{1-x}In_xS_2$, soln. growth using In solvent 2−74679
$CuGaS_2$, soln. growth using In solvent 2−74679
CuO, single cryst. prep. by sublimation 2−74678
^{163}Dy, and neutron diffraction expts. 2−74667
^{163}Dy, techniques and isotope preparation 2−56613
ErOF, flux method 2−60717
$Er(OH)_3$, hydrothermal growth 2−47244
^{170}Er, and neutron diffraction expts. 2−74667
^{170}Er, techniques and isotope preparation 2−56613
EuS, by H_2S-Eu_2O_3 reaction at high-temps. 2−50569
EuS, high temp. high press. chem. transport 2−47218
Eu_3SiO_5 synthesis by chem. transport 2−48173
Fe-Mn system, b.c.c. martensite growth 2−64591
Fe, whiskers, morphologies, lattice twists 2−80561
$FeAs_2$, chem. vapour transport 2−47219
$FeBO_3$, fluxed melt. technique, and $Fe_2O_3B_2O_3$ phase relations 2−50594
Fe_3C, growth texture 2−43872
$FeCr_2S_4$, by chem. vapour transport 2−71371
$FeNbO_4$, flux method 2−60717
Fe_xO-MnO solid solns., rel. to optical props. 2−48174
$FeSb_2$, chem. vapour transport 2−47219
$FeSi_x$, chem. transport reaction, rel. to structural study 2−47206
GGG, epitaxial magnetic film, prep. by chem. vapour deposition 2−77527
$Ga_{1-x}Al_xAs$, liquid phase epitaxial, composition, elec. microprobe obs. 2−47286
GaAs:Si, amphoteric impurity distrib. equilib. calc. 2−83981
GaAs, Czochralski method, temp. profile and thermal stress effects on dislocation structure formation 2−53615
GaAs, dislocation-free, by liq. encapsulation 2−50596
GaAs, for γ-ray detector 2−46052
GaAs, from gas phase, cryst. morphology 2−56656
GaAs, impurity incorporation, effect of surface space charge layer 2−47428
GaAs, open flow quartz systems, Si contamination 2−43529
GaAs, single crystals grown by Bridgeman method 2−60724
GaAs, temp. fluctuation effect on nonuniformities 2−47267
GaAs, thin platelet crysts., growth by forced- convection open-tube technique 2−67935
GaAs Schottky-barrier diode preparation for differential capacitance meas. rel. to dopant conc. profile determ. 2−83905
$GaAs_{1-x}P_x$, epitaxial 2−43528
$GaAs_{1-x}P_x$, melt-growth under controlled vapour pressure 2−56611
$GaAs_{1-x}P_x$, vapour growth, thermodynamic calc. 2−47220
$GaAs_{1-x}Sb_x$, from vap. phase 2−43511
GaN, from vap. phase 2−43511
GaN, vapour phase, mass spectrometric obs. 2−53606
GaP, from soln., for red emitting diode manufacture 2−60711
GaP, heteroepitaxial growth on Si substrates 2−83864
GaP, liq. encapsulated growth from non-stoichiometric melts 2−47268
GaP, melt growth, defect characteriz., S-pits 2−50595
GaP, open flow quartz systems, Si contamination 2−43529
GaP crystals grown by vapour transport, 780-935°C, thermodynamics, kinetics, rate of transport, nucleation and crystal size 2−71372
GaS from vapour phase, sublimation and chem. transport 2−71373
GaSe, vapour growth and morphology 2−50574
$Gd_2(MoO_4)_3$, π-GMO, X-ray amorphous, prepn. and physical parameters 2−84136
A-Gd_2S_3, from gaseous phase by chemical transport with I_2, physical properties 2−53607
Ge, profiled crystals drawn from melt, deflection of orientation 2−47425
Ge, single crystal ribbon, from melt, commercial scale processes, equipment development 2−60725
Ge, Stepanov method, effect of dopant conc. 2−47270
Ge ribbon crystal, Stepanov method 2−47269
Ge ribbon crystals, morphology, Stepanov method 2−47328
Ge single crystals, effect of growth parameters on dislocation density 2−47414
GeO_2 polymorphs, solution top-seeding 2−50583
$GeSe_2$, Czochralski pulling under liquid encapsulation 2−50597
$GeSe_{(2)}(Te)$, by vapour transport 2−50575
α-HIO_3, from aqueous solution 2−43520
$HfS_2(Se_2)$, vapour transport technique 2−50577
$Hg(CN)_2$, through slow decomp. of tetrahydrofuran solvate crystal to the air 2−47208
$Hg_{1-x}Cd_xTe$ alloy, using Te as solvent 2−47271
HgI_2, red tetragonal phase, sublimation growth in vacuum 2−74671
HgI_2 for nuclear particle detection 2−46037
α-HgS, cinnabar, hydrothermal growth 2−47235
$Hg_3Te_2Cl_2$, optically active, sublimation method 2−71374
$Hg_2V_2O_7$, high press. prep. 2−71367
InAs, deposition rate rel. to I conc., transport processes kinetics 2−74673
InAs, vapour phase, supersaturation of InI as process control parameter 2−74672
$InAs_xP_{1-x}$:Zn, by Bridgman method, laser diode fabrication 2−59185
$In_xGa_{1-x}As$:Zn, by Bridgman method, laser diode fabrication 2−59185
$In_xGa_{1-x}As$ prep. and props. rel. to electroluminescent diodes 2−68708
$In_xGa_{1-x}As$, vapour growth, equilib. calc. 2−47222
$In_{1-x}Ga_xP$, from vap. phase 2−43511
$In_{1-x}Ga_xP$, liquid epitaxy, stimulated emission, luminescence, laser operation 2−45747
$In_xGa_{1-x}P$, vapour growth, equilib. calc. 2−50576
InP, group IV doped, by liq. encapsulation 2−47272
InSb:Fe, crystallisation features rel. to dopant, hole and acceptor distribution 2−53604
InSb:Te, growth from melt under destabilizing thermal gradients 2−74708

Crystals continued
- **growth** continued
  - InSb, doped, growth rate depend. of impurity distrib. 2–47209
  - InSb, from melt, conc. depend. of impurity distrib. 2–47438
  - $KBe_2(BO_3)F_2$, synthesis and physicochemical props. 2–47210
  - KCN, of single crysts., Czochralski method 2–67944
  - KCl:Pb, rapidly grown from melt, thermal stress defect model 2–50649
  - $KCl:Pb^{2+}$ from soln., inhomogeneous impurity distrib., spectrophotometric obs. 2–74796
  - KCl, Czochralski method, functional dependence of dislocation function 2–53616
  - KCl, from soln., in presence of Pb^{2+} 2–47237
  - KCl, growth spirals on crysts. grown from soln. 2–50586
  - KD_2PO_4, in solns. containing acetate ions 2–60712
  - KH_2PO_4, soln. growth by gradual addition of reactant 2–47238
  - $KMnF_3$, by Czochralski method, dislocation density determ. 2–53605
  - $K_{0.5}Nd_{0.5}TiO_3$, perovskite, prep., mag. susceptibility, cryst. field effects, 2-600K 2–54294
  - K_2SO_4, nucleation and growth in fluidized bed crystallizer 2–47282
  - $KSbSe_2(S_2)$, Bridgman method 2–47273
  - KVO_3, melt growth and characteriz. 2–47261
  - $LaCo_2$, high-press., high-temp., prepn. 2–83901
  - $LaCoO_3$, flux method 2–60717
  - $LaCuO_3$, prepn. under oxygen pressure and props. 2–83897
  - $La_2Li_{0.50}Cu_{0.50}O_4$, prepn. under oxygen pressure and props. 2–83897
  - LaOCl, flux method 2–60717
  - $La_2Ti_2O_4$, flux method 2–60717
  - LiF, single crystal ribbon, by edge-defined film-fed growth technique, for dosimetry 2–67943
  - $LiIO_3$, from saturated soln., solubility study 2–50584
  - $LiNbO_3$, ferroelec. material 2–65063
  - $LiNbO_3$, single-domain, pulling method using h.f. induction furnace, crystal properties, applications 2–77528
  - $Li_{0.5}Nd_{0.5}TiO_3$, perovskite, prep., mag. susceptibility cryst. field effects, 2-600K 2–54294
  - $LiTaO_3$ single crystal, pulling, dielec., thermal and optical props. 2–72008
  - $LiVO_3$, melt growth and characteriz. 2–47261
  - $Li_7Y_3(MoO_4)_8$, prep., decomp. at 735°C to solid and liq. phase 2–74904
  - $MgAl_2O_4$, modified Verneuil technique 2–47274
  - $Mg_{0.5}Fe_{0.5}Ti_2O_5$, armalcolite, growth from glass initially having composition of lunar rock sample 2–44928
  - $MgGa_2O_4$, by Czochralski method, substrate for direct liq. phase epitaxy 2–71380
  - MgO, by chem. vapour deposition 2–47223
  - $6MgO.As_2O_5$, Mn activated phosphor, flux growth method 2–43525
  - $MgSO_4.7H_2O$, formation in presence of seed 2–74681
  - $MgSO_4.7H_2O$, growth rate of artificial vicinal faces 2–74680
  - $MnCoP_4$, high-press. synthesis and props. 2–83899
  - Mn_3O_4, flux method 2–60717
  - MnTe, from nonstoichiometric melts by liq. encapsulation 2–50598
  - $MnWO_4$, flux method 2–60717
  - $MoAs_2$, Mo_2As_3, Mo_5As_4, by halogen chem. transport 2–67936
  - $MoS_2(Se)_2$, direct vapour transport optimum conditions 2–60707
  - $MoTe_2$, Br transport, optimum conditions 2–60707
  - NH_4Cl, dendritic growth under influence of electric fields 2–43486
  - $NaBe_2(BO_3)F_2$, synthesis and physicochemical props. 2–47210
  - NaCN, of single crysts., Czochralski method 2–67944
  - NaCl, growth spirals on crysts. grown from soln. 2–50586
  - $NaClO_3$, from soln. 2–47240
  - $NaClO_3$, from superaturated soln., contact nucleation mechanism 2–50585
  - $Na_2HPO_4.12H_2O$, rates of growth in aqueous solutions and kinetics of crystallization 2–71376
  - $NaIn(WO_4)_2$, from soln. 2–43586
  - $NaNH_4SeO_4.2H_2O$, prep. and analysis 2–43521
  - $NaNbO_3$, flux method 2–60717
  - $Na_{0.5}Nd_{0.5}TiO_3$, perovskite, prep., mag. susceptibility, cryst. field effects, 2-600K 2–54294
  - $Na_5P_3O_{10}.6H_2O$, growth rate from soln. 2–47241
  - $NaVO_3$, melt growth and characteriz. 2–47261
  - Na_xWO_4, cryst. growth by fused salt electrolysis 2–48341
  - $NaY(WO_4)_2$, growth conditions 2–74955
  - Nb, energy required for twinning 2–64588
  - $Nb_{1-x}Ta_x$ alloy, $0<x<0.25$, growth by electron beam float zoning 2–50599
  - $Nd(OH)_3$, preparation from Nd_2O_3 in H_2O vapour 2–80598
  - $NiAl_2O_4$, growth on sapphire, orientation relations 2–71333
  - $NiFe_2O_4$, growth rate variation with supersaturation in fluxed melts 2–47255
  - NiO, dendritic growth from vapour phase 2–64592
  - $Ni(OH)_2$, prep. from turbostratic hydroxide 2–47211
  - $NiWO_4$, flux method 2–60717
  - Pb dendrites, growth kinetics in gels 2–47137
  - Pb thin film, growth kinetics near melting point 2–60652
  - PbI_2, for nuclear particle detection 2–46037
  - $Pb(N_3)_2$, growth from solution 2–83900
  - $PbO-GeO_2$ system single crystal growth 2–74666
  - PbO, for nuclear particle detection 2–46037
  - $Pb_{1-x}Sn_xTe$ alloy, Bridgman technique, cryst. perfection, composition, carrier conc. obs. 2–53618
  - $PbTiO_3$, plate-like growth and exam. of domain struct. 2–71398
  - $PbTiP_2O_6$, flux method 2–60717
  - $PbZrO_3$, from solutions in $PbO-ZrO_2-PbF_2-B_2O_3$ system 2–81140
  - Pr oxides, higher, hydrothermal growth 2–47243
  - $PtGa_2$, equipment and parameters 2–50600
  - $RbBe_2(BO_3)F_2$, synthesis and physicochemical props. 2–47210
  - $RbFeCl_3$, Bridgman technique, and mosaic spread of neutron diffr. 2–47224
  - $RbMnF_3$ by Czochralski method, dislocation density determ. 2–53605
  - $RbNiCl_3$, Bridgman technique, and mosaic spread of neutron diffr. 2–47224
  - $RbSbS_2$, Bridgman method 2–47273
  - Sb_2O_3, valentinite and senarmontite polymorphs, crystalliz. under hydrothermal cond. 2–74683

Crystals continued
- **growth** continued
  - Si, doping, during whisker growth by gas transport 2–47430
  - Si, from pedestal, adaptations using combined heating 2–53601
  - Si, pedestal technique using electron beam heating 2–43512
  - Si, profiled crystals, e.m. field in system inductor-concentrator-pedestal 2–47275
  - Si, ribbons, by edge-defined film-fed growth technique 2–71381
  - Si growth from solution, 2-dimensional nucleation and corner growth 2–74684
  - Si growth twins grown by pulling method 2–74688
  - SiC, synthesis of C-free crysts. 2–47212
  - SiC single crystals, monitoring gas medium during growth 2–60704
  - SiO_2, tridymite, from $Li_2MoO_4-MoO_3$ flux 2–77529
  - ^{154}Sm, and neutron diffraction expts. 2–74667
  - ^{154}Sm, techniques and isotope preparation 2–56613
  - SnF_2, from soln. 2–47245
  - SnSSe, vapour transport method 2–67937
  - $SnS_2(Se_2)$, vapour transport method 2–67937
  - SnS_xSe_{2-x}, (x=0-1), vapour transport technique 2–50577
  - $SrAlF_5$, pure and Eu^{2+}-doped single crysts. 2–60726
  - $Sr_2Nb_2O_7$, by floating zone technique 2–47276
  - $SrSO_4$, from silica gels 2–43519
  - TaS_2, 1S and 2S polymorphs, chem. transport 2–47226
  - $TaSe_2$, direct vapour transport, optimum conditions 2–60707
  - Tb oxides, higher, hydrothermal growth 2–47243
  - ThC, ThS, electron beam melting of material synthesised by direct reaction between element 2–53620
  - Ti, low dislocation density, phase transform. technique 2–77526
  - Ti_xO_y, controlled stoichiometry and order 2–50570
  - $TiS_2(Se_2)(Te_2)$, vapour transport technique 2–50577
  - Ti_3SiC, preparation from gaseous phase, chemical and physical properties 2–53580
  - Tl_2Te, and semicond. props. 2–64990
  - UC, US, electron beam melting of material synthesised by direct reaction between element 2–53620
  - UO_2, form melt, stoichiometry variations 2–53621
  - V-C alloys, floating zone melting apparatus with r.f. heating, volatilization loss reduction 2–71378
  - $VC_x(O_x)(N_x)$, by floating zone technique 2–47277
  - V_2O_5, large crystals for dielectric relaxation measurements 2–68463
  - V_nO_{2n-1} (n=3,4, ..., 8) single cryst., by chem. transport reaction 2–43509
  - $VOPO_4$, prep. and cryst. chem. 2–50627
  - WC dendrite, chemical vapour deposition 2–43487
  - WSe_2, direct vapour transport, optimum conditions 2–60707
  - WTe_2, Br transport, optimum conditions 2–60707
  - YAG:Nd, boule defects, and Nd distrib. obs. 2–47246
  - YAG:Nd garnet, grown by Czochralski method, cryst. perfection rel. to melt comp. and rot. speed 2–67945
  - $Y_3Al_5O_{12}:SiO_2$ garnet, from melt, habit modification by doping 2–74751
  - $Y_3F3_{5-x}Cr_xO_{12}$, fluxed melt technique 2–47289
  - $Y_3Fe_5O_{12}:SiO_2$ garnet, from melt, habit modification by doping 2–74751
  - $YFeO_3$, by Czochralski pulling, characteriz. 2–50605
  - $Y_2Fe_5O_{12}$, grown from soln., dislocation density rel. to conditions 2–56715
  - $Y_3Ge_5O_{12}:SiO_2$ garnet, from melt, habit modification by doping 2–74751
  - YIG, Ca-Si substituted, flux growth and mag. characterization 2–47278
  - YIG, chem. transport 2–43513
  - YIG, epitaxial magnetic film, prep. by chem. vapour deposition 2–77527
  - YIG, flux growth, local cooling and accelerated crucible rotation effects on quality 2–50602
  - YIG, fluxed melt method, effects of oxygen pressure 2–50603
  - YIG, viscosity and density of melts 2–60713
  - YVO_4, modified pulling method 2–50604
  - YbFe garnet, Ca-Si substituted, flux growth and mag. characterization 2–47278
  - Zn-Cd alloy, microsegregation of Cd during growth, partition coefficient 2–47648
  - Zn-Cd dilute alloy, dendritic morphology 2–43488
  - Zn-In-S system polytypes, vapour growth 2–50579
  - $ZnCd_{1-}S$, steeply graded, photoluminescence 2–72444
  - $ZnGeP_2$, Bridgman method 2–80599
  - ZnO, by ZnF_2 + water reaction, inversion twin obs. 2–50581
  - ZnO, chemical transport method, semicond. props. 2–43516
  - ZnO, from vapour phase, influence of multicomponent conc. 2–43515
  - ZnO, pure and doped, vapour phase growth 2–50580
  - ZnO single crystal, hydrothermal growth rate and morphology 2–47247
  - ZnS, hexagonal, melt growth, defect elimination by donor impurity doping 2–47279
  - ZnS, hollow crystals by pulling sealed tube method 2–43527
  - ZnS, luminophors, prep., 36–180°C 2–78141
  - ZnS, stacking order, X-ray obs. 2–47213
  - ZnS, vapour phase growth, polytype form., and perfection rel. to photovoltaic props. 2–47227
  - ZnS(Se), chem. vapour deposition of transparent polycrysts. 2–50578
  - ZnSe, vapour phase growth under controlled partial press. 2–64594
  - $ZnSiP_2$, sublimation technique 2–64593
  - $ZnWO_4$, effect of struct. charact. on penetration of Cr and Gd impurities 2–71542
  - ZrO_2, hydrothermal growth and etching in HF 2–50588
  - $ZrS_2(Se_2)$, vapour transport technique 2–50577
  - $ZrSiO_4$, zircon, hydrothermal and flux growth 2–47248
- **hyperfine field interactions**
  - alkali halides, e.s.r. of irrad. paramag. centres 2–81467
  - anthracene, dye-sensitized, delayed fluorescence, magnetic hyperfine modulation 2–65309
  - biotite, Mossbauer effect, ^{57}Fe nuclei 2–75266
  - coupling consts. for $S=1/2$ system, determ. of relative signs through e.p.r., ENDOR, double ENDOR 2–70674
  - N,N′-dimethyl-piperazine, ^{14}N quadrupole interaction 2–84603

Crystals continued
hyperfine field interactions continued
dipolar spin-lattice relax. rates of quadrupole interacting spin system 2−84452
electron spin echo envelope, amplitudes of superhyperfine freq. 2−78168
e.s.r. triplet spectra, hyperfine anomaly from nuclear spin-forbidden transition, abs. sign determination of zero-field splitting constant 2−57388
europium dibenzoylmethide chelate, cryst. field splitting of electronic transitions 2−65239
F-centre, high pressure ENDOR cavity 2−82412
ferroelectric, order-disorder type, elec. field gradient from nucl. double reson. studies 2−81481
ferromagnetic metal, magnetization, temp. depend. 2−48066
glass, containing metal ions, structure, Mossbauer effect 2−64526
group II-VI compound, e.p.r. theory of group IV ion 2−51399
ion implantation, study of radiation damage involving Mossbauer effect 2−50631
lead acetate hydrate, X-irradiated, e.p.r., Pb^+ and PbH^{2+} identification 2−75347
liquid metals and alloys, nucl. quadrupole relaxation, ionic motion contrib. 2−43316
magnetic alloy, dilute, crystal field effects on e.s.r. line splitting 2−51401
magnetic dipole and elec. quadrupole study by nuclear orientation with and without n.m.r. 2−63758
metal, ferromag., temp. depend., rel. to magnetiz. 2−54323
metal (h.c.p.):^{57}Fe electric field gradients 2−80986
metal systems, data compilation, NBS Permuted Materials Index 2−68155
metals, mag. impurities, mag. hyperfine interaction studies, review 2−84397
methyl malonic acid, tunnelling sidebands of methyl group hyperfine structure, e.s.r. obs. 2−57389
molecular cryst., low symmetry, quantitative simulation of ENDOR 2−65354
Mossbauer absorber spectra, analysis of five line hyperfine split 2−65227
Mossbauer hyperfine spectra, temp. depend. line shape rel. to mag. orders 2−75263
Mossbauer line broadening, many closely spaced internal fields 2−61601
Mossbauer line shape in coupled hyperfine interactions 2−75264
nontransition metal fluorides, ^{19}F mag. screening, tetrahedral and octahedral environments 2−48120
nuclear spin, rel. to polarization of impurity luminesc. 2−44405
nuclear spin-lattice relaxation due to the orbital interaction 2−84585
optical spectra, $4f^{13}$ ions 2−61625
orthorhombic symmetry spin hamiltonian eigenvalues 2−81316
palladium benzoylacetonate, VO^{2+} doped, e.p.r., ^{51}V quadrupole coupling 2−61741
paraelectric crysts., hyperfine interaction consts. ENDOR of A-centre electrons rel. to external elec. field 2−78176
paramagnetic, perturbed γ-γ angular correl., effect of spin-lattice relax. and ultrasound 2−72241
permalloy, magnetic hyperfine field at ^{57}Fe, Mossbauer spectra 2−54386
potassium hydrogen di-trifluoracetate, deuteron quadrupole coupling const. 2−72528
powder, n.m.r. pattern, graphic analysis in the presence of quadrupole interactions 2−48300
pyrene, Davydov splitting of first triplet state 2−61660
radioactive impurities, radiation characs. 2−61568
rare earth ions in metals, metal props. rel. to cryst. elec. field splitting 2−57315
rare earth orthochromites, n.m.r. of ^{53}Cr 2−48307
rare earth trichlorides under hydrostatic press., n.q.r., elec. field gradient 2−54519
recoil nuclei interacting with solids, effects 2−68587
S-state ion, covalency effects in e.s.r. obs. 2−48272
sodium methylammonium tungstovanadate, VO^{2+} doped, e.p.r., ^{51}V quadrupole coupling 2−61741
spin Hamiltonian hyperfine operator with axial symmetry 2−54374
texture effects and differential perturbed angular correlations 2−78055
transition metal ions, core polarization, semiempirical law 2−84577
transition metals with actinide impurities, rel. to cond. electron polarization and d-electron contribs. 2−68588
triglycine fluoroberylate:Cu^{2+}, e.p.r. obs. 2−51409
triglycine fluoroberylate, Cu^{2+} aggregate e.p.r. spectrum, h.p. and temp. influence 2−84575
π-tropyliumvanadium tricarbonyl, ^{51}V quadrupole relax., coupling const. 2−84453
vitrinite, e.p.r. obs. 2−68731
zeolite, cation-exchanged, Mossbauer effect of Fe^0-atoms 2−54390
Ag-Tb dil. alloys, perturbed ang. correl. on ^{169}Tm 2−72247
Ag, time-differential perturbed ang. correl., ^{111}Cd quadrupole interaction 2−57316
Al, interactions of implanted ^{220}Rn and ^{224}Ra studied by α-γ angular correlations 2−81341
β As_4S_4, nuclear quadrupole resonance of ^{75}As 2−84595
Au-Yb dilute alloy, localized moments, Mossbauer obs. 2−81210
$BaBr_2$, F-centre, e.s.r. obs. 2−51336
$BaCl_2$, F-centre, e.s.r. obs. 2−51336
$BaSO_4$:MnO_4^{2-}, polarized optical absorption and e.s.r. spectra, crystal field transition e-t_2 assignment 2−48274
Be, negative cond. electron contrib. to field gradient 2−68277
BeO, irrad., V_1 centre, hyperfine parameters, ENDOR obs. 2−54498
BeO, n.m.r. of ^{9}Be, quadrupole splitting 2−44453
Be_2SiO_4:Cr_2O_3, e.s.r. of Cr^{5+} 2−72477
Bi, interaction of implanted ^{220}Rn and ^{224}Ra studied by α-γ angular correlations 2−81341
$BiCl_3$, ^{209}Bi quadrupole coupling const., temp. and press. depend. 2−78177
$Bi_4Ge_3(Si_3)O_{12}$ electro-optic crysts., quadrupole coupling consts. 2−84604
BiSb, narrow band emission, nuclear electric quadrupole radiative transitions 2−78118

Crystals continued
hyperfine field interactions continued
$Bi_{92}Sb_{08}$, dc-pumped, line narrowing of microwave radiation caused by nuclear electric quadrupole transition in ^{209}Bi 2−44403
CaF_2, ENDOR spectrum of U^{3+}-F- 2−84607
$Ca^{181}HfO_3$, perovskite type, nucl. quadrupole interactions, perturbed angular-correlation meas. 2−72244
Cd, interactions of implanted ^{220}Rn and ^{224}Ra studied by α-γ angular correlationss 2−81341
CdF_2:Mn^{2+}, obs. of hyperfine and superhyperfine splittings in e.p.r. spectra 2−48276
CdS ligand hyperfine interaction of Ti^{2+} on sites with trigonal symmetry C_{3v} 2−80977
$CdS_{1-x}Se_x$:Mn^{2+}, temp. and comp. depend., e.p.r. study 2−81456
CdSe ligand hyperfine interaction of Ti^{2+} on sites with trigonal symmetry C_{3v} 2−80977
$Cd_{1-x}Zn_xS$:Mn^{2+}, temp. and comp. depend., e.p.r. study 2−81456
$CeAl_x$, n.m.r. and magnetic susceptibilities 2−84594
CeO_2, u.v. irrad. paramag. hole centres, e.s.r. obs. 2−65322
Ce_xLa_{1-x} Sb, crystal field splitting of Ce^{3+}, magnetic. obs. 2−61570
Ce_xY_{1-x} Sb, crystal field splitting of Ce^{3+}, neutron scatt. and magnetic. obs. 2−61570
Co:As, hyperfine mag. fields as As, meas. by ^{75}Se γ-γ cascade decay 2−78018
Co:^{42}Ca, perturbed angular correlation studies, g-factor of 3.19 MeV 6^+ state in ^{42}Ca 2−72243
Co-As dilute system, internal hyperfine mag. field determ. 2−44321
Co-Cr dilute alloy, n.m.r. and nuclear relaxation study of satellite lines 2−44454
Co-Mn dilute alloy, n.m.r. and nuclear relaxation study of satellite lines 2−44454
Co-V dilute alloy, n.m.r. and nuclear relaxation study of satellite lines 2−44454
$Co_xZn_{1-x}Fe_2O_4$, ferrite, Fe^{3+} spin fluctuations mag. hyperfine splitting, relax. effects, Mossbauer spectra 2−81287
Cr_2O_3, crystal field splitting Cr^{3+} ion, wavelength modulated reflectivity, obs. 2−65257
Cs alums, interpretation of Ti^{3+} e.s.r. spectra 2−81445
Cu-Ni:^{57}Fe, Mossbauer doublets, time-differential perturbed angular correlations 2−72275
Cu, nuclear mag. field interaction with μ^+meson 2−57090
Cu, nuclear mag. field interaction with μ^+meson 2−57090
Cu dil. alloys, elec. field gradients 2−51413
Cu^{2+} tetragonal complexes, covalency effects in anisotropic h.f.s. 2−84580
Cu(II) complex, bis- diethyldithiophosphate, hyperfine couplings of ^{33}S 2−81446
Cu(II) complex, bis(O,O′-di-iso-propyl-dithiophosphato) copper(II), s.h.f. splitting, e.p.r. 2−81510
$DyAsO_4$, Splitting of Dy^{3+} levels, Jahn Teller effect, Raman spectra 2−48198
$DyVO_4$, splitting of Dy^{3+} levels, Jahn Teller effect, Raman spectra 2−48198
$ErCl_3$, transferred effect obs. 2−72242
Eu ions in aromatic acids 2−75324
EuSe:Gd(La), Mossbauer effect, mag. struct. effect 2−48145
Fe: ^{169}Tm, hyperfine field at Tm temp. depend. from perturbed angular correl. expts., 4.2-450K 2−81252
Fe:As, hyperfine mag. fields at As, meas. by ^{75}Se γ-γ cascade decay 2−78018
Fe:^{42}Ca, perturbed angular correlation studies, g-factor of 3.19 MeV 6^+ state in ^{42}Ca 2−72243
Fe:^{183}Re, magnetic hyperfine splitting constants 2−72245
Fe:^{184}Re, magnetic hyperfine splitting constants 2−72245
Fe-Al dil. alloy, ave.-moment-internal field variations 2−78008
Fe-Co dilute alloy, ^{57}Fe n.m.r. study 2−65344
Fe-Cr dil. alloy, field reduction produced by solute 2−44354
Fe-Ga alloys, magnetic props. and Mossbauer investigations 2−84416
Fe-Ga solid solns., Mossbauer lineshape effects 2−44353
Fe-Rh alloy, f.c.c., rel. to Mossbauer determ. of Neel temp. 2−78072
Fe-Rh alloy, hyperfine field at Rh nuclei by Coulomb excitation 2−61572
Fe-Si dil. alloy, ave.-moment-internal field variations 2−78008
$(Fe,Zn)_2Mo_3O_8$, Mossbauer study 2−75270
Fe, $^{188,\ 190,\ 192}$Os g-factor meas., comparison of IMPACT, PAC and Mossbauer techniques 2−42534
Fe, anomalous temp. depend. of hyperfine field for Os impurity 2−48121
Fe, electron spin density meas. by combined Mossbauer and electron spectroscopy technique 2−81343
Fe, interactions of implanted ^{220}Rn and ^{224}Ra studied by α-γ angular correlations 2−81341
Fe, matrix, hyperfine fields at Al, P, Sc and Ta nuclei, spin echo obs. 2−72229
Fe, Mossbauer effect, ^{127}I mag. moment obs. 2−63812
Fe, Mossbauer effect, high pressure obs. between 300-20K 2−72283
Fe, n.m.r. and nucl. polarization of ^{74}As, mag. moment, internal field 2−76796
Fe, of ^{31}P, ^{75}As, ^{93}Nb, ^{121}Sb, ^{123}Sb, n.m.r. obs. 2−75354
Fe, sign of hyperfine fields for rare earth impurities 2−44322
Fe film, magnetic h.f.i. in u.h.v. Mossbauer emission spectra 2−72284
Fe garnet, magnetic hyperfine field interaction of Ce^{3+} by angular correlations 2−81320
$FeBO_3$, ^{57}Fe Mossbauer h.f. splitting, mag. struct. 2−54355
$FeCl_3$ frozen aqueous soln., Mossbauer spectra, investigation of glass to crystal transformation at 200 K 2−72280
$FeCl_3.6H_2O$, spontaneous magnetization, mag. ordering, mag. hyperfine fields, Mossbauer reson., $T<4.2$ K 2−75272
$FeCr_2S_4$ spinel, e.f.g., dynamic Jahn-Teller effect interpret. 2−57331
FeF_2, mag. interactions of Fe^{2+}, core polarization field 2−61604
Fe(II) complex, bis(thiosemicarbazide)iron(II) sulphate, large quadrupole splitting 2−61605
Fe(IV) complex, interactions in $t_{2g}{}^4$ config. of ^{57}Fe 2−84472

- **Crystals** continued
  - **hyperfine field interactions** continued
    - α-Fe_2O_3, haematite, quadrupolar interaction const., paramag. state 2−65234
    - α-Fe_2O_3 microcrysts., chem. modification of quadrupole interaction 2−65231
    - FeS, Mossbauer spectra obs. 2−48146
    - FeS antiferromagnetic, Mossbauer determ. of spin arrangements, quadrupole interaction, internal magnetic field, chemical shift 2−81344
    - FeSi-CoSi system, itinerant ferromag., ^{59}Co n.m.r. obs. 2−61745
    - ^{57}Fe, det. of electric field gradient parameters from Mossbauer spectra 2−54387
    - ^{57}Fe in powdered absorbers, h.f.s. coupling and Mossbauer spectra parameters 2−75265
    - Gd, ferromag., transient mag. field at Gd, ion implantation angular correlation obs. 2−65143
    - $GdAl_2$, mag. induced elec. field gradient, spin echo obs. 2−72509
    - $Gd_{1-x}La_xZn$, n.m.r., zero-field resonances, hyperfine field contribs. 2−72510
    - $Gd_{1-x}Y_xZn$, n.m.r., zero-field resonances, hyperfine field contribs. 2−72510
    - Ge-Hf alloy, electric quadrupole interaction of ^{181}Ta 2−75359
    - GeO_2:V^{4+}, e.p.r., g and A tensors, orbital mixing parameter, radial average, core polarization 2−72503
    - Hf, quadrupole interaction of ^{181}Ta, Mossbauer obs. 2−61607
    - Hf (IV) complexes, octocoordinated, differential perturbed ang. correl., ^{181}Ta quadrupole coupling 2−61571
    - Hf polycrystalline sample, influence of Zr on the quadrupole interaction of ^{181}Ta 2−84593
    - HfF_4:^{181}Ta, in dilute HF, time differential perturbed γ-γ angular correlation, temp. dependence 2−81321
    - $HfOCl_2.xH_2O$, static elec. quadrupole interaction of ^{181}Ta 2−78057
    - HfV_2, n.m.r., quadrupole parameter anomaly 2−54507
    - ^{181}Hf cpds., ABO_3-type, perovskite type, nucl. quadrupole interactions, perturbed-angular-correlation meas. 2−72244
    - In-Cd alloy, quadrupole interactions of ^{111}Cd and quadrupole moment of 247-keV state 2−75246
    - In, quadrupole interactions of ^{111}Cd and quadrupole moment of 247-keV state 2−75246
    - InSb, narrow band emission, nuclear electric quadrupole radiative transitions 2−78118
    - n-InSb Knight shift in the extreme quantum limit 2−84597
    - InSb microwave emission explained in terms of nuclear electric quadrupole radiative transitions of $^{121,123}Sb$ 2−44404
    - $KAu(CN)_2$, elec. hyperfine alignment of ^{197}Au 2−44355
    - $KAu(CN)_2$, Mossbauer effect, elec. alignment of ^{197}Au 2−44356
    - KCl(Br), F-centre interactions, press. depend., ENDOR 2−83986
    - $KFeF_4$, planar antiferromagnet, quadrupole splitting, Mossbauer obs. 2−78043
    - KH_2AsO_4, X-irradiated at 4.2 K, obs. of proton superhyperfine structure in ENDOR spectrum 2−72469
    - $K_3IR^{III}(CN)_6$, electron irradiated in KCl single crystals, e.s.r. studies of ligand hyperfine structure in $Ir^{II}(CN)_5$ species 2−61735
    - $KMgF_3$:$^{53}Cr^+$, ENDOR of $^{53}Cr^+$, hyperfine const., covalency depend. 2−68753
    - K_2MnF_4, planar antiferromagnet. contrib. to ^{19}F n.m.r. lineshift 2−54510
    - K_2SO_4:Tl^{2+}, e.p.r. obs. 2−72470
    - K_2ZnF_4:Mn^{2+}, spin Hamiltonian parameters, e.s.r. obs. 2−65323
    - $KZnF_3$:V^{2+}, e.p.r. and ^{19}F ENDOR study 2−75353
    - La and Y ethylsulphates: ^{166}Er $\gamma\gamma$ cascade, crystal orientation effect 2−78053
    - LiCl, gradient-elastic consts. determ. by n.m.r. 2−77637
    - LiF(Cl), F-centre interactions, press. depend., ENDOR 2−83986
    - $Li_{0.5}Fe_{2.5-x}Al_xO_4$ $(0 \leqslant x \leqslant 1)$ and $Li_{0.5}Fe_{2.5-x}Ga_xO_4$ $(0 \leqslant x \leqslant 1.63)$, electric fields at lattice points and magnetic anisotropy 2−72194
    - $Li_{0.5}Fe_{2.5-x}Ga_xO_4$, supertransferred hyperfine fields at ^{69}Ga and ^{71}Ga 2−54511
    - $Li_{0.5}Fe_{2.5}O_4$, supertransferred hyperfine field at ^{57}Fe, n.m.r. study 2−78169
    - $LiYF_4$:Er^{3+}, g-value and quadrupole splitting calc. 2−51240
    - M centre triplet state, quadrupole interactions, ENDOR obs. 2−72533
    - Mg-Mn alloy, relaxation bottleneck suppression, e.p.r. obs. 2−44438
    - MgF_2, static electric quadrupole interaction of beta emitter ^{20}F produced by capture of polarized neutrons, n.m.r. obs. 2−75356
    - MgO:Cr^+, γ irrad., e.p.r. obs. 2−75346
    - Mn (II), complex, tris(octamethylpyrophosphoramide) manganese (II) perchlorate, h.f. splitting parameter 2−81513
    - Mn_{1-x} Cr_xSb, ^{55}Mn n.m.r. and ^{121}Sb Mossbauer obs. 2−54514
    - MnAlGe, ferromagnetic, n.m.r. studies 2−84586
    - $Mn_2(CO)_{10}$ single crystal, quadrupole coupling, broadline n.m.r. study 2−57397
    - MnF_2, mag. interactions of Fe^{2+}, core polarization field 2−61604
    - $Mn_xMg_{1-x}Al_2O_4$ spinel, e.s.r. parameters 2−48290
    - $(NH_4,Rb)_2CuBr_4.2H_2O$, mag. and elec. quadrupole interactions 2−65144
    - NH_4Br:Cu^{2+}, e.p.r., covalency, core polarization 2−78154
    - $(NH_4)_2SO_4$, paraelectric, ^{14}N quadrupole coupling 2−44456
    - ^{14}N, n.m.r. in $Ce_2Mg_3(NO_3)_{12}.24H_2O$ 2−48305
    - Na, nuclear contact densities for electrons 2−61569
    - $NaClO_3$, acoustic excitation of ^{23}Na n.m.r. 2−78166
    - Nb-Mo:Fe alloy, localized moments on Fe, Mossbauer obs. 2−48149
    - Nb, Mossbauer spectrum of ^{57}Fe, hydrogen conc. effects 2−78075
    - $NdNi_2$, $NdAl_2$, $NdCo_2$, Laves phases, contrib. to low temp. specific heat, cryst. field and exchange effect model 2−57067
    - Ni: ^{206}Bi, mag. hyperfine field at Bi 2−81251
    - Ni:As, hyperfine mag. fields at As, meas. by ^{75}Se γ-γ cascade decay 2−78018
    - Ni:^{42}Ca, perturbed angular correlation studies, g-factor of 3.19 MeV 6^+ state in ^{42}Ca 2−72243
    - Ni-As dilute system, internal hyperfine mag. field determ. 2−44321
    - Ni-Pd alloys, ^{61}Ni Mossbauer effect obs., conc. depend. 2−72285
    - Ni-Pd(Pt) alloys, matrix and impurity cluster polarization 2−44358
    - Ni-W alloy, conc. depend. of hyperfine field at ^{182}W 2−75273
    - Ni, $^{188,\ 190,\ 192}Os$ g-factor meas., comparison of IMPACT, PAC and Mossbauer techniques 2−42534
    - Ni, at ^{181}Ta nuclei, $\gamma-\gamma$ angular correl. obs. 2−44320
    - Ni, hyperfine field at ^{181}Ta, perturbed ang. correl. study 2−65204
    - Ni, mag. field at recoil implanted ^{41}K 2−65205
    - $Ni_{1.2}Fe_{1.7}Sb_{0.1}O_4$, supertransferrred fields and covalency at diamag. cations 2−48150
    - Os, quadrupole interaction of ^{181}Ta, Mossbauer obs. 2−61607
    - $Pb^{181}HfO_3$, perovskite type, nucl. quadrupole interactions, perturbed-angular-correlation meas. 2−72244
    - PbI_2, quadrupole coupling, Mossbauer obs. 2−68614
    - Pb_2MnSb, ferromagnet, n.m.r. study 2−61750
    - Pd:^{163}Dy, hyperfine splitting, consts., e.s.r. 2−72497
    - Pd:^{167}Er, hyperfine splitting, consts., e.s.r. 2−72497
    - Pd:Er^{3+}, e.s.r. obs. 2−61732
    - Pd:Gd^{3+} single crystal, e.p.r. obs. 2−68733
    - Pr, hyperfine sp. ht., mag.-ground-state props. of single crysts. 2−48078
    - Pr, nuclear cooling 2−65121
    - $PrCu_2$, spontaneous mag. order, 54 mK 2−44225
    - PrO_2, Mossbauer scattering obs. using ^{141}Pr 2−48151
    - Pt-Co dil. alloys, nucl. sp. ht., low temp. 2−43986
    - RbBr(Cl), gradient elastic consts. determ. by n.m.r. 2−77637
    - Re, quadrupole interaction of ^{181}Ta, Mossbauer obs. 2−61607
    - $Re_2(CO)_{10}$ single crystal, quadrupole coupling, broadline n.m.r. study 2−57397
    - $ReMn(CO)_{10}$ single crystal, quadrupole coupling, broadline n.m.r. study 2−57397
    - Ru, quadrupole interaction of ^{181}Ta, Mossbauer obs. 2−61607
    - Si, hyperfine structure of the e.s.r. spectrum of A centre 2−81005
    - $Sn^{181}HfO_3$, perovskite type, nucl. quadrupole interactions, perturbed-angular-correlation meas. 2−72244
    - Sn(II) materials, lattice contribution to electric field gradient 2−65206
    - SnO_2, ENDOR meas. on ^{53}Cr and ^{57}Fe 2−48309
    - $SrCl_2$:$^{151}Eu^{2+}$, $^{153}Eu^{2+}$, temp. dependence, e.p.r. spectra 2−72471
    - $SrCl_2$:Ti^{2+}, e.p.r. investigation, obs. of double quantum transitions, determ. of spin- Hamiltonian parameters 2−81454
    - $SrCl_2$, e.p.r. of Ag^{2+}, superhyperfine structure of equivalent chlorine nuclei 2−84579
    - SrF_2, ENDOR spectrum of U^{3+}-F^- 2−84607
    - $Sr^{181}HfO_3$, perovskite type, nulc. quadrupole interactions, perturbed-angular-correlation meas. 2−72244
    - $SrMoO_4$:Er^{3+}, g-value and quadrupole splitting calc. 2−51240
    - $TbVO_4$, splitting of Tb^{3+} levels, Jahn Teller effect Raman spectra 2−48198
    - ThO_2, e.s.r. absorpt. spectrum of monovalent iron 2−48296
    - ThO_2, hyperfine splitting of Gd^{3+}, temp. depend., Debye temp. obs. 2−84581
    - Tm_3Al_2, n.m.r. and Mossbauer spectra, quadrupole coupling, EFG tensor 2−48155
    - $UO_2(NO_3)_2.6H_2O$:VO^{2+}, rel. to e.p.r. linewidths variations in single crysts. 2−57392
    - WO_3-P_4O_{10}-V_2O_5 , e.p.r. obs. 2−54495
    - YIG:Cr^{3+},Cu^{2+} garnet, hyperfine interactions of Cr^{3+} and Cu^{2+} ions, n.m.r. obs. at 4.2 K 2−72504
    - YIG, electrostatic forces, elec. field gradient, mol. orbitals construct. 2−68615
    - YbFe garnet, perturbed ang. correl. on ^{169}Tm 2−72247
    - $YbPd_3$, Mossbauer effect of ^{170}Yb, mag. field, temp. depend. 2−54393
    - Zn complex, 2,6-pyridinedicarboxylate, Cu-doped, e.p.r. obs. 2−78155
    - ZnF_2, mag. interactions of Fe^{2+}, core polarization field 2−61604
    - ZnSe:Co^{2+}, ligand hyperfine struct., molecular orbital approx. calc. 2−51294
    - $ZrFe_2$:Np, hyperfine splitting of ^{239}Np 2−46207
  - **imperfections** *see Crystal imperfections*
  - **internal fields**
    - *see also Crystal field theory*
    - alkali bromides, gradient-elastic tensor, n.m.r. acoustic saturation study 2−44457
    - alkali halides, rel. to lattice distortion produced by edge disloc., photoconductivity spectra obs. 2−74777
    - aromatic mols., vibronic coupling in emission spectra revealed by crystal field distortion 2−75243
    - excitons, Frenkel theory, exchange interactions, local field effects 2−77834
    - F-centre radiative decay, effects of random fields 2−74800
    - glass, containing metal ions, mag., rel. to struct., Mossbauer obs. 2−64526
    - metal (h.c.p.):^{57}Fe electric field gradients 2−80986
    - paramagnetic ions in axial fields, magnetothermodynamic props. 2−44220
    - rare earth ions is combined mag. and hexagonal cryst. fields, energy levels and moments 2−72117
    - resonant γ-ray nuclear Bragg reflection, azimuthal depend. elec. field determ. 2−81342
    - semiconductor, amorphous, rel. to thermally stimulated capacitor discharge expt. 2−54188
    - semiconductor, electroreflectance line shapes, local-field effects, contact exciton effects 2−68618
    - thulium ethyl sulphate, splitting of $p_{3/2}$ core levels of Tm^{3+} 2−44318
    - $Al_2Fe_3(SiO_4)_3$, almandite, garnet, elec. field gradient, internal mag. field, Mossbauer obs. 2−54388
    - BeO, field gradient parameter, applied field depend., n.m.r. obs. 2−44453
    - CdSe, elec. field distrib., subjected to 0-600 V applied voltages 2−64960
    - Co:As, hyperfine mag. fields at As, rel. to host mag. moments 2−78018
    - Co, effective mag. field on ^{67}Zn 2−84404
    - Co_3S_4, n.m.r. of Co^{3+}, apparent hyperfine field 2−81475
    - Dy_xCo_y, critical fields, ordering temps., magnetization curves at 4.2K 2−68544
    - Er^{3+} in phosphate and borate glasses, spectra rel. to cryst. field 2−75307
    - Eu ions in aromatic acids 2−75324

Crystals continued
internal fields continued
EuTe, Eu_3Te_4, Eu_4Te_7, Eu_3Te_7, Mossbauer spectra, sublattice covalent bonding, isomer shift, internal mag. field at Te nuclei 2−54389
Fe: ^{169}Tm, hyperfine field at Tm temp. depend. from perturbed angular correl. expts., 4.2-450K 2−81252
Fe:As, hyperfine mag. fields at As, rel. to host mag. moments 2−78018
Fe, effective mag. field on ^{67}Zn 2−84404
Fe, interactions of implanted ^{220}Rn and ^{224}Ra studied by α-γ angular correlations 2−81341
Fe film, e.f.g. in u.h.v. Mossbauer emission spectra 2−72284
$FeCl_3.6H_2O$, spontaneous magnetization, mag. ordering, mag. hyperfine fields, Mossbauer reson., $T<4.2$ K 2−75272
$Fe_{0.95}O$, wustite, mag. field, Mossbauer obs., 300, 223 and 80K 2−75269
FeS, antiferromagnetic, Mossbauer studies of internal magnetic field 2−81344
Ga, single cryst., elec. field gradient tensor from high field n.m.r. spectra 2−57396
$GdCl_3$, low temp. cooperative behaviour, n.m.r. obs. 2−72166
GeO_2:V^{4+}, e.p.r., g and A tensors, orbital mixing parameter, radial average, core polarization 2−72503
$K_{0.5}Nd_{0.5}TiO_3$, perovskite, prep., mag. susceptibility, cryst. field effects, 2-600K 2−54294
$Li_{0.5}Nd_{0.5}TiO_3$, perovskite, prep., mag. susceptibility cryst. field effects, 2-600K 2−54294
$Mo_{1-x}M_xGa_4$, M=Nb, Ru, Mn, Fe, Co, exchange field on conduction electron spins due to paramagnetic impurities 2−77862
NaCl, stressed, electric field gradient using molecular wavefunctions 2−80973
$Na_{0.5}Nd_{0.5}TiO_3$, perovskite, prep., mag. susceptibility, cryst. field effects, 2-600K 2−54294
Nb-Mo:Fe alloy, local moments on Fe, Mossbauer obs. 2−48149
NdP, NdAs, NdSb, crystalline electric field levels detn., neutron spectroscopy obs. 2−68585
Ni: ^{206}Bi, mag. hyperfine field at Bi 2−81251
Ni:As, hyperfine mag. fields at As, rel. to host mag. moments 2−78018
Ni, effective mag. field on ^{67}Zn 2−84404
$PbZnO_3$, internal electric field gradient by perturbed angular correlations 2−81156
$PrCl_3$, low temp. cooperative behaviour, n.m.r. obs. 2−72166
SiO amorphous, rel. to thermally stimulated capacitor discharge expt. 2−54188
SmF_3, effect of strong fields on n.m.r. behaviour 2−84589
Te, nuclear quadrupole diffr. of resonant γ-rays by ^{125}Te 2−57335
Tm^{2+} in phosphate and borate glsses, spectra rel. to cryst. field 2−75307
YAG:Nd^{3+}, random variation of static crystalline field, e.s.r. line width obs. 2−44441
YIG rod, internal field distrib., magnetoelastic reson. determ. 2−57285

lattice mechanics
see also Debye-Waller factors; Electron-phonon interactions; Ferroacoustic resonance; Mossbauer effect; Phonons; Spin-lattice relaxation
adiabatic approximation formulation 2−64830
alkali fluorides, Raman spectra, phonon modes 2−48196
alkali halide, higher anharmonic contribs. to diffuse X-ray scatt. 2−61059
alkali halide, method of moments for U-centre localised freq. 2−50984
alkali halide, surface optical modes obs. 2−51344
alkali halide crystals, limiting optical freq. calc. and temp. variation 2−72311
alkali halide Frenkel defect, lattice statics and deformation dipole model 2−60789
alkali halides: CrO_4^{2-}, optical and i.r. vibrational absorption spectra used to study defects in the host crystal 2−48171
alkali halides, B-2 type, three body force shell model calcs. 2−50993
alkali halides, $Co(CN)_6^{3-}$ doped, vibr. props. 2−54413
alkali halides, F-centre, relaxed excited state, vibronic model 2−43647
alkali halides, high press. and temp. props. 2−61072
alkali halides, local and gap modes due to substitutional impurity 2−47731
alkali halides, resonant phonon modes of Ag^+ and Au^+ 2−54018
alkali metals, dynamical struct. factor calc. using Krebs model 2−75052
alkaline earth fluorides, point defects vibr. spectra, thermal cond., i.r. absorpt., Raman scatt. obs. 2−71724
alkaline-earth halide crystals, vibronic spectra exam. 2−71705
ammonium thiocyanate and ammonium thiocyanate-d_4, far i.r. and Raman spectra 2−48201
amorphous, vibration effects on light absorpt., review 2−72293
amorphous substances, frequency spectrum moment method for study of vibrational properties 2−50981
anharmonic, thermodynamic properties 2−68207
anharmonic, thermodynamic properties 2−68208
anharmonic crysts. with singular interactions, phonon propagator and displacement field 2−61478
anharmonic lattices, stability 2−80882
anharmonic monoatomic linear chains, stability 2−80881
anharmonicity, estimation from X-ray interference intensity coeff. 2−54017
anharmonicity and Jahn-Teller effect 2−80957
anisotropic relax. of cryst. momentum transport in Umklapp-dominated regime 2−43997
attenuation due to spin-phonon interactions in a conc. paramag. crystal, $S={}^{1}._{2}$ 2−64846
p-azoxyanisole, temp. dependence of intermolec. interaction 2−50335
band modes in semiconductors and insulators, colour centre behaviour 2−54448
benzene and hexadeuterobenzene impurity, absorption spectra and exciton-phonon interaction 2−71717
benzene D_{2h}^{15}, Raman line strengths of lattice vibrations 2−44394
biphenyl crystal, lattice dynamics using 6-exp potential function 2−57043

Crystals continued
lattice mechanics continued
Born-von Karman theory, self-force matrix symmetry 2−80901
Brillouin zone sums on cubic lattices, evaluation 2−57115
bromoform, polycryst., combination scattering spectra 2−57339
caesium methanesulphonate meas. of Raman and i.r. spectra, correlation with crystal structure 2−72375
centred cubic, mean square displacement of atoms, simple conc. 2−57037
p-chloroaniline D_{2h}^{16}, Raman line strengths of lattice vibrations 2−44394
chloroform, polycryst., combination scattering spectra 2−57339
cluster model, variational Jahn-Teller groundstate 2−72234
conductor, microscopic formulation, long-wavelength limit 2−84186
critical phenomena, intermediate and h.f. sound propag. theory 2−54027
cross-relaxation between paramagnetic ions 2−68578
crystal surface, perturb. of vibrational props. by steps 2−57036
crystals, effects of external force gradients on i.r. and Raman activity of long wavelength optical phonons 2−84513
cubic crystals, anisotropic thermal conduction in phonon boundary scattering regime 2−68260
cubic crysts., localized polariton modes, continuum approx., variational approach 2−80885
cubic monatomic lattice, surface mode dispersion relations and surface sp. ht. 2−77487
cyclopentane-d_0 and -d_{10} cryst., vibr. assignment 2−84485
Debye frequency tensor of single crystals 2−80891
Debye model exam. using Born-von Karman theory 2−50983
defect crystal, with singular defect submatrix 2−61066
detective system, shell model dynamics, Green's function method 2−50989
diamond, Keating's model calcs. 2−71708
diatomic lattice, diagrammatic method analysis, Helmholtz free energy 2−80888
diatomic linear lattice, local and gap modes due to surface or substitutional impurity 2−74963
diatomic molecular crystal, model for lattice vibrs. 2−43960
diatomic molecular crystal, model for lattice vibrs. 2−43959
dielectric crystals, Lyddane-Sachs-Teller relation in the thermodynamic theory of dispersion theory 2−81148
dielectric thin layers and plates, thermal cond. and Poiseuille flow of phonons 2−61058
dilute quantum alloys, theory of vibrations 2−43948
disordered material, small polaron hopping and lattice relaxation 2−61144
disordered system, many site theory 2−47723
durene, phonon spectrum, Raman scatt. obs. 2−54022
durene, vib. and rot. freqs. distrib. from neutron scatt. 2−50999
dynamics, new exptl. methods using neutron and X-ray scattering 2−74706
dynamics, Raman theory, review 2−61054
feldspar, force field obs. 2−43955
ferroelectric, displacive-type, model for phase transition, polarization correlation 2−81127
ferroelectric, order-disorder transform., dynamic wave-vector-depend. susceptibility 2−81151
ferroelectric soft mode represented as motion of coupled sublattices 2−81152
ferromagnet, Heisenberg model, spin-lattice interactions 2−61497
ferromagnetic metal, hyperfine field, magnetization, temp. depend. 2−48066
ferromagnetic phase transformation, effect of lattice vibrations 2−68524
films, ionic crystal, microscopic theory of surface vibrations 2−80552
first order displacive phase transition, soft heat diffusion mode 2−61028
fluorides, perovskite type, i.r. absorpt. freq. rel. to cryst. parameters 2−61053
fluorite structure, Gruneisen parameters an interatomic forces 2−51050
fluorite-type crystals, doped spin- phonon interaction 2−72235
formamide crystals, i.r. and Raman vibrational spectra 2−44395
Franck-Condon displacements, effects on mobility edge and energy gap in disordered materials 2−54014
frequency spectrum of an isobaric disordered one-dimensional chain 2−64826
glass, chalcogenide, vibrational modes, molecular model 2−61057
graphite, pyrolytic, vibr. mode freqs., force consts. 2−43954
graphite, thermal vibs. of C atoms 2−54020
group III-V compound, amorphous, Raman scatt., phenomenological explanation 2−61665
group III-V compounds, amorphous, phonon density of states, Raman scatt. obs. 2−61664
group theoretical considerations 2−61069
group theory applic. and irreducible representations of a point group 2−64825
halides, heavier metal type, ionic Rydberg function 2−47727
halides, heavy, Born theory of i.r. eigenfrequencies and lattice props. 2−74961
hard core quantum crystal, point transformed self consistent harmonic treatment 2−61065
hexamethylbenzene, vib. and rot. freqs. distrib. from neutron scatt. 2−50999
hydrocarbons, crystalline, intermolecular interaction potential from incoherent scattering of slow neutrons 2−47738
hydroxyapatites, OH ions i.r. spectra, stretching and librational modes, H-bonding 2−61650
ice, hexagonal, atomic vibrs. 2−47730
ice, permittivity, low temp. meas., rel. to translational vibrs. 2−82414
ice, three dimensional eight vertex model and proton-proton correlation function 2−47726
impurity atom, thermal vibr. amplitude found using scattering of channelled ions 2−80897
inelastic scatt. and diffl. cross sect. of slow neutrons by localized vibrations of interstitial atoms 2−71722
inert gas crystals, review 2−61070

Crystals continued
lattice mechanics continued
infinite lattice with Coulomb interactions, long-wavelength normal modes 2−61056
insulating crystal with paramagnetic impurities, spin-phonon modes, change in thermal cond. 2−71706
interstitial impurities lattice dynamics, response function, interactions 2−77759
ionic cryst., Anderson-Gruneisen parameter 2−47724
ionic cryst., models, compressibility and dielec. props. 2−43952
ionic crystal, generalized shell model 2−61064
ionic crystal, realistic models for surface phonons 2−50988
ionic crystal plate, surface optical vibrations 2−71704
isomorphous proustite pyrargyrite series, vibrational spectra 2−44387
lattice model, two-body interatomic pots., rel. to elastic constants 2−68212
lattice resonant mode, effect on nuclear quadrupole spin-lattice relax. 2−51284
lattice vibration and group theory 2−77763
lattice vibrations in terms of group theory 2−80899
LEED rel. to lattice vibrs. 2−61062
linear defects, inelastic neutron scatt. cross sections calc. 2−50997
local states, iterative procedure 2−77824
longitudinal vibration modes and activation energy of self-diffusion 2−64827
magnetically ordered crystal, long wavelength optical phonons, morphic effects 2−72359
magnon-phonon interaction, microscopic theory of Raman scatt. modifications caused by mag. ordering 2−72360
mean square displacements of vol. and surf. atoms of fcc crystals, calc. 2−71307
metal, ang. force models 2−43945
metal, cohesive force conjugate to uniform expansion 2−67929
metal, cubic, lattice statics of vacancy-screw disloc. interact. 2−56687
metal, ferromag., vibrs. effect on temp. depend. of magnetiz. and hyperfine field 2−54323
metal, mech. forces caused by relativistic electron beams 2−57089
metal, simple, phonon spectra, electron-ion interaction higher order effects 2−47728
metal, vibr. behaviour of point defects 2−53723
metal halides, force constants and restrahlen frequencies, calc. from modified logarithmic form of overlap repulsion 2−43502
methyl group rotation and proton spin symmetry 2−68715
molecular cryst., anharmonicity due to exciton-exciton interaction 2−57338
molecular crystal, determination of general coupling parameters from classical theory of stimulated Stokes generation 2−51315
molecular crystal, neutron scatt. and vibrational spectra 2−54012
molecular crystals, calc. of small vibration spectra on basis of atom-atom representation of energy interaction 2−43947
molecular crystals, electron-vibrational spectra, review 2−57345
molecular solids, classical and quantum dynamical treatments, review. 2−61070
molecular solids, quantum lattice dynamics for translational and vibrational modes 2−71703
molecular solids, vibrational spectra, librational, torsional and translational modes 2−72362
momentum autocorrelation function of limited crystals 2−64832
multiphonon quantum theory of adatom desorption 2−50523
network models, derivation of difference eqn., study of energy spectrum and dispersion curves 2−77520
noble metal alloy, β-brass type, lattice vibrs. rel. to martensite struct. 2−56930
one dimensional anharmonic lattice model, specific heat and thermal expansion, high temp. calc. 2−57058
order-disorder phenomena, position, orientation, magnetic disorder, experimental techniques 2−50991
organic semiconductors with narrow conduction band, soln. of kinetic eqn. 2−81011
organic semiconductors with narrow conductivity zones, electron-phonon interaction 2−77810
orientationally disordered systems, atomic vibrs., hexagonal ice 2−47730
orientationally disordered systems, atomic vibrs., two-dimens. model 2−47729
oxide glass, alkali metal cation vibrs., far i.r. spectra study 2−71284
paramagnet, perturbed γ-γ angular correl. eff. of spin-lattice relaxation and ultrasound 2−72241
perovskite type crystal, self consistent theory of structural phase transitions 2−77767
phase transitions, decoupled-mode dynamic scaling theory 2−52103
phonon polarization vectors meas. with triple-axis spectrometers 2−64838
phonon spectra of crystal with imperfections of stacking fault type 2−68209
phonon states, symmetry labelling, orientation depend. 2−61134
pivalic acid, plastic, Brillouin doublets assignments 2−57366
plastic crystal, molecular rotation models, cold neutron scatt. obs. 2−80590
polariton Raman scattering, anisotropy effect 2−44388
polyethylene, lattice vibration dispersion curves 2−71718
polyethylene, localized and resonance modes below 700 cm^{-1}, due to kinks and folds, calc. 2−61153
polyglycine, extended form, calc. of two-dimensional lattice vibrations 2−68210
polymer, thermal fluctuations, valency angle stiffness, and Debye-Waller factors 2−74972
polymeric crystals, vibrs. of antiparallel chain sheet structs. 2−80884
polystyrene, example of three-dimensional damped Debye lattice 2−60104
polytetrafluorethylene, low temp. lattice bands in far i.r. 2−81353
quantum cryst., coherent state formalism and phonon freqs. 2−74960
quantum cryst., low temp. localized single particle formalism 2−61061
quantum crystal, neutro scatt. data interpretation 2−61060
quantum solids, phonon dispersion relation 2−77766

Crystals continued
lattice mechanics continued
quantum transport processes and quantization of Bloch function in strong elec. fields 2−61147
α-quartz, A_2 vibr. modes, i.r. lattice bands, classical oscill. model 2−74977
Raman spin-lattice relax. rel. to localized and quasilocalized vibrs. due to paramag. impurities 2−80896
rare earth fluorides, l.f. lattice vibrs. 2−43963
rare earth oxides, A-type, vibr. spectra 2−51355
rare earth oxyhalides, i.r. spectra, vibrs. assignments 2−57348
rare earth trichlorides under hydrostatic press., soft-sphere model for n.q.r. 2−54519
rare gas crystal, zero point energy, contrib. of high order multipole three body forces 2−74962
rare-earth fluoride crystals, vibronic spectra exam. 2−71705
rare-earth oxides, temp. spikes following Coulomb excitation 2−71719
reciprocal lattice determ. using goniometer stage and electron microscope 2−80614
Renner-type system, with strong vibr. coupling, optical absorpt. band shape determ. 2−65248
resonance vibrational states of crystal with point defects, influence of small perturbations 2−74761
Rochelle salt, far i.r. spectra, using Fourier transform spectrometer 2−72319
rutile struct. crysts., short range force consts. for rigid ion model from elastic consts. 2−50982
semiconductor, diamond-type, phonon induced quadrupole potential 2−71772
semiconductor, impurity conc. profiles and site distrib. determ. using i.r. localized vibr. modes 2−47433
semiconductors, cubic, nonpolar- lattice scattering effect on Ohmic conductivity of holes 2−51131
semiconductors, II-VI, deep Cu impurity, optical spectra, vibr. struct. 2−80954
Sharma and Joshi model applied to the thermal props. of Cs 2−47749
simple cubic lattice Green function 2−61050
slow vibrational relaxation, effect on Stokes shifted luminesc. and energy transfer 2−51374
sodium ammonium tartrate, ferroelec. phase transition mechanism 2−81139
sodium methanesulphonate meas. of Raman and i.r. spectra, correlation with crystal structure 2−72375
solid solns., metallic, application of Lindemann's rule for melting 2−74582
solid solution, X-ray diffr. and model of interatomic force equil. 2−74965
solid state physics, an overview 2−57093
sound wave-soft mode resonant interaction, rel. to displacive transitions 2−54026
sphalerite semiconductors, group III-V, charact. temps. 2−54013
spodiosite analogues, i.r. and Raman spectra 2−51318
strontium formate, i.r. and Raman spectra 2−61661
superconductor, A15 cpds., phonon linewidths, supercond. influence on Kohn anomaly 2−43951
surface, inelastic scatt. of low energy electrons by one phonon processes, theory 2−50986
surface dynamics, mean-square displacements of atoms in continuum approx. 2−43461
surface phonons and gas surface interactions 2−50522
surface phonons and magnons, review 2−50985
surface vibrational spectra, inelastic law energy electron scatt. 2−71706
surface vibrations, low energy electron spectroscopy obs. 2−50987
surface vibrs. of model h.c.p. cryst. 2−50456
TCNQ complexes, with quinolinium and triethylammonium, i.r. spectra, vibronic effects 2−81387
TCNQ cpds., Debye lattice contrib. to low temp. sp. ht. 2−54052
p-terphenyl, rigid mol., librational motion temp. factor 2−54025
thermal plane wave dispersion and polarization 2−43949
thermodynamics of crystals, book 2−43950
thiourea, librational mode linewidth, Raman spectra obs. 2−75314
transition metal carbides, phonon anomalies 2−64836
transition metals, h.c.p., noncentral force model 2−80887
vibration, mean square amplitude matrix, low-temperature limit 2−59970
vibration symmetry determ. using method of ascent in symmetry 2−57038
vibrational edge modes, long wave acoustic phonons at edge 2−61063
vibrational properties of harmonic solids, consistency requirements 2−74964
vibrational spectra of isotropically disordered crystals 2−64828
vibrations, freqs., polarization vectors and dynamic matrix elements relations 2−61055
wurtzite type crystal, spontaneous distortion from tetrahedral struct. 2−67981
X-ray thermal scattering, Model Q-function descrip., linear lattice approx. 2−53630
XY_6 octahedral mol., normal vibration modes from group theoretical considerations 2−61068
XY_6 octahedral molecule, group theory applications 2−61067
zincblende cpds., local-mode frequencies of isoelectronic impurities, molecular model 2−54016
zincblende semiconductor, Debye-Waller factor calc. from mod. rigid ion model 2−84199
Ag, Compton effect scatt. power, thermal vibr. freqs. 2−68213
Ag, phonon dispersion curves, by coherent inelastic scattering of thermal neutrons 2−80900
Ag, total energy, pseudopot. theory, applic. to phonon spectra 2−61137
AgCl(Br), anharmonicity, far i.r. dielec. response study 2−61071
AgI, wurtzite-type, fund. optic lattice modes, Raman scatt. 2−61662
Al, thermal vibr. freqs., X-ray scatt. obs. 2−61073
Al_2MgO_4 spinel, lattice dynamics, elastic properties, seismic velocity and density profiles 2−72636
AlN, interaction of i.r. luminescence centre with natural transverse acoustic vibrations 2−75336

Crystals continued
lattice mechanics continued
α-Al_2O_3, anharmonic coeffs. of sp. ht. and entropy, Gruneisen parameter 2−51047
Ar-O_2 system, Raman spectra and luminesc. sideband obs. 2−75310
Ar, static lattice energies, PV relation, at T=0K 2−80889
As_2S_3, vitreous, Raman scatt. obs. 2−61663
As_2S_3, vitreous, vibration spectra, computer generated 2−74966
$As_2S_3(Se_3)$, amorphous, refl. spectra study 2−61614
As_2Se_3, vitreous, vibration spectra, computer generated 2−74966
Au, and specific heat 2−61074
Au, total energy, pseudopot. theory, applic. to phonon spectra 2−61137
Au single crystals, electron microscopy at low temps. 2−80892
Ba_2CaMO_6 ordered perovskites, M=Mo, Te, W, meas. of vibrational spectra, assignment of internal vibrations 2−81370
BaF_2, force fields, contrib. of three-body overlap effects 2−77765
BaF_2, low temp. plasma produced radiational defects 2−71452
BaF_2, second-order Raman spectra correl. with two-phonon density of states 2−57040
Ba_2MgWO_6 ordered perovskite, meas. of vibrational spectra, assignment of internal vibrations 2−81370
$Ba_2NaNb_5O_{15}$, Raman spectra, vibr. props., characterization 77-843K 2−72364
$BaTiO_3$, ferroelectric, acoustic- mode-soft-optic mode interactions, press. depend. 2−71707
$BaTiO_3$, lattice dynamics 2−61412
$BaTiO_3$, lattice vibr. of monatomic linear chain, double min. potential, computer simulation 2−54019
$BaTiO_3$, Raman scatt. line shape of soft E polariton mode 2−78112
$BaTiO_3$, vibr. amplitude, calc. 2−68215
$BaTiO_3$, vibr. amplitudes and Debye-Waller factors from elastic consts. and Raman freqs. 2−50983
$Be_2Al_2Si_6O_{18}$, beryl, anharmonicity of i.r. vibration modes, reflectivity obs. 2−51317
BeF_2, Raman spectra to 630°C 2−48197
BeO, vibr. amplitudes and Debye-Waller factors from elastic consts. and Raman freqs. 2−50983
Bi, diffusive propagation of heat pulses, second sound 2−47762
BiOBr(Cl)(F)(I), i.r. spectra, vibrs. assignments 2−57348
C X-ray diffraction intensity effective temperature factor 2−53655
CO, model for lattice vibrs. 2−43960
CO_2, symmetry of vibrs., group theoretical study 2−43953
CO_2 librational modes, application of quantum mechanical lattice dynamics formalism 2−71709
CaF_2:H-, local modes studied with intense CO_2 laser 2−61632
CaF_2, low temp. plasma produced radiational defects 2−71452
CaF_2, neutron scatt. anal. 2−71723
CaF_2, rare earth doped, interstitial ion vibr. freqs. 2−60790
CaF_2, second-order Raman spectra correl. with two-phonon density of states 2−57040
CaF_2, surface optical modes obs. 2−51344
CaF_2, vibr. amplitudes and Debye- Waller factors from elastic consts. and Raman freqs. 2−50983
CaF_2 film, spectral emission by polaritons 2−65252
CaF_2 force fields, contrib. of three-body overlap effects 2−77765
CaO, phonon dispersion, three body force shell model 2−68216
CaO, shell model calc. of Gruneisen parameter and thermal expansion 2−47756
Cd, Keating's approach 2−84182
$CdCl_2:Co^{2+}$, obs. of vibrational-electronic coupling in high resolution spectrum of spin forbidden band 2−81356
CdF_2, surface optical modes obs. 2−51344
CdS, boson echos obs. 2−65071
CdS hot electron mobility 2−84276
CdS_xSe_{1-x} mixed crystal, study of lattice dynamics, phonon-phonon interactions by Raman spectra 2−51353
CdSe:S, local impurity and lattice vibrs., Fermi reson., absorpt. spectra obs. 2−80895
Cl_2 i.r.-active intermol. translational band intensities, intermol. bonding obs. 2−74967
$Co_3B_7O_{13}I$, rel. to press. depend. of ferroelec. transition temp. 2−47984
Cr-1.6%W alloy, phonon freqs., neutron scatt. obs. 2−74973
Cr, theory of surface atom mean square displacements 2−61075
Cr complexes, Cr(III) dimethylsulfoxide compounds, low temp. luminescence and vibrational spectra 2−51375
CrO_2, Raman scatt., phonon spectra rel. to VO_2 2−65277
$Cr(ur)_6I_3$, ${}^4A_2 \rightarrow {}^2E$ transition, spin-orbit interaction and Jahn-Teller distortion effects in calc. of vibronic spectra 2−51291
Cs, lattice vibration based on Toya's electron-phonon interaction 2−64834
Cs, thermal props. calc. model 2−47749
CsBr, cation impurity, i.r. absorp. obs. 2−61635
CsBr(Cl)(I), three body force shell model calcs. 2−50993
$CsCl:K^+(Rb^+)$ impurity- induced i.r. absorpt. calcs., 2−54419
CsCl, phonon-dispersion, neutron spectrometer study and shell model anal. 2−84192
CsCl(Br)(I), vibr. absorpt. spectrum of NO_2^- and NO_3^- 2−77769
CsF, phonon dispersion relations, neutron scatt. study 2−64840
$CsICl_4$, normal modes of vibr. 2−71427
Cs_2PtCl_6, rotary lattice mode freq. over Brillouin zone, temp. depend. 2−77748
Cs_2UBr_6, force constants, vibronic structure 2−74968
$Cs_2ZrB_6:Re^{4?}$, vibr. mode energies of ground state 2−57370
Cu, total energy, pseudopot. theory, applic. to phonon spectra 2−61137
CuCl and CuBr, anomalous thermal expansion with i.r. spectroscopy 2−43993
Cu_2O, i.r. absorp. and light scattering obs. 2−61636
Cu_2O, resonant Raman scatt. near 1S exciton level 2−54434
Dy, lattice excitation and magnon spectra, magnetoelastic effects 2−65141
EuO:Gd, lattice vibrations, dopant effects 2−68397
F_2, model for lattice vibrs. 2−43960
F_2, model for lattice vibrs. 2−43959
α-Fe, modified lattice statics approach to point defect calcs. 2−60784
Fe, Mossbauer effect, high pressure obs. between 300-20K 2−72283
α-Fe 2−84178

Crystals continued
lattice mechanics continued
$FeCr_2S_4$ spinel, Debye model deviations of isomer shift in Mossbauer spectra 2−57331
Fe(III) complexes, vibrations of T_{1u} mode, magnetic circular dichroism analysis 2−48176
GaAs:Si, boatgrown and pulled, B impurity, i.r. local mode absorption spectra, comparison 2−61640
GaAs, mean square atomic displacement study by LEED 2−71318
GaAs, surface and bulk atomic vibrs., calc. 2−80894
GaAs, zinc-blende lattice, anharmonic props. 2−80898
GaP:B, i.r. spectra, localized mode frequencies and gap mode vibrations 2−80883
GaP:N, localized vibr. modes due to N isotopes, i.r. absorp. obs. 2−68639
GaP, phonon damping func. freq. depend., polariton Raman scatt. obs. 2−61076
GaP, surface and bulk atomic vibrs., calc. 2−80894
Gap, two phonon Raman spectra 2−48156
$Gd(MoO_4)_3$, calc. rel. to ferroelec. domains and condensed soft mode 2−68470
$Gd_2(MoO_4)_3$, ferroelec., ferroelastic, elastic constants and soft optic modes 2−65061
$Gd_2(MoO_4)_3$, ferroelec. transition parameters 2−78068
$Gd_2(MoO_4)_3$, Raman spectrum, temp. depend., calc. 2−68660
Ge, amorphous, phonon density of states, Raman scatt. obs. 2−61664
Ge, amorphous, Raman scatt., phenomenological explanation 2−61665
Ge, dispersion curves and specific heats, angular force model 2−74969
Ge, Keating's model calcs. 2−71708
Ge, tetrahedrally bonded, vibr. states from Keating model, Raman line intensity 2−68224
Ge III polymorph, vibrational props., Raman scatt. obs. 2−72372
$Ge_xAs_{40-x}S_{60}$ glass, rel. to heat capacity 2−51045
o-H_2, f.c.c. and h.c.p. phases, phonon state density 2−64839
H_2, ortho, zero-phonon IR Q-branch absorpt. theory 2−74975
H_2, self-consistent eqn, of state 2−71711
o-H_2 librational modes, application of quantum mechanical lattice dynamics formalism 2−71709
$HCl.2H_2O$, $H_5O_2^+$ ion vibrations from i.r. and Raman spectra 2−61667
He, Umklapp thermal relax. time tensor, thermal cond. anisotropy 2−74579
${}^3He$, b.c.c., ground state props., localized single particle and correlated function calcs. 2−53482
${}^3He$, b.c.c., thermal excitations 2−43434
${}^4He$, b.c.c., anomalous Debye- Waller factor 2−67865
${}^4He$, b.c.c., phonon freq. dispersion curves and group widths 2−53483
${}^4He$, b.c.c., scatt. function for inelastic neutron scatt. 2−67867
${}^4He$, h.c.p. and b.c.c. phases, single-particle scatt. phenomena 2−67866
Ho, non-central force model 2−74970
InP-InAs solid solns., i.r. lattice vibrs. 2−47739
InP, vibr. amplitudes and Debye-Waller factors from elastic consts. and Raman freqs. 2−50983
InSb, zinc-blende lattice, anharmonic props. 2−80898
KBr, analysis of R_2 absorp. struct. 2−51342
KBr, effect of melting on multiphonon i.r. absorp. spectra 2−68220
KBr, phonon energies at Van Hove crit. pts. 2−71712
KBr film, i.r. reflectivity, dielectric response obs. 2−72304
KBr(Cl)(I), reson. phonon modes of Ag^+ 2−50994
$KCl:Co(CN)_6^{3-}$, vibr. props. 2−54413
KCl, analysis of R_2 absorp. struct. 2−51342
KCl, sylvite, thermal oscillation freqs., 295, 80 and 5K 2−64835
KCl,SO_4^{2-}, internal vibr. modes, rel. to anion vacancy trapping 2−43620
KCl(I), local and gap modes due to substitutional impurity 2−47731
$KClO_3$, irrad., Raman spectra, radiation damage obs. 2−57361
KD_2PO_4, ferroelectric vibrations obs. in Raman scattering spectra 2−48200
KH_2AsO_4, ferroelectric vibrations obs. in Raman scattering spectra 2−48200
KH_2PO_4, ferroelectric mode, proton-phonon coupling effects, Raman spectra obs. 2−65279
KH_2PO_4, ferroelectric vibrations obs. in Raman scattering spectra 2−48200
KH_2PO_4, mode interactions 2−55680
$K_2Ir(Pd)(Pt)Cl_6$, incipient phase transitions, rotary lattice mode freq. over Brillouin zone 2−77748
KN_3, Raman active librational modes, anharmonic self energy shift 2−71726
K_2PtBr_6, rotary lattice mode softening, n.q.r. obs. 2−61756
K_2SO_4, laser Raman spectra, lattice vibration modes 2−72368
$KTa_xNb_{1-x}O_3$, l.f. zone boundary lattice vibr. modes, Debye-Waller factor anisotropy 2−80902
$KTa_xNb_{1-x}O_3$, Raman scatt. study 2−54425
Kr, Mossbauer recoilless fractions calc. with central-force rigid-atom model 2−74974
La complex, lanthanide (III) tropolonates, crystal field effects in i.r. spectra 2−61644
Li b.c.c., lattice dynamics, phonon freqs., sp.ht., Debye temp., from Krasko-Gurskii model 2−68227
LiCl, Hartree-Fock wave function and localized orbital calcs. of elastic consts. 2−50726
LiCl, heat capacity, size-disparity anharmonicity 2−71748
LiD:H, localized lattice vibrations, Raman scattering 2−61668
LiD, phonon dispersion, three body force shell model 2−68217
LiF, analysis of R_2 absorp. struct. 2−51342
LiF, assignments of two-phonon i.r. absorpt. spectrum 2−61645
LiF, deformable shell model studies 2−50995
LiF, effect of melting on multiphonon i.r. absorp. spectra 2−68220
$LiIO_3$, near and far i.r. investigations for α and β crystals 2−84511
$LiIO_3$, polariton dispersion, light scatt. associated with photons 2−68617
$LiNbO_3$, Raman scattering and obs. of polaritons by photographic method 2−81374
$LiNbO_3$ single crystal, lapping characts. 2−71603

Crystals continued
lattice mechanics continued
Mg, phonon freqs. from Krasko and Gurshii model potential 2–74976
MgO, lattice dynamics, elastic properties, seismic velocity and profiles 2–72636
MgO, second-order Raman scatt. tensor calc. 2–71713
MgO, three body interactions in shell model 2–61077
MgO film, spectral emission by polaritons 2–65252
Mg_2SiO_4 spinel, lattice dynamics, elastic properties, seismic velocity and density profiles 2–72636
MgTe-CdTe mixed crystals, vibrs., Raman spectra study 2–71714
$Mg_yU_{1-y}O_{2-x}$, B value of thermal vibrations observed by X-ray meas. 2–47336
$(Mn, Fe)_3O_4$, i.r. absorp. spectra obs. 2–61648
MnO, dispersion props., three body force shell model 2–61078
Mo 2–84178
Mo:^{57}Fe, impurity-host to host-host coupling const. ratio, Mossbauer study 2–84183
MoO_2, Raman scatt., phonon spectra rel. to VO_2 2–65277
MoS_2, rigid layer lattice vibrations and van der Waals bonding 2–84194
$MoSe_2$, i.r. absorpt. spectra, transverse optic lattice vibr. freq. 2–78105
α-N_2, librational anharmonicity 2–47733
N_2, model for lattice vibrs. 2–43960
N_2, model for lattice vibrs. 2–43959
α-N_2 librational modes, application of quantum mechanical lattice dynamics formalism 2–71709
NH_3 and ND_3, Raman spectra, metastable phase obs., lattice modes 2–72370
NH_4Br, critical fluctuation enhanced Raman scatt. by phonons 2–43956
NH_4Br, l.f. soft vibr. modes, stress effects, phase transforms 2–71696
$(NH_4)_2Cd_2(SO_4)_3$, non-homogeneous lattice vibr. modes instability under press. 2–77958
NH_4Cl, analysis of lattice vibrations in low-temp. ordered phase using rigid-molecule model 2–68219
NH_4Cl, phase transitions, pseudospin and stochastic model description 2–43923
$NH_4H_2PO_4$, antiferroelectric, long-wavelength polarization fluctuations 2–78113
$(NH_4)_2S_2O_8$, vib. and rot. freqs. distrib. from neutron scatt. 2–50999
$(NH_4)_2SiF_6$, vib. and rot. freqs. distrib. from neutron scatt. 2–50999
NaBr(Cl), local and gap modes due to substitutional impurity 2–47731
NaCl:$Co(CN)_6^{3-}$, vibr. props. 2–54413
NaCl, effect of melting on multiphonon i.r. absorp. spectra 2–68220
NaCl, equation of state, 0-8kbar, 300-800K, u.s. determ. 2–68065
NaCl, one-phonon Green function, anharmonic contribs. 2–50996
NaCl film, i.r. reflectivity, dielectric response obs. 2–72304
NaCl surface, mean-square amplitudes of vibr. 2–50454
NaCl surface, vibr. modes in rigid-ion model 2–50455
$NaClO_3$, ferroelectric phase transition, relation to phonon structure 2–61431
$NaClO_3$, irrad., Raman spectra, radiation damage obs. 2–57361
NaF slabs, for-i.r. emission assignment 2–61649
$NaMnF_3$, vibration frequency determ. from absorp. spectra at 300K and 80K 2–65262
NaN_3, rhombohedral, lattice dynamics 2–43957
$NaNO_2$, piezoelec, and birefringent, Brillouin scatt. at room temp. 2–48204
$NaNO_3$, Raman scatt. tensors detn. 2–75312
$NaNbO_3$, soft phonon modes, rel. to cryst. struct., 480-575°C 2–80649
Nb, diffusion of H and D, application to quantum theory 2–80718
NbH_x, neutron scatt. obs. of hydrogen motions 2–77771
Nb_3Sn-type compounds, phonon spectrum calc. 2–84187
Nb_3Sn, phonon linewidths, supercond. influence on Kohn anomaly 2–43951
Ne, anharmonic, interference effects in neutron inelastic scatt. 2–54023
$Ni_xZn_{1-x}Cr_2O_4$, cooperative Jahn-Teller transition, thermal expansion and sound velocity study 2–71693
O_2, model for lattice vibrs. 2–43960
O_2, model for lattice vibrs. 2–43959
Pb-In dilute alloy, supercond., phonon spectra detn., elec. tunnelling obs. 2–54142
PbF_2, thermal expansion and phase transition, shell model 2–84216
$Pb_5Ge_3O_{11}$, ferroelec., soft optic phonon mode 2–43961
PbTe, TO lattice mode, low temp. far i.r. detn. 2–65265
Pd_3Fe, vibr. mode freqs., 80K 2–43962
PrF_2, second-order Raman spectra correl. with two-phonon density of states 2–57040
RbBr, reorientation rates of OH- defects, calc. from phonon spectra 2–61080
RbCl, phonon dispersion relations, shell model calc. 2–61079
RbCl, surface phonon branch distrib., shell model 2–47734
RbCl, vibr. absorpt. spectrum of NO_2^- and NO_3^- 2–77769
RbF, surface phonon branch distrib., shell model 2–47734
$RbMnF_3$, phonon struct. of absorp. spectra in 3900 Å region 2–65266
Rb_2PtCl_6, rotary lattice mode freq. over Brillouin zone, temp. depend. 2–77748
ReF_7, vibr. spectrum, normal coord. analysis, logarithmic steps methods 2–54024
SbSI, boson echos obs. 2–65071
SbSI, far i.r. reflectivity, complex dielec. const. deriv., soft mode in paraelec. phase 2–61619
Se, trigonal, modified valence force field approach 2–57041
Si, amorphous, Raman scatt., phenomenological explanation 2–61665
Si, anharmonicity, rel. to forbidden (442) refl. temp. depend. 2–83885
Si, clean and doped, mean square atomic displacement study by LEED 2–71318
Si, Keating's model calcs. 2–71708
Si, phonon energy assignments, multiphonon Raman spectra obs. 2–68221

Crystals continued
lattice mechanics continued
Si, Raman scatt., one and two phonon struct. obs. 2–61081
Si, tetrahedrally bonded, vibr. states from Keating model, Raman line intensity 2–68224
Si, two phonon spectra, three independent components detn. two phonon Raman spectra 2–48156
Si III polymorph, vibrational props., Raman scatt. obs. 2–72372
SiC:H(D), implanted, recomb. radiation of excitons and vibr. spectrum 2–68688
SiC, H- and D-implanted, CH and CD bond-stretching modes 2–65296
SiO_2, vitreous, lattice vibrational spectra, pressure densification effects 2–74971
Si(111) surfaces, lattice vibrations 2–43467
Sn base dilute alloy, ^{119}Sn nuclei vibrations, Mossbauer obs. 2–71721
SrF_2, Gruneisen function, shell model calcs. 2–84216
SrF_2, low temp. plasma produced radiational defects 2–71452
SrF_2, phonon dispersion curves, harmonic vibr. props. 2–77760
SrF_2, second-order Raman spectra correl. with two-phonon density of states 2–57040
SrF_2 force fields, contrib. of three-body overlap effects 2–77765
SrO, Raman scatt. spectrum 2–44393
SrO, shell model calc. of Gruneisen parameter and thermal expansion 2–47756
$SrTiO_3$, electric polarization of crystals by inertial forces 2–54238
$SrTiO_3$, l.f. soft vibr. modes, stress effects, phase transf. 2–71696
$SrTiO_3$, lattice dynamics, normal mode freqs., harmonic models, calc. of props. 2–77761
$SrTiO_3$, response function of soft zone boundary phonon, microscopic calc. 2–61082
TaC, phonon anomalies 2–64836
TaC_x, lattice instability, effects on superconducting and mechanical props. 2–68349
Tb, lattice excitation and magnon spectra, magnetoelastic effects 2–65141
$Tb_2(MoO_4)_3$, low freq. phonon dispersion rel. to ferroelectric phase transition, neutron scatt. obs. 2–65066
Te, amorphous, vibrational density of states, Raman spectra obs. 2–65281
TeO_2, active modes, i.r. refl. and Raman scatt. study 2–71716
Ti-V-O and Ti-V-Al-O solid solutions, charact. temp. and elasticity modulus 2–50844
TiO_2, rel. to temp. depend. of elastic consts. 2–84042
TlBr, TlCl, thermal expansion obs. 2–57076
TlCl(Br), anharmonicity, far i.r. dielec. response study 2–61071
$UO_2(NO_3)_3$, anisotropy of i.r. vibrations 2–75308
V_2O_5, long wave optical vibrational spectrum 2–68629
V_3Si, lattice stabilization in high magnetic fields 2–77869
W 2–84178
Xe, elastic-force model, ang. force effects 2–61083
$Zn_xCd_{1-x}Se$ solid solution, phonons and structure, Raman scatt. obs. 2–64837
$Zn_xCd_{1-x}Te$ solid solution, phonon freq. detn. from reflection spectra 2–72308
ZnS:Be, i.r. lattice absorption spectra, localized mode sidebands obs. 2–72385
ZnS, vibr. amplitudes and Debye-Waller factors from elastic consts. and Raman freqs. 2–50983
ZnS polytypes, Raman scatt. obs. 2–61084
$ZnSiP_2$, optical phonons, polaritons, mode freqs., strengths, damping factors 2–61621
Zr, Keating's approach, elastic consts. and thermal expansion calc. 2–43964
orientation
by cleavage plane reflected laser beam 2–74656
crystal surface orientation meas. by u.s. beam displacement 2–56604
elastomers, effect on strength and toughness at low temperatures 2–60886
f.c.c. polycrystals, viscoelastic properties, grains disorientation effects 2–53786
goniometer for implantation and channelling exprts. 2–74788
preparation by lapping 2–80587
and shape, absorption corrections, checking method 2–64628
X-ray diffraction goniometer, symmetrically moving θ-θ 2–53635
α-Al_2O_3, corundum, Verneuil grown cryst., cryst. axis orientation 2–60701
Au single crystals, electron microscopy at low temps. 2–80892
Co-Fe, electrolytically deposited films 2–53561
β-Co, electrolytically deposited films 2–53561
GaAs, growth from gas phase, cryst. morphology 2–56656
Ge, profiled crystals drawn from melt, deflection of orientation 2–47425
La and Y ethylsulphates: ^{166}Er, effect on $\gamma\gamma$ cascade ang. correlation 2–78053
Mo single crysts., surface orientation effects on yield 2–74842
polarons *see Crystal electron states/polarons*
twinning
– 2–77522
b.c.c. lattice, accommodation of deform. twins by screw dislocations 2–74782
5,5'- biisoxasole, Weissenberg photographs 2–83964
brass, fatigue cracking, effects of grain and twin boundaries, slip mode behaviour 2–71598
coherent twin boundaries interaction with grain boundaries, review 2–68032
deformation, law, and applic. to reciprocal lattice 2–67932
diamond, deform. twinning and twinning plane identification 2–50684
diamond, framesite, microstructural aspects 2–50877
diamond, intersecting twins 2–80692
dislocation model 2–47410
electron microscope intensity calculations at joint 2–80626
enstatite, X-ray topographic studies of natural and deformed crystals 2–61970
fluorite, natural X-ray topographic obs. 2–80669
2- iododibenzoyl peroxides, conservative twinning, topotaxy 2–77525

Crystals continued
twinning continued
- metal coatings, X-ray exam. of fault probability 2−50473
- metal film deposition on alkali halides, multiply-twinned particles 2−47101
- phase transformations, rel. to elastic constants and the ΔE effect 2−77664
- rare earth oxides, types of. twinning process 2−53739
- snowflake crystals 2−62245
- steel, austenitic stainless, precip. at twin boundaries 2−43850
- steel, high temp. fracture, influence of annealing twins 2−56833
- steel, high-C martensitic, electron diffr. obs. 2−56934
- steel, martensitic, field ion microscope obs. 2−64779
- topotaxy, templates and twinning 2−77525
- Zircaloy-4, deform. mechanism 2−50747
- Al_2O_3, alumina, kinetics of twin boundary grooving on single cryst. surfaces 2−50432
- Al_2O_3 ceramic, rel. to deformation processes 2−60993
- Au-Cu ordered alloys, dislocation mechanisms of twinning 2−68033
- $BaSO_4$, interpenetrating in cryst. grown from silica gels 2−43519
- Be, rel. to anisotropy of deform. after programmed loading 2−80775
- Bi-Zn(Ag) eutectic alloy, electron diffr. obs. 2−60976
- Bi whisker, deform. twinning, nucleation and propag. stresses 2−47424
- $CaCO_3$, calcite, twinning boundaries, thermal shift after annealing 2−77573
- CsCl B2 type struct., transform. twinning, inhomogeneous shear model, reply to comments 2−64810
- CsCl B2 type struct., transform. twinning, inhomogeneous shear model, comments 2−61032
- Cu, fatigue cracking, effects of grain and twin boundaries, slip mode behaviour 2−71598
- Cu, growth of twin free crystals by secondary recrystn. and zone refining 2−47580
- Cu and Cu-Zn alloys, development of texture 2−80849
- Cu single crystals, mech. twinning during elongation or torsion at 78 K and room temp. 2−74783
- Fe-Co-C, suppression in martensite flow stress 2−56941
- Fe-Co-V alloy, ordered and disordered, recovery behaviour 2−50804
- Fe-Cr-Ni, low temp. deform. characts. 2−43693
- Fe-Mn-(B)-C, suppression in martensite flow stress 2−56941
- Fe, fast neutron irrad. at 77K, twinning suppression 2−80689
- Ge, profiled crystals, anisotropy of layered growth 2−47425
- GeTe-SnTe alloy, epitaxial film, electron diffr. obs. 2−53574
- GeTe epitaxial film, electron diffr. obs. 2−53574
- In, rolled, influence on texture 2−80774
- $K_4Fe(CN)_6.3H_2O$, ferroelectric, proton mag. resonance obs. 2−74655
- KIO_3, detwinning method 2−74733
- $KNbO_3$, ferroelectric single crystals, deformation and stress relaxation behaviour 2−80743
- Mg, plane strain extrusions, texture control and yield anisotropy 2−80848
- Mn-Al alloy, rel. to effect of $\varepsilon \to \tau$ transform. on mag. props. 2−57280
- Mo-34%Re, deform. struct. obs. 2−43624
- Mo-35%Re alloy, deform. twins, nucleation and growth 56720 2−56720
- Mo-Ru alloy, rel. to deform. mechanism 2−50840
- MoC, foil, electron diffr. obs. 2−43641
- Nb, energy required for twinning 2−64588
- Ni-Ni_3Nb, directionally solidified eutectic alloy, slip and mech. twinning 2−56796
- Ni, work hardened in tension, double texture, twinned growth influence 2−60985
- Ni coatings, electrolytically obtained, transmission electron microscopy 2−50519
- Ni stacking fault propagation from a coherent twin boundary 2−80670
- $NiAl_2O_4$, grown on sapphire 2−71333
- $RbIO_3$ crystal struct. determ. 2−77548
- Si growth twins grown by pulling method 2−74688
- SiC whiskers, twin morphology 2−53581
- Sn, shisker, deform. twinning, nucleation and propag. stresses 2−47424
- Sn whisker, mech. twinning rel. to supercond. behaviour 2−47869
- $SrSO_4$, interpenetrating in cryst. grown from silica gels 2−43519
- Ti-Ta alloys, martensitic transform. 2−47696
- U, β phase, microstress behaviour during quenching, relaxation 2−77659
- VO_2, transformation to tetragonal phase, X-ray obs. 2−47698
- X-ray intensity statistics, twin identification 2−47184
- (Zn, Mn, Fe)Ti_3O_7, landauite, Baumhauer type twins 2−71499
- Zn, whisker, deform. twinning, nucleation and propag. stresses 2−47424
- ZnO, cryst. growth, inversion twin obs. 2−50581
- ZnS, melt grown, hexagonal, defect elimination by donor impurity doping 2−47279
- ZnS epitaxial film, on GaAs 2−71339
- ZnSe, grown from vapour phase under controlled partial press. 2−64594
- ZnTe epitaxial film, on Ge substrate 2−50515
- ZrO_2, calcia stabilized, thermal stress induced microstruct. modifications 2−50901
- ZrO_2, martensitic transform. struct. 2−50953

whiskers
- snowflake crystal surface rel. to internal elec. field 2−62245
- tensile strength, apparatus for testing 2−80789
- tensile testing machine 2−43759
- viscoelastic parameters, effect of adhesive flow, viscoelastic three element elastic modes 2−63087
- Ag-Hg amalgam, growth on Hg surface from aqueous solns. 2−60669
- Ag, filamentary growth from Ag compounds, solid state ionics technique 2−47133
- Ag, growth and dissolution 2−50517
- α-Al_2O_3, growth during Al oxidation 2−74637
- Al_2O_3, poor efficiency in reinforcing Ni for high temp. use 2−47668
- α-Al_2O_3, role of water in formation reaction 2−74638

Crystals continued
whiskers continued
- Al_2O_3, sapphire filaments, strength enhancement due to continuous flame polishing 2−80867
- Bi, deform. twinning, nucleation and propag. stresses 2−47424
- Bi, resist. oscills. in mag. field at 4.2 K 2−68338
- Cd, vapour growth in various atmospheres 2−47134
- Co, martensitic transformations, constitution and dislocation structure 2−71340
- Cu, ductility determ. 2−56810
- Cu, growth by halide reduction, and defect struct. 2−80570
- Cu, vacancy formation 2−47397
- Fe, lattice twists, growth morphologies 2−80561
- Fe, mag. stray fields of 180° Bloch walls, Permalloy probe study 2−78015
- InSb, growth by InSb gas transport morphology 2−75366
- KCl, growth on KCl crysts., and struct. 2−67914
- KCl, slightly deformed, etch pit distrib. 2−71490
- MnAs, phase boundary motion at coupled lattice- and spin-disorder transition, resist. study 2−78021
- NaCl whiskers inelastic phenomena 2−80575
- Rb, gas-phase growth 2−74639
- Rb, growth rate obs. rel. to surface diffusion near m.p. 2−60629
- Si, doping, during growth by gas transport 2−47430
- SiC, twin morphology 2−53581
- Si_3N_4, Ni-coated, high temp. stability, gaseous environment effects 2−74640
- Sn, deform. twinning, nucleation and propag. stresses 2−47424
- Sn, mech. twinning rel. to supercond. behaviour 2−47869
- Te, vapour grown, morphology and dislocation structure 2−67915
- Zn, deform. twinning, nucleation and propag. stresses 2−47424

Curie temperature *see Ferroelectric materials; Ferroelectric phenomena; Magnetic properties of substances*

Curie-Weiss law *see Magnetic properties of substances/paramagnetic; Paramagnetism*

Curium
- in Ap star HD 25354, spectral obs. 2−72994
- atom, L_2 subshell, fluoresc. yield 2−79924
- biological damage, interactions with cells and tissues 2−78659
- magnetic properties and valence 2−48037
- in nuclear fuels determ. during reprocessing 2−74178
- nuclear targets, electrodeposition methods of prep. for cross section obs. and accelerator bombardment 2−73919
- ^{244} Cm, production based on neutron irradiation of Pu 2−49987
- ^{244}Cm, applications as radioisotopic power fuel 2−49252

Curium compounds
- CmF_3, magnetic properties 2−48037
- CmO_x-O_2, phase reactions during isobaric thermogravimetric analysis 2−74927
- CmOCl, magnetic properties 2−48037
- $^{248}CmO_2$, thermal coeff. of expansion, 25°-450°C 2−84207

Current, electrical
- air-earth current, diurnal variation at Kyoto, Japan 2−78379
- balances, temperature rise in coil former due to resistance in windings and corrections 2−41896
- conservation, distinction from charge conservation and flux integral forms 2−55652
- frequency analysis method, for current fluctuation in plasma 2−53198
- h.v. breakdown, Z-pinch, low pressure formative phase in gases 2−67650
- impulse surface discharge rel. to applied voltage and specific capacitance, obs. 2−71017
- ionospheric Sq currents, north south asymmetry 2−58114
- kiloampere current monitor for 2 MeV pulsed electron source 2−79694
- magnetron, c.w., dark current and electron energy spread obs. 2−49328
- particle beam analysis of spatial current distrib. using rotating probe 2−52388
- picoammeters, characteristics 2−49232
- plasma, fully ionized, generation of third harmonic current density 2−43135
- plasma accelerator, crossed field, circulating currents 2−56339
- porous gas electrodes, current generation distribution 2−59044
- sinusoidal filament parallel to half-space, e.m. field calc. 2−69811
- small ion current detection, using photomultipliers 2−45689
- solar quiescent prominences, calc. method 2−73145
- in special relativity, definition 2−55396
- toroidal conductor, variation, rel. to optimization of field uniformity 2−59070
- X-ray tube anode current stabilizer circuit using a triac 2−45652
- CdS, acoustoelectronic effect at large acoustic intensity 2−80915
- InSb single crystals, conversion of low voltage electric current 2−45634

Current algebra
- axial vector current and PCAC in σ-model, explicit opera construction in perturbation theory 2−76579
- axial vector current conservation in world of massless pions, investigation of two-body decays of vector and tensor mesons 2−63637
- bilocal, testing using $e^{\pm} + e^{-} \to e^{\pm} + e^{-} +$ hadrons 2−49478
- bilocal algebra on light cone calc. of structure functions for $\gamma N \to \gamma' +$ anything, comparison with parton model calc. 2−49498
- bilocal operators, test using electroproduction of massive muon pairs 2−76582
- bilocal operators, tests for connected part 2−70109
- broken chiral symmetry 2−73736
- canonical representation of modified Sugawara theory 2−82659
- commutation of axial charge with axial divergence 2−70125
- commutator matrix element saturated, derivation of Callan-Treiman type equations 2−49544
- commutators and Khuri amplitudes, light-cone behaviour 2−70122
- Compton amplitudes, fixed poles and Pomeranchukon coupling 2−49537
- Compton scattering, light core approach to fixed poles 2−59409
- covariant T* products and Schwinger terms 2−52528
- creation or annihilation currents, criteria for excistence 2−70102
- current-current Lagrangian model for nonleptonic hyperon decays 2−82782

Current algebra continued
- dual resonance model of vector currents, representation of current algebra 2−79516
- e.m. current and its time derivatives, equal-time commutators 2−49467
- energy density-current density commutators, constraints 2−63482
- equal-time and null-plane commutators of conserved currents on light cone 2−79487
- factorizable, infinite momentum limit 2−70124
- field theory, transformation properties under broken symmetry 2−45850
- Fritzch-Gell-Mann, application to connection between structure function of $eN \to e\gamma +$ anything and $eN \to e +$ anything 2−42340
- gauge invariance and Ward identities in massive-vector-meson model, study by normal product techniques 2−79481
- generalized 'similarity' relation 2−70126
- global charges as integrals over density 2−73707
- guage-invariance restrictions on pole models for $K_l \to \gamma\gamma$ decay 2−79567
- hadron interactions, exotic e.m. currents 2−59459
- hadron weak interactions, $\Delta I = {}^{1}._{2}$ rule in three-triplet and paraquark models 2−59460
- hyperon decay, nonleptonic weak 2−52643
- hyperon nonleptonic decays, consequences of current algebra in limit $q^2 = 0$ 2−52641
- inequalities for structure functions of deep inelastic lepton-nucleon scattering 2−42329
- interactions, weak and e.m., divergence compensation in $\Delta T = 2$ isotopic mass differences 2−45844
- internal and conformal symmetrics, necessary and sufficient conditions for conservation of generating currents 2−70113
- Lie algebra common to dual models, current algebra, dynamical groups, gauge groups 2−45854
- light cone, current densities and operator phenomenology 2−49462
- light cone algebra and parton model relationships 2−70166
- light-cone approach to structure function inequalities for inelastic lepton nucleon scattering 2−66935
- light-cone commutators, tests 2−82663
- light-cone dominance approach to exclusive approach 2−66932
- light-cone dominance of time-ordered products and fixed singularities in J-plane 2−79473
- light-cone expansion of commutators of bilocal currents in relativistic quark oscillator model 2−73706
- light-cone singularities in classical and quantum field theories with interaction 2−70114
- light-cone singularities of bilocal operations, application to scalar-gluon model 2−82661
- local, representations without constraints, construction of physical spares, covariance 2−59354
- meson interactions, broken scale invariance in tree and seagull approx., massive gravitation 2−79482
- meson-nucleon dynamics, Ward identity for axial current, Wilson expansions and commutators 2−49461
- n currents, covariant time ordered products 2−45857
- neutrino interactions, inelastic low-q^2, comparison of exptl, results with PCAC hypothesis 2−59415
- Nevue-Schwarz dual model, axial currents which satisfy local SU mult SU algebra 2−82615
- null-plane commutators, derivation of generalized sum rules 2−52536
- null-plane current commutator algebra and the e.m. self-mass of hadrons 2−45899
- $O_{4,2}$, relation between lepton and hadron currents 2−42330
- one-particle singularities of current matrix elements, physical symmetries 2−73728
- operator tower of canonical dimensions, implication of smoothly broken scale invariance 2−79488
- parton model and dual hadron model, relationship 2−79520
- PCAC, gravitational correction 2−59381
- PCAC, prediction of $\Sigma(\Lambda)$ production cross sections and polarization phenomena in $\pi N \to \pi\Sigma(\Lambda)$ reaction 2−52644
- PCAC, relation to chiral $SU(3) \times SU(3)$, study of strong interactions 2−63489
- PCAC and chiral $SU(2) \times SU(2)$ symmetry 2−79478
- PCAC relations in renormalized nonlinear σ-model 2−73732
- perturbation Lagrangian theory for Dirac fields, Ward-Takahashi identity and current algebra 2−82622
- perturbation Lagrangian theory for scalar fields, Ward-Takahashi identity and current algebra 2−82621
- pion physics, low energy theorems 2−59525
- pion production in nuclear collisions, application of current algebra 2−63862
- quark light-cone, of Fritzsch and Gell-Mann, implications for existence of quarks 2−59435
- quark model light-cone algebra, implication for existence of real quarks 2−79513
- quark-gluon light cone, implications for neutrino scattering 2−42335
- radiative hyperon decay, second class current contributions 2−49597
- representations of local currents, general properties 2−63480
- $SU(2) \times SU(2)$ chiral dynamics, invariant functional formulation 2−70127
- SU(4) bilocal, application to inclusive reactions 2−73756
- Sugawara model, dynamical soln., behavior of current commutator with respect to Lie identities 2−76578
- Sugawara model, dynamical solution 2−49464
- Sugawara model, modification in which all currents have scale dimension three 2−82658
- sum rules, by hard-meson technique 2−70123
- sum rules, in two-particle bases and single- particle inclusive processes 2−49514
- sum rules at quark level, evaluation of low- energy parameters in πN scattering 2−63529
- symmetries, dynamic and algebraic, review 2−63485
- Thirring model in terms of currents, solution and light-cone expansions 2−66893
- triplet quark model light-cone algebra of currents, lepton-nucleon scattering sum rules 2−76708
- ultralocal free current theory 2−42294
- unified model, weak and e.m. interaction symmetry 2−55809
- vector particle scattering, current conservation 2−49490

Current algebra continued
- Veneziano model constructions of current amplitudes which satisfy local current algebra 2−55838
- vertex functions with arbitrary spin, analytic decomposition 2−82660
- Yang-Mills' type gauge field, properties and applications 2−45852
- , PCAC application 2−76654
- A_1 $\rho\pi$ coupling constants, determination using collinear dispersion relations 2−63639
- $e\pi \to e +$ anything, deep-inelastic scattering, PCAC 2−73758
- K pionic decay formulas, symmetry-breaking corrections calc. in framework of SU(3) σ model 2−52595
- $K \to \pi\mu(e)\nu$, form factors determ. from current algebra sum rules using Veneziano model 2−73802
- $K \to \pi\pi$, PCAC application 2−76654
- $K_l \to \mu^+ + \mu^-$, role of weak neutral currents 2−42373
- $K\pi$ scattering, calc. of consts. and parameters, Pade approx. 2−79556
- ν scattering, sum rules and scale dimension of the chiral symmetry breaking Hamiltonian 2−55818
- πK scatt., low-energy, compatibility between current algebra and unitarity constraints 2−67030
- $\pi^+ p \to \rho^0 \Delta_{1236}{}^{++}$, near threshold, study using method of effective Lagrangians 2−67025
- $\pi\pi$ scattering, low-energy parameters determ. from current algebra, unitarity corrections 2−55860
- $\pi\pi$ scattering processes, analysis using hard- pion constraints of current algebra and current conservation in the Veneziano model 2−63632
- $\rho\pi\pi$ coupling constants, determination using collinear dispersion relations 2−63639

Curvature measurement *see Mechanical measurement*

Cutting *see Forming processes*

Cyanogen (C_2N_2) *see Carbon compounds*

Cyclotron resonance
- — 2−62372
- Azbel'-Kaner, effect of strong elec. field 2−71821
- Azbel-Kaner, line shape, splitting, influence of mass spread 2−57139
- Azkel'-Kaner reson., retardation effects 2−51094
- collision frequency and resonance width comparison, short range scatt. force case 2−61213
- electron, anal. of plugging and confinement of hot-electron plasma by microwaves 2−80284
- electron beam interaction with e.m. field, non- linear treatment 2−69879
- and electronic transitions, review 2−72294
- group II-VI compounds, excited state laser spectroscopy of impurities 2−64997
- group III-V compounds, excited state laser spectroscopy of impurities 2−64997
- induction, magnetic dipole resonance of semiconducting sphere placed in cavity 2−71820
- ion cyclotron resonance mass spectrometer, electron impact excitation spectra 2−80135
- ion cyclotron resonance spectroscopy, equations of motion for ion 2−70558
- ion waves in magnetoactive plasmas 2−74396
- ion-molecule collisions, freq. in gases determined by phase coherent pulsed ion cyclotron resonance 2−43027
- ion-molecule reaction rate constants by ion cyclotron resonance mass spectrometry 2−61768
- ionosphere, nf_h, frequency shifts 2−51647
- magnetoplasma, collisionless linear damping of e.m. waves 2−53193
- metal, Azbel-Kaner resonance 2−57384
- metal, thin film, free-electron-like, Doppler-shifted, semiclassical approach 2−54120
- metal films in magnetic field, microwave absorption peaks due to Doppler-shifted cyclotron resonances 2−80941
- metallic electrons in magnetic fields 2−61155
- plasma, relativistic heating 2−70905
- plasma accelerator as ion beam source 2−60253
- plasma heating in magnetic trap, asymptotic particle distribution function 2−74365
- projectile ion thermal energy charge transfer rate consts. determ. by ion cyclotron reson. spectroscopy 2−80132
- rare gas ion thermal energy charge transfer rate consts. determ. by ion .cyclotron reson. spectroscopy 2−83399
- semiconductor, harmonics, plasmon-assisted i.r. absorpt. 2−54409
- semiconductor, magnetooptical transitions, plasmon assisted, line-shape calcs. 2−68320
- semiconductor, of hot electrons, recomb. effects on line profile 2−84282
- semiconductors, mag. field dependence of linewidth in quantum limit 2−51148
- solid state physics, an overview 2−57093
- from surface-bound electrons on liquid He 2−80513
- technique and appl. to meas. of μ_p/μ_n and $H_2{}^+ - D^+$ mass difference 2−70254
- uniaxial conducting crystal, in magnetic field, e.m. wave propagation and coupled cyclotron-plasma resonance 2−84280
- Be, ang. depend. of effective masses 2−84257
- Bi-Sb low-concentration alloy, determ. of cyclotron effective masses of carriers, mass parameters of electron pockets 2−47807
- Bi, determ of cyclotron effective masses of carriers, mass parameters of electron pockets 2−47807
- CdS, of piezoelec. polarons, far i.r. 2−71924
- Ga, retardation effects, Fermi surface orbits 2−51094
- n-$Ga_xIn_{1-x}As$ alloy, effective mass compositional depend., sub mm. cyclotron resonance obs. 2−64982
- GaP, hole effective masses detn. 2−75041
- n-Ge, in quantizing mag. field 2−71942
- Ge rel. to scatt. of holes by neutral acceptors 2−71941
- He ion motion in magnetic field in presence of induced electric field 2−70959
- HgTe, magnetoabsorpt. of i.r. and submillimetric waves rel. to mag. field, band struct. 2−68294
- n-InSb, electric field modulated laser induced, impurity and cond. electron resonance obs. 2−81021

Cyclotron resonance continued
n-InSb, hot electron resonance, nonlinear transport props. obs. 2−77845
InSb, small spheres, cyclotron reson. type absorpt. due to induced mag. moment at 35 GHz and 77K 2−68326
Si, electrons generated by impurity excitation with CO_2 laser 2−71947
Si, microwave absorpt. spectra, anisotropy, hole reson. rel. to wave vector 2−71822
Te, valence band Landau levels obs. 2−81019
Te, valence band Landau levels obs. 2−81017
Te, valence band structure and transitions between Landau levels determ. 2−68321
TlBr, electron and hole resons., carrier mobilities 6.5-14K 2−68322
TlBr(Cl), of electrons and holes, polaron effective mass 2−47830
ZnO, anomalous shallow bound states 2−51349

Cyclotrons *see Particle accelerators/cyclotrons*

Czochralski method *see Crystals, growth*

D-layer *see Ionosphere/D-region*

Damping
see also Internal friction
acoustic damping coefficients in loudspeaker-excited closed cylindrical tube 2−55529
adiabatic perturbations, expanding universe 2−72954
amplitude-phase-frequency characteristics of vibrating system, dependence on dissipative properties 2−82296
atmospheric gravitational oscillations, and forecast models including orography 2−51571
beams with hysteresis damping, transient vibration problem 2−73400
bisphenol-A-polycarbonate, compression yield stress rel. to mech. loss peak 2−47506
characteristics of certain steels, cast irons and other metals 2−69703
charged drops, oscillations, EHD stability 2−80227
combustion instability oscillation by short rocket nozzles 2−55516
cubic crysts., of elastic waves, effective anharmonicity consts. 2−80913
cylinder in fluid, oscillatory damping 2−45473
cylindrical shells, dynamic responses to concentrated radial loads 2−55457
device for pressure gauges 2−76164
Dorrestein wave equation, physical interpretation for surface active materials 2−56466
dynamic vibration neutralizer with motion limiting stops, theory 2−66589
Earth and planets oscillations, law of creep 2−58482
eddy motion, pregalactic turbulence 2−81810
elastically supported sandwich plates 2−78909
element characteristic, determ. method 2−69690
e.l.f. noise, ionosphere, Q-type bursts, damping coefficients 2−78394
ferromagnetic materials, stress depend. damping at stresses to fatigue limit 2−74826
free flexural vibrations of damped plates 2−45463
full modal matrix, construction from exptal. obs. 2−46501
galactic density waves by induced shocks 2−48660
instability of equilibrium of nonlinearity damped holonomic mechanical systems 2−76240
internal friction due to point defect dragging with dislocation interaction, hysteresis damping 2−64704
interstellar spiral density waves by induced shocks 2−81827
Landau, effect on nonlinear wave modulation in plasma 2−53224
Landau, in finite amplitude obliquely propagating waves 2−80317
Landau, of plasma longitudinal oscillations 2−46779
Landau and collisional, of plasma lines, numerical computations of linewidths and intensities 2−43143
l.f. ionization recombination, oscillations in bounded low density plasma 2−80352
l.f. mechanisms in mechano-acoustical networks 2−41652
liquid waves, forced resonant second-order interaction 2−83738
lower ionosphere layer, effect on propagation characteristics 2−81719
magnetoplasma, collisionless linear damping of e.m. waves 2−53193
material, stability of rotating systems 2−52130
metal, damping capacity meas. under direct cyclic stresses 2−53861
natural oscillations of a bar, suppression by dynamic vibfation absorbers 2−52203
noise, on Rhine cruise ship 2−45530
nonlinear nonconservative systems, subject to step fn. excitation 2−58894
nonlinear system with two degrees of freedom 2−55489
particulate damping in solid propellant rockets 2−44792
plasma, coherent waves individual linear damping effects on nonlinear instability 2−60269
plasma, collisional damping of transverse waves 2−80357
plasma, collisionless, damping of finite-amplitude electron waves 2−77293
plasma, fast wave, at second harmonic of ion cyclotron freq. 2−56369
plasma, ion acoustic waves and Landau damping electrostatically driven in ideal Q-machine 2−67671
plasma, nonlinear time depend. Landau damping of finite amplitude wave 2−83626
plasma, spatial and temporal of quasi-longitudinal oscillation near lower hybrid resonance 2−60276
plasma, transition from amplitude oscill. to linear Landau damping 2−83545
plasma drift waves, effect on mag. shear 2−70946
plasma echo, Landau 2−53229
plasma explosive instability, role of linear damping 2−70960
polyethylene oxide, mechanical damping index obs. with torsional braid analyser 2−71547
precessing vortex cores, by combustion in swirl generators 2−83427
repeated impacts, transmissibility and damping 2−55468
shell, dynamic stability 2−66494
shock waves, nonlinear theory of resonances in continuous system 2−77327

Damping continued
silicone based electrons, dynamic shear properties over wide temp. ranges 2−47488
small disturbances in radiating gray gas 2−80404
stellarator confined plasma viscosity damping of convective cells 2−80276
thin viscoelastic layers, measurement techniques 2−76342
Timoshenko beams, clamped and free, dynamic responses 2−82342
Tokamak, major radius oscill., theory 2−70936
vibrations, optimal control 2−82347
vibrodamping treatment distrib. on structs., optimization methods 2−45497
viscous, longitudinal vibrations of prismatic bars 2−76350
viscous of oscillatory flow 2−53349
Ziegles model and cantilever beam, stability, external and internal damping effects 2−45454
Cu-Al-Ni alloy, damping characts. and causes 2−80776
Cu, stress pulse damping in region of propagating brittle crack 2−60801
Fe-C alloy, recovery of internal friction after strain ageing 2−47481
Fe-(30.3 wt.%)Ni alloy, damping of oscillations during heating after martensitic transform. 2−43791
Fe, cast, capacity, from the variation of its dynamic modulus with strain amplitude 2−77674
Nb, internal friction, vibr. freq., β-process, 20-170°C 2−56778
Ni, electrolytic, anisotropic effects in magnetoelastic damping 2−54337
W, elastic oscillations, orientation depend. 2−43671

Dark space *see Discharges, electric*

Data tables *see Collections of physical data; Tables, mathematical*

Dating *see Earth/age; Radioactive dating*

Daughter *see Nucleus; Radioactivity*

Dawn chorus *see Atmospherics; Ionosphere*

Dayglow *see Airglow*

de Haas-Shubnikov effect *see Magnetoresistance*

de Haas-van Alphen effect
see also Diamagnetism; Magnetic properties of substances/diamagnetic
conduction electron, relax. times and spin props. determ. from oscillatory amplitudes 2−77847
electron gas, longitudinal dielectric tensor in uniform magnetic field 2−75038
Fermi surface orbits, integral calc. method 2−44028
graphite, majority and minority carrier masses and freqs. 2−57121
oscillations amplitude reduction by signal dephasing by strain fields round impurities 2−77846
Ag, Fermi surface, infinite field phase 2−61182
Ag alloy, impurity scatt., electron lifetimes., Fermi surface 2−61148
Al, Fermi surface press. depend. 2−61180
Al, influence on directly generated standing sound wave 2−51018
Al, rel. to audio freq. helicon resons. 2−57136
Al, uniaxial compression effects on Fermi surface third zone obs. 2−71790
Au, Fermi surface, infinite field phase 2−61182
Au, Fermi surface, uniaxial stress effects 2−54108
$AuGa_2$, Fermi surface cross sections 2−51078
Be-transition metal alloys, Fermi surface, electron scatt. 2−71791
Bi, bulk, rel. to nonextremal Fermi-surface orbits 2−77828
Cu, Fermi surface, infinite field phase 2−61182
Cu, obs. of electron scatt. by dislocations 2−61214
Cu Kondo alloys, exchange splitting of electron spins 2−77848
Hg, amplitude meas. between 1 and 17K 2−57140
InSb, electron lifetime detn. 2−71909
Ir, Fermi surface obs. 2−61215
Pb, Fermi surface press. depend. 2−44034
Sn, white, Fermi surface cross sections stress derivatives 2−75033
SnTe, 1.6-7.9K, Fermi surface determ. 2−68420
Zr, fields up to 57 kG 2−84249

Debye-Huckel theory *see Conductivity, electrical/liquids, electrolytic; Electrochemistry; Solutions*

Debye-Scherrer cameras *see Cameras; X-ray crystallography/apparatus*

Debye temperature
see also Specific heat and subheadings
electron microscope determ., applic. of high voltage metallography 2−56632
energy depend., LEED meas. 2−61062
halides, heavier metal type, calc. using ionic Rydberg function 2−47727
halides, heavy, Born theory of i.r. eigenfrequencies and lattice props. 2−74961
metal, and heat capacity at low temperature, review 2−47747
metal, close-packed, relation to cohesive energy 2−60697
metal halides, calc. from modified logarithmic form of overlap repulsion 2−43502
rare gas, solid, calc. from higher order elastic consts. 2−50990
semiconductor, cubic relation with energy band gap 2−51147
transition metal binary alloys, low-temp, sp. Lt. parameters γ and θ_d, inverse scaling, rel. to phase stability 2−68248
transition metal nitrides, calc. 2−61112
transition metals, h.c.p., noncentral force model 2−80887
weighting coeffs. in approx. of Debye temp. in cubic crystals 2−74991
zeolite, cation-exchanged, Mossbauer effect of Fe^0-atoms 2−54390
Ag film, X-ray diffraction study 2−61102
$AgMo_4S_5$, superconducting properties 2−81051
Al, determ. from temp. depend. of LEED intensity 2−60624
Au-Sn alloy, rel. to Mossbauer effect 2−51308
Bi, from low temp. sp. ht. data analysis using magnetically smoothed temp. scale 2−68249
$CaCO_3:Fe^{3+}$, spin-lattice relax obs. 2−65177
Cd, from low temp. sp. ht. data analysis using magnetically smoothed temp. scale 2−68249
$CdS:Co^{2+}$, spin-lattice relax. obs. 2−54367
CdSb, charact. temp. det. from elastic modulus 2−64854
Cr (100) surface, LEED obs. 2−50992
Cs, computed in terms of sharma and Joshi lattice dynamical model 2−47749

Debye temperature continued
α-Cu-Au alloys, conc. depend. 2−51044
Cu-Cu_3Au alloy, elastic moduli, elec. cond., 4.2-293K 2−47752
Cu film, electron diffraction study 2−61102
$ErH_{1.81}$, acoustic velocity obs. 2−57047
Fe, Mossbauer effect, high pressure obs. between 300-20K 2−72283
$FeSb_2$, from analysis of Mossbauer spectra isomer shift 2−61606
GaAs, from low temp. sp. ht. data analysis using magnetically smoothed temp. scale 2−68249
GaSb, from low temp. sp. ht. data analysis using magnetically smoothed temp. scale 2−68249
GaSb single crystal, elasticity versus temp., calc. 2−60843
n-Ge rel. to carrier conc. 2−77772
H_2, D_2, and H_2-D_2 system, specific heat obs. 2−43985
He, solid h.c.p. crystal, from elastic consts. by sound propagation 2−43972
He complete monolayer on graphite 2−71253
InSb, from low temp. sp. ht. data analysis using magnetically smoothed temp. scale 2−68249
KBr-Ki solid solution single crystals, u.s. pulse method obs. 2−71550
Li, b.c.c., from Krasko-Gurskii model 2−68227
Li_2WO_4, anhydrous, ^{183}W Mossbauer effect obs. 2−71720
Mg-Cd and h.c.p. alloys, rel. to supercond. 2−47859
Mo (100) surface, LEED obs. 2−50992
Nb-Mo alloy, from elastic consts., 83-373K 2−60845
Ne, solid, X-ray drift. obs. 2−47753
$PbMo_6S_7$, superconducting properties 2−81051
RbBr(Cl)(I), temp. depend. 2−61111
$ScH_{1.99}$, acoustic velocity obs. 2−57047
Sn, from low temp. sp. ht. data analysis using magnetically smoothed temp. scale 2−68249
$SnMo_5S_6$, superconducting properties 2−81051
Ta-Nb alloys, superconducting, sp. ht. and mag. meas. 2−71875
Tb, from elastic consts., 70-300K 2−60846
$Te_{15}Ge_3As_2$ glass, calc. from u.s. velocity 2−47742
ThO_2, e.s.r. meas. 2−84581
TlCl pressure dependence of elastic constants 2−84035
$YH_{1.93}$, acoustic velocity obs. 2−57047
Zn, from low temp. sp. ht. data analysis using magnetically smoothed temp. scale 2−68249

Debye-Waller factors
alkali metals optical absorpt., phonon effects 2−61628
crystal, deformed, resonant absorption of X-rays 2−84474
diatomic molecular crystal, calc. from lattice vibr. model 2−43959
liquid metal, rel. to hard-sphere interference function temp. depend. 2−67796
phase transform, Mossbauer fraction anomaly 2−68211
polymer crystal, thermal fluctuations, valency angle stiffness 2−74972
quantum crystal, from neutron scatt. data 2−61060
semiconductor, III-V, rel. to band struct. calc. 2−68415
Sn gase dilute alloy, rel. to ^{119}Sn nuclei vibrations, Mossbauer obs. 2−71721
spinel structure compounds, off centre ions, model for local distortions 2−80646
zincblende semiconductor, mod. rigid ion calc. 2−84199
Al, thermal shifts of electron energies 2−54414
$BaTiO_3$, from elastic consts. and Raman freqs. 2−50983
BeO, from elastic consts. and Raman freqs. 2−50983
CaF_2, from elastic consts. and Raman freqs. 2−50983
Cr (100) surface, LEED obs. 2−50992
F_2, calc. from lattice vibr. model 2−43959
α-Fe lattice dynamics 2−84178
^4He, b.c.c., anomalous factor, Gaussian function 2−67865
^4He, b.c.c., scatt. function for inelastic neutron scatt. 2−67867
Hg films deposited on LiF substrate, rel. to scattering of thermal He atoms 2−56573
HoPtSn and related intermetallics, Mossbauer study 2−50621
InP, from elastic consts. and Raman freqs. 2−50983
$KTa_xNb_{1-x}O_3$, l.f. zone boundary lattice vibr. modes, Debye-Waller factor anisotropy 2−80902
Mo (100) surface, LEED obs. 2−50992
Mo lattice dynamics 2−84178
N_2, calc. from lattice vibr. model 2−43959
Nb_3Sn, Mossbauer obs. 2−44357
O_2, calc. from lattice vibr. model 2−43959
$SrTiO_3$, from phonon freq. distribs. 2−77761
Te cryst., 296 K 2−47736
W lattice dynamics 2−84178
Xe (111) surface, LEED thermal scatt. obs. 2−50470
ZnS, from elastic consts. and Raman freqs. 2−50983

Decay periods *see Hyperons/decay; Kaons/decay; Mesons/decay; Pions/decay; Radioactivity/decay periods*

Decay schemes *see Hyperons/decay; Kaons/decay; Mesons/decay; Pions/decay; Radioactivity/decay schemes*

Decomposition
see also Chemical reactions
alloy, supersaturated solid soln. decomp., review 2−43928
ethane in reactions with methyl radical, theoretical critical configuration 2−57420
ethylene, adsorp. on W surface, flash desorp. obs. 2−50552
eutectoid, lamellar eutectoid growth, stepwise growth model 2−50814
excited molecules, dynamic model, lifetime determ. 2−78188
gas discharges, organic reactions leading to polymer deposits 2−74408
metal/hydrogen systems, h.p. thermodynamics 2−77715
nimonic alloy, ageing, solid sln. decomp. and volume change 2−50805
photochemical, of large molecules theoretical results 2−81525
refractory carbides, nitrides and borides, NASA research 2−64801
rhombohedral system, spinodal decomp., modulated phase orientation 2−47676
spinodal, diffuse interface expansion, higher derivative terms 2−56951
spinodal, mean field pair interaction theory 2−56952
steel, low-C low-alloy, fine struct. and phase comp. at elevated temps. 2−53898

Decomposition continued
steel, α- martensite decomp., second stage, X-ray obs. 2−50938
Al-Mg-Zn alloy, influence of Zn 2−43911
Al-(1.8 wt.%)Mn alloy, decomp. products 2−47615
$As_2S_3(Se_3)$ cryst., photodecomp. 2−51463
CO_2, adsorbed on W 2−77513
CO_2, on W(100) surface, flush desorp. mass spectrometry obs. 2−50551
Co-Mn-Al system, DTA, microstruct. and cryst. struct. studies 2−64816
Co-Ni-Ti system, decomp. and formation of modulated struct. in coherent phase zone of stability 2−57030
Co-Ti alloy, solid soln. decomp. 2−56933
$(Cr_{0.8}Fe_{0.2})(OH)_3$, thermal conversion to $(Cr_{0.8}Fe_{0.2})O_3$, Mossbauer parameters variation 2−72547
Cu-Be-Ag alloys, structural states in decomposition process, e. diffr., e. micro. and microhardness exam. 2−80782
Fe-Co(Ni)-Ti-Al alloy, solid soln. decomp. 2−56933
Fe-Cr steel, embrittlement at 475°C, ordering, decomp. of ferrite 2−47634
Fe_2O_3, heat of transformation, decomposition temp. Gibbs free energy of formation determ. by EMF method 2−51425
β-FeOOH, thermal conversion to α-Fe_2O_3, Mossbauer parameters variation 2−72547
GaAs-Cu, supersaturated solid solution, interaction of Cu atoms with residual impurities and structural defects 2−83836
$GdCo_5$, powder, coercive force rel. to sintering temp., decomp. stability 2−68511
KCl-NaCl solid solns., supersaturated 2−43921
LiF:Mg, impurity associations decomp., light scatt. obs. 2−83983
$Li_7Y_3(MoO_4)_8$, prep., decomp. at 735°C to solid and liq. phase 2−74904
Mn-Ga alloys, γ solid soln. decomp., rel. to internal friction 2−50735
NH_3, decomposition behind reflected shock waves 2000-4500K, obs. of i.r. emission 2−48324
N_2O molecular beam, reactive scatt. from clean and C covered Pt(100) surface 2−50547
Na_2O-SiO_2 glass, morphological changes produced by amorphous phase decomp. 2−47060
Nb-O solid soln., form. of Nb_4O during decomp., annealing effects, 500-700°C 2−53902
Ni compound, non-metallic, thermal decomp., photostimulated exoelectron emission obs. 2−57408
$PbBr_2$ pressed discs, u.v. irrad., photodecomposition 2−44491
SF6, current interruption, gas circuit breakers 2−74489
Sc_2O_3-MgO solid. soln., phase diagram, disintegration mechanism 2−74906
$SmCo_5$, powder, coercive force rel. to sintering temp., decomposition stability 2−68511
Ti b.c.c. solid solutions, $\beta \rightarrow \omega$ transform. 2−68204
U-9.5 wt %Nb alloy, gamma phase decomp., discontinuous precip., 450-600°C 2−80802
$YAlO_3:Nd^{3+}$, high temp. phase instability 2−74958
29 at.% Zn-Al alloy, spinodal decomp., metastable rhombohedral form., elastic anisotropy effects 56923 2−56923
Zr b.c.c. solid solutions, $\beta \rightarrow \omega$ transform. 2−68204

thermal *see Chemical reactions*

Decoration techniques *see Crystal imperfections/dislocations; Crystals/etching*

Defects *see Crystal imperfections*

Deformation
see also Bending; Elastic deformation; Plastic deformation
acoustic emission, generic discussion 2−49134
Alfianello meteorite, shock metamorphism and dynamic deformation 2−44970
alpha-constant stiffness method for analysis of nonlinear problems 2−58850
aluminium cylinders strain analysis, by holographic interferometry 2−50787
anisotropic cylindrical shells, pure bending, stretching and twisting 2−45374
arcs in transverse magnetic field, cut off model 2−60321
astronomical mirror flexure, influence of cell deformation 2−48819
astronomical mirrors, method of determining thermal deformations 2−48820
astronomical telescope, optical aberrations due to temperature deformations and convective fluxes, interferometric investigations 2−48821
automatic static deformation recorder 2−56854
bar, incremental wave effects, effect of strain rate history 2−45477
bifurcation buckling as approximations of collapse load for general shells 2−45357
bone, considered as solid-liquid composite 2−69220
cholesteric struct., planar, mag. field induced distortions 2−46927
circular cylinders, elastic wave propagation 2−76337
circular cylindrical shells axially compressed 2−52160
circular discs and cylinders, symmetrical deflection 2−41564
cladding rel. to mechanical interaction with fuel 2−49894
clamped circular plates with central blast loading, algorithm 2−73356
composite steel concrete beams with welded stud shear connectors 2−58836
cones, produced by kinetic forming 2−52141
contact problem of two thin spherical shells 2−82065
at crack tips, interferometric technique for viewing zones 2−60903
creep, of asteroids and major planets satellites 2−78491
creep buckling of plates and shells 2−76318
crustal deformation due to dislocation in multi-layered medium 2−78284
crystalline rocks in Tazin Group, Canada, multiple deformation 2−51514
cyclic straining, subgrain formation 2−80763
cylinder with plane faces displacement-free, eigenfunctions for symmetrical deformations 2−58867
Debye-Scherrer lines of deformed crystals, profile analysis 2−53629

Deformation continued
- deformed body, holographic interferometry used to determine surface displacement components 2−66552
- diamond, cathodoluminescence changes, electron microscopic obs. 2−81428
- dilatancy in rock under hydrostatic pressure 2−68860
- disc, rotating, accelerating, displacements, closed form deform. solns. 2−66490
- drops conveyed by gas flow 2−60335
- Earth, multilayered sphere model, static deformation by internal sources 2−51492
- Earth's crust, around volcanoes, model 2−78285
- Earth-model with a rigid core, deformation and stresses 2−51521
- elastic-plastic buckling, variational method 2−78891
- finite deflections of uniform beams using Euler-Bernoulli law of bending 2−52145
- flat membranes, large deflection analysis, numerical methods 2−73346
- flat plates, due to surface couples 2−52158
- fragile material microsamples, machine for det. 2−56846
- free shape problem for closed ring under two opposing point loads 2−45354
- graphite, Gilsocarbon, irrad. behaviour, dimens. changes 2−56994
- graphite, neutron irrad. at 715°C, dimens. stability 2−56047
- graphite, nuclear, high fluence neutron irrad. behaviour, two-phase model 2−56048
- graphite, nuclear, nat. graphite filler, neutron irrad. behaviour rel. to comp. 2−56049
- graphite, pyrolytic, highly oriented, high dose fast neutron effects dimensional changes 2−57072
- holographic interferometric meas. 2−82150
- hydrodynamic perturbation in uniform magnetc field for plane flow in circular region 2−60198
- indentation of a consolidating half-space 2−78236
- in interface, dislocations, between two isotropic phases, stress fields and strain energies 2−80668
- kaolinite rods, elastic consts. from adsorptive length changes 2−77641
- kIlauea Volcano summit area 2−57828
- liquid drops in high speed gas flow 2−43303
- Lower Devonian sandstone, strain rate effects 2−54735
- materials response meas. holographic interferometric techniques 2−49402
- materials with memory, thermo-mechanical coupling 2−76291
- metal film, longitudinal and transverse strain coeff. of resistance 2−61218
- metal forming processes, tensile creep 2−76262
- metal surface, of asperities, profilometric obs. 2−50452
- metal swelling implications in fast reactor design 2−49900
- metal-matrix composite materials, development 2−43900
- MG cylinder, stress and deflection meas. 2−43811
- moire interferometry applics. to study of large deformations 2−42139
- multilayer shells, transverse normal layer deformations 2−63061
- non-Newtonian media, deformation velocity, relationship with strain, applications in lubrication 2−50162
- nonlinear membrane shell, applic. to noncircular cylinders 2−45364
- nonlinear membranes subjected to internal pressure 2−76312
- nonsteady inelastic, stress anal. 2−76298
- optical orientation of excitons in crystals with wurtzite struct., infl. of deform. 2−71804
- Pacific Basin, tidal element 2−57715
- parametric stability of thin-walled beams of open section under axial load 2−45380
- periodic and transient, study by double pulsed holographic interferometry 2−41665
- plane strain consolidation in saturated clays, finite element method 2−76314
- plate bending, triangular finite element analysis 2−52164
- plate bending problem, applic. of dual analysis principle 2−52167
- plate bending problem, local solution approach in finite element methods 2−52166
- plates, circular with limited thickness, minimum weight design 2−76311
- plates and shells, law of thickness variation for stationary value of stiffness functional 2−41596
- plates of arbitrary planform, bending, analysis using triangular, rectangular finite elements based on hybrid formulation 2−66495
- polycarbonate, uniaxial strain rate and yield locus det. 2−43778
- polyethylene spherulites and origin of contrast effects in electron microscopy 2−60782
- polyimide films, uniaxially drawn orientation studied by IR spectroscopy and X-ray diffraction analysis 2−43677
- polymer systems, conc., constitutive equations for nonlinear viscoelasticity 2−82316
- polymers, effect of form of inelastic deformation on intermolecular reaction 2−80119
- polyolefins, variation in sound velocity rel. to deformation 2−80750
- polytetrafluoroethylene, cyclic loading effect on morphology 2−60870
- rational reduction of large scale eigenvalue problems 2−69695
- rock fracture zone rel. to penetration of trapezoidal- shaped body 2−75425
- rocks, pre-Caledonian, Mullet Peninsula, County Mayo, Ireland 2−61842
- rotating cylinder, effects of non-homogeneity 2−73377
- rubber, swelling by sorted gas expansion during tensile testing at low temp. 2−43710
- rubber cylinder, swelling under torsion 2−60876
- rubber cylinder in torsion, swelling 2−60875
- salt media, analysis of time-dependent deformations of openings 2−62012
- shallow spherical shells, impulsive loading 2−76292
- simply supported skew plates under combined loading, stability 2−45391
- space eqn. of free surface of viscous and viscoelastic deformed layer 2−52194
- stability of elastic continuous media, sufficient conditions 2−45409
- static, beams and plates subjected to fluctuating loads 2−41662

Deformation continued
- steel, annealed low carbon, dislocation model for delayed yielding phonomenon, strain-time history 2−80813
- steel, mild, thermal activation parameters during non-uniform and uniform deformation 2−80814
- steel, stainless, solution treated type 304, empirical representation of irradiation-induced swelling 2−43609
- steel beam column connection due to welding 2−58855
- strain gauge, strain distrib., interaction with substratum 2−66527
- stress analysis, finite element method 2−45429
- stress wave emission, review 2−69745
- stress-strain-temperature behaviour of fatigue prone structure, model 2−56887
- tension/compression stage for scanning electron microscope 2−79120
- thermoluminescence changes following 2−84554
- thin layer structure, spreading resistance det. 2−45402
- three-dimensional body, tensor wave theory considering small deformation 2−76336
- twisting of non-homogeneous sphere, stress anal. using surface couple 2−73376
- two dimensional flow, geometrical interpretation 2−53123
- volcanism associated, numerical modelling 2−57829
- water drop response to sudden acceleration 2−83739
- Ag, films, indentation and impact studies of loading 2−77708
- Al-Mg alloys, viscous glide in solid solution, dislocation climb and Newtonian viscous deformation mechanisms 2−64718
- Al, sub-grain boundary migration 2−80824
- B sheath, chem. vap. deposited on C monofilament, elongation on deposition 2−53956
- BaTiO$_3$ single crystals influence of the amplitude of free vibrations on the permittivity 2−81154
- C, lampblack, dimens. stability rel. to graphitization 2−56995
- C, poorly crystn. isotropic, fast neutron irrad. induced dimens. changes 2−56767
- C products, graphitization effects on neutron irrad. induced dimensional changes 2−56996
- C−C biaxial test specimens, holometric obs. 2−82145
- Cu, single cryst., depend. of deform.-resist. on rate and temp. of prev. loading 2−84010
- Cu and Cu-Zn alloys, development of texture 2−80849
- Fe, yield stress damage function for neutron irradiation, determ. using SAND II code for data analysis 2−79840
- KNbO$_3$, ferroelectric single crystals, movement of twin boundaries, load-deformation curves 2−80743
- α-U, radiation-induced size changes 2−52845
- UC$_x$, nuclear fuel, fission gas swelling, external diametrical swelling, $T \leqslant 1900$°C 2−43614
- UN$_x$, nuclear fuel, fission gas swelling, external diametrical swelling, $T \leqslant 1900$°C 2−43614
- UO$_x$, nuclear fuel, fission gas swelling, external diametrical swelling, $T \leqslant 1900$°C 2−43614
- WC-Co composite, non-elastic stress-strain behaviour 2−47670

Delay lines, ultrasonic *see Acoustics; Ultrasonics*

Delbruck scattering *see Photons/scattering*

Demagnetization
- *see also Magnetization process*
- cerium ethyl sulphate, low temp. mag. behaviour 2−68551
- heated rock sample, demagnetization using astatic magnetometer 2−66695
- Permalloy film, effective demag. field rel. to thickness and mag. moment 2−61539
- rocks, apparatus using alternating magnetic field 2−51662
- steel, Fe-Si, domain struct. rel. to demagnetizing field freq. 2−84412
- EuB$_6$, effects on e.p.r. and g-factor measurements 2−84565
- Na$_3$[Ce(C$_7$H$_3$NO$_4$)$_3$].15H$_2$O, mag. and thermometric props. in 2-20 mK range 2−82079
- Ni, internal demangetizing factor, temp. and alternating field direction depend. 2−48074
- YIG, shock induced, method for investigation 2−48081

Dember effect *see Photoelectromagnetic effects*

Demonstrations *see Teaching/demonstrations*

Dendrites
- *see also Crystal growth*
- alloy, dendritic coarsening during solidification, model 2−50818
- growth in flowing liquid metal in magnetic field 2−64576
- ice (snow), growth mechanisms 2−47207
- metal, spherical cryst. dendritic growth from highly supercooled liq. metals 2−60966
- solid-liquid growth fronts, solute distrib., contrib. to interfacial undercooling 2−43517
- Ag, on amorphous substrates, disclinations 2−53582
- Ag filament, growth from Ag compounds, solid state ionics technique 2−47133
- Al-Cu alloy, di-directional solidification and dendritic growth 2−50823
- Al-Mn alloy, structural features of a plane strip obtained directly from melt by Stepanov method 2−50821
- Al, di-directional solidification and dendritic growth 2−50823
- Cr, galvanostatically obtained from CrO$_3$-H$_2$SO$_4$- dimethylsulphoxide-H$_2$O solution 2−47135
- Cu-Sn alloys, unidirectionally solidified, columnar dendrite structure 2−74641
- Cu, habit and morphology, crystn. mode effects 2−47136
- Mg-Zn and Mg-Zn-Zr dendritic and nondendritic structs., soln. kinetics of secondary phases 2−47640
- NH$_4$Cl, growth under influence of electric fields 2−43486
- NiO, dendritic growth from vapour phase 2−64592
- Pb, growth in gels, kinetics 2−47137
- WC, chemical vapour deposition 2−43487
- Zn-Cd dilute alloy, growth and morphology 2−43488

Densification
- alumina from vapour-deposited powders, reactive hot pressing 2−68171
- cermet steels, dynamic hot pressing, effect on struct. and mech. props. 2−84146
- ferrite, 1000 NN, compaction kinetics during hot pressing 2−53882

Densification continued
graphite powder, fine-disperse, effects of oxidation on pressing ability 2−77737
hot pressing of orientated glass filament 2−77703
metal powder, rolling mechanism in initial nonstationary period 2−50908
mullite, press.-sintering kinetics and mechanism 2−50874
oxide fuel struct. evolution, modelling using BEHAVE-2 code 2−52858
powder metallurgy, structural aspects 2−56946
two-phase systems, sintering, shrinking rel. to conc. 2−43886
Ag powder, expt. and theory 2−50909
β-Al_2O_3, alumina, hot pressing and characteriz. 2−50875
Al_2O_3, plastic deformation in hot-pressing 2−77735
BeO, obs. and mechanism 2−74914
BeO, powder, glass-sealed, by hot isostatic pressing 2−53940
BeO powder, initial stage sintering mechanism determ. 2−47662
CoO, pure and Li-doped, final stage densification kinetics 2−50879
Cu, elimination of pores by hydrostatic pressures and density increase at 20 kbar 2−71626
Cu powder, vibr. packing, inertial loading effect 2−50911
Fe fine powder, sintering 2−61000
HfN-ZrB_2 cutting tool materials characteriz. 2−50883
$MgAl_2O_4$ polycryst. ceramic prep. and characteriz. 2−50887
$MgAl_2O_4$ spinel, final stage kinetics 2−50889
Ni-Fe powder compact, structural aspects 2−56946
Ni-Zn ferrite powder, hot-pressing 2−43893
Ni powder metallurgy, structural aspects 2−56946
SiO_2 vitreous, radiation compaction mechanism 2−50410

Densitometry
bone densitometer using transmitted and scattered γ-rays 2−69222
by decoding grille, for photographic spectrograph 2−42281
laser microdensitometry of photographic film, noise meas. 2−59333
mass spectra of solids, computer aided automation of analysis 2−84688
microdensitometer, multiple sine-slit, eval. of m.t.f. of photographic emulsions 2−45807
optical density meas. of hidden photographic image 2−52499
photographic transparencies, modulation transfer function from edge analyses 2−79295
radiographic film detail evaluation, significance of light density 2−73695
spectrophotometer attachment for gel electrophoretic meas. 2−73680
stero pair scanning electron micrograph meas. conversion to real 3D data 2−43563
vesicular film, standardization 2−58692
Ag conc. under variable exposure for latex, nitrocellulose, polyvinyl butyryl rel. to optical density 2−52500

Density
coronal enhanced region 2−73150
film granularity, colour films, black and white films 2−82595
gas-fluidized beds, fluctuations detected by microwave beam 2−83505
glass, pyroxene type, effect of heat treatment 2−53533
hard-sphere gas, thermal fluctuations 2−76224
lunar interior 2−85036
plasma, streaming along uniform mag. field, fluctuations, dependence on electrical field controlled by metal ends 2−43127
polyethylene, bulk modulus and density in 30 kbar, glass transition temp. press. coeff. 2−83352
waves, M51 galaxy, spiral structure 2−58234
waves, streaming, in spiral galaxies 2−58232
H_2, equilibrium saturated state, equation 2−64517
He monolayer formation on graphite, densities at completion 2−71253
Hg, crit. fluid, effect on thermoelec. power 2−60377
NaCl aerosols formed by condensation 2−60530
Xe, critical, law of rectilinear diameter employed 2−53502

gases
jet, distribution obs. by laser induced gas breakdown 2−46823
mass meas. of flowing liquids and gases, electronic apparatus 2−77341
rarefied, electron-optical investigation methods 2−60343
HCl thermal dissociation in shock waves, gradient meas. 2−44473
Hg, effect on cond. in metal-insulator transition range 2−60378
N_2, det. from equations of state representing all saturated state variables 2−53332
S, up to 800°C, apparatus for obs. 2−47045

liquids
acetone-cyclohexane, meas. at 25°C 2−53408
acetone-methanol, meas. at 25°C 2−53408
benzene-methanol mixtures, meas. in temp. range 10°-50°C 2−60450
composite dilatometer for meas. 2−62962
α,ω-dichloroalkanes, rel. to molar activation energy for viscous flow 2−60489
from isobaric ensemble formalism in Monte Carlo calcs. 2−64428
mass meas. of flowing liquids and gases, electronic apparatus 2−77341
measurement device for determ. level, density and interface of liquids 2−77376
methane, from 1.8 ρ_c to freezing liquid 2−80448
methanol-cyclohexane, meas. from 25 to 50°C 2−53408
methanol-cyclohexane-acetone, meas. at 25°C 2−53408
optical density, continuous-flow ultraviolet microdensitometer 2−56504
sea water, specific gravity, instrumental obs., comparison with tables 2−62022
water, second order fluctuations in particle no., integration over X-ray scattering interactions 2−74517
water, specific volume calc. using hydrol-polyhydrol model 2−43317
Ag, elevated temperature changes by measurement of thrust 2−64699
Al_2O_3, correl. with covalent bonding 2−43338
AsSI and AsSeI, vitreous and molten, temperature dependence, structure and chemical bond changes in transition 2−84393
Bi-Zn alloys, m.p. to 600°C obs. 2−43339

Density continued
liquids continued
Bi, m.p. to 600°C obs. 2−43339
Co, at elevated temperatures exptl. results 2−64505
Cu, elevated temperature changes by measurement of thrust 2−64699
Cu binary alloy, max. bubble pressure method 2−56488
Cu_2S-CuCl melt, rel. to elec. and structural props. 2−46983
Fe, at elevated temperatures exptl. results 2−64505
FeS-$FeCl_2$ melt, rel. to elec. and structural props. 2−46983
In-Bi alloy, rel. to transport processes 2−46939
In-Ga(Sn) alloys, comp. depend., 700K 2−67815
Na, density response function from Mori's generalized Langevin eqn. 2−83776
Na alloy, rel. to compressibility determ. 2−77415
Ni, at elevated temperatures exptl. results 2−64505
Pb, elevated temperature changes by measurement of thrust 2−64699
Rb, calc. using sound velocity data at high pressures 2−71195
Se, elevated temperature changes by measurement of thrust 2−64699
Sn, elevated temperature changes by measurement of thrust 2−64699
Tl-Te system, melting point to 1300 K 2−56490
$Y_3Fe_5O_{12}$-BaO-B_2O_3-Fe_2O_3 melt, for $Y_3Fe_5O_{12}$ cryst. growth 2−60713

solids
— 2−60573
alkali metals, zero-press. density calc. 2−83884
alloys containing ZrC_x and HfC_x, effects of protective atmos. during sintering 2−77721
aluminate glass, densification behaviour 2−53526
composite dilatometer for meas. 2−62962
diepoxy-cyclohexane 2−43598
Earth near base of mantle and centre, distrib. meas. 2−72678
glass, rel. to oxide content, computer calcs. 2−44500
glasses, Se enriched, Ge-Se system, (4-16.7 at.% Ge), temp. depend.84209 2−84209
graphite, Gilsocarbon, irrad. behaviour, dimens. changes 2−56994
graphite, isotropic, influence on creep strain 2−56963
graphite, neutron irrad. at 715°C, dimens. stability 2−56047
graphite, nuclear, high fluence neutron irrad. behaviour, two-phase model 2−56048
graphite, pyrolytic, bulk and thin film 2−60648
graphite, pyrolytic, highly oriented, high dose fast neutron effects 2−57072
graphite composite, Pyrostrand, rel. to fabrication and struct. 2−53960
graphite from isotruxene carbons 2−61023
hypotaurocyamine 2−43600
metal, neutron damage simulation by ion bombardment, void form. 2−53692
metal, neutron damage simulation by ion bombardment, void form. 2−53693
metal, neutron irrad., void form. 2−50641
metal, pure and impure, irrad., void form., temp. effect 2−50642
metal, quenched or irrad., void form. mechanisms 2−53696
metal, radiation-induced void form. 2−50638
metal, swelling data analysis using displacement rates from Lindhard model 2−52880
metal, void nucleation and growth, computer simulation 2−53699
metallic materials, neutron irrad., void form. and growth, theory 2−53701
metallic materials, void nucleation during high-energy irrad. 2−53703
Moon, large-scale variations in interior 2−73064
mullite, stoichiometric ceramic compact 2−50873
polymers, effct of form of inelastic deformation 2−80119
polymorphic transitions under pressure, strain gauge obs. of volume changes 2−47678
radiation-induced void growth, applied stress effects 2−53704
rare earth monochalcogenides, press. induced electronic collapse and struct. changes 2−68297
reactor cladding and struct. materials, irrad. induced void form. 2−49901
refractory, high alumina, rel. to thermal shock resistance, and hot modulus of rupture 2−56961
sample preparation variables, X-ray spectrochemical analysis 2−65416
steel, dense struct. form. in the powder during stationary hot pressing in Cr steel 2−77698
steel, prep. by powder metallurgy, rel. to sintering conditions 2−43892
steel, stainless, deuteron generated void form., in-reactor damage simulation 2−53714
steel, stainless, irrad., fluence and temp. depend. of void form. 2−50647
steel, stainless, irrad., void form. 2−50646
steel, stainless, proton irrad., swelling, displacement damage depend. 2−53716
steel, stainless, proton- and nickel-irrad., void form. 2−53715
steel, stainless, suppression of void form. 2−50648
steel, stainless, void form. on quenching 2−53717
steel, stainless, void nucleation and growth during fast neutron irrad. 2−50645
swelling in fast-neutron-irrad. materials, theory 2−53702
Ag, elevated temperature changes by measurement of thrust 2−64699
Al, neutron irrad., void annealing 2−53705
Al, neutron irrad., void distrib., struct. imperfections in fluence 2−53736
AlN-Al_2O_3-Mo cermet, rel. to sintering conditions 2−43869
α-Al_2O_3, prepared from Al_2O_3 with AlF_3 additive 2−47704
Al_2O_3 ceramic, fine grain, Cr_2O_3 additions effect 2−50867
$AlPO_4$, high quartz solid solution glass ceramics, influence of composition 2−56562
Al_2SiO_5, high and low pressure polymorphs, rel. to thermal conductivity 2−65582
C-Si alloys, co-deposited, high-fluence irrad.-induced dimens. changes 2−53776
C, lampblack, rel. to graphitization obs. 2−56995
C, poorly crystn. isotropic, fast neutron irrad. induced dimens. changes 2−56767

Density continued
 solids continued
  C glassy monofilament, prep. and props. 2−56982
  C products, graphitization effects on neutron irrad. induced dimensional changes 2−56996
  C pyrolytic, fluidized-bed, mech. rel. to struct. props. 2−56768
  CaF_2:Gd very small specimens, precision meas. 2−47473
  CaF_2, density change on proton irrad. 2−71454
  $CaSiO_3$-$NdSiO_5$ system, homogeneous phase 2−47707
  Cd, with Sb or Bi impurity, annealing effects 2−71665
  Cd_3As_2-2CdTe system, rel. to phase diagram determ. 2−47708
  Cd_3P_2-2CdSe system, rel. to phase diagram determ. 2−47708
  Ce_2Se_3-GeS_2 system, rel. to phase diagram determ. 2−61043
  Co, at elevated temperatures exptl. results 2−64505
  $Co(PO_3)_2$-$NaPO_3$ and $Co(PO_3)_2$-KPO_3, glasses and melts, effect of temp. on optical density and comp. on excess molar volume 2−84481
  $Co(PO_3)_2$, molten, meas. in temp. range 1100-1200°C, relation to bonding and coordination 2−84034
  $CsPO_3$, molten, meas. in temp. range 800-1050°C, relation to bonding and coordination 2−84034
  Cu, elevated temperature changes by measurement of thrust 2−64699
  Dy_2O_3-WO_3 solid soln., of phases 2−57013
  Fe, at elevated temperatures exptl. results 2−64505
  Fe_2O_3, density changes and pore distribution during heat treatment 2−68140
  Fe_2SiO_4, high and low pressure polymorphs, rel. to thermal conductivity 2−65582
  $Gd_2O_3.GaO_2,Ge_2O_3.2GeO_2$, from phase diagram of Gd_2O_3-GeO_2 system 2−84097
  a-Ge film, rel. to u.v. dielectric consts., reflectance obs. 2−61586
  Ge films, X-ray total refl. obs. 2−74630
  GeO_2, high and low pressure polymorphs, rel. to thermal conductivity 2−65582
  $LiAlO_2$, high quartz solid solution glass ceramics, influence of composition 2−56562
  $Li_{0.93}Na_{0.07}Fe_5O_8$, effect of sintering conditions 2−64790
  Li_2O-B_2O_3-GeO_2 glass, rel. to struct. 2−47059
  Mg, neutron irrad., struct. damage and annealing 2−80683
  $MgAl_2O_4$, high quartz solid solution glass ceramics, influence of composition 2−56562
  Mo, ion irrad., void lattice obs. 2−53720
  Ne-p-H_2, Ne-n-D_2 solutions, low temps. 2−57027
  Ni-Al system, increase due to vacancy filling on high temp. compression 2−43939
  Ni-Al system phases 2−43938
  Ni-Fe, powder compact, struct. charact. 2−56946
  Ni, at elevated temperatures exptl. results 2−64505
  Ni, powder compact, struct. charact. Poisson's ratio 2−56946
  $POBr_3$, vibrational spectra and crystal structure 2−44380
  Pb, elevated temperature changes by measurement of thrust 2−64699
  Pb, with Ag impurity, annealing effects 2−71665
  PbO-RO-GeO_2, R=Mg, Ca, Sr, Ba, glass, rel. to structure 2−53540
  Se, elevated temperature changes by measurement of thrust 2−64699
  Si-As-Te amorphous semiconductor, relation to energy band gap 2−65003
  Si amorphous films, density detn. by backscattering of 2500 keV alpha parts. 2−80559
  SiO_2, high quartz solid solution glass ceramics, influence of composition 2−56562
  Sn, elevated temperature changes by measurement of thrust 2−64699
  SnF_2, soln. grown crysts. 2−47245
  $Te_{15}Ge_3As_2$ glass, calc. from u.s. velocity 2−47742
  $TeO_2-V_2O_5-Fe_2O_3$ glass, obs. 2−64534
  TiO_2 film, chemical vapour deposited, as function of processing temp. 2−50511
  UO_2 sintered bodies, effect on open pore distrib. 2−61025
  V-Ti(Cr)(Sn)(Al) alloy, comp. depend. 2−53912
  W single crystal, changes induced by neutron irradiation 2−52849
  $W_xNb_{1-x}Se$, (x=0-1) 2−60767
  $ZnAl_2O_4$, high quartz solid solution glass ceramics, influence of composition 2−56562
  ZrC-NbC, solid solution, creep meas. in compression, temp. range 2600-3150 K 2−84033
  $Zr_2Si_2Se_2$, rel. to nonstoichiometry 2−43505
Density measurement
  apparatus for obs. to 10^{-4}, by hydrostatic weighing 2−58691
  Archimedes, principle technique 2−78756
  Archimedes apparatus for small samples 2−52034
  composite dilatometer for meas. of liquids and solids 2−62962
  device for determ. level, density and interface of liquids 2−77376
  oceanographic velocity microstructure, free fall probe for determining velocity and density gradients 2−48415
  optical, continuous-flow ultraviolet microdensitometer 2−56504
  radioactive materials, differential method for small density change meas. 2−42662
  small samples, apparatus 2−41451
  soil, obs. using X-rays, models 2−61964
  thermal plasma densities in magnetosphere, digital sonograms of hydromagnetic whistlers 2−48535
  CaF_2:Gd very small specimens, precision meas. 2−47473
Desorption
  see also Sorption
  adatoms from solid surfaces, multiphonon quantum theory 2−50523
  benzene flash desorption and decomp. from clean or contaminated W polycryst. 2−84624
  electron bombardment surface ion desorption apparatus 2−43491
  gas, chemisorbed, thermal desorption kinetics, review 2−67918
  gases on a cathode investigating using vacuum micro-balance 2−85176
  graphite, heats of immersion rel. to degassing behaviour 2−53549
  graphite, isotropic nuclear and 'Poco', of oxygen, reactivity obs. 2−59843
  metal, effects on hydrogen permeation 2−77608
  metal surface, contaminated, spatial distrib of H_2 2−50526
  metallic-field effect consequences 2−54206
  molecules from surface following recombination of atoms, vel. distrib., model 2−47148
  porous material, of N_2 gas at liq. N_2 temps. 2−50541
Desorption continued
  powder, surface area meas. by nitrogen desorption, apparatus 2−56969
  pressure effects on magnetron press. gauge on satellite O VI-15 2−58148
  spectra, in presence of strong wall interaction interpretation 2−46409
  synthetic zeolite, of ^{4}He, for desorption cooling 2−52009
  Ag, mass changes and gases evolved during thermal desorption 2−47151
  C fibre, surface area changes on outgassing and desorpt. product composition 2−53951
  CO_2, on W(100) surface, rel. to decomposition 2−50551
  Cu-Ni alloy, adsorption of CO and O_2, flash desorption obs. 2−50536
  Cu wires, degassing in ultrahigh vacuum 2−60679
  Ge(100) substrate, of Na and Cs submonolayers, laser- induced 2−67921
  H-metal interaction, piezoelectrical quartz crystal micro-balance 2−74643
  H, in a LEED vacuum chamber of stainless steel and molec. beam assembly 2−67922
  H_2, photoactive agent in emission from freshly treated surfaces 2−81538
  H_2O_2, photoactive agent in emission from freshly treated surfaces 2−81538
  Mo in H_2 atmos. removal of C from Mo 2−64763
  N, in a LEED vacuum chamber of stainless steel and molec. beam assembly 2−67922
  NaCl, of Sn or In, activation energy, rel. to thin film deposition 2−43480
  Ni (111) plane, flash desorption spectroscopy study of H_2 adsorption 2−80568
  Ni film, desorption spectrum of H adsorbed under ultra-high vacuum conditions 2−53590
  Pt, chemisorpt. of H_2, adsorpt. and desorpt. kinetics 2−77514
  Si, surface Auger electron spectroscopy and electron impact desorpt. combined studies 2−64556
  SiO_2, of CO_2, u.h.v. studies 2−71353
  Si(111) surface, chemisorbed O_2, electron bombardment surface ion desorption study 2−71351
  TiO_2, of water, and adsorption 2−60688
  UO_2, entrapped noble gas ion obs. 2−60815
  W, energy, of O_2, as function of coverage 2−47171
  W, field desorption of CO in FIM, image gas enhancement 2−60673
  W, flash and electron stimulated desorption of CO on (100) planes 2−71356
  W, of CO, electron stimulated 2−47153
  W, of CO, field emission microscope obs. 2−71355
  W, of CO, quantitative analysis rel. to chemisorption states 2−47173
  W, of Cs^+, mol. beam study 2−60691
  W, of O, mass spectrometric obs., chemisorption 2−48327
  W, of O_2, M_2 CO, SIMS, EID, flash filament obs., binding states 2−47170
  W, of O_2, thermionic electron emission and work function obs. 2−47172
  W, of Si, activation energy, field emission obs. 2−47085
  W (100) surface, H-adatom flash desorp. spectrum 2−50555
  W crystal face, of ethylene, flash desorp. and decomposition 2−50552
Detonation
  see also Exploding wires; Explosions; Shock waves
  acetylene-oxygen-nitrogen mixtures, divergent spherical detonation propag. speed 2−52258
  Chapman Jouguet surface in multiheaded gaseous detonation 2−83648
  Chapman-Jouguet, unicity 2−58934
  Chapman-Jouguet detonation, self-similar blast waves 2−80392
  energy transfer in confined combustions and detonations 2−84618
  exothermic hypersonic flows about blunt projectiles, periodicity 2−83650
  explosives, laser radiation use, obs. 2−69784
  filled explosives in charges of small diameter 2−73454
  flow behind detonation with lateral confinement 2−83652
  gas dynamics, blast wave and finite kinetic rate models, review 2−80378
  gasdynamic theory, book 2−41837
  gasdynamics, conference (Marseille, France, Sept. 1971) 2−80375
  gaseous, free, quasi one-dimensional analysis 2−52259
  initiation by laser beam focused in gaseous medium 2−80377
  initiation by shock wave of mechanically inhomogeneous explosives 2−73453
  instabilities in reaction zones of detonation waves 2−83646
  ionizing wave propagating into gas, study of self similar flow patterns 2−45563
  isopropyl nitrate, effect of confinement 2−80422
  laser generated shock waves for detonation of insensitive explosives 2−49174
  liquid explosives, low velocity mechanism 2−83723
  local heat build-up in process of destruction of thin layers on impact 2−73455
  Mach stem induced, rel. to structure of detonation waves 2−80379
  MHD waves, props. 2−80220
  mild steel and plexiglass, loading, breakage and stress waves 2−84048
  nitromethane, divergent cylindrical detonation 2−83722
  nitromethane, effect of confinement 2−80422
  observation with fibre optics 2−55746
  one-dimensional, pulsating, with induction zone kinetics 2−45565
  propagation speeds in gaseous mixtures 2−83647
  propane-oxygen-nitrogen mixtures, divergent spherical detonation propag. speed 2−52258
  radial oscillations of gas cavity in compressible fluid rel. to underwater detonation of TNT 2−60174
  shell motion subsequent to detonation, numerical soln. 2−76383
  shock tubes with imploding detonation drivers, performance and limitations 2−69778
  solid explosive, CO_2 gas-dynamic laser production 2−45722
  tubular casing projection by cylindrical explosive cavity 2−58935
  two-phase, rotating, in liquid rocket motors 2−82372

Detonation continued
two-phase, with bimodal drop distrib. 2-80489
underwater shock wave pressures 2-46899
velocity in iso-atomic gas mixtures 2-83649
waves, local vel. meas. by Schlieren interferometry of Doppler shifted laser light 2-63138
waves, transient studies 2-82368

Deuterium
— 2-64127
adsorbed on W, field emitted electrons energy distrib. as function of coverage 2-48016
arc lamp, recalibration of spectral radiance in near u.v. 2-79450
in atmospheric precipitation model 2-62240
atom, hyperfine structure, αm/M correction 2-66902
atomic beams, charge fractions and excited atom populations of 8 to 100 keV beams from solid films of C, Mg, Nb, Au 2-49981
atoms, trapped, interpretation of microwave power dependence of differential saturation of hyperfine components 2-49946
Born-Oppenheimer approx. breakdown 2-56151
bubble chamber, background due to tritium decay 2-79682
burning, stellar evolution, pulsational instability 2-62505
coaxial plasma focus gun, current sheath obs. 2-80271
collision effects on Raman line profiles 2-43039
compressed, Rayleigh-Brillouin scatt. and relaxing thermal cond. 2-56171
cubic phase, orientational order parameter, 0.4-4K 2-60755
D-T plasma, laser heating to thermonuclear temps., by ion-ion collisions 2-64289
D-T reactor, thermal stability of spatially non-uniform plasma 2-80309
D-T reactors blanket chemistry 2-63953
diffusion in Nb, application to quantum theory 2-80718
electron density determination, spatial and temporal 2-67624
ergonic fusion, controlled thermonuclear reactions, power production 2-70930
first toroidal pinch, electron beam injection, low pressure operation 2-83598
foam chamber for charged particle detection by X-ray transition radiation, 300 GeV 2-73903
fusion by laser driven flame propagation in solid DT targets 2-64308
gas, Brillouin scattering, analysis of spectrum using kinetic model based on Wang Chang-Uhlenbeck eqn. 2-80409
hadrons pair production cross section for γ, 265-4215 MeV in hydrogen and deuterium 2-63497
heat of adsorption on Ni film, comparison with H_2 2-43497
heavy water enrichment, separation factor, current density, cathode material, temp. effects 2-42820
interstellar, production by cosmic rays 2-84970
isotope mixture separation using critical state method 2-56134
isotopic H_2 molecules, gas chromatographic separation and quantitative det. 2-52956
laser heated pellets, decoupling of corona and core 2-46770
liquid target system development, use of closed cycle refrigerator 2-46034
molecular beam, scatt. from W surface 2-47084
molecular collisional dissociation, DWBA theory 2-43033
molecule, core excited resonances, electron transmission spectroscopic investigation 2-46547
molecule, hyperfine temp. shift in Ne and Ar buffer gas 2-50033
molecules, polarisability temp. dependence 2-46546
neutron yield from Zr target fed with ^{3}H 2-42443
neutrons precision monitoring from TD and DD reactions 2-70305
photo-disintegration assay, determ. of total body water in man 2-69269
plasma, θ-pinch, laser-beam-scattering meas. of ion temperature 2-56364
plasma, estimation of Coulombian transparency as a function of temperature 2-42593
plasma, laser generation and heating to thermonuclear temps. 2-43179
plasma, X-ray fine structure in coaxial accelerator 2-80270
plasma ion heating and sheath formation in low density h.v. θ pinch 2-83580
plasma production, by laser heating of special gas target 2-80293
solid, heating by laser pulse 2-43152
solid, laser heating and production of DD reactions 2-43140
solid, self-diffusion and vacancies 2-43656
solid, sound velocity at 4.2K and pressures up to 200 bar 2-80910
solid, specific heat, Debye temp. and EQQ interactions 2-43985
solid pellet, laser irrad., parametric instabilities of plasma 2-67679
solubility and electromigration in Pd-Ag alloys 2-83990
spectral lamp, lowering of ignition voltage by addition of Ne and He 2-42284
substitution in acetylene, effect on n.m.r. parameters 2-77096
target, preparation techniques 2-49624
vibrational relaxation, transient stimulated Raman scatt., obs. 2-56150
wavelength dependence of laser light absorption by solid target 2-43176
Z-pinch, high pressure confinement, losses 2-83600
D_2:Xe, solid, vacuum u.v. study of Wannier states, obs. of host isotope effect on linewidths 2-51341
D/H ratio in Jovian atmosphere 2-66172
D-H ratio in Jupiter 2-75885
D_2-He, quantum mechanical scatt., comparison with He-HT system 2-60115
D_2-He collisionally induced vibrational excitation, effects of rotational motion 2-80139
n-D_2-Ne solutions, density at low temps. 2-57027
D_2-Ne(N_2)(Ar) systems, conc. depend. of binary diffusion coeffs., 300K 2-64399
D-T fusion reactor review of recent progress in mag. confinement 2-79843
D^+, mass-identified, mobility in He 2-43203
D_2, collisional de-excitation of vibrationally excited 2,4-dimethylpentyl-2*(-d_1*) 2-46648
D_2, vibrational relaxation, studied by laser induced vibrational fluorescence technique 2-80134

Deuterium continued
D_2, vibrationally excited, collisions with Na atoms, excitation of D-line radiation 2-70627
D_2 and ethylene mixed adsorption on polycrystalline W 2-44484
D_2 dissociative excitation, by electron impact, absolute meas. of 2S atom production 2-42889
D_2 vibrational level linewidths due to predissociation 2-79999
$D + Cl_2$, energy distribution among reaction products 2-65370
$D_2 + F$, energy distribution among reaction products 2-65368
$D + H_2 \rightarrow HD + H$, cross-section 2-61773
$D + H_2 \rightarrow HD + H$, molec. beam study 2-72546
$D + H_2 \rightarrow HD + H$, quantum cross section 2-61772
$D_2 + H_2 \rightarrow 2DH$, reaction paths 2-44466
H_2-D_2 solid system, specific heat, Debye temp. and EQQ interactions 2-43985
HD, Dicke narrowing and collision broadening of depolarized Rayleigh and Raman line 2-70700
$H_2 + D_2 \rightarrow 2HD$ four-centre exchange reaction ab initio calcs. of orbitals, contragradience and reaction surface 2-48323
$KH_{2(1-x)}D_{2x}PO_4$, ferroelectric crystal importance of D conc. on dielec. and thermal properties 2-84364
in Nb, interstitial site location by deuteron channelling 2-60811
SiC:D, implanted, recomb. radiation of excitons and vibr. spectrum 2-68688

Deuterium compounds *see Hydrogen compounds*

Deuterons
see also Cosmic rays/deuterons; Nuclear reactions and scattering due to/ deuterons
channelling in Ni foil, polarization 2-47784
inclusive reactions mechanism and inelastic screening 2-42363
low energy beam, angular spreading in neutralizer cell 2-79697
magnetic moment, review 2-70269
NE 230 and NE 231 liquid scintillators, response to deuterons and protons 2-79653
production, 25-70 GeV/s pulse, from internal target in accelerator 2-42480
relativistic charge form factor calc. from exptl. n-p phase shifts 2-42427
stopping power in Al, Ni, Cu, Rh, Ag, Pt, Au at 7.2 MeV and 14.4 MeV 2-54098
Ge, electron scattering in planar dechannelling 2-61128
Nb, location of interstitial D sites by deuteron channelling 2-60811
Si, electron scattering in planar dechannelling 2-61128
effects
graphite, production of electron spin centers, e.s.r. obs. 2-78152
thin target, fast particle damage production, theory 2-50636
Au, radiation damage, energy depend. 2-50643
Ay, radiation damage, energy depend. 2-50643
Er, secondary electron emission 2-61468
ErD_3, secondary electron emission 2-61468
Pt, radiation damage, energy depend. 2-50643
Sc, secondary electron emission 2-61468
ScD_3, secondary electron emission 2-61468
interactions
photographic emulsions, inelastic collisions with nuclei 2-55997
ad→b'pn, differential cross-sections in impulse approximation 2-55883
ad→bpp, differential cross-sections in impulse approximation 2-55883
dn→pnn, unitary model for three-body collisions 2-82992
dp→^{3}H(mm)$^+$, 2.8 to 3.8 GeV/c, high statistics missing mass spectroscopy 2-76727
dp→^{3}He (mm)^0, 2.8 to 3.8 GeV/c, high statistics missing mass spectroscopy 2-76727
ed→e$\Delta\Delta$, electromagnetic props. of Δ(1236) 2-82784
γ + d, ρ meson production, Glauber-model formalism 2-63638
γd, charged pion production, Khuri Treiman formalism applied 2-42386
γd, photoproduction of ρ^0 and ω at 4.3 GeV, determ. of direct vector meson photon coupling 2-49579
γd, $\pi^\pm$ production, π^-/π^+ ratio 2-49559
γd, total cross section for hadron production in 0.265-4.215 GeV region 2-46020
$\gamma d \rightarrow \Delta\Delta$, electromagnetic props. of Δ(1236) 2-82784
$\gamma d \rightarrow \pi^0 d$, differential cross section, coherent photoprod. of π^0 obs. 2-82671
$\gamma d \rightarrow \pi^0 p(n_s)$, 400 to 800 MeV, cross section comparison with $\gamma p \rightarrow \pi^0 p$ 2-42383
$\gamma d \rightarrow \rho^0 d$ cross sections interpret., coherent photoprod. of ρ 2-82676
K-d→K-π-π^+np$_s$ 7.3 GeV/c, K$\pi\pi$ enhancement in Q region 2-42370
K-d→K$^0\pi$-d, final state obs., 4.9 GeV/c 2-70222
K-d→K$^0\pi$-π^0d, final state obs., 4.9 GeV/c 2-70222
K$^-$d, 3.4 GeV/c, final states with K° or Λ hyperon 2-67011
K$^-$d, 4.9 GeV/c, total and differential cross-sections for various final states 2-42375
K$^-$d, 5.5 GeV/c, bubble chamber analysis of final states 2-63594
K$^-$d, ~400 MeV/c, $\Sigma\pi$ and ΣN final states 2-66998
K$^-$d→K$^-\pi^-\pi^+$d, 7.3 GeV/c, production of K$\pi\pi$ enhancement in Q region (1200-1450 MeV), structure and decay properties of Q 2-82770
K$^-$d→K$^-\pi^-\pi^+$np$_s$, 7.3 GeV/c, production of K$\pi\pi$ enhancement in Q region (1200-1450 MeV), structure and decay properties of Q 2-82770
K$^-$d→K$^-\pi^+\pi^-$n p$_s$ 5.5 GeV/c, cross section meas., production of K^{*0}(890) K^{*0}(1420) and Δ^-(1236) resonances 2-59515
K$^+$d, one and two prong interaction of K$^+$ on deuterium at 5.5 GeV/c, meas. of partial cross section 2-63595
K$^+$d→K^{0}pp, 0.64-1.51 GeV/c, cross-sections for K$^+$n→K^{0}p deduced 2-49550
K$^+$d→K^{0}pp$_s$, 3.8 GeV/c, total and differential cross sections rel. to K$^+$n charge exchange 2-70213
K$^+$d→KπN(N$_s$), 4.6 GeV/c, K*(892) and K*(1420)prod. 2-67040
K$^+$d→dK$^0\pi^+\pi^0$, 3.8 GeV/c, study of final state 2-66999
K$^+$d→dK$^+\pi^+\pi^-$, 3.8 GeV/c, study of final state 2-66999
μ-d→n,nν_μ, non-relativistic approx. using Primakoff weak interaction Hamiltonian 2-63525
n 14 MeV high intensity pulse generation using d beam 2-79656
nd total cross sections, 25-60 MeV 2-82982

Deuterons continued
interactions continued
nd → nnp, n-d initial-state interaction 2−82991
$\nu d \to \mu$-pp quasi-elastic reaction, forward cross-section determ., relativistic effects, one-pion exchange contribs. 2−42334
pd, 3.5 GeV/c, transverse and longitudinal momentum spectra of resultant pions 2−49591
pd, Impulse Approx. validity 2−59582
pd, p annihilation and study of pn bound states with detn. of nonzero orbital momenta 2−70262
pd annihilations, low energy phenomena 2−59586
pd → ^{3}He + X^0, study of missing mass spectra, 2 GeV protons 2−42410
pd → n(NN), bound states of (NN) system 2−46005
pd → $p_s pn\pi^+\pi^-$, 5.55 GeV/c, meas. of cross section for pn reaction and production of $\Delta n\pi^+$ and $\Delta p\pi^+$ final states 2−63663
pd → $\pi\Delta X$, new cross-section relations 2−63545
π^-d, 7 GeV/c, search for multipion resonances and validity of spectator model 2−67019
π^+d, 7 GeV/c, two pion final states 2−45957
π^+d, coherent A_2 production 2−59555
$\pi^\pm$d, total cross sections in momentum region 15 to 60 GeV/c, Glauber correction 2−45968
Σ^-d total cross sections at 19 GeV 2−79625
photodisintegration
coherent production of π^0 by polarized γ-rays, asymmetry ratio 2−70229
differential cross-sections and polarization of photonucleons 2−63672
π^-/π^+ production ratio between 240 and 400 MeV 2−67017
polarization
light nuclei, analysis of reactions 2−46307
in nd elastic scatt., P-wave interactions and tensor force effects 2−67060
nd scattering, simultaneous effect of P-wave interactions and tensor force 2−63666
^{12}C(d, d), 20-30MeV polarized beam, meas. of angular distribs., vector polarization, differential cross sections, optical model parameters 2−74106
^{12}C(d,d), 1.6 to 2.7 MeV, tensor polarization of deuterons 2−42580
scattering
see also Protons and antiprotons/scattering, proton-deuteron
hadron-deuteron, quasi-elastic, recoil effect 2−63565
recoil and Fresnel corrections determ. by analysis of double scattering term in Watson multiple-scattering series 2−73857
Z-dependence of level intervals in $2s^22p^2$, $2s^22p^3$ and $2s^22p^4$ 2−73114
, $K^+d \to K^+K^+d$, 3 GeV/c, meas. of differential cross sections, investigation of K^+n elastic scattering 2−63577
ed, at squared four momentum transfers of 1.0 and 1.5 (GeV/c)^2, neutron e.m. form factors 2−42418
$K^+d \to K^0pp$, 3 GeV/c, meas. of differential cross sections, investigation of K^+n elastic scattering 2−63577
$K^+d \to K^+pn$, 3 GeV/c, meas. of differential cross sections, investigation of K^+n elastic scattering 2−63577
Nd, elastic scatt., polarization calc. 2−67046
nd, low energy elastic scatt., effective range approx. 2−63665
nd, SU(3) basis of representation for Faddeev eqns. for three particles 2−76722
nd, spin structure in cross-section defect 2−82771
nd cross sections, 3-nucleon problems, two-term nonlocal separable potentials 2−82845
nd S-wave scattering studied using N/D approximation 2−52081
p + d → ^{3}He + X^0, analysis of π^0, η^0 and ω^0 production 2−42411
pd, elastic, investigation in diffraction cone region at energy 10 to 70 GeV 2−52635
pd, elastic scatt., phase shift analysis, 2.0 to 3.8 MeV 2−67055
pd, production of high energy polarized neutrons 2−70264
pd, real part of amplitude of elastic scattering at 70 GeV 2−46002
pd, spin structure in Glauber theory 2−59755
pd near- backward elastic scattering at high energies calc. of second order correction to first order baryon exchange formula 2−63661
πd, elastic, in πN resonance region, use of Glauber formulas incorporating Fermi motion 2−45972
πd, generalised Glauber formula with recoil 2−59487
πd scattering length, formula obtained by summing infinite series of nonrelativistic Feynman graphs 2−45970
Σ^-d, 30 to 90 MeV/c, quartet elastic and reaction cross sections 2−59590
nd, polarization, simultaneous effect of P-wave interactions and tensor force 2−63666
Nd elastic scatt., perturbative calc. of spin observables, tensor force 2−82960
Development, photographic *see Photographic process/development*
Diamagnetic resonance *see Cyclotron resonance*
Diamagnetism
see also Cyclotron resonance; de Haas-van Alphen effect; Magnetic properties/diamagnetic
Coulomb gas, many-body effects, free and Bloch electrons 2−68518
optokinetic, via optoelectrical effect, theoret. expressions, applic. to stars 2−66656
semiconductor, amorphous, diamag. enhancement of susceptibility, mechanisms 2−44219
Cd alloys, types and magnitudes of structures 2−81203
Diamonds
abrasion resist. during polishing and grinding, microscopic cleavage mechanism 2−74868
cathodoluminescence, changes caused by deformation, electron microscopy obs. 2−81428
crack structure, atomistic study 2−56831
deformation twinning and twinning plane identification 2−50684
diamond-metal system, compaction during liq.-phase sintering 2−80829
elastic moduli, press. and temp. coeffs. 2−50728
electrical conductivity of heavily doped (B, Al and Ti) samples 2−68396
electron irrad., bremsstrahlung spectra 2−49499
electron irrad., photocond., spectra 2−77962
e.p.r. of free and bound holes in B doped diamond 2−81458

Diamonds continued
framesite, plastic deform. and microstructure 2−50877
graphite-diamond transition, diffusional mechanism in strong elec. field 2−47706
graphitization at zero pressure and at high pressure 2−47677
ion machining 2−50811
irradiated, N impurity effects on annealing, optical absorp. obs. 2−71453
lattice dynamics, Keating's model calcs. 2−71708
lattice parameter changes, fast electron irrad. 2−60775
lattice vibrations, anharmonicity estimation from X-ray interference intensity coeff. 2−54017
molecular cryst., group theoretical classif. of mol. arrangements 2−71358
morphology, origin of features 2−74654
Mossbauer effect of ^{57}Fe 2−48152
optical absorption, first-principles energy-band calc. 2−84464
plastically deformed, intersecting twins 2−80692
powder, oxygen chemisorption, kinetics 2−65374
radiation damage, review 2−47371
radiation defects, theory of vacancies 2−47364
sliding friction with soft metal stylus 2−84044
structure-property relations, molecular orbital cluster calcs. 2−53516
synthesis in metal-C-X system, influence of third component 2−68782
synthetic, Ni inclusions, determ. of Curie points for different coloured diamonds 2−81213
three-wave mixing, resonant and nonresonant, interference 2−82507
vacancy, localized levels, LCAO-MO treatment 2−47808
X-ray topographic studies 2−64613

Dichroism *see Pleochroism*

Dielectric constant *see Permittivity*

Dielectric devices
capacitor, metallic-field effect consequences on capacitance 2−54206
ferroelectric display devices, multiple scattering of light by inhomogeneities 2−79350
i.r. thermometer with pyroelectric detector 2−55590
megavolt energy concentrating device, use of water as dielec. 2−46974
optical filters, optical control during preparation of thin films 2−52472
$Pb_xLa_{1-x}(Zr, Ti)O_3$ ceramics for selectively erasable image storage and display 2−79454
piezoelectric transducer, mechanical response under influence of body force 2−69749
piezoelectrical quartz crystal micro-balance for H-metal interaction studies 2−74643
$PbTiO_3$, pyroelectric i.r. detector 2−55572

Dielectric loss *see Dielectric relaxation*

Dielectric measurement
biological materials, three-terminal bridge with well defined sample field 20 kHz to 500 kHz 2−55206
cell, high temp., appl. to alumina 2−72012
complex dielectric constant meas. method, patent 2−82424
crystalline powers, piezoelectricity tester, description 2−59031
detection of high frequency absorption from microwave data 2−43381
high or low loss materials, short- circuited waveguide meas., computer program 2−49236
low and high loss materials, 0° to 70°C, method 2−49235
microwave absorption heated samples, dynamic high-temp. complex permittivity meas. 2−49237
permittivity, at audio frequencies, elimination of contact phenomena 2−72009
permittivity, microwave, modified infinite sample method 2−49238
permittivity, partial discharges, instrumentation 2−45639
polymers 2−81133
quartz, X-cut, strain dependence of permittivity det. by shock compression 2−51207
rocks, complex dielectric permittivity meas. method 2−54718
static dielec. const., press., temp. and freq. depends., meas. technique 2−65046
static dielec. const., press., temp. and freq. depends., meas. technique 2−65046
surface charge distributions in carnauba wax electrets 2−72046
thermally stimulated currents and voltages, theory for linear nonisothermal effects 2−45632
time domain reflection behaviour of transmission line partly filled with polar dielectric 2−63213
volume charge distributions in carnauba wax electrets 2−72046
$Bi_{12}GeO_{20}$, constant meas. 2−51203
Dielectric phenomena
see also Dielectric relaxation; Electric strength; Paraelectric resonance
charges in media with dielectric function 2−57103
Cole-Cole dielec. eqn., causality 2−59024
diagnostic radiography, e.s. imaging methods 2−69369
dielectric crystals, Lyddane-Sachs-Teller relation in the thermodynamic theory of dispersion theory 2−81148
discharge and partial discharges, air gap between dielectrics, space and time picture 2−74426
e.s. capacitance, circular disc near plane containing aperture 2−73496
fundamental characteristics describing all dielectric processes under electric field influence 2−41897
ketones, aliphatic, in benzene, dielec. absorpt. of microwaves, dielec. props. 2−60509
metallic system, one-dimens., Gor'kov- Eliashberg effect 2−57095
metals, charging effects in electron gas undergoing p-polarized optical excitation, surface plasmons 2−68317
nonpolar fluids, mol. model approach to permittivity 2−83803
particle charging in vibrofluidized bed 2−53110
plasma, dielec. response function calc. 2−60240
plasma density meas., calibration procedure to correct for effects of dielectric containers 2−67655
polar systems, phenomenological theory 2−81147

Dielectric phenomena continued
polymer film, electrochemical model for capacitance effects 2−57228
ring in uniform axial electrostatic field, exact and truncated solns. 2−58978
shock induced polarization, effects of non-uniform dynamic loading of test piece 2−76382
u.h.f. phase sensitive moisture gauge 2−52352
van der Waals interactions between macroscopic bodies having inhomogeneous dielec. susceptibilities 2−74561
NaBrO$_3$, optical phonon spectrum by laser Raman spectroscopy 2−84495
RbBr:OH, paraelastic alignment, optical absorp. pressure depend. obs. 2−61596
RbI:OH, paraelastic alignment, optical absorp. pressure depend. obs. 2−61596
ferroelectric *see Ferroelectric phenomena*

Dielectric properties of substances
see also Dielectric relaxation; Electric strength; Paraelectric resonance; Permittivity
biological materials 2−48839
crosslinked polyethylene, discharge-type treeing phenomena 2−57237
dipole moments, relaxation times, tables 2−45631
electrical insulation testing, analysis of gaseous decomposition products, gas chromatography applications 2−68828
fluids, electroconvection under alternating electric field 2−53151
insulating materials, aging, i.r. absorption spectroscopy measurements 2−68827
liquid cryst., cholesteric, dielec. loss and const., function of temp. and freq. 2−71229
liquid crystal, nematic, with negative dielec. anisotropy, rel. to cond. regime 2−60494
liquid crystals, nematic, angular depend. studies of anisotropy 2−80459
literature digest, book 2−45638
oil-paper insulation systems, chemical analysis of gaseous decomposition products, mass spectrometer applications 2−68824
polymer dielectric constant and loss tangent measurements, coaxial-resonator setup 2−81133
polyvinylchloride-nitrile butadiene rubber system 2−75144
rutile, point defect effects 2−61412
semiconductors, photodielectric effect, instrument for obs. 2−77907
snow, frequency dependence and relaxation times of complex dielectric constant 2−53466
gases
atomic, molecular and ionic interacions, book contrib. 2−46862
breakdown, ionization 2−46802
F compressed, meas. of dielectric const. and molar polarizability in 100-300 K range at 21 MN/m^2 2−67736
NH$_3$ variation of static dielectric permeability in strong resonance field 2−77369
O$_2$, compressed, meas. between 100 and 300K and 55 and 154K, calc. of Clausius-Mosotti function 2−50274
liquids and solutions
acrylates, permittivity and loss factor, microwave 2−60491
alcohol in heptane solns., dielec. relax. times, permittivities, loss tangent, rel. to comp. and temp. at 9.3477 GHz 2−74555
alcohol solns. with nonpolar solvents, dispersion behaviour 2−80487
alcohols in n-heptane soln., microwave absorpt.obs. 2−84611
n alkanes, from n pentane-n decane, relative permittivity as function of pressure and temperature 2−43384
alkyl acetates, relax. in aromatic and aliphatic solvents at microwave freqs. 2−60488
atomic, molecular and ionic interacions, book contrib. 2−46862
p-azoxyanisole, dielectric anisotropy of liquid crystal produced by magnetic field 2−50336
benzylamine, complex dielectric constants by microwave absorption 2−74553
benzylbromide, complex dielectric constants by microwave absorption 2−74553
benzylchloride, complex dielectric constants by microwave absorption 2−74553
benzylcyanide, complex dielectric constants by microwave absorption 2−74553
breakdown rel. to vapour bubble formation 2−56509
bromoalkanes in cyclohexane soln., mean relax. times, Cole-Cole plots, dipole moments 2−71221
bromonaphthalene solutions, microwave properties 2−43381
charge transmission through dielectric interfaces, application to liquid He 2−43413
6-chloro-1-hexanol, variation of complex dielectric const. with frequency in 300 MHz-24 GHz region at −42° and +20°C 2−64468
chloronaphthalene solutions, microwave properties 2−43381
complex dielectric constant det. at submillimeter wavelengths 2−56508
complex dielectric constant meas. method, patent 2−82424
complex molecules in solution, molec. structure and formation constant, determination from polarisation meas. 2−60486
conduction and breakdown, book contrib. 2−46978
conduction phenomena, book contrib. 2−47958
constants meas. having high losses in 3 cm wavelength range 2−56507
detection of high frequency absorption from microwave data 2−43381
α,ω-dichloroalkanes, relax. behaviour rel. to intramol. cooperative phenomena 2−60489
dimethyl siloxane fluids, photoinjection from metal-free phthalocyanine film 2−56512
electrical insulation and dielectric phenomena, conference, Williamsburg (1971) 2−57222
electrolyte soln., compressibility rel. to dielec. const. 2−50342
ethylene glycol, Debye effect and relax. time distrib. 2−46971
hydrated electron struct. and electron affinity of water 2−80013
hydrocarbon, electronic conduction 2−56511
hydrocarbon, photoinjection from metal- free phthalocyanine film 2−56512
hydrogen-bonded, nonlinear dielec. effect, significant struct. theory 2−46970

Dielectric properties of substances continued
liquids and solutions continued
o-hydroxyacetophenone solutions, microwave properties 2−43381
ionic solution, dielectric coeffs. in interphase with electrode 2−48335
ketones, aliphatic, in benzene, dielec. absorpt. of microwaves, dielec. props. 2−60509
luminescence decay law, effect of dielectric properties on transfer of excitation energy 2−53439
2-methylbutanol-2 solutions, polarization 2−46975
myglobin in water, dielectric dispersion due to molecular rotation 2−46976
n-octyl bromide, relative permittivity as an indication of molecular interactions, short range ordering 2−56476
nonpolar systems, electron dynamics 2−81531
oil, cond. current statistics, stress-induced motion effect 2−43383
organic solvent, effect on H-bond polarity of phenol-triethylamine complexes 2−46621
pentanol isomers, pressure dependence of static permittivity 2−56510
N- phenyl-α-naphthylamin in n-heptane-n-butanol mixtures, effective local dielectric constant and spectra 2−56149
N-phenyl-β-naphthylamin in n-heptane-n-butanol mixtures, effective local dielectric constant and spectra 2−56149
polar molecules in non-polar solvents, dilute solution, theory of dielectric constant 2−74551
polaron viewpoint of solvated electrons 2−78180
prebreakdown, stat. analysis of emitted light pulses 2−43382
silicone thermal breakdown under pulsed h.f. fields 2−56513
solvated electrons, absorpt. spectrum resolution, band shapes 2−67831
thermal convection under central force field, laboratory model 2−52279
water, static dielec. const. to high temps. and press. from Mean Spherical Model 2−83793
water, use in megavolt energy concentrating device 2−46974
F, saturated, meas. of dielectric const. and molar polarizability in 70 to 140 K range at 21 MN/m^2 2−67736
H$_2$O, dielectric absorption around 70 MHz, meas. of total impedance and phase angle 2−74552
O$_2$, compressed, meas. between 100 and 300K and 55 and 154K, calc. of Clausius-Mosotti function 2−50274
solids
8/65/35 PLZT fine grained ferroelec. ceramic, dielec. and optical fatigue effects 2−77953
A$_1$B$_2$ crystal, fluorite struct., theoretical analysis 2−72003
alkali halide crystals, polarization by inertial forces 2−54238
amorphous semiconductor, photodielec. effect, rel. to trapping 2−61443
atomic, molecular and ionic interacions, book contrib. 2−46862
benzophennone molecular crystal, polarizabilities and dipole moments for lowest singlet and triplet $n\pi^*$ excited states 2−81136
breakdown properties, electrical and thermal, book contribs. 2−47959
cellulose and similar fibrous materials, dielectric constant and crystallinity 2−61408
charge transport 2−57186
chrysene, dielectric tensor components derived from energy loss spectra 2−81138
conduction phenomena, book contrib. 2−47958
crystals, thermally stimulated current and voltage techniques 2−72004
cyclopentanol, solid, unusual dielectric behaviour and molecular motion, dielectric and visual studies 2−57224
dicalcium lead propionate, spin-lattice relax. near crit. point 2−65196
dipolar entropy and heat capacity of ionic crystal with paraelectric dipolar impurities for E∥[100], [110] and [111], E=applied field 2−57221
dipole-dipole interaction effects, model, Monte Carlo method 2−77943
electrical insulation and dielectric phenomena, conference, Williamsburg (1971) 2−57222
electron gas in metals, longitudinal dielectric tensor in uniform magnetic field 2−75038
epoxy resins, rel. to effect of fillers and plasticizers on molecular mobility 2−47062
films, fabrication, nucleation, epoxy, book contrib. 2−47961
films, review of conducting props. 2−64907
glass, chalcogenide, i.r. cond., 10^9-10^{13}Hz 2−61638
glass ceramics, workability and dielec. props. 2−43868
ice:KOH, dielec. dispersion and phase transition 2−72014
ice, proton distribution, Kirkwood correlation factor 2−80642
ice I$_h$ crystals, dielectric relaxation spectra, effects of dislocations, multicrystallinity, HF doping, space-charge pile-up 2−72013
inorganic glasses, polarization, empirical relationship with electrical conduction 2−57188
insulated crystal, kinetics of screening, metal-dielectric-semiconductor-dielectric system 2−72002
insulator, charging during LEED 2−64547
insulator, thermal switching behaviour 2−61268
insulators, irreversible local breakdown and electric stress, reln. 2−68466
interatomic spacings, nonlinear algebraic equations and formation of a complete set 2−71400
metallic conductors, permittivity, phenomenological model 2−75253
molecular crysts., local elec. field and charge-carrier mobilities 2−81129
multilayer coatings for high power laser 2−55699
naphthalene, persistent internal polarization temp. and electric field dependence 2−75138
niobates, ABCNb$_2$O$_{15}$, A=Ca, Sr, Ba; B=Ca, Sr, Ba, C=Na, K 2−75251
nonlinear response of electrons to X-rays 2−61576
organic, geminate recombination of charge carriers 2−57187
oxide films, stored charges 2−44166
paraelectric crysts., ENDOR of A-centre electrons rel. to elec. field 2−78176
perspex magnetoelectrets, effect of forming magnetic field on dielectric behaviour 2−65074

Dielectric properties of substances continued
solids continued
phenanthrene, dielectric tensor components derived from energy loss spectra 2−81138
Pippard's relations applied to λ transitions 2−61490
plate for polarization control in He-Ne laser 2−82474
polar substances in n-pentane, rel. to solid soln. struct. 2−72016
poly(4-chlorostyrene,4-methylstyrene)copolymers 2−68462
poly (N-vinyl carbazole) film, transient space charge perturbed current 2−57229
polyethylene foil, degradations induced by ion bombardment and partial discharges 2−44148
polyethylene terephthalate film, crystallinity effects 2−61410
polyethylene terephthalate film, dielec. obs. of stress relaxations 2−56779
polyimide, aromatic, secondary dynamic dispersions 2−83366
polymer, depolarization spectra, thermal treatment effect 2−47974
polymer, ionic cond. temp. depend., struct. factors influence 2−72019
polymer, linear chain, spontaneous polarization and pyroelec. coeff. 2−72045
polymer, normalized relax. spectrum construc. in log/log coords. 2−47972
polymer, polarization and cond., conf., Bratislava, Czechoslovakia [May 1972] 2−47962
polymer, surface states and polarization 2−47971
polymer, thermostimulated depolarizing currents and thermoelectret effect 2−47973
polymer films, breakdown 2−47980
polymer films, electrical conductivity, use as dielectric layers in m.i.m. structures 2−83859
polymer films, internal struct. of single hole breakdown 2−47981
polymer films solvent cast, dielectric relaxation rel. to residual solvent and crystallinity effect 2−57227
polymer surfaces, humidity effect 2−57223
polymers, book contrib. 2−47960
polymers, thermally stimulated current and voltage techniques 2−72004
polymers conductivity and diffusion rel. to mechanical strain 2−57232
polymers-Hg contact, electric field effect 2−57236
polyolefins, electric strength, effect of impregnation with various viscous materials 2−57234
polyoxymethylene, absorption, analyses of anisotropy due to defects 2−61417
polypropylene film, crystallinity effects 2−61410
polystyrene films, passage of transient currents along surface 2−72001
polythene, irreversible local breakdown and electric stress, reln. 2−68466
powder and bulk materials, correl. over range of permitt. and packing fraction 2−61411
for reactor use, conductivity changes due to irradiation 2−52851
saline aqueous frozen solns., permittivity obs. of cooperative phenomena 2−75139
sectioned insulator made of semiconductor sitall 2−61441
semiconductor, AB type, third moment of imaginary part of dielectric const. 2−68461
semiconductor, amorphous, trap levels, thermally stimulated capacitor discharge study 2−54188
semiconductor with contacting bands, dielec. function, transverse and longit., RPA approx. 2−77941
semiconductor with contacting bands, transversal dielec. function in mag. field, RPA approx. 2−77942
semiconductors, dielectric matrix computed in pseudopotential scheme 2−47933
semiconductors, dielectric screening 2−61217
semimetals, excitonic- insulator phase, effect of interband scattering 2−81003
static dielectric const., accurate determ. 2−72011
stearic acid films, high-field transient behaviour 2−77950
steatite materials, dielectric resistance, effect of defects 2−53933
sugarcane wax electrets, heterocharge mechanism 2−75157
surface charge decay in insulators with nonconst. mobility and deep trapping 2−51193
thin films, interference method for meas. of dispersion in refractive index 2−44342
time depend. polarization and current after voltage applic. 2−47965
triglycine sulphate, ferroelec., temp. depend. in far i.r. 2−61435
triglycine sulphate, structural inhibition of ferroelec. switching, X-irrad. field treatment 2−77952
Ag film, dielectric const. changes, piezoreflectivity obs. 2−54382
AlN_x films, prepared by reactive r.f. sputtering, dielectric characteristics 2−77507
Al_2O_3, 0-1000°C 2−72012
Al_2O_3 film, in m.i.m. struct., transients, capacitance variation with temp. 2−57219
As_2S_3 and As_4S_4 films, rel. to a.c. cond. 2−68392
As_2Se_3 film, rel. to a.c. cond. 2−68392
Au-Bi_2O_3-Al, capac. and loss tangent, freq. depend. 2−80594
BaF_2, l.f. consts., press. and temp. derivatives 2−51189
$Ba_2NaNb_5O_{15}$, characterization, vibr. props. 2−72364
$Ba_xSr_{1-x}ZrO_3$, high-permittivity temp.-stable, low microwave loss 2−51190
Bi, thin films, permittivity meas. 2−47975
C film, insulating charact. and dielectric const. 2−56588
CaF_2, l.f. consts., press. and temp. derivatives 2−51189
Ca(Zr,Ti)O_3, high-permittivity temp.-stable, low microwave loss 2−51190
CeF_3 film, evap., a.c. props. 2−44153
KBr(Cl), l.f. consts., press. and temp. derivatives 2−51188
KCN, permittivity, temp. depend., anomalies at transition points 2−75141
KCl-ice, high concentration, dielectric dispersion 2−75142
KCl, OH^- substituted, paraelectric centres with low zero field splitting 2−75147
$KH_{2(1-x)}D_{2x}PO_4$, study in ferroelectric and paraelectric phases 2−84364
K(Ta,Nb)O_3 crystals, paraelectric electro-optical, optical damage analysis 2−79226
Dielectric properties of substances continued
solids continued
LiF, l.f. consts., press. and temp. derivatives 2−51188
LiF, radiation-induced thermally activated depolarization 2−72007
$LiGaO_2$, rel. to electromech. coupling factor and reson. freq. 2−51206
Li(N_2H_5)SO_4 dielectric const., 6 to 5.10^6 Hz, 20 to 200°C 2−77931
$(NH_4)_2SO_4$, paraelectric, ^{14}N quadrupole coupling 2−44456
NaBr(Cl)(F), l.f. consts., press. and temp. derivatives 2−51188
NaCl, static const., anharmonic contribs. 2−50996
$NaNO_3$, optical props. in vacuum u.v. region 2−84487
$NaNO_3$, phase transition, X-ray diffr. obs. 2−65048
$Ni_xZn_{1-x}Fe_2O_4$ ferrites, 10^2-10^6 Hz; −60-0°C, dispersion regions 2−84358
$PbBr_2$, elec. cond. in cell arrangement, space charge effects, elec. polarization 2−61420
$PbBr_2$, electronic cond., hole cond., elec. polarization 2−61419
$PbTiO_3$-$Pb(Cd_{0.5}W_{0.5})O_3$ ceramic, electromechanical props. 2−64788
$PbZrO_3$, growth and obs. of intermed. ferroelec. phase 2−81140
RbBr:Ag^+, static and dynamic paraelec. props., low temp., electrooptical study 2−61422
RbCl:Ag^+, static and dynamic paraelec. props., low temp., electrooptical study 2−61422
RbCl, Arrhenius relax. of OH- ions, dielec. susceptibility study 2−65050
RbCl, susceptibility of CN^- ions from 1 to 26 GHz 2−51192
SbSi, naturally polarized crysts., photodomain effect on illumination 2−77940
Se film, rel. to a.c. cond. 2−68392
Si dielectric matrix computed in pseudopotential scheme 2−47933
SiO, amorphous trap levels, thermally stimulated capacitor discharge study 2−54188
SiO films, electron-beam-evaporated, microwave relax. phenomena 2−54231
SiO_2 and SiO films, moisture stability 2−72015
SiO_2 r.f. sputter deposited, electrical characteristics uniformity 2−61407
$SrCl_2$:K^+(Na^+), dielec. const., loss angle, cond., Frenkel defect form. 2−47969
SrF_2, l.f. consts., press. and temp. derivatives 2−51189
Sr(Zr,Ti)O_3, high-permittivity temp.-stable, low microwave loss 2−51190
Ta-Al anodic oxides, correlation between temp. coeff. of capac. and dielectric loss 2−77946
Ta anodic oxides, correlation between temp. coeff. of capac. and dielectric loss 2−77946
Ta_2O_5 film, in m.i.m. struct., transients, capacitance variation with temp. 2−57219
TiO film, amorphous, sputtered, equiv. elec. cct. 2−47970
TiO film, in m.i.m. struct., transients, capacitance variation with temp. 2−57219
$Tl_2Cd_2(SO_4)_3$ ferroelectric Langbeinite 2−51199
Y_2O_3, low loss dielec. film, use of mag. fields in electron beam evaporation 2−77947
ZnO-Al_2O_3-SiO_2 glass-ceramics, dielec. props. and effects of adding (CaO, SrO, BaO) 2−65045
ZnO, decay of pyroelectrically induced polarization charges 2−54241
solids, ferroelectric *see Ferroelectric materials*
Dielectric relaxation
2,3-dimethylbutane, crystalline, dielec. loss meas., different relaxations above and below glass temp. 2−81144
— 2−72027
acetic acid in benzene solution, deuterated and non-deuterated 2−71219
acetophenone, 2-hydroxy-5-methyl derivative, computation from permittivity and loss meas. in benzene solution at 37.4 GHz 2−60487
acrylates, microwave region, 30-70°C 2−60491
alcohol in heptane solns., dielec. relax. times, permittivities, loss tangent, rel. to comp. and temp. at 9.3477 GHz 2−74555
alcohol solns. with nonpolar solvents, dispersion behaviour 2−80487
alcohols in n-heptane soln., microwave absorpt.obs. 2−84611
alkyl acetates, in aromatic and aliphatic solvents at microwave freqs. 2−60488
anisole mols. in polystyrene, mobility study 2−83387
anthraquinone-pyrometallic anhydride polymer 2−81143
benzophenone, 2-hydroxy-5-methyl derivative, computation from permittivity and loss meas. in benzene solution at 37.4 GHz 2−60487
bromoalkanes in cyclohexane soln., mean relax. times, Cole-Cole plots, dipole moments 2−71221
camphor, solid, molecular rotation at dielectric relaxation transition 2−61414
caprylophenone, 2-hdyroxy-5-methyl derivative, computation from permittivity and loss meas. in benzene solution at 37.4 GHz 2−60487
ceramic matrix, chemically reacted, for fibre reinforced composites 2−56972
composite system, nonlinear losses and behaviour of ions 2−54228
cyclohexanol, crystalline, dielec. loss meas., different relaxations above and below glass temp. 2−81144
4,4′-di-n-heptyloxyazoxybenzene, nematic phase, anomalous alignment due to elec. fields 2−77412
α,ω-dichloroalkanes, rel. to intramol. cooperative phenomena 2−60489
dipole moments, tables 2−45631
dipole-dipole interaction effects, model, Monte Carlo method 2−77943
emulsion with cond. dispersed phase, dipolar type Debye relax. 2−43408
emulsion with dipolar Debye absorpt. Hanai formula 2−80490
epoxy resins, rel. to effect of fillers and plasticizers on molecular mobility 2−47062
ethylene glycol, Debye effect and relax. time distrib. 2−46971
ethylene-carbon monoxide copolymer, anisotropy of relaxation for dipolar orientation change 2−75140
fibrin, elongated, films, piezoelectricity and viscoelasticity 2−85087

Dielectric relaxation continued
  n-GaAs, anisotropy of the submillimeter conductivity of warm carriers 2−84330
  gases of linear molecules in magnetic field, time correlation functions 2−46853
  generalized model of dielectrics with time dependent polarization 2−68460
  ice I_h crystals, dielectric relaxation spectra, effects of dislocations, multicrystallinity, HF doping, space-charge pile-up 2−72013
  insulating layers on contaminated Langmuir probes 2−50206
  ionic crystals, orientation mechanism and theory of dielec. loss 2−77933
  ketones, aliphatic, in benzene, dielec. absorpt. of microwaves, dielec. props. 2−60509
  liquid compound of asymmetric top molecules, calc. of collective molecular orientation correlation functions 2−50313
  liquid cryst., cholesteric, dielec. loss and const., function of temp. and freq. 2−71229
  liquid crystal, and EHD instabilities 2−53395
  liquid crystal, cholesteric, rapid conical-helical perturb., a.c.-d.c. technique obs. 2−71217
  liquid crystal, nematic, with negative dielec. anisotropy, rel. to cond. regime 2−60494
  loss model, based on interfacial electron tunnelling 2−47964
  losses in rectangular waveguide loaded with dielectric slab in H-plane 2−59001
  macroscopic theory, appl. to anal. of phenomenological model 2−83792
  maximum absorpt. freq. eval. expression 2−57176
  methoxy benzylidene butyl aniline, nematic, bend oscillations in dielectric electrohydrodynamical instability 2−46931
  p-methyoxybenzilidene p-n-butylaniline, nematic phase, rel. to anomalous alignment and domains 2−71161
  myristophenone, 2-hydroxy-5-methyl derivative, computation from permittivity and loss meas. in benzene solution at 37.4 GHz 2−60487
  naphthalene compressed pellets, electrical conductivity, 1 kc/s to 100 Mc/s range 2−61415
  α-naphthylamine compressed pellets, electrical conductivity, 1 kc/s to 100 Mc/s 2−61415
  non-linear dielectric loss (imaginary part of susceptibility) at high elec. fields 2−77944
  nylon 66, hexamethylene adipamide, space charge, Maxwell-Wagner effect 2−65051
  nylon 66, thermodepolarization current study 2−77938
  polar substances in n-pentane, rel. to solid soln. struct. 2−72016
  poly(hexamethylene sebacamide) (nylon 610), effects of melting 2−44151
  polychlorotrifluoroethylene, meas. and mechanism 2−61416
  polycrystalline solids, dynamics of losses using diagrammatic technique 2−72010
  polyethylene terephthalate, oriented anisotropy of α and β relaxations 2−60856
  polymer, normalized relax. spectrum construc. in log/log coords. 2−47972
  polymer crystalline, anisotropy of relaxation for dipolar orientation change 2−75140
  polymer films solvent cast, rel. to residual solvent and crystallinity effect 2−57227
  polymers, cryogenic loss peaks, assignment of molecular mechanisms 2−71557
  polypentene, rel. to struct. and morphology 2−60613
  polyvinyl acetate solution in toluene u.s. absorption 2−83376
  snow, times of computer dielectric constant 2−53466
  thin films, tangent of loss angle, determination by contactless method 2−57225
  time depend. polarization and current after voltage applic. 2−47965
  triglycine sulphate, multi-domain single crystal 2−61434
  water emulsion, dipolar Debye type relax., −40 to −15 degrees C 2−43409
  $AgNa(NO_2)_2$, temp. depend., hydrostatic press. effect 2−77955
  $AgNa(NO_2)_3$, crit. slowing down of relax., thermal noise study 2−72029
  $Al-Al_2O_3-Al$, effect of reactor radiation 2−81114
  $Al-MoO_3-Al$ structure, dielec. relax. current obs. of defect nature 2−68453
  $Al-SiO_x-Al$, effect of reactor radiation 2−81114
  As-Se glass, Ag doped, rel. to d.c. cond. 2−64975
  As_2S_3 and As_4S_4 films, rel. to a.c. cond. 2−68392
  As_2Se_3 film, rel. to a.c. cond. 2−68392
  $Ba_2Bi^{5+}Bi^{3+}O_6$, phase transition obs. 2−75150
  $BaO-B_2O_3-Fe_2O_3$ glass, microstruct. effects 2−65113
  $BaTiO_3$ ceramic, sintering parameter effects 2−57241
  Bi:Te deposits, relaxation time of carriers 2−75255
  Bi_2WO_6, temp. depend. 2−47263
  CaF_2, rare earth doped, interstitial dipole relax., thermal depolarization obs. 2−60790
  CeF_3 film, evap., mechanism of relax. 2−44153
  KCl, OH^- substituted, paraelectric centres with low zero field splitting 2−75147
  KH_2AsO_4 ferroelectric, correlation with n.m.r. 2−57243
  KH_2PO_4, molecular dynamics study and ferroelec.-antiferroelec. transitions 2−72032
  K_2O-SiO_2 glass, as function of thermal history 2−54229
  $Li_2O-Fe_2O_3-SiO_2$ system, dispersion, composition depend. 2−54333
  Li_2SO_4, polycryst. pellet, radio and microwave freqs. 2−61413
  MoS_2 layer structures, a.c. conductivity in high and low frequency limit 2−81062
  NaCl, doped with Bi^{3+} coordinately bound on O, loss factor 2−51191
  Na_2O-SiO_2 glass, loss peak and phase separation 2−54230
  $PbBr_2$, pure and Cu^+-doped, defect studies 2−47402
  $PbCl_2$, pure and K^+-doped, defect studies 2−47402
  Sc_2O_3 film, loss peak, predicted by hopping model for a.c. cond. 2−61324
  Se film, rel. to a.c. cond. 2−68392
  Si_3N_4 film, relatively sputtered onto Cu substrate, dissipation factor 2−43481
  SiO films, electron-beam-evaporated, microwave relax. phenomena 2−54231

Dielectric relaxation continued
  SiO_2, vitreous, dielec. loss rel. to struct. props. 2−47061
  SiO_2 and SiO films, loss tangent, moisture stability 2−72015
  $SrCl_2$:K^+(Na^+), loss angle, dopant conc. depend. 2−47969
  Ta-Al anodic oxides, correlation between temp. coeff. of capac. and dielectric loss 2−77946
  Ta anodic oxides, correlation between temp. coeff. of capac. and dielectric loss 2−77946
  V_2O_5, large crystals 2−68463
Differential analysers *see Calculating apparatus*
Differential equations
  — 2−72965
  — 2−58707
  acceleration waves of arbitrary shape, behaviour 2−45242
  advanced interactions, existence theorem 2−55806
  approximate Z-transform technique, transient anal. of lumped and distributed parameter systems 2−55440
  asymptotic, for entropy of mixing 2−83714
  asymptotic methods for solution of nonlinear eqns. in dynamics 2−52125
  beam and shell deflection, numerical soln. of boundary value problem 2−82314
  Bessel functions, computation in high scattering studies 2−70022
  Blasius eqn. for solving mixed layer flow 2−46656
  Bloch equations, solution method 2−69841
  blunt bodies, supersonic nonequilibrium flow 2−83678
  boundary layer, method of solution 2−53119
  boundary value problem in gas dynamics, variational soln. and error bound 2−77340
  Brown's lunar theory, different methods of derivation of differentials 2−84938
  Burgers eqn. for turbulent flow, table of solns. 2−77179
  Cauchy problems soln. using reproducing kernel method 2−58710
  Cauchy problems soln. using reproducing kernel method 2−58709
  cavity distortions in massive liquid due to inertial effects, numerical soln. of differential eqn. on MINSK-22 2−83745
  in celestial mechanics, eqns. of motion, power series solns., transforms, applic. 2−62453
  comparison for cascade theory of 2-dimensional flow fields and elastic theory of 2-dimensional stress fields 2−52044
  corneal topography, differential equation used with diffused ring photokeratoscope 2−66314
  coupled mode, unbounded solns. 2−58704
  diffraction of plane waves by a strip, exact and asymptotic solns. 2−82177
  diffusion, moving-boundary problem for oxygen in absorbing medium 2−83997
  diffusion, numerical soln. of problem 2−66481
  digital computer for incremental integration with serial-paralllel processing 2−82283
  dimensional perturbation of contraction coefficient 2−46894
  dual integral eqn. system soln. 2−45238
  Duffing's, occurrence of second higher harmonic oscillations 2−73289
  expansion of underwater cylindrical gas bubble, approximation 2−43306
  functional-derivative, method of characts. adaptation 2−58706
  Gibbs adsorption equation for multicomponent solutions 2−83874
  Gibbs adsorption equation for multicomponent solutions 2−83873
  glow curve numerical solution using Runge-Kutta method 2−84535
  Green's function, asymptotic soln. for wave eqn. with variable vel. and boundary conditions 2−82176
  Hamilton equations of motion, canonical transformations and quadratic Hamiltonians 2−41456
  Hamiltonian partial, canonical transforms. and generating functionals 2−66421
  Hardy-Lebesgue space approach to polynomial solns. 2−58705
  harmonic oscillator, free damped, soln. of eqn. of motion 2−78809
  heat eqn., semi-linear n-dimensional boundary-value problem, existence, uniqueness 2−76168
  heat prod. in semi-infinite cylinder and generalized hypergeometric function 2−82256
  heat production in cylinder, analysis using Gegenbauer polynomials 2−41855
  Hills, general, stability boundaries, anal. by perturbation method 2−45234
  hyperbolic, second-order difference method 2−69716
  integration of boundary layer eqns. through region of reverse flow 2−43219
  intrinsic momentum computation of charged particle in magnetic field 2−45675
  inversion-free methods for finding nonlinear operator equation solutions 2−58708
  kinetic, with stiffness, numerical solution 2−45347
  Lagrange eqns. of motion, 2 degrees of freedom, simplified soln. 2−82288
  laminar boundary layer with continuous or local injection and variable wall temp., analytical soln. 2−83688
  Liapunov stability of hybrid dynamical systems with multi-elastic domains 2−76251
  Lienard equations for 2nd order mass-spring system graphical treatment 2−78870
  linear hyperbolic partial, for two-dimensional impulsive waves in linear acoustic medium, integration 2−73427
  linearization and Liapunov stability analysis 2−45230
  local potential energy eigenvalues calc. method 2−82224
  Mac method, homogeneous boundary condition for pressure 2−46655
  minimality props. of local pot. 2−63052
  multidimensional gas dynamics, boundaries characteristics, in time dependent finite difference analysis 2−74478
  neutron transport props. of regular lattices 2−83058
  non-linear rate eqn. for analysis of world population problem 2−69545
  nonlinear, for electric arc modelling 2−64361
  nonlinear, for reflection coefficient of inhomogeneous transmission line, linearization technique 2−69824
  nonlinear, generation of approximate periodic solutions, error minimization criteria 2−45233
  nonlinear, mixed Cauchy problems, method for exact soln. 2−66417

Differential equations continued
nonlinear, partial, for transverse oscillations of travelling string, soln. by Panavko's linearisation method 2−49089
nonlinear, phase shift, numerical calculation, variable phase method 2−45869
nonlinear, whose orthogonal trajectories satisfy Riccati equations, determination 2−62971
nonlinear elastic constitutive equations 2−76320
nonlinear interaction between three waves, 1st initially absent. 2−83620
nonlinear optics, N-soliton soln. 2−82503
nonlinear ordinary, validity of averaging methods for oscillatory solutions 2−76167
nonlinear parametric interactions, instabilities, numerical study 2−78780
nonlinear wave propagation, asymptotic theory 2−76169
nonlinear wave-wave interacting systems with well- defined phase description, bounds for solution 2−45241
nuclear reactor transients, space dependent, closed-form analysis 2−83096
numerical methods and computational problems in MHD 2−80267
ordinary differential eqn. model of chemical reactions, comparison with Markov chain model 2−75364
partial, buckling of thin plate, hybrid displacement methods 2−82311
partial, finite element solution for seepage problem 2−74310
partial, for torsion of shafts with elliptic inner boundaries, by perturbation techniques 2−73351
partial, in mathematical model of sea pollution 2−44632
partial, parabolic, similarity and generalized finite difference solutions 2−66418
partial, soln. by use of fast Fourier transforms 2−55442
partial, soln. with hybrid computers 2−69628
partial, third order, for ocean currents near equator 2−84707
partial, upwind difference scheme for solution of transport problems 2−58811
partial, validity of averaging methods for wave-type solutions 2−76167
partial derivatives, pseudo true connexion 2−69544
Poisson equation solution 2−48977
radiation conditions, intrinsic approach to solution 2−66415
reduction to Lagrangian form, for non-holonomic mechanics 2−52124
Reynolds, for three-dimensional flows of gaseous lubricants 2−60336
rheology nonlinear buckling of cylindrical shells, numerical soln. 2−73360
sets of automorphic structure, field eqns. and automorphic solns. 2−78827
stochastic, for dispersion of material in slowly moving fluids 2−46664
Stokes problem, computational algorithm 2−60173
Stokes problem, computational algorithm 2−56311
structural mechanics, boundary value problems, integral equation method of solution 2−58826
structural mechanics boundary value problems, integral equation method of solution 2−58825
thermoelastic, potential function for integration 2−69687
three-body problem, new form of differential equations of relative motion of planets 2−81756
trajectories of plane autonomous nonconservative dynamical systems 2−76250
turbulence solutions of p.d.e. 2−53118
two-dimensional electron trajectories analysis by numerical analysis 2−76449
variational principle based on spatial variation 2−52039
variational principle for irreversible phenomena 2−76239
variational principles for Navier-Stokes equation 2−43047
viscous fluid motion past impulsively started semi-infinite flat plate, numerical soln. 2−83459
wave eqn. incident on 2 vertical parallel barriers, approx. soln. 2−83737
weak explosion propag. in quasi-linear systems 2−66634
$y'=f(x,y)$, approx. construction of soln. 2−82152

Diffraction
corrections in radiometry 2−78951
dynamal theory, for ideal cryst., equivalence of Darwin and Ewald-Laue methods 2−47294
elastic waves, by two coplanar Griffith cracks in infinite elastic medium 2−41671
elastic waves, by two coplanar parallel rigid strips 2−78900
of elastic waves by rigid ellipsoid, integral eqn. method 2−52219
electron microscope, real space diffraction analysis 2−82450
flexural waves, thin blades, electromechanical filters 2−52355
Fraunhofer, focusing of optical and electron microscopes, optimal picture 2−76533
geometrical theory validity, by star shaped cylinder 2−78770
interatomic spacings, nonlinear algebraic equations and formation of a complete set 2−71400
parallel and perpendicular polarized wave from echelette grating 2−49422
phase evaluation in generalized diffraction, application to electron microscopy 2−79158
plane wave, by a strip, exact and asymptotic solns. 2−82177
scattering of charged particles, quantitate criteria for transfer and Fresnel scattering 2−63859
rel. to scattering phenomena, theory 2−45246
shock waves, by sharp edge, semiempirical formulation 2−58933
shock waves on yawed wedge, supersonic outflow 2−76380
shock waves underwater by semi-infinite plane 2−56465
strong shock waves, at wall surface, pressure and temp. change 2−83655
waves, bending, diffr. and scatt. by mass impedance loadings of plane plate 2−63099
of waves incident obliquely on half-plane 2−73293
wedge, of scalar pulse waves, closed solutions 2−45245
zone plate, construction 2−62935

acoustic waves
aircraft wake vortices, acoustic ray deflection 2−56430

Diffraction continued
acoustic waves continued
by annular spherical cap, perfectly rigid, integral equation technique 2−45514
circular disc in neighbourhood of spherical source 2−58915
continuous and impulsive, by sphere, in range 0.5-20 kHz, comparison of theory and expt. 2−69742
by elastic wedge, Kirchhoff soln. 2−41733
by Griffith cracks, coplanar, in infinite elastic medium 2−41671
interior diffr. problems, numerical soln. 2−45554
later potentials of multilayers 2−63116
by moving or stationary plate, theory 2−73439
piston transducers, pulsed operation, corrections in liquid medium 2−69754
plane, by two coplanar parallel perfectly soft or rigid strips 2−45513
plane wave by sphere of small radius, angular dependence of field 2−69741
propagating diffraction field due to reflection from plate edge of elastic surface waves 2−55507
sound reduction by barriers on ground 2−55553
spherical, by longitudinally slotted conical surfaces 2−63117
bystationary blade, velocity domains 2−52236

acoustic waves, ultrasonic
anisotropic crystals, diffraction and focusing 2−61595
broad-band pulses, u.s. diffraction loss and phase change 2−73436
NaCl, laser beam optical probing for sound intensity distribution 2−51026

electromagnetic waves
10.6 mkm radiation, by Ge cryst. at 13 MHz u.s. modulation efficiency 2−49201
by aperture between two wedges,, asymptotic soln. for large spacing 2−63184
apertures, circular and rectangular 2−78963
asymptotic solution, long planar e.m. wave 2−55610
Cauchy integral method of analysis 2−55613
by circular dielectric discs at X-band, modified Kirchhoff theory 2−49212
circular disk between two different media 2−58993
by circular helical conducting waveguide 2−63194
conducting crystals, by sound, electron conc. wave contrib. 2−54396
cross-sectional semi- infinite conductor, comments 2−52322
crossed periodic arrays on dielectric substrates, reflection and transmission coefficients 2−63188
by cylindrical object of arbitrary cross section and finite conductivity 2−69819
dielectric coated gratings, effects of polarization on transmission intensity for mm waves 2−69827
dielectric corrugated surface, amplitude and angular distribution calc. 2−69828
dielectric layer influence on efficiency of perfectly conducting gratings 2−79383
E-, H-polarized waves, normal incidence on array rectangular dielectric rods 2−63187
E-polarized plane waves, in infinitely-thin longitudinally slotted cylindrical waveguide with coaxial metal inner conductor 2−63186
E-region, reflected radio waves, ground diffraction pattern 2−72887
Earth's surface, h.f. charact. 2−49214
e.m. radiation from electron beam crossing diffraction grating 2−55614
e.m. radiation of electron beam passing through diffraction grating 2−55615
Fabry-Perot resonators, props. of two closely-spaced apertures 2−58982
field expansion into Eigenfunctions, scattering matrix analysis 2−55611
finite conductivity gratings diffracting plane waves 2−78970
grating of conducting cylinders with arbitrary cross section 2−58992
by grating placed at interface of two dielectric layers, E-, H-polarized waves, oblique incidence 2−63189
by infinite dielectric cylinder, differential method of obs. 2−69829
infinite slit perforated in conducting screen with finite thickness 2−82393
by infinitely conducting lamellar grid 2−55609
l.f. wave diffraction on stratified Earth surrounded by thin gyrotropic ionosphere 2−72852
metal arrays, effect of losses 2−63183
microwave diffraction loss due to spherical Earth, calc. 2−69830
microwaves, theory and experiment, new emphasis 2−62945
moving conducting strip, h.f. case 2−78960
near field of medium slit 2−59236
oblique incident waves, scatt. by inhomogeneous fibres 2−78967
odd symmetry wave front deformations effects on diffractograms of e.m. images in electron microscope 2−82446
open dielectric resonator, diffractional losses 2−78974
optical, periodically modulated media 2−63380
by periodic two-element grating, dimensions comparable with wavelength, longwave asymptotic analysis 2−63185
plane, moving conducting medium, calc. 2−52310
plane semi-infinite impedance systems, three dimensional problems 2−55608
Raman-Nath diffraction in semiconductors 2−54396
ray theory of diffraction by open-ended waveguides 2−41886
space-fluctuating radiation diffraction on scattering object 2−78959
steady state self-focusing, with saturating nonlinearity 2−69817
by thin conducting strip, dual integral equations 2−78976
truncated cylinder, R-function appl. 2−55612
two-dimensional aperture with arbitrary cross-section 2−58994
two-dimensional diffraction by slit in conducting screen 2−58995
upper and lower bounds, admittance, impedance matrices, scattering matrix 2−69831

electrons *see Electron diffraction*

light
see also Holography
− 2−61595
acoustic velocity meas. in datelike elastic materials, Bragg diffraction imaging 2−43970
by acoustic waves consisting of fundamental tone and first n−1 harmonics 2−63398

Diffraction continued
  light continued
    acousto-optical deflector, coupled transducers 2−69753
    amplitude variations control in computer generated holograms 2−79271
    analysis formulae, angular dependence, discussion 2−82555
    annular aperture with amplitude filter partially space coherent diffr. 2−82551
    beam, modulated by circular aperture, Fourier spectra 2−79315
    bleached holograms, aerial reconnaissance photographic emulsion, diffraction efficiency 2−63390
    Bragg, by standing ultrasonic waves with application to optical demultiplexing 2−49421
    Bragg imaging of ultrasonic waves, nonlinearity 2−41788
    calculation of object corresponding to given diffraction image 2−42204
    circular aperture, by partially coherent light, with spherical aberration 2−45794
    circular aperture, radiometric errors 2−63387
    circular aperture, truncated Gaussian asymptotic expansion 2−79340
    circular aperture diffraction limited MTF 2−63385
    data processor, u.s. light diffractors, high speed printer 2−76116
    by defocused circular aperture illuminated by partially coherent light 2−52458
    defocussed circular aperture, in partially space coherent light 2−45792
    diffraction system, for phase-object observing double diffraction system use in interferometer 2−70019
    diffractomter, laser light source 2−63405
    diffusing surfaces, coherent light diffraction 2−59235
    electron micrograph analysis by optical diffraction and filtering 2−79145
    far-field diffraction by apodized slit apertures, coherent light 2−59234
    film with rough boundaries ellipsometric parameters 2−79328
    effects in focused truncated gaussian beams 2−79339
    Fourier images, paradox 2−49423
    Fourier transform techniques in optical metrology 2−45793
    Fraunhofer, at regular polygon shaped apertures 2−79327
    Fraunhofer, complex momentum and energy transfer 2−76520
    Fraunhofer, partially coherent, by circular aperture with pupil of non uniform transmission 2−42201
    Fraunhofer, partially coherent light, by apodized slit aperture 2−70020
    Fraunhofer, studies in schools 2−62934
    Fraunhofer and Fresnel approximations, regions of validity 2−79344
    Fraunhofer pattern analysis, image quality assessment 2−79407
    Fresnel, experiment using laser 2−62933
    Fresnel, of partially coherent light by circular aperture 2−76508
    Fresnel diffraction patterns, obs. during total solar eclipse 2−58001
    Gaussian beam, propagation and focusing effects 2−79342
    generalized theory, application to second harmonic generation 2−63368
    granulation around rough objects, linear systems 2−63391
    hologram reconstruction by incoherent light, expt. 2−69969
    holographic emulsion diffraction efficiency determ. using latent image technique 2−66786
    holographic imaging of point object in higher diffraction orders 2−52437
    images of partially coherent phase discs with variable phase plates 2−76519
    Kirchhoff theory of thermal lensing in solids 2−55727
    Kirchhoff-Fresnel, in turbulent atmosphere 2−45791
    Laguerre Gaussian beams by aperture 2−63388
    laser, semicond., electron beam pumped, spatial modes far-field diffr. patterns time variations 2−79211
    laser beam, by high acoustic power levels from n-GaAs ultrasonic amplifier 2−64847
    lens design for optical Fourier transform systems 2−49409
    magneto-optical, at periodic mag. structs. 2−61590
    measurement technique, laser applic. 2−49424
    modulation transfer function of camera lenses, slit shutter effects 2−59329
    moire fringes, cross gratings as sensors in industry 2−55741
    MTF estimation for imaging system from edge response 2−49420
    near field of medium slit 2−59236
    obscured circular apertures, far field patterns 2−79343
    off-axis Fresnel zone plate as coded aperture for imaging incoherent sources 2−70021
    optical data processing, Fourier transform operation 2−55739
    partially coherent, by high numerical aperture system obeying sine condition 2−45795
    pattern reconstruction on closed circuit TV 2−78736
    patterns, d.c. bias suppression 2−73640
    in periodically modulated media 2−63380
    polycrystalline minerals, review of Raman theories 2−61594
    pulsed Bragg diffraction method of ultrasonic visualization 2−49164
    pulsed Bragg imaging, U.S. visualization 2−63126
    resonators, low loss, modes and losses, diffr. formulas 2−79375
    resonators, with round spherical mirrors, diffraction loss of radiation 2−66738
    ribosome microcrystals, optical diffraction from electron micrographs 2−82000
    ring laser, diffraction frequency splitting of oppositely traveling waves 2−66740
    ring laser, diffraction splitting of frequencies 2−59138
    of scalar wave by thin screen changing phase randomly and regularly, caustics, statistical moments of wave field 2−42200
    scattered objects image transformation in holography 2−59195
    scattering by weak acoustic waves, Huygens' expression for diffr. field 2−55742
    slit diaphragm photometer errors 2−73648
    sound beam visualization utilizing Raman-Nath diffr. of light 2−78991
    sound field probing 2−45525
    spatial filtering, predictions of Fourier transformations and development of general transformations 2−79314
    speckle patterns, historical retrospect 2−79299
    speckling in diffraction and image field of rough objects, statistical functions for linear systems 2−52455
    spectrometer entrance slit, fast beam spectral line broadening 2−45816
    supersonic waves, oblique incidence case, Raman-Nath eqns. 2−66822
    surface profiles reconstruction from diffraction spectra 2−55732
    target edge response viewed through atmospheric turbulence over water 2−81648
    teaching demonstration using gas laser as light source 2−66399
    theory and experiment, new emphasis 2−62945
    three dimensional phenomena using N regularly spaced exposures on photographic plate 2−42203
    u.s. field, rel. to optical images of two-dimensional object 2−45790
    u.s. imaging by Bragg diffr., acoustic phase conservation 2−49447
    u.s. waves, adjacent, parallel with arbitrary frequencies 2−55738
    $Gd_2(MoO_4)_3$ diffracted light obs. from domain wall 2−84467
    La flint glass, Bragg diffraction rel. to acousto-optic applications 2−66839
    Mg-Mn ferrite film, transparent, light diffraction by mag. stripe domains 2−65220
    YIG domains, of laser beams 2−44348
    YIG single crystal film, domain wall mobility meas. by light diffraction 2−84434
  neutrons *see Neutron diffraction*
  X-rays *see X-ray diffraction*
Diffraction by acoustic waves *see Acoustic waves/effects; Diffraction/light*
Diffraction gratings
    coarse, freq. determination by Moire fringe technique 2−63384
    coherent light, far-field diffraction by apodized slit apertures 2−59234
    concave, sensitive visual test 2−49419
    concave toroidal, for spectrographs using Iglya scheme and normal incidence 2−73679
    crossed, as sensors in industry, technology of moire fringes 2−55741
    crossed periodic arrays on dielectric substrates, reflection and transmission coefficients 2−63188
    dielectric coated effects of polarization on transmission intensity for mm waves 2−69827
    echelette, diffraction of parallel and perpendicular polarized wave 2−49422
    echelette, far i.r. obs. and production 2−42282
    echelette in constant deviation, efficiency, quantitative study 2−42202
    electron microscope manufacturing process with Stereoscan Mk II 2−59095
    e.m. radiation from electron beam crossing diffraction grating 2−55614
    e.m. resonators with, eigenmodes of periodic structure, waveguide damped resonance 2−63176
    e.m. waves, infinitely conducting lamellar grid 2−55609
    finite conductivity, diffraction of plane e.m. waves 2−78970
    generalized ellipsometry for surfaces with direction preference, application 2−79357
    holographic, efficiency and stigmatism for unpolarized light in vac. u.v. 2−63352
    manufacture of reflection monochromator sine drive, cam and linkage design 2−55770
    Moire grating, with pseudo-random sequences, use in contouring meas. 2−79372
    multiple imaging in optical systems using incoherent monochromatic light 2−66802
    N-layer periodic, acoustic waves, waveguide approach 2−78923
    nematic liquid crystals, application as phase grating of electrically tunable spatial frequency 2−64443
    optical grating coupler waveguide system, response 2−66808
    pattern reconstruction on closed circuit TV 2−78736
    perfectly conducting influence of dielectric layer on efficiency 2−79383
    polarization characts. of scatt. radiation, ellipsometric obs. 2−44343
    precision, VEB Carl Zeiss JENA 2−55740
    reflection, use in mechano-optic polarization modulator 2−70036
    ruling engine, 750 mm, for producing large gratings and echelles 2−42221
    Smith-Purcell effect, Al and Ag gratings 2−73526
    spacing errors reduction 2−73654
    spectrometer using constant transmission grating 2−42277
    spectroscopy by grating synthesis 2−42267
    spread functions, distortions caused by random manufacturing errors 2−70041
    subtraction of Fourier transformed waves 2−45789
    three-reflection-grating system, interference-generated moire fringes, rel. to linear displacement meas. 2−59256
    triangular, with 100° apex angle, calc. 2−63386
    Wadsworth mounting, three-dimensional theory 2−63389
    X-ray line grating, possible violation of extinction law 2−52020
Diffrimoscopy *see Diffraction/light; Optical images*
Diffusion
    see also Neutrons and antineutrons/diffusion; for diffusion of matter, see Diffusion in gases; Diffusion in liquids; Diffusion in solids
    − 2−60212
    adsorbed grains, internal diff. coeff. calcs. for arbitrary isotherms 2−47143
    atmospheric, crosswind shear effects 2−57961
    atmospheric, tensor diffusion equation, numerical solution 2−72781
    binary mixture, asymptotic behaviour of Green Kubo integrands 2−74308
    bronchial tree, diffusion deposition of small-sized particles 2−85123
    Brownian particles, sedimentation rate, diffusion coeff., holographic interferometry 2−45767
    classical fluids, diffusive and collective motion 2−74314
    concentration depend., one dimens., surface conc. 2−64687
    crystal growth by diffusion method, mathematical model 2−60708
    dispersion layers, 2-current approx. analysis of thermal diffusion 2−49179
    electron diffusion-controlled gas breakdown meas. using microwave cavity 2−50231
    electron swarms at low E/p_0, longitudinal coeff. 2−71008

Diffusion continued
electropolishing soln., diffusion control necessary characteristic for universal application 2−80547
e.m. fields, transient, in inhomogeneous media 2−44536
f.c.c. crystal, (110) interface, surface diffusion 2−50426
flow, laminar, through circular tubes, low Peclet number entrance-region mass transfer of diffusing matters 2−77226
gas into porous material 2−80394
gelatin gels, of water, interfacial contact resist. 2−60533
general solution of diffusion equation for semiinfinite geometries 2−73343
hydraulic, heterogeneous confining bed 2−78308
incompressible fluid, diffusive force effect of large eddies 2−77173
incompressible fluid, diffusive force exerted by large eddies 2−46697
insoluble monolayer leakage across movable barriers, radiotracer detection method 2−53416
interacting particles system, diffusion wave propag. 2−45334
ion diffusion coeffs. in gas mixtures at arbitrary field strengths, comp. depend. 2−77265
ion getter pump and oil diffusion pump comparison 2−76720
ionic, through excitable membranes, theory, obs. using equivalent electrical circuit 2−48843
Knudsen cell orifices, conical, divergent particulate fluxes, Monte Carlo analysis 2−50136
lattice wind-tree models, absence of diffusion 2−45289
lattice wind-tree models, analytic functions 2−63025
load diffusion from bar embedded in semi infinite elastic medium 2−69653
macromolecules, study by photon correlation spectroscopy using digital PDP-9 computer 2−79443
magnetospheric protons, by turbulent electrostatic oscillations 2−68940
modelling and control 2−73344
molecular coefficient for gas absorption into a turbulent liquid 2−50298
molecules, optically pumped, rel. to probing of excited species interaction 2−60106
monolayers, surface coeffs., theory and expt. obs. 2−71179
moving boundary problem with variable diffusivity, soln. using method of successive approximations 2−49045
moving-boundary problem for oxygen in absorbing medium 2−83997
myristic acid monolayer on water surface coeffs., theory and expt. obs. 2−71179
N-interacting Brownian particles, extension of Einstein diffusion relation 2−66465
numerical soln. of problems 2−66481
plane-polygonal polymer, translational coeff., applic. of modified Oseen tensor 2−64200
plasma, axially decaying collisional, anomalous diffusion 2−70884
plasma, elliptical torus, neoclassical diffusion 2−67645
plasma, in axisymmetric torus in intermediate region 2−50187
plasma, spectral dependence in magnetic field 2−46720
plasma, three-dimensional magnetized equil., transverse spatial diffusion coeffs. 2−56333
plasma, toroidal, with helical mag. field, stationary equilib. and diffusion 2−77278
plasma drift-dissipative instability development 2−60284
plasma in toroidal Z-θ pinch at Padova 2−83571
plasma turbulence, probabilistic models 2−56371
poly-kind particle systems, diffusion for gradient of vacancy conc., thermodynamic consideration 2−64688
resonance excitation, in gas, stimulated emission effect 2−59903
resonant in strong plasma turbulence 2−70943
rodlike polymers, translational coeff., applic. of modified Oseen tensor 2−64199
self-diffusion, simulation of obstruction effect by random walk methods 2−58777
self-diffusion coefficient, force correlation function representation 2−49046
solar magnetic fields, in weak plage regions 2−78605
solid/liquid interface, conc. depend. rel. to linear stability analysis of phase transform. 2−68181
stearic acid monolayer on water, surface coeffs., theory and expt. obs. 2−71179
stochastic quantum mechanics, derivation of diffusion coefficient 2−63009
surface, field emission microscopy of $A^{I}B^{V}$ coated W monocrystal 2−83872
surface, pore migration and coalescence, rel. to swelling during postirrad. annealing 2−53548
surface, rel. to vapour deposition 2−50475
surface diffusion rates, determ. from thermal transpiration meas. 2−83719
suspension of particles, convective diffusion for case of Stokes flow of fluid 2−64481
turbulent, across density interface in ocean, model 2−84706
turbulent, variational methods of quantum mechanics in theory 2−46677
two-dimensional diffusion with extraction of fluid on diverging walls, flow fields 2−74340
two-phase systems, rel. to shrinkage conc. depend. during sintering 2−43886
upwind difference scheme for solution of transport problems 2−58811
variational principle for irreversible phenomena 2−76239
waves induced by high intensity sources 2−83699
weakly coupled quantum oscillators 2−73329
wind-tree model with overlapping scatterers, abnormal diffusion 2−52114
Ag film, annealed, hillock and island form, by surface diffusion 2−67896
Al_2O_3, alumina, grain boundary grooving on single cryst. surfaces 2−50432
Al_2O_3, powder, initial sintering rel. to surface diffusion, neck growth obs. 2−43887
Ar substrate, mobility of adsorbed He atoms near 2K 2−67920
CO_2 in caves, gaseous subterranean diffusion and air circulation 2−48412

Diffusion continued
Cu, surface diffusion of Ag on (100), (111) and (110) planes 2−60626
Cu, surface diffusion of Ni, 600 and 900°C 2−53761
Fe-Ni, surface, enhancement by heating at 1385°C 2−68052
H_2O adsorbed layer on silica, self-diffusion obs. 2−60686
^{3}He abundance in 3 Cen A 2−58266
Mo, cathode, flashing effect, surface atom migration, field ion microscopy 2−53557
Mo powder, sintering mechanism, mass transfer by diffusion- viscous flow 2−53941
Na, in d.c. arc plasma, obs. using intensity distrib. of emitted light 2−60211
Nb, diffusion of H and D, application to quantum theory 2−80718
O atoms, collision integrals 2−83184
Rb, surface diffusion near m.p. 2−60629
Rh surface self-diffusion on Rh, low temp. 2−64555
^{90}Sr, Great Lakes, sediments, diffusional transport 2−65564
UC, surface diffusion, rel. to surface smoothing kinetics 2−53556
W, cathode, flashing effect, surface atom migration, field ion microscopy 2−53557
W, surface self-diffusion rel. to C adsorpt., field emission obs. 2−64582
W surface, interactions between Re atoms 2−50469
W surface, of Ni, coeff. determ., mass transfer method 2−50466
Xe, afterglow plasma, electron temp. lowering by diffusion cooling 2−70882

acoustic waves
see also Scattering/acoustic waves
stochastic transmission system diffusion function 2−78915

electromagnetic waves
see also Scattering/electromagnetic waves
magnetosphere, whistler wave amplification, pitch angle and energy diffusion coefficients 2−48516

light
see also Reflectivity; Scattering/light
benzene, forced combination diffusion in laser resonator 2−41976
diffuse reflectors, effective reflection 2−52451
diffusing surfaces, coherent light diffraction 2−59235
exponential diffusers, power spectrum analysis 2−49428
multiple, by assembly of spheres 2−70023
noncoherent radiation transfer, across isothermic medium 2−66817
planetary atmospheres, diffusely reflected photons rel. to absorption lines, probability distribution 2−78529
powder, Kubelka-Munk diffuse reflectance remission function rel. to fund. optical parameters 2−79329
stars, stellar shell expanding with constant velocity 2−69073
surface diffusers' transmittance, design of near band limited binary diffusers 2−59237
three-dimensional, theory, for spectrophotometric instrumentation design 2−45824

Diffusion columns *see Diffusion in gases/thermal; Isotope separation*

Diffusion in gases
see also Flow/gases
airborne particles, diffusional separation 2−80496
atmosphere, in 10-100 km range 2−51592
atmosphere, numerical study of diffusion of ^{222}Rn daughter ions in fair weather and thunderstorms 2−62184
atmosphere, Rn steady-state turbulent diffusion 2−65669
atmosphere and air pollution control 2−62090
atmospheric, conference (Las Cruces, USA, Dec 1971) 2−62146
atmospheric pollutants propagation over large distances rel. to vertical diffusivity with time and height 2−81661
atmospheric surface layer, turbulent diffusion 2−62092
barodiffusion, binary mixture on infinite rotating disk, isotope separation 2−77196
binary, interpolation of effective diffusion coeff. 2−56445
binary diffusion of jet embedded in boundary layer 2−71072
binary mixtures, diffusion slip velocity phenomena 2−80421
capillary, diffusive press. effect for all ranges of Knudsen number 2−83717
cylindrical diffusator, gas press. distrib. 2−46865
diffusion controlled breakdown, in rectangular microwave cavity 2−80412
electron group drift between plane parallel electrodes, mathematical model 2−83715
flow in diffusers for centrifugal turbomachines 2−80383
under gravitation, appl. to F-region processes 2−58091
under gravity action 2−56446
homologous series in binary mixtures with common gas, regularities in coeffs. 2−80420
ions, elec. field effects, relay race model 2−50224
minor atmospheric components stationary diffusion at night, allowing for recombination 2−72773
mixtures with internal degrees of freedom classical mech. calcs. 2−50281
multicomponent system of polyatomic molecules, rotational diffusion coeff. 2−50280
polar binary mixtures, calc. using Stockmayer force consts. 2−83716
self, velocity-correlation functions in two and three dimensions, low density limit 2−53329
stepped vapor concentration in binary gas mixture 2−53342
supersonic free jet, diffusion of filament of injected gas 2−74457
turbulent mixing, co-flowing streams, diffusion flames 2−77349
urban area source pollutants, numerical modelling 2−51605
vapour diffusion coefficients in a ternary gaseous system 2−83718
velocity, influence on gas mixture flows 2−77333
CO_2 diffusion laser, interaction kinetics of diffusion mixing of CO_2 and N_2 2−73565
D_2-Ne(N_2)(Ar) systems, conc. depend. of binary diffusion coeffs., 300K 2−64399
H_2-Ne(N_2)(Ar) systems, conc. depend. of binary diffusion coeffs., 300K 2−64399
He-Ar system, conc. depend. of diffusion coeff. at 300 K and 1 atm. press. 2−71121
He-Co_2 (N_2O)(SF_6) systems, binary diffusion coeffs. conc. depend. 2−67737
He-Ne mixtures, binary coeff. meas. in temp. range 25 to 700°C 2−50278

Diffusion in gases continued
He, atmosphere, gas, instantaneous point source diffusion within turbulent boundary layer 2—72780
He, diffusion coefficient of $N_2(A^3\Sigma_u^+)$ state in afterglow of He-N_2 mixture 2—50132
K ions, reduced mobility, apparent pressure dependence 2—56448
Ne-N_2 mixtures, binary coeff. meas. in temp. range 25 to 700°C 2—50278
O_2, lateral diffusion of mass identified O^{2+} 2—43204
thermal
atmosphere, computation of steady-state supersaturations in diffusion chamber 2—62235
jet, homogeneous free, turbulence characteristics meas., investigation of the peculiarities of the heat diffusion method 2—80196
mixtures with internal degrees of freedom classical mech. calcs. 2—50281
multicomponent gases, theory and review 2—56447
H_2-^{4}He system, thermal diffusion factor and quantum collision integrals, effect of inelastic collisions 2—56449
He-Kr system at 300K, 1 atmosphere pressure, composition dependence of diffusion coefficient 2—50279
Ne, diffusion factor calc. using scattering potential of Siska 2—46863
Diffusion in liquids
see also Flow/liquids
accelerating diffusion with mixed solvents 2—83779
acetone-water liquid system, relationship between self-diffusion and inter-diffusion coeffs. 2—50350
acetonitrile, rotational diffusion, i.r. spectra 2—83323
alkali metal, self-diffusion, temp. depend. 2—67817
alkali metals, self-diffusion, significant liquid-structure theory 2—56489
alloy, electrotransport, rel. to amorphous semiconductors 2—60455
binary-liquid phase transition 2—53407
blood, flowing, effect of shear rate, model anal. 2—55215
blood, flowing, platelet diffusion, effect of hematocrit and shear rate 2—55214
blood and plasma, of oxygen, protein conc. effect 2—51886
boundary-laer characteristics, determ. by solution of solid-method 2—80426
carbon tetrachloride-cyclohexane, liquid system, relationship between self-diffusion and inter-diffusion coeffs. 2—50350
coastal currents of Great Lakes, complex diffusion processes 2—62038
constant measurement, by simple and fast method 2—53412
coupled diffusion fluxes and changes in diffusion rates 2—53413
cyclohexane, cyclohexanol, cyclohexanone, self-diffusion coeffs. 2—80446
dichloromethane, self-diffusion coeffs., freezing to boiling point, rotational correlation times 2—56472
electrolyte in soln., eqn. for effect of appl. mag. field 2—83782
electrolytes, higher terms in concentration dependence of self-diffusion coeffs. 2—72563
electron transfer reactions in solution, generalized mobility theory 2—84648
emulsion, restricted diffusion, pulsed n.m.r. obs., droplet size distrib. 2—74573
gas bubble, consideration of moving boundary 2—64421
glycerol, meas. of diffusion const. on pyrene molecules in triplet state from -17 to +15°C 2—68804
glycerol, pulse n.m.r. meas. of self- diffusion 2—60453
glycerol, viscous, self-diffusion coeff., rotating frame proton spin relaxation 2—56526
ionic solns., diffusion of small particles, electrostatic effects 2—71250
2,6-lutidine-water, tracer diffusion coefficients of tritiated water 2—46941
measurement, of constant, by simple and fast method 2—53412
metals, self-diffusion model 2—46944
molecular theory of diffusion consts. 2—74536
nematic liquid crystals, self-diffusion and spin-lattice relaxation 2—56524
neutron scatt. obs., quasielastic, book 2—64456
ocean, mesoscale double diffusivity effect 2—57856
one way, flow and mass transfer, laws 2—50347
poly(vinyl cinnamate), hydrodynamic, optical props. 2—83388
poly-4-vinylpyridine in solution, hydrodynamic and optical props. 2—60452
poly-γ-benzyl-L-glutamate conc. solns. in diphenylanthracene, rotational diffusion 2—60451
polymeric solns., dilute, mutual diffusivity of liq. solutes, conc. depend. 2—53411
polystyrene in ethyl acetate ethyl alcohol mixtures 2—60458
polystyrene-anisole solution, temp. depend. of spin-lattice relaxation obs., study of molecular mobility 2—60514
pyridine, self-diffusion coeffs., freezing to boiling point, rotational correlation times 2—56472
rotational, of spherical-top molecules, comment on paper by McClung (1969) 2—71178
sea, application of diffusion process to the dispersion of pollutants 2—44631
sea, use of tracers, dependence of eddy diffusion coefficients on scale of phenomena 2—44630
self-diffusion, pulse n.m.r. meas. technique for viscous liquids 2—60453
self-diffusion current pulse generator for n.m.r. obs. by pulsed gradient technique 2—73502
submerged heated jet discharging into lake or river, turbulence 2—78304
turbulent, analogy with molecular diffusion, features of turbulent motion in sea 2—44629
viscoelastic relaxation, defect-diffusion model 2—64449
water, crystal dissolution velocity 2—74650
Ag-In molten alloy, of Ag, capillary reservoir technique 2—56491
Ag-Sn melt, electrotransport, current density effects 2—50348
AgI particle dissolving in H_2O drop 2—60434
Al, review 2—83992
$CsNO_3$, of Ag^+, interdiffusion coeff. 2—65383
$Fe/Al_{(l)}$ system, solid/liquid diffusion 2—80715
Fe, abs. rates of N and calc. chem. diffusion coeffs. 2—64694
Diffusion in liquids continued
Fe, liquid of O_2 potentiostatic electrochemical measurements 2—60456
Fe, of C, O, H, N and S, temp. depend. 2—43661
Fe, of C, O, N and S, effective radii of diffusing particles, diffusion mechanisms 2—50709
$Ge_{15}Te_{85}$, atomic transport 2—60457
H_2O, absorption of CO_2 2—67816
^{3}He-^{4}He dil. solns., const. meas. and ^{3}He-roton cross section 2—53471
^{4}He, diffusion of ^{3}He, investigation by thermal neutrons 2—64492
Hg-Cd(Ga)(In)(Tl)(Sn)(Sb)(Bi) amalgams, dil., small-step diffusion theory, rel. to comp. depend. of viscosity 2—64451
In-Bi alloy equi-atomic 2—46939
KNO_3, of Ag^+, interdiffusion coeff. 2—65383
$LiNO_3$, of Ag^+, interdiffusion coeff. 2—65383
$NaNO_3$, of Ag^+, interdiffusion coeff. 2—65383
$RbNO_3$, molten, isotope effect of electromigration of Rb ions, temp. depend. 2—64457
Si, of C, using polycryst. SiC in soln. 2—56487
Sn-Ag alloy, determ. of interdiffusion coeffs. 2—53415
Sn-Ag(Sb) alloys, interdiffusion coeffs. 2—50349
Sn-Sb alloy, determ. of interdiffusion coeffs. 2—53415
$TlNO_3$, of Ag^+, interdiffusion coeff. 2—65383
V_3Ga, supercond. cpds. formation by a new diffusion process 2—84301
V_3Si, supercond. cpds. formation by a new diffusion process 2—84301
thermal
Boussinesq fluid, temperature adjustment process via buoyancy-induced meridional circulation 2—67742
flow, laminar, incompressible, viscous, in a porous straight channel, temperature distribution 2—56458
growth of spherical bubble controlled by heat diffusion, approximate soln. including convective flow 2—83729
n-heptane in n-hexadecane, effect of temp. gradient on diffusion coeff. 2—77418
metal, of Tl, phonon scatt. 2—46945
mixtures with temperature gradient, Soret effect with laminar flow 2—67758
Soret effect, laminar flow considerations 2—60454
water-ethanol liq. layer, heated from below, temp. field oscills. due to thermal diffusion 2—67821
Ag, thermotransport of Co, heat of transport 2—53414
He mixtures, superfluid transition temp. gradient with heat flow 2—43424
Diffusion in solids
see also Permeability, mechanical
acetylene cryst., mol. motions, plastic behaviour 2—83881
alkali borate and silicate glasses, n.m.r. obs. of ^{7}Li ionic motion 2—64690
alloy, binary, interdiffusion coeffs. determ. by electron microprobe analysis 2—80719
alloy, binary, isothermal reaction stage influence on cpd. growth 2—64686
alloy, binary, of hydrogen, struct. influence 2—77611
alloy, chem. diff. coeff. determ. method using soln. treatments and metallography 2—56748
alloy, disordered binary, self-diffusion coeff. calc. from vacancy equilibrium conc. 2—53688
alloy, f.c.c., dil., vacancy jump freq. ratio, determ. by electromigration 2—83995
anodic sectioning technique for distrib. and diffusion profile obs. 2—60817
binary arsenosilicate glass film diffusion source, vapour deposition 2—71324
borate glass, He migration 2—53759
ceramic-metal systems, ion tunnelling 2—51183
chemical diffusion, phenomenological theory 2—74808
composite, Ni-Cr base alloy, Mo alloy or W filament reinforced, matrix-filament interaction 2—56988
composite, nichrome, W or Mo reinforced, interdiffusion at filament-matrix interface 2—53966
creep, grain boundary sliding contrib. to axial strain 2—47509
crystal lattice and chemical potential regarding vacancy diffusion eqn. 2—74807
defects, crystal lattice, diffusional relaxation, in the fields of local lattice disturbances 2—84000
diamond type cryst., impurity correl. factors 2—60827
diffusional creep, atomic mechanisms 2—56730
diffusional creep, atomistic aspects 2—56729
dolomite, self-diffusion of C and O_2, obs. using isotopic exchange 2—68855
electrochemical methods for diffusion coeff. meas. 2—77602
electrotransport of C, N_2 and O_2 2—80716
film, metallic, electromigration, grain boundary contribs. 2—56751
films, X-ray obs. of composition profile and diffusion generated substructure 2—56585
fluorapatite, of Ca, P, and OD^- ions 2—77609
gas bubbles, voids, nucleation 2—50632
glass, K^+ ion migration from K^+ ion-exchanged layer under reverse electric field 2—75388
glass-forming oxides, He migration 2—50707
graphite, self-diffusion, interstitials as diffusing defect 2—53760
hydrides, spin-lattice relax. times of diffusing hydrogen 2—54369
impurity diffusion and effect of stresses on dislocations 2—71481
intermetallic diffusion and deterioration of reflection coatings 2—55764
Kirkendall effect, study using Darken's equations 2—68045
lattice defect, effect of trapping on annihilation 2—56678
mass and temp. depend., quantum and anharmonic effects 2—74806
metal, creep and sintering rate reduction by oxide dispersions 2—47512
metal, dislocation loop migration as coarsening mechanism 2—53698
metal, f.c.c., grain boundary, computer calc. 2—50701
metal, of gases, coeff. determ. from rate of change of elec. resist. 2—47452
metal, of hydrogen, by lattice expansion method 2—77606
metal, of hydrogen, review 2—77604
metal, of hydrogen, theory 2—77605

Diffusion in solids continued
metal, of oxygen, from oxide film 2−71533
metal, solute segregation around growing voids 2−53697
metal, vacancy annihilation in oxidation reactions in gases 2−53756
metal film, rel. to relax. of elastoresist. 2−56765
metal systems, mechanisms review 2−68044
metal thin films, electromigration, interface reactions 2−74622
metal/hydrogen systems, conf., Julich, Germany (Mar 1972) 2−77713
metal/hydrogen systems, Gorsky effect 2−77603
microcline perthite, of K 2−68859
moisture transfer in porous elastic solids, stress development 2−46889
molecular crystals, irradiated, e.s.r. study using recombination of free radicals 2−80722
Mossbauer spectra of impurity atoms in crystals, correlation influence in diffusion 2−65228
neopentane, plastic crysts., mol. rot motion and diff. consts. 2−53513
neutron scatt. obs., quasielastic, book 2−64456
neutron spectroscopy at high resolution 2−77607
oxidation, internal and precipitation phenomena 2−68187
perfluorocyclohexane plastic crystal, self- diffusion study by n.m.r. 2−50702
piezoelectric semiconductors, impurity diffusion coefficients, ultrasonic meas. method 2−50691
point defects, stress-assisted diffusion to dislocations, eigenfunction expansion description 2−43652
Poisson's equation, soln. for pure cryst. 2−60816
polyethylene, low-density, determ. of diffusion coeffs. of O_2 by radiothermoluminescence method 2−84004
polyethylene doped with I, h.f. Gunn domains 2−57202
polymer membranes, organic vapours, self- diffusion, obs. using radio tracer technique 2−71180
polymers, glassy, of organic vapours 2−83362
polymers, rel. to mechanical strain effect 2−57232
polypropylene, large- and small-spherulite, determ. of diffusion coeffs. of O_2 by radiothermoluminescence method 2−84004
porous glass, counterdiffusion of adsorbed hydrocarbons 2−60685
powder, models, for initial sintering 2−50904
powder, rel. to initial combined sintering analysis 2−50903
pyrolytic graphite, oxidation of prism plane, effect of diffusion in grain boundaries and in bulk on reactivity rate 2−51448
quantum theory, temp. depend. of interstitial diffusion in Debye solids 2−43653
quantum theory for low temps. 2−68046
quartz, of water, temp. depend. 2−50716
quartz, radiation-induced diffusion of alkali ions and protons and formation of colour centres 2−71532
radioactive tracers, diffusion coeffs. calc. method 2−56749
rocks, of Ar, det. of source material for ultramafic minerals 2−65583
rocks, of He, det. of source material for ultramafic minerals 2−65583
self-diffusion, longitudinal vibration modes and activation energy 2−64827
semi-infinite medium, from thin layer, conc. depend. diffusion coeff. 2−71513
semiconductor, two-stage diffusion, layer parameters calc. allowing for evaporation 2−71512
silica, self-diffusion of Si and O and ionic transport 2−64696
sintering models and volume diffusion controlled pore shrinkage 2−50854
solid solns., dilute b.c.c., calc. of partial correlation factors 2−80717
solid solns., ternary, of C, C conc. curve, at interface 2−47454
solution-grown crystal, movement of solvent inclusions by centrifugation 2−47465
steel, cementite, Ostwald ripening, diffusion rate 2−50936
steel, film, C distrib., study by spectroscopy 2−47435
steel, H content determination, using diffusion kinetics 2−64780
steel, Ni martensite, of C, effect of dislocations 2−56758
steel, of C, rel. to hot pressing conditions 2−43793
steel, of Si, porosity of siliconized layer rel. to holding time and C content 2−47635
steel, stainless, types 304 and 316, of ^3H, 25-222°C 2−47458
supersaturated constituents, migration to surface sinks 2−80720
transition metal/hydrogen systems, quasielastic neutron scatt. obs. 2−77623
transition metals, n.m.r. obs. of hydrogen diffusion 2−77622
transition metals, of tritium, time-lag method obs. 2−77624
αU, of Fe, 645°C 2−50719
viscoelastic material, gas bubble behaviour in creep process 2−50699
Zircaloy-2(-4), of hydrogen, 275-700°C 2−53773
Ag-Au alloys, vacancy flow, effect and Kirkendall shift meas. 2−74809
Ag-In solid solution, Zener relaxation 2−47453
Ag, grain boundary self-diffusion, isotope effects, correl. effects, vacancy model 2−56752
Ag, of Co and Cd, 375-650°C, near-surface effects 2−68049
Ag, of O_2 in chemisorption, effect on surface behaviour 2−51442
Ag microsection preparation, electrochemical technique 2−50429
AgBr, impurity ions and vacancies interaction, diffusion mechanism 2−80699
AgCl, impurity ions and vacancies interaction, diffusion mechanism 2−80699
Ag_4RbI_5, of I_2, electrochemical cell obs. 2−84657
Al-Mg system, interdiffusion, 325-425°C 2−64692
Al-Si contacts, electromigration failure 2−50706
Al-6.8%Zn alloy, and effects of Ag, Si, or Mg, X-ray small angle scatt. obs. 2−56753
6Al-4V-Ti, surface embrittlement charact. during diffusion bonding 2−68160
Al, Al-0.5 wt.%)Fe alloy, high temp.-low stres, directional diffusion vs. dislocation process mechanisms 2−50755
Al, of Co, temp. depend., 400-640°C 2−64691
Al, of Mg, Fe, Cu, Zn, Ge and Ag, interpreted rel. to oscill. form of inter-ion potential 2−64691
Al, review 2−83992

Diffusion in solids continued
Al film, electromigration, effect of oxygen 2−50703
Al of Ga, 100−310°C, solid solubility, X-ray diffr. obs. 2−74810
Al_2O_3, grain boundary enhanced diffusion 2−50705
Al_2O_3, sapphire, grain boundary migration 2−50704
Al_2O_3, sintering kinetics, effect of iron oxide 2−50865
As_2S_3/Ag system, of Ag^+ in photochem. transform. phenomena 2−57433
Au-Ag alloy, electromigration of Au and Ag 2−83996
Au-Pb system, interstitial dissolution and compound formation 2−43826
Au-Sn solid solns., dil., correl. factor and self-diffusion 2−64693
Au film, of Cr, backscatt. obs. 2−56754
Au nucleation on an ionic crystal 2−71534
BCl_3, diffused p-n junction material, meas. by electron beam microprobe 2−44133
B_2O_3, glass, of Ar and Ne, mass spectrometry obs. 2−53758
Be-(1 wt.%)Fe alloy, of Be and Fe, rel. to precip. mechanism, Mossbauer obs. 2−50931
Be, of C, electromigration 2−43657
Bi-Te unit crystals, determ. Sb diffusion rate on function of composition 2−68051
Bi, electron diffusion through shock wave front 2−71771
BiTe, of Cd and In effect of distrib. of diffusing element, thermal e.m.f. and orientation relative to basal plane, creation of p-n junctions 2−83991
C fibrous structures, pyrolytic C infiltration 2−53957
C film, impermeability to Na^+, diamond-like props. characterization 2−56588
C pyrolytic, impregnation with graphite, neutron irrad. stability 2−56997
Cd, impurity diffusion in single crysts. 2−43658
Cd, of Ag, tracer diffusion 2−56755
CdF_2, thermal defect order, mobility and complex form., ionic cond. mechanism 2−51194
CdS, of Ag, Cu and In, thermal diffusion method for photosensitive material 2−72059
CdS, of Se, optical waveguide fabrication 2−66842
CdS, self-diffusion of Cd, radiotracer study 2−83993
CdTe, of Cu, from evaporated and chemically plated Cu layers, He ion backscatt. obs. 2−64676
Co-Ni-Fe alloy, ^{60}Co self-diffusion, Fe content effects 2−43659
Co-(31.8 wt.%)W alloy, excess vacancy conc. effect on grain boundary diffusion 2−47455
β-Co, of O and Si, 1000-1300°C, internal oxidation studies 2−74811
CoO, volume diffusion rel. to sintering 2−50878
$CrCl_2.3AlCl_3$, chem. transport of $CrCl_2$, $CrCl_2$ prep. method 2−65361
Cr_2O_3-TiO_2 system, rutile struct. solid soln., interdiffusion and solubility limits 2−47618
CsCl:Ba^{2+}, ionic cond., 250-500°C 2−54232
CsCl, pure and Ba^{2+}-doped, self-diffusion, 360-460°C 2−74813
CsI, Xe diffusion and calc. of activation energies 2−74812
Cu-Au alloy, of Au, misfit dislocation behaviour 2−71497
Cu-Au bimetallic film, interdiffusion, X-ray obs. 2−60828
Cu-(30 wt.%)Zn alloy, relax. of diffused Zn during short-range-ordering 77705 2−77705
Cu-Zn solid solution, of Zn, residual activity method 2−47457
Cu-Zn system, deform. influence on diffusion processes during electron irrad. 2−47456
Cu, of Au, comp. profiles near grain boundaries, electron diffr. obs. 2−56757
Cu, of Nb by an electrical-resistance method 2−53762
Cu, of Pt, 750-1075°C 2−56756
Cu, of Zn, residual activity method 2−47457
Cu, superficial autodiffusion 2−71535
Cu_3Au, free vacancy no. determ. in fission-neutron displacement cascade 2−53712
D_2, self-diffusion and vacancies 2−43656
Er anisotropic self-diffusion rate is temperature range 1202-1412°C 2−56750
Fe/Al system, barrier effect of intermediate Ag layers 2−47461
Fe/$Al_{(l)}$ system, solid/liquid diffusion 2−80715
Fe/Ni and Fe/Ti diffusion couples, atomic mobility in Kirkendall plane 2−53763
Fe-C-i-j-...-n multicomponent solid solution, of C, thermodynamic interpretation 2−43662
Fe-C system, of impurities, theory 2−50708
Fe-Mn alloy, oxidation kinetics, diffusion model 2−48333
Fe-Ni-C, quenching and hydrogenation effects on mechanical props. and brittleness 2−43723
Fe-Ni, of N and C along austenite/ferrite phase boundary 2−68052
Fe-Ni alloy, of hydrogen, struct. influence 2−77611
Fe-3.1 wt.%Si, electrodiffusion activation energy of polygonization substruct. 2−53764
β-Fe-Ti, of Fe, Mossbauer study 2−77612
Fe-Zn system, influence of ultrasonic strains on diffusion growth of various phases 2−43655
Fe, cast, of C, rel. to bainite growth kinetics 2−43920
α-Fe, impurities, influence on self- diffusion coeffs. 2−47462
Fe, of C, O, H, N and S, temp. depend. 2−43661
Fe, of C, O, N and S, effective radii of diffusing particles, diffusion mechanisms 2−50709
α-Fe, of C, press. effect 2−43660
Fe, of Zn, determ. of Fe-Zn interdiffusion coeffs. 2−47459
α-Fe, pure and alloyed, of Mn, 778.3-901°C 2−83994
α-Fe, rel. to elastic consts., 25-900°C 2−60842
α-Fe, zone melted, of hydrogen 2−77610
Fe alloys, abs. rates of N and calc. chem. diffusion coeffs. 2−64694
Fe alloys, partitioning of transition metals in oxide scales, chem. diffusion model 2−78197
Fe(16 wt.%)Cr alloy, electromigration of Fe and Co 2−47460
FeO, point defects, thermodynamic analysis, migration processes 2−56684
α-Fe_2O_3, of Fe, O_2 partial press. depend., high temp. 2−51138
GaAs-CdS heterojunction, isotypic, diffusion of Ga and Cd across junc. 2−71956
GaAs, impurity diffusion, technological aspects 2−71514
GaAs, N^+ layer formation by Sn diffusion 2−71515
GaAs, of Fe, Cr and Co, 800-1100°C 2−60829

Diffusion in solids continued
n-GaAs, of Fe and Co, temp. depend. 2−47463
GaAs, of Sn, effect of mask edges 2−54205
GaAs, of Zn, diffusion profile anal. 2−47464
GaSb:Te, segregation coeff. of Te 2−74798
GaSb, of Zn, temp. and conc. depend., radioactive tracer obs. 2−74799
n-Ge, electron irrad., low temp. annealing, diffusion limited recovery 2−47378
Ge, impurity atom diffusion enhancement by light ion implantation 2−60814
Ge, interstitial diffusion of Li, press. depend. 2−47442
Ge, migration energy of quenched-in defects, specimen size effect 2−71536
Ge, of Cu, temp. depend. 2−77613
Ge, of Li, hydrostatic press. effect 2−47443
Ge, of Sb, influence of In concentration gradient 2−71516
Ge, self diffusion of interstitials and vacancies 2−47399
H_2, self-diffusion and vacancies 2−43656
p- H_2 quantum diffusion, jump freqs. of o-H_2 impurities 2−60830
He, of isotopic impurities, quantum theory 2−68046
β-Hf, mechanism 2−68044
InSb, thermal etch pattern form. during diffusion 2−47440
KBr, mass transport along grain boundary pipelines, comments 2−56760
KBr, mass transport along grain boundary pipe lines 2−56759
KBr, of He, permeation, gas release and ion implantation studies 2−84002
$K_2CO_3 + 2PbSiO_3$ subsolidus reaction, kinetics and mechanism 2−60996
$K_2CO_3 + 2(4PbO.SiO_2)$ reaction, kinetics and mechanism 2−50884
KCl, diffusion coeff. of self-trapped holes and migration to thallium centres 2−68709
KCl, migration of water drops, under various driving forces 2−47466
KCl, of ion-implanted ^{85}Kr, effects of channeling, radiation damage and divalent doping 2−68053
KCl, of water mols., influence of OH^- ions 2−60831
KI, diffusion coeff. of self-trapped holes and migration to thallium centres 2−68709
K_2O-SrO-SiO_2, interdiffusion coeffs. matrix 2−80724
K_2O-SrO-SiO_2 glass, cation self-diffusion coeffs. 2−53765
Li dil. alloys, translation diffusion rel. to nucl. spin relax. 2−44317
Mg-Zr alloy, of Ni, 350-500°C 2−47467
MgO, anion doped, grain boundary diffusion of Ni^{2+} 2−50710
MgO, cation self-diffusion up to 2350C 2−56761
$MgO.Al_2O_3$ spinel, oxygen self-diffusion 2−50711
Mn_xO-MgO system, interdiffusion 2−50714
MnO, point defects, thermodynamic analysis, migration processes 2−56684
Mo, of C to surface removal by further desorption 2−64763
Mo, of Cr, bulk and boundary diffusion 2−53766
$MoO_3 + SrCO_3 \rightarrow SrMoO_4 + CO_2$ reaction kinetics 2−54536
Mo_5Si_3, of Si, oxide coating form., at 1700°C 2−53769
NH_3, self-diffusion, rotating frame relaxation time 2−47451
$(NH_4)_4Fe(CN)_6.H_2O$, of ions, Arrhenius activation energy, n.m.r. obs. 2−74814
Na borosilicate glass, rel. to Na^+-K^+ ion exchange 2−53537
NaCl, of Mn^{2+}, diffusion coeff. meas. using e.p.r. 2−50700
NaI, diffusion coeff. of self-trapped holes and migration to thallium centres 2−68709
Na_2O-B_2O_3-Al_2O_3, nabal glass, self-diffusion of Na ions and interdiffusion coeffs. 2−60832
Na_2O-K_2O-SiO_2 glass, Na and K self diffusion, rel. to internal friction 2−50712
$Na_2O.3SiO_2$ glass, of Na, effects of annealing atmosphere 2−53767
Nb-Al system, diffusion in $NbAl_3$, Nb_2Al and Nb_3Al phases 2−74815
Nb, of H, low temp., determ. by Gorsky effect 2−80847
Nb, of H, phase equil. and evolution kinetics of dil. solns. 2−53903
Nb, of H, quantum interpret. 2−71537
Nb, of H absorption, solubility 2−50542
Nb, of hydrogen, anelastic obs. 2−77616
Nb, of oxygen, under neutron irrad. 2−53768
Nb, oxide growth in matrix 2−47468
β-NbH, proton jump rate determ. by neutron scatt. and n.m.r. 2−77614
NbH_x, neutron scatt. obs. of hydrogen motions 2−77771
NbH_x, quasielastic neutron scatt., diffusive motions of hydrogen 2−77615
Nb_5Si_3, of Si, oxide coating form., 1700°C 2−53769
Ne, high purity crystalline, equilibrium vacancy formation self-diffusion 2−71470
Ni-Co, coarse grained polycrystalline, Co self-diffusion at low temp. 2−47450
Ni-Mo system, interdiffusion coeffs., temp. and conc. depend. 2−56762
Ni, hydrogen migration energy 2−53792
Ni, of H, quantum interpret. 2−71537
Ni, self-, width of wide-angle grain boundaries 2−47469
Ni, solubility of U, low limit determ. from heterodiffusion coeffs. 2−43654
Ni_xO-Co_xO system, interdiffusion 2−50714
NiO, of Cr, temp. depend. 2−50713
NiO, polycryst., self-diffusion of Ni, intercryst. diffusion 2−80721
Pb-Sn alloy, of Ag 2−56763
Pb, of ^{124}Sb, temp. depend., 188-315°C 2−77617
Pb, of ^{22}Na meas. by sectioning diffusion couples, 249-313°C, vacancy mechanism 2−77600
Pb, of Ag, isotope effect in dissociative mechanism 2−68044
Pb, of Cu, 0 to 56 kbars 2−47470
Pb, of Cu, evidence for two simultaneous mechanisms 2−84001
Pd-Ag alloys, of hydrogen, neutron scatt. obs 2−77618
Pd-Ag alloys, solubility and electromigration of H_2 and D_2 2−83990
Pd-Mo system, interdiffusion coeffs., temp. and conc. depend. 2−56762
Pd-V system, inter- and intrinsic processes, phase obs. 2−53770
Pd, of H, at elevated press. 2−77620
Pd, of H, quantum interpret. 2−71537
Pd, of hydrogen, equil. and kinetic isotope effects 2−77619

Diffusion in solids continued
Pd, of hydrogen, jump-model, neutron quasielastic scatt. obs. 2−83999
Pd and Pd-Ag alloys, of H, coeff. meas. by electrochem. methods 2−77602
Pt-Si contacts, solid-solid reactions 2−50715
Pu, of Cu 2−71539
^{240}Pu, self-diffusion under hydrostatic pressure 2−64695
RbCl, anion self diffusion, tracer and sectioning technique 2−47471
RbI, diffusion coeff. of self-trapped holes and migration to thallium centres 2−68709
Rn in lunar regolith, model for diffusion by random walk method 2−44921
Sb, electron diffusion through shock wave front 2−71771
Sc-H solid solution, diffusion parameters from n.m.r. obs. 2−72517
Se, amorphous, of Pt rel. to threshold and memory switching effects 2−57196
Se, of Tl, 60-210°C, cpd. formation 2−53771
Si:B impurity enhanced diffusion 2−50693
Si:K, doped surface layers, donor props. and diffusion 2−65019
Si:P impurity enhanced diffusion 2−50693
Si-SiO_2 system, of B 2−68037
Si, anomalous diffusion of B and P 2−50694
Si, As, Sb, Au impurities, concentrations, lattice locations using He-ion backscattering technique 2−64675
Si, impurity atom diffusion enhancement by light ion implantation 2−60814
Si, impurity diffusion using emulsion type doped oxide 2−71517
Si, of As, of props. of SiO_2:As and Ge/SiO_2:As diffusion sources 2−83979
Si, of Au, at 1000°C, rel. to dislocations, reaction rate limited 2−60833
Si, of Au, surface cpd. formation, refl. electron diffr. obs. 2−50463
Si, of B, effect of mask edges 2−54205
Si, of B, from doped oxide layers 2−64677
Si, of B, from localized surface source 2−56739
Si, of B, Si-B phase influence 2−77523
Si, of B, using B_2H_6-CO_2 system 2−43645
Si, of implanted B and P, effect on charge carrier distrib. 2−47432
Si, of Li, drift and precipitation obs. 2−50692
Si, of P, coeff. determ. by Boltzmann-Matano method 2−71540
Si, of P, impurity profile kink form. mechanism 2−56742
Si, of Sb and P, enhancement by proton irrad, dose rate effects 2−80707
Si, self diffusion of interstitials and vacancies 2−47399
Si, variable coeffs. for B impurities 2−56745
Si film, epitaxial, of Sb, temp. and dislocation density depend. 2−74816
Si low conc. diffusion of P and B under sealed tube conditions 2−74792
Si p-n junction, reactor irrad., broadening of Zn and Ga impurity profiles 2−84355
Si wafer, surface defect generation on reoxidation in H_2O vapour during B diffusion 2−64672
SiC, of B, distribution, elec. cond. and p-n junc. obs. 2−74797
SiGe/W film, interface reactions, effects of p- or n-type substrates, ion backscattering analysis 2−71951
SiO_2-K_2O system, binary interdiffusion coeffs. and O_2 self-diffusion 2−53772
SiO_2-Na_2O system, binary interdiffusion coeffs. and O_2 self- diffusion 2−53772
SiO_2, steam grown on Si, cation transport 2−61405
Sn, of Hg, obs. and mechanism 2−68054
Sn, self-, width of wide-angle grain boundaries 2−47469
Ta, proton motion, temp. depend. 2−43653
TaH_x, quasielastic neutron scatt. obs. of hydrogen diffusion 2−77621
Ta_5Si_3, of Si, oxide coating form., 1700°C 2−53769
Th, bulk to surface equilib. of surface impurities 2−50465
Ti/Al chem. diffusion couple, Al_3Ti growth and solubility limits 2−53757
Ti, diffusional saturation with O_2, residual stresses introduced 2−56949
β-Ti, mechanism 2−68044
Ti, of H, quantum interpret. 2−71537
α-Ti, ultra-fast diffusion of ^{63}Ni 2−64697
Ti hydrides, ternary and binary, temp. and freq. depend. of proton spin relax. 2−78052
TiN-MgO solid soln., solid phase interaction, diffusion of Ti, 1700-2000 K 2−53907
TiO_2-SiO_2 glass, He migration 2−50718
TiO, cation self-diffusion 2−50717
TlCl, pulse n.m.r. investigation of vacancy and interstitial diffusion 2−71471
γ-U, mechanism 2−68044
UC-ZrC solid solns., radioactive isotope study, boundary diffusion, activation energy 2−71541
UC, rel. to surface smoothing kinetics 2−53556
UO_2, fission sintering and irrad. induced diffusion 2−52855
UO_2, neutron irrad., fission gas bubble nucleation and gas migration 2−63971
V-H(D) systems, n.m.r., β- and δ-phase behaviour 2−78175
V_6C_5, disordered, C self-diffusion 2−60834
VH_x, quasielastic neutron scatt. obs. of hydrogen diffusion 2−77621
W, interdiffusion in emitters of thermionic converters 2−53560
W, of Fe and Co along grain boundaries 2−47472
W, of interstitial He, lattice damage prod. by He ion irrad. 2−47394
W, self-, width of wide-angle grain boundaries 2−47469
W_5Si_3, of Si, oxide coating form., at 1700°C 2−53769
ZnS, of Cd, formation of steeply graded $ZnCd_{1-}S$, and luminescence 2−72444
ZnS, of Mn, Au and S 2−56764
$ZnWO_4$, effect of struct. charact. on penetration of Cr and Gd impurities 2−71542
Zr-Nb alloys, phase transform, mechanisms 2−53999
Zr-Y syst., H_2 diffusion through layers, calc. by eigenfunction method 2−50720
α-Zr, bulk diffusion of ^{51}Cr 2−67357
β-Zr, mechanism 2−68044
Zr, of hydrogen, 275-700°C 2−53773
α-Zr, of oxygen, coeff. variations 2−71543

Diffusion in solids continued
α-Zr, ultra-fast diffusion of ^{59}Fe, ^{60}Co, and ^{63}Ni 2−64697
thermal
alloy, numerical calc. of redistribution of interstitial solute in thermal gradient 2−77601
diffusivity meas., small specimen, incandescent temp., by electron beam 2−85162
metal, of hydrogen, isotope effects 2−77605
semiconductors, heat treatment and props. of doping element 2−84321
semiconductors with nonparabolic bands, study of transport props. and thermal diffusion coeff. 2−81101
steel, decarburized, diffusion of hydrogen at low-temps., effect of grain boundaries 2−68047
α-Fe-Sn, solid solns., effect of third alloy component on precip. kinetics 2−80812
Cu, (111) oriented, of Ni, 600 and 900°C 2−53761
MgO, plastically deformed, pipe diffusion prod. of prismatic dislocation loops after annealing 2−64689
Ni-Co alloys, diffn. of Co at temps. up to 1000°C 2−71538
Zn activated vacancy, self-diffusion coefficients and thermal coeff. of expansion 2−68048
Diffusion pumps *see Vacuum pumps*
Digital computer applications *see Computer applications*
Digital computers *see Calculating apparatus/digital computers*
Dilatometers *see Length measurement; Volume measurement*
Dimensions
see also Units
chiral invariant scale breaking part of Hamiltonian density 2−49481
and decibels, standards 2−41444
linear, pneumatic gauging at low temps. 2−76156
physical quantities, mathematical theory of units and dimensions 2−62956
reactor fuel elements, irrad., radiograph prod. and automatic meas. 2−42659
three dimensional location, using planar X-ray system 2−62960
Ge, length change on electron irrad. 2−68016
Dimers *see Molecules; Polymers*
Dineutrons *see Neutrons and antineutrons*
Diodes *see Electron tubes; Plasma devices; Rectifiers; Semiconducting devices/diodes and /tunnel and interface devices*
Dipole moments *see Molecules/moments; Nucleus/electric moment; Nucleus/magnetic moment*
Diquarks *see Quarks*
Dirac electron theory *see Electron theory*
Dirac equation
amplified, non-relativistic limit 2−69587
amplified, reduction to Pauli formalism 2−69586
central potential, exact soln. in semi-relativistic approx. 2−58750
charged particle motion in field of transverse e.m. plane wave, group theoretical analysis 2−63262
delta function, integral representation 2−78735
electron interacting with plane e.m. field, algebraic soln. 2−82227
electron-atom scattering, amplitudes and spin polarizations for incident energies 100 to 1500eV 2−52940
external electromagnetic field interaction 2−69588
free particle with spin /2, transformation teaching to absence of zitterbewegung 2−70103
generalized covariant for 5-dimensional model universe, elementary spinaxial excitations 2−41455
integral approximation, rel. to elastic scattering 2−41522
LorentzlDirac equation, for charged particle motion 2−82172
Maxwell-Dirac equations, coupled, Cauchy problem 2−42297
perturbation Lagrangian theory for Dirac fields, Ward Takahashi identity and current algebra 2−82622
relativistic Kepler problem with magnetic charges, quaternionic solutions 2−52060
in Riemann-Cartan space-time 2−73294
solution for four new configurations of external magnetic field, use of quaternionic formalism 2−41502
solutions, construction from solutions of two-component spin-$^{1}._{2}$ wave equation 2−59382
spectra, even and odd, of one-dimensional symmetrical potential 2−41493
spinor field, modified quantiz. in external e.m. field 2−79461
stigma equation, Poincare noninvariance proved 2−42331
strong external fields, solution rel. to heavy ionic and molec. collisions 2−42769
superoperator theory, zitterbewegung as subdynamics 2−73321
two component alternative, new equation 2−73753
two-component spin-1/2 wave equations 2−78824
vertex functions with arbitraty spin, analytic 2−82660
Weinberg equation, rel. to calc. of e.m. interactions between particles with arbitrary spin 2−49485
H atom, formulation in Friedman universe 2−49972
Discharge tubes *see Electron tubes; Gas-discharge tubes; Ion sources; Particle accelerators; X-ray tubes*
Discharges, electric
see also Arcs, electric; Breakdown,electric; Corona, electric discharge; Plasma; Sparks, electric
a.c. arc, wall stabilized, current zero behaviour 2−71057
a.c. arcs, wall stabilized, current zero behaviour 2−71056
air gap between dielectric, space and time picture 2−74426
air-gaps, prebreakdown current meas. 2−43216
arcs, cathode erosion, displacement of arc support points 2−80367
arcs, square wave power pulses, transient parameter calculation 2−67696
breakdown in l.p. gas gaps 2−80416
breakdown streamer, guidance by laser induced rarefaction channels 2−80362
capillary, instability with evaporating wall 2−56385
cathode dark-space distance in d.c. sputtering system 2−50226
cathode sputtering during discharge with oscillating electrons, investigation using vacuum micro-balance 2−85176
charge production and discharge phenomena rel. to supertankers and supersonic aircraft 2−77310
condensed spark, spectrochemical analysis, spectra excitation using shunting capacitor 2−65414

Discharges, electric continued
constricted induction, theoretical formulation 2−80364
crossed field plasma discharge at low press., and plasma accumulation in electrostatic potential well 2−46755
current, induction of motion in conducting fluid 2−56305
cylindrical magnetron diode, pulse discharge, spectroscopic investigation 2−60299
detector of partial discharges, automatic measurement of magnitude and inception and extinction voltage 2−82417
development in homogeneous and heterogeneous fields 2−70993
effect on propag. of flames 2−82373
electrode material losses in low pressure gas discharge lamps 2−70999
electrodeless lamp, device for precise temperature control 2−82586
electron and ion beam gun form. rel. to welding 2−60296
electron drift velocity meas. using microwave dragging technique 2−80268
electron gas in positive column, non-hydrodynamic props., reson. behaviour 2−74420
electron temperature, current dependence and shape of volt-ampere characteristic 2−53263
exploding-wire, neutron prod. 2−67665
fast transverse, for gas laser pumping, simple model 2−52416
flash tubes, time, peak power and spectral advantages 2−76539
formation in flow, initial boundary value problem 2−50227
free fall column, theory, noble gas ion laser 2−73551
gas, conference, London (1972) 2−70990
gas dynamic loading of microparticles for pulsed discharge interactions 2−53250
gas laser electron beam controlled, elec. field and secondary electron distribs., Monte Carlo calcs. 2−80360
H-pressed, configurations and modes 2−43207
He, bremsstrahlung in strong electric field 2−80368
heavy rare gases, radiation properties 2−71004
h.f., resonant, effect of constant electric field on stability 2−64342
h.f. resonance and h.f. single electrode in coaxial resonator in longitudinal mag. field 2−64341
high power double discharge TEA laser, analysis of amplification process 2−76479
high-β reversed field discharges with extended lifetimes 2−83563
hollow cathode, mode to explain local overpressure 2−46795
h.v. arrangements uniform description 2−70985
h.v. Z-pinch, formative phase analysis of low pressure gases 2−67650
hydrodynamics current driven instability in electrodeless induction discharge 2−80356
impulse, electrode dissociation studies 2−64343
impulse surface discharge rel. to applied voltage and specific capacitance, obs. 2−71017
induction, stability analysis 2−80365
inductive ring, breakdown behaviour 2−53249
inert gas, low current ioniz. wave theory 2−77312
inert gas alkali MHD generator 2−80374
inhomogeneous positive column, distrib. of charged particles and potential 2−80366
ionization current between parallel plane electrodes growth computation 2−67689
ionization waves (striations), exact theory 2−64349
Langmuir probes, low electron temp. meas. in afterglow plasma rel. to ionospheric meas. inaccuracies 2−83555
large spheregaps, analysis of volt-time characteristics by integration method 2−71031
laser, pulser/sustainer, stable uniform lasing 2−59137
laser beam triggering 2−74406
leader channel of long air gap discharge investigation by probe electrode 2−70992
l.f. oscillation of diffusion constricted discharge 2−74394
lightning, causing forest fires 2−65795
in liquids, study using X-ray flash tube 2−85181
long air gaps under positive linearly rising voltages, predischarge phenomena 2−77315
longitudinal diffusion coeff. for electron swarms at low E/p_0 2−71008
low pressure, anode adjustment in transverse mag. field 2−74416
low pressure, argon mixture, properties 2−71011
low pressure, electron density meas. with microwave reflectometer system 2−74380
low pressure, retrograde motion in transverse magnetic fields 2−70996
machining advances 2−83639
magnetogasdynamics, current and heat dissipation 2−53186
magnetron diode, potential distribution effect on critical mag. field 2−60300
medium pressure column, impedance, equivalent circuit and stability behaviour 2−67690
metal chloride molecular discharges, thermodynamic and kinetic considerations 2−64354
microwave, mag. field stabilized plasma 2−64271
moving striations, in tapered tube 2−43205
negative ion interactions under swarm conditions, apparatus for study 2−71000
nonlinear heat transfer problems, analytic solns. 2−56329
optically dense plasma, passage of powerful laser emission 2−43154
organic insulating materials, rel. to corona 2−71006
organic reactions leading to polymer deposits 2−74408
Penning, high power crossed field, for h.v.d.c. interruption 2−74413
Penning, plasma, l.f. oscillations 2−50216
Penning discharge ion source for plasma diffusion studies 2−52401
Penning gap, Laplace equation solution by method of nonlinear parameters 2−80371
Penning source, formation position of ions, dependence on mag. field 2−53262
pinched, pumping of rhodamine 6G laser 2−42046
plasma, inductance, influence of cooling gas layer on geometric sizes, calc. 2−64340
plasma afterglow, one-dimensional model, numerical solution 2−70894
plasma bunch, effective electron temp. from self-radiation in bunch discharge 2−60208

Discharges, electric continued
plasma focus type, obs. of second compression 2—56344
plasma limiters, radioactive (tritium) ignitors 2—50204
plasma potential in positive column of low-pressure discharge 2—60254
plasma-beam discharge, dynamics of freq. spectra of oscillations 2—70952
point electrodes, field distribution effect in solids 2—72020
polyatomic gas, influence of dissociative recombination on spectral sharpness 2—60297
positive column, steady-state theory in mag. field, finite cylinder separable solns. 2—50225
positive column field and electrode falls, external probe meas. 2—71010
positive column self contraction, plasma filament radius detn. 2—46796
positive point-plane, effect on electrode surfaces in air 2—74415
powdered samples, evaporation temp. in arc discharge 2—53508
pre-breakdown phenomena between heated W electrodes 2—71028
previous discharge effects in positive point to plane gap 2—70997
pulsed, generation of blast waves in plasma 2—74360
pulsed, heavy current, volt-ampere characteristic 2—60301
pulsed, in dielectric chamber 2—70989
pulsed, in rarefied gases, mag. field meas. by Faraday effect 2—78992
pulsed ablation accelerator plasma, electron density measurement 2—80297
pulsed toroidal discharge, energy balance and spectroscopic study 2—53216
radiation sources, gas plasmas 2—60307
reactive oscillations, longitudinal mag. field effects 2—80363
r.f. preionization in supersonic transverse electrical discharge laser 2—59146
rod-plane gaps, behaviour under positive ramp voltages 2—71009
rod-plane gaps under positive switching impulses 2—74431
in sea water, spectral characteristics of generated pressure pulse 2—62056
secondary electron resonance, computer study of phase conditions of excitation, in three-electrode system 2—59107
self-sustained, form., electron-ion recomb. influence, nonlinear eigenvalue problem 2—56384
shock tube, electric discharge, as plasma flow source for MHD expts. 2—60252
spark gap triggered by TEM_{00}-mode mode-locked ruby laser, switching jitter 2—74409
stagnant, dissociation model for H_2 2—53007
standing striations as solns. of Pekarek equation 2—70986
static electricity from insulator surface 2—82390
stimulated v.u.v. and soft X-ray emission from optical transitions of multiionized atoms in high current density discharges 2—41961
streamer propagation in atmospheric air, mathematical model 2—64359
striations in electron-energy-deposition profiles from high-current field-emission diodes 2—49325
superalloy, powder, elec. discharge activated press. sintering, composite struct. bonding 2—53938
surface flashover charact. 2—74407
thermionic converter, with long electrodes, instability 2—49274
thyratron employing orthogonal electric and magnetic fields 2—70994
Tokamaks, neoclassical transport theory in banana/plateau regimes 2—70919
Townsend Huxley expt. lateral diffusion expt., theory and practice 2—69627
Townsend-Huxley diffusion expt. two-term Lorentz approx. 2—83705
u.v. lamps, visible emission obtained by using fluorescent plastics 2—63421
vortex confined pumping discharge in dye laser solution 2—49371
water vapour, formation of rotationally excited $OH(^2\Sigma^+)$ radicals 2—60027
wire explosions, electrode effects 2—69785
Ag vapour, high-current hollow cathode discharge, radiation, effect of reson. and recomb. 2—74423
AlI_3, continuum radiation 2—74421
Ar-He, separation of constituents in discharge 2—77313
Ar-Hg, voltage frequency influence on instantaneous densities of excited Hg atoms and electronic energies 2—74424
Ar-K, flowing, heat transfer between electrodes 2—60209
Ar, dynamics of inverse pinch 2—56358
Ar, hollow cathode, electron density obs. 2—70988
Ar, hollow cathode, electron temp. and density profiles 2—77307
Ar, hollow cathode, excitation mechanisms, electron and ion temp. and density 2—77308
Ar, low pressure, self excited running layers and noise phenomena 2—43209
Ar, noise temperature variation with mount style, meas. at 147 MHz 2—60304
Ar, plasma temp. meas. 2—58971
Ar, pulsed, in cylindrical magnetron diode, spectral obs. 2—71007
Ar, radial distrib. of temp. and density of charged particles 2—50228
Ar, self excited striations in tube of varying diameter 2—71012
Ar, Townsend, electron energy distribs., expt. 2—43211
Ar, Townsend discharge, electron energy distributions 2—70987
Ar arc, investigation at 950 atm. 2—67662
Ar high-gain neutral laser lines in pulsed discharge 2—41979
Ar luminescent-arc discharge, meas. of OH rotational temperature 2—43210
Ar multiply ionized ions, Z-pinch, laser oscill. 2—49352
Ar plasma, flowing, radial and axial characteristics 2—70896
Ar plasma, high current, pulsed, electron density obs. in early stages 2—60261
Au vapour, high-current hollow cathode discharge, radiation, effect of reson. and recomb. 2—74423
CO_2-O_2 mixture, high voltage, relative intensity meas. on Fox-Duffendack-Barker and u.v. doublet band systems of CO_2^+ 2—56162
CO gas dynamic laser, operating parameters 2—45720
CO_2, elec. discharge laser gas mixture, energy conversion, plasma kinetic processes 2—59151

Discharges, electric continued
CO_2, microwave discharge, spectroscopic and photometric study 2—77303
CO_2 convection laser, model of expt. 2—45716
CO_2 laser, pulse discharge development and generation process 2—45717
CO_2 laser media, parametric studies of electron beam controlled discharge 2—41996
CO_2 MHD laser charact. ionization instabilities and discharge characteristics 2—79207
CO_2 transversely pulsed discharge, effect of discharge driving capacitance on small signal gain 2—79190
Cs-Ba filled thermionic converter, influence of magnetic pressure 2—49282
Cs, cold cathode pulsed, current maxima 2—74422
Cs, low voltage arc, excitation and ionization processes 2—53265
Cs, resonance radiation effects on plasma 2—70908
Cs filled thermionic converter, discharge modes, polarization and interferometric investigations 2—49288
Cs low voltage arc, Maxwellization of precathode electron distrib. fn. 2—53264
Cs vapour, ionization in nuclear reactor 2—53252
Cs vapour, peculiarities of photoresonance perturbation relaxation in low-temp. discharge plasma 2—64320
Cs vapour Q-switches for synchronizing mode-locked laser pulse trains with external events 2—73546
Cu vapour, high-current hollow cathode discharge, radiation, effect of reson. and recomb. 2—74423
Cu vapour laser, effective generation of visible band, with high ave. power 2—82475
H, pulsed, plasma diagnostics, maximum electron conc. 2—67692
H thyratron pulse discharges, arc pot. obs. 2—56399
H_2, streamer formation, anal. of mechanisms 2—64344
H_2^+ charge-exchange analysis of cathode dark-space data 2—67693
He/N_2/CO_2 mixture, atmospheric pressure uniform d.c. discharge using gas additives 2—43214
He-CO_2 mixture, atmospheric pressure, ionization instability 2—60305
He-CdI_2, laser action of I II at 6127 Å 2—45738
He-Ne, streamers, in homogeneous fields induced by laserlight 2—74419
He-Ne mixture, frequency spectrum and dispersion relation of moving striations in narrow tubes 2—64346
He, frequency spectrum and dispersion relation of moving striations in narrow tubes 2—64346
He, h.f., props. rel. to purity of gas 2—46797
He, hollow cathode, effect of mag. field on V-I characteristics 2—64347
He, hot-probe investigation of spatial fine structure in plasma potential 2—60255
He, Langmuir paradox region, electron energy distrib. and striations 2—64350
He, postlum., metastable atom creation by electro-ion recomb. 2—64345
He, pulsed, electrical and optical measurements 2—60306
^{3}He, optically pumped, detection of orientation of $^3He^+$ by absorption of 10830Å line of ^{4}He 2—74245
Hg-Ar-Ne, probe measurements in positive column 2—74425
Hg-Ar, l.p., mass spectrometric analysis of Hg_2^+ form. in positive column 2—83640
Hg-Ar and Hg-Ar-N_2, electrodeless, r.f., electrical characteristics 2—71014
Hg-Ar arc, cathode spaces, influence of cathode qualities 2—60324
Hg-Ga vapour discharge, high press, gallium ionide 2—53251
Hg, high pressure, incremental impedance 2—71015
Hg, pulsed, vapour density decay 2—70991
Hg axially uniform column, arc chopping 2—70995
Hg lamp, for illuminating people 2—42251
Hg lamp, recalibration of spectral radiance in near u.v. 2—79450
Hg positive column, microwave scattering from ion acoustic waves 2—74387
Hg vapour, ionization in nuclear reactor 2—53252
Hg vapour, l.p., secondary ioniz. coeff. 2—53253
Hg vapour long capillary positive column 2—60303
I_2-He, electronegative gas laser discharges, characteristics of system 2—71016
Kr, pulsed, electrical and optical characteristics 2—43212
Kr, pulsed, obs. of high gain neutral laser lines 2—41979
Kr, radial distrib. of temp. and density of charged particles 2—50228
N_2-methane mixture, cathode-directed streamer, secondary avalanche development 2—60298
N, dependence of high-current pulsed discharge on initial pressure and current 2—56387
N multiply ionized ions, Z-pinch, laser oscill. 2—49352
N_2, bremsstrahlung in strong electric field 2—80368
N_2, instationary, at high overvoltages 2—71005
N_2, ionized, pulsed discharge production in visible range, use for laser pumping 2—69890
N_2, mechanism of spark breakdown 2—60318
N_2, positive ion drift velocities at high pressure 2—74411
N_2 plasma stationary microwave discharge at atmos. pressure 2—64293
N_2 relative populations of $C^3\Pi_u$ and $B^2\Sigma_u^+$ states 2—80121
N_2^+, mechanism of electron-ion dissociative recombination in gas discharge 2—74272
N_4^+ form. mechanism 2—67685
Na vapour, high pressure, radial temp. distribution 2—71065
Na vapour, high pressure, radiance at centre of D-lines, obs. value rel. to calc. value 2—71019
Ne-Br_2 mixtures, r.f. discharge spectrum, excitation mechanisms 2—71018
Ne-Xe, gyroscopic effect in constricted discharge 2—74410
Ne, frequency spectrum and dispersion relation of moving strations in narrow tubes 2—64346
Ne, hot-probe investigation of spatial fine structure in plasma potential 2—60255
Ne, in hollow cathode, effect of nonlinear absorption at 0.63 m. wavelength 2—83641
Ne, low current ioniz. wave theory 2—77312

Discharges, electric continued
- Ne gas discharge in magnetic field, optical pumping with multimode laser, saturation resonances by magnetic mode crossing 2−46436
- Ne low-pressure column, tail of electron, energy distribution function 2−50229
- Ne multiply ionized ions, Z-pinch, laser oscill. 2−49352
- O_2, ionized, pulsed discharge production in visible range, use for laser pumping 2−69890
- O_2, mechanism of spark breakdown 2−60318
- Rb vapour Q-switches for synchronizing mode-locked laser pulse trains with external events 2−73546
- SF_6, compressed, voltage time characteristics 2−70998
- SF_6, mechanism of spark breakdown 2−60318
- Xe, high pressure, initial stage 2−67691
- Xe, laser action on unclassified transitions in highly ionized plasma 2−59142
- Xe, pulse discharge radiation, space-time distrib. 2−56389
- Xe, pulsed, parameter time depend. obs. 2−53254
- Xe, pulsed, rel. between electrical conductivity and current density 2−60302
- Xe, radial distrib. of temp. and density of charged particles 2−50228
- Xe impulse lamp, emission effects on organic dye solutions 2−53378
- Xe plasma, pulsed, basic parameters, optical and electrical props. 2−74381
- Xe pulsed discharge, meas. of plasma temp. 2−56388
- **glows**
  - afterglow at low pressure, three-body recombination 2−80372
  - air, obs. of near i.r. emission spectrum 2−46798
  - anode oscillations, optical studies by photomultiplier 2−71020
  - ball lightning, new theory, seed for linear lightning 2−65802
  - chemical analysis of O_2 and CO_2 by metastable ion detection 2−65402
  - cold cathode, normal, problems in obs. 2−71021
  - contact glow-discharge electrolysis, study in water containing various electrolytes 2−54551
  - convectively unstable random ionization waves 2−60309
  - current oscillations in subnormal glow discharges 2−74427
  - d.c., plasma diagnostics and energy transport rel. to sputtering 2−50230
  - electron beam production 2−49318
  - electrophoresis phenomena, in gases and metal vapours, review 2−84645
  - galvanoluminescence during electrolysis 2−77305
  - high pressure, gas heating effects in constriction 2−80361
  - laser capillary discharge tubes, l.f. oscillations due to moving striations 2−77314
  - lewis Rayleigh N_2 afterglow, excitation of Al and Cu atoms 2−77011
  - low pressure, growth and sputtering of SiO_2 films 2−74634
  - in low-current, low-pressure gas, critical capacitance, effect of inductance on stability 2−43213
  - metastable atom density in afterglow plasmas in neon 2−67629
  - metastable atom production rel. to hollow cathode arc discharge 2−74211
  - microbeam electron gun, performance 2−66707
  - neutral component, macroscopic velocity obs. in crossed folds 2−70976
  - noble gas mixtures, emission in short wavelength vacuum region 2−83642
  - plasma electron energy analysis 2−74379
  - positive column, distrib. of impurity vapour 2−64351
  - predischarge negative currents, under variable pressure, obs. 2−60308
  - rare gas mixtures, impedance variation of positive column 2−43206
  - sputtering, plasma diagnostics, obs. 2−53214
  - sputtering systems for thin film production 2−71323
  - striations, random, in positive column 2−46799
  - transition and line shapes, meas. method 2−70080
  - vapour deposition of high work function materials, fabrication of thermionic emitters 2−49273
  - Al_2O_3, rapid sintering by glow-discharge apparatus 2−80804
  - Ar-He mixture, spectroscopic measurements of cataphoresis 2−71022
  - Ar afterglow, benzene $^1B_{2u}\rightarrow{}^1A_{1g}$ emission obs. 2−70747
  - CO_2, electron energy distrib., new probe technique 2−64348
  - F gas, voltage-current characts., 60 to 150 torr, obs. 2−71013
  - H, spectral line intensity in mag. field 2−52919
  - He-Cd, gas mixture, laser action in Crookes region 2−79196
  - He-Cd gas mixture glow discharge, distribution functions and kinetic coeffs. 2−71024
  - He-Cd mixture, electron distrib. fns. 2−74429
  - He-Ne, average electron energy in positive column 2−60310
  - He-Zn, gas mixture, laser action in Crookes region 2−79196
  - He, radial structure of cathodic region 2−64352
  - He, spectral line intensity in mag. field 2−52919
  - He with hollow cathode in mag. field, photoemission effect 2−43215
  - Hg, spectral line intensity in mag. field 2−52919
  - Hg afterglow plasma, transition from free-fall to ambipolar diffusion 2−60212
  - Mo controlled electrode surfaces, prebreakdown current 2−80370
  - N rotational temp. in rarefied supersonic flow in glowing-discharge 2−60311
  - N_2, electron energy distrib., new probe technique 2−64348
  - N_2, electronegative gases, light emission in electron avalanches 2−74428
  - N_2, microwave discharge, pink afterglow, vibrational relaxation 2−53255
  - N_2 afterglow, O_2 and temp. effect on first positive bands 2−77304
  - N_4^+ ions frequency in positive column 2−71023
  - N_2+O_2, electron energy distrib., new probe technique 2−64348
  - Ne, electron distrib. function, ioniz. waves influence 2−74430
  - Ne, p and s ionization waves, nonlinear interaction 2−71025
  - Xe, afterglow plasma, electron temp. lowering by diffusion cooling 2−70882
- **high frequency**
  - beam-plasma, hot electron prod. 2−53236
  - ethyl isocyanate, emission spectra 2−42990
  - formic acid, emission spectra 2−42990
  - generators of condensed sparks, electrical processes 2−53258
  - large quiescent collisionless plasma, production 2−56365

Discharges, electric continued
- **high frequency** continued
  - re-ignition, influence of metastable states 2−43217
  - r.f. plasma, electrostatic probe props. 2−50207
  - space charge in initial stages, photoelectric investigation 2−74443
  - in supersonic gas flow, breakdown voltage and electric field strength 2−74418
  - in weakly ionized plasma in presence of magnetic field, l.f. oscillations due to 2−77294
  - Ar, high pressure, under magnetic field, r.f. break down potential 2−71036
  - Ar + N_2, cross sections for excitation of $N_2(C^3\Pi u)$ 2−43041
  - H_2, re-ignition, influence of metastable states 2−43217
  - N_2, re-ignition, influence of metastable states 2−43217
  - N_2 microwave discharge, plasma sampling diagnostics 2−60258
  - Ne, re-ignition, influence of metastable states 2−43217

Disintegration *see Beta-decay theory; Nuclear decay theory; Radioactivity*

Disintegration energies *see Radioactivity*

Dislocations *see Crystal imperfections/dislocations*

Disperse systems
- *see also Aerosols; Colloids; Emulsions; Foams; Powders; Sols; Suspensions*
- acoustical particle counter, evaluation 2−51597
- adhesion of particles, effect of flattening 2−74560
- agitated, fluid-fluid interac. and hydrodynamics, simulation model 2−53363
- air-water-glass bead three phase flow system, exptl. investigation of hold-up 2−67605
- analysis, aerosol sampler 2−53463
- anomalous viscosity of disperse systems in shear stress zones 2−60515
- atmospheric particulate matter, isokinetic sampler for use on aircraft 2−57943
- atmospheric surface layers, dispersion of matter, eddy diffusivity approximation analysis 2−78369
- axial dispersion in beds of small particles, chromatographic techniques 2−71239
- benzene lenses at air-water interface, with translational and rotational symmetry 2−74510
- bubbly liquids, one-dimensional flow, dynamic props. 2−80436
- coaxial high temperature jet radiation with Ti dispersive particles, energy loss 2−80497
- colloidal dispersions, viscoplastic deposit formation in turbulent pipe flow 2−83826
- concentration, fluctuations, correlation theory, local disturbance 2−83811
- correlation theory, fluctuations, local disturbance 2−83811
- Couette flow of viscous fluid with particle injection, determ. of velocity and temp. distrib. 2−77225
- crude oil, with high paraffin content at low temps., hydrodynamic resistance 2−83751
- dispersed-phase axial mixing, statistical model of residence time distribution 2−67763
- dispersion of material in slowly moving fluids 2−46664
- electron density of particles in colloidal suspensions, X-ray study under different collimation conditions 2−71285
- frequency contrast characteristics 2−46991
- gas-liquid droplet system, model for shock wave propag. 2−83656
- immiscible liquid mixtures, continuous and dispersed phases, viscosity nomogram 2−43392
- inclusion, spherical, transitive process of d.c. field 2−43394
- Indian ink particles, in water and $FeCl_3$, aq. soln., Brownian motion in uniform mag. field 2−67846
- interaction forces between condensed bodies in contact 2−74566
- jet, two-phase, turbulence intensity 2−46995
- jets, colliding, motion of solid particles, computer anal. 2−56310
- latex interpenetrating networks, theory and effects of synthetic detail 2−64490
- Lifshitz-Van der Waals constant calcs. from optical states 2−53457
- light scattering, data inversion information theory 2−64476
- light-scattering, particle size analysis, use of automated laser light photometer 2−63307
- liquid-liquid dispersion, drop size measurement by photographic technique 2−71240
- magnetic moments of dust particles, microscopic determination 2−53456
- magnetite, magnetic characteristics rel. to palaeomagnetism 2−58139
- magneto- and electro-rheology 2−58854
- marine sediments, acoustic props. 2−57834
- mass transfer rates from spherical particle boundary-layer injection suction considerations, variational analysis 2−77397
- mono-dispersed drops, production by vibration- atomization 2−71246
- monodisperse lattices, rheology, review 2−74565
- monodisperse spray deflagration, burning velocity distrib. 2−84619
- monostatic reflection by elastic spheres in water 2−43398
- N. Atlantic deep sea sediments, Cd distrib. 2−81618
- 2-naphthol particles, mass transfer to flowing water 2−71129
- nepheloid layer characteriz., correl. between light scatt. and suspended material analysis 2−57913
- nonlinear, stability of solitary waves, anal. by Korteweg-de Vries eqn. 2−46898
- nuclear fuel element, randomly dispersed discontinuous phase, temp. distrib. 2−49889
- osmometry, salt free polydisperse polyelectrolyte, possible source of error 2−56492
- particle retention in filters 2−66361
- particle size determ. by sequential X-ray fluorescence 2−64485
- particulate material dispersing and disaggregating method 2−43884
- phase transformation of vapour, study by microwave abs. 2−56543
- photography of particles by scattered light at low levels of intensity 2−50376
- polydisperse polymers, undiluted, stress relaxation after steady-state shear flow 2−64482
- polyethylene oxide supermolecules, electron microscope meas. of size and growth in solution 2−64204
- polymer in soln., refr. index increments, conc. depend. 2−60520

Disperse systems continued
- polymer latex, particle size analysis, angular light scattering data 2−43411
- polymer solution, having draining effect, normal stress effect 2−71164
- polystyrene in cyclohexane soln., conc. fluctuation dynamics near critical pt. 2−46996
- polystyrene latex, freeze-etched, electron microscope study of particle size 2−60522
- polystyrene latexes, multiple scattering of light, determ. of coeffs. of scattering and absorption 2−43400
- polystyrene lattices, surface conductance, comparison of theory and expt. 2−60521
- polystyrene solution and latex, nonlinear viscoelasticity 2−83368
- portland cement paste, microstruct. effects on deform. and fracture 2−60995
- powder layer, finely dispersed, vibration effects 2−43393
- relaxation coefficients, dependence on size of particles, effect of optical constants 2−53461
- rheology, conference, Nagoya, Japan, Oct. (1971) 2−82315
- rheology, role of particle interactions 2−64484
- saturation phenomena of elec. light scatt. by large strongly elongated disperse particles 2−74562
- scattering media, light beam attenuation, exponential low limits, scatt. indicatrix 2−56527
- sediments, role of Brownian motion in control of detrital remanent magnetization 2−74564
- sediments, seismic wave amplification, det. of shear velocity using surface wave dispersion 2−57526
- sludges and slurries, aqueous effect of freeze/thaw treatment on precip. 2−84807
- solid-in-liquid non-Newtonian viscometry, translating or rotating cylinder 2−71168
- solid-liquid-vapour system, medium effects on interfacial energy 2−60519
- spectra, link with solid state spectra through weak absorption 2−53460
- spectral density, random field, concentration fluctuations 2−83810
- spherical cells with compressible elastic membrane, bulk modulus calc. 2−67847
- stainless steel with Al_2O_3 dispersoid, prep. of thin foils for transmission electron microscopy 2−80549
- statistical props. of conc. in disperse systems 2−83435
- Stokes flow in and around fluid sphere in presence of another sphere or plane boundary 2−80164
- tetrahymena culture systems, bioconvective fluid instabilities 2−77451
- thermal diffusion, 2-current approx. analysis of kinetics 2−49179
- three-phase flow, vertical, one-dimensional theory for predicting average hold-up 2−67606
- titanomagnetite, magnetic characteristics rel. to palaeomagnetism 2−58139
- transient mass transport of sphere in finite volume of homogenized fluid 2−46990
- turbid water, multiple scattering of laser light 2−43391
- turbidity spectrum, determ. of size and refractive index of particles 2−43399
- turbulent combustion processes, acoustic noise generated by, analytical results 2−69774
- van der Waals forces between immersed particles 2−60516
- van der Waals interactions between macroscopic bodies having inhomogeneous dielec. susceptibilities 2−74561
- water droplets produced by u.s. 2−71241
- zircaloy-2 with Y_2O_3 dispersoid, prep. of thin foils for transmission electron microscopy 2−80549
- $Al:Al_2O_3$, dispersion-hardened prep. of thin foils for transmission electron microscopy 2−80549
- $Fe:Al_2O_3$, dispersion hardened, prep. of thin foils for transmission electron microscopy 2−80549
- Li dispersion in vaseline, r.f. Faraday effect 2−43410
- Pt dispersed electrode, electrochemical activity 2−45656
- $Zr:Y_2O_3$, dispersion hardened, prep. of thin foils for transmission electron microscopy 2−80549

Dispersion, acoustic
- effects on cross correlograms 2−55517
- cyclotron waves in plasma 2−67673
- geometric spreading loss, invariance with changes in ray parametrization 2−55524
- liquid and solid aerosols 2−74569
- in multicomponent fluid systems near critical point 2−67574
- Navier-Stokes eqn., modified, consequences in sound dispersion 2−53130
- ocean waters, coastal, sound-speed dispersion and fluctuations 2−44661
- piezoelectric plates $PbTiO_3$, $BaTiO_3$, ZnO, CdS, $Pb(Ti, Zr)O_3$, flexural modes 2−84205
- Rayleigh waves, crustal structure of Bahama platform 2−65546
- solid waveguides, dispersion relations in normal modes 2−66624
- sound velocity in mag. field at low temp., meas. 2−61092
- InSb, dispersion relations, meas. by heat-pulse technique using supercond. bolometer 2−80911

ultrasonic
- carboxylic acid series, velocity dispersion 2−71192
- fibre reinforced composite, stress wave dispersion 2−47743
- nitrobenzene-n-hexane binary mixture near critical point, meas. in 5-55 MHz range 2−71196
- polymethyl methacrylate, epoxy formulations, u.s. dispersion, acoustic characterization 2−80905

Dispersion, optical
- *see also Optical constants; Refractive index/light*
- air, i.r. 2−60376
- atmospheric dispersion of telescope images, automatic compensation 2−48825
- calcite, infrared dispersion parameters determination from reflectivity, Kramers-Kronig relations and damped oscillator theory 2−57322
- chlorinated polyethylene supramolecular structures morphology 2−50413
- classical theory recapitulated 2−73632

Dispersion, optical continued
- controllable dispersion interference-polarization filter, design method 2−66845
- dialogite, infrared dispersion parameters determination from reflectivity, Kramers-Kronig relations and damped oscillator theory 2−57322
- dielectric thin film, interference method for meas. of dispersion in refractive index 2−44342
- dolomite, infrared dispersion parameters determination from reflectivity, Kramers-Kronig relations and damped oscillator theory 2−57322
- dyes, semicolloidal solns., intense light 2−50360
- f.c.c. cryst., antiferromag., by magnons 2−61550
- ferrite garnets, distribution of electromagnetic waves near compensation temp. 2−65211
- fibre dispersion meas. using a mode locked Kr laser 2−79235
- fibre dispersion meas. using self pulsing GaAs laser 2−79233
- focused unstable laser beams, wind, thermal distortion effects 2−82520
- forces of oscillats,meas. by more sensitive method of ‘hooks’ 2−49928
- gases, non-linear optical obs. 2−71117
- in hard dielectric film optical waveguides 2−42238
- Kerr liqs., optical filaments, pulse distortion, optical shock, dispersion effects 2−79234
- Kramers-Kronig dispersion anal. method for obtaining optical indices from i.r. transmittance data 2−73643
- mixed polymers of diethylene glycol- bis-allyl carbonate and isophthalic acid diallyl ester, with controlled optical refraction and dispersion 2−55752
- molecular band intensity, fringe shift and fringe slope band analysis procedures 2−49992
- polymethylene dyes, laser pulses 2−49377
- refractive index measurement by interference microscopy and corrections for dispersion 2−70016
- resonance dispersion and Faraday rotation in self induced transparency 2−44324
- Runge mode-locked dye laser, dispersive explanation of spectral behaviour 2−66758
- Siderite infrared dispersion parameters determination from reflectivity, Kramers-Kronig relations and damped oscillator theory 2−57322
- smithsonite, infrared dispersion parameters determination from reflectivity, Kramers-Kronig relations and damped oscillator theory 2−57322
- theory, rel. to light shifts 2−76979
- turbid medium, rel. between optical parameters and dispersion indicatrices 2−73641
- visual photoreceptors, light absorpt. rel. to anomalous dispersion 2−82062
- $AgGaS_2$, i.r. dielectric dispersion 2−44364
- $Ba_2NaNb_5O_{15}$, far-i.r., room temp. reflectivity spectrum analysis 2−68622
- GaSe single crystal, anomalous dispersion study by Rozhdestvenskii hook method 2−78099
- $LiNbO_3$ spontaneous parameteric scattering, idler absorption and dispersion 2−44337
- NO-$\gamma(A^2\Sigma$-$X^2\Pi)$ system, oscillator strength of (0,0) band, meas. technique 2−50062
- TiC-TiN solid solution, 0.6-5.5 eV, band struct. determ. 2−51080

Dispersion relations
- *see also Field theory, quantum; S-matrix theory*
- Cerenkov radiation of moving test particle in magnetoplasma 2−80250
- charged particles elastic scatt. from nuclei low-energy forward relations 2−67205
- circular waveguide, relativistic dispersion eqn. for rotating tubular beam under space charge conditions 2−82396
- cold magnetoactive plasma, low-freq. potential oscills. in field of e.m. wave 2−80349
- Coulomb T matrix 2−76972
- cut to cut extrapolations and weighted relations 2−42295
- dielectric wedge, electrostatic edge modes 2−84363
- dipole gas, kinetic equation 2−80415
- E-region ionosphere dispersion, Antarctic obs. 2−62370
- e.m. wave interaction with radially divergent electron beam 2−49327
- e.m. waves in random nonlinear dispersive medium 2−73622
- ferromagnet, associated magnetoelastic waves, dispersion laws and polarization 2−57294
- fixed-t, in πN change-exchange scattering 2−63624
- flow, plane parallel convective, oscillatory instability 2−83472
- fluid, surface and internal waves in inhomogeneous ocean 2−81636
- gravitational waves 2−73295
- gravity wavefield, random, nonlinear relation 2−54784
- hadron dynamics interpret., composite theory 2−52576
- hard sphere gas, hydrodynamic disturbances, nonanalytic dispersion relations 2−66477
- hot magnetoplasma with collisions 2−50192
- isotropic turbulence, angular dispersion of fluid line element 2−80170
- iterative evaluation for determ. of analytic continuation of scattering amplitudes 2−59396
- Kramers-Kronig relations and sum rules 2−82646
- linear waves in geophys. fluids 2−54785
- longitudinal plasma waves in h.f. electric field 2−46785
- magnetoplasma, v.l.f. waves 2−50197
- magnetoplasma containing negative ion, dispersion characteristics for Lorentz, Cauchy and Maxwell distribs. 2−80229
- magnetoplasma waves in strongly curved configurations 2−70953
- mass-dispersion, and broken scale invariance 2−66911
- meson scatt., partial wave relations from fixed-u dispersion relations 2−59505
- meson-meson low energy interactions, inverse amplitude dispersion relns. 2−82733
- modification due to piecewise-analytic scattering amplitude of indefinite-metric quantum field theory 2−63457
- moving striations in laser discharge tubes 2−77314
- multipole expansion of retarded interatomic dispersion energy, derivation from quantum electrodynamics 2−49935

Dispersion relations continued
nonlinear dispersive wave problems, multiphase modes 2−52037
nuclear spectroscopic factors determ. 2−67127
optimized data extrapolation off the boundary of an analytic function 2−49475
partial wave, with Kantor amplitude, analysis of nucleon-nucleon scatt. 2−55873
particle velocity dispersion in magnetic field of prism spectrometer 2−73521
periodic structures 2−49198
plasma, bi-Maxwellian, numerical solution 2−80330
plasma, collisional, scattering function 2−50191
plasma, dispersion of longitudinal electric waves rel. to photon rest mass 2−55073
plasma, He^+/He_2^+, electron drift-excited ion-acoustic waves 2−67684
plasma, ion wave propagation, perpendicular longitudinal, effects of collisions 2−56370
plasma, Landau's dispersion equation, asymptotic soln. 2−56374
plasma, relativistic Vlasov, self-consistent e.m. waves 2−70904
plasma, threshold of ionization instability in unbounded low temp. plasma 2−46788
plasma drift waves 2−53226
plasma echoes, numerical simulation 2−70954
plasma surface waves 2−53227
plasmas, ion motion and return currents 2−56376
plasmons, prop. in periodic lattices 2−77803
radiowave reflection from ionosphere, ground pattern irregularities, obs. 2−78390
rectangular waveguide in nonhomogeneous plasma, modelling of dispersive propagation of symmetric magnetic waves 2−83534
resonance saturated fixed-t, used in improvements to static model for πN and $\pi\Delta$ elastic scattering 2−42399
seismic surface waves in ice cap 2−81573
sidewise, consistent resonance dominance of form factors 2−70121
solids, surface plasmons, microscopic theory 2−84277
two-body scattering, transverse momentum for fixed s 2−49491
unsubtracted, for baryon e.m. mass differences 2−76705
waves, nonlinear weakly dissipative 2−58715
weighted and cut-to-cut extrapolations 2−63570
$e\mu$ scattering, invariant amplitudes and double dispersion relations 2−45884
$\gamma \rightleftharpoons rp\pi^-$, in 33 resonance region, dispersion relation predictions 2−52550
KN, modified dispersion relation, constant scattering length parametrization 2−49557
Kp, model independent calculation 2−79569
K^+p, backward dispersion relations 2−45946
K^+p elastic scattering below 1.3 GeV/c, partial-wave dispersion relation analysis 2−52609
K^+p partial wave dispersion relations, role of ε exchange 2−63597
K^+p scatt. below 1.3 GeV/c 2−55848
K^+p scattering, study of phase shifts for consistency with backward dispersion relations 2−52608
$N^{**} \to N^*\gamma$, sum rules for isovector e.m. transition moments, derivation using combined back and forward dispersion relations 2−49601
π, photoproduction, s-plane invariant amplitudes for evaluation of t-channel singularities 2−63504
π^0 electroproduction in resonance region, dispersion relation calculation 2−55851
πN, dispersion relations, soln. by Pade approximant method 2−49569
πN form factor, corrections to Goldberger-Treiman relation 2−59530
πN resonance, dynamics, review 2−46015
π^-p forward elastic scattering near 1 GeV/c, comparison of predictions with expt. 2−73823
$\rho\pi\pi$, $A_1\rho\pi$ coupling constants, determination using collinear dispersion relations 2−63639
$^4He(p,p)He$ elastic scatt. below 50 MeV, forward dispersion relation 2−67205
InSb, dispersion near band gap nonlinear susceptibility and second harmonic generation, model 2−44334
N, threshold dominated relations for form factors, rel. to mass radius 2−52631

Dispersions *see Disperse systems*

Displacement measurement *see Length measurement; Strain gauges*

Dissociation
see also Decomposition; Heat of dissociation; Ionization; Molecules/dissociation
electrode, during impulse discharge 2−64343
gas flow, variation of flow quantities along streamlines 2−43236
gases, asymptotic behaviour of the external fringes of compressible laminar boundary layers 2−67698
metastable ions, determ. of lifetimes by field ionization mass spectrometry 2−46789
photodetachment of electrons from major negative ions 2−78403
polyatomic gas, influence of dissociative recombination on spectral sharpness 2−60297
rare earth tetraborides, thermal stability 2−53995
spiropentane, energy nonrandomized decomposition initiated by recoil T substitution reactions 2−81533
C_2-exchange reactions of gaseous dicarbides of rare earth metals 2−65359
CO, on W, dissociative chemisorption, field emission microscope obs. 2−71355
CO_2, on W(100) surface, flush desorp. mass spectrometry obs. 2−50551
CO_2 MHD laser, ionization instabilities and discharge characteristics 2−79207
CaH_2-LaH_3 system, dissoc. press., temp. and comp. depend. 2−50958
CdO, dissociation and form. equilib. const. from saturation v.p. temp. depend. 2−75371
H_2, in cool supergiants, equilibrium 2−62499
$H_2O^+(H_2O)_n$, photolysis in range 5800 Å to 6100 Å 2−84679
NH_3 photodissociation, separation of N and H isotopes 2−43198
O_2 photodissociation rates in mesosphere in lower thermosphere 2−65830
Pt electrode on alkali-containing glass, model of electrode 'polarization' by d.c. potential applic. 2−81141

Dissociation continued
SF6, current interruption, gas circuit breakers 2−74489
Sb_2S_3, dissoc. energy determ. 2−74595
Sc monoauride, rel. to bond energy calc. for Sc diatomic intermetallic 2−50557
SiO, dissoc. energy determ. from $Ge + SiO \rightleftharpoons GeO + Si$ study 2−72548
Y monauride, rel. to bond energy calc. for Sc diatomic intermetallic 2−50557

electrolytic
see also Ions; Electrolytic
galvanoluminescence cathode glow described 2−77305

Dissolution *see Solubility; Solutions*

Distillation
see also Isotope separation
fractionation effects on polymer crystal growth, dilute soln. theory 2−81501
multi-component column design, nonideal phase equilibria data prediction 2−75361
multicomponent vapour-liquid equilibrium data computation 2−74589
vacuum devices, packings, comparative separation performance 2−45196
vapour-liquid, multicomponent separation calculations, modified Newton's method 2−68756

DNA *see Macromolecules*

Domains
p-n-alkoxybenzoic acid, periodic oriented oscillations of domain struct. in alt. elec. fields 2−71159
alloy, AuCu-ype, breaking through of dislocations across domain boundaries, activation energy 2−56692
anti-phase domain mats., X-ray diffraction theory 2−67973
antiferromagnetics, uniaxial, parity effect, 90° model 2−68536
antiferromagnets, biaxial domain structure in tilted mag. field 2−81306
Bloch walls, cold neutron diffraction, nonelastic scatt., macroscopic anal. 2−51248
boundary deformation in magnetic field with transverse bonding 2−68537
boundary displacement under deformation, effect of dislocations 2−72143
bubble and strip, dynamics rel. to wall mobility and wall coercivity 2−61506
bubble domain materials, wall mobility and velocity saturation 2−81221
bubble garnets, magnetiz. reversal due to annealing 2−51253
conductivity of ferromagnets, infl. of domains 2−72147
copolymers, A-B type, domain formation mechanisms 2−57419
copolymers, amorphous blocks cast from soln., domain struct. 2−83848
cylindrical, dimens. in presence of wall coercivity and wall energy anisotropy computer studies 2−81232
dicalcium strontium propionate, ferroelectric 180° domain struct., electron mirror microscope obs. 2−65060
$Fe_{36}Cr_{22-x}Ti_x$, χ-phase alloy, $8<x<10$, inversion domain obs. 2−64637
ferrimagnet, hysteresis loop, wall displacement and bulging in magnetization mechanism 2−65167
ferrite discs, resonance phenomena in presence of domain structure 2−68714
ferrite epitaxial films, prep. for mag. bubble domain memories 2−72192
ferroceramics, microstruct., domain struct. 2−53925
ferroelectric, second harmonic scatt., domain shape effects 2−82508
ferroelectric, transverse acoustic wave reflection, influence of piezoelectric effect 2−74982
ferroelectric domain structures, phase transition, scanning electron microscope 2−57240
ferroelectric switching, domain wall motion kinetics, general formulation 2−72025
ferroelectric switching, nucleation model for sidewise wall motion, validity for TGS 2−72041
ferroelectrics, domain structure, temp. effects, scanning electron microscope obs. 2−81132
ferroic crystals and ceramics, effect of lower order couplings 2−57238
ferromagnet, domain struct., calc. for various types of anisotropy 2−81270
ferromagnet, dynamic effects, nucl. paramag. reson. 2−61488
ferromagnet, periodic distrib. of magnetization, theory 2−81222
ferromagnet, rel. to dislocation theory of energy loss during mag. reversal 2−72144
ferromagnet, uniaxial, Bloch wall mag. moment, domain width depend. 2−57281
ferromagnet, uniaxial, domain width thickness depend., theory 2−65145
ferromagnetic, electron images of two-dimensional domain walls 2−51247
ferromagnetic, motion, from Landau-Lifshitz-Gilbert equation 2−48059
ferromagnetic film, band periodic domain struct., spin wave spectrum 2−72183
ferromagnetic film, Lorentz microscopy and spatial filtering 2−48088
ferromagnetic film, polarization of domain boundaries of Neel type 2−57297
ferromagnetic film, stripe-domain width, longitudinal field intensity depend. 2−57296
ferromagnetic film, supercrit. props. of stripe structs. 2−61520
ferromagnetic film, theory of wall mobility 2−78031
ferromagnetic films, electron microscopy of magnetic structure, review 2−84428
ferromagnetic plate, in mag.field, ground state and phase transition 2−72159
ferromagnetic resonance, domain wall structure effect in films 2−68717
ferromagnetic superconductor, micromagnetic theory 2−77870
ferromagnetics, weak, parity effect 2−68536
film, Bloch walls, interacting, transversal shift 2−72181

Domains continued
film, cross-tie-Neel domain wall transition, hysteresis change, in mag. field 2−48090
film, domain wall parameters from Lorentz electron microscopy 2−72182
film, ferromagnetic, with periodic banded domain structure, spin wave spectrum 2−68553
film, magnetic domain boundary creep, thickness and props. influence 2−72179
film, subject to quasistatic reversal, influence of domain structure on SHF susceptibility 2−68554
formation in crystals, geometrical aspects 2−68021
garnet film, epitaxial, magnetic bubble mobility measurement 2−57303
garnet mag. films, domain interaction with laser beams, domain writing 2−75230
garnet multilayer epitaxial films for magnetic bubble devices, hard bubble suppression 2−65162
garnets bubble films, elimination of hard bubbles by second magnetic layer 2−65164
half-bubble static stability, equilibrium properties, variational model 2−84391
hardening, statistical problem, Bloch wall motion and pinning 2−68125
high anisotropy multi-domain particles, magnetization reversal 2−44243
insulating ferroelectric crystals, surface potential variation with scanning electron microscope 2−81157
irreversible displacement phenomena in cylindrical ferromagnetic, Barkhausen effect meas. 2−81227
liquid crystal, nematic film, wall motion 2−74521
magnetic, and appl. 2−81262
magnetic, materials for domain wall devices, review in book 2−57282
magnetic bubble, twisted wall structure in films, variational method calc. 2−72142
magnetic bubble in uniaxial mag. sheet, stray fields calc. 2−45668
magnetic bubble materials, cryst. growth 2−47199
magnetic bubbles, domain-wall config. 2−78009
magnetic bubbles, hard, dynamic props. 2−78010
magnetic bubbles, materials, properties, applications, review 2−78035
magnetic domain-wall mobility, Bloch line effects 2−78011
magnetic film, wall mass and crit. velocity calcs. 2−68558
magnetic garnet films, hard bubble suppression by ion implantation 2−65163
magnetic reversal in magnetically hard ferromagnetic substances, investigating method 2−54322
magnetic thin uniaxial film, stripe-domain config., magnetization and thickness determ. method 2−68559
magneto-optic and domain wall device materials, review in book 2−57282
magneto-optical diffr. at periodic mag. structs. 2−61590
manganese spinels, domain formation due to atomic displacements 2−68021
p-methoxybenzilidene p-n-butylaniline, nematic phase, relationship with anomalous alignment 2−71161
Neel wall in stray fields, wall creeping mechanism 2−61522
Permalloy field access bubble domain drive ccts., magnetostatic pot. wells, drive fields, meas. technique 2−73507
permalloy film, changes in domain structure during pulsed a.c. magnetization, thermofluctuational character 2−68556
Permalloy film, cross-tie walls, motion threshold field and behaviour at inhomogeneities 2−77994
Permalloy film, oxidized, slow domain wall motion 2−54340
Permalloy films, l.f. slip of domain boundaries 2−61528
Permalloy films and perfect monocryst. laminae, stripe struct., magneto-optical obs. 2−61531
Permalloy films with supercrit. hysteresis loop, stripe struct. 2−61532
Permalloy plated-wire memory, electron microscope obs. 2−75231
permalloy supercritical films, banded domain structure 2−68557
Permalloy thin wires, Bitter pattern obs. 2−61535
Permalloy-SiO- Permalloy multilayer systems, stripe domain struct. 2−61530
phase transformations, rel. to elastic constants and the ΔE effect 2−77664
piezo-semiconductors, waveguide effect of surface domains 2−54029
piezoelectric semiconductor, moving acoustoelectric domain nucleation 2−68237
piezosemiconductor, fluctuating elec. field and Franz-Keldysh effect inside domains acoustoelec. domains 2−54033
piezosemiconductor, narrow propagating domains of acoustic flux, prod. method 2−43978
platelet, uniaxial, criteria for magnetostatic behaviour 2−81250
PLZT ceramics, crystal structure and enhanced ordering of ferroelec. domains 2−80760
polydomain ferromagnets, singularities of elastic and inelastic scattering of neutrons 2−81226
polyethylene doped with I, Gunn type oscillations 2−57202
pyroxene, lunar and terrestrial minerals antiphase, polymorphic transformation on cooling 2−62689
pyrrohotite, formation rel. to structural vacancy ordering 2−68021
Q bubble materials, interacting Bloch lines, wall energy mechanism 2−72141
rare earth iron garnet, damping of domain wall motion 2−57304
rare earth orthoferrites, domain size during phase transform. 2−81291
semiconductor, elec. domain, nL criterion 2−51133
semiconductor, Poisson and transport equations, high field domain solns. 2−54167
$SmCo_5$ spacing at low temps. 2−51250
steel Fe-Si, domain struct. rel. to demagnetizing field freq. 2−84412
structure, effect on thermodynamic parameters near Curie point 2−72146
structure, one-dimensional antiphase, interpretation with non-integral half period 2−53625

Domains continued
structure in presence of magnetic fields, e. microscope investig. 2−68503
symmetry props. of transform. twins, ferroelec. and ferromag. domains 2−77522
transformer steel, effect of induced magnetic anisotropy on magnetic properties and domain structure 2−68539
triglycine sulphate, irrad., domains, electron microscope exam. mats. 2−65067
triglycine sulphate, reshaping of ferroelec. domains after heat treatment 2−54234
triglycine sulphate, second-harmonic scatt., domain shape effects 2−82508
triglycine sulphate, vanadyl-doped, domain struct. changes, e.p.r. obs. 2−77937
triglycine sulphate pyroelectric detector, laser study of nucleation sites 2−44165
wall movement retardation, due to interaction with dislocations 2−68540
wall movement retarded by interaction with dislocations 2−68540
9 Al_2O_3-AlN, periodic antiphase domain struct. 2−50618
$BaTiO_3$, abnormal birefringence due to lamellar domains 2−81128
$BaTiO_3$, ferroelec., relaxation rel. to light emission due to uniaxial stress pulses 2−72440
$BaTiO_3$, ferroelec. domain studies by scanning electron microscopy 2−47983
$BaTiO_3$, phase transitions, domain interactions 2−61427
$BaTiO_3$ film, polarization change, stroboscopic elec. microscope obs. 2−75149
$BaTiO_3$ single crystals influence of the amplitude of free vibrations on the permittivity 2−81154
$BaTiO_3$ surface, ferroelec. struct., photoemission microscopy obs. 2−61428
C, isotropic pyrolytic, formed below 1500° C., crystallite orientation in μ-sized optic domains annealing 2−61022
CdS, acoustic domains, optical modulation 2−61088
CdS, Brillouin scatt. from longit. acoustoelec. domains 2−43974
CdS, h.f. propagation, two-dimensional charact. 2−51156
CdS high-field domains, propagation characteristics 2−61099
Co, domain wall movement retarded by interaction with dislocations 2−68540
Co, electron images of two-dimensional domain walls 2−51247
Co, mag. domains, electron microscope obs. 2−44262
Co, magnetization process, h.v. electron microscopy 2−84402
Co film, epitaxial growth and mag. domain config. 2−61524
Co wall movement retardation, due to interaction with dislocations 2−68540
$CoFe_2O_4$ films, monocryst., domain struct. and mag. polarity reversal 2−61523
Cr, antiferromagnetic, Q-switch and polarization domains, obs. with neutron diffraction topography 2−65179
Cr, magnetic struct. intensity, temp. hysteresis, sign change 2−54328
Cu-Pd alloys, influence of domain size and ordering on mech. props. and elec. resist. 2−68506
Dy_3Al_2, DyCoNi, magnetic after effect associated with narrow domain walls 2−54318
$Dy(Co,Ni)_2$, intrinsic mag. aftereffect 2−44274
$ErFeO_3$, with high coercivity surface layer, domain struct., magnetooptical study 2−81284
Fe-Co layers with intermediate LiF layer, electron microscope study of interacting interdomain boundaries 2−61534
Fe-Ni alloy film, domain boundaries, energy of stabilization 2−57300
Fe-Ni alloy film, rel. to elastic stress effects on crit. field 2−51264
Fe-Ni film, structure, influence of temp., elec. microscope obs. 2−72185
Fe-Ni single crystals, Kerr effect obs. 2−78017
Fe-Si, domain width, sample thickness and cryst. orientation depend. 2−48061
Fe-Si, Neel lines, magnetooptic Kerr effect obs. 2−78014
Fe-Si, obs. of domain changes under cyclic tensile loading for specimens in remanent cond. 2−65147
Fe-Si alloy, ferromag. domain spatial replication, anisotropic decomp. struct. 2−72149
Fe, electron images of two-dimensional domain walls 2−51247
Fe, freq. spectrum of Barkhausen noise 2−61515
Fe film, asymmetric 180° domain walls, Lorentz microscopy obs. 2−48092
Fe film monocrystalline, inter-domain boundaries 2−61533
Fe wall movement retardation, due to interaction with dislocations 2−68540
Fe whiskers, mag. stray fields of 180° Bloch walls, Permalloy probe study 2−78015
$FeBO_3$, amplified n.m.r. signal from inside domains 2−68745
Fe_3C, mag. domains, electron microscope obs. 2−44262
FeSi, electron images of two-dimensional domain walls 2−51247
Fi-Si sheet Goss-oriented, elastic properties rel. to magnetostriction 2−53778
GaAs, acousto-electric, origin and properties 2−54034
GaAs, acoustoelectric, elec. and optical props. 2−80912
GaAs dielectric-surface-loaded elements, high field domain propagation 2−51141
n-GaAs diodes, high-resist., high-field domain propag. 2−54220
$(Gd,Tb,Eu)_3Fe\ O_{12}$ ferrite garnet, optical anisotropy and cylindrical domains 2−68602
GdFe garnet, bubble domains, flux switching 2−57305
Gd_2MoO_4, det. of thickness of walls by Raman scattering 2−72366
$Gd_2(MoO_4)_3$ diffracted light obs. from domain wall 2−84467
GdTbFe garnet cylindrical magnetic bubbles, properties 2−65169
Ge, electron irrad., 8.5MeV, high field domain instability 2−57208
α-GeTe, domain struct., twin and interface boundary interface types 2−72150
GeTe film, superstruct. and domain struct., electron microscope obs. 2−80574
InSb, acousto-electric, origin and properties 2−54034
InSb, Gunn domain formation rel. to contact effect on microwave emission 2−47897
n-InSb, Gunn effect threshold in transverse mag. field, travelling domain form. 2−71908

Domains continued
- n-InSb, magnetoacoustoelectric effect, acoustoelec. domain form. and instabilities 2−64850
- KD_2PO_4, domain wall mobility, temp. depend. 2−71740
- KD_2PO_4, u.s. stress wave interaction with domain walls 2−71740
- $KH_{2(1-x)}D_{2x}PO_4$, domain contrib. charge to dielec. constant value in ferroelectric phase 2−84364
- KH_2PO_4, dense domain structure at ferroelectric transition, stress-induced birefringence 2−75260
- KH_2PO_4, molecular dynamics study and ferroelec.-antiferroelec. transitions by NMR and dielec. relax. 2−72032
- $KNbO_3$, ferroelec., mech. switching of domain walls 2−44160
- $KNbO_3$, ferroelectric domain investigations using pseudocubic {001} cleavage planes 2−61429
- $Li_{0.5}Fe_{2.5-x}Al_xO_4$, magnetization process, domain wall reson. study 2−72198
- $Li_{0.5}Fe_{2.5}O_4$, reson. phenomena at moving domain boundaries 2−72456
- $LiNbO_3$, ferroelec. domain struct., growth 2−65063
- Mg-Mn ferrite film, transparent, light diffraction by mag. stripe domains 2−65220
- MgO cleavage face, elec. field domains, rel. to LEED pattern 2−60627
- Mn-Al-Ge alloy, nucleation centres and hysteresis 2−68550
- Mn-Bi alloy, nucleation centres and hysteresis 2−68550
- Mn-Bi films, intermediate cpds., polarization microscope images 2−57301
- MnBi film, domain struct. 2−44263
- $Mn_{1.92}Cr_{0.08}Sb$, Bitter pattern technique obs. 2−65148
- $MnFe_2O_4$, reson. phenomena at moving domain boundaries 2−72456
- $MnO\text{-}Fe_2O_3$ single-crystal films, static and dynamic domain structure 2−68561
- $NbTe_2$, domain formation due to atomic displacements 2−68021
- $NbTe_3$, structure and dislocation config. 2−60804
- NdS, antiferromagnet, domain struct. obs. 2−81307
- Ni-Co alloys, magnetic structure during electrodeposition in presence of magnetic field 2−77995
- Ni-Fe, f.c.c., domain struct. after different annealing treatments, Kerr effect obs. 2−78016
- Ni-Fe alloy films, open stripe struct. model interpret. of mag. props. 2−61538
- Ni-Fe film, wall mobility, rel. to field and freq. depend. of coercive force 2−78033
- Ni-Fe films, polycryst., edge anisotropy 2−61527
- Ni-Fe films, wall creep, effects of fields, film thickness 2−77993
- Ni, ferromag. domains, anisotropy of depolarization of neutron beams 2−61509
- Ni, mag. domain struct. after plastic deform. 2−44244
- Ni ⟨110⟩ single cryst., domain struct., rel. to n.m.r. 2−78173
- Ni domain wall movement retardation, due to interaction with dislocations 2−68540
- Ni magnetic domain walls, 180°, tilted, struct. from Lorentz electron images 2−72151
- Ni wall movement retardation, due to interaction with dislocations 2−68540
- $NiFe_2O_4$, reson. phenomena at moving domain boundaries 2−72456
- Ni_3Mo, antiphase boundary configurations 2−68021
- Ni_4Mo, structure and types of interfaces 2−68021
- Pb, supercond., Landau domain struct., motion induced by electric transport current 2−75074
- $Pb_5Ge_3O_{11}$ single crystal, ferroelec. optical rotation domains 2−44164
- $PbTiO_3$, plate-like growth and exam. of domain struct. 2−71398
- SbSI, ferroelec. semicond., influence of nonequilib. carriers on domain struct. 2−72036
- SbSi, naturally polarized crysts., photodomain effect on illumination 2−77940
- Si-Fe laminations, dynamic ferromag. domain wall response to a.f. field, rel. to eddy current losses 2−48062
- Si-Fe textured sheet, permeability, eddy current loss, angle and field depend. rel. to domains 2−65153
- $SrTiO_3$, uniaxially stressed, domain struct. at 2K 2−61433
- $TmFeO_3$, orthoferrite, domain struct., effect on mag. field 2−57306
- $V_{2-x}Cr_xO_3$, form. during Mott metal-insulator transition, geometry and crystallography 2−71785
- VO_2 switching device, influence of high-conducting bubble 2−54208
- $Y_{3-x}Eu_xAl_yFe_{5-y}O_{12}$ films, epitaxial, characteriz. for bubble devices 2−61541
- $YFeO_3$, intrinsic domain-wall damping 2−65176
- $YFeO_3$, with high coercivity surface layer, domain struct., magnetooptical study 2−81284
- YIG, hysteresis loop, wall displacement and bulging in magnetization mechanism 2−65167
- YIG, laser beam diffraction 2−44348
- YIG, light-induced Bloch wall pinning 2−48060
- YIG, reson. phenomena at moving domain boundaries 2−72456
- YIG garnet, sound wave absorpt. effects, magnetoelasticity, domain wall motion 2−61097
- YIG single crystal film, domain wall mobility meas. by light diffraction 2−84434

Domains, antiphase *see Alloys; Crystal structure/microstructure; Solids/structure*

Doping *see Crystal electron states/impurity states and effects; Crystal imperfections/impurities; Semiconducting materials; Semiconductors*

Doppler effect
- acoustic, sound field of sources in motion 2−73422
- acoustic holography 2−69979
- anomalous, in medium with wave phase velocity exceeding velocity of light 2−78776
- aurora, Doppler radar signatures 2−58069
- blueshifted absorption lines of Fe I in type I supernovae 2−75765
- broadening of spectral lines as indication of temp. of upper atmos. 2−72816
- 3C 279 radiosources, at hypervelocities 2−78482
- driven Doppler line, spontaneous emission 2−42833
- Fabry-Perot spectrometer adjustment for compensation of Doppler shift from rapidly rotating and flowing sources 2−70081
- flow meas., laser velocimeter 2−83510

Doppler effect continued
- gamma-rays scatt. from atomic electrons, student demonstration of electron velocity in atom 2−78722
- gas, spectral line shapes, kinetic theory, transition between Doppler and collision broadening 2−64091
- gas velocity meas. technique 2−83690
- ionosphere, backscatt. obs. of nighttime maintenance 2−58094
- ionospheric topside electron temp. determ. from Doppler splitting of diffuse resonance 2−62355
- laser anemometer, automatic data processing system 2−84789
- laser beam, remote sensing strain-rate meter 2−84148
- laser Doppler velocimeter, for MHD boundary layer studies 2−80217
- laser Doppler velocimeters, unified analysis 2−62958
- laser velocimeter, factors affecting accuracy 2−45220
- lunar motion, errors, lasers 2−84939
- metal, Doppler-broadened annihilation radiation spectra, electron effective mass 2−61216
- metal films in magnetic field, microwave absorption peaks due to Doppler-shifted cyclotron resonances 2−80941
- microwave transhorizon propagation, angle and Doppler spectrum obs. 2−54869
- moored temp. spectra, Doppler shift in frequency of inertial waves 2−81598
- nonrelativistic expressions, derivation without assumptions concerning plane wave phase 2−55376
- nuclear level lifetimes, apparatus for meas. 2−82794
- optical Doppler meas. of turbulent flow velocity 2−77236
- plasma instability and multiloop electron stream interaction with plasma 2−74400
- plasma osc. generation by beam-plasma interaction, light emission 2−70945
- plasma vel. meas. 2−64296
- positron annihilation in 29 elements, Doppler broadening obs. 2−68324
- radar, hail meas. 2−75578
- radar Doppler spectrum of meteorological echoes, uncertainties in coherent meas. of mean frequency and variance 2−75507
- radar obs. of wind gradients in convective storms 2−75560
- severe storms, with high reflectivity cores, Doppler radar obs. 2−75559
- shift, study of effect on perceived noiseness, computer analysis of data 2−66631
- shock and detonation waves, local vel. meas. by Schlieren interferometry of Doppler shifted laser light 2−63138
- space optics and time dilation 2−79433
- squall line, Doppler velocity obs. 2−75561
- structural materials of fast reactors, Doppler effect analysis 2−83104
- theoretical interpretations and experimental evidence 2−66659
- turbulence meas. using Laser Doppler Velocimeter system 2−71087
- TWERLE, TIROS-N, Doppler systems 2−62116
- underwater surface backscatter of acoustic waves 2−55532
- u.s. Doppler blood flowmeter, theory 2−85092
- u.s. Doppler technique for imaging blood vessels 2−62828
- u.s. flowmeter, vol. blood flow meas. 2−51901
- u.s. wave backscatter from rough water surface 2−68861
- velocity structure in interstellar H Doppler profiles rel. to spiral arm features 2−81818
- waveguide with density modulated electron beam pumped by strong field 2−69836
- $(AgBr + AgCl(5\%)):C^{5+}(N^{5+})(O^{6+})(S^{6+})$ high energy implantations, Doppler broadening of positron annihilation photons 2−71507
- $AgCl:C^{5+}(N^{5+})(O^{6+})(S^{6+})$ high energy implantations, Doppler broadening of positron annihilation photons 2−71507
- Au neutron Doppler effect studies in unresolved resonance region 2−67233
- Ba plasma, laser-generated, spectral line parameters 2−67643
- CO_2 laser, single-mode, Doppler Q-switching by rot. mirror 2−69914
- ^{50}Cr lifetimes of 9 states by Doppler shift attenuation method 2−76794
- Mg, A=24, 26 static quadrupole moment meas. via reorientation effect using Doppler-shift 2−74010
- Na, Doppler temp. meas. of D_1 line excited in N_2 afterglow 2−49951
- Ne, A=20, 22, static quadrupole moment meas. via reorientation effect using Doppler-shift 2−74010
- ^{28}Si, static quadrupole moment meas. via reorientation effect using Doppler-shift 2−74010
- ^{46}Ti, lifetimes of 9 states by Dopper shift attenuation method 2−76794

Dosimetry
- *see also Radiation monitoring; Radioactivity measurement; X-ray measurement*
- absorbed dose in lung and lymphonodes by inhalation of radioactive insoluble aerosols 2−55266
- absorbed exit dose from patient radiation exposure, film techniques 2−69413
- absorbed fractions for photon emitters within the body 2−55268
- accelerator beam flatness computer-aided evaluation 2−67103
- accident simulation with phantom, real neutron dose compared to badge meas. 2−52893
- adsorbed dose of fast neutrons, obs. using ionization and calorimetric methods 2−69380
- aerosol particles, primary deposition in human respiratory tract in relation to particle size, breathing parameters, region 2−55242
- albedo-type personnel neutron dosimeter 2−73208
- albedos of intermediate energy bremsstrahlung on reactor shielding materials 2−76958
- alpha source plane, simulating skin, microstructure of dose 2−85134
- angular dependence of dose and hadron yields from targets in extracted proton beams 2−46254
- application of resistivity of water under irradiation 2−69402
- for artificial heart pacemaker using ^{238}Pu energy source 2−51949
- beam flattening in moving field therapy with electrons 2−69438
- beta dose rate in vivo det. by in vitro meas. 2−66286
- betatron X-rays, 42 MeV, calc. of dose distrib. for treatment planning 2−69406
- body burden meas. by urine analysis for exposure in atomic energy operations 2−58627
- body organs, model for estimating space proton dose 2−58590

Dosimetry continued
- bone contamination by β emitters ^{89}Sr, ^{90}Sr, calc. of local and average doses 2−55265
- cell survival curves, damage and recovery 2−69327
- cellulose nitrate as rapid neutron dosimeter material 2−63709
- cerebral circulation, digital dynamic radionuclide studies, automatic analysis 2−76094
- clinical, temp. response of Si surface barrier semiconductor detector 2−69399
- clinical thermoluminescence, experience gained at Radiumhemmet, Stockholm 2−69429
- cobalt metabolism by normal human male, retention data 2−58589
- colorimeter for radiation dosimetry in WR-1 nuclear reactor 2−46396
- compensation for large irregular ^{60}Co fields in radiation therapy 2−69395
- complex dosimetry in radiotherapy using PDP8/I computer 2−69394
- dental X-ray dose obs. 2−69426
- depth dose calorimeter, for high intensity, l.v., flash X-ray machines 2−66285
- diagnostic radioisotopes procedures, obs. of radiation doses to children 2−69244
- dose delivered to rats' bone marrow by X-irradiation 2−58576
- dose distrib. obs. if field is larger than patient 2−69409
- dose effect and transmission curve, new aspects of interpretation 2−55299
- dose reduction, in X-ray fluoroscopy, use of scanning beams 2−69445
- dose-rate effects rel. to use of Cathetron ^{60}Co after-loading unit 2−69331
- electron, high energy, obs. using ionization chamber free of polarity effect 2−69397
- electron beam radiotherapy of entire skin 2−69440
- electron energy spectrum in water irradiated with 10 to 20 MeV beams 2−78649
- electrons with initial energies between 1 and 50 MeV, fluence, adsorbed dose and mass stopping power obs. 2−76961
- energy dependence of differential W-value of α-particles in tissue-equivalent gas 2−66283
- energy deposition produced by fast neutron irradiation in equivalent-tissue volumes 2−73182
- exoelectron, optical stimulation 2−68489
- by exoelectronemission 2−77974
- exposed dose units for X and gamma radiation, USSR state primary standard 2−76734
- exposure to natural radiation in USA, dose equivalent distribution 2−57803
- farmer dosemeter, design of thimble chamber 2−45049
- fast neutron personnel dosimetry, integral methods, survey 2−85129
- fast neutron personnel monitoring by fission fragment registration in ^{237}Np 2−79676
- fast neutrons, exposure estimation using direct counting ^{32}P in hair 2−85130
- fingers, skin and bone, dose from handling radioisotopes in a syringe 2−58621
- fission fragments, gas core nuclear rocket, lead shielding 2−85127
- fission track dosimeter monitoring of neutron flux incident on Ge(Li) detector 2−74191
- fractional cell survival rel. to depth of tissues exposed to high energy ions 2−69330
- Fresnel zone plate imaging 2−58583
- fundamental, current trends, review 2−69396
- gradients at material interfaces, meas. with thermoluminescent detector 2−82822
- gynecologic radiation therapy, dose distrib. by meas. and computer 2−69411
- health physics problems, book 2−73177
- health physics problems of instant contamination, 2nd European congress on radiation protection, Budapest (3-5 May 1972) 2−55219
- heavy particle radiation, nuclear emulsions and solid track detectors 2−46062
- helical scanning, computerized, location of radionuclides in human body 2−76099
- high energy electron beams, dose distrib. 2−69437
- high resistivity thermoluminescent dosimeter, operational evaluation 2−85081
- in-vivo, tissue equivalent semiconductor detector 2−46049
- incorporation measurements, dosimetric interpretations 2−52889
- integral recurrence relations for finite order scattering and transmission functions 2−76097
- internal contamination hazard involved in industrial application of nuclear tracer technique 2−58599
- internal contamination of patient caused by radioactive impurities in generator produced radionuclides, estimation of absorbed dose 2−55273
- internal contamination risk, influence on monitoring programmes 2−58628
- intrauterine monitor 2−76093
- ionization chamber construction and response, patient X-ray dose meas. 2−78667
- ionization chamber for γ-ray energy deposition meas. in nuclear reactors 2−42699
- ionization chamber in water phantom, control by direct connection to digital computer 2−69384
- ionizing radiation, using exoelectron emission obs. 2−70550
- irradiation doses due to tritiated pharmacological substances 2−55276
- irregularly shaped fields, central axis tissue-air ratios as function of area/perimeter at depth 2−66284
- isodose meter 2−69386
- isodose scanner, computerized 2−69355
- kapis shells as possible thermoluminescent dosimeter 2−82823
- lens opacification in mice, dose dependence of fast neutron RBE 2−78671
- LET spectra, obs. using detector of infinite slab shape, pulse height obs. 2−69398
- LET-spectra det. for gamma-neutron radiation with low efficiency counters 2−58622
- linear energy transfer analysis, algorithm 2−45051

Dosimetry continued
- low-temperature monitoring using thermoluminescent materials 2−67085
- luminescence, conference part II, Denmark, 1971 2−68675
- luminescence, third international conference, 1971 2−82819
- man, radiation dose from galactic cosmic rays 2−58595
- mantle, para-aortic and neutral axis radiation fields, errors in dosage calcs. 2−69405
- mathematical procedures for estimating dose from internally deposited emitter 2−55263
- medical dose rel. to Hiroshima and Nagasaki A-bomb doses 2−76100
- medical X-rays and population dose 2−58580
- metabolic processes induced by new radiopharmaceuticals on small animals 2−55223
- metaphosphate glasses, silver-activated, influence of base glass on radiophotoluminescence 2−57383
- mixed field of neutrons and photons, by aid of TLD system 2−42697
- modifying factors and dose equivalent in radiation protection 2−78646
- monitoring of external radiation, technical standards 2−56080
- neutron, Al_2O_3-CoO and MgO-CoO detectors 2−49684
- neutron, conference (Gatlinburg USA, Oct 1971) 2−49617
- neutron, practical fast systems 2−69392
- neutron, preparation of dosimeters for nuclear reactor applic. 2−49909
- neutron, research reactor, intensity obs. 2−70541
- neutron, using $FeSO_4$ 2−69390
- neutron, using solid-state detectors 2−69393
- neutron activation prediction program system 2−63947
- neutron and γ-ray personnel dosimeters at critical assemblies, comparison 2−67368
- neutron beam, obs. using CaF_2:Mn and ^{7}LiF thermoluminescent dosimeters 2−69382
- neutron beam intensity estimation, biological and medical applications 2−76079
- neutron dosimeter prep. for reactors 2−74187
- neutron dosimeters, high temp. preparation methods 2−73949
- neutron fields produced by d bombardment of Be 2−67320
- neutron radiation normalization 2−62871
- neutron radiation on human body, expt. with tissue equivalent substance 2−55239
- neutron using multisphere spectrometer for Pu-Be source 2−59878
- non-luminescent methods in solid-state 2−70308
- nuclear accident dosimetry meas. at Oak Ridge 2−52892
- nuclear power plant following reactor accident 2−67370
- nuclearly simulated reservoirs, radiological impact from use of contaminated neutral gas 2−56077
- organ and tissue burdens and doses resulting from acute and continuous exposure to radioactive aerosol 2−55277
- organ doses due to internal γ emitters, Monte Carlo calcs. and thermoluminescent measurements 2−55264
- organism transfer functions expressed in servomechanism theory, application to calc. of urinary excretion of inhaled nuclide 2−55221
- patient radiation protection, conference, Copenhagen, (1972) 2−69347
- pelvimetry, fluoroscopic polaroid technique for dose reduction 2−69446
- personal monitoring dosimeter characts. 2−70553
- personnel dosimeters, present status 2−85125
- personnel monitoring, application of luminescence methods 2−69428
- phosphate glasses, Ag-activated, beta rays 2−55927
- phosphors, thermally stimulated exoelectron emission and thermoluminescence 2−82821
- photoelectrons contribution to dose across bone-tissue interface due to x-irradiation 2−76098
- photoresistor characteristics, nuclear radiation detectors 2−82800
- polycarbonate films for 10-100 Mrad range 2−42700
- population exposure from planned or accidental releases of radioactivity to environment, estimation method 2−55298
- positron camera, MGH, medical use with, short-lived cyclotron produced radionuclides 2−69444
- proportional counter response versus Linear Energy Transfer 2−59609
- quantities and units in health physics 2−58625
- RAD radiation energy dose unit, extrapolation chamber construction 2−56079
- radiation, absorbed dose obs. in graphite using heat-loss-compensated calorimeter 2−67366
- radiation, in nuclear medicine 2−69427
- radiation energy dose unit, German agency of weights and standards 2−67080
- radiation exposure in manned spaceflight 2−51947
- radiation protection criteria and recommendations 2−76082
- radiation therapy, use of radiologic films 2−69416
- radiation therapy at AAPM radiological physics center 2−69324
- radioactivity of spring-waters in Hungary, dose originating from consumption 2−58634
- radiodiagnostic dose reduction 2−73201
- radiological treatment planning, compensation for tissue heterogeneity and contours 2−69414
- radionuclide meas. in body or excreta, calc. of dose 2−55269
- radionuclides, medically applied, effect on radioresistance of red blood cells, determ. of dose dependence 2−55237
- radiopharmaceutical, pediatric, diagnostic, procedures and radiation protection 2−69379
- radiophotoluminescent glass, high-sensitive and soil-insensitive, using u.v. N_2 gas laser 2−67094
- radiophotoluminescent glass, response to ^{60}Co γ and 10 to 30 MeV electron radiation 2−67095
- radiophotoluminescent glass dosimeters, formation kinetics of colour centres 2−67092
- radiophotoluminescent system, with fully automated data evaluation 2−67093
- radiotherapy depth dose scanning system electrometer amplifier system 2−69302
- radiotherapy dosage calculator 2−69408
- rat, major organs exposed to 4 X-ray energies 2−62873

Dosimetry continued
ratio circuit for plotting dose distribution in radiation field of 8 MV linear accelerator 2-59653
reactor, WR-1, flux density determination 2-83159
reactor accident, field radiological monitoring system 2-63979
reactor fuel radiation dose rates 2-59876
redistribution of internal exposure doses, effect of radio-deterioration procedures 2-55297
rodent phantom models, u.h.f. cavity exposure chamber, dosimetry 2-52003
scanning-be whole-body counter, design and evaluation 2-85080
shadow-shield whole-body counter calibration for use in psychiatric hospital 2-69422
skin, permissible exposure tested using relationship between absorbed dose, mithotical activity, chromosome aberrations 2-55230
skin surface doses from 4 MV linear accelerators 2-69385
solid-state and film dosimeters, fading kinetics at increased temps. and humidities 2-69403
spaceflight neutron, Ir and Ta foils 2-58147
specially collimated scintillation detector, reduction of extrathyroidal neck radioactivity 2-76095
specific absorbed dose and inhomogeneity 2-55267
standards in Germany 2-49912
telecentric electron pendulum irradiations 2-69439
teletherapy, optimization by regression methods 2-69410
thermally stimulated conductivity technique 2-69401
thermally stimulated exoelectron emission, use of open window G.M. counter and proportional counter 2-67090
thermally stimulated exoelectron emission dosimeters, use in exptl. and incorporational dosimetry 2-55300
thermoluminescence, for clinical use in radiation therapy 2-69430
thermoluminescence, non-linearity and LET effects of response, releasing probability change model 2-68697
thermoluminescence, with photon counting 2-49340
with thermoluminescence associated 2-42696
thermoluminescence dosimeter characts. as personnel monitor 2-70552
thermoluminescence from adhesive coated teflon tape 2-62872
thermoluminescent, det. of atmospheric contamination 2-62291
thermoluminescent, for automatic large-scale monitoring at Riso, Denmark 2-69433
thermoluminescent, in medical physics laboratory 2-73264
thermoluminescent, in vivo, clinical radiation therapy 2-69415
thermoluminescent, personnel monitoring 2-58620
thermoluminescent dosimeter, uniform extremely thin, manufacture by liquid moulding technique 2-67086
thermoluminescent dosimeter with digital readout 2-55924
thermoluminescent dosimeters, response to fast neutrons 2-85082
thermoluminescent dosimeters, responses in D$^+$ on Be neutron fields 2-69391
thermoluminescent dosimeters, TLD-700, response to protons and α-particles 2-81979
thermoluminescent dosimetry for dose meas. in hands of nuclear medicine technicians 2-73207
thin biological samples, electron irradiated 2-51946
thorotrast cases in Czechoslovakia, study of radiotoxicological effects 2-55238
timer error in patient daily dose 2-69418
tissue air ratio, backscatter and field size 2-73205
tissue doses, nucleons up to 30 GeV 2-63984
tissue-equivalent materials, freq. distribution of energy loss by protons 2-58624
underground uranium miners in USA, dose-effect relationship of radiation and induction of lung cancer 2-55240
wearable pocket noise dosimeter with digital readout 2-41826
whole body counting, γ-rays, Anger camera 2-78663
whole body counting systems, performance and applications 2-69419
whole body dose from absorption of inhaled noble gas, calc. 2-78661
whole-body counter with high sensitivity, clinical applications 2-69420
whole-body counting, nature and control of external sources of variation 2-69378
whole-body radioactivity monitor, effect of deposited Rn daughter products on background count rate 2-69421
X-ray, eye in carotid angiography 2-69334
X-ray diffraction and fluorescence analysis equipment, monitoring and dose limits 2-78657
X-ray films, theoretical and practical 2-69447
X-ray spectral distribution in roentgens 2-82021
X-rays, 250 kVp and 65 kVp, energy deposition spectra 2-82026
X-rays and γ-rays, instrument for calibration of monitoring instruments 2-69243
Ag activated phosphate glasses, radiation induced photoluminescence, laser pulse excitation 2-68713
Al$_2$O$_3$-solids, exoelectronic properties, use in TSEE dosimetry 2-68490
^{241}Am, estimation of permissible radiation dose to gonads and foetus 2-55280
^{241}Am, estimation of relative role of penetration into critical organs through intact skin 2-55295
^{241}Am biological action of compounds as function of dose, routes and character of intake 2-55281
^{41}Ar, derivation of maximum emission rate from nuclear stack 2-70551
BF$_3$ tubes, correction factors for neutron monitoring 2-59636
α-Be neutron sources, neutron spectra 2-55928
BeO:Si for environmental and personnel dosimetry in tropical countries 2-85133
BeO, dependence of TSEE on various oxide and silicate admixtures after high temperature pretreatment 2-68493
BeO, role of Si activator in exoelectron emission 2-59635
BeO ceramic, chemically, thermally and radiation-induced changes in TSEE characteristics 2-68492
BeO ceramic, effect of different absorbing materials during γ- and X-ray irradiation on TSEE response 2-68491
BeO low-Z activated, use as high sensitivity radiation detector in TSEE dosimetry 2-67089
^{11}C, in vivo metabolism meas. 2-69388

Dosimetry continued
^{11}C, use in clinical research 2-69387
^{14}C labelled compounds, production, control of surface and internal contamination 2-58604
CaF$_2$:Dy detectors, 80 kVp X-rays 2-55925
CaF$_2$:Dy phosphor, thermoluminescent for thermal neutron dosimetry 2-83160
CaF$_2$:Dy thermoluminescence dosimeter meas. of background radiation in USA 2-84859
CaF$_2$:Mn response to n, γ irradiation 2-83161
CaF$_2$:Mn thermoluminescent dosimeters, influence of size on ^{60}Co γ-ray dosimetry in extended media 2-67088
CaF$_2$:Mn thermoluminescent γ-dosimeter, sensitivity to neutrons 2-82820
CaF$_2$, neutron, using thermoluminescence 2-69345
CaF$_2$ dosimeter in sunburn range 2-85136
CaF$_2$ dosimeters, thermoluminescent, preparation and props. 2-82824
CaF$_2$ power phosphor, characteristics for thermally stimulated exoelectron emission dosimetry 2-67091
CaF$_2$ thermoluminescent dosimeter, for meas. natural background radiation 2-42698
CaF$_2$natural phosphor, thermoluminescent for thermal neutron dosimetry 2-83160
CaSO$_4$:Dy phosphor, thermoluminescent for thermal neutron dosimetry 2-83160
CaSO$_4$:Dy phosphor for meas. of u.v. irradiances 2-82561
CaSO$_4$:Dy thermoluminescence dosimeters for environmental monitoring 2-79675
CaSO$_4$:Mn response to n, γ irradiation 2-83161
CaSO$_4$:Mn thermoluminescence, dose relationship, energy response and rate dependence from 8 keV-30 MeV 2-68701
CaSO$_4$:Tm phosphor for meas. of u.v. irradiances 2-82561
CaSO$_4$:Tm phosphor powder use for fast neutron dosimetry 2-78666
CaSO$_4$:Tm thermoluminescent dosimeter construction and characts. 2-55923
Cd loaded 9 and 10 inch sphere, correction factors for neutron monitoring 2-59636
^{115m}Cd, retention and elimination in man, meas. using whole body counting technique 2-55285
^{144}Ce, influence of irradiation on incorporation in hair and other tissues of rabbits and rats 2-55293
^{252}Cf, implantable, calc. neutron dose rates 2-66287
^{252}Cf brachytherapy program 2-69381
^{252}Cf medical neutron source, ion chamber dosimetry 2-69441
^{252}Cf spontaneous fission neutron source for medical implant therapy, dose tables and modified distribution system 2-69442
^{252}Cf therapeutic sources, absorbed dose and linear energy transfer distributions 2-45039
Co radioisotopes in Man 2-62870
Co tissue-air ratios and orthovoltage depth doses calc. 2-69407
^{60}Co, absorption and retention in man, det. by whole body counting 2-62841
^{60}Co, γ-ray irradiation of malignant lymphopathies 2-69412
^{60}Co, teletherapy, skin doses 2-69417
^{60}Co and 6 MeV photons, computer calculation of dose for irregularly shaped fields 2-69434
^{60}Co gamma rays energy, deposition spectra 2-82026
^{60}Co teletherapy two dimensional dose distributions with coplanar beams 2-78665
^{132}Cs, comparative behaviour in males and females following oral administration 2-55292
^{137}Cs, estimation of relative role of penetration into critical organs through intact skin 2-55295
^{18}F, production and use in metabolic studies 2-69389
^{18}F internal radiation dose, use in bone scanning 2-55274
^{59}Fe absorption in man, whole-body counting 2-55282
^{67}Ga, ^{111}In and ^{75}Se in tumours, Ge(Li) detector for simultaneous meas. 2-73206
^{3}H, estimation of relative role of penetration into critical organs through intact skin 2-55295
^{3}H, influence of irradiation in incorporation in hair and other tissues of rabbits and rats 2-55293
^{3}H labelled compounds, production, control or surface and internal contamination 2-58604
I isotopes, internal contamination in isotope production heat laboratory, Budapest 2-58632
I radionuclides and precursors inhaled into human body, calc. of radiation dose to thyroid 2-55275
^{131}I, estimation of permissible radiation dose to gonads and foetus 2-55280
^{131}I human serum albumin, intrathecal administration 2-55262
^{131}I production laboratories, radiation monitoring and risk of internal contamination 2-58630
^{131}I production risks, routine thyroid monitoring 2-58631
^{111}In, ^{67}Ga and ^{75}Se in tumours, Ge(Li) detector for simultaneous meas. 2-73206
^{192}Ir hairpin interstitial radiation therapy, dosimetric considerations 2-69424
^{140}La, contamination of monkeys by inhalation exposure, DTPA treatment 2-55259
Li$_2$B$_4$O$_7$:Mn application, preparation of samples with optimum thermoluminescent properties 2-49913
Li$_2$B$_4$O$_7$:Mn thermoluminescent dosimeter, energy response 2-58623
Li$_2$B$_4$O$_7$, mass attenuation and energy absorption coeffs. for 1 to 150 keV photons 2-64871
LiF-100, (-7) thermoluminescence, dose relationship, energy response and rate dependence from 8 keV-30 MeV 2-68701
LiF, based on radiophoto luminescence 2-55926
LiF, clinical radiation dose measurements 2-69431
LiF, dose rate dependence for exposures above 15000 R per pulse 2-59634
LiF, mass attenuation and energy absorption coeffs. for 1 to 150 keV photons 2-64871
LiF, single crystal ribbon prod. by edge-defined film-fed growth technique and thermoluminesc. 2-67943
LiF, thermoluminescent, protection in radiodiagnosis 2-48888
LiF, thermoluminescent response to 1.7-3.7 MeV α and 2.4-13.3 MeV p 2-85135

Dosimetry continued
- LiF and natural fluorite, mixed field of gamma-rays and neutrons 2–73948
- LiF in teflon discs, consistency of properties over repeated cycles of use 2–67087
- LiF personal thermoluminescent dosimeter system 2–69432
- LiF powder phosphor, characteristics for thermally stimulated exoelectron emission dosimetry 2–67091
- LiF response to n, γ irradiation 2–83161
- LiF teflon rods, calibration for internal β-ray obs. 2–45050
- LiF thermolum. mechanism 2–61720
- LiF thermoluminescence dosimeters, response to fast neutrons 2–79671
- LiF thermoluminescent dose meter 2–67068
- LiF thermoluminescent dosimeter, for obs. during radiotherapy 2–69400
- LiF thermoluminescent dosimetry grade 100 powder incorporated in silicone rubber, dependence of energy response on grain size 2–68702
- LiF undoped power, high-level dosimetry, radiation induced optical absorption and photoluminescence 2–67096
- ^{7}LiF, dosimeter, changes in gamma sensitivity 2–85084
- N ion beam at 3.9 GeV, meas. of physical and radiobiological parameters 2–69425
- ^{13}N, in vivo metabolism meas. 2–69388
- ^{13}N, production and use in metabolic studies 2–69389
- $^{13}N_2$, use in clinical research 2–69387
- ^{237}Np, biological action of compounds as function of dose, routes and character of intake 2–55281
- ^{237}Np fission fragment registration for fast neutron personnel monitoring 2–79676
- O_2 ion beam, from Bevatron, depth dose characteristic 2–69404
- ^{15}O, in vivo metabolism meas. 2–69388
- ^{15}O, production and use in metabolic studies 2–69389
- $^{15}O_2$, use in clinical research 2–69387
- ^{32}P content in breast cancer, surface detection of diurnal variation 2–69266
- ^{203}Pb, kinetics of retention and distribution in young rats meas. with scintillation counter 2–55284
- ^{210}Pb, in area of Roumania with increased natural background, meas. of absorption levels in population 2–58633
- ^{210}Pb, influence of irradiation on incorporation in hair and other tissues of rabbits and rats 2–55293
- ^{147}Pm containing luminous paint, metabolism following inhalation by mice, removal of radioactive materials 2–55288
- ^{210}Po, kinetics of metabolism in body after radionuclide intake through skin and determ. of contamination levels 2–55283
- Pu systematic burden, manual and computer evaluation 2–78664
- ^{238}Pu, used in cardiac pacemakers 2–51948
- ^{239}Pu, biological action of compounds as function of dose, routes and character of intake 2–55281
- ^{239}Pu, estimation of relative role of penetration into critical organs through intact skin 2–55295
- ^{239}Pu, in lungs, determ. of effective tissue thickness 2–85124
- ^{239}Pu, influence of irradiation on incorporation in hair and other tissues of rabbits and rats 2–55293
- ^{239}Pu late phase lung clearance in vivo det. 2–58588
- Ra Crowe and ^{90}Sr nasopharyngeal applicators, dose distributions 2–69436
- Ra daughters, lung cancer risk in relation to long-term exposure 2–55231
- Ra linear sources, simplified method for dose calculations 2–69423
- ^{224}Ra, ^{226}Ra, kinetics and decay products in mice, dose-effect relation 2–55279
- ^{226}Ra, influence of irradiation on incorporation in hair and other tissues of rabbits and rats 2–55293
- ^{226}Ra, time course of distribution in some bones of mice 2–55286
- Rn and daughters, dose to epithelium and upper respiratory tract 2–82020
- Rn(A=220, 222) activity and potential alpha energy in different air atmospheres 2–56078
- ^{222}Rn- and ^{220}Rn-daughters, inhaled α-energy rel. to absorbed 2–82019
- ^{222}Rn, ^{220}Rn, and daughters, radiation dose to inhabitants of radon-spa from air contamination 2–58014
- ^{222}Rn and daughter products, dependence of chromosomal aberrations in peripheral blood lymphocytes on inhaled internal dose 2–55272
- ^{222}Rn inhalation in rats, meas. of body accumulation of ^{210}Po, ^{210}Pb and increase of activity with time 2–55287
- ^{222}Rn short-lived daughters, maximum permissible doses by inhalation in mines and radon spas 2–55271
- ^{222}Rn short-lived daughters, recommendation of maximum permissible intake by inhalation 2–55270
- ^{75}Se, ^{67}Ga and ^{111}In in tumours, Ge(Li) detector for simultaneous meas. 2–73206
- Si photodiodes for fast neutrons, properties 2–46057
- ^{85}Sr, changes of passage and absorption in gastrointestinal tract of irradiated rats 2–55294
- ^{85}Sr internal radiation dose, use in bone scanning 2–55274
- ^{89}Sr, estimation of relative role of penetration into critical organs through intact skin 2–55295
- ^{89}Sr and ^{90}Sr determination by liquid scintillation beta spectroscopy 2–85083
- ^{90}Sr, estimation of permissible radiation dose to gonads and foetus 2–55280
- ^{90}Sr, internal contamination in isotope production heat laboratory, Budapest 2–58632
- ^{90}Sr nasopharyngeal applicator, photographic determ. of dose rate distribution 2–69435
- ^{87m}Sr radiation dose calculation, evidence for calculation errors 2–76096
- T, organic-bound, in mice as increasing tissue dose after single or daily administration of tritiated water 2–55291
- T beta particles energy, deposition spectra 2–82026
- THO, transport kinetics in human body, use of compartment analysis 2–55290
- T_2O, estimation of permissible radiation dose to gonads and foetus 2–55280
- ^{99m}Tc polyphosphate, internal radiation dose, use in bone scanning 2–55274

Dosimetry continued
- Th and daughters in body following spinal injection determ. of quantitative location 2–58626
- U, determ. of content in body and critical organs for underground miners, assessment of radiation safety standards 2–55241
- U deposition in human organs by chronic exposure, mathematical model 2–55278
- U miners, investigation of immunoglobin levels in blood serum after high exposure to ionizing radiation 2–55296
- ^{238}U, in area of Roumania with increased natural background, meas. of absorption levels in population 2–58633
- ^{133}Xe, radioactive, nonlinear relation between inhaled activity and whole-body activity, retention in man and rat 2–55289
- ^{90}Y determination by liquid scintillation beta spectroscopy 2–85083

Double refraction
- *see also Electromagnetic wave propagation; Optical constants; Optical rotation; Polarization/light*
- birefringent laser polarizer, high efficiency 2–82556
- birefringent polymer films on substrates for integrated optics 2–80592
- birefringent prism, for luminance subtraction 2–66805
- calcite crystal 2–82113
- collisionless gases, transient orientational birefringence 2–43267
- ferrite-garnets, magnetic birefringence 2–65216
- gases of linear molecules, flow birefringence in magnetic field 2–46853
- glass, acoustic birefringence under strong uniaxial compression 2–54028
- glass, tempered, plate, residual surface stress measurement using birefringence 2–60989
- Kerr cell, multiple refl., for liq. birefringence obs. 2–76524
- laser beams, propagation through thermally distorted windows 2–82524
- laser modulation, automatic optical bias control, p.c.m. communication 2–66797
- liquid crystals, nematic, applied a.c. voltage effects on birefringence 2–53431
- liquid crystals, nematic optical birefringence, application as phase grating of electrically tunable spatial frequency 2–64443
- macromolecular solution, electric birefringence, relaxation spectrum, decay curve, numerical method 2–74543
- MBBA, Kerr const. temp. depend. near isotropic-liq. cryst. transition 2–77430
- methane, solid, obs. of second transition due to spin isomerisation 2–64814
- microcline, shock effects 2–61843
- molecular optical anisotropy dispersion obs. using laser induced birefringence 2–63394
- nylon 6 monofilament, model for deform. and fracture from creep and birefringence obs. 2–84021
- nylon 6 monofilament, model for deform. and fracture from creep and birefringence obs. 2–84022
- optical birefringence, analysis of generalized expts. based on photon statistics of scattered light 2–63308
- plane wave propagation in biaxially anisotropic layered media 2–42209
- polyethylene crystallization at high temp. and pressure, birefringence obs. 2–47064
- polymer chain elongational flow calc. of intrinsic birefringence 2–46870
- polypropylene, T-die film, mechanical props. and mol. orientation, birefringence method 2–47537
- polyurethane block polymers, meas. of birefringence relaxation 2–74850
- reflected-shadow method for constrained zone study of cracks in birefringent media 2–68101
- superimposed birefringence and optical activity of medium polariscope investigation 2–66835
- suspension of oriented particles, birefringence determ. from polarizability coeffs. 2–56532
- $AgGaS_2$, direct obs. using fringe technique 2–75259
- $BaTiO_3$, abnormal birefringence due to lamellar domains 2–81128
- CaF_2, stress induced, dependence on growth technique 2–47396
- $CdGeAs_2(P_2)$, birefringence, 2-10μ 2–72261
- $CdSiAs_2$, birefringence, 2-10μ 2–72261
- $(Gd,Tb,Eu)_3Fe\ O_{12}$ ferrite garnet, optical anisotropy, birefringence obs. 2–68602
- $Gd_2(MoO_4)_3$, ferroelec., spontaneous birefringence 2–78068
- $Gd_2(MoO_4)_3$, improper ferroelec., induced and spontaneous birefringence 2–61588
- n-InSb, hot electron Kerr effect birefringence phase shift calc. 2–51303
- $LiIO_3$, α and β forms compared 2–81326
- $NaNO_2$, rel. to Brillouin scatt. at room temp. 2–48204
- Nd:YAP solid laser, polarization and crystal direction effects 2–42067
- SiO_2, acoustic birefringence under strong uniaxial compression 2–54028
- SiO_2, vitreous, induced birefringence, nonlinear variation with uniaxial stress to 7 kbar 2–68600
- $ZnGeP_2$, birefringence, 2-10μ 2–72261
- ZnS, birefringent striations, X-ray obs. 2–47213

electric *see Electro-optical effects*

flow
- arterial branching in models using flow birefringence 2–66250
- photoviscosity, velocity profile, strain rate, shear stress 2–60393
- poly(vinyl cinnamate), hydrodynamic, optical props. 2–83388
- poly-4-vinylpyridine in solution, hydrodynamic and optical props. 2–60452
- polyethylene, molten, flow birefringence obs. of flow through parallel slit 2–71142
- polyisobutylene in decaline, in concentric cylinders, rheo-optical analysis 2–56457
- stress-optical coeff. calc. from fine structure in depolarized light scatt. 2–50358

magnetic *see Magneto-optical effects*

mechanical
- *see also Photoelasticity*
- elastomers, by Hertzian waves 2–68601

Double refraction continued
mechanical continued
hypoelastic dielectric, birefringence calc. 2−45416
hypoelastic dielectric, birefringence in simple shear 2−45417
parameters, determination in stress analysis by photoelasticity method 2−82331
polyisobutylene in decaline, in concentric cylinders, rheo-optical analysis 2−56457
polymethylmethacrylate, plastically deformed 2−51301
As$_2$S$_3$, amorphous, piezobirefringence freq. depend., one-oscillator model 2−54383
KH$_2$PO$_4$, dense domain structure at ferroelectric transition, stress-induced birefringence 2−75260

Double resonance *see Nuclear magnetic resonance and relaxation; Paramagnetic resonance and relaxation*

DPPH (Diphenylpicrylhydrazyl) *see Free radicals; Organic compounds*

Drawing *see Forming processes*

Drops
— 2−71276
acetone, heat transfer from small diameter channel in film boiling temp. range 2−53379
breakup of columns by shock waves 2−83806
carbon tetrachloride, settling process of unstable dispersed droplets 2−80435
charged, oscillations, EHD stability 2−80227
chlorobenzene, rate of fall in water column subjected to sinusoidal pulsations 2−46904
cloud, laboratory, size distribution obs. 2−57978
cloud droplets gravitational coagulation, numerical simulation 2−65739
in clouds, collisions, gas kinetic effects 2−78370
clouds, effect on solar radiation absorption by atm. dust 2−84806
coalescence, effect of applied force 2−71147
combustion in super-critical conditions and gas pockets, model 2−81487
condensation, heat transfer, numerical simulation 2−77471
conveyed by gas flow, breakup 2−60335
deformation and mass loss in high speed gas flow, capillary surface wave mechanism 2−43303
drizzle, effect of fluctuations in vertical acceleration on coalescence growth 2−48491
droplet atomization in convective gas stream 2−46908
droplet growth in nucleation, kinetic theory 2−60551
droplet or ice particle formation on aerosol particles, temp. and humidity conditions 2−51612
dynamics of small droplets near mouth of pitot tube and interpretation of pressure for two-phase flow 2−50141
electrically suspended water droplets, wind correction to evaporation rate and Rayleigh instabilities 2−56531
ethanol, homogeneous nucleation and growth in supersonic flow 2−80393
evaporating liquid, maximum relaxation times 2−43302
expansion and heating by internal heat sources 2−43300
fall in non-Newtonian media 2−46905
filters, rotary impaction, with tapered filaments, design 2−43402
finite-difference cloud droplet collection equation, critique and reply 2−68904
fluid circulation in and round dielec. fluid in elec. field 2−83524
forced convection evaporation with finite vaporization kinetics and liquid heat transfer 2−77398
freon 11, 113 droplet splattering on hot surface, heat transfer rates 2−55575
fuel, chemical aspects of shock initiation 2−83724
gas-liquid droplet system, model for shock wave propag. 2−83656
gas-liquid flow, annular, mean vels. calc. 2−53345
generator with electronic control of size, production rate and charge 2−67790
glycerine, in castor oil, wake obs., deflection mapping with Babinet compensator 2−64405
growing water drop rel. to diffusion-kinetic approach 2−56471
growth, heat conduction constraint 2−43301
homogeneous nucleation theories, droplet approach 2−80520
immiscible, moving in liquid, vaporization mechanism 2−83834
liquid, atomization and freezing in biphase gas system, adiabatic expansion 2−71111
liquid, evaporation in turbulent air stream, impurities effect 2−71279
liquid, suspension in cylindrical tube, viscous flow 2−64419
liquid-liquid dispersion, drop size measurement by photographic technique 2−71240
menisci, axisymmetric, tables of profiles 2−60413
methanol, heat transfer from small diameter channel in film boiling temp. range 2−53379
mono-dispersed, production by vibration-atomization 2−71246
motion of drop in pulsated medium under nonlaminar conditions 2−46904
organic liquids, fall in polymer solutions 2−46905
passage of liquid drop through liquid-liquid interface 2−50305
passage through liquid-liquid interface 2−50305
polymer solution atomization by grooved-core nozzle 2−50377
rain, erosion model, effect on supersonic flight 2−43252
rain, size changes inferred from underwater noise 2−57979
rain drop size, time dependent distribution, model 2−57930
rain drop size distribution and rainstorm type rel. to radar raingauge accuracy 2−75593
rain drop size distribution determ. by radar, errors rel. to vertical air motion 2−75592
rain drop size distributions using 35 GHz Doppler radar 2−75591
raindrops, terminal fallspeeds 2−75603
rainfall rate and drop size distributions, simultaneous meas. using radar and raingauges 2−75590
reacting liquid sprays, in-line holography 2−83755
removal from fast flowing airstream, rotary impaction filter efficiency 2−67849
satellite droplets formed by liquid atomization by rotating disk 2−60404
sessile, surface and interfacial tensions, from profile 2−67789
sessile lenticular configs., translationally and rotationally symmetric lenses 2−74510

Drops continued
sessile profiles, corrected methods for surface tension and spreading coeffs. 2−83785
size in power law non-Newtonian systems 2−46906
solid, 0.5-10 μm, evaporation of soln. in high temp. column 2−67788
solvent inclusions, in KCl cryst., movement by centrifugation 2−47465
spherical, motion on flow of viscous fluid 2−60406
steel, solidification in oil 2−43440
supercooled cloud droplets and distribution, airborne obs. 2−54848
suspension of drops in elec. field, stress system 2−83819
temperature measurement of individual droplets in cloud of drops 2−67784
ultrasonic atomization 2−74507
water, AgI particle dissolving in, contrib. of diffusion and interfacial kinetics rate of solution 2−60434
water, contact angle rel. to drop size at b.p. for 50-760 Torr 2−77474
water, disruption by electric forces 2−64426
water, formation in deep cloud cover 2−68875
water, freely suspended, oscillation freq. 2−64427
water, freely suspended supercooled, freezing by contact nucleation 2−47036
water, freezing, ejection of microdroplets 2−50401
water, freezing by contact with CuS particles 2−48499
water, heat transfer from small diameter channel in film boiling temp. range 2−53379
water, in air and CO$_2$, drop evaporation rate meas., conditions of thermostatic drop surface 2−77406
water, internal circulation for drops falling at terminal velocity in air 2−64414
water, migration through KCl crysts. 2−47466
water, rate of soln. of ice nuclei, effects on nucleation 2−75600
water, scavenging of aerosol by falling droplet, particle size effect 2−75599
water, scavenging of aerosol particles 2−46998
water, stationary, in superheated vapour atmosphere, condensation characteristics 2−53500
water, supercooled, shattered by shock waves, freezing 2−47037
water drop response to sudden acceleration 2−83739
water droplets produced by u.s. 2−71241
water-drop impacts, electro-acoustic meas. of drop size, shape and velocity 2−63129
Al, supercooling and spheroidizing, effect of Cu inclusions 2−43441
Bi droplets, crystallization and nucleation 2−71382
Fe, solidification in oil 2−43440
Hg droplets, crystallization and nucleation 2−71382

Drying
freeze, in vacuum, using homogeneous beds of sand and beef 2−73249
freeze dryer with improved standards of biological safety, design and construction 2−78638
porous medium with internal heat generation 2−45573
specimen preparation with freeze-drying technique for electron microscopy 2−79098
sponge, elec. field effects on heat and mass transfer 2−52282
Cu powder, effect of temp. and ambient 2−80828

Dual resonance model
— 2−66988
absorptive, applic. to two-body elastic scattering 2−59483
absorptive model analysis of vector meson photoproduction and Compton scattering 2−76694
absorptive model for separation of helicity-nonflip amplitude of πN scattering at 6 GeV/c 2−70240
amplitude, crossing symmetric, with geometrical structure, applic. to $A_1\pi\to\pi\pi$ process 2−59474
amplitudes with Mandelstam analyticity, asymptotic behaviour 2−70194
bi-Regge-pole duality 2−45926
class of dual models with SL(2,C) symmetry, generalization of Virasoro-Shapiro type model 2−73786
combustion, which improves mass spectrum of Neveu Schwarz model is Kola Nielsen formulation 2−49531
conformal models, local gauge principle 2−66891
coupling parameter sum rule, unitarization of dual models and bootstrap 2−55834
Deck effect 2−49528
deep inelastic hadronic scattering 2−59486
dual absorptive model, helicity conserving and nonconserving pomeron exchange amplitudes 2−59467
dual pion model, physical states and pomeron poles 2−70227
dual quark-parton model for single-particle distribs. in deep elastic electroproduction 2−70160
dual-position-space kernels, operator formalism 2−66971
dual-tube model, one-loop graph 2−49533
duality and absence of exotic resonances, deduction of hadronic internal symmetry groups 2−76637
duality and pion electromagnetic form factor 2−59524
duality and positivity in zero-width approx., exptl. consequences 2−76636
duality concept and development of Veneziano model 2−66975
duality for real and virtual photons 2−59401
duality in current interaction tested by analysis of ep inelastic scattering 2−42343
duality in deep inelastic electroproduction 2−59420
dynamics underlying duality and gauge invariance 2−55784
e.m. interaction, generalized minimum interaction principle 2−49523
exclusive processes, one-current dual model 2−66932
factorizable models without tachyons 2−79512
Feynmann rules for massive gauge fields with dual diagram topology 2−73733
field theory, position-space propagators and functional fields 2−76571
fixed poles, unitarity and duality, charge exchange applic. 2−79533
Freund-Harari duality tests, evidence against resonance saturation in finite-energy sum rules 2−63568
generalization, group-theoretical approach 2−63556
generalized duality, relationship between three body forward scattering and two-body scattering 2−63558

Dual resonance model continued
generalized interference model, exchange degeneracy and duality 2−73792
ghost-free model with leading intercept minus one 2−79534
graphical duality and algebra of Regge vertex strengths 2−70195
hadronic prod. in e^+e^- annihilation processes 2−63518
hadronic vector currents, representation of current algebra 2−79516
impact parameter description, compatibility with s-u symmetry constraint 2−49529
inclusive cross sections and dual topology 2−70186
inclusive distributions, in thermodynamic model 2−70175
inclusive distributions 2−49534
inclusive electroproduction, single particle, scaling in dual model 2−42338
inclusive interactions, phenomenological duality 2−59437
inclusive processes at high energy 2−59450
inclusive reactions, duality constraints, role of Harari-Freund conjecture 2−79528
inclusive reactions, implications of duality in missing mass for polarisation effects 2−52577
inclusive reactions, single-particle spectra at fixed angle and duality 2−66979
intermediate-energy bootstrap dynamics based on average nonlinear duality, calcs. of Pomeranchuk residue at $t=0$ 2−66986
iso-vector 0^+ meson, ‘near universality’ of struct. functions and form factors 2−66970
large angle scattering, invariant 4-point amplitudes satisfying mathematical duality constraints 2−42366
loop amplitude structure in terms of Mandelstam variables S_{ij} 2−45915
Lorentz invariance and duality 2−70198
mass levels, physical and spurious states 2−42362
meson-baryon scatt., backward amplitudes and average radius of interaction on duality basis 2−66997
meson-baryon scatt., multiple scatt. model duality breaking effects 2−63572
multi-pomeron selection rules in dual loop models with spin 1/2 partons 2−66983
multiparticle processes at high-energy, application of dual-parton model 2−63547
multiparticle theory with nonlinear trajectories, first and second factorization 2−59485
multiperipheral configuration, dual amplitude construction based on general field theory vertices and propagators 2−59470
N-point amplitude, off-shell 2−55839
n-point Virasoro model, Lorentz invariance and duality 2−70198
narrow resonance and ‘tachyon’ approximation of scattering amplitudes 2−76634
nonplanar helicity pole couplings, duality and Feynman graph 2−45843
O(n) relations for coupling consts. and space-time dimens. 2−79540
off-shell amplitude, derivation 2−59466
P′ Regge singularity phenomenological anal. 2−79537
parton, for lepton-hadronic and colliding- beam inclusive reaction 2−66931
parton model, light-cone structs. and sum rules 2−59478
perturbation series for dual amplitudes 2−73705
photonlike particles, sum rules for Compton scattering 2−59469
physical states, construction 2−70111
pions, factorizable dual model based on a coupling of dual spin fields with $J_s=-\frac{1}{2}$ and $J_s=-1$ 2−42379
quality and Regge complex pole model as basis for taking Regge cuts into account 2−66989
quantum number assignments to external particles by formalism based on broken SU(12) symmetry 2−63560
quark diagrams, inclusion of spin, L-excitation and elimination of ghosts 2−59479
quark model developed from Veneziano model by inclusion of Dirac spin 2−63530
quark models for high-energy forward, backward, and large-angle scattering 2−76642
Regge cut corrections to absorpt. models from duality diagrams 2−79535
Regge models and duality, review 2−63569
Regge-behaved dual amplitudes satisfying the Mandelstam representation 2−76635
resonance model for inclus. distribs. in high-energy electron-positron annihilation 2−82685
resonant width, multiplicity, statistical calc. 2−70185
scalar currents, analogue model extension 2−79532
semilocal duality, application to $a+b+c \rightarrow a+b+c$ process in double-Regge region 2−76639
single-particle prod., dual-model analysis at intermediate energies 2−79526
spectrum of physical states, implications in statistical approach 2−79544
spectrum-generating algebra and no-ghost theorem 2−79515
spin distribution function calc. in analytical form assuming number of level N tends to infinity 2−42358
spin J resonance production 2−45922
Thirring model constitution of dual models 2−49530
time-like extension and difference eqn. 2−76572
triple Regge vertex, nonplanar couplings 2−45925
two fermion vertices, for excited fermion states 2−82631
two particle distributions 2−45918
two-body processes, generalization of geometrical duality 2−76624
two-component duality consequences for πN and KN total cross sections 2−76646
two-current dual amplitudes and fishing-net diagrams 2−79520
two-particle production, dual-amplitude analysis 2−63536
with unit intercept, construction of currents and Green’s functions 2−45914
unitarization and absorpt. Regge cut 2−66981
vector currents; form factors 2−79538
vector-meson scattering, application of quark-model like results from duality 2−45984
vertex describing transition of Ramond fermion into Neveu Schwarz meson 2−76617
Virasoro gauge conditions, relation to geometrical and mechanical props. of classical two-dimensional media 2−42360

Dual resonance model continued
Virasoro operators, identification of finite transformations 2−55837
virtual scalar photon, single particle distribution 2−70143
zero-slope limit reduction to φ^3 theory, and tree graphs 2−73710
eN, deep inelastic scattering and geometric duality, virtual photon nucleon scatt. 2−42406
ep scatt. and single particle distribs. due to virtual phonon in dual reson. model 2−76607
$K^+K^-pn\pi^-$ system, application to reactions $K^+p \rightarrow K^+\pi^+n$, $K^+n \rightarrow K^+\pi^-p$, $K^-n \rightarrow K^-\pi^-p$ 2−76659
KN scattering, consequences of local duality, specific solution in exact SU(3) limit 2−67012
$k\text{-}p \rightarrow \Lambda\eta$, 1.25-1.85 GeV/c, duality 2−73810
$k\text{-}p \rightarrow \Lambda\pi$, 1.25-1.85 GeV/c, duality 2−73810
NN annihilation into pions, possibility of determining spin for resonances in direct channel 2−73843
$NN \rightarrow 3\pi$, duality and final-state-interaction approach 2−52634
p annihilation analysis 2−59577
$pn \rightarrow \pi^+\pi^-\pi^-$, 1.2 GeV, investigation using dual amplitude with Mandelstam analyticity 2−52636
π^0 photoprod., cut contribs. in dual cut model 2−55852
$\pi\Delta \rightarrow \omega\Delta$, dual amplitudes and relations between coupling consts. 2−76684
πN, backward amplitudes, dual absorptive model 2−79580
πN forward scattering amplitude, duality and high-energy limit 2−76664
πN scatt., dual geometrical model 2−67031
πN scatt., dual Regge cut amplitudes 2−55856
$\pi N \rightarrow \omega N(\Delta)$, dual amplitudes and relations between coupling consts. 2−76684
$\pi N \rightarrow \rho N$, dual amplitudes 2−67020
πp backward elastic scattering, fluctuations, dips and duality 2−82759
$\pi^-p \rightarrow \pi^0n$ amplitudes, estimate in terms of direct-channel resonances and dual absorptive requirements 2−82761
$\pi^\pm p$, elastic scatt., Pomeron and f exchange amplitudes 2−59540
ρ^0, forward slope in photoproduction and electroproduction, application of dual-absorptive model 2−73837

Ductility *see Plastic flow; Plasticity*

Dusts *see Aerosols; Powders*

Dynamics
see also Ballistics; Kinematics; Rotating bodies; Vibrations
air cushion expts. for teaching of school physics 2−62930
asymptotic methods for solution of nonlinear equations with partial derivatives 2−52125
atmosphere, re-entry vehicle dynamics, effects on atmospheric data 2−75528
atmospheric vortices, tropical cyclones 2−78367
Bay of Bengal, storm surges rel. to dynamics and storm-tide tables 2−75483
bubbles, nonspherical 2−43305
bubbles and vapour cavities 2−43304
buoyant vortex rings and thermals 2−77189
celestial mechanics, cascade dynamics, simulation of collective motion 2−81779
clamped plastic circular plates, dynamics 2−52139
classical, noncommutative representation, connections with classical dynamics 2−41561
classical nonlinear, review of recent progress 2−63059
comets, perturbation by planets and stars close to solar system 2−81783
connected rigid-body systems, gyroscopic phenomena 2−76253
continuum model of dynamical systems 2−76246
Coriolis forces, effect on water flow in pipe 2−74496
curved and twisted rod, equations of motion 2−41560
cylinders rolling on viscoelastic plane, contact area rel. to vel. 2−66488
cylindrical panels, moderately thick, dynamic response 2−55447
discrete Cosserat media, general equations of non-linear theory 2−52120
discrete Cosserat media, non-linear theory. constrained rotations 2−52121
explicit discrete mechanics using difference equations, with applics. 2−73348
extremum principles for rigid plastic dynamic loading problems 2−69681
fluid, techniques for numerical solution of problems, review 2−43056
forced system with hysteresis, periodic solutions 2−45341
general classical mechanical variables, fluctuations under external force 2−45339
geometrically nonlinear structural analysis 2−41559
gyrostat, motion about centre of gravity in central field 2−55450
harmonically bound semi-infinite and infinite chains with friction and applied forces 2−63058
high-speed rotating devices 2−58828
impact, rigid sphere on elastic layer, force time investigations 2−69633
impact phenomena in spatial mechanisms, analogy between gyrodynamics and elastostatics 2−73378
Lagrange eqns. of motion, 2 degrees of freedom, simplified soln. 2−82288
large-scale cosmic n-body problem with variable gravitational constant, dynamical consequences 2−81769
Liapunov stability of hybrid dynamical systems with multi-elastic domains 2−76251
lumped and continuous dynamic systems, bounds on motion 2−45459
magnetosphere, radial diffusion of He^+ and protons 2−65849
many non-rigid bodies system, translational dynamical equations for relative motion 2−69632
molecular, of dilute gases, computer experiments 2−83704
multiple synchronization in system of weakly coupled objects with one degree of freedom 2−52211
non-circular stiffened cylindrical shells 2−69657
nonlinear continuous media, approximations of models 2−52119
nonlinear perturbations of motions, rel. to eqns. of motion solns. props. 2−45346

Dynamics continued
- nonlinear self-oscillatory systems, determ. of dynamic characteristics 2—82294
- oscillogyro, dynamical characteristics 2—78871
- plane parallel motion of rigid body, dynamic effects of arbitrary order 2—52131
- plate, rigid, on elastic-plastic foundation with variable plasticity limit, elastic unloading dynamics 2—45495
- point mass past large mass of prolate ellipsoid of revolution, motion 2—55451
- polymer molecule 2—53090
- principle of least action, physical foundation 2—45344
- pulse phase-locked systems dynamics 2—82500
- reactor, soln. of nonlinear space time problems using eigenfunction expansions 2—83101
- relativistic, of rigid test body in curved space-time 2—52050
- resolution of forces using a linear air track 2—55348
- response of discrete linear systems to forcing functions with inequality constraints 2—76249
- response of linearly elastic rods 2—41615
- rods, multi-indical system, elastic buckling, Lagrange eqns., mech.-stereomech. analogy 2—45343
- rolling contact between elastic bodies, dynamic response to random roughness 2—58829
- rolling contact of rigid cylinder over elastic or viscoelastic layer 2—41608
- rotating body, slender, aeroelastic equations 2—50257
- rough vibrating inclined plane, motion of body on surface 2—66575
- second order system, monotonic nature of phase trajectories, bifurcation curves 2—66414
- self gravitating magnetized cylinders and stellar formation 2—66072
- spinning bodies containing elastic rods 2—52123
- stability of systems with constraints and integrals of motion 2—76245
- statics, interrelation 2—55448
- stellar, vertex deviation 2—44849
- stellar, water bag model in cylindrical two dimensional stellar system 2—44850
- straight shaft of non-circular cross section housing rotor centre-of-symmetry trajectory 2—49053
- stress functions in three-dimensional elastodynamics 2—69663
- symmetries, 1/r potential 2—58830
- third integral of motion; problem solutions 2—78802
- three-body systems, relativistic grand orbital momentum 2—69630
- trajectories of plane autonomous nonconservative dynamical systems 2—76250
- vibrations of dynamic system with dry friction 2—82287

Dynamometers *see Force measurement*

Dynamos *see Electrical machines*

Dysprosium
- — 2—57380
- lattice excitation and magnon spectra, magnetoelastic effects 2—65141
- magnetic crit. scatt. role in elec. resist. 2—57271
- magnetic structure, of single cryst., near Curie point, from neutron depolariz. meas. 2—51251
- paramagnetic susceptibility anisotropy, 5 to 750°C 2—44227
- recrystallization, X-ray diffr. and metallographic obs. 2—80773
- solubility in $ZrSiO_4$, isomorphous substitution of Zr 2—74913
- CaF_2:Dy thermoluminescence dosimeter meas. of background radiation in USA 2—84859
- $CaF_2:Dy^{3+}$, spin lattice relax. rate rel. to temp. 2—84198
- Dy II in solar spectrum 2—66200
- Dy II spectrum interpret., odd levels 2—67389
- Dy II spectrum interpret., even levels 2—67390
- Dy^{2+} effect of core polarization on f-f interactions 2—52929
- Dy^{3+} in lanthanum ethyl sulphate, crystal field energy levels and Zeeman spectra 2—80951
- Dy^{3+} in SiO_2-CaO-MgO-Na_2O-AlF_3 glass system, luminesc., effect of heat treatment 2—48228
- ^{163}Dy, production and crystal growth, neutron diffraction expts. 2—74667
- Ir:Dy, localized moment-cond. electron exchange interaction, e.s.r. 2—68737
- Pd:^{163}Dy, hyperfine splitting, consts., e.s.r. 2—72497
- SrF_2:Dy, axial distrib. of impurities, neutron activation analysis 2—56744

Dysprosium compounds
- ethyl sulphate, caloric and mag. obs. 2—68523
- $DgVO_4$, cryst. struct., refined 2—60756
- Dy-Au alloy system, phase diagram, intermetallic form. 2—50973
- Dy-Nd alloys, struct., mag. and elec. props. 2—51237
- Dy-Zr alloys, form. of low temp. metastable allotropic solid solns. 2—47646
- DyAl garnet, mag. sp. ht. 2—43983
- $DyAl_2$, elec. resist. behaviour in crit. region 2—57279
- Dy_3Al_3, magnetic after effect associated with narrow domain walls 2—54318
- DyAlG, resonant cancellation of Raman scattering from electronic levels 2—68657
- $DyAsO_4$, Jahn Teller induced phase trans., Raman scatt. study, 12K 2—48198
- $DyCl_3.6H_2O$, caloric and mag. obs. 2—68523
- $Dy(Co,Ni)_2$, intrinsic mag. aftereffect 2—44274
- $DyCo_2$, Co atom paramagnetic moments 2—72116
- $DyCo_2$ mag. behaviour in ordering region 2—44280
- Dy_xCo_y, critical fields, ordering temps., magnetization curves at 4.2K 2—68544
- DyCoNi, magnetic after effect associated with narrow domain walls 2—54318
- $DyCo_{3-x}Ni_x$, mag. ordering 2—51256
- $DyFe_{3-x}Ni_x$, mag. ordering 2—51256
- DyGa, mag. props. 2—48079
- DyGa, magnetization and suceptibility, temp. depend. 2—72170
- $DyIn_3$, indirect exchange parameters 2—81299
- $DyIn_3$ magnetic properties 2—72223
- $DyNi_2$, magnetization mechanisms 2—72107
- $DyNi_3$, mag. struct. 2—48080
- Dy_2O_3-BaO solid soln., phase diagram 2—54005

Dysprosium compounds continued
- Dy_2O_3-WO_3 solid soln., phase equilib., transform., phase diagram, densities, m.p. 2—57013
- $Dy(OH)_3$, ferromag. relax. 2—54334
- Dy_sO_2Se, mag. props. 2—44228
- DySb, mag. struct. 2—44292
- $DyVO_4$, cooperative Jahn-Teller distortions 2—43926
- $DyVO_4$, elastic consts. anomalous behaviour at Jahn-Teller induced phase transition 2—84038
- $DyVO_4$, Jahn-Teller phase transitions, acoustic mode anomalies 2—71681
- $DyVO_4$, Jahn Teller induced phase trans., Raman scatt. study, 14K 2—48198
- $DyVO_4$, quadratic-orthorhombic transition 2—43915
- $DyVO_4$, uniaxial stress effects on absorp. spectra 2—51338
- $DyVO_4$, uniaxial stress in co-operative Jahn-Teller distortion, theory 2—51292
- $Er_{0.6}$-$Ho_{0.2}$-$Dy_{0.2}$ alloy, magnetization curves, study at 4.2 K 2—65174

E-layer *see Ionosphere/E-region*

Ear
- *see also Hearing*
- acetylcholine release by olivocochlear bundles on electrical stimulation 2—45166
- acoustic reflex of animal's middle ear using high speed photography 2—45829
- aquatic animals, cochlear hair cells, microsensitivity enhancement by environmental K ions 2—66306
- artificial mastoids, threshold values for audiometric bone conduction calibration 2—82056
- basilar membrane, simulated, bandpass noise stimulation 2—82041
- basilar membrane vibr., fuzziness detection, using laser light 2—82033
- basilar membrane vibrs., frequency response curve in living guinea pig 2—82035
- basilar membrane vibrs., vibratory amplitude and phase pattern along membrane 2—82034
- binaural loudness balance, unequal duty cycles 2—69455
- cat, tympanic membrane vibrations obs. using time averaged holography 2—51955
- central auditory masking 2—66293
- channel capacity and speech intelligibility, computation using information theory and conventional circuit theory 2—69451
- cochlea, fractional distortion pairs 2—66297
- cochlear membrane, resistance obs. analysis 2—48898
- cochlear microphonic potential rel. to stapes velocity, recording with micropipets 2—51953
- cochlear partition, hybrid computer model 2—48880
- computer simulation of cochlear microphonic potential augmentation during intercochlear perfusion 2—45167
- derivative relationship between stapes movement and cochlear microphonic 2—82055
- domestic pigs, measurements on inner ear 2—55316
- equilibrium organs, infrasonic effect 2—73216
- external acoustics, influence on acoustic impulses arriving at ear drum 2—45096
- guinea pig, cochlear degeneration following impulse noise exposure 2—45157
- guinea pig cochlea, cochlear microphonics, summating and endocochlear potentials and K^+ conc. obs. 2—45149
- guinea pig middle ear, acoustical impedance and effects of middle ear muscles 2—45097
- guinea pigs, AC cochlear potential, effects of choline salicylate 2—45163
- guinea pigs, cochlear partition, effects of electrical biasing 2—66305
- human cadaver, tympanic membrane vibs. obs. by time-averaged holography 2—82052
- human cochlear partition, stiffness, mathematical model 2—45080
- insert earphone pressure response in real ears and Zwislocki couplers 2—48899
- interaural time and level differences, detectability signal duration 2—66298
- lateral inhibition, rippled noise investigations 2—45105
- man and guinea pig, acoustic behaviour of outer-middle-ear complex 2—45147
- monaural phase effects, tone on tone masking 2—69454
- monkey, integration time constant from period histograms 2—45160
- music, understanding and appreciation 2—66294
- noise meas., individual's exposure 2—45082
- Peterson-Bogert model of cochlea, new boundary condition 2—45081
- pigeon, cochlear potentials, relation to age, cholesterol and sclerosis 2—45162
- pigeon cochlear nerve, response patterns 2—45161
- poststimulatory masking, pure tones 2—62876
- poststimulatory masking, thresholds as fn. of probe tone duration 2—62877
- primary auditory neuron, response to human speech 2—45103
- pure-tone masking in normal and cochlear-impaired ears 2—48917
- pure-tone masking in normal and cochlear-impaired ears 2—48917
- residue pitch perception, model prediction 2—45104
- slow fluid waves in cochlea and action in pitch feedback and lateralisation 2—58638
- sound pressure levels from stereo components, damage risk 2—66292
- squirrel monkey, inner ear changes caused by intense auditory stimulation 2—82046
- tomography, X-ray exam. 2—62874
- tympanometry in normal and pathalogical ears 2—69452
- K deficiency effects on cochlear potentials and cation content in endolymph 2—45165
- O_2 availability, in tunnel of Corti, microelectrodes 2—66307

Earphones *see Transducers*

Earth
- *see also Geodesy; Geophysics*
- Aegean region, morphology and activity of seismic zone 2—78229
- African plate tectonics, hot spots in mantle 2—81617
- Alaskan Jurassic palaeomagnetic pole and Alaskan orocline 2—54943
- albedo of surfaces, as fn. of solar zenith angle 2—75485
- albedo X-rays, from hard solar burst, spectral characteristics 2—62752

Earth continued
Aleutian trench, config. of underthrust oceanic plate from gravity and mag. anomalies 2—54687
Arizona, regional Bouguer gravity anomaly map 2—54686
Atlantis fracture zone, Mn crusts 2—78230
Australian-Antarctic continental drift, paleocirculation changes and oligocene deep sea erosion 2—78290
Bahama platform, crustal structure from Rayleigh wave dispersion 2—65546
basement anomaly, seismic, gravity and mag. surveys 2—57777
Bay of Biscay, mantle reflections of seismic waves 2—72621
Beaufort Sea, seismic vel. analysis 2—78255
Bedford, Massachusetts, crustal tilt from three borehole tiltmeters 2—54688
California, Devil's Playground area of Mojave Desert, stratigraphy and tectonic framework of Mesozoic rocks 2—57739
capture resonance of asteroid 1685 Toro 2—69169
central Alaska, crustal morphology, seismic data 2—57741
chandlerian wobble (1900-1970) 2—65425
coastal southwestern Oregon, sedimentation, erosion and man. 2—57737
core, MHD, model 2—81640
core, viscosity at boundary on inner and outer regime 2—65542
core structure, multiple longitudinal waves from distant earthquakes 2—44588
core-mantle boundary, effect of magnetic field on SH reflection 2—72639
creep, law which accounts for damping 2—58482
crust, anisotropy, obs. of tidal strains 2—78281
crust, gravimetric model in Eastern Alpine area 2—54597
crust, sedimentary cover and depth structure from natural electromagnetic field probing 2—44596
crust, structure and physical props. in Fennoscandia 2—51511
crust, uppermost part, gradient layer as waveguide of body waves 2—54645
crust movement, causes 2—54667
crust rel. to lunar and Martian crusts, three-dimensional model 2—81917
crust-mantle structure infered from SH and SV wave spectra 2—78276
crustal and upper-mantle-structure beneath Colorado Plateau, determ. from Rayleigh-wave dispersion 2—78278
crustal deformation due to dislocation in multi-layered medium 2—78284
crustal deformations around volcanoes, model 2—78285
crustal movement, three-dimensional geodetic monitoring 2—54611
crustal movements, techniques for obs. 2—57712
crustal movements and anomalous deformation as earthquake forerunners 2—65511
crustal structure from surface load tilts using finite element method 2—72665
crustal structure of Red Sea, gravity meas. in north-eastern Sudan 2—51516
deformation and stresses in non-homogeneous Earth-model with a rigid core 2—51521
deformation by surface loads 2—75430
deformations, postglacial rebound 2—75448
density distrib. near base of mantle and centre 2—72678
density stratification and diapirism, theoretical models 2—65543
depth of magma sources, obs. using thermomagnetic studies of pliocene basalts 2—78283
dynamical properties and internal structures, review 2—51520
Earth resource rockets, first firing in Australia using Skylark 2—75640
Earth-atmosphere-ocean system, intransitive model 2—44518
Earth-Moon gravity tie 2—62650
Earth-Moon system evolution rel. to satellite swarm accretion 2—58484
eastern Canada, possible plate contact in Precambrian 2—57703
eastern Indonesia, tectonic development rel. to Gondwanaland dispersal 2—75429
effect of deviations from spherical symmetry on frequency of torsional vibrations 2—61838
elastic dislocation theory, small elastic gravitational disturbances 2—61958
Emperor Seamounts, Alkali volcanic suite 2—57734
European plate igneous chains, movement over thermal plumes or hotspots in mantle 2—72673
evolution of atmosphere and surface temperature 2—73083
evolution of continents rel. to endogenous processes 2—57708
fault displacement meas. by optical parallax 2—54683
free oscillations, lateral variations of density and elastic moduli 2—51493
free oscillations, toroidal, splitting of eigenfrequencies due to lateral heterogeneities 2—51500
free oscillations for order numbers higher than 50 from earthquakes 2—84704
geodynamical constants, reevaluation from space tracking data 2—58441
geological massif, effect of rheological props. on stress concentration round supported elliptical tunnel 2—44590
global tectonics and ancient trench deposits 2—57754
Gosses Bluff airborne magnetic survey 2—57701
gravity field, 300 n.m. mean anomalies 2—54685
Hawaiian volcanic rifts, influence of gravitational stress on operation and growth 2—57736
Hawaiian-Emperor chain rel. to Cenozoic circumpacific tectonics 2—57735
hydromagnetic oscillations of core rel. to geomagnetic secular variation 2—62378
hypervelocity impacts on Earth and the Moon 2—66195
ice age, commencement and duration 2—48411
Indian Ocean, evolution since Late Cretaceous 2—54691
Indian Ocean floor, hydrothermal ore 2—78291
inner solar nebula, physical conditions 2—81948
interior structure and evolution, det. from differential travel time data 2—57762
internal structure, models 2—57716
inverse theory w. grossly inadequate data 2—72664
joint formation with Moon 2—58444

Earth continued
Jurassic island arc-continental margin collision, Californian model 2—57756
Kodiak Island, Alaska, marine refraction data 2—78258
Lac St. Jean, Quebec, analysis of vertical crust movement 2—81595
land subsidence in Venice, subsoil one dimensional model 2—57817
laterally heterogeneous, theory for elastic-gravitational oscillation 2—78286
latitude obs. for 1935.0-1947.0 at Muzusawa, Kitab, Gaithersburg and Ukiah 2—44514
layering in intrusive rocks, effects of earth tremors and convection currents 2—75436
Leduc reefs, Alberta, seismic wave vel. variation 2—78254
liquid core, dynamics 2—84724
lithospheric slab behaviour as anchors 2—61975
lithospheric tearing beneath Aleutian arc, seismic obs. 2—44578
lower mantle inhomogeneities 2—72680
mantle, lateral inhomogeneities and petrological interpretation 2—54682
mantle anelasticity, attenuation of surface and body waves 2—57522
mantle convection and new global tectonics 2—81639
mantle convection rel. to global gravity 2—57468
marine sediments, compressional wave attenuation 2—78256
mass, refinement from obs. of artificial satellite motion 2—55139
minerals, elastic props. from u.s. and compression data 2—68848
minerals and rocks, equations of state 2—72681
model consistent with free oscillation and surface wave data 2—84726
movement relative to microwave background 2—48656
New Hampshire, gravity evidence for shallow-floored plutons 2—54684
North and South Atlantic, evolution from magnetic data 2—54692
northeast Pacific and Western North America, Cenozoic plate movements and interactions 2—54693
orbital velocity, determination from stellar radial velocity 2—44938
origin and evolution of Earth-Moon system 2—73077
origin rel. to core models and thermal history, review 2—57448
orography, influence on synoptic-scale atm. motion 2—65680
Osakayama, crustal strains, secular and annual changes 2—78295
P-wave propagation from Longshot nuclear explosion, lithospheric slab model 2—68838
Pangea, assemblage and fragmentation, palaeomagnetic evidence 2—54695
phlogopite + enstatite, stability at high pressures, model of micas in upper mantle 2—78221
plain strain with hydrostatic initial stress field, Galerkin representation 2—84718
plate tectonics and the Hercynian Orogeny 2—72674
polar asymmetry 2—69146
polar motion, variations in annual component at individual observatories 2—54689
Precambrian geology rel. to shield development and renewal 2—57707
quarternary tephrochronology of western Canada 2—61967
radiation, determ. of total outgoing intensity of earth-atmosphere system 2—54810
radiation balance mapping 2—48506
radiation budget from satellites during five-year period, critique and reply 2—57478
Rangely anticline, northwestern Colorado, absolute stress meas. 2—72671
remote sensing of Earth resources and environment, seminar (Palo Alto, USA, Nov. 1971) 2—84767
resistance curves of anisotropic layer of finite thickness 2—61962
Resources Technology Satellite model, testing 2—51676
rock elasticity, effects of pressure 2—68849
rock fracture and flow, effect of triaxial stress system 2—72679
San Andreas Fault movement, laser satellite meas. 2—54690
San Francisco Bay area, crustal models from transfer function ratios 2—57740
seabed sand transport and whistling beaches 2—61959
seamounts, palaeomagnetism 2—54947
sedimentary stratum, density inhomogeneities, gravitational core sampling 2—44525
seismic modelling, crustal structure 2—61963
SH-wave propagation in anisotropic inhomogeneous crustal layer 2—51512
Shikoku, Japan, Permian oceanic crust and plate junction 2—75434
Smithsonian Standard Earth (II), 1969, empirical data and variance-covariance matrix 2—72601
solar wind flow past Earth rel. to interactions with Mars and Venus 2—78574
southeastern California, petrography and statistical analysis of late Precambrian-Cambrian quartzites 2—57563
southern Alaska, uplifted trench sediments, circumpacific comparisons 2—57755
static deformation of multilayered spherical model by internal sources 2—51492
structure, non-stationary mag. fields probing, curves transformation 2—44589
structure, obs. using differential travel times 2—57696
structure, pseudo-aftershocks from underground nuclear explosions rel. to upper mantle and outer core 2—84728
subsurface pollution, waste disposal sites 2—62005
surface tilting obs. in Koyna-Pophali region, India 2—65531
Tasman Sea, Macquarie Ridge, Alpine Fault, plate tectonic considerations of evolution 2—54671
Tasmania, plate tectonics model rel. to lower Palaeozoic 2—84723
tectonic processes, relation between Earth and Moon, rel. to orogenetic cycles 2—48392
tectonic stress variations, effect on geyser activity 2—65572
thermal radiation field, spectral angular and height distribution 2—72798
Tidal analyses of simultaneous records taken by 2 Askania borehole tiltmeters 2—54598
tidal time series, spectral techniques for Fourier analysis 2—51494
tide pendulum, Askania borehole tiltmeter, ball-calibration 2—54599
time and latitude observations for July 1971, Tokyo Astronomical Observatory 2—44814
1685Toro asteroid, capture resonance by Earth 2—58518

Earth continued
  total magnetic energy, changes external to core 2−44758
  upper mantle, fourth-order anharmonic theory for prediction of equations of state, high compression and temp. 2−72676
  upper mantle flow rel. to dislocation mechanisms of olivine 2−65533
  upper mantle seismic anisotropy 2−72662
  upper mantle structure det. from seismic wave velocity obs. 2−57643
  upper mantle structure in Western USA from body wave obs. 2−57717
  upper mantle velocity distribution rel. to P-wave travel times 2−57519
  velocity rel. to absolute space, suggested meas. method 2−82204
  western Oregon and Washington, stratigraphic evidence for rifting 2−57738
  western Pacific in Late Mesozoic, mag. anomaly limitations and plate tectonics 2−54694
  Rn exhalation from ground 2−61988
  ^{222}Rn and ^{220}Rn exhalation from ground, technique for meas. 2−65565
  Th exhalation from ground 2−61988
 age
  see also Radioactive dating
  Alps, summary of magmatic history 2−57709
  continental evolution rel. to lunar thermal history and mare basalts 2−57449
  igneous rocks from ophiolitic complexes, paleozoic ages 2−62002
  Kiaman magnetic interval lower boundary, palaeomagnetic and radiometric det. 2−48408
  Lewisian basement gneisses from Scotland, discordant zircon age patterns 2−61997
  metamorphosed belt-series sediments, discordant radiometric ages 2−61999
  meteorites, small bodies in Solar System 2−66190
  mica pairs, coexisting, K-Ar ages 2−62001
  Mountsche Toundra Pluton, USSR, secular evolution limits of ^{87}Sr/^{86}Sr in mantle 2−62000
  oceanic basin, rel. to continental drift 2−57773
  paragneisses, polymetamorphic and anatectic, zircon ages interpret. 2−61998
  Precambrian rocks, Northern New Mexico, Rb-Sr geochronology 2−61995
  volcanics of Southern High Plains, K-Ar dates and nature 2−62003
  zircon U-Pb and whole rock Rb-Sr age lowering during metamorphism of Grenville Province 2−61996
  Rb-Sr geochronolgy data, use of two-error linear regression treatments 2−61994
 composition
  — 2−61966
  acoustical holography, detection of geological formations, digital computer processing 2−44554
  amino acid abundance 2−57729
  asthenosphere, CO$_2$ rich, model 2−57705
  Atlantis Fracture Zone, Mn crust chemistry and mineralogy 2−61983
  basalts from East Pacific Rise, compressional and shear wave vels., 10 kbars 2−65481
  Bryan field, sediment cored anticline 2−44584
  Canada, upper mantle and deep crust 2−65552
  carbonatite magma, nature and composition 2−75427
  core, inhomogeneous accretion hypothesis, early melting 2−51518
  crater impact genesis rel. to geometric similitude of lunar and terrestrial craters 2−78510
  crust and upper mantle structure, large aperture seismic array, teleseismic residuals 2−65528
  deep crustal seismic reflections, complex structure of southern Alberta, Canada 2−51498
  Denali Fault, Alaska, crustal deformation 2−65544
  density anomalies, satellite observations and gravity measurements 2−57714
  equatorial Mid-Atlantic Ridge, rare earth element distrib. in gabbros 2−54676
  geochemistry of stable isotopes and radiochemistry rel. to geology, report 2−63954
  Hawaiian Ridge, origin, K-Ar dating 2−57725
  inferences from He content obs. in S bank fumarole of Kilauea Volcano 2−57742
  interior, det. from differential travel time data 2−57762
  Jan Mayen island, geochemistry of alkali olivine basalts from eruption 2−54669
  late Cainozoic shoshonitic lavas from Torres Strait, Papua and Queensland 2−54670
  lithosphere, possibility of e.m. waveguide 2−75428
  lower oceanic crust, evidence for seismic anisotropy 2−51519
  Lyra basin, structural geology from reflection profiles 2−57723
  magmatic activity as major process in chemical evolution of crust and mantle 2−57480
  magmatic silicate liquids, viscosity prediction 2−78222
  mantle, applic. of solid eqn. of state eval. scheme for h.p. phases 2−61981
  mantle, lower, rel. to elastic props. of periclase, wustite and stishovite 2−61980
  marine sediments, compressional and shear wave velocities 2−57697
  Mid Atlantic Ridge near 45°n, electron microscope obs. of magnetic minerals in basalt samples 2−61870
  New Caledonia Basin, possible folded structure 2−57721
  New Guinea-Solomon Islands area, crustal structure and tectonics 2−57542
  North American upper mantle, seismic wave attenuation and partial melting 2−65527
  Pacific Ocean, anisotropy of oceanic upper mantle 2−57540
  seismic studies of crustal structure beneath the seas and oceans 2−61894
  tectonic features, relation to mineral deposits 2−57724
  Tonga, volcanic island, submarine eruptions 2−65545
  upper mantle, mineralogy rel. to seismic properties 2−57695
  upper mantle, role of exptal., physical acoustics 2−57450
  upper mantle in western Europe, study using long-range seismic refraction 2−84705
  Walvis ridge, volcanics, in situ rocks 2−81621

Earth continued
 composition continued
  West Philippine Basin, structural framework 2−57722
  Ar, radiogenic, excess in metamorphic amphibotes and biotites in Norwegian Caledonides 2−44601
  Fe, distribution in upper mantle 2−72675
  Fe compounds and minerals in deep interior 2−72677
  K occurrence in Fe-FeS core 2−44582
  MgO-FeO-SiO$_2$ system in mantle minerals, phase equilibria and elastic properties 2−57711
  Pb isotope ratios in conformable ores and oceanic rocks, evolutionary model 2−61991
  Sr isotopic disequilibrium in lherzolites from Puerco necks, New Mexico 2−65537
  U and Th conc- in wind-borne Saharan dust over N.Atlantic Ocean 2−44583
  Xe, in terrestrial and extraterrestrial matter 2−66040
 electricity
  aerial induction method, conducting body, parameters det. simplification 2−54702
  air-earth current, diurnal variation at Kyoto, Japan 2−78379
  anomalies above conducting sphere, comparison for electrical geophysical exploration methods on land 2−48407
  anomalous conductivity, magnetovariational profiling in quasi-steady approximation 2−54701
  apparent resistivity calc. for laterally inhomogeneous semi-infinite conducting half-plane 2−57783
  audio frequency magnetotellurics application to mineral exploration 2−57800
  Barringer INPUT data, digital processing 2−54723
  conducting earth rel. to auroral zone geomag. variations 2−58113
  conducting sphere in e.m. input field prospecting 2−72626
  conductive structure, N.W. USA and S.W. Canada, determination from geomagnetic variation data 2−54706
  conductive structure, rel. to magnetometer array study of daily geomagnetic variation 2−54916
  conductive structure in S. Central Australia, magnetometer array study 2−54917
  conductivity, geomagnetic variation studies in Ethiopia 2−57792
  conductivity, magnetic and telluric field obs. in Azores 2−54708
  conductivity, sloping and shelving discontinuities, geomagnetic effects 2−65540
  conductivity, under Great Plains region of USA, derivation from fluctuation geomagnetic field properties 2−57791
  conductivity inhomogeneities, perturbation of alternating geomagnetic fields 2−54934
  conductivity profile, inverse problem of geomagnetic induction 2−65563
  conductivity structure, deep electrical soundings of crust-upper mantle in South Africa 2−54707
  core-mantle boundary, effect of magnetic field on SH reflection 2−72639
  covered permeable inhomogeneous cylinder, transient response to line current source 2−57786
  crust, cond. profile in resistant part 2−57799
  crust and upper mantle in Siberia from natural electromagnetic field probing 2−44596
  Dar Zarrouk curves and differential resistivity soundings 2−57502
  d.c. resistivity well logging 2−65541
  depth of investigation of direct current methods 2−78292
  Dhanbad, quartz reefs, resistivity profiles 2−68850
  differential resistivity sounding, equivalent field system 2−51523
  dipping contact effects on behaviour of electromagnetic field 2−54696
  Dykes of Dhanbad, resistivity profiles 2−57780
  Earth, square array resistivity meas., effects of anisotropy 2−72623
  Earth valleys with elliptic cross-section, resistivity meas. 2−72630
  Earth-crust waveguide from e.l.f. to v.l.f. 2−52334
  electrical conductivity, determ. from secular geomag. field variations data 2−72686
  electromagnetic airborne prospecting systems, analogue model studies 2−54722
  electromagnetic airborne system for light aircraft 2−54725
  electromagnetic field, dipping layers effect 2−61986
  electromagnetic prospecting, airborne system, time domain, field checks and model results 2−54726
  electrotelluric field, rel. to strong earthquakes 2−78264
  e.m. depth sounding experiment across Santa Clara Valley 2−54697
  e.m. fields of thunderstorms, information about ore objects 2−72647
  e.m. induction, finite element method of solution 2−54705
  e.m. induction problem, boundary conditions and calc. of surface values 2−48400
  field in sea, instruments and methods of obs. 2−44595
  geoelectric profile containing nonconductive layer, e.m. field 2−72644
  geoelectric sounding curves, multilayer, computer processing and representation 2−44562
  geomagnetic induction problems, method for soln. computation 2−68973
  horizontal polarization in arrays, anomalous geometric variations 2−58110
  Icelandic basalt, resistivity measurements 2−65562
  impedance measurements, effect of anisotropy 2−57784
  induced field, battery operated electrographs 2−57790
  induced polarization and resistivity instrument 2−54699
  induced polarization and resistivity instrument 2−54700
  induced polarization depth location 2−54698
  induced polarization field phase meas. 2−54720
  induced polarization using physical-and-mathematical model, nonlinear phenomenon 2−57779
  induced potentials method, hydrogeological and engineering-geological possibilities 2−54721
  induction currents due to electrojet 2−54913
  Khor Kundi El-Bahan, electrical sounding on water surface 2−72627
  magnetotelluric method, transfer fns. with lateral variation of electrical conductivity 2−57788
  magnetotelluric sounding, impedance for inhomogeneous surface waves 2−78282

Earth continued
electricity continued
magnetotelluric soundings in sea by difference arrangements 2−72714
magnetotelluric type meas. using artificial source 2−57801
micropulsations, polarization characteristics, effect of geoelectric structure 2−66010
New England, magnetotelluric study of elec. cond. anomalies near Atlantic Ocean 2−57798
nonlinear conductivity in boreholes, observation of effects 2−54703
northern France and along the channel coast, electrical conductivity anomalies 2−54704
ore-zone excited by current carrying cable, induction anomaly 2−57781
permeable inhomogeneous cylindrical conductor surrounded by thin shell, Turam response 2−72687
plains of Alberta, interpretation of magnetotelluric data 2−57778
prospecting method for highly conducting bodies and discrimination between ionic and electric conduction 2−54719
resistance obs., point of assignment 2−75437
resistivity, magnetotelluric obs. of lateral changes beneath Iceland 2−57793
resistivity mapping, airborne, using E-PHASE 2−54727
resistivity sounding data, linear filter method interpretation 2−72633
resistivity sounding on three-dimensional transitional model 2−72625
r.f. interference depth sounding for electrical parameters and surface layer thickness estimation 2−55137
rocks, complex dielectric permittivity meas. method 2−54718
rocks, elec. and electrochem. characts., equivalent network 2−65524
rocks, mountain, seismoactive areas, electrical resistivity variation 2−65561
seismoelectric effects in rocks, borehole and lab. studies 2−54641
self potential anomalies, due to spherical ore bodies 2−57785
soil, specific electrical conductivity along power transmission lines 2−61985
South Australia, polarization sensitive magnetic variation anomaly 2−81744
sub-surface magnetic fields produced by line current source on nonflat Earth 2−51665
transient e.m. response of conducting infinite cylinder, surveys for elongated ore deposits 2−44594
Turam modelling, veins of finite length in conducting half-space 2−54724
two concentric spherical shell model, transient e.m. stressing 2−44597
upper mantle conductivity structure in Nigeria 2−57782
upper mantle geomagnetic induction studies and electrical state 2−57787
Upper Rhine Graben, preferred directions of polarization 2−57789
Wenner three-electrode and dipole-dipole d.c. resistivity methods, investigation depth 2−72629
Fe liquid core, calc. of electrical resistivity 2−54674
heat
aeromagnetic survey of Mexicali-Cerro Prieto geothermal area 2−54928
BOMEX core experiment rel. to total atmospheric radiative heating 2−65444
boreholes near Orlando Florida and Uvalde Texas heat flow from well cuttings 2−61866
Colorado, New Mexico, Texas, Utah and Wyoming, heat flow and radioactive prod. 2−57486
continental drift, moving heaters model 2−57479
convection of mantle and polar ice sheets, critical Rayleigh number 2−51517
convective heat transport with strongly temp. variable viscosity 2−57492
crust, heat flow anomaly associated with dyke intrusion 2−61867
crustal heat sources, statistical thermodynamic model for distribution 2−54678
deep mantle, dynamical processes 2−57713
eastern equatorial Pacific, heat flow and bottom water temperature tectonic interpretation 2−48374
energy budget, deconvolution of wide-field radiative meas. from satellites 2−65447
enstatite, anisotropic lattice thermal conductivity as function of pressure and temperature 2−54619
equilibrium temp. of centre, calc. 2−57487
flow map of Germany 2−54621
fumeroles, physical properties of discharged steam 2−78247
geyser activity, regulation by 18.6-year Earth tidal component 2−81633
Geysers geothermal area, technique for det. of seismic noise 2−57598
global radiation and energy budget, historical review 2−61864
heat-flow and geothermal gradient in N.E. Poland 2−72608
hot-spots, plate motions and polar wandering 2−57733
hydrothermal percolation at ridge-crest and oceanic crust form. 2−57495
Idaho batholith, vertical distrib. of heat generation 2−65452
Imperial Valley California, anomalies 2−57454
lava pond surface heat and mass transfer, obs. 2−78249
limb radiance obs., improved algorithm for inversion 2−62250
limb radiance obs., radiative response of atmos. 2−62249
limb radiance profiles, inference of stratospheric temp. structure 2−62128
lithosphere, descending, frictional heating 2−57491
lower mantle, temp. estimation 2−51496
magmas and fluid ascending in crust and upper mantle, pressure and temp. gradients 2−65557
mantle, plate tectonics implications 2−54622
mantle, upper, convecting, temp. distrib. 2−57493
mantle hotspot tendency to cluster 90° from relative rot. poles 2−57494
mean temperature of Earth's surface with atmosphere interface balance 2−65449
Melanesia, arc heat flow meas. rel. to plate boundaries 2−57488

Earth continued
heat continued
melting temperatures in mantle, olivine, spinel and periclase melting curves 2−57481
Mesa and Dunes geothermal anomaly, S. California, heat flow and temp. distrib. 2−61868
Mid Atlantic Ridge at 43°N, heat flow 2−65453
Mid Atlantic Ridge near 45°N, heat flow obs. 2−65454
Nibmus 4 i.r. spectroscopy, calibrated thermal emission spectra 2−65765
Norway, south and central, heat flow meas. in drill holes 2−57483
outgoing i.r. flux meas. from SIRS radiance measurements 2−65446
Pacific catastrophy and ocean floor convergence considerations 2−57489
radiation budget, measurements from satellites, natural variations 2−65445
radiation fluxes measured by Cosmos-320, satellite 2−61865
radiation interaction with atm. aerosols. 2−65653
radiative energy budget, analysis of non-isothermal spherical detector 2−62259
Rio Grande rift, heat flow meas. 2−57485
Rio Grande rift, heat flow meas. 2−57484
sea surface i.r. radiance meas. off tropical east-coast Australia 2−65764
seafloor spreading model studies 2−62087
shallow mantle convection, one- dimensional model 2−65450
South Australia, polarization sensitive magnetic variation anomaly 2−81744
surface radiative energy budget, effect of atmospheric aerosols on long-wave irradiance 2−65448
surface temperature from satellite radiometric measurements, water vapour absorption problems 2−54821
tectonics of regional and ocean-floor metamorphism 2−57710
temp. of apparatus during borehole descent, calc. 2−44537
terrestrial flow in N.E. England 2−48375
thermal balance of mid ocean ridge and sea floor spreading 2−48398
thermal convection within mantle, linear stability problem 2−78248
upper mantle, role of exptal., physical acoustics 2−57450
upper mantle and lithosphere, terrestrial heat flow 2−57482
volcanology rel. to composition and processes of upper mantle 2−57514
Zambia, heat flow meas. in boreholes 2−61869
magnetic field
activity correl. with gravitational signals in Weber's expt. 2−44824
aeromagnetic survey of Liberia, West Africa 2−78294
ancient field, influence of chemical magnetization on intensity determ. 2−78409
anomalies along fracture zones 2−54942
anomalies due to two-dimensional structures 2−65993
Arizona, deeper crust obs. 2−57745
automatic method of compilation and mapping of high resolution aeromagnetic data 2−65994
Baffin Bay, magnetic anomaly map of central oceanic area 2−57457
Block Island Sound, geomagnetic and seismic measurements 2−57760
Bristol Bay, Alaska, crustal lineations based on mag. and gravity surveys 2−57797
component obs. at sea, corrections for deviations 2−72906
components and moduli in ocean, latitude distribution 2−44769
conductivity profile, inverse problem of geomagnetic induction 2−65563
conformal-grid method for analytic continuation of two-dimensional fields 2−72604
conjugate points, real height variations of ionospheric F2 layer 2−51653
continental margin of Africa off Liberia, magnetic anomalies 2−57459
continental margin off Norway rel. to magnetic quiet zone 2−57456
continental shelf off southern Baffin Island, reflection seismic and magnetic profiles 2−57458
control of thermospheric energy sources 2−58021
current systems of weak geomagnetic disturbances at polar caps 2−84923
Darnley Bay, N.W.T., magnetic profiles of large magnetic anomaly 2−75632
data processing and interpretation methods, 1964-71, review 2−78242
dayside limit of closed field lines rel. to solar particles 2−68982
Deccan trap lavas of Aurangabad region, remanent magnetic direction and tectonic significance 2−54946
depth to magnetic layer, det. by maximum likelihood estimation from aeromagnetic fields spectrum 2−51522
disturbed zone between Murray and Molokai fracture zones, origin 2−44771
dyke, interpretation by characteristics 2−54905
dynamo theory of origin, computer applications 2−84712
dynamo theory of terrestrial magnetism, numerical soln. to MHD eqn. of Earths core 2−48594
effects of sloping and shelving discontinuities of Earth conductivity 2−65540
electrical conductivity studies in Azores 2−54708
electromagnetic field, dipping layers effect 2−61986
electron whistler coupling to ion whistler at crossover level 2−72849
e.m. induction in non-uniform conducting half space by external line current 2−58105
external, theories and obs. 2−78387
field distortions rel. to radiation belt particles 2−62382
geoelectric profile containing nonconductive layer, e.m. field 2−72644
geomagnetic pulsations, system of spectral and energetic indices 2−54932
geomagnetic tail, internal structure of neutral sheet 2−65836
geomagnetic tail model, consequences of isotropic static plasma sheet 2−54887
Gulf of Alaska and Bering Sea areas development, model based on earth expansion 2−54716
horizontal component meas. using direction controllable magnet variometer 2−82425

Earth continued
  magnetic field continued
    induction problems, method for soln. computation 2−68973
    interaction with solar wind plasma 2−80225
    international geomagnetic reference field, accuracy and adjustment 2−54911
    International Geomagnetic Reference Field, derivation 2−72903
    International Geomagnetic Reference Field, evaluation 2−54908
    Jurassic Dufek intrusion, Antarctica, palaeomagnetism and magnetic polarity zones 2−58126
    kinematic dynamo in liquid core, Maxwells eqns. 2−68974
    Kosmos-219 satellite, combined meas. of components of mag. field and proton flux and energy spectra 2−72829
    Laschamp polarity event, confirmation in sedimentary cores of latest Pleistocene period 2−54950
    line tracing by Ba vapour in ionosphere 2−65995
    linear magnetic anomalies, intrusives and extrusives 2−58106
    lineated magnetic anomalies near sea floor rel. to geomagnetic chronology of Gilbert epoch 2−58125
    liquid core precession effects 2−54909
    magnetic equator, obs. by POGO spacecraft 2−58044
    magneto-telluric field in nonhomogeneous medium 2−72904
    in magnetosphere, ring current particle injection investigated using dynamical model of radiation belt in self-consistent magnetic field 2−62349
    effect of magnetosphere deformation discontinuities and models 2−48603
    magnetotelluric anisotropy rel. to spreading tectonics 2−54910
    magnetotelluric data, obs. of lateral changes in elec. properties beneath Iceland 2−57793
    magnetotelluric soundings in sea by difference arrangements 2−72714
    magnetotelluric type meas. using artificial source 2−57801
    mathematical models, palaeointensity distrib. 2−44760
    Meanook Magnetic Observatory, obs. for (1969) 2−72902
    measurement, Rb magnetometer operation and performance 2−73511
    monopole term in spherical harmonic reduction of geomagnetic data 2−65996
    Mount Girnar, India, Deccan trap activity 2−81738
    New England, magnetotelluric study of elec. cond. anomalies near Atlantic Ocean 2−57798
    nonstationary field of vertical magnetic dipole in beds of limited thickness 2−54907
    observatory system under test by Institute of Geological Sciences 2−48593
    Oceanic Magnetized Layer, limits and estimates of props. from near-bottom meas. 2−54776
    Ogo 5 magnetic-field data rel. to low-frequency magnetic wave theory in bow shock region 2−65840
    outer magnetosphere, magnetic-field measurements in high geomagnetic latitudes 2−68931
    Pacific Ocean floor, near-bottom mag. lineations 2−54712
    paleomagnetic directions and pole positions, pole numbers 12/1 to 12/180 2−48608
    paleomagnetic evidence for centred dipole source of geomagnetic field 2−58101
    plains of Alberta, interpretation of magnetotelluric data 2−57778
    polar cusp F-layer, magnetic control 2−54902
    pole movements, solar activity effects 2−66226
    potential field, Fourier method for regional residual problem 2−57464
    projection of midday magnetospheric boundary with diverse geomagnetic dipole orientation 2−54879
    reconnection of lines of force with interplanetary mag. field 2−72907
    reconnection rate with interplanetary field meas. using interplanetary solar particle discontinuities 2−62727
    reversal, c.28000 BC, evidence from Australian aboriginal fireplaces 2−58133
    reversals, and palaeomagnetic investigation of Icelandic lava flows 2−44777
    reversals, search in ferromanganese nodules 2−54951
    reversals, stationary solutions of kinematic-dynamo equations 2−51654
    sea floor spreading magnetic anomalies in Central North Atlantic Ocean 2−57898
    solutions representing dipole field immersed in plasma 2−43130
    sounding by singular point method, phase curve interpretation 2−84925
    spectral analysis of geomagnetic var. rel. to tidal and storm modulation effects 2−84920
    spectral power density variations in frequency range 1 to 10^{-4} Hz 2−72905
    spherical analysis from angular data, extrapolated g_{1}^{0} value 2−48592
    Steinheim Basin, cryptoexplosion struct. type locality 2−57761
    sub-surface fields produced by line current source on nonflat Earth 2−51665
    Swider 3-hour-range indices and mag. character figures, April to June (1971) 2−51655
    Tasman Sea, central, early opening evidence 2−54711
    telluric potentials recorded simultaneously at 3 sites near Canberra 2−54906
    total magnetic energy, changes external to core 2−44758
    transient e.m. field of current carrying loop over homogeneous Earth 2−51666
    unequal coaxial dipole pair as geomagnetic source, hemispherical contrasts as support for offset dipole hypothesis 2−58100
    upper mantle geomagnetic induction studies and electrical state 2−57787
    upward continuation from uneven track 2−78404
    Urals, inclination, archeomagnetic data 2−84918
    variable field induced in coastal zone 2−48596
    Victoria Magnetic Observatory, record of obs. (1970) 2−72901
    Ba cloud, mag. field meas. 2−62297
  magnetic field, variations
    see also Magnetic storms; Micropulsations
    'intermediate' anomalies in COSMOS-49 and OGO-2, 4, 6 data, determ. of locations and amplitudes 2−54929

Earth continued
  magnetic field, variations continued
    activity, effect on magnetospheric structure and low energy electron fluxes 2−65858
    activity index for short-period fluctuations 2−58109
    activity rel. to interconnection of interplanetary mag. force lines and magnetosphere 2−51659
    aeromagnetic data, design of spatial filters 2−44764
    aeromagnetic strip across NW United States interpretation 2−58103
    aeromagnetic studies north and east of the Azores Islands 2−54918
    aeromagnetic study of Oceanographer Fracture zone-Mid-Atlantic ridge 2−54919
    aeromagnetic survey of Mexicali-Cerro Prieto geothermal area 2−54928
    Alaskan Jurassic palaeomagnetic pole and Alaskan orocline 2−54943
    Aleutian Islands, Quarternary and late tertiary lava flows, geomag. field palaeosecular variation 2−62406
    Aleutian trench, config. of underthrust oceanic plate from anomalies 2−54687
    Algero-Provencal basin, mag. cartography 2−54912
    annual polar field vars. rel. to interplanetary mag. field 2−78572
    annual variation rel. to two-component model of geomagnetic field 2−84916
    anomalies, global, explanation for existing distribution 2−48597
    anomaly on continental rise off Cape Haltteras 2−68980
    archeomagnetic data rel. to geomagnetic field for last 350 years 2−81741
    AU and AL indices on international quiet days and geomagnetic field variations at high latitudes 2−48602
    auroral oval, rel. to field aligned currents 2−65912
    auroral zone, conducting earth effects on standard observatory records 2−58113
    Baker Lake observatory, record of obs. (1969) 2−68977
    basement anomaly, seismic, gravity and mag. surveys 2−57777
    British Columbia and N.E. Pacific ocean, anomaly maps, aeromagnetic survey (1969) 2−68983
    Canadian Arctic Archipelago aeromagnetic results 2−58102
    Cannikin, quasistatic changes, underground nuclear explosion 2−58112
    Central Asia, seismically active region 2−72909
    cosmic noise absorption at 24.6 MHz, effect of magnetic activity at low latitudes 2−54935
    daily, magnetometer array study, related conductive structures 2−54916
    daily, sources, current and induction 2−84926
    daily ranges, dependence on geomag. activity index A_p 2−44766
    daily variation, rel. to determination of conductive structure in N.W. USA and S.W. Canada 2−54706
    daytime irregular pulsation, relation to magnetospheric substorm 2−72914
    deep magnetic-variation sounding theory 2−81740
    deformation of sea floor, meas. from Tufts Abyssal Plain to Washington-Oregon coast 2−54646
    depth extent estimates of magnetized bodies from vertical gradient or multilevel data 2−58121
    disturbances, obs. of energy releases in upper atm. 2−81717
    disturbances in polar cap S_q^p and DP-2 2−72910
    diurnal, at polar caps, caused by critical component of interplanetary magnetic field 2−62385
    diurnal, low latitude, solar wind associated component 2−44768
    diurnal, rel. to determination of polarity of interplanetary mag. field 2−66194
    diurnal and semidiurnal components, amplitudes 2−62380
    diurnal at high latitudes, rel. to. polarity of interplanetary mag. field 2−78571
    DP-2 and equivalent current system 2−72911
    electrical conductivity and equatorial electrojet studies in Ethiopia 2−57792
    e.m. induction effects on equitorial electrojet region, Zaria, Nigeria 2−65998
    e.m. induction in equatorial electrojet region, magneto-telluric relations 2−62386
    energy spectra changes of anomalous magnetic fields 2−48595
    equatorial variability, longitudinal spread 2−66001
    fluctuation properties, rel. to derivation of elec. conductivity under Great Plains region of USA 2−57791
    fluctuations during magnetospheric substorms 2−81713
    fluxgate magnetometer for geomagnetic variations in shallow seas 2−69851
    Fort Churchill mag. observatory, records of obs. (1969) 2−62381
    geomagnetic excursion 30000 b.p., aboriginal fireplace meas. 2−81743
    geomagnetic pole wandering rel. to palaeomagnetism 2−44761
    Gosses Bluff airborne magnetic survey 2−57701
    Great Whale River observatory, record of obs. (1969) 2−66003
    Greenland, west coast, ground based measurements 2−68979
    height and temp. variations of F_2-region max. as function of geomagnetic activity 2−48591
    Honolulu volcanic series, palaeosecular variation 2−65997
    horizontal polarization in arrays, anomalous geometric variations 2−58110
    hot-spots, plate motions and polar wandering 2−57733
    hydromagnetic oscillations of core rel. to geomagnetic secular variation 2−62378
    indian Ocean, evolution since Late Cretaceous, anomaly data 2−54691
    induction, wide frequency band measurements 2−58111
    international geomagnetic reference field, accuracy and adjustment 2−54911
    ionospheric electron content dependence on geomagnetic activity 2−54894
    Jurassic and Cretaceous reversal chronology from marine magnetic anomalies in western north atlantic 2−58117
    K_p index, correlation with solar photospheric activity 2−75992
    Kaena and Mammoth polarity reversal events, palaeomagnetic obs. 2−44600
    Kiaman interval, field reversal during upper Carboniferous and Permian periods 2−44762
    L at Potsdam, Seddin and Niemegk, rel. to sunspots 2−44770
    l.f. oscillations, characteristics 2−65999

Earth continued
magnetic field, variations continued
lines-of-force of anomalous magnetic field used for locating and delineating magnetized bodies 2−54927
low latitude asymmetric disturbance, high time resolution 2−66000
lunar and luni-solar variations in the Indian region 2−51657
lunar and solar daily variations, effect of sunspot cycle 2−75633
lunar daily variation and error analysis 2−66011
lunar magnetic variations and effect of solar activity 2−66013
lunar semidiurnal variations, from 2.5 min. data scalings 2−51656
MAGI, magnetics and gravity compilation-interpretation system 2−57474
magnetic observatory, obs. (1969) 2−68976
magnetometer array study, rel. to conductive structure in S. Central Australia 2−54917
magnetosphere, three dimensional, analytical model with defined magnetopause 2−65813
magnetospheric fluctuating magnetic fields, u.l.f. waves 2−75622
magnetotail changes rel. to geomag. pulsations 2−66005
magnetotelluric method, petroleum exploration of sedimentary basins 2−44765
magnetotelluric method, transfer fns. with lateral variation of electrical conductivity 2−57788
Mesozoic reversal stratigraphy 2−58130
micropulsations, polarization characteristics, effect of geoelectric structure 2−66010
micropulsations meas. by induction coils, digital computation of spectra by power spectral density method 2−62389
micropulsations mid-latitude, octave-bandwidth analysis covering period range 16-24 secs 2−62388
Miyake-jima Island, anomaly 2−58108
Mould bay observatory, record of observations (1969) 2−68978
multi component magnetic survey in areas of ultra low Z and location of dip equator 2−48604
neutral sheet, magnetic effects 2−68975
noise near L∼4, quiet-day power spectra 2−62384
North and South Atlantic, evolution from magnetic data 2−54692
northeast Pacific and western North America, Cenozoic plate movements and interactions, magnetic anomaly data 2−54693
northern France and along the channel coast, electrical conductivity anomalies 2−54704
NW Turkey, seismo-magnetic effect 2−58107
O, component of lunar daily variation 2−44767
ocean areas, airborne meas. of equatorial electrojet effects 2−54913
ore exploration using 3-component drill hole magnetometers 2−58122
palaeomagnetic field variations of intermediate term in ocean crust 2−54968
palaeomagnetic latitudes, investigation using oceanic sediments of lower tertiary age 2−54952
palaeomagnetic poles from sea floor spreading anomalies 2−54948
palaeomagnetic stratigraphy, nomenclature problems 2−62398
palaeomagnetism rel. to field reversals and dipole characteristics 2−58132
paleomagnetic differences between normal and reversed field sources, pole position problem 2−62405
Pangea, assemblage and fragmentation, palaeomagnetic evidence 2−54695
Pc 4 pulsations, observations at Tottori 2−78407
perturbation of alternating geomagnetic fields by three dimensional conductivity inhomogeneities 2−54934
polar cap, rel. to interplanetary mag. field direction 2−62728
polar substorms, correlation with interplanetary magnetic field structure 2−66006
polar substorms, signatures of growth and expansion phases 2−66007
post, Palaeozoic magnetic reversal 2−58115
power spectra meas. at conjugate points, study of electron radial diffusion coeff. 2−62383
pulsation data rel. to long-term statistical forecast of type Pc 1 activity 2−48598
pulsations, high speed spectrum analyser, S-type hissa 2−72920
pulsations, pi2 and pc5, on north-south profile through Europe 2−54933
quiet day diurnal, study at low latitude stations equidistant from dip equator 2−54914
quiet zone in Western Atlantic, meas. of surface and deep tow magnetic profiles 2−54922
Raff-Mason anomaly area extension to 144° W, resolution of fracture zones 2−54924
reversal, evidence from palaeomagnetism of lower cretaceous lava 2−58137
reversal, evidence from palaeomagnetism of lower Jurassic sandstone 2−54957
reversal, evidence from palaeomagnetism of upper cretaceous ash flows 2−54956
reversal, indications in magnetic properties of lower tertiary basalt 2−54962
reversal chronology for tertiary, reviews 2−58116
reversal studies, deep Pacific Ocean cores, susceptibility stratigraphy and paleomagnetism 2−44763
secular, determ. of electrical conductivity of Earth 2−72686
secular, effect on inner proton belt 2−65926
secular, in Pacific Ocean region 2−62379
secular, recording by remanent magnetization of lake sediments, applic. as chronological index 2−54954
secular, response of trapped particles 2−68957
secular, westward drift, planetary waves in rotating global fluid shells 2−81745
secular variation and offset dipole models, applic. of Brunhes epoch palaeomagnetic data 2−54953
secular variations during Brunhes epoch in igneous rocks from Indian and Atlantic Oceans 2−58104
semiannual component of magnetic field rel. to two-component generating mechanism 2−84919
short polarity events in geomagnetic time scale: 55 to 70 million years 2−54923
smooth zones in South Atlantic observed in aeromagnetic profiles, origin 2−54920

Earth continued
magnetic field, variations continued
solar activity effects, variations over 1955-1965 period tabulated 2−44774
solar activity effects 2−66226
solar flare producing regions statistical analysis of relationship to geomagnetic storms, Forbush decreases and SC + Si events 2−54925
South Australia, polarization sensitive magnetic variation anomaly 2−81744
south east Australian coast, magnetic variometer array 2−72908
Sq currents, north south asymmetry, study using ionospheric dynamo model 2−58114
storm, modulation of geomagnetic records 2−54915
storms, sporadic, rel. to solar flare activity 2−75634
sub-auroral activity, associated with changes in sunspot area to number ratio 2−62792
sudden impulses in geomagnetic tail and magnetosheath, propagation 2−72913
surface equatorial variations, on disturbed days 2−66002
Upper Carboniferous to Eocene, polar wandering 2−54949
vector mag. anomalies from single component meas. of field 2−58118
Western Channel diabase, stable remanent magnetization rel. to polar wandering 2−75637
western Pacific in Late Mesozoic, mag. anomaly data 2−54694
world distribution of disturbances 2−81712
zone of magnetic anomalies obs. between East Coast anomaly and Smooth Zone (36°-31° N) 2−54921
rotation
ballistic motion in gravitational field, Coriolis deflection 2−73270
Chandler wobble, changes in inertia tensor due to faulting 2−72657
Foucault's pendulum 2−54582
geodynamic and astronical research in France (CERGA) 2−62641
geostrophic adjustment of rotating homogeneous or stratified fluid 2−61861
gravitational potential and derivatives for non-spherical body 2−54607
latitude obs. using Danjon astrolabe at Paris observatory, (1956.5 to 1970.8) 2−44515
motion about centre of mass, appl. of action-angle variables perturbation theory 2−82289
non-gravitational process and acceleration of Earth's spin 2−58477
origin of angular momentum of Earth-Moon system, satellite swarm accretion 2−58484
paleontological evidence for rotational history since early Precambrian 2−58478
polar motion, long term components 2−61836
pole movements, astronomical determination 2−62691
projectile range, effect of rotation 2−73276
rate variation, hemispheric zonal wind mechanism 2−54584
secular, solar system origin, geological evidence 2−85038
secular deceleration, effect of oceanic tides 2−78240
space vehicle meas. system 2−54614
spin and obliquity variations from al-Biruni's solar data 2−65427
velocity, solar activity effects 2−66226
and zonal kinetic energy balance 2−51569
Earth satellites *see Satellites, artificial*
Earthquakes *see Seismology*
Eberhard effect *see Photographic materials*
Ebullition *see Boiling*
Echelons *see Diffraction gratings*
Echo
see also Architectural acoustics; Reverberation; Sound ranging
atmosphere, stably stratified, sound beam zenith angle depend. 2−44742
atmospherics, line type angel echo, formation, X-band radar obs. 2−62276
bats, echolocating and target-ranging rel. to sonar receiver 2−55546
conjugate ducted echoes observed on Alouette 2 ionograms 2−78391
lower troposphere acoustic sounder experiments 2−48521
open-air theatre, multiple echo reflectors 2−45551
orientation of animals and insects on sensory basis, conference, N.Y., USA (1971) 2−58646
radar echo distributions rel. to Arizona summer thunderstorm regime 2−65700
radar echo from precipitation, spectrum shape at 3.2 centimetre wavelength 2−81658
u.h.f. ionospheric propagation, scattered weak delayed 2−51641
volume reverberation, mathematical model 2−44665
volume reverberation simulation 2−44666
Eclipses *see Moon; Sun/eclipses*
Eddy-currents
e.m. fields in thin conducting strips, integral equations 2−52332
inductive method for cond. meas. of metallic cylinders 2−49239
nondestructive testing of irrad. fuel pins 2−42661
sea of finite depth, modelling 2−44639
semiconductor, electron-hole plasma, in oscill. mag. field 2−80995
$Mn_xFe_{3-x}O_4$, rel. to ferromag. reson. linewidth 2−44430
Si-Fe laminations, losses, dynamic ferromag. domain wall response to a.f. field 2−48062
Si-Fe textured sheet, permeability, eddy current loss, angle and field depend. rel. to domains 2−65153
Edge emission *see Luminescence/solids, inorganic; Luminescence/solids, organic*
Education *see Teaching*
Effective mass *see Crystal electron states/band structure; Crystal electron states/transport processes*
Effusion *see Flow/gases*
Eightfold way *see Elementary particles/symmetry; Field theory, quantum*
Einstein-de Haas effect *see Gyromagnetic effect*
Einsteinium
nuclear targets, electrodeposition methods of prep. for cross section obs. and accelerator bombardment 2−73919
Einsteinium compounds
No entries

Elastic constants
see also Compressibility; Stress/strain relations
acrylonitrile butadiene styrene, Poisson's ratio 2−53784
aedotropic bodies, number of elastic coeff. 2−49066
alkali halides, extrapolation of elastic props. to high pressure 2−65575
alkali halides, high press. and temp. props. 2−61072
alkali silicate glasses, static longitudinal modulus, u.s. study 2−56773
ammonium hydrogen oxalate hemihydrate, rel. to cryst. struct. 2−84005
ammonium oxalate, from triboluminesc. intensity obs. 2−51396
ammonium oxalate hydrate, rel. to cryst. struct. 2−84005
Araldites, polycrystalline specimens, edge effect in moduli 2−60854
p-azoxyanisole, nematic phase, calc. based on lattice model 2−50325
bone, considered as solid-liquid composite 2−69220
bulk modulus loss factor determ. using ultrasound, of small specimens 2−71615
ceramic tile bodies, effect of polymer impregnation on physical and mech. props. 2−80759
composite, unidirectional C-fibre reinforced plastic, shear modulus 2−74921
composite materials, uniqueness of effective moduli 2−66546
cubic crystal, sixth order, method of symmetry operations 2−53779
Debye frequency tensor of single crystals 2−80891
diamond, press. and temp. coeffs. 2−50728
diamond structure crystal, temp. depend., Born method calc. 2−68059
dilute semi-crystalline polymer, elastic model calc. 2−60840
disperse system of spherical cells with compressible elastic membrane, bulk modulus calc. 2−67847
dynamic constants of solids under pressure 2−76326
from elastic wave velocity det. 2−55511
ferrite memory cores, porosity depend. 2−84431
ferrous alloys, strength-differential effect, effective modulus interpretation 2−74853
Gilsocarbon, neutron irrad. effects rel. to high temp. reactor design 2−52871
glass, comp. depend., stratification effects 2−47478
glass, polycrystalline optical specimens, edge effect in moduli 2−60854
glass fibre, high modulus, prep. and crystn. kinetics 2−43902
glass fibre reinforced plastic beams, dynamic moduli and loss factors 2−47487
graphite, Gilsocarbon, irrad. behaviour, Young's modulus 2−56994
graphite, isotropic, influence on creep strain 2−56963
graphite, isotropic, Young's modulus porosity depend. up to 1800°C 2−56772
graphite, nuclear, high fluence neutron irrad. behaviour, two-phase model 2−56048
graphite, oriented, rigidity and limiting strength, comparative estimates 2−47475
graphite, porosity effects 2−50926
graphite, pyrolytic, ribbon for reinforcement 2−56999
graphite, pyrolytic, u.s. transmission technique obs. 2−43664
graphite fibre, fast neutron irrad. effects 2−56992
graphite from isotruxene carbons 2−61023
higher order coeff. calcs. for 32 crystal classes, group theoret. method 2−68058
independent tensor somponents, number determ. for cryst. with n-fold symmetry axes 2−83915
inert gas solids, polycryst., bulk modulus 0K 2−74817
Invar, elastic consts. anomalous temp. depend. in ferromag. state 2−84053
ionic crystal, Brugger-type consts., electrostatic contrib. 2−84057
kaolinite rods, from adsorptive length changes 2−77641
liquid crystal, nematic, calc. based on lattice model 2−50325
liquid crystal, nematic, normal deform. determ. 2−53399
liquid crystal, nonsingular model for screw disclinations 2−56482
liquid crystal, smectic-C, quasielec. Rayleigh 2−67833
liquid crystals, nematic 2−46926
lithium acetate, Brillouin effect obs. 2−50732
lunar samples from Apollo mission 2−66158
metal, Brugger-type consts., electrostatic contrib. 2−84057
metal, bulk moduli calc. from methods of homogeneous deofrm. and long waves 2−47177
metal, calc. from microscopic theory of lattice dynamics 2−84186
metal, f.c.c., point detect-extended disloc. interaction, elastic modulus effect calc. 2−50652
metal, high-damping, dynamic modulus under direct cyclic stresses 2−53861
metal, shear modulus near the melting point and internal pressure 2−80746
metal during bending at low freq., meas. from 20 to 800°C 2−64749
metals, dislocation line tension, effects of elastic anisotropy 2−74772
metals, simple, elastic consts. det. using pseudopotential methods 2−60836
p-methoxybenzylidene-p-n-butylaniline, nematic phase electric const. 2−60427
minerals, u.s. and compression data 2−68848
mullite, press.-sintered, porosity depend. 2−50722
mullite, Young's modulus rel. to porosity 2−43906
muscovite crystals, elastic modulus and deformation, X-ray diffraction study 2−80733
noble metals, temp. and press. derivatives, calc. from equation of state 2−68063
nonionic anharmonic dielec. crysts., second order elastic consts., self consistent theory 2−84056
nonlinearity parameters det. from ultrasonic second harmonics in resonant nonlinear elastic solids 2−41750
pentaerythritol, high temp. phase, u.s. velocity 2−57049
Perspex, Young's modulus, press. depend., stimulated Brillouin scatt. obs. 2−47480
phase transformations, the ΔE effect 2−77664
piezoelectric materials, ultrasonic method of determ. 2−65069
Poisson coefficient for thinly layered medium 2−60862
Poisson ratio of polycarbonate, yield processes, moire-grid anal. 2−84084

Elastic constants continued
poly(2,6-diphenyl-p-phenylene-oxide), molecular motion study by meas. of Young's modulus and mechanical damping 2−74819
polycrystalline ferrites of Mg, Co, Ni, Zn, temp. dependence of Young's and rigidity moduli in range 90-570 K 2−68064
polyethylene, bulk modulus and density in 30 kbar, glass transition temp. press. coeff. 2−83352
polyethylene, rigidity and limiting strength, comparative estimates 2−47475
polyethylene terephthalate, structural characterization of tensile and dynamic loss moduli 2−50721
polyimide moulding, dynamic modulus determ. from stress relax. data 2−43667
polyisoprenes, relaxation modulus, influence of entanglements 2−47484
polymer, drawn, mech. anisotropy represent. as spherical tensors 2−77627
polymer, press. effects, finite strain theory 2−68094
polymer, uniaxially and biaxially drawn, directional props. of compliance consts. 2−77628
polymer cryst., morphology influence 2−60860
polymeric rod, influence of cold working on elastic modulus of nylon 6-6, polycarbonate and high density polyethylene 2−80810
polystyrene-organic liquid system, meas. of Young's modulus in 4-250 K range 2−74820
pressure derivatives calculation in alkali metals 2−60839
pyrocarbon coating, neutron irrad. effects on Young's modulus 2−56771
pyrrone moulding, dynamic modulus determ. from stress relax. data 2−43667
quartz single crystal, edge effect in moduli 2−60854
rare earth oxides, Ln_2O_3, rel. to twinning 2−53739
rare gas crystal, contrib. of high order multipole three body forces 2−74962
rigid modulus det. using free and forced vibrations 2−63079
rochelle salt, from triboluminesc. intensity obs. 2−51396
rock as composite material 2−56974
rocks, effects of pressure 2−68849
rubber blocks, bonded, compressed, elastic stress strain eqns. dynamic relax. solns., Poissons ratio effects 2−66528
rutile struct. cryst., short range force consts. for rigid ion model 2−50982
semiconductor, and low temp. Gruneisen parameter 2−71752
semiconductors, cubic, stress dependence of the Raman frequencies and elastic constants 2−84497
sodium tartrate, from triboluminesc. intensity obs. 2−51396
solid, effect on pressure pulse propagation 2−68074
solid solutions, B2 and $L1_2$ superstruct., antiphase boundary effects 2−47416
steel, carbon, chromizing effects 2−53780
steel, sintered, model to explain behaviour near yield point 2−84128
stress investigation, variable modulus of elasticity 2−78755
sugar, from triboluminesc. intensity obs. 2−51396
tartaric acid, from triboluminesc. intensity obs. 2−51396
transition metal nitrides, Young's modulus determ. 2−61112
rel. to two-body interatomic potentials in lattice model 2−68212
vibrational amplitudes and Debye-Waller factors derivation 2−50983
viscoelastic composites, isotropic, improved bounds for real and imaginary parts of complex moduli 2−56776
wear parameters rel. to Young's modulus to hardness ratio 2−68111
wood, meas. of Poisson's ratio and Young's moduli 2−60841
Young's modulus of filamentary materials, meas. as function of temp. by flexural meas. 2−84112
Young's modulus of muscle during development of rigor mortis 2−66252
Young's modulus of polycarbonate, yield processes, moire-grid anal. 2−84084
zinc-blende type crysts., calc. of third-order and temp. depend. of second-order elastic constants 2−80898
Ag, bulk modulus, influence of neutron irrad. 2−77642
Ag, high pressure effects, meas. using torsional oscillatory method 2−68061
Ag, modulus anomaly during recrystalliz. 2−47577
Ag film, Poissons ratio, X-ray obs. 2−67904
Al, high pressure effects, meas. using torsional oscillatory method 2−68061
Al, high purity, and dil. alloys, review 2−68076
Al alloy, NS.5, Young's modulus and Poisson's ratio, X-ray values 2−71643
Al alloy strip with steel rod inserts, transverse tensile properties and Young's modulus 2−64701
Al single crystal, elastic behaviour under uniaxial stress 2−60837
Al_2O_3, hugoniotelastic limit, rel. to viscosity and loss angle of Young's modulus calc. 2−84055
β-Al_2O_3, Na, K, Rb, and Na-K substituted, rel. to mech. behaviour 2−56770
AlSb, recalculation 2−77626
Ar, compressed, Monte Carlo calc. 2−84058
Ar, solid, Monte Carlo calcs. 2−68062
Ar, solid, stimulated Brillouin scatt. obs. 2−68231
Ar solid, from Monte Carlo calculations along solid-vapour coexistence curve 2−57055
As, Young's modulus and Poisson's ratio, orientation depend. 2−74821
Au-47.5 at.%Cd alloy, Young's modulus, shear modulus, Poisson's ratio, in cubic-orthorhombic phase transform. region 2−77643
B-epoxy fibre reinforced composite, static elastic moduli 2−47743
BN, hexagonal, rigidity and limiting strength, comparative estimates 2−47475
Ba-mica/Al_2O_3 composite 2−56977
$3BaO.5SiO_2$ glass-ceramic, mechanical props. 2−53930
Bi, adiabatic stiffness consts., room temp. to m.p., u.s. determ. 2−74822
Bi, Young's modulus and Poisson's ratio, orientation depend. 2−74821
C, pyrolytic, γ-irrad. stress-graphitized, dynamic mech. props. 2−53775
C composite, chem. vap. deposited felts, compressed 2−61018
C composites, fibre reinforced resin matrix, from u.s. obs. 2−53964

Elastic constants continued
C fibre, diamagnetism rel. to tensile modulus and structure depend. 2—57270
C fibre, fast neutron irrad. effects 2—56992
C fibre, neutron irrad. effect 2—43708
C fibre, S impurity effects 2—50913
C fibre, thermal expansion anisotropy effects 2—54054
C fibre monofilament substrate/chem. vap. deposited B composite 2—53956
C fibre reinforced chem. vap. deposited C composites 2—53955
C fibre reinforced plastic beams, dynamic moduli and loss factors 2—47487
C fibres and composites, u.s. obs. 2—50723
C pyrolytic, fluidized-bed, rel. to struct. 2—56768
$CaCO_3$, monocryst., u.s. obs. 2—80727
$CaCO_3$, rel. to generalized Gruneisen parameters and thermal expansion determ. 2—74996
$CaMg(CO_3)_2$, monocryst., u.s. obs. 2—80727
$CaMoO_4$, u.s. determ. 2—77773
CaO, temp. depend. 2—74823
$CaWO_4$, adiabatic eleastic stiffness moduli, u.s. pulse superposition meas., 15-300K 2—84037
$CaWO_4$, u.s. determ. 2—77773
Cd, third order, Keating's approach 2—84182
$CoAl_2O_4$, porosity effect 2—50729
CoO-MgO solid solns., porosity effect 2—50729
Cs, lattice vibration based on Toya's electron-phonon interaction 2—64834
Cu-Au alloys, press. depend. up to 7 kbar 2—74824
Cu-Cr alloys, Young's modulus, after isochronal annealing 2—77633
Cu-Cu_3Au alloy, Debye temp., elec. resist., comp. and temp. depend., 4.2-293K 2—47752
Cu, high pressure effects, meas. using torsional oscillatory method 2—68061
$CuSO_4$, from triboluminesc. intensity obs. 2—51396
$DyVO_4$, anomalous behaviour at Jahn-Teller induced phase transition 2—84038
$DyVO_4$, rel. to anomalies in Jahn-Teller phase transitions 2—71681
$ErH_{1.81}$, acoustic velocity obs. 2—57047
Fe-Ni alloy, thermal stability, contrib. of Invar anomaly and ΔE-effect 2—50724
Fe-Ni alloy, Young's and shear modulus anomalies, in Invar region, origin 2—77632
Fe-Ni Invar alloy, anomalous temp. depend. 2—80751
Fe-Si alloy, at high temp., and phase stability 2—71546
Fe-Si alloys, conc. depend. 2—74818
α-Fe, rel. to spin order and diffusion, 25-900°C 2—60842
$FeCO_3$, polycrystalline, elastic props. to 10 kbars 2—65573
$Fe_{0.98}O$, wustite, u.s. vel. obs., rel. to upper mantle comp. 2—61980
Ga, determ. by u.s. pulse method 2—71549
GaAs, calc. of third-order elastic constants 2—80898
Gd, meas. of C_{33}, 13 kOe max., 270-320 K 2—44260
$Gd_2(MoO_4)_3$, ferroelec., ferroelastic, rel. to phase transitions and soft optic modes 2—65061
Ge, rel. to homology with Si 2—84190
He, h.c.p. solid, anisotropic rel. to sound velocities 2—50394
He, solid h.c.p. crystal, sound propagation obs. 2—43972
Ho-50%Tb, antiferromag. spiral spin state64843 2—64843
InSb, calc. of third- order and temp. depend. of second-order elastic constants 2—80898
KBr-KI solid solution single crystals, u.s. pulse method, temp. depend. 2—71550
KBr, pure and doped, Young's modulus 2—56835
KCl, pure and doped, Young's modulus 2—56835
Kr, solid, isothermal compressibility and u.s. velocity obs. 2—50725
Kr, solid, Monte Carlo calcs. 2—68062
$LiBaF_3$, mean stiffness and refr. index, u.s. obs. 2—53781
LiCl, gradient-elastic consts. determ. by n.m.r. 2—77637
LiCl, Hartree-Fock wave function and localized orbital calcs. 2—50726
LiF, deformable shell model studies 2—50995
$LiGaO_2$, rel. to electromech. coupling factor and reson. freq. 2—51206
$MgCO_3$, monocryst., u.s. obs. 2—80727
$MgCO_3$, polycrystalline, elastic props. to 10 kbars 2—65573
MgO, hot-pressed, annealing effect 2—50888
MgO, shocked, press. derivatives 2—60853
Mn-Cu-Mo alloy, cold worked, heat treated, Young's modulus, rigidity modulus 2—47476
Mn-Cu-W alloy, cold worked, heat treated, Young's modulus, rigidity modulus 2—47477
$MnCO_3$, polycrystalline, elastic props. to 10 kbars 2—65573
Mo, deformed, Young's modulus and Poisson ratio, annealing time and temp. depend. 2—84054
$(NH_4)_2SO_4$, Brillouin spectra obs. 2—43665
NaBr, pure and doped, Young's modulus 2—56835
NaCl, pure and doped, Young's modulus 2—56835
NaCl, third order constants C_{144}, C_{166}, new inertial loading technique 2—71551
NaCl, u.s. determ., rel. to equation of state, 0-8kbar, 300-800K 2—68065
NaF, third-order u.s. determ. 2—60844
Na_2O-SiO_2 glass, pressure depend. 2—53782
Na_2O-TiO_2-SiO_2 glasses press. and temp. depend. of elastic moduli, ultrasonic interferom. meas. 2—80741
Nb-Mo alloy, effect of comp., 83-373K 2—60845
Nb-Mo alloys, anomalous temp. depend., rel. to Fermi surface features 2—47479
Nb, Young's modulus in normal and supercond. states 2—77635
Nb_3Sn-type compounds, lattice dynamical calc. 2—84187
Nb_3Sn, temp. depend., band model interpret., behaviour near cubic-tetragonal transform. 2—51117
Ni-Fe, powder compact, struct. charact., Poisson's ratio 2—56946
Ni, powder compact, struct. charact. Poisson's ratio 2—56946
Ni, shear modulus, shear strain amplitude depend. 2—78028
$Pb_{1-x}La_x(Zr_yTi_z)_{1-x/4}O_3$ ceramic, Poissons ratio variations and det. of radial mode coupling factor 2—51195
δ-Pu, Young's modulus, elastic limit, dislocation interstitial interaction, meas. apparatus, 4-300 K 2—80739
RbBr(Cl), gradient-elastic consts. determ. by n.m.r. 2—77637

Elastic constants continued
RbH_2PO_4, effect of deuteration, sound velocity obs. 2—74979
Sb, Young's modulus and Poisson's ratio, orientation depend. 2—74821
$ScH_{1.99}$, acoustic velocity obs. 2—57047
Se amorphous, Young's, rigidity moduli, u.s. propagation. 0-60°C 2—57051
n-Si, heavily doped, under uniaxial stress 2—68066
Si, rel. to homology with Ge 2—84190
SiC, polycryst., effects of crystallite size 2—56774
SiC, rigidity and limiting strength, comparative estimates 2—47475
SiO_2, stishovite, u.s. vel. obs., rel. to upper mantle comp. 2—61980
Sn, adiabatic stiffness consts., room temp. to m.p., u.s. determ. 2—74822
Sn and Sn-In dil. alloy, third-order consts. 2—50727
SnF_2, soln. grown crysts. 2—47245
$SrMoO_4$, u.s. determ. 2—77773
SrO, temp. depend. 2—74823
Tb, u.s. wave vel. obs., 70-300K 2—60846
$TbVO_4$, anomalous behaviour at Jahn-Teller induced phase transition 2—84038
$TbVO_4$, rel. to anomalies in Jahn-Teller phase transitions 2—71681
$Te_{15}Ge_3As_2$ glass, calc. from u.s. velocity 2—47742
Ti-V-O and Ti-V-Al-O solid solutions, effect of O content 2—50844
TiO_2, temp. depend., 4-583K 2—84042
TlCl pressure dependence of elastic constants 2—84035
UN, 278K, u.s. determ. 2—53783
VC_x, rel. to fracture surface energy determ. 2—50776
W, sintered, porosity influence 2—84145
W filament, rel. to appl. to composite reinforcement 2—53970
WC-Co cemented carbide, Young's modulus recovery obs., dislocation config. 2—68070
WC-Co hard metal, X-ray stress meas. at carbide phase 2—74910
Xe, solid, Monte Carlo calcs. 2—68062
Xe single cryst., Brillouin spectrum obs. 2—47737
$YH_{1.93}$, acoustic velocity obs. 2—57047
Zr, calc. using Keating's approach 2—43964
ZrO_2-Y_2O_3, current blackening effects, u.s. wave vel. obs. 2—43666

measurement
bars and discs, reson. method 2—45464
Brillouin scatt. method 2—50731
bulk modulus loss factor of small solid specimens 2—47572
continuous recording high temp. system 2—53852
diorites, effects of specimen size 2—57820
dynamic modulus testing apparatus for use under direct cyclic stresses 2—53861
electrostatic driving method, eval. of precise meas. of shear and Young's modulus 2—50791
high pressure effects, ultrasonic method 2—68060
longitudinal, third and fourth order det. by shock compression techniques 2—47567
modulus nondestructive determ. by electroacoustic techniques using computer 2—53785
nematics method for meas. twist elastic constant 2—50329
quartz, X-cut, third and fourth order longitudinal constants det. by shock compression 2—51207
radiation effects, apparatus for reactor meas. 2—84062
reactor fuel particles, irrad., Young's modulus meas. 2—43772
single crystal meas., room temp.-1400K, apparatus 2—56769
snow and ice, l.f. Young's modulus, using double pendulum 2—74878
strain, by holographic interferometry 2—73609
torsional oscillatory method for high pressure effect obs. on elastic constants 2—68061
ultrasonic attenuation and moduli meas. in wires at elevated temp. and ultrasonic thermometry 2—49189
wood, vibration method of det. 2—56844
Bi, resonance electrostatic meas. of temp. depend. 2—71545
$Bi_{12}GeO_{20}$, acoustic resonances of thin plates, frequency meas. 2—51203
CoO, sound velocity and acoustic absorption coefficients 2—43971
Cu, third order, nonlinearity constant D, temp. depend. 2—47744
$KZnF_3$, elastic consts., u.s. vel. meas. 2—84007
MnO, sound velocity and acoustic absorption coefficients 2—43971
NiO, sound velocity and acoustic absorption coefficients 2—43971

Elastic deformation
see also Bending; Stress/strain relations; Torsion
alkaline earth fluorides, point defects vibr. spectra, thermal cond., i.r. absorpt., Raman scatt. obs. 2—71724
anisotropic work hardening materials, elasto plastic analysis 2—76265
ball indentation analysis, elastic-plastic soln., finite element method 2—66496
balloon, of Mooney material, spherelike deformations 2—76275
bending, finite, of a compressible anisotropic rectangular block into a hyperbolic shell, exact solution 2—55455
bonded toroid, finite inflation 2—66544
Boussinesq problem for thick elastic layer under a punch of arbitrary profile 2—58862
buckling, elastic cylindrical shell during longitudinal impact against target 2—66548
cantilevered columns under periodic loads, stability and non-stationary vibration digital simulation 2—69705
Cauchy material, slowness surface, energy propag. vector of second-order discontinuity 2—76276
circular annulus, depression due to load uniformly distributed 2—52156
circular plate loaded along a circle by uniformly distributed transverse load, compact ring, analysis 2—82332
composite, fibre-reinforced, stress boundary value problem for plane strain deform. 2—58868
compressed circular plates, load carrying capacity 2—66492
compressible rubberlike solids, large deformation isotropic elasticity 2—53774
crack tip, finite deformation analysis of elastostatic stresses and displacement 2—77639
creep buckling analysis incorporating elastic deformation and time-hardening creep 2—58863
critical points and stability boundary determination for nonlinear structural systems undergoing loading 2—52151

Elastic deformation continued
- crystals, effects of external force gradients on i.r. and Raman activity of long wavelength optical phonons 2—84513
- cylinders, solid and tubular of incompressible isotropic elastic material, strain-energy functions 2—52174
- disclinations, relation between continuous and discrete 2—76267
- displacement, caused by propagating crack in infinite medium, exact solution and seismological applications 2—61940
- domain boundary displacement under deformation, effect of dislocations 2—72143
- elastic membrane, homogeneous, incompressible, isotropic 2—78880
- elastic plastic, generalised theory for thin membrane shells 2—45414
- elastic plastic solids, resistance to rolling 2—41630
- elastic solids, perfectly conducting in presence of magnetic field, discontinuity expansion solution 2—66603
- elastic-plastic shells of revolution, finite element large deflection anal. 2—78875
- elasto-plastic plates, finite element analysis 2—76254
- elastoplastic medium isotropic, finite deformation, growth of acceleration wave 2—55504
- elastoplastic thick-walled cylinder, incremental stress analysis method 2—55469
- elliptic opening in elastoplastic body, stress conc. 2—52154
- equivalence of F^eF^p and F^pF^e 2—49075
- film, polycryst., anisotropy of deform. 2—80730
- finite deformation of elastic- plastic solids 2—76304
- finite elastic-plastic deflections in circular plates, numerical analysis 2—41629
- finite element analysis 2—52185
- finite-element soln. for large deformation, discontinuous fields 2—76274
- flexible elastic plates, geometric nonlinear theory relationships 2—82326
- glasses, elastic recovery and hardness testing 2—64739
- half-space, indentation by rigid axisymmetric punch, formulation as mixed boundary value problem 2—76303
- hardness, general class for elasto-plastic deformations 2—63068
- hollow sphere, axially symmetric deformation, soln. of boundary value problem 2—82329
- homogeneous prestressed cylinders, stability under small twist 2—52138
- hyperboloid of revolution, single-cavity, under given boundary forces 2—76322
- incompressible bodies, three-dimensional stability problems 2—63062
- incompressible highly elastic bodies, Hu-Washizu type variational principle 2—41594
- indentation of elastic-perfectly-plastic half- space by a hard sphere 2—47498
- laminated arch under mech. and thermal action 2—76324
- laminated fibre-reinforced plates, plane strain bending 2—66543
- linear and nonlinear theories of elastic slender curved rods 2—76289
- liquid crystal, nematic, normal deform. in elec. and mag. fields 2—53399
- membranes, stability 2—58872
- membranes, stability under finite deformation 2—52181
- metal film, elastoresist., relax. phenomena 2—56765
- metal spheres, internal displacements meas. method 2—77644
- microhardness tester attachment for meas. of deformation of wire in coiling 2—82129
- mirrors, light weight, under various support conditions 2—79392
- muscovite crystals, elastic modulus and deformation, X-ray diffraction study 2—80733
- orthotropic bodies, three-dimensional, stability of equilibrium with small deformations 2—41619
- plane region with irregular hole 2—82334
- plastic distortion and disclinations, semi-microscopic 2—76263
- plate, calc. of equilibrium, boundary conditions by combination of displacement fields 2—76269
- plate on viscoelastic foundation, deflection in variable temp. field 2—41639
- plates, anal. of vibrational modes, finite element method 2—82341
- polycrystalline metals, slow elastic plastic deformation with micro stresses 2—76260
- polyethylene, linear, affine deformation during stretching and transformation to original state 2—64703
- polyethylene filled with randomly oriented glass fibres, stress-strain curve 2—77690
- polyethylene films, changes in crystal orientation with time following stretching 2—83381
- polymer films dynamic light scattering study 2—83382
- polymeric materials, diffractometer measurements 2—43749
- polymethyl methacrylate, oriented, relax. rate depend. on struct. transform. 2—47485
- printer type piece, due to impact of print hammer, study using holographic interferometry 2—69666
- prismatic rods, automatic solution of elastoplastic twisting problem 2—82328
- rectangular beam, stress calc. on flexure 2—45401
- Reiner fluid, yield value 2—76264
- rock-joint deformation, modelling 2—72668
- rubber, under small uniaxial extension and compression 2—64705
- rubber elasticity on chemical relaxation 2—83378
- rubberlike materials, stored energy function derived from simple tensile data 2—53787
- rubbery polymers, extension and compression behaviour 2—43681
- sandwich shells of revolution, large elastic plastic deflections 2—76266
- semi-infinite porous medium, two-dimens. 2—58860
- semiinfinite body containing spherical cavity, subjected to uniform pressure 2—41581
- sensing elements, optical projection microscopes for det. 2—45805
- slightly compressible materials, finite deforms., screw dislocations governing eqns. 2—78881
- solid surface, thermoelastic deform. by laser beam 2—43459
- spherical shells, numerical soln. 2—58861
- static, elastic half space by surface pressure, review 2—75430
- steel, annealed low C, at high strain rates 2—71565
- steel, effect of strain rate and temperature on yielding 2—47524
- stretched circular plates, load carrying capacity 2—66492

Elastic deformation continued
- thermoelastic continua, gradient perturbations, stability criteria for perturbations 2—52200
- thin shell surface charging on external (deformational) loading 2—49234
- thin shells, asymptotic solutions for stress concentrations 2—76294
- time dependent in elastic material, small vibrations 2—52188
- time dependent materials, plastic behaviour 2—76256
- Timoshenko type shells, due to transverse displacements 2—66500
- torsion of elastic layers, initial value approach 2—49057
- transverse impact of sharpened body against elastic or elastoplastic membrane 2—78893
- variational principle for finite displacements 2—66537
- viscoelastic Maxwellian media, finitely deformed, evolutionary conditions for mechanics equations 2—52190
- vulcanizates, SBR, temp. depend. of mech. props. under large deformation 2—83379
- zinc-blende type crysts., determ. of anharmonic props. 2—80898
- Al, high purity and dil. alloys, elastic deform., review 2—68076
- BeO high pressure effects on single crysts. and polycrystalline mat. 2—68082
- Fe alloys, grain growth, second max. and nonuniformity after deform. 2—83961
- Ga_2O_3-TiO_2 solid soln., crystallographic shear struct., planar boundaries 2—74768
- KCl, computation of electronic structure of colour centres and electronic polarization fields 2—71520
- NaCl, computation of electronic structure of colour centres and electronic polarization fields 2—71520
- Ni alloys, grain gowth, second max. and nonuniformity after deform. 2—83961
- SiO_2, vitreous, induced birefringence, nonlinear variation with uniaxial stress to 7 kbar 2—68600
- V_3Si, elastic softening and supercond. 2—44081

Elastic fatigue *see Fatigue*

Elastic limit
- *see also Slip*
- alloys, body centred cubic, theory of solid solution hardening 2—77691
- cracking stress of glass fibre reinforced inorganic cement, use of fracture mechanics 2—64726
- cylindrical tube under pressure, elastic-plastic and thick-walled, effect of non-homogeneity on yield pressure 2—49064
- failure criteria of concrete rel. to incremental constitutive laws 2—58864
- fine wire, with small remanent strain 2—43676
- generalized isotropic yield criterion 2—66520
- initial yield surface of unidirectionally reinforced composite 2—66507
- mild steel and plexiglass, yield zone caused by detonative loading, breakage patterns and stress waves 2—84048
- model, nonlinear defect, to explain generation of cracks at breakdown 2—84047
- nylon-epoxide adhesive 2—47673
- post yield fracture mechanics, crack model for high and low strength materials 2—64727
- rocks, yield condition and hardening rule 2—57818
- ruby, h.p. absorpt. spectra studies 2—61630
- steel, annealed low carbon, dislocation model for delayed yielding phenomenon 2—80813
- steel, effect of strain rate and temperature on yielding 2—47524
- steel, effects due to stress fields around inclusions 2—47491
- steel, Mn-Cr-B spring, tempering behaviour 2—77688
- steel, sintered, model to explain behaviour of elastic moduli 2—84128
- surface layer effects in exptal. det. 2—43675
- unidirectionally reinforced composite, determ. using von Mises yield criterion 2—66507
- yield surface, buckling stress, elastic/plastic compressed plate 2—76301
- Fe-Ti-Si alloy, yield stress, during age hardening 2—43806
- Fe, strain ageing and length of yield plateau 2—71624
- UC, polycrystalline, high-temp. deformation and yielding 2—67348

Elastic losses *see Internal friction*

Elastic relaxation
- *see also Creep*
- alloy, ternary, b.c.c., Snoek effect, rel. to substitutional solute atom pairing 2—43672
- heterophase systems, phase nucleation, internal stress relax., coherent loss, thermodynamics 2—60859
- metal during bending at low freq., meas. from 20 to 800°C 2—64749
- poly(1,4-phenylene ether), transitions and relax. of phenomena, 100-800K 2—83355
- polydisperse polymers, undiluted, stress relaxation after steady-state shear flow 2—64482
- polyethylene, high density, melt rheology 2—83371
- polyethylene, X-ray diffraction relaxation 2—43674
- polyethylene films, nonlinear viscoelastic behaviour 2—83375
- polyethylene terephthalate, oriented anisotropy of α and β relaxations 2—60856
- polyethylene terephthalate film, dielec. and dynamic mechanical obs. 2—56779
- polymer solutions, concentration depend. of steady state compliance 2—83373
- polymers, narrow distribution, relation between mol. wt. and non Newtonian viscosity 2—83372
- polymers, undiluted linear narrow molecular weight distrib. samples in terminal zone, viscoelasticity 2—83336
- polymethyl methacrylate, relaxation effects, fracture mechanics 2—80821
- rubber elasticity on chemical relaxation 2—83378
- squalane, viscoelastic relaxation study 2—46987
- squalene, viscoelastic relaxation study 2—46987
- 5,5,11,11-tetramethylhexadecane, spin-lattice relaxation rates meas., cf. with viscoelastic relaxation 2—46987
- thermal, rel. to transient thermoelastic waves in half-space 2—58905
- vulcanizates, SBR, temp. depend. of mech. props. under large deformation 2—83379

Elastic relaxation continued
Al_2O_3, hugoniotelastic limit, rel. to viscosity and loss angle of Young's modulus calc. 2−84055
Au-Cu alloys, Zener relax., internal friction obs. 2−60852
Co, mag. after-effect of hydrogen 2−78029
Fe-V-N alloy, abnormal Snoek peak 2−47482
Nb, O and N Snoek peaks, grain size effect 2−50736
Ni, mag. after-effect of hydrogen 2−78029
Ta, Snoek effect absence for H 2−77647

Elastic waves
see also Acoustic waves; Magnetoelastic waves; Seismic waves
absorption and velocities in saturated porous media, calc. using Frenkel-Biot theory 2−82343
acceleration, in strained α-quartz 2−45487
acceleration wave growth in isotropic elastoplastic medium in state of finite deformation 2−55504
acceleration wave propagation in anisotropic hyperelastic materials 2−78911
acceleration waves in deformed elastic nonconductors of heat 2−45483
acceleration waves in nonlinear viscoelastic materials, prediction of response using steady shock waves 2−49080
acoustic emission, generic discussion 2−49134
anisotropic, two-dimensional, wave-front singularities 2−49115
in anisotropic media, Q-ellipsoid derivation 2−65503
anisotropic plates, solution of wave equation and coupled thermoelastic problem 2−55506
Araldites, polycrystalline specimens, edge effect in wave velocities 2−60854
in beams, hyperbolic differential equations, second- order difference method 2−69716
bending waves, multiple scattering by random inhomogeneities 2−73416
blood vessel wave propagation, application of prestressed shell theories 2−82338
circular cylinders subject to finite deformation, propagation 2−76337
circular cylindrical shells, dispersion of flexural waves 2−63108
composite viscoelastic layer, propagation in magnetic field 2−55462
coupled thermoelastic waves in solids 2−43673
crystals, imperfections, scanning electron microscopy 2−80623
in cubic and tetragonal crysts., external conical refr. 2−74825
cubic crystals, shear horizontal surface waves on (001) face 2−80745
cubic crysts., damping, effective anharmonicity consts. 2−80913
curved beams, pulse propagation theory 2−76362
deformation, time-dependent, generation in elastic material 2−52188
diffraction, l.f., by Griffith crack 2−49068
diffraction by rigid ellipsoid, integral eqn. method 2−52219
diffraction by two coplanar Griffith cracks in infinite elastic medium 2−41671
diffraction by two coplanar parallel rigid strips 2−78900
dispersive Rayleigh waves, harmonic generation as sensitive meas. of thin film elastic properties 2−50472
dynamic contact problem, effective method of solution 2−76284
elastic half-space, surface displacements due to surface dipole 2−58903
elastic half-space, vertical surface displacements due to buried dipole 2−58904
elastic plate, effect of surface irregularity 2−55464
elastic stress pulse reflection at interface between elastic rod and elastic half-space 2−73414
elastic-plastic medium, propagation of two-dimensional waves 2−66572
elasto-plastic medium with Mises plasticity, single waves and shock break-up 2−52218
elastodynamic representation theorems, propagator matrices 2−78898
elastoplastic wave propag. in bar for nonlinear stress/strain case 2−82345
electromagneto-thermoelastic plane waves in solids with thermal relaxation 2−45435
elliptical discontinuity effects on stress distribution 2−45485
emulsions, semi-solid, viscoelastic props., dynamic meas. by Weissenberg rheogoniometer 2−83817
equations of motion for infinite isotropic homogeneous elastic media, multipole expansions 2−55513
explosion inside oblate spheroidal and circular cylindrical cavities considered from circular disc source 2−51503
ferrimagnetic crystals interactions with magnetic fields 2−43673
ferromagnetic alloys interactions with magnetic fields 2−43673
ferromagnetic crystal, interaction between elastic oscillations and precessing mag. moment 2−81208
fibre reinforced composite materials 2−43673
finite amplitude in rods, subject to impact loading, Bell's parabolic law study 2−58901
flexural in prismatic bars, effect of initial stress 2−45492
glass, polycrystalline optical specimens, edge effect in wave velocities 2−60854
guided, leaky wave couplers for devices 2−73413
guided, propagation problems, h.f. asymptotic solutions 2−66606
harmonic, propagation through composite media with periodic structure 2−66604
helical Rayleigh waves, excitation and reception on rods of contactless electrodynamic transducers for nondestructive testing 2−50634
helical spring for reverberation devices, propag. of struct. borne waves 2−45489
h.f., refraction by major crustal and upper mantle horizons in Earth 2−68842
on impedance bodies of resolution 2−52226
infinite rectangular elastic bars, effect of surface mass distribution 2−73415
inhomogenous anisotropic media, intensities, numerical techniques 2−72635
isotropic body with initial stresses, propagation 2−41673
Lamb, guided propagation problems, h.f. asymptotic solutions 2−66606
Lamb's problem, leaking modes 2−44576
laminated composite materials, simple thickness modes 2−73438
laterally inhomogeneous media, numerical calculations 2−63106

Elastic waves continued
layered micropolar isotropic elastic half space, surface wave propagation 2−55463
leaking modes, real frequency complex wave number analysis 2−45480
l.f. biaxial loads effects on stress concentration factors in plates 2−41599
longitudinal, plane, reflection from boundary of elastic half-space covered by particle layer 2−76359
longitudinal, propagation in composite bar with conical sections 2−41668
longitudinal stress pulse amplification in elastic bars with intermediate tapered region 2−41678
Love, guided, propagation problems, h.f. asymptotic solutions 2−66606
Love type, propagation in infinite cylinder with rigidity and density varying linearly with radial distance 2−75418
Love wave, surface excitation 2−63111
Love waves dispersion, heterogeneous layer lying over homogeneous half space 2−72617
metals, interactions with magnetic fields 2−43673
micropolar elastic half space, reflection laws and amplitude ratios 2−41667
mixed surface waves at boundary between elastic medium and fluid 2−52216
motion of rigid disc in contact with plastic solid 2−55509
nonhomogeneous isotropic media, propagation at surface, of spherical opening 2−78899
nonstationary SH waves in elastic sphere with waveguide 2−61889
overlay elastic waveguides, thickness effects on higher modes 2−49109
P, S and Rayleigh waves in plexiglass and plaster of paris 2−41674
photoelastic, linear and nonlinear theories 2−66602
in piezoelectric composite transducer, mechanical response in thermal field 2−41756
in piezoelectric crystals, nonlinear acoustic parameters 2−61087
piezoelectric film surface wave transducers, coupling factor, capacitance and phase velocity 2−49111
piezoelectric substrate, phase and amplitude distrib., electrostatic surface probe obs. 2−63093
plane, interaction with embedded circular cylindrical shell 2−78912
plane harmonic, propagation in fibre reinforced elastic material 2−66611
plane wave admittance of elastic half space 2−41680
plastic, with discontinuous loading conditions, hodograph transformation 2−66609
plate, laminated, harmonic propag. 2−49095
plate with circular holes, dynamic stresses 2−45484
polycrystalline material, effective moduli and attenuation in presence of phase transform. 2−60851
pressure pulse propagation in solid, effect of mechanical props. 2−68074
propagation from cylindrical waves, effects of couple stresses 2−55508
propagation in anisotropic half-space 2−57506
propagation in circular cylinder when torsional shear stress is applied to end surface 2−52220
propagation in discretely inhomogeneous elastic cylindrical rods, comparison of two theories 2−45488
propagation in elastic medium with surface Coulomb friction 2−76364
propagation in finite length bar with variable cross section 2−45486
propagation in laterally inhomogeneous media 2−68844
propagation in nonlinearly elastic rods, perturbation solutions 2−58902
propagation in prestressed Mooney material, response to impulsive lines of force 2−82339
propagation in truncated conical shell 2−69717
pseudo-Stoneley waves, line source on a solid solid interface 2−81577
pulse propagation, nonlinear viscoelastic rod of finite length 2−45482
quartz, free surface, reflection 2−41681
quartz single crystal, edge effect in wave velocities 2−60854
quartz with thin surface film of Ge, electron microscope obs. of propagation 2−80732
Rayleigh, axial, on cylindrical surfaces of transversely isotropic material and varying density in mag. fields 2−73418
Rayleigh, dispersion in inhomogeneous medium, rel. to Love waves in crust and upper mantle 2−73419
Rayleigh, guided, propagation problems, h.f. asymptotic solutions 2−66606
Rayleigh, numerical model for propagation around corners 2−57619
Rayleigh surface wave coupling, tunable matching 2−50417
Rayleigh wave propagation in nonhomogeneous layer between two homogeneous semi infinite media 2−49106
Rayleigh waves, analysis 2−58900
Rayleigh waves, isotropic half space, moving thrust fault 2−72613
Rayleigh waves excitation on unphased interdigital structure 2−69732
Rayleigh waves on concave cylindrical surface, two-dimensional models 2−82337
reflection and transmission by moving slab 2−52215
rock, undergoing phase transitions, det. of velocity and attenuation 2−57594
scattering by interface irregularities, unified treatment 2−61884
scattering by movable rigid sphere in infinite elastic solid 2−52252
scattering by moving objects 2−55514
seismoelectric effects in rocks, borehole and lab. studies 2−54641
SH, in inhomogeneous wedge, Green's function 2−73420
shear finite amplitude, energy propagation 2−52222
shock, one-dimensional, amplitude governing equation 2−52221
shock activity during injection of water into stressed rock 2−55510
silicone based electrons, dynamic shear properties over wide temp. ranges 2−47488
solid granules, effect of grain size on absorption and velocity 2−84204
spherical, acoustic, transient interaction with spherical elastic shell, Cesaro mean appl. 2−66614
spherical, dilatational, scattering by spherical cavity 2−66610

Elastic waves continued
spherical, in viscoelastic media, numerical computation 2−66608
spherical resonance obs. on medium Q materials 2−55512
stability of nonlinear oscillations of elastic rod 2−73399
Stoneley wave equation, complex roots 2−45479
Stoneley wave equn., solid liquid interfaces 2−41676
strain, on centre line of Al bar, resulting from impact, expt. and numerical obs. 2−66605
stress, propagation in cylindrical shells, perturbation analysis 2−66607
stress, reflection and transmission at interfaces between elastic materials 2−41677
stress release, initial front, emitted by suddenly expanding crack in elastic solid 2−66612
stress waves, laser generated in circular elastic ring 2−45436
stress waves, thermally induced in laminated composite 2−47665
surface, on multilayered anelastic media 2−63105
surface, reflection from periodic arrays on YZ $LiNbO_3$ 2−51022
surface, reflection from plate edge and generation of propagating acoustic diffraction field 2−55507
surface, wedge transducers, high efficiency, excitation by bulk-wave beam 2−49113
surface probe, electrostatic, waveform distortion meas. 2−49170
surface velocity meas., coherent pulse superposition technique 2−49108
surface wave encoders and decoders, temp. and Doppler shift effects 2−49107
surface wave filters in integrated circuits 2−49112
surface wave propagation, guided by ridges calc. by finite element technique 2−76335
surface wave radiation from buried volume relaxation source in multilayered half-space 2−57639
surface waveguide effect for wave equation 2−41669
surface waveguides, single mode, large aperture 2−49110
thermochemical effects on propagation 2−45481
thermoelastic, diffr. at cylindrical cavities 2−76363
thermoelastic, diffraction on cylindrical and spherical surfaces 2−55505
thermoelasticity, new theory, plane wave propagation 2−73394
thin hollow cont., propagation, by finite elements 2−76361
three-dimensional body, tensor wave theory 2−76336
torsional wave in rod, stability under initial stress 2−41675
transient, in Voigt solid, boundary condits. 2−63107
transient, theory, nonlinear and thermal effects 2−76340
transient linear, propagation in shells, analysis by finite difference method 2−63109
transient thermoelastic, in half-space with thermal relaxation 2−58905
two and three dimensional, transition between in seismic models 2−65459
U.S devices, h.f., review in book 2−57046
velocities in solid materials, pressure depend., porosity effects 2−54635
velocity det. in materials from phase delays corresponding to transmission times 2−55511
velocity in Indian rocks rel. to others 2−75453
visco-elastic half-plane, Rayleigh waves 2−66573
viscoelastic material, linear, longitudinal waves 2−58906
wave-propagation in biaxially-stressed elastic media 2−49116
weak, acceleration, propagation in elastic-plastic strain-hardening rate-independent solid 2−41672
Al_2O_3, light scatt. by elastic waves and rotation of polarisation plane 2−72358
B-epoxy laminated composite plates, holographic stress analysis 2−78895
Cu, stress pulse damping in region of propagating brittle crack 2−60801
He/Cu interface, Rayleigh waves influence on Kapitza resistance 2−47764
KH_2PO_4, light scatt. by elastic waves and rotation of polarisation plane 2−72358
$LiNbO_3$, dispersion of elastic waves and permittivity along trigonal axis 2−72033
$LiNbO_3$, light scatt. by elastic waves and rotation of polarisation plane 2−72358
MgO, shocked, vel. meas., press. derivatives 2−60853
RbH_2PO_4, light scatt. by elastic waves and rotation of polarisation plane 2−72358
SiO_3, light scatt. by elastic waves and rotation of polarisation plane 2−72358
ZnO film, d.c. triode sputtered, u.s. surface elastic waves, coupling factor phase velocity, propag. loss 2−80560

Elasticity
see also Compressibility; Mechanical strength; Stresses, internal; Thermoelasticity; Viscoelasticity
— 2−58875
aeolotropic elastic rotating disc, study of transverse vibrations 2−52204
aeroelastic stability of flat anisotropic sandwich-type plates 2−49073
aeroelasticity, trends and achievements 2−50254
anisotropic, dynamic Green's tensor calculation 2−76302
anisotropic nonlinearly elastic body, strain stability, applicability of Euler approach 2−69672
anisotropic shells, classical linear theory 2−49072
anisotropic shells, concentrated forces effects 2−78883
arbitrarily shaped solids, solution of fundamental three-dimensional problem 2−76282
Babuska's paradox of simply supported Kirchhoff plate and finite element method 2−78894
beam cantilever, Saint-Venant bending, closed form elasticity solns. 2−66505
beam-columns, computer programs 2−66599
borate glass, separation of delayed elasticity from viscous flow 2−56781
boundary problem of asymmetric theory, quasi- classical approximation 2−52177
boundary problems, Laplace's equation appl. 2−82309
boundary value problem, couple stresses in circ. region 2−41618

Elasticity continued
boundary value problems of elastic media, Fourier-Laplace transform 2−76293
boundary-initial-value problems, semidiscrete approx. 2−63053
boundary-value problems, radiation property 2−45411
brittle materials, crack propag. rel. to nonrecoverable elastic energy, Griffith criteria 2−71595
buckling of elastic systems, stability theory 2−76242
buckling of thin plate, hybrid displacement methods 2−82311
Cauchy material, slowness surface, energy propag. vector of second-order discontinuity 2−76276
circular cylindrical shells axially compressed 2−52160
circular hollow beam problems 2−66549
classical elastic sphere problems, numerical solution by integral equations 2−45383
classical theory, applied to contact problem in multilayer medium 2−78889
composite elastic sphere and cylinder, vibrations 2−66583
composite fuel annular bodies, fracture and elastic props. 2−71588
composite materials, variational methods for obs. of props. 2−66604
composite materials multi-continuum theory 2−71655
compressibility effects for nearly incompressible elastic solids 2−52170
compressible rubberlike solids, large deformation isotropic elasticity 2−53774
computation, plane elastic systems 2−41614
conical shell, fastened in screen, effect of sound press. wave 2−69712
contact problem, axisymmetric, for elastic half-space with cylindrical hole 2−58843
continuum mechanics, role of thermodynamics 2−52191
Cosserat, theory, stress wave propagation in elastic rods 2−41679
crack originating at edge of circular hole, stress intensity factor 2−82336
crack propag. in elastic material strips under plane extension 2−45407
crack propagation in elastic solid subjected to general loading, constant rate of extension 2−55470
crack propagation in elastic solid subjected to general loading, non-uniform rate of extension 2−55471
cracks, radial, in a circular ring, elastic anal. and comparison to internally pressurized cylinders 2−69647
crystal class 6m2, standard choice of axes 2−68474
cylinder with plane faces displacement-free, eigenfunctions for symmetrical deformations 2−58867
cylindrical and spherical layers, one-dimens. stationary elastic field 2−76323
cylindrical cavity in infinite elastic medium, dynamic and impact responses 2−69665
cylindrical configurations, elastic analysis with stress singularities 2−66515
cylindrical shell, finitely deformed, stability 2−49069
cylindrical shell, with liquid, motion under axial shock loadings 2−73385
cylindrical shell finite element based on independent strain functions 2−49067
cylindrical shells, dynamic responses to concentrated radial loads 2−55457
cylindrical shells with arbitrary closed periphery 2−63072
deformed material, spatial energy propagation vectors 2−45415
diffraction contrast from coherent precipitates in elastically-anisotropic materials 2−80671
discrete, theory of variated states 2−41611
discs, blocks, point loaded, plain stress, plane strain elasticity, numerical approx. method 2−66526
dislocations in non-parallel slip planes, elastic interaction 2−71479
doubly-folded plate, fractured 2−41610
dynamic contact problem, effective method of solution 2−76284
dynamic contact problems theory 2−45412
dynamic forms of loss of stability in intense loading over finite time interval 2−76325
Earth, elastic dislocation theory, small elastic gravitational disturbances 2−61958
Earth, fourth-order anharmonic theory for prediction of equations of state 2−72676
elastic bodies, distribution of natural frequencies, applic. to random vibration problems 2−41656
elastic field of rotating disc with eccentric elliptic insert 2−55465
elastic space, spherical cut under action of internal pressure 2−41620
elastic-gravitational oscillations, of laterally heterogeneous Earth 2−78286
elastic-plastic buckling, variational method 2−78891
elastic-plastic constitutive models 2−69635
elastic-plastic surface, rolling resistance of rigid cylinder 2−41630
elastic-plastic systems, shakedown theorem under dynamic loadings 2−66511
elastic/plastic compressed plate, buckling stress, yield surface 2−76301
elasto-plasticity, general variational theorem for rate problem 2−45418
elastohydrodynamic lubrication problem, finite element numerical solution 2−68114
elastomechanics, bounds on field quantities in natural vibration problems 2−41609
elastoplastic material, eqn. of state 2−82300
elastostatics, uniqueness and existence of solution for inhomogeneous materials 2−73379
equations of motion for elastic rings and helical coils of small pitch 2−41625
essential features of inelastic behaviour, effects of geometry change 2−76295
failure criteria of concrete rel. to incremental constitutive laws 2−58864
finite, strain energy function and boundary value problems 2−73381
finite deformation theory, arterial constitutive relations 2−55199
flexible elastic plates, geometric nonlinear theory relationships 2−82326
frictionless elastic contact, minimum principle, with applic. to non-Hertzian half-space contact problems 2−45408

Elasticity continued
- geometrically nonlinear theory, one-dimens. problems, boundary conditions 2−62970
- Griffith crack, li.f. diffr. of elastic waves 2−49068
- half-space, indentation by rigid axisymmetric punch, formulation as mixed boundary value problem 2−76303
- half-space, plate contact problem 2−78884
- half-space, response to dynamic expansion of embedded spherical cavity 2−41670
- half-space with circular lines of division of marginal modes, compound problems 2−66540
- helicoidal shells, spirally sinusoidal stress distribution 2−52182
- Helmholtz eqns., approx. reduction, for nonuniform media 2−82319
- hollow sphere subjected to dynamic pressure on inner or outer surface 2−73380
- hyperboloidal shell of revolution, numerical method and computer program 2−66550
- hyperelastic media, laminated, control vol. approach to propagating shock front 2−47486
- hypoelastic dielectric, birefringence in simple shear 2−45417
- hypoelastic dielectric, constitutive equations 2−45416
- impact, rigid sphere on elastic layer, force time investigations 2−69633
- impulsively loaded, uniformly expanding ring of elastic-perfectly plastic material, transient and final deformation 2−41631
- infinite Bernoulli-Euler beam, on elastic foundation, dynamic response 2−66585
- infinite elastic solid, thermoelastic, interactions due to concentrated heat sensor 2−69688
- infinite plate containing axisymmetric hole, extension problem 2−66545
- infinite plate with crack along circular arc, mixed boundary value problem 2−52172
- inhomogeneous bodies, bending 2−66541
- interaction between wedge disclination 2−50658
- isotropic layer with shear stresses in contact region, punch problem 2−76319
- isotropic medium weakened by congruent groups of arbitrary holes, periodic problem 2−82321
- laminated anisotropic circular plate, stability 2−41650
- layer, series soln. of three dimens. problem 2−66539
- linear, equations, dynamical torsion theory of rods 2−45397
- linear, uniqueness theorems, book 2−52184
- linear and nonlinear theories of elastic slender curved rods 2−76289
- linear shell theory, pointwise displacement errors due to errors in stress/strain relations 2−82335
- linear theory, completeness of three function set 2−58866
- linear theory, strains in region of special pts. 2−78882
- linearized and linear problems in theory with uniform initial states 2−52178
- linearized systems, subject to nonconservative forces, onset of divergence 2−45413
- local equivalence and frame indifference generalizations 2−52056
- long cylindrical shell, rel.to creep collapse under external pressure at elevated temp. 2−76329
- magneto-elasticity, extremum principle for nonlinear problem 2−58835
- magnetoelasticity of thin solids 2−76283
- magnetomechanical materials, constitutive theory 2−63077
- mantle anelasticity, attenuation of surface and body waves 2−57522
- mass tensor, uniqueness, general relativity study 2−45405
- mathematical model used in theory of structures 2−52134
- mechanical problems, book 2−66569
- mechanotronic dynamometer for testing elastic elements 2−69541
- membrane, curved, geometry induced equil. hysteresis 2−43668
- metal, cubic, lattice statics of vacancy-screw disloc. interact. 2−56687
- micromagnets, continuum theory, dissipative processes 2−84394
- micromorphic materials with memory, constitutive theory 2−49070
- micropolar theory, plane static problem soln. 2−45394
- minimum weight beams and frames under random loading 2−58853
- modulus nondestructive determ. by electroacoustic techniques using computer 2−53785
- molecular crystals, calc. by method of atom-atom potentials 2−71548
- moment theory, singularities of homogeneous solns. of plane problem with semiinfinite cut 2−69674
- multilayer media, impact and contact stress analysis in classical electricity theory, computer calcs. 2−82304
- multilayer shells, theory 2−63061
- multilayered bidirectional composites 2−69664
- nematic crystal, elastic strain and alignment on solid surface 2−53397
- non-simple materials, non-polar kinetics 2−52179
- nonlinear elastic constitutive equations 2−76320
- nonlinear elastic suspension, linear isolation mounts 2−45399
- nonlinear interactions in free-shear layer transitions 2−76338
- nonlinear theory, transient wave propagation problems 2−76340
- nonlinear theory of elastic beams 2−69667
- nonuniform layer on elastic half-space, stress state 2−41621
- oriented and multipolar discrete media 2−45400
- oriented elastic continuum as model of magnetoelastic body 2−69668
- penny-shaped crack on interface, stress analysis 2−66542
- perfectly locking bodies, limit displacements and solids parameters optimization 2−45393
- piezoelastic bodies, dynamic problems for bounded bodies 2−76288
- plane, linear, nonclassical theories 2−78896
- plasmodium actin polymers, flexibility, obs. by quasielastic scattering of laser light 2−60606
- plate, Berger eqns. for large deflections 2−52173
- plate, infinite, with parabolic crack, mixed boundary value problem 2−41617
- plate, isotropic, twisted by rigid circular stamp, mixed problem 2−45410
- plate, rigid, on elastic-plastic foundation with variable plasticity limit, elastic unloading dynamics 2−45495
- plate, trapezoidally corrugated, shear stiffness calc. 2−41626
- plate, trapezoidally corrugated, shearing, theory 2−41627
- plates, accurate practical theories 2−52176

Elasticity continued
- cis-polybutadiene, cross-linked in swollen state, elastic behaviour 2−60835
- cis-1,4-polybutadiene rubber vulcanizates, elastic hysteresis, obs. 2−60855
- polyolefins, variation in sound velocity rel. to deformation 2−80750
- porous elastic medium, semi-infinite, two dimensional deformation under load 2−58860
- porous solids fluid saturated, single constitutive theory 2−68179
- pulmonary alveolar microvascular sheet of cat 2−51877
- pulmonary alveolar sheet of cat 2−51878
- α- quartz, based on interatomic force model 2−68854
- random linearly elastic rods, pressure signals, dynamic response 2−41615
- reduction of integral eqns. to systems with infinite no. of degrees of freedom 2−82320
- repeated impacts, transmissibility and damping 2−55468
- rocks, effects of pressure 2−68849
- rocks, in uniaxial strain 2−75454
- rocks and polycrystals, mantle minerology 2−65569
- rods, multi-indical system, elastic buckling, Lagrange eqns., mech.-stereomech. analogy 2−45343
- rolling contact of rigid cylinder over elastic layer 2−41608
- rubberlike slightly compressible circular cylinders, finite torsion 2−76321
- rupture, path-independent integral for perfectly elastic materials 2−58874
- second order, magnetostriction effects 2−44259
- second order theory, solution of some problems 2−41624
- semiinfinite rod, longitudinal impact, stability loss 2−69673
- semispace, contact problems of pressure exerted by smooth punch 2−76297
- shell, dynamic stability 2−66494
- shell, shallow, nonlinear theory, existence of solns. 2−82322
- shell, shallow crit. loads for loss of stability, asymptotic method 2−82323
- shell, thin, with inner constraints, conformation field represent. 2−78885
- shock waves of finite amplitude, in elastodynamics influence of non-linearity on reflection 2−52256
- snap through analysis of curved plates using discrete elements 2−45395
- stability, nonconservative problems, approximate methods 2−58893
- stability of elastic continuous media, sufficient conditions 2−45409
- stacking faults, continuum theory of high-speed propagation, dynamic singularity 2−50680
- stiffened plates containing one longitudinal or transverse girder under compression, buckling strength 2−66536
- stress analysis contact surface integration, finite element analysis 2−73383
- stress conc. in layer weakened by circular slot 2−45406
- stress fields, two-dimensional, differential equations comparison with flow fields 2−52044
- stress functions in three-dimensional elastodynamics 2−69663
- stress/strain relations for anisotropic bodies in cylindrical and polar co-ordinates 2−52171
- stresses around one or two holes subjected to internal pressures in semi-infinite or infinite elastic mediums 2−76273
- string, nonlinear vibrations, investigation 2−55503
- structural non-homogeneous bodies, tensional elasticity, mechanical model 2−49074
- structures under dynamic load, design optimization 2−73386
- suspension of spherical particles in isotropic matrix. elastic behaviour 2−53458
- thin elastic plate in bipolar coordinates, circular plate with eccentric circular hole 2−69671
- thin elastic plate in bipolar coordinates, solution of biharmonic equation 2−69670
- thin films, elastic properties, sensitive meas. by harmonic generation of dispersive Rayleigh waves 2−50472
- thin shells, asymptotic solutions for stress concentrations 2−76294
- thin shells, construction and itegration of equilibrium equations 2−76281
- thin-walled compression members, optimum design 2−52175
- three dimensional equations, exact and approximate solutions 2−66553
- torsional spring subjected to sinusoidal oscillations, heat generation 2−55501
- trusses, nonlinear elastic analysis, control theory formulation 2−45398
- trusses for alternate loads, optimization 2−58865
- twist disclination loop elastic behaviour near free surface 2−50664
- two phase materials, circular disclination, elastic fields, interface effects 2−76272
- two-dimensional, inverse method 2−76327
- two-dimensional half-space model of welded quarter- spaces, seismograms 2−65469
- two-dimensional solids, determ. of elastic stresses at notches and corners by integral equations 2−82306
- ultrasonic techniques of meas. 2−64752
- unbalanced angle-ply rectangular plates under transverse normal loading, analytical solution by Fourier series 2−82305
- uncoupled instantaneous, nonlinear solid mechanics, thermodynamic foundations 2−56766
- variational principle for finite displacements 2−66537
- vibrations of laminated honeycomb structures, adhesive layer, elastic properties 2−50927
- volume dilatation caused by dislocations, applics. 2−50660
- wood, vibration method of det. 2−56844
- Al, nonlinear behaviour, acoustic shock pulse generation obs. 2−64842
- C, glassy fibres, derived from phenolic resin, mech. props. 2−84100
- CdSb, Debye charact. temp. det. from elastic modulus 2−64854
- CsCl, based on interatomic force model 2−68854
- Fe, strain ageing and effective elasticity modulus 2−71624
- GaSb single crystal, elasticity versus temp., calc. 2−60843
- glass, As-S, As-S-I, As-S-Tl, in transition region and viscosity 2−84049

Elasticity continued
KNiF$_3$, Neel point determ., elastic, magneto-optical and heat capacity meas. 2−72219
NaCl, based on interatomic force model 2−68854
SbSI, ferroelec., resonance method obs. 2−54240
SiO$_2$, fused fibres, nonlinear elasticity at room temp. 2−60847
Sn, white, elastic and plastic anisotropy 2−80726
29 at.% Zn-Al alloy, spinodal decomp., metastable rhombohedral form., elastic anisotropy effects 2−56923
liquids
see also Compressibility/liquids
flow, free convective, of elastico-viscous liquid past infinite porous plate 2−46881
polymer solution, time-dependent elongational viscosity calc. using elastic dumbbell model 2−71171
Weissenberg rheogoniometer data rel. to viscoelastic liquids 2−77391
Elastomers *see Rubber*
Elastoplasticity *see Plasticity*
Elastoresistance *see Piezoresistance*
Electrets
see also Electrostatics
capacitive microphone element, miniature applics. 2−41759
Carnauba wax, surface and volume charge distributions 2−72046
dipolar, heteropolar, homopolar and monopolar, characteristics, review 2−44168
dosimetry, formation, discharge and depolarization obs. 2−70308
epoxy resin polymerization in elec. field 2−47991
microphone, optimization of ridge backplate 2−41761
naphthalene thermoelectrets, X-ray diffraction structural studies 2−65075
oxide films, stored charges 2−44166
perspex, characteristics of cubical thermo-electrets 2−61439
perspex magnetoelectrets, effect of forming magnetic field on dielectric behaviour 2−65074
photoelectret state, non isothermal relax. 2−57247
photoelectrets as memory photon detectors 2−42219
poly(methyl methacrylate) thermoelectrets, thermodepolarization currents 2−83348
polyethylene terephthalate, atmosphere effect on polariz. and thermally stimulated current obs. 2−65076
polyethylene thermoelectrets, heterocharge and depolarization current 2−72047
polymer, depolarization spectra, thermal treatment effect 2−47974
polymer, thermostimulated depolarizing currents and thermoelectret effect 2−47973
polypropylene thermoelectrets, heterocharge and depolarization current 2−72047
polyvinylidene fluoride, depolarization current and surface potential decay 2−51208
PVC(SR$_{11}$), thermal current meas. 2−44167
pyrene, photoelectret effect 2−81131
shellac wax, surface charge formation and decay characteristics 2−61440
sugarcane wax, heterocharge mechanism 2−75157
thermally stimulated current obs. 2−51193
thermoelectret, fabrication, changing mechanism; appl. 2−75156
thermoelectret behaviour under different humidity conditions 2−81145
transducer, characteristics and special applics. 2−41760
transducers, operation and applics., review 2−41758
BiI$_3$, non isothermal relax. of photoelectret state 2−57247
BiI$_3$, photopolariz., localized states and electron-hole processes obs. 2−61706
CdS film, photoelectret state formation and temp. depend. 2−77939
CdS films, shift in lux-ampere and I-V characts. due to photoelectret effect 2−81170
SbSI, photoelectret state, trapping levels, thermally stimulated photocurrents obs. 2−75154
Electric breakdown *see Breakdown, electric*
Electric cells
dielectric, low temp., for permittivity meds. 2−82414
electrochemical concentration cell, anisotropic, system based on β-alumina (NaAl$_{11}$O$_{17}$) solid electrolyte 2−61799
electrorefining cell, mass transfer, effect of uniform mag. field, expt. 2−54550
galvanic, high-energy direct conversion 2−84652
International Society of Electrochemistry, 23rd meeting, Stockholm (1972) 2−68792
ionic mass transfer in parallel plate unit 2−59040
Leclanche, with couple Zn/MnO$_2$ and electrolyte Mg(ClO$_4$)$_2$-Mg(OH)$_2$ 2−59038
secondary cells Li/Cl, Na/Cl, Li/S, Na/S and Li/CuF$_2$ with inorganic electrolyte 2−66689
tangential stresses of two-phase flow on wall of vertical tube 2−64425
thermoelectric isotope battery for pacemakers 2−76064
CdSO$_4$, 'acid' standard cell, e.m.f.-temp. coeff., 15° to 40°C 2−82130
Cu electrowinning in coupled electric and magnetic field 2−68796
Li/S secondary cells 2−66687
Li organic electrolyte batteries with high energy densities 2−66688
Zn/air battery, Zn passivation and mass transfer effect in flowing electrolyte 2−59039
Electric charge
see also Space charge
aerosol charging theories, comments 2−50385
Carnauba wax electrets, surface and volume distribution 2−72046
in conducting medium, density rel. to relaxation time 2−49197
conservation and flux integral forms, distinction from current conservation 2−55652
dickite ground, negative surface charges 2−78235
electrophotographic developers, measurement methods 2−70100
insulator, charging during LEED 2−64547
insulators, electrostatic charging after contact with metals 2−72005
kaolinite ground, negative surface charges 2−78235
m.a.o.s. structure, partial charge accumulation 2−61401
monitor for 2 MeV pulsed electron source 2−79694
Electric charge continued
nonradiating bunched charges, particle-like spherically symmetric distribution, nonlinear relativistic equation 2−63171
point charges, teaching paper, computer plotting of equipotential lines 2−78744
synchronous satellite charging in orbit rel. to magnetosphere 2−66025
thermoelectret behaviour under different humidity conditions 2−81145
Al film, normal-state cond. and supercond. transition temp., electrostatic charging effects 2−71845
Au, boundary layers, transmission of struct. information 2−77494
Ge surface, slow relax., surface cond. and contact potential studies 2−81105
KNbO$_3$, ferroelec., surface change layers, obs. by AF electrolum. 2−75151
MgO cleavage face, elec. field domains, rel. to LEED pattern 2−60627
NH$_4$Cl(I) aq. solns., elec. pots. generated on freezing at uniform rate, substrate effects 2−53495
NaCl, electrical processes occurring at moment of cleavage 2−74659
Si, m.i.s., inversion layer, hole field effect mobility rel. to dielec. charge 2−71992
ZnO, decay of pyroelectrically induced polarization charges 2−54241
Electric discharges *see Discharges, electric*
Electric domains *see Domains*
Electric fields
see also Electromagnetic fields
anode, field ionization tip, meas. 2−59119
atmospheric, penetration into ionosphere and magnetosphere 2−62347
atmospheric, variations during substorms, OGO 6 obs. 2−81714
aurora, parallel elec. field obs. 2−65913
in bipolarly charged aerosol, effect on dispersion 2−80492
computation, derivatives of elliptic integrals of the third kind 2−45232
critical breakdown strength in solids 2−75146
distribution in massive conductors, applic. to resistivity meas. and nondestructive testing 2−45643
Earth, in sea, instruments and methods of obs. 2−44595
Earth, induced field, battery operated electrographs 2−57790
electrohydrodynamics, macroscopic coupling between electric fields and fluids 2−77210
flowing gas, free unipolar, field distribution in phase plane 2−64365
fluid in transverse non-uniform magnetic field 2−60182
gas laser, longitudinal elec. field rel. to internally modulated light beam 2−49367
gas laser electron beam controlled, elec. field and secondary electron distribs., Monte Carlo calcs. 2−80360
graphite, surface polarity when covered by oxygen complexes, evaluation using heats of immersion 2−64550
horizontal, in enclosed charged fog or mist, ungrounded electronic field meter for obs. 2−66680
ionosphere, at high latitude 2−72866
ionosphere, fields and zonal currents induced by merging of field lines 2−62351
ionospheric, balloon meas. during Ba cloud release in magnetosphere 2−62365
ionospheric, during pulsating auroras 2−48572
ionospheric electric field pot. distrib., world-wide meas. 2−65963
magnetopause, structure in dawn to noon quadrant from Explorer 43 meas. 2−62316
magnetosphere, decaying ring current as origin 2−78386
magnetospheric, computer model 2−65879
magnetospheric convection fields, high latitude satellite obs. 2−75626
measurement using pulsed laser Kerr system polarimeter 2−55744
metal-semiconductor contact, surface elec. field, determ. by differential electroabsorpt. 2−65036
in MHD channels for anisotropic non uniform conductivity 60217 2−60217
in microwave tube interaction gaps, analytic expressions 2−69880
ocean floor, using self-contained recording system 2−68862
oscillating in absorbent dielectric medium, time- averaged Maxwell stress tensor 2−73495
particle accelerator low phase velocity supercon. resonant cavities 2−49700
plasma, singularities in electric field 2−80237
plasma, temporal profile 2−83545
polar cusp, electric fields and electron fluxes 2−54895
ring electrets, application to state selection of masers 2−78955
Schrodinger-Pauli-type eqn. for constant homogeneous electric and magnetic fields, Green's function 2−69589
snowflakes, replicas, electric field and symmetry 2−62245
surface of revolution, Green's functions 2−45637
transmission electron microscope imaging of electric field regions associated with p-n junctions 2−79134
Ar atmospheric cascade arc, intensity meas. 2−46804
He atmospheric cascade arc, intensity meas. 2−46804
N$_2$ atmospheric cascade arc, intensity meas. 2−46804
effects
AgBr layer sensitivity, fog, speed, polarity 2−84674
atmospheric effects of nuclear explosion 2−62277
coagulation kinetics of polydisperse emulsion in electrostatic field 2−74572
convective heat and mass transfer, horizontal surface under forced convection 2−52282
crystals, effects of external force gradients on i.r. and Raman activity of long wavelength optical phonons 2−84513
cyclotron resonance, Azbel'-Kaner, effect of strong elec. field 2−71821
dichlorobenzophenone crystal, singlet and triplet exciton states 2−44385
dielectric loss theory and orientation mechanism 2−77933
dipolar entropy and heat capacity of ionic crystals with paraelectric dipolar impurities 2−57221

Electric fields continued
effects continued
dye molecules in solid lipid layers, effect of electric field on absorption spectrum 2−68801
electrohydrostatic stability of fluid surface, two-dimensional problem 2−46651
electron group drift between plane parallel electrodes, in gases, mathematical model 2−83715
electron moving in vertical metallic pipe, effect of electric field arising in shield due to gravitational field 2−66705
ethyl alcohol counterflow diffusion flame in transverse electric field, optical study of temperature profiles 2−83703
film, chalcogenide glass, high field effects, Poole-Frenkel emission 2−44097
film, metallic, electromigration, grain boundary contribs. 2−56751
films grown by evaporation, effect on resistance 2−71341
fluid circulation in and round dielec. fluid in elec. field 2−83524
h.f. resonant discharge stability 2−64342
ice film on cooled surface, microstruct. rel. to deposition rate, elec. field, vacuum breakdown 2−83866
ion diffusion in own gas, relay race model 2−50224
liquid cryst. smectic, type A, elec. induced hydrodynamic instabilities 2−80462
liquid crystal, nematic, field induced distortions 2−53399
liquid crystal modulation of coherent light 2−42160
liquid crystals, nematic, applied a.c. voltage effects on birefringence 2−53431
macromolecules, transient scattering from absorbing solutions in pulsed elec. fields 2−50378
mass spectrometer, transverse displacement of ions 2−74198
metal film growth, vacuum vapor deposition 2−60634
non-linear dielectric loss (imaginary part of susceptibility) at high elec. fields 2−77944
non-uniform r.f. field influence on ion trajectories in omegatron 2−59650
nuclear emulsion, concealed image distrib., pulsed field effects 2−46061
nuclear emulsion, track shortening in fields of 1.5-6.0 × 10^4 V/cm 2−42476
optically inactive crystals, opt. rotat. induced by crossed elec. and mag. fields 2−78066
organisms, physiological and metabolic changes 2−48851
p-n junction, photoluminesc., quenching by elec. field in space charge region 2−65290
paraelectric crysts., ENDOR of A-centre electrons rel. to external elec. field 2−78176
photographic emulsion sensitivity control 2−52506
photographic films, exposure conditions 2−72464
plasma, fully ionized, generation of third harmonic current density 2−43135
plasma, ion-acoustic and electron wave parametric coexcitation by h.f. field 2−67684
plasma density fluctuations, streaming along uniform mag. field 2−43127
plasma heating, computer simulation 2−64334
plasma toroidal transport with azimuthal fields 2−46719
plasma with flow, steady-state diffusion controlled, effect of nonuniformity of applied h.f. electric field 2−67635
polymers-Hg contact 2−57236
quantum domain, effects on quasibound states, integral equation method 2−52077
quantum transport and quantization of Bloch oscillations in strong elec. fields 2−61147
recording of ionizing particles in photographic emulsion 2−59642
rhodamin B molecules in cadmium arachidate multilayers in thin capacitors, electrochromic spectra 2−68802
semiconductor, coupled electron-phonon system evolution in strong elec. field 2−61291
semiconductor, heated by h.f. elec. field, hot electron recomb. 2−64972
semiconductor, narrow band, current rel. to elec. field 2−77891
semiconductor, supercond., rel. to state mixing between bands due to e.m. field 2−77872
semiconductors with nonparabolic bands, transport props. 2−81101
silicone liquids thermal breakdown under pulsed h.f. fields 2−56513
stearic acid films, high-field transient behaviour of dielec. props. 2−77950
step motion on crystal surfaces under electric fields 2−74613
streamer propagation in divergent electric fields 2−74412
superconductor, gap, equilib. value, rel. to weak alternating fields 2−57157
thermocouples, temperature measurement errors due to improper grounding 2−66652
thyratron employing orthogonal electric and magnetic fields 2−70994
two photon absorption by a crystal in elec. field 2−65243
type II superconductor in crossed electric and magnetic fields, coherent quasiparticle excitation 2−84307
u.s. amplification by interaction with electrons 2−77776
water drop disruption 2−64426
CdS, photosensitivity rel. to elec. field 2−75167
CdSe, elec. field distrib., subjected to 0-600 V applied voltages 2−64960
Cr dendrites, galvanostatically obtained from CrO_3-H_2SO_4-dimethylsulphoxide-H_2O solution 2−47135
Cu electrowinning in coupled electric and magnetic field 2−68796
Cu_2O, $\Gamma^{+}{}_{5}$ exciton quadrupole transition rel. to static elec. field, Stark splitting 2−81406
n-GaAs, negative photocond. when illuminated with impurity absorbed light, recomb. mechanism 2−65083
Ge, galvanomagneto-recombination effect kinetics rel. to elec. and mag. fields 2−65015
Ge, indirect exciton ground state, exciton line broadening by elec. field 2−77841
He,liq., charge carrier mobilities near vapour press. 2−53472
InP, electroreflection spectrum shape for uniform and inhomogeneous fields 2−81433
p-InSb:Ge, electrical instability in presence of elec. field 2−71884
InSb, recomb. rate rel. to elec. field, drifted Maxwellians approx. 2−81077
KCl film, vapour deposited, form. rel. to elec. field 2−64570
LiCl, hyperfine spectra in zero magnetic and low electric fields using new electric resonance molecular beam apparatus 2−46557
Pt electrode on alkali-containing glass, model of electrode 'polarization' by d.c. potential applic. 2−81141
Se, field effect rel. to temp., field mobility, surface cond. 2−71933
Si hole, drift velocity rel. to band struct., elec. field effects, at 5K 2−81107
SiO_2 and diatomite suspension in kerosene, mechanical behaviour during shearing in electric field 2−60531
$SrTiO_3$, anomalous reson. in permittivity on cooling in elec. field 2−77935
Ti sputter ion pumps, influence of asymmetry 2−62899
ZnS, extinction of luminescence 2−75331
$ZnWO_4$:Cr^{3+}, e.p.r. line splitting, temp. variation 2−72473

Electric strength
see also Breakdown, electric
epoxy resins, losses during thermal ageing 2−83394
polyethylene, for use in h.v. pulse generators 2−65055
polyolefins, effect of impregnation with various viscous materials 2−57234
transformer oil, for use in h.v. pulse generators 2−65055
water, distilled, for use in h.v. pulse generators 2−65055
$BaTiO_3$ ceramic, sintering parameter effects 2−57241
He, pressurized, obs. 2−50233
SiO_2 and SiO films, moisture stability 2−72015

Electrical conduction *see Conductivity, electrical*

Electrical current *see Current, electrical*

Electrical machines
compensation methods for assigning small linear and angular speeds 2−76160
conducting plate, in uniform mag. field, free vibrs., theory 2−41900
continuous current motor, discontinuous current operation 2−52357
continuous current motor driven by thyristor interrupter, operation stability 2−41902
electromechanical conversion, energy efficiency 2−41901
electrostatic generator, charge collection, theory 2−52711
magnetic field calc. 2−63217
motor drives and guidance of small radio telescopes 2−85066
motorized drive for double tilting specimen holder of electron microscope 2−55641
polyphase hysteresis motor with non-mag. core, mag. field and couple determ. 2−73503
quasistationary theory, approximations and appl. 2−58981
rotary electrostatic field meas. 2−52347
rotating, noise and vibrs. 2−45655
selsyn-type electric machines, error determinations 2−76437
static power convertors, numerical simulation method 2−52358
stepping motor drive system, solid state, providing constant angular motor shaft velocity 2−45653
superconducting, developments, review 2−66686

Electrical measurement
Entries describing measurement methods for specific electrical quantities and effecte may also be found listed under the various headings for the subjects concerned
atmospheric electricity using aircraft borne cylindrical field meas. 2−58004
breakdown voltage measurement apparatus for semiconductor device testing 2−82423
bridge silicon mag. diode, volt-tesla charact., 0-1.3 T 2−82416
capacitance meter for artificial lipid bilayer membranes 2−82422
characteristics of MIS structures, apparatus for automatic meas. and recording 2−63214
contact potential difference measurements on oxidised Si surfaces 2−77914
contact potential differences, u.h.v. guarded Kelvin probe 2−45647
current balance, temperature rise in coil former due to resistance in windings and corrections 2−41896
cylindrical electrostatic fluxmeter for corona discharge obs. 2−45646
d.c., corona discharge, electric field measurements by e.s. fluxmeter 2−74444
d.c. ratio transformer, low-temp., standardisation and current detection 2−82421
diagnostic X-ray tubes, kV measurement 2−69350
electrodynamic force moment, effect of a non-magnetic conducting cylindrical case 2−59026
electrometric characterization of tarnish films on Cu-Zn alloys 2−77717
electronic instrumentation, conference, Hobart, Tasmania (1972) 2−52356
field ionization tip, field strength measurement using fragmentation of n-heptane ions 2−59119
Hall effect in high resistivity samples, double a.c. meas. techniques 2−82415
Hall mobilities, amorphous semiconductors, meas. by Corbino disc 2−68426
impedance, thermal noise analysis 2−73497
instruments, utilization of draw springs as support for moving system 2−59036
intense relativistic beam device, impedance and spot-size meas. 2−63295
Kerr system electrical measurement techniques, recent developments 2−78990
linear passive circuit elements, by measurement of third harmonics 2−82420
of magnetosphere, south magnetic pole region, automatic measuring station using isotopic generator 2−51637
mass spectrometer, spark-source, semi- automatic system for operation of electrical detection 2−84700
moisture gauge, u.h.f., phase sensitive 2−52352
moving coil ballistic galvanometer, calibration 2−45654
non-magnetic conducting monolithic and laminar bodies, electrodynamic effect 2−59027

Electrical measurement continued
  ocean floor field, self contained recording system 2−68862
  particle mag. diodes, volt-amp-characts. 0-1 tesla 2−82416
  picoammeters, characteristics 2−49232
  potential modulation differntiation, instantaneous response functions 2−76435
  primary standards, techniques in Netherlands 2−78745
  recording track, electron-optical meas. of dynamic fields 2−63278
  Schottky-barrier diode, differential capacitance meas. for dopant conc. profile determ. in epitaxial GaAs 2−83905
  semiconducting thermoresistors, volt-ampere characts. for different velocities and flux temps. 2−55589
  semiconductor device props., 77 to 300 K, cryostat 2−85169
  semiconductor impurity, profiles, capacitance- voltage meas. 2−64673
  using semiconductor thermoelectrical materials 2−76432
  solid electrolyte cells in liquid metals, e.m.f. meas. 2−66681
  thermoelectric materials, rapid meas. of temperature dependence of thermal e.m.f. and electrical conductivity 2−52351
  thin specimen, resistivity measurement using electrical-contact four-electrode transducer, measurement errors 2−45642
  vertical velocity of water surface, registration using e.m. induction method 2−72717
  voltage fluctuations in resistor, Nyquists theorem and its generalizations 2−45630
  voltage pulse proportional to particle volume 2−44489
Electrical properties of substances
  see also individual properties, e.g. Conductivity, electrical; Dielectric properties of substances, etc.
  film, metal, discontinuous, rel. to strain 2−64908
  lunar samples from Apollo mission 2−66158
  lunar surface, obs. using coherent radar 2−51814
  rocks, elec. and electrochem. characts., equivalent network 2−65524
  squid giant axon, propagated subthreshold oscillatory response and classical electronic response 2−55204
  steatite materials, effect of modifying agents on electromechanical behaviour 2−53933
  $CaRuO_3$, orthorhombic perovskites, metallic elec. props. of single crystals 2−84291
  p-Ge-n-CdS_xSe_{1-x} epitaxial heterojunction 2−77924
  Hg, review, evidence for pseudogap 2−77445
  $MoO_{3-x}F_x$, characterization 2−57146
  $PbTiO_3$-$Pb(Cd_{0.5}W_{0.5})O_3$ ceramic, electromechanical props. 2−64788
  $PbZrO_3$, growth and obs. of intermed. ferroelec. phase 2−81140
  $SrRuO_3$, orthorhombic perovskites, metallic elec. props. of single crystals 2−84291
  $VO_{3-x}F_x$, characterization 2−57146
  $WO_{3-x}F_x$, characterization 2−57146
Electrical units *see Units*
Electricity
  conversion to light, thermal and electroluminescent, principles 2−68439
  feedthrough, spherical, for high pressure vessels 2−62895
  vacuum feedthrough, doubly insulated, guarded ultrahigh resistance 2−62902
Electricity, direct conversion
  see also Electric cells; Plasma diodes
  electrochemical, math. anal. and feasibility of air electrode in organic systems 2−84652
  Gipsie radioisotopic generator for use in cardiac pacemakers 2−51906
  isotope powered generators in UK, economics 2−49302
  isotope thermoelectric battery for cardiac pacemakers 2−49290
  isotopic fuels, ^{238}Pu, ^{244}Cm production 2−49987
  isotopic power generators regulatory aspects 2−49243
  nuclear batteries for cardiac pacemakers, fabrication techniques for thermoelements 2−51907
  nuclear cells for cardiac pacemaker, dosimetry 2−51949
  nuclear energy sources for implantable biomedical devices 2−51914
  from nuclear radiation energy, book 2−83145
  power from radioisotopes, symposium, Madrid (1972) 2−49242
  radio photovoltaic power conversion systems, efficiency and power limits 2−49255
  radioisotope generator for polar based automatic measuring station 2−51637
  radioisotope power generators for cardiac pacemakers, legal and administrative problems in Italy 2−51916
  radioisotope power source development by AECL, MAPLE generators using ^{60}Co, review 2−49298
  radioisotope thermoelectric, for artificial hearts, USAEC development programme 2−51915
  radioisotope thermoelectric generator for TRANSIT navigational satellite 2−49296
  radioisotope thermoelectric generator systems for space vehicles, safety systems 2−51681
  radioisotope thermoelectric generators, Stirling engine applications 2−49305
  radioisotopic converters 2−49244
  radioisotopic power generators, oceanography appl. 2−49301
  radioisotopic power source, accident analysis 2−55218
  radioisotopic thermoelectric generator SNAP 19, laboratory testing 2−49291
  radioisotopic thermoelectric generators for submerged oil installations, results of experimental tests 2−49295
  radiosiotope cardiac pacemakers, fuel capsule resistivity against fire-arms 2−49250
  radiovoltaic energy from tritium 2−49247
  solar energy, large-scale concentration 2−73506
  space vehicle nuclear power systems using ^{238}Pu, safety systems 2−51667
  thermal accumulator, stores energy by melting and solidifying storage body, applications, difficulties 2−49256
  thermocell, molten salt, thermoelec. pot. 2−52379
  thermoelectric generator, isotope powered, description 2−59046
  thermoelectric isotope battery for pacemakers 2−76064
  thermoelectric transverse thin film device fabrication using Te 2−54249
Electricity, direct conversion continued
  thermophotovoltaic radionuclide battery, model 2−49294
  Bi film thermoelectric figure of merit 2−55642
  ^{244}Cm power fuel, compound preparation techniques 2−49252
  Ge thermophotovoltaic cell efficiency rel. to Er_2O_3 radiator performance 2−66693
  ^{3}H-fuelled batteries, leak testing 2−49254
  ^{3}H battery connected to electrically driven mechanical vibrator, direct charge collection, principles 2−49251
  ^{3}H cell using Ti^3H, with β-particle collection, design 2−49253
  ^{3}H miniature batteries medical appl. 2−49248
  ^{3}H nuclear cardiac pacemaker battery using electron voltaic effect 2−51908
  ^{3}He battery, for submicrowatt range 2−49245
  Ni-Cd cell, 20 Ah, for orbiting astronomical observatory 2−85075
  ^{238}Pu battery for artificial heart system 2−49246
  ^{238}Pu for cardiac pacemakers 2−49249
  ^{238}Pu fuelled thermoelectric battery for cardiac pacemaker 2−51888
  ^{238}Pu thermoelectric generator, comparison with ^{90}Sr, milliwatt thermoelectric generator 2−49297
  ^{90}Sr, milliwatt thermoelectric generator, comparison with ^{238}Pu thermoelectric generator 2−49297
  ^{90}Sr thermoelectric generator TRISTAN 2−49293
  UN fueled convertors, performance evaluations 2−63242
 fuel cells
  alkaline-matrix H_2/O_2 cells, mathematical model of H_2O transport 2−69847
  anodic oxidation of binary compounds of transition elements in H_2SO_4 2−61790
  Bacon H_2/O_2 cells, mathematical model of H_2O transport 2−69847
  with bipolar, non-noble metal electrodes and acid electrolyte 2−66690
  current-voltage characteristics using a mathematical model 2−41903
  electrolyte stabilization in wetproofed pores of electrodes 2−45657
  electrolyte- phobic molten carbonate electrodes 2−59045
  high temp., with ceramic electrolytes for conversion of cheap fuels 2−59041
  high temp. fuel cell, electrode development, test results 2−49258
  high temperature, series connections utilising Allox conductors 2−41904
  high temperature solid electrolyte, maximum power output per unit volume 2−66691
  hydrocarbon conversion, high temperature fuel-cell battery 2−49257
  zirconia electrolyte appl., oxygen ion conduction 2−49259
  C-HO fuels, production from molten alkali carbonates, initial mixtures 2−59042
  O alkali gas diffusion electrodes fabricated from Pt, PTFE and porous nickel, model 2−59043
  Pt dispersed electrode, electrochemical activity 2−45656
 magnetohydrodynamic
  blow-in, influence on power characteristics 2−52360
  Carter's coefficient calculation for cylindrical MHD machines 2−45658
  channel ionization instabilities in nonlinear regime 2−80264
  combustion gas plasma, in elec. fields, heat transfer, obs. 2−80300
  compensating current in winding or single phase MHD machine with parallel branches in phase 2−49260
  conduction pump, single phase single section, model in electrodynamic approximation 2−52361
  convertor with inductive cylinder-symmetrical cryogenically cooled 2−69848
  cylindrical induction machine, end effects on e.m. field, power and efficiency 2−59051
  dynamo, hydromagnetic, convection driven 2−73504
  end effect in generator with optimum load distribution 2−63218
  explosive driven multimegajoule pulse generation feasibility 2−59052
  Faraday type generator, two-dimensional flow gasdynamics, calc. 2−80260
  field distribution along channel axis in magnet system of conduction pump 2−49261
  generator, patent 2−69850
  generator, piston-type, liquid metal, dynamic characteristics 2−41906
  generators of open cycle, in USSR 2−41905
  induction pumps and bearings, efficiency 2−50169
  inert gases, plasma parameters for nonequilibrium generator 2−59049
  ionization instability control by feedback 2−80263
  linear inductors, single phase rotor with variable phase velocity 2−53152
  liquid metal and plasma secondary machines, design and operation 2−52359
  liquid metal induction converter, energy loss due to discrete tooth-slot arrangements 2−63219
  nuclear MHD electric power system, space applications 2−59050
  plane linear induction pumps with side bars, e.m. field distrib. 2−50170
  plasma subjected to electrothermal instability, two-point correlation description 2−80266
  power generator, effect of heterogeneity and Hall current 2−69849
  power system feasibility 2−52362
  U-02 power installation, prolonged continuous working tests 2−59047
  Ar-K plasma generator, nonequilibrium effects, obs. 2−59048
  Ar-N_2 plasma MHD generator, spectroscopic temp. detn. 2−46716
  He-Cs gas plasma MHD, fluctuations calc. 2−80265
 solar cells
  arrays atmospheric drag cross section, inclination nodal regression, solar declination 2−83677
  heterojunction type, characteristics of ZnSe-GaAs solar cells 2−63253
  honeycomb absorbers on collecting base surface, absorption efficiency 2−41909
  space vehciles solar sail and electric propulsion systems compared 2−72929
  Bi_2Te_3, performance as solar thermoelectric generator material 2−59058
  CdS, thin film solar cells, state of the art and space applications 2−59059

Electricity, direct conversion continued
solar cells continued
CdTe layers and solar cells 2–41907
GaAs, Si, efficiency comparison on spacecraft in range 0.2 to 10 a.u. 2–49306
PbTe, performance as solar thermoelectric generator material 2–59058
Si, 1 MeV electron radiation of TiO_x and SiO_x antireflective coatings 2–59056
Si, effect of series resistance on power output at low intensities 2–73505
Si, effects of storage temperatures on contacts 2–41908
N/P Si, encapsulated in fluorinated ethylene propylene, effect of simulated micrometeoroid exposure 2–52380
Si, performance improvement using passivated Ti(Pd)Ag contacts 2–59057
Si, series resistance methods of determ. 2–66692
Si, short-circuit current rel. to minority carrier diffusion length 2–59060
Si crystals obtained by Stepanov method 2–45660
thermionic
additive convertors, formation of metal oxides, effect on emitter work function 2–63233
arc drop suppression 2–63246
arc mode, influence of collector material work funct. 2–49281
arc mode, nonequilibrium electron distrib. funct. 2–49275
asymptotic stability of thermionic reactor 2–63221
caesium, plasma characteristics meas., spectrographic method 2–59055
closed loop reactor control schemes 2–63225
conference, San Diego (1971) 2–63223
converter characteristics, with constant input power 2–52374
converter using ^{227}Ac fuel 2–49292
current instability and contraction in thermionic converter 2–52371
cylindrical diode characteristics with sublimed electrode surfaces 2–63240
discharge instability around long electrodes 2–49274
electron temp. effect on electron density of Cs plasma 2–63244
electron work function in binary and ternary transition metal-nonmetal systems 2–63235
emitters, tungsten- coated, thermionic convertors 2–49289
external fuel reactor system 2–63224
flame heated convertor 2–52363
fuel cladding systems, material development 2–52369
fuel element development for in-core thermionic reactor for space applications 2–49263
fuel element testing 2–49264
fuel-rod development 2–49266
high melting point electrode materials 2–54272
in core thermionic reactors, applications to space and underwater technologies 2–49269
incore thermionic reactor, out of pile investigations 2–52370
incore thermionic reactor emitters, irradiation tests 2–52368
irradiated converters, mechanical and electrical properties 2–52364
Isomite thermionic radioisotope battery, Pm, Pu heat source, development, construction, output and life characteristics 2–49267
Knudsen mode, sinusoidal potential distributions 2–49284
mathematical calculations simplified 2–63245
maximum attainable efficiency, theoretical limits 2–52373
multicell reactor power supply design 2–63226
nuclear reactors, alumina insulators, neutron damage reduction using hydrogenous moderator 2–63228
nuclear reactors, dielectric breakdown in ceramic insulators, 300 to 1200°K, mechanisms 2–65056
nuclear reactors, effects of fast neutron irradiation on b.c.c. refractory metals 2–63229
parallel plane convertor, (110) oriented W emitter, polycrystalline W collector, power generation measurement 2–63237
performance comparison with several collector materials 2–63239
performance data, fixed spaced planar diodes 2–63238
performance data with Nb collector and chloride vapour deposited tungsten emitter 2–63247
plasma calorelectric diode 2–52367
plasma diode, nonlinear current oscillations rel. to high cathode temperature, low Cs pressure and Coulomb collisions 2–52365
preset generation, conference Julich, Germany (1972) 2–49268
radioisotope fuelled batteries, plutonium 238 and strontium 90 2–49303
radioisotope thermoelectric generator, underwater appl. 2–49299
refractory metal single crystals, emitter and collector work function measurement 2–63234
short discharge plasma diodes, physical properties 2–52366
space missions, electric propulsion employing nuclear reactor power systems 2–66031
space propulsion employing reactor power system 2–66033
spacecraft propulsion employing nuclear reactor system, power conditioner design 2–66034
transient pressures in arc plasma, during ignition and quenching 2–52377
transport phenomena in gaseous mixers and plasma, improved formalism 2–63248
triple diode, irradiation expt. 2–49271
unmanned space missions for outer planet exploration employing nuclear reactor power systems 2–66032
vapour deposition of refractory metals, performance of deposits 2–49272
^{227}Ac fueled generator 2–49262
Al_2O_3, ceramic to metal seal for thermionic fuel elements 2–53928
Al_2O_3, fast neutron irradiation, thermionic reactor design 2–53707
Al_2O_3 ceramic insulator, swelling in neutron irradiation 2–53706
Ba-Cs filled, current voltage characteristics 2–49286
Ba-Cs filled, ignited mode 2–49285
Ba-Cs thermionic diodes with polycrystalline Mo electrodes 2–63236
Cs-Ba filled, influence of magnetic pressure 2–49282
Cs-Ba filled, optimization 2–49283
Cs-O_2-W electrode system, statistical mechanical model 2–63230
Cs-O_2 sources, increasing electrical output 2–63222
Cs-W-O convertor adsorption phenomenology, analytical model 2–63231

Electricity, direct conversion continued
thermionic continued
Cs, cylindrical converter, I-V characteristics 2–52375
Cs, diode plasmas, collision processes, model improvements 2–49277
Cs, ignited mode, charge influence of V-I characteristics 2–52378
Cs, low vapour pressures, arc mode 2–52376
Cs, nonequilibrium relaxation phenomena, near emitter region 2–49276
Cs, plasma probe measurements, space coeff. power source 2–54991
Cs arc mode theory, assumptions, parameters 2–63249
Cs convertors, equilibrium Cs adsorption on polycrystalline W, ellipsometry measurement technique 2–63232
Cs diode diffused electronic and ionic currents through grid type anode 2–45659
Cs discharge tube, ionization in nuclear reactor 2–53252
Cs filled, discharge modes, polarization and interferometric investigations 2–49288
Cs low voltage arc, ion loss and electron temp. 2–80369
Cs plane parallel diode, I-V characteristics 2–49287
Cs plasma convertors, arcing mode and energy rating 2–59054
Cs vapour source, for Cs-graphite system 2–52372
Cs_2O-Cs soln., as source of Cs and O_2 2–49280
Hg discharge tube, ionization in nuclear reactor 2–53252
Mo/UO_2 emitter-fuel system technology and test results 2–63251
Mo, chemical vapour deposition 2–53559
Mo, monocrystal, electrical characteristics, thermionic converter emitter 2–54275
Mo, Nb cylindrical convertor, parametric optimization 2–63243
Mo, sublimed collector coatings, additive diode operation 2–49278
Mo electrode diodes for incore thermionic fuel elements 2–49270
ThO_2 as heat source in thermionic conversion rel. to ^{228}Th radioactive decay simulations 2–52787
UN fueled, out of core evaluation 2–49265
UO_2 clad fuel element swelling at high temp., factors 2–63250
UO_2 fueled and unfueled cylindrical thermionic convertor 2–63241
W-Nb, CVD, variable spacing, thermionic performance 2–59053
W, chemical vapour deposition 2–53559
W, monocrystal, electrical characteristics, thermionic converter emitter 2–54275
W compatibility with buffered hyperstoichiometric UC alloys 2–63252
W electrodes, interdiffusion in emitters 2–53560
W oxides, formed on emitter, additive thermionic converters 2–49279
Y_2O_3, fast neutron irradiation, thermionic reactor design 2–53707
Electro-deposition *see Electrolytic deposition*
Electro-optical effects
see also Electroluminescence; Electroreflectance; Optical constants; Piezo-optical effects
aromatic hydrocarbons, anisotropic polarizability eval. 2–80108
biexciton theory, spectrum analysis 2–47817
carbon tetrachloride, Kerr effect induced by fluctuational statistical processes 2–46955
circular scan deflectors 2–66830
crystals, electro-optical activity from piezomagnetic tensor 2–72258
cyclohexanol, polar liquid, microwave Kerr effect, Kerr const. 2–80470
disperse particles, large strongly elongated, saturation phenomena of elec. light scatt. 2–74562
distance meas. using electrooptical instruments 2–82533
electro-optical light modulator, use with nonlaser light sources 2–76528
electro-optical spatial light modulator for optical data processing, two dimensional, adaptive, online 2–79418
ethoxybenzylidene-p'-n-butylaniline: 1-menthol (racemic menthol), liquid crystals, optical storage effects 2–43365
glass, self-focusing rel. to electrostriction and Kerr effect, damage threshold 2–75249
gradientless temp. cell for optical study of cpds. in elec. fields 2–82588
guided wave structures for electrooptical modulation at 10.6 μm 2–42157
interdigital electro-optic thin film modulator using nitrobenzene 2–79376
interferometric method for meas. of coeffs. in crystals 2–63397
Kerr cell, multiple refl., for liq. birefringence obs. 2–76524
Kerr cell shutter with ten picosecond time resolution, application to particle accelerators 2–42291
Kerr effect, isotropic phase of some nematogenic compounds, investigation, temperature dependence and relaxation times 2–53430
Kerr effect, meas. of absolute phase delay using polarization interferometer 2–42197
Kerr effect, rel. to simultaneous passive mode-locking and Q-switching of high power lasers 2–66737
Kerr effect, u.h.f., quadratic law verification 2–43355
Kerr effect in glass fibre waveguide 2–42239
Kerr effect self-focusing of picosecond laser pulses 2–52431
Kerr system electrical measurement techniques, recent developments 2–78990
laser modulation, automatic optical bias control, p.c.m. communication 2–66797
laser pulses self trapping in Kerr liquids 2–42112
leaky wave couplers for devices for guided elastic and optical wave devices 2–73413
light modulation in anisotropic waveguides 2–63410
liquid cryst., nematic, dynamic scatt., effect of charge transfer acceptors, voltage transmission characts. 2–71201
liquid cryst., nematic, elec. field quenching of thermal fluctuations of orientation 2–43332
liquid cryst., nematic, orientation behaviour, elec. and optical behaviour 2–80444
liquid crystal, nematic, appl. to p-n junction and insulating layer investigation 2–77918
longitudinal Kerr effect in 4 layer system of ZnS, Fe, MgF_2 in Ag base, calculation 2–42216
macromolecular solution, electric birefringence, relaxation spectrum, decay curve, numerical method 2–74543

Electro-optical effects continued
- macromolecules, transient scattering from absorbing solutions in pulsed elec. fields 2—50378
- MBBA, Kerr const. temp. depend. near isotropic-liq. cryst. transition 2—77430
- MBBA nematic liquid films with free surfaces, and hydrodynamic props. 2—67804
- metal-semiconductor contact, surface elec. field, determ. by differential electroabsorpt. 2—65036
- methyl group stretching and bending vibrs., substituent effect on i.r. absorpt. intensities 2—56245
- modulator, developments 2—73657
- nematic liquid crystals, homeotropic geometry, soln. of boundary-value problem associated with electro-optic mode 2—71150
- m-nitroaniline, linear props. and rel. to crystal structure 2—72271
- nitrobenzene, Kerr effect, meas. of absolute phase delay using polarization interferometer 2—42197
- nonlinear luminous interactions in electro-optical media excited by travelling circular modulating field 2—69995
- optical pulse generator with Fabry-Perot electro-optic modulator as output coupler of laser reson. 2—79175
- p-methoxybenzylidene-p′-amino phenyl acetate, nematic, dynamic scatt. life, current density effects 2—71203
- palygorskite colloid soln., stability, transient elec. light scatt. obs. 2—74567
- particle size spectrometer, submicron aerosol, meas. from aircraft 2—82579
- piezosemiconductor, Franz-Keldysh effect inside acoustoelec. domains 2—54033
- polar molecules, Kerr effect and dielec. saturation formulation 2—52971
- poly-γ-benzyl-L-glutamate solns., i.r. elec. dichroism 2—60083
- processing of phased array antenna data 2—42226
- pulsed laser Kerr system polarimeter, for electro-optical fringe pattern obs. of transient electrical parameters 2—55744
- quartz, calc. from light wave intensity reduction 2—65222
- quartz, dispersion and temp. dependence in static fields 2—65224
- quartz, gyrotropy and asymmetric electro-optic props., two beam refraction obs. 2—72269
- α- quartz, Pockels effect 2—52461
- semiconductor, cubic, spectral depend. of electro-optic coeffs. calc. 2—81335
- semiconductor, disordered, theory of electroabsorption 2—51330
- semiconductor, electro-transmission in visible and near i.r., charge carrier obs. 2—51323
- semiconductor, two-photon interband transition in arbitrary elec. field 2—61623
- semiconductor electrode surface, determ. of recombination rate and term distribution using internal reflection spectroscopy 2—68423
- shutter for Q-switching lasers emitting unpolarized radiation 2—69959
- small polaron absorption, in high elec. fields 2—57344
- solid state plasma, magnetised, submillimetre wave propagation 2—82394
- thermal and electric field broadening, calc. 2—57327
- tri-o-cresylphosphate, polar liquid, microwave Kerr effect, Kerr const. 2—80470
- t.w. electro-optic modulators, performance 2—73661
- two-photon absorption by excitons, elec. field effect 2—65221
- Ar, liq., Kerr effect induced by fluctuational statistical processes 2—46955
- $Bi_{12}SiO_{20}$ electro-optic image modulator for optical processing 2—79416
- $Bi_{12}SiO_{20}$ electro-optic image modulator, sensitivity and resolution 2—79417
- CS_2, u.h.f. Kerr effect detection and obs. at 9227.12 MHz 2—74544
- $CaWO_4$-Nd laser, active Q switching technique for high power in single longitudinal mode 2—63337
- CdS:Cu, trapping parameters, photocond. response, i.r. quenching, photochem. effects 2—65000
- CdTe, electroabsorpt., light quanta with energy less than forbidden bandwidth 2—78059
- GaAs, elec. field induced interference effects at ground exciton level 2—78084
- GaAs, impurity electroabsorption 2—65258
- GaAs film, epitaxial, guiding and electrooptic modulation of light 2—68608
- GaAs p-si-n structure, electroabsorption, polarization effects 2—70666
- GaP, linear effect, wavelength range 0.55-1.3μ 2—68607
- GaSe, linear electro-opt. eff. at room temp., photon energy 1.25-1.96eV 2—72270
- $Gd_2(MoO_4)_3$, ferroelec., coeffs. temp. depend. 2—78068
- n-Ge, light modulation by non-equilib. optical phonons in pulsed elec. fields 2—78069
- Ge, n-type, infrared birefringence on hot electrons 2—81328
- α-HIO_3, meas. of ratio of electroopt. const. for coeff. up to 20MHz 2—72267
- n-InSb, Faraday and Kerr effects of hot electrons in i.r. 2—57326
- n-InSb, hot electron Kerr effect birefringence phase shift calc. 2—51303
- KD_2PO_4, Pockels effect, light valve device for image storage and processing 2—66847
- KH_2PO_4-type crystal, optimum cut for transversal modulation 2—61592
- KH_2PO_4, calc. from light wave intensity reduction 2—65222
- KH_2PO_4, z cut and electrode configuration effects on control voltage for switching shutter 2—69894
- $KTa_xNb_{1-x}O_3$, absorpt. edge splitting, paraelec. and ferroelec. phases 2—48184
- $La_2Ti_2O_7$, paraelec. crystal 2—51205
- $LiNbO_3$, calc. from light wave intensity reduction 2—65222
- $LiNbO_3$ crystals, light modulation applications 2—69988
- $LiNbO_3$ single domain crystals, growth by pulling method in h.f. induction furnace, properties, applications 2—77528
- Mn ferrite, Kerr effect and optical consts., magnetooptical reson. in visible 2—81337
- MnO:Li, electro-transmission in visible and near i.r., charge carrier obs. 2—51323

Electro-optical effects continued
- $(NH_4)_2C_2O_4.H_2O$, meas. of ratio of electroopt. const. for coeff. up to 20MHz 2—72267
- $NH_4H_2PO_4$, Pockels effect above 90°C 2—54381
- $(NH_4)_xK_{1-x}H_2PO_4$ epitaxial film, electro-optic waveguide 2—70058
- $NaNH_4SeO_4.2H_2O$, ferroelec. temp. depend. of electro-pt. coeffs. 2—72268
- NiO:Li, electro-transmission in visible and near i.r., charge carrier obs. 2—51323
- $(Pb,La)(Hf,Ti)O_3$, hot-pressed 2—56966
- $(Pb,La)(Zr,Ti)O_3$, electrooptic ceramic, fabrication by atm. sintering 2—56967
- $PbMg_{1/3}Nb_{2/3}O_3$-$PbTiO_3$-$PbZrO_3$ solid solution, hot-pressed 2—57328
- $PbMg_{1/3}Nb_{2/3}O_3$ crystals, change in refractive index as function of electric field strength, use of prisms as light beam deflectors 2—42215
- $Pb(Zn_{0.33}Nb_{0.67})O_3$ ceramic, props. rel. to sintering conditions 2—65223
- $RbBr:Ag^+$, paraelec. props. study 2—61422
- $RbCl:Ag^+$, paraelec. props. study 2—61422
- SbSI, effect on absorp. edge 2—81379
- Si, doping inhomogeneities, obs. by electroreflectance 2—71510
- Si, low field electroabsorpt., split-off exciton and phonon-depend. lineshape 2—72349
- SiC, 6H electroabsorption due to indirect excitons 2—81331

Electroacoustic transducers *see Transducers*

Electrocataphoresis *see Electrophoresis*

Electrochemistry
- *see also Chemical analysis/electrochemical; Electrolysis; Electrolytic deposition*
- alkali metals, molten, interionic interaction and thermodynamic potl. analysis 2—84650
- alkaline solns., nonlinear effects and transient phenomena, pot. barrier height 2—61795
- alloy, electron charge transfer and electrochem. effects 2—64884
- arodic sectioning technique 2—60817
- austenitic stainless steels, susceptibility to stress-corrosion cracking, evaluation by electrochemical methods 2—68104
- book, electro-chemical science 2—84651
- cathodic protection, stress corrosion cracking 2—78194
- colloid, electrical double layer round spherical particle, functional representatinal of properties 2—60525
- colloid, Esin-Markov coefficient for elec. double layer 2—60524
- concentration cell, anisotropic, system based on β-alumina ($NaAl_{11}O_{17}$) solid electrolyte 2—61799
- coulometric titrator with feedback controlled electrolysis current 2—65404
- diffusion coeff. meas. methods for metals 2—77602
- diffusion of 1:1 electrolyte, eqn. for effect of appl. mag. field 2—83782
- Eighth International Power Sources Symposium, Brighton (1972) 2—84653
- electrolyte, charged particle system, statistical theory, osmotic model 2—51459
- electrolyte, Gouy layer, ion-size corrections of Poisson-Boltzmann equation 2—61792
- electrolyte solutions, limitations of analogy with point defects in ionic crystals 2—64657
- electrolyte solutions, Rayleigh and Brillouin scattering studies 2—43360
- electrolytes, higher terms in concentration dependence of self-diffusion coeffs. 2—72563
- electrolytes, van der Waals forces 2—51458
- electron transfer reactions in solution, generalized mobility theory 2—84648
- electropolishing procedure for Debye-Scherra camera specimen prep. 2—43544
- ellipsometric-electrochemical cell, surface film form. on Ti obs. 2—50510
- high-conductivity solid electrolytes, thermoelectric powers 2—77961
- International Society of Electrochemistry, 23rd meeting, Stockholm (1972) 2—68792
- iodination of human serum albumin at alkaline pH 2—55213
- $LiNO_3$, molten, interdiffusion coeff. of Ag^+ 2—65383
- local natural convection mass transfer, electrochemical technique obs. 2—50288
- mass transfer in flowing electrolyte with quasi porous electrode 2—68794
- mass transfer rates, meas. at rough surfaces 2—54552
- materials for cardiovascular implants, electrochemical methods for selection and eval. 2—69226
- metal melts, thermodynamic props., determ. by e.m.f. meas. 2—77421
- metal surface roughness factor determ. method 2—47067
- metal-electrolyte solution interface, electron photoemission 2—68496
- metal-powder formation at metal-electrolyte interfaces, determ. of potential barriers and eqns. of tunnelling limiting current 2—57426
- mixed conductors, polarization measurement methods 2—68464
- Nernst-Planck eqns. for ionic diffusion at conditions near equil. 2—78198
- pH meas. using glass electrodes 2—57427
- phase-discrimination methods β—phase in Ti alloys, comparison with X-ray diffraction 2—77669
- photoeffect obs., applic. of phase selective detector system 2—59032
- polyelectrolyte macromolecules, adsorption on flat interface, approx. theory for low potentials 2—61793
- reactions, proposed use of electrode potential control of ZnO green luminescence as probe 2—61717
- rocks, elec. and electrochem. characts., equivalent network 2—65524
- solid electrolyte cells in liquid metals, e.m.f. meas. 2—66681
- solid electrolytes, applications to measure solubility and diffusion in nuclear materials 2—49904
- solid-state galvanic cell technique, for thermodynamic study of rare earth carbides 2—43865
- stainless steels, susceptibility to intergranular corrosion by potentiodynamic polarization 2—68788
- unsymmetrical electrolyte, linearized potential eqn. for interfacial region 2—75385

Electrochemistry continued
Ag complex, $[C_5H_5NH]Ag_5I_6$, solid electrolyte, struct. and cond. 2−43574
Ag_4RbI_5, solubility and diffusion of I_2, e.m.f. obs. 2−84657
Al_2O_3 film, growth by plasma anodization 2−43477
$CdCl_2$, adiabatic compressibility and sound propag. speed, reln. to molec. struct. 2−72564
$CdFe_2O_4$, specific saturation magnetization depend. on pH of soln. 2−84432
CdTe, electrochem. preparation 2−75384
$CoCl_2$, adiabatic compressibility and sound propag speed, reln. to molec. struct. 2−72564
$CsNO_3$, molten, interdiffusion coeff. of Ag^+ 2−65383
Cu coatings' hardness and conductivity 2−84647
GaAs, controlled sectioning by anodic oxidation and removal of oxide layer 2−64544
H bonded materials, proton migration studies, experimental methods, review 2−83998
HgO/Zn cell, reaction thermodynamics, electrochemical processes 2−84655
HgTe, electrochem. preparation 2−75384
In-Ga alloy, component activities detn. using a solid oxide electrolyte technique 2−78201
InSb, anodic dissolution potentials and activation energies in HCl 2−71366
KNO_3, molten, interdiffusion coeff. of Ag^+ 2−65383
Mg-Li alloys, thin Foil prep. using a non aqueous electrolyte 2−80548
$MgCl_2$, adiabatic compressibility and sound propag. speed, reln. to molec. struct. 2−72564
$NaNO_3$, molten, interdiffusion coeff. of Ag^+ 2−65383
$NiCl_2$, adiabatic compressibility and sound propag. speed, reln. to molec. struct. 2−72564
Pb, anodic dissolution in H_2SO_4 2−84658
ThO_2 and solid solns., electrolyte transport props. 2−65053
$TlNO_3$, molten, interdiffusion coeff. of Ag^+ 2−65383
ZrO_2-Y_2O_3, current blackening, effect on elastic consts. 2−43666
ZrO_2, Y_2O_3-stabilized, current blackening effects, defect struct. obs., e.s.r. spectra 2−61740

electrodes
see also Electrodes
adsorption of org. cpds. in double layer 2−84646
air in organic systems, feasibility for energy conversion 2−84652
dielectric coeffs. in interphase between electrode and ionic solution 2−48335
electrolyte-phobic molten carbonate fuel cell 2−59045
Faraday and two-layer impedances relationship 2−81507
fuel cells, high temp. electrode development, test results 2−49258
ion selective electrodes, properties and uses in seawater 2−54549
kinetics of charge transfer, quantum-statistical mechanics approach 2−65385
liquid-iron and platinum-air electrodes oxygen diffusivity, potentiostatic electrochemical measurements 2−60456
metal, with one cryst. plane only, prep. 2−48337
metal dendrite formation at limiting current 2−68795
porous, current generation distribution 2−59044
potentials comparison in solid and liq. ionic media 2−54548
selective ion-sensitive, development 2−48336
transient straining electrodes for study of stress corrosion cracking of metal-environment systems 2−68103
vitreous C electrode material, electrochemical evidence for structure 2−84649
water, electrochemical photolysis at semiconductor electrode 2−57428
Ag, sintered, morphology, electrical characteristics, KOH concentration effects 2−84654
Ag, with one cryst. plane only, prep. 2−48337
C, glassy, in coulostatic analysis 2−72587
porous Cd, passivation in KOH solution 2−84656
CdS(Se) anodes, electron injection 2−61797
GaP electrodes, selective etching and anodic dissolution 2−75386
Ge, equilibrium and nonequilibrium effect near semiconductor-electrolyte boundary 2−61798
Hg, metal dendrite formation at limiting current 2−68795
Ni-Ni hydroxide, sintered plate, behaviour in lithiated electrolyte solution 2−84659
Pt/PTFE/porous Ni fuel cell, oxygen/ alkali gas diffusion, model 2−59043
Pt, dispersed, for fuel cell, electrochemical activity 2−45656
Si, equilibrium and nonequilibrium effect near semiconductor electrolyte boundary 2−61798
Zn secondary cell electrode active material migration obs. 2−65386
ZnO anode, electron injection 2−61797

Electrodes
see also Anodes; Cathodes; Electrochemistry/electrodes
a.c., polarization in neurological recording, signal distortion 2−51895
air gaps in nonuniform fields, a.c. corona inception voltage calc. 2−71048
arcs, recovery, refractory region, effect of arc gas 2−74451
bioelectric event obs., book 2−55216
bioelectrode systems, interface design 2−85085
cardiac catheter electrode, very flexible, development 2−51898
diffusion, for elimination of liquid dielectric breakdown 2−77444
e.c.g. and spray-on, for biomedical transducers 2−73180
e.m.g., indwelling wire, histological response of rat skeletal muscle 2−55211
film, chalcogenide, amorphous, elec. props. rel. to electrode comp. 2−61309
film, chalcogenide, amorphous, pre- and postswitching characts., rel to electrode comp. 2−61310
fuel cell, electrolyte stabilization in wetproofed pores of electrodes 2−45657
glass for pH meas. 2−57427
graphite, mech. strength at high temp., integrated evaluation 2−56813
LEED-AES system, electrodes and circuits 2−74612
macroparticle detachment rel. to vacuum breakdown initiation at pulsed voltage 2−62898
material losses in low pressure gas discharge lamps 2−70999

Electrodes continued
materials, effects in wire explosions 2−69785
microelectrodes, reduction of tip potential artefacts 2−61796
paint-on, for surface electromyography 2−45037
paste, for determ. of Ag in various stages of oxidation 2−65384
photoelectric emission, space charge limited, in plane parallel electrode geometry 2−68494
plasma, contact pot. between emitting electrode and probe 2−74376
point, field distribution effect rel. to partial discharge channels in solids 2−72020
rotating Sparkonite, in triggered spark gap 2−79643
semiconductor, electrooptical method for determ. of recombination rate and term distribution at surface 2−68423
silicone liquids thermal breakdown under pulsed h.f. fields 2−56513
spot welding, electrode fault-free life 2−69479
steel, stainless, subjected to very high positive and negative voltages, struct. 2−71042
surface waves reflection from transducer electrodes, meas. and modeling 2−49142
thin needle, shape, structure and evolution of a.c. coronas 2−74442
vacuum gap, elec. characts., prebreakdown current, breakdown voltage, 4-300K 2−63294
W, heated, pre-breakdown phenomena 2−71028
welding, heat content and size distrib. of electrode metal droplets 2−69483
Ar-K, flowing, heat transfer between electrodes 2−60209
C, present and future applic. 2−68172
KH_2PO_4, z cut and electrode configuration effects on control voltage for switching electro-optical shutter 2−69894
Mo-Cu-Co cermet contact, elec. erosion characts. working surface struct., rel. to Co content 2−47659
Mo, in diode for incore thermionic fuel elements 2−49270
Mo, in vacuum, elec. breakdown rel. to electrode surface finish 2−75190
Pt electrode on alkali-containing glass, model of electrode 'polarization' by d.c. potential applic. 2−81141
Rh film electrodes on glass, deposition by sputtering 2−64573
SF_6 breakdown, surface conditions effects 2−74439

Electrodynamics
see also Eddy-currents; Quantum electrodynamics
— 2−69562
action-at-a-distance, solution of two-body straight-line motion 2−55655
arbitrarily moving charge, radiation indicatrix 2−69858
atmosphere, charged particle flux interactions 2−48549
Boltzmann eqn. for charge particle transport in magnetic field, simplified soln. 2−73492
Born-Infeld, exact plane wave solution 2−49313
Born-Infield nonlinear e.m. theory, Newman-Penrose conserved quantities 2−82163
charge moving in isotropic transparent medium in field of intense e.m. wave, emission 2−78775
charged particle, uniformly moving in time-dependent magnetoactive plasma, radiation 2−53180
charged particle drift velocity, effect of small magnetic field 2−55653
charged particle motion and radiation in rapidly oscillating mag. fields 2−69861
charged particle motion near neutral plane, Hamiltonian analysis 2−69862
charged particle stream, transverse instabilities growth rates 2−66704
charged particles, equation of motion 2−82173
charged particles, equations of motion 2−82172
charged particles, symmetry relation between radiative properties in attractive and repulsive Coulomb fields 2−45608
Cherenkov radiation of charged particle creation, e.m. field and rate of increase of field energy 2−63260
Chladni forces, generalized concept 2−49312
classical, with classical e.m. zero-point radiation, derivation of unretarded London van der Waals forces between atoms 2−46464
coupled e.m. and mesonic fields; calc. of cross section for interacting particles 2−78774
current conservation, distinction from charge conservation and flux integral forms 2−55652
disc and ring conductors, rel. to field penetration depth 2−76433
dust particles, influence of polarizability on oscillatory behaviour in a.c. fields 2−49311
electro- and magneto-rheology in dispersive systems 2−58854
electron, Poincare's Rendiconti paper on relativity 2−41426
electron, with anomalous mag. moment, induced radiation in field of e.m. wave 2−45674
electron beam with relativistic energy spread, limiting currents 2−79022
electron motion at synchrotron output, nonlinear resonance of betatron oscill. obs. 2−70329
electron moving in vertical metallic pipe, effect of electric field arising in shield due to gravitational field 2−66705
electron ray tracing under e.m. field influence 2−73523
electron undergoing synchrotron radiation, quantum-mechanical treatment 2−49320
e.m. field prod. in mag. field of arbitrary config., classical eval. 2−49315
energy flow from atomic dipole in classical electrodynamics 2−79942
energy flow from atomic dipole in classical electrodynamics 2−59891
equation of motion of charged particle in symmetric magnetic field 2−78778
in expanding universe, co-determined Einstein- Maxwell equations, soln. 2−76193
Faraday ring currents in low-pressure ring-shaped duct with radial mag. field 2−60219
field equations and equations of motion, generalization 2−69859
force acting on sphere in travelling magnetic field 2−49195
forced radiation from electron in e.m. wave, effect of vaccum mag. moment 2−76166
forces in e.m. stirrer for molten metals 2−50183

Electrodynamics continued
  free electron interaction with circularly polarized laser pulse 2—55657
  gauge group of electrodynamics and general relativity, semidirect product. 2—76191
  Hamiltonian formulation of charged particle motion in neutral sheet type magnetic field 2—59077
  harmonic generation due to electron retardation in presence of intensive light wave 2—66796
  Helmholtz eqns., approx. reduction, for nonuniform media 2—82319
  hydrodynamical analogy of equations 2—63264
  intrinsic momentum computation of charged particle in magnetic field 2—45675
  Landau gauge soln. for wave packet motion for charged particle in magnetic field 2—78807
  levitation and stabilization of single particle using negative feedback 2—63263
  light pulse scattering by spherical particle, theoretical considerations 2—79320
  macroscopic bodies, Van der Waals forces, electrodynamic theory, fluctuation dissipation theorem 2—66679
  magnetoelasticity of thin solids 2—76283
  Maxwell's eqns., soln. in periodic laminated media, Green's function method 2—82398
  moving media, Minkowski's equations 2—73478
  nonlinear, shock relations 2—52387
  nonlinear field eqns. for particles interacting with coupled e.m. and mesonic fields, soln. method 2—78773
  oscillating charge, in inhomogeneous medium, radiation, perturbation theory 2—41917
  oscillator, moving along interface, radiation 2—41916
  particles trapped by Whistler wave, detrapping by second wave 2—69860
  point particle eqns. of motion, analogy with quantum eqns. for high spins 2—55658
  pulsar rotating magnetic field, Hamiltonian anal. of charged particle motion 2—62613
  quantum, synthesis with classical electrodynamics 2—78766
  rel. to quantum theory, soft quanta approach 2—55793
  quasiclassical wavefunctions for charged particles in uniform magnetic field, geometrical relations 2—78761
  quasistationary theory, approximations and appl. 2—58981
  quasistationary theory, Maxwell equations, Lorentz force in moving matter, models 2—45677
  radiation from free electron interacting with circularly polarized laser pulse 2—78772
  radiation from oscillating charge crossing boundary between two dielectrics 2—69863
  radiation from particle, in equal mutually perpendicular static elec. and mag. fields 2—63261
  radiation of charged particle moving in hyperbolic motion in vacuum 2—76416
  relativistic, duality principle 2—76179
  relativistic electron motion in spatially modulated magnetic field 2—66703
  spin-1 theory consistency for motion of particle in external e.m. field 2—49314
  in strong magnetic field, phenomena studied by perturbation formalism 2—63265
  symmetrical theory of electricity and magnetism 2—41871
  synchrotron instability of modulated beam of charged particles 2—78777
  synchrotron radiation, from electron in uniform helical motion 2—45676
  TEM plane wave field, group-theoretical analysis of charged particle motion 2—63262
  transition radiation, generation by inclined flight through waveguide 2—41930
  ultra-high-energy particles with anisotropic mass, interaction with e.m. field 2—45678
  unidimensional motion in an electric nonhomogeneous field with Coulomb potential 2—76215
  Vavilov-Cerenkov effect, in medium with wave phase velocity exceeding velocity of light 2—78776
Electroendosmosis *see Electrophoresis*
Electrogasdynamics *see Electrohydrodynamics*
Electrohydrodynamics
  see also Magnetohydrodynamics
  charged drop, oscillations, relaxation and damping, EHD stability 2—80227
  closed-loop liquid system, interaction of two injection diodes 2—60493
  flow, two dimensional potential cases 2—77222
  fluid electrically charged, some solns. to Einstein Maxwell equations 2—69563
  free flow of unipolar gas, electric field distribution in phase plane 2—64365
  ion source for mass spectrometry 2—74203
  liquid crystal, instability phenomena and dielec. const. relax. 2—53395
  liquid crystal, nematic, instabilities in elec. fields, domains and reorientation 2—56477
  liquid crystal, nematic, oscillation modes 2—50321
  liquid crystal, nematic, transition between cond. and dielec. regimes of instabilities 2—43330
  liquid crystal, nematic, Williams domain and variable grating mode boundary value soln. 2—50319
  liquids, insulating, in elec. field, hydrodynamic stability conditions 2—83527
  liquids, propoagation and stability of electro-fluid-mechanical space charge and polarization waves 2—46872
  macroscopic coupling between electric fields and fluids 2—77210
  nematic liquid crystal, instabilities in low-freq. fields 2—43326
  nematic liquid crystal, instabilities under a.c. fields, special effects near cut-off freq. 2—56478
  one-dimensional flow with variable mobility coeff., evap. and condensation jumps 2—83528
  probe under floating pot., perturbation analysis 2—64223
  shock waves structure 2—77254
  stratified liquids with space charge, dynamics 2—56453
Electrohydrodynamics continued
  weak waves around thin body 2—67608
Electrojet *see Atmosphere/upper; Atmospheric electricity; Ionosphere*
Electrokinetic effects
  see also Electrophoresis
  a.c. electroosmosis 2—72562
  alumina, zero point of charge, temp. depend. 2—72567
  charge transfer on electrodes, quantum-statistical mechanics approach 2—65385
  charge-mosaic membranes, piezodialytic salt flux reduction, geometric effects 2—53419
  electro-osmotic energy conversion in glass/n-propanol system 2—66678
  haematite, crystalline, zero point of charge 2—72566
  hydrodynamic coupled flow in porous media, finite element solution 2—74310
  magnetite, zero point of charge, temp. depend. 2—72567
  palygorskite colloid soln., zeta pot. rel. to stability 2—74567
  streaming potential meas. technique 2—72566
  suspended colloids in flowing medium, expt. obs. 2—71127
Electroluminescence
  — 2—57380
  alkali halide crystals, nonactivated, luminescence centres formation in very strong electric fields 2—84542
  anthracene diode, double injection electrolum., and carrier injection props. of C fibres 2—75338
  anthracene films and crystals current/voltage charact. rel. to thickness, temperature and light emission 2—57201
  Avzel effect fluoresc. process, diodes, visualisation applications 2—84530
  book collection of 5 papers 2—68705
  capacitor, brightness, temp. depend. 2—72435
  cells, obs. of non-linear effects using computer 2—63420
  crystals, phenomena, coloured light, ageing 2—51384
  Destriau effect kinetics, investig. method 2—68706
  diodes, light emitting, response time 2—51385
  film, electrode current rel. to applied stress 2—81435
  graphitic diamonds, 480-780 nm, determ. of voltage and frequency dependence of intensity 2—84546
  image storage panel, characts. 2—70068
  injection, groups III-V luminescent materials 2—44417
  light source, principle of energy conversion 2—68439
  light sources, apparatus for obs. of quantum efficiency 2—55759
  mim and mis structures, characteristics 2—68448
  phosphors, EL 460, EL 510 and EL 580, energy absorpt. mechanism 2—48264
  physical processes, review 2—65315
  review 2—48265
  semiconductor, with nipi superstruct., critical and electrical props. 2—65237
  $Al_xGa_{1-x}As$ grown-diffused planar monolithic diodes 2—51386
  $Al_xGa_{1-x}As$ heterojunction, characteristics 2—81431
  CdS:Cu powder phosphors, a.c. characts. 2—44420
  CdS:Cu powder phosphors, d.c. characts. 2—44419
  CdS, optical cavity, total internal refl. and Fabry-Perot configs., electrolum., spectra, laser action 2—81413
  CdS powder, brightness, effect of nonstoichiometric deviations 2—61716
  $Ga_{1-x}Al_xAs$:Si diodes, substrate orientation depend. 2—51153
  $Ga_{1-x}Al_xAs$, indirect gap semicond., direct band recombination 2—75337
  $Ga_{1-x}Al_xAs$ epitaxial layer growth 2—47288
  GaAs:Zn light emitting diodes 2—65031
  GaAs-$Al_xGa_{1-x}As$ p-n heterojunction, current flow during electrolum. 2—72438
  GaAs, electrolum. diode, electron diffusion length, internal quantum efficiency, temp. depend. 2—61725
  GaAs, electrolum. diode, sinusoidal modulated, recomb. emission phase shifts rel. to injection levels 2—72400
  $GaAs_{1-x}P_x$, electrolum. diode, Zn diffusion in open-tube system 2—75126
  $GaAs_{1-x}P_x$, light emitting diodes characteristics, applications 2—44422
  $GaAs_{1-x}P_x$, light emitting diodes 2—44421
  $GaAs_{1-x}P_x$ light emitting diodes, reliability 2—44423
  GaAsP(N), diodes, light emitting, N doping effects, 77-300K 2—81411
  GaN:Mg, diode, fabrication, props. 2—72387
  GaN m.i.s. diodes, radiative recombination due to electric field polarity reversal 2—71990
  GaP: Zn, Al, 1.7 to 2.3eV 2—75321
  n-GaP:Te,Zn,O, and mean electron conc., influence of Te content 2—57381
  GaP:Zn, diode, red. prep. 2—44424
  GaP-ZnSe alloy, cond. hopping contrib., ionized impurity scatt., electrolum. and cathodolum. 2—81415
  GaP, green electrolum. efficiency, weak photolum. band 2—84548
  GaP, melt-grown, S-pit correl. with reduced efficiencies 2—50595
  GaP, switches, p-n-p-n, controlled rectifiers, blocking voltages, electrolum., $0 \leqslant T \leqslant 500C$ 2—61392
  GaP green emitting diode fabrication by double- bin liquid-phase epitaxy 2—72437
  GaP light emitting diode, props. for green and red emission, quantum efficiency 2—44418
  GaP p-n-p-n diode, green emission, quantum efficiency 2—72436
  GaP p-n junction growth by liq. phase epitaxy 2—47287
  GaP red-emitting diode manufacture, cryst. growth technique 2—60711
  GaP red-emitting diodes, scanning electron microscope characteriz. 2—51389
  $In_xGa_{1-x}As$, p-n diodes with efficient 1.06 μm emission 2—61726
  $In_xGa_{1-x}As$ prep. and props. rel. to electroluminescent diodes 2—68708
  $In_{1-x}Ga_xP$, diode, vapor grown 2—49386
  $In_{1-x}Ga_xP$ p-n junction, bright yellow emission 2—44425
  InP, properties with view to use in injection laser 2—42096
  n-InSb, recomb. radiation from impact-ionized shallow donors 2—68707
  KCl, diffusion coeff. of self-trapped holes and migration to thallium centres 2—68709

Electroluminescence continued
KI, diffusion coeff. of self-trapped holes and migration to thallium centres 2–68709
$KNbO_3$, ferroelec., surface change layers, obs. by AF electrolum. 2–75151
NaI, diffusion coeff. of self-trapped holes and migration to thallium centres 2–68709
$POCl_3$ solns., of trivalent rare earth ions, emission mechanism 2–46966
PbTe epitaxial thin film diode, evaporated, injection luminesc. and laser action 2–57382
RbI, diffusion coeff. of self-trapped holes and migration to thallium centres 2–68709
Se-CdS(Se) heterojunction diodes 2–54481
Si, radiative recomb. rate, 300K, carrier conc. depend. 2–81430
α-SiC, influence of struct. defects on elec. props. and luminescence 2–71774
ZnCdS-Cu, Mn powder crystallophosphors, interaction of electrolum. and photocond. during switching 2–68710
ZnO, electrode potential control, possible use as probe for electrochemical reactions 2–61717
ZnS:Cu, Cl, changes in brightness wave during ageing 2–65316
ZnS:Cu, Pb, Cl film temp. depend. of electrolum. and thermal quenching 2–84533
ZnS-Cu crystallites, centres of luminescence, radiation intensity, influence of milling 2–51390
ZnS, role of Cu and Cl impurities 2–51394
ZnS, temp. depend., thermal extinction mechanism 2–48267
ZnS film, in electrolum. device, high field a.c. electrolum. rel. to field clamping 2–81412
ZnS luminophor, Gudden-Pohl effect, optical quenching 2–51393
ZnS p-n junction, electronic behaviour obs. 2–68711
ZnS phosphor, abnormality with variable impedance 2–48268
ZnS phosphor, abnormality due to variable d.c. bias, obs. 2–51392
ZnS photoelectroluminescence following u.v. irradiation, confliction with Fischer model 2–51391
ZnS single crystal, homogeneous, u.v. spectrum, electronic behaviour 2–68712
ZnTe, low efficiency d.c., due to avalanche ionization and recombination 2–64962

Electrolysis
see also Conductivity, electrical/liquids, electrolytic; Dissociation/electrolytic; Electrochemistry; Electrolytic deposition; Ion velocity/electrolytic
bi-polar electrolyte flow cell for electrolysis of organic and/or inorganic depolarizers 2–68797
contact glow-discharge, study in water containing various electrolytes 2–54551
electrolytes in porous systems, subject to MHD pressure, kinetic steady-state and transient phenomena 2–71133
Faraday's law, irreconcilable results 2–75387
foil preparation, for electron microscopy, electrolytic jet thinning procedures 2–71415
galvanoluminescence cathode glow described 2–77305
glass, K^+ ion migration from K^+ ion-exchanged layer under reverse electric field 2–75388
heavy water enrichment, H-D separation factor, current density, cathode material, temp. effects 2–42820
heterogeneous proton transfer, mechanism and rate transfer 2–61794
iodination of human serum albumin at alkaline pH 2–55213
jet thinning apparatus, for electron microscopy, specimen holder design 2–67959
kinetic phenomena in electrolytes in porous systems subject to MHD pressure 2–71132
mass transfer, effect of uniform mag. field, expt. 2–54550
quartz, i.r. spectra obs. and colour centres 2–74802
quartz, purification method 2–61800
water, electrochemical photolysis at semiconductor electrode 2–57428
Ag crystal transmission electron microscopy sample prep. 2–80619
Cu electrowinning in coupled electric and magnetic field 2–68796
Cu refining, behaviour of $(NH_2)_3CS$ 2–75389
$CuSO_4$ aqueous solution with concentration polarization, exptl. determ. of critical Rayleigh number 2–48338
Mo-Cu-Co cermet contact, elec. erosion characts., rel. to Co content 2–47659
$(NH_3)_2CS$ behaviour in electrolytic refining of Cu 2–75389

Electrolytes, theory *see Electrochemistry; Solutions*

Electrolytic conductivity *see Conductivity, electrical/liquids, electrolytic*

Electrolytic deposition
Co, electrodeposited with [0001] axis of preferred orientation, dependence of magnetic properties on texture perfection 2–54327
epitaxial, two dimensional nucleation effect on electrocrystalliz. rate 2–71320
metal, prep. of electrodes with one cryst. plane only 2–48337
nucleation, probabilistic aspects 2–50474
permalloy film electrodeposited on Cu wire, and e.m. props. 2–77990
Ag, prep. of electrodes with one cryst. plane only 2–48337
Ag_3Sn, preparation of electrodeposits 2–53569
Co-Fe films, structure and orientation 2–53561
β-Co films, structure and orientation 2–53561
CrH_x, electrodeposited from chromic acid soln., struct., lattice consts., deposition conditions 2–47320
Cu-Sn alloys, composition and crystal structures 2–84085
Cu, cathodic impedance study 2–48339
Cu, epitaxial, growth defects 2–47107
Cu, growth morphology, current density and substrate orientation effects 2–48340
Cu purification and single cryst. prep. 2–72565
Fe-Co-Ni alloy powder, highly disperse, effect of electrolytic prep. variables on mag. props. 2–68543
Fe-Ni-Mo alloy, dispersed, optimal conditions 2–77725
Fe foils, electrocrystn. structures 2–83862
on InP, for study of electroreflection spectrum 2–81433
Na_xWO_4, cryst. growth by fused salt electrolysis 2–48341
Ni-B coatings, particle distrib., heat treatment effects 2–77730
Ni-Fe film, mag. props. optimization 2–61540

Electrolytic deposition continued
Ni-Fe(18 wt%) film, substrate relief rel. to anisotropy fluctuations 2–84409
Ni, cathodic impedance study 2–48339
NiO films, deposition conditions depend. of optical consts. 2–61618
Pd colloid particle struct. depend. on prod. parameters 2–83818
Pd powder, from chloride solutions 2–68799
TiB_2 coatings, characteriz. 2–51460

Electrolytic tanks *see Calculating apparatus/analogue apparatus*

Electromagnetic fields
anomalous interaction with gravitational fields, analysis of astronomical data 2–54994
Bethe-Salpeter equation for field correlation function to discrete scattering medium 2–55593
Born-Infield nonlinear e.m. theory, Newman-Penrose conserved quantities 2–82163
boundary-initial value problem, variational formulation, convolution bilinear form 2–69806
charge moving in field of arbitrary config., classical eval. 2–49315
classification, analogous to Petrov classification of gravit. field 2–82194
coupled e.m. and mesonic fields; calc. of cross section for interacting particles 2–78774
depth sounding experiment across Santa Clara Valley 2–54697
diffracted, expansion in terms of eigenfunctions of d'Alembert operator 2–69808
dipping contact effects on behaviour of electromagnetic field 2–54696
Dirac eqn. for electron interacting with plane e.m. field, algebraic soln. 2–82227
dispersive medium, linearized field energy and momentum conservation laws 2–63269
Earth, dipping layers effects 2–61986
electrodynamic force acting on sphere in travelling magnetic field 2–49195
electrodynamic forces in e.m. stirrer for molten metals 2–50183
electron beams interaction, cyclotron resonance, non-linear treatment 2–69879
electron in uni-accelerated frame, non-inertial frame of reference 2–78783
electron ray tracing method 2–73523
energy transport 2–76410
Faraday's law coils for teaching purposes 2–48960
field induced by vertical harmonic dipole in anisotropic medium 2–69805
force interaction with current conducting, dielectric bodies, materials handling applications 2–69812
gauge independent gravit.-coupled e.m. field 2–42303
generalized Manley-Rowe relations, energy balance in double periodic e.m. fields 2–82389
generation during movement of conducting fluid in mag. field 2–43103
geoelectric profile containing nonconductive layer 2–72644
geophysical studies, magnetic receivers freq. characteristics 2–54581
gravitational field effects of collapsed bodies 2–58162
Green's function, enclosed cylindrically symmetric 2–49194
helical antenna buried inside earth 2–52337
Huygens's sources, radiative field formulas 2–63168
integral formulas analysis 2–55594
intensity calc. for arbitrarily changing sphere radius, vector pot. function 2–63169
intensity in open resonators determ. from field in waveguide for different coupling iris sizes 2–82404
interaction theory 2–73477
ionospheric D layer, calc. 2–59007
kinetic theory of e.m. field fluctuations in anisotropic plasma half-space 2–80235
lens, stigmatic, structure of e.m. field near focus 2–69826
linear nonconducting bianisotropic media 2–69810
liquid crystals, e.m. hydrodynamics 2–50330
magnetic dipole immersed in cond. half space, e.m. surface fields 2–78966
magnetotelluric fields in 3-dimensional bounded electrical structures 2–55596
Maxwell, local independence, investigation using classical field theory 2–58977
measurement, ferrite antenna use 2–45624
microwave field perturbation by animals and apparatus 2–52004
multiple coherence, quantum optics 2–49336
multipolar decomp., generalized, space-time multipolar sources 2–52530
multipolar represent. of field pot. 2–45853
multipole expansion for field generalized by localized current distribution 2–78980
nonlinear field eqns. for particles interacting with coupled e.m. and mesonic fields, soln. method 2–78773
nonuniform lossless transmission lines, field calc. methods 2–82407
optical waveguide, calc. 2–58999
periodic structures, dispersion equations 2–49198
pulsar magnetosphere, rotating fields, model 2–58415
pulsars, special relativistic treatment 2–58386
randomized, autocorrelation and spectrum of intensity fluctuations 2–41870
scaler Debye potentials for fields in spherical gravity and spherical media 2–82401
simple coupling with gravitational fields 2–73311
sinusoidal current filament parallel to half-space 2–69811
spatial localization of equivalent forces, in weakly polarizable liquids 2–77252
spinning particles in gravitational and e.m. fields, canonical dynamics 2–41479
static, in general relativity, effects of massive bodies 2–78799
stationarity, homogeneity and isotropy in presence of random sources 2–58738
subsurface of circular loop of current located above ground 2–52309
thunderstorms, information about ore objects 2–72647

Electromagnetic fields continued
transient diffusion in inhomogeneous conducting media, geophysical prospecting applications 2−65523
transient diffusion in inhomogeneous media 2−44536
transient sounding over stratified earth 2−57816
transverse plane wave field, group theoretical analysis of charged particle motion 2−63262
TWT, localized, effect in cutoff intermediate section 2−59106
unified field theory, Einstein's eqns., soln. for spatially flat field of e.m. origin 2−82193
of waveguides filled with inhomogeneous isotropic dielectrics, coupled transmission line equations 2−41888
weak, around rotating black holes, Maxwell's eqns. in Kerr geometry 2−55388
Si, profiled crystal growth, field in system inductor-concentrator-pedestal 2−47275

Electromagnetic oscillations
see also Magnetohydrodynamics; Masers; Plasma/oscillations
amplitude in open resonators determ. from field in waveguide for different coupling iris sizes 2−82404
cavity resonators, freq. insensitive to axial elongation 2−69814
E_{010} cavity resonator, temp. variation of resonant frequency, resonance curves 2−58985
gas prism resonator, toroidal as energy stores 2−71119
Helmholtz eqns., approx. reduction, for nonuniform media 2−82319
microwave cavity excited in TM_{0n0} mode, diffusion-controlled gas breakdown meas. 2−50231
microwave open resonator with spherical mirrors, variational calc. of resonant freq. to test beam-wave theory 2−58984
microwave resonator, open, with axial corrugated metal rod, theory 2−49224
open dielectric resonator, diffractional losses 2−78974
parametric, phase matched in GaAs thin-film waveguides, theory 2−73483
polymer-solid adhesion breakdown rel. to radio emission parameters 2−52314
resonant cavity, cylindrical, lossless, transient elec. field 2−78965
resonator coaxial, for dielec. meas. on polymers 2−81133
resonators with diffraction arrays, eigenmodes of periodic structure 2−63176
superconducting resonators, harmonic generation 2−73485
sustained plasma in microwave cavity 2−60234
three field mode model, statistical props., quantum theory 2−45696
waveguide resonator struct., props. in semicond. laser with electron beam pumping 2−52335

Electromagnetic radiation *see Electromagnetic waves; Gamma-rays; Light; Radiation; X-rays*

Electromagnetic wave propagation
see also Absorption; Diffraction, etc.; Plasma/electromagnetic waves
in anisotropic media, field structure analysis 2−41872
Antarctic ice sheet permittivity meas. using v.l.f. band 2−54731
antennas and propagation, international symposium, Sendai (1971) 2−41874
Appleton-Hartree equation generalization of collision frequency theories 2−82400
azimuthal, over curved anisotropic dielectric sheet 2−45611
coaxial and coplanar loops in uniform dissipative media, e.m. coupling 2−59006
cold isotropic plasmas, pulse propagation space-time ray methods 2−43142
conducting media, MHD effects, taking into account kinematic viscosity 2−50171
conducting region moving at light velocity 2−55598
crystal, polariton mode propagation in bounded media 2−68307
dispersive media, energy relations 2−49208
edges with angular dielectric, e.m. wave analysis 2−49204
e.m. field of Gaussian beam with elliptical cross section 2−73597
ferromagnet, coupled e.m. and spin waves in quantized mag. field 2−68525
finite incoherent source in random medium 2−69818
frequency-time analysis of e.m. waves in magnetosphere 2−84703
geology, airborne resistivity mapping using E-PHASE 2−54727
geophysical prospecting, time domain airborne system, model results and field checks 2−54726
geophysical surveying, airborne, electromagnetic system for light aircraft 2−54725
homogeneous dispersive rock, frequency dependence effect of conductivity and permittivity 2−52317
in inhomogeneous media, solution of ray equations using successive perturbation theory 2−69813
inhomogeneous waves contribution in angular spectrum representations 2−79349
interaction with irrotational fluids 2−41873
interplanetary plasma, monochromatic radio waves 2−55601
interstellar space, dispersion phenomena 2−48734
ionospheric reflection polarization, determ. using Stokes parameter 2−84904
light, in anisotropic media, evolution of ellipse of polarization 2−79322
loops, ground constant calculation 2−49206
magnetic dipole immersed in cond. half space, e.m. surface fields 2−78966
magnetoplasma, v.l.f. waves 2−50197
magnetotelluric sounding, impedance for inhomogeneous surface waves 2−78282
metal, point meas. of Fermi vels. by time-of-flight method 2−51075
microwave field visualization, $CoCl_2$ solution water evaporation 2−55605
modular ray trace program, Fortran program 2−79345
modulation by electron beam passing above sawtooth grating, energy characteristics 2−63181
moving lossless inhomogeneous medium reflection and transmission 2−82402
moving plane-stratified medium 2−69815
nondispersive homogeneous time-varying media invariant imbedding 2−49205
in nonhomogeneous isotropic medium 2−41877
nonlinear dielectric, const. amplitude plane wave phenomena 2−76415

Electromagnetic wave propagation continued
nonlinear medium, interaction between microwaves and short laser pulses 2−42128
nonuniform medium, random e.m. propagation 2−52320
nonuniformly moving medium, relativistic effects 2−63182
one-dimensional model random medium comprising dielectric slabs 2−76412
optical waves, mutual coherence function propag. in random medium 2−78968
optically thin anisotropic media, theory 2−79332
plane waves, in biaxially anisotropic layered media 2−42209
plasma surrounding Crab pulsar 2−62610
prospecting, airborne systems, analogue model studies 2−54722
quasi static approx., validity 2−55597
radar echo intensity and modified coeff. for weather radar eqn. 2−75508
random discrete scatterer, limiting cases 2−76413
random nonlinear dispersive medium 2−73622
ray optics, principles and applications 2−69821
reflectance and transmittance of light by a thin inhomogeneous dielectric film, new formulae 2−54378
relativistic e.m. and gravit. wave, propag. of tensor discontinuities 2−78782
semiconductor, band struct. and elec. field effects 2−77892
semiconductor, space charge waves and progressive amplification 2−55599
semiconductor layer, microwave field parameters, thickness and resistivity depend. 2−49207
series soln. for nonuniform media, geometrical optics approximation 2−58987
shock discontinuity, in nonlinear isotropic material 2−58990
in sinusoidally space-time periodic dielectric 2−52318
solar, proportional counter expt., resultant ionisation in mesosphere 2−73118
solid state plasma, magnetised, electro-optic effects on submillimetre waves 2−82394
statistical theory of light propagation in turbulent medium, review 2−82553
statistically inhomogeneous nonlinear medium with weak regular inhomogeneity, slightly diverging beam propagation 2−78972
steady state self-focusing, with saturating nonlinearity 2−69817
sum-frequency amplitudes formulae for propagation of e.m. waves from nonlinear multilayer film 2−58989
synchrotron radiation by electrons moving in weakly focusing magnetic field 2−58983
thermoelastic plane waves in solids with thermal relaxation 2−45435
thin wire parallel to interface, boundary value problem 2−52333
transition layer effects in gyrotropic and nongyrotropic media 2−69820
transmission lines, nonuniform, wave propagation analysis 2−49221
uniaxial conducting crystal, in magnetic field, coupled cyclotron-plasma resonance 2−84280
uniform media, stochastic fields charact. 2−78961
upstreaming in solar wind, excitation and propagation 2−66211
wave analysers, elliptically polarized, phase differences 2−63179
whistler mode signals from v.l.f. transmitter in Australia 2−78396
Al, e.m. wave transmission, helicon waves, Gantmakher- Kaner excitations, sound waves, quantum effects 2−57135
KCl containing material, dielectric dispersion 2−75142
n-Si, 16GHz obs. of cond. anisotropy in mag. field 2−84343

atmosphere
adsorption by impurity gases O_3, CO, N_2O 2−48518
aerosol interaction with outgoing terrestral radiation 2−65653
aerosols of irregular particles, scattering 2−62254
angle-of-arrival fluctuations of spherical wave propagated near ground level 2−81684
atmospheric turbulence model, scintillation of spherical and plane waves 2−81680
attenuation compensation analysis rel. to radar meas. of rain rate 2−75501
attenuation in showfall, at centimetre and millimetre wavelengths 2−51628
beam shape effects on phase fluctuations of e.m. propagation in turbulent medium 2−44728
Benard convetion with black and mirror boundaries, radiative stabilization 2−68890
buoyant thermals, dynamics with radiative cooling 2−65657
clear air convection, radar reflectivity and refractive index spectra 2−75614
clear air scatter layers, meteorological structure meas. by ultra high resolution radar 2−75540
climate studies with radiation model, comparison with Mintz- Arakawa model 2−68907
cloud multispectral identification technique using satellite meas. 2−65758
cumulonimbus clouds, effects on airborne 30-mm radar at long ranges 2−81664
delay in satellite to earth communication at 1 to 15 GHz 2−54866
dispersive auroral hiss, m.f. whistler mode 2−68954
distortions produced by turbulence, h.f. plane wave filter function for folded path 2−75609
Doppler radar data interpretation 2−75509
Earth's radiative energy budget, analysis of non-isothermal spherical detector 2−62259
evaporation duct propagation, simple analytical modelling 2−45609
extinction of e.m. energy in 8-12 μm window by particulate matter 2−65772
ground clutter effects on Z-v_{rms} relationship for statiform rain at vertical incidence 2−75595
i.e. transfer, effect of particulate layers 2−62130
inhomogeneous atm., arbitrary profile of refr. index, linear-segment approximation 2−45625
i.r. flux, effect of aerosols 2−62129
i.r. laser beam, 10.6 μm, attenuation coefficents in real, artificial fog 2−72804
i.r. radiance meas. off tropical east-coast Australia 2−65764
i.r. radiation transfer profiles in presence of aerosols and clouds 2−65755
i.r. radiative transfer, effect on vertically propagating planetary waves 2−65684

Electromagnetic wave propagation continued
atmosphere continued
laser beam, spot dancing, obs. 2—54800
laser beam charact. 2—69955
laser beams, Maxwell's eqn. 2—59190
laser radiation, 10.6, 0.63 μm, attenuation coefficients for snow, rain, drizzle 2—75611
light beam gravity centre floating, correlation meas. 2—48435
line-of-sight propagation expt. for atmospheric turbulence 2—68897
magnetosphere, amplitude variations in artificially stimulated v.l.f. emissions 2—54881
magnetosphere, application of results for weakly ionized warm magnetoplasma 2—53189
magnetosphere, v.l.f. in whistler mode 2—78384
magnetosphere, v.l.f. waves in ducts, theoretical investigation of leakage 2—65861
magnetospheric v.l.f. and u.l.f. waves, monochromatic, circularly polarized, nonlinear theory 2—68930
magnetospheric whistler propag. at low latitudes 2—84884
meteoric reflection, for synchronizing frequency standards and relating time scales 2—58693
microwave absorption in submillimeter region, obs. of significant low-J lines in rotational spectrum of $H_2{}^{18}O$ 2—70706
microwave transhorizon propagation, angle and Doppler spectrum obs. 2—54869
model choice for turbulent atmosphere 2—44736
motion with radiative dissipation, linear harmonic analysis 2—68891
mountainous region, elec. field intensity, computation 2—48519
Nibmus 4 i.r. spectroscopy, calibrated thermal emission spectra 2—65765
nonequilibrium energy constants associated with large amplitude electron whistlers 2—50196
northeastern Colorado, radar climatology of thunderstorms 2—65702
phase fluctuations investigation using Zhamen's type interferometer 2—72740
plasmapause, Cerenkov instability and v.l.f. emissions 2—72827
polar ionosphere waveguide studies 2—54799
precipitable water meas. w. SIRS-b radiation profiles 2—62258
precipitation media radar obs. of anisotropy 2—62238
quasiperiodic v.l.f. emissions, hydromagnetic modulations, relation to micropulsations 2—72921
radar, rocket tracking, refraction corrections 2—78381
radar climatology of Gauhati airport and its neighbourhood 2—62228
radar echo from precipitation, spectrum shape at 3.2 centimetre wavelength 2—81658
radar propagation characteristics in dust haze preceding thunderstorm 2—75512
radar wave propagation and sea evaporation effects 2—65629
radiation balance at tropical station 2—68908
radiative interactions in tropical disturbance 2—65762
radio noise meas. rel.to lightning flashes in India 2—84790
radio waves, statistical signal model parameter determ. from quantile ratios 2—72812
radiometer, dual-channel polarizing, high-precision computer controlled 2—62260
rain attenuation meas. at 10 GHz using ADA 2—54865
rain attenuation on slant-path at 10 GHz, radar-derived statistics 2—54867
raindrop size distribution in Florida summer showers, simultaneous radar reflectivity and rainfall data 2—62214
rainfall crosspolarisation at microwave frequencies 2—48514
remote sensing technique, effects of layers 2—44738
resonance interaction of electrostatic wave with electrons in current sheet 2—72826
resonant interaction of electrostatic wave with electrons in current sheet 2—72826
satellite meas. of atm. thickness 2—62256
scintillation obs. using ground-aircraft path 2—81682
scintillation of upward directed laser beams, wave front curvature and beam waist effects 2—81681
over snowfield at elevated site, radiation meas. 2—65761
solar radiation, multiple scattering calc. in atm.—ocean system 2—65756
solar radiation, simultaneous meas. from aircraft and satellites during BOMEX 2—62255
s.w. link stability rel. to ionospheric disturbances 2—72813
synoptic-scale moisture using Nimbus 4 THIR 6.9 micrometer obs. 2—62257
temperature wave propagation in non-grey radiative fluid 2—65656
temporal spectra of phase difference fluctuations 2—81685
tropical, long-wave radiative transfer model 2—65654
troposphere, precipitation attenuation, obs. 2—81652
troposphere, radiowave troposcatter time dependence over mountainous path, radiometeorological interpretations 2—68922
troposphere and upper atmosphere, aerosol distribution and optical transmission, laser radar study 2—62281
troposphere range error parameter, latitude variation 2—54868
tropospheric fading, s.h.f. signals, obs. 2—44737
tropospheric propagation, ultra short waves, long distance 2—48520
tropospheric radio-refractivity gradient over Japan, obs. 2—65803
tropospheric slant path, attenuation at 11.75 and 17 GHz, in UK 2—72811
turbulence resolution by line-of-sight microwave propagation expt. 2—68897
turbulent atmosphere, fluctuations of submillimeter waves 2—51629
upper tropospheric cold core cyclones, numerical model of parametrized i.r. cooling 2—68900
vertical circulation of troposphere, radiation induced, magnitude and character 2—68889
v.h.f. and u.h.f. over Mediterranean Sea, field strength meas. 2—51627
v.l.f. field variations in polar region, diurnal and seasonal patterns 2—48517
v.l.f. Wait and Walters model, surface impedance concept 2—58009
v.l.f./e.l.f., transpolar propagation, laboratory simulation 2—65942
Whistler mode waves, quasi-linear interaction with nonthermal electrons 2—58043
wind field analysis using Nimbus 4 THIR 6.9 micrometer obs. 2—62257
windows, radiative props. 2—65793

Electromagnetic wave propagation continued
guided waves
annular lens optical waveguide, reflection and absorption losses and misalignment sensitivity 2—45618
arbitrarily shaped aperture, scattering parameters, calc. 2—78971
birefringent polymer films on substrates for integrated optics 2—80592
Cherenkov MHD waves due to moving source 2—83525
circular cylindrical tube, Maxwell's equations 2—59004
circular waveguide, relativistic dispersion eqn. for rotating tubular beam under space charge conditions 2—82396
circular waveguide in anisotropic medium 2—69835
circular waveguides lined with artificial anisotropic dielectrics 2—49219
coaxial waveguide, screened surface waves of dipole family 2—41887
coherent light, intensity distrib., rectangular waveguide 2—63413
core transition zone, vel. depth curves from PKP travel times 2—72658
dielectric thin film waveguides, TE_0 and TM_0 modes spectral props., coupling 2—78969
discontinuity impedance in circular waveguide 2—78975
Doppler effect in waveguide with density modulated electron beam pumped by strong field 2—69836
E_{01} wave, excitation by bunches passing through dielec. waveguide 2—41931
E-polarized, plane, diffraction in infinitely-thin longitudinally slotted cylindrical waveguide with coaxial metal inner conductor 2—63186
Earth crust waveguide, normal mode model 2—78962
Earth-crust waveguide, e.l.f. absorption mode 2—45616
Earth-crust waveguide, u.l.f. absorption modes 2—45617
Earth-ionosphere waveguide, e.l.f., v.l.f. and l.f. waves 2—54892
eddy currents in thin conducting strips, integral equations 2—52332
effective field in irregular slowing down system 2—69837
e.m. field of waveguide filled with inhomogeneous isotropic dielectrics, using coupled transmission line equations 2—41888
evanescent wave interactions in optical wave-guiding structures 2—70056
evanescent-field-pumped dye laser, pumping scheme using waveguide mode 2—79184
ferrite-waveguide configuration, anomalous loss 2—59000
fibre optical waveguide with low-loss liquid-core 2—58998
film, waveguide, phase matching of nonlinear optical interactions 2—70012
film asymmetric wave guides, fund. transverse elec. field (TE_0) mode selection 2—73481
film optical waveguides, distributed feedback laser prod. 2—79210
flat waveguide with magnetoactive plasma, scattering due to electron charge fluctuations 2—77275
glass-fibre waveguide fused junctions 2—45615
guided wave structures for electrooptical modulation at 10.6 μm 2—42157
gyromagnetic coaxial, characteristic eqn. 2—49218
in hollow conducting waveguides of arbitrary cross section, solution of nonlinear integral eigenvalue equation, computer programs 2—63198
hollow dielectric waveguide for distributed feedback laser 2—45714
hollow waveguide gas laser resonators, coupling losses rel. to mirror position and radius 2—79177
along horizontal wire above ground using field approach 2—63193
infinitely long wire in magnetoplasma 2—83533
intense waves, focusing in ducts with parabolic, saturating nonlinearity 2—69838
interdigital electro-optic thin film modulator using nitrobenzene 2—79376
ionospheric, hydromagnetic pulse propagation 2—84897
in irregular grooved waveguides with asymmetric cross-section 2—63196
laser beam scattering by slowly varying leaky wave structures 2—79337
laser beam slow TM modes on double film waveguide 2—79338
leaky wave couplers for devices for guided elastic and optical wave devices 2—73413
lenslike medium and circular TE_{01} wave guide analysis 2—49217
light beam along lenslike medium 2—76510
light guides, automatic device for inspecting and sorting in terms of cross sectional dimensions 2—63414
light-beam, temperature difference reduction in shielding pipes 2—76511
lithosphere, cooling, causing subsidence by thermal contraction 2—72649
low loss optical waveguides, spectral response, attenuation obs. 2—55619
metal clad dielec. waveguide, mode selective props., attenuation, phase consts. 2—78964
metal-film-substrate optical waveguides, propagation loss calc. 2—73482
millimeter waveguide line attenuation, meas. by shuttle pulse method and pulse single reflection method 2—63192
modulated light, information carrying, wave guides, optical circuits, design 2—82546
multibeam transmission 2—70008
nonuniform lossless transmission lines, field calc. methods 2—82407
normal waves, complete system in waveguide 2—78973
open periodic disc-line, propagation const. detn. 2—78956
open waveguide resonator excitation by coupling aperture 2—63197
optical, electrically induced migration of ions in glass plates 2—42229
optical, epitaxial $(NH_4)_xK_{1-x}H_2PO_4$ mixed crystal electro-optic film waveguide 2—70058
optical, glass multimode waveguide, attenuation obs. 2—70060
optical, in garnet single cryst. epitaxial films 2—70059
optical, response of grating coupler-waveguide system 2—66808
optical angular scattering from fibre waveguides with irregular core surfaces 2—79335
optical fibres, mode propag., coupled mode theory, coupling coeffs. 2—79323
optical guidance and control in semiconductor epitaxial films 2—42236

Electromagnetic wave propagation continued
- **guided waves** continued
  - optical propagation in anisotropic waveguides, applications of electrooptic effect to guided wave modulation 2−63410
  - optical scattering in polycrystalline waveguides from grain boundaries and surface defects 2−79336
  - optical semiconductor waveguide 2−70014
  - optical waveguide, fabrication by ion implantation through electron resist masks 2−59268
  - optical waveguide, modes props. 2−49412
  - optical waveguide, multimode fibres, filtering 2−41885
  - optical waveguide, self focusing, using nitrocellulose film 2−63412
  - optical waveguide, transmission behaviour, calc. 2−58999
  - optical waveguide's information carrying capacity, backscattering effects 2−49425
  - optical waveguides, ion-bombarded fused quartz, optical properties 2−50688
  - optical waveguides coupling 2−79400
  - optical-fibre waveguide, multimode, pulse dispersion, obs. 2−41884
  - periodic cylinder waveguides, e.m. field eqns., operator coeff. props. 2−82405
  - plasma, inhomogeneous transport of r.f. energy to lower hybrid resonance 2−74362
  - plasma, modelling of dispersive propagation of symmetric magnetic waves 2−83534
  - plasma electron frequency greater than wave frequency, TE_0 mode 2−76420
  - propagation mode and scattering loss, dielectric waveguides, gradual refractive index 2−49220
  - quasi static approx., validity 2−55597
  - ray theory of diffraction by open-ended waveguides 2−41886
  - rectangular oversized waveguides, scattering characteristics of a cross junction 2−59002
  - in rectangular waveguide, scattering by thin elliptical rods, function of position, orientation of rod 2−63190
  - rectangular waveguide loaded with dielectric slab in H-plane 2−59001
  - rotating tubular stream confined by magnetic field, Coulomb field and space charge waves 2−73484
  - in round waveguide with longitudinal slots, dispersion equation 2−63195
  - sea floor spreading rel. to progressive alteration of basalts, seismic vel. 2−72656
  - SELFOC fibre, axial field component, multiple reflections 2−58988
  - semiconductor filled rectangular guide, nonlinear effects 2−58997
  - in space-time periodic media, dispersion and propagation 2−55620
  - strip line loaded with magnetized ferrite, propagation constant 2−49216
  - surface waves, characteristics of cylindrical metallic corrugated structure excited in E_0 mode 2−49223
  - Tatra Mountains, fission-track age determinations of accessory apatite 2−72661
  - TE_{01} mode, negotiation of curves in curved, circular cross-section waveguide 2−45614
  - TEM and lowest order mode in ferrite filled coaxial line or resonator 2−49222
  - thin organic film optical waveguides, essential thickness calc. 2−83860
  - transition radiation, generation by inclined flight through waveguide 2−41930
  - transmission line, in transient regime, analogue and digital computer analysis 2−82406
  - wave guiding props. of double heterostruct. injection laser 2−59003
  - waveguide, beam, of rectangular symmetry, E- and H-wave superposition 2−63191
  - waveguide, cylindrical with moving medium, dyadic Green's functions 2−41883
  - waveguide filled with compressible magneto plasma, excitation 2−52331
  - waveguide resonator struct., props. in semicond. laser with electron beam pumping 2−52335
  - $Al_xGa_{1-x}As$ solid solns., in heterostructs., optical and electronic channelling rel. to comp. 2−63341
  - CdS, optical waveguide fabrication by Se diffusion 2−66842
  - Fe garnet film magnetooptic waveguide, light modulation and switching 2−81323
  - GaAs-$Al_xGa_{1-x}As$ dielec. waveguide, fabrication by mol. beam epitaxy 2−80593
  - n-GaAs, optical waveguiding by proton implantation 2−66841
  - GaAs film, epitaxial, guiding and electrooptic modulation of light 2−68608
  - GaAs thin film waveguide, theory of phase matched parametric oscillation 2−73483
  - GaAs waveguide, fabrication by proton bombardment 2−79413
  - Ge films, 10.6 μm guided waves obs. 2−55749
  - Ge films, 10.6 μm guided waves obs. 2−55748
  - n-InSb filled waveguide, in mag. field, controlling effect on phase and amplitude of microwave signals 2−82395
  - ZnO optical waveguides, epitaxial, low losses, below 5dB/cm 2−79377
  - ZnO single crystal optical waveguides, sapphire substrate, properties, technology 2−52463
- **ionosphere**
  - A_1 absorption, rel. to solar X-ray flux 2−58078
  - abrupt scintillation boundary, beacon satellite 2−72857
  - absorption, winter anomaly, LF A3 measurements 2−51643
  - absorption at 2.0, 2.5, 3.0 MHz, seasonal anomaly 2−78395
  - absorption obs. by radio astronomic polarization method 2−48567
  - amplitude probability distribution rel. to reflections from travelling ionospheric disturbances 2−48569
  - Antarctic D-region, at v.l.f., average reflection heights based on waveguide dispersion 2−54900
  - application of results for weakly ionized warm magnetoplasma 2−53189
  - artificial heating with 1-MW 40-MHz transmitter 2−68961
  - biexponential model of electron density profile, u.h.f. radiowaves, refraction, group delay 2−69840

Electromagnetic wave propagation continued
- **ionosphere** continued
  - circumterrestrial signal generation allowing for ionospheric inhomogeneities 2−72850
  - conjugate ducted echoes observed on Alouette 2 ionograms 2−78391
  - cosmic radio noise absorption, riometry 2−84902
  - D- and E-region absorption at 2.2 MHz over Haringhata 2−65968
  - D-layer, reflection and transmission coeff. calc. 2−59007
  - D-layer absorpt. and geomag. activity 2−81730
  - D-region, cross modulation at l.f. and v.l.f. 2−58079
  - D-region, model for midlatitude summer noon during sunspot maximum, l.f., v.l.f. 2−55625
  - D-region, radio wave absorpt. correl. with total atmospheric ozone content 2−78399
  - D-region, reflection coefficients, from thin parabolic layer 2−72889
  - D-region, satellite- borne earth-refl. sounder expt. 2−58080
  - D-region, signal partial reflection, h.f. dynamic phase metering instrument 2−65967
  - D-region, simultaneous satellite meas. of precipitating particles and r.f. absorpt. 2−58081
  - dayside auroral particle precipitation mechanism, mid-latitude v.l.f. emissions 2−48538
  - daytime and nighttime electron temperatures from topside resonances 2−68963
  - dipole antennas, nonlinear sheath admittance 2−45610
  - dispersion motions, surface gravity waves in D- and E-regions 2−51644
  - disturbance of ionospheric plasma by strong radio waves 2−72892
  - drift measurements, comparison with radar meteor wind measurements 2−72870
  - drift measurements, signal coupling among spaced sensor channels 2−51646
  - drifts and irregularities, meas. by large aerial arrays, analysis 2−68965
  - E-layer recombination coeff. meas., solar flares 2−44756
  - E-region, reflected radio waves, ground diffraction pattern 2−72887
  - Earth-ionosphere waveguide, e.l.f., v.l.f. and l.f. waves 2−54892
  - electron cyclotron resonances, nf_h, frequency shifts 2−51647
  - electron density measurements using rocket c.w. radio propagation method 2−48571
  - e.l.f. and v.l.f., circularly polarized, negative ion effects 2−48561
  - e.l.f. noise, Q-type bursts, damping coefficients 2−78394
  - e.l.f. reson. freqs. rel. to lower ionospheric changes 2−62353
  - equatorial electrojet, irregularities 2−65919
  - equatorial spread F, 10 cm waves on grand circle 2−48562
  - excitation of parametric instabilities by radiowaves 2−44750
  - F2, FO, lunar variations at low latitude 2−62376
  - F2-layer, e.m. wave reflection 2−65980
  - F_2 layer, disturbances, strong spread reflections 2−72900
  - F-region, e.l.f. and v.l.f., ionospheric fields stable solutions 2−48584
  - F-region, ionization irregularities, direct backscatter reflections 2−72893
  - F-region, scintillations, seasonal, diurnal and magnetic dependence 2−65991
  - F-region, spread-F theory 2−48583
  - F-region irregularities, scintillations of satellite beacons 2−65983
  - F-region modification, by high power h.f. radiowave 2−81733
  - Faraday rotation, rel. to total electron content detn. 2−48570
  - fundamental indices, φ and φ_2, mean values 2−81718
  - h.f., threshold of F-region modifications 2−65981
  - h.f. absorption calc. 2−84905
  - h.f. radiowave analytic ray solutions, plane stratified ionosphere models 2−41891
  - incoherent scatter spectrum, h.f. induced enhancements above Arecibo 2−65941
  - incoherent scattering, ionosphere characterization 2−78392
  - ion, cyclotron whistlers, p and He, satellite obs. over 400 km, 100-500 Hz. 2−72849
  - ionosphere, electron resonances, topside sounder obs. 2−81727
  - l.f. wave diffraction on stratified Earth surrounded by thin gyrotropic ionosphere 2−72852
  - lower ionosphere, drift of ionization inhomogeneities 2−68964
  - lower ionosphere layer, effect on propagation characteristics 2−81719
  - lower ionospheric absorption, magnetic control at lower latitudes 2−51645
  - Martian ionosphere, effective collision freq., h.f. cond. and complex refr. index calc. 2−51828
  - maximum usable frequency rel. to electron content and slab thickness 2−72861
  - modification by radio waves 2−68962
  - N(h) profiles, equivalent delay determination from regions below f_{min} 2−44749
  - nighttime, latitudinal variations of field strength 2−48566
  - nighttime E-region, radiowave propagation, stratification effects 2−51652
  - nonequilibrium energy constants associated with large amplitude electron whistlers 2−50196
  - oblique incidence of radio waves on isotropic inhomogeneous plasma 2−72854
  - oblique sounding, mechanism of formation and form of scattered signal 2−72853
  - partial reflection analysis, phase shift meas. 2−52319
  - pc 1 hydromagnetic whistler diurnal effects rel. to early afternoon source model 2−84922
  - plasma containing irregularities, excess electron density due to irregularities 2−75629
  - polarization of mean field of reflected wave 2−72860
  - propagation and application of waves in ionosphere, review 2−62352
  - proton whistlers, meas. of wave-normal vector by Ogo 6 satellite 2−65940
  - radio auroral aspect sensitivity and plasma two stream instability 2−68948
  - radio noise characteristics of auroral ionosphere 2−72840
  - radio scintillation observations, power spectral analysis of intensity fluctuations from discrete sources 2−54898
  - radiowave absorption on 1.725 MHz and winter anomaly during sunspot minimum 2−54891

Electromagnetic wave propagation continued
ionosphere continued
radiowave noncoherent scattering and satellite signal simultaneous meas. of total number of electrons 2−54893
radiowave reflection, ground pattern irregularities, obs. 2−78390
reflection height computation from oblique backscatter soundings at two frequencies 2−48565
remote sensing systems, applic. of Monte Carlo method 2−44751
remote sensing technique, effects of layers 2−44738
r.f., reflection due to time-varying irregularities 2−72856
r.f., refraction due to time-varying irregularities 2−72856
riometer absorpt. during solar cosmic ray effects 2−62765
satellite beacon transmissions scintillations, distrib. of ionospheric irregularities 2−68967
solar X-ray flare effects on 164 kHz radio-wave propagation 2−81736
spread F, electrostatic turbulence 2−65982
spread-F, at magnetic equator 2−48582
sunrise effects in low ionosphere 2−68959
TBF waves, nonguided, near lower hybrid reson. freq. maximum 2−65939
three- dimensional nonuniform magnetoactive ionosphere, propagation effects 2−81720
transequatorial propagation circuit, time delay measurements 2−51642
transequatorial propagation of decametric waves rel. to ionospheric irregularities 2−84895
transequatorial propagation studied by ray tracing procedures including magnetic field 2−48563
two-dimensional ray tracing, computer program 2−65944
u.h.f., scattered weak delayed echoes 2−51641
universal dimensionless formulae for spherical media 2−78712
v.h.f., reflections from sporadic E-layer 2−72888
v.l.f., reflection coefficients, effect of positive ions 2−78393
v.l.f. and e.l.f. waves in whistler mode, variation in absorption with solar activity and latitude 2−72855
v.l.f. auroral hiss rel. to precipitating low-energy electrons 2−68952
v.l.f. disturbances assoc. with solar X-ray bursts 2−73119
v.l.f. emission and propag., sources 2−68960
v.l.f. phase, sliding effect and anomalies of diurnal phase cycles 2−72851
v.l.f. phase changes due to proton flux 2−41875
v.l.f. radio waves, D-region propagation at sunrise 2−72883
wavelike ionospheric disturbances and signal phase characteristics 2−72869
whistler mode reflection coeff., wave interference effect 2−58072
whistler- mode signals in conjugate region, 200 kHz satellite observations 2−65943
whistler-mode wave refraction by large-scale gradients in middle-latitude ionosphere 2−84893
Whistlers, refractive index and attenuation surfaces in vicinity of cross-over level 2−72858
whistlers and gyroelec. echoes, monthly and diurnal occurrences in conjugated regions 2−84896

Electromagnetic waves
see also Diffraction; Reflection, etc.; Light/electromagnetic theory
amplification by uniaxial plane- parallel slab of quartz crystal, effect of two-element metal arrays 2−63177
charges in motion, relativistic treatment 2−82399
coherence theory rel. to radiative transfer eqn. 2−78834
cosmic medium, dispersion, rel. to Brans-Dicke cosmology 2−62437
duration and coherence time in pulsed fields 2−45697
effects on vision during welding 2−69461
production by electron beam diffraction, linear self-consistent theory 2−63174
and electron beam interaction, dispersion equation 2−49327
energy density in media with strong temporal dispersion, generalized expression 2−63180
evanescent, Fresnel, Zeeman spectrum and mag. reson., TEM case 2−73476
excitation by electron beam moving sinusoidally above ribbon diffraction grating 2−63175
forced radiation from electron in e.m. wave, effect of vaccum mag. moment 2−76166
Fresnel evanescent wave, Zeeman spectrum and mag. reson. 2−63306
Galactic Centre, e.m. spectrum as proton synchrotron emission 2−81796
h.f. intensity meas. for radiation protection, accuracy limitation 2−78989
light, polarization distribution transformation, synthesis of a field with angular depend. of exp (j2θ) 2−76521
light, polarization distribution transformation, synthesis of circular symmetry 2−76522
magnetic insulators, modes coupling 2−72191
Maxwell's equation solution rel. to limiting polarization 2−45606
metals, antiferromagnetic, particle scattering by coupled electromagnetic-magnon waves 2−84443
metals, indirect exchange and s-d model, dispersion and attenuation of spin waves, effect of e.m. wave 2−72132
nonionizing, lower r.f. through optical spectrum, effects in biological materials, systems 2−45038
oscillations in variable velocity electron beam 2−79019
plate tectonics, n plate problem 2−72663
polarized, nonconservative Rayleigh scatt., Milne problem 2−52459
radiation by sources moving with velocity greater than light in vacuum 2−48642
radiation from free electron interacting with circularly polarized laser pulse 2−78772
resonant medium, interaction of 2 waves 2−82397
scalar Debye potentials for waves in spherical gravity and spherical media 2−82401
s.h.f. transmitting power meas. by magneto-resistance sensors 2−78993
spin-electromagnetic waves in antiferromagnetic with small exchange constants 2−81290
spin-electromagnetic waves in ferromag. semicond. and metals, theory 2−81225

Electromagnetic waves continued
stimulated emission due to electron moving in weak wave field 2−63311
submillimetre, generation by difference frequency mixing in GaAs 2−49200
transformation to acoustic waves by piezoelectric plate 2−65070
undulator radiation theory 2−69816
wave shapes, surfaces 2−63178
radiators
— 2−59006
admittance of two collinear antennas, asymptotic theory 2−66660
antenna, 36-m dipole, in topside ionosphere, admittance meas. 2−72859
antenna, in plasma, appl. to diagnostics 2−74375
antenna, infinite, admittance expressions 2−55621
antenna, receivers, rad. pattern determ. by holography and optical processing 2−45623
antenna behaviour as function of frequency of excitation, summary 2−80291
antenna feeder system, electrodynamic analysis 2−45622
antenna surface contour meas. 2−73601
antennas and propagation, international symposium, Sendai (1971) 2−41874
antennas in plasma, characteristics as functions of frequency 2−80290
broadband antenna excitation patterns, mathematical synthesis, optimization in Hilbert space 2−41889
charged particles, symmetry relation between radiative properties in attractive and repulsive Coulomb fields 2−45608
charged particles in gravitational field, rel. to quasar luminosity 2−44890
coaxial solids of revolution excitation, computer appl. 2−55622
cylindrical cavity, isothermal and diffusely reflecting, normal emissivity 2−78939
cylindrical homogeneous lenses 2−49211
diffraction characteristics of metal arrays, losses 2−63183
dipole antennas, nonlinear sheath admittance, ionosphere 2−45610
electron beam moving over ribbon diffraction grating 2−63173
ferrite antenna, for e.m. field meas. 2−45624
finite cylindrical dipole antenna, arbitrary orientation in uniaxial medium, solution as boundary problem, numerical technique 2−49225
finite incoherent source in random medium 2−69818
helical antenna buried inside earth, far- zone e.m. fields 2−52337
human body in resonance region, rel. to admittance and radiation efficiency meas. in 30 to 70 MHz 2−49227
integral equation solution, narrow strongly radiating slot 2−55603
interferometer, 136/138 MHz using steerable antennas 2−52321
linear antennas, centre fed with displaced feed points, analysis 2−45621
loop antenna, in isotropic compressible plasma, radiation impedances, calc. 2−52336
metal-to-metal point contact diode, i.r. generation by laser and microwave freq. mixing 2−69839
microwave, frequency variable semiconductor oscillator 2−73479
microwave antenna near field amplitude-phase meas. using photocontrolled semiconductor plates 2−55624
moving e.m. sources in gyromagnetic plasma, dipoles 2−53195
multipole radiation in optically uniaxial media 2−52311
one-dimensional examples 2−49226
optical simulation of radiation patterns, Frensal zone radiohologram 2−55623
radially symmetric planar homogeneous lens antenna, e.m. analysis using Green's function approach 2−52338
radiation resistance of cylindrical antenna in ionized magnetoplasma 2−41890
reflector antenna array, design 2−73156
smooth conducting bodies, arbitrary shape, in presence of known external source, numerical analysis of e.m. radiation properties 2−63202
surface waves in corrugated conical horn 2−52316
toroid-coupled tree antenna efficiency rel. to foliation 2−63199
underwater communication using magnetic loop transmitter-receiver 2−81631
vertical antenna, analysis in free space near conducting half space 2−45619
VORTAC task 2 TACAN antenna, weather and snow effects 2−68880
n-InSb Corbino disc, in mag. field, r.f. wave generation 2−84333
YIG cylindrical rod, mode separation of magnetostatic waves 2−59005

Electromagnetism
see also Electrodynamics; Magnetic monopoles; Quantum electrodynamics
Bohm Aharanov effect, explanation 2−73475
Born-Infeld theory, peeling and conservation laws 2−58980
boundary conditions and surface-effects from phenomenological point of view 2−78977
charge decay in conducting medium 2−49197
charged media, nonlinear relativistic equations of motion, Maxwell's equations 2−63170
classical, e.m. energy transfer in material, Maxwell's tensor 2−63167
classical zero-point radiation, with classical electrodynamics, derivation of unretarded London van der Vaals forces between atoms 2−46464
composite cylindrical shell, radial vibration in magnetic field 2−66581
conducting plate, in uniform mag. field, free vibrs., theory 2−41900
conformally invariant Maxwell eqns. with source terms and eqns. of motion for massive particles 2−52308
constitutive map for replacement of relation $D=\varepsilon E$ and $B=\mu H$ 2−52307
application of covariant Hamilton's principle 2−63172
dielectric ring in uniform axial electrostatic field, exact and truncated solns. 2−58978
electrodynamics of moving media, Minkowski's equations 2−73478
e.m.-point energy of cond. spherical shell 2−63166
emission on electron flow over nonsymmetric lattices 2−55595

- **Electromagnetism** continued
  - equations, transform, from Gaussian to International System of units 2−45607
  - Faraday's law coils for teaching purposes 2−48960
  - Faraday's law paradoxes 2−49196
  - Faraday as natural philosopher, book 2−41427
  - force moment, effect of a non-magnetic conducting cylindrical case 2−59026
  - Gelfand-Yaglom equations, causality problems 2−76409
  - generalized Manley-Rowe relations, energy balance in double periodic e.m. fields 2−82389
  - geomagnetic field, kinematic dynamo in liquid core 2−68974
  - high-energy e.m. phenomena rel. to astrophysics 2−78442
  - local equivalence and frame indifference generalizations 2−52056
  - magnet moving near thin conductor, drag force 2−78953
  - magnetoelastic interaction, relativistic theory 2−41616
  - Maxwell's equations, a self-contained derivation of their invariance 2−49193
  - Maxwell's equations, relativistic solution, algebraic method 2−69807
  - Maxwell equations, derivation, symmetrical theory of electricity and magnetism 2−41871
  - Maxwell-Minkowski and De Broglie-Geheniau tensors, rel. to photon impulse flux density 2−59123
  - Maxwells equations, Amperes law derivation and displacement current 2−49192
  - non-magnetic conducting monolithic and laminar bodies, electrodynamic effect 2−59027
  - nonmagnetic conducting monolithic and laminal bodies, electrodynamic effect 2−78954
  - nonradiating bunched charges, particle-like spherically symmetric distribution, nonlinear relativistic equation 2−63171
  - oscillators in electromagnetic field, dispersion forces, semi-classical treatment 2−74302
  - photon absorption by electron in high magnetic fields 2−52306
  - Poisson equation solution 2−48977
  - potentials, reality of 2−73475
  - radiant cavity, Maxwell-Newton equations of motion, classical solvable model 2−69809
  - transversely isotropic finite cylindrical magnetic field 2−66582
  - vector potentials defn. and limit 2−58979
  - Fe liquid and Ni alloy, thermodynamic study by electromagnetic levitation melting in inert atmosphere 2−67871
- **Electromagnets** *see Magnets*
- **Electromechanical effects** *see Electrostriction; Piezoelectricity*
- **Electrometers** *see Electrical measurement*
- **Electromotive force**
  - induced, solution of expression by computer 2−62925
  - standard unit, volt 2−58688
  - thermocouple, press. effect, meas. method 2−49190
  - thermoelectric materials, rapid meas. of temperature dependence of thermal e.m.f. and electrical conductivity 2−52351
  - CdSO$_4$, 'acid' standard cell, e.m.f.-temp. coeff., 15° to 40°C 2−82130
  - Fe$_2$O$_3$, thermodynamic properties determ. by EMF method 2−51425
  - O$_2$ concentration cells, meas. 2−66681
- **Electron affinity** *see Atoms; Ionization; Molecules; Solids*
- **Electron annihilation** *see Electron pairs/annihilation*
- **Electron avalanches** *see Breakdown, electric*
- **Electron beams**
  - *see also Electron optics; Particle accelerators*
  - 2 MeV pulsed source, kA current and charge meas. 2−79694
  - 500 kV electron microscope gun, brightness, 200-500 kV accel. volt. 2−55660
  - accelerator with increased stability for h.v. electron microscopy 2−79034
  - alkali halide films, charact. energy losses by slow electrons 2−81532
  - analysis of thick biological tissue samples 2−69299
  - Astron-type E layer, magnetic compression 2−56356
  - backscattered, average energy loss fraction, empirical eqn. 2−64868
  - backscattering by solid targets, 0.5-10 keV, rel. to angle of incidence 2−83855
  - backscattering coeff. determ. for incident energies of 10-50 keV 2−80922
  - backscattering from semi-infinite targets, spectral ang. distrib. meas. 2−84218
  - betatron, energy spread, in cylindrically symmetrical mag. field, equation 2−79690
  - Bloch wave channelling, extended Lindhard's theory 2−60737
  - bremsstrahlung, in atmospheric density meas. expt. 2−58018
  - Brillouin, large-signal velocity-modulated, radial, axial r.f. current distribution, velocity distribution 2−45681
  - channelling pattern, scanning electron microscopy of surfaces 2−47074
  - charge deposition in water from high energy beam 2−55984
  - chrysene, dielectric tensor components derived from energy loss spectra 2−81138
  - circulating, in synchrotron, vertical polarization rotation into horizontal plane by imperfection resonance excitation 2−76756
  - cold cathode, to initiate atmospheric pressure carbon dioxide laser 2−69915
  - current density distribution at object 2−78998
  - current monitoring system, ferrite, absolute calibration 2−41919
  - cylindrical, moving, scattering of e.m. waves from, velocity dependence 2−52327
  - cylindrical electron-ion beam, self focusing, stationary state 2−63273
  - deflection, aberration correction using quadrupole, hexapole and octupole lenses 2−63282
  - defocusing, due to filament mag. fields in electron guns of linear accelerators 2−49691
  - diameter measurement 2−76450
  - dielectric target, ang. distrib. of scattered electrons, elec. field effect 2−47068
  - differentially pumped cold field emission gun interfaced to scanning electron microscope 2−79030
  - display method contrast improvements for electron beam scanning system 2−63276

- **Electron beams** continued
  - electron microscope gun, mean brightness 2−41918
  - electron waves, modulation by laser beam 2−59082
  - electrostatic parallel plate spectrograph for relativistic particles, optical props. 2−63691
  - e.m. fields interactions, cyclotron resonance, non- linear treatment 2−69879
  - e.m. oscillations in variable velocity electron beam 2−79019
  - e.m. radiation from electron beam crossing diffraction grating 2−55614
  - e.m. radiation of electron beam passing through diffraction grating 2−55615
  - and e.m. wave interaction, dispersion equation 2−49327
  - emission of radiation by charged particles reflected from solid surfaces 2−54397
  - energy analyzer, on-line, for linear accelerator 2−63724
  - energy broadening of electron beam in electron microscope 2−79094
  - energy loss and bremsstrahlung in 59 elements and 55 compounds, calc. 2−54095
  - energy spectrum in water irradiated with 10 to 20 MeV beams 2−78649
  - evaporator, multiple source 2−66376
  - Faraday cup to measure kA/cm^2 distributions 2−82792
  - fast electron gun from tetrode nuvistor for atomic decay studies 2−45682
  - field emission gun, electrostatic lens aperture effect 2−63279
  - field emission gun as source for 100 kV transmission scanning microscope 2−79029
  - field emission gun for 100 kV electron microscope 2−79032
  - field emission gun for scanning electron microscope 2−79031
  - field emission guns, design of electrostatic lenses 2−79033
  - field emission guns for electron microscopy 2−79025
  - first toroidal pinch, low pressure operation 2−83598
  - focusing, using optimum control 2−78995
  - gas, dense, beam spreading behaviour 2−66709
  - glow discharge microbeam gun, performance 2−66707
  - glow discharge source 2−49318
  - gun, with inert replaceable filament 2−45683
  - gun with 200 KV accelerating potential 2−63267
  - guns, problems of computation and design 2−76454
  - guns with locally heated cathode 2−79026
  - high brightness boride emitter electron gun, design and performance 2−79027
  - high current, quasi-onedimensional solutions of equations 2−76455
  - high intensity electron beam, stability 2−83618
  - high power bombardment system for ioniz. of atomic beams 2−63271
  - high-current, self-focusing, relativistic, mirror capture on closed orbit 2−52391
  - high-current relativistic, trapping in magnetic mirror trap 2−63270
  - high-current relativistic, use in thermonuclear synthesis, acceleration technique, non-destructive testing 2−45680
  - high-energy passage through crystals, reduction of coherence area 2−54096
  - h.v. electron microscopy, energy loss and aberrations 2−79137
  - h.v. gas discharge, electron and ion beam gun form., rel. to welding 2−60296
  - injection into compressor, accompanying transients 2−59651
  - intense relativistic, propagation 2−74404
  - interacting with plasma, Fokker-Planck equation 2−80283
  - ion-electron generators, experimental study 2−63268
  - kV electron energy dissipation vs. penetration distance in high at. no. mats. 2−56634
  - laser modulation, interference effects 2−59081
  - limiting currents with relativistic energy spread 2−79022
  - linear accelerator injection conditions effects on transverse instability of beam 2−73960
  - linearized e.m. field, energy and momentum conservation laws 2−63269
  - metal, coupled helicon-magnon wave scattering 2−68314
  - metal surface backscatter obs. for 12.25 MeV oblique incidence 2−52389
  - metallic small particles, reln. between polarization tensor and inelastic differential cross section 2−68262
  - microprobe, h.v. sweep and controlled magnetic lens current supplies 2−66718
  - modulated beam spectrometer for ionization cross-section meas. 2−76456
  - modulation by laser beam in dielec. crystal, Schwarz-Hora effects 2−59083
  - monoenergetic, instability in plasma, non-linear theory 2−46778
  - multipurpose tool 2−59084
  - narrow, formation theory 2−79035
  - object structure determ., using high and low energy electrons 2−79009
  - optimum waveguide electron buncher, numerical design 2−79018
  - organic thin films, charact. energy losses by slow electrons at 77K 2−84669
  - parallel electron beam production with beam energy below 6 keV and beam intensity 100 μA 2−84382
  - phenanthrene, dielectric tensor components derived from energy loss spectra 2−81138
  - in plasma, dissipative instability, nonlinear theory 2−64338
  - polymethylmethacrylate, Monte Carlo simulation of energy dissipation 2−62826
  - polystyrene, ang. distrib. of scattered electrons, elec. field effect 2−47068
  - polystyrene slabs, finite, electron depth-dose distrib. meas. 2−61130
  - positron focussing and selection, geometrical ray tracing for astigmatic sector spectrograph 2−52673
  - pulsed, compact Faraday cup array for current distrib. obs. 2−63272
  - quantum field theory approach to interaction of electrons with cavities 2−76414
  - radiation above bifurcation, energy characteristics 2−63181
  - radiation from electron bunches interacting with iris loaded waveguide 2−79020
  - radiotherapy, from linear accelerator, dose distrib., stability, contamination 2−69377
  - ranges, Z-depend. and geometry effects 2−44017

Electron beams continued
- recording track, electron-optical meas. 2−63278
- relativistic, emission of coherent microwaves in modulated magnetic field 2−52313
- relativistic, intense, mag. confined, flow disruption by drift tube walls radius changes 2−69866
- relativistic, interaction with axial and convergent magnetic guide fields 2−70320
- relativistic, mag. focusing by mirror mag. field 2−79012
- relativistic, microsecond duration 2−82434
- relativistic, transit through strong mag. field 2−81897
- relativistic beam, mag. focusing by mirror mag. field 2−79011
- relativistic model, equilibrium 2−80322
- relativistic propag. in h.p. gases 2−53241
- relativistic propag. in l.p. gases 2−50220
- scanning, production using dynamically switched Gray- scale coded structures 2−49338
- scanning electron microscope, electron trajectory and virtual source of field emission gun 2−69877
- Schwartz-Hora effect 2−69865
- Schwarz-Hora effect, obs. in crystalline media 2−49319
- secondary emission monitor of accelerated electron beam position, design and sensitivity 2−55944
- self-consistant stationary state of relativistic beam in drift space 2−73527
- self-phasing in slow-wave system 2−79017
- semiconductor, ferromagnetic, coupled helicon-magnon wave scattering 2−68314
- semiconductor technology applications 2−61371
- separation from other particles by synchrotron radiation, for 100 GeV beam 2−73959
- solid, inelastic electron scatt. by excitation of deep atomic levels, energy loss spectra 2−44012
- stabilty of neutralized high intensity beams 2−41920
- straggling of moderately relativistic electrons due to inelastic scattering and bremsstrahlung 2−68266
- in synchrotron, meas. of freq. of coherent oscills. 2−59652
- total reflection at potential barrier, shift of beam position 2−69869
- transmission, reflection, and absorption, high current density pulses, in Al thin film 2−84223
- transmission through gases voltage and pressure dependence 2−83713
- velocity distribution in beams formed by high-perveance three-electrode guns 2−63277
- velocity spread rel. to initial electron velocities and emitter roughness 2−69867
- volume defect, analysis using electron energy loss spectra 2−80654
- in waveguide, Coulomb field and space charge waves 2−73484
- X-Y deflection system for retrofit on welding guns 2−66706
- Al grating, interaction radiation of moving electron 2−73526
- Au grating, interaction radiation of moving electron 2−73526
- C materials, calc. of thermal cond. at high temps. 2−84210
- Ge, electron spectroscopy of amorphous films at energy losses below 1 eV 2−80934
- Ge, irrad., pair-prod. energy for free carriers 2−61351
- LaB$_6$ cathode gun, brightness and energy distrib. 2−73525
- NaCl, backscatt. and transmission yields 2−57091
- Ni, energy loss spectra as function of surface impurities, electronic transition characts. 2−47079
- Pd film, low-energy transmission orientation depend. 2−47787
- Si, electron spectroscopy of amorphous films at energy losses below 1 eV 2−80934
- Si, irrad. pair-prod. energy for free carriers 2−61351

absorption *see Electrons/absorption*

effects
- *see also Beta-rays/effects*
- n-Ge, low temp. annealing, diffusion limited recovery 2−47378
- amorphous material, imaging by structural alteration 2−60568
- anthracene single crystal irradiated, hole trap 2−51126
- beam-plasma instability suppression, effect of beam modulation on ion acoustic waves 2−70963
- beam-plasma system, nonlinear interaction of waves excited 2−74355
- breakdown triggering of vacuum spark gap 2−71027
- copper-phthalocyanine, reduced radiation damage in electron microscopy 2−80635
- coronene, radiation damage occuring in electron microscope 2−43617
- cross sections for excitation of Ar II laser lines in electron-ion collisions 2−69954
- diamond, electron irrad., photocond. spectra 2−77962
- diamond, fast-electron, irrad., lattice parameter changes 2−60775
- electromagnetic wave prod. in solid 2−71817
- electronographic emulsion, characteristic curve 2−42442
- electrostatic instability excited by electron beam trapped in magnetic mirror of magnetosphere 2−48537
- excitation of monochromatic plasma wave 2−46778
- excitation of plasma potential oscillations by phased oscillators 2−64318
- excitation of superradiant gas laser 2−42024
- gas laser electron beam controlled, elec. field and secondary electron distribs., Monte Carlo calcs. 2−80360
- graphite, displacement damage, high voltage microscopy 2−56683
- graphite, electron beam deposition, sublimation energies 2−60644
- graphite, h.v. electron microscope damage 2−47370
- graphite, irrad. damage, electron microscope obs. 2−53710
- graphite, pyrolytic, low temp. irrad. damage and recovery, resist. study 2−80659
- heat propagation from beam pulse to thin disk 2−66708
- HELA cell survival at ultra high dose-rates of high energy electrons 2−69339
- high β fusion plasmas, formation by intense relativistic electron beams 2−83607
- hot electron plasma generation 2−53217
- information storage, elec. irrad. defect inhibition of cathodoluminescence 2−57379
- ion emission from solids, and mass spectrometer applications 2−75201
- ion plasma oscillation, excitation 2−80343

Electron beams continued

effects continued
- ionized water cluster production by electron bombardment of ice films 2−84221
- linear pinches, interaction with intense relativistic electron beams 2−83608
- malonic acid, electron spin-lattice and cross relaxation 2−44442
- medical articles, throw-away sterilisation using Van de Graaff generator 2−85119
- metal, irrad., void formation 2−47361
- metal, mech. forces caused by relativistic beams 2−57089
- metal, plastic deform., radiation induced 2−47363
- metal, point defect stability, low-energy- recoil events and vibr. behaviour 2−53723
- metal, surface plasmons, collective mode excitation 2−51087
- metal, void and point defect agglomerate studies using h.v. electron microscopy 2−53695
- metal surface, ion source electron beam bombardment of metal surface 2−41934
- multiloop stream interaction with plasma, instability due to Doppler effects 2−74400
- nichrome, resistive thin film, evaporated from liquid phase by electron beam gun 2−71332
- oxide film destruction 2−71322
- penetration in extended media, calculation by computer 2−47777
- plasma, beam-plasma interaction beyond linear stage 2−67628
- plasma, excitation of ion waves, turbulent like spectrum 2−64316
- plasma, injection of dense beam and motion along magnetic field 2−74358
- plasma, ion acceleration by electron beam-plasma interaction in a mirror machine 2−50214
- plasma heating in mirror trap, oscill. spectra 2−56368
- plasma heating with and without magnetic field. quasi-linear theory 2−46714
- plasma interaction rel. to nonlinear oscillation development 2−70934
- plasma interaction with small cold beam 2−56337
- plasma modified ordinary wave in presence of contrastreaming beams, macroscopic model and stability 2−46780
- plasma oscillations excited by relativistic beam beam 2−64338
- plasma oscills. excited by modulated electron beam in mirror machine, nonlinear effects 2−50217
- plasma resonant interaction inducing h.f. electrostatic wave instability 2−53239
- plasma temp. distribution heated by relativistic electron beams 2−53183
- plasma wave excitation by relativistic beam 2−53228
- plasma-beam system, plasma oscill. damping in modulation by l.f. signal 2−50215
- poly(vinyl chloride), electron and γ-irrad. at 77K, e.s.r. 2−83360
- polyethylene, electron irrad., traps, thermally stimulated current obs. 2−83363
- polyethylene spherulites, deformation and origin of contrast effects in electron microscopy 2−60782
- polymer, irrad., elec. cond., temp. and electron dose effects 2−84316
- propagation of high energy electron beams 2−69868
- pumping of CdS laser, photon loss and gain 2−42077
- radiation damage in polymers, effect on electron microscope image 2−80700
- radiation damage induced by channelling effect of high energy electrons 2−43604
- radiation damage studies of crystals in 8-300 K range using h.v. electron microscopy 2−79141
- radioactivity induced in earth 2−52888
- resist material, sensitivity change due to backing material 2−55661
- restricted plasma, longitudinal wave excitation by relativistic electron beam injection 2−80348
- rubin, irrad., phosphoresc. 2−72429
- semiconductor, amorphous film, read and write processes 2−61260
- semiconductor, group II-VI cpds., radiation damage 2−47366
- semiconductor, pulsed electron beam excited, β-conductive signal 2−71887
- semiconductor thin bar, β-conductive signal, effect of surface recomb. velocity 2−51130
- silicone resin hardening and electron beam resists for microimaging 2−59297
- steel, stainless, damage induced by high energy electron channelling 2−53713
- super radiant light source produced by electron beam pumping 2−79215
- surface atoms, inner shell ionization 2−50553
- surface ion desorption, apparatus 2−43491
- Teflon, electron irrad., traps, thermally stimulated current obs. 2−83363
- therapy techniques, megavolt, review 2−69318
- thermal diffusivity meas. incandescent temps., by stepwise modulated beam 2−85162
- thermonuclear reaction initiation by high current electron beams 2−46722
- thin-walled tubular electron beams theory 2−55659
- topaz, microstructural breakdown 2−60776
- upper atmosphere, meas. of density and temperature from obs. of local fluorescence produced by electron gun 2−48524
- welding, between dissimilar metals, evaluation of weld metal composition 2−69482
- zeolite surfaces, low-temperature emission excited by electron impact, rel. to adsorption and energy of surface states 2−77973
- Al, damage induced by high energy electron channelling 2−53713
- Al, displacement damage, high voltage microscopy 2−56683
- Al, electron beam deposition, sublimation energies 2−60644
- Al, irrad. induced pt. defect clustering, high- voltage electron microscopy 2−56682
- Al, microstructure effects on subsequent dislocation loop formation during electron irrad. 2−53733
- Al, point defect prod., annealing 2−60785
- Al foil, stage III recovery obs. 2−43805
- α-Al$_2$O$_3$, polymorphic transform., thermodifferential analysis 2−47681
- Au, irrad. damage, h.v. electron microscope obs. 2−80650

Electron beams continued
- **effects** continued
  - Ba atomic beam excitation at low energies, spectrometry with high resolving power 2—63426
  - BaF_2 colour centre interconversion induced by electron irradiation 2—77598
  - CO_2 laser media, parametric studies of electron beam controlled discharge 2—41996
  - CO_2 long pulse laser, excitation by short pulse longit. electron beam 2—55682
  - CaF_2, colour centre interconversion induced by electron irradiation, changes in adsorption spectrum 2—77598
  - CaF_2, mechanism of intrinsic radiational defect formation 2—56680
  - CdS, 10 MeV irradiated, photocond. 2—57254
  - CdS, irrad., stage III_n recovery, activation energy 2—71455
  - CdS, polymorphic transform., thermodifferential analysis 2—47681
  - CdTe, radiation damage and cathodolum. edge emission 2—48254
  - CdTe, radiation effects, carrier conc., Hall mobility, photocond. 2—47892
  - Cds, irrad. damage, effects on donor-acceptor pair cathodolum. 2—54478
  - CsBr, photostimulated emission, rel. image storage targets 2—48023
  - CsCl, photostimulated emission, rel. image storage targets 2—48023
  - Cu-Zn system, diffusion processes during irrad. 2—47456
  - Cu, electron, lattice parameter and resistivity changes 2—60777
  - Cu, irrad. induced pt. defect clustering, high-voltage electron microscopy 2—56682
  - GaAs:Si(Te), irrad., carrier removal, mobility changes, annealing characts. 2—47917
  - GaAs, asymmetric damage regions, elec. props. obs. 2—74759
  - GaAs, electron and neutron irrad., i.r. absorpt. 2—72332
  - n-GaAs, irrad., annealing behaviour of elec. props. and photolum. 2—47918
  - GaAs, irrad., i.r. absorpt. band obs. 2—48180
  - GaAs, n- and p-type, irrad., defect levels, Hall effect and resist. study 2—80992
  - p-GaAs, spontaneous emission, internal quantum efficiency, effect of beam voltage increase 2—72433
  - GaAs laser, generation of controllable light pulses by spatial scanning of pumping electron beam 2—42090
  - Gd thin single crystal films, dislocation loops formed during electron microscopy 2—71489
  - Ge:Li, low temp. irrad., Hall effect and minority carrier diffusion length obs. 2—47927
  - Ge:P, bombardment induced interstitial P, e.p.r. obs. 2—48279
  - Ge:Sb, irrad. damage, phonon scatt. and induced energy levels, thermal cond. obs. 2—47766
  - n-Ge, annealing impurity depend., vacancy-interstitial pair effects 2—47379
  - Ge, asymmetric damage regions, elec. props. obs. 2—74759
  - Ge, change in length and elec. resist. 2—68016
  - p-Ge, defect prod., annealing and conductivity obs. 2—47377
  - n-Ge, disordered region prod. by 28 MeV electrons 2—47931
  - Ge, excess minority carriers generated by pulsed beam, diffusion length 2—51165
  - n-Ge, impurity depend. of low temp. annealing 2—47376
  - Ge, irrad., 8.5MeV, high field domain instability 2—57208
  - Ge, irrad. damage, Mossbauer type photoluminesc. spectra obs. 2—48243
  - Ge, K_α X-ray prod., by 350 keV electron irrad. 2—48208
  - p-Ge, low temp. irrad., 220K defect, resistivity and Hall obs. 2—47928
  - p-Ge, low temp. irrad., point defect annealing 2—47381
  - n-Ge, radiation damage, annealing kinetics 2—47380
  - In film, heating during diffraction 2—83920
  - InSe film, crystalliz., elec. microscope obs. 2—56594
  - KBr, colour centre, transient form., pulsed electron beam 2—53753
  - KCL:Tl, electron pulse irrad., colour centre formation 2—71524
  - KCl, surface, polygonization, produced by electron bombardment and illumination 2—50457
  - $KMgF_3$-$KMnF_3$ mixed crysts., single defect involving F-centre, prod. mechanism 2—68040
  - Mo, irrad. at 4.2K, stage I recovery, resist. study 2—53718
  - Mo surrace, Auger electron spectra obs. 2—50453
  - N_2 laser, pumped by intense electron beam 2—73569
  - $Na_8Al_6Si_6O_{24}X_2$ sodalite (X=Cl, Br, I), cathodochromism, elucidation of damage mechanism by ESCA 2—47447
  - NaCl, surface, polygonization, produced by electron bombardment and illumination 2—50457
  - $Nb_{1-x}Ta_x$ alloy, $0<x<0.25$, growth by electron beam float zoning 2—50599
  - Ni-Fe-Cr based alloy, γ'-hardened, electron irrad., void swelling 2—80684
  - Ni, electron irrad., void form., effect of injected gas atoms 2—43613
  - Ni, ferromagnetic after effect at 55K 2—78026
  - Ni, irrad., mag. after-effect and elec. resist., recovery 2—64655
  - Ni, point defect interactions with dislocations, high-voltage electron microscopy 2—56686
  - Pb-GaAs Schottky barrier tunnel junction, zero bias anomaly, irrad. effects 2—71960
  - Pb, sound excitation by electrons and positrons 2—61089
  - Si:C, irrad. damage, i.r. absorp. obs. 2—48191
  - Si:Ge, O, C, irrad. damage, i.r. spectra obs. 2—48192
  - Si:Li, electron irrad., luminesc., annealing and Li impurity effects 2—48229
  - n-Si:Li, irrad., Li-defect interactions, e.p.r. obs. 2—48293
  - n-Si:Li, irrad. induced defects, impurity effects 2—47385
  - Si:Mg, irrad., donor levels, excitation spectra 2—72351
  - Si:P(As) radiation-induced infrared absorption bands 2—68650
  - Si, asymmetric damage regions, elec. props. obs. 2—74759
  - Si, defect prod., liquid He temp., a.c. hopping cond. obs. 2—47936
  - Si, defects, electron microscope examination 2—64656
  - p-Si, irrad., Hall coeff. and elec. cond. 2—71944
  - p-Si, irrad., Hall effect and elec. cond. 2—54201
  - p-Si, irrad., hole emission rates, activation energy and annealing of defects 2—54199
  - p-Si, irrad., low temp. photocond. 2—47999
  - Si, irrad., recomb. luminesc., uniaxial stress effects and temp. depend. 2—48230

Electron beams continued
- **effects** continued
  - Si, irrad., recomb. luminesc., annealing and impurity effects 2—48231
  - n-Si, vacancy capture and transfer between defect complexes 2—80694
  - Si film and bulk, electron irrad., defect prod., resist. change 2—80655
  - Si n^+-p diode, fast electron irrad., capacitance 2—71978
  - β-SiC, irrad. effects on luminesc. 2—48232
  - SiO_x antireflective coatings for Si solar cells, effects of electron irradiation 2—59056
  - Si(111) surface, chemisorbed O_2, electron bombardment surface ion desorption study 2—71351
  - α-Sn, irrad., atomic displacement process evidence 2—53722
  - α-Sn, irrad., damage production and thermal annealing, resist. study 2—80682
  - SrF_2 colour centre interconversion induced by electron irradiation 2—77598
  - Ti alloys, radiation induced transformations in h.v. electron microscope 2—80874
  - TiO_2 film, crystallization 2—47129
  - TiO_x antireflective coatings for Si solar cells, effects of electron irradiation 2—59056
  - W, electron stimulated desorption of CO 2—47153
  - Y_2O_3, low loss dielec. film, use of mag. fields in electron beam evaporation 2—77947
  - ZnS, cathodoluminescence, rel. to S atom displacement by electron irrad. 2—48263
  - ZnTe, threshold energy for Te displacement, cathodoluminesc. obs. 2—68018
  - znSe cathodlum., Se atom displacement 2—61723
- **ionization** *see Electrons/ionization*

Electron capture *see Ions/recombination; Radioactivity/electron capture*

Electron density
- arc plasma electron density alteration effect on temp. distribution 2—46726
- artificial cloud in ionosphere, electron density increase in E-layer 2—68969
- atmosphere, profile for height range 80-170 km 2—54875
- auroral D and E layers, incoherent scatter radar obs. 2—81735
- bone, determ. using transmitting and scattering 2—69222
- cascaded arc, meas. using scattered laser light 2—53260
- CGCG 1622+4112 extremely compact galaxy 2—55018
- colloidal suspension particles, X-ray study under different collimation conditions 2—71285
- coronal enhanced region 2—73150
- D-region, method for determ. of density profile 2—62369
- D-region, profiles during sudden ionospheric disturbance 2—72879
- D-region profiles from extraordinary component of partial reflections from lower ionosphere 2—84906
- decay in afterglow at low pressure discharges, three-body recombination 2—80372
- Earth's bow shock obs. from lunar orbit, meas. of electron plasma properties across shock and in magnetotail 2—62313
- electron density affected by visible light flux 2—48577
- electrons and dust densities in solar system rel. to F and K components of solar corona 2—62803
- F_2 region, disturbances during magnetic storms 2—75631
- flowing transient plasma, Lecher wire microwave probe 2—77283
- galactic disk, mean-square electron density and early-type stars 2—44836
- geomagnetic storm, topside electron density measurements 2—72867
- Hall current effect on hydromagnetic flow near accelerated plate 2—43131
- height profile, auroral ionosphere model 2—81723
- inductive ring discharge, development rel. to breakdown behaviour 2—53249
- interferometric obs., circuit for direct registration 2—67658
- interstellar clouds, model 2—75785
- in ionizing shock waves, i.r. techniques for obs. 2—82562
- ionograms reduction to true height-electron density profiles 2—84898
- ionosphere, density measurements using rocket c.w. radio propagation method 2—48571
- ionosphere, distrib. about F_2 peak determ. by analysis of ground echoes 2—54903
- ionosphere, effect on radio maximum usable frequency 2—72861
- ionosphere, excess in random irregularities 2—75629
- ionosphere, incoherent scatter sounder obs. 2—78392
- ionosphere, influence of whistler mode reflection 2—58072
- ionosphere, irregularities near aurorae 2—81725
- ionosphere, large scale periodic disturbances 2—65945
- ionosphere, low, profile at high latitudes from riometer obs. 2—72862
- ionosphere, lower, average electron density height profile 2—75630
- ionosphere, magnetic storms effects 2—44772
- ionosphere, regular horizontal gradients, along satellite orbit 2—75628
- ionosphere, rel. to topside plasma flow inside and outside of plasmasphere 2—58095
- ionosphere, satellite spin effects on cylindrical probe obs. 2—65951
- ionosphere, spread-F, producing structures, incoherent scatter radar obs. 2—48588
- ionosphere, topside, sunrise effects 2—81734
- ionosphere D- and E-regions, profiles for all seasons and varying solar activity 2—44755
- ionosphere D-region, equatorial electron densities, rocket measurements 2—84914
- ionosphere D-region, meas. of electron densities and collision frequencies 2—65971
- ionosphere D-region, meas. partial reflection method 2—51651
- ionosphere D-region, sunrise conditions 2—72883
- ionosphere E- and F-regions, drifts over magnetic equator, solar cycle effects 2—44757
- ionosphere E-region, describing function of diurnal variation 2—65975
- ionosphere F region, seasonal anomaly, computer simulation 2—78402

Electron density continued
- ionosphere F-region, det. of vertical velocity 2−48589
- ionosphere F-region, variation above N. America during magnetic disturbance 2−65986
- ionosphere Langmuir probe obs. 2−72876
- ionosphere large-scale electron density gradients, refraction of whistler-mode waves 2−84893
- ionospheric, meas., r.f. probe 2−48574
- ionospheric D-region, exponential model 2−84910
- ionospheric D-region rel. to ion pair production rate 2−48576
- ionospheric E-region, time depend. of profiles 2−58089
- ionospheric E-region seasonal anomaly rel. to regression-line studies 2−65976
- ionospheric electron content in subtropical regions, diurnal and seasonal variations 2−84900
- ionospheric F-region, density disturbance by strong radio waves 2−72892
- ionospheric seasonal variations 2−51649
- ionospheric soundings, $P'(f)$ to N(h) inversion problem 2−72874
- ionospheric total electron content rel. to movements of mid-latitude trough 2−72864
- Jamin interferometer modified to measure electron density gradients 2−66771
- laser interferometer with harmonically matched cavities 2−66811
- liquids, effective Kerr constant for short laser pulses, rel. to steric effects and compressibility 2−71200
- longitudinal plasma wave, wave vector in direction of electron stream, two stream electrostatic instability 2−80311
- magnetosphere, electron cyclotron and Langmuir frequency ratio and electron and ion densities 2−72841
- magnetosphere, variations during one solar cycle 2−44744
- magnetospheric density profiles deduced from plasmapause whistlers 2−68939
- Me-OH (Me=Cr, Mn, Fe, Co, Ni, Cu, Zn,) molecule, Mulliken population analysis 2−42867
- MEVARC device, obs. using electron collisional half width of 5153 Å line 2−71060
- microwave plasmas, calc. 2−77271
- plane plasma capacitor in crossed fields 2−64304
- plasma, afterglow, single Langmuir probe technique appraisal 2−53211
- plasma, determination by measurement of electroacoustic resonances broadband short pulse technique 2−43173
- plasma, distrib. from bending of laser beam 2−67657
- plasma, from laser-produced gas breakdown, interferometric holography 2−83559
- plasma, high temperature, from intensity calibration using continuum emission in vacuum u.v. 2−53196
- plasma, Langmuir probe and r.f. capacitance probe meas. 2−50209
- plasma, meas., calibration procedure to correct for effects of dielectric containers 2−67655
- plasma, meas. by laser radiation scattering in Tuman-2 2−70925
- plasma, meas. using direct reading microwave interferometer 2−60257
- plasma, rel. to voltage pulse profile of pulsed ioniz. chamber 2−52686
- plasma, time varying, meas. with microwave reflectometer system 2−74380
- plasma diagnostics using microwave resonant cavity 2−43169
- plasma focus, highly localized X-ray source 2−83585
- plasma in collisionless flows, obs. using positively biased electrostatic probes 2−77282
- plasma in pinch discharges, probe, Thompson scattering and photographic obs. 2−83564
- plasma surrounding atmospheric re-entry body, simulation 2−72931
- projectile wake, fluctuation meas. 2−60352
- pulsed ablation accelerator plasma 2−80297
- pulsed toroidal discharge, energy balance and spectroscopic study 2−53216
- Q-pinch torus, Scylac 5-meter, helical equilibria 2−83561
- r.f. plasma diagnostics using electrostatic probes 2−50207
- solar corona, det. from Faraday rotation of Crab radiowaves 2−66236
- solar corona, distrib. obs. from K-coronameter data 2−76025
- solar flares with flat microwave spectrum 2−75995
- solar wind, Explorer 35 obs. 2−66215
- solar wind, irregularity spectrum 2−58552
- Sun, thermal radio burst regions 2−44980
- sun, XUV meas. 2−73116
- topside ionosphere, effects of disturbances on night side 2−48586
- two-, three- and four-electron ions, Hartree-Fock and Hartree-Fock-Slater atomic form factors, radial electron density in momentum space 2−74205
- Ar, arcs, effect on local thermodynamic equilibrium 2−77306
- Ar, electrodeless discharge, determ. of radial distrib. 2−50228
- Ar, pulsed plasma, containing 1-2% H_2, particle conc. from spectral meas. 2−49941
- Ar, Townsend discharge, electron energy distribs., expt. 2−43211
- Ar discharge, hollow cathode, electron temp. and density profiles 2−77307
- Ar discharge, hollow cathode, using electrostatic probe 2−70988
- Ar discharge, hollow cathode, excitation mechanisms, electron and ion temp. and density 2−77308
- Ar plasma discharge, obs. in early stages 2−60261
- Ar^+ plasma obs. following shock wave formation in interaction of plasma with transverse mag. field 2−77268
- CdO, method using T activity 2−71934
- CdS, method using T activity 2−71934
- Cs, ionized vapour, spectral line mixing meas. 2−46792
- Cs plasma, reson. absorpt. produced, radial distrib. 2−46727
- Cs plasma in thermionic convertor, electron temp. effect 2−63244
- D spatial and temporal electron density determination 2−67624
- Ge, n-type, infrared birefringence on hot electrons 2−81328
- H discharge, pulsed, plasma diagnostics, maximum electron conc. 2−67692
- H plasma, model obs. 2−64278
- H plasma, time-resolved diagnostics 2−53209
- He-Cd mixture, glow discharge, electron distrib. fns. 2−74429
- He-Ne laser output power rel. to electron temp. and density 2−45737
- He, pulsed, electrical and optical measurements 2−60306

Electron density continued
- Hg afterglow plasma, model 2−60212
- K plasma, laser obs. using selective excitation spectroscopy 2−70928
- Kr, electrodeless discharge, determ. of radial distrib. 2−50228
- LiI, emission spectra analysis 2−60247
- NaCl, irradiated, method using T activity 2−71934
- W, neutron electron scatt. obs. 2−57138
- Xe, e.m. T tubes, Mach 5 shocks, precursor ionization 2−78932
- Xe, electrodeless discharge, determ. of radial distrib. 2−50228
- ZnO, method using T activity 2−71934

Electron diffraction
- *see also LEED*
- apparatus in schools 2−62936
- camera , UEG-150, high voltage, accelerating voltage up to 150 kV 2−59085
- computer simulation of Lorentz micrograph 2−79135
- cooling effects on electron diffraction pattern of beam-sensitive specimens 2−79140
- cylindrical system with diaphragms and thick electrodes, combined focusing and deflecting 2−69873
- dielectric target, ang. distrib. of scattered electrons, elec. field effect 2−47068
- e.m. wave production, linear self- consistent theory 2−63174
- fluxon contrast calculations rel. to specimen thickness and defocus distance 2−79136
- LEED and RHEED in ultrahigh vacuum electron emission microscope 2−79096
- Lorentz microscopy, in-focus, wave optical theory for thin ferromagnetic films 2−76458
- low angle diffraction patterns from C fibres, interpretation by optical analogue techniques 2−80613
- plasmon energy loss shifts rel. to specimen contamination 2−80935
- ribbon grating, diffraction radiation due point charges moving above grating 2−63173
- by ribbon grating, e.m. wave excitation 2−63175
- slit apertures, calc. of field of system 2−66713
- slits and thick electrodes with rectangular apertures, calc. of field 2−66714
- slow electrons in mirror electron microscope 2−79167
- small angle by gases, apparatus with electron counting devices 2−64133

Electron diffraction crystallography
- *see also Debye-Waller factors; Crystal structure, atomic; LEED*
- bend contours, Bloch wave calcs. 2−83939
- Bloch wave channelling, extended Lindhard's theory 2−60737
- bombardment, information gain aspects 2−60744
- charge density determ. in crystals desirability of absolute scale 2−77535
- computer-generated transmission diffr. patterns 2−43549
- continuous random network cluster, diffr. props., calc. 2−64618
- contrast of perfect and imperfect crystals, SEM backscatt. electrons, dynamical theory 2−56628
- critical voltage measurement, electron form factors 2−80628
- crystal containing plate shaped crystal, theory and computer expression of elec. microscope image 2−53641
- crystal lattice, theory and computer expression of elec. microscope image 2−53641
- decoration method, determ. of electrically active point defects and lattice structure 2−80604
- defect contrast, weak beams at 1 MV 2−80632
- defects, diffraction contrast micrographs, transmission and reflection 2−80621
- energy analysing and selecting systems and applics. 2−56635
- fine structure, limits on diffr. anal. 2−74697
- HEED cross-grating 2−83940
- intergranular precipitates identification by double diffraction 2−80615
- intersecting overlapping stacking faults, computer simulation method display 2−80625
- Kikuchi band and abnormal absorption, exchange effects, calc. 2−64631
- Kikuchi band contrast reversal in transmission mode 2−83921
- Kikuchi map for c.p.h. structure 2−67956
- Kikuchi patterns, displaced lines 2−53636
- Kikuchi patterns, influence of thermal diffuse scattering 2−83935
- Klein-Gordon eqn., soln. for periodic lattice 2−67975
- Kossel patterns, reading 2−64617
- laser-illuminated crystal, dynamical theory 2−50612
- low and high energy research instrument 2−47304
- medium energy diffraction, state-of-the-art 2−50421
- multiple diffuse scattering contributions to Kikuchi line contrast 2−83934
- order-disorder investigation 2−50991
- orientation relationships, data processing 2−74709
- phase change on electron wave scattering from thin objects 2−80636
- reciprocal lattice determ. using goniometer stage and electron microscope 2−80614
- reciprocity theorem 2−82445
- reflection intensities of point electron diffraction patterns in det. of crystal structures 2−80641
- scanning high-energy, review 2−74710
- scanning transmission diffraction techniques 2−80622
- single crystals, UNESCO teaching project 2−69528
- speciment manipulator for LEED camera with two-axis gonimeter 2−60739
- transmission electron microscopy contrast, strong beam to weak beam conditions 2−80631
- two dimensional images, contrast features 2−80627
- UNESCO teaching project 2−69528
- Al critical strains, Bloch waves 2−80629
- Cu critical strains, Bloch waves 2−80629
- GaAs, (110)-surface, LEED obs. 2−76739

Electron diffraction examination of materials
- acetyl bromide and chloride, zero-point average structures determination 2−77136
- acetylacetone, gas phase determination of molecular geometry 2−60045
- adatoms, thermal disorder, 1-dimens. model, LEED pattern calc. 2−60672

Electron diffraction examination of materials continued
amorphous materials,scattering, transition matrix approach 2–83936
biological objects, reconstruction of spatial structure 2–81980
coronene, radiation damage occuring in electron microscope 2–43617
domains, interface geometry, contrast effects 2–56718
graphite, Xe adsorption, LEED obs. 2–50533
group II-VI compound film, epitaxial, structure 2–56582
interphase interfaces, strain fields, epitaxial dislocations, steps, electron diffr. contrast 2–56625
low angle electron scattering of films with anisotropic distribution of crystallites 2–80640
maleic anhydride, molecular structure, gas phase 2–42992
metal, f.c.c., {001} surface, LEED, expt. and theory 2–50428
metal oxide structures, microanalysis 2–77540
metals, antiferromagnetic, scattering cross section by electromagnetic-magnon waves 2–84443
methyl isothiocyanate, molecular structure, gas phase 2–43001
molecular force constants calculation from diffraction data 2–77043
neopentane, molecular structure determ. in gas phase 2–70796
pearlite electron diffraction patterns, orientation determinations using computer 2–68188
polytetrafluoroethylene, emulsion-grade, electron diffraction studies of ribbons and rods 2–71295
porous materials, improvement of pore image by collection of secondary electrons 2–80606
semibullvalene, tricyclo[3,3,0,$0^{2,8}$]octa-3,6-diene, structure determ. in gas phase 2–77154
Si, transmission electron diffraction, contrast reversal of Kikuchi bands 2–83921
silyl isocyanate, determ. of molecular dimensions and large amplitude vibration by electron diffraction 2–80080
silyl isocyanate, determ. of molecular dimensions and large amplitude vibrations by electron diffraction 2–80080
sphalerite, e. microdiffraction exam. of microscopic impurity inclusions 2–71408
spiropentane, molecular structure determ. in gas phase 2–70796
steel, austenitic, stainless, microstructure determ. of oxide film due to corrosion 2–81505
steel, carbide form. during low temp. isothermal tempering 2–43842
steel, high-C martensitic, fine struct. 2–56934
steel, nitrided by ion bombardment 2–56935
steel stainless, high- tensile, cryst. struct. determ. 2–77672
thick crysts., stacking fault contrast at high voltages, Bloch wave interactions 2–71407
transition metal carbides and nitrides (Gp IV and V), nonstoichiometry 2–61029
tri-tert-butylmethane, gas phase determination of structure 2–77108
tricyclopropylphosphine, molecular structure determ. in gas phase 2–70796
trifluoroacetone, gas phase determination of molecular geometry 2–60045
trifluoroacetylacetone, gas phase determination of molecular geometry 2–60045
trimethylazidosilane, electron diffraction determ. of molecular structure 2–80109
V_2MoO_8, cryst. shear struct. 2–47352
vinyl chloride, gas-phase study of molecular- structural parameters 2–67524
β-Ag-Al alloys, splat quenched, martensitic transform 2–71672
Ag_3TlTe_2, crystal structure 2–74722
Al, (100) face, LEED rotation diagram, calc. 2–74618
Al, {111} and {110} surfaces, LEED spectra, calc. 2–83857
Al, diffusion, review 2–83992
Al, expt. and theoretical LEED rotation diagrams 2–50433
Al, Kikuchi band and abnormal absorpt., exchange effects, calc. 2–64631
Al, Kikuchi patterns, displaced lines 2–53636
Al, temp. depend. of LEED intensity, Debye temp. calc. 2–60624
Al films, electron multiwave scattering at 70 keV, scatt. intensity detn. 2–71451
Ar-Kr(Xe) film, 6K to sublimation temp. 2–80573
Au, meas. of complex structure potentials by convergent electron diffraction 2–83932
Au, surface struct., 5×20 struct., RHEED obs. 2–77482
Au film, bicryst., electron diffr. by grain boundary dislocation networks 2–77593
Au films, electron multiwave scattering at 70 keV, scatt. intensity detn. 2–71451
B, rhombohedral, α→β transform. 2–47680
$BaTiO_3$ (OOl) systematic reflections 2–84367
Be cleaved surface, LEED intensity-energy curves 2–60625
Bi-Zn(Ag) eutectic alloy, crystallographic relations and morphology 2–60976
C columnar growth analysis 2–80603
C fibre, low angle aptterns, interpretation by optical analogue techniques 2–72307
C fibres, lattice fringes rel. to defects and diffraction geometry 2–80634
C fibres, thinned, low energy electron diffr. 2–64634
Cd, electron transmission, det. of lattice potentials 2–83942
CdSe vacuum evaporated films, structure on mica, NaCl, PbSe film substrates 2–71327
Cr, atomic scatt. factor, determ. by vanishing Kikuchi line electron diffr. method 2–74750
Cr dendrites, galvanostatically obtained from CrO_3-H_2SO_4-dimethylsulphoxide-H_2O solution 2–47135
Cu-Au, diffused comp. profiles near grain boundaries, selected-area obs. 2–56757
Cu-Au film, epitaxial growth by r.f. sputtering, microstruct. 2–67908
Cu-Be alloy, extra spots in diffr. pattern, obs. during G.P. zone formation 2–77578
Cu-Sb alloys, long period superstructures with hexagonal symmetry near 20 at.% 5b 2–71430
Cu, chemisorption of oxygen on (110) and (100) faces 2–60678
Cu film, lattice consts. of small nuclei, rel. to surface stress 2–60655
Cu trichites, orientation and degree of perfection 2–47321
$CuAgTe_2$, synthesis and struct. detn. 2–71431

Electron diffraction examination of materials continued
$Cu_{2-x}S$ film, on NaCl substrate 2–60653
1,1-dimethylcyclohexane, gas-phase mol. struct. 2–70765
Er film, f.c.c. struct. and oxidation, HEED obs. 2–50490
Fe, (100) surface, LEED and photoelec. work function study 2–50443
$FeSi_2$, $\alpha \rightleftharpoons \beta$ transition mechanism 2–43919
GaAs, HEED, surface stoichiometry and struct. obs., surface vacancy model 2–50445
Gap, HEED, surface stoichiometry and struct. obs., surface vacancy model 2–50445
Ge, amorphization during ion bombardment, HEED obs. 2–80685
Ge film, amorphous, metal contact induced crystalliz. 2–56590
Ge_xSe_{1-x} alloy film, amorphous, radial distrib. 2–60659
GeTe-SnTe alloy, epitaxial film, twinning faults 2–53574
GeTe epitaxial film, twinning faults 2–53574
$GeTe_2$ film, amorphous, local order and microstructure 2–60660
H_2O molecule, small angle diffr., chemical binding energy detn. 2–64133
In-Te system, film, phase studies 2–60662
In film, heating 2–83920
In films, polycryst. thin melting e diffr. study 2–83845
InSb, p-n junction, minority carrier diffusion 2–81111
K adsorbed layer, on Ni (001), specular electron refl. 2–50544
Kr-Xe film, 6K to sublimation temp. 2–80573
Li particles, technique for transfer to electron microscope 2–43555
Mg, electron transmission, det. of lattice potentials 2–83942
MgO, periclase, energy distrib. in Kikuchi band 2–60761
MgO cleavage faces, LEED beam splitting, model 2–60627
MnBi film, struct. and orientation 2–47119
$Mn_xFe_{3-x}O_4$, Jahn Teller domains, obs. 2–43922
Mo, ion irrad., surface damage, LEED obs. 2–50468
MoC, foil, stacking faults, twins 2–43641
MoS_2 intercalation compound, struct. obs. 2–64643
Na adsorbed layer, on Ni (001), specular electron refl. 2–50544
Na montmorillonite, isolation monocrystalline particles, selected area electron diffraction patterns 2–68001
$Nb(O, F)_x$, cryst. shear struct. 2–47352
$NbSe_2$ intercalation compound, struct. obs. 2–64643
Ni-Au alloy, compositional changes, critical voltage effect applic. 2–56944
Ni-Be alloy, extra spots in diffr. pattern, obs. during G.P. zone formation 2–77578
Ni-P chemically deposited films, structure in relation to elec. conductivity 2–77510
Ni, (001) surfaces, absolute intensity energy LEED spectra 2–50459
Ni, (111) surface, averaged LEED intensities 2–50460
Ni, effect of disordered Na, K, Cs and Ba overlayers on specular electron refl. 2–60681
Ni, low index surface, adsorped Pb layer, LEED obs. 2–60682
Ni, with adsorbed O, thermal disorder, LEED pattern interpretation 2–60672
Ni_3Al-Ni_3Nb eutectic alloy, interface between two ordered lattices obs. 2–71647
P_2H_4, molecular structure 2–42937
Pb, influence of thermal diffuse scattering on Kikuchi patterns 2–83935
PbTe meas. of complex structure potentials by convergent electron diffraction 2–83932
Pt film, lattice consts. of small nuclei, rel. to surface stress 2–60655
Sb-Cs photocathode study using scanning electron diffraction system 2–75195
Si, Au-diffused, surface cpd. formation, refl. diffr. obs. 2–50463
Si, cleaning in H_2O_2 soln., HEED obs. 2–53555
Si, Kikuchi band and abnormal absorpt., exchange effects, calc. 2–64631
Si, Kikuchi patterns, displaced lines 2–53636
Si, small spherical voids, diffr. contrast profile, calc. 2–77571
Si film, amorphous, metal contact induced crystalliz. 2–56590
Si_2H_6, molecular structure 2–42937
SiO film, radial distrib. analysis 2–53577
SiO_2 film, grown by oxidation of silane, struct., electron diffr. and i.r. absorp. obs. 2–60664
SiO_2 film, pyrolytic, struct. determ. 2–80571
SiO_2 thermally grown film 2–71999
SnSe film, epitaxial on KCl, boundary struct., rotational Moire method obs. 2–74635
TaC film epitaxially grown by electron beam evap. 2–67916
Te-Ge based memory glass film, thermal crystn. 2–47128
Te vapour grown whiskers, disloc. struct. 2–67915
Ti-22at.%Nb, containing unequal amounts of ω-phase variants 2–53908
Ti alloys, β→ω transform. 2–68204
TiC, surface struct., ultrahigh vacuum obs. 2–43469
TiO_2-Cr_2O_3 system, solid solns. and cryst. shear struct. 2–47406
U_3Si, in-pile irrad. effects, obs. 2–47393
V-C alloys, ordering effects in struct. obs. comp. depend. 2–71378
V-N system, V_3N phase 2–50978
V, atomic scatt. factor, determ. by vanishing Kikuchi line electron diffr. method 2–74750
V_6C_5, superlattice, C vacancy ordered distrib. 2–43621
VO short range ordering of defects 2–80701
W, adsorption of CO, LEED obs. 2–60692
W, ion irrad., surface damage, LEED obs. 2–50468
WO_x and $(W, M)O_x$, (M=V, Nb, Ta, Mo), cryst. shear struct. 2–47352
Zn, electron transmission, det. of lattice potentials 2–83942
Zn cleaved surface, LEED intensity-energy curves 2–60625
ZnO, epitaxial layer, on Ge and GaAs 2–74636
Zr alloys, β→ω phase transform. 2–68204

Electron emission
see also Noise/electrical; Photoelectricity
atom, excited by fast electrons, ejected electron spectra, reson. line shapes 2–67384
Auger emission, kinematic theory, dynamic theory 2–48010
aurora, magnetic bay accompanied, rocket meas. of keV electron spectra 2–58064
aurora, type-A red, low energy electron meas. 2–58063
dosimetry phosphors, 6, thermally stimulated exoelectron emission and thermoluminescence following β-irradiation 2–82821

Electron emission continued
dynamic field emission, model of cathode phenomena in cold cathode arcs 2−71059
exo-emission, detection using pulsed breakdown in gas 2−56390
exoelectron, optical stimulation 2−68489
exoelectron emission obs. for dosimetry of ionizing radiation 2−70550
exoemission with no ionostimulation 2−48009
film, multilayer, porous and nonporous, discrete frontal electron emission, ratio of pair production 2−68488
film, surface states by thermally stimulated exo-emission 2−48008
functions $\Theta(y)$, $t(y)$ and $\varphi(y)$ evaluated for $1 \leqslant Y \leqslant 5$ 2−65097
glass, and practical applications 2−65109
insulating solids surfaces, exoemission optically and thermally stimulated, review 2−84383
light elements, LMM Auger transitions vs. LLM transition 2−48015
metal, optical field emission, influence on nonlinear photoelec. effect 2−48020
metal surface, exo-emission detection using open counters 2−44187
metal vapour, production of constant stream by control of electron emission 2−67890
metallocenes, electron spectra, electronic configs. 2−64187
mica, Auger emission, relative intensities of lines 2−72081
microscope, construction and applics. to deform. and recrystn. obs. 2−43779
polymers, exoelectronemission 2−77974
thermal exo-electron detection by proportional counters 2−67079
ultrahigh vacuum, combined with LEED microscopy 2−79048
zeolite surfaces, low-temperature emission excited by electron impact, rel. to adsorption and energy of surface states 2−77973
Al-Al_2O_3-Al thin film, cold emission, distribution 2−81125
Al-borosilicate glass-Al thin film sandwich, elec. cond. props., negative resist., electroforming and electron emission 2−71989
Al, exo-emission, threshold illumination intensity 2−44189
Au, elongated, depend. of exoemission on work function 2−54269
Ba formates, formation and surf. props. of electron emissive coatings 2−65365
BeO, role of Si activator in exoelectron emission 2−59635
Ca formates, formation and surf. props. of electron emissive coatings 2−65365
CaF_2:Mn, thermal exoelectrons, trapping centres 2−68699
CaF_2 power phosphor, characteristics for thermally stimulated exoelectron emission dosimetry 2−67091
$CaSO_4$:Sm, Mn, thermally stimulated exoelectron glow curves, role of activators 2−48255
CdS, in m.i.s.m. and m.s.i.m. structures 2−57218
Cu-Al alloy, exoemission, interdependence with annealing processes 2−48011
Cu-Al alloy, exoemission kinetics and hardness depend. on strain or elongation 2−74836
Cu, Auger spectra, LMM, fine struct., L-S coupling interpretation 2−61453
Cu, plastically deformed, exo-emission rel. to surface struct. 2−77975
GaAs-(AlGa)As cold cathode structure, factors affecting extended operation 2−48012
He atom, excited by fast electrons, ejected electron spectra, reson. line shapes 2−67384
$Li_2B_4O_7$:Sm, Mn, thermally stimulated exoelectron glow curves, role of activators 2−48255
LiF powder phosphor, characteristics for thermally stimulated exoelectron emission dosimetry 2−67091
M-CdS-I-M, thin film device 2−68450
Mg, exo-emission, threshold illumination intensity 2−44189
MgO, high resolution Auger electron spectra meas. with new Auger spectrometer 2−77972
Mo, Auger spectra, chem. shift on adsorption of O_2 2−51223
Nb-C system, work function measurement, pulsing voltage procedure 2−63235
NbC_x, work function, correl. with surface recomb. of H atoms 2−50549
Ni compound, non-metallic, thermal decomp., photostimulated exoelectron emission obs. 2−57408
Pb, exo-emission, threshold illumination intensity 2−44189
Pd, elongated, depend. of exoemission on work function 2−54269
Pt, elongated, depend. of exoemission on work function 2−54269
Sr formates, formation and surf. props. of electron emissive coatings 2−65365
TiC_x, work function, correl. with surface recomb. of H atoms 2−50549
W, cathode, in Cs plasma, electron emission rel. to temp. and current density 2−75191
W wires heated in vacuum, effect of surface contamination 2−65098
Y, Auger spectra, chem. shift on adsorption of O_2 2−51223
Zn, Auger spectra, LMM, fine struct., L-S coupling interpretation 2−61453
Zn, exo-emission, threshold illumination intensity 2−44189
Zr-Nb-C system, work function measurement, pulsing voltage procedure 2−63235
Zr-Ta-C system, work function measurement, pulsing voltage procedure 2−63235

field emission
adsorbate-covered surfaces, total energy distrib. 2−48013
breakdown mechanisms in h.p. gases 2−67695
Cambridge surface states, tunnelling and electron field emission theory 2−47814
differentially pumped cold field emission gun interfaced to scanning electron microscope 2−79030
gun for 100 kV electron microscope 2−79032
guns, design of electrostatic lenses 2−79033
guns for electron microscopy, and materials 2−79025
metal, energy distrib., effect of lattice potential 2−61457
metallic-field effect consequences 2−54206
microscopy of A^IB^V coated W monocrystals 2−83872
m.i.m. structures, surface roughness effect on distribution 2−47948
p-Si, photokinetic charact. of photofield emission 2−84389
solids, rel. to multiple particle tunneling 2−77976
spike cathode, field conc. and emission pattern from a regular array of spikes 2−48014
in vacuum, IV characs. and breakdown 2−44188

Electron emission continued
field emission continued
C fibres of 7 μ diameter, characteristics as electron source 2−72086
D_2, adsorbed on W, energy distrib. as function of coverage, electronic states 2−48016
p-Ge, influence of adsorption of sIo molecs. on field emission 2−72076
p-Ge, obs. in impulse and stationary conditions 2−61458
H_2, adsorbed on W, energy distrib. as function of coverage, electronic states 2−48016
Hi, electron spin polarization, band-structure calculation 2−44190
Mo, electrode, in vacuum, elec. breakdown rel. to electrode surface finish 2−75190
Si, point arrays, photosensitive field emission, quantum efficiencies 2−81186
p-Si photosensitive cathode, temp. depend for various volume doping 2−57260
Si transmissive mode field emission array photoemitter, photosensitivity 2−81187
W/Ge, adsorbed layer electronic props. determ. 2−71349
W-SiO_2:C-Au tunnel cathode, using amorphous dielectric, threshold emission and elec. switching 2−81122
W, (211) and (110) planes, Cl adsorption effects 2−60693
W, Ag absorption study 2−60690
W, coated with Si, surface diffusion obs. 2−47085
W, modified pot. barrier effect 2−54270
W, surface self-diffusion rel. to C adsorpt., field emission obs. 2−64582
W single crystal planes thermal-field emission, meas. by probe hole FEM 2−72085
ZnO, (0001) surface, field emission and surface states 2−54271

photoelectric
— 2−75185
alkali azides, X-ray photoelectron spectra, core and valence electronic levels 2−67466
alkali halide ionization pot. meas. by X-ray photoelectron spectroscopy 2−83259
alkali halides, photoelectron spectra interpretation 2−79933
alkali metal atoms, ang. distrib. and spin orientation of photoelectrons 2−56107
alkyl iodides, X-ray photoelectron spectra, comparison of valence shell and core ionization potentials 2−64167
alloy, change due to chemisorption 2−50524
apparatus with monochromatized X-ray source, for ESCA 2−57261
atmospheric mols., including N_2, O_2 and CO_2, 304 Å photoelectron spectra 2−80058
atom, electronic struct. comparison in X-ray and electron spectroscopy 2−46455
atom, X-ray stimulation in 100 to 1000 eV region 2−46416
atoms, Auger lines in X-ray photoelectron spectrometry 2−52937
atoms, intermediate and high Z, analytical formula of K-shell photoeffect 2−79885
Auger electron spectroscopy, general topics 2−57264
benzenes, fluorinated, X-ray photoelectron spectra, binding energy shifts 2−83289
bromoethylenes, photoelectron spectra, π interaction 2−77140
2-bromopropene, photoelectron spectra, π interaction 2−77140
chalcogenide glass, evidence for states in band gap 2−61334
charge transfer complexes, photoelectron energy spectra 2−64163
chlorophyll-a microcrystal suspension, photoelectric response 2−51469
cyanine dyes, adsorbed, external yield and ioniz. energy 2−48025
cyanometalate complexes in aqueous solns. photoelectron emission spectroscopy 2−68808
cyclopentadiene, photoelectron spectra, electronic struct. 2−70761
cyclopropane, photoelectron spectra, orbital structs. 2−64175
d-band metals, clean and cesiated samples, photoemission verification of resonance formulation 2−84386
data analysis, in terms of scattering phase shifts 2−72320
diazirine and difluordiazirine, photoelectron spectra, orbital structs. 2−64175
electron density states of materials obs. 2−75193
electron-molecule interactions in photoelectron spectroscopy 2−83402
ESCA, u.v. photoexcitation, review 2−54567
ESCA, X-ray photoexcitation, review 2−54568
F-region of ionosphere, photo-electron energy distrib. and its variation with sunspot activity 2−65984
Fowler universal photoemission curve, operational equivalent 2−72087
fulvene, photoelectron spectra, electronic struct. 2−70761
furan quinone pigments, DFC and DF, energy level obs. 2−54256
GEOS satellite, electric field perturbations caused by photoemission on sunlit side 2−54982
group IIB-VIA semiconductor compounds, X-ray induced, core electron energy levels detn. 2−48019
group III-V semiconductor, X-ray photoemission, core levels detn. 2−65240
group III-V semiconductor, X-ray photoemission, outermost core d and p electrons obs. 2−81195
H I clouds, heating by u.v. photoemission from grains 2−58351
hield and photoabsorption spectra in soft X-ray range, close similarity 2−61675
hollow cathode in magnetic field, photoemission rel. to discharge glow in He 2−43215
hydrocarbons, interpretation of photoelectron spectra using SPINDO calc. 2−77114
hydrocarbons, photoelectron spectra interpret. using MINDO method 2−67501
ionosphere, photoelectron flux meas. by radar and satellite methods, comparison 2−62374
ionosphere, photoelectron flux meas. with ISIS 1 and 2 satellites 2−62361
isoquinoline, photoelectron spectra, perfluoro effect 2−70790
linear mols., photoioniz. cross sections in valence electron approx., photoelectron spectra intensities 2−79976
low light intensity features, emission probability 2−84381
magnesium phthalocyanine film, impurity level energies from photoemission and cond. obs. 2−81028
many body theory, quadratic response formalism 2−61461

Electron emission continued
photoelectric continued
metal, nonlinearity, optical field emission effects 2−48020
metal cathode, nonlinear effect due to optical field emission 2−44193
metal-electrolyte solution interface 2−68496
microscopy, analytical methods 2−56636
molecular crysts., bibliography 2−48159
molecule, photoelectron bandshapes depend. on ionizing radiation freq. 2−67440
natural or inverted order discrimination of delocalized orbitals 2−77051
negative electron affinity emitters 2−44194
nitrobenzene, and $-d_5$, electronic structure determ. using photoelectron spectroscopy 2−56251
nitromethane, and $-d_3$, electronic structure determ. using photoelectron spectroscopy 2−56251
nitroxide radicals, photoelectron spectra and mol. orbital calcs. 2−80073
phonon energy loss effect on photoemissive yield model 2−61460
photocathode, using alkaline earth metals, energy structure 2−44195
photocount distrib. in partially coherent Gaussian light 2−55674
photoelectron spectroscopy, applications 2−53862
photoelectron spectroscopy, det. of branching ratios and transition probabilities 2−50032
poly-N-vinylcarbazole (acid-doped): o-dinitrobenzene charge transfer complex films, photoelectronic properties 2−78212
α-quartz, emission spectrum in neighbourhood of Si $L_{2,3}$ threshold 2−72094
quinoline, photoelectron spectra, perfluoro effect 2−70790
rare earth atoms, 34f energy determination by photoelectron spectroscopy 2−49926
semiconductor, conf., Warsaw, Poland, July (1972) 2−68384
solid, electronic struct. elucidation, book contrib. 2−72088
solutions, energy distrib. curves of emitted photoelectrons 2−81189
space charge limited, in plane parallel electrode geometry 2−68494
spectrometry of low concentration samples, measurement method 2−84695
surface states obs. technique 2−48018
c- tetrazine, photoelectron spectra, structure interp., Rydberg transitions 2−70737
thiazole and derivatives, photoelectron spectra obs. of ioniz. pots. 2−83305
thiazyl fluoride, photoelectron spectra, vibr. analysis, comparison with LCAO calcs. 2−53083
thymine and other mols., ESCA spectra, assignments and interpretation 2−77156
transition metal halide complexes valence regions by X-ray photoelectron spectroscopy 2−83247
trialkali-Sb photocathodes technology 2−44196
triglycine sulphate, forbidden band, width determ. 2−77932
X-ray and u.v. spectroscopy and electron structure of matter 2−68495
AU, computer simulation using band structure data 2−48022
Ag, valence band density of states, X-ray photoemission spectroscopy obs. 2−65104
Ag_2F, estimation of work function from threshold value of photoelectric emission and by photoelectron spectroscopical method 2−72089
AgPd system, X-ray excited, density of states obs. 2−61179
Al, determination of attenuation lengths 2−44201
Al, internal photoemission, struct. on high energy side of $KL_{23}M$ Auger peak 2−44212
Al, two-photon photoelec. effect 2−48021
Al, valence-electron excitation by internal X-ray photoemission 2−54276
Al film, due to nonradiative surface plasma waves 2−44200
Al_2O_3, escape depth of X-ray excited electrons and Auger electrons 2−51224
Au, electrodes, due to cold cathode He and N glow discharges 2−65105
Au, energy distrib., relation to band structure 2−61462
Au, energy distributions, study using 10 to 40 eV synchrotrons radiation 2−44202
Au, escape depth of X-ray excited electrons and Auger electrons 2−51224
Au, high-resolution X-ray photoemission spectrum of valence bands 2−44203
Au film, on glass, photoelectron spectrometric investigation 2−80572
Ba, oxidation kinetics, spectra of chemisorbed levels 2−51446
$BaTiO_3$ surface, ferroelec. struct., photoemission microscopy obs. 2−61428
Bi-Cs layers, photoemission properties 2−65102
BiOBr, photoemission, determ. of optical transitions and Fermi level 2−81197
BiOCl, photoemission, determ. of optical transitions and Fermi level 2−81197
BiOI, photoemission, determ. of optical transitions and Fermi level 2−81197
C, band struct. from X-ray photoelectron spectra, amorphization effects 2−57262
CO, photoelectron spectra, search for core electron satellites 2−42876
CO_2^+, predissoc., photoelectron- photoion coincidence spectroscopy and photoion kinetic energy analysis 2−67470
Ca films, elec. field influence 2−81188
Cd, L-shell photoelec. cross sections of gamma-rays 2−76967
CdS crystal, auto-photoemission, spectral investig. under pulsed and const. voltage condits. 2−72090
Ce, u.v. photoelectron spectroscopy, oxidation process obs. 2−72557
Ce film, core level binding energies, X-ray photoelectron spectra study 2−72096
Co compounds, chemical bonding study using X-ray photoelectron spectroscopy 2−53002
Cr complex, hexacarbonyl X-ray photoelectron spectra, multiple peak structure 2−46538
Cr complex, hexacarbonyl X-ray photoelectron spectra, multiple peak structure 2−46538

Electron emission continued
photoelectric continued
Cr compounds, chemical bonding study using X-ray photoelectron spectroscopy 2−53002
CrO_4^{2-}, valence region X-ray photoelectron spectra, energy spread of ioniz. pots. 2−80004
CrO_4^{2-}, X-ray photoelectron spectra, ground state obs. 2−77095
Cs film, 3.7-21.2eV 2−54277
CsBr, in ultra high vac., emission from colour centres 2−48023
CsCl, in ultra high vac., emission from colour centres 2−48023
Cs_3Sb, integral sensitivity 2−65103
Cu, two-photon photoelec. effect 2−48021
Cu, valence band density of states, X-ray photoemission spectroscopy obs. 2−65104
Cu, valence states produced by ion-sputtering reduction, X-ray photoelectron spectroscopic obs. 2−57263
CuCl, valence bands studied by emitted X-ray photoelectron 2−44204
EuO, EuO:Gd, high resolution meas., p-band excitations and dopant effect on band structure 2−68497
Fe-2.89%Si (100) face, work function rel. to surface composition 2−61463
Fe, (100) surface, LEED and photoelec. work function study 2−50443
Fe, electron spin density meas. by combined Mossbauer and electron spectroscopy technique 2−81343
Fe, valence states produced by ion-sputtering reduction, X-ray photoelectron spectroscopic obs. 2−57263
Fe compounds, chemical bonding study using X-ray photoelectron spectroscopy 2−53002
(Ga,In)As:Cs-O , surface escape probability, 0.9-1.6 μm range 2−72091
GaAs, cathode, negative electron affinity, photoemission rel. to Cs-O layers thickness 2−75194
GaAs, Cs adsorption effect 2−53595
GaAs, energy levels, X-ray photoemission study 2−84387
GaAs, intrinsic surface states, densities 2−44207
GaAs, synchrotron radiation, valence band and surface state obs. 2−81194
GaAs, X-ray photoemission valence-band spectra, valence-band densities of states 2−81192
GaP, energy levels, X-ray photoemission study 2−84387
GaS, low energy spectra and direct interband transitions 2−51225
GaS, surface electronic props. detn. 2−65106
GaSb/Cs-O, electronic states, yield and energy distrib. 2−44205
GaSe, surface electronic props. detn. 2−65106
GaSe, surface struct., surface states 2−48024
GaTe, surface electronic props. detn. 2−65106
GdS, magnetic coupling and band structure studies 2−72139
Ge_x-Si_{1-x}, mixed crystals, work function, quantum efficiency, threshold of emission, energy distribution 2−72092
Ge, amorphous, energy distrib. curves rel. to band struct. 2−61464
Ge, amorphous and crystalline, density of states obs. 2−77977
Ge, intrinsic surface states, densities 2−44207
Ge, quantum effic. of int. photoelec. eff. and impact ioniz. 2−71907
Ge, synchrotron radiation, valence band and surface state obs. 2−81194
Ge, valence bands, X-ray photoelectron spectra 2−81191
Ge, X-ray photoemission valence-band spectra, valence-band densities of states 2−81192
GeTe, amorphous and polycryst., energy distrib., electronic struct. obs. 2−61465
Ge_xTe_{1-x} alloy, amorphous, X-ray photoemission, structure and bonding 2−60575
p-InAs, ang. distrib. of photoemitted electrons, mag. field determ. 2−51226
InAs, energy levels, X-ray photoemission study 2−84387
$InAs_{0.4}P_{0.6}$/Cs-O i.r. photocathode, wavelength depend. of Cs-O optimum thickness 2−68498
$InAs_{0.4}P_{0.6}$, cathode, negative electron affinity, photoemission rel. to Cs-O layers thickness 2−75194
InBr photoelectron spectra, bonding in group III monohalides 2−80027
InCl photoelectron spectra, bonding in group III monohalides 2−80027
InI photoelectron spectra, bonding in group III monohalides 2−80027
InSb, energy levels, X-ray photoemission study 2−84387
K, surface photoelectric effect of alkali materials 2−65107
KCl, in ultra high vac., emission from colour centres 2−48023
KI, in ultra high vac., emission from colour centres 2−48023
La film, core level binding energies, X-ray photoelectron spectra study 2−72096
Mg, determination of attenuation lengths 2−44201
Mn compounds, chemical bonding study using X-ray photoelectron spectroscopy 2−53002
$Mn(CO)_5H$ and $Mn(CO)_5CH_3$ photoelectron spectra, ab initio SCF MO calcs. of electronic structure 2−70713
MnO_4^-, valence region X-ray photoelectron spectra, energy spread of ioniz pots. 2−80004
MnO_4^-, X-ray photoelectron spectra, ground state obs. 2−77095
Mo, changes due to exposure to Co, N_2 and O_2 2−51227
Mo, photoelectron energy distribution and photocurrent meas. 2−72093
Mo complex, hexacarbonyl X-ray photoelectron spectra, multiple peak structure 2−46538
Mo complex, hexacarbonyl X-ray photoelectron spectra, multiple peak structure 2−46538
NO^-, laser photodetachment and photoelectron spectrometry, determ. of molecular constants and electron affinity of NO 2−53027
NSF, photoelectron spectrum 2−42946
Nb, photoelectron energy distribution and photocurrent meas. 2−72093
Ne 2p shell photoelectron angular distrib. parameter, 0.20 eV region above threshold 2−67405
Ni, energy distrib. above and below Curie temp. 2−65108
Ni, valence band density of states, X-ray photoemission spectroscopy obs. 2−65104
Ni film, rel. to surface potential of adsorbed Xe 2−47163

Electron emission continued
photoelectric continued
O_2^-, laser photodetachment and photoelectron spectroscopy determ. of structure of O_2^- and electron affinity of O_2 2−53028
P_4, valence shell structure study using HeI photoelectron spectroscopy 2−46574
Pb, determ. of shell-wise photoelectric cross-sections at 100 and 279 keV by indirect method 2−49925
PbO-SiO_2 glass, hopping cond. obs. 2−44206
PbS, refl. spectra, X-ray photoemission, spin-orbit splitting 2−78092
PbSe, refl. spectra, X-ray photoemission, spin-orbit splitting 2−78092
PbTe, refl. spectra, X-ray photoemission, spin-orbit splitting 2−78092
Pd to Xe, X-ray photoemission spectra, evolution of core states from energy bands in 4d5s5p region 2−64891
Pt, determ. of shell-wise photoelectric cross-sections at 100 and 279 keV by indirect method 2−49925
Rb film, 3.7-21.2eV 2−54277
Re, photoelectron energy distribution and photocurrent meas. 2−72093
ReO_3, density of states by X-ray photoelectron spectroscopy 2−54111
Sb-Cs photocathode study using scanning electron diffraction system 2−75195
Sb_2Se_3, electron energy states for amorphous and cryst. material 2−68627
Sb_2Se_3 film, amorphous, rel. to transport props. 2−61323
Se, amorphous, valence band density of states determ. 2−84258
Se, effects of cryst. disorder on electronic struct. 2−61466
Si/Cs-O, neg.-electron-affinity surface obs. 2−81185
Si/Pt interface-state density, photoelectric measurement 2−44128
Si, amorphous, electronic structure obs. 2−61454
Si, amorphous, energy distrib. curves rel. to band struct. 2−61464
Si, intrinsic, photoemission processes analysis and band bending profiles as a function of caesium coverage 2−72082
Si, intrinsic surface states, densities 2−44207
Si, n-type, surface states, energy distribution of emitted electrons 2−44208
Si, p-type, role of surface states 2−44199
p-Si, photokinetic charact. of photofield emission 2−84389
Si, point arrays, photosensitive field emission, quantum efficiencies 2−81186
Si, single crystal surfaces, under influence of external accelerating electric field 2−68499
Si, synchrotron radiation, valence band and surface state obs. 2−81194
Si, valence bands, X-ray photoelectron spectra 2−81191
Si field cathodes on illumination from reverse side 2−44209
Si surface, effect of annealing on electronic properties and atomic structure 2−72095
Si transmissive mode field emission array photoemitter, photosensitivity 2−81187
SiO_2, thin layer on Si, hot electron energy losses, photoemission obs. 2−81061
Sr, u.v. photoelectron spectroscopy, oxidation process obs. 2−72557
Sr oxidation kinetics, spectra of chemisorbed levels 2−51446
Ta, photoelectron energy distribution and photocurrent meas. 2−72093
Ta, two-photon photoelec. effect 2−48021
Te, effects of cryst. disorder on electronic struct. 2−61466
Te films, amorphous, localized states, photoemission quantum yield 2−68422
TeAsGeS glass, electronic struct. obs. 2−61329
Ti surface, from sorbed gases, energy levels detn. 2−47166
U, X-ray photoelectron spectra 2−54278
UO_2, X-ray photoelectron spectra 2−54278
UO_3, X-ray photoelectron spectra 2−54278
U_3O_8, X-ray photoelectron spectra 2−54278
VO_4^{3-}, X-ray photoelectron spectra, ground state obs. 2−77095
V_2O_3, band struct. below Fermi level, X-ray photoelectron spectra obs. 2−61193
W, obs. of photoemission from surface state 2−75198
W, photoelectron energy distribution and photocurrent meas. 2−72093
W, point, field effect, pot. barrier lowering 2−54279
W, two-photon photoelec. effect 2−48021
W complex, hexacarbonyl X-ray photoelectron spectra, multiple peak structure 2−46538
W complex, hexacarbonyl X-ray photoelectron spectra, multiple peak structure 2−46538
W complex, hexamethyl tungsten, photoelectron spectrum and electronic struct. 2−64160
W obs. of photoemission from surface state 2−75197
WO_3 cryst. surface, photoemission microscopy obs. 2−60631
Y film, core level binding energies, X-ray photoelectron spectra study 2−72096
$Zn_xMFe_{2-x}O_{4-x}F_x$, M = Ni, Co, ferrite, synthesis, magnetization, hopping cond. 2−75234
ZnO, band struct. determ. 2−75196
ZnSe, X-ray photoemission valence-band spectra, valence-band densities of states 2−81192

secondary
electron yield stat. distrib., meas. technique 2−51228
films, thin, examination 2−77978
graphite, band struct. determ. 2−51150
at low primary beam energies, LEED-Auger system for obs. 2−45687
metal surface, by metastable atoms, energy and ang. distribution of ejected electrons 2−48026
metals, for oblique incidence in 12 to 25 MeV range, energy dependence 2−52389
negative electron affinity emitters 2−44194
oxide film destruction by electron beam 2−71322
photo-semiconductors, high resistivity, meas. of dark current using electron beam contact 2−75166
piezoelectric crystal, rel. to charge storage of acoustic r.f. signals 2−61085
due to primary and backscatt. electrons, model 2−65110

Electron emission continued
secondary continued
retarding field analyser, electrostatic 2−46040
scanning electron microscope exam. of hot and electron emitting surfaces, techniques 2−47305
solid surface spectroscopic study 2−67891
solid target, ion bombarded, Auger electrons and surface plasmon characteristic losses 2−51229
spatial distrib. of secondary electrons, calcs. 2−68500
three-electrode system, computer study of phase conditions of excitation 2−59107
transmission secondary electron emitters resolution rel. to backscatter of electrons 2−81184
whole angle of slow and medium fast electrons 2−44198
Ag, charact. energy loss and gain, Auger peaks, fine struct. 2−54280
Ag, chemisorption of O_2, rel. to surface struct. LEED and secondary electron spectroscopy 2−51442
$AgPO_3-X^{n+}(PO_3)_n$, $X^{n+} = Mg^{2+}, Ca^{2+}, Sr^{2+}, Ba^{2+}, Pb^{2+}, Al^{3+}$ use for multichannel image convertors and amp. 2−68501
Al films, angular distribution measurement 2−44213
Al_2O_3, ion bombarded, electron yield 2−51228
Au films, angular distribution measurement 2−44213
Be film, structure effects 2−57265
Cu (001) and (011) faces, H ion induced 2−75199
Er, deuteron bombarded 2−61468
ErD_3, deuteron bombarded 2−61468
Fe single and polycrystals, LEED obs. rel. to rocking curves 2−54281
p-GaAs, refl. mode gains, escape depth, photoresponse 2−75200
GaP, Ar^+ 40KeV ion bombardment, energy distrib. of secondary electrons 2−72097
Ge, amorphous and crystalline, density of states obs. 2−77977
Ge film, amorphous, electron states and disorder 2−61353
Ge film, structure effects 2−57265
He, electron impact ionization, energy and ang. distrib. of secondary electrons 2−64031
InP, Ar^+ 40 KeV ion bombardment, energy distrib. of secondary electrons 2−72097
KCl film, porous, energy distrib. of transmitted secondary electrons 2−81190
KCl films, controllable emission, applic. to particle detectors 2−72098
Kr, electron impact ionization, energy and ang. distrib. of secondary electrons 2−64031
Li, Auger spectra, relative intensities determ. and interpret. 2−65111
Mg, Auger satellite rel. to plasmon absorpt. and duble ionization processes 2−77971
Mo, anisotropy, raster method with modulation and deflection 2−81198
Mo, by keV K^+ ions, sharp threshold obs. 2−54282
Mo, plasma satellites obs. 2−72099
Na, Auger spectra, relative intensities determ. and interpret. 2−65111
Pb-glass with semiconducting surface layer, delayed electron emission after electron bombardment 2−84384
Sc, deuteron bombarded 2−61468
ScD_3, deuteron bombarded 2−61468
Si, amorphous, electronic structure obs. 2−61454
Si, anisotropy, raster method with modulation and deflection 2−81198
Si surface, effect of annealing on electronic properties and atomic structure 2−72095
TiO, ion bombarded, electron yield 2−51228
W, (100) face, under action of slow electron beam 2−72100
W, by keV K^+ ions, sharp threshold obs. 2−54282
Zn, surface bombarded with low-frequency ions, energy spectrum structure 2−48027

thermionic
see also Cathodes
cathode with Wehnelt cylinder, electron beam energy distrib. 2−45686
cermetelectrodes, bare and covered surfaces 2−54273
discontinuous thin metal films, mechanisms of conduction, nucleation 2−54127
electron work function from plasma immersion probe measurements 2−54263
emitter fabrication by vapour deposition of high work function materials in glow discharge 2−49273
fluctuating microfields effects on emission characteristics of hot cathodes 2−63293
high melting point electrode materials, thermionic converters 2−54272
microscopy, and applic. to phase transform. obs. 2−57016
oxide cathodes, effect of axial mag. field on Boltzmann temp. 2−59103
surface properties, investigation and recording equipment 2−75192
transition metal borides, of IVA-VIA metals, 1300-2100K 2−48017
transport and electron current equation development 2−64878
trialkali photocathode, Richardson and effective work functions 2−61459
vapour deposition of refractory metals, performance of deposits 2−49272
work function of carburized W-Re alloys in 1600-1800 K range 2−54267
Al_2O_3-solids, exoelectronic properties, use in TSEE dosimetry 2−68490
Ba-W_{110} system, temperature dependence of work function 2−75186
BeO, dependence of TSEE on various oxide and silicate admixtures after high temperature pretreatment 2−68493
BeO ceramic, chemically, thermally and radiation-induced changes in TSEE characteristics 2−68492
BeO ceramic, effect of different absorbing materials during γ- and X-ray irradiation on TSEE response 2−68491
BeO low-Z activated, use as high sensitivity radiation detector in TSEE dosimetry 2−67089
BiI_3, thermionic work function, effect of adsorption 2−47993
CrB, properties, obs. 2−44191
Cs covered surfaces, work fn. determ., with plane parallel Cs diode, technology 2−61455

Electron emission continued
 thermionic continued
  Cs covered surfaces, work fn. determ., with plane parallel Cs diode, physical basis 2—61456
  Ir(111)-C film, with two- dimensional phase transitions, props. 2—65100
  KCl:Ag(In), retarding potential curves 2—54274
  K_2CsSb photocathode, Richardson and effective work functions 2—61459
  LiF dosimetric grade powders, influence of thermal and chemical treatment on TSEE phenomena 2—67090
  Mo, annealed electrodes, room temp. ductility and intergranular cracking 2—53875
  Mo, monocrystal, electrical characteristics, thermionic converter 2—54275
  Mo, sublimed collector coatings, additive diode operation 2—49278
  Nb-C thermionic emission constants and electron work function changes 2—54268
  NiO, true work function, A constant, normal energy distribution 2—44192
  Si single-crystal cathode, anisotropy obs. 2—65101
  Ta-O thermionic emission constants and electron work function changes 2—54268
  ThO_2 on Ir cathodes for electron bombarded semiconductor devices 2—65099
  W/Cs(Cs-O) work function theory 2—54262
  W, adsorption of O_2, thermionic electron emission and work function obs. 2—47172
  W, monocrystal, electrical characteristics, thermionic converter 2—54275
  W oxides, formed on emitter, additive thermionic converters 2—49279
  W single crystal surface work function change rel. to adsorption of O and Cs and O-Cs co-adsorption 2—54266
  W single crystals, work function dependence on crystal orientation 2—54264
  W work function change as function of Mo coverage of single crystal surface 2—54265
  Zr-O (B)(C) thermionic emission constants and electron work function changes 2—54268
  Zr-Ta(Nb)-C thermionic emission constants and electron work function changes 2—54268
Electron energy states *see Crystal electron states*
Electron gas
  see also Metals/theory; Plasma; Solids/theory; Superconductivity
  classical one-component plasma, crystallization, Monte Carlo equations of state calc. 2—78843
  correlation energy, Monte Carlo approach 2—49041
  Debye approx., dressed particle description 2—78839
  degenerate, magnetic props., implications for metals, white dwarfs and neutron stars 2—47823
  degenerate, quasi-particle and plasmaron properties 2—68315
  degenerate, specific heat 2—57102
  diamagnetism of free and Bloch electrons, many-body effects 2—68518
  electron plasma, static dielec. const. in presence of strong e.m. wave 2—77843
  electron-phonon interaction effect on X-ray hole correlation function via polarization propagator 2—48167
  elementary excitations, book 2—71806
  energy-density functional in locally linear approx. of one-body pot. 2—76228
  exchange energy, Liberman approx. correction 2—68312
  exchange polarized, dielectric const., magnetic susceptibility 2—77842
  Fermi, neutron rich nuclei, equation of state 2—79723
  ferrromagnetism, ground state energy calcs. 2—71816
  Fokker-Planck equation, electron distribution in elec. field 2—58809
  free, const. m.f.p., magnetoresist. 2—80971
  general-relativistic interior metric for stable static charged matter fluid with large e/m 2—48997
  Grad's thirteen moment method 2—41547
  ground state, method of correlated basis functions 2—63044
  ground state energy anomaly 2—47825
  interacting, orbital susceptibility 2—65120
  interacting, vertex eqn. and dielec. function, variational soln. 2—63045
  linked cluster theorem for Abriskov pseudo-fermion represent. of spin operators 2—54106
  longitudinal dielectric tensor in uniform magnetic field 2—75038
  magnetic, semi-infinite, inhomogeneous, polarized, generalized Hohenberg-Kohn theory 2—54118
  magnetoactive, collective effects 2—58810
  metal, charges embedded in surface, self-consistent screening, jellium model 2—47813
  metal, localized modes of excitation in vicinity of an impurity 2—64902
  metal, paramag. spin susceptibility, calc. for interacting electron gas 2—75207
  metal, passage of a positron, energy loss 2—80967
  metal, positron correl. energy 2—57142
  metallic densities, spin-up-spin-down pair distrib. function 2—71815
  in metals, semi-infinite undergoing p-polarized optical excitation, charging effects 2—68317
  orbital magnetisation at absolute zero in external magnetic field 2—45333
  periodic lattice, dielec. function, self-consistent calc. 2—54116
  plasma of d.c. discharge, non-hydrodynamic props., reson. behaviour 2—74420
  plasmons, prop. in periodic lattices 2—77803
  screening of positive particles 2—61135
  semiclassical theory of transport in disordered materials 2—41548
  semiconductor, field free heating, expressions for vel., pressure and temp. 2—51089
  semiconductor, heated by h.f. elec. field, hot electron recomb. 2—64972
  semiconductors, temp. determ. 2—51121
  spherical and cylindrical symmetry, equilibrium state and pulsation frequency spectrum 2—52112
  spin polarized case, local exchange-correlation potential 2—57266
Electron gas continued
  thermodynamics, characts. in parallel elec. and mag. fields 2—45332
  Townsend Huxley expt. lateral diffusion expt., theory and practice 2—69627
  two-band model, magnetic and excitonic instabilities 2—64881
  two-dimensional, electron-electron interactions continuously variable in range $2.1>r_s>0.9$ 2—57134
  unstable, population and oscillations of two level system 2—63266
  $Li(NH_3)_4$, model for magnetic susceptibility behaviour below 15 K 2—43389
Electron guns *see Electron beams*
Electron lenses
  see also Electron microscopes; Electron optics
  condenser system of electron microscope resolving power 2—79008
  coupled, double focusing, calcs. 2—66716
  electromagnetic cathode, stabilization of accelerating voltages 2—69876
  immersion, spherical and chromatic aberration, magnification depend. 2—49321
  longitudinal spherical aberration, distortion in pupil plane and wave aberration 2—52392
  mirrors, compound cylindrical, theory 2—69872
  multipole, for image distortion 2—69871
  objective lens design for transmission microscope 2—79063
  optimization of antisymmetric quadrupole rel. to aperture and chromatic aberrations 2—79062
  quadrupole, third order aberration coeffs. 2—79058
  ray path tracing through lenses for spherical aberration determ. in scanning electron microscope 2—41928
  ring shaped, correction of spherical aberration by two round lenses 2—79051
  selected area diffraction in scanning microscope, 3-lens electron optical system 2—79093
  spherical aberration rel. to coma, function of object and position 2—59089
  superconducting, optics, book 2—66715
  wide field imaging with aberration minimised JEM-100B electron microscope 2—79071
 electrostatic
  3 coaxial tubes, computer analysis, real and virtual cardinal points, aperture and aberration constants 2—76453
  aperture effect, Crewe field emission gun 2—63279
  aperture lens, design and computer evaluation 2—79066
  astigmatic, 5-electrode quadrupole-octupole lens 2—79003
  cathode, electron image minification 2—59090
  charged vortex ring focusing, in liquid He II 2—80503
  design, for field emission guns 2—79033
  electrostatic electron optical systems, synthesis 2—76457
  five electrode quadrupole-octupole triplet with reduced spherical aberration 2—78999
  Johansson objective, pot. distrib. on axis, calc. method 2—76448
  microprobe system, axially asymmetric elements 2—63280
  modulation transfer function calculation case with geometrical aberrations 2—69875
  potential and field analysis, method using electrode surface charges 2—69874
  quadrupole, asymmetric, third order geometric aberrations 2—63281
  quadrupole multiplets, potential distribution calc. 2—79057
  single, axially-symmetrical, field aberrations 2—76452
  symmetrical three-aperture, analysis 2—66717
  W cathode surface temp. det. in electrostatic field of immersion objective 2—41923
 magnetic
  aberration correction in two stage magnetic deflection system for electron microscope 2—79061
  alignment of pole pieces with initially not coinciding pole piece axes 2—59094
  annular pole pieces, microscope centralization 2—73531
  asymptotic aberration coefficients 2—79060
  coma free round lenses, minimum spherical aberration 2—79059
  condensor objective, for l.v. electron microscope 2—79072
  crossed slits magnetic pseudo-quadrupoles 2—79056
  e.m. quadrupole lenses, parameters and construction 2—59092
  field aberrations, third order of axially symmetric lenses 2—59091
  field meas. using cylindrical search coil 2—79065
  Gaussian dioptrics of e.m. cylinder lenses 2—59093
  MER-3 scanning electron microscope, triple lens system 2—78997
  optical demagnification with long field lens and strong short lens 2—59102
  permanent magnet lenses for electron microscope 2—79067
  pole piece system alignment 2—79054
  probe effects on accuracy of deflection 2—64532
  quadrupole, hexapole, octupole, as aberration correctors for electron beam deflection 2—63282
  size reduction and design optimization 2—79068
  spherical aberration, calc. 2—41924
  spherical and chromatic correction, influenced charges on gauze or thin foil 2—59080
  superconducting, 400 kV electron optical testing system 2—79070
  superconducting, field distribution 2—45684
  superconducting, in 400 kV electron microscope, cryostat cooling system 2—63291
  superconducting, in 400 kV microscope, electron-optical and operating characts. 2—63292
  superconducting, objective for 300 kV microscope, properties and applications 2—79069
  superconducting lenses, shielding and rings 2—79064
  superconducting objective, phase contrast transfer functions 2—52393
  superconducting shielding lens for electron microscope 2—41922
  transmission reduction in image point converters 2—79073
  wave mechanical approach to electron motion 2—79055
Electron microscope examination of materials
  see also Ion microscopes
  — 2—71430
  absorption scanning technique 2—67946
  aerosol, latex, detection of emulsifier particles using grid shadowing 2—71249

Electron microscope examination of materials continued
- alloy, hard metal, fracture surfaces, crack path electron microscope replica obs. 2—50773
- authigenic pyrite from Pacific deep-sea core 2—44579
- biological analysis of atomic and molecular level, role of computers in collection and pouring of data 2—83340
- biological objects, reconstruction of spatial structure 2—81980
- biological specimens 2—66265
- β- brass type alloys, quenched, structure and microstructure 2—84106
- breccia, lunar and terrestrial minerals, deform. substruct. 2—62688
- cavities, defocusing contrast 2—83930
- cellulose and modified cellulose, study of fine structure 2—64624
- ceramic matrix, chemically reacted, for fibre reinforced composites 2—56972
- ceramic substrate, effect of surface chem. on TaN adhesion 2—57005
- ceramics, SEM applications 2—56956
- ceramics and mineralogy, inc. lunar rocks 2—56954
- chromosomes, X-ray irrad. electron microscope obs. 2—62853
- clays, yield and failure 2—76268
- column approximation and defocus contrast 2—83929
- copper-phthalocyanine, reduced radiation damage in electron microscopy 2—80635
- coronene, radiation damage occuring in electron microscope 2—43617
- crystal microstructure and inhomogeneities, quantitative examination 2—80605
- decoration method, determ. of electrically active point defects and lattice structure 2—80604
- diamond, cathodoluminescence changes caused by deformation 2—81428
- dicalcium strontium propionate, ferroelectric 180° domain struct., electron mirror microscope obs. 2—65060
- diffraction contrast from coherent precipitates in elastically-anisotropic materials 2—80671
- dislocation structures in metals, large angle specimen tilting device 2—82438
- domains, interface geometry, contrast effects 2—56718
- double tilting specimen holder, motorized drive 2—55641
- elastomers, scanning microscopy of fatigue fractured surfaces 2—60899
- epoxy resins, correl. of supermol. struct. stability with electrophys. props. 2—83394
- etched $A^{II}B^{VI}$ compounds, surface structure, scanning mode obs. 2—64540
- ferroelectric domain structures, phase transition, scanning electron microscope 2—57240
- ferroelectrics, domain structure, temp. effects, scanning electron microscope obs. 2—81132
- ferromagnetic films, electron microscopy of magnetic structure, review 2—84428
- ferromagnetic thin film, Lorentz microscopy and spatial filtering 2—48088
- fibre/fibre friction meas. with s.e.m. 2—82441
- film, domain wall parameters from Lorentz electron microscopy 2—72182
- film thickness determination by electron backscattering 2—79116
- glass:Nd, phase separation degree, rel. to optical props. 2—57372
- glass, effect of high pressure organic impregnation, surface microstruct. obs. 2—53520
- glass, exam. and surface structure 2—60587
- glass, glass-ceramics, elemental analysis, using scanning elec. microscope 2—60579
- glass, laser irrad., struct. transforms. 2—60588
- glass fibre/polyester resin composite, cracking and debonding on water uptake 2—61020
- glow polymer layers, formation study 2—53564
- grain boundaries, energy analysis 2—53743
- graphite, artificial, anisotropic and isotropic, struct. distrib. 2—53972
- graphite, electron displacement damage, high-voltage electron microscopy 2—56683
- graphite, electron irrad. damage obs. 2—53710
- graphite, high resoln., sample prep. and technique improvement 2—53637
- graphite, high temp. fracture, scanning mode obs. 2—56829
- graphite, highly oriented pyrolytic, effects of oxidation on basal and edge surfaces 2—56572
- graphite, h.v. microscope damage 2—47370
- graphite, laser effects at mod. Ar press., crater formation 2—53552
- graphite, neutron irrad. defect struct., single cryst. 2—53709
- graphite, oxidized pyrolytic, kinetic study 2—68118
- graphite, Poco, high temp. creep obs. using sequential scanning mode 2—56803
- graphite, pyrolytic, effects of oxidation 2—60620
- graphite, pyrolytic siliconated, fracture surface obs. 2—74861
- graphite, stacking fault- halogen impurity interactions 2—53738
- graphite, thin film, struct. characts. scanning mode obs. 2—60648
- heat resistant alloys, development of grain boundaries 2—56721
- high temp. straining stage for s.e.m. 2—79121
- igneous, characteristics of microstructures, planetary surface simulation studies 2—58483
- illite, microstructure and chemical comp. 2—84710
- ilmenites, from Mare Tranquillitatis, morphology 2—44905
- intergranular precipitates identification by double diffraction 2—80615
- keratin fibre surfaces, s.e.m. examination 2—82442
- latex particles size distribution meas. 2—43405
- lattice defects, SEM backscatt. electrons, dynamical theory 2—56628
- magnetic minerals in basalt samples, Mid Atlantic Ridge near 45°N 2—61870
- magnetic oxide powders, sub- micron range, particle size distribution measurement 2—71654
- Mars simulation samples, size classification 2—69160
- metal, close packed, Burgers vectors determ. using g.b=2 contrast 2—60792
- metal, fatigue mechanism, scanning mode obs. 2—56787
- metal, grain boundary ordered struct., boundary dislocations, transmission electron microscopy 2—53651
- metal, in situ electron irrad., void formation 2—47361

Electron microscope examination of materials continued
- metal, void and point defect agglomerate studies using h.v. microscope 2—53695
- metal fibre/refractory oxide matrix, composites, growth and characterization 2—56990
- metal film, significance of electric field on growth 2—60634
- metal oxide structures, microanalysis 2—77540
- metal powder, contact stresses 2—56970
- metal systems, deformation and recrystallization, emission mode obs. 2—43779
- metallic solid/liquid interface micromorphology 2—47194
- metals, 'in situ' study of heavy ion radiation damage 2—74756
- metals, obs. of normal wear 2—43754
- mica and granite, weathering, scanning electron microscope study of morphological aspects 2—56667
- micro grid techniques, specimen prep. 2—60742
- microcrystals in polycrystalline object, investigation of form 2—60741
- nuclear reactor structural mat., swelling under neutron irrad. 2—59868
- out-of-focus effects, phase contrast and related effects 2—83931
- particulate matter, handling, mounting and exam. techniques for SEM 2—43565
- periclase brick, microstruct. of hot fracture surface 2—77661
- Permalloy film, cross-tie walls, motion threshold field and behaviour at inhomogeneities 2—77994
- Permalloy plated- wire memory, domain struct. obs. 2—75231
- polyethylene, crysts., slip traces, dislocation motion 2—83847
- polyethylene, direct obs. of screw dislocations 2—43640
- polyethylene films formed by evaporation and deposition in vacuum, crystal morphology 2—50516
- polyethylene spherulites, origin of contrast effects 2—60782
- polyethylenes, linear, melt blended with atactic polystyrenes, microstructure 2—67848
- polypropylene, crystn. on solid surfaces 2—83392
- polystyrene, atactic, melt blended with linear polyethylenes, microstructure 2—67848
- polystyrene, crazing behaviour, obs. 2—64736
- polystyrene latex, freeze-etched, study of particle size 2—60522
- pore formation in weld deposits made from low alloyed steel welding rods 2—50809
- porosity networks, determ. of infiltration of epoxy mixture 2—80819
- portland cement paste, microstruct. effects on deform. and fracture 2—60995
- pressure cell, structure of thin films of condensed gas 2—79117
- pyrocarbon coated reactor fuels, anisotropy determination 2—74145
- pyroxene, lunar and terrestrial minerals, microstruct. on cooling 2—62689
- α-quartz, direct-recording electronograph in study of objects giving increased background 2—53639
- quartz, synthetic, Dauphine microtwins 2—68003
- quartz, synthetic, plasticity stages of single crysts. 2—56797
- quartz with surface Ge film, elastic wave propagation 2—80732
- radiation- induced defects, contrast calcs. 2—50640
- reactor cladding and struct. materials, irrad. induced void form. 2—49901
- refractories, microstruct. 2—56955
- ribosome microcrystals, optical diffraction from electron micrographs 2—82000
- semiconductor, group II-VI cpds., radiation induced and growth defect obs. 2—47372
- semiconductor, lattice damage prod. by ion implantation 2—47374
- semiconductor amorphous film morphology 2—44129
- Si, electron beam irradiation induced defects 2—64656
- sintering, method of obs., without use of substrate 2—43879
- stacking faults complementary images 2—77541
- stainless steel, dislocations in ferritic phase 2—80873
- stainless steel, types 304 and 316 low-cycle fatigue behaviour at LMFBR operating temps. 2—60945
- steel, 18—8 stainless, cross slip in fatigue deformation 2—77686
- steel, γ'-phase precip., influence of quenching temp. 2—80768
- steel, AISI type 310, transformation characteristics for ferrite, sigma phase and carbides, e. microscope study 2—68189
- steel, AISI type 310, transformation characteristics for ferrite, sigma phase and carbides, e. microscope study 2—68189
- steel, austenitic, irradiated, obs. of nucleation of voids 2—71466
- steel, austenitic stainless, rel. to stress corrosion testing, mech. behaviour 2—50765
- steel, austenitic vanadium nitrogen type, fine precipitates struct. 2—53893
- steel, Cr-Mn-Mo-Ti type, carbides identification 2—47627
- steel, ductile-brittle transition, deform. mode influence 2—43694
- steel, Kh18N10T, fine structure changes for degree of deformation in creep 2—83956
- steel, low-C, hot-rolled, quenched transformation effects on microstruct. 2—57017
- steel, low-C, low-alloy, AlN precip. 2—50833
- steel, low-C and low-alloy, neutron irrad., radiation- and anneal-hardening 2—80681
- steel, low-carbon, topography on fatigue fractured surface 2—84126
- steel, martensitic, effect of lath boundary precip. on fracture toughness 2—57018
- steel, martensitic, Fe-plated fracture edge obs. 2—56940
- steel, martensitic, low-C Mn, effect of Sb on high temp. tempering 2—56905
- steel, martensitic, tempered, crack initiation and propag. 2—43734
- steel, Mn-Cr-B spring, tempering behaviour 2—77688
- steel, stainless, 18-8, fatigue props. at cryogenic temp. 2—56939
- steel, stainless, AISI 304 and 316, substructure correlation with elevated temperature low cycle fatigue 2—56819
- steel, stainless, crack formation, in situ obs. in 500 kV microscope 2—80853
- steel, stainless, dislocation dipole, obs. using systematic reflections 2—80666
- steel, stainless, effect of explosive load on struct. 2—43836
- steel, stainless, electrodes subjected to very high positive and negative voltages 2—71042
- steel, stainless, irrad., cold work effects on void form. 2—50646

Electron microscope examination of materials continued
steel, stainless, irrad., fluence and temp. depend. of void form. 2−50647
steel, stainless, proton irrad., swelling, displacement damage depend. 2−53716
steel, stainless, proton- and nickel-irrad., void form. 2−53715
steel, stainless, void nucleation and growth during fast neutron irrad. 2−50645
steel, stainless, void nucleation and growth obs. using h.v. microscope irrad. 2−53694
steel, structural, fracture behaviour rel. to inclusion orientation and shape 2−43713
steel wire, annealing struct. of heavily drawn pearlite 2−64760
structure and props. of grain boundaries and interfaces, conference, Yorktown Heights, N.Y., USA, Aug (1971) 2−56722
structure property relationships 2−56908
superalloys, precipitation hardened, extraction replica technique, study of submicroscopic particles 2−80817
superconductor, possibility of fluxon obs. by transmission microscope 2−77867
surfaces, irregular, magnification calibration technique 2−79013
tendon collagen, fractography 2−43016
tensile stage for adhesion meas. during s.e.m. obs. 2−82440
tension/compression stage for scanning electron microscope 2−79120
thin films, quantitative analysis in EMMA 4 using block standards 2−81563
thin metal foils, quantitative analysis by ratio technique 2−81562
three-dimensional object reconstruction by improved stereo micrometry 2−79118
Ti-Mo binary alloys, phase separation processes in beta phase during aging 2−80816
ticonal annealed at 800°C electron microscope exam. of struct. 2−80781
topaz, thermal and electron beam induced microstructural breakdown 2−60776
transition metal carbides and nitrides (Gp IV and V), nonstoichiometry 2−61029
4d transition metals, vapour deposited, struct. obs. 2−60594
triglycine sulphate, electron microscope examination of fine structure of irradiated crystals 2−65067
V_2MoO_8, cryst. shear struct. 2−47352
wear obs., scanning technique 2−43741
Zircaloy-4, neutron irrad., deform. parameters, 300°C 2−50749
Ag-15% Ge alloy, splat-cooled, martensitic transformation of structure 2−56921
Ag, crack formation, in situ obs. in 500 kV microscope 2−80853
Ag, filament, grown from Ag compound, crystal morphology obs. 2−47133
Ag, growth processes on alkali halides 2−47096
Ag, radiation damage, nature and annealing characts. 2−47368
AgBr, emulsion, Ag formation in single emulsion grains 2−81546
Al/Cu/Al films, electromigration obs. by transmission electron microscopy 2−64879
Al-1.2 wt%Mg_2Si alloy, two-step ageing study 2−64765
Al-4%Cu alloy, ageing, effects of additional elements 2−56910
Al-Mg-Si alloy, structure of metastable precipitates formed during ageing 2−56909
Al-Mg-Zn alloy, decomp., phase transform. 2−43911
Al-Mg alloys, β, γ phases, atomic structure 2−71642
Al-Mg and Al-Mg-Zn alloys, preprecip. zone obs. 2−53885
Al-9%Mg alloy, rel. to effects of additional elements on clustering and precip. during ageing 2−50801
Al-(3 at.%)Mg alloy, high temp. deformation, lattice rotation, dislocation dragging 2−74835
Al-(1.8 wt.%)Mn alloy, decomp. products 2−47615
Al-Zn-Mg-Cu-Mn forging, alloy, microstructure rel. to fracture toughness 2−53826
Al-Zn-Mg alloy, precipitate free zone obs. 2−56902
Al, crit. stress effect on contrast 2−67983
Al, cross slip in fatigue deformation 2−77686
Al, deformed, dislocation loop struct. rel. to deform. method 2−77574
Al, electron displacement damage, high-voltage electron microscopy 2−56683
Al, electron irrad. induced pt. defects clustering, high voltage electron microscopy 2−56682
Al, integranular flow, effect on grain boundaries, role of imperfections 2−43643
Al, intergranular corrosion in HCl, symmetrical flexion boundaries 2−72561
Al, nucleation during recrystn. 2−80859
Al, plastic deformation, dislocation dynamics, high voltage electron microscopy 2−56785
Al, plastically deformed, dislocation arrangement in surface layer 2−43465
Al foil, α-irrad., growth of very small He bubbles 2−80688
Al foil, direct-recording electronograph in study of objects giving increased background 2−53639
Al neutron irrad., pt. defect clustering, low temp. obs. 2−60783
Al polycrystalline films, on NaCl substrate, effect of annealing 2−80566
AlN-Y_2O_3, sintered, with fibrous struct., textural determ. 2−47666
Al_2O_3:Ti, precip. hardening kinetics 2−50872
9 Al_2O_3-AlN, periodic antiphase domain struct. 2−50618
Al_2O_3, alumina, phosphate bonded, strength props. 2−77662
Al_2O_3, ceramic, microstruct. rel. to deform. processes 2−60993
α-Al_2O_3, cleavage on {1011} planes 2−74657
Al_2O_3, porous compact, grain growth 2−43905
Al_2O_3 crystals, subsurface damage due to abrasion 2−80870
Al_2O_3 film, plasma and gas plasma deposited, struct. determ. 2−64563
$As_2S_3(Se_3)$ cryst., photodecomp. products 2−51463
As_2Te_3-As_2Se_3 glass, microstructural props. 2−61299
Au-Cu, quantitative microanalysis with combined electron microscope-microanalyser (EMMA-3) 2−81561
Au, bicrystals, grain boundary dislocation behaviour 2−56732
Au, h.v. obs. of electron irrad. damage 2−80650
Au, quenched, stacking fault tetrahedra growth and annealing 2−77590

Electron microscope examination of materials continued
Au, quenching velocity influence on vacancy clusters obs. 2−71630
Au, radiation damage, nature and annealing characts. 2−47368
Au, stacking fault energy, determ. using weak beam technique 2−77591
Au bicrystal, ion irrad., g.b. disloc. climb obs. 2−56731
Au film, growth processes on alkali halides 2−47096
Au film, large angle rotation boundaries 2−56736
Au film growth, on alkali halide, from nuclei with fivefold symmetry 2−47102
Au single crystals, electron microscopy at low temps. 2−80892
Au struct. of coincidence and near-coincidence tilt boundaries 2−60810
B_4C, neutron irrad. damage obs. 2−47369
B_4C, neutron radiation induced defects, transmission e. microscope obs. 2−67355
$Ba_2NaNb_5O_{15}$ ceramic, sintering behaviour 2−53929
$Ba_4SrNb_{10}O_{30}$, solidification structs. 2−47654
$BaTiO_3$, ferroelec. domain 2−47983
$BaTiO_3$, ferroelectric surface obs. using electron mirror microscopy 2−65060
$BaTiO_3$, phase transitions, domain interactions 2−61427
$BaTiO_3$ film, polarization change, stroboscopic e.m. obs. 2−75149
$BaTiO_3$ single crystal film, microstruct. of domains and domain walls 2−68469
Be, deformation obs. by synergy of TEM, selected area X-ray topography and line profile analysis 2−56791
BeO powder, direct-recording electronograph in study of objects giving increased background 2−53639
BeO powder, initial stage sintering mechanism determ. 2−47662
Bi-Ag eutectic alloy, surface damage after polishing, e. microscope study 2−67898
C, glassy fibres, derived from phenolic resin, mech. props. 2−84100
C, high-resoln. obs. on coals, chars, evaporated films 2−53532
C, high resoln., sample prep. and technique improvement 2−53637
C black, paracryst. distortions 2−53974
C fibre, PAN-based, fine struct. 2−53948
C fibre, struct., neutron irrad. effects 2−56991
C fibre, struct. obs. 2−53950
C fibre and composites, topography 2−53951
CdI_2, growth characts., stacking faults distrib. and stability, polytypism 2−74781
CdS single crystals, polytypic growth 2−60769
CdSe vacuum evaporated films, structure on mica, NaCl, PbSe film substrates 2−71327
Co-Ni-Ti system, decomp. and formation of modulated struct. in coherent phase zone of stability 2−57030
Co-P film, electroless deposited, growth and struct. 2−53566
Co-Ti alloy, solid soln. decomp., obs. 2−56933
Co-base alloys, microstruct. obs. of phase transformations, photoemission e. micro. obs. 2−68193
Co, electron images of two-dimensional ferromag. domain walls 2−51247
Co, magnetic domains 2−44262
Co, magnetization process, domain nucleation 2−84402
Co film, epitaxial, mag. domain config. obs. 2−61524
Cu-AL(10 wt%), high fluence neutron irrad. damage 2−80686
α-Cu-Al alloy, stacking fault energy detn. 2−50682
Cu-Au film, epitaxial growth by r.f. sputtering, microstruct. 2−67908
Cu-Au system, superdislocation in Cu_3Au, obs. using systematic reflections 2−80666
Cu-(30 wt.%)Ni-0.3 wt.%)Be alloy, age hardening precipitate phases, struct. and morphology 2−50934
Cu-Ni alloy, film, growth, struct., epitaxial temp. rel. to comp. 2−60654
Cu, crit. stress effect on contrast 2−67983
Cu, electron irrad. induced pt. defects clustering, high voltage electron microscopy 2−56682
Cu, foil, heavy ion irrad., rad. damage 2−43608
Cu, high fluence neutron irrad. damage 2−80686
Cu, point defect clusters, effect on fatigue hardening 2−53724
Cu, precip. of Fe_3O_4 impurities, effect on residual resist. 2−71832
Cu, radiation damage, nature and annealing characts. 2−47368
Cu by halide reduction, defect struct. obs. 2−80570
Cu film, condensed in presence of residual gases, oxidation 2−71328
Cu film, epitaxial, microstruct., orientation and imperfections 2−67909
Cu film, vacuum-deposited, substruct., determ. 2−50489
Cu foil recrystallization in a high voltage electron microscope 2−80825
Cu neutron irridiated, cleared channels, correl. with surface slip steps 2−50761
Cu_6Sn_5 fibres, brittle fracture surface morphologies 2−80744
Fe-1%C-0.5%As alloy, anomalous precip. obs.50940 2−50940
Fe-C, Fe-C-X, phase transforms., thermionic emission electron microscopy applic. 2−57016
Fe-1%C alloy, effect of As and Sn on tempering stages 2−50796
Fe-Co layers with intermediate LiF layer, electron microscope study of interacting interdomain boundaries 2−61534
Fe-Co(Ni)-Ti-Al alloy, solid soln. decomp., obs. 2−56933
Fe-Mn-C, alloy, long period stacking order structure formed by thermal cycling 2−67990
Fe-(6 at.%)Mo alloy, precip. 43849 2−43849
Fe-Ni-Co-Mo, maraging alloy, coherent precip. 2−57019
Fe-Ni film, domain struct., influence of temp. obs. 2−72185
Fe-Si, plastic deformation, dislocation dynamics, high voltage electron microscopy 2−56785
Fe-Ta alloy, ductility enhancement using allotropic phase change scanning and transmission obs. 2−57020
Fe, electron images of two dimensional ferromag. domain walls 2−51247
Fe, interstitial H-dislocation interaction 2−53735
α-Fe, neutron irrad., radiation- and anneal-hardening 2−80681
Fe, plastic deformation dislocation dynamics, high voltage electron microscopy 2−56785
Fe, strengthening mech., dynamic strain ageing, dislocation struct. 2−56911

Electron microscope examination of materials continued
Fe film, asymmetric 180° domain walls, obs. 2−48092
Fe foils, electrocrystn. structures 2−83862
α-Fe irradiated, structure obs. 2−60965
Fe_3C, magnetic domains 2−44262
Fe_2O_3-TiO_2 solid soln., crystallographic shear structs., planar boundaries 2−74768
Fe_2O_3 and Fe_3O_4, morphological and struct. changes during reduction 2−50881
γ-FeOOH, lepidocrocite, cryst. struct. and mag. props., at temp. of conversion to α-Fe_2O_3, hematite 2−57287
FeSi, electron images of two-dimensional ferromag. domain walls 2−51247
$FeSi_2$, $\alpha \rightleftharpoons \beta$ transition mechanism 2−43919
GaAs:Ar, Te ion implanted, radiation damage obs. 2−60821
GaAs, amorphous, e. micro. exam of struct. and short-range order 2−71433
GaAs, etched surface morphology 2−56575
GaAs, interfacial defect obs. using high voltage transmission mode, device manuf. considerations 2−54215
n-GaAs, surface barrier diode, hole diffusion length 2−61387
Ga_2O_3-TiO_2 solid soln., crystallographic shear structs., planar boundaries 2−74768
GaP, characterization of epitaxial layers on insulating substrates 2−47111
GaP electroluminescent diode, preferential etching, SEM obs. 2−71972
GaP red-emitting diode characteriz. 2−51389
Gd thin single crystal films, dislocation loops formed during electron microscopy 2−71489
Ge-Se-Te-As system, amorphous bulk and thin film, composition and physical props. 2−60573
Ge-Te alloy film, amorphous struct. obs. 2−50479
Ge, amorphous film, dark-field obs. 2−60593
Ge film, amorphous struct. obs. 2−50479
a-Ge film, crystalliz. processes 2−60658
Ge metal contact induced crystalliz. film, amorphous 2−56590
α-GeTe, domain struct., twin and interface boundary interface types 2−72150
GeTe film, superstruct. study 2−80574
$GeTe_2$ film, amorphous, local order and microstructure 2−60660
Hg on polymer thin films, contact angle meas. 2−46942
HgS single crystals, polytypic growth 2−60769
In film, vapour deposited, growth and nucleation rel. to thickness and substrate temp. 2−77512
InSe film, electron bombardment crystalliz. 2−56594
Ir, interfacial structure obs. using transmission mode 2−56576
KBr, colour centres in cathode luminescence mode 2−80708
KBr crystals, u.v. irrad. and colour centre prod. from exciton decay 2−71527
KCl, of colour centres in cathode luminescence mode 2−80708
KCl, surface polyonization by electron bombardment and illumination 2−50457
KCl whiskers, growth on KCl crysts., and struct. 2−67914
Li films, structure causing absorption bands 2−65260
Li particles, technique for transfer to electron microscope 2−43555
LiBr shortened glycerinated muscle fibres 2−62825
LiF, colour centres in cathode luminescence mode 2−80708
LiF, dislocation loops and radiation colloids 2−74760
LiF, spark discharge induced damage 2−68013
Mg-Li alloys, thin foil prep. using non-aqueous electrolyte 2−80548
Mg-Th, Mg-Th-Mn, Mg-Mn, Mg-Zr alloys, precipitation processes 2−53993
Mg, neutron irrad., distortion and swelling, effects of alloying additions 2−60778
Mg, neutron irrad., pt. defect clustering, low temp. obs. 2−60783
Mg, neutron irrad., struct. damage and annealing 2−80683
Mg, pyramidal slip, dislocation configs. 2−47420
MgO with sulphur dioxide adsorbents, struct. features 2−83871
$Mg_yU_{1-y}O_{2-x}$, structural analysis by X-ray and electron microscope meas. 2−47336
Mn-Al alloy, τ phase, microstruct. 2−50838
MnBi film, props., struct., domain struct. 2−44263
MnBi film, struct. and orientation 2−47119
$Mn_xFe_{3-x}O_4$, Jahn Teller domains, obs. 2−43922
Mo-35%Re alloy, deform. twins, nucleation and growth 2−56720
Mo-Ru alloy, α, β and σ phases 2−50840
Mo-Zr, Mo-Ru alloys, vapour deposited, struct. obs. 2−60594
Mo, ion irrad., void lattice obs. 2−53720
Mo, neutron irrad., void formation during annealing 2−77575
Mo alloy, cellular struct. development during hydroextrusion 2−47642
Mo spray coatings and base metal, scanning electron micrograph of boundary surface peculiarity 2−64748
MoS_2 intercalation compound, struct. obs. 2−64643
NaCl, deformed, dislocation arrangement and glide 2−53807
NaCl, electrical processes occurring at moment of cleavage 2−74659
NaCl, laser induced breakdown 2−54376
NaCl, of colour centres in cathode luminescence mode 2−80708
NaCl, single slip and double slip 2−80749
NaCl, surface polygonization by electron bombardment and illumination 2−50457
Na_2O-SiO_2 glass, with small additions of Al_2O_3 and Ga_2O_3, immiscibility temp. 2−53539
Nb-40% Ti, alloy, supercond., mag. irreversibility and microstruct. 2−47855
Nb-Fe system, plastic deformation, microhardness, emission microscopy 2−74843
Nb-H foil, microcracks, transmission microscope obs. 2−68106
Nb-Hf alloys, fracture morphology, transmission and scanning electron microscopy 2−56834
Nb-N alloy, prismatic loop generation by nitride precip. 2−53994
Nb-O solid soln., form. of Nb_4O during decomp., annealing effects, 500-700°C 2−53902
Nb-Zr-Ti alloy, supercond., struct. determ. 2−50842
Nb-Zr, Nb-Mo alloys, vapour deposited, struct. obs. 2−60594
Nb, stressed, dislocation struct. form. mechanism 2−71494
$Nb(O, F)_x$, cryst. shear struct. 2−47352
$NbSe_2$/organo intercalation compounds, electron microscope examination of lattice, and superconductivity 2−53676

Electron microscope examination of materials continued
$NbSe_2$ intercalation compound, struct. obs. 2−64643
$NbTe_2$, domain structure and dislocation config. 2−60804
Ni-Al alloy, dislocation struct. changes rel. to flow-stress recovery 2−74888
Ni-Al alloy, high temp. deformed, dislocation density, rel. to flow-stress recovery 2−74889
Ni-Co, alloy, f.c.c., dislocation bands produced by electrolytic hydrogen charging 2−56713
Ni-Fe-Cr based alloy, γ'-hardened, electron irrad., void swelling 2−80684
Ni-(5wt.%)Fe-(5wt.%)W, powder composite, fracture micromechanism obs. 2−56947
Ni-Fe, powder compact, densification structural aspects 2−56946
Ni-Fe film, ripple spectrum, depend. on anisotropy, crystallite size, thickness and field 2−81279
Ni-P chemically deposited films, structure in relation to elec. conductivity 2−77510
Ni-P film, electroless deposited, growth and struct. 2−53566
Ni, interfacial structure and energy using transmission and scanning modes 2−56576
Ni, neutron irrad., pt. defect clustering, low temp. obs. 2−60783
Ni, point defect interactions with dislocations, high-voltage electron microscopy 2−56686
Ni, powder compact, densification structural aspects 2−56946
Ni, vacancy clusters after quenching 2−64661
Ni alloy, rel. to strength and alloy design, transmission mode obs. 2−56945
Ni and alloys, void nucleation and growth obs. using h.v. microscope irrad. 2−53694
Ni coatings electrolytically obtained, dislocations and twinning 2−50519
Ni film on NaCl substrate, effect of annealing on dislocation struct. 2−80565
Ni magnetic domain walls, 180°, tilted, struct. from Lorentz electron images 2−72151
Ni particles, sintering obs. using new hot stage for scanning EM 2−56641
Ni stacking fault propagation from a coherent twin boundary 2−80670
β-NiAl, ordered b.c.c. alloy, creep obs. 2−56807
$Ni_2(AlTi)$, $Ni_2(AlNb)$, ordered ternary b.c.c. alloys, creep obs. 2−56807
$NiSiO_2$ cermet films, granular, microstruct. 2−50498
Pb-Sb alloy, precip. mechanism study 2−80858
PbTe/PbS interface, misfit dislocations, image contrast 2−71483
$Pb(Zr,Ti)O_3$ ceramic, microstruct., role of Fe_2O_3 2−50895
Pd-H and Pd 24% Ag-H foils, production of dislocations 2−56948
Pt cermet cathodes, electron microscope study of thermal activation 2−81506
ReO_2, monoclinic to orthorhombic transition 2−47695
Rh, imaging of atoms, with convention electron microscope 2−56665
RuO_2 film 1-5 μm thick 2−47123
Si, amorphous film, dark-field obs. 2−60593
Si, epitaxial film, lattice resolution e. microscopy obs. of struct. of twin boundaries, faults and dislocats. 2−74779
Si, ion damage obs., high resolution replica technique 2−56629
Si, P-implanted, annealing characts. 2−64678
Si, small spherical voids, diffr. contrast profile, calc. 2−77571
Si film, amorphous, metal contact induced crystalliz. 2−56590
Si film, amorphous struct. obs. 2−50479
SiC, stacking faults and dislocations 2−47423
SiC whiskers, twin morphology 2−53581
Si_3N_4, microstruct., transmission high-voltage electron microscope obs. 2−60998
SiO_2-Al_2O_3 glass, crystallization obs. 2−53542
SiO_2-B_2O_3-Na_2O-Al_2O_3 system, comp. fluctuation and phase decomp. 2−53543
SiO_2 film, amorphous struct. obs. 2−50479
SiO_2 film, dielec., defects, local junction form 2−71964
SiO_2 glass, ion irrad., surface topography 2−50462
Sn,, finely dispersed, supercond. crit. temp., particle size effect study 2−61230
Sn film, vapour deposited, growth and nucleation rel. to thickness and substrate temp. 2−77512
Ta-H system, ordering in β-Ta_2H 2−54003
TaC film epitaxially grown by electron beam evap. 2−67916
TaC_{1-x}, plastic deform. up to 2200°C 2−60869
TaC_x film, on needle-like W microcrysts. 2−50509
TaS_2/organo intercalation compounds, electron microscope examination of lattice, and superconductivity 2−53676
Te-Ge based memory glass film, thermal crystn. 2−47128
Te on alkali halides, growth of thin layers at 100°C 2−47120
$Te_{85}Ge_{15}$, $Te_{81}Ge_{15}Sb_4$, $Te_{81}Ge_{15}As_4$ glasses, struct. and crystalliz. 2−60598
Ti-Al-Mo-Zr alloy, influence of β-phase on ductility 2−50746
Ti alloys, $\beta \rightarrow \omega$ transform. 2−68204
Ti alloys, radiation induced transformations in h.v. electron microscope 2−80874
$TiNb_{24}O_{62}$, n-beam lattice images 2−56669
TiO_2-Cr_2O_3 system, solid solns. and cryst. shear struct. 2−47406
TiO_2 powder compact, abrupt shrinkage on sintering 2−43895
$TlSbS_2$, thin films on NaCl, determ. of cryst. struct. 2−80564
$(U,Pu)O_2$ microspheres and pellets, sol-gel derived, microstructure 2−47610
U, β phase, multiquenched rods, microstress behaviour 2−77659
U alloy, ion etched, scanning mode exam. 2−56578
U_3Si, in-pile irrad. effects, obs. 2−47393
U_3Si, irradiated, effect of electropolishing on voids 2−67354
V-C alloys, ordering effects in struct. obs. comp. depend. 2−71378
V-H system, low temp. phase transform. 2−53998
V-N system, V_3N phase 2−50978
V foil, quenched, vacancy detects obs. 2−71472
VC_x:B, precipitation and dislocation struct., electron microscope obs. 2−61038
$V_{2-x}Cr_xO_3$, domain form. during Mott metal-insulator transition, geometry and crystallography 2−71785
W, foil, 60 kev Au ion irrad., dislocation loop prod. 2−43615

Electron microscope examination of materials continued
W, foil, Au ion irrad., vacancy-type dislocation loop, prod. 2−43616
W, foil, Au ion irrad., vacancy-type dislocation loop prod. 2−43616
W film, chem. vapour deposited 2−47131
WC-Co cermets, plasticity, slip, grain boundary sliding 2−47505
WC-Co hard metals, mixed milling effect on sintering, electron microscope investigation 2−56899
$W_4Nb_{26}O_{77}$, n-beam lattice images 2−56669
WO_x and $(W, M)O_x$, ($M=V$, Nb, Ta, Mo), cryst. shear struct. 2−47352
Zn-0.1%Cd, single crystal, deformed, slip lines obs. 2−47421
Zn, condensed particle size, determ. using time discrete sampling apparatus 2−77454
ZnS single crystals, polytypic growth 2−60769
$ZnSe_xTe_{1-x}$ p-n junction diodes, struct., props., electron microscope and cathodolum. obs., 77-300K 2−81118
ZnTe epitaxial film, on Ge, struct. 2−50515
ZnTe film on NaCl, KCl, determ. migration length, 1.5 to 10 K 2−80563
Zr-Al dilute alloy, ordering and stacking faults 2−47354
Zr, neutron irrad., dislocation loops characteriz. 2−43639
Zr alloy, stress corrosion cracking in Hg, fracture surface study 2−43737
Zr alloys, $\beta \rightarrow \omega$ phase transform. 2−68204
Zr and Zr-O alloy, strain ageing study 2−47599
ZrO_2, martensitic transform. struct. 2−50953

Electron microscopes
see also Ion microscopes
3 MV, accelerating tube and microscope column 2−79133
3MV, improvements and image quality 2−52394
3MV microscope, construction and performance 2−55664
100 kV, high resolution, development of field emission gun 2−79032
500 kV electron microscope gun, brightness, 200-500 kV accel. volt. 2−55660
aberration correction in two stage magnetic deflection system 2−79061
accelerating voltages det. by electron diffraction method 2−82452
active X-ray shielding of viewing head 2−45201
advances 2−59096
aperture lens, design and computer evaluation 2−79066
apparent image enhancement through coherent defocusing 2−79023
channel plate detector for scanning microscope 2−79085
charge production in specimen, method of elimination 2−63284
column, 1000 kV, characteristics 2−79039
condensed opjective of microscope with 300 KV accelerating potential, optical characteristics 2−63286
condensor objective lens for l.v. electron microscope 2−79072
conference (Manchester, Sept 1972) 2−79024
cryogenic emission, design and specimen prep. 2−79049
cryostat cooling system for supercond. lenses 2−63291
diffraction unit, electrostatic type, with intermediate electron accelerator 2−52395
displaced aperture dark field images by an aberration correction technique 2−79053
electron gun, mean brightness 2−41918
electrostatic collectors, improved sensitivity, meas. of surface electric potential 2−79000
Elmiskop 101, small probe techniques 2−79041
EM 201, development, modifications and attachments 2−79040
EM 201, operating characts., design concepts 2−55665
EM-150, accelerating voltage increased to 150 kV 2−63288
EM-150 industrial microscope with 150 KV accelerating potential 2−63285
EM-450, accelerating potential 200 KV 2−63267
EMB-100L, low angle diffraction 2−64616
emission-type, with deformation device, construction and applications 2−43779
EMMA for carrying out X-ray spectroscopic analysis 2−61829
energy analysing and selecting systems and applics. 2−56635
energy broadening of electron beam in electron microscope 2−79094
field emission, scanning, NPL-VG, design and performance 2−79046
Fourier analysis of images 2−79160
freeze drying and low temp. stage 2−79110
goniometer stage, JEM-7A, inclined specimen cartridge 2−79114
Grenoble CEN laboratory, principles and applications 2−73533
high resolution magnetic spectrometer for energy selecting electron microscope 2−82431
h.v., illumination system 2−63287
h.v., modified environmental cell 2−79112
image contrast, anal. study of effect of initial electron vel. 2−79010
image formation, aberrations, defocusing and ultimate resolution 2−82448
image resolution 2−82449
immersion objective as secondary electron collector in s.e.m. 2−79088
ion beam and u.v. light sources for use with 2−79004
LEED and RHEED in ultrahigh vacuum electron emission microscope 2−79096
magnetic, centralization, pole adjustment 2−73531
magnetic screening with soft Fe 2−79078
MER-3, scanning, description 2−78997
microfield analysis by scanning microscope 2−55667
micrograting manufacture in Stereoscan Mk. II 2−59095
million volt microscope, h.v. generator 2−55668
mirror, charge distribution in isolated layers 2−79128
mirror, diffraction of very slow electrons 2−79167
mirror, peculiarities of optical systems 2−59097
mirror, sensitivity to surface electrical inhomogeneities 2−79036
objective lens design for transmission microscope 2−79063
odd symmetry wave front deformations effects on diffractograms of e.m. images 2−82446
permanent magnet lenses 2−79067
photographic equipment for ZEISS EM 10, high-resolution 2−79084
REM-3, MER-3, improvements to videocontrol and power supply units 2−78996
resolution, convolution integral two dimens. soln., deconvolution 2−73529

Electron microscopes continued
resolution improvement 2−79028
resolution with single-field condenser objective 2−79076
retarding field electron energy analyzer 2−79079
scanning, 1 MeV, optical system 2−79043
scanning, automatic 2−79016
scanning, charging artifacts, occurrance and effects 2−43558
scanning, conductive mode amplifier 2−55639
scanning, design using modular system 2−79044
scanning, electron trajectory and virtual source of field emission gun 2−69877
scanning, EM 300 G, attachment 2−79042
scanning, field emission, model 2−79047
scanning, field emission gun 2−79031
scanning, image contrast 2−82453
scanning, image contrast effects from superimposed submicron structural networks 2−79127
scanning, interfaced to differentially pumped cold field emission gun 2−79030
scanning, medium resolution, 'Stereoscan 600', for surface morphology study 2−66720
scanning, ray path tracing through lenses for spherical aberration determ. 2−41928
scanning, transmission, field emission source 2−79045
scanning, ultrahigh vacuum, differentially pumped, construction, operation 2−63289
scanning, unchanged images of insulators 2−79129
scanning electron microscope, electron trajectory and virtual source of field emission gun 2−69877
scanning electron microscope-probe analyser combination, use in examination and anal. of ceramics 2−71414
scanning transmission, 100 kV high resolution, design 2−79029
scanning transmission, probe size and current 2−59101
scanning transmission diffraction techniques 2−80622
secondary electron scanning electron microscope, collector with magnetic field 2−79090
selected area diffraction in scanning microscope, 3-lens electron optical system 2−79093
side entry single tilt specimen holders for heating and stress corrosion cracking 2−79109
side entry soft straining and heating stages for in situ dynamic obs. 2−79108
specimen chamber for in situ obs. on mag. materials 2−79111
specimen stage for low temp. obs. 2−64623
stereo viewing, direct, in s.e.m. 2−79086
Stereoscan, optimum working conditions 2−73532
stereoscopic, patent 2−66721
stroboscopic electron mirror microscope for operation up to 100 MHz 2−66719
superconducting electron lens testing using 400 kV electron optical system 2−79070
with superconducting lenses, electron-optical and operating characts. 2−63292
superconducting objective, phase contrast transfer functions 2−52393
superconducting objective for 300 kV microscope, properties and applications 2−79069
superconducting shielding lens 2−41922
superposition effects in energy analysing electron microscope 2−79015
surface scanning electron microscope, low loss images 2−79126
three-dimensional image construction of small objects 2−52397
transmission, emission and mirror, optical systems 2−79038
transmission, straining holder for deformation obs., using piezoelectric effect 2−79107
transmission and scanning, optics, book 2−66715
transmission scanning, Arizona 1MeV, design features 2−41927
turbomolecular pumps application 2−55331
turbomolecular vacuum pump for Siemens Elmiskop 101 2−45194
vacuum pump system, 10^{-8} to 10^{-9} mm Hg 2−79007
voltage contrast mechanism 2−82454
wide field imaging with aberration minimised JEM-100B electron microscope 2−79071
Al, (100) and (111) faces, LEED intensities, quantum field theory calc. 2−74712
LaB_6 rod cathode low power heater 2−62888
Li-glass scintillator tip for detection of secondary electrons in electron microscopes, long life 2−82430

Electron microscopy
see also Crystal structure, atomic
accidental reflections effects on contrast of extinction contours 2−83933
additive difference image method 2−79156
amorphous materials 2−83937
anomalous absorption effects on image contrast of stacking faults in wedge shape crystals 2−43551
apparatus for rapid processing techniques for biophysics 2−45043
astigmatic, 5-electrode quadrupole-octupole lens 2−79003
effects of atomic elastic and inelastic scattering 2−83207
Auger spectroscopy in emission microscope 2−81196
automation of structural analysis of images 2−71417
autoradiography, monolayer prep. technique 2−80616
biological macromolecular complexes by dark field microscopy 2−82001
biological objects, reconstruction of spatial structure 2−81980
biological systems, beam efficiency, inelastic scatter and radiation damage in h.v. microscope 2−50613
bombardment, information gain aspects 2−60744
cathode system, resolution under homogeneous e.s. field 2−59087
ceramics, textured studies by scanning electron microscopy, examples of use 2−71413
channel plates as image intensifiers for transmission microscopy 2−79083
channelling patterns, meas. of image contrast changes 2−83944
chemical polishing technique for prepn. of thin foils for e. microscopy 2−67963
chemically active materials, technique 2−43555
cold stage units for Hitachi microscopes 2−53640
computer enhancement of high resolution electron micrographs with weak periodic information 2−79143

Electron microscopy continued
- computer simulation of Lorentz micrograph 2−79135
- conference, Berkeley, USA, Sep. (1971) 2−56630
- contrast of image of unextended object 2−79005
- contrast of perfect and imperfect crystals, SEM backscatt. electrons, dynamical theory 2−56628
- contrast transfer function, effect on coma or astigmatism 2−82444
- contrasts, diffraction, theor. comput. for obs. of groups of two dislocations 2−67960
- controlled atmosphere, use of gas- reaction stage 2−65363
- crack formation and propagation, in situ obs. in high voltage microscope 2−80853
- crystallographic defects, diffraction constant micrographs, transmission and reflection 2−80621
- darkfield, imaging of heavy atoms using hollow cone illumination 2−59100
- differentially pumped environmental cell in AEI EM7 high voltage microscope 2−82437
- differentially pumped environmental cell in AEI EM7 high voltage microscope 2−82437
- direct-recording electronograph in study of objects giving increased background 2−53639
- dislocation behaviour and contrast effects rel. to grain boundaries and internal boundaries 2−56701
- dislocation loops, small perfect, characterisation by transmission electron microscopy 2−80674
- dislocation loops, small perfect, characterization by transmission electron microscopy 2−80673
- dissociated dislocations, analysis of images 2−80624
- domain structure obs., interface geometry 2−68021
- elastically scattered electrons, technique for direct recording 2−79087
- electron beam-induced radiation damage in polymers, effect on electron microscope image 2−80700
- electron energy loss spectrum meas. by electron microscopy and energy analyser, statistical analysis of errors 2−73524
- electron gun, field emission, 75 and 100 kV, optical aberrations 2−69878
- electron microscope with prism spectrometer for selected area electron spectrometry 2−79095
- electropolishing apparatus for foils at -50°C 2−43553
- electrostatic collectors, s.e.m. investigation 2−79089
- emission, analysis of microstructure and topography of Al alloys 2−80875
- emission, obs. of deformation and recrystallization phenomena 2−79115
- emission, research instrument 2−47304
- emission microscope with deformation device, construction and applications 2−43779
- emission rel. to diffraction using u.h.v. instruments 2−79048
- energy analysing and selecting systems and applics. 2−56635
- energy dispersive analysis of biological thin sections 2−82002
- energy loss problems and contrast preservation 2−79091
- environmental cell, for high voltage obs. of wet biological materials 2−73168
- epitaxial growth of metals and non-metals, obs. 2−60727
- equipment and techniques, conference (Manchester, Sep 1972) 2−79024
- Fe-3%Si foil specimens, low temp. tensile tests 2−80872
- ferromagnetic domain walls, electron images 2−51247
- field emission, two-dimensional crystallization obs. 2−53622
- field emission guns and materials 2−79025
- field emission investigation of A^{IV} coated W monocrystals 2−83872
- film nucleation and growth obs. 2−74624
- film/substrate interface, misfit dislocations, image contrast 2−71483
- fine mesh hemispherical grids, cold forming process 2−82435
- fluxon contrast calculations rel. to specimen thickness and defocus distance 2−79136
- focusing, automatic, of scanning microscopes, using image analysers 2−79014
- foil prep., 3 mm discs, at subzero temps. 2−73656
- fractography by crack replication 2−47545
- freeze-etching technique, temperature vacuum and fracturing considerations 2−79100
- fundamental phenomena, Lewis' scatt. theory, Monte Carlo technique 2−80608
- Gerchberg-Saxton algorithm application to Lorentz microscopy 2−82447
- Harwell 1MV microscope, high-voltage use for texture study of ceramics 2−71412
- heating element for freeze etching 2−56626
- high resolution, improving phase constant transfer properties by special apertures 2−79163
- high resolution replica technique for ion damage obs. 2−56629
- at high temperatures 2−64620
- high voltage, applic. to fractography, straining device incorp. 2−56825
- high voltage, environmental chamber design 2−56642
- high voltage, plastic deform. obs. on thick foils 2−56785
- high voltage metallography, and applics. 2−56632
- h.v., defect contrast and resolution 2−80633
- h.v., optimum voltage and specimen penetration 2−47307
- h.v., penetration and contrast, for crystalline materials 2−79132
- h.v. electron accelerator with increased stability 2−79034
- h.v. electron microscopy, energy loss and aberrations 2−79137
- h.v. electron microscopy applied to 8-300 K radiation damage studies of crystals 2−79141
- h.v. electron microscopy of crystalline polymers 2−79139
- hydraulic-type tensile device for transmission microscopy 2−60743
- image accuracy, multiple diffr. effects 2−43554
- image analysis, two dimensional correlation functions 2−79155
- image contrast, inelastic scattering of electrons 2−79021
- image deblurring by holographic deconvolution 2−55666
- image filtering with fast Fourier transformation using digital computer 2−79142
- image formation, parametral effects 2−82443
- image quality, electron scatt. effects 2−79002
- image reconstruction methods, review and comparisons 2−79149
- images, holographic recording 2−79225

Electron microscopy continued
- images of periodic objects, effect of spherical aberration and defofussing 2−79124
- imaging of heavy atom patterns in monomolecular layers 2−80639
- imaging of light waves using electron microscope and stimulated Compton scattering 2−82451
- imaging of single atoms in scanning microscopy 2−79162
- in situ expts. review 2−80620
- increased penetration in specific voltage ranges, semiclassical prediction 2−83938
- insulating-ferroelectric crystals, surface potential variation, observation with scanning electron microscope 2−81157
- kV electron energy dissipation vs. penetration distance in high at. no. mats. 2−56634
- LEED, selected area, in emission microscope 2−79080
- light optical model, in-line holography 2−59099
- living plant cell walls, sample preparation for scanning electron microscopy 2−78641
- Lorentz microscopy, in-focus, wave optical theory for thin ferromagnetic films 2−76458
- Lorentz microscopy by laser diffraction, quantitative determ. of magnetization ripple 2−79144
- low-angle diffraction in EMB-100L microscope 2−64616
- low-angle dispersion 2−64615
- l.v., intermediate deceleration of electrons 2−79037
- magnification system, new aspects in design 2−79074
- metallography, developments in UK, (1948-1960) 2−67958
- micro grid techniques, specimen prep. 2−60742
- micrographs, reduction of noise by tilting a crystalline supporting film 2−59098
- microholography, single beam method 2−64629
- microprobe system, axially asymmetric elements 2−63280
- mirror, image contrast formation in piezoelectric fields 2−84368
- mirror, resolving power and electron optical characteristics of condenser system 2−79008
- modulation function meas. for electron sensitive films 2−79154
- muscle phosphorylases a and b, electron micrograph analysis by optical diffraction and filtering 2−79145
- n-beam lattice image technique and applic. to complex oxides 2−56669
- object structure determ., using high and low energy electrons 2−79009
- object-image relationship in transmission microscope 2−79123
- optimal picture, from focusing by means of Fraunhofer diffraction 2−76533
- phase change on electron wave scattering from thin objects 2−80636
- phase contrast enhancement by single sideband modulation transfer 2−79122
- phase contrast zones, relative phases obs. with aid of optical diffractometer 2−52396
- phase evaluation in generalized diffraction 2−79158
- photoemission, analytical methods 2−56636
- preparation techniques effects on statistical analysis of metallographic electron micrographs 2−43550
- projecting functions, synthesis 2−74717
- pulse height analysis, network method 2−61830
- quantitative defectoscopy, and computer-simulation of images 2−60745
- reactor cladding and struct. materials, post-irrad. exam. 2−42669
- reactor fuel element specimen prep. 2−42685
- real space diffraction analysis 2−82450
- reciprocal lattice determ. using goniometer stage and electron microscope 2−80614
- reciprocity theorem and diffraction 2−82445
- reconstruction of complex image function from electrons micrographs 2−79157
- recording, processing and correction of images 2−79152
- recovery of functions from their projections, theory 2−74716
- reflection microscopy, measurement of inclined steps 2−60740
- replica techniques for scanning microscopes 2−64622
- resolution and contrast in 1 MV electron microscope environmental cell 2−79138
- resolution limit of holographic reconstruction methods 2−79161
- resolution of image, effect of object scattering props. 2−79006
- resolution test, spectrum of spatial frequencies of electron micrographs 2−79146
- resolving power for very thin specimens 2−79125
- review, techniques and appls. 2−53638
- ring diffraction patterns on-line analysis 2−79153
- sample polishing, thinning and cutting using jet 2−67957
- sample position semi-automatic control 2−43552
- sample preparation, for scanning microscopy of fine particulates 2−50905
- scanning, applic. to wear obs. 2−43741
- scanning, bibliography 2−43567
- scanning, biological and medical appls. and techniques 2−76074
- scanning, biological sample preparation 2−78642
- scanning, channelling pattern technique 2−56637
- scanning, charging artifacts, occurrance and effects 2−43558
- scanning, contrast separation possibility 2−47983
- scanning, defect obs. using diffraction contrast, theory and practice 2−43562
- scanning, defectoscopy, review 2−56700
- scanning, electron channelling patterns in cryst. surface studies 2−47074
- scanning, fractography applic. 2−56640
- scanning, freeze-fracture of biological samples 2−82080
- scanning, hot and electron emitting surface exam. technique 2−47305
- scanning, hot stage development 2−56641
- scanning, low-loss image, electron scatt. theory 2−43530
- scanning, metals, Lilienfeld radiation 2−79131
- scanning, multiple inelastic scattering in channelling patterns 2−80936
- scanning, obs. on uncoated, nonconducting or thermally sensitive specimens using fast scan field emission source 2−43559
- scanning, particulate matter exam. techniques 2−43565
- scanning, preparation of non-conducting objects 2−67961
- scanning, preparation of porous material 2−80540
- scanning, quantitative, crystal imperfections, elastic waves 2−80623

Electron microscopy continued
- scanning, selected area channelling patterns, rocking angle and working distance effects 2−53642
- scanning, selected area channelling patterns from 1μ specimen areas 2−53643
- scanning, selected-area electron channelling patterns and applic. 2−56638
- scanning, stereo pair micrograph meas. conversion to real 3D data 2−43563
- scanning, summary of SEM symposium, 1968-71 2−43566
- scanning, technique for exam. of irrad. mats. 2−43560
- scanning and transmission, comparison for height and depth meas. using shadow casting 2−43564
- scanning fractography as microstruct. determ. technique 2−56639
- scanning microscope facility at NBS 2−47306
- scanning transmission image, for thick specimen 2−79130
- self supporting micro grids production using Elmiskop 101 2−79166
- semiconductor and device characterization 2−61372
- shadow effect in 3-dimens. crystal model rel. to channelling 2−71768
- simulation of shadow width distributions for protein molecules 2−79099
- space charge correction of spherical aberration 2−79075
- space frequency spectra of images at same resolution 2−64621
- specimen holder for electrolytic jet thinning apparatus 2−67959
- specimen prep., critical point drying apparatus 2−56627
- specimen prep., multi-jet technique 2−80618
- specimen prep. by sputter-thinning 2−80617
- specimen prep. for transmission obs., technique for dispersion hardened mats. 2−80549
- specimen preparation, ion-thinning, effects on surface of SiO_2 glass 2−50462
- specimen preparation with freeze-drying technique for electron microscopy 2−79098
- stacking faults complementary images 2−77541
- stereometric analysis with micro-videomat 2−41926
- superdislocation and dislocation dipole, obs. using systematic reflections 2−80666
- target temp. indicators, ultrathin Sn layers 2−71416
- techniques for improved resoln. of carbon and graphite samples 2−53637
- tensile testing device, usable from room temp. to −150°C in electron microscope 2−71613
- thermionic emission, applic. to phase transform. obs. 2−57016
- thin foil prep., semiautomatic double jet polisher 2−79105
- three dimensional image reconstruction by object illumination from discrete set of directions 2−79159
- three dimensional reconstruction at high resolution 2−79164
- three dimensional reconstruction from electron micrographs, iterative method 2−79148
- three dimensional reconstruction from electron micrographs of tilted objects 2−79147
- three-dimensional reconstruction of structure from electron micrographs 2−79151
- three-dimensional reconstructions from electron micrographs by holography 2−79150
- three-dimensional struct. reconstruct. from projections by direct methods 2−71410
- tissue preparation for light and electron microscopy 2−78643
- topographic step height evaluation using electron mirror microscopy and applic. 2−65060
- transient phenomena, direct filming with closed circuit TV as view finder 2−79082
- transmission, Ag crystal specimen prep. using electrolytic technique 2−80619
- transmission, appl. to pulmonary pathophysiologic obs. 2−76073
- transmission, applics. and recent developments incl. high voltage work 2−56631
- transmission, defectoscopy, review 2−56700
- transmission, foil prep., electrolytic jet thinning procedures 2−71415
- transmission, ion beam thinning of cylindrical objects 2−79104
- transmission, sputter thinning of specimen foils review 2−79101
- transmission, system for in situ nucleation obs. 2−79113
- transmission automatic device for perforation-free polished specimen prep. 2−79106
- transmission EM imaging of electric field regions associated with p-n junctions 2−79134
- transmission image simulation for random and periodic arrays of coherency strain centres 2−56633
- transmission scanning, physical limits to thick specimen work 2−43561
- transmission scanning electron microscopy and energy analysis 2−79092
- TV monitor picture, modulation transfer 2−79081
- twin crystal joint, intensity calculations 2−80626
- weak beam method, high resolution 2−80630
- Wien filter, double-focusing, as full-image energy analyzer 2−79077
- X-ray, scanning with shadow image 2−79001
- Al, diffusion, review 2−83992
- Al_2O_3, transmission e. microscopy obs. of subsurface damage caused by mech. polishing and grinding 2−71418
- Al_2O_3 films on glycerol as specimen support film 2−43556
- Au apertures, self cleaning, preparation with varied contours 2−79165
- CdS evaporated layers, thinning for transmission electron microscopy 2−67962
- Fe, cast, ion beam thinning, graphite/pearlite interface microstructure 2−74877
- Ge, field-emission cathode, preparation technique 2−82433
- He liquid cooled stage for s.e.m. 2−82439
- He liquid stage for s.e.m. 2−79119
- Rh, imaging of atoms, with convention electron microscope 2−56665
- Si field-emission cathode, preparation technique 2−82433
- Si rubber membranes as supporting medium for cells for electron microscopy 2−79097
- U atoms imaging by phase contrast, specimen preparation 2−80637
- U atoms imaging by phase contrast 2−80638

Electron mobility, solids *see Crystal electron states/transport processes*

Electron multiplier phototubes *see Photomultipliers*

Electron multipliers *see Electron tubes; Photomultupliers*

Electron nuclear double resonance (ENDOR) *see ENDOR*

Electron optics
- *see also Beta-ray spectrometers; Electron lenses; Ion optics; Particle optics*
- aberration correction in two stage magnetic deflection system for electron microscope 2−79061
- aberration correction using quadrupole, hexapole and octipole lenses 2−63282
- apparent image enhancement through coherent defocusing 2−79023
- asymmetric quadrupole lenses, third order geometric aberrations 2−63281
- beam defocusing due to filament fields in gun 2−49691
- cathode system, resolution under homogeneous e.s. field 2−59087
- compression of high current relativistic beams by converging magnetic fields 2−73530
- condenser system of electron microscope resolving power 2−79008
- contrast of image of extended and unextended objects 2−79005
- contrast transfer function in electron microscope, effect on coma or astigmatism 2−82444
- current density distribution at object 2−78998
- cylindrical analyser for energy analysis in ESCA studies 2−84382
- cylindrical electron energy analyzer, instrument function 2−66712
- cylindrical system with diaphragms and thick electrodes, combined focusing and deflecting 2−69873
- demagnification using long magnetic field lens and strong short magnetic lens 2−59102
- devices on display at 1972 Physics Exhibition 2−55662
- digital electro-optical displacement sensor 2−59086
- electostatic prism spectrometer with quadrupole lenses 2−49632
- electron gun, field emission, 75 and 100 kV, optical aberrations 2−69878
- electron mirror microscope, charge distribution in isolated layers 2−79128
- electrostatic electron optical systems, wide-aperture, design 2−76451
- electrostatic parallel plate spectrograph for relativistic particles 2−63691
- electrostatic sector, cylindrical, for energy analysis 2−69870
- electrostatic systems, synthesis 2−76457
- equipment and techniques, conference (Manchester, Sept 1972) 2−79024
- field aberrations, third order of axially symmetric lenses 2−59091
- fluxon contrast calculations rel. to specimen thickness and defocus distance 2−79136
- guns, problems of computation and design 2−76454
- high brightness boride emitter electron gun, design and performance 2−79027
- image intensifiers, basic characteristics 2−73673
- imaging systems, transmission, emission and mirror, microscopes 2−79038
- imaging systems of rotational symmetry with off axis ray paths 2−79052
- light pipe, generalized Chladni forces concept applic. 2−49312
- magnetic probe of lens, effect on accuracy 2−64532
- microscope image contrast, effect of initial electron vel. 2−79010
- microscopical installation, resolution improvements 2−79028
- modulation transfer function of proximity focused image tube, effects of photon energy 2−52390
- optical grid systems error analysis 2−66711
- oscillator gauge, electron trajectories 2−76128
- phase vibrations of electrons in synchrotrons, effect of synch. rad. 2−79689
- photomultiplier, locating light events randomly distributed in plane 2−49330
- progress review 2−79050
- ray tracing under e.m. field influence 2−73523
- reconstruction of optical signal as electron image 2−66710
- relativistic beam, mag. focusing by mirror mag. field 2−79011
- relativistic beam, mag. focusing by mirror mag. field 2−79012
- resolution of image, effect of object scattering props. 2−79006
- scanning electron microscope, field emission, model 2−79047
- scanning electron microscope, image contrast effects from superimposed submicron structural networks 2−79127
- scanning electron microscope, unchanged images of insulators 2−79129
- scanning electron microscopes, videocontrol and power supply units 2−78996
- selected area diffraction in scanning microscope, 3-lens electron optical system 2−79093
- slit apertures, calc. of field of system 2−66713
- slits and thick electrodes with rectangular apertures, calc. of field 2−66714
- spectrometer, distortion of differentiated deflection analyser current 2−45685
- spherical aberration, reduction in 5 electrode quadrupole- octupole triplet 2−78999
- spherical aberration correction in electron microprobe by non axially symmetric elements 2−81560
- spherical grid retarding potential analyzer, optimization of geometry 2−55663
- surface scanning electron microscope, low loss images 2−79126
- system for 1 MeV scanning electron microscope 2−79043
- trajectories in arbitrary static e.m. fields, computer technique eliminating integration truncation errors 2−73528
- transmission and scanning microscopes, book 2−66715
- transmission reduction in image point converters with magnetic lenses 2−79073
- transmission secondary electron emitters resolution rel. to backscatter of electrons 2−81184
- transmission spectroscope 2−59088
- two-dimensional electron trajectories analysis by numerical analysis 2−76449
- GaP(Cs) dynode photomultipliers 2−49677

Electron pairs
see also Positronium
colliding beams as tool for quantum electrodynamic processes and hadronic e.m. current investig. 2−76609
ferrocyanide in glasses produced by freezing NaOH-H_2O solutions, photoelectron emission spectra 2−44210
ionic crystal, defective, positron centres 2−71823
photoproduction, improved Weizsacker Williams method for calc. of energy-angle distrib. 2−66930
annihilation
annihilation, fundamental ideas, measurement techniques and annihilation radiation, review 2−59428
atomic matter-antimatter rearrangement and annihilation cross sections 2−62433
α-brass, Fermi surface, positron annihilation study 2−80955
cross-section difference between $e^+e^-\to$hadrons and $e^+e^-\to\pi^+\pi^-$, rel. to hadronic contrib. to muon magnetic moment 2−76612
differential cross section, meas. at 1.0 GeV, test for validity of quantum electrodynamics 2−63521
Doppler broadening for 29 elements, Fermi energy calc. 2−68324
electron scattering, deep-inelastic, continuation to deep electron-positron annihilation 2−79504
graviton prod. processes 2−78784
hadron final states by pair production and multiple production, 1400-2400 MeV expts. at ADONE storage ring 2−73761
hadron multiplicities in scaling model 2−82686
to hadrons, high energy data review 2−76611
into hadrons, isospin and SU(3) equalities 2−49484
high energy limit, hadron prod. and virtual photon phenomena 2−76605
high polymers, positron annihilation 2−68265
hydrocarbons, solid, anomalous annihilation 2−68264
ice, mag. quenching of o-positronium 2−77849
ice, pure and doped, positron lifetimes 2−54091
ionic crystal, defective, positron lifetime 2−71823
liquid crystals, phase and temp. dependence of positron annihilation 2−64439
metal, Doppler-broadened annihilation radiation spectra, electron effective mass 2−61216
metal, electron gas, passage of a positron, energy loss 2−80967
metal, Fermi surface determ. from photon annihilation spectrum 2−61171
metal, monovacancy, formation energy, determ. from temp. depend. positron annihilation 2−56689
metal, positron annihilation, theory 2−54122
metal, positron correl. energy in electron gas 2−57142
metal, positron trapping rate, temp. depend. 2−80675
metal, positron vertex renormalization of effective electron-positron interaction 2−54115
metal, trapping obs. of defects, error sources 2−80676
metals, electron momentum distrib., from Doppler-broadened annihilation lineshapes 2−71782
nitrate glasses, positron lifetimes, temp. depend., phase transitions influence 2−47772
perturbation theory, connection with deep inelastic ep scattering 2−52562
polyethylene under static electric field, positron lifetimes rel. to polariz. 2−61409
positron lifetime spectra analysis using FORTRAN program 2−52561
positronium, in molecular liquids and solids 2−43311
quantum electrodynamics, experimental tests 2−82609
rate enhancement in periodic fields 2−77801
single graviton annihilation, in ext. e.m. field 2−49507
single-quantum annihilations of positrons by screened K- and L-shell electrons 2−76981
structure and properties determination technique, review 2−47771
structure functions, scaling 2−82689
transition metal monoxides, positron lifetime spectra, rel. to cond. and nonstoichiometry 2−71825
tristearin, polymorphism, positron annihilation study 2−60773
two particle annihilation, ang. distrib., theory 2−75042
water, light and heavy, positron lifetimes 2−54091
e^+e-, into hadrons; resons., Regge poles, fixed poles, scaling and duality 2−63518
$e^+e\text{-}\to W_0{}^\pm W_1{}^\pm$, colliding beams, one-photon process, determ. of total cross section 2−45979
e^+e^-, hadrons production, consequences of energy-momentum conservation 2−73764
e^+e^-, study of amplitudes for production of two and four charged pions by photons in low-energy region 2−52612
$e^+e^-\to$ hadron + anything, calc. of single particle distrib. in one-photon approx. from dual-resonance model 2−82685
$e^+e^-\to K^+K^-$, 1.18 to 1.34 GeV, cross-section 2−79510
$e^+e^-\to N+$anything colliding-beam reaction, parton dual resonance model 2−66931
$e^+e^-\to 3\pi$, high energy limit in Feynman graph framework 2−76603
$e^+e^-\to e^+e^-$, 1400-2400 MeV expts. at ADONE storage ring, confirmation of quantum electrodynamical predictions 2−73761
$e^+e^-\to e^+e^-e^+e^-$, calc. of differential cross section for two-photon annihilation contribution using new technique for Feynmann graph evaluation 2−73731
$e^+e^-\to h^\pm h^\mp$, exptl. obs. in 1400 to 2400 MeV range 2−59429
$e^+e^-\to h+$anything, conformal invariance and scaling 2−70163
$e^+e^-\to$hadrons, oscillations in total cross section 2−63520
$e^+e^-\to\gamma\to V$ (vector meson) quark model coupling constants 2−73834
$e^+e^-\to\gamma\gamma$, 1400-2400 MeV expts. at ADONE storage ring, confirmation of quantum electrodynamical predictions 2−73761
$e^+e^-\to\mu^+\mu^-$, 1400-2400 MeV expts. at ADONE storage ring, confirmation of quantum electrodynamical predictions 2−73761
$e^+e^-\to\mu^+\mu^-$, interference between weak and e.m amplitudes 2−42344
$e^+e^-\to\mu+\mu^-$ meas. of muon polarization as test of weak-interaction models 2−73762
$e^+e^-\to n\pi^+n\pi^-$ via 2 photons, total cross section calc. 2−42345
$e^+e^-\to\nu\nu\gamma$, 2 × 200 GeV, study of weak e.m. processes, radiative and higher order weak corrections to amplitude 2−42344
$e^+e^-\to p+$anything, asymptotic scaling function deduced from that for $e^-p\to e+$anything 2−45890

Electron pairs continued
annihilation continued
$e^+e^-\to\varphi\to K_l\to\pi^+\pi^-$, φ mass determination from pion ang. distrib. 2−59553
$e^+e^-\to\pi^+\pi^-$, 1.18 to 1.34 GeV, cross-section 2−79510
$e^+e^-\to\pi^+\pi^-$ (KK), influence of two photon terms on cross section 2−73763
$e^+e^-\to\pi^+\pi-\pi^0\pi^0$, 990 MeV, cross section meas. at Orsay Storage Ring 2−66943
$ee\to ee\pi\pi$ colliding beam expt., meas. of even partial-wave π-π phase shifts 2−63608
γ, timelike statistical constituent model 2−63519
π production and boson resonance with spin J, validity of vector-meson dominance model 2−70230
$\rho\omega$ mixing 2−59552
(AgBr + AgCl(5%)):$C^{5+}(N^{5+})(O^{6+})(S^{6+})$ high energy implantations, Doppler broadening of positron annihilation photons 2−71507
AgCl:$C^{5+}(N^{5+})(O^{6+})(S^{6+})$ high energy implantations, Doppler broadening of positron annihilation photons 2−71507
Al-(1.7 at.%) Zn, positron- annihilation study of vacancy-impurity binding energy53727 2−53727
Al, positron and dislocation binding 2−83977
Al, positron lifetimes and trapping probabilities at vacancies and dislocations 2−44010
Al_2O_3, positron lifetime spectra, temp. depend. 2−75003
Cd, positron angular distributions using positron wavefunctions with proper crystal symmetry 2−80942
Co-Al alloy, near equiatomic, conc. depend. of relative probability 2−77804
Cu-Al alloy, α-phase, position annihilation, Fermi surface obs. 2−64888
Cu-Ge(Ni)(Zn) dil. alloys, rel. to vacancy-impurity complexes 2−47398
Cu-Mn dil. alloys, neck effect in ang. correl. 2−44046
Cu, ang. correl., plastic deform. influence 2−51063
Cu, annihilation radiation, angular correl. 2−80968
Cu, liq. and solid, positron annihilation, ang. correl. curves 2−75004
Cu, plastically deformed, annealing temp. depend. 2−54123
Cu, positron angular distributions using positron wavefunctions with proper crystal symmetry 2−80942
$e^+e\text{-}\to\pi^0\gamma$, bound for cross section 2−45882
Fe-Ni alloy, invar, areas of Fe conc., positron annihilation obs. 2−80524
Fe alloys, γ-phase and α-modified compared 2−68325
FeRh, first-order antiferromag.-ferromag. transition, electronic struct. changes 2−84438
GaAs, positron lifetime spectra, temp. depend. 2−75003
He, positron elastic scattering, annihilation and positronium formation 2−42800
KBr, positron annihilation, electron density anisotropy and effective charge 2−54100
KCl:Ca^{2+}, positron annihilation, temp. and mag. field effects 2−77850
KCl, positron capture by colour centres, tempering effect 2−54092
KI, positron lifetime spectra, temp. depend. 2−75003
Mo, annihilation characteristics rel. to void size 2−71469
Mo, annihilation obs. of crystal defects, effects of voids 2−71468
Mo, surface electronic struct., positron annihilation study 2−54114
Mo, two-phonon ang. correl. and band struct. 2−71824
NH_4Cl, positron lifetimes, temp. depend., phase transitions influence 2−47772
Nb_3Al, density of states variation, positron annihilation obs. 2−47860
$Nb_3Al_xGe_{1-x}$, density of states variation, positron annihilation obs. 2−47860
Ni, ultrasonically treated, imperfections obs. 2−43612
$No_{(2)}$, positronium quenching rate, free annihilation rate 2−77070
Pb-Sn alloy, dependence of γ ang. correlation of positron annihilation on composition 2−71766
Pb single crystal γ-irradiated temperature dependence of positron annihilation spectrum 2−71767
Si, positron lifetime spectra, temp. depend. 2−75003
Zn, positron angular distributions using positron wavefunctions with proper crystal symmetry 2−80942
production
using alternating field in vacuum 2−82691
angular correlation detection, technique for meas. of γ-ray polarization 2−79645
atomic field screening effects at intermediate and high energies 2−83201
collision of laser beam with bremsstrahlung beam, determ. of intense-field mass shift of electron 2−66904
double/single pair-creation cross sections ratio for 6.6 MeV photons 2−76610
in electric field, variable, in vacuum, probability calc. 2−82632
film, multilayer, porous and nonporous, discrete frontal electron emission, ratio of pair production 2−68488
photoproduction, on nuclei, polariz. phenomena 2−70147
photoproduction on nuclei, Born-approximation analysis taking account of form factors of e.m. multipole moments 2−49782
$e^+e^-\to e^+e^-e^+e^-$ double pair production, colliding beam expt., cross-section meas. 2−82692
$pp\to ppe^+e^-$, for calibrating cross-sections in colliding p beams 2−45997
Pb, scattering of 40 MeV-120 MeV photons, cross section for electron pair production 2−67207

Electron paramagnetic resonance *see Paramagnetic resonance and relaxation*

Electron-phonon interactions
— 2−61204
alkali metals, rel. to anisotropic transport scatt. times 2−75014
alloy, concentrated strong scatt. disordered, elec. resist., temp. depend. 2−44049
alloy, dil., rel. to cond., Green function calc. 2−61219
anharmonic metal, solution of transport equations for coupled electron-phonon system in collision free regime rel. to sound propagation 2−43966

Electron-phonon interactions continued
anharmonic metal, solution of transport equations for coupled electron-phonon system in collision-dominated regime rel. to sound propagation 2−43965
anisotropy and spin effects of electrons and holes on phonon instability in a magnetic field 2−84180
anomalous, quantum transport and quantization of Bloch oscillations in strong elec. fields 2−61147
electron-hole-phonon quasiparticle bound states in strong mag. fields 2−68302
ferromagnet, itinerant, spin wave energy temp. depend., electron-phonon interact. influence 2−61498
ferromagnetic alloy, rel. to anomalous Hall effect 2−81223
film, semicond., transverse quantum galvanomag. effects rel. to elastic scatt. by optical phonons 2−64973
ionic crystals, plasma echo 2−44041
Ising magnet, compressible, spin-phonon interactions 2−72124
longitudinal optical phonon, coupled with Stark ladder electron, current charact. 2−68276
metal, alkali, Hall const. temp. depend. rel. to electron-phonon interaction anisotropy 2−57104
metal, anisotropic quantum fluctuations, rel. to linear magnetoresist. 2−57141
metal, monovalent, rel. to high temp. thermal resistivity 2−68258
metal, phenomenological model of superconductivity 2−57160
metal oxides, rel. to elec. cond., characts. 2−57106
metal-superfluid He interface, low temp. thermal cond. anomalies 2−54065
metals, theory of infrared divergence 2−48167
Mott expression, discussion 2−75009
Nb-Sn alloys, vacuum deposited, constants detn. and penetration depth of low freq. field 2−68365
noble metals, coupling and mass enhancements, pseudopot. obs. 2−51069
phonon- impurity centre-exciton bound states, theory of dielec. modes 2−68303
photoemissive yield, phonon energy loss effects, band-theoretic model 2−61460
piezoelectric polaron, simultaneous strong and weak coupling 2−84268
piezosemiconductor, u.s. second harmonic generation 2−51039
polar crystals, photon drag effect, generated elec. field 2−68274
polaron conductions from band to hopping types, Hall effect 2−84230
rare earth garnets, LnAlG and LnGaG, phonon induced electronic transitions 2−77786
self-consistent coupling construct., elastic consequences, supercond. applic. 2−57098
semi-metal, rel. to investigation of excitonic phase 2−64897
semiconductor, conf., Warsaw, Poland, July (1972) 2−68384
semiconductor, coupled system evolution in strong elec. field 2−61291
semiconductor, diamond-type, phonon induced quadrupole potential 2−71772
semiconductor, hot electron distrib. func. and energy losses on interacting with optical phonons 2−71894
semiconductor, polar, electron-hole interaction, effective mass eqn., optical phonon effects 2−68306
semiconductor, polar, electron-hole interaction, optical phonon interactions 2−68305
semiconductor, polar, oscill. struct. of magnetophonon effect, transverse config. 2−57179
semiconductor, rel. to many photon absorp. by carriers 2−84521
semiconductor, resonant coupling effects in magneto-optical props., many-body theory 2−68604
spin-phonon interaction, ground state 2−68272
superconductor, neutron scatt. spectral function reln. 2−71861
superconductor, with strong coupling, transition temp., rel. to energy gap 2−57158
symmetric contribs. to transport phenomena 2−47792
thermodynamics of crystals, book 2−43950
transfer phenomena in electron-phonon system in strong mag. field at low temp. 2−57100
transition metal oxides, role in metal-insulator transitions 2−57120
Urbach rule, unified mechanism 2−54430
Ag-Au-Cu alloy, rel. to sp. ht. 2−75051
Ag-Au alloy, rel. to sp. ht. 2−75051
Ag, elec. resist., evidence of phonon drag 2−64909
AgBr, photocarrier mobility electron-lattice interaction effects 2−81181
AgCl, photocarrier mobility electron-lattice interaction effects 2−81181
AgF, photocarrier mobility electron-lattice interaction effects 2−81181
Al, normal and supercond., u.s. attenuation obs. 2−81049
CdS, rel. to current stabilization 2−47891
CdS, resonant interaction of LO phonon and donor electron 2−68278
CdSe, resonant interaction of LO phonon and donor electron 2−68278
$Cd_{2.8}Zn_{0.2}As_2$, high mobility, scattering processes 2−81090
Cs, lattice vibration based on Toya's electron-phonon interaction 2−64834
Cu, anisotropy of electron-phonon renormalization 2−84256
Cu, magnetic surface levels and electron-phonon scatt. rate determ. 2−68290
GaAs, rel. to energy gap temp. depend. 2−80964
GaAs magnetic enhancement of acoustoelectric gain, obs. by Brillouin scattering 2−51034
GaSb, LO phonon scatt., rel. to photoelectromag. effect in quantizing field 2−68484
Ge, acoustoelec. effects, quadrupole and octupole electron phonon coupling 2−61101
n-Ge, Debye temp. rel. to carrier conc. 2−77772
Ge, effect on radiative recomb., 2-77K 2−68684
p-Ge, rel. to impurity scatt. of warm holes 2−44124
n-Ge, rel. to transverse magnetoresist. in quantizing mag. fields, calc. 2−71939
n-Ge, thermal magnetocond., electron-phonon scatt., doping effects 2−81084

Electron-phonon interactions continued
He, superfluid, hydrodynamic approx. approach to charge carrier scatt. by phonons 2−77459
K, rel. to r.f. size effect calc. 2−71835
K, umklapp processes in low-temp. thermal resist. 2−51061
K elec. conductivity calc., electron-phonon scatt., soln. of Boltzmann eqn. 2−71830
$KTaO_3$, Urbach's tail behaviour, unified mechanism 2−54430
n-Mg_2Ge, intravalley acoustic-mode scatt. 2−51143
Na, thermal cond., 40 to 360 K 2−57086
Nb, supercond., thermal cond. 2−47767
Nb_3Sn, high-T_c superconductor, tunnelling, phonon spectrum 2−81048
Pb-In dil. alloy, phonon spectra and supercond. parameters 2−47865
Pb-In dilute alloy, supercond., elec. tunnelling 2−54142
n-$Pb_{1-x}Sn_xTe$, rel. to hot-electron cond. 2−68407
p-PbTe, high field transport, current-field curves, mixed scatt. by phonons 2−81068
n-PgSe(Te), rel. to hot-electron cond. 2−68407
SbSI, paraelec. region, rel. to illumination effects on V-I characts. 2−81163
Si:P, phonon and electric field influence on extrinsic photocond. 2−81179
Si, acoustoelectric effects, quadrupole and octupole electron phonon coupling 2−61101
p-Si, rel. to impurity scatt. of warm holes 2−44124
Si n-channel m.o.s.f.e.t., electron mobility, electron surfon interact. calc. 2−51172
n-SiC, coupling const., Raman scatt. 2−51356
inSiO_2, three terminal electron Hall mobility measurements 2−54178
SiO_2 thin layer, rel. to hot electron energy losses, photoemission obs. in SiO_2/Si 2−81061
Sn-Cd dilute alloy, rel. to lattice thermal cond. 2−84295
$SrTiO_3$, Urbach's tail behaviour, unified mechanism 2−54430
Ta-Nb alloys, superconducting, sp. ht. and mag. meas. 2−71875
Tl, discrepancy between supercond. tunnelling and neutron scatt. data 2−84189
V_3Si, lattice stabilization in high magnetic fields 2−77869
Zn, anisotropy in the phonon limited resistivity 2−64919

Electron probe analysis
(U,Pu)C and $(U,Pu)_2C_3$, distribution coeffs. of U and Pu, microprobe analysis 2−67352
achondrites, Basaltic, microprobe analysis of pigeonites 2−58533
alloy, binary, interdiffusion coeffs. determ. 2−80719
alloy, quantitative, applic. of Monte Carlo calcs. 2−68830
bombardment, information gain aspects 2−60744
ceramics, textural studies by electron probe microanalysis 2−71411
ceramics, texture and phases in spark plugs, e. probe anal. and X-ray diffr. study 2−71390
computer applications 2−58823
computer applics. at Oak Ridge National Laboratory 2−64606
fundamental phenomena, Lewis' scatt. theory, Monte Carlo technique 2−80608
glass, glass-ceramics, using scanning electron microscope 2−60579
high spatial resolution x-ray analysis 2−81564
Kossel patterns, reading 2−64617
lattice constant determ., wide angle transmission method 2−56617
metal, correction for absorption and atomic number 2−65417
metal thin foils, solute concs., applic. of EMMA-4 2−56924
microanalysis, grazing incidence grating monochromator, description 2−63275
microanalyzer, electron probe X-ray, high resolution system 2−65411
microanalyzer, seven channel, design and performance 2−63274
microprobe X-ray analyzer, progress and developments 2−65410
periclase-chrome brick, empirical correction procedure for chromites 2−77663
photographic detail determ. by scanning electron microdensitometry 2−81553
polyethylene melts, thermal motion obs. from solid specimen spectra 2−80536
quantitative microanalysis, present state-of-art 2−48363
rarefied gas flows, density distrib. determ. 2−60343
reactor fuel, irrad., micro-analyzer problems 2−44510
reactor fuel elements, irrad., radiation background reduction methods 2−44511
refractory carbide/liquid metal contact interactions 2−68190
scanning, acceleration potential det. 2−63290
scanning electron microscope-probe analyser combination, use in examination and anal. of ceramics 2−71414
spherical aberration correction in electron microprobe by non axially symmetric elements 2−81560
steel, press. vessel type, radiation sensitivity, effect of impurities 2−53895
styrene-butadiene rubber mixture, electron microprobe study of chemical bond 2−64536
surface distribution of elements, analyzing system using electron probe microanalyzer 2−65412
thin films, network scheme of pulse height anal. 2−61830
thin films, quantitative analysis in EMMA 4 using block standards 2−81563
thin metal foils, quantitative analysis by ratio technique 2−81562
X-rays from crystals, dependence on crystal orientation 2−83943
Al_2O_3-ZrO_2-SiO_2 fused grain refractories, rebonded, characteriz. 2−53926
$As_2S_3(Se_3)$ cryst., photodecomp. products 2−51463
Au-Cu, quantitative microanalysis with combined electron microscope-microanalyser (EMMA-3) 2−81561
Au-SiO_2 r.f. cosputtered films 2−80576
BCl_3, diffused p-n junction mat. 2−44133
C-Fe film on Al, Zr, or steel reactor material, thickness determ. 2−44509
C film on Al, Zr, or steel reactor material, thickness determ. 2−44509
Ca-Si system, phase diagram determ. 2−71700
Cu-based alloy contamination by oxided nonmetallic inclusions, scale for point evaluation 2−84684
Fe-Ta alloy, ductility enhancement using allotropic phase change 2−57020
FeSi films, e microprobe analysis 2−77509

Electron probe analysis continued
at low operating voltage, problems in achieving analyt. accuracy 2—78213
MgO (001) single crystal with Fe deposit, LEED-AES system analysis 2—74612
NiFe films, e microprobe analysis 2—77509
O_2, CO_2 metastable ions detection, discharge glow 2—65402
Pd-V system, diffusion processes, phase obs. 2—53770
Si, p-n, minority charge carrier diffusion length meas. 2—44133
Ti-Ni-Cu alloy, homogeneity range 2—43858
$(U,Pu)O_2$ microspheres and pellets, sol-gel derived, microstructure studied by microprobe analysis 2—47610
U alloy, inclusions in relief in ion etched sample 2—56578
UC, oxidation in liq. Na with small O content 2—51452
Uo_2-PuO_2 mixed fuels, advanced characteriz. 2—52870

Electron probe microanalysis *see Electron probe analysis*

Electron resonance *see Cyclotron resonance; Paramagnetic resonance and relaxation*

Electron spin resonance *see Paramagnetic resonance and relaxation*

Electron states in solids *see Crystal electron states*

Electron structure of solids (crystallography) *see Crystal structure, atomic*

Electron structure of solids (energy structure) *see Crystal electron states*

Electron theory
see also Quantum electrodynamics
anomalous moment calc. through 4th order perturbation theory 2—82616
cohesive force, vibrations about equilibrium position 2—70157
in curved geometry, for Dirac particle near Schwarzschild black hole 2—41482
Dirac electron, dynamics in electromagnetic and uniform magnetic fields 2—55801
Dirac eqn. for electron interacting with plane e.m. field, algebraic soln. 2—82227
electron wave functions in strong e.m. field, quantized dimensions 2—82219

Electron theory of metals *see Crystal electron states; Metals/theory*

Electron traps
see also Crystal electron states/impurity states and effects
alkali halide, electrons trapped in edge dislocations rel. to mag. behaviour 2—81200
alkali halides, γ-irrad., aquoluminesc., energy levels of trapped electrons 2—43376
anthracene, dimer clusters as sites 2—75105
chalcogenide, amorphous film, thermally stimulated cond. 2—57189
dielectric, near interface with metal electrode, electron tunnelling rel. to dielectric loss model 2—47964
dielectric film, Poole-Frenkel pre-exponential factor 2—57217
hydrogen-bonded glasses, Frohlich polaron model for Compton electron trapping 2—44040
ice, KF and NH_4F doped and irradiated, role of F- in increased colouring 2—60823
ice, trapped electron, optical absorption spectra 2—75295
maleic acid, irrad., electron trapping centre obs. in single cryst. 2—78211
naphthalene crystals, trap density calc. using space charge limited theory 2—84325
poly N-vinylcarbazole, investigation of trap structure by thermally stimulated currents 2—54182
polyethylene, electron irrad., traps, thermally stimulated current obs. 2—83363
s-triazine isotopic mixed crystal, variable trap problem 2—75043
semiconductor, amorphous, localized state density, energy depend. determ. using field effect 2—47911
semiconductor, effect on acoustoelectric field 2—47746
semiconductors and insulators, amorphous, statistics, recomb. processes and photocond. 2—61290
space charge limited current, with coulombic trapping, trap filled limit 2—57183
Teflon, electron irrad., traps, thermally stimulated current obs. 2—83363
thermally stimulated conductivity, alternating current method 2—75113
Ag halides, grains, photographic sensitizing and desensitizing by electron traps 2—81023
AgBr reduction sensitization, effect of electron and positive hole traps 2—66862
As_2Se_3, trap density at Fermi level and high field cond. 2—68394
As_2Se_3 glass, rel. to high field conductivity 2—51134
CdS, rel. to relax. oscill. induced by laser irrad. 2—64979
CdS(Se)(Te) films, a.c. photocond. on excitation with intensity-modulated light 2—57255
CdSe, photoconducting, effect on acoustoelec. props. 2—61100
CdSe film, rel. to photoelec. props. 2—51212
D_2O crystals, pulse radiolysis at -150°C optical absorption spectrum of trapped electrons, visible and i.r. 2—48348
GaAs interface, n-type, model 2—65039
$Ga_{2x}In_{2(1-x)}$, thermostimulated cond. study 2—84317
He II rotating superfluid, obs. of single vortex lines, detection of trapped charge 2—53479
In_2S_3, thermostimulated cond. study 2—84317
$NaNO_3$, capture cross-section and trap. parameters, thermoluminesc. glow curve obs. 2—48257
SbSI, semicond. ferroelec., thermally stimulated photocurrent obs. 2—75154
Se, amorphous, kinematics of deep trapping 2—61344
Si, neutron irrad., divacancy obs. 2—48194
Si, neutron irrad., space-charge-limited current obs. of trapping and detrapping 2—51168
Si_3N_4-GaAs m.i.s. capacitor, insulator traps 2—77919
$Zn_2In_2S_5$ single crystal, rel. to photocond. relax. 2—75175
ZnS:Cu, Al, Br film, rel. to temp. depend. of electrolum. and thermal quenching 2—84533
ZnS:Cu, Pb, Cl film, rel. to temp. depend. of electrolum. and thermal quenching 2—84533
ZnS-Cu,Co,Cl, differences between optical and thermal depths 2—51395

Electron traps continued
ZnS, disappearance of electron traps under influence of pressure 2—61722
$ZnS_{1-x}Se_x$, thermoluminesc. rel. to stimulated cond. with persistent memory 2—75104
ZnSe, trapping and detrapping times, time of flight mobility obs. 2—44107

Electron tubes
see also Plasma diodes; X-ray tubes
beam flow disruption by drift tube wall radius changes 2—69866
channel electron multipliers, saturation current rel. to applied voltage, space charge saturation 2—74609
c.r.o. for balancing electrical-measurement circuits 2—41929
c.r.t. optical film recorder with optical feedback exposure control 2—42223
diode, high-current field-emission plasma instabilities 2—49325
double gap klystron, obs. of working range for ion beam bunching 2—45688
electron multipliers performance in field ion microscope atom probes 2—66723
image tube, development of Echelle spectrograph, optimization of optics 2—76543
intense relativistic beam device, impedance and spot-size meas. 2—63295
klystron, 50 kW, 2450 MHz, high efficiency 2—49329
LM-2, modified, Franck-Hertz experiment 2—69527
magnetron, c.w., dark current and electron energy spread obs. 2—49328
magnetron, natural oscillations of electron cloud 2—49326
magnetron amplifier frequency multiplying properties 2—59105
modulation transfer function of proximity focused image tube, effects of photon energy 2—52390
multicolour CRT phosphors, voltage-controlled, prep. and charact. 2—75329
photoelectronic image-brightness intensifier, multielectron noise and remanent gas pressure and composition 2—59273
residual gas sorption, using Ta getter, mass spectrometer obs. 2—76130
second generation image intensifiers, signal to noise ratio measurement 2—69882
space charge flow with unrestricted variation of current density and energy range 2—49324
spectroscope, patent 2—82816
spiral electron multiplier operation characts. for positive ions in atm. 2—66724
storage vidicon electrophotographic spectrum imager for visible spectrum 2—59345
TWT, coupled cavity, axially symmetrical, analytic expressions for interaction gap electric fields 2—69880
TWT, localized, effect in cutoff intermediate section 2—59106
vacuum gap, elec. characts., prebreakdown current, breakdown voltage, 4-300K 2—63294
$AgPO_3-X^{n+}(PO_3)_n$, $X^{n+}=Mg^{2+}$, Ca^{2+}, Sr^{2+}, Ba^{2+}, Pb^{2+}, Al^{3+} use for multichannel image convertors and amp. 2—68501
Be-Cu electron multiplier dynodes, cleaning and activation 2—82793
Cs plane parallel diode, work fn. determ., of Cs covered surfaces 2—61456
Cs plant parallel diode, work fn. determ. of Cs covered surfaces 2—61455
Cs thermionic diode, diffused electronic and ionic currents through grid type anode 2—45659
Si transmissive mode field emission array photoemitter, photosensitivity 2—81187

Electrons
see also Beta-rays; Cosmic rays/electrons; Crystal electron states; Noise/ electrical; Nuclear reactions and scattering due to/electrons; Photoelectricity; Plasma; Positronium; Positrons; Space charge
This heading includes both negative and positive electrons when the differences between them are of no special significance
in air, plasma, velocity distribution function 2—77262
anomalous gyromagnetic ratio, sixth-order contribution 2—63509
anomalous magnetic moments, quantum electrodynamics review 2—63471
bunches in dielec. waveguide, excitation of E_{01} wave 2—41931
drift velocity and characteristic energy, meas. method 2—64397
drift velocity in neutral gas under influence of uniform electric field 2—56382
electron-graviton vertex, low-energy e.m. corrections determ. using Feynmann graphs 2—76559
electron-ion oscillation discharge, potl. distrib., temp. and density detn. 2—64319
electron-muon mass doublet, lifetime of muon state 2—59422
energy loss meas. in 90-550 MeV region 2—66939
energy spectra in the magnetopause and magnetotail meas. using electrostatic analysers on satellite 2—62323
energy-loss cross sections, scattering in O_2 and CO continuum 2—83410
form factors up to fourth order 2—82612
form factors up to fourth order 2—82611
free trapped, spin polariz. detection in r.f. spectroscopy 2—79898
in Hulthen potential, solution of Schrodinger eqn. in SO(2,1) representation69596 2—69596
intense-field mass shift determ. from vacuum polarization on mass shell 2—66904
ionospheric electron temperature enhancement in wake of Explorer 31 satellite 2—54899
lepton-triplet prod. in Coulom field 2—79500
low energy flux in magnetosphere, midnight-dawn sector 2—62321
magnetic dipole moment, in ladder approx. 2—45880
magnetic dipole moment calc. in ladder approx. 2—73755
mass, meas. of increase with velocity, verification of special relativity predictions 2—55394
mass difference rel. to muons 2—76606
mass origin from study of lepton inner structure 2—49502
measurability of spin, reply to comments 2—82233
in neutral gases, drift velocity and runaway phenomena 2—46794
photon absorption in high magnetic fields 2—52306
radiative polarization in storage rings 2—70338
Rydberg, molecular autoionization, semiclassical theory 2—77032
solvated, polarization energy 2—46914

Electrons continued
solvated, spectra in methanol and ethanol, semicontinuum model applied to pressure effects 2—61807
solvated in ethanol, pressure effects on reaction rates 2—61812
spin, interaction with photons in presence of static magnetic field 2—52551
spin motion in magnetic mirror trap 2—45881
spin of free electron, measurability 2—70156
Thomson's e/m expt. using cathode ray tube 2—78730
trapping and solvation, optical absorption and e.s.r. meas. in ethanol glass at 4K 2—61810
Ne low-pressure discharge, tail of electron, energy distribution function 2—50229
absorption
see also Beta-rays/absorption
electron-photon showers caused by 50-400 MeV electrons and γ-quanta in Pb 2—67065
interactions
baryon resonance, electroproduction, form factors 2—55881
charged pion production, pseudovector pion-nucleon coupling 2—45952
coincidence electroproduction above resonance region 2—49503
deep inelastic electroproduction, sum rules, parastatistics 2—70158
deep-inelastic scattering, continuation to deep electron-positron annihilation 2—79504
electropeoduction of nucleon isobars in quark model 2—42423
electroproduction, connection with photoproduction examined from consideration of duality 2—59401
electroproduction, isospin and SU(3) equalities 2—49484
electroproduction, microcausality consequences for matrix element of $\langle p|[A(x)B(0)]|p\rangle$ commutator 2—76587
electroproduction, nonforward fixed mass sum rules 2—52559
electroproduction of N* in harmonic- oscillator quark model 2—52647
electroproduction processes, tests of hadron models 2—82679
electroproduction scaling function for protons and neutrons, Regge behaviour 2—63511
electroproduction sum rule, model independent deep inelastic 2—55821
energy transfer to electrons in fast proton collisions 2—55986
hadron electroproduction, violation of scale invariance due to contribution of cuts 2—63534
hadrons, inclusive production 2—70159
highly inelastic electroproduction, light-cone dominance in presence of singularities elsewhere in coordinate space 2—73754
inclusive electroproduction, single particle, scaling in dual model 2—42338
K-, L-shell electrons, single-quantum annihilations of positrons 2—76981
light-cone limit sequences in electroproduction 2—66940
meson electroproduction, survey of exptl. information 2—82694
neutrinoproduction, nonforward fixed mass sum rules 2—52559
with neutrinos, Population II stars 2—78459
nucleon isovector axial form factor 2—79509
pair electroproduction, vacuum polarization corrections 2—63474
resonance electroproduction, longit./transverse cross sections ratio, quark model 2—59546
stimulated emission due to electron moving in weak wave field 2—63311
vector meson electroproduction, simple diffraction considerations and relations between σ_t and slope 2—59548
$e^{\pm} + e- \to e^{\pm} + e- +$ hadrons, test for bilocal current algebra 2—49478
$ed \to e\Delta\Delta$, electromagnetic props. of $\Delta(1236)$ 2—82784
ee, C-even resonance production 2—82693
e^+e^-, intermediate boson production cross section calcs. 2—73832
$e^+e^- \to$ hadrons, oscillations in total cross section 2—63520
$e^+e^- \to \mu^+\mu^-$, weak neutral cureent obs. 2—76604
$e^{\pm}e^- \to e^{\pm}e^-W^+W^-$, total cross section determ. 2—79508
eN, as test for algebra of nonlocal operators 2—70109
eN, intermediate boson production cross section calcs. 2—73832
eN, parton description of forward peak as function of photon mass 2—79505
eN, vector meson dominance model 2—59406
$e^-N \to e^- +$ anything electroproduction, parton dual resonance model 2—66931
$eN \to e +$ soft pion + anything, SU(4) bilocal current algebra 2—73756
$eN \to e\gamma +$ anything, SU(4) bilocal current algebra 2—73756
$e\nu$, relativistic interacting particle system, asymptotic limit for speed of sound 2—66429
ep, vector meson prod., triple-Regge formulae 2—79494
e^-p, coincidence π^0 electroprod. in second reson. region 2—67015
$e^-p \to e +$ anything, analytic continuation of scaling function gives asymptotic scaling function for $e^+e^- \to p +$ anything 2—45890
$ep \to e'X(e'AX)$, applic. of dual parton model 2—63512
$ep \to e\mu^+\mu^-X$, test of algebra of bilocal operators 2—76582
$ep \to en\pi^+$, rel. to nucleon charge form factor determ. 2—42405
$ep \to ep\pi^o$, dispersion relation calc. of π^o production in resonance region 2—55851
$ep \to e\pi^+ +$ anything, inclusive pion distributions 2—70231
$e\pi \to e +$ anything, deep-inelastic, PCAC current 2—73758
μ pair creation via two-photon exchange in electron collisions, QED investigation 2—82684
π electroproduction near threhold, current algebra description 2—59525
π production, form factor 2—70225
πN cross section through extrapolation of deep inelastic electroproduction data 2—67021
ρ and decay to 2π 2—79601
$e^+e- \to \pi^0\gamma$, bound for cross section 2—45882
ionization
— 2—67686
atoms, excitation of characteristic X radiation, polarization determ. 2—76975
atoms adsorbed on W substrate, backscattering cross sections for K-shell ionization 2—79919
heterocyclic cpds., negative ion form. by electron interaction 2—80154
K-shell ionization cross sections for 2.04 MeV electrons for elements from Z=23-83 2—74204

Electrons continued
ionization continued
modulated electron beam spectrometer for ionization cross-section meas. 2—76456
tetracyanoethylene, negative-ion form. by electron bombardment 2—67687
Ar, outer s shell role in single ioniz. 2—67399
CO, C^- and O^- production by dissociative resonance electron capture 2—83415
CO_2, partial ioniz. cross sections by electrons (25-600 eV) 2—70979
CO_2 clusters, model for ionization cross section including energy losses inside cluster 2—80150
H, electron impact cross sections, correl. approx. modification 2—67422
H_2 clusters, model for ionization cross section including energy losses inside cluster 2—80150
He, collisional ioniz. by 250 eV electrons, ang. correl. meas. 2—83213
He, electron impact, ang. and energy distrib. of secondary electrons 2—64031
He, electron impact, excitation of autoionized $^3P^-$ states and resonance ionization, Fano's theory 2—79953
He, reson. ioniz. by fast electrons 2—67432
He, simultaneous excitation and ionization by electron impact, calc. of cross sections and nuclear charge dependence 2—79954
Kr, electron impact, ang. and energy distrib. of secondary electrons 2—64031
Kr, outer s shell role in single ioniz. 2—67399
N_2 clusters, model for ionization cross section including energy losses inside cluster 2—80150
Ne, outer s shell role in single ioniz. 2—67399
Xe, outer s shell role in single ioniz. 2—67399
radiation
see also Bremsstrahlung; Cherenkov radiation; Electrodynamics; Synchrotron radiation
bremsstrahlung spectra of irrad. diamond 2—49499
E_{01} wave, excitation by bunches passing through dielec. waveguide 2—41931
electrons, nonrelativistic, in single crystal, origin of oriented maxima in spectrum 2—80932
microwave frequency spectrum emitted by relativistic electron moving in spatially modulated magnetic field 2—66703
in nuclear emulsion, radiation length meas. 2—70164
oscillating charge, in inhomogeneous medium, perturbation theory 2—41917
oscillator, moving along interface, far zone fields, energy losses 2—41916
synchrotron, quantum-mechanical treatment 2—49320
synchrotron, second-order correction to first-order quantum mechanical treatment 2—82617
transition, generation by inclined flight through waveguide 2—41930
transition, generation by inclined flight through waveguide 2—41930
scattering
see also Atoms/electron scattering; Beta-rays/scattering; Molecules/electron scattering
100 MeV facility at University of Glasgow 2—55943
νe and νe, polarization effects 2—76602
ABFST model, ω-scale breaking as $q^2 \to 0$ 2—79503
backscattering by solid targets, 0.5-10 keV, rel. to angle of incidence 2—83855
backscattering from metal and dielectric foils, thickness det. 2—41921
coincidence electroproduction and scaling in the Regge region 2—63515
Compton, with laser photons 2—52435
Compton amplitudes, Regge behaviour and tests of complex scaling 2—59426
cross-section in ferromag. semicond. and metals, theory 2—81225
deep inelastic, approach to scaling and e.m. mass differences 2—49506
deep inelastic, on polarized targets, light-cone quark algebra 2—52584
deep inelastic electroproduction, hadron final-states 2—59423
deep inelastic electroproduction, single-particle distributions 2—70160
deep-inelastic, scaling properties 2—67044
elastic in an intense field, vacuum polarization corrections 2—63474
electron microscopes, electron scatt. effects on image quality 2—79002
electron-hadron, high energy, review 2—82678
electroproduction, deep inelastic, duality 2—59420
electroproduction of one particle, application of light cone expansion, generalization for many particle production 2—59421
film, electron elastic plural scatt. by atoms, intensity-angular distribs. 2—84220
of hadrons, quark mass and structure functions 2—73787
higher-order corrections, field-theories perturbation methods, for $e\text{-}\nu_e$, $e\text{-}\nu_e$ 2—79472
inelastic, radiative corrections in coincidence measurement 2—82683
inelastic, space-time phenomenology 2—55811
inelastic narrow-resonance approx. calc. using gauge-field theory of fermions 2—82623
metal surface backscatter obs. for 12.25 MeV oblique incidence 2—52389
microscopes, image resolution effects 2—79006
multiple, energy loss by ionization and excitation, knock-on, backscattering coeff. transmission coeff. energy spectra, simulation 2—80926
nucleons, relation between from factors in elastic and inelastic electron scatt. 2—70162
polarization effects, in gravitational field of rotating source 2—55381
scanning electron microscope, multiple inelastic scattering in channelling patterns 2—80936
scanning electron microscopy, electron probe microanalyzer, fund. phenomena Monte Carlo technique 2—80608
single-particle electroproduction at high energy in covariant parton model 2—55822

- **Electrons** continued
  - **scattering** continued
    - structure function, possible exchange degeneracy on light cone 2–55825
    - ed, at squared four momentum transfers of 1.0 and 1.5 $(GeV/c)^2$, neutron e.m. form factors 2–42418
    - ee, differential cross-sections using page geometry 2–55824
    - e^+e^-, Bhabba scatt., acoplanarity and radiative corrections 2–59424
    - $e^\pm e^- \rightarrow e^\pm e^-$, interference between weak and e.m. amplitudes 2–42344
    - ee → ee + hadrons, study of scaling behaviour in off-shell $\gamma^*\gamma^*$ scattering 2–45870
    - $e\text{-}\gamma \rightarrow e\text{-}n\pi^+ n\pi\text{-}$ deep inelastic process, calc. of differential cross section and photon structure functions 2–63514
    - $e\gamma$, inclusive soft pion production 2–42384
    - $e\gamma$ Compton scattering, calc. of spectral forms for invariant amplitudes to order e^4 2–76597
    - $e\gamma$ Compton scattering, polarized target, calc. of differential cross section to order e^6 and left-right asymmetry 2–76598
    - $e\mu$, invariant amplitudes and double dispersion relations 2–45884
    - eN, deep-inelastic, breaking of scaling behaviour in multi-triplet quark models 2–66949
    - eN, deep inelastic, parton model and ratio $\nu W_2^n/\nu W_2^p$ 2–70251
    - eN, deep inelastic expts., comparison with high-order Feynman diagram model for hadrons 2–42347
    - eN, deep inelastic region, partons, virtual photon mass parameters 2–70167
    - eN, deep inelastic region, role of one-pion exchange 2–45888
    - eN, deep inelastic scattering and geometric duality, virtual photon nucleon scatt. 2–42406
    - En, determ. of sum rules from triplet quark model light-cone algebra of currents 2–76708
    - eN, inelastic, scaling behaviour of structure function, parton model 2–82674
    - eN, inelastic scatt., proton data analysis 2–79506
    - eN deep inelastic, inequalities for structure function derived from quark parton model and quark model with neutral gluons 2–42329
    - eN deep inelastic, interpretation of exptl. data in proton model, Regge pole analysis 2–59427
    - eN deep inelastic scaling properties and bound state nature of physical nucleon 2–45991
    - eN inclusive electroproduction in target fragmentation region, consequences of light-cone dominance 2–79607
    - eN inelastic, connection between structure function of $eN \rightarrow e\gamma$ + anything and $N \rightarrow e$ + anything using Fritzch- Gell-Mann algebra 2–42340
    - eN inelastic, vector dominance and n/n ratio 2–82687
    - eN inelastic electroproduction, possible relation between prominent resonances and limiting scaling data 2–76608
    - eN inelastic structure functions, field theoretic models 2–66941
    - eN scaling of structure functions and compositeness 2–55823
    - en structure function calc. in leading logarithm approx. to perturbation theory and massive g.e.d. Lagrangian 2–73752
    - ep, inelastic, nature of scale-invariance breaking term determ. from DGS representation 2–59425
    - νe (νe),elastic, weak interaction of photons 2–55817
    - νe and νe scattering, anal. on assumption of ν-proton interaction 2–82680
    - νe forward scatt. amplitudes, sum rules 2–79498
    - $\nu_e e$-, search for reaction 2–45878
    - $\nu_\mu e \rightarrow \nu_\mu e$, amplitude of reaction in unified models, induced neutral current effects 2–70155
    - ω-scale breaking as $q^2 \rightarrow 0$, modified ABFST model 2–79503
    - π^0 electroproduction at first resonance at momentum transfers $q^2 = 0.6$, 1.0 and 1.56 GeV^2 2–73817
    - ρ^0 electroproduction, forward slope, application of dual-absorptive model 2–73837
    - Al, angular distrib. of inelastically reflected electrons 2–80551
    - Ar, backscattering of electrons, Monte Carlo simulation 2–70892
    - Cu, angular distrib. of inelastically reflected electrons 2–80551
    - Mo, angular distrib. of inelastically reflected electrons 2–80551
    - W, angular distrib. of inelastically reflected electrons 2–80551
  - **scattering, electron-proton**
    - Callan-Gross sum rule, rederivation from light-cone commutator 2–45889
    - Compton scatt., virtual, off forward direction, scaling limit 2–63510
    - cross section data, rel. to scale relation for proton form factors 2–55874
    - cross-sections longitudinal and transverse determ., magnetic dipole transition form factor 2–45887
    - deep inelastic, massive quantum electrodynamics 2–42341
    - deep inelastic, perturbation theory, connection with e^+e^- annihilation 2–52562
    - deep inelastic, two-photon exchange affects 2–73759
    - deep inelastic electroproduction, meas. of inclusive hadron momentum distribution 2–73777
    - deep inelastic light-cone analysis of soft-pion production 2–45954
    - elastic, large angle, parity violation 2–45885
    - elastic, phenomenological use of Callan-Symanzik eqn., obs. of scaling law 2–66922
    - exclusive scattering, Bjorken limit, scaling behaviour 2–42342
    - hadron electroproduction distribution, one photon exchange part, Regge behaviour 2–70171
    - inelastic, and single particle distribs. due to virtual phonon in dual reson. model 2–76607
    - inelastic, at small four- momentum transfers, test of finite-energy sum rules 2–45883
    - inelastic, comparison of differential cross section data with μp meas. at 12 GeV/c 2–66946
    - inelastic, generalized vector dominance, model 2–49505
    - inelastic, test for duality in current amplitudes 2–42343
    - inelastic structure functions in gluon model 2–63513
    - parton model, scaling behaviour 2–52560
    - radiative corrections to cross-section for small angle scattering when detecting recoil protons 2–66942
    - S-matrix, Fourier transform of elements, effect of light cone singularities 2–82650
    - spin dependent deep inelastic, light cone analysis 2–55826
    - structure function calc. in leading logarithm approx. to perturbation theory and massive g.e.d. Lagrangian 2–73752

- **Electrons** continued
  - **scattering, electron-proton** continued
    - structure functions, non-scaling corrections 2–49504
    - sum rule connecting resonance region of virtual Compton amplitude to deep inelastic region 2–70161
    - super-eikonal model, calc. of νW_2 structure function 2–63516
    - ep → ep + anything, t and q^2 dependence, triple-Regge formalism application 2–73757
    - $ep \rightarrow ep\rho^\circ$, yield of $p + \rho^\circ$ rel. to other hadron final states 2–63517
    - $ep \rightarrow e\pi^+ +$ anything, inclusive electroproduction 2–79502
    - $ep \rightarrow e\pi n\pi$, study of multiparticle final states using spectrometer with spark chambers 2–76738
- **Electrophoresis**
  - alumina, zero point of charge, temp. depend. 2–72567
  - biological cells and particles, det. from Doppler shift of scattered laser beams 2–79385
  - charged colloidal particles deposition, kinetics studies 2–68793
  - densitometer attachment for Unicam SP800 spectrophotometer for gel electrophoretic meas. 2–73680
  - glow discharges in gases and metal vapours review 2–84645
  - magnetite, zero point of charge, temp. depend. 2–72567
  - palygorskite colloid soln., zeta pot. rel. to stability 2–74567
  - paper electrophoresis separation of ^{141}Cs prior to γ-ray energies and half-life determ. 2–76812
  - pseudoboehmites in dil. nitrate electrolytes, point of zero charge 2–75390
  - Ar-He discharge, cataphoresis separation of constituents 2–77313
- **Electrophotography** *see Photography*
- **Electrophotoluminescence** *see Electroluminescence*
- **Electropolishing** *see Surface structure*
- **Electroproduction** *see Beta-rays/effects; Electrons; Nuclear reactions and scattering/due to electrons*
- **Electroreflectance**
  - band struct. analysis, review 2–72298
  - line-shape analysis 2–78090
  - modulation spectroscopy, optical and first-derivative, surface elec. field effects determ. 2–78089
  - semiconductor, effective mass eqn. for Wannier exciton examined 2–72320
  - semiconductor, local-field effects on line shapes, contact exciton effects 2–68618
  - $AgGaS_2(Se_2)$, band struct. study 2–75276
  - $CdSnAs_2$, $CdSnP_2$, band struct. obs. 2–81404
  - $CuInSe_2$, transitions from Cu of levels in valence band 2–80974
  - Cu_2O, electric field effects on excitons 2–51320
  - n-GaAs, flatband electrorefl. spectra, elec. field modulation 2–68623
  - GaAs reactor irradiation effect on the optical transitions 2–83976
  - $Ga_xIn_{1-x}P$ alloy, band struct. 2–61641
  - Ge, direct-edge electrorefl., curve fitting using one-electron theory 2–78091
  - Ge, heavily doped n- and p-type, Franz-Keldysh and electron-distrib. effects 2–51321
  - Ge, reactor irradiation effect on the optical transitions 2–83976
  - HgSe, $\Lambda_3 - \Lambda_1$ transition 2–68624
  - InP, n-type, spectrum shape under depletion and enhancement conditions in surface layer 2–81433
  - n-GaAs, 1.2-5.3 eV photon energy range 2–68619
  - Se reactor irradiation effect on the optical transitions 2–83976
  - Si, in m.o.s. struct., surface barrier obs. 2–65241
  - WSe_2, line shape of electroreflectance spectra 2–84510
  - $ZnSnAs_2$, $ZnSnP_2$, band struct. obs. 2–81404
- **Electrostatic generator** *see High voltage techniques; Particle accelerators/linear*
- **Electrostatic lenses** *see Electron lenses/electrostatic; Ion optics*
- **Electrostatics**
  - *see also Electrets; Electric charge; Electric fields*
  - boundary value problem, field between two spherical conductors, by H-function 2–45636
  - charge in fluidized bed, data on how charge may be lowered 2–50134
  - circular disc near plane containing aperture, capacitance 2–73496
  - circular discs, closely separated at equal potential, solution to boundary value problem 2–52346
  - contact electrification due to material separation 2–45640
  - cylindrical film, charged, bursting 2–52349
  - diagnostic radiography, e.s. imaging methods 2–69369
  - dielectric particle charging in vibrofluidized bed 2–53110
  - dielectric ring in uniform axial electrostatic field, exact and truncated solns. 2–58978
  - discharge of static from insulator surface 2–82390
  - electron optical systems, wide-aperture, design 2–76451
  - equations, transform, from Gaussian to International System of units 2–45607
  - equilibrium potential of magnetospheric satellite in eclipse situation 2–72933
  - external field of localized charge in unified field theory 2–76202
  - field computation, derivatives of elliptic integrals of the third kind 2–45232
  - field of ring electrets, application to state selection of masers 2–78955
  - gas-dust medium, meas. of shock relaxation time by electrostatic suspension system 2–46834
  - harmonic principle functions, applications 2–69844
  - ionic solns., diffusion of small particles, electrostatic effects 2–71250
  - ionospheric satellite, phase-plane solution 2–52348
  - machines, rotary electrostatic field meas. 2–52347
  - macroscopic bodies, Van der Waals forces, electrodynamic theory, fluctuation dissipation theorem 2–66679
  - mixed boundary value problem 2–45635
  - modelling of plane sources of neutrons 2–70500
  - oscillating electric field in absorbent dielectric medium, time-averaged Maxwell stress tensor 2–73495
  - parallel plate spectrograph for relativistic particles, optical props. 2–63691
  - potential distribution in uniaxial anisotropic layered media 2–59023
  - potential of plane, electrostatic field, estimation from above 2–76434

Electrostatics continued
precipitation, particle charging time 2−62142
precipitation techniques in cloud seeding 2−62191
probe for elastic surface wave meas. 2−63093
quadrupole energy filter with plane electrodes 2−82391
synchronous satellite charging in orbit rel. to magnetosphere 2−66025
tank filling operations, hazards due to generation and accumulation of electrostatic changes 2−69845
thin shell surface charging on external (deformational) loading 2−49234
van der Waal's forces between macroscopic bodies calc. 2−82170
Electrostriction
see also Piezoelectricity
dielectric plate, pure bending 2−65068
electromechanical filters, flexural waves, thin blades 2−52355
film, surface oxide, electromech., photomech. and conc. effects 2−51155
glass, rel. to self-focusing 2−75249
laser beam self-focusing simulation 2−65207
PbZrTiO$_4$ electrostrictive transducer material, fatigue testing 2−71625
SbSI, ferroelec., resonance method obs. 2−54240
Electroviscous effect *see Colloids; Viscosity*
Elementary particles
see also Baryons; Chirality; Energy loss of particles; Field theory, quantum; Hadrons; Leptons; Magnetic monopoles; Mass differences; Mass formulae; Nucleons and antinucleons; Nucleus; Particle detectors; Quantum theory; Quarks; Strange particles; Tachyons; and individual particles e.g. Electrons; Mesons
antimatter, expt. work, state-of-the-art 2−63481
book, current theoretical and exptl. topics 2−59383
book, semi-popular exposition 2−42308
Brandeis University Summer Institute lectures (1970) 2−63459
Brandeis University Summer Institute lectures (1970) 2−63461
collection of review articles, book 2−42310
conference, Fribourg, Switzerland [Sept. 1972] 2−60563
conference, Honolulu, Hawaii (1971) 2−49474
conference, Jerusalem, Israel (May 1972) 2−70340
conference on particle physics, Irvine, Calif., Dec 1971 2−59380
data analysis, computerised, software strategies 2−46029
definition as irreducible unitary representations of group of asymptotically flat space-times in general relativity 2−73737
empirical mass relation 2−73740
European Phys. Soc. conf., Wiesbaden, Germany (Oct. 1972) 2−76139
experimental developments in particle research 2−66905
experiments, Triangle Seminar (Budapest, Feb. 1972) 2−76575
machine recognition of patterns 2−82637
major problems of contemporary physics 2−42309
masses and magnetic moments, determ. using exotic atoms with small overlap orbitals 2−77027
meson factories, accelerators and experiments 2−82640
production in strong interactions, new model for particle multiplication 2−59391
research in high energy physics, computer applications 2−41422
spectroscopy, use of wide aperture multiparticle spectrometers with spark chambers 2−76737
Springer Tracts in Modern Physics 2−82639
tadpole model, faster-than-light inertial frames and interacting tachyons 2−78788
interactions
see also Field-theory, quantum/interactions; Nuclear reactions and scattering. Entries on interactions involving named particles are listed under the particles concerned, e.g. Mesons/interactions; Cosmic rays/effects and interactions
3 identical spinless particles with Yukawa potential, variational approach 2−73743
100 GeV and above, relations between energies of charged and neutral particles produced 2−73742
A + B → A + B, CPT invariance if particles are identical and crossing is valid operation 2−55803
advanced, existence theorem for differential equations 2−55806
Bethe-Salpeter spinor eqns., partial-wave analysis for single particle exchange 2−73724
boson boson → boson boson crossing equations and spin structure, construction of kinematically regular amplitudes 2−79483
boson boson-fermion fermion, crossing eqns. and spin structure, construction of kinematically regular amplitudes 2−79484
cluster decomposition approach to phenomenology of high energy inclusive and exclusive processes 2−42355
differential cross sections of direct and crossed reactions, new proof of asymptotic quality based on Meyman theorem 3 2−70130
diffraction dissociation, mechanism of kinetic coupling between momentum transfers 2−63488
eikonal formalism for multiparticle production 2−42319
exclusive processes, study of form factors, dimensionalities of operators, fixed singularities and Bjorken limit 2−66932
fermion boson → fermion boson, crossing eqns. and spin structure, construction of kinematically regular amplitudes 2−79484
fermion fermion → fermion fermion, crossing equations and spin structure, construction of kinematically regular amplitudes 2−79483
final-state, review 2−63487
formalism for description of ab → cde type reactions 2−76626
high energy, spectra, interpolation formula 2−70129
high energy collision systematics recent developments 2−76583
hypercharge exchange, peripheral production of resonances 2−76691
inclusive, application of analytic representations of conformal group and connection to distrib. on Minkowski space 2−52517
inclusive, kinematics and direct channel expansions in 1-particle and 2-particle processes, review 2−45862
inclusive cross-section sum rules for various kinds of particles in final state 2−49483
inclusive reactions in high energy multiparticle production phenomena, kinematics 2−45908
inclusive spectra and correlations, numerical calculation in phi^3 ladder model 2−52542
many-particle production, review 2−66915
models, exchange, resonance and duality types 2−52569

Elementary particles continued
interactions continued
multichannel processes, interdependence of reactions 2−63501
multiparticle production, angular distribution fluctuations, high energy collisions, bimodality 2−76589
multiparticle production at high-energy, Feynmann fluid analogy 2−66914
multiperipheral dynamics, behaviour of average multiplicity 2−45901
multiperipheral dynamics beyond models 2−76588
multiple production of secondary particles, meas. of angular distrib. for t-cut phase volume 2−70277
neutral particle production, missing momentum analysis 2−79522
pair production in e.m. field, particles with arbitrary spin 2−52543
quasi-elastic, below prod. threshold, unitarity eqn. 2−66913
s-channel resonant amplitude, real part 2−70131
statistical quantities for collision defined using analogy between phase-space integral in multiparticle collisions and in relativistic quantum statistics 2−42320
thermodynamics of multiple- particle production, remarks on paper by Wayland 2−49482
three particle final state, use of scatterplots 2−79527
two and quasi two body reactions, properties of pion exchange contribution 2−73779
two-body, production of three-meson resonances in relativistic Faddeev approach 2−76696
unitary statistical weight, SU(3) and SU(6) symmetry models 2−59385
vertex functions in convergent relativistic model theories 2−70132
interactions, electromagnetic
— 2−66917
arbitrary spin particles, calculations based on Weinberg equation 2−49485
chiral Lagrangian models, minimal coupling and nonlinearization 2−45864
finite theory of weak and e.m. interactions, correction to muon magnetic moment 2−66944
high energy interactions, neutral current and heavy lepton models 2−82641
inclusive processes, isospin and SU_3 equalities 2−49484
lepton number conserving and non-conserving 2−79477
particles with arbitrary spin, propagators and higher-order processes using Weinberg's equation 2−82651
renormalizable model of weak and e.m. interactions with CP violation 2−79489
renormalizable theories, mixing angle in SU(3) × SU(3) and SU(2) × U(1) models 2−49486
stellar energy-loss rates for neutrino pair production mechanisms calc. in Weinberg's theory 2−69071
structure functions in theory of weak and e.m. interactions, structure functions 2−82657
SU(2) × U(1), models of weak and e.m. interactions based on spontaneously broken gauge 2−79476
SU(3) × SU(3) symmetry violations 2−76590
unified model, weak and e.m. interaction symmetry 2−55809
unified theory of e.m. and weak, with broken gauge symmetry 2−70145
Unified weak and electromagnetic, without neutral currents 2−45861
weak and electromagnetic interactions, model 2−82652
Weinberg's model, calc. of static quantities of charged intermediate bosons 2−73744
Weinberg model, photon lepton scatt. and lepton mag. moment 2−59408
interactions, strong
see also Dual resonance model; Veneziano model
(3.3+) + (3+.3) symmetry breaking model in pole-dominance approximation 2−82710
baryon-antibaryon pairs and quarks, production, modified peripheral model 2−82711
broken symmetries of strongly interacting particles, recent developments 2−76583
chiral symmetry approach, relation to current algebra and PCAC 2−63489
Coulomb and strong interaction amplitudes expression for phase difference 2−45900
dynamical theory 2−42321
inclusive processes, isospin and SU_3 equalities 2−49484
inclusive reactions, kinematically corrected correl. functions 2−59389
inclusive reactions, polarization and spin effect 2−59390
Pade approximation applications 2−73291
production processes, new model for particle multiplication 2−59391
unitary multiperipheral models 2−82728
vector meson dominance model, applications 2−66916
interactions, weak
cosmological time dependence 2−73299
CP violation, neutral currents and weak equivalence 2−59393
CPT-violating model 2−63490
current, second kind, tensor constant 2−76591
current × current Lagrangian modification with nonpolynomial factor 2−73760
current theory, elementary outline 2−45866
currents of second kind 2−52718
divergence of weak parity-nonconserving NNP amplitude pion-pole dominance 2−82662
electromagnetic and weak interactions, model 2−82652
Fermi Lagrangian, Bogoliubov-Parasiuk-Hepp renormalization 2−59394
field theoretic models 2−59392
finite theory of weak and e.m. interactions, correction to muon magnetic moment 2−66944
heavy lepton concept., model of weak interactions 2−52556
high energy interactions, neutral current and heavy lepton models 2−82641
higher order with CP- invariance violating amplitudes, neutral K system 2−73801
higher-order corrections, field-theories perturbation methods 2−79472
inclusive processes, isospin and SU_3 equalities 2−49484

- **Elementary particles** continued
  - **interactions, weak** continued
    - lepton number conserving and non-conserving 2−79477
    - leptonic and semileptonic, lowest order V-A perturbation theoretic predictions 2−52555
    - leptonic and semileptonic processes, lepton-number and chirality non-conservation 2−45865
    - meson-dominance model for weak interaction Hamiltonian 2−73833
    - mesonic currents of second class 2−66993
    - model of weak and e.m. interactions based on O(3) × O(2) 2−66917
    - muon magnetic moment, weak contributions calc. in theory of weak and e.m. interactions 2−49510
    - parity-nonconserving $\Delta S=0$ nonleptonic processes in presence of second class currents 2−82656
    - quarks, scalar coupling and kaon decay parameters 2−59510
    - renormalizable model of weak and e.m. interactions with CP violation 2−79489
    - renormalizable theories, mixing angle in SU(3) × SU(3) and SU(2) × U(1) models 2−49486
    - reviews of work 1965-72 2−63491
    - scalar-boson-mediated theories, test in high-energy ν-scattering processes 2−82682
    - stellar energy-loss rates for neutrino pair production mechanisms calc. in Weinberg's theory 2−69071
    - structure functions in theory of weak and e.m. interactions, structure functions 2−82657
    - SU(2) × U(1), models of weak and e.m. interactions based on spontaneously broken gauge 2−79476
    - SU(3) × SU(3) symmetry violations 2−76590
    - theories, review 2−42322
    - unified model, weak and e.m. interaction symmetry 2−55809
    - unified theory of e.m. and weak, with broken gauge symmetry 2−70145
    - Unified weak and electromagnetic, without neutral currents 2−45861
    - vector coupling const. for beta decay 2−59395
    - Weinberg's model, calc. of static quantities of charged intermediate bosons 2−73744
    - Weinberg's theory, higher order weak and e.m. connections to strangeness-conserving β decay 2−79518
    - Weinberg's theory of interactions in unitary gauge, renormalization, higher-order corrections to leptonic processes 2−79497
    - Weinberg model, applic. to $\nu_\mu + p \to \nu_\mu + p + \pi^0$ 2−59417
    - Weinberg model, photon lepton scatt. and lepton mag. moment 2−59408
    - Weinberg model applied at nonzero temps. 2−70133
    - $e^+e^- \to \mu^+\mu^-$ meas. of muon polarization as test of weak-interaction models 2−73762
  - **scattering**
    - *see also Regge poles and trajectories*
    - — 2−70140
    - amplitude bounds, high energy, backward scatt. t-channel singularities estimation 2−76593
    - amplitude expansion in transverse- momentum plane 2−70135
    - amplitudes, in Bloch-Nordsieck model field theory 2−76573
    - amplitudes at physical Landau singularities, algebraic factorization 2−49489
    - amplitudes with positive imaginary part, lower bound problems for elastic cross-section 2−70137
    - analytic continuation of amplitudes determ. by iterative resolution of usual dispersion relation and inverted one 2−59396
    - Ball-Pinsky variable, physical interpretation 2−45868
    - bounds on deep inelastic structure functions for virtual photon and neutrino reactions 2−55872
    - Callan Symanzik eqn., phenomenological use 2−66922
    - charged centres, long-range coulomb pot. 2−62976
    - Compton and deep-inelastic, analysis of finite-energy sum rules using Regge-pole model including cuts 2−63494
    - cut to cut extrapolations and weighted dispersion relations 2−42295
    - deep inelastic processes, application of canonical light-cone commutators 2−59397
    - deep inelastic structure functions calc. from infinite component wave eqn. 2−55871
    - deep inelastic with fixed states, scaling 2−59421
    - diffraction scattering of charged particles, quantitate criteria for transfer and Fresnel scattering 2−63859
    - diffraction slopes, high energy, Chou-Yang model 2−49488
    - diffractive dissociation of composite particles, proton model 2−70138
    - elastic, of slow particles, due to long-range potential 2−76580
    - elastic amplitudes, derivation of finite energy bounds 2−70139
    - elastic processes, s-channel helicity conservation 2−55840
    - error-affected data, bias-free method for detecting bound, antibound and resonant states 2−45867
    - extragalactic X-ray sources, Compton scattering of electrons and photons rel. to extended and compact sources 2−51798
    - forward and backward, in eikonal approximation 2−66918
    - forward scattering amplitude, analyticity and integral equations 2−59388
    - four-fermion amplitude free from kinematical singularities 2−59399
    - free particle system, kinematical symmetry 2−82665
    - Glauber's multiple diffraction theory, S-matrix approach 2−73746
    - Glauber approx., relationship with Watson multiple scattering theory 2−52544
    - heavy ion, inverse problem, connection between parametrized phase-shift and optical-potential models 2−73747
    - helicity amplitude expansion in terms of unitary representations of the Lorentz group 2−55810
    - helicity amplitudes, Fourier-Bessel transforms 2−70136
    - high energy bounds, derivation from low energy data 2−59398
    - identical particles, unitarity and K-matrix solution to inhomogeneous eqn. method 2−63492
    - impact parameter represents. for scatt. amplitude 2−73745
    - Khuri amplitudes, light-cone behaviour 2−70122
    - Levinson's theorem, connection with singular integral equations 2−82606
    - multiparticle production, solvable relativistic unitary model 2−76592
    - multiparticle scattering function, derivation from field theory of basic discontinuity equation 2−66921
    - multiperipheral ABFST model, for $\gamma\gamma$ scattering 2−79496

- **Elementary particles continued**
  - **scattering** continued
    - multiple, high energy collision, comparison of approximate methods 2−49494
    - multiple-production processes, impact parameter formalism 2−76581
    - n-point functions, IU(3.1) invariant analytic extensions, analyticity domains 2−76563
    - N/D solution, singular power potentials and singular Yukawa potentials 2−59400
    - partial-wave transition amplitude, off-shell extension, Marchenko approach 2−79486
    - potential, resonance and phase shift calc. using Pade approximation theory 2−49019
    - quasi-eikonal approximation and scattering amplitudes 2−70134
    - quasi-elastic scattering amplitude, negative energy time-like states 2−49487
    - in relativistic field theory, of charged particles 2−73722
    - spin 0-spin $^1/_2$, unitarity bounds 2−49493
    - standard free air chamber effect of beam path length on photon scatter correction in low-energy X-radiation meas. 2−55907
    - sum rules, constraints of helicity amplitudes from analyticity, crossing symmetry, unitarity 2−52545
    - three body problem, amplitudes, Hilbert-Schmidt expansion 2−66920
    - three-body, application of method of moments 2−73748
    - three-body, unitary parametrization 2−63495
    - three-body problem, Faddeev−Lovelace equations in eikonal approximation 2−70348
    - three-particle production, relation with coupling constant in S-matrix theory 2−52546
    - total cross- section, relation to diffraction peak of elastic scattering 2−66919
    - two-body, dispersion relations in transverse momentum for fixed s 2−49491
    - two-body processes, high energy, charge independence restrictions 2−49492
    - two-body scatt. amplitude, normal threshold approx. to analyticity and Mandelstam represent. 2−76594
    - two-channel problems, coupled form factors 2−79485
    - unequal-mass amplitude, expansions in terms of Poincare representations and complex ang. momentum at zero energy 2−42323
    - vector particles, current conservation 2−49490
  - **symmetry**
    - *see also CPT conservation; SU(n) theory*
    - (3, 3) model, consistent soln. to K_{l3} problem 2−82747
    - (8,8) chiral symmetry model, dimensionality of δ 2−49481
    - (8, 8) chiral symmetry breaking parameter determ. from spectral-function sum rule 2−63484
    - ABFST model, ω-scale breaking as $q^2 \to 0$ 2−79503
    - baryons, ladder U(6,6) symmetry, classification and mass formulae 2−45990
    - book, chiral dynamics 2−82667
    - book, symmetry principles in particle physics 2−82666
    - boson boson→boson boson, crossing equations and spin structure, construction of kinematically regular amplitudes 2−79483
    - boson boson-fermion fermion, crossing eqns. and spin structure, construction of kinematically regular amplitudes 2−79484
    - breakdown, spontaneous in neutral gauge and scalar field interactions 2−82633
    - breaking, possible origin 2−55805
    - breaking for two-body processes energy dependence 2−79514
    - broken, applic. of effective Lagrangians, review 2−63462
    - broken scale invariance, applications 2−42317
    - broken scale invariance and mass-dispersion relations 2−66911
    - broken symmetries of strongly interacting particles, recent developments 2−76583
    - Callan Symanzik eqn., phenomenological use 2−66922
    - chiral approach to strong interactions 2−63489
    - chiral Lagrangian models, minimal coupling and nonlinearization in presence of e.m. interaction 2−45864
    - chiral SU(2)$\otimes$SU(2) symmetry, nonuniqueness of effective Lagrangian, $\pi\pi$ and πN interactions 2−45845
    - chiral SU(3) × SU(3) mass breaking, effect of 'weighted' linear transforms 2−49480
    - chiral symmetry (8,8) model for meson-baryon scatt., σ-terms 2−45928
    - chiral symmetry breaking, W-parity, octet dominance 2−73739
    - conformal, in single-meson production processes 2−63612
    - conjugation symmetry of baryon number and lepton number 2−76701
    - de Sitter space-time and harmonic oscillator 2−63016
    - dual models with SL(2,C) symmetry 2−73786
    - dual resonance model, assignment of spin and internal symmetry to external particles 2−63560
    - dually charged particles and dual invariance, classical description 2−52539
    - dynamic and algebraic, review 2−63485
    - fermion boson→fermion boson, crossing eqns. and spin structure, construction of kinematically regular amplitudes 2−79484
    - fermion fermion→fermion fermion, crossing equations and spin structure, construction of kinematically regular amplitudes 2−79483
    - free particle system, kinematical symmetry, geometric approach 2−82665
    - gauge symmetry, spontaneously broken, convergence of lowest order $\gamma\gamma$ scatt. 2−70145
    - hadronic internal, effect of weak interactions on breaking 2−63535
    - hadrons, classification in ladder U(6,6)-symmetry scheme 2−63527
    - hadrons, internal symmetry breaking, mathematical characterisation 2−45894
    - hadrons, weakly broken subsymmetries 2−66952
    - hypothesis of threshold dominance in renormalized linear SU(2) × SU(2) σ model 2−66912
    - isotopic symmetry violation in $\pi N \to \omega(N,\Delta)$ 2−63615
    - Lie theory and Lauricella functions 2−62974
    - mass formulae for resonances with identical strangeness, parity, ordinary and isotopic spin 2−73741
    - meson-baryon total cross sections, comparison of Johnson Treiman Banger Rubic symmetry relations 2−66963
    - n currents, covariant time ordered products 2−45857

Elementary particles continued
symmetry continued
nonrelativistic composite elementary particles and conformal Galilei group 2—82655
O(4), X-particle interpret. 2—55844
O(n) relations for coupling consts. and space-time dimens. in dual models 2—79540
oscillator algebra represent., SO(3,2) 2—66907
Poincare noninvariance of stigma eqn., an alternative to Dirac eqn. 2—42331
relativistic quark model, symmetries and nonsymmetries 2—79517
s-channel helicity conservation in ABFST multiperipheral model 2—42398
scale invariance and scale breaking 2—42316
scaling law conformally covariant description 2—82637
SU(3)×SU(3), chiral, weakly broken subsymmetries 2—63532
SU(3)×SU(3) spontaneous breaking, mass relations and particle mixings 2—66910
SU(3) σ model of $0^{\pm}$ fields, effects of adding $1^{\pm}$ gauge fields, chiral and scale symmetry breaking 2—79469
$U_{n,1}$ and IU_n representation matrix elements, props. 2—82164
U(6,6)⊗O(3,1) peripheral absorption model and production of the $5/2^+$ nucleon resonance 2—55882
U(6,6)⊗O(3,1) peripheral absorption model for production of 2^+ and 1^+ mesons 2—55863
U(6,6) symmetric kinematic factors, combination with generalized Veneziano model, application to $K^-p \to K^{*-}\pi^+n$ 2—67010
unified model, weak and e.m. interaction symmetry 2—55809
unitary, appls. in high energy scatt. 2—42361
unitary groups, symmetric tensor operators 2—62973
unstable particles, time reversal 2—66908
W-parity, octet dominance and breaking of chiral symmetry 2—66909
A_1 isomultiplet, dynamic chiral symmetry and cancellation of divergences in mass differences 2—52628
$\Delta I=1/2$ rule and $K \to \pi\pi$, electromagnetic effects 2—79559
ep, inelastic scattering, nature of scale-invariance breaking term determ. from DGS representation 2—59425
$\eta' \to \eta\pi\pi$, breaking of scale symmetry 2—55866
KN scattering, chiral symmetry braking 2—49554
ν scattering, current algebra sum rules and scale dimension of chiral symmetry breaking Hamiltonian 2—55818
νN scattering, dimension of symmetry breaking Hamiltonian 2—42336
π isomultiplet, dynamic chiral symmetry and cancellation of divergences in mass differences 2—52628
ρ isomultiplet, dynamic chiral symmetry and cancellation of divergences in mass differences 2—52628

theory
see also Form factors; Sum rules
angular correlation theory for double reson. prod. 2—45863
arbitrary spin, generalized multipole parameters by ALGOL 2—42315
bounds on deep inelastic structure functions for virtual photon and neutrino reactions 2—55872
broken scale invariance, applications 2—42317
canonical light-cone commutators, application to deep inelastic processes and derivation of sum rules 2—59397
causality violation in the motion of high spin particles in an e.m. field 2—82664
charged-particle multiplicity distributions, predictions for higher moments 2—70128
chiral invariant scale breaking part of Hamiltonian density, dimensionality 2—49481
chiral tensors and axial charge 2—76585
conformal invariant theory, construction of 2, 3 point functions from quark diagram 2—70163
covariant field theory 2—52522
current commutators and Khuri amplitudes, light-cone behaviour 2—70122
deep inelastic structure functions calc. from infinite component wave eqn. 2—55871
Dirac particle, geometrodynamical charge in curved geometries 2—41482
dual N-point functions in PGL(n-2,C)- invariant formalism 2—49477
duality in the proton model of hadrons 2—59441
dually charged particles and dual invariance, classical description 2—52539
flux loop model quantized 2—73772
form factors, consistent resonance dominance, using sidewise dispersion relation 2—70121
Gell-Mann formula restricted to pseudo orthogonal algebras 2—42313
gravitation propagator, potentials, gauge transformation 2—45855
identical particles with crossing, CPT invariance of $A+B \to A+B$ reaction 2—55803
invariant mass spectrum of Dalitz pair, radiative corrections 2—55807
invariant tensors in SU(3) constructed in terms of λ matrices 2—49479
lepton number conservation, test proposal 2—73749
Levinson's theorem, connection with singular integral equations 2—82606
Lie algebra common to dual models, current algebra, dynamical groups, gauge groups 2—45854
local saturation of commutator matrix elements 2—59356
longitudinal phase space, volume 2—63479
low-energy theorems, nonperturbative evaluation of anomalies, applic. to $\pi^0 \to 2\gamma$ decay 2—45856
mass formulae for resonances with identical strangeness, parity, ordinary and isotopic spin 2—73741
mass quantization theory where different particles are regarded as excited positive-energy states of fundamental extensible object 2—45860
mass splitting in relativistic SU(3) 2—76584
matrix elements of permutation group, calc. in 'trees' basis 2—63483
microcausality consequences for matrix element of $\langle p|[A(x)B(0)]|p\rangle$ commutator 2—76587
multiproduction of distinguishable particles, solvable unitary model with cluster decomposition 2—82722

Elementary particles continued
theory continued
n-point functions, IU(3.1) invariant analytic extensions, analyticity domains 2—76563
optimized data extrapolation off the boundary of an analytic function 2—49475
optimized integral continuation methods 2—42314
Pade approximation applications 2—73291
Poincare group representations on functions of eigenvalues of Casimir operators 2—52045
polarizabilities from exotic atoms 2—67439
quantum numbers, algebraic approach 2—59384
radius, by general relativity 2—69567
relativistic equations for nonzero mass particles 2—58720
s-channel resonant amplitude, real part 2—70131
scale invariance and scale breaking 2—42316
scaling and resonances 2—76586
scaling function, continuation from deep electroproduction to deep electron-positron annihilation 2—45890
scaling law conformally covariant description 2—82637
strangeness-changing structure functions, light-cone relations 2—63493
three particle bound state equivalence, sufficiency of condition of vanishing renormalization constants 2—73708
two-component spin-$^1/_2$ wave equation, properties and connection with Dirac equation 2—59382
unstable particle, spin spectrum 2—42312
vertex functions in convergent relativistic model theories 2—70132
weak and electromagnetic interactions, model 2—82652
Wigner supermultiplet scheme, construction of basis states 2—52537

Elements
atomic coordination valency 2—80591
CNDO method for mols. with second row atoms, invariance 2—83225
cosmic origin and distribution of biologically important elements, conf., London (1968) 2—55001
E184, calcs. on influence of quantum electrodynamical effects on chemistry 2—49929
fifth period, e.u.v. spectra, energy levels 2—64001
light elements prod. and solar system origin 2—66141
nearest-neighbour distance rel. to quantum and atomic nos. and valence 2—47178
polymorphic transitions of the elements and system of structural types 2—71397
superheavy, in meteorites, attempted characterization 2—44973
superheavy, new, search for in secondary reactions in U 2—70379
superheavy, prod. and nucl. props. 2—59893
superheavy, with atomic number 114, search in nature 2—82837
transuranium, prod. and nucl. props. 2—59893

origin
see also Cosmology; Thermonuclear reactions
antimatter particles, expt. work, state-of-the-art 2—63481
expanding universe, proton-neutron concentration ratio at stages preceding element formation 2—51691
generalized Taub solution as Universe model 2—78428
light element production rel. to extragalactic cosmic rays 2—55003
mechanisms, review 2—58159
nucleosynthesis and formation of superheavy elements 2—84947
nucleosynthesis theory and formation of elements up to Fe group 2—72949
nucleosynthetic chronologies rel. to ^{146}Sm and p-process nucleosynthesis 2—51686
stellar, nuclear laboratory investigation 2—48695
Universe, from obs. of objects in Universe, book 2—55000
He, abundance in primordial matter 2—48647

relative abundances
atmospheric aerosols, Pasadena 2—51587
cosmogenic radionuclides in stones rel. to meteorite orbits 2—73097
CY Cygni, irregular variable star, spectrum and element abundances 2—78465
F131, star in galactic cluster M67, metal deficiency and reddening 2—84991
F90, star in galactic cluster M67, metal deficiency and reddening 2—84991
Fe abundances in evolved stars, det. from narrow band indices 2—66090
Galaxy, heavy element synthesis, separation of r- and s-process abundances 2—66052
He, in cosmos 2—72955
HR 465, identification of trace elements in Ap stars 2—75733
Johnstown meteorite, analysis of bulk composition of hypersthene achondrite 2—44972
K giant stars, metal abundances from synthetic stellar spectra 2—69083
lunar rare earths and liquid type and solid type materials 2—55122
magnetic star atmospheres, possible separation of elements 2—62498
metal abundances in galactic star cluster NGC 752 2—48723
rare earths in stellar systems, symmetric fission of superheavy nuclei as explanation of overabundance 2—54998
solar chromosphere, metallic abundances as function of height 2—55191
solar corona active region models and relative abundances rel. to soft X-ray emission and continuum fluxes 2—78628
solar coronal abundances and quiet Sun model from radio observations 2—78623
solar flares, He enrichments rel. to solar wind, He/H relative abundance measurements 2—55189
stars, late-type giants, metal abundances detn. from narrow band photometry 2—69051
stellar, nuclear laboratory investigation 2—48695
stellar nucleosynthesis, giant stars 2—66084
stone meteorites, elemental abundances for chondrites and achondrites 2—75930
Sun, e.u.v. quiet solar spectrum, emission measure and relative abundances for 10 elements 2—75943
superheavy nuclei, evidence for previous existence in solar system 2—62643
trace element profiles in Sargasso Sea, from Geosecs II test station 2—75471

- **Elements** continued
  - **relative abundances** continued
    - very heavy nuclei, overabundance accelerated by solar flares 2−76001
    - Al-Ir abundance association in L chondrites 2−73099
    - Am, in Ap star HD 25354, spectral obs. 2−72994
    - Ar excess in submarine basalts rel. to Earth-atmosphere evolution model 2−72689
    - Au/H ratio in Sun from spectral synthesis of λ3123 AuI line 2−44977
    - Ba abundance profiles in Pacific and Mediterranean sea water 2−75467
    - Ba concentrations at oceanographic stations Geosec I and III 2−75468
    - Ba profiles in southwest Pacific from Geosecs III station near Tonga 2−75466
    - C total content and abundance in Apollo 11, 12 and 14 lunar samples 2−78513
    - Ca/H ratio in solar corona from observations of Ca XV lines 2−55159
    - Ca surface abundance in high velocity A-stars, from Ca II 3933 Angstrom line 2−48702
    - Cm, in Ap star HD 25354, spectral obs. 2−72994
    - Eu in sunspots, high resolution spectral obs. 2−73135
    - Fe/H ratio from binary star observations, Mv(K) dependence in late-type giants 2−73036
    - Fe/Mg cosmic abundance ratio rel. to Type I carbonaceous meteorites 2−69175
    - Fe, in sun and stars 2−62748
    - Fe in sun and solar curve of growth 2−44974
    - Fe solar abundance det. from weak Fe I line λ5127.7 2−75944
    - Fe solar coronal abundance and electron temperature meas. during 1966, November 12 eclipse 2−76027
    - Ga, solar, spectrum synthesis 2−75946
    - H I, atomic, in globular clusters, upper limits 2−75783
    - He, in horizontal branch stars 2−75714
    - He, in solar cosmic rays 2−75971
    - He, in young O and B stars rel. to old hot subdwarfs in galactic halo and nebulae 2−81859
    - He, Kilauea Volcano S bank fumarole, content and significance 2−57742
    - He content of globular cluster, M92, subgiant luminosity function 2−55065
    - He solar wind relative abundance ratio rel. to solar activity 2−75975
    - Ir-Al abundance association in L chondrites 2−73099
    - K/Ar data rel. to origin of feldspar megacrysts in alkali basalt 2−54729
    - La in sunspots, high resolution spectral obs. 2−73135
    - ^{176}Lu and s-process nucleosynthesis 2−58158
    - Mn solar abundance determinations 2−55158
    - O/N_2 ratio in thermosphere rel. to density-temperature phase delay 2−65816
    - O/O_2 ratio in thermosphere rel. to density-temperature phase delay 2−65816
    - O atmospheric concentrations from OI 5577 Å line emission at auroral zone latitude 2−84890
    - O concentrations in Venus' upper atmosphere from O I 1304 and 1356 Angstroms lines intensity 2−78567
    - O in population II horizontal branch stars HD 86986, HD 109995, HD 161817 2−66095
    - O profiles in North Atlantic Ocean from Geosecs II 2−75413
    - O_2 Martian abundance upper limits and mixing ratio with CO_2 from photoelectric spectra 2−78550
    - Si and trace elements in seawater, in-situ analysis using synthetic fibres 2−75469
    - Sm in sunspots, high resolution spectral obs. 2−73135
    - Sr abundance profiles in Pacific and Mediterranean sea water 2−75467
    - Sr distributions in seawater profiles at oceanography test stations Geosecs I and II 2−75472
    - Th, in Ap star HD 25354, spectral obs. 2−72994
    - Ti/Fe ratio in A-type supergiant stars 2−62537
    - U-distribution in basaltic fragments of five lunar rock samples 2−75849
    - U, in Ap star HD 25354, spectral obs. 2−72994
    - W, in Ap star HD 25354, spectral obs. 2−72994
    - Xe, in terrestrial and extraterrestrial matter 2−66040
- **Ellipsometry**
  - barium behenate molec. film, ellipsometric study of optical constants and refractive index detn. 2−78064
  - barium margarate molec. film, ellipsometric study of optical constants and refractive index detn. 2−78064
  - biological systems, obs. of surface reactions by ellipsometry, review 2−69203
  - data analysis with small programmable desk calculator 2−42208
  - diffusion pump oil on Au mirrors, ellipsometric meas., simulation of space effects on optical surfaces 2−79431
  - ellipsometer with oscillographic presentation of pattern 2−66834
  - ellipsometric-electrochemical cell, surface film form. on Ti obs. 2−50510
  - exact first order ellipsometric calcs. range of applicability 2−42210
  - film, thickness and optical consts., calc. method 2−44339
  - film thickness and optical const. meas. method 2−47095
  - film with rough boundaries, ellipsometric parameters 2−79328
  - generalized, for surfaces with directional preference, application to diffraction gratings 2−79357
  - interferometry with elliptically polarized light beams, application 2−79359
  - metal, liq., optical consts. determ. 2−43359
  - metal deposits, optical consts. determ. meth. 2−79379
  - multiple null spacing 2−42212
  - plasma diagnostics, microwave interference polarimeter-ellipsometer for resolution of ambiguity of meas. between rotation and ellipticity 2−83557
  - polarimetry applic. to mag. reson. problems 2−78984
  - polarization characts. of scatt. radiation from diffr. grating, applic. to surface roughness 2−44343
  - randomly rough surfaces, Helmholtz Kirchhoff integral 2−73647
  - surface temperature measurement, in ultrahigh vacuum 2−76387
  - transmission, coupling effect of systematic errors 2−55743
- **Ellipsometry** continued
  - u.h. vacuum system, oil pumped, surface contamination, ellipsometric obs. 2−48941
  - u.h. vacuum system, oil pumped, surface contamination, ellipsometric obs. 2−48941
  - Hg, surface-induced vectorial optical props. 2−77436
  - Si, irrad. with 400 eV ions, surface damage, change in optical consts., ellipsometric obs. 2−47081
  - Si, surface cleaning by ion irrad., ellipsometric obs. 2−47082
  - W surface, Cs adsorption obs. 2−50550
- **Emission spectra** *see Luminescence; Spectra; X-ray spectra/emission*
- **Emissivity**
  - — 2−58969
  - Arctic Sea ice, aircraft meas. of microwave emission 2−81632
  - atmospheric, effective, under clear skies, contrib. of H_2O, CO_2 and O_3 2−51616
  - automatic meas. apparatus 2−52264
  - blackbodies, general analysis 2−78858
  - cavity radiators, det. by reflection meas. 2−41844
  - clouds, variation in i.r. 2−65738
  - conductor material, temp. distrib. in d.c. heated conductors, calc. 2−57054
  - cylindrical cavity, isothermal and diffusely reflecting function of inside radius 2−78939
  - directional, opaque surfaces, influence of surface roughness 2−55574
  - emission spectra by Fourier transform spectroscopy, 1000-2300°C 2−54086
  - flames containing Al_2O_3 particles, i.r. emission and temperature measurements 2−73468
  - ion source emission meter 2−76464
  - light source, incandescent, principles of electronic energy conversion to light 2−68439
  - lunar fines, total emittance as fn. of temp. 2−66152
  - lunar surface fields, thermal emission spectrum, wavelength depend. 2−58462
  - lunar surface layer, calc. 2−48763
  - Mars, thermal emission, Mariner 9 i.r. radiometer obs. 2−58498
  - measurement apparatus, high temps. 2−52265
  - metal, refractory, high temp. measurement 2−57077
  - metal layers on insulating substrates, low. temp., phonon emission 2−54084
  - metal ribbon with surface macrostruct., thermal spectral radiation 2−72309
  - moving radiometers, response when passing over field of varying emittance or reflectance 2−66637
  - nonmetallic materials, meas. at high temps. 2−55570
  - overlap emissivity of CO_2 and H_2O 2−57947
  - planetary atm. and lunar soil, generalized Kirchhoff's law 2−75854
  - quartz glass, integral normal emissivity meas. 2−54085
  - radiation thermometry, compensatory techniques for unknown variations in emissivity 2−73467
  - radiative thermal cond. meas. technique 2−51052
  - Rayleigh approx., absorption and emission cross sections of nonspherical particles 2−64477
  - sea foam at microwave freq. 2−65602
  - semiconductor, polycryst, laser-induced burst emission of i.r. radiation 2−61575
  - semitransparent materials, at high temps. 2−54069
  - thermal emission from a rough lunar surface, directionality 2−44915
  - thermophysical properties at high temperatures, conf., Turin, June (1972) 2−54035
  - thick plate, inverse methods of heat conduction 2−49181
  - Al film, integrated radiating power 2−74999
  - Al_2O_3/Al ribbon system, thermal spectral radiation 2−61629
  - Al_2O_3-Cr_2O_3-P_2O_5 coating, radiative capacity rel. to struct., 600-2000K 2−57087
  - Al_2O_3 particles, radioactive props., high temp. 2−78183
  - Au film on quartz, low temp., phonon emission 2−54084
  - CO_2, i.r. spectral emissivity data, comparison with total emissivity charts 2−83702
  - GaAs, split, negative differential cond., i.r. emission 2−61311
  - H_2O vapour, i.r. spectral emissivity data, comparison with total emissivity charts 2−83702
  - In film on quartz, low temp., phonon emission 2−54084
  - Mo, spectral radiance, 1000 to 2000K 2−64019
  - NaF slabs, for-i.r. emission assignment 2−61649
  - Nb, normal spectral, at melting point, pulse heating method 2−53487
  - O_2, compressed, 100 to 1000 K, Planck mean absorption coeff. 2−76391
  - Sn film on quartz, low temp., phonon emission 2−54084
  - Ta-10%W alloy, pulse heating obs., 1500-3200K 2−57069
  - $Tl_2SeAs_2Te_3$ glass, switching rel. to radiation emission 2−64981
  - W-Y_2O_3 two-phase system, black-body radiation 2−43875
  - W, as spectral emissivity standard 2−54087
  - W, high temp. total emittance 2−54083
  - ZrO_2, stable white pigment, for space environment 2−44799
- **Emulsions**
  - *see also Colloids*
  - coacervate formation by aerosol OT with NaCl 2−74570
  - with cond. dispersed phase, dipolar type Debye relax. 2−43408
  - dielectric relaxation in systems with dipolar Debye absorpt., Hanai formula 2−80490
  - electronographic emulsion, characteristic curve 2−42442
  - emulsifier particles in latex aerosol, detection procedure using shadowing of electron microscope grids 2−71249
  - flow behaviour, droplet-size distribution effect 2−50388
  - holographic, diffraction efficiency determ. using latent image technique 2−66786
  - i.r., for recording images 2−52501
  - photographic, effects of u.s. radiation, formation of impurity centres, mechanisms 2−70094
  - photographic, electric field effect as function of exposure conditions 2−72464
  - polydisperse, calc. of coagulation kinetics in electrostatic field 2−74572
  - PVC-filler composites, influence of fillers on dynamic mechanical props. 2−64792
  - restricted diffusion, pulsed n.m.r. obs., droplet size distrib. 2−74573

Emulsions continued
sound attenuation, theory and experiment 2−43395
stability, film thinning behaviour studies 2−60532
thermoplastic recording, local deformation due to ponderomotive forces 2−73235
thermoplastic recording layers with regular image element structure, optimum resolution 2−73236
u.s. wave scattering characteristics 2−71251
viscoelastic props., dynamic meas. by Weissenberg rheogoniometer 2−83817
water, dipolar Debye type relax., −40 to −15 degrees C 2−43409
water, dipolar type Debye relax. 2−43408
AgBr in gelatin monodisperse, r.m.s. granularity 2−66869
AgBr monodisperse photographic emulsions, development, fixing rate measurements 2−66870
AgCl emulsion microcrystals dichroism, spectral reversal 2−84470
Emulsions, nuclear *see Nuclear track emulsions*
Emulsions, photographic *see Nuclear track emulsions; Photographic materials*
ENDOR
see also Nuclear magnetic resonance and relaxation; Paramagnetic resonance and relaxation
π-radicals in soln., mechanisms for β-protons 2−71235
alkali halides, F-centre relaxed-excited state detection 2−53749
arsenates, H-bonded ferroelectrics, ENDOR and double ENDOR 2−68734
8-chloroquinoline, excited triplet states; optically detected ^{35}Cl and ^{37}Cl spectra 2−46518
dilute spins in solids, high resolution pulsed double resonance analogue Fourier transform spectroscopy 2−68752
DL-serine, X-ray irradiated, 153 to 340K, free radicals 2−75350
dynamically polarized spin system overhauser effect autostabilization of reson. conditions 2−84583
electric effects, review 2−68728
ferromagnet, dynamic effects of domain struct. 2−61488
free radicals in solution, temp. and conc. depend. 2−80480
galvinoxyl radical, g-factor, solvent effects 2−53064
high pressure cavity, F centre hyperfine interactions 2−82412
hyperfine coupling consts. for $S=1/2$ system, determ. of relative signs through e.p.r., ENDOR, double ENDOR 2−70674
imidazole free radical, determ. of hyperfine tensors for protons of H bond 2−65394
mechanism applicable to homogeneously broadened lines 2−55629
methanol glass at 77K, matrix ENDOR linewidths of trapped electrons 2−57402
methyl malonic acid, rel. to tunnelling sidebands of methyl group hyperfine structure 2−57389
2-methyltetrahydrofuran glass at 77K, ENDOR linewidth of trapped electrons 2−57402
molecular cryst., low symmetry, quantitative simulation and electron cross relax. 2−65354
noncrystalline solids, theoretical and exptl. spectra, molecular dynamics 2−65353
organic nitroxide radicals, quadrupole splitting obs. in liquid crystals 2−50103
paradichlorobenzene, excited triplet states, optically detected ^{35}Cl and ^{37}Cl spectra 2−46518
paraelectric crysts. of A-centre electrons, elec. field effects 2−78176
ruby, investigation of instabilities in e.p.r. behaviour 2−44436
ruby, photon echo-nuclear double reson. 2−61733
ruby, spin-echo modulation 2−47963
spectrometer, description and operation 2−63205
spectrometer, slow wave resonance system 2−82411
spectrometer description 2−82408
spectrum analysis, appl. of tensor operators 2−78156
1,2,4-triazole free radical, determ. of hyperfine tensors for protons of hydrogen bonds 2−65394
triple resonance technique 2−68734
Tutton salts, spin system dynamics obs. 2−84445
BeO, irrad., V_1 centre, hyperfine parameters 2−54498
CaF$_2$, ENDOR spectrum of U^{3+}-F- 2−84607
Cu(II) zeolites, meas. of enhancement of proton resonance line on saturation of e.p.r. at liquid He temp. 2−54517
Ga$_x$Al$_{1-x}$As, optical electron-nuclear reson. 2−61695
KCl, F′ to F centre conversion obs. 2−71529
KCl(Br), F-centre hyperfine interactions, press. depend 2−83986
KH$_2$AsO$_4$, X-irradiated in ferroelectric phase at 4.2 K, study of AsO$_4^{4-}$ centre 2−72469
KI, relaxed-excited state of F-centre, wave function determ. 2−68738
KMgF$_3$:^{53}Cr$^+$, of ^{53}Cr$^+$, hyperfine const., covalency depend. 2−68753
KZnF$_3$:V^{2+}, hyperfine interactions, ^{19}F study 2−75353
KcL, M centre triplet state, quadrupole interactions obs. 2−72533
La$_2$Mg$_3$(NO$_3$)$_{12}$.24H$_2$O, spin system dynamics obs. 2−84445
LiF(Cl), F-centre hyperfine interactions, press. depend 2−83986
NaOH ice glass at 77K, matrix ENDOR linewidth of trapped electrons 2−57402
^{29}Si data, assignment to lattice sites 2−61361
SnO$_2$, hyperfine interactions of ^{53}Cr and ^{57}Fe 2−48309
SrF$_2$, ENDOR spectrum of U^{3+}-F- 2−84607
Energy bands *see Crystal electron states/band structure; Metals/theory; Semiconducting materials; Semiconductors*
Energy gaps *see Crystal electron states/band structure; Semiconducting materials; Semiconductors; Superconducting materials; Superconductivity*
Energy levels *see Atoms/structure; Molecules; Nucleus/energy levels; Spectra*
Energy loss of particles
see also Channelling
in air of ^{210}Po α-parts, obs. 2−56433
alkali halide films, charact. energy losses by slow electrons 2−81532
anomalous straggling of α-particles in Al 2−49911
backscattered electrons, average energy loss fraction, empirical eqn. 2−64868
blocking dips in crysts., extended cut-off model 2−68261
charged particle collisions with atoms, stopping power 2−64026

Energy loss of particles continued
charged particles, energy loss by ionization, FORTRAN-4 computer program 2−64870
Cherenkov effect is alternating electric field in dielectric media 2−69822
chrysene, dielectric tensor components derived from energy loss spectra 2−81138
continuum potential from planar channelling 2−44006
crystal surface, low energy electron energy loss spectrum 2−50986
crystal surface, of low energy electrons rel. to surface phonons and gas surface interactions 2−50522
dielectric film, surface phonons and electron energy losses, metal contact influence 2−47829
dispersion of high energy charged particle beam in matter, multiple nuclear scattering effects, possibility of mass separation 2−82429
displacement cascades caused by elastic and inelastic collisions of charged particle in substance 2−44016
electron energy loss spectra, volume defect analysis 2−80654
electron energy loss spectrum meas. by electron microscopy and energy analyser, statistical analysis of errors 2−73524
electron energy spectroscopy, chemical analysis 2−81565
electron microscope, energy analysing, superposition effects 2−79015
electron ranges, Z-depend. and geometry effects 2−44017
electron spectrometry, low energy, book 2−41925
electrons, extrapolated range, generalized semiempirical equations 2−70281
electrons, high-energy passage through crystals, reduction of coherence area 2−54096
electrons, in 90-550 MeV region 2−66939
electrons, in collisions with photons in CTR 2−83100
electrons, in plasma 2−46723
electrons, scattering in O$_2$ and CO continuum, energy loss cross sections 2−83410
electrons in nucl. emulsion, radiation length meas. 2−70164
fission fragment ranges in U-Al alloys, UO$_2$, U$_3$O$_8$ 2−83028
fission fragment stopping in gases, kinetic energy deficit and energy distrib. width 2−63937
fission fragment stopping in gases, range distrib. 2−63936
group III-V semiconductor, characteristic electron energy loss, core levels detn. 2−65240
hydrocarbons, influence of mol. binding on alpha-particle stopping power 2−64869
inert gas ions on glass, 5.6 keV 2−61123
ion penetration profiles meas. in solids using (p,γ) reactions 2−61122
ion ranges in solids 2−74765
ion scattering from crystals, angular distributions 2−75005
ionization loss of heavy nuclei traversing matter 2−44015
ions, small-angle scattering from Ne and Ar target gases meas. of inelastic energy loss 2−64045
kV electron energy dissipation vs. penetration distance in high at. no. mats. 2−56634
lattice disorder profiles determ. by nucl. backscatt. 2−53689
magnetoplasma, collisional, e.m. radiation from test charge 2−46725
metal, stopping cross sections rel. to irrad. induced displacement cascades 2−53691
metal, thick target, protons scatt. by Pb, Ta, Yb, Ce, Ag and Mo 2−80928
metal films, fast electron energy loss in phonon spectral range 2−47828
muon local prod. underground, stopping rate meas. 2−82788
muons, stopping particles underground 2−59594
naphthalene vapour, electron energy-loss spectroscopy 2−80131
neutron absorpt. during slowing down, correl. between Resonance and Greuling Goertzel Approx. 2−42608
neutron displacement cross sections for stainless steel, Fe, Cr, Ni and Ta bases on Lindhard model 2−83053
neutron slowing down in infinite medium, generalized formulation 2−42607
nomograms for computing charge particle losses in absorber materials 2−56072
organic thin films, charact. energy losses by slow electrons at 77K 2−84669
oscillating charge, in inhomogeneous medium, radiation energy losses 2−41917
oscillator, moving along interface, radiation energy loss 2−41916
phenanthrene, dielectric tensor components derived from energy loss spectra 2−81138
plasmon energy loss shifts rel. to specimen contamination 2−80935
polystyrene slabs, finite, electron depth-dose distrib. meas. 2−61130
positrons, in plasma 2−46723
proton beam separation in CERN Proton Synchrotron 2−42483
protons, 66 and 100 MeV, fluctuations in energy loss in thin proportional counter 2−49634
protons, freq. distribution of loss after passage through tissue-equivalent materials 2−58624
scanning electron microscope, multiple inelastic scattering in channelling patterns 2−80936
shielding for ultrarelativistic muons, calc. of survival probability by Monte Carlo method 2−79845
slowing down spectra of secondary electrons in H$_2$O, Al, Cu 2−75006
solid, collective excitations, fast-electron spectroscopy, quantized formulation 2−68313
solid, inelastic electron scatt. by excitation of deep atomic levels, energy loss spectra 2−44012
steel, stainless, energy spectrum of slow monoenergetic reflected electrons 2−50441
stopping and straggling, moment theory bounds on mean energies 2−46496
stopping power, for proton and ion channelling 2−44014
stopping power mean excitation energy calc. for all elements 2−49922
stopping power of media for heavy ions, effective charge 2−54097
stopping power of pure metals for 25-250 keV H ions 2−47774
stopping powers of solids for 30-90 MeV ^{238}U ions 2−47773

Energy loss of particles continued
  straggling of moderately relativistic electrons due to inelastic scattering and bremsstrahlung 2−68266
  surface vibrational spectra, low energy electron scatt. theory 2−71706
  Vavilov distribution, difference between average and most probable energy loss 2−80925
  e beams, 10 keV-100 MeV, calc., in 59 elements, 55 compounds and soft tissue 2−54095
  Ag, 21.6 MeV I ions, axial channelling phenomenon 2−44007
  Ag, and Ag on Be, Auger electron ranges 2−71304
  Ag, ranges and range straggling of ^{150}Sm 2−68269
  Ag, stopping power for protons and deuterons at same velocity 2−54098
  Ag, stopping powers for ^{4}He, ^{16}O, ^{35}Cl at 1 to 3 MeV 2−80921
  Al, characteristic energy loss for low energy electrons 2−51091
  Al, characteristic energy loss 2−51091
  Al, range of ^{235}U fission fragments 2−61125
  Al, stopping power for 28 MeV α-particles 2−54099
  Al, stopping power for protons and deuterons at same velocity 2−54098
  Al (100) surface, LEED, elastic and inelastic scatt., bulk and surface plasmon excitation 2−50434
  Al thin absorbers, loss of protons 2−80924
  Ar, loss and straggling of 6.05 and 8.78 MeV α-particles meas. using Si surface barrier detector 2−79626
  Ar ions, meas. of range-energy relations in Ar, N_2, O_2 and air, 0.3-1.0 MeV 2−79917
  Au, electron energy loss spectra, surface plasmon excitation 2−44043
  Au, stopping power for 28 MeV α-particles 2−54099
  Au, stopping power for protons and deuterons at same velocity 2−54098
  Au, stopping powers for ^{4}He, ^{16}O, ^{35}Cl at 1 to 3 MeV 2−80921
  Au, Xe ion penetration 2−61124
  Be, and Be on Ag, Auger electron ranges 2−71304
  Be, range of ^{235}U fission fragments 2−61125
  Be, stopping power for 28 MeV α-particles 2−54099
  Bi films, charact. electron energy loss spectra 2−44044
  C, range of ^{235}U fission fragments 2−61125
  in CO_2, of ^{210}Po α-parts, obs. 2−56433
  CdS, electron energy loss spectra, rel. to interband transitions, bulk and surface plasmons 2−68318
  CdSe, electron energy loss spectra, rel. to interband transitions, bulk and surface plasmons 2−68318
  CdTe, electron energy loss spectra, rel. to interband transitions, bulk and surface plasmons 2−68318
  ^{252}Cf fission fragments energy loss in argon 2−59800
  Cs ions beam traversing Cs and near- thermal equilibrium plasma 2−43112
  Cu, and Cu on Ag, Auger electron ranges 2−71304
  Cu, dipole interactions and diffusion of μ^+ meson 2−57090
  Cu, range of energetic Xe ions 2−61126
  Cu, ranges and range straggling of ^{150}Sm 2−68269
  Cu, stopping power for 28 MeV α-particles 2−54099
  Cu, stopping power for protons and deuterons at same velocity 2−54098
  Cu thin absorbers, loss of protons 2−80924
  Ge, electron energy loss, determination of optical props. from loss function 2−71769
  Ge, electron spectroscopy of amorphous film at energy losses below 1 eV 2−80934
  Ge, stopping powers for ^{4}He, ^{16}O, ^{35}Cl at 1 to 3 MeV 2−80921
  in He, of ^{210}Po α-parts, obs. 2−56433
  K, on W(100), surface plasmon losses, energy loss spectra obs. 2−64903
  KCl:KI, films, slow electron impact, luminescence excitation and characteristic energy losses 2−81417
  KI films, slow electron impact, luminescence excitation and characteristic energy losses 2−81417
  $Li_2B_4O_7$, mass attenuation and energy absorption coeffs. for 1 to 150 keV photons 2−64871
  LiF, mass attenuation and energy absorption coeffs. for 1 to 150 keV photons 2−64871
  Mo, stopping power for 0.50-1.75 MeV protons meas. by backscattering method 2−64872
  Mo, stopping power for 28 MeV α-particles 2−54099
  ^{99}Mo, fragment from neutron fission of ^{235}U, range in W 2−47786
  N ions, meas. of range-energy relations in N_2 and air, 0.3-2.0 MeV 2−79917
  Na ions, meas. of range-energy relations in air, 0.3-2.0 MeV 2−79917
  Ni, stopping power for protons and deuterons at same velocity 2−54098
  Ni, stopping powers for ^{4}He, ^{16}O, ^{35}Cl at 1 to 3 MeV 2−80921
  Ni (111) surface, in Curie temp. region, band struct. changes 2−51267
  Ni(110), N or S adsorbate-covered, electron energy loss spectra, elastic scatt. 2−84222
  Pd film, low-energy electron beam transmission, orientation depend. 2−47787
  Pt, stopping power for protons and deuterons at same velocity 2−54098
  Rb, on W(100), surface plasmon losses, energy loss spectra obs. 2−64903
  Rh, stopping power for protons and deuterons at same velocity 2−54098
  Si, electron energy loss, determination of optical props. from loss function 2−71769
  Si, electron spectroscopy of amorphous film at energy losses below 1 eV 2−80934
  Si, range of ^{235}U fission fragments 2−61125
  Ta, stopping power for 0.50-1.75 MeV protons meas. by backscattering method 2−64872
  Ta, stopping power for 28 MeV α-particles 2−54099
  ^{132}Te, fragment from neutron fission of ^{235}U, range in W 2−47786
  Ti, stopping power for 0.50-1.75 MeV protons meas. by backscattering method 2−64872
  TlBr, electron spectra, optical constants detn. 2−61129
  TlCl, electron spectra, optical constants detn. 2−61129

Energy loss of particles continued
  TlI, electron spectra, optical constants detn. 2−61129
  ^{235}U fission fragment deceleration in light media 2−56013
  W, stopping power for 0.50-1.75 MeV protons meas. by backscattering method 2−64872
  W thick target, protons and α-particles 2−80928
  Y, stopping powers for ^{4}He, ^{16}O, ^{35}Cl at 1 to 3 MeV 2−80921
  ZnS, electron energy-loss spectra 2−75111
  ZnSe, electron energy-loss spectra 2−75111
  ZnTe, electron energy-loss spectra 2−75111

Enthalpy *see Thermodynamic properties*

Enthalpy measurement *see Calorimetry*

Entropy
  see also Thermodynamics
  bond entropy in activated complexes, calc. method 2−84638
  communal, theory 2−41539
  crystals, monatomic, of melting 2−53488
  decomposition, transfer matrix problems 2−41529
  definition for any state on C* algebra 2−73335
  density of large system at low temperatures, lower limits 2−55429
  dichlorofluoramine, calc. from spectroscopic data 2−60372
  fluid mixture, stagnation point flow effect on entropy variation rate 2−80162
  Gibbs paradox 2−66472
  Glansdorff and Prigogine's stability theory, ambiguities in entropy production 2−69617
  irreversibility and second law of thermodynamics 2−78943
  kinetic theory in closed rotating cosmologies, entropy production in collision time approx. 2−48648
  lunar rocks and minerals, following impact 2−51821
  maximum entropy spectra and maximum likelihood spectra relationship 2−54628
  mixing, nonideal solutions 2−45305
  mixing of ideal gases, asymptotic differential equation 2−83714
  non-Newtonian fluids, time-dependent and time-independent, rel. to generalised rheological equations 2−67559
  perfect gas, multidimensional simple wave flow and entropy 2−60342
  polyethyleneoxalate, polyethylenesuccinate, intramolec. contributions to entropy of fusion 2−46637
  polymer, matrix method of calc. for confined circular chain 2−60099
  product of entropies, mechanical analogue 2−66473
  production in irreversible processes and Liapunov function method. 2−76390
  radiation-matter interaction considerations 2−76222
  reactive molecular collisions, characterization of product energy distribs., information and entropy deficiency 2−54529
  simple materials, non equilibrium thermodynamic theory, single integral entropic functional 2−76257
  small-crystal, number dependence of entropy on crystal size and shape 2−68245
  small-crystal, number dependence of vibrational entropy 2−68244
  statistical, comparison with thermodynamic entropy 2−45310
  successive time derivatives, nonlinear BGK model 2−73336
  superconductor, entropy production density calc. using methods of thermodynamics of irreversible processes 2−77865
  thermal radiation, formulae derivation 2−58816
  in thermodynamics and information theory, not identical 2−76389
  Cs vapour, by statistical theory 2−50264
 properties of substances
  alloy, binary, config. entropy of mixing 2−43820
  B-2 type phase, rel. to disorder 2−43819
  cholesteryl esters, effect of substituent location at transitions 2−80452
  difluorocyanamide gas, calc. 2−71114
  dipolar of ionic crystal with paraelectric dipolar impurities for E‖[100], [110] and [111], E=applied field 2−57221
  eutectics containing compound phases, correl. with morphology 2−47600
  grain boundaries, computer calcs. 2−56727
  high-conductivity solid electrolytes, transport entropies 2−77961
  ice, low entropy form obtained from a linear step growth model 2−83906
  liquid metal, from ion-ion pot. effective interaction 2−60415
  metal, entropy of fusion, rel. to cryst. struct. 2−64506
  microcrystallite replacement entropy 2−68206
  α-Al_2O_3, anharmonic coeffs. 2−51047
  Au-Co alloys, nucl. spin entropy changes during ageing 2−43798
  Bi, phenomenological relationship between solid and liquid phases 2−74581
  CaH_2-LaH_3 system, entropy of solution 2−50958
  CrSi, $CrSi_2$, Cr_3Si, Cr_5Si_3, isobaric-isotherm. potl., entropy and heat of formation detn. by meas. galvanic e.m.f. 2−68246
  β-Gd_2MoO_4, from 0.4 to 4.2K along b crystal axis 2−51277
  β-$Gd_2(MoO_4)_3$, electrically polarized, 0.4 to 4.2K, up to 90 kG along a crystal axis, and heat capacity 2−44290
  He II, entropy transport by vortices, and second sound vel. modifications 2−64500
  ^{3}He, λ transition to ordered antiferromag. phase 2−56537
  ^{3}He, thermodynamic interaction functions 2−77462
  ^{4}He, thermodynamic interaction functions 2−77462
  $KH_{2(1-x)}D_{2x}PO_4$, excess entropy of ferroelec.-paraelectric phase charge increase with D conc. 2−84364
  LiBr, aqueous, equilibrium phases, entropy-temp. diagram 2−58942
  NaCl:Cd^{2+}, determ. of dissolution entropy of precipitates 2−83844
  $Ni_{3\pm x}Te_2$, transition behaviour, entropy of transformation 2−57068
  Rb, liquid, change with temp. and pressure, calc. from PVT data 2−71195
  $SOBr_2$, mol. parameters 2−56169
  Sb_2S_3, entropy of vaporization 2−74595
  TiC_xO_{1-x} solid solns., low temp. obs. 2−43989
  XeF_4, 5 to 350K, heat capacity, thermodynamic functions 2−80411
  ZnTe, entropy of melting, DTA determ. 2−47033

Epitaxy
  see also Crystals/growth
  — 2−56597
  bicrystal, epitaxial, interface struct., effect of misfit, bonding and cryst. dimens. 2−56690

Epitaxy continued
$Co_xMg_{1-x}O$, single crystal film, epitaxial growth method 2−60650
$Co_xMg_{1-x}O$, single crystal film, epitaxial growth method 2−60650
electrodeposition, two dimensional nucleation effect on electrocrystalliz. rate 2−71320
electrodeposition, two-dimensional nucleation effect on electrocrystallization rate 2−71320
epitaxial island alignment rel. to misfit dislocations, misfit strain 2−56697
epitaxial islands, equilib. elastic strains, misfit dislocations, size dependence 2−56696
ferrite and garnet crysts. for bubble domain memories 2−47199
ferrite films, prep. for mag. bubble domain memories 2−72192
films, chemical vapour deposition by organometallic sources 2−74621
$GaAs_{1-x}P_x$ epitaxial growth by thermal decomposition 2−64597
GaAs layer, liquid phase epitaxy 2−71385
garnet multilayer films for magnetic bubble devices, hard bubble suppression 2−65162
group II-VI compound, epitaxial, struct., composition 2−56582
group II-VI semiconductor, by decomp. of group II metalorganic 2−47091
group III-V semiconductor, by decomp. of group III metalorganic 2−47091
growth definition rel. to terminology of mutual crystal orientation 2−83888
layers, growth from soln., theory 2−77505
liquid phase, growth of GaAs on ZnSe substrates from Ga, Sn solutions 2−53573
metal and non-metal epitaxial growth, electron microscope obs. 2−60727
metal and non-metal growth, electron microscope obs. 2−60727
metal evap. on alkali halides, multiply-twinned particles 2−47101
metal films on alkali halides, electron surface scatt. influence on cryst. orientation 2−53565
misfit dislocation energy of finite thickness overgrowths 2−60798
nucleation and growth, LEED-Auger instrument and u.h. vac. electron microscope 2−74624
optical data processor, coherent and noncoherent, space invariance conditions 2−79368
overgrowths of finite thickness, misfit dislocation energy 2−60798
poly γ-benzyl L-glutamate, growth stages in epitaxial crystallisation 2−60605
polyoxymethylene, temperature dependence of overgrowth thickens on NaCl 2−43485
rare gases on graphite, molecular beam system and specimen holder for t.e.m. obs. 2−79113
surface quality improvement for solution grown layers 2−60656
surface quality improvement of layers 2−60656
transition layer, structure and props. 2−47093
Ag, growth on substrates, various modes 2−77530
Ag single crystal charact. and preparation 2−74627
Al, growth from the melt, nucleation by Tl cpds. 2−47098
Al film, on KCl, rel. to nucleation 2−67905
Al film, on NaCl and KBr substrates 2−77501
AlAs, on GaAs, elec. props. and optical absorp. 2−71881
$Al_xGa_{1-x}As$-GaAs heterojunction, prep. by multiple layer liq. phase epitaxy 2−50482
$Al_xGa_{1-x}As$ grown- diffused electroluminescent planar monolithic diodes 2−51386
AlGaAsP solid soln., prep. by liq. epitaxy methods, use in lasers 2−63343
Au, growth on substrates, various modes 2−77530
Au, on rocksalt, influence of interfacial amorphous C layers 2−77503
Au, rel. to use as self-supporting targets in channelling expts. 2−71326
Au film, on KCl, rel. to nucleation 2−67905
Au film growth, rel. to use as self-supporting targets in channelling expts. 2−71326
BeO film growth and characterisation for microacoustoelectronic applications 2−51042
CdS film, growth under isothermal conditions 2−47106
CdS film, liquid phase growth 2−47104
CdS film, optimum conditions 2−47105
CdS single crystal films, epitaxial growth 2−53572
CdSe film, growth under isothermal conditions 2−47106
CdTe, on CdS, closed-tube chem. transport technique 2−77498
CdTe film, growth under isothermal conditions 2−47106
CdTe film, optimum conditions 2−47105
Co-P film, electroless deposition 2−53566
Co, epitaxial growth on LiF substrate 2−61524
Cu-Au film, epitaxial growth by r.f. sputtering, microstruct. 2−67908
Cu-Ni alloy, film, growth, struct., epitaxial temp. rel. to comp. 2−60654
Cu, electrodeposition, growth defects 2−47107
Cu, epitaxial, microstruct., orientation and imperfections 2−67909
Cu, microstruct., orientation and imperfections 2−67909
Cu, oxide nucleation on (001) face, off angle effect 2−64566
$EuEr_2Fe_{4.3}Ga_{0.7}O_{12}$, liquid-phase epitaxial growth 2−83902
$EuEr_2Fe_{5-x}Ga_xO_{12}$ film, liquid phase epitaxy, optimum conditions 2−47108
$Fe_{1-x}O$ film, on CaF_2 2−47109
$Ga_{1-x}Al_xAs$:Si layer growth, Al conc. effect on amphoteric behaviour of Si 2−51153
$Ga_{1-x}Al_xAs$, light emitting diode growth on GaP substrate 2−51388
$Ga_{1-x}Al_xAs$, liq. phase epitaxial growth from unstirred soln., simulation by numerical methods 2−74693
$Ga_{1-x}Al_xAs$, liq. phase epitaxial growth from unstirred soln., simulation by numerical methods 2−74693
$Ga_{1-x}Al_xAs$, liquid phase, composition, elec. microprobe obs. 2−47286
$Ga_{1-x}Al_xAs$ layer growth 2−47288
n-GaAs:Ge film, alloy regrowth process, degenerate, forbidden gap, traps 2−44114
GaAs-$Al_xGa_{1-x}As$ double heterostruct. laser diodes, reproducible liq. phase epitaxial growth 2−49385
GaAs-$Al_xGa_{1-x}As$ dielec. waveguide, fabrication by mol. beam epitaxy 2−80593

Epitaxy continued
GaAs-GaP heterojunction, prep. by multiple layer liq. phase epitaxy 2−50482
GaAs, anisotropy obs. using abrupt changes in doping level 2−47112
GaAs, electrical props. 2−71882
GaAs, epitaxial growth kinetics 2−60635
GaAs, epitaxial layer growth from soln. in Ga, rel. to undercooling 2−74694
p-GaAs, gas transport system, orientation effects 2−71387
GaAs, growth morphology obs. by sequential changes in doping level 2−47113
GaAs, impurity incorporation, effect of surface space charge layer 2−47428
GaAs, layers, influence of gas phase comp. on electrical properties 2−83893
GaAs, open flow quartz systems, Si contamination 2−43529
GaAs, origin of high resistance region at substrate interface 2−71883
GaAs, perfection of single crysts. and epitaxial layers, X-ray obs. 2−74767
GaAs, selective growth, morphological studies 2−50493
GaAs, solution growth, surface quality improvement 2−60656
GaAs, using liquid phase epitaxy method, optimum kinetics and conditions 2−71384
GaAs, vapour phase growth 2−83891
GaAs crystal growth, using liquid phase epitaxy method, optimum kinetics and conditions 2−71384
GaAs epitaxial layers, surface quality improvement 2−60656
GaAs film, from soln., growth kinetics 2−60635
GaAs film, liq. phase epitaxy on ZnSe, elec. characts. rel. growth conditions 2−67910
GaAs layer, optical props. by photoluminescence method 2−72442
GaAs layer growth from vapour phase 2−50492
GaAs layers, growth by liquid phase epitaxy 2−71385
GaAs photodiode, feasibility of production on single-crystal strip of Ge 2−54260
GaAs vapour-phase, epitaxial 2−71386
GaAs vapour-phase, growth techniques 2−71386
$GaAs_{1-x}P_x$ layers, on GaAs, by pyrolysis of $Ga(CH_3)_3$, AsH_3 and PH_3 2−50496
$GaAs_{1-x}P_x$, on GaAs, surface struct., cross-hatch pattern due to misfit disloc. array 2−47110
$GaAs_{1-x}P_x$ crystal growth 2−43528
$GaAs_{1-x}P_x$ layers, vapour phase epitaxial growth kinetics 2−50494
$GaAs_xP_{1-x}$, growth on GaAs substrate, anisotropic bending 2−80567
$GaAs_xSb_{1-x}$-$Al_yGa_{1-y}As_xSb_{1-x}$ double heterojunction laser prep. 2−59184
$GaAs_{1-x}U_x$, growth by thermal decomp. method 2−64597
$Ga_xIn_{1-x}As$, growth on GaAs substrate, anisotropic bending 2−80567
$Ga_xIn_{1-x}P$ on GaAs substrate, lattice mismatch effects 2−60728
GaN layer growth from vapour phase 2−50495
GaP, growth on insulating substrates and characterization 2−47111
GaP, heteroexpitaxial growth on Si substrates 2−83864
GaP, liquid phase, coprecipitation of Ga_2O_3 2−50609
GaP, open flow quartz systems, Si contamination 2−43529
GaP, p-n-p-n green light emitting diode fabrication 2−72436
GaP green emitting diode fabrication by double- bin liquid-phase epitaxy 2−72437
GaP p-n junction growth 2−47287
Ge-GaAs heterojunction, liquid phase growth 2−71957
Ge-GaAs heterojunction, liquid phase growth 2−71957
Ge-Si structure, u.h.v. evaporation 2−56591
n-Ge, degenerate, on GaAs, growth conditions 2−47115
Ge, layer growth by hydrogen reduction of $GeCl_4$ 2−64598
Ge, layer growth by thermal decomp. of GeH_4 2−64598
Ge, thermodynamic calc. of the Ge-H-Cl system 2−53623
Ge layers, epitaxial growth by thermal decomposition of GeH_4 2−64598
Ge layers, epitaxial growth by hydrogen reduction of $GeCl_4$ 2−64598
InAs, on ZnTe substrate, heterojunction prep. 2−57213
Ir, vapour deposition, low temp. 2−53575
Mg/MoS_2 film/substrate system, curvilinear dislocations 2−80554
$MgGa_2O_4$, growth by Czochralski method, substrate for direct liq. phase epitaxy 2−71380
Ni-P film, electroless deposition 2−53566
Ni film on NaCl substrate, effect of annealing on dislocation struct. 2−80565
Ni films, epitaxial, planar Hall effect 2−72186
Pb film, on Ni, azimuthal disorientation of elementary nuclei 2−47122
$Pb_{1-x}Sn_xTe$, solution growth, surface quality improvement 2−60656
$Pb_{1-x}Sn_xTe$ epitaxial layers, surface quality improvement 2−60656
Pd, vapour deposition, low temp. 2−53575
Pt, vapour deposition, low temp. 2−53575
Rh, vapour deposition, low temp. 2−53575
ScN layer growth 2−50503
Si:P, doping during growth 2−47431
Si-Ge, single crysts., epitaxial growth from vapour phase 2−64599
Si-$ZnSiP_2$ solid solution, epitaxial growth on Si 2−60665
Si-$ZnSiP_2$ solid solution, on Si, new technique 2−60665
p-Si, dual rate deposition on spinel, hole mobilities detn. 2−43482
Si, effect of substrate impurity absorption 2−74647
Si, epitaxial, diffusion of Sb, temp. and dislocation density depend. 2−74816
Si, epitaxial film, lattice resolution e. microscopy obs. of struct. of twin boundaries, faults and dislocats. 2−74779
Si, from dichlorosilane 2−71389
Si, growth rate calc. for barrel reactor 2−71388
Si, growth using SiH_4-H_2 system 2−71335
Si, using hydrogen reduction in $SiCl_4$, two dimensional growth 2−47125
Si film, gas doping during deposition 2−50690
Si film growth using SiH_4-H_2 system 2−71335
Si layers, effect of substrate impurity adsorption 2−74647
Si X-band double-drift IMPATT diode fabrication by consecutive epitaxy 2−71976
SiC layers, system for chem. vapour deposition 2−50507
SnSe, on KCl, boundary struct., rotational Moire method 2−74635
TaC film, growth by electron beam evap. 2−67916
Te on alkali halides, growth of thin layers at 100°C 2−47120

Epitaxy continued
- YAG films, Nd^{3+} site preferences for growth by liquid phase epitaxy, spin-reson. meas. 2−83867
- YIG, heteroepitaxy, flux method and hydrothermal synthesis 2−50513
- YIG film, chem. vapour deposited, substrate growth band and core struct. replication 2−71338
- YIG film growth by chem. vapour deposition 2−47132
- ZnO/Al$_2$O$_3$, heteroepitaxial layer struct., surface acoustic props. rel. to delay line behaviour 2−68235
- ZnO, on Ge and GaAs, electron diffr. obs. 2−74636
- ZnO, on Ge and GaAs, electron diffr. obs. 2−74636
- ZnS, on GaS, struct. 2−71339
- n-ZnS, vapour phase growth on pGaP, electrical characteristics 2−80596
- ZnS film, on Si by forced vapour transport 2−50514
- n-ZnSe, vapour phase growth, on pGaP, electrical characteristics 2−80596
- ZnTe film, on Ge substrate 2−50515
- ZnTe film, optimum conditions 2−47105
- ZnTe film on NaCl, KCl, determ. migration length, 1.5 to 10 K 2−80563

Equations
- *see also Differential equations; Integral equations*
- boundary value problems in optically thick media, Lie series treatment 2−83112
- Chandrasekhar's equation and correlation functions for isotropic turbulence, resolution of equation 2−70871
- dimensional analysis with similarity considerations 2−82161
- Hamilton-Jacobi equation, validity in quantum mechanics 2−41497
- ill conditioned linear equations used in astronomy solution method 2−69195
- interatomic spacings, nonlinear algebraic equations and formation of a complete set 2−71400
- Karplus, for vicinal coupling in molecules, functional form 2−83230
- Lagrange, for holonomic systems, crit. cases 2−66416
- Legendre's eqn., simple proof for teaching 2−41438
- linear algebraic, method of successive refinements for solving infinite systems 2−73290
- many non-rigid bodies system, translational dynamical equations for relative motion 2−69632
- MHD duct flow, corner regions in asymptotic solution of $\varepsilon\mathrm{grad}^2 u = \partial u/\partial y$ 2−50180
- nonlinear dispersive waves, asymptotic solution 2−45243
- quasi-linear hyperbolic system, second order, boundary problems 2−62970
- Ricatti, integrable, for motion of a point 2−45428
- Sturm Liouville eigenvalue problem, error in calc. of coeffs. in paper by S.N. Singh, 1958 2−62969

Equations of state
- *see also Thermodynamics*
- adsorption layers, convergence and first-order approx. for fugacity expansions 2−53584
- adsorption of solute from dilute liquid solution, derivation of virial equation 2−53585
- Burnett-isochoric coupled data, applic. to adsorbing gases 2−67868
- BWR, development and applic. for c.-a.d. of cryogenic plant 2−76121
- classical one-component plasma, crystallization, Monte Carlo calc. 2−78843
- critical point vicinity, an improved eqn. 2−80522
- dense medium, thermodynamic functions in model of higher order 2−49036
- diatomic molecular crystal, calc. using lattice vibr. model 2−43960
- elastoplastic material, stress analysis 2−82300
- fluid at critical point 2−56538
- fluids, from Ursell-Mayer density expansion 2−53108
- hadronic, rel. to ultimate temperature 2−54997
- hadronic matter at ultrahigh densities, model 2−52571
- hard sphere fluid, inverse power pots., radial distrib. functions, virial coeffs. 2−73341
- hard-sphere eqn. in form of Pade approximant, modifications to give fluid and solid behaviour 2−67550
- intermolecular potential in theory of equilibrium of classical fluids 2−53128
- Ising-like ferromagnet, scaling eqn. of state near crit. pt., Feynman-graph expansion 2−68526
- Lennard-Jones 6-12 potential, self-consistent approximation and fourth virial coefficients 2−58783
- linear and nonlinear state-space eqns., Lagrange and Hamilton methods 2−53485
- linear model parametric, rel. to gravity effect analysis in gas-liquid critical point region 2−47040
- magnetic phase transition, 2nd order, determ. by computer simulation 2−78948
- molecular dynamics for parallel hard squares, comparison with two simple models 2−52105
- neutron star matter at subnuclear densities 2−66096
- neutron stars, equilibrium configuration, transport props. 2−44866
- non-Newtonian fluids, time-dependent and time-independent 2−67559
- penetrable sphere model of liquid- vapour equilib. calcs. 2−80523
- phase equilibria and complex reaction problem calculation by computer 2−74580
- plasma, relativistic 2−70876
- plasma, superdense, correlation effects 2−70874
- predictive capabilities study, using inversion curves determ. 2−84609
- quantum theory of second virial coeffs. 2−78822
- rigid sphere, calc. of absorption coeff. of sound due to thermal and viscous losses 2−55435
- second virial coefficient, equations 2−53333
- solids with U_s-u_p linear relationship, melting line determ. 2−80518
- stars, physical state of interior, virial theorem for simple evolution curve 2−66083
- stellar interiors 2−58271
- superdense matter and threshold of disintegration in degenerate electron neutron gas 2−58255
- thermal, unified, for single component substance, parameter det. taking into account exptal. data at saturation line 2−60538

Equations of state continued
- from unit-compressibility line 2−53330
- virial, determination of excess Gibbs function from total vapour pressure measurements 2−81485
- virial expansion, summation to infinity 2−82384
- virial expansion for non-ideal reference system, compared with perturbation theory 2−45298
- virial theorem 2−45311
- Yvon-Born-Green square well equation, critical point behavior and scaling laws 2−50396
- Yvon-Born-Green square-well equation 2−50395
- CO crystal, calc. using lattice vibr. model 2−43960
- F$_2$ crystal, calc. using lattice vibr. model 2−43960
- N$_2$ crystal, calc. using lattice vibr. model 2−43960
- O$_2$ crystal, calc. using lattice vibr. model 2−43960

gases
- 83706
- associated, derivation 2−46856
- carbon tetrachloride-gas mixtures at high pressures, second cross virial coeffs. determ. from solubilities 2−43262
- carbon tetrafluoride, octopole moments and dielec. second virial coeffs. 2−83294
- carbon tetrafluoride, Percus-Yevick and Lennard-Jones (7-28) potential calc., comparsion with exptl. data 2−43259
- classification by consideration of internal pressure 2−53331
- dense, second virial coefficients, method of irreducible spherical tensors employed 2−71118
- diatomic, second virial coeff. determ. from atom-atom pots. 2−77366
- ethylene, contributions of nonspherical and nonadditive molecular interactions to third virial coeff. 2−71110
- generalized, with 6 virial coeffs. 2−80417
- in high temp. range, method of determ. of intermolecular potential constants 2−60111
- imperfect classical, virial theorem 2−45569
- imperfect quantum gas 2−45326
- methane, based on unit compressibility line 2−53330
- methane, octopole moments and dielec. second virial coeffs. 2−83294
- new condition which any proposed equation of state must fulfil 2−43260
- non-ideal reference system, virial expansion, chain approximations 2−55436
- non-polar polyatomic, m-6-8 pot. analysis of second virial coeff. 2−77370
- nonpolar-polar mixtures, contribution of interactions to second order coefficient 2−80413
- polyatomic, contributions of nonspherical and nonadditive molecular interactions to third virial coeff. 2−71110
- Redlich-Kwong, modified, determination of equilibrium constants 2−50265
- second virial coefficients, undergraduate apparatus 2−52026
- self-consistent theory 2−60366
- virial coeff., second, of polyatomic gases, calc. from atom-atom intermolecular potential 2−46855
- virial coefficients, Burnett apparatus for accurate determination 2−56439
- virial coefficients rel. to association constants, rigorous expressions 2−43261
- virial coeffs. calc. 2−50266
- virial coeffs. for potential (12-7) 2−56437
- virial coeffs. from exp. (p,v,t) data 2−56438
- virial coeffs. of compressed mixtures, calc. 2−56441
- virial expansion, convergence for assoc. gas 2−83711
- virial expansion for a binary mixture model 2−82257
- water vapour, from triplet point to critical point, droplet model 2−67869
- Yvon-Born-Green square well equation, critical point behavior and scaling laws 2−50396
- Yvon-Born-Green square-well equation 2−50395
- Ar, adaption of van der Waals eqn., prediction of PVT behaviour, application to simple substances 2−71109
- Ar, calc. of second virial coeffs. using various interatomic potential models 2−64393
- Ar, calc. of third virial coeffs. at low temps. 2−56440
- Ar, isotope separation factor between liq. and vapour 2−80521
- Ar, third virial coeff. and nonadditivity 2−60367
- Ar, third virial coefficients 2−74482
- CO$_2$, m-6-8 pot. analysis of second virial coeff. 2−77370
- CO$_2$ from triplet point to critical point, droplet model 2−67869
- He, path integral calc. of three-particle direct and exchange contribs. to pair distrib. function and third virial coefficient 2−53334
- Kr, calc. of third virial coeffs. at low temps. 2−56440
- Kr, from 120 to 423K at pressures from 0 to 1000b 2−67732
- N$_2$, contribution of nonspherical and nonadditive molecular interactions to third virial coeff. 2−71110
- N$_2$, m-6-8 pot. analysis of second virial coeff. 2−77370
- N$_2$, representing all saturated state variables 2−53332
- Ne, third virial coeff. and non additivity 2−60367
- Ne second virial coeff. calc. using scattering potential of Siska 2−46863
- O$_2$, m-6-8 pot. analysis of second virial coeff. 2−77370
- Xe, calc. of third virial coeffs. at low temps. 2−56440

liquids
- benzene, nonlinear U(u) Hugoniot below 15kb 2−53390
- Berthelot mixture, excess functions 2−56473
- boiling, rel. to diaphasic resistance variations 2−53504
- cavitating, nucleation models 2−53503
- chloroform, nonlinear U(u) Hugoniot below 15kb 2−53390
- cyclohexane, nonlinear U(u) Hugoniot below 15kb 2−53390
- diiodomethane, nonlinear U(u) Hugoniot below 15kb 2−53390
- dynamical equation, struct. relax. time evaluation 2−46919
- Kirkwood, Born, Green eqn., derivation and solution of 1-dimensional analogue 2−71153
- methane, nonanalytic eqn., up to 350 bar, 400 K 2−80448
- non-electrolyte liquids and solutions, thermodynamic properties 2−46913
- polymer solns., dil., virial coeffs. for interactions 2−60437
- rigid sphere equation, appl. to acoustic props. calc. 2−46918

Equations of state continued
liquids continued
second virial coeffs., determ. from osmotic pressure meas., numerical treatment of data 2−43343
self-consistent theory 2−60366
statistical theory of salts in solvents with low dielect. const. 2−84617
thermal relaxation times using imoroved rigid sphere equation of state rel. to sound absorption 2−56499
Van der Waals model correction 2−64429
rel. to viscosity, calc. in terms of internal press. 2−46937
water in metastable region, thermodynamic stability boundary 2−60418
Yvon-Born-Green square well equation, critical point behavior and scaling laws 2−50396
Yvon-Born-Green square-well equation 2−50395
Ar, adaption of van der Waals eqn., prediction of PVT behaviour, application to simple substances 2−71109
Ar, isotope separation factor between liq. and vapour 2−80521
CS_2, nonlinear U(u) Hugoniot below 15kb 2−53390
^4He, λ transition phenomena 2−80502
n- hexane, nonlinear U(u) Hugoniot below 15kb 2−53390
solids
alkali metals, calc. from volume depend. of dynamical matrix 2−74997
antiferroelectric connecting field strength, temp. and polarization 2−84360
Birch-Murnaghan, seismic data for testing 2−61893
continuous heteroplastic medium 2−76296
Earth, fourth-order anharmonic theory at high compression and temp. 2−72676
fourth-order anharmonic, appl. to shock waves and temp. derivation along Hugoniot curves 2−84188
heteroplastic medium 2−82301
lunar samples from Apollo mission 2−66158
mantle minerals, eval. scheme for h.p. phases 2−61981
metallic system, dynamic compressibility curve determ. from eqn. of state of constituents 2−60861
minerals and rocks, geophysical applications 2−72681
noble metals, based on elastic and cohesive props. 2−68063
two parameter equations, comparison with Murnaghan eqn. 2−47051
viscoelastic suspensions, rheological equation of state 2−83824
Ar, static lattice energies, PV relation, at T=0K 2−80889
Cu-Al alloy, α-phase, calc. 2−56929
H, ground-state energy at high density 2−43501
H_2, molecular solid, anisotropic interactions 2−64824
H_2, self-consistent formulation 2−71711
Mg_2SiO_4-Fe_2SiO_4 olivine transformed spinel system, det. using Birch's law 2−43504
NaCl, 0-8kbar, 300-800K, u.s. determ. 2−68065

Erbium
atom, relative isotope shifts in u.v. region, determ. of coeff. of nuclear deformation and internal quadrupole moment 2−49947
deuteron bombarded, secondary electron emission 2−61468
film, f.c.c. struct. and oxidation HEED obs. 2−50490
film, maximum sorption capacities and gettering action 2−43495
laser, propagation in CO_2 atmos. in near i.r. 2−42131
laser material, Ho versus Er rel. to visual safety 2−45750
luminescence sensitizing with Mo, patent 2−82486
magnetic reson., microwave absorpt., 24 GHz and 100 GHz 2−65318
microwave absorpt. obs. of mag. transitions 2−51257
oxidation, film form. 2−50491
paramagnetic susceptibility anisotropy, 5 to 750°C 2−44227
photoabsorption spectra in vicinity of 3d edges 2−76988
self-diffusion rate is single crystals in temperature range 1202-1412°C 2−56750
solar photospheric abundance det. from spectrum synthesis 2−58554
$Ca_3(VO_4)_2:Er^{3+}$ ions, luminescence spectra, energy levels from diffuse reflection spectra 2−84534
$CdF_2:Er^{3+}$, correlated e.p.r. and optical study 2−78164
$CdF_2:Er^{3+}$ i.r. quantum counter, noise effects 2−59631
$Er^{3+}:LiYF_4$ pulsed laser operation at 0.85 μm at room temperature 2−42062
Er, Ho, Yb, Tm:YAG laser, recirculating liquid N_2 system for cooling 2−63339
Er III, emission spectrum analysis 2−70580
Er^{3+}, e.p.r. spectra, in $ZnSiO_4$, $HfSiO_4$ and $ThSiO_4$ hosts 2−48278
Er^{3+}, in alkali silicate glass, multiple sites, absorpt. study 2−54429
Er^{3+}, in BaY_2F_8, laser emission in the visible 2−61704
Er^{3+}, in glass, fluoresc. quenching by OH^- ions 2−54467
Er^{3+}, in $LaCl_3$ and lanthanum ethyl sulphate, spin-lattice relax. at zero mag. field 2−65194
Er^{3+}, in Pd single cryst., e.s.r. 2−61732
Er^{3+}, in Y_2O_2S and Er_2O_2S, energy levels and crystal field splittings detn. 2−51339
Er^{3+}, in YF_3, Y_3OCl_7 and YOCl, i.r. to visible conversion 2−54470
Er^{3+}, spectra in phosphate and borate glasses, emission and absorpt. cryst. field effects, luminesc. efficiency 2−75307
Er^{3+} doped oxides, visible luminesc., i.r. excited, effect of host lattice 2−78140
Er^{3+} effect of core polarization on f-f interactions 2−52929
Er^{3+} glass, stimulated emission cross section, relative gain coeff., absorpt. and fluorescence spectra obs. 2−75323
Er^{3+} in CdF_2, absorpt. and fluoresc. spectra, ion site obs. 2−54416
Er^{3+} in CdF_2, i.r. transitions, fluoresc. 2−65305
Er^{3+} ions in silicate glass, photoinduced absorption spectra 2−75291
Ev^{3+}, in $SrMoO_4$ and $LiYF_4$, crystal parameters verified 2−51240
^{170}Fr, production and crystal growth, neutron diffraction expts. 2−74667
$GdAlO_3$:Er, Zeeman optical absorp. spectra, Er^{3+}-Gd^{3+} exchange interaction obs. 2−57349
Ir:Er, localized moment cond. electron exchange interaction, e.s.r 2−68737
$NaYF_4$:Yb, Er, phosphor, upconversion, i.r.-pumped visible luminesc. 2−72413
Pd:^{167}Er, hyperfine splitting, consts., e.s.r. 2−72497
ZnS-CdS:Er^{3+} mixed fluorescent compounds spectroscopic investigation 2−84545

Erbium compounds
erOOH, monoclinic, mag. struct. 2−44296
ethyl sulphate, caloric and mag. obs. 2−68523
ethyl sulphate, low temp. calorimetry 2−44229
tritide film, ageing, bubble form. and rupture 2−43478
Ag-Er alloy, dilute, exchange interact. with cond. electrons, e.p.r. obs. 2−72467
Er-B system, phase diagram and props. 2−50964
Er-H system, gas pressure standard 2−52016
$Er_{0.6}$-$Ho_{0.2}$-$Dy_{0.2}$ alloy, magnetization curves, study at 4.2 K 2−65174
Er-Zr alloys, form. of low temp. metastable allotropic solid solns. 2−47646
$ErAg_2$, magnetic structure, 297-1.5K, neutron powder diffraction study 2−61551
$ErAl_2$ and $Er_xY_{1-x}Al_2$, mag. struct., neutron diffr. obs. 2−81275
$ErAl_3$, mag. struct., neutron diffr. obs. 2−81275
$ErAsO_4$, a.c. susceptibility, absence of phase transition down to 0.6K 2−65187
$ErAu_2$, mag. struct. 2−72216
ErB_6, form. and stability 2−50965
ErC_2, crystal and mag. struct., 297-2K, neutron diffr. obs. 2−72217
$ErCl_3$, n.q.r., hydrostatic press. coeffs., soft sphere model 2−54519
$ErCl_3$, transferred hyperfine effect 2−72242
$ErCl_3.6H_2O$, caloric and mag. obs. 2−68523
$ErCl_3.6H_2O$, spectra, optical absorption, J levels 2−51340
$ErCo_2$, Co atom paramagnetic moments 2−72116
$ErCo_2$, mag. bheaviour in ordering region 2−44280
ErD_3, deuteron bombarded, secondary electron emission 2−61468
$Er_2EuGa_{0.7}Fe_{4.3}O_{12}$ garnet mag. films, domain interaction with laser beam, domain writing 2−75230
$ErFeO_3$, mag. struct., Mossbauer obs. 2−44351
$ErFeO_3$, spin reorientation transition phenomena, sound propag. 2−54026
$ErFeO_3$, with high coercivity surface layer, domain struct., magnetooptical obs. 2−81284
ErGa, mag. props. 2−48079
ErGa, magnetization and susceptibility, temp. depend. 2−72170
ErGa garnets, metamagnetism 2−61557
$ErH_{1.81}$, acoustic velocity, limiting Debye temp. and elastic consts. detn. 2−57047
ErNiAl, mag. props., metamagnetism 2−72162
$Er_2O_3:Er^{3+}$, electronic excitation, far i.r. and optical spectrosc. obs. 2−81369
Er_2O_3 film form. on oxidation of Er 2−50491
Er_2O_3 radiator performance effect on Ge thermophotovoltaic convertor efficiency 2−66693
ErOF, flux growth 2−60717
$Er(OH)_3$, hydrothermal growth 2−47244
$Er_2O_2S:Er^{3+}$, energy levels and crystal field splittings detn. 2−51339
Er_2O_2Se, mag. props. 2−44228
$ErPO_4$, a.c. susceptibility, absence of phase transition down to 0.6K 2−65187
$ErTe_{3-x}S_x$ solid solns., high temp. homogeneity regions 2−53905
$ErVO_4$, a.c. susceptibility, absence of phase transition down to 0.6K 2−65187
$EuEr_2Fe_{5-x}Ga_xO_{12}$ film, liquid phase epitaxy, optimum conditions 2−47108
$Ho_xEr_{1-x}Fe_2$ system, spin orientation diagram 2−72197
$KMnF_3ErF_3$ system, phase diagram, existence of $KMnEr_3F_{12}$ 2−50622
Mg-Er alloy, dilute, exchange interact. with cond. electrons, e.p.r. obs. 2−72467
$(Y,Yb,Er)F_3$ phosphor., i.r. convertor, prep. by coprecipitation 2−48248
Ergodic theorem *see Statistical mechanics*
Errors *see Measurement errors; Random processes*
Esaki diodes *see Semiconducting devices/tunnel and interface devices*
Esaki effect *see Semiconducting devices/junctions*
Etalons *see Interferometers*
Etching *see Crystals/etching*
Ether drift *see Relativity/special; Velocity/light*
Ettingshausen effect *see Magnetothermal effects*
Europium
Galaxy, heavy element synthesis, separation of r- and s-process abundances 2−66052
magnetic crit. scatt. role in elec. resist. 2−57271
sunspot abundances, using high resolution spectra 2−73135
thermal resist., electronic, critical divergence at Neel point 2−57124
AlN:Eu,Mn, radical recomb. luminesc. and photoluminesc. 2−57371
BaF_2:Er, spin lattice relax. of ^{19}F in laboratory frame and rot. frame 2−68582
$Ca_3(VO_4)_2:Eu^{3+}$ ions, luminescence spectra, energy levels from diffuse reflection spectra 2−84534
Eu:YVO_3, excitation induced anisotropy of local environment 2−81440
Eu^{2+}-Sm^{2+} exchange coupling problems in chalcogenides 2−54373
Eu I, interstellar, effect of radiation pressure round stars, galactic evolution 2−48730
Eu^{2+}, e.p.r. in $CaWO_4$, elec. field effect 2−48287
Eu^{2+}, in $PbCl_2$, luminesc. 2−54447
Eu^{2+}, in $SrCl_2$, hyperfine interactions, temp. depend., e.p.r. obs. 2−72471
Eu^{2+}, luminesc. in $SrCaAlF_7$ and $BaCaAlF_7$ 2−72420
Eu^{2+} activated luminophores, oxidation 2−54483
Eu^{2+} in BaF_2, diffusion vanishing spin-lattice relax. of ^{19}F 2−44315
Eu^{2+} in crystal field config., $4f^6$ 5d, electronic interactions 2−72237
Eu^{2+} ion alkali halide, Z-centres, optical absorpt. and e.p.r. at 77K 2−71526
Eu^{3+}, in $Ba_2MgGe_2O_7$ glass and crystal matrices, luminesc. props. 2−72423
Eu^{3+}, in phosphate glass, energy transfer with Sm^{3+} 2−48238
Eu^{3+}, luminescence in NaF, Ce^{3+} impurity effect 2−65295
Eu^{3+} fluorescence in organic solvents subject to quenching 2−50369

Europium continued
Eu^{3+} in glass, emission spectra, comp. and temp. depend., effective cryst. field props. 2−78130
Eu^{3+} in rare earth oxides, flame excited luminesc., temp. depend. 2−48270
Eu^{3+} in silicates, spectral characts. and quantum efficiencies 2−48233
Eu^{3+} in Y_2O_2S, luminesc., sensitization by Pr^{3+} and Tb^{3+} 2−51371
Gd_2O_3:Eu^{3+} transparent phosphor, prep. and optical props. 2−72409
KCl:Eu^{2+}, impurity-vacancy dipole relax. and aggregation, and X-ray effects 2−83982
La_2O_2S:Eu, luminescence and photoconductivity 2−72064
Na_2ZrSiO_5:Eu^{3+}, cryst. struct. and luminesc. 2−72414
$SrAlF_5$:Eu^{2+}, cryst. growth and characterization 2−60726
Y_2O_3 and Y_2O_2S phosphors, emission spectra rel. to Eu^{3+} conc. 2−48235

Europium compounds
complexes with β-diketones, Tb sensitized luminescence 2−74549
EuO, ferromag. semicond., Redfield technique detn. of Hall mobility of photoelectrons 2−81060
EuS:Sn, nonmag. impurity effects, first and second neighbour exchange 2−65138
Eu-Fe-O system, phase relations and cpd. formation 2−47710
Eu-Th-Bi soln., mutual solubilities, 350-700°C 2−67809
Eu-W-O, subsolidus phase relations and cryst. chem., phase diagram 2−74952
(Eu,Sm)Fe and (Eu, Ho)Fe garnets, mixed, easy magnetiz. direction Mossbauer obs. 2−51314
Eu chelates, comparison of Mossbauer resonant intensities used to determine structure differences 2−48142
Eu complex, tris(2,2,6,6-tetramethyl-3,5-heptadionato-) europium dimer, magnetic susceptibility down to 4.2 K 2−61481
Eu compounds with aromatic acids, luminescence and i.r. spectra 2−75324
Eu^{3+}, in organic solvents, quenching effect of →C-H and -O-H groups, from spectra 2−53436
Eu^{3+}, luminesc. quenching by dyes at 77 and 293 K 2−54460
$EuAg_2Si$, prep. and cryst. struct. 2−74735
$EuAlO_3$:Mn^{4+}, Raman luminescence 2−44428
EuB_6, e.p.r. g-factor and linewidths 2−84565
EuB_6, exchange interactions, e.p.r. obs. 2−81468
$Eu_2B_5O_9Br(Cl)$, cryst. struct. 2−53657
$EuCl_2$, vaporization thermodynamics 2−64515
$EuCrO_3$, n.m.r. of ^{53}Cr, h.f.s., mag. props. 2−48307
$EuEr_2Fe_{4.3}Ga_{0.7}O_{12}$, liquid-phase epitaxial growth 2−83902
$EuEr_2Fe_{5-x}Ga_xO_{12}$ film, liquid phase epitaxy, optimum conditions 2−47108
$EuEr_2Ga_{0.7}Fe_{4.3}O_{12}$ film, epitaxial, magnetic bubble mobility measurement 2−57303
EuF_2, electronic interactions in 4f^6 5d config. 2−72237
$Eu_{1-x}Gd_xO$, metal-nonmetal transition 2−71899
EuH_2, mag. ordering, sensitivity to hydrogen conc. 2−77986
Eu(III) complex, chelate, Mossbauer obs. of polymerization 2−51309
Eu(III) complexes, hexahalo, Mossbauer parameters 2−51310
$EuLnAlO_4$, (Ln=La, Ce, Pr, Nd, Sm, Eu, Gd), cryst. struct. 2−56664
$Eu(NH_3)_6$, thermodynamic properties and gaseous ammoniation energies of Eu^{2+} 2−61774
Eu_3NbO_7, crystal structure 2−47346
EuO:Gd, bidirectional threshold and memory type switching 2−81081
EuO:Gd, exchange-induced imperfection ionization, investigation using optical absorption and Faraday rotation 2−68598
EuO, doped, metal-semiconductor transition 2−77842
EuO, effect of hydrostatic press. on ferromagnetic and antiferromagnetic interactions 2−48057
EuO, $Eu_{0.97}Gd_{0.03}O$, and $Eu_{1-x}Ca_xO$, magnetic props. exchange interactions, temp. depend. of magnetization 2−68545
EuO, EuO:Gd, high resolution photo- emission meas., p-band excitations and dopant effect on band structure 2−68497
EuO, insulator-metal transition and bound mag. polarons 2−80975
EuO, m.p. determ. by sealed crucible technique 2−67872
EuO, mag. order-disorder transition phenomena, sound propag. 2−54026
EuO, Mossbauer effect of ^{15}Eu after Coulomb excitation with 3.3 MeV α-particles 2−84473
EuO, spin-spin relax. of ^{151}Eu and ^{153}Eu, field depend. relax. rates 2−72230
EuO film, transparent, prep. by oxid. of Eu film, absorp. obs. 2−64568
EuS-EuF_2 films, prep. for magneto-optical obs. at low temps. 2−64567
EuS, cryst. growth by high temp. high press. chem. transport 2−47218
EuS, effect of hydrostatic press. on ferromagnetic and antiferromagnetic interactions 2−48057
n-EuS, elec. resist. and Hall effect, 140 kOe, Curie pt. phenomena 2−47895
EuS, growth by H_2S-Eu_2O_3 reaction at high-temps. 2−50569
EuS, m.p. determ. by sealed crucible technique 2−67872
EuS, slightly Eu rich, systematics of conduction in band tail 2−75094
EuS film, effective exchange parameters and surface anisotropy 2−68532
EuSe:Gd(La) Mossbauer effect, ^{151}Eu hyperfine interactions, mag. struct. effect 2−48145
EuSe, effect of hydrostatic press. on ferromagnetic and antiferromagnetic interactions 2−48057
EuSe, m.p. determ. by sealed crucible technique 2−67872
EuSe(Te) films, co-evap. and characteriz. 2−50502
Eu_3SiO_5, prep. and phys. props. 2−48173
EuTe, e.p.r. linewidth near crit. point 2−75341
EuTe, effect of hydrostatic press. on ferromagnetic and antiferromagnetic interactions 2−48057
EuTe, Eu_3Te_4, Eu_4Te_7, Eu_3Te_7, Mossbauer spectra, sublattice covalent bonding, isomer shift, internal mag. field at Te nuclei 2−54389
EuTe, m.p. determ. by sealed crucible technique 2−67872
EuTe, para- and antiferromag. resonances, critical phenomena near Neel temp. 2−61728

Europium compounds continued
EuTe, press. induced electronic collapse and struct. changes 2−68297
EuTe, press. induced struct. and electronic transform. 2−50948
Eu_2TiO_4, mag. props. rel. to cryst. chem. 2−51249
$Eu_3Ti_2O_7$, mag. props. rel. to cryst. chem. 2−51249
$Y_{3-x}Eu_xAl_yFe_{5-y}O_{12}$ films, epitaxial, characteriz. for bubble devices 2−61541

Evaporation
see also Vaporization
aerosol, in low temp. flame photometry 2−48358
air-liquid interface, wind tunnel study using isotopic techniques 2−56544
atmospheric, over France, Penman's and Ivanov's methods 2−65676
CdS film growth by evaporation, inclined orientation 2−71370
continuum gas flows over heated sphere, kinetic effects 2−80403
cooling of body of water 2−77475
difluorochloromethane bubbles, influence of pressure 2−73244
drops, generation of uniform 0.5 to 10 μm particles 2−67788
electrically suspended water droplets, wind correction to evaporation rate and Rayleigh instabilities 2−56531
energy and mass transfer through wavy air-water interface over which turbulent wind is passing 2−72748
evapotranspiration in Douglas fir forests, calculation using average Bowen-ratio method 2−72767
films with salt deposition on horizontal cylindrical surface 2−77408
forced convection droplet, with finite vaporization kinetics and liquid heat transfer 2−77398
graphite, method of determining thermodynamic properties and kinetic parameters 2−56545
humidity sensor for meas. evaporation by pulsation method 2−54822
from lake in warm dry environment and suppression by inversion 2−54740
liquid droplets, maximum relaxation times 2−43302
liquid droplets in turbulent air stream, impurities effect 2−71279
lower atmosphere, turbulent flow, effects of evaporation on stability, and radiation on temp. fluctuations 2−44699
meniscus, 2-dimensional, extended, adsorbed on superheated glass plate 2−67876
metal, meas. by atomic reson, absorption 2−50406
metal vapour, production of constant stream by control of electron emission 2−67890
metallurgical vacuum melting and degassing, activated reactive evaporation 2−55336
microwave field visualization, $CoCl_2$ solution water evaporation 2−55605
moisture, process and transport factors det. order instationary conditions 2−64509
moisture from wet surface, determ. of flux of vapour in terms of humidity potential and wet-bulb depression 2−83833
multiple input dynamic stochastic model of rainfall evapotranspiration - runoff process 2−54845
one-dimensional EHD flow with variable mobility coeff. 2−83528
powdered samples, temp. in arc discharge 2−53508
rate measurement, ultrahigh vacuum quartz spring microbalance 2−85175
sea surface cooling mechanisms, surface stress 2−65593
sea surface layer film and droplet formation 2−78323
seawater, migration of chemical components from ocean to atmosphere, ratios 2−62151
solids into vac., kinetics 2−77465
thermic, dipolar interaction forces, effect on grains in thin metal layers 2−64559
transient concentration profile, exact solution for semi-infinite region with nonvolatile solute 2−53507
turbulent fluxes over open water, trivane measurements, tilt errors and precipitation effects 2−72783
vacuum, of metal films 2−47087
vapour bubble, thermal equilibrium, effects of liquid motion induced by condensation and evaporation 2−77399
water drops with monomolecular surface films 2−60557
water-air interface energy transport in liquid surface waves 2−77395
wind velocity and atmospheric relative humidity effects on evaporation from large body of water 2−57891
C, thin film production 2−74629
CdSb, of Cd atoms during annealing, effect on elec. props. 2−47890
$CsBO_2$, thermodynamics, heat of sublimation and saturation vapour pressure using mass spectrometer 2−64512
Cu-Be alloy, mass spectrometer control 2−73233
GaAs by laser, mass spectrometric analysis of ions in vapour 2−75409
GaP by laser, mass spectrometric analysis of ions in vapour 2−75409
H_2O in clouds, acceleration of ice phase in supercooled water 2−62236
He II, stimulated evaporation of atoms by heat pulses 2−67860
He II phase space analysis of evaporation spectrum 2−50390
$InBr_2$, heterogeneous equilib. 750-1050 K, enthalpy, entropy of evaporation, boiling point 2−74593
KBO_2, thermodynamics, heat of sublimation and saturation vapour pressure using mass spectrometer 2−64512
$LiBO_2$, thermodynamics, heat of sublimation and saturation vapour pressure using mass spectrometer 2−64512
$NaBO_2$, thermodynamics, heat of sublimation and saturation vapour pressure using mass spectrometer 2−64512
Pt, promoted evap. rel. to H adsorption, field ion microscopy obs. 2−50548
$RbBO_2$, thermodynamics, heat of sublimation and saturation vapour pressure using mass spectrometer 2−64512
ZrC-W compounds, vacuum, high temp. from open surface and through W coating 2−73239

Evershed effect *see Sunspots*

Examination of materials *see Electron diffraction examination of materials; Electron microscope examination of materials; Neutron diffraction examination of materials; X-ray examination of materials*

Exchange interactions
— 2−72115
— 2−72154
alloy, dil., s-d model, electron energy renormalization and resist. 2−51274

Exchange interactions continued
antiferromagnet, magnetic impurity atom located between magnetic sublattices, effects 2−72458
antiferromagnet, mechanism in four-magnon excitation in Raman scatt. 2−54433
antiferromagnetic-ferromag. transform., mag. moment oscill., mag. dipole radiation 2−78007
antiferromagnets, Raman scatt. by four magnons, excited state exchange mechanism 2−65276
antiferromagnets, two-sublattice, indirect exchange parameters 2−81299
canted ferrimagnet, intrinsic biquadratic exchange and sublattice magnetizations 2−54346
Coulomb correlation effects and the exchange correlation energy, atomic and band struct. calc. 2−61157
dilute alloys, exchange enhancement, transport properties 2−68334
dilute mag. system, Schrieffer-Wolff transform., Kondo model rel. to Anderson model, diagrammatic eqns. 2−48042
doubly degenerate band, electron correlation 2−84425
electron gas, exchange energy, Liberman approx. correction 2−68312
electron gas, exchange-polarized, magnetic susceptibility 2−77842
exchange coupled ferromag.-antiferromag. pair, transverse susceptibility rel. to field 2−72155
excitons, Frenkel theory, rel. to exchange interactions 2−77834
f.c.c. spin lattice system, mag. struct. exchange and dipolar interactions, mean field approx. 2−84426
f.c.c. type-2 antiferromagnetic ordering, stability and exchange constant calc. 2−61549
ferromagnet, influence of biquadratic exchange 2−48065
ferromagnet, micromagnetic continuum theory, for cryst. with indirect exchange coupling 2−78001
ferromagnet, model with narrow s-band, rel. to temp. depend. of magnetization 2−65140
ferromagnet, uniaxial, rel. to mag. field induced phase transitions 2−65149
ferromagnetic metal, elementary spin excitations 2−44238
ferromagnetic two-magnon bound states, biquadratic exchange effect 2−72120
ferromagnetic-antiferromag. coupled film systems, interfacial exchange coupling, thermal fluctuation aftereffect model 2−81231
ferromagnetism model, estimation of critical parameters 2−44233
hexaferrites, Y-structures and more complex structures anti-symmetric exchanges between spins of cations 2−84436
insulator, electronic correlation, field-theoretic model 2−68411
ion, with orbital ang. momentum, interactions in insulators, review 2−65112
ions with partly filled 3d shells, generalized Heitler-London model 2−68529
linear chains, alternate, of inequivalent coupled nuclei, n.m.r. line shape 2−43019
magnetic alloy, dil., rel. to spin reson. theory 2−78160
magnetic centres in effective energy band, Hubbard model, functional integral approach 2−77983
magnetic structures, between electric and magnetic polarizations 2−81212
magnetically doped tunnel junctions, mag. interactions 2−68449
measurement, e.s.r. and optical techniques 2−61730
metal, rel. to retardation effects in longitudinal spin relaxation 2−65190
metals, indirect exchange and s-d model, dispersion and attenuation of spin waves, effect of e.m. wave 2−72132
molecular crystal, in contact with ferromagnet, emission due to exchange interaction 2−77838
non-Heisenberg magnet 2−72133
nuclear relaxation, effect of electron exchange interactions 2−65189
nuclear spin-lattice relaxation due to the orbital interaction 2−84585
Permalloy film spin wave expts. below saturation magnetization 2−78034
rare earth chalcogenides, divalent ion coupling problems, cryst. field aspects 2−54373
rare earth metals, effective f-f exchange interactions, temp. depend. 2−54317
rare earth orthoferrites and orthochromites, ang. depend. of superexchange interactions 2−68569
rare earths, spin wave energy rel. to interatomic exchange Heisenberg parameters, exchange coupling 2−61505
rare earths in metals, indirect exchange 2−44217
semiconductor, in bound excitons 2−81009
semiconductor, paramagnetic, magnetic polaron props., d-d interactions 2−47880
semimetal, indirect, interband susceptibility calc. 2−75022
specific heat anomalies due to simultaneous effects of exchange and mag. fields 2−57308
spin system, S=1, paramag. reson. shift due to exchange interaction 2−72465
spin-paired symmetric exchange systems, orbited magnetism 2−75211
spinel structure compounds, off centre ions, model for local distortions 2−80646
superconductivity, rel. to Fermi liquid model of s-d electrons 2−71856
superconductivity in s-d exchange model, effect of localized magnetic moment 2−47840
superexchange models based on factorization of orbital matrix elements 2−48103
superexchange ordering of degenerate orbitals and mag. structure of crysts. with Jahn-Teller ions 2−68565
theory, generalized Heitler-London method 2−68528
titanomagnetites, effect of annealing on exchange anisotropy 2−72927
triplet exciton spin systems, Heisenberg exchange 2−68729
weak ferromagnetism, s-d exchange model 2−81257
Ag-Er alloy, dilute, exchange interact. with cond. electrons, e.p.r. obs. 2−72467
Ag-Mn dilute alloys, s-d exchange interaction constant from electrical resistivity measurements 2−44214
Al pseudopotential calcs. of bulk props., effect of statistical approx. 2−80960
Al_2O_3-Fe_2O_3 solid solution, e.p.r. study 2−75351

Exchange interactions continued
Au-Gd alloy, dilute, exchange interact. with cond. electrons, e.p.r. obs. 2−72467
$Ca_3(VO_4)_2$, between rare earth elements, interionic interaction of activator-activator type as exchange-dipole 2−84534
CdS, rel. to strain splitting of bound excitons 2−68678
CdSe, bound exciton to ionized centre, magneto-optical obs. 2−68636
α-Ce, exchange-enhanced, resist. temp. and press. depend., spin-fluctuation resist. 2−81219
$CeAl_x$, n.m.r. and magnetic susceptibilities 2−84594
CeB_6, sp.ht. studies, 1 to 22 K 2−54339
$Ce_xY_{1-x}Sb$, $Ce_xLa_{1-x}Sb$ solid solutions, antiferromagnetically ordered, dependence on lattice constants 2−72212
$Ce_7\square Te_8$, rel. to press. depend. of Curie point 2−54336
Cr complex, $[Cr_3O(CH_2COO)_6(H_2O)_3]^+$, insufficiency of Heisenberg model 2−44294
CrTe thin film, ferromag. reson. study 2−57387
$Cr_3\square Te_4$, rel. to press. depend. of Curie point 2−54336
$CsCrCl_3$, ligand field, magnetic coupling between Cr ions 2−81363
Cu complex, Cu(II) croconate trihydrate, spin-spin interactions between Cu(II) ions 2−72106
Cu Kondo alloys, exchange splitting of electron spins 2−77848
$CuCl_2.2H_2O$, antisymmetric, rel. to spin-spin relax. 2−68579
Cu(II) complex, diammine-(o-phthalato) Cu(II), e.s.r. study 2−65335
Cu(II) complexes, tetrameric, $Cu_4OX_6L_4$, $X=Cl$, $L=(C_6H_5)_3PO$ and $X=Br$, $L=(C_6H_5)_3PO$ or C_5H_5N, and spin coupling 2−51233
$Cu(NH_3)_4SO_4.NH_3$, exchange integral variation with lattice spacing, sp. ht. obs. 2−54353
$Cu(NO_3)_2.2^1/_2H_2O$, differential susceptibility, energy levels and relaxation effects 2−48106
Er_2O_3, rel. to level splitting in internal and external fields 2−81369
EuB_6, e.p.r. obs. 2−81468
EuO:Gd, exchange-induced imperfection ionization, investigation using optical absorption and Faraday rotation 2−68598
EuO, effect of hydrostatic press. on ferromagnetic and antiferromagnetic interactions 2−48057
EuO, $Eu_{0.97}Gd_{0.03}O$, and $Eu_{1-x}Ca_xO$, magnetic props. exchange interactions, temp. depend. of magnetization 2−68545
EuS, effect of hydrostatic press. on ferromagnetic and antiferromagnetic interactions 2−48057
EuS film, effective exchange parameter determination from ferromagnetic and spin-wave resonance curves 2−68532
EuSe, effect of hydrostatic press. on ferromagnetic and antiferromagnetic interactions 2−48057
EuTe, effect of hydrostatic press. on ferromagnetic and antiferromagnetic interactions 2−48057
Fe-Co alloy, metamagnetic character, rel. to temp. depend. of mag. props. 2−51258
Fe-Pd alloys, f.c.c., mixed interaction, neutron scatt. obs. 2−84421
Fe, ferromagnetism, model for origin and ave.-moment-internal field variations in dil. Fe-Si(Al) alloys 2−78008
α-Fe, rel. to elastic consts., 25-900°C 2−60842
Fe, with rare earth impurities f-d exchange 2−44322
Fe dil. alloys, indirect interactions effect on Curie temp. 2−44248
Gd-Ni intermetallic compounds, paramagnetic resonance meas. of g_s values, study of exchange interactions 2−84568
Gd^{3+}, isotropic exchange interactions from e.p.r. measurement in rare earth insulators 2−72487
GdAg, e.p.r. obs. 2−51404
$GdAlO_3$:Er, Er^{3+}-Gd^{3+} exchange, Zeeman optical absorp. spectra obs. 2−57349
$GdAlO_3$, resonant, between spin waves and u.s. waves, obs. 2−54348
GdB_6, e.p.r. obs. 2−81468
GdCu, e.p.r. obs. 2−51404
H_2+D_2+2HD four-centre exchange reaction ab initio calcs. of orbitals contragradience and reaction surface 2−48323
^3He, Neel temp., triple exchange effects 2−83830
^3He solid, theoretical approaches and Monte Carlo calc. 2−53484
Ho, paramag., spin-phonon interaction via modulation of exchange interaction 2−68522
$HoCrO_3$, mag. props., 4.2-300 K 2−48070
Ir:Dy (Er), localized moment cond. electron exchange interaction, e.s.r. 2−68737
K_2CuF_4, two-dimens. ferromagnet 2−81239
K_2CuF_4, two dimensional ferromagnet temp. and frequency dependence of the e.s.r. line width 2−85663
$KMnCl_3.2H_2O$, mag. phase boundaries, anisotropy exchange fields, mol. field theory 2−68574
$KMnF_3$, resonance behaviour 2−84556
$LiCuCl_3.2H_2O$, mag. phase boundaries, anisotropy exchange fields, mol. field theory 2−68574
$LiCuVO_4$, n.m.r. and long-range superexchange interactions via Cu-O-V-O-Cu linkages 2−72511
$Li_{0.5}Fe_{2.5}O_4$, supertransferred hyperfine field at ^{57}Fe, n.m.r. study 2−78169
Mg:Gd, dil. mag. alloy, exchange narrowing of fine structure 2−72496
Mg-Er alloy, dilute, exchange interact. with cond. electrons, e.p.r. obs. 2−72467
Mg, pseudopotential calcs. of bulk props, effect of statistical approx. 2−80960
Mn-permalloy film, exchange anisotropy, ferromag. to anitoferromag., thermomag. recording 2−57286
Mn complex, di-μ-oxo-tetrakis(2,2′-bipyridine)dimanganese(III,IV) perchlorate trihydrate, antiferromagnet, superexchange coupling 2−44303
Mn complex, Mn-amine, Faraday effect obs. 2−65124
MnAlGe, ferromagnetic, n.m.r. studies 2−84586
$Mn_{1-x}Cr_xSb$ films, ferromag. reson. study 2−72450
$MnF_2:Fe^{2+}$, exchange field obs. under press. 2−44304
$MnF_2:Fe^{2+}$, exchange polariz. in superexchange interactions, far i.r. obs. 2−81297
MnF_2, exchange polariz. in superexchange interactions, far i.r. obs. 2−81297
$MnFe_2O_4$, ferrite, single cryst. film, spin wave resonance 2−72454
MnO, exchange polariz. in superexchange interactions, far i.r. obs. 2−81297

Exchange interactions continued
MnO, rel. to spin waves, inelastic neutron scatt. obs. 2−61558
$Mn_{1-x}Zn_xFe_2O_4$, Neel type interactions 2−78022
$(NH_4,RB)_2CuBr_4.2H_2O$, mag. interactions 2−65144
$NaMnF_3$, powder, magnetization, susceptibility, canting, effective exchange, anisotropy fields 2−48098
$NdCrO_3$, optical spectroscopy 2−84512
$NdNi_2$, $NdAl_2$, $NdCo_2$, Laves phases, low temp. specific heat, cryst. field and exchange effect model 2−57067
Ni-Co alloys, exchange consts. and saturation magnetiz. 2−44265
Ni^+ in $CsMgCl_3$, $CsMgBr_3$, interionic coupling effects on exchange spectra 2−84483
NiFe permalloy, film, oxidized, exchange anisotropy effects, hysteresis loop, 5-300 K 2−81230
NiO, magnetic insulator, crystal field theory 2−68564
NiO, rel. to spin wave dispersion 2−81303
$PrCu_2$, cooperative nuclear magnetic order below 54 mK 2−51282
$PrCu_2$, spontaneous mag. order, 54 mK 2−44225
Tb-Sc alloys, consts. and derivs. 2−68576
Tm_3Al_2, indirect s-f interaction in paramag. state 2−48155
$Tn_xMn_{1-x}O$, $0.07 \leqslant x \leqslant 0.9$, superexchange interaction, mag. props., 100-1000 K 2−54364
Y-Fe garnet, between mag. Fe^{3+} ions, determ. of absorption props. 2−81392
Y orthoferrites and orthochromites, ang. depend. of superexchange interactions 2−68569
YIG, rel. to temp. depend. of magnetooptical coeffs. 2−72266
YIG epitaxial film, coupling between dipole and exchange dominated spin waves 2−72189
YbFe garnet, stat. mol. field interpret. of mag. props. 2−72205

Exchanges, chemical
see also Isotope exchanges
benzene flash desorption and decomp. from clean or contaminated W polycryst. 2−84624
electron transfer reactions in solution, generalized mobility theory 2−84648
gas phase chain reactions in photochemical, radiolytic batch reactors 2−68760
glass, soluble, surface stabilization by alkali ion exchange 2−53519
ion exchange membrane/electrolyte solution system, Hall mobility 2−43386
methyl iodide fixation by silver zeolites 2−84640
multi-site, principles of n.m.r. investigations 2−61763
n.m.r. spectra, molec. reorganization effects on line shapes 2−54524
reactive scattering calculations, exact quantum mechanical method 2−69602
seawater evaporation, migration of chemical components from ocean to atmosphere, ratios 2−62151
sequential ion exchange separation in mixed oxide nuclear fuels, burn-up and isotopic distribution meas. 2−75401
zeolite, adsorpt. of ethane and ethylene, effects of size, charge and conc. of exchange cation 2−74646
B isotope separation, ion exchange process 2−64082
$CO_2 + N_2O$ collisions, vibr.-translation and vibr.-vibr. exchanges 2−43034
$CS_2 + S = CS + S_2$ gaseous equil., heat of form. of CS 2−72544
$CrCl_2.3AlCl_3$, chem. transport of $CrCl_2$, $CrCl_2$ prep. method 2−65361
$F + H_2 \rightarrow HF + H$, Monte Carlo calcs. of reaction rates and energy distribs. among products 2−57410
H atom exchange in reactive scattering, quantum mechanical calculations 2−69602
$H_2 + D_2 \rightarrow 2DH$ reaction paths 2−44466
$H_2 + I_2$, dynamics of mol. and atomic processes 2−51423
InSb-I_2 system, gas transport reactions, whisker growth, morphology 2−75366
$Li_2O.Al_2O_3.2SiO_2$, glass, fibres, ion exchanged, internal friction, Li and Na conc. profiles 2−80754
$N + N_2$ collision, exptl. investigation 2−54528
Na borosilicate glass, Na^+-K^+ ion exchange 2−53537
Na silicate glass, surface stabilization by ion exchange 2−53538

Excimers *see Molecules/excitation*

Excitation *see Atoms/excitation; Molecules/excitation; Nuclear excitation; Vibrations/excitation*

Excitons *see Crystal electron states/excitons*

Excitons, molecular *see Molecules; Polymers*

Exoelectron emission *see Electron emission*

Exosphere *see Atmosphere/upper*

exp-6 potential *see Kinetic theory; Molecules/intermolecular mechanics*

Expanding universe *see Cosmology*

Expansion, thermal *see Thermal expansion*

Exploding wires
aerosol generator, evaluation for use in inhalation obs. 2−85160
discharge, neutron prod. 2−67665
electrode or end effects, influence of electrode materials 2−69785
generation of cylindrical stress waves 2−41600
multipole radiation source, exploding wire Sn 2−46441
radiation multipole, ultra high speed photography 2−45620
W, in vacuo, X-ray production 2−76135

Explosions
see also Detonation; Exploding wires; Shock waves
above-ground and underground, calc. of surface and ground waves 2−81566
in atmosphere os arbitrary density distrib. 2−84817
atmospheric, seismic and microbarographic signals 2−57633
blast wave problems, evolution of discontinuity in self-similar flows 2−73458
brittle body fracture by explosion, anal. 2−69782
calculation in media with polymorphic phase transitions 2−58937
conbustible gas, propagation of blast waves 2−80380
detonation, of secondary explosives, laser radiation use obs. 2−69784
earthquakes, low power, low cost station 2−81575
elastic waves from circular disc source, explosion inside oblate spheroidal and circular cylindrical cavities 2−51503
electric discharge phenomena in supertankers and supersonic aircraft 2−77310

Explosions continued
explosimeter, instrument for predicting explosions by det. of explosible atmosphere 2−58938
explosive driven MHD multimegajoule pulse generation feasibility 2−59052
extragalactic phenomena, energy source for violent events 2−81865
fracture of triangular plaster of Paris plates due to contact explosive pressure 2−53793
galactic, model based on blast waves in rotating media in gravitational field 2−55014
gasdynamics, conference (Marseille, France, Sept. 1971) 2−80375
geophysical prospecting, marine exploration 2−84753
geophysics, prestressed media, stress wave radiation from explosions 2−81604
ground motions of initial ejection phase of underground explosions, X-ray photography 2−78931
hardening of two phase solids 2−80725
jet formation on collision of metals, explosive welding model 2−69783
meteor, gas dynamics 2−81900
molten metal interaction with water 2−73457
nonsymmetric dynamic expansion of cylindrical cavities 2−73456
porous NaCl, spherical charge, shock wave parameters 2−58936
in radio galaxies, dynamics 2−58401
reactions, decoupling of physical and chemical mechanisms 2−81486
S- and P-wave travel times and amplitudes, northern Australia 2−61883
self modelling motion during sudden liberation of energy in viscous and heat conducting gas 2−67705
supernova explosions, remaining ionization zones 2−81856
thermoluminescence changes following 2−84554
tubes, visco-plastic deformation as a function of the properties of the surrounding medium 2−60866
underground, wave propagation in nearly elastic range 2−57641
underwater, acoustic scattering from expanding bubbles, velocity effects 2−52237
underwater, deconvolution of refraction seismograms 2−65474
underwater, intense, shock wave calc., model 2−78930
underwater, total pressure waves, apparent transmission gain 2−41713
Upper Mantle Project, explosion seismology 2−57515
in water under impulse heavy current, shock wave pressure meas. 2−73452
weak, propag. in quasi-linear systems 2−66634
ν and νe, polarization effects 2−72696
H_2-air and methanol-air mixtures, thermal explosion, boundary of flame propagation region 2−75378

nuclear
aquifer systems response 2−57826
atmosphere, lightning induced by detonations 2−65794
atmospheric, exciting Rayleigh waves in ground below 2−65485
atmospheric, model for generation of hydromagnetic waves 2−65686
atmospheric electric field effects obs. 2−62277
Canadian seismograph network, P- and Rayleigh amplitude 2−57567
Cannikin, long period water wave meas. 2−62068
Cannikin, near field seismic motion 2−61937
Cannikin, P-wave residuals, anomalous upper mantle velocities det. 2−57642
Cannikin, reaction of shallow surface waters to ground shocks 2−57552
Cannikin, seismic and acoustic signal obs. using l.f. sonobuoys in aircraft 2−57592
Cannikin, strain and tilt records 2−61930
Cannikin, strain release characteristics and tectonic effects 2−61931
Cannikin, T-phase signal obs. 2−57593
CANNIKIN and MILROW, induced ground motion obs. 2−57551
Cannikin strain and tilt steps, interpretations 2−61929
CANNIKIN underground, of 1971, seismic effects 2−57607
Chinese tests, ^{90}Sr and ^{89}Sr fallout obs. 2−62285
decay of P waves, epicentral distance 2−81583
double fission isomer population kinetics 2−74124
earthquakes and underground explosions, P-wave amplitude spectra 2−57566
geothermal systems, effects upon 2−83041
high-altitude, fission fragment localization method 2−51630
inner core reflections, core mantle boundary diffraction 2−81580
JORUM underground explosion, stress changes in nearby rock 2−65468
Longshot, global tectonic implications from anomalous seismic *P* travel times 2−65500
Longshot, short period P-wave propagation 2−68838
Longshot, source parameters det. from teleseismic P-waves 2−57444
Milrow, source parameters det. from teleseismic P-waves 2−57444
MILROW underground, of 1969, seismic effects 2−57607
multisite estimation of source parameters 2−65494
nuclear debris cloud, temporal charges in horizontal diffusion parameters 2−65745
pseudo-aftershocks from underground nuclear explosions rel. to upper mantle and outer core 2−84728
radiation belt disturbance, hard radiation meas. 2−51639
radioactive fallout from test, γ-ray spectra and fractionation effect 2−79819
S-device, e.m. pulse and time-dependent escape of neutrons and gamma rays 2−56074
seismic amplitude yield scaling for underground explosions 2−57568
seismic data from 12 nuclear explosions detonated underground 2−65525
seismic signal comparison of earthquake and detonation 2−57570
short period seismic discrimination between earthquakes and underground explosions 2−72650
Starfish, decay lifetimes of artificial electrons 2−72846
Starfish electron decay time limits 2−65934
surface-wave and body-wave magnitudes, rel. to natural earthquakes 2−61877
teleseismic P-wave amplitude obs. 2−48382
trigger faulting, vertical displacement 2−81574
underground, Amchitka, seismic effects 2−57548
underground, anal. of P-wave amplitude spectra 2−65504

Explosions continued
  nuclear continued
    underground, body wave magnitudes at 1 Hz and 2 Hz, discrimination from earthquakes 2−48385
    underground, Cannikin, ground deformation measurements 2−57470
    underground, Cannikin, quasistatic magnetic field changes 2−58112
    underground, Cannikin, seismic effects 2−57550
    underground, collapse structure obs. 2−57830
    underground, compressional wave arrivals 2−57565
    underground, discrimination from earthquakes using improved M_s scale 2−68836
    underground, Love wave excitation 2−65491
    underground, model anal. of gas flow in backfill 2−53276
    underground, pseudo-aftershock obs. 2−57591
    underground, seismic source energies 2−72614
    underground, temporal change of travel times 2−57629
    underground, U.S.A., seismic source survey (1961-1970) 2−65466
    ^{214}Fr isomeric ratio determ. in ^{12}C and ^{16}O reactions on ^{205}Tl, ^{209}Bi 2−74123
    ^{237}Nb fission cross-sections by 20 eV to 7 MeV neutrons, nuclear explosive expt. 2−70492
    ^{115}Te, ^{117}Te, short-lived isomers obs. by pulse activation of enriched Sn isotopes using α-particles and ^{3}He beams 2−74036

Extensive air showers *see Cosmic rays/showers and bursts*

Extensometers *see Strain gauges; Thermal expansion*

Extra-terrestrial radiation *see Cosmic radiations, radiofrequency; Sun/radiation*

Extrusion *see Forming processes*

Eye
    see also Vision
    accommodation control circuit, continuous objective measurement 2−78674
    accommodative response times using histogram information 2−66378
    action spectra of retinomotor and pupillary responses 2−51971
    albino rats, monkeys and man, isolated retinas, optical modulation 2−78684
    alpha activity, change in freq. following eye opening and closure 2−78672
    animal holding platform for slit lamp exam. 2−55325
    artificial eye unit, review 2−51959
    autonomic effector control loop, qualitative model 2−76107
    bee photoreceptor, light absorption 2−62886
    carotid angiography, X-ray doses 2−69334
    cat, anaesthetized paralyzed, torsion meas. during receptive field studies 2−51997
    cats, ERG and late receptor potential depression by light deprivation 2−51994
    central and peripheral ganglion cells, differential effects of refractive errors and receptive field organization 2−69474
    characteristics from lighting viewpoint 2−85154
    chicks, growth pattern, light induced alterations 2−66322
    childhood optic neuritis, electroencephalographic changes 2−73227
    colour contrast borders, visibility 2−62885
    contrast sensitivity, influence of reference cues 2−78678
    cornea-retinian electrical fields, instrumentations for obs. of potential difference caused 2−69458
    corneal configuration by meas. of derivatives 2−66318
    corneal thickness control, unsteady state description of corneal mass transport 2−78670
    corneal topography, differential equation used with diffused ring photokeratoscope 2−66314
    corneal topology, meas. 2−66319
    cortical evoked potential from visual stimulus 2−62878
    dark adaption, early phase, threshold rise after bleaching 2−51970
    diagnosis of diseases, mathematical model for flicker e.r.g. 2−69469
    drosophila, transient and receptor potentials in electroretinogram 2−85153
    eccentric fixation in amblyopia ex anopsia, entoptic method 2−66313
    electroretinogram, components 2−51940
    e.m. radiation effects during welding 2−69461
    evoked cortical potential, photopic and scotopic contribution 2−85143
    evoked responses in visual pathway of cat with elevation of intraocular pressure 2−78685
    frog's cone system suppression in dark 2−51996
    frog retina, lateral spread of signals, light adaption and excitation 2−51998
    fundus oculi obs. using retinophot 2−45830
    fundus reflectometer 2−66312
    glass spectacle lenses with back surface vinyl membrane, fracturing and safety properties 2−70066
    goldfish, optic nerve fibres, rod and cone input 2−66352
    honey bee, compound, long wave photoreceptor distrib. 2−62887
    human visual system, edge detector neurones 2−51962
    interpupillary distance meas. with pupillometers 2−51956
    intraocular noise, origin and characteristics 2−66357
    isolated frog retina, cone system, adaptational changes 2−51995
    lamellar structure of bleached and unbleached rod photoreceptor membranes 2−48925
    lamellar structure of bleached and unbleached rod photoreceptor membranes 2−48925
    lens change in rabbit, X-ray and proton induced 2−78673
    lens opacification in mice, dose dependence of fast neutron RBE 2−78671
    lesion detection, applic. of Cherenkov phenomenon 2−69459
    light adapted retina, changes of psychophysical organization 2−51957
    Limulus, nerve impulses in eccentric cells, variability in firing 2−73228
    mammalian retina, isolated, fast intraretinal potentials 2−51960
    mesopic region, differential sensibility and black light density 2−78682
    monkey optic tract fibers maintained activity and lateral geniculate nucleus cells 2−52000
Eye continued
    monkey optic tract fibres response to monochromatic lights 2−51999
    monochromatic aberration, effect of spherical spectacle lenses 2−78676
    Movement, effect of target contrast variation 2−66321
    movement, pursuit, release using after image, uncancelled corollary discharge 2−66323
    movement quantity during fast sleep, time variations 2−48923
    movement quantity during fast sleep, time variations 2−48923
    movements, role in perception of apparent motion 2−76106
    mudpuppy retina sensitization 2−82073
    nervous system model 2−85141
    ocular interdependence studied by electroretinography 2−76108
    oculomotor imbalance investigation using electro-oculography 2−51941
    off axis imaging 2−62879
    oil droplets in passerine birds, distribution localization and absorption characts. 2−69475
    ophthalmology, average visual evoked potentials 2−62835
    perimetry information theoretic basis for computer control of automated perimetry 2−85142
    photographic obs. using 35 mm camera 2−85138
    photokeratoscopy, eye adjustment method 2−66320
    pigeon, elec. responses to wavelength changes of stimulating light 2−51990
    primary receptor cells, excitatory mechanisms 2−82064
    protection from i.r. laser radiation 2−76109
    protective lens materials, ballistic testing 2−48926
    protective lens materials, ballistic testing 2−48926
    pupil diameter changes in dark, age dependence 2−66316
    pupil diameter role in contact lens data 2−55320
    pupil light reflex, adaptation 2−51966
    pupil size, bleaching and backgrounds 2−51965
    rabbit corneas, light scattering obs. 2−69477
    rabbit eye lens opacities after 2.45 GHz irradiation 2−51926
    rat retina, electroretinogram 2−52001
    rat schematic eye, revision 2−51961
    resolution and contrast sensitivity at low luminance 2−51964
    retina, diffusive properties, aberrations 2−78675
    retina, oculomotor error signal 2−51979
    retina, peripheral, spatio-temporal integration 2−51967
    retina, visual acuity testing using Moire fringes 2−45171
    retina model 2−78680
    retinal and cephaline in α-tocopherol membrane, photovoltaic e.m.f. 2−85089
    retinal image and excitability of retinal ganglion cells, linear systems theory description 2−51981
    retinal lesions caused by microwave exposure 2−69460
    retinal photopigments photoproducts and visual adaptation 2−51963
    retinal receptor orientation and role of fibre optics in vision 2−73226
    retinoscopic reflex, videotape recording, methodology and instrumentation 2−45172
    rhodopsin content and visual threshold, bleach regeneration and dark adaption 2−51969
    saccadic behaviour, effect of foveal and non-foveal after-images 2−51968
    safety, effects of laser beam scintillation in atmosphere 2−48924
    safety, effects of laser beam scintillation in atmosphere 2−48924
    scotopic transmittance variability for red and blue filters 2−66324
    sheeps electroretinagram component analysis 2−85145
    signal detection, confidence and cortical evoked potential 2−82074
    single binocular vision, Panum's limits, low scotopic luminance 2−78679
    soft contact lenses, visual acuity, astigmatism 2−66325
    spectacle lenses, comparison of reliability and durability for glass and plastic lenses 2−58647
    star tracing, sex and eye-hand preferential difference 2−66315
    tinted ophthalmic lenses, function, evaluation and evaluation 2−62881
    tissue photocoagulation, therapy 2−48876
    tissues, nonionizing radiation effects 2−48875
    tonometry, contact problem of two thin spherical shells 2−82065
    Troxler's effect, total disappearance time in peripheral vision 2−78677
    vergence movements to pairs of disparity stimuli with shape selection cues 2−62880
    vertebrate retina model, spatio-temporal information processing operations 2−76110
    visual system and neuronal specificity 2−51958
    voluntary saccadic movements, kinematic characteristics 2−69457
    wide angle optical model 2−66317
    Ar retinal vascular and macular diseases, photocoagulation, 4W laser, design and construction, clinical results 2−82018
    $Na_2{}^{75}Se$ disappearance rate in rat's eye, comparison of meas. with CdTe and Si(Li) probes 2−51992

F-centres
    alkali halides, absorpt. band, spin mixing and circular dichroism, electron spin memory 2−53750
    alkali halides, dynamical Jahn-Teller effect in relaxed excited state 2−43647
    alkali halides, emission mechanisms 2−80709
    alkali halides, F_{a1}, F_{a2}, U centres, temp. depend. of peak position of absorpt. and emission bands 2−75298
    alkali halides, optical pumping cycle dynamics, relaxed-excited state detection 2−53749
    alkali halides, spin-orbit effects in absorpt. bands 2−51335
    alkali halides, temp. dependence of peak position of absorption and emission bands 2−75298
    alkali halides, X-ray scatt., quantum theory 2−47444
    band mode exam. in semiconductors and insulators 2−54448
    electronic structure, theoretical developments, review 2−56746
    electronic wave functions calcs. for ionic crystals 2−84247
    hyperfine interactions, high pressure ENDOR cavity 2−82412
    ionic cryst., defect form. mechanism and struct. 2−80702
    ionic crystals, multistage formation of irradiation-induced defects 2−78087
    radiative decay, effects of random fields 2−74800
    reactive tunnelling, classical S-matrix theory 2−72551

F-centres continued
  BN, hexagonal, paramag. centre identification 2−72430
  $BaBr_2$, optical absorp. and e.s.r. spectra obs. 2−51336
  $BaCl_2$, optical absorp. and e.s.r. spectra obs. 2−51336
  BaFCl, X-irrad. and additively coloured, absorpt. 2−64680
  BaO, F, F^+ centres obs. at 77 K 2−74803
  BeO, electron irrad., e.p.r. obs. 2−47366
  CaF_2:La,Ce, X-irrad., rel. to charge transfer processes 2−65253
  CaF_2, $\langle 100 \rangle$ and $\langle 110 \rangle$ oriented F_2-centres 2−53751
  CaF_2, coloured, zero-phonon line obs. 2−53752
  CaO, excited state of F-centres, optical detection, of paramagnetic resonance 2−44437
  CaO, F^+ and F-centres, absorpt. and emission, temp. depend. 2−84537
  CaO, F^+ and F′ centres 2−71523
  CaO, Jahn-Teller coupling in excited level of F^+ centre, uniaxial stress effects 2−68635
  CaO, neutron irrad., F_a^+ centre, emission and absorp. band obs. 2−71522
  CaO, neutron irrad., F_a^+ centre, emission and absorp. band obs. 2−71522
  $CdCr_2S_4$, red shift peak in absorpt. band, mag. F′ centre model 2−80712
  CsBr, electric field effects on F-band 2−51347
  Csbr, photoemission and photostimulated emission rel. to image storage targets 2−48023
  Cscl, photoemission and photostimulated emission rel. to image storage targets 2−48023
  KBr:Na, F_b centres, absorpt. and emission study 2−64682
  KBr:PO_2, recombination luminescence, F-centre accumulation during β-irradiation 2−78136
  KBr, computation of electronic structure of colour centres and electronic polarization fields 2−71520
  KBr, transient form., pulsed electron beam 2−53753
  KCl:Ca, Sr, X- irradiated, thermal annealing of defects 2−50696
  KCl:Na, F_b centres, absorpt. and emission study 2−64682
  KCl:Na, X-irradiation, room temperature, effect of Na impurity 2−77595
  KCl:OH^-, X-irrad., temp. effect on F-centre formation 2−47449
  KCl:Tl, electron pulse irrad., absorpt. study 2−71524
  KCl:Tl, KBr:Tl detection of Tl^+ centres by recombination radiation from F centers 2−81001
  KCl, computation of electronic structure of colour centres and electronic polarization fields 2−71520
  KCl, F-centre g_{orb} factor determ. by mag. circular dichroism and Faraday effect 2−77596
  KCl, F′ to F centre conversion, ENDOR obs. 2−71529
  KCl, γ-ray induced, strain effects 2−71528
  KCl, photoemission in ultra high vac. 2−48023
  KCl, thermal aggregation mechanisms 2−64683
  KCl, thermal transform. into colloids, dislocation induced precip. 2−71525
  KCl, transformations on flash light excitation, absorpt. spectra obs. 2−43649
  KCl(Br), press. depend. of F-centre hyperfine interactions, ENDOR 2−83986
  KI:Tl, recomb. and capture probabilities of F-centre electrons 2−84285
  KI, photoemission in ultra high vac. 2−48023
  KI, relaxed-excited state of F-centre, wave function determ. 2−68738
  $KMgF_3$-$KMnF_3$ mixed crysts., electron irrad., prod. suppression by Mn, new defect obs. 2−68040
  LiCl possibility of regeneration of wave functions of localized electrons for F-centres 2−68041
  LiF, possibility of regeneration of wave functions of localized electrons for F-centres 2−68041
  LiF(Cl), press. depend. of F-centre hyperfine interactions, ENDOR 2−83986
  MgF_2, radiation damage process 2−56747
  MgO, $F^+ \rightleftarrows F$ centre conversion obs. 2−68043
  MgO, MeV Ne^+ irrad., F-type centre prod., absorpt. band obs. 2−68042
  NaCl:Sr^{2+} F to Z_1 transition 2−84515
  NaCl, computation of electronic structure of colour centres and electronic polarization fields 2−71520
  NaCl, conversion to X-centre, lattice and disloc. mechanism 2−50698
  NaCl, decay of F_2 centres, 330 K luminescence maximum 2−51380
  NaCl, γ-irrad., plastic deform. effects, optical absorp. obs. 2−53755
  NaCl crystals containing colour centres, flow stress spectroscopy 2−81396
  RbCl:Na, F_b centres, absorpt. and emission study 2−64682
  RbCl, F_a(Li) centre, a.c. photocond. study 2−71530
  $SrCl_2$, mag. circular dichroism on F-centre absorpt. band, $g_{orbital}$ factor 2−74805
  SrF_2:La,Ce, X-irrad., rel. to charge transfer processes 2−65253
  SrF_2, $\langle 100 \rangle$ and $\langle 110 \rangle$ oriented F_2-centres 2−53751
  SrF_2, coloured, zero-phonon line obs. 2−53752
  ZnO, electron irrad., e.p.r. obs. 2−47366
  ZnS, electron irrad., e.p.r. obs. 2−47366
F-layer *see Ionosphere/F-region*
Faculae *see Sun*
Fallout
  see also Atmosphere/radioactivity; Nuclear reactions and scattering; Radioactivity
  A-bomb, effect on chromosomes 2−62846
  atmospheric electricity, secular effects 2−65805
  atmospheric radioactivity, conference (Mishima, Japan, Nov. 1971) 2−62284
  fission fragments localization from high- altitude nuclear explosion 2−51630
  gamma ray anti-Compton spectrometer for marine environmental radionuclide analysis 2−82806
  and precipitation, relationship investigated 2−62282
  in rain, Melbourne, (1958-1970) 2−72814
  and release from nuclear power stations, γ-spectroscopic obs. 2−72690
  Ag, patterns from seeded convective storms 2−62220
  ^{90}Sr, bearing on weather conditions 2−62286
Fallout continued
  ^{90}Sr and ^{89}Sr, from Chinese nuclear tests 2−62285
Faraday effect
  anisotropic crystals, rotation tensor components, extraction 2−61587
  balance for low temp. mag. susceptibility obs. 2−73512
  biaxial crystals., diachroism rel. to Faraday rotation, transform. matrix 2−72259
  compact Faraday cup array for current distrib. obs. from pulsed electron beams 2−63272
  cosmology, Brans-Dicke, rot. concepts. 2−62436
  and electronic transitions, review 2−72294
  ferromagnetic materials, anisotropy of g-factor of rare-earth ions, low temp. study 2−65217
  ferromagnetic metal films, meas. of longitudinal effect 2−54379
  internal conical refraction, effects of optical activity of Faraday rotation 2−49430
  ionosphere, radio wave rotation, total electron content detn. 2−48570
  n.q.r. Faraday effect technique 2−84606
  paramagnetic crystal, Mossbauer dispersion and nuclear Faraday effect 2−78073
  paramagnetic materials, anisotropy of g-factor of rare-earth ions, low temp. study 2−65217
  probe for plasma magnetic flux density meas. 2−77279
  pulsed discharges in rarefied gases, mag. field meas. 2−78992
  rare earth ethyl sulphates, paramg. relax. obs., interactions contrib. to sp. ht. 2−57314
  rare earth iron garnets, temp. and field depend. 2−81286
  rotation, in self induced transparency 2−44324
  rotation by intergalactic magnetic field and steady state and Einstein-de Sitter cosmologies 2−54999
  solar bursts, Faraday rot. and tangled mag. fields 2−62806
  transition metals, in soln., const. of stability and specific mag. rotation determ. 2−66823
  CaF_2:Ce^{3+}, paramag. relax., obs. by magnetooptic Faraday effect 2−72231
  $CrBr_3$, three-dimens. magnetization struct. obs. 2−78013
  EuO:Gd, rotation rel. to exchange-induced imperfection ionization 2−68598
  $FeBr_2$, temp. and field depend., of mag. rot. power 2−65218
  GaAs film, epitaxial, heavily doped 2−65214
  GaSe, in exciton absorpt. region 2−72263
  GaSe, near absorpt. edge 2−72262
  n-Ge, effect of ionized impurity scattering 2−51302
  Ge, i.r., hot electron transfer between equivalent valleys obs. 2−78067
  Ge, magneto-microwave free-carrier absorpt. in Faraday config. 2−68605
  n-Ge microwave Faraday effect, multiple reflections and lattice and impurity scatt. effects 2−75257
  α-HgS, synthetic, rotation 2−75258
  n-InSb, of hot electrons in i.r. 2−57326
  KCl, F-centre g_{orb} factor determ. 2−77596
  Li dispersion in vaseline, r.f. effect 2−43410
  Mg-Mn ferrite film, transparent, light diffraction by mag. stripe domains 2−65220
  Mn complex, Mn-amine, exchange interactions, mag. susceptibility 2−65124
  MnBi films, Ti-substitution effect 2−51265
  PbSe, free carrier dependence 2−84469
  n-Si, microwave measurement 2−61591
  Tm orthoferrite, obs. of stripe struct. 2−54384
  YIG, 1.15μ 2−72266
Fatigue
  8/65/35 PLZT fine grained ferroelec. ceramic, dielec. and optical fatigue effects 2−77953
  alloy 800, low-cycle fatigue and stress relaxation at elevated temps. 2−60947
  alloys, heat resistant, testing at elevated temperatures and aeronautical application 2−56870
  alloys, high temperature, design for use with gas turbines 2−56882
  aluminium alloy (2618-T6), fatigue testing at elevated temperatures and aeronautical application 2−56870
  bending, low-cycle, machine for testing 2−64740
  brass, cracking effects of grain and twin boundaries, slip mode behaviour 2−71598
  brass, u.s. fatigue inhibition 2−50767
  brittle materials, dependence of test results on nature of stress state 2−56841
  brittle materials, fatigue failure probability determ. 2−60994
  cermet, fatigue testing at elevated temperatures and aeronautical application 2−56870
  cobalt superalloy, FSX 414, thermal fatigue crack propagation testing 2−56878
  composite, fatigue crack damage, vibr. testing 2−60921
  composite, fibre-reinforced, graphite/epoxy, compressive fatigue 2−61021
  composite materials, fibrous and laminates review 2−43901
  $^1/_2$Cr-Mo-V steels, high-strain fatigue properties 2−60948
  crack, instrument for recording time of initiation of fatigue crack and rupture of specimens 2−71610
  crack growth rate and crack opening displacement 2−84019
  crack initiation and propagation, review 2−60892
  crack propagation analysis 2−77655
  cracks, growth in A286 at 1100°F effects of frequency and environment 2−56861
  cumulative shock loading using ballistic impact 2−60939
  cyclic straining, subgrain formation 2−80763
  damage, steel and cast-iron, microhardness method 2−77670
  damage due to nonstationary random vibration of nonlinear structures 2−76347
  damage indicator, conducting polymer of epoxy matrix with graphite particles 2−53971
  deformation and fracture under cyclic and steady loads 2−56816
  deformation kinetics criteria of low cyclic creep fatigue at high temps. 2−56886
  ductility exhaustion model for prediction of thermal fatigue and creep interaction 2−60896
  elastomers, electron microscope investigation of fractured surfaces 2−60899

Fatigue continued
- elevated temperatures, conference, Storrs, USA, June (1972) 2−56859
- epoxy resins, (Epon 828), cyclic fatigue stress behaviour 2−64798
- extensometry, optical, for elevated temperature fatigue testing, survey 2−56871
- failure, materials under broad band random vibrations 2−77707
- failure at elevated temperatures, nucleation and cracking 2−60893
- failure of materials under narrow band random vibrations 2−48623
- fatigue-crack front straightness in K_{Ic} testing 2−71591
- fatigue-crack growth under cyclic loads, theory 2−69643
- fatigue-crack initiation from flaws using fracture mechanics theory 2−69649
- fatigue-crack propagation in metals and polymers, review 2−64728
- fracture toughness, in zone of stress concentrators 2−80787
- fracture under dynamic interactions 2−63063
- fretting, effects of contact pressure and hardness 2−43712
- glass, crack tip profile and static fatigue 2−53521
- glass reinforced plastics, debonding and cracking under tensile and fatigue loading 2−64725
- glass-reinforced plastics, behaviour in water under high stress 2−84083
- graphite, fatigue failure probability 2−53827
- graphite, fatigue failure probability determ. 2−60994
- high temperature low cycle fatigue, phenomenological theory 2−77682
- high temperature phenomenological mechanisms 2−56818
- high-pressure component fatigue failure evaluation, design features 2−69502
- high-temperature, monitoring using acoustic emission 2−56872
- impact fatigue testing machine, rotating disc type and applic. 2−80809
- incipient, ultrasonic techniques of meas. 2−64752
- Inco 713C alloy, low cycle fatigue tests and crack propagation rate at 1400F 2−56885
- Incoloy 800, high cycle fatigue properties at elevated temperatures 2−60951
- Inconel 718, surface integrity effect on fatigue at elevated temps. 2−60944
- Inconel alloy, X-750, fracture and creep-fatigue behaviour 2−56860
- lifetime predictions in turbine blades, stress calc. 2−56890
- limit definition 2−53832
- low-cycle, under random loads at elevated temperatures 2−56894
- low-cycle creep fatigue testing, method and equipment 2−56874
- low-cycle fatigue cracking, prediction method including biaxial stress and notch effects 2−56888
- magnesium alloy, fatigue failure, material properties control 2−60893
- mechanism, scanning electron microscope obs. 2−56787
- metal, characteriz. for reactor core applic. 2−59862
- metal, high-damping, stress level determ. up to fatigue limit 2−53861
- metal fatigue in liquid metal reactor component design 2−56893
- metallic materials microfractographic characteristics 2−50730
- metals, high power ultrasonics, uses 2−50794
- metals, temperature obs. during testing, radiation method 2−63157
- 9Ni-4Co-0.30C, fracture mechanics of crack growth at elevated temperatures 2−56867
- nickel superalloy, Rene' 77, thermal fatigue crack propagation testing 2−56878
- notch root radius effects on fatigue crack propagation and initiation 2−69648
- notched parts with compressive mean load, fatigue crack growth 2−47543
- notched specimens, fatigue strength estimation method 2−73390
- nucleation and growth of fatigue cracks from root of a notch 2−56817
- plastic, C-fibre reinforced, interlaminar-shear fatigue props. 2−71656
- plastic, crack tip profile and static fatigue 2−53521
- plastics, effect of frequency and loading history on bheaviour 2−64823
- polyester resins, (Paraplex P43), cyclic fatigue stress behaviour 2−64798
- polymers, failure under stress 2−53829
- polyvinyl chloride, fatigue crack propag. mechanism, comparison with polypropylene and ABS blend polymer 2−71601
- quartz, earthquake phenomena 2−65499
- quartzite, static fatigue, axial crack growth 2−60898
- refractive materials, programmed testing 2−41593
- Rene 80, Inconel 718, surface integrity effect on fatigue at elevated temps. 2−60944
- Rene 95, Inconel 718, surface integrity effect on fatigue at elevated temps. 2−60944
- resistance, effect of loading frequency at high temps. 2−56839
- rolled steel plate, anisotropy of fatigue limit 2−74872
- rubber components, tearing energy detn. for estimation of fatigue life 2−68102
- service life prediction in a fatigue creep environment 2−60953
- shafts, coefficient of reliability 2−52133
- solid propellant, simulated, low-cycle dynamic fatigue-curve for dynamic shock wave loading 2−84027
- stability tests, sensitivity estimates for asymmetrical loading cycles from strain diagrams 2−56840
- stainless steel, 20% cold-worked Type 316, fatigue- crack growth at elevated temps. 2−84141
- stainless steel, types 304, 316 estimates of creep-fatigue interaction in irradiated and unirradiated samples 2−83121
- stainless steel, types 304 and 316 low-cycle fatigue behaviour at LMFBR operating temps. 2−60945
- stainless steel electrodes, strength 2−80762
- steel, 0.16% low carbon, microstructure changes during thermal and low-cycle fatigue 2−60894
- steel, 08kp, kinetics of failure 2−53828
- steel, 18−8 stainless, cross slip, elec. microscope obs. 2−77686
- steel, 1%C, crack propagation, stress intensity and microstruct. effects 2−71645
- steel, alloys, fracture mechanics of crack growth at elevated temperatures 2−56867
- steel, austenitic stainless, effect of loading at high temp. 2−60946

Fatigue continued
- steel, ball bearing, rolling fatigue life, retained austenite effects 2−64764
- steel, carbon strain energy during rotatory bending fatigue, effect of pearlite patches 2−84125
- steel, deformed by reverse bending 2−50769
- steel, effect of cyclic bending, at 20 and −60°C 2−84080
- steel, effects due to stress fields around inclusions 2−47491
- steel, fatigue lifetime and Wohler curves, statistical study 2−43714
- steel, fatigue-crack growth, effects of oxygen, water-vapour and hydrogen 2−68067
- steel, heat treated, cyclic strain softening at various hydrostatic pressures rel. to short-life fatigue 2−68142
- steel, heat treatment depend. 2−60962
- steel, impact fatigue effect on microstructure 2−80809
- steel, low carbon, inelastic phenomena and kinetics of damage for cyclic loading 2−60915
- steel, low-C, bending fatigue tests, Wohler curves, slip lines, cracks 2−50979
- steel, low-c, yielding and fatigue reln. under static and dynamic loading 2−84023
- steel, low-carbon, study on fractured surface with different crack propagation rates, tip profile of cracks 2−84126
- steel, maraging, plane strain fracture toughness tests 2−60979
- steel, maraging weldments, sustained load failures 2−71590
- steel, martensitic, low-cycle, rel. to X-ray microstruct. 2−43715
- steel, mild, fatigue cracking, initiation, growth, rel. to thickness 2−53833
- steel, press. vessel material, time-depend. embrittlement phenomena 2−59849
- steel, quenched, quench-aged, fatigue behaviour rel. to microstruct. instability 2−50768
- steel, simulation of infrequent cycling, fatigue life data 2−71593
- steel, stainless, AISI 304, low-cycle fatigue, effect of strain rate and hold periods 2−60954
- steel, stainless, AISI 304 and 316, substructure correlation with elevated temperature low cycle fatigue 2−56819
- steel, stainless, fatigue failure, material properties control 2−60893
- steel, stainless, high cycle fatigue properties at elevated temperatures 2−60951
- steel, stainless, low-cycle fatigue and stress relaxation at elevated temps. 2−60947
- steel, stainless 18-8, at cryogenic temps., elec. microscope obs. 2−56939
- steel, stainless weldments, type 304, fatigue crack growth at elevated temperatures 2−56865
- steel, thick-walled cylinders, fatigue strength 2−64781
- steel, type 403, influence of NaCl in steam on v.h.f. high- cycle fatigue 2−60955
- steel in hydrogen atmosphere or vacuum, low-cycle fatigue 2−60891
- steels, austenitic, fatigue crack growth at high temperatures for types 304, 316, 321 and 348 2−56864
- steels ferritic, fatigue crack growth, threshold at 300°C 2−56863
- strainrange partitioning approach for creep fatigue analysis 2−56889
- strength, alternating tension and compression, plain and notched high strength mats., 500-700°C 2−74870
- strength and lives of press-fitted shafts under two-step pulsating load 2−69639
- superalloys, thermal fatigue behaviour, effect of metallurgical variables 2−56879
- supersonic transport, materials testing using simulated flight-by-flight loading 2−60952
- testing apparatus for simultaneous handling of four flat specimens 2−53854
- testing apparatus for use in controlled atmospheres 2−47566
- testing apparatus for use in controlled atmpspheres 2−47565
- testing at elevated temperatures, review 2−56869
- testing at high temp. in liquid corrosive medium 2−53848
- testing machine with programmed amplitude and frequency variation, temp. range 4.2 to 1000 K 2−53853
- testing temp. effects, on nodular cast iron 2−60923
- testing under bending and rotation, gripping collet design 2−53855
- theory of successive stochastic processes, analysis under variable stress amplitudes 2−73393
- thermal, general theory 2−60895
- thermal and low-cycle, relationship at elevated temperatures 2−60894
- thermal fatigue resistance of metals using fluidized beds 2−56877
- thermoacoustic fatigue testing of space shuttle thermal protection panels 2−56873
- thermomechanical, method of determ. for materials in contact with melts 2−64741
- thermoplastics, long term strength, fatigue failure 2−43718
- thick tube fatigue test apparatus using external and internal pressures 2−69500
- thick walled cylinder failure test-machine using fracture mechanics on pressure cycling 2−69501
- thin section material, low cycle fatigue bend test method 2−47570
- two-axial stress state specimens, machine for testing 2−43755
- Udimet 500, low cycle and fracture modes 2−56820
- Udimet 710, nickel-base superalloy, effect of mean stress on high-cycle fatigue at 1000°F 2−60950
- under combined stresses, review 2−47539
- u.s. transducer material fatigue testing of magneto- and electrostrictive materials 2−71625
- welded joints, assessment criteria 2−64768
- Zircaloy-2, containing ZrH_x, fatigue fracture 2−47649
- Zircaloy-2, low-cycle fatigue behaviour at 573 K 2−60943
- Al/B(C) fibre composites 2−56976
- 97.4%Al-Mg alloy, fatigue crack dependence, temperature dependence 2−56866
- Al-Mg alloy, slip struct. and crack growth 2−47519
- Al-Zn-Mg-Cu alloy, fatigue behaviour of bolted joints 2−71622
- Al-6Cu, DTD 5014 (RR58), L65, 2024-T 81, heat effects on fatigue of structural elements 2−60949
- Al, cross slip, elec. microscope obs. 2−77686
- Al, high purity, and dil. alloys, review 2−68076
- Al, slip struct. and crack growth 2−47519
- Al alloys, crack growth rate, special gauges for det. 2−60934
- Al alloys, fatigue damage at high temps. 2−80808

Fatigue continued
Al alloys in thick sections, fatigue-crack propagation characteristics 2−71592
Al_2O_3, static and cyclic fatigue behaviour 2−50766
$BaTiO_3$, dynamic fatigue, ageing of switching props. 2−72031
Co-base composite materials, superalloys with fibres obtained by directed solidification, properties 2−64793
Co-base superalloys, thermal fatigue crack propagation under strain-temperature cycles 2−56868
$2^1/_4$Cr-Mo ferritic steel, high cycle fatigue properties elevated temperatures 2−60951
Cu-Al alloys, cyclic fatigue damage, thermal cond. meas. 2−50672
Cu, cracking, effects of grain and twin boundaries, slip mode behaviour 2−71598
Cu, inelastic phenomena and kinetics of damage for cyclic loading 2−60915
Cu, point defect clusters, effect on fatigue hardening 2−53724
Fe-Ni superalloys, bend fatigue testing at elevated temperatures 2−56884
Ni-Al-W alloy, γ' matrix, fatigue fracture 2−43716
Ni-Cr lamellar composite alloy, fatigue deformation, crack propag., fracture energy 2−56821
Ni-base composite materials, superalloys with fibres obtained by directed solidification, properties 2−64793
Ni-base superalloy, dispersion strengthened, rotating bending fatigue tests 2−56883
Ni-base superalloy, low-cycle fatigue with thermal and strain cycling 2−56880
Ni-base superalloys, thermal fatigue crack propagation under strain-temperature cycles 2−56868
SiC ceramic, resistance to dynamic fatigue at room temp. in air 2−80761
Si_3N_4, ceramic, high density, fatigue behaviour, 250-1200°C 2−60897
steel, low C, changes of dislocation arrangement during fatigue process 2−84162
Ti-Al-V alloy, mill-annealed, fatigue crack growth, temp. effects 2−60904
WC-(25 wt.%)Co alloy, surface finish effects 2−43717

Fermi gas *see Quantum fluids/fermion systems*
Fermi level *see Crystal electron states/Fermi level*
Fermi surface *see Crystal electron states/Fermi surface*
Fermion systems *see Quantum fluids/fermion systems*

Fermions
see also Elementary particles; Quantum fluids/fermion systems; Statistical mechanics/quantum
closed fermion loops, gauge-invariant analytic regularization investigation 2−73730
current commutator algebra null-plane, abstracted from fermion theory 2−45899
dual model, two fermion vertices, for excited fermion states 2−82631
dually charged particles and dual invariance, classical description 2−52539
e.m. and weak masses, cancellation of divergences 2−63486
field, fermion source term, scaling props. of spin-1/2 operator 2−79459
fields introduced for renormalization purposes 2−73714
ground state, invariant cones and uniqueness 2−76558
nonlinear fermion-field equation of motion, exact nonperturbative soln. with compounds lying on Regge trajectory 2−79467
nuclear, ground state energy, many fermion, correction to 2-hole line-approximation eqns. 2−63752
pair creation in alternating external field, group theoretical aspects 2−52540
pair production in vacuum under electric field 2−82632
quantum fields with cut-off self-interaction, spin- momentum distribution observables and asymptotic fields 2−63456
Ramond fermion transition into Neveu Schwarz meson, general dual vertex 2−76617
scalar, Gupta-Bleuler formalism in massless Yang-Mills theory 2−73725
scattering, four-fermion amplitude free from kinematical singularities 2−59399
second quantization fermion operators, diagonalization of quadratic linear form 2−82629
urfermion represent. of boson creation and annihilation 2−79470

Fermium
nuclear targets, electrodeposition methods of prep. for cross section obs. and accelerator bombardment 2−73919

Fermium compounds
No entries

Ferrimagnetic resonance
see also Ferromagnetic resonance
$Li_{0.5}Fe_{2.5-x}Al_xO_4$, magnetization process, domain wall reson. study 2−72198
$Li_{0.5}Fe_{2.5}O_4$, reson. phenomena at moving domain boundaries 2−72456
$MnFe_2O_4$, reson. phenomena at moving domain boundaries 2−72456
$NiFe_2O_4$, reson. field reduction due to iodine additives 2−44279
$NiFe_2O_4$, reson. phenomena at moving domain boundaries 2−72456
YIG:Ru, magnetostriction consts. 2−44281
YIG, nonmag. ion substituted, polycryst., mag. parameters and lattice consts. obs. 2−61547
YIG, parallel pump spin wave instab., discrete magnon resonances 2−48271
YIG, reson. field reduction due to iodine additives 2−44279
YIG, reson. phenomena at moving domain boundaries 2−72456
YIG, substituted, ultra-low bandwidth, microwave loss 2−44435
YIG single cryst./polycryst. composites, amplified Hahn-type echoes 2−44270

Ferrimagnetism
see also Ferromagnetism
excitations, ordering, spin interactions, spin one ion Hamiltonian 2−48101
Heisenberg magnet, high-temp. susceptibility and crit. pt. behaviour 2−48099
hysteresis loop, magnetization mechanism, role of wall displacement and bulging 2−65167

Ferrimagnetism continued
spin waves and generalized susceptibilities for classical models 2−44269
susceptibility meas. on ferrimagnets, graphical analysis 2−81280

Ferrites
see also Magnetic properties of substances/ferrimagnetic
bubble domain materials, wall mobility and velocity saturation 2−81221
compaction kinetics during hot pressing 2−53882
cone, magnetostatic solns. of ferrimagnetic resonance 2−68724
core, fast magnetization reversal by external magnetostatic field 2−61542
cores, internal effective field during nonuniform rotation 2−69857
crystal growth, flux-pulling crystalliz. with heterogeneous seeds for hexagonal ferrites 2−71379
crystal growth for bubble domain memories 2−47199
cylindrical layered ferrite-metal medium, independent propagation of magnetostatic surface waves 2−81285
disaccommodation phenomena, nature of dissipative behaviour 2−72190
epitaxial films for mag. bubble domain memories prep. 2−72192
ferrite garnets, distribution of electromagnetic waves near compensation temp. 2−65211
ferrite-garnets, magnetic birefringence 2−65216
ferromagnetic reson., stress effect on linewidth 2−68720
ferromagnetic resonance, moments of absorpt. line, spin-wave and independent-grain approx. 2−72449
field ion microscopy exam. comparing orientation to nitrided samples of Fe and Fe-Mn alloys 2−64777
garnet film, epitaxial, magnetic bubble mobility measurement 2−57303
hexaferrites, Y-structures and more complex structures anti-symmetric exchanges between spins of cations 2−84436
hexagonal, with planar anisotropy under perpendicular pumping, first-order nonlinear theory 2−51269
for inductance cores, automatic testing apparatus for long term permeability loss measurement 2−45661
interface with dielectric, gyromag. surface waves 2−44271
magnetic bubbles, properties, applications, review 2−78035
magnetic phenomena of surface gas-solid interactions 2−84395
magnetostrictive ferrite transducer material, fatigue testing 2−71625
memory cores, strength, firing time depend. 2−84431
memory cores, strength rel. to water environment, comments 2−80756
memory cores, strength rel. to water environment 2−77652
nickel zinc ferrites, hot-pressed, flame-sprayed, permeability, temperature coefficient changes 2−84430
asparticle detectors, use of generation of u.s. waves, spin waves, and Cherenkov radiation 2−73941
permeability, relative, teaching expt. for determ. 2−41433
polycrystalline of Mg, Co, Ni, Zn, temp. dependence of Young's and rigidity moduli in range 90-570 K 2−68064
rare earth iron garnet, damping of domain wall motion 2−57304
rare earth ortho-ferrite, substituted, mag. non equivalent states, Mossbauer obs. 2−61602
rare earth orthoferrites, cryst. growth and phase relationships in R_2O_3-Fe_2O_3 melts 2−50601
rare earth orthoferrites, possibility of intermediate state existence for first order phase transformation 2−81291
rare earth orthoferrites and orthochromites, ang. depend. of superexchange interactions 2−68569
resonance phenomena in discs in presence of domain structure 2−68714
spin echo enhancement by double freq. pumping, mechanism 2−68740
spinel, ferromag. relax. of parametric spin waves 2−72228
spinel, time variation of electrical conductivity 2−47882
spinel, validity of Hall effect theory of small polaron 2−75083
spinel structure, magnetostriction constants, mag. dipolar interact. contrib. 2−78036
spinel type, magnetic and electrical props. 2−48100
steel, AISI type 310, transformation characteristics for ferrite, sigma phase and carbides, e. microscope study 2−68189
steel, AISI type 316, transformation characteristics for ferrite, sigma phase and carbides, e. microscope study 2−68189
strip line, loaded, propagation constant 2−49216
in waveguide, anomalous loss 2−59000
wustite, oxidation and reduction in H_2O vapour and H_2 mixtures, kinetics and mechanism 2−75381
wustite, reduction, crystal diminution 2−75380
YIG, nature of spin echo and obs. at 1.3 and 9.4 GHz 2−72522
δ-$AgFeO_2$, cryst., struct. 2−53652
$Ba_5Co_2(Cu_2)Ti_3Fe_{12}O_{31}$, magnetiz. and anisotropic props., rel. to microwave applic. 2−44273
$BaCo_xTi_xFe_{12-x}O_{19}$, mag. struct. 2−48102
$BaF_{12}O_{13}$, grinding and thermal treatment effects 2−54342
$BaFeO_{19}$, saturation magnetization, reduced temp. depend. by As or P substitution 2−78019
$BaFe_{12}O_{19}$, deform. texture 2−56962
$BaFe_{12}O_{19}$, high temp. enthalpy and specific heat 2−54049
$BaFe_{12}O_{19}$, sintering kinetics 2−77738
$BaFe_2O_4$, high temp. enthalpy and specific heat 2−54049
$BaFe_{12-x}Ti_xZn_xO_{19}$, mag. props., Ti-Zn cation distrib. effects, mag. saturation and neutron diffr. obs. 2−72195
$Ba_3Zn_2Fe_{24}O_{41}$, hexagonal, anisotropy, comparison with $BaMg_2Fe_{12}O_{22}$ 2−72451
Ca-Bi-V, excitation of longit. acoustic waves in rods 2−43968
CaO-FeO-Fe_2O_3, synthesis and physico-chem. props. 2−43871
$CdFe_2O_4$, specific saturation magnetization depend. on prep. conditions 2−84432
Co, cation re-ordering, temp. depend. of cond. time variation obs. 2−75145
$CoFe_2O_4$ films, monocryst., domain struct. and mag. polarity reversal 2−61523
$Co_xNi_{1-x}Fe_2O_4$, magnetostriction and mag. parameters, temp. variation 2−72196
$Co_xZn_{1-x}Fe_2O_4$, Fe^{3+} spin fluctuations, mag. hyperfine splitting, relax. effects, Mossbauer spectra 2−81287
Cu, cation re-ordering, temp. depend. of cond. time variation obs. 2−75145

Ferrites continued
$Cu_{0.5}Fe_{2.5}O_{4|x}$, spinel ferrite, neutron-diffraction study, with and without mag. field 2−61543
$ErFeO_3$, mag. struct., Mossbauer obs. 2−44351
$ErFeO_3$, with high coercivity surface layer, domain struct., magnetooptical obs. 2−81284
Fe rich, induced anisotropy and disaccommodation, mag. relax. obs. 2−48112
$Fe_{3-x}Mg_xO_4$, ferrite-spinels, Mossbauer spectra and effect of admixture 2−72282
$Fe_{3-x}Sc_xO_4$, electronic struct. of ions 2−48207
$(Gd,Tb,Eu)_3Fe\,O_{12}$ garnet, optical anisotropy and cylindrical domains 2−68602
Li, magnetostriction, effect of Co ions 2−65158
$Li_{0.5}Fe_{2.5-x}Al_xO_4$, lattice const., comp. depend. 2−47334
$Li_{0.5}Fe_{2.5-x}Al_xO_4$, magnetization process, domain wall reson. study 2−72198
$Li_{0.5}Fe_{2.5-x}Al_xO_4$ $(0 \leqslant x \leqslant 1)$ and $Li_{0.5}Fe_{2.5-x}Ga_xO_4$ $(0 \leqslant x \leqslant 1.63)$, spinel ferrites, electric fields at lattice points and magnetic anisotropy 2−72194
$Li_{0.5}Fe_{2.5-x}Ga_xO_4$, supertransferred hyperfine fields at ^{69}Ga and ^{71}Ga 2−54511
$Li_{0.5}Fe_{2.5}O_4$, ferromag. relax. of parametric spin waves 2−72228
$Li_{0.5}Fe_{2.5}O_4$, mag. props., synthesis conditions influence 2−44277
$Li_{0.5}Fe_{2.5}O_4$, reson. phenomena at moving domain boundaries 2−72456
$Li_{0.5}Fe_{2.5}O_4$, supertransferred hyperfine field at ^{57}Fe, n.m.r. study 2−78169
$Li_{0.45}Mn_xFe_{2.55-x}O_4$, anisotropy contrib. of Mn^{3+} and related directional orders 2−65170
$Li_{0.93}Na_{0.07}Fe_5O_8$, sintering, effect of conditions on density and particle size 2−64790
$LiO_2(5-2t)Fe_2O_3tCr_2O_3$, crystallographic struct., influence of heat treatment 2−57021
$Li_{1-x}Zn_{2x}Fe_{5-x}O_8$, high temp. enthalpy and specific heat 2−54049
Mg-Mn, electronic struct. of Mn and Fe ions 2−47182
Mg-Mn film, transparent, light diffraction by mag. stripe domains 2−65220
Mg-ferrite, spin-wave instability, obs. 2−78151
Mg, magnetostriction, effect of Co ions 2−65158
$Mg_{1-y}Co_yFe_2O_4$, mag. anisotropy, ferromag. reson. study 2−81283
$MgFe_2O_4$, exchange anisotropy and relax., degree of treatment depend. 2−72156
$MgFe_2O_4$, ferromag. relax. of parametric spin waves 2−72228
$MgFe_2O_4$, temp. depend. of permeability, anomaly at Curie temp. 2−72167
$MgFe_2O_4$ films, mag. polarity reversal, temp. effect 2−61537
Mn-Fe-Ti-O system, mag. props. and crystallochem. 2−44254
Mn-Mg-Fe film, flash evaporated, chem. comp., X-ray fluoresc. obs. 2−71331
Mn-Zn-Fe, permeability, thermal change, resonance type profiles 2−61545
Mn-Zn, powders, comp. effects on technological props. 2−68163
Mn-Zn, single crystal, signal processing technique to obtain Kerr effect M-H loops 2−48064
Mn, Kerr effect and optical consts., magnetooptical reson. in visible 2−81337
$MnFe_2O_4$, acoustic magnon dispersion, neutron diffr. obs. 2−61544
$MnFe_2O_4$, reson. phenomena at moving domain boundaries 2−72456
$MnFe_2O_4$, single cryst. film, spin wave resonance 2−72454
$Mn_xFe_{3-x}O_4$, ferromag. reson., 77-350K, 9.3 GHz 2−44430
MnZn ferrites, influence of Ti ions on mag. props. 2−84405
$Mn_{1-x}Zn_xFe_2O_4$, mag. order 2−78022
$Mn_{1-x}Zn_xFe_2O_4$, magnetic order 2−65168
$NdFeO_3$, spontaneous magntiz., moment temp. depend., effective field 2−72221
Ni-Co-Zn, h.f. mag. props., temp. depend. 2−68723
Ni-Zn-Co ferrite film, anisotropy induced by thermomagnetic treatment 2−81228
Ni-Zn, mag. losses in h.f. fields 2−84435
Ni-Zn, powder, quality characterization 2−57312
Ni-Zn , powder, hot-pressing and densification 2−43893
Ni, cation re-ordering, temp. depend. of cond. time variation obs. 2−75145
Ni ferrites, iron rich, Hall mobility measurements, room temp. to 600°C, activated hopping process 2−81069
NiFe, freq. effect, torque obs. 2−44278
$NiFe_{0.8}Cr_{1.2}O_4$, statistical angular spin configurations 2−72200
$NiFe_{0.8}Cr_{1.2}O_4$, structural transition at mag. transformation, Mossbauer and X-ray obs. 2−72201
$NiFe_2O_4$, cryst. growth rate variation with supersaturation in fluxed melts 2−47255
$NiFe_2O_4$, ferromag. relax. of parametric spin waves 2−72228
$NiFe_2O_4$, magnetocryst. anisotropy, reson. fields, iodine additive effects 2−44279
$NiFe_2O_4$, reson. phenomena at moving domain boundaries 2−72456
$NiFe_2O_4$ films, ferromag. reson., etching effect 2−44431
$Ni_{1.2}Fe_{1.7}Sb_{0.1}O_4$, supertransferre d hyperfine fields and covalency at diamag. cations 2−48150
$Ni_{1-x-y}Fe_x{}^{2+}Zn_yFe_2{}^{3+}O_4$, spinel, Fe^{2+} cation distrib., i.r. spectra and Mossbauer obs. 2−72341
$Ni_{1-x}Zn_xFe_2O_4$, high temp. enthalpy and specific heat 2−54049
$Ni_xZn_{1-x}Fe_2O_4$, thermal expansion coeffs. at Curie pt., conc. depend. 2−81281
$Ni_xZn_{1-x}Fe_2O_4$ dielectric properties, 10^2-10^6Hz; −60-0°C, dispersion regions 2−84358
$PbFe_{12}O_{19}$, saturation magnetization, reduced temp. depend. by As or P substitution 2−78019
Sc, struct. rel. to spectral props. 2−54440
$SrF_{12}O_{19}$, saturation magnetization, reduced temp. depend. by As or P substitution 2−78019
$SrFeO_3$, mag. struct., neutron diffr. obs. 2−81282
$SrFe_{12}O_{19}$, crystallized from B_2O_3-SrO-Fe_2O_3 glasses 2−54345
$SrO(6-x)Fe_2O_3xAl_2O_3$, influence of thermal history on Mossbauer spectra 2−48144
$TbFeO_3$, mag. struct., shape effects 2−61559
Tm orthoferrite, Faraday effect, periodic stripe struct. 2−54384
$TmFeO_3$, orthoferrite, domain struct., effect on mag. field 2−57306
$TmFeO_3$, spin reorientation, n.m.r. study 2−44460

Ferrites continued
Y orthoferrites and orthochromites, ang. depend. of superexchange interactions 2−68569
$Y_3Fe_{5-(x\|y)}Al_xGa_yO_{12}$ garnet, magnetiz. and ferromag. resonance 2−72204
$YFe_{1-x}Al_xO_3$, local mag. field at ^{57}Fe, effect of Fe^{3+} exchange linkages, Mossbauer obs. 2−72288
$YFe_xCr_{1-x}O_3$, mixed, x=0, 0.3, 0.5, 0.7, 1 mag. props., 78K to Neel point 2−77996
$YFeO_3$, cryst. growth and characteriz. 2−50605
$YFeO_3$, with high coercivity surface layer, domain struct., magnetooptical study 2−81284
$Y_3Ga_{1.1}Fe_{3.9}O_{12}$ layer, laser beam thermomagnetic recording 2−51273
YIG/Ge interface, interaction of surface magnetostatic waves with carriers 2−84420
YIG-Si, thermally induced negative resistance 2−51145
YIG, ferroacoustic surface wave resonance 2−51035
YIG, parallel pump spin wave instab., discrete magnon resonances 2−48271
YIG, polycryst., spin wave transit time, limitation by pores 2−75232
YIG, reson. phenomena at moving domain boundaries 2−72456
YIG, single crystals, surface nonlinearities, obs. 2−51270
YIG, surface spin wave propagation in inhomogeneous fields 2−78037
YIG, tangentially magnetized substrate, magnetoelastic, Rayleigh type surface wave 2−43976
$(Y_2O_3)_3(Fe_2O_3)_5$ garnet, photocond., 280-800 nm 2−84380
$Zn_xMfe_{2-x}O_{4-x}F_x$, M=Ni, Co, synthesis, magnetization, hopping cond. 2−75234

Ferroacoustic resonance
No entries

Ferroelectric devices *see Dielectric devices*

Ferroelectric materials
see also Antiferroelectric materials
8/65/35 PLZT fine grained ferroelec. ceramic, dielec. and optical fatigue effects 2−77953
— 2−72041
— 2−72367
$(C_2NO_2H_5)_3H_2SO_4$, triglycine sulfate, second order ferroelec. transitions, calorimetric exam. 2−77951
applications and physical study 2−68467
arsenates, H-bonded, EPR and ENDOR 2−68734
bibliography, 315 refs. 2−77954
bibliography, October to December 1971 2−44158
ceramic, transparent, elec. and optical props., grain size and porosity effects 2−57244
ceramics, effect of nonlinearities, on design of sonar and industrial transducers 2−49156
dicalcium strontium propionate, 180° domain struct., electron mirror microscope obs. 2−65060
dielectric const., complex, frequency and temperature dependence near Curie point 2−84365
displacive type, phase transition, lattice dynamics, polarization correlation 2−81127
domain structure, effect on thermodynamic parameters near Curie point 2−72146
domain structure, temp. effects, scanning electron microscope obs. 2−81132
domain structures, phase transition, scanning electron microscope 2−57240
domains, symmetry props. 2−77522
$Fe_{1-x}S$, semicond. uniaxial ferroelec. qualitative model 2−77956
ferroic crystals and ceramics, coupled props. 2−57238
film, critical thickness and thermodynamic stability 2−61425
glycine silver(I) nitrate, cryst. struct. 2−47356
hydrogen bonded, random phase approx., Blinc-De Gennes model 2−57239
hydrogen-bonded, harmonic generation, tunnelling model 2−44326
hypersonic wave propag., nonlinear effects, slowly varying amplitudes method 2−77775
ice, polariz. and depolariz. current obs. at low temp. 2−57242
interband absorption, in quasi-classical random field, theory 2−48166
$KDHPO_4$ ferroelectric transition, molecular field approx. study 2−65062
Langbeinites, structural phase transitions 2−61423
lithium ammonium tartrate, n.m.r., ferroelec. paraelec. transition phenomena 2−72527
model of ferroelectric soft mode based on lattice dynamics, dielectric properties 2−81152
order-disorder type, dielec. dispersion 2−72027
order-disorder type, nucl. double reson. studies 2−81481
order-disorder type, temp. dependence of n.m.r. spectra second moment 2−81150
permittivity and pyroelec. coeff. from pyroelec. response to step radiation signals 2−81126
phase transition dynamics, spin-lattice relax. meas. by double reson. 2−84450
piezoelectric and electrooptic materials 2−45641
PLZT ceramics, crystal structure and enhanced ordering of ferroelec. domains 2−80760
Rarita-Schwinger field with spin $^3/_2$, gauge props. 2−73702
Rochelle salt, far i.r. spectra, using Fourier transform spectrometer 2−72319
Rochelle salt, sp. ht. anomaly, two sublattice treatment 2−43990
Rochelle salt, thermal cond., Curie pt. phenomena 2−44001
second harmonic scattering of light, domain shape effects 2−82508
semiconducting alloy, doped, transition temp. rel. to ferroelec. Curie temp. 2−44071
sodium ammonium tartrate, ferroelec. phase transition mechanism 2−81139
solid solution, thermodynamic theory 2−61424
solid solutions, phase transition, thermodynamics 2−65057
switching, domain wall motion kinetics, general formulation 2−72025
thiourea, paraelec. and ferroelec. phases, i.r. absorpt. 2−75309
thiourea, Raman spectra above and below ferroelectric transition point, 169K 2−75314

Ferroelectric materials continued
transformation, material with temp. independent elec. susceptibility in prototypic phase 2−72026
triclycine sulphate, semiconductor electrodes on insulators, aftereffects 2−77905
triglycerine sulphate, effect of growth rate on defect struct. and dielec. props. 2−47987
triglycine fluoroberyllate, thermal expansion in ferroelec. transition region 2−71751
triglycine selenate, thermal and elastic props., deuteration effects 2−72042
triglycine sulphate, absorpt. spectra, photoemission, band struct., ionic cond. 2−77932
triglycine sulphate, coercive force, freq., amplitude and temp. depend. 2−47988
triglycine sulphate, critical behaviour, thermal noise study 2−72040
triglycine sulphate, electromech. coupling near T_c 2−68475
triglycine sulphate, field effect and Hall mobility of Te and PbTe 2−77814
triglycine sulphate, irrad., domains, electron microscope exam. mats. 2−65067
triglycine sulphate, L-alanine doped, induced growth anisotropy 2−53608
triglycine sulphate, multi-domain, dielec. relaxation 2−61434
triglycine sulphate, reshaping of domains after heat treatment 2−54234
triglycine sulphate, second-harmonic scatt., domain shape effects 2−82508
triglycine sulphate, structural inhibition of ferroelec. switching, X-irrad. field treatment 2−77952
triglycine sulphate, surface potential variation, observation with scanning electron microscope 2−81157
triglycine sulphate, temp. depend. of dielec. props. in far i.r. 2−61435
triglycine sulphate, temp. depend. of switching rate 87-300K 2−72041
triglycine sulphate, thermal and elastic props., deuteration effects 2−72042
triglycine sulphate, thermal cond. near Curie point 2−44002
triglycine sulphate, vanadyl-doped, domain struct. changes, e.p.r. obs. 2−77937
triglycine sulphate pyroelectric detector, laser study of nucleation sites 2−44165
triglycinefluoroberylate, l.f. spectra, −115 to 36°C 2−51357
triglycineselenate, l.f. spectra, −115 to 36°C 2−51357
triglycineselenate, l.f. spectra, −115 to 36°C 2−51357
u.s. anomalies, attenuation and ferroelectric anomalies 2−74988
with vanishing $\Gamma_{jk}{}^{l}$ invariants, boundary conditions 2−73699
$AgNa(NO_2)_2$, crit. slowing down of dielec. relax., thermal noise study 2−72029
$AgNa(NO_2)_2$, dielec. relax. time, temp. depend., press. effects 2−77955
$AgNa(NO_2)_2$, hydrostatic pressure effects on ferroelectric transition 2−61426
$AgNa(NO_2)_2$, hysteresis loop in quasi-static elec. field 2−72030
$AgNa(NO_2)_2$, spontaneous polariz., pyroelec. obs. 2−54235
$(Ba, Pb)TiO_3$ ceramic, light emission by surface microplasma new Curie temp. 2−65303
$Ba_2Bi^{5+}Bi^{3+}O_6$, phase transition, dielectric constant. and loss obs. 2−75150
$Ba_2KNb_5O_{15}$, Ta-substituted, Curie temp. decrease 2−47315
$Ba_2LiNb_5O_{15}$, cryst. growth, Czochralski method 2−60721
$BiFeO_3$, lattice parameters, thermal expansion, elec. Curie temp. 2−47317
Bi_2WO_6, growth, cryst. struct. and dielec. props. 2−47263
$Co_3B_7O_{13}I$, transition temp., hydrostatic press. depend. 2−47984
$CsPbCl_3$, cubic-tetragonal transition temp., press. depend. 2−71676
$Fe_{1-x}S$, semicond. uniaxial ferroelectric, phase diagram 2−77957
$Gd(MoO_4)_3$, ferroelec. domains and condensed soft mode 2−68470
β-Gd_2MoO_4, heat capacity, entropy, magnetic moment from 0.4 to 4.2K along b crystal axis 2−51277
$Gd_2(MoO_4)_3$, elastic constants and soft optic modes 2−65061
β-$Gd_2(MoO_4)_3$, electrically polarized, 0.4 to 4.2K, up to 90 kG along a crystal axis, magnetothermodynamics 2−44290
$Gd_2(MoO_4)_3$, electro-optical props. 2−78068
$Gd_2(MoO_4)_3$, improper ferroelec., induced and spontaneous birefringence 2−61588
$Gd_2(MoO_4)_3$, π-GMO, X-ray amorphous, prepn. and physical parameters 2−84136
$Gd_2(MoO_4)_3$, Raman spectrum, temp. depend. 2−68660
β-$Gd_2(MoO_4)_3$, second harmonic generation, pseudotetragonal symmetry effects 2−51298
$Gd_2(MoO_4)_3$ diffracted light obs. from domain wall 2−84467
$Gd_2(MoO_4)_3$ piezoelectric d_{36} coefficient 2−81149
guanidinium aluminium sulphate hexahydrate, optical and interferom. studies of cleavages and etch patterns 2−64670
KD_2PO_4, growth and etching in solns. containing acetate ions 2−60712
KD_2PO_4, monoclinic, cryst. struct., X-ray obs. 2−64640
KD_2PO_4, Raman scattering from crystals and solutions, anomalous temp. dependence of low frequency lines caused by Cochran's shift 2−48200
KD_2PO_4, u.s. stress wave interaction with domain walls 2−71740
$K_4Fe(CN)_6.3H_2O$, anomalous spin-lattice relax. by quasi-spin waves 2−75152
$K_4Fe(CN)_6.3H_2O$, twinning and polymorphism, proton mag. resonance obs. 2−74655
KH_2AsO_4, Raman scattering from crystals and solutions, anomalous temp. dependence of low frequency lines caused by Cochran's shift 2−48200
KH_2AsO_4, X-irradiated at 4.2 and 77 K, obs. of domain splitting in e.p.r. spectra, determ. of hysteresis curve 2−72469
KH_2AsO_4 and KD_2AsO_4, thermodynamic props., first order transitions, spontaneous polarization 2−47985
KH_2AsO_4 n.m.r. correlation with dielectric relaxation 2−57243
$KH_{2(1-x)}D_{2x}PO_4$, Curie const., comp. depend. 2−54236
$KH_{2(1-x)}D_{2x}PO_4$, study of dielec. and thermal props. in ferroelec. and paraelectric phases 2−84364
KH_2PO_4, dense domain structure at ferroelectric transition, stress-induced birefringence 2−75260

Ferroelectric materials continued
KH_2PO_4, electron delocalization weight of H bond 2−71359
KH_2PO_4, ferroelectric mode, proton-phonon coupling effects, Raman spectra obs. 2−65279
KH_2PO_4, molecular dynamics study and ferroelec.-antiferroelec. transitions by NMR and dielec. relax. 2−72032
KH_2PO_4, Raman scatt., oscillatory intensity behaviour with temperature 2−65280
KH_2PO_4, Raman scattering from crystals and solutions, anomalous temp. dependence of low frequency lines caused by Cochran's shift 2−48200
KH_2PO_4, transition order experiments 2−81155
$KNbO_3$, dielec. const. under biasing conditions 2−61430
$KNbO_3$, domain investigations using pseudocubic {001} cleavage planes 2−61429
$KNbO_3$, mech. switching of domain walls 2−44160
$KNbO_3$, single crystals, deformation and stress relaxation behaviour 2−80743
$KNbO_3$, surface charge layers, obs. by AF electrolum. 2−75151
$KTa_xNb_{1-x}O_3$, cond. band. edge splitting and lattice dynamics 2−54425
$KTa_xNb_{1-x}O_3$, l.f. zone boundary lattice vibr. modes, Debye-Waller factor anisotropy 2−80902
$KTa_xNb_{1-x}O_3$, absorpt. edge splitting, paraelec. and ferroelec. phases 2−48184
$KTaO_3$, paraelec., press. depend. of static dielec. const. 2−44161
$LiH_3(SeO_3)_2$ thermal expansion rel to band arrangement, -150 to +25°C 2−68253
$LiNbO_3:Mn^{2+}$ e.s.r. studies of crystal field parameters 2−81451
$LiNbO_3$, dispersion of elastic waves and permittivity along trigonal axis 2−72033
$LiNbO_3$, ferroelec. domain struct., growth 2−65063
$LiNbO_3$, laser irrad., surface damage, ferroelec. props. effects 2−79252
$LiNbO_3$, spin-lattice relaxation times determ. by tone- bursting technique in quadrupolar nuclei 2−48312
$LiTaO_3$, ferroelec.-paralec. phase transition 2−44162
$LiTaO_3$, laser irrad., breakdown threshold at Curie temp. 2−79252
$LiTaO_3$, spin-lattice relaxation times determ. by tone- bursting technique in quadrupolar nuclei 2−48312
$(NH_4)_2BeF_4$-$(NH_4)_2SO_4$ concentration and temp. dependence of dielectric constant and spontaneous polarization 2−68471
NH_4Br, soft vibr. modes, stress effects, phase transforms. 2−71696
NH_4Br and ND_4Br, two-phase region in lambda transition 2−44163
$(NH_4)_2Cd_2(SO_4)_3$, ferroelec. phase transition temp. shift at press. to 1400 bar, 20-300K 2−77958
NH_4HSO_4, γ-irrad., e.s.r. of $HNSO_3^-$ radical, ferroelec. transition mechanism, dielec. const. 2−84369
$(NH_4)_2SO_4$, Brillouin spectra, elastic and photoelastic consts. 2−43665
$NaClO_3$, relation between phonon structure and phase transition 2−61431
$NaNH_4SeO_4.2H_2O$, ferroelec. temp. depend. of electro-pt. coeffs. 2−72268
$NaNO_2$, modulation of millimeter wave absorp. by polariz. reversal 2−48212
$NaNO_2$, order-disorder transition 2−61432
$NaNO_2$, polarization in reversal of applied field, 10^{-2} to 10^7 V/cm.sec 2−65064
$NaNbO_3$-$BaTiO_3$-$BaNb_2O_6$ system, tungsten bronze field, lattice parameters and Curie point 2−72034
$NaNbO_3$, anisotropic diffuse X-ray scatt. and phase transitions 2−71715
$NaTh_2(PO_4)_3$, temp. depend. of permittivity, rel. to struct. 2−54237
$(Pb,La)(Hf,Ti)O_3$, hot-pressed, material and electrooptic props. 2−56966
$(Pb,La)(Zr,Ti)O_3$, electrooptic ceramic, fabrication by atm. sintering 2−56967
$(Pb,La)(Zr,Ti)O_3$, phase boundary and defect struct. 2−56968
$PbFe_{2/3}W_{1/3}O_3-PbTiO_3$, phase diagram and transition temp. 2−81229
$Pb_5Ge_3O_{11}$, pyroelectric properties 2−57246
$Pb_5Ge_3O_{11}$, soft optic phonon mode 2−43961
$Pb_5Ge_3O_{11}$ single crystal, ferroelec. optical rotation domains 2−44164
$Pb_{1-3x/2}La_x(Zr_{0.65}Ti_{0.35})O_3$ ceramic acoustic detection of phase changes 2−51196
$Pb_{1-3x/2}La_xZr_{0.65}Ti_{0.35}O_3$, phase transitions 2−57245
$PbMg_{1/3}Nb_{2/3}O_3$-$PbTiO_3$-$PbZrO_3$ solid solution, hot-pressed, electrooptic props. 2−57328
$5PbO.3GeO_2$, ferroelec. material, acousto-optical figure of merit, acoustic attenuation 2−64849
$5PbO.3GeO_2$, Raman scatt. by low freq. temp. depend. modes 2−61669
$PbTiO_3$ in m-i-m structure Seebeck effect 2−44169
$Pb(Zr, Ti)O_3$, shock induced electromech. conversion, additives influence 2−84359
$Pb(Zr,Ti)O_3$, thermodynamic theory of morphotropic phase transition 2−75153
$Pb(Zr,Ti)O_3$ type, static dielec. const. and dissipation factor, nonlinear field depend. 2−72035
RbH_2PO_4, effect of deuteration, sound velocity obs. 2−74979
$RbH_3(SeO_3)_2$, improper ferroelec. phase transition, group theoretical analysis 2−51197
$SbNbO_4$, hydrothermal growth and ferroelec. props. 2−72037
SbSI, critical light scatt. phenomena 2−61612
SbSI, electrostriction, piezoelectricity, and elasticity 2−54240
SbSI, far i.r. reflectivity, complex dielec. const. deriv., soft mode in paraelec. phase 2−61619
SbSI, ferroelec. semicond., photoluminescence of single crystals 2−72443
SbSI, ferroelec. semicond., influence of nonequilib. carriers on domain struct. 2−72036
SbSI, one dimensional mech. stress effect on phase transition, permittivity obs. 2−75155
SbSI, p-T phase diagram rel. to critical point 2−72038
SbSI, paraelec. region, voltage-current characts., illumination effects 2−81163
SbSI, phase transition, illum. and rate of coding depend. 2−47986

Ferroelectric materials continued
- SbSI, Seignette semicond., thermal currents induced by light 2−72039
- SbSI, semicond., temp depend. of photoelec. e.m.f. 2−72078
- SbSI, trapping levels, thermally stimulated photocurrents obs. 2−75154
- $Sr_2KNb_5O_{15}$, Ta-substituted, Curie temp. decrease 2−47315
- $Sr_{2-x}K_{1+x}Nb_5O_{15-x}F_x$, synthesis, struct., and comp. depend. of Curie temp. 2−51198
- $Sr_2Nb_2O_7$, cryst. growth by floating zone technique 2−47276
- $SrTeO_3$, growth, structure and dielec. props. 2−68472
- $SrTiO_3$, anomalous reson. in permittivity on cooling in elec. field 2−77935
- $SrTiO_3$, dynamics of struct. transitions above T_c 2−65065
- $SrTiO_3$, electric polarization of crystals by inertial forces 2−54238
- $SrTiO_3$, l.f. soft vibr. modes, stress effects phase transformations 2−71696
- $SrTiO_3$, lattice dynamics, normal mode freqs., harmonic models, calc. of props. 2−77761
- $SrTiO_3$, uniaxially stressed, domain struct. at 2K 2−61433
- $Tb_2(MoO_4)_3$, ferroelectric phase transition, neutron scatt. obs. 2−65066
- β-$Tb_2(MoO_4)_3$, second harmonic generation, pseudotetragonal symmetry effects 2−51298
- Te films on uhv-cleaved TGS, aftereffects in field eff. at large gate charges 2−77900
- $Tl_2Cd_2(SO_4)_3$, Langbeinite, optical and dielectric props. 2−51199
- **barium titanate**
  - acoustic-mode-soft-optic mode interactions, press. depend. 2−71707
  - ceramic, dielec. props., sintering parameter effects 2−57241
  - domain studies by scanning electron microscopy 2−47983
  - dynamic fatigue, ageing of switching props. 2−72031
  - electrical noise characteristics det. for confirmation of internal stress model of polycrystalline ferroelectric materials 2−44159
  - electron diffraction, OOl systematic reflections 2−84367
  - film, polarization change, stroboscopic elec. microscope obs. 2−75149
  - film, r.f. sputtered on Si, elec. props. 2−75148
  - films, discrete vacuum evaporation method for ferroelectric behaviour, study of comp. and structure 2−83894
  - lamellar domains and abnormal birefringence 2−81128
  - laser irradiated, breakdown threshold at Curie temp. 2−79252
  - lattice vibrations, monatomic linear chain, double min. potential, computer simulation 2−54019
  - light emission, due to uniaxial stress pulses 2−72440
  - phase transitions, domain interactions 2−61427
  - piezoeffect rel. to semicond. props. and work function 2−77959
  - point defect effects, optical properties and lattice dynamics 2−61412
  - proton channelling, above and below Curie temp. 2−65059
  - single crystal film, microstruct. of domains and domain walls 2−68469
  - specific heat, near T_c, d.c. calorimetry technique 2−64853
  - surface domain reorientation prod. by abrasion and annealing, X-ray diffraction exam. 2−80544
  - surface domain struct., photoemission microscopy obs. 2−61428
  - surface obs. using electron mirror microscopy 2−65060
  - surface potential variation, observation with scanning electron microscope 2−81157
  - vibrational amplitude, calc. 2−68215
  - $Ba_{1-x}Sr_xTiO_3$, permittivity and hysteresis loop, temp. dependence in range 4.2 to 600K in flux-grown single crysts. 2−47966
  - $BaTiO_3$:Y and reduced single crystal, phase transition effects on d.c. conductivity 2−68468
  - $BaTiO_3$-Bi_2O_3, La doped composite ceramic, two-step anomalous resistivity increase 2−68395
  - $BaTiO_3$-$NaNbO_3$-$BaNb_2O_6$ system, tungsten bronze field, lattice parameters and Curie point 2−72034
  - $BaTiO_3$, mobility meas. in ferroelectric and paraelectric phases 2−81100
  - $BaTiO_3$ ceramics, La doped, Bi_2O_3 as grain boundary element, resistivity temperature characteristic anomaly at transitions 2−84366
  - $BaTi_{1-x}{}^{4+}Ti_x{}^{3+}O_{3-x}F_x$, formation and dielec. props. 2−47705

Ferroelectric phenomena
- Devonshires approach of minimum free energy rel. to polarization field calc. 2−48189
- disaccommodation phenomena, nature of dissipative behaviour 2−72190
- internal stress model of polycrystalline materials, confirmation from noise characteristics of $BaTiO_3$ 2−44159
- nonlinearities, effect on design of sonar and industrial transducers 2−49156
- order-disorder transformation, dynamic wave-vector-depend. susceptibility 2−81151
- oscillatory system, effect of automatic temp. stabilization 2−44157
- phase transition, sixteen vertex lattice model 2−65058
- phase transitions, displacive, by exciton phonon interactions 2−81153
- phase transitions, models 2−58799
- photoconductor/ferroelectric memory device, switching and remanence 2−47982
- Rochelle salt, second order ferroelec. transitions, calorimetric exam. 2−77951
- semiconductor electrodes on insulators, aftereffects 2−77905
- Shubrikov point groups and ferroelasticity 2−84006
- spectroscopic and laser study 2−72028
- surface potential variation, observation with scanning electron microscope 2−81157
- transitions, Lyddane-Sachs-Teller relation in the thermodynamic theory of dispersion theory 2−81148
- transverse acoustic wave reflection at domain boundaries, influence of piezoelectric effect 2−74982
- $(C_2NO_2H_5)_3H_2SO_4$, triglycine sulfate, second order ferroelec. transitions, calorimetric exam. 2−77951
- $LiN_2H_5SO_4$, anomalous neutron scatt. and absence of ferroelectricity 2−84357
- $(NH_4)_2Cd_2(SO_4)_3$, ferroelec. phase transition temp. shift at press. to 1440 bar, 20-300K 2−77958
- $Pb_{1-3x/2}La_x(Zr_{0.65}Ti_{0.35})O_3$ ceramic acoustic detection of phase changes 2−51196
- $PbZrO_3$, ferroelectric phase obs. 2−81140

Ferroelectricity *see Phase transformations/solid state; Plastic deformation*

Ferromagnetic relaxation
- ferrite, Fe rich, induced anisotropy and disaccommodation, mag. relax. obs. 2−48112
- spinel ferrites, parametric spin wave relax. 2−72228
- $Dy(OH_3)$, a.c. susceptibility study 2−54334
- $Ho(OH)_3$, a.c. susceptibility study 2−54334
- $Li_{0.5}Fe_{2.5}O_4$, parametric spin wave relax. 2−72228
- $MgFe_2O_4$, parametric spin wave relax. 2−72228
- MnZn ferrites, influence of Ti ions on magnetic properties 2−84405
- $NiFe_2O_4$, parametric spin wave relax. 2−72228
- $Tb(OH)_3)$, a.c. susceptibility study 2−54334

Ferromagnetic resonance
- *see also Ferrimagnetic resonance; Ferroacoustic resonance*
- condensed matter theory, transmission reson. in zero field 2−47822
- crystals with anisotropic g-factor, theory 2−72446
- domain wall structure effect in films 2−68717
- ferrite, moments of absorpt. line, spin-wave and independent-grain approx. 2−72449
- ferrite, stress effect on linewidth 2−68720
- ferrite garnets, lineshape near Curie pt. 2−72445
- ferromagnet, magnetoelastic phenomena in parametric mode magnetiz. oscillation 2−68719
- film, Heisenberg ferromagnet 2−51263
- film, nonlinear phenomena in parametric cct. 2−68721
- film, spin wave reson., stability conditions 2−48089
- frequency and width at finite temp. calc. method 2−68718
- lunar rocks and fines 2−62648
- magnetostatic solns. in a ferrite cone 2−68724
- magnon parametric instability due to three-magnon processes 2−48050
- metal, bulk, surface spin-wave mode 2−54486
- nonlinear magnetoelastic phenomena and threshold of magnetoacoustic instability 2−72447
- Permalloy film, effective demag. field rel. to thickness and mag. moment 2−61539
- permalloy films epitaxially grown on fcc metals, structural and standing spin wave resonance props. 2−78149
- polarization of spin waves and hf pumping in thin ferromag. films 2−78150
- spin wave excitation threshold anisotropy 2−72448
- students measuring apparatus 2−57385
- supermalloy, anomalous behaviour of antireson. transmission at 23.7 GHz 2−81442
- $Ba_3Zn_2Fe_{24}O_{41}$, hexagonal, anisotropy, comparison with $BaMg_2Fe_{12}O_{22}$ 2−72451
- $CdCr_2S_4:Fe^{2+}$, anisotropy of tetrahedral Fe^{2+} ions 2−72161
- $CdCr_2Se_4$, ang. depend., 4.2-293K 2−68722
- $CdCr_2Se_4$, anisotropy, impurity ion contrib. 2−54487
- Co fine particles, 4-300K, 10-47GHz 2−57386
- CoS_2 powder, line with, freq. depend. 2−72452
- CrTe thin film, g-value and exchange coupling const. 2−57387
- Er, microwave absorpt. obs. of mag. transitions 2−51257
- EuS film, rel. to determination of effective exchange parameters 2−68532
- FeGe, cubic, obs. of resonances using e.s.r. spectrometer 2−84557
- GdFe garnet with Tb^{3+} impurity, reson. field and absorpt. linewidth anisotropy 2−72453
- Mg-ferrite, spin-wave instability, obs. 2−78151
- $Mg_{1-y}Co_yFe_2O_4$, mag. anisotropy determ. 2−81283
- $MgFe_2O_4$, exchange anisotropy and relax., degree of treatment depend. 2−72156
- $Mn_{1-x}Cr_xSb$ thin films, $(0\leqslant x\leqslant 0.6)$ 2−72450
- $MnFe_2O_4$, ferrite, single cryst. film, spin wave resonance 2−72454
- $Mn_xFe_{3-x}O_4$, 77-350K, 9.3 GHz 2−44430
- Ni-Co alloys, standing spin wave reson., exchange consts. determ. 2−44265
- Ni-Zn-Co ferrite film, anisotropy induced by thermomagnetic treatment 2−81228
- Ni single crystal film, ripple effects 2−65317
- $NiFe_2O_4$ films, etching effect on reson. modes 2−44431
- Ni(100) film, magnetoelastic consts. h_3 and h_4 determ. 2−44264
- $PbO.6Fe_2O_3$, unsaturated crystals, 36-52 GHz 2−72455
- Tb, free lattice model behaviour, at 24 GHz 2−65318
- Y-Fe garnet, l.f. magnetization oscillations where absorption maximum coincides with ferromagnetic resonance 2−75340
- Y garnets, magneto-elastic bonding of Fe^{3+} and Cr^{3+} ions 2−65321
- $Y_3Fe_{5-(x+y)}Al_xGa_yO_{12}$ ferrite garnet 2−72204
- $Y_3Fe_{5-x}Al_xO_{12}$, garnet, obs. of natural anisotropy 2−78148
- YIG, Al^{3+}-substituted, Ru^{3+}-doped 2−81444
- YIG, magnetostriction consts. determ. 2−72176
- YIG, substituted, ultralow-linewidth, microwave loss 2−51397
- YIG, thin single-crystal distrib., magnetoexchange branch repulsion 2−44433
- YIG discs, epitaxial, anisotropy effects on magnetostatic modes 2−44432
- YIG thin film disks, anisotropic excitations of magnetostatic modes 2−44434

Ferromagnetics *see Magnetic properties of substances/ferromagnetic*

Ferromagnetism
- *see also Antiferromagnetism; Exchange interactions; Ferrimagnetism; Ferromagnetic relaxation; Ferromagnetic resonance; Heisenberg models; Ising lattices and models; Magnetic properties of substances/ferromagnetic; Magnetization process; Magnetization state; Metamagnetism; Superparamagnetism*
- alkali halide, ferro-associated props. rel. to electrons trapped in edge dislocations 2−81200
- amorphous ferromagnet, free energy lower bound 2−78006
- amorphous ferromagnets, condition for existence, const. coupling approx. 2−81274
- amorphous Ising model, thermodynamical behaviour 2−57273
- anisotropic chain with S=1/2, energy spectrum 2−81261
- anisotropy due to anisotropic impurity spin, theory 2−81237
- antiferromag.-ferromag. transform., mag. moment oscill., mag. dipole radiation 2−78007
- b.c.c. lattice sums applic. 2−48051
- biquadratic exchange, influence on Curie temp., correlation length and spin diffusion 2−48065

Ferromagnetism continued
Blume-Capel Ising ferromagnet, tricritical point, droplet model 2−65135
cluster treatment of itinerant electron ferromagnet 2−68531
complex lattice, bound state energy, using boson Hamiltonian 2−51245
conducting ferromagnetic plates, analogue computer study 2−73509
cooperative processes, correlated fluctuations in equil. and steady-state systems 2−78841
critical behaviour, comparison with nematic-isotropic transition in liq. crysts. 2−53401
critical fluctuations, neutron scatt. 2−54309
critical phenomena, conf., New York, USA (June 1970) 2−52102
critical phenomena, static correl. function selfconsistent singularities 2−54296
critical spin dynamics, symmetry and conservation laws 2−54308
cubic system, mag. anisotropy represented by lines of const. cryst. energy 2−78000
Curie point, crit. depolarization of neutrons 2−81268
d-dimensional spherical model, scaling theory for finite size effects in critical region 2−45303
degenerate band models, absence of complete ferromagnetism 2−72127
degenerate electron gas, implications for metals, white dwarfs and neutron stars 2−47823
dilute ferromagnet with four-spin interaction, critical behaviour 2−72128
dilute magnet, critical behaviour, term struct. of series expansions 2−52090
dislocation theory of energy loss during magnetic reversal 2−72144
disordered systems, correlation phenomena 2−64815
domain boundary deformation in magnetic field with transverse bonding 2−68537
domain structure, calc. for various types of anisotropy 2−81270
domain structure, periodic distrib. of magnetization, theory 2−81222
double exchange, quantum theory 2−54295
double exchange ferromagnet, one-particle states of hole, Green function 2−81236
dynamic effects of domain struct., nucl. paramag. reson. 2−61488
dynamical spherical model, phase transitions 2−52104
electron gas, ground state energy calcs. 2−71816
electron gas, two-band model, magnetic and excitonic instabilities 2−64881
electron gas theory, effect on work function 2−54118
electron-magnon interaction, energy and lifetime 2−48056
ergodic and non-ergodic systems, crit. slowing down, nonlinear dynamical response 2−54310
exchange interaction model, estimation of critical parameters 2−44233
exciton behaviour in singlet ground state, soft modes 2−51244
film, polarization of domain boundaries of Neel type 2−57297
film, theory of domain wall mobility 2−78031
film, uniaxial unpinned, Green's function theory, review 2−78003
finite systems, scaling laws 2−54314
Gaussian spin model, with long range interactions, renormalization group and critical exponents 2−81248
Green's function solution for 2 spin 1/2 ferromagnet 2−78726
Green function approach to anisotropic ferromagnet 2−72123
Greens function theory based on two-spin systems 2−75210
Hall effect, side-jump model 2−65133
Heisenberg chains, impure linear, spin correls. 2−48048
Heisenberg diluted system, transition temp. depend. 2−48046
Heisenberg ferromagnet, Green function methods 2−45283
Heisenberg ferromagnet, partially finite, long-range order and phase transitions 2−75212
Heisenberg ferromagnet, thermodynamic properties by self-consistent Monte Carlo method 2−68530
Heisenberg magnet at infinite temp., two-time spin-pair correl. function 2−61548
Heisenberg magnet at infinite temperature, two-time spin-pair correlation function 2−44232
Heisenberg model, computer simulation 2−81272
Heisenberg model, deformed cubic ferromagnet, localized impurity states 2−81273
Heisenberg model, energy spectrum and magnetization, monoionic anisotropy effects 2−51243
Heisenberg model, longitudinal dynamic susceptibility and cross-relax. 2−78002
Heisenberg model, scaling function calc. using high-temp. series expansions 2−54315
Heisenberg model, scaling functions, universality rel. to lattice struct. and spin quantum number 2−54316
Heisenberg spin 1/2 model, using anticommutator Green's functions 2−65132
Hubbard model, ground state energy 2−54291
Hubbard model, one-dimens., susceptibility at zero temp. 2−54303
inhomogeneous system, Gibbs free energy and related props. 2−61502
intinerent electron magnetization at low temps., band splitting 2−78005
Ising ferromag., with nonmag. impurities, susceptibility, high temp. expansion techniques 2−61491
Ising ferromagnet, mag. susceptibility rel. to nonmag. impurities, series expansion 2−77992
Ising ferromagnets, spin correl. functions, hierarchy of inequalities, critical temp. bounds 2−68538
Ising magnet, critical isotherm analysis 2−54297
Ising model, 3-dimens., spin-spin correl., high temp. series and crit. amplitude 2−81260
Ising model, of restricted dimensionality, susceptibility 2−81235
Ising model, one-dimensional with single ion anisotropy 2−57274
Ising model, scaling function calc. using high-temp. series expansions 2−54315
Ising model, scaling functions, universality rel. to lattice struct. and spin quantum number 2−54316
Ising model, scaling relations in Wilson theory 2−61495
Ising model, three-dimens., critical behaviour 2−54300
Ising model, two-dimens., high temp. susceptibility bounds 2−54299
Ising spin system, sp. ht. density 2−61486

Ferromagnetism continued
Ising system, three-dimens., sp. ht. density asymptotic behaviour for $T \geqslant T_c$ 2−61487
Ising systems on anisotropic lattices, crit. behaviour 2−84423
Ising-like magnet, scaling eqn. of state near crit. pt., Feynman-graph expansion 2−68526
itinerant, intermediate-coupling theory 2−54301
itinerant electron model, behaviour thermodynamic quantities near critical point 2−84427
itinerant electron model, spin wave energy temp. depend., electron-phonon interact. influence 2−61498
itinerant ferromagnet, theory of magnetic fluctuations 2−65157
itinerant model, dynamical scaling violation 2−54312
Kondo problem, renormalization-group techniques 2−81259
liquids, self propagating thermal convection, MHD 2−53160
magnetoelastic waves, associated, dispersion laws and polarization 2−57294
magnetostatic mode pattern and mode spectrum analysis, in finite circular disc 2−48053
micromagnetic continuum theory, for cryst. with indirect exchange coupling 2−78001
model with narrow s-band, temp. depend. of magnetization 2−65140
multiaxial system, magnetization and mag. reversals, mag. texture effect 2−51252
Neel wall in stray fields, wall creeping mechanism 2−61522
non-Heisenberg magnet, exchange interaction effects 2−72133
nonergodicity of spin systems 2−54311
one-band model, const.-coupled, with finite site number, exact eigenvalues 2−54305
one-dimensional model, phase transitions, transfer-matrix approach 2−61489
phase transitions, decoupled-mode dynamic scaling theory 2−52103
phase transitions, model studies 2−58798
planar magnet, longit. susceptibility, RPA obs. 2−54313
point-group symmetry and localized impurity problem 2−54304
s-band models, absence of complete ferromagnetism 2−72126
scaling laws and crit. phenomena, geometrical interpret. 2−72119
screening in a spin polarized electron liquid 2−61499
small particles, remanence, influence of curling 2−77999
spherical model, dynamic props. in low temp. and crit. regions 2−48047
spherical samples, of single crysts., form effect of magnetostriction 2−78027
spin lattice systems interacting through arbitrarily many-body and indefinitely-long-range interactions 2−54298
spin systems at zero temperature, phase transitions 2−81267
spin systems with mixed ferro- and antiferromag. coupling, crit. temps. 2−65131
spontaneous magnetization, Hall effect measurement 2−75219
superconductor, micromagnetic theory 2−77870
susceptibility of ferromagnet, with single-ion anisotropy Green function calc. 2−84555
thermally activated relax. and Jordan aftereffect 2−54307
transition elements, fermion theory of 3d band 2−76232
two dimensional Ising model, external force on boundary atoms 2−48055
uniaxial magnet, Bloch wall mag. moment, domain width depend. 2−57281
weak, s-d exchange model 2−81257
XY chain, excitations of single spin 2−77997
XY magnet at infinite temperature, two-time spin-pair correlation function 2−44232
CeB$_2$, exchange interactoon and fluctuation effects 2−54339
Fe-Ni, ferromagnetic resonance line width, effect of Ni content after quenching or annealing 2−72174
Fe, model for origin and ave.-moment-internal field variations in dil. Fe-Si(Al) alloys 2−78008

spin wave theory
see also Spin waves
amorphous magnet, ground state instability and long-wavelength spin wave form. 2−48043
antiferromagnets, two-sublattice, indirect exchange parameters 2−81299
coupled e.m. and spin waves in quantized mag. field 2−68525
crystals with equivalent sublattices, spin wave correction to ground state energy 2−61496
doubly degenerate band, electron correlation 2−84425
electron fluid, anisotropic, dispersion equation 2−57275
ferrite, moments of ferromag. reson, absorpt. line, spin-wave approx. 2−72449
film, stability conditions 2−48089
film, surface free-energy for spin-wave and molecular field models 2−75229
fluctuations, neutron scatt. 2−54309
Heisenberg, bound spin waves 2−44234
Heisenberg, spin half, second order Tyablikov treatment, low temp. 2−44236
Heisenberg chains, disordered, density of spin wave states 2−48044
Heisenberg ferromagnet, dilute, spin-waves, percolation theory, critical conc. 2−81240
Heisenberg ferromagnet, effects of finite conc., of impurities 2−65134
Heisenberg magnet, dilute, rel. to critical conc. 2−44230
Heisenberg magnet, disordered anisotropic, Green's function theory 2−48054
Heisenberg magnet, kinetic equation for critical spin fluctuations 2−44235
Heisenberg magnet, longit. waves 2−72121
Heisenberg model, algebraic realization 2−44237
Heisenberg model, interference effect between two impurity spins 2−65130
Heisenberg model, long wavelength surface spin waves, effect on mag. props. 2−44231
Heisenberg model, magnon relax. and second sound propag. 2−65129
Ising-model metamagnet, high-temperature expansions study 2−54302
magnetization, low-temp. spontaneous, of spin 1/2 b.c.c. ferromagnet. 2−61514

Ferromagnetism continued
spin wave theory continued
magnetocrystalline anisotropy consts. temp. depend. interpret. 2−54321
magnetoelastic phenomena in parametric mode magnetiz. oscillation 2−68719
magnon oscillation, weakly bonded impurity spins 2−54306
magnon parametric instability due to three-magnon processes 2−48050
magnon spectra in multidomain materials 2−61488
magnon-electron interaction in itinerant electron ferromagnet 2−44239
metal, anomalous spin-wave damping 2−72129
metal, bulk, surface spin-wave mode in f.m.r. 2−54486
metal, elementary spin excitations 2−44238
molecular-field ferromagnets, phenomenological theory of spin transport 2−51242
paramagnetic-ferromagnetic phase transition, spontaneous symmetry breaking and propagating hydrodynamic wave in the initial region 2−84413
polarization of spin waves and hf pumping in thin ferromag. films 2−78150
semiconductor, spin wave-helicon wave interactions 2−51122
spectrum of spin vibrs. in isotropic layer 2−72122
spin system, $S=1$, with uniaxial single-ion anisotropy 2−78002
$SU(3) \times SU(3)$ field algebra amplitudes, unitarization 2−73720
transition element oxide glasses, amorphous antiferromagnets, absence of ordering 2−81301
two-dimensional magnet, spin-wave spectrum, temp. depend. 2−44240
two-dimensional spin one Ising ferromagnet, spontaneous magnetization by Peierls method 2−73275
two-magnon bound states, biquadratic exchange effect 2−72120
Van der Waals spin systems, thermodynamic equivalence 2−48045

Ferromagnets *see Magnetic properties of substances/ferromagnetic*

Feynman diagrams *see Field theory, quantum/interactions*

Fibre optics *see Fibres/optical*

Fibres
alumino silicate refractory fibre, props. and applicatons 2−56953
composite, Al_2O_3/B, high temp. bearing characts. 2−47558
composite, brittle matrix, strength, thermal shock resist., impact and abrasion resist. 2−53968
composite, UO_2/W system, eutectic structs., influence of growth parameters 2−53969
composite porous fibre material, strength rel. to porosity 2−43707
composites, longitudinal tensile failures 2−64745
crystals, formation using CO_2 laser as heat source 2−74664
discontinuous in composite, matrix stress conc. factor rel. to modulus ratio 2−61012
electron diffraction patterns from C fibres, interpretation by optical analogue techniques 2−80613
fibrous systems, small-angle equatorial X-ray scattering, methods of extracting physical parameters 2−50616
filaments, high temp. testing of strength 2−60956
friction between fibres, meas. with scanning electron microscope 2−82441
glass, aluminoborosilicate, B coordination number heat treatment effects 2−64528
glass, for composites strengthening, physcal properties 2−71658
glass, fragmented, in polymer films, mechanical anisotropy 2−84131
glass, high modulus, prep. and crystn. kinetics 2−43902
glass, reinforced nylon 6, dynamic viscoelasticity temp. depend., two-phase blend system model applic. 2−71556
glass reinforced polyester, fatigue crack damage, vibr. testing 2−60921
glass reinforced polyester, fracture energy determ. 2−50780
glass-reinforced polyester, work of fracture 2−74863
graphite, fast neutron irrad. effects on mech. props. 2−56992
graphite, three dimensional C structure synthesis at one atmosphere 2−56979
graphite, transverse thermal expansion 2−53954
graphite, with C-C unidirectionally reinforced composites, exam. of props. 2−68176
graphite reinforced composite, compressive fatigue 2−61021
keratin surfaces, scanning electron microscope examination 2−82442
laminated fibre-reinforced plates, plane strain bending 2−66543
metal, in reinforced ceramics, manufacture, applications, props. 2−43866
in metal matrix, precise alignment and uniform distrib. 2−77666
metallic for compposites strengthening, physical properties 2−71658
nylon 66, drawn, effect of high-temperature annealing on structure and morphology 2−74602
nylon 6, reaction rate model of fracture 2−74854
nylon-6, structure property, relationship from viscoelastic analysis 2−56775
polyacrylonitrile, effect of heat treatment on morphology and structure 2−71293
polyethylene filled with randomly oriented glass fibres, stress-strain curve 2−77690
polyethyleneterephthalate, determ. of degree of crystallinity by X-ray methods 2−74607
pulling of mounting pins from glass rods, device 2−64769
reinforced composite, elimination of coupling effects 2−74917
reinforced composite, fracture toughness 2−77667
reinforced composite, shrinkage stresses near discontinuity 2−71659
reinforced composite, state-of-the-art 2−47663
reinforced composite, stress boundary value problem for plane strin deform. 2−58868
reinforced metal composite, resist., calc. 2−50915
reinforced plates, optimum design 2−55456
reinforced resin, metal incorporation using organometallics 2−50923
sapphire filament growth, void-free at rates up to 3 cm/min, effect of using W growth orifices 2−60720
stainless steel, tensile strength 2−77742
steel, stainless, in Sn-Pb alloy matrix, fracture behaviour 2−50921
steel reinforced Al, thermal and elec. cond. 2−53946
steel wire reinforced polyester resin, fracture toughness 2−47528

Fibres continued
suspension, stock flow 2−77220
synthetic, properties and applic. 2−77702
tendon collagen, fractography 2−43016
tobacco mosaic virus, heavy atom positions from X-ray diffraction diagrams 2−56621
X-ray crystallography, math. problems 2−71405
$AlN-Y_2O_3$, sintered, with fibrous struct., textural determ. 2−47666
Al_2O_3, poor efficiency in reinforcing Ni for high temp. use 2−47668
Al_2O_3, sapphire filament, fracture strength in tension 2−50917
Al_2O_3, sapphire filament, growth and microstruct. 2−50916
C-reinforced polyester, work of fracture 2−74863
C, (hk) interferences linewidth, effects of preferred orientation 2−53627
C, appl. for carrier injection in anthracene electrolum. diodes 2−75338
C, diamagnetism rel. to tensile modulus and structure depend. 2−57270
C, elec. resistivity and diamag. susceptibility, meas. 2−68331
C, electron microscopy 2−53950
C, fast neutron irrad. effects on mech. props. 2−56992
C, field emission source 2−72086
C, gas chromatographic obs. of surface reactivity 2−60623
C, glassy fibres, derived from phenolic resin, mech. props. 2−84100
C, in composite materials, book 2−43904
C, ion beam thinning for t.e.m. 2−79104
C, mech. and crystallographic props., S impurity effects 2−50913
C, micromechanics rel. to chem. vap. deposited C composites 2−53955
C, microporosity 2−53952
C, monofilament substrate for chem. vap. deposited B composites 2−53956
C, neutron irrad. effect on mech. props. 2−43708
C, neutron irrad. effects on elec., mag. and thermal props. 2−56998
C, PAN-based, fine struct. 2−53948
C, preferred lattice orientations, three-dimensional crystallinity 2−53973
C, present and future applic. 2−68172
C, produced from lignin and PVA, voids, X-ray obs. 2−47667
C, property changes during fast neutron irradiation 2−53965
C, radiation effects on mech. props. based on 'sheath' and 'core' model of fibre structure 2−64702
C, reinforced Ni composite, prep., thermal expansion, high temp. deformation characts. 2−74919
C, Royal Aircraft Establishment review 2−43903
C, size effects on radial distribution analysis, influence of atomic bonding 2−64630
C, strengthening by fast neutron irradiation fibres, strengthening by fast neutron irradiation 2−71662
C, struct., neutron irrad. effects 2−56991
C, surface props. 2−53951
C, tensile strength, fast neutron irrad. effects 2−80830
C, thermal expansion, room temp. −1800°C 2−53953
C, thermal expansion anisotropy effects on struct. and mech. strength 2−54054
C, thinned, low energy electron diffr. 2−64634
C, two dimensional lattice orientation and three dimensional crystallinity 2−68177
C, unidirectionally reinforced plastic, shear strength and modulus 2−74921
C, wettability 2−64802
C, with C-C unidirectionally reinforced composites, exam. of props. 2−68176
C, X-ray preferred orientation obs. 2−53949
C fibre reinforced glass, fracture energy 2−84104
C fibres, adhesion to organic matrices 2−84101
C fibres electron diffraction studies, lattice fringes rel. to defects and diffraction geometry 2−80634
C fibrous structures, pyrolytic C infiltration 2−53957
C glassy monofilament, prep. and props. 2−56982
C reinforced ceramics and glass, discontinuous fibres, fabrication and props. 2−50918
C reinforced ceramics and glass, continuous fibres, mech. props. 2−50919
Co-base composite materials, superalloys with fibres obtained by direct solidification, props. 2−64793
$CrSi_2$, in Si matrix, composite, anisotropy columnar structs., resist. anisotropy 2−74920
Cu_6Sn_5 fibres, brittle fracture surface morphologies 2−80744
$Li_2O.Al_2O_3.2SiO_2$, glass, ion exchanged, internal friction, Li and Na conc. profiles 2−80754
Mo, pressed part formation 2−53883
Mo alloy reinforced Ni-Cr base alloy, mech. props. 2−56988
Mo reinforced nichrome, filament-matrix interface struct. 2−53966
Ni-base composite materials, superalloys with fibres obtained by direct solidification, props. 2−64793
SiO_2, fused fibres, nonlinear elasticity at room temp. 2−60847
W, high temp. mech. props. and struct., rel. to composite reinforcement 2−53970
W feinforced nichrome, struct. and props. 2−53967
W reinforced Ni-Cr base alloy, mech. props. 2−56988
W reinforced nichrome, filament-matrix interface struct. 2−53966
ZrC_x fibres, physical and mech. props. detn. 2−68178
optical
airport installations, applications of fibre optics 2−70061
angular scattering from fibre waveguides with irregular core surfaces 2−79335
application in kinetic obs. in discharge flow systems 2−48319
array for radial distrib. of light intensity obs. for particle size anal. 2−70057
bundle communication systems, advantages of semiconductor lasers over lamps 2−42088
catheter for obs. of blood pressure and O_2 2−51897
coupling in high power semiconductor laser arrays 2−42089
design and aberrations 2−63372
detonation obs. 2−55746
dispersion meas. using a mode locked Kr laser 2−79235
dispersion meas. using self pulsing GaAs laser 2−79233
for electronics, developments 2−76536

Fibres continued
- **optical** continued
  - evanescent wave interactions 2—70056
  - flexible bundles, quality criteria, measurement 2—42235
  - glass, effect of phys. props. on light propag. 2—42242
  - glass, pulse broadening, obs. 2—49438
  - glass, reinforced polycarbonates, mechanical reliabilities 2—73665
  - glass, stimulated backward Brillouin scattering 2—44398
  - integrated optics, status report 2—63406
  - interferometrically prepared structures, ray anal. of image transfer props. 2—73666
  - Kerr effect in glass waveguide 2—42239
  - liquid-filled, pulse delay variation meas. 2—70062
  - low loss optical waveguides, spectral response, attenuation obs. 2—55619
  - mode propag., coupled mode theory, coupling coeffs. 2—79323
  - modulation transfer functions of real devices 2—59269
  - multimode, direct obs. of frequency response 2—55761
  - multimode, glass, coupling losses with laser diodes 2—73602
  - plastic, glow areas due to light scattering along fibre, theory, applications 2—82581
  - sapphire filament, void-free, light pipe applic. rel. to growth technique 2—60720
  - Selfoc lens, imaging properties 2—70003
  - transmission line, suitability of synthetic quartz 2—48136
  - waveguide, high order modes, filtering 2—41885
  - waveguide, multimode, pulse dispersion, obs. 2—41884
  - waveguide with low-loss liquid-core 2—58998
  - waveguides fused junctions 2—45615

Field emission *see Electron emission/field emission*

Field emission microscopes *see Electron microscopes; Ion microscopes*

Field ion microscopy
- alloy, obs. of surface reconstruction due to chemisorption 2—50524
- contrast across interfaces, geometrical theory 2—43622
- development, application to metallurgy, image form., construction, operation 2—56643
- field-ion image formation, comments 2—69887
- imaging processes, review 2—67964
- liquid He vapour cooled field ion microscope 2—66726
- metal, defects produced by method of exam. 2—56567
- metal, low temp. epitaxy by vapour deposition 2—53575
- metal, quenched or irrad., void form. mechanisms 2—53696
- methane, adsorpt. on W, field ion microscopy obs. imaging props. 2—64583
- microanalyzer in geochem., application to Juvinas meteorite 2—44504
- orientation relationships analysis from micrographs, method 2—47308
- specimen preparation, automatic electropolishing control unit 2—47309
- steel, martensitic, fine struct. obs. 2—64779
- surface and interface obs. in mats. science 2—56571
- two-dimensional crystallization obs. 2—53622
- Fe-Mo-C alloy, quenched and tempered, microstruct. obs. 2—47581
- Fe, Fe-Mn alloy, nitrided, orientation relationships with α ferrite and iron nitride 2—64777
- Ga-In-Sn alloy, liquid-solid interface obs. 2—67900
- Ge surface, H and Ar ion images, at 80K 2—64554
- Ir, and alloys, of dissociated dislocations, geometrical contrast theory analysis 2—77592
- Ir, brittle fracture and grain boundary struct. obs. 2—56576
- Ir, ion implantation obs. 2—56740
- Ir, ion implantation obs. 2—56741
- Mo, cathode, flashing effect, surface atom migration 2—53557
- Pt, adsorption of H rel. to promoted evap. 2—50548
- Pt film, vapour deposited on W, field ion microscopy, 78K 2—50500
- W:O, grain boundary segregation obs. 2—53746
- W, adsorpt. of O, low coverage, at 78K 2—64584
- W, adsorption and dissoc. of CO 2—71355
- W, cathode, flashing effect, surface atom migration 2—53557
- W, contrast patterns produced by self-interstitial ions 2—64625
- W, field desorption of CO in FIM, image gas enhancement 2—60673
- W (110), polarizability of W adatoms 2—60689
- W surface, interactions between Re atoms 2—50469

Field theory, classical
- *see also Electromagnetism; Gravitation; Relativity*
- $\lambda\varphi^4$ theory, infinite sets of classical solutions 2—73717
- canonical formalism of algebra of observables 2—82151
- canonical transforms. and generating functionals 2—66421
- coupled e.m. and mesonic fields; calc. of cross section for interacting particles 2—78774
- Hamiltonian variational principle, applic. to nonlinear heat transfer and fluid flow 2—45240
- Helmholtz eqn. in exterior of convex curve, Neumanns problem, Green's function 2—45239
- with interaction, light-cone singularities 2—70114
- itinerant ferromagnet, theory of magnetic fluctuations 2—65157
- Maxwell field, investigation of local independence 2—58977
- nonlinear field eqns. for particles interacting with coupled e.m. and mesonic fields, soln. method 2—78773
- scalar field gradient 2—48983
- solenoidal field represent. by poloidal and toroidal. pots. 2—82179
- stationary orbits in central gravitational fields 2—76165
- three-body problem, symmetries, Lagrangian and Euler eqns. 2—82285
- Yang-Mills equations, exact solutions 2—41465

Field theory, quantum
- *see also Bethe-Salpeter equation; Brillouin zones; Bootstrapping; Chirality; Dispersion relations; Elementary particles; Lee model; Perturbation theory; Physics fundamentals; Quantum theory*
- — 2—66954
- $\lambda\varphi^4$ theory, infinite sets of classical solutions 2—73717
- σ model in tree approx., analytic properties of symmetry-breaking 2—79466
- φ^3 analyticity and finite-energy sum rules for inclusive reactions 2—66960

Field theory, quantum continued
- φ^3 theory, high energy scattering and breakdown of eikonal approx. 2—79545
- φ^3 theory and the zero-slope limit of the dual resonance model 2—73710
- φ^4 model, quasisecular clothing transformation 2—73716
- φ^4 model in one space dimension, Heisenberg equation analysis, renormalization 2—73715
- ABFST equation, strong coupling solutions 2—45840
- algebraic, central decomposition of invariant states applications to groups of time translations and Euclidean transformations 2—66887
- algebraic methods, textbook 2—45336
- anharmonic oscillator with polynomial self-interaction, equivalence 2—63015
- anomalous Ward identities, closed-loop regularization 2—73730
- axial-vector anomalies and scaling prop., Adler-Bardeen theorem 2—79480
- axiomatic, analysis of unitarity, locality, Lorentz covariance and the spectrum condition 2—59379
- axiomatic, observables and fields, review 2—63476
- axiomatic, perturbation expansions 2—59376
- axiomatic, vacuum vector uniqueness 2—63475
- bivectorial fields, energy tensors and spinors 2—45832
- Bjorken, Johnson and Low theorem, equal-time commutators in perturbation theory 2—63478
- book, introduction to theory and application 2—82635
- book 2—58795
- box graph singularities, position and strength 2—76560
- Brandeis University Summer Institute lectures (1970) 2—63461
- Brandeis University Summer Institute lectures (1970) 2—63459
- broken scale invariance Ward identities and asymptotic behaviour 2—59368
- broken symmetries, applic. of effective Lagrangians, review 2—63462
- Callan Symanzik eqn., phenomenological use 2—66922
- canonical light-cone commutators, application to deep inelastic processes and derivation of sum rules 2—59397
- Clebsch-Gordan coeffs. for coupling states, from Wigner supermultiplet scheme 2—45846
- complex masses and acausal propag. 2—55790
- complex-ghost relativistic theory, covariant formulation 2—49470
- compositeness and light-cone singularities 2—66894
- conformal algebra, shadow operator formalism, vacuum expectation values and operator products 2—45837
- conformal covariant, self-consistency conditions 2—70105
- conformal covariant correlation functions 2—49463
- conformal covariant operator- product expansions 2—70112
- conformal covariant Wilson expansion, nonequivalence in Euclidean and Minkowski space 2—73719
- conformal invariance and the energy-momentum tensor 2—59369
- conformal invariance in perturbation theory, disorientation of Ward identities 2—49466
- conformal symmetry and reverberations for zero-mass fields 2—55783
- conformal-covariant expansion on light cone 2—59367
- Correspondence Principle, scalar-tensor gravitation and perihelion advance 2—70117
- covariant, for elementary particles with mass 2—52522
- covariant theory for stable and unstable particle fields 2—59366
- creation or annihilation currents, criteria for excistence 2—70102
- de Sitter groups, contractions of representations 2—66885
- dilatation invariance, breakdown 2—82627
- dilatation invariance, spontaneous violation, in relativistic theories 2—59365
- dilation invariance, spontaneous breakdown and massive particles 2—82628
- discontinuity equation for multiparticle scattering function, derivation 2—66921
- distributions on Minkowski space and their connection with analytic representations of the conformal group 2—52517
- dual reson. models, position-space propagators and functional fields 2—76571
- effective Lagrangian formulation 2—82634
- eikonal methods in classical bound-state problems, rel. to H spectrum 2—82618
- e.m. and weak masses, cancellation of divergences 2—63486
- energy momentum tensor of spin-1/2 particle, restrictions 2—79458
- energy-momentum tensor, correl. function, Ward identities 2—55791
- energy-momentum tensors, Z-diagrams 2—49460
- equal-time commutators of e.m. current and its time derivatives 2—49467
- Euler Lagrange operators, mathematical props. 2—70101
- f-g theory 2—73704
- f-g vacuum field equations, generation of more exact solutions using work of Kundt 2—49473
- fermion fields with cut-off self- interaction, spin-momentum distribution observables and asymptotic fields 2—63456
- Feynman's path integral 2—78817
- Feynman diagram calc. of ground states of mols. with closed shells 2—77052
- Feynman graph treatment of $e^+e^-\rightarrow 3\pi$ 2—76603
- field algebra and its positive linear functionals 2—66888
- field equation and Hamiltonian approaches, relationship 2—76568
- finite energy sum rules and light cone dominance 2—70188
- fixed singularities in T_1 2—55786
- Fock representations, theorem on unitarity equivalence 2—49459
- four point function, analyticity, box diagram study 2—76560
- frame-dependent cutoff, t^{-2} law for effective Sachs e.m. form factors 2—63458
- gauge fields, new regularization and renormalization procedure 2—59352
- gauge independent gravit.-coupled e.m. field 2—42303
- gauge problem, electromagnetic field 2—52521
- gauge theories, anomaly free 2—73713
- gauge-dependent fields, rel. to scaling and scale invariance in gravitation theory 2—55404
- gauge-field theory of fermions, construction of Lagrangians 2—82623
- gauge-invariant regularization 2—52531

Field theory, quantum continued
- generalized Goldstone theorems in effective-Lagrangian framework 2−55785
- global charges as integrals over density 2−73707
- GNS construction, pedagogical example 2−63477
- gravitational field in unified spinor field theory 2−66438
- helicity states in infinite momentum frame 2−49468
- Higgs-Kibble theories, anomalous Ward identities, appearance of ghosts and gauge variance 2−45842
- Hilbert spaces, rigged, and charge operators 2−59360
- homogeneous space of Poincare groups, nucleon form factors calc. 2−63650
- indefinite metric, probabilistic interpretation based on Bogolyubov's unitarization mechanism 2−70115
- infinite component and parton-quark, perturbation series for dual amplitudes 2−73705
- infinite mass renormalization and $Z=0$ condition 2−79456
- infinite-component, describing oscillator bound states of quarks, study of light-cone behaviour 2−73706
- in infinite-momentum frame 2−66896
- internal and conformal symmetrics, necessary and sufficient conditions for conservation of generating currents 2−70113
- Klein-Gordon equation, Hulthen and Schwarzschild potentials 2−59351
- Klein-Gordon type equation, zero meas., conformal invariance 2−52520
- Lagrangian, gyroscopic system, eigenvalue problem 2−42298
- Lagrangian, infinitesimal invariance transformation 2−76569
- Lagrangian formulation and current algebra in Nevue-Schwarz dual model 2−82615
- LEED, inelastic, dynamical theory 2−74711
- LEED, inelastic, intensity calc. for Al(100) and Al(111) 2−74712
- Lie algebra derivation of analytic unimodular matrix group containing image D^j of rotation group 2−41463
- Lie identities, behavior of current-current comutator in Sugawara model 2−76578
- Lienard-Wiechert fields, generalized, multipole structure of radiation from moving multipole source 2−45833
- light cone singularities, Fritzsch Gell Mann algebra test 2−49504
- light-cone limit sequences in electroproduction, calc. to higher order of approx. in $\lambda 0^3$ model 2−66940
- Lippmann-Schwinger kernel for exponential pot., S-wave eivenvalues 2−59361
- local, transformation properties of operators 2−73721
- local gauge principle in conformal dual models 2−66891
- local saturation of commutator matrix elements 2−59356
- lowest order 'divergent' graphs in ν-dimensional space 2−66903
- magnetic lattice, 1 dimensional, field theoretical structure 2−52094
- massive $\lambda\varphi$-theory, 'equal-time' and 'equal light-cone' commutator between the dilatation charge and the field 2−59347
- massive gauge field theories 2−42301
- massless, analytic renormalization of experimental interaction, three-point time-ordered product with minimum light cone singularity 2−45836
- Maxwell-Dirac equations, coupled, Cauchy problem 2−42297
- Migdal-Polyakov Conformal invariant bootstrap theory, currents, stress tensor, generalized unitarity 2−73698
- model constructions 2−59355
- multiplicative renormalization group, critical behaviour in $d=4-\varepsilon$ dimensions 2−69622
- on multiply connected and homogeneous spaces 2−52065
- neutral gauge-scalar interaction, solution with spontaneous symmetry breakdown 2−82633
- non-polynomial Lagrangians, renormalization in Jaffe's class 2−66886
- nonderivative nonpolynomial Lagrangians, finiteness 2−73701
- nonlinear, ambiguity elimination using Carleman theorem 2−73734
- nonlinear chiral Langrangians invariant under K(n), construction 2−76561
- nonlinear fermion-field equation of motion, exact nonperturbative soln. with compounds lying on Regge trajectory 2−79467
- nonlinear Lagrangians, procedure for divergent expressions, unitarity relation 2−79465
- nonlinear realization of groups on its subgroup, symmetry violation 2−45841
- nonlinear spinor theory, functional, eigenvalue calcs. 2−63466
- nonlinear spinor theory, functional defn. and global observables calc. 2−63467
- nonlinear theories, conservation of kinks and spin, Feynman approach 2−59377
- nonlocal higher-derivative, generalized theory 2−63464
- nonlocality and generalized analyticity, microcausality at high energies 2−82604
- nonplanar helicity pole couplings, duality and Feynman graph 2−45843
- nonpolynomial with zero mass, techniques 2−59348
- nonrenormalizable containing scalar field derivative coupled to nonconserved vector current of massive fermion, finite predictions 2−55782
- one dimensional, exact solutions to field equations and boson commutation relations 2−66890
- $P(\varphi)_2$, Nelson's symmetry and infinite volume behaviour of vacuum 2−52535
- $P(\varphi)_2$ model, vacuum energy shift and Wightman functions 2−82607
- particle boundedness in $\Gamma^i_{jk;l}=0$, $g_{ij;k}=0$ field theory 2−76566
- perturbation Lagrangian theory for Dirac fields, Ward-Takahashi identity and current algebra 2−82622
- perturbation Lagrangian theory for scalar fields, Ward-Takahashi identity and current algebra 2−82621
- perturbative renormalization, role of locality 2−59370
- phenomenological, equal time commutators 2−42301
- Rayliegh-Ritz procedure, use in determ. of effective fidld equations for one-electron multiphoton stationary states 2−52534
- relativistic, hadron structure in self-consistent dynamical mechanism 2−66951
- relativistic wave equations for particles of arbitrary spin, Poincare and CPT invariance 2−45848
- renormalizable, Noether theorem and Ward identities 2−45839
- renormalizable model of weak and e.m. interactions with CP violation 2−79489
- renormalizable when gauge invariance present, anomaly removal by introducing fermion fields 2−73714
- renormalization, analytic, via continuous space dimension 2−59378
- renormalization, local operator products, review 2−63460
- scalar electrodynamics, calculations of Z_3^{-1} to fourth order 2−66898
- self-energies and light-cone singularities, pathological features 2−70110
- simple loop diagrams, validity of infinite momentum frame canonical formalism 2−42299
- spin-1/2 field, expressions for equal-time commutators, fermion source term 2−79459
- spin-two field, minimally coupled 2−55787
- spin-zero electrodynamics, fourth-order charge renormalization 2−66899
- spinor field, conformally covariant equations in six-dimensional space 2−79457
- spinorial field defn. in presence of gravitation field 2−78784
- spinorial fields, energy tensors and spinors 2−45832
- spontaneously broken gauge symmetries, perturbation theory and renormalization 2−59372
- spontaneously broken gauge symmetries, renormalizability 2−59371
- spontaneously broken gauge symmetries, S-matrix equivalence in R- and U-gauge formulations 2−59373
- state vectors with vanishing norm and probability distrib. 2−79471
- statistical physics methods, applic. to Bose fluids 2−44705
- stochastic space concept and phase fluctuations of propagating wave 2−78763
- stress-energy tensor, Ward identities and trace identities 2−45838
- structure functions 2−82689
- structure functions in theory of weak and e.m. interactions, structure functions 2−82657
- SU(3) σ model of $0^\pm$ fields, effects of adding $1^\pm$ gauge fields, chiral and scale symmetry breaking 2−79469
- superpropagators for scalar massless fields, construction and uniqueness 2−82614
- symmetry breaking and gauge invariance 2−63465
- tachyon fields, commutator and anticommutator calc. 2−73712
- Thirring model, massive, absence of Callan Symanzik coupling constant renormalization 2−63455
- Thirring model in terms of currents, solution and light-cone expansions 2−66893
- transformation properties under broken symmetry 2−45850
- ultralocal free current theory 2−42294
- vanishing of renormalization constants, sufficiency for elementary particle equivalence to three particle bound state 2−73708
- Ward identities and current-stress-tensor commutators 2−73718
- Ward identities for local gauge symmetries 2−70108
- Weyl algebra, equivalent of Glimm's and unitary dressing transformations 2−45835
- Wheeler-Feynman, extension to relativistic domain, emission processes 2−52525
- Wightman functions in space-like directions, asymptotic behaviour 2−66889
- Wigner supermultiplet scheme, derivation of coupling coeffs. 2−45846
- Yang-Mills' type gauge field, properties and applications 2−45852
- Yang-Mills field, massive two masses concept. in Lagrangian 2−70118
- Yang-Mills field mass and radiative corrections 2−55799
- Yang-Mills theory, massive, Ward-Takahashi relations 2−63463
- Yukawa in two-dimensional space-time, estimates, renormalized currents and field equations 2−55788
- $A_1\rho\pi$ coupling constants, determination using collinear dispersion relations 2−63639
- eN inelastic structure functions, field theoretic models 2−66941
- N e.m. form factors in perturbation theory, field-theoretical model 2−79608
- $\rho\pi\pi$ coupling constants, determination using collinear dispersion relations 2−63639

electromagnetic field *see Quantum electrodynamics*

interactions
- *see also Elementary particles/interactions; Elementary particles/interactions, electromagnetic; Nuclear reactions and scattering; SU(n) theory. Entries on interactions involving named particles are listed under the particles concerned*
- $^2H(\alpha, \alpha p)n$, new impulse approx. reaction mechanism 2−79796
- φ^3 ladder model, numerical calc. of inclusive spectra and correlation 2−52542
- anomalous Ward identities, coherent production, low-energy theorems 2−63502
- rel. to black hole quantum numbers nonmeasurability 2−55406
- charged particle interaction with electromagnetic fields, algebraic approach 2−52523
- Coulomb Green's function, nonrelativistic, construction 2−42300
- covariant T* products and Schwinger terms 2−52528
- differential cross sections of direct and crossed reactions, new proof of asymptotic quality based on Meyman theorem 3 2−70130
- effective Lagrangian, nonuniqueness in chiral $SU(2)\otimes SU(2)$, symmetry, $\pi\pi$ and πN interactions 2−45845
- electromagnetic, massive spin one particle, equivalence theorems 2−73700
- electron-graviton vertex, low-energy e.m. corrections determ. using Feynmann graphs 2−76559
- e.m., current algebra, divergence compensation in $\Delta T=2$ isotopic mass differences 2−45844
- e.m. factor calc. in renormalizable theory using cluster expansion 2−55792
- external field problems, vacuum definition 2−59353
- Feynman amplitudes, renormalization 2−59379
- Feynman diagram derivation of Glauber series, generalization to nonzero scattering angles 2−74056
- Feynman diagram model for hadrons, high-order planar, comparison with expts. on deep inelastic eN scattering 2−42347
- Feynman gas and multiperipheral models, relations between N-particle production of inclusive cross sections 2−45847
- Feynman necklace graph, monodromy rings 2−73729
- Feynman triangular diagram for calc. of energy distrib. of α-particles from (n,α) reactions on doubly deformed even nuclei 2−42568

Field theory, quantum continued
interactions continued
Feynmann graph technique for analysis of ^{12}C-^{16}O elastic scattering 2−74117
Feynmann graphs new method of evaluation, application to electrodynamic processes 2−73731
Feynmann rules for massive gauge fields with dual diagram topology 2−73733
Galilei and Lorentz invariant systems, conservation laws 2−63468
gauge fields, Feynman rules for effective Lagrangians 2−52527
Goldberger-Treiman relation corrections, πN form factor 2−59530
homogeneous, perturbation theory, derivation of Green's function 2−76567
indicatrices of Wightman functions as definition of time ordered products of renormalized and unrenormalized interactions 2−82613
Kadyshevsky momentum representation for boson-boson, boson-photon interactions, S-matrix theory method 2−55789
Lagrangian, rel. to NN interaction 2−45992
Lagrangian construct. of pionic processes for arbitrary SU(2) × SU(2) breaking 2−82603
Lagrangian interaction choice, rel. to s-matrix for field-field interactions 2−66895
leptonic processes, highly inelastic, comparison of parton and light cone analyses 2−55816
Lie algebraic struct. of commutation bracket exam. 2−52526
light cone, current densities and operator phenomenology 2−49462
light cone and multi-Regge theory for inclusive processes at large mass 2−73782
light-cone singularities 2−70114
massive spin one particle, equivalence theorem 2−52519
meson field with e.m. field, multipole singularities in nonlinear cases 2−59364
meson-nucleon dynamics, Ward identity for axial current, Wilson expansions and commutators 2−49461
quartic Boson interaction in three dimensions, representation of CCR and uniqueness of Hamiltonian 2−42296
relativistic three-particle eqns. with arbitrary pots. 2−59444
scalar boson trilinear coupling in small mass limit, S-matrix and field-theoretical arguments 2−59387
scalar in two space and one time dimension, soln. to renormalization problem 2−73711
spin-3/2 field in presence of interactions, quantisation 2−82618
spin-two fields, minimal electromagnetic coupling 2−66892
unified model, weak and e.m. interaction symmetry 2−55809
vertex function of virtual photon interactions with scalar field 2−76565
virtual photon-hadron, vanishing longitudinal cross sections and operator Schwinger terms 2−59458
Wick-Cutkosky model, Regge poles for large coupling constants 2−59350
Yang-Mills field interacting with nucleons, Feynman rules 2−73735
$\omega\rho\pi$ nonrenormalizable, ladder approximation for vertex function 2−52627

interactions, strong
see also Dual resonance model; Elementary particles/interactions, strong; Veneziano model
No entries

interactions, weak
see also Elementary particles/interactions, weak
CP-violating gauge interactions, derivation of Lagrangian 2−63453
current algebra, divergence compensation in $\Delta T=2$ isotopic mass differences 2−45844
divergence cancellation in simplified weak interaction model using Higgs mechanism 2−42307
higher-order corrections, field-theories perturbation methods 2−79472
model, coupling of boson to spinor field, renormaliz. 2−82654
unified model, weak and e.m. interaction symmetry 2−55809
virtual process, light-cone analysis, mechanisms for finite mass differences 2−49469

meson field
see also Mesons; Nuclear forces
φ theory, form factor in eikonal approx., determ. of bound state poles of two interacting particles 2−42304
baryon non-local field, construction of mesons 2−79463
rel. to black hole quantum numbers nonmeasurability 2−55406
boson fields, uniqueness of vac. energy density and van Hove phneomenon 2−42306
divergence cancellation in simplified weak interaction model using Higgs mechanism 2−42307
gauge invariance and Ward identities in massive-vector-meson model, study by normal product techniques 2−79481
interaction with e.m. field, multipole singularities in nonlinear cases 2−59364
massive gauge fields, variant of Stuckelberg formalism, applications to hadron electrodynamics 2−42305
neutral scalar field, Hamiltonian as graph limit, infinite renormalization 2−59363
renormalization and symmetry of massive vector fields 2−82610
Sakata-Taketani field assoc. with Kemmer field under symmetry breaking 2−66897
scalar, axially symmetric massive, nonexistence 2−59359
spin-one mesons, tensor approach for quantization 2−82625
spin-one mesons, tensor approach to magnetic dipole moment and electric quadrupole moment 2−82626
zero mass meson, interaction with charged dust in axially symmetric fields 2−42302

quantization
see also Quantum theory/quantization
de Sitter space, scalar massless field 2−70104
dual quark theory as second quantiz. of Thirring model 2−66947
dynamics in the 'infinite- momentum frame' 2−45849
Einstein equation, linearized, local and covariant quantization 2−59362
electrodynamics, mass spectrum in pure Coulomb field 2−49471
fermion operators, second quantiz., diagonalization of quadratic linear form 2−82629
Foldy-Wouthuysen quantized field, commutation rules 2−70116
magnetic charge quantiz. rules 2−59357

Field theory, quantum continued
quantization continued
massive spin one particle, equivalence theorem 2−52519
Maxwell-Dirac field in Coulomb gauge, covariant generalization of quantization 2−69578
rel. to noncommutative representation of classical, dynamics 2−41561
renormalizable gauge model of lepton interactions 2−76599
renormalized theory on light 2−82616
spin-3/2 field in presence of interactions 2−82620
spin-$^3/_2$ field, causal coupling 2−70106
spin-one mesons, tensor approach for quantization 2−82625
spinor field, modified quantiz. in external e.m. field 2−79461
spontaneously broken gauge symmetries, perturbation theory and renormalization 2−59372
tachyon fields, free, spin/statistics relation 2−79464

scattering
see also Elementary particles/scattering
— 2−66433
amplitude determination from differential cross-section and unitarity 2−82636
amplitudes, in Bloch-Nordsieck model 2−76573
charged intermediate vector boson scatt. by Yukawa pot. 2−55808
Compton effect s-channel helicity conservation, a critical test 2−79491
cut to cut extrapolations and weighted dispersion relations 2−42295
Dirac spinor amplitudes, expression in terms of invariants 2−73723
Eckmann model, asymptotic nucleon fields constructed 2−76570
elastic processes, s-channel helicity conservation 2−55840
electron scatt. structure function, possible exchange degeneracy on light cone 2−55825
ep, spin dependent deep inelastic, light cone analysis 2−55826
finite energy bounds on elastic scattering amplitude, desication 2−70139
Fock space, time-independent perturbation theory 2−45834
gauge theories, convergence props. of lowest order diagrams 2−70145
hadrons, high energy scatt. in φ^3 theory, eikonal approx. breakdown 2−59477
high-energy, pole positions for large coupling consts. 2−59501
indefinite-metric theories, physical unitarization 2−70107
indefinite-metric theory, consequences of piecewise-analytic scattering amplitude 2−63457
infinite momentum QED, applic. to high energy scattering 2−63473
Levinson's theorem, connection with singular integral equations 2−82606
light cone commutations used to derive finite energy sum rules 2−63557
multiperipheral configuration, dual amplitude construction based on general field theory vertices and propagators 2−59470
n-particle amplitude, local analyticity properties. 2−76564
n-point functions, IU(3.1) invariant analytic extensions, analyticity domains 2−76563
optical model at high energies 2−49465
relativistic eikonal dynamics 2−45851
relativistic theory, charged particle scattering 2−73722
Schwinger variational principle and Pade approximants 2−52516
variational Pade solution of Bethe-Salpeter eqn. 2−73709
virtual Compton amplitude and fixed-pole 2−52552
Yukawa pot., Regge poles for large coupling consts. 2−59500
νN scattering, operator product expansions and dimension of symmetry breaking Hamiltonian 2−55820
GeTe, thin film, amorphous polycrystalline phase transformation, radial distrib. of atoms 2−71686

Films
air, thickness measurement using white light interferometry 2−70015
fluid, squeeze film behaviour between two parallel annular disks, one with porous facing, mathematical analogue 2−67562
Indium, electron diffraction beam heating 2−83920
liquid cryst., vacuum deposited, surface orientation 2−71157
liquid crystal, nematic, domain wall motion 2−74521
liquid crystal, nematic, polarimetry and interferometry studies 2−43329
nematic liquid crystal in variable magnetic field, transient distortions 2−53396
photographic, frequency contrast characteristics measurement 2−70093
photographic, granularity, density, colour films, black and white 2−82595
polyethylene terephthalate films, observations of optical irregularities 2−52452
thermoplastic, local deformation of free emulsion surface 2−73235
thin film analysis using two beam interferometer 2−79354
thin film system, inhomogeneous field generated by total reflection of plane wave 2−52450
liquid
see also Adsorbed layers; Contact angle; Helium/liquid; Superfluidity; Surface tension
— 2−67876
axisymmetric liquid-fluid interfaces, stability towards general disturbances 2−67794
boiling, steady, laminar, natural convection on vertical surface, stability analysis 2−43448
calcium stearate lubricant monolayers, shear strength 2−53383
charged cylindrical, bursting 2−52349
circular, smallest stable radius rel. to contact angle and line tension 2−60412
condensation of binary vapours, effects of forced flow and variable properties 2−77411
condensation of pure and binary vapours at forward stagnation point of horizontal cylinder 2−77410
cooling and mass transfer data, correlation, for protecting solid surface in hot gas streams 2−67795
drainage and evaporation of film with salt deposition on horizontal cylindrical surface 2−77408
electric double layers, wave motion of low-tension interfaces 2−83740
entry-region flow, finite difference numerical solutions to Navier-Stokes eqns. 2−67793
flow and stability on rotating horizontal disc 2−43309

Films continued
liquid continued
flow on flat plate, enhancement of heat transfer by waves 2−56494
free liquid films, rheological features of thinning process 2−60408
free vertical, medium effects in equilibrium thickness 2−60411
friction on inclined plane, polarographic obs. 2−83728
gas-liquid flow, annular, mean vels. calc. 2−53345
glycerine solutions, wave inception in falling film 2−50287
hydrodynamic stability of two component fluid layer heated from below 2−56452
laminar, vapour shear boundary condition for condensation 2−53501
laminar falling, mass transfer balance equations 2−71149
laminar free liquid film flow, theory and expt. 2−74497
lifting of liquids by withdrawal 2−43276
mass loss from thin liquid surface films exposed to re-entry heating and shear 2−54976
MBBA nematic liquid films with free surfaces, electro-optic and hydrodynamic props. 2−67804
menisci, axisymmetric, tables of profiles 2−60413
methylene blue dye film waveguides, optical absorption 2−63416
MHD, thin film of conducting liquid in transverse magnetic field, wave flow regime 2−53162
rigid surface films, apparatus for thickness measurement 2−53382
sheets, disintegration and aerodynamic instability 2−67779
single gas absorption, mass transfer into sheared interface with and without chemical reaction 2−67749
soap, stabilised with ionic surfactants, impurity effects in meas. of very small contact angles 2−60410
soap, transition regions, line tensions and contact angles 2−60409
superfluid, size effects near second order phase transition 2−83869
supersonic streams interactions, nonlinear stability 2−78934
surface waves on water with depths less than boundary layer thickness 2−74503
thermoplastic, local deformation of free emulsion surface 2−73235
thickness meas. by Moire fringe contouring 2−79371
thickness measurement, electrical contact method, hysteresis, statistical profile 2−83733
thin, wavy flow 2−53381
thin film flow on curved surfaces, application to determ. downstream boundary condition for flow on flat plate 2−43308
water, wave inception in falling film 2−50287
wave roughened gas-liquid interface, heat and mass transfer to annular two-phase two-component flow 2−77409
He, acoustic interference applic. to thickness meas. 2−47008
He, acoustic multiple beam scattering 2−83832
He, anomalous attenuation of third sound, microscopic origin for apparent uncertainty principle 2−71252
He II, non-pot. flow at sub-crit. vels. 2−47022
He II, rotating, thickness changes 2−64496
He II, surface tension, temp. depend., surface excitations contrib. 2−53473
He II film flow, thermally driven, 1.7-2.1 K, dissipation 2−67862
He II film flow transfer over Plexiglas ampoules, singularities 2−67856
He superfluid, wave processes 2−80516
^{4}He, adsorbed, superfluid, quartz microbalance obs. 2−64497
^{4}He, thermally driven superfluid film, saturation of fluctuation dissipation in flow 2−80507
^{4}He adsorbed on graphite, flow 2−74575
N$_2$, boiling, heat transfer in plug stage, expt. 2−56546

Films, solid
see also Thickness measurement; Thin film devices
acoustic transducer, thin film mosaic for bulk waves 2−49135
adhesion mechanics, elastic and elastic-plastic behaviour 2−71666
Ag, prep. and characterization 2−56586
alkali halide, charact. energy losses by slow electrons 2−81532
alloy layer, on hot dip Al coated, stainless steel, struct. and composition 2−56937
amorphous, chalcogenide, grown by vapour deposition, contribs. to growth temp. 2−64564
anodic oxide film formed on Ti, effect of formation electrolyte on no. of imperfections 2−50518
antistatic agent, on plastic, thickness recovery processes, ellipsometry obs. 2−65073
BDPA, organic free radical, vapour deposition 2−56598
Bi, charact. electron energy loss spectra 2−44044
binary arsenosilicate glass, diffusion source, thermal stresses 2−71325
CdCr$_2$Se$_4$, prep. by simultaneous vacuum deposition from separate sources 2−60649
CdS film growth by evaporation, inclined orientation 2−71370
CdS film growth by evaporation, inclined orientation 2−71370
chalcogenide, amorphous, dielec. const., elec. cond., struct. features 2−61309
chalcogenide alloy, amorphous, sputtered, thermally stimulated Ar release study 2−43472
chemical polishing technique for prepn. of thin foils for e. microscopy 2−67963
Co$_x$Mg$_{1-x}$O, single crystal film, epitaxial growth method 2−60650
coatings, high temp., deposition from fused salts and by ion plating 2−50860
compact, spectral energy distribution (rel. to Markarian 205) 2−73000
condensed gas, electron microscope pressure cell 2−79117
conference, Jerusalem, Israel (May 1972) 2−70340
curved surface acoustic waveguides, propagation 2−49122
deposition on cylindrical substrates by asymmetric a.c. sputtering 2−80600
deposition rate monitoring by quartz crystal microbalance 2−69512
dielec., multilayer, for 1700-2500 Å bands 2−42191
dielectric, deposition by h.f. sputtering 2−78695
dielectric, spot size dependence of laser- induced damage thresholds 2−48123
dielectric, surface phonons and electron energy losses, metal contact influence 2−47829
dielectric layers with imposed spectral characts., control and preparation 2−63418
diffusion zones, X-ray obs. of composition profile and diffusion generated substructure 2−56585

Films, solid continued
dispersion hardened materials, prep. for transmission of electron microscopy by spark machining and electropolishing 2−80549
DPPH, organic free radical, vapour deposition 2−56598
elastic properties, sensitive meas. by harmonic generation of dispersive Rayleigh waves 2−50472
electromigration, grain boundary contribs. 2−56751
electron elastic plural scatt. by atoms, intensity-angular distribs. 2−84220
electron probe analysis, network scheme of pulse height anal. 2−61830
element profiles across oxide films by Auger electron spectroscopy 2−56580
epitaxial, structure and props. of transition layer 2−47093
epitaxial layers, growth from soln., theory 2−77505
f.c.c., epitaxial, stacking fault determ. 2−77588
garnet, bubble domain, epitaxial, effect of substrate defects on struct. 2−47092
garnet, chem. vapour deposition, product phase control 2−71321
garnet, chemical vapour deposition by organometallic sources 2−74621
gas discharges, organic reactions leading to polymer deposits 2−74408
glass, chalcogenide, high field effects, current voltage characts., Poole-Frenkel emission 2−44097
glow polymer layers, electron microscopy study of formation 2−53564
graphite, pyrolytic, ribbon production and mech. props. 2−56999
graphite, pyrolytic, struct. characts. 2−60648
group II-VI semiconductor, epitaxy by decomp. of group II metalorganic 2−47091
group III-V semiconductor, epitaxy by decomp. of group III metalorganic 2−47091
growth, review of techniques 2−60638
holographic recorder for monitoring deposition 2−76494
ice, ionized water cluster production by electron bombardment 2−84221
ice, on cooled surface, microstruct. rel. to deposition rate, elec. field, vacuum breakdown 2−83866
insulating, defects, obs. using elec. field induced light scatt. in liq. cryst. 2−77918
interference filter, reflex, conjugate, within Fabry-Perot cavity 2−79346
ionic crystal, microscopic theory of surface vibrations 2−80552
layered media on sapphire substrates, surface acoustic wave propagation 2−51000
Lorentz microscopy, in-focus, wave optical theory for thin ferromagnetic films 2−76458
low angle electron scattering of films with anisotropic distribution of crystallites 2−80640
magnesium phthalocyanine, impurity level energies from photoemission and cond. obs. 2−81028
magnetostrictive, prep. by tetrode plasma sputtering 2−43473
metal, cond. e.p.r. line shapes, theory 2−81450
metal, deposition by h.f. sputtering 2−78695
metal, electromigration, interface reactions 2−74622
metal, epitaxial, on alkali halides, electron surface scatt. influence on cryst. orientation 2−53565
metal, morphological changes due to illumination during deposition 2−74620
metal, significance of electric field on growth 2−60634
metal, surface plasmon excitation by transmission of fast electrons 2−47828
metal, time taken for laser pulse to make hole 2−79255
metal and dielectric foils, electron backscattering thickness det. 2−41921
metal coating, twinning fault probability X-ray exam. technique 2−50473
metal evap. on alkali halides, multiply-twinned particles 2−47101
metal layers, dipolar interaction forces effect on grains after thermic evaporation 2−64559
metal silicide formation, on Si from thin metal films 2−43861
metal tritide, ageing, bubble form. and rupture 2−43478
metal/SiO$_2$ cermet, recoil atom implantation produced, microstruct. 2−53578
misfit dislocations, at film/substrate interface, image contrast 2−71483
monolayer, prep. for autoradiography 2−80616
multilayer, porous and nonporous, discrete frontal electron emission, ratio of pair production 2−68488
nichrome, prod. by multiple sublimation, vacuum system, props. 2−47121
nichrome, resistive, evaporated from liquid phase by electron beam gun, prep. and props. 2−71332
nichrome, sintering 2−68151
noncrystalline solid prep. by r.f. sputtering 2−47114
nuclear target preparation 2−73921
nucleation and growth, exptl. approach to well controlled studies 2−56583
nucleation and growth, LEED-Auger instrument and u.h. vac. electron microscope 2−74624
optical components for integrated optics, fabrication, review 2−79413
organic, charact. energy losses by slow electrons at 77K 2−84669
organosilicon, r.f. plasma polymerization 2−43484
overlays for, time delay trimming in delay lines 2−51006
oxide, on metal, diffusion of oxygen into metal 2−71533
oxide film destruction by electron beam 2−71322
oxide layer on α-brass, rel. to stress corrosion cracking 2−64734
paraffin, i.r. holograms using pulsed high power lasers 2−55713
Permalloy, creep rel. to thickness 2−56806
permalloy films epitaxially grown on fcc metals, structural and standing spin wave resonance props. 2−78149
permeability of H$_2$O vapour in coatings, measurement technique 2−80757
phonon generation in metal films in an electric field 2−54015
piezoelectric interdigital transducers, impedance and capacity for Rayleigh and SV modes 2−49151
plasma sprayed coating, variables influencing characteristics, review 2−53562

Films, solid continued
- polarization of spin waves and hf pumping in thin ferromag. films 2−78150
- polycarbonate, as dosimeter for 10-100 Mrad range 2−42700
- polycrystalline, anisotropy of elastic deform. 2−80730
- polyethylene, formed by evaporation and deposition in vacuum, crystal morphology 2−50516
- polyethylene films, changes in crystal orientation with time following stretching 2−83381
- polyethylene terephthalate, mech. props., influence of liq. media 2−50750
- polyethylene terephthalate, stress relaxations, dielec. and dynamic mechanical obs. 2−56779
- polyimide, aromatic, secondary dynamic dispersions 2−83366
- polymer, contact angle meas. of Hg scanning electron microscope obs. 2−46942
- polymer, electromechanical model for capacitance effects 2−57228
- polymer, filled with fragmented glass fibres, mechanical anisotropy 2−84131
- polymer, mech. props. rel. to mol. orientation, sound vel. obs. 2−47536
- polymer, tensile, rupture and elongation props. 2−60887
- polymer insulator synthesis and deposition for Josephson tunnelling applics. 2−71877
- polymer layers, crystn., electron-microscopic study 2−83392
- polymer layers, supermol., struct. form. 2−60637
- polymers, dynamic light scattering study 2−83382
- polypropylene, T-die film, mechanical props. and mol. orientation 2−47537
- preparation, conference (Gatlinburg USA, Oct 1971) 2−49617
- production by evaporation in elec. field, effect of resistance 2−71341
- production by glow discharge sputtering systems 2−71323
- protective layer in d.c. diode sputtering 2−60643
- protective properties of anodic oxide films on Al and its alloys 2−53886
- PTFE, transfer in sliding 2−53820
- PVA, uniaxially stretched films, mech. anisotropy 2−83365
- pyrofoil tape, production and characterisation for reactor use 2−56050
- radiation source production by radiofrequency sputtering 2−74046
- radiation sources, production by r.f. sputtering 2−49334
- rare earth monochalcogenides, co-evap. and characteriz. 2−50502
- rare earth oxide, martensitic phase transformation 2−50949
- refractory metals, zone decorations in field evaporated surface 2−53551
- refractory prep. using plasma jet in vacuo 2−83889
- rubber, crystallization at high pressures 2−60603
- scanning high energy electron diffraction, review 2−74710
- secondary electron emission exam. 2−77978
- self supporting, role parting agents in production 2−56584
- semiconducting surface oxide, electronic properties and pitting susceptibility of underlying type 304 stainless steel 2−57422
- semiconductor, amorphous, electron beam interaction, read and write processes 2−61260
- semiconductor, amorphous, morphology exam. by scanning electron microscopy 2−44129
- semiconductor, multilayer, thermal cond., rel. to thermoelec. props. 2−51054
- semiconductor, single crystal, electrical conductivity and adsorption, combined meas. 2−71932
- Seyfert and related types, i.r. photometry 2−73051
- sputter deposition, energy analysis of particles on substrate 2−61118
- sputter deposition, focussing effects 2−60642
- sputtering, r.f., target processes 2−60640
- sputtering, r.f., transport and deposition processes 2−60641
- stable layer systems, diffusion barrier arrangements, ageing, stability rel. to comp. 2−75120
- steel, diffusion layer, C distrib., study by spectroscopy 2−47435
- steel, high tensile strength, chemical grinding prep. 2−71636
- stress and mass change obs. using quartz resonators 2−50786
- structure, effects of ion bombardment and implantation 2−53568
- substrate role in det. crystallinity of organic thin films 2−77533
- sum-frequency amplitudes formulae for propagation of e.m. waves from nonlinear multilayer film 2−58989
- superconductor, thermal cond., mag. field depend. 2−68344
- surface acoustic wave velocity meas. change caused by thin conducting film 2−51017
- surface density meas. by proton excited X-rays, Fredholm expression 2−80542
- surface oxide, electromech., photomech. and conc. effects 2−51155
- surface states calc. by Green function's technique 2−75036
- targets, preparation techniques 2−49624
- tetraethoxysilane, dielectric film growth by low temperature oxidation 2−60636
- thermionic emitter fabrication by vapour deposition of high work function materials in glow discharge 2−49273
- thickness, ellipsometry, calc. method 2−44339
- thickness, maximum uniformity, algorithm for experimental parameters optimizations 2−50478
- thickness determination by electron backscattering 2−79116
- thickness meas., ellipsometric method 2−47095
- thickness meas. by holographic interferometry 2−50477
- thickness meas. of lubricating, insulating and protective coatings on metals and semiconductors 2−55357
- thickness measurement, solid solutions, X-ray diffraction 2−82125
- thickness measurement, X-ray glassy halo obs. 2−64557
- thickness measurement by elastic backscattering 2−80923
- thickness measuring, photoelectric, of optical thin films 2−59225
- thickness uniformity on rotating substrates 2−67903
- thin, internation converence, Venice, May 1972 2−77504
- thin layer, X-ray fluorescence method for thickness determination 2−43470
- transition metals, amorphous, deposition and annealing, resist. study 2−77499
- 4d transition metals, vapour deposited, electron microscope obs. 2−60594
- triphenylmethane dyes in films of poly(methylmethacrylate), photochemistry 2−65387
- trisiloxane, electron beam polymerization, physical props. 2−47909

Films, solid continued
- vacuum decoration method, study of growth processes and defect structure 2−80538
- vacuum deposited, cross-section obs. by replication 2−56579
- vacuum deposited, optical thickness monitor for control 2−47094
- vacuum deposition, technology and state of art 2−78693
- vacuum deposition 2−66384
- by vacuum evaporation, charact. 2−47087
- vapour deposited, nucleation kinetics, analytical formula 2−64562
- vapour deposited, nucleation theories, capture number evaluation 2−64561
- vapour deposition, adatom capture and nuclei growth 2−50475
- vapour deposition, computer simulation 2−50476
- vapour deposition, nucleation, role of active centres 2−47089
- Vickers type ultra-microhardness tester 2−43471
- viscoelastic behaviour, nonlinear, of polyethylene films 2−83375
- X-ray diffractometer, URS-501M, vacuum attachment 2−62907
- Ag, annealed, hillock and island form. by surface diffusion 2−67896
- Ag, Debye characteristic temp. 2−61102
- Ag, films, indentation and impact studies of loading 2−77708
- Ag, growth process on alkali halides, electron microscope obs. 2−47096
- Ag, on mica, oriented recrystallization on annealing 2−47097
- Ag, Poissons ratio, X-ray obs. 2−67904
- Ag, single crystal, prep. and characterization 2−56586
- Ag, single crystal charact. and preparation 2−74627
- Ag, stresses in vacuum evaporated films 2−80569
- Ag, thickness det., comparison of multiple beam Fizeau interferometry, photoelectric shearing interferometry and stylus instrument methods 2−47118
- Ag, vacuum deposition on Ni, secondary ion-ion emission obs. 2−50481
- Ag films on mica substrates, exam. of internal stresses 2−77650
- AgCl photolysis, temp. depend., 77-400K 2−61803
- Ag$_2$Se, formation for substrate temperature 20°C-120°C, effect of heat treatment on properties 2−53570
- Ag$_3$Sn, preparation of electrodeposits 2−53569
- Al-Cu alloy, precip., G.P. zone form., rel. to bulk alloy props. 2−47099
- Al-Mg oxide films, structural analysis, electron microscope examination 2−71642
- Al-Si dilute alloy, Si precip., resist. study 2−50825
- Al, adsorption of Cl, Auger spectrosc., ellipsometry and surface potl. meas. of clean films 2−71345
- Al, Ar$^+$ bombardment, transmission sputtering and recoil implantation 2−54090
- Al, deposited on Nb, LEED and Auger spectroscopy obs., 22-1200°C 2−50484
- Al, growth from the melt, nucleation by Ti cpds. 2−47098
- Al, hillock growth 2−77506
- Al, laser beam hole ('bit') creation, physical processes 2−69989
- Al, multilayer structures, internal stresses, X-ray and Newton's rings obs. 2−43475
- Al, oxidation, LEED obs. 2−51445
- Al, thermal cond. and integrated radiating power 2−74999
- Al, transmission, reflection, and absorption of high current density electron pulses 2−84223
- Al, vacuum evaporated into polymer, adhesion mechanism 2−43476
- Al coating on U-Nb alloy, effect on stress corrosion cracking 2−53911
- Al epitaxial growth on NaCl and KBr substrates 2−77501
- Al films, electron multiwave scattering at 70 keV, scatt. intensity detn. 2−71451
- Al foil, direct-recording electronograph in study of objects giving increased background 2−53639
- Al polycrystalline films, on NaCl substrate, effect of annealing 2−80566
- Al single crystals, possibility of use of oscillating film spectrometer for detn. of dislocation density homogeneity 2−77582
- Al thin absorbers, loss of protons 2−80924
- Al with interlayered transition metals, effect on ^{27}Al n.m.r. 2−68743
- Al$_x$Ga$_{1-x}$As, multiple layer liq. phase epitaxy on GaAs, junction prep. 2−50482
- AlN, deposition on Si, m.i.s. struct. prep. 2−54225
- AlN$_x$, preparation by reactive r.f. sputtering, optical and electrical properties 2−77507
- Al$_2$O$_3$, crystn. of amorphous anodic film by heating in vac. 2−83861
- Al$_2$O$_3$, electron beam produced, electrostatic potential effects 2−60645
- Al$_2$O$_3$, in m.i.m. struct., film struct. rel. to transient phenomena 2−57219
- Al$_2$O$_3$, plasma and gas plasma deposited, struct. determ. 2−64563
- Al$_2$O$_3$, plasma anodization 2−43477
- Al$_2$O$_3$, struct. and props., effect of chem. vapour deposition temp. 2−50483
- Al$_2$O$_3$ amorphous anodic films, partial model for structure from X-ray scattering data 2−47100
- Al$_2$O$_3$ on glycerol as specimen support film for atomic resolution electron microscopy 2−43556
- Ar-Kr(Xe), struct., 6K to sublimation temp., electron diffr. obs. 2−80573
- As$_2$Se$_3$, crystalline and amorphous, ion bombardment effects 2−60646
- Au-Al, α-phase dil. alloy, band struct., refl. study, 1.1-11.5 eV 2−75278
- Au-SiO$_2$ r.f. cosputtered films, combined electron microscopy X-ray microanalysis obs., and preparation 2−80576
- Au, {100} orientated, surface struct., LEED, RHEED 2−77500
- Au, band struct., refl. study, 1.1-11.5 eV 2−75278
- Au, bicryst., electron diffr. by grain boundary dislocation networks 2−77593
- Au, boundary layers, transmission of struct. information 2−77494
- Au, Cr low temp. migration, backscatt. obs. 2−56754
- Au, growth process on alkali halides, electron microscope obs. 2−47096
- Au, large angle rotation boundaries, electron micrographs 2−56736
- Au, on amorphous C, oriented crystn. mechanism, rel. to interaction forces at interface 2−77502
- Au, on glass, photoelectron spectrometric investigation 2−80572

Films, solid continued
Au, temp. rise during film deposition as a function of applied power for sputtering 2−67913
Au, thickness det., comparison of multiple beam Fizeau interferometry, photoelectric shearing interferometry and stylus instrument methods 2−47118
Au, u.s. velocity, attenuation and internal friction meas. 2−77780
Au, X-ray diffraction, internal strain and crystallite size rel. to spitaxial growth 2−50485
Au films, electron multiwave scattering at 70 keV, scatt. intensity detn. 2−71451
Au ion alkali halide, growth from nuclei with fivefold symmetry 2−47102
B filament chem. vap. deposition on C monofilament substrate 2−53956
BP layers, vapour growth using open and closed tube processes 2−50486
BaTiO$_3$, single crystal, microstruct. of domains and domain walls 2−68469
BaTiO$_3$, vacuum evaporation technique 2−83894
Be, condensation on cold substrate, crit. thickness determ. 2−56587
Be, condensed on glass, amorphous to cryst. transition temp. 2−43474
Be, structure effects on secondary electron emission 2−57265
BeO, epitaxial film growth and characterisation for microacoustoelectronic applications 2−51042
Bi, condensation on cold substrate, crit. thickness determ. 2−56587
Bi, condensed on glass, amorphous to cryst. transition temp. 2−43474
Bi, i.r. holograms using pulsed high power lasers 2−55713
Bi, in picosecond holography using Nd:glass laser 2−55714
Bi, vacuum evap., selective condensation on macroinhomogeneous surface 2−74628
Bi$_2$O$_3$, amorphous and polycrystalline film prep. by cathode reactive sputtering 2−80594
Bi$_8$Te$_7$S$_5$ layered material, thickness distrib. in cleaved single cryst. films 2−47103
C-Fe, on Zr, Al, or steel reactor material, electron probe anal. 2−44509
C, amorphous, graphitization by light pulses 2−61030
C, amorphous, struct., elec. props. and absorpt. study 2−61302
C, deposition and diamond-like props. characterization 2−56588
C, evaporation production technique 2−49625
C, graphitization under light pulse irrad. 2−57002
C, graphitized, anisotropy of g-value 2−78153
C, on Zr, Al, or steel reactor material, electron probe anal. 2−44509
C, production using evaporation method 2−74629
C on glass laser damage rel. to surface film 2−82504
Cd coating on U-Nb alloy, effect on stress corrosion cracking 2−53911
CdS, c-axis orientation modification, evaporation by reflection 2−50487
CdS, deposition on GaAs-CdS to form isotypic heterojunction 2−71956
CdS, epitaxial growth under isothermal conditions 2−47106
CdS, evaporated in vacuum, crystal structure 2−77508
CdS, liquid phase epitaxy 2−47104
CdS, optimum conditions for epitaxial growth 2−47105
CdS, sputter deposition 2−53571
CdS epitaxial growth, single crystal films 2−53572
CdS evaporated layers, thinning for transmission electron microscopy 2−67962
CdS films, evaporated in vacuum 2−77508
CdS transducer deposition, parameters controlling device usefulness 2−67906
CdS$_x$Se$_{1-x}$, band gap, optical transmission study 2−61633
CdSe-SiO$_x$, electron transport study in space charge layer of vacuum-deposited film 2−77852
CdSe, epitaxial growth under isothermal conditions 2−47106
CdSe, residual gas analysis during vapour deposition 2−78697
CdSe, vacuum evaporated, structure on mica, NaCl, PbSe substrates, electron microscopy, electron diffraction techniques 2−71327
CdSe films, energy spectrum and nature of trapping centres detn. by induced impurity photocond. method 2−71501
CdTe, epitaxial growth, on CdS, closed-tube chem. transport technique 2−77498
CdTe, epitaxial growth under isothermal conditions 2−47106
CdTe, optimum condition for epitaxial growth 2−47105
Cd$_x$Zn$_{1-x}$S, prep. and comp. depend. of energy gap 2−54169
Ce, core level binding energies, X-ray photoelectron spectra study 2−72096
Co-Fe, electrolytically deposited, structure and orientation 2−53561
Co-P, electroless deposited, growth and struct. 2−53566
β-Co, electrolytically deposited, structure and orientation 2−53561
Co, two-layer, bonding energy determ. 2−57298
Co n.m.r., effect of constitution and temp. 2−81471
Cr-Si-Fe-W ceramic electron microscope study of laser produced holes 2−80780
Cr-SiO ceramic electron microscope study of laser produced holes 2−80780
Cr, condensation on NaCl, nucleation 2−50488
Cr, electrodeposited, internal stresses 2−64565
CrSe, vacuum deposited, struct. 2−67907
CrTe, vacuum deposited, struct. 2−67907
Cu-Au bimetallic, interdiffusion, X-ray obs. 2−60828
Cu-C alloy, prep. by vac. deposition, microstruct. 2−56928
Cu-Ni alloy, growth, struct., epitaxial temp. rel. to comp. 2−60654
Cu, condensed in presence of residual gases, oxidation 2−71328
Cu, Debye characteristic temp. 2−61102
Cu, deposition on cold substrate, fibre texture formation 2−50480
Cu, electrodeposited, morphology, current density and substrate orientation effects 2−48340
Cu, electrodeposition, cathodic impedance study 2−48339
Cu, electroplated and vapour deposited, struct. rel. to annealing 2−77497
Cu, epitaxial electrodeposited, defect obs. 2−47107
Cu, growth kinetics near melting point 2−60652
Cu, lattice consts. of small nuclei, rel. to surface stress 2−60655
Cu, r.f. sputtered, film thickness distrib. 2−60651
Cu, vacuum-deposited, substruct., deposition rate effects 2−50489

Films, solid continued
Cu films in storage, ageing effects on substruct. and mech. props. 2−83863
Cu thin absorbers, loss of protons 2−80924
Cu$_{2-x}$S, on NaCl, deposition and phase struct. 2−60653
Er, f.c.c. struct. and oxidation, HEED obs. 2−50490
Er, maximum sorption capacities and gettering action 2−43495
Er$_2$O$_3$ film form. on oxidation of Er 2−50491
EuEr$_2$Fe$_{5-x}$Ga$_x$O$_{12}$, liquid phase epitaxy, optimum conditions 2−47108
EuO, prep. by oxid. of Eu film 2−64568
EuS-EuF$_2$, prep. for magneto-optical obs. at low temps. 2−64567
Fe, condensed on glass, amorphous to cryst. transition temp. 2−43474
Fe, corrosion products in NaNO$_2$, internal conversion electrons, Mossbauer study 2−72281
Fe foils, electrocrystn. structures 2−83862
Fe$_3$C, condensed, carbide grain growth 2−56932
Fe$_{1-x}$O, epitaxy on CaF$_2$ 2−47109
FeSi, e microprobe analysis 2−77509
GGG, epitaxial magnetic film, prep. by chem. vapour deposition 2−77527
Ga, condensed on glass, amorphous to cryst. transition temp. 2−43474
n-GaAs:Ge, epitaxial, degenerate, forbidden gap, traps 2−44114
GaAs, controlled sectioning by anodic oxidation and removal of oxide layer 2−64544
GaAs, epitaxial, doping level and impurity distrib., substrate orientation effects 2−47436
GaAs, epitaxial, growth morphology obs. by sequential changes in doping level 2−47113
GaAs, epitaxial growth, anisotropy obs. using abrupt changes in doping level 2−47112
GaAs, epitaxial growth on Ge, feasibility of photodiode production 2−54260
GaAs, epitaxial growth on ZnSe substrates from Ga, Sn solutions 2−53573
GaAs, multiple layer liq. phase epitaxy on GaP, junction prep. 2−50482
GaAs, selective growth, morphological studies 2−50493
GaAs, vapour phase epitaxy, layer characteriz. 2−50492
on GaAs substrate, meas. using split-beam ellipsometer 2−71329
GaAs$_{1-x}$P$_x$, comp., effects of deposition conditions in GaAs-AsCl$_3$-PCl$_3$-H$_2$ system 2−60657
GaAs$_{1-x}$P$_x$, epitaxial growth on GaAs by pyrolysis on Ga(CH$_3$)$_3$, AsH$_3$ and PH$_3$ 2−50496
GaAs$_{1-x}$P$_x$ layers, vapour phase epitaxial growth kinetics 2−50494
GaN, prep. by cathode sputtering 2−56589
GaN epitaxial layer growth from vapour phase 2−50495
GaP, epitaxial growth on insulating substrates and characterization 2−47111
GaP, heteroepitaxial growth on Si substrates 2−83864
Ge-Se-Te-As system, amorphous, composition and physical props. 2−60573
Ge-Si heteroepitaxial structure, u.h.v. evaporated, structure 2−56591
Ge-Te alloy, amorphous, structure, elec. microscope obs. 2−50479
Ge, amorphous, crystalline transform. rel. to thickness and environment 2−67882
Ge, amorphous, dark-field electron microscope obs. 2−60593
Ge, amorphous, metal contact induced crystalliz. 2−56590
Ge, amorphous, microcrystallite struct. 2−43479
Ge, amorphous, secondary electron emission spectrum obs. of disorder 2−61353
Ge, amorphous, small angle X-ray scatt. obs. 2−60661
Ge, amorphous, structure, elec. microscope obs. 2−50479
Ge, amorphous, structure 2−60577
Ge, amorphous, technique for Hall voltage obs. 2−64963
Ge, amorphous, thick self supporting production and bulk prop. obs. 2−56592
Ge, amorphous, void structure and optical sum rules 2−78063
a-Ge, crystalliz. processes, elec. microscope obs. 2−60658
n-Ge, degenerate, on GaAs, epitaxial growth 2−47115
Ge, density meas. by X-ray total refl. 2−74630
Ge, deposition and annealing parameters, influence on strain sensitivity 2−77709
Ge, electron spectroscopy of amorphous film at energy losses below 1 eV 2−80934
Ge, evaporated amorphous, anisotropic microstructure, X-ray study 2−47116
Ge, structure effects on secondary electron emission 2−57265
Ge, thick amorphous self-supporting 2−74631
Ge, thick film, amorphous, self supporting, production and bulk prop. obs. 2−56592
Ge amorphous, struct. rel. to angle of evaporation 2−71330
Ge epitaxial, on GaAs, differential thermal expansion detn. 2−57075
Ge$_3$N$_4$, vapour deposition on Ge, dissolution rate 2−54224
GeSe thin film, amorphous polycrystalline phase transformation, radial distrib. of atoms 2−71686
Ge$_x$Se$_{1-x}$ alloy, amorphous, radial distrib., elec. diffr. obs. 2−60659
GeTe-SnTe alloy, epitaxial, twinning faults 2−53574
GeTe, epitaxial, twinning faults 2−53574
GeTe, superstruct., consistent with electron microscope obs. 2−80574
GeTe$_2$, amorphous, local order and microstructure 2−60660
Hg, deposited on LiF substrate, thermal He atom scattering 2−56573
In-Mn alloys, superconducting thin films, electronic thermal conductivity 2−68352
In-Te system, 33-45%Te, phase studies 2−60662
In, deposition on NaCl, island density 2−43480
In, on Si substrate, condensation and nucleation, mass spectrometer obs. 2−47117
In, polycryst., melting, e. diffr. study 2−83845
In, vapour deposited, growth, nucleation rel. to thickness and substrate temp. 2−77512
In superconducting thin films, electronic thermal conductivity 2−68352
InSe, electron bombardment crystalliz., elec. microscope obs. 2−56594

Films, solid continued
InSe, flash evaporated thin films, eff. of thermal treatment on props. 2—77853
In_2Se_3, flash evaporated, props. 2—56593
In_2Se_3, flash evaporated thin films, eff. of thermal treatment on props. 2—77853
Ir, epitaxy by vapour deposition, low temp. 2—53575
Ir, surface ionization of CsCl, effect of C adsorption on (111) face 2—64543
KCl, vapour deposited, elec. field effects 2—64570
Kr-Xe, struct., 6K to sublimation temp., electron diffr. obs. 2—80573
La, core level binding energies, X-ray photoelectron spectra study 2—72096
Mg-Li alloys, prep. using a non aqueous electrolyte 2—80548
MgF_2, thickness det., comparison of multiple beam Fizeau interferometry, photoelectric shearing interferometry and stylus instrument methods 2—47118
Mn-Mg-Fe ferrie, flash evaporated, chem. comp., X-ray fluoresc. obs. 2—71331
MnBi, prep., props., domain struct. 2—44263
MnBi, struct., Ti-substitution effect 2—51265
MnBi, struct. and orientation, electron microscope an diffr. obs. 2—47119
Mo:C, supercond. transition temp., struct. 2—57169
Mo-Zr, Mo-Ru alloys, vapour deposited, electron microscope obs. 2—60594
Mo, chemical vapour deposition, for thermionic converters 2—53559
Mo, sputter deposition on W, Auger spectroscopy study 2—50520
MoO_2, prepared by reactive sputtering 2—55335
MoS_2, sputtered, slip ring contact lubricant 2—56596
MoS_2 coating, applied to steel by detonation, heat and friction resist. 2—43744
Nb-Zr, Nb-Mo alloys, vapour deposited, electron microscope obs. 2—60594
NbN, prepared by d.c. sputtering, props. 2—84311
NbN, reactive high-vacuum codeposition 2—50497
NbO_x, Nb_2O_5, oxidation of Nb, stresses involved in oxid. process., annealing flexure obs. 2—43735
Ni/SiO_2 cermet, granular, microstruct. 2—50498
Ni-P, chemically deposited, structure in relation to elec. conductivity 2—77510
Ni-P, electroless deposited, growth and struct. 2—53566
Ni, electrodeposition, cathodic impedance study 2—48339
Ni, electrolytically obtained dislocations and twinning observed by transmission electron microscopy 2—50519
Ni, heat of adsorption of H_2 and D_2 2—43497
Ni, on Si (111) surface, adsorp. and condensation obs. using mass spectrometer 2—50499
Ni, on W, high temp. behaviour rel. to sintering of W/Ni powder 2—43897
Ni, origins of stress, interference obs. 2—43679
Ni films, intrinsic stress obs. by optical interference method 2—77649
$NiAl_2O_4$, growth on sapphire, orientation relations 2—71333
NiFe e microprobe analysis 2—77509
NiO, mechanisms of low temp. oxid. of polycryst. Ni 2—72558
Pb-Ag-Pb layers, heat capacity at ^3He temps., proximity effect obs. 2—81041
Pb, epitaxial, on Ni, azimuthal disorientation of elementary nuclei 2—47122
Pb, growth kinetics near melting point 2—60652
Pb, on W(100) surface, struct., LEED obs. 2—77511
Pb, supercond., 9.4 GHz u.s. attenuation 2—61229
Pb evaporated layers, oxidation by low energy O_2^+ bombardment 2—61791
PbS, struct. rel. to substrate surface struct. 2—64571
PbS film on semiconductor substrate, crystallization from aqueous solution 2—80562
PbSe, struct. rel. to substrate surface struct. 2—64571
PbSe film on semiconductor substrate, crystallization from aqueous solution 2—80562
PbTe, struct. rel. to substrate surface struct. 2—64571
Pd, epitaxy by vapour deposition, low temp. 2—53575
Pd, low-energy electron beam transmission, orientation depend. 2—47787
Pd, temp. rise during film deposition as a function of applied power 2—67913
Pt-Co alloy, electrodeposited, mag. props., dispersity, struct. 2—44268
Pt, epitaxy by vapour deposition, low temp. 2—53575
Pt, lattice consts. of small nuclei, rel. to surface stress 2—60655
Pt, vapour deposited on W, field ion microscopy, 78K 2—50500
Re, struct. and microhardness, condensation temp. effects 2—50501
Rh, electrodes on glass, deposition by sputtering 2—64573
Rh, epitaxy by vapour deposition, low temp. 2—53575
RuO_2, 1-5 μm thickness, prep. and struct. 2—47123
Sb_2Se_3, amorphous, controlled composition by vac. evap. 2—53576
Sc, optical sensitivity to energetic ions, tuning of ion microprobes 2—45691
ScN, epitaxial growth 2—50503
Se, crystalline and amorphous, ion bombardment effects 2—60646
Se, rolling texture, X-ray and elec. resist. study 2—64574
Si:P, epitaxial, doping during growth 2—47431
Si, amorphous, characteriz. as function of decreasing spin conc., e.p.r. obs. 2—78162
Si, amorphous, dark-field electron microscope obs. 2—60593
Si, amorphous, localized state distrib., field effect study 2—68437
Si, amorphous, metal contact induced crystalliz. 2—56590
Si, amorphous, microcrstallite struct. 2—43479
Si, amorphous, structure, elec. microscope obs. 2—50479
Si, electron spectroscopy of amorphous film at energy losses below 1 eV 2—80934
Si, epitaxial, gas doping 2—50690
Si, epitaxial growth, using hydrogen reduction in $SiCl_4$, two-dimensional growth 2—47125
p-Si, epitaxial growth on spinel, dual rate deposition 2—43482
Si, oriented growth on ZnS single crystal 2—56597
Si, prep. using plasma source 2—67912

Films, solid continued
Si amorphous films, density detn. by backscattering of 2500 keV alpha parts. 2—80559
Si electron irrad., defect. prod., resist. change 2—80655
Si layers, homoepitaxial, influence of substrate on interface props. 2—77495
Si wafers, thickness determ. using optical method 2—67902
Si with predeposition of B, charact. and mechanisms 2—71503
SiC, heterostruct., prod. by irrad. of Si by C^+ ions 2—50504
β-SiC, on Si substrate, chemical conversion with hydrocarbon, growth mechanisms 2—60663
SiC layers, system for chem. vapour deposition 2—50507
Si_3N_4, chemical vapour deposited on Si, dislocation generation 2—68031
Si_3N_4, detection of silicon oxynitride layers on surface by Auger elec. emission 2—50506
Si_3N_4, for semicond. devices, high prod. system for deposition 2—71952
Si_3N_4, on Cu substrate, reactive sputtering 2—43481
Si_3N_4, suppression of ionic contamination during deposition, rel. to m.n.o.s. struct. 2—71336
Si_3N_4 film on Si substrate, ammonia free, props. at low temps. 2—74633
SiO_2-Si_3N_4 syst., phase composition and thickness determ. by spectrophotometry 2—47086
SiO-SiO_2, thickness and composition, nondestructive meas. 2—50508
SiO, electron diffr., radial distrib. analysis 2—53577
SiO_2, amorphous, structure, ele. microscope obs. 2—50479
SiO_2, dielec., defects, local junction form 2—71964
SiO_2, grown by oxidation of silane, struct., electron diffr. and i.r. absorp. obs. 2—60664
SiO_2, on planar struct., flower-like defects 2—47124
SiO_2, on Si by tetraethoxysilane oxidation 2—47126
SiO_2, prep. by oxygen bombardment of Si, use in p-n junction protection 2—51176
SiO_2, pyrolytic, electron diffr. obs. 2—80571
SiO_2, pyrolytic decomposition of silicon compounds 2—74632
SiO_2, thermally grown, struct., i.r absorpt. study 2—53579
SiO_2, ultra thin layers on Si, kinetics of thermal growth 2—71337
SiO_2 formation over Au layer on Si substrates 2—67911
SiO_2 growth and sputtering in low pressure glow discharge 2—74634
SiO_2 on Ge, deposition and post-deposition treatments rel. to applic. of interface system 2—61402
SiO_2 thin films, atomic structure 2—74623
SiO_x, stoichiometric analysis by obs. of (d,p) reactions on Si and O 2—61835
Sn, deposition on NaCl, island density 2—43480
Sn, vapour deposited, growth, nucleation rel. to thickness and substrate temp. 2—77512
Ta, deposition in d.c. sputtering system 2—50226
Ta, low density, strain gauge factor study 2—77710
Ta, sputtering, triode config. with rotating base 2—78694
Ta, sputtering with uniform thickness 2—47127
Ta, temp. rise during film deposition as a function of applied power 2—67913
TaC_x, on needle-like W microcrysts., electron and field emission microscope obs. 2—50509
TaN, adhesion to ceramic, effect of substrate surface chem. 2—57005
Ta_2N resistor, relative nitrogen doping level by Seeback effect 2—74793
Ta_2O_5, in m.i.m. struct., film struct. rel. to transient phenomena 2—57219
Ta_2O_5 anodic, precise sectioning method for conc. profiles 2—43483
Te-As-Ge-S glass, four-element quantitative analysis 2—72593
Te-Ge based memory glass, thermal crystn. 2—47128
Te, large grained, prep. techniques 2—64575
Te based memory glass, sputtered, thermal crystalliz. 2—60668
Th, photon appearance potential spectroscopy 2—54441
Ti-Zr-Al-N, sputtered, struct., elec. resist. props. 2—47130
Ti, maximum sorption capacities and gettering action 2—43495
Ti surface film, formed in water and methanol solns., ellipsometric-electrochemical cell obs. 2—50510
TiB_2 coatings, electrodeposition and characteriz. 2—51460
TiC_x, chemical vapour deposition on Ta substrates 2—80597
TiO_2, chemical vapour deposition, properties as function of processing temp. 2—50511
TiO_2, crystallization, by electron beam irradiation 2—47129
TiO_2, in m.i.m. struct., film struct. rel. to transient phenomena 2—57219
TiO_2 reactive cathode sputtering, optimal conditions 2—45197
Ti_3SiC, preparation from gaseous phase, chemical and physical properties 2—53580
$TlInSe_2$:Cu,Sn, photosensitivity, optical absorpt., dark cond., forbidden band width 2—57197
$TlSbS_2$, thin films on NaCl, determ. of cryst. struct. 2—80564
U-Nb and U-Nb-Zr systems, oxide layer formation and characts. 2—48334
UO_2 thickness determ. using reflectivity 2—79412
V_2O_3, VO_2, V_2O_5, prep. by pyrolysis of vanadium acetylacetanate 2—44106
W, 110 orientation, deposition using WCl_6 gas discharge 2—50512
W, chem. vapour-deposition, substrate temp. and gas press. effects 2—47131
W, chemical vapour deposition, for thermionic converters 2—53559
W, interdiffusion in emitters of thermionic converters 2—53560
W, on SiGe, interface reactions, effects of p- or n-type substrates, ion backscattering analysis 2—71951
Xe, on Ir, use in determ. of Ir surface struct. by LEED 2—47077
Y, core level binding energies, X-ray photoelectron spectra study 2—72096
YAG films, Nd^{3+} site preferences for growth by liquid phase epitaxy, spin-reson. meas. 2—83867
YIG, epitaxial growth by chem. vapour deposition 2—47132
YIG, epitaxial magnetic film, prep. by chem. vapour deposition 2—77527
YIG, Fe-deficient, comp. variation 2—72202
YIG, heteroepitaxy, flux method and hydrothermal synthesis 2—50513

Films, solid continued
YIG chem. vapour deposited, substrate growth band and core struct. replication 2−71338
Y_2O_3, low loss dielec. film, use of mag. fields in electron beam evaporation 2−77947
Yb, condensed on glass, amorphous to cryst. transition temp. 2−43474
Yb, phase transform. on annealing 2−50952
ZnO, d.c. triode sputtered, u.s. surface elastic waves, coupling factor phase velocity, propag. loss 2−80560
ZnO, surface acoustic wave transducers, coupling constants and film thickness 2−49152
ZnS-CdS, evaporated layers, mosaic heterojunction photo-emf 2−77970
ZnS, epitaxial on Si by forced vapour transort 2−50514
ZnSe, vapour phase deposition to improve contrast in metallographic obs. of transition zones 2−43780
ZnTe, on Ge substrate, epitaxial growth and struct. 2−50515
ZnTe, optimum conditions for epitaxial growth 2−47105

electrical properties
— 2−68479
amorphous chalcogenide threshold and memory devices, preswitching props., forming and switching 2−77920
amorphous polymer, geminate recombination of charge carriers 2−57187
amorphous semicond. films, physical background of applic. 2−77885
anthracene, current/ voltage charact. rel. to thickness, temperature and light emission 2−57201
antistatic agent, on plastic, surface cond. recovery 2−65073
barium behenate, built-up films dielec. constant study 2−77948
barium margarate, built-up films dielec. constant study 2−77948
barium palmitate, built-up films dielec. constant study 2−77948
borosilicate glass, current-voltage characts. 2−47950
bulk and surface states 2−44037
CdSe photoconductive films, field quenching 2−77964
chalcogenide, amorphous, pre- and postswitching characts. 2−61310
chalcogenide, amorphous, Seebeck coeff. 2−61442
chalcogenide, amorphous, thermally stimulated cond. 2−57189
chalcogenide, heterogeneous materials, electronic transport 2−64959
chalcogenide, noncrystn., threshold and memory switching at low temps. 2−61308
chalcogenide, on SnO_2 coated glass, polarized memory effect 2−64971
chalcogenide glass, amorphous, switching behaviour 2−81071
dielectric, Poole-Frenkel pre-exponential factor 2−57217
dielectric constant and tangent of dielectric loss angle 2−57225
diphenylpolyene, elec. cond. temp. depend. 2−84338
electrical insulation and dielectric phenomena, conference, Williamsburg (1971) 2−57222
electroluminescent, electrode current rel. to applied stress 2−81435
electron mobility, space quantization effects 2−81078
ferroelectric, critical thickness and thermodynamic stability 2−61425
fibrin, elongated, piezoelectricity, dielectricity and viscoelasticity 2−85087
furan quinone pigments, DFC and DF, photoinjection and photoemission, energy levels 2−54256
furan-quinone pigment, DFC, charge transport props. 2−51219
galvanomagnetic size effects, magnetoresistance, Hall coefficients 2−54126
glass, chalcogenide, thick and thin, switching temp. depend., onset of breakdown 2−77895
glass, thermally switching, pulse response of cond. channel 2−51129
group II-VI compound, epitaxial, specific resistance and mobility 2−56582
insulating films, fabrication, nucleation, epoxy, book contrib. 2−47961
insulator with nonconst. mobility and deep trapping, surface charge decay 2−51193
insulators, m.i.m. struct., d.c. conduction mechanisms, thermally stimulated current analysis 2−61394
ion bombardment and implantation effects 2−53568
metal, 1/f noise, physical process 2−68335
metal, anomalous skin effect 2−54121
metal, discontinuous, non-ohmic behaviour 2−57150
metal, discontinuous, rel. to strain 2−64908
metal, elastoresist., relax. phenomena 2−56765
metal, longitudinal and transverse strain coeff. of resistance 2−61218
metal, size effect of transverse magnetoresist. 2−51095
metal, supercond. transition temp. change due to noble gas adsorption 2−47856
metal, surface impedance under anomalous skin effect conditions 2−51096
metal, transport props., Halperns theory of size effects rel. to m.f.p. method 2−57149
metal, with adsorbed gas layer, demetallization phenomenon 2−47150
metal films in magnetic field, microwave absorption peaks due to Doppler-shifted cyclotron resonances 2−80941
metal/SiO_2 cermet recoil atom implantation produced, conduction 2−53578
multilayer insulating films 2−75136
Mylar, negative resistance charact. 2−57203
oxide, stored charges 2−44166
p-i-n junction anodic film on Ti 2−47138
permalloy films, thin, influence of plasma and cathode sputtering on struct. elec. and mag. props. 2−84410
phthalocyanine, photoinjection of negative charge carriers into hydrocarbon and dimethyl siloxane fluids 2−56512
poly(N-vinyl carbazole), transient space charge perturbed current 2−57229
poly-N-vinylcarbazole complexed with trinitrofluorenone, bulk recomb. of charge carriers 2−72073
polyethylene, I doped, elec. cond., form of current transients 2−64994
polyethylene terephthalate, crystallinity effects on dielec. props. 2−61410
polymer, dielec. breakdown 2−47980
polymer, internal struct. of single hole breakdown 2−47981

Films, solid continued
electrical properties continued
polymer, linear chain, spontaneous polarization and pyroelec. coeff. 2−72045
polymer films amorphous and crystalline, electrical conductivity in strong electric fields 2−84340
polymer solvent-cast, dielectric relaxation rel. to residual solvent and crystallinity effect 2−57227
polymers-Hg contact, electric field effect 2−57236
polypropylene, crystallinity effects on dielec. props. 2−61410
polystyrene films, passage of transient currents along surface 2−72001
polyvinyl chloride films, pulsed photoconductivity, obs. of transient photocurrents with oscillations 2−72074
polyvinylcarbazole, dye sensitized photoinduced voltage decay 2−81165
polyvinylidene fluoride, far i.r. spectral investigations of structural conformations rel. to piezoelectric props. 2−61438
resistance of films grown in electric field 2−71341
review of metallic semiconducting and dielectric props. 2−64907
rhodamine 6G, amorphous, carrier trapping, thermostimulated cond. study 2−54180
semiconducting thin films, electrical conductivity theory high electrical field 2−64558
semiconductor, amorphous, ohmic and non-ohmic cond. 2−61289
semiconductor, carrier conc. 2−71931
semiconductor, epitaxial, steady state surface photovolt., interpretation 2−75177
semiconductor, kinetics of small charge currents and carrier lifetime determ., from time depend. of photocurrent 2−81088
semiconductor, magnetoresist. and Hall coeff., calc. 2−71892
semiconductor, multilayer, cond., rel. to thermoelec. props. 2−51054
semiconductor, nonlinear h.f. conductivity 2−44089
semiconductor, single crystal, electrical conductivity and adsorption, combined meas. 2−71932
semiconductor, transport, coeffs. rel. to surface states, Hall and Seebeck coeffs. 2−47884
semiconductor, transverse quantum galvanomag. effects rel. to elastic scatt. by optical phonons 2−64973
semiconductor electrodes on insulators, aftereffects 2−77905
shielded superconducting, current distribution 2−81057
stearic acid films, high-field transient behaviour of dielec. props. 2−77950
superconducting, phase reversal and modulated flux motion 2−54138
superconducting Dayem bridge, I-V charact. near transition temp. 2−71844
superconductors condensed on cold substrates, surface resistance meas. 2−64924
surface layer on metal parameters, effect of substrate stress state 2−71966
surface states, thermally stimulated exo-emission obs. 2−48008
tetracene, investigation of high and low conductivity stable states and switching 2−54181
transition metals, amorphous, resist. during deposition and annealing 2−77499
Ag, epitaxial, temp. coefficient of resistance 2−61221
Ag, induced supercond., energy gap and electron-electron interaction 2−44072
Ag, size effect, rel. to cond. electron mean free path in bulk material 2−75012
Ag, size effect on strain coefficient of resistance 2−57151
Ag film on mica, modulation of conductance due to changing interface, metallic field effect 2−75047
Ag on W, work function determ. by employing retarding-field diode technique 2−72083
Ag_2S epitaxial, variation of resistance with temp., photoconductivity, spectral sensitivity of photocurrent 2−53567
Ag_2Se variation of resistance with temperature, determ. of phase transformation temp. and activation energy for semiconducting phase 2−53570
Al/Cu/Al films, electromigration obs. by transmission electron microscopy 2−64879
Al-Al_2O_3-Al field emission and cold emission of electrons, electron distrib. 2−81125
Al-Al_2O_3 granular films, superconducting, sp. ht. obs., T_c enhancement 2−77878
Al-Si dilute alloy, Si precip., resist. study 2−50825
Al, ang. distrib. meas. of secondary electrons 2−44213
Al, electromigration, effect of oxygen 2−50703
Al, normal-state cond. and supercond. transition temp., electrostatic charging effects 2−71845
Al, photoelec. emission due to nonradiative surface plasma waves 2−44200
Al, supercond. transition temp. depression by noble gas overlayers 2−61228
Al, superconducting, thermodynamic fluctuations in resistive transition 2−71858
Al, temp. coeff. of resist. 2−74999
Al superconducting film, density of states change due to adsorbed molecular oxygen 2−51111
AlAs epitaxial layer, on GaAs, elec. props. and optical absorp. 2−71881
AlN, in m.i.s. struct. 2−54225
AlN_x, preparation by reactive r.f. sputtering, dielectric and resistance characteristics 2−77507
Al_2O_3, annealing effects on MAS characteristics 2−71997
Al_2O_3, anodic, breakdown by impact ionization 2−57235
Al_2O_3 step and ramp voltage breakdown tests 2−72024
As_2S_3 and As_4S_4, amorphous, a.c. cond., temp. depend. 2−68392
As_2Se_3, amorphous, a.c. cond., temp. depend. 2−68392
As_2Se_3, amorphous, charge transport, photocond. and dark current obs. 2−68393
As_2Se_3, amorphous, dark discharges 2−49458
As_2Se_3, amorphous, memory switching rel. to thickness 2−81072
$3As_2Se_3$,$2Sb_2Se_3$, amorphous semicond., cond., photocond., band struct. 2−54187
$As_2Se_3(Te_3)$, amorphous, trap-limited processes 2−61325
$3As_2Se_3.2Sb_2Se_3$, amorphous semicond., band struct. 2−54186

Films, solid continued
- **electrical properties** continued
  - As_2Te_3, amorphous, a.c. cond. rel. to localized tail states 2−61288
  - Au-SiO, cermet, struct., elec. props., rel. to deposition condition 2−64976
  - Au-SiO cermet post-deposition resistance increase, obs. 2−61222
  - Au, ang. distrib. meas. of secondary electrons 2−44213
  - Au, discontinuous, on soda-lime substrate, resist. rel. to ion drift in substrate 2−47833
  - Au, discontinuous, post deposition resistance increase, obs. 2−61222
  - Au, size effect, rel. to cond. electron mean free path in bulk material 2−75012
  - Au, thermoelec. power rel. to surface scatt., Matthiessen's rule 2−64895
  - Au island films on insulators magnetoresistance 2−84298
  - discontinuous Au thin films, Au-SiO cermets mechanisms of conduction, nucleation 2−54127
  - Au thin films obtained by sputtering, changes of electrical and structural properties changes during annealing process 2−60647
  - $BaTiO_3$, discrete vacuum evaporation method for ferroelectric behaviour prod. 2−83894
  - $BaTiO_3$, polarization change, stroboscopic electron microscope obs. 2−75149
  - $BaTiO_3$ on Si substrate by r.f. sputtering 2−75148
  - Be, Hall const., rel. to crit. thickness determ. 2−56587
  - Be, on dielec. substrate, elec. resist., supercond. transition temp., absorpt. spectra 2−72323
  - Bi, disordered, supercond. transition temp. and normal state cond., effects of surface charge 2−44070
  - Bi, Hall const., rel. to crit. thickness determ. 2−56587
  - Bi, magnetoresistance as function of thickness 2−84332
  - Bi, permittivity meas. 2−47975
  - Bi, thermo-e.m.f. rel. to struct. 2−81161
  - Bi, thermoelectric figure of merit 2−55642
  - C, amorphous, cond., piezoresist. and thermopower 2−61302
  - C, amorphous, cond. change on graphitization by light pulses 2−61030
  - Ca, photoelec. props., elec. field influence 2−81188
  - Cd, disordered, supercond. energy gap and transition temp. 2−54134
  - CdO, reactively sputtered, transparent electrodes for CdS 2−54209
  - CdS, amorphous, in m.i.m. structs., electroforming and elec. cond. props. 2−64978
  - CdS, electron mobility and scatt. rel. to grain boundaries and surfaces 2−61149
  - CdS, electron scatt. by stacking faults rel. to elec. props. 2−61150
  - CdS, Hall Mobility, thickness depend., effects of Cu impurity 2−77894
  - CdS, photocond., prolonged relax. of dark current after illumination 2−81173
  - CdS, photocond. with gain in through thickness operation 2−44173
  - CdS, photoelectret state formation and temp. depend. 2−77939
  - CdS, photorectification in longitudinal quasi unipolar photocond. with non uniform illumination 2−81172
  - CdS, shift in lux-ampere and I-V characts. due to photoelectret effect 2−81170
  - CdS, sputter-deposited, photocond. 2−53571
  - n-CdS, thin compound semicond., sorption-induced conductivity changes 2−77886
  - CdS(De)(Te), a.c. photocond. on excitation with intensity-modulated light, trapping levels 2−57255
  - CdSe:Cu, a.c. photocond. in negative photocond. region 2−65081
  - CdSe, conductivity, influence of Se vapour annealing 2−44094
  - CdSe, effect of O_2 and N_2 on Hall and field effect mobilities 2−57191
  - CdSe, elec. props. rel. to substrate temp., 25-200°C 2−64980
  - CdSe, l.f. noise, obs. 2−51136
  - CdSe, photoelec. props. 2−57253
  - CdSe, photoelectronic props. 2−51212
  - CdSe, thin film transducer, operation characteristics and anomalous behaviour 2−77922
  - CdSe on $LiNbO_3$, surface states effect on surface wave amplification 2−84201
  - CdSe vacuum deposited, Hall mobility 2−83868
  - n-Cd_2SnO_4, amorphous, cond., carrier mobility, effective mass 2−51137
  - p-CdTe, photocond. 2−48217
  - CdTe, with anomalously high photovolt., photomag. effect 2−75178
  - CdTe layers and solar cells 2−41907
  - $Cd_xZn_{1-x}S$, resist. comp. depend 2−54169
  - CeF_3, evap., a.c. elec. props. 2−44153
  - Cr, sputtered, supercond. props. rel. to deposition conditions 2−81045
  - Cs, photoemission, 3.7-21.2eV 2−54277
  - Cu, rel. to uniform thickness 2−84647
  - Cu thermoelec., resist., cond. electron m.f.p. 2−68477
  - CuCl(Br)(I), on Ag or Cu, light sensitivity spectra 2−77966
  - CuS, semiconducting, supercond. transition temp. obs. 2−51112
  - Ga, disordered, supercond. transition temp. and normal state cond., effects of surface charge 2−44070
  - n-GaAs:Cu, epitaxial, carrier mobility, impurity effects, scatt. by space charge centres 2−64983
  - GaAs, epitaxial, carrier conc., Hall mobility 2−53573
  - GaAs, epitaxial, microwave meas. of velocity-elec. field charact. 2−51140
  - GaAs, epitaxial, photocond., substrate orientation effects 2−47436
  - GaAs epitaxial layers, free carrier conc. and mobility 2−50492
  - Ge-Au quench-condensed, supercond. energy gap, tunnelling obs. 2−51115
  - Ge-Cr, amoprhous, hopping cond. 2−61313
  - Ge, amorphous, anisotropy in resist. 2−68430
  - Ge, amorphous, effects of substrate temp. 2−64987
  - Ge, amorphous, ohmic and non-ohmic cond. 2−61289
  - Ge, amorphous, secondary electron emission spectrum obs. of electron states 2−61353
  - Ge, cond. and Hall effect, thickness depend. 2−54192
  - Ge_3N_4, vapour deposition on Ge, dielec. const. 2−54224
  - Ge_xSi_{1-x} solid soln., photoelec. props. 2−65090
  - HgTe, temp. dependence of Hall coeff. and electrical conductivity 2−54174

Films, solid continued
- **electrical properties** continued
  - In, e.m. generation of transverse acoustic waves, supercond. parameters 2−71866
  - In, supercond., intermediate state struct., magneto-optical study 2−81050
  - In superconducting, noise props., r.f. generation 2−68348
  - In_2O_3/SnO_2, reactively sputtered, transparent electrodes for CdS 2−54209
  - InP, epitaxial, photocond. 2−72410
  - InSb, flash deposited, Hall electron mobility parameters 2−54176
  - n-InSb, transport phenomena, 20-100 K and 300-500 K 2−71911
  - InSb films, thickness dependence of electron mobility, model based on surface accumulation layer 2−68403
  - In_2Se_3, flash evaporated resistivity rel. to structure 2−56593
  - K elec. conductivity calc., electron-phonon scatt., soln. of Boltzmann eqn. 2−71830
  - KCl, porous, energy distrib. of transmitted secondary electrons 2−81190
  - La superconducting, phonon structure in tunnelling density of states 2−75059
  - Li film, bulk and surface states 2−44037
  - MgF_2, thermally assisted hopping mechanism, Poole-Frenkel cond. 2−68279
  - $Mn_xHg_{1-x}Te$, Hall coeff., Hall mobility and electrical conductivity 2−71885
  - Mo:C supercond. transition temp. effect of C coating 2−54145
  - Mo-Re, A-15 struct., supercond. transition temp. 2−71867
  - Mo, cond. and Hall const., size effect 2−81030
  - MoO_3, a.c. elec. props. and I-V characts. under d.c. bias 2−68454
  - MoO_3, donor band and Schottky barrier obs. using dielectric relax. currents 2−68453
  - NbN, crit. current anisotropies rel. to columnar structure 2−68366
  - NbN, sputtered, supercond. characteriz. 2−50497
  - NbN, supercond., lower crit. field meas. 2−54146
  - NbN, superconductive critical field 2−84310
  - Nb_2O_5, conductivity and switching time obs. 2−61320
  - Nb_2O_5, prep. by anodic oxid., field depend. of dielec. const. ellipsometric obs. 2−44150
  - Nb_2O_5, r.f. sputtered, elec. instability in m.o.s. struct. 2−71995
  - $Nb_{0.88}Ti_{0.12}N$, fluctuation broadening of supercond. transition 2−71850
  - Ni-B, obtained by oxidation-reduction in liquid phase, conductivity 2−77860
  - Ni-P, chemically deposited, relation with structure 2−77510
  - Pb-In alloy, supercond., electronic thermal cond. 2−81042
  - Pb, disordered, supercond. transition temp. and normal state cond., effects of surface charge 2−44070
  - Pb, superconducting, mag. flux penetration 2−71871
  - Pb, superconducting energy gap, photocurrent temperature dependence due to, 2.5 to 12°K 2−68354
  - PbS layers, photocond. mechanism, elec. cond. and Hall effect obs. 2−81166
  - PbSe epitaxial films on NaCl substrate, effects of ambient gases 2−65008
  - $Pb_{0.8}Sn_{0.2}Te$, epitaxial, photoconductivity 2−65085
  - PbTe, effect of O_2 and N_2 on Hall and field effect mobilities 2−57191
  - PbTe, epitaxial, photoconductivity 2−65085
  - PbTe, optical and elec. props., and comparison with bulk 2−57172
  - Pt/SiO cermet, elec. resist. in a.c. 2−75095
  - Pt, cond. rel. to temp., 77-573 K, adsorpt. effects 2−64917
  - Pt, discontinuous, current noise 2−68340
  - Pt island films on insulators magnetoresistance 2−84298
  - PtSi on single crystal Si substrate, thermal stability, sheet resistivity meas. 2−71334
  - Rb, photoemission, 3.7-21.2eV 2−54277
  - RuO_2, 1-5 μm thickness, cond. 2−47123
  - $Sb_{1-x}Se_x$, amorphous, photocond. spectral response rel. to comp. 2−81167
  - Sb_2Se_3, amorphous, transport props. 2−61323
  - Sc, cond. and Hall const., size effect 2−81030
  - ScN, epitaxial, Hall mobility, optical energy gap 2−50503
  - Sc_2O_3, a.c. conductivity, hopping model 2−61324
  - Se: Cl, As, vacuum evap., transport props., time resolved drift technique 2−44104
  - Se, amorphous, a.c. cond., temp. depend. 2−68392
  - Se, amorphous, one- and two-carrier space-charge-limited currents 2−75097
  - Se, amorphous layers, photoeffect 2−84374
  - Se, vitreous, trap-limited processes 2−61325
  - n-Si:P, epitaxial, on $MgO.Al_2O_3$, cond., Hall effect, and photocond. 2−77910
  - Si-Ge alloy, oxide layer etched away reoxidation, production of MOS transistors 2−75132
  - Si, amorphous, effects of thermal neutron irrad. 2−60666
  - Si, amorphous, elec. cond., 77-300K, annealing effects 2−61360
  - Si, amorphous, photocond. spectra rel to band struct. 2−61655
  - Si, amorphous, rel. to localized state distrib. determ. 2−68437
  - p-Si, dual rate epitaxial deposition on spinel, hole mobilities 2−43482
  - Si, epitaxial, nonequilibrium carrier lifetime, photoelectric obs. 2−84331
  - Si, on sapphire, determ. using m.o.s. Hall technique 2−51169
  - Si, surface oxide layer influence 2−51325
  - SiO, electron-beam-evaporated, microwave relax. phenomena 2−54231
  - SiO, permittivity, investigation of anomalous behaviour 2−44149
  - SiO_2, Na^+ ion transport, m.o.s. C-V characts. study 2−77936
  - SiO_2, on Si, Fowler-Nordheim tunnelling and dielec. breakdown 2−47955
  - SiO_2, prep. by oxygen bombardment of Si, dielectric strength obs. 2−51176
  - SiO_2, r.f. sputter deposited, electrical characteristics uniformity 2−61407
  - SiO_2, thermally grown, breakdown rel. to oxidation temp. and atmosphere 2−71999
  - SiO_2 and SiO, dielec. props., moisture stability 2−72015
  - SiO_2 thickness effect on MAOS charact. 2−71997
  - SiO_x, r.f. sputtered in Ar-O_2, m.o.s. obs., O_2 conc. effects 2−60667

Films, solid continued
electrical properties continued
Sn-Mn, mag. state of Mn rel. to supercond. 2−68512
Sn, cylindrical, supercurrent stability 2−47850
Sn, Josephson effect 2−61248
Sn, quantum oscill. amplitude, temp. depend. 2−71838
Sn, quantum size effect and supercond. crit. temp., oscillatory depend. on thickness 2−57164
Sn, supercond., nonlinear flux flow resistivity 2−47849
Sn, supercond. transition temp. depression by noble gas overlayers 2−61228
Sn, superconducting, mag. flux penetration 2−71871
Sn superconducting, noise props., r.f. generation 2−68348
SnTe, epitaxial, carrier conc. and mobility, effect of atomic H 2−54179
SnTe, polycryst., vacuum deposited, semiconducting props., temp. depend. 2−71916
Ta_2O_5, prep. by anodic oxid., field depend. of dielec. const. ellipsometric obs. 2−44150
Te-As-Si-Ge, amorphous, a.c. cond. rel. to localized tail states 2−61288
Te, amorphous, localized states, photoemission quantum yield 2−68422
Te, on glass, temp. depend. of cond., below 300 K 2−75099
Te, polycryst., on mica, elec. transport props. 2−61330
Te films on uhv-cleaved TGS, aftereffects in field eff. at large gate charges 2−77900
Te thermoelectric power, Hall and Seebeck coeffs., resistivity 2−54249
Ti-Au, conductor stripes, electromigration damage rel. to pulsed d.c. powering 2−80940
TiO, amorphous, sputtered, dielec. props. equiv. elec. cct. 2−47970
TiO_2, amorphous, photocond. 2−72068
Tl-Te alloy, amorphous, cond., band struct. model 2−61328
trisiloxane, electron beam polymerized, conductivity, photocond., and dielec. const. 2−47909
V_2O_3, VO_2, V_2O_5 prep. by pyrolysis, temp. depend. of resistance 2−44106
W_2O_5, prep. by anodic oxid., field depend. of dielec. const. ellipsometric obs. 2−44150
Y, cond. and Hall const., size effect 2−81030
Zn, disordered, supercond. energy gap and transition temp. 2−54134
Zn, on dielec. substrate, elec. resist., supercond. transition temp., absorpt. spectra 2−72323
ZnCdS evaporated layers as photoresistors in u.v. 2−44179
ZnO:Cu, amorphous, band struct. and impurity state energy spectrum 2−68421
ZnS:Cl, photovolt. polarity reversal by excess Zn 2−51222
ZnS, amorphous, in m.i.m. structs., electroforming and elec. cond. props. 2−64978
ZnS, in electrolum. device, high field a.c. electrolum. rel. to field clamping 2−81412
ZnSe (Cu, Ga), epitaxial thin films, photoluminescent, oscillations of photocurrent 2−78147
n-ZnSe(Cu,Ga) film, photolum., photocurrent oscills., 80-220K, luminesc. field quenching 2−81168
ZnTe, in m.i.m. device, switching and memory props. 2−44142
magnetic properties
antiferromagnet, spin wave spectrum, calc. 2−81289
BDPA, organic free radical, vapour deposited, e.p.r. obs. 2−56598
binary arsenosilicate glass, vapour deposition for diffusion source 2−71324
Bloch walls, interacting, transversal shift 2−72181
bubble domain, twisted wall struct., variational method calc. 2−72142
bubble domains, domain-wall config. 2−78009
bubble domains, hard, dynamic props. 2−78010
bubble garnets, magnetiz. reversal due to annealing 2−51253
coupled two-layer system, hysteresis loops, calc. 2−48087
cross-tie-Neel domain wall transition, hysteresis change, in mag. field 2−48090
domain boundary creep, thickness and props. influence 2−72179
domain wall. mass and crit. velocity calcs. 2−68558
domain wall parameters from Lorentz electron microscopy 2−72182
domain-wall mobility, Bloch line effects 2−78011
DPPH, organic free radical, vapour deposited, e.p.r. obs. 2−56598
ferrite epitaxial films, prep. for mag. bubble domain memories 2−72192
ferro-antiferromagnetic exchange coupled films, microscopic mag. switching 2−78030
ferromagnet, electron microscope obs. of mag. struct., review 2−84428
ferromagnet, factors influencing realization of trigger effect 2−75228
ferromagnet, Lorentz microscopy and spatial filtering 2−48088
ferromagnet, magnetoresist., effect of angular dispersion of magnetization 2−48086
ferromagnet, stripe-domain width, longitudinal field intensity depend. 2−57296
ferromagnet, supercrit. props. of stripe structs. 2−61520
ferromagnet, theory of domain wall mobility 2−78031
ferromagnetic, band periodic domain struct., spin wave spectrum 2−72183
ferromagnetic, polarization of domain boundaries of Neel type 2−57297
ferromagnetic, spin wave polarization and h.f. pumping 2−71380
ferromagnetic, surface free-energy for spin-wave and molecular field models 2−75229
ferromagnetic, uniaxial unpinned, Green's function theory, review 2−78003
ferromagnetic film, surface spin-wave excitation 2−68716
ferromagnetic films, Lorentz microscopy by laser diffraction, quantitative determ. of magnetization ripple 2−79144
ferromagnetic metals, meas. of longitudinal Faraday effect 2−54379
ferromagnetic reson., nonlinear phenomena in parametric cct. 2−68721
ferromagnetic resonance, domain wall structure effect in films 2−68717
ferromagnetic thin film, spin waves and resonance, stability 2−48089

Films, solid continued
magnetic properties continued
ferromagnetic with anomalous surface anisotropy, static magnetic susceptibility 2−72178
ferromagnetic with periodic banded domain structure, spin wave spectrum 2−68553
garnet, domain interaction with laser beams, domain writing 2−75230
garnet, epitaxial, magnetic bubble mobility measurement 2−57303
garnet multilayer epitaxial films for magnetic bubble devices, hard bubble suppression 2−65162
garnets, elimination of hard bubbles by second magnetic layer 2−65164
garnets, hard bubble suppression by ion implantation 2−65163
Hall effect and magnetoresistance, size effect theory in thin metallic films 2−77984
Heisenberg ferromagnet, magnon specific heat and ferromag. resonance 2−51263
holography of mag. moment in h.f. field 2−68555
magnetic moment, hodograph in high frequency magnetic field 2−68555
magnetic ordering, Hubbard model, Stoner mol. field approx. 2−72180
magnetization and thickness determ. method for thin uniaxial films 2−68559
magnetostrictive, anisotropy skew patterns, temperature gradient effects 2−72177
metal, fluctuation enhancement of mag. moment 2−81209
metal, monocryst., orientational magneto-optic effect 2−61589
microprobe analyzer for thin films 2−66702
multilayer system, interaction energy 2−84403
Neel wall in stray fields, wall creeping mechanism 2−61522
Permalloy, anisotropy, annealing depend. 2−61525
Permalloy, cross-tie walls, motion threshold field and behaviour at inhomogeneities 2−77994
Permalloy, domain boundary motion, effect of struct. factors 2−61526
Permalloy, electrodeposited, comp. and depositing current effects 2−57302
permalloy, electrodeposition on Cu wire, stress meas. and effects on e.m. props. 2−77990
Permalloy, ferromag. reson., mag. moment, thickness, magnetization pinning 2−61539
Permalloy, l.f. slip of domain boundaries 2−61528
Permalloy, oxidized, slow domain wall motion 2−54340
Permalloy, spin waves, 0.8-16 GHz, below saturation magnetization 2−78034
Permalloy, stripe domain struct. 2−61531
Permalloy, with supercrit. hysteresis loop, domain struct. 2−61532
Permalloy field access bubble domain drive ccts., magnetostatic pot. wells, drive fields, meas. technique 2−73507
permalloy film, changes in domain structure during pulsed a.c. magnetization, thermofluctuational character 2−68556
permalloy films, thin, influence of plasma and cathode sputtering on struct. elec. and mag. props. 2−84410
Permalloy plated-wire memory, domain struct., electron microscope obs. 2−75231
permalloy supercritical films, static and dynamic properties, domain structure 2−68557
Permalloy thin wires, Bitter pattern obs. 2−61535
Permalloy-SiO- Permalloy multilayer systems, stripe domain struct. 2−61530
susceptibility, SHF, influence of domain structure 2−68554
uniaxial, ang. dispersion of anisotropy effect on hysteresis loop 2−61521
V395 Herculis, optical variability 2−75681
$CdCr_2Se_4$, vacuum deposited, saturation magnetization 2−60649
Co-P, hysteresis characts. rel. to heat treatment conditions 2−48091
Co, anisotropy, rel. to n.m.r. 2−81471
Co, electrodeposited with [0001] axis of preferred orientation, dependence on texture perfection 2−54327
Co, electron microscope study of magnetic domains 2−44262
Co, epitaxial, domain config. 2−61524
Co, evaporated at oblique incidence, mag. contrib. of columnar grains 2−72184
Co, n.m.r. level inversion of ^{59}Co in 2-phase Co films 2−68744
Co, two-layer, magnetization vectors, rel. to bonding energy determ. 2−57298
$CoFe_2O_4$, monocryst., domain struct. and mag. polarity reversal 2−61523
CrTe, ferromag. reson. 2−57387
Cu-Mn dilute alloy, e.s.r. study 2−44446
Cu films, Hall coeff. detn. and existence of size effect 2−77985
EuS, effective exchange parameters and surface anisotropy 2−68532
Fe/LiF/Fe-Co system, quasistatic mag. reversals 2−84408
Fe-Co layers with intermediate LiF layer, electron microscope study of interacting interdomain boundaries 2−61534
Fe-Ni, domain struct., influence of temp., elec. microscope obs. 2−72185
Fe-Ni, grown by thermal evaporation, exam for 0-100% Ni 2−77496
Fe-Ni, perpendicular anisotropy from galvanomag. meas. 2−61529
Fe-Ni alloy, crit. fields, effect of elastic stresses 2−51264
Fe-Ni alloy, rotating anisotropy, temp. depend. 2−57300
Fe-Ni alloys, elimination of Barkhausen effect in electrodeposited films 2−72169
Fe, asymmetric 180° domain walls, Lorentz microscopy obs. 2−48092
Fe, monocrystalline, inter-domain boundaries 2−61533
Fe, u.h.v. Mossbauer emission spectra, mag. behaviour rel. to particle size 2−72284
Fe thin films, Mossbauer spectra, 15-350 K, superparamagnetic fluctuations 2−68611
Fe_3C, electron microscope study of magnetic domains 2−44262
Fe_xGd_y, amorphous, ferrimag. 2−44275
$Fe_{16}N_2$, deposited in N_2 atmosphere, ultrahigh mag. moment 2−57299
Gd, superferromagnetism 2−48093
GdTbFe garnet, cylindrical magnetic domains, hard bubbles 2−65169
In cylindrical layers, crit. mag. field 2−84299

- **Films, solid** continued
  - **magnetic properties** continued
    - Mg-Mn ferrite, transparent, light diffraction by mag. stripe domains 2−65220
    - $MgFe_2O_4$, mag. polarity reversal, temp. effect 2−61537
    - Mn-Bi system, intermediate cpds., domain patterns 2−57301
    - Mn-Permalloy, coercivity, influence of driving field 2−81278
    - Mn-Permalloy bimetal film, mag. after-effect 2−81224
    - Mn-permalloy, exchange anisotropy, ferromag. to antiferromag., thermomag. recording 2−57286
    - MnBi, Ti-substitution effect 2−51265
    - MnBi thin films, preparation by Williams method effects of residual gas pressure, evaporation rate on magnetization 2−68560
    - $MnBi_{(1-x)}Te$, magneto-optical props. 2−72264
    - $Mn_{1-x}Cr_xSb$, ferromag. reson., $(0 \leqslant x \leqslant 0.6)$ 2−72450
    - $MnFe_2O_4$, ferrite, epitaxial, spin wave resonance 2−72454
    - MnO-Fe_2O_3 single-crystal films, static and dynamic domain structure 2−68561
    - $Mn_{0.8}Ti_{0.2}Bi$, Curie-temp. writing 2−78032
    - NbN, supercond., lower crit. field meas. 2−54146
    - Ni-Co alloys, exchange consts. and saturation magnetiz. 2−44265
    - Ni-Fe/Fe-Co alloy, layers, permeability, intrinsic magnetization, coercivity, remanence 2−61536
    - Ni-Fe, coercive force, field and freq. depend. 2−78033
    - Ni-Fe, domain wall creep effects of fields, film thickness 2−77993
    - Ni-Fe, electrodeposition, props., optimization 2−61540
    - Ni-Fe, polycryst., edge anisotropy 2−61527
    - Ni-Fe, ripple spectrum, depend. on anisotropy, crystallite size, thickness and field 2−81279
    - Ni-Fe alloy, complex spinwave patterns 2−48077
    - Ni-Fe alloy, multilayer systems, interaction energy 2−84403
    - Ni-Fe alloys, temp. depend and transverse anisotropy 2−61538
    - Ni-Fe(Pd), magnetoresist. anisotropy 2−44266
    - Ni-Fe(18 wt%), electrodeposited, hyper-crit. thickness, anisotropy fluctuations 2−84409
    - Ni-Re alloys, elimination of Barkhausen effect in electrodeposited films 2−72169
    - Ni-Zn-Co ferrite film, anisotropy induced by thermomagnetic treatment 2−81228
    - Ni, adsorption of H_2, effect on saturation magnetization 2−48094
    - Ni, magnetoresist., thickness depend. 2−51266
    - Ni, porous, magnetostriction, field depend. 2−72187
    - Ni, residual magnetization, susceptibility, anisotropy, Hall effect 2−48095
    - Ni, spontaneous magnetization rel. to Hall effect 2−48096
    - Ni films, epitaxial, planar Hall effect 2−72186
    - Ni single crystal, ripple effects in ferromag. resonance 2−65317
    - NiFe permalloy, oxidized, exchange anisotropy effects, hysteresis loop, 5-300 K 2−81230
    - $NiFe_2O_4$, ferromag. reson., etching effect 2−44431
    - Ni(100) single crystal, magnetoelastic coefficients at room temp. 2−44264
    - Pb, superconducting, mag. flux penetration 2−71871
    - Pb, superconductor current- induced intermediate state mag. struct., magneto-optical obs. 2−54151
    - Permalloy, oxidized antiferromag. surface layer, mag. after effect 2−44267
    - PtSi on single crystal Si substrate, thermal stability 2−71334
    - Sn-Mn, mag. state of Mn rel. to supercond. 2−68512
    - Sn, superconducting, mag. flux penetration 2−71871
    - Tb, phonon emission at 15 GHz, dynamic magnetoelastic coupling obs. 2−68562
    - $Y_{3-x}Eu_xAl_yFe_{5-y}O_{12}$ epitaxial, characteriz. for bubble devices 2−61541
    - $Y_{2.5}Gd_{0.5}Fe_4Ga_1O_{12}$ garnet, magnetization orient. depend., induced anisotropies, magnetooptic Faraday effect obs. 2−72188
    - YIG/dielectric/conductive plane, magnetostatic propag. 2−51268
    - YIG, epitaxial, coupling between dipole and exchange dominated spin waves 2−72189
    - YIG, Fe-deficient, magnetization 2−72202
    - YIG, thin single-crystal distrib., magnetoexchange branch repulsion 2−44433
    - YIG discs, epitaxial, anisotropy effects on magnetostatic modes 2−44432
    - YIG disks, anisotropic excitations of magnetostatic modes 2−44434
    - YIG single crystal film, domain wall mobility meas. by light diffraction 2−84434
  - **optical properties**
    - ABA block copolymer films, light scattering from anisotropic regions 2−44325
    - ammonium thiocyanate and ammonium thiocyanate-d_4, far i.r. spectra 2−48201
    - antistatic agent, on plastic, refractive index recovery, ellipsometry obs. 2−65073
    - applications, present and future 2−73660
    - barium behenate molec. film, ellipsometric study of optical constants and refractive index detn. 2−78064
    - barium margarate molec. film, ellipsometric study of optical constants and refractive index detn. 2−78064
    - BDPA, organic free radical, vapour deposited, absorp. obs. 2−56598
    - birefringent polymer films on substrates for integrated optics 2−80592
    - β-carotene, gas adsorption effect on absorpt. spectra 2−57355
    - CdSe photoconductive films, field quenching 2−77964
    - chloroform, i.r. spectra in polarized light 2−84484
    - coatings, detection of laser induced damage 2−63415
    - cyanine dyes, luminescence of solid films 2−75327
    - deposition, optimal conditions for uniform thin films 2−60639
    - dielectric, sputtered and evap., as function of deposition conditions 2−48131
    - dielectric optical constant determ. from reflectances 2−78062
    - dielectric thin film, interference method for meas. of dispersion in refractive index 2−44342
    - dielectric thin film waveguides, TE_0 and TM_0 modes spectral props., coupling 2−78969
    - diffusion pump oil on Au mirrors, ellipsometric meas., simulation of space effects on optical surfaces 2−79431
    - DPPH, organic free radical, vapour deposited, absorp.obs. 2−56598
    - electroluminescent, electrode current rel. to applied stress 2−81435

- **Films, solid** continued
  - **optical properties** continued
    - ellipsometric method for consts. meas. 2−47095
    - ellipsometry determ. of optical consts., calc. method 2−44339
    - e.u.v., evaporated films stored in ultra light vacuum 2−48133
    - filters, optical control during preparation of stacks of thin dielectric films 2−52472
    - fused quartz, ion-bombarded, refractive index and optical loss variations 2−50688
    - Gaevachrome film type 6.00 and 6.05, rel. to physicochemical processing methods 2−52502
    - garnet, epitaxial single crystl., optical waveguides 2−70059
    - glasses, binary borosilicate, vapour-deposited films, infrared absorption vibrational spectra 2−48169
    - integrated optics, progress review 2−49437
    - integrated optics, propagation of light in thin films 2−42190
    - interdigital electro-optic thin film modulator using nitrobenzene 2−79376
    - interference filters, simulated space radiation effects 2−49440
    - lasers for high power 2−55699
    - lenses, photolithographic fabrication 2−73629
    - metal, absorption displaying quantum size effect 2−72314
    - metal, monocryst., orientational magneto-optic effect 2−61589
    - metal, on opaque substrate, thickness uniformity determ. by optical transmission microscopy 2−64560
    - metal oxide, reflection and emission coeff., thickness meas. 2−54398
    - metallic, optical consts., Vasiceks theory, Murman-Forsterling theory, single refl. theory 2−48132
    - motion picture black and white negative films, light sensitivity 2−66873
    - multilayer, low loss reflection coatings using absorbing materials 2−42244
    - multilayer system, reflectance and transmittance performance evaluation using computer 2−59222
    - nitrocellulose, self focusing by controlled thickness distrib. 2−63412
    - optical coatings, Multilayer Automatic Coater for deposition 2−73659
    - optical constant determ. from reflectances 2−78062
    - optical waveguides, distributed feedback laser prod. 2−79210
    - organic, optical waveguides, essential thickness calc. 2−83860
    - permalloy, on CaF_2, optical absorpt., polarization anisotropy rel. to thickness and orientation 2−57324
    - phenanthrene-naphthacene thin layer, u.v excited sensitized luminesc. 2−48251
    - photochromic, acousto-optical effects, acoustic wave mapping and holography 2−55548
    - photoelastic coatings, full-field isopachic generation 2−60938
    - photoluminescence spectra, freq. shift gap struct. 2−68687
    - polarizers, single wavelength 2−79381
    - poly-N-vinylcarbazole films, doped, spectral response and sensitometric curves, positive and negative modes 2−66884
    - polymer fracture surface layer, optical thickness determ. 2−70013
    - polymers, optical characterization 2−56599
    - polyoxymethylene dioxide, structure studies using small angle polarized light scattering 2−84526
    - polyvinylalcohol, irradiated by ^{60}Co γ-rays, trapped radicals in u.v. and visible absorption spectra 2−57437
    - Raman scattering by size quantization levels 2−81394
    - rare earth monochalcogenides, characteriz. 2−50502
    - rare earth oxysulphide multilayers, luminescent props. 2−48224
    - reflectance and transmittance of light by a thin inhomogeneous dielectric film, new formulae 2−54378
    - refractive index and thickness of thin films calc. from X-ray specular reflection data 2−53563
    - refractive index thickness and extinction coeff. det. 2−59224
    - with rough boundaries, ellipsometric parameters 2−79328
    - r.p. sputtered glass film for light guide 2−44013
    - salicylideneaniline, coherent optical props. as hologram recording medium 2−82530
    - sprayed metal films, absorption spectra 2−75392
    - thickness calc. from elippsometric values and intensity meas. using Drude equations 2−56581
    - transparent film- absorbing substrate, reflection polarization 2−73644
    - vacuum deposition, meas. and control for coating different from $\lambda_0/4$ 2−80602
    - vacuum unit for coating deposition by sputtering 2−62903
    - wave guides, fund. transverse elec. field (TE_0) mode selection 2−73481
    - waveguide, phase matching of nonlinear optical interactions 2−70012
    - Ag, piezorefl. and piezotransmission, rel. to electron states 2−81366
    - Ag film, dielectric const. changes, piezoreflectivity obs. 2−54382
    - AgI, optical constants of thin films in exciton band region, meas. 2−65209
    - Ag_2S, epitaxial, photoconductivity, spectral sensitivity of photocurrent, optical absorption at room and liquid nitrogen temps. 2−53567
    - Al, automatic apparatus for preparation of MIM interference filters 2−70029
    - Al, struct. change effects on opt. absorpt. 2−54415
    - AlAs epitaxial layer, on GaAs, elec. props. and optical absorp. 2−71881
    - AlN_x, preparation by reactive r.f. sputtering, absorption spectra 2−77507
    - As-S-Ge glass, laser induced refractive index changes 2−61583
    - As-Se-Ge glass, amorphous to crystalline state conversion by light irradiation 2−75077
    - As_2S_3 crystals, self-absorption edges, effect of temperature and polarization 2−84479
    - As_2Se_3, crystalline and amorphous, ion bombardment effects on absorp. spectrum 2−60646
    - $3As_2Se_3.2Sb,Se_3$, amorphous, transmittance, absorpt., refr. index 2−54186
    - Au-Al, α-phase dil. alloy, refl., 1.1-11.5 eV, rel. to band struct. determ. 2−75278
    - Au, discontinuous, photon emission on applic. of strong electric field 2−48266
    - Au, refl., 1.1-11.5 eV, rel. to band struct. determ. 2−75278

Films, solid continued
- **optical properties** continued
  - Au black deposit, i.r. transmission, rel. to prep. conditions 2−57347
  - Au evaporated films, optical constants, variation with time 2−75254
  - Be, on dielectric substrate, absorpt. spectra 2−72323
  - C, amorphous, absorpt. 2−61302
  - C, amorphous, transmission, change on graphitization by light pulses 2−61030
  - C, turbostratic, spectra, effects of thermal treatment, comparison with graphite 2−78080
  - CaF_2, spectral emission by polaritons 2−65252
  - CdS, optical absorpt. edges, rel. to pot. barriers at microcryst. boundaries 2−65256
  - CdS_xSe_{1-x}, transmission, 7000-21000 cm^{-1}, band gap calc. 2−61633
  - n-Cd_2SnO_4, refl. and transmission spectra, optical band gap .2−51137
  - p-CdTe, photolum. spectrum 2−48217
  - Cu-Ni alloy, soft X-ray absorpt., band struct. interpretation 2−65286
  - Cu, far-i.r. transmission, surface plasma oscillation obs. 2−54401
  - γ-CuI, piezo-optical effect at 77K in fundamental absorption band region 2−48172
  - CuO optical consts. wavelength depend., 450-800 mμ thickness 2−48135
  - EuO, transparent, prep. by oxid. of Eu film, optical absorp. obs. 2−64568
  - Fe, garnet film magneto-optic film waveguide, light modulation and switching 2−81323
  - n-$Ga_{1-x}Al_xAs$, epitaxial, edge photoluminesce, free exciton annihilation contrib. 2−81432
  - GaAs, epitaxial, cathodolum., carrier mobility effects 2−72434
  - GaAs, epitaxial, guiding and electrooptic modulation of light 2−68608
  - GaAs, epitaxial, photolum., substrate orientation effects 2−47436
  - GaAs, heavily doped, Faraday effect 2−65214
  - Ge, 10.6 μm guided waves obs. 2−55748
  - Ge, 10.6 μm guided waves obs. 2−55749
  - Ge, amorphous, void structure and optical sum rules 2−78063
  - Ge, amorphous film, u.v. reflectance depend. on deposition temp. 2−54403
  - a-Ge, u.v. dielectric consts., reflectance obs. 2−61586
  - Ge_xSi_{1-x} solid soln., photoelec. props. 2−65090
  - In-Te system, 33-45%Te, absorpt. and optical density 2−60662
  - In, absorption, ellipsometry obs. rel. to electronic struct. 2−72334
  - InP, epitaxial, free and bound exciton decay 2−72410
  - In_2Se_3, flash evaporated, optical gap, absorp.obs. 2−56593
  - KBr, i.r. reflectivity, dielectric response obs. 2−72304
  - KCl:KI, slow electron impact, luminescence excitation and characteristic energy losses 2−81417
  - KI, slow electron impact, luminescence excitation and characteristic energy losses 2−81417
  - Li, absorption and structure 2−65260
  - Li, optical consts., 2-3.8 eV, meas. by excitation of nonradiative surface plasmons 2−75256
  - LiF, overcoat on Al, effect on u.v. refl. 2−79370
  - LiF on Al, thickness monitoring by reflectance meas. using 1216 Å line of H 2−55733
  - Mg-Mn ferrite, transparent, light diffraction by mag. stripe domains 2−65220
  - MgF_2, overcoat on Al, effect on u.v. refl. 2−79370
  - MgF_2 on Al, thickness monitoring by reflectance meas. using 1216 Å line of H 2−55733
  - MgO, evaporated, refr. index and absorpt., 0.22-8μ 2−79369
  - MgO, spectral emission by polaritons 2−65252
  - MnBi, Ti-substitution effect 2−51265
  - $MnBi_{(1-x)}Te$, magneto-optical props. 2−72264
  - Mo, complex index obs. 2−56595
  - $(NH_4)_xK_{1-x}H_2PO_4$, epitaxial, electro-optic waveguide 2−70058
  - NaCl, i.r. reflectivity, dielectric response obs. 2−72304
  - Nb_2O_5, prep. by anodic oxidation, field depend. of refractive index, ellipsometric obs. 2−44150
  - Ni, colour phenomena, explt. obs. and mechanisms 2−59243
  - Ni, on CaF_2, optical absorpt., polarization anisotropy rel. to thickness and orientation 2−57324
  - Ni, opaque coatings for code modulating disks and grids 2−70047
  - NiO, optical consts., electrochem. deposition conditions depend. 2−61618
  - Os, evaporated, reflectance and optical constants in v.u.v. from 300 to 2000 Å 2−81336
  - $PbBr_2$ thin film, optical constants and exciton states, 2-10 eV at 4.2 K 2−57321
  - PbI_2, influence of nature of substrate and preparation conditions on exciton spectrum 2−48188
  - PbO, absorp., band edge and acceptor levels detn. 2−57352
  - PbS, prep. by chem. precip., transmission spectra, optimum prep. conditions 2−75304
  - PbS layers, photocond. mechanism, elec. cond. and Hall effect obs. 2−81166
  - PbS photosensitive layers, prepared by different methods, adsorption properties 2−61652
  - PbTe, optical and elec. props., and comparison with bulk 2−57172
  - Pt, for u.v. reflectance 2−61653
  - Re evaporated film, reflectance in v.u.v. from 300-2000 Å 2−44345
  - Sb_2S_3 single cryst., absorp. edge obs. 2−81390
  - $Sb_{1-x}Se_x$, amorphous, photocond. spectral response rel. to comp. 2−81167
  - Sb_2Se_3, amorphous, absorp. and reflectivity 2−61323
  - Sb_2Se_3, amorphous, absorpt., transmission, and optical energy gap 2−53576
  - Se, amorphous, optical const. determination from reflectivity spectra 2−61620
  - Se, crystalline and amorphous, ion bombardment effects on absorp. spectrum 2−60646
  - Se thin films, i.r. laser radiation recording characteristics 2−69960
  - n-Si:P, epitaxial, on $MgO.Al_2O_3$, refl. and transmission 2−77910
  - Si, amorphous, effects of thermal neutron irrad. 2−60666
  - Si, amorphous, optical absorp. and photocond. spectra 2−61655
  - SiO_2-Si_3N_4 syst., freq. depend. of abs. coeff. 2−47086
  - SiO, evaporated, i.r. spectra 2−50505

Films, solid continued
- **optical properties** continued
  - SiO, evaporated films, interference meas. of refractive index 2−65212
  - SiO_2, r.f. sputtered, i.r. absorpt., effect of substrate temp. 2−83865
  - SiO_2, study of transparency by luminescent method 2−44340
  - SiO_2, thermally grown, i.r. absorpt. meas. 2−71999
  - SiO_2, thermally grown, struct., i.r absorpt. study 2−53579
  - SiO_x, r.f. sputtered in Ar-O_2, i.r. absorp., O_2 conc. effects 2−60667
  - SmSe, prep., structure, optical and magneto-optical props. 2−81324
  - SmTe prep., structure., optical and magneto-optical props. 2−81324
  - Ta_2O_5, prep. by anodic oxidation, field depend. of refractive index, ellipsometric obs. 2−44150
  - TiO_2, amorphous, photolum. 2−72068
  - TiO_2 chemical vapour deposited, refractive index as function of processing temp. 2−50511
  - W evaporated film, reflectance in v.u.v. from 300-2000 Å 2−44345
  - W_2O_5, prep. by anodic oxidation, field depend. of refractive index, ellipsometric obs. 2−44150
  - Zn, on dielectric substrate, absorpt. spectra 2−82323
  - ZnCdS evaporated layers as photoresistors in u.v. 2−44179
  - ZnO, Burstein-Moss effect 2−51350
  - ZnO, photocurrents and photovoltages obs. 2−51218
  - ZnO Electrofax layers, effect of emission on print quality 2−66883
  - ZnO optical waveguides, epitaxial, low losses, below 5dB/cm 2−79377
  - ZnS:Cu, Pb, Cl, temp. depend. of electrolum. and thermal quenching 2−74533
  - ZnS:Cu, Pb, Cl temp. depend. of electrolum and thermal quenching 2−84533
  - ZnS:Mn films, energy level scheme from reflectivity and transmission meas. 2−71799
  - ZnS, in electrolum. device, high field a.c. electrolum. rel. to field clamping 2−81412
  - ZnS, vapour phase deposited interference layers used to identify inclusions 2−56737
  - ZnS dielectric thin film, interference method for meas. of dispersion in refractive index 2−44342
  - ZnS with Cu and Cl impurities, photo- and electroluminescent props. 2−51394
  - ZnSe (Cu, Ga), epitaxial thin films, photoluminescent, oscillations of photocurrent 2−78147
  - n-ZnSe(Cu,Ga) film, photolum., photocurrent oscills., 80-220K, luminesc. field quenching 2−81168

Filters
- acoustic surface wave, analysis 2−49144
- acoustic surface-wave, piezoelectric devices 2−58924
- acoustic surface-wave pulse compression corrections for diffraction effects 2−49158
- adaptive, time varying, long period seismic signal enhancement 2−57616
- aerosol, collection efficiency, as fm. of particle size and velocity 2−56530
- continuously adjustably hole size, biological cell separation 2−85088
- digital, type curve computation for e.m. depth sounding on horizontal transmitting coil 2−72634
- digital dual window for gamma radioactive decay meas. 2−46032
- fan, equiripple approximation, seismic data processing 2−78253
- high pass mechanical velocity filter for molecular beams 2−42862
- immiscible fluids, first boundary value problem for one dimensional filtration 2−60388
- i.r. matched configuration for sensor 2−79284
- linear, transient mode of output variance affected by commutation, application to nuclear pulse shaping 2−49689
- linear digital, comparison with Fourier truncation 2−78342
- linear low-pass, for gravity waves 2−57903
- liquid filtration, soil, electro osmosis 2−83783
- magnetic filtration, high intensity, for selective separation of micron-size particles 2−41912
- mechanical l.f. band pass 2−49150
- noise, distortion of spectral lines 2−52339
- nuclepore and golden membrane for radioactive aerosol meas. 2−84819
- polycrystalline Be filter, chopper monochromator neutron spectrometer, time of flight, wavelength resolution 2−82565
- porous media, flow, models 2−74499
- pressure cell for filtering and use as pressure membrane 2−68757
- quadrupole energy filter with plane electrodes 2−82391
- rotary impaction, droplet removal from fast flowing air stream, efficiency 2−67849
- rotary impaction filters with tapered filaments, design 2−43402
- sampling, for drawing interstitial water from marine sediments 2−62086
- sound waves, sea surface as random filter 2−57838
- spatial, application to aeromagnetic data 2−44764
- velocity, three-dimensional optimum multichannel, for seismic waves 2−57498
- viscoelastic plastic, filtration of nonlinear viscous liquids 2−53357
- Wiener, digital image processing, nucl. medicine 2−82810
- wire screens for 0.001 μ particles 2−85159
- X-ray bandpass, nanosecond resolution of plasma spectra 2−67659
- B and B + Cd, for neutrons in nondestructive activation anal. 2−72598
- Cd, for neutrons in nondestructive activation anal. 2−72598
- ^{131}I monitor for nuclear plants 2−67364
- $LiIO_3$, elastic surface wave props. and device applics. 2−77778
- Rb maser, isotopic filter 2−59126

Filters, electrical *see Circuits*

Filters, optical
- *see also Absorption/light; Films, solid/optical properties*
- absorbing multilayers, transmittance and reflectance 2−66843
- amplitude, rel. to partially space coherent diffr. of defocussed circular aperture 2−45792
- annular aperture with amplitude filter partially space coherent diffr. 2−82551
- arc welding radiation meas. rel. to protective filter glass standardization 2−73668
- bleachable absorber-laser amplifier-detector combination, wide-angle low-noise laser receiver 2−45755

Filters, optical continued
coherent optical processing, spatial frequency diversity 2−79292
colorimetric receptor set correction 2−52462
complex obtained as a Fresnel hologram with a converging reference beam 2−42151
confocal interference, imaging 2−66844
controllable dispersion interference- polarization, design method 2−66845
dichroic, colour props. 2−70064
dielec., multilayer, for 1700-2500 Å bands 2−42191
electron microscope, retarding field electron energy analyzer 2−79079
Fresnel zone plate spectrometer with central stop 2−59283
glass, for colour temperature improvement of incandescent lighting 2−73669
glass and thin film interference, simulated space radiation effects 2−49440
high pass, transmission echelette, optical props. 2−70063
holographic image-deblurring, high-resolution extended-range, realization method 2−45766
holographic matched filter systems for pattern recognition using correlation method 2−76495
holography, selectivity and noise effects in applications of optical correlation 2−69963
inholography, spatial filtering using double diffr. mounting 2−82514
I_2 absorption filler for reduction of parasitic light in Raman and Brillouin spectroscopy 2−52471
image filtering with fast Fourier transformation using digital computer 2−79142
induced-transmission, symmetrical containing absorbing layers, equiv. layers concept 2−79445
intensity spatial filtering for inspection of periodic arrays 2−79424
interference, high-contrast, 10 to 30 A half-width 2−70065
interference, reflex, conjugate, thin-film, within Fabry-Perot cavity 2−79346
interference coatings, multilayer, optical monitoring 2−79408
interferential, Lyot-Ohman, tuning results 2−51875
i.r. thin film filters rel. to developments in optical equipment 2−73667
multicolour imagery from holograms by spatial filtering 2−79273
multilayer, low loss reflection coatings using absorbing materials 2−42244
multilayer, tandem arrays, radiant transmittance, attenuation optimization 2−79382
multilayer coatings, graphical displays of complex reflectance based on circle diagrams 2−49439
multilayer system, optical props. calc. 2−45810
optical data processor, coherent and noncoherent, space invariance conditions 2−79368
organic dye, for visible and i.r. region methods of production and properties 2−55745
organic glass, as u.v. radiation filter 2−72357
parasitic flux transmitted, estimation from transfer function 2−42247
polymethylacrylate, for visible and i.r. region methods of production and properties 2−55745
PVC, for visible and i.r. region methods of production and properties 2−55745
reflection, 'Irtran-1' for 20μ atmospheric window in astronomical photometers 2−73163
Reusch piles, propag. phenomena 2−82552
review of some definitions 2−70038
rotatory dispersive, dye laser wavelength tuning 2−55696
selectively absorbing for contrast enhancement of light sources 2−55763
spatial, for detection of particular shape in aerosols 2−48462
spatial, optimization, use in scanning optical detection system 2−42245
spatial filtering and correlation unit for processing of electron micrographs 2−42241
spatial filtering of interfering waves 2−66814
spectral microscopy, high resolution filter system 2−42246
stearate multilayer struct. 2−46633
thermocontrolled, construction principle 2−52473
thin dielectric films, optical control during preparation 2−52472
time domain configuration of narrow frequency- bandwidth pulses 2−49441
u.v. bandpass, alkali alloys 2−66846
Al film thickness control, automatic apparatus for preparation of MIM interference filters 2−70029
MgF_2, multilayer, quarter wave, generalized Brewster angle condits. at non-normal incidence 2−79410
MgF_2 low temp. filter for photometry in 20 μ atmospheric window 2−63399
ZnO low temp. filter for photometry in 20 μ atmospheric window 2−63399
ZnS, multilayer, quarter wave, generalized Brewster angle condits. at non-normal incidence 2−79410

Finlay-Freundlich red-shift hypothesis *see Astronomical spectra; Cosmology; Gravitation; Relativity*

Fireball model *see Cosmic rays; Elementary particles; Field theory, quantum/interactions; Nuclear reactions and scattering*

Fission *see Nuclear fission*

Flames
acetylene-air, impingement heat transfer rates 2−52288
acoustic vibrations effects on combustion 2−52285
aerodynamics of laminar diffusion flames formed by jet emanating from narrow extended slit 2−53303
air excess coeff. computation from electrical props. for laminar flames for gas fuels 2−58964
asymmetrical turbulent flame, burning characteristics 2−61789
atomic levels, spectral measurements of population in atomic absorption spectrometry 2−49939
autostabilization in combustion chamber of liq. rocket engine 2−52287
burner, flat-flame, motion of gases in open flame 2−58970
convective heat transfer, soln. of conservation eqns. 2−76401
diffusion, in homologous turbulent shear flows 2−69786

Flames continued
diffusion, velocity distrib. in boundary layer over flat plate 2−83659
diffusion H_2, supersonic flow in closed channel, temp. influence on burning characteristics 2−67703
ethyl alcohol counterflow diffusion flame in transverse electric field, optical study of temperature profiles 2−83703
free-burning, rel. to detection of pulsed laser radiation 2−42162
heat distrib. analysis by method of spliced asymptotic expansions 2−82269
heat loss by radiation, calorimetric meas. 2−58965
heat transfer from, laser interferometer for obs. 2−73635
inhomogeneous positive column, distrib. of charged particles and potential 2−80366
moving-flame phenomenon by propagating periodic heat source 2−67819
natural gas-O_2, impingement heat transfer rates 2−52288
oxyacetylene, temp. and particle flight velocity in gas-powder build-up 2−52286
in particle suspension in gas, propagation characts. 2−48326
photometry, book on laboratory practice 2−48359
photometry, effects of rate of entry and composition of soln. 2−48358
photometry, TV recording methods 2−57442
probe measurements of oscillating flames 2−82356
propagation, effect of electric discharges 2−82373
propane, cold, math. model 2−61781
spectrometry, use of novel sample modulation technique 2−84696
stabilization of diffusion flames from industrial natural gas in axial flow 2−58967
temperature meas. by atomic fluoresc. spectrometry 2−84691
temperature measurement by i.r. emission from flames containing Al_2O_3 particles 2−73468
temperature obs. using β-radiation 2−58966
turbulent, jets, structure, effect of rotation 2−80376
turbulent combustion processes, acoustic noise generated by, analytical results 2−69774
turbulent struct., chemilum. meas. applic. 2−61780
turbulent swirling boundary layer flow, inverse solution method 2−46671
u.s. wave prod. by activated flame plasma 2−83531
velocity and size of particle measurement photographic method 2−66879
volcanic gas burning at Kilauea Volcano 2−57928
welding torch, burning natural gas, temp. distrib. 2−69484
Al_2O_3 particles, radioactive props., high temp. 2−78183
$H_2/O_2/N_2$, radical recomb. reactions, HO_2 participation 2−65373
$H_2/O_2/N_2$, with Cr and K additives, electron attachment and negative ion form. 2−72555
H_2-O_2-N_2, premixed, emission noise spectrum obs. in Na and K flame spectra 2−49952
H_2-air diffusion flames, structure 2−61787
H, quenching of atomic Sr fluorescence 2−42715
$H + H + OH \rightleftharpoons H_3O^+ +$ e- reactions in flames, kinetics and heats of reactions 2−54541

Flare stars *see Stars*

Flares, solar *see Sun/flares*

Flash photolysis *see Photochemistry*

Flicker noise *see Electron tubes; Noise/electrical*

Floating zone refining *see Zone melting and refining*

Flocculation *see Sedimentation*

Flow
see also Boundary layers; Diffusion; Jets; Plastic flow; Turbulence; Viscosity
absolute stability of fluid conduit connected to mass and spring system 2−74316
acoustic ray theory for inhomogeneous moving medium 2−45503
aerosol aspiration study by photographing particle tracks under flash illuminations 2−43404
air jet, of fluidics, observation by optical method 2−73653
air-water-glass bead system, exptl. investigation of hold-up 2−67605
annular, co-current and counter-current, in vertical tubes 2−43090
around blunt bodies, near stagnation point, streamline behaviour 2−74341
around disc rotating in non-Newtonian fluid 2−83485
asymmetric, due to motion of a sphere, rel. to rotation and mag. field 2−60133
atmosphere stationary barotropic flow crossing meridional mountain barrier 2−54835
attached, fluidic logic study by optical visualization 2−73664
axial compressor in nuclear power reactor, hub/tip ratio rel. to cost 2−49871
axially-symmetric, Baecklund transforms. and invariance props. 2−70833
axisymmetric creeping flow, force on accelerating body 2−83478
axisymmetric potential, past annular aerofoils and bodies of revolution, surface vorticity theory 2−67577
axisymmetric stagnation point flow with uniform suction 2−83447
axisymmetric turbulent boundary layers in zero pressure-gradient flows 2−46691
axisymmetrical rotational flows, jet path determ., numerical soln. 2−46674
benzoic acid/water, mass transfer coeffs. on flat plate by parallel channel flow and turbulence promoter 2−67601
between eccentric rotating cylinders, stability and growth of Taylor vortices 2−80210
between two rotating fixed discs, general structure 2−80215
bidimensional channel, measurement of statistical distribution of boundary gradient of longitudinal velocity 2−74322
binary diffusion of jet embedded in boundary layer 2−71072
Bingham type non-Newtonian fluids, laminar flow in square duct 2−83491
blood, red cell rotation model, verification using holography 2−85096
blood coronary circulation in conscious dog with cardiac neural ablation 2−85121
bluff body, influence of taper 2−80212
Boltzmann eqn. soln. in weakly nonlinear region 2−78837

low continued
  boundary free, in n-dimensional space, general invariance of hydrodynamic equations, classical symmetry breaking 2—80183
  boundary layer, inverse problem, numerical computation 2—67576
  boundary layer, on circular cylinder moving in fluid at rest 2—83477
  boundary layer, past magnetized plate, mag. field oscillations effects 2—83530
  boundary layer, thermal laminar with arbitrary surface temp. distrib., exact solutions 2—60150
  boundary layer effects on travelling shock waves 2—80211
  boundary layer on bodies of revolution 2—67573
  boundary layer transition induced by two dimensional roughness element 2—50157
  boundary layers, hydrodynamic stability analysis 2—77208
  boundary layers, over surface of const. catalytic efficiency, diffusion of species 2—68769
  withboundary layers, use of nonuniform grids in finite-difference equations 2—82281
  boundary layers in ducts, numerical predictions 2—70843
  capillary, Oldroyd rate type fluid, Bagley end correction factor and die swell 2—67600
  Cauchy-Poisson wave problem in rotating fluid 2—50149
  cavitation damage, dimensional anal. 2—67776
  cavitation erosion testing and cutting, using simple cavitating nozzle 2—77388
  cavity and wake, free-streamline theory, review 2—80205
  cerebral blood flow, sympathetic control in dogs 2—85122
  characteristics of small diameter orifices in series 2—83517
  chemically reacting, irreversible thermodynamics and continuous mechanics 2—80203
  in circular pipes, errors in velocity-area method of obs. 2—83522
  circulating, in vessel with screw agitator, numerical anal. 2—83488
  cocurrent oblique crossflow transfer, angle between flow directions between 0 and 90 degrees 2—50146
  collapsible tubes, steady pressure characteristics 2—46698
  companion flows in presence of recirculation zone channel with constant cross section 2—64233
  compressible, computation of the adiabatic wall temperature for laminar boundary layers 2—53129
  compressible, simple quadrature method for computing laminar boundary layers 2—74315
  computer simulations, especially of incompressible flows 2—83440
  condensation heat transfer in horizontal tubes, prediction of mean Nusselt number 2—83444
  condenser cooling water discharge into adjacent water body 2—80201
  conducting, stratified, with mag field, propagation of Alfven-gravitational waves 2—60195
  conducting fluid, induced by elec. current discharge 2—56305
  conducting source flow in inhomogeneous magnetic field, nonlinear boundary value problem 2—80222
  conical flow, structure rel. to streamline patterns 2—80199
  with constant stretch history, generalization of fundamental relations 2—80159
  convection, forced and free, heat transfer from vertical thin needles in uniform stream 2—80179
  convective in box of porous material saturated with fluid 2—56308
  convective instability in hydrodynamically coupled vertical channels 2—77221
  convective plane-parallel in vertical slot, oscillatory instability 2—83472
  Couette, dipolar fluids, in annular space between two concentric cylinders 2—43074
  Couette, forces on flat plate 2—60169
  Couette, inviscid plane, distribution-theoretic approach to stability problem of Orr 2—53136
  countercurrent systems, method for numerical determination of transients 2—60142
  creeping, in screw channel at screw agitator 2—83486
  creeping, through clusters of spheroids and elliptical cylinders, numerical solutions to Navier-Stokes equations 2—67568
  cross, in tubes, influence of Coulombic damping on susceptibility to vibr. damage 2—53112
  cross flow, fluid mechanics, heat and mass transfer 2—43097
  cross-flow, heat transfer from cylinders to liquids, correlation equation for forced convection 2—55577
  crossflow, wakes of cylinders, sensitivity to freestream turbulence of heat transfer 2—55576
  current dependence of convection in electrolytically heated fluid layers 2—49182
  curve det. in extremely low shear velocity range 2—60161
  cylindrical anemometer probes, heat transfer in yawed flows 2—58949
  cylindrical tube, laminar combustion stability 2—56284
  decay of swirl in annulus, series solution 2—46695
  deformation of velocity profile in turbulent boundary layer in water and oil 2—74492
  developing, from short tubes and nozzles, non Newtonian fluid 2—83489
  differential rotation of right circular cylindrical depression in one of two rapidly rotating parallel plates 2—50154
  dimensional perturbation of contraction coefficient 2—46894
  discrete numerical approach to fluid dynamics 2—80218
  dispersion of material in slowly moving fluids 2—46664
  drag reduction in fluids rel. to wavelength of flow-oriented wall eddies 2—53172
  duct, acoustics conference, Southampton, Jan 1972 2—55539
  ducts, acoustic impedance of holes in wall 2—78922
  eccentric rotating cylinders, Taylor vortices 2—77240
  EHD, one-dimensional flow with variable mobility coeff., evap. and condensation jumps 2—83528
  EHD, two dimensional potential cases 2—77222
  elastico-viscous fluid, stability 2—53143
  electro-diffusion method of meas. of spectral characteristics by turbulent flow 2—77234
  electrokinetic and hydrodynamic coupled, finite element solution 2—74310
  elliptic cylinders unsteady starting flow 2—50163
  expansion flow, vibrational relaxation of anharmonic oscillators 2—66422

Flow continued
  Falkner-Skan, unsteady, finite difference method of solution 2—53144
  Falkner-Skan problem with mass transfer, parametric study 2—70837
  finite flat plate parallel to uniform flow, drag, calc. 2—70846
  over flat plate in entrance region, variational method, hybrid computer soln. 2—67572
  on flat plate normal to two-dimensional laminar jet from nozzle of finite height 2—77224
  fluid, compressible swirling, through annular nozzles 2—53141
  fluid, ideal, isentropic flow eqns. exact solns. 2—46805
  fluid, micropolar, unsteady boundary layer flow along an infinite plate 2—80165
  fluid, on flat plate at zero incidence receiving a single free jet 2—43070
  fluid, viscoelastic, non-viscometric flows, review 2—46659
  fluid, viscous incompressible around slowly rotating sphere, steady state forced convection 2—64228
  fluid line transients, survey of modelling techniques 2—67593
  fluid through random particulate bed, local flows 2—83435
  fluid turbulent flow heat transfer near pseudo-critical temp. in supercritical pressure 2—74320
  fluid viscous compressible in spherical cavity, nonstationary motion 2—67570
  fluidized beds, flow velocity and space fraction, correlation 2—43401
  fluids, applic. of Hamiltonian variational principle for classical field theory 2—45240
  fluids, generation of thrust, continuum mechanics, book 2—70825
  fluids, in acoustically lined circular ducts sound attenuation 2—58913
  fluids, point source in rotating stratified fluid 2—43099
  fluids, through semi-infinite circular transmission line, step response, time domain solutions 2—67592
  fluids in straight tube, effect of axial boundary motion on pressure surge generation 2—67591
  fluids with antisymmetric stress, constitutive relations and extension of Curie principle 2—60157
  forced-convection, buoyancy effects, anal. by perturbation method 2—74319
  formation of regular components in random field of turbulent fluctuations with unsteady growth of boundary layer 2—74327
  free and forced convection through vertical noncircular ducts 2—60135
  free convection, three-dimensional, near two-dimensional isothermal surface 2—46672
  free shear layers, instability considerations 2—80198
  free stream which oscillates without reversing, two-dimensional boundary layer 2—80172
  free surface, theory of optimum shapes, minimum drag profiles in infinite cavity flow 2—80175
  free surface, theory of optimum shapes, optimum profile of sprayless planing surface 2—80174
  free surface, time dependent, inviscid irrotational, exact solutions 2—80176
  fully developed, laminar free convection between vertical plates heated asymmetrically 2—56287
  Gaussian isotropic turbulent flow, velocity field and temperature distribution 2—74334
  general MHD duct flow problems, numerical method of solution 2—46707
  geostrophic, MHD of Earth\s core 2—81640
  gradually and spatially varied, numerical integrations 2—77243
  grain, modes during gravitational discharge 2—60148
  Hagen-Poiseuille nonlinear stability, theory 2—70848
  half jet mixing, linearized solns. of Blasius eqn. 2—60136
  headpieces conically converging, input angle and length effect 2—83446
  heat and mass transfer in entrance section of circular tube 2—64236
  heat propag. in relativistic fluid dynamics, linear solns. 2—70840
  heat transfer, conference (Lucas Heights, Australia Aug. 1971) 2—43077
  heat transfer laminar, in horizontal rectangular channel large Prandtl number fluid, buoyancy effects 2—67549
  heat transfer with dissipation, effects of vorticity, displacement speed and curvature 2—53125
  heated ellipsoid of revolution, steady laminar free convection boundary layer, flow characteristics 2—56286
  heated films and wires for flow angle and shear stress meas. 2—46686
  helical, homogeneous, about rot. self excitation, stability 2—46683
  heterogeneous, stability to nonaxisymmetric disturbances 2—71125
  horizontal wind, vertical ongitudinal shear fluctuations, probability distribution, stochastic process, mean wind profile, aerospace vehicles 2—83465
  hydraulics and fluid mechanics, conference, Melbourne Australia (1971) 2—77207
  hydroelastic stability of flat panel in fluid flow, influence of free surface 2—46701
  hydromagnetic, about curved neutral sheet 2—80225
  hydromagnetic boundary layer, around oscillating axisymmetric body 2—60192
  hydromagnetic flow between 2 rotating discs with noncoincident parallel axes of rotation 2—56322
  hydromagnetic free convection in electrically conducting nonmagnetic fluid flowing past flat plate 2—53150
  hydromagnetic unsteady, near accelerated plate, effect of Hall currents 2—43131
  hydrostatic new condition in generalization of Richardson's turbulence 2—53145
  hypersonic flow, internal, inviscid, about unyawed cones, closed form solutions 2—56428
  ideal incompressible fluid, classes of quasi-stationary flow 2—64240
  ideal relativistic fluid, Friedmann and Helmholtz equations 2—67555
  incident, longitudinal, drag and mass and heat transfer on plates 2—46663
  inclined adversely heated fluid layer, thermal instability and formation of stationary secondary rolls 2—46693

Flow continued
- incompressible, instabilities of limiting laminar layer 2−43069
- incompressible, potential, for axisymmetric body duct configurations 2−64246
- incompressible fluid, homogeneous isotropic turbulence studies using eddy representation of Navier-Stokes equation 2−46697
- incompressible fluid, turbulent wake behind plane plate 2−50144
- incompressible fluid theory of homogeneous isotropic turbulence, eddy description of Navier-Stokes eqn. 2−77173
- incompressible fluids, interaction of two flows in flat duct 2−77217
- incompressible Newtonian fluid, between two rotating discs, determ. of heat transfer 2−76394
- incompressible Newtonian fluids behind slot grid 2−83492
- incompressible past bodies with permeable walls, Navier Stokes equations solutions 2−77182
- incompressible turbulent, in permeable-walled duct 2−70856
- incompressible turbulent, resolution of split flows at thick bodies, numerical method for computer solution 2−64231
- incompressible two dimensional wall jet characts. 2−50158
- infrasonic, three-dimensional, in nozzles and channels of variable cross section 2−53285
- in inlet region of a channel, effect of injection 2−64229
- instability on rotating disc, electrochemical obs. 2−67579
- integral calc. of skin friction on porous plate 2−43068
- inviscid fluid, between rotating cylinders under circular magnetic field, stability of non-rotationally symmetric disturbances 2−43111
- inviscid fluid, design of axisymmetric convergent cones with plane sonic outlets 2−50244
- inviscid fluid, heat transfer from sphere immersed in stream, at small Peclet number 2−45596
- inviscid parallel, homogeneous stratified fluids, linear stability, eigenvalue bounds 2−50155
- isocorrelation curves rel. to longit. vel. fluctuations in circular pipe 2−83434
- isothermal, self similar solns. 2−80387
- jet like, cylinder oscillating in stationary fluid 2−43100
- jet penetration into subsonic stream, model 2−60164
- Kelvin-Helmholtz, nonlinear waves 2−80171
- laminar, between parallel plates, effect on non-uniform inlet velocity profile on development 2−70841
- laminar, between stationary surfaces of revolution with common axis of symmetry 2−67595
- laminar, boundary layer, on rotating sphere 2−80185
- laminar, developing, between parallel plates, effect of buoyancy 2−74318
- laminar, development with combined forced-free convection in directional vertical tube, numerical analysis of gravity effect 2−53138
- laminar, fluid heat transfer in tubes and ducts, with wall mass transfer 2−83443
- laminar, free oscillatory movement 2−77195
- laminar, fully developed in vertical tube, of non-Newtonian fluid, buoyancy effects 2−70844
- laminar, incompressible, near separation point 2−77201
- laminar, lateral rod displacement effect on heat transfer 2−53137
- laminar, non-isothermal, heat transfer 2−83487
- laminar, of non-Newton fluid through circular pipes, heat transfer and hydrodynamics 2−60124
- laminar, past bluff body with separated wake 2−46675
- laminar, pressure drop in spherical and cylindrical packings 2−83442
- laminar, through circular tubes, low Peclet number entrance-region mass transfer of diffusing matters 2−77226
- laminar, unsteady, in tube, incompressible fluid 2−77246
- laminar and turbulent boundary layers, theory of small disturbances 2−77187
- laminar axial, in annulus with rotating inner cylinder, tangential flow development 2−43075
- laminar boundary layer, flow behaviour in pre-separation zone, effect of free-stream variables and wall temperature 2−60146
- laminar cross flow, turbulent plume growth and rise 2−67701
- laminar flow development and heat transfer in converging plane-walled channels 2−53117
- laminar in tubes with constriction 2−74335
- laminar incompressible, analysis method 2−50150
- laminar maxwell fluid near oscillating porous infinite plane 2−60154
- laminar MHD boundary layer during blowing and suction 2−67614
- laminar mixing of two uniform parallel semi-infinite streams 2−77227
- laminar nonisothermal contracted flow, theoretical analysis 2−83423
- laminar of incompressible fluid in conduit, computer-oriented solution 2−46684
- laminar pipe jet, instabilities, flow props., expt. study 2−83422
- laminar radial flow between parallel plates 2−53116
- laminar transient freezing in laminar tube-flow 2−83731
- laminar transitional and turbulent flow, compressible nonadiabatic boundary layers calc. 2−70861
- laminar viscous, past infinite porous flat plate with sudden suction change, Laplace transform soln. 2−83434
- laser anemometer, tracer behaviour in turbulent flow 2−43054
- laser Doppler velocimeter, instantaneous turbulence velocity measurement 2−43230
- laser Doppler velocimeter meas. 2−66408
- laser interferometer, boundary layer study in fluids 2−59228
- layered viscous fluids, accelerated motion of sphere 2−77248
- limiting turbulent layer, primary vel. distrib. in dihedron interior 2−50143
- linear viscoelastic fluid, pulsatile flow in elastico- viscous tubes 2−80167
- linearized stationary plane flow, shear waves and perturbations for perfect fluid 2−83457
- liquid crystal, nematic, flow alignment 2−60426
- liquid metal fast breeder reactor single subassembly accident, inertial contribution of fluid in plenum to rapid coolant-expulsion process 2−70524
- logarithmic throttle valve, design and working performance 2−53140
- long bore orifices, low Reynold's numbers 2−83515
- longitudinal velocity fluctuation in smooth circular pipes 2−60125

Flow continued
- magnetohydrodynamic, at low and moderate Hartmann numbers, application of Gringberg's soln. to design of duct 2−67613
- magnetohydrodynamic flow past flat plate with nonaligned mag. field 2−53155
- mass, in pipe systems, iterative calc. using digital computer 2−64232
- mean velocity profile thick turbulent boundary layer, along circular cylinder 2−70835
- measurement, auroral industrial practice, review 2−83509
- measurement, laser velocimeter, Doppler effect 2−83510
- measurement, long bore orifices, low Reynolds number 2−83515
- measurement, microwave Doppler meter 2−83513
- measurement, molumetric, optical anemometer 2−83512
- measurement, n.m.r. technique, velocity distribution for 2−83757
- measurement, nonnewtonian fluids, pressure difference meters 2−83516
- measurement, volumetric, u.s. methods 2−83514
- measurement in strong swirl, with laser doppler anemometer 2−83511
- measurements by current meters, propeller weight and shape effects 2−60144
- meter, slotted, cylindrical, circulating calorimetric schemes 2−80388
- metering, developments and prospects, review 2−83523
- MHD, development in entrance region of channel 2−64253
- MHD, in circular pipe in transverse mag. field, linear stability 2−67616
- MHD, laminar boundary layers along infinite porous plate 2−60204
- MHD, past a hollow sphere, in a mag. field 2−80219
- MHD, perfectly conducting fluid, multiplicity theorem 2−50173
- MHD, two-dimensional, gasdynamics, calc. 2−80260
- MHD channel between conducting walls, heat transfer 2−43108
- MHD channel entrance flow, linearized analysis 2−70869
- MHD channel flow with arbitrary inlet. vel. profile 2−56323
- MHD entrance flow in channel, in Prandtl approx. 2−60205
- MHD fluctuating along infinite flat wall with variable suction 2−53168
- MHD of liquid metals through dendritic conducting filler 2−64576
- minimum drag in free-molecular flow, determination of optimum non-slender bodies of revolution 2−53122
- mixing layer, boundary layer problem, Blasius eqn. 2−46656
- modes of submerged jet 2−70852
- naphthalene/air, mass transfer coeffs. on flat plate by parallel channel flow and turbulence promoter 2−67601
- Navier stokes, evolution, existence and stability of secondary periodic solution 2−77188
- Navier Stokes equation, invariant solns., motion with a free boundary 2−60167
- Navier-Stokes eqn., modified, consequences in sound dispersion 2−53130
- Navier-Stokes eqns., incompressible, exact vorticity solns. 2−83456
- Navier-Stokes eqns., numerical soln. 2−67558
- Navier-Stokes eqns., solns. for hydrocyclone with central air column 2−83454
- Navier-Stokes eqns., two-dimensional unsteady compressible, numerical scheme 2−56291
- Navier-Stokes eqns. existence of periodic weak solutions in regions with periodically moving boundaries 2−74333
- Navier-Stokes equation, periodic solution of non-linear mixed problem 2−50142
- Navier-Stokes equation of continuity, existence and uniqueness theorems 2−74321
- near-wall collateral flow in three-dimensional turbulent boundary layers 2−43063
- Newtonian through truncated sector ducts, momentum transfer coeffs. 2−83439
- n.m.r. studies, pulsed field-gradient spin echo technique 2−56303
- Noll's fluid, between two infinite planes with suction, solution by method of singular perturbations 2−53126
- non-isothermal, turbulence obs. 2−43081
- non-Newtonian, in tube with sinusoidal deformation 2−53127
- non-Newtonian fluids, economic optimization for laminar pipe flow 2−60143
- non-Newtonian inelastic viscous fluid between two concentric spheres, slow steady motion 2−43060
- non-Newtonian media, deformation velocity, relationship with strain, applications in lubrication 2−50162
- non-viscometric rotational, used to determ. material parameters of viscoelastic fluids 2−50140
- nonisoenergetic compressible free shear layer, initial development 2−70863
- nonisothermal, pipe, turbulence obs. behind attached ring-type turbulence promoter 2−43087
- nonisothermal, simultaneous measurement of temperature and velocity 2−74337
- nonlinear heat-conducting viscoelastic fluid 2−67599
- nonlinear incompressible, between rot. coaxial disks, algorithm 2−56292
- nonlocal fluid mechanics, continuum theory 2−46654
- nonstationary, in tubes, coefficient of frictional resistance 2−50148
- nonstationary, of viscous and ideal fluids in R^3 2−46680
- nonstationary shear flow of visco-plastic medium 2−77235
- nonuniform, linearized profile theory 2−43058
- nonviscometric with proportional stretch history 2−77206
- nuclear fuel core exit, subchannel flow 2−76929
- nuclear fuel rod assembly, utilizing helical wire wrap spacer, turbulent flow pressure drop model 2−76930
- nuclear fuel rod assembly, utilizing helical wire wrap spacer, forced flow interchannel mixing model 2−76931
- nuclear reactors, effect on stability and dynamics 2−42646
- obstacle in nonuniform motion, solution of three-dimensional laminar boundary layer equation 2−53133
- one-dimensional unsteady compressible fluid, MCCOY and SIMLA computer programs 2−70865
- open channel surges and bores, numerical simulation 2−43277
- orifices, short lines, transient response behaviour 2−67594
- Orr-Sommerfeld problems, numerical solution 2−46667
- oscillations, high-frequency, of second-order fluids near a sphere, calculation 2−56313

Flow continued
oscillatory, in pipe, similarity treatment 2−60162
OSEEN solution, modified, extension for laminar viscous flow past a semi-infinite plate 2−83452
parabolic, response of heat transfer from moving flat plate 2−55581
paradichlor benzene/air and ammonia/air, mass transfer coeffs. on flat plate by parallel-channel flow and turbulence promoter 2−67601
parallel flow stability, effect of nonlinearity, viscosity in critical layer 2−80195
parallel shear, stability of a coupled wave-turbulence system in 2−68892
partial differential equations, turbulence solutions 2−53118
particle velocity determ. using holography 2−82539
particulate fluidized beds, fluid mixing, hydrodynamic mathematical model 2−67567
passive scalar dispersion in non-uniform turbulent flow, Wiener-Hermite expansion 2−56325
past circular cylinder, incompressible laminar boundary layers, curvature and displacement speed effects 2−74331
periodic, nonlinear stability theory 2−53132
periodic phenomena, in aeronautics or architectural aerodynamics 2−80207
peristaltic MHD, in slotted channel 2−60180
photolysis of rapid flow processes 2−75391
pipe, instability pattern, produced by turbulence promoter on viscous sublayer 2−43088
pipe, radioactivity cloud rel. to u.s. and thermodynamic methods of velocity obs. 2−83760
plane, rectilinear vortices, stationarity and stabilization 2−60141
plane Couette, nonlinear stability, theory 2−70848
plane Couette and Poiseuille, bounds on flow quantities 2−83479
plane potential, round rotational circle blade lattice 2−70834
plane steady, around profile situated between straight parallel lines 2−64230
plane turbulent wakes, applic. of model Reynolds stress equation 2−56294
plasma, caused by plasma emitter 2−53240
plasma, characteristics in arc channel 2−64294
plasma, collisional, axial, in θ-pinch 2−50202
plasma, collisionless, electron density obs. using positively biased electrostatic probes 2−77282
plasma, collisionless, Rayleigh's problem 2−80252
plasma, continuous pinch in coaxial plasma device, flow process energy balance 2−83538
plasma, effects on toroidal confinement 2−64285
plasma, polarization interaction in transverse magnetic field 2−56334
plasma, recombining, population inversion of atomic C 2−46452
plasma, resistive, toroidally confined, effects of thermal conductivity and viscosity on containment 2−46756
plasma, steady-state diffusion controlled, effect of nonuniformity of applied h.f. electric field 2−67635
plasma streams, rel. to ideal conductive liquid flows 2−80339
plate, porous, heat and mass transfer, using Laplace transform. 2−49176
plate heat exchanger, heat transfer coeffs. 2−66641
over plates, analogy between buckling and flutter 2−41566
Poiseuille, in circular cross section pipe, stability det. 2−56297
Poiseuille, pipe, linear spatial stability 2−56298
Poiseuille, two dimensional laminar, heat transfer 2−53115
Poiseuille, with viscous heating, uniqueness of solns. 2−70832
Poisson equation solution 2−48977
polar fluids, simple oscillatory 2−64243
polar fluids, simple shearing flows 2−64244
poly(dimethyl siloxane), in high shear rate region, relation between mol. wt. and viscosity 2−83374
polymer systems, conc., constitutive equations for nonlinear viscoelasticity 2−82316
polyphase, conference (San Francisco March 1972) 2−67603
polytropic, velocity coefficient, with friction and heat transfer 2−74344
in porous media, swelling and nonswelling 2−77244
power law fluid in rotation straight pipe, study of heat transfer 2−50151
power-law non-Newtonian fluid on slender cylinder, axisymmetrical boundary layer 2−67566
prediction in rectangular wall cavity with turbulent flow 2−67596
pressure driven Stewartson layers, rotating circular cylinder in viscous fluid 2−77198
pressure gradient effects, atmospheric applications 2−78341
primary and secondary compressions, deviations of pressure-velocity adiabatics 2−64234
process, device for comparison of friability 2−53939
pseudoplastic fluids, power requirements, rheology 2−83754
pulsating, interpretation of heat exchange by meas. of velocity gradient at wall 2−60166
pulsating of viscous incompressible fluid under uniform transverse magnetic fields 2−64250
quasi-liquid, of spherical particles, pressure loss equation 2−60139
radioisotope constant rate injection method of velocity obs., hydraulic machine performance 2−83761
rate obs., using orifices, for non-Newtonian fluids 2−83490
Rayleigh-Benard convection, dynamics and stable flows 2−77205
reacting and non-reacting, rotation effects, structure of swirling jets and flames 2−80376
rectangular channel, two immiscible viscoelastic Maxwell fluids with transient pressure gradient 2−50161
reverse, and integration of boundary layer eqns. through region of reverse flow 2−43219
Reynolds numbers, turbulent kinetic energy prod. in wall jets 2−83455
Reynolds stress near wall in turbulent boundary layer flow 2−77260
rheology, conference, Nagoya, Japan, Oct. (1971) 2−82315
Rivlin-Ericksen fluid, oscillations by rotating sphere about fixed diameter 2−60155
Rivlin-Ericksen fluids, channel bounded by 2 flat parallel plates, axial press. gradient 2−83448
rocks, stress-strain relations 2−57822
rotating, axial, side-wall boundary layer studies 2−83460

Flow continued
rotating, axisymmetric, upstream influence of dipole 2−64238
rotating, hydraulically critical, transition of subcritical geostrophic flow 2−80184
rotating, structure of turbulence 2−77202
rotating and stratified, finite amplitude disturbances 2−80202
rotating black hole, energy and angular momentum flow 2−78436
rotating fluid dynamics, ultrastable air bearing turntable 2−77232
rotating fluid under weightless conditions, natural frequencies 2−77218
rotation of circular cylinder about eccentric parallel axis in viscous fluid 2−56296
second-order fluids, steady flow in entrance region of straight channel 2−83450
secondary, in confined rotating fluids 2−60149
secondary, induced by transverse resonant acoustic field in circular duct 2−67590
secondary, turbulence induced, in square-sectioned ducts 2−60156
self-similar, evolution of discontinuity, point explosion problem 2−73458
semi-fluid, non-uniform flow, motion analysed by holographic interferometry 2−52436
separated, ideal fluid and gas 2−77193
shallow rectangular cavity flow 2−60151
shear, growth and maintenance of turbulent field 2−80181
shear, laminar wake of flat plate 2−77245
shear, perfectly conducting, momentum transport by gravity waves 2−60196
shear, turbulent, mechanics of controlled wave disturbances 2−60171
shear, turbulent, small amplitude wave disturbances, models rel. to expts. 2−60172
shock computations, self-adjusting hybrid schemes 2−55560
skin-friction meas. in laminar and turbulent flows using heated thin film gauges 2−60138
slightly viscous rotating fluid trapped oscillations 2−67582
slow viscoelastic flow at large distance from an axis of symmetry 2−46694
slow viscous, between rotating concentric spheres, thermal effects 2−56285
smooth cylindrical pipe, turbulence, temp. distrib. obs. 2−80160
solids and slurries, velocity determ. by neutron activation anal. 2−83518
sound transmission in a duct with flow 2−66619
sound transmission in ducts with thin shear layers, convergence to uniform flow case 2−55521
spheres, unsteady starting flow 2−50163
stability of compressible boundary layer at subsonic velocities 2−64247
stability of fluid motion in ellipsoidal cavity, laboratory study 2−60152
stability of magnetic baroclinic flow of unbounded fluid with linear velocity profile 2−78585
stability of non-stationary circular jet of ideal incompressible fluid 2−77233
stability of stratified rotating boundary layer 2−67575
stability of thin non-rotating Hadley circulations 2−66167
stagnation point flow effect on entropy variation rate of fluid mixture 2−80162
stagnation temperature in natural convection flow 2−62137
standing periodic waves, existence in perfect inviscid incompressible fluid 2−56289
starting-vortex length for circular cylinders, unsteady flows 2−53134
steady, above infinite rot. disc with suction, asymptotic soln. 2−67586
steady, between rotating and stationary disc with uniform suction at stationary disc 2−60168
steady, heat transfer from fine hot wires 2−80173
steady laminar, produced by rot. disk in viscous fluid 2−80168
steady neutral planetary boundary layer forced by horizontally non uniform flow 2−62642
steady two-dimensional viscous flow in jet due to point source 2−77229
stochastic modelling and time series analysis techniques 2−41860
Stokes problem, computational algorithm, applic. to erythocyte 2−60173
Stokes problem, computational algorithm 2−56311
stratified fluid, in wavy channel 2−46678
stratified fluids in lakes, thermal bar circulation 2−44606
stream in limited space, distribution of average temp. along the direct and reverse stream 2−46696
subsonic, characteristics of a cylindrical probe, mach 0.3 to 0.79 2−83683
subsonic, compressible, past an obstacle, expansion soln. 2−60134
superfluid past plane boundary, solution for Ginzburg- Landau theory equations for neutron-star-matter 2−51755
surface waves due to periodic-in-time source under surface 2−50156
suspension, of rigid particles, turbulent drag reductions, expt. 2−53373
swirling, structure of blunt base wakes 2−80157
Taylor columns in rotating stratified fluids 2−67581
tectonic stresses and interstitial fluid flow 2−72659
temperature distribution along tube, applic. to reactor fuel element circulating system 2−52840
around thin body in electrohydrodynamics, charact. 2−67608
three dimensional laminar boundary layer, calc. 2−43066
three dimensional parabolic flow, calc. procedure for heat mass and momentum transfer 2−67571
three-dimensional ideal fluid, small perturbations in initial vel. field 2−53131
three-dimensional turbulent boundary layer, low-speed, flow characts. 2−70859
three-phase, vertical, one-dimensional theory for predicting average hold-up 2−67606
three-phase in round cylindrical tube in presence of boundary layers 2−43072
time variable dispersion from prescribed concentration distribution 2−67583
torque on sphere inside rot. cylinder 2−83476

Flow continued
traffic flow, kinematic waves, analytical solns. 2—69626
in tubes and channels, turbulent friction 2—53124
turbulence, effect of mag. field 2—70873
turbulence, pressure fluctuations at boundary 2—74326
turbulence and flow stability in M shaped velocity profiles with application to laminar MHD flow 2—60206
turbulence and pressure gradient effects on boundary layer transition 2—50152
turbulence distortion approaching two-dimensional bluff body 2—46676
turbulence in viscous sublayer near plane wall 2—74325
turbulence measurement by laser anemometer measuring individual realizations 2—80182
turbulent, associating recording of head fluctuations 2—70854
turbulent, conditional sampling 2—43080
turbulent, density stratified fluids, heat transfer 2—77249
turbulent, experimental methods, review 2—77238
turbulent, flow with weak drag reducing solutions of polymers 2—77373
turbulent, fluids, study using light dispersion techniques, evaluation 2—77216
turbulent, homogeneous, statistical theory 2—70842
turbulent, in long, strainght rectangular duct of high aspect ratio 2—43085
turbulent, in rough tubes, heat transfer 2—56282
turbulent, in smooth and rough pipes, Reynolds numbers from 30000 to 480000 2—67589
turbulent, isotropic and Gaussian exact Gaussian soln. of passive scalar 2—70851
turbulent, kinetic theory 2—70853
turbulent, mean period fo fluctuations near wall 2—83425
turbulent, model, laws for boundary layers and pipes 2—77190
turbulent, near rough surface 2—74324
turbulent, over rigid half plane, sound radiation 2—74311
turbulent, prediction of constant property flow and heat transfer in rectangular wall cavity 2—67596
turbulent, reversion to laminar flow in highly accelerated boundary layers 2—77191
turbulent, time mean values, equations 2—56288
turbulent, uniformly sheared, review 2—43078
turbulent around bluff bodies 2—77186
turbulent axisymmetric, past a long cylinder, analysis using law-of-the-wall approach 2—46689
turbulent boundary layer, effects of strong axial pressure gradients 2—83481
turbulent boundary layer, memory effect due to axial variation of meas. velocity gradient 2—77185
turbulent boundary layer separation 2—43084
turbulent boundary layer separation in strong adverse pressure gradients with injection through porous flat plate 2—74317
turbulent boundary layer with positive pressure gradient and injection 2—74328
turbulent boundary layers, calc. 2—74305
turbulent boundary layers, highly nonequilibrium, velocity and shear stress obs. and calc. 2—80214
turbulent boundary layers, intermittent structure of wall region 2—77181
turbulent boundary layers, large Reynolds number, asymptotic expansion of eqns. of motion 2—74330
turbulent boundary layers, three dimensional, hodograph models for cross flow velocity components 2—67587
turbulent boundary layers, with heat transfer and press. gradient using compressibility transform. 2—70862
turbulent boundary layers, with heat transfer and press. gradient using compressibility transform. 2—70864
turbulent boundary layers along curved surfaces 2—67602
turbulent channel, micromorphic description 2—56290
turbulent heat transfer processes 2—77219
turbulent in pipes, burst signatures 2—77184
turbulent intermittent nature 2—77183
turbulent mixing in pipes acceration using jet mixers 2—83441
turbulent pipe and channel, eddy viscosity model 2—43065
turbulent shear, conditional sampling 2—70860
turbulent shear, hot film obs. of wall region 2—56295
turbulent shear, in wall region 2—77203
turbulent shear, local transport eqns., determ. of mean velocity, kinetic energy, shear stress 2—83468
turbulent shear, model equation 2—64239
turbulent shear layer prediction on basis of transport equations for Reynolds stresses 2—77237
turbulent shear wakes, equilibrium and relaxation 2—56293
turbulent swirling boundary layer flame, inverse solution method 2—46671
turbulent two dimensional separation, numerical experiment 2—70839
two-dimensional, of non-Newtonian fluid in channel with rectangular cavities 2—67563
two-dimensional, optimal successive overrelaxation technique, triangular meshes 2—74332
two-dimensional, with conduction and convection, convergence and accuracy of finite difference schemes 2—60153
two-dimensional and viscous, past semi-infinite plate and obstacle, force relationship 2—56309
two-dimensional channel, self-oscill. regimes in Poiseuille flow 2—70855
two-dimensional diffusion with extraction of fluid on diverging walls, flow fields 2—74340
two-dimensional fields, cascade theory, differential equations comparison with stress fields 2—52044
uniform field, vibrations of flexible cable, coupling of longitudinal and transverse motions 2—55492
unilateral, nonlinear transfer eqns. 2—78945
unsteady, along infinite porous flat plate, time-dependent suction 2—50159
unsteady, Cauchy-Poisson wave problem in rot. fluid 2—50149
unsteady, convective instability 2—56300
unsteady, cylindrical shock tube, hot wire anemometer 2—77242
unsteady boundary layer, in convergent channel 2—60137

Flow continued
unsteady free convective, past infinite vertical porous plate with constant suction, viscous dissipation effects 2—46869
unsteady magnetohydrodynamic, over yawed infinite cylinder 2—70872
unsteady MHD slip flow past infinite flat plate 2—53169
using-body aerodynamic interaction 2—80401
variational principle for irreversible phenomena 2—76239
variational principles for Navier-Stokes equation 2—43047
velocity and mass flow obs. using natural turbulence signals 2—83762
visco-plastic ferromagnetic hydrodynamics, laminar flow equation of motion soln. 2—60197
viscoelastic, in V-shaped duct, constitutive eqn. 2—43057
viscoelastic fluid, in disc and cylinder system, orthogonal collocation analysis 2—70857
viscoelastic fluid, stability of plane Poiseuille flow to finite-amplitude perturbations 2—46666
viscoelastic fluid in annulus, effect of radial magnetic field on heat transfer 2—52268
viscoelastic fluids, generalized measures of deformation rates in secondary flows between rotating spheres 2—50147
viscoelastic fluids, unsteady flow through circular, coàxial circular ducts, press. function of time 2—83451
viscoelastic Maxwell fluid, oscillatory motion in annular channel under periodic pressure gradient 2—74343
viscoelastic medium, flow in constant cross-section tubes, pressure drop in viscometers 2—60128
viscosity of suspension for doublets of two equal sized spheres 2—74559
viscous, between 2 coaxial ref. cylinders different permeab. 2—83449
viscous, between two rotating coaxial cylinders, effect of radial temp. gradient on stability 2—67597
viscous, due to impulsive motion of flat plate 2—70847
viscous, slow axisymmetric, past arbitrary convex body of revolution 2—83463
viscous, two-dimensional exact statistics with random forcing 2—83464
viscous flowfield calcs. on pointed bodies at angle of attack in nonuniform free streams 2—46662
viscous fluid, high frequency oscillations of sphere 2—70866
viscous fluid, nonlinear baroclinic instability 2—83461
viscous fluid, streamlining of spherical drop 2—60406
viscous incompressible fluid, between two parallel flat plates, unsteady flow, temp. distribution 2—56304
viscous incompressible fluid, two-dimens., slow and steady motion 2—46670
viscous separated, numerical solution by non-uniform finite-difference net 2—46668
viscous sublayer, intermittent character, with interpretation of probability density measures 2—83432
viscous three-dimensional, numerical calculation application to hypersonic leading edge 2—46835
visualization, u.s. schlieren method 2—49433
visualization by holography, data reduction 2—83507
vortex, steady axisymmetric 2—43071
vortices induced in jet by subsonic cross flow 2—43067
vorticity distribution and cancellation in two dimensional incompressible periodic wake 2—77192
vorticity divergence and deformation, geometrical interpretation for two dimensional flow 2—53123
wakes, behind two dimensional square cylinders, at low Reynolds numbers 2—77247
wakes, boundary layers, definition by vortex sheets 2—77239
wakes, flat plate in uniform flow, velocity fluctuations 2—80407
wave packet propagation in baroclinic shear flow 2—62094
wave patterns produced by point disturbance, calc. 2—50153
Ar-K plasma, heat transfer between electrodes 2—60209
Mo powder, sintering mechanism, mass transfer by diffusion- viscous flow 2—53941

gases
see also Acoustic streaming;Aerodynamics; Anemometers; Supersonic flow
absolute, near impeller inlet of centrifugal turbomachine 2—80381
absorption of gases of varying solubility in laminar gas and liquid flow 2—50290
acoustic linings, optimization in presence of wall shear layers 2—71077
aerodynamic throttling of two-dimens. nozzle flows 2—60357
aerofoils, flow around leading edge 2—77362
air, contraction effect on turbulent channel flow 2—60345
air, developing laminar free convection between vertical flat plates with asymmetric heating 2—76402
air, distrib. of shear stresses in incompressible turbulent boundary layer 2—60333
air, in square channel with partially heated sides, temp. field 2—53336
air, ionized, MHD unsteady free convection flow past infinite vertical plate, variable suction 2—83526
air, nonequilibrium, mass spectrometric anal. at high temps. and pressures 2—48354
air, subsonic turbulent jets, pressure fluctuations 2—60347
air, supersonic around thin shaped tail group edges 2—71096
air, turbulent, time-interval and amplitude analyser, control of chronophotographic analyser 2—67708
air, turbulent flow in plain tube, heat and mass transfer 2—76397
air, velocity obs. using reverse flow sensing hot wire anemometer 2—67707
air and H_2 turbulent streams, optical method for concentration measurement 2—67704
air flow across mountain barrier, numerical shallow fluid model with variable grid 2—48478
air flow over mountains, three-dimensional effects 2—84814
air flow over sudden change of surface roughness, numerical computation 2—48480
air in storm basin, technical and regime characteristics 2—44716
air over heated horizontal plane, mixed convection 2—80391
air turbulence intensity and time-mean velocity distributions in low Reynolds number pipe flows 2—46832

Flow continued
 gases continued
  air turbulence round raingauge causing catch variations 2−78246
  air turbulent flow through porous tube with suction, friction factors 2−60338
  air with injected species, heat transfer in two- dimensional stagnation point flows 2−45576
  air-cooled heat exchanger in box plenum chamber 2−71088
  aircraft and missiles, three-dimensional flow separations 2−56422
  artificial satellites, aerodynamic forces, drag and lift, theoretical determination 2−62419
  atmosphere, maintenance of axisymmetric part 2−51608
  atmosphere, with and without shear, free convection similarity 2−78358
  atmospheric type boundary layers with large Reynolds number 2−43235
  axial, motion of vortex filament 2−60361
  axial compressors, secondary flows 2−53294
  axial flow compressor, subsonic, off design performance 2−53293
  axial flow turbomachines, annulus wall boundary layer development 2−77351
  axisymmetric hypersonic flow, subsonic and supersonic regions 2−60346
  axisymmetric jets and wakes, implicit finite difference soln. 2−60325
  baroclinic annulus waves at large Taylor numbers atmospheric applications 2−62093
  Be stars, envelopes, temporal variations of flow parameters 2−75711
  BGK Boltzmann equation, finite element analysis 2−58766
  bidimensional stationary, around obstacle, under gravity 2−50240
  binary gas mixtures, calculation of slip velocity 2−53273
  blunt body heat transfer, effects of slip 2−60359
  boundary layer stability for flow over porous surface 2−64377
  boundary layers, numerical computation 2−53266
  boundary value problem, variational soln. and error bound 2−77340
  buffet phenomena applic. of miniature pressure transducers 2−46827
  burner, flat-flame, motion of gases in open flame 2−58970
  capture area ratio effect on a propagating shock into a flowing duct 2−41835
  channel conductance estimation using optical analogue 2−53282
  Chapman Jouguet surface in multiheaded gaseous detonation 2−83648
  chemically reacting, over base 2−43240
  circular arc using profiles with critical asymptotic Mach number 2−60349
  circular compressible flow, extension of Miles- Howard theorem 2−77319
  behind circular cylinder in subcritical Reynolds number region, spanwise correl. meas. 2−71075
  clear air turbulence, generation by nonlinear waves 2−54831
  Coanda type, of three dimensional curved wall air jets issuing tangentially to wall surface 2−71083
  cocurrent gas-liquid flow in coil; pressure drop and void fraction meas. 2−83437
  compounding of transmission probabilities for composite systems 2−67578
  conbustible gas, propagation of blast waves 2−80380
  conductance, in molecular flow range, dynamic method of obs. 2−46817
  continuous induced-ionization meter 2−77348
  continuum flows due to kinetic effects 2−80403
  convective, self-preserving, energy deficiencies 2−44689
  coordinate perturbation and multiple scale techniques 2−50249
  corner of intersecting wedges at high Reynolds number 2−56410
  Couette flow of viscous fluid with particle injection, determ. of velocity and temp. distrib. 2−77225
  cross, laminar, turbulent plume growth and rise 2−67701
  cylinders, rough and smooth, obs. rel. to flow past a thunderstorm 2−62185
  detonation velocity in iso-atomic gas mixtures 2−83649
  behind detonation with lateral confinement 2−83652
  developing laminar and turbulent duct flow with chemical reactions 2−83658
  differential manometer gas flowmeter with automatic pressure and temp. correction 2−71079
  diffusers for centrifugal turbomachines, aerodynamic parameters 2−43243
  in diffusers for centrifugal turbomachines 2−80383
  diffusion flame in homologous turbulent shear flows 2−69786
  diffusion flames, turbulent mixing 2−77349
  discharge formation, initial boundary value problem 2−50227
  dissociating gas, asymptotic behaviour of the external fringes of compressible laminar boundary layers 2−67698
  dissociative, nonequilibrium flow, curved shocks 2−46821
  dissociative, three dimens., variation of flow quantities along streamlines 2−43236
  drop removal, design of rotary impaction filters with tapered filaments 2−43402
  dusty gas model, growth props. of solns. 2−83687
  dynamic and transport phenomena in two dimensional jet interaction flow field 2−46807
  dynamics, kinetic theory treatment 2−77365
  effusion of gaseous mixtures, application of failure-of-isotropy theory 2−77339
  effusion orifice transmission probabilities determ. as function of pressure for near ideal and right-circular cylindrical orifices 2−74464
  energy transfer in thermally developing and radiating gas 2−43229
  entrance region of cooled tube, heat transfer in v. high temp. flow 2−46818
  ethanol drops, homogeneous nucleation and growth in supersonic flow 2−80393
  external flow jet flap, trailing vortex wake downwind 2−80385
  field behind reflected shock, calc. by perturbation method 2−78933
  flow reactor for chem. vapour deposition props. rel. to gas flow pattern and mass transfer 2−83896
  flowfield meas. using total temperature probe at Mach numbers 2, 6 and 25 2−43234
  forced, effect on binary film condensation 2−77411

Flow continued
 gases continued
  forced, effect on film condensation of pure and binary vapours at forward stagnation point of horizontal cylinder 2−77410
  free-molecular stream, force moments det., photoelectric instrument 2−55725
  frictional heating and surface temp. due to flow over plate 2−64366
  galloping and vortex excitation of rectangular block in uniform flow 2−53316
  gas-dust medium, shock relaxation 2−46834
  gasdynamics eqns., exact solns. 2−46805
  heat transfer characteristics from inherent temperature perturbations 2−43238
  heat transfer of sphere with blow, effects on temp. field 2−77345
  heat transfer to laminar flow of non-grey gases through circular tube 2−43228
  heating of driven gas, in shock tube, high stagnation temperatures 2−56403
  heating/cooling channel perturbation dynamics in gas cooled reactor 2−59818
  heterogeneous, conjugate flow theory 2−67709
  high speed jets, turbulence, noise radiation 2−77350
  holographic visualization, single pulse technique 2−83694
  hot, temperature obs. using β-radiation 2−58966
  hypersonic, asymmetrical triangular plate with blunt edges 2−56414
  hypersonic, over flat plate 2−43239
  hypersonic, over flat plate at zero angle of incidence, beam continuum model 2−43231
  hypersonic, round body of rotation with injection from ring slot 2−56419
  hypersonic internal, numerical method for blunt leading edges and two blunt bodies 2−56407
  hypersonic model flow with strong shock waves, boundary layer method 2−83686
  hypersonic of ionized gas around blunt ended bodies and leading radiation 2−77347
  hypersonic past wedge, effects of upstream unsteadiness 2−74466
  hypersonic rarefied, over sharp slender cones drag, heat transfer and number flux measurements 2−74470
  hypersonic turbulent boundary layers structure 2−50247
  hypersonic unsteady compressible boundary layer depend. on Prandtl number 2−56416
  hypersonic wings, thin shock layer approx. applic. to non-conical shapes 2−64371
  hypersonic with massive blow in, asymptotic theory 2−77328
  impact tube method for meas. of period of thermal relaxation of vibration of polyatomic mols. 2−83398
  incompressible, bluntness of nose shape, effect on pitching moment of bodies of revolution 2−53325
  incompressible, mixing of cocurrent gas jets 2−74463
  incompressible potential, lift forces on plane aerofoil 2−53328
  incompressible thin wing flow, vortex lattice numerical solution, accuracy 2−53271
  injection through porous surface effects on turbulent boundary layer 2−74458
  inlet system, adjustable, for isotope mass spectrometer 2−74202
  instabilities in reaction zones of detonation waves 2−83646
  internal, determination by transient numerical technique 2−56406
  inviscid, boundary layers on axisymmetric bodies at small angles of attack 2−50243
  inviscid, in tube, displacement effects of laminary boundary layer developed within unsteady expansion and compression waves 2−46808
  inviscid hypersonic flow around cone at angles of attack 2−53296
  jet, high pressure, density distrib. obs. by laser induced gas breakdown 2−46823
  jet, turbulent, pot. core, entrainment region, intrinsic struct. 2−64237
  jet noise, theory using method of matched inner and outer expansions 2−77326
  jets, two-dimens., coalescing, vortex formation processes 2−67712
  kinetic energy spectrum of large scale atmospheric flow, power law 2−84844
  Knudsen, in a tube with arbitary gas-wall interaction 2−64372
  Knudsen cell results, calc. of flux gradients and effusive flow patterns 2−71068
  laminar, condensation of vapour with arbitrary pressure gradients 2−47042
  laminar, in molecular laser, calc. of temp. ranges 2−45715
  laminar, longitudinal, steady, electric arc 2−71055
  laminar, sphere drag in subsonic wind tunnel, sting free meas. 2−67719
  laminar, stationary processes in kinetic combustion 2−84635
  laminar, through rotating vertical cylinder, vel., friction loss, press. gradient 2−67714
  laminar, transitional and turbulent boundary-layer profiles on wedge at local Mach numbers 6.5 and 20 2−71103
  laminar boundary layer with continuous or local injection and variable wall temp., analytical soln. 2−83688
  laminar flow through orifice, two-dimens. 2−83671
  laminar in annulus of falling cylinder viscometer, effect of local drag on viscosity 2−46864
  laminar mixing of homogeneous gas streams with pressure gradient 2−53272
  laser Doppler velocimeter design for use in turbomachinery 2−46826
  laser technique, use of gasdynamic flows 2−73554
  lava pond surface heat and mass transfer, obs. 2−78249
  Laval type nozzles, non-symmetric flow 2−83684
  l.f. subsonic stream, convective heat transfer of sphere 2−53305
  linear gas/oil system, simultaneous unsteady flow through porous media 2−80389
  past liquid drops, deformation and mass loss, capillary surface wave mechanism 2−43303
  local skin friction evaluation 2−53299
  low speed wind tunnel, turbulent separated flow downstream of rearward-facing step, heat transfer 2−50242
  low velocity nonuniform flow, average pressure measurement, computer program 2−53268
  lubricants, three-dimensional, Reynolds differential equations 2−60336

Flow continued
gases continued
magnetogasdynamic, nonstationary uniform 2–67615
Martin-Ludford gas, expansion to vac. 2–80397
mass flow rate and mean density obs. in separated laminar boundary layers 2–46820
mechanism of blocking in stratified atmos. 2–67710
MHD, oscillatory flow of electrically conducting gas, numerical solution 2–46708
MHD, perfectly conducting fluid, multiplicity theorem 2–50173
MHD, subsonic, in annular channels with curvilinear walls 2–50176
MHD, transverse field effects on high temp. flow in channel with high thermal insulations 2–77258
mixing of different density jets, low initial turbulence level 2–56404
mixtures, influence of diffusion velocity 2–77333
modulation during leak detection 2–78710
molecular region, resistance concept in transmission probability 2–60344
motion about strongly heated bodies 2–77346
multidimensional, entropy and simple waves 2–60342
natural gas, industrial type, stabilization of diffusion flames 2–58967
near wake of a slender body, decay rate of boundary layer turbulence 2–56411
nearly free-molecular channel flow at finite pressure ratio 2–43237
non stationary in MHD channel with continuous electrodes 2–60201
non-equilibrium dissociative, curved shocks 2–46821
non-steady flow direction generation and obs. 2–46847
nonequilibrium, dissociative, variation of flow quantities along streamlines 2–43236
nonequilibrium condensation with gas flow in supersonic nozzles and jets 2–60331
nonequilibrium dissociating, laminar high speed mixing 2–83657
nonlinear panel response, turbulent boundary layer 2–71090
nonstationary, conducting, conduction MHD channel, numerical computation 2–60189
nonstationary unidimensional, velocity vector sign and modulus meas. 2–50241
nonuniform plug nozzle flowfields calc. for closed wake 2–60340
nonviscous, polyatomic, radial flow, N-dimensional travelling waves 2–56418
nozzle wall boundary layers, at high Mach numbers 2–71069
nozzles and channels of variable cross section, 3-dimens. subsonic and supersonic flow 2–74468
ogive-cylinder bodies at high angles of attack, side forces in transonic flow 2–64383
one-dimensional stationary, across normal shock wave, numerical soln. procedure 2–71078
optical anemometer, volumetric flow measurement 2–83512
optical thick radiating gas, past smooth boundary, asymptotic theory 2–53279
packed beds, axial heat transfer between 20 and 650C 2–45575
parallel-walled radial diffusor, flow analysis 2–53290
particulate damping in solid propellant rockets 2–44792
patterns during strong shock wave diffraction 2–83655
plane nonstationary, exact solution of equation 2–50250
pneumatic tube system for fast transport of sample in half-life electrons in millisecond region 2–79634
Poiseuille, through capillary tube, thermokinetic potentials, current-affinity relations, nonequilibrium thermodynamics 2–49031
polytropic, anisotropic non-steady flow 2–43101
porous layers, air resistance meas. 2–56405
pressure and temperature behind blunt bodies in supersonic flow with supply of inert and reacting gases to base region 2–60332
pressure distribution meas. on air foil at high subsonic speed in transonic wind tunnel 2–56431
pressure gradient effects on hypersonic turbulent skin friction 2–83662
propagation of cylindrical magnetogasdynamic shock in nongravitating system 2–53185
propane $+ 5O_2 + 10N_2$ mixtures, shock and detonation speeds 2–83647
propane-air mixture, turbulent flow, burning stability 2–67702
propellants, coaxial orifices, adjacent orifices 2–83676
pseudostationary, inviscid, unsteady, vortexline geometry 2–56413
pulsating, in pipes, numerical soln. 2–77344
pulsed ionization flowmeter, development 2–83696
quasi-biennial cycle of tropical stratosphere 2–84798
radial laminar flow between two coaxial discs 2–50260
radial symmetric motion and stationary regime of laser heated vapours 2–77343
radioisotope constant rate injection method and integrated pulse velocity method of velocity obs. 2–83697
rarefied, density distrib., electron-optical investigation methods 2–60343
rarefied, external, hydrodynamic equations derivation 2–46830
rarefied, external, low speed past circular cylinder 2–46831
rarefied, induced by thermal stress 2–53277
rarefied flow through slits 2–71082
rarefied gas, flow induced by thermal stress 2–56417
rarefied large scale from molecular jets effusing from perforated boundary 2–77335
rarefied slightly ionized supersonic, flow field diagnostics 2–50245
real gases, boundary-layer laminar flow on flat plate, local heat transfer 2–60369
rectangular block, flow patterns and aerodynamic characteristics 2–50262
rectangular cylinders, base press. and drag coeffs., Strouhal number 2–64364
rocket, nuclear, open cycle gaseous core, flow visualization studies 2–72932
S-shaped ducts, total press., static press., surface shear stress, yaw angle 2–71086
saturated, stably-stratified shear layer, stability 2–62169
saturated vapour, across porous horizontal plate with large suction, laminar film condensation 2–60552
second order stress in dense gas 2–71081
secondary injection ratio supersonic stream application to thrust vector control 2–60339

Flow continued
gases continued
secondary losses in axial turbine stages, reduction 2–53295
self preserving convective flow, energy deficiencies 2–44689
self-similar pattern arising from ionizing shock and detonation waves 2–45563
past semi-infinite flat plate, const. temp., optically thick case 2–64368
semiautomatic double jet polisher for thin foil prep. for t.e.m. 2–79105
in shallow fluidized beds, meas. of concentration profiles and mass transfer coeffs. 2–60330
shock heated gas outflowing into evacuated space, formation of jets 2–83654
shock wave, numerical calc., particle in cell method 2–49173
shock-induced flow in Ar, acceleration measurements 2–53297
slender cone at angle of attack, boundary layer separation 2–56409
slender wing in uniform stream, vortices over leading edge 2–77332
sonic, round wing profile, calc. 2–53300
sonic flow around wing profiles, numerical calculation 2–74476
sonic flow through multihole probes using multidimensional approximations to aerodynamic and thermodynamic values 2–53292
space vehicle entry simulation, arc-heated duct facilities for turbulent flow 2–66028
steady, aeroelastic instability of hot-wire filaments 2–80406
steam, condensation heat transfer under stratified flow conditions, empirical correlation 2–83670
stellar, winds and breezes, radial flow of inviscid heat conducting gas with gravitational effects 2–62527
straight suction duct with deflected inflow, momentum analysis 2–67700
stratified, over extended obstacles, application to topographical effect on vertical wind shear 2–62183
subsonic, about nonaxial symmetric bodies 2–53327
subsonic and supersonic boundary layer flow past wavy wall 2–56408
subsonic wind tunnels, displacement correction and limits of operation 2–67724
supersonic, over convex and concave shapes, with radiation and ablation effects 2–77337
supersonic free jet, diffusion of filament of injected gas 2–74457
supersonic gas flow, velocity measurement 2–77342
supersonic jets, incompletely expanded, form of boundaries 2–64388
supersonic turbulent boundary layer in adverse pressure gradient 2–46806
supersonic turbulent boundary layer in adverse pressure gradient, data analysis 2–56426
supersonic turbulent jet, aerodynamic study of two-stream propulsive systems 2–50256
swirling flow in long tubes, stability 2–83673
telemetry of respiratory air flow 2–85098
temp. meas. errors 2–69803
three-dimensional, perfect and compressible viscous 2–77322
three-dimensional stagnation point flows, heat and mass transfer from foreign gas injection 2–64370
thunderstorm weak echo regions, obs. using slowfall chaff 2–75565
tornado dynamics, obs. using lab. model 2–84809
tornado-like vortex, simulated, velocity field meas. using three-dimensional velocity probe 2–44712
torsion balance, effect on motion 2–72605
towed vehicle system in coordinated turn by towing vehicle 2–43245
trailing edge of oscillating airfoil 2–80382
transformations in gas- and magnetogas-dynamics 2–77259
transient flow field produced by secondary injection, numerical solution 2–43255
transient mass flow rate obs., device development 2–83695
transonic, aeroelasticity, trends and achievements 2–50254
transonic, steady, calc. using small disturbance theory 2–80402
transonic, two-dimensional and axisymmetric stability, nonlinear approximation of hyperbolic system near bicharacteristic curve 2–53283
transport through packed bed, dispersion model 2–43242
transverse, through graphite is high temperature gas-cooled reactors, effect on fission product movement 2–42642
tube vehicle systems, aerodynamic analysis 2–43246
tubular reactor for high temp. kinetic obs. 2–48318
turbulence, homogeneous, plane deform. 2–80390
turbulence degeneration in wake of square mesh grids in wind tunnel 2–74459
turbulence meas. using Laser Doppler Velocimeter system 2–71087
turbulent, complex and non-self-similar 2–77321
turbulent, hot wire anemometer corrections 2–64369
turbulent, hypersonic, construction of hot-wire anemometer 2–64373
turbulent, optical Doppler meas. of velocity 2–77236
turbulent, predictability 2–84795
turbulent, study of heat transfer properties, effect of gas physical properties variation 2–41851
turbulent air, meas., three component dynamic wind tunnel balance design 2–46829
turbulent air flow through concentric annuli 2–53280
turbulent boundary layer, separation influenced by blowing 2–46810
turbulent boundary layer response to step change in surface roughness, rough-to-smooth 2–50248
turbulent boundary layers, meas. of Reynolds shear stress fluctuations 2–64385
turbulent boundary layers, three-dimens., behind yawed separation bubbles 2–67699
turbulent cocurrent jets, isothermal and nonisothermal mixing 2–74462
turbulent compressible subsonic separated jet, numerical method of description 2–83674
turbulent flow in aircraft design 2–60353
turbulent free shear, errors in intermittency obs. 2–46811
turbulent mixing layer between streams of gases 2–80208
turbulent wake, asymmetrical, generated by pairs of cylinders 2–50246

Flow continued
gases continued
two component vortex flow studies of colloid core nuclear rocket 2−62414
two dimensional retarded cascade, cascade testing method 2−74473
two dimensional retarded cascade, contraction effect 2−74472
underexpanded exhaust plumes, flowfield interactions 2−43232
uniformly sheared free stream, influence on turbulent boundary layer 2−77353
unipolar, free flow, electric field distribution in phase plane 2−64365
unsteady, at branched duct junction, press. wave behaviour 2−67713
unsteady, through semi-finite porous medium, variational soln. of nonlinear boundary value problem 2−74465
unsteady anisentropic, study of rectilinear, cylindrical spherical-symmetric flows 2−67706
unsteady loadings caused by trailing edge control surface motions 2−71106
vapour jet, in cathode region of vacuum arc discharge 2−77309
velocity meas. from Doppler shift of spectral line 2−83690
velocity potential eqn. analysis 2−66417
vertical cylinder, laminar boundary layer, pure and simultaneous heat and mass transfer 2−53270
vibrational relaxation of anharmonic oscillators in nozzle flow 2−80142
viscous, through capillaries at large pressure differences 2−83672
viscous and heat conducting, self modelling motion during sudden liberation of energy 2−67705
viscous compressible, laminar, in shallow ducts of variable section 2−53289
viscous interaction over concave and convex surfaces at hypersonic speeds 2−77357
visualization at weak inhomogeneities, with holograph interferometer 2−64374
visualization by Raman effect 2−46824
volume flowmeter, gasdynamic method for calibrating 2−74467
vortex wake system, motion through stratified atmosphere 2−81670
wake density fluctuations meas. using pulsed laser holographic interferometer 2−46833
wedges and cones, hypersonic leading edge 2−83636
wind tunnel for subsonic periodically varying flow 2−56412
wind tunnel models design for aeroelastic studies in transonic flow 2−46838
wind tunnel wall interference reduction by streamwise porosity distrib. 2−46812
wind velocity obs. using pattern velocity computers 2−57968
Ar/He, transmission through activated C adsorbent 2−43242
Ar, partially ionized, heat transfer in laminar flow in pressure of transverse mag. field 2−53298
CO, CO-Ar, CO-N_2 gas mixtures, vibrational relaxation rate in nozzle flow 2−80142
CO, laminar flow with radiative interaction 2−43229
CO_2 and vibrationally excited N_2, high velocity mixing 2−83661
CO_2 electric discharge convection laser, electrical power deposition control 2−59152
CO_2 through stainless steel tubes, heat transfer 2−43228
H_2, O_2, Cl_2, photochemical initiation of combustion 2−84660
He, atmospheric arc, determ. of thermal conditions in asymptotic model using equilibrium flow model 2−77317
He, in bed of non-porous particles, one-dimensional dispersion model 2−60337
Hg, partially ionized, boundary layer growth in shock tube flow 2−64389
N rotational temp. in rarefied supersonic flow in glowing-discharge 2−60311
N_2, atmospheric arc, determ. of thermal conditions in asymptotic model using equilibrium flow model 2−77317
N_2, blunt body, effects of nonequilibrium dissociation 2−77361
N_2, outflow under 4-12 kbar press. through small aperture nozzle 2−74474
Ne-Kr, separation by ambipolar effusion, mass spectrometric obs. 2−74475
O_2, condensation in boundary layer 2−77354
O_2 blasts, industrial systems, compensation differential manometers 2−56415
SF_6, temp. profile around arc column 2−71049
liquids
see also Acoustic streaming; Double refraction/flow; Hydrodynamics; Superfluidity
absorption of gases of varying solubility in laminar gas and liquid flow 2−50290
alternative flow regimes in agitated vessels 2−53362
analytical flow nets in channel seepage 2−57825
annular, with rotating core, frictional resistance 2−83750
aquifer overlain by water table aquitard, numerical simulation of flow 2−78307
arterial branching in models using flow birefringence 2−66250
axial mixing in liquid-fluidized beds, correlations 2−67565
axial mixing in packed columns, effect of packing below flooding point 2−64412
axisymmetric rotating flow past circular disk 2−50291
p-azoxyanisole nematic liquid crystal in Poiseuille flow, apparent viscosity calc. by continuum theory 2−50337
biopolymer, flow dichroism spectra applic. to molec. studies, review 2−53089
blood, aortic disturbances, in vivo study 2−48842
blood, arterial velocity profiles, direct numerical calc. 2−48845
blood, characteristics in mild arterial stenosis 2−51882
blood, collateral, inaccuracy of retrograde flow and peripheral coronary pressure methods of obs. 2−48844
blood, control system to vascular bed of awake baboon, occlusion cuff system 2−85128
blood, dynamics at aortic bifurcation 2−48841
blood, evaluation in liver using dynamic scintigraphy 2−48884
blood, in arterial stenoses models, geometry influence 2−51904
blood, in arterials, effects of continuous obstruction 2−48848
blood, in renal vascular and tubular compartments, digital simulation 2−51903
blood, in small curved glass tubes 2−48849

Flow continued
liquids continued
blood, laminar, time dependent, effect of high molecular weight additive 2−48850
blood, n.m.r. flowmeter for pulsatile flow, analysis 2−81981
blood, optical technique for continuous monitoring of haemolysis 2−51883
blood, pulmonary, alveolar 2−51879
blood, pulsatile, in arteries, nonlinear anal. 2−82024
blood, regional organ flow, radioisotope technique, mathematical model 2−78637
blood, subendocardial distrib., effect of antianginal drugs 2−76061
blood, tumour, meas. by ^{133}Xe clearance rel. to capillary 2−62863
blood acceleration and peak velocity in aortic arch, transcutaneous meas. 2−48889
blood circulation, biomechanics, numerical studies 2−78644
blood in capillaries, analysis 2−48840
blood multichannel e.m. flowmeter telemetry system 2−82008
blood velocity profiles, real-time obs. using u.s. multigated pulsed Doppler velocimeter 2−69311
boundary currents in rot. β-plane water tunnel 2−53353
boundary layers, turbulent and laminar, development on circular cylinder, separation bubbles 2−80437
branched pipe flow, separation surface 2−53352
cabbeling instability under oceanic conditions 2−57919
cambered hydrofoil with jet flap, characteristics 2−67748
capillary-gravity waves, flow over wavy bottom 2−77374
carboxymethyl cellulose, water soln., laminar flow, heat transfer 2−74498
cavitation scheme application to flow over step 2−60391
cavity, unsteady, anal. using linearized free streamline theory within incompressible inviscid flow approx. 2−67759
centrifugal chamber, calc. taking into account boundary layers 2−71126
cetyltrimethylammmonium, bromide, velocity profile in turbulent pipe flow 2−53350
through circular orifice with central cylindrical pin with axis perpendicular to orifice plane 2−74504
circular tank with centrally located drain at flat bottom, unsteady axisymmetric flows 2−67757
cocurrent gas-liquid flow in coil; pressure drop and void fraction meas. 2−83437
coefficient of entrainment, of horizontal buoyant jet in calm ambient fluid 2−60400
column obs. using ^{24}Na labelled Na_2CO_3 solution 2−56456
compressible boundary layer eqns., Stewartson type, transformations 2−80194
concentric cylinder viscometer with curvilinear flow patterns 2−71166
through contractions, numerical model 2−77377
convection in electro-winning cell, decrease in mass-transfer rate obs. due to opposing flows 2−46868
convective, at bottom of system with axial mixer and radial baffles 2−83752
convective heat transfer in turbulent flow in pipe 2−60461
converging flat plates, flow between, numerical analysis 2−67777
core-annular, fluid mechanics 2−80439
core-annular, of two ideal liquids, hydrodynamic stability 2−64401
Couette, of viscoelastic fluid, stability 2−46871
crude oil, with high paraffin content at low temps., hydrodynamic resistance 2−83751
dense packing of drops in liquid-liquid spray column, hydrodynamic study, influence of viscosities of liquids 2−43280
density-stratified, channel flow about immersed bodies 2−46874
dielectrophoretic Poiseuille, overstability in thin annulus 2−64404
differentially-heated, in rot. annulus, time depend. general circulations 2−53354
disc and cylinder, viscometric flow, exp. 2−67754
disc and cylinder, viscometric flow 2−67753
displacement of liquid by a miscible liquid in a porous bed 2−53356
earthquake effect on pore-water pressure 2−78280
eccentric rotating cylinders, non-local effects in stability 2−67741
effect on axial mixing of liquid in bubble column 2−67762
elastico-viscous, free convective flow past infinite porous plate 2−46881
electrically conducting, rate obs., transducer 2−60384
electroconducting, unsteady laminar motion under transverse magnetic field 2−60194
electrolytes, in porous systems, subject to MHD pressure, kinetic phenomena 2−71132
electrolytes in porous systems, subject to MHD pressure, kinetic steady-state and transient phenomena 2−71133
erosion focuses, primary and secondary, structure of cavitation zones 2−60390
estuaries, partially stratified, mass transport mechanisms 2−51535
in evaporator tubes, stability, pressure drop in horizontal tubes 2−71123
film, entrance effect, finite difference numerical solutions to Navier-Stokes eqns. 2−67793
films, vertical falling, classification of flow regimes 2−74490
filtration in porous media, models 2−74499
fixed annulus, rel. to moving internal heat source 2−67819
flooding criteria for liquids with high density and high interfacial tension 2−50294
fluidized beds, study of axial dispersion 2−60387
glass, energy transport in cylindrical channels 2−56552
gravity current head, lower boundary effects 2−53344
groundwater systems, rel. to subsurface pollution 2−62005
groundwaters with free surface, equation of motion 2−72697
heart valves flow patterns, numerical solution of Navier-Stokes equations 2−85126
hemisphere on infinite plane, boundary layer growth 2−43283
horizontally oscillating liquid with beds of dense particles, study of transitions between flow regimes 2−83741
hydraulic measuring bridge, theory 2−45649
ideal, conductive, rel. to plasma streams 2−80339
immiscible drops, vaporization mechanism 2−83834
impinging circular jets, flow pattern 2−71146
incomplete wells, flow from free pools and captive pools in stratified rocks 2−44516

Flow continued
liquids continued
inhomogeneous turbulent, large eddies, calculation by extension of classical energy method for stability analysis 2—43286
isotropic turbulence generated by mechanically agitated grid, decay 2—60389
jet in rotating flows, velocity profile and flow characts. 2—53370
lake circulation around island, finite element investigation 2—74493
laminar, in conducting pipes under magnetic field, extremum principles 2—60203
laminar, in rotating cylinder cell, mass transfer 2—53346
laminar, incompressible, viscous, in a porous straight channel, temperature distribution 2—56458
laminar, Soret effect obs. 2—60454
laminar, stable, single gas mass transfer into sheared interface with and without chemical reaction 2—67749
laminar cross flow, turbulent plume growth and rise 2—67701
laminar elastico-viscous source, between parallel porous disks 2—50295
laminar falling films, mass transfer balance equations 2—71149
laminar free liquid film flow, theory and expt. 2—74497
laminar to turbulent transition, spheres transportation at very high Reynolds numbers 2—67750
laminar transient freezing in laminar tube-flow 2—83731
lava flows, dynamics and spreading distance 2—65435
lifting of liquids by withdrawal 2—43276
linear gas/oil system, simultaneous unsteady flow through porous media 2—80389
liquid mixture with temperature gradient, stability of laminar flow 2—67758
liquid-liquid co-current flow in a packing, statistical model for dispersed-phase axial mixing 2—67763
local natural convection mass transfer, electrochemical technique obs. 2—50288
low Reynolds number drag on sphere 2—67745
measurement of rapidly varying hydraulic flow rates by ultrasonic waves 2—46890
meltwater, in snow cover, flow measurement 2—75443
meniscus, vel. profiles for plate withdrawal, Navier-Stokes eqns. 2—60383
metal forming, upper bound approach for conical flows 2—46882
metals, e.m. flowmeters 2—83763
MHD, in region of discontinuity in conductivity of wall 2—53165
MHD, near time-varying accelerated plate 2—67611
MHD, stabilization by distributed feedback system 2—53163
MHD, thin film of conducting liquid in transverse magnetic field, wave flow regime 2—53162
model of topography effects, applic. to Antarctic Circumpolar Current 2—54783
muscle induced ejection flows, model 2—48832
1-naphthol, velocity profile in turbulent pipe flow 2—53350
nematic liquid crystals, optical method of obs. 2—71141
non-Newtonian, convective mass transfer in circular tube, velocity and concentration fields 2—46883
non-Newtonian flow, transport in fluids containing high molecular weight polymers 2—50289
nonequilibrium flow of weakly conducting liquid, near critical point in magnetic field 2—53164
ocean, transverse circulation, near coast, anal. 2—62034
ocean current meas. in passages of Lesser Antilles 2—65596
offshore tidal stream, residual flow 2—62037
oil slick spreading over water, dynamics 2—46866
open channel, turbulence, suspension wire-probe and hot film anemometer 2—77386
open water channel with slotted walls, self induced oscillations 2—80432
optical anemometer, volumetric flow measurement 2—83512
oscillatory, viscous damping 2—53349
poly sodium acrylate, shear stress and normal stress meas. on moderately concentrated solutions 2—60395
polyacrylamide aqueous soln., pulsation velocity in turbulent boundary layers 2—74491
polybutadienes, narrow distribution, flow rate through capillaries 2—60394
polydisperse polymers, undiluted, stress relaxation after steady-state shear flow 2—64482
polyethylene, molten, flow through parallel slit, flow birefringence obs. 2—71142
polyisobutylene in decaline, in concentric cylinders, rheo-optical analysis 2—56457
polyisoprenes, narrow distribution, flow rate through capillaries 2—60394
polymer chain elongational flow calc. of intrinsic birefringence 2—46870
polymer melts, non-isothermal flow in round tubes 2—83749
polymer melts, nonlinear thermodynamics 2—83748
polymer solutions, dilute, drag-reducing, degradation 2—53351
polymer solutions, dilute laser velocimeter obs. of Reynolds stress and turbulence 2—71128
polymer solutions, laminar and turbulent entry flow 2—46884
polymer solutions in curved pipe, det. of normal stress coefficients 2—60385
polymers, solutions and melts, review of recent non-linear viscoelasticity expts. 2—83364
polypropylene melt, end corrections in capillary flow with positive exit pressure 2—64408
polypropylene melt, mol. wt. dependence of capillary flow props. 2—46885
polystyrene, sheared, flow in capillaries, concept of molecular migration 2—50293
porous media of second type, circle theorem applic. 2—71130
properties rel. to fluidized beds 2—83502
pumping systems for use with flow calorimeters 2—83736
reacting liquid sprays, in-line holography 2—83755
rheoviscometer study of polymer solutions rel. to rheological properties and changes during two-phase separation 2—60392
river pattern variability, models 2—57821
rotating system, apparent field of gravity 2—50282
round spherical bubbles with internal circulations 2—83730
salt solution linearly stratified, laminar wake obs. 2—67751

Flow continued
liquids continued
seawater, direction, speed and temp. meas. using thermistor and laser techniques 2—54775
shear, energy exchange with internal waves of finite amplitude 2—43292
ship hydrodynamics, theoretical models, review 2—77379
ship resistance, Havelock-Oseen theory 2—77375
siphon type flow meter, discrete flows of liquid 2—56461
small disturbance stability of plane Poiseuille flow of viscoelastic Oldroyd fluid 2—50292
solutions, continuous neutron activation anal., optimal measuring conditions 2—72596
stability of liquid interfaces in porous media 2—71131
steady state turbulent flow of liquids with bubbles asymptotic theory applics. 2—43310
stirred tanks with turbine impeller, flow patterns 2—46867
stirring, applic. of theory of Markov's processes 2—83753
stirring with rotating agitator, radial component of vel. vector 2—60382
Stokes flow, material tensors symmetries for a particle 2—67743
in strata bordering on weakly permeable seams 2—60381
stratified water in duct, two dimensional sink flow 2—43281
streamflow hydrographs, derivation of base flow recession curves and parameters 2—51528
streamflow simulation, broken line process as potential model for hydrologic simulation 2—78314
streamflow simulation, Markovian models, fractional gaussian noise and crossing theory 2—78313
streamflow simulation, monthly, long memory, by broken line model 2—78311
streams, channel capacity as indication of mean flow and flood magnitudes 2—51529
streams, groundwater basin, finite difference model 2—51531
submerged orifices, regimes of bubbling and jetting 2—60399
about supercavitating lifting hydrofoils, second order results 2—46895
supercritical flow in curved channels, hydraulic model obs. 2—83747
surface profile above fully developed Poiseuille channel flow-undular bore 2—71145
surface waves, generated by submerged periodic point source, motion 2—53369
suspensions, turbulent, agglomeration rate/deposition rate relationship 2—43396
swirling flow vel. profiles, fluid resist. in duct, expt. 2—80197
telemetric obs. of local blood flow by heat conduction probes 2—82007
thermocapillary flows near hemispherical bubble on heated wall 2—50303
thin film flow on curved surfaces, application to determ. downstream boundary condition for flow on flat plate 2—43308
thin films, stability on rotating horizontal disc 2—43309
thin films, thickness measurement, electrical contact method, hysteresis, statistical profile 2—83733
three dimensional disturbances in boundary layer along concave wall 2—74495
transient seepage of ground water with free surface studied by finite element method 2—53359
tube flow, vel. profiles 2—64407
in tube systems with H-flow, flow distribution, thermal inequalities 2—71124
turbopump inducers for rocket engines, internal streamliner flow analysis 2—43288
turbulent, in pipe, separation of binary mixtures by freezing 2—46878
turbulent, in rotating cylinder cell, mass transfer 2—53347
turbulent boundary layers, time scales and correlations 2—64403
turbulent motion in liquid-filled precessing spherical cavity, rigid body approximations 2—46892
turbulent optical Doppler meas. of velocity 2—77236
turbulent shear, burst rates 2—77384
turbulent wake, large scale instabilities 2—67771
two-dimensional unsteady, forced heat transfer from hot film 2—80431
unconfined aquifer, unsteady radial flow 2—78309
unconfined aquifers, flow theory considering delayed response of water table, model 2—78234
unsteady, axisymmetric, draining from circular tank 2—77380
unsteady, in pipes, review of calc. by numerical methods 2—67752
unsteady, open channel, parameter identification 2—77382
u.s. Doppler blood flowmeter, theory 2—85092
vapour bubble, thermal equilibrium, effects of liquid motion induced by condensation and evaporation 2—77399
velocity determ. by neutron activation anal. 2—83518
viscoelastic, between 2 circular cylinders under periodic pressure gradient 2—53365
viscoelastic, in pipes, turbulent, theory of heat transfer 2—46877
viscoelastic, linear stability of plane Poiseuille flow 2—67755
viscoelastic, nonlinear stability of plane Poiseuille flow 2—67756
viscoelastic, through abrupt contraction, rheological props. 2—64406
viscous, down inclined plane, similarity soln., rel. to boundary currents in ocean 2—57910
viscous, impulsive flow past semi-infinite flat plate, boundary layer equations 2—46873
viscous, in ducts, drag rel. to pressure grad. 2—43282
viscous, of suspension of drops in cylindrical tube 2—64419
viscous, photoviscosity and double exposure bubble techniques 2—60393
viscous, slow flow down wavy inclined plane 2—60380
viscous fluid motion past impulsively started semi-infinite flat plate, numerical soln. 2—83459
viscous liquid flow on rotating disk, atomization effects 2—74509
viscous sublayer effect of drag-reducing polymers on turbulence 2—46880
water; effect of polymer additions on turbulent friction 2—53361
water, bounded turbulent jet, mean flow properties 2—77396
water, in pipe, under influence of Coriolis forces 2—74496
water, laminar, mixed convection 2—53343
water, mass transfer of 2-naphthol particles 2—71129

Flow continued
- **liquids** continued
  - water, nonsteady flow at high speeds 2–77371
  - water, nonuniform, in rivers and estuaries, longit. dispersion 2–67747
  - water, parameters meas. in tank reactor 2–42681
  - water, Schlieren obs. of laminar boundary layer separation 2–67760
  - water, temp. distribution of viscous gravity flow in horizontal pipes 2–64402
  - water, transit time methods in underground hydrology 2–46887
  - water, turbulent free jet flow, amplitude modulation of ultrasound 2–74494
  - water, turbulent velocity fluctuation meas. using cell flowmeter based on variation of electrical resistance 2–71137
  - water, wave-induced mean flow, interaction between surface waves and currents 2–83726
  - water and solute, in extracellular channels with filtration, osmosis and active transport 2–46879
  - water containing bubbles, convective heat transver enhancement 2–60464
  - water flow velocity meas. using H_2 bubble apparatus 2–71135
  - water through heterogeneous and anisotropic saturated porous media 2–84714
  - water-Freon 113 system, stratified flow with simultaneous interfacial boiling, direct contact heat transfer 2–50285
  - wavy, of thin films 2–53381
  - weirs and flumes, flow measurement 2–83756
  - Al-Cu alloy solidification, two-dimensional flow of liquid with liquid solid region considered as porous medium 2–47038
  - H_2O periodic cortex formation in rear of fixed plate, comparison with solution of Navier-Stokes equation 2–53348
  - He II, critical flow through holes 2–47020
  - He II, laminar and turbulent flow 2–47017
  - He II, liquid, superfluid, thermohydrodynamic conditions at peak flux of horizontal heaters 2–67859
  - He II, torque on Rayleigh disc 2–53478
  - He II film flow, thermally driven, 1.7-2.1 K, dissipation 2–67862
  - He II films, non-pot. flow at sub-crit. vels. 2–47022
  - HeII, counter flow, onset of turbulence 2–43420
  - ^{4}He, thermally driven superfluid film, saturation of fluctuation dissipation in flow 2–80507
  - ^{4}He adsorbed on graphite 2–74575
  - Hg, MHD unsteady free convection flow past infinite vertical plate, variable suction 2–83526
  - Hg, rapid mean flow in annular channel produced by moving heat source 2–53355
  - Hg in tube, temp. fluctuation spectra 2–64413
  - Na corrosion deposits in reactor cooling systems, effect on heat transfer coeffs. 2–83117
  - Na liquid cooling problems of fast breeder reactor 2–52843
- **two-phase**
  - — 2–71280
  - — 2–67786
  - absorption and rectification in rotary film columns, mass transfer 2–83494
  - aerosols, mass transfer with radial axial diffusion in laminar flow in narrow rectangular channel 2–53269
  - air entrained water flows, under reduced ambient pressure 2–77404
  - air-water, horizontal, pressure as stochastic parameter 2–43096
  - air-water, in simulated rod bundle geometries, turbulent mixing rates, meas. 2–53120
  - air-water cocurrent flow on flat plate, enhancement of heat transfer by waves 2–56494
  - air-water mixture in two-dimensional diffuser, pressure recovery performance 2–46910
  - alkali metals, temp. inversion with boiling in tubes 2–64514
  - annular, two-component, heat and mass transfer at wave roughened gas-liquid interface 2–77409
  - annular-mist condensing, interfacial shear stress 2–53288
  - asymptotic theory, steady state turbulent flow of liquids with bubbles 2–43310
  - axial mixing of liquid in bubble column, effect of liquid flow 2–67762
  - baroclinic instability, laboratory study 2–53113
  - beds of dense particles in horizontally oscillating liquid, transitions between flow regimes 2–83741
  - bentonite-water suspensions, flow behaviour for time-dependent non-Newtonian fluid 2–60159
  - bimodal drop distrib., detonations 2–80489
  - binary film condensation, effect of forced flow down vertical plate 2–77411
  - bubble column cascade reactor, unidirectional flow of gas and liquid 2–67783
  - bubbles, in fluidized beds, slug flow regime 2–77401
  - bubbles in liquids, conjugate flow theory appl. 2–67709
  - bubbly, turbulence characteristics 2–80440
  - bubbly liquids, one-dimensional flow, dynamic props. 2–80436
  - classification rel. to matter props. 2–70849
  - clay-H_2O suspensions, flow behaviour 2–83816
  - coaxial high temperature jet radiation with Ti dispersive particles, energy loss 2–80497
  - cocurrent gas-liquid flow in coil; pressure drop and void fraction meas. 2–83437
  - colloidal dispersions, viscoplastic deposit formation in turbulent pipe flow 2–83826
  - colloids, gravitational deposition from laminar channel flow 2–83814
  - condensation heat transfer im horizontal tubes, prediction of mean Nusselt number 2–83444
  - condensation heat transfer under one-component stratified flow conditions, empirical correlation 2–83670
  - core-annular, of two ideal liquids, hydrodynamic stability 2–64401
  - correlations for void fraction and pressure drop 2–83438
  - Couette flow of viscous fluid with particle injection, determ. of velocity and temp. distrib. 2–77225
  - crossed electric and magnetic field effects on motion in MHD separator 2–60190
  - dense packing of drops in liquid-liquid spray column, hydrodynamic study, influence of viscosities of liquids 2–43280
  - density-wave oscillations, fundamental and higher mode 2–53286

Flow continued
- **two-phase** continued
  - diffusive, gas into porous material 2–80394
  - dispersion phenomena through porous media, using random mode model 2–56459
  - displacement of liquid by a miscible liquid in a porous bed 2–53356
  - droplet entrainment, det. of velocity of inception 2–60405
  - dusty gas, flow past body 2–53278
  - electrolytes, in porous systems, subject to MHD pressure, kinetic phenomena 2–71132
  - electrolytes in porous systems, subject to MHD pressure, kinetic steady-state and transient phenomena 2–71133
  - emulsions, droplet-size distribution effect 2–50388
  - film condensation of binary vapours 2–77410
  - fluid, flow over porous flat plate in transverse mag. field, Hall current effects 2–46704
  - fluid and gas bubbles, mutually migrating mixture 2–67785
  - fluid pore pressure, changes induced by earthquakes, after shock 2–44521
  - fluidization, bottom restrained countercurrent, of binary particle mixtures 2–80193
  - fluidized bed, solids motion caused by a bubble 2–80191
  - fluidized bed, three phase, caused by size distribution of gas bubbles 2–80192
  - fluidized beds, liquid, mixing processes 2–80189
  - fluidized beds, properties rel. to liquids 2–83502
  - fluidized beds, rheological props. and particle number densities 2–83501
  - friction in gas saturated liquid, turbulent boundary layers 2–53375
  - fuel element heating channel, meas. of local void fraction at high pressure 2–49907
  - gas distributors design, and prediction of bubble size in large gas-solids fluidized beds 2–80186
  - gas in shallow fluidized beds, meas. of concentration profiles and mass transfer coeffs. 2–60330
  - gas jet impinging on free liquid, interfacial stability, taking into account surface tension 2–56299
  - gas liquid, heat transfer, pressure drop for 2–70845
  - gas transfer from bubbles in fluidized bed to dense phase 2–80163
  - gas-liquid, annular, in vertical tubes, residence times in liquid 2–53345
  - gas-liquid, breakup of liquid droplet columns by shock waves 2–83806
  - gas-liquid, breakup of liquid jets and drops 2–60335
  - gas-liquid, concurrent, sampling error in mass transfer, calc. 2–53121
  - gas-liquid, laminar in horizontal channel, absorption of different solubility gases 2–50290
  - gas-liquid, obs. of voidage and slip distribution 2–43094
  - gas-liquid, tangential stresses on wall of vertical tube in electrolytic cell 2–64425
  - gas-liquid, without interphase slip or mass transfer 2–43095
  - gas-liquid droplet system, model for shock wave propag. 2–83656
  - gas-non-Newtonian, without mass transfer, model 2–50251
  - gas-solid, vortex dust removal apparatus, velocity field obs. 2–60334
  - gas-solid fluidized bed, exptl. technique for solid flow behaviour 2–60160
  - gas-solid suspension, particle vel. profiles, air vel. profiles, local particle flux profiles 2–67711
  - gas-solids suspensions, turbulent pipe flow, particle slip velocity 2–53284
  - gas/liquid, flow pattern in multistage vibrating disk contactor 2–67564
  - gases in granular media at low pressures, grain size matching that found at Apollo 12 landing site 2–56420
  - granular solid, velocity distrib. in gravity flow in inclined open channel 2–74338
  - granular solid in gas, pneumatic transport through pipes 2–77338
  - gravity current head, lower boundary effects 2–53344
  - groundwater, in inhomogeneous aquifer, groundwater head 2–67768
  - groundwater flow, transient, finite element method soln. 2–67769
  - growth of spherical bubble controlled by heat diffusion, approximate soln. including convective flow 2–83729
  - heat transfer, conference (Lucas Heights, Australia Aug. 1971) 2–43077
  - heat transfer in gas fluidized bed, limiting factors 2–80190
  - homodyne microwave radar technique for flow meas. 2–60158
  - horizontal, pressure as stochastic parameter 2–43096
  - hydrodynamic dispersion in porous media, apparatus induced dispersion 2–67767
  - hydrology, ρ_1 estimation from small sample 2–67766
  - immiscible drops in liquid vaporization mechanism 2–83834
  - immiscible fluids, first boundary value problem for one dimensional filtration 2–60388
  - incompressible fluid through tubes with porous walls 2–43076
  - infinite, plane, porous wall, viscoelastic fluid with time-dependent suction 2–50160
  - interfacial stability, taking into account surface tension 2–56299
  - jet, homogeneous free, turbulence characteristics meas., investigation of the peculiarities of the heat diffusion method 2–80196
  - jet, turbulence intensity 2–46995
  - Knudsen cell orifices, conical, divergent particulate fluxes, computer simulation 2–50136
  - laminar, airborne particles, diffusional separation 2–80496
  - laminar, between parallel porous plates, thermal and combined entry problems 2–53139
  - laminar boundary layer, over flat plate, Karman- Pohlhausen approx. 2–46822
  - linear gas/oil system, simultaneous unsteady flow through porous media 2–80389
  - liquid dispersions, exhibiting slip effect, peculiarities 2–83820
  - liquid through porous media, soil physics, theoretical mechanics 2–77383
  - liquid-air ejector system system, horizontal, momentum transfer 2–67781
  - liquid-fluidized beds, correlation for axial mixing 2–67565
  - Lockhart and Martinelli flow model, calculation of pressure drop and hold up 2–56455

Flow continued
- **two-phase** continued
  - Marangoni convection at liquid-liquid interface, effect of heats of solution 2—77381
  - mass transport in porous media, nonlinear multidimens. problems, method of homogeneous zones 2—46888
  - MHD, between concentric rotating porous cylinders, soln. of eqns. 2—56320
  - mixing, influence of feedpoint location and viscosity on mixing time 2—83493
  - moisture transfer in porous elastic solids, stress development 2—46889
  - monodisperse spray deflagration, burning velocity distrib. 2—84619
  - 2-naphthol particles, mass transfer to flowing water 2—71129
  - Newtonian and non-Newtonian liquids in spray 2—83500
  - non-Newtonian suspensions in water, rheological model 2—83823
  - nuclear reactor coolants, hydrodynamics, neutron fluctuations 2—76936
  - oil and water simultaneous flow through cracked porous medium of small inclination, finger-imbibition phenomenon 2—53358
  - packed beds, non-uniform porosity causing flow maldistribution 2—46665
  - particle ejection and entrainment from gas-fluidized beds 2—77177
  - particle motion behind oblique shock in two-phase supersonic flow past a wedge 2—60145
  - particle paths in curvilinear flow, numerical results for industrial processes 2—74323
  - particle size and size distribution effect on the behaviour of gas-fluidized beds 2—80187
  - particle trajectories with spherical particles 2—80169
  - particle velocity det. using optical methods 2—60165
  - pattern at wall of fluidization column induced by single bubbles 2—80188
  - percolation of fluid through porous dam, numerical treatment of singularity in free boundary problem 2—83469
  - pitot pressure interpretation, dynamics of small droplets near mouth of tube 2—50141
  - pointed bubbles in viscous fluid, slow flow 2—80494
  - porous media, hydraulic conductivity, pore struct. modelling 2—67765
  - porous medium, fluid-filled, nonequilib. thermodynamics 2—50137
  - porous medium containing filtering fluid, equations of behaviour, using thermodynamics principles 2—50286
  - porous partitions, capillary osmosis 2—46902
  - porous visco-elastic plastic media, filtration of nonlinear viscous liquids 2—53357
  - post dry-out heat transfer, influence of curvature of tube 2—77223
  - pressure wave velocity calc. 2—67604
  - Rayleigh-Taylor instability, effects of heat and mass transfer 2—46687
  - rheoviscometer study of polymer solutions rel. to rheological properties and changes during two-phase separation 2—60392
  - Rivlin-Ericlsen dust fluid, unsteady flow through circular cylinder 2—83808
  - rotating bubble bed, hydrodynamics 2—83498
  - saturated vapour flow, heat exchangers, tube bundles, void fraction 2—82247
  - simple fluid, steady Couette flow between porous plates 2—67585
  - soil, inhomogeneous, anisotropic, Darcy's law, tensor form transform. 2—67770
  - solid-gas, non-Newtonian flow under laminar conditions 2—83821
  - solid-gas, reactive nozzle flow 2—83660
  - solids weighing, in hydrotransportline 2—46700
  - spheroidal gas bubble rising in water, effect of periodic nature of drag, vortex structure 2—80425
  - spout diameter prediction in a spouted bed 2—77176
  - stability of liquid interfaces in porous media 2—71131
  - steady, in porous media with several cavities, anal. 2—43073
  - steady velocity field, motion of small particle 2—43397
  - steam and water, discharged from geothermal ground, physical properties 2—78247
  - steam-air system, aerosol transport in naturally convected boundary layers 2—67786
  - stock flow of fibre suspensions 2—77220
  - Stokes flow in and around fluid sphere in presence of another sphere or plane boundary 2—80164
  - structural and hydrodynamic characteristics of flow past bodies in fluidized media 2—74339
  - structure and mixing length theory 2—43092
  - submerged orifices, regimes of bubbling and jetting 2—60399
  - suspension, instability, discontinuous and dilatant viscosity behaviour 2—64245
  - suspension of drops in cylindrical tube 2—64419
  - suspension of particles, convective diffusion for case of Stokes flow of fluid 2—64481
  - suspension of solids in non-Newtonian liquids, viscosity 2—83822
  - suspension of variable concentration, unsteady flow 2—77452
  - suspensions, rigid dumbbell, hydrodynamic interaction effects 2—67738
  - system with drag-reducing polymer solns. 2—83424
  - transient, gas in porous column, model anal. 2—53276
  - transient in boiling channel, finite difference scheme 2—59838
  - transient seepage of ground water with free surface studied by finite element method 2—53359
  - transport of solid particles by turbulent flows 2—74329
  - turbulence meas. in hydraulic jump 2—64235
  - turbulent, liquid droplet evaporation, impurities effect 2—71279
  - turbulent, of liquids with bubbling, method of limited expansions 2—56462
  - turbulent, transverse migration of suspended particles 2—74571
  - turbulent wall jet interaction with shear flow, mixing flow 2—83482
  - two component, horizontal and vertical, surface friction obs. 2—43093
  - two dimensional fluidized bed, bubble formation 2—77403
  - two-component critical flow in a venturi 2—46825
  - two-dimensional, in tube with permeable and deformable wall 2—43284

Flow continued
- **two-phase** continued
  - unsteady, oscillatory, generation by interaction of liquid jet and free liquid surface 2—43285
  - unsteady gas flow through semi-infinite porous medium, variational soln. of nonlinear boundary value problem 2—74465
  - velocity distribution and pressure drop characteristics det. using Prandtl mixing length concepts 2—43091
  - vertical, one-dimensional theory for predicting average hold-up 2—67606
  - viscoplastic inhomogeneous fluid, in porous media anal. in horiz. plane 2—46886
  - vortex flow studies of colloid core nuclear rocket 2—62414
  - water containing bubbles, convective heat transver enhancement 2—60464
  - water flow velocity meas. using tracer of H_2 bubbles 2—71135
  - water table aquifer, two-dimens., Boussinesq eqn., computer simulation 2—67764
  - watershed subsurface response, surface runoff rel. to subsurface flow, base flow contribs. 2—67761
  - wet vapour, in relaxation zone behind front of shock wave, parameters and structure 2—60407
  - Al-Cu alloy solidification, two-dimensional flow of liquid with liquid solid region considered as porous medium 2—47038
  - B particle nonequilibrium effects, air augmented combusting ducted flows 2—70836
  - Hg and N_2 or He in packed bed system, criteria for flooding in counter-current flow 2—50294

Flow birefringence *see Double refraction/flow*

Flowmeters
- *see also Anemometers*
- blood, hepatic flow measurement, removal efficiency of dyes 2—58607
- blood, review of technique and instruments 2—78645
- cell, for turbulent velocity fluctuation meas. in water, based on variation in electrical resistance 2—71137
- clamplon for obs. in hydraulic lines 2—46699
- conference, Harwell, England (1971) 2—83508
- continuous flow autoanalyser, single or dual channel 2—83466
- correlation methods for flow speed meas. 2—77230
- current industrial practice, review 2—83509
- for deposition of water drops on steam turbine blades, flow rate determined by electrical resistance measurement 2—46891
- differential manometer gas flowmeter with automatic pressure and temp. correction 2—71079
- differential pressure, linear response 2—83759
- Doppler u.s., vol. blood flow meas. 2—51901
- electrical pulse generation type, patent 2—70858
- electrically conducting liquids, transducer 2—60384
- e.m., developments and appls. 2—83521
- e.m. for liquid metals 2—83763
- e.m. multichannel telemetry system for blood flow 2—82008
- e.m. water-current velocity meter, oceanographic applications 2—71138
- float-area-type, characteristics for turbulent region 2—71134
- fluid velocity meas., using acoustic wave transducers, patent 2—83480
- flumes, for liquids, general introduction 2—74500
- free piston circumfluent flow gauge, parameters 2—46681
- free precession of magnetization in moving liquid and application to flowmetering 2—74502
- gas, continuous induced-ionization meter 2—77348
- gas, transient mass flow rate obs., development 2—83695
- gases, using nonstandard diaphragms, adsorption pilot equipment 2—43227
- homodyne microwave radar technique for flow meas. 2—60158
- hydraulic measuring bridge, theory 2—45649
- induction, principle of operation, general properties and applications 2—64409
- industrial development in techniques and applications 2—64410
- industrial flow meas. and control, review 2—80158
- input edge of diaphragm, obs. of change of sharpness during use 2—77231
- laser Doppler velocimeter, instantaneous turbulence velocity measurement 2—43230
- level signalling device, using transformer transducer 2—56460
- mass, with elastically coupled vanes, parameters of transducers 2—56396
- mass flow meas. device 2—70850
- mass meas. of flowing liquids and gases, electronic apparatus 2—77341
- measurement principles and techniques 2—64411
- MHD flows, laser Doppler velocimeter, obs. 2—80217
- multiple gate pulse Doppler flowmeter for spatial velocity profiles in blood vessels 2—51934
- multiple-venturi system, application to design of flow-rate meter 2—46685
- nonisothermal flows, simultaneous measurement of temperature and velocity 2—74337
- nuclear reactor coolant, flow vel. fluctuations 2—76918
- ocean current velocity meas. with BPV type current recorders, dispersion 2—62054
- one path ultrasonic fluid flowmeter using electroacoustic feedback 2—55549
- optical Doppler meas. of velocity of turbulent fluids 2—77236
- pitot traverses, accuracy of air flowrate measurements, comparison with orifice plates 2—74471
- Pitot-tubes, anomalous indications in solid particle suspensions and polymer solns. 2—53360
- pressure difference, nonNewtonian fluids 2—83516
- primary elements with non-constant area of flowpath 2—83473
- pulsatile flow simulator design and applics. 2—51900
- pulsed gas ionization, development 2—83696
- quadrant-edged orifice plate, for low Reynolds Number flow with viscosity as factor 2—74501
- siphon type, discrete flows of liquid 2—56461
- for solids 2—56302
- standard orifice plates, determination of edge sharpness using silicone rubber impressions 2—60140
- thermal, operating from pulsed heat injection source 2—66640

Flowmeters continued
- thermoelectric, rapid response and small sensor size 2−83758
- turbine, flow characteristics 2−83519
- turbine-type, tip clearance loss obs. 2−83520
- u.s., and applic. 2−76370
- u.s., meas. of variations in circulation 2−71136
- u.s. Doppler blood flowmeter, theory 2−85092
- u.s. meter for water flow measurement 2−64242
- vacuum gauge calibration system 2−76129
- variable orifice, in anaesthetic machines, prevention of inaccuracies due to electrostatic charges 2−69281
- volume, gasdynamic method for calibrating 2−74467
- vortex rate sensors, theoretical analysis of angular momentum conservation and signal transmission 2−60327
- water, slow rates, automatic device 2−50296
- water flow velocity meas. using H_2 bubble apparatus 2−71135
- weirs and flumes, generalized flow equation 2−83756
- O_2 blasts, industrial systems, compensation differential manometers 2−56415

Fluctuations
- *see also Brownian motion; Random processes*
- concentration, spectral density, disperse systems random field 2−83810
- constant pressure systems, fluctuations of thermodynamic variables 2−45570
- cooperative processes, correlated fluctuations in equil. and steady-state systems 2−78841
- disperse systems concentration, correlation theory, local disturbance 2−83811
- fluctuation-dissipation theorems, review 2−58793
- fluctuation-regression hypothesis for one-dimensional system of hard rods under gravitational potential 2−69621
- fluidised beds, liquid solid, local porosity fluctuations, study by elec. conductance meas. 2−77178
- frequency modulation of laser by fluctuations in chemical reaction 2−41977
- gas lasers, intensity fluctuation meas. threshold oscillations 2−63320
- hard-sphere gas, thermal fluctuations 2−76224
- head, in turbulent flows 2−70854
- higher order moment functions 2−78846
- horizontal wind, vertical longitudinal shear fluctuations, probability distribution, stochastic process, mean wind profile, aerospace vehicles 2−83465
- isolated systems, fluctuations of thermodynamic variables 2−45570
- Kirchhoff-Fresnel diffraction in turbulent atmosphere 2−45791
- Langevin eqn. in a non-linear system 2−78850
- laser beam propagated in turbulent atmosphere 2−57995
- light beam in turbulent atmosphere, mean illumination and intensity 2−49413
- multiplicative stochastic processes, dissipative behaviour 2−58773
- Onsager systems, linear phenomenological fluctuation 2−49037
- optical field, coherence and fluctuation props. 2−82463
- plasma, diagnostics using digital spectral analysis 2−70926
- randomized e.m. fields, autocorrelation and spectrum of intensity fluctuations 2−41870
- submillimeter waves in turbulent atmosphere 2−51629
- system with internal degrees of freedom, relaxation matrix 2−45304
- thermal radiation, energy fluctuations formulae derivation 2−58816
- turbulent flows, mean period of fluctuations near wall 2−83425
- ultrashort pulse generation by laser with saturable absorber 2−73545
- viscous compress. flow, electrically and thermally conducting, weak fluctuation modes in homogeneous mag. field 2−53153
- voltage, in resistor, Nyquists theorem and its generalizations 2−45630
- He II, rel. to a.c. Josephson effect 2−64499
- p-InSb:Ge, electrical instability in presence of elec. field 2−71884
- Sc_3In, itinerant ferromagnet, theory of magnetic fluctuations 2−65157

Fluctuons *see Quasi-particles*

Fluid flow *see Flow*

Fluid mechanics *see Hydrodynamics*

Fluidized beds
- axial mixing in liquid-fluidized beds, correlations 2−67565
- binary particle mixtures, bottom restrained countercurrent fluidization 2−80193
- capacitance probes, appl. in gas beds 2−50906
- dense particles in horizontally oscillating liquid, transitions between flow regimes 2−83741
- dielectric particle charging in vibrofluidized bed 2−53110
- dispersion, axial, determ. 2−60387
- electrostatic charge, data on how charge may be lowered 2−50134
- flow velocity and space fraction, correlation 2−43401
- freely bubbling, gas distrib. between bubble and suspension phase and spatial bubble distrib. 2−83503
- gas, density fluctuations detected by microwave beam 2−83505
- gas bubble, slug flow regime 2−77401
- gas bubbles, size distribution, leaving a three phase fluidized bed 2−80192
- gas distributors design, and prediction of bubble size 2−80186
- gas fluidization of large spherical particles 2−67569
- gas transfer from bubbles to dense phase 2−80163
- gas-solid, behaviour of bubbles, theory for initial bubble formation 2−50145
- gas-solid, exptl. technique for solid flow behaviour 2−60160
- gas/liquid interface, transfer of oxygen 2−67547
- glass beads, horiz. vel., stat. meas. using piezoelec. prop. 2−43883
- rel. to glossy sphere production from particles, by processing through plasma stream 2−56971
- heat transfer from horizontal tube in presence of unheated tubes 2−45572
- heat transfer in a high temp. bed 2−60120
- heat transfer in gas fluidized bed, limiting factors 2−80190
- heat transfer in semifluidized beds, glass and Al spheres in water, obs. 2−60130
- heat transfer to immersed objects 2−83506
- hydrodynamics and rectification kinetics in column 2−83496
- instability, discrete particle contributions 2−56283
- kinetics, appl. to theory of Markov random processes 2−83499

Fluidized beds continued
- liquid solid, local porosity fluctuations, study by elec. conductance meas. 2−77178
- mixing processes in liquid fluidized beds 2−80189
- packed small dia., mass transfer from wall to fluid 2−83436
- particle ejection and entrainment 2−77177
- particle size and size distribution effect on the behaviour of gas-fluidized beds 2−80187
- particulate, fluid mixing, hydrodynamic mathematical model 2−67567
- percolation of fluid through porous dam, numerical treatment of singularity in free boundary problem 2−83469
- properties rel. to liquids 2−83502
- random particulate bed, local flows 2−83435
- residence time distribution study 2−60386
- rheological props. and particle number densities 2−83501
- shallow, gaseous flow, meas. of concentration profiles and mass transfer coeffs. 2−60330
- solid flow pattern at wall of fluidization column induced by single bubbles 2−80188
- solids motion caused by a bubble 2−80191
- spout diameter prediction in a spouted bed 2−77176
- thermal fatigue resistance of metals using fluidized beds 2−56877
- two dimensional, bubble formation 2−77403
- two dimensional, high speed photographic obs. 2−83504
- wetted spherical particles, mass transfer 2−83497
- NbC_x, production in fluidized layer 2−68168

Fluidized powders *see Flow; Fluids; Powders*

Fluids
- *see also Fluidized beds; Gases; Liquids; Non-Newtonian fluids*
- — 2−67549
- — 2−66478
- aerospace sciences progress, theory and experimental techniques, book 2−81748
- binary mixture, asymptotic behaviour of Green Kubo integrands 2−74308
- Born-Green theory, inclusion of triplet potentials 2−70823
- Boussinesq, nonlinear motions induced by moving thermal waves 2−56301
- Boussinesq. perfectly conducting, propagation in stratified perfectly conducting flow with mag. field 2−60195
- buoyancy-surface tension instability due to internal heat source 2−64248
- Burgers eqn. one-dimensional, table of solns. 2−77179
- cavitation, book 2−71140
- cavitation damage, in rotating disc 2−77390
- circular fluid transmission line, semi-infinite, step response, time domain solution 2−67592
- classical, diffusive and collective motion 2−74314
- classical, in critical region, effect of rotation on number density 2−46658
- classical, optimized cluster expansion, application to molecular liquids 2−67554
- classical, optimized cluster expansions, variational formulation of mean spherical model and hard sphere Percus-Yevick eqns. 2−67553
- classical, perturbation theory for repulsive forces 2−43044
- cnoidal waves, generated by moving pressure field 2−67610
- cocurrent oblique crossflow transfer, angle between flow directions between 0 and 90 degrees 2−50146
- computer simulation of ocean currents rel. to two fluid media model 2−78320
- confined rotating, secondary flow in 2−60149
- corresponding state theories, one fluid type, from perturbation theories 2−53107
- creeping flow through clusters of spheroids and elliptical cylinders numerical solutions to Navier-Stokes equations 2−67568
- deflection of impinging jets in fluidic devices 2−70828
- dense, calc. of transport coeffs. using modified Enskog theory 2−64227
- dense classical, projection operators and interaction representation 2−55438
- dispersion of material in slowly moving fluids 2−46664
- drag reduction rel. to wavelength of flow-oriented wall eddies 2−53172
- dynamics, generation of thrust, continuum mechanics, book 2−70825
- dynamics, techniques for numerical solution of problems, review 2−43056
- dynamics, variational analysis, finite element method 2−77211
- electrically charged, some solns. to Einstein Maxwell equations 2−69563
- electrohydrodynamics, macroscopic coupling between electric fields and fluids 2−77210
- electrohydrostatic stability of fluid surface, two-dimensional problem 2−46651
- equations of state at critical point 2−56538
- near equilibrium, relativistic Boltzmann equation, supplementary conditions 2−49024
- extended press., consistent eqn. 2−46652
- flow, compressible swirling, through annular nozzles 2−53141
- flow, point source in rotating stratified fluid 2−43099
- flow chemical engineering, equipment design and automation (conference Prague, Sept. 1972) 2−83483
- formulation of rheological equations of structured systems rel. to fluids 2−58842
- free shear layers, instability considerations 2−80198
- functional equation in fluid theory 2−43046
- and gas bubbles, mutually migrating mixture 2−67785
- Gaussian isotropic turbulent flow, velocity field and temperature distribution 2−74334
- Gaussian molecule mixture, correlation functions 2−64205
- general relativity, Lagrangian density for perfect fluids 2−82196
- geostrophic adjustment of rotating homogeneous or stratified fluid 2−61861
- gradually and spatially varied flows, numerical integrations 2−77243
- gyroscopic behaviour for fluids with internal angular momentum 2−56312
- hard sphere, drag of pair correlations 2−64221

Fluids continued
hard sphere model, transport process, carbon tetrachloride obs. 2−74525
high pressure handling techniques 2−69503
horizontal layers, thermally induced instabilities 2−43050
hydraulics and fluid mechanics, conference, Melbourne Australia (1971) 2−77207
hydroelastic stability of flat panel in fluid flow, influence of free surface 2−46701
ideal relativistic fluid, Friedmann and Helmholtz equations 2−67555
inclined adversely heated fluid layer, thermal instability and formation of stationary secondary rolls 2−46693
incompressible, flow through tubes with porous walls 2−43076
incompressible, homogeneous isotropic turbulence studies using eddy representation of Navier-Stokes equation 2−46697
incompressible, interaction of two flows in flat duct 2−77217
incompressible, laminar flow in conduit, computer oriented solution 2−46684
incompressible, unsteady laminar flow in tube 2−77246
incompressible theory of homogeneous isotropic turbulence, eddy description of Navier-Stokes eqn. 2−77173
incompressible turbulent flow in permeable-walled duct 2−70856
interactions in agitated dispersion, simulation model 2−53363
interfaces near critical point, continuum theory 2−67813
internal gravity waves, convective instability 2−53146
inviscid incompressible, stability of heterogeneous layer heated from above 2−70824
irrotational, e.m. wave interaction 2−41873
isotropic systems of nonspherical mols., hydrodynamic eqns. and expressions 2−80178
jet like flow, cylinder oscillating in stationary fluid 2−43100
laminar boundary layer equations from differential- difference method 2−80398
laminar mixing of two uniform parallel semi-infinite streams 2−77227
laminar thermal boundary layers on continuous surfaces, heat transfer characteristics 2−41849
laser anemometer, tracer behaviour in turbulent flow 2−43054
layered, accelerated motion of sphere 2−77248
light scattering from n-particle system non-Gaussian 2−73541
line transients, survey of modelling techniques 2−67593
linear viscoelastic, pulsatile flow in elastico-viscous tubes 2−80167
longitudinal velocity fluctuation in smooth circular pipes 2−60125
mass and momentum transfer in 3-dimensional parabolic flow, calc. procedure 2−67571
Maxwell viscoelastic, oscillatory motion in annular channel under periodic pressure gradient 2−74343
mechanics, and logics for automation 2−74456
mechanics, harmonic principal functions applic. 2−70826
micromorphic materials with memory, constitutive theory 2−49070
micropolar, unsteady boundary layer flow along an infinite plate 2−80165
mixed hard spheres, perturbation calc. of distribution function 2−78941
molecular, hydrodynamic model calc. of momentum correlation functions at long times 2−50138
multi-component mixtures of hard spheres, determ. of pair distribution functions 2−69625
Newtonian, incompressible, laminar flow between stationary surfaces of revolution with common axis of symmetry 2−67595
Noll's, flow between two infinite planes with suction, solution by method of singular perturbations 2−53126
nonbuoyant vortex ring, hot wire anemometer meas. 2−77250
nonhomogeneous, thermal instability 2−60121
nonlocal mechanics, continuum theory 2−46654
with nonspherical molecules, Ornstein-Zernike equation and mean spherical model 2−66466
one path ultrasonic fluid flowmeter using electroacoustic feedback 2−55549
perfect, linearized stationary plane flow, shear waves and perturbations 2−83457
perfect relativistic, symplectic theory 2−53106
physical properties data base system 2−74309
Poiseuille flow with viscous heating, uniqueness of solns. 2−70832
polar, comparison of two-particle distribution function theories 2−43045
polar, simple oscillatory flow obs. 2−64243
polar, simple shearing flows 2−64244
power law, axisymmetric free laminar jet, solution of boundary layer equations 2−60170
pressure driven Stewartson layers, rotating circular cylinder in viscous fluid 2−77198
pure, conformal solution theory 2−46650
radial oscillations of gas cavity in compressible fluid rel. to underwater detonation of TNT 2−60174
radially bounded rotating, heated from below, stability 2−64224
randomly stratified rotating, internal wave propagation 2−80213
real, eqns. of state, from Ursell-Mayer density expansion 2−53108
Reiner-Rivlin, incompressible, obeying orthogonality condition 2−56275
relativistic, nonlinear dispersive waves 2−45243
relativistic fluid dynamics, concepts of mean force, mean vel. and total vel. 2−83431
relativistic perfect fluid, Einstein field equations, spherically symmetric solns. 2−56277
rigid dipole fluid, existence of dielectric constant 2−74306
rigid particles, statistical mechanics 2−41549
rotating, axisymmetric inertial oscillations 2−74342
rotating, Cauchy-Poisson wave problem 2−50149
rotating, equations of motion for slow-moving boundary layers 2−53142
rotating and stratified, flow over obstacles, finite amplitude disturbances 2−80202
rotating dynamics, ultrastable air bearing turntable 2−77232
rotation of perfect fluid with gravitational, electromagnetic and thermodynamic props. about fixed axis 2−69577
shallow rectangular cavity flow 2−60151
shock wave propagation and growth in inhomogeneous fluids 2−56314

Fluids continued
simple fluid, steady Couette flow between porous plates 2−67585
slow viscoelastic flow at large distance from an axis of symmetry 2−46694
solitary wave development on shelf, variable coefficient Korteweg-de Vries equation 2−56276
squeeze film behaviour between two parallel annular disks, one with porous facing, mathematical analogue 2−67562
stability of fluid motion in ellipsoidal cavity, laboratory study 2−60152
stability of stratified rotating boundary layer 2−67575
standing wave parametric amplification 2−46839
steady capillary gravity waves, generated by press. periodically distrib. along flow surface 2−70867
supercritical, effect of diameter of heated wire on free convective heat transfer 2−41865
surface waves, nonlinear effects when resonantly driven 2−80161
symposium on fluid mechanics, Warsaw (1972) 2−43049
tectonic stresses and interstitial fluid flow 2−72659
temperature-stagnation temperature difference in Navier Stokes system 2−62137
thermal instability in centrifugal force field 2−60129
thermo-convective instability of radiating and thermally conducting fluid layer 2−60176
thermodynamic theory of curved boundary layers of uni-phase, -component fluids 2−82382
thermohaline convection, oblique gradients effects 2−77212
transient flow in straight tube, effect of axial boundary motion on pressure surge generation 2−67591
trapped oscillations of rotating fluid in thin spherical shell 2−83474
turbulence, homogeneous, statistical theory 2−70842
turbulence meas. using optical recording of acoustic wave phases 2−60123
turbulent entrainment, across density discontinuities 2−77241
turbulent flow, study using light dispersion techniques, evaluation 2−77216
turbulent fluid heat transfer near pseudo-critical temp. in supercritical pressure 2−74320
turbulent shear layers, calculation method 2−67588
two phase flow, in porous media, swelling and nonswelling 2−77244
two-dimensional model, thermodynamics and hydrodynamics 2−46649
two-phase, pressure wave velocity 2−67604
two-phase interface at equilibrium, continuum model 2−53109
uniform sphere, properties in general relativity 2−66425
van der Waals generalized theory 2−67546
viscoelastic, determ. of material parameters by rotational non-viscometric flows 2−50140
viscoelastic, flowing through abrupt contraction, rheological props. 2−64406
viscoelastic, non-viscometric flows, review 2−46659
viscoelastic flow, orthogonal collocation analysis 2−70857
viscoplastic, inhomogeneous, motion in porous media, anal. in horiz. plane 2−46886
viscosity, absolute measurements comparison of results using channel flow and torsional pendulum techniques 2−60132
viscosity coeffs. eval. using perturbation theory 2−77213
viscous, rotating, slow oscill. of axially symmetric body 2−46679
viscous, secondary flow induced by transverse resonant acoustic field in circular duct 2−67590
viscous, steady laminar flow produced by rot. disk 2−80168
viscous, transient and steady state vorticity generated by horizontal temp. gradients 2−67561
viscous and, free oscillatory movement 2−77195
viscous compressible, in spherical cavity, nonstationary motion 2−67570
viscous incompressible around slowly rotating sphere, steady state forced convection 2−64228
vortices, vector analysis, analogies in other physical systems 2−60122
wakes, behind two dimensional square cylinders, at low Reynolds numbers 2−77247
wave propagation in uniformly rotating fluid, surface and inertial waves 2−50164

Fluorescence
see also X-ray fluorescence
— 2−66731
(anthracene)-$(CH_2)_n$-(N, N-dimethylaniline) systems, intramol. electron donor-acceptor interactions 2−60047
adatom position in surface from fluoresc., adsorbed atoms determ. 2−77488
alkali halides, Cu doped, spectra obs. 2−61712
alkanes, x-ray excited, lifetime meas. 2−42951
3-amino-N-methylphthalimide exiplexes with acetone, pyridine and dimethyl formamide 2−64169
3-aminobenzaldehyde, and 3-aminobenzoic acid, in aprotic solvents 2−54538
aniline vapour, vibrational analysis of absorption bands in resonance fluorescence spectra 2−70742
anthracene, auto-association of frozen solns. 2−54558
anthracene, dye-sensitized, delayed fluorescence, magnetic hyperfine modulation 2−65309
anthracene, effect of neutron induced crystal defects 2−44411
anthracene, mag. field effect on prompt fluoresc., singlet exciton fission obs. 2−81521
anthracene, quenching by CCl_4, wavelength effects 2−68694
anthracene, quenching of triplet excitons by trapped carriers used to determ. charge density gradient 2−47907
anthracene, singlet exciton collision fluorescence decay following laser stimulation 2−78144
anthracene, triplet exciton annihilation fluorescence changes induced by neutron radiation damage 2−84553
anthracene, two-photon absorption 2−44410
anthracene, two-photon excitation fluoresc. polarization 2−60039
anthracene and derivatives, gas phase, sensitized anti-Stokes delayed annihilation fluoresc. 2−74284
anthracene crystal, rel. to photoconduction and depend. on surface quenching of triplet excitons 2−81169
anthracene crystals, calculation of light reabsorption 2−61715

Fluorescence continued
anthracene crystals and solutions, quenching under intense excitation 2—54471
anthracene crysts., carrier-exciton interactions, delayed fluoresc. quenching 2—65308
anthracene derivatives in toluene, monomeric and exomeric fluorescence, concentration quenching 2—53445
anthracene dyes in alcohol soln., fluoresc. correl. with photochem. activity 2—77432
anthracene single crystal, intensity depend. on triplet exciton generation, decay and surface quenching 2—81427
aromatic and heteroaromatic molecules, meas. of quantum yields, study of radiative and radiationless transitons 2—53039
aromatic hydrocarbon aliphatic amine systems, exciplex formation studies 2—68691
aromatic hydrocarbons, nonradiative decay of lowest triplet state 2—80074
aromatic hydrocarbons fluorescence quenching by carbon tetrachloride, wavelength effects and complex formation 2—78205
aromatic mols., triplet deactivation parameters determ. 2—80075
2-(N-arylamino)-6-naphthalene sulphonates, fluoresc. emission and quenching analysis 2—80077
atmosphere, OH conc. detn. using dye laser 2—72765
atmospheric aerosol characterization and monitoring 2—81692
atom, X-ray fluorescence, intermediate state proximity effects 2—70563
atomic fluorescence spectrometry, combined hollow cathode and h.f. discharge as excitation source 2—72589
atomic system, Hanle effect rel. to coherence effects 2—59912
atoms, mean yields in heavy ion-atom collisions obtained by comparison of X-ray emission and Auger excitation cross sections 2—42777
atoms, unlike, collective radiation processes 2—79926
atoms, yields in K, L, and M shells, review of exptl. and theoretical techniques 2—42755
aurora, efficiencies for electron and proton induced processes 2—58061
Avzel effect, electrolum. diodes, visualisation applications 2—84530
azulene in frozen n-pentane, quasilinear structure of spectra 2—53046
benzene, Franck-Condon factors for predissoc. 2—80079
benzene solutions of aromatic hydrocarbons, radiation-induced fluorescence 2—53447
benzene solutions of aromatic hydrocarbons radiation-induced fluorescence 2—53448
benzene triplet yield in dil. cyclohexane soln., temp. depend. 2—57429
benzene vapour, fluorescence lifetime and quenching 2—83285
benzenes, methylated and fluorinated, decay times and rates of first excited singlet states 2—53050
benzenes, methylated and fluorinated, quenching by singlet energy transfer, mechanisms 2—56219
3,4-benzophenanthrene, bimolecular quenching, interaction between excited molecules in solution 2—56506
benzophenone, prompt and delayed fluorescence 2—50081
benzoquinoline, 7,8- and 5,6-, dipole moments 2—74281
5,6- and 7,8- benzoquinoline trapped in n-paraffins at 77K, vibrational analysis of quasilinear spectra 2—50080
benzoxazolyl-substituted aromatic hydrocarbons 2—57375
biophysics, diagnosis, recent developments 2—81995
biphenyl, influence of chloro substitution 2—46595
bromoacetylene, electronically excited, competition between photon emission and photodissociation 2—42969
build-up in complex formation, effect on nonradiation transitions 2—78207
carbon tetrafluoride, surrounding CO_2 laser induced sparks 2—74440
β-carotene, obs. using tunable dye laser 2—42262
chloroacetylene, electronically excited, competition between photon emission and photodissociation 2—42969
chlorophyll, obs. using tunable dye laser 2—42262
complex molecule solutions, dependence on exciting light 2—60480
complex molecules, two-photon excitation, determ. of polarization limits of emission 2—83237
complex mols., two-photon excitation fluoresc. polarization 2—60039
concentration quenching of fluorescence polarization in two and three dimensional solution 2—64462
coronene, bimolecular quenching, interaction between excited molecules in solution 2—56506
cryptocyanine illuminated by ruby laser, calc. of deviation from Beer-Lambert's law 2—81416
cryptocyanine soln., quantum yield, 140—300K 2—77441
cyanine dyes, luminescence of solid films 2—75327
cyanine dyes, regularities in radiating transition from second excited singlet state, polarization characteristics of fluorescence band 2—53054
cyclobutanone ($^1A_2$), fluorescence excitation, photodecomposition, of first excited singlet 2—48343
cyclohexane solutions of aromatic hydrocarbons, radiation induced fluorescence 2—53446
cyclohexane solutions of aromatic hydrocarbons, radiation- induced fluorescence 2—53449
cyclohexane solutions of aromatic hydrocarbons, radiation-induced fluorescence 2—53447
cyclohexane solutions of aromatic hydrocarbons radiation-induced fluorescence 2—53448
decay, evaluation of distribution of distances between energy donors and acceptors 2—74252
decay curves measurement, single-photon method, evaluation of rate parameters 2—68690
decay time meas. rel. to physical limitations of observation region 2—79435
diatomic mols., Hg*-sensitized, vibr. distrib. in electronic- vibr. energy transfer 2—59988
1,4-diazabicyclo (2.2.2) octane and methyl analogue, struct. effects on photophys. processes 2—81512
dibenzanthracenes, complex electronic spectra interpret. 2—53055
dibenzofuran excimer emission 2—46967
dichlorodifluoromethane, surrounding CO_2 laser induced sparks 2—74440

Fluorescence continued
diffusion constants of triplet states, modification of Avakian-Merrifield method 2—68800
diphenylamine, two-photon fluorescence patterns, absorption cross sections and picosecond relaxation times 2—43379
9, 10-diphenylanthracene photoperoxidation, quantum yield and intersystem crossing 2—72576
2,5-diphenyloxazole-1,3 and derivatives eximeric fluorescence 2—53075
diplenyl crystal, and electron excitation energy migration 2—72425
distyryldurene derivatives synthesis as wavelength shifters in plastic scintillators 2—61703
erythrosin molecule in alcohol and isopropanol solvents, dynamics of ultrafast decay processes 2—43367
ethanol glass, trapped electrons produced by biphotonic photoioniz. rel. to delayed emission of indole ring 2—54559
ethanol-dye soln., fluoresc. depolarization, vitreous transition obs. 2—60602
ethylene, laser induced combination band luminescence, vibration-rotation energy transfer 2—60066
excitation master equation to multi-shell-model of polarization quenching, applic. 2—78142
fatty acid molecules, monomolecular layers, improved resolution technique 2—55765
fine structure obs. in fluorescence spectra of laser-excited complex molecules, solid solvent selection 2—68693
flame temp. meas. by atomic fluoresc. spectrometry 2—84691
flavins, excited states 2—46605
fluoranthene, bimolecular quenching, interaction between excited molecules in solution 2—56506
fluoranthene, quenching due to exciton-exciton interaction, determ. of rate const. and exciton migration rate 2—81426
fluoranthene crystal, spectral response of lifetime, to determine purity 2—84536
fluorescein solns. luminance, rel. to contact lens practice 2—55318
glass:Nd, effect of phase separation 2—57372
glass:Nd, ion-ion energy transfer temp. depend. laser induced line narrowing obs. 2—65307
glass:Nd, laser induced line narrowing 2—48247
glass, rare earth doped, quenching by OH^- ions 2—54467
glycerol, meas. of diffusion const. on pyrene molecules in triplet state from -17 to +15°C 2—68804
halogens, obs. using tunable dye laser 2—42262
hydrocarbons, aromatic, non-Born—Oppenheimer coupling and D effect on $T_1 \rightarrow S_0$ radiative transitions 2—43002
hydrocarbons, surrounding CO_2 laser induced sparks 2—74440
indole, interaction with methanol, kinetics 2—53069
indole and derivatives in aqueous salt solns., effect of adding salt on deactivation of excited state 2—77442
indolizine and azaindolizines, quantum yields, lifetimes, energy gaps influence 2—68815
intensity and decay meas., effect of fluorescence polarization 2—46504
ketone energy transfer to rare earth ions, mechanism 2—60482
laser, dye, quenching by absorption from excited singlet state 2—79970
laser saturated atomic reson. fluoresc. non-quenching collisions influence 2—83199
laser-induced, rel. to reaction product internal state distrib. meas., applic. to $Ba+O_2 \rightarrow BaO_2$ 2—61770
laser-induced fluorescence line narrowing in gases and solids 2—48241
lithium formate monohydrate, u.v. N_2 laser pumped parametric 2—48130
macromolecular, polarized fluoresc., rel. to rot. Brownian motion 2—60091
macromolecule, polarization dynamics 2—56266
methyl fluoride, laser excitation and equilibration of excited vibrational states 2—50101
1-methylnaphthalene, excimer-monomer equil., deactivation processes, temp. effects 2—71214
microscope, FLUOVAL, design and construction 2—59250
microscopy, laser flying spot scanner in antibody instrumentation 2—66264
microscopy with acridine orange, demonstration of tumour cells in cerebrospinal fluid 2—55256
microspectrofluorimeter, intensity excitation and absorption spectra measurement of small samples 2—63434
minerals, rock forming, obs. using tunable dye laser 2—42262
molecular cryst., impurity one-phonon spectra, mirror symmetry breakdown 2—65271
molecular resonance fluorescence, cross sections and quantum yields, general expressions 2—74251
NA, excited collision-induced rot. and vibr. transfer laser-induced fluoresc. obs. 2—83412
noise, signal to noise ratio, temperature, scintillation counters 2—82801
n-nonane:coronene, 77K, complex struct. of doublets 2—78145
one-electron atoms, metastable, radiative decay rates 2—79958
optical parametric, tuning in uniaxial crystals 2—82529
organic dye solutions in far anti-Stokes region, correspondence with absorption spectra 2—74546
organic molecule collisions, meas. of sensitized anti-Stokes annihilation bremsstrahlung fluorescence 2—53094
organic solns., temp. depend. of non-radiative, deactivation processes 2—80070
organoluminor solution, obs. of stimulated emission by exciplexes 2—67836
ovalene in condensed media at room and liquid N temp. obs. of two-level emission as function of pressure 2—50105
oxacarbocyanine, excimer and related emission at low temp. 2—66861
2,3-pentanedione, photolysis emission and deactivation of excited states 2—54561
2,3-pentanedione, yield on photolysis 2—54560
phenanthrene, excited dimer fluorescence of pairs of molecules 2—56253
phenanthrene, two-photon absorption 2—44410
phenanthrene-naphthacene thin layer, u.v excited sensitized luminesc. 2—48251

Fluorescence continued
phenylcyclopropanes and phenylethanes, emission spectra, 77K 2-84663
phosphate glass, energy transfer between Sm^{3+} and Eu^{3+} 2-48238
phthalimide derivatives, two-photon excitation fluoresc. polarization 2-60039
phthalimide derivatives, vapour phase, dependence of duration on frequency of emitted light 2-53073
phthalimide solution, double-band generation 2-43377
phthalocyanine and derivatives, fluoresc. and photocond. 2-72426
planetary nebulae, Bowen mechanism, He II Lα radiation 2-58235
poly(1-vinylnaphthalene), excimer fluorescence obs. 2-54564
poly(1-vinylnaphthalene) and copolymers, excimer fluorescence obs. 2-54564
poly-γ-benzyl-L-glutamate, local viscosity of conc. solns. meas. by fluorescence depolarization 2-60451
polyadenylic acids, influence of triplet energy trapping on decay kinetics of delayed fluorescence produced by triplet-triplet annihilation 2-51471
polymethine dyes, stimulated fluorescence depend. on exciting illumination 2-77443
polyphenylene, energy transfer mechanism 2-71209
polypropylene, T-die film, mechanical props. and mol. orientation 2-47537
polystyrene, excimer fluorescence obs. 2-54564
polystyrene, structure in glassy state determ. by fluorescence depolarization 2-60615
propynal, laser-excited, collision-induced radiationless transitions 2-83298
pyrazine, vibronic coupling, bending vibr. progression 2-80066
pyrazine vapour, investigation of long lifetime component by study of pressure dependence 2-50113
pyrazine-h$_4$, -d$_4$, in benzene, 4.2 K, Frank-Condon patterns 2-77121
pyrene, rel. to energy transfer from perylene 2-60109
pyrene solutions, quenching under intense excitation 2-54471
pyrene solutions, under pulsed excitation 2-60483
pyridazine vapour, single vibronic level fluoresc., excited states 2-80078
pyrimidine-benzene mixed crystals, spectra at 4.2K 2-44412
radiative lifetimes, device for det. based on phase-shift technique 2-55366
Raman spectra by pulsed Raman technique, fluoresc. background reduction 2-79446
rare earth complexes with acetylene bonds 2-51373
rare earth ion aqueous solns., fluoresc. quenching by vibrs. of solvent mols. 2-60481
rare earth ions, in Y_2O_2S, La_2O_2S, Gd_2O_2S, X-ray excited optical fluoresc. 2-72418
reacting system, thermodynamic concentration fluctuations by fluorescence correlation spectroscopy 2-72540
reserpine, fluoresc. detection reaction, sensitivity increase by Th ion addition 2-71215
rhodamine 6G, two-photon fluorescence patterns, absorption cross sections and picosecond relaxation times 2-43379
rhodamine B, in aqueous soln., excitation spectra 2-64465
rhodamine B solution in methanol, anti-Stokes fluorescence in organic dye solutions 2-43378
rhodamine solutions, quenching by anthracene compounds 2-43380
ruby, effect of magnetic field on intensity, decay time 2-72419
selenacarbocyanine, excimer and related emission at low temp. 2-66861
selfdepolarization, construction and analysis of models 2-70656
semiconductor II-VI cpds., donor and acceptor identification 2-50573
singlet-exciton energy transfer, generalized random walk model 2-84270
solution electron transfer photoprocesses, extinction and exiplex formation 2-48346
solutions illuminated by ruby laser, calc. of deviation from Beer-Lambert's law 2-81416
spectrophotofluorometer, computerized data acquisition system 2-82584
stilbene, effect of neutron induced crystal defects 2-44411
tetracene crysts., exponential decay time, singlet fission 2-54472
s- tetracyanobenzene-benzene complex, fluorescence decay process, laser-induced photocurrent 2-72579
1,2,4,5-tetracyanobenzene-durene complex, quenching due to exciton-exciton interaction, determ. of rate const. and exciton migration rate 2-81426
thiacarbocyanine, excimer and related emission at low temp. 2-66861
thianthrene complexes in solution, fluorescence study, enthalpies 2-84637
trinitrofluorenone-poly(N-vinylcarbazole), photogeneration efficiency, field depend. 2-65399
triphenylamine in alkane, ion recombination fluorescence, viscosity dependent rate 2-46968
triphenylmethane, exciton splitting in electronic spectra 2-81523
upper atmosphere, meas. of density and temperature from obs. of local fluorescence produced by electron gun 2-48524
1-vinylpyrene and poly(1-vinylpyrene), quantum yields and excimer emission 2-65400
X-ray, Apollo-16 geochemical experiment 2-78497
X-ray, quantitative analysis using solid solution specimens, influence of quality of primary radiation 2-51485
X-ray, quantitative analysis using solid solution specimens, influence of quality of primary radiation 2-51486
X-ray analysis, theory of double concentration method for liquid and solid solutions 2-51487
Z=35-85, calc. of Auger group rates and fluorescence yields for vacancy in 3p or 3d shell using nonrelativistic HFS model 2-70572
$[Al(ha)_6]Br:Ti^{3+}$, $^2E \rightarrow ^2T_2$ transition mechanism 2-65302
Ar, resonance absorption and fluorescence 2-52933
B, K-shell fluorescence yield by synchrotron radiation 2-77012
BF_3, surrounding CO_2 laser induced sparks 2-74440
BO_2, band enhancement, chemiluminescent reaction of O with triethyl boron 2-44475
$Ba_2NaNb_5O_{15}$, stimulated parametric, tunable, induced by picosecond pump pulses 2-69889

Fluorescence continued
$Ba_2ZnGe_2O_7:Nd^{3+}$, absorpt. and fluorescence spectra, Nd^{3+} stimulated emission and laser action 2-61705
Be, K-shell fluorescence yield by synchrotron radiation 2-77012
$BuF_2:Sm^{2+}$, one phonon sidebands, theory 2-65304
C, K-shell fluorescence yield by synchrotron radiation 2-77012
C atom K-shell X-ray fluorescence, effect of molecular environment 2-49995
CO, isolated in solid Ne and Ar matrices, vibrational fluorescence laser excited low temp. study 2-59994
CO A $^1\Pi$ state, zero-field level crossing spectrosopy, obs. of fluorescence of resolved rotational features 2-70691
CO excited singlet state, vibr. relax. cross sections, quenching 2-56159
CO Hg*-sensitized, vibr. distrib. in electronic-vibr. energy transfer 2-59988
CO_2 polyatomic mixtures, laser-excited vibrational fluorescence measurements 2-43035
CO_2 TEA amplifier 2-41995
$CaCO_3$, rare earth doped, X-ray excited 2-61707
$CaF_2:Nd_2O_3$ (NdOF), optical spectra of Nd^{3+}, Stark effect obs. 2-61702
CaF_2, ⟨100⟩ and ⟨110⟩ oriented F_2-centre obs. 2-53751
CaI_2:K, Pb, Mn, investigation using 365 nm u.v. irradiation 2-51387
CaO, excited state of F-centres, paramagnetic resonance 2-44437
CaO, rare earth doped, X-ray excited 2-61707
Cd, magnetic depolarization of fluorescence lines, Hanle effect 2-79860
$CdF_2:Er^{3+}$, i.r. transitions, Stark dissoc. by cryst. field 2-65305
CdF_2, of Er^{3+}, ion site obs. 2-54416
Cl_2CS, laser excited $^1(\pi^*$-n) eigenstates 2-83282
Cm, L_2 subshell, fluoresc. yield 2-79924
Cs_2HfCl_6, of Yb^{3+} in octahedral cryst. field 2-72482
DF and DF-CO_2 chemical lasers, vibrational fluorescence 2-66751
Er^{3+} glass, stimulated emission cross section, relative gain coeff., absorpt. and fluorescence spectra obs. 2-75323
$Er_2O_2S:Er^{3+}$, energy levels and crystal field splittings detn. 2-51339
Eu^{3+}, in organic solvents, quenching effect of →C-H and -O-H groups 2-53436
Eu^{3+} fluorescence in organic solvents subject to quenching 2-50369
FeO, after release of $Fe(CO)_5$ in upper atmosphere 2-65825
Gd, L subshell yields using X-rays emitted by ^{155}Eu 2-70581
H_2-phthalocyanine in 1-chloronaphthalene, solutions, decay curves meas. by single-photon method 2-68695
H, radiative decay of 2P state, exponential decay law 2-79959
HBr, vibr.-vibr. energy transfer and collisional pumping 2-80129
HCl, vibrational fluorescence, vibrational energy transfer from molecule to molecule 2-83256
HF, vibrational, vib.-vib. energy transfer time detn. 2-60005
HF, vibrational relaxation measurements using combined shock tube and laser-induced fluorescence technique 2-53011
HF and HF-CO_2 chemical lasers, vibrational fluorescence 2-66751
$He_2(3p^3\pi)$, fast reaction system for obs. 2-46552
Hg-Cd sensitized fluoresc., amplitude modulation 2-64014
Hg 2537 Angstroms fluorescence rel. to remote sensing of oil pollution on water 2-84771
Hg_2 mol., transitions between vibr. levels and ground state 2-53020
I_2, excited by 6328 Å He/Ne laser, magnetic quenching, determ. of O_u^- repulsive potential energy wave 2-77085
I_2, laser induced line narrowing 2-74267
I_2, saturation microscopy by intermodulated fluorescence 2-67502
I_2, vapour, reson. Raman scatt. change to reson. fluoresc., intensity distrib. 2-67485
I_2 vapour, excited by Kr ion laser, transitions assignment 2-80016
I_2 vapour excited by Ar ion laser, obs. of progressive change from resonance fluorescence to resonance Raman effect 2-56181
$La_{1-x-y}Ce_xTb_yPO_4$, quantum efficiency 2-48246
$LaF_3:Ho^{3+}$, optical transition probabilities for Ho^{3+} 2-54468
$LaGaO_3:Bi^{3+}$, u.v. 2-48245
Li, K-shell fluorescence yield by synchrotron radiation 2-77012
Li_2O-Tb_2O_3-SiO_2, glass, intensity rel. to heat treatment and crystalline phases 2-51376
MgO, in thermally stimulated luminesc. under u.v. excitation 2-57378
MgO, rare earth doped, X-ray excited 2-61707
N_2-CO, laser excited, vibration to vibration energy transfer, laser excited fluorescence obs. 2-67489
NO_2, collisionally induced excitation, radiative lifetime 2-80015
NO_2, dynamics of electronic states excited by tunable dye laser 2-50059
NO_2, obs. using tunable dye laser 2-42262
NaI:Tl, intensity changes during X-ray dynamical diffr. 2-65301
NaK molecule, laser-induced resonance fluorescence, rotational and vibrational consts. determ. 2-64149
NaLi, heat-pipe oven applic. 2-49453
NdP_5O_{14}, laser material 2-73587
OH reactions with H_2, D_2 and CO, pulsed vacuum u.v. obs. using reson. fluoresc. 2-84665
OH + NO + M reaction, flash photochemical study using reson. fluoresc. detect. of OH 2-84666
O(^{1}S), quenching by O(^{3}P) 2-49970
Pb metastable and excited states, alignment monitored by detecting polarization of fluorescence 2-42785
Pb_2, new molecular constants for ground electronic state determ. from laser excited resonance fluorescence 2-42929
Rb, $6^2P_{1/2}$-$6^2P_{3/2}$ excitation transfer induced in noble gas collisions 2-74231
Rb, coherently excited, spontaneous decay 2-67403
Rb, resonance 2-44328
SF_6 and SF_6-air mixtures, pressure dependence of resonance lifetimes 2-42932
SiF_4, surrounding CO_2 laser induced sparks 2-74440
Sr, excited atoms, quenching in H flames 2-42715
Sr fluorophosphate, Mn^{2+} doped, optical excitation and fluoresc. spectra of Mn^{2+} 2-81421
SrF_2, ⟨100⟩ and ⟨110⟩ oriented F_2-centre obs. 2-53751
SrS phosphors, activated by Zr, Sn, Pb and Th 2-61713

Fluorescence continued
Tl^+-Gd^{3+} energy transfer, in inorganic glasses 2−61709
$Y_2O_2S{:}Er^{3+}$, energy levels and crystal field splittings detn. 2−51339
(Zn, Cd)S:Ag, Ni, efficiency curves, investigation of Klasens' simple thermal quenching theory 2−48250
ZnS-CdS:Er^{3+} mixed fluorescent compounds, spectroscopic investigation 2−84545
Fluorescent screens *see Luminescent devices*
Fluorimetry *see Chemical analysis*
Fluorine
atom, pulsed stimulated emission 2−79194
atomic, Li-like, spectra of autoionization electrons 2−49953
atomic stopping cross sections of α particles by application of Bragg additive rule to molecular stopping cross sections 2−70820
Chesapeake Bay, mixing model of fluoride distribution 2−65610
contamination, on Zr alloy nuclear fuel element, proton activation analysis 2−52876
gas, corona discharge at 100 torr to 1 atm, voltage-current characts. 2−71013
gas, glow and intermittent discharges at 60 to 150 torr, voltage-current characts. 2−71013
liquid, Raman spectra, fund. vibr. freqs. 2−43369
liquid and gaseous, meas. of dielectric const. and molar polarizability 2−67736
molecule, dissoc. energy, shock tube calorimeter studies 2−83253
photolytic atom sources for chem. lasers 2−68807
pressure change monitor for HF chemical laser 2−82509
refractive index, interferometric obs. rel. to wavelength 2−74488
F- in CaF_2 and SrF_2, ENDOR spectrum of U^{3+}-F- 2−84607
F + HCl → HF + Cl, effecr of excess reagent vibr. excitation on reaction dynamics 2−84629
F VIII in D plasma, meas. of depopulation of $2^3P_{0,1,2}$ triplet levels by electron collisions 2−79961
F^-, hydrated, binding energy calc. by ab initio semi-empirical MO and classical methods 2−50030
F^-, self-consistent symmetries, stability 2−76986
F^+, spurious ion currents in electron impact ion sources 2−74200
F_2, solid, model for lattice vibrs. 2−43959
F_2, vacuum u.v. absorption spectrum, determ. of dissociation energy and ionization potential 2−70696
^{18}F, production and use in metabolic studies 2−69389
^{19}F nuclear acoustic resonance in $RbMnF_3$, magnetoelastic theory and lattice imperfections 2−51412
$F+H_2$ laser oscillator, closed-form solution for rate equations 2−69922
$F+H_2 \rightarrow FH+H$, potential energy surface including electron correlation, refined linear surface 2−78189
$F+H_2 \rightarrow HF+H$, Monte Carlo calcs. of reaction rates and energy distribs. among products 2−57410
F_2+H_2 mixture excited by short electrical discharge, population of HF vibration-rotation levels, pulse laser investigation 2−66750
F_2+H_2 pulsed laser, computer modelling and parametric study 2−41978
$F+H_2(D_2)$, energy distribution among reaction products 2−65368
$F+H_2(D_2)$ reaction, exoergic, product static distrib. and temp. concept 2−68761
F + HF collisions, temp. dependence of vibrational energy transfer probability, 300 to 1500K 2−43037
HD + ^{18}F hot-atom reactions, classical dynamics 2−81497
Fluorine compounds
fluorides, perovskite type, lattice dynamics 2−61053
fluorite-type crystals, doped spin- phonon interaction 2−72235
halogenosilane bis-pyridine and o-phenanthroline complexes, vibr. spectra, normal coord. analysis, struct. 2−77081
Mf_6, ions (M=P, As, Sb, Si, Ge, Sn), force constant determination and correction for nonactive frequencies 2−64125
F^--F^- interionic potential, computation using Hartree-Fock and semiempirical methods 2−74651
$F_2HP.BH_3$, electronic structure and molecular conformation, CNDO/2 calculations 2−53032
$FNSF_2$ vibrational spectra, tentative assignments band shape and G-matrix elements calc. 2−70697
$F_3P.BH_3$, electronic structure and molecular conformation, CNDO/2 calculations 2−53032
$MeF_2{:}Ce^{3+}$ (II) crystal,, optical properties of quasi-tetragonal Ce centres 2−61646
XF_3 (X=N, B, P, As), ambiguities in harmonic force fields 2−50063
Foams
see also Bubbles
air bubbles in water, acoustic scattering strength meas. 2−74511
air-water mixture in two-dimensional diffuser, pressure recovery performance 2−46910
cavitation bubble implosion pressure pulses and cavitation damage 2−56469
i.r., ultrahigh luminosity, obs. at 10 microns 2−73051
liquid hold up in steady state froth bed 2−80498
polystyrene, foamed, thermal cond., H_2O vapour permeability, mech. props. 2−43412
sea, emissivity at microwave freq. 2−65602
structure, dissimilarity to polycryst. struct. 2−47313
syntactic, u.s. wave velocity as function of temp. 2−57048
Focusons *see Crystals/lattice mechanics; Sputtering*
Focussed collision sequences *see Sputtering*
Fog
— 2−72770
atmospheric electric fog effect and forecasting 2−51582
cold fog seeding at Oslo Airport using dry ice 2−72793
detection by acoustic echo sounding 2−62234
dispersal, at airports in US, potential economic benefits 2−72751
dispersal, evaluation of operations and cost effectiveness 2−65723
dispersal at airport, numerical model of ground based heating system 2−65722
dispersal by wide area low concentration airborne hygroscopic particle seeding 2−65721
dispersal from airport by airborne hygroscopic particle seeding using urea 2−65720
electric field effects, AgBr layers, polarity, speed 2−84674
Fog continued
element length, horizontal transmittance discontinuities 2−75602
holography through fog image reconstruction, incoherent scattering and vision improvement 2−79259
laser beam attenuation 2−57998
laser beams, 10.6 μm, attenuation coefficients, artificial real fog 2−72804
Los Angeles, transfer of near u.v. through smog 2−57992
low-temperature fog, urban growth effects over airports 2−44717
modification at several temps. using physico-chemical methods 2−72796
modification with organic surface films in laboratory 2−65743
multiple scattering obs. in synthetic foggy atmosphere 2−64478
warm, meteorological condits. for artificial dissipation 2−65719
warm, modification by seeding, numerical simulation model 2−62197
Fokker-Planck equation *see Transport processes*
Foldy-Wouthuysen transformation *see Field theory, quantum*
Forbush decreases *see Cosmic rays/variations*
Force *see Dynamics*
Force constants *see Molecules/vibration*
Force measurement
dynamometer wattmeter for power loss obs. in Si iron 2−73501
gravity meas. with noiseproof torsional system 2−76161
mechanotronic dynamometer for testing elastic elements 2−69541
springs, choice of parameters and calcs. 2−76162
van der Waal's force between curved mica surfaces, meas. in range 1.5-130 nm 2−82169
Form factors
— 2−63767
$\Lambda \rightarrow pe^-\nu_e$, induced pseudoscalar term due to SU(3) symmetry breaking 2−79624
atomic, diffraction studies desirability of absolute scale 2−77535
atoms and ions, 2-, 3- and 4-electron, Z^{-1} expansion for X-ray form factor 2−46460
baryon gravitational behaviour 2−73767
baryon resonance, electroproduction on nucleons 2−55881
bilocal operators, rel. to light-cone commutators 2−82663
bound state poles in eikonal approx. and infinite component wave equations 2−42304
charge, in summing of leading terms of vector-gluon model 2−79519
consistent resonance dominance, using sidewise dispersion relations 2−70121
coupled, in two-channel problem 2−79485
decomposition of symmetric tensor currents 2−82605
deformed nuclei, two-nucleon transfer form factors 2−63860
deuteron, relativistic charge, calc. from exptl. n-p phase shifts 2−42427
dual reson. model of vector currents 2−79538
elastic nucleon electromagnetic, excitations of nucleon in relativistic quark model 2−55870
electromagnetic, asymptotic behaviour, exchange forces in quark bound states 2−63554
electromagnetic, of hadrons in parton model 2−73811
electron magnetic dipole moment, in ladder approx. 2−45880
electron scattering, from nucleons, elastic and inelastic scatt. 2−70162
electrons, critical voltage measurement 2−80628
e.m., calc. in normalizable theory using cluster expansion 2−55792
e.m., effective Sachs, t^{-2} law in context of frame-dependent cutoff quantum field theory 2−63458
e.m., meromorphic function interpret. 2−52579
e.m., of $\pi^\pm$ and $K^\pm$ meas. using NAL and ISR 2−73812
e.m., power behaviour in hadron structure 2−66950
e.m. in quantum electrodynamics, study of asymptotic behaviour by functional methods 2−79468
e.m. of hadrons, calc. using Miyazaki's representation of Yang-Mills' field current 2−45852
exclusive processes, one-current dual model 2−66932
generator-coordinate analysis of nuclear reactions 2−52828
hadron, e.m. factors and parton model 2−59503
interacting Bose gas, moments of dynamic form factors for excited states generated by densities and currents 2−69623
intermediate Reggeon, form decomposition of scattering amplitude in Zachariasen-like model 2−52587
iso-vector 0^+ meson, 'near universality' of functions in dual reson. model 2−66970
isovector axial, of nucleon in electroproduction at threshold 2−79509
Lorentz-invariant, for structure of higher baryon couplings in resonance transitions 2−45983
magnetic dipole transition form factor for ep scatt. 2−45887
metal, binding energy in pseudo-ion approx. 2−83883
microscopic for charge exchange reactions to unbound residual states 2−49778
neutron, dipole behaviour of e.m. form factor 2−49588
neutron, e.m. form factors, from electron deuteron scattering meas. at squared four momentum transfers of 1.0 and 1.5 $(GeV/c)^2$ 2−42418
neutron charge form factor contrib. to elastic electron scatt. from nuclei 2−82955
neutron charge study of octet dominance of baryon matrix elements, explanation of vanishing charge radius 2−67059
in non-local quantum electrodynamics 2−59375
nuclear currents, relation between invariant form factors and impulse approximation 2−67113
nucleon, relation between axial vector and magnetic moment form factors 2−67043
nucleon-transfer, relative to microscopically specified core 2−46222
nucleus, c.m. spuriosity effects on charge form factor 2−67145
physical arguments, Callan-Treiman type equations 2−49544
pion, electromagnetic form factor, unitarization in smoothed Veneziano model 2−55850
pion electromagnetic, duality 2−59524
pion pair production, inelastic contribs. 2−42382
proton, connection between large q^2 behaviour and transverse momentum dependence of pp scattering studied in parton model 2−42407
proton, dipole behaviour of e.m. form factor 2−49588
proton, e.m. form factor in parton model 2−59564

Form factors continued
- proton, scale relation 2−55874
- proton, strong-interaction form factor in proton proton elastic scatt. 2−59568
- scalar, in K_{l3} decay 2−73804
- scaling, averaging over resonances 2−76586
- Seyfert galaxies, structure and luminosity rel. to quasars 2−72974
- single nucleon transfer reactions, form factor calc. 2−70427
- stripping DWBA amplitude to isobaric analog resonances 2−63861
- stripping reactions, Sturmian function applic. in calculations 2−46308
- symmetric tensor currents, decomposition into form factors 2−82605
- trinucleon bound state, charge form factor from exact solution of Faddeev equations with realistic nuclear forces 2−46077
- two-, three- and four-electron ions, Hartree-Fock and Hartree-Fock-Slater atomic form factors, electron momentum distributions 2−74205
- ur-citon scheme, derivation by operator method 2−52582
- Weizsacker Williams improved method, application to calc. of energy-angle distrib. of photoproduced lepton pairs 2−66930
- , π, Veneziano-like represent. 2−79594
- (p,d), complex form factors in nucleon transfer reaction 2−49791
- (p,t), complex form factors in nucleon transfer reaction 2−49791
- $\Delta(1236)$ isobars, possible meas. method for e.m. form factors 2−46017
- e, fourth order eval., asymptotic and threshold behaviours 2−82611
- e, fourth order eval., discontinuities and zero-momentum-transfer values 2−82612
- $e^+e^- \to K^+K^-$, 1.18 to 1.34 GeV, ρ- and φ-meson region 2−79510
- $e^+e^- \to \pi^+\pi^-$, 1.18 to 1.34 GeV, ρ- and φ-meson region 2−79510
- ^{3}He, analysis of π^0, η^0 and ω^0 production in $p + d \to {}^3He + X^0$ reaction 2−42411
- K e.m. form factor in Veneziano-type represent. 2−63578
- $K^+ \to \pi^0\pi^0 e + \nu$, branching ratio and form factor 2−42374
- $K \to l\nu_l\gamma$ decay, Q^2 depend 2−76669
- $K \to \pi\mu(e)\nu$, derivation of bounds on form factor using soft-pion theorem as input 2−55845
- $K \to \pi\mu(e)\nu$ decay, corrections to theorem 2−63583
- $K \to \pi\mu(e)\nu$ decay, rel. to κ meson 2−70209
- $K \to \pi\mu(e)\nu$ determ. from current algebra sum rules using Veneziano model 2−73802
- $K \to \pi\mu(e)\nu$ using massless pion method 2−45857
- $K \to \pi\pi\mu(e)\nu$, effective Lagrangian model 2−66953
- $K \to \pi\pi\mu(e)\nu$, form factor deviation from chiral symmetry value, light cone corrections 2−63582
- $K \to \pi\pi\mu(e)\nu$, form factor of vector current calc. 2−63576
- K_{l3} divergence form factor elastic region phase rel. to bound for decay parameters 2−63589
- $K^o \to \pi e\nu$, study of vector form factor 2−82739
- $K_l^0 \to \pi^\pm e^\mp \nu$, energy dependence of form factor, wide-gap spark chamber study 2−67008
- $K_\rho \to \pi eV$, strong interaction form factors 2−82740
- N, asymptotic behaviour, solution of Bethe-Salpeter eqn. 2−79606
- N, charge form factor determ. using $ep \to en\pi^+$ process 2−42405
- n, e.m. form factors, dipole behaviour 2−76711
- n, e.m. form factors, dipole behaviour 2−76712
- N, estimation from dispersion model for $\pi^- p \to e^+e^- n$, 275 MeV 2−63602
- N, in field theory on homogeneous space of Poincare groups 2−63650
- N, t-dependence 2−59557
- N e.m. form factors in perturbation theory, field-theoretical model 2−79608
- $NN\pi$, calc. as function of square of momentum exchange, Goldberger-Treiman relation 2−59558
- p, e.m. factor, rel. to inelastic p-p scatt. 2−55877
- p, e.m. form factors, dipole behaviour 2−76712
- p, e.m. form factors, dipole behaviour 2−76711
- π, Bethe-Salpeter model 2−63601
- π, contribution of ρ and ρ' vector mesons, determ. of charge radius 2−76663
- π, e.m. factor, sum rules 2−79498
- π, possible heavy vector meson 2−70226
- π charge, study by analysis of $\pi^\pm$ elastic scattering on ^{4}He 2−63604
- π e.m., new constraints derived using Chou-Yang model 2−70224
- π estimation from dispersion model for $\pi^- p \to e^+e^- n$, 275 MeV 2−63602
- $\pi \to l\nu_l\gamma$ decay, Q^2 depend 2−76669
- πN, corrections to Goldberger-Treiman relation 2−59530
- ^{12}C, elastic and inelastic electron scatt. form factors in Hartree-Fock approx. 2−82956
- ^{12}C, elastic scatt. of neutrons, elastic scatt., microscopic approach, coupled channel calcs. 2−76855
- ^{12}C quadrupole and octupole vibrations, form factors and transition densities of 4.34 and 9.64 MeV levels 2−82881
- ^{114}Cd, ^{3}He inelastic scatt., form factor phase and shape 2−59777
- Cu, charge density form factor, X-ray scatt. determ. 2−84251
- Fe, A=54, 56, 58, quadrupole and octupole transitions 2−70393
- ^{3}H, attractive form factor for exactly phase- equivalent separable potentials 2−55956
- ^{3}H, Reid potential calc., of binding energy admixture probabilities and charge form factor 2−76779
- ^{3}He, charge, with Reid soft-core potential 2−63764
- ^{3}He, charge and magnetic electromagnetic structure 2−70372
- ^{3}He, S′- and D-state effects 2−42497
- ^{4}He, c.m. spuriosity effects on charge form factor 2−67145
- ^{4}He, elastic electron scatt. form factor in local density approx. 2−83004
- ^{6}Li high energy limit for ^{4}He-^{2}H and ^{3}He-^{3}H form factors and nodes of wavefunctions 2−67146
- ^{6}Li(p,2p)^{5}He 100 MeV ground and 16.7 MeV states of ^{5}He 2−82966
- N, matrix elements of contacted energy-momentum tensor, rel. to mass radius 2−52631
- ^{62}Ni. quadrupole and octupole transitions 2−70393
- ^{16}O, c.m. spuriosity effects on charge form factor 2−67145
- Pb, from electron-ion interaction pseudopot. model 2−77812
- Tb^{4+}, mag. form factor in $BaTbO_3$ neutron diffr. detn. 2−81217
- TmSb, cryst. field effects in mag. form factor 2−81254

Forming processes
- — 2−71628

Forming processes continued
- actinide metal target preparation using tilt-pour and injection casting techniques 2−73907
- alloy, casting characts. and solidification morphology 2−64770
- arc welding, square wave current pulses 2−69480
- arc welding, steel, fracture, obs. 2−56919
- arc welding, weld pool stability study using gas-liq. interface analysis 2−43224
- automatic welding, mild steel plates, plastic deformation kinetics 2−69481
- brass, extrusion behaviour rel. to solidification texture 2−43809
- centrifugal casting of accelerator tubes 2−70318
- ceramic shapes, plastic deform. applic. 2−47493
- clad fissionable foil manufacture for ZPR obs. 2−74148
- cold-rolling, isotope target preparation, stable and active 2−73909
- cutting and thinning disk specimens for electron microscopy 2−67957
- defects in fusion welds rel. to basic metallurgy for non-destructive testing 2−53845
- deformation and restraint stress of steel beam column connection due to welding 2−58855
- diamond, ion machining 2−50811
- diffusion brazing, graphite joints, high temperature strength 2−71627
- electron beam welding, between dissimilar metals, evaluation of weld metal composition 2−69482
- electron beam welding of metals, ions emission 2−68144
- extrusion, flow function analysis of visioplasticity data 2−66560
- extrusion and plastic deformation of high polymers in solid state 2−84051
- ferrite, 1000 NN, compaction kinetics during hot pressing 2−53882
- fine mesh hemispherical grids, cold forming process 2−82435
- forging, fault position by u.s. testing 2−84156
- graphite, nuclear, production by mixing different cokes 2−68174
- hot rolling, determ. of roll forces 2−53881
- isostatic compression for metal forming including sheet metal 2−68128
- isotopic accelerator target prep. techniques 2−73962
- metal, upper-bound approach for conical flows 2−46882
- metal powder, rolling mechanism in initial nonstationary period 2−50908
- minerals, grinding, change in props. 2−68148
- oriented microsections of single crysts., prep. method 2−43534
- polymeric rod, cold extrusion and cold drawing, mechanical props. by tension and compression tests 2−80810
- powder metallurgy of high-temp. materials, conference, Tyrol, Austria, June 1971 2−53937
- pulling of mounting pins from glass rods, device 2−64769
- rock grinding model, thermal stresses in spheres 2−62010
- rolling techniques for prep. of target foils 2−49621
- rolling techniques for target foil fabrication 2−73910
- rubber, relationships between viscosity meas. at variable rates of shear and processing behaviour 2−53788
- shielded gas welding, pore formation in weld deposits from low alloyed steel welding rods 2−50809
- spot welded joints, stress analysis using photoelastic coating technique 2−68143
- spot welding, electrode fault-free life 2−69479
- steel, ausformed by extrusions, mech. props. and form. of struct. 2−47327
- steel, drawing, martensite form., mechanism and kinetics 2−43917
- steel, low temp. isothermal drawing, carbide formation 2−43810
- steel, rolling conditions, heat affected zone properties 2−68132
- steel, shear behaviour in heavy forming apparatus 2−53823
- steel, welding and hardfacing, with twin plasma jets 2−68147
- steel, with high N content, formed by melting under high press., metallography 2−50812
- steel film preparation by chemical grinding 2−71636
- steel targets, effect on ballistic behaviour 2−60980
- steel welding, restraint stress effect on delayed cracks 2−77711
- superalloy, powder, elec. discharge activated press. sintering, composite struct. bonding 2−53938
- thermo-plastics, long-period rupture strength and time welding factors 2−53880
- thermoluminescence changes following grinding 2−84554
- thin film micromachining, focused Q-switched YAG laser beam 2−73605
- welded joints, crack formation in stress relieving annealing 2−64759
- welded joints, fatigue behaviour 2−64768
- welded joints, finite element method of strength assessment 2−63065
- welded joints of wires made of alloys Nb+Zr+Ti and Nb+Ti, properties 2−61227
- welded pressure vessels, loading capacity, stressed at high temps. 2−64771
- welding, electron and ion beam gun form. in h.v. gas discharges 2−60296
- welding, heat content and size distrib. of electrode metal droplets 2−69483
- welding, structural steel, effect on microstructural region in weld transition area 2−50808
- welding, surface tension of molten metal pool, meas. method 2−71618
- welding dissimilar metals with two electron beams 2−68145
- welding of cored electrode wire, metal pool surface tension determ. 2−71618
- Al-Mg-Si alloy, extrusion temp. effects on toughness 2−60974
- Al-Zn-Mg alloy, extrusion temp. effects on toughness 2−60974
- Al-based materials, hot formability criteria 2−80852
- Al, lateral rolling, dislocation struct. and fracture 2−74837
- Al alloy tubes, production by cold extrusion, technical problems and factors influencing extrusion pressure 2−68157
- Al sheet, rolling and annealing texture of outer layer 2−64756
- Al_2O_3, transmission e. microscopy obs. of subsurface damage caused by mech. polishing and grinding 2−71418
- Al_2O_3 ceramics, microwave machining and piercing characteristics 2−53867
- C, grinding effect on effective temperature factor 2−53655
- CO_2 cutting of various materials by gas laser, techniques, advantages and disadvantages 2−82497

Forming processes continued
  - Cr-Ni steel, weldability to C steels, gas pressure process 2−68146
  - Cu-based materials, hot formability criteria 2−80852
  - In, rolled, influence of twinning on texture 2−80774
  - Mg, and props. and applications, book 2−60936
  - Mg alloy, props. and applications, book 2−60936
  - Mg extrusions, plane strain, yield anisotropy and texture control 2−80848
  - Mo fibres, pressed part formation 2−53883
  - Ni-Fe alloy, sheets, heavily rolled, annealing textures, recryst. mechanism 2−74886
  - Se film, rolling texture, X-ray and elec. resist. study 2−64574
  - TiC-Nb cermet, hot pressing kinetics 2−56914
  - WC-Nb cermet, hot pressing kinetics 2−56914
  - Zr-(2.5 wt%)Nb press, tubes, texture development 2−50848

Fortran *see Calculating apparatus/digital computer programmes*

Fountain effect *see Helium-liquid; Superfluidity*

Fourier analysis
  - *see also X-ray crystallography/calculation methods*
  - achromatic Fourier transformation 2−42225
  - double series soln. to general anisotropic plates 2−69669
  - electro-optical Fourier transforms of leukocytes 2−51884
  - electromechanical synthesizer, demonstration 2−48957
  - electron microscope images, recording, processing and correction 2−79152
  - electron microscope images 2−79160
  - Fourier images, paradox 2−49423
  - gravity anomaly data manipulation using Fourier series 2−48370
  - harmonic field contents of pulsed quadrupole magnets using stepping search coil 2−76444
  - high resolution micrographs computer enhancement of weak periodic information using Fourier synthesis techniques 2−79143
  - holographic Fourier transform spectroscopy, Moire technique for hologram recording 2−73614
  - incoherent Fourier transform technique for determ. of optical transfer function 2−66804
  - LEED intensities for surface struct. determ. 2−47073
  - magnetosphere, substorm depression and expansion phases 2−62334
  - n.m.r., partially relaxed Fourier transform ^{11}B spectra 2−56521
  - nuclear reaction cross-section fluctuations, use of weighting functions in Fourier analysis 2−52791
  - optical metrology, Fourier transform techniques 2−45793
  - phase evaluation in generalized diffraction, application to electron microscopy 2−79158
  - plasma, laser produced, heat cond., Fourier's theory, applicability 2−80245
  - plasma-beam discharge oscillations, frequency spectra construction 2−70952
  - plate, isotropic, twisted by rigid circular stamp, mixed problem 2−45410
  - plotted functions, direct optical spectral anal. 2−70077
  - p.m.r., delayed Fourier transform method 2−55631
  - reconstruction of holograms using digital computer 2−69982
  - series, harmonic summation 2−69543
  - spectrometry, diaphragm geometry effect on instrumental function 2−59284
  - spectroscopy, digital data handling of spectra 2−52485
  - spectroscopy, high resolution 2−63429
  - spectroscopy, rapid scan i.r. Fourier transform, review of techniques and applications 2−52486
  - square wave targets used in lens MTF meas. 2−59221
  - teaching method by discovery approach, use of computer as calculational aid 2−78734
  - time domain configuration of narrow frequency- bandwidth pulses 2−49441
  - transform method for 2D and 3D neutron transport problems 2−70507
  - transform method for periodogram anal. for quasi-periodic variable stars 2−75764
  - transform proton n.m.r. in aqueous solution 2−77448
  - transform spectrometer from all reflection interferometer 2−59282
  - transform spectrometry, interface effects 2−70074
  - transform spectroscopy, using Michelson interferometer 2−55344
  - transform spectroscopy, using Michelson interferometer 2−55771
  - transform technique applic. to anal. of dynamic and impact responses in cylindrical cavity in infinite elastic medium 2−69665
  - transformed waves, subtraction using diffraction gratings 2−45789
  - truncation and linear digital filtering compared 2−78342
  - X-ray line profiles for talc from sepiolite 2−64627
  - ^{13}C Fourier transform n.m.r. study of trimethyl(phenylethynyl)-silane, Si-C bonding 2−83312
  - ^{29}Si Fourier transform n.m.r., exptl. techniques 2−65355
  - W, emission spectra by Fourier transform spectroscopy, 1000-2300°C 2−54086

Fourier series *see Series; Transformations, mathematical*

Fourier-transform spectroscopy *see Fourier analysis; Spectroscopy*

Fractionation *see Distillation*

Fracture
  - *see also Cleavage; Mechanical strength*
  - alloy, ductile fracture prediction under discrete loading 2−43728
  - alloy, hard metal, fracture surfaces, crack path electron microscope replica obs. 2−50773
  - aluminosilicate ceramic, thermomechanically strengthened, thermal-stress fracture 2−50738
  - BORSIC aluminium fibre-matrix interfacial region, exam. 2−64546
  - brittle, in compression 2−84018
  - brittle bodies, by impact, fracture mech. study 2−69642
  - brittle body fracture by explosion, anal. 2−69782
  - brittle fracture faces, interpretation in physics and geology 2−47540
  - brittle fracture initiation under triaxial stress conditions, Gibbs free energy 2−84016
  - brittle materials, crack propag. rel. to nonrecoverable elastic energy, Griffith criteria 2−71595
  - brittle materials, dependence of test results on nature of stress state 2−56841
  - brittle materials, fatigue failure probability determ. 2−60994
  - ceramic, notched beam test for fracture energy meas. 2−50858
  - ceramic, strengthened by surface compression, thermal stress fracture 2−50871

Fracture continued
  - ceramic, subcritical crack growth and fracture energy 2−50857
  - ceramic, surface condition influence on thermal fracture behaviour 2−47521
  - ceramic polycryst. topography, mirror obs. 2−50855
  - ceramics, texture with ref. to mech. props. 2−67949
  - characteristics, electron-fractographic obs. 2−43751
  - Charpy specimens, precracked, dynamic fracture toughness from impact hammer tests 2−71609
  - Chelmsford granite, cylindrical specimens 2−75456
  - Coconino sandstone under confining pressure, influence of pore-fluid chemistry, temperature 2−68858
  - composite, C continuous fibre reinforced ceramics and glass 2−50919
  - composite, C discontinuous fibre reinforced ceramics and glass, fracture strength 2−50918
  - composite, fibre-reinforced, graphite/epoxy, compressive fatigue 2−61021
  - composite, filament reinforced, multiple fracture 2−56975
  - composite, glass fibre reinforced polyester, fracture surface energy determ. 2−50780
  - composite, glass-crystal two-phase, theory 2−74860
  - composite, steel wire reinforced polyester resin, fracture toughness 2−47528
  - composite fuel annular bodies, fracture and elastic props. 2−71588
  - composite materials, fibrous and laminates review 2−43901
  - crack energy release rates and stress-intensity factors, by finite-element method 2−66531
  - crack tip diffraction of tension stress wave 2−69654
  - cracking stress of glass fibre reinforced inorganic cement, use of fracture mechanics 2−64726
  - creep, due to diffusional growth of grain boundary voids 2−47523
  - creep fracture, secondary, influence on fatigue failure at elevated temperatures 2−60893
  - cumulative shock fatigue using ballistic impact 2−60939
  - cyclic stress and derivation of a formula for failure in creep fracture 2−56862
  - delayed, in solids, criteria and experimental verification 2−71585
  - dispersion strengthening effects on hydrogen susceptibility, deformation and fracture 2−74862
  - dynamic fracture toughness meas. technique 2−82124
  - elastomers, electron microscope investigation of fatigue fractured surfaces 2−60899
  - electron microscope obs., applic. of high voltage fractography 2−56825
  - environmental chamber for hertzian fracture testing 2−56855
  - fatigue, high temperature phenomenological mechanisms 2−56818
  - fatigue deformation and fracture under cyclic and steady loads 2−56816
  - fatigue under dynamic interactions 2−63063
  - fatigue-crack growth under cyclic loads, theory 2−69643
  - fatigue-crack initiation from flaws using fracture mechanics theory 2−69649
  - ferrite memory cores, fracture stress, firing time depend. 2−84431
  - fibre composite, fracture toughness 2−77667
  - fibre composites, plane-strain model 2−43898
  - flaws, inherent, effect of microstruct. on stress to propagate at room temp. 2−68096
  - freeze-fracture of biological samples for scanning electron microscopy 2−82080
  - fretting fatigue, effects of contact pressure and hardness 2−43712
  - glass:Nd laser, damage mechanism and improvement of damage threshold 2−42050
  - glass, $Na^+ \rightarrow K^+$ ion exchanged 2−64787
  - glass, optical, relation between abrasion, micro indentation hardness and maximum fracture velocity, expts. 2−56550
  - glass, strengthened by surface compression, thermal stress fracture 2−50871
  - glass, subcritical crack growth and fracture energy 2−50857
  - glass ceramic, lithium silicate, fracture energy as function of struct. 2−50886
  - glassy polymers, characteristics of brittle fracture and viscous flow 2−60889
  - granite, low porosity, biaxial compression test implications 2−57765
  - graphite, fatigue failure probability determ. 2−60994
  - graphite, fracture strength and fatigue failure 2−53827
  - graphite, high temp. process 2−56829
  - graphite, mechanics 2−56828
  - graphite, physically based statistical theory 2−56827
  - graphite, pyrolytic siliconated, fracture surface, electron microscope obs. 2−74861
  - graphite polycrystalline, environment effect on mech. anisotropy 2−68173
  - high pressure container, duct seal break, reaction force calc. 2−62893
  - Inconel alloy, X-750, fracture and creep-fatigue behaviour 2−56860
  - jade, toughness 2−50856
  - linear fracture thermodynamics of solids, convolution inverse variational principles applics. 2−55466
  - Lower Devonian sandstone, strain rate effects 2−54735
  - lucite cones, by shock waves 2−68055
  - lunar glass, interferometric evidence for low temp. shock 2−55124
  - mechanics, progressive failure of clay slopes, growth of slip surfaces 2−78238
  - metal, b.c.c., brittle fracture, theory 2−43720
  - metal, brittle, surface energy from phonon freqs. 2−60902
  - metal, brittle fracture, ductile-brittle transition 2−43730
  - metal, by superimposing stress waves generated by electron pulses techniques 2−56812
  - metal, ductile fracture prediction under discrete loading 2−43728
  - metal, embrittled, Auger spectrographic analysis 2−47541
  - metal, fractography by crack replication 2−47545
  - metal, in tension, under hydrostatic press., time depend. 2−80728
  - metal, mixed visco-brittle fracture 2−47507
  - metal, shock spallation, appl. of phonon theory of brittle fracture 2−80747
  - metallic materials, due to force loading, fatigue, microfractographic characteristics 2−50730
  - mica glass-ceramics, rel. to microstruct. 2−60999

Fracture continued
mild steel and plexiglass, tensile zone caused by detonative loading, breakage patterns and stress waves 2–84048
mullite, press.-sintered, porosity depend. 2–50722
Nimonic 90, rel. to appl. stress, using creep equation 2–71575
nylon 66, monofilament, pure torsion, combined torsion and tension bondings for fracture 2–60858
nylon 6 fibres, reaction rate model 2–74854
nylon 6 monofilament, model for deform. and fracture from creep and birefringence obs. 2–84022
nylon 6 monofilament, model for deform. and fracture from creep and birefringence obs. 2–84021
oceanic basalt, brittle fracture 2–61971
periclase brick, microstruct. of hot fracture surface 2–77661
Plaster of Paris, fracture of triangular plates due to contact explosive pressure 2–53793
plastics, deformation to fracture, review 2–60863
plates or tubes, plastic instability and growth of grooves and patches 2–55474
polycarbonate longitudinal crazing 2–53840
polychloroprene, gel fracture rate, crystallinity effects 2–47483
polyester, glass- or C-fibre reinforced, work of fracture 2–74863
polygraphites, obs., modes and criteria 2–56830
polymer cryst., morphology influence 2–60860
polymer fracture surface layer, optical thickness determ. 2–70013
polymeric glass, environmental crazing mechanics and mechanism 2–64735
polymeric substances, impact fracture 2–84052
polymers, isotropic, longitudinal crazing 2–53840
polymethyl methacrylate, longitudinal crazing 2–53840
polymethyl methacrylate, relaxation effects 2–80821
polymethylmethacrylate, tensile creep behaviour and fracture mechanics, liquid environment 2–53819
polypropylene, effects of cooling rate from melt 2–56908
polystyrene, craze yielding and stress-strain characts. of crazes 2–64736
polystyrene, low-angle X-ray scattering from crazes and fracture surfaces 2–74855
polyvinyl chloride, fatigue crack propag. mechanism, comparison with polypropylene and ABS blend polymer 2–71601
portland cement paste, effects on microstructure 2–60995
post yield fracture mechanics, crack model for high and low strength materials 2–64727
quartz, static fatigue, earthquake phenomena 2–65499
quartz, thermal fracture probability 2–50897
radial cracks emanating from pin loaded hole, strain energy release 2–84017
radiation involved brittle fracture in structural materials 2–68099
reactor fuel element sheathing problems 2–59866
refractory, high alumina, hot modulus of rupture 2–56961
refractory oxide, oxide filament reinforced 2–56973
resistance of materials, particularly metal alloys, physical and technological significance 2–71580
rock fracture zone rel. to penetration of trapezoidal- shaped body 2–75425
rock-joint deformation, modelling 2–72668
rocks, effect of stress gradient on brittle fracture initiation 2–72667
rocks, static uniaxial deformation to 30 kb 2–62013
rocks, statistical theory of polyaxial compressive strength 2–72670
rocks, stress-strain relations 2–57822
rocks in Earth, effect of triaxial stress system 2–72679
rocks under axial loading, seismic wave velocities 2–57654
rubber, during tensile testing at low temp. 2–43710
scanning electron microscope fractography applic. 2–56640
scanning electron microscope fractography as microstruct. determ. technique 2–56639
solid propellant, simulated, low-cycle dynamic fatigue-curve for dynamic shock wave loading 2–84027
solid soln., crack propag. rate 2–43729
speed meas. using u.s. fractography applic. to Si and Ge 2–82123
steel, 11% Cr, rel. to appl. stress, using creep equation 2–71575
steel, austenitic stainless, stress corrosion testing, mech. behaviour 2–50765
steel, brittle fracture, effect of grain boundary form 2–80765
steel, brittle fracture, theory 2–43720
steel, brittle fracture resist., tempering temp. effects 2–53838
steel, brittle fracture susceptibility, effect of V alloying 2–53896
steel, En 24, soln. between microstructure and fracture toughness 2–71586
steel, fracture probability, rel. to stress amplitude 2–43714
steel, fracture toughness, effect of heat treatment temp. 2–53842
steel, fracture toughness, effect of rare earth alloying 2–53900
steel, fracture toughness, u.s. vibr. effects 2–53877
steel, high temp. fracture, influence of annealing twins 2–56833
steel, high-speed W-Mo, fracture toughness, effects of Co 2–53992
steel, impact props, rel. to FeO type inclusions 2–47530
steel, Kh18N10T, fine structure changes for degree of deformation in creep 2–83956
steel, low carbon, microstructure and embrittlement 2–43783
steel, low temp., notched specimens preloaded at room temp. 2–64783
steel, low-alloy, brittle fracture, effect of Ce addition 2–53831
steel, low-alloy, temper-brittle fracture and grain boundary segregation 2–47624
steel, low-C, fracture rel. to microstruct., embrittlement, bend tests 2–56823
steel, low-carbon, fatigue study on surface with different crack propagation rates 2–84126
steel, maraging, plane strain fracture toughness tests 2–60979
steel, martensitic, effect of lath boundary precip. on fracture toughness 2–57018
steel, martensitic, Fe-plated fracture edge, elec. microscope obs. 2–56940
steel, martensitic, intercryst. mechanism, incompat form. 2–56815
steel, mech. props. at elevated temps. and pressures 2–60917
steel, quenched, aged, cooled, dislocation substruct. rel. to fracture behaviour 2–47413
steel, quenched, tempered, resist. to plastic deform. and cold brittle failure 2–47502
steel, shear behaviour in heavy forming apparatus 2–53823

Fracture continued
steel, sintered, mechanical behaviour, model to explain behaviour of elastic moduli 2–84128
steel, stainless 18-8, at cryogenic temps., elec. microscope obs. 2–56939
steel, stainless austenitic 25%Ni 20%Cr, rel. to tertiary creep processes 2–47514
steel, structural, fracture behaviour rel. to inclusion orientation and shape 2–43713
steel, synthetic weld structure, obs. 2–56919
strength, influence of temperature, weld procedure, test piece location, heat treatment, embrittlement and loading rate 2–74852
stress intensity factors for cracked bodies from Buekner's formulation 2–84015
stresses in bonded materials with perpendicular crack at interface 2–60901
styrene-butadiene block copolymers, mechanically induced bond rupture, e.p.r. 2–43711
superplastic alloy, metallographic obs. 2–56786
surface, effects of creep and fatigue loading on steel at high temp. 2–60946
tearing energy, penny shaped cracks between two bonded dissimilar materials 2–45390
tendon collagen of rat tail 2–43016
theories rel. to plasticity theories, phenomenological approach 2–76317
thermoplastics, amorphous, hydrogen bonding influence on stress crazing and cracking 2–60908
thick walled cylinder, plane strain toughness method 2–60937
thick walled cylinder failure test-machine using fracture mechanics on pressure cycling 2–69501
titanium alloy OT4, influence of hydrogen on fracture structure 2–60888
toughness, fatigue cracks, in zone of stress concentrators 2–80787
toughness test specimen, finite element analysis in nonlinear range 2–43758
transition metals, b.c.c., cold brittleness 2–43726
tuff, high porosity, biaxial compression test implications 2–57765
Udimet 500, surface topography rel. to low cycle fatigue 2–56820
untempered ultrahigh strength steels of high fracture toughness 2–53872
vulcanizates, oil-extended SBR, large elastic behaviour and fracture 2–84050
wustite, fracture energy invariance with grain size 2–50880
yielding and size effects, fracture of plates and pressure vessels 2–84013
Zircaloy-2, containing ZrH_x, fatigue fracture 2–47649
Zircaloy-4, localized shear mechanism 2–50747
Al/α-Al_2O_3 composite, effect of filament length 2–53947
Al-9.5 wt.%Mg:Ti,Zr,Mo,B alloy, rel. to alloy additions 2–47546
Al-Cu-Mg-Mn-Fe-Si-Ni-Zr-Ti alloy, D16T, recryst. and uncryst. structure, in static and cyclic conditions 2–47527
Al-Zn-Mg-Cu-Mn forging alloy, fracture toughness rel. to microstructure 2–53826
Al, plastically deformed by lateral rolling 2–74837
Al alloy, multiphase, microstructure rel. to topography of fracture surfaces 2–80820
Al alloy, shear creep fracture prediction, complex stress creep characts. 2–53813
Al alloy hand forgings, fracture toughness and stress corrosion cracking 2–60905
Al alloy hand forgings, fracture toughness and stress corrosion cracking 2–60906
$Al_2O_3/ZrO_2/Y_2O_3$ eutectic, directionally solidified 2–47526
β-Al_2O_3, alumina, hot-pressed, characteriz. 2–50875
Al_2O_3, sapphire, role of plastic deform. 2–50762
Al_2O_3, sapphire, surface analysis 2–50774
Al_2O_3, sapphire filament, fracture strength in tension 2–50917
Ar, stability and mode of fracture of highly stressed ideal crystal 2–77631
Ba-mica/Al_2O_3 composite 2–56977
$3BaO.5SiO_2$ glass-ceramic, mechanical props. 2–53930
Be, basal slip effects on fracture 2–64753
BeO high pressure effects on single crysts. and polycrystalline mat. 2–68082
C, glass like, thermal shock and crack propagation 2–56822
C composite, chem. vap. deposited felt and filament wound, flight-tested, phys. props. 2–61017
C fibre, thermal expansion anisotropy effects 2–54054
C fibre monofilament substrate, on chem. vap. deposition of B 2–53956
C fibre reinforced glass, fracture energy 2–84104
C pyrolytic, fluidized-bed, rel. to struct. 2–56768
Co, large grain size specimens, 3 kbar range pressure effects 2–68097
Co alloys, metallurgical structure and properties 2–71667
Cu-Al alloys, mechanical properties and ductility as a function of temperatures 2–64776
Cu-Ni-Fe alloy, intergranular fracture on spinodal decomp., mechanism 2–57012
Cu-W composite, surface energy det. 2–55475
Cu, creep fracture of cylindrical bars under pure torque 2–64754
Cu_6Sn_5 fibres, brittle fracture surface morphologies 2–80744
Fe-Mg-Ni alloy, austenite transform., cooling rate effects 2–53991
Fe-Ni-C alloy, martensitic, intercryst. mechanism, incompat form. 2–56815
Fe-Ni and Fe-Ni-C martensitic alloys, delayed fracture formation during cathodic charging under static stress 2–64731
Fe-Ta alloy, ductility enhancement using allotropic phase change 2–57020
Fe, grain size and temperature effects on cyclic strength and fracture 2–56896
FeCo-(2 wt.%)V alloy, crack propagation and nucleation in ductile fracture 2–53835
Ge, speed meas. using u.s. fractography 2–82123
Ir, anomalous brittle, scanning electron and field ion microscope obs. 2–56576
KH_2PO_4 nonlinear crystal, fracture by ruby laser radiation 2–79254
$LiNbO_3$ nonlinear crystal, fracture by ruby laser radiation 2–79254
MgO-$MgAl_2O_4$ system eutectic struct. 2–47658

Fracture continued
MgO, hot-pressed, strength and fracture reln. to annealing rates 2—71589
MgO, plastic deform. during cleavage fracture 2—71570
Mo, polycrystalline, role of impurity atmospheres in brittle fracture 2—71587
NaCl, stability and mode of fracture of highly stressed ideal crystal 2—77631
Nb-Hf alloys, morphology, transmission and scanning electron microscopy 2—56834
Ni-Al-W alloy, γ' matrix, fatigue fracture 2—43716
Ni-Cr lamellar composite alloy, fatigue deformation, crack propag., fracture energy 2—56821
Ni-(5wt.%)Fe-(5wt.%)W, powder composite, fracture micromechanism obs. 2—56947
Si, speed meas. using u.s. fractography 2—82123
Si crystal, brittle-fracture and crack propag., atomistic computer simulation 2—84036
SiC, fracture energy relation, thermal shock behaviour, acoustic damping 2—60890
Si_3N_4, ceramic, hot pressed, fracture energy at high temps. 2—60907
Si_3N_4, ceramic, hot pressed, strength fracture energy, microstruct. relationships 2—60883
Sn-Pb alloy stainless steel fibre reinforced, fracture behaviour 2—50921
Ti-Al-Mo-V alloys, fatigue fracture behaviour in dry Ar environment 2—84118
Ti-Al-V alloy, mill-annealed, fatigue crack growth, temp. effects 2—60904
Ti-Cr alloy, fracture modes, effect of ω phase 2—47547
Ti-(13 wt.%)V-(11 wt.%)Cr-(3 wt.%)Al, mech. property-fracture-microstruct. reins.56950 2—56950
Ti alloys, comparison with theoretical investigation of plastic deformation peculiarities in planar stress state 2—43698
U-Mo alloy, stress corrosion cracking in humid aid, C content effects 2—53839
UO_2, rel. to porosity 2—43699
VC_x, fracture surface energy determ. 2—50776
W single crystal, brittle fracture, rel. to {110} cleavage in ⟨110⟩ axis 2—56606
WC-(25 wt.%)Co alloy, surface finish effects 2—43717
Zn, large grain size specimens, 3 kbar range pressure effects 2—68097
Zr alloy, stress corrosion cracking in Hg, fracture surface study 2—43737
ZrO_2, calcia-stabilized, fracture toughness 2—50777

Francium
No entries

Francium compounds
No entries

Franck-Condon factors *see Spectra*
Frank-Read sources *see Crystal imperfections/dislocations*
Fraunhofer lines *see Astronomical spectra; Spectra; Sun/spectra*
Free field rooms *see Acoustical laboratories*

Free radicals
acetylene dicarboxylic acid dihydrate crystal, irradiated, e.s.r. 2—75348
1-adamantyl, induced by radiolysis of adamantane 2—54562
L-alanine, irradiated, unstable radical CH_3CHR, temp. dependence of ESR spectrum 2—68818
amino and γ-irradiated crysts., study of u.v.-induced free radical conversion using EPR 2—84667
butatrienyl, e.s.r. in Ar matrices 2—83286
t-butyl, e.s.r. evidence for planarity 2—74288
tert-butylperoxy, prep. and e.s.r. spectrum 2—65391
carbazyl, recrystallised samples, e.s.r. line width and exchange narrowing 2—65330
chemically induced dynamic polarization in thin films 2—51461
in chrysene, X-irradiated, e.s.r. examination to investigate stable free radicals formed 2—57393
cyclohexene and formic acid, step-growth polymerization of polyester 2—83351
cysteine hydrochloride monochydrate, u.v. and γ-irrad., radical recomb., mag. reson. obs. 2—72575
1,1-difluoroalkyl, solution e.s.r. spectra, asymmetric line-width effects in presence of resolved second order splittings 2—56519
elastomers, detected by e.p.r. during mechanical testing at low temperatures 2—60886
electron-spin polarization, generated by radical-pair mechanism, calc. of limiting polarization 2—54543
ENDOR, of free radicals in soln, temp. and conc. depend. 2—80480
fluoromethyl, ab initio calculations and α-F spin coupling parameters 2—77148
hydrazil, recrystallised samples, e.s.r. line width and exchange narrowing 2—65330
hydrocarbon 40 keV $CH^+ \to C^+ + H$, $C + H^+ C^+ + H^+ + e$, fragment kinetic energy meas. 2—70772
hydrocarbons of form $CH_n{}^+$, $n=2, 3, 4, 5$, dissociation, kinetic energy of H^+, $H_2{}^+$, $H_3{}^+$ fragments 2—70771
1 and 2hydronaphthyl radicals in naphthalene single crystals, e.p.r. study 2—54499
hyperfine coupling constants 2—42854
imidazole, produced by γ-irradiation of single crystals, ENDOR determ. of hyperfine tensors for protons in H bonds 2—65394
iminoxyl, n.m.r. spectra interpret. 2—80110
iminoxyl radical with ^{15}N isotope, mol. reorientation character effect on e.s.r. lineshape 2—70773
inorganic, calculation of hyperfine coupling constants 2—42863
malonamide, X-irradiated, confirmation of σ-radical, e.s.r. spectra obs. 2—64185
methyl, ab initio calculations of hyperfine coupling 2—77148
methyl radical + $Cl_2(Br_2)$ collisional reaction, molec. beam study 2—61779
methylchlorosilyl radical, meas. of ^{29}Si coupling consts. effect of degree of CH_3 substitution on planar structure 2—56241
methylene, low-lying electronic states, nonempirical CI study 2—53025
in molecular crystals, irradiated, recombination used for diffusion process study 2—80722

Free radicals continued
nitroxide, slowly tumbling adiabatic rapid passage e.p.r. spectra 2—83339
nitroxide radicals, photoelectron spectra and mol. orbital calcs. 2—80073
organic nitroxide, quadrupole splitting obs. by ENDOR in liquid crystals 2—50103
phenyl, photoionization, determ of heat formation and ionization potential 2—67520
photoproduction in ethanol glasses, e.s.r. studies 2—81509
pi hydrocarbon, ^1H and ^{13}C hyperfine splitting, unrestricted Hartree-Fock calc. 2—67453
poly(methyl methacrylate), prod. by radiation, effect on u.v. absorpt. 2—84671
polymer, formation during fluorination, e.s.r. detection 2—61771
in polymers under uniaxial tension, mechanism for submicrocrack generation 2—74858
polystyryl chain length dependence of coupling reaction 2—72556
propargyl, e.s.r. in Ar matrices 2—83286
reactions, preexponential factors calc. using bond entropy additivity 2—84638
recombination reactions in $H_2/O_2/N_2$ flames 2—65373
recrystallized PAC powder, meas. of line shapes, line widths, g factors of e.s.r. spectra 2—81484
rubber, formed during tensile testing at low temp., e.p.r. 2—43710
sonoluminescence of liquids, due to recombination 2—71210
succinic acid, ESR studies on radical conversions 2—81528
thiocarbonyl anion, e.s.r. studies of structure 2—53082
1,2,4-triazole, produced by γ-irradiation of single crystals, ENDOR determ. of hyperfine tensors for protons in H bonds 2—65394
trimethyl-lead radical, e.s.r. spectra, determ. of g tensors and hyperfine coupling 2—70795
vinyl, e.s.r. in Ar matrices 2—83286
vinyl-type radical in irrad. maleic acid matrix, e.s.r., geom. and electronic struct. 2—64195
BF_2, ab initio calc. of electronic struct. and geometry 2—83244
BH_2, ab initio calcs. including electron correl. of lowest states 2—80011
BH_2, structure of transition dipole moment 2—80025
$BrO_3{}^-$, vibrational spectra and force constants 2—59996
$CF_3 + NH_3$, Arrhenius parameters, kinetic isotope effects and tunneling corrections 2—81496
CH, ab initio valence bond treatment 2—50025
CH, excited states, Rydberg and valence shell character as functions of internuclear distance 2—50056
CH_2, structure of transition dipole moment 2—80025
$CH(^2\Pi)$, pulse radiolytically produced, reaction with methane, kinetics of ethylene production 2—48347
$CH_3 + NH_3$, Arrhenius parameters, kinetic isotope effects and tunneling corrections 2—81496
CN red band system, shock tube determ. of electronic transition moment 2—77083
ClCO, ClOO, e.s.r. spectra, g-factor and h.f.s. tensors and nucldar quadrupole coupling constants 2—50031
$ClO_3{}^-$, vibrational spectra and force constants 2—59996
ClOO in Venusian atm., structure and stability 2—78559
Cn, level anticrossing 2—42878
$CrO_4{}^{2-}$, resonance Raman spectra, analysis of ν_1 breathing mode 2—50054
D_3O, matrix stabilised, comparison of e.s.r. spectra with INDO calculations 2—42892
Fe(III) complexes with oxyacids, low temperature photolysis, e.p.r. spectra 2—75393
HO_2, i.r. spectrum, vibr. funds., electronic struct. 2—56174
H_3O, matrix stabilized, comparison of e.s.r. spectra with INDO calculations 2—42892
HOO, nonempirical LCAO MO SCF and CI studies of low lying electronic state 2—50040
$IO_3{}^-$, vibrational spectra and force constants 2—59996
$MnO_4{}^-$, resonance Raman spectra, analysis ν_1 breathing mode 2—50054
$N_3{}^{2-}$ and $N_3{}^0$, molecular orbital calc. of isotropic hyperfine interactions 2—64144
NF_2, ab initio calc. of electronic struct. and geometry 2—83244
NH, excited states, Rydberg and valence shell character as functions of internuclear distance 2—50056
NH_2 structure of transition dipole moment 2—80025
$NH_2{}^+$, low-lying electronic states, nonempirical CI study 2—53025
NS, microwave spectra, transitions 2—76542
OH, kinetic behaviour in excess NO at 5-82 torr He 2—84666
OH, mirowave spectra, transitions 2—76542
$OH + NO_2 + Ar \to HNO_3 + Ar$ reaction rate const. determ. by u.v. fluorescent scatt. 2—81491
OH groups, dependence of torsional vibration frequency on H bond energy 2—42857
OH radicals formed from water of crystallization, role of H-bonding 2—81495
OH reactions with H_2, D_2 and CO, pulsed vacuum u.v. obs. using reson. fluoresc. 2—84665
$OH(^2\Sigma^+)$, rotationally excited, formation in water vapour discharge 2—60027
PH_4, trapped in solid Kr, e.s.r. obs. 2—64154
SO, microwave spectra, transitions 2—76542
SiH_2, ab initio calcs. for potential curves, description of geometry and electronic spectrum 2—46584
So_3F normal coordinate analysis in Urey-Bradley force field 2—56198

Freezing
see also Melting; Nucleation; Supercooling
— 2—67878
alloy, binary, dendritic coarsening, model 2—50818
alloy, binary, phase diagram 2—53509
alloy, dil. binary, solute redistrib. in melt, conc. and temp. gradient effects 2—47260
alloy, solidification morphology and casting characts. 2—64770
alloy, solidification rate rel. to thermal contact resist. 2—74586
alloy, ternary, monovariant solidification, and zone melting 2—47601
alloy, ternary, solidification behaviour, microsegregation and precip. mechanism 2—56915

Freezing continued
alloy solidification, growth morphology, in-situ radiographic obs. 2−47605
alloys, unidirectional solidification, review 2−80850
aqueous systems using temp. gradient microscope stage 2−74585
cloud droplets, rel. to ice form. mechanism in seeded convective storms 2−84856
disperse syst., of vapour, study by microwave abs. 2−56543
eutectic solidification, thermodynamics 2−47035
freeze-etching technique, temperature, vacuum and fracturing considerations in electron microscopy 2−79100
Green's functions for solving problems in cylindrical coordinate system 2−47030
hail formation in steady convective cloud 2−72792
ice, classical wire expt., heat conduction mechanism 2−45587
ice growth on cold metal from low pressure water vapour condensation 2−53498
ice-water system, Stephan problem solution 2−77470
Kirkwood-Alder transition, evidence for existence in colloidal system 2−67874
lattice theory, Lennard-Jones and $1/r^{12}$ system 2−77468
liquid drops in biphase gas system, adiabatic expansion 2−71111
lunar basalts, rate of solidification rel. to Hawaiian lava lakes 2−66144
mean field theory, formulation in terms of variational principle, description of freezing transition and frozen state 2−53494
melt, setting, calc. of thermal convection 2−60547
membrane-filter ice nucleus chamber, numerical estimates of humidity 2−65671
metal, solidification, effects of shock, vibration and flow 2−80851
metal, spherical cryst. dendritic growth from highly supercooled liq. metals 2−60966
off-eutectic composite growth, transient composition changes, calc. 2−60548
polluted water drops and atmospheric aerosols, freezing temperatures 2−71276
porous material, capillary, of vapour, study by microwave abs. 2−56543
pressurization of solidifying sphere of molten material 2−47039
rain drops with different solutes and anomalous ice concentrations in clouds 2−54843
seawater, freezing point, resolution of discrepancies in existing data 2−57896
seawater interferometry meas. or convection currents 2−65601
semiconductor pseudobinary alloy, diffusional freezing for cryst. growth 2−47702
sludges and slurries, aqueous, effect of freeze-thaw treatment on precip. 2−83807
solid-liquid growth fronts, solute distrib., contrib. to interfacial undercooling 2−43517
solidification processes, effects of thermal oscillations 2−47028
specimen preparation with freeze-drying technique for electron microscopy 2−79098
steel, austenitic stainless, containing delta ferrite, solidification 2−43847
steel, MnS inclusion size, effect of solidification rate and S content 2−43852
steel, unidirectional solidification, growth rate rel. to fluid flow speed. 2−47620
steel drops, solidification in oil 2−43440
supercooled liquid, approx. cryst. growth rate estimation 2−56540
temperature-gradient microscope stage, aid in teaching solidification phenomena 2−58680
thermodynamics of freezing of small solution droplets containing insoluble particles 2−54841
transient, in laminar tube-flow 2−83731
turbulent flow in pipes, separation of binary mixtures 2−46878
water, in porous glass, freezing point lowering 2−80880
water, porous rocks, periglacial zone, freezing-thawing process 2−75446
water, sp. ht. near crit. point and Ornstein-Zernike fluctuation corrections 2−60541
water droplets, supercooled shattered by shock waves 2−47037
water drops, by contact with CuS particles 2−48499
water drops, ejection of microdroplets from surface 2−50401
water drops, freely suspended supercooled, by contact nuclation 2−47036
Ag-15% Ge alloy, splat-cooled, martensitic transformation of structure 2−56921
Ag-Cu alloy, eutectic, freezing and melting point determ. 2−53486
Al-Cr range extension in equilibrium diagram 2−43824
Al-(4.5wt.%)Cu alloy, late stage of solidification, two-dimensional flow of liquid 2−47038
Al-Cu alloy, di-directional solidification and dendritic growth 2−50823
Al-Mn range extension in equilibrium diagram 2−43824
Al-Si alloy, solidification in shell mould, and effects of additional elements 2−84134
Al, di-directional solidification and dendritic growth 2−50823
Al alloy, pressurization of solidifying sphere 2−47039
Al alloys, eutectic, microstructures for unidirectional solidification 2−67985
Al drops, supercooling and spheroidizing, effect of Cu inclusions 2−43441
$Ba_4SrNb_{10}O_{30}$, solidification 2−47654
Bi-Cd, eutectic, unidirectional solidification 2−43442
Bi-Cd eutectic, cellular solidification, plane front- cell transition 2−43443
$Ca^{181}HfO_3$, perovskite-type, nucl. quadrupole interactions, perturbed-angular-correlation meas. 2−72244
CdTe, optical grade cryst. prod. by directional solidification 2−50607
Co-Cu-Fe-Ce permanent magnet prep. by directional solidification 2−43787
Co-base composite materials, superalloys with fibres obtained by direct solidification, props. 2−64793
Co, Cr-$Cr_{7-x}Co_xC_3$, monovariant eutectic, faceted-nonfaceted, strongly coupled growth 2−57010
Co_2Si, solidification characts. 2−43924
Cu, point determ. 2−53496
Fe, cast, melt solidification, nodular graphite formation, additive effects 2−74881
Fe, cast, nodular, solidification process and quenching technique and relation to austenite shell 2−60549
Fe, cast, solidification of elbows 2−74587
Fe drops, solidification in oil 2−43440
Fe(II) salt solutions, frozen at normal pressure 2−78178
H_2O, adsorbed layer on silica, n.m.r. obs. 2−53596
^{3}He, solidification press. below 3 mK 2−56537
KCl-H_2O, solns., permittivity discontinuities at crit. pt. 2−53499
Mg-Zn alloys, Ostwald ripening during solidification of nondendritic spherical structures, model 2−64508
MgO-$MgAl_2O_4$ system, eutectic solidification 2−47658
MnSb-(Sb,Bi) and MnSb-(Sb,Sn) eutectics, growth rate effect on morphology 2−47641
NH_4Cl-H_2O, solns., permittivity discontinuities at crit. pt. 2−53499
NH_4Cl(I) aq. solns., elec. pots. generated on freezing at uniform rate, substrate effects 2−53495
Ni-base composite materials, superalloys with fibres obtained by direct solidification, props. 2−64793
Ni_3Al-Ni_3Ta eutectic, directional solidification growth 2−47644
Ni_3(Al,Ti), Ni-rich γ'-phase, solidification behaviour and γ-precip. 2−53904
Ni_2Si, solidification characts. 2−43924
Pb-Bi alloys, nonequilib. freezing, quantitative predic. by classical eqn. 2−47032
Pb-Bi peritectic alloy, heat of solidification, calc. 2−43444
Sb-Sn alloy, peritectic crystn., pore form. 2−53906
Sn-Pb(Zn, Sb) alloys, unidirectional solidification, equiaxed crystal origin 2−74882
UO_2/W composite, unidirectional solidification behaviour 2−47669
Zn inogt, unidirectional solidification, uniaxed crystal origin 2−74882

Frenkel defects *see Crystal imperfections/interstitials*

Frequency *see Time measurement*

Friction
see also Internal friction
— 2−57589
— 2−67572
abrading surface shape, microscopic probability model 2−47562
air turbulent flow through porous tube with suction, friction factors 2−60338
AK-4 alloy, strengthening and roughness of rubbing surfaces, effect on wear and bearing capacity 2−60916
atmospheric drag cross section solar cell arrays, nodal regression, solar declination 2−83677
ceramic, fund. review 2−47554
ceramic and cermet characts. 2−47555
ceramic coupled with surface-hardened metallic alloy 2−47556
cermet, Fe-based, antifriction props. rel. to sintering in various protective atmospheres 2−77727
cermet, Fe-based, effects of protective sintering atmos. on antifriction props. 2−68166
contact parameters, surface films and microprojection hardening influences 2−47557
cylinders, glass and plastic, contact stresses, elastohydrodynamic lubrication 2−47559
cylinders rolling on viscoelastic plane, contact area rel. to vel. 2−66488
drag, plate in incident longitudinal flow 2−46663
drag of cylinder with air blowing in air stream 2−71074
drop weight expts., impact kinetics, energy dissipation rel. to heating 2−64737
elastic bodies, wave losses 2−52129
elastic wave propagation in elastic medium with surface Coulomb friction 2−76364
fibre/fibre, meas. with scanning electron microscope 2−82441
flow, laminar, through rotating vertical cylinder, vel., friction loss, press. gradient 2−67714
gas flow over plate, heating and surface temp. 2−64366
glass, hot viscous, sliding on metal surfaces, mechanics 2−56553
granite, stable sliding stick-slip transition, seismological implications 2−61941
graphite, anti-friction AG-T type, 150 to 600°C 2−43743
gyroscope suspension bearings, effect of friction on motion with forced rotation of mounting 2−82137
harmonically bound semi-infinite and finite chains, dynamics 2−63058
Hertzian partial elastohydrodynamic contacts between real surfaces 2−68117
hypersonic turbulent flow, film cooling effectiveness and skin friction 2−83666
liquid film on inclined plane, polarographic obs. 2−83728
local skin friction evaluation in compressible flow 2−53299
lubricated sliding point contacts, load, traction, film thickness meas. device 2−53864
lubrication ball and peg testing machine, friction monitoring 2−68123
machine for testing antifriction materials up to 700°C 2−56848
magnetically suspended rotating spheres, residual drag torque 2−73350
metal stylus, sliding friction under negative load on graphite and diamond 2−84044
minimum drag in free-molecular flow, determination of optimum non-slender bodies of revolution 2−53122
nonstationary flow in tubes, coefficient of frictional resistance 2−50148
plastic flow with Coulomb friction, equilib. method and upper bound theorem in plane problems 2−45419
polyethylene, high density, static and kinetic friction over clean surfaces, transfer and molecular structure 2−64738
polyethylene, surface, anomalous low friction for steel-polymer friction by helium atom irradiation 2−56837
polyfluoroethylene, filler content influence 2−47553
polymer with inorg. chain mols., self-lubricating heat-resisting antifriction props. 2−43745
polymers, three section single-contact roller machine for det. 2−56850

Friction continued
polypropylene, surface, anomalous low friction for steel-polymer friction by helium atom irradiation 2−56837
powder, effect of temp. and press. 2−43880
PTFE, static and kinetic friction over clean surfaces, transfer and molecular structure 2−64738
PTFE, transfer in sliding. occurrence of thin film 2−53820
rocks, model of fault behaviour 2−57728
rod/spring/block system, impulse driven, mech. self-oscillation 2−78867
rolling contact, surface roughness effects 2−68116
scanning electron microscope obs. 2−43741
seizure resistance between sliding surfaces under high, low loads, factors influencing 2−43742
self induced vibration elimination 2−60914
sheet drawing, analysis of effects 2−60913
steel, 38KRM Yu A, strengthening and roughness of rubbing surfaces, effect on wear and bearing capacity 2−60916
steel, heat treatment depend. 2−60962
steel, lubricated friction against Al, oxidation influence 2−53844
surface deformation and destruction, statistical structural model 2−43746
temperature anomaly in surface layers of sliding surfaces 2−53843
Tennessee Sandstone, exptl. investigation of stick-slip 2−62089
Tennessee Sandstone, influence of surface roughness and gouge on frictional sliding 2−65521
vinyl chloride-acetate copolymer, wear resist. and frictional props. 2−47561
Al, energy loss, rel. to projectile penetration forces 2−53803
Al_2O_3 and Al_2O_3/B fibre composites, high temp. bearing characts. 2−47558
Be, temp. depend. of friction stress for basal dislocations, 300-500K 2−64753
C-metal composite, high strength, evaluation as sliding material 2−61019
Co alloys, metallurgical structure and properties 2−71667
MoS_2 coating, applied to steel by detonation, friction resist. 2−43744
WSe_2-$NbSe_2$ alloys, antifriction and elec. props., comp. depend. 2−68115
Frictional electricity *see Electric charge; Electrostatics*
Fuel cells *see Electricity, direct conversion/fuel cells*
Fugacity *see Diffusion in gases; Kinetic theory/gases*
Functions
analytic, on hyperspheres, harmonic analysis 2−45236
analytic, optimized data extrapolation off the boundary 2−49475
analytic, optimized data representation, statistical extrapolation 2−78860
Bessel, computation in high scattering studies 2−70022
Bessel, cylindrical, for neutron ang. distrib. analysis 2−82978
Bessel, for torsional vibrations of orthotropic cylindrical shell 2−73411
Bessel, FORTRAN subroutine for calculating $j_l(\rho)$, $J_{l+1/2}(\rho)$ and derivatives 2−41459
Bessel functions, generalized of first kind 2−45235
Cauchy problem, rel. to thermal cond. of rigid conductors 2−82272
Coulomb, FORTRAN IV subroutine, numerical accuracy 2−45237
Dirac delta function, integral representation 2−78735
eigenfunction expansions, appl. to problems in nonlinear space time reactor dynamics 2−83101
eigenfunctionals of one-dimensional transport operator in modal approx. 2−76217
functional analysis, text book for first year graduate student 2−82182
Gegenbauer (ultraspherical) polynomial applic. to cooling of heated cylinder 2−82242
Gegenbauer polynomials, appl. to heat production in cylinder 2−41855
Green Kubo autocorrelation functions, asymptotic behaviour of Green Kubo integrands 2−74308
H-function, for boundary value problem in electrostatics 2−45636
harmonic, analytic continuation to points of lower half-space which lie outside given sphere 2−45228
harmonic principal, applic. to fluid mechanics and thermodynamics 2−70826
hypergeometric, confluent, for Coulomb wave functions 2−49006
Jacobi polynomial, for Coulomb wave functions 2−49006
$K_n(\tau)$ in nongrey radiative transfer, mathematical properties 2−76238
Laplace transform of neutron age in perpendicular direction in slab lattices 2−83059
Meijer's G-function, expansion formula 2−41855
modulated, normal, generalization of Hagen theory of elementary errors 2−62966
multidimensional Newtonian method for flutter equations 2−73288
organism transfer functions expressed in servomechanism theory, application to calc. of urinary excretion of inhaled nuclide 2−55221
orthogonal, generated by M-sequence, appl. 2−76171
projecting, synthesis, rel. to electron microscopy 2−74717
pseudo stream, for natural convection in confined porous medium 2−55583
recovery, from projecting function, theory 2−74716
spherical, for irreducible tensors 2−48981
Thomae-Whipple functions, for Wigner coeffs. 2−41464
Ursell-Mayer, functional calculus approach 2−41530
Fundamental concepts *see Physics fundamentals*
Fundamental constants *see Constants*
Fundamental particles *see Elementary particles*
Furnaces *see Heating; High temperature technique*
Furry theorem *see Quantum electrodynamics*
Fusion *see Heat of fusion; Melting; Nuclear fusion*
g-factor *see Elementary particles; Gyromagnetic ratio; Nucleus; Spectra*
G-matrix *see Molecules/internal mechanics*
Gadolinium
atom, L subshell fluoresc. using X-rays emitted by ^{155}Eu 2−70581
burnable poison for light water reactors 2−59844

Gadolinium continued
dislocation loops formed during electron microscopy of thin single crystal films 2−71489
elastic const., C_{33}, meas., 13 kOe max., 270-320 K 2−44260
electrical resist. anomaly near Curie pt. 2−57291
electrotransport of C, N_2 and O_2 2−80716
energy band theory, derived from group theory 2−57114
ferromagnetic, transient magnetic precession of Gd 2−65143
film, in Al-Al_2O_3-GD supercond. junc., electron spin polariz. detn. 2−64958
film, superferromagnetism 2−48093
Hall effect, elec. resist., galvanomag. effect of press., 77-400K 2−77858
Hall effect, pressure effect on single crystals 2−68547
magnetic anisotropy consts. temp. depend. 2−54321
magnetic crit. scatt. role in elec. resist. 2−57271
magnetic interactions, e.p.r. obs. 2−75352
magnetic permeability rel. to plastic deform. and recrystn. 2−81234
magnetoresistance in strong effective fields at 4.2K 2−77859
paramagnetic resonance, in YAl_2 and $Y_{1-w}Th_wAl_2$ 2−65327
paramagnetic susceptibility anisotropy, 5 to 750°C 2−44227
sound attenuation, meas., 13 kOe max., 270-320 K 2−44260
spin reorientation transition phenomena, sound propag. 2−54026
$CaF_2:Gd^{3+}$, second order spin-lattice coeffs., temp. depend., e.p.r. obs. 2−80890
$CdF_2:Gd^{3+}$, ionic thermocurrents, temp. depend. 2−81089
$CdF_2:Gd^{3+}$, second order spin-lattice coeffs., temp. depend., e.p.r. obs. 2−80890
$CeRu_2:Gd^{3+}$, supercond. transition temp. rel. to Gd^{3+} conc. 2−84302
EuO:Gd, bidirectional threshold and memory type switching 2−81081
Gd-Ti alloy, thermal conductivity and electrical resistivity 2−64866
Gd^{3+}, e.p.r. below 40G in single crystals of $Bi_2Mg_3(NO_3)_{12}.24\ H_2O$, lanthanum ethylsulphate and samarium ethylsulphate 2−51405
Gd^{3+}, e.p.r. in europium benzoylacetonate 2−81469
Gd^{3+}, e.p.r. spectra, in $ZnSiO_4$, $HfSiO_4$ and $ThSiO_4$ hosts 2−48278
Gd^{3+}, e.p.r. spectra, review 2−72485
Gd^{3+}, e.p.r. spectrum in SrF_2, Ce^{3+} codopant effect 2−61737
Gd^{3+}, in CaO, CaF_2, ThO_2 and CeO_2, spin-lattice coeffs. calc. 2−51286
Gd^{3+}, in chalcogenide glass, e.p.r., fine struct. 2−72476
Gd^{3+}, in hexagonal CdS, axial centres, e.p.r. obs. 2−65333
Gd^{3+}, in Pd single cryst., paramag. resonance, resolved fine structure 2−68733
Gd^{3+}, in rare earth ethyl sulphate, e.p.r. obs. 2−75349
Gd^{3+}, in zircon struct., ground state splitting, ligand contribs. to quadrupole components 2−84235
Gd^{3+}, isotropic exchange interactions from e.p.r. measurement in rare earth insulators 2−72487
Gd^{3+}, isotropic g-factor for e.p.r. of GdB_6, at 9.16 Ghz 2−72486
Gd^{3+} e.s.r. centres in SrF_2 and BaF_2, hydrolysis effects 2−84582
Gd^{3+} impurity in Al_2O_3-Fe_2O_3 system, effects on spin relax. time of ferric ions 2−54368
Gd^{3+} in CaF_2, thermolum. glow curves, hole activation energies, 4.2 to 600K 2−57377
Gd^{3+} in SrF_2 possible existence of separate cubic symmetry 2−80705
Gd^{3+} in ThO_2, hyperfine splitting 2−84581
Gd^{3+} ion aqueous solns., fluoresc. quenching by vibrs. of solvent mols. 2−60481
$La_2O_2S:Gd^{3+}$, e.s.r. 2−72491
$PbMoO_3$:Cu, Gd, site occupancies of dopant and trace impurity 2−68739
Tl^+-Gd^{3+} energy transfer, in inorganic glasses, fluorescence obs. 2−61709

Gadolinium compounds
— 2−72462
Au-Gd alloy, dilute, exchange interact. with cond. electrons, e.p.r. obs. 2−72467
$Ce_{1-x}Gd_xRu_2$ alloys, supercond. and normal, magnetiz. curves 2−44073
Fe_xGd_y alloy films, amorphous, mag. props. 2−44275
GGG, epitaxial magnetic film, prep. by chem. vapour deposition 2−77527
Gd-B system, phase behaviour 2−50969
Gd-Ni intermetallic compounds, paramagnetic resonance meas. of g, values, study of exchange interactions 2−84568
Gd-Th alloys, elec. resist., mag. ordering effects 2−84294
Gd-Y alloys, Hall effect, 4.2-340K 2−68332
Gd-Zr alloys, form. of metastable low temp. allotropic solid solns. 2−47646
$(Gd,Tb,Eu)_3Fe\ O_{12}$ ferrite garnet, optical anisotropy and cylindrical domains 2−68602
Gd^{3+} ions in solutions of complex compounds, luminescence 2−71211
$GdAl_2$, mag. induced elec. field gradient, spin echo obs. 2−72509
$GdAl_2(Co_2)(Ni_2)(Pt_2)(Rh_2)$, elec. resist. behaviour in crit. region 2−57279
$GdAlO_3$:Er, Zeeman optical absorp. spectra, Er^{3+}-Gd^{3+} exchange interaction obs. 2−57349
$GdAlO_3$, obs. of u.s. attenuation in high magnetic field, spin wave interactions 2−54348
GdAs, antiferromag. ordering, exchange consts. calc. 2−61549
GdB_6, exchange interactions, e.p.r. obs. 2−81468
GdB_6, nonstoichiometry 2−47183
GdB_6, polycrystalline, e.p.r. spectrum at 9.16 Ghz, using reflection type cavity spectrometer 2−72486
$Gd_2(CO_3)_3.xH_2O$, standard heats of form. 2−43335
$GdCl_3$, ferromag., dipole-dipole interact. theory 2−68534
$GdCl_3$, low temp. cooperative behaviour n.m.r. obs. 2−72166
$GdCl_3$, n.q.r., hydrostatic press. coeffs., soft sphere model 2−54519
$GdCl_3$, single-ion-induced absorpt. lineshapes, magnon and exciton states dispersion 2−48181
$GdCo_2$, Co atom paramagnetic moments 2−72116
$GdCo_5$, powder, coercive force rel. to sintering temp., decomp. stability 2−68511
$Gd(Co_{1-x}Ni_x)_3$ and $Gd(Fe_{1-x}Ni_x)_3$, transition metal moment obs. 2−51271
GdFe garnet, bubble domains, flux switching 2−57305
GdFe garnet polished platelets, uniaxial anisotropy 2−44276

Gadolinium compounds continued
GdFe garnet with Co^{2+} substituted, magnetooptical props. 2−84460
GdFe garnet with Tb^{3+} impurity, ferromag. reson. 2−72453
$Gd_3Fe_{5-x}Al_xO_{12}$ garnet, cation distrib. detn., Mossbauer obs. 2−48147
GdGa, mag. props. 2−48079
GdGa, magnetization and susceptibility, temp. depend. 2−72170
$GdGa_xCu_{1-x}$, electronic struct., rel. to mag. order 2−78020
GdIG, high temp. high press. phase formation 2−57024
GdIG, sublattice rotation near mag. compensation point, sp. ht. study 2−61508
GdIG, substituted, compensation temp., applic. to beam- addressable magneto-optic memory 2−72193
Gd(III) complexes in dimethylformamide solution, electron spin relaxation 2−64474
$GdIn_3$ magnetic properties 2−72223
$GdIn_xAg_{1-x}$, electronic struct., rel. to mag. order 2−78020
$Gd_{1-x}La_xZn$, n.m.r., zero-field resonances, hyperfine field contribs. 2−72510
$GdLiO_2$, luminesc. of Eu^{3+}, energy levels 2−48226
$Gd(MoO_4)_3$, ferroelec. domains and condensed soft mode 2−68470
Gd_2MoO_4, det. of thickness of domain walls by Raman scattering 2−72366
β-Gd_2MoO_4, heat capacity, entropy magnetic moment from 0.4 to 4.2K along b crystal axis 2−51277
β-$Gd_2(MoO_4)_3$, electrically polarized, 0.4 to 4.2K, up to 90 kG along a crystal axis, heat capacity, entropy, magnetic moment 2−44290
$Gd_2(MoO_4)_3$, ferroelec., electro-optical props. 2−78068
$Gd_2(MoO_4)_3$, ferroelec., ferroelastic, elastic constants and soft optic modes 2−65061
$Gd_2(MoO_4)_3$, improper ferroelec., induced and spontaneous birefringence 2−61588
$Gd_2(MoO_4)_3$, π-GMO, X-ray amorphous, prepn. and physical parameters 2−84136
$Gd_2(MoO_4)_3$, Raman spectrum, temp. depend. 2−68660
β-$Gd_2(MoO_4)_3$, second harmonic generation, pseudotetragonal symmetry effects 2−51298
$Gd_2(MoO_4)_3$ diffracted light obs. from domain wall 2−84467
$Gd_2(MoO_4)_3$ piezoelectric d_{36} coefficient 2−81149
Gd_3NF_6, mag. props. 2−48110
Gd_3NbO_7, crystal structure 2−47346
$Gd_2O_3:Eu^{3+}$ transparent phosphor, prep. and optical props. 2−72409
$Gd_2O_3:Eu^{3+}(Tb^{3+})$, flame excited luminesc., temp. depend. 2−48270
Gd_2O_3-GeO_2 system, phase diagram obtained by high temp. microscopy, microstructural and X-ray phase anal. 2−84097
$Gd(OH)_2$, magnetic specific heat, and ac susceptibility measurements using a r.f. tunnel diode oscillator 2−68513
$Gd(OH)_3$, single-ion-induced absorpt. lineshapes, magnon and exciton states dispersion 2−48181
$Gd_2O_2S:Tb$ as phosphor for X-ray image intensifier screen 2−73251
Gd_2O_2Se, mag. props. 2−44228
GdP, antiferromag. ordering, exchange consts. calc. 2−61549
$GdRu_2$, struct., high press. effects 2−71689
GdS, magnetic coupling and band structure, electron photoemission studies 2−72139
GdS, magnetic coupling and band structure, electron photoemission studies 2−72139
A-Gd_2S_3, crystal growth from gaseous phase, physical properties 2−53607
$Gd_2(SO_43.8H_2O$ paramag. relax. times meas. 2−84455
GdSi 2−68568
Gd_5Si_3, antiferromagnetic properties, magnetic structure 2−68568
GdTbFe garnet, cylindrical magnetic domains, hard bubbles 2−65169
$GdTiO_3$, resist. and Seebeck coeff., 77-1500 K 2−57144
$GdVO_4$, luminescence dependence on electronic transitions in VO_4^{3-} 2−65300
Gd_xY_{1-x}, e.p.r. of Gd, g-shift and linewidths 2−81462
$Gd_{1-x}Y_xZn$, n.m.r., zero-field resonances, hyperfine field contribs. 2−72510
$GdZn_xAg_{1-x}$, electronic struct., rel. to mag. order 2−78020
La-Gd dil. alloys, supercond., temp.-depend. pair breaking 2−54144
(La,Gd)Al_2, dilute system, n.q.r. and relax. obs., ordering onset 2−68754
$La_{1-x}Gd_xAl_s$, nuclear spin lattice relax. 2−54370
Mg:Gd, dil. mag. alloy, exchange narrowing of fine structure 2−72496

Galaxies
see also H I regions; H II regions; Intergalactic matter; Nebulae
0620-52, radio, redshift values 2−66061
A262 cluster, morphology of galaxies 2−58190
Abell 2147 region, redshifts 2−55009
Abell 2199 cluster of galaxies, static properties of 170 objects 2−69030
absorption of light, statistical evaluation 2−72978
activity, interpreted in terms of plasma processes 2−58220
activity, plasma MHD processes 2−58193
Andromeda, high velocity HI regions in centre 2−51705
Anon 0947 + 31, bright u.v. knots, H II regions 2−84962
asymmetrically rotating fluid disc model 2−56279
blue emission-line galaxies in rich clusters 2−84961
bright, correlation with 3C QSO's 2−48742
bright, integrated magnitude, colours, USV photometry 2−84956
3C 120, Seyfert, rapid expansion of radiosource at 3.8 cm wavelength 2−58400
3C 120, Seyfert galaxy, optical spectrum 2−58203
3C 273, circular polarization obs. 2−58405
Cassiopeia, nebulae, investigation by Fabry- Perot interferometer 2−75695
CGCG 1622+4112 extremely compact galaxy, spectral analysis 2−55018
cluster Abell 31, distrib. obs. 2−75677
clusters, Abell's, evolutionary effect 2−75676
clusters, as X-ray sources, review of current theories 2−55102
clusters, description by approx. solutions of relativistic gravitational field eqns. 2−58197
clusters, n-body problem 2−58233
clusters, relation between X-ray luminosity and velocity dispersion 2−58202

Galaxies continued
clusters of galaxies, estimation of masses of individual components 2−66054
clusters of galaxies rel. to extended X-ray sources and Compton scattering of electrons 2−51798
collapsing, variations of stellar orbits 2−81784
collisions, mass loss and formation of giant systems 2−44841
collisions and charges in gravitational energy 2−58200
Coma cluster, absence of Lyman α emission 2−58227
Coma cluster, correlation of redshift with magnitude and morphology 2−51706
Coma cluster, density data and emission measure 2−75680
Coma Cluster, distribution of orientations, selection effects 2−58225
Coma cluster, E and S0 galaxies, absolute magnitudes 2−58192
Coma cluster, infall of matter, effect on evolution 2−58191
Coma cluster, ionized intergalactic gas, models and mass estimates 2−51700
Coma cluster, radial velocities, structure and stability 2−51707
Coma Cluster, redshift, morphology and integrated magnitude relationships 2−58224
Coma Cluster, reidentification of 5C4 radiosources 2−48748
compact, Zwicky's list, correlation with radiosources in Ohio Survey 2−51787
with complex blue nuclei, inner part of flat subsystem 2−72977
concentration indices and central surface brightness, surface photometry 2−55017
current studies 2−66065
Cyg A, emission-line spectrum 2−66060
damping of galactic density waves by induced shocks 2−48660
diameter-redshift relationship 2−75690
disk galaxy studies, construction of static self-consistent model 2−58229
disk like stellar systems, constant models 2−81774
distances rel. to expanding universe, Hubble constant and Freidmann time 2−69039
distribution of orientations, selection effects 2−58225
dust grains, radiation-driven efflux and circulation in spiral galaxies 2−81802
dynamic astronomy, meeting (College Park, USA, March 1972) 2−58166
elliptical, 10 colour photometry 2−58216
elliptical, multiple systems, photometry 2−69040
elliptical, search for H I regions 2−75678
evolution, collapse of massless, non-rotating cloud around point nucleus 2−84953
evolution, models 2−78453
extragalactic distance determinations using classical Cepheids 2−69095
extragalactic radiosources, emission mechanisms 2−48754
extragalactic rings, spectra 2−58207
faint blue objects at high galactic latitude 2−58201
Faraday depolarization of radio galaxies and quasars 2−73042
flat, gravitational field calc. 2−55010
flat, nonlinear spiral structure 2−75683
flat, speed distribution function 2−81773
formation, evolution of expanding hot universe 2−51712
formation, from thermal instability in expanding universe 2−51714
formation, role of intergalactic mag. fields 2−66049
formation from primeval universal turbulence 2−62465
formation in anisotropic cosmologies 2−69014
Galaxy and the distance scale, Woolley symposium, Herstmonceaux, Aug (1972) 2−69015
gas content and density rel. to efficient star formation 2−58230
gas content hypothesis, star formation, Jeans instability 2−62466
gravitationally interacting binary systems, computational models 2−55012
groups, instability explained by presence of intergalactic ionized H 2−48665
IC342, Scd, global HI distrib. obs. at 21 cm 2−58223
IC 10 heavily obscured, 21 cm line study 2−44896
IC 450, Markarian 6, H line activity 2−69028
identification with radiosources in 4C catalogue 2−81786
II Zw 40, neutral H study of compact galaxy 2−81793
IIIZw43 compact, spectrum, recession velocity obs. 2−72976
infalling matter effect on heavy element content of galaxy 2−55015
intergalactic reddening 2−66051
internal kinematics of two compact galaxies 2−58210
internal motions in 'spiral nebulae', historical perspective of Adriaan van Maanen's work 2−55019
i.r. obs 2−58212
Large Magellanic Cloud, catalogue of spectral classifications, radial velocities and u.b.v. photometry of stars 2−62548
Large Magellanic Cloud, for u.v. imagery from Moon by Apollo 16 crew 2−75685
Large Magellanic Cloud, Hα emission stars 2−58204
Large Magellanic Cloud, photometry of bright stars 2−48697
Large Magellanic Cloud, positions, dimensions and photometric props. of dark nebulae 2−62474
Large Magellanic Cloud, spectroscopic study of blue globular clusters 2−81804
Large Magellanic Cloud, supergiants and galactic foreground stars 2−66059
Large Magellanic Cloud, supernova remnant obs. 2−69090
Large Magellanic Cloud, tilt, galactical binary 2−75673
Large Magellanic Cloud, topography of 1830 variable stars 2−75691
Large Magellanic Cloud, UBV photoelectric photometry of 160 O-B supergiants 2−62546
Large Magellanic Cloud, van Wijk sequence, UBV photometry obs. 2−69033
Large Magellanic Cloud, X-ray observation 2−62467
Local Supercluster, intergalactic extinction, selective 2−44840
M101, Scd, global HI distrib. obs. at 21 cm 2−58223
M101, spiral, density wave streaming 2−58232
M101, type II supernova, polarization measurements 2−73020
M31, nuclear region, energy distrib. in i.r. 2−72975
M31, nucleus, spiral structure and elliptical companion obs. at 1415 MHz 2−69031
M31, stellar motions in nuclear disk 2−58209
M31, velocity dispersion of stars in nucleus 2−75682
M31, Wing-Ford band at 9910 Å as population indicator 2−58217

Galaxies continued

- M31 (Andromeda galaxy) and halo, radio observations in v.h.f. range 2−81787
- M32, nuclear region, energy distrib. in i.r. 2−72975
- M51, emission line strength in nucleus, greater magnitude than galactic HII regions 2−75688
- M51, structure of small sources at 2695 MHz 2−72973
- M51, UBV photoelectric obs. 2−58215
- M51 spiral structure, density wave nature 2−58234
- M5, study of W Virginis type variables V42 and V84 2−58321
- M64, emission line strength in nucleus, greater magnitude than galactic HII regions 2−75688
- M81, emission line strength in nucleus, greater magnitude than galactic HII regions 2−75688
- M81, photometric obs. 2−58214
- M82, linear polarization of $H\alpha$ emission line in halo 2−58194
- M82, peculiar exploding galaxy, millimetre observations, loop stability 2−55011
- M 31, M 32, M 81, population synthesis, quadratic programming 2−81799
- M 32, mass determination, from radial velocity distrib. of stars 2−58196
- M 81, photoelectric study 2−66055
- M 82, polarization and velocity field, model 2−66056
- Maffei 1 and 2, interstellar absorption, UBV photometry 2−55016
- Maffei 2, radio maps 2−55013
- Maffei 2, spiral, radio map at 1415 MHz 2−69032
- Magellanic Cloud orbits rel. to rotation speed of the Galaxy 2−69037
- Magellanic Clouds, barred spiral structure 2−48667
- Magellanic clouds, distance scale, SMC Cepheids anomaly 2−69038
- Magellanic Clouds, photometry of Cepheids 2−62580
- Magellanic Clouds, props. of developing stellar systems 2−66062
- Magellanic Clouds, X-ray sources 2−62597
- Magellanic Clouds gamma radiation flux rel. to metagalactic origin of primary component of cosmic rays 2−72959
- magnetic field structures 2−51690
- Markarian, spectra 2−58189
- Markarian, spectroscopic, photometric and photographic obs. 2−58205
- Markarian, u.v. continuum, Seyfert galaxies 2−69027
- Markarian 231, absorption-line Seyfert, spectra 2−66057
- Markarian 231, i.r. photometry of the Seyfert galaxy 2−66063
- Markarian 78, violent mass motions 2−58206
- metagalactic background radiation, red shift losses and evolutionary effects 2−48649
- Molonglo Cross, pulsar declinations and periods 2−48749
- NGC2403, Scd, global HI distrib. obs. at 21 cm 2−58223
- NGC6946, Scd, global HI distrib. obs. at 21 cm 2−58223
- NGC 1052 nuclei, stellar population and continuum study 2−69034
- NGC 1068, circular polarization obs. 2−58405
- NGC 1068, circular polarization of u.v. 2−81794
- NGC 1068, Seyfert galaxy, structure of nucleus 2−72974
- NGC 1068 and 1566, Seyfert, comparison of nuclear luminosity, surface brightness and galactic disk colours 2−44842
- NGC 1275, radio gas ejection from nucleus 2−48664
- NGC 2403, spiral, density wave streaming 2−58232
- NGC 253, i.r. obs. of nucleus 2−58213
- NGC 253, obs. at 80 MHz 2−81795
- NGC 2655 nuclei, stellar population and continuum study 2−69034
- NGC 2903, stellar velocity fields 2−58208
- NGC 2903 nuclei, stellar population and continuum study 2−69034
- NGC 3115, nuclear region, energy distrib. in i.r. 2−72975
- NGC 3115 and 4472, absorption features in spectra, radial variations in strength 2−51709
- NGC 3516, Seyfert, variations in nuclear luminosity 2−81790
- NGC 4051, circular polarization obs. 2−58405
- NGC 4151, circular polarization obs. 2−58405
- NGC 4151, circular polarization of u.v. 2−81794
- NGC 4151, nuclear region, energy distrib. in i.r. 2−72975
- NGC 4151, Seyfert Galaxy, nonnuclear regions 2−75689
- NGC 4151, Seyfert galaxy, structure of nucleus 2−72974
- NGC 4151, Seyfert galaxy static photoionization models for emission line regions 2−69024
- NGC 4319, spiral, evidence for physical connection with Markarian 205 2−66058
- NGC 4406, nuclear region, energy distrib. in i.r. 2−72975
- NGC 4486, gas ejection and nuclei activity obs. 2−84963
- NGC 4486, radio, gas ejection from nucleus 2−48664
- NGC 4569 nuclei, stellar population and continuum study 2−69034
- NGC 45, obs. at 21 cm using radiotelescope of Parkes, meas. of line profiles 2−58198
- NGC 4881, electrographic photometry, possible lenticular S0 classification 2−81788
- NGC 5128, radio gas ejection from nucleus 2−48664
- NGC 5194 and 5195, model of encounter 2−58211
- NGC 5194/5195 double system, multicolour photometric analysis 2−51710
- NGC 520 chain, discrepant redshift of cluster galaxies 2−58375
- NGC 5253, bright supernova, optical polarization 2−69091
- NGC 5253, interstellar lines in supernova spectrum 2−81828
- NGC 5253 rel. to NGC 5408, emission line type, velocities and N_2/H_2 ratio 2−51699
- NGC 5253 supernova, optical obs. 2−62574
- NGC 5548, Seyfert, variations in nuclear luminosity 2−81790
- NGC 55, for u.v. obs. by Apollo 16 from Moon 2−75699
- NGC 5866, stellar velocity fields 2−58208
- NGC 6814, Seyfert, brightness variations 2−66064
- NGC 6946, spiral, density wave streaming 2−58232
- NGG 1068, Seyfert, emission line profiles 2−58219
- non-velocity redshifts, systematic measurement errors 2−69036
- nuclei, collapse of gas into centre, time-dependent stability anal. 2−58221
- nuclei, ejection of massive objects 2−48661
- nuclei, energy source for violent events, explosive phenomena 2−81865
- nuclei, stellar population and continuum study 2−69034
- nucleus, model, stability of gas-star system 2−81895
- OJ 287, circular polarization obs. 2−58405
- optical circular polarization, search 2−75800

Galaxies continued

- optical identifications of radiogalaxies in the B2 catalogue of radiosources 2−62607
- peculiar in NGC 520 chain of quasars discrepant redshift of cluster galaxies 2−58375
- Perseus spiral arm, shock wave embedded in background density wave 2−58231
- physical associations with quasi stellar objects 2−51782
- PKS 2053-20, elliptical, radiosource, structure 2−58383
- PKS 2057-17, elliptical, radiosource, structure 2−58383
- population synthesis, quadratic programming 2−81799
- pregalactic turbulence, damping of eddy motion 2−81810
- proto-galaxies, formation in expanding universe, gravitational instability 2−51713
- protoclusters, formation, cosmology 2−75679
- protogalaxy, collapse, with rotation and capacity in later stages 2−58178
- radial flow of perfect gas with a central gravitating source 2−78433
- radial velocities of several groups of galaxies 2−69029
- radiation, elliptical polarization search 2−75724
- radio, dynamics of multiple explosions 2−58401
- radio, evolution and source 2−62599
- radio, luminosity-spectral index relationship 2−78481
- radio, optical position meas. 2−81872
- radio, redshift values 2−66061
- radio, role in observational cosmology 2−75804
- radio, rotation measures, interpretation 2−62602
- radio, rotation measures, redshift dependence 2−81871
- radio, source counts and evolution 2−62600
- radio astronomy, electrooptical processing 2−62813
- radio trails of active galaxies in clusters, rel. to interacting galaxies hypothesis 2−51711
- radiosource 3C 272.1 associated with M84 elliptical galaxy obs. at 2.7 and 5.0 GHz 2−58409
- radiotelescope interferometer expts., between US and USSR 2−58566
- redshift anomalies, photon-photon inelastic interaction as explanation 2−48643
- resonant stellar orbits in spiral galaxies 2−75684
- rich cluster, inverse Compton mode of X-ray emission 2−48757
- rich clusters, statistical assoc. with quasi-stellar radiosources 2−62609
- Scd, global HI distrib. obs. at 21 cm 2−58223
- Scd, HI distributions and rotation curves from obs. at 21 cms. 2−62464
- Seyfert, 3C 120, optical spectrum of nucleus 2−58195
- Seyfert, NGC 6814, brightness variations in nucleus 2−66064
- Seyfert nuclei images rel. to quasars 2−69035
- short lived phenomena, evidence from real-time image orthicon surveys 2−58218
- Small Magellanic Cloud, colour-magnitude diagram of NGC 419 star cluster 2−81803
- Small Magellanic Cloud, $H\alpha$ emission survey of main sequence stars 2−69106
- Small Magellanic Cloud, N_2 deficiency in planetary nebulae 2−44844
- Small Magellanic Cloud, search for absorption of soft X-ray diffuse flux 2−81816
- southern, with bright nuclei optical survey 2−58222
- spherical systems, predominant motions, instability 2−58199
- spiral, dynamics of self-gravitating gaseous discs 2−81815
- spiral arm mechanisms rel. to wave patterns in galactic disks 2−58228
- spiral arms, direction of winding in spiral galaxies 2−81811
- spiral structure, development and application of computer models, obs. of density waves 2−78444
- spiral structure, generating mechanism 2−48666
- Stephan's Quintet, radio continuum emission at 21 cm 2−81806
- tidal interactions in multiple galaxies and gas cloud tails 2−78447
- triple gravitational systems, evolution, termination of binary 2−58175
- Ursa major, distribution of orientations, selection effects 2−58225
- u.v. continuum, observational list 2−69025
- u.v. continuum, spectral and colour characteristics 2−69026
- violent events in nuclei, model based on blast waves in rotating media in gravitational field 2−55014
- Virgo Cluster, distribution of orientations, selection effects 2−58225
- Virgo cluster, E and S0 galaxies, absolute magnitudes 2−58192
- Virgo cluster, optical luminosities and diameters of galaxies, inclination corrections 2−81805
- water vapours, microwave radiation obs. rel. to maser mechanism 2−69016
- X-ray background radiation rel. to distributions and clustering of galaxies 2−58436
- X-ray emission near galaxies from accretion of hot gas 2−66050
- X-ray galaxies, possibility for high galactic latitude sources 2−75837
- IZw 129, compact, internal kinematics 2−51704
- IIZw 70, compact, internal kinematics 2−51704
- Zw Cl 0152+33, cluster of compact galaxies, redshifts 2−66104
- II Zwicky 40, age and structure 2−81800
- Zwicky catalogue, brightness distributions 2−58226
- CN band strength gradients, radial, near nuclei of galaxies 2−51708
- Fe spectral line identification and abundance 2−62748
- FeSi, electron microprobe analysis 2−75686
- NiFe, electron microprobe analysis 2−75687

the Galaxy

- background continuum at 15 GHz, thermal and nonthermal components 2−58187
- background radiation spectrum between 0.2 and 2.6 MHz 2−75675
- Carina spiral arm, H I velocities and stellar obs. 2−48662
- carina spiral features, structure and motions 2−72970
- centre region, high energy γ-radiation 2−62636
- Cepheus extension of Perseus spiral arm from 1500 stellar observations 2−78445
- constants, a discussion 2−69022
- continuum radio structure of galactic disk 2−69023
- cosmic γ-ray obs. above 250 MeV 2−62628
- cosmic ray production of D_2, ^{3}He, Li, Be and B 2−84970
- cosmic ray source, magnetic white dwarf theory 2−69007

Galaxies continued
the Galaxy continued
Cygnus Loop, brightness and polarization meas. at 6-cm. wavelength 2—69017
diffuse f.u.v. radiation, interstellar dust grains 2—75668
disk, mean-square electron density and early type stars 2—44836
distance from centre using exponential disc models 2—72972
distance scale determinations, methods and accuracy 2—69019
dynamical model with 3 kpc, arm rel. to density and galactic shock waves 2—58184
e.m. spectrum of Galactic Centre, proton synchrotron emission 2—81796
expanding ring 270 pc in radius at galactic centre 2—66053
extinction in Carina-Centaurus region, photoelectric UBV observations 2—73038
foreground stars rel. to observations of Large Magellanic Cloud 2—66059
galactic distances using early-type stars 2—69057
galactic halo in direction of SA 71, star density, 3 colour photometric obs. 2—62461
galactic radio sources at metre wavelength and the galactic disc radiation 2—81898
galactic spurs, HI region, linear polarization, measurement, antenna radiation patterns 2—85060
gamma rays from galactic centre 2—62451
gamma-radiation between 200 MeV and 10 GeV, balloon-borne observations 2—58439
gas kinematics near galactic centre 2—72971
gaseous component, equilibrium configuration 2—51701
gravitational acceleration perpendicular to galactic plane 2—51702
gravitational wave, emergence from centre 2—84964
gravitational waves from cosmic energy sources 2—44825
halo, RR Lyrae star distrib. survey 2—69096
heavy element synthesis, separation of r- and s-process abundances 2—66052
high velocity HI regions rel. to continuuum jets near galactic centre 2—55008
high-velocity interstellar H I up to high galactic latitudes, survey 2—58355
infall of intergalactic matter and soft X-ray emission 2—75666
inner regions, density wave model 2—44837
intergalactic gas, soft X-ray emission 2—55007
intermediate age galactic population stars, kinematics near North Galactic Pole 2—58182
interstellar extinction laws in spiral arms and field regions 2—84980
i.r. survey, suspected supergiant M stars 2—66134
kinematic parameters from star clusters rel. to galactocentric distance to Sun 2—84959
Loop III, extension into southern latitude 2—48663
low energy diffuse cosmic X-rays, origin, galactic component 2—51797
magnetic field, origin and form, primordial-field model 2—69018
map of centre region, high resolution and sensitivity at 15.5 GHz 2—75818
Milky Way, southern, atlas of identified stars, nebulae and open clusters 2—75669
Milky way spiral structure 2—51703
molecular clouds near galactic centre, kinematics 2—58180
North Galactic Pole, reddening effects of interstellar medium 2—84993
novae, frequency estimate, indirect classification 2—73023
nuclear bulge, obs. of stellar population 2—44839
nucleus, mass distribution 2—44835
OB stars in Norma Milky Way region, UBV and Hβ photometry 2—69075
outer spiral structure and high velocity clouds 2—44838
photon rest mass and dissipation of magnetic fields 2—75674
radial composition gradient in disk, distribution of CN stars 2—58181
radio emission, non-thermal, Galactic supernova remnants 2—78452
radio pulses rel. to gravitational waves from the Galactic Centre 2—58369
recombination line emission from galactic ridge, excess H II regions 2—66123
red variables, in globular clusters, galactic centre, solar neighbourhhod 2—73019
rolling motions of spiral arms, and bending of galactic plane 2—75670
rotation and precession constant
rotation constants from stellar proper motions 2—69021
rotation speed from observations of Magellanic Cloud orbits 2—69037
spiral and halo structure using three colour photometry of stars 2—69020
spiral arms, formation, computer obs. 2—81792
spiral arms, maintenance mechanisms 2—58188
spiral arms rel. to motion of stars and gas, review 2—58183
spiral structure, theoretical 21 cm. line profiles 2—58186
spurs, linear polarization survey at 1415 MHz 2—84950
stability and galactic halo and disc masses 2—75671
statistical investigation, classification of M-type giants 2—66092
steady-state galactic magnetic field, azimuthal component 2—81814
structure, open clusters, UBV-Hβ photometry 2—84954
surface photometry, from space vehicle, obs. procedures 2—45003
third integral, approximate form 2—81801
tilt of Large Magellanic Cloud, galactical binary 2—75673
two component model of local region 2—75672
velocity structure in H Doppler profiles rel. to spiral arm features 2—81818
X-ray production, diffuse flux from galactic sources 2—55104
X-ray sources, discrete, Uhuru obs. 2—62463
H I velocity-longitude diagram for southern Milky Way 2—84984
H_2, interstellar clouds, velocity structures and streaming 2—58364
H_2, kinematic distribution 2—62462
H_2 motions, in center and 3 Kpc arm 2—58185
HI distributions rel. to spiral arms and HII regions 2—78446
Hα, two new large diameter regions of faint emission 2—58179

Gallium
amorphous, strong coupling superconductor, crit. mag. field temp. variation 2—68356
amorphous state, Hall effect 2—75048

Gallium continued
atom, lifetime meas. using beam-foil technique 2—42730
chemical classification of Fe meteorites, conc. rel. to Ge 2—75925
chondrites, H-group, distribution in metal and silicate portions 2—62719
diffusion, in Si p-n junction, profile broadening by reactor irrad. 2—84355
diffusion in Al, 100—310°C, solid solubility, X-ray diffr. obs. 2—74810
elasticity moduli, determ. by u.s. pulse method 2—71549
Fermi surface, retardation effects in cyclotron reson. 2—51094
film, condensed on glass, amorphous to cryst. transition temp. 2—43474
film, disordered, supercond. transition temp. and normal state cond., effects of surface charge 2—44070
film, supercond. transition temp. change due to noble gas adsorption 2—47856
Gantmakher-Kaner effect 2—47797
Hall mobility meas. apparatus using Corbino method 2—71224
lattice vibrs., freqs., polarization vectors and dynamic matrix elements relations 2—61055
liquid, compressibility, statistical mechanical perturbation theory calc. 2—80461
liquid, diffusion of Tl 2—46945
liquid, filling of ultrafine channels in zeolites 2—84153
liquid, multiple neutron scatt., effective scatt. factors 2—60422
liquid, optical consts. 2—43359
liquid, struct. factor rel. to entropy of melting 2—64434
molten, embrittlement of Al 2—43721
n.m.r. high field spectra, elec. field gradient tensor, single cryst. 2—57396
scintillography with ^{67}Ga, detection of metastatic lung tumors 2—48886
single crystal, containing additions, substructure, X-ray obs. 2—71474
solar abundance, spectrum synthesis 2—75946
solubility and alloying effects in Fe-Ni-Al-Cu alloys 2—43845
superconducting, energy gap. cryst. orientation depend. 2—68358
superconducting transition, anisotropy in length change of single crystals 2—71846
surface struct. rel. to plastic deform. by unidirectional abrasion and rolling 2—83856
γ-Ga, cryst. struct. 2—53661
Ga, thermal cond. from Lorenz number and elec. cond. 2—71188
Ga^+ lifetime meas. using beam-foil technique 2—42730
GaSb, piezoemission, stress effects on impurity and bound exciton lines 2—48179
^{67}Ga, calibration of 1383A ionization chamber 2—59613
^{67}Ga for tumour localization 2—69297

Gallium compounds
epitaxial, dopant conc. profile determ. by Schottky-barrier diode differential capacitance meas. 2—83905
GaSb, band struct., critical point detn., wavelength modulation derivative spectroscopy obs. 2—48160
GaSb and GaSb:Cs, electronic properties of surface, exam. by photoemission meas. 2—71312
II Zwicky 40, age and structure 2—71372
rare earth intermetallics, LnGa, magnetization and susceptibility, temp. depend. 2—72170
Al-Ga liquid alloy, Cr or Mn impurity, susceptibility near nonmag.-mag. transition 2—80486
$Al_yGa_{1-y}As_xSb_{1-x}$-$GaAs_xSb_{1-x}$ double heterojunction laser, prep. and emission spectra 2—59184
Cu-Ga alloy, cold-worked, defects, X-ray obs. 2—80861
ErGa garnets, metamagnetism 2—61557
Fe-Ga-Sb system, constitution and mag. props. 2—64821
Fe-Ga alloy, molten, paramag. props. 2—80488
Fe-Ga alloys, magnetic props. and Mossbauer investigations 2—84416
Fe-Ga solid solns., Mossbauer lineshape effects on hyperfine fields 2—44353
Ga-Ag alloy, liquid, free enthalpy of mixing 2—53422
Ga-Au alloy, liquid, free enthalpy of mixing 2—53422
Ga-Au alloys, metallurgical properties, contact characteristics 2—84069
Ga-Cr alloy, phase diagram, intermetallic cpds. 2—64817
Ga-Hg alloy, liq., sp. ht. anomaly near phase separation critical pt. 2—50354
Ga-In-As-Sb system, props. with view to use in injection laser 2—42096
Ga-In-Sn alloy, field ion microscope obs. of liquid-solid interface in vacuum 2—67900
Ga-Sb system, solid and liq., constitution and mag. props. 2—64820
Ga-V(Cr)(Mn)(Fe)(Co)(Ni) dilute liquid alloys, mag. susceptibility 2—80485
GaAlAs, close confinement laser diodes using, structure, performance, applications 2—82490
GaAlAs injection laser materials, application to moderate power i.r. laser diode array light sources 2—82491
$Ga_{1-x}Al_xAs$, indirect gap semicond., direct band recombination, electroluminesc. obs. 2—75337
$Ga_{1-x}Al_xAs$, liq. phase epitaxial growth from unstirred soln., simulation by numerical methods 2—74693
$Ga_{1-x}Al_xAs$, liquid phase epitaxial growth, composition, elec. microprobe obs. 2—47286
$Ga_{1-x}Al_xAs$, pseudobinary system, solidus boundary, thermodynamic analysis 2—50968
n-$Ga_{1-x}Al_xAs$ epitaxial film, edge photoluminesce, free exciton annihilation contrib. 2—81432
GaAs-AlAs, solid solution heterojunction injection laser, 7400-9000 Å range 2—73596
GaAs-GaP alloy, i.r. lattice absorption, thermodynamic props. detn. 2—57074
GaAs-GaP pseudobinary, phase diagram, solidus boundary 2—83841
GaAs, layer compound, valence electron density and band struct. 2—81016
$GaAs_{1-x}P_x$, compositionally graded cryst., like-sign asymmetric dislocations 2—71478
$GaAs_{1-x}P_x$, p- and n-type, direct and indirect gap, photoluminesc. spectra 2—84538

Gallium compounds continued
$GaAs_{1-x}P_x$, vapour growth, thermodynamic calc. 2−47220
$GaAs_{1-x}P_x$ epitaxial layer, on GaAs, surface struct., cross-hatch pattern due to misfit disloc. array 2−47110
GaBi, mass spectrometric determ. of dissociation energy 2−64126
GaCl, hyperfine structure in rotational spectrum 2−46540
$Ga(ClO_4)_3$ aqueous solns., relax. rates of ^{69}Ga and ^{71}Ga 2−77449
$GaFeO_3$, crystal growth, from the flux systems $PbO\text{-}V_2O_5$ and $Bi_2O_3\text{-}V_2O_5$ 2−50589
GaGe-V(Cr)(Mn)(Fe)(Co)(Ni) dilute liquid alloys, mag. susceptibility 2−80485
GaH, potential energy curves and dissociation energies 2−60000
GaI_3 use in high press. Hg-Ga discharge 2−53251
$Ga_{0.6}In_{0.4}As/Cs$, photoemissive yield, phonon energy loss effects 2−61460
n-$Ga_xIn_{1-x}As$ alloy, effective mass compositional depend., sub mm. cyclotron resonance obs. 2−64982
$Ga_{1-x}In_xN$, fundamental absorpt. edge and energy gap 2−72329
$Ga_xIn_{1-x}P$ alloy, band structure, electroreflectance obs. 2−61641
$Ga_xIn_{1-x}P$, cryst. growth, vapour phase 2−43511
$Ga_{2x}In_{2(1-x)}S_3$ thermostimulated cond. 100-350K 2−84317
GaN:Mg, diode, electrolum., fabrication, props. 2−72387
GaN:Zn(Cd), luminescence, acceptor site location and new emission band obs. 2−72398
GaN, band struct. calc. 2−71925
GaN, cryst. growth, vapour phase 2−43511
GaN, electrolytic etching, device fabrication 2−71365
GaN, epitaxial growth from vapour phase 2−50495
GaN, equilibrium pressure of N_2 over GaN 2−47049
GaN, fundamental absorpt. edge and energy gap 2−72329
GaN, luminesc. bands, positions, half-widths, intensities, rel. to temp. 2−65299
GaN, vapour phase crystal growth, mass spectrometric obs. 2−53606
GaN film, prep. by cathode sputtering 2−56589
GaN m.i.s. diodes, radiative recombination due to electric field polarity reversal 2−71990
GaO_x-Ag alloy, dispersion strengthened, creep 2−53814
$Ga_2O_3\text{-}TiO_2$ solid soln., crystallographic shear structs., planar boundaries 2−74768
Ga_2O_3, coprecipitation during liquid phase epitaxy of GaP 2−50609
$\beta\text{-}Ga_2O_3$, crystal growth, from the flux systems $PbO\text{-}V_2O_5$ and $Bi_2O_3V_2O_5$ 2−50589
Ga_2O_3, effect on immiscibility temp. of $Na_2O\text{-}SiO_2$ glass 2−53539
$Ga_2O_3(c)$, heat capacity, drop calorimetry and diff. scanning calorimetry 2−54047
GaP: Zn, Al, photolum. and electrolum., 1.7 to 2.3eV 2−75321
GaP:B, i.r. spectra, localized mode frequencies and gap mode vibrations 2−80883
GaP:Bi, luminesc., kinetics due to bound excitons, 77.3K 2−65292
p-GaP:Cu,O, bound exciton luminesc., emission and excitation spectra 2−78131
GaP:Ge, e.p.r., linewidth and g-value 2−72484
GaP:Mn, i.r. luminesc. due to $^4T_1 \rightarrow {}^6A_1$ internal transition, dynamic Jahn-Teller effect 2−81424
GaP:Mn,S, Mn-S nearest neighbour complex, e.s.r. obs. 2−75344
GaP:N, localized vibr. modes due to N isotopes, i.r. absorp. obs. 2−68639
GaP:N, null field splitting of B-line 2−61692
GaP:N, Zeeman effect on bound exciton-complex 2−61693
GaP:Sb, recomb. radiation involving isoelectronic centres 2−72407
GaP:Sn, strain-depend. e.p.r. and spin-valley coupling of donors 2−84570
n-GaP:Te,Zn,O, electrolum., mean electron conc.; influence of Te content 2−57381
p-GaP:Zn,O, donor electron capture cross sections, rel. to quantum efficiency limits 2−68681
GaP:Zn,O, luminesc. time response rel. to multiple trapping at Zn-O impurity centres, 4-120K 2−61696
p-GaP:Zn,O, photolum. efficiency and kinetics of Zn-O complex formation 2−51368
p-GaP:Zn,O, recomb. of excitons bound to deep neutral donors and acceptors 2−68682
GaP-GaAs alloy, epitaxial growth on GaAs, by pyrolysis of $Ga(CH_3)_3$, AsH_3 and PH_3 2−50496
GaP-GaAs film, comp., effects of deposition conditions 2−60657
GaP-GaAs heterojunction, prep. by multiple layer liq. phase epitaxy 2−50482
GaP-GaAs mixed crystal, multiphonon Raman scatt. 2−68659
GaP-ZnSe alloy, cond. hopping contrib., ionized impurity scatt., electrolum. and cathodolum. 2−81415
GaP, 40 keV Te implantation damage and annealing 2−80706
GaP, amorphous, absorption edge, temp. depend. 2−75293
GaP, amorphous, band struct., optical props. pressure effects obs. 2−61333
GaP, amorphous, phonon density of states, Raman scatt. obs. 2−61664
GaP, Ar^+ 40KeV ion bombardment, energy distrib. of secondary electrons 2−72097
GaP, band struct., critical point detn., wavelength modulation derivative spectroscopy obs. 2−48160
GaP, band struct., X-ray photoemission study 2−84387
GaP, chem. shift in binding energies of Zn and Cd 2−65001
GaP, coprecipitation of Ga_2O_3 during liquid phase epitaxy 2−50609
GaP, core levels, spectral obs. 2−65240
GaP, crystal growth, open flow quartz systems, Si contamination 2−43529
GaP, diffuse reflection spectra, energies of E_1, E_0' and E_2 peaks 2−75275
GaP, donor-acceptor emission energy shift on varying the excitation intensity 2−72388
GaP, donor-acceptor pairs, config. interaction 2−84260
GaP, electron mobility, theoretical calc. 2−77889
GaP, energy gap, temp. depend., calc. using Brooks-Yu theory 2−68415
GaP, epitaxial growth on insulating substrates and characterization 2−47111
GaP, GaAsP, injection luminescence 2−44417
GaP, green electrolum. efficiency, weak photolum. band 2−84548
GaP, growth defects, S-pits, luminesc. efficiency 2−50595

Gallium compounds continued
GaP, heteroepitaxial growth on Si substrates 2−83864
GaP, i.r. dispersion of second order electric susceptibilities 2−61581
GaP, i.r. lattice absorption, thermodynamic props. detn. 2−57074
GaP, ion implantation of S, junction form. 2−47429
GaP, ionicity, dispersion, and optical spectra 2−44374
GaP, linear electro-optical effect 2−68607
GaP, liq. encapsulated growth from non-stoichiometric melts 2−47268
n-GaP, metal-semicond. barrier obs., surface levels detn. 2−84352
GaP, pair photolum., peak energy, excitation intensity depend. 2−75318
GaP, phonon damping func. freq. depend., polariton Raman scatt. obs. 2−61076
GaP, photoluminescence and optical absorption 2−57343
GaP, physics of radiative centres 2−61724
GaP, polariton dispersion and damping temp. depend. from k vector space non-linear spectra 2−71710
GaP, soln. growth, for red emitting diode manufacture 2−60711
GaP, surface and bulk atomic vibrs., calc. 2−80894
GaP, surface stoichiometry and structure, surface vacancy model 2−50445
GaP, wavelength modulatd refl spectra, band struct. 2−61616
GaP electrodes, selective etching and anodic dissolution 2−75386
GaP electroluminescent diode, preferential etching, scanning elec. microscope obs. 2−71972
GaP evaporation by laser, mass-spectrometric analysis of ions in vapour 2−75409
GaP green emitting diode fabrication by double- bin liquid-phase epitaxy 2−72437
GaP light emitting diode, props. for green and red emission, quantum efficiency 2−44418
GaP p-n-p-n green light emitting diode, fabrication and characts. 2−72436
GaP p-n junction growth by liq. phase epitaxy 2−47287
GaP red-emitting diodes, scanning electron microscope characteriz. 2−51389
GaP(Cs) dynode photomultipliers, electron optics and time broadening 2−49677
GaP(Cs) dynodes photomultipliers, performance and characteristics 2−49678
p-GaP(Zn,O), p-GaP(N), minority carrier lifetime, luminesc. decay time obs. 2−48221
GaS, direct interband transitions, low energy photoemission spectra 2−51225
GaS, growth from vapour phase, sublimation and chem. transport 2−71373
GaS, surface electronic props. detn. 2−65106
$\beta\text{-}Ga_2S_3$, photolum. and photocond. 2−84532
GaSb:Te, lightly doped, photolum. at high excitation levels 2−72402
GaSb:Te, segregation coeff. of Te 2−74798
GaSb:Te,Zn, thermal e.m.f. rel. to carrier conc., 300K 2−54248
GaSb:Te(Zn)(Te + Zn), heavily doped, photolum. at high excitation levels 2−72403
GaSb/Cs-O, electronic states, photoemission yield, energy distrib. 2−44205
GaSb/Cs, photoemissive yield, phonon energy loss effects, band-theoretic model 2−61460
GaSb-GaAs system, phase diagram, thermodynamic analysis 2−44086
n-GaSb-Pb contact, tunnelling spectroscopy and band struct. press. effects 2−84351
n-GaSb, cond. band parameters from high-temp. transport meas. 2−57206
GaSb, core levels, spectral obs. 2−65240
GaSb, diffusion of Zn, temp. and cond. depend., radioactive tracer obs. 2−74799
p-GaSb, doped, heavy/light hole mobility ratio 2−81063
GaSb, energy gap, temp. depend., calc. using Brooks-Yu theory 2−68415
GaSb, heavily doped, phonon scatt., thermal cond. obs. 2−47765
GaSb, i.r. dispersion of second order electric susceptibilities 2−61581
GaSb, Landau levels at saddle point, diff. reflectivity in mag. field obs. 2−71795
GaSb, Landau transition at E_1 edges, excitonic effects 2−68404
GaSb, photoelectromag. effect in quantizing mag. field 2−68484
GaSb, radiation damage, review 2−47365
GaSb, specific heat below 30 K 2−68249
GaSb, transition metal doped, anomalous elec. and mag. props. 2−68405
p-GaSb, undoped, acceptor states and excitons, photocond. and photoluminesc. obs. 2−61708
GaSb, variation of energy bands with hydrostatic pressure 2−61393
GaSb single crystal, elasticity versus temp., calc. 2−60843
GaSe, band struct., pseudopot. calc. 2−61341
GaSe, exciton absorpt. peak shift and phase change induced by hydrostatic press. 2−72330
GaSe, Faraday effect in exciton absorpt. region 2−72263
GaSe, interband Faraday effect 2−72262
GaSe, linear electro-opt. eff. at room temp., photon energy 1.25-1.96eV 2−72270
GaSe, luminesc. of free and bound excitons, 4.2 and 1.8K 2−72406
GaSe, optical consts. anisotropy near band edge 2−48178
GaSe, surface electronic props. detn. 2−65106
GaSe, surface struct., surface states LEED, photoemission, Auger spectroscopy obs. 2−48024
GaSe, under two-photon excitation, stimulated emission 2−72405
GaSe, vapour growth and morphology 2−50574
GaSe crystals, reflection spectra, similarity with zone structure 2−84480
GaSe liquid and solid, thermal cond. 2−64865
GaSe single crystal, anomalous light dispersion in exciton line 2−78099
Ga_2Se_3, i.r. refl. spectra at 290K, phonon freqs. and dielec. consts. 2−75279
$Ga_2Te_3\text{-}As_2Te_3$ system, phase diagram 2−47713
Ga_2Te_3-Cu system, phase diagram and elec. props. 2−47715

Gallium compounds continued
GaTe, forbidden band width and exciton binding energy, optical absorp. obs. 2−75294
GaTe, surface electronic props. detn. 2−65106
$Ga_{1-x}Te_x$ alloy, liq., n.m.r., Knight shift, mag. relax., quadrupole relax., Fermi level 2−60512
Ga_2Te_3, semicond., radiation stability due to stoichiometric vacancies 2−71906
^{67}Ga-citrate and scintillation camera in detection of liver tumours, computer scintigraphy 2−73198
^{67}Ga citrate, isotope scanning of Hodgkin's disease 2−55246
Gap, two phonon Raman spectra 2−48156
Hg-Ga amalgam, dil., viscosity comp. depend., 0-100°C 2−64451
In-Ga alloy, component activities detn. using a solid oxide electrolyte technique 2−78201
In-Ga alloy, surface tension and density, comp. depend., 700K 2−67815
$In_xGa_{1-x}P$, vapour growth, equilib. calc. 2−50576
$In_xGa_{1-x}P$ alloys, thermal expansion coeff. temp. depend., 15-650°C 2−71750
InP-GaP system, component distrib. coeffs. and phase diagram 2−47716
Mn-Ga alloys, internal friction 2−50735
Nb-Ga system, constitution diagram 2−43937
Sn-Ga, liquid binary alloys, absolute thermoelectromotive force 2−56518
V-Ga-Al alloy, A15 struct., superconducting crit. temp. and current density 2−57168
Zn-Ga, liquid binary alloys, absolute thermoelectromotive force 2−56518
gallium arsenide
see also Semiconducting materials/gallium arsenide
amorphous, phonon density of states, Raman scatt. obs. 2−61664
atomic vibrations, surface and bulk, calc. 2−80894
bound exciton photoluminescence spectra 2−57373
cathode, negative electron affinity, photoemission rel. to Cs-O layers thickness 2−75194
crystal growth, using liquid phase epitaxy method, optimum kinetics and conditions 2−71384
crystal modulator, phase characteristics 2−63362
Czochralski growth, temp. profile and thermal stress effects on dislocation structure formation 2−53615
diffusion of Fe, Cr and Co, 800-1100°C 2−60829
dislocation-free cryst. growth by liq. encapsulation 2−50596
electron and neutron irrad., i.r. absorpt. 2−72332
epitaxial, plane defect at interface and dislocations, X-ray obs. 2−71488
epitaxial, selective growth, morphological studies 2−50493
epitaxial growth, from soln., surface quality improvement 2−60656
epitaxial layer growth from soln. in Ga, rel. to undercooling 2−74694
epitaxial layer growth from vapour phase 2−50492
epitaxy, anisotropy obs. using abrupt changes in doping level 2−47112
epitaxy, growth morphology obs. by sequential changes in doping level 2−47113
etched surface morphology, elec. microscope obs. 2−56575
etching, anisotropic behaviour of etchants 2−74660
evaporation by laser, mass spectrometric analysis of ions in vapour 2−75409
exciton-phonon coupling, optical absorp. obs. 2−61642
film, epitaxial, guiding and electrooptic modulation of light 2−68608
film, epitaxial growth from soln., kinetics 2−60635
film, liq. phase epitaxy on ZnSe, elec. characts. rel. growth conditions 2−67910
films, epitaxial, heavily doped Faraday effect 2−65214
frequency mixing, 2 and 3 wave anisotropic interference 2−75250
function laser, coefficient of superlinear dependence of gain on current density 2−59183
growth, impurity incorporation, effect of surface space charge layer 2−47428
growth from gas phase, cryst. morphology 2−56656
injection luminescence 2−44417
ion implantation lattice disorder, low temp. channelling obs. 2−47373
ionic Brillouin effect, theory 2−84502
i.r. absorpt., impurity induced, calc. by Green's function technique 2−61639
i.r. lattice absorption, thermodynamic props. detn. 2−57074
i.r. radiation modulation at piezoresonance 2−57329
laser, narrow junction, fabrication techniques 2−73595
lasers, tunable monochromatic injection, fabrication 2−73593
layers, growth by liquid phase epitaxy 2−71385
light emitting diodes, optical fluctuations 2−75180
mean square atomic displacement study by LEED 2−71318
platelet crystal growth by forced-convection open-tube technique 2−67935
polishing by gaseous etching, during growth from gas phase in chloride system 2−83853
resistance thermometers, characteristics 2−49188
room-temperature radiation detector possibilities 2−52692
single cryst., internal friction temp. depend., 20-540°C 2−53790
single crystals grown by Bridgeman method 2−60724
single mode laser, in external cavity 2−73594
specific heat below 30 K 2−68249
strain induced phonon line broadening observed by surface reflection Raman scattering 2−83858
submillimetre wave generation, by difference freq. mixing 2−49200
surface props., obs. by Rutherford scatt. and channelling 2−64553
surface stoichiometry and structure, surface vacancy model 2−50445
thin film waveguide, theory of phase matched parametric oscillation 2−73483
waveguide, fabrication by proton bombardment 2−79413
X-ray photoemission valence-band spectra, valence-band densities of states 2−81192
Ga-As-Te system, GaAs-Te polythermal section determ. 2−61047
Ga-As-Zn system, GaAs-Zn polythermal section determ. 2−61046
(Ga,In)As:Cs-O, photoelectron surface escape probability, 0.9-1.6 μm range 2−72091

Gallium compounds continued
gallium arsenide continued
$Ga_{1-x}Al_xAs$, liquid phase epitaxial growth, composition, elec. microprobe obs. 2−47286
GaAs:Ar, Te ion implanted, radiation damage, elec. microscope obs. 2−60821
GaAs:Mg-Li, i.r. absorpt. due to pair defects, absorpt. cross section 2−81360
GaAs:Si, amphoteric impurity distrib. equilib. calc. 2−83981
GaAs:Si, boatgrown and pulled, B impurity, i.r. local mode absorption spectra, comparison 2−61640
GaAs:Te, Se and S, effect of doping on struct. 2−71432
$GaAs\text{-}As_2Te_3$ system, phase diagram 2−47713
GaAs-Cu in supersaturated solid solution, differences in laws of decomposition 2−83836
$GaAs\text{-}Ga_{1-x}Al_xAs$, single heterostructure laser diode, interferometric obs. of evaluation of thermal mirror deformation 2−73592
GaAs-Sn quasi-binary system, phase diagram 2−43934
GaAs, amorphous, e. micro. exam of struct. and short-range order 2−71433
GaAs, calc. of third-order elastic constants 2−80898
$GaAs_{1-x}P_x$, vapour growth, thermodynamic calc. 2−47220
$GaAs_{1-x}P_x$ epitaxial layer, on GaAs, surface struct., cross-hatch pattern due to misfit disloc. array 2−47110
$GaAs_{1-x}P_x$ layers, vapour phase epitaxial growth kinetics 2−50494
$GaAs_xP_{1-x}$, epitaxial growth on GaAs substrate, anisotropic bending 2−80567
$Ga_xIn_{1-x}As$, epitaxial growth on GaAs substrate, anisotropic bending 2−80567

Galvanomagnetic effects *see Magnetoelectric effects*

Galvanothermomagnetic effects
semiconductor, with low mobility charge carriers, rel. to Hall field detn. 2−47883
Bi-Sb alloy, temp., mag. field and cryst. direction depend. 2−75161
Bi-Sb solid soln., thermomagnetogalvanic props. 2−54245
$p\text{-}Bi_2Te_3$, magneto-Seebeck effect, second valence bound obs. 2−61339
$Cd_{2.8}Zn_{0.2}As$, high mobility, rel. to scattering parameter determ. 2−81090
n- GaAs, magneto-thermal e.m.f., pressure depend., rel. to effective electron mass. 2−44098
n-GaSb, conduction band minima energy separation temp. depend., p-n junc. tunnelling current obs. 2−75109
n-InAs, thermoelec. power in quantizing mag. fields 2−84372
n-InSb, coeffs. at high temp., degeneracy and screening effects 2−68378

Gamma-ray astronomy *see X- and gamma-ray astronomy*

Gamma-ray sources *see Gamma-rays*

Gamma-ray spectra
see also Nuclear decay theory
— 2−59732
anisotropy, general formula by Gorter-Rose method 2−42494
capture and fission gamma rays from epithermal neutron irradiation of ^{235}U 2−52820
coated irrad. kernels, burn-up obs. 2−42665
compound nucleus, exit states role in high-energy γ-ray emission 2−59763
computer code for searching attributions, use in neutron activation analysis 2−82859
computer method for peak analysis 2−61564
cosmological, from matter-antimatter annihilation in universe 2−69004
cosmological annihilation in Omnes model 2−62434
data-handling system, multi-purpose 2−52667
gaseous effluents from nuclear facilities, use of γ spectroscopy, to identify isotopes, estimate off. gas holdup times 2−42690
hypernuclear spectroscopy, obs. of γ-rays from excited states, consequences for Λ-N interactions 2−76775
neutron capture reaction, 14 MeV, mass depend. of cross sections 2−67282
neutron radiative capture widths, departures from statistical theory 2−46095
neutron-gamma competition following (d,d′) reaction 2−46325
nucleus-heavy ion reactions, γ-spectroscopy determ. of e.m. matrix elements 2−83023
radiation from galactic centre 2−62629
radiative capture of 14 MeV neutrons on 11 medium and heavy nuclei, γ spectra meas. 2−67261
radioactive fallout from test, γ-ray spectra and fractionation effect 2−79819
reactor fuel post-irrad. exam. techniques 2−42670
reactor room obs. 2−63983
secondary cosmic rays, 0.2-5 GeV, 0-16 km altitude in atmosphere 2−51660
stopped kaon nucl. γ-rays intensity and identification 2−59773
transmission, Monte Carlo calculation of low energy spectra 2−80927
unbound states in nucleon-induced reactions, γ-decay 2−79780
(d,pγ) reaction, proton ang. distrib. determ. from spectral shapes 2−79802
(n,γ), radiative capture mechanism, compound nucleus exit states model 2−67262
(n,γ) reactions, meas. of circular γ-ray polarization for primary transitions 2−49801
$^{143(m+g)}$Sm 2−46200
$^{93g+m}$Ru, produced by ^{92}Mo(^{3}He, xn), obs. of γ transitions 2−49768
^{a}Ge, A=70, 72, 74, 76, γ-ray spectra following thermal neutron capture 2−46286
^{a}Ho, A=164m, 164g, decay to ^{164}Dy, ^{164}Er meas. of energies and relative intensities of γ-rays and X-rays 2−52785
^{a}Sb, A=110-114, product and decay consts. of γ transition, β-γ, γ-γ coincidence meas., β spectra and point meas. 2−46191
^{a}Sn, A=123, 125, 128, cumulative yields from thermal-neutron induced fission of ^{235}U deduced from γ-ray intensities 2−46345
^{a}Sn, A=129-132, half-lives determ. from X- and γ-ray emissions 2−46196

Gamma-ray spectra continued
- (AgBr + AgCl(5%):$C^{5+}(N^{5+})(O^{6+})(S^{6+})$, high energy implantations, Doppler broadening of positron annihilation photons meas. with Ge(Li) detector 2−71507
- AgCl:$C^{5+}(N^{5+})(O^{6+})(S^{6+})$, high energy implantation, Doppler broadening of positron annihilation photons meas. with Ge(Li) detector 2−71507
- ^{110}Ag, decay study of γ-transitions to elucidate low-spin excited states in ^{110}Cd 2−74035
- ^{25}Al, population of $3/2^+$, 945 keV level in ^{2}H(^{24}Mg, nγ) reaction, meas. of mean lifetime for γ-ray decay 2−79736
- ^{27}Al high-spin states produced in ^{12}C(^{16}O,p) and ^{24}Mg(α,p) reactions, meas. of γ-ray branching ratio, p-γ angular correlation 2−42504
- ^{27}Al(n,n)^{27}Al, inelastic, 0.8-9.0 MeV, cross-section for production of de-excitation γ-rays 2−67243
- ^{240}Am→^{240}Pu electron capture decay, meas. of γ-ray and conversion electron spectra, determ. of conversion coeffs. and multipolarities 2−79770
- ^{34}Ar, γ-decay and lifetime of low-lying states populated in ^{32}S(^{3}He, n) reaction 2−74012
- ^{71}As→^{71}Ge decay scheme 2−63848
- ^{197}Au(n,γ), resonances 2−67305
- Au(n,γ), fast neutron capture, γ-rays, intensity distribs., 5.5 MeV anomaly 2−67304
- ^{134}Ba, multipole mixing ratios of γ-transitions following β-decay of ^{134}Cs 2−70404
- ^{138}Ba, γ-ray and conversion electron spectra, spin-parity assignments 2−46155
- ^{138}Ba(n,γ), 14 MeV radiative capture, mass depend. of direct- semi-direct theory calcs. 2−67270
- Ba(n,γ), capture of 5-80 keV neutrons, transition obs. 2−67286
- ^{198}Bi→^{198}Pb, ^{200}Bi→^{200}Pb, γ-ray and conversion electron spectra 2−46174
- ^{205}Bi→^{205}Pb decay, level scheme of ^{205}Pb 2−82928
- ^{78}Br decay, rel. to energy level determ. of ^{78}Se 2−74050
- ^{81}Br(^{16}O, ^{16}O$'\gamma$), 33 MeV, Coulomb excitation of low-lying levels, meas. of γ-ray energies, yields, angular distribs., Doppler broadening 2−74032
- ^{81}Br(α, $\alpha'\gamma$) 2.5-8.2 MeV, Coulomb excitation of low-lying levels, meas. of γ-ray energies, yields, angular distribs., Doppler broadening 2−74032
- ^{40}Ca(n,γ), 14 MeV radiative capture, mass depend. of direct- semi-direct theory calcs. 2−67270
- ^{131}Ca, level scheme, transitions 2−42521
- ^{107}Cd, study of levels populated in β^+/EC decay of ^{107}In by obs. of γ-ray spectra 2−82934
- Cd(n,γ), capture of 5-80 keV neutrons, transition obs. 2−67286
- ^{140}Ce, angular correlation of γ-cascade 2−49748
- ^{145}Ce, 3.0 min. γ-decay studied by method of separation, determ. of energies and relative intensities 2−42524
- ^{37}Cl(n, γ)^{38}Cl, meas. of γ radiation, excitation energies for ^{38}Cl levels, Q-value 2−49808
- ^{37}Cl(n,γ)^{38}Cl, γ-ray spectra obs., correlation with E1 reduced intensities 2−67272
- ^{245}Cm, groundstate rotational band, γ branching and total conversion coeffs. of intraband transitions 2−52772
- ^{57}Co, γ decay of levels populated in ^{56}Fe(^{3}He,dγ) reaction 2−46138
- ^{59}Co, M1 and E2 characters of transitions between levels populated in ^{59}Fe β-decay 2−79769
- ^{60}Co, intensity ratio of 2158 keV and 2505 keV γ-rays 2−76811
- ^{50}Cr(p, pγ)^{50}Cr 7 MeV, γ-ray spectra, Doppler shift attenuation of lifetimes in ^{46}Ti 2−76794
- ^{54}Cr(n,γ)^{55}Cr, thermal neutron capture, meas. of γ-ray spectra and level structure of ^{55}Cr 2−42510
- Cs, mapping of correlation between neutron width and radiative capture 2−67292
- ^{129}Cs decay, γ-ray energy determ. 2−42546
- ^{134}Cs→^{134}Ba decay scheme study by meas. of γ-γ coincidences 2−52781
- ^{135}Cs, ^{137}Cs, ^{139}Cs, γ-ray and conversion electron spectra, spin-parity assignments 2−46155
- ^{141}Cs, direct meas. of half-life and energies 2−76812
- ^{163}Dy(d, 2nγ), 13.5 MeV, meas. of γ-ray spectra, deduced ^{163}Ho level scheme 2−63820
- ^{163}Dy(n,γ)^{164}Dy, nonstatistical aspects in 4s giant resonance 2−67300
- ^{163}Dy(p, nγ) 6.7 MeV, 13.5 MeV, meas. of γ-ray spectra, deduced ^{163}Ho level scheme 2−63820
- ^{156}Eu→^{156}Gd, decay scheme study 2−49751
- ^{158}Eu→^{158}Gd, decay scheme study 2−49751
- ^{152m}Eu→^{152}Sm decay, level scheme obs. 2−59730
- ^{56}Fe(n,n)^{56}Fe, inelastic, 0.8-9.0 MeV, cross-section for production of de-excitation γ-rays 2−67243
- ^{57}Fe(n,γ)^{58}Fe, meas. of circular γ-ray polarization for primary transitions, interference of spin components of capture state 2−42572
- ^{65}Ga, β-decay to ^{65}Zn 2−63847
- ^{156}Gd, conversion electron intensities and γ-ray intensities obtained 2−46162
- ^{156}Gd, meas. of energies and intensities of γ-rays depopulating low spin levels of β- and γ-vibrational bands 2−52766
- ^{158}Gd, meas. of energies and intensities of γ-rays depopulating low spin levels of γ-vibrational band 2−52766
- Ge(Li), automatic anal. on small computers 2−82082
- ^{73}Ge, γ-ray decay modes and reduced upward transition probabilities following Coulomb excitation, test of quasiparticle-phonon coupling theories 2−74030
- ^{1}H(n,γ)^{2}H, possible test for capture via $^1S_0\rightarrow{}^2S_1$ transition 2−46283
- ^{174}Hf, role of K-quantum number in de- excitation following Yb(α,xnγ)^{174}Hf 2−46328
- ^{177}Hf(n,γ)^{178}Hf, quantum no. influence on partial γ transitions 2−67303
- Hg(n,γ), fast neutron capture, γ-rays intensity distribs., 5.5 MeV anomaly 2−67304
- ^{165}Ho(α, 4nγ)^{165}Tm, 38 and 50 MeV, determ. of rotational bands by meas. of γ-γ coincidences 2−74039
- I, mapping of correlation between neutron width and radiative capture 2−67292
- ^{126}I→^{126}Te,^{126}Xe, energies and intensities of γ-rays meas. using Ge(Li) spectrometer 2−52780

Gamma-ray spectra continued
- ^{112}In decay, study of γ-transitions to elucidate low-spin excited states in ^{112}Cd 2−74035
- ^{115}In(n,γ)^{116}In, obs. of γ-rays in spin-assigned capture resonances 2−67290
- ^{115}In(n,γ)^{116}In, thermal neutron capture, γ-ray spectroscopy study of ^{116}In level scheme 2−67168
- ^{191}Ir, and electron conversion line compared, conversion coeffs. 2−76806
- ^{192}Ir, γ-ray spectra, K-shell internal conversion coeffs. 2−70423
- ^{39}K(n,γ)^{40}K, meas. of circular γ-ray polarization for primary transitions, interference of spin components of capture state 2−42572
- ^{41}K, γ-decay nonconservation of P-parity studied by meas. of γ-transition circular polarization 2−49739
- ^{139}La (n, γ), correlation with (d, p) reaction 2−59768
- ^{7}Li, γ-rays from first excited state populated by ^{7}Be radiative electron capture transition 2−46184
- ^{175}Lu(n, γ)^{176}Lu slow neutron capture, study of ^{176}Lu excited levels by obs. of γ-ray spectra 2−79744
- ^{176}Lu (n,γ), study of high-energy region of γ spectrum, search for correlations with (d,p) reactions 2−70456
- ^{176}Lu(n, γ)^{177}Lu, level scheme, transitions 2−59769
- ^{24}Mg yield meas. following μ^- capture 2−63870
- ^{25}Mg, population of $3/2^+$, 975 keV level in ^{2}H(^{24}Mg, pγ) reaction, meas. of mean lifetime for γ-ray decay 2−79736
- ^{92}Mo(n,γ)^{93}Mo, γ-ray spectra meas., test of valency model 2−67283
- ^{101}Mo→^{101}Tc decay, energy levels of ^{101}Tc 2−74051
- Mo(n,γ), capture of 5-80 keV neutrons, transition obs. 2−67286
- ^{15}N, γ-ray decay, lifetime determ. by Doppler shift attenuation method using ^{12}C(^{3}He,p) reaction 2−70375
- ^{23}Na, γ-decay of levels populated in β-decay of ^{23}Ne 2−79773
- ^{90}Nb, γ-decay scheme studied using ^{90}Zr(p,nγ) reaction 2−42515
- ^{143}Nd(n,γ), resonance neutron capture 2−67295
- ^{144}Nd(n,γ)^{145}Nd, thermal neutron capture, γ-ray spectroscopy study of ^{145}Nd 2−67172
- ^{20}Ne(d,pγ)^{21}Ne, study using p-γ and γ-γ coincidence techniques, determ. of levels in ^{21}Ne 2−79762
- ^{20}Ne(p,γ)^{21}Na, meas. of γ-ray branching ratios and lifetimes, search for missing $J^\pi=3/2^+$ level in ^{21}Na 2−79761
- ^{58}Ni(α, pγ)^{61}Cu, compound satistical theory computation of cross-section for level population, γ-ray emission 2−79804
- ^{58}Ni(α, ppγ)^{60}Ni compound statistical theory computation of cross-section for level population, γ-ray emission 2−79804
- ^{58}Ni(p, nγ)^{58}Cu, 12.0-13.03 MeV, determ. of γ-ray decay modes of low-lying states of ^{58}Cu by n-γ and γ-γ coincidence techniques 2−74026
- ^{60}Ni, γ transitions of levels populated in β^+ decay of ^{60}Cu(II) 2−63846
- ^{64}Ni(p,nγ)^{64}Cu, 3.47-5.19 MeV, study of structure and γ-decay of levels excited near isobaric analogue resonances 2−67160
- ^{16}O, π^- scattering, 250 MeV, γ spectra study 2−70459
- ^{189}Os(n_{th},γ)^{190}Os, meas. of γ-ray spectra, evidence for K=0 excited states 2−67179
- ^{31}P(n,n)^{31}P, inelastic, 0.8-9.0 MeV, cross-section for production of de-excitation γ-rays 2−67243
- ^{31}P(p, γ)^{32}S, $E_p=1100$-1600 keV, gamma-decay of resonance levels 2−74090
- ^{230}Pa→^{230}Th decay meas. of γ and electron singles-spectra and γ-γ coincidences, study of bands in ^{230}Th 2−70416
- ^{208}Pb(n,γ), 14 MeV radiative capture, mass depend. of direct- semi-direct theory calcs. 2−67270
- ^{208}Pb(n,γ)^{209}Pb, radiative capture cross section, $E_n=6.2$-14.7, reson. struct. 2−67307
- ^{105}Pd, gamma ray spectrum in ^{104}Ru(α,3n) reaction, determ. of multipolarities 2−49744
- ^{108}Pd(n,γ)^{109}Pd*, gamma-ray spectrum, resonance spin determ. 2−67288
- ^{141}Pr(n,γ)^{142}Pr, test of valency neutron model 2−67294
- Pt, A=188, 190, 192, excited level study 2−70410
- ^{194}Pt(d,p), threshold region yields 2−67225
- ^{195}Pt(p,p$'$), threshold region yields 2−67225
- ^{239}Pu, asymmetry of E1 and M1 γ transitions, multipole mixing ratios 2−46207
- ^{239}Pu(n,γ)^{240}Pu, 2keV neutron capture, γ-ray studies of ^{240}Pu 2−67187
- ^{239}Pu(n,γ)^{240}Pu, thermal neutron capture, γ-spectroscopy study of ^{240}Pu 2−67186
- ^{241}Pu(n,γ)^{242}Pu, thermal neutron capture, γ-ray spectroscopy study of ^{242}Pu level structure 2−67188
- ^{224}Ra, ^{226}Ra, analysis of γ spectra in non-equilibrium with decay products, application to retention in mice 2−58615
- ^{224}Ra, ^{226}Ra, kinetics and decay products in mice, dose-effect relation 2−55279
- ^{185}Re, multipole mixing ratios of γ-transitions from levels populated in ^{185}Os electron capture decay 2−67178
- ^{92}Ru, 3.6 min produced by ^{92}Mo(^{3}He,xn), obs. of new weak γ transitions 2−49768
- ^{92}Ru→^{92}Tc, new neutron-deficient isotope, meas. of energies and relative intensities of γ-rays 2−76813
- ^{104}Ru(n_{th},γ)^{105}Ru, thermal neutron capture, spin assignments of ^{105}Ru levels 2−67287
- ^{30}S, γ-decay and lifetime of low-lying states populated in ^{28}Si(^{3}He, n) reaction 2−74012
- ^{32}S(γ,nγ'), influence of γ-cascade on population of low-lying levels of residual nucleus 2−42505
- ^{32}S(γ,pγ'), influence of γ-cascade on population of low-lying levels of residual nucleus 2−42505
- ^{32}S(n,n)^{32}S, inelastic, 0.8-9.0 MeV, cross-section for production of de-excitation γ-rays 2−67243
- ^{34}S(n,γ)^{35}S, thermal neutron capture, meas. of γ-ray spectra, transition scheme for ^{35}Si 2−49807
- Sb, mapping of correlation between neutron width and radiative capture 2−67292
- Sb(n,γ), A=121, 123, resonances 2−67291
- ^{77}Se(n,γ)^{78}Se, thermal n, singles and coincidence spectra, decay scheme for ^{78}Se 2−52779
- ^{28}Si, psec. lifetime of 9.699 MeV(5^-) level, delayed coincidence meas. 2−55959
- ^{28}Si yield meas. following μ^- capture 2−63870

Gamma-ray spectra continued
^{28}Si(n,γ), 14 MeV radiative capture, mass depend. of direct- semidirect theory calcs. 2−67270
^{30}Si(n,γ)^{31}Si, thermal neutron capture, meas. of γ-ray spectra, transition scheme for ^{31}Si 2−49807
Si(n,γ), gamma-ray spectra meas., cross-sections for γ-transitions 2−67269
^{140}Sm 2−46200
^{142}Sm 2−46200
^{141m}Sm 2−46200
S(n,γ), gamma-ray spectra meas., cross-sections for γ-transitions 2−67269
Sn(n,γ), capture of 5-80 keV neutrons, transition obs. 2−67286
^{86}Sr(^{3}He, $\alpha\gamma$)^{85}Sr, 17 MeV meas. of $\alpha\gamma$ coincidences, mean lives of low lying levels in ^{85}Sr deduced 2−42514
^{88}Sr(n,γ), 14 MeV radiative capture, mass depend. of direct- semidirect theory calcs. 2−67270
^{88}Sr(n,γ), radiative capture cross sections for 14 MeV neutrons mass depend. 2−67282
Ta(n,γ), fast neutron capture γ-rays, intensity distribs., 5.5 MeV anomaly 2−67304
^{154}Tb, decay scheme, γ-ray and γ-γ coincidence spectra 2−52784
^{91}Tc, 3.2 min produced in ^{92}Mo(p,xn), obs. of γ transitions 2−49768
^{92}Tc, growth and decay of gamma-rays obs. following decay of ^{92}Ru neutron-deficient isotope 2−76813
^{101}Tc→^{101}Ru decay, energy levels of ^{101}Ru 2−74051
^{99m}Tc decay, obs. of weak γ transition of 322 keV, determ. energy and intensity ratio to 140 keV transition 2−49769
^{46}Ti(p, pγ)^{46}Ti, 7 MeV, γ-ray spectra, Doppler shift attenuation of lifetimes in ^{46}Ti 2−76794
^{205}Tl(n,γ)^{206}Tl, anomalous 5.5 MeV γ-radiation 2−46289
Tl(n,γ), fast neutron capture, γ-rays intensity distribs., 5.5 MeV anomaly 2−67304
^{169}Tm(α, 2n)^{171}Lu, high spin rotational levels obs. 2−59717
^{169}Tm(α, 2n)^{171}Lu, rel. to validity of rotor motor for ^{171}Lu 2−59718
^{169}Tm(n,γ), γ-ray spectra, study of resonances 2−46288
^{235}U(n,γ)^{236}U, thermal neutron interaction, meas. of G-ray spectra 2−67310
^{133}Xe, ^{135}Xe, ^{136}Xe, γ-ray and conversion electron spectra, spin-parity assignments 2−46155
^{173}Yb(n,γ)^{174}Yb, nonstatistical aspects in 4s giant resonance 2−67300
Zn, A=73, 74, decay characteristics 2−79746
Zr(n,γ), capture of 5-80 keV neutrons, transition obs. 2−67286

Gamma-ray spectrometers
see also Beta-ray spectrometers; X-ray spectrometers
air-borne data, computer simulation 2−65440
analysis of irradiated reactor fuels, properties of operating reactors 2−76925
Anger camera system, improvement of intrinsic resolution 2−63707
angular correlation meas. of positron annihilation gamma-ray pairs, continuous scanning method using multiple channel analyser 2−42447
asymmetric linear Ge(Li)-Ge(Li) sum-peak coincidence spectrometer 2−79648
band-filter, for neutron capture studies 2−67077
Compton construction with Si(Li) and Ge(Li) detectors for obs. of lower energy γ-rays in complex spectra 2−79642
Compton summing, improvement of accuracy 2−59632
curved crystal, at Grenoble high- flux reactor 2−67076
curved crystal as energy band selector 2−63687
dead-time correction system for γ-ray spectrometry of short lived isotopes 2−70304
electronically gated calibration scheme 2−52679
fuel elements apparatus for studying radial migration of radioactive products 2−52847
high resolution, using Ge(Li) detectors, for nuclear technology 2−42441
Mossbauer, application to structural mechanics 2−55901
Mossbauer, based on A1-256 analyzer 2−59630
Mossbauer, multichannel, using multiwire proportional counters 2−42446
Mossbauer effect spectroscopy, backscatter detector 2−79659
Mossbauer spectra, recording by current method 2−59620
polarization meas. using symmetrical two-crystal Compton polarimeter 2−79641
precision spectroscopy of short lived nuclides using He jet recoil transport method 2−70290
resonance, constant velocity, with normalization from reference obs. 2−70289
semiconductor detector, Compton scattering suppression, guard scintillator, pulse shape discriminator, isotope determination 2−82796
soft, using semiconductor detectors, review 2−70287
solar flare meas. between 50 and 500 MeV from satellite 2−73142
Cd Te, halogen doped 2−55920
GaAs detector and two semiconductor thermoelements 2−49667
dual Ge(Li)-dual NaI(Tl) 2−63688
Ge(Li) anticoincidence shielded spectrometer for marine environmental radionuclide analysis 2−82806
Ge(Li) coaxial detectors used as spectrometer, pulse shape analysis 2−46054
Ge(Li) large-volume device 2−52678
Ge(Li) total absorption, for (n, xγ) cross section meas. 2−46039
HgI$_2$, conducting type, obs. of two carrier collection 2−49627
HgI$_2$, crystal growth and detection props. 2−46037
TiO$_2$, thin film production, study of optimal conditions 2−45197

Gamma-rays
see also Cosmic rays/photons
atmospheric, generation by cosmic rays, collective interactions 2−73887
cosmic ray interactions in atmosphere, 10^{14} eV, production of families of γ-quanta 2−73890
distribution at large distances from source 2−63978
high pressure apparatus, study of geometrical stability 2−85170
laser, based on crysts. of long lived nuclear isomers 2−66762
pinhole channelling patterns and applic. to cryst. defect studies 2−43605
self absorption in disc shaped source, Monte Carlo calc. 2−52663
source containers, commercial aspects 2−70546

Gamma-rays continued
vector meson production from γ-rays, quark model coupling constants 2−73834
Al, scatt., symmetry of Compton profile 2−71764
^{54}Fe, Eo decay of 2561 keV O^{+} level 2−82907
^{16}N decay, disc radiator with uniform high energy 2−46395

absorption
see also Mossbauer effect
crystal, deformed, resonant absorption of X-rays 2−84474
electron-photon showers caused by 50-400 MeV electrons and γ-quanta in Pb 2−67065
porosity meas. by γ-ray absorpt., optimum conditions calcs. 2−68180
radioactivity in building materials, background reduction measures outside spectrometric facilities 2−56076
resonant γ-ray nuclear Bragg reflection, azimuthal depend. elec. field determ. 2−81342
self absorption in large cylindrical samples 2−74190
shielding by two types of concrete 2−79846
Al, 250-1000MeV photons, absorpt. cross sections 2−72272
C, 250-1000MeV photons, absorpt. cross sections 2−72272
^{22}Ne(p, γ)^{23}Na, resonant absorpt., ^{23}Na level widths, Rutherford scatt. effect 2−76843
Ti, 250-1000MeV photons, absorpt. cross sections 2−72272

angular distribution
— 2−70411
angular correlation detection in pair production for meas. of γ-ray polarization 2−79645
correlations perturbation by stochastic Gaussian-Markov process 2−55946
detection of γ-ray pairs arising from positron annihilation, continuous scanning method using multiple channel analyser 2−42447
differential perturbed angular correlations and crystallographic texture effects 2−78055
directional correlation for γ cascade from nucleus bound to asymmetric-top molecule in soln., effect of molecular shape and flexibility 2−51474
1-3 directional correlations with mixed unobserved transitions and parity 2−73963
even-even nuclei, method for γ-γ directional correlation measurements 2−79673
high-spin states excited in (α,xγ) reactions, spin determ. method 2−79721
linear polarization coeffs., graphical representation 2−70365
metal, effect of heating and positron annihilation 2−81002
multiplicity comparison for compound nucleus and direct reaction mechanisms 2−67224
paramagnet, perturbed γ-γ angular correl. eff. of spin-lattice relaxation and ultrasound 2−72241
perturbation for study recoil nuclei interaction with solids 2−68587
perturbed following nuclear reactions, review 2−67206
rare earth nuclei implanted in Cu matrix, excitation by heavy ions, meas. of angular distrib. of de-exciting γ-rays 2−63927
time reversal, validity tests, optimization 2−63750
e-γ angular correlation, effect of higher approx. 2−82667
γ-γ directional correlation experiment 2−73266
γ-ν ang. correls. in muon capture 2−79778
n-γ ang. correl. technique for spectroscopic meas. 2−59738
pp collisions, data analysed to deduce angular distrib. of π° and multiplicity of all created charged particles 2−49561
^{59}(n,γ) ^{60}Co, thermal neutron capture 2−67278
^{a}Os, A=188, 190, 192, comparison of IMPACT, PAC and Mossbauer effect meas. of g-factor, ferromagnetic host effects 2−42534
Ag-Yb dil. alloys, perturbed ang. correl. on ^{169}Tm, h.f.s. 2−72247
Ag, time-differential perturbed ang. correl., ^{111}Cd quadrupole interaction 2−57316
Al, positron and dislocation binding 2−83977
^{27}Al high-spin states produced in ^{12}C(^{16}O,p) and ^{24}Mg(α,p) reactions, meas. of γ-ray branching ratio, p-γ angular correlation 2−42504
^{28}Al, γ-γ ang.-correl. on low-lying levels, PAC determ. of 2^{+} state moment 2−76790
^{36}Ar, lifetimes of bound states and resonances in ^{35}Cl(p,γ) reaction determ. from γ-ray angular distribs. 2−52747
^{37}Ar, γ decay of levels below 3 MeV excitation populated in ^{34}S(α,n) reaction 2−63790
^{81}Br(^{16}O, ^{16}O$'\gamma$), 33 MeV, Coulomb excitation of low-lying levels, meas. of γ-ray energies, yields, angular distribs., Doppler broadening 2−74032
^{81}Br(α, $\alpha'\gamma$) 2.5-8.2 MeV, Coulomb excitation of low-lying levels, meas. of γ-ray energies, yields, angular distribs., Doppler broadening 2−74032
^{12}C, alpha-gamma ang. correlation studies 2−70477
^{12}C(^{6}Li,d)^{16}O, meas. of 6.92- and 7.12 MeV γ radiation as function of bombarding energy, determ. of reaction mechanism 2−46332
^{12}C(n,n$'\gamma$)^{12}C, improved statistics for angular correlation measurements 2−46273
Ca^{181}HfO$_3$, perovskite type, nucl. quadrupole interactions, perturbed angular-correlation meas. 2−72244
^{48}Ca(p, p$'\gamma$), particle-γ angular correlation and lifetime studies of 4.61 and 5.15 MeV levels 2−82889
^{140}Ce, ang. correlation meas. on cascades 2−52763
^{140}Ce, angular correlation of γ-cascade 2−49748
^{252}Cf triple fission, angular meas. of γ-radiation yield 2−49852
^{37}Cl(p,nγ)^{37}Ar, 3.25-5.90 MeV, meas. of γ-ray angular distribs. and mean lifetimes of levels in ^{37}Ar 2−74015
^{51}Cr, ang. distrib. of ground state e.m. transitions 2−79751
^{51}Cr, in transitions from excited states populated in (p,n) and (p,nγ) reactions on ^{51}V 2−46265
^{54}Cr(p, nγ)^{54}Mn, 2.0-3.9 MeV, meas. of excitation functions and angular distributions of gamma rays, determ. of ^{54}Mn level structure 2−79743
^{131}Cs decay, gamma gamma directional correl. meas. 2−46197
^{63}Cu, ^{65}Cu(α,$\alpha'\gamma\gamma$) Coulomb excitation, 5.5, 7.0 MeV, meas. of angular distrib. and $\gamma\gamma$ angular correlations 2−63802
^{19}F(d,pγ)^{20}F, p,γ ang. correl., low-lying states of ^{20}F 2−79801
Fe: ^{169}Tm, hyperfine field at Tm temp. depend. from perturbed angular correl. expts., 4.2-450K 2−81252
Fe-Rh alloy, proton irrad., hyperfine field at Rh nuclei detn. 2−61572

Gamma-rays continued
angular distribution continued
Fe garnet, magnetic hyperfine field interaction of Ce^{3+} by angular correlations 2−81320
^{54}Fe(p,p'γ)^{54}Fe, $E_p = 10$ MeV, spectroscopy of ^{54}Fe 2−76836
^{57}Fe, 122-14KeV cascade, ang. correl. obs. 2−70395
^{58}Fe(p, nγ)^{58}Co 3.9 MeV, meas. of nγ correlations and g-factors, determ. lifetimes and magnetic moment of ^{58}Co levels 2−79742
n-Ga$_{1-x}$Al$_x$As, metal-semicond. surface barrier struct., energy band diagram 2−75134
GaP:N(Bi), exciton binding to impurities, uniaxial stress effects 2−75108
^{151}Gd, meas. of angular γ-γ correlations and multipolarities of transitions 2−46160
^{154}Gd, γ-transitions, by γ-γ angular correlation measurements 2−82919
^{154}Gd, time differential perturbed ang. correlation studies in liquid environment at different temp. 2−60511
Hf (IV) complexes, octocoordinated, differential perturbed ang. correl., ^{181}Ta quadrupole coupling 2−61571
HfF$_4$:^{181}Ta, in dilute HF, time differential perturbed γ-γ angular correlation, temp. dependence 2−81321
^{181}Hf cpds., ABO$_3$-type, perovskite type, nucl. quadrupole interactions, perturbed-angular-correlation meas. 2−72244
^{165}Ho (n,nγ new γ-ray transition 2−46159
^{39}K(n,γ)^{40}K, circular polarization of capture γ-radiation, spin assignment 2−67273
^{39}K(n,γ)^{40}K, thermal neutron capture, ^{40}K level scheme 2−67274
^{42}K, spins of states determ. by γ-γ correlations in ^{41}K(d,p) reaction at 6 MeV 2−46131
^{79}Kr γ-ray transition meas. 2−79758
^{81}Kr γ-ray transition meas. 2−79758
^{82}Kr, spins of excited states, γ-γ correlation study 2−46145
^{83}Kr γ-ray transition meas. 2−79758
^{85}Kr γ-ray transition meas. 2−79758
La and Y ethylsulphates: ^{166}Er γγ cascade, crystal orientation effect 2−78053
^{54}Mn, spin assignments of low lying levels, from ^{54}Cr(p,nγ) 2−46134
^{55}Mn(α, nγ)^{58}Co, 10 MeV, meas. of n-γ angular correlations and lifetimes using Doppler-shift attenuation method 2−82890
^{94}Mo(p,p'γ)^{94}Mo, angular correlation obs., analog resonance in ^{95}Tc 2−74078
^{14}N, meas. of γ-ray production cross sections at 4.2, 5.9 and 6.9 MeV for (n,n'γ), (n, αγ) and (n,pγ) reactions 2−79507
^{93}Nb(n,γ), resonant neutron capture 2−67284
^{93}Nb(n,n'γ)^{93}Nb, de-excitation γ-rays, ^{93}Nb level scheme 2−67164
^{20}Ne(^{3}He,nγ)^{22}Mg, 4.3-11.5 MeV, angular correlation and coincidence meas., ^{22}Mg deduced levels 2−63784
^{20}Ne(t, pγ)^{22}Ne, 3 MeV, p-γ ang. correl., spin assignments 2−79739
^{21}Ne, level struct., ^{18}O(α,nγ) obs. 2−55958
Ni, hyperfine field of ^{181}Ta, γ−γ angular correl. obs. 2−44320
^{58}Ni, alpha-gamma ang. correlation studies 2−70477
Pb-Sn alloy, dependence of γ ang. correlation of positron annihilation on composition 2−71766
Pb^{181}HfO$_3$, perovskite type, nucl. quadrupole interactions, perturbed-angular-correlation meas. 2−72244
PbZnO$_3$, internal electric field gradient by perturbed angular correlations 2−81156
^{206}Pb, perturbed ang. correl. obs. of isomeric state g-factor 2−59720
^{139}Pr γ-γ angular correlations for 114-708 and 114-738 keV cascades, lifetime of 822 keV level 2−46158
^{141}Pr(n,nγ) new γ-ray transition 2−46159
^{224}Ra α decay, study of hyperfine interactions when implanted in Fe, al, Cd, Bi, α-γ correlation meas. 2−81341
^{185}Re, γ-γ direction correlation expts. on cascades populated from electron capture decay of ^{185}Os 2−67178
^{187}Re 72-134 keV cascade, ang. correl. coeff. 2−82885
^{220}Rn α decay, study of hyperfine interactions when implanted in Fe, Al, Cd, Bi, α-γ correlation meas. 2−81341
^{102}Ru(n,γ)^{103}Ru, thermal neutron capture, ^{103}Ru level scheme obs. 2−67166
^{34}S(α,γ)^{38}Ar, 3.6-4.8 MeV, meas. of cross sections, angular distributions and angular correlations ^{38}Ar levels deduced 2−63791
^{125}Sb→^{125}Te decay, γ−γ directional correlation expts. concerning negative and positive parity levels 2−46195
^{45}Sc(n,γ)^{46}Sc, γ spectroscopic obs. of ^{46}Sc level scheme 2−67156
^{75}Se, γ-γ cascade decade, meas. of hyperfine mag. fields at As in Fe, Co and Ni 2−78018
^{29}Si(α,p)^{32}P, 10.4-11.0 MeV, pγ angular correlation and Doppler-shift meas. 2−49735
^{30}Si(α,nγ)^{33}S, 6.0-9.5 MeV, study of ^{33}S levels up to 4.3 MeV excitation, analysis of γ-ray angular distribs. 2−70385
^{152}Sm, static hyperfine interactions at free atoms 2−70560
Sn^{181}HfO$_3$, perovskite type, nucl. quadrupole interactions, perturbed-angular-correlation meas. 2−72244
^{117m}Sn, perturbed ang. correl. meas. of g-factor 2−63811
Sr^{181}HfO$_3$, perovskite type, nulc. quadrupole interactions, perturbed-angular-correlation meas. 2−72244
^{181}Ta 133-keV γ-rays cascade, perturbed ang. correl. obs. 2−78057
^{125}Te, γ-γ ang correlation of 171 to 427 keV cascade 2−52758
^{227}Th decay, α-γ coincidence and directional correlation studies 2−63852
^{227}Th→^{223}Ra decay, α-γ coincidence and directional correlation studies 2−49776
^{43}Ti de-excitation γ-rays meas. and used to give spin assignments 2−46132
^{46}Ti(d, p)^{47}Ti, 5 MeV, study of spin-dependent reaction mechanism from pγ correlation 2−63919
^{235}U, thermal-neutron-induced fission, emission of prompt. γ-rays 2−76892
^{186}W(n,γ)^{187}W, nsec. isomeric transitions, γ-γ coincidence obs. 2−67176
^{186}W(n,γ)^{187}W, nsec. isomeric transitions, γ-γ coincidence obs. 2−67176
YbFe garnet, perturbed ang. correl. on ^{169}Tm, h.f.s. 2−72247
detection, measurement
see also Dosimetry; Gamma-ray spectrometers; Particle detectors; Radioactivity measurement
camera-computer systems, maximum frame rates 2−78652

Gamma-rays continued
detection, measurement continued
celestial nuclear γ-ray monitoring from OSO-7 2−58438
Compton polarimeters, relative peak efficiencies 2−76743
extensive air showers, γ-ray point source search by registration of Cherenkov light 2−51801
fluctuations, giving nucl. reactor local power 2−83102
ground level background, absence of fluctuations 2−63675
imaging system for diagnostic radiography using pulse compression techniques 2−51930
intrinsic γ detection efficiencies for cylindrical Geiger Muller tubes by Monte Carlo methods 2−73933
luminescence, visual control of γ-ray sources 2−85177
momentum distribution of γ rays produced by high energy K^{+} interactions with nuclei in heavy liquid bubble chamber 2−52704
noise, meas. rel. to reactor parameter determination 2−49908
nuclear reactor stochastic two-group model including neutron and gamma detection 2−83095
photonucleon cross section det. for separate residual nuclei states utilizing continuum γ sources 2−74061
photoresistors, dosimetric characteristics 2−82800
pin hole camera, wide angle 2−67069
probe, for high temp. industrial applications 2−67083
quality control of p-type and intrinsic Ge monocrystals 2−46044
radionuclide imaging, three dimensional, using detection of cascading γ-rays in coincidence at 90° 2−69284
reactor room, spectral obs. 2−63983
scintigraphic device, Autoimager 2−69283
semiconductor devices 2−46043
shielding calcs. eval. and parameters determ. with bremsstrahlung radiation 2−83156
snow water equivalent meas. using attenuation of natural γ radiation emission from soil 2−54742
solid angle optimization in angular correlation measurements 2−73905
tomographic scintillation camera, performance and reliability 2−69285
variable baseline scanner, medical application 2−78653
wire spark chamber γ-ray imaging system for biomedical use 2−69290
(n,γ), thermal neutron capture, absolute γ-ray efficiencies of Ge(Li) detectors 2−67256
CaF$_2$:Mn dosimeter response 2−83161
CaF$_2$:Mn thermoluminescent γ-dosimeter, sensitivity to neutrons 2−82820
CaSO$_4$:Mn dosimeter response 2−83161
GaAs detector, crystal growth and material quality obs. 2−46052
Ge, very pure, new detector 2−52694
Ge(Li) coaxial detector, local efficiency variations 2−70301
Ge(Li) detectors, method for controlling surface properties 2−59625
Ge(Li) γ-ray detectors, evaluation procedures 2−55919
Ge(Li) total absorption spectrometer for (n, xγ) cross section meas. 2−46039
Ge(Li)γ-ray detector for college laboratories, nonsensitive area determ. 2−62929
LiF and natural fluorite, mixed field with thermal neutrons 2−73948
LiF detector, thermoluminescent, for neutron and gamma radiation 2−52691
LiF dosimeter response 2−83161
PbO, crystal growth and detection props. 2−46037
pbI$_2$, crystal growth and detection props. 2−46037
effects
see also Nuclear reactions and scattering due to/photons
alkali halides, irrad., aquoluminesc., energy levels of trapped electrons 2−43376
alkali silicate glass, irrad., thermolum. 2−81410
amino acids, irrad., effect of cryst. struct. on stability, yield and shape of e.s.r. spectra 2−81536
cellulose triacetate, e.s.r. obs. of radicals formed 2−44494
cysteine hydrochloride monohydrate, irrad., radical recomb. mag. reson. obs. 2−72575
dipeptides, irrad., effect of cryst. struct. on stability, yield and shape of e.s.r. spectra 2−81536
DNA single-strand breaks produced by γ-ray after treatment with 2, 4-dinitrophenol 2−66272
glasses containing La and Ce, optical stability 2−70071
graphite, X-irrad., dynamical mech. props. 2−53777
hexachloroethane, irrad., thermolum. and e.s.r. 2−48259
ice, trapped electron, optical absorption spectra 2−75295
ice forming activity of γ irradiated AgI particles 2−48498
memory device, amorphous film, radiation effects 2−61365
methane, solid, spin species conversion by paramag. impurities 2−84446
PMMA, irrad., induced optical density rel. to dosage 2−72357
poly(vinyl chloride), electron and γ-irrad. at 77K, e.s.r. 2−83360
polypropylene, formation of γ-form crystals from melt 2−60614
pulsed γ-neutron radiation, monkeys, brain blood flow, vascular resistance, blood pressure and heart rate obs. 2−69316
ruby laser, stimulated radiation props., ^{60}Co radiation effects 2−73585
stimulated emission from ruby laser 2−69935
thermoluminescence in quartz, determ. of geological origin 2−84709
Al-Al$_2$O$_3$ and Al-SiO$_x$-Al, dielec loss and conductivity variations 2−81114
Al, irrad. induced variations in linear dimens. 2−43607
Al$_2$O$_3$:V, before and after γ-irrad., phonon scatt., thermal cond. study 2−68214
BeO, irrad. damage, e.s.r. obs. 2−44445
C, pyrolytic, γ-irrad. stress-graphitized, dynamic mech. props. 2−53775
CaF$_2$, optical absorption following intense γ- irradiation 2−84529
CdCl$_2$ crystals, e.p.r. spectra of impurity ions at 5 eV, radiation effects 2−84475
CdTe:Li, interaction of impurity with radiation-induced defects 2−75107
^{60}Co, γ-ray irradiation of malignant lymphopathies, dose distribution 2−69412
CsI:Tl, scintillation growth times 2−73938
Cu, irrad. induced variations in linear dimens. 2−43607

Gamma-rays continued
effects continued
n-GaAs, irrad., effects on current instabilities caused by recomb. centres 2-81092
n-Ge:O, irrad., Hall mobility, anisotropy 2-54196
Ge, donor-vacancy complexes, prod. kinetics and energy spectrum 2-47382
Ge, irrad. damage, Mossbauer type photoluminesc. spectra obs. 2-48243
n-Ge, irrad. damage, recombination parameters 2-47929
Ge, γ-irrad., O-free, divacancy-donor complexes 2-71943
KCl, F-centre colouring, γ-ray induced, strain effects 2-71528
KCl, voltametric behaviour of soln., aquoluminesc. phenomena 2-84662
KCl crystals, critical resolved shear stress 2-47492
$KClO_3$, radiation damage, Raman spectra obs. 2-57361
Mo, irrad. induced variations in linear dimens. 2-43607
NH_4HSO_4, irrad., e.s.r. of $HNSO_3^-$ radical, ferroelec. transition mechanism 2-84369
NaCl, NaCl:Ca, d.c. conductivity obs., room temp. −70°C, electronic and ionic contribs. 2-57231
$NaClO_3$, radiation damage, Raman spectra obs. 2-57361
Pb single crystal γ-irradiated temperature dependence of positron annihilation spectrum 2-71767
p-Si:B, Li-compensation influence on irrad. defect form. 2-47390
Si, irrad. induced defect obs. 2-47937
n-Si, photoconductivity obs. 2-72066
Si p-n diode, irrad., impurity effects, photovolt. effect obs. 2-61358
$Y_3Al_5O_{12}$:Pr(Tb)(Eu)(Yb) colour centre investigation of absorption and thermal de-excitation 2-80714

internal conversion
see also Beta-ray spectra/conversion electrons
— 2-59705
E1 internal conversion, study based on Saxon-Woods potential 2-49719
M1-intranuclear conversion analysed on basis of Saxon-Woods potential 2-46089
total internal conversion coefficients meas. using Ge(Li) detector 2-73982
^{113*}Tn (100 min) decay, internal conversion, M4, E5 character 2-74052
^{73}As, coeffs. of low level transitions, using ^{75}As(p,n) 2-52752
^{197}Au, 77 keV transition, internal conversion process 2-55968
^{115m}Cd, decay to ^{115}In, internal conversion electrons 2-70420
Co containing ^{57}Fe, contact charge density of conduction electrons 2-51307
^{154}Gd, 123 keV transition, conversion coeff. meas. 2-46161
^{156}Gd, K conversion coeffs. for 80 transitions obtained 2-46162
^{177}Hf, 113 keV transition, relative internal conversion electron intensities 2-63825
^{177}Hf coefficients for E1 transitions with energies 71.6, 208.3, 321.3 keV 2-49754
^{198}Hg, K-shell internal conversion coeffs. meas. with X-ray scintillation spectrometer 2-79737
^{191}Ir, conversion coeffs. for prominent transitions 2-76806
^{192}Ir, γ-ray spectra, K-shell internal conversion coeffs. 2-70423
^{139}La, det. of total coeff. 2-59711
^{175}Lu(n, e)^{176}Lu slow neutron capture, study of ^{176}Lu excited levels by obs. of conversion electron spectra 2-79744
^{177}Lu penetration matrix elements for 150 keV transition 2-82914
^{191m}Os, K conversion coefficient near threshold 2-42535
^{141}Pr, K-shell internal conversion coeffs. meas. with X-ray scintillation spectrometer 2-79737
^{153}Sm, effective g_s factor determ. by internal conversion processes 2-52765
^{203}Tl, K-shell internal conversion coeffs. meas. with X-ray scintillation spectrometer 2-79737
^{169}Tm, penetration effects in internal conversion of transitions 2-63822
^{171}Tm, penetration effects in internal conversion of transitions 2-63822
^{138}Xe fission product, β- and γ-decay study using ARIEL on-line isotope separator, meas. of internal conversion and Auger L spectra 2-82924

scattering
see also Compton effect
approximate calculation techniques for the design of geometries specific to industrial applications 2-79847
crystal perfection, precise measurement 2-47297
electron velocity in atoms, Compton effect demonstration for students 2-78722
fermion pair and γ quantum, photoprod. on nuclei, polariz. phenomena 2-70147
Mossbauer spectra interference rel. to polarization 2-54385
nuclei, and absorption cross-section calc. 2-76774
$\gamma\gamma$, virtual, and new type of scaling 2-82675
$\gamma\gamma$, virtual, asymptotic form of amplitude 2-59411
Ag, incoherent, by K-shell electrons 2-59931
^{57}Fe, asymmetries, h.f.s., vectorial relations, interference 2-74025
Sm, incoherent, by K-shell electrons 2-59931
Ta, incoherent, by K-shell electrons 2-59931
TiO, Compton profiles, scatt. factors, determ. of electron state 2-68628

Gamow-Teller transitions *see Beta-decay theory; Nucleus/energy levels*

Garnets
see also Ferrites
almandine, optical absorpt. spectra of Fe, cubic field approx. 2-72328
bubble domain type, epitaxial film, effect of substrate defects on struct. 2-47092
bubble films, elimination of hard bubbles by second magnetic layer 2-65164
bubble materials, magnetiz. reversal due to annealing 2-51253
crystal growth for bubble domain memories 2-47199
ferrite, distribution of electromagnetic waves near compensation temp. 2-65211
ferrite-garnets, magnetic birefringence 2-65216
ferromagnetic reson. lineshape near Curie pt. 2-72445

Garnets continued
film, chem. vapour deposition, product phase control 2-71321
film, epitaxial, magnetic bubble mobility measurement 2-57303
film, epitaxial single cryst., optical waveguides 2-70059
film, magnetic, domain interaction with laser beams, domain writing 2-75230
magnetic bubbles, domain-wall config. 2-78009
magnetic bubbles, hard, dynamic props. 2-78010
magnetic bubbles, properties, applications, review 2-78035
magnetic domain-wall mobility, Bloch line effects 2-78011
magnetic films, hard bubble suppression by ion implantation 2-65163
multilayer epitaxial films for magnetic bubble devices, hard bubble suppression 2-65162
Raman scattering from electronic levels, identification of Raman active photons 2-68657
rare earth, LnAlG and LnGaG, phonon cond. 2-77786
rare earth, with ions on dodecahedral and octahedral sites, mag. ordering 2-44226
rare earth iron, damping of domain wall motion 2-57304
rare earth iron, isomer shifts of ^{57}Fe 2-57333
rare earth iron, mixed, easy magnetiz. direction, Mossbauer obs. 2-51314
rare earth iron, physical props. near compensation temp. 2-81286
rare earth metal, containing Fe ions, absorp. spectra 2-75305
YAG laser, Ge photodiode detecting head 2-66761
YIG sphere under parallel pumping condits., anisotropy of above-threshold susceptibility 2-72140
$[YCa_2][Zr_2](Fe_{2.75}Ge_{0.25})O_{12}$, mag. struct., neutron diffr. obs. 2-78038
$Al_2Fe_3(SiO_4)_3$, almandite, mag. struct., cryst. struct. 2-54349
$Al_2Fe_3(SiO_4)_3$, almandite, elec. field gradient, internal mag. field, Mossbauer obs. 2-54388
$Ca_3Al_2[SiO_4]_3:Fe^{3+}$ optical spectra calc. 2-72295
$Ca_3Fe_{2-x}M_xGe_3O_{12}$, $M=Al^{3+}$, Ga^{3+}, Cr^{3+}, Sc^{3+}, In^{3+}, Mossbauer study of lattice 2-72278
$Ca_3Fe_2[SiO_4]_3:Fe^{3+}$, optical spectra calc. 2-72295
$Cd_3Fe_{2-x}M_xGe_3O_{12}$, $M=Al^{3+}$, Ga^{3+}, Cr^{3+}, Sc^{3+} In^{3+}, Mossbauer study of lattice 2-72278
DyAl, mag. sp. ht. 2-43983
ErGa, metamagnetism 2-61557
(Eu,Sm)Fe and (Eu,Ho)Fe, mixed, easy magnetiz. direction, Mossbauer obs. 2-51314
$EuEr_2Fe_{4.3}Ga_{0.7}O_{12}$, liquid-phase epitaxial growth 2-83902
$EuEr_2Fe_{5-x}Ga_xO_{12}$ film, liquid phase epitaxy, optimum conditions 2-47108
$EuEr_2Ga_{0.7}Fe_{4.3}O_{12}$ film, epitaxial, magnetic bubble mobility measurement 2-57303
Fe, magnetic hyperfine field interaction of Ce^{3+} by angular correlations 2-81320
Fe, magneto-optic film waveguide, light modulation and switching 2-81323
FeMg garnet, ^{27}Al and ^{29}Si n.m.r. studies 2-65341
GGG, epitaxial magnetic film, prep. by chem. vapour deposition 2-77527
$(Gd,Tb,Eu)_3Fe\ O_{12}$ ferrite, optical anisotropy and cylindrical domains 2-68602
GdFe, bubble domains, flux switching 2-57305
GdFe, with Tb^{3+} impurity, ferromag. reson. 2-72453
GdFe garnet with Co^{2+} substituted, magnetooptical props. 2-84460
GdFe polished platelets, uniaxial anisotropy 2-44276
$Gd_3Fe_{5-x}Al_xO_{12}$, cation distrib. detn., Mossbauer obs. 2-48147
GdIG, high temp. high press. phase formation 2-57024
GdIG, sublattice rotation near mag. compensation point, sp. ht. study 2-61508
GdIG, substituted, compensation temp., applic. to beam- addressable magneto-optic memory 2-72193
GdTbFe, hard bubbles, new cylindrical magnetic domain 2-65169
$La_{2.97}In_{1.94}Ga_{3.09}O_{12}$, spectral transmission and refractive index 2-75300
Mg-rich, compression to 100 kbars 2-65581
Nd:YAG, Q-switched laser, pumping CdSe i.r. parametric oscillator 2-42061
Nd:YAG new laser transitions $^4F_{3/2}$ to $^4I_{9/2}$ 2-42066
Nd^{3+}:YAG intracavity phase modulated laser separation of mode locked states 2-42048
Nd^{3+}:YAG solid laser, generation of subnanosecond 10 μ pulses 2-42068
$Nd_{3-y}R_yR_xGa_{2-x}Ga_3O_{12}$ garnet, R=Yb, Tm, Er, Ho, Dy, mag. props., 1.6-300K 2-61485
$Tb_3Al_5O_{12}$, luminesc. time depend., dipolar transfer 2-54459
TbIG, high temp. high press. phase formation 2-57024
Y-Fe, l.f. magnetization oscillations where absorption maximum coincides with ferromagnetic resonance 2-75340
Y, diamagnetically displaced, magnetostriction constants 2-65161
Y, magneto-elastic bonding of Fe^{3+} and Cr^{3+} ions, EPR and FMR study 2-65321
YAG:Ho, Yb, Er, Tm laser, recirculating liquid N_2 system for cooling 2-63339
YAG:Nd, crystal growth, boule defects, and Nd distrib. obs. 2-47246
YAG:Nd, grown by Czochralski method, cryst. perfection rel. to melt comp. and rot. speed 2-67945
YAG:Nd electro-optically Q-switched laser, multipulsing behaviour 2-59173
YAG:Nd laser, CW pumped, output fluctuations 2-45751
YAG:Nd laser, diode-pump-modulated, response to pump intensity sinusoidal modulation 2-52427
YAG:Nd laser, harmonic mode locking 2-59172
YAG:Nd laser, meas. of start photon number 2-52428
YAG:Nd laser, props. rel. to Nd:YALO, Nd:Yttralox, Nd:apatites 2-63338
YAG:Nd laser, pulsed, organic dyes as filters 2-73588
YAG:Nd laser, single freq. travelling wave, output 2-73581
YAG:Nd laser, space qualified, design 2-69940
YAG:Nd laser material, holographic interferometry meas. of thermal refractive index and expansion coefficients 2-59174
YAG:Nd laser system for generation of controllable reproducible giant pulses 2-69925
YAG:Nd lasers bibliography 2-42065

Garnets continued
YAG:Nd^{3+}, random variation of static crystalline field, e.s.r. line width obs. 2−44441
YAG:Nd^{3+} laser, effect of pressure in Xe and Kr arc lamps on pumping efficiency 2−42072
YAG:Nd^{3+} laser, recirculating liquid N_2 system for cooling 2−63339
YAG:Nd^{3+} laser target designators and range finders 2−42064
YAG:Nd^{3+} quasicontinuous laser, spectral characts. and oscill. dynamics 2−79216
YAG:Pm laser, radiative transition probabilities rel. to YAG:Nd 2−59186
YAG-YALO:Nd^{3+} laser, hybrid operation at 1.064 μ 2−69939
YAG, crystallization from PbO-YF_3-Al_2O_3 melts, det. of stability range for YAG 2−74692
YAG, luminesc. of Tb^{3+}, quenching by direct transfer and migration 2−54459
YAG films, Nd^{3+} site preferences for growth by liquid phase epitaxy, spin-reson. meas. 2−83867
$Y_3Al_5O_{12}$:SiO_2, grown from melt, habit modification by doping 2−74751
$Y_{3-x}Ca_xFe_{5-x}Sn_xO_{12}$ noncollinear spin config., Mossbauer spectra obs. 2−54344
$Y_{3-x}Eu_xAl_yFe_{5-y}O_{12}$ films, epitaxial, characteriz. for bubble devices 2−61541
$Y_3Fe_{5-(x+y)}Al_xGa_yO_{12}$ ferrite, magnetiz. and ferromag. resonance 2−72204
$Y_3Fe_{5-x}Al_xO_{12}$, mag. anisotropy, natural ferromag. reson. obs. 2−78148
$Y_3Fe_{5-x}Cr_xO_{12}$, crystal growth, fluxed melt technique 2−47289
$Y_3Fe_5O_{12}$:SiO_2, grown from melt, habit modification by doping 2−74751
$Y_3Fe_5O_{12}$, mag. phase transition, polarized neutrons and RF susceptibility obs. 2−57284
$Y_3Ga_{1.1}Fe_{3.9}O_{12}$ layer, laser beam thermomagnetic recording 2−51273
$Y_{2.5}Gd_{0.5}Fe_4Ga_1O_{12}$, film, magnetization orient. depend., induced anisotropies, magnetooptic Faraday effect obs. 2−72188
$Y_3Ge_5O_{12}$:Si, grown from melt, habit modification by doping 2−74751
YIG:Cr^{3+}, Cu^{2+}, hyperfine interactions of Cr^{3+} and Cu^{2+} ions, n.m.r. obs. at 4.2K 2−72504
YIG:Ru, magnetostriction consts. 2−44281
YIG:Si, photoinduced dichroism, model 2−72260
YIG:Si^{4+},Ca^{2+} magnetostriction rel. to mag. field inclination to crystallographic axes at 4.2K, 77K and room temp. obs. 2−84437
YIG/Ge interface, interaction of surface magnetostatic waves with carriers 2−84420
YIG/dielectric/conductive plane, magnetostatic propag. 2−51268
YIG, Al^{3+}-substituted, Ru^{3+}-doped, ferromag. reson. 2−81444
YIG, Ca-Si substituted, flux growth and mag. characterization 2−47278
YIG, cryst. growth, chem. transport 2−43513
YIG, cryst. growth, viscosity and density of melts 2−60713
YIG, crystal growth, fluxed melt method, effects of oxygen pressure 2−50603
YIG, d.c. magnetization produced by parallel optical pumping 2−72203
YIG, diamagnetically substituted, Mossbauer spectra in crit. region 2−78077
YIG, effect of magnetic ordering on optical absorption spectrum 2−81392
YIG, electrostatic forces, elec. field gradient, mol. orbitals construct. 2−68615
YIG, epitaxial film growth by chem. vapour deposition 2−47132
YIG, epitaxial magnetic film, prep. by chem. vapour deposition 2−77527
YIG, ferroacoustic surface wave resonance 2−51035
YIG, flux growth, local cooling and accelerated crucible rotation effects on quality 2−50602
YIG, heteroepitaxy, flux method and hydrothermal synthesis 2−50513
YIG, high temp. high press. phase formation 2−57024
YIG, hysteresis loop, wall displacement and bulging in magnetization mechanism 2−65167
YIG, light-induced Bloch wall pinning 2−48060
YIG, magnetocryst. anisotropy, reson. fields, iodine additive effects 2−44279
YIG, magnetooptical coeffs., temp. depend. 2−72266
YIG, magnetostriction consts., meas. by ferromag. reson. 2−72176
YIG, nonmag. ion substituted, polycryst., ferrimag. resonance obs. 2−61547
YIG, nucl. gamma reson. study of mag. anisotropy 2−81266
YIG, parallel pump spin wave instab., discrete magnon resonances 2−48271
YIG, photomechanical effect 2−81332
YIG, polycryst., spin wave transit time, limitation by pores 2−75232
YIG, reson. phenomena at moving domain boundaries 2−72456
YIG, shock induced demagnetization, method for investigation 2−48081
YIG, sound wave absorpt. effects, magnetoelasticity, domain wall motion 2−61097
YIG, spin relaxation near Curie temp. studied by high frequency magnetic susceptibility 2−84417
YIG, substituted, ultra-low bandwidth, microwave loss 2−44435
YIG, substituted, ultralow-linewidth, microwave loss 2−51397
YIG, surface spin wave propagation in inhomogeneous fields 2−78037
YIG, tangentially magnetized substrate, magnetoelastic, Rayleigh type surface wave 2−43976
YIG cylindrical rod, mode separation of magnetostatic waves 2−59005
YIG discs, epitaxial, anisotropy effects on magnetostatic modes 2−44432
YIG domains, laser beam diffraction 2−44348
YIG epitaxial film, coupling between dipole and exchange dominated spin waves 2−72189
YIG film, chem. vapour deposited, substrate growth band and core struct. replication 2−71338

Garnets continued
YIG film, chem. vapour deposited, comp. variation and magnetization 2−72202
YIG magnetostatic echo analysis 2−57313
YIG rod, internal field distrib., magnetoelastic reson. determ. 2−57285
YIG single cryst./polycryst. composites, amplified Hahn-type echoes 2−44270
YIG single crystal film, domain wall mobility meas. by light diffraction 2−84434
YIG thin film disks, anisotropic excitations of magnetostatic modes 2−44434
YIG thin single-crystal distrib., magnetoexchange branch repulsion 2−44433
YIG(Si), reversible photomagnetic effects, microscopic theory 2−54259
$(Y_2O_3)_3(Fe_2O_3)_5$ ferrite, photocond., 280-800 nm 2−84380
YbFe, perturbed ang. correl. on ^{169}Tm, h.f.s. 2−72247
YbFe, stat. mol. field interpret. of mag. props. 2−72205
YbFe garnet, Ca-Si substituted, flux growth and mag. characterization 2−47278

Gas analysis *see Chemical analysis*

Gas-discharge tubes
see also Counters; Ion sources
capillary gas lasers, l.f. oscillations due to moving striations 2−77314
flashlamp of rectangular cross-section 2−77311
heavy rare gases, radiation properties 2−71004
lamp, straight tubular gas-discharge, effect of bulb on brightness distrib. 2−43208
laser discharge tube with capillary section, patent 2−63335
mirrors and windows, shielding from electrode disintegration products 2−55684
moving striations, in tapered tube 2−43205
thyratron employing orthogonal electric and magnetic fields 2−70994
thyratron pulse discharges, arc pot. obs. 2−56399
Ar, d.c. arc constricted horiz. column motion due to buoyancy 2−71051
Ar Z pinch discharge electron density gradients meas. using modified Jamin interferometer 2−66771
Cs, thermionic converter, nonequilibrium relaxation phenomena, near emitter region 2−49276
Hg, anode glow oscillations, optical studies 2−71020
N_2, electronegative gases, light emission in electron avalanches 2−74428
Ne flash tube, location of particle along length 2−70314

Gas flow *see Flow/gases*

Gases
see also Kinetic theory/gases
absorption in laminar gas-liquid flow in horizontal channel 2−50290
acoustic wave propagation in waveguide filled with gas mixture with transverse concentration gradient 2−41719
aerosol conversions, classification of physical nature 2−43406
air, fully developed turbulent flow through concentric annuli 2−53280
atomization and mixing of gas/liquid coaxial injector elements 2−62415
binary mixture, asymptotic theory for steady source expansion 2−71108
binary mixture, composition meas. with fast-response probe 2−56401
binary mixture, stepped vapour concentration 2−53342
binary mixtures, acoustic propagation from plane wave solns. of coupled linearized Boltzmann eqns. 2−50272
biphase system, adiabatic expansion, liquid drop atomization and freezing 2−71111
in bubble columns, dynamic meas. by X-ray absorpt. 2−64420
bubbles, behaviour in gas-solid fluidized beds, theory for initial bubble formation 2−50145
chemisorbed, thermal desorption kinetics, review 2−67918
chromatography, injection apparatus under vacuum 2−61820
classical gas, dynamical correlation function, first order perturbation calculation 2−43258
classical of hard discs at high density, investigation using De Boer cell-cluster theory 2−64391
collisionless, transient orientational birefringence 2−43267
dense, paired correlation function, integral equations 2−60207
dense, spreading of large current electron beam 2−66709
dense, transport phenomena, Greens function theory 2−43275
dew point, containing low conc. of H_2SO_4 2−75536
diatomic, thermal radiation interaction, model kinetic eqn. for internal fluid 2−43263
diatomic gas in shock front and wake, relaxation equations for vibrational and rotational energy including transport processes and chemical reactions 2−52966
diffusion into porous materials and viscous loss 2−80394
dissipative, one dimensional nonlinear acoustic wave propagation 2−52229
dissociating, asymptotic behaviour of the external fringes of compressible laminar boundary layers 2−67698
dynamics, application of invariant difference methods 2−77334
electron drift velocity in neutral gas under influence of uniform electric field 2−56382
electron transmission, voltage and pressure dependence 2−83713
equations of state, from Ursell-Mayer density expansion compressibility factors 2−53108
equations of transfer mechanically reacting nonhomogeneous gases 2−68765
expansion in rarefied atmosphere, simularity solutions 2−80396
free jets, turbulent mixing 2−74461
freons, Raman spectroscopy 2−80418
heat of mixing and integral Joule-Thomson effect, relation 2−50267
hot, temperature measurement up to 1600°C using thermocouples 2−73471
hydrocarbons, Raman spectroscopy 2−80418
micro-scale for meas. over eight decades 2−66411
mixture, light scatt. 2−67735
mixtures, chem. reacting, transport processes 2−48320

Gases continued
- molecular, nongrey radiation, formulation in terms of slab band absorptance 2−77367
- noncondensable, effect on film condensation of pure and binary vapours at forward stagnation point of horizontal cylinder 2−77410
- nonhomogeneous, volume interchange factors rel. to radiative heat transfer 2−53335
- polar gases, viscosity dependence on pressure 2−56444
- polyatomic, phys. props. prediction from mol. struct. 2−83698
- radiating, straight oblique shock waves 2−46837
- range pair counting method application to oxidation in combustion chamber exhaust gases 2−57421
- resonance excitation diffusion, stimulated emission effect 2−59903
- self gravitating, shock wave propag., rel. to stellar models 2−84987
- separation using 'light pump' 2−71120
- shock wave propagation in gases with discrete velocity distributions 2−53301
- shock wave structure using nonlinear model Boltzmann eqns. 2−50258
- simple, statistical mechanical description of depolarized light scattering and many-body effects 2−53338
- solubility in liquids 2−53405
- sonic discontinuities in a radiative gas, growth and decay of waves for second and third order compatibility 2−56442
- spectral line shapes, kinetic theory, transition between Doppler and collision broadening 2−64091
- stability of plane 2-dimensional vortex sheet separating thermally radiating gases 2−67733
- surface interaction, effects of roughness 2−77363
- temperature oscillations undergoing free correction, effect on solidification 2−47028
- thermal accommodation coeffs. det. by temp. jump and free molecular flow methods 2−77368
- thermal diffusion for multicomponent gases, theory and review 2−56447
- thermally driven oscillations, heat balance, acoustic streaming 2−80358
- turbulent jets, cryogenic discharges into gaseous medium 2−74460
- turbulent wakes, temp. fluctuations, measurement by probe 2−77330
- u.s. methods of investigation, short review 2−60374
- vapour diffusion coefficients in a ternary gaseous system 2−83718
- weak shock waves propagation in relaxing gas 2−83653

Gegenschein *see Zodiacal light*

Geiger counters *see Counters/Geiger*

Gelatin
- dichromated, phase hologram applications, properties and requirements 2−63357
- gel, diffusion of water, interfacial contact resist. 2−60533
- relief capacity for acid photographic dyes 2−70092

Gels
- aqueous, effect of freeze/thaw treatment on precip. 2−83807
- compact gel-growth technique for cryst. growth 2−50566
- gelatin, diffusion of water, interfacial contact resist. 2−60533

Generators *see Electrical machines*

Geochemistry *see Earth/composition*

Geochronology *see Earth/age; Radioactive dating*

Geodesy
- *see also Gravity*
- 'intermediate' anomalies in COSMOS-49 and OGO-2, 4, 6 data, determ. of locations and amplitudes 2−54929
- adjustment of free networks, generalization of least squares method 2−65429
- airborne thermal scanner, intermittent film advance in camera 2−70091
- anholonomity, generalized Riemannian geometry 2−81587
- astrogeodetic geoid determination, least squares prediction and collocation 2−72607
- Atlantic Ocean, satellite surveys 2−54612
- atmospheric gravitational potential, effect on geoid 2−54801
- baseline determination using v. long baseline interferometry 2−54617
- Cannikin, underground nuclear explosion, ground deformation measurements 2−57470
- distance meas., electronic methods and instruments 2−81637
- Earth crustal movement, three-dimensional monitoring 2−54611
- earthquake forerunner detection 2−65511
- Eurasia, geophysical geoid 2−54600
- geoid form and isostasy 2−54589
- GEOLE system 2−61862
- GEOS-2 spacecraft, Goddard Range and Range rate system 2−54985
- gravitational field, sea surfaces using space systems 2−54614
- gravity anomaly detection, satellite to satellite tracking data 2−54616
- gravity field, 300 n.m. mean anomalies 2−54685
- gravity field from range meas. between two satellites 2−54613
- level ellipsoid, simple layer potential 2−81588
- marine, role in ocean physics 2−54610
- marine geoid, undulation spectra 2−54601
- Mariner-Mars 1971, use in unified S-band tracking 2−54984
- point position solutions for geoceiver stations in the US 2−54987
- positioning data, location of underwater acoustic transponders 2−62088
- pseudoinverse of sparse matrices, algorithm 2−54605
- radar altimetry data from GEOS-C, orbit accuracy requirement for geoid improvement 2−54615
- San Andreas Fault movement, laser satellite meas. 2−54690
- Santa Barbara Channel, California, seismic and aseismic horizontal strain 2−57699
- satellite, functional analysis and formula manipulation 2−54606
- satellite altimetry data analysis, local surface fitting method 2−54604
- SPARCENT, Karachi, Pakistan, geodetic parameters, Doppler satellite geodesy and classical method compared 2−65441
- standard printing colour identification system 2−59298
- standard printing screen system 2−59299
- sub-vehicle point and height of space vehicle 2−62411
- three-dimensional, for terrestrial network adjustment 2−65432
- vertical deflection processing 2−54603

Geodesy continued
- weight function approach to surface modelling 2−54609

Geoelectricity *see Earth/electricity*

Geomagnetism *see Earth/magnetic field*

Geometrical optics *see Optics/geometrical*

Geometry
- charge-mosaic membranes, piezodialytic salt flux reduction, geometric effects 2−53419
- generalized Riemannian anholonomity in geodesy 2−81587
- hypersurfaces of conformally flat space 2−69546
- K-contact Riemannian manifold 2−82166
- orientable hypersurfaces of 7-dimensional Euclidean space 2−69547
- quasars, geometrical interpretation of luminosity distributions rel. to separate big bang 2−55079
- Riemannian, celestial mechanics, dynamic space, curvature and ergodicity 2−81778
- stochastic space concept and phase fluctuations of propagating wave 2−78763

Geons *see Gravitation*

Geophysical prospecting
- acoustical holography, detection of geological formations, digital computer processing 2−44554
- aerial, instruments freq. distortions, transients 2−54739
- aerial induction method, conducting body, parameters det. simplification 2−54702
- aeromagnetic and aeroradioactivity survey of Liberia, West Africa 2−78294
- Barringer INPUT data, digital processing 2−54723
- borehole quadrupole curves, effect of horizontal boundary layers 2−72685
- borehole variometry, det. of small perturbing bodies 2−44526
- common depth surface profiling from multiple reflections, statistical algorithm 2−44567
- compressional wave velocity, dependence on porosity in unsaturated rocks 2−44555
- conducting sphere in e.m. input field 2−72626
- core-sampling, electrical probe properties, analysis 2−44519
- covered permeable inhomogeneous cylinder, transient response to line current source, elongated conducting mineral deposits 2−57786
- Dar Zarrouk curves and differential resistivity soundings 2−57502
- d.c. resistivity well logging 2−65541
- deep electrical soundings of crust-upper mantle in South Africa 2−54707
- deep sea drilling project (DSDP), progress report 2−84713
- depth extent estimates of magnetized bodies from vertical gradient or multilevel data 2−58121
- depth of investigation of direct current methods 2−78292
- differential resistivity sounding, equivalent field system 2−51523
- digital instrumental and methodological development, concepts 2−44560
- digital microbarography array data, frequency domain processing 2−65484
- Earth resources satellite mission planning, orbital photography 2−65510
- Earth resources technology satellites, digital image processing techniques 2−81624
- Ekco mineral analyser, radio-isotopic X-ray fluorescence 2−81643
- electrical method for highly conducting bodies and discrimination between ionic and electronic conduction 2−54719
- electrical methods on land, anomalies above a conductive sphere, comparison 2−48407
- electromagnetic, time domain airborne system, model results and field checks 2−54726
- electromagnetic airborne prospecting systems, analogue model studies 2−54722
- electromagnetic airborne system for light aircraft 2−54725
- e.m. depth sounding on horizontal transmitting coil, type curve computation with digital linear filter 2−72634
- e.m. fields of thunderstorms, information about ore objects 2−72647
- e.m. sounding, transient, over stratified earth 2−57816
- fissured media models, streaming potentials 2−57702
- frequency sounding above electrical reference horizon of infinitely high resistance 2−84738
- gas bearing formations, resolution of neutron-γ logging 2−84746
- geoelectric profile containing nonconductive layer, e.m. field 2−72644
- geoelectric sounding curves, multilayer, computer processing and representation 2−44562
- geothermal systems, effect of nuclear explosions 2−83041
- Gosses Bluff airborne magnetic survey 2−57701
- gravimetry and seismic combined use for gently sloping structures 2−44524
- gravitational and magnetic body calcs., unambiguity 2−44563
- gravity anomalies, interpretation by non-linear optimization 2−57462
- gravity anomaly, interpretation over causative body with circular symmetry 2−57466
- gravity dot charts in two and three dimensions 2−72631
- induced polarization field phase meas. 2−54720
- induced potentials method, hydrogeological and engineering-geological possibilities 2−54721
- isotope geology, optimal adjustment of mass spectrometer ion source 2−46398
- Khor Kundi El-Bahan, electrical sounding on water surface 2−72627
- magnetic and gravitational potential field, Fourier method for regional residual problem 2−57464
- magnetic body location and delineation 2−54927
- magnetotelluric exploration, identification of inhomogeneous conducting media from transient diffusion of e.m. fields 2−65523
- magnetotelluric exploration, using penetration of e.m. fields 2−44536
- magnetotelluric interpretation and field results in geologically complex areas 2−58120
- magnetotelluric method, petroleum exploration of sedimentary basins 2−44765
- marine sediments, compressional and shear wave velocities 2−57697
- marine seismic energy source, secondary pulses 2−84753

Geophysical prospecting continued
mineral exploration, audio frequency magnetotellurics application 2—57800
multicoil aerial e.m. prospecting system, helicopter stowed 2—65479
neutron activation analysis logging in mineral exploration programmes 2—57805
New Hampshire, gravity evidence for shallow-floored plutons 2—54684
oceanography conference, Brighton, England, (1972) 2—62058
oil, data processing, analogue digital conversion 2—84754
ore deposits flooding in karst regions, geophysical methods for studying conditions 2—57461
ore exploration using 3-component drill hole magnetometers 2—58122
ore methods, non-stationary mag. fields probing, curves transformation 2—44589
ore-zone excited by current carrying cable, induction anomaly 2—57781
ores, problems in regions of and climate, techniques 2—75422
potential field continuation between general surfaces 2—72624
pulsed neutron logging source, use of pseudonoise, sequences to code 2—65478
remote sensing, impact on earth science 2—57500
resistivity sounding data, linear filter method interpretation 2—72633
resistivity sounding on three- dimensional transitional model 2—72625
rocks, elec. and electrochem. characts., equivalent network 2—65524
seismic electroprospecting by resistance method, inverse problem solution 2—84739
seismic exploration, investigation of rock mass mechanical strength, system to measure wave front travel time 2—51509
seismic exploration, multi-channel, practical r.f. telemetry system 2—57672
seismic noise meas. in geothermal area 2—57499
seismic waves, operational frequency analysis, infrasonic spectrometer-analyzer 2—57507
seismographic geophysical exploration, h.f. filtering and nonlinear distortions in apparatus 2—48394
seismovac monopulse pneumatic rebound seismic source 2—44558
sounding, acoustic field created by radially oscillating cylindrical emitter in elastic medium 2—61890
South India, categorization of Precambrian 2—72628
square array resistivity meas., effects of anisotropy 2—72623
taconites, discovery by natural remanent magnetism 2—68989
Texas, gravity survey correction by vertical gradient obs. 2—57463
transient e.m. response of conducting infinite cylinder, surveys for elongated ore deposits 2—44594
Turam modelling, veins of finite length in conducting half-space 2—54724
valleys with elliptic cross- section, resistivity meas. 2—72630
well-logging, computer anal. of data 2—84748
well-logging equipment, design problems 2—84745
Wenner three-electrode and dipole-dipole d.c. resistivity methods, investigation depth 2—72629
^{252}Cf neutron activation, mineral analysis on ocean floor 2—65522
K, drill core scanning by gamma ray spectrometry 2—78293
Th, drill core scanning by gamma ray spectrometry 2—78293
U, drill core scanning by gamma ray spectrometry 2—78293
U economic geology, radioactive series disequilibrium 2—61871
U ores low grade, advances 2—61989
U well logging, pulsed neutron method 2—44598

Geophysics
see also Atmosphere; Earth; Oceanography; Seismology
— 2—61916
— 2—68856
— 2—62023
M waves, examination with registering gravimeter 2—72606
acid volcanism, phenocrysts, charnockites 2—84719
Africa, uplift, rifting and break-up mechanisms 2—57769
African Euler pole of rotation rel. to E. African rift system, review 2—61957
African plate tectonics, hot spots in mantle 2—81617
albedo of surfaces, as fn. of solar zenith angle 2—75485
Alboran Sea, evidence for rigid plate separation 2—54752
Aleutian Islands, large Earth strain episodes 2—57547
Aleutian Islands, late Holocene vertical stability 2—57726
the Alps, crustal structure, explosion seismology 2—81586
Alps, summary of magmatic history 2—57709
Amchitka, underground nuclear explosion, seismic effects 2—57548
analytical flow nets in channel seepage 2—57825
anhydrous upper mantle, melting relations of hornblende eclogite, water effect 2—61852
anorthite, Si-O and Al-O bond length parameters analysis 2—61850
aquifer overlain by water table aquitard, numerical simulation of flow 2—78307
aquifer systems, response to explosions 2—57826
Archaean greenstone belts rel. to terrestrial equivalents of lunar maria 2—65535
Arizona, deeper crust obs. 2—57745
asthenosphere, CO_2 rich, model 2—57705
Atlantic Ocean floor, geomorphological aspects 2—72684
attenuation of ground accelerations in vicinity of faults 2—57530
automatic contouring using bicubic functions 2—78239
automatic terrain classification from aerial photography 2—84769
azimuthal variation in directional reflectance of vegetative canopies 2—78232
Azores-Gibraltar region, plate tectonics 2—57704
Baffin Bay, gravity and magnetic data analysis 2—57457
Baffin Bay and Lancaster Sound, geology 2—65532
Baffin Island, increased glacierization and climatic cooling trend 2—51527
Bismarck-Solomon Seas region, crustal plates, triple junction analyses and models 2—54709
Block Island Sound, geomagnetic and seismic measurements 2—57760
blueschist belts, occurrence and mineralogic evolution 2—61956
borehole quadrupole curves, effect of horizontal boundary layers 2—72685

Geophysics continued
Bristol Bay, Alaska, crustal lineations based on mag. and gravity surveys 2—57797
Cache Valley, ground-water potential rel. to integrated geophysical study 2—81642
Calavera's fault creep event 2—57599
California, fault creep along San Andreas fault, geomag. obs. 2—65560
California, southern, strain obs. 2—78288
Canada, upper mantle and deep crust, structure and composition 2—65552
Canadian Cordillera, evolution, plate-tectonic model 2—61953
carbonatite magma, nature and composition 2—75427
Caribbean, origin and struct. 2—57770
Caribbean Laramide Island Arc polarity determ. by petrology 2—61984
Carpathian system, global tectonics 2—78297
Cascade Mountains, quaternary andesitic volcanoes, coherent and divergent lava suites 2—57543
Caucasus, seismic activity and major earthquakes 2—78225
Ceara Rise in Western Equatorial Atlantic, geophysical data 2—57758
Central Aleutians, secular strain measurements 2—57546
Chandler wobble, changes in inertia tensor due to faulting 2—72657
chandlerian wobble (1900-1970) 2—65425
channel networks and network patterns, props. of link magnitudes 2—78312
China Basin, tectonic evolution 2—57772
chondrule-like spherule preparation from supercooled molten oxide and silicate droplets 2—44581
Clipperton Ridge and Mathematicians Ridge, topographic interpret. 2—54714
coastal beach, energy balance microclimatic variations 2—72716
coastal dynamics, problems 2—62052
Coconino Sandstone, deformed, Luders bands and cataclasis 2—57763
Coconino sandstone, fracture under confining pressure, effects of pore-fluid chemistry, temperature 2—68858
communication process examined 2—78241
computer systems, balanced, data transfer capabilities 2—54587
conf. 1972 Washington 2—54583
continental drift, rel. to metalliferous sediment formation 2—72682
continental drift and age of oceanic basin 2—57773
continental drifting rel. to plate tectonics 2—68847
continental margin of Africa off Liberia, magnetic anomalies 2—57459
continental margin off Norway rel. to magnetic quiet zone 2—57456
continental shelf off southern Baffin Island, reflection seismic and magnetic profiles 2—57458
continental USA, inversion of isostatic Green function and lateral density changes 2—65426
convergent plate margins 2—61974
Cordilleran tectonics and North America plate motion 2—61954
Corner Seamounts area, evolution of sea floor 2—65550
Corsica-Sardinia microplate rotation and the Ligurian Sea 2—54673
crust, anisotropy, obs. of tidal strains 2—78281
crust-mantle structure infered from SH and SV wave spectra 2—78276
crustal and upper-mantle-structure beneath Colorado Plateau, determ. from Rayleigh-wave dispersion 2—78278
crustal deformations around volcanoes, model 2—78285
crustal flake tectonics and continental collision mechanisms 2—75426
crustal model parameters from P-wave spectra 2—65458
crustal movements, vertical, rel. to eustatic changes in sea-levels 2—57775
crustal movements in tectonic areas 2—65559
crustal tilt preceeding aftershock due to strain accumulation 2—81571
crystalline rocks in Tazin Group, Canada, multiple deformation 2—51514
Darien Province, Panama, radar imagery, cumulative frequency curves 2—44530
deep crust lateral continuity 2—61976
deep crustal seismic reflections, complex structure of southern Alberta, Canada 2—51498
deep ocean drill site temp. distrib. meas. 2—54777
deep sea drilling project, Japan to Fiji 2—61966
deep structure of S-W Europe and P-wave residuals at Iberic stations 2—44585
deformation and stresses in non-homogeneous Earth-model with a rigid core 2—51521
depth to magnetic layer, det. by maximum likelihood estimation from aeromagnetic fields spectrum 2—51522
Devon Island, small Arctic catchment, annual hydrological regime 2—51532
digital image processing of Earth Resources Technology Satellite data 2—81641
digital recording mass spectra in geologic studies, digital recording using magnetic tape 2—72600
displacement and strain fields of nonuniform dislocations 2—57727
displacement measurement, holographic interferometry applic. 2—61845
dynamo theory of terrestrial magnetism, numerical soln. to MHD eqn. of Earths core 2—48594
Earth, laterally heterogeneous, toroidal free oscillations 2—51500
Earth, multilayered sphere model, static deformation by internal sources 2—51492
Earth's free oscillations for order numbers higher than 50 from earthquakes 2—84704
Earth resources data handling and automatic correlation, pilot system design 2—84770
Earth Resources Survey Program and remote sensing 2—84768
earth resources technology satellite, agriculture 2—84929
Earth resources technology satellite 2—61841
Earth resources using aerospace photography 2—61853
Earth strainmeter transducer, interferometric calibration 2—65530
Earth-atmosphere evolution model rel. to Ar excess in submarine basalts 2—72689
earthquake activity rel. to crustal pressure of reservoirs 2—61881
earthquake stress, friction, heat generation and spectra 2—57544

Geophysics continued
earthquake-tide correlation 2−57503
earthquakes, circum Pacific arcs, tsunamis and tectonic deformation 2−57545
earthquakes, stress distribution beneath island arcs 2−81602
Eastern Alps, gravimetric investigation along profile strip 2−57469
Eastern Indian Ocean and Caroline Basin, fracture zones and sea-floor spreading 2−54710
education and opportunities in India 2−54578
education and opportunities in India 2−54579
eigenfrequency perturbation of a cylinder due to ridge on surface 2−51505
elastic wave propagation in laterally inhomogeneous crustal structures 2−68844
electromagnetic field, dipping layers effect 2−61986
electromagnetic scattering from two dimensional earth models 2−54717
e.m. induction problem, boundary conditions and calc. of surface values 2−48400
Empress Group of sedimentary deposits in southern Saskatchewan 2−51513
eocene emplacement of Colebrooke thrust plate, Oregon 2−57750
eolian-modified craters, simulation 2−61844
Ethiopia, lower Omo basin, late Cenozoic molloscan assemblages 2−75461
European plate igneous chains, movement over thermal plumes or hotspots in mantle 2−72673
evaporation from lake in warm dry environment and suppression by inversion 2−54740
evaporative heat losses from water bodies 2−77475
evolution of continents rel. to endogenous processes 2−57708
exploration geophysics, meeting, Houston, Tex., USA (1971) 2−54585
fault creep and tectonic stress release 2−57728
fault plane determ. method rel. to earthquake focus of Hindukush zone 2−78226
fault stability and pore press. 2−65471
faults, stick-slip obs., applic. to earthquakes 2−65558
feldspar megacrysts in basalt, K-Ar ages and origin 2−61992
Fennoscandia, structure and physical properties of Earth's crust 2−51511
field variations near focal zones of Kamchatka 2−65516
filter obs. series, statistical analysis using white noise as basis 2−54577
finite amplitudes convection in self gravitating fluid sphere 2−41864
fluid dynamics application to layered systems with flexible boundaries affected by gravity 2−75432
fluid pore pressure, changes induced by earthquakes, after shock 2−44521
fossil bone dating using racemization of isoleucine 2−65568
free oscillations, nonlinear effects 2−81584
free oscillations of laterally heterogeneous spherical Earth model, variations of density and elastic moduli 2−51493
frequency-impedence soundings, for geological structure obs. 2−61899
frost heaving, meas. of heat flow 2−75447
fumeroles, physical properties of discharged steam 2−78247
GAG-2 gravimeters rel. to gravimetric reference network 2−78228
gas-hydrated strata, thermal method of exploitation, math. model 2−75464
generalized inverse gravimetric problem for contact surface 2−61857
geochemical ocean sections (Geosecs) program, 1970-1 period 2−75412
geology, conference, (Hawaii USA March 1972) 2−57451
geology, interpretation of physics fracture faces 2−47540
geology, structural educational game 2−57455
geomorphological development and post-Pleistocene sea level changes in Northumberland straits 2−72660
geophone arrays, theoretical and practical design 2−57690
geopotential, correlation functions for isobaric surfaces 2−44713
geopotential, time-dependent, atmospheric contribution 2−48406
Georgia, crustal seismic anisotopy 2−57627
geostrophic adjustment of rotating homogeneous or stratified fluid 2−61861
Gerstner's trochoidal waves, first-order irrotationality, gravity wave motion 2−50284
geyser activity, fluctuations caused by variations in Earth tides, barometric pressure and tectonic stress 2−65572
glacial deposits, late ordovician glacial marine sediments from N. Sierra Leone 2−57810
glaciology, anomalous moraine heights, range-front faulting 2−57812
glaciology, deep ice temperatures, theoretical and experimental profiles correlation 2−54730
global plate tectonics, naturally occurring model 2−65551
global tectonics obs. and earthquake prediction using seismicity 2−57516
Gondwanaland, positioning of Madagascar 2−78287
Gondwanaland Precambrian and plate tectonics, paired metamorphic belts 2−78289
granite, low porosity, biaxial compression test implications 2−57765
gravity attraction of right rectangular prism, nomograms 2−57467
gravity measurements over Gorda and Juan de Fuca Rises westward to Surveyor and Sedna Fracture Zones 2−54618
gravity model of crustal and upper mantle struct. of Central Aleutian Arc 2−54715
Grenville province Ontario, metamorphic facies series 2−48405
ground motions of initial ejection phase of underground explosions, X-ray photography 2−78931
groundwater basin, transient saturated-unsaturated flow, model 2−51531
groundwaters with free surface, equation of motion 2−72697
Gulf of Alaska and Bering Sea areas development, model based on earth expansion 2−54716
Gulf of California, northern and central, tectonic elements obs. 2−57796
Gulf of Mexico, crust and mantle structure 2−68846
Gulf of Mexico, micropaleontological, tephrachronological and paleomag. studies 2−61968

Geophysics continued
Gulf of Mexico, Pleistocene paleoclimatology 2−75462
Hawaiian lava lake samples, rate of solidification rel. to lunar basalts 2−66144
Hawaiian volcanic rifts, orientation and growth, effect of regional structure and gravitational stresses 2−65428
heat flow through Black Sea floor 2−54738
Hokkaido, land block movement rel. to main island of Japan 2−44586
Holocene, lower boundary in terms of European sequence 2−75439
hydrograph anal. using channel length frequency distrib. 2−78303
hydrology, digital radar data applics. 2−75495
hydrology, operational, multilay multivariate autoregressive model 2−78310
hydrology, parameter identification in unsteady open channel flows 2−77382
hydromagnetic oscillations of core rel. to geomagnetic secular variation 2−62378
ice, photogalvanic effect, geophysical implications 2−54258
ice thickness det., e.m. sounding 2−44604
imaging spectral radiometer, optical design for Earth resources applications 2−84775
impedance measurements, effect of anisotropy 2−57784
Imperial Valley, California, gravity and geothermal anomalies 2−57454
incomplete wells, flow from free pools and captive pools in stratified rocks 2−44516
India, coastal deformation, earthquakes and secular creep 2−78298
Indian Peninsula, crust-mantle structure 2−65482
indices of crustal thickness and depth to Benioff zone 2−57731
induction logging in inhomogeneous media, numerical solution 2−78261
inertial mass variation, exp. test 2−52118
inner core solidity studies, inferences from PKP- amplitudes 2−57650
inverse mag. and gravitational exploration problems, analytic continuation of 2-dimensional potential fields using bipolar coordinates 2−54591
inverse problem, errors, resolution and separation of variables, application to mantle and crust in S. Africa and Scandinavia 2−48399
inverse theory w. grossly inadequate data 2−72664
island arc calc-alkaline rock suite in Lesser Antilles 2−65534
isostatic compensation of mountains, least square criterion 2−68831
isotope geology, importance of electronics, demands upon instrumentation 2−84725
Italy, seismicity, plate tectonics 2−81589
Jan Mayen island, geochemistry of alkali olivine basalts from eruption 2−54669
Japan, position for new crustal-deformation observatory 2−75423
Japanese Paleozoic geosynclinal basalt, measure of hydration 2−65536
jet discharging horizontally into lake or river, heat transfer, diffusion and mixing 2−78304
Juan de Fuca ridge, crustal struct. 2−61973
Kilauea Volcano, contrasting rift zones 2−57831
Kilauea Volcano, deformation 2−57828
Kilauea Volcano, He content of S bank fumarole 2−57742
Kilauea volcano eruption, as naturally occurring model of global plate tectonics 2−65551
Kilauea Volcano lava entry into sea 2−57587
la Coste-Romberg gravity meters, calibration factors, time variations 2−81590
Lake Superior, long range seismic refraction observations, predictive deconvolution 2−57513
Lake Superior region, snowmelt energy exchange 2−57811
landform evolution, mathematical models 2−65547
landslide remote sensing techniques 2−57744
laser strainmeter, methane absorption stabilized, design and operation 2−65439
late and neoglacial deposits in Quaternary, northern Cumberland Peninsula, Canada 2−51525
late Cainozoic shoshonitic lavas from Torres Strait, Papua and Queensland 2−54670
late glacial deposits in Quaternary, northern Cumberland Peninsula, Canada 2−51524
lateral structure-foundation interaction of structures with base masses 2−61873
latitude obs. using Danjon astrolabe at Paris observatory, (1956.5 to 1970.8) 2−44515
lava flows, dynamics and spreading distance 2−65435
layering in intrusive rocks, effects of earth tremors and convection currents 2−75436
least-squares method in signal filtration and in inverse geophysical problem 2−78768
lherzolite inclusions and host basaltic rocks, $^{87}Sr/^{86}Sr$ geochemistry 2−57827
Lipari arc, deep structure det. from S-wave attenuation of deep focus earthquakes 2−75433
liquid core, dynamics 2−84724
lithospheric slab behaviour as anchors 2−61975
Loch Ness, internal surge obs. 2−44607
lower mantle inhomogeneities and origin of Hawaiian Islands, teleseismic obs. 2−81622
lower oceanic crust, evidence for seismic anisotropy 2−51519
Lyra basin, structural geology from reflection profiles 2−57723
magmas and fluid ascending in crust and upper mantle, pressure and temp. gradients 2−65557
magmatic activity as major process in chemical evolution of crust and mantle 2−57480
magnetic receivers freq. characteristics 2−54581
magnetized dyke, interpretation by characteristics 2−54905
magneto-telluric profiling in Arctic Ocean 2−78265
magnetotelluric anisotropy rel. to spreading tectonics 2−54910
magnetotelluric sounding, impedance for inhomogeneous surface waves 2−78282
magnetotelluric soundings, smoothing of results 2−61892
mangle convection, rel. to global gravity 2−57468
mantle, upper, deform. mechanisms 2−61978

Geophysics continued
mantle beneath S. Pacific Basin, evolution, det. from $^{87}Sr/^{86}Sr$ ratios 2−57730
mantle convection and new global tectonics 2−81639
mantle materials, yield strength meas. method under high pressure 2−60879
mantle plume activity on ocean crust 2−57897
marine deposits, Mg content and crystal habits in ancient carbonates 2−54754
Massif of Lanzo, plastic deformations in lhorzolite 2−54681
measurement data, simultaneous interpretation 2−57447
measuring base, 10 m, for crustal strain meas. 2−44517
melting temperatures in mantle, olivine, spinel and periclase melting curves 2−57481
Mesozoic plate motions in Eastern Central North Atlantic 2−57757
metamorphic belt through Black Hills of S. Dakota 2−65506
methodological aspects 2−61840
microreleif of ocean floor, obs. using anal. of photo- and stereomaterials 2−72683
mid Atlantic Ridge at 43N, heat flow and bathymetry 2−65453
Middle East, active plate boundaries 2−57768
Middle East, focal mechanism of earthquakes, plate tectonics 2−72618
Midway Atoll latitude of form. determ. from paleomag. meas. 2−57771
mineralogy, transmission elec. microscopy applic. 2−56954
minicomputer systems for computer controlled field systems and office playback systems 2−54588
model earthquake sequence, stochastic analysis 2−81600
Morocco, major strike-slip fault of Hercynian age 2−44587
Mount Etna and Stromboli geologic and photoballistic obs. 2−81567
mountain building in plate tectonics theory 2−81619
Mozambique Channel, seafloor spreading 2−54675
multiscanner spectral data processing, suitability of normal density assumption 2−81608
multispectral scanner system, 24-channel, for remote sensing 2−48397
multispectral scanning from airborne stations and satellites, applics. 2−75416
muscovite melting in $KAlSi_3O_8$-Al_2O_3-SiO_2-H_2O system 2−61851
N. American-Eurasian plate motions from astronomical photographic zenith tube observations 2−75424
Nasca Plate, crustal struct. obs. 2−57795
N.E. USA, tectonic stresses 2−57577
nematatis and absolute drift of crystal plates 2−57732
neutron moisture meter response to stony soils 2−54732
New Caledonia Basin, possible folded structure 2−57721
normal faulting related to mountain flank thrusting 2−57700
north circum Pacific belt, earthquake probability analysis 2−57549
Northern Algeria, morphology, trench formation by compression 2−44580
northern Midwest USA, postglacial climatic change, fossil pollen spectra 2−75463
northern Skye and Little Minch, negative gravity anomaly rel. to deep sedimentary basin 2−54596
nuclear spectroscopy of geological materials 2−61846
observations, discrepancies in interpretation, international Upper Mantle Project of 1969/1970 2−61839
ocean floor underthrusting and Indonesian Island Arc form. 2−57490
oceanic crust, geologic model, rel. to compressional wave velocities of dredged samples 2−57899
oceanization, isostasy, sea floor spreading 2−78332
operational hydrology, use of radar data from D/RADEX 2−75581
Osakayama, crustal strains, secular and annual changes 2−78295
Pacific Basin deformation, tidal element 2−57715
Pacific deep-sea core, distribution and scanning electron microscope obs. of authigenic pyrite 2−44579
Pacific Ocean floor, near-bottom mag. lineations 2−54712
palaeomagnetism rel. to geomagnetic field reversals and dipole characteristics 2−58132
Pan-African orogenic belt, subduction process of mountain-building 2−65539
periodicities, stochastic processes, biophysics, meteorology, stochastic processes, periodicities 2−52084
Peru earthquakes of 1966 and 1970, mechanisms and tectonic implications 2−84727
Phillipine Sea plate, sinking along western boundary 2−54679
photogrammetry and mapping appls. of holography 2−84780
piston core, device for obs. of behaviour 2−61965
plagioclase feldspars, phase diagram 2−61849
plane Lamb's problem line load suddenly applied in a magnetoelastic initially stressed conducting half-space 2−51504
planets formation and volcanic activity 2−66169
plate motions rel. to deep mantle and development of subduction zones 2−65554
plate tectonic model 2−57774
plate tectonics, metamorphism and related magmatism 2−61955
plate tectonics, rel. to deep earthquake distrib. 2−61942
plate tectonics and orogenic belts in S.E. Pacific 2−48403
plate tectonics and the Hercynian Orogeny 2−72674
plate theory, epeirogenesis and eustatic sea level changes 2−75431
plate-tectonic theory, review 2−61952
polar motions and tides 2−57861
potential field, design of small operators 2−65431
potential field, location of singularities two dimensional field extension using Taylors series 2−61858
potential fields, singular points det. by integral functions approximation 2−44523
potential fields, two-dimensional, net methods using conformal meshes for analytic continuation 2−61854
pre-Caledonian rocks, Mullet Peninsula, County Mayo, Ireland 2−61842
pre-Mesozoic continental drift and plate tectonics as Mesozoic catastrophe 2−57767
precambrian development in E. Africa 2−44522
Precambrian geology rel. to shield development and renewal 2−57707
progressive failure of clay slopes, growth of slip surfaces 2−78238
Project Sand, remote sensing of Mississippi Delta 2−44529

Geophysics continued
pulsed neutron gamma method for highly absorbing media 2−54728
quartz, determ. of geological origin from thermoluminescence prod. by gamma rays 2−84709
quartz sand and sandstone recognition by two-channel i.r. imagery 2−65438
quartz-sand layers in N. Atlantic basin, with high thermal conductivity 2−65553
radar data remoting and recording system SCEPTRE for distributing CAPPI maps 2−75414
radionuclides ^{134}Cs, ^{85}Sr and ^{65}Zn released to water basins, accumulation 2−57833
rainfall and runoff data, conceptual anal. with hybrid computer 2−78302
Rayleigh waves, Earth flattening procedure for propagation in crust and mantle 2−57511
REACTION program for multicomponent geological system studies 2−61847
reconnaissance of soils and rocks, colour aerial photography 2−44535
recording device, deviation of actuator, conversion to binary code 2−44520
red sandstone, effect of heat treatment on magnetic minerals 2−81601
reflectance model for mature corn, application to corn blight detection 2−78233
Reid's Passage, northeast of Samoa, evidence for erosion during late Tertiary 2−57864
remote sensing, i.r. and multispectral 2−44577
remote sensing, subject outline 2−81606
remote sensing, United Nations resource exploration and evaluation programs 2−81607
remote sensing of Earth resources and environment, seminar (Palo Alto, USA, Nov. 1971) 2−84767
remote sensing of Earth resources with solid state multispectral imager 2−84776
remote sensing of moisture of specular soils with multifrequency microwave radiometry 2−84778
resources, NASA satellite research and development program 2−48371
resources information systems using satellites, aircraft and ground teams 2−48372
Reykjanes Ridge, seismic reflection survey of oblique aseismic basement trend 2−65526
river pattern variability, models 2−57821
rock burst mechanics study 2−72696
rock structures of northeastern Newfoundland, geotectonics 2−51515
rock systems, Fe^{2+}-Fe^0-Si relations 2−61848
rock U assays, neutron activation method 2−84690
rock weathering profiles, distinguishing modern from relict. 2−54580
Rockall Plateau, igneous rocks with unexpected magnetic props. 2−54677
Rockall Plateau and Continental Shelf subsidence 2−48401
Rockall Plateau microcontinent, crustal structure obs. 2−48402
rocks, complex dielectric permittivity meas. method 2−54718
rocks, partial melting and subsequent creep under low stresses 2−57764
rocks, residual elastic strains, reflecting crystal distortions 2−78299
rocks, similarity anal. of process of movement 2−62004
rocks, simultaneous meas. of u.s. vel. and compression 2−61982
Rocky Mountain Trench, geology, paleocology, and palynology of Oligocene rocks 2−54666
Ross Sea, evidence for widespread submarine erosion 2−57706
runoff volumes from small urban watersheds 2−57824
Salt Lake Crater, Hawaii, ultramafic minerals, nature of source material from He and Ar diffusion obs. 2−65583
San Gabriel anorthosite complex, aeromagnetic survey 2−57746
sandstones from India, age determ. from paleomag. data 2−68985
Santa Barbara Channel region, late cenozoic structure and sedimentary history 2−57719
Santa Catalina and Rincon Mountains, turtleback structures 2−57747
Santa Monica Basin, late Tertiary tectonic development 2−57720
Savonoski Crater, Alaska, possible meteorite impact structure 2−78296
scanning radiometer, for orbiting satellite, meteorological applications 2−84865
sea floor acoustic props. remote det. 2−44533
sea floor spreading, viscous dissipation and periodicity, Benard convection expts. 2−65549
sea floor spreading magnetic anomalies in Central North Atlantic Ocean 2−57898
seafloor spreading, thermal aspects 2−62087
secondary sea floor spreading centre S. of Murray fracture zone 2−57718
seismic data, optical processing, description 2−72622
seismic s-wave spectra analysis method rel. to layered structure inferences 2−78271
seismic S-wave spectra rel. to structure studies in regions of Japan 2−78272
seismomagnetic effect, possibility of using magnetic methods to study tectonic processes 2−65513
self potential anomalies, due to spherical ore bodies 2−57785
SH-wave propagation in anisotropic inhomogeneous crustal layer 2−51512
shale beds, regularities in compaction with depth 2−84744
shallow earthquakes, wide scattering in continents 2−57512
shallow-faulting model, particle motion along surface trace 2−61837
Shikoku, Japan, Permian oceanic crust and plate junction 2−75434
shoreline behaviour of active pahoehoe lava at Kilauea Volcano 2−57832
singular points nearest to Earths surface of harmonic functions describing anomalous mag. and gravitational fields 2−61856
Siqueiros and Clipperton fracture zones, eastern extension, Farallon-Pacific Plate motions 2−54713
snow-ball growth in minerals, theory 2−61961
soft sediment glacial grooving of Dwyka age 2−57814
Solenhofen Limestone, deformed, Luders bands and cataclasis 2−57763

Geophysics continued
solid earth tide and phase vel. variations 2−61979
solid tidal measurements in New England area of Australia 2−54593
Solomon Sea Junction, tsunamigenic earthquakes, seismotectonics 2−57582
South America, seismicity and Q-structure 2−57645
South Australia, polarization sensitive magnetic variation anomaly 2−81744
South Fiji basin, complex crustal structure, ASTPER refraction data 2−57541
southern Nevada, regional secular strain fields 2−48404
southern Rocky Mountain region, geochemistry of Sr isotopes 2−57698
southern Rocky Mountain region, upper Cenozoic basalts 2−57693
southwestern New Mexico, midtertiary Mogollon Datil volcanic province, volcano tectonic timing 2−57692
southwestern New Mexico, Mogollon Datil volcanic province, petrology and petrogenesis 2−57694
Soviet Union, current status of applied geophysics 2−54586
space research, photography 2−84750
spectrophotometry of Earth from manned spacecraft 2−48373
spelaeology, applic. to past climate obs. 2−62118
statistical estimation precedure for Monte Carlo inversion 2−57446
statistical model of processes having probability density function with skewness and excess 2−48365
statistical test methods and effective number of independent sample values 2−54576
Steinheim Basin, cryptoexplosion struct. type locality 2−57761
strain meas. at Sandy, Texas 2−61977
strain patterns around fold hinge zones 2−54680
stream channels and flow relations 2−51529
stream systems, analogy to entropy in thermodynamics 2−51530
streamflow hydrographs, derivation of base flow recession curves and parameters 2−51528
streamflow simulation, broken line process as potential model for hydrologic simulation 2−78314
streamflow simulation, Markovian models, fractional gaussian noise and crossing theory 2−78313
streamflow simulation, monthly, long memory, by broken line model 2−78311
stress changes in rocks due to nucl. explosions 2−65468
stress control of processes at extensional plate margins 2−65555
stress distribution around single underground opening in layered medium under gravity loading 2−75459
stress systems at young continental margins 2−54668
stress wave profile meas. using Yb piezoresistive transducers 2−61943
stresses around single underground opening near traction free surface 2−75458
structural geology of northern Silver Peak Mountains 2−57748
subcrustal phase transition in mantle model, surface readjustment 2−84729
superficial seismic noises, anomalous potentials using Grandinetti's type soundings 2−81585
supersonic faulting, far-field radiation 2−65461
surface electroprospecting methods for cartography 2−61855
surface tilting obs. in Koyna-Pophali region, India 2−65531
Tasman Oragenic Zone in Lower Palaeozoic, model 2−84723
Tasman Sea, central, early opening evidence 2−54711
Tasman Sea area, sea floor struct. 2−57794
Tasmania, plate tectonics model rel. to lower Palaeozoic 2−84723
tectonic fault and rock contact tracing and detection 2−84740
tectonic implications of presence of Edna Mountain formation in Nevada 2−57749
tectonic processes, relation between Earth and Moon, rel. to orogenetic cycles 2−48392
tectonic stress, great earthquakes earthquake swarm relationships, model for Philippine Sea plate 2−48396
tectonic stresses and interstitial fluid flow 2−72659
tectonics from obs. of p-travel time residuals from Cannikin explosion 2−57590
tectonics of regional and ocean-floor metamorphism 2−57710
tectonophysics, solution of problems rel. to mechanics of solid deformable bodies 2−81614
telluric signals, amplifier and filter system for obs. 2−81627
tensioned-wire Earth strainmeters 2−81603
terrain remote sensing, effect of angular variation on spectral reflectivity 2−44534
terrigenous formations, reservoir characteristics estimation on basis of classification 2−84747
thin sand aquifer, hydraulic diffusivity 2−78308
three dimensional map display with stereo-orthophoto 2−51491
three variable closed array, nonuniform density of data points 2−81594
tidal time series, spectral techniques for Fourier analysis 2−51494
tidal triggering of eruptions from Mt. Stromboli, Italy 2−78321
torsion balance effect of convection and nonequilibrium flow on motion 2−72605
Tottori earthquake of 1943, determ. of effective tectonic stress rel. to earthquake faulting 2−84730
Troodos Massif, evidence for magmatic processes at ocean ridges 2−61960
truncated sinusoids, maximum entropy power spectrum 2−63047
tuff, low porosity, biaxial compression test implications 2−57765
unconfined aquifer, unsteady radial flow 2−78309
unconfined aquifers, flow theory considering delayed response of water table, model 2−78234
upper mantle, role of exptal., physical acoustics 2−57450
upper mantle and lithosphere, terrestrial heat flow 2−57482
upper mantle flow rel. to dislocation mechanisms of olivine 2−65533
Upper Mantle Project, explosion seismology 2−57515
vegetation mapping, radar backscatter obs. 2−44532
vegetation mapping using side looking airborne radar 2−44531
Venezuela, gravity fields and plate boundaries 2−57472
Venezuelan borderland survey 2−57452
vertical crustal movements along U.S. east coast, sea level measurements 2−57759
vertical deformation through underground nuclear explosions 2−81574
volcanic collapse structures and man-made analogues 2−57830
volcanic eruptions triggered by tides 2−57776
volcanic gas, H burning at Kilauea Volcano 2−57928
volcanism, numerical modelling of deformations 2−57829
volcanology rel. to composition and processes of upper mantle 2−57514
W. Pacific guyots, geology 2−57453
water, transit time methods in underground hydrology 2−46887
water quality data analysis using spectral analysis 2−78300
wave propagation in uniformly rotating fluid, surface and inertial waves 2−50164
Weber Sandstone at Rangely Oil Field, local stress meas. 2−57658
well depth det. in surveys 2−62016
West Philippine Basin, structural framework 2−57722
Woodlark Basin, sea-floor spreading evidence 2−57904
Wright's Point, inverted topography region 2−57743
Yakutat Bay, Alaska, coastal piedmont deglaciation 2−57815
CO_2 in caves, gaseous subterranean diffusion and air circulation 2−48412
Fe, melting temp. with pressure in Earths core 2−56542
K/Ar data rel. to origin of feldspar megacrysts in alkali basalt 2−54729
K-Ar ages, volcanic stratigraphy and geomagnetic polarity in Canary Islands, Tenerife, La Palma and Hierro 2−78220
Pb isotope ratios in conformable ores and oceanic rocks, evolutionary model 2−61991
Rb-Sr geochronolgy data, use of two-error linear regression treatments 2−61994
^{222}Rn and ^{220}Rn exhalation from ground, technique for meas. 2−65565
S in air and soil and crop yields 2−78301
Sr isotopic disequilibrium in lherzolites from Puerco necks, New Mexico 2−65537
Germanium
see also Semiconducting devices; Semiconducting materials/germanium
absorption edge under pressure, high resolution meas. 2−48182
absorption of H and O on (111) face of single crystal 2−80583
adsorbed layer on W, electronic props. determ. from field emission 2−71349
adsorption and nucleation, of Cd, by mol. beam technique 2−47158
adsorption of Cd, mol. beam technique 2−50534
amorphization during ion bombardment, HEED obs. 2−80685
amorphous, atomic arrangement, computer simulation 2−60574
amorphous, diffr. props., consistency with continuous random network model 2−64618
amorphous, phonon density of states, Raman scatt. obs. 2−61664
amorphous, Raman scatt., phenomological explanation 2−61665
amorphous, struct., extended X-ray absorpt. fine struct. determ. 2−71283
amorphous, temp. dependence of elec. conductivity 2−47924
amorphous film, u.v. reflectance depend. on deposition temp. 2−54403
amorphous region form. by neutron irrad. or ion bombardment 2−47384
amorphous state, different forms 2−60572
chemical classification of Fe meteorites, conc. rel. to Ni, Ga, and Ir 2−75925
chondrites, H-group, distribution in metal and silicate portions 2−62719
correlated successive collisions of 5-30 keV Ar ions, ion scatt. processes 2−47775
covalent-metallic phase transition under pressure 2−83886
crack structure, atomistic study 2−56831
dechannelling of 0.3-1.5 MeV protons, Lindhard's multiple scatt. 2−47788
defects, formation and annealing during bombardment with Kr ions 2−71461
deposition and annealing parameters, influence on strain sensitivity 2−77709
desorption of Na and Cs submonolayers, laser-induced 2−67921
detector, ion-implanted, high purity 2−46047
diffusion and solubility of Li, hydrostatic press. effect 2−47443
diffusion in Al, interpreted using oscill. form of inter-ion potential 2−64691
dislocation density, effect of growth parameters, single crystals 2−47414
dislocation vel., stress and temp. depend. 2−47415
dislocation velocity, dopant influences 2−50674
donor-vacancy complexes, γ-irrad. prod. kinetics and energy spectrum 2−47382
elastic wave damping, effective anharmonicity consts. 2−80913
electromodulation study of forbidden indirect transitions 2−72333
electron energy loss functions, determination of optical props. 2−71769
electron irrad., changes in length and elec. resist. 2−68016
electron irrad., K_α X-ray prod. 2−48208
electronic scattering in planar dechannelling, protons and deuterons 2−61128
epitaxial layers, tripyramid growth 2−64569
epitaxy, thermodynamic calc. of the Ge-H-Cl system 2−53623
etched pits on (111), (110) and (001) surfaces, symmetry and form 2−50446
etched surfaces, kinetics of development of first- order network 2−50447
etching, gas phase with water vapour 2−67933
film, amorphous, crystalline transform. rel. to thickness and environment 2−67882
film, amorphous, metal contact induced crystalliz. 2−56590
film, amorphous, microcrystallite struct. 2−43479
film, amorphous, struct. rel. to angle of evaporation 2−71330
film, amorphous, structure 2−60577
film, amorphous, structure small angle X-ray scatt. obs. 2−60661
film, amorphous, technique for Hall voltage obs. 2−64963
film, amorphous, void structure and optical sum rules 2−78063
film, amorphous struct., elec. microscope obs. 2−50479
film, heteroepitaxial structure on Si, structure 2−56591
film, structure effect on secondary electron emission 2−57265

Germanium continued
films, evaporated amorphous, anisotropic microstructure, X-ray study 2−47116
films, thick amorphous self-supporting 2−74631
foil, multiple scatt. of H, He, Li, Ne, Ar and Kr ions, 100-1000 keV 2−47781
fracture speed meas. using u.s. fractography 2−82123
g-factors of B impurity 2−54402
impurities Au and Sb, absorption and movement of melted zone in the solid phase 2−83892
impurity atom diffusion enhancement by light ion implantation 2−60814
internal friction at low temp., dislocation behaviour 2−68068
interstitial diffusion of Li, press. depend. 2−47442
irradiation damage, electrons and γ-rays, Mossbauer type photoluminesc. spectra obs. 2−48243
1 2−77772
lattice dynamics, angular force model 2−74969
lattice dynamics, Keating's model calcs. 2−71708
Laue case of X-ray diffraction in nearly perfect crystals, 111 and 440 reflections 2−71403
liquid, structure, X-ray diffr. obs. 2−60424
low temp. meas. using thermal noise in Ge sensor 2−62889
metastable polycryst III, photon Raman spectra 2−68664
morphology of ribbon crystals grown by Stepanov method 2−47328
mosaic structure during testing, X-ray and e. microscope exam. 2−71475
Mossbauer effect of ^{57}Fe 2−48152
n-type, electron irrad., annealing kinetics 2−47380
n-type, electron irrad., impurity depend. of annealing, vacancy-interstitial pair effects 2−47379
n-type, electron irrad., impurity depend. of low temp. annealing 2−47376
orientation deflection, profiled crystals drawn from melt 2−47425
p-type, electron irrad., low temp. annealing 2−47378
p-type, electron irrad. defect prod., annealing and cond. obs. 2−47377
p-type, low temp. elec. irrad., point defect annealing 2−47381
p-type, low temp. electron irrad., 220K defect 2−47928
p-type, radiation defect annihilation centre, photocond. obs. 2−83978
phonon dispersion relations, homology with Si 2−84190
phonon lifetimes 2−71725
photoelasticity, in cryst., at 13 MHz u.s., modulation of 10.6 mkm radiation 2−49201
point defects, investigation by non-irrad. techniques 2−47399
pure, singly doped and compensated n-type, far i.r. props. 2−72384
quenched-in defect, migration energy, specimen size effect 2−71536
radiation effects, defect models, review 2−47375
refractive index, X-ray interferometric determ. 2−72256
ribbon crystal growth, Stepanov method 2−47269
slip system, effects of crystal anisotropy and cryst. struct. 2−71577
stopping powers for ^{4}He, ^{16}O, ^{35}Cl at 1 to 3 MeV 2−80921
surface, field ion microscopy at 80K 2−64554
surface, metal metal spreading kinetics 2−67814
surface, monomolecular layers exam. using ellipsometry 2−56601
surface, Ne adsorbed layer, mol. beam scatt. 2−47159
surface, sputtered atom ejection and ion bombardment induced disorder 2−43466
surface reaction, with O_2, LEED and conductivity obs. 2−50448
surface relief, photogoniography 2−47076
thermal cond., three phonon resist., second upper bound 2−71759
thermal expansion, rel. to stress in epitaxial Ge on GaAs 2−57075
thermal resistivity, due to three-phonon scatt., Ziman limit 2−75000
thermometer, cryogenic, interpolation routines for calibration 2−52294
thick film, amorphous, self supporting, production and bulk prop. obs. 2−56592
thin films, 10.6 μm guided waves obs. 2−55749
thin films, 10.6 μm guided waves obs. 2−55748
vacancies, estimation of true formation energy 2−47400
vacancy equilibrium configuration, computer calc. 2−71467
vacancy mobility and conc., high-temp. behaviour 2−64659
X-ray diffraction, absorption and excitation in multiple Borrmann diffraction 2−60736
X-ray diffraction, peculiarities of multiple beam Borrmann effect 2−47330
X-ray photoelectron spectra of valence bands 2−81191
X-ray photoemission valence-band spectra, valence-band densities of states 2−81192
X-ray transmission pattern, anomalous, effect of simultaneous refl. 2−53662
Al-4%Cu alloy, vacancy-Ge binding energy 2−50824
GaAs:Ge p-n junction, Zn- diffused, photolum., 8100-8500 Å 2−72404
GaP:Ge, e.p.r., linewidth and g-value 2−72484
^{67}Ga, imaging agent, dynamic vascular scintiphotography of liver 2−58609
Ge:P, electron irrad., bombardment induced interstitial P, e.p.r. obs. 2−48279
Ge:Sb, phonon propag. characts. 2−47735
Ge/H_2O/H_2 system, etching rate, average reaction enthalpy, 950-1200K 2−74661
Ge-Se system (4-16.7 at.% Ge), glasses, temp. depend. of density and thermal expansion 2−84209
p-Ge-n-CdS_xSe_{1-x} epitaxial heterojunction, prep., struct. and elec. props. 2−77924
p-Ge, influence of adsorption of sIo molecs. on field emission 2−72076
a-Ge film, crystalliz. processes, elec. microscope obs. 2−60658
a-Ge film, u.v. dielectric consts., reflectance obs. 2−61586
Ge III, polymorphs, Raman scattering from phonons 2−72372
Ge surfaces, heat-treated in various atmospheres, e.s.r. obs. 2−72488
Ge^{3+} in SrF_2, possible existence of separate cubic symmetry 2−80705
Ge(Li) detector, well-type, semitoroidal configuration, performance 2−46046
Ge(Li) γ-ray spectra automatic anal. on small computers 2−82082
GeSe, amorphous, struct. by Fourier analysis of EXAFS 2−60576

Germanium continued
$Ge + SiO \rightleftharpoons GeO + Si$, heat of reaction, mass spectrometric determ. 2−72548
InSB:Ge, energy levels of shallow acceptors, far i.r. absorp. obs. 2−75296
Si:Ge, O, C, low temp. electron irrad. damage, i.r. obs. 2−48192

Germanium compounds
— 2−60573
— 2−61242
germania, vitreous, structure, neutron and X-ray diffr. obs. 2−53534
tetraphenyl germanium, defect struct. determ. 2−53731
Ag-15% Ge alloy, splat cooled, martensitic transformation of structure 2−56921
Ag-Ge alloy, laser irrad., metastable phase formation 2−50929
Al-Ge, vacancy-solute binding energies 2−74763
Al-Ge alloys, microstruct. and metastable phases, detn. 2−71675
Al-Ge alloys, rapidly solidified, constitution and microstruct. 2−43929
Al-Ge liquid alloy, Cr or Mn impurity, susceptibility near nonmag.-mag. transition 2−80486
As-S-Ge glass film, laser induced refractive index changes 2−61583
As-Se-Ge glass film, amorphous to crystalline state conversion by light irradiation 2−75077
As-Te-Ge-Se glass switching device, small signal behaviour 2−61376
As-Te-Ge-Si glass, thermal breakdown 2−61298
Ce_2Se_3-GeS_2 system, phase diagram, intermediate cpd. formation 2−61043
Cu-Ge dil. alloys, vacancy-impurity complexes and positron annihilation 2−47398
Cu-Ge solid soln. single crysts., growth and characteriz. 2−53614
Cu-Ge solid solution, cryst. growth, for neutron monochromator appl. 2−47205
Fe-Ge alloy, molten, paramag. props. 2−80488
Fe-Ge α' solid solution, precipitation behaviour 2−64819
Fe-Ge system, constitution and mag. props. 2−64821
Fe_3(Al,Ge), influence of Ge on struct. changes, nuclear γ-reson., X-ray diffract. and dilatometric analyses 2−80779
Ge-Ag alloy, impurity scatt., electron lifetimes, Fermi surface, de Haas-van Alphen meas. 2−61148
Ge-Ag alloy, liquid, free enthalpy of mixing 2−53422
Ge-As-Se-Pd(Cd) glass, microstruct. and immiscibility temp. 2−56561
Ge-As-Se glass chalcogenide system, atomic distribution and coordination numbers 2−56559
Ge-As-Te, amorphous, cryst. layer form., effect of water during heat treatment 2−60571
Ge-As solid soln., absorpt. and scatt. of X-rays by cluster defects and dislocation loops 2−77584
Ge-Au alloy, liquid, free enthalpy of mixing 2−53422
Ge-Au films, quench-condensed, supercond. energy gap, tunnelling obs. 2−51115
Ge-Cr film, amorphous, hopping cond. 2−61313
7at.%Ge-Cu alloy, deformed, neutron irrad., dislocation strain fields, low. temp. lattice thermal cond. obs. 71498 2−71498
Ge-Cu alloy, liquid, struct., X-ray diffr. interference functions 2−83774
Ge-Hf alloy, electric quadrupole interaction with ^{181}Ta 2−75359
Ge-$MgSi_{1.72}$ solid soln., prep., thermal e.m.f., elec. and thermal cond. 2−74905
Ge-Mn-Te alloy, degenerate semicond., e.s.r. obs. 2−48273
Ge-Na liquid solution, thermodynamic props., e.m.f. cell obs. 2−71183
Ge-Sb-S-I glass system, glass forming regions 2−80533
Ge-Sb system, struct. and alloy chem. of metastable GeSb 2−47329
Ge-Se-Sn system glasses, chem. comp., struct. units, Mossbauer obs. 2−43452
Ge-Se glass, microphase separation and semicond. behaviour 2−60592
Ge-Si-As-Te glass, comp. vs. glass transition temp. 2−60597
Ge-Si, single crysts., epitaxial growth from vapour phase 2−64599
Ge_x-Si_{1-x}, mixed crystals, photoelectric emission 2−72092
Ge-Sn-Se-As glass, Mossbauer effect, isomeric shift, quadrupole splitting, phase diagram 2−75267
Ge-Sn alloy, Shubnikov-de Haas oscills. rel. to carrier heating in cond. band 2−81080
Ge-Sr system, phase diagram 2−47714
Ge-Te-As glass, high current density path shape 2−57193
Ge-Te, memory glass system, glass forming regions, transition temps., melt crystn. temps. 2−80805
Ge-Te alloy film, amorphous struct., elec. microscope obs. 2−50479
Ge-Te non-crystalline phases, structural differences 2−60577
Ge-Te system, noncrystalline film prep. by sputtering 2−47114
Ge-Ti-O system, noncrystalline film prep. by sputtering 2−47114
Ge-V(Cr)(Mn)(Fe)(Co)(Ni) dilute liquid alloy, susceptibility 2−80485
GeAs-V(Cr)(Mn)(Fe)(Co)(Ni) dilute liquid alloy, susceptibility 2−80485
$Ge_xAs_{40-x}S_{60}$ glasses and liquids, heat capacity 2−51045
$Ge_{10}As_{20}Te_{70}$, amorphous semiconductor, electrical/thermal/optical properties 2−61262
$Ge_{16}As_{35}Te_{28}S_{21}$, amorphous, semiconductor- metal contact, photovoltaic effect and space charge capacitance 2−61374
GeF_2, vacuum u.v. spectra, vibr. assignments 2−80040
GeF_2 microwave spectrum, determ. of nuclear quadrupole coupling consts., and effect of centrifugal distortion 2−70698
GeF_4, nucl. spin relax. obs. of spin-rot. interaction 2−56199
GeH, multiplet struct. and centrifugal distortions, rot. energy levels 2−79991
GeH_4, in Jovian atmosphere, hypothetical chemical and spectroscopic activity 2−44942
GeH_3Br, u.v. photolysis and i.r. spectra of matrix-isolated products 2−61804
GeH_3F, GeD_3F, microwave spectrum, molec. properties 2−60001
Ge(Li) detectors, trap parameters of Ag, Co, Cr and Te impurities 2−46045
$GeMnO_3$, magnetoelec. susceptibilities and sp. ht. 2−44300
Ge_3N_4 film, vapour deposited on Ge, depend. of props. on deposition temp. 2−54224

Germanium compounds continued
$GeO_2:V^{4+}$, e.p.r., g and A tensors, orbital mixing parameter, radial average, core polarization 2—72503
GeO_2-B_2O_3 glass, n.m.r. of ^{11}B 2—54506
GeO, layers, defective, hopping cond., elec. cond., 77-453 K, 20-100 MHz 2—54173
GeO_2, amorphous, struct. by Fourier analysis of EXAFS 2—60576
GeO_2, amorphous, struct. extended X-ray absorpt. fine struct. determ. 2—71283
GeO_2, glass-forming, He migration 2—50707
GeO_2, glassy, struct., small-angle X-ray scatt. obs. 2—43453
GeO_2, high and low pressure polymorphs, rel. to thermal conductivity 2—65582
GeO_2 and $Si_{1-x}Ge_xO_2$, recrystn. in hydrothermal fluoride solns. 2—47285
GeO_2 network, depolymerization in presence of two cations 2—53535
GeO_2 polymorphs, crystal growth, solution top-seeding 2—50583
GeO_2 tetragonal, on Ge, effect on surface elec. props. 2—47939
Ge_xS_{1-x} alloys, radial distrib. studies 2—53536
$GeS_2(Se_2)(Te_2)$, refl., 1-12.5 eV, rel. to band struct. calc. 2—48161
GeS(Te), refl., 1-12.5 eV, rel. to band struct. calc. 2—48161
GeSe, amorphous, struct., extended X-ray absorpt. fine struct. determ. 2—71283
GeSe, amorphous, struct. by Fourier analysis of EXAFS 2—60576
GeSe, semicond. liq., Hall effect 2—60498
GeSe and GeTe, thin film, amorphous polycrystalline phase transformation, radial distrib. of atoms 2—71686
$GeSe_2$, cryst. growth, Czochralski pulling 2—50597
$GeSe_2$, liquid semiconductor, switching, thermal breakdown mechanism 2—81096
Ge_xSe_{1-x} alloy film, amorphous, radial distrib., elec. diffr. obs. 2—60659
$GeSe_{(2)}$(Te), cryst. growth and morphology 2—50575
$Ge_{1-x}Si_x$, indirect phononless optical transitions, wavelength modulated absorp. obs. 2—68640
Ge_xSi_{1-x} solid soln., film, photoelec. props. 2—65090
GeTe-Bi_3Te_3 solid soln., Hall carrier conc., elec. cond., thermal e.m.f., thermal cond., struct., hardness 2—74903
Ge_2Te_3-Hg_3Te_3 alloy, transport processes, Hall mobilities, near semimetal-semicond. transition at high press. 2—68406
GeTe-SnTe alloy, epitaxial film, twinning faults 2—53574
GeTe, amorphous and polycryst., electronic struct., photoemission and reflectivity obs. 2—61465
α-GeTe, domain struct., twin and interface boundary interface types 2—72150
GeTe, efficiency criterion for thermogenerators 2—75158
GeTe epitaxial film, twinning faults 2—53574
GeTe film, superstruct., consistent with electron microscope obs. 2—80574
$GeTe_2$ film, amorphous, local order and microstructure 2—60660
$Ge_{0.17}Te_{0.83}$, amorphous, neutron and X-ray diffr. radial distrib. functions 2—56548
$Ge_{15}Te_{85}$, liquid, atomic transport 2—60457
Ge_xTe_{1-x} alloy, amorphous, structure and bonding 2—60575
Ge_xTe_{1-x} alloy, amorphous, energy level scheme, optical and electrical obs. 2—77904
$Ge_{15}Te_{80}As_5$ semiconducting glasses, thermally induced surface and bulk electrical effects 2—68401
GeTeI, glass forming region 2—60592
GeTeSi, glass forming region 2—60592
$Ge_{15}Te_{81}X_4$, amorphous, memory device model 2—61375
$Ge_{15}Te_{81}X_4$, X=Ga, P, As, switching glass, n.m.r. 2—61752
GeTe—Bi solid soln., regions of existance at 250, 400, 500 and 600°C 2—53888
$K_2Ge(IO_3)_6$ crystal struct. determ. 2—77549
Mn-Al-Ge alloy, domain structure and nucleation centres 2—68550
Nb-Al-Ge system, phase equilib. and supercond. props. 2—43936
$Pb_{1-x}Ge_xTe$, lattice const., and phase transform. 2—84108
PbO-GeO_2 system single crystal growth 2—74666
PbO-RO-GeO_2, R=Mg, Ca, Sr, Ba, glass, struct. and props. 2—53540
5PbO.3GeO_2, Raman scatt. by ferroelec. modes 2—61669
Sb-Ge alloy, etch pit orientation determ. 2—47187
Si-Ge alloy, He^+ irrad., atomic displacements, Rutherford scatt. obs. 2—47388
Si-Ge alloy, oxide layer etched away reoxidation, production of MOS transistors 2—75132
Si-Ge alloy thermocouples, precip. of dopants 2—51210
Sn-Ge, saturated melt spreading over Ge surface 2—67814
Te-As-Ge-S glass films, four-element quantitative analysis 2—72593
Te-As-Ge amorphous alloy, negative differential capacitance 2—64961
Te-As-Si-Ge film, amorphous, a.c. cond. rel. to localized tail states 2—61288
Te-Ge-As glass, u.s. velocity, hydrostatic press. effects 2—47742
Te-Ge based memory glass film, thermal crystn. 2—47128
Te-Se-Ge glass, threshold type, thermal effects 2—71917
$Te_{60}As_{25}Ge_{13}M_x$, M=S, Se, chalcogenide glass, interdepend. between, switching memory and thermal behaviour 2—47901
TeAsGeS glass, structural and electrical props. 2—61329
V-Ge-Al alloy, Knight shift meas. 2—57398

Getters
selective, for metal halide lamps 2—52478
Er film, maximum sorption capacities and gettering action 2—43495
Ta, sorption of residual gases in evacuated valve, mass spectrometer obs. 2—76130
Ti film, maximum sorption capacities and gettering action 2—43495

Giant pulsations *see Earth/magnetic field; Magnetic storms*

Gibbs function *see Thermodynamic properties*

Ginzberg-Landau theory *see Superconductivity*

Glaciers
Amery Ice Shelf, Antarctica, evidence for bottom freezing from $^{18}O/^{16}O$ ratio 2—68852
Antarctic ice sheet permittivity meas. using v.l.f. band 2—54731
Antarctic ice sheets, radio echo method of measuring thickness changes 2—84722

Glaciers continued
Athabasca Glacier, time lapse cinematographic obs. of geologic processes 2—57813
Baffin Island, increased glacierization and climatic cooling trend 2—51527
deep ice temperatures, theoretical and experimental profiles correlation 2—54730
Fleming Glacier, Antarctic Peninsula, movement obs. using radio echo technique 2—72691
icebergs, containing rock fragments, structure and texture 2—75445
late and neoglacial deposits in Quaternary, northern Cumberland Peninsula, Canada 2—51525
late glacial deposits in Quaternary, northern Cumberland Peninsula, Canada 2—51524
McCall glacier, northern Alaska, atmospheric turbidity measurements 2—62273
melting, eustatic sea level change and deformation of Earth 2—75448
movement obs. using radio echo technique 2—72691
piedmont, recession, coastal features produced at Yakutat Bay, Alaska 2—57815
stagnation, steam vent explosion, microearthquakes 2—81582
as structural models 2—57751

Glass
see also Optical materials; Vitreous state
a.c. conductivity, atomic and electronic hopping 2—47881
acoustic birefringence under strong uniaxial compression 2—54028
activated, thermo-optic constants 2—59276
alkali alumino borosilicate, growth rate of silver halide liquid particles 2—77478
alkali borate, containing nickel oxide, spectrophotometric studies rel. to struct. 2—67885
alkali borate, e.s.r. spectrum, hole and electron centres obs. 2—54489
alkali borate, rheological props., effects of water 2—53795
alkali borate, rheological props. 2—53794
alkali borate and silicate, n.m.r. obs. of ^7Li ionic motion 2—64690
alkali borate glass containing Fe, Mossbauer effect and magnetic props. 2—65230
alkali borate glasses, Ni^{2+}-containing, absorpt. anomalies, ligand field approach 2—75303
alkali halide-alkali borate, e.s.r. spectrum, hole and electron centres, and halogen atoms obs. 2—54489
alkali silicate, γ-irrad., thermolum. 2—81410
alkali silicate, Brillouin scatt. 2—57365
alkali silicate, Er^{3+} sites, absorpt. study 2—54429
alkali silicate, static longitudinal modulus, u.s. determ. 2—56773
aluminas, polycrystalline, influence of texture on mechanical props. 2—68093
aluminate, densification behaviour 2—53526
aluminoborosilicate fibre, B coordination number heat treatment effects 2—64528
analysis, batch and raw materials, computer controlled X-ray fluorescence 2—64525
analysis, problems with automatic X-ray spectrograph 2—64523
Aouelloul crater, ^{26}Al content, rel. to Zli sandstone, formation theories 2—65584
arc welding radiation meas. rel. to protective filter glass standardization 2—73668
arsenosilicate diffusion source, use in As doping of Si, 1000-1200°C 2—83980
atomic arrangements and chemical bonding, n.m.r. obs. 2—54500
autoradiography, water in glass obs. 2—53517
basaltic, failure in sea, palagonite formation 2—57753
beryllate systems, glass formation 2—53528
binary, effect of a third component upon the immiscibility 2—60607
binary arsenosilicate film, diffusion source, thermal stresses 2—71325
binary arsenosilicate film, vapour deposition for diffusion source 2—71324
binary borosilicate, vapour-deposited films, infrared absorption vibrational spectra 2—48169
borate, analysis of water content 2—56555
borate, binary, crystallization of tetranates from melt 2—53612
borate, He migration 2—53759
borate, non-destructive method for ceric/cerous ratio determ. 2—48362
borate, separation of delayed elasticity from viscous flow 2—56781
borate, struct. changes, e.p.r. 2—54496
borate, X-ray irrad., Ti induced centres, e.p.r. spectra 2—44450
boric oxide, rheological props. 2—53794
borophosphate, e.p.r., radiation colour centres 2—44444
borosilicate, containing La_2O_3, radiation and optical stability 2—70071
borosilicate films, current-voltage characts. 2—47950
breakdown by mode-locked laser radiation, i.r. 2—79251
bubble formation in glass melts 2—64531
ceramic, high quartz solid solution, fine grained crystallization rel. to nucleation agents 2—50411
ceramic, lithium silicate, fracture energy as function of struct. 2—50886
ceramic, Nd^{3+} doped, lasing threshold and efficiency 2—73589
ceramic, strength, review 2—47520
ceramic, workability, thermal and dielec. props. 2—43868
—ceramic capacitance thermometer, performance in 0.007 to 0.040 K range 2—66371
chalcogenide, elec. changes in surface region 2—54190
chalcogenide, film, amorphous, switching behaviour 2—81071
chalcogenide, film, thick and thin, switching temp. depend., onset of breakdown 2—77895
chalcogenide, i.r. cond., 10^9-10^{13}Hz 2—61638
chalcogenide, Mn^{2+}-, Fe^{3+}-, or Gd^{3+}-doped, e.p.r., fine struct. 2—72476
chalcogenide, parasitic absorpt. bands elimination 2—54411
chalcogenide, solid and liq., struct., n.m.r. and i.r. vibr. spectra obs. 2—60595
chalcogenide, states in the gap, expt. evidence 2—61334
chalcogenide, structural features rel. to elec. conductivity and electron transport processes, review 2—61267
chalcogenide, switching behaviour between Ge electrodes, firing 2—81074

Glass continued
- chalcogenide, threshold and memory types, thermal effects 2−71917
- chalcogenide, vibrational modes, molecular model 2−61057
- chemical analysis, oxide content, by physical methods, computer calcs. 2−44500
- composite, C continuous fibre-reinforced, mech. props. 2−50919
- composite, C discontinuous fibre-reinforced, fabrication and props. 2−50918
- composite, glass-crystal two-phase, fracture, theory 2−74860
- contact behaviour between glass and metal in forming of hot viscous glass 2−56554
- corrosion, automatic analysis techniques 2−65379
- crack propag., subcritical growth and fracture energy 2−50857
- crack propagation, effect of aqueous solns. 2−64730
- crack tip profile; static fatigue and stress corrosion 2−53521
- crystallizing, frozen elastic stresses 2−56784
- cylinder, contact stresses, elastohydrodynamic lubrication 2−47559
- decoration effects by evaporation of gold 2−64527
- defect and dioptric effect det. using holography 2−45776
- elastic deformations in hardness testing 2−64739
- electron microscope examination 2−60587
- elemental analysis, using scanning elec. microscope 2−60579
- emission spectra of Eu^{3+}, comp. and temp. depend., effective cryst. field props. 2−78130
- enthalpy meas. and calc. of sp. ht. 2−74992
- ethanol, electron trapping and solvation at 4K, optical absorption and e.s.r. meas. 2−61810
- ethanol, trapped electrons produced by biphotonic photoioniz. rel. to delayed emission of indole ring 2−54559
- ethanol, vitreous transition, fluoresc. depolarization obs. in soln. 2−60602
- ethanol glasses, free radical photoproduction, e.s.r. study 2−81509
- exponential absorp. edge, theory review 2−78078
- fibre, effect of phys. props. on light propag. 2−42242
- fibre, high modulus, prep. and crystn. kinetics 2−43902
- fibre, reinforced nylon 6, dynamic viscoelasticity temp. depend., two-phase blend system model applic. 2−71556
- fibre filled polymer films, mech. anisotropy 2−84131
- fibre optical waveguide with low-loss liquid-core 2−58998
- fibre reinforced composite materials, tensile and bending strength 2−84123
- fibre reinforced polyester, fracture energy determ. 2−50780
- fibre waveguide, optical Kerr effect 2−42239
- fibre-reinforced polyester, work of fracture 2−74863
- film, amorphous, chalcogenide, grown by vapour deposition, contribs. to growth temp. 2−64564
- film, chalcogenide, high field effects, current voltage characts., Poole-Frenkel emission 2−44097
- film, chalcogenide, noncrystn., threshold and memory switching at low temps. 2−61308
- film, thermally switching, pulse response of cond. channel 2−51129
- filters, structure of pore area, separation of solid and liquid components of a mixture 2−80786
- fission tracks, thermal stability in Standard Reference Materials 2−79686
- fission tracks stability rel. to water effects 2−67097
- flowing in cylindrical channels, energy transport 2−56552
- fluor-richterite composition, treatment for obtaining high strength polycryst. material 2−47651
- fluor-richterite composition ceramic, high mechanical strength, microstructure determ. 2−77704
- fluorescent lamps, performance improvement through additives to glass 2−52474
- formation, kinetic treatment based on time-temp.-transform. curves 2−53523
- germania, vitreous, structure, neutron and X-ray diffr. obs. 2−53534
- glass: Nd, laser induced fluorescence line narrowing spectroscopy 2−48247
- glass: Nd laser, investigation of two-photon amplification using organic dyes 2−61808
- glass:Nd laser, cylindrical rod plano-convex cavity, mirror transmission 2−76492
- glass:Nd laser, damage mechanism and improvement of damage threshold 2−42050
- glass:Nd laser, set-up for plasma production 2−80294
- glass-ceramic, viscosity changes during nucleation and crystallization 2−53923
- glass-ceramic capacitance thermometer for obs. in 1.7 to 300K range 2−76404
- glass-reinforced plastics, behaviour in water under high stress 2−84083
- high quartz solid solution glass ceramics, influence of composition on density 2−56562
- high refractive index with low dispersion, correction of medium and high ametropia 2−66329
- hot pressing, densification of orientated glass filaments 2−77703
- hot stage microscope applications 2−56838
- hot viscous, sliding on metal surfaces, mechanics 2−56553
- hydrogen-bonded, Frohlich polaron model for Compton electron trapping 2−44040
- inorganic, correlation between electrical conduction, dielectric polarization 2−57188
- inorganic, Tl^{+}-Gd^{3+} energy transfer, fluorescence obs. 2−61709
- interionic distance rel. to temp., stratification, 800-1900K 2−56563
- isopaustic, u.s. delay lines 2−78928
- laser, Nd:glass, thermal lensing effects 2−63336
- laser damage rel. to surface film 2−82504
- laser doped with Er or Er-Yb having luminescence sensitized with Mo, patent 2−82486
- laser heating, internal focusing and defocusing 2−82526
- laser irradiated, struct. transforms., electron microscope obs. 2−60588
- laser self-focusing damage tracks, anatomy and thermal history 2−82501
- laser with zig-zag beam, power improvement 2−69932
- laser-induced destruction of surface and interior 2−79256
- for lasers and optical transmission media 2−82563
- $Li_2O.Al_2O_3.2SiO_2$, fibres, ion exchanged, internal friction, Li and Na conc. profiles 2−80754

Glass continued
- liquid-glass transition, bond-lattice model, configurational excitations in condensed matter 2−50408
- low temperature vacuum chamber for obs. of luminescence 2−58670
- lunar, Fra Mauro comp., sintering 2−62671
- lunar, interferometric evidence for low temp. shock 2−55124
- lunar, terrestrial, tektites, mag. susceptibility, 1050-4.2K 2−73073
- lunar glass spherule comparison with microtektites 2−62670
- lunar particles, micrometeorite craters, radial fracture zones and spall zones 2−51822
- in lunar soil, effect on spectrum of moon 2−58464
- lunar ultramafic green glasses 2−78483
- melts, bubble formation and removal 2−56551
- metaphosphate glasses, silver-activated, influence of base glass on radiophotoluminescence 2−57383
- mica glass-ceramics, microstruct. and mech. props. 2−60999
- microcraters, profile and depth 2−60582
- microhardness load dependence, microstresses and effects 2−74864
- migration of K^{+} ion from K^{+} ion-exchanged layer under reverse electric field 2−75388
- mixed alkali effect, electrodynamic interaction 2−53524
- molecular motion, Mossbauer scatt. obs. 2−61609
- molten, radiative and conductive heat transfer, exptl. and analytical study 2−52270
- multilayer films as directional coupler 2−42237
- Na-Sn silicates, elec. props., effect of Sn content, Mossbauer effect 2−47055
- Nd^{3+} activated laser, struct. of radiation 2−59170
- nitrate, positron lifetimes, temp. depend., phase transitions influence 2−47772
- nontransport quartz, colour changes investigated by e.p.r. and elec. cond. meas., importance of melting temp. and atmosphere and impurity ions Ti^{3+} in formation 2−84482
- optical, homogeneity 2−42224
- optical, polycrystalline specimens, edge effect in elastic wave velocities and moduli 2−60854
- optical, relation between abrasion, micro indentation hardness and maximum fracture velocity, expts. 2−56550
- optical, striae solubility in melts 2−59260
- optical, surface layer, purification and preparation of melt surfaces, two-strength spectacle glass 2−82564
- optical fibres stimulated backward Brillouin scattering 2−44398
- optical finishing by ion-beam sputtering machining 2−82571
- optical grade, relative intensities of Rayleigh and Brillouin scatt. 2−57364
- optical multimode waveguide, attenuation obs. 2−70060
- optical waveguides, electrically induced migration of ions in glass plates 2−42229
- organic, electronic spectra of trapped electrons 2−81516
- organic, influence of annealing on thermal behaviour in glass transition region 2−71744
- oxide, alkali metal cation vibrs., far i.r. spectra study 2−71284
- oxyfluorphosphate, alkali free, elec. resist., 250-500°C 2−57192
- particle detection, effect of mass and energy on track diameters 2−79681
- particle track detector materials characteriz. 2−63714
- phase separation, X-ray study under different collimation conditions 2−71285
- α- phenyl o- cresol, crystn., growth rate vs. temp. 2−50606
- phosphate, Ag-activated, trapezoidal shaped, beta-dosimetry 2−55927
- phosphate, energy transfer between Sm^{3+} and Eu^{3+} 2−48238
- phosphate, Nd^{3+} doped, time development of wide-band generation spectra in resonator with diffusion 2−42073
- photochromic, containing AgCl, darkening, effects of heat treatment, u.v. irrad. and CuO additive 2−78065
- photoelastic scattering of light from a non-alkali alumino silicate glass 2−65226
- physical analysis of small changes in composition 2−44499
- plastics, porosity influence on tensile strength 2−47522
- plexi-glass cylinders, density profiles during non-regular reflection of shock waves 2−66570
- PMMA, γ-irrad., absorpt. spectrum, optical density increment, u.v. filter 2−72357
- polishing by ion beam 2−50444
- polyethylene filled with randomly oriented glass fibres, stress-strain curve 2−77690
- polymer-solid adhesion breakdown rel. to radio emission parameters 2−52314
- polymeric, environmental crazing mechanics and mechanism 2−64735
- polymers, relation between expansion coefficients and glass temperature 2−60604
- porous, counterdiffusion of adsorbed hydrocarbons 2−60685
- porous, water freezing point lowering 2−80880
- porous glass desalination membrane, NMR, function of external salt concentration 2−56522
- preparation and optical properties of Ag particles in glass matrix 2−54412
- Pyrex sinter in cascade electro-osmotic cell 2−66678
- pyroxene type, crystn., effect of Cr_2O_3 content 2−53533
- quartz, glassy sphere production from particles by processing through plasma stream 2−56971
- quartz, integral normal emissivity meas. 2−54085
- quartz, tubular and bulk specimens, crystn., 1350-1550°C 2−64529
- quartz, with diminished heat flux, increased rate of ablation 2−73466
- radiophotoluminescent dosimeters, formation kinetics of colour centres 2−67092
- radiophotoluminescent dosimeters, response to ^{60}Co γ and 10 to 30 MeV electron radiation 2−67095
- radiophotoluminescent dosimetry of high sensitivity and soil insensitive 2−67094
- rare earth doped, fluoresc., quenching by OH^{-} ions 2−54467
- raw material analysis, by X-ray fluorescence spectroscopy 2−64524
- refractive index determination, non-immersion method 2−70048
- reinforced composite, fatigue crack damage, vibr. testing 2−60921
- roughness factor changes with heating in vacuum 2−60618
- safety lenses, drop-ball testing 2−42228
- scanning electron microscope applications 2−56956

Glass continued
  secondary electron emission and practical applications 2−65109
  self-focusing rel. to electrostriction and Kerr effect, damage threshold 2−75249
  semiconductor, mag. susceptibility, temp. and comp. depend. 2−61480
  semiconductor, perturbed bands, model 2−61335
  semiconductor, pseudobinary section $P_2Se_3-As_2Se_3$, n.m.r. of ^{31}P, comp. depend. of width of spectral lines, second moment and chemical shift 2−84584
  shock waves due to internal focusing of laser beam 2−42124
  silica glass, anomalous properties, interpretation 2−67884
  silicate, binary, structure of corroded surface 2−53541
  silicate, containing CeO_2, radiation and optical stability 2−70071
  silicate, crysn., effect of synthesis conditions 2−64530
  silicate, hydrogen-alkali exchange with aqueous solutions, theory 2−53518
  silicate, ligand field spectra of Ni^{2+} and struct. 2−50409
  silicate, struct. transform., oxides influence 2−53525
  silicate, wetting of Pt, contact angle meas. 2−53371
  silicate glasses K-8, F-5, volumetrical damage due to laser 2−76541
  silicates, luminesc. of Eu^{3+}, spectral characts. and quantum efficiencies 2−48233
  silicon, vitreous, structure, neutron and X-ray diffr. obs. 2−53534
  sintered metal containing, phase comp., X-ray obs. 2−50862
  slag, bending strength, softening temp., conc. depend. 2−56814
  sliding of metal and hot viscous glass, mechanics of 2−56553
  soda glass:Tb^{3+}, optical characts. 2−57374
  soda lime, Fe^{2+}-doped, phonon scatt., low temp., elec. and mag. field depend. 2−51056
  soda lime, slow environment sensitive crack growth 2−64729
  soda lime silicate, trace transition metal analysis by neutron activation 2−60580
  sodium borosilicate melt, critical-composition fluctuation in real space 2−67812
  sodium phosphate, heat of formation from heat of solution obs. 2−74598
  sodium phosphate melt, condensed, vitrifaction, effect of cooling rates 2−77479
  solder, in system $CaO-Al_2O_3-SiO_2-MgO$, use for Al oxide-Nb metal seals 2−66377
  soluble, surface stabilization by alkali ion exchange 2−53519
  spectacle lenses with back surface vinyl membrane, fracturing and safety properties 2−70066
  sputtering and energy losses of inert gas ions 2−61123
  steatite materials, sintered, effect of modifying agents on struct. and electromech. props. 2−53933
  stimulated Raman gain in single mode waveguides 2−42130
  stratification, effects on comp. depend. of elasticity modulus 2−47478
  strength, effect of high pressure organic impregnation 2−53520
  strength and fracture for $Na^+ \rightarrow K^+$ ion exchange 2−64787
  strengthened by surface compression, thermal stress fracture 2−50871
  stress corrosion failure under dynamic loading conditions 2−50771
  stress relaxation mechanism of $NaPO_4$ glasses 2−77636
  striae in glass, optical microscope system for obs. 2−59253
  structure, contrib. of classical magnetic measurements 2−60581
  structure, crystallite hypothesis 2−80532
  structure, e.p.r. spectra obs. 2−54488
  structure, Mossbauer obs. 2−60583
  structure-property relations, molecular orbital cluster calcs. 2−53516
  superbroadening of ultrashort pulse spectrum 2−43368
  surface adsorption of ^{19}F, time depend curve 2−83877
  surface tension measurement 2−83780
  suspension in turbulent air flow, trajectories and velocity of particles 2−76395
  temperature meas. of surface, elimination of effect of radiant heat transfer 2−55588
  tempered, plate, residual surface stress measurement using birefringence 2−60989
  tempered, residual stresses 2−77648
  thermal diffusivity and cond. simultaneous meas. by flash method 2−43996
  thermal expansion and props. around 1K 2−61107
  thermometers, capacitance, glass-ceramic, low temp., equations 2−49187
  torch holder for use away from glass laboratory 2−85157
  transparent, filamentary tracks formed by laser-beam self-focusing 2−65207
  tridimensional fibres for composites strengthening physical properties 2−71658
  viscosity of molten glass of mixed alkali $PbSiO_3$ 2−77416
  vtrifaction of condensed sodium phosphate melts, effect of cooling rates 2−77479
  window and optical, melt, dynamic viscosity, effect of CO_2, 1400−1700°C 2−74527
  windows, thin hemispherical, construction for nuclear and optical expts. 2−82573
  AL-Si-O prep. and processing, i.r. spectra, crystn. products, mineral species form. 2−56557
  Ag activated phosphate dosimetry props. rel. to melting and heat treatment 2−51381
  Ag activated phosphate glasses, radiation induced photoluminescence, laser pulse excitation 2−68713
  $Ag_2O-B_2O_3$ system, n.m.r. B sites obs. 2−65342
  $AgPO_3-X^{n+}(PO_3)_n$, $X^{n+}=Mg^{2+}, Ca^{2+}, Sr^{2+}, Ba^{2+}, Pb^{2+}, Al^{3+}$ use for multichannel image convertors and amp. 2−68501
  Al-borosilicate glass-Al thin film sandwich, elec. cond. props., negative resist., electroforming and electron emission 2−71989
  As-S, As-S-I, As-S-Tl viscosity in the transition region 2−84049
  As-S, mechanism of hologram formation 2−59204
  As-Se-Ge-Sn, Mossbauer effect, isomeric shift, quadrupole splitting, phase diagram 2−75267
  As-Se, Ag doped, elec. props. 2−64975
  As-Te-Ge-Se, switching device, small signal behaviour 2−61376
  As-Te-Ge-Si system, thermal breakdown 2−61298
  As-Te, memory glass system, glass forming regions, transition temps., melt crystn. temps. 2−80805
  As_2S_3, local struct. order, ^{75}As n.q.r. obs. 2−57404

Glass continued
  As_2S_3 glassy state, n.q.r. obs. 2−84605
  $As_2Se_3-As_2Te_3(Tl_2Se)(Sb_2Se_3)(As_2S_3)$, e.s.r. and X-ray studies 2−61734
  $1-xAs_2Se_3.xSb_2Se_3$ semiconductor system, devitrification characs. 2−71286
  $As_2Te_3-As_2Se_3$, elec., thermal and structural props. 2−61299
  $As_2Te_3-As_2Se_3$, microstruct. a.c. and d.c. cond. 2−60589
  $As_2Te_3-As_2Se_3$, switching rel. to comp. and thermal treatment 2−61295
  As_2Te_3, switching characts., cond. exponential temp. depend. 2−81073
  As_xSey, e.s.r. spin conc. and signal intensity 2−65332
  B, refractive index control by selective applic. of neutron irradiation 2−59226
  $B_2O_3-BaO-Fe_2O_3$, microstruct., ultrastruct., mag. props. 2−56558
  B_2O_3, diffusion of Ar and Ne, mass spectrometery obs. 2−53758
  B_2O_3, hydrostatically compacted, X-ray scatt., electron radial distrib. obs. 2−53527
  B_2O_3, refractive index variation with hydrostatic press. up to 7 kbar, prep. history and structure 2−68595
  B_2O_3 photo- and X-ray luminescence, obs. of luminescent centres 2−84547
  Ba silicates, phase relations 2−54006
  $BaO-B_2O_3-Fe_2O_3$, elec. and mag. props., microstruct. effects 2−65113
  $3BaO-5SiO_2$ glass, controlled spherulitic crystallization, 800-950°C 2−80530
  $3BaO.5SiO_2$ glass-ceramic, mechanical props. 2−53930
  X BaSe-$Ge_{1.5}As_{0.5}Se_3$, pseudobinary system, glass formation 2−80531
  Bi-Se system, formation, effects of phase separation 2−60591
  C, glassy, optical consts., 0-82 eV, refl. meas. 2−61584
  C fibre reinforced glass, fracture energy 2−84104
  C fibre reinforced plastic beams, dynamic moduli and loss factors 2−47487
  C monofilament, prep. and props. 2−56982
  C precursor, prep. under pressure from organometallic complexes 2−61014
  $CaO-Al_2O_3-SiO_2$ syst., i.r. spectra, struct. study 2−47057
  $CaO.Al_2O_3.CaF_2$, coordination numbers from i.r. spectral data 2−64587
  Cd-Ge-As-Se, microstruct. and immiscibility temp. 2−56561
  Cd-Si-As system, glass-forming region determ. by differential thermal analysis 2−74599
  $CdAs_2$, i.r. spectra in range 2 to 25 mk 2−61627
  $CdGeAs_2$, $CdGeP_2$, i.r. spectra in range 2 to 25 mk 2−61627
  CdP_2, i.r. spectra in range 2 to 25 mk 2−61627
  X CdSe-$Ge_{1.5}As_{0.5}Se_3$, pseudobinary system, glass formation 2−80531
  Ce, series 100 glasses, spectral analysis, monitoring of radiation resistance 2−63981
  $CoO-Al_2O_3-SiO_2$ system, low field mag. suscept. 2−65178
  $(CoO)_{1.4}.P_2O_5$, glasses, antiferromag. interactions 2−75237
  $Co(PO_3)_2-KPO_3$ system, absorption spectra and volume properties of melts 2−84481
  $Co(PO_3)_2-NaPO_3$ system, absorption spectra and volume properties of melts 2−84481
  Cu-As-Se compositions, voltage controlled switching 2−67886
  Er^{3+} ions in silicate glass, photoinduced absorption spectra 2−75291
  ^{18}F adsorption on surface, time depend curve 2−83877
  $55Fe-45P_2O_5$ glass, a.c. and d.c. characteristics, correlation with structure 2−81142
  Fe, crystalliz. kinetics of magnetic 2−54329
  $FeCl_3$ frozen aqueous soln., Mossbauer spectra, investigation of glass to crystal transformation at 200 K 2−72280
  $Fe_2O_3-P_2O_5$, glass forming range and magnetic suscept. 2−54354
  $(Fe_2O_3)_{0.79}.P_2O_5$, glasses, antiferromag. interactions 2−75237
  Ge-As-Se, chalcogenide system, atomic distribution and co-ordination numbers 2−56559
  Ge-Sb-S-I system, glass forming regions 2−80533
  Ge-Se-Sn system, chem. comp., struct. units, Mossbauer obs. 2−43452
  Ge-Se, microphase separation and semicond. behaviour 2−60592
  Ge-Te-As, high current density path shape 2−57193
  Ge-Te, memory glass system, glass forming regions, transition temps., melt crystn. temps. 2−80805
  $Ge_xAs_{40-x}S_{60}$, heat capacity 2−51045
  $GeO_2-B_2O_3$, glass, n.m.r. of ^{11}B 2−54506
  GeO_2 network, depolymerization in presence of two cations 2−53535
  $Ge_{15}Te_{80}As_5$ semiconducting glasses, thermally induced surface and bulk electrical effects 2−68401
  GeTeI, glass forming regions detn. 2−60592
  GeTeSi, glass forming regions detn. 2−60592
  $Ge_{15}Te_{81}X_4$, X=Ga, P, As, switching glass, n.m.r. 2−61752
  glass:Nd laser, mini face-pumped, free from thermal distortion 2−73582
  glass:Nd laser, pulsed, beam parameter obs. using holographic interferometry 2−79218
  glass:Nd laser, Q-switching a convex optical cavity 2−76467
  K_2O-SiO_2, irrad., nature of hole centres, e.p.r. obs. 2−65336
  $K_2O-SrO-SiO_2$ system, cation self-diffusion coeffs. 2−53765
  $xK_2O(1-x)SiO_2$, u.s. vel. and absorpt., meas. apparatus, 0−300K 2−74983
  $KX-K_2O-B_2O_3$, (X=F,Cl,Br,I,O), X-irrad., colour centres, e.p.r. obs. 2−81463
  La flint glass, Bragg diffraction rel. to acousto-optic applications 2−66839
  $XLa_2Se_3-Ge_{1.5}As_{0.5}Se_3$, pseudobinary system, glass formation 2−80531
  Li-glass scintillator tip for detection of secondary electrons in electron microscopes, long life 2−82430
  $Li_2B_4O_7$, crystallization from melt 2−53617
  $Li_2O-Al_2O_3-SiO_2$ glass-ceramic, strength and microstruct. 2−53931
  $Li_2O-B_2O_3-GeO_2$, struct. and props. 2−47059
  $Li_2O-MgO-Al_2O_3-SiO_2$, crystallization, F addition effects 2−47058
  Li_2O-SiO_2, phase separation and crystn., X-ray obs. 2−56560
  $Li_2O-Tb_2O_3-SiO_2$, fluorescence rel. to crystalline phases 2−51376

Glass continued
Li_4SiO_4-Zn_2SiO_4-Mg_2SiO_4-SiO_2 glass, phase equilibria and crystallization 2−64520
MgO-Al_2O_3-ZrO_2-SiO_2, complex particle growth, small-angle X-ray scatt. obs. 2−67887
MgO-Li_2O-Al_2O_3-SiO_2-TiO_2, glass-ceramic, crystn., microstruct., indentation hardness 2−80535
MgO.Al_2O_3.SiO_2 glass-ceramic, ZrO_2-nucleated, phase transitions 2−47691
2 MgO.5SiO_2.2Al_2O_3.nCr_2O_3, crystn. due to Cr_2O_3 additions, e.s.r. obs. 2−83850
Mn phosphate, mag. props. and structure 2−57292
Na_2-CaO-MgO-SiO_2, phase equilib. in glass forming region 2−57023
Na borosilicate, boron coordination det. by n.m.r. 2−60586
Na borosilicate, Na^+-K^+ ion exchange 2−53537
Na silicate, surface stabilization by ion exchange and chemical vapour deposition 2−53538
Na_2O-AL_2O_3-SiO_2, X-ray diffraction study 2−60585
Na_2O-B_2O_3-Al_2O_3, nabal glass, self-diffusion of Na ions and interdiffusion coeffs. 2−60832
Na_2O-B_2O_3-SiO_2 system, struct. 2−43454
Na_2O-B_2O_3 system, n.m.r. spectra, structural obs. 2−48301
Na_2O-K_2O-SiO_2, Na and K self diffusion, rel. to internal friction 2−50712
Na_2O-P_2O_5, containing metal ion impurities, u.v. transparency 2−65225
Na_2O-SiO_2, elastic moduli and i.r. absorp. spectra, pressure depend. 2−53782
Na_2O-SiO_2, ion exchanged, internal friction, effect of water 2−53791
Na_2O-SiO_2, nucleation process in the metastable region 2−60584
Na_2O-SiO_2, phase separation rel. to dielec. loss 2−54230
Na_2O-SiO_2 system, morphological changes produced by amporphous phase decomp. 2−47060
Na_2O-TiO_2-SiO_2 glasses press. and temp. depend. of elastic moduli, ultrasonic interferom. meas. 2−80741
NaOH-H_2O solutions frozen, photoelectron emission spectra of ferrocyanide 2−44210
Nd:glass laser, aqueous Cu(II) sulphate gel target to produce coherent X-rays 2−66765
Nd^{3+}:glass laser, production of super-dense plasmas 2−77286
Nd-activated, laser excitation of luminescence 2−78135
Nd-doped, lasing efficiency, fluoresc. and absorpt., effect of phase separation 2−57372
Nd laser, meas. of start photon number 2−52428
P_2O_5-B_2O_3-Cs_2O, struct., e.p.r. obs. of Cu(II) paramag. centres 2−48291
P_2O_5-V_2O_5 struct., elec. resist., thermal expansion, rel. to comp. 2−60601
Pb-Ge-As-Se, microstruct. and immiscibility temp. 2−56561
Pb-glass with semiconducting surface layer, delayed electron emission after electron bombardment 2−84384
PbO-Al_2O_3-SiO_2-B_2O_3, between metal electrodes, memory effect 2−71915
PbO-RO-GeO_2, R=Mg, Ca, Sr, Ba, structure and props. 2−53540
PbO-SiO_2, hopping cond., photoemission obs. 2−44206
XPbSe-$Ge_{1.5}As_{0.5}Se_3$, pseudobinary system, glass formation 2−80531
$Pd_{0.775}Cu_{0.06}Si_{0.165}$ glassy alloy, electronic and lattice contribs. to sp. ht., excess, 2-18K 2−80916
Pr-Cr_2O_3, absorption spectra 2−75286
Pt electrode on alkali-containing glass, model of electrode 'polarization' by d.c. potential applic. 2−81141
Sb-Se system, formation, effects of phase separation 2−60591
Se-As, temp. distribution, effect of optical characteristics 2−68256
Se-As glasses, thermal characteristics near glass transformation point 2−61104
Se, impurity effects on struct. and elec. props. 2−61326
Se enriched, Ge-Se system, (4-16.7 at.% Ge), temp. depend. of density and thermal expansion 2−84209
Si-Ge-As-Te, comp. vs. glass transition temp. 2−60597
SiO_2-Al_2O_3-K_2O-Na_2O, thermal expansion and formation of leucite 2−74994
SiO_2-Al_2O_3-Na_2O-K_2O-CaO-MgO glass, viscosity-temp. relations 2−67883
SiO_2-Al_2O_3-R_xO, struct. state of Al ion, complex stability 2−56556
SiO_2-Al_2O_3, crystallization, DTA, elec. microscope and X-diffr. obs. 2−53542
SiO_2-B_2O_3-Na_2O-Al_2O_3 system, comp. fluctuation and phase decomp. 2−53543
SiO_2-CaO-Al_2O_3, stratification, liquation, opalescence 2−56564
SiO_2-CaO-MgO-Na_2O-AlF_3:Dy^{3+}, syst., luminesc., effect of heat treatment 2−48228
SiO_2-K_2O system, binary interdiffusion coeffs. and O_2 self- diffusion 2−53772
SiO_2-Na_2O system, binary interdiffusion coeffs. and O_2 self- diffusion 2−53772
SiO_2, fused, development of new variety 2−70046
SiO_2, ion irrad., surface topography 2−50462
SiO_2, silica, mechanically crushed, paramag. centres, e.p.r. obs. 2−67888
SrO.xB_2O_3, n.m.r. of ^{11}B, struct. 2−54504
Te-As-Ge-S, films, four-element quantitative analysis 2−72593
Te-Ge-As system, superconductivity and structural features 2−61242
Te-Ge based memory glass film, thermal crystn. 2−47128
Te based film, sputtered, thermal crystalliz. 2−60668
Te systems, chemical aspects of glass formation 2−60599
$Te_{60}As_{25}Ge_{13}M_x$, M=S, Se, chalcogenide, interdepend. between switching, memory, and thermal behaviour 2−47901
TeAsGeS, structural and electrical props. 2−61329
$Te_{85}Ge_{15}$, $Te_{81}Ge_{15}Sb_4$, $Te_{81}Ge_{15}As_4$, struct. and crystalliz. 2−60598
$Te_{15}Ge_3As_2$, u.s. velocity, hydrostatic press. effects 2−47742
$Te_{81}Ge_{15}As_4$, struct. of laser written lines, elec. microscope obs. 2−60600
$TeO_2-V_2O_5-Fe_2O_3$, glass formation 2−64534
TiO_2-SiO_2, He migration 2−50718
^{47}Ti and ^{49}Ti impusities, hyperfine structure and e.p.r. centres 2−84571

Glass continued
Tl germanat glasses with high Tl_2O content, revised refractive indices 2−61585
$Tl_2SeAs_2Te_3$, switching rel. to radiation emission 2−64981
$Tl_2SeAs_2Te_3$ chalcogenide semiconductor, struct., n.m.r. and i.r. absorp. obs. 2−60420
V_2O_5-P_2O_5, microstruct., mag. ordering, mag. props., e.s.r. 2−44310
WO_3-P_4O_{10}-V_2O_5, elec. cond. and mag. resonance 2−54495
Xe adsorption on quartz glass, isotherms meas. 2−50529
ZnO-Al_2O_3-SiO_2 glass-ceramics, dielec. props. and effects of adding (CaO, SrO, BaO) 2−65045
XZnSe-$Ge_{1.5}As_{0.5}Se_3$, pseudobinary system, glass formation 2−80531

Glass-metal seals *see Seals*

Glow discharges *see Discharges, electric/glows*

Goks *see Hypernuclei*

Gold
adsorption of water, detn. by meas. of work function 2−71347
atom, absolute total cross section for K-shell ionization by electron impact, 90-140 keV 2−46458
atom, electron-bremsstrahlung cross-section meas. at incident energy 0.2 MeV, photon energies 0.02-0.2 MeV 2−70613
atom, L X-ray production by 0.5-3.0 MeV protons, relativistic effects 2−52913
atom, neutral, elastic scattering by Ar, 5-90 eV, determ. of interaction potential 2−56114
band structure, crit. point detn., wavelength mod. derivative spectroscopy obs. 2−48160
band structure, critical ooint determ., wavelength modulation derivative spectroscopy obs. 2−48160
beam foil spectroscopy, search for channelling effect 2−80930
beta-ray self-absorption correction factors in foil 2−76956
bicrystals, grain boundary dislocation behaviour, electron microscope obs. 2−56732
black deposit, i.r. transmission, rel. to prep. conditions 2−57347
boundary layers, transmission of struct. information 2−77494
channelling effects on transmission of MeV H_2^+ ions through thin single crystals 2−44011
channelling of 1.8 MeV α-particles in planar directions, continuum potentials deduced 2−44006
complex structure potentials meas. by convergent electron diffraction 2−83932
conduction electron mean free path determ. from size effect of thin films 2−75012
contact resistance on NiO 2−61370
cover on ceramic BeO during γ- and X-ray irradiation, effect on TSEE response 2−68491
decoration g radiation damages alkali halide crysts. 2−80607
diffusion in Cu, comp. profiles near grain boundaries, electron diffr. obs. 2−56757
diffusion in Cu-Au alloy of Au, misfit dislocation behaviour 2−71497
diffusion in Si, cpd. formation, refl. electron diffr. obs. 2−50463
diffusion in ZnS single cryst. 2−56764
diffusion into Si slices at 1000°C rel. to dislocations 2−60833
electrodes, electron photoemission due to cold cathode glow discharges 2−65105
electromigration in Au-Ag alloy 2−83996
electron energy loss spectra, surface plasmon excitation 2−44043
electron irrad. damage, h.v. electron microscope obs. 2−80650
electron microscope self cleaning apertures with varied contours, preparation 2−79165
electron microscopy of single crystals at low temps. 2−80892
electron momentum distribution, from Doppler-broadened annihilation lineshapes 2−71782
epitaxial growth on substrates, various modes 2−77530
epitaxy on rocksalt, influence of interfacial amorphous C layers 2−77503
equation of state, based on elastic and cohesive props. 2−68063
Fermi surface, de Haas-van Alphen meas., infinite field phases 2−61182
Fermi surface, phase shift parametrization 2−44030
Fermi surface, uniaxial stress effects, de Haas-van Alphen obs. 2−54108
film, {100} oriented, surface struct., LEED, RHEED 2−77500
film, ang. distrib. meas. of secondary electrons 2−44213
film, bicryst., electron diffr. by grain boundary dislocation netorks 2−77593
film, discontinuous, photon emission on applic. of strong electric field 2−48266
film, epitaxial growth, rel. to use as self-supporting targets in channelling expts. 2−71326
film, evaporated, optical consts. variation with time 2−75254
film, growth processes on alkali halides, elec. microscope obs. 2−47096
film, large angle rotation boundaries, electron micrographs 2−56736
film, low temp. migration of Cr, backscatt. obs. 2−56754
film, on amorphous C, oriented crystn. mechanism, rel. to interaction forces at interface 2−77502
film, on glass, photoelectron spectrometric investigation 2−80572
film, on KCl, epitaxy rel. to nucleation 2−67905
film, radioactive tracer self-diffusion, T<200°C 2−56751
film, significance of electric field on growth 2−60634
film, thermoelec. power rel. to surface scatt., Matthiessen's rule 2−64895
film, thickness det., comparison of multiple beam Fizeau interferometry, photoelectric shearing interferometry and stylus instrument methods 2−47118
film, u.s. velocity, attenuation and internal friction meas. 2−77780
film, X-ray diffraction, internal strain and crystallite size rel. to spitaxial growth 2−50485
film deposition by sputtering, temp. rise as a function of applied power 2−67913
film deposition on alkali halides, multiply-twinned particles 2−47101
film growth, on alkali halide, from nuclei with fivefold symmetry 2−47102

Gold continued
- film on quartz, heat transport, phonon emission, low temp. 2−54084
- film on Si, ion channelling 2−54094
- films, discontinuous, post-deposition resistance increase, obs. 2−61222
- films, electron multiwave scattering at 70 keV, scatt. intensity detn. 2−71451
- films obtained by sputtering, changes of electrical and structural properties changes during annealing process 2−60647
- foil, multiple scatt. of 300-1000 keV ions with $1 \leqslant Z \leqslant 18$ 2−47779
- foil cover on ^{252}Cf source, effect on fission fragment energy loss and spectrum parameter changes 2−42445
- grain boundary, struct. of coincidence and near coincidence tilt boundaries, elec. microscope obs. 2−60810
- grain boundary dislocation climb, in ion irrad. bicrystals 2−56731
- grating, interaction radiation of moving electron 2−73526
- Hall and Righi-Leduc coeffs., 4-125 K, Weidemann- Franz law 2−61224
- hyperchannelling of ^{127}I and ^{4}He ions, orientation rel. to intensity and energy loss 2−47778
- impurity in Ge, absorption and movement of melted zone in the solid phase 2−83892
- ion penetration of Xe 2−61124
- ion sources, laboratory, low intensity 2−55672
- liquid, optical consts. 2−43359
- mineral deposits, relation to tectonic features 2−57724
- nucleation on an ionic crystal, diffusion mechanism 2−71534
- optical props. and interband transitions, review 2−72292
- ore, elemental anal. using neutron capture γ-rays 2−44513
- ore, neutron capture gamma ray studies 2−61846
- phase picture production by metallographic examination with ZnSe coating 2−56918
- photoelectric emission, electronic struct. 2−72088
- photoemission electron energy distributions, study using 10 to 40 eV synchrotron radiation 2−44202
- plastically deformed after quenching, resist. recovery 2−56790
- point detect-extended dislocation interaction, elastic modulus effect calc. 2−50652
- primary photoemission spectra, rel. to band struct. 2−61462
- quenched, stacking fault tetrahedra growth and annealing 2−77590
- radiation damage, atomic displacement cascades, computer simulation 2−53700
- radiation damage, nature and annealing characts. 2−47368
- radiation damage, proton, deuteron and He-ion, energy depend. 2−50643
- reflectance, 1.1-11.5 eV, rel. to band struct. determ. 2−75278
- stacking fault energy from Shockley partial dislocations separation meas. 2−77591
- stacking fault tetrahedra formation, models 2−60808
- stopping power for 25-250 keV H ions 2−47774
- stopping power for 28 MeV α-particles 2−54099
- stopping power for protons and deuterons at same velocity 2−54098
- stopping powers for 30-90 MeV ^{238}U ions 2−47773
- stopping powers for ^{4}He, ^{16}O, ^{35}Cl at 1 to 3 MeV 2−80921
- surface, {100}, focusing in sputtering 2−64542
- surface, MgO coated, positron backscatt. as conversion method 2−64078
- surface, sputter deposition and sputter removal of Mo, Auger spectroscopy 2−50520
- surface struct., 5×20 struct., RHEED obs. 2−77482
- surface struct., kinematic LEED intensities extraction from averaged data 2−43462
- surfaces, radiation heat interchange 2−55578
- target, micrometeoroid simulation, Fe microparticles from Van de Graaff accelerator 2−66187
- thermal resistivity, high temp., and electron-phonon interaction 2−68258
- thermoelectric power rel. to Fermi surface shape and sample dimens. effects 2−68296
- thin oxide formation in aqueous electrolyte solutions passing anodic current, reaction kinetics 2−68784
- total energy, pseudopot. theory 2−61137
- trace elements analysis by spark source mass spectroscopy 2−61823
- u.s. attenuation, Gruneisen mode and const., phonon viscosity and thermoelastic effects 2−68234
- u.s. attenuation, quantum oscillation 2−51037
- u.v. photoemission emission, computer simulation using band structure data 2−48022
- vacancy clusters, influence of quenching velocity, elec. microscope obs. 2−71630
- valence bands, high-resolution X-ray photoemission spectrum 2−44203
- vapour, high-current hollow cathode discharge, radiation, effect of reson. and recomb. 2−74423
- Al$_2$O$_3$, escape depth of X-ray excited electrons and Auger electrons 2−51224
- Au:Cu, impurity-vacancy binding energy, equilib. resistivity obs. 2−71465
- Au/CO adsorbed layer, i.r. refl.- absorpt. spectra study 2−60676
- Au/H abundance ratio in Sun from spectral synthesis of λ3123 AuI line 2−44977
- Au/W-SiO$_2$-Si, m.o.s. system, effect of bias-temp. treatments 2−84345
- Au-Al alloy, dilute, Mathiessens rule deviation due to scatt. processes 2−80969
- Au-Cu bimetallic film, interdiffusion, X-ray obs. 2−60828
- Au-Cu foils, quantitative microanalysis with combined electron microscope-microanalyser (EMMA-3) 2−81561
- Au-SiO cermet film, post-deposition resistance changes 2−61222
- Au-SiO$_2$ r.f. cosputtered films, combined electron microscopy X-ray microanalysis obs., and preparation 2−80576
- Au-lacquer-Se structure, current passage mechanism 2−84348
- Au island films on insulators magnetoresistance 2−84298
- Au$^+$ in alkali halides, resonant phonon modes 2−54018
- Au$_2$ mol., true pot. energy curves, r-centroids, Franck- Condon factors 2−56155
- CdS-Au, study of anode hole injection 2−84346
- p-Ge:Au, photocond., electron capture coeff., excess free carrier distrib., surface recomb. effects 2−81164

Gold continued
- Ge:Au diode, fabrication, double injection negative differential resist. 2−71974
- I ion-Au, Th, U collisions, 10 to 60 MeV, X-ray spectra of temporarily formed superheavy quasiatoms 2−74236
- in Nb-Sn sinter material, supercond., effect on screening behaviour 2−75061
- Pb:Au, relax. effects, internal friction obs. 2−68069
- Si:Au, Ag, Co, trapped minority carrier thermal emission rates, meas. technique 2−71784
- Si:Au, m.o.s. capacitance meas. of Au levels 2−61362
- Si:Au, near i.r. absorpt. 2−72348
- p$^+$-n Si:Au diode, current filament behaviour in mag. field 2−71975
- Si:Au diode, thermally-stimulated current from deep-lying trapping levels 2−68419
- in Si diodes, p$^+$-n and n$^+$-p, barrier capacitance during exchange between Au levels 2−71979
- onSi single crystal substrate, SiO$_2$ formation 2−67911

Gold compounds
- − 2−71831
- alloy, β-brass type, lattice vibrs. rel. to martensite struct. 2−56930
- Ag-Au-Cu alloy, sp. ht. and residual resist. 2−75051
- Ag-Au alloy, effects of pressure on resistivity 2−51097
- Ag-Au alloy, electronic struct., reflectance obs. 2−61174
- Ag-Au alloy, sp. ht. and residual resist. 2−75051
- Ag-Au alloys, vacancy flow, effect and Kirkendall shift meas. 2−74809
- Ag-Au dilute alloy, Righi-Leduc and Hall coeff., 2.5-120 K 2−75050
- Ag-Au system, coherent pseudopotential model 2−75025
- Ag-(28 at.%) Au thermocouple wire, Standard Reference Material 733, thermoelec. voltage comparison with common materials, 4 to 273K obs. 2−65080
- Ag$_3$AsS$_3$ single crystal, vibrational spectra 2−44387
- Al-Au alloy, electronic struct., soft X-ray emission obs. 2−68671
- Au-Ag alloy, electromigration of Au and Ag 2−83996
- Au-Ag alloy, impurity scatt., electron lifetimes, Fermi surface, de Haas-van Alphen meas. 2−61148
- Au-Al, α-phase dil. alloy, band struct., refl. study, 1.1-11.5 eV 2−75278
- Au-Co alloys, nucl. spin entropy changes during ageing 2−43798
- Au-Cr alloy systems, optical absorpt., band struct. 2−44371
- Au-Cu alloy, diffusion of Au, misfit dislocation behaviour 2−71497
- Au-Cu alloy, melting, strain energy effects 2−53492
- Au-Cu alloys, Zener relax., internal friction obs. 2−60852
- Au-Cu film, epitaxial growth by r.f. sputtering, microstruct. 2−67908
- Au-Cu ordered alloys, dislocation mechanisms of twinning 2−68033
- Au-Fe alloy, precip. rel. to G.P. zone form., dislocations, vacancies 2−43851
- Au-Fe thermocouples, calibration rel. to KP, Ag, Cu, temp. range 4K-280K 2−81158
- Au-Fe(Mn)(Co)(Ni)(Ti) dilute alloys, resist., deviation from Matthiessen's rule, 0.5-60 K 2−77854
- Au-Ga alloy, liquid, free enthalpy of mixing 2−53422
- Au-Ga alloys, metallurgical properties, contact characteristics 2−84069
- Au-Gd alloy, dilute, exchange interact. with cond. electrons, e.p.r. obs. 2−72467
- Au-Ge alloy, liquid, free enthalpy of mixing 2−53422
- Au-In alloy, liquid, free enthalpy of mixing 2−53422
- Au-Pb system, interstitial dissolution and compound formation 2−43826
- Au-Pd alloy, short-range order formation, resistivity obs. 2−74894
- Au-Pt alloy, low field Hall coeffs. at 4.2K and 300K, two band model 2−61188
- Au-Si, mixed phase formation at interface, Auger electron spectroscopy, 100-300C 2−74619
- Au-SiO film, cermet, struct., elec. props., rel. to deposition condition 2−64976
- Au-Sn alloy, Mossbauer oscills 2−51308
- Au-Sn solid solns., dil., correl. factor and self-diffusion 2−64693
- Au-Ti dil. alloys, weak resist. minimum 2−44052
- Au-Ti film conductor strpes, electromigration damage rel. to pulsed d.c. powering 2−80940
- Au-V alloy, dil., field depend. of mag. susceptibility 2−61475
- Au-V alloy systems, optical absorpt., band struct. 2−44371
- Au-V dil. alloys, mag. susceptibility, 2-293K, local behaviour 2−68517
- Au-47.5 at.%Cd alloy, elastic and anelastic props. near cubic-orthorhombic phase transform. 2−77643
- Au-Yb dilute alloy, localized moments, Mossbauer obs. 2−81210
- Au-Zn alloy, β' phase, liquidus and solidus temps. 2−80838
- Au-Zn dilute alloys, optical and piezo- optical properties from reflectivity measurements 2−68621
- AuAl$_2$, density of states and anomalous Knight shift 2−47806
- AuBe band system, Morse Franck-Condon factors and re-centroids 2−67467
- AuCN anomalously narrow Mossbauer linewidth in ^{197}Au 2−78074
- AuCu$_3$, effect of ordering on lattice heat capacities 2−57060
- AuCu$_3$, elastic moduli, antiphase boundary and long-range order effects 2−47416
- AuCu$_3$, superdislocations and antiphase boundaries 2−47417
- AuFe alloy, Mossbauer effect, reducing point charge model analysis 2−65229
- AuFe dilute polycrystalline alloy, negative transverse magnetoresistance 2−64911
- AuGa$_2$, density of states and anomalous Knight shift 2−47806
- AuGa$_2$, Fermi surface, hydrostatic press. and Pd doping effect 2−51078
- AuIn$_2$, density of states and anomalous Knight shift 2−47806
- AuX$_2$, X = Al, Ga and In, single cryst. growth and prep. 2−50600
- Cr-Au alloy pressure transducers, influence of high pressure H$_2$ on resistance, compared with manganin 2−76122
- (Cu-Au)-Fe dilute alloy, mag. susceptibility 2−61483
- Cu-Au, diffused, comp. profiles near grain boundaries, electron diffr. obs. 2−56757
- Cu-Au alloy, elastic consts., press. depend. up to 7 kbar 2−74824
- Cu-Au alloy, electrical resistivity, temp. dependence 2−75049

Gold compounds continued
  Cu-Au alloy, electronic struct., reflectance obs. 2−61174
  α-Cu-Au alloys, low temp. sp. ht., conc. depend. 2−51044
  Cu-Au alloys, side bands of fundamental reflections and diffuse superstructure lines, detection 2−64614
  Cu-Au disordered alloys, correlation phenomena 2−64815
  Cu-Au system, superdislocations in Cu_3Au, electron microscope obs. 2−80666
  Cu-Cu_3Au alloy, Debye temp., elastic moduli, elec. resist., temp. depend., 4.2-293K 2−47752
  CuAu, Cu_3Au, effect of ordering on optical properties, reflectance measurements 2−72303
  Cu_3Au alloy, flow stress temp. depend. 2−43692
  $Cu_{80}Au_{20}$, model of structure periodically modulated in three dimensions 2−50615
  Dy-Au alloy system, phase diagram, intermetallic form. 2−50973
  Fe-Au alloy, intraband absorpt., anomalous temp. depend. 2−81388
  Ge-Au films, quench-condensed, supercond. energy gap, tunnelling obs. 2−51115
  $KAu(CN)_2$, elec. hyperfine alignment of ^{197}Au 2−44355
  Na-Au dilute alloy, liq., compressibility determ. 2−77415
  Ni-Au alloy, compositional changes, elec. diffr. critical voltage effect obs. 2−56944
  Sm-Au alloy system, phase diagram, intermetallic form. 2−50973
Goniometers *see Crystals/orientation; X-ray crystallography/apparatus*
Grain boundaries
  alloy, grain boundary precip. coarsening, cumulative distrib. functions 2−47603
  alloy, grain boundary precip. coarsening, cumulative size distrib. function 2−47604
  bismuth oxide in semiconducting barium titanate, resistivity temperature characteristic anomaly at transitions 2−84366
  boundary sliding, diffusional creep, atomistic aspects 2−56729
  brass, fatigue cracking, effects of grain and twin boundaries, slip mode behaviour 2−71598
  α+β brass, rel. to superplastic props. 2−64714
  coincidence-ledge-dislocation model, supporting evidence 2−47426
  crystalline interfaces struct., 0-lattice theory 2−56616
  cyclic straining, subgrain formation 2−80763
  diffusion models for initial sintering, effect of particle size distrib. 2−50904
  diffusional creep, vacancy source via dislocation climb, interface reaction control conditions 2−50752
  disclination model 2−56723
  dislocation behaviour and contrast effects 2−56701
  domains, interface geometry, contrast effects, electron microscope and diffr. obs. 2−56718
  electron microscopy and energy analysis 2−53743
  energy measurement, isothermal calorimetry method, appl. to Cu alloys 2−83967
  entropy, Einstein cryst. model and Morse pot., computer calcs. 2−56727
  f.c.c. bicrystal, grain boundary kinking 2−74784
  f.c.c. crystal, two-dimens. model, interaction with edge dislocations 2−80652
  f.c.c. metal, wide-angle, props and at. struct. 2−53740
  feldspar, rel. to axial growth of inclined en echelon cleavage cracks during compression 2−61972
  film, metallic, electromigration, grain boundary contribs. 2−56751
  free volume, and relation to grain boundary props. 2−71500
  heat resistant alloys, electron microscope of degree of development 2−56721
  heterophase dislocation theory, high temp. behaviour 2−56733
  high angle, structure, phase matching vs. dislocation model 2−74785
  interaction with lattice defects, review 2−68032
  large angle, structure factor calc. using coincidence superlattice 2−47427
  metal, f.c.c., diffusion, computer calc. 2−50701
  metal, grain boundary ordered struct., boundary dislocations, transmission electron microscopy 2−53651
  metal, order struct. and dislocations in bubble-raft boundary 2−53741
  metal, rel. reversed creep deformation behaviour 2−77629
  metal, velocity, effect of impurity atoms 2−43785
  migration, rel. to struct., review 2−56728
  models, free volume concept 2−56724
  motion under action of own curvature, theory 2−74786
  mullite, press.-sintering kinetics and mechanism 2−50874
  nickel silvers, fire-cracking mechanism 2−43794
  quartz in prograde metamorphic sequence, rel. to preferred orientation 2−57766
  relaxed coincidence model 2−68034
  sliding contrib. to axial strain during diffusion creep 2−47509
  sliding rel. to diffusional creep 2−56730
  steel, annealed low carbon, dislocation model for delayed yielding phenomenon, pile-up time 2−80813
  steel, austenitic, stainless, grain boundary penetration by Cs-O solutions and caesium oxide, out-of-reactor study 2−67356
  steel, austenitic Cr-Mn, intergranular corrosion susceptibility 2−71646
  steel, decarburized, diffusion of hydrogen at low-temps., effect of grain boundaries 2−68047
  steel, effect of boundary form on impact strength and brittle fracture 2−80765
  steel, low C, effect of microstructure on embrittlement 2−84158
  steel, low-alloy, grain boundary segregation rel. to temper embrittlement 2−47624
  steel, low-carbon, fracture on surface with relatively low crack propag. rate 2−84126
  steel, martensitic, fracture mechanism, incompat form. at grain boundaries 2−56815
  steel, martensitic, low-C Mn, effect of Sb 2−56905
  steel, stainless, melted by different methods, O impurity effects 2−53899
  steel, structural, migration, rel. to austenite grain growth mechanism 2−53988
  steel, transformer, precip. at grain boundaries, rel. to coercive force 2−47632
Grain boundaries continued
  structure and energy, pairwise interactions, Morse, Lennard-Jones 6-12 and 4-7 pots. 2−56726
  structure and properties, review 2−53742
  structure and props. of grain boundaries and interfaces, conference, Yorktown Heights, N.Y., USA, Aug (1971) 2−56722
  structure and segregation, conf., London, England [Nov. 1971] 2−47606
  structures and energies, computer calcs., minimum free energy criterion 2−56725
  superplasticity mechanism, metallographic obs. 2−56786
  surface energy, zero creep condition, grain boundary term 2−56569
  void growth on grain boundaries, rel. to creep 2−50685
  voids, diffusional growth rel. to creep fracture 2−47523
  Yttralox ceramic characteriz. as laser material 2−49381
  Ag-Cu alloy, migration, rel. to discontinuous precip. kinetics 2−80856
  Ag, grain boundary self-diffusion, isotope effects, correl. effects, vacancy model 2−56752
  Al-Mg alloy, intergranular corrosion susceptibility 2−71646
  Al-Zn-Mg alloy, precipitate free zone, elec. microscope obs. 2−56902
  Al-Zn-Mg alloy, rel. to stress corrosion crack paths 2−43732
  Al, deformed, resistivity changes obs. 2−53744
  Al, high angle boundaries, rel. to nucleation during recrystn. 2−80859
  Al, integranular flow, effect on grain boundaries, role of imperfections 2−43643
  Al, intergranular corrosion in HCl, symmetrical flexion boundaries 2−72561
  Al, intergranular flow effects 2−43643
  Al, neutron irrad., influence on void form. 2−53736
  Al, sub-grain boundary migration 2−80824
  Al alloy, multiphase, microstructure rel. to distrib. of sliding boundaries 2−80820
  Al non-isoaxial bicrystal, tensile deformation, effect of tilt boundaries 2−50740
  Al non-isoaxial bicrystal, tensile deformation, effect of twist boundaries 2−50741
  Al_2O_3, alumina, grain boundary grooving on single cryst. surfaces 2−50432
  Al_2O_3, alumina, high temp. creep, and grain boundary sliding 2−50753
  Al_2O_3, grain boundary enhanced diffusion 2−50705
  Al_2O_3, porous polycrystalline, rel. to compressive creep mechanism 2−47513
  Al_2O_3, sapphire, grain boundary migration 2−50704
  Al_2O_3 bicrysts., porosity distrib. and pore growth 2−60991
  Al_2O_3 ceramic, shear rel. to deformation processes 2−60993
  Au, bicrystals, grain boundary dislocation behaviour, electron microscope obs. 2−56732
  Au, struct. of coincidence and near-coincidence tilt boundaries, elec. microscope obs. 2−60810
  Au bicrystal, ion irrad., g.b. disloc. climb, elec. microscope obs. 2−56731
  Au film, bicryst., electron diffr. by grain boundary dislocation networks 2−77593
  CdS cathodoluminescence, electron beam microprobe exam. of crystal structure defects 2−53745
  CdS film, electron mobility and scatt. rel. to grain boundaries and surfaces 2−61149
  Co-(31.8 wt.%)W alloy, excess vacancy conc. effect on grain boundary diffusion 2−47455
  Cr interfacial free energies meas. 2−80795
  CrV steels, free energy changes and boundary segregation of Sn and Sb 2−71309
  Cu-Au, diffused, comp. profiles near grain boundaries, electron diffr. obs. 2−56757
  Cu-Bi alloy, fragility and segregation 2−53830
  Cu-CR alloy, f.c.c.-b.c.c. interphase boundary dislocation structs. 2−56734
  Cu, fatigue cracking, effects of grain and twin boundaries, slip mode behaviour 2−71598
  Cu, Ni diffusion, grain boundary coeff. 2−53761
  Cu, void growth on grain boundaries, rel. to creep 2−50685
  Cu base solid solution, strengthening 2−53891
  Fe:Sn, hardening, micro-indentation elastic recovery obs. 2−60910
  Fe-Cr(8%) alloy, martensite, rel. to substruct. strengthening 2−84071
  Fe-Ni-C alloy, martensitic, fracture mechanism, incompat form. at grain boundaries 2−56815
  Fe-Ni-Si alloy, temper brittleness development, grain boundary adsorption of P, internal friction study 2−80767
  Fe-Ni alloy, hardening at high strain rates, subgrain boundary changes 2−47593
  Fe foils, electrocrystn. structures 2−83862
  α-Fe single crystal, rel. to high temp. creep 2−56804
  Ir, structure obs. using field ion microscopy 2−56576
  KBr, mass transport along grain boundary pipelines, comments 2−56760
  KBr, mass transport along grain boundary pipe lines 2−56759
  LiF bicrystal, interaction of stress waves with a boundary 2−84061
  Mg, neutron irrad., rel. to damage production and annealing 2−80683
  Mg alloy, superplastic, sliding as rate controlling mechanism 2−74841
  MgO, anion doped, grain boundary diffusion of Ni^{2+} 2−50710
  MgO, coincidence twist boundaries energies, Born-Mayer pot. and rigid lattice approx. 2−56735
  mischmetal-Mg alloys, dilute, metallographic study of phase transformations 2−80794
  Mo, bulk and boundary diffusion of Cr 2−53766
  Mo, refining, effect of B addition 2−56943
  Mo interfacial free energies meas. 2−80795
  NaCl, in dislocation generation, expt. obs. in singel and polycrystalline mat. under hydrostatic pressure 2−68029
  NaF, impurity content, etching obs. 2−67934
  Ni, free energy obs. using electron microscopy 2−56576
  Ni, rel. to disloc. generation during premacroyield deform. 2−47418
  Ni, wide-angle, diffusion width 2−47469

Grain boundaries continued
Ni alloys, dispersion hardened, role of grain size and shape in strengthening 2—71648
Ni film, intrinsic stress origins, interference obs. 2—43679
Pb(Zr,Ti)O_3 ceramic, role of Fe_2O_3 2—50895
Sn, wide-angle, diffusion width 2—47469
Ti alloy, grain boundary etching, grain surface etching 2—50686
α-U, rel. to Fe diffusion, 645°C 2—50719
UO_2-PuO_2 mixed fuel, grain boundary sliding 2—53808
W:O, g.b. segregation, field ion microscopy obs. 2—53746
W, diffusion of Fe and Co along grain boundaries 2—47472
W, wide-angle, diffusion width 2—47469
W interfacial free energies meas. 2—80795
W wire, drawn, micropore pinning effect on grain boundary motion during recrystn. 2—47647
WC-Co cermet, grain boundary sliding 2—47505
Zn bicrystal, motion, expt. configuration of theory 2—74786

Gramophones *see Sound reproduction*

Granato—Lucke theory *see Crystal imperfections/dislocations*

Granular structure
elastic wave velocity and absorption, effect of grain size 2—84204
grain diameter, true volume calculation 2—67977
grained solid, grains/unit volume, determ. from theory of stochastic processes 2—43877
refractory carbide cemented alloys, carbide grain shape 2—53889
X-ray diffr., intensity rel. to granularity 2—74700
K, anomalous i.r. absorpt. and collective oscills. in small metal particles 2—65210
MgO refractories, effect of stress on grain growth 2—74915
Na, anomalous i.r. absorpt. and collective oscills. in small metal particles 2—65210
$Ni(OH)_2$ powder, crystallite struct. from X-ray diffr. profiles 2—74739

Graphite
absorbed dose obs., using heat-loss-compensated calorimeter 2—67366
adsorption, of CO and H_2 in high vac. range 2—43494
adsorption, of rare gases or CH_4, film formation stages 2—47152
adsorption, of Xe, LEED obs. 2—50533
adsorption of He monolayer, densities and compressibilities on completion 2—71253
adsorption of normal liq. paraffins, quasicryst. layer form. 2—50532
anisotropic electronic correlations 2—57108
anti-friction AG-T type, friction and wear, 150 to 600°C 2—43743
arc electrode temps. and reignition characts. 2—50236
artificial, anisotropic and isotropic, struct. distrib. 2—53972
artificial, neutron irrad. effects on thermal conductivity 2—54073
atmospheric aerosol constituent, optical consts. 2—57946
band structure, secondary electron emission study 2—51150
boronated, irradiation-induced dimensional change 2—76949
brazed joints, high temperature strength 2—71627
composite, graphite/SiC, thermal expansion, 300 to 800 K 2—54057
composite, Pyrostrand, fabrication, struct., mech. and thermal props. 2—53960
composite material, graphite—ZrC_x(—Zr) systems, durability props. rel. to comp. and struct. 2—77741
creep under neutron irrad. in Dragon reactor, high temp. 2—56802
crystal polarimeter, for stellar X-ray astronomy 2—62640
crystalline prisms, space dependent neutron spectra 2—70506
electrode, mech. strength at high temp., integrated evaluation 2—56813
electron beam deposition, sublimation energies 2—60644
electron displacement damage, high-voltage electron microscopy 2—56683
electron irrad., h.v. electron microscope damage obs. 2—47370
electron irrad. damage, electron microscope obs. 2—53710
electron momentum distribution, from Doppler-broadened annihilation lineshapes 2—71782
electronic carrier location and identification 2—57107
electronic density of states perturbed, calcs. 2—57123
electronic properties of very thin crysts. 2—54102
electrothermal, crystallite size 2—57001
energy band calcs. using tight-binding approx. 2—68287
energy band parameter calcs. 2—57121
energy band struct., tight binding approx., optical absorpt. 2—84234
Esaki effect, I-V characts. in mag. field 2—44093
e.s.r. obs. effect of irradiation with heavy ions 2—78152
etch pitting by atomic and mol. H_2, O_2 and N_2 2—53553
evaporation, method of determining thermodynamic properties and kinetic parameters 2—56545
fatigue failure probability 2—53827
fatigue failure probability determination 2—60994
fibre, fast neutron irrad. effects on mech. props. 2—56992
fibre, transverse thermal expansion 2—53954
fibre and composites, u.s. elastic consts. 2—50723
fibre reinforced composite, compressive fatigue 2—61021
fibre strength and Griffith equation 2—53944
fibre synthesis, three dimensional C structure synthesis at one atmosphere 2—56979
fibre-reinforced polyester, work of fracture 2—74863
fracture, physically based statistical theory 2—56827
fracture at high temp. 2—56829
fracture mechanics 2—56828
Gilsocarbon, characts. rel. to high temp. reactor design 2—52871
Gilsocarbon, irrad. behaviour 2—56994
graphite, pyrolytic, highly oriented, high dose fast neutron irrad. 2—57072
graphite, thermal diffusivity, 650-2700K 2—54082
graphite-Bi mixture obs. on neutron diffusion lengths 2—49861
graphite-Br intercalation compound, Fermi surface, Shubnikov-de Haas oscill. obs. 2—68288
graphite-diamond transition, diffusional mechanism in strong elec. field 2—47706
graphite-epoxy composites, radiation effects on mech. props. 2—64795
graphite-Ge switch, asymmetric, and light sensitivity 2—61272
graphitization in C film under light pulse irrad. 2—57002
Hall effect and magnetoresistance, rel. to struct. imperfections 2—57190

Graphite continued
heats of immersion rel. to degassing behaviour 2—53549
high temperature gas-cooled, effects of transverse flow through graphite on fission product movement 2—42642
HTGR fuel block, struct. props. and mech. strength due to irradiation 2—56045
inert gas nucleation, growth and epitaxy, molecular beam system and specimen holder for t.e.m. obs. 2—79113
interlayer force, Thomas-Fermi calc. 2—77823
interlayer props., effect of interstitial atoms, simple model 2—56605
isotropic, creep strain, effect on elastic modulus, cryst. orientation and density 2—56963
isotropic, Young's modulus porosity depend. up to 1800°C 2—56772
from isotruxene carbons, formation and microstruct. from X-ray exam. 2—61023
laser beam irrad., chaoite formation in craters 2—56574
laser effects at mod. Ar press., crater formation 2—53552
LCAO band structure calculation rel. to chemisorption 2—50525
light pressure efficiency factor for spherical particles 2—45772
magnetoelectric props., pressure effects, energy level and carrier scattering models 2—57110
magnetoreflection spectrum at high fields 2—57340
microscopy at high resolution, sample prep., technique improvement 2—53637
neutron diffusion length, depend. on temp. 2—76898
neutron irrad., sp. ht., 0.6-5 K 2—57062
neutron irrad., sp. ht., 1.4-4.4 K, strong mag. field effects 2—57063
neutron irrad., sp. ht. obs., low temp., rel. to heat treatment 2—54045
neutron irrad. at 715°C, dimens. stability 2—56047
neutron irrad. at high-temp., mech. interactions among crystallites 2—56679
neutron irrad. damage, dose rate effects 2—53708
neutron irrad. defect struct., single cryst. 2—53709
neutron irradiated, thermal cond., 50-1000°C 2—54075
neutron wave propagation, analysis of total response 2—42603
nodular, formation rel. to cast Fe melt solidification and additives 2—74881
nuclear, from coke mixtures, props. and irrad. effects 2—59841
nuclear, high fluence neutron irrad. behaviour, two-phase model 2—56048
nuclear, isotropic, reactivity to oxygen 2—59843
nuclear, nat. graphite filler, neutron irrad. behaviour rel. to comp. 2—56049
nuclear, production by mixing different cokes 2—68174
nuclear, reaction with hydrogen 2—59842
nuclear, strength distrib. functions, effect of high temp. fast neutron irrad. 2—53822
nuclear fuel element for NUGG reactor 2—56067
nuclear reactor core, calc. of thermal resistance between hexagonally arrayed channels 2—42651
nuclear reactor structures, problems, conference, London (1972) 2—56052
ordering, effect of Zr and Si additives 2—50829
oriented, rigidity and limiting strength, comparative estimates 2—47475
oxidation effects in highly oriented pyrolytic graphite 2—56572
oxidation effects in pyrolytic graphite 2—60620
oxidation in a reactor due to irradiation obs. 2—52850
oxidized pyrolytic, scanning e microscope kinetic studies 2—68118
phonon drag thermoelec. low temp., rel. to struct. imperfection 2—44170
phonon-drag thermoelectricity rel. to structural imperfections 2—57248
Poco, high temp. creep 2—56803
Poco, reactivity to oxygen 2—59843
POCO grade HPD-1, high temperature creep, comparison with polycrystalline graphites 2—77625
polycrystalline, environment effect on mech. anisotropy 2—68173
polygraphites, fracture obs., modes and criteria 2—56830
porosity, effect on thermal and elec. cond. and elastic consts. 2—50926
porous, high temp. thermal cond. meas. 2—54074
positron annihilation, appl. to struct. and props. determ. 2—47771
powder, fine-disperse, effects of oxidation on pressing ability 2—77737
prism, neutron wave propag. effect of cold neutrons 2—83044
pyrofoil tape, production and characterisation for reactor use 2—56050
pyrolitic and stress recrystallized, present and future applications 2—68172
pyrolytic, c-axis conduction mechanism from galvanomagnetic obs. 2—57109
pyrolytic, effect of B doping on thermal conductivity 2—57084
pyrolytic, elastic consts., Gruneisen parameters, 80-300K 2—43664
pyrolytic, high temp. thermal diffusivity 2—54066
pyrolytic, lattice dynamics 2—43954
pyrolytic, low temp. electron irrad. damage and recovery, resist. study 2—80659
pyrolytic, meas. over wide temp. range of thermal and electrical conductivities, thermal expansion and heat capacity 2—84208
pyrolytic, neutron reflectivity and use as analyzer and higher order filter in neutron scattering 2—55891
pyrolytic, oxidation of basal plane with modulated molecular beam 2—51447
pyrolytic, oxidation of prism plane, effect of diffusion in grain boundaries and in bulk on reactivity rate 2—51448
pyrolytic, spreading critical surface energy, from liq. metal wetting obs. 2—80558
pyrolytic, thermal conductivity and diffusivity above 1500 K 2—57083
pyrolytic, thin film, production and mech. props. 2—56999
pyrolytic, thin film struct. characts. 2—60648
pyrolytic siliconated, fracture surface, electron microscope obs. 2—74861
pyrolytic stress-annealed, surface tension 2—60621
radiolytic reaction with CO_2, effect of CO, 225-375°C 2—57434
reaction with oxygen, at high temp., molecular beam and mass spectrometer 2—48332
review of work at Royal Aircraft Establishment 2—43903

Graphite continued
self-diffusion, interstitials as diffusing defect 2−53760
shock wave compression, X-ray diffr. obs. in single crystals 2−56646
single crystal, use as X.U.V. polarizer 2−42211
sliding friction with soft metal stylus 2−84044
sorbed layers, Rb-Cs mixtures, vapour press. 2−53592
stacking fault-halogen impurity interactions 2−53738
structural, removal from coated particles in spent nucl. fuel, electrolytical cell performance 2−83070
sublimation of bulk mat., effect on microstruct. on characts. 2−60560
surface, metal metal spreading kinetics 2−67814
surface impurities, detect. by ^{4}He$^+$ and H$^+$ ion beams backscatt. 2−77485
surface polarity when covered by oxygen complexes, evaluation using heats of immersion 2−64550
surface study of gases prod. by thermal decomposition from acidic surface oxides 2−64551
surface/oil/water/air system, forced spreading 2−53380
thermal cond. at high temps., modulated electron beam technique 2−84210
thermal expansion parallel to basal plane, high temp. coeff. 2−57073
thermal expansion theory applied to basal planes 2−64859
thermal expansion theory applied to expansion coefficients, electronic contribution 2−64860
thermal expansion theory applied to hexagonal axis 2−68251
thermal pulsed-neutron experiments 2−74131
thermal vibs. of C atoms 2−54020
thermoelectric and thermomagnetic effects 2−57249
thermomagnetic effects, coupled Boltzmann eqn. 2−54243
tunnelling spectroscopy, state density near Fermi level 2−57122
X-irrad., dynamical mech. props. 2−53777
in C, pyrolytic, neutron irrad. stability 2−56997
C products, graphitization effects on neutron irrad. induced dimensional changes 2−56996
composite, graphite matrix, C fibre reinforced, microstruct. effects on mech. props. 2−61015
Cs-graphite thermionic converter, Cs vapour source 2−52372
Cu plated, cermet on Fe base, sintering 2−53863
^{4}He adsorbed on graphite, flow 2−74575
POCl$_3$, adsorbed, effect on oxidation behaviour 2−68783
SiO$_2$-graphite system, phase equilib. 2−43930
UO$_2$-dispersed, fission gas release, obs. 100-950°C, release mechanisms discussed 2−70534

Graphitisation *see Annealing*

Graphs
see also Nomograms
plotting computer output on line printer using high density plotting symbols 2−66485
undirected, for molecule representation, algorithm 2−64103

Gratings *see Diffraction gratings; X-ray diffraction*

Gravimeters *see Gravity*

Gravitation
see also Gravitational collapse; Red shift; Relativity/general
— 2−62990
axially symmetric fields and the Kerr metric 2−82199
axially symmetric fields with discs of matter at source, study of counter-rotating discs 2−55401
Brans-Dicke theory, general relativity 2−78430
Brans-Dicke theory, gravitational collapse 2−69558
Brans-Dicke theory test using cold neutron star model 2−73308
bremsstrahlung radiation from charge falling in strong field, relativistic treatment 2−78797
canonical formalism, static and two-body pots. 2−58732
central classical fields, creation and annihilation of spin pairs by photons and gravitons 2−82178
charged particle mass rot. around axis, relative equil. 2−72946
constant, possible variatio over elements 2−48986
curvature of physical space and difference between gravitational and inertial fields 2−78804
deflection of light by Sun and velocity and wavelength changes, wave theory 2−45247
Deser and Laurent nonlocal linear theory, possible experimental tests 2−66423
dilaton theory, effect on G and solar neutrino flux 2−79632
Einstein's eqn., generalized, solns. containing Yukawa type terms 2−82190
Einstein's field theory, use of Lorentz- covariant procedure for motion of particles interacting through gravitational field 2−49000
Einstein's principle of equivalence, configuration of atoms due to hydrostatic pressure inside matter 2−69556
Einstein effect, fourth, bending and retardation of light in a gravitational field 2−66426
Einstein field equation, quadratic first integral for charged particle orbits in Kerr solution 2−73296
Einstein-Cartan equations 2−41470
Einstein-Cartan equations 2−73294
electron moving in vertical metallic pipe, effect of electric field arising in shield due to gravitational field 2−66705
electron scattering, in gravitational field of rotating source, polarization effects 2−55381
electrovac fields with geodesic eigenrays 2−41471
e.m. radiation generation from charged particles, rel. to quasar luminosity 2−44890
energy-momentum tensor as source of tensor gravitation, spin-1/2 particles 2−79458
exact field, infinitely long rotating hollow cylinder 2−48992
experimental tests using radar and radio waves 2−76198
field, interaction with fermions, anal. 2−82252
field, structure in asymptotic limit at spatial infinity 2−45248
field equations, Yang Mills type theory with SL(2,C) invariance 2−52049
field existence in unified spinor field theory 2−66438
fields; construction and characterisation in unified field theory 2−66437
fields, degenerate, with twisting rays 2−69565
fields, evidence for anomalous interaction with e.m. fields from analysis of astronomical data 2−54994

Gravitation continued
fields, simple coupling with e.m. fields 2−73311
finite range theories, inconsistency 2−58733
fluctuating-regression hypothsis for one-dimensional system of hard rods 2−69621
fluid, perfect, with electromagnetic and thermodynamic props. rotating about fixed axis 2−69577
fluid, rotating, with finite resistivity, self- gravitat. instability 2−50167
galaxies, flat, field calc. 2−55010
gas diffusion, appl. to processes in ionospheric F-region 2−58091
gas diffusion in gravitational field 2−56446
generalized equations, central symmetric solutions 2−69570
gravitational constant, possible anisotropy effects on celestial orbits 2−81755
higher spin rest-mass zero fields, properties 2−73304
and inertial mass equivalence meas. by torsion balance method 2−82184
instability, rel. to proto-galaxy formation in expanding universe 2−51713
intermediate-range gravity, generally covariant model 2−55400
internally stressed body in gravitational field, general relativity theory 2−78803
Jeans instability criterion, finite amplitude sound propagation in general relativity 2−52053
Kerr Schild type vacuum gravitational fields 2−62984
light interacting with gravitational field 2−55383
linear conservative theories, gauge groups 2−78792
linear theories 2−45249
locally Lorentz-invariant curved-space theory 2−62989
Lorentz-covariant reference-tetrad theories 2−69555
lunar circular maria, mascons rel. to isostatic adjustment 2−69135
lunar gravitational field measurement from Lunar Orbiter 2−44917
Lyra type, connection with scaling and scale invariance 2−55404
Mach's principle and gauge freedom in Brans- Dicke theory 2−41477
Mach's principle connection, rel. to universe 2−58736
many-body forces and the effect of the matter distrib. in the universe on the gravitational constant 2−58156
massive bodies, effects on static e.m. fields in general relativity 2−78799
massive gravitational field theory, zero-mass limit 2−41481
massive two-tensor theory, generally covariant 2−62991
metric-space formulation of Newtonian fields 2−73298
n-body problem with variable gravitational constant, dynamical consequences 2−81769
negative mass concept, exptl. detection methods 2−78785
neutrino gravitational scatt. in one-graviton-exchange approx. 2−79499
neutrinos in spherically symmetric gravitational fields 2−58727
Newton's law, closed orbits of solar system 2−48985
Newtonian theory, Poincares generalization 2−62946
non-Newtonian gravity, astrophysical test for dilation theory 2−78796
nonvacuum field eqns., conservation of energy-momentum 2−82200
perihelion advance of planets, calc. by field approach to gravitation 2−48765
planets, perihelion motion from new theory 2−62977
plasma, non-Markovian time evolution, weakly oscillatory relax. process 2−68999
propagator, gravitational potentials and gauge transformation 2−45855
quantum theory, semantic foundations of quantization procedure 2−63002
radiation, upper limit on X-ray flux 2−44826
redshift rocket probe experiment rel. to theories of gravitation 2−69571
relativistic field eqns. approx. solutions to describe clusters of galaxies 2−58197
relativity-gyroscope expt., precession in Einstein and arbitrary theories of gravitation 2−76187
retarded interactions, two-body problem 2−82186
Riemannian space, pseudo-geodesic and pseudo-Riemannian coordinate systems 2−55380
Salam two-theory, exact Kerr-Schild type vacuum solutions 2−48991
satellite, axisymmetric, in gravitational field, rapid-rotation stability 2−75648
scalar covariant theory of Nordstrom, its implications for general relativity 2−76174
scalar-tensor theory, formalism in general relativity theory 2−82208
scalar-tensor theory, Taub-Kazner cosmological metric generalization 2−78435
solar field, obs. using twin probe method 2−85052
space dilation in spherically symmetrical gravitational field 2−69557
spherical rotating layers, field in linear approximation 2−76190
spherical shells of ideal gas in central gravitational field, motion in framework of general relativity 2−48984
spherically symmetric fields, Hamiltonian formulation 2−55389
spin-spin interaction 2−73300
spinning particles in gravitational and e.m. fields, canonical dynamics 2−41479
stationary orbits in central gravitational fields, field theory 2−76165
stellar convection envelope response to tidal variations of gravitation field 2−85008
stochastic space concept and phase fluctuations of propagating wave 2−78763
SU(1,1) spinor algebra, spin coeffs. 2−82213
synchrotron radiation, effect of Peres gravitational field 2−69823
theoretical research, review 2−62992
theory, iteration solution 2−76189
theory, non-local linear 2−76177
tidal effects of planets rel. to solar activity during 200 year period 2−75984
translation-rotational motion of triple rod in a Newtonian field 2−45348
Treder theory, cosmological solution 2−48644

Gravitation continued
two-tensor theory, constraint relations 2−55379
two-tensor theory, generation of exact solutions to vacuum field equations using work of Kundt 2−49473
weak interactions, cosmological time dependence 2−73299
weak linearized radiation field, measurability analysis of electric type components 2−45250
weak-field approx. and range of gravitational force 2−76186
Weber's expt., correl. between gravitational signals and solar and terrestrial mag. activity 2−44824

Gravitational collapse
— 2−69006
black hole, quantum numbers nonmeasurability 2−55406
black hole, rotating, gravitational wave radiation, review 2−48652
black hole development, extension of Oppenheimer-Snyder dust cloud solution 2−62445
black holes, det. in eccentric binary systems 2−58350
black holes, interstellar gas accretion and emergent radiation spectrum 2−75661
black holes, nonexistence of baryon number, agreement with Israel Carter conjecture 2−55385
black holes, radiation 2−44828
black holes, relativistic Roche problem 2−58161
black holes, review 2−78437
black holes, rigidity 2−62444
black holes, time symmetric initial value problem 2−58726
black holes, white holes and particle creation 2−78438
black holes and second law of thermodynamics 2−72957
black holes and temporal ordering 2−81764
black-hole bomb, floating orbits and superradiant scattering 2−62443
in Brans-Dicke theory of gravity 2−69558
charged black holes, gravitational radiation 2−78439
electromagnetic field equations for charges in Schwarzschild geometry 2−58162
galactic evolution, collapse of massless, non-rotating cloud around point nucleus 2−84953
homogeneous spheres, adiabatic contraction 2−69005
massive body, black holes formation 2−58163
nebula to neutron star, stages reviewed 2−84985
nonspherical perturbations, fadeaway of multiple moments 2−78799
polytropic sphere with negative index, crit. masses 2−66041
protogalaxy, collapse, with rotation and capacity in later stages 2−58178
relativistic, nonspherical perturbation in integer spin of zero-rest-mass fields treated in Newman-Penrose formalism 2−55387
relativistic, nonspherical scalar of gravitational perturbations 2−55386
rotating black hole, energy and angular momentum flow 2−78436
rotating black hole, study of surrounding weak e.m. fields 2−55388
rotating black holes, separable wave equations for gravitational and electromagnetic perturbations 2−84945
rotating cloud, formation of multiple stars 2−48733
rotating star, theoretical formulation 2−62495
Schwarzschild black hole, gravitational radiation pulses of particle falling radially 2−55405
static black holes in Brans-Dicke theory, Schwarzschild solution 2−52051
stellar evolution endpoints, discussion of various possibilities and relation to phenomena of high energy astrophysics 2−78460
stellar matter, black hole and expanding universe 2−66042
supermassive nonrotating 0.75×10^6 M$_\odot$ star, hydrodynamic model calc. for collapse to black hole 2−44821
two gravitationally bound black holes, upper limits on gravitational radiation 2−81763
wave production and detection, theoretical 2−44822
X-ray sources, accretion disc models 2−85014

Gravitational red shift *see Red shift*

Gravitational waves
acoustic-gravity waveforms in laterally inhomogeneous media, large scale meteorological influences 2−54809
anisotropic Euclidean homogeneous cosmology, perturbation calc. 2−72956
astrophysical sources, detection of radiation on Earth 2−62439
binary system containing dense object, pointless limits to gravitational radiation 2−58345
black hole, rotating, gravitational wave radiation, review 2−48652
Crab pulsar, upper limit on gravitational flux reaching earth, laser interferometer expt. 2−81894
detection, review of developments 2−44823
detection, using neutron scatt. effect, theory 2−52054
detection methods, using fluids or solutions 2−66424
detector coincidences, computer analysis local disturbance elimination 2−82202
dispersion in vacuo 2−73295
emergence from centre of the Galaxy 2−84964
energy sources in Galactic centre 2−44825
galactic production, detection 2−44822
galactic radiation and effects on calculated lifetime of universe 2−81765
general relativity, invariant criterion, tetrad formulation 2−82192
gravitational synchrotron radiation, analysis in terms of Stokes parameters 2−72958
induced, due to energy-momentum conservation laws 2−78793
neutron star, v.h.f. gravitational radiation 2−73007
positive signature for recognition 2−76042
pulse detector, transmission line analysis of response functions 2−52062
radiation, emission, propagation and absorption 2−76188
radiation, upper limit on X-ray flux 2−44826
radiation by sources moving with velocity greater than light in vacuum 2−48642
radiation damping existence in linearized general relativity 2−66455
radiation detection, coincidences between outputs of new detectors at 1661 Hz and 1581 Hz, determ. of bandwidth, energy flux 2−76182
radiation detection limit, mech. matching condition 2−82195
radiation detector, based on Weber's but with enhanced time resolution 2−76184
radiation from charged black holes 2−78439

Gravitational waves continued
radiation from relativistic systems, calcs. for circular orbits and extreme hyperbolic trajectories 2−55390
radio pulses rel. to gravitational waves from the Galactic Centre 2−58369
relativistic e.m. and gravit. wave, propag. of tensor discontinuities 2−78782
review of recent experiments, theoretical implications 2−78805
scattering by relativistic neutron stars, connection between scattered amplitude and nonradial vibrational modes 2−69088
self-focusing and self-trapping 2−55384
shock wave energy considerations 2−62987
spherical wave propagation in weak statical field 2−55391
spinning mass, exact sonl. for gravitational field reducing to one of Weyl metrics at J=0 2−82206
synchrotron gravitational radiation, Regge-Wheeler formalism 2−44827
synchrotron radiation 2−58721
theory and detection, binary stars 2−66037
third and higher order, for tensor and scalar-tensor fields 2−73307
two gravitationally bound black holes, upper limits on gravitational radiation 2−81763
vibrating bar, contactless paremeter measurements of changes in length 2−52210
water waves, small amplitude shallow, effect of bottom irregularities 2−83732
Weber-type detector, construction and operation, comparison with divided-bar prototype 2−69566
H atom excitation, semiclassical treatment 2−77021

Gravitons
dilaton-graviton coupling, an astrophysical test 2−78796
electron-graviton vertex, low-energy e.m. corrections determ. using Feynmann graphs 2−76559
emission in scatt. of nonrelativistic particles, rel. to solar thermal gravitational radiation 2−73007
energy-momentum tensor, connection with conformal invariance 2−59369
neutrino gravitational scatt. in one-graviton-exchange approx. 2−79499
PCAC, gravitational correction 2−59381
photon-graviton vertex, e.m. corrections 2−82207
production by electron-positron pair annihilation 2−78784
e-e$^+$ pair, single graviton annihilation, in ext. e.m. field 2−49507

Gravity
see also Geophysical prospecting
M waves, examination with registering gravimeter 2−72606
absolute and relative determ. 2−65437
acceleration effects on organisms using zero g and hyper-g 2−45025
acoustic-gravity waves, obs. using Hg tiltmeter 2−65810
Aleutian trench, config. of underthrust oceanic plate from anomalies 2−54687
Alfven-gravitational waves, momentum transport in perfectly conducting shear flow 2−60196
Alfven-gravitational waves, propagation in stratified perfectly conducting flow with mag. field 2−60195
anomalies, depth of sources 2−54595
anomalies, improvements in convergency in iterative gravity interpretation 2−48368
anomalies, interpretation by non-linear optimization 2−57462
anomalies, satellite determined, explanation of sources 2−57602
anomaly, interpretation over causative body with circular symmetry 2−57466
anomaly data manipulation using Fourier series 2−48370
anomaly models; statistical models for vertical deflection 2−65434
Arizona, deeper crust obs. 2−57745
Arizona, regional Bouguer anomaly map 2−54686
artificial, centrifugally obtained in space craft 2−62423
atmosphere, internal gravity waves, rel. to turbulence 2−58038
atmosphere, upper, gravity wave perturbation models 2−72822
atmospheric, internal gravity wave, self destructing 2−78355
atmospheric potential, effect on geoid 2−54801
Baffin Bay, free air and Bouguer gravity anomaly maps 2−57457
basement anomaly, seismic, gravity and mag. surveys 2−57777
borehole variometry, det. of small perturbing bodies 2−44526
boreholes, gravimetric obs. handling 2−44525
Bristol Bay, Alaska, crustal lineations based on mag. and gravity surveys 2−57797
capillary-gravity waves, flow over wavy bottom 2−77374
Chan Scrap Fault Survey 2−48369
changes associated with San Fernando earthquake 2−57471
compendium of metric theories and post Newtonian limits 2−62978
conformal-grid method for analytic continuation of two-dimensional fields 2−72604
constant of gravity, meas. with noiseproof torsional system 2−76161
crustal and upper mantle struct. of Central Aleutian Arc, model 2−54715
curved space cosmological bounds on time variation 2−58157
data, standard format-prerequisite to routine computer applications 2−57476
data processing and interpretation methods, 1964-71, review 2−78242
deformation of sea floor, meas. from Tufts Abyssal Plain to Washington-Oregon coast 2−54646
demonstration in lift 2−55354
density anomalies of Earth, satellite observations 2−57714
digital automatic gravimeter, construction and operation 2−84741
diurnal and semidiurnal tidal components, obs. using superconducting gravimeter 2−65433
dot charts in two and three dimensions for prospecting 2−72631
downhole meters, data applications 2−61863
Earth's crust, gravimetric model in Eastern Alpine area 2−54597
Earth's external field, new technique for calcs. 2−65430
earth tidal forces, effect on geyser activity 2−65572
Earth tide pendulum, Askania borehole tiltmeter, ball-calibration 2−54599
earthquake-tide correlation 2−57503
Earths field, obs. using numerical relationship between orbits, of planets 2−85042
Eastern Alps, gravimetric investigation along profile strip 2−57469

Gravity continued
Eastern Alps, gravimetric measuring Salzburg, Karnten and Tyrol 2−65442
elastic-gravitational oscillations, of laterally heterogeneous Earth 2−78286
energy spectra changes of anomalous gravitational fields 2−48595
expanding universe, gravitational influence of homogeneous neutrino sea 2−68994
free air anomalies over Gorda and Juan de Fuca Rises westward to Surveyor and Sedna Fracture Zones 2−54618
GAG-2 gravimeters rel. to gravimetric reference network 2−78228
geodesic information from range meas. between two satellites 2−54613
geodetic information using space systems 2−54614
geopotential coeffs., 15th order from orbit of transit 1B 2−75417
geopotential modelling, truncation effects 2−54608
global, rel. to mantle convection 2−57468
gradient, effect of contact surface relief 2−61860
gradiometer, orbiting satellite requirements 2−54986
gravimeters, polygonal methods of calibration, developments and prospects 2−84742
gravimeters, small dial scale factor instability, causes 2−44528
gravimeters, with photoelectric indication, use of light diodes as radient energy sources 2−61900
gravimetric and reflection seismic profiles, combined interpretation 2−57691
gravimetry and seismic exploration and prospecting of gently sloping structures 2−44524
gravitational absorption 2−51495
15^{1h} orderharmonics of Earths potential, det. from satellite orbit 2−54594
Hawaiian volcanic rifts, influence of gravitational stress on operation and growth 2−57736
Imperial Valley California, anomalies 2−57454
internal waves, refl. by small density variations 2−60397
interpretation calc. approximations 2−57475
ionosphere, gravity wave induced irregularities, receiver drift expt. simulation 2−62364
la Coste-Romberg gravity meters, calibration factors, time variations 2−81590
LaCoste-Romberg gravimeter, simplified theory 2−48968
laminar flow, development with combined forced-free convection in isothermal vertical tube, numerical analysis of gravity effect 2−53138
laminar flow, development with combined forced-free convection in isothermal vertical tube, numerical analysis of gravity effect 2−53138
linear filtering applications 2−78244
lunar, anomaly det. using orbiting gravity gradiometer expt. 2−51813
lunar, Apollo 14 and 15 missions 2−55134
lunar, Apollo 15 S-band transponder expt. 2−62657
lunar gravity transverse expt. 2−62650
MAGI, magnetics and gravity compilation-interpretation system 2−57474
Mars gravity field from Mariner 9 tracking data 2−58499
Martian field, from Mariner 9 tracking 2−75904
mass distribution from anomalies 2−57465
Mauritanian craters of explosive origin, gravity reconnaissance 2−51842
modelling, quantitative examples 2−57477
Moon, C_{20} and C_{22} in expansion of gravity field 2−75852
Moon, large-scale density variations in interior 2−73064
New Hampshire, evidence for shallow-floored plutons 2−54684
non-spherical rotating body, uniform representation 2−54607
northern Skye and Little Minch, negative gravity anomaly rel. to deep sedimentary basin 2−54596
ocean ridges, positive anomalies 2−57473
offshore obs. with sealed gravimeters, techniques for improving accuracy and productivity 2−84743
optimal gravimetric survey network 2−61901
pion e.m. mass difference calc. in presence of scalar gravity 2−42381
plane inverse potential theory problems, uniqueness of solutions 2−78245
potential energy of vertically stratified water columns 2−57860
potential field, Fourier method for regional residual problem 2−57464
potential fields, two-dimensional, analytic continuation using bipolar coordinates in solution of gravitational exploration problem 2−54591
potential fields, two-dimensional, net methods using conformal meshes for analytic continuation 2−61854
Potsdam correction from satellite determined geopotential 2−75415
rapidly rotating stars, detection of gravity darkening and axial inclination from photographic line profiles 2−75745
reduction of meas. by numerical solns. of Molodenskiy integral equation 2−54592
reduction of unevenly spaced potential field data to horizontal plane by finite harmonic series 2−78243
right rectangular prism, nomograms for calculating attraction 2−57467
Rio Grande rift, Bouguer gravity anomalies 2−57485
satellite for meas. of time variation of G 2−72603
satellite to satellite tracking data, detection of anomalies 2−54616
satellites, gravity-gradient momentum management 2−66026
second derivative, generalized computing method 2−72602
secular variations, detection in USSR 2−61859
solid tidal measurements in New England area of Australia 2−54593
space vehicle mission analysis and Trajectory Simulation model 2−54990
spherical, scalar Debye potentials for em fields 2−82401
surface gravity of early-type stars from forbidden He I 4045 Angstroms line 2−55027
terrestrial, 300 n.m. mean anomalies 2−54685
Texas, survey correction by vertical gradient obs. 2−57463
Tidal analyses of simultaneous records taken by 2 Askania borehole tiltmeters 2−54598
tidal effects on artificial satellite motion 2−84933
tidal profiles, trans-US and trans-Europe link 2−54602

Gravity continued
tides, modulation of geomagnetic records 2−54915
triaxial rigid satellite in precessing elliptic orbit, effects of gravity-gradient torque on rotational motion 2−81752
two-dimensional interpretation using frequency analysis 2−54590
Venezuela continental margin, Bouguer anomaly maps 2−57472
vertical gradient, effect of relief of interred density boundary 2−44527
vertical gradient, exptal. investigations 2−78223
VSA gravity meter system, development and tests 2−65436
wave, inertia-gravity, propag. during geostrophic adjustment, variable Coriolis parameter 2−54790
wave, nonlinear, phase and group vel. 2−54786
wave field interaction with mean vel. and buoyancy field 2−54788
wave interaction with capillary waves 2−62084
wave scatt. by irregular bottom 2−54787
wavefield, random, nonlinear dispersion relation 2−54784
waves, atmospheric, effect on ionospheric parameters determined during vertical sounding 2−72877
waves, atmospheric, nighttime obs. at Arecibo 2−65687
waves, atmospheric, rel. to dynamics 2−72777
waves, internal, nonlinear, in slowly varying medium 2−60131
waves, internal standing, breaking mechanism, in atmos. and ocean 2−72776
waves, linear low-pass filter development 2−57903
waves, neutral, magnetic storms 2−44772
waves, Stokes expansion by computer 2−77197
waves, weakly nonlinear surface and internal, interaction 2−54789
western Canadian anomalies, seismic refraction profile 2−81593
Western Germany, tests for isotropy of vertical deflections 2−65443
white dwarf variables, model with non-radial oscillations of gravity modes 2−55055

Green's function methods
— 2−69562
acoustic radiation from two spheroids 2−55519
alloy, disordered, X-ray spectra 2−61671
alloy, disordered, X-ray spectra intensity, Green's function method 2−51359
alloy dil., low temp. cond., calc. 2−61219
amorphous system, electronic Green's function, density of states 2−71786
anharmonic oscillator, density matrix 2−76216
anisotropic dislocation theory, isotropic limiting behaviour 2−50668
anisotropic elasticity, dynamic Green's tensor calculation 2−76302
anisotropic ferromagnet, mag. props. 2−72123
asymptotic soln. for wave eqn. with variable vel. and boundary conditions 2−82176
atomic and molec. physics, review 2−49919
band structure computation 2−84227
benzene, orbital energy calc. 2−50083
Brueckner theory, interpretation 2−78855
Coulomb Green's function, nonrelativistic, construction for two-body system 2−42300
Coulomb-Green method for calc. of cross section for Compton scattering by K-shell electrons in hydrogen- like atom 2−70610
crystal, deformed, resonant absorption of X-rays 2−84474
crystal electron system linear response investigation 2−77834
cubic crystal, KKR formulation, struct. consts. 2−54107
cubic lattice, Watson sum 2−58772
cut-off potentials, scattering and bound states, energy power expansion of Green function and Pade approximation 2−45278
damping-modified many-time functions rel. to magnon parametric instability 2−48050
defect crystal, with singular defect submatrix, lattice dynamics 2−61066
deformation potentials at symmetry points for shear strains, derivation 2−80976
dense gases, transport phenomena 2−43275
diffraction geometrical theory validity, by star shaped cylinder 2−78770
diffusional relaxation of crystal lattice defects in the fields of local lattice disturbances 2−84000
dislocation theory, anisotropic, isotropic limiting behaviour of six dimensional formalism 2−61727
dislocations, elastic Green's function, Debye cutoff 2−64663
disordered force constant systems, effect of disorder on absorption of light 2−43958
disordered system, three-dimens., definition of degree of localization 2−47799
double exchange ferromagnet, one-particle states of hole 2−81236
doubly degenerate band, electron correlation 2−84425
dual models with unit intercept, construction of currents and Green's functions 2−45914
dyadic, for cyclindrical waveguides with moving media 2−41883
electronic function for heavily doped cryst., self energy derivation 2−61156
electronic Green functions calc. using nonorthogonal basis functions, crystal applic. 2−61131
e.m. fields, enclosed cylindrically symmetric Green's function 2−49194
Faddeev equations, relaxation method of solution 2−59473
Fermi gases, dilute, infinite volume limit of Green's function 2−76233
Fermi system, interacting, Green's function eqns. of motion as Feynman diagrams partial sums 2−52110
ferromagnet, with single-ion anisotropy ferromag. reson. calc. 2−84555
ferromagnetic film, uniaxial unpinned, review 2−78003
ferromagnetic resonance, frequency and width at finite temp., calc. method 2−68718
ferromagnetism theory, two-spin system 2−75210
force constant calc., comparison with L-matrix approx. method 2−49998
force constants, constraint for calc. using Green's function formalism 2−46506
free electron, in uniform mag. field, Green's function calc. 2−55411
frequency spectrum of an isobaric disordered one-dimensional chain 2−64826
graphite, perturbed electronic density of states calcs. 2−57123

Green's function methods continued
harmonic oscillators, integral representation of Green's function 2−82232
Hartree-Fock Hamiltonian Green's function, occupation numbers computed 2−58788
h.c.p. metals, band struct. calc. by Kohn-Rostoker determinant method 2−80959
Heisenberg chains, short linear 2−41523
Heisenberg ferromagnet, 2 spin 1/2, exact solution 2−78726
Heisenberg ferromagnet, effects of finite conc. of impurities spin-wave theory 2−65134
Heisenberg ferromagnet, f.c.c., with second- neighbour interactions, Green's functions calc. procedure 2−72131
Heisenberg ferromagnet, Kubo formula, general formalism 2−45283
Heisenberg ferromagnet, spin 1/2 model, using anticommutator Green's functions 2−65132
Heisenberg ferromagnet theory 2−48054
Helmholtz eqn. in exterior of convex curve, Neumanns problem, Green's function 2−45239
high-energy quantum electrodynamics, series expansion 2−55798
homogeneous interactions in quantum field theories 2−76567
hopping impurity conduction, Hall effect 2−57178
inelastic and reactive scattering, effective separable approx. for multichannel Green's functions 2−46639
inelastic atom-surface scattering, quantum theory 2−46465
lattice function for diatomic alternating lattices 2−61051
lattice functions, exact calcs. 2−55428
lattice Green's function of square lattice in diagonal direction, asymptotic form 2−69608
lattice Green function for simple cubic lattice 2−61050
lattices, time dependent excitation function for incoherent exciton quenching 2−45290
Lee model with Fermi coupling, explicit solution in low sectors 2−52524
linear homopolymers and copolymers, analysis of vibrational spectra by Green's function method, effect of defects 2−43021
linear transport theory, general theory of spherically symmetric boundary value problems 2−46361
linked cluster theorem for Abriskov pseudo-fermion represent. of spin operators 2−54106
localized defects in solids, asymptotic behaviour of static Green's function 2−43618
magnetohydrodynamic approx. for double-time Green's functions of conducting fluid in magnetic field 2−74346
many-body functions for closed shell atoms 2−59913
many-body systems, transport equations 2−71779
many-time, calc. of nonlinear polarizability tensors of interacting quasiparticles 2−84197
Maxwell's eqns., soln. in periodic laminated media 2−82398
melting or solidification problems in cylindrical coordinate system 2−47030
molecular orbital energies, calc. method 2−50003
molecular vibrations, analysis of XY_4 isotopic substitutions 2−77029
multiatom systems, radiative cooperative effects 2−66729
multiple-scattering expansion and Glauber approximation 2−45279
n.m.r. lineshape in rot. solids 2−68741
nonrelativistic electron in field of plane wave, generation of harmonics 2−66796
one-particle, one-hole nuclei, core excitations by six-point Green function 2−79712
one-phonon function of NaCl, anharmonic contribs. 2−50996
photon function, rel. to non-local quantum electrodynamics 2−59375
polyethylene, localized and resonance modes below 700 cm^{-1}, due to kinks and folds, calc. 2−61153
ring, stiffened, in-plane flexural vibr. 2−63100
scalar and spinor electron in plane-wave field, eikonal methods 2−82618
scattering, free Reimann Green function of inverse problem 2−63019
scattering, Riemann method for inverse problem 2−63018
scattering of intense light by two-level system 2−49938
Schrodinger eqn. in const. and homogeneous elec. and mag. fields 2−49007
Schrodinger-Pauli-type eqn. for constant homogeneous electric and magnetic fields, time delay 2−69589
Schwinger's proper-time method and eikonal approx, for electrons Green's function in plane-wave field 2−82618
semiconductor, heavily doped, magnetoresistance at low temps. and weak mag. field 2−51132
SH waves in inhomogeneous wedge 2−73420
shell model dynamics, defective system 2−50989
singular oscillator problem 2−52075
spatial charge displaced by impurity scattering, T-matrix approach 2−51074
spin half Heisenberg ferromagnet, second order Tyablikov treatment, low temp. 2−44236
spontaneously broken gauge symmetries, perturbation theory and renormalization 2−59372
spontaneously broken gauge symmetries, renormalizability 2−59371
spontaneously broken gauge symmetries, U-gauge functions 2−59373
stress state in plane shaped disc with circular hole 2−41579
structural phase transition, two-fluid model, heat diffusion mode 2−84185
sturmian function, applic. to calc. of third harmonic generation coeff. 2−46478
SU(2) × SU(2) chiral dynamics, invariant functional formulation 2−70127
substituted and perturbed molecules, analysis of vibrations 2−52974
surface function calcs. for Ge electronic surface states 2−51164
for surfaces of revolution, elect. field intensity calc. 2−45637
thin film, calc. of surface states with δ-function array model potential 2−75036
three dimensional diffraction problems for plane semi-infinite impedance systems 2−55608
transition metal, supercond. with non-mag. impurities, specific heat calc. 2−44061
transition metals optical absorption, a model calc. 2−84498
triangular and honeycomb lattice functions 2−61052

Green's function methods continued
two-magnon Raman scatt., two-time Green function decoupling, heat-bath damping effects 2−68654
two-particle self-energy expansion 2−52068
Ward identities for functions involving arbitrary number of vector and axial vector currents 2−79481
Yang-Mills field mass and radiative corrections 2−55799
(d, p), reaction study 2−83012
GaAs, calc. of impurity induced i.r. absorpt. 2−61639
InSb density of states in impurity bands 2−80961
KCl crystal, with a divalent activator, localized one-electron states 2−84287
Li-Mg(Al) solid solution, electronic props. calc. 2−75029
Pr, mag. props., double time Green's func. calc. 2−75205
X_3Y_4, XY_3Z_2, molecular models, mixing of normal vibrations and isotropic freq. rules 2−56137
Grey atmosphere *see Radiative transfer; Stars/radiation*
Grinding *see Forming processes*
Group theory
see also SU(n) theory
analytic unimodular matrix group containing image D^j of rotation group 2−41463
atomic shell theory applic. 2−59908
branching rule evaluation, for linear groups using mappings between weight spaces 2−58712
canonical bases of Lie groups, use in atomic spectroscopy theory 2−79935
charged particle in field of transverse e.m. plane wave group theoretical analysis 2−63262
coherent states for arbitrary Lie group 2−41508
conformal symmetry, spontaneous breaking and causality 2−58731
constitutive map for replacement of relation $D=\epsilon E$ and $B=\mu H$ 2−52307
continuous groups rel. to ligand field theory 2−78815
Coulomb problem applic., book 2−63017
cubic harmonics as linear combinations of spherical harmonics 2−82180
D_2^+ double group, isomorphic to quaternion group, reln. to approx. eigenfunctions 2−63012
de Sitter space-time and harmonic oscillator 2−63016
dual N-point functions in PGL(n-2,C)- invariant formalism 2−49477
dual reson. models generalization 2−63556
Eilenberg's and Maclane's cohomology theory of group prolongations, study of Newtonian space-time 2−73301
electron interacting with plane e.m. field, algebraic soln. by Poincare group generators 2−82227
equations with partial derivatives, pseudo true connexion 2−69544
fine structure constant, mathematical description in terms of group theory 2−78779
general relativity, co-ordinate group symmetries 2−55399
group theoretical classification of repeating representations in quantum-mechanical problems with point-group symmetry 2−83928
harmonic oscillator group, Clebsch-Gordan coefficients and special function identities 2−41513
inner structure of hadrons 2−52565
invariance prop. of Lagrange function, rel. to virial theorem 2−82298
irreducible representations, decomp. of direct products 2−58714
isometry group of a compact manifold of negative curvature 2−76173
isotropy group of simple solids, exponential form 2−47050
lattice mechanics application 2−77763
lattice vibrations, applic. 2−61069
lattice vibrations and normal molecule vibrations 2−64825
lattice vibrations in terms of group theory 2−80899
Lie algebra common to dual models, current algebra, dynamical groups, gauge groups 2−45854
Lie algebra of general linear group in five dimens., weight diagrams 2−78762
Lie algebras, classification of semisimple algebras up to rank 6 2−82165
Lie groups, boson state symmetry props. 2−59909
Lie theory and Lauricella functions 2−62974
Lorentz covariant anal. functions and scatt. functions 2−82648
Lorentz group, deformation of SO(2,C) subgroup 2−82183
Lorentz group, homogeneous, unitary represents. in O(1,1)⊗O(2) basis 2−63024
Lorentz groups, Laplace transform, quasiregular representations 2−82156
matrix elements of permutation group, calc. in 'trees' basis 2−63483
molecular term symbol determination 2−52981
multigroup, generalization to determ. eigendistributions of linear Boltzmann operator in modal approx. 2−76217
N-body problem, non-relativistic, construction of kinematic angular functions 2−52070
n-electron problem and matrices representing symmetric groups 2−52896
nonrelativistic composite elementary particles and conformal Galilei group 2−82655
nuclear rotational motion, symmetry approach 2−49706
O*, irreducible tensor theory, V and W coeffs. 2−42830
O(2,3) algebra, unitary representation constructed using bound state H atom radial functions 2−42791
O(2, 1) × O(3), solution to generalised quantum mechanical Kepler problem 2−58761
O(n), explicit form of invariant operators 2−41462
orthogonal and unitary group methods, applic. to N-body problem, review 2−58804
oscillator algebra represent., SO(3,2), applic. to quark model 2−66907
parametrization of orthogonal and unitary groups, rel. to random unit vector components 2−62979
Poincare dilation group of Zeeman-order topology on Minkowski space 2−73292
Poincare group, homogeneous space field theory 2−63650
Poincare group on light cone, Galilean struct. 2−82653
Poincare group reduction with respect to Lorentz group 2−82649
Poincare group representations on functions of eigenvalues of Casimir operators 2−52045
Poincare type groups, unitary irreducible representation 2−58711

Group theory continued
- quantum mechanical three-body problem, complete set of functions 2−41490
- quantum mechanics, hemitian sum operators, and tensor operators 2−58740
- quantum mechanics, relativistic, relation of space-time to material symmetry 2−66440
- Regge group, for Wigner coeffs. and Thomae-Whipple functions 2−41464
- relativistic quasi-exchange, finite transforms 2−48982
- rotation and Lorentz groups represent. on model of non-cantorian set theory 2−82174
- rotation matrices, simple solution 2−77039
- SL(2,C) invariance and gravitational field 2−52049
- SO(2,1) representation by solution to Schrodinger eqn. for electron in Hulthen potential 2−69596
- SO(2q+1) group, invariant operators, true values 2−69551
- special Lorentz group, spinor equivalents of irreducible tensors 2−41458
- spectral terms classification applications 2−69550
- symmetrized powers of irreducible representations of point groups 2−52046
- symmetry of space 2−69549
- symmetry problems in cosmology 2−62435
- symplectic group, finite dimens. irreducible represent. space, lowering operators 2−82175
- three-dimensional rot. group, symmetries of Wigner coeffs. and Thomae-Whipple functions 2−78813
- $U_{n,1}$ and IU_n representation matrix elements, props. 2−82164
- U(n), evaluation of multiplicity-free Wigner coeff. 2−41460
- unitary groups, symmetric tensor operators 2−62973
- XY_6 octahedral molecule, group theory applications to molecular and lattice vibrations 2−61067
- H atom, radial-angular factorized, ‘natural’ group scheme and selection rules 2−59944

Gruneisen relation
- alcohols, compressional study through pseudo-Gruneisen parameters 2−83789
- alkali halides, constant at absolute zero 2−61113
- alkali halides, high press. and temp. props. 2−61072
- alkali metal liqs., determ. of pseudo-Gruneisen parameters 2−74540
- alkali metals, calc. 2−74997
- rel. to anharmonicity estimation, using X-ray interference intensity coeff. 2−54017
- fluorites, Gruneisen parameter calc. 2−51050
- graphite, pyrolytic, parameters, 80-300K, thermoelastic stress obs. 2−43664
- halides, heavy, Gruneisen and Anderson-Gruneisen parameters, Born theory 2−74961
- ionic cryst., Anderson-Gruneisen parameter 2−47724
- rel. to melting pt./volume relation 2−47031
- rare earth metal chalcogenides, Mie Gruneisen interatomic pot. model, detn. analysis 2−57053
- rare gas, solid, calc. from higher order elastic consts. 2−50990
- semiconductor, low temp. parameter determ. from elastic cnstants 2−71752
- Ag, u.s. attenuation, Gruneisen mode and const. 2−68234
- α-Al_2O_3, mean parameter temp. depend. 2−51047
- As, parameters, and thermal expansion, 2-30K, 55-90K, and at 283K 2−77784
- Au, u.s. attenuation, Gruneisen mode and const. 2−68234
- Ba, parameter, thermal expansion studies 2−74993
- Bi, parameters, and thermal expansion, 2-30K, 55-90K, and at 283K 2−77784
- Ca, parameter, thermal expansion studies 2−74993
- $CaCO_3$, generalized Gruneisen parameters of elastic waves, calc. 2−74996
- CaO, press. depend. shell model calcs. 2−47756
- Cr (100) surface, rel. to Debye-Waller factor and thermal exp. coeff. 2−50992
- Cu-Cu_3Au alloy, Debye temp., elastic moduli, elec. resist., temp. depend., 4.2-293K 2−47752
- Cu, u.s. attenuation, Gruneisen mode and const. 2−68234
- GaAs-GaP alloy, i.r. lattice absorpt. obs. 2−57074
- GaAs, i.r. lattice absorpt. obs. 2−57074
- GaP, i.r. lattice absorpt. obs. 2−57074
- KN_3, Gruneisen parameter from Raman active librational modes 2−71726
- Li thermal expansion coefficient and Gruneisen parameter, lattice dynamical calculation 2−84179
- Mo (100) surface, rel. to Debye-Waller factor and thermal exp. coeff. 2−50992
- NaCl, vol. and temp. depend., u.s. study 2−68065
- NaF, calc. from third-order elastic consts. 2−60844
- PbF_2 thermal expansion and phase transition 2−84216
- Sb, parameters, and thermal expansion, 2-30K, 55-90K, and at 283K 2−77784
- Sr, parameter, thermal expansion studies 2−74993
- SrF_2, and thermal expansion 2−84216
- SrO, press. depend. shell model calcs. 2−47756
- Te, low temp., and thermal expansion 2−68254
- $Te_{15}Ge_3As_2$ glass, parameter, calc. from u.s. velocity 2−47742
- TlBr, TlCl, rel. to thermal expansion obs. and lattice dynamics 2−57076
- V_3Si, anomalous constants, change in soft mode sound velocity under shear strain 2−74980

Gudden-Pohl effect *see Electroluminescence*

Guiner-Preston zones *see Crystal structures/microstructure*

Gunn devices *see Gunn effect; Microwave techniques and devices; Semiconducting devices*

Gunn effect
- bulk instabilities, book contrib. 2−57184
- device study 2−77927
- diode, construction, v.h.f. power generation 2−47943
- diode, instability characteristics for negative differential conductivity 2−71982
- diode, switching behaviour interpret. rel. to instabilities 2−54166
- impact ionization, high field domain 2−65034

Gunn effect continued
- negative differential mobility elements, linearized equation for current flow 2−84319
- oscillator-piezoelectric structure, u.s. transduction, acousto-optic deflection effects 2−84458
- polyethylene, iodine doped, h.f. 2−57202
- $CdSnP_2$, rel. to current controlled negative resist. 2−61304
- GaAs acoustoelectricity, ultrasonics 2−77774
- GaAs bulk element, static negative resistance due to geometrical effect, computer analysis 2−84320
- GaAs diode, ultrasonic generation 2−77774
- GaAs electron density ratio in valleys, elec. field depend. 2−81093
- GaAs epitaxial diodes, coaxial resonant cavity mounted, low temperature characteristics 2−71983
- GaP:O p-n junction, deep double electron O trap transitions, photocapacitance obs. 2−75013
- InSb, domain formation rel. to contact effect on microwave emission 2−47897
- n-InSb, threshold in transverse mag. field, travelling domain form. 2−71908

Gyromagnetic effect
- coaxial waveguide, characteristic eqn. 2−49218

Gyromagnetic ratio
- α-amino acid crystals, g-tensors for VO^{2+} impurities 2−84566
- bound electron g-factor, nuclear mass. correction 2−67386
- chloroacetylene, mol. g-value, Zeeman effect obs. 2−70758
- dimethylsulphide-d_6, rot. Zeeman effect, g-tensors 2−64177
- E1 comversion transitions, determ. of g_s factors by comparison of theory and expt. 2−49719
- electron spin motion in magnetic mirror trap, anomaly 2−45881
- electrons, sixth-order anomaly contribution 2−63509
- even rare-earth nuclei, calcs. of moments of inertia and g_r factors including residual p-h and p-p interaction 2−73988
- ferromagnetic film, rel. to realization of trigger effect 2−75228
- ferromagnetic materials, anisotropy of g-factor of rare-earth ions, low temp. study 2−65217
- ferromagnetic resonance in crystals with anisotropic g-factor, theory 2−72446
- flavoproteins, analysis of in vivo and in vitro e.s.r. spectra of intrinsic spin label ^{2}H-flavin 2−83338
- g-values for various organic molecules from microwave Zeeman effect 2−70739
- galvinoxyl radical, g-factor, solvent effects 2−53064
- group II-VI compound, e.p.r. theory of group IV ion, g-shift 2−51399
- Lande g-factor, from mag. moment ratio for $2^{3}S$, ^{4}He level and fundamental ^{3}He level 2−56127
- muon, sixth-order anomaly contribution 2−63509
- orbital g-factor, change due to exchange currents, rel. to E1 sum rule for photoabsorption 2−63757
- paramagnetic materials, anisotropy of g-factor of rare-earth ions, low temp. study 2−65217
- S-state ion, g-value, covalency effects in e.s.r. obs. 2−48272
- thioformaldehyde, obs. of high-field rotational Zeeman effect, determ. of molecular g values 2−43010
- ytterbium ethylsulphate, g-value 2−51241
- yttrium ethyl sulphate:Yb^{3+}, phonon field contrib. to g shift 2−68586
- ^{a}Os, A=188, 190, 192, comparison of IMPACT, PAC and Mossbauer effect meas. of g-factor, ferromagnetic host effects 2−42534
- ^{107}Ag, ^{109}Ag, g-factors of low-lying $3/2^-$ and $5/2^-$ levels 2−70371
- Al_2O_3:Ti^{3+}, corundum, e.p.r. g-value calc., Jahn-Teller theory 2−65331
- ^{78}Br isomeric states, g-factor meas. by time differential methods and stroboscopic obs. 2−74029
- ^{81}Br isomeric states, g-factor meas. by time differential methods and stroboscopic obs. 2−74029
- C, graphitized film, anisotropy of g-value 2−78153
- ^{42}Ca, g-factor of 3.19 MeV 6^+ state 2−72243
- ^{42}Ca, lowest 6^+ state, ^{40}Ca(α,2p) study 2−59700
- CdS, hexagonal, hexagonal, Gd^{3+} centres at sites of axial geometry 2−65333
- ^{110}Cd, g-factor expt. on first excited 2+ state 2−52742
- Ce^{3+} in crystalline cerium dipicolinate, measurement of g-values and g-axes 2−72487
- ^{140}Ce, of 2083 keV 4^+ state, meas. 2−52763
- ClCO, ClOO radicals, g-factor from e.s.r spectra 2−50031
- CrTe thin film, ferromag. reson. study 2−57387
- Cs, determ. of g_j factor in $7^{2}P_{3/2}$ state by optical double resonance in strong magnetic field 2−52916
- EuB_6, g-factor determ. from e.p.r. 2−84565
- Fe:^{183}Re, g-factor 2−72245
- Fe:^{184}Re, g-factor 2−72245
- ^{54}Fe, g-factor of first excited 2^+ state 2−70392
- ^{66}Ga isomeric states, g-factor meas. by time differential methods and stroboscopic obs. 2−74029
- Ge, g-factors of B impurity 2−54402
- GeO_2:V^{4+}, e.p.r., g and A tensors, orbital mixing parameter, radial average, core polarization 2−72503
- H, effect of nuclear mass on bound electron g factor determ. using pulsed double-mode maser 2−42796
- KCl, F-centre g_{orb} factor determ. by mag. circular dichroism and Faraday effect 2−77596
- K_2SO_4:Tl^{2+}, g-factor, e.p.r. obs. 2−72470
- Mg-Mn alloy, g-shift, relaxation bottleneck suppression, e.p.r. obs. 2−44438
- MgO:Cr^+, γ irrad., g-factor, e.p.r. obs. 2−75346
- Mn_3As_2, MnAs, Mn_2Sb, e.s.r. and thermomagnetic meas. rel. to determination of Lande factor 2−51411
- NF_2, calc. of g values 2−50066
- NO_2^{2-}, calc. of g values 2−50066
- ^{14}N, $^{4}S_{3/2}$ g_j factor, by atomic-beam magnetic resonance technique 2−76984
- Na-NH_3, density of states, Mott g ratios, self consistence, significance in MNM transition 2−44033
- Nd, A=143, 145, g_j values of $^{5}I_{4,5,6,7,8}$ atomic states, hyperfine structure const. 2−76990
- Nd even nuclei, first (2^+) and second (4^+) states, g-factor function of neutron number 2−42522
- Ne, Lande-factor of $2p_4$ level meas. with He-Ne laser 2−63428

Gyromagnetic ratio continued
- O II, mean lives and g values of beam-foil excited levels, suppression of optical cascading effects 2−79910
- O_3^-, calc. of g values 2−50066
- ^{188}Os, g-factors of several excited states determ. from perturbed angular correlation following ion implantation by Coulomb excitation 2−63829
- ^{192}Os, g-factors of several excited states determ. from perturbed angular correlation following ion implantation by Coulomb excitation 2−63829
- ^{206}Pb, g-factor of 12^+ isomeric state and effective orbital g-factor of neutron 2−59720
- ^{106}Pd, g-factor expt. on first excited 2+ state 2−52742
- ^{147}Pm, g-factor of 91keV state, meas. using 319 to 91 keV gamma cascade 2−59712
- ^{192}Pt, g-factor of first 2^+ state 2−70411
- ^{194}Pt, nucl. g-factor 2−76807
- ^{195}Pt, g-factors of 211 and 240 keV states 2−63830
- ^{196}Pt, nucl. g-factor 2−76807
- Rb I, electronic g_J factors for ^{87}Rb in $np^2P_{3/2}$ series 2−46439
- ^{103}Rh, g-factors of low-lying $3/2^-$ and $5/2^-$ levels 2−70371
- ^{102}Ru, g-factor expt. on first excited 2+ state 2−52742
- ^{117}Sb, isomeric level 2−59708
- Sm even nuclei, first (2^+) and second (4^+) states, g-factor function of neutron number 2−42522
- ^{153}Sm, effective g_s factor determ. by internal conversion processes 2−52765
- ^{117m}Sn, g-factor of 158.6 keV level 2−63811
- $SrCl_2$, mag. circular dichroism on F-centre absorpt. band, $g_{orbital}$ factor 2−74805
- SrF_6:Tm^{2+} g values within $(TmF_8)^{6-}$ cluster framework 2−78054
- ^{125}Te, of 462 keV $5/2^+$ state, meas. 2−52758
- Tm I, $4f^{13}5d6s$ and $4f^{12}6s^26p$ config., Lande g-factor, theory 2−56104
- ^{49}V, g-factor of $3/2^-$ 153 keV state, ^{48}Ti(p,γ) obs. 2−67157
- ^{182}W, K^π=2- octupole vibration band, g-factor of ground state meas. using integral PAC method 2−42533

Gyroscopes
- autonomous mechanical system, stability theory 2−76242
- dynamics, connected rigid-body systems, gyroscopic phenomena 2−76253
- equation of motion in general relativity 2−69569
- fluids with internal angular momentum, gyroscopic behaviour 2−56312
- gyrostabilized sights for use in firing control and observation from moving vehicles 2−52466
- gyrostat, motion about centre of gravity in central field 2−55450
- high-speed rotating devices 2−58828
- motion of rigid-body systems, new classes of solutions 2−76241
- oscillogyro, dynamical characteristics 2−78871
- precession in Einstein and arbitrary theories of gravitation 2−76187
- relativity expt. at arbitrary orbit inclinations, calc. of total precession and optimum orbit 2−66430
- spacecraft isotensoid flywheels, applic. to spacecraft energy and ang. momentum storage 2−72928
- stabilization conditions including elasticity internal friction, transient phenomena in electric circuits 2−82293
- stochastic methods in solutions of analysis problems 2−78872
- suspension bearings, effect of friction on motion with forced rotation of mounting 2−82137
- tuned, multigimbal elastically supported, theory of errors 2−82121
- tuned, multigimbal elastically supported, theory of operation 2−82120
- two-gimbal, motion in artificial satellite 2−66489

H I regions
- in Andromeda galaxy central region 51705 2−51705
- black hole accretion of gas, emergent radiation spectrum 2−75661
- cold HI clouds with hotter possible inter-cloud medium, high resolution obs. 2−58244
- in elliptical galaxies, 21 cm obs. 2−75678
- galactic spurs, linear polarization, measurement, antenna radiation patterns 2−85060
- in globular clusters, upper limits on abundance 2−75783
- Gum 67, catalogue and identification maps 2−44878
- Gum 68, catalogue and identification maps 2−44878
- high velocity clouds, high resolution obs. 2−48727
- high velocity regions rel. to continuum jets near galactic centre 2−55008
- high-velocity clouds in directions of globular clusters 2−51780
- high-velocity interstellar H I up to high galactic latitudes, survey 2−58355
- II Zw 40, compact galaxy 2−81793
- intercloud HI gas, 21 cm line profiles 2−66117
- interstellar, heating by u.v. photoemission from grains 2−58351
- interstellar, strong polarization shocks 2−48735
- low emission regions and baseline determination problems in 21-cm. H line observations 2−55193
- optical depths, by polarization techniques 2−58352
- positive velocity, above galactic plane between l=252° and l=322°, survey 2−48729
- in Scd galaxies, distrib. obs. at 21 cm58223 2−58223
- southern Milky Way, velocity-longitude diagram 2−84984
- u.v. absorption-line spectra, charge exchange reaction effects 2−58243
- velocity structure in H Doppler profiles rel. to spiral arm features 2−81818
- C I, C II and C III, interstellar, ionization structure 2−81829

H II regions
- anomalously excited, search for early type stars 2−58253
- Anon 0947 + 31, bright u.v. knots 2−84962
- Anon 1242+28, bright u.v. knots 2−84962
- atomic collisions, 10 to 75 keV, outer shell excitations 2−74238
- black hole accretion of gas, emergent radiation spectrum 2−75661
- η Carinae nebula, Hα and NII profiles from high interferometric resolution observations 2−55024
- circumstellar dust particles, grain mass and protonic accretion 2−44847
- cosmic-ray heating 2−51720
- fine structure synthesis obs. at 11 and 3.7 cms. 2−62475

H II regions continued
- galactic disk, mean-square electron density and early-type stars 2−44836
- galactic HI distributions rel. to spiral arms and HII regions 2−78446
- IC 4628, and RCW 113, evidence for origination from same gas cloud 2−62476
- II Zw 40, compact galaxy 2−81793
- interstellar lines in u.v. spectrum of Ophiuchi 2−66088
- i.r. sources at 100 μm, grain temperatures 2−55025
- M81, M64, M51 galactic nuclei, emission line strengths 2−75688
- massive main sequence stars, effective temperatures 2−66075
- motion rel. to associated young stars 2−44848
- NGC 2264, optical obs, of i.r. source 2−69044
- NGC 7538, microwave spectroscopic mapping 2−75696
- Orion A, recombination line obs. at Ku band 2−69048
- Orion Nebula, λ4686 He II line intensity, reln. to cosmic ray flux 2−69043
- partially ionized interstellar cloud, microwave observations 2−81807
- radio emission at 1400 MHz from galactic H II regions 2−58252
- radio recombination lines, diffuse interstellar medium 2−66068
- RCW 38, RCW 49, RCW 57(b), RCW 74, absorption profiles, 21 cm H I obs. 2−84949
- recombination line emission from galactic ridge, excess H II regions 2−66123
- recombination lines at decimetre wavelengths 2−69046
- Sco OB 1 association, RCW 113 and IC 4628 nebulae 2−62476
- Sharpless 266, i.r. photometry 2−48673
- W22, W37, absorption profiles, 21 cm H I obs. 2−84949
- W3, recombination line obs. at Ku band 2−69048
- W49, recombination line obs. at Ku band 2−69048
- W51, high resolution radio obs. 2−48674
- W51, recombination line obs. at Ku band 2−69048
- water vapour emission sources, interferometric positions 2−51719
- H 109α recombination line obs. on 13 southern regions 2−69045
- H 3 cm. fine structure transition, detection attempt 2−58251
- H_2O maser, at HII region boundaries, gain parameters 2−69047
- He II 4686 Å intensity obs. and cosmic ray flux 2−58254
- OH maser, at HII region boundaries gain parameters 2−69047

Hadrons
- *see also Lee model*
- angular dependence of dose and hadron yields from targets in extracted proton beams 2−46254
- axial charge commutation with axial divergence decuplet contribution to sum rules 2−73766
- charge superselection rule nonexistence 2−52572
- chiral lagrangian theories, canonical second rank SU(3) tensor 2−42311
- classification, ladder U(6,6)-symmetry scheme 2−63527
- composite model, correlation effects and quantization 2−79511
- cosmic ray cascades and interactions, Monte Carlo simulations in multiplate cloud chambers 2−42436
- dual parton model, applic. to $ep \rightarrow e'X(e'AX)$ 2−63512
- dual reson. model, time-like extension and difference eqn. 2−76572
- dual-parton model, applications to multiparticle processes at high-energy 2−63547
- early universe implications of Hagedorn's exponentially increasing mass spectrum for baryon on temperature maximum 2−81767
- electrodynamics, application of variant of Stuckelberg formalism for massive gauge fields 2−42305
- electroproduction, violation of scale invariance due to contribution of cuts 2−63534
- electroproduction in deep inelastic region, meas. of inclusive momentum distribs. 2−73777
- electroproduction in e^+e^- annihilation 2−73764
- electroproduction in ep scatt., distribution, one photon exchange part, Regge behaviour 2−70171
- electroproduction processes, parton description of forward peak 2−79505
- e.m. mass difference, deep inelastic contrib. 2−66955
- e.m. self- masses, null-plane current commutator algebra for 2−45899
- e.m. self-mass, criteria on finiteness 2−59433
- Feynman diagram model, high-order planar, comparison with expts. on deep inelastic eN scattering 2−42347
- gravitational relativistic field eqns. used to deduce props. 2−69564
- high-energy production, multiresonance model 2−52573
- high-transverse-momentum hadron jet production, cross-section in parton model 2−70180
- inclusive electroproduction 2−70159
- inner structure, group theory and quark model employed 2−52565
- internal structure, boson missing mass spectrum interpret. 2−55829
- internal symmetry breaking, mathematical characterisation 2−45894
- isomers, possible existence, heuristic considerations 2−52564
- isomers, possible existence of high spin states having relatively low excitation and long lifetimes 2−42348
- limiting-temperature concept, implications for production of massive exotic hadron states 2−76618
- Markoffian model and solution of basic Kolmogorov's eqn. 2−73773
- mass spectrum, relativistic derivation, calc. of thermodynamic quantities for system with this spectrum 2−42320
- matter at ultrahigh densities, model 2−52571
- minimum-uncertainty wave packet description, scaling variables and Poincare group 2−76619
- multiple prod. model 2−59463
- new event in cosmic ray expt., interpret. 2−52651
- pair production cross section for γ, 265-4215 MeV in hydrogen and deuterium 2−63497
- parton dual resonance model for lepton-hadronic and colliding-beam inclusive reaction 2−66931
- parton model, difficulties in application to internal symmetries 2−59431
- parton model, dynamical, with independent tension 2−45895
- parton model, e.m. mass shifts and approach to scaling 2−55827
- parton model, lepton-nucleon inelastic structure functions, scaling 2−70150
- parton model, massive lepton pair production in hadron collisions 2−70178
- parton model, nonperturbative, bilocal commutators 2−45898
- parton model and deep-inelastic scattering 2−73776

Hadrons continued
parton model and ratio $\nu W^n{}_2/\nu W^p{}_2$ 2−70251
parton model calc. of structure functions for $\gamma N \rightarrow \gamma' +$ anything, comparison with bilocal algebra on light cone 2−49498
parton model for deep elastic scattering 2−42407
parton model for diffractive dissociation of composite particles 2−70138
parton model for inclusive electroproduction in target fragmentation region 2−79607
parton model is deep-inelastic electroproduction 2−59423
parton models, phenomenological consequences for photon processes 2−66923
parton structure, predictions for inclusive reactions 2−63539
parton-model of Nachtmann connection with light-cone approach to structure function inequalities 2−66935
partons, test of existence of pointlike coupling of photon to partons 2−49532
partons and bilocal operators 2−73776
partons in proton, charge distributions and scaling in deep inelastic scattering 2−45916
partons with integral charge 2−63528
phase transitions 2−59432
phonon system picture, application to determ. of inelastic excitation function of proton 2−70170
production in Coulomb field of the nucleus 2−42550
production in e^+e^- interactions at ADONE storage ring, 1400-2400 MeV 2−73761
production in e^+e^- annihilation processes 2−63518
proton model for deep inelastic eN scattering data 2−59427
quark model and tensor coupling, helicity conservation 2−70168
quark structure 2−66951
quark-boson model of internal structure 2−66956
quark-gluon model, chiral symmetry realization 2−45897
quartet model, leptonic decay of charmed mesons 2−70201
quartet model leading to satisfactory theory of weak interactions 2−42349
quartet scheme in chiral U(4)xU(4) 2−45896
scalar-gluon model, anomalies of bilocal operators, determ. of light-cone singularities 2−82661
scaling, cosmic-ray interactions with dense targets 2−67063
single-particle electroproduction at high energy in covariant parton model 2−55822
soft partons, Feynman distribution, multiperipheralisms and degeneracy of vacuum 2−66954
structure, state-of-the-art review 2−59665
structure and 'wrong statistics' 2−73769
structure probing using neutrinos 2−59418
SU(3) × SU(3), chiral, limit of no explicit breaking 2−63532
superfluid phase, derivation of critical temp. 2−59434
superfluidity of hadronic matter 2−73775
superluminal urbaryon model 2−79464
symmetry and spontaneous breakdown 2−73768
symmetry models for gauge theory of weak and electromagnetic interactions of leptons and hadrons 2−42332
thermodynamic and dual resonance model, relationship 2−70175
triplet quark models, distinguishing tests 2−59436
ultradense matter, properties 2−55828
urbaryon model use to explain cosmic ray cut-off 2−73868
urbaryon models, new Nagoya and Hiroshima, discrimination proposal 2−73771
urbaryon rearrangement diagrams, contribution to inelastic two-body processes 2−70192
urbaryon size determ., applicability of scaling law 2−70169
vector-gluon model, summing of leading terms, consequences for form factors 2−79519
weakly broken subsymmetries 2−66952
$e^+e^- \rightarrow$ hadrons, oscillations in total cross section 2−63520

current
broken algebra and Cabibbo angle 2−63533
divergence under scale and conformal transformations, consequences for baryon matrix elements 2−73767
dual hadron model, relationship with parton e.m. model 2−79520
dual models with unit intercept, construction of currents and Green's functions 2−45914
dual reson. model of vector currents, form factors 2−79538
e.m. current struct., e^+e^- colliding beams applic. 2−76609
gluon-quark-type models for currents, light-cone dominance of time-ordered products 2−79473
meson, in space-time analysis of hadronic inclusive reactions 2−70176
mesonic of second class, existence in weak interactions 2−66993
parity-nonconserving $\Delta S=0$ nonleptonic weak processes in presence of second-class currents 2−82656
products, short distance singularity estimate using free quark model 2−73801
in quark model, relation with lepton currents in $O_{4.2}$ current algebra 2−42330
quark model, strengths and currents 2−52568
scalar currents, analogue model extension 2−79532
symmetry relation for elastic neutrino reactions on neutrons and protons 2−52557
triangle anomaly in divergence of axial-vector current, second-order radiative corrections to π-γ-γ vertex 2−79589
vector, dual resonance model, representation of current algebra 2−79516
vector and axial vector, derived from relativistic quark model with harmonic dynamics 2−63531
vector current annihilation into spinless particles 2−82686
weak interaction current of second kind, tensor const. 2−76591

decay
inclusive process, Regge behaviour 2−59492
new event in cosmic ray expt., weak decay interpret. 2−52651
non-leptonic, structure and 'wrong statistics' 2−73769
relativistic quark model, symmetries and nonsymmetries 2−79517
strangeness-conserving β decay in Weinberg's theory of weak interactions, higher order weak and e.m. connections 2−79518

interactions
see also Veneziano model
ρ exchange invariant amplitude estimates 2−63544

Hadrons continued
interactions continued
(3.3+) + (3+.3) symmetry breaking model in pole-dominance approximation 2−82710
angular distrib. and multiplicity of pionization particles and scaling law 2−42352
annihilation, Regge behaviour for inclusive processes 2−59492
baryon-antibaryon pairs and quarks, production, modified peripheral model 2−82711
charge exchange reactions, inclusive single particle spectra using multi-Regge model 2−79560
charge exchange reactions with t-dependent residues, differential cross sections 2−52574
cluster decomposition approach to phenomenology of high energy inclusive and exclusive processes 2−42355
compensation theory of elementary couplings 2−70181
composite theory dynamics 2−52576
correlation functions in high-energy multiple production and extension of Feynman's gas analogue 2−45905
coupling parameter sum rule, unitarization of dual models and bootstrap 2−55834
current algebra sum rules, in two-particle bases and single-particle inclusive processes 2−49514
diffractive, review of phenomenology 2−66966
diffractive models in non-diffractive regions 2−82714
diffractive-excitation model and multiperipheral model, tests by two-particle analysis 2−45903
double Regge model, spin and parity analysis 2−49517
double resonance production, phase of helicity amplitudes 2−82705
double-peripheral dynamics, momentum transfer dependence in diffraction dissociation 2−49526
dual models, resonant width, multiplicity, statistical calc. 2−70185
dual multiparticle theory with nonlinear, trajectories, twist relation, third factorization and general vertex 2−73781
dual systems, e.m. interaction investigation by generalized minimum interaction principle 2−49523
duality incorporated in parton model of hadrons 2−59441
electro-inclusive reaction, general approach to scaling 2−59457
e.m., exotic currents 2−59459
e.m., review, properties of e.m. currents, photoproduction and electroproduction 2−82674
e.m. form factors, meromorphic function interpret. 2−52579
equilibrium concentrations for relativistic spheres for zero total baryon number 2−69060
exclusive and inclusive cross sections, interrelations investigated by efficiency matrices 2−59443
exclusive and inclusive reactions interrel., urbaryon rearrangement diagrams 2−76623
exclusive processes, study of form factors, dimensionalities of operators, fixed singularities and Bjorken limit 2−66932
exotic exchange processes, resonance overlap and energy dependence 2−66961
Feynman gas model for semi-inclusive reactions 2−82704
formalism for description of ab→cde type reactions 2−76626
gauge theory of strong, weak and e.m. interactions 2−76629
hadrodynamics, hard and soft precesses 2−63543
hadron-hadron, super-high-energy, possible bounds on muon pair and $W^\pm$ production 2−63537
hadron-hadron total cross sections, empirical scaling behaviour 2−73778
Harari-Freund theory, avoidance of factorization of Regge residues 2−70174
high energy, zero pion mass limit 2−63603
high energy collisions, vol. 1, Oxford, England (Apr. 1972) 2−82715
high-energy total cross sections, comparison of Johnson Treiman Banger Rubic symmetry relations 2−66963
high-transverse-momentum hadron jet production, cross-section in parton model 2−70180
inclusive, φ^3 analyticity and finite-energy sum rule 2−66960
inclusive, CERN Intersecting Storage Rings expts. 2−82716
inclusive, duality constraints, role of Harari-Freund conjecture 2−79528
inclusive, exotic fragmenting states 2−76627
inclusive, finite mass sum rules 2−49516
inclusive, hierarchy of exotic channels and early scaling 2−70174
inclusive, in multiperipheral mode, π and K distrib. in pionization region 2−76625
inclusive, interrelation between background and resonances 2−63548
inclusive, one- and two-particle, new isospin predictions 2−63545
inclusive, phenomenological duality 2−59437
inclusive, polarisation effects, absorption model 2−52577
inclusive, polarisation effects 2−59446
inclusive, predictions based on parton structure 2−63539
inclusive, Regge phenomenology, review 2−66967
inclusive, relevance of internal symmetries 2−59431
inclusive, single particle distribution and multi-particle correlations 2−55832
inclusive, soft-pion results 2−66962
inclusive, space-time analysis 2−70176
inclusive, superconvergence relations 2−63550
inclusive, two particle correlations and boundary conditions, incorporation of energy and momentum conservation in factorization tests 2−59445
inclusive, two-particle correlations 2−82707
inclusive π^+ electroproduction, hypothesis of limiting fragmentation 2−79502
inclusive cross sections and dual topology 2−70186
inclusive cross sections depend. on missing mass squared 2−82713
inclusive cross-section sum rules, derivation from charge and strangeness conservation 2−70172
inclusive cross-sections, isospin sum rules 2−66968
inclusive distribs., π and K prod. in multiperipheral model 2−79525
inclusive distributions, analysis using generalization of Fermi statistical model 2−82708
inclusive distributions in central region, triple Regge couplings 2−59447
inclusive electroproduction, single particle, scaling in dual model 2−42338

- **Hadrons** continued
  - **interactions** continued
    - inclusive exchange region, symmetry considerations 2−79524
    - inclusive expts., relation of model for Pomeranchuk singularity 2−45907
    - inclusive model for production of resonance like objects novas 2−45906
    - inclusive process, controlling factors, 20-1500 GeV 2−66957
    - inclusive process, general properties of correlation functions 2−63538
    - inclusive processes, application of spectral representations, pp$\rightarrow\mu^+\mu^-$ + anything and pp$\rightarrow\pi$ + anything considered 2−55835
    - inclusive processes, effect of virtual photon mass on transverse momentum distributions 2−49515
    - inclusive processes, energy momentum conservation 2−59439
    - inclusive processes, pion exhange dominated, elementary pion and transverse momentum cut-off 2−59442
    - inclusive processes and urbaryon rearrangement 2−45910
    - inclusive processes at high energy 2−59450
    - inclusive reaction spectra, calc. by urbaryon rearrangement 2−82700
    - inclusive reactions, diffraction model, leading-particle and momentum conservation effects 2−70179
    - inclusive reactions, factorization and exchange degeneracy of secondary trajectories 2−42356
    - inclusive reactions, factorization and scaling 2−63542
    - inclusive reactions, finite-energy sum rules, Reggeon-particle scattering amplitudes 2−73849
    - inclusive reactions, predictions based on parton structure 2−42354
    - inclusive reactions, produced particle fluxes at very high energies 2−59449
    - inclusive reactions, single particle production test of mass dependence in triple Reggeon graphs 2−42353
    - inclusive reactions, spin rotation-parameters 2−73784
    - inclusive reactions and diffractive production processes 2−70183
    - inclusive reactions and Gribov's triple-Pomeranchukon vertex 2−66969
    - inclusive reactions at CERN ISR for 0.4 GeV/c transverse momentum, charged particle production ratio 2−76631
    - inclusive reactions in high energy multiparticle production phenomena, kinematics 2−45908
    - inclusive reactions in Regge pole model and exotic resonances 2−45909
    - inclusive single particle spectra in fragmentation and pionization regions 2−42357
    - inclusive spectra, Regge phenomenology in central region 2−59448
    - inclusive sum rules for isotopic spin 2−66958
    - inelastic, high energy, e.m. mechanism 2−82712
    - interference models with good analytic properties 2−79530
    - lepton pair production, scaling model 2−82688
    - lepton-hadron, theory 2−82679
    - lepton-hadronic inclusive reactions, parton dual-resonance model 2−66931
    - leptonic weak processes, review 2−63553
    - light cone and multi-Regge theory for inclusive processes at large mass 2−73782
    - limiting fragmentation, double Regge boundary condition 2−49520
    - longitudinal phase space plots in arbitrary frames for analysis of high energy production processes 2−76621
    - many-body, high energy, review 2−82717
    - many-body problem, review 2−82719
    - many-particle production, review 2−66915
    - massive lepton pair production and parton model 2−70178
    - multiparticle, at high energies, review 2−49521
    - multiparticle amplitude, unitary models 2−59456
    - multiparticle processes at high-energy, application of dual-parton model 2−63547
    - multiparticle prod. processes, model-independ. analysis of density-matrix element meas. 2−79523
    - multiparticle production at high energy, thermodynamic characteristics 2−66965
    - multiperipheral configuration, dual amplitude construction based on general field theory vertices and propagators 2−59470
    - multiperipheral dynamics, behaviour of average multiplicity 2−45901
    - multiperipheral model, inclusive reaction, 2-particle distribution function 2−73783
    - multiperipheral model, systematics of odd isospin combination of n-particle production cross sections 2−49518
    - multiperipheral model used to study effect of Pomeron exchange 2−63540
    - multiperipheral models with charged particles 2−45902
    - multiperipheral-thermodynamic model, rapidity correlations in inclusive two pion production 2−49563
    - multiple generation, statistical theory 2−55836
    - multiple particle prod., generating functionals 2−55830
    - multiple prod. model 2−59463
    - N-body inclusive reactions in Veneziano model 2−70177
    - neutral particle production, missing momentum analysis 2−79522
    - Neveu-Schwarz model, generalization to include arbitrary intersection of ρ trajectory 2−59438
    - nuclear star production 2−52891
    - one pion exchange model in inclusive framework 2−59454
    - p_t limited phase space predictions 2−55831
    - paired spectra of particles in colliding beams at high energies 2−42350
    - partially inclusive reactions limiting behaviour 2−59440
    - particle production spectra, derivation of longitudinal momentum distrib. from quark-boson model 2−66956
    - parton-parton interaction and hadron structure in partial bootstrap model 2−66950
    - photon-hadron, high energy photoprod. processes, hadronic nature of photon 2−82677
    - photon-hadron, high energy pseudoscalar meson production models, review 2−59504
    - photon-hadron, Int. Summer Inst., Hamburg (1971) 2−59405
    - photon-hadron, theoretical aspects, conference, Hamburg July 1971 2−59404
    - with photons, analytic equivalence of Gupta- Bleuler formalism and S-matrix formalism 2−52578
    - photoproduction on hadrons, test of $\Delta I \leqslant 1$ rule 2−63499
    - photoproduction processes, high-energy quasi-inclusive, multi-Regge model applic. 2−52575
    - pionization struct. function for inclusive processes 2−66959
    - production processes, eikonal treatments, formal solns. 2−59462
    - quark bound states, exchange factors, asymptotic behaviour of form factors 2−63554
    - real processes, high energy amplitudes from FESR 2−42351
    - Regge analysis and dual absorptive model, review 2−59451
    - relativistic three-particle eqns. with arbitrary pots. 2−59444
    - resonance excitation, scaling, simple potential-theoretic parton model 2−79529
    - S-matrix perturbation theory for electromagnetic corrections in strong interactions and field-theoretic self-energy calculations 2−52518
    - scaling method for high energies from data below 30 GeV 2−73738
    - scaling of interaction radius 2−70184
    - scaling of semi-inclusive distrib., Feynman gas model 2−73780
    - scaling variables, extended hadrons and Poincare group 2−76619
    - semi-inclusive cross section correlations 2−79521
    - semi-inclusive cross sections, derivation of properties using unitarity and Regge-pole analysis 2−63551
    - semi-inclusive cross-section, Feynman gas and liquid models 2−82704
    - single particle distributions near kinematical limits, phenomenological study 2−45904
    - single-particle inclusive, triple-Regge phenomenology from finite-mass sum rules 2−76622
    - single-particle inclusive cross sections, phenomenology of triple-Regge region 2−76628
    - single-particle prod., dual-model analysis at intermediate energies 2−79526
    - single-particle spectra, comparison at accelerator and cosmic-ray energies, evidence for clustering 2−63549
    - statistical treatments, Ericson fluctuations and Bohr model 2−82702
    - strong, application of ideas to deuteron stripping reactions at high energies 2−76633
    - strong, at very high energy, review of expts. at IHEP and ISR 2−59453
    - strong, canonical anomalies and broken scale invariance 2−59455
    - strong core, possible explanation by composite model 2−45911
    - strong exptl. and theoretical aspects, review 2−49522
    - strong interaction amplitudes, parametrization of Coulomb interference 2−45900
    - SU(4) weak interaction quark model modification 2−79531
    - symmetry breaking for two-body processes energy dependence 2−79514
    - tachyonic resonances in differential cross sections, phenomenology of high-energy processes 2−63546
    - thermodynamic inclusive single particle spectra 2−82706
    - thermodynamic inclusive single particle-spectra, particle production ratios at ISR 2−82706
    - three particle final state, use of scatterplots 2−79527
    - threshold enhancements and statistical bootstrap 2−70189
    - total cross sections and cone slope, exptl. data rel. to theory 2−82699
    - total cross-section, relation to slope of diffraction cone 2−66964
    - triple Regge vertex, eigenvalue integral equation 2−82724
    - two-body, review 2−82718
    - two-body processes, generalization of geometrical duality ·2−76624
    - two-particle correlation, associated multiplicity 2−49519
    - two-particle inclusive, new plot for study of transverse momentum correlations 2−76620
    - two-particle production, dual-amplitude analysis 2−63536
    - uncorrelated jet model, multiplicity distributions 2−70182
    - unitary multiperipheral models 2−82728
    - urbaryon rearrangement and impact parameter represent. of reson. correl. 2−55833
    - vacuum transfer in 3 region domain 2−76630
    - vector meson dominance rel. to coupling of Reggeized ρ to 'charged' photons 2−79539
    - vector mesons photoproduction, quark model predictions for angular decay distributions in inclusive processes 2−52624
    - Virasoro algebra, one physical state in each irreducible representation 2−63541
    - virtual photon reactions, analogy 2−70187
    - virtual photons, vanishing longitudinal cross sections and operator Schwinger terms 2−59458
    - weak, $\Delta I={}^1/_2$ rule in three-triplet and paraquark models 2−59460
    - weak, CP violation, review of exptl. studies 2−49525
    - weak, effect on breaking of hadronic internal symmetry 2−63535
    - weak, e.m. divergences 2−59452
    - weak, satisfactory theory using quartet model of hadrons 2−42349
    - weak and electromagnetic, lepton and quark symmetry 2−73750
    - weak and electromagnetic, models for gauge theory of lepton and hadron interactions 2−42332
    - weak and e.m., review of theoretical aspects 2−49524
    - weak and e.m. interaction symmetry 2−66933
    - Wick-Cutkosky model, Regge poles for large coupling constants 2−59350
    - e + hadron (p) ex, inified light-cone treatment of scaling, positivity constraint on short-distance behaviour 2−82690
    - μ pair creation via two-photon exchange in charged hadron collisions at very high energies 2−82698
    - π^- inclusive reactions, factorization in central region 2−70228
    - GaP, cyclotron resonance of holes 2−75041
  - **scattering**
    - − 2−63570
    - ρ exchange invariant amplitude estimates 2−63544
    - ABFST model, relationship between Regge slopes and Lorentz poles 2−59497
    - absorptive effects in multipheral models 2−59471
    - absorptive parts of elastic amplitudes, asymptotic bounds 2−52583
    - Adler sum, rule for inelastic lepton-hadron processes 2−82642
    - amplitude, reson. and Regge descriptions, role of duality 2−45913
    - amplitudes, ambiguities resulting from insufficient experimental data 2−59476
    - amplitudes at low, intermediate and high energies, rigorous constraints, bounds, analyticity 2−79551
    - charge and hypercharge exchange, polarization relations 2−55841
    - composite theory at large angles, tests of parton concepts 2−49532

Hadrons continued
scattering continued
Compton amplitudes, fixed poles and Pomeranchukon coupling 2−49537
current-hadron scattering, finite energy sum rule 2−70188
deep inelastic, in dual resonance model 2−59486
deep inelastic electroproduction, single-particle distributions 2−70160
deep-inelastic, description of anomalies in terms of canonically determined bilocal operators 2−82661
deep-inelastic processes, symmetry relations 2−66973
diffraction dissociation, inclusive bootstrap constraints 2−59475
diffraction scattering inside $|t| \sim 4m_\pi^2$, structure 2−70200
diffraction scattering with fixed pole and shielding cut, models discussed 2−45923
diffractive inclusive processes, relation to two-Pomeranchukon cut 2−66987
diffractive prod. processes, helicity conservation 2−76641
diffractive production in hadron-hadron collision at high energies, model 2−76632
dual absorptive model, helicity conserving and nonconserving pomeron exchange amplitudes 2−59467
dual amplitudes and Thirring model 2−49530
dual amplitudes with Mandelstam analyticity, asymptotic behaviour 2−66988
dual model, unitarization and absorpt. Regge cut 2−66981
dual multiparticle theory with nonlinear trajectories, first and second factorization 2−59485
dual N-point amplitude, off-shell 2−55839
dual quark models 2−59479
dual resonance amplitude, off-shell derivation 2−59466
dual resonance model, inclusive distributions 2−49534
dual resonance model, sum rules for Compton scatt. of photonlike particles 2−59469
dual resonance model, two particle distributions 2−45918
dual scattering amplitudes, unitarity effects 2−63562
dual-resonance model without tachyons 2−79512
duality, Deck effect 2−49528
duality, reson. and Regge descriptions of amplitude 2−45913
duality and positivity in zero-width approx., exptl. consequences 2−76636
eikonal model 2−82729
elastic, dual absorpt. models, peripherality assumption 2−52585
elastic diffraction peaks, 'Pomeranchuk' theorem 2−66984
elastic processes, s-channel helicity conservation 2−55840
electromagnetic form factors in parton model 2−73811
exchange, resonance and duality models 2−52569
exchange degeneracy and duality in generalized interference model 2−73792
exclusive production amplitudes, light- cone expansion for vertex functions 2−45920
Faddeev equations, relaxation method of solution 2−59473
Faddeev equations with local interactions, solutions by variational Pade method 2−59465
fixed poles, unitarity and duality, charge exchange applic. 2−79533
fixed-pole Pomeron shielding-cut mechanism, diffr. scatt. asymptotic behaviour 2−52588
fixed-pole Pomeron with shielding branch-cuts 2−59489
form factors and parton model 2−59503
functions of order p, Veneziano and Coon representations 2−79552
generalized duality, relationship between three body forward scattering and two-body scattering 2−63558
Glauber formula, generalized with recoil 2−59487
hadron-^{12}C elastic scatt., cross sections analysis 2−82723
hadron-deuteron, quasi-elastic, recoil effect 2−63565
hadron-hadron, elastic slope parameters 2−45919
hadron-hadron elastic, cross-over and shrinkage, defects of simple optical model 2−70191
hadron-neutron, shadow correction 2−42363
helicity amplitudes, unitary constraints 2−59468
helicity conservation at high energies in diffraction scattering and diffractive production of unstable particles 2−49527
high energy, ABFST model 2−45912
high energy, unitarization and OBE contrib. 2−76638
high energy, unitary symmetry, appls. 2−42361
high energy elastic, simple description of Pomeron exchange 2−59494
high energy elastic scatt., Pomeron exchange in Regge language 2−59480
high-energy, character of asymptotic regime studied in generalized multiperipheral model 2−42359
high-energy, in φ^3 theory, breakdown of eikonal approx. for exchange of two or more ladders 2−79545
high-energy, in φ^3 theory, eikonal approx. breakdown 2−59477
high-energy, summation of direct-channel resonances by SW method, connection of 'parabolic' mass and width trajectories 2−63564
high-energy exchanges based on multiperipheral ideas, phenomenological study 2−70199
high-energy forward, backward, large-angle, construction of dual quark models 2−76642
high-energy scatt. phenomenology 2−63566
hypercharge-exchange reactions, octet Pomeranchukon component and absorption 2−79547
impact parameter description, compatibility with s-u symmetry constraint 2−49529
inclusive and exclusive cross sections and cluster decomposition, general connections 2−79546
inclusive cross sections, bounds, unitarity 2−79548
inclusive differential cross-section in pionization region, non-leading behaviour 2−49536
inclusive reactions, single-particle spectra at fixed angle and duality 2−66979
inclusive single-particle spectra calc. using thermodynamic model 2−79549
inclusive spectra in central region, Regge analysis 2−59481
inclusive sum rules for discontinuities of multiparticle amplitudes, diagonalization, possibility of inclusive bootstrap 2−66992
inclusive transverse momentum distrib. studied using multiperipheral models, correlation lengths 2−66974

Hadrons continued
scattering continued
inelastic, role of lower lying exchanged trajectories studied in framework of two-fire-ball model 2−59482
inelastic partial-wave amplitudes, improved N/D method 2−73789
inelastic phase-shift analysis, removal of ambiguities 2−63555
inelastic two-body processes, urbaryon rearrangement diagrams 2−70192
interaction scaling radius hypothesis, comparison with data for 6-14 GeV/c 2−73788
large angle, invariant 4-point amplitudes satisfying mathematical duality constraints 2−42366
lepton-hadron, deep inelastic, weak interaction processes 2−59392
lepton-hadron, duality, scaling and fixed poles in virtual Compton scatt. 2−63506
lepton-hadron scatt., high energy, review 2−82678
Lorentz invariance and duality 2−70198
mesh-point inversion in scattering region 2−82624
meson-hadron scattering, finite energy sum rule 2−70188
multi-particle reactions, partial wave amplitudes, sum rules from crossing symmetry 2−66977
multiperipheral boostrap model, statistical generalization of one-dimensional version 2−70197
multiperipheral bootstrap model, self-consistent diffraction 2−59502
multiperipheral dynamics, diffractive dissociation 2−73790
multiperipheral model, unitarity effects 2−66972
multiperipheral model with constant total cross-section 2−82725
multiple-scattering Regge units, phase problem and signature rule 2−52589
narrow resonance and 'tachyon' approximation of scattering amplitudes 2−76634
Neveu Schwarz model mass spectrum improved by combustion of dual resonance model 2−49531
non-Pomeranchukon amplitudes, evidence against resonance saturation in finite energy sum rules 2−63568
nonlinear integral eqn. for high-energy scattering, numerical solns. 2−79543
nonlinear integral eqn. for high-energy scattering, solutions, existence theorem 2−79542
parity doublet elimination in Regge amplitudes 2−66990
particle number distrib. function rel. to multi-pomeron exchange 2−66978
parton dual reson. model, light-cone structs. and sum rules 2−59478
parton model for inelastic lepton-hadron scattering coherent contrib. to breaking of Bjorken's scaling law for small Q^2 2−82727
parton model of inelastic lepton scattering 2−59414
partons in proton, charge distributions and scaling in deep inelastic scattering 2−45916
piecewise-analytic scattering amplitude of indefinite-metric quantum field theory, consequences 2−63457
polarization in deep inelastic electron and neutrino scattering from light-cone quark algebra 2−52584
production processes, multiplicities and correlations 2−52580
quark-orbital Regge trajectories 2−76644
quark-parton model for application of duality in deep inelastic electroproduction 2−59420
quasi two-body and two-body inelastic processes 2−82732
quasi-potential and eikonal approximation to high energy scattering 2−70193
real parts of amplitudes, corrective term to Regge model 2−59472
Regge exchange amplitude, ρ-P cut, partial bootstrap and phenomenological pole 2−59496
Reggeon perturbation theory in Zachariasen-like model 2−52587
resonances, introduction of effective mass and effective width 2−63561
rising cross sections shrinking diffraction peaks and Pomeranchuk trajectories 2−45917
selection rule, quark diagrams 2−49535
semilocal duality, application to $a+b+c \to a+b+c$ process in double-Regge region 2−76639
Shapiro-Virasoro model, construction of physical states, especially DDF states 2−73785
single particle distribs., emission model analysis 2−79536
spin structure at high-energy multiple scattering 2−73791
string model, breaking and connection approach 2−52581
sum rules, finite energy related to light-cone commutator of currents 2−63557
t-channel discontinuity in scattering amplitude due to ρ meson exchange calc. in resonance approx., eikonal form 2−42365
total cross-sections and elastic scatt. at high energies 2−82731
triple pomeranchukon vertex, consequence of vanishing at zero mass 2−59495
triple Regge couplings, unitarity bound 2−59461
triple Regge vertex, eigenvalue integral equation 2−82724
triple-Regge amplitude 2−42368
two particle elastic scattering in presence of inelastic processes, relativistic potential scattering 2−52586
two-body, systematic struct. and reson. correl., urbaryon rearrangement 2−63563
two-body, Toller pole analysis of dip struct. 2−66976
two-body amplitude, origin of hierarchy 2−76640
two-body amplitudes, properties in absorptive model 2−59484
two-body inelastic, dual absorptive model and structure 2−59483
two-body processes, generalization of geometrical duality 2−76624
ur-citon scheme, amplitude derivation by operator method 2−52582
Veneziano model, dual Pomeron compatibility with unitarity and absence of ghosts 2−59491
Virasoro partial wave amplitude, fixed and moving poles shown to be multiplicative 2−70196
e scatt., quark mass and structure functions 2−73787
Haemoglobins *see Proteins*
Hafnium
atom, collisions with CO_2, non-resonant energy transfer 2−53101
diffusion mechanism in β-modification 2−68044
electric quadrupole interaction of ^{181}Ta, Mossbauer obs. 2−61607
electrical and thermal cond., 20 to 1200°C 2−47769
phonon dispersion, Debye temp., noncentral force model 2−80887
thermal diffusivity, thickness effects 2−57085
Hf, electron scattering mechanisms at high temps. rel. to kinetic properties 2−81035

Hafnium continued
^{181}Ta, in Hf polycrystalline sample, quadrupole interaction, influence of Zr 2—84593
Hafnium compounds
HFC-Re system, meas. of lattice consts., solubility relations and phase diagram 2—84096
Hf-B system, phase diagram 2—50957
Hf-Ge alloy, electric quadrupole interaction with ^{181}Ta 2—75359
Hf-Nb-B alloy, phase equilibria, at 1400°C, X-ray obs. 2—43912
Hf-O system, near $HfO_{1/6}$, interstitial order-disorder transform. 2—68205
Hf-Ta alloys, superconductivity under pressure 2—81058
Hf (IV) complexes, octocoordinated, differential perturbed ang. correl., ^{181}Ta quadrupole coupling 2—61571
HfB_2-ZrN alloy, microhardness and resist., conc. depend. 2—47638
HfB_2, thermionic emission, rel. to electronic struct. 2—48017
$HfBr_4$, orbital valence force field consts. 2—77075
HfC, band struct. calc. 2—57126
HfC, hot pressing for high temp. bearing applications, NASA research 2—64801
$HfCl_4$, orbital valence force field consts. 2—77075
$Hf_3Cu_4Si_2(Ge_2)$, cryst. structure 2—43597
HfF_4:^{181}Ta, in dilute HF, time differential perturbed γ-γ angular correlation, temp. dependence 2—81321
HfH_x, electron-nuclear interactions rel. to spin-lattice relax. 2—78047
HfI_4, orbital valence force field consts. 2—77075
HfN-ZrB_2 cutting tool materials characteriz. 2—50883
HfN, hot pressing for high temp. bearing applications, NASA research 2—64801
HfN, microhardness and thermal expansion, 80-300K 2—61112
HfO_2-W composite, thermal shock resistance 2—56989
HfO, electronic band spectra interpret. 2—77069
HfO_2, dispersion strengthening phase in Ni powder, effect on thermal stability 2—77739
HfO_2, elec. cond., 1600-1900K 2—54233
HfO_2 particle growth in Ni ceramic, matrix density effects 2—68169
$HfOCl_2.xH_2O$, static elec. quadrupole interaction of ^{181}Ta 2—78057
HfS_2, nearly perfect cryst., growth and X-ray obs. 2—50577
Hf_2S, metalic bonding, Brewer Engel correl. 2—47180
$HfSe_2$, cryst. growth by vapour transport 2—50577
$HfSiO_4$:M^{3+} (M=Er, Yb, Gd), e.s.r. spectra 2—48278
HfV_2, lattice transition, supercond., cryst. struct., alloying effects 2—71865
HfV_2, n.m.r. and mag. susceptibility anomaly 120 K 2—54507
^{181}Hf cpds., ABO_3-type, perovskite-type, nucl. quadrupole interactions, perturbed-angular-correlation meas. 2—72244
Mo-Hf, internal nitriding, high-temp. props. 2—60968
Nb-Hf alloys, fracture morphology, transmission and scanning electron microscopy 2—56834
Nb(38 at.%)Hf alloy, supercond., fluxoid pinning rel. to precipitate dispersion 2—44076
Ta-W-Hf alloy, tensile props., effects of O contamination 2—43862
Half-lives *see Radioactivity/decay periods*
Hall effect
see also Semiconducting materials; Semiconductors
— 2—68424
alpha-effect calc. rel. to gyromotion of electrons and ions 2—60214
anisotropic conductor, long needle coeff. 2—51065
anomalous, in ferromagnetic semiconductors with strong s-d coupling 2—71879
carbons irradiated by neutrons and annealed, props. changes 2—68137
disordered system, Hall coeff. in narrow band, random phase model 2—75008
EuO, ferromag. semicond., Redfield technique detn. of Hall mobility of photoelectrons 2—81060
ferromagnet, spontaneous magnetiz. measurement 2—75219
ferromagnetic, side-jump model 2—65133
ferromagnetic alloy, anomalous Hall effect, phonon scatt. effects 2—81223
ferromagnetic metal, anomalous effect, contrib. of electron-electron collisions 2—57147
ferromagnetic metals and alloys, anomalous spin-orbit interaction effect on electron scatt. 2—72157
ferromagnetics, near compensation temp. T_k 2—72158
film, semicond., transport coeffs. rel. to surface states, Hall and Seebeck coeffs. 2—47884
fluid, flow over porous flat plate in transverse mag. field, Hall current effects 2—46704
frequency dependence of Hall e.m.f. in varying magnetic field meas. 2—52383
graphite, pyrolytic, 1.2-300 K, c-axis conduction mechanism 2—57109
graphite, rel. to struct. imperfections 2—57190
graphite very thin crysts., total carrier density behaviour 2—54102
high resistivity samples, double a.c. meas. technique 2—82415
hopping impurity conduction 2—57178
Hubbard model, low-field regime calcs. 2—77903
p-InSb, 2-300 K 2—72050
ion exchange membrane/electrolyte solution system 2—43386
liquid metals, method of determ. 2—64469
liquids, semiconducting, method of determ. 2—64469
magnetic conductor, anomalous effect, band struct. influence on skew scatt. 2—47791
magnetometer, elimination of temp. influence on flux density meas. accuracy 2—49309
metal, alkali, Hall const. temp. depend. rel. to electron-phonon interaction anisotropy 2—57104
metal-NHz solns., transport props. in the non-metal-metal transition range 2—80484
metals, meas. method for rectangular plates 2—59029
MHD power generator, effect of heterogeneity and Hall current 2—69849
mica, surface conduction and surf. Hall coeff. dependence on temp. and mag. field 2—80541
mobilities, amorphous semiconductors, meas. by Corbino disc 2—68426
m.o.s. technique for elec. prop. determ. of Si on sapphire 2—51169
organic materials, rel. to conduction mechanism determ. 2—47905
Hall effect continued
plasma, rotating, thermal instability 2—70967
plasma, stratified, with tensor cond., coeff. determ. 2—83542
plasma flow in travelling magnetic field 2—60216
plasma of combustion products, and turbulence 2—64265
polaron conductions from band to hopping types 2—84230
rare earth dodecaborides 2—47838
Ru, low temp. dependence 2—68333
semiconducting crystals, Hall coeff. meas. by four-probe method 2—54191
semiconductor, amorphous, Hall cond., random phase model 2—61277
semiconductor, cubic, polaron Hall mobility calc. 2—68383
semiconductor, heterogeneous, carrier mobility measurement 2—54164
semiconductor, III-V, transition metal doped, anomalous temp. depend. 2—68405
semiconductor, impurity level activation energy determ. 2—80958
semiconductor, polar, AC meas. apparatus 2—57174
semiconductor, strongly doped, model interpret. 2—77880
semiconductor, with low mobility charge carriers 2—47883
semiconductor film, calc. 2—71892
size effect theory in thin metallic films 2—77984
size effects in thin films 2—54126
solid and disordered system, Hall resistivity expression using nonequilib. statistical operator 2—71776
spinel ferrites, validity of Hall effect theory of small polaron 2—75083
sum frequency method of obs. in belt apparatus 2—57267
transition metal nitrides, hot pressing, sintering, Hall coeff. 2—47661
triglycine sulphate, field effect and Hall mobility of Te and PbTe 2—77814
turbulent MHD, effect of conductivity 2—43110
VB_2, one and two-zone model and measurements, comparison 2—77881
Ag-Au(Cd)(In) dilute alloy, 2.5-120 K 2—75050
Ag, Hall and Righi-Leduc coeffs., 4-125 K, Weidemann- Franz law 2—61224
AgCl(Br), molten, effective mobility 2—67839
α-AgI solid electrolyte, ionic Hall effect 2—83988
n-Ag_2Te, rel. to Lorenz number and electron scatt. inelasticity obs. 2—84337
Ag_2Te at m.p. and to 1500 K 2—60495
Al-Ag alloy, preprecip. study 2—77692
Al, coeffs., from audio freq. helicon resons. 2—57136
$As_2Se_3-xAs_2Te_3$, amorphous, as func. of temp. and subsequent annealing 2—77893
AsTeI glass, mobility obs. 2—61296
Au, Hall and Righi-Leduc coeffs., 4-125 K, Weidemann- Franz law 2—61224
Be film, crit. thickness determ. 2—56587
Bi-Sb alloy, effects of Ag, In and Pt addition 2—71896
Bi, amorphous state, free electron model 2—75048
Bi, polycrystalline, obs. by sum frequency method in belt apparatus 2—57267
Bi film, crit. thickness determ. 2—56587
n-Bi_2S_3, coeff. temp. depend. 2—44092
$Bi_{1-x}Sb_x$:Cd(In)(Sn), (x=0-0.2), 180-420K 2—61301
p-Bi_2Se_3, Hall and cond. mobilities, carrier compensation, galvanomag. effects, 4.2-300K 2—81076
p-Bi_2Te_3, low- and high-field props. 2—51135
$Bi_8Te_7S_5$, single crystal film, Hall eff. meas. and detn. of carrier mobility 2—77851
$Bi_2Te_{3-x}Se_x$, temp. depend. of electron effective mass and mobility, using Hall density expression 2—81099
C, multiphase system, mag. field depend. 2—57112
C, soft pregraphitic, Hall coeff. depend. on heat treatment and doping 2—44113
Ca-NH_3, solution, 203-243K 2—46984
Ca semimetal, temp. and uniaxial stress dependence obs. 2—71840
Cd-Hg alloy, 0-14 at.% Hg, room temp. 2—77855
$Cd_xPb_{1-x}Se$ alloy, Hall coeff., Hall mobility, thermoelec. power, optical energy gap, 77-450 K 2—64977
CdS film, Hall mobility, thickness depend., effects of Cu impurity 2—77894
CdSb:Te, with low Te content, 78-293K 2—61307
CdSe-SiO_x, electron transport study in space charge layer of vacuum-deposited film 2—77852
CdSe, mobility obs., elec. behaviour between room temp. and 600C 2—61305
CdSe film, effect of O_2 and N_2 on mobility obs. 2—57191
CdSe films vacuum deposited, Hall mobility 2—83868
CdSe(Te), high temp. defect. equilib., elec. transport props. 2—44096
CdTe:Li, rel. to self-compensation and interaction of Li with defects 2—75107
$Cd_{2.8}Zn_{0.2}As$, high mobility, rel. to scattering parameter determ. 2—81090
CrSi, elec. cond., thermal e.m.f.. and Hall coeff. detn 2—77797
$CrSi_2$ thermoelectric props. and crystal growth 2—84370
Cu, Hall and Righi-Leduc coeffs., 4-125 K, Weidemann-Franz law 2—61224
Cu films, Hall coeff. detn. and existence of size effect 2—77985
CuCl, molten, effective mobility 2—67839
$CuCr_2Se_4$, temp. depend., 100-650K 2—81091
Cu_2Te-Ag_2Te system, comp. and temp. dependence of Hall mobility 2—84323
n-EuS, 140 kOe, negative magnetoresist. obs. 2—47895
EuS, slightly Eu rich, Hall coeff. calc. using model for transport in band tails 2—75094
Fe-Co alloy, temp. ⩽4.2K 2—47836
Fe-Cr alloy, temp. ⩽4.2K 2—47836
Fe-Ni alloy, Invar, temp. depend., 100-300°C 2—72164
Fe, temp. ⩽4.2K 2—47836
FeSi, elec. cond., thermal e.m.f. and Hall coeff. detn. 2—77797
Ga, amorphous state, free electron model 2—75048
Ga, apparatus for mobility meas. by Corbino method 2—71224
p-GaAs:C ion implanted, carrier conc. and Hall mobility obs. 2—64986

Hall effect continued
- n-GaAs:S ion implanted, carrier conc. and Hall mobility obs. 2–64986
- n-GaAs:Si ion implanted, carrier conc. and Hall mobility obs. 2–64986
- p-GaAs, effect of pressure, 10000 kg/cm^2 2–44099
- n-GaAs, electron irrad., annealing behaviour 2–47918
- n-GaAs, epitaxial, Hall coeff. and mobility 300-800 K, valley energy separation 2–68398
- GaAs, epitaxial layers, influence of gas phase comp. 2–83893
- GaAs, heat treated, acceptor centres obs. 2–61343
- n-GaAs, low field galvanomag. transport, Hall mobility, magnetoresist. coeff., 77-300K 2–71902
- n-GaAs, mag. field effect on impurity cond. 2–81085
- GaAs, n- and p-type, electron irrad., defect levels determ. 2–80992
- n-GaAs, rel. to impurity distrib. coeff. anisotropy 2–47437
- GaAs, undoped, point defect conc. effects on temp. depend. 2–71905
- GaAs epitaxial layer 2–71882
- GaP, epitaxial on insulating substrate, electrical characterization 2–47111
- n-GaSb, coeff. temp. and mag. field depend., cond. band parameter obs. 2–57206
- Gd-Y alloys, 4.2-340K 2–68332
- Gd, pressure effect on single crystals 2–68547
- Gd, rel. to press., 77-400K 2–77858
- Ge:Cu, donor compensation density determ. 2–51166
- Ge:Li, electron irrad., mobility and minority carrier diffusion length obs. 2–47927
- n-Ge:O, γ-irrad., Hall mobility, anisotropy 2–54196
- Ge:Sn heavily doped, mobility, temp. and concentration effects 2–77911
- n-Ge, disordered region prod. by 28 MeV electrons 2–47931
- N-Ge, even and odd effect in strong electric fields 2–81108
- Ge, heavily doped, 2-300 K 2–81109
- p-Ge, low temp. elec. irrad., point defect annealing 2–47381
- p-Ge, low temp. electron irrad., 220K defect obs. 2–47928
- Ge, n-type, measurement with cubic type high- pressure multianvil apparatus 2–76431
- p-Ge, neutron irrad. effects, 77K 2–47930
- n-Ge, rel. to laser generated carrier mobility, transient behaviour 2–47925
- p-Ge, theory extended to include optical phonon scatt. 2–65011
- Ge film, thickness depend. 2–54192
- Ge films, amorphous, small voltage obs. 2–64963
- Ge minority carrier mobility, influence of majority carriers 2–75114
- GeSe, semicond. liq. 2–60498
- $Ge_{15}Se_{85}$, Hall mobility meas. by double a.c. technique 2–82415
- $GeTe-Bi_2Te_3$ solid soln., Hall carrier conc. 2–74903
- H bonded solids, proton migration study, review 2–83998
- Hg, apparatus for mobility meas. by Corbino method 2–71224
- p-$Hg_{1-x}Cd_xTe$, carrier freeze-out and acceptor energies determ. 2–57194
- $Hg_3Te_3-Ge_2Te_3$ alloy, transport processes, Hall mobilities, near semimetal-semicond. transition at high press. 2–68406
- $Hg_3Te_3-In_2Te_3$ alloys, cond. types of h.p. phases 2–54175
- HgTe, Hall coeff. and self-conc. of carriers 2–61314
- HgTe, in high mag. field, 4.2, 77 and 300 K 2–64988
- HgTe films, temp. dependence of Hall coeff. and electrical conductivity 2–54174
- Ho single crystals, 4.2-300K extremum values of magnetoresistance and Hall field at magnetic transition temperatures 2–68548
- n-InAs, rel. to thermoelec. power in quantizing mag. fields 2–84372
- n-InSb, coeffs. at high temp., degeneracy and screening effects 2–68378
- n-InSb, Hall mobility, impact ionization phenomena, mag. field effects 2–61317
- InSb, n-type study of electronic structure by a microwave beat method 2–84246
- InSb film, flash deposited, electron mobility parameters 2–54176
- InSb single crystals, conversion of low voltage electric current 2–45634
- $K-NH_3$, solution, 203-243K 2–46984
- La:Ce, skew scattering of electrons obs. 2–75055
- $Li-NH_3$, solution, 203-243K 2–46984
- $Li(NH_3)_4$, carrier mobility determ., Hall coeff. 1.5-89K 2–47894
- n-Mg_2Ge, mobility temp. depend. and scatt. mechanism 2–51143
- $Mg_xPb_{1-x}Se$ alloy, Hall coeff., Hall mobility, thermoelec. power, optical energy gap, 77-450 K 2–64977
- Mg_2Sn pressure dependence of electrical resistance and Hall data 2–84326
- $Mn_xHg_{1-x}Te$ films, Hall coeff., Hall mobility and electrical condutivity 2–71885
- MnSi, elec. cond., thermal e.m.f.. and Hall coeff. detn. 2–77797
- Mo film, size effect 2–81030
- MoS_2, layer struct., contact annealing effect 2–54177
- $NbSe_2$, low-temp. cryst. modification 2–81052
- Ni ferrites, iron rich, Hall mobility measurements, room temp. to 600°C, activated hopping process 2–81069
- Ni film, residual magnetization, susceptibility, anisotropy, Hall effect 2–48095
- Ni film, spontaneous magnetization rel. to Hall effect 2–48096
- NiB, room temp. 2–51099
- $Ni_3(Mn,Co)$ and $Ni_3(Mn,Fe)$ alloys, electron and hole mobility obs. 2–47837
- NiS, Hall coeffs., 80–400 K, semicond.-semimetal transition 2–81097
- Pb-In alloys, thermal Hall effect and the Righi-Leduc angle, observations 2–68370
- Pb, amorphous state, free electron model 2–75048
- Pb, intermediate state, isotropic and anisotopic galvanomag. props. 2–47866
- Pb, temp. $\leqslant$4.2K 2–47836
- PbO, autocompensated photoconductor, rel. to inversion of the sign of conductivity 2–44175
- PbS layers, photocond. mechanism, elec. cond. and Hall effect obs. 2–81166

Hall effect continued
- PbSe epitaxial films on NaCl substrate, effects of ambient gas uptake 2–65008
- p-PbTe, rel. to room temp. transport props. 2–54161
- PbTe film, effect of O_2 and N_2 on mobility obs. 2–57191
- Pd-Ag alloy, low field Hall coeff., at 4.2K and 300K 2–61188
- Pd-Pt alloy, low field Hall coeff., at 4.2K and 300K 2–61188
- Pd-Rh alloy, low field Hall coeff., at 4.2K and 300K 2–61188
- Pd-Ru alloy, low field Hall coeff., at 4.2K and 300K 2–61188
- Pt-Au alloy, low field Hall coeff. at 4.2K and 300K, two band model 2–61188
- Pt-Ir alloy, low field Hall coeff. at 4.2K and 300K, two band model 2–61188
- Pt-Os alloy, low field Hall coeff. at 4.2K and 300K, two band model 2–61188
- Pt-Pd alloy, low field Hall coeff. at 4.2K and 300K, two band model 2–61188
- $RbAg_4I_5$ single crystals, of Ag ions 2–77949
- Ru, 4.2 K, interpreted rel. to Fermi surface 2–51103
- Sb_2Se_3, semicond., liq. 2–60498
- Sc film, size effect 2–81030
- Si:Na(K), impurity atomic radius effects 2–71948
- Si:P, implanted, annealing characts. 2–77594
- n-Si:P, piezo-Hall effect, 4.2, 77 and 300K 2–71945
- n-Si:P epitaxial film, on $MgO.Al_2O_3$, 76-350K 2–77910
- Si, anisotropy and hot electron effects, 1-300 K 2–84342
- n-Si, doped, rel. to microwave propag. 2–54197
- p-Si, electron irrad. effects 2–54201
- p-Si, electron irrad. effects 2–71944
- Si, γ-ray and neutron irrad. induced defect obs. 2–47937
- Si film, epitaxial, gas doped during deposition 2–50690
- n-Si proton bombardment induced shallow donors, elec. props. 2–61355
- SiO_2, three terminal electron Hall mobility measurements 2–54178
- Sn, amorphous state, free electron model 2–75048
- SnTe polycrystalline film, elec. props., temp. depend. 2–71916
- Tb, pressure effect on single crystals 2–68547
- Tb, rel. to press., 77-400K 2–77858
- Te, electron irrad. damage obs. 2–47392
- Te, liquid, rel. to n.m.r. obs. 2–71237
- Te film, and thermoelectric power Seebeck coeff., resistivity 2–54249
- Te valence band structure from Shubnikov-de Haas expts. 2–84245
- TiO_2, AC meas., polaron mass obs. 2–57174
- Tl-Te liquid, semicond., Hall mobility, electronic struct., two band model 2–60506
- $TlBiTe_2$ and TlTe, mobility temp. depend. 2–51144
- $Tl_2Se.As_2Te_3$, amorphous, mobility detn. 2–61331
- VO_x, 300K 2–64991
- V_2O_5 bronzes, electrical conductivity in solid and liquid state 2–84339
- Y film, size effect 2–81030
- Yb semimetal, temp. and uniaxial stress dependence obs. 2–71840
- ZnO, mobility detn. on crystals grown by chemical transport method 2–43516
- ZnTe, high temp. defect. equilib., elec. transport props. 2–44096

Hall generators *see Electricity/direct conversion; Semiconducting devices*

Hall mobility *see Hall effect*

Halogens
- atoms, neutral, spectra and structural obs. 2–79933
- halide minerals and rocks, visible and near i.r. spectra 2–72672
- interstitial atoms in KCl and KBr, ionization of In^{2+} and Tl^{2+} centres 2–81001
- metal halides, overlap repulsion, modified logarithmic form 2–43502
- mixtures with dioxan, v.l.f. far i.r. spectra 2–83322
- negative halide ions, decay and charge exchange cross sections in 300-3000 eV range 2–64052
- Raman, resonance Raman and fluorescence spectra obs. using tunable dye lasers 2–42262
- Van der Waals potential between halogen and inert gas atoms 2–80123
- X + HY (X = Cl, Br; Y = Br, I), energy distribution among reaction products 2–65369
- W-halogen lamps, thermodynamic study 2–61764

Hamidashi effect *see Ferroelectric materials; Ferroelectric phenomena*

Hard-sphere gases *see Quantum fluids; Statistical mechanics*

Hardness
- *see also Abrasion; Work hardening*
- alloys, body centred cubic, theory of solid solution hardening 2–77691
- austenitic stainless steel, effect of neutron irradiation on strain hardening exponent 2–77719
- bismuth oxide ceramics, rel. to use in nuclear reactors 2–83064
- brittle surface layers, det. using u.s. oscillations 2–56845
- ceramic alloy B2Zh, prep. and mech. characterization 2–77720
- cermet alloys based on Ni-containing titanium carbonitrides 2–68152
- Cu, inelastic phenomena and kinetics of damage for cyclic loading 2–60915
- diamond, abrasion resist. during polishing and grinding, microscopic cleavage mechanism 2–74868
- dispersion hardening, particle shape effects 2–74887
- elasto-plastic deformations, general class 2–63068
- engineering materials, hot hardness testing, mech. props. detn. 2–77680
- epoxy resin hardener HN 2200 2–77657
- film, Vickers type ultra-microhardness tester 2–43471
- fretting fatigue, effects of contact pressure 2–43712
- glass, optical, relation between abrasion, micro indentation hardness and maximum fracture velocity, expts. 2–56550
- glass ceramic, lithium silicate, fracture energy as function of struct. 2–50886
- glasses, elastic deformations in hardness testing 2–64739
- ionic crysts., NaCl type struct., anisotropy, Knoop hardness meas. 2–56836
- Knoop indentation testing, resolved shear stress distrib. calcs., computer program 2–60941

Hardness continued
measurement, British Standard methods 2−58684
metal, refractory hard, correlation with d-electron to atom ratio 2−47550
microhardness load dependence, microstresses and effects, tests on glasses and other non-metals 2−74864
microhardness meas. by method of small penetration of indentor 2−47549
microhardness tester attachment for meas. of deformation of wire in coiling 2−82129
pyrophyllite, firing temp. depend. 2−50890
quartz optical contacts, hardening by heat treatment 2−59252
radiation hardening of structural materials, review of developments in understanding 2−43803
reactor absorber materials performance in HFIR control cylinders 2−83129
rocks, indentation by rough wedge 2−57819
rocks, yield condition and hardening rule 2−57818
Rockwell α hardness ASTM D 785 and ball indentation hardness DIN 53456, conversion formula 2−57004
scale of hardness for Rockwell Superficial HR 30T test 2−43771
sea floor in nearshore waters 2−65619
shock stress amplitude and duration effects on residual hardness 2−68072
snow, temperature dependence 2−74865
solid solutions, hardening, statistical theories 2−50813
steatite, firing temp. depend. 2−50890
steel, ε-carbide phase form. and struct. 2−43844
steel, austenitic, high Mn, microhardness determ. 2−71638
steel, effect of heat treatment temp. 2−53842
steel, high carbon, workhardened, ageing and recovery obs. 2−47597
steel, high-speed W-Mo, effects of Co 2−53992
steel, low carbon, inelastic phenomena and kinetics of damage for cyclic loading 2−60915
steel, low-C martensitic, alloying element effects 2−50834
steel, mild, effect of high energy ultrasonic waves 2−77673
steel, mild, scratch and indentation hardness 2−53841
steel, Mn-Cr-B spring, tempering behaviour 2−77688
steel, nitrided by ion bombardment 2−56935
steel, prep. by powder metallurgy, microhardness rel. to sintering conditions 2−43892
steel, stainless, effect of explosive load 2−43836
steel, trasnsform. of austenite, obs. of hardness and microhardness 2−47690
steel martensitic, low-C Mn, effect of Sb on high temp. tempering, hardness testing 2−56905
steel rolls hardening depth, ultrasonic device for measurement 2−60928
steel targets, effect on ballistic behaviour 2−60980
steels, carbon, dynamic strengthening singularities under infl. of shock waves 2−84075
superficial Rockwell reading, use of diamond indenter 2−43747
system, plastic deformation, microhardness, emission electron microscopy 2−74843
tester, cast iron abrasive wear, obs. 2−50792
transition metal germanides, group IV-VI, microhardness, rel. to atomic volume change, structural loosening 2−74866
transition metal nitrides, 80-300K 2−61112
ultrasonic techniques of meas. 2−64752
wear parameters rel. to Young's modulus to hardness ratio 2−68111
welded joints, strength figures from metal hardness, meas. method 2−71617
Ag alloys, soln. hardening, stress equivalence 2−80834
Al-Ag alloy, precipitation process study 2−84133
Al-4%Cu alloy, rel. to effects of additional elements on ageing 2−56910
Al-Fe alloy, microhardness rel. to precip. of Fe and annealing out of lattice defects 2−50828
Al-Mg-Zn alloy, soln. softening effect of Zn additions at high temps. 2−47613
Al-9%Mg alloy, rel. to effects of additional elements on clustering and precip. during ageing50801 2−50801
Al-(N at.%) Mg, N=10, 8, alloy, age hardening and related properties 2−47612
Al, high purity, and dil. alloys, review 2−68076
Al, Knoop hardness anisotropy 2−43738
AlN-Al_2O_3-Mo cermet, and microhardness 2−43869
Al_2O_3, alumina, coupled solute solid soln. softening with MgO and TiO_2 2−47653
As_2Te_3-GaAs(Ga_2Te_3) system, rel. to phase diagram determ. 2−47713
Ba-mica/Al_2O_3 composite 2−56977
Be bronze, cold worked, precipitation hardening, press. induced thermal activation 2−43781
C, glassy fibres, derived from phenolic resin, mech. props. 2−84100
C film, diamond-like props. characterization 2−56588
Cd_3As_2-2CdTe system, rel. to phase diagram determ. 2−47708
$CdGeP_2$, CdGeAs, sphalerite-chalcopyrite transition, struct. of phases, micro-hardness 2−57025
$CdGeP_{2x}As_{2-2x}$, comp. depend. 2−47616
$CdGe_xSi_{1-x}P_2$, comp. depend. 2−47616
Cd_3P_2-2CdSe system, rel. to phase diagram determ. 2−47708
$CdSnAs_2$, sphalerite-chalcopyrite transition, struct. of phases, microhardness 2−57025
Ce_2Se_3-GeS_2 system, rel. to phase diagram determ. 2−61043
Co alloys, metallurgical structure and properties 2−71667
Cr-Ni alloy, stress rupture test, alloying additions effect 2−74856
Cr, high-purity phase obs. 2−47531
Cr, O-enriched, effect of Ce, Pr, or Nd 2−43830
Cu-Al alloy, exoemission kinetics and hardness depend. on strain or elongation 2−74836
Cu-Al alloy, plastically deformed, rel. to solute segregation to stacking faults 2−50681
Cu-Al alloy, two-phase struct., microhardness 2−71678
Cu-(0.6 at.%)Cr alloy, precip.-hardening, neutron irrad. effect 2−43833
Cu-Ni:Mn, Cr, Al, struct. and props. with ageing and hardening 2−83954

Hardness continued
Cu-(30 wt.%)Ni-0.3 wt.%)Be alloy, age hardening precipitate phases, struct. and morphology 2−50934
Cu-Zr, dil. alloys., softening resistance mechanism 2−56709
Cu, dynamic strengthening singularities under infl. of shock waves 2−84075
Cu, intermetallic compounds, obs. 2−50782
Cu, scratch and indentation hardness 2−53841
Cu, single cryst., depend. of deform.-resist. on rate and temp. of prev. loading 2−84010
Cu, single crystals deformed in tension, effect of strain rate upon hardening 2−84160
Cu alloys, soln. hardening, stress equivalence 2−80834
Er-B system phases, microhardness 2−50964
Fe:Sn, grain-boundary hardening, micro-indentation elastic recovery obs. 2−60910
Fe-Mg-Ni alloy, austenite transform., cooling rate effects 2−53991
Fe-Mn alloy, austenitic, singularities of hardening 2−50783
Fe-Ni-Nb-C alloy, effect of ageing 2−47596
Fe-Ni alloys, deform. martensite obs. 2−43838
Fe-Si single crystal, hardening, effect of dimensional factors 2−71568
Fe-Ta alloy, initial softening on annealing 2−57020
Fe, cast, spheroidal graphite at elevated temperature 2−43739
Fe, dynamic strengthening singularities under infl. of shock waves 2−84075
α-Fe, structure studies, neutron irradiation, transmission electron microscopy 2−60965
Gd-B system phases, microhardness 2−50969
GeTe-Bi_2Te solid soln. 2−74903
HFC-Re system, microhardness meas. of lattice const., solubility relations and phase diagram 2−84096
HfB_2-ZrN alloy, conc. depend. 2−47638
InBi, hot hardness and indentation creep 2−71602
$IrB_{1.1}$ characterization 2−47657
KBr, pure and doped 2−56835
KCl, pure and doped 2−56835
KCl crystals, effect of γ-irradiation on critical resolved shear stress 2−47492
$LiNbO_3$ single crystal, lapping characts. 2−71603
Li_2O-B_2O_3-GeO_2 glass, rel. to struct. 2−47059
Mg alloys, soln. hardening, stress equivalence 2−80834
Mg substitutional soln. hardening 2−43855
MgO-Li_2O-Al_2O_3-SiO_2-TiO_2, glass-ceramic, crystn., microstruct., indentation hardness 2−80535
Mn-Cu-Mo alloy, cold worked, heat treated 2−47476
Mn-Cu-W alloy, cold worked, heat treated 2−47477
Mo-Cr-alloyed or unalloyed case hardened steel, residual stresses in carbonized layers for different thermal treatments 2−56931
Mo-Ru alloy, high purity as-cast 2−50840
Mo alloy, rel. to struct. changes during deform. 2−50839
Mo alloy, strengthening by precip. of Ti and Zr carbides during ageing 2−47643
NaBr, pure and doped 2−56835
NaCl, pure and doped 2−56835
Nb, cold-worked or irrad., stage III recovery study 2−47404
Ni-Cr-Ti alloys, strengthening by precip. of intermetallic phases 2−43859
Ni-Cr steels, as measure of Cu additive effect on tempering 2−60957
Ni-40%Cr alloy, effects of Al and Ti on age hardening 2−64767
Ni-Cu-Al-Ti alloy, age hardening, precip. 2−53878
Ni-Fe-Nb alloy, and magnetic characts. 2−57293
Ni, dynamic strengthening singularities under infl. of shock waves 2−84075
Ni, recovery after 300 kbar shock wave loading 2−56794
Ni_3Al, effect of Cr, Ti or W alloying 2−43740
Pb-Ag alloys, ageing, softening mechanism and kinetics 2−43860
Pb-Sb alloy, precip. mechanism study 2−80858
Pb, scratch and indentation hardness 2−53841
PbS(Se)(Te), carrier conc. effect 2−50784
PbTe-UTe system, rel. to phase diagram determ. 2−47717
Re film, microhardness, condensation temp. effects 2−50501
Si:P, Knoop hardness and hardness anisotropy, impurity conc. effects 2−71604
SnF_2, soln. grown crysts. 2−47245
SnTe-UTe system, rel. to phase diagram determ. 2−47717
Ta-N, interstitial hardening orientation dependence 2−74844
Ta-W-Hf alloy, effects of O contamination, 1204°C 2−43862
Ti, dislocation structure effects in hardening 2−56714
Ti, dynamic strengthening singularities under infl. of shock waves 2−84075
Ti alloy surface, effect of gas saturation 2−53909
TiB_2 coatings characteriz. 2−51460
TiC-Mo_2C-Ni alloy, rel. to microstruct. 2−47538
TiC-Ni-Mo alloy, cermet, Mo alloying effects 2−47534
TiC, changes in microhardness following neutron irradiation 2−52848
U, β phase, function of number of quenching cycles 2−77659
V-Ti(Cr)(Sn)(Al) alloy, comp. depend. 2−53912
V, neutron irrad., anneal and radiation hardening, tensile props. 2−80665
W filament, rel. to appl. to composite reinforcement 2−53970
W filaments, reinforced in nichrome 2−53967
W film, chem. vapour deposited, effect of deposition conditions 2−47131
Zn-Al eutectic alloy, room-temp. deform. characts. rel. to superplasticity 2−43701
$ZnGeAs_2$, $ZnGeP_2$, sphalerite-chalcopyrite transition, struct. of phases, microhardness 2−57025
$ZnSiAs_2$, sphalerite-chalcopyrite transition, struct. of phases, microhardness 2−57025
$ZnSnAs_2$, $ZnSnP_2$, sphalerite-chalcopyrite transition, struct. of phases, microhardness 2−57025
Zr and Zircaloy tubular materials, texture and anisotropy rel. to plastic deform. 2−53916
ZrC-NbC, solid solution, creep meas. in compression, temp. range 2600-3150 K 2−84033

Hardness, magnetic *see Magnetic properties of substances/ ferromagnetic*

Harmonic analysis *see Acoustic analysis; Calculating apparatus; Fourier analysis*
Harmonic generation, optical *see Lasers; Nonlinear optics*
Harmonic oscillators *see Quantum theory*
Hartree-Fock method
  13 basis function calc. for water molecule based on selection of proper canonical orbitals 2−67477
  A=8-28 4n nuclei, calcs. of multipole deformations, static quadrupole moments, e.m. transitions 2−70364
  atom correlation models, Hartree-Fock functions and correlation splitting model 2−49933
  atomic, Brillouin's theorem for intershell correlations 2−70596
  atomic central-field models for open shells 2−64025
  atomic core-electron binding energies from orbital energies 2−79861
  atomic valence shell orbitals, optimization of transferability 2−70564
  atomic wavefunctions, full correl. approach 2−59910
  atoms, energy interactions for p^{n} configuration excited states, B to Br atoms 2−76964
  atoms, energy interactions in 3d^{n}4s^{0} and 3d^{n}4s^{2} configuration excited states in transition elements 2−76965
  atoms, numerical soln. 2−64010
  Auger and X-ray transition probabilities, calc. for elements Z=4-54 2−64008
  bubble nuclei in spherical configs., density calcs. 2−82905
  complex and unrestricted HF wavefunctions, conditions for instability 2−74197
  decoupled H-F method applied to atoms with orthogonalized orbitals 2−52904
  diagonalization of Hartree- Fock Hamiltonian for occupied states 2−45273
  double excitation of atoms by electron impact, construction of target wave functions 2−70607
  double-closed-shell nuclei, using modified delta interaction 2−63747
  electric quadrupole transitions in Fe XVI, Co XVII, Ni XVIII, calc. of multiplet strengths using HF orbital wave functions 2−42728
  electron scatt. form factors calc. for ^{12}C 2−82956
  electron spin-spin contact interaction in many-electron atoms 2−59905
  excited states, extended method orbitals 2−79971
  extended method using corresponding orbitals, application to LiH 2−53021
  extended SCF methods, cusp conditions 2−59939
  finite nuclei A=16−208, calc. of density dependent effective interactions using HF theory and local density approx. 2−79709
  formaldehyde with Slater basis sets, magnetic susceptibility and ^{17}O and ^{13}C n.m.r. shielding constants 2−50094
  frozen-core type wave function calcs. of elec. quadrupole transitions of Na isoelectronic sequence 2−56102
  inorganic radicals, calculation of hyperfine coupling constants 2−42863
  iterative solution of equations with improved stability 2−83181
  large molecules, numerical computation with dynamical basis set 2−83232
  light nuclei, $4 \leqslant A \leqslant 41$ unrestricted HF approx. calcs. of ground state properties 2−63733
  magic nuclei, shell effects, self-consistent calc. 2−63783
  methane molecule, electronic structure, analysis of formation in Hartree-Fock model 2−60074
  molecular systems, ten-electron, united-atom many-body perturbation procedure 2−67480
  molecules, energy expectation value of Hamiltonian, direct minimization 2−70651
  Newton-Kantorovic procedure consistent symmetry 2−70342
  nonlinear eqn., rigorous method of solution, application to ^{16}O 2−76761
  nuclear charge distribution calc. tested by electron scattering data 2−74016
  nuclear many body problem, generalization incorporating 2 body correlations 2−63730
  nuclear rotational states, stability condition determ. using procedure of Hartree-Fock-Bogoliubov method 2−63755
  nuclear single nucleon transfer reactions, form factor calc. 2−70427
  nuclear states structure and systematics, relation of collective motion 2−82863
  nuclear struct. applic., cranked Hamiltonian concept 2−59682
  nuclei, binding energy, relativistic Hartree- Fock approximation 2−42490
  nuclei, practical angular momentum projection method in multishell Hartree-Fock calc. 2−46119
  nucleon-nucleus potential, Hartree-Fock approx. with Skyrme interaction 2−63891
  oscillator strength calculations in frozen core HF approx. length and velocity formulae 2−46408
  pairing tendencies of T=1 and T=0 interactions 2−79719
  perturbation theory for spherical gaussian SCF-MO wavefunctions, applic. to LiH, Li$_2$, BH 2−50052
  perturbation theory of magnetic shielding and susceptibility developed using basis set of gauge invariant atomic orbitals 2−42850
  projected, for elastic and inelastic electron scattering on nuclei 2−82957
  projected wave functions in inelastic nucleon-nucleus scattering, coupled-channel treatment 2−70443
  relativistic atomic energies, fine structure splitting 2−42713
  renormalized approach to perturbation theoretic study of many-fermion systems 2−78855
  Roothaan-Hartree-Fock, selection of proper canonical orbitals for particular applications 2−67373
  SCF calcs. on large molecules using molecular fragments, construction of initial P-matrices 2−70667
  SCF field molecular wave functions, approximations 2−42851
  SCF wavefunctions for sequence depend. of DNA hypochromism 2−80118
  self-consistent field theory, equations of motion approach to nuclear spectroscopy 2−82947
  (s,d)-shell nuclei, α-type, single effective interaction calculations 2−49710
  spherical nuclei, HF calcs. in local density approx., saturation properties 2−79710

Hartree-Fock method continued
  spin densities, unrestricted Hartree-Fock calc. with orthogonalized atomic orbitals 2−67453
  superheavy nuclei, radii and binding energies 2−63838
  thermodynamic Green's functions, occupation numbers computed 2−58788
  transition metals optical absorption, a model calc. 2−84498
  two particle-two hole excitation, stability of solutions 2−42493
  two-, three- and four-electron ions, Hartree-Fock and Hartree-Fock-Slater atomic form factors, electron momentum distributions 2−74205
  variation after projection method tested on ^{44}Ti 2−74019
  variation-perturbation uncoupled scheme applic. to polarizability calcs. of 12- and 18-electron systems 2−79929
  virtual orbital approach to description of excited states 2−64070
  Z=35-85, calc. of Auger group rates and fluorescence yields for vacancy in 3p or 3d shell using nonrelativistic HFS model 2−70572
  N-N effective interaction, RPA renormalization in HF basis 2−73971
  π-electron approx., justification from Hartree-Fock method 2−79988
  Ar, energy bands calc. 2−84272
  Be atoms in small aggregates, calculation of electron states 2−80978
  ^{8}Be rotational states, properties of projected HF functions of ground state bands 2−73992
  C 2p3p, term dependence of Hartree-Fock results 2−56092
  CH, diatomic, calc. of Hartree-Fock photoionization cross section using many body perturbation theory 2−80018
  CO electric dipole moment calc. configuration interaction calc. near HF limit 2−74258
  ^{12}C rotational states, properties of projected HF functions of ground state bands 2−73992
  Ca 3d4d, term dependence of Hartree-Fock results 2−56092
  F^{-}, deformated H-F states, correlation effects 2−76986
  FeH, electronic states, approx. calc. using single-centre basis state 2−67474
  He, nsms ^{1}S states with orthogonal orbitals, theorem on Hartree-Fock eqns. 2−56128
  He 1s2s, term dependence of Hartree-Fock results 2−56092
  Li atoms in small aggregates, calculation of electron states 2−80978
  NH$_3$, force const., dipole moment derivatives 2−80029
  Ne-Ne^{+} inelastic collisions, ab initio H.F. calcs. for Ne$_2$, Ne$_2^{+}$, Ne$_2^{++}$ systems for different interatomic distances 2−49969
  Ne, deformed H-F states, correlation effects 2−76986
  ^{20}Ne rotational states, properties of projected HF functions of ground state bands 2−73992
  O^{-}, deformed H-F states, correlation effects 2−76986
  ^{16}O, Hartree-Fock intrinsic states 2−63776
  ^{16}O, rigorous method for soln. of Hartree Fock equation 2−76761
  ^{16}O rotational states, properties of projected HF functions of excited 8p-8h band 2−73992
  ^{44}Ti, Hartree-Fock variation after projection method, test 2−74019

Hearing
  see also Ear; Speech
  aquatic animals, cochlear hair cells, microsensitivity enhancement by environmental K ions 2−66306
  audiometer for meas. ability 2−76103
  audiometric l.f. threshold levels, field survey 2−66299
  auditory adaption, relative magnitude changes with additional management conditions 2−45128
  auditory evoked potential in man, review 2−62875
  auditory evoked potentials, stimulus sequencing and late components 2−45095
  auditory short term memory, limiting conditions 2−82050
  auditory system modelling in USA 2−82058
  bats, echolocating and target-ranging rel. to sonar receiver 2−55546
  Bekesky thresholds using single sweep frequency modulation 2−48919
  Bekesky thresholds using single sweep frequency modulation 2−48919
  Bekesy thresholds and amplitude meas., effects of testing methods 2−45146
  binaural analysis as function of physiological masking 2−45126
  binaural detection in sequential detection paradigm 2−45121
  binaural equal-loudness contours for normal hearing observers 2−45130
  binaural interaction in l.f. stimuli 2−51951
  binaural l.f. medullary neurons, input-output functions, kangaroo rat 2−45152
  binaural loudness balance, unequal duty cycles 2−69455
  cat, parametric obs. of neutrons in inferior colliculus using stimuli of varying informational value 2−45151
  cats, evoked tactile and auditory central nervous system responses after 915 MHz microwave irradiation 2−51923
  cats, primary evoked potentials, effects of medial geniculate lesions 2−45153
  central auditory masking 2−66293
  characteristics of violin tone, research potentials 2−48911
  characteristics of violin tone, research potentials 2−48911
  chimpanzees, chronic exposure to impusive noise, bheavioral effects 2−45154
  chinchilla, temporary threshold shift, electrophysiological correlates 2−82038
  chinchilla, tone deletion from tonal pattern, detectability 2−45168
  chinchilla's response to auditory change, latency 2−45169
  chinchillas, comparison between hair cell losses and permanent threshold shifts for impulse noise 2−45156
  chirps, frequency modulated, of various bandwidths, frequency discrimination 2−45114
  cochlea, fractional distortion pairs 2−66297
  cochlear microphonics and action potentials, difference between inner and outer cell populations in generation 2−45094
  combination bands of even order, masking effects, levels of difference bands estimation 2−82044
  combination tones, audibility region 2−66300
  combination tones, elevated threshold 2−66301
  conference, 83rd meeting Acoustical Society of America, (New York, April 1972) 2−41683
  consistency of hearing for speech across diverse listening conditions 2−55314

Hearing continued
consonant confusions, effect of broad band masking noise 2—45092
constant loudness preservation with interaural amplitude asymmetry 2—82047
contralateral reflex elicited by wide-band noise and pure tones, dynamic characteristics 2—82045
contralateral white-noise masking effects on auditory thresholds 2—45145
critical band development 2—66304
critical masking interval, masking brief signal by noise 2—45110
deafness risk rel. to noise levels on aircraft carrier flight decks 2—41825
dichotic fusion along acoustic continuum 2—48914
dichotic fusion along acoustic continuum 2—48914
dichotic scores of temporal lobectomies, hemispherectomies, and normals, effect of competing CVs, vowels or bleats 2—45136
dichotic speech perception, interaural intensity differences 2—45135
discrimination, combinations of amplitude and frequency differences 2—58642
distortion products f_2-f_1 and $2f_1$-f_2 2—48901
distortion products f_2-f_1 and $2f_1$-f_2 2—48901
diver auditory sensitivity and bone conduction 2—45124
dolphins, atlantic bottlenose, auditory frequency discrimination 2—66310
ear defender, amplitude sensitive 2—73219
ear protection in factory environment 2—73218
earphone coupling system for acute physiological obs. 2—82054
earphone enclosure for communication in noise, enhanced noise reduction 2—45083
earplugs, custon-fitted, attenuation 2—45122
echolocating bats, horizontal angle resolution 2—48930
echolocating bats, horizontal angle resolution 2—48930
effective perceived noise level, duration correction 2—73450
equal loudness contours derived from sensory magnitude judgments 2—48909
equal loudness contours derived from sensory magnitude judgments 2—48909
exact scale prejudging using tolerance 2—55310
forward masking dependence on masker duration 2—55311
frequency discrimination changes caused by leading and trailing tones 2—48908
frequency discrimination changes caused by leading and trailing tones 2—48908
funneling mechanism and two-tone inhibition 2—76104
gerbils, effect of short term adaptation on incremental responses of auditory neurons 2—45150
goldfish, auditory threshold, temporal summation 2—66308
goldfish, perception of a.m. auditory signals 2—66309
guinea pig, cochlear degeneration following impulse noise exposure 2—45157
guinea pigs, cochlear partition, effects of electrical biasing 2—66305
guinea pigs, detection threshold discrepancy, electrophysiologic obs. 2—45148
guinea pigs, noise exposed, temporary threshold shifts and action potential amplitude obs. 2—45159
head related stereophony for psychological hearing comparisons of different rooms 2—58645
hearing aid evaluations, factor analysis of competing message testing 2—45143
hearing aids, time constant of compression, comparison measurements 2—45142
hearing-aid acoustics, semantic labelling in quality questionnaire 2—45141
human auditory system modelling 2—76105
impairment to noise exposure and age, relation 2—45140
intelligibility, interaural delay 2—45137
interaural phase and level differences in detection and lateralization at 1000 and 2000 Hz 2—82048
interaural time and level differences, detectability signal duration 2—66298
intonation display system, for deaf people 2—55303
kangaroo rat and man, magnetically coupled stimulation of ossicular chain 2—66303
lateral inhibition, psychophysical evidence 2—48904
lateral inhibition, psychophysical evidence 2—48904
lateral inhibition, rippled noise investigations 2—45105
lateralization, dichotic listening data for children 5 to 10 years old 2—45134
lateralization degree of dichotically presented stimuli, unbiased procedure 2—45133
lateralization thresholds, left- and right-ear and median plane, interaural intensity relations 2—45129
l.f. masking, physiological noise, cardiac cycle effects 2—82051
l.f. sound, annoyance effects 2—69775
l.f. sounds, audibility measurements 2—55312
l.f. threshold effects, infrasound 2—73220
listening rate preferences of adults, normative study 2—45102
localization of front and rear sound source 2—82036
loudness, relation to averaged electroencephalic response 2—55315
loudness as a fu. of tone duration 2—45106
loudness discomfort levels for pure tones and noise 2—45125
loudness enhancement following contralateral stimulation 2—82040
loudness enhancement of tone burst by preceding tone burst 2—45107
masked threshold at reduced ambient pressures 2—45123
masking by combination bands, level estimation 2—82043
masking level difference, gating from uncorrelated to correlated noise 2—66296
masking level difference for uncorrelated noise, effect of signal frequency 2—48907
masking level difference for uncorrelated noise, effect of signal frequency 2—48907
masking obs. in landscaped office 2—41832
masking of narrow bands of noise near h.f pure tones, combination band levels 2—82042
masking with continuous and gated sinusoids 2—48905
masking with continuous and gated sinusoids 2—48905
missing harmonic detection in continuous or pulsed harmonic complex 2—45109
monaural and antiphasic binaural psychometric functions, invariance 2—82049

Hearing continued
monaural distortion product estimation, algorithm for anal. of phase effects 2—82039
monaural localization of noise 2—45132
monaural phase effect, cancellation and reinforcement of distortion products 2—48902
monaural phase effect, cancellation and reinforcement of distortion products 2—48902
monaural phase effects, tone on tone masking 2—69454
monaural phase effects for two tone signals 2—48903
monaural phase effects for two tone signals 2—48903
monkey, integration time constant from period histograms 2—45160
monkeys, impairment following exposure to noise 2—45158
multidimensional tonal dissimilarity, direct estimation 2—51950
music, ear and brain 2—66294
musical timbre recognition based on auditory system model 2—69456
mutual interference between two linguistic dimensions 2—45138
negative afterimage, Zwicker's experimental studies 2—48906
negative afterimage, Zwicker's experimental studies 2—48906
neural phase locking to combination tones, transducer model 2—45108
noise, in-ear meas., individual's exposure 2—45082
noise annoyance, individual differences 2—45139
noise annoyance, jet aircraft takeoff 2—73222
noise annoyance susceptability 2—55313
orientation of animals and insects on sensory basis, conference, N.Y., USA (1971) 2—58646
owl monkey, auditory sensitivity 2—45170
paradigms, one- and two-interval, intensity and frequency discrimination 2—45112
patients with sensorineural hearing loss, consonant confusion 2—45091
pattern discrimination in absence of spectral cues 2—45116
perceived pitch of prevocalic consonants 2—45067
perceived sound level calc., rel. to perceived light 2—73221
perception of pulse-modulated u.h.f. electromagnetic energy, psychophysical obs. 2—51954
perception using coarticulation 2—45101
perceptual asymmetry, cross language obs. 2—45085
perceptual features of English consonants det. by choice reaction time 2—45086
perceptual features of prevocalic Hindi consonants 2—45087
phase-locked pure-tone octave masking, sensorineural hearing obs. 2—48918
phase-locked pure-tone octave masking, sensorineural hearing obs. 2—48918
pigeon, cochlear potentials, relation to age, cholesterol and sclerosis 2—45162
pitch of noise 2—58641
pitch of pure tone, effects of masking tones and noises 2—55309
pitch of short sinusoidal pulses as function of initial phase 2—55515
pitch of single period tones, perception 2—45113
pitch perception due to slow fluid waves in cochlea 2—58638
pitch perception impairment by temporally continuous stimuli 2—45115
pitch perception of complex tones, functional model 2—58644
pitch perception of complex tones 2—58643
polststimulatory masking, pure tones 2—62876
post stimulatory masking phenomena, tests on model 2—73225
post-stimulatory masking phenomena, model 2—73224
poststimulatory masking, thresholds as fn. of probe tone duration 2—62877
protectors in industrial noise, variation with noise spectra and with people 2—73217
pulsed stimuli, rate changes, correct detections 2—45119
pure-tone central masking, low frequency, temporal relations 2—45127
pure-tone masking in normal and cochlear-impaired ears 2—48917
pure-tone masking in normal and cochlear-impaired ears 2—48917
recovery from sound exposure rel. to cat 2—45100
residue pitch perception, model prediction 2—45104
sensitivity, influence of external ear acoustics 2—45096
sensorineural acuity level testing, system with clinical applications 2—45144
short tone pulses, pitch estimation, dependence in duration 2—69453
signal detection as function of contralateral sinusoid-to-noise ratio 2—48910
signal detection as function of contralateral sinusoid-to-noise ratio 2—48910
signal detection of uncertain frequency, individual alternative signals analysis 2—45120
silent gap discrimination in two-tone sequences of different frequencies 2—45117
simultaneous two-channel signal detection, correlated and uncorrelated signals 2—51952
single unit response to f.m. tones, inhibitory effect of two tone stimuli 2—78669
sinusoids in noise, detection as fn. of S/N ratio 2—45111
sonic boom startle, field study in West Germany 2—85137
sound analyser, adaptive processes in cases of minor brain injury 2—78668
sound pressure levels from stereo components, damage risk 2—66292
speaker recognition, efficient acoustic parameters 2—48913
speaker recognition, efficient acoustic parameters 2—48913
speech discrimination loss and masking by low-frequency vowel formants 2—48915
speech discrimination loss and masking by low-frequency vowel formants 2—48915
speech feature perception by listeners with severe sensorineural hearing loss 2—48916
speech feature perception by listeners with severe sensorineural hearing loss 2—48916
speech perception, articulator rate and acoustical invariants 2—45089
speech perception, obs. of stress patterns and errors 2—45090
speech perception under conditions of spectral transformation, phonetic characteristics 2—55305
speech/nonspeech perceptual contrasts 2—45084
spoken German consonants, automatic recognition of spectrum features 2—58639

- **Hearing** continued
  - squirrel monkey, hearing losses caused by intense auditory stimulation 2−82046
  - stimulus bandwidth effects on listener judgements of vocal loudness and effort 2−66290
  - temporal gap discrimination, silent durations 2−66295
  - temporal integration at relatively high masked threshold levels 2−48900
  - temporal integration at relatively high masked threshold levels 2−48900
  - temporal order perception, special rules for initial and terminal sounds of sequences 2−45118
  - temporary and permanent threshold shifts produced by 3 levels of impulse noise 2−45155
  - temporary threshold shift, changes associated with humming and non-vocal activities 2−82037
  - temporary threshold shift from impulses 2−45099
  - temporary threshold shift from l.f. and h.f. intermittent noise as function of off time 2−45098
  - tone detection, absence of masking noise, signal intensity and freq. 2−66302
  - tone-on-tone masking for binaural listening conditions 2−82053
  - underwater hearing, absolute thresholds and sound localisation 2−82059
  - verbal transformation effect, consistency of subjects' reported verbal transformation 2−45093
  - voice identification, two year expt. 2−48912
  - voice identification, two year expt. 2−48912
  - wavetrain signals and equal loudness pressures, frequency 250 to 6000Hz 2−45131
  - Pb induced auditory impairment and VDL and AP charges in chronically poisoned guinea pigs 2−45164
- **Heat**
  - *see also Radiation/heat; Thermodynamics*
  - boundary-initial-value problems, semidiscrete approx. 2−63053
  - distortion of semi infinite solid due to transient surface heating 2−58963
  - generation in torsional spring subjected to sinusoidal oscillations, heat generation 2−55501
  - lines, nonuniform, asymmetry coeff. of pulse 2−55565
  - production in cylinder, analysis using Gegenbauer polynomials 2−41855
  - pulse, asymmetry coeff. for non-uniform heat lines 2−55565
- **Heat capacity** *see Specific heat*
- **Heat conduction**
  - *see also Conductivity. thermal*
  - — 2−68256
  - — 2−60176
  - Black Sea floor 2−54738
  - circular cylinder, semi-infinite, containing heat sources 2−82256
  - contact thermal resistances, non-steady, determination by inverse methods of heat conduction 2−58953
  - cylinder, anal. using Gegenbauer polynomials 2−41855
  - differential equation, modification when temperature changes within mean free path 2−58958
  - droplet growth, constraint 2−43301
  - dual analysis, by finite element method 2−73464
  - eddy conductivity in turbulent flow in heated channel 2−76396
  - glass, molten, exptl. and analytical study 2−52270
  - heat-pipe performance, steady-state, model 2−76398
  - helically heated tube, steady state temp. distribution 2−66645
  - hyperbolic equation, geometrized theory 2−45588
  - ice, explanation of classical wire expt. 2−45587
  - Kampe de Feriet expansion formulae evaluation of integrals 2−55373
  - laser heating of plasma 2−64258
  - low gravity environment, expts. to demonstrate heat conduction mechanisms 2−58954
  - numerical soln. of heat eqn. using Chebyshev series 2−58957
  - plasma instability analysis 2−80359
  - polystyrene, polystyrene +20% by weight divinylbenzene, 1°K to 115°K 2−71732
  - relativistic formulation for conduction between bodies in relative motion 2−55567
  - relativistic thermodynamics, co-moving, equivalence of two major formulations 2−41475
  - sinusoidally modulated heat flow in multilayer and pyroelectric effect 2−52275
  - slab, absorbing, emitting, scattering, with reflecting boundaries 2−45580
  - sphere, approx. soln. to heat conduction equation 2−76220
  - sphere, thermal stress at its boundary surface 2−78878
  - steel laminate stacks, surface texture effects 2−49180
  - Stefan problem, axisymmetric, with boundary condition of second kind 2−63151
  - superposition in the approximation solution 2−63153
  - terrestrial, during frost heaving, meas. 2−75447
  - terrestrial flow in N.E. England 2−48375
  - thermal diffusivity, meas., heat pulse methods, apparatus, 20-300°C 2−55573
  - two-dimensional flow with conduction and convection, convergence and accuracy of finite difference schemes 2−60153
  - two-temperature plasma, laser heating 2−64259
  - unbounded plate with arbitrary initial temp. distribution 2−58956
  - wires, thermokinetic potentials, curent-affinity relations, nonequilibrium thermodynamics 2−49031
  - He II, critical heat flux density and thermal quenching in long channels 2−47021
  - $NaNO_3$, thermal diffusivity, critical parameters 2−57052
- **Heat exchange** *see Heat transfer*
- **Heat flow** *see Convection; Heat conduction; Heat transfer*
- **Heat losses** *see Heat transfer*
- **Heat measurement** *see Calorimeters; Calorimetry*
- **Heat of adsorption**
  - glass, of Xe, isosteric heat meas. 2−50529
  - Ar monolayer, of ^{3}He and ^{4}He, low temp. 2−43493
  - Au, of CO, determ. from i.r. refl.-absorpt. study 2−60676
  - Ge, of Cd, mol. beam technique 2−50534
- **Heat of adsorption** continued
  - He monolayer adsorbed on surface of Ar crystal, calcs. of heat of absorption and band widths 2−43490
  - MgO, of sulphur dioxide, 423K, adiabatic calorimetric obs. 2−83871
  - Ni, of hydrogen, cryst. oreintation influence 2−60680
  - Ni film, of H_2 and D_2, isotope effect 2−43497
  - Pt, of H_2, rel. to coverage 2−77514
  - S sensitizers for photographic AgBr, AgCl and Ag_2S 2−73686
  - W, of Cd, mol. beam technique 2−50534
- **Heat of combustion**
  - propane, heat release in multistage reaction 2−58146
- **Heat of crystallization** *see Crystallization*
- **Heat of dissociation**
  - unimolecular reaction, kinetic energy release, thermochemical aspects 2−75368
  - Ce_xS_y, heats of atomization, from mass spectrometric studies 2−72545
  - $EuCl_2$, dissociation energy calc. 2−64515
  - N_2O_4, liq., ioniz. enthalpy determ. from cond. and permittivity 2−84612
  - $Sb_4 \rightleftharpoons 2Sb_2$, mass spectrometric determ. 2−72554
- **Heat of formation**
  - carbonium ions, MINDO/2 calc. 2−77112
  - cyclopropanes, protonated, MINDO/2 calc. 2−77112
  - organic F containing σ-bonded molecules, MINDO/2 calc. 2−77111
  - phenyl radical, photoionization, determ. of heat formation and ionization potential 2−67520
  - sodium phosphate glasses, from heat of solution obs. 2−74598
  - Ag-Ga(In)(Ge)(Sn) solid solns., partial free enthalpies of form. determ. in galvanic cells 2−64887
  - AlF_2, by reaction $2AlF(g) \rightleftharpoons Al(g) + AlF_2(g)$ 2−72543
  - $AlOF_2$, by reaction $AlF(g) + AlOF(g) \rightleftharpoons Al(g) + AlOF_2(g)$ 2−72543
  - BP, calc. from heat of reaction $9BCl_3.PCl_5(s)$ 2−48330
  - CS, from $CS_2 + S$ gaseous equil. 2−72544
  - $Ce_2(CO_3)_3.6H_2O$, standard heats 2−43335
  - CrSi, $CrSi_2$, Cr_3Si, Cr_5Si_3, isobaric-isotherm. potl., entropy and heat of formation detn. by meas. galvanic e.m.f. 2−68246
  - Fe_2O_3, heat of transformation, decomposition temp. Gibbs free energy of formation determ. by EMF method 2−51425
  - $Gd_2(CO_3)_3.xH_2O$, standard heats 2−43335
  - $LuC_2(s)$, rel. to investigations of Lu-C system vaporization 2−64518
  - $RhC_{(2)}$, heats of atomization determ. by high temp. mass spectrometry 2−84623
  - SbS, from reaction $Sb_2S_3(s) \rightarrow 2SbS(g) + 1/2S_2(g)$ 2−74595
  - $Sm_2(CO_3)_3.xH_2O$, standard heats 2−43335
  - TiC_2, heats of atomization determ. by high temp. mass spectrometry 2−84623
  - VO, effusion mass spectrometric determination 2−44476
  - VO_2, effusion mass spectrometric determination 2−44476
  - V_4O_{10}, effusion mass spectrometric determination 2−44476
  - V_4O_8, effusion mass spectrometric determination 2−44476
- **Heat of fusion**
  - energy of melting from nonlocal pseudopotential theory 2−60544
  - metal, rel. to cryst. struct. 2−64506
  - metals, rel. to liq. struct. factor, Percus-Yevick formulation 2−64434
  - nuclear, rel. to laser heating of plasma in focus-type system 2−77288
  - nuclear, rel. to laser heating of plasma in focus-type system 2−77289
  - polyethylenes, chlorinated, differential scanning calorimetry 2−50400
  - Al_2O_3, alumina, condensed phase near melting point 2−54044
  - α-Al_2O_3, corundum, high temp. calorimeter obs. 2−53490
  - BeO, determination by mixing method 2−56496
  - LiH, det. from meas. of enthalpy 2−64507
  - Nb, from enthalpy in liquid and solid states 2−54038
  - V, determ. by obs. of liq. and solid state near melting point 2−47029
  - ZnTe, DTA determ. 2−47033
- **Heat of mixing** *see Heat of solution*
- **Heat of reaction**
  - ceramics, determ. by direct calorimetric anal. 2−54522
  - cyclopentadiene, negative ion formation and negative ion-molecule reactions, estimation of thermochemical parameters 2−46986
  - protonation of acetate ion, 20°C 2−48314
  - protonation of tris-(hydroxymethyl)-aminomethane, 20°C 2−48314
  - thermochemical model of ESCA shifts, near equivalence of quantum mechanical potential model 2−72535
  - thianthrene complexes in solution, fluorescence study, enthalpies 2−84637
  - $Ce_2S_2(g) \rightarrow 2CeS(g)$, rel. to heat of atomization determ. for Ce_xS_y cpds. 2−72545
  - $Ce_2S(g) \rightarrow Ce(g) + CeS(g)$, rel. to heat of atomization determ. from Ce_xS_y cpds. 2−72545
  - $CeS_2(g) + Ce(g) \rightarrow 2CeS(g)$, rel. to heat of atomization determ. for Ce_xS_y cpds. 2−72545
  - $Ce_2S_3(g) + Ce(g) \rightarrow 3CeS(g)$, rel. to heat of atomization determ. for Ce_xS_y cpds. 2−72545
  - Cl^-, heat of hydration, SCF Dirac-Slater calcs. 2−53403
  - $Ge + SiO \rightleftharpoons GeO + Si$, mass spectrometric determ. 2−72548
  - $HNO_3 + NaOH \rightarrow NaNO_3 + H_2O$, 20°C 2−48314
  - $H + H + OH \rightleftharpoons H_3O^+ + e-$ reactions in flames, kinetics and heats of reactions 2−54541
  - Na^+, heat of hydration, SCF Dirac- Slater calcs. 2−53403
  - $P(s) + 2.5Cl_2(g) + BCl_3(g) \rightarrow BCl_3.PCl_5(s)$, rel. to BP heat of formation calc. 2−48330
  - $Sb_4 \rightleftharpoons 2Sb_2$, mass spectrometric determ. 2−72554
- **Heat of solution**
  - alloy, binary, at infinite dilution, pseudopotential perturbation method 2−56495
  - benzene-xylene, heat of mixing determ. by microcalorimetry 2−77426
  - liquid-liquid interface, unsteady state transfer of solute, effect of heat of solution on Marangoni convection 2−77381
  - polymer, free energy of mixing 2−60436
  - polymer solution, press. and temp. depend. 2−64446
  - sodium phosphate glasses and heat of formation determ. 2−74598
  - tris-(hydroxymethyl)-aminomethane, in 0.1 M HCl, 20°C 2−48314
  - CaH_2-LaH_3 system 2−50958

Heat of solution continued
  $Ce_2(CO_3)_3.6H_2O$, standard heats 2−43335
  Cs-K alloy, pseudo alloy atom model 2−74897
  Cs-Rb alloy, pseudo alloy atom model 2−74897
  $Gd_2(CO_3)_3.xH_2O$, standard heats 2−43335
  KCl, in water, 20°C 2−48314
  Li-Bi liquid alloy, of Nd and Th 2−43334
  NH_3, enthalpies of solution and formation by direct solution calorimetry 2−77422
  Nb-H, dil., entropy and enthalpy of soln. 2−53903
  Nb-H solns., nondil., equil. press.- comp.-temp. relationships 2−50843
  Sb-Sn-Zn system, heats of mixing, 650°C 2−43336
  $Sm_2(CO_3)_3.xH_2O$, standard heats 2−43335

Heat of sublimation
  naphthalene, enthalpy of sublimation, calorimetric detn. 2−77477
  Bi_3, third law anal. 2−72554
  $EuCl_2$, second-law values for condensed state, calc. 2−64515
  In_2S, and of formation 2−74485
  Sb_3, third law anal. 2−72554

Heat of transformation
  ^3He-^4He soln., liquid-liquid transition 2−43422
  Pb-Bi peritectic alloy, heat of solidification, calc. 2−43444

Heat of vaporization
  alkali halide vapours, vapour pressures and enthalpies of vaporization, detn. 2−77473
  metal, single-atomic 2−71152
  water calc. using hydro-polyhydrol model 2−43317
  Sb_2S_3, thermogravimetric Knudsen effusion vaporization studies 2−74595

Heat of wetting *see Wetting*

Heat pumps *see Heat transfer*

Heat radiation *see Radiation/heat*

Heat transfer
  see also Convection; Heat conduction; Radiation/heat; Radiative transfer
  — 2−67548
  — 2−67878
  — 2−71280
  — 2−67571
  absorbing emitting, isotropically scattering medium, simultaneous ablation and radiation studied by normal-mode-expansion technique 2−41854
  acetone drops, from small diameter channel in film boiling temp. range 2−53379
  aerodynamic, blunt bodies, effects of slip 2−60359
  air, transpired turbulent boundary layer 2−45577
  air mass transformation experiment, East China Sea 2−62164
  air with injected species, two-dimensional stagnation point flows 2−45576
  air-cooled exchanger, flow characts. in box plenum chamber 2−71088
  air-sea interface, unified model for heat and gas exchange 2−62069
  air-water cocurrent flow on flat plate, enhancement of heat transfer by waves 2−56494
  air-water interface, rel. to sea surface temp. meas. 2−65625
  alkali metal boiling, temp. inversion in tubes under annular flow 2−64514
  analytical solns. to eqns. in finite regions 2−49175
  annular flow condensation in horizontal tubes, prediction of mean Nusselt number 2−83444
  annular transfer, transmission probabilities and radiosity 2−66636
  atmosphere, homogeneous, above basement layer 2−48444
  atmospheric geostrophic drag, heat and mass transfer coefficients for the diabatic Ekman layer 2−57957
  atmospheric total static energy classification, comparison with energy flux classification at sea surface 2−54815
  axially symmetric bodies, laminar, transition and turbulent heat transfer to leeward side 2−53306
  Baffin Bay and Labrador Sea 2−68869
  bibliography, Russian publications 2−45583
  bibliography 2−45584
  bibliography of polish works (1969-1970) 2−58951
  bibliography of Soviet work in 1970 2−55579
  boiling from small cylinders in water and organic liquids, identification of heat removal modes 2−77472
  boundary layer, three dimensional, iterative calculation 2−53275
  boundary layers, improved Lighthill analysis 2−45574
  bubble, vapour, growing 2−53377
  capillary discharge, instability with evaporating wall 2−56385
  carboxymethyl cellulose, water soln., laminar flow 2−74498
  to CO_2 at supercritical pressure 64394 2−64394
  cocurrent oblique crossflow transfer, angle between flow directions between 0 and 90 degrees 2−50146
  combustion gas plasma, in electric fields, obs. 2−80300
  compressed gas, losses in adiabatic compression unit 2−56402
  compressible turbulent boundary layer, to rough surfaces in pressure gradient 2−56425
  computation for laminar boundary layer without pressure gradient 2−53129
  condensation of steam under stratified flow conditions, empirical correlation 2−83670
  contact thermal resistances, non-steady, determination by inverse methods of heat conduction 2−58953
  control of binary gas mixture condensation 2−77466
  convection, forced and free, heat transfer from vertical thin needles in uniform stream 2−80179
  convective, from flames, soln. of conservation eqns. 2−76401
  convective, of MHD jet flow near wall 2−60200
  convective, radiative, CO_2-N_2 mixture, hypersonic flow, shock wave, stagnation point 2−82250
  convective and radiative wall heat flux delineation, calorimetric gauge 2−41850
  convective field in clean air, plume theory 2−44686
  Couette flow of viscous fluid with particle injection, determ. of velocity and temp. distrib. 2−77225
  coupled materials, thermal contact resist., sinusoidal press. variation influence 2−74998

Heat transfer continued
  cross-inclined tube bundles, thermal performance meas. by transient method 2−55580
  cylinder, with time varying coeff., calc. of temp. transients 2−42615
  cylindrical anemometer probes 2−58949
  Czochralski crystal growth, rel. to temp. distrib. in growing crystal 2−47256
  data acquisition and processing 2−63148
  deep ocean drill site temp. distrib. meas. 2−54777
  density stratified fluids, turbulent flow 2−77249
  in dispersion layers, 2-current approx. analysis of kinetics 2−49179
  with dissipation, surface curvature effects for large Prandtl no. 2−76219
  dissipative, effects of vorticity, displacement speed and curvature 2−53125
  dropwise condensation, numerical simulation 2−77471
  eddy conductivity in turbulent flow in heated channel 2−76396
  eigenfunctions of Sturm Liouville eqn., error in calc. of coeffs. in paper by S.N. Singh, 1958 2−62969
  exchange in recuperators, criterial equation 2−58947
  exchanger design, performance advantage of roughened tubes 2−58948
  ferromagnetic visco-plastic fluid, mag. field influence on heat exchange 2−80466
  film condensation of pure and binary vapours, effect of variable thermophysical properties 2−77410
  films and wires for flow angle and shear stress meas. 2−46686
  fin approximation, criterion for validity 2−66648
  fine hot wires in steady flow 2−80173
  from flames, laser interferometer for obs. 2−73635
  flames, natural gas-O_2 and acetylene-air, impingement rates 2−52288
  flat plate at zero incidence receiving a single free jet 2−43070
  on flat plate normal to two-dimensional laminar jet from nozzle of finite height 2−77224
  flow, analogy with electric flow in model 2−52277
  flow in entrance section of circular tube 2−64236
  flow in tubes and ducts with wall mass transfer, development of temperature field 2−83443
  in flow of power law fluid in rotating straight pipe, study of heat transfer 2−50151
  fluid containing high molecular weight polymer, non-Newtonian flow 2−50289
  fluid flow, conference (Lucas Heights, Australia Aug. 1971) 2−43077
  fluid turbulent heat transfer near pseudo-critical temp. in supercritical pressure 2−74320
  fluidized bed, from horizontal tube in presence of unheated tubes 2−45572
  fluidized bed at high temp. 2−60120
  forced, over thin needles 2−52271
  forced convection from heated surfaces to liquids, influence of property variation 2−55577
  forced-convection flow, buoyancy effects, anal. by perturbation method 2−74319
  free stream flow which oscillates without reversing, two- dimensional boundary layer 2−80172
  freon 11, 113 droplet splattering on hot surface, heat transfer rates 2−55575
  Freon 11, condensation, finned tubes 2−82248
  Freon water modeling of critical heat flux in uniformly heated annuli 2−41857
  freon-113, meas. of local transfer during boiling on nonisothermal surface 2−64516
  freons, boiling, smooth tubes, finned tubes 2−82249
  fuel rod, with time varying coeff., calc. of temp. transients 2−42615
  fusible material, with diminished heat flux, increased rate of ablation 2−73466
  gas flow, v. high temp., entrance region of cooled tube 2−46818
  gas flows, det. from inherent temperature perturbations 2−43238
  gas possessing internal energy influence of inter-mode exchange on heat flux at boundary 2−74483
  gas-liquid two-phase flow, theoretical model 2−70845
  glass, flowing, energy transport in cylindrical channels 2−56552
  glass and metal contact behaviour in the forming of hot viscous glass 2−56554
  glass particles in turbulent air flow, suspension trajectories, velocity of particles 2−76395
  glass surface temp. meas., elimination of effect of radiant heat transfer 2−55588
  heat equation, spatial decay of solutions 2−52272
  heat exchanger ribs, irregularity effect on efficiency 2−82251
  heat-pipe performance, steady-state, model 2−76398
  hollow cylinders, thermal characts. in contact planes 2−69794
  hot air to wetted ribbed tube, by convection, solution by enthalpy difference 2−69801
  hot film in two-dimensional unsteady flow 2−80431
  in HTR, He cooled, components of THTR 300 heat transfer system 2−42688
  hypersonic rarefied gas flow over sharp slender cones 2−74470
  incompressible flow, second order effects of curvature and displacement 2−77182
  infinite plate, temp. distrib. heat source depend. on temp. 2−82255
  insulators and structural materials, thermal conductivity and diffusivity and specific heat 2−57080
  interacting particles system, thermal and diffusion wave propag. 2−45334
  interferometer long path difference, 30 cm diameter for mass and heat transfer aerodynamics 2−59231
  interferometric investigation of transfer between parallel walls 2−49178
  Jovian atmosphere, vertically inhomogeneous scattering models 2−58489
  laminar, in horizontal rectangular channel large Prandtl number fluid, buoyancy effects 2−67549
  laminar, with axial conduction, error in paper by Chia-Jung Hsu, 1967 2−66639
  laminar flow, lateral rod displacement effect 2−53137
  laminar flow development and heat transfer in converging plane-walled channels 2−53117

Heat transfer continued
laminar flow of non-grey gases through circular tube 2—43228
laminar flows with radiative interaction using total band absorptance model 2—43229
laminar thermal boundary layers on continuous surfaces, heat transfer characteristics 2—41849
lava pond surface heat and mass transfer, obs. 2—78249
light-diffusing layer heating kinetics from radiant heat exchange calc. 2—82465
liquefied gases supercritical state, maximum coefficient 2—83788
liquid, high-temp. heating of flows 2—60462
liquid in forced convection droplet evaporation 2—77398
liquid metal heat pipes, vapour transport limits 2—83128
liquid-gas system, Marangoni instability 2—60550
low gravity environment, expts. to demonstrate heat conduction mechanisms 2—58954
Mars, flow from atmosphere and soil to north polar cap 2—73084
methanol drops, from small diameter channel in film boiling temp. range 2—53379
in MHD channel flow between conducting walls 43108 2—43108
MHD Couette flow between cond. walls, effects of ext. circuit 2—46703
Moon, flow obs., Apollo Lunar Surface Experiment 2—62656
moving flat plate in parabolic flow, response 2—55581
multi-region problems, improved point-matching techniques 2—52269
Navier-Stokes eqn., modified, consequences in sound dispersion 2—53130
Newtonian fluids in agitated vessels 2—67818
non-Newtonian, non-isothermal laminar flow 2—83487
non-Newtonian fluids in laminar flow through circular pipes 2—60124
non-Newtonian liquids in agitated vessels 2—74538
nonlinear, applic. of Hamiltonian variational principle for classical field theory 2—45240
nonlinear, Hamiltonian variational principle 2—45578
nonlinear equations, numerically stable solution using Gauss-Seidel system relaxation method, Newton-Raphson root evaluation technique 2—69795
nonlinear heat eqn., uniform convergence of finite difference scheme 2—69796
nonstationary, between simply shaped bodies and surrounding medium by radiation 2—41853
Norwegian Sea, from N. Atlantic current 2—44640
nuclear reactor cooling systems, effect of Na corrosion deposits on heat transfer coeffs. 2—83117
nuclear reactor core, multichannel mixing effect 2—83080
nuclear reactor critical heat flux, compensated- distortion fluid model 2—46370
nuclear reactor fuel rod bundle-geometries, with streamline coolant flow 2—74146
nuclear reactor fuel rod cluster and coolant channel performance 2—42644
nuclear reactor nucleate and film boiling 2—53510
nuclear reactors, effect on stability and dynamics 2—42646
nucleate boiling, heat transfer function tested by temp. control feedback system 2—53506
nucleate boiling, varying levels of subcooling and acceleration 2—47043
objects immersed in fluidised bed 2—83506
operational heat pipe, internal temp. distrib. 2—69802
optimization in ducts, efficiency factor determination 2—41858
packed beds, axial transfer, gas flow between 20 and 650 C 2—45575
packed beds, small diameter 2—41859
phonon generation in metal films in an electric field 2—54015
planetary atmospheres, momentum and heat transports, non-geostrophic baroclinic stability 2—58481
plasma, analytic soln. for nonlinear problem 2—56329
plasma, in combustion MHD generator, heat flux density, obs. 2—80257
plasma, thermally ionized, heat transfer to wires, rel. to ionization 2—56330
plasma, two-dimensional flow at toroidal inclusion 2—53177
plasma jet, stagnation point, heat pipes calorimetry 2—43164
plate, porous, in fluid flow, using Laplace transform. 2—49176
plate heat exchanger, heat transfer coeffs. 2—66641
plate in incident longitudinal flow 2—46663
Poiseuille flow, two dimensional laminar, adiabatic forced convection 2—53115
porous convection, variational problem 2—67820
porous medium, abrupt change at supercritical Rayleigh number 2—55584
post dry-out, influence of curvature of tube 2—77223
power station condenser cooling water discharge 2—80201
prediction in rectangular wall cavity with turbulent flow 2—67596
pulsating flow, interpretation of heat exchange by meas. of velocity gradient at wall 2—60166
radiation with free convection, investigation in absorbing emitting and scattering medium 2—45582
radiative, electrical simulation 2—58971
radiative, flows over convex and concave shapes 2—77337
radiative heat exchanger, transient processes 2—58955
Rayleigh-Taylor instability, effects 2—46687
reactor fuel rods adjacent to subassembly walls, laminar- and slug-flow heat transfer characts. 2—83114
reactor rod fuel element, effect of surface roughness on heat transfer 2—76911
real gases, boundary-layer laminar flow on flat plate 2—60369
rear of cylinder in crossflow 2—43097
regenerative heat exchange in multifluid systems, internal thermal conditions 2—66642
regenerators, prediction of coupled heat and mass transfer 2—45581
relativistic fluid dynamics, linear solns. of heat propag. 2—70840
review of 1971 literature 2—76393
r.f. surgical brain probe, model for analysis 2—51899
ribbed surfaces, influence of wall thickness, thermal conductivity and method of heat input 2—45579
rod surface, effect of boiling transition regime on propagation of temp. oscillations 2—64513

Heat transfer continued
rotating bubble bed 2—83498
from rotating naphthalene disc in uniform forced stream, and laminar mass transfer 2—73465
roughed surfaces used in nuclear reactors, heat transfer and pressure drop performance 2—59872
sea surface, sensible and latent heat fluxes rel. to temperature fluctuations 2—57890
sea surface cooling mechanisms, surface stress 2—65593
semi-transparent solids, radiant conduction, temp. field 2—68256
semifluidized beds, of glass and Al spheres in water 2—60130
shallow ducts of variable section, laminar flow of viscous compressible gas 2—53289
solid, in high temp. gas flow, during initial stages, heat flux meas. 2—55566
solid bodies heated by radiation 2—63146
solid-liquid suspensions, agitated 2—83827
sounding rockets, aerodynamic heating effects 2—53309
sphere slowly rotating in viscous incompressible fluid, steady state forced convection 2—64228
stationary in thermal input section of annular channel with third type boundary conditions 2—41852
steady state flow of Newtonian fluid between two rotating discs, solution of Navier-Stokes eqn. 2—76394
steel, melting in Fe-C melts, with natural convection, rates for various C concentrations 2—43438
stellar interiors 2—58271
stellar polytropic atmospheres, radiation heat exchange 2—58263
stochastic identification and modelling in nuclear reactor channels and heat exchangers 2—42647
stochastic modelling and time series analysis techniques 2—41860
submerged heated jet discharging into lake or river, turbulence 2—78304
supercritical fluid, effect of diameter of heated wire on free convective heat transfer 2—41865
supersonic turbulent boundary layer, incipient separation 2—71070
between surfaces of solid materials, thermal radiation process, enclosed space method 2—58946
terrestrial, Colorado, New Mexico, Texas, Utah and Wyoming 2—57486
terrestrial, Mesa and Dunes geothermal anomaly, S. California, heat flow 2—61868
terrestrial, Rio Grande rift, meas. 2—57484
terrestrial, Rio Grande rift 2—57485
terrestrial, Zambia, borehole meas. 2—61869
terrestrial heat-flow and geothermal gradient in N.E. Poland 2—72608
terrestrial in Norway, drill hole obs. 2—57483
thermal fatigue resistance of metals using fluidized beds 2—56877
thermal flowmeter operating from pulsed heat injection source 2—66640
thermonuclear reactors, controlled, review 2—42645
thermosyphon, two-phase closed, performance 2—58950
three-dimensional stagnation point flows, transfer from foreign gas injection 2—64370
tube bundles, saturated air, void fraction 2—82247
turbulent, from large body of water 2—57891
turbulent, to non-Newtonian liquids 2—50297
turbulent boundary layer, discontinuity in wall temp. and concentration 2—53274
turbulent boundary layer, heat flux from wall 2—43082
turbulent compressible boundary layer 2—43061
turbulent flow heat transfer of liquid in tube 2—60461
turbulent flow in plain tube, radial and tangential eddy diffusivities 2—76397
turbulent flow in rough tubes 2—56282
turbulent flow of viscoelastic liquids in pipe, theory 2—46877
turbulent flows 2—77219
in turbulent gas flow, effect of gas physical properties variation 2—41851
turbulent separated flow downstream of rearward- facing step in low speed wind tunnel 2—50242
unsteady-state temperature distrib. in convecting fin of constant area 2—63154
vapour condensation, laminar flow with arbitrary pressure gradients 2—47042
vapour-cooling water under film-type condensation, over-all coefficient 2—43446
variational principle for irreversible phenomena 2—76239
vertical cylinder, laminar boundary layer, pure and simultaneous heat and mass transfer 2—53270
from vertical plates to conducting fluid in magnetic field 2—60181
viscoelastic fluid in annulus, effect of radial magnetic field 2—52268
wakes of cylinders in crossflow, sensitivity to freestream turbulence 2—55576
wall/vaporizable liq. system, thermokinetic analysis 2—63145
water, radiation energy transfer, local radiant flux, radiant energy loss or gain 2—67827
water and glycerol-water mixture, boiling in trapezoidal channel 2—60556
water containing bubbles, convective heat transfer enhancement 2—60464
water cooled nuclear reactors 2—49883
water drops, from small diameter channel in film boiling temp. range 2—53379
water-Freon 113 system, in stratified flow with simultaneous interfacial boiling 2—50285
wave roughened gas-liquid interface in annular two-phase two-component flow 2—77409
wet vapour flow in relaxation zone behind front of shock wave 2—60407
Al surfaces to boiling He 2—66362
Ar-K plasma, heat flow meas. to electrodes 2—60209
Ar, meas. of wall transfer in atm. cascade arc 2—46804
Ar, partially ionized, heat transfer in laminar flow in pressure of transverse mag. field 2—53298
Ar plasma, flowing, anode heat transfer at elevated temp. 2—67626
CO_2 liquid, heat transfer at supercritical pressure and temp. heads up to 850°C 2—60463

Heat transfer continued
- He, meas. of wall transfer in atm. cascade arc 2−46804
- He II, energy transfer from pulsed thermal source below 0.3K 2−71263
- He II, entropy transport by vortices, and second sound vel. modifications 2−64500
- N_2, meas. of wall transfer in atm. cascade arc 2−46804
- N_2 liq. film, boiling, plug stage, expt. 2−56546
- N_2O_4, liquid, convective heat exchange at precritical and supercritical pressures 2−46947
- N_2O_4 nucleate boiling, criterial equation 2−45586
- $N_2O_4.2NO_2$ nucleate boiling, heat transfer regularity 2−47044

Heat treatment
- *see also Annealing*
- — 2−60668
- alloy, low stacking fault energy, interaction between quenching defects and dislocations 2−64662
- amorphous chalcogenide threshold and memory devices., effect of preswitching heat treatment 2−77920
- austenitic stainless steels, sensitized between 500 and 900°C, inergrannular corrosion tests based on potentiokinetic polarization curves 2−68791
- carbon phenolic, two dimensionally reinforced, re-entry material, characterization 2−56980
- carbons, soft and neutron-irrad. graphite, low temp. sp. ht. obs. 2−54045
- cermet steels, dynamic hot pressing, effect on struct. and mech. props. 2−84146
- Co-Ni-Cr-Ti alloy, quench-ageing behaviour, 700-900°C 2−68138
- composite, nichrome, W or Mo reinforced, hot pressing 2−53966
- crack formation in heat affected zones of welded joints 2−71596
- ferrite, 1000 NN, compaction kinetics during hot pressing 2−53882
- forging apparatus for temps. up to 1900°C under vacuum or inert atmospheres 2−58655
- glass, Ag activated phosphate, dosimetry props. rel. to melting and cooling rate 2−51381
- glass, crystallizing, frozen elastic stresses 2−56784
- glass, fluor-richterite comp., treatment for obtaining high strength polycryst. material 2−47651
- glass, photochromic, containing AgCl, effects on darkening 2−78065
- glass, pyroxene type, crystn., density, acid stability 2−53533
- glass, tempered, residual stresses 2−77648
- glass fibre, aluminoborosilicate, effect on B coordination number 2−64528
- hardening of quartz optical contacts 2−59252
- INCO 713C, thermal stability and corrosion of Al coatings after heat treatments 2−60959
- influence on fracture strength of material 2−74852
- low-temp., relief of stresses in tube welds 2−71629
- metal, polygonized struct., conditions of formation of recrystn. nuclei 2−56901
- metal, quenched, void form. mechanisms 2−53696
- metal, recrystn., effect of impurity atoms on grain boundary motion 2−43785
- metal recrystallization and transition bands 2−68135
- poly(vinylidene chloride), effect of heat treatment on morphology and structure powder 2−71293
- polyacrylonitrile, effect of heat treatment on morphology and structure of crystals powders and fibres 2−71293
- polymer, effect on dielec. depolarization spectra 2−47974
- polymer, effect on morphological struct. 2−60611
- polystyrene polyvinyl methyl ether mixtures, thermally induced phase separation 2−61041
- pyrofoil tape, production and characterisation for reactor use 2−56050
- pyrophyllite, mech. props., effect of firing temp. 2−50890
- recrystallization of cold-worked metals, new grain nucleation 2−68134
- recrystallization of metals, emission electron microscopic 2−79115
- Saran, effect of heat treatment on morphology and structure of powder 2−71293
- semiconductors, doped, properties of doping element 2−84321
- silicate glass, effect of synthesis conditions on crystn. 2−64530
- simulated safety lenses, on impact resistance 2−48927
- simulated safety lenses, on impact resistance 2−48927
- steatite, mech. props., effect of firing temp. 2−50890
- steel, austenitic, creep behaviour, obs. 2−56920
- tempering, anal. of stressed and strained states in surfaced components 2−71607
- topaz, microstructural breakdown 2−60776
- transition metal nitrides, hot pressing, sintering, compaction kinetics 2−47661
- triglycine sulphate, reshaping of ferroelec. domains after heat treatment 2−54234
- Ag dispersion hardened, recryst. temp. rel. to particle vol. fraction, separation deform. 2−56900
- Al-pyrolytic SiO_2-Si system, effect on density of fast surface states 2−77915
- Al, conditions of formation of recrystn. nuclei 2−56901
- Al, effect of tempering on internal friction 2−77699
- Al, foil, recrystn., effect of small alloying additions 2−47578
- Al, recrystn., electron microscope obs. 2−80859
- Al, sub-grain boundary migration 2−80824
- Al crystal, dislocation config. as result of cooling rate 2−47411
- Al_2O_3-$Ni(NO_3)_2.6H_2O$ system, effect of heating in oxidizing and reducing media 2−60992
- α-Al_2O_3 formation, in presence of AlF_3 2−47704
- As-Te-Ge amorphous, cryst. layer form., effect of water 2−60571
- As_2S_3/Ag system, effects on photochemical transf. rate 2−57433
- Au, quenching velocity influence on vacancy clusters, elec. microscope obs. 2−71630
- B_2O_3-MgO, phase relations determined by quenching 2−74936
- Ba_2MReO_6, (M=Mn,Re,Co,Ni), perovskites, synthesis and characteriz. 2−50876
- Be-(1 wt.%)Fe alloy, precip., Mossbauer obs., mechanism 2−50931
- Be, increase of microplastic deform. resist. by thermocyclic treatment 2−53871
- BeO, powder, glass-sealed, densification by hot isostatic pressing 2−53940

Heat treatment continued
- Bi, quenching effects on thermoelectric power and magnetoresistivity 2−68336
- C, effect of treatment temp. (600-1600°C) on sp. ht., 0.5-5 K 2−57061
- C, glassy, temp. rel. pore size, X-ray small-angle scatt. obs. 2−53530
- C, lampblack, rel. to graphitization 2−56995
- C, microstructure, high-resoln. electron microscopy obs. 2−53532
- C, soft pregraphitic, effect on Hall coeff. 2−44113
- C, turbostratic film, opt. spectra obs. 2−78080
- C fibre, effects on surface props., thermal behaviour and reactivity 2−53951
- C fibre, thermal expansion anisotropy effects on struct. and mech. strength 2−54054
- C fibres 2−53951
- CaF_2 powder, sintering activity, effect of calcination 2−61004
- Cd, liquisol quenching, effect on lattice parameters and vacancy conc. 2−77572
- $CdCr_2Se_4$ film, prep. 2−60649
- Ce_2O_3-ZrO_2, phase relation by quenching between 1350 and 1900°C 2−74935
- Co-10%Cr alloy, thermal stability and corrosion of Al coatings after heat treatments 2−60959
- Cu, growth of twin free crystals by secondary recrystn. and zone refining 2−47580
- Cu, high purity, recrystn. 2−68136
- Cu foil recrystallization in a high voltage electron microscope 2−80825
- Cu wire, recrystallization, cold worked, press. induced thermal activation 2−43781
- Cu_2O, recrystn. and grain growth kinetics 2−43788
- Cu_xS-CdS photovoltaic cell, effect on performance 2−54261
- Dy, recrystn., X-ray diffr. and metallographic obs. 2−80773
- Fe-Al-C alloys, influence of ordering and martensitic transformations during quenching 2−84073
- Fe-12.3 at.%-Al, Mossbauer determination of quenching effect on short-range order 2−51311
- Fe, high purity, recrystn. 2−68136
- Fe, recrystn., internal friction obs. 2−47626
- Fe, recrystn., internal friction obs. 2−47625
- Fe cermet, highly porous, thermophysical properties 2−71651
- Fe cermets, thermal stability of sulphides of some metals 2−68164
- Fe_2O_3, density changes and pore distribution during heat treatment 2−68140
- GaAs epitaxial layer, origin of high resistance region at substrate interface 2−71883
- Gd, mag. permeability rel. to plastic deform. and recrystn. 2−81234
- Gd_2O_3:Eu^{3+}, transparent ceramic phosphor, hot pressing 2−72409
- Ge surfaces, in various atmospheres, e.s.r. obs. 2−72488
- InSb, elec. transport props., changes, field effect and elec. cond. obs. 2−64989
- InSe, flash evaporated thin films, eff. of thermal treatment on props. 2−77853
- In_2Se_3, flash evaporated thin films, eff. of thermal treatment on props. 2−77853
- KBr, quenching of cathodoluminescence as a function of colour centres, at 90 and 300 K 2−68704
- KCl-NaCl mixed single crystals, phase separation during heat treatment 2−74884
- KCl, quenching of cathodoluminescence as a function of colour centres, at 90 and 300 K 2−68704
- KCl, tempering effect and positron annihilation ang. correl. 2−54092
- KI, quenching of cathodoluminescence as a function of colour centres, at 90 and 300 K 2−68704
- K_2O-SiO_2 glass, rel. to conductivity and dielec. relax. 2−54229
- $LiAl_5O_8$, ceramic, transparent, prod. by hot-pressing 2−43873
- LiF, rel. to disloc. loops and radiation colloids, elec. microscope obs. 2−74760
- Li_2O-Al_2O_3-SiO_2 glass-ceramic, effect on microstruct. 2−53931
- Li_2O-Tb_2O_3-SiO_2 glass, fluorescence rel. to crystalline phases 2−51376
- $LiO_2(5-2t)Fe_2O_3tCr_2O_3$ ferrite, influence of crystallographic struct. 2−57021
- MgF_2, influence of hot pressing temp. on elec. cond. 2−47898
- MgO-B_2O_3, phase relations determined by quenching 2−74936
- MgO, $F^+ \rightleftharpoons F$ centre conversion obs. 2−68043
- $MgO.Al_2O_3.SiO_2$ glass-ceramic, ZrO_2 nucleated, phase transitions 2−47691
- Mn-Zn ferrite powders, calcination and effects in crack reduction on core production 2−68163
- Mo, before and after neutron irradiation, physical mechanical properties 2−53730
- Mo, removal of C by heating with atmos. 2−64763
- Mo, removal of C by heating with atmos. 2−64763
- Mo, room temp. ductility and intergranular cracking after annealing 2−53875
- Nb, multi-mechanical-thermal- treatments, role of oxygen and nitrogen solutes 2−64722
- Nb, struct. sensitive mech. props., review 2−43697
- $Nd(OH)_3$, preparation from Nd_2O_3 in H_2O vapour 2−80598
- Ni-HfO_2 powders, effect of dispersion strengthening phase on thermal stability 2−77739
- Ni-Zn-Co ferrite film, anisotropy induced by thermomagnetic treatment 2−81228
- Ni, recrystan., texture variation 2−50806
- Ni, textures produced by primary and secondary recrystn. 2−84070
- Ni, vacancy clustering after quenching, electron microscope obs. 2−64661
- Ni, work hardened in tension, secondary recrystn. 2−60986
- Ni steels, 40N25, 60N20 and 80N15, amplitude-dependence of int. frict. 2−84076
- Ni wire, recrystallisation, cold worked, press. induced thermal activation 2−43781
- Ni(001), surface impurity segregation, work function and Auger electron spectroscopy obs. 2−53554
- Pt, vacancy conc. rel. to press., quenching effects, excess resist. obs. 2−60788
- PtSi-Al Schottky diode, effect on barrier height 2−75131

Heat treatment continued
- SiO_2-CaO-MgO-Na_2O-AlF_3:Dy^{3+} glass syst., effect on luminesc. 2−48228
- SrO(6−x)Fe_2O_3xAl_2O_3, influence of thermal history on Mossbauer spectra 2−48144
- U, β phase, multiquenched rods, microstress behaviour 2−77659
- U, recrystallization after annealing and cold rolling at room temp. 2−68141
- V foil, quenched, vacancy detects, electron microscope obs. 2−71472
- W, before and after neutron irradiation, physical mechanical properties 2−53730
- W swaged and drawn deform. textures 2−53868
- W wire, drawn, micropore pinning effect on grain boundary motion during recrystn. 2−47647
- Zr, vacancy formation energy, quenching obs. 2−53728
- ZrO_2-Ce_2O_3, phase relation by quenching between 1350 and 1900°C 2−74935
- **alloys**
  - austenite, static recrystalliz. between intervals of hot working 2−47575
  - α-brass, recrystn. texture, X-ray obs. 2−68139
  - casting characteristics and solidification morphology 2−64770
  - grain boundary development, exam. by electron microscope 2−56721
  - hot rolling, determ. of roll forces 2−53881
  - hot workability, review 2−50795
  - nickel silvers, fire-cracking mechanism 2−43794
  - rapid cooling by laser melt quenching 2−56897
  - recrystallization, dynamic 2−68133
  - recrystallization, electron emission microscope examination 2−43779
  - SAP-1 plate, fine struct. and recrystn. 2−53870
  - steel, γ′-phase precip., influence of quenching temp. 2−80768
  - steel, austenitic, grain coarsening temp., hot rolling effects 2−47582
  - steel, austenitic, strengthening by ageing, optimal conditions 2−53876
  - steel, austenitic, substruct., effect of deform. temp. during thermomech. treatment 2−80770
  - steel, austenitic vanadium nitrogen type, fine precipitates struct. 2−53893
  - steel, brittle fracture resist., tempering temp. effects 2−53838
  - steel, carbide form. during low temp. isothermal tempering 2−43842
  - steel, carbon, elastic and relax. characts., chromizing effects 2−53780
  - steel, Cr-Mn-Mo-Ti type, carbides identification 2−47627
  - steel, dislocation-additive interaction during tempering 2−43790
  - steel, effect of isothermal treatment on mech. props. 2−53874
  - steel, effect on mech. props. 2−60962
  - steel, effect on mech. props. and struct. 2−53842
  - steel, eutectoid, mech. props., rel. to directional growth of pearlite and rolling 2−47529
  - steel, high C, low temp. tempering, retained austenite, X-ray obs. 2−74883
  - steel, high carbon, recovery and ageing, hardness and resistivity obs. 2−47597
  - steel, high-C martensitic, tempering, carbide precip. 2−64762
  - steel, high-C martensitic, tempering, carbide precip. 2−64761
  - steel, high-speed, thermal expansion, partial coeffs. 2−54059
  - steel, high-speed deformed low-C, dilatometric behaviour 2−43839
  - steel, hot pressing, C diffusion, dislocations, internal stresses, mosaic struct. 2−43793
  - steel, hot working temp. ranges for optimum ductility and strength 2−60978
  - steel, hot-worked austenitic and ferritic, recrystn. during continuous cooling 2−53873
  - steel, hypereutectoid, low carbon martensite struct., prod. by heat treatment 2−47585
  - steel, impact strength variation, role of cryst. distortions 2−43792
  - steel, low alloy, microduplex processing effects on strength-toughness 2−43835
  - steel, low-alloy, temper-brittle fracture and grain boundary segregation 2−47624
  - steel, low-C, hot-rolled, quenched, effects on microstruct. and mech. props. 2−57017
  - steel, low-C, low-alloy, AlN precip. 2−50833
  - steel, low-C low-alloy, fine struct. and phase comp. at elevated temps. 2−53898
  - steel, low-C low-alloy pipe, formation of abnormal struct. 2−53897
  - steel, maraging with 18%Ni, flow behaviour 2−84068
  - steel, martensitic, effect of lath boundary precip. on fracture toughness 2−57018
  - steel, martensitic, low-C Mn, effect of Sb on high temp. tempering 2−56905
  - steel, medium carbon, effects of forge quenching treatment on mech. props. 2−80806
  - steel, phase transforms. during laser beam heating, effect of original struct. 2−53990
  - steel, quenched, cooling rate rel. to struct. and mech. props. 2−47587
  - steel, quenched, fracture behaviour rel. to dislocation substruct. 2−47413
  - steel, quenched, quench-aged, fatigue behaviour rel. to microstruct. instability 2−50768
  - steel, quenched, tempered, resist. to plastic deform. and cold brittle failure 2−47502
  - steel, rel. to grain boundary form effects on impact strength and brittle fracture 2−80765
  - steel, retarding recrystn. during thermomech. treatment at high temp. 2−60961
  - steel, stainless, elimination of ridging phenomenon in sheets 2−68131
  - steel, stainless, void form. on quenching 2−53717
  - steel, strength and ductile-brittle transition, effect of cold rolling and heat treatment 2−80777
  - steel, structural, austenite grain growth 2−53988
  - steel, structural, single crystal temper brittleness 2−60982
  - steel, tempering, transform. of retained austenite 2−47689
  - steel, tempering effect on mech. props. after ausforming 2−43801

Heat treatment continued
- **alloys** continued
  - steel, transformer, hot rolling, effect of S content on recrystn. 2−47586
  - steel targets, effect on ballistic behaviour 2−60980
  - steel tempering, Ostwald ripening obs., grouping errors in data analysis 2−60942
  - steels, constructional, effect on hydrogen permeability and diffusion 2−64757
  - thermomechanical treatment, review 2−80854
  - weld metal, toughness below 0°C, effect of metallurgically conditioned inhomogeneities 2−74890
  - Zircaloy tubing, recrystn., effect of oxygen and fabrication variables 2−53915
  - Zircaloy-2, stress orientation and circumferential ductility, thermal cycling effect 2−53914
  - Ag-Cu, 7.5 wt% Cu, discontinuous precip. kinetics, 200-500°C 2−80856
  - Al-Cu-Mg-Ni, forged after quenching, recovery treatment, creep strain mechanisms 2−43804
  - Al-Cu-Mn, homogenization, precip. 2−43786
  - Al-Si, dil., film, Si precip., resist. study 2−50825
  - Al-Zn-Mg-Mn, strength rel. to rest between quenching and ageing, effect of additions 2−50803
  - Al-Zn-Mg, ageing process after quenching, resistometric obs. 2−71632
  - Al-Zn-Mg alloy, precipitate free zone, elec. microscope obs. 2−56902
  - Al-Zn alloys, X-ray central diffusion study of Guinier Preston zones after quenching 2−64632
  - Al-based materials, hot formability criteria 2−80852
  - Al-1.2 wt%Mg_2Si, two-step ageing behaviour 2−64765
  - Al, superstrength, by continuous cyclic thermomech. treatment 2−47614
  - Co-P film, rel. to hysteresis characts. 2−48091
  - Co alloys, metallurgical structure and properties 2−71667
  - $CoFe_2O_4$-Co_3O_4, quenched, aged, saturation magnetization, intrinsic coercive force, rel. to microstruct. 2−81233
  - Cu-Al, two-phase struct. formation 2−71678
  - Cu-Be evaporation, mass spectrometer control 2−73233
  - Cu-Cr, effect of precip. size on recrystalliz. temp. 2−56927
  - Cu-Cr alloy, rel. to dispersion struct. production 2−43832
  - Cu-X, X=Mg,Cd,Zr,Cr,Ag, weakening resist. rel. to deform., heating time and temp. 2−50764
  - Cu-Zr-Cr, effect of precip. size of recrystalliz. temp. 2−56927
  - Cu-Zr, effect of precip. size on recrystalliz. temp. 2−56927
  - Cu-based materials, hot formability criteria 2−80852
  - Cu-40 at.% Ni, sp, ht. below 3K, effect of clusters and quenching 2−61103
  - Fe-Al-C, martensite cryst. struct. change, −196 to 20°C 2−80766
  - Fe-C, quench ageing and reversion 2−56903
  - Fe-1%C, effect of As and Sn on tempering stages50796 2−50796
  - Fe-Co-Ni-Ti-Al-Cu alloy, YuNDK42T8, homogenizing, rel. to phase comp., mag. and mech. props. 2−47688
  - Fe-Cr steel, embrittlement at 475°C, ordering, decomp. of ferrite 2−47634
  - Fe-Cr(8%), martensite, substruct., quenching and tempering temp. effects, rel. to strengthening 2−84071
  - Fe-Mn-C, long period stacking order structure formed by thermal cycling 2−67990
  - Fe-Mo-C, quenched and tempered, microstruct., field ion microscopy obs. 2−47581
  - Fe-N, quench ageing and reversion 2−56903
  - Fe-(30.3 wt.%)Ni, damping of oscillations during heating after martensitic transform.43791 2−43791
  - Fe-Ni-C-Mo-Cr, tempering, effect on struct. and mech. props. 2−43853
  - Fe-Ni-C, phase transform., martensite to austenite, rel. to heating rate 2−53985
  - Fe-Ni-C, quenching and hydrogenation effects on mechanical props. and brittleness 2−43723
  - Fe-Ni-C, tempering, effect on struct. and mech. props. 2−43853
  - Fe-Ni, Fe-Ni-Co and Fe-Ni-Mo, cumulative thermal cycling behaviour, 300°C/hr. 2−60960
  - Fe-Ni martensitic transformation study by internal friction 2−43916
  - Fe-(3 wt.%)Si, surface films influence on effectiveness of thermomag. treatment 2−44261
  - Fe, cast, nodular, solidification process and quenching technique and relation to austenite shell 2−60549
  - Fe, dil., recrystn., internal friction obs. 2−47626
  - Fe, dil., recrystn., internal friction obs. 2−47625
  - Fe, spheroidal graphite and common grade grey, hardness and dilatation 2−43739
  - Fe nitrided zone refined, ductile-brittle transition 2−47629
  - Mn-Cu-Mo, cold worked, heat treated, Young's modulus, rigidity, hardness, thermal expansion 2−47476
  - Mn-Cu-W, cold worked, heat treated, Young's modulus, rigidity, hardness, thermal expansion 2−47477
  - Mo-Cr-alloyed or unalloyed case hardened steel, residual stresses in carbonized layers for different thermal treatments 2−56931
  - Mo alloy TZM, sintered compact production, solid state reactions 2−56906
  - Nb-Al, rel. to supercond. transition temp. 2−47589
  - Nb-(40 wt.%)Zr, metallurgical variables influence on supercond. 2−47861
  - Nb_3(Al-Ge) compound tapes, supercond., prep. and props. 2−64949
  - Ni-B electrolytic coatings, particle distrib. 2−77730
  - Ni-Be, recrystn., texture variation 2−50806
  - Ni-Cr steels, effect of Cu additive on tempering 2−60957
  - 81%Ni-Fe, Barkhausen effect, after heat treatment 2−78023
  - Ni-Fe sheets, heavily rolled, annealing textures, recryst. mechanism 2−74886
  - Ni base, Zr effect on hot workability and boundary-phase plasticity 2−47645
  - NiTi, non-stoichiometric, elec. resist., comp. and temp. depend. 2−74885
  - PtSi film on single crystal Si substrate, thermal stability 2−71334
  - Ta-H alloy, quenching at liq. He temps. 2−56907
  - TiC-WC, effect on short-range order 2−84072
  - Zr-(1.5wt.%)Cr-(0.1wt.%)Fe tubing, recrystn. 2−53918

Heat treatment continued
alloys continued
Zr-(2 at.%)Cr-(0.16 at.%)Fe, precip. reactions rel. to corrosion resist. 2—53919

Heating
— 2—60716
aerodynamic heating of shell in supersonic turbulent flow 2—60368
aerodynamic heating stresses of solid isotropic sphere, transient axisymmetric thermoelastic problem, two-temperature theory 2—45433
atmospheric aerosols, climatic effects rel. to direct solar radiation heating 2—65767
atmospheric radiative heating rel. to BOMEX core experiment 2—65444
compression heating of classical particles in ID box 2—62948
controlled thermonuclear fusion and heating by laser 2—70486
D-T plasma to thermonuclear temps., by ion-ion collisions due to laser radiation 2—64289
diabatic, airflow over arbitrary mountain ridge 2—78364
driven gas in shock tube, high stagnation temperatures 2—56403
drops, by internal heat sources 2—43300
electric oven for studying mag. props. of rocks 2—73241
electrolytic, Cu powder sintering 2—74891
electron beam on thin disk 2—66708
e.u.v. heating of atmosphere, annual and sub-annual effects rel. to density variations 2—84841
flap turbulent heating, skin friction and pressure data from hypersonic shock tunnel 2—53314
flow discharge column constriction, gas heating effects 2—80361
frictional and surface temp. due to gas flow over plate 2—64366
furnace, for use in materials testing reactor at temps. up to 2000°C 2—49905
furnace, high temp., for Weissenberg camera 2—76119
furnace for obtaining high temp. Raman spectra 2—55775
fusion reactors, engineering problems of l.f. heating 2—46373
gas flame equipment producing temps. up to 2300C for X-ray diffractometer 2—67800
ionosphere, ambient electron heating calcs. 2—62373
ionospheric E-region and lower F-region 2—48580
liquid in container, subject to periodic heating, temp. fluctuations 2—71181
loudness det. by power summation 2—58640
lower ionosphere, artificial heating with 1-MW 40-MHz transmitter 2—68961
metals, effect on O_2 content, spectrochemical determination 2—72590
microwave processes, heterogeneous materials containing water 2—54037
perception of segments of spoken Hindi vowel-consonant-vowel syllables 2—45088
plasma, and parametric instability near lower hybrid resonance 2—80327
plasma, application of parametric instabilities in magnetic field 2—46785
plasma, CO_2 laser produced, magnetic field enhanced 2—70929
plasma, collisionless, due to transit time magnetic pumping, resonances 2—64314
plasma, conduction heating and hydrodynamic expansion, derivation of joint equations 2—64258
plasma, conduction type laser heating 2—64259
plasma, cyclotron, heating in magnetic trap, asymptotic particle distribution function 2—74365
plasma, electric arc produced, by i.r. laser beam 2—43148
plasma, high β, of ions by oblique shock waves 2—80280
plasma, high density θ pinch, transverse irradiation by pulsed CO_2 laser 2—50200
plasma, in mirror trap, oscill. spectra 2—56368
plasma, in solar flares, by high energy electrons and non-thermal X-ray emission 2—81951
plasma, in Tuman-2, microwaves in upper hybrid range 2—74367
plasma, ion energy distribution resulting from turbulent heating 2—70927
plasma, laser heating, averaged equations of hydrodynamic expansion and conduction-type heating, case of spherical symmetry 2—77277
plasma, laser heating for spherical wave 2—77276
plasma, laser induced 2—56375
plasma, laser produced, in magnetic field 2—43134
plasma, relativistic cyclotron resonance heating 2—70905
plasma by electric field, computer simulation 2—64334
plasma by microwaves 2—43139
plasma by relativistic electron beams, temp. distribution 2—53183
plasma in fast theta pinch, shock heating 2—83578
plasma in pinch discharges 2—83564
plasma in toroidal Z-θ pinch at Padova 2—83571
plate heat exchanger, heat transfer coeffs. 2—66641
salt systems binary and ternary, simultaneous recording of electrical conductivity and DTA 2—78179
semiinfinite piezoelectric rod due to prescribed heat flux 2—41856
solar e.u.v. heating in upper atmosphere, annual and sub-annual effects 2—84840
solar plasma, type II meter bursts 2—75963
solar wind, review of models 2—69187
solid, in high temp. gas flow, heat flux meas. 2—55566
sonic vibrations in heated channels 2—58920
space shuttles, aerodynamic heating, surface oil flow patterns 2—83679
stellar atmospheres, radiation field effects 2—58268
stress waves induced in laminated composite 2—47665
thermostat heater for preparations beneath microscope 2—45180
Ti alloy VT14, phase transf. during heating and cooling 2—68201
torch holder for use away from glass laboratory 2—85157
Ucera meteorite, determ. of differential atmospheric heating using natural thermoluminescence 2—75926
water, superheated to 279.5°C at atmospheric pressure 2—60558
X-ray diffraction single-crystal studies, heating stage for temps. 20-1000°C 2—60732
zunyite, structural changes 2—75451
Bi superheating, anomaly between small particles and bulk 2—77467
CO_2 laser as heat source for forming single crystal fibres 2—74664

Heating continued
D, plasma ion heating and sheath formation in low density h.v. θ pinch 2—83580
^2H plasma, laser heating to thermonuclear temps. 2—43179
^2H solid by laser pulse and production of DD reactions 2—43140
He^+/Ar^+ plasma simultaneous ion heating in linear turbulent-heating expts., mass dependence 2—80288
He II, stimulated evaporation of atoms by heat pulses 2—67860
In film during diffraction 2—83920
KDP, cooled, heating by 337 μm laser radiation 2—63347

Heaviside layer *see Ionosphere*

Heavy water *see Water*

HEED *see Electron diffraction; Electron diffraction crystallography; Electron diffraction examination of materials*

Height measurement *see Length mwasurement*

Heisenberg model
alloy, CPA approx. with random off-diagonal elements, Heisenberg ferromagnet 2—78004
anisotropic, high temp. series expansion 2—57276
anisotropic n-vector model, critical phenomena 2—65136
antiferromag. chain, study on basis of Fermi representation 2—81298
antiferromagnet, insufficiency for polynuclear clusters 2—44294
antiferromagnet, linear chain, short range order effect on anisotropy 2—44295
antiferromagnet, principal susceptibilities, spin wave theory 2—65172
antiferromagnet, two-dimens., with nearly continuous symmetry, low temp. behaviour 2—44288
antiferromagnet, two-magnon Raman scatt. at finite temp. 2—54431
antiferromagnetic chain, uniform, thermodynamic props. and magnetostriction 2—84439
antiferromagnets, spin waves and generalized susceptibilities for classical models 2—44269
b.c.c. lattice at infinite temp., two-time spin-pair correl. function 2—61548
cooperative assemblies, with many body interactions, first order and critical point phase transitions 2—69605
cooperative phenomena 2—45295
critical exponents, recursion relation 2—48052
critical spin dynamics, symmetry and conservation laws 2—54308
diluted system, transition temp. depend. 2—48046
electron spin resonance spectra triplet exciton spin systems 2—68729
ferrimagnet, high-temp. susceptibility and crit. pt. behaviour 2—48099
ferrimagnet, rel. to acoustic magnon dispersion in $MnFe_2O_4$ 2—61544
ferrimagnets, spin waves and generalized susceptibilities for classical models 2—44269
ferro- and antiferromagnets, algebraic realization of spin wave theory 2—44237
ferromagnet, amorphous, conditions for existence, const. coupling approx. 2—81274
ferromagnet, amorphous susceptibility and Curie temp. rel. to spin-fluctuations 2—57277
ferromagnet, computer simulation 2—81272
ferromagnet, deformed cubic, localized impurity states 2—81273
ferromagnet, dilute, spin waves 2—44230
ferromagnet, dilute, spin-waves, percolation theory, critical conc. 2—81240
ferromagnet, disordered anisotropic, Green's function theory 2—48054
ferromagnet, effects of finite conc. of impurities, spin-wave theory 2—65134
ferromagnet, energy spectrum and magnetisation, monoionic anisotropy effects 2—51243
ferromagnet, equation for magnetization, equivalence to Hubbard model 2—65140
ferromagnet, f.c.c., with second-neighbour interactions, Green's functions calc. procedure 2—72131
ferromagnet, Green function methods 2—45283
ferromagnet, interference effect between two impurity spins 2—65130
ferromagnet, long wavelength surface spin waves, effect on mag. props. 2—44231
ferromagnet, longit. spin waves 2—72121
ferromagnet, longitudinal dynamic susceptibility and cross-relax. 2—78002
ferromagnet, nonmag. impurity effects, first and second neighbour exchange 2—65138
ferromagnet, partially finite, long-range order and phase transitions 2—75212
ferromagnet, spin 1/2 model, using anticommutator Green's functions 2—65132
ferromagnet, spin-lattice interactions 2—61497
ferromagnet, thermodynamic properties by self-consistent Monte Carlo method 2—68530
ferromagnet, three-dimens. b.c.c., mag. interactions 2—65144
ferromagnet with antiferromag. impurity spin, localized magnons 2—84424
ferromagnetic chains, disordered, density of spin wave states 2—48044
ferromagnetic film, magnon specific heat and ferromag. resonance 2—51263
ferromagnets and antiferromagnets, bound spin waves 2—44234
Green's function solution for 2 spin 1/2 ferromagnet 2—78726
Heisenberg-Ising ring for $|\Delta|\geqslant 1$, low-temperature thermodynamics 2—69611
Heisenburg-Ising ring, $|\Delta|<1$, thermodynamics, improved eqns. 2—69606
isotropic spin systems, critical exponents 2—65137
kinetic equation for critical spin fluctuations 2—44235
linear chains, short, Green's function methods 2—41523
magnet at infinite temperature, two-time spin-pair correlation function 2—44232
magnon relax. and second sound propag. 2—65129
magnon-phonon interaction, microscopic theory of Raman scatt. modifications caused by mag. ordering 2—72360
paramagnet, anisotropic, n.m.r. line shape calcs. using kinetic energy 2—72111

Heisenberg model continued
Potts model at critical point, equiv. to linear Heisenberg chain 2—81253
rare earths, spin wave energy rel. to interatomic exchange Heisenberg parameters, exchange coupling 2—61505
scaling function calc. using high-temp. series expansions 2—54315
scaling functions, universality rel. to lattice struct. and spin quantum number 2—54316
second-order phase transitions, universality, scale factor for correl. length 2—63029
spatially random spins at very low temp., dilute ferromagnet 2—72135
spatially random spins at very low temps., dilute antiferromagnet with nearest neighbour SRO 2—72136
spatially random spins at very low temps., multicomponent ferromag. alloy with SRO 2—72137
spin correls. in impure linear chains 2—48048
spin diffusion at infinite temperature, theoretical criterion 2—81207
spin half ferromagnet, second order Tyablikov treatment, low temp. 2—44236
spin system on a 1 dimensional lattice, field theory 2—52094
spin-paired symmetric exchange systems, orbited magnetism 2—75211
spin-spin correl. function, eqn. of state, droplet model 2—77991
$Fe(Pd_xPt_{1-x})_3$, phase diagram model showing quadrupole point 2—51234
Helicity *see Elementary particles; Field theory, quantum*
Helicons
degenerate solid state plasmas, Landau damping 2—54119
ferromagnetic semiconductor, spin-wave-helicon wave interactions 2—51122
instability in solid state plasma 2—71818
magneto-optical obs., review 2—72294
metal, coupled helicon-magnon wave, neutron and electron scatt. 2—68314
metal, helicon reson., meas. by obs. of spatially decaying fields 2—80949
metal, resonance obs. of Fermi surface 2—57384
plasma helicon wave radial structure depend. on electron inertia, dispersion 2—68376
semiconductor, ferromagnetic, coupled helicon-magnon wave, neutron and electron scatt. 2—68314
uniaxial conducting crystal, in magnetic field, e.m. wave propagation 2—84280
Al, e.m. wave transmission, helicon waves, Gantmakher- Kaner excitations, sound waves, quantum effects 2—57135
Al, resons., audio freq., magnetoresist., Hall coeff. 2—57136
Cu, e.m. wave transmission, helium propag., Gantmakher-Kaner oscill. 2—61211
GaAs, wave propagation in mag. fields up to 200 kG 2—47910
Ge, wave propagation in mag. fields up to 200 kG 2—47910
InSb, InAs, wave propagation in mag. fields up to 200 kG 2—47910
Si, wave propagation in mag. fields up to 200 kG 2—47910
Helions *see Alpha-particles; Helium-3*
Heliotron *see Plasma/devices*
Helium
— 2—67435
abundance in cosmos 2—72955
adsorption on Ar monolayer, binding energy, low temp. 2—43493
alpha particle energy loss and stopping power 2—56433
antiprotonic atoms, X-ray lines, strong-interaction effects 2—79965
arc at atmospheric pressure, spectroscopic intensity measurement 2—43225
atom, 1s2s, term dependence of Hartree-Fock results 2—56092
atom, 2^1S_0 metastable state, laser light interaction 2—46489
atom, 2 ^3P fine-structure splittings 2—52951
atom, application of various forms of second Born approximation to electron collisions in range 200-500eV 2—56132
atom, autoionization states, computation using Feshbach formalism 2—46487
atom, beam-foil excited, 40 keV, meas. of relative level populations 2—52955
atom, collisional ioniz. by slow electrons 2—64074
atom, collisions with CO_2, N_2, methane, ethane, translational spectra due to collision induced overlap moments 2—50129
atom, collisions with H^+ at 4 keV, probability ratio for neutralization of H^+ to H(2p) or H(1s) 2—42802
atom, collisions with Na and depolarization cross-sections of D lines 2—59957
atom, double photoionization, Roths threshold law 2—79956
atom, dynamic polarizabilities and mean excitation potentials 2—77026
atom, elastic reson. energy 2—74230
atom, electron and positron scatt., effective potentials 2—67423
atom, electron impact excit. to metastable states, Born-Oppenheimer approx. 2—46490
atom, electron impact excitation, high energy limit, differential cross sections 2—59950
atom, electron impact excitation function from threshold to 200 eV for formation of metastable states 2—70640
atom, electron impact excitation functions for singlet and triplet levels 2—67431
atom, electron impact excitation of 2^1S state, 26.5-83 eV, calc. of Glauber cross sections 2—70642
atom, electron impact excitation of autoionized $^3P^-$ states and resonance ionization, Fano's theory 2—79953
atom, electron impact ioniz., slow electron obs. 2—64033
atom, electron impact ionization, energy and ang. distrib. of secondary electrons 2—64031
atom, electron scatt., inelastic cross section calc., adiabatic approx. 2—46481
atom, electron scatt., second Born scatt. amplitude considerations 2—64077
atom, energies and wavefunctions for unbound $2s^2$ ^1S and $2p^2$ ^1S states and ground and excited bound states calc. using least squares method 2—56129
atom, excited by fast electrons, ejected electron spectra, reson. line shapes 2—67384
atom, excited states, virtual orbital approach 2—64070
Helium continued
atom, Feshback-type $^{1,3}P^e$ autoionization states, applic. of multiconfiguration energy bound method 2—46486
atom, fine structure splitting of deepest triplet P state, quantum-electrodynamical corrections 2—42810
atom, fine-struct. splittings, nucl.-motion corrections 2—77020
atom, ground state, effects of correlation in target wavefunction on cross section 2—70639
atom, ground state spin rearrangement in strong mag. field 2—67383
atom, Hartree approx., variational principles for single-particle expectation values 2—66450
atom, influence of electron correlation on one-particle electron density and radial expectation values 2—52950
atom, integral eqn. approach, energy values 2—70630
atom, ionization by proton impact 2—59955
atom, Li^+ elastic scattering cross sections, repulsive potential derivation 2—59934
atom, magnetic moment, ratio for 2^3S; ^4He level and fundamental ^3He level 2—56127
atom, many-body Green's functions, orbitals, ioniz. pots., ground state energies 2—59913
atom, meas. of lifetimes of excited states 2—52926
atom, metastable, deexcitation in collisions with gases, cross sections 2—64054
atom, metastable, elec. field effect 2—83215
atom, multiphoton ioniz. from excited states 2—46492
atom, nsms ^1S states with orthogonal orbitals, theorem on Hartree-Fock eqns. 2—56128
atom, Penning-ionizing collisions, excited-ion lifetimes 2—67433
atom, photoionization, cross-section for triplet metastable state 2—79957
atom, photoionization calc. using Brueckner-Goldstone perturbation theory 2—46493
atom, position of lowest D autoionization states calc. using Feshbach's Q-operator formalism 2—49982
atom, positron collisions, total cross sections meas. 2—64078
atom, positron scattering, swarm- and beam-technique meas. of positron annihilation, ortho-positronium quenching, cross sections 2—42812
atom, pseudo particle state calc. of hyperpolarizability and third harmonic generation coeff. 2—79880
atom, quench radiation and transition probability 2—77025
atom, reson. ioniz. by fast electrons 2—67432
atom, scattering of K^+, 150-2350 eV, effective total cross section meas. 2—67415
atom, second-order Rayleigh-Schroedinger perturbation energy for ground state 2—64072
atom, simultaneous excitation and ionization by electron impact 2—79954
atom, simultaneous excitation and ionization of 4^2S and 4^2P states by electron impact, meas. of relative cross sections 2—64076
atom, triplet metastable, reson. multiphoton ioniz. 2—46491
atom beam, scatt. from W surface 2—47084
atom excitation transfer effects on population of 3^3D state 2—42819
atom singlet + triplet mixing in $n=3$ states excited by proton impact 2—56130
atom-atom fast collisions, electron loss cross sections 2—70645
atom-electron impact ionization, double and triple differential cross-sections 2—74246
atom-positron elastic scattering, annihilation and positronium formation 2—42800
atomic, Stark quenching of 2S states, time-dependent theory 2—49974
atomic, vac. u.v. meas. of electron impact excitation 2—49983
atomic ground state, effect of Pauli-forbidden intermediate states and operator identities 2—64003
atomic oscillator strengths for isoelectronic sequence 2—56126
atomic polarisability, ground state wavefunctions calc. 2—83211
atomic projectile interaction with Hg, pot. cross sections 2—77015
atomic spectra, 4471.48 AA line, plasma broadened, distant electron collisions effects 2—67429
atomic spectra, standard for unknown transition in Ne 2—59915
atomic spectrum, relative absorpt. of 3889 and 10830 Å lines 2—59949
atomic structure calcs., polarized core approx. 2—70565
atoms, $1^1S \rightarrow 4^1D$ transition, excited by inelastically scattered electrons, absolute differential cross sections 2—74247
atoms, adsorbed on Ar, mobility near 2K 2—67920
atoms, scatt. by Ag surface 2—50430
atoms, scattering from Hg film deposited on LiF substrate 2—56573
atoms, triplet metastable, resonance multiphonon ionization 2—42811
atoms and He-like ions, ^1S ground states, algebraic 1 matrices and radial momentum distribs. from Hylleraas-type wavefunctions 2—52953
atoms collisional ioniz. by 250 eV electrons, ang. correl. meas. 2—83213
atoms perturbation energies by multidimensional WKB method 2—82221
autoionization, projection-operator approximation in inelastic scattering region 2—77019
breakdown, laser-induced, electron cascade theory 2—60312
carbon tetrachloride-He system, surface tension, 1-71 atm., room temp. 2—64453
chondrites, ^3He production rate by solar protons 2—62721
core He burning, massive stars evolution 2—62518
CPD-31°1701, subluminous O-type star 2—75734
cusp-satisfying orbitals effect on electron densities at nucleus 2—83208
diffusion in rocks, det. of source material for ultramafic minerals 2—65583
diffusion in TiO_2-SiO_2 glass 2—50718
discharge, hot-probe investigation of spatial fine structure in plasma potential 2—60255
discharge, narrow tube, freq. spectrum and dispersion relation of moving striations 2—64346
discharge glow, hollow cathode in mag. field, photoemission effect 2—43215
electron impact excitation, broad P-wave reson. obs. 2—64075
electron scatt., inelastic collisions, adiabatical approx. 2—64064

Helium continued
- energy accommodation coeffs. for one-phonon inelastic scatt. from W 2−50528
- equation of state, improved, in vicinity of critical point 2−80522
- excitation by fast proton impact, Born cross-sections 2−79949
- globular clusters and Hartwick's two-dimensional classification 2−75781
- high pressure medium, speech intelligibility 2−73212
- ion motion in magnetic field in presence of induced electric field 2−70959
- ionization by H^+ impact 2−42817
- ions, dipolar polarizability, variational calc. 2−74206
- ions, fine struct., singlet-triplet correction 2−83210
- ions, hyperchannelling in Au and Ag, orientation rel. to intensity and energy loss 2−47778
- ions, irrad. of W, interstitial diffusion 2−47394
- ions, scatt. from solid surface, surface analysis technique 2−47072
- ions, scattering, multiple, by C and Ge foils 2−47781
- isoelectronic sequence, coherent atomic scatt. factor for ground state 2−64071
- isoelectronic sequence, electron impact excitation of ions interpolation formulae 2−74244
- isoelectronic sequence, oscillator strength for allowed nd-n′f transitions 2−56125
- isoelectronic sequence, upper and lower bounds of excited states 2−64073
- isotope mixture separation using critical state method 2−56134
- Jupiter, adiabatic model for gaseous-liquid H and He, temperature distributions 2−81933
- massive stars, advanced evolution 2−66086
- in metals, migration and release after implantation 2−50639
- metastable atom creation by electro-ion recomb. in postlum. of discharge 2−64345
- migration, in borate glass 2−53759
- migration in glass-forming oxides 2−50707
- monolayer adsorbed on Ar, correlation energy 2−74644
- optical breakdown, formation of non-stationary radiation driven detonation 2−80377
- Orion Nebula, 85α recombination line survey 2−81797
- Orion Nebula, total abundance 2−58238
- βOrionis, supergiant star, differential shifts in He I lines, atmospheric motion 2−62538
- plasma, cryogenic, electron-ion recomb. coeff. 2−77264
- plasma, electron-ion recombination, produced by laser 2−67631
- plasma, influence of atom-atom collisions on collisional- radiative ionization and recombination coeffs. 2−67630
- plasma, thermal, absorption and emission line shapes for Stark broadened He II resonance line 2−79952
- plasma potential in positive column of low-pressure discharge 2−60254
- plasma produced by $^{10}B(n,\alpha)$ reaction 2−70887
- plasma with 0.01%H, observed discrepancies in central region of Hβ profile at low electron densities 2−70631
- positron scatt., total cross sections, 15 to 23 eV 2−59951
- primordial cosmological abundance 2−48647
- pulsating stars, instability strip in HR diagram 2−58326
- recoil spectrometer for α particles 2−73932
- scattering by LiF, one-phonon transitions 2−50451
- scattering of He and Ar atoms from a W(112) single crystal, effect of O adsorption 2−67894
- shock wave downstream propagation in electrical shock tube with curved end wall 2−77356
- solar cosmic rays, relative abundance 2−75971
- solar emission regions, temp. in atmosphere 2−62747
- solar flares, D_3 emission obs. using narrow band filtergrams 2−62795
- solar wind, abundance variations 2−62780
- solar wind, velocity and flux dependence of He abundance 2−62779
- solar wind flux rel. to intensity of resonantly backscattered HeII solar radiation at 304 angstroms 2−55157
- solar wind relative abundance ratio rel. to solar activity 2−75975
- speech convertor operating in time domain 2−73215
- Stark profiles of forbidden and allowed transitions in dense laser produced plasma 2−42805
- stars, characteristics and spectra 2−51739
- in steel, neutron irrad., rel. to LMFBR development 2−49902
- steel-polymer friction, anomalous reduction by irradiation 2−56837
- stellar abundances, globular clusters, R-method 2−81808
- stellar chromospheres, obs. of He I D_3 line 2−58295
- stellar production, nuclear laboratory expts. 2−48695
- stellar spectrum in large mag. fields 2−62535
- triplet metastable, 5 photon ionization probability light intensity depend. 2−74248
- triplet radiation in prominences, response to increase in u.v. flux from flares 2−75996
- Ar/He, transmission through activated C adsorbent 2−43242
- Ar-He discharge, cataphoresis separation of constituents 2−77313
- CO_2+N_2+He, active medium in tuned prismatic resonator, selective properties 2−52411
- H-He pairs, retarded van der Walls pot. 2−67412
- H-He plasma, absorption coefficients of i.r. radiation 2−46744
- H-He plasmas, thermodynamic properties for stagnation shock layer of spacecraft entering atmosphere of Jupiter 2−46718
- H^--He, collisions, anglular distribution of autodetached electrons 2−77024
- H^+-He, differential scattering cross-sections, calculation and measurement at 8.826 hartrees 2−46484
- H_2O-He system, surface tension, 1-71 atm., room temp. 2−64453
- $H^+ + He$ impact, metastable H ang. distrib. 2−64069
- H(2s)-He charge-changing collisions, 20-120 keV, meas. of absolute cross sections 2−70638
- He^+/Ar^+ simultaneous ion heating in linear turbulent-heating expts., mass dependence 2−80288
- He/H_2 mixing ratio determination in giant planets 2−62693
- He-Ar mixture, glow discharge, spectroscopic measurements of cataphoresis 2−71022
- He-Ar mixtures, collision induced- absorpt. near $\lambda = 1$ mm 2−77084
- He-CO_2-N_2 deexcited plasma, quantitative emission spectroscopy 2−79206
- He-Cd mixture glow discharge, distribution functions and kinetic coeffs. 2−71024
- He-Cs plasma, oscillations and stability in mag. field 2−60267
- He-H mixtures in Jupiter's core rel. to statistical mechanics of light elements at high pressure 2−58779
- He-H_2, total scattering cross section of thermal energies 2−64212
- He-HD, low energy collisions, HD rotational transitions calc. 2−46644
- He-He fast collisions, metastable atom influence on excitation 2−42814
- He-He pairs, retarded van der Waals pot. 2−67412
- He-He scattering, intermolecular potential determ. from energy depend. of cross section 2−64079
- He^+-He collisions, formation of doubly charged ions 2−59954
- He^+-He collisions, meas. of differential cross section for excitation of inelastic processes in energy range 1-3keV 2−56133
- He-I_2, inelastic non-reactive energy transfer, calc. and analysis of probabilities and cross sections 2−60116
- He-Kr, He-Xe, mixtures, i.r. absorption spectrum, temp. dependence, determination of intermolecular potentials 2−50131
- He-Ne glow discharge, average electron energy in positive column 2−60310
- He-Ne laser, cathode glow discharge in transverse hollow cathode structure 2−79205
- He-Ne laser, effects of axial magnetic fields on mode intensity spectrum and output 2−79208
- He-Ne laser, elimination of unwanted lasing at 640.1 nm 2−79183
- He-Ne laser open cavity, aerosol particle detection and size obs. 2−56528
- He-Ne mixture, excitation of 2p-3s Ne lines 2−42742
- He-like ions, observability of hyperfine structure and Lamb, nuclear-volume shifts in 1snl-1snl′ transitions 2−52952
- He, He^+ ionizing collisions with Ne, Ar, Kr, Xe, 100eV-5000eV 2−56119
- He 584 Angstroms emission from magnetosphere, e.u.v. resonance radiation 2−68934
- He and H bulk speeds in solar wind, interplanetary shocks 2−62764
- He I, energies and lifetimes of doubly excited states meas. using beam-foil technique 2−52954
- He I, interstellar, effect of radiation pressure round stars, galactic evolution 2−48730
- He I and H lines in solar prominence, intensity ratio and chromosphere 2−66229
- He I line widths and shifts, line broadening calculations 2−52918
- He I λ10830 sunspot umbral line profile, photoelectric measurement 2−44989
- He I profiles in 56 Ari, Si Ap variable star 2−81853
- He I spectral lines of B-type supergiant-stars, new identifications in i.r. spectra of B-type supergiants 2−62544
- He I triplet lines in B-stars, influence of u.v. line blanketing 2−84976
- He II, improved Stark profile calc. for lines between 256 and 4686 Å 2−46477
- He II 4686 Å intensity in H II regions 2−58254
- He II in O star spectra, spectrophotometric luminosity criteria 2−58290
- He II Lα radiation, Bowen fluorescence mechanism nebulae 2−58235
- He II λ10124 line obs. in O and Of stars 2−51744
- He^- electron detachment cross sections in H, He, Ar, 4-30 keV 2−77017
- He^+, absolute differential ion and charge transfer scattering cross sections for collisions with He, Ne, Ar, Kr, 500-5000 eV 2−46485
- He^+, angular distributions in electron impact ionization 2−56108
- He^+, backscattering and channelling effects in crystalline solids 2−84224
- He^+, intensity decay curves, cascade-induced alignment changes 2−42753
- He^+, lifetime of $2^2S_{1/2}$ state 2−70641
- He^+, lifetime of 2S state 2−67430
- He^+, meas. of rate coeff. for recombination with electrons in pulsed afterglow 2−70643
- He^+ 304 Angstroms emission from magnetosphere, e.u.v. resonance radiation 2−68934
- He^+ collisions with Ne, 20-180 keV, meas. of absolute excitation cross sections 2−70628
- He^+ concentrations in magnetospheric light ion trough, satellite measurements 2−84889
- He^+ inelastic scattering on Ne atoms differential cross sections 2−59956
- He^+ ion, high energy, backscatt. and channelling in crystalline solid 2−77791
- He^+ ion scattering on Si (111) crystal surface, study of chemical reaction with bromine 2−50416
- He^+ polar wind distributions, model 2−81698
- He_2, attractive well, meas. by crossed beam differential elastic scatt. technique 2−50133
- He_2, energy barriers in excited states 2−56178
- He_2, exchange and Coulomb energies, dependence on wave functions of interacting systems 2−56180
- ^3He-^3He atomic cross-section meas. 1.5-2.1K 2−67437
- ^3He, relativistic contribution to the hyperfine interval of metastable triplet state 2−42808
- ^3He, weak hyperfine struct. interaction consts., determ. by mag. depolarization 2−59902
- ^3He abundance, 3 Cen A, diffusion 2−58266
- ^3He abundances and ratio to D and H in solar wind and sun, comparison with ratios on Earth 2−44982
- ^3He balance and thermal loss of atmosphere during 1947-68 period 2−78433
- ^3He discharge optically pumped, detection of orientation of $^3He^+$ by absorption of 10830Å line of ^4He 2−74245
- ^3He excess in Atlantic Ocean 2−75473
- ^3He interstellar, production by cosmic rays 2−84970
- $^3He + {}^3He$ interaction pots. from low-energy scatt. cross-section meas. 2−67434
- ^4He-^4He atomic cross-section meas. 2−67437
- ^4He-H_2 system, thermal diffusion factor and quantum collision integrals, effect of inelastic collisions 2−56449

Helium continued
$^4He^-$, r.f. reson. obs. of fine struct. transitions 2−67428
^{4}He flux precip. meas. in aurora 2−65910
$^4He + {}^4He$ interaction pots. from low-energy scatt. cross-section meas. 2−67434
$^4He + He$ interaction pot. from low energy total cross section meas. 2−59953
He + Ar collisions, chemi-ionization cross sections 2−64080
$He + H_2$ inelastic scattering, effective separable approx. of multichannel Green's functions 2−46639
$He + H_2^+ \rightarrow HeH^+ + H$, reaction cross-section, enhancement by vibrational excitation of H_2^+ 2−81500
$He^+ + H_2$ collisions, low-energy, optical excitation and polarization 2−67436
He + He scatt., long range retarded dipole forces, exptl. detection feasibility 2−67408
$He^+ + He$ collisions, inelastic, time-of-flight analysis of neutral products 2−70807
$He^+ + He$ collisions, very-small-angle charge exchange, technique for studying structure 2−42818
$He + Li^+$, elastic and inelastic scattering, charge exchange channels 2−42790
$He + h\nu = He^+(n=2) + e$, simultaneous ionization and excitation, 100-200 eV, meas. of cross section ratio 2−56131
$He(2^3S) + CO \rightarrow (CO^+)^* + He + e[C^* + O + He]$, excitation transfer and Penning ionization reactions, determ. rate constants for production of excited products 2−54535
$He_2(3p^3\pi)$, excitation transfer and quenching reactions 2−46552
He_{II} 4686 in quiescent and loop prominences and in chromosphere 2−73144
$He(s=1)$, $He^+(s=1/2)$, electron polarization by exchange scattering 2−59952
Li^+-He, oscillation of charge exchange cross section 2−64053
Na-He collision depolarization cross-sections for D lines 2−83169
Na-He collisions, broadening of D_2 line at high temp. 2−74237
Na-He collisions, broadening of D lines and relaxation of resonance levels of Na 2−42784
O_2^+-He collisions, vibrational excitation of diatomic Morse- oscillator 2−70806
in W, entrapment at vacancies 2−50651

gas
absorption into turbulent distilled water 2−50298
abundance in extreme population I matter rel. to Sun 2−81838
abundance in young O and B stars rel. to old hot subdwarfs in galactic halo and nebulae 2−81859
adsorption on solid Xe, energy spectrum calculation method 2−43499
arc, atm. cascade, electric field intensity and wall heat transfer meas. 2−46804
atmospheric arc, determ. of thermal condition in asymptotic region using spectroscopy and equilibrium flow model 2−77317
B subdwarf content, models 2−78450
B-type supergiants, He I lines at 8776.74 and 8582.65Å 2−69077
binary mixtures with methane, ultrasonic absorption meas. of rotational relaxation 2−64219
breakdown at very low temperature, obs. 2−50233
bubble form, in α-irrad., Al 2−50644
burning, stellar evolution, thermal pulses, calc. including neutrino energy losses 2−62512
cloud diffusion, neutral turbulent boundary layer simulated point-source, downstream cross sections, statistical parameters, concentration 2−84825
counter-current flow with Hg in packed bed system, criteria for flooding 2−50294
diffusion coefficient of $N_2(A^3\Sigma_u^+)$ state in afterglow of He-N_2 mixture 2−50132
discharge, hollow cathode, effect of mag. field on V-I characteristics 2−64347
discharge, Langmuir paradox region, electron energy distrib. and striations 2−64350
discharge, props. rel. to gas purity 2−46797
effect on $7^2S_{1/2}$Tl lifetime, coherence measuring and resonance broadening 2−49955
electric discharge, bremsstrahlung in strong electric field 2−80368
electron mobility, semiclassical calc. 2−41548
elimination of refraction effects in optical free surface motion detector 2−45439
embrittlement by neutron reaction-produced He in structural mats. at high temps. 2−68100
gaseous nebulae, line spectra and level populations 2−48672
glow discharge, radial structure of cathodic region 2−64352
for HTR coolant, conservation safety, economic and resource utilization criteria, design considerations 2−42621
ionization meas., pre-breakdown, influence of gas sampling techniques 2−50221
Kilauea Volcano S bank fumarole, content and significance 2−57742
laser, He-Ne, permeation of old laser to improve performance 2−42017
laser magnetometers, directional sensor errors 2−52382
Martian exosphere, thermal and non-thermal loss mechanisms 2−58509
monolayer adsorbed on surface of Ar crystal, calcs. of heat of adsorption and band widths 2−43490
nuclear reactor cooling, comparison with CO_2 cooling 2−56032
pair distribution function and third virial coefficient, path integral calc. of three-particle direct and exchange contribs. 2−53334
photoionization, by extreme u.v. radiation of laser produced plasma 2−53242
pulsating star, instability strip for $2M_\odot$ model 2−48709
pulsed discharge, electrical and optical measurements 2−60306
pulsed with 10.6 μm laser radiation, gas breakdown thresholds 2−83707
solar line intensity ratios, E(Hα)/E(He D3) and E(Hβ)/E(He D3) 2−76006
solubility and mobility in KBr, permeation, gas release and ion implantation studies 2−84002
sound velocity meas. at low frequency by resonance tube method 2−43265
spallogenic gas in Weston chondrite 2−73098

Helium continued
gas continued
spectral line intensity in glow discharge in transverse mag. field 2−52919
stellar, abundance in horizontal branch 2−75714
stellar abundance, main sequence B-stars 2−62488
stellar evolution, burning, solar mass stars 2−75721
thermally driven gas oscillations, heat balance, acoustic streaming 2−80358
thermospheric, longitudinal variations in density indicating magnetic control of polar heat input 2−65827
ultra-cold neutron attenuation 2−67084
upper atmospheric distributions, transport mechanisms 2−78383
D^+, mass identified, mobility 2−43203
He-Ar mixtures, sound dispersion as test for linearized Boltzmann eqns. 2−60375
He-Ar system, conc. depend. of diffusion coeff. at 300 K and 1 atm. press. 2−71121
He-CO_2 laser, chemical, pulsed, output pulse obs., pumping mechanism 2−73561
He-CO_2 mixture, atmospheric pressure discharge 2−60305
He-Cd, gas mixture, glow discharge, laser action in Crookes region 2−79196
He-Cd laser, 4416 Å, excitation mechanism, and operation parameters 2−79181
He-Cd laser, determ. of wavelength for centre of Lamb dip 2−66754
He-Cd laser, pumping mechanism and plasma parameters 2−76474
He-Cd laser generating at 4416 Å 2−45749
He-Cd lasers using recirculation geometry 2−59157
He-Cd mixture, glow discharge, electron distrib. fns. 2−74429
He-Cd vapour-ion laser, CW, developments, review 2−42021
He-Co_2 (N_2O)(SF_6) systems, binary diffusion coeffs. conc. depend. 2−67737
He-Cs gas plasma MHD, two-dimensional calc. of ionization fluctuations 2−80265
He-D_3 spectroheliograms, distrib. of photospheric mag. field 2−73103
He-H_2, meas. of absolute integral total cross sections and interaction potential 2−70814
He^+-He^{2+}-e plasmas, calc. of collisional-radiative volume recombination and ionization coefficients 2−50193
He-I_2 electronegative gas laser discharges, characteristics of system 2−71016
He-I_2 mixture, cw laser oscillation of singly ionized I_2 2−69923
He-Kr system at 300K, 1 atmosphere pressure, composition dependence of diffusion coefficient 2−50279
He-Kr^+ laser, ring shaped beam form., mechanism 2−63327
He-Mg mixture, double ionization of Mg by thermal collisions with He 2−70980
He-N_2-CO_2 TEA laser, double discharge trigger circuit 2−79199
He-N_2-O_2-CO laser, CW operation in some CO lines below 5.0 μ 2−45726
He-N mixture, decaying plasma, collision processes 2−50189
He-Ne, in magnetic field, use for Zeeman spectroscopy 2−63428
He-Ne, laser, with dispersive cavity 2−49353
He-Ne, streamers, in homogeneous fields induced by laserlight 2−74419
He-Ne 250 mW laser with Hg cathode 2−76482
He-Ne colour TV laser display system wide screen and high definition, NHK Model 101C, 525 line 2−82506
He-Ne laser, 0.63 μ, radiation fluctuations, parasitic generation influence 2−45736
He-Ne laser, atm. influence on wavelength, correction to laser interferometer 2−69957
He-Ne laser, automatic optical bias control, p.c.m. communication 2−66797
He-Ne laser, coupling modulation charact. 2−49368
He-Ne laser, freq. and wavelength meas., speed of light 2−78758
He-Ne laser, freq. stabilization using inverted Lamb dip and mode interaction effects 2−66753
He-Ne laser, frequency stabilization by saturated absorption in I_2 vapour 2−66752
He-Ne laser, gradual transition from single frequency to multifrequency 2−63328
He-Ne laser, hysteresis, production by conversion from single to double frequency 2−73558
He-Ne laser, impulse linear mag. field effect on generating power at $\lambda_{gen} = 1.15$ μm 2−63329
He-Ne laser, intensity correlation function, interferometry determ. 2−79200
He-Ne laser, methane stabilized, frequency and wavelength det. at 3.39 microns, speed of light det. 2−42018
He-Ne laser, output power, optimum tube diameter 2−59159
He-Ne laser, output power intensity dips, use in Zeeman spectroscopy 2−66857
He-Ne laser, single frequency operation and change to multifrequency 2−69909
He-Ne laser, transverse mag. field effect on radiated power 2−59161
He-Ne laser, variation of longit. elec. field by internally modulated beam 2−49367
He-Ne laser, with internal nonlinearly absorbing methane cell, 3.39μ freq. standard 2−59158
He-Ne laser active element using external mirrors 2−49356
He-Ne laser coupling to active rhodamine B doped polyurethane thin films 2−42055
He-Ne laser frequency measurement rel. to speed of light determination 2−48974
He-Ne laser mode selection and polarization control using dielectric plate 2−82474
He-Ne laser output power rel. to electron temp. and density 2−45737
He-Ne mixtures, viscosity and binary diffusion coeff. meas. in temp. range 25 to 700°C 2−50278
He-Ne output powers, experimental values 2−59160
He-Xe laser 3.508 μ transition, freq. stabilization methods 2−63330
He-Zn, gas mixture, glow discharge, laser action in Crookes region 2−79196
He-Zn, He-Cd, He-Se, He-Mg lasers, role of thermal energy-charge exchange 2−42019

Helium continued
gas continued
He I density in upper atmos., 10830Å obs. in tropical latitudes 2-65823
HeI interstellar gas in solar system, backscatter of solar resonance radiation 2-55078
^{3}He-^{20}Ne, laser magnetic field effect at 3.39 μ on ring lasers 2-45734
^{3}He-^{4}He dilution refrigerator, acoustic device of ^{3}He concentration monitoring 2-82574
^{3}He-^{4}He dilution refrigerator, acoustic device of ^{3}He concentration monitoring 2-85165
^{3}He-^{4}He mixture, study of specific heat near gas- liquid critical point 2-71255
^{3}He-^{4}He ratio at stellar surfaces, spallation processes 2-48692
^{3}He-CO_2-N_2 laser, high press., preionized in a reactor, performance 2-69916
^{3}He, near critical point, meas. of thermal relaxation times 2-80514
^{3}He, primordial, in Sun, reduction of neutrino flux 2-81947
^{3}He monolayer film adsorbed on graphite, motional narrowing in NMR 2-64578
^{4}He, desorption from synthetic zeolite, for desorption cooling 2-52009
^{4}He proportional counters, Monte Carlo of α-particle recoil spectra for incident neutrons 2-42454
He + Li^{+}, elastic and inelastic scattering 2-42815
He + Li^{+}, elastic and inelastic scattering, rotational coupling 2-42816
He + Ne laser, output-power fluctuations reduction 2-55692
He + Ne lasers, automatic frequency control and frequency fluctuations of difference wave 2-55691
I_2-He mixture, interaction of dissoc. and vibr. relax. behind shock wave 2-77168
liquid
see also Quantum fluids; Statistical mechanics/quantum; Superfluidity
^{3}He-^{4}He solns., osmotic press. along phase separation curve near absolute zero 2-80500
automatic level regulator in cryostat 2-69488
boiling, heat transfer from Al surfaces 2-66362
breakdown at very low temperature, obs. 2-50233
charge carrier mobilities near vapour press. 2-53472
charge carrier mobility at vapour pressure obs. 2-43415
charge transmission through dielectric interfaces 2-43413
charged vortex rings, focusing using electrostatic lenses 2-80503
collective modes in streams of charged vortex rings 2-53476
in cryostat, bypass valve for transfer 2-58657
cryostat, for X-ray analysis of single crysts. 2-43546
Dewar, all glass, using no auxiliary 2-58653
electron transport, non-ohmic, in image-potential-induced surface states 2-56534
films, acoustic multiple beam scattering 2-83832
heat exchanger props. in dilution refrigerator 2-73243
HeI, ^{3}He mass transport, obs. by thermal-neutron method 2-67855
interface, liquid-solid, reflection of phonons 2-74576
interface with metallic layers, low temp. thermal cond. anomalies 2-54065
interface with solid, Kapitza resist., phonon absorpt. 2-54072
interface with solid, Kapitza resistance, effect of low energy vibr. modes 2-51053
Kapitiza resist., phonon attenuation effects, acoustic mismatch model 2-67853
Kapitza resistance, transfer hamiltonian approach 2-56533
level indicator for dewars 2-55327
level indicator for small metal Dewar vessels 2-58651
level sensor, operating conditions for NbTi filaments 2-66368
low temp. physics, conf., Freudenstadt, Germany (Apr. 1972) 2-45183
monolayer formation on graphite, densities at completion 2-71253
phonon dispersion under press. 2-80510
phonon-like excitations and roton spectrum 2-77461
production techniques 2-66365
Raman scatt. by two roton bound states, roton binding energy 2-83828
Raman scatt. modified Stephen's theory 2-80504
roton energy temp. depend. 2-80517
roton lifetime in superfluid 2-43428
roton lifetime theory, inclusion of two-roton resonances in final-state interaction 2-71262
scanning electron microscope, cooled stage 2-82439
scanning electron microscope stage 2-79119
superfluid, application of equation-of-motion method to two-branch excitation spectrum 2-71260
superfluid, dissipative flow theory 2-71257
superfluid, force exerted b charged vortex rings 2-80508
superfluid, hydrodynamic approx. approach to charge carrier scatt. by phonons 2-77459
superfluid, phonon emission and absorpt. due to rotons 2-64495
superfluid, quantized charged vortex rings, electromagnetic field dependence 2-74577
superfluid, vortices, comparison with other physical systems 2-60122
superfluid application of equation-to-motion method to two-branch excitation spectrum 2-71261
superfluid baths coupled through a small hole, oscillations 2-47014
superfluid films, wave processes 2-80516
superfluid flow channel, extrinsic dissipation, mechanism 2-56535
superfluid transition temp. gradient with heat flow in mixtures 2-43424
superfluid vortices and turbulence as ultrasonic cavitation nucleation mechanism 2-43426
superfluidity at densities higher than 10^{6} g/cm^{3} 2-78851
surface bound electrons, lifetime and mobility 2-53468
surface-bound electrons, obs. of cyclotron resonance 2-80513
tricritical exponents and scaling fields for two-component systems 2-63035
two-dimensional, ground state, physically adsorbed monolayer model 2-77457
vortex expt. for detection at known location 2-67861

Helium continued
liquid continued
He/Cu interface, Kapitza resist., Rayleigh waves influence 2-47764
He/metallic layer/He bath system, energy flux calc. 2-47010
He/metallic layer/He bath system, energy flux eval. 2-53474
He I, acoustic cavitation at 10 kHz 2-56464
He I, heat transfer modes 2-64491
He II, acoustic cavitation at 10 kHz 2-56464
He II, boundary pressures and forces generated by moving vortices 2-47016
He II, critical flow through holes 2-47020
He II, critical heat flux density and thermal quenching in long channels 2-47021
He II, electronic bubble surface tension, press. depend. 2-77463
He II, emission and absorpt. of phonons by rotons 2-43425
He II, energy transfer from pulsed thermal source below 0.3K 2-71263
He II, evaporation spectrum, phase space analysis 2-50390
He II, flow, torque on Rayleigh disc 2-53478
He II, flow stabilization by modulation 2-43421
He II, fluctuations and a.c. Josephson effect 2-64499
He II, forces in superfluid flow 2-80501
He II, growing collective modes in vortex rings 2-53477
He II, heat capacity at const. vol. near λ pt. 2-47012
He II, injected K^{+} mobility, iron-roton scatt. cross sections 2-67863
He II, interaction of charged vortex rings with superfluid surface 2-50392
He II, laminar and turbulent flow 2-47017
He II, Landau parameters for rotons 2-43418
He II, light scattering by ultrasonic cavitation 2-43427
He II, liquid, superfluid, thermohydrodynamic conditions at peak flux of horizontal heaters 2-67859
He II, long-wavelength phonon dispersion 2-60534
He II, low temp. superfluid density in restricted geometries 2-47019
He II, meas. of effective mass of positive and negative charge carriers by resonance technique 2-80512
He II, negative charge carriers 2-47024
He II, onset of turbulence for counter flow 2-43420
He II, phonon emission rate of rotons 2-47011
He II, phonon spectrum, thermodynamic evidence against quadratic term 2-77456
He II, positive impurity ion mobility 2-60535
He II, pressurized turbulent, escapt of negative ions and vortex annihilation model 2-67857
He II, relaxation phenomena at rotation acceleration in spherical vessel, rel. to pulsar relaxation 2-81893
He II, second sound velocity, scaling and universality, under pressure near superfluid transitions 2-43419
He II, stimulated evaporation of atoms by heat pulses 2-67860
He II, superfluid currents, persistent, linear velocities and role of vortex lines 2-47015
He II, superfluid flow in restricted geometries 2-47013
He II, two-roton bound states 2-50393
He II, vortex core radius, temp. depend. 2-71264
He II, vorticity by obs. of current at a grid in an ion cell 2-83829
He II bath, low temp. thermal exchange 2-64498
He II film, rotating, thickness changes 2-64496
He II film flow, thermally driven, 1.7-2.1 K, dissipation 2-67862
He II film flow transfer over Plexiglas ampoules, singularities 2-67856
He II films, non-pot. flow at sub-crit. vels. 2-47022
He II films, surface tension, temp. depend., surface excitations contrib. 2-53473
He II in rotating bucket, origin of quantized vortices 2-67858
He II rotating superfluid, obs. of single vortex lines, detection of trapped charge 2-53479
He II superflow, saturated dissipation 2-53475
^{3}He-^{4}He dil. mixtures, osmotic press. thermometry 2-45184
^{3}He-^{4}He dil. mixtures, osmotic press. 2-47005
^{3}He-^{4}He dil. solns., diffusion const. meas. and ^{3}He-roton cross section 2-53471
^{3}He-^{4}He dil. solns., equil. theory, low temp. 2-43416
^{3}He-^{4}He dilute mixtures, osmotic press., 20-400 mK 2-73242
^{3}He-^{4}He dilute solutions, ion motion at ultralow temp. 2-47003
^{3}He-^{4}He mixture, diagram of state singularities due to hydrostatic effect 2-43414
^{3}He-^{4}He mixture, study of specific heat near gas- liquid critical point 2-71255
^{3}He-^{4}He mixture superfluid density near tricritical point 2-74578
^{3}He-^{4}He mixtures, Landau theory test 2-63040
^{3}He-^{4}He saturated mixtures, osmotic press. below 300 mK 2-43423
^{3}He-^{4}He soln., dilute, viscosity, 0.03-0.6K 2-71254
^{3}He-^{4}He soln., heat of transition 2-43422
^{3}He, below 3 mK, magnetic phenomena 2-77460
^{3}He, cooling by Pomeranchuk effect, cryostat construct. 2-45191
^{3}He, diffusion in liquid ^{4}He, investigation by thermal neutrons 2-64492
^{3}He, near critical point, meas. of thermal relaxation times 2-80514
^{3}He, specific heat singularity near critical point 2-47004
^{3}He, thermodynamic interaction functions 2-77462
^{3}He adsorbed monolayer form. and struct., n.m.r. obs. 2-80509
^{3}He and ^{3}He-^{4}He mixtures, obs. of critical point phenomena 2-64493
^{3}He liquid-solid mixture, interpretation of NMR and thermodynamic data below 3 mK, new liquid phase 2-80511
^{3}He refrigerator, 200 mW recirculating 2-52008
^{3}He solid interface, Kapitza resist., single- particle vs zero-sound couplings 2-47006
^{3}He + ^{4}He solutions, saturated vapour pressure and specific heat below λ temp. 2-52108
^{4}He, calc. of ground-state Bijl-Jastrow wave function using bridge diagram sums in Euler Lagrange eqn. 2-71256
^{4}He, compressibility, correl. length, near critical point, temp. depend. 2-80505
^{4}He, eqn. of state in λ transition region 2-80502
^{4}He, ground-state energy, liquid structure function, three-particle correlation factors 2-80506
^{4}He, hydrodynamic operators in atomistic model theories 2-64494

Helium continued
liquid continued
^{4}He, ionic mobilities, λ point phenomena 2−47007
^{4}He, Kapitza cond. with Cu, rel. to Khalatnikov model, at 1.9 K 2−67854
^{4}He, light scatt. near λ line, intensity peak, rel. to isothermal compressibility 2−50391
^{4}He, phonon dispersion and contribution to heat capacity 2−47001
^{4}He, superfluid, ^{3}He limited drift of charge carriers 2−77458
^{4}He, superfluid, phonon spectrum, self-energy 2−71258
^{4}He, thermal expansion, 0.1 to 0.7K 2−47002
^{4}He, thermally driven superfluid film, saturation of fluctuation dissipation in flow 2−80507
^{4}He, thermodynamic interaction functions 2−77462
^{4}He adsorbed on graphite, flow 2−74575
^{4}He energy excitation spectrum, comparison with high-density calcs. on interacting Bose system 2−63042
^{4}He film, adsorbed, superfluid, quartz microbalance obs. 2−64497
^{4}He superfluid calc. of roton-limited mobility of ions at temps. below 1.7 K 2−71259
^{4}He under press., superfluid density near λ point 2−43417

liquid, sound propagation
see also Second sound; Zero sound
film, acoustic interference applic. to thickness meas. 2−47008
films, anomalous attenuation of third sound, microscopic origin for apparent uncertainty principle 2−71252
second sound velocity and superfluid density near tricritical point of ^{3}He-^{4}He mixture 2−74578
He II, charged impurities conc. waves as type of second sound waves 2−53480
He II, entropy transport by vortices, and second sound vel. modifications 2−64500
He II, fourth sound, thermal excitation, 0.8K to λ point 2−67864
He II, h.f. u.s. attenuation, press. depend. of phonon dispersion 2−47025
He II, second sound, mutual friction force obs. 2−47018
He II, thermally excited sound waves 2−47023
He II, u.s. damping and vel. shift in Landau model 2−60536
He II films, third sound waves, rel. to surface tension temp. depend. 2−53473
^{3}He-^{4}He liquid mixture, light scatt. study 2−53481
^{3}He-^{4}He mixture, thermodynamic relationship between second sound velocity and osmotic pressure 2−64501
^{4}He, acoustic vel. under press., temp. depend. 2−47009
^{4}He, excitation spectrum, absence of quadratic term 2−53469
^{4}He, superfluid, light scatt. study 2−53481

solid
b.c.c., Brillouin scatt. from transverse phonons 2−84509
coherent state formalism and phonon freqs. 2−74960
conducting phase, high pressure conversion calc. 2−68293
diffusion of isotopic impurities, quantum theory 2−68046
electron mobility, pressure effects 2−43431
interface, liquid-solid, reflection of phonons 2−74576
lattice dynamics, non-central force model 2−74970
sound propagation, elastic consts., Debye temp., and compressibility detn. 2−43972
sound velocities, anisotropic, in h.c.p. solid 2−50394
submonolayer, adsorbed on Ar and Ne, two phase model 2−80581
thermal conductivity anisotropy 2−56536
thermodynamic, elastic and mag. props., review 2−80515
Umklapp thermal relax. time tensor, thermal cond. anisotropy 2−74579
^{3}He-^{4}He mixture, anomalous n.m.r. data 2−43429
^{3}He-^{4}He mixtures, phase separation, review 2−80515
^{3}He-^{4}He mixtures, thermal cond. in phase separation region 2−47027
^{3}He, b.c.c., ground state energy 2−71266
^{3}He, b.c.c., ground state props., localized single particle and correlated function calcs. 2−53482
^{3}He, b.c.c., thermal excitations 2−43434
^{3}He, exchange, Monte Carlo calc. 2−53484
^{3}He, ground state properties 2−43430
^{3}He, Neel temp., triple exchange effects 2−83830
^{3}He, solidification press., λ transition to ordered antiferromag. phase 2−56537
^{3}He, spectral density function, longit. and transverse nucl. relax. times 2−43433
^{3}He, spin diffusion and transverse relax. time 2−47026
^{3}He adsorbed monolayer form. and struct., n.m.r. obs. 2−80509
^{3}He liquid-solid mixture, interpretation of NMR and thermodynamic data below 3 mK, new liquid phase 2−80511
^{4}He, apparatus for production 2−64502
^{4}He, b.c.c., anomalous Debye- Waller factor 2−67865
^{4}He, b.c.c., phonon freq. dispersion curves and group widths 2−53483
^{4}He, b.c.c., scatt. function for inelastic neutron scatt. 2−67867
^{4}He, compressibility, correl. length, near critical point, temp. depend. 2−80505
^{4}He, ground state properties 2−43430
^{4}He, h.c.p., crystallographic angles 2−53663
^{4}He, h.c.p. and b.c.c. phases, single-particle scatt. phenomena 2−67866
^{4}He, hypersonic phonons 2−43432
^{4}He, isotopic impuritons 2−71267
^{4}He, Kapitza cond. with Cu, rel. to Khalatnikov model, at 1.9 K 2−67854
^{4}He, submonolayer on Cu and Ar and Ne monolayers on Cu, low temp. specific heat 2−80580
^{4}He, temp. pulse propag. in diffusive, second sound and ballistic regions 2−71268

Helium-3
change distrib. in external beam of Hamburg isochronous cyclotron 2−79691
interactions
$\pi^-{}^3\text{He} \rightarrow \pi^+(3n)$, resonances in three- nucleon system at low energies 2−42424
scattering
No entries

Helium compounds
He-H_2 system, population and natural spin orbital analyses 2−67540

Helium compounds continued
He-Ne, laser LG 68 for building industry 2−66755
HeH, mol. with just H atom in ground state, translational absorption spectrum 2−74266
HeH^+, electron correl. influence on vibr. and rot. consts. 2−64139
$(HeH)^+$ dissociation by electron impact, distortion polarization of orbitals and asymmetry in forward-backward scattering fragments 2−56179
HeH^+ molecule, ground state electronic struct., calc. 2−46542
HeH^{++}, floating one-centre perturbation treatment 2−67455
$HeH_2{}^+$, ab initio potential energy surface calcs., diatomics-in-mols. method 2−83246
HeNe absorption spectrum in vacuum u.v. region 2−77090

Hellmann-Feymann theorem *see Quantum theory*

High-pressure phenomena and effects
see also High-pressure techniques
anvil apparatus, tetrahedral, high pressure and temperature generation 2−78689
behaviour of materials in relation to dynamical properties of Earth and planets, Bullen's hypothesis 2−51520
carbon tetrachloride gas mixtures, second cross virial coeffs. determ. from solubilities 2−43262
containers, duct seal break, reaction force calc. 2−62893
Cu, elimination of pores by hydrostatic pressures and density increase at 20 kbar 2−71626
dilatancy in rock under hydrostatic pressure 2−68860
dislocations, hydrostatic pressure effects 2−60797
elastic property changes, u.s. meas. method 2−68060
engineering solids, conf., Aviemore, Scotland, May (1972) 2−68127
fracture of triangular plaster of Paris plates due to contact explosive pressure 2−53793
freons, viscosity, isotherms 2−83784
gas in porous column, transient effects on nuclear expl., model anal. 2−53276
granular rocks, u.s. wave vel. and compression simultaneous meas., porosity depend. 2−61982
Hall constant measurement of n-type Ge by cubic type high-pressure multianvil apparatus 2−76431
Hg_3Te_3-Ge_2Te_3 alloy, elec. transport processes, near semimetal-semicond. transition at high press. 2−68406
hydrostatic soaking, influence on structural change of deformed polycrystalline metals, X-ray study 2−84127
ionic substances, polymorphism predictability, empirical rules 2−68191
manganin pressure transducers, influence of H_2 on electrical resistance, compared with Au-Cr alloy 2−76122
melting, pair pots. rel. to melting curves 2−56541
metal, structural changes and effect on mech. characts. 2−68079
plastic behaviour of single crystals 2−68080
plastic yielding in crystn. and amorphous solids 2−68081
polyethylene, bulk modulus and density in 30 kbar, glass transition temp. press. coeff. 2−83352
polyethylene, crystallization and melting 2−50414
polyimide, hydrostatic press. effect on mech. behaviour 2−83347
polymer, elastic modulus, yield strength and deformation up to 50000 lbf/in^2 2−68094
polytetrafluoroethylene, cryst. struct. at high press., transition at 4.5kbar 2−83849
pressure transmitting media, low temp. behaviour of talc and teflon 2−73248
pulse propagation in solid, effect of mechanical props. 2−68074
rocks, static uniaxial, to 30 kb 2−62013
rocks, static uniaxial deformation to 30 kb 2−62013
rubber, crystallization 2−60603
ruby, absorpt. spectra below elastic limit 2−61630
semiconductor, amorphous, lone pair, refr. index press. depend. 2−68594
solid polymers, relaxation and d.c. conduction 2−74604
steel, heat treated, cyclic strain softening at various hydrostatic pressures 2−68142
steel, with high N content, formed by melting under high press., metallography 2−50812
steel thick-walled cylinders, microstrain obs. under internal pressure up to 6 kbar 2−68156
thick-walled cylindrical vessels, creep testing under internal pressure rel. to design 2−69497
transition metal dichalcogenide layers, spectra, press. to 6Kbars 2−44378
vacancy motion and clustering under pressure 2−68020
welded pressure vessels, loading capacity, stressed at high temps. 2−64771
Ag-Au alloy, effect on resistivity 2−51097
Ag, elastic constants, meas. by torsional oscillatory method 2−68061
Al, elastic constants, meas. by torsional oscillatory method 2−68061
AlMn, supercond transition temp., 0-20 kbar press. 2−47870
Ar arc discharge at 950 atm. 2−67662
BeO, plastic deform. in single and polycrystalline mat. 2−68082
Bi-Cd binary system, pressure effect on eutectic temp. 2−76124
Bi-Sb alloys, pressure-temp.-comp. diagrams 2−68192
Cd, Fermi surface topology rel. to hydrostatic press., magnetoacoustic meas. 2−77806
Co, large grain size specimens, fracture under 3 kbar pressure 2−68097
Cu, elastic constants, meas. by torsional oscillatory method 2−68061
Cu, removal internal porosity on sintering 2−68130
n-GaSb(Te), galvanomag. props. rel. to hydrostatic press. at 4.2K 2−68400
Gd, Hall effect, elec. resist., galvanomag. effect, effect of press., 77-400K 2−77858
HfV_2, supercond. transition temp. changes 2−71865
Mg_2Sn pressure dependence of electrical resistance 2−84326
$(NH_4)_3Cd_2(SO_4)_3$, ferroelec. phase transition shift at press. to 1400 bar, 20-300K 2−77958
NH_4F, shock wave accompanying induced phase change, seismological implications 2−78268
Na, liquid, coherent X-ray diffraction patterns at very high pressures, along melting curve 2−67803

High-pressure phenomena and effects continued
- NaCl, dislocation generation, grain boundary mechanism, expt. obs. in single and polycrystalline mat. 2−68029
- NaClO$_3$, n.q.r. of Cl, press. depend. to 20 kbar 2−51419
- Ni olivine to Ni spinel, reaction rate of phase change, seismological implications 2−78270
- Pb-Bi alloy, supercond. under high press., supercond. transition 2−47868
- Pt, vacancy conc. rel. to press., quenching effects, excess resist. obs. 2−60788
- Rb, liquid, sound velocity meas., 0-20000 p.s.i. 2−71195
- Si, band edge position, uniaxial stress effects, Schottky barrier obs. 2−51167
- SiC-B alloy, phase composition rel. to press., 50-60 kbar 2−53996
- SiO$_2$, vitreous, induced birefringence, nonlinear variation with uniaxial stress to 7 kbar 2−68600
- SnO$_2$-TiO$_2$ mixed crystals, exsolution obs. 2−74746
- Tb, Hall effect, elec. resist, galvanomag. effect, effect of press., 77-400K 2−77858
- ^{99}Tc, effect of high hydrostatic pressure (100 kbar) on decay constant 2−46190
- ThCe, supercond transition temp., 0-20 kbar press. 2−47870
- ThU, supercond. transition temp., 0-20 kbar press. 2−47870
- Zn, large grain size specimens, fracture under 3 kbar pressure 2−68097

High-pressure techniques
- *see also High-pressure phenomena and effects*
- absorption spectra meas. apparatus for mineral studies 2−61828
- apparatus, calibration 2−76124
- apparatus for obs. of chemical reactions involving changes in conductivity 2−66373
- autoclave for obs. of effects of deformation on high temp. aqueous corrosion of metals 2−66375
- biological systems, high resolution microscopy in high pressure chamber 2−85086
- component fatigue failure evaluation, design features 2−69502
- conductivity cell for liquid obs. 2−48940
- conductivity cell for liquid obs. 2−48940
- deadweight free piston gauge with electromagnetic equilibrium 2−69492
- diamond-anvil high-pressure cell, ruby sharp-line luminescence employed 2−58658
- electrical feedthrough, spherical 2−62895
- ENDOR cavity, F centre hyperfine interactions 2−82412
- fluid handling techniques 2−69503
- force displacement meas. apparatus contained entirely within pressure vessel 2−68080
- furnace, for cryst. growth, at up to 150 atm. gas press. 2−60716
- hydraulic press, tap for controlling motion of plunger 2−78690
- hydrostatic pressure, for creep deformation obs. 2−68088
- hydrostatic pressure attainable at low temp. with a pressure cylinder 2−76123
- hydrostatic pressure production at low temp., rel. to investigation of pressure effects on metal Fermi surface 2−57118
- internal insulation testing for high-pressure vessels 2−69498
- isentropic materials compression technique and apparatus 2−52010
- isostatic compression for metal forming including sheet metal 2−68128
- liquid structure, X-ray diffraction studies along melting curves 2−67799
- low electrical conductivity meas. 2−59030
- manometer, differential with tensometer, for 100 to 300 bar absolute pressure 2−55372
- mass spectrometric anal. of nonequilibrium air flows 2−48354
- mass spectrometric system 2−49920
- measurement, 15 to 35 Kb, high temps., piston cylinder apparatus 2−76163
- micropump for steady state synthesis of gas mixtures at very dilute concs. 2−69493
- microreactor, magnetically stirred, for obs. up to 138 bar 2−57407
- multi-anvil apparatus, study of geometrical stability by gamma rays 2−85170
- nondestructive testing of filament wound pressure vessels and composites 2−64791
- O-ring design 2−69495
- optical cell for spectroscopy, for obs. in temp. range 77 to 500 K 2−66856
- optimal parameters of high pressure cryogenic fluid storage systems 2−76120
- safety precaution, cubicle for containing blast effects on vessel rupture 2−69504
- safety precautions, design for equipment 2−69491
- safety precautions for containing ballistic fragments 2−69499
- seals, cone for electrical leads in high pressure systems 2−69494
- seals, self sealing, design calcs. 2−66374
- shock wave pressures meas. in solid bodies, manganin pressure gauge 2−62894
- solid state studies 2−85171
- spark isostatic pressing for metallic materials 2−68129
- spectrophotometer cell, i.r.-u.v.- visible, high pressure, high temp., for in situ catalyst obs. 2−59290
- thick tube fatigue test apparatus using external and internal pressures 2−69500
- thick walled cylinder failure test-machine using fracture mechanics on pressure cycling 2−69501
- thick-walled cylindrical vessels, creep testing under internal pressure rel. to design 2−69497
- thick-walled vessels, finite element analysis of threaded end closures 2−69496
- three stage high-pressure apparatus, working vol. 100 cm^3, operational details 2−62897
- torsional oscillatory method for high pressure effect obs. on elastic constants 2−68061
- unit for phase transformation obs. up to 40 kbar in 2 to 400 K range 2−78691
- vessel and plates fracture, yielding and size effects 2−84013
- X-ray camera diffraction pattern recording w. two film cassette 2−66872
- X-ray device for thermodynamic investig. of metal/hydrogen systems 2−77715

High-pressure techniques continued
- Al pressure vessels, porosity 2−62896
- Hg$_2$V$_2$O$_7$, high press. prep. 2−71367

High-speed photography *see Cinematography; Photography/high-speed*

High-temperature phenomena and effects
- *see also High-temperature techniques; Refractories*
- air, i.r. emission, absorpt. coeffs., 6000-8500K 2−73240
- anvil apparatus, tetrahedral, high pressure and temperature generation 2−78689
- Earth, fourth-order anharmonic theory for prediction of equations of state of rocks 2−72676
- fuel cells with ceramic electrolytes for conversion of cheap fuels 2−59041
- gas flow, initial heating of solid, heat transfer, heat flux meas. 2−55566
- gas flow through entrance region of cooled tube, heat transfer 2−46818
- liquid flow, heat transfer 2−60462
- plasma production, efficiency of laser set-up 2−80294
- space vehicle entry simulation, arc-heated duct facilities for turbulent flow 2−66028
- Al alloys, fatigue damage 2−80808
- CO$_2$ continuous spectrum, calculation of absorption coeffs. oven temp. range 20000-100000°K 2−70692
- D plasma production by laser heating of special gas target 2−80293
- Ni olivine to Ni spinel, reaction rate of phase change, seismological implications 2−78270
- UO$_2$, polycryst., plasticity, 1400-2100°C 2−53810
- UO$_2$ clad fuel element swelling, factors 2−63250

High-temperature techniques
- *see also High-temperature phenomena and effects*
- arc furnace for thermal analysis of super-refractories 2−66363
- electric oven for studying mag. props. of rocks 2−73241
- extensometering 2−58687
- forging under vacuum or inert atmospheres 2−58655
- furnace, high temp., for Weissenberg camera 2−76119
- furnace for obtaining high temp. Raman spectra 2−55775
- furnace up to 800°C for heating of specimens in electron microscopy 2−85161
- gas flame heating equipment producing temps. up to 2300C for X-ray diffractometer 2−67800
- gradientless temp. cell for optical study of cpds. in elec. fields 2−82588
- high temps., precise meas. apparatus 2−52291
- liquid metal heat pipes, vapour transport limits 2−83128
- magnetic measurements, changes of magnetisation of weakly magnetic substances 2−59062
- mass spectrometric anal. of nonequilibrium air flows 2−48354
- physical property measurements above 2000°K 2−71616
- scanning electron microscope, straining stage 2−79121
- thermal analysis of volatile cpds. to 2500°C, sealded crucible technique 2−67872
- thermal cond. of ceramics obs. 2−77734
- thermal diffusivity meas. incandescent temps., by stepwise modulated beam 2−85162
- thermal expansion meas. at high-temps. by dilatometer reference materials 2−57071
- thermometry, review 2−52289
- thermophysical quantities, meas., at high temps., fast system 2−52299
- u.s. attenuation and velocity meas in steel at 1200°C using momentary contact method 2−74978
- Verneuil furnace, oxidation-reduction potential of environment, thermodynamic calc. 2−60705
- X-ray diffractometer attachment for high temp. obs. 2−77536
- CeO$_2$ thermal conductivity determ. 2−61116
- ZrC-W compounds vacuum evaporation 2−73239
- ZrC, meas. of thermal conductivity 2−61117

High voltage techniques
- electron and ion beam gun form., in gas discharges, rel. to welding 2−60296
- electrostatic generator, charge collection, theory 2−52711
- gas breakdown, Z-pinch, low pressure formative phase 2−67650
- Van de Graaff accelerator and accessories 2−59644
- X-ray tubes with a.c. heated filaments, emission current stabilizer 2−69518

History
- air-sea interaction, state-of-art 2−61840
- balloons in scientific experiments, review 2−72743
- Bose, S.N., co-founder of quantum statistics 2−62916
- cosmogony of solar system, nebular hypothesis of Isaac Orr, historical aspects 2−81926
- electron metallography, developments in UK, (1948-1960) 2−67958
- geometrical theory of measurement 2−52030
- George Ellery Hale, astronomical history, book 2−84946
- holography, development of principles 2−66391
- interstellar absorption, research development (1900-30 period) 2−81842
- life, atmospheric ozone, biological screen 2−78348
- loudspeaker horns, for sound reproduction, review 2−41763
- Matthiessen's rule, deviations from, review and critical evaluation 2−71753
- metallurgy, physico-chemical, progress 1871-1971 2−47569
- of nuclear physics, 2 discussion conferences 2−82085
- nuclear single-particle shell model 2−69523
- ocean currents and status of research 2−62048
- oceanography, contemporary trends originating with the floating marine research institute 2−62046
- photographic techniques, electrophotography 2−70099
- physical and astrophysical problems of current interest 2−82086
- Poincare's Rendiconti paper on relativity of electron dynamics 2−41426
- pretelescopic stellar outbursts, novae and supernovae 2−73022
- special relativity, Einsteins discovery 2−82093
- stellar parallax, first measurements 2−69521
- structure of space in physics 2−73252
- thermonuclear fusion, controlled 2−59789
- Titius-Bode law of planetary distances 2−48952

History continued
- wave mechanics, role of Louis de Broglie in founding it described by himself 2−58678
- X-ray crystallography history of development of direct methods 2−64612
- ^{14}C dating method employing emulsion 2−75438
- Pt pyrometers of Guyton de Morveau 2−69522

Hodoscopes *see Cosmic rays/apparatus; Particle detectors*

Hole theory of liquids *see Liquids/theory*

Holes *see Crystal electron states; Semiconducting materials; Semiconductors*

Hollow cathode *see Discharges, electric*

Holmium
- atom, arc spectrum, configs. determ. 2−64015
- atomic spectra, u.v. absorpt. and i.r. emission, classification 2−52920
- galvanomagnetic phenomena in single crystals 2−68548
- laser material, Ho versus Er rel. to visual safety 2−45750
- magnetic crit. scatt. role in elec. resist. 2−57271
- magnetoresistance in strong effective fields at 4.2K 2−77859
- paramagnetic, quadratic field depend. of attenuation coeff. of u.s. waves 2−68522
- paramagnetic susceptibility anisotropy, 5 to 750°C 2−44227
- thin phase holograms, noise effects of granularity 2−73610
- Ho^{3+}: apatite lasers, properties and performance 2−42063
- Ho, Er, Yb, Tm:YAG laser, recirculating liquid N_2 system for cooling 2−63339
- Ho^{3+}, in LaF_3 and $YAlO_3$, optical transition probabilities 2−54468
- $LiTmF_4$:Ho^{3+}, optical absorpt., emission and excitation spectra 2−81418
- YF_3: Yb, Ho, diffusion and transfer of optical excitation 2−61714

Holmium compounds
- tritide film, ageing, bubble form. and rupture 2−43478
- $Er_{0.6}$-$Ho_{0.2}$-$Dy_{0.2}$ alloy, magnetization curves, study at 4.2 K 2−65174
- Ho-50%Tb alloy, u.s. propagation 2−64843
- Ho-Zr alloys, form. of low temp. metastable allotropic solid solns. 2−47646
- Ho^{3+} in yttrium ethyl sulphate spin-lattice relaxation rate measurement using electron paramagnetic resonance techniques 2−68584
- $HoAl_2$, mag. struct., neutron diffr. study 2−75217
- $HoAu_2$, mag. struct., neutron diffr. obs. 2−72218
- $HoCo_2$, Co atom paramagnetic moments 2−72116
- $HoCo_2$, mag. behaviour in ordering region 2−44280
- $HoCo_{3-x}Ni_x$, mag. ordering 2−51256
- $HoCrO_3$, spontaneous magnetization, susceptibility, exchange interactions, 4.2-300 K 2−48070
- $Ho_xEr_{1-x}Fe_2$ system, spin orientation diagram 2−72197
- $HoFe_3$, mag. struct., neutron diffr. and thermal magnetiz. obs. 2−51272
- $HoFe_{3-x}Ni_x$, mag. ordering 2−51256
- $Ho_3Fe_5O_{12}$ garnet, cell parameters, X-ray powder data 2−74745
- HoGa, mag. props. 2−48079
- HoGa, magnetization and susceptibility, temp. depend. 2−72170
- $Ho(OH)_3$, ferromag. relax. 2−54334
- Ho_2O_2Se, mag. props. and struct. 2−44228
- HoPtSn and related intermetallics, crystallographic and Mossbauer study 2−50621
- $HoVO_4$, cryst. struct., refined 2−60756
- $HoZn_2$, mag. struct., ordering 2−68573
- $Tb_xHO_{1-x}FeO_3$, magnetic properties, rare-earth grids, Neel temps. of sublattices, easy magnetization axis, rare earth ion interactions 2−65033

Holography
- absolute flatness det, by combination of standard and compensating hologram 2−79244
- accuracy of holographic images 2−63350
- acoustic, application of photochromic films 2−55548
- acoustic, by sector scanning 2−79280
- acoustic, capacitor-transducer array for liquid and gas operation 2−69765
- acoustic, current and potential appls. 2−82536
- acoustic, Doppler effects 2−69979
- acoustic, Pohlman cell applic. to reconstructing complete sound fields in hollow cylinders 2−69977
- acoustic, synthetic aperture sonar, principles and performance 2−73444
- acoustic, with scanned linear detector array and electronically stimulated reference wave 2−76368
- acoustic 2−42153
- acoustic imaging, for medical diagnosis 2−76089
- acoustical, detection of geological formations, digital computer processing 2−44554
- acoustical, Huygens' expression for diffr. field of light scatt. by weak acoustic waves 2−55742
- acoustical, methods and applications, book 2−63363
- aerospace applics., data processing, review 2−48639
- aerospace testing applics. 2−46848
- amplitude holograms, diffraction efficiency effect of emulsion thickness 2−42141
- amplitude transmittance, linear and nonlinear effects 2−52432
- analysis of general displacement field 2−82541
- antenna, receivers, rad. pattern determ. by holography and optical processing 2−45623
- applications, conference (Los Angeles, Feb. 1972) 2−82534
- artificial hologram as optical compensator 2−76503
- aspherical surface control method 2−52433
- associative reproduction of pictures by optical correlation 2−79242
- automatic surface mapping, recording and image projection 2−79274
- automatic surface mapping, tracking and measurement 2−79275
- binary mixtures, investigation of critical phenomena 2−71269
- biomedical applications 2−78662
- bleached holograms, aerial reconnaissance photographic emulsion, diffraction efficiency 2−63390
- broad band characteristics of zone plate and holographic lens systems and hologram illumination 2−79264
- Brownian particles, sedimentation rate, diffusion coeff., holographic interferometry 2−45767

Holography continued
- chromatic aberration of reconstructed image, compensation by dispersive lens 2−42133
- cinematographic developments 2−69967
- coding plate, application of holographic memory 2−79270
- complex filter obtained as a Fresnel hologram with a converging reference beam 2−42151
- computer based analysis of hologram imagery, aberrations 2−52439
- computer generated holograms recording methods and noise charact. 2−82498
- computer restoration of optical holograms 2−69981
- contouring, surface evaluation of airfoils 2−82537
- correlation detection of data 2−73615
- crystal growth studies using microscopy system 2−47193
- deconvolution, image deblurring of electron micrographs 2−55666
- deformation meas., materials, response, holographic interferometric techniques 2−49402
- development of holograms recorded in photoresist 2−42137
- diffraction efficiency estimation of holographic material using latent image technique 2−66786
- diffraction method of controlling amplitude variations in computer generated holograms 2−79271
- digitally generated memories, spectrum shaping with parity sequences 2−66782
- discrete hologram, minimum element number 2−55720
- displacement meas. 2−41446
- double exposure, time ordered 2−69974
- double exposure hologram, for three orthogonal displacement component determination 2−66787
- double exposure holograms, applic. of mode-locked ruby laser 2−66781
- double exposure holograms for meas. spatial dependence of index of refraction 2−73616
- double exposure holograms of rapidly changing object, using mode-locked laser 2−63365
- double pinhole holography analysis 2−59193
- double pulsed holographic interferometry for study of periodic and transient deformation 2−41665
- dye induced desensitization of AgBr phase holograms to Ar laser light 2−42132
- electron micrographs, three-dimensional reconstructions by holography 2−79150
- electron microholography, single beam method 2−64629
- electron microscope images, holographic recording 2−79225
- erasable recording of optical information on alkali halide crystal, patent 2−66793
- fabrication of metallic gratings on photoresist by recording 2−82544
- far-field, theoretical calc. of edge smear 2−82539
- film thickness meas. by holographic interferometry 2−50477
- filter selectivity and noise effects in applications of optical correlation 2−69963
- flaw det. with mechanical impact excitation 2−56676
- flow visualization, single pulse technique 2−83694
- flow visualization and data reduction 2−83507
- focussed-image holograms using radiation scattered by the defect as the reference wave 2−42150
- throughfog, image reconstruction, incoherent scattering and vision improvement 2−79259
- Fourier holograms, synthesized in white light using biprism 2−79241
- Fourier transform spectroscopy, Moire technique for hologram recording 2−73614
- Fraunhofer holograms, wavelength dependent distortion 2−63358
- front surface detail recording from scene moving at high vel. 2−69964
- generation using superposition of plane waves, patent 2−82517
- grating, efficiency and stigmatism for unpolarized light in vac. u.v. 2−63352
- guitar, acoustical and hologram interferometric meas. of top plate vibrations 2−52244
- high density information storage, dynamic system 2−79257
- high resolution photomaterials for, requirements 2−66790
- history and development of principles 2−66391
- holo-diagram for interpretation of fringe patterns 2−45760
- hologram cross section, electron micrographs 2−66784
- hologram interferometry, real-time, for vibration pattern visualization 2−66788
- hologram reconstruction by incoherent light, expt. 2−69969
- hologram recording, 20 double exposure sequence 2−42144
- hologram transmission using random phase reference, computer simulation 2−73606
- holograms, large format, using He-Ne laser, obs. 2−49404
- holograms recorded with pulsed, continuous sources exposure characteristics 2−69983
- homothetic images, interference between two superposed images 2−63383
- image location and magnification determ. method 2−63349
- image multiplexing using random diffuser 2−63366
- image position, calc. 2−45761
- image structure produced by nonlinear distortions during hologram recording, spatial filtering 2−59201
- image transformation, of scattered objects 2−59195
- image-deblurring filter, high resolution extended-range, realization method 2−45766
- imagery by ray-tracing method 2−69896
- imaging, projective transformations 2−69971
- imaging and magnification properties 2−42146
- imaging of point object in higher diffraction orders 2−52437
- in-line, reacting liquid sprays 2−83755
- in-line expts., light optical model for electron microscopes 2−59099
- in-line Fraunhofer hologram image, intensity distribution, errors, focal tolerance 2−79222
- incohrent optical correlation system for integration of functions of one variable 2−55441
- information content in hologram interferometry 2−79262
- information storage applications, plane, volume holograms, review 2−63354
- inspection of aerospace materials 2−84169
- intensity distribution approximation 2−42136
- interference microscope, optical configuration and performance 2−73619

Holography continued
interference microscopy of biological cells 2−62827
interferogram analysis from single view 2−79269
interferogram of laser wavefront, det. of degree of spatial coherence 2−42125
interferogram of phase object using achromatic fringe system 2−76507
interferometer, visualization at weak inhomogeneities, in gas flows 2−64374
interferometer and fringe analyser, study of supersonic flow in wind tunnels 2−46836
interferometric, laser-produced gas breakdown 2−83559
interferometric, recording onto photochromic spiropyran 2−55719
interferometric anal. of contaminant deposits on optical surfaces 2−45809
interferometric deformation obs. of C−C biaxial test specimens 2−82145
interferometric technique for meas. of absolute retardation in photoelasticity 2−41623
interferometry, anal. of static deflections 2−66576
interferometry, appl. to ultrasonic wire bonder device motion 2−63128
interferometry, applic. to small displacement measurement rel. to geophysical studies 2−61845
interferometry, application to printer type piece deformation study 2−69666
interferometry, closed loop, real time 2−66791
interferometry, cylinders under hoop stress, flaw detection applications, sensitivity 2−84167
interferometry, determ. of influence coeffs. for composite structures 2−82143
interferometry, displacement and deformation meas. 2−82150
interferometry, examination of impact loaded objects 2−45765
interferometry, for aluminium cylinders train analysis 2−50787
interferometry, for strain meas. 2−73609
interferometry, method of stationary phase for anal. of fringe functions 2−66783
interferometry, motion analysis of semifluid nonuniform flow 2−52436
interferometry, noncylindrical Z-pinch density profiles 2−83597
interferometry, obs. of laser beam parameters 2−79218
interferometry, obs. of resonances of treble viol plates 2−45520
interferometry, printed circuit board evaluation 2−73617
interferometry, quantitative data reduction using fringe control techniques 2−82540
interferometry, use of matte scatterer 2−69980
interferometry, use of Moire patterns for enhancing sensitivity 2−76504
interferometry employing spherical mirrors 2−69978
interferometry for vibration meas. 2−49103
i.r., using pulsed high power lasers, Bi and paraffin films 2−55713
isochromatic and isopachic fringe patterns for dynamic loadings, simultaneous det. by holographic photoelasticity 2−66551
laser speckle used to measure small tilts of optically rough surfaces 2−73613
lecture demonstration of reconstruction of image of a plane object 2−66398
light scattering in photographic materials 2−63438
linear optimization in sequential information storage of holographic data 2−79261
linear recording, method retaining reconstruction efficiency 2−69972
long-range, for improving telescope resolution through distorting atmos. 2−66780
longwave, three-dimensional visualization of information acquired by longwave carrier 2−82542
loudspeaker diaphragm, dynamic behaviour obs. 2−45519
magneto-optic memories, materials, review 2−63345
matched filter systems for pattern recognition using correlation method 2−76495
measuring technology and metrology applications 2−58681
medicine and biology applics., book 2−73178
memory, effect of film grain noise on performance 2−42140
memory design, geometrical design 2−49398
microscopy, time resolved differential holography 2−55715
microscopy of small parts 2−55747
microwave, applications in modern aviation 2−82543
microwave, liquid-crystal display for concealed weapon detection 2−69975
microwave, reconstruction by electronic spatial frequency analysis 2−79278
microwave, resolution of defects 2−84171
microwave, scanning technique 2−49403
microwave hologram radar system, design and operation 2−82535
microwave holograms, optically reconstructed enhancement 2−59200
microwave holographic interferometry applications 2−79279
millisecond pulsed, applications to NDT strain and vibration analysis 2−79277
moire, applics. to study of large deformations 2−42139
multicolour imagery from holograms by spatial filtering 2−79273
multiple hologram optical elements, with low dispersion and low aberrations, anal. 2−66779
n.d.t., engineering appls. 2−84170
nematic liquid crystal used as instantaneous medium 2−79243
non-destructive testing applic. 2−71608
nondestructive monitoring for optimization of in-service performance tests 2−60924
nondestructive testing, metrological techniques, laser holography and speckle patterns 2−45763
object motion compensation using reflection holography 2−79276
optical, appls. to applied mechanics 2−84168
optical elements consideration 2−82545
optical elements design using phase holograms 2−69965
optical elements interferometric testing, computer generated holograms 2−82572
optical holographic interferometry, underwater, acoustically induced mutual coupling effects 2−79229
optical memories for computers 2−79219

Holography continued
optical simulation of radiation patterns, Frensal zone radiohologram 2−55623
in optically inhomogeneous medium, effect of scattering 2−79253
optimal construction geometry 2−59196
pattern recognition, parallel and time sequential optical multiplex systems 2−59198
phase holograms as optical elements 2−42143
phase holograms in dichromated gelatin applications 2−63357
phase mapping in holographic vibration analysis 2−79281
phase modulation noise in reconstructed image of Fourier transform plane phase hologram 2−79246
phase object visualization using Moire patterns 2−69973
photoanodically engraved holograms, data storage, retrieval and replication 2−69966
photoelastic, physical explanation in terms of warped- wavefront 2−52438
photogrammetry and mapping appls. 2−84780
photographic emulsion bleaching technique 2−55712
photographic materials, modulation transfer for 2−82527
photographic phase holograms, low noise processing technique 2−79245
photographic phase holograms, technique for reduction of scattering 2−42149
photopolymer recording films for real time image formation without processing 2−69968
photopolymer recording materials, nonlinear effects 2−49397
photoresist noise 2−49400
picosecond holography, using Bi thin film and Nd:glass laser 2−55714
plasma neutron meas. in focus, interferometric 2−83583
polarization, photoelastic analysis 2−82148
process of production, patent 2−66792
pulsed laser beam adjusting application 2−63353
quantization and other nonlinear distortions of transmittance 2−55718
quantization of transmission function, effect on quality of reconstructed image 2−66785
read only memory system 2−59203
reading of holograms by semiconductor injection laser 2−42142
real time, hologram types compared 2−79265
real time and double exposure microholographic interferometry for phase variation dynamics obs. 2−42148
real time depth gated acoustic image holography 2−42138
real-time contouring of gear tooth surfaces 2−82538
reconstruction of electron micrographs 2−45777
reconstruction of holograms using digital computer 2−69982
reconstruction using heterodyne detection 2−79260
recorder for transient and high speed events 2−76494
recording Fresnel holograms with broad spectral bandwidth light source 2−42134
recording materials, photochromic CaF_2, La doped 2−66789
recording materials, review 2−55716
recording medium, 3d character of photosensitive materials 2−42145
red blood cell rotation, model verification using holography 2−85096
without reference wave, two dimensional raster- like objects 2−73618
refractive index meas., three-dimensional, interferometric techniques 2−82582
relief phase holograms of photographic transparencies, practical arrangements 2−63359
remote real time reconstruction of holograms by Lumatron 2−42135
resolution limit of holographic reconstruction methods in electron microscopy 2−79161
review (1948-1971) 2−79249
r.f. modulation, for large volume scenes 2−59202
rigid body motion fringes control in live fringe holographic interferometry 2−79263
salicylideneaniline, coherent optical props. as hologram recording medium 2−82530
scalar coherent millimetre wave imaging based on Fresnel- Kirchhoff diffraction formulation 2−63364
scanned for study of paper loudspeaker cones 2−55541
seismic, underground objects, size and general shape det. 2−57679
seismic acoustical holography for underground objects identification 2−72655
seismic wave anal., energy distrib. and time variation obs. 2−76502
side band, with electrons compensation of magnetic lens wavefront aberrations 2−45764
Skylab contamination ground test, particle size distribution and velocities 2−78416
space division multiplexed holographic appts., patent 2−82516
spatial filtering using double diffr. mounting 2−82514
speckle pattern interferometry, application to engineering meas. 2−82557
stability test for system 2−42147
stabilizing techniques for holographic recording 2−73608
storage media, recyclable, performance parameters, review 2−63361
strain anal. using spline functions 2−82142
strain measurement, optical correlation method 2−82141
strain obs. on tensile specimen 2−82144
stress analysis of anisotropic composite plates 2−41598
subtraction of complex spatial function from another holographically 2−73611
subtraction with circularly polarized light 2−79247
superresolution, optical system 2−76501
surface displacement components det. for deformed body 2−66552
surface plasmon resonance effect 2−59197
technique for obs. of dioptric effect and defects in glasses 2−45776
technology and applications, book 2−42154
telephone diaphragm vibrs. study 2−45475
telescope main mirror, holographic correction of deformational aberrations 2−59251
testing of industrial plastic pipe products 2−79282
thermoplastic photoconductor storage media, structure, fabrication, recording techniques 2−63360
three dimensional display techniques 2−82580
time average, with thin phase recording materials 2−55717

Holography continued
- time average holographic interferometry, damped oscillations 2-63094
- time averaged, obs. of tympanic membrane vibrations in cats 2-51955
- time averaged, obs. of vibs. of tympanic membrane of human cadaver ears 2-82052
- tomography, variable depth display, holographic methods 2-69371
- total measurement 2-42152
- two element off axis lens system design 2-79272
- ultrasonic, real time image reconstruction techniques 2-49166
- ultrasonic, underwater viewing system and acoustical hologram reconstruction 2-49165
- ultrasonic imaging, synthetic aperture 2-82367
- ultrasonic multiplexing technique to construct 3-D images 2-79250
- ultrasonic with large phase disturbances using stochastic processing 2-73607
- u.s., visualization of holograms using Pohlman cell 2-69976
- u.s. transducer improvement, macrosonics 2-76497
- vibration analysis by real time and time average methods, bibliography 2-58885
- vibration and deflection meas., projected ruling Moire method 2-82149
- vibration measurement applic. 2-58897
- vibrational pattern of solid surface, real-time/time averaged interferometry 2-82147
- vibrations of segmented shells 2-82146
- vibratory mode shape patterns of cored mirrors det. by holographic interferometry 2-52434
- wake density fluctuations meas. using pulsed laser holographic interferometer 2-46833
- wave front reconstruction 2-59194
- weak signal enhancement technique 2-49401
- X-ray, of lensless Fourier-transform type 2-59199
- and X-ray radiography for materials research 2-69970
- Zeiss Jena stereoplanigraph, apparatus description 2-63351
- As-S-Ge glass film, laser induced refractive index changes obs. 2-61583
- As-S glass, mechanism of hologram formation 2-59204
- B-epoxy laminated composite plates, stress analysis 2-78895
- KCl:Na M_a centres, information storage using photodichroic effect 2-49399
- $LiNbO_3$:Rh, reversible holographic storage 2-69984
- $LiNbO_3$, doped, as erasable optical recording medium 2-73612
- $LiNbO_3$, transition metal doped, recording sensitivity, maximum diffraction efficiency, erase behaviour 2-63356
- $LiNbO_3$ applications, physical model, transport theory 2-63355
- $LiNbO_3$ for multiple storage of thick phase holograms 2-45762

Hot-atom chemistry *see Chemical analysis/radioactive; Nuclear reactions and scattering/chemical effects; Radiochemistry*

Hubble model *see Cosmology*

Hugoniot diagrams *see Equations of state*

Humidity
- *see also Atmosphere/humidity; Hygrometers; Moisture*
- effects on breakdown of sphere, rod gaps under short, long waveform impulse voltages 2-74433
- controlled humidity generator for X-ray struct. determ. of clay minerals 2-56623
- membrane-filter ice nucleus chamber, numerical estimates of humidity 2-65671
- moisture evaporation from wet surface, determ. of vapour flux in terms of humidity potential 2-83833
- photographic films, apparatus for meas. of humidity dependent internal stress and strain 2-52497
- polymer surfaces, effect 2-57223
- simulated atmospheric aerosols, effects on light scattering 2-57991

Hydrodynamics
- *see also Flow/liquids; Jets; Liquid oscillations; Liquid waves; Magnetohydrodynamics; Viscosity/liquids*
- 2 sink flow of stratified fluid duct 2-43281
- acoustic field coupling with plate vibrs. 2-45472
- acoustic ray theory for inhomogeneous moving medium 2-45503
- acoustic resonance phenomena produced by the non- stationarity of singular charge losses in pipes 2-56278
- asymmetrically rotating fluid disc, application to galaxies and solar system 2-56279
- atmospheric frontal motions, instability 2-84799
- axisymmetric creeping flow, force on accelerating body 2-83478
- bioconvective fluid instabilities in tetrahymena culture systems 2-77451
- boiling channel, l.f. stability, D marking method, computer calc. 2-56454
- boundary layer eqn., solns., appl. for non-zero wall vel. 2-83458
- boundary layer flows, stability analysis 2-77208
- Boussinesq fluid, temperature adjustment process via buoyancy-induced meridional circulation 2-67742
- cambered hydrofoil with jet flap, characteristics 2-67748
- carbon tetrachloride, settling process of unstable dispersed droplets 2-80435
- cavitation damage, in rotating disc 2-77390
- cavity distortions in massive liquid due to inertial effects, numerical soln. of differential eqn. on MINSK-22 2-83745
- cholesteric liquid crystals, governing equations 2-50332
- classical fluid, in critical region, effect of rotation on number density 2-46658
- computational topics computer simulation of various flow types 2-83440
- computer implementation of problems, using IBM system/360 operating system 2-43043
- computer simulation of ocean currents rel. to two fluid media model 2-78320
- convective instability in fluid layer, light scatt. obs. 2-46660
- convective stellar envelopes 2-62477
- core annular flow 2-80439
- coronal streamer during 7th March, 1970 eclipse 2-76036
- crude oil, with high paraffin content at low temps., hydrodynamic resistance 2-83751
- current driven instability in electrodeless induction discharge 2-80356

Hydrodynamics continued
- deformation of velocity profile in turbulent boundary layer in water and oil 2-74492
- disc rotating in non-Newtonian fluid 2-83485
- discrete numerical approach for prototype fluid flow 2-80218
- dispersion, agitated, by simulation model 2-53363
- dispersion in porous media, apparatus induced dispersion 2-67767
- elastohydrodynamic lubrication problem, finite element numerical solution 2-68114
- electrodynamic forces, volumetric and superficial, spatial localization in weakly polarizable liquids, applied electromagnetic field 2-77252
- electrodynamical analogy of equations 2-63264
- electrokinetic coupled flow in porous media, finite element solution 2-74310
- evaporation of solids into vac., kinetics 2-77465
- experimental, modern instrumentation advances 2-77209
- fall of drops in non-Newtonian media 2-46905
- flow, helical, homogeneous, about rot. self excitation, stability 2-46683
- flow measurements by current meters, propeller weight and shape effects 2-60144
- flow past bodies in fluidized media 2-74339
- fluid, convective instability, spectral anal, study 2-67609
- fluid, two-dimensional model 2-46649
- fluid circulation in and round dielec. fluid in elec. field 2-83624
- fluid mechanics and automation 2-74456
- fluidized bed of fine spiral packing 2-83496
- fluids, generation of thrust, continuum mechanics, book 2-70825
- fluids with antisymmetric stress, constitutive relations and extension of Curie principle 2-60157
- foundations, views of Predvoditelev 2-67548
- free-surface, initial value techniques 2-56467
- gas injection into vac., fast ionisation gauge 2-84928
- gases, application of invariant difference methods 2-77334
- general conservation theorem 2-67556
- general invariance of hydrodynamic equations, classical symmetry breaking 2-80183
- geophysical application to layered systems with flexible boundaries affected by gravity 2-75432
- geostrophic adjustment of rotating homogeneous or stratified fluid 2-61861
- Gosiewski's theorem, vorticity tensor, stretching tensor 2-46653
- Great Lakes, modified sigma equations' approach to numerical modeling 2-65597
- groundwater flow in inhomogeneous aquifer, groundwater head 2-67768
- gyroscopic behaviour for fluids with internal angular momentum 2-56312
- hard sphere gas, hydrodynamic disturbances, nonanalytic dispersion relations 2-66477
- heat disposal from power generation 2-80201
- p-n-hexyloxybenzylidene-p'-aminobenzonitrile, temp. depend of flow alignment 2-50339
- homogeneous turbulence associated with purely plane deformation, velocity-pressure correlations 2-56281
- hydraulics and fluid mechanics, conference, Melbourne Australia (1971) 2-77207
- hydrocyclone mechanics, basic theory 2-83454
- hydroelastic stability of flat panel in fluid flow, influence of free surface 2-46701
- hydrology, ρ_1 estimation from small sample 2-67766
- ideal relativistic fluid, Friedmann and Helmholtz equations 2-67555
- inertial effects in motion driven by hydrodynamic fluctuations 2-70827
- instability of parabolic problems, rel. to eigenvalues problems 2-77199
- internal waves around body moving curved path 2-80216
- ion mobility in liquid, hydrodynamic determ. 2-71163
- isocorrelation curves rel. to longit. vel. fluctuations in circular pipe 2-83434
- isotropic fluid systems of nonspherical mols., hydrodynamic eqns. and expressions 2-80178
- jet stability, rel. to small pot. perturbations, on escaping from slit 2-83470
- Kelvin-Helmholtz instability, nonlinear development 2-56468
- lake circulation around island, finite element investigation 2-74493
- lifting of liquids by withdrawal 2-43276
- linear viscoelastic fluid, pulsatile flow in elastico- viscous tubes 2-80167
- liquid crystals, e.m. hydrodynamics 2-50330
- liquid films, vertical falling, classification of flow regimes 2-74490
- liquid transition layers, calculations on model rel. to boundary layer characts. 2-80426
- loaded hydraulic cylinder with step inputs, cavitation effects 2-77389
- Mac method, homogeneous boundary condition for pressure 2-46655
- matter-antimatter, coalescence effect 2-44820
- MBBA nematic liquid films with free surfaces, electro-optic and hydrodynamic props. 2-67804
- p'-methoxybenzylidene-p-n-butylanilene, temp. depend of flow alignment 2-50339
- minimum drag in free-molecular flow, determination of optimum non-slender bodies of revolution 2-53122
- mixing layer, vel. distrib. using Blasius diff. eqn. 2-46656
- molecular fluids, hydrodynamic model calc. of momentum correlation functions at long times 2-50138
- motion of drop in pulsated medium under nonlaminar conditions 2-46904
- multiple-venturi system, application to design of flow-rate meter 2-46685
- Navier-Stokes eqn., modified, consequences in sound dispersion 2-53130
- nematic liquid crystals, applic. of unified formulation for normal liquids, liquid crystals and solids 2-43325
- non-Newtonian fluids in laminar flow through circular pipes 2-60124

Hydrodynamics continued
nonisoenergetic compressible free shear layer, initial development 2−70863
nonlinear interactions in Kelvin pattern 2−77378
nonlinear interactions problems 2−77194
nonlinear modelling eqn. for finite disturbances 2−74313
nonlinear motions induced by moving thermal waves 2−56301
nonlinear spin up and spin down of contained fluid 2−77204
nonlocal fluid mechanics, continuum theory 2−46654
nonstationary hydrodynamical accretion onto neutron star 2−81852
nonuniform flow, linearized profile theory 2−43058
nuclear reactor coolants, neutron fluctuations 2−76936
nuclear reactor fuel rod in vertical coolant tube, hydrodynamics, vibration and wear obs. 2−52844
numerical solution of cylindrical shock problem, computer oriented 2−67557
ocean, conference Liege, Belgium (1971) 2−44625
oil slick spreading over water 2−46866
oscillatory damping of cylinder in fluid 2−45473
parallel flow stability, effect of nonlinearity, viscosity in critical layer 2−80195
paramagnetic-ferromagnetic phase transition, spontaneous symmetry breaking and propagating hydrodynamic wave in the initial region 2−84413
penetration of density interface by heavy vortex rings 2−77214
plane problems, using semi-inverse and semi-indirect methods 2−43051
planetary waves, in rotating global fluid shells 2−81745
Poisson equation solution 2−48977
pressure effect at arbitrary Knudsen numbers 2−74312
radial oscillations of gas cavity in compressible fluid rel. to underwater detonation of TNT 2−60174
rarefied gas flow, external, unified kinetic theory approach 2−46830
relativistic, finite amplitude sound propagation in general relativity, gravitational instability 2−52053
relativistic perfect fluid, Einstein field equations, spherically symmetric solns. 2−56277
reservoir capacity design, rel. to inflow generation mechanism 2−67746
review, book 2−80200
Riccati transformation in numerical soln. of Orr-Sommerfeld problems 2−46875
rotating bubble bed 2−83498
rotating liquid, isothermal bubble motion 2−46912
rotation of circular cylinder about eccentric parallel axis in viscous fluid 2−56296
Schwarzschild interior soln., conformally flat system 2−78429
sea pollution, mathematical modelling, hydrodynamical and biochemical state variables, evolution equation 2−44632
second gradient theory leading to capillarity theory of Laplace 2−56280
self-gravitating gaseous discs, review 2−81815
self-similar solutions as intermediate asymptotics 2−80206
ship, theoretical models of flow, review 2−77379
shock wave propagation in compressible medium, hydrodynamic theory and scheme for incompressibility 2−82370
SO(3) × SO(3) symmetry, closed system specified press.- density relation 2−77174
spherical shell, translatory motion under the effect of spherical wave in compressible liquid 2−71122
spout diameter prediction in a spouted bed 2−77176
stability criterion for hydrodynamical transport states 2−49044
stability of core-annular flow of two ideal liquids 2−64401
stability of horizontal two component fluid with positive vertical temp. gradient 2−70831
stability of radially bounded rotating fluid heated from below 2−64224
stability of two component fluid layer heated from below 2−56452
steepening of long internal waves in stratified fluid influenced by vertical density profile curvature 2−53148
stellar and planetary atmospheres, motions in stratified convective zones 2−78455
stirred tanks with turbine impeller, dynamics and flow patterns 2−46867
stochastic point processes 2−41532
Stokes flow, material tensors symmetries for a particle 2−67743
Stokes resistance, multiparticle systems in linear shear field 2−56451
stratified liquids with space charge 2−56453
stratified ocean, coastal upwelling 2−57907
supercavitating hydrofoils with rounded noses 2−67775
suspensions, rigid dumbbell, hydrodynamic interaction effects for steady shear flow 2−67738
swimming of elastic slender bodies excited by external force, analysis 2−50283
symposium on fluid mechanics, Warsaw (1972) 2−43049
thermo-hydrodynamical model of ocean circulation 2−62027
thermohaline convection, oblique gradients effects 2−77212
thermoplastic films, amplitude of local deformation due to ponderomotive forces 2−73235
tides and storm surges, numerical solution of three dimensional hydrodynamical eqns. 2−44634
tornadoes and hurricanes, steady and unsteady, review 2−81644
transport coeff. determ., connection with molecular dynamics processes 2−82245
turbopump inducers for rocket engines, internal streamliner flow analysis 2−43288
turbulent entrainment, across density discontinuities 2−77241
turbulent flow over rigid half plane, sound radiation 2−74311
turbulent spiralling flow, in short tube, hydraulic resist. 2−80197
two fluid horizontal layers, thermally induced instabilities 2−43050
urinary tract flow analysis 2−51902
variational analysis, finite element method 2−77211
variational principle for irreversible phenomena 2−76239
velocity autocorrelation function, extension of hydrodynamics to binary dynamics 2−43278
vibrating circular hydrofoil in stream of ideal liquid, determ. of lifting force and longitudinal momentum 2−83744

Hydrodynamics continued
vortices, interacting line, negative temp. instability for two-dimens. motions 2−53111
vorticity divergence and deformation, geometrical interpretation for two dimensional flow 2−53123
water, flow, nonuniform, in rivers, and estuaries, longit. dispersion 2−67747
water, transit time methods in underground hydrology 2−46887
water, turbulent flows, amplitude modulation of ultrasound 2−74494
water drop response to sudden acceleration 2−83739
watershed subsurface response, surface runoff rel. to subsurface flow, base flow contribs. 2−67761
wave propagation in uniformly rotating fluid, surface and inertial waves 2−50164
weather forecasting using hydrodynamic barrier flow 2−65635
$CuSO_4$ liquid electrolyte horizontal layer exhibiting concentration polarization, hydrodynamic stability w.r.t. natural convection 2−48338
He II, liquid, superfluid, thermohydrodynamic conditions at peak flux of horizontal heaters 2−67859
^{4}He liquid, hydrodynamic operators in atomistic model theories 2−64494

Hydrogen
see also Deuterium; Protons and antiprotons; Tritium
absorption on (111) face of Ge single crystals 2−80583
adsorbate structure, on W surface 2−50554
adsorbed layer, ortho-para conversion on paramag. surfaces 2−43496
adsorbed on ferromagnetic catalyst, ortho-para conversion, surface magnetization orientation effect 2−71342
adsorbed on Ni film, effect on saturation magnetization 2−48094
adsorbed on Ti, photoemission energy level meas. 2−47166
adsorbed on TiC_x and NbC_x, surface recomb. rel. to carbide work function 2−50549
adsorbed on W, field emitted electrons energy distrib. as function of coverage 2−48016
adsorption, on graphite in high vac. range 2−43494
adsorption, on Nb polycryst. wire, u.h.v. technique 2−47161
adsorption and absorption by Nb, solubility 2−50542
adsorption enthalpy on Ni, cryst. orientation influence 2−60680
adsorption on (111) face of Ge single crystals 2−74934
adsorption on Ni films, under ultra-high vacuum conditions, meas. of desorption spectrum 2−53590
adsorption on Pt, promoted evap., field ion microscopy obs. 2−50548
adsorption state, W (100) surface, and flash desorp. spectrum 2−50555
air flames, diffusion, structure 2−61787
atomic and mol., interaction with Ne, Ar and ice surfaces at 4.2K 2−50539
austenite to martensite transform., effects of hydrogen 2−74923
cathodic, influence on Matteucci effect in electrolytic Ni 2−48084
in cellulose acetate detection by neutron radiography 2−65408
chemically induced dynamic electron polarization phenomenon in γ-irrad. solns. 2−78204
chemisorpt. on Pt, absorpt. and desorpt. kinetics 2−77514
chemisorption, on Cu, weak adsorp. obs. 2−50537
chemisorption on ZnO, i.r. studies of isotope effects 2−65375
concentration anal. of H_2 atoms in third order reactions to determ. rate consts. 2−84625
corona discharge between concentric hemispheres, positive ion species determ. 2−43220
crack propagation, induced, decohesion theory testing 2−74859
cryopumping with liquid H_2, advantages over He refrigerator 2−78705
desorption, from contamined metal surface, spatial distrib. obs. 2−50526
desorption and adsorption on W, SIMS, EID, flash-filament obs. 2−47170
desorption phenomena for stainless steel LEED and molec. beam assembly 2−67922
diffusion, in Zr and Zircaloy-2(-4), 275-700°C 2−53773
diffusion flames, temp. influence on burning characteristics 2−67703
diffusion in binary systems, struct. influence 2−77611
diffusion in Fe, solid and liq. states 2−43661
diffusion in metals, lattice expansion method 2−77606
diffusion in metals, review 2−77604
diffusion in metals, theory 2−77605
diffusion in Nb, anelastic obs. 2−77616
diffusion in Nb, application to quantum theory 2−80718
diffusion in Nb, Pd, Ti and Ni, quantum interpret. 2−71537
diffusion in Pd, equil. and kinetic isotope effects 2−77619
diffusion in Pd, jump model, neutron quasielastic scatt. obs. 2−83999
diffusion in Pd and Pd-Ag alloys, coeff. meas. by electrochem. methods 2−77602
diffusion in Pd at elevated press. 2−77620
diffusion in transition metals, quasielastic neutron scatt. obs. 2−77623
diffusion in zone melted α-Fe 2−77610
diffusivity in Nb, low temp., determ. by Gorsky effect 2−80847
discharge, h.f., re-ignition, influence of metastable states 2−43217
discharge, pulsed, plasma diagnostics, maximum electron conc. 2−67692
electrolytic charging of f.c.c. Ni-Co alloy, dislocation band production 2−56713
embrittlement, stress corrosion cracking, catalytic dissociation as primary process 2−84020
embrittlement of heat-treated Zr-(2.5 wt.%) Nb press. tubes 2−50770
embrittlement of Ni-ThO_2, dispersion strengthening effects 2−74862
embrittlement of steel, mechanistic model 2−77653
embrittlement of zone-refined Fe 2−43725
environmental effects on stress corrosion cracking of plastic solid 2−77654
etch pitting of graphite 2−53553
gas, absorption into turbulent distilled water 2−50298

Hydrogen continued
gas, Brillouin scattering, analysis of spectrum using kinetic model based on Wang Chang-Uhlenbeck eqn. 2−80409
gas, diffusion in Zr-Y layers, calc. by gen. eigenfunction method 2−50720
gas, elec. breakdown due to large number of electrons 2−83709
gas, pulsed with 10.6 μm laser radiation, gas breakdown thresholds 2−83707
gas laser, v.u.v. radiation 2−42012
gas laser, Werner band stimulated v.u.v. emission 2−42013
generators for neutron tubes 2−46035
heat of adsorption on Ni film, comparison with D_2 2−43497
interstellar, molecular, formation on ice and solid CO, physical adsorption energy 2−55076
isotope mixture separation using critical state method 2−56134
isotopes, separation during photodissociation of NH_3 2−43198
laser, Lyman and Werner band v.u.v. emission 2−42014
laser compression to super-high densities, thermonuclear applications 2−70487
liquefier 2−45188
liquid, 3 metre nuclear targets 2−59601
liquid, 50 cm target with Lawsonite windows 2−52670
liquid, bubble chamber Mirabelle, use with Serpukov accelerator 2−76746
liquid, conical nuclear target 2−59602
liquid, superfluidity 2−53470
liquid target system development, use of closed cycle refrigerator 2−46034
Markarian 6 galaxy, IC 450, H line activity 2−69028
metallic phase, influence of expression for dielectric function in structure calcs. 2−77521
in metals, determ. using an omegatron partial- pressure gauge 2−53866
neutral, motions in galactic center and 3 Kpc arm 2−58185
Ni:H, hydrogenated, thermo-e.m.f., 3d band shape 2−72052
in nuclear fuels, chemical analysis techniques 2−74168
permeation, stress corrosion cracking, brittle delayed failure 2−78194
permeation through Ni, Fe, Pt, Nb, Cu and stainless steel, surface effects 2−77608
planetary atmospheres, exospheric temp. of 2-component diffusive equilibrium model 2−44935
plasma, Faraday ring currents in low-pressure ring-shaped duct with radial mag. field 2−60219
plasma, ion energy distribution resulting from turbulent heating 2−70927
plasma, observed discrepancies in central region of Hβ profile at low electron densities 2−70631
plasma, Stark broadening of Balmer lines 2−64278
plasma in focus device, flow in a pulsed mag. compressor 2−83593
plasma line electron broadening, boundary of quasistatic region 2−77022
plasmoid purification by mag. field in injector-diverter 2−80298
positive column plasma, population density and local thermal equilib. of excited atoms 2−43128
pressure and temperature behind blunt bodies and supersonic flow with supply of reacting gases to base region 2−60332
pyrolysis on W filaments, atomization, e.s.r. obs. 2−72550
reaction with nuclear graphites 2−59842
recombination lines, partially ionized interstellar cloud, microwave observations 2−81807
shell H burning, massive stars evolution 2−62518
shock waves, normal ionizing, press. jump 2−67721
solar abundance, collision broadening of Ca I and Ca II lines 2−75948
solar line intensity ratios, E(Hα)/E(He D3) and E(Hβ)/E(He D3) 2−76006
solid, anisotropic molecular interactions 2−64824
solid, coherent state formalism and phonon freqs. 2−74960
solid, ground-state energy, pressure, compressibility and phase transition at high densities 2−43501
solid, h.c.p., Raman spectrum, fund. and overtone vibr. transitions 2−61666
solid, metal-insulator transition 2−68282
solid, n.m.r. spin echoes, ortho H_2 conc. depend. 2−48306
solid, normal, permittivity meas. 4.2-13.1K 2−77934
solid, nucl. spin-lattice relax., temp. depend., 0.075-1.5K 2−68583
solid, ortho, zero-phonon IR Q-branch absorpt. theory 2−74975
solid, ortho-enriched, fundamental, i.r. absorption band meas. above and below order-disorder phase transition 2−81346
solid, possibility of supplying missing cosmological mass 2−75667
solid, self-consistent eqn. of state 2−71711
solid, self-diffusion and vacancies 2−43656
solid, sound velocity at 4.2K and pressures up to 200 bar 2−80910
solid, specific heat, Debye temp. and EQQ interactions 2−43985
solubility and electromigration in Pd-Ag alloys 2−83990
solubility in β-Ti and alloys, alloying element effect 2−74909
solubility in metals and non-ideal soln. behaviour 2−77716
solubility in Mo, 905-1521°C 2−50841
sound absorption, rotational relaxation effects 2−46858
spectral lamp, lowering of ignition voltage by addition of Ne and He 2−42284
spectrochemical determination Ti alloys 2−72592
in steel, conc. determ. using diffusion kinetics 2−64780
stellar burning, nuclear laboratory expts. 2−48695
stellar spectra, highly excited lines, gas density determ. 2−75725
superradiant gas laser, field emission electron beam emission 2−42024
thyratron pulse discharges, arc pot. obs. 2−56399
upper atmospheric distributions, transport mechanisms 2−78383
viscosity and thermal conductivity coeffs. calc. using modified Enskog theory over wide temp. and density range 2−64227
in Co, mag. after-effect 2−78029
H_2:Xe, solid, vacuum u.v. study of Wannier states, obs. of host isotope effect on linewidths 2−51341
H/Fe abundance ratio from binary star observations, Mv(K) dependence in late-type giants 2−73036
H_2/He mixing ratio determination in giant planets 2−62693
$H_2/O_2/N_2$ flames, radical recomb. reactions, HO_2 participation 2−65373

Hydrogen continued
$H_2/O_2/N_2$ flames, with Cr and K additives, electron attachment and negative ion form. 2−72555
$H_2/O_2/N_2$ mixtures, self-inflammation rates 2−81488
H_2/air and H_2/O_2 combustion, shock-induced 2−83651
H-Ar plasma, blast waves generation, by pulsed electric discharges 2−74360
H_2-D_2 solid system, specific heat, Debye temp. and EQQ interactions 2−43985
H-He mixtures in Jupiter's core rel. to statistical mechanics of light elements at high pressure 2−58779
H-He plasmas, thermodynamic properties for stagnation shock layer of spacecraft entering atmosphere of Jupiter 2−46718
p-H_2-Ne solutions, density at low temps. 2−57027
H_2-Ne(N_2)(Ar) systems, conc. depend. of binary diffusion coeffs., 300K 2−64399
H_2-air mixtures, thermal explosion, boundary of flame propagation region 2−75378
H_2-methane-Ar mixtures, mean ionization energy 2−60290
H + H_2 collinear reaction probability in threshold region, DWBA study 2−81489
H and He bulk speeds in solar wind, interplanetary shocks 2−62764
H^+ polar wind distributions, model 2−81698
o-H_2, rot. relax., 170-300K, sound absorpt. meas. 2−80909
o-H_2, solid, f.c.c. and h.c.p. phases, phonons, librons and rot. state 2−64839
p- H_2, solid, quantum diffusion, jump freqs. of o-H_2 impurities 2−60830
H_2 chemisorption on (111) plane of Ni, flash desorption spectroscopy study 2−80568
H_2 effect of VV transfer processes on rate of thermal dissociation 2−67456
o-H_2 librational modes, application of quantum mechanical lattice dynamics formalism 2−71709
HD, temp. dpeendence of Scott thermomagnetic torque 2−46861
H_2 + F laser oscillator, closed-form solution for rate equations 2−69922
Hγ and δ equivalent widths measurement for det. absolute magnitudes of young stars 2−48701
Nb:H, X-ray diffr. pattern, anomalous line broadening due to H 2−64642
in Ni, interaction with dislocations, internal friction obs. 2−53792
in Ni, mag. after-effect 2−78029
Pd-H and Pd 24% Ag-H foils, electron microscope examination 2−56948
SiC:H, implanted, recomb. radiation of excitons and vibr. spectrum 2−68688
in Ta, Snoek effect absence 2−77647

ions
electron impact cross-sections, representation for ionization and excitation 2−64063
intergalactic gas, explanation of instability of nearby groups of galaxies 2−48665
ionospheric density, topside obs. 2−58074
isoelectronic sequence, electron impact excitation of ions interpolation formulae 2−74244
metastable, formation by dissociation of H_2^+, meas. of angular distribs. 2−70816
microwave ion source 2−69884
microwave source construction, operation and principles 2−63299
Orion Nebula, 85α recombination line survey 2−81797
plasma, dense, Lyman-α line asymmetry 2−70635
plasma, expanding, population inversion of excited atomic levels 2−46709
plasma, non-equilibrium, axially symmetric free expansion 2−77270
projectile interaction with Hg, pot. cross sections 2−77015
radio recombination line data rel. to non-LTE theory 2−69113
scattering, multiple, by C and Ge foils 2−47781
sintering of Cu powder by electrolytic heating 2−74891
stopping power of pure metals for 25-250 keV ions 2−47774
Cu, induced electron emission from (001) and (011) faces 2−75199
H^+-H collisions, differential cross-section for H(n=2) direct excitation 2−46482
H^+-H high-energy scattering, pseudo-state expansion applications 2−42762
H^+-H interactions, Gaussian representations of charge overlap effects in intermolecular forces 2−43026
H^+-H_2 collisions, vibrational excitation, 15-1000 eV, semiclassical theory 2−80152
H^+-H_2 vibrational excitation, application of theory of small-energy-transfer collisions in dominant long-ranged forces 2−70817
H^--He, collisions, anglular distribution of autodetached electrons 2−77024
H^+-He, differential scattering cross-sections, calculation and measurement at 8.826 hartrees 2−46484
H^+-Xe charge exchange collisions, 15 eV, three-state calcs. of spin polarization 2−79918
H_2^+-atom superelastic collisions, vibrational excitation of H_2^+ 2−70815
H_2^+-molecule superelastic collisions, vibrational excitation of H_2^+ 2−70815
H-, autoionization states, computation using Feshbach formalism 2−46487
H-, position of lowest D autoionization states calc. using Feshbach's Q-operator formalism 2−49982
H- spectrum, calc. of low-lying resonance in 2^1P state 2−46476
H, ^2H abundances and ratio to ^3He in solar wind and sun, comparison with ratios on Earth 2−44982
H^-, autoionization, projection-operator approximation in inelastic scattering region 2−77019
H^-, energies and wavefunctions of ground state calc. using least squares method 2−56129
H^-, h.f. source prod. without parasitic behaviour 2−79168
H^-, influence of electron correlation on one-particle electron density and radial expectation values 2−52950
H^-, photodetachment, variational calculation 2−46448
H^-, proof that 2 $^{1,3}S$ states are not bound 2−42807
H^-, proton-ion electron capture collisions 2−64067
H^-, pulsed duoplasmatron source 2−79169

Hydrogen continued
ions continued
H^- collisions with inert-gas atoms and diatomic molecules, coincidence studies of elementary processes 2−42804
H^- electron detachment cross sections in H, He, Ar, 4-30 keV 2−77017
H^- in CaF_2, local modes studied with CO_2 laser 2−61632
H^+, absolute differential ion and charge transfer scattering cross sections for collisions with He, Ne, Ar, Kr, 500-5000 eV 2−46485
H^+, collisions with He, Ne, Ar and H_2, probability ratio for neutralization of H^+ to H(2p) or H(1s) 2−42802
H^+, elastic scatt. by Ar, excited states 2−64051
H^+, H_2^+ impact on H_2 gas, H atom electron capture into $n=3,4$ states, cross sections 2−70637
H^+, identification in corona discharge between concentric hemispheres 2−43220
H^+, negative absorption of light 2−70910
H^+ collisions with inert-gas atoms and diatomic molecules, coincidence studies of elementary processes 2−42804
H^+ collisions with Ne, 20-180 keV, meas. of absolute excitation cross sections 2−70628
H^+ concentrations in magnetospheric light ion trough, satellite measurements 2−84889
H_2, vibrationally excited, collisions with Na atoms excitation of D-line radiation 2−70627
H_2 labile negative ion, electronic and nuclear magnetic resonances 2−74264
H_2^+, bound-state calcs. use of regional wavefunctions 2−49937
H_2^+, charge shifts in formation of covalent bonds 2−80034
H_2^+, diamagnetic properties, variation-perturbation calculation 2−53008
H_2^+, diamagnetic properties, variation- perturbation calculation, effect of varying internuclear separation 2−53009
H_2^+, finite-difference soln. of united atom, one centre expansion of molecular wavefunctions 2−80048
H_2^+, floating one-centre perturbation treatment 2−67455
H_2^+, perturbation and perturbation-variation treatments of $1s_g$ and $2p_u$ states 2−53010
H_2^+, perturbed generalized eigenvalue equation 2−64128
H_2^+, proton prod. by electron collision, Rundel's discussion 2−50041
H_2^+, spherical limit symmetry dilemma 2−42894
H_2^+, two-parameter wavefunctions for iso ground state 2−80032
H_2^+, wavefunctions in momentum space, effect of nuclear vibrational motion 2−46545
H_2^+ beam, MeV range, transmission through thin Au single crystal, channelling effects 2−44011
H_2^+ collisions with Ne, 20-180 keV, meas. of absolute excitation cross sections 2−70628
H_2^+ discharge charge-exchange analysis of cathode dark-space data 2−67693
H_2^+ dissociation by impact On He, Ar, H_2, N_2 at 4-12 keV, meas. of cross sections for angular distribs. of H(2s) 2−70816
H_2^+ rotational states, upper limits studied using potential energy functions of Morse and Hulburt-Hirschfelder 2−46543
H_3^+, identification in corona discharge between concentric hemispheres 2−43220
H_3^+, observability of fundamental spectrum, comment on paper by Kawaoka and Borkman (1971) 2−70705
H_5+, identification in corona discharge between concentric hemispheres 2−43220
HD^+, collision induced dissociation by electron impact, effect of dipole moment studied using Born-Oppenheimer approx. 2−56173
H-H^+, H_2^+, H_3^+ reactions with electrons in dark interstellar clouds 2−75786
$H_2^+ - D^+$ mas difference meas. using ion cyclotron resonance technique 2−70254
$H^+ + Ar$, total differential cross-section, energy depend. 2−79858
$H^+ + Ar$ collision at 5 eV, interatomic potential determination by inversion of elastic differential cross section data 2−59930
$H_2^+ + CO_2$, $H_2^+ + CO$, $H_2^+ + N_2$ reaction rate constants by ion cyclotron resonance mass spectrometry 2−61768
$H- + H^+ \rightarrow H(n,l) + H^+ + e$, electron detachment by charged particle collision 2−59947
$H^+ + H(1s) \rightarrow H(1s) + H^+$, charge transfer scatt. at high energies 2−77023
$H^+ + Kr$ total differential cross-section, energy depend. 2−79858
H_2^+ + electron collisions, proton prod. cross sections, low energy 2−64132
H^+ + noble gas collisions, differential cross sections, 500-3000 eV 2−64068
H(2p) vacuum u.v. excitation by electron impact on H_2, polarization free meas. of Lyman α radiation 2−80120
He ionization by H^+ impact 2−42817
$He + H_2^+ \rightarrow HeH^+ + H$, reaction cross-section, enhancement by vibrational excitation of H_2^+ 2−81500
$p + H- \rightarrow H(nl) + H$ recombinations in slow collisions 2−59948

neutral atoms
— 2−66450
adiabatic theory of Stark broadening used to describe transitional frequency band between impact and quasi-static limits 2−46474
adsorption on C, rel. to work function variation 2−60677
in 56 Arietis spectrum, variations 44860 2−44860
Balmer jumps in spectra of B-type supergiants temperature scale 2−58273
beam production by microwave discharge and mass spectrom. detection 2−67427
beam-foil excited, obs. of fine structure interference effects in Lyman β radiation 2−64062
inbinary solutions of liquids, meas. of total neutron cross sections 2−79823
binding energy, lowest excitation energy, in mag. field 10^8-10^{11} gauss 2−67419
bound electron g factor, effect of nuclear mass determ. using pulsed double mode maser 2−42796
bound state radial functions used to construct basis for unitary representation of algebra O(2,3) 2−42791
bound states, rel. to four-dimens. harmonic oscillator 2−42792
bound-state spectrum, treatment using eikonal methods 2−82618

Hydrogen continued
neutral atoms continued
charge exchange collision with proton, Coulomb T matrix calc. 2−46483
charge-changing cross sections in collisions with I ions, 5-25 MeV 2−70623
collision with Ar, N_2, O_2, meas. of cross section for electron capture in 1.4-8 keV range 2−56123
collisional excitation and ionization rates rel. to classical and quantum mechanical formulae in astrophysical calculations 2−49977
collisional excitation by alkali metal atoms 2−67426
collisions with electrons, Stark broadening, one-electron approximation 2−42757
collisions with H_2, N_2 and O_2, electron loss cross sections 2−64216
collisions with inert-gas atoms and diatomic molecules, coincidence studies of elementary processes 2−42804
collisions with positive mesons, muonium form 2−83217
densities at exobase 2−65832
Dirac equation, formulation in Friedman universe 2−49972
electron and positron scatt., effective potentials 2−67423
electron and proton scatt. four-channel approx. approach 2−83212
electron capture cross sections for collisions of protons and deuterons with atoms 2−67411
electron capture into $n=3,4$ states by H^+, H_2^+ impact, cross sections 2−70637
electron impact cross sections, correl. approx. modification 2−67422
electron impact cross-sections, representation for ionization and excitation 2−64063
electron scatt., elastic phase shifts comput. 2−64065
electron scatt., Fredholm optical potential calc. of elastic phase shifts 2−46480
electron scatt., inelastic collisions, adiabatical approx. 2−64064
electron scatt., inelastic cross section calc., adiabatic approx. 2−46481
electron scatt., virial theorem generalization 2−64066
electron scattering, applications of quasiminimum principle to calcs. of variational lower bounds 2−49979
electron scattering, complex coordinate space calculations for position and width of lowest ^1S resonance 2−70636
electron scattering, coupled channels with square well potentials, Fredholm-Pade approx. 2−76205
electron scattering, elastic, variational principles for multichannel Feshbach equations 2−52898
electron scattering, elastic differential cross sections, off-shell Coulomb T matrix 2−42797
electron scattering, Glauber type eikonal approximation for 'angle' trajectories 2−79876
electron scattering, threshold behaviour of ionization interval function calc. using classical three body computer programme 2−56122
electronic energy levels, emission spectrum 2−45206
emission spectrum in rotating electric field 2−59941
energy level relativistic shift, operator domain paradox 2−63014
energy levels and wave functions, momentum representation treatment 2−56120
e.p.r. spectrum, spin-relaxation effects 2−79950
excitation by electron and positron impact calc. in eikonal approx. 2−52944
excitation by gravitational wave, semiclassical treatment 2−77021
excitation of $n=2$ levels by electron impact, eikonal theory 2−42758
exciton ground and first excited states of excitons in mag. field 2−64060
exosphere, calc. of H distribution 2−75621
frequency dependent properties, generalized eigenvalue equation approach 2−56121
galactic HI distributions rel. to spiral arms and HII regions 2−78446
gas, viscosity and thermal conductivity in range 1 to 10^5K 2−50276
gas, viscosity calculations, comparison with exptl. results 2−50277
in globular clusters, upper limits on abundance 2−75783
ground state, translational absorption spectrum 2−74266
ground-state energy, u.v. convergence of e.m. correction 2−42795
hadrons pair production cross section for γ, 265-4215 MeV in hydrogen and deuterium 2−63497
inert gas-H dispersion forces, improved rigorous bounds 2−42801
injector for fast atom bunches 2−53204
integral eqn. approach, energy values 2−70630
interaction energy, first-order, non-additive effects 2−49980
interaction with intense laser radiation, time- dependent approach 2−79955
interplanetary distribution, extraterrestrial Lyman α radiation distribution 2−62731
interstellar, 21cm absorption profile towards W3 radio nebula, radial velocity and Cnα recombination line 2−44897
interstellar, angular distrib., columnar density obs. using 21 cm radiation 2−81837
interstellar, effect of radiation pressure round stars, galactic evolution 2−48730
interstellar, self absorption in large region toward galactic centre 2−44885
interstellar H_2 and H and He fluxes from planetary nebulae 2−78448
interstellar Hi in solar system, backscatter of solar resonance radiation 2−55078
interstellar HI resonant scattering of solar Lyman α radiation 2−78433
interstellar matter volume density within 500 pc of sun 2−55074
isoelectronic sequence, radiative decay rates of metastable systems 2−79958
linear Stark effect due to resonant interactions of static and dynamic fields 2−64061
Lyman α solar radiation, backscatter by interstellar gas in direction of solar apex 2−85006
Lyman-α absorption rel. to upper atmosphere pressure, density and scale height 2−65817
Lyman-α interstellar equivalent widths in OB-stars, Mariner 9 observations 2−58362
Lyman-α line profile meas. in arc experiment 2−74243
maser, physical processes, review 2−49342
mass determ. from 21 cm obs. of NGC 45 2−58198
matrix elements and selection rules exact 2−42794

Hydrogen continued
neutral atoms continued
metastable, 2.5 keV produced by charge- exchange process in Cs vapour, absolute detection and collisional destruction 2−56124
metastable, form. by proton impact on He target, ang. distrib. 2−64069
multiphoton ionization in presence of intense e.m. field 2−49978
multiphoton ionization of ground-state, semiclassical treatment of intense e.m. field 2−79960
multiphoton transitions between 1S and 2P levels 2−67418
n=3 state, r.f. spectroscopy meas. of resonance narrowed Lamb shift 2−52947
one dimens., repulsive core term in Coulomb pot., energy levels in strong mag. field 2−59940
plasma, continuum emission in visible and u.v. 2−80247
in plasma, line broadening, quasistatic and impact approx. 2−52948
polarization interaction of two atoms in ground and first excited state 2−67425
population inversion in laser plasmas 2−49973
position scattering, elastic, calc. by optical potential method 2−46421
positron elastic scattering, inclusion of long range effects via pseudostate expansion 2−42798
positron elastic scattering, test of approximate methods, positronium formation 2−42800
positron pickup, treated by theory of sequential projections and quasi-minimum principle 2−42803
positron scatt., elastic, calc. with Kohn variational method 2−46479
radial-angular factorized, 'natural' group scheme and selection rules 2−59944
radiative decay of 2P state, exponential decay law 2−79959
reaction with W inhibition due to O adsorption on W surface 2−71344
reactions with electrons in dark interstellar clouds 2−75786
reactive scattering, quantum mechanical calculations 2−69602
S-like energy spectrum, analytic treatment of Coulomb potential in path integral formalism 2−46473
scattering by rare gases, absolute total cross sections, interatomic forces 2−67424
scattering of low energy electrons and high energy protons, pseudo-state expansion applications 2−42762
Scd galaxies, HI distributions and rotation curves from obs. at 21 cms. 2−62464
Sco X-1, Balmer H line profiles in spectrum 2−58431
semiconductor detector measurements of free H atom concentrations 2−52693
solar chromosphere, spectral line profiles of H lines on the disk 2−48810
solar flare spectra, OSO-7 obs. 2−78593
solar wind flux rel. to intensity of resonantly backscattered Lyman α radiation 2−55157
spectral line intensity in glow discharge in transverse mag. field 2−52919
spectrum generating current including spin-orbit and Lamb shift 2−59943
spin polarized, production in Xe-H^+ collisions, three-state calculations 2−79918
Stark broadened Lyman-α lines, electronic shifts 2−64059
Stark broadening, time evolution operator in semiclassical theory 2−42793
Stark profile of Ly-α line in the region of transition from impact to quasi-static broadening 2−46475
Stark quenching of 2S states, time-dependent theory 2−49974
stars, Lorentz line broadening, overestimation of gas densities 2−75742
stimulated emission, third harmonic generation coeff. calc. using sturmian function 2−46478
target, preparation techniques 2−49624
trapping in X-irradiated glasses and ices 2−81535
two-quantum photon-plasmon $2S_{1/2}-1S_{1/2}$ transition 2−79962
Van der Waals forces for systems involving non-spherical atoms 2−63998
variational bounds for imaginary frequency polarizability and dispersion interaction constant 2−52943
velocity structure in interstellar H Doppler profiles rel. to spiral arm features 2−81818
wings of Stark-broadened lines, Holtsmark's 5/2 power law 2−74242
Fe/H ratio in F1-F5 stars, by model atmos. anal. 2−66077
H/D ratio in Jovian atmosphere 2−66172
H-D ratio in Jupiter 2−75885
H-H, long-range interaction 2−42813
H-H collisions, spin-change frequency shifts 2−42770
H-H interactions, Gaussian representations of charge overlap effects in intermolecular forces 2−43026
H-H pairs, retarded van der Waals pot. 2−67412
H^+-H collisions, differential cross-section for H(n=2) direct excitation 2−46482
H-H_2 collinear collisions, reaction probabilities and high energy trajectories 2−50130
H-He pairs, retarded van der Waals pot. 2−67412
H-He plasma, absorption coefficients of i.r. radiation 2−46744
H-Hg elastic scatt., orbiting resons., rel. to vibr.-rot. levels obs. of diatomic mol. 2−77018
H, excited state wavefunctions, comparison of Messmer and Rayleigh-Ritz- variational methods 2−59942
H and He I lines in solar prominence, intensity ratio and chromosphere 2−66229
H I regions in II Zw 40, compact galaxy 2−81793
H I reson. lines in far-u.v. spectrum of Venus 2−58515
H I velocity-longitude diagram for southern Milky Way 2−84984
p-H_2, polycrystalline parahydrogen and n-D_2, comparison and influence of zero energy on plastic deformation 2−71569
H_α, optical resolution of fine structure and obs. of Lamb shift by laser saturation spectroscopy 2−52946
H_α fine structure, intensity oscill. in sun 2−66202
H_α loops, rel. to filaments in sun 2−66203
H_α mottles in sun 2−66201
H_α profiles for G-type dwarfs and subgiants 2−84978
H_α solar flares rel. to chromospheric response to downward propagating shock waves 2−78620
H_γ astronomical spectral lines, influence of shock waves 2−58314
H+ formaldehyde, abs. rate constant, investigation using formaldehyde photolysis 2−54539
H + H interaction, higher multipole coeffs. determ. from dynamic multipole polarizabilities 2−59945
H + H_2 linear collisions, classical S-matrix theory 2−72551
H + H_2 linear reactive collisions below the classical threshold complex-valued classical trajectories determ. from S-matrix theory 2−44474
H + H_2 planar reaction, hindered rotor states, natural bifurcation coordinates 2−75372
H + H_2 reaction, planar reactive collisions, classical trajectory studies 2−75373
H + H_2 vibr. excitation process, rate const. 2−67537
$H^+ + H(1s) \rightarrow H(1s) + H^+$, charge transfer scatt. at high energies 2−77023
H + X_2 (X=Cl_2Br), energy distribution among reaction products 2−65370
H(2s) charge-changing collisions with N_2, Ar, He at 20-120 keV 2−70638
Hα, Hβ lines, night sky emission, local and galactic contributions 2−62338
Hα and Ca II K-line, solar chromospheric short-lived brightening event 2−78612
Hα emission stars in the Large Magellanic Cloud 2−58204
Hα profile of η Carinae nebula from high interferometric resolution observations 2−55024
Hα solar emission, total flux, rel. to type IV bursts at 1.5 metres, time profile comparisons 2−51850
Hα sunspot umbral line profile, photoelectric measurement 2−44989
InBi, hot hardness and indentation creep 2−71602

neutral molecules
$^1\Sigma^+$ states, lowest, adiabatic potential energies, frozen-core approximation 2−42898
— 2−67538
— 2−67436
adsorption on C, rel. to work function variation 2−60677
air and H_2 turbulent streams, optical method for concentration measurement 2−67704
arc, rotating helical 2−74449
astrophysics, highly excited electronic levels, radio band 2−48732
beam, interaction with Pt and Mo surfaces, scatt., chemisorption 2−50461
binding energy curve, calc. by contracted gaussian type function 2−83243
bonding molecular orbitals 2−50013
Born-Oppenheimer approx. breakdown 2−56151
Brueckner orbitals applic. to ground state, determ. of one-electron operators 2−50006
bubble apparatus for water flow velocity measurements 2−71135
clusters, model for electron impact ionization cross section including energy losses inside cluster 2−80150
coherently driven by light waves, obs. of anharmonic Raman scattering, determ. second order polarizability 2−42899
collision effects on Raman line profiles 2−43039
collision induced-absorpt. near λ=1 mm 2−77084
collisional dissociation, DWBA theory 2−43033
collisions with H^+ at 4 keV, probability ratio for neutralization of H^+ to H(2p) or H(1s) 2−42802
collisions with H atoms, electron loss cross sections 2−64216
compressed, Rayleigh-Brillouin scatt. and relaxing thermal cond. 2−56171
cool supergiants, dissociation equilibrium and convection 2−62499
core excited resonances, electron transmission spectroscopic investigation 2−46547
cusp-satisfying orbitals effect on electron densities at nucleus 2−83208
density in dark interstellar clouds 2−75786
dissociation by electron impact, linear momentum transfer effects 2−67460
dissociation in elec. discharge, model 2−53007
electron collisions, differential and total cross section calcs. for models 2−64136
electron elastic scattering, 30-912 eV, calc. of differential and total cross sections in plane wave approx. 2−77167
electron impact dissociative excitation, polarization free vacuum u.v. meas., obs. of Lyman α radiation 2−80120
electron scattering intensity, vibrational correction calc. using five term CI wavefunction 2−50036
equilibrium, equation for saturated density 2−64517
exchange perturbation theories for interaction energies calc. 2−83421
exchange perturbation theory applic. to intermol. forces calc. 2−83420
excited states, Rydberg and valence shell character as functions of internuclear distance 2−50056
free, determ. of fraction of π^--p interaction heavy liquid bubble chamber 2−70313
galactic kinematic distribution 2−62462
gas, with decreasing density, strong shock propagation 2−60358
ground-state energy calc. by new transcorrelated method, comparison with variational method 2−64134
interstellar, intercloud H I gas, 21 cm line profiles 2−66117
interstellar H_2 and H and He fluxes from planetary nebulae 2−78448
Io atmosphere, upper limits 2−75867
ionization cross sections for high- energy electrons and positrons, comparison of H_2 and D_2 2−70598
isotopic, gas chromatographic separation and quantitative det. 2−52956
Jovian atmosphere absorption bands, obs. using Galilean satellite eclipse obs. 2−58490
in Jovian visible clouds, spectral obs.75875 2−75875
Jupiter, adiabatic model for gaseous-liquid H and He, temperature distributions 2−81933
Jupiter, level of formation of quadrupole lines 2−75874

Hydrogen continued
neutral molecules continued
Jupiter, quadrupole H_2 absorption 2−75872
line profile of $Q_{01}(1)$ vibr. resonance in Dicke narrowing zone 2−56176
lines in interstellar spectrum of ξ Persei 2−81836
Lyman band absorptions, equivalent widths 2−56170
Lyman-α obs. in outer geocorona and interplanetary space 2−65856
magnetic, susceptibility, ground state, calc. upper and lower bounds 2−46524
microwave absorpt. at high press., Uranus atmos. obs. 2−55150
Morse potential, optimised calculations 2−56142
multiphoton dissoc., predissoc., autoionization 2−83263
multiphoton ioniz. and dissoc. due to 1.06 μm laser radiation 2−80051
multiphoton ionization, temp. depend. 2−60004
muon interactions, multichannel neutron recording system using computer 2−70296
normal and para, low temp. shock waves 30K min. 2−46550
nuclear-spin relaxation in low-density molecular H_2 at room temp. 2−70707
perturbation theory of intermolec. forces in small overlap region 2−70813
perturbation theory of intermolec. forces in small overlap region 2−70812
photoactive agent in emission from freshly treated surfaces 2−81538
photoelectric cross-section meas. at 5.41 keV 2−67483
photoionization, effects of rotational autoionization on angular distrib. of photoelectrons 2−50045
photoionization and photoexcited autoionization, cross section calc. 2−50037
photoionization cross sections of singly excited states 2−70703
planetary atm. validity of Dicke approximation for computing collision narrowed profiles of quadrupole lines 2−75856
planetary atmospheres, Rayleigh and Raman scattering 2−58512
polarisability, temp. dependence 2−46546
quadrupole moment functions, vibrational matrix elements 2−64129
reactive collisions with ions, effect of reactant internal energy on spectator stripping 2−44472
rotational Raman lines, anisotropy of Dicke narrowing 2−42893
rotational relaxation, isotopic spaces, effect on sound absorption 2−46858
rotational states, upper limits studied using potential energy functions of Morse and Hulburt-Hirschfelder 2−46543
Saturn, quadrupole H_2 absorption 2−75872
Slater basis set difference density maps, minimum and expanded, comparison 2−77088
stimulated Raman emission by tunable dye laser 2−77078
streamer formation, anal. of mechanisms 2−64344
target, liquid, 150 cm, for synchrophasotron 2−67072
three-body recomb. dynamics via reson. complex mechanism 2−80130
Titan's atm., greenhouse effect 2−78488
vibration-rotation props., screening and polarization effects 2−64130
vibrational and rotational analysis of eight simple models 2−46549
vibrational excitation by collision with Li^+, model potential 2−43038
vibrational excitation by H^+ and e^- impact, cross section calc. 2−70817
vibrational excitation by Li^+, quantum mechanical studies 2−77171
vibrational force const. and electron relax. 2−60002
vibrational relaxation, transient stimulated raman scatt. obs 2−56150
volcanic gas burning at Kilauea Volcano 2−57928
X-ray scattering, 5.41 keV, obs. of differential scattering cross-section 2−64138
CF_4, collisional de-excitation of vibrationally excited 2,4-dimethylpentyl-2*(-d_1*) 2−46648
CO_2-H_2 mixtures, simultaneous vibr.-translation, vibr.-rot. and rot.-translation exchanges 2−53099
$D + H_2 \rightarrow HD + H$, cross-section 2−61773
$D + H_2 \rightarrow HD + H$, quantum cross section 2−61772
$F + H_2 \rightarrow FH + H$, potential energy surface including electron correlation, refined linear surface 2−78189
$F + H_2 \rightarrow HF + H$, Monte Carlo calcs. of reaction rates and energy distribs. among products 2−57410
$F + H_2(D_2)$ reaction, exoergic, product static distrib. and temp. concept 2−68761
H-H_2 collinear collisions, reaction probabilities and high energy trajectories 2−50130
H_2-H^+ collisions, vibrational excitation, 15-1000 eV, semiclassical theory 2−80152
H_2-H_2 long range potential, analysis of SCF-Mo calcs. 2−64217
H_2-He collisionally induced vibration, effect of rotational motion 2−80139
H_2-Ne Van der Waals complexes in collision-induced fund. bands of hydrogen, spectra 2−64127
H_2, Dicke narrowing and collision broadening of depolarized Rayleigh and Raman line 2−70700
H_2, H_6 ring system, electron density and correlation in ground states, simple LCAO approx. 2−67476
H_2, O_2, Cl_2 subsonic flow, photochemical initiation of combustion 2−84660
H_2, oscillator orbitals in CI calculations 2−59883
H_2, shock waves, low temp., 30K min. 2−46550
H_2, valence bond Aufbau principle for excited states 2−80008
H_2 dissociative excitation, meas. of time-of-flight spectrum of metastable H(2S) atoms, evidence of predissociation 2−46551
H_2 hyperfine structure of N=1 rotational state of $^3\Pi_u$ electronic state 2−64137
H_2 in Ar, multiple quantum transition effects on dissociation constant 2−50035
H_2 in He and Ne, rotational relaxation, approx. soln. to Boltzmann eqn. 2−80137
H_2 inert gas binary mixtures, proton spin lattice relaxation times in 165-265K range 2−46645
H_2 Lyman band lines in interstellar spectrum of Ophiuchi, expected equivalent width calculations 2−55072
$\mu^+ + H_2 \rightarrow H^+ + \mu H$, differential cross section 2−67481
$\mu^+ + H_2 \rightarrow \mu H + H^+$, total cross- section 2−67482

Hydrogen continued
neutral molecules continued
H_3, self-consistent procedures for generalized valence band wavefunctions 2−53012
H_3 potential surfaces in atom-H_2 collision, saddle point 2−51429
H_4, lowest $^1\Sigma_g{}^+$ state calc. 2−50039
HD, compressed, Rayleigh-Brillouin scatt. and relaxing thermal cond. 2−56171
HD, Dicke narrowing and collision broadening of depolarized Rayleigh and Roman line 2—70700
HD, nucl. spin-spin coupling const., perterbation calc. based on bare-nucleus pot. 2—70702
HD, rotational transitions in low energy HD-He collisions 2—46644
Hd lines in interstellar spectrum of ξ Persei 2—81836
HD* colliding with HD or He, collision-broadened cross-sections from peak-absorbency meas. 2—67479
HD+ ^{18}F hot-atom reactions, classical dynamics 2—81497
H_2-^4He system, thermal diffusion factor and quantum collision integrals, effect of inelastic collisions 2−56449
HT-He, quantum mechanical scatt., comparison with He-D_2 system 2−60115
H_2 + Ar plasma, stabilized arc, cylindrical, emission line profile 2−64307
$H_2 + Ar^+$ reaction, spin-orbit states of Ar^+ 2−81498
$H_2 + CO_2{}^+$, $H_2 + CO^+$, $H_2 + N_2{}^+$ reaction rate constants by ion cyclotron resonance mass spectrometry 2−61768
$H_2 + D_2 \rightarrow 2DH$ reaction paths 2−44466
$H_2 + D_2 \rightarrow 2HD$ four-centre exchange reaction ab initio calcs. of orbitals, contragradience and reaction surface 2−48323
$H_2 + D \rightarrow HD + H$, molec. beam study 2−72546
H_2 + F, energy distribution among reaction products 2−65368
$H_2 + F_2$ in pulsed laser, computer modelling and parametric study 2−41978
$H + H_2$ linear collisions, classical S-matrix theory 2−72551
$H + H_2$ linear reactive collisions below the classical threshold complex-valued classical trajectories determ. from S-matrix theory 2−44474
$H + H_2$ planar reaction, hindered rotor states, natural bifurcation coordinates 2−75372
$H + H_2$ reaction, planar reactive collisions, classical trajectory studies 2−75373
$H + H_2$ vibr. excitation process, rate const. 2−67537
$H_2 + H_2$, structure of linear symmetric molecule H_4 2−50039
$H_2 + H_2$ reactive vibr. nonequil. effects 2−84627
$H_2 + I_2$, dynamics of mol. and atomic exchange reaction 2−51423
$H_2 + O_2$ on Cu surface, mechanism 2−54531
$H_2 + e^+$, 45-500 eV, cross sections for positronium-negative-ion formation by double electron capture 2−50044
Hα characteristics of luminous late type stars 2−62550
He-H_2, meas. of absolute integral total cross sections and interaction potential 2−70814
He-H_2, total scattering cross section of thermal energies 2−64212
He + H_2 inelastic scattering, effective separable approx. of multichannel Green's functions 2−46639
O_2-H_2 mixtures, ioniz., non-attaching gas behaviour of oxygen 2−53246
O_2, dissociative excitation of vacuum u.v. emission by electron impact, cross section meas. 2−42900
vibrational level linewidths due to predissociation 2−79999

Hydrogen compounds
see also Ice; Steam; Water
acid environment for austenitic stainless steel, cold plastic deformation effect in corrosion 2−68790
acid hydrates, hydronium ion struct. and dynamics 2−84601
acids, MO SCF calcs. of proton affinities 2−83220
elastic induction interaction, calc. through fifth-order perturbation theory, applic. to HF + HF collision 2−50126
halide mols., Born-Oppenheimer approx. breakdown 2−56151
halides, CO_2 mixtures, vibration-to-vibration energy transfer 2−43036
HCN, investigation of bands at 14 μ 2−50042
hydrides, spin-lattice relax. times of diffusing hydrogen 2−54369
magnetic phenomena of surface gas-solid interactions 2−84395
metal-H system, applied stress field effects, thermodynamic analysis 2−71640
metal/hydrogen systems, conf., Julich, Germany (Mar 1972) 2−77713
metal/hydrogen systems, due to elastic interaction 2−77744
metal/hydrogen systems, electronic struct. 2−77822
metal/hydrogen systems, Gorsky effect 2−77603
metal/hydrogen systems, h.p. thermodynamics 2−77715
metal/hydrogen systems, thermodynamics, review 2−77714
Ag-Pd-H system, phase diagram 2−74953
Cl + HI(DI) reaction, exoergic, product state distrib. and temp. concept 2−68761
Cs + HBr, rotational polarization of reaction products and reprojection of angular momentum in molecular beam expts. 2−65367
Cs + HI, rotational polarization of reaction products and reprojection of angular momentum in molecular beam expts. 2−65367
$(DBNH)_3$, ^2H n.m.r., quadrupole coupling constants 2−44461
DBr-Br_2 system, hot atom reactions rates 2−72549
DBr, matrix-isolated, i.r. obs. at cryogenic temp., hindered rotation 2−68637
DBr, Raman and Rayleigh scattering, molecular motions when dissolved in solvents 2−46962
DBr, Raman and Rayleigh scattering, molecular motions in liquid phase 2−46961
DBr, Raman and Rayleigh scattering, molecular motions, self-broadening and broadening in inert gases 2−46544
DBr(I), matrix-isolated, i.r. obs. at cryogenic temps., interactions 2−68638
DCN liquid and crystalline, i.r. spectra 2−57351
DCl, Raman and Rayleigh scattering, molecular motions when dissolved in solvents 2−46962
DCl, Raman and Rayleigh scattering, molecular motions in liquid phase 2−46961
DCl, Raman and Rayleigh scattering, molecular motions, self-broadening and broadening in inert gases 2−46544
$D_3Co(CN)_6$, hydrogen bonds, potential energy wells 2−42895

Hydrogen compounds continued
DF, DF-CO_2, chemical lasers, vibrational energy transfer and de-excitation 2−49366
DF, i.r. chemilum. quenching, vibr. energy transfer to CO_2 and HF 2−65371
DF, vibr. relax., catalytic efficiencies of NO 2−77163
DF and DF-CO_2 chemical lasers, vibrational energy transfer processes 2−66751
DF chemical laser, pulsed, performance 2−73567
DI + Cl, energy distribution among reaction products 2−65369
D_2O, angular dependent leakage spectra 2−76906
D_2O, dipole moment determ. from Stark effect meas. on microwave transitions 2−80045
D_2O, u.s. structural absorption and adiabatic volume viscosity 2−56500
D_2O crystals, pulse radiolysis at -150°C optical absorption spectrum of trapped electrons, visible and i.r. 2−48348
D_2O ice, ^2H spin-lattice relaxation 2−61744
D_3O, matrix stabilised, comparison of e.s.r. spectra with INDO calculations 2−42892
DOF, i.r. spectra, vibr.-rot. analysis 2−77062
Er-H system, gas pressure standard 2−52016
Fe-Pd-H system, phase diagram and Mossbauer spectrum 2−74953
H-Nb system, equilibrium pressures, secondary standard for ultra high vacuum gauge calibration 2−78692
HBr-Br_2 system, hot atom reaction rates 2−72549
HBr, chemisorption on PbO layers, examination 2−75377
HBr, effect of resonance on vibr. distrib. charge transfer reactions with Kr^+ and Ar^+ 2−51424
HBr, intensity of vibr.-rotation spectra, foreign gas density depend. 2−74263
HBr, Martian atmosphere, minor constituents, Mariner borne i.r. spectrometer 2−69156
HBr, Raman and Rayleigh scattering, molecular motions in liquid phase 2−46961
HBr, Raman and Rayleigh scattering, molecular motions, self-broadening and broadening in inert gases 2−46544
HBr, Raman and Rayleigh scattering, molecular motions when dissolved in solvents 2−46962
HBr, vibr.-vibr. energy transfer and collisional pumping 2−80129
HBr chemical laser, TEA, performance, effect of gas additives 2−42015
HBr in condensed phases, first harmonic of vibration-rotation spectrum 2−53014
HBr in condensed phases, second harmonic of vibration rotation spectrum 2−53015
HBr in condensed phases, spectra of vibration rotation fundamental 2−53013
HBr.$4H_2O$, solid and liquids, H-bonds, Raman and i.r. spectra 2−43314
HCN, bond lengths in ground state 2−46513
HCN, general quartic force field, calc. using Parr-Brown anharmonic potential function 2−52999
HCN, infrared matrix isolation spectra 2−70708
HCN, microwave emission from C stars 2−58301
HCN, minimal basis set LCGO calcs. 2−79989
HCN, semi-empirical analysis of electronic spectra and molecular structure 2−42891
HCN beam type maser, operation, frequency stability measurements at 88.6 GHz 2−52408
HCN hypersonic molecular beam, electric resonance spectroscopy 2−67478
HCN laser, high power, pulsed, optimization of discharge parameters 2−66749
HCN laser, modes obs. using liq. cryst. image convertor 2−42011
HCN laser, stabilization of output, automatic power control system and automatic frequency control system 2−45733
HCN laser, submillimeter wavelength measurements 2−79171
HCN laser, thermally stabilized, mode gain and visualiz. 2−52421
HCN liquid and crystalline, i.r. spectra 2−57351
HCN meas. of resonant wavelengths at 311 and 337 μm using resonator interferometry 2−41985
$H^{13}C^{14}N$ and $H^{12}C^{15}N$ in Orion A i.r. nebula 2−66135
HCNO, elec. dipole moment, iterative extended Huckel theory calc. 2−56187
HCP, calc of K-type doubling in $B^3\Pi$ electronic states 2−46510
HCP, dipole moments of $^1A''$ and $^3\Delta_1$ states 2−42897
HCP, Zeeman effect in 2782Å band 2−70699
HCl-HCl and DCl-DCl collisions, evidence for neutral collision complexes, computer- graphics studies 2−67533
HCl, absorption in extreme u.v. 2−46586
HCl, effect of resonance on vibr. distrib. charge transfer reactions with Kr^+ and Ar^+ 2−51424
HCl, HBr, reactions with NO_2-, NO_3-, rate const. meas. in flowing afterglow system 2−61775
HCl, i.r. sunspot spectrum, fundamental vibration rotation bands and ^{35}Cl abundance 2−55163
HCl, in SF_6 solution, i.r. absorption bands, effect of vibration-rotation interaction 2−42841
HCl, intensity of vibr.-rotation spectra, foreign gas density depend. 2−74263
HCl, Martian atmosphere, minor constituents, Mariner borne i.r. spectrometer 2−69156
HCl, mol., selective laser excitation of high vibr. levels 2−53017
HCl, parameters of proton shielding function determ. from temperature dependence meas. of proton chemical shift 2−80046
HCl, population on vibr.-rot. levels during NOCl + H_2 reaction 2−53005
HCl, Raman and Rayleigh scattering, molecular motions when dissolved in solvents 2−46962
HCl, Raman and Rayleigh scattering, molecular motions in liquid phase 2−46961
HCl, Raman and Rayleigh scattering, molecular motions, self-broadening and broadening in inert gases 2−46544
HCl, thermal dissociation in shock waves, density gradient meas. 2−44473
HCl, Venus clouds, containing dissolved Fe compounds 2−58514
HCl, vibrational energy transfer, optical parametric oscillator pumped 2−80155

Hydrogen compounds continued
HCl, vibrational fluorescence, vibrational energy transfer from molecule to molecule 2−83256
HCl + F → HF + Cl, effect of excess reagent vibr. excitation on reaction dynamics 2−84629
HCl chem. lasers with $SOCl_2$, SO_2Cl_2, Cl_2CNCl and ClCN, pumping mechanisms 2−79192
HCl effect of VV transfer process on rate of thermal dissociation 2−67456
HCl in CO_2 atmosphere, line shape parameters 2−42879
HCl in condensed phases, first harmonic of vibration-rotation spectrum 2−53014
HCl in condensed phases, second harmonic of vibration rotation spectrum 2−53015
HCl in condensed phases, spectra of vibration rotation fundamental 2−53013
HCl with soluble and insoluble Fe compounds as possible composition of Venus clouds 2−44963
$HClO_4$, time differential perturbed ang. correlation studies using ^{154}Gd 2−60511
HCl.$2H_2O$, $H_5O_2{}^+$ ion vibrations from i.r. and Raman spectra 2−61667
$H_3Co(CN)_6$, hydrogen bonds, potential energy wells 2−42895
HD, absorption spectrum in vac. u.v., Rydberg states and ionization energy 2−50038
HD, vibrational relaxation, studied by laser induced vibrational fluorescence techniques 2−80134
HD Brillouin scattering, analysis of spectrum using kinetic model based on Wang Chang-Uhlenbeck eqn. 2−80409
HD in He and Ne, rotational relaxation, approx. soln. to Boltzmann eqn. 2−80137
HDO, rotational dependence of dipole moment determ. from Stark effect meas. on microwave transitions 2−80045
HF-HCN dimer, H-bonding and structure, prediction by ab initio molecular orbital methods 2−80005
HF, calc. of magnetic shielding and spin-rotation constants associated with nuclei using molecular orbital theory 2−42850
HF, correlation energy calc. using linked cluster many body perturbation theory 2−67484
HF, HF-CO_2, chemicl lasers, vibrational energy transfer and de-excitation 2−49366
HF, HF^+, HF-, pot. energy curves of ground states 2−60026
HF, i.r. chemilum. quenching, vibr. energy transfer to CO_2 and HF 2−65371
HF, intensity of vibr.-rotation spectra, foreign gas density depend. 2−74263
HF, liq., heat capacity 2−60465
HF, perturbed by compressed gases, rot. line broadening 2−53006
HF, polarizability anisotropy 2−42907
HF, refractive index, interferometric obs. rel. to wavelength 2−74488
HF, vib.-vib. energy transfer time. vib. fluorescence obs. 2−60005
HF, vibr. relax., catalytic efficiencies of NO, H_2O, D_2O and HCl 2−77163
HF, vibration-rotation level population during elementary act of F + H_2 reaction 2−66750
HF, vibrational relaxation measurements using combined shock tube and laser-induced fluorescence technique 2−53011
HF and HF-CO_2 chemical lasers, vibrational energy transfer processes 2−66751
HF chemical laser, 1J, pulse discharge initiated 2−42020
HF emission power in F + H_2 laser oscillator 2−69922
HF gas, anisotropic ultrahigh gain emission in rotational transition, optical pumping 2−50047
HF in CO_2 atmosphere, line shape parameters 2−42879
HF in He, rotational relaxation, approx. soln. to Boltzmann eqn. 2−80137
HF laser, transversely excited, gain and relaxation obs. 2−45732
HF laser rate eqns., closed-form soln. 2−82479
HF optical pumping of low-pressure gas sample, laser-induced line narrowing spectroscopy 2−45819
HF production efficiency in H_2:SF_6 gas laser 2−79191
HF pulsed chemical laser, spectroscopy using i.r. vidicon camera tube 2−59140
$(HF)_n$, microwave spectrum and bond lengths 2−56177
HF + F collisions, temp. dependence of vibrational energy transfer probability, 300 to 1500K 2−43037
HI, mechanisms for vibrational relaxation 2−70704
α-HIO_3, Fermi resonance in Raman scatt. of light by polaritons 2−84493
A-HIO_3, meas. of ratio of electroopt. const. for coeff. up to 20MHz 2−72267
α-HIO_3 crystals, growth from aqueous solution 2−43520
HNC, interstellar, identification of 3.306 mm line 2−58360
H_2NCN, elec. dipole moment, iterative extended Huckel theory calc. 2−56187
HNCO, elec. dipole moment, iterative extended Huckel theory calc. 2−56187
HNCS, u.v. spectrum, vibr. analysis 2−56175
HNNN, elec. dipole moment, iterative extended Huckel theory calc. 2−56187
HNO_3-Pu solns., radiolytic generation of H_2 and O_2 during storage 2−48350
HNO, microwave spectrum, interstellar matter, laboratory obs. 2−50034
HNO_2, electronic struct., cis and trans isomer obs. 2−56172
HNO_3, heat of neutralization with NaOH, 20°C 2−48314
HNO_3 u.v. absorption intensity at 22°C 2−64135
HNO_3 vapour in stratosphere 2−51596
H_2O-atom collisions, classical rotational excitation probabilities of H_2O 2−80136
HO_2 radical, i.r. spectrum, vibr. funds., electronic struct. 2−56174
H_2O, calc. of force constants by Hellmann-Feynman theorem 2−80055
H_2O, correlation energy calc. using linked cluster many body perturbation theory 2−67484
H_2O 8200 Angstroms band in Martian atmosphere, ground based photoelectric observations during Mariner 9 mission 2−78551
H_2O 8200 Angstroms band studies in Martian atmosphere with gound-based Varo image tube 2−78552

Hydrogen compounds continued
H_2O and D_2O, correspondence of fundamental and combination bands in i.r. spectra 2-50365
H_2O Raman scattering cross sections and depolarization ratio 2-53026
H_2O_2, photoactive agent in emission from freshly treated surfaces 2-81538
H_2O_2 decomposition on Ag particles and heterogeneous catalysis of image forming vesicular reaction products 2-59315
H_2O_2 molecule, interpretation of barriers to internal rotation 2-83249
H_3O, matrix stabilized, comparison of e.s.r. spectra with INDO calculations 2-42892
H_3O^+ ion in flames rel. to kinetics and heats of reductions 2-54541
$H_5O_2^+$, SCF-MO-LCGO calculations of properties of H-bond 2-56147
HOF-H_2O mixed dimer, LCAO-MO-SCF calcs. of equilibrium structures and energies 2-67491
HOF-H_2O mixed dimer, LCAO-MO-SCF calcs. of equilibrium structures and energies 2-67491
HOF, i.r. spectra, vibr.-rot. analysis 2-77062
$(HOF)_2$ dimer, LCAO-MO-SCF calcs. of equilibrium structures and energies 2-67491
$H_2O^+(H_2O)_n$, photolysis in range 5800 Å to 6100 Å 2-84670
HOO, nonempirical LCAO MO SCF and CI studies of low lying electronic state 2-50040
H_2S-O_2 balance in water of Black Sea 2-44645
H_2S, absorption in extreme u.v. 2-46586
H_2S, i.r. absorption coeffs. 2-56156
H_2S, kinetic energy of dissociation 2-80028
H_2S, MO LCAO-CNDO calc. of electronic structure, comparison with X-ray spectra 2-60034
H_2S, Martian atmosphere, minor constituents, Mariner borne i.r. spectrometer 2-69156
H_2S, solubility in liqs. 2-53405
H_2S and D_2S, infrared matrix isolation spectra 2-70708
H_2S fine structure of ultrasoft X-ray absorption spectra of S in 160-210 eV range 2-42939
H_2SO_4, force constants, normal coordinate treatment 2-74262
H_2SO_4 as solvent and perylene radical cation as solute, solvation shell relaxation and ion-electron recombination 2-46934
H_2SO_4 effects on dew point of gases at low concentrations 2-75536
H_2SO_4 liquid, 100%, X-ray determ. of molecular density correlation function and mean amplitude variation, geometric model 2-67801
HSO_3F as solvent and perylene radical cation as solute, solvation shell relaxation and ion-electron recombination 2-46934
HSSH, direct obs. of anomalous K doubling caused by centrifugal distortion 2-64131
$H_2Te_2O_6$ single crysts., cryst. struct. 2-74747
HY + X, (X = Cl, Br; Y = Br, I), energy distribution among reaction products 2-65369
^2H_2O and H_2O, correspondence of fundamental and combination bands in i.r. spectra 2-50365
^{2}HF-CO_2 chemical transfer laser, model predictions and exptal. results 2-42016
H_25 in interstellar medium, obs. at 168.7 GHz 2-66118
Hf, solid, struct. refinement from ^{19}F n.m.r. data 2-71434
K + HBr, rotational polarization of reaction products and reprojection of angular momentum in molecular beam expts. 2-65367
LiO_2-Sc_2O_3-SiO_2-H_2O, hydrothermal crystallization 2-71383
Lu-H(D) system, α-phase characts. 2-77749
Mo-H system, H solubility, 905-1521°C 2-50841
NH_2OH-H_2O mixed dimer, LCAO-MO-SCF calcs. of equilibrium structures and energies 2-67491
N_2 + HCl collisions, vibr.-vibr. energy exchange 2-83407
Nb-H dil. solns., phase equil. and evolution kinetics of dil. solns. 2-53903
Nb-H foil, microcracks, transmission electron microscope obs. 2-68106
Nb-H solns., nondil., equil. press.- comp.-temp. relationships 2-50843
Nb-H system, H-dislocation interaction, cold work peak study 2-80841
Nb-H system, phase diagram, 80-500 K 2-77756
OH, atmospheric conc., resonance fluoresc. obs. using dye laser 2-72765
Pd-H system, isotope equilib., 77K 2-68154
Pd-H system, superconductivity, elec. resist. study 2-54135
Pd-Ni-H system, superconductivity, elec. resist. study 2-54135
Sc-H, n.m.r. obs. Korringa product, diffusion parameters determ. 2-72517
THO, transport kinetics in human body, use of compartment analysis 2-55290
T_2O, estimation of permissible radiation dose to gonads and foetus 2-55280
Ta-H alloy, quenching at liq. He temps. 2-56907
Ta-H system, ordering in β-Ta_2H 2-54003
Ta-H system, resist. rel. to solute conc. 2-80857
Ti^3H, applications in direct β particle collection electrical cell, design 2-49253
V-H system, low temp. phase transform. 2-53998
V-H(D) systems, n.m.r., β- and δ-phase behaviour 2-78175
Zr-H dil. alloys, internal friction peaks 2-50737

Hydrogen ion concentration *see Electrochemistry*

Hydromagnetics *see Magnetohydrodynamics*

Hydrometry *see Flowmeters*

Hydrophones *see Oceanography; Transducers*

Hydrostatics
electrohydrostatic stability of fluid surface, two-dimensional problem 2-46651
fluid, extended press., consistent eqn. 2-46652
fluids, generation of thrust, continuum mechanics, book 2-70825
liquid hold up in steady state froth bed 2-80498
normal liquids, mechanical properties and internal energy 2-56450
pressure soaking, influence on structural change of deformed polycrystalline metals, x-ray study 2-84127
volume coefficient of expansion of metals, use of hydrostatic microbalance 2-80785

Hydrostatics continued
^{3}He-^{4}He mixture, diagram of state singularities due to hydrostatic effect 2-43414

Hygiene *see Medical science*

Hygrometers
absorption type, for atmospheric water vapour measurement, models 2-84864
calibration and testing for horizontal soundings of troposphere and lower photosphere 2-57934
troposphere, water vapour, troposphere, fluctuations in water vapour content, from microwave observations of celestial radiosources 2-51591
u.h.f. phase sensitive moisture gauge 2-52352
LiCl heated hygrometer, phase transition between solid hydrate and saturated soln. 2-56486

Hyperfine structure *see Crystals/hyperfine field interactions; Paramagnetic resonance and relaxation; Spectra*

Hyperfragments *see Hypernuclei*

Hypernuclei
heavy spallation hyperfragments, lifetime 2-63841
light, binding energies, applic. of Garvey-Kelson mass formulas 2-46115
p-shell, shell-model analysis of Λ binding energies, numerical fitting and hypernuclear predictions 2-63760
p-shell props., Majorana forces influence 2-59685
production by meson scattering, direct interaction theory 2-63761
production in K^- irradiation of photonuclear emulsions 2-76576
spectroscopy, obs. of γ-rays from excited states, consequences for Λ-N interactions 2-76775
spectroscopy, review 2-67139
$k^- + \text{nucleus} \rightarrow \pi^- + \text{charged particle} + \text{hypernucleus}$ 2-79732
$\Lambda^{12}C \rightarrow {}^1H + \Lambda^{11}B$, unstable resonant state of ^{12}C obs. 2-79732
$^3{}_\Lambda H$ binding energy, ΛN, ΛNN potentials and Λp scatt. 2-82876
$^4{}_\Lambda H$ binding energy, ΛN, ΛNN potentials and Λp scatt. 2-82876
$^4{}_\Lambda He$ binding energy, ΛN, ΛNN potentials and Λp scatt. 2-82876

Hyperons
see also Mesons; Nuclear reactions and scattering due to/hyperons
hyperonic matter composition, effect of tensor forces 2-46008
meson nucleon sigma terms, theoretical estimate 2-63571
$\gamma p \rightarrow \kappa^+ \Lambda$, 5 GeV, recoil polarization in $K^+\Lambda$ 2-66926
$KN\Lambda$, $KN\Sigma$ coupling consts., upper bounds 2-76652
Σ channel in ΛN low energy S-wave interaction, separable potential 2-46012

absorption
No entries

capture
No entries

decay
$\Lambda \rightarrow pe^-\nu_e$, induced pseudoscalar term due to SU(3) symmetry breaking 2-79624
current algebra in broken chiral symmetry 2-73736
nonleptonic, consequences of current algebra in limit $q^2 = 0$ 2-52641
nonleptonic, construction of pole model for decays where exchanged particles of all spins are included 2-52642
nonleptonic, current-current Lagrangian model 2-82782
nonleptonic, generalized similarity relation and trilinear matrix elements 2-76724
nonleptonic, in current-current quark model 2-76723
nonleptonic weak, current algebra 2-52643
radiative, second class current contributions 2-49597
weak radiative, pole model considerations 2-59589
Λ, non-leptonic, s-wave and p-wave, pole model 2-70266
Λ produced in π-$p \rightarrow K^{*o}\Lambda$ 3.9 GeV/c, amplitude structure determ. from decay correlations 2-42391
λ^0 lifetime, decaying in flight at 100 GeV, predictions of CPT-violating model 2-63490
$\Lambda \rightarrow pP^-$, polarization of Λ 2-66926
$\Lambda \rightarrow p\mu$-ν, meas. of branching ratio 2-46011
$\Lambda(1520) \rightarrow \Sigma(1385)\pi$, meas. of decay width 2-42420
Ω, octet baryon nonleptonic decay 2-70267
Ω^- nonleptonic decay in current-current quark model 2-76723
Ω^- nonleptonic decays investigated in framework of phenomenological chiral Lagrangian model 2-52642
Σ-$\rightarrow ne$-ν, meas. of ratio of axial vector to vector coupling 2-46013
$\Sigma^- \rightarrow p\mu^-e^-$ as test for lepton number conservation 2-73749
$\Sigma^+ \rightarrow p\gamma$, pole model considerations 2-59589
$\Sigma^+ \rightarrow p\pi^0$, test of $\Delta 1 = {}^1{}_{\cdot 2}$ rule and Lee-Sugawara relation 2-42421
$\Sigma^\pm \rightarrow \Lambda$, contribution of weak mesonic currents to axial vector form factor 2-66993
Ξ, lifetimes and α parameters 2-73855
Ξ, non-leptonic, s-wave and p-wave, pole model 2-70266
Ξ lifetimes and α parameters 2-79623
$\Xi^- \rightarrow \Sigma^+\mu^-e^-$ as test for lepton number conservation 2-73749
$\Xi \rightarrow N\pi$, ΔS_2 transitions 2-46014

detection, measurement
No entries

effects
No entries

interactions
see also Hypernuclei
features and potential applications 2-63662
hyperon-nucleon, exact SU(3) symmetry and unitarity of S-matrix 2-79622
with nucleons, review of theoretical concepts and exptl. knowledge 2-59587
ΛN potential, two-pion exchange 2-59588
Λp, Λn, Λp, Λn, 6 to 21 GeV/c, total cross sections 2-52645
Λp, one boson exchange potential model including ΣN channel 2-82783
Σ^-d total cross sections at 19 GeV 2-79625
Σ^-p total cross sections at 19 GeV 2-79625
ΞN, estimate of cross section for $\Lambda\Lambda$ production 2-49598

magnetic moment
No entries

mass
No entries

Hyperons continued
- **production**
  - negative hyperons, by 24 GeV/c proton bombardment of W target 2−42419
  - single rel. to $^{3}._{2}{}^{+}$ decuplet weak decays 2−46009
  - Δ resonance production on nuclei, determ. ΔN total cross section 2−42425
  - $\gamma p \to K^+\Lambda$, K*-K** absorbed exchanges, F/D ratio 2−70210
  - $\gamma p \to K^+\Sigma$, K*-K** absorbed exchanges, F/D ratio 2−70210
  - Λ, cross-section on protons by antineutrinos 2−67061
  - Λ, cross sections in inclusive photoproduction 2−49562
  - Λ, hyperon-antihyperon yields in pp scattering studied by absorbed Regge pole model with exchange degeneracy 2−42408
  - Λ, in K^-p interactions at 3.95 GeV/c, meas. of Λ polarization for $\eta\Lambda$ and $\eta'\Lambda$ final states 2−59518
  - Λ, in π-p interactions at 4.5 and 6 GeV/c, determ. of polarization 2−79599
  - Λ photoproduction near proton fragmentation region, inclusive cross section predicted via factorisation 2−59403
  - Λ production in $KN \to \pi\pi\Lambda$, usefulness of meas. of Λ polarization 2−63667
  - Λ production in $\pi N \to K\pi\Lambda$, usefulness of meas. of Λ polarization 2−63667
  - λ^0 in K^- N interactions in nucleus, production of hypernuclei 2−76576
  - $\Lambda\Lambda$ invariant mass spectrum enhancement in events produced by K^- interactions in bubble chamber 2−49598
  - Ω, in K^-p interaction, review of recent results 2−42377
  - Ω^-, meson coherent dissociation on nuclei, spin and parity 2−76725
  - Ω^+, in K^+p at 10 GeV/c, production cross-section obs. 2−63668
  - Σ, hyperon-antihyperon yields in pp scattering studied by absorbed Regge pole model with exchange degeneracy 2−42408
  - Σ, in π-p interactions at 4.5 and 6 GeV/c, determ. of polarization 2−79599
  - Σ (1385) production in final state with Λ in 3.4 GeV/c K-d interactions 2−67011
  - Σ^0, cross-section on protons by antineutrinos 2−67061
  - $\Sigma^\pm$, in K^-d interactions near 400 MeV/c 2−66998
  - $\Sigma(\Lambda)$, in $\pi N \to \pi\Sigma(\Lambda)$ reaction, PCAC prediction of cross sections and polarization phenomena 2−52644
  - Ξ-, in K^+p at 10 GeV/c, production cross-section obs. 2−63668
  - Ξ, in K^-p interactions, review of recent results 2−42377
  - Ξ, meson coherent dissociation on nuclei, spin and parity 2−76725
  - Ξ^+, in K^+p at 10 GeV/c, production cross-section obs. 2−63668
- **resonances**
  - Λ^* production search in pp interactions, from 24.9 and 28.6 GeV/c 2−67053
  - Λ(1520) production in K^-d interactions at 5.5 GeV/c 2−63594
  - Σ (1385) production in final state with Λ in 3.4 GeV/c K-d interactions 2−67011
  - Σ(2030), in 7+/2 multiplet 2−42422
  - Y_0^* (1405) in K^-d interactions near 400 MeV/c 2−66998
  - Y_1^* (1385) in K^-d interactions near 400 MeV/c 2−66998
- **scattering**
  - ΛN, two-channel separable potentials to represent low-energy S-wave interaction 2−46012
  - ΛN two-channel $^3S_1$-$^3D_1$ separable potential 2−55880
  - ΛN two-channel separable potentials, restrictions 2−46010
  - Λp and binding energy of $^{3}_{\Lambda}$H, $^{4}_{\Lambda}$H and $^{4}_{\Lambda}$He 2−82876
  - $\pi\Lambda$, sum rules for elastic scatt. amplitudes, threshold behaviour 2−70242
  - $\pi\Sigma$, sum rules for elastic scatt. amplitudes, threshold behaviour 2−70242
  - Σ^-d, 30 to 90 MeV/c, quartet elastic and reaction cross sections 2−59590
- **spin and parity**
  - Ω^-, production, coherent meson dissociation on nuclei 2−76725
  - Ξ, production, coherent meson dissociation on nuclei 2−76725

Hypersonics *see Ultrasonics*

Hypertritons *see Hypernuclei; Tritons*

Hypervirial theorem *see Quantum theory*

Hypochromism *see Absorption/light; Polymers*

Hysteresis
- *see also Dielectric phenomena; Dielectric properties of substances; Ferroelectric phenomena; Magnetization process*
- adamantane, solid, press, induced, solid-solid transition 2−61563
- alloy 79 NM, influence of thermomagnetic treatment on mag. props. 2−72048
- closed ferromagnetic cores, dynamic characteristics, apparatus for plotting hysteresis curves 2−82426
- curve automatic recording apparatus 2−82427
- elastic membrane, curved, geometry induced equil. hysteresis 2−43668
- elastomeric foams 2−71552
- ferrimagnet, magnetization mechanism, role of wall displacement and bulging 2−65167
- ferromagnetic films, coupled two-layer system, calc. 2−48087
- ferromagnetic material, loss measurement error, pulsed magnetiz. 2−75220
- ferromagnetic materials, dynamic cycles direct recording on X-Y recorder using apparatus based on sampling techniques 2−45664
- film, cross-tie-Neel domain wall transition, hysteresis change, in mag. field 2−48090
- film, uniaxial, ang. dispersion of anisotropy effect on hysteresis loop 2−61521
- forced system, periodic solutions 2−45341
- gas laser, produced by conversion from single to double frequency 2−73558
- hysteresigraph, l.f., Preisach's theory verification 2−66694
- internal friction due to point defect dragging with dislocation interaction, hysteresis damping 2−64704
- loops, analytic description from magnetic induction 2−45666
- loss in isotropic sheet magnetic material, mechanical stress 2−77998
- magnetic reversal in magnetically hard ferromagnetic substances, investigating method 2−54322
- magnetic thin uniaxial film, magnetization and thickness determ. method from loop meas. 2−68559
- materials with memory, thermodynamic theory 2−52097
- metal during bending at low freq., meas. from 20 to 800°C 2−64749

Hysteresis continued
- nonconductive ferromagnets, hysteresis loop tracer 2−66697
- Permalloy films with supercrit. hysteresis loop, domain struct. 2−61532
- permalloy supercritical films, supercriticality 2−68557
- plasma, magnetised, and helical instability 2−80342
- cis-1,4-polybutadiene rubber vulcanizates, elastic hysteresis, obs. 2−60855
- superconductor, hard, hysteretic model for magnetiz. 2−68364
- superconductor, type II, magnetic 2−68363
- thickness measurement, thin fluid films, electrical contact method, statistical profile 2−83733
- triglycine sulphate, 0°C to Curie temp. 2−47988
- viscoelastic nonlinear materials 2−71552
- $AgNa(NO_2)_2$, ferroelec., in quasi-static elec. field 2−72030
- $Ba_{1-x}Sr_xTiO_3$, loop temp. dependence in range 4.2 to 600K in flux grown single crysts. 2−47966
- $BaTiO_3$ film, polarization change, stroboscopic electron microscope obs. 2−75149
- Co-P film, characts. rel. to heat treatment conditions 2−48091
- Co, electrodeposited with [0001] axis of preferred orientation, dependence on texture perfection 2−54327
- Co_5Sm magnet alloy, 24 MG Oe energy product 2−51254
- Cr, magnetic struct. intensity, temp. hysteresis, sign change 2−54328
- Fe-Pd alloy, powder, rel. to magnetically soft α phase 2−48097
- Fe alloy, in martensitic transform. 2−50943
- H_2O, adsorbed layer on silica, thermal hysteresis obs. rel. to freezing process 2−53596
- In-Cd alloy, type II superconductor 2−71863
- KH_2PO_4, transition order experiments 2−81155
- $Li(NH_3)_4$. investigation of 88.8 K and 82.2 K phase transitions 2−43389
- Li_2O-Fe_2O_3-SiO_2 system, ferromag., composition depend. 2−54333
- Mh-Zn ferrites single crystal, signal processing technique to obtain Kerr effect M-H loops 2−48064
- Mn-Al-Ge alloy, domain structure and nucleation centres 2−68550
- Mn-Bi alloy, domain structure and nucleation centres 2−68550
- ND_4Cl, first order phase transition 2−84150
- $NaNO_2$, polarization in reversal of applied field, 10^{-2} to 10^7 V/cm.sec 2−65064
- Ni-Fe-Nb alloy, mag. characts. 2−57293
- Ni-Fe alloy films, loop parameters, temp. depend. 2−61538
- Ni-Zn ferrites, mag. losses in h.f. fields 2−84435
- Ni film shape of loop of planar Hall effect 2−72186
- Ni powders, monocrystalline, temp. depend. of rotational hysteresis 2−68508
- $PbZrO_3$, growth and obs. of intermed. ferroelec. phase 2−81140
- UAsS(Se, Te), magnetization rel. to temp. and mag. field, 3 K to Curie point, hysteresis loop, anisotropy 2−72172
- V_2O_5-P_2O_5, glass of e.s.r. line intensity vs. temperature 2−44310
- YIG, magnetization mechanism, role of wall displacement and bulging 2−65167

Ice
- *see also Glaciers; Snow*
- adsorption of H at 4.2K 2−50539
- Alberta hailstorms, aircraft seeding using pyrotechnic flare system 2−65746
- Amery Ice Shelf, Antarctica, evidence for bottom freezing from $^{18}O/^{16}O$ ratio 2−68852
- Antarctic ice sheets, radio echo method of measuring thickness changes 2−84722
- Arctic pack, under and upper surface profiles det. by remote sensing, automatic data processing 2−44602
- Arctic Sea, Arctic Sea ice, aircraft meas. of microwave emission 2−81632
- atmosphere, ice nucleus and chloride particle concentrations at Mauna Loa Observatory 2−65672
- atmospheric, electrodynamic models, for radar probing 2−44674
- atmospheric, nuclei, time lag in activation 2−57973
- broadband complex refractive index between −20 and 0°C 2−64460
- concentration of crystals in clouds meas. using Cannon particle camera 2−54851
- for contact nucleation of freely suspended supercooled water drops 2−47036
- contrail sheets of ice spheres in atmosphere, effects on radiation budget 2−62148
- crystal growth, from the vapour in an electric field 2−47221
- crystal growth from vapour phase study of abrupt habit changes as function of temperature 2−54847
- crystals, formation in deep cloud cover 2−68875
- deep ice temperatures, theoretical and experimental profiles correlation 2−54730
- dielectric correlation factor 2−81137
- ferroelectric behaviour, polariz. and depolariz. current obs. at low temp. 2−57242
- film, on cooled surface, microstruct. rel. to deposition rate, elec. field, vacuum breakdown 2−83866
- floes, radar obs. of drift 2−78331
- formation of two dimensional ice embryos on basal and prismatic faces of ice crystal 2−48497
- forming aerosols, downward transport from stratosphere 2−62165
- frost heaving, meas. of heat flow 2−75447
- Georgian Bay ice regimes and surface water temp. 2−57862
- growth of particles in atmosphere from vapour and cloud drop accretion 2−54849
- hail growth by stochastic collection in cumulus model 2−44719
- hail rel. to organized updrafts at thunderstorm bases 2−65748
- hail seeding, simple technique for determining location of AgI particles 2−65747
- hailstones, air bubbles 2−78371
- haloes on ice crystals, photographs taken in Antarctica 2−68913
- heterogeneous nucleation of ice clouds rel. to AgI-bearing smoke activity curves 2−57971
- hexagonal, atomic vibrs. 2−47730
- high concentration, containing KCl, dielectric dispersion 2−75142
- hoar crystals forming on cooling pipes, X-ray Laue examination 2−74732
- ice:KOH, dielec. dispersion and phase transition 2−72014
- ice water system, freezing, Stephan problem solution 2−77470

Ice continued
icebergs, containing rock fragments, structure and texture 2-75445
ionized water cluster production by electron bombardment of ice films 2-84221
irradiated, KF and NH_4F doped, role of F- in increased colouring 2-60823
Jupiter IV, Callisto, thermal radio-emission rel. to thick icy surface layer 2-75870
l.f. Young's modulus, using double pendulum 2-74878
light scattering by ice clouds in visible and i.r. regions 2-58000
low entropy form obtained from a linear step growth model 2-83906
low pressure water vapour condensation and growth of ice on cold metal 2-53498
magnetic quenching of o-positronium 2-77849
membrane-filter ice nucleus chamber, numerical estimates of humidity 2-65671
microwave brightness temp. of natural sea ice and salt water ice 2-84777
microwave dielectric const. 2-81134
n.m.r, strong collision relaxation in rotating frame 2-61747
nucleation, obs. of ice crystal conc. in natural cap clouds 2-48488
nucleation centres, smoke particles, method of generating for weather modification 2-62099
nucleation mechanism, using AgI 2-62192
nuclei, rel. to inadvertent weather modification in Los Angeles smog 2-51572
nuclei generation, ground based solution burner 2-62100
nuclei generator, airborne, dynamic calibration 2-62193
optical absorption spectrum due to trapped electron 2-75295
particle formation on aerosol particles, temp. and humidity conditions 2-51612
particles coexisting with supercooled cloud droplets, airborne obs. of distribs. 2-54848
particles in clouds over Pacific Northwest, techniques for collection and automatic counting 2-54850
permittivity, low temp. meas., rel. to translational vibrs. 2-82414
permittivity evolution in premelting stage 2-53497
phase transitions, models 2-58799
photogalvanic effect, geophysical implications 2-54258
plastic deformation, associated activation volume 2-64698
p.m.r., review of recent investigations 2-61746
polar ice sheets thermal convection and empirical flow laws of ice 2-48410
polar masses, movement obs. using radio echo technique 2-72691
porous rocks, periglacial zone, freezing-thawing process, frost damage 2-75446
precipitation from orographic clouds, numerical model 2-65730
proton distribution, Kirkwood correlation factor 2-80642
pure and doped, positron lifetimes 2-54091
quadrupole reson. of ^{17}O at 77 K, quadrupole coupling constants 2-75360
radar returns from sea ice, data interpretation 2-48431
rate of soln. in water drops, nucleation 2-75600
Rayleigh approximation, and emission cross sections of nonspherical particles 2-64477
recrystallization under mechanical strain 2-74691
regelation, heat conduction mechanism for classical wire experiment 2-45587
sea, surface roughness and resistance coeff. 2-65567
sea, thermal tension cracking, source of underice noise 2-65578
sea, thickness det., theory and field tests of microwave radiometer 2-44603
sea cover, air drag coefficients and roughness length 2-65566
sea ice, satellite i.r. location, image enhancement techniques 2-65574
sea ice research, important problems from marine expeditions 2-62050
seeded convective storms, ice form. mechanism 2-84856
seeding, cumulus clouds 2-94933
snowflake crystals, symmetry rel. to electric field 2-62245
stalactites growth under sea ice 2-57915
terminal velocities of ice crystals in air, equivalent metal disk models 2-57972
thickness det., e.m. sounding 2-44604
three dimensional eight vertex model and proton-proton correlation function 2-47726
Venus, atmospheric clouds, spectroscopic evidence against pure H_2O ice particles 2-78564
whiskers, growth, nuclei and crystal concentrations 2-84855
wind direction and speed meas. over ice drift during aerial photo survey 2-57967
β-AgI crystal shapes rel. to ice nucleation properties 2-64589
AgI particles, γ irradiated, ice forming activity 2-48498
CO_2 and H_2O ice layers in Martian polar cap. rel. to theory of formation 2-81931
H_2O and CO_2 ice layers in Martian polar cap rel. to theory of formation 2-81931
I_h crystals, dielectric relaxation spectra, effects of dislocations, multicrystallinity, HF doping, space-charge pile-up 2-72013

Ignition *see Combustion*

Illumination
see also Brightness
applied photometry, lighting industry usefulness, equipment, cost, data 2-79360
coherent, nonuniform, of circular aperture focusing system, resolution 2-59246
computational methods 2-82559
condenser systems, dispositive plane, light intensity distribution calc. 2-59217
distribution produced by optical system in arbitrary plane, computer program 2-59258
holograms with polychromatic source, broad band characteristics of zone plate and holographic lens systems 2-79264
light field in scattering media a long time after illumination by pulse source 2-79321
photographic, strobe lighting for action- stopping problems 2-59326
tutorial paper, rel. to optical aberrations 2-66800
underwater illumination, statistical characteristics rel. to sea roughness 2-81609

Image convertors and amplifiers
amorphous material, imaging by structural alteration 2-60568
camera driven by giant pulse laser 2-73672
cathode lens, electron image minification 2-59090
channel plates as image intensifiers for transmission electron microscopy 2-79083
diffraction pattern reconstructed on closed circuit TV, teaching demonstration 2-78736
electroluminescence storage panel, characts. 2-70068
electron optical brightness intensifiers, basic characteristics 2-73673
electron-optical, with microchannel intensification stage, modulation transfer function 2-70069
image intensifier for direct viewing and brief-time recording of crystallographic events 2-56620
intensifier tube scanner, calc. of photon loss 2-42256
intensifier-with-eye, performance characts. 2-66337
intensifiers, second generation, signal to noise ratio measurement 2-69882
i.r. upconverter, synchronously pulsed, conversion efficiency, peak power 2-79378
liquid crystal, obs. of HCN laser modes 2-42011
liquid crystal, plasma diagnostics applic. 2-53208
liquid crystal camera for visual obs. of laser modes 2-52421
liquid crystal displays, matrix-addressed, discrimination problems 2-52480
optical adaption of camera to image intensifier 2-73674
optical arrangement with large angle aperture for conversion from i.r. to visible region 2-42255
optical array for restoring astronomical images degraded by atmospheric turbulence 2-85074
photoelectrochemical image conversion, i.r. to visible 2-42254
photoelectronic image-brightness intensifier, multielectron noise and remanent gas pressure and composition 2-59273
radiodiagnostics, applications to photography 2-70070
radiographic automatic exposures with use of image intensifier method 2-76087
real time image enhancement and processing on Mariner 9 2-78412
scan amplifier, near confocal, angular deflection enhancement 2-59274
solid state, pickup and display devices, review in book 2-55767
storage vidicon electrophotographic spectrum imager for visible spectrum 2-59345
thermal, det. of thermal sensitivity, time and space constants and dissymmetry factor 2-52479
thermal image parametric upconversion, theory 2-69792
tomographic and section imaging devices, quantification of depth effect 2-45032
u.s. imaging by Bragg diffr., acoustic phase conservation 2-49447
viewers with image intensifiers, minimum brightness gain 2-66338
wafer image intensifier for photographic cameras 2-59275
Westinghouse Electric Corporation products, review 2-42222
wide angle i.r. to visible image conversion system using pumping of KH_2PO_4 crystal 2-45815
X-ray, using Gd_2O_2S:Tb as phosphor for input screen 2-73251
$AgPO_3-X^{n+}(PO_3)_n$, $X^{n+}=Mg^{2+}$, Ca^{2+}, Sr^{2+}, Ba^{2+}, Pb^{2+}, Al^{3+} use for multichannel image convertors and amp. 2-68501
$In_{1-x}Ga_xP$, compositionally graded cryst., like-sign asymmetric dislocations 2-71478
KD_2PO_4 electro-optic light valve device, image storage and processing 2-66847
N intensifier, nonlinear light intensification 2-42257
$Te_{81}Ge_{15}As_4$ glass, struct. of laser written lines, elec. microscope obs. 2-60600

Image intensifiers *see Image convertors and amplifiers*

Image orthicons *see Electron tubes*

Impact
see also Ballistics
— 2-58875
aerosol spectral impactor, size distribution meas. 2-64488
axial hollow nonhomogeneous cone 2-45388
bar, energy relations during shock impact 2-69634
basaltic rocks, high-velocity impact experiments 2-74851
C steels, fatigue, effect on microstructure 2-80809
Charpy impact specimens, irradiated, testing 2-60926
crater impact genesis rel. to geometric similitude of lunar and terrestrial craters 2-78510
crater shape dependence on particle velocity and material of target and particle, application to space vehicle meteorite collisions 2-54974
drop weight expts., impact kinetics, energy dissipation rel. to heating 2-64737
elastic semiinfinite rod, longitudinal impact, stability loss 2-69673
fatigue testing machine, rotating, disc type and applic. 2-80809
fibre composite, brittle matrix, impact resist. 2-53968
first impulse in dynamic destruction, device for studying action 2-56851
glass, microcraters, profile and depth 2-60582
high-speed impacts in solids and induced shock waves, theoretical model 2-41836
hypervelocity impacts on Earth and the Moon 2-66195
local heat build up in process of destruction of thin layers 2-73455
lunar regolith evolution mechanisms from impact experiments and computer simulations 2-81943
lunar rock microcraters, classification of crater type and impact theory 2-81942
mechanics, spherical tool against sonic transmission line 2-55446
metallic solids, high speed collisions, wave phenomena 2-76252
meteorites, detector, cactus micro-accelerometer 2-73100
meteorites, simulation, release of energy 2-75924
microparticles in space, position sensing and momentum evaluation 2-66022
multilayer elastic media, contact problem 2-78889
phenomena in spatial mechanisms, analogy between gyrodynamics and elastostatics 2-73378
plate impact expts., compression- release phenomena 2-66508
polymeric substances, impact fracture 2-84052
rain, erosion model, effect on supersonic flight 2-43252
resistance of simulated safety lenses, effect of thermal toughening 2-48927

- **Impact** continued
    - resistance of simulated safety lenses, effect of thermal toughening 2−48927
    - response of elastic media with cylindrical cavity 2−69665
    - response of finite crack in plane extension 2−45366
    - rigid sphere on elastic layer, force time investigations 2−69633
    - rutile powder, X-ray line profile analysis of particle size and strain 2−74831
    - Savonoski Crater, Alaska, possible meteorite impact structure 2−78296
    - sound emission meas. device for use with metals and alloys 2−80783
    - steel, fully heat treated low alloy, effects of sulphide morphology 2−56908
    - steel, synthetic weld structure, obs. 2−56919
    - steel ball on nylon and rubber layers over granite base 2−78889
    - steel strips, notched, dynamic stress concentration 2−80807
    - steel target, ballistic behaviour, effect of metallurgical factors and mech. props. 2−60980
    - testing of eye protector lens materials 2−48926
    - testing of eye protector lens materials 2−48926
    - transverse, sharpened body against elastic or elastoplastic membrane 2−78893
    - water-drop impacts, electro-acoustic meas. of drop size, shape and velocity 2−63129
    - Ag, films, indentation and impact studies of loading 2−77708
    - Al, high purity, and dil. alloys, review 2−68076
    - Al, projectile penetration forces 2−53803
    - Al, surface, impingement erosion 2−68113
    - Cu, single crystals deformed in tension, effect of strain rate upon hardening 2−84160
- **Impedance, acoustic** *see Acoustic impedance*
- **Imperfections in solids** *see Alloys; Crystal imperfections; Solids/structure*
- **Impurities** *see Crystal imperfections/impurities; Crystals/growth; Semiconducting materials*
- **Impurity electron states and effects** *see Crystal electron states/impurity states and effects*
- **Indentation** *see Hardness*
- **Independent particle model** *see Nucleus/models*
- **Indeterminacy**
    - Heisenberg relations for nonsimultaneous measurements 2−41506
    - linear harmonic oscillator, Heisenberg relation for time and energy 2−66451
    - probability uncertainty and its relation to other physical quantities 2−62995
    - quantum mechanical measurement, omission from basic postulates 2−73312
    - quantum theory of measurement probability generation in infinite systems 2−76213
- **Indium**
    - atom, lifetime meas. using beam-foil technique 2−42730
    - atomic spectral lines temperature effects in pressure broadening in flames 2−67413
    - deconvoluted spectra and higher resolution for Auger electron spectroscopy 2−72082
    - diffusion in BiTe, effect of distrib. of diffusing element, thermal e.m.f. and orientation relative to basal plane, creation of p-n junctions 2−83991
    - film, C adsorption on (111) face, effect on surface ionization of CsCl 2−64543
    - film, deposition on NaCl, island density 2−43480
    - film, e.m. generation of transverse acoustic waves, supercond. parameters 2−71866
    - film, on Si substrate, condensation and nucleation, mass spectrometer obs. 2−47117
    - film, optical absorption, ellipsometry obs. rel. to electronic struct. 2−72334
    - film, vapour deposited, growth, nucleation rel. to thickness and substrate temp. 2−77512
    - film on quartz, and alumina, heat transport, phonon emission, low temp. 2−54084
    - films, electron diffraction beam heating 2−83920
    - films, polycryst., thin, melting, e. diffr. study 2−83845
    - fine particles, superconductivity 2−71847
    - flow stress, meas. in normal and superconducting state 2−47857
    - liquid, diffusion of Tl 2−46945
    - liquid, thermal cond., Lorenz no. 2−43347
    - liquid, u.s. velocity, theory and expt. 2−80469
    - melting of small particles, size effect 2−43439
    - optical constants ε_1 and ε_2, absolute values 2−48134
    - quadrupole interactions of 247-keV state of ^{111}Cd, perturbed ang. correl. studies 2−75246
    - r.f. size effect in cylindrical samples 2−44053
    - Righi-leduc effect, 3.5-8K 2−75163
    - rolled, influence of twinning on texture 2−80774
    - seals, below 300°C, for joining pyrex to various materials 2−66385
    - solubility and alloying effects in Fe-Ni-Al-Cu alloys 2−43845
    - spaceflight neutron dosimetry 2−58147
    - superconducting cylindrical layers, crit. mag. field 2−84299
    - superconducting film, demonstration of flux quantization 2−41432
    - superconducting film, intermediate state struct., magneto-optical study 2−81050
    - superconducting film, noise props., r.f. generation 2−68348
    - superconducting thin films, penetration depth and flux creep 2−68345
    - superconductor, thin film, electronic thermal conductivity 2−68352
    - surface tension, 142°C 2−56577
    - transition in properties at 170K 2−68198
    - $Bi_{1-x}Sb_x$:In, elec. props., (x=0-0.2), 180-420K 2−61301
    - CdF_2:In^{3+}, ionic thermocurrents, temp. depend. 2−81089
    - CdS:In, photosensitive material, spectral characts. 2−72059
    - CdS:In laser, spin flip, visible, operation at liq. He temps. 2−66768
    - CdTe:In, Cu, high temp. cond., impurity effects 2−61303
    - CsBr:In, luminesc. crystals, exciton and hole migration 2−48242
    - Ge:In, conc. gradient influence on diffusion of Sb 2−71516
    - In$^+$, in CsBr, i.r. absorp. 2−61635
    - In$^+$ lifetime meas. using beam-foil technique 2−42730
    - Ir(111)-C film emitter with two-dimensional phase transitions, props. 2−65100
- **Indium** continued
    - KCl:In, ionization of In$^+$ centres by interstitial halogen atoms 2−81001
    - KCl:In, thermostimulated electron emission, retarding field depend 2−54274
    - PbTe:In, donor level above the bottom of the cond. band 2−84281
    - Si:In, ion implanted, photoelectromag. effect rel. to dose and annealing 2−72077
    - Si:In, spectral depend. of extrinsic photocond. 2−51216
- **Indium compounds**
    - Pb-In alloys, surface resistance variations with applied field 2−64942
    - Ag-In molten alloy, diffusion of Ag, capillary reservoir technique 2−56491
    - Ag-In solid solution, Zener relaxation 2−47453
    - cc $In_{1-x}Ga_xP$, diode, vapour grown, bright electroluminesc. and orange laser emission 2−49386
    - Cd-In system, liq., elec. resist. 2−46981
    - Cd-Tl, binary liquid metals, electrotransport and elec. resist. detn. for density of states at Fermi level 2−80476
    - $Cu_{64}In_{36}$, phase bundles and homogeneity detn. 2−71680
    - Ga-In-Sn alloy, field ion microscope obs. of liquid-solid interface in vacuum 2−67900
    - $Ga_{0.6}In_{0.4}As$/Cs, photoemissive yield, phonon energy loss effects 2−61460
    - $Ga_{1-x}In_xN$, fundamental absorpt. edge and energy gap 2−72329
    - $Ga_{2x}In_{2(1-x)}S_3$ thermostimulated cond. 100-350K 2−84317
    - Hg-In amalgam, dil., viscosity comp. depend., 0-100°C 2−64451
    - Hg-In liquid alloy, partial struct. factors and atomic distribs. 2−64437
    - Hg-In liquid alloy, reflectivity meas. from 0.31 to 9 eV 2−64467
    - Hg_3Te_3-In_2Te_3 alloys, h.p. phases, cond. types, band struct. 2−54175
    - In-Ag alloy, liquid, free enthalpy of mixing 2−53422
    - In-Au alloy, liquid, free enthalpy of mixing 2−53422
    - In-Bi alloy, thermodynamic props., calorimetric obs. 2−57056
    - In-Bi alloys, liq., longit. spin relax. of ^{115}In 2−50370
    - In-Bi alloys, supercond., flux flow state props. 2−44074
    - In-Bi liquid alloy equi-atomic, transport props. 2−46939
    - In-Cd alloy, quadrupole interactions of 247- keV state of ^{111}Cd, perturbed ang. correl. studies 2−75246
    - In-Cd alloy, type II superconductivity and mag. hysteresis 2−71863
    - In-Cd dilute alloy, pressure and strain derivatives of supercond. transition temp., Fermi surface topology effects 2−71859
    - In-Cu alloy, liquid, struct., X-ray diffr. interference functions, 700°C 2−83775
    - In-Ga alloy, component activities detn. using a solid oxide electrolyte technique 2−78201
    - In-Ga(Sn) alloy, surface tension and density, comp. depend., 700K 2−67815
    - In-Hg-Pb alloy, supercond., thermodynamics, role of electron scatt. 2−81038
    - In-Hg alloy, supercond., thermodynamics, role of electron scatt. 2−81038
    - In-Hg alloy, thermodynamic props., calorimetric obs. 2−57056
    - In-Hg amalgam, liq. diluted, cond. near metal-nonmetal transition of pure Hg 2−53451
    - In-Mn alloy, superconductor, thin film, electronic thermal conductivity 2−68352
    - In-Pb alloy, Seebeck coeff., comp. depend., 120°C 2−81162
    - In-Pb alloys, liq., longit. spin relax. of ^{115}In 2−50370
    - In-Sn-Pb ternary alloy superconducting wire, magnetic properties, flux flow voltages 2−81037
    - In-Sn alloy, Seebeck coeff., comp. depend., 100°C 2−81162
    - In-Te alloy, molten, elec. cond. and thermoelec. power 2−77446
    - In-Te system, films, phase comp. and band struct of In_2Te_3 2−60662
    - In-Tl alloys, liq., longit. spin relax. of ^{115}In 2−50370
    - In-Zn, liquid binary alloys, absolute thermoelectromotive force 2−56518
    - $In_xAl_{1-x}P$, cryst. growth, vapour phase 2−43511
    - InAs-ZnTe heterojuction, prep. by liq. phase epitaxy, optical and elec. props. 2−57213
    - InAs, amorphous, phonon density of states, Raman scatt. obs. 2−61664
    - p-InAs, ang. distrib. of photoemitted electrons, mag. field determ. 2−51226
    - InAs, band struct., critical point detn., wavelength modulation derivative spectroscopy obs. 2−48160
    - InAs, band struct., X-ray photoemission study 2−84387
    - InAs, by low temp. Gruneisen parameter from elastic consts. 2−71752
    - n-InAs, compensated, absorpt. edge obs. 2−75297
    - InAs, core levels, spectral obs. 2−65240
    - InAs, crystal growth from vapour phase, supersaturation of InI as process control parameter 2−74672
    - InAs, deposition, transport processes kinetics, I conc. depend. 2−74673
    - InAs, energy gap, temp. depend., calc. using Brooks-Yu theory 2−68415
    - n-InAs, heavily doped, impact ionization, elec. field depend. 2−81087
    - InAs, helicon wave propagation in magnetic fields up to 200 kG 2−47910
    - InAs, i.r. dispersion of second order electric susceptibilities 2−61581
    - n-InAs, photolum., 77-200K, temp. effects 2−72412
    - InAs, surface structure, LEED and Auger spectroscopy obs. 2−50449
    - n-InAs, thermoelec. power in quantizing mag. fields 2−84372
    - $InAs_xP_{1-x}$:Zn, growth, laser diode fabrication, lasing action 2−59185
    - $InAs_{0.4}P_{0.6}$/Cs-O i.r. photocathode, wavelength depend. of Cs-O optimum thickness 2−68498
    - InAsP, semiconductor laser, thin platelet, mode coupling in edge to edge cavity config. 2−69946
    - $InAs_{0.4}P_{0.6}$, cathode, negative electron affinity, photoemission rel. to Cs-O layers thickness 2−75194
    - $InBO_3$, i.r. absorpt. spectra 2−75292
    - InBi, elec. resist. and morphology, thermal cycling effects 2−51101

Indium compounds continued
In$_2$Bi, magnetic properties, deduced to be intrinsic type II superconductor 2−75072
In$_5$Bi$_3$ phase, thermodynamic props. 2−71687
InBr, cryst. struct., elec. cond., optical props. 2−64638
InBr photoelectron spectra, bonding in group III monohalides 2−80027
InBr$_2$, heterogeneous equilib. 750-1050 K, enthalpy, entropy of evaporation, boiling point 2−74593
In$_{6.6}$Ca$_{3.1}$S$_{13}$, cryst. struct. and cryst. chem. 2−60758
InCl, electric dipole moment, Stark effect measurement 2−46555
InCl photoelectron spectra, bonding in group III monohalides 2−80027
InF, photoluminescence spectra of excitons bound to group II acceptors 2−84279
InF band systems, vibr. transition probabilities and r-centroids 2−60006
In$_x$Ga$_{1-x}$As:Zn, growth, laser diode fabrication, lasing action 2−59185
In$_x$Ga$_{1-x}$As prep. and props. rel. to electroluminescent diodes 2−68708
In$_x$Ga$_{1-x}$As, vapour growth, equilib. calc. 2−47222
In$_{1-x}$Ga$_x$P p-n junction, bright yellow luminesc. 2−44425
In$_{1-x}$Ga$_x$P, cryst. growth, vapour phase 2−43511
In$_{1-x}$Ga$_x$P, solution growth, stimulated emission, liminescence, laser operation 2−45747
In$_x$Ga$_{1-x}$P, vapour growth, equilib. calc. 2−50576
In$_x$Ga$_{1-x}$P alloys, thermal expansion coeff. temp. depend., 15-650°C 2−71750
InI, cryst. struct., elec. cond., optical props. 2−64638
InI photoelectron spectra, bonding in group III monohalides 2−80027
InN, fundamental absorpt. edge and energy gap 2−72329
In$_2$O$_3$/SnO$_2$ film, transparent electrode for CdS 2−54209
InP-GaP system, component distrib. coeffs. and phase diagram 2−47716
InP-InAs solid solns., i.r. lattice vibrs. 2−47739
InP, [110] surface Brillouin zone, intrinsic localized states, calc. 2−65007
InP, amorphous, phonon density of states, Raman scatt. obs. 2−61664
InP, Ar$^+$ 40KeV ion bombardment, energy distrib. of secondary electrons 2−72097
InP, band struct., critical point detn., wavelength modulation derivative spectroscopy obs. 2−48160
InP, core levels, spectral obs. 2−65240
InP, energy gap, temp. depend., calc. using Brooks-Yu theory 2−68415
InP, excitonic recomb. and photocond. 2−72410
InP, free and bound electron transitions to acceptors, 1.3776 eV emission 2−72411
InP, group IV doped, cryst. growth, luminesc., donor and acceptor levels 2−47272
InP, high resistance, doped with Cu, Fe or Cr, preparation aid props. 2−83895
InP, i.r. dispersion of second order electric susceptibilities 2−61581
InP, impure, multiphoton luminesc. satellites in strong e.m. field 2−61679
n-InP, magnetophonon spectroscopy study 2−68385
InP, n-type, electroreflection spectrum under depletion and enhancement conditions in surface layer 2−81433
InP, n-type, electroreflection spectrum under depletion and enhancement conditions in surface layer 2−81433
InP, photoluminesc. of bound excitons 2−68685
InP, photoluminesc. of excitons bound to neutral acceptors, strain effects 2−48223
InP, second order Raman spectrum and phonon frequencies detn. 2−81367
n-InP, velocity-field charact., calc. 2−71912
InP, vibrational amplitudes and Debye-Waller factors from elastic consts. and Raman freqs. 2−50983
InP, wavelength modulated refl. spectra, band struct. 2−61616
InP bound exciton photoluminescence spectra 2−57373
InP electron transfer 2−61315
InP injection laser, photoluminescent and electroluminescent props. 2−42096
In$_2$S$_3$-Ag$_2$S solid soln., coprecip. diagram 2−53901
In$_2$S vapour, thermodynamic functions, electronic and i.r. spectra, heats of sublimation and formation, 273-2000 K 2−74485
In$_2$S$_3$ thermostimulated cond. 100-350K 2−84317
InSb, degenerate, attenuation variation of 9 GHz u.s. waves 2−64845
In$_2$Se$_3$-Sb$_2$Te$_3$ system, phase diagram, intermediate cpd. formation 2−61048
InSe, absorpt., 300K and 70K, 2.3 to 3.0 eV, hyperbolic excitons 2−81398
InSe, exciton-phonon interaction, absorption edge obs. 2−84518
InSe, flash evaporated thin films, eff. of thermal treatment on props. 2−77853
InSe, liquid and solid, thermal cond. 2−64865
InSe crystals, reflection spectra, similarity with zone structure 2−84480
InSe film, electron bombardment crystalliz., elec. microscope obs. 2−56594
InSe single crystals reflection and absorption in the i.r. region 2−81395
In$_2$Se$_3$, flash evaporated thin films, eff. of thermal treatment on props. 2−77853
In$_2$Se$_3$ film, flash evaporated, props. 2−56593
In$_2$Se(Te), molten, elec. cond. and thermoelec. power, temp. depend. 2−67837
In$_2$Se$_{3x}$Te$_{3(1-x)}$ single crystal, optical props. detn. 2−54422
In$_2$Te$_3$-Cu system, phase diagram and elec. props. 2−47715
In$_2$Te$_3$-Hg$_3$Te$_3$ alloy, negative magnetoresist., 77-400K 2−44102
In$_2$Te, refl., 1-12.5 eV, rel. to band struct. calc. 2−48161
In$_2$Te$_3$, semicond., radiation stability due to stoichiometric vacancies 2−71906
InTe$_{0.5}$Se$_{0.5}$, molten, elec. cond. and thermoelec. power, temp. depend. 2−67837

Indium compounds continued
InTlSe(Te), molten, elec. cond. and thermoelec. power, temp. depend. 2−67837
In$_2$(WO$_4$)$_3$-K$_2$WO$_4$ solid soln., phase diagram 2−57033
MgIn, structural energy, pseudopot. and perturbation theory calc. 2−50623
Na-In dilute alloy, liq., compressibility determ. 2−77415
Pb-In, superconducting alloys, strong coupling, mag. meas. 2−64950
Pb-In alloy, superconductor, microwave surface resist. 2−54133
Pb-In alloy film, supercond., electronic thermal cond. 2−81042
Pb-In alloy supercond., electronic thermal conductivity, temp. and mag. field depend. 2−47867
Pb-In alloys, superconducting, thermal conductivity, temp. and mag. field depend. 2−71872
Pb-In alloys, thermal Hall effect and the Righi-Leduc angle, observations 2−68370
Pb-In dil. alloy, phonon spectra and supercond. parameters 2−47865
Pb-In dilute alloy, supercond., phonon spectra detn., elec. tunnelling obs. 2−54142
Pb-In superconducting alloy, phonon spectrum, hydrostatic pressure effects, tunnelling obs. 2−64936
Pb-Ir superconducting wire, microwave absorpt., rel. to mag. field and temp., 9.2GHz 2−84306
Sn-In, superconducting, flux-trapping, structural sensitivity 2−54152
Sn-In dil. alloy, third-order elastic consts., u.s. vel. obs. 2−50727
Sn-In superconducting microbridge, transition from bulk like behaviour to Josephson junction like behaviour 2−64951

indium antimonide
see also Semiconducting materials/indium antimonide
acoustic wave dispersion meas. by heat-pulse technique using supercond. bolometer 2−80911
amorphous, phonon density of states, Raman scatt. obs. 2−61664
bolometer, hot electron, props. for submm. astronomy 2−73158
elastic wave damping, effective anharmonicity consts. 2−80913
impurity distribution, for Te, Zn and Cd, conc. depend. 2−47438
p-InSb, galvanomagnetic and thermomagnetic effects 2−72050
magneto-Raman scattering obs. 2−45730
n-type, uniaxial stress, obs. of tunable component in spectrum 2−82488
nonlinear susceptibility dispersion near band gap and second harmonic generation model 2−44334
photoconductivity, effect of light and X-rays at 77K 2−47996
resonance Raman scatt. near E$_1$ transition 2−68661
seeding dislocations, related to solid dopant inclusions, X-ray investigation 2−50675
single crystals, growth of 'star' defects and effect of seeding on clustering 2−71476
specific heat below 30 K 2−68249
superconductivity, crit. temp. determ. 2−71848
surface, sputtered atom ejection and ion bombardment induced disorder 2−43466
thermal etch pattern form. during diffusion 2−47440
InSb:^{57}Co, Mossbauer effect 2−65235
InSb:Te, growth from melt under destabilizing thermal gradients 2−74708
InSb-I$_2$ system, gas transport reactions, whisker growth, morphology 2−75366
InSb-NiSb eutectic, thermomag. props., rel. to device appl. 2−59064
InSb, calc. of third- order and temp. depend. of second-order elastic constants 2−80898
n-InSb magnetoresistance meas. 2−46729
InSb microwave emission explained in terms of nuclear electric quadrupole radiative transitions of ^{121,123}Sb 2−44404

INDOR
benzene solution w. tanone free radical, resonant helix and coil 2−66666
2,2-dichloroethane, weakly coupled three-spin system, relaxation effects 2−50116
dimethyl phosphite, neat and in dilute soln., effect of deuterium substitution on ^{1}J(^{31}P-H) 2−80104
diphenylsilane, Overhauser effect, ^{29}Si Fourier transform n.m.r. study 2−65355
homonuclear, rel. to determination of amino acid conformation 2−50078
magnetic double resonance Overhauser and solid state effect in methods of high frequency spectroscopy 2−54516
metal-ammonia solutions, relaxation times and Overhauser enhancements for protons 2−46988
octamethylcyclotetrasiloxane, Overhauser effect, ^{29}Si Fourier transform n.m.r. study 2−65355
organomercury compounds, heteronuclear double magnetic resonance studies of ^{199}Hg nuclear shielding consts. 2−57403
Overhauser effect in proton-decoupled n.m.r. spectra of ^{13}C, suppression 2−67463
paramagnetic spin systems, internucl. Overhauser effect, theory 2−59984
tetramethylsiloxane, Overhauser effect, ^{29}Si Fourier transform n.m.r. study 2−65355
1,1,2-trichloroethane, weakly coupled three-spin system, relaxation effects 2−50116
D chemical shifts measurement by ^{1}H-{^{2}H} 2−42947
^{14}N-proton double resonance, ^{14}N sites in paraelectric (NH$_4$)$_2$SO$_4$ 2−44456
NaCl, of ^{23}Na-^{35}Cl spin system, rotating frame by non resonant oscill. field, energy matching condition modification 2−81473

Inductance
Earth, inverse problem of geomagnetic induction 2−65563
induction flowmeters, principle of operation, general properties and applications 2−64409
jumping ring expt., teaching 2−48963
magnetic, for toroidal plasma confinement systems 2−83568
nonlinear, charact. curves 2−66677
ore-zone excited by current carrying cable, induction anomaly 2−57781
superconducting point contacts, effect on static and microwave props. 2−81054

Inductance continued
transformer coil, self-inductance meas. by moving coil galvanometer 2−52350

Inert gases
see also the individual gases
abundance in extreme population I matter rel. to Sun 2−81838
adsorbate structure, on W surface 2−50554
adsorbed layer, on graphite, formation stages 2−47152
adsorption on Pt, accommodation coeffs. 80-450K 2−56603
alkali MHD generator, discharge structure 2−80374
atom, collision-induced excitation transfer in alkali vapours 2−74231
atom, collisional induction of m_j mixing in oriented $6^2P_{1/2}$ Cs 2−46468
atom, collisions with H^+, differential cross sections, 500-3000 eV 2−64068
atom, electron scatt. lengths and Fermi press. shifts 2−64038
atom, outer s shell role in single ioniz. by electron impact 2−67399
atom, proton impact double ioniz. 2−83176
atom-electron scatt., 0-12 eV, failure of exchange potentials to satisfy data 2−73332
atom-H atom dispersion forces improved rigorous bounds 2−42801
atoms, coincidence studies of elementary processes in collisions with H°, H^+, H^- 2−42804
atoms, collisional broadening of Cs resonance lines, determ. of extreme-wing line broadening and adiabatic potentials 2−70622
atoms, constant acceleration approx. in collision-induced absorption 2−53096
atoms, elastic reson. energy 2−74230
atoms, photoionization, interference effect from $ns^2np^6 \rightarrow ns^2np^5\varepsilon d$ transition 2−67401
atoms, pot. parameters of interaction 2−60375
atoms, scattering of K, total cross section meas. 2−83192
atoms, study of satellite bands caused by perturbation of alkali metal atoms 2−70568
atoms and ions with inert gas structure, repulsive interactions in 0.1-10 eV 2−42773
atoms colliding with Cd in 5^3P_1 state, meas. of relaxation consts. 2−42783
atoms collisions with excited alkali atoms, transfer of excitation between fine-structure levels 2−42776
Auger spectrum, correlation effects 2−46456
binary mixtures with H2, proton spin lattice relaxation times in 165-265K range 2−46645
bubbles in irrad. Al-Li alloys, effects on mech. props. 2−43688
bubbles in solids, computer simulation of precipitation kinetics 2−64424
150 Kg chondrite of Keyes, Oklahoma, depth variations in cosmic ray spallation produced noble gases 2−58534
chondrites, recently fallen, noble gas analysis, ages 2−58535
cluster beams, multiple ionization by electron impact 2−60287
creep, thermal, expts. 2−74484
crystals, Brillouin scatt. from transverse phonons 2−84509
crystals, lattice mechanics, review 2−61070
differential scattering of H^+, He^+ from He, Ne, Ar, Kr, 500-5000 eV, meas. of absolute cross sections 2−46485
discharge, low current ioniz. wave theory 2−77312
electronic energy transfer in atomic and molecular collisions 2−79868
electrostatic interaction between p^4l and p^4l', matrix element calculation 2−56093
glow discharge emission in short wavelength vacuum region from gas mixtures 2−83642
hydride ions, realistic single-function potential models 2−50046
inhaled, absorption, whole body dose calc. 2−78661
ion entrapment in UO_2 2−60815
ion lasers, NeII, AsII, KrII, XeII, exptl. and theoretical studies including spectroscopic data 2−52422
ions, collision-induced ioniz., ion kinetic energy spectra 2−83175
ions, sputtering and energy losses on glass 2−61123
ions, thermal energy charge transfer reactions to methane, ethane, propane and silane 2−83399
isotopes fission yields in 14 MeV neutron fission, on-line meas. 2−59792
linear polarizability at ruby laser freqs. 2−52909
lunar regolith, noble gas variations with depth 2−58461
mixed interaction, test for Munn potential 2−67414
multiphoton ionization, role of excited states 2−46446
nonisothermal plasmas, mean energy, mobility and atom bremsstrahlung of electrons 2−43118
nucleation, growth and epitaxy on graphite, molecular beam system and specimen holder for t.e.m. obs. 2−79113
ocean distrib. in east equatorial and southeast Pacific 2−65603
Pacific equatorial undercurrent as revealed by inert gas profiles 2−57895
photoionization, ang. distrib. of photoelectrons with many-electron correls. 2−49958
plasma parameters for nonequilibrium MHD generator 2−59049
positive discharge column, impedance variations 2−43206
pressure and temperature behind blunt bodies in supersonic flow with supply of inert gases to base region 2−60332
rare gas crystal, elastic consts. and zero point energy, contrib. of high order multipole three body forces 2−74962
scattering of H atoms, absolute total cross sections, interatomic forces 2−67424
scattering of positrons, below inelastic threshold, determ. of elastic and annihilation cross sections 2−74233
scintillation counters, design and development 2−82825
solid, Debye temp. and Gruneisen parameters 2−50990
solid, electronic polarons, correl. formulae 2−51086
solid, polycryst., bulk modulus 0K 2−74817
solid, specific heat, anharmonic corrections at high temp. 2−68247
solubility in liq. Na, 600°C 2−56041
spectroscopic investigations of pulse discharge in cylindrical magnetron diode 2−60299
Van der Waals potential between halogen and inert gas atoms 2−80123
van der Walls interactions between rare gas atoms in a dense classical fluid 2−74234
Kr, liquid longitudinal phonons, law of corresponding states 2−71156

Inert gases continued
Xe, liquid longitudinal phonons, law of corresponding states 2−71156

Inflammability *see Combustion*

Information theory
see also Entropy; Random processes; Statistical analysis/applications
aerosol size distribution, informational entropy appl. 2−67851
channel capacity of human ear, speech intelligibility 2−69451
coherent optical processing, spatial frequency diversity 2−79292
conservation of information, energy storage 2−69552
counters, Poisson distributed random events, errors 2−49615
entropy in thermodynamics and information theory, not identical 2−76389
eye, perimetry, information theoretic basis for computer control of automated perimetry 2−85142
film information, automatic readout, optical scanning computer monitoring 2−82566
i.r. sensors, matched filter configuration 2−79284
light scattering, data inversion 2−64476
linear optical data processors used with coherent or incoherent light 2−79293
modulation transfer function from edge analyses techniques 2−79295
optical, rate distortion fn., resolution 2−79306
optical beam width-divergence product, maximization 2−79290
optical transfer function of lens, signal dependent noise 2−79294
optimum array photocounting receivers rel. to aperture integration types for log normally distributed irradiance 2−79173
real time processing system employing nonlinear optics 2−79425
space bandwidth product of multichannel coherent processors 2−79291
stochastic processes, non stationary spectral relationships for energy and power bounded functions 2−66457
system response to transient random excitation, smoothing mean square estimates 2−63051
three-dimensional image reconstruction rel. to information theory 2−66803
transfer channel, maximum capacity, rel. to thermography 2−82378

Infrared astronomy
application of i.r. system 2−84764
asteroid surface composition from spectral reflectivities obs. in 0.3 to 1.1 range 2−81909
B2 1212+30 variable radio source, obs. 2−69123
Bamberga, visible and i.r. photometric obs. 2−78493
BL Lac, coordinated multiwavelength obs. of intraday variability 2−75812
bolometric Bond albedo and size determ. from photometric models 2−78492
3C 120, coordinated multiwavelength obs. of intraday variability 2−75812
VV Cephei-type and symbiotic stars, i.r. excess measurements 84995 2−84995
chopper improvement for use in i.r. photometry 2−85067
R Cor Aust, i.r. source, HCN and CS obs. at 3mm and 6mm 75825 2−75825
R Coronae Australis and surrounding young stellar group, i.r. and optical obs. 2−78468
Crab nebula rel. to neutron star models 2−75692
Cyg X-3 region, i.r. emission four weeks after radio flare 2−81887
NML Cygnus, OH i.r. emission 2−55045
diffuse interstellar features in stars with circumstellar dust shells 2−84992
30 Doradus, size and radiation charact.58418 2−58418
galaxies and quasars 2−58212
Galilean satellites, brightness temp. obs. at 20 microns 2−78487
Galilean satellites, Io and Ganymede, thermal properties from 20 μm eclipse radiometry 2−78538
Galilean satellites, i.r. observations and eclipse measurements 2−78537
H2-3, i.r. source, HCN and CS obs. at 3mm and 6mm 2−75825
H II regions, sources at 100 μm, grain temperatures 2−55025
HBV 475, i.r. photometry 2−69126
Hoffman sources, OH emission 2−81870
Iapetus albedo, radius and temp. obs. at 20μ 2−81905
IRC+10216, polarimetry and photometry 2−58280
IRC object identification 2−75824
Iris, visible and i.r. photometric obs. 2−78493
K- and M-type stars, correlation coefficients for micron colour and band intensities 2−75737
BL Lacertae, i.r. obs. 2−69123
APLib. variable radio source, obs. 2−69123
lunar surface, bistatic radar obs., Apollo 14 and 15 2−78495
M 1, far i.r. flux meas. 2−55023
M 42, far i.r. flux meas. 2−55023
Markarian 231, i.r. photometry of the Seyfert galaxy 2−66063
Mars, i.r. spectroscopy from Mariner 9, temp. profiles of Southern Hemisphere 2−75905
Mars, surface materials rel. to i.r. spectrophotometric mapping 2−78544
Mercury, surface composition from reflection spectrum, 0.32−1.05 microns 2−78556
MHα, 238-116, i.r. photometry 2−69126
new astronomy, conference, March 1972, Bloemfontein, S. Africa 2−66071
NGC 2024, far i.r. flux meas. 2−55023
NGC 2024, flux obs. 2−73052
NGC 2264, i.r. source, HCN and CS obs. at 3mm and 6mm 2−75825
NGC 2264, optical obs, of i.r. source 2−69044
NGC 253, obs. of nucleus 2−58213
NGC 7538, i.r. source, HCN and CS obs. at 3mm and 6mm 2−75825
NML Cyg, polarimetry and photometry 2−58280
NML Tau, polarimetry and photometry 2−58280
Nova Serpentis 1970, infrared spectrum 2−78454
OJ 287, coordinated multiwavelength obs. of intraday variability 2−75812
OJ 287 variable radio source, obs. 2−69123
ON 231 variable radio source, obs. 2−69123
Orion A nebula, ^{15}N and U169.3 methanol line 2−66135

Infrared astronomy continued
- Orion Nebula, flux obs. 2−73052
- planetary nebulae, obs. from 1.65-3.4 microns 2−51715
- R hor OH source, correlation of i.r. colour with velocity separation of emission peaks 2−48755
- Rhea, albedo, radius and temp. obs. at 20μ 2−81905
- Saturn, methane bands rel. to Titan's spectrum 2−81906
- Seyfert and related galaxies, OSO's, photometry at 10 microns 2−73051
- solar spectrum, Arizona NASA atlas, 12187-17731 Å 2−69179
- solar spectrum, Arizona NASA atlas, 19374-20930 Å 2−69181
- solar spectrum, Arizona NASA atlas, 21492-25583 Å 2−69182
- solar spectrum, Arizona NASA atlas, 25583-30920 Å 2−69183
- solar spectrum, Arizona NASA atlas, 4 m spectrometer 2−69180
- solar spectrum, Arizona-NASA atlas, 1.4 μ H_2O band 2−69178
- source detection in 40 to 350 micron range 2−73052
- southern Milky Way, suspected supergiant M stars 2−66134
- stellar observations rel. to i.r. techniques 2−66136
- IKTauri, period and near i.r. variability 2−75762
- telescope, two-element, high collecting efficiency, for submm. obs. 2−73158
- Titan, brightness temp. obs. at 20 microns 2−78487
- Titan, methane bands rel. to Saturn's spectrum 2−81906
- V Mic OH source, correlation of i.r. colour with velocity separation of emission peaks 2−48755
- Vesta, visible and i.r. photometric obs. 2−78493
- VX Sgr OH source, correlation of i.r. colour with velocity separation of emission peaks 2−48755
- VY CMa, polarimetry and photometry 2−58280
- W3, i.r. source, HCN and CS obs. at 3mm and 6mm 2−75825
- water of hydration on Martian surface, high altitude aircraft i.r. spectrometric observations 2−78553
- Wolf-Rayet stars, northern, i.r. photometry 2−81833
- young star clusters, i.r. studies rel. to circumstellar envelopes 2−75774
- C stars, micron colour indices rel. to colour temp. and spectral type determ. 2−75736
- H_2O 8200 Angstroms band in Martian atmosphere, ground based photoelectric observations during Mariner 9 mission 2−78551
- OH stars, maser emission at 1612 MHz 2−81830

Infrared convertors *see Image convertors and amplifiers*

Infrared detectors *see Bolometers; Radiation detectors*

Infrared sources *see Light sources; Radiation/heat*

Infrared spectra *see Spectra*

Instruments
- *see also Laboratory apparatus and technique; Measurements; Recording; and under specific subjects, e.g. Astronomical instruments. Some specific instruments are listed separately, e.g. Spectrometers; Thermometers. Where no separate headings exist, entries describing instruments may be found included under the headings of the appropriate quantities or subjects*
- adaptation of apparatus to variable working conditions, theoretical considerations 2−82134
- aerodynamical, wind tunnel, problems due to high power and temp., techniques 2−83685
- air pollution monitoring, state of the art 2−81694
- apparatus for testing materials for wear in liquid and vaporised alkali metals at temps. up to 700°C 2−82127
- atmospheric isokinetic sampler for det. of particulate matter, for use on aircraft 2−57943
- contamination in space environmental test chambers, real time detection 2−78417
- dielectric meas., permittivity, partial discharges 2−45639
- electrogeophysical aerial prospecting, instruments freq. distortions, transients 2−54739
- electronic instrumentation, conference, Hobart, Tasmania (1972) 2−52356
- electronics in isotope geology, demands upon instrumentation 2−84725
- explosimeter, instrument for predicting explosions by det. of explosible atmosphere 2−58938
- i.r. scanner, integrator, properties of output 2−76385
- Martian gravity simulator for Viking landing tests 2−78420
- planetary emitted radiation and albedo simulator 2−78517
- recovery methods from deep ocean 2−48427
- spring, for linear obs., improvements 2−76157
- for thermophysical investigation 2−63156
- unit for determining the elastic limit in pure bending under the action of surface and corrosion active media 2−85156

Insulating materials, acoustic *see Noise abatement*

Insulating materials, electrical *see Dielectric properties of substances*

Insulating materials, thermal *see Conductivity, thermal*

Integral equations
- Abmarzumian, initial value method 2−41550
- anisotropic elasticity, dynamic Green's tensor calculation 2−76302
- dual type, initial value method 2−48980
- elasticity of isotropic medium weakened by congruent groups of arbitrary holes, periodic problem 2−82321
- elasticity theory, reduction to systems with infinite no. of degrees of freedom 2−82320
- e.m. three-dimensional quasistationary fields 2−52332
- e.m. wave scatt. from dielectric ring, technique 2−52323
- first kind, with logarithmic singularity numerical soln. 2−48976
- flat galaxy, speed distribution function, Abel integration 2−81773
- for ocean currents near equator, derivation from 3rd order differential eqn. 2−84707
- Fredholm, simultaneous pair, for mixed boundary value problem in electrostatics 2−45635
- Fredholm, stress intensity factor of crack originating at edge of circular hole 2−82336
- Fredholm's, in elasticity 2−82309
- Fredholm equations, least-squares method in signal filtration and in inverse geophysical problem 2−78768
- functional analysis methods for stat. mech. of infinite systems 2−58796
- functional methods applic. in stat. mech. 2−58800
- generalized Kepler motion, motor integrals 2−84936
- Kampe de Feriet expansion formulae evaluation of integrals 2−55373

Integral equations continued
- mechanics of continuous media problems, Hankel and Miller-Fok transforms. 2−63056
- minimality props. of local pot. 2−63052
- neutron transport props. of regular lattices 2−83058
- nonlinear, for high-energy scattering, numerical solns. 2−79543
- nonlinear, for high-energy scattering, solutions, existence theorem 2−79542
- for plane potential flow, round rotational circle blade lattice 2−70834
- point reactor kinetics, direct integral formulation 2−83097
- quasibound states in quantum domain, electric field effects 2−52077
- radiation field charged particle moving uniformly in cryst. 2−82162
- with singular kernel, for temp. transients in fuel rod 2−42615
- Tarasov specific heat model, evaluation method 2−43979
- third integral of motion; problem solutions 2−78802
- three body problem, hyperbolic-elliptic motion, energy integral 2−81776
- transform method for 2D and 3D neutron transport problems 2−70507
- two-dimensional solids, determ. of elastic stresses at notches and corners by integral equations 2−82306
- underwater sound, integral soln. of sound field in interbedded liq.-solid half space 2−82366
- vibration theory of supporting surface, boundary value problems 2−55486
- Volterra, linear and nonlinear, solution by power series 2−82310
- Volterra type integrodiff. eqn. use in approx. construction of soln. to $y'=f(x,y)$ 2−82152
- waveguides, integral equation solution, narrow strongly radiating slot 2−55603

Integrals
- *see also Calculus; Green's function methods*
- — 2−60102
- σ and π electron interactions in free electron model, revised integrals for 3-dimensions 2−77813
- action, relation to first order adiabatic invariant for harmonic oscillator with time varying coeffs. 2−52073
- atomic, Coulomb and hybrid, over Slater-transform- Preuss functions 2−42702
- convolution, two dimens. soln., deconvolution, application to electron microscope 2−73529
- Dirac delta function, integral representation 2−78735
- electron-repulsion, spin-spin and spin-orbit, over Slater functions 2−79980
- elliptic, third kind, derivatives in magnetic and electrostatic field computation 2−45232
- e.m. field calc., analysis 2−55594
- folding, for nonspherical distributions, radial moments 2−58701
- Fox's H-function, hypergeometric function, rel. to heat conduction in cylinder 2−82256
- function space, applic. to wave propagation in random media 2−58716
- general three body problem, numerical integration 2−81777
- gradually and spatially varied flows, numerical integrations 2−77243
- incohrent optical correlation system for integration of functions of one variable 2−55441
- inequalities with mathematical structure of expectation values 2−76211
- ionosphere, numerical integration method, chemical and charge balance conservation 2−81721
- linear wave theory, asymptotic expansion of integrals 2−82154
- molecular one-electron integrals 2−42848
- nonholonomic mech. system with uniform linear couplings, first integral derivation 2−66420
- nonlinear viscoelastic solid, single integral constitutive law 2−76332
- numerical integration for matrix elements between localized molecular orbitals 2−52978
- optimized integral continuation methods, application to elementary particle calcs. 2−42314
- orbit-orbit integrals for diatomic molecules, evaluation of integrand 2−49988
- phase-space, in multiparticle collisions and in relativistic quantum statistical mechanics, analogy 2−42320
- reactor theory, Cd cutoff energies 2−83113
- Talmi, for contrib. of central, spin-orbit and tensor forces to effective interaction 2−76764
- transient wave in anisotropic plasmas, steepest descent evaluation 2−56351
- two-electron integrals in LCAO-MO calculations, economic storage and processing method 2−52979

Intensity measurement
- ancient geomag. field, influence of chemical magnetization 2−78409
- e.m. waves, scattered from rough surfaces 2−78978
- focused light beam in gravity centre 2−55723
- laser pulse, short duration, peak intensity and energy content estimation using saturable absorbers 2−66775
- light beam, instrument for correlation function obs. 2−73662

acoustics
- levels meas. from distant source 2−52248
- loudness evaluation, comparison with bangs 2−58907
- loudness of transients, effect of rise time and repetition rate 2−45531
- portable sound analyzer and recording system 2−55550
- random noise, loudness calculations, ISO R-532 (Method B), optimal algorithms 2−73446
- single number noise rating for $^1/_3$-octave band sound power levels 2−73447
- sound power level meas. in semireverberant rooms 2−41692
- sound signal level indicators, operation 2−66629
- u.s., Radiation Control for Health and Safety Act 2−45041
- u.s. field meas. by liquid surface relief method 2−63110
- u.s. powers, in microwatt-milliwatt range 2−41794

Interatomic forces, between bound atoms *see Bonds; Molecules/internal mechanics; Solids*

Interatomic forces, between free atoms *see Collision processes/atoms*

Interface phenomena
see also Surface phenomena
adhesive layer in laminated honeycomb structures, elastic vibrations 2−50927
air-sea, unified model for heat and gas exchange 2−62069
air-water, heat transfer and thermal struct., rel. to sea surface temp. meas. 2−65625
bicrystal, epitaxial, interface struct., effect of misfit, bonding and cryst. dimens. 2−56690
BORSIC aluminium fibre-matrix interfacial region, exam. 2−64546
boundary profile between two phases, formulating using square approx. of cluster variation method 2−52087
boundary structure between two phases, boundary free energy in lattice model, general formulation 2−52085
boundary structure between two phases, determ. of boundary free energy in lattice model 2−52086
bubbles, surface waves and subharmonics, thresholds for acoustic excitation 2−43307
ceramic-metal systems, chem. bonding 2−50861
ceramic-metal systems, ion tunnelling 2−51183
colloid, electrical double layer round spherical particle, functional representatinal of properties 2−60525
colloid, Esin-Markov coefficient for elec. double layer 2−60524
coupled materials, thermal contact resist., sinusoidal press. variation influence 2−74998
crystal/melt, free energy calc. from radial distrib. function 2−43463
dielectric interfaces, charge transmission, applic. to liquid He 2−43413
dislocations, between two isotropic phases, stress fields and strain energies 2−80668
equidistant mol. plane model, surface tension 2−84630
equidistant mol. plane model, surface tension 2−84631
ferrite-dielectric, gyromag. surface waves 2−44271
ferrite/semiconductor interface, interaction of surface magnetostatic waves with carriers 2−84420
fluid interfaces near critical point, continuum theory 2−67813
fractional crystallization in ternary systems, distribution of isomorphous salts between aqueous, solid phases 2−50582
gas-liquid, stability analysis, rel. to weld pool stability 2−43224
gas-liquid, wave roughened, heat and mass transfer to annular two-phase two-component flow 2−77409
gelatin gels, diffusion of water, interfacial contact resist. 2−60533
gravitational instability of two streams 2−84930
heat exchange coeffs. for materials in contact, transient region meas. method 2−78832
immiscible polymers, interface theory 2−60441
interaction forces between condensed bodies in contact 2−74566
interference between direct, head and interface waves 2−81577
Kapitza resist., phonon absorpt. 2−54072
Kapitza resistance, effect of low energy vibr. modes 2−51053
Kapitza resistance, transfer hamiltonian approach 2−56533
liquid, dynamic meas. of dilational properties 2−50302
liquid wave motion of low-tension interfaces with electric double layers 2−83740
liquid-liquid, effects of heats of solution on Marangoni convection 2−77381
magnetic phenomena of surface gas-solid interactions 2−84395
mass transport between finite vol. of homogenized fluid and sphere with finite transport coefficients 2−46990
metal powder, contact stresses, electron microscope obs. 2−56970
metal-electrolyte solution interface, electron photoemission 2−68496
metal-powder formation at metal-electrolyte interfaces, determ. of potential barriers and eqns. of tunnelling limiting current 2−57426
metal-superfluid He, low temp. thermal cond. anomalies 2−54065
metallic solid/liquid interface micromorphology, electron microscopy obs. 2−47194
metallic-field effect calc., rel. to field emission, ioniz. and capacitor capacitance 2−54206
ocean density interface, entrainment and turbulent diffusion model 2−84706
p-anisylidene p-aminophenylacetate, nematic, influence on thermal cond. 2−80467
in precipitation kinetics 2−68187
refractory carbide/liquid metal contact interactions 2−68190
rod surface, effect of boiling transition regime on propagation of temp. oscillations 2−64513
Si-SiO_2 interface, e. scatt. by surf. oxide charges and lattice vibrat. 2−71317
solid surfaces, conference, Boston Mass., USA, Oct. (1971) 2−47070
solid-liquid, roots of Stoneley wave equn. 2−41676
solid-liquid growth fronts, solute distrib., contrib. to interfacial undercooling 2−43517
solid-solid, nonelectronic thermal cond. at low temp. 2−43998
stress waves, reflection and transmission at interfaces between elastic materials 2−41677
structure and props. of grain boundaries and interfaces, conference, Yorktown Heights, N.Y., USA, Aug (1971) 2−56722
two phase materials, circular disclination, elastic fields, interface effects 2−76272
two-phase fluid interface at equilibrium, continuum model 2−53109
unsymmetrical electrolyte, linearized potential eqn. for interfacial region 2−75385
water/Al, u.s. refl., surface wave creation 2−64851
Ag film on mica., modulation of conductance due to changing interface, metallic field effect 2−75047
AgI particle dissolving in H_2O drop, interfacial kinetics 2−60434
As_2S_3/Ag system, photochem. transformation rate temp. depend., ht. treatment and ageing effects 2−57433
Au film, on amorphous C, oriented crystn. mechanism, rel. to interaction forces at interface 2−77502
Bi liquid-solid interface, damping of oscillations by magnetic field 2−71303
C fibre reinforced glass, fracture energy 2−84104
C fibres, adhesion to organic matrices 2−84101
CdSe-SiO_x, electron transport study in space charge layer of vacuum-deposited film 2−77852
Cr interfacial free energies meas. 2−80795
Cu, with liq. and solid ^{4}He, Kapitza cond. at 1.9 K 2−67854

Interface phenomena continued
Ga-In-Sn alloy, field ion microscope obs. of liquid-solid interface in vacuum 2−67900
Ge electrode, equilibrium and nonequilibrium effect near semiconductor electrolyte boundary 2−61798
He/metallic layer/He bath system, energy flux eval. 2−53474
He/solid, low energy modes in acoustic propag. 2−47008
He liquid-solid, reflection of phonons 2−74576
Mg/MoS_2 film/substrate system, curvilinear dislocations 2−80554
Mo interfacial free energies meas. 2−80795
Mo_2C-$Fe_{(l)}$, contact interactions 2−77728
Si-Au, mixed phase formation at interface, Auger electron spectroscopy, 100-300C 2−74619
Si-SiO_2 interface, ion implanted, deep energy level detn. by m.o.s. technique 2−80938
Si electrode, equilibrium and nonequilibrium effect semiconductor electrolyte boundary 2−61798
Si layers, homoepitaxial, influence of substrate on interface props. 2−77495
TaC, wetting by liq. Ag and liq. Cu, surface energy 2−43468
W/Ni, rel. to sintering 2−43897
W interfacial free energies meas. 2−80795

Interface tension *see Surface tension*

Interference
carrier conc. meas. by i.r. interference 2−82567
coatings, multilayer, optical monitoring 2−79408
electron beam. laser modulation, interference effects 2−59081
fibre optics structure production, ray anal. of image transfer props. 2−73666
gas flow, wind tunnel wall, reduction by streamwise porosity distrib. 2−46812
holography, double exposure, time ordered 2−69974
laser beams, complex coherence factor eval. by superposition of two systems of stationary waves 2−73603
magnetized plasma, Fresnel-like interference and ion wave decay 2−70939
photoelectron-conversion electron, effect of absorber thickness in Mossbauer effect 2−55953
Rayleigh waves, large aperture seismic array obs. 2−65455
superconducting point contact quantum interference device, model for operation 2−82554
visibility of spectral modulation in white light interference 2−79421
zone plate, construction 2−62935
GaAs frequency mixing, 2 and 3 wave anisotropic interference 2−75250

acoustic waves
amplitude and phase fluctuations of field in waveguide with rough walls 2−41688
holography by sector scanning 2−79280
interaction with coherent light beam, phase fluctuations 2−73435
interference pattern method for meas. reflection from uneven surfaces 2−69740
surface wave propagation in monolayers of soluble polymers using Moire fringes 2−73445
two transducer frequency analysis technique to characterize discontinuities 2−41791
u.s., pattern visualization in front of radiating quartz by optical illumination in direction of propagation 2−55547

electromagnetic waves
interaction of opposite e.m. wave beams in transparent nonlinear medium 2−78958
Moire patterns from X-rays, depend. on wavelength 2−85178
odd symmetry wave front deformations effects on diffractograms of e.m. images in electron microscope 2−82446
r.f. depth sounding for electrical parameters and surface layer thickness estimation 2−55137
teaching demonstration, standing microwaves by oblique incidence on mirror 2−41431

light
see also Films, solid/optical properties
— 2−59265
analytical ultracentrifuge, alignment with schlieren system 2−61819
atmospheric phase difference spectra for 10.6 μ laser beam 2−81673
atmospheric seeing conditions on Mt. Wilson rel. to Agassiz Station, interferometric study 2−68909
broad source, surface flatness meas. rel. to mechanical face seal 2−66405
coherently illuminated rough surface, structure of interference field 2−42207
complex momentum and energy transfer 2−76520
controllable dispersion interference-polarization filter, design method 2−66845
deforming light path ring laser expts., based on von Laue thought expt. 2−79239
dielectric thin film, interference method for meas. of dispersion in refractive index 2−44342
dielectrics, transparent, laser surface damage thresholds rel. to Fresnel reflections 2−79228
diffraction images of partially coherent phase discs with variable phase plates 2−76519
double exposure holograms from meas. spatial dependence of index of refraction 2−73616
filter, induced-transmission, symmetrical containing absorbing layers, equiv. layers concept 2−79445
filters, high-contrast, 10 to 30 A half-width 2−70065
filters, reflex, conjugate, thin-film, within Fabry-Perot cavity 2−79346
fluid film thickness meas. by Moire fringe contouring 2−79371
forces of oscillats,meas. by more sensitive method of ‘hooks’ 2−49928
fringe-visibility for anti-phase amplitude modulated beams 2−45788
full-field compensation, Tardy’s principle modification 2−52456
holographic microscope, optical configuration and performance 2−73619
homothetic images, interference between two superposed images 2−63383
independent sources of laser beams 2−52453
laser speckle patterns, wavelength diversity technique for speckle size reduction 2−66774

Interference continued
light continued
moire anal. of strain, polycarbonate 2−84084
Moire fringe effect, det. of freq. of coarse gratings 2−63384
moire fringe method, for high velocity motion recording photographically 2−50788
Moire fringe method in shaft torsion problem 2−49056
Moire fringe patterns formed by polarization gratings 2−49429
Moire fringe system, automatic high-speed scanner 2−66815
moire fringes, crossed gratings as sensors in industry 2−55741
moire fringes, rel. to aspherical surface control method 2−52433
Moire fringes for testing visual acuity of retina 2−45171
moire fringes in three-reflection-grating system, rel. to linear displacement meas. 2−59256
moire gauging of in-plane displacement using double aperture imaging 2−66403
Moire grating, with pseudo-random sequences, use in contouring meas. 2−79372
Moire patterns for enhancing sensitivity of holographic interferometry 2−76504
Moire technique for recording spectroscopic holograms in photographic film 2−73614
multiple spherical wave interference patterns, computation of asymmetrical profiles 2−42195
nonselective, using twin-discharge multielement lamps 2−52492
optical surfaces parallelism using c.w. gas laser 2−82532
patterns as confocal conic sections, teaching aid 2−49418
phase distribution meas. of field on laser output mirror 2−66776
phase object visualization using Moire patterns 2−69973
phase shifts and visibility variations due to multiple internal reflections in beam splitter of two beam interferometer 2−42199
polyethylene terephthalate films, observations of optical irregularities 2−52452
polymer fracture surface layer, optical thickness determ. 2−70013
refractive index measurement by interference microscopy and corrections for dispersion 2−70016
Reusch piles, propag. phenomena 2−82552
single-photon double-slit, teaching demonstration 2−48959
spatial filtering of interfering waves 2−66814
speckle patterns, atmos. induced, information retrieval 2−66812
speckle patterns, historical retrospect 2−79299
teaching demonstration using gas laser as light source 2−66399
technique for detecting fast displacements of small areas in beam direction 2−73592
technique for meas. of coherence of single laser pulse 2−79348
thickness, optical, meas. method 2−70013
white light multiple beam for surface microtopographies 2−73636
white light source, spectral modulation visibility meas. method 2−73675
zone plates, third order and chromatic aberrations 2−59227
AgGaS$_2$, birfrngence obs. using fringe technique 2−75259
Al film thickness control, automatic apparatus for preparation of MIM filters 2−70029
Ni film, intrinsic stress obs. 2−43679
OH, interstellar, interferometric obs. of $^2\pi_{3/2}$ $J=5/2$ microwave transition 2−75792
ZnS, vapour phase deposited interference layers used to identify inclusions 2−56737

Interference spectroscopy *see Spectroscopy*

Interferometers
electron beam, using laser modulation 2−59081
Fabry-Perot etalon use for weak line profile investigations with spectrophotometer 2−76546
holographic, visualization at weak inhomogeneities, in gas flows 2−64374
Josephson junction interferometers, critical current periodicity, interf. patterns, mag. field effects 2−61254
Mach Zehnder, for meas. of isotherms of SF$_6$ in critical region 2−80519
Mach-Zehnder, measurement of aerodynamic force on oscillating aerofoil section 2−77358
Moire fringe system, automatic high-speed scanner 2−66815
acoustic waves
swept frequency resonant, for acoustic dispersion parameter obs. in 1 MHz frequency range 2−66623
electromagnetic waves
136/138 MHz using steerable antennas 2−52321
band-width synthesis, radio astronomical 2−58388
i.r. Fourier transform spectrometer with 500-5000 cm^{-1} bandwidth 2−62818
microwave, analysis for plasma density meas. 2−46728
microwave, X-band for meas. electron density in a plasma 2−60257
radio, for astronomical meas., description 2−81965
radio, on super-long base line, sensitivity, signal freq. depend. rel. to digital information processing 2−81970
radio interferometer at K$_u$-band 2−55197
radio thermal signal processing of moving emitters in near zone of interferometer 2−79316
X-rays, depend. of Moire patterns on wavelength 2−85178
Ag-In dilute alloy, Righi-Leduc and Hall coeff., 2.5-120 K 2−75050
Bi-In alloy, induced high press. phases, X-ray and specific volume studies 2−74926
light
a.c. shearing interferometer using white light extended source 2−79355
all-reflection, use as Fourier transform spectrometer 2−59282
automatic regulation of SISAM interferometer 2−55737
common path, testing long focus optical systems 2−73637
digital, using linear displacement conversion principle 2−59230
using double diffraction system for phase-object observing 2−70019
Fabry-Perot, for meas. of Raman spectra of gases under high resolution 2−74250
Fabry-Perot, obs. of weak signals by press. scanning 2−79437
Fabry-Perot, scanning, using air bearings, design and construction 2−70018
Fabry-Perot, surfacing polishing and quality evaluation 2−76509
Fabry-Perot etalon interferograms method of determ. real contour parameters from observed contour 2−66836
Fabry-Perot oscillating, use in atomic flame spectroscopy 2−84693

Interferometers continued
light continued
Fabry-Perot surface defects compensation using SiO$_2$ compensating layers 2−70017
forces of oscillats,meas. by more sensitive method of 'hooks' 2−49928
Jamin, use in investigating transverse and longitudinal spatial coherence of radiation field 2−66813
Jamin interferometer modified to measure electron density gradients 2−66771
laser, based on schlieren system, design and performance 2−73635
laser, boundary layer study in fluids 2−59228
laser, differential, for fire research 2−42159
laser, for θ-pinch plasma 2−50201
laser, for length obs. 2−59229
laser, for optical systems control 2−42127
laser, high sensitivity meas. on transient phase objects 2−42192
laser, study of plane-stress-wave propagation in solids 2−59233
laser beams, wavefront studies 2−59129
laser with harmonically matched cavities, plasma diagnostics 2−66811
Llyod mirror, determination of velocity of light from moving source 2−42174
long path difference, 30 cm diameter for mass and heat transfer and aerodynamics obs. 2−59231
Mach Zehnder, direct phase detecting system 2−55735
Mach-Zehnder, for meas. of laser linewidth due to quantum phase and quantum amplitude noise 2−49396
Michelson, applic. to high resolution astronomical spectrometry 2−62812
Michelson, for analysis of complete spectrum of collision induced light scattering 2−80408
Michelson, for Fourier transform spectroscopy 2−55771
Michelson, polarizing, laser frequency selection applications 2−73639
Michelson, underwater vibrational meas. 2−55481
Michelson for study of frequency behaviour of lasers 2−69987
microscope systems, for refractive index, thickness and surface struct. obs. 2−55736
moire, applics. to study of large deformations 2−42139
Moire fringe system, automatic high-speed scanner 2−66815
multi-pass Michelson, for length 2−76518
multiple beam interference refractometer and comparator 2−45787
multiple use, for testing opaque and transparent samples 2−42194
phase shifts and visibility variations due to multiple internal reflections in beam splitter 2−42199
photoelectric stabilized, for obs. of amplitude-frequency responses of piezotransducers 2−76515
polarization, use for meas. absolute phase delay in Kerr effect 2−42197
polarization rotating interferometer for Sagnac effect meas. 2−79358
Sagnac, in optical autocorrelator for lens testing 2−76532
scanning microinterferometer, laser illuminated, for det. of dry mass of living cells 2−45785
stellar, i.r., heterodyne detectors 2−81975
stellar rotation and simulation of intensity interferometer 2−58270
thickness gauge 2−70031
thin film analysis using two beam interferometer 2−79354
Tolansky microinterferometer, transmission like interference fringes 2−45786
Twyman Green, for testing large aperture optical systems 2−63402
ultravariable resolution single interferometer echelle scanner 2−42266
visibility, brightness and fringe shifts at different ports as function of polarization states 2−52454
Zhamen's type, for phase fluctuations of coherent optical radiation in atmosphere 2−72740
He-Ne laser, effect of atm. on wavelength, correction methods 2−69957
In$_x$Ga$_{1-x}$P ternary phase diagram and band gap energy obs. 2−74949

Interferometry
calibration of Earth strainmeter transducer 2−65530
correction of off centre sampled interferograms by change of origin, effect of overlapping aliases 2−45783
geodetic application, baseline determination 2−54617
gravitational flux reaching earth from Crab pulsar, reach for minimum detectable signal using laser interferometer 2−81894
heat transfer between parallel walls, det. 2−49178
holographic, noncylindrical Z-pinch density profiles 2−83597
methods of counting and interpolating interference fringes rel. to length and angle measurement 2−76155
nondestructive film thickness meas. technique 2−50508
Cr interfacial free energies meas. 2−80795
Mo interfacial free energies meas. 2−80795
W interfacial free energies meas. 2−80795
acoustic waves
guitar, acoustical and hologram interferometric meas. of top plate vibrations 2−52244
electromagnetic waves
astronomical obs. technique, effects of irregular propagation media 2−58560
long coherence intercontinental, for detection of fine structure in compact radio sources 2−62814
lunar surface topography obs. Earth based radar technique 2−62649
phase errors in interferometry, identification and removal 2−66241
plantary nebulae, radio flux obs. 2−62469
plasma electron density obs., circuit for direct registration 2−67658
satellite tracking of ATS-3 by v. long baseline technique 2−54988
signal processing with positive constraint 2−55198
very long baseline, mapping of radiosources 2−58564
X-ray, refractive index determ. for Si and Ge 2−72256
light
— 2−66788
— 2−62159
astronomical telescope, optical aberrations due to temperature deformations and convective fluxes, interferometric investigations 2−48821
atmospheric pollution aerosol monitoring using high-resolution interferometric techniques 2−51600

Interferometry continued
light continued
Brownian particles, sedimentation rate, diffusion coeff., holographic interferometry 2−45767
coherence using interferometric contrast fringes 2−76517
coherent obs. of gear tooth surfaces 2−82538
computer program for analysis 2−79353
convection in rectangular air filled cavities, meas. 2−76400
direct phase detecting system 2−55735
discharge, plasma focus type, obs. of second compression 2−56344
displacement, by holographic interferometry 2−41446
distance measuring process, increase in accuracy 2−41448
double pass Fabry Perot technique for Brillouin scattering in nitrobenzene-n-hexane critical mixtures 2−46965
double pulsed holographic interferometry for study of periodic and transient deformation 2−41665
double-beam method of obs. of axisymmetric configurations of dense plasma 2−43170
elastic and plastic strains, using symmetrical telecentric lens 2−45784
electro-optic coefficients in crystals meas. 2−63397
elliptically polarized light beams 2−79359
ethyl alcohol counterflow diffusion flame in transverse electric field, optical study of temperature profiles 2−83703
Fabry-Perot, for Fourier spectroscopy 2−49450
film thickness meas. by holographic interferometry 2−50477
obs. of freezing of sea water 2−65601
fringe shape meas. accuracy, effects of interference field and analyzer 2−76516
hologram, double exposure type, for three orthogonal displacement component determination 2−66787
hologram, obs. of resonances of treble viol plates 2−45520
holographic, appl. to ultrasonic wire bonder device motion 2−63128
holographic, applic. to small displacement measurement rel. to geophysical studies 2−61845
holographic, application to printer type piece deformation study 2−69666
holographic, appls. to applied mechanics 2−84168
holographic, displacement and deformation meas. 2−82150
holographic, electron density in plasma from laser-produced gas breakdown 2−83559
holographic, examination of impact loaded objects 2−45765
holographic, for aluminium cylinders strain analysis 2−50787
holographic, for strain meas. 2−73609
holographic, La doped CaF_2 recording materials 2−66789
holographic, laser wavefront obs. det. of degree of spatial coherence 2−42125
holographic, printed circuit board evaluation 2−73617
holographic, real-time/time averaged interferometry 2−82147
holographic, recording onto photochromic spiropyran 2−55719
holographic, technique for meas. of absolute retardation in photoelasticity 2−41623
holographic, technology, book 2−42154
holographic, vibration and deflection meas., projected ruling Moire method 2−82149
holographic, vibration meas. 2−49103
holographic, vibrations of segmented shells 2−82146
holographic anal. of contaminant deposits on optical surfaces 2−45809
holographic deformation obs. of C-C bioxal test specimens 2−82145
holographic interferometer and fringe analyser, study of supersonic flow in wind tunnels 2−46836
holographic interferometry, surface displacement components of deformed body 2−66552
holographic interferometry, underwater, acoustically induced mutual coupling effects 2−79229
holographic interferometry, use of Moire patterns for enhancing sensitivity 2−76504
holographic n.d.t., engineering appls. 2−84170
holographic obs. of semi-fluid material flow and audio speaker modes 2−52436
holographic strain obs. on tensile specimen 2−82144
holography, anal. of static deflections 2−66576
holography, closed loop, real time 2−66791
holography, determ. of influence coeffs. for composite structures 2−82143
holography, measuring technology and metrology applications 2−58681
holography, method of stationary phase for anal. of fringe functions 2−66783
holography, obs. of laser beam parameters 2−79218
holography, quantitative data reduction using fringe control techniques 2−82540
holography, three-dimensional refractive index field, meas. 2−82582
holography, use of matte scatterer 2−69980
holography application to stress analysis of anisotropic composite plates 2−41598
holography employing spherical mirrors 2−69978
interferogram of phase object using achromatic fringe system 2−76507
interferometric spectropolarimetry determ. of intensity and state of polarization 2−79436
for kinematics transducers calibration 2−73634
laser, for meas. of strain amplitudes in internal friction exprts. 2−73395
laser interferometer dilatometer, for thermal expansion meas. 2−49183
laser interferometer dilatometer, for thermal expansion meas. 2−49183
laser resonator interferometry for accurate meas. of cyanic resonant wavelengths at 311 and 337 μm 2−41985
lateral shearing interferograms evaluation 2−79351
lateral shearing interferometry data reduction, application to turbulent medium 2−79352
lens system evaluation by interferometric fan trace plotter 2−79420
liquid crystal, nematic film studies 2−43329
materials response meas. holographic interferometric techniques 2−49402

Interferometry continued
light continued
Michelson technique for obs. of thermal elongation of laser diodes 2−42095
mirror testing, flatness and sphericity 2−55757
multiple beam Fizeau and photoelectric shearing, film thickness det. 2−47118
optical flats inspection, methods and instruments 2−59232
optical instrument testing, roughness and scratch determination 2−73638
phase modulation, longitudinal optical localization 2−42193
photoelastic, physical explanation in terms of warped-wavefront 2−52438
photographic materials, resolving power determination 2−70095
plasma diagnostics of CO_2 TEA laser produced plasma 2−64310
plasma diagnostics using Axicon-scanned Fabry-Perot spectrometer, non-homogeneity brightness of fringes 2−60262
plasma neutron meas. in focus, holographic 2−83583
plexiglass plate cracks, interferometric determination of opening and edge sliding mode stress-intensity factors 2−47544
scan interferometry, interference meas. on moved faces 2−63401
shock and detonation waves, local vel. meas. by Schlieren interferometry of Doppler shifted laser light 2−63138
solar small scale features 2−55164
spatially rough surfaces illuminated by high intensity source, far field intensity distrib. 2−79347
speckle pattern, application to engineering meas. 2−82557
speckle pattern, application to study of phase objects 2−79330
technique for viewing deformation zones at crack tips 2−60903
time average holographic interferometry, damped oscillations 2−63094
vibratory mode shape patterns of cored mirrors det. by holographic interferometry 2−52434
white light, application to thin air film thickness measurement 2−70015
CH^+ molecules, interstellar 2−75798
CdS electronic fringe counter 2−42198
guanidinium aluminium sulphate hexahydrate, optical and interferom. studies of cleavages and etch patterns 2−64670
He-Ne laser interference fringe counting in high accuracy length measurement 2−55358
$KNbO_3$, ferroelectric domain investigations using pseudocubic {001} cleavage planes 2−61429
SF_6 liquid-vapour transition, interferometric meas. of isotherms in critical region 2−80519
Sf_6, liquid-vapour coexistence curve, interferometric obs. 2−74591

Intergalactic matter
Coma cluster, infall of matter, effect on evolution 2−58191
Coma cluster of galaxies, not gravitationally bound by ionized gas 2−58227
compact extragalactic radio sources rel. to radio cloud pairs 2−78485
dust grains, radiation-driven efflux from spiral galaxies rel. to intergalactic extinction 2−81802
extragalactic rings, spectra 2−58207
gas, mixing time scale of newly made material, spatial inhomogeneities of nucleosynthesis 2−66048
gas, soft X-ray emission in neighbourhood of Galaxy 2−55007
gas heating and photocluster fragmentation 2−75679
H II regions, 3 cm. fine structure transition of H, detection attempt 2−58251
infall into the Galaxy and soft X-ray emission 2−75666
infalling matter effect on heavy element content of galaxy 2−55015
inner bremsstrahlung, X-ray background, steady state universe 2−58434
ionized gas, in Coma cluster, models and mass estimates 2−51700
magnetic field causing Faraday rotation and steady state and Einstein-de Sitter cosmologies 2−54999
magnetic fields, upper strength limits, role in hot model of Universe and galaxy formation 2−66049
massive object moving supersonically through galaxy, X-ray and optical radiation 2−48661
photoionization by hot white swarfs 2−81791
protogalaxy, collapse, with rotation and capacity in later stages 2−58178
radiative shock waves, propagation in inhomogeneous cosmic medium 2−68995
radio trails of active galaxies in clusters, rel. to interacting galaxies hypothesis 2−51711
reddening of galaxies 2−66051
relativistic perfect fluid, Einstein field equations, spherically symmetric solns. 2−56277
X-ray emission near galaxies from accretion of hot gas 2−66050
H_2 solid, missing cosmological mass 2−75667

Intermediate bosons
charged, in weak and e.m. interactions, calc. of static quantities in Weinberg's model 2−73744
charged vector boson, anomalous mag. moment 2−55808
massive and massless vector particles, current conservation, Lorentz condition, weak gauge invariance 2−70248
production cross section calcs. 2−73832
theory, radiative corrections to muon decay 2−45891
vector, rel. to mirror asymmetry of Fermi β decay 2−79772
weak-interaction model, renormaliz. 2−82654
ν-lepton interaction, and intermediate vector boson 2−55819
νp scatt., elastic, with strong W-boson interactions 2−79501
W pair production in high energy electron collisions 2−79508
$W_{0,1}$ production cross sections for $\nu_e(\nu_e)+Z$ resonant process at high energies 2−45980
W_0 production by colliding e+e- beams 2−45979
W_1 production by colliding e^+e- beams 2−45979
$X^0(3.1,3.4,3.6)$ obs. in $pp \rightarrow X^0\pi^0 \rightarrow n\pi^+ \; n\pi\text{-}\pi^0$, $n=3,4$ 2−63645

Intermetallic compounds *see Alloys; Semiconducting materials and under the compounds and alloys of the individual metals*

Intermolecular forces *see Molecules/intermolecular mechanics*

Internal conversion *see Beta-ray spectra/conversion electrons; Gamma-rays/internal conversion*

Internal friction
brass polycrystals doped with zinc, meas. of amplitude independent internal friction 2−64706

Internal friction continued
continuous recording high temp. system 2-53852
Earth and planets oscillations, law of creep 2-58482
ferromagnetic materials, stress depend. damping at stresses to fatigue limit 2-74826
Hasiguti peaks, thermal unpinning of dislocations 2-68023
Maxwell solid body, generalized, free vibrs., internal friction limiting value 2-55487
metal, negative reversing effect, elimination 2-53789
metal during bending at low freq., meas. from 20 to 800°C 2-64749
metals, high resolution automatic apparatus 2-68122
point defect dragging with strong dislocation interaction 2-64704
polyethylene, linear, anomalous internal friction at low temps. 2-84107
polymers, method for finding effect of inelastic deformation on hydrogen bonds 2-80119
radiation effects, apparatus for reactor meas. 2-84062
rocks, effects of temperature variation 2-65577
steel, carbon, chromizing effects 2-53780
steel, dislocation-additive interaction during tempering 2-43790
steel, low carbon, inelastic phenomena and kinetics of damage for cyclic loading 2-60915
in straight shaft of non-circular cross section housing rotor 2-49053
strain amplitudes meas. by laser interferometer 2-73395
Ag, influence of neutron irrad. 2-77642
Ag, γ-irrad., recrystn. behaviour 2-64758
Ag, rel. to recrystalliz. on annealing 2-47577
Ag, work hardened, anelastic phenomena at low temp. 2-60848
Al, effect of tempering 2-77699
Al, neutron-irradiated, comparison with values for annealed Al 2-60850
Al, workhardened and irrad., defect. movements 2-43669
β-Al_2O_3, Na, K, Rb, and Na-K substituted, rel. to mech. behaviour 2-56770
Al_2O_3 ceramic, temp. depend. 2-71553
Au-Cu alloys, Zener relax. obs. 2-60852
Au-47.5 at.%Cd alloy, anelastic props. in cubic-orthorhombic phase transform. region 2-77643
Au films, internal friction detn. from u.s. attenuation meas. 2-77780
$BaTiO_3$ single crystals influence of the amplitude of free vibrations on the permittivity 2-81154
C, pyrolytic, γ-irrad. stress-graphitized, dynamic mech. props. 2-53775
c V-Ti alloy, rel. to scavenging of interstitials 2-50845
Cu-Cr alloys, after isochronal annealing, conc. depend. 2-77633
Cu-Mg(Mo)(W) solid solns., dislocation-impurity binding energy determ. 2-43630
Cu-(30 wt.%)Zn alloy, relax. of diffused Zn during short-range-ordering 2-77705
Cu, inelastic phenomena and kinetics of damage for cyclic loading 2-60915
Fe-1%C-0.5%As alloy, anomalous precip. obs.50940 2-50940
Fe-C alloy, precipitation obs. 2-56903
Fe-C alloy, strain ageing obs. 2-56904
Fe-N alloy, precipitation obs. 2-56903
Fe-N alloy, strain ageing obs. 2-56904
Fe-Ni-C-Mo-Cr alloy, effect of tempering 2-43853
Fe-Ni-C alloy, effect of tempering 2-43853
Fe-Ni-Si alloy, temper brittleness development, grain boundary adsorption of P, obs. 2-80767
Fe-Ni alloys, martensitic transformation study with heat treatment 2-43916
Fe-V-N system, abnormal Snoek peak 2-47482
Fe, strain ageing and amplitude dependence 2-71624
Fe and dil. alloys, recrystn. obs. 2-47626
Fe and dil. alloys, recrystn. obs. 2-47625
GaAs:Te, heavily-doped, defect studies 2-71926
GaAs, single cryst., temp. depend., 20-540°C 2-53790
Ge, low temp., dislocation behaviour 2-68068
$Li_2O.Al_2O_3.2SiO_2$, glass, fibres, ion exchanged 2-80754
Mn-Ga alloys, rel. to phase equilib. 2-50735
Mo, microdeform. under dynamic loading, temp. and impurities influence 2-43696
Mo, neutron irrad., rel. to stress induced ordering of stage I defects 2-64654
Mo, polycrystalline, role of impurity atmospheres in brittle fracture 2-71587
Mo, single crystals, influence of surf. states and Ti coatings on dislocat. struct. 2-83969
NaCl whiskers inelastic phenomena 2-80575
NaF, vibr. depend., dislocation-point defect interaction, 4.2-295 K 2-71554
Na_2O-K_2O-SiO_2 glass, rel. to Na and K self diffusion 2-50712
Na_2O-SiO_2 glass, ion-exchanged, effect of water 2-53791
Nb-Zr alloys, peaks due to nitrogen impurity 2-60849
Nb, diffusion of hydrogen, anelastic obs. 2-77616
Nb, in normal and supercond. states 2-77635
Nb, vibr. freq., damping, β-process, 20-170°C 2-56778
NbH_x, α-peak interpret., acoustical loss mechanism, kink generation on dislocations 2-77645
Ni, containing H, effect of relax. and trapping of dislocations 2-53792
Ni, shear strain amplitude depend. 2-78028
Ni steels, 40N25, 60N20 and 80N15, amplitude-dependence after thermomech. treatment 2-84076
Ni_4Mo, rel. to dislocation density 2-43670
Pb:Au, relaxation effects 2-68069
β-PdH, temp. depend., peak interpret., 4-200 K 2-77646
Ta, Snoek effect absence for H 2-77647
WC-Co cemented carbide, recovery obs., dislocation config. 2-68070
Zr-H(O) dil. alloys, peaks due to interaction of substitutional and interstitial atoms 2-50737
Zr and Zr-O alloy, strain ageing study 2-47599
liquids *see Liquids; Viscosity/liquids*
Internal stresses *see Stresses, internal*
Internuclear double resonance (INDOR) *see Nuclear magnetic resonance and relaxation*

Interplanetary magnetic fields
anomalies in lunar wake 2-62730
cosmic ray diurnal effect correls. with equatorial anisotropy 2-62396
critical component, rel. to diurnal geomagnetic field variation at polar caps 2-62385
cycle vars., annual and solar magnetic, of inferred field 2-78572
direction, effect on magnetospheric structure and low energy electron fluxes 2-65858
direction, rel. to polar cap magnetic variations 2-62728
direction changing, effect on auroral morphology 2-81716
discontinuities, tangential and rotational, orientation in space 2-62737
effect on propagation of flare generated interplanetary shock waves 2-66119
field direction rel. to high-latitude ionospheric currents 2-68966
flare induced shocks and corotating streams, sources of geomagnetic storms 2-62723
fluctuations, correlation with trapped particle redistribution 2-65925
Forbush decrease, March 1966, and discontinuous struct. 2-62393
galactic cosmic ray modulation 2-62458
geomagnetic trail, possible crossing at 3000 earth radii by automatic interplanetary station, Mars-3 2-75623
interaction with Moon, effect of boundary condition asymmetries 2-51816
large-scale, mapping from multispacecraft solar wind data 2-62729
lunar wake in solar wind flow, magnetic-field anomalies 2-69134
magnetospheric interconnection, rel. to geomagnetic activity 2-51659
MHD discontinuities, statistical properties 2-62738
nonlinear interaction with galactic cosmic rays 2-48653
orientation, rel. to nonuniform structure of Earth's bow shock 2-65847
pitch angle distrib. of particle fluxes, calc. method based on rocket and satellite data 2-72825
polar cusp depend. on N-S field component 2-65874
polarity, determination from geomagnetic obs. 2-66194
polarity distribution, rel. to active longitude persistence for metric continuum noise sources 2-58545
proton injection onto field lines, relation to times and positions of solar radio bursts 2-62759
reconnection of lines of force with geomagnetic tail 2-72907
reconnection rate with geomagnetic field meas. using interplanetary solar particle discontinuities 2-62727
sector structure at solar maximum 2-66120
sector structure during sunspot cycles 2-78571
soft electron zone depend. on field direction 2-65903
rel. to solar mag. field (1969) 2-75937
solar particle event configs. 2-62774
solar proton access effects during interplanetary field section boundary crossing 2-62767
solar proton polar cap structs. during passage of interplanetary discontinuities 2-62766
solar wind, relative role of limiting factors 2-73129
spectral power density variations in frequency range 1 to 10^{-4} Hz 2-72905
spiral, model of collisionless solar wind in 2-66207
structure, relationship to development of polar magnetic storms 2-66006
turbulent, heat cond., applic. to solar wind electrons 2-66220
variations and substorm activity 2-66012

Interplanetary matter
cluster growth in space and particles bonding 2-58539
co-rotating struct. obs. using radio star intensity scintillation technique 2-62726
Coal Sack, southern, formaldehyde absorption 2-69042
colliding plasmas, e.m. instability 2-60213
cosmic dust, reliability of data from Pioneers 8 and 9 2-62732
cosmic-ray electrons in 3 to 12 MeV range, temporal variations 2-66192
diffusion model of solar cosmic radiation through interplanetary medium 2-75974
dust, heavy ions, evaporation 2-66121
dust in deep sea sediments 2-73101
dust particles, Pioneer spacecraft, astronomical interpretation 2-78573
electron component, 200 keV, source models 2-81929
electron component from 18 keV to 1.8 MeV during solar quiet time 2-78496
electrons, from coronal site of type III burst 2-62758
electrons and dust densities in solar system rel. to F and K components of solar corona 2-62803
flare induced shocks and corotating streams, sources of geomagnetic storms 2-62723
Forbush decreases in spaces 2-62394
high energy electrons from solar flares rel. to propagation conditions in interplanetary space 2-55190
hyperbolic microparticles, analysis of data from Pioneer cosmic dust sensor 2-62733
interstellar gas in Solar System in direction of solar apex 2-85006
interstellar HI and HeI in solar system, backscatter of solar resonance radiation 2-55078
jet stream formation rel. to solar system development and Bode's Law 2-66140
macrostructure, correlation with tropospheric circulation 2-44704
MHD waves, oblique nonlinear, correlation with local solar wind plasma density fluctuations 2-62784
modulated, cosmic rays, idealized model for radial gradient in interplanetary medium 2-66191
plasma, monochromatic radio propagation 2-55601
plasma irregularities rel. to small scale diameter radiosources scintillation spectra 2-58408
proton injection onto field lines, relation to times and positions of solar radio bursts 2-62759
quiet-time electron increases rel. to outer solar system modulating mechanism 2-66193
radio scintillation observations, power spectral analysis of intensity fluctuations from discrete sources 2-54898
radio wave propagation, Venera-7 data 2-55151

Interplanetary matter continued
radiosource scintillation, theoretical study of higher moments 2−85029
radiosource scintillations, obs. of higher moments 2−85028
scintillation, Besselian spectral analysis 2−62724
scintillation at 74 MHz 2−66122
scintillation of radiosources, power spectrum, solar wind obs. 2−66205
scintillation studies at Molonglo radio observatory 2−62725
shock, interaction with Earth's bow shock 2−62294
shock normals, thermal anisotropy influence on best-fit estimates 2−62739
shock wave, solar-flare associated, fine structure obs. 2−62736
shock wave thickness 2−62734
shock waves, flare generated, effect of interplanetary mag. field on propagation 2−66119
shock waves, Pioneer 8 obs. near 1 a.u., interpretation 2−62735
shock waves, rel. to closed mag. structs. in solar wind 2−66219
shock waves, role of gasdynamic processes in transfer of solar material in solar system 2−81899
shock-wave ensemble caused by solar flare 2−69177
solar activity delays, effect on solar-terrestrial space processes 2−85031
solar electron and proton content during solar particle event 2−65842
solar nebula, low temp. condensation accretion process rel. to planetary formation 2−44903
solar wind, relative role of limiting factors 2−73129
H and He bulk speeds in solar wind, interplanetary shocks 2−62764
H distribution, extraterrestrial Lyman α radiation distribution 2−62731
H_2 Lyman-α obs. 2−65856
He^+ ion flux in solar wind rel. to intensity of resonantly backscattered HeII solar radiation at 304 angstroms 2−55157
Hi atoms flux in solar wind rel. to intensity of resonantly backscattered Lyman α radiation 2−55157

Interstellar magnetic field
cosmic ray propagation, diffusion by galactic mag. field 2−81761
cosmic ray source location on galactic mag. field lines, rel. to anisotropy 2−72961
dust grains, alignment and orientation rel. to magnetic field and gas 2−78477
metagalactic, evidence from radiosource obs. 2−51690

Interstellar matter
see also H I regions; H II regions; Interstellar magnetic field
albedo of particles det. from reflection nebulae 2−75794
aligned grains, circular polarization 2−69110
average interstellar radiation density calc, 1250-4250Å 2−75796
black hole accretion of gas and emergent radiation spectrum 2−75661
carina spiral features, structure and motions 2−72970
circular polarization in Crab Nebula direction 2−69111
circumstellar shells with SiO_3 excesses, i.r. spectra 2−51742
cloud formation in cooling medium 2−51767
clouds, molecular astronomy obs. 2−75788
cold HI clouds with hotter possible inter-cloud medium, high resolution obs. 2−58244
colour excess in Carina-Centaurus region, photoelectric UBV observations 2−73038
cosmic matter-antimatter annihilation in universe and γ-ray background spectrum 2−69004
cosmic plasmas, nonlinear dissipation of Alfven waves 2−75784
damping of spiral density waves by induced shocks 2−81827
dark clouds, density of H_2 molecules 2−75786
dark dust clouds, 21 cm line obs. 2−81826
diffuse absorption bands obs. from reddened B supergiant spectra 2−58361
diffuse interstellar absorption feature, λ4430, polarization obs. 2−44854
diffuse interstellar features in stars with circumstellar dust shells 2−84992
dust, det. of distances to planetary nebulae 2−58236
dust, presence of trivalent transition- metal ions 2−81848
dust clouds, mm wavelength molecular line obs. 2−75825
dust clouds in the Large Megallanic Cloud 2−58248
dust grain origin of cosmic ray air showers 2−55886
dust grains, alignment and orientation rel. to magnetic field and gas 2−78477
dust grains, and neutral atoms, effect of radiation pressure round stars 2−48730
dust grains, cosmic ray electron bombardment, contrib. of transition radiation produced to diffuse-X-ray background 2−51778
dust grains, diffuse galactic f.u.v. radiation 2−75668
dust grains, radiation-driven efflux and circulation in spiral galaxies 2−81802
dust particles, grain mass and protonic accretion 2−44847
electron density, mean-square, in galactic disk and early type stars 2−44836
e.m. wave dispersion phenomena 2−48734
extinction in Carina-Centaurus region, photoelectric UBV observations 2−73038
extinction laws in spiral arms and field regions 2−84980
formaldehyde in dark nebulae, 2 cm isotropic background radiation absorption 2−75789
formaldehyde in direction of Cygnus X-3, 6 cm. obs. 2−81849
as fuel for ramjet type space vehicle 2−48613
furan, 6 cm search, in galactic sources 2−48725
galactic diffusion coefficient rel. to extragalactic cosmic rays and production of light elements 2−55003
galactic supernova remnants, 80 MHz emission absorption 2−69089
gas, effect on continuum spectrum of radiosource 3C391 2−58390
gas ejection from active nuclei of galaxies 2−48664
gas motions in galactic spiral arms, review 2−58183
gas surrounding Sco X-1, ionization 2−73054
grains, alignment, momentum exchange between small particles and light 2−62596
grains, twisted alignment causing stellar obs. polarization 2−73002
H I clouds, heating by u.v. photoemission from grains 2−58351
heavy element content, effect of infalling matter 2−55015
Heiles Cloud 4, mm wavelength molecular line obs. 2−75825

Interstellar matter continued
high-velocity interstellar H I up to high galactic latitudes, survey 2−58355
IC 410, linear filaments of diffuse nebulosity rel. to stellar winds 2−58363
imidazole, 6 cm search, in galactic sources 2−48725
interstellar H_2 and H and He fluxes from planetary nebulae 2−78448
ionized by supernova 2−58365
law of interstellar extinction, influence of surface roughness of grains 2−84972
light propagation, theory 2−79332
local condition, influence on star formation 2−58279
Lyman-α interstellar equivalent widths in OB-stars, Mariner 9 observations 2−58362
Magellanic clouds, electronographic photometry of NGC 2257 2−48722
molecular clouds near galactic centre, kinematics 2−58180
molecule formation by association reactions 2−44884
molecule formation via negative ions 2−58357
molecules, abundances 2−51779
molecules and dust in Ophiuchus cloud and total-to-selective extinction ratio 2−75793
molecules in dense clouds of H_2, emission and absorption of spectral lines, numbers, densities, isotopic abundances 2−75799
Monoceros field, obscuring matter 2−78473
near resonant charge transfer processes at thermal energies 2−58353
neutral H clouds, optical depths, by polarization techniques 2−58352
organic molecules and their chemistry 2−78476
partially ionized interstellar cloud, microwave observations 2−81807
phase transition, spiral arm density wave, star formation 2−62591
photoelectric meas. of 6284 Å diffuse interstellar line 2−58367
plasma, dispersion of longitudinal electric waves rel. to photon rest mass 2−55073
plasma, electrostatic l.f. waves, negative press. effect 2−46773
Pleiades, circumstellar molecules, observation of CH^+ line 2−58354
polarization, wavelength dependence in direction of zeta Oph. 2−58366
polarized 10μ radiation from cool stars with circumstellar shells 2−51743
profiles of diffuse interstellar lines 2−48728
radio recombination lines, giant H II regions 2−66068
radio recombination lines and low energy cross sections for transitions between highly excited states of atoms 2−46405
radioastronomy spectral lines and information on interstellar and galactic matter 2−66124
recombination line emission from galactic ridge, excess H II regions 2−66123
reddening curve, absorption feature at 2200 angstroms 2−55071
reddening effects near North Galactic Pole, observations of B-, A-, and F-type stars 2−84993
reddening law, wavelength dependence in u.v. for BO stars 2−58292
reddening within 200 pc of Sun 2−69112
research development in interstellar absorption during 1900-30 period 2−81842
rotating and expanding ring of gas 2.4 kpc from galactic centre 2−44886
rotating cloud, collapse, formation of multiple stars 2−48733
scattering effects on apparent size of masers 2−75787
scintillation pattern of PSR 0329+54 2−66130
self gravitating gas cloud, effect of tangential shippage on hydromagnetic stability 2−55077
self gravitating nonrotating gas layer, with stellar, magnetic and cosmic-ray components, stability 2−51777
Sharpless 157, diffuse nebula, exciting star and spectra of bright knot inside 2−55020
solar wind interaction, model 2−51853
space, absorption of longitudinal electric waves and photon rest mass 2−62595
spectral distrib. of amplified spontaneous emission 2−45695
structure and stability of shocks in two component medium 2−75797
thioformaldehyde, laboratory characterization by microwave techniques and detection in space 2−44888
third thermally stable phase 2−78475
transition radiation from passage of relativistic charged particles through interstellar grains as source of cosmic X-rays 2−48726
two component model of local region of the Galaxy 2−75672
u.v. stars effects on interstellar medium 2−75716
X-ray attenuation 2−62594
B, possible production by low energy cosmic rays 2−62593
B production by cosmic rays 2−84970
Be, possible production by low energy cosmic rays 2−62593
Be production by cosmic rays 2−84970
C, abundance det. from u.v. stellar spectra 2−58359
C I, C II and C III, ionization structure 2−81829
C I, effect of radiation pressure round stars, galactic evolution 2−48730
CH abundance discussed with reference to Franck-Condon factor measurements 2−44887
CH^+ abundance discussed with reference to Franck-Condon factor measurements 2−44887
CH^+ molecules, interferometric obs. 2−75798
CN, detection of 1.32 mm background radiation in spectrum of Ophiuchi 2−48736
CO, collisional excitation, particle densities 2−66115
CO, SiO, CS, H_2 and HD lines in interstellar spectrum of ξ Persei 2−81836
CO molecular lines in interstellar spectrum of Ophiuchi, equivalent width measurements 2−55072
CS molecular lines in interstellar spectrum of Ophiuchi, expected equivalent width calculations 2−55072
$^{12}C/^{13}C$ ratio in CH^+ molecules towards various stars 2−48731
$^{12}C/^{13}C$ ratio obs. at 4232 Å 2−73039
$^{12}C^{32}S$, $^{12}C^{34}S$, $^{13}C^{32}S$, $^{12}C^{33}S$, isotopic abundance ratio and CS optical depth 2−75791
Ca II, interstellar line in supernova spectrum in NGC 5253 2−81828
CaI lines, photoelectric obs. and CaI/CaII ratio 2−78474
Co II lines in southern sky, comparison with 21 cm absorption line 2−75795
D production by cosmic rays 2−84970

Interstellar matter continued
Eu I, effect of radiation pressure round stars, galactic evolution 2−48730
Fe I, effect of radiation pressure round stars, galactic evolution 2−48730
H, angular distrib., columnar density obs. using 21 cm radiation 2−81837
H atoms, volume density within 500 pc of sun 2−55074
H I, effect of radiation pressure round stars, galactic evolution 2−48730
H self absorption in large region toward galactic centre 2−44885
H_2, Lyman band absorptions, equivalent widths 2−56170
H_2, molecular formation on ice and solid CO, physical adsorption energy 2−55076
H_2, velocity structures and streaming 2−58364
H_2 Lyman band lines in interstellar spectrum of Ophiuchi, expected equivalent width calculations 2−55072
H_2 mol., highly excited electronic levels, radio band 2−48732
H_2CO molecule, obs. of 4830 MHz in direction of discrete radio sources 2−69109
HI in solar system, backscatter of solar Lyman α 2−55078
HNC 3-306 mm line identification 2−58360
HNO, microwave spectrum, laboratory obs. 2−50034
H_25, obs. at 168.7 GHz 2−66118
He I, effect of radiation pressure round stars, galactic evolution 2−48730
HeI in solar system backscatter of solar line at 584 angstroms 2−55078
^3He production by cosmic rays 2−84970
Li, possible production by low energy cosmic rays 2−62593
Li production by cosmic rays 2−84970
^{15}N and U169.3 methanol line in Orion A i.r. nebula 2−66135
Na I, interstellar line in supernova spectrum in NGC 5253 2−81828
Na^o/Ca^+ ratio interpretation, model of clouds 2−75785
O_2, abundance det. from u.v. stellar spectra 2−58359
OH, amplified spontaneous emission 2−55075
OH, excited potential states, thermal and maser emission obs. 2−75790
OH, interferometric obs. of $^2\pi_{3/2}$ $J=5/2$ microwave transition 2−75792
OH, interstellar, excited potential states, thermal and maser emission obs. 2−75790
OH abundance in intercloud medium, upper limits in high-latitude directions 2−81817
OH emission regions, apparent size reduction 2−58356
OH in direction of Cygnus X-3 18 cm. obs. 2−81849
OH masers, parametric down conversion 2−62590
OH molecule, pumping by polarized i.r. radiation, maser emission 2−81851
OH radiation, models 2−62592
Si, abundance det. from u.v. stellar spectra 2−58359
SiH^+ abundance discussed with reference to Franck-Condon factor measurements 2−44887
SiO, detection of $J=2\rightarrow1$ rotational transition 2−58358
SiO, in Sgr B2 and Ori A, at 87 GHz 2−48745
SiO molecular lines in interstellar spectrum of Ophiuchi, expected equivalent width calculations 2−55072

Interstitials *see Crystal imperfections/interstitials*

Invariance (CP, CPT) *see Elementary particles/symmetry*

Iodine
absorption filter for reduction of parasitic light in Raman and Brillouin spectroscopy 2−52471
atomic stopping cross sections of α particles by application of Bragg additive rule to molecular stopping cross sections 2−70820
doped polyethylene films, elec. cond., form of current transients 2−64994
doping in polyethylene, h.f. Gunn domains 2−57202
fluorescence, laser induced line narrowing 2−74267
ions, charge states 2^+ to 18^+, meas. of charge-changing cross sections in H and O, 5-25 MeV 2−70623
ions, hyperchannelling in Au and Ag, orientation rel. to intensity and energy loss 2−47778
laser, photochem., energy transfer obs. 2−55693
laser, photochem., kinetic processes 2−52440
laser induced fluorescence line narrowing 2−48241
liquid, surface tension 2−71175
molecular beam spectra excited by 5145 Å Ar ion laser 2−67486
molecular vapour, optically pumped, stimulated emission and laser action 2−49369
molecular vapour excited by Kr ion laser, transitions assignment 2−80016
molecule, angular scattering of superthermal K atoms 2−42787
molecule, Raman resonance, effect of excitation freq. on overtone intensities 2−56182
molecule, reactive collision cross section with Cs 2−70738
molecule, saturation microscopy by intermodulated fluorescence 2−67502
molecule, thermal decomp. in inert gas, diffusion theory approach 2−80059
solubility and diffusion, in Ag_4RbI_5, electrochemical cell obs. 2−84657
solubility in benzene-cyclohexane mixtures 2−43333
vapour, 5145Å excited anti-Stokes resonance Raman spectra, vibrational-rotational structure 2−77086
vapour, reson. Raman scatt. change to reson. fluoresc., intensity distrib. 2−67485
vapour, vibr.-rot. struct. in reson. Raman effect 2−80037
vapour light source, photon no. and lifetime 2−55776
AgCl:I-, decay mechanism of bound exciton, luminesc., 4.2-80K 2−72392
He-I_2, inelastic non-reactive energy transfer, calc. and analysis of probabilities and cross sections 2−60116
He-I_2 mixture, cw laser oscillation of singly ionized I_2 2−69923
I_2-He, electronegative gas laser discharges, characteristics of system 2−71016
I_2-He mixture, interaction of dissoc. and vibr. relax. behind shock wave 2−77168
I-, accurate analytical wave functions 2−42733
I II, to CW laser action at 6127 Å 2−45738
I IX, e.u.v. spectra, energy levels 2−64001

Iodine continued
I_2, absorption spectra 2−76147
I_2, in aqueous CH_3I solns., (n, γ) reactions 2−81537
I_2, magnetic quenching of fluorescence excited by 6328 Å He/Ne laser 2−77085
I_2, rot. Lande factors in $B^3\Pi_{0(+)(u)}$ state 2−50049
I_2, spontaneous predissoc. 2−70710
I_2 double scatt. investigated with Glauber theory 2−42831
I_2 recombination in Ar using flash photolysis 2−80009
I_2 vapour excited by Ar ion laser, obs. of progressive change from resonance fluorescence to resonance Raman effect 2−56181
I_2 vapour laser, optically pumped, performance 2−42022
I_2^+, spin-orbit coupling 2−70709
I_2^{127} and I_2^{129} hyperfine structure near 6328 Angstroms by laser saturated absorption spectroscopy 2−46554
I_3^-, resonance Raman effect laser excited, vibration enhancement 2−80007
I_3^- Raman spectrum resonance laser excited spectrum 2−79998
^{125}I radiology, bone mineral content, in vivo measurement 2−69313
$^{127}I_2$,$^{129}I_2$, hyperfine interactions in optical transitions 2−50050
^{131}I-triolein excretion test for steatorrhoea using unabsorbed radioactive marker 2−69267
^{131}I, normal take-up by humans 2−66257
^{131}I labelled triolein, absorption test for fat balance obs. in man 2−45029
^{131}I monitor for nuclear plants 2−67364
$I+Ar\rightarrow IAr$, equilibrium constant 2−80009
I_2+H_2, dynamics of mol. and atomic exchange reaction 2−51423
InSb-I_2 system, gas transport reactions, whisker growth, morphology 2−75366
ion-Au, Th, U collisions, 10 to 60 MeV, X-ray spectra of temporarily formed superheavy quasiatoms 2−74236
ion channelling in Ag at 21.6 MeV, axial phenomenon 2−44007
$K+I_2$ reaction, exoergic, product state distrib. and temp. concept 2−68761

Iodine compounds
iodide, charge-transfer- to-solvent absorpt. bands in far-u.v. 2−56505
AsTeI glass, electronic transport props. 2−61296
$Cl+IBr\rightarrow ClI+Br$ or $\rightarrow I+ClBr$, quantum mech. model calc. 2−65366
Cr-I system, phase diagram and phase identification 2−71701
glass, As-S-I, viscosity in transition region 2−84049
I-S-Sb-Ge glass system, glass forming regions 2−80533
ICl, dipole moment by Stark effect meas. 2−42902
ICl interhalogen, vacuum u.v. spectrum 160-130 nm obs. of Rydberg transitions 2−83272
IF_7, nonrigid D_{5h} molecule, vibrational assignment from i.r. and Raman spectra 2−42901
IFe, Mossbauer expt., meas. of magnetic moment of 57.6 keV state of ^{127}I, and hyperfine field 2−49747
IO, electron resonance spectra in $J=5/2$ rotational levels 2−46530
IO_3^-, vibrational spectra and force constants 2−59996
Sb-Se-I-R-H_2O system, R=solvent=HI, HCl, Na_2Se, hydrothermal crystn. process, 300-450°C 2−74682

Ion beams
see also Energy loss of particles; Ion optics; Mass spectrometers; Particle accelerators; Sputtering
— 2−60296
beam-plasma system, instability control 2−74403
bunching, double gap klystron, obs. of working range 2−45688
channelling, stopping power, position depend. 2−44014
channelling patterns recorded with heavy radioactive ions 2−61121
cluster injection into D-T mirror fusion power system 2−64262
collection techniques, prep. of nuclear materials laboratory type isotope separator 2−73917
collective ion acceleration by intense relativistic electron rings 2−55942
cyclotron, auxiliary monitor using proton reactions with Cu 2−70334
cyclotron, excited state lifetime obs. in 300 nsec range 2−70311
cylindrical electron-ion beam, self focusing, stationary state 2−63273
density distrib. of accel. particles, meas. 2−59112
for electron emission microscope 2−79004
electrostatic gun for specimen thinning, design and operation 2−79102
heating of confined plasma causing electrostatic instabilities 2−43187
high current, large area, production 2−63299
high current, with laminated flow, extraction from duoplasmatron 2−55673
high energy, props. for radiotherapy 2−69274
instability of two-ion-beam, meas. of self-stabilisation by microturbulent ion heating 2−43195
linear stability in ferromagnetic channel, kinetic equation 2−63283
medical heavy ion beams, composition 2−69321
metal single crysts., low energy ion refl., energy and angular distribs. 2−67895
metastable state population det. by beam attenuation method 2−59113
microprobe, tuning using Sc thin film targets 2−45691
monitor for nanoampere currents 2−73537
nuclear research material prep. with isotope separator 2−49335
plasma, patent 2−41935
plasma, positive and negative beams, nonlinear effects 2−80344
plasma-beam system, in longitudinal mag. field, drift-beam instability 2−80345
polarized, production and applic. 2−73536
polycrystalline solids, backscatt. of keV ions, Monte Carlo calc. 2−77792
production by electron cyclotron resonance plasma accelerators 2−60253
scattering, multiple, by C and Ge foils 2−47781
scattering, multiple, of 300-1000 keV ions with $1\leqslant Z\leqslant 18$ by Au foils 2−47779
scattering by metal surface, dynamic screening effects 2−64892
scattering from crystals, angular distributions 2−75005
scattering of low energy ions, surface analysis technique 2−47072
scintillation efficiency for random and heavy channelled ions at intermed. vels., track-account theory 2−70316

Ion beams continued
semiconductor technology applications 2−61371
slowing down spectra of secondary electrons 2−75006
solar wind, interpenetrating beams 2−66221
sputtering, application to production of insulators and semiconductor layers in microelectronics 2−58667
stopping power of media, effective charge 2−54097
stopping powers of solids for 30-90 MeV ions 2−47773
thinning machine, obs. of faceted structures formed on Ag-Zn crystals 2−79103
thinning of cylindrical objects for t.e.m. 2−79104
trajectories in omegatron, influence on non-uniform r.f. field 2−59650
Ar^{+}, optical spectra Zeeman splitting 2−70577
Ar^{18+}, accelerated to 1.17×10^{10} eV, Princeton synchrotron accelerator 2−79701
Au, beam foil spectroscopy, search for channelling effect 2−80930
Au, Xe ion penetration 2−61124
Au film, low temp. migration of Cr, backscatt. obs. 2−56754
C, multiple scattering in solid, anomalous Z_1 depend. of interaction potential 2−77794
Cs, neutral atom rate meas. 2−53207
Cs low energy traversing Cs plasma 2−43112
Cs^{+} sputtering ion source for mass spectrometer 2−69885
Cu, range of energetic Xe ions 2−61126
H^{+}, backscatt. by Si and graphite surfaces, impurity and disorder obs. 2−77485
H_2 from microwave ion source 2−69884
He^{+}, channelling in Si:B, impurity lattice location 2−60819
$^{4}He^{+}$, backscatt. by Si and graphite surfaces, impurity and disorder obs. 2−77485
N, high energy, production at Bevatron of California Univ. 2−70319
N ion beam at 3.9 GeV, meas. of physical and radiobiological parameters 2−69425
N^{+}, det. of metastable state population 2−59114
Nb, backscatt. of H^{+}, Ne^{+}, Ar^{+}, energy and ang. distrib. 2−50467
Ne^{+}, 600 eV, backscatt. by Ni surface, chain effect 2−77484
Ni surface, multiple scatt. of low energy noble gas ions 2−50458
Ni with adsorbed O, He^{+} backscatt. study 2−50543
O^{+}, optical spectra Zeeman splitting 2−70577
O_2, ion beam, from Bevatron, depth dose characteristic 2−69404
Si:B, ion implanted lattice disorder distribs., He ion channelling analysis 2−68036
Si, dechannelling of 7.15 MeV He ions 2−61120
Si overlaid with Al and Au films, channelling 2−54094
U ions, charge states in emergent beams from solid foils, 29.2 - 45.7 MeV 2−49971
W, backscatt. of H^{+}, Ne^{+}, Ar^{+}, energy and ang. distrib. 2−50467
W surface, low angle scatt. of 275 keV He^{+} ions and surface channelling 2−80929

effects
amorphous target, range profiles, damage distribs. 2−47776
cross sections for excitation of Ar II laser lines in electron-ion collisions 2−69954
crystal, calc. of atom collisions and trajectories 2−74795
crystalline solid, backscattering and channelling of high energy He^{+} ions 2−77791
defects, formation and annealing during bombardment with Kr ions 2−71461
diamond, radiation damage, review 2−47371
etched $A^{II}B^{VI}$ compounds, surface structure, scanning mode obs. 2−64540
films, bombardment and implantation effects 2−53568
fractional cell survival rel. to depth of tissues exposed to high energy ions 2−69330
fused quartz, refractive index and optical loss variations 2−50688
glass, polishing 2−50444
graphite, production of electron spin centers, e.s.r. obs. 2−78152
heavy ion radiation damage of metals, 'in situ' expts. in electron microscope 2−74756
heavy ions, channelling, abnormal stopping power in low velocity region, from Firsovs theory 2−68268
heavy ions, charge states and charge changing cross sections for penetration through gaseous and solid media, review 2−60294
implantation, mass depend. of crit. amorphizing dose, calc. 2−56677
inert gas ions, sputtering and energy losses on glass 2−61123
lattice disorder profiles determ. by nucl. backscatt. 2−53689
machining of diamond 2−50811
metal, He migration and release after implantation 2−50639
metal, irrad., void formation 2−47361
metal, radiation- induced void form. 2−50638
metal, surface plasmons, collective mode excitation 2−51087
metal, void form. during bombardment, neutron damage simulation 2−53692
metal, void prod. by high-energy bombardment, neutron damage simulation 2−53693
metal crystals, effect of ion bombardment on surface roughness 2−74614
metal/SiO_2 cermet film, produced by recoil atom implantation 2−53578
metallic materials, void nucleation during high-energy irrad. 2−53703
plasma longwave instability 2−74401
plasma wave field excitation, electron capture 2−70951
polyethylene foil, degradations induced by ion bombardment and partial discharges 2−44148
radiation damage study by Mossbauer effect 2−50631
sapphire, ion beam polished, increased laser surface damage threshold obs. 2−57317
semiconductor, implantation induced lattice disorder 2−47367
semiconductor doping, lattice damage prod. 2−47374
solid, destruction by heavy ionizing particles, electronic subsystem excitation 2−68014
solid target, secondary electron spectra, Auger electrons and surfsce plasmon characteristic losses 2−51229
sputtering, for etching, in solid state device manuf. 2−43458
sputtering, substrate currents 2−58668
steel, nitrided by N-ion bombardment 2−56935

Ion beams continued
effects continued
steel, stainless, deuteron generated void form., in-reactor damage simulation 2−53714
steel, stainless, proton- and nickel-irrad., void form. 2−53715
steel, stainless, void nucleation and growth obs. using h.v. electron microscpe irrad. 2−53694
surface topography during ion bombardment, computer simulation 2−60619
vacuum gap conditioning 2−67694
void formation in reactor materials, study using accelerator simulation 2−76922
Ag, He-ion damage, energy depend. 2−50643
Ag, radiation damage, nature and annealing characts. 2−47368
Al, calc. of ^{85}Kr implantation profile 2−74795
Ar^{+}, 5-30 keV, correlated successive collisions on Cu, Ge, Si, ion scatt. processes 2−47775
Ar^{+}, irrad. of semicond., cond., noncond. targets, secondary ion emission 2−48029
Ar^{+} interacting with surface, obs. of mass spectrum 2−79849
Au, channelling effects on transmission of MeV H_2^{+} ions through thin single crystals 2−44011
Au, He-ion damage, energy depend. 2−50643
Au, radiation damage, nature and annealing characts. 2−47368
Au bicrystal, rel. to g.b. disloc. climb, elec. microscope obs. 2−56731
C amorphous, ion irrad., nuclear ion-atom interactions, Z_1 oscills., non-evidence 2−47780
C ions, stopping powers in Cr, Fe, Co, Ni, Cu, Zn 2−47782
C^{+}, irrad. of Si for prod. of SiC heterostruct. film 2−50504
CdTe, ion implantation doping 2−74790
Cu, Ar^{+} and Ne^{+}, angular and temp. depend. of sputtering 2−51064
Cu, foil, heavy ion irrad., rad. damage, electron microscope 2−43608
Cu, H ion induced electron emission from (001) and (011) faces 2−75199
Cu, radiation damage, nature and annealing characts. 2−47368
Fe, cast, ion beam thinning, graphite/pearlite interface microstructure, electron microscopy 2−74877
GaAs:Ar, Te implanted, radiation damage, elec. microscope obs. 2−60821
GaAs, implantation lattice disorder, low temp. channelling obs. 2−47373
n-GaAs, luminesc. from implanted Zn ions 2−48222
GaP, 40 keV Te implantation damage and annealing 2−80706
GaP, Ar^{+} 40KeV ion bombardment, energy distrib. of secondary electrons 2−72097
Ge, bombardment induced disorder, annealing 2−43466
Ge, irrad. induced damaged region form. 2−47384
Ge crystal, irrad., amorphization dose, temp. and atomic number depend. 2−80685
InP, Ar^{+} 40KeV ion bombardment, energy distrib. of secondary electrons 2−72097
InSb, bombardment induced disorder, annealing 2−43466
Ir, implantation, field ion microscope obs. 2−56741
Ir, implantation, field ion microscope obs. 2−56740
KBr, ion bombardment, mass spectrometer obs. of sputtering and ion emission 2−71765
KBr, solubility and mobility of He, implantation effects studies 2−84002
KCl, diffusion of ion-implanted ^{85}Kr, effects of radiation damage 2−68053
LiF, excited particle velocity spectrum, Ar-ion bombardment, energy level struct. obs. 2−48030
$LiNbO_3$, thinning by ion etching for acousto-optic deflectors 2−63417
MgO, MeV Ne^{+} irrad., F-type centre prod., absorpt. band obs. 2−68042
Mo, irrad., surface damage, LEED obs. 2−50468
Mo, irrad., void lattice obs. 2−53720
MoO_3, bombardment enhanced elec. cond. 2−68408
MoO_3, ion impact effects on electrical conductivity 2−60779
N ions, stopping power in Cr, Fe, Co, Ni, Cu, Zn 2−47782
NaCl, damage, backscatt. obs. 2−43611
NaCl, excited particle velocity spectrum, Ar-ion bombardment, energy level struct. obs. 2−48030
NaCl, La surface contamination, O ion induced X-rays obs. 2−60628
Nb_2O_5, ion impact effects on electrical conductivity 2−60779
Ni and alloys, void nucleation and growth obs. using h.v. electron microscope irrad. 2−53694
O ions, stopping power in Cr, Fe, Co, Ni, Cu, Zn 2−47782
O^{+} interacting with surface, obs. of mass spectrum 2−79849
Pb evaporated layers, oxidation by low energy O_2^{+} bombardment 2−61791
Pt, He-ion damage, energy depend. 2−50643
Si:As, He ion min. backscatt. yield variation obs. 2−60820
Si:O, lattice damage due to ion implantation, e.p.r. obs. 2−60780
Si:P, implantation damage annealing, resist. and electron microscope study 2−64678
Si:P, implanted, annealing characts. 2−77594
Si:P, implanted, carrier density and mobility, depth distrib. 2−80993
Si-ge alloy, He^{+} irrad., atomic displacements, Rutherford scatt. obs. 2−47388
Si, amorphous layer prod. 2−71456
Si, apparent damage induced optical absorp., scatt. from defect zones 2−48158
Si, bombardment induced disorder, annealing 2−43466
Si, calc. of ^{10}B implantation profile 2−74795
Si, He^{+} irrad., atomic displacements, Rutherford scatt. obs. 2−47388
Si, implantation, mass depend. of crit. amorphizing dose calc. 2−56677
Si, implantation damage and impurity location, channelling obs. 2−71511
Si, ion-implanted, radiation damage under channelling conditions 2−68017
Si, irrad., divacancy formation and annealing, i.r. absorpt. study 2−71457
Si, irrad. induced damaged region form. 2−47384

Ion beams continued
  effects continued
    Si, irrad. with 400 eV ions, surface damage, change in optical consts., ellipsometric obs. 2−47081
    Si, surface cleaning by ion irrad., ellipsometric obs. 2−47082
    Si single crystal, H_2^+ ion bombarded, bicrystal formation, X-ray obs. 2−47386
    α-SiC, residual lattice disorder due to ion bombardment 2−47391
    SiO_2, Au implantation rel. fabrication of floating gate devices 2−68458
    SiO_2 glass, irrad., surface topography 2−50462
    SiO_2 vitreous, radiation compaction mechanism 2−50410
    Ti, bombarded, X-ray Kα and Kβ spectra 2−57368
    Ti, excited particle velocity spectrum, Ar-ion bombardment, energy level struct. obs. 2−48030
    TiO_2, ion impact effects on electrical conductivity 2−60779
    U alloy, etching and scanning electron microscopy 2−56578
    V_2O_5, bombardment enhanced elec. cond. 2−68408
    V_2O_5, ion impact effects on electrical conductivity 2−60779
    W, foil, 60 kev Au ion irrad., dislocation loop prod. 2−43615
    W, foil, Au ion irrad., vacancy-type dislocation loop prod. 2−43616
    W, foil, Au ion irrad., vacancy-type dislocation loop, prod. 2−43616
    W, irrad., by He, lattice damage, interstitial diffusion 2−47394
    W, irrad., He entrapment at vacancies 2−50651
    W, irrad., surface damage, LEED obs. 2−50468
    W bombardment by alkali metal ions, secondary emission of W^+ 2−48031
    WO_3, bombardment-induced amorphization and mean damage rates determ. 2−77576
Ion counters *see Counters*
Ion emission
    in electron beam welding of metals 2−68144
    ion source emission meter 2−76464
    metals, field evaporation theory, Mie potential 2−72101
  secondary
    from electron bombarded solids, and mass spectrometer applications 2−75201
    ion-ion emission, mass spectrometric technique for studying processes on surface and in bulk of solids 2−61469
    polycrystalline, metallic and semiconductor, energy distribution and mean energy, Ar^+ ion bombardment 2−61470
    semiconducting, conducting and nonconducting targets, bombarded with Ar^+ 40 keV ions, comparative yields 2−48029
    transition metal, cleaned and oxidized surfaces, absolute yields 2−61471
    Ag/Ni film/substrate system, vacuum deposition study 2−50481
    Ag, acid-treated surfaces, absolute yields 2−61471
    (Al, Cu), influence of asymmetrical correlations 2−68502
    (Al, O), influence of asymmetrical correlations 2−68502
    Al, cleaned and oxidized surfaces, absolute yields 2−61471
    GaAs evaporation by laser, mass spectrometric analysis of ions in vapour 2−75409
    GaP evaporation by laser, mass spectrometric analysis of ions in vapour 2−75409
    KBr, ion bombardment, mass spectrometer obs. of sputtering and ion emission 2−71765
    LiF, excited particle velocity spectrum, Ar-ion bombardment, energy level struct. obs. 2−48030
    Mg, cleaned and oxidized surfaces, absolute yields 2−61471
    NaCl, excited particle velocity spectrum, Ar-ion bombardment, energy level struct. obs. 2−48030
    Ti, excited particle velocity spectrum, Ar-ion bombardment, energy level struct. obs. 2−48030
    W^+, from W, following bombardment by alkali metal ions 2−48031
  thermionic
    No entries
Ion exchange *see Exchanges, chemical; Ions, electrolytic*
Ion implantation
    critical amorphizing dose, mass depend., calc. 2−56677
    Cu:Mn giant e.s.r. transmission through one-sided and two-sided ion implanted Cu foil 2−84569
    diodes, mesa, planar, measurement techniques 2−71970
    films, implantation equipment 2−53568
    fused quartz, refractive index and optical loss variations 2−50688
    goniometer for implantation and channelling exprts. 2−74788
    implantation profiles determ. by secondary ion mass spectrometry 2−74794
    magnetic garnet films, hard bubble suppression 2−65163
    metal ion source 2−63301
    optical waveguide, fabrication, implantation in fused silica through electron resist masks 2−59268
    perturbed angular correlation method for determ. of heavy ion ranges and range straggling 2−68269
    semiconductor doping, lattice damage prod. 2−47374
    semiconductor technology applications of ion beams 2−61371
    semiconductors, ion gun 2−60812
    SiC film, prod. by irrad. of Si by C^+ ions 2−50504
    technology, specific features 2−74789
    (AgBr + AgCl(5%)):$C^{5+}(N^{5+})(O^{6+})(S^{6+})$ high energy implantations, Doppler broadening of positron annihilation photons 2−71507
    AgCl:$C^{5+}(N^{5+})(O^{6+})(S^{6+})$ high energy implantations, Doppler broadening of positron annihilation photons 2−71507
    Al films, Ar^+ bombardment, transmission sputtering and recoil implantation 2−54090
    GaAs, of S, junction form. 2−47429
    GaAs with Cd, residual bombardment disorder and atom location 2−60813
    GaP, 40 keV Te implantation damage and annealing 2−80706
    GaP, of S, junction form. 2−47429
    Ge, impurity atom diffusion enhancement by light ion implantation 2−60814
    Ge, of S, junction form. 2−47429
    KCl, diffusion of ion-implanted ^{85}Kr 2−68053
    Si:B, lateral spread of implanted ions, obs. by junction delineation 2−71508
    Si:In, ion implanted, photoelectromag. effect rel. to dose and annealing 2−72077
    Si:O, lattice damage, e.p.r. obs. 2−60780
Ion implantation continued
    Si:P, implanted, carrier density and mobility, depth distrib. 2−80993
    Si:P thermometers for 10 mK to 20 K 2−48938
    Si:P thermometers for 10 mK to 20 K 2−48938
    Si-SiO_2 interface, ion implanted, deep energy level detn. by m.o.s. technique 2−80938
    Si, B ions, self-consistent results for dechannelling mechanism 2−68036
    Si, crit. amorphizing dose, mass depend., calc. 2−56677
    Si, implantation damage and impurity location, channelling obs. 2−71511
    Si, impurity atom diffusion enhancement by light ion implantation 2−60814
    Si, ion-implanted, radiation damage under channelling conditions 2−68017
    Si, ion implanted, lateral strains, X-ray topographic obs. 2−80704
    Si, of B ions, channelling, depth distrib., computer simulation 2−47439
    Si, or B and P, channelling and anomalous diffusion effects on charge carrier distrib. 2−47432
    Si, radiation hardening of thermal oxides by displacement damage 2−50689
    Si planar technology 2−53747
    SiO_2 layers on Si, ion implant and annealing effects, ir abs. and ellipsometric meas. 2−74791
Ion microscopes
    see also Field ion microscopy
    atom probes, performance of electron multipliers 2−66723
    beam thinning machine, obs. of faceted structures formed on Ag-Zn crystals 2−79103
    field, Indian, construction and operation 2−59117
    field, liquid He vapour cooled, for vapour deposition obs. 2−66726
    field ion microscopy, development, applications to metallurgy, image form., construction operation 2−56643
    mass-spectra, magnification 150 times 2−59118
    microprobe, performance evaluation 2−63296
    microprobe mass analyzer, description of instrument 2−63298
    microprobe mass analyzer, microanalysis use 2−63297
    shadow effect in 3-dimens. crystal model rel. to channelling 2−71768
    sputtering, uniform, means for obtaining, in ion microprobe 2−71300
    tip field strength measurement using fragmentation of n-heptane ions 2−59119
    Si:B, ion microprobe analysis of implanted ion distribs. 2−64674
Ion mobility *see Ion velocity*
Ion optics
    see also Alpha-particle spectrometers; Ion microscopes; Mass Spectrometers; Particle optics.
    — 2−62368
    beam extraction from duoplasmatron 2−55673
    cyclotron beam transporting system design, ion optics principles utilization 2−55945
    collimating system for gas ion source 2−69883
    cyclotron resonance spectroscopy equations of motion for ion 2−70558
    electric hexapole, use as correction device for image curvature of optical instrument 2−45693
    electrostatic hexapole lens, third-order transfer matrix 2−59078
    electrostatic particle guide for time-of- flight spectroscopy of low energy ions 2−52402
    field-ion image formation, comments 2−69887
    image transfer by ions at atmospheric press. 2−79453
    magnetic analyzer, 270°, double focusing 2−52677
    mass spectrometer with magnetic dispersion field, patent 2−83167
    microprobe, performance evaluation 2−63296
    microprobe mass analyzer, description of instrument 2−63298
    microprobe mass analyzer, microanalysis use 2−63297
    quadrupolar focusing lens for heavy ion accelerator 2−42485
    quadrupole lenses, mag. and electrostatic, third order transfer matrices for fringing field 2−69886
    retarding potential analyzer errors due to pot. nonuniformities in grid planes 2−62366
    superconducting lenses, field distribution 2−45684
    toroidal condenser, electrostatic potential 2−52403
Ion pumps *see Vacuum pumps*
Ion sources
    see also Ion emission/thermionic
    back-diffusion type source of monoenergetic ions 2−45692
    compact polarized, atomic beam aspects 2−66725
    electrohydrodynamic, for mass spectrometry of liquids 2−74203
    electron cyclotron resonance plasma accelerators 2−60253
    for electron emission microscope 2−79004
    electron impact, spurious F^+ signals, source and behaviour 2−74200
    electron-ion generators, experimental study 2−63268
    electrostatic gun for specimen thinning, design and operation 2−79102
    emission meter 2−76464
    gun, semiconductor ionic doping 2−60812
    high vapour pressure metal, use in sputter ion pump 2−45193
    ion-mol. reactions, low energy, suitable source for their study 2−82458
    laboratory, low intensity for Ag, Au, Ni, Fe, Pt ions 2−55672
    laser ion source for mass spectrographic laser microanalysis of solids 2−82456
    low energy ion-molecule scattering apparatus 2−63302
    low energy with high current density 2−59115
    mass spectrometer, adapted to analyser 2−56084
    in mass spectrometer, patent 2−63991
    for mass spectrometer, patent 2−59890
    in mass spectrometer, stabilizer of current which heats tapes 2−56085
    mass spectrometers, optimal adjustment for isotope geology applic. 2−46398
    mass spectrometric analysis, corrosive gases 2−81555
    metal, electron beam bombardment of metal surface 2−41934
    metal, for ion implantation system 2−63301
    metal 2−76463
    multicharged phosphor ions, generation and acceleration 2−63300

Ion sources continued
multiple beam and wide beam 2−55671
multiply charged source, hot electron plasma heated by Lisitano coil 2−63303
patent 2−41935
Penning discharge for plasma diffusion studies 2−52401
Penning source, high power, for multiply charged heavy ions 2−49333
polarized beams production and applic. 2−73536
pulsed-field ion source in combination with mass spectrometers 2−59886
r.f., compact transistorized pulser 2−49332
thin film, production by r.f. sputtering 2−49334
triplasmatron, for negative and positive ion prod. 2−82455
H ions, microwave, construction, operation and principles 2−63299
H^-, h.f. source prod. without parasitic behaviour 2−79168
H^-, pulsed duoplasmatron source 2−79169
H_2 ions from microwave ion source 2−69884
$^{202}Hg^+$ collimating system for mass spectrometer, with distributed ionization region 2−69883
Li^+, exp. investigation 2−59116
N, high energy, production at Bevatron of California Univ. 2−70319
$^{14}N^+$, collimating system for mass spectrometer, with distributed ionization region 2−69883
$^{28}Ni^+$, collimating system for mass spectrometer, with distributed ionization region 2−69883
Zn ions, generation and acceleration 2−63300

Ion velocity
diffusion in gas, elec. field effects, relay race model 2−50224
drift tube, design and construction 2−70982
drift tube, variable length, ionic reaction meas. 2−60292
field dependence of gaseous-ion mobility, theoretical tests of approx. formulas 2−70984
joint ion-gas speed distribution, two temperature representation 2−70983
laser plasma, ion energy spectrum, rel. to accel. and recombination effects 2−53215
liquid, hydrodynamic determ. of ion mobility 2−71163
mobility of ions in parent gases 2−56383
multi-charge ions moving in an impulse discharge 2−50223
plane plasma capacitor in crossed fields 2−64304
roton-limited mobility in superfluid ^4He at temps. below 1.7 K 2−71259
streaming motion in laser produced plasma 2−80272
sub-thermal, spectrometer requirements 2−60293
transport phenomena in ionized gases, non-equilibrium thermodynamics kinetic theory 2−83701
Ar, photo-ion drift vel., diffusion coeffs. and temps. 2−64339
He, mobility of mass-identified D^+ 2−43203
He II, positive impurity ion mobility 2−60535
^3He-^4He dilute solutions, ion motion at ultralow temp. 2−47003
K^+, mobility in He II, ion-roton scatt. cross sections 2−67863
K^+ mobility in N, effect of clustering 2−67688
Kr multi-charge ions moving in an impulse discharge 2−50223
N, photo-ion drift vel., diffusion coeffs. and temps. 2−64339
$N_2{}^+$, positive ion drift velocities in high pressure discharge 2−74411
O, photo-ion drift vel., diffusion coeffs. and temps. 2−64339
O^-, $O_2{}^-$, $O_3{}^-$, mobilities and ion-mol. reaction rates 2−53248
O^{2+}, lateral diffusion in O_2 2−43204
Xe multi-charge ions moving in an impulse discharge 2−50223

electrolytic
see also Conductivity, electrical/liquids, electrolytic; Electrophoresis
Nernst-Planck eqns. for ionic diffusion at conditions near equil. 2−78198

Ionic conduction, solids
amorphous materials, rel. to high field conductivity 2−54168
crosslinked epoxy polymers, effect of free volume on electrical conductivity 2−57233
electrolytes, transport entropies 2−77961
glass, alkali-containing, model of electrode polarization by d.c. potential application 2−81141
hopping cond., freq. depend. 2−61270
ionic thermo currents, reciprocal heating scheme, current rel. to dipole reorientation enthalpy 2−72017
mixed conductors, polarization measurement methods 2−68464
polymer, temp. depend., struct. factors influence 2−72019
polymers, rel. to mechanical strain effect 2−57232
polymers under high pressure 2−74604
pyridinium salt, fused, specific cond. and n.m.r. spectra 2−72018
superionic conductors, properties 2−47977
triglycine sulphate, Curie pt. phenomena 2−77932
undergraduate research project, thermoconductivity in dielectrics 2−41437
Ag complex, $[C_5H_5NH]Ag_5I_6$, −63-129°C 2−43574
AgBr emulsion, latent image centres displacement 2−80723
AgCl, Frenkel defects, equilibr. conc. perturbation by microwave pulse, ionic cond. change 2−80698
AgCl, up to 25°C below m.p. 2−68050
α-AgI electrolyte, ionic Hall effect 2−83988
$Ag_{19}I_{15}P_2O_7$, high cond. solid electrolyte from AgI-$Ag_4P_2O_7$ system 2−44152
$Ag_7I_4PO_4$, high cond. solid electrolyte from AyI-Ag_3PO_4 system 2−44152
Al_2O_3, single and polycryst., high temp. 2−47978
Au film, discontinuous, on soda-lime substrate, resist. rel. to ion drift in substrate 2−47833
Bi_2O_3-$SrO(CaO)(La_2O_3)$ sintered system, and ion transference no. determ. 2−61418
CaF_2:Na, conc. and mobility of F ion vacancies 2−47979
CaF_2, proton irrad., elec cond. 300-800K, anion vacancy cond. mechanism 2−57230
$CdF_2:Na^+(Ag^+)(Li^+)(La^{3+})(In^{3+})(Gd^{3+})$, ionic thermocurrents, temp. depend. 2−81089
CdF_2, thermal defect order, mobility and complex form. 2−51194
Co ferrite, cation re-ordering, temp. depend. of cond. time variation obs. 2−75145
$CsCl:Ba^{2+}$, 250-500°C 2−54232
Cu ferrite, cation re-ordering, temp. depend. of cond. time variation obs. 2−75145

Ionic conduction, solids continued
CuCl, Frenkel defects, equilib. conc. perturbation by microwave pulse, ionic cond. change 2−80698
α-CuI, electrolyte, 2-40 GHz, freq. depend. 2−83989
Cu_xTe, thermal e.m.f., electronic and ionic cond. at 400°C, composition 2−54247
H bonded materials, proton migration studies, experimental methods, review 2−83998
KBr(Cl), press. depend. 2−44154
KHF_2, a.c. impedance, 50Hz-20kHz 2−68465
MgO, 800-1300°C 2−81065
MgO single crystal, Faraday law employed 2−65052
NH_4ClO_4, effects of annealing and partial decomp. 2−44155
NH_4ClO_4, proton transfer cond. 2−84361
NaBr(Cl), press. depend. 2−44154
$NaCl:Cd^{2+}$, meas. for dissolution of precipitates study 2−83844
NaCl, ionic conduction with temperature 2−44156
NaCl, NaCl:Ca, γ-irrad., d.c. conductivity obs., room temp. −70°C, electronic and ionic contribs. 2−57231
Ni ferrite, cation re-ordering, temp. depend. of cond. time variation obs. 2−75145
$PbBr_2$, pure and Cu^+-doped, defect studies 2−47402
$PbBr_2$, pure and Tl^+-doped, vacancy parameters determ. 2−47401
$PbCl_2$, pure and K^+-doped, defect studies 2−47402
$RbAg_4I_5$ single crystals, Hall effect of Ag ions 2−77949
SiO_2 film, Na^+ transport, m.o.s. C-V characts. study 2−77936
ThO_2 and solid solns., rel. to solid electrolyte applic. 2−65053
$ZrO_2.CaO$ solid electrolyte, ion transport number 2−65054

Ionization
see also Dissociation; Electrons/ionization; Photoionization
β-decay, probability of K-shell internal ionization calc. using theory of Stephas and Crasemann 2−70566
angular distribution anisotropy of ions from dissociative attachment of electrons to molecules 2−59929
angular distributions of secondary electrons in dipole approximation, relation between photon and charged particle impact 2−52931
associative ionization in slow collisions between atoms 2−83180
atom, inner shell ioniz. by violent ion-atom collisions at moderate nucl. vels. 2−77014
atom, K-shell ioniz. by high energy electrons 2−52928
atom-atom collisions, Drawin formula 2−46466
atomic and molecular production by electron scattering 2−42760
atomic beam, using high power electron bombardment system 2−63271
atomic Coulomb excitation by heavy charged particles 2−79911
atoms, ejection of electrons by protons, character of interference of resonances with continuum in spectra 2−70618
atoms, electron impact, differential cross-sections 2−56108
atoms, electron impact cross-sections, velocity distrib. of bound electron in classical impulse approx. of binary encounter theory 2−67395
atoms, K- and L-shell ionization by single-quantum annihilations of positrons 2−76981
atoms, K-shell ionization by protons, impact parameter dependence of angular distribution of scattered fragments 2−79909
atoms, test of invariance of ionization-energy threshold value with ejection energy 2−52930
atoms and molecules, cross sections for electron and positrons, 0.1-2.7 MeV 2−70598
atoms and molecules, in mass spectrometer chamber, in current and ion distrib. 2−49921
benzenes, substituted, electron attachment and excitation processes 2−42949
beta decay L-shell auto-ionization, model 2−46181
bromomethane, pulse radiolysis, electron disappearance 2−61816
carbonyl compounds, electron attachment and excitation processes 2−60055
carbonyls, electron attachment and excitation processes 2−42949
chloromethane, pulse radiolysis, electron disappearance 2−61816
double-continuum Coulomb wave function, asymptotic expansions 2−76973
electron affinity of water and struct. of hydrated electron 2−80013
electron impact, double and triple differential cross sections 2−74246
electron impact, secondary-electron-production cross sections 2−76963
elements, Z=23-83, K-shell ionization cross sections for 2.04 MeV electrons 2−74204
equilibrium and stability of quantum plasma 2−64327
ethyl bromide and chloride, pulse radiolysis, electron disappearance 2−61816
fission product atoms, ionization probabiliites for K- and L-shells calc. 2−46351
heterocyclics, six-membered with O and N, electron affinity, AVE CI SCF calculation 2−56204
hydrogenic atoms, multiphoton ionization, using non-perturbation method 2−79951
inert gas atoms, proton impact double ioniz. 2−83176
inert gas ions, collision-induced ioniz., ion kinetic energy spectra 2−83175
ion-atom collisions, inner shell ionization, X-ray production, review 2−83198
ionospheric E_s region, solar eclipse effect 2−65972
ionospheric E-region and lower F-region 2−48580
ions, multiply charged, trapped in hollow electron beam, meas. of electron impact cross sections, threshold −500eV 2−70609
K-shell internal ioniz. probability, accompanying β decay, direct collisions contrib. 2−59919
MHD channel, instabilities in nonlinear regime 2−80264
molecule, photoelectron bandshapes depend. on ionizing radiation freq. 2−67440
molecules, autoionization, Rydberg electron, semiclassical theory 2−77032
molecules, electron impact, differential cross-sections 2−56108
multiphoton, effect of spatio-temporal laser light structure 2−63309
multiphoton, role of excited states 2−46446
negative ionization mode modification for high resolution mass spectrometer 2−84680
one-electron ions, coeff. of ionization 2−52949
perfluoropropane, dissociative electron capture 2−60079

Ionization continued
perfluoropropylene, dissociative electron capture 2−60079
plasma in toroidal Z-θ pinch at Padova 2−83571
plasma instability, feedback control 2−80263
polarized nuclei, ang. distrib. of K-electrons ejected during K-capture 2−64027
rare earths, doubly and triply ionized, ionization energies 2−79947
relativistic heavy nuclei traversing matter 2−44015
supernova explosions, remaining ionization zones 2−81856
threshold of ionization instability in unbounded low temp. plasma, dispersion relation 2−46788
transparent liquids, avalanche ionization and limiting diameter of filaments by light pulses 2−77435
two-photon process, analysis using Laplace transformation theory 2−64029
universal function for ionization by structureless charged particles of arbitrary mass and charge 2−52925
Ag, absolute total cross section for K-shell ionization by electron impact, 30-140 keV 2−46458
Ag, K-shell ionization by electron impact, absolute cross-sections 2−79931
Ag, K-shell ionization by electron impact, absolute cross-sections 2−79931
AgBr, nuclear track emulsion, track formatin, analog theory 2−81543
Al, autoionizing levels, far-u.v. absorpt. spectra analysis 2−67388
Al, K-shell ionization cross sections by ^{20}Ne and ^{22}Ne bombardment, isotope effect 2−74216
Al L-shell, by inelastic collisions of fast particles 2−64026
Ar-Ar collisions, production of electrons by autoionization 2−76993
Ar^{2+}-Ar collisions, 2-8 keV, meas. of cross sections, competition between single and double electron transfer prócesses 2−79870
Ar, autoioniz. by slow electron impact 2−74229
Ar, behind strong shocks, multi-level initial ionization and average atom-atom cross sections 2−67398
Ar, electron impact, efficiency curves 2−59921
Ar, electron impact ioniz., slow electron obs. 2−64033
Ar, in slow collision with He and He^+ meas. of energy spectra and angular distrib. of ejected electrons 2−56119
Ar discharge, motion of ionization front in microwave e.m. field 2−60238
Ar electron impact, double and triple differential cross- sections 2−74246
Ar VIII, Na-like, collisional-rate coeff. meas. in plasmas 2−46450
$^{15}Ar^+$, highly excited, metastable autoionizing states, electronic energies and electron emission lifetimes 2−42749
Au, absolute total cross section for K-shell ionization by electron impact, 90-140 keV 2−46458
B, autoionizing levels, far-u.v. absorpt. spectra analysis 2−67388
B, by electron impact, calc. for $1s^22s^22p$ configuration 2−46451
Ba I, auto-ionization resonance structures, high resolution photometry 2−79943
Ba^+, meas. of absolute cross section for single ionization by electron impact in 10-1000 eV range 2−70601
Be, autoionizing levels, far-u.v. absorpt. spectra analysis 2−67388
Be, K-shell ionization by protons and heavy ions 2−83179
C, autoionizing levels, far-u.v. absorpt. spectra analysis 2−67388
C, in solar atmosphere density dependent ionization balance 2−66231
C, K-shell ionization by fast protons 0.3-2.0 MeV 2−42748
C I, C II and C III, interstellar, ionization structure 2−81829
C II, by electron impact, calc. for $1s^22s^22p$ configuration 2−46451
C_4H_8 isomers ionisation efficiency at 123.6 nm 2−83302
CO_2, metastable anions 2−42875
Cd, Penning ioniz. by collisions with He metastables, excitation mechanism of He-Cd laser 2−79181
^{109}Cd, charge states of ions prod. by electron decay capture 2−79884
Cl fast ion beams, beam-foil excitation, metastable X-ray emitters 2−42788
Cl_2, electron affinity 2−68774
Cl^{6+}, metastable autoionizing states 2−49945
$^{14}Cl^+$, highly excited, metastable autoionizing states, electronic energies and electron emission lifetimes 2−42749
Cs seeded Ar, nonequilibrium MHD plasma 2−80262
^{131}Cs decay, double K-shell ionization 2−64028
Cu, absolute total cross section for K-shell ionization by electron impact, 20-135 keV 2−46458
Cu arc, 1-15A current, autoionized and non-autoionized spectra 2−71064
^{185}Er decay, double K-shell ionization 2−64028
F, Li-like, classification of spectra of autoionization electrons 2−49953
Fe I ionization and excitation equilibrium in solar atmosphere 2−66230
$H_2/O_2/N_2$ flames, with Cr and K additives, electron attachment and negative ion form. 2−72555
H-, autoionization states, computation using Feshbach formalism 2−46487
H-, position of lowest D autoionization states calc. using Feshbach's Q-operator formalism 2−49982
H, electron impact cross-sections, representation for ionization and excitation 2−64063
H, electron scattering, threshold behaviour of ionization internal function calc. using classical three body computer programme 2−56122
H atoms, collisional excitation and ionization rates rel. to classical and quantum mechanical formulae in astrophysical calculations 2−49977
H^-, autoionization, projection-operator approximation in inelastic scattering region 2−77019
H^- electron detachment cross sections in H, He, Ar, 4-30 keV 2−77017
H_2, miltiphoton dissoc., predissoc., autoionization 2−83263
H_2, photoexcited autoionization cross section calc. 2−50037
H_2O, by electron bombardment, electronic states of resultant H_2O^+ 2−42896
H_2O vapour, electron impact cross sections, atmospheric applications 2−53019
hd, absorption spectrum in vac. u.v., ionization energy 2−50038
He-Cs gas plasma MHD, fluctuations calc. 2−80265

Ionization continued
He, autoionization, projection-operator approximation in inelastic scattering region 2−77019
He, autoionization states, computations using Feshbach formalism 2−46487
He, by H^+ impact 2−42817
He, by proton impact 2−59955
He, collisional ioniz. by slow electrons 2−64074
He, direct, in inelastic collision with He^+, obs. of oscillatory structure in energy distrib. of ejected electrons 2−56133
He, electron impact, ang. and energy distrib. of secondary electrons 2−64031
He, electron impact, double and triple differential cross-sections 2−74246
He, electron impact ioniz., slow electron obs. 2−64033
He, Feshbach-type $^{1,3}P^3$ autoionization states, applic. of multiconfiguration energy bound method 2−46486
He, Penning-ionizing collisions, excited-ion lifetimes 2−67433
He, position of lowest D autoionization states calc. using Feshbach's Q-operator formalism 2−49982
He atom, simultaneous excitation and ionization of 4^2P and 4^2S states by electron impact, meas. of relative cross sections 2−64076
He atom, triplet metastable, reson. multiphoton ioniz. 2−46491
He atoms, multiphoton ioniz. from excited states 2−46492
He atoms, triplet metastable, resonance multiphonon ionisation 2−42811
He ground state, effects of correlation in target wavefunction on cross section 2−70639
He triplet metastable, 5 photon ionization probability light intensity depend. 2−74248
He^- electron detachment cross sections in H, He, Ar, 4-30 keV 2−77017
He + Ar collisions, chemi-ionization cross sections 2−64080
He + (2^3S and 2^1S) + Ar total cross section 2−67435
I-, electron affinity accurate analytical wave functions 2−42733
K^+-Ar collisions, ionization processes 2−79925
K, by laser impact, ion energy spectra 2−52921
Kr, electron impact, ang. and energy distrib. of secondary electrons 2−64031
Kr, in slow collisions with He and He^+ meas. of energy spectra and angular distribs. of ejected electron 2−56119
Kr, oscillator strengths for multiple ioniz. in outer and first inner shells 2−79891
Li, Li^-, electron affinity from approximate natural orbitals for groundstates 2−46433
Li, model potential calc. of electron affinity 2−42752
$LiScF_4$, relative ionization cross-section determ. 2−46556
Mg, autoionizing levels, far-u.v. absorpt. spectra analysis 2−67388
N, autoionizing levels, far-u.v. absorpt. spectra analysis 2−67388
N discharge, motion of ionization front in microwave e.m. field 2−60238
N III, by electron impact, calc. for $1s^22s^22p$ configuration 2−46451
N^+, N_2^+, N_2^{2+}, cross sections, prod. from N_2 by 16 to 600 eV electrons 2−83404
N_2, autoionising levels, converging to $A^2\Pi_u$ and $B^2\Sigma_u^+$ limits 2−83403
N_2, by slow electrons, rotational level distrib. of N_2^+ 2−80053
N_4^+ form. in swarm expts. and gas discharges 2−67685
NH_3, aqueous, enthalpy of ionization, by solution calorimetry 2−77423
NO, electron affinity determ. by laser photodetachment and photoelectron spectrometry on NO^- 2−53027
NO, Penning ionization by $Ar(^3P_1)$ 2−53041
NO, Rydberg series of bands in 680−560 Å region, ionization of σ*2s orbital 2−74271
NO_2, electron affinity 2−68774
Ne, electron impact excitation, 42-51 eV obs. of autoionizing $2s^22p^43s3l$ states and related Ne^- resonances 2−67402
Ne, electron impact ioniz., slow electron obs. 2−64033
Ne, in slow collision with He and He^+ meas. of energy spectra and angular distribs. of ejected electrons 2−56119
Ne, in solar atmosphere, density dependent ionization balance 2−66231
Ne, simultaneous ionization and excitation by electron impact 2−49960
Ni K-shell and beta-decay, summing-energy spectrum meas. 2−46186
O, Li-like, classification of spectra of autoionization electrons 2−49953
O and O^-, calc. of electron affinity using symmetry-adapted pair correlations 2−42709
O IV, by electron impact, calc. for $1s^22s^22p$ configuration 2−46451
O^-, O_2^-, O_3^- ions, mobilities and ion-mol. reaction rates 2−53248
O_2, electron affinity determ. from binding energy of O_2^- by Hess cycle 2−50019
O_2, in solar atmosphere, density dependent ionization balance 2−66231
O_2 ($^1\delta_g$), Penning ionization by $Ar(^3P_1)$ 2−53041
O_2 electron affinity determ. by laser photodetachment and photoelectron spectroscopy of O_2^- 2−53028
O_2 ion-pair production of O^+ and O^- by $He(2^12^3S)$ metastables 2−83260
O_2^+, O_4^+ formation and loss in Kr-O_2 afterglow plasmas, possible ionospheric implications 2−70889
SO_2, attachment cross-sections by electron collision 2−60035
Si, autoionizing levels, far-u.v. absorpt. spectra analysis 2−67388
Sn, inner-shell ioniz. cross sections calc. 2−52936
^{204}Tl, K-shell internal ionization accompanying β-decay, obs. 2−63850
U atom, electron impact ionization cross-section 2−46588
UO, UO_2, UO_3, electron impact ionization cross-sections and fragmentation 2−46588
$U + O_2 \rightarrow UO_2^+ + e$ chemi-ionization, determ. probability of occurrence 2−68766
xe, in slow collisions with He and He^+, meas of energy spectra and angular distribs. of ejected electron 2−56119
Xe, oscillator strengths for multiple ioniz. in outer and first inner shells 2−79891

- **Ionization** continued
  - **gases**
    - *see also Charge exchange; Plasma*
    - air, associating atmospheric electricity rel. to human biological behaviour 2−58591
    - air, ionization extrapolated ranges for N, Na and Ar ions 2−79917
    - air, temporal growth of ionization in long uniform field gaps 2−71029
    - atmosphere, air traffic control laboratory, personnel performance 2−75612
    - atmosphere, due to meteor trails, effect on meteoroid radio obs. 2−69172
    - charged particle transport by stream of gas or steam 2−60295
    - combustion, nonequilibrium phenomena, calc. 2−80261
    - conference, Split, Yugoslavia (1972) 2−60291
    - cross-sections, effects of excited ions and crossed electric and mag. fields 2−60289
    - current growth between parallel plane electrodes computation 2−67689
    - efficiency curves for electron impact ionization, inverse convolution computation 2−70977
    - electric breakdown 2−46802
    - electron energy distribution functions, asymptotic solns., in stationary and homogeneous medium 2−70981
    - e.m. signal transmission through ionized media, distortion, obs. 2−45626
    - glow discharge, convectively unstable random ionization waves 2−60309
    - He-Cs plasma, MHD, fluctuationc calc. 2−71773
    - high current ion accelerator, optimization 2−79704
    - high pressure, breakdown, field emission mechanisms 2−67695
    - h.v. breakdown, Z-pinch, low pressure formative phase 2−67650
    - inert gas clusters, multiple ionization by electron impact 2−60287
    - interstellar, surrounding Sco X-1 2−73054
    - interstellar material, by supernova explosions 2−58365
    - ionosphere lower, nighttime, obs. using e.m. wave absorption patterns 2−48579
    - laser-induced disequilibrium in vapours 2−77343
    - longitudinal diffusion coeff. for electron swarms at low E/p_0 2−71008
    - mine air anal., using cross section ionization detector 2−68821
    - mobility of ions in parent gases 2−56383
    - monatomic, strong normal shock waves, impurity effects on ionization-relaxation zone 2−50239
    - multiphoton, optical breakdown, at high pressures 2−43199
    - neutral component, macroscopic velocity obs. in crossed folds 2−70976
    - nonisothermal, sound propagation 2−66618
    - plasma atomic level populations, distribution function 2−77269
    - relativistic electron beam propag. in h.p. media 2−53241
    - relativistic electron beam propag. in l.p. media 2−50220
    - r.f. preionization in transversely excited supersonic flow CO_2 laser 2−59146
    - by shock and detonation waves 2−45563
    - in shock tube, magnetically driven, steady-state current sheet speed obs. 2−52253
    - striations, at low currents, exact theory 2−64349
    - sudden ionospheric disturbances caused by solar flares, review 2−84903
    - tissue equivalent, distribution obs. 2−51918
    - Ag vapour, high-current hollow cathode discharge, Penning ionization, effect on radiation 2−74423
    - Ar-N_2, −CO mixtures, heteronuclear associative ionization, formation of ArN_2^+, $ArCO^+$, Ar_2^+ following 30 eV electron impact 2−51430
    - Ar-methane-Kr and Ar-methane-H_2 mixtures, mean energy 2−60290
    - Ar, ionization extrapolated ranges for Ar ions, 0.3-1.0 MeV 2−79917
    - Ar, shock-heated, ionization relax. time calc. 2−70978
    - Ar, steady state electron mean energy between parallel plates 2−43201
    - Ar electron capture collisions with H(2s), cross section meas. 2−56123
    - Ar gas, electron momentum transfer cross section from Boltzmann eqn. 2−83708
    - Au vapour, high-current hollow cathode discharge, Penning ionization, effect on radiation 2−74423
    - CO_2-N_2-^3He laser, high press., preionized in a reactor, performance 2−69916
    - CO_2, partial ioniz. cross sections by electrons (25-600 eV) 2−70979
    - CO_2 laser, high press., pulsed, gas breakdown, ionization by rad., operating press. limit 2−69919
    - CO_2 long pulse laser, excitation by short pulse longit. electron beam 2−55682
    - Cl_2-Kr mixtures, shock tube heated, dissoc. relax. times 2−53244
    - Cl_2-Kr mixtures, shock tube heated, electron affinity continuum 2−53243
    - Cs vapour, electron density determ. from spectral line mixing 2−46792
    - Cu vapour, high-current hollow cathode discharge, Penning ionization, effect on radiation 2−74423
    - Fe I in solar atmosphere 2−58559
    - H, axially symmetric free expansion of non-equilibrium plasma 2−77270
    - He-CO_2 mixture, atmospheric pressure discharge 2−60305
    - He-Cd laser, pumping mechanism and plasma parameters 2−76474
    - He^+-He^2+ -e plasmas, calc. of collisional-radiative volume recombination and ionization coefficients 2−50193
    - He, pre-breakdown, meas., influence of gas sampling techniques 2−50221
    - He plasmas, collisional-radiative ionization and recombination coefficients, influence of atom-atom collisions 2−67630
    - $He(2^3S) + CO \rightarrow (CO^+)^* + He + e[C^* + O + He]$, excitation transfer and Penning ionization reactions, determ. rate constants for production of excited products 2−54535
    - Hg, l.p. discharge, secondary ioniz. coeffs. 2−53253
    - K vapour, multiphoton resonant processes under laser irradiation 2−42750
    - K vapour, using dye laser beam 2−74215
    - Mg-He, double ionization of Mg by thermal collisions with He 2−70980

- **Ionization** continued
  - **gases** continued
    - N_2-O_2 mixtures, behind shock waves 2−77302
    - N_2, ionization extrapolated ranges for N and Ar ions 2−79917
    - N_2, temporal growth of ionization in long uniform field gaps 2−71029
    - N_2, Townsend first ionization coeff. at low values of E/p 2−74405
    - N_2 electron capture collisions with H(2s), cross section meas. 2−56123
    - Ne-Ar discharge, detection of Penning ionization by laser perturbation spectroscopy 2−80373
    - Ne, p and s ionization waves, nonlinear interaction 2−71025
    - Ne, Townsend primary ionisation coefficient, determination by luminous flux method 2−46790
    - O_2-CO systems, current growth meas. 2−60288
    - O_2-H_2 mixtures, non-attaching gas behaviour of oxygen 2−53246
    - O_2, ionization extrapolated ranges for Ar ions, 0.3-1.0 MeV 2−79917
    - O_2, low energy electron attachment at v. high gas density 2−50222
    - o_2 electron capture collisions with H(2s), cross section meas. 2−56123
    - O_2 three-body electron attachment coeff., low temp. meas. 2−53247
    - O_2^- labile ions, vibration and rotation during d.c. discharge 2−46793
    - SF_6, electron diffusion and drift 2−43202
    - SF_6, pressure dependent electron attachment process 2−71039
    - SF_6, thermal energy effect on ioniz. efficiency curves of negative ions 2−67686
    - Xe, e.m. T tubes, Mach 5 shocks 2−78932
    - Xe, laser action on unclassified transitions in highly ionized plasma 2−59142
    - Xe, shock-heated, ionization relax. time calc. 2−70978
  - **liquids**
    - cyclopentadiene, negative ion formation by electron impact studied using mass spectrometer 2−46986
    - dielectric, prebreakdown, stat. analysis of emitted light pulses 2−43382
    - electron transfer reactions in solution using Kubo linear response theory 2−84648
    - hydrocarbons, localized electron theory 2−67840
    - Mg, K-shell ionization cross sections by ^{20}Ne and ^{22}Ne bombardment, isotope effect 2−74216
    - N_2O_4, ioniz. enthalpy determ. from cond. and permittivity 2−84612
  - **solids**
    - alkali halide films, electron affinities 2−81532
    - Auger spectroscopy, comparison of X-ray and electron impact ionization 2−61467
    - Gunn devices, impact ionization, high field domain 2−65034
    - ion-ion emission, mass spectrometric technique for studying processes on surface and in bulk of solids 2−61469
    - laser, X-ray, soft, rel. to ionization, inversion, stimulated emission and Auger effect 2−79209
    - organic films, electron affinities 2−84669
    - semiconductor, amorphous, avalanche ionization, Shockley hot-electron model 2−61287
    - semiconductor, impact ioniz. coeff., Schottky barrier obs. 2−44091
    - semiconductor junctions, multiplication factor analysis 2−51180
    - surface atoms, inner shell ionization by electron impact 2−50553
    - thermal ionization of deep centers in the space charge of semicond. 2−71921
    - transparent, avalanche ionization and limiting diameter of filaments by light pulses 2−77435
    - AgCl electron impact ionisation species, and dissociation energies 2−50021
    - Al_2O_3 film, anodic, elec. breakdown 2−57235
    - $Fe_{3-x}Mg_xO_4$, ferrite-spinels, Mossbauer spectra and effect of admixture 2−72282
    - GaAs, photothermal ioniz. of shallow donors, photocond. obs. 2−81177
    - Ge, quantum effic. of int. photoelec. eff. and impact ioniz. 2−71907
    - $NaNO_3$, rel. to thermoluminesc. glow curves 2−48257
    - PbS quantum yield of internal photoelec. effect and impact ioniz. 2−72065
    - Si, free hot carrier impact ionization obs. 2−54203
    - Si impact ioniz. coeff., Schottky barrier obs. 2−44091

- **Ionization, atmosphere**
  - *see also Atmosphere/radioactivity; Ionosphere*
  - aurora, low energy ion composition measurements 2−68950
  - auroral ionosphere model, electron density height profile 2−81723
  - D-region, cluster, switch and rearrangement reactions for positive ions 2−58084
  - D-region, impulsive variations rel. to polar substorms 2−58083
  - D-region, relation of theory and experiment 2−78401
  - D-region, theoretical models, ion pair production 2−78400
  - dawn and dusk conductivity gradients effects on equatorial electrojet 2−54885
  - daytime F-region, coupling between electron density and electron temp. 2−48585
  - density fluctuations of small and large ions 2−48436
  - E-region, numerical model for profiles 2−58087
  - electron density trough, magnetic shell alignment, Ariel 3 data 2−72863
  - e.l.f. and v.l.f. propagation in ionosphere, negative ion effects 2−48561
  - equatorial D-region electron and positive ion density distributions 2−72880
  - equatorial ionosphere above Thumba, rocket meas. of ionization irregularities and plasma instabilities 2−84901
  - evening anomaly in F-layer ionization 2−72897
  - F_2 region, disturbances during magnetic storms 2−75631
  - F-layer, nighttime maintenance mechanism 2−58092
  - F-region, ionization irregularities, direct backscatter reflections 2−72893
  - F-region, nighttime maintenance, backscatt. obs. 2−58094
  - F-region, nighttime maintenance, horizontal transport influence 2−58096
  - F-region, nighttime maintenance, models 2−58093
  - F-region, numerical model for profiles 2−58087

Ionization, atmosphere continued
F-region, topside, charge exchange mechansim, rel. to nighttime maintenance 2—58098
ion annihilation by aerosol particles up to 60 km. altitude 2—65953
ion concentration distribution in ionosphere at 600 km. low and middle latitudes 2—75627
ion temperature errors in retarding potential analyzers, grid-plane potential 2—68927
ionosphere, composition 220 to 4360 km, vertical space probe meas. 2—54873
ionosphere, dynamics, model, interhemispheric coupling 2—81722
ionosphere, effective height integrated conductivity 2—65949
ionosphere, electron densities, regular horizontal gradients, along satellite orbit 2—75628
ionosphere, field aligned ion cloud, Gaussian distrib. of ionization density 2—72868
ionosphere, ionization cross sections, secondary electron distributions 2—78389
ionosphere, level after sunrise, continuous sounding obs. 2—84908
ionosphere, photoionization and photoabsorption cross sections calculations 2—78388
ionosphere, sudden increases in total electron content after solar radio bursts 2—51648
ionosphere D-region, diurnal models, transient conditions, photochemical computer code 2—81731
ionosphere E-region, model parameters 2—81732
ionosphere electron cyclotron resonances, nf_h, frequency shifts 2—51647
ionospheric, interaction with atmospheric waves 2—44671
ionospheric absorption, winter anomaly, LF A3 measurements 2—51643
ionospheric D-region, solar corpuscular flux in central latitudes 2—51650
ionospheric electron content, graviety waves, frequency spectra 2—57983
ionospheric electron density, predawn airglow enhancement 2—48542
ionospheric layer formation, transient, rel. to sudden disturbances in 20-50km range 2—54888
lower ionosphere, drift of ionization inhomogeneities 2—68964
lower ionosphere, r.f. impedance probe, electron density and temp. determ. 2—65954
lower ionospheric absorption, magnetic control at lower latitudes 2—51645
mesosphere, produced by solar X-rays 2—73118
mobility spectra of atmospheric ions under various conditions 2—62354
molecular ion concentrations in F_2-layer 2—72895
neutral wind charge, effect on low-latitude F-region 2—65989
plasmapause, Cerenkov instability and v.l.f. emissions 2—72827
plasmapause, light ion trough characts. 2—58047
polar wind model, O^+, H^+ and He^+ distributions 2—81698
thermal positive ions in outer ionosphere and magnetosphere 2—65844
thermosphere, quenching of vibr. excited N_2 by CO_2 2—58029
topside, electron densities, sunrise effects 2—81734
total electron content rel. to movements of ionospheric mid-latitude trough 2—72864
variations, ionospheric 2—51649
O^+ ion distribution and vertical motions in lower part of F-region 2—72894

Ionization, surface
see also Electron emission/thermionic; Ion emission/thermionic; Work function
atoms adsorbed on W substrate, backscattering cross sections for K-shell ionization by electron impact 2—79919
ion-ion emission, mass spectrometric technique for studying processes on surface and in bulk of solids 2—61469
metal/vacuum surface, ioniz. probability for crossing atom 2—48032
metallic-field effect consequences 2—54206
negative ion formation, mass spectra 2—79851
tetracyanoethylene, negative-ion form. by electron bombardment 2—67687
work function change, meas. methods 2—48028
C and C compounds, polyatomic negative ions 2—79928
CsCl on Ir film, effect of C adsorption on (111) face 2—64543
Si, energy, effect of annealing 2—72095
$^{235}U/^{238}U$ isotope ratio meas., technique using mass spectrometry 2—83216

Ionization chambers
1383 A type, calibration for ^{67}Ga 2—59613
air circulation type, calibration 2—70293
beta ray calibration at protection levels 2—42449
calibration, mobile system, for nuclear reactors 2—67362
calorimeter for investigation of ultrahigh energy muons 2—73862
exoelectrons, thermally stimulated, meas. 2—59614
free of plarity effect, obs. in high energy electron dosimetry 2—69397
gas, transient electron current 2—79646
gas ΔE chamber for fission fragments 2—70294
high resolution fast neutron spectrometry 2—67075
using internal proportional gas multiplication, high spatial resolution 2—42455
multi-wire proportional chamber for nuclear medicine applications 2—49639
multiwire proportional chamber readout, coaxial and pointed circuit delay lines 2—49636
multiwire structures rel. to recent progress in large detector systems 2—49637
nuclear reactor radiation dosimetry, gamma-ray energy deposition meas. 2—42699
parallel plate using contact potential difference 2—73936
pulse, fission, in reactor controllers, characts. 2—42678
pulsed, analytical model for voltage pulse profile characts. with space charge 2—52686
radiation energy dose unit, German agency of weights and standards 2—67080
radiation monitoring of gaseous effluents from nuclear facilities 2—42690

Ionization chambers continued
in reactor, for controlling irradiation times in pneumatic transport system 2—74189
rectangular, impulse due to relativistic particle, expt. 2—49642
Rontgen unit determ., magnetic field chamber 2—58675
spherical, for faster indicial response 2—49641
stability improvement 2—79664
standard free air chamber effect of beam path length on photon scatter correction in low-energy X-radiation meas. 2—55907
wire counters using chamber with new gas mixture 2—49635
x-ray machines, controlling and recording radiation exposure 2—58596
X-ray patient dose meas., construction and response 2—78667

Ionization gauges *see Vacuum gauges*

Ionization potential
alcohols, and proton-acceptor properties in H bonds 2—50076
alkali halides, meas. by X-ray photoelectron spectroscopy 2—83259
alkyl iodides, comparison of valence shell and core potentials, X-ray photoelectron spectroscopy study 2—64167
anthracene, from photoelectron spectra 2—60048
appearance spectroscopy of Cr surface, L_3/L_2 intensity ratio 2—51230
aromatic hydrocarbons from photoelectron spectra 2—60048
associative ionisation in slow collisions between atoms 2—83180
atomic systems with closed core plus two electrons 2—46421
atoms, term splittings, electron affinities, Bethe-Goldstone calculations based on configurational excitations 2—76983
atoms with $Z \leqslant 18$, method for determ. of total binding energies and their derivatives 2—56094
benzenes, dihydroxy- and diamino-substituted, and electron affinities 2—70749
biphenylene, from photoelectron spectra 2—60048
closed shell system, many-body Green's functions 2—59913
cyanoacetylene, determ. from Rydberg series in vacuum u.v. spectrum 2—46600
cyclopentadiene, electronic struct., SPINDO calc. and photoelectron spectra 2—70761
diphenyl acetylene, from photoelectron spectra 2—60048
formaldehyde, semi-empirical SCF-LCAO calculations 2—42986
fulvene, electronic struct., SPINDO calc. and photoelectron spectra 2—70761
heterocyclics, six-membered with O and N, AVE CI SCF calculation 2—56204
hydrocarbons calc. using new bond length-resonance integral relationship 2—50009
1-iodoalkanes, far u.v. spectra, obs. of Rydberg series leading to one of first two ionization potentials 2—74292
ion, relation between ionic radius and ionization potential 2—83200
isoquinoline, shift in π ionization potential due to F substitution 2—70790
isothiazole and derivatives, photoelectron and mass spectra obs. 2—83305
light atoms, decoupled Hartree-Fock calculations 2—52904
linear mols., photoioniz. cross sections in valence electron approx., photoelectron spectra intensities 2—79976
mass spectrometric determ., effects of repeller voltage and shield voltage 2—79850
metallocenes, electron spectra, adiabatic first ioniz. pot. 2—64187
methane, lowest potential, ab initio calc. 2—56244
methane molecule, electronic structure, analysis of formation in Hartree-Fock model 2—60074
molecules, statistical total energy in multiple scattering formalism 2—42828
nitroxide radicals, photoelectron spectra and mol. orbital calcs. 2—80073
onset potential, mass spectrometric determination method 2—46399
organic F containing σ-bonded molecules, MINDO/2 calc. 2—77111
phenanthrene, from photoelectron spectra 2—60048
phenyl radical, photoionization, determ. of heat formation and ionization potential 2—67520
phosgene 2—43006
quinoline, shift in π ionization potential due to F substitution 2—70790
Scheibe's rules for molecules first and higher excited states, atomic nature 2—50013
sulphuryl molecules, photoelectron spectra, vibrational spectra 2—64156
s tetrazine, electronic structure obs. in electron impact energy loss spectrometer, ionization potential 2—70737
thioformaldehyde, pyrolysis products of dimethyldisulphide, first ionization potential 2—72538
thionyl molecules, photoelectron spectra, vibrational spectra 2—64156
thiophosgene 2—43006
third derivative method for determining electron impact onset potentials 2—60286
$B_{10}H_{14}$, SCF study 2—64115
B_2H_6, comparison of calc. using minimum basis set and extended Slater orbital wave functions 2—64114
Be many-body Green's functions 2—59913
CS, vertical pot. meas. 2—72544
ClO_3F, photoelectron spectrum, determ. of vertical and adiabatic ionization potentials 2—46587
CrO_4^{2-}, valence region X-ray photoelectron spectra, energy spread of ioniz. pots. 2—80004
Cs_2, determ. from ionization of Cs vapour by method of space charge amplification 2—70603
F_2, vacuum u.v. absorption spectrum, determ. of dissociation energy and ionization potential 2—70696
He, many-body Green's functions 2—59913
He isoelectronic sequence, excited state calcs. 2—64073
MnO_4^-, valence region X-ray photoelectron spectra, energy spread of ioniz. pots. 2—80004
MoVIII, spectral analysis 2—74217
Nb VII, spectral anal., configurations and levels determ. 2—74219
SO_2F_2, photoelectron spectrum, determ. of vertical and adiabatic ionization potentials 2—46587
Th, photon appearance potential spectroscopy 2—54441
ZrVI, spectral anal., configurations and levels determ. 2—74225

Ionized gases *see Ionization/gases; Plasma*

Ionosondes *see Ionosphere measuring apparatus*

Ionosphere
see also Electromagnetic wave propagation/ionosphere
— 2—62357
abrupt scintillation boundary, beacon satellite 2—72857
aeronomic ion-neutral molecule reactions rel. to direct ionospheric measurements 2—83397
Appleton magneto-ionic eqns., quasi-longitudinal and quasi-transverse approximations for large Z 2—50190
Arctic ionosphere auroral precipitation patterns, airborne observations 2—84907
AU and AL indices on international quiet days and geomagnetic field variations at high latitudes 2—48602
auroral, mapping of proton and alpha particle distribs. 2—65909
auroral belt ionospheric currents, Harang discontinuities 2—68947
auroral electrojet polarization, idealized model 2—65901
auroral model, electron density height profile 2—81723
Birkeland currents intensification due to elec. fields 2—65904
Booker's theorem on solution of refractive index profiles, generalization to under range of profiles 2—54889
characterization using incoherent scatter sounder 2—78392
charged particle motion and radiation in rapidly oscillating mag. fields 2—69861
composition 220 to 4360 km, vertical space probe meas. 2—54873
computer model of magnetospheric elec. fields 2—65879
cosmic radio noise absorption, riometry 2—84902
critical frequency variability statistical model 2—48365
dawn and dusk conductivity gradients effects on equatorial electrojet 2—54885
day glow, intensity and polarization, measurements made during 1965 total solar eclipse 2—72832
dayside, effects of magnetosheath particle precipitation 2—58073
daytime and nighttime electron temperatures from topside resonances 2—68963
deep magnetic-variation sounding theory 2—81740
detection of cosmic X-ray phenomena 2—68968
diffusive coupling with plasmasphere 2—58049
disturbances affecting s.w. link stability 2—72813
drift, meas. method for determ., variation of similarity method 2—65955
drift analysis using full correlation methods for general observing triangle 2—84894
drift measurements, comparison with radar meteor wind measurements 2—72870
drift measuring method, applic. to middle latitudes 2—72875
drifts and irregularities, meas. by large aerial arrays, analysis 2—68965
dynamics, model, interhemispheric coupling 2—81722
dynamo currents and interaction with ocean, effects on daily geomag. variations 2—84926
Earth's lower region, average electron density height profile 2—75630
effective height integrated conductivity, current flow with magnetosphere 2—65949
effects of solar flares 2—81955
electric current, rel. to field-aligned and ring currents in magnetosphere 2—81712
electric field pot. distrib., world-wide meas. 2—65963
electric fields, horizontal, air electric meas. 2—54890
electric fields, meas. techniques and props. 2—72878
electric fields and ionization drift in F_2 regions 2—84911
electric fields and precipitating particles meas. by balloon during release of Ba cloud in magnetosphere 2—62365
electric fields at high latitude 2—72866
electric fields during pulsating auroras 2—48572
electrodynamic coupling with magnetosphere, rel. to quiet auroral arcs 2—65905
electrojet, equatorial, rel. to magnetic equator obs. by POGO spacecraft 2—58044
electrojet, rel. to conducting earth effects on standard observatory records on auroral zone geomagnetic variations 2—58113
electrojet region, instability, generation of potential waves by transverse current 2—44752
electron, ion and neutral density obs. during magnetic storms 2—44772
electron content, gravity waves, frequency spectra 2—57983
electron content in subtropical regions, diurnal and seasonal variations 2—84900
electron content with respect to solar and geomagnetic activity 2—54894
electron cyclotron resonances, nf_h, frequency shifts 2—51647
electron densities, regular horizontal gradients, along satellite orbit 2—75628
electron density, P′(f) to N(h) inversion problem 2—72874
electron density, predawn airglow enhancement 2—48542
electron density, satellite spin effects on cylindrical probe obs. 2—65951
electron density and temp., Langmuir probe obs. 2—72876
electron density excess in random irregularities 2—75629
electron density irregularities, large-scale disturbances, observations at Haringhata field station, Calcutta, India 2—65945
electron density irregularities near aurorae 2—81725
electron density measurements using rocket c.w. radio propagation method 2—48571
electron density profile, biexponential model, u.h.f. radiowave refraction, group delay for 2—69840
electron density profile at high latitudes from riomenter obs. 2—72862
electron density trough, magnetic shell alignment, Ariel 3 data 2—72863
electron energy transfer rates 2—72865
electron impact excitation cross sections, analytic models 2—81724
electron precipitation from magnetosphere, at time of sudden commencement, theory 2—65837
electron resonances, topside sounder obs. 2—81727
electron temp., suprathermal electron flux and 6300 Å airglow, predawn enhancement 2—62360
electron temp. determ. from plasma wave phenomena 2—62355
electron temp. obs., a.c. Langmuir probe technique, rocket borne instrumentation 2—81726

Ionosphere continued
electron temp. obs. with Langmuir probe and electron temp. probe 2—44753
electron temperature, empirical model from satellite meas., 500-3500 km 2—62359
electron temperature enhancement in wake of Explorer 31 satellite 2—54899
electron temperature gradient instability 2—65956
equatorial anomaly rel. to OI (6300 Å) night airglow 2—62339
equatorial anomaly rel. to OI (6300 Å) nightglow 2—62340
equatorial electrojet and solar flux effects on diurnal development of total electron content of equatorial anomaly 2—65921
equatorial electrojet current system rel. to ionospheric processes 2—84791
equatorial ionosphere above Thumba, rocket meas. of ionization irregularities and plasma instabilities 2—84901
equatorial spread F, 10 cm waves on grand circle 2—48562
field aligned ion cloud, Gaussian distrib. of ionization density 2—72868
global distrib. of parameters, unified coordinate system for describing 2—72847
gravity wave induced irregularities, receiver drift expt. simulation 2—62364
gravity wave perturbation models 2—72822
height structure of tidal winds, incoherent scatter obs. 2—72872
high latitudes, elec. fields and zonal currents induced by merging of field lines 2—62351
high-latitude ionospheric currents rel. to interplanetary magnetic-field direction 2—68966
inhomogeneous determ. of polarization of reflected radio-waves using Stokes parameter 2—84904
ion concentration distribution at 600 km. low and middle latitudes 2—75627
ion density profiles for Project Aladdin 2—58075
ion profiles, numerical modelling for ALADDIN expt. 2—58076
ionization cross sections, secondary electron distributions 2—78389
ionization interaction with atmospheric waves 2—44671
ionograms reduction to true height-electron density profiles 2—84898
irregularities, distribution, scintillations in satellite beacon transmissions 2—68967
irregularities, over Huancayo, upward moving 2—72871
layer during oblique soundings, critical frequency and geometric parameters of parabolic model 2—72848
lower, drift of ionization inhomogeneities 2—68964
lower ionosphere layer, effect on propagation characteristics 2—81719
lower thermosphere, variation with latitude 2—72817
magneto-ionospheric effects of substorms 2—48601
magnetopause, speed and thickness of current sheet determ. by meas. of energetic proton flux gradient 2—62317
magnetosphere interactions, conference review 2—48568
micropulsations from finite source, ground signal rel. to Pc 1 disturbances 2—65960
mid-latitude trough movements rel. to scintillation boundary 2—72864
model, axially symmetric, relationship between ray path derivations in azimuth and elevation 2—44747
model development, specified solar flux and boundary conditions 2—81697
modification by radio waves 2—68962
modification expts., variability of plasma line enhancement 2—65947
neutral-particle wake method for satellite-borne temperature measurements 2—68925
numerical integration method, chemical and charge balance conservation 2—81721
oblique sounding, mechanism of formation and form of scattered signal 2—72853
parameter variations, correlation with solar activity 2—48560
parameters determined during vertical sounding, effect of gravity waves 2—72877
partial ring current rel. to positive geomagnetic bays 2—78405
particles trapped by Whistler wave, detrapping by second wave 2—69860
photoelectron flux in 3-50 eV range, effect of 1970, March 7 solar eclipse 2—65948
photoelectron flux meas. with ISIS 1 and 2 satellites 2—62361
photoelectron transport equations 2—65952
photoionization and photoabsorption cross sections calculations 2—78388
plasma, inhomogeneous, purely growing parametric instability 2—65957
plasma diagnostic phenomena 2—78397
plasma diagnostics, method based on potential meas. around embedded high freq. antenna 2—74375
plasma resonances, book 2—60251
plasma resonances time durations rel. to latitude, altitude and ratio of electron plasma and cyclotron frequencies 2—48573
polar cap elec. fields, effects on magnetospheric convection 2—65962
polar cusp, electric fields and electron fluxes 2—54895
Polar magnetic substorms, meas. of MeV electrons during recovery phase 2—68981
polar thermospheric winds, convection electric fields in ionospheric model 2—65855
polarization of Pcl micropulsations propagated through ionospheric ducts 2—54930
potential variations rel. to 11-year solar cycle 2—65961
probing, possibility of using low-intensity relativistic electron beam, theory 2—80348
propagation of oblique hydromagnetic plane waves at micropulsation frequencies 2—65959
proton fluxes with ISIS-1 and 2 at mid-latitudes, association with plasmapause and SAR arcs 2—62327
radio drift velocities, point source effect in time- averaged correlations 2—65964
radio noise characteristics of auroral ionosphere 2—72840
reflection height computation from oblique backscatter soundings at two frequencies 2—48565

Ionosphere continued
review of developments (1925-1955) 2−68958
shock front from Apollo 15 launching 2−54897
signals, spectral props. obs. with multichannel field recorder 2−48564
simulation using plasma accelerator 2−77280
solar activity effects 2−66226
spaced receiver drift records, study of methods of analysis 2−84899
storm, rel. to geomag. disturbances 2−62363
substorms, rel. to auroral absorption substorm development, models 2−81729
sudden disturbances, interpretation using solar X-ray flux obs. 2−75954
sudden disturbances caused by solar flares, review 2−84903
sunrise effects on meteor region and radio echoes from Quadrantid meteors 2−44748
thermal positive ions in outer ionosphere and magnetosphere 2−65844
thermosphere, chem. release obs. from high flying aircraft 2−58035
thermosphere, diurnal variations of temp. and density, influence of vertical motions 2−65820
thermosphere, equatorial, neutral comp. 2−58033
thermosphere, global mean temp. maintenance by EUV flux absorpt. 2−58026
thermosphere, lower, neutral comp. meas. in ALADDIN I program 2−57952
thermosphere, lower, quiet day Joule heating rate 2−58023
thermosphere, mass spectrometry and incoherent scatter sounding 2−65824
thermosphere, minor constituents meas. by mass spectra 2−62295
thermosphere, molecular O_2 densities from Ariel 3 measurements 2−51631
thermosphere, neutral composition above Fort Churchill 2−65828
thermosphere, neutral heating efficiency 2−58025
thermosphere, neutral particle temp. meas. from San Marco III 2−58020
thermosphere, one- and three-dimens. model obs. 2−58039
thermosphere, photodissociation rates of O_2 2−65830
thermosphere, positive ion composition obs. during summer at high latitude 2−65829
thermosphere, theoretical and empirical approaches 2−58031
thermosphere, tidal temp. oscillations from incoherent scatter obs. 2−58024
thermosphere dynamics, heat input and eigenfunctions 2−81699
thermosphere dynamics, planetary waves 2−81701
thermosphere dynamics, tidal waves 2−81700
thermosphere energy source, convection elec. fields 2−58041
thermosphere explorer program 2−58032
thermospheric composition, longitudinal variations indicating magnetic control of polar heat input 2−65827
thermospheric density, annual and semiannual variations 2−48525
thermospheric dynamics, obs. using travelling ionospheric disturbances 2−65958
thermospheric heating and energetics 2−58022
thermospheric model, satellite orbital decay densities, incoherent scatter temps. 2−81702
thermospheric O_2 abundance variation, 6300Å twilight airglow obs. 2−58055
thermospheric temperature, measurements in polar zone 2−48523
thermospheric winds from exptl. density data 2−58042
thundercloud, calc. of electric field in ionosphere and magnetosphere 2−62347
topside, electron temp. vertical gradients 2−62358
topside, oxygen and hydrogen ion densities 2−58074
topside electron density measurements during geomagnetic storm 2−72867
total electron content, radio wave Faraday rotation obs. using ionospheric beacon satellite 2−48570
total electron content, sudden increases after solar radio bursts 2−51648
total number of electrons, simultaneous meas. by radiowave noncoherent scatterng and satellite signals 2−54893
transequatorial propagation of decametric waves rel. to ionospheric irregularities 2−84895
transient ion layer formation rel. to sudden disturbances in 20-50km range 2−54888
transient responses, resonance spikes of topside sounders 2−81728
travelling disturbances, as diagnostic tool for thermospheric dynamics 2−65958
travelling disturbances, directional filtering by strong thermospheric winds 2−54896
travelling disturbances, theory and expt. 2−72873
trough regions, thermalization of colliding ion streams 2−65946
TV techniques appl. for data acquisition in auroral and ionospheric research 2−84892
upper, electron temp. anisotropy 2−62356
variations in ionization, diurnal and seasonal 2−51649
v.l.f. reflection coefficients, effect of positive ions 2−78393
waveguide, hydromagnetic pulse propagation 2−84897
wavelike ionospheric disturbances and signal phase characteristics 2−72869
whistler mode signals from v.l.f. transmitter in Australia 2−78396
whistlers, fractional hop, OGO-6 obs. of wave normal vectors 2−62362
wind fields, vertical profiles 2−58077
Ba cloud growth in highly conducting medium 2−65950

D-region
A_1 absorption, rel. to solar X-ray flux 2−58078
absorption at 2.2 MHz over Haringhata 2−65968
aurora, electron density, incoherent scatter radar obs. 2−81735
average reflection heights, by v.l.f. trans-Antarctic propagation based on waveguide dispersion meas. 2−54900
cross modulation at l.f. and v.l.f. 2−58079
diurnal models, transient conditions, photochemical computer code 2−81731
electron densities and collision frequencies 2−65971
electron density affected by visible light flux 2−48577
electron density and collision frequency meas. by partial reflections method 2−51651
electron density profile, determ. method 2−62369

Ionosphere continued
D-region continued
electron density profiles during sudden ionospheric disturbance 2−72879
electron density profiles for all seasons and varying solar activity 2−44755
electron density profiles from extraordinary component of partial reflections 2−84906
electron number density rel. to ion pair production rate 2−48576
e.m. fields calc. 2−59007
e.m. propag. and total electron content, satellite-borne earth-refl. sounder expt. 2−58080
equatorial, electron and positive ion density distributions 2−72880
equatorial electron densities, rocket measurements 2−84914
exponential model, electron distribution profile 2−84910
incoherent scatter measurements, 1290 MHz aurural zone radar, Chatanika, Alaska 2−72884
incoherent scatter observations at Arecibo using pulse compression techniques 2−72885
ion chemistry, effect of sudden disturbances caused by solar flares 2−84903
ion-ion neutralization reactions, obs. using merged beam technique 2−65969
ionization and neutral constituents, relation of theory and experiment 2−78401
ionization by solar corpuscular flux in central latitudes 2−51650
magnetic storm induced anomalies in absorpt. phenomena 2−81730
magnetosphere-ionosphere interactions, conference 2−48568
midlatitudes, model for summer noon during sunspot maximum, l.f., v.l.f. propagation 2−55625
partially reflected signals from, statistical characteristics 2−44754
photodetachment of electrons from major negative ions 2−78403
plasma diagnostics using symmetric double-probe technique 2−58086
polar, impulsive variations in ioniz. 2−58083
positive ions, cluster, switch and rearrangement reactions 2−58084
pre-sunrise, positive ion comp. 2−58085
precipitating energetic electrons at mid- latitudes due to minor mag. activity 2−58082
precipitating particles and r.f. absorpt., simultaneous satellite meas. 2−58081
radio wave absorpt. correl. with total atmospheric ozone content 2−78399
reflection coefficients, from thin parabolic layer 2−72889
r.f. impedance probe, electron density and temp. determ. 2−65954
signal partial reflection, h.f. dynamic phase metering instrument 2−65967
Solar protons effect rel. to riometer absorption during polar cap absorption events 2−48575
sunrise, photodetachment rates of negative ions 2−72882
sunrise, time variation of O_3, metastable O_2, O densities 2−72881
sunrise conditions, time variations of negative ion, electron densities, model 2−72883
theoretical models, ion pair production 2−78400
upper atmosphere wind speed and direction, air density and temperatures up to 95 km, simultaneous meas. using chaff cloud sensors 2−54876
v.l.f. disturbances assoc. with solar X-ray bursts 2−73119
X-radiation detection, emission from solar subflares 2−66228
NO, eddy diffusion coefficient, chemistry of NO densities 2−65970

E-region
absorption at 2.2 MHz over Haringhata 2−65968
aurora, electron density, incoherent scatter radar obs. 2−81735
drift dispersion, Antarctic obs. 2−62370
electrojet effects, lab. simulation 2−58071
electron density increase below artificial Ba cloud 2−68969
electron density profiles, time depend. 2−58089
electron density profiles for all seasons and varying solar activity 2−44755
electron drifts over magnetic equator, solar cycle effects 2−44757
equatorial sporadic E, plasma instabilities 2−54901
height-frequency characteristics forecasting for normal E-layer 2−72890
horizontal drift of ionospheric plasma above Millstone Hill 2−65974
incoherent scatter measurements, 1290 MHz aurural zone radar, Chatanika, Alaska 2−72884
incoherent scatter observations at Arecibo using pulse compression techniques 2−72885
ion chemistry and thermal balance 2−48580
ionization profiles, numerical model 2−58087
maximum electron density, describing function of diurnal variation 2−65975
model parameters, ionization and recombination 2−81732
motion, study from measurements of ground diffraction patterns produced by 300 kHz radio wave reflections 2−68970
neutral temp., from twilight and nightglow O λ6300 and λ5577 profiles 2−65973
night time studies, 1/25 MHz and 50/2000 KHz ionogram 2−51652
nighttime, absorption patterns, indication of ionization processes 2−48579
nighttime, stratifications variations, 1/25 MHz & 50/2000 kHz ionogram 2−51652
Peruvian electrojet, lunar variations using E-region electron-drift measurements 2−68955
radio pulse amplitude probability distrib. 2−78398
recombination coeff. meas., solar flares 2−44756
reflected radio waves, ground diffraction pattern 2−72887
r.f. impedance probe, electron density and temp. determ. 2−65954
seasonal anomaly rel. to regression- line studies 2−65976
sporadic, movement and spreading 2−48581
sporadic, v.h.f. wave propagation 2−72888
sporadic E, high latitude, patterns of occurrence 2−72886
sporadic E, ion density profiles for Project Aladdin 2−58075
sporadic E, positive ion comp. 2−58085
sporadic E, positive ion comp. meas. 2−58088
sporadic E appearance, frequency distribution at polar latitudes a function of limiting frequency 2−72899
sporadic E detection during electron density measurements 2−48571
sporadic E ionization, solar eclipse effect 2−65972
sporadic E region, vector mag. obs. of Sq currents 2−65977

Ionosphere continued
E-region continued
sporadic-E, blanketing, seasonal occurrence near geographic equator 2−48578
sporadic-E formation, role of meteors 2−72891
spread E, conditions causing rel. to F-region irregularities causing scintillation, magnetic field line connection 2−65978
tidal motions, radar obs. 2−58090

F-region
altitude dependence of various parameters 2−68971
ambient electron heating calcs. 2−62373
atmospheric gravity waves, perturbation profiles in F-region 2−65987
critical frequency, small-scale fluctuations, observations at Delhi, India 2−62371
dawn effects, simultaneous conjugate point measurements 2−65988
daytime, coupling between electron density and electron temp. 2−48585
east-west ion drifts, polarization fields 2−58097
electron density, disturbances during magnetic storms 2−75631
electron density distrib. about F_2 peak, determ. by analysis of ground echoes 2−54903
electron density disturbance by strong radio waves 2−72892
electron density disturbance effects on night side 2−48586
electron density variation above N. America during magnetic disturbance 2−65986
electron drifts, horizontal and vertical at Thumba 2−84915
electron drifts over magnetic equator, solar cycle effects 2−44757
electronic collision frequency in F-region, ground-based measurements 2−84913
e.l.f. and v.l.f. waves propagation, ionospheric fields stable solutions 2−48584
equatorial phenomena, rel. to soft particle flux characts. up to 1200 km 2−65834
e.s. turbulence, spread F 2−65982
evening anomaly in F-layer ionization 2−72897
F2, FO, lunar variations at low latitude 2−62376
F2 layer, importance of nonlinear term in equation of motion 2−48474
F2 layer, nighttime maitenance, models 2−58093
F2 layer, real height variations above geomagnetically conjugate points 2−51653
F2-layer, e.m. wave reflection 2−65980
f_1 layer, at medium to high latitudes, diurnal and seasonal model 2−65985
F_2 layer, disturbances, strong spread reflections 2−72900
F_2 layer parameters, computer forecasting 2−84912
geomagnetic control over evolution of F_2-layer at sunrise 2−84909
height variations of F_2-region max. and temp. variations as function of solar and geomagnetic activity 2−48591
horizontal drift of ionospheric plasma above Millstone Hill 2−65974
incoherent scatter measurements, 1290 MHz aurural zone radar, Chatanika, Alaska 2−72884
ion admixture distribution, one-dimensional nonisothermal diffusion for stationary case 2−48587
ion chemistry and thermal balance 2−48580
ionization irregularities, direct backscatter reflections 2−72893
ionization level after sunrise, continuous sounding obs. 2−84908
ionization profiles, numerical model 2−58087
irregularities, scintillations of satellite beacons 2−65983
Jicamarca, magnetic storm of March 8, 1970, synthesis using computer 2−72916
magnetic apex coordinate system for F_2-layer 2−65979
MHD wave interpret. of motions 2−62377
modification, by high power h.f. radiowave 2−81733
modification by h.f. radio waves, determ. of threshold 2−65981
molecular ion concentrations in F_2-layer 2−72895
neutral wind charge, effect on low-latitude F-region 2−65989
nighttime, absorption patterns, indication of ionization processes 2−48579
nighttime 6300 Angstroms airglow emission at magnetic equator rel. to F-layer peak movement 2−84880
nighttime maintenance, backscatt. obs. 2−58094
nighttime maintenance, horizontal transport influence 2−58096
nighttime maintenance mechanism 2−58092
orientation of irregularities causing scintillation of Earth satellite signals 2−65990
parameters, correlation with 6300Å line intensity in nightglow 2−65890
parameters, relation with 6300 Å airglow 2−48543
photo-electron energy distrib. and its variation with sunspot activity 2−65984
photoelectron flux meas. by radar and satellite methods, comparison 2−62374
plasma drift and electron concentrations 2−48590
polar cusp, magnetic control 2−54902
predawn effect, calc. of energy flux transmitted from local electron heating in plasma 2−54904
processes rel. to appl. of gas diffusion in gravitational field 2−58091
radio pulse amplitude probability distrib. 2−78398
radiowave refraction from F-layer in transequatorial propagation obs. by ray tracing procedure 2−48563
range spreading type spread-F, producing structures, incoherent scatter radar obs. 2−48588
recombination, effect of excited states of atomic oxygen ions 2−62375
response to v.l.f. ion-acoustic waves rel. to sudden geomagnetic storms 2−83614
ring current effect on F-region disturbance 2−72896
scintillation, irregularities causing rel. to conditions causing spread E magnetic field line connection 2−65978
scintillations, seasonal, diurnal and magnetic dependence 2−65991
seasonal anomaly, computer simulation 2−78402
spread-F, at magnetic equator 2−48582
spread-F, theory 2−48583
stability of dynamic model 2−72898
storms, theoretical models 2−65992
tidal motions, radar obs. 2−58090

Ionosphere continued
F-region continued
topside, continuity eqn. calcs., ioniz. loss, charge exchange, plasmasphere coupling 2−58098
topside, dynamical processes, plasma drifts 2−68972
topside, electron densities, sunrise effects 2−81734
topside, reson. obs. on rocket-borne advanced radio sounder 2−62372
topside plasma flow inside and outside of plasmasphere 2−58095
vertical velocity det. from nighttime electron density-true height profiles 2−48589
F_2 layer, neutral temp., from twilight and nightglow O λ6300 and λ5577 profiles 2−65973
O/N_2, O/O_2 abundance ratios in thermosphere rel. to nighttime F_2 region 2−65816
O^+ ion distribution and vertical motions in lower part of F-region 2−72894

Ionosphere measuring apparatus
admittance meas. of 36-m dipole antenna in topside ionsphere 2−72859
auroral-zone incoherent-scatter radar, Chatanika, Alaska, 1290 MHz 2−72884
automatic recording system for amplitude, phase measurements of ground diffraction, patterns 2−68970
double-probe technique for plasma diagnostics 2−58086
electron density meas., r.f. probe 2−48574
electron temp. meas. IC apparatus design 2−65966
ground observatory for predicting radio communication conditions 2−62293
h.f. dynamic phase metering instrument for partially reflected e.m. signals from D-region 2−65967
incoherent scatter sounder, characteristics, computer optimization 2−78392
ionosonde receiver with automatic noise suppression and digital-analogue recording 2−65965
Langmuir probes, low electron temp. meas. in afterglow plasma rel. to ionospheric meas. inaccuracies 2−83555
multichannel field recorder, effect of dephasing of channels on correlation characteristics of signal 2−48564
negatively biased conical probes in supersonic flow, current drawn and det. of ion density 2−46758
pulse compression radar for incoherent scatter observations 2−72885
radio drift measurements, signal coupling among spaced sensor channels 2−51646
retarding potential analyzer errors due to pot. nonuniformities in grid planes 2−62366
retarding potential analyzer operation in directional flux mode 2−62367
retarding potential analyzers, ion trajectory perturbations due to pot. nonuniformities in grid plane 2−62368
r.f. impedance probe, electron density and temp. determ. 2−65954
riometer absorpt. during solar cosmic ray effects 2−62765
satellite electrostatic field, phase-plane solution 2−52348
scanning f.m.-CW radar sounder, for clear air structure obs. 2−84842
spaced receiver drift records, study of methods of analysis 2−84899

Ions
see also Atoms; Ion emission/thermionic; Molecules; Plasma
anode plasma of pulsed vacuum arc, energy distributions 2−46803
atmosphere, detection with spiral electron multiplier, operation characts. 2−66724
atomic, repulsive potentials 2−67379
corona point discharge in air at atmospheric pressure, obs. of small ion clusters 2−53259
n-decane, metastable ions 2−59884
electron-ion oscillation discharge, potl. distrib., temp. and density detn. 2−64319
energies in laser produced plasma 2−74385
hydrocarbon negative ions, CNDO calculations and reactions 2−64184
ion-sensitive plate response, depend. on ion struct. and comp. 2−83163
ionization potential-ionic radius relationship 2−83200
Jahn-Teller dynamic interaction of an ion in a crystal, simple approach 2−61565
metastable, determ. of lifetimes by field ionization mass spectrometry 2−46789
metastable data collection, modification of commercial mass spectrometer 2−59884
molecular-ion reactions, mechanism, relative cross-section rel. to collision ion energy 2−50122
molecule-ion reaction studies with quadrupole ion storage trap 2−83405
negative ion interactions under swarm conditions, apparatus for study 2−71000
neutralization theory, Laplace transform method, applic. to scavenging probability calc. in gamma radiolysis of dielectric liquids 2−44493
quartz, radiation-induced diffusion of alkali ions and protons and formation of colour centres 2−71532
rare earth, in crystal matrices, moments of radial function distributions, dependence on calc. method 2−65199
small ion current detection, using photomultipliers 2−45689
solar wind, extended power spectra of charge flux 2−62777
suprathermal, detection near lunar surface 2−44913
tetrahedral, force constants by orbital release force field and Urey-Bradley force field 2−77077
two-, three- and four-electron ions, Hartree-Fock and Hartree-Fock-Slater atomic form factors, electron momentum distributions 2−74205
uronium, CNDO/2 calculations of structure 2−60089
CO_2^+, predissoc., photoelectron- photoion coincidence spectroscopy and photoion kinetic energy analysis 2−67470
Er^{3+} ions in silicate glass, photoinduced absorption spectra 2−75291
Fe group, analytic wave functions consisting of 2 Slater type orbitals 2−83205
Gd^{3+}, isotropic exchange interactions from e.p.r. measurement in rare earth insulators 2−72487
$H_3O^+.H_2O$, rate constants and kinetic analysis for formation in inert gases 2−84622

Ions continued
- He II liquid, meas. of effective mass of positive and negative charge carriers by resonance technique 2—80512
- O^- production in dissociative electron capture by CO_2 2—80026
- SF_6, breakdown, electrode surface conditions and dust particle effects 2—74439

recombination
- afterglow at low pressure, 3 body recomb. 2—80372
- electron capture cross-sections, calc. by approximation procedures, book 2—63986
- ion-electron, in strongly associated solvents, solvation shell relaxation 2—46934
- ionospheric F-region, rel. to excited states of atomic oxygen ions 2—62375
- l.f. ionization recombination, oscillations in bounded low density plasma 2—80352
- plasma atomic level populations, distribution function 2—77269
- polyatomic gas, influence of dissociative recombination on spectral sharpness 2—60297
- Sagittarius B_2 radio complex, physical and kinematic properties 2—75814
- three-body recombination of positive and negative ions, reviews 2—74228
- triphenylamine in alkane solvent, viscosity dependent rate, fluorescence following pulse irradiation 2—46968
- Ar_2^+ afterglow, dissociative recomb. at elevated temp. 2—83262
- BaO, F centres reported, recombination by tunnelling 2—74803
- C, 85α line survey in Orion Nebula 2—81797
- Fe^+ in solid Xe, time meas. 2—46426
- H, 85α line survey in Orion Nebula 2—81797
- H, axially symmetric free expansion of non-equilibrium plasma 2—77270
- He^+-He^{2+}-e plasmas, calc. of collisional-radiative volume recombination and ionization coefficients 2—50193
- He, 85α line survey in Orion Nebula 2—81797
- He plasma, electron-ion recombination, produced by laser 2—67631
- He^+, meas. of rate coeff. for recombination with electrons in pulsed afterglow 2—70643
- He_2^+, with electrons, in postlum. of discharge 2—64345
- Kr_2^+ dissociative recombination at elevated temperatures in Kr afterglow 2—70888
- N_2^+, mechanism of electron-ion dissociative recombination in gas discharge 2—74272
- Ne_2^+ afterglow, dissociative recomb. at elevated temp. 2—83262
- O_2^+, O_4^+ formation and loss in Kr-O_2 afterglow plasmas, possible ionospheric implications 2—70889

scattering
- from crystals, angular distributions 2—75005
- He^+, backscattering and channelling effects in crystalline solids 2—84224
- NaCl before and after Cu vapour deposition, ion scatt. study 2—71314
- SiGe/W film, interface reactions, effects of p- or n-type substrates, ion backscattering analysis 2—71951

Ions, electrolytic
- *see also Conductivity, electrical/liquids, electrolytic; Dissociation/electrolytic*
- glass, strength and fracture for $Na^+ \rightarrow K^+$ ion exchange 2—64787
- Gouy layer, ion-size corrections of Poisson-Boltzmann equation 2—61792
- heterogeneous proton transfer, mechanism and rate transfer 2—61794
- lanthanide ions in solution, pseudocontact contribution to n.m.r. shifts 2—80481
- separation by hyperfiltration through charged collodion-polybase membranes 2—50352
- separation by hyperfiltration through charged membranes, calculation based on Teorell-Meyer and Sievers model 2—50351
- solutions, aqueous, i.r. spectra, freq. shifts 2—46959
- unsymmetrical electrolyte, linearized potential eqn. for interfacial region 2—75385
- Gd^{3+} in solutions of complex compounds, luminescence 2—71211
- $NiFe_2O_4$-Fe_3O_4-Fe_2TiO_4, ternary solid soln., cations distrib., in tetrahedral and octahedral positions 2—83840
- ZrO_2.CaO solid electrolyte, ion transport number 2—65054

Irasers *see Lasers*

Iridium
- cathodes, ThO_2 coated, as electron emitter for electron bombarded semiconductor devices 2—65099
- chemical classification of Fe meteorites, conc. rel. to Ge 2—75925
- chondrites, H-group, distribution in metal and silicate portions 2—62719
- de Haas-van Alphen effect, Fermi surface obs. 2—61215
- epitaxy by vapour deposition, low temp. 2—53575
- field ion microscopy, dissociated dislocations, geometrical contrast theory analysis 2—77592
- film, significance of electric field on growth 2—60634
- interfacial and grain boundary struct., brittle fracture, obs. using SEM, TEM and FIM 2—56576
- ion implanted, field ion microscope obs. 2—56741
- ion implanted, field ion microscope obs. 2—56740
- optical props. meas. in range 15-0.302 μm at 77 and 295 K 2—81359
- surface struct., use of Xe film in determ. by LEED 2—47077
- thermal expansion, high temp. obs. 2—51049
- thin oxide formation in aqueous electrolyte solutions passing anodic current, reaction kinetics 2—68784
- Ir:Dy(Er), e.s.r. of Dy and Er, localized moment-cond. electron exchange interaction 2—68737
- Ir-Al abundance association in L chondrites 2—73099
- Ir^{4+} in Cs_2ZrCl_6, high resolution MCD, and absorption spectra 2—57342
- ^{192}Ir hairpin interstitial radiation therapy, dosimetric considerations 2—69424
- in Pb-Ir-Pb structure, BCS interaction parameter determ. 2—71849

Iridium compounds
- alloy, field ion microscopy, dissociated dislocations, geometrical contrast theory analysis 2—77592
- pyrochlores, $M_2Ir_2O_7$, (M=Ln,Bi,Pb,Tl), struct. and props. 2—60987
- Fe-Rh-I, magnetic contrib. to electronic sp. ht. 2—64856

Iridium compounds continued
- Ir-Pt alloy, chemisorbed CO, i.r. spectra 2—68645
- Ir-Pt alloys, low field Hall coeffs. at 4.2K and 300K, two band model 2—61188
- $IrB_{1.1}$, prep. and elec. props. 2—47657
- $IrCr_3N$, crystallographic parameters and struct. transforms. 2—60759
- IrO, band spectrum, rotational and vibrational analysis, 4200 to 6400 Å 2—77065
- IrO_2, high-field magnetoresistance obs., Fermi-surface model 2—68295
- $K_2Pt(CN)_4Cl_{0.3}.xH_2O$, organometallic, thermoelec. analysis of elec. cond. 2—72055
- Th-Ir system, 66-83% Ir, phase relations 2—50976
- Th-Os-Ir system, comp. range of stability of $ThOs_2$-ThIr phase 2—50976

Iron
- — 2—67391
- — 2—69175
- — 2—67400
- abundances in evolved stars, det. from narrow band indices 2—66090
- adsorption of CO, change in work function 2—71348
- analysis, in glass raw materials, X-ray fluorescence spectroscopy 2—64524
- annealed in H_2 atmosphere, magnetic properties, effects of annealing temperature, holding time, cooling rate 2—81271
- atom, collisions with atmospheric ions, meas. of charge transfer cross sections for formation of Fe ions, 2-500 eV 2—79866
- atom, in $3d^64s^2$ and unstable Fe^+ $3d^7$ states, produced by decay of ^{57}Co in Xe 2—46426
- atom, K X-rays produced by heavy ions, energy shifts and relative intensities 2—64013
- atomic, Fe IX to XVI, classification of transitions 2—49948
- atomic central-field models for open shells, SCF calcs. 2—64025
- atoms in YuNDK24 alloy, exam. by nuclear γ reson. after thermomagnetic treatment 2—84471
- Barkhausen noise, freq. spectrum 2—61515
- b.c.c., electronic wavefunctions, rapid calculation 2—75018
- b.c.c., four-fold dislocation node formation 2—77583
- bombarded by C, N and O ions, 0.5-2 MeV, stopping power 2—47782
- cast, annealing, spheroidal graphite precip. 2—47584
- cast, damping characteristics 2—69703
- cast, ion beam thinning, graphite/pearlite interface microstructure, electron microscopy 2—74877
- cast, melt solidification, nodular graphite formation, additive effects 2—74881
- cast, solidification of elbows, numerical methods analysis 2—74587
- cast, spheroidal graphite, segregations rel. to microstruct. 2—50836
- cermets, thermal stability of sulphides of some metals 2—68164
- chemical polishing technique for prepn. of thin foils for e. microscopy 2—67963
- in composite, fibre-reinforced resin, incorporation using organometallics 2—50923
- cosmic ray muons multiple scattering in 10 to 70 GeV/c 2—73859
- creep, high temp., in α-phase single crystals 2—56804
- creep testing during thermal cycling for high purity and Swedish pure 2—56881
- critical and spin wave fluctuations, neutron scatt. 2—54309
- crystal, centred cubic, mean square displacement of atoms, simple calc. 2—57037
- crystals, effect of impurity concentration on type of deformation at 77K 2—64713
- in Cu and Cu-Al alloys, liq., cond.-electron spin polarization obs. 2—53455
- deformation temp. effect on changes of the mech. props. of α-Fe and low C steels 2—84159
- density at elevated temps., exptl. results for liquid and solid phases 2—64505
- desorption, of H_2, spatial distrib. obs. 2—50526
- diffusion along grain boundaries in W 2—47472
- diffusion in α-Fe_2O_3, O_2 partial press. depend., high temp. 2—51138
- diffusion in α-U, 645°C 2—50719
- diffusion in Al, interpreted using oscill. form of inter-ion potential 2—64691
- diffusion in Fe/Al solid/liquid system 2—80715
- diffusion in GaAs, 800-1100°C 2—60829
- diffusion in n-GaAs, temp. depend. 2—47463
- diffusion of C, O, H, N and S, solid and liq. states 2—43661
- diffusion of C, O, N and S, effective radii of diffusing particles, diffusion mechanisms 2—50709
- diffusion of hydrogen in zone melted α-phase rod 2—77610
- diffusion of Zn, determ. of Fe-Zn interdiffusion coeffs. 2—47459
- dislocation line tension, effects of elastic anisotropy 2—74772
- domain wall movement retardation, due to interaction with dislocations 2—68540
- Doppler effect due to structural material for fast reactor systems 2—83104
- drops, solidification in oil 2—43440
- dynamic strengthening singularities under infl. of shock waves 2—84075
- Earth's liquid core, calc. of electrical resistivity 2—54674
- effective magnetic field on ^{67}Zn 2—84404
- Ekco mineral analyser, radio-isotopic X-ray fluorescence 2—81643
- electrical resist. behaviour in crit. region 2—57279
- electron spin density meas. by combined Mossbauer and electron spectroscopy techniques 2—81343
- emission line wavelengths, and solar far u.v. spectrum and forbidden line identity 2—42729
- e.s.r. absorpt. spectrum in ThO_2 2—48296
- fatigue, high power ultrasonics 2—50794
- fatigue damage, steel and cast-iron, microhardness method 2—77670
- ferromagnetic host for $^{188, 190, 192}Os$ g-factor meas., comparison of IMPACT, PAC and Mossbauer techniques 2—42534
- ferromagnetism, model for origin and ave.-moment-internal field variations in dil. Fe-Si(Al) alloys 2—78008
- film, amorphous, deposition and annealing resist. study 2—77499
- film, asymmetric 180° domain walls, Lorentz microscopy obs. 2—48092
- film, condensed on glass, amorphous to cryst. transition temp. 2—43474

Iron continued
- film, corrosion products in $NaNO_2$, internal conversion electrons, Mossbauer study 2 72281
- film, in Al-Al_2O_3-Fe supercond. junc., electron spin polariz. detn. 2 64958
- film, meas. of longitudinal Faraday effect 2−54379
- film, single-crystal, inter-domain boundaries 2−61533
- film, u.h.v. Mossbauer emission spectra, mag. behaviour rel. to particle size 2−72284
- film, Xe adsorp., roughness and surface potential 2−50556
- films, monocryst., orientational magneto-optic effect 2−61589
- films, thin, Mossbauer spectra, 15-350 K, superparamagnetic fluctuations 2−68611
- finely divided, suspension in toluene, magnetization, temp. depend., 20-105 C 2−77450
- foil, electrocrystn. structures 2−83862
- foil, extended in electron microscope, cell formation obs. 2−71487
- green bodies, porous and sintered parts, polished metallographic specimen production 2−60933
- Hall effect, magnetoresist., $T \leqslant 4.2K$ 2−47836
- high purity, recrystn., polygonization 2−68136
- high strain rate behaviour using split Hopkinson bar method 2−53796
- hyperfine, interactions of implanted ^{220}Rn and ^{224}Ra studied by α-γ angular correlations 2−81341
- hyperfine field, at Al, P, Sc and Ta nuclei, spin echo obs. 2−72229
- hyperfine field for Os impurity, anomalous temp. depend 2−48121
- hyperfine fields, of ^{31}P, ^{75}As, ^{93}Nb, ^{121}Sb, ^{123}Sb, n.m.r. obs. 2−75354
- hyperfine fields for rare earth impurities 2−44322
- interstitial H-dislocation interaction 2−53735
- ion, in $FeFe_{2-x}Sc_xO_4$, Sc-containing magnetite, K emission and absorp. spectra 2−44400
- ion, in rare earth metal garnet, absorp. spectra 2−75305
- ion sources, laboratory, low intensity 2−55672
- Kerr effect meas. for increasing accuracy of magneto-opt. parameters 2−84461
- latent hardening, 110 extension axis 2−43799
- lattice dynamics 2−84178
- LEED and photoelectric work function measurement, (100) surface 2−50443
- liquid, abs. rates of N and calc. chem. diffusion coeffs. 2−64694
- liquid, diffusivity of oxygen, potentiostatic electrochemical measurents 2−60456
- liquid and Ni alloy, thermodynamic study by electromagnetic levitation melting in inert atmosphere 2−67871
- lunar breccias and soils, possible origin for excess 2−55127
- magnetic anisotropy, represented by lines of const. cryst. energy 2−78000
- magnetic crit. phenomena, sp. ht. and thermopower obs. 2−57290
- magnetic moment, atomic, dependence on the lattice parameter 2−81256
- magnetic moment, temp. depend., $T/T_c < 0.5$ 2−65154
- magnetic permeability calc. from optical spectra 2−65155
- magnetized Fe muon shield for high energy neutrino laboratory, design 2−83157
- magnetoelasticity, dislocation theory applic. 2−61519
- melting, thermodynamic properties, significant structure theory 2−56542
- meteorites, chemical classification, Ge conc. rel. to Ni, Ga and Ir 2−75925
- micrometeoroid simulation on metal targets microparticles from Van de Graaff accelerator 2−66187
- mineralogic distribution in upper mantle 2−72675
- Mossbauer effect, ^{127}I mag. moment obs. 2−63812
- Mossbauer effect, high pressure obs. between 300-20K 2−72283
- Mossbauer examination of internal mag. field variation with temp. and pressure 2−68330
- Mossbauer spectra of foils, high freq. mag. field effects 2−57332
- multidomain, neutron irradiation effects on remanent magnetism rel. to magnetization of lunar samples 2−58458
- neutron displacement cross sections, based on Lindhard model 2−83053
- neutron irradiated, low temp., softening and anneal hardening 2−80689
- αneutron irradiation, structure studies 2−60965
- nitrided zone refined, ductile-brittle transition 2−47629
- n.m.r. and nucl. polarization of ^{74}As, mag. moment, internal field 2−76796
- nodular cast, testing temp. effects fatigue strength 2−60923
- optical absorpt. spectra in almandine garnet 2−72328
- paramagnetic and ferromagnetic, structural features within d bands 2−61672
- permeation of hydrogen, surface effects 2−77608
- pitting, intergranular corrosion and stress corrosion cracking, significance of protection potential 2−68787
- plastic deform. of polycryst. foil, small-angle X-ray scatt. obs. 2−71567
- plastic deformation, dislocation dynamics, high voltage electron microscopy 2−56785
- plastically deformed, defects, resist. study 2−80740
- point defect calculations, α-phase, modified lattice statics approach 2−60784
- polycrystalline, meas. of longitudinal and transverse magnetoresistance at 4.2K, 77K, 273K 2−48063
- porous, shock response, Hugoniot elastic limits, model 2−61024
- powder, fine, sintering 2−61000
- radiation damage, atomic displacement cascades, computer simulation 2−53700
- reactor shielding, meas. of dose albedos of intermediate energy bremsstrahlung 2−76958
- reactors, atomic displacement rate and displacement cross section 2−42643
- recrystallization, internal friction obs. 2−47625
- recrystallization, internal friction obs. 2−47626
- refining, floating zone melting 2−47266
- resonance lines, intensities using different spectral lamps 2−52492
- RR Telescopii spectrum 2−58297
- secondary electron emission, from single and polycrystals, LEED obs. rel. to rocking curves 2−54281

Iron continued
- single crystal, H induced plastic strain, divergent X-ray beam obs. 2−64715
- sintering activator, role in W powder sintering 2−50899
- solar abundance, deduced from particle obs. made with nuclear emulsions 2−62745
- solar abundance det. from weak Fe I line $\lambda 5127.7$ 2−75944
- solar and stellar abundance and spectra 2−62748
- solar curve of growth and abundance 2−44974
- solar flares, 1971, January and September, composition and energy spectra of heavy nuclei, 0.5 to 40 MeV per nucleon 2−58556
- solar overabundance, accelerated by solar flares 2−76001
- solute in liq. Sn, thermoelec. power 2−71227
- spin waves, small-angle magnon scatt. collapse 2−44242
- spin-density asphericity, temp. depend. 2−44250
- steel plates, cold rolled Si, Fe loss due to rotating magnetic field 2−84422
- stellar radial velocity evaluations using standard wavelengths in Fe spectrum 2−48687
- stellar reaction rates, influence of excited states of target nuclei in vicinity 2−62507
- strain ageing, first stages 2−71624
- strain ageing, stress-assisted diffusion to dislocations, theory 2−43652
- strengthening mech., dynamic strain ageing, dislocation struct. 2−56911
- surface, cleaned and oxidized, secondary ion yield 2−61471
- tensile strength of single crystal plates, surface orientation depend. 2−71583
- transformations, α-γ-α, dilatometric behaviour 2−53987
- two-dimensional ferromagnetic domain walls, electron images 2−51247
- u.s. properties during solidification 2−71669
- valence states produced by ion-sputtering reduction, X-ray photoelectron spectroscopic obs. 2−57263
- whiskers, lattice twists, growth morphologies 2−80561
- whiskers, mag. stray fields of 180° Bloch walls, Permalloy probe study 2−78015
- yield stress damage function for neutron irradiation, determ. using SAND II code for data analysis 2−79840
- zone-refined, hydrogen embrittlement 2−43725
- α-Al_2O_3:Fe, α-Al_2O_3, Ti and α-Al_2O_3(Fe,Ti), polarized and high resolution UV, visible and IR spectra, e.s.r. spectra 2−78082
- Cu-Ni:^{57}Fe, Mossbauer doublets, time-differential perturbed angular correlations 2−72275
- Fe: ^{169}Tm, hyperfine field at Tm temp. depend. from perturbed angular correl. expts., 4.2-450K 2−81252
- Fe:Al_2O_3, dispersion-hardened, prep. of thin foils for transmission electron microscopy 2−80549
- Fe:As, hyperfine mag. fields at As, rel. to host mag. moments 2−78018
- Fe:^{42}Ca, hyperfine fields, perturbed angular correlation studies, g-factor of 3.19 MeV 6^+ state in ^{42}Ca 2−72243
- Fe:^{183}Re, ^{184}Re, nuclear orientation, mag. hyperfine splitting consts. 2−72245
- Fe/Al system, diffusion, barrier effect of intermediate Ag layers 2−47461
- Fe/H abundance ratio from binary star observations, Mv(K) dependence in late-type giants 2−73036
- Fe/H ratio in F1-F5 stars, by model atmos. anal. 2−66077
- Fe/LiF/Fe-Co film system, quasistatic mag. reversals 2−84408
- Fe/Ni diffusion couples, atomic mobility in Kirkendall plane 2−53763
- Fe/Ti diffusion couples, atomic mobility in Kirkendall plane 2−53763
- Fe/boride coating system, thermal expansion anisotropy 2−54058
- Fe-NbC, pseudobinary, phase equilib., phase diagram 2−68199
- Fe-Si textured sheet, permeability, eddy current loss, angle and field depend. rel. to domains 2−65153
- Fe^{3+}-centre, in SnO_2:Ni, e.p.r. 2−84564
- Fe-constantan junction, e.m.f. generated by shock wave propag. 2−75010
- α-Fe, cube edge dislocations, strain displacement field, linear elastic Volterra soln. 2−77568
- α-Fe, diffusion of C, press. effect 2−43660
- α-Fe, edge dislocation, elastic field, computer simulation 2−56710
- α-Fe, edge dislocations, core characts., computer simulation 2−60803
- α-Fe, elastic consts. rel. to spin order and diffusion, 25-900°C 2−60842
- Fe, grain size and temperature effects on cyclic strength and fracture 2−56896
- α-Fe, high temp., dislocation struct. and stresses 2−43637
- α-Fe, impurities, influence on self- diffusion coeffs. 2−47462
- α-Fe, neutron irrad., radiation- and anneal-hardening 2−80681
- α-Fe, plastically deformed, nature of debris loops 2−74778
- α-Fe, pure and alloyed, diffusion of Mn, 778.3-901°C 2−83994
- Fe and Cr simultaneous estimation in stainless steel by polarographic method 2−48352
- Fe I, 5049.83 Å, solar photospheric fluctuations, radial veloc., coherence and phase spectra 2−75950
- Fe I, Fe II resonance transitions, radiative lifetimes, applic. to Fe abundance det. in sun and QSO PHL 938 2−58547
- Fe I, first order analysis of variations of limb darkening and shapes for solar Fraunhofer lines 2−66199
- Fe I, interstellar, effect of radiation pressure round stars, galactic evolution 2−48730
- Fe I 5250.216 Angstroms solar line profiles rel. to sunspot models 2−75989
- Fe I in HD 188041, periodic magnetic variable, magnetic intensification and starspots 2−75747
- Fe I ionization and excitation equilibrium in solar atmosphere 2−66230
- Fe I ionization and excitation equilibrium in solar atmosphere 2−58559
- Fe I lines in solar spectrum rel. to saturation of Fraunhofer lines 2−78587
- Fe XIII ion, intensity ratios of i.r. lines in solar spectrum 2−55168
- Fe XIII line in solar corona, abundance and electron temperature meas. during 1966, November 12 eclipse 2−76027

Iron continued
Fe XIV, XV, XXIV lines in e.u.v spectra of solar flares 2−58546
Fe XV, solar e.u.v. spectrum rel. to theory and collisional excitation 2−78586
Fe XVI, multiplet strengths for electric quadrupole transitions calc. using HF orbital wave functions 2−42728
Fe XXV and Fe XXVI, high temp. obs. in minute plasma pts. 2−53179
Fe XXV in solar flares, calc. of wavelengths in X-ray region 2−85050
Fe XXV line emission from Scorpius X-1, high resolution search 2−85013
Fe XXVI, highly ionized, X-ray spectra 2−52917
Fe^{+} e.p.r. linewidth in MgO, temp. depend. 2−48289
Fe^{+} spin-lattice relax. in ThO$_2$ 2−84581
Fe^{2+}, in CdTe and MgO, phonon conductivity 2−64864
Fe^{2+}, in MnF$_2$, exchange polariz. in superexchange interactions, far i.r. obs. 2−81297
Fe^{2+}, level splitting, effect of configuration interaction 2−51293
Fe^{2+} impurity in Al$_2$O$_3$-Fe$_2$O$_3$ system, effects on spin relax. time of ferric ions 2−54368
Fe^{2+} in CaO, energy of first excited electronic levels 2−72478
Fe^{2+} in CdCr$_2$S$_4$, anisotropy of tetrahedral Fe^{2+} ions 2−72161
Fe^{2+} in MgO, higher order acoustic paramagnetic resonance transitions 2−51406
Fe^{2+} in MnF$_2$, exchange field obs. under press. 2−44304
Fe^{2+} in ruby, a.p.r. and spin-lattice relax. obs. 2−51285
Fe^{2+} in soda lime glass, thermal cond. 2−51056
Fe^{2+} ion, in Ni$_x$Fe$_{3-x}$O$_4$, Mossbauer obs., Zeeman patterns 2−54391
Fe^{2+} substitution in RbMnF$_3$, effect on e.p.r. linewidth and g-values 2−48292
Fe^{3+}, charge transfer bands in MgO, magneto-opt. struct. 2−72339
Fe^{3+}, e.p.r. in V$_2$O$_5$-Fe$_2$O$_3$ 2−48297
Fe^{3+}, e.p.r. in ZnWO$_4$ and MgWO$_4$, elec. field effect 2−48286
Fe^{3+}, exchange linkages in YFe$_{1-x}$Al$_x$O$_3$, effect on local mag. field at ^{57}Fe 2−72288
Fe^{3+}, in CaO or MgO, spin-lattice coeffs., relativistic cryst. field contrib. 2−65203
Fe^{3+}, in chalcogenide glass, e.p.r., fine struct. 2−72476
Fe^{3+}, in LiNbO$_3$, Hamiltonian parameters detn., e.p.r. obs. 2−65324
Fe^{3+}, spin-lattice relax. in TiO$_2$ 2−81459
Fe^{3+} e.p.r. in perovskites 2−81465
Fe^{3+} e.p.r. linewidth in MgO, temp. depend. 2−48289
Fe^{3+} in α-Al$_2$O$_3$, forbidden e.s.r. transitions 2−78158
Fe^{3+} in CaCO$_3$, spin-lattice relax. obs. 2−65177
Fe^{3+} in SnO$_2$, e.p.r. 2−48309
Fe^{3+} site assignment in low symmetry crystals 2−44439
FeI←CaII resonance, T-Tauri stars 2−75744
^{52}Fe production for medical use 2−69270
^{57}Fe, det. of electric field gradient parameters from Mossbauer spectra 2−54387
^{57}Fe in powdered absorbers, h.f.s. coupling and Mossbauer spectra parameters 2−75265
^{59}Fe, ultra-fast diffusion in α-Zr 2−64697
MgO, plastic yielding, high pressure effects 2−68081
Mn^{2+} in lunar plagioclases, e.p.r. obs. 2−62686
Mo:^{57}Fe, impurity-host to host-host coupling const. ratio, Mossbauer study 2−84183
Nb-Mo:Fe alloy, localized moments on Fe, Mossbauer obs. 2−48149
Ti/Fe abundance ratio in A-type supergiant stars 2−62537
TiO$_2$:Fe^{3+}, hole trapping by surface ferric acceptor states, Mossbauer obs. 2−84236
TiO$_2$:Li,V,Cr,Mn,Fe, transition metal impurity levels, esr determ. 2−44117
Y-Fe garnets, exchange interactions between mag. Fe^{3+} ions to determine absorption props. 2−81392
(ZnO-MgO):Fe,O photoconductor transient effect, shallow trap obs. 2−84377

Iron alloys
see also Iron compounds; Steel
absorption rates of N and calc. chem. diffusion rates 2−64694
Armco, grain size depend. of tensile strength 2−43846
Armco iron, plastic deform. influence on electronic struct. 2−75028
austenite, C content of small regions and transformation mechanism of Mo$_2$C fibres 2−77675
cast, bainite growth kinetics 2−43920
cast, cavitation erosion mechanism 2−71606
cast, damping capacity and dynamic modulus meas. under direct cyclic stresses 2−53861
cast, damping capacity from the variation of its dynamic modulus with strain amplitude 2−77674
cast, nodular, 4-5% Si, high wear resistance 2−74869
cast, nodular, solidification processes and quenching technique and relation to austenite shell 2−60549
cast, with graphite, decarburising, effect of S, Al, or Mg 2−43837
cast iron, abrasive wear tester, obs. 2−50792
cast iron, spheroidal graphite and common grade grey, hardness at elevated temperature 2−43739
dilute, Curie temp., effect of indirect exchange interactions 2−44248
dilute, recrystn., internal friction obs. 2−47625
dilute, recrystn., internal friction obs. 2−47626
dilute liquid Fe in Cu, CuZu, Zn, ZnGa, Ga, GaGe, GeAs, As, mag. susceptibility 2−80485
Fe$_{36}$Cr$_{22-x}$Ti$_x$, χ-phase alloy, $8<x<10$, inversion domain obs. 2−64637
ferrous metals, phases, stresses, Mossbauer spectroscopy 2−51312
grain growth, second max. and nonuniformity after deform. 2−83961
gray cast, rolling mild wear, Amsler machine obs. 2−56938
Hastelloy-X, neutron irrad., void form. and swelling resist. 2−53721
Incoloy-800, neutron irrad., void form. and swelling resist. 2−53721
Inconel-625, neutron irrad., void form. and swelling resist. 2−53721
Invar, elastic consts. anomalous temp. depend. in ferromag. state 2−84053
Invar, mag. moment temp. depend., $T/T_c<0.5$ 2−65154
Invar, spontaneous magnetostriction, itinerant electron model interpret. 2−48085
Invar, thermal expansion, low temp., Fermi liquid props. 2−84217

Iron alloys continued
invars, neutron diffraction study of crystal structure 2−68002
liquid, equilib. between Mn and O$_2$ 2−77676
martensitic structures, classification based on morphological criteria 2−83955
martensitic transform., martensite temp. 2−50943
martensitic transform. activation by stimulated emission of phonons 2−43909
oxide scales, partitioning of transition metals, chem. diffusion model 2−78197
permalloy, film, on CaF$_2$, optical absorpt., polarization anisotropy rel. to thickness and orientation 2−57324
Permalloy field access bubble domain drive ccts., magnetostatic pot. wells, drive fields, meas. technique 2−73507
Permalloy film, appl. of networks method for electron probe anal. 2−61830
permalloy film, coercive force and anisotropy, influence of substrate 2−84411
Permalloy film, creep rel. to thickness 2−56806
Permalloy film, cross-tie walls, motion threshold field and behaviour at inhomogeneities 2−77994
Permalloy film, electrodeposited, mag. anisotropy and magnetostriction 2−57302
Permalloy film, ferromag. reson., mag. moment, thickness, magnetization pinning 2−61539
Permalloy film, oxidized, slow domain wall motion 2−54340
Permalloy film, oxidized antiferromag. surface layer, mag. after effect 2−44267
Permalloy film, spin waves, 0.8-16GHz, below saturation magnetization 2−78034
Permalloy films, domain boundary motion, effect of struct. factors 2−61526
Permalloy films, l.f. slip of domain boundaries 2−61528
Permalloy films, mag. anisotropy, annealing depend. 2−61525
Permalloy films, monocryst., orientational magneto- optic effect 2−61589
Permalloy films, stripe struct., magneto-optical obs. 2−61531
Permalloy films with supercrit. hysteresis loop, domain struct. 2−61532
Permalloy plated-wire memory, domain struct., electron microscope obs. 2−75231
Permalloy thin wires, Bitter pattern obs. 2−61535
permalloy-Mn film, exchange anisotropy, thermomag. recording 2−57286
Permalloy-SiO- Permalloy multilayer systems, stripe domain struct. 2−61530
pig iron, antimony content neutron activation analysis, spectral method 2−78215
positron annihilation in γ-phase and α-modified compared 2−68325
solid solns., serrated yielding between 500 and 775 K 2−74839
spectrographic determination of Ag 2−57443
and steel, trace nonferrous metals analysis, sample particle size effect 2−51476
strength-differential effect, effective modulus interpretation 2−74853
superalloy, vacuum melted, Ce additions to control residual S 2−47637
system, plastic deformation, microhardness, emission electron microscopy 2−74843
Udimet 500, low cycle fatigue and fracture modes 2−56820
Vanadium Permendur, dimens. stability 2−43994
Al-Fe, liq., resist., conc. depend., 1650°C 2−46980
Al-(0.5 wt.%)Fe, creep, high temp.-low stress, directional diffusion vs. dislocation process mechanisms 2−50755
Au-Fe, dil., deviation from Matthiessen's rule, 0.5-60 K 2−77854
Au-Fe, dilute polycrystalline, negative transverse magnetoresistance 2−64911
Au-Fe thermocouples, calibration rel. to KP, Ag, Cu, temp. range 4K-280K 2−81158
AuFe, Mossbauer effect, reducing point charge model analysis 2−65229
α-Fe-Sn, solid soln., precip. of Fe-Sn by dislocations, effect of third component on morphology and kinetics 2−80812
Be-(1 wt.%)Fe alloy, precip., Mossbauer obs. 2−50931
Co-Cu-Fe-Ce permanent magnet, sintered, prep. and props. 2−50910
Co-Cu-Fe-Ce permanent magnet prep. by directional solidification 2−43787
Co-Fe, structure and orientation of electrolytically deposited films 2−53561
Co-Fe (8 at.% Fe) alloys, anisotropic magnetization and magnetic anis. 2−81255
Co-Ni-Fe ^{60}Co self-diffusion, Fe content effects 2−43659
Co$_{0.91}$Fe$_{0.09}$, f.c.c., temp. dependence of mag. moment distrib. 2−65165
Cu-Al-Fe bronze, superplastically deformed, textures and anisotropic flow 2−43831
(Cu-Au)-Fe, dil., mag. susceptibility 2−61483
Cu-Fe, dil., paramag. susceptibility, 1.7-300K 2−61483
Cu-Fe, distrib. of nearest neighbour atoms, Mossbauer obs. 2−74900
Cu-Fe, liquid, density, max. bubble pressure method 2−56488
Cu-Ni-Fe, intergranular fracture on spinodal decomp., mechanism 2−57012
Fe:Sn, grain-boundary hardening, micro-indentation elastic recovery obs. 2−60910
Fe-0.3% Nb, dynamic strain ageing47598 2−47598
Fe-30 wt.% Ni, surface martensite obs. 2−68196
Fe-Al-C, martensite cryst. struct. change, −196 to 20°C 2−80766
Fe-Al-C alloys, influence of ordering and martensitic transformations during quenching 2−84073
Fe-Al-Cr effect of zirconium on mechanical props. and oxidation resistance 2−60935
Fe-Al-Cu-Mg-Mn-Si-Ni-Zr-Ti, D16T, recryst. and uncryst. struct., fracture under static and cyclic conditions 2−47527
Fe-Al-Mg-Cu-Si-Mn, AK6, ageing, temp.-time ranges 2−50802
Fe-Al-Ni-Co-Ti, prod. by Magnicol process, reaction mechanisms 2−43834
Fe-Al, diffuse X-ray scatt. and temp. depend. of sp. ht. 2−56654
Fe-Al, magnetic anisotropy 2−54319

Iron alloys continued
Fe-Al, microhardness rel. to precip. of Fe and annealing out of lattice defects 2−50828
Fe-Al, quantitative microanalysis, applic. of Monte Carlo calcs. 2−68830
Fe-Al, struct., mech. and elec. props., precip. of Fe 2−50827
Fe-Al dil. alloy, ave.-moment-internal field variations 2−78008
Fe-Al system, β-solid solns., order-disorder processes, sp.ht. obs. 2−54002
Fe-Au, intraband absorpt., anomalous temp. depend. 2−81388
Fe-Au, precip. rel. to G.P. zone form., dislocations, vacancies 2−43851
Fe-B-metal melts, mag. behaviour 2−72138
Fe-B system, phase diagram 2−50957
Fe-Be, Fermi surface, electron scatt., de Haas-van Alphen and residual resist. obs. 2−71791
Fe-1%C-0.5%As, anomalous precip., resistivity, internal friction and elec. microscope obs. 50940 2−50940
Fe-C-W, precipitation of eutectic carbide, and microsegregation obs. 2−74929
Fe-C-i-j-…-n multicomponent solid solution, C diffusion coeff., thermodynamic interpretation 2−43662
Fe-C, baikovite, a new struct., produced by ultra rapid heating and cooling by laser beam 2−47630
Fe-C, Fe-C-X, phase transforms., thermionic emission electron microscopy applic. 2−57016
Fe-C, quench ageing and reversion 2−56903
Fe-C, recovery of internal friction after strain ageing 2−47481
Fe-C, strain ageing, internal friction obs. 2−56904
Fe-C system, diffusion of impurities, theory 2−50708
Fe-1%C, effect of As and Sn on tempering stages 2−50796
Fe-(0.11 wt.%)C austenite grain size effects on Widmanstatten start temp. of proeutectoid ferrite reaction 2−68195
Fe-Co/LiF/Fe film system, quasistatic mag. reversals 2−84408
Fe-Co-C, struct. and strength 2−56941
Fe-Co-Ni-Ti-Al-Cu, YuNDK42T8, homogenizing rel. to phase comp., mech. and mag. props. 2−47688
Fe-Co-Ni, coherent potential approx. calc. 2−71794
Fe-Co-Ni, powder, highly disperse, effect of electrolytic prep. variables 2−68543
Fe-Co-V, ordered and disordered, recovery behaviour 2−50804
Fe-Co-V , plastic deform. and brittleness 2−60868
Fe-Co, dil., hyperfine fields, ^{57}Fe n.m.r. study 2−65344
Fe-Co, equiatomic, magnetic anisotropy energetics, order determ. 2−61507
Fe-Co, Hall effect, magnetoresist., $T \leqslant 4.2K$ 2−47836
Fe-Co, metamagnetic character, rel. to temp. depend. of mag. props. 2−51258
Fe-Co, ordering effects on electronic struct. 2−44249
Fe-Co, very dil., 25 mK, spin-lattice relax. of ^{60}Co, field depend. 2−72232
Fe-Co layers with intermediate LiF layer, electron microscope study of interacting interdomain boundaries 2−61534
Fe-Co(Ni)-Ti-Al, solid soln. decomp. 2−56933
Fe-Cr-Al, potentiodynamic curves as function of tensile stress 2−44488
Fe-Cr-Co system, phase boundary $\alpha+\gamma/\gamma$ determ. 2−84164
Fe-Cr-Mn α-γ phase equilib., effect of transition metal additions 2−47687
Fe-Cr-Mn system, phase boundary $\alpha+\gamma/\gamma$ determ. 2−84164
Fe-Cr-N, microstructure revealing nitride phase 2−53894
Fe-Cr-Ni, plastic deform., low temp. 2−43693
Fe-Cr-Ni system, phase boundary $\alpha+\gamma/\gamma$ determ. 2−84164
Fe-(16 wt.%)Cr, electromigration of Fe and Co 2−47460
Fe-Cr, dil., Mossbauer effect, lattice disturbance produced by solute 2−44354
Fe-Cr, sp. ht. and thermopower near mag. crit. pts. 2−57290
Fe-Cr Hall effect, magnetoresist., $T \leqslant 4.2K$ 2−47836
Fe-Cr system, computed low temp. phase equilib. 2−50966
Fe-Cr σ-phase, atomic distrib. and mag. props., Mossbauer obs. 2−44253
Fe-Cr(8%), martensite, substruct., quenching and tempering temp. effects, rel. to strengthening 2−84071
Fe-Cu-O system, equilib. phase diagram detn. 2−64818
Fe-Cu, dispersion strengthening model, slip dislocation precipitate interaction 2−50744
1 at.%Fe-Cu, precip. of Fe during ageing, Mossbauer obs. 2−77724
Fe-Fe$_3$C-Si, phase diagram, white cast iron and carbon equivalent 2−74954
Fe-Ga-Sb and Fe-Sb systems, constitution and mag. props. 2−64821
Fe-Ga alloys, magnetic props. and Mossbauer investigations 2−84416
Fe-Ga solid solns., Mossbauer lineshape effects on hyperfine fields 2−44353
Fe-Ge α' solid solution, precipitation behaviour 2−64819
Fe-Ge system, constitution and mag. props. 2−64821
Fe-Mg-Ni, austenite transform. 2−53991
Fe-Mg-O system, activities, calc. by Darken's method 2−43815
Fe-Mn-C, long period stacking order structure formed by thermal cycling 2−67990
Fe-Mn-C alloy, orientation relationship of the (225) martensitic transform. 2−74928
Fe-Mn-Ni system using semihard magnetic alloys 2−84407
Fe-Mn-O system, activities, calc. by Darken's method 2−43815
Fe-Mn-Ti, ferritic and martensitic, hardening 2−47592
Fe-Mn-(B)-C, struct. and strength 2−56941
Fe-(3o wt.%)Mn, austenitic, strengthening by shock loading 2−43841
Fe-Mn, austenitic, singularities of hardening 2−50783
Fe-Mn, b.c.c., shock deformed, recovery 2−56912
Fe-Mn, kinetics of manganeseo-wustite scale formation 2−48333
Fe-Mn alloy, field ion microscopy exam. comparing orientation to ferrite α and iron nitride 2−64777
Fe-Mn alloys, $\gamma \rightleftarrows \varepsilon$ transformations, austenite stabilisation, effect of interstitials and substitutional atoms 2−71682
Fe-Mn and Fe-Mn-C alloys, martensitic transformations and temp. conc. boundaries 2−71683
Fe-Mn system, b.c.c. martensite growth 2−64591
Fe-(6 at.%)Mo, precip. 2−43849

Iron alloys continued
Fe-Mo, precip. rel. to G.P. zone form., dislocations, vacancies 2−43851
Fe-Mo alloys, nitrided, substitutional interstitial G.P. zones 2−80826
Fe-Mo solid solution, creep type, variation with applied stress 2−43703
Fe-MoC, quenched and tempered, microstruct., field ion microscopy obs. 2−47581
Fe-3.1 wt.%Si, electrodiffusion activation energy of polygonization substruct. 2−53764
Fe-N, quench ageing and reversion 2−56903
Fe-N, strain ageing, internal friction obs. 2−56904
Fe-(30.3 wt.%)Ni, damping of oscillations during heating after martensitic transform. 2−43791
Fe-Nb-Al bearing steel, dynamic strain ageing 2−47598
Fe-Ni/Fe-Co layers, permeability, intrinsic magnetization, coercivity, remanence 2−61536
Fe-Ni-Al-Cu, struct. and mag. props., alloying additive effects 2−43845
Fe-Ni-Al, martensite transform, effect of disperse particles 2−50942
Fe-Ni-Al, martensitic transformation, effect of dispersion particles 2−57015
Fe-Ni-C-Mo-Cr, tempering, effect on struct. and mech. props. 2−43853
Fe-Ni-C, deform.-induced martensitic reaction, kinetics 2−80833
Fe-Ni-C, deform. martensite formation, effect on mech. props. 2−71684
Fe-Ni-C, isothermal and athermal, deform. induced martensitic transform. 2−71685
Fe-Ni-C, martensite, surface plastic deform., X-ray obs. 2−80769
Fe-Ni-C, martensitic, microplastic deform. and isothermal transform 2−43807
Fe-Ni-C, martensitic, microplastic deform. and isothermal transform. 2−43808
Fe-Ni-C, phase transform., martensite to austenite, rel. to heating rate 2−53985
Fe-Ni-C, quenching and hydrogenation effects on mechanical props. and brittleness 2−43723
Fe-Ni-C, tempering, effect on struct. and mech. props. 2−43853
Fe-Ni-C martensitic, intercryst. mechanism, incompat form. 2−56815
Fe-Ni-Co alloys, dilatometric study of vol. exp. for fcc to bcc transformations 2−65146
Fe-Ni-Cu, spinodal, interphase interfaces, interfacial dislocations 2−56719
Fe-Ni-Mn, isothermal martensitic transform. rel. to mag. field 2−50937
Fe-Ni-Mn martensitic alloys, reversion behaviour 2−77747
Fe-Ni-Mo, dispersed, electrolytic deposition 2−77725
Fe-Ni-Mo, powder metallurgy, carbonyl prod. method 2−68159
Fe-Ni-Nb-C, ageing, 700 and 800°C 2−47596
Fe-Ni-Si, temper brittleness development, grain boundary adsorption of P, internal friction study 2−80767
Fe-Ni, atom redistrib. on ageing, Mossbauer obs. 2−60981
Fe-Ni, deform. martensite obs. 2−43838
Fe-Ni, diffusion of hydrogen, struct. influence 2−77611
Fe-Ni, dislocations, mobile, strain rate sensitivity and density 2−56711
Fe-Ni, Fe-Ni-Co and Fe-Ni-Mo, cumulative thermal cycling behaviour, 300°C/hr. 2−60960
Fe-Ni, ferromagnetic resonance line width, effect of Ni content after quenching or annealing 2−72174
Fe-Ni, film, rotating mag. anisotropy, temp. depend. 2−57300
Fe-Ni, hardening at high strain rates, rel. to microstruct. changes 2−47593
Fe-Ni, invar, areas of Fe conc., positron annihilation obs. 2−80524
Fe-Ni, Invar, elastic consts., anomalous temp. depend. 2−80751
Fe-Ni, Invar, Hall and Nernst-Ettinghausen effect, 100-300°C 2−72164
Fe-Ni, martensite, morphology and cryst. geometry, comp. effects 2−80771
Fe-Ni, martensitic transformation study by internal friction during heat treatment 2−43916
Fe-Ni, martensitic transform., interphase boundary shifting 2−43910
Fe-Ni, para processes, high field susceptibility, conc. depend. 2−72114
Fe-Ni, surface diff. and diff. of N and C along austenite/ferrite phase boundary 2−68052
Fe-Ni, thermal stability of elastic modulus, contrib. of Invar anomaly and ΔE-effect 2−50724
Fe-Ni, Young's and shear modulus anomalies, in Invar region, origin 2−77632
Fe-Ni alloys, elimination of Barkhausen effect in electrodeposited films 2−72169
Fe-Ni alloys, magnetisation and magnetostriction in strong magnetic fields 2−68507
Fe-Ni and Fe-Ni-C martensitic alloys, delayed fracture formation during cathodic charging under static stress 2−64731
Fe-Ni doped invar, f.c.c. lattice, main magnetic moment and effective magnetic field of ^{57}Fe 2−68533
Fe-Ni film, crit. fields, effect of elastic stresses 2−51264
Fe-Ni film, domain struct., influence of temp., elec. microscope obs. 2−72185
Fe-Ni films, perpendicular anisotropy from galvanomag. meas. 2−61529
Fe-Ni films, thermal evaporation prepn., detn. of lattice parameters and mag. props., 0-100% Ni 2−77496
Fe-Ni magnon heat conduction and scattering processes 2−65142
Fe-Ni melt in deep interior of Earth 2−72677
Fe-Ni quenched alloys, short-range order detn. in first and second coord. spheres from n. scatt. 2−81199
Fe-Ni sheets, heavily rolled, annealing textures, recryst. mechanism 2−74886
Fe-Ni single crystals, domain struct., Kerr effect obs. 2−78017
Fe-Ni strip as sensor for two-dimensional magnetic field distributions 2−73508
Fe-Ni superalloys, bend fatigue testing at elevated temperatures 2−56884
Fe-Pd-H system, phase diagram and Mossbauer spectrum 2−74953

Iron alloys continued
Fe-Pd, powder, remag. mechanism, hysteresis characts. 2−48097
Fe-Pd alloys, f.c.c., mixed exchange interactions, neutron scatt. obs. 2−84421
Fe-Rh, f.c.c., Neel temp., Mossbauer study 2−78072
Fe-Rh, Fe-Rh-Ir, magnetic contrib. to electronic sp. ht. 2−64856
Fe-Rh, magnetoresist., temp. depend 2−54330
Fe-Rh hyperfine field at Rh nuclei by Coulomb excitation 2−61572
Fe-S solid solution, thermodynamic props. 2−50837
Fe-(3(wt.%)Si, grain-oriented strips, saturation approach law of longitudinal magnetostriction 2−54335
Fe-(3 wt.%)Si, surface films influence on effectiveness of thermomag. treatment 2−44261
Fe-Si, dislocation, dynamics on plastic deformation, high voltage electron microscope obs. 2−56785
Fe-Si, domain width, sample thickness and cryst. orientation depend. 2−48061
Fe-Si, elastic props. and model atomic interactions 2−74818
Fe-Si, ferromag. domain spatial replication, anisotropic decomp. struct. 2−72149
Fe-Si, magnetization and mag. reversals, mag. texture effect 2−51252
Fe-Si, mech. props., influence of microstruct. 2−80778
Fe-Si, Neel lines, magnetooptic Kerr effect obs. 2−78014
Fe-Si, obs. of domain changes under cyclic tensile loading for specimens in remanent cond. 2−65147
Fe-Si, temp. depend. of specific energy loss during remagnetization 2−48069
Fe-Si alloys, remagnetization specific energy losses rel. to specimen thickness and mag. induction amplitude 2−72163
Fe-Si dil. alloy, ave.-moment-internal field variations 2−78008
Fe-Si phase stability and high temp. elastic consts. 2−71546
Fe-Si sheet Goss-oriented, elastic properties rel. to magnetorestriction 2−53778
Fe-Si single crystal, slip and hardening, effect of dimensional factors 2−71568
Fe-Si solid solns., b.c.c., ordered atomic configs. 2−47326
Fe-2.89%Si (100) face, surface composition rel. to photoelec. work function 2−61463
Fe-Sn-C system, formation and stability range of ternary cpds. 2−43933
Fe-Sn system, phase boundaries of γ-loop 2−47712
Fe-Ta, ductility enhancement using allotropic phase change 2−57020
Fe-Ti-Si, age hardening, precipitation and yield stress 2−43806
β-Fe-Ti, diffusion of Fe, Mossbauer study 2−77612
Fe-V-C steel, fibrous vanadium carbide occurrences after thermal or continuous cooling transformation 2−61033
Fe-V-C system, phase diagram, pseudo-binary section at 0.5 wt-%V 2−47711
Fe-V-N system, abnormal Snoek peak 2−47482
Fe-V, Fe-rich, ^{57}Fe n.m.r. 2−75355
Fe-V, meas. of longitudinal and transverse magnetoresistance at 4.2K, 77K, 273K 2−48063
Fe-V σ-phase, atomic distrib. and mag. props., Mossbauer obs. 2−44253
Fe-Zn, phase diagram, obs. of Fe rich side 2−50967
Fe-Zn, solid soln., interdiffusion coeffs. determ. 2−47459
α-Fe-Zn solid solution, precip., influence of P 2−80855
Fe-12.3 at.%-Al, Mossbauer determination of short-range order, heat treatment and cold rolling effects 2−51311
Fe-3%Si foil specimens, low temp. tensile tests, h.v. electron microscope obs. 2−80872
Fe-(B-metal), molten, paramag. props. 2−80488
Fe-rich solid solutions, summary of magnetic properties 2−81243
(Fe,Cr)-(Cr,Fe)$_7$C$_3$ composite, growth and props. 2−50920
armco Fe, 20-900°C magnetization and magnetic susceptibility 2−68546
Fe 30% Ni, martensitic transform, plasticity 2−68197
Fe$_3$(Al,Ge), influence of Ge on struct. changes, nuclear γ-reson., X-ray diffract. and dilatometric analyses 2−80779
Fe$_3$Al, compression induced mag. anisotropy and superlattice dislocations 2−61516
FeCo-(2 wt.%)V, crack propagation and nucleation in ductile fracture53835 2−53835
Fe^{60}Co, single- passage resonance obs. by β-emission and spin-lattice relax. meas. 2−72508
(Fe$_{1-x}$Co$_x$)Si solid solns., moment form., n.m.r. obs. 2−44223
Fe$_x$Gd$_y$ films, amorphous, mag. props. 2−44275
Fe$_{1-x}$Mn$_x$Si solid solution, mag. props. 2−48068
FeNi permalloy, film, oxidized, exchange anisotropy effects, hysteresis loop, 5-300 K 2−81230
Fe$_x$Pd$_{80-x}$P$_{20}$ ($13 \leqslant x \leqslant 44$), amorphous alloy, magnetic properties study from Mossbauer effect of ^{57}Fe 2−65114
Fe(Pd$_x$Pt$_{1-x}$)$_3$, mag. phase transitions, Mossbauer obs. 2−48108
FeRh, first-order antiferromag.-ferromag. transition, electronic struct. changes 2−84438
FeRh, mag. field depend. of antiferromag.-ferromag. transition temp. 2−81288
FeSi, two-dimensional ferromagnetic domain walls electron images 2−51247
Fe$_{1-x}$Ti$_{1||x}$, magnetization and sp. ht., rel. to resist. minimum 2−44252
Mn-Permalloy film, coercivity, influence of driving field 2−81278
Nb-Mo-Fe, discontinuous formation of localized moments, Mossbauer study 2−78076
Ni-(5wt.%)Fe-(5wt.%)W, powder composite, fracture micromechanism obs. 2−56947
Ni-Fe-Cr, based, γ'-hardened, electron irrad., void swelling 2−80684
Ni-Fe-Mo alloys, thin strips, magnetic properties and texture 2−68509
Ni-Fe-Nb, magnetic characteristics 2−57293
Ni-Fe-W, mag. props., magnetostriction and elec. resistivity 2−48076
81%Ni-Fe, Barkhausen effect, after heat treatment 2−78023
Ni-Fe, f.c.c., domain struct. after different annealing treatments, Kerr effect obs. 2−78016
Ni-Fe, multilayer films, interaction energy 2−84403

Iron alloys continued
Ni-Fe, quenched, aged, toughness, ductility, inverse temp. depend. 2−47501
Ni-Fe, spinwave dispersion coeff. in the Invar region, compositional depend. 2−48077
Ni-Fe alloy (around 75-25), behaviour in neighbourhood of order-disorder transform. temp. 2−84137
Ni-Fe alloys with f.c.c. structure, Curie temp. conc. depend. 2−68541
Ni-Fe film, coercive force, field and freq. depend. 2−78033
Ni-Fe film, electrodeposition, mag. props. optimization 2−61540
Ni-Fe film, ripple spectrum, depend. on anisotropy, crystallite size, thickness and field 2−81279
Ni-Fe films, domain wall creep effects of fields, film thickness 2−77993
Ni-Fe films, mag. props. temp. depend. and transverse anisotropy 2−61538
Ni-Fe films, magnetoresist. anisotropy 2−44266
Ni-Fe films, polycryst., edge anisotropy 2−61527
Ni-Fe powder compact, densification structural aspects 2−56946
Ni-Fe system, Ni$_3$Fe ordered alloy, 4-s band struct., perturbation calc. 2−71801
Ni-Fe(18 wt%) electrodeposited film, hyper- crit. thickness, anisotropy fluctuations 2−84409
Ni-Fe(50-50) alloy, mag. annealing effects 2−81241
NiFe films, e microprobe analysis 2−77509
Ni$_3$Fe, long range order parameter 2−60984
Pd-Fe, dil., elec. resist. behaviour in crit. region 2−57279
Pd-Fe, dil., mag. ordering obs. 2−81246
Pd$_3$Fe, lattice dynamics, 80K 2−43962
Pd$_3$Fe spin wave dispersion relation, neutron scatt. obs. 2−61503
Permalloy-Mn bimetal film, mag. after-effect 2−81224
Rh-Fe, Coles alloy, temp. depend. of resist. due to localized spin fluctuations 2−75056
Si-Fe laminations, dynamic ferromag. domain wall response to a.f. field, rel. to eddy current losses 2−48062
TiFe system, electron energy spectrum of equiatomic cpd., X-ray emission study 2−75316
Y-Co-Fe system, CaCu$_5$-type phase stabilities 2−43944
Zn-Fe, dilute, Kondo effect and localized spin fluctuations 2−64918
Zr-(1.5wt.%)Cr-(0.1wt.%)Fe tubing, hydrided, mech. props. and struct. 2−53918
Zr-(2 at.%)Cr-(0.16 at.%)Fe, precip. reactions rel. to corrosion resist. 2−53919
Zr-Cr-Fe alloy, correl. of microstruct. with properties 2−53922

Iron compounds
see also Ferrites; Iron alloys; Steel
chemical bonding study using X-ray photoelectron spectroscopy 2−53002
complexes, nitroprussides, purity of samples tested by obs. of line widths in ^{57}Fe Mossbauer spectra 2−44352
complexes, polar and nonpolar in benzene and hexafluorobenzene, p.m.r. study of solvent induced shifts 2−83264
Fe$_{1-x}$S, semicond. uniaxial ferroelec. qualitative model 2−77956
ferrice amphibole, pressure induced reduction 2−84721
ferromanganese nodules, thermomagnetic behaviour 2−58142
ferrous formate-magnesium formate system, mixed crystn., Mossbauer obs. 2−56673
garnet film magnetooptic waveguide, light modulation and switching 2−81323
haematite, crystalline, zero point of charge 2−72566
magnetite, crystalliz. from high Fe glass 2−54329
magnetite, zero point of charge, temp. depend. 2−72567
Mg$_2$SiO$_4$-Fe$_2$SiO$_4$ olivine transformed spinel system, equations of state det. using Birch's law 2−43504
pyrrhotite, cryst. growth, use of deformed greigite as seed cryst. 2−60723
pyrrhotite, domain structure formation rel. to structural vacancy ordering 2−68021
Staurolite, Fe^{2+} site distribution, Mossbauer spectrum 2−48143
wustite, fracture energy invariance with grain size 2−50880
Al$_2$O$_3$-Cr$_2$O$_3$-Fe$_2$O$_3$ system, orientation of modulated structs. 2−50853
Al$_2$O$_3$-Fe$_2$O$_3$ solid solns., impurity ion effects on spin relax. time of ferric ions 2−54368
Al$_2$O$_3$-Fe$_2$O$_3$ solid solution, mag. interactions , e.p.r. study 2−75351
BaO-B$_2$O$_3$-Fe$_2$O$_3$ glass, elec. and mag. props., microstruct. effects 2−65113
Eu-Fe-O system, phase relations and cpd. formation 2−47710
Fe-Ca olivines, X-ray diffraction study 2−47325
Fe-Ni carbonyl powders, phase composition 2−77726
Fe-Si sheet, grain oriented, magnetostriction meas. by optical lever method 2−65160
Fe-Si single crystals deformed by tensile forces, slip polygonization 2−84060
Fe-Si solid solns., ordering reactions and meas. of specific heat capac. 2−71745
Fe-Y garnet, l.f. magnetization oscillations where absorption maximum coincides with ferromagnetic resonance 2−75340
Fe-Zn system, influence of ultrasonic strains on diffusion growth of various phases 2−43655
55Fe-45P$_2$O$_5$ glass, a.c. and d.c. characteristics, correlation with structure 2−81142
(Fe,M)$_2$Mo$_3$O$_8$, (M=Mg, Zn, Mn, Co, Ni), Mossbauer spectra interpretation 2−75270
Fe cermet, highly porous, thermophysical properties 2−71651
Fe complex, aminoacid, Mossbauer spectra obs., 82 and 298K 2−57336
Fe complex, diarsine complexes, Mossbauer absorption spectra, after effects of electron capture decay 2−65232
Fe complex, diarsine complexes, Mossbauer emission spectra, after effects of electron capture decay 2−65233
Fe complex, FeN$_2$ electronic and geometric structure 2−77073
Fe complexes, Fe^{II}Fe$_2$^{III}(CH$_3$COO)$_6$.O.X, X=5H$_2$O, py$_{3.5}$, thermal electron transfer, Mossbauer spectra study 2−72276
Fe complexes, iron(II) naphthyridines, Mossbauer parameters and mag. moments 2−81340
Fe nitride, field ion microscopy exam. comparing orientation to nitrided samples of Fe and Fe-Mn alloys 2−64777
Fe oxides, lunar surface, solar wind darkening 2−66154

Iron compounds continued
$FeAs_2$, cryst. growth chem. vapour transport 2−47219
$FeAs_2$, prep., diamag. semicond., band gap, band model 2−61340
FeB_x, rel. to elec. resist., 300-1200K 2−51100
FeB_x coating, on Fe, thermal expansion anisotropy 2−54058
$FeBO_3$, amplified n.m.r. signal from inside domains 2−68745
$FeBO_3$, antiferromag. reson. above Neel temp., reson. absorpt. line obs. 2−72461
$FeBO_3$, antiferromagnetic resonance in an ordered state, induced by external magnetic field over the Neel temp. 2−84558
$FeBO_3$, crystal growth, fluxed melt technique, and Fe_2O_3-B_2O_3 phase relations 2−50594
$FeBO_3$, high-frequency obs. of antiferromagnetic resonance 2−72459
$FeBO_3$, i.r. absorpt. spectra 2−75292
$FeBO_3$, mag. field induced antiferromag. 2−54355
$FeBO_3$, n.m.r. and weak ferromag. temp depend. 2−72523
$FeBO_3$ single crystals, in mag. field, 77-300°K, magnetic and magnetoelastic properties 2−72175
$FeBr_2$, specific heat study, 4-70 K and detn. of Neel temp. 2−64852
$FeBr_2$, temp. and field depend., of mag. rot. power 2−65218
Fe_3C, electron microscope study of magnetic domains 2−44262
Fe_3C, electron structure, Fe X-ray K-emission obs. 2−72379
Fe_3C, growth texture 2−43872
Fe_3C condensed films, carbide grain growth 2−56932
$Fe_3(CN)_5NO.2H_2O$, i.r. spectra, cryst. chem. 2−78081
$Fe(CN)_5(OH_2)^{2-}$-$Fe_2(CN)_{10}{}^{4-}$ equilibrium mixture in aqueous solution, study by magnetic circular dichroism 2−71231
$FeCO_3$, Ising behaviour, magnon-phonon coupling 2−44297
$FeCO_3$, magnetic structure, nonuniformities at metamagnetic transformation 2−65219
$FeCO_3$, polycrystalline, elastic props. to 10 kbars 2−65573
$Fe(CO)_5$, catalytic effect on CO oxidation in shock waves 2−57417
$Fe(CO)_5$, release in upper atm. 2−65825
$Fe(CO)_5$, vibrational spectra of isotopic species, potential constants 2−67473
$FeCl_2$, specific heat study, 4-70 K and detn. of Neel temp. 2−64852
$FeCl_2$, X-ray $K\beta$ emission and K absorpt. spectra 2−65287
$FeCl_3$ frozen aqueous soln., Mossbauer spectra, investigation of glass to crystal transformation at 200 K 2−72280
$FeCl_4{}^-$ containing compounds, luminescence at 85K 2−51367
Fe_2Cl_6, normal coordinate anal. and thermodynamic props. 2−42945
$FeClO_4$ frozen solns., mag. props. of Fe^{3+} ion 2−78070
$Fe(ClO_4)_2.6H_2O$, phase transition, Mossbauer spectra electric quadrupole interaction rel. to temp. and mag. field 2−75271
$FeCl_3.6H_2O$, spontaneous magnetization, mag. ordering, mag. hyperfine fields, Mossbauer reson., $T<4.2$ K 2−75272
$FeCr_2S_4$, cryst. growth, by chem. vapour transport 2−71371
$FeCr_2S_4$ spinel, Mossbauer spectra, h.f.s., e.f.g. Debye model, Jahn-Teller effect 2−57331
FeF_2, covalency parameters 2−77057
FeF_2, mag. hyperfine interactions of Fe^{2+} interpret. 2−61604
FeF_2, magnon-phonon interaction 2−44298
FeF_2, magnon-phonon interactions, coupling, spin Hamiltonian 2−80886
FeF_2, neutron scatt. struct. factor, nonlinearity effect 2−48107
FeF_2, two-magnon Raman scatt., temp. depend., calc. 2−81304
FeF_3, transparent antiferromagnet, n.m.r., nuclear echo 2−54505
$FeFe_{2-x}Sc_xO_4$, Sc-containing magnetite, K emission and absorp. spectra 2−44400
FeGe, cubic ferromagnet, obs. of magnetic resonances using e.s.r. spectrometer 2−84557
FeH, ground and low-lying excited electronic states 2−67474
Fe(II) complex, bis(thiosemicarbazide)iron(II) sulphate, large quadrupole splitting 2−61605
Fe(II) complex, $Fe(phen)_2(NCS)_2$, mag. heat capacity due to low spin ${}^1A_1 \rightleftharpoons$ high spin ${}^5T_2$ transition 2−75240
Fe(II) complexes, octahedral, halogen- bridged, Raman and far i.r. spectra 2−46558
Fe(II) salt solutions, frozen at normal pressure 2−78178
Fe(III) complexes, magnetic circular dichroism of d-d transition, ligand field theory analysis 2−48176
Fe(III) complexes with oxyacids, low temperature photolysis, e.p.r. spectra 2−75393
Fe(IV) complex, paramagnetic hyperfine interactions in $t_{2g}{}^4$ config. of ${}^{57}Fe$ 2−84472
$Fe(KSO_4)_2.6H_2O$, magnetic susceptibility, anisotropy and ligand fields 2−54292
FeMg garnet, ${}^{27}Al$ and ${}^{29}Si$ n.m.r. studies 2−65341
$(Fe_xMg_{1-x})_2SiO_4$, mag. transitions, comp. depend., 4-300K 2−68987
$(Fe_{0.64}Mn_{0.36})_3C$ X-ray K-emission obs. 2−72379
Fe_2MoO_4, spinel, X-ray and neutron diffraction studies 2−84414
FeN_x, hexagonal, magnetic and Mossbauer obs. 2−54331
$Fe_{16}N_2$ film, deposited in N_2 atmosphere, ultrahigh mag. moment 2−57299
$Fe(NH_4SO_4)_2.6H_2O$, magnetic susceptibility, anisotropy and ligand fields 2−54292
$FeNbO_4$, flux growth 2−60717
$Fe_{0.9}Nb_{1.1}O_4$ magnetic structure, neutron diffr. obs. 2−65181
Fe_2O_3-Al_2O_3-CaO, phase comp. analysis by X-ray diffr. 2−74725
Fe_2O_3-B_2O_3-BaO glass, microstruct., ultrastruct., mag. props. 2−56558
Fe_2O_3-B_2O_3, phase relations rel. to applic. to $FeBO_3$ crystal growth 2−50594
Fe_2O_3-FeO-$Li_{0.5}Fe_{0.5}O$, coexisting phases equilibrium and thermodynamics, 900-1200°C 2−74931
α-Fe_2O_3-β-FeOOH, disperse system, high surface area, Mossbauer obs. 2−68612
Fe_3O_4-Fe_2TiO_4, lattice parameter calc. 2−56655
$0.35Fe_3O_4$-Fe_2TiO_4, self-reversal of thermoremanent magnetization 2−48609
Fe_xO-MnO solid solns., optical props. 2−48174
Fe_2O_3-P_2O_5 glass, forming range and mag. suscept. 2−54354
FeO-SiO_2-MgO system in mantle minerals, phase equilibria and elastic properties 2−57711
Fe_2O_3-TiO_2 solid soln., crystallographic shear structs., planar boundaries 2−74768
FeO, absorption coeff. for i.r. vibration-rotation spectrum 2−42890
FeO, point defects, thermodynamic analysis, migration processes 2−56684

Iron compounds continued
FeO and Fe_3O_4, artificial meteor ablation obs. 2−66188
FeO chemiluminescence and resonance fluorescence on release of $Fe(CO)_5$ in upper atm. 2−65825
$Fe_{0.95}O$, wustite, Mossbauer spectra, isomeric shift, mag. field, at 300, 223 and 80K 2−75269
$Fe_{0.98}O$, wustite, elastic consts., rel. to upper mantle comp. 2−61980
$Fe_{1-x}O$ film, epitaxy on CaF_2 2−47109
α-Fe_2O_3, antiferromag. and nucl. mag. reson. freq. shift phenomena 2−81482
α-Fe_2O_3, c-axis moment obs. 2−44299
α-Fe_2O_3, crystal growth, from the flux systems PbO-V_2O_5 and Bi_2O_3-V_2O_5 2−50589
α-Fe_2O_3, d.c. cond. and Fe diffusion, high temp. 2−51138
Fe_2O_3, density changes and pore distribution during heat treatment 2−68140
Fe_2O_3, elemental anal., using neutron capture γ-rays 2−44513
Fe_2O_3, experimental sintering kinetics, approx. equation 2−47652
Fe_2O_3, from α-, β-, γ- and δ-FeOOH, cryst. struct. and Morin point determ. 2−81292
α-Fe_2O_3, haematite, magnon energy of optic mode, Morin transition 2−51278
α-Fe_2O_3, haematite, Mossbauer effect of ${}^{119}Sn$ and ${}^{57}Fe$, Morin transition obs. 2−65234
Fe_2O_3, isomer shifts of ${}^{57}Fe$ 2−57333
Fe_2O_3, piezomagnetic properties, effect of annealing 2−48083
γ-Fe_2O_3, superparamagnetism, magnetiz. and Mossbauer obs. 2−48038
Fe_2O_3, thermodynamic properties determ. by EMF method 2−51425
γ-Fe_2O_3, vacancy distrib. over tetrahedral and octahedral sites 2−60786
α-Fe_2O_3 (haematite) from oxidation of basaltic magnetite rel. to surface colour of Mars 2−78546
Fe_2O_3 and Fe_3O_4, morphological and struct. changes during reduction 2−50881
α-Fe_2O_3 and natural haematite, true heat capacity, mag. component 2−43984
Fe_2O_3 effect on sintering kinetics of Al_2O_3 2−50865
Fe_2O_3 in $Pb(Zr,Ti)O_3$ ceramic, effect on microstruct. 2−50895
α-Fe_2O_3 microcrysts., chem. modification of quadrupole interaction 2−65231
Fe_3O_4, high temp. polaronic semicond. i.r. reflectivity obs. 2−61265
Fe_3O_4, magnetite, metal-insulator transition, Verwey temp. 2−57125
Fe_3O_4, one-electron energy levels 2−68292
Fe_3O_4 micropowders, grain-size dependence of anhysteresis susceptibility 2−54341
Fe_xO, non-stoichiometric, magnetite-wustite boundary, order-disorder problem 2−84067
Fe_xO, wustite, lattice parameters, at high temps. 2−43580
FeOCl, mag. struct., Mossbauer obs. 2−44351
FeOOH, cryst. struct. and neutron diffr. studies 2−81292
γ-FeOOH, lepidocrocite, cryst. struct. and mag. props., at temp. of conversion to α-Fe_2O_3, hematite 2−57287
β-FeOOH, thermal conversion to α-Fe_2O_3, Mossbauer parameters variation 2−72547
$(Fe_2O_3)_{0.79}.P_2O_5$, glasses, antiferromag. interactions 2−75237
Fe_3P, mag. struct. anomalous n.m.r. spectrum 2−44251
$Fe(Pd_xPt_{1-x})_3$, mag. phase diagram model showing quadrupole point 2−51234
FeRh, first-order transition, demonstration experiment 2−61476
FeS-$FeCl_2$ melt, electrical and structural props. 2−46983
FeS, hyperfine interactions, Mossbauer spectra obs. 2−48146
FeS antiferromagnetic, Mossbauer determ. of spin arrangements, quadrupole interaction, internal magnetic field, chemical shift 2−81344
$Fe_{1-x}S$, semicond. uniaxial ferroelectric, phase diagram 2−77957
Fe_3S_4, synthetic samples, magnetic properties, Mossbauer spectra 2−81338
$FeSO_4$, for neutron dosimetry 2−69390
$FeSb_2$, cryst. growth, chem. vapour transport 2−47219
$FeSb_2$, Mossbauer spectra, quadrupole splitting, isomer shift, Debye temp., 6.4-540K 2−61606
$FeSb_2$, prep., elec. and mag. props., band model 2−61340
$Fe_{1\|\delta}Sb$, antiferromagnetism, Mossbauer effect meas. 2−84440
$Fe_{3-x}Sc_xO_4$, electronic struct. of ions 2−48207
FeSi-CoSi system, itinerant ferromag., ${}^{59}Co$ n.m.r. obs. 2−61745
FeSi, elec. cond., thermal e.m.f. and Hall coeff. detn. 2−77797
FeSi films, e microprobe analysis 2−77509
$FeSi_2$, $\alpha \rightleftharpoons \beta$ transition mechanism 2−43919
$FeSi_2$, high temp. phase stability 2−47685
$FeSi_x$, growth by chem. transport, rel. to structural study 2−47206
Fe_2SiO_4-Mn_2SiO_4 phase diagram and ideal soln. behaviour 2−50852
Fe_2SiO_4, high and low pressure polymorphs, rel. to thermal conductivity 2−65582
Fe_2SiO_4, olivine and spinel forms, pressure- induced elec. conductivity increase and red shift in absorption spectrum 2−54421
Fe_2Ti, elec. resist. thermo-hysteresis rel. to martensitic transform., 4.2−1200K 2−71834
$FeTiO_3$, Mossbauer spectra below Neel temp. 2−57330
Fe_2TiO_4, i.r. absorpt. spectra, ionic ordering 2−72342
$(Fe_2TiO_4)_c(NiFe_2O_4)_{1-c}$, $0 \leqslant C \leqslant 1$, binary solid soln., effect of comp., lattice parameter, saturation mag. moment and Curie temp. on solubility 2−83840
Fe_2TiSn, Heusler alloy, mag. properties 2−51255
FeV_2Te_4, prep., struct., elec. and mag. props. 2−60757
Fe_2WO_6, lattice parameters, space group 2−83950
Fe(II) complexes of 2-methyl-1, 10-phenanthroline, ${}^{57}Fe$ Mossbauer spectrum obs., 298-4.2K 2−51306
Fe^{III} complex, in $K_3Co_{1-x}Fe_x(CN)_6$, $3d(t_{2g})$ density distrib. Mossbauer and e.p.r. obs. 2−68613
GdFe garnet with Co^{2+} substituted, magnetooptical props. 2−84460
LiO_2-Fe_2O_3-SiO_2 system, dielec. and magnetic props. 2−54333
Mn-Mg-Fe ferrite film, flash evaporated, chem. comp., X-ray fluoresc. obs. 2−71331
Mn-Zn-Fe ferrite, permeability, thermal change, resonance type profiles 2−61545
$(Mn, Fe)_3O_4$, i.r. absorp. and cation distrib. 2−61648
MnZn ferrites, influence of Ti ions on mag. props. 2−84405
Ni/Fe/H system, form. and decomp. equil. 2−77715

Iron compounds continued
  $NiFe_2O_4$-Fe_3O_4-Fe_2TiO_4, ternary solid soln., effect of lattice parameter on solubility 2−83840
  $(Ni_2TiO_4)_c(Fe_3O_4)_{1-c}$, $O \leqslant C \leqslant 1$, binary solid soln., effect of comp., lattice parameter, saturation mag. moment and Curie temp. on solubility 2−83840
  $PbO.6Fe_2O_3$, unsaturated crystals, ferromagnetic resonance, 36-52 GHz 2−72455
  $TbNbO_4$, crystal growth, from the flux systems PbO-V_2O_5 and Bi_2O_3-V_2O_5 2−50589
  V_2O_5-Fe_2O_3 system, e.p.r. of Fe^{3+} 2−48297
  V_2O_5-Na_2O-Fe_2O_3 system, liq., n-type semicond. and ionic cond. props. 2−83796
  (Zn, Mn, Fe)Ti_3O_7, landauite, Baumhauer type twins 2−71499

Irradiation effects *see Biological effects of radiations; Chemical effects of radiations; Physical effects of radiations*

Ising lattices and models
  antiferromagnetic finite chains, order and correlation 2−75235
  Ashkin-Teller and eight-vertex models, symmetry props. 2−52092
  Blume-Capel ferromagnet, tricritical point, droplet model 2−65135
  boundary free energy for square-lattice Ising model 2−52086
  cluster expansion, determination of first ten high temp. coeff. 2−45291
  compressible, cooperative order- disorder phenomena, pressure effects, double interaction model 2−45297
  compressible magnet, spin-phonon interactions 2−72124
  cooperative assemblies, with many body interactions, first order and critical point phase transitions 2−69605
  cooperative phenomena, new approximation method based on independent particle picture 2−69607
  cooperative phenomena 2−45295
  critical behaviour, term. struct. of series expansions 2−52090
  critical behaviour rel. to dimensionality, scaling theory 2−78849
  critical point exponents, inequalities for spin- spin and energy-energy correlation functions 2−63030
  critical slowing down, nonlinear dynamical response 2−54310
  cubic lattice, phase transition, correl. functions near crit. temp. 2−78840
  density matrices, linear inequalities 2−82262
  duality relation for model with four- spin interactions 2−41527
  effective critical exponents and confluent singularities, temperature-dependence 2−69616
  ferromagnet, 3-dimens., spin-spin correl., high temp. series and crit. amplitude 2−81260
  ferromagnet, amorphous, thermodynamical behaviour 2−57273
  ferromagnet, amorphous susceptibility and Curie temp. rel. to spin-fluctuations 2−57277
  ferromagnet, critical isotherm analysis 2−54297
  ferromagnet, mag. susceptibilitiy rel. to nonmag. impurities, series expansion 2−77992
  ferromagnet, of restricted dimensionality, susceptibility 2−81235
  ferromagnet, one-dimensional with single ion anisotropy 2−57274
  ferromagnet, phonon polarization operator, calc. using spin-phonon interaction Hamiltonian 2−81265
  ferromagnet, scaling eqn. of state near crit. pt., Feynman-graph expansion 2−68526
  ferromagnet, scaling relations in Wilson theory 2−61495
  ferromagnet, sp. ht. density 2−61486
  ferromagnet, three-dimens., critical behaviour 2−54300
  ferromagnet, three-dimens., sp. ht. density asymptotic behaviour for $T \gg T_c$ 2−61487
  ferromagnet, two dimensional model, external force on boundary atoms 2−48055
  ferromagnet, two-dimens., high temp. susceptibility bounds 2−54299
  ferromagnet, with nonmag. impurities, susceptibility, high temp. expansion techniques 2−61491
  ferromagnet with $S > {}^1/_2$, critical isotherm, series expansion analysis 2−84419
  ferromagnetic, crit. behaviour of quadratic lattices 2−84423
  ferromagnets, spin correl. functions, hierarchy of inequalities, critical temp. bounds 2−68538
  Fisher droplet model in simulated two dimensional cluster distribs. 2−72130
  Heisenberg-Ising ring for $|\Delta| \geqslant 1$, low-temperature thermodynamics 2−69611
  Heisenburg-Ising ring, $|\Delta| < 1$, thermodynamics, improved eqns. 2−69606
  high temp. expansions, weighting of graphs 2−52091
  idealised Ising model, 1st, 2nd order transitions, computer simulation 2−78948
  impurity problem, internal energy of lattice 2−69609
  instabilities and phase transitions, review 2−63031
  insulating crystal, magnetic side bands induced by zero point motion 2−81376
  isotropic spin systems, critical exponents 2−65137
  Kerr liq., spectral broadening of light filament, meas. with laser pulses 2−71204
  kinetic model, critical slowing down, dynamical scaling hypothesis 2−78852
  lattices with $S=1$ and $S=1/2$ and site impurities, partition functions relations 2−66461
  long-range interactions, critical exponents 2−76230
  long-range interactions, determ. of partition functions, thermodynamic functions, diagram expansions 2−45296
  metamagnet, and tricritical susceptibility exponent 2−54302
  models with lattice anisotropy, crossover behaviour 2−66459
  nearest neighbour model with added local 4-spin interaction 2−75213
  one-dimensional, rel. to cooperativity in biological systems 2−58579
  pair correl., functions decay at high temp. 2−52096
  phase transition, Ising type model of excitonic state 2−45321
  phase transition, sixteen vertex ferroelectric model 2−65058
  phase transitions, model studies 2−58798
  phase transitions, zero temp. 2−81267
  phase transitions and static spin correlations, models with free surfaces 2−78854
  phase transitions and transfer matrix method 2−58799
  polymers, of relaxation of cooperative binding 2−46635

Ising lattices and models continued
  quasi−two-dimensional and quasi− one-dimensional systems, crossover behaviour 2−76231
  random one-dimensional transverse model, magnetic susceptibility 2−52093
  scaling function calc. using high-temp. series expansions 2−54315
  scaling functions, universality rel. to lattice struct. and spin quantum number 2−54316
  second-order phase transitions, universality, scale factor for correl. length 2−63029
  self-dual relation for triplet interactions 2−75209
  size effect in three dimensional Ising lattice 2−66464
  spin system dynamics, Monte Carlo calc. 2−81272
  spin systems, property of zeros of partition function 2−44283
  spin-phonon coupled system, theory of phase transitions of NH_4Br 2−47700
  spin-phonon interaction effect of lattice vibration on magnetic phase transformation 2−68524
  spin-spin correl. function, eqn. of state, droplet model 2−77991
  spin-spin correlation functions, asymptotic behaviour 2−81269
  square and s.c. Ising magnet, spin orderings, energy per spin 2−72125
  stochastic chain, kinetics in two flip model 2−45292
  stochastic model, transport processes, computer simulation 2−45335
  superantiferromagnetism, lattice model 2−72206
  three dimens. assembly, self dual relation, singularity location 2−58771
  three dimensional, phase diagram involving first and second neighbour interactions 2−72134
  two dimensional, with pure 3 spin interactions, exact soln. 2−81247
  two-dimensional, duality and asymptotic behaviour of correlation functions 2−58774
  two-dimensional model, decay of order 2−52095
  two-dimensional model, phase separation line 2−58767
  two-dimensional model, phase separation line and relationship with nonfree random walk problem 2−63028
  Van der Waals spin systems, thermodynamic equivalence 2−48045
  XY model, partition function, distrib. of zeros 2−66462
  ErGa garnet, rel. to magnetic curves and metamagnetism 2−61557

Isobaric analogue states
  see also Nucleus/excitation
  channel correlation effects for fragmented analog states 2−46096
  dipole IAS in even-even nuclei, two classes of proton channels 2−59741
  double and single analog resons., total widths 2−82939
  magic, transitional and strongly deformed nuclei, proton scattering, energies of resonances 2−46148
  in proton induced reactions, rel. to nucl. spectroscopy 2−59754
  radiative pion absorpt. processes in complex nuclei 2−82987
  resonances, survey of statistical neutron decay for nuclei in A=91-97 range 2−67131
  spherical and collective nuclei, modified Fano approach 2−70367
  spherical nuclei, I^+ reson. in charge exchange reactions 2−42491
  spherical nucleus, 0^+-states, proton- neutron hole 2−76770
  stripping DWBA amplitude to isobaric analog resonances, form factor 2−63861
  ^{a}Sn(γ,p), A=116-118, 120, 122, 124, meas. of spectra and yeild curves 2−46233
  ^{71}As, of ^{71}Ge in ^{70}Ge(p,p)^{70}Ge, evidence for intermediate structure 2−46143
  ^{73}As of ^{73}Ge in ^{72}Ge(p,p)^{73}Ge, evidence for intermediate structure 2−46143
  ^{209}Bi, E1 radiative widths 2−76809
  ^{209}Bi, proton decay of isobaric analogs of ground states 2−63888
  ^{209}Bi analog resons., compound spreading widths 2−63835
  ^{209}Bi antianalogue states, calc. of compound spreading width of analogue resonance 2−42539
  ^{209}Bi(p,n)^{209}Po(IAS), 28, 35 and 45 MeV, angular distributions and excitation function 2−70446
  ^{13}C, e.m. transitions 2−46111
  ^{142}Ce(p, p_0), 9.5 to 12 MeV, excitation functions 2−67332
  ^{142}Ce(p, p_1), 9.5 to 12 MeV, excitation functions 2−67332
  ^{57}Co, obs. of resonance states in ^{56}Fe(p,γ) reaction, isobaric analogs of states in ^{57}Fe 2−63882
  ^{57}Co analogs of low-lying states in ^{57}Fe 2−46138
  ^{59}Co, of 3/2- excited state in ^{59}Fe, fine structure 2−46140
  ^{50}Cr(^{3}He, t) 70 MeV, isobaric analog ground state obs. 2−83009
  ^{52}Cr, low-lying, study from (p,γ) and (p,n) reaction in ^{51}V 2−76795
  ^{59}Cu, core excitation of $g_{9/2}$ analogue and anti-analogue states 2−74027
  ^{65}Cu elastic and inelastic widths of resonances excited in ^{64}Ni(p,p′) reaction 2−63804
  ^{168}Er structure studied through formation and decay of isobaric analogues of ^{169}Er 2−46169
  ^{19}F, e.m. transitions 2−46111
  ^{54}Fe(p,γ)^{55}Co, reson. identification, $E_p=1$ to 3 MeV 2−59754
  ^{55}Fe, γ-decay of analogue states excited in ^{54}Fe(p,γ)^{55}Co reaction 2−46135
  Ge crystal, blocking of protons, effect on lifetime of compound nucleus fine structure 2−52811
  ^{116}In, formation in ^{115}In (p,p), properties 2−67215
  ^{86}Kr-^{87}Kr system, level structure investigated by inelastic proton scattering through isobaric analog resonances 2−46147
  ^{86}Kr(p,p)^{86}Kr, 4.76-10.10 MeV, obs. of isobaric analog resonances, study of core coupling in ^{87}Rb 2−46146
  ^{24}Mg, formation in 1.7-3.0 MeV proton bombardment of ^{23}Na, γ-ray decay props. 2−70384
  Mo isotopes, hole-strength variations in neutron pick-up reactions 2−46151
  ^{91}Nb,^{93}Nb, total and partial widths 2−59703
  ^{91}Nb+n, polarization effects in isospin- coupled reaction channels 2−63884
  ^{20}Ne, β^+-decay of ^{20}Na 2−59729
  ^{58}Ni, ^{60}Ni(^{3}He, t), population of 0^+ and 2^+ states in ^{58,60}Cu, meas. of angular distribs. 2−63918
  ^{60}Ni, intermediate states of dipole analogue resons. 2−59702
  ^{64}Ni(p,nγ)^{64}Cu, 3.47-5.19 MeV, study of structure and γ-decay of levels excited near isobaric analogue resonances 2−67160
  ^{15}O and ^{15}N, identification of analogue states with corresponding theoretical negative-parity states 2−70375

Isobaric analogue states continued
- ^{31}P, e.m. transitions 2−46111
- ^{206}Pb, proton decay of isobaric analogs of ground states 2−63888
- ^{206}Pb(p,p′)^{206}Pb*($2_1{}^+$), compound particle-core coupled states 2−59721
- ^{207}Pb, E1 radiative widths 2−76809
- ^{207}Pb, proton decay of isobaric analogs of ground states 2−63888
- ^{208}Pb, ground state, analogue state in ^{208}Bi, population and decay 2−52770
- ^{208}Pb, proton decay of isobaric analogs of ground states 2−63888
- ^{209}Po produced in ^{209}Bi(p, n)^{209}Po(p)^{208}Bi reaction p,n ang. distrib. obs., compared to Becchetti-Greenlees optical potential 2−46266
- ^{210}Po, T=23 double analogue states, obs. in ^{209}Bi(p,2p)^{208}Pb reaction 2−70446
- ^{87}Rb, total and partial widths 2−59703
- ^{49}Sc, by elastic and inelastic proton scatt. from ^{48}Ca 2−70390
- ^{119}Sn(p, n), 28 and 35 MeV, populating IAS, angular distribution meas. 2−70444
- ^{119}Sn(p, np), total cross section, excitation function 2−70444
- Ta, study by ^{178}Hf(p,p) reaction at 11.2 to 12.6 MeV 2−42532
- Tc isotopes, stripping reaction study 2−46180
- ^{93}Tc,^{97}Tc, total and partial widths 2−59703
- ^{93}Tc, (^{3}He,d) population, DWBA analysis 2−49743
- ^{95}Tc, $^{5}.{}_{2}{}^{+}$(g.s.) analog in ^{94}(Mo(p,p′γ)^{94}Mo 2−74078
- ^{46}Ti, ^{48}Ti(^{3}He, t), population of 0^+ and 2^+ states in ^{46,48}V, meas. of angular distribs. 2−63918
- ^{205}Tl, levels populated in inelastic proton scattering on ^{204}Hg, study of isobaric analogue strength 2−74080
- ^{47}V, proton resonances, study by ^{46}Ti(p, p) and ^{46}Ti(p, p_1) reactions 2−70389
- ^{49}V, proton resonances, study by ^{48}Ti(p, p) and ^{48}Ti(p, p_1) reactions 2−70389
- ^{49}V obs. in elastic and inelastic scattering of protons on ^{48}Ti 2−79783
- ^{51}V, proton resonances, study by ^{50}Ti(p, p) reaction 2−70389
- ^{51}V(p,p)^{51}V obs. of 2.335 MeV isobaric analog resonance 2−46265
- ^{52}V, low lying levels, study by ^{51}V(p, γ)^{52}Cr reaction at 1.567 and 1.629 MeV 2−74023
- ^{188}W, rel. to interpretation of forbidden $0^+ \rightarrow 0^+$ β transition to ^{188}Re 2−59731
- ^{89}Y, isobaric analog resons., proton inelastic scatt. 2−76846
- ^{89}Y, total and partial widths 2−59703
- ^{90}Y, formation in ^{89}Y (p,p), properties 2−67215
- ^{90}Zr, intermediate states of dipole analogue resons. 2−59702
- ^{90}Zr(^{3}He,t), 70 MeV isobaric analog ground state obs. 2−83009
- ^{91}Zr(p, n), 28 MeV, populating IAS, angular distribution meas. 2−70444
- ^{91}Zr(p, np), total cross section, excitation function 2−70444

Isomer shift
- biotite, Mossbauer effect, ^{57}Fe nuclei 2−75266
- group V_2-VI_3 semiconducting Sb compound, Mossbauer effect of ^{121}Sb and ^{125}Te nuclei 2−75274
- group V-VI-VII semiconducting Sb compound, Mossbauer effect of ^{121}Sb and ^{125}Te nuclei 2−75274
- Mossbauer line broadening, many closely spaced internal fields 2−61601
- Mossbauer spectra, determination of explicit value 2−61598
- rare earth iron garnets, of ^{57}Fe, for inequivalent sites 2−57333
- B:Fe, Mossbauer investigation 2−51305
- ^{209}Bi, muonic atom shifts, analyzed in terms of single particle or hole coupled to collective vibrations 2−70579
- EuO, Mossbauer effect of ^{15}Eu after Coulomb excitation with 3.3 MeV α-particles 2−84473
- EuTe, Eu_3Te_4, Eu_4Te_7, Eu_3Te_7, Mossbauer spectra, sublattice covalent bonding 2−54389
- ^{153}Eu, muonic and Mossbauer isomer shifts of gamma transitions 2−59714
- ^{153}Eu, theoretical investigation of muonic and Mossbauer isomer shifts 2−42526
- $FeCr_2S_4$ spinel, Mossbauer spectra, Debye model deviations 2−57331
- $Fe_{0.95}O$, wustite, Mossbauer obs., 300, 223 and 80K 2−75269
- Fe_2O_3, of ^{57}Fe, for equivalent sites 2−57333
- $FeSb_2$, in Mossbauer spectra 2−61606
- ^{57}Fe, in solid N_2, Mossbauer obs. 2−48148
- Gd, A=158, 160, Mossbauer effect study 2−70407
- ^{178}Hf 93.2 keV transition, Mossbauer isomer shift, shrinking of nucl. charge radius in rot. state 2−76804
- HoPtSn and related intermetallics, Mossbauer study 2−50621
- $KFeF_4$, planar antiferromagnet, Mossbauer obs. 2−78043
- Nb, Mossbauer spectrum of ^{57}Fe, hydrogen conc. effects 2−78075
- PbI_2, Mossbauer obs. 2−68614
- ^{207}Pb, muonic atom shifts, analyzed in terms of single particle or hole coupled to collective vibrations 2−70579
- ^{141}Pr, Mossbauer scatt. obs. in Pr^{4+} and Pr^{3+} compounds 2−48151
- ^{195}Pt Mossbauer effect obs. 2−59719
- $RbCaF_3$, Mossbauer effect of ^{57}Fe at substitution sites 2−81339
- Sm ionic, semicond. and metallic cpds., Mossbauer shifts 2−48154
- Sn halides, electronegativity correlations with ^{119}Sn Mossbauer shift 2−44360
- Sn halides, Mulliken electronegativities rel. to ^{119}Sn Mossbauer shifts 2−44359
- ^{119}Sn, in solid N_2, Mossbauer obs. 2−48148
- Te hexahalides, ^{125}Te Mossbauer isomer shifts and quadrupole splittings 2−61608
- ^{203}Tl, muonic shift 2−59961
- ^{205}Tl, muonic shift 2−59961
- Yb, A=170, 172, 174, 176, Mossbauer effect study 2−70407

Isomerism
- *see also Nuclear isomerism*
- acetylacetone, tantomerism 2−60045
- n-alkylbenzenes, l.f. vibr. spectra interpret. rel. to rot. isomerism 2−56213
- allyl chloride and bromide, rotational isomers 2−42952
- azobenzene and substituted derivatives, reversible orientational photodichroism and photoisomerization in viscous solutions 2−42959
- benzene, Dewar structure CNDO/2 calculation 2−60051
- bromoacetyl bromide, energy differences between rotational isomers by absolute i.r. intensity method 2−46598
- 2-bromoethanol, normal coordinate analysis on rotational isomerism 2−42981

Isomerism continued
- 1,3-butadienes, 1-substituted and 1,4-disubstituted, electronic spectra, comparisons between geometric isomers 2−42965
- chloracetyl chloride, energy differences between rotational isomers by absolute i.r. intensity method 2−46598
- chloralides, optically active, conformation 2−42971
- 2-chloroethanol, normal coordinate analysis on rotational isomerism 2−42981
- conformational isomer detection using internal rot. effect on band contours in oscillation spectra 2−83239
- 2-cyanoethanol, normal coordinate analysis on rotational isomerism 2−42981
- cyclohexane, ring interconversion 2−42974
- decay isomers in Z=88, 89 region produced by neutron bombardment of ^{226}Ra 2−70458
- dichloracetyl chloride, energy differences between rotational isomers by absolute i.r. intensity method 2−46598
- 1,2-ethane dithiol, Raman spectrum meas. in liquid and solid state, determ. of rotational isomerism 2−53061
- 2-furanaldehyde, conform., rot. isomerism, nematic-phase n.m.r. obs. 2−77147
- furfural, electronic structure calc. for rotational isomers 2−50096
- glyoxal, LCAO-MO-SCF calc. determ of energy for cis-trans isomerization 2−53065
- hadrons, possible existence, heuristic considerations 2−52564
- hot-atom substitution products, decomposition, RRKM theory, methyl isocyanide paradox 2−51428
- isomerization reactions, examination of underlying stochastic process 2−51426
- methane, solid, second transition due to spin isomerisation, obs. by optical birefringence 2−64814
- methyl nitrite, i.r. spectra 2−77149
- methyl sulphite, i.r. spectra 2−77149
- monoalkylbenzenes, conformers 2−42953
- olefines, trisubstituted, regiospecific and stereoselective isomerization 2−77105
- permutational isomerization reactions, enumeration 2−42827
- poly-L-proline I chain, cis-trans isomerism effect on vibr. modes 2−80113
- 11-cis-retinal, PCILO calculation and conformation 2−77153
- succinic acid, radical isomerization following conformational change 2−81528
- succinyl chloride, meas. of Raman spectrum in solid and liquid states, determ. of rotational isomerism 2−53079
- thioamides, cis-trans isomerism 2−43011
- triallyl amine, rotational 2−43012
- trifluoroacetone, tantomerism 2−60045
- trifluoroacetylacetone, tantomerism 2−60045
- 1,1,1-trimethoxyethane, rotational isomerism 2−43013
- CH_4 solid, spin isomer conversion, n.m.r. obs. 2−68749
- HNO_2, electronic struct., cis and trans isomer obs. 2−56172
- XeF_6, electronic isomerism rel. to electronic states and molecular geometry 2−42940

Isomerization *see Isomerism*

Isomorphism
- between algebra 0(n,n+1) and para-Fermi algebra 2−55374
- dickite ground, negative surface charges 2−78235
- kaolinite ground, negative surface charges 2−78235
- $NaICl_4.2H_2O$ with $NaAuCl_4.2H_2O$ 2−84590
- $SrAl_2SiO_8$-$BaAl_2SiO_8$ solid soln., phase diagram, polymorphic species 2−54009

Isotope effects
- *see also Isotope shifts*
- acetoxime, ^{13}C n.m.r., chem. shift 2−64165
- acetylene, effects of deuterium substitution on n.m.r. parameters 2−77096
- benzene, pure and isotropic mixed crystals, absorption spectroscopic study of isotope effects intermolecular interactions 2−81357
- benzene-chloroform weak complexes, radiationless decay of benzene triplet state, external deuterium isotope effect 2−84661
- dichloroethane-d_0 and -d_4, chem. activated, cascade deactivation and nonequil. kinetic isotope effects 2−83408
- diffusion mechanisms in metals 2−68044
- dimethyl phosphite, neat and in dilute soln., effect of deuterium substitution on ^{1}J(^{31}P-H) 2−80104
- ethylamine, effect of D substitution on vapour pressure 2−43450
- formic acid, spin-lattice relax. time differences between ^{12}C-H and ^{13}C-H 2−60069
- hydrides, spin-lattice relax. times of diffusing hydrogen 2−54369
- hydrocarbons, aromatic, non-Born−Oppenheimer coupling and D effect on Ti→S_0 radiative transitions 2−43002
- methane mass spectra 2−83321
- methane-d_4 + silane ion molecule reactions, hydride ion transfer and isotope effects 2−68778
- methylamine, effect of D substitution on vapour pressure 2−43450
- methylchloride, variation of Cl quadrupole coupling on deuteration 2−80091
- propylamine, effect of D substitution on vapour pressure 2−43450
- triglycine selenate, thermal and elastic props., deuteration effects 2−72042
- triglycine sulphate, thermal and elastic props., deuteration effects 2−72042
- Ag, during grain boundary self-diffusion 2−56752
- Al, K-shell ionization cross sections by ^{20}Ne and ^{22}Ne bombardment 2−74216
- AlN, emission spectrum, rotational analyses and isotopic studies 2−42868
- Ar, isotope separation factor between liq. and vapour 2−80521
- CF_3 + NH_3, Arrhenius parameters, kinetic isotope effects and tunneling corrections 2−81496
- Ch_3 + NH_3, Arrhenius parameters, kinetic isotope effects and tunneling corrections 2−81496
- Cu ion, influence of ethanol on first hydration shell, e.s.r. obs. 2−64123
- D_2-He collisionally induced vibration, effect of rotational motion 2−80139
- DBr-Br_2 system, hot atom reaction rates 2−72549
- GaP:N, localized vibr. modes due to N isotopes, i.r. absorp. obs. 2−68639

Isotope effects continued
- H_2-He collisionally induced vibration, effect of rotational motion 2−80139
- HBr-Br_2 system, hot atom reaction rates 2−72549
- H_2O in aqueous and hydrated solid $CuSO_4$ 2−47324
- $LiHC_2O_4.H_2O$, X-ray diffraction study of isotope effect and structure 2−56657
- Mg, K-shell ionization cross sections by ^{20}Ne and ^{22}Ne bombardment 2−74216
- $N^{16}O$-$N^{17}O$-$N^{18}O$ gaseous mixture, e.p.r. spectra 2−80031
- Ni film, heat of adsorption of H_2 and D_2 2−43497
- $RbNO_3$, molten, electromigration of Rb ions, temp. depend. 2−64457
- Sb_2, vibrational and rotational analysis of $B \rightarrow X$ system 2−50068
- SnI in emission bands 2−53037
- ^{203}Tl, muonic, of μ-capture rates 2−59961
- ^{205}Tl, muonic, of μ-capture rates 2−59961
- ZnO, chemisorption of H_2, i.r. studies 2−65375

Isotope exchanges
- hot-atom substitution products, decomposition, RRKM theory, methyl isocyanide paradox 2−51428
- N_2, gas phase chain reactions for radiolytic, photochemical batch reactors 2−68760
- ^{75}Se-selenourea, preparation 2−54527
- T, penetration in Atlantic thermocline, advection rates 2−72705

Isotope separation
- *see also Radiochemistry*
- ^{210m}Bi microgram quantities of low isotopic abundance 2−42444
- binary mixture on infinite rotating disk, barodiffusion 2−77196
- critical state separation method 2−56134
- e.m. separator, nuclear material preparation 2−49614
- e.m. separator for preparation of nuclear research samples 2−73918
- formaldehyde, isotopic separation of H and D by photopredissociation 2−67438
- Haeffner effect, theory giving rate 2−57425
- heavy water, H-D separation factor, current density, cathode material, temp. effects 2−42820
- ion source, magnetron radioactivity, high temperature techniques 2−82457
- laboratory type isotope-separator for preparation of nuclear research materials 2−73917
- nuclear research material preparation 2−49335
- on-line facility at Buenos Aires IALE project 2−52957
- plasma centrifuge, MHD processes 2−70648
- using radiation pressure of laser light 2−42172
- rare earth metals, large single cryst. growth 2−47225
- rare gas fission yields in 14 MeV neutron fission, on-line meas. 2−59792
- three stage separator design, and review of history of separators 2−74249
- ^{a}Cs, A=117-120, half-lives determ. using on-line isotope separator techniques 2−42545
- ^{227}Ac gram scale production, irradiated radium 2−49300
- B, ion exchange process 2−64082
- ^{244}Cm, chemical separation processes 2−49987
- ^{163}Dy production and crystal growth, neutron diffraction expts. 2−74667
- ^{170}Er production and crystal growth, neutron diffraction expts. 2−74667
- H_2-D_2, H_2-T_2, D_2-T_2 mixtures, using critical state separation method 2−56134
- H_2 molecules, gas chromatographic separation and quantitative det. 2−52956
- ^{3}He-^{4}He mixtures, using critical state separation method 2−56134
- K-Ar dating, orifice correction 2−59959
- Kr, short-lived isotopes, e.m. method 2−70647
- ^{238}Pu, chemical separation processes 2−49987
- Rn, short-lived isotopes, e.m. method 2−70647
- ^{154}Sm production and crystal growth, neutron diffraction expts. 2−74667
- U, power reactor applic. 2−63961
- U enrichment, calc. of flow rate in cascade separator 2−83082
- Xe, short-lived isotopes, e.m. method 2−70647
- ^{138}Xe fission product, β- and γ-decay study using ARIEL on-line isotope separator, meas. of internal conversion and Auger L spectra 2−82924

Isotope shifts
- − 2−80950
- aromatic mols., of electronic origins and ring vibrs. 2−56207
- atomic spectroscopy, relativistic effects 2−77005
- hexamethyldisiloxane, in vibrational spectra by CD_3 substitution 2−46632
- methylamine, ^{14}N shift in i.r. spectrum, force constant determination 2−60075
- molecule, freq. shifts, perturbation theory calc. 2−64094
- small molecules, i.r. matrix isolation spectra, isotopic shift and structure determ. 2−70708
- trifluoroethane and trifluoroethane-d_3, ^{19}F n.m.r. chemical shifts in gas phase 2−83308
- trimethylchlorosilane, in vibrational spectra by CD_3 substitution 2−46632
- trimethylchlorosilane, in vibrational spectra by CD_3 substitution 2−46632
- Cd, relative isotope shift (112-114)/(110-112) of 4416Å spectral line 2−64016
- Ce, isotopes, arc and spark spectra obs. 2−79892
- Ce isotopes, arc and spark spectra, ^{140}Ce-^{142}Ce shifts 2−79893
- Er, relative isotope shifts in u.v. region, determ. of coeff. of nuclear deformation and internal quadrupole moment 2−49947
- $Fe(CO)_5$, vibrational spectra of isotopic species, potential constants 2−67473
- HCN, i.r. matrix isolation spectra 2−70708
- HCl, shift between ^{27}Cl and ^{35}Cl determ. from proton shielding function parameters 2−80046
- H_2S and D_2S, i.r. matrix isolation spectra 2−70708
- $HgAr^+$, u.v. emission spectrum 2−46553
- ^{193}Hg 3.5h, determ. by Zeeman scanned optical pumping 2−46429
- NeI, specific isotope shift of 1s-2p and 2p-2s lines, calc. 2−77007
- O-H-O hypothetical linear mol., isotopic shift for large-amplitude vibrs. 2−83227

Isotope shifts continued
- ^{87}Rb-^{85}Rb D, line isotope shift, laser spectroscopic obs. 2−74222
- $SbCl_3(Br_3)$, molecular vibr. freq. 2−80022
- $SiCl_4$, ^{35}Cl and ^{37}Cl shifts, exact force field determ. 2−42936
- SnF, (1,0) band of (A−X) system 2−77093
- ^{203}Tl, muonic, of 10.35 keV state 2−59961
- ^{205}Tl, muonic, of 10.35 keV state 2−59961
- $Zn(py)_2X_2$ complexes, py=pyradine, X=halogen, band assignments from far i.r. and Raman spectra based on isotope shifts 2−70731

Isotopes
- alpha radioactive, target preparation 2−49623
- cardiac pacemakers, fuel capsule resistivity against fire-arms 2−49250
- converter for thermal energy 2−49244
- determination, semiconductor gamma ray spectrometer pulse shape discriminator, Compton scattering suppression 2−82796
- force const. matrices, prop. satisfying vibr. eqns. of two isotopic species 2−83219
- medical nuclear devices, safety analysis 2−51911
- Mossbauer isotope, table of data 2−63759
- mwteorites, preatmospheric dimensions from isotopes analysis 2−58530
- neutron deficient, of nuclei with Z=69-89, search for γ-ray isomerism 2−55970
- power from radioisotopes, symposium, Madrid (1972) 2−49242
- power generators regulatory aspects 2−49243
- power sources, accident analysis 2−55218
- radionuclide production by charged particle bombardment, units and quantities 2−42554
- safety regulations and standards, radioisotopic batteries 2−49304
- synthesis of nuclei with excess of neutrons 2−63872
- thermoelectic generator SNAP 19, laboratory testing 2−49291
- thermoelectric battery for cardiac pacemakers 2−49290
- thermoelectricity, radioisotope fuelled batteries, plutonium 238 and strontium 90 2−49303
- transporting device, mass spectrometers semiconductor detectors 2−83164
- transuranium, in vivo counting in human body 2−58616
- yield from intranuclear cascades in light nuclei, dependence on changes in density of target nucleus 2−55977
- ^{11}C, production with 3 MeV Van de Graaff 2−70646
- ^{252}Cf thermal flux subcrit. multiplication 2−83062
- ^{244}Cm, applications as radioisotopic power fuel 2−49252
- ^{137}Cs, ^{133}Cs, distrib. of radioactive and stable isotropes to human body 2−55224
- ^{3}H for energy conversion 2−49247
- ^{3}He battery, for submicrowatt range 2−49245
- ^{43}K production for medical use 2−73173
- ^{24}Mg, ^{25}Mg, ^{26}Mg, coherent neutron-scatt. amplitudes 2−67995
- Ne, liq., shear viscosity 2−53406
- ^{238}Pu, for nuclear powered artificial hearts, potential availability, encapsulation, USAEC development programme 2−51915
- ^{238}Pu battery for artificial heart system 2−49246
- ^{238}Pu sealed for cardiac pacemakers, safety studies 2−51905
- ^{90}Sr thermoelectric generator TRISTAN 2−49293

detection
- *see also Mass spectra; Radioactivity*
- geology, rock ages, importance of electronics, demands upon instrumentation 2−84725
- ionization chamber with air circulation 2−70293
- surface regions, nuclear densities isotopic tracing, by charged particle beam 2−80556
- ^{189}Tl, and energy levels 2−55967

relative abundances
- *see also Elements/relative abundances*
- gases, mass spectrometry, bakable changeover valve 2−74201
- mass spectrometric determ., systematics of double spiking 2−64081
- mass spectrometric meas., peak area comparison, instrumental modifications 2−49985
- ratio measurements rel. to isotope geology, optimal adjustment of mass spectrometer ion source 2−46398
- ^{40}Ar/^{36}Ar ratio and Ar excess in submarine basalts rel. to Earth-atmosphere evolution model 2−72689
- ^{7}Be concentrations in Atlantic Geosecs II water column rel. to oceanic circulation 2−75475
- ^{12}C/^{13}C abundance ratio in SgR A and SgrB2 and absorption spectrum of ^{13}C isotope of formaldehyde 2−48671
- ^{12}C/^{13}C interstellar ratio, obs. at 4232 Å 2−73039
- $^{12}C^{32}S$, $^{12}C^{34}S$, $^{13}C^{32}S$, $^{12}C^{33}S$, interstellar, isotopic abundance ratio and CS optical depth 2−75791
- ^{64}Ge, synthesis by α-capture during explosive stellar events 2−55963
- ^{3}H profile in Atlantic Ocean from Geosecs test cruise station 2−75474
- ^{3}He concentration monitor, ^{3}He-^{4}He gas mixture, acoustic device 2−85165
- ^{3}He concentration monitor, ^{3}He-^{4}He gas mixture, acoustic device 2−82574
- ^{3}He excess in Atlantic Ocean 2−75473
- (^{14}N/^{15}N)/(^{12}C/^{13}C) in orion A i.r. nebula 2−66135
- ^{18}O/^{16}O ratio, ocean isotope evolution and growth, model 2−84749
- ^{18}O/^{16}O ratio in Amery Ice Shelf, Antarctica, evidence for bottom freezing 2−68852
- Pb isotope ratios in conformable ores and oceanic rocks, evolutionary model 2−61991
- ^{228}Ra profile at Geosecs II in North Atlantic 2−75477
- Rb-Sr geochronolgy data, use of two-error linear regression treatments 2−61994
- Rb-Sr isotope characts. of lunar soils 2−66139
- S, balance in oceans, model 2−57863
- ^{87}Sr/^{86}Sr, det. of evolution of mantle beneath S. Pacific Basin 2−57730
- ^{87}Sr/^{86}Sr in fresh South African kimberlites 2−75452
- ^{87}Sr/^{86}Sr ratio in lherzolites from Puerco necks, New Mexico 2−65537
- ^{90}Sr in seawater from Geosecs II, shipboard analysis techniques 2−75476
- ^{235}U/^{238}U ratio meas. using mass spectrometry 2−83216

Jahn-Teller effect
alkali halide phosphors, dynamic interaction in excited electronic states 2−57346
alkali halides, F-centre, relaxed excited state 2−43647
anharmonicity and effective potentials in cluster approximation 2−80957
benzene in cyclohexane matrix, sensitivity of pseudo-distortion of benzene to host lattice, study at 1.6K 2−80952
book 2−48118
cluster model, variational Jahn-Teller groundstate 2−72234
cobaltocene, dynamic effect in orbitally degenerate $^2E_{1g}$ ground state determ. by e.p.r. and optical studies 2−56226
cyclohexane, sensitivity of pseudo-distortion of benzene to host lattice, study at 1.6K 2−80952
diamond, rel. to LCAO-MO treatment of vacancy 2−47808
dynamic effect, review 2−77809
dynamic interaction of an ion in a crystal, simple approach 2−61565
dynamical, numerical analysis 2−78056
elastic consts. anomalous behaviour at Jahn-Teller induced phase transition 2−84038
insulating crystal, magnetic side bands induced by zero point motion 2−81376
manganese spinels, and domain structure formation 2−68021
optical absorption band shapes of Jahn-Teller systems with orbital doublet, semiclassical approx. 2−65197
optical absorption band shapes of Jahn-Teller systems with orbital doublet, path integration method 2−65198
phonon-induced shift of spectral lines 2−75245
rare earth cpds., phase transitions, thermodynamic props. 2−64806
rare earth vanadates, arsenates, and phosphates, low temp. phase transform. 2−77746
rare earth vanadates, cooperative Jahn-Teller distortions 2−43926
Renner-type system, with strong vibr. coupling, optical absorpt. band shape determ. 2−65248
semiconductor, II-VI, deep Cu impurity, e.s.r. and optical spectra 2−80954
superexchange ordering of degenerate orbitals and mag. structure 2−68565
symmetry and degeneracy, particle is perturbed box, teaching techniques 2−82098
s-triazine absorption spectra, obs. of Jahn-Teller distortion in lowest excited singlet state 2−46631
vibronic interactions in doubly degenerate electron states 2−49991
$(Al,Cr)(ur)_6(ClO_4)_3$ low temp. polarized absorption spectrum, 7500-3500 Å, Jahn-Teller distortion 2−51289
$(Al,Ti)(ur)_6X_3$, X=Cl, Br, I, low temp. polarized absorption spectrum, 7500-3500 Å, Jahn-Teller distortion 2−51289
$Al_2O_3:Ti^{3+}$, corundum, rel. to e.p.r. g-value calc. 2−65331
$Al_2O_3:V$, thermal cond. and e.p.r. study 2−68214
$CaO:Fe^{2+}$, strong orbital reduction from obs. of energy of first excited electronic levels 2−72478
CaO, coupling in excited level of F^+ centre, uniaxial stress effects 2−68635
CaO rel. to temp. depend. of F^+ and F-centre luminesc. 2−84537
$Cr(ur)_6I_3$, $^4A_2 \rightarrow {}^2E$ transition, spin-orbit interaction and Jahn-Teller distortion effects in calc. of vibronic spectra 2−51291
$Cr(ur)_6I_3$ low temp. polarized absorption spectrum 7500-3500 Å, Jahn-Teller distortion 2−51289
$CsCrCl_3$, crystal structure, Jahn-Teller distortion 2−81363
Cu(II) complexes, six-coordinated, simple model of dynamic effect, determ. of associated vibrational degrees of freedom 2−53004
$DyAsO_4$, induced phase transtiion, 12K, study by Raman scatt. 2−48198
$DyVO_4$, elastic consts. anomalous behaviour at Jahn-Teller induced phase transition 2−84038
$DyVO_4$, induced phase transition, 14K, study by Raman scatt. 2−48198
$DyVO_4$, Jahn-Teller phase transitions, acoustic mode anomalies 2−71681
$DyVO_4$, rel. to uniaxial stress effects on absorp. spectra 2−51338
$DyVO_4$, uniaxial stress in co-operative Jahn-Teller distortion, theory 2−51292
$FeCr_2S_4$ spinel, dynamic effect, rel. to e.f.g. in Mossbauer spectra 2−57331
GaP:Mn, i.r. luminesc. due to $^4T_1 \rightarrow {}^6A_1$ internal transition, dynamic Jahn-Teller effect 2−81424
GaP:N, null field splitting of B-line 2−61692
$KBr:Tl^+$, magneto-optical obs. on C band 2−68606
KI, relaxed-excited state of F-centre, wave function determ. 2−68738
K_2OsBr_6 Raman spectra, obs. of dynamic Jahn-Teller effects, and quenching by charge transfer and spin-orbit coupling 2−72369
K_2OsCl_6 Raman spectra, obs. of dynamic Jahn-Teller effects and quenching by charge transfer and spin-orbit coupling 2−72369
$MgO:V^{3+}$, energy from model for effect of strains on e.p.r. spectrum 2−72495
MgO, ground state of Cr^{2+} from thermal cond. meas. 2−72238
$(Mn, Fe)_3O_4$, i.r. absorp. spectra obs. 2−61648
Mn complex, di-μ-oxo-tetrakis(2,2′-bipyridine)dimanganese(III,IV) perchlorate trihydrate, antiferromagnet, superexchange coupling 2−44303
$Mn_xFe_{3-x}O_4$ Jahn-Teller domains, electron microscope obs. 2−43922
$Na_2Cd(SO_4)_2.2H_2O$ vibrational frequencies assigned 2−83270
$Na_2Cd(SO_4)_2.2H_2O$ vibrational frequencies assigned 2−83270
$Na_2Cu(SO_4)_2.2H_2O$ vibrational frequencies assigned 2−83270
$Na_2Mn(SO_4)_2.2H_2O$ vibrational frequencies assigned 2−83270
$Na_2Mn(SO_4)_2.2H_2O$ vibrational frequencies assigned 2−83270
$Na_2(SO_4)_2.2H_2O$ vibrational frequencies assigned 2−83270
Ni II complexes, low-spin trigonal bipyramidal, electronic spectra, temp. dependence of lowest energy ligand field band 2−53031
$Ni_xZn_{1-x}Cr_2O_4$, cooperative Jahn-Teller transition, thermal expansion and sound velocity study 2−71693
P_4, valence shell structure, distortion obs. using photoelectron spectroscopy 2−46574
Pd II complexes, low-spin trigonal bipyramidal, electronic spectra, temp. dependence of lowest energy ligand field band 2−53031
Pt II complexes, low-spin trigonal bipyramidal, electronic spectra, temp. dependence of lowest energy ligand field band 2−53031
$RbMnF_3$, in Mn^{2+}, spectrum uniaxial stress effects, obs. 2−65267

Jahn-Teller effect continued
$RbMnF_3$, in Mn^{2+}, spectrum obs. 2−65268
Si, neutron irrad., rel. to piezospectroscopic obs. 2−48193
Si, rel. to isolated vacancy elec. struct., many electron molecular orbital method 2−47935
$SrTiO_3$, e.p.r. of Mo^{5+}, dynamic effect 2−48295
$TbVO_4$, Jahn-Teller phase transitions, acoustic mode anomalies 2−71681
$TbVo_4$, induced phase transition, 34K, study by Raman scatt. 2−48198
$TmAsO_4$, heat capacity, near Jahn-Teller transition, evidence of low-lying excited state 2−61105
$TmAs(V)O_4$, cooperative phase transitions, Raman scatt. obs. 2−54436
$TmVO_4$, magnon-exciton processes, absorp. spectra obs. 2−81377
$TmVO_4$, optical obs. spectrum obs. of cooperative Jahn-Teller transition 2−65269
V^{3+} complexes, trigonally distorted octahedral, lattice-ion interactions in the ligand field theory 2−81205
$ZnO:Nb^{2+}$, e.s.r. obs. 2−48284
$ZnSe:Cr^{2+}$, optical absorp. spectrum obs. 2−65270

Jet stream *see Atmosphere/movements*

Jets
see also Sprays
− 2−60136
− 2−70828
aerodynamic throttling of two-dimens. nozzle flows 2−60357
air, as acoustic lens or waveguide 2−45508
air, flow observation of fluidics by optical methods 2−73653
air, incompressible, turbulent, three dimensional issuing tangentially to and flowing along curved wall, mean velocities 2−71083
air, subsonic turbulent, pressure fluctuations 2−60347
air-natural gas, aerodynamical characteristics for combustion in transitional flow region 2−53317
arc material ablation studies, channel test device 2−53313
atmospheric streams over India in winter 2−65685
axisymmetric free laminar, power-law fluid, solution of boundary layer equations 2−60170
axisymmetrical rotational flows, jet path determ., numerical soln. 2−46674
binary diffusion of jet embedded in boundary layer 2−71072
boundary turbulence, application of Reichardt model 2−53304
chemical solutions for cutting disk specimens for electron microscopy 2−67957
circular, aerodynamic noise obs. 2−64387
coaxial high temperature jet radiation with Ti dispersive particles, energy loss 2−80497
compressed air, fluid mechanics for automation 2−74456
cylinder oscillating in stationary fluid 2−43100
dimer and cluster formation in free jets 2−84626
discharging horizontally into lake or river, heat transfer, diffusion and mixing 2−78304
discrete, output impedance, experimental determination 2−83428
dispersive syst., colliding jets, motion of solid paraticles, computer anal. 2−56310
exhaust plume/boundary layer interactions at supersonic speeds 2−56423
external flow jet flap, trailing vortex wake downwind 2−80385
flame spectrophotometry, use with heating chambers 2−44503
flow and heat transfer of flat plate at zero incidence receiving a single free jet 2−43070
flow of laminar, incompressible jet along a parabola 2−46900
fluidic logic study by optical visualization 2−73664
formation on collision of metals, explosive welding model 2−69783
free and emitted ih wake of cylinder parallel to hypersonic flow, comparative study 2−93669
free gases, turbulent mixing 2−74461
free shear layers, instability considerations 2−80198
gas, as mixing devices theory 2−83693
gas, axisymmetric, implicit finite difference soln. 2−60325
gas, different densities, mixing, low initial turbulent level 2−56404
gas, impinging on liq. surface, interfacial stability 2−43224
gas dynamic and transport phenomena in two dimensional jet interaction flowfield 2−46807
gas high pressure, density distrib. obs. by laser induced gas breakdown 2−46823
headpieces conically converging, input angle and length effect on flow coefficient 2−83446
high speed, turbulence, noise radiation 2−77350
horizontal buoyant, in calm ambient fluid, coefficient of entrainment 2−60400
hypersonic flow round body of rotation with injection from ring slot in body 2−56419
idealized, transient acoustical sources 2−55536
impingement of two jets and liquid atomization 2−74505
incompressible gases, mixing of cocurrent gas jets 2−74463
incompressible two dimensional wall jet characts. 2−50158
inviscid cylindrical, electric current effect on capillary instability 2−60401
laminar coaxial, recircularing cells 2−83667
laminar pipe, instabilities, flow props., expt. study 2−83422
liquid, conveyed by gas flow, breakup 2−60335
liquid, flow pattern at two impinging circular jets 2−71146
liquid, flow through circular orifice with central cylindrical pin with axis perpendicular to orifice plane 2−74504
liquid, interaction with free liquid surface, generation of unsteady oscillatory two phase flow 2−43285
liquid, momentum transfer in a horizontal ejector 2−67781
liquid vibration-atomization, production of monodispersed drops 2−71246
local mass transfer, over a flat plate with laminar air jet impinging normally 2−53267
low density aerodynamic tube, cryogenic pump calc. 2−82078
mass spectrometric study of vapour, errors due to dimer formation 2−68825
MHD flow near wall, convective heat transfer 2−60200
modes of submerged jet 2−70852
molecular effusing from perforated boundary producing large scale rarefied flows 2−77335
multitube multishroud supersonic jet noise suppressor 2−43233

- **Jets** continued
  - noise, generalized theory 2−55552
  - noise, simple pressure source model 2−56429
  - noise, theory, using method of matched inner and outer expansions 2−77326
  - noise field of supersonic Mach 1.5 cold model jet 2−41801
  - noise generated by air flow through circular nozzles 2−46845
  - noise intensity perturbed by screen, near field pressure and hot wire meas. 2−41820
  - nonequilibrium condensation with gas flow in supersonic nozzles and jets 2−60331
  - nonuniform plug nozzle flowfields calc. for closed wake 2−60340
  - penetration into airstream using swept back injectors at angle of attack 2−71085
  - penetration into subsonic stream, model 2−60164
  - plasma, d.c., arc constriction 2−74374
  - plasma, generator with cathode sleeve 2−53206
  - plasma, powerful light erosion plasmatron 2−53218
  - plasma generator, pulsed injector and conical electrode geometry 2−64292
  - plasma stagnation point heat transfer, heat pipe calorimetry 2−43164
  - propagation in transverse magnetic field, degeneration to elliptical shape 2−60183
  - quarter circle nozzles, expansion figures, opening ratios 2−77175
  - in rotating flows, velocity profile and flow characts. 2−53370
  - in shallow rectangular cavity flow 2−60151
  - shock heated gas outflowing into evacuated space, formation 2−83654
  - sonic, viscous interaction with supersonic external flows 2−71089
  - stability, rel. to small pot. perturbations, on escaping from slit 2−83470
  - stability of coaxial rotating jet and vortex of different densities 2−74336
  - stability of non-stationary circular jet of ideal incompressible fluid 2−77233
  - steady two-dimensional viscous flow in jet due to point source 2−77229
  - streams, numerical simulation 2−85027
  - submerged orifices, regimes of bubbling and jetting 2−60399
  - subsonic, turbulent, fluctuating pressure, space correlations 2−71076
  - supersonic, effects of nozzle plenum pressure fluctuations on noise 2−69771
  - supersonic, incompletely expanded, form of boundaries 2−64388
  - supersonic, velocity and temperature 2−77352
  - supersonic air ejectors, performance and noise characts. 2−46843
  - supersonic free jet, diffusion of filament of injected gas 2−74457
  - supersonic nozzle, turbulent boundary layer meas. with and without wall cooling 2−53287
  - supersonic nozzle flow, influence of contraction section shape and inlet flow direction 2−66023
  - supersonic spherical source flow with finite back pressure 2−80395
  - supersonic surface, hypersonic flow interaction with axial symmetry 2−56424
  - swirling, structure, effect of rotation 2−80376
  - thermal plumes, model for predicting temps. 2−78305
  - three-dimensional wall, from circular orifice, mean vel. and turbulence intensity 2−64380
  - turbulence characteristics meas., investigation of the peculiarities of the heat diffusion method 2−80196
  - turbulent, gases, cryogenic discharges into gaseous medium 2−74460
  - turbulent, in cross flow, distribs. of vel., press., temp. and intensity 2−71084
  - turbulent, pot. core, entrainment region, intrinsic struct. 2−64237
  - turbulent, sound influence, vortex generation 2−46842
  - turbulent, three dimensional, growth on flat plate 2−77200
  - turbulent cocurrent, isothermal and nonisothermal mixing 2−74462
  - turbulent combustion processes, acoustic noise generated by, analytical results 2−69774
  - turbulent compressible subsonic separated jet, numerical method of description 2−83674
  - turbulent wall jet interaction with shear flow, mixing flow 2−83482
  - twin plasma jet, welding and hardfacing of steel 2−68147
  - two-dimensional laminar from nozzle of finite height onto flat plate, flow and heat transfer 2−77224
  - two-dimensional turbulent jet attachment on plane wall 2−83689
  - two-phase, turbulence intensity 2−46995
  - vacuum prod. of thin refractory films 2−83889
  - vapour flow in cathode region of vacuum arc discharge 2−77309
  - vibrational relaxation of anharmonic oscillators in nozzle flow 2−80142
  - viscous flow down inclined plane, similarity soln., rel. to boundary currents in ocean 2−57910
  - vortex form. processes in two-dimens. coalescing jets 2−67712
  - in vortices, columnar, concentrated, structure and dynamics 2−80156
  - vortices induced by subsonic cross flow 2−43067
  - VTOL aircraft, jet impingement, flow field meas. 2−83664
  - wall, turbulent kinetic energy prod., Reynolds numbers 2−83455
  - water, bounded and turbulent, mean flow properties 2−77396
  - water, mass and phase spectrometry 2−49986
  - water, turbulent flows, amplitude modulation of ultrasound 2−74494
  - wave generation in magnetically confined and field-permeated axisymmetric jet 2−77256
  - Ar freejet plasma, nonequilibrium effects, shock wave formation 2−70900
  - Ar plasma, radial temp. distrib. meas. 2−46767
  - CO, CO-Ar, CO-N_2 gas mixtures, vibrational relaxation rate in nozzle flow 2−80142
  - CO_2 laser, plasmotron excitation by plasma jet injection 2−69917
  - H_2O, circular, energy spectrum and turbulent scales 2−46901
- **Jets, cosmic-ray** *see Cosmic rays/showers and bursts*
- **Jogs** *see Crystal imperfections/dislocations*
- **Johnsen-Rahbek effect** *see Adhesion; Electrostatics*
- **Johnson noise** *see Noise/electrical*
- **Jordan-Thiry field** *see Cosmology; Relativity/general*
- **Josephson junction** *see Superconducting devices*
- **Josephson tunelling effect** *see Superconductivity; Superconducting devices*
- **Joshi effect** *see Discharges, electric/glows*
- **Joule-Thomson effect**
  - integral, rel. to heat of mixing for gas mixtures 2−50267
  - inversion curves, determ., eqns. of state predictive capabilities study 2−84609
  - steam, coeff. meas. by throttling element for radial flow of fluid 2−67825
  - water, coeff. meas. by throttling element for radial flow of fluid 2−67825
- **Jupiter**
  - absorption line formation models rel. to observations of methane equivalent widths 2−78535
  - adiabatic model for gaseous-liquid H and He, temperature distributions 2−81933
  - atmosphere, application of atomic collision processes to study of composition 2−44941
  - atmosphere, basic optical scattering props., obs. using occultation expts. 2−75878
  - atmosphere, clouds, semi-transparent, radiative transfer props. in thermal i.r. 2−65737
  - atmosphere, collisional deactivation of NH_2 2−50060
  - atmosphere, computation of transmission profiles in ν_4 band of methane 2−48769
  - atmosphere, minor constituents, u.v. spectroscopy from Orbiting Astronomical Observatory 2−69140
  - atmosphere, obs. of singly deuterated methane in 4- to 5-micron spectrum 2−51826
  - atmosphere, physical props. from 1971 eclipse of Galilean satellites 2−75860
  - atmosphere, physicochemical and meteorological explanation 2−44940
  - atmosphere, vertically inhomogeneous scattering models 2−58489
  - atmosphere obs. by occultation of β Scorpii 2−75863
  - atmospheric absorption bands, obs. using Galilean satellite eclipse obs. 2−58490
  - atmospheric aerosol distrib. determ. from satellite eclipse obs. 2−75877
  - atmospheric entry probe missions, scientific objectives 2−75871
  - atmospheric temp. sounding 2−78539
  - brightness temperature, at 2 and 8 mm wavelengths 2−66184
  - brightness temperature in frequency interval 18.5 to 24.0 GHz 2−62698
  - Callisto, thermal radio-emission rel. to thick icy surface layer 2−75870
  - cloud system, models 2−44943
  - clouds, greenhouse effect, atmospheric composition 2−44944
  - cloudy atm., spectral line formulation 2−62710
  - comets, short period, effect of multiple encounters with Jupiter on orbits 2−58523
  - decametric pulse distribution 2−75858
  - decametric radio emission, model for control by Io 2−48770
  - decametric radio emission as indicator of high velocity fluxes and shock waves in solar wind 2−48801
  - decametric radio emission rel. to Great Red Spot 2−81903
  - decametric radiosources, two-dimensional probability and flux from 1957 to 1970 obs. 2−75862
  - decimetre flux density, long-term variations 2−69147
  - deuterated methane abundance and D-H ratio 2−75885
  - EAS as cause of sporadic decameter radio emission 2−81932
  - emission at 12.6 cm, beaming obs. 2−75873
  - energetic proton fluxes trapped in Jovian magnetosphere, upper limits 2−73080
  - entry probe rel. to atmospheric measurements 2−75642
  - environmental simulation 2−78569
  - equatorial acceleration mechanism 2−78534
  - far u.v. emission spectrum between 1200 and 1950Å 2−75879
  - formation as star of mass 0.001 $M_\odot$ 2−55138
  - Galilean satellites, brightness temp. obs. at 20 microns 2−78487
  - Galilean satellites, i.r. observations and eclipse measurements 2−78537
  - Ganymede, thermal properties from 20 μm eclipse radiometry 2−78538
  - Halileys satellites, influence on motion of artificial Kallisto satellite 2−58491
  - Hestia (VI), photometric obs. 2−75859
  - inhomogeneous atmospheric models with two cloud layers 2−78540
  - Io, diameter determination from occultation of β Scorpii 2−75864
  - Io, electrical conductivity 2−75868
  - Io, motion causing decametric radio emission 2−69148
  - Io, obs. of occultation of β Scorpii C 2−75866
  - Io, plasma sheath effects and related charged-particle acceleration 2−51825
  - Io, thermal properties from 20 μm eclipse radiometry 2−78538
  - Io, triaxial figure and apparent equatorial radius from β Scorpii C occultation 2−78536
  - Io, upper limits for an atm. 2−75867
  - Io's triaxial figure 2−75865
  - Io controlled Jovian decametric radiation, variation of highest cutoff 2−55141
  - ionospheric winds and radiation belt, meas. of dawn-dusk potential differences, average wind velocity 2−62695
  - i.r. spectrum and radiative props. of clouds 2−75884
  - isolated 5μ source obs. 2−75881
  - Kirkwood gap located at 1:2 resonance with Jupiter, evolution of orbits 2−62457
  - model, atmosphere 2−85048
  - momentum and heat transports, non-geostrophic baroclinic stability 2−58481
  - occultation by β Scorpii 2−62697
  - occultation of β Sco, flashing phenomena 2−66171
  - occultation of β Scorpii, obs. of atmosphere 2−55142
  - origin of short-period meteor orbits rel. to perturbations of Jupiter 2−58525
  - photometric characteristics of regions of disk in 0.33-0.48 microns region 2−58486
  - Pioneer spacecraft project 2−48771
  - planetary and lunar laboratory obs. 2−44945

Jupiter continued
radiative-dynamical model for static stability of rotating atmospheres 2−58480
radio emission at 102 MHz and measure of brightness temperature 2−81936
radio wave bursts and interaction of Io with magnetosphere 2−66174
Red Spot, isodensity and photometric profiles for 1971 2−69149
Red Spot and disturbances, 1970-1971 photoelectric obs. 2−75861
satellites, eclipse light curve calcs. 2−81908
β Scorpii, occultation on 1971, May 13-14, by Jupiter and its satellite Io 44879 2−44879
secular variations of asculating elements 2−62696
spacecraft and mission 2−85049
spacecraft missions to Jupiter as part of Pioneer series 2−72935
spectrum in 3200 to 11200Å region 2−75880
surface activity maps for 1963-67 period 2−58488
surface activity maps for 1965-70 period 2−58487
thermal radio emission, model atm. 2−75882
transit of Jovian system across the multiple star β Scorpii 2−44874
turbopause probe, applicability to Saturn atmospheric investigations 2−78557
Turbopause Probe and atmospheric experiments 2−75644
upper atmosphere, hypothetical chemical and spectroscopic activity of GeH_4 2−44942
upper atmosphere thermal structure with convective heat transfer 2−44939
u.v. absorption in continuous spectrum, time variations 2−75869
visible clouds, structure determ. from methane and H_2 quadrupole lines 2−75875
X-ray emission survey 2−66173
^{13}C methane and $^{12}C/^{13}C$ ratio estimation in atm. 2−66170
^{13}C methane identification and $^{12}C/^{13}C$ ratio in atm. 2−75883
D/H ratio in atmosphere 2−66172
H-He mixtures in core rel. to statistical mechanics of light elements at high pressure 2−58779
H-He plasmas, thermodynamic properties for stagnation shock layer of spacecraft entering atmosphere of Jupiter 2−46718
H_2 absorption, quadrupole, spectral obs. 2−75872
H_2 quadrupole lines, level of formation 2−75874
NH_3 aerosol layer rel. to optical properties and structure of Jupiter's atmosphere 2−58485
NH_3 variations over disk, spectrophotometric obs. at 1.5μ window 2−75876

K-capture *see Radioactivity/electron capture*

Kaons
CPT and T violation in interactions with π, $l\nu$ pair, Onsager relation 2−73799
electromagnetic mass splitting, possible origin for symmetry breaking 2−55805
gas Cherenkov counter with large aperture for distinguishing between pions kaons and protons 2−76742
mass relations, on pion-muon model 2−79555
neutral system, $\eta_{\parallel} \approx \eta_{00}$ from weak interaction theory 2−73801
review of published works in 1−1.4 GeV and 1.75 GeV mass region 2−76647
$\gamma p \to \kappa^+ \Lambda$, 5 GeV, recoil polarization in $K^+ \Lambda$ 2−66926
K^o-K^o system, microscopic irreversibility, check of necessity of time-reversal symmetry for Onsager relations 2−70208
$K^\pm$ e.m. form factors and inelastic structure function meas. using NAL and ISR 2−73812
$KN\Lambda$, $KN\Sigma$ coupling consts., upper bounds 2−76652
K_l-K_s mass difference in a chiral approach, two-pion contribution 2−70219
$K^0{}_l$-$K^0{}_s$ mass difference, connection to pole approximation calcs. 2−67009
$K^- p \to K^0 \pi^- p$, 3.95 GeV/c, meas. of differential cross sections and density matrix elements for production of $K^{*-}(890)$ p and $K^{*-}(1400)$p final states 2−70221

decay
see also CPT conservation
apparent T violation, restriction on conclusions 2−66908
current algebra in broken chiral symmetry 2−73736
$K \to \pi\mu(e)\nu$, consistent soln. in (3, 3) model 2−82747
2π magnetic spectrometer for study of K^+ decays 2−73931
mass distribs., CPT invariance of CT-noninvariant and CP-invariance theories 2−67000
microscopic causality and reversibility rel. to neutral decays 2−82734
symmetry, limits on variances 2−76651
weak radiative, possibility of unified description 2−76655
$|\eta_{00}|/|\eta_{\parallel}-|$ meas. in terms of K_l, K_s decay rates 2−49545
K^0-K^0 states in K_l-K_s phenomenological S matrix 2−82745
K^0, meas. by cylindrical wire spark chamber system 2−55935
K^0, mixing parameter ε in frame of Ulu and Yang's theory 2−70216
K^0 weak decay amplitudes, unitarity and CPT properties in S-matrix approach 2−70215
$K^0 \to \pi^+\pi^-\gamma$, experimental test of CP non-invariance 2−79561
$K^0 \to \pi^+\pi^-\pi^0$, exptl. study of time-dependence of decay rate 2−67003
$K^0 \to \pi^+\pi^-\pi^0$, measured in parallel with K_{l3} decay using large surface impulse chambers 2−42369
$K^0 \to \pi\mu(e)\nu$, search for fine structure, leptonic resonances 2−49543
$K^0 \to \pi\mu(e)\nu$, tests of weak interaction $\Delta S = \Delta Q$ selection rule in time distrib. of decay 2−67004
$K^0 \to \pi\mu(e)\nu$ $\Delta S = \Delta Q$ weak-interaction selection rule tested 2−45933
$K^0 \to \pi\mu\nu$, CP-violating charge asymmetry 2−76615
$K^0{}_s \to \mu\mu$, schizon model of CP nonconservation 2−79557
K^+, in flight meas. of branching ratios and phase-space distrib. for three-body semileptonic modes 2−79571
$K^+ \to e^+\nu$, branching ratio meas., rel. to V-A theory 2−79565
$K^+ \to e^+\nu\gamma$, search for description of weak radiative decays 2−76655
$K^+ \to \mu^+\nu\nu^-\nu^*$, search for process in counter expt. at Bevatron determ. of upper limit on branching ratio 2−67002
$K^+ \to \pi^- e^+ \mu^+$, doubly charged weak currents, branching ratios to $\pi^+ e^+ \mu^-$ and $\pi^+ e^+ e^-$ model 2−70217
$K^+ \to \pi^0\pi^0 e^+\nu$, branching ratio and form factor 2−42374
$K^+ \to \pi^0\pi^0 e^+\nu$ stopped decays, exptl. search 2−82748
$K^+ \to \pi^+\gamma\gamma$, current algebra application 2−76654
$K^+ \to \pi^+\gamma\gamma$, search for unified description of weak radiative decays 2−76655

Kaons continued
decay continued
$K^+ \to \pi^+\gamma\gamma$ stopped decays, exptl. search 2−82748
$K^+ \to \pi^+\pi^0\gamma$ stopped decays, exptl. search 2−82748
$K^\pm \to \pi^+\pi^- e^\pm \nu_e$, discrete symmetries test 2−67001
$K^\pm \to \pi^\pm\pi^0\gamma$, direct emission amplitude 2−45935
$K^\pm \to \pi^\pm\pi^0\gamma$, evidence for direct emission 2−79564
$K^\pm \to \pi^\pm\pi^0\gamma$. search for direct processes 2−59514
$K^\pm \to \pi^\pm\pi^\pm\pi^\mp$, Dalitz-plot distrib., expt. 2−45931
$K^\pm \to \pi^\mp\mu^\pm e^\pm$ as test for lepton number conservation 2−73749
$K^\pm \to \pi\pi\pi$, search for violation of CP invariance by comparison of Dalitz-plot distrib. for τ^+ and τ^- decays 2−52598
$K_2{}^0 \to \gamma\gamma$, Steinberger fermion-loop model 2−52593
$K_2{}^0 \to \pi^+\pi^-\gamma$, search for unified description of weak radiative decays 2−76655
$K_2 \to \pi^0 e^+ e^-$, second-order weak amplitude calc. 2−82746
$K_2 \to \pi^0\gamma\gamma$ model, unitarity constraint on decay rate 2−67005
$K \to 2\pi$, symmetry-breaking corrections to current algebra formula calc. in framework of SU(3) σ model 2−52595
$K \to 3\pi$, Moffat's model applic. 2−55843
$K \to 3\pi$, symmetry-breaking corrections to current algebras formula calc. in framework of SU(3) σ model 2−52595
$K \to l^+ l^-$, corrections for second order effects in weak interaction 2−67006
$K \to l\nu_l\gamma$, form factors, Q^2 depend 2−76669
$K \to \mu^+\mu^-$, lower bound for CP nonconservation 2−73803
$K \to \mu\mu$, anomalous $K \to \pi\pi\gamma \to \mu\mu$ interaction 2−63585
$K \to \pi l^+ l^-$, corrections for second order effects in weak interaction 2−67006
$K \to \pi\mu(e)\nu$, bounds determ. for parameters 2−63581
$K \to \pi\mu(e)\nu$, corrections to theorem on decay form factors 2−63583
$K \to \pi\mu(e)\nu$, derivation of bounds on form factor using soft-pion theorem as input 2−55845
$K \to \pi\mu(e)\nu$, $\Delta S = \Delta Q$ law of Fermi interaction verified by expt. in advanced statistics, used to meas. $K^0 \to \pi^+\pi^-\pi^0$ 2−42369
$K \to \pi\mu(e)\nu$, form factors determ. from current algebra sum rules using Veneziano model 2−73802
$K \to \pi\mu(e)\nu$, simple bound for parameters using $\pi K(s=0, T=1/2)$ phase shift 2−82744
$K \to \pi\mu(e)\nu$, sum-rule from SU(3) × SU(3) light-cone commutators 2−79558
$K \to \pi\mu(e)\nu$ decay parameters, weak κ-dominance model and bounds 2−76656
$K \to \pi\mu(e)\nu$ form factors, rel. to κ meson 2−70209
$K \to \pi\mu(e)\nu$ form factors, using massless pion method 2−45857
$K \to \pi\mu(e)\nu$ parameters, calc. by Pade approximations 2−79556
$K \to \pi\mu(e)\nu$ parameters and weak interactions of urbaryons 2−59510
$K \to \pi\pi$, current algebra application 2−76654
$K \to \pi\pi$, $\Delta I = 5/2$ contributions, S-wave $\pi - \pi$ phase shifts 2−79570
$K \to \pi\pi$, electromagnetic effects in symmetrized soft pion limit 2−79559
$K \to \pi\pi$, $K \to \pi\pi\pi$, difference in interference formulas for CPT or T invariance 2−82738
$K \to \pi\pi$, $K \to \pi\pi\pi$ difference in interference formulas for CPT or T invariance 2−82738
$K \to \pi\pi\mu(e)\nu$, decay widths, effective Lagrangian model 2−66953
$K \to \pi\pi\mu(e)\nu$, form factor deviation from chiral symmetry value, light cone corrections 2−63582
$K \to \pi\pi\mu(e)\nu$, form factor of vector current calc. 2−63576
$K \to \pi\pi\pi$, Dalitz-plot distribution, analysis by two- variable expansions 2−55846
$K \to \pi\pi\pi$, model satisfying analyticity, crossing symmetry and approximate unitarity 2−76649
K_{l3}, equivalence of Klein-Gordon and Kemmer formulations 2−73805
K_{l3}, inequivalence of Klein-Gordon and Kemmer formulations 2−73804
K_{l3}, relation slip between parameters 2−49544
K_{l3}, simple bound for decay parameters using πK phase shift 2−63589
$K_{\mu 3}{}^0$, $\Delta S = \Delta Q$ selection rule tested, K^9 produced by π-$p \to \Lambda K^0$ at 3 GeV/c 2−45934
$K_{\mu 3}{}^+$, correlations among products 2−45936
K^o, long-lived, precision meas. on mean lifetime 2−63587
$K^o \to \pi e\nu$, study of vector form factor 2−82739
$K_s{}^0 \to \pi^+\pi$-π^0, search for decay, K^0 produced in reaction π-$\to \Lambda K^0$ at 3 GeV/c 2−45932
$K_s{}^0 \to \pi^+\pi^- / K^0 \to \pi^0\pi^0$, branching ratio meas. 2−52594
$K_s \to 2\gamma$ rate calc. on CP invariance basis 2−59512
$K_s \to \mu\mu$, 2π-2μ interaction, CP noninvariance, decay widths 2−59509
$K_s \to \pi^0\pi^0$, charged-neutral branching ratio 2−63590
$K_s \to \pi^+\pi^- / K_s \to \pi^o\pi^o$ branching ratio 2−82736
$K_s \to \pi^+\pi^-$, charged-neutral branching ratio 2−63590
$K^0 \to \pi^\mp e^\pm \nu$, test of $\Delta S = \Delta Q$ rule in heavy liquid bubble chamber expt. 2−63588
$K^\circ \to \pi\mu\nu$, test of $\Delta S = \Delta Q$ selection rule and CP symmetry 2−45940
K_l, meas. of branching ratio $\Gamma(K_l \to 3\pi^0)/\Gamma(K_l \to \pi^+\pi^-\pi^0)$ 2−52597
$K_l{}^0$, mean life meas. in scintillation-counter by obs. of exponential decrease in $K_l{}^0$ flux 2−82741
$K^0{}_{l,s} \to \pi^0\pi^0$, reevaluation of relative decay rate and CP violation 2−76653
$K^0{}_l \to \mu^+\mu$ effect of CP violation 2−73800
$K_l{}^0 \to \mu^+\mu^-$, possibility of anomalous intermediate $\pi^0 \to 2\mu$, $3\pi \to 2\mu$ 2−63584
$K_l{}^0 \to \nu\pi\mu$ where π and μ form a mesic atom, probability calc. 2−64085
$K_l{}^0 \to \pi^+\pi^-\gamma \to \mu\mu$, calc. of contribution of intermediate state to absorptive part of decay 2−63586
$K_l{}^0 \to \pi^+\pi^-\pi^0$, slope parameter meas. 2−49542
$K_l{}^0 \to \pi^\pm e^\mp \nu$, energy dependence of form factor, wide-gap spark chamber study 2−67008
$K_l{}^0 \to \pi^\pm\mu^\pm\nu$, charge asymmetry meas. system 2−52690
$K_l{}^0 \to \pi^\pm\mu^\mp\nu$, exptl. study, Dalitz plot 2−63580
$K_l \to 2\mu$, hypothesis for existence of light vector meson as cause of negative exptl. result 2−67007
$K_l \to 2\mu$, possible CPT breaking effects 2−45938
$K_l \to 3\pi$, $K_l \to 2\gamma$, intermediate η meson production 2−45937
$K_l \to \chi^0\gamma(\chi^0 \to \pi^0\gamma)$, exptl. search for neutral vector meson 2−52596
$K_l \to e^+e^-\gamma$, exptl. search for neutral vector meson 2−52596

Kaons continued
- **decay** continued
  - $K_l \to \gamma\gamma$, gauge-invariance restrictions on pole models 2−79567
  - $K_l \to \mu^+ + \mu^-$, role of weak neutral currents 2−42373
  - $K_l \to \mu^+\mu^-$, neutral current and higher order weak effects 2−59392
  - $K_l \to \mu^-\mu^-$, possible CPT violation 2−59511
  - $K_l \to \mu\mu$, test for possible class of CP invariant solutions 2−63579
  - $K_l \to \pi^0\pi^0$, ratio η_{00}/η_{+-} measured 2−49546
  - $K_l \to \pi\pi\gamma$, experimental test of CP non-invariance 2−79561
  - $K_\rho \to \pi\mu\nu$, strong interaction form factors 2−82740
  - $K_l - K_s$ regeneration amplitude on hydrogen, high energy 2−79609
  - $K^0{}_l\rho\mu\mu$, search for new vector meson intermediate state 2−82769
  - K_s-K_l decay, equivalence between S-matrix and potential formalism 2−49547
  - $K_{s,l} \to \gamma\gamma$, branching ratio 2−59513
  - $K \to \pi\pi$, nonlocal effects, violation of CP, T, and CPT invariance 2−70214
  - $K_l \to 2\mu$, effect of e.m. interaction of muon 2−45939
- **interactions**
  - atomization by impingement of two jets 2−74505
  - free precession of magnetization in moving liquid and application to flowmetering 2−74502
  - internal gravity waves, effects of microstructure of ocean density fields 2−75478
  - ultrasonic atomization 2−74507
  - K^- interactions in bubble chamber, 2.1 GeV/c, search for final states $K\Lambda\Lambda$ 2−49598
  - K^+ one and two prong interactions on deuterium at 5.5 GeV/c, partial cross sections for k^+p, K^+n and K^+d reactions 2−63595
  - $K^\pm$ $p \to cX$ inclusive reaction spectra, calc. by urbaryon rearrangement 2−82700
  - $K^\pm$ strong interactions below 5 GeV/c, Rutherford Laboratory Meeting, Nov. 1971 2−52592
  - K^0K^0 system, temporal evolution from relax. eqn. of density matrix 2−70218
  - KN, 2-5 GeV/c, review including polarization, R parameter data, cross sections 2−52602
  - KN, 2-5 GeV/c, review including polarization, R parameter data, cross sections 2−52602
  - KN, partial wave analyses, multichannel scatt. 2−73806
  - KN, study using track sensitive targets 2−52669
  - KN charge exchange reactions, effects of correction to real part of Regge amplitudes 2−59472
  - KN parametrizations below 2 GeV/c 2−52601
  - KN production of 2^+ and 1^+ mesons studied in $U(6,6)\otimes O(3,1)$ peripheral absorption model 2−55863
  - $KN \to \pi\Lambda$, 1.54 to 2.15 GeV, duality and role of daughter resonances 2−79568
  - $KN \to \pi\Lambda$, energy independent coupled channel phase shift analysis 2−79563
  - $KN \to \pi\Sigma$, energy independent coupled channel phase shift analysis 2−79563
  - $KN \to \pi\Sigma$, Λ, strangeness-exchange interactions at high-energy, cross-section and polarization 2−76650
  - $KN \to \pi\Sigma$, new Regge absorption model fits to polarization and cross section data 2−73794
  - $KN \to \pi[\Sigma,\Lambda]$, hypercharge exchange reaction, amplitude analysis 2−42389
  - $KN \to \pi\pi\Lambda$, usefulness of meas. of Λ-polarization 2−63667
  - K^+N, 0.6-1.5 GeV/c, phase shift analysis of I=0 and I=1 states 2−76660
  - $K^+(K^-)p \to K^0(K^0)$ + anything, inclusive spectra calc. according to thermodynamic model 2−59517
  - K-d$\to$K-π-π^+np, 7.3 GeV/c, $K\pi\pi$ enhancement in Q region 2−42370
  - K-d$\to K^0\pi$-d, final state obs., 4.9 GeV/c 2−70222
  - K-d$\to K^0\pi$-π^0d, final state obs., 4.9 GeV/c 2−70222
  - K^-d, 3.4 GeV/c, final states with K° or Λ hyperon 2−67011
  - K^-d, 4.9 GeV/c, total and differential cross-sections for various final states 2−42375
  - K^-d, 5.5 GeV/c, bubble chamber analysis of final states 2−63594
  - K^-d, ~400 MeV/c, $\Sigma\pi$ and ΣN final states 2−66998
  - $K^-d \to K^-\pi^-\pi^+d$, 7.3 GeV/c, production of $K\pi\pi$ enhancement in Q region (1200-1450 MeV), structure and decay properties of Q 2−82770
  - $K^-d \to K^-\pi^-\pi^+np_s$, 7.3 GeV/c, production of $K\pi\pi$ enhancement in Q region (1200-1450 MeV), structure and decay properties of Q 2−82770
  - $K^-d \to K^-\pi^+\pi^-n\,p_s$ 5.5 GeV/c, cross section meas., production of $K^{*0}(890)$ $K^{*0}(1420)$ and $\Delta^-(1236)$ resonances 2−59515
  - $K^+d \to K^0pp$, 0.64-1.51 GeV/c, cross-sections for $K^+n \to K^0p$ deduced 2−49550
  - $K^+d \to K^0pp_s$, 3.8 GeV/c, total and differential cross sections rel. to K^+n charge exchange 2−70213
  - $K^+d \to K\pi N(N_s)$, 4.6 GeV/c, K*(892) and K*(1420)prod. 2−67040
  - $K^+d \to dK^0\pi^+\pi^0$, 3.8 GeV/c, study of final state 2−66999
  - $K^+d \to dK^+\pi^+\pi^-$, 3.8 GeV/c, study of final state 2−66999
  - $K^0{}_lN$, cross-sections and ang. distrib., compilation of 13 papers 2−82749
  - K-n$\to K^0\pi$-MM, final state obs., 4.9 GeV/c 2−70222
  - K-n$\to K^0\pi$-n, final state obs., 4.9 GeV/c 2−70222
  - K-n$\to \pi^\circ\Sigma$-, 1850 to 2160 MeV, resonant states 2−59516
  - $K^-n \to K^-\pi^-p$, application of dual resonance model for $K^+K^-pn\pi^-$ system 2−76659
  - $K^-n \to \pi^-\Lambda$, partial wave analysis between 1.9 and 2.2 GeV 2−52600
  - $K^-n \to \pi^-\Lambda$ real process, use of FESR gives EXD residues with WSNZ 2−42351
  - $K^+n \to K^0p$, cross section deuced from observation of $K^+d \to K^0pp$ 2−49550
  - $K^+n \to K^0p$, cross section difference with $K^-p \to K^0n$, Regge analysis 2−76658
  - $K^+n \to K^+N^{*0} \to K^+\pi^-p$, 12 GeV/c, study of $p\pi^-$ mass enhancement 2−82742
  - $K^+n \to K^+\pi$-p analysis of $K\pi$ scattering 2−49558
  - $K^+n \to K^+\pi^-p$, application of dual resonance model for $K^+K^-pn\pi^-$ system 2−76659
  - K-p, 5.5 GeV/c, elastic scatt. and single-pion production 2−49551
  - K-p charge exchange, differential cross sections, evidence for tachyonic resonances 2−63546

Kaons continued
- **interactions** continued
  - K-p$\to K^0n$, 1700-2100 MeV c.m. energies, meas. of cross sections, angular distribs., polarizations 2−79572
  - K-p$\to K^+\Xi$-, consequences of exchange degeneracy with respect to polarization 2−49548
  - k-p$\to \Lambda\eta$, 1.25-1.85 GeV/c, duality 2−73810
  - k-p$\to \Lambda\pi$, 1.25-1.85 GeV/c, duality 2−73810
  - K-p$\to \Lambda\pi^0$, 1700-2100 MeV c.m. energies, meas. of cross sections, angular distribs., polarizations 2−79572
  - K-p$\to \Xi$-$K^0\pi^+$, investigated at 2.18 GeV/c 2−45942
  - K-p$\to \pi^\pm\Sigma^\mp$, 1.73 to 2.11 GeV, partial wave analysis 2−45943
  - K-p$\to \pi Y_1^*(1385)$, study of baryon decays involving two partial waves, test for basic violations of $SU(6)_w$ 2−63642
  - Kp, high-energy, asymmetry of pion distrib. 2−45967
  - K^-p, 10 GeV/c, obs. of central emission of pions, search for symmetry system 2−73816
  - K^-p, 3.9 and 4.6 GeV/c, study of production and decay of nonstrange mesons 2−66994
  - K^-p, 3.95 GeV/c, f and f′ production 2−79604
  - K^-p, 8.25 GeV/c, average transverse momentum of pions from final states 2−79566
  - K^-p, existence of M(953) meson 2−73831
  - K^-p, quasi-two body and multiple body reactions at 10 GeV/c, Ω and Ξ production, review of recent results 2−42377
  - K^-p experiments of Vienna Bubble Chamber Group at 10 GeV/c, 8.25 GeV/c, 16.6 GeV/c 2−76577
  - $K^-p \to K^-\pi^-\Delta^{++}(1236)$, 8.25 GeV/c, CLA model, Pomeron and K* exchange 2−55847
  - $K^-p \to K^-\pi^+n$, 3.9 and 4.6 GeV/c, study of interference effects of K*(890) and K*(1420) resonances with background 2−63647
  - $K^-p \to K^-\pi^+\pi^-$ 10 GeV/c s-channel and t-channel helicity conservation tested 2−82753
  - $K^-p \to K^0n$, cross section difference with $K^+n \to K^0p$, Regge analysis 2−76658
  - $K^-p \to K^0p$ + anything, 10 GeV/c, correlations between longitudinal momenta of p and E^0 2−63659
  - $K^-p \to K^{*-}p$, 10.9, 13.4, 15.9 GeV/c, meas. of differential cross sections, K^{*-} spectrum 2−49585
  - $K^-p \to K^{*-}\pi^+n$, U(6,6) symmetry and generalized Veneziano model 2−67010
  - $K^-p \to K^*(890)\pi N$, 10 GeV/c, isospin analysis, diffractive dissociation 2−82735
  - $K^-p \to K\pi N$, 10 GeV/c, isospin analysis, diffractive dissociation 2−82735
  - $K^-p \to \Lambda\eta'$, 2.2 GeV/c, η^1 parameters determ. 2−76692
  - $K^-p \to \Lambda\omega$, exchange mechanisms, 3.95 GeV/c 2−63592
  - $K^-p \to \Lambda\omega$, quasi-two body reaction, 1.26- 1.84 GeV/c partial wave analysis 2−52599
  - $K^-p \to \Lambda\varphi$, exchange mechanisms, 3.95 GeV/c 2−63592
  - $K^-p \to NK^*(890)$, quasi-two body reaction, 1.26-1.84 GeV/c, partial wave analysis 2−52599
  - $K^-p \to \Sigma^0\varphi$, exchange mechanisms, 3.95 GeV/c 2−63592
  - $K^-p \to \Sigma^0\rho$, exchange mechanisms, 3.95 GeV/c 2−63592
  - $K^-p \to \Sigma(1385)\pi$, quasi-two body reaction, 1.26-1.84 GeV/c, partial wave analysis 2−52599
  - $K^-p \to (\omega,\varphi)\Lambda$, meas. of joint density-matrix elements, study of vector-meson production with hypercharge exchange 2−82743
  - $K^-p \to (\omega,\varphi)\Lambda$, polarization and unnatural parity exchange 2−42376
  - $K^-p \to \eta\Lambda$, 3.95 GeV/c, meas of cross section, angular distributions and Λ polarizations 2−59518
  - $K^-p \to \eta'(958)\Lambda$, 3.95 GeV/c, meas. of cross section, angular distributions and Λ polarizations 2−59518
  - $K^-p \to \omega\Lambda$, 1915-2168 MeV, partial wave analysis, resonance formation 2−70220
  - $K^-p \to pK^-\pi^+\pi^-$, study of resonance production in two- and three-particle systems at 10 GeV/c, analysis of spin structure 2−76657
  - $K^-p \to pK^0\pi^+\pi^-\pi^-(\pi^0)$, 10 GeV/c, study of resonance production and three-body states 2−73808
  - $K^-p \to p\pi^+\pi^-$ s-channel and t-channel helicity conservation tested 2−82753
  - $K^-p \to \pi^-Y^{*+}(1385)$, amplitude analysis of reaction 2−70211
  - $K^-p \to \pi^+\pi^-\pi^-$, 10 GeV/c, s-channel and t-channel helicity conservation tested 2−82753
  - $K^0p \to Q^0p$, 4 to 12 GeV/c, Q-enhancement phenomena 2−67034
  - $K^0p \to Q^0p$, 4 to 12 GeV/c, Q-enhancement phenomena 2−67034
  - K^+p, 10 GeV/c, production cross section for Ξ^+, Ξ-, Ω^+ 2−63668
  - K^+p, 12-28 GeV, correlations between produced π^- particles 2−55832
  - K^+p, 12 GeV/c, investigation of low mass $K\pi\pi$ systems 2−59519
  - K^+p, backward produced Q obs. 2−79562
  - K^+p, comparison of multiperipheral model with inclusive data 2−49552
  - K^+p, four- and five-body, reson. prod. 2−73809
  - K^+p, inclusive $\pi^-\pi^-$ production, rapidity correlations 2−49563
  - K^+p, p_t limited phase space predictions 2−55831
  - K^+p, relation between GGLP effect and particle pair mass distribution 2−49549
  - K^+p, resonances produced in bubble chamber 2−45941
  - K^+p, search for weakly decaying S= +2 exotic meson 2−59549
  - K^+p, systematic methods analysis 2−63593
  - $K^+p \to K^0$ + anything, momentum spectrum of K^0 2−79560
  - $K^+p \to K^0\pi^0\Delta^{++}$, 3-13 GeV/c, analysis of observed $K\pi$ scattering 2−42378
  - $K^+p \to K^0\pi^+\pi^-\pi^+p$, 5 and 8.25 GeV/c, analysis of $K\pi$ inelastic scattering 2−49555
  - $K^+p \to K^0\pi^+\pi^0p$, 5-12.7 GeV/c, longitudinal phase space analysis 2−73807
  - $K^+p \to K^+\pi^+n$, application of dual resonance model for $K^+K^-pn\pi^-$ system 2−76659
  - $K^+p \to K^+\pi^+\pi^-p$, 5-12.7 GeV/c, longitudinal phase space analysis 2−73807
  - $K^+p \to K + n$ charged + anything neutral, Feynman gas model 2−82704
  - $K^+p \to pK^+\omega$, momentum transfer and ang. decay spectra 2−63591
  - $K^+p \to pK^+\varphi$, momentum transfer and ang. decay spectra 2−63591
  - $K^+p \to \pi^-$ + anything inclusive process comparison of π^- distributions for γp and pp collisions 2−67052
  - $K^\pm p$ total cross-section, relation to slope of diffraction cone 2−66964

Kaons continued
interactions continued
$K^{\pm}p$ total cross-sections, empirical scaling behaviour 2−73778
π-K^{+}, 2.45 GeV/c, meson and baryon reson. prod. 2−42403
$\pi K\rightarrow\omega K$, finite-energy sum rules 2−63635
$\pi K\rightarrow\varphi K$, finite-energy sum rules 2−63635
K^{-} capture by nuclei, negative relative kinetic energy region interpret. 2−63901
K-N$\rightarrow\pi$-π-$\pi^{+}\Lambda$, 4.9 GeV/c, cross sections meas. 2−42371
K-N$\rightarrow\pi$-π-$\pi^{+}\Sigma^{0}$, 4.9 GeV/c, cross sections meas. 2−42371
K-N$\rightarrow\pi$-π-$\pi^{0}\Lambda$, 4.9 GeV/c, cross sections meas. 2−42371
K-n, 4.91 GeV/c, prod. of K*-(890) and N*-(1236) 2−42372
$K^{+}p$, single-particle and two-particle inclusive reactions at 12.7 GeV/c 2−45944
production
Bose distribution in p-p collisions at 12-30 GeV/c, determ. of scaling behaviour 2−76717
in inclusive processes, multiperipheral model approach 2−79525
in proton interactions in nuclei at 24 GeV/c 2−63606
two-body strange particle final states in π-p interactions at 4.5 and 6 GeV/c 2−79599
$\gamma p\rightarrow K^{+}\Lambda$, K*-K** absorbed exchanged, F/D ratio 2−70210
$\gamma p\rightarrow K^{+}\Sigma$, K*-K** absorbed exchanged, F/D ratio 2−70210
K/π ratio in single particle inclusive processes at cosmic ray energies 2−67051
K^{+} beam, 25-70 GeV/s pulse, from internal target in accelerator 2−42480
K^{+} inclusive spectra in pp collisions, quantitative Regge expressions with scaling 2−45953
$K^{\pm}$, ratios at 21, 31, 45, 53 GeV in centre of mass 2−49564
K_{1}^{0}, in pp annihilation final states at 1.6 to 2.2 GeV/c 2−49596
$K^{-}p\rightarrow K^{0}p$ + anything, 10 GeV/c, correlations between longitudinal momenta of p and E^{0} 2−63659
pN$\rightarrow$NNKK, total cross- sections, model with single kaon exchange 2−76719
K^{+}/p diffractive excitation model adjustment of relative normalization 2−82756
K-/π- diffractive excitation model adjustment of relative normalization 2−82756
resonances *see Mesons/resonances*
scattering
— 2−59556
e.m. form factor in Veneziano-type represent. 2−63578
$K\pi$ phase shifts, cross section and moment extrapolations to π pole 2−73824
$K^{\pm}$ e.m. form factors and inelastic structure function meas. using NAL and ISR 2−73812
K-^{12}C elastic scatt., cross sections analysis 2−82723
K-^{12}C forward scatt. amplitudes, K_{s}^{0} regeneration amplitude 2−82737
KN, absorption model construction 2−63651
KN, amplitudes analysis in intermediate energy region 2−63596
KN, amplitudes analysis in intermediate energy region 2−63596
KN, calc. of magnitude of nucleon expectation value of σ commutator 2−63598
KN, chiral symmetry braking 2−49554
KN, consequences of local duality, specific solution in exact SU(3) limit 2−67012
KN, elastic and charge exchange, phenomenological analysis, Regge contributions 2−42400
KN, modified dispersion relation, constant scattering length parametrization 2−49557
KN, sum rules for elastic scatt. amplitudes, threshold behaviour 2−70242
KN, sum rules for elastic scatt. amplitudes, threshold behaviour 2−70242
KN, urbaryon rearrangement and reson. correl. 2−63563
KN, urbaryon rearrangement and reson. correl. 2−63563
KN inelastic channels below 3 GeV/c, review 2−52611
KN total cross sections, resonance and background contributions, 1-4 GeV/c 2−76646
KN$\rightarrow$KN, energy independent coupled channel phase shift analysis 2−79563
KN$\rightarrow$K*(890)N, Regge pole ρ_{10} production, unnatural parity exchange 2−49586
$K^{+}N$, below 2 GeV/c, review of I=0 state 2−52610
$K^{+}N$, I=0 state, phase shift analyses 0.6-1.5 GeV/c 2−49556
$K^{+}d\rightarrow K^{0}pp$, 3 GeV/c, meas. of differential cross sections, investigation of $K^{+}n$ elastic scattering 2−63577
$K^{+}d\rightarrow K^{0}pn$, 3 GeV/c, meas. of differential cross sections, investigation of $K^{+}n$ elastic scattering 2−63577
$K^{+}d\rightarrow K^{+}d$, 3 GeV/c, meas. of differential cross sections, investigation of $K^{+}n$ elastic scattering 2−63577
$K^{-}n\rightarrow\Lambda\pi^{-}$, backward analysis of differential cross sections and polarization using trajectory parameters 2−70223
$K^{+}n$ elastic scattering parameters studied in $K^{+}d\rightarrow K^{+}d$, $K^{+}d\rightarrow K^{+}pn$ and $K^{+}d\rightarrow K^{0}pp$ interaction 2−63577
$K^{+}n\rightarrow K^{0}p$, multiple scatt. model, duality breaking effects 2−63572
$K^{+}n\rightarrow K^{0}p$, total and differential cross sections inferred from $K^{+}d$ data 2−70213
K-p backward elastic, 1.2-2.5 GeV/c, cross section analysis by resonance and Reggeized baryon exchange 2−63599
Kp, Chou Yang model for high energy diffraction slopes 2−49488
Kp, transition regeneration amplitude meas., 14-42 GeV 2−79609
Kp dispersion relations, model independent calculation 2−79569
Kp interaction scaling radius hypothesis, comparison with data for 6-14 GeV/c 2−73788
Kp polarization, interpretation in terms of optical model 2−67056
$K^{-}p$, charge exchange cross section at 1.8 GeV/c 2−59521
$K^{-}p$, differential cross sections, unitarization and OBE contrib. 2−76638
$K^{-}p$, elastic scattering, 10 GeV/c, review of recent results 2−42377
$K^{-}p\rightarrow K^{0}n$, multiple scatt. model, duality breaking effects 2−63572
$K^{-}p\rightarrow\pi^{-}\Sigma^{+}$, multiple scatt. model, duality breaking effects 2−63572
$K^{+}p$, 2.11 to 2.72 GeV/c, elastic channel analysis 2−49553
$K^{+}p$, backward dispersion relations 2−45946
$K^{+}p$, backward elastic, relation to quantitative Regge expressions for $\pi^{\pm}$, K^{+} inclusive spectra 2−45953
$K^{+}p$, below 1.3 GeV/c, dispersion relations 2−55848

Kaons continued
scattering continued
$K^{+}p$, below 2.5 GeV/c, diffractive and elastic interactions 2−49541
$K^{+}p$, elastic, 0.9-1.9 GeV/c, meas. of differential cross section in computer expt. 2−52607
$K^{+}p$, elastic, 430-940 MeV/c, meas. of differential cross sections 2−52606
$K^{+}p$, elastic, below 1.3 GeV/c, partial-wave dispersion relation analysis 2−52609
$K^{+}p$, elastic, below 2 GeV/c, review of regions below and above 0.9 GeV/c, partial wave analysis 2−52604
$K^{+}p$, elastic, differential cross sections in momentum range 0.9 to 1.9 GeV/c 2−59523
$K^{+}p$, elastic, threshold 2.5 MeV/c, application of Cutcofsky-Deo method 2−52605
$K^{+}p$, partial wave dispersion relations, role of ε exchange 2−63597
$K^{+}p$, Pomeron exchange amplitude and existence of Z* 2−70212
$K^{+}p$ backward dispersion relations 2−52608
$K^{+}p$ backward dispersion relations 2−45945
$K^{+}p$ elastic, in range 0.9 to 1.9 GeV/c, meas. of differential cross sections 2−55849
$K^{\pm}p$, elastic, total cross sections 2−59522
$K^{\pm}p$, elastic charge exchange scatt., s-channel helicity amplitudes 2−59520
$K^{\pm}p$, large angle contribution of direct channel resonances 2−42366
$K^{\pm}p$, Regge fit with Veneziano residues 2−52603
$K\pi$, analysis in $K^{+}n\rightarrow K^{+}\pi$-p reaction 2−49558
$K\pi$, calc. of consts. and parameters, Pade approx. 2−79556
$K\pi$, off-shell scatt., effects from linear dynamical zeros 2−73825
$K\pi$, phase-shift solutions in model satisfying analyticity, crossing symmetry and approx. unitarity 2−67032
$K\pi$, saturation of commutator matrix element, local approx. 2−49544
$K\pi$, sharp changes in behaviour of $\langle Y_{1}^{0}\rangle$ moment 2−45971
$K\pi$ angular distribs. obs. in $K^{+}p\rightarrow K^{+}\pi^{-}\pi^{+}p$ and $K^{+}p\rightarrow K^{0}\pi^{0}\pi^{+}p$ reactions from 3-13 GeV/c 2−42378
$K\pi$ elastic scattering cross-section in I=3/2 state studied using $K^{-}d$ interaction at 5.5 GeV/c 2−63594
$K\pi$ phase shifts, duality structure 2−59543
$K^{+}\pi^{-}\rightarrow K^{0}\pi^{+}\pi^{-}$, cross section determ. using Chew-Low extrapolation method 2−49555
πK, bootstrap calc. of K* using effective potential method 2−45989
πK, low-energy, compatibility between current algebra and unitarity constraints 2−67030
πK, low energy, inverse amplitude dispersion relations 2−82733
$\pi K(s=0,T=1/2)$ phase shift for simple bound on $K\rightarrow\pi\mu(e)\nu$ decay parameters 2−82744
KDP *see Potassium compounds*
Keratin *see Proteins*
Kerr effect *see Electro-optical effects; Magneto-optical effects*
Kicksorters *see Counting circuits*
Kikuchi lines *see Electron diffraction crystallography; Electrons/scattering*
Kinematics
acceleration analysis in complex mechanisms 2−45350
automobile, elastic, stability in critical case 2−41562
cosmological nonrelativistic, Hooke's symmetries, relation to Galilei group 2−54996
disclinations, general equations 2−74780
gas kinematics near centre of the Galaxy 2−72971
heavy filament in satellite orbit, transverse oscillations 2−73349
inclusive reactions in high energy multiparticle production phenomena 2−45908
Lagrange's equations and balances of linear and angular momentum for rigid body system 2−58833
liquid crystals 2−43279
molecular force field models 2−52976
motion of a point subject to forces depending on its position and friction 2−45428
nonholonomic systems, virtual displacements with arbitrary constraints 2−58834
nonlinear perturbations of motions, rel. to eqns. of motion solns. props. 2−45346
optimal transfer trajectory in central Newtonian field of forces 2−52128
projectiles, teaching expt. using spring-gun portion of ballistic pendulum 2−78733
rigid body, angular velocity 2−58832
rigid body in constrained motion, path of inertia pole 2−78869
rigid-body systems, new classes of solutions 2−76241
technical stability of motion relative to separately given coordinates 2−41563
three body restricted problem, periodic orbits of collision 2−49054
translation-rotational motion of triple rod in a Newtonian field 2−45348
IZw 129, compact galaxy, intwnal kinematics 2−51704
IIZw 70, compact galaxy, internal kinematics 2−51704
Kinetic theory
— 2−67551
anisotropic plasma half-space, kinetic theory of e.m. field fluctuations 2−80235
Bogoliubov's functional assumption, math. validity 2−76223
in closed rotating cosmologies, entropy production in collision time approx. 2−48648
diamagnetic diatomic molecules, evaluation of kinetic theory collision integrals 2−53095
disperse systems, van der Waals forces between immersed particles 2−60516
droplet growth in nucleation 2−60551
elastic particle collisions, max. number under Newtonian and relativistic laws 2−82292
electrolytes, van der Waals forces 2−51458
electron mean energy between parallel plates in Ar, variation of steady state value 2−43201
e.m. plane wave scattering from plasma cylinder 2−83537
equations stiffness, numerical solution 2−45347
exponential-6 potential, mixture rule 2−45302
fatigue crack propag., activation energy estimation 2−73391
Grad's thirteen moment method, appl. to electron gas 2−41547

Kinetic theory continued
hard sphere fluids, distrib. functions, theorem 2−73342
hard-sphere gas, thermal fluctuations 2−76224
laser line width, kinetic theory for spectrally heterogeneous medium 2−55679
Lennard-Jones 6-12 potential, self-consistent approximation and fourth virial coefficients 2−58783
Lennard-Jones (12-6) potential, empirical equations to calculate 16 transport collision integrals $\Omega^{(l,s)*}$ 2−58812
Lifshitz-Van der Waals constant calcs. from optical states 2−53457
moving particle, relativistic kinetic temperatures 2−66474
multilevel system, theory of spectrophone effect 2−80410
non-ideal reference system, virial expansion, chain approximations 2−55436
particle diffusive growth, kinetic equation 2−71248
plasma, chemically reacting 2−70875
plasma, kinetic equations for strong turbulence 2−53221
plasma, systematic derivation of wave kinetic equation 2−64256
plasma, weakly-turbulent, kinetic equations by multiple scattering theory 2−70903
plasma collision dominated regime and azimuthal electric fields in toroidal transport 2−46719
rarefied gases, exact solution of temperature slip problem 2−50270
relativistic, lecture notes 2−52101
relativistic, supplementary conditions 2−49024
retarded van der Waals forces between macroscopic particles, theory and exptl. evidence 2−58803
soft sphere fluid, inverse-12 potential, radial distribution functions 2−49039
spatially inhomogeneous system, structure propagation theorem 2−52083
turbulent flow 2−70853
van der Waals forces calc. from dispersion relations 2−78816
van der Waals generalized theory for dense fluids 2−67546
van der Waals interactions between macroscopic bodies having inhomogeneous dielec. susceptibilities 2−74561
weak-coupling approx. renormalization 2−74481
He, path integral calc. of three-particle direct and exchange contribs. to pair distrib. function and third virial coefficient 2−53334

gases
see also Association/gases; Brownian motion; Collision processes; Diffusion in gases; Equations of state/gases; Joule-Thomson effect; Molecules/intermolecular mechanics
acoustic propagation in gas of Maxwell molecules 2−41707
binary gas mixture, time-dependent correlation functions 2−56436
binary mixtures, diffusion slip velocity phenomena 2−80421
Boyle's law air track demonstration 2−62949
carbon tetrafluoride, Percus-Yevick and Lennard-Jones (7-28) potential calc., comparsion with exptl. data 2−43259
classical gas dynamics, new set of axioms 2−60364
classical hard discs at high density, investigation using De Boer cell-cluster theory 2−64391
classical ideal, Maxwell-Boltzmann distribution, different proof 2−62941
compression heating of classical particles in ID box 2−62948
degeneracy of spectra of linearized Boltzmann collision operated for Maxwellian molecules 2−46852
diatomic, second virial coeff. determ. from atom-atom pots. 2−77366
diatomic, thermal radiation interaction, model kinetic eqn. for internal fluid 2−43263
dilute gas, collision integrals, FORTRAN IV program adapted to run on IBM computers 2−53340
dynamics, leading edge problem, shock structure and sound propagation 2−77365
effusion of gaseous mixtures, application of failure-of-isotropy theory 2−77339
effusion orifice transmission probabilities determ. as function of pressure for near ideal and right-circular cylindrical orifices 2−74464
Enskog dense gas theory, self-consistency 2−56434
fugacity and equation of state derivation for associated gases 2−46856
gas mixture, with arbitrary intermolecular potentials 2−46850
gas possessing internal energy influence of inter-mode exchange on heat flux at boundary 2−74483
gasdynamic equations in presence of oscillatory relaxation 2−77364
inert gases, mixed interaction, test for Munn potential 2−67414
isotropic, stationary gas, free path and displacement of foreign molecule 2−46854
joint ion-gas speed distribution, two temperature representation 2−70983
Knudsen cell, effective effusion cross section determ. 2−60365
Knudsen gas, rarefied, equilib. state, effect of adsorbing surfaces 2−50263
lunar atmosphere calc. of density and flux distributions of neutral gases 2−66156
mixture, linearized collision operator, modelling theory 2−56435
molecular, kinetic model based on Wang Chang- Uhlenbeck eqn., application to Brillouin scattering 2−80409
molecular dynamics of dilute gases, computer experiments 2−83704
molecular randomicity propagation 2−58780
multipole interaction effects on rotational energy exchange in molecular collisions 2−50269
neutral and ionized, study of transport phenomena 2−83701
nonequilibrium dynamics for single-component, binary mixtures and chemically reacting systems 2−64390
polar, preaveraged pot. model and equil. props. 2−83706
polarization oscills. for dipole gases 2−80415
rarefied flow, external, low speed past circular cylinder 2−46831
rarefied flow external, hydrodynamic equations derivation 2−46830
reacting and high temp., kinetic studies by chemical analysis 2−71107
relativistic, reciprocal relations for a resistive mixture 2−64392
second order stress in dense gas 2−71081
thermodynamic rel. to dynamic stability, Van der Waals gas 2−49034
transport collision integrals, evaluation using rigid core model 2−60363

Kinetic theory continued
gases continued
velocity-correlation functions in two and three dimensions, low density limit 2−53329
H_2, rel. to sound propagation rotational relaxation effects on absorption 2−46858
N_2 theory of thermomagnetic torque based on classical Boltzmann equation 2−50271
liquids *see Liquids/theory*
Kink bands *see Crystal imperfections/dislocations; Plastic deformation*
Kirkendall effect *see Diffusion in solids; Precipitation*
Klystrons *see Electron tubes; Microwave techniques and devices*
Knight shift
alkali metals and their liquid alloys, rel. to contact density determ. 2−72515
Ga, single cryst., tensor behaviour in high field spectra 2−57396
liquid metal, temp. depend. and electronic struct. 2−67842
metal, deformed, due to contactless electron-nucleus interaction 2−44451
metal, fast magic-angle rot. technique 2−81480
metal systems, data compilation, NBS Permuted Materials Index 2−68155
Al, solid and liq., n.m.r. obs., room temp.-1100°C 2−54503
Al based liquid alloy, Cr or Mn impurity 2−80486
$AuAl_2(Ga_2)(In_2)$, anomalous shift, rel. to density of states 2−47806
$CeAl_x$, n.m.r. and magnetic susceptibilities 2−84594
$CeSn_3$, rel. to absence of magnetic ordering 2−84588
Cu and Cu-Al alloys, liq. with Mn and Fe impurities, cond.-electron spin polarization obs. 2−53455
CuBr, as reference cpd. 2−44455
$Ga_{1-x}Te_x$ alloy, liq., n.m.r., temp. and conc. depend., Fermi level 2−60512
InSb, direct meas. of wave function in extreme quantum limit 2−68746
n-InSb Knight shift in the extreme quantum limit 2−84597
$LaIn_3$, n.m.r. obs. 2−65346
$LaPb_3$, n.m.r. of ^{139}La and ^{207}Pb obs. 2−65346
Na, rel. to nuclear contact densities for electrons 2−61569
Pb from electron-ion pseudopot. model 2−77812
PdH_x, of ^{105}Pd and proton n.m.r. lines 2−78174
PtSi, n.m.r. obs. 2−65348
Sc-H solid solution, Korringa product, diffusion parameters determ. 2−72517
SmF_3, anomalous ^{19}F shift 2−84589
Te, liquid, temp. depend. obs. rel. to electronic transport behaviour 2−71237
$Tl_{1-x}Te_x$ alloy, liq., n.m.r., temp. and conc. depend., Fermi level 2−60512
V-Ge-Al alloy, n.m.r. determ. 2−57398
V-Ru alloys, temp. and mag. field depend. 2−61753
$V_{1-x}Cr_xBe_2$, ^{51}V and ^{9}Be n.m.r. 2−72520
$(V_{1-x}Cr_x)_3Si$, ternary alloys, physical props. and electron struct. 2−68514
Knudsen number *see Flow; Hydrodynamics*
Kohn effect *see Crystal electron states; Crystals/lattice mechanics*
Kondo effect
— 2−71831
alloy, dilute, rel. to localized spin fluctuations 2−57148
anomalous charge oscill. around resonant scatt. impurities, theory 2−81029
dilute alloys, exchange enhanced, transport properties 2−68334
dilute mag. system, Schrieffer-Wolff transform., Kondo model rel. to Anderson model, diagrammatic eqns. 2−48042
$Fe_xPd_{80-x}P_{20}$ ($13 \leqslant x \leqslant 44$), amorphous, weakly coupled Fe atoms and spin-flip scattering process 2−65114
finite impurity spin lifetime concept. and resist. calc. 2−54287
Kando Hamiltonian, pseudo-fermion Hamiltonian representation 2−73340
magnetic impurity, symmetric Anderson model and Mattis' model 2−75021
magnetically doped tunnel junctions, mag. interactions 2−68449
random impurity potential, high temp. effect 2−72102
renormalization-group techniques, ferromag. and antiferromag. cases 2−81259
superconducting alloys, critical field and temp. behaviour below 0.1K 2−44082
superconducting alloys with paramag. impurities and local states in gap 2−71857
superconductor, specific heat, influence of mag. impurities 2−64929
temperature of strongly coupled pair of magnetic impurities 2−72103
transition metal alloys, dil., two-band model interpret. 2−61145
Ag, with mag. impurities, elec. resist. 2−64909
Al-3d transition metal dil. alloys, validity of Kondo model 2−81029
Au-Ti dil. alloys, weak resist. minimum 2−44052
Au-V dil. alloys, mag. susceptibility, 2-293K, local behaviour 2−68517
$CeAl_2$, $CeAl_3$, resistance minimum of Kondo-type numerical soln. for self-energy of conduction electrons 2−75054
$CeAl_2$, resistivity under pressure obs. 2−77857
$Ce_xLa_{1-x}Pd_3$ alloy, elec. resistivity and heat capacity 2−51098
CoSi, near-stoichiometric susceptibility, Kondo behaviour 2−68521
Cu-Co, n.m.r. and double resonance studies of electron spin density near Co atoms, obs. of satellite lines 2−75204
Cu-Ni-Mn, dil. alloy, resist., magnetoresist., Z-100K 2−47835
Cu-Ni(Cr) alloy, resistivity and magnetoresistance obs. 2−64913
Cu alloys, validity of Kondo model 2−81029
Cu dil. alloys, exchange splitting of electron spins 2−77848
Ge:As tunnel diode, mag. scatt. 2−71973
La-Ce(Gd) dil. alloys, temp.-depend. pair breaking 2−54144
$(La,Ce)Al_2$, re-entrant supercond.—normal phase boundary obs. 2−75060
$LaAl_2$, resistivity under pressure obs. 2−77857
$(La_{1-x}Ce_x)Al_2$, Kondo supercond., anomalous crit. field curves 2−61238
$(La_{1-x}Ce_x)Al_2$ alloys, supercond. vanishing below second transition pt. 2−44075
Ni-Pd-P-base amorphous alloy containing Fe, resistivity-temperature relationship, $T^{-1/2}$ singularity 2−44215

Kondo effect continued
- Pb-Mn superconducting film, temp. determ. from tunnelling conductance curves 2–71851
- Y-Ce, line widths and satellite positions detn. using susceptibility meas. 2–65350
- Y-Ce alloy, decrease in elec. resist. under press. 2–71839
- Zn-Cr(Mn) alloys, supercond. below 0.1K 2–44082
- Zn-M dilute alloy, M=Mn, Cr, Fe 2–64918

Kramers-Kronig relations *see Dielectric phenomena; Optical properties of substances*

Krypton
- afterglow exptl. meas. of dissociative recombination at elevated temperatures 2–70888
- afterglow plasma, diffusion cooling 2–56336
- atom, absorption spectra in range 330 to 600Å 2–49949
- atom, elastic reson. energy 2–74230
- atom, electron impact ionization, energy and ang. distrib. of secondary electrons 2–64031
- atom, ionization in slow collisions with He and He^+, meas. of energy spectra and angular distribs. of ejected electron 2–56119
- atom, metastable, collisional excitation of Xe atoms 2–59936
- atom, oscillator strengths for multiple ioniz. in outer and first inner shells 2–79891
- atom, outer s shell role in single ioniz. by electron impact 2–67399
- atomic collisions with N_2 and O_2, Lennard-Jones potentials determ. 2–56272
- atoms, Hanle effect meas. of lifetimes of excited states 2–42751
- discharge, radial distrib. of temp. and density of charged particles 2–50228
- equations of state, from 120 to 423K at pressures from 0 to 1000b 2–67732
- high gain neutral laser lines in pulsed discharge 2–41979
- implantation profile in Al, calc. 2–74795
- ions, scatt., multiple, by C and Ge foils 2–47781
- ions, yhree-body conversion to mol. ions 2–83188
- laser, mode-locking of coupled transitions 2–82478
- laser lights attenuation charact. in water 2–76512
- liquid, longitudinal phonons and the law of corresponding states 2–71156
- liquid 145-240 K, sound velocity adiabatic compressibility and specific heats 2–83790
- liquid and solid doped with ethylene, absorption spectra 2–46603
- multi-charge ions moving in an impulse discharge, method of measuring velocity 2–50223
- photoionization by X-rays, relative abundances of multiply charged ions 2–53245
- plasma, electron thermal conductivity temperature dependence 2–60263
- pulsed discharge, electrical and optical characteristics 2–43212
- relative transition probabilities 2–63996
- scattering of H atoms, absolute total cross sections, interatomic forces 2–67424
- short-lived isotopes, e.m. separation 2–70647
- singly ionized laser, optimum conditions for emission of 5208.3 Å, 5681.9 Å and 6470.9 Å lines 2–42023
- solid, elastic const. calcs. using Monte Carlo procedure 2–68062
- solid, elastic constants, isothermal compressibility and u.s. velocity obs. 2–50725
- solid, Mossbauer recoilless fractions calc. with central-force rigid-atom model 2–74974
- solid, specific heat, anharmonic corrections at high temp. 2–68247
- solidified, sublimation activation energy, cryst. thickness depend. 2–60562
- solubility in liq. Na, 600°C 2–56041
- thermal cond., 800-2000K meas. 2–71112
- third virial coeff. calc. at low temps. 2–56440
- viscosity, temp. depend. of coeffs. on saturation line of liq. and vapour phases at const. density 2–71170
- $H^+ + Kr$ total differential cross-section, energy depend. 2–79858
- He-Kr mixtures, i.r. absorption spectrum, temp. dependence, determination of intermolecular potentials 2–50131
- He-Kr system at 300K, 1 atmosphere pressure, composition dependence of diffusion coefficient 2–50279
- Kr-Cl_2 mixtures, shock tube heated, electron affinity continuum 2–53243
- Kr-Cl_2 mixtures, shock tube heated, dissoc. relax. times 2–53244
- Kr^+-He laser, ring shaped beam form., mechanism 2–63327
- Kr^+-Kr, charge transfer cross section and effect of initial J-states in ions 2–70624
- Kr^+-Kr collisions, inelastic energy losses in electron transitions 2–64034
- Kr-Ne, separation by ambipolar effusion, mass spectrometric obs. 2–74475
- Kr-O_2 afterglow, formation and loss of O_2^+ and O_4^+ ions 2–70889
- Kr I, e.u.v. spectra, energy levels 2–64001
- Kr I isoelectronic sequence, Hartree Fock predictions of ^1p term in p^5d configurations 2–46422
- Kr II laser, cross modulation effects 2–66756
- Kr^+, effect of reson. on vibr. distrib. in charge transfer reactions with HCl and HBr 2–51424
- Kr_3, binding energies, calc. for Lennard-Jones 12-6 pair potentials 2–60023
- ^{85}Kr inhaled, absorption, whole body dose calc. 2–78661
- $Kr^+ + Kr$ collisions, charge transfer and fine struct., transitions 2–46462
- $Kr^{**} + CCl_4 \rightarrow Kr^+ + CCl_3 + Cl^-$, rate const. prediction 2–80145
- N_2-Kr mixture, viscosity, 25 to 500°C 2–80419

Krypton compounds
- Kr-Ar(Xe) film, struct., 6K to sublimation temp., electron diffr. obs. 2–80573
- KrF_2, electronic struct. and props. 2–83251
- Rb-Kr, Van der Waals molecule, action of r.f.field 2–56194

Kuhn-Thomas sum rule *see Molecules/electronic structure*

Kurie plots *see Beta-decay theory; Beta-ray spectra*

Kyropoulos method *see Crystals/growth*

Laboratories
- *see also Acoustical laboratories*
- computer application to laboratory automation 2–84699
- engineering metrology laboratories, design and equipping 2–69530

Laboratories continued
- modern physics laboratory, senior flexible scheme 2–73255
- reactor fuel development lab. in Japan 2–70533
- school-research laboratory liaison 2–82102
- teaching, philosophy for selection of experiments 2–78720
- Vanderbilt planetarium, available facilities 2–66396

Laboratory apparatus and technique
- — 2–67852
- abridged supporting block set for optical expts. 2–78737
- adhesive bonded metal-to-metal joints, n.d.t. 2–47674
- aerosol particle counter, self contained automatic portable apparatus 2–67850
- air cushion expts. for teaching of school physics 2–62930
- air table for basic dynamics 2–62932
- all-glass-mercury static equilibrium still for vapour pressure meas. of solutions 2–53511
- animal holding platform for slit lamp exam. 2–55325
- anvil apparatus, tetrahedral, high pressure and temperature generation 2–78689
- apparatus for superhigh freqs. studies up to 1°K 2–58656
- Burnett apparatus for accurate determination of gas compressibility and second virial coefficients 2–56439
- Camac system controller 2–78688
- capillary support apparatus for use in glove bags and dry boxes, X-ray powder pattern system 2–64604
- chemical analysis, computerised data treatment system 2–84699
- current balance, classroom instrument 2–48962
- current carrying tensioning spring for high temp. ribbon filament 2–82418
- data acquisition system for residual gas analyzer 2–58649
- data acquisition system for underwater light and bioluminscence obs. 2–52005
- data acquisition system with isolated output voltage for acquiring events-versus-voltage spectra 2–48933
- data acquisition system with isolated output voltage for acquiring events-versus-voltage spectra 2–48933
- detector of partial discharges, automatic measurement of magnitude and inception and extinction voltage 2–82417
- diaphragm cell for determination of semi-permeable characteristics of charged membranes 2–68758
- diffraction experiments, new emphasis 2–62945
- Doppler effect, simple experiment 2–82108
- electron diffraction in schools 2–62936
- electron microscopes at Grenoble CEN 2–73533
- electron microscopy foil prep., 3 mm discs, at subzero temps. 2–73656
- electropolishing foils at -50°C for electron microscopy 2–43553
- fine mesh hemispherical grids, cold forming process 2–82435
- fission fragment transport from fission sources by He-jet technique 2–73900
- flame photometry, book on laboratory practice 2–48359
- flow investigation using TV camera rotating with agitator 2–53362
- fluorescence, decay curves measurement, single-photon method, evaluation of rate parameters 2–68690
- forced oscillation system, mechanical 2–62937
- forging apparatus for temps. up to 1900°C under vacuum or inert atmospheres 2–58655
- gas dynamic loading of microparticles for pulsed discharge interactions 2–53250
- glass windows, thin hemispherical, construction for nuclear and optical expts. 2–82573
- glassware with conductive coatings 2–58650
- heatable specimen handler for evaporation system 2–82376
- h.f. irradiation of biological specimens, differential power meas. 2–52002
- holder for preparation of sections from steels and refractory alloys 2–73238
- interactive computer graphics system in spark chamber events display 2–48936
- interactive computer graphics system in spark chamber events display 2–48936
- isolated and cooled, targets, for cathodic sputtering devices 2–45189
- laboratory furniture, University of Edinburgh 2–66395
- liquid level regulator, patent 2–73234
- liquid metals, supercooling, homogeneous nucleation study 2–71275
- lunar crater simulation 2–44924
- medical physics laboratory, thermoluminescent dosimetry 2–73264
- metallurgical microscope and television system for educational purposes 2–55350
- microreactor, high pressure, magnetically stirred 2–57407
- mixer for free flowing materials in spectral analysis 2–84681
- motorized drive for double tilting specimen holder of electron microscope 2–55641
- mounting of Peltier elements, stress-free system 2–76117
- multianvil apparatus, high pressure, cubic type, Hall constant measurement of n-type Ge 2–76431
- multiple crystal folder, u.s. measurements 2–82360
- nondestructive monitoring for optimization of in-service performance tests 2–60924
- on line digital analysis system 2–48932
- on line digital analysis system 2–48932
- optical bench, apparatus for making x and y adjustments 2–41436
- photoelastic bench 2–82112
- photomultiplier housing, liquid N_2 cooled for use with side window tubes 2–52399
- physics experiments for school teachers 2–52028
- plasma waves, simulation in transmission line 2–73263
- plug cutting from CaF_2 plates 2–45182
- pressure filtering and membrane cell 2–68757
- programmer for control of operation of power circuits over wide range of time intervals 2–48935
- programmer for control of operation of power circuits over wide range of time intervals 2–48935
- projectile loader for gas gun 2–66360
- pulse height analyzer-card punch interface 2–73950
- recording creep apparatus 2–52027
- red blood cells, automatic washing machine 2–85120
- rubbers, testing for wear in liquids 2–82128
- sample position semi-automatic control for electron microscope 2–43552

Laboratory apparatus and technique continued
sampling valve for gas chromatography, high temps. and pressures 2−44497
second virial coefficients, undergraduate apparatus 2−52026
signal averaging at modest cost 2−62918
source strength of ^{60}Co, ^{46}Sc using scintillation detectors and γ-γ coincidence, student expt. 2−78738
specimen stage allowing high resolution electron microscope at low temps. 2−64623
substrate design incorporating single crystal disc for LEED and AES studies in ultra high vacuum 2−60617
temperature-gradient microscope stage, aid in teaching solidification phenomena 2−58680
thermogravimetric apparatus for pressures up to 70 atoms. 2−61759
thermoluminescent dosimetry, in medical physics laboratory 2−73264
thermostat heater for preparations beneath microscope 2−45180
three parameter nuclear coincidence data collection and magnetic recording system 2−76735
tissue preparation for light and electron microscopy 2−78643
tubular fast flow reactor for high temp. gas kinetic obs. 2−48318
vibrating quartz balance, very sensitive, appl. to gas-solid interactions 2−69538
zone plate, construction 2−62935
γ-γ directional correlation experiment 2−73266
GaAs, controlled sectioning by anodic oxidation and removal of oxide layer 2−64544
LaB_6 rod cathode low power heater 2−62888
Si surface barrier detector, low-cost fabrication for laboratory use, characteristics 2−78731
Lamb shift *see Spectra/atoms*
Lambda (λ) point *see Helium/liquid; Phase transformations*
Lamps *see Light sources*
Lande splitting factor *see Spectra; Zeeman effect*
Langmuir probes
a.c., ionospheric electron temp. determ., rocket borne instrumentation 2−81726
automatic plotting of susceptance- and conductance-voltage curves 2−53210
contaminated, l.f. admittance meas. and dielec. relax. in insulating layers 2−50206
d.c. second derivative system, electron energy distrib. 2−67656
electron density meas., comparison with r.f. capacitance probe obs. 2−50209
electron temp. obs. in ionosphere 2−44753
electrostatic, electron temp. meas., effect of plasma resist. 2−60260
I-V characteristics, in afterglow plasma, technique for recording 2−64299
ion density and plasma potential, probe current, calculation 2−43174
low electron temp. meas. in afterglow plasmas rel. to ionosphere meas. inaccuracies 2−83555
plasma, fixed-bias floating double probe techniques 2−60259
in plasma flow, saturation current behaviour, obs. 2−56361
single probe technique appraisal for afterglow plasma diagnostics 2−53211
spherical, classical theory 2−64303
Ne-Hg-Ar discharge, probe measurements in positive column 2−74425
Lanthanides *see Rare earth metals*
Lanthanons *see Rare earth metals*
Lanthanum
film, core level binding energies, X-ray photoelectron spectra study 2−72096
film superconducting, phonon structure in tunnelling density of states 2−75059
flint glass, Bragg diffraction rel. to acousto-optic applications 2−66839
optical absorpt. spectra, 4d→4f transition, 4d level binding energy 2−75301
photoabsorption spectra in vicinity of 3d edges 2−76988
steel, spectral analysis of residual content 2−54572
sunspot abundances, using high resolution spectra 2−73135
surface contamination of NaCl, O ion induced X-rays obs. 2−60628
$BaTiO_3$-Bi_2O_3, La doped composite ceramic, two-step anomalous resistivity increase 2−68395
CaF_2:La,Ce, uncoloured and X-irrad., optical absorpt., charge transfer processes 2−65253
$CdF_2:La^{3+}$, ionic thermocurrents, temp. depend. 2−81089
La:Ce, skew scattering of electrons, Hall effect obs. 2−75055
La IV, Hartree-Fock calc. for $4d^95s^25p^64f$ configuration 2−46431
SrF_2:La,Ce, uncoloured and X-irrad., optical absorpt., charge transfer processes 2−65253
Lanthanum compounds
complex, lanthanide (III) tropolonates, crystal field effects in i.r. spectra 2−61644
hydrides, empirically derived band diagrams 2−77833
(b,La)(Zr,Ti)O_3, cold pressing and low temp. sintering 2−50892
CaH_2-LaH_3 system, dissoc. press. and thermodynamic props. 2−50958
$Ce_xLa_{1-x}Pd_3$ alloy, Kondo effect, elec. resistivity and heat capacity 2−51098
$Ce_xLa_{1-x}Sb$, antiferromagnetically ordered, Neel temp. dependence on lattice constants 2−72212
$Ce_{0.25}(Y,La)_{9.75}Al_2$, inelastic neutron scatt. determination of cryst. field levels of Ce^{3+}, susceptibility calc. 2−72105
La-Ce dil. alloys, supercond., temp.-depend. pair breaking 2−54144
La-Gd dil. alloys, supercond., temp.-depend. pair breaking 2−54144
La-Ni system, 50-100 at.% Ni, phase equilib. and H_2 absorpt. 2−74934
La-Th-Bi soln., mutual solubilities, 350-700°C 2−67809
(La,Ce)Al_2, Kondo system, re-entrant supercond.−normal phase boundary obs. 2−75060
(La,Gd)Al_2, dilute system, n.q.r. and relax. obs., ordering onset 2−68754
La complex, lanthanum ethylsulphate: ^{166}Er, $\gamma\gamma$ cascade, crystal orientation 2−78053
$LaAg_2Si$ and $LaAu_2Si$, prep. and cryst. struct. 2−74735
$LaAl_2$, Laves phase, low temp. specific heat, electronic contrib. 2−57067

Lanthanum compounds continued
$LaAl_2$, resistivity under pressure, Kondo effect and Ce crystalline field variations 2−77857
$LaAlO_3:Nd^{3+}$ laser crystal, luminescence and absorp. spectra 2−75302
$LaAlO_3$, self consistent lattice dynamical theory of structural phase transitions 2−77767
$LaAlO_3$, static and dynamic crit. phenomena near struct. phase transitions, e.p.r. 2−81465
LaB_6 cathode electron gun, brightness and energy distrib. 2−73525
LaB_6 rod cathode low power heater 2−62888
(LaCa)MnO_3; ^{119}Sn, Mossbauer eff. mag. fields and transfer of spin density to electronic shells 2−72287
$(La_{1-x}Ce_x)Al_2$, Kondo supercond., anomalous crit. field curves 2−61238
$(La_{1-x}Ce_x)Al_2$ alloys, supercond. vanishing below second transition pt. due to Kondo effect 2−44075
$La_{3-x}Ce_xIn$ alloys, supercond. and mag. props. 2−64946
$La_{1-x-y}Ce_xTb_yPO_4$, fluoresc. quantum efficiency 2−48246
$LaCl_3:Pm^{3+}$, absorption spectrum in 12000 to 28000 cm^{-1} range 2−81405
$LaCl_3$, spin-lattice relax. at zero mag. field of Nd^{3+} and Er^{3+} 2−65194
$LaCo_2$, high-press., high-temp., prepn. 2−83901
$LaCo_5$, permanent mag. 2−52385
$LaCoO_3$, flux growth 2−60717
$LaCoO_3$, high-spin-low spin equil. and localized-collective electron transition 2−54288
$LaCrO_3$; ^{119}Sn, Mossbauer eff. mag. fields and transfer of spin density to electronic shells 2−72287
$LaCuO_3$, prepn. under oxygen pressure and props. 2−83897
$LaF_3:Er^{3+}$, spectra, optical absorption, J levels 2−51340
$LaF_3:Ho^{3+}$, optical transition probabilities for Ho^{3+} 2−54468
LaF_3-P_2O_5-PF_2, R=Ba, Mg, triangular diagrams, crystn. and vitrification regions 2−57035
LaF_3, X-ray luminesc. excitation efficiency of lanthanide ions 2−84549
$LaGaO_3:Bi^{3+}$, luminesc. props. 2−48245
$La_{1-x}Gd_xAl_s$, nuclear spin lattice relax. 2−54370
$La_{1-x}Gd_xRu_2$, mixed cryst., supercond. and mag. props., T_c depression 2−68549
La_3In:Gd, e.s.r. obs. in type II supercond. 2−72475
$LaIn_3$, n.m.r., Knight shifts, spin-lattice relax. obs. 2−65346
$La_{3-x}InCe_x$, supercond. and magnetic props., conc. depend. 2−47854
$La_{2.97}In_{1.94}Ga_{3.09}O_{12}$, garnet, spectral transmission and refractive index 2−75300
$La_2Li_{0.50}Cu_{0.50}O_4$, prepn. under oxygen pressure and props. 2−83897
$La_2Mg_3(NO_3)_{12}$:Sm, dynamic nuclear polarization 2−68590
$La_2Mg_3(NO_3)_2.24H_2O:Ce^{3+},Pr^{3+}$, spin-phonon interaction, e.p.r. obs. 2−44316
$La_2Mg_3(NO_3)_{12}.24H_2O$:Nd, spin diffusion props. from spin heat bath relax. time 2−78049
$La_2Mg_3(NO_3)_{12}.24H_2O$, spin system dynamics obs. 2−84445
$La_2Mn_3(NO_3)_{12}.24H_2O$, paramag. relax. at liq. He temps. 2−68736
$LaMnO_3$, doped, double exchange ferromagnet, quantum theory 2−54295
$La_2(MoO_4)_3$, cryst. struct. 2−74736
$La(NO_3)_3$, aqueous solution at 25°C, u.s. relaxation 2−53427
$La^{18}O$ emission spectrum at 5600 Å, determ. of rotational constants of B−X band system 2−80019
La_2O_3, effect on lattice distortion of $CaTiO_3$ 2−74724
La_2O_3, vibr. spectra and space groups 2−51355
La_2O_3 in Bi_2O_3, ion conduction obs. 2−61418
La_2O_3 in borosilicate glasses, radiation and optical stability 2−70071
LaOBr(Cl), i.r. spectra, vibrs. assignments 2−57348
LaOCl, flux growth 2−60717
La_2O_2S:Eu, luminescence and photoconductivity 2−72064
$La_2O_2S:Gd^{3+}$, e.s.r. 2−72491
$LaOs_2$, high press. phase transition 2−71689
$LaPb_3$, n.m.r., Knight shifts, spin-lattice relax obs. 2−65346
$La_{1-x}Pr_xRu_2$, mixed cryst., supercond. and mag. props., T_c depression 2−68549
$LaRu_2$, superconductor, low temp. ht. capacity 2−77879
XLa_2Se_3-$Ge_{1.5}As_{0.5}Se_3$, pseudobinary system, glass formation 2−80531
$LaSn_3$ type compounds, band struct., impossibility of simple metal description 2−44032
$La_{1-x}Sr_xCrO_3$, volatile oxidation kinetics for optimum material characteriz. 2−50885
$LaTaO_4$, cryst. struct., X-ray obs. 2−53669
$LaTaO_4$, luminescence, fergusonite crystal struct. 2−61711
La_2Te_3-La_3Te_4 system, thermal and electrical cond. meas., semiconducting nature of La_3Te_4 2−80919
La_3Te_4, thermal and elec. cond., thermal e.m.f., 80−680 K, complex cond. band 2−80918
$LaTiO_3$, resist. and Seebeck coeff., 77-1500 K 2−57144
$La_2Ti_2O_7$, electrooptic and piezoelec. props. 2−51205
$La_2Ti_2O_7$, flux growth and single cryst. X-ray diffr. 2−60717
La_3Tl-Pr_3Tl, paramagnetic region, superconductivity and onset of ferromagnetism 2−72115
La_xTl-$Pr_{3-x}Tl$, induced-moment system, effects of 7 at.% La substitution 2−72154
La_3X, (X=Al, Ga, In, Tl, Sn, Pb), supercond. and mag. props. 2−61244
(Pb,La)(Hf,Ti)O_3, hot-pressed, material and electrooptic props. 2−56966
(Pb,La)(Zr,Ti)O_3, electrooptic ceramic, fabrication by atm. sintering 2−56967
(Pb,La)(Zr,Ti)O_3, phase boundary and defect struct. 2−56968
$Pb_{1-3x/2}La_xZr_{0.65}Ti_{0.35}O_3$, phase transitions 2−57245
Laser beams
1 nanosecond pulse prod. at 10.6 μ by CO_2 mode locked oscill. and pulsed selection scheme 2−79195
acoustic wave interaction with coherent light beam, phase fluctuations rel. to acoustic noise 2−73435
acousto-optical laser beam modulation 2−59128
acoustooptic diffraction grating modulators, design theory 2−79221
acoustooptic laser beam deflector, performance, optical analysis 2−79220

Laser beams continued
amplified systems, far field brightness 2−79224
angular divergence det. by transforming system of prisms 2−42161
anisotropic dispersion of nonlinear susceptibility in four wave i.r. mixing 2−42107
area modulated signal recordings for coherent optical correlators 2−49407
atmospheric coherence meas. of laser beams at 10.6 and 0.63μ 2−81674
atmospheric propagation, Maxwell's eqn. 2−59190
atmospheric propagation, phase difference spectra at 10.6 μ 2−81673
in atmospheric propagation, spot dancing, obs. 2−54800
atmospheric propagation, turbulence effects 2−84861
atmospheric slant path scintillation in planetary boundary layer of laser beam 2−81675
attenuation charact. in water 2−76512
attenuation coefficients in atmospheric precipitation, 10.6, 0.63 μm radiation 2−75611
bleachable absorber-laser amplifier-detector combination, wide-angle low-noise laser receiver 2−45755
calorimetric meas. of optical power from pulsed lasers 2−79232
camera with rapidly rotating mirrors for determ. beam properties 2−52510
chaotic and coherent radiation, superposed, simulation using h.f. signal processor 2−49406
chondrule-like spherule preparation from supercooled molten oxide and silicate droplets 2−44581
clouds, backscattering, first and second order, illuminated by lidar beam 2−51610
coherence determ. using interferometric method 2−76517
complex coherence factor eval. by superposition of two systems of stationary waves 2−73603
continuous tunable source of u.v. by frequency doubling output of dye laser 2−42030
continuously tunable 2500-3250Å radiation by frequency doubling dye lasers 2−79198
continuously tunable coherent source by beam mixing in ADP 2−45758
coupling of rhodamine B doped polyurethane film ring laser and He-Ne radiation 2−42055
cross sections for excitation of Ar II laser lines in electron-ion collisions 2−69954
c.w., high power, calorimeter for total energy measurement 2−78937
deflection by phase objects, obs. using speckling 2−69958
deforming light path ring laser expts., based on von Laue thought expt. 2−79239
depolarization from H_2O clouds for monostatic Lidar 2−78377
detection by current changes in gas laser discharge tube 2−42163
detection by flame 2−42162
detector frequency response of m.o.m. diodes at 1.15 μm radiation with a d.c. bias 2−45769
diffraction effects in focused truncated gaussian beams 2−79339
digital light beam deflector, 20-stage, design and performance 2−66826
efficient generation with elliptic cross section 2−55708
electro-optical shutter for Q-switching lasers emitting unpolarized radiation 2−69959
e.m. field of Gaussian beam with elliptical cross section 2−73597
energy measurements, reference calorimeter 2−49395
energy monitor with digital output 2−66794
fast pulse detection using photodiode assembly 2−57215
focused unstable beams, wind, thermal distortion effects 2−82520
focusing by geodesic thin film lens, application to integrated optics 2−49393
focussing characteristics of CO_2 laser beam 2−52420
frequency selection, polarizing Michelson interferometer applications 2−73639
frequency shift during amplification of narrow spectrum signal 2−59189
frequency tunable i.r. source, nonlinear mixing of lasers 2−73599
Gaussian beam optics rel. to conventional optics 2−79296
Gaussian fields, sequential photon counting statistics and maximum likelihood estimation techniques 2−79266
glass, optical grade, relative intensities of Rayleigh and Brillouin scatt. 2−57364
guided wave structures for electrooptical modulation at 10.6 μm 2−42157
harmonic generation, change of axial intensity 2−66778
high power pulses, energy obs. using tubular calorimeter 2−73474
high-power facility for hire 2−73600
integrated optics, thin film geodesic lenses 2−79401
intensity oscillations associated with beam splitters 2−49345
interference, fringe-visibility for anti-phase amplitude modulated beams 2−45788
i.r., 10.6 μm, attenuation in artificial, real fog 2−72804
i.r. recording on Se films and magnetic films, comparison 2−69960
i.r. to visible parametric upconversion in proustite 2−49388
i.r. upconverter, synchronously pulsed, conversion efficiency, peak power 2−79378
irradiance fluctuations in transmission through atmosphere 2−51619
light pulses, picosecond, techniques for detect and meas. 2−82512
liquid, low dispersive, enhanced optical four photon parametric interaction 2−79237
liquids, nonlinear response to laser pulses, effect of steric effects and compressibility, rel. to diameters of self-trapped filaments 2−71200
longitudinal displacements near total reflection, photon mass and new exptl. results 2−45759
Mandel'shtam-Brillouin scatt., stimulated, wavefronts of reflected and exciting light 2−42123
mixing with X-rays, parametric conversion and nonlinear X-ray scattering 2−41937
mode locked signal detection 2−69985
mode-locked, compressed spatially non- Gaussian pulse obs. 2−49394
mode-locked pulses, higher order correlation meas., fluctuations effects 2−42122

Laser beams continued
mode-locked ultrashort, duration and intensity meas. by different order photoelectric effect 2−69962
mutual coherence function of finite cross section optical beam propagating in turbulent medium 2−49390
nonlinear medium, interaction between microwaves and short laser pulses 2−42128
nonlinear propagation, analytic and numerical solns., comparison 2−82522
output pulse charact., fast gas switch 2−69952
pair production by collision of laser beam with bremsstrahlung beam 2−66904
phase distribution meas. of field on laser output mirror 2−66776
phase modulated fields, statistical props. 2−45698
photocount problem, exact soln. near threshold 2−41949
photocounting receiver performance for detection of multimode laser or scattered radiation 2−41948
photons scattered by electrons 2−52435
picosecond light pulses, statistical properties using two-photon absorbing semiconductors 2−41950
picosecond pulse shape meas. by 3-photon fluorescence 2−42120
picosecond pulses, substructured and nonlinearly broadened, mode-locking characteristics 2−42121
in plasma, i.r. inverse bremsstrahlung and photoionization absorption 2−43147
Pockel cell Q-switched Nd:glass oscillator, amplified output, picosecond structure 2−42070
propagation in optically inhomogeneous medium, scattering 2−79253
propagation in turbulent atmosphere, beam wander phenomenon 2−84862
propagation in turbulent weak drizzles, intensity fluctuations spectra 2−75607
propagation through atmosphere 2−42155
propagation through turbulent atmosphere, spot dancing 2−76500
pulse chirping in self-induced transparency 2−59205
pulse duration, using variable ultrafast photographic shutter based on polymethane cyanide dyes 2−49405
pulse duration meas. using optical bridge 2−73563
pulse propagation in molecular absorber and minimizing of heating effects 2−84860
pulse shortening using saturable absorbers 2−42104
pulse storage system, studying properties of laser photons 2−42110
pulsed, holographic adjusting 2−63353
pulses, short duration, peak intensity and energy content estimation using saturable absorbers 2−66775
Q-switched, frequency and spatial shift 2−42126
Q-switching by passive shutter 2−59192
radially polarized mode generation, expt. 2−69901
radiometry of coherent light sources 2−79172
relative energy monitor for pulsed systems, using photodiode-operational amplifier 2−52441
r.f. modulation and demodulation for communication 2−52444
scattering by slowly varying leaky wave structures 2−79337
scattering from cyclotron-harmonic waves in plasma 2−56350
scattering from high density low temp. plasmas 2−67623
scattering from turbid water, depolarization 2−64486
Schwartz-Hora effect, rad. from modulated electron beam 2−69865
scintillation in Earth to space propagation path 2−51618
scintillation of upward directed laser beams, wave front curvature and beam waist effects 2−81681
second harmonic generation, applic. of generalized theory of diffraction 2−63368
second harmonic generation of ruby laser radiation by organic crystals 2−68592
self defocusing by Rb vapour 2−43273
self focusing, beam diameter limitation due to stimulated Raman scattering 2−42117
self focusing in inhomogeneous nonlinear dielectric media 2−59206
self focusing of picosecond pulses, Kerr orientational effect obs. 2−52431
self focusing threshold of gaussian elliptic beams 2−42116
self induced thermal lens effects on imaging or tracking systems viewing along same path, image quality degradation 2−49391
self induced transparency in semiconductors 2−44329
self-focusing, limiting diameters, explanation 2−67832
self-focusing effect, effect on spatial characts. of stimulated Raman scatt. 2−77437
self-induced transparency of e.m. pulse, rot. of plane of polarization 2−52443
semiconductor laser, electron beam pumped, spatial modes far-field diffr. patterns time variations 2−79211
shock and detonation waves, local vel. meas. by Schlieren interferometry of Doppler shifted laser light 2−63138
slow TM modes on double film waveguide 2−79338
space correlation, photon coincidence obs. 2−55677
spatial coherence meas. using speckle patterns 2−52442
speckle reduction using multicolour illumination 2−79267
spectral broadening of light in filament induced by moving focus 2−42115
steady state filament formation in self focusing 2−42114
stimulated thermal scatt. of psec. pulses by liquids 2−67830
stimulated thermal scattering, frequency response 2−59238
thermal blooming, computer simulation 2−82521
time division demultiplexer for twenty four channels using sinusoidal polarization switches 2−49434
total reflection and separation into two circularly polarized beams 2−52430
transient, photocount statistics 2−66777
travelling wave light intensity modulator using polarization rotated reflection 2−42158
triglycine sulphate pyroelectric detector, nucleation sites study 2−44165
turbulent absorbing media, refractive attenuation of intensity, analyses 2−49389
turbulent atmosphere, field fluctuations 2−57995
two laser mixing and direct frequency meas. using m.i.m. point-contact diodes 2−45757
ultrashort pulse generation by optical coupling of two cavities 2−79176

- **Laser beams** continued
  - wavefronts, study by interferometer 2−59129
  - Ar 4880 Å output, scintillation obs. using ground- aircraft path 2−81682
  - GaAs, use in glass fibres, pulse broadening, obs. 2−49438
  - He-Ne, atm. influence on wavelength, correction to laser interferometer 2−69957
  - He-Ne laser, resonant absorption by methane behind shock wave front 2−64396
  - $NH_4H_2PO_4$ polarizers for, modified Wallaston prism 2−42105
  - YAG laser, Q-switched, irradiation characts. for thin film micromachining 2−73605
  - **applications**
    - acoustic shear wave probe, in $LiNbO_3$ surface wave device 2−68232
    - acoustic wave visualization by acoustic stroboscopy 2−78927
    - acousto-optic modulators and deflectors 2−55709
    - activated ferroelectric study 2−72028
    - aerosol, urban, St. Louis, Mo., Lidar obs. 2−62145
    - aerosol particle detection and size det. using open cavity of He-Ne gas laser 2−56528
    - air pollution, detection of pollutant gases by CO and CO_2 lasers 2−81668
    - air pollution mapping, Q-switched ruby laser radar 2−78350
    - alignment and straightness meas., two-aperture method 2−70035
    - anemometer, Doppler difference method, automatic data processing system 2−84789
    - anemometer, tracer behaviour in turbulent flow 2−43054
    - antenna surface contour meas. 2−73601
    - astronomical telescope RM-700 Coude focus adjustment using laser beam 2−48822
    - atmosphere, OH conc. detn. using dye laser 2−72765
    - atmospheric aerosols, meas. of complex refr. index 2−62252
    - atmospheric O_2 concentration, vertical profile, 2-wavelength lidar method 2−62135
    - atmospheric pollution aerosol monitoring by scatter of Ar-ion laser beam, interferometry 2−51600
    - atmospheric scattering data using large laser radar equipment 2−84867
    - atmospheric scintillation, laser beam meas. from 1.5 to 10.5 km altitude 2−81672
    - atmospheric surface layer, location and attenuation coeff. detn. 2−57998
    - atmospheric turbidity meas. w. laser radar 2−62272
    - atmospheric turbulence detection, rel. to air traffic control 2−78337
    - atomic absorption analysis, sample production for use in graphitic cell 2−54571
    - atomic and mol. spectroscopy, high spectral resolution 2−77004
    - atomic and molecular spectroscopy, tunable dye lasers 2−79941
    - bacteria, meas. of chemotactic response 2−58577
    - biological and medical uses and fundamentals of interaction 2−69961
    - biology and medicine, book 2−73178
    - birefringence induced by high energy laser waves for molecular optical anisotropy dispersion obs. 2−63394
    - bouncing light beam in sugar soln. unusual effect obs. 2−41435
    - CAT, detect using lidar 2−81649
    - coherence, light source characteristics 2−82547
    - coherent optical processing, spatial frequency diversity 2−79292
    - communication, charact. in water and atmospheric media 2−69955
    - cone calorimeters, spectral response 2−73473
    - construction machine guidance 2−82513
    - controlled nuclear fusion using laser compression of matter to superhigh density 2−70487
    - controlled thermonuclear fusion and heating by laser 2−70486
    - crystal growth, Czochralski method, optical diameter control 2−60715
    - crystal orientation by cleavage plane reflected laser beam 2−74656
    - detonation initiation in gaseous medium 2−80377
    - differential interferometer for fire research 2−42159
    - diffraction meas. technique 2−49424
    - diodes, coupling losses with multimode glass fibres 2−73602
    - discharge control 2−74406
    - displacement meas. from double exposure laser photographs 2−52032
    - distance meas. using electrooptical instruments 2−82533
    - Doppler anemometer, flow meas. in strong swirl 2−83511
    - Doppler meas. of turbulent flow velocity 2−77236
    - Doppler vel. meter, application to turbulence charact. 2−69540
    - Doppler velocimeter, design for use in turbomachinery 2−46826
    - Doppler velocimeter, factors affecting accuracy 2−45220
    - Doppler velocimeter, fluid flow meas. 2−66408
    - Doppler velocimeter, for MHD boundary layer studies 2−80217
    - Doppler velocimeter, instantaneous turbulence velocity measurement 2−43230
    - Doppler velocimeters, unified analysis 2−62958
    - double pinhole holography analysis 2−59193
    - dye lasers, use in two-photon spectroscopy 2−72354
    - Earth-Moon distance measurements 2−44932
    - electric breakdown triggering, effects of spark gap geometry and laser components 2−71034
    - electron density distrib. in plasma from bending meas. 2−67657
    - electron density gradients meas. using modified Jamin interferometer 2−66771
    - electrophoresis of particles and biological cells, det. from Doppler shift of scattered laser beams 2−79385
    - engineering applics. 2−45707
    - engineering meas. 2−49392
    - erasable holographic recording, patent 2−66793
    - explosives, light detonation, obs. 2−69784
    - Fabry-Perot resonator excitation of natural oscillations 2−45711
    - fibre dispersion meas. using a mode locked Kr laser 2−79235
    - fibre dispersion meas. using self pulsing GaAs laser 2−79233
    - filtering of defects in integrated circuits 2−42103
    - flash technique for thermal diffusivity det. of liquid metals at elevated temps. 2−46946
    - flow direction, speed and temp. meas. in geophys. fluid dynamics expts. 2−54775
    - flow meas., laser velocimeter, Doppler effect 2−83510
    - fluorescence production, rel. to reaction product internal state distrib. meas., applic. to $Ba + O_2 \rightarrow BaO_2$ 2−61770

- **Laser beams** continued
  - **applications** continued
    - flying spot scanner, for use in automated fluorescence microscopy 2−66264
    - frequency gain profile of CO laser obs. 2−45718
    - fusion by laser driven flame propagation in solid DT targets 2−64308
    - fusion reaction excitation, potential as thermal neutron source 2−56020
    - gain line shape of CO laser, using tunable semicond. laser 2−45728
    - gas temp. meas., by Raman laser scattering 2−50268
    - gases, separation using 'light pump' 2−71120
    - geodetic distance measurement 2−81637
    - glass transmission media, material technology 2−82563
    - gravitational flux reaching earth from Crab pulsar, reach for minimum detectable signal using laser interferometer 2−81894
    - heat source, focussing characteristics of CO_2 laser beam 2−52420
    - high-speed photography 2−76556
    - hole ('bit') creation in Al film, physical processes 2−69989
    - holographic interferometry, examination of impact loaded objects 2−45765
    - hyperballistics, laser optical system 2−82578
    - illumination system, frequency-doubled four- level, for stopaction photos 2−55781
    - image converter camera control 2−73672
    - image multiplexing using random diffuser 2−63366
    - imaging of light waves by electron microscope and stimulated Compton scattering 2−82451
    - induced gas breakdown, method of obs. density distrib. in high pressure gas jet 2−46823
    - industrial metrology in mechanical systems 2−76493
    - industry, for heating 2−82531
    - instrumentation used in aerospace test facilities 2−46848
    - integrated optics, status report 2−63406
    - interference between two light sources, obs. 2−52453
    - interferometer, based on schlieren system, design and performance 2−73635
    - interferometer, boundary layer study in fluids 2−59228
    - interferometer, for length obs. 2−59229
    - interferometer for θ-pinch plasma 2−50201
    - interferometer for high sensitivity meas. on transient phase objects 2−42192
    - interferometer for optical systems control 2−42127
    - interferometer with harmonically matched cavities, plasma diagnostics 2−66811
    - interferometry, study of plane- stress-wave propagation in solids 2−59233
    - ion temperature in θ-pinch deuterium plasma, laser-beam-scattering meas., evidence for thermonuclear reaction 2−56364
    - i.r. heating of dense electric arc plasma 2−43148
    - i.r. laser system for long path air pollution monitoring 2−62150
    - laser canes for blind persons, design improvements 2−51893
    - laser radar system, rocket mounted, for upper atmosphere aerosol obs. 2−54878
    - laser Raman spectroscopy, for small samples 2−61825
    - laser-generated shock waves for detonation of insensitive explosives and testing reliability of printed circuits 2−49174
    - lidar backscatter and extinction meas. of urban aerosols in atmosphere 2−51622
    - lidar location of light reflector on Lunokhod-1 vehicle on Moon's surface, distance measurements 2−69953
    - lidar probing of troposphere, comments 2−62266
    - light scattering photometer for particle size analysis 2−63307
    - light source in Raman spectrometer 2−59291
    - Lorentz microscopy by laser diffraction, quantitative determ. of magnetization ripple 2−79144
    - low loss optical glasses, absorption measurement 2−63407
    - lunar altimetry, Apollo 15 meas. 2−62682
    - lunar laser ranging expt., single photon detection and timing 2−48973
    - lunar laser ranging expt. 2−44930
    - lunar motion, errors, Doppler effect 2−84939
    - Lunar Motion analysis, ranging, filtering 2−58448
    - lunar orbital, laser ranging data, trial solns. 2−58449
    - lunar ranging expts. with decimeter accuracy 2−58447
    - magneto-optical expts., opt. behaviour of solids, review 2−72294
    - materials processing 2−42106
    - measurement, industrial, alignment, length, granularity, angle, velocity 2−82494
    - metal plasma production 2−74382
    - metastable isomeric nuclear levels, energy meas. by laser spectroscopy of mol. vibr. transitions 2−79713
    - metrology, systems description and examples of applications 2−69950
    - microdensitometry of photographic film, noise meas. 2−59333
    - microprobe analysis, background and energy corrections, statistical evaluation 2−68826
    - microspectral analysis of PAWEL meteorite 2−48786
    - microvibration anal., basilar membrane vibr. 2−82033
    - mode locked laser, short light pulse generation, operation, applications 2−41975
    - molecular beam mass spectrometry, i.r. laser modulated 2−81490
    - moon, laser range meas. 2−55131
    - Moon distance measurement using subnanosecond pulses, optical radar 2−85068
    - multiphoton ionization at high pressures 2−43199
    - nonequilibrium, superconductors, photoexcitation of quasiparticles 2−77868
    - nonlinear behaviour of material, determ. by self-focussing, trapping 2−79258
    - nuclear fission 2−43175
    - nuclear fusion reactors 2−56037
    - nuclear industry, possible uses of beams with foreseeable power output increase 2−63313
    - optical communication, M-ary laser detection, optimization 2−55721
    - optical images recording on magnetic plate 2−52469
    - optical memory matrices, resolution in recording information systems 2−55710
    - optical resonator, for lenses long focal length measurement 2−76537

Laser beams continued
applications continued
optical surface microtopography measurement and/or automatic focusing 2−73655
optical surfaces parallelism using nonlocalized fringes 2−82532
organic liquid laser based on Rhodamine 6J for spectrochemical analysis 2−84702
pair production in vacuum 2−82691
particle velocity det. in fluid flow 2−60165
Penning ionization detection by laser perturbation spectroscopy 2−80373
picosecond and subpicosecond light pulse generation 2−42104
picosecond electrical pulse generation by rectification of Nd:glass laser by LiTaO$_3$:Cu^{++} 2−79268
plasma, conduction type laser heating 2−64259
plasma diagnostics, electron temp. and density meas. in cascaded arc using scattered laser light 2−53260
plasma diagnostics, light scatt. technique 2−70924
plasma diagnostics, transient phenomena analysis using pulsed laser and liquid cryst. detector 2−53208
plasma diagnostics in i.r. 2−82562
plasma electron temp. and density meas. by scattering in Tuman-2 2−70925
plasma for X-ray flash tube 2−76134
plasma generation and containment, power production 2−70930
plasma heating, averaged equations of hydrodynamic expansion and conduction-type heating, case of spherical symmetry 2−77277
plasma heating 2−64258
plasma heating for spherical wave, fusion energy taken into consideration 2−77276
plasma prod., fusion, review of conditions, expt. work, prospects 2−80299
plasma production, ion temp. detn. 2−43167
plasma production, laser radiation use 2−70931
plasma production, magnetic field enhanced heating 2−70929
plasma production, set-up for high temp. heating of solid target 2−80294
plasma production by nanosecond and picosecond pulses, comparison 2−80269
plasma production from solid target, parametric dependence of temp. 2−43149
plasma single-spike laser-generated, spectroscopy, rel. to spectrochemical analysis 2−60241
plasma waves, excitation 2−70947
plasmatron, jet production by powerful light erosion 2−53218
pollution monitor for NO, laser device based on Zeeman modulation of absorption 2−61826
pressure transducers, laser technique for study of thermal transients on performance characteristics 2−66413
pressure transducers, temp. change response testing using laser 2−73286
printing and reading of part numbers 2−82577
propynal, fluorescence, collision-induced radiationless transitions 2−83298
pulse method of meas. of specific heat and thermal conductivity 2−63163
pulsed laser Kerr system polarimeter, for electro-optical fringe pattern obs. of transient electrical parameters 2−55744
radar, 10.6 μ, parametric obs. 2−55681
radar for upper atmosphere obs. 2−62281
radar obs. of dust influx into atmosphere above 30 km 2−48470
radiative and lattice thermal cond. meas. technique 2−51052
Raman backscatter obs. of atmospheric temperature profiles 2−44691
Raman difference spectroscopy using chopped laser beam 2−70072
Raman spectra by pulsed Raman technique, fluoresc. background reduction 2−79446
Raman spectroscopy, introductory presentation 2−73261
Raman spectroscopy, laser-excited for polymer struct. characterization 2−83343
Raman spectroscopy and fluorescence obs. of gases and liquids 2−42262
range meas., accuracy of atmospheric corrections 2−54857
rapid cooling by laser melt quenching 2−56897
rarefaction channels, guidance of electrical breakdown streamer 2−80362
reading of holograms by semiconductor injection laser 2−42142
reflected energy from nsec laser produced plasma 2−43177
retroreflectors, lunar physical librations obs. 2−51817
ruby lidar, remote obs. of smoke plume transmittance 2−68910
saturation spectroscopic det. of fine structure and Lamb shift or H$_\alpha$ line 2−52946
saturation spectroscopy of atomic systems, theory 2−79907
scanned microscope for photoluminescence obs. of semiconductor wafers 2−55706
scanning microinterferometer, laser illuminated, for det. of dry mass of living cells 2−45785
Schlieren techniques applied to high current arc investigations 2−64360
seismic data, optical processing, description 2−72622
single subpicosecond light pulse generation 2−46958
soldering and machine finishing, types of lasers and characteristics 2−82496
spatial frequency range scanning using zoom objective 2−63346
speckle pattern interferometry, application to study of phase objects 2−79330
spectra excitation, pulse and continuous operation, review 2−45818
spectroscopy, applic. to elastic scatt. cross section determ. in gases, Lamb dip features 2−83414
spectroscopy, developments 2−79447
spectroscopy, i.r., atm. water vapour absorpt. lines 2−84843
spectroscopy, optical-acoustic method 2−42259
spectroscopy developments 2−70076
speed of light, laser frequency and wavelength meas. 2−78758
strain-rate meter, remote sensing, based on Doppler shift 2−84148
strainmeter, methane absorption stabilized, design and operation 2−65439
stroboscopic visualiz. of u.s. waves in liq. media 2−82492
submillimetre wave generation, CO$_2$ laser radiation difference freq. mixing in GaAs 2−49200

Laser beams continued
applications continued
target designators and range finders 2−42064
teaching demonstration of wave optics using gas laser as light source 2−66399
TEM$_{00}$-mode mode-locked ruby laser triggering spark gap, switching jitter 2−74409
thermal diffusivity measurement technique, for liq. metals 2−53423
thermal expansion meas. 2−49183
thickness measurement of bloom slabs, beam triangulation, CCTV scanning 2−82495
thin film micromachining, focused Q-switched YAG laser beam 2−73605
three dimensional sequential information storage, nonlinear absorption 2−73663
time average holographic interferometry, damped oscillations 2−63094
torch, use as light source for spectral isotopic determ. of gases in metals 2−84701
tropospheric aerosols obs. 2−57942
tunable dye lidar technique for meas. of atmospheric constituents 2−84868
turbulence meas. using Laser Doppler Velocimeter system 2−71087
ultrafast radiation and nonradiative relaxations of molecules 2−79979
underwater heterodyne detection systems, S/N ratio 2−69951
unit for cutting glass beam 2−41999
unseeded supersonic airflow meas. using a laser anemometer 2−83682
upper atmospheric studies, laser radar, atmospheric backscatter 2−51638
u.s. phase gratings, laser visualization 2−60469
u.s. transducer improvement, macrosonics 2−76497
velocimeter, operation, accuracy and performance 2−66409
velocimeter, two dimensional, optical configuration 2−55368
velocimeter for Reynolds stress and turbulence meas. 2−70838
velocimeter obs. of Reynolds stress and turbulence in dil. polymer solutions 2−71128
velocimeters, atmospheric Doppler methods, performance analysis 2−62964
velocity meas., noise-cancelling signal difference method 2−66772
velocity meas. one-, two- and three- dimensional, self-aligning comparison beam method 2−66773
velocity of light meas. by det. of laser radiation wavelengths 2−78759
vibration meas. using laser-interferometry for calibration of detectors 2−55479
video processing film converter 2−59300
video recording, colour, TV film, apparatus 2−76496
wake density fluctuations meas. using pulsed laser holographic interferometer 2−46833
X-ray tube, high power, pulsed 2−85183
Zeeman spectroscopy, using He-Ne laser in magnetic field 2−63428
Ag activated phosphate glasses, radiation induced photoluminescence 2−68713
Ar 4W, photocoagulation therapy; retinal diseases, design and construction, clinical results 2−82018
Ar breakdown, threshold conditions at superhigh- pressure 2−64355
CO$_2$, for power transmission 2−73620
CO$_2$, heating of small θ-pinch plasma 2−83606
CO$_2$ cutting of various materials, gas laser, techniques, advantages and disadvantages 2−82497
CO$_2$ laser as heat source for forming single crystal fibres 2−74664
CO$_2$ laser as industrial tool 2−55687
Cl$_2$CS fluorescence, laser excited $^1(\pi^*\text{-n})$ eigenstates 2−83282
D electron density determination, spatial and temporal 2−67624
D high temperature plasma production, by laser heating of special gas target 2−80293
HCN and H$_2$O, submillimeter wavelength measurements 2−79171
^{2}H, solid, heating by laser pulse 2−43152
^{2}H plasma generation and heating to thermonuclear temps. 2−43179
He-He, Ar colour TV display system, wide screen and high definition, NHK Model 101C, 525 line 2−82506
He-Ne laser interference fringe counting in high accuracy length measurement 2−55358
K plasma diagnostics, selective excitation spectroscopy 2−70928
K vapour ionization and three-photon excitation 2−74215
Li plasma production, ion energy, retarding potential probe obs. 2−43168
LiTaO$_3$:Cu^{2+}, optical generation of intense picosec. electrical pulses 2−45768
Mn$_{0.8}$Ti$_{0.2}$Bi film, Curie-temp. writing 2−78032
NO$_2$, laser magnetic resonance at 311 and 337 μm 2−42912
Na atmospheric layer, daytime laser radar obs. 2−81703
Na atomic resonance excitation by tunable dye laser 2−59920
NaBrO$_3$, optical phonon spectrum by laser Raman spectroscopy 2−84495
NaCl, optical probing for sound intensity distribution 2−51026
Nd^{3+}:glass, production of super-dense plasmas 2−77286
Nd laser, for two photon excitation of CaF$_2$:Er^{3+}(Ho^{3+}) 2−48216
OH in atmosphere, meas. of small relative concentrations using high-power frequency-controlled dye laser 2−42109
^{87}Rb-^{85}Rb D, line isotope shift, laser spectroscopic obs. 2−74222
TePb$_{1-x}$Sn$_x$ diode, current tunable, detection of SO$_2$ pollution 2−57940

effects
absorbing plasma absorbing capacity 2−43154
air, optical breakdown in presence of elec. discharge 2−50232
air breakdown induced by pulsed CO$_2$ TEA lasers 2−46800
anthracene, singlet exciton collision fluorescence decay following laser stimulation 2−78144
atomic ionization by low-energy photons in intense laser fields 2−52927
birefringence, propagation through thermally distorted windows 2−82524
breakdown induced by CO$_2$ laser, numerical solutions 2−46801
cavitation, bubble collapse and rebound 2−43289
chemical reaction induction, mass spectrometric obs. 2−44501
D-T plasma heating to thermonuclear temps., by ion-ion collisions 2−64289

- **Laser beams** continued
  - **effects** continued
    - damage to thin film coating, detection 2−63415
    - desorption of Na and Cs submonolayers from Ge(100) substrate 2−67921
    - dielectric thin films, spot size dependence of laser induced damage thresholds 2−48123
    - dielectrics, transparent, laser surface damage thresholds rel. to Fresnel reflections 2−79228
    - double resonance of 3.5 μm He-Xe radiation in formaldehyde 2−46607
    - electric surface stress and laser surface damage 2−59191
    - electron beam modulation by laser beam in dielec. crystal, Schwarz-Hora effects 2−59083
    - electron beam modulation interference effects 2−59081
    - electron diffraction by illuminated crystal, dynamical theory 2−50612
    - electron wave modulation, crystalline media 2−59082
    - energy density distribution monitoring of mode-locked 1.06 micron beams 2−55707
    - explosives, light detonation, obs. 2−69784
    - eye, i.r. radiation, protection equipment 2−76109
    - eye, safety considerations, atmospheric inhomogeneities causing scintillation 2−48924
    - eye, safety considerations, atmospheric inhomogeneities causing scintillation 2−48924
    - fracture of nonlinear crystals, Q-switched ruby laser 2−79254
    - free electron interaction with circularly polarized pulse 2−55657
    - garnet mag. films, domain interaction with laser beams, domain writing 2−75230
    - gas breakdown, laser-induced, electron cascade theory 2−60312
    - glass, irrad., struct. transforms., electron microscope obs. 2−60588
    - glass, laser damage rel. to surface film 2−82504
    - glass, Nd-activated, excitation of luminescence 2−78135
    - glass, transparent, destruction of surface and interior 2−79256
    - glass, transparent, filamentary tracks formed by self-focusing 2−65207
    - glasses, heating, internal focusing and defocusing 2−82526
    - trans-glyoxal ^3A_u, phosphorescence obs. 2−48345
    - graphite, at mode. Ar press., crater formation 2−53552
    - intense radiation interaction with H atom, time- dependent approach 2−79955
    - laser saturation spectroscopy of alkali ground-state atoms, fine and hyperfine structure 2−46411
    - liquid, breakdown, high speed photography of cavitation and bubbles 2−56470
    - liquid, refr. index gradients due to ultrashort pulses 2−43358
    - luminescence of carbonyl compounds in crystalline state with exciting pulse of 3rd harmonic of Nd laser 2−54463
    - luminophors, organic, pumped by solid state lasers, bleaching 2−59164
    - metal film, time taken for pulse to make hole 2−79255
    - molecule, excitation of predissoc. states, selective photochem. reactions possibility 2−68803
    - multiphoton ionization, effect of spatio-temporal light struct. 2−63309
    - multiple scattering from turbid water 2−43391
    - neutron yields from spherical targets heated by spherically symmetric irrad. from multiple-beam laser 2−67339
    - nonlinear absorption and optical breakdown of liquid laser attenuators 2−42119
    - nonlinear responses and self trapped filament diameters, influence of steric interference 2−42113
    - optical pumping by multimode laser beams, saturation resonances by magnetic mode crossing 2−41955
    - photosensitive materials response to He-Cd laser radiation 2−59310
    - plasma, conduction type laser heating 2−64259
    - plasma, electron-heavy particle collisional relax. in strong radiation field 2−53182
    - plasma, high density θ pinch, heating on transverse irradiation by pulsed CO$_2$ laser 2−50200
    - plasma, superdense, high-temp. heating, radiation energy feeding problem 2−67667
    - plasma characteristics with TEA CO$_2$ laser and wavelength scaling law 2−43150
    - plasma heating, thermal decay phenomena 2−67625
    - plasma heating 2−64258
    - plasma heating in focus-type system and heat of nucl. fusion 2−77288
    - plasma in focus-type system and heat of nucl. fusion 2−77289
    - plasma instability, induced anomalous heating 2−56375
    - plasma prod. and excitation 2−49973
    - plasma production, electron density meas. using interferometric holography 2−83559
    - plasma production, ion energies 2−74385
    - plasma production, laser radiation use 2−70931
    - plasma production, obs. of nonlinear excitation of waves in meas. of X-radiation and scattered light 2−56366
    - plasma production by irradiation of polyethylene foil, determ. of ion and velocity structure 2−80272
    - plasma subsonic motion in continuous laser light, thermal expansion, plasma extinction 2−74353
    - plasma waves, excitation 2−70947
    - plastic, damage threshold, stimulated Brillouin scatt. obs. 2−68668
    - pulse in solid, two-dimensional thermal attenuation 2−75247
    - pulsed radiation, excitation of signals on electrodes in free-burning flame 2−42162
    - Q-switched ruby laser energy, photographic film response to. 2−84679
    - relativistic particle interaction with free e.m. waves in presence of helical magnet 2−52709
    - resonance dispersion and Faraday rotation in self induced transparency 2−44324
    - response of photosensitive materials to He-Cd laser radiation 2−59310
    - ruby, phase relaxation and self induced transparency 2−42118
    - ruby, photon echo-nuclear double reson., Cr-Al interaction parameters 2−81474
    - sapphire, ion beam polished, increased surface damage threshold obs. 2−57317

- **Laser beams** continued
  - **effects** continued
    - sapphire, relationship between laser induced surface damage and surface plasmas 2−60266
    - sapphire, self focusing threshold enhancement with elliptical beams 2−61578
    - saturated atomic reson. fluoresc. non-quenching collisions influence 2−83199
    - Schwarz-Hora effect, obs. in crystalline media 2−49319
    - self induced transparency from coherent interaction with absorbing systems 2−44328
    - self induced transparency in NH$_3$ at 10 μ, extrapolation to CO$_2$ laser radiation atmospheric propagation 2−43268
    - self trapping of short pulses in Kerr liquids 2−42112
    - self-defocusing of light by adiabatic following in Rb vapour 2−70608
    - self-focusing damage tracks, in glass, anatomy and thermal history 2−82501
    - self-focussing -trapping, -phase modulation, prod. by nonlinear change in refractive index 2−79258
    - semiconductor, amorphous, reversible optical effects 2−60569
    - semiconductor, impure, multiphoton luminesc. satellites in strong e.m. field 2−61679
    - semiconductor, nonlinear forward drift of electrons in a laser beam 2−57252
    - semiconductor, polycryst., induced transmittance and emission phenomena 2−61575
    - shock waves in glass due to internal focusing 2−42124
    - solid surface, thermoelastic deform. 2−43459
    - solid surface interaction studies, shock wave propagation 2−43136
    - solutions illuminated by ruby laser, calc. of deviation from Beer-Lambert's law 2−81416
    - sparks in molecular gases, obs. of surrounding fluorescence 2−74440
    - speckle, linear systems, ideally rough objects 2−73598
    - speckles, statistics, removal and applications, bibliography 2−49387
    - spiropyrans, 2 photon excitation of molecule under laser radiation 2−78208
    - Stark shifted molecular levels, optical nutation and free induction decay 2−42834
    - stationary regime and radial symmetric motion, laser-induced, thermal and ionization disequilibrium 2−77343
    - steel, phase transforms. during laser beam heating, effect of original struct. 2−53990
    - stress waves generated in circular elastic ring 2−45436
    - temperature distribution in solids under laser irradiation, calc. using Carlslaw-Yaeger method 2−74990
    - thermal lensing in solids, vector Kirchhoff approach 2−82525
    - thermonuclear plasma prod. on interaction with small particles 2−70879
    - transient stimulated Raman scattering in binary mixed liquids 2−80472
    - transparent dielectrics, breakdown by mode-locked radiation, i.r. 2−79251
    - transparent liquids and solids, avalanche ionization and limiting diameter of filaments by light pulses 2−77435
    - turbulence, spectral law of temp. fluctuations 2−82523
    - in turbulent atmosphere, broadening along sloping traces 2−45756
    - two-level atom in intense multimode radiation field, excited states population 2−66730
    - ultrasonic waves thermal excitation in methanol by laser beams interference 2−41737
    - volumetrical damage in silicate glasses K-8, F-5 and polymethylmetacrylate 2−76541
    - X-ray emission from laser plasma from high Z target 2−43151
    - X-ray emission meas. from laser produced plasma 2−43165
    - Ag-Ge alloy, irrad., metastable phase formation 2−50929
    - Al, 7075, shock-induced microstruct. and mech. prop. changes 2−68075
    - Al film, hole ('bit') creation, physical processes 2−69989
    - Ar, breakdown, by 0.35μ picosecond laser pulse 2−60314
    - Ar gas, cw breakdown using 10.6 μm laser radiation 2−60313
    - Ar gas, pulsed with 10.6 μm laser radiation, gas breakdown thresholds 2−83707
    - As-S-Ge glass film, refractive index changes 2−61583
    - BaTiO$_3$, laser irrad., breakdown threshold at Curie temp. 2−79252
    - Be, elec. resist, laser irrad. and annealing effects 2−81036
    - C, chaoite formation in craters 2−56574
    - CO$_2$-TEA laser produced plasma, interferometric obs. 2−64310
    - CO$_2$, optical breakdown in presence of elec. discharge 2−50232
    - CO$_2$ high powered laser, momentum transfer and plasma formation above a surface 2−67663
    - CaCO$_3$, optical strength and damage caused by laser radiation 2−72273
    - Cr-Si-Fe-W ceramic film, electron microscope study of laser produced holes 2−80780
    - Cr-SiO ceramic film, electron microscope study of laser produced holes 2−80780
    - Cs atom, three-quantum photoionization 2−70604
    - D$_2$ pellet, irrad., parametric instabilities of plasma 2−67679
    - Fe-C alloy, baikovite, a new struct. produced by ultra rapid heating and cooling by laser beam 2−47630
    - GaAs, laser irrad., 0.694-1.06μ surface damage 2−61574
    - Ge, photocond., surface excitation by Nd laser pulse, surface transport props. obs. 2−84379
    - glass:Nd, fluorescence line narrowing 2−48247
    - H$_2$, miltiphoton dissoc., predissoc., autoionization 2−83263
    - H$_2$, multiphoton ioniz. and dissoc. due to 1.06 μm laser radiation 2−80051
    - H$_2$, temp. depend. of multiphoton ionization 2−60004
    - H$_2$ gas, pulsed with 10.6 μm laser radiation, gas breakdown thresholds 2−83707
    - HCl, mol., selective laser excitation of high vibr. levels 2−53017
    - ^{2}H, solid target, wavelength dependence of laser light absorption 2−43176
    - ^{2}H laser heated pellets, decoupling of corona and core 2−46770
    - ^{2}H solid target, thermonuclear reaction and measurement of neutron flux 2−43153
    - He gas, pulsed with 10.6 μm laser radiation, gas breakdown thresholds 2−83707

Laser beams continued
effects continued
He plasma, electron-ion recombination 2−67631
I_2 fluorescence, laser induced line narrowing 2−74267
I_3^- Raman spectrum resonance laser excited spectrum 2−79998
n-InP, photon replicas in the induced luminescence spectra under the conditions of two photon excitation 2−81429
InSb exciton-hole plasma prod. by laser irrad., two-photon absorpt., direct recomb., 77K 2−80972
K^+ energy spectra, laser-produced ions 2−52921
KDP, cooled, heating by 337 μm laser radiation 2−63347
$K(Ta,Nb)O_3$ crystals, paraelectric electro-optical, optical damage analysis 2−79226
$LiIO_3$, noncollinearly phase matched second harmonic generation using Nd:YAG laser 2−79230
$LiNbO_3$, surface damage, ferroelec. props. effects 2−79252
$LiNbO_3$ luminescence irradiated by ruby laser 2−44426
$LiTaO_3$, laser irrad., breakdown threshold at Curie temp. 2−79252
N_2, breakdown, by 0.35μ picosecond laser pulse 2−60314
N_2 gas, pulsed with 10.6 μm laser radiation, gas breakdown thresholds 2−83707
NH_3 molecules, two-step photodissociation and excitation by laser irrad. 2−72572
NO_2, photodissociation by pulsed laser light at 6943A 2−44490
NaCl, laser induced breakdown 2−54376
Ne, optical pumping, nonlinear effects in weak magnetic field 2−46453
Ni, vacancy condensate prod. on irrad. 2−53726
O_2, laser magnetic resonance lines obs. 2−74274
SF_6, saturation behaviour at high pressure and laser intensity 2−74277
Si-SiO_2 interface, photoemission from Si to SiO_2 during laser irrad., photocurrents 2−81119
Si, cyclotron reson. of electrons generated by impurity excitation with CO_2 laser 2−71947
Te, CO_2 laser induced photoeffects 2−81178
Te, second harmonic generation with CO_2 Q-switched laser, 290-370K 2−79238
$Te_{81}Ge_{15}As_4$ glass, struct. of written lines, elec. microscope obs. 2−60600
V, vacancy condensate prod. on irrad. 2−53726
$Y_3Ga_{1.1}Fe_{3.9}O_{12}$ layer, thermomagnetic recording by laser beam heat pulse 2−51273

Laser transitions *see Stimulated emission*

Lasers
see also Light/coherence; Q-switching; Stimulated emission
amplification and spectral dip shape analysis 2−73548
amplification of sterically hindered pulse in isotropic medium 2−73539
amplifier spectral linewidth and amplified spontaneous emission, rel. to intersteller media 2−45695
amplifiers driven by cw oscillator, gain saturation 2−41966
angle-tuned optical parametric oscillators, bandwidth and threshold calculations 2−59130
beam modes, open resonators filled with anisotropic uniaxial crystals 2−45710
cavity, unstable, centreline laser radiation intensity variation 2−79174
cavity pulling in passive frequency standards 2−63304
conference, Jerusalem, Israel (May 1972) 2−70340
cooperative processes, correlated fluctuations in equil. and steady-state systems 2−78841
electro-optical systems design conference 1971 West 2−82473
energy and time duration of self pulses 2−41962
European Phys. Soc. conf., Wiesbaden, Germany (Oct. 1972) 2−76139
focal length of pump induced lenses in laser media meas. 2−41959
frequency behaviour det. using Michelson interferometer 2−69987
frequency modulation of laser by fluctuations in chemical reaction 2−41977
high power, pulsed, single mode TEM_{00q} operation 2−82472
high power, simultaneous passive mode locking and Q-switching using optical Kerr effect 2−66737
inductive store for 20MJ, construction and operation 2−59021
injection pulse, with adjustable combined resonator, characteristics 2−52409
interactions between generating lines in a cascade 2−66735
i.r. sources, review of tuning methods 2−76469
kinetics of single pulse production and second harmonic conversion efficiency 2−66739
light amplification principles and laser cavity 2−69893
line fine struct. in homogeneous line width limit 2−55678
line width, kinetic theory for spectrally heterogeneous medium 2−55679
linewidth due to quantum phase and quantum amplitude noise above and below threshold 2−49396
locking phenomena in ring, Zeeman and multimode lasers 2−41965
M-ary laser detection, optimization 2−55721
matching flashlamps for pulsed lasers 2−63312
mode locking using intracavity modulators 2−41971
mode-locked, dynamics, statistical model 2−41972
mode-locked, short light pulse generation, operation, applications 2−41975
mode-locked pulsed and c.w., production of intense light pulses, meas. of picosecond duration 2−76470
mode-locking and short pulse generation, bibliography 2−82469
molecular amplifiers, influence of relaxation on amplification 2−41963
multimode, cavity field, theory of wave packet 2−41967
multimode oscillations, buildup from quantum noise 2−63315
noise, quantum phase and quantum amplitude, above and below threshold 2−63314
optical pulse generator with Fabry-Perot electro-optic modulator as output coupler of laser reson. 2−79175
optical quality improvement device, patent 2−82549
optimized TEM_{00} output from uniformly pumped four level laser 2−41958
output formulation based on photon packets 2−69895
parametric oscillator, behaviour 2−49344

Lasers continued
polariton phase matching for 100W tunable power in i.r. at room temps. 2−42108
polarizer, birefringent for, high efficiency 2−82556
power output, possible future increases and applications of such powerful beams 2−63313
pulse modulation, for returning auxiliary passive resonator by u.s. 2−69900
pulsed, synchronisation of Q switched pairs 2−69905
Q-switched, pulse duration extending for heterodyning expts. 2−45709
quantum electronic conference, (Montreal 1972) 2−41957
quasi-c.w. parametric light generator for active Raman- scatt. spectroscopy 2−66853
radiation, coherent, harmonic generator system, patent 2−42171
radiation pressure of light, review of expts. 2−42172
recombinational, light enhancement by mol. ground state vibr. transitions 2−69897
resonant cavity, freq. shift of intense pulses 2−79180
resonator, confocal spherical, excitation, theory 2−49346
resonator, equivalence relations with a lens-like medium, approx. from Huygens-Fresnel principle 2−69899
resonators, transverse modes, diffractive calculations 2−82471
ring, improved model for self-pulsing 2−79178
rod support, optical contact approach 2−69904
saturated optical absorption technique for meas. of optical resonances 2−79231
second harmonic generation of twin frequency laser 2−42129
self-synchronized, using polarization modulating cells and polarization beam splitter in optical cavity, patent 2−66795
single quasimode oscillations 2−41968
soft X-ray emission, pumping methods 2−41960
solid state physics, an overview 2−57093
speckle patterns, wavelength diversity technique for speckle size reduction 2−66774
spectral density calc., characteristic function 2−41986
spectral line contour of optical transition at resonance with strong field on adjacent transition 2−49343
spontaneous mode locking using circuit model 2−59132
stellar atmospheres, laser action 2−48699
superradiant level shift, in N 2-level molecules 2−41964
theory, operation, main applications 2−59131
transverse mode suppression using rimmed unstable resonators 2−41970
tunable, operation and applications, review 2−59127
two level atom in arbitrarily strong sinusoidal field, Liouville eqn. soln. 2−66736
two-mode, spectral linewidths 2−73549
ultrashort pulse generation with saturable absorber, fluctuation mechanism 2−73545
unstable resonator modes, large Fresnel numbers 2−82470
variable output coupling device for far i.r. 2−59135
v.u.v. and soft X-ray emission from optical transitions of multiionized atoms in high current density discharges 2−41961
wavefront conservation in strongly deformed media 2−82468
Westinghouse Electric Corporation products, review 2−42222
CdSe, pumped by $CaF_2:Dy^{2+}$, parametric generation 3.37-7.86μ 2−69937
HF chemical, F_2 pressure change monitor 2−82509
KH_2PO_4, mode interactions 2−55680
Nd, single pulse, one mode, with frequency stabilization 2−76490

gaseous
— 2−68807
active element using external mirrors 2−49356
alkali metal vapours, phase matched, generation of u.v. radiation 2−42027
alkyl iodide photodissociation, criterion for quenching 2−79201
capillary discharge tubes, l.f. oscillations due to moving striations 2−77314
chemical, flash photolysis, thermal actinometer construct. 2−81518
chemical, review 2−41981
chemicals, that operate on vibrational- rotational transition in molecules 2−52413
CO_2, intense, for study of resonance in CaF_2:H- 2−61632
cross relaxation effect on behaviour of gas laser oscillators 2−59156
CW, automatic mode locking by internal loss modulation 2−73556
c.w., patent 2−63317
c.w., use of photorecombination of radicals and atoms 2−42038
CW gasdynamic, theory formulation 2−76477
CW gasdynamic, with unstable resonator, approximate theory 2−76471
discharge tube with capillary section, patent 2−63335
discharge tubes, mirrors and windows, shielding from electrode disintegration products 2−55684
distributed feedback, using hollow dielectric waveguide 2−45714
dynamic, pulsed detonation driven, operation 2−45721
electric discharge, pulser/sustainer, stable uniform lasing 2−59137
electron beam controlled, elec. field and secondary electron distribs., Monte Carlo calcs. 2−80360
formaldehyde, far i.r. emission 2−45740
frequency control, role of hole burning in self-stabilisation method 2−55683
gasdynamic flows in laser technique 2−73554
high power double discharge TEA, analysis of amplification process 2−76479
high-power homogeneously broadened, mode competition 2−49351
hollow waveguide gas laser resonators, coupling losses rel. to mirror position and radius 2−79177
hysteresis, production by conversion from single to double frequency 2−73558
inert gas ion, NeII, ArII, KrII, XeII, exptl. and theoretical studies including spectroscopic data 2−52422
intensity fluctuation meas., statistics, threshold oscillations 2−63320
magnetometers, helium lasers, directional sensor errors 2−52382
metal vapour, techniques and developments, review 2−42021
metal-vapour ion, CdII, MgII, exptl. and theoretical studies including spectroscopic data 2−52422
methyl fluoride, 10W at 496 microns 2−42029

Lasers continued
gaseous continued
methyl fluoride, ten watts at 496 microns, pumped by CO_2 TEA laser 2−42028
microwave excited, with external magnetic field 2−49349
mode selection in helical transversely excited and atmospheric pressure laser 2−45712
molecular, calc. of temp. ranges, gas transport characts. 2−45715
molecular, c.w., technique for temp., inversion ratio and pressure broadened line width obs. 2−73574
molecular, technique for sequential Q-switching 2−55686
multifrequency, variation of emission spectrum due to small harmonic signals 2−69908
multisectional CW gasdynamic, internal efficiency, radiation density 2−76472
narrow bore, folded, plural gas filled discharge tubes optically connected by three element corner cube reflector, patent 2−63332
noble gas ion laser, theory of free fall discharge column 2−73551
optical polarization effects 2−59139
optical surfaces parallelism using nonlocalized fringes 2−82532
organic scintillators, frequencies of molecular electronic transitions 2−76484
oscillation types, stability, nonlinear selective losses 2−49355
oscillators, effect of cross-relaxation effects on behaviour 2−41982
plasma, prod. by photoionization with u.v. light 2−79193
pulsed, transverse excitation, in gas dynamically cooled mixtures 2−45713
pulsed discharge, review 2−66742
pumping, simple model for fast transverse discharges 2−52416
radiation field, characteristic function 2−41986
r.f. preionization in transversely excited supersonic flow CO_2 laser 2−59146
rhodamine B, xanthene dye vapours, optical and discharge excitation 2−42042
ring, diffraction frequency splitting of oppositely traveling waves 2−66740
ring, diffraction splitting of frequencies 2−59138
ring, freq. stabilization, as optical freq. standard 2−69906
ring, polarising effect of decrease of competition by outer waves 2−63318
ring, radiation trapping rel. to mode competition and dispersion, Lamb eqns. 2−79182
ring laser, polarization characteristics of opposite direction travelling waves, He-Ne plasma tube 2−45735
ring laser with mixture of active gas isotopes, detuning region 2−76478
ring laser with naturally active cell, radiation polarization 2−73557
rotational relaxation, resonator loss coeff. and original degree of inversion effects on form of impulse 2−49354
with saturable absorber, nonlinear polarization calc. 2−41983
self-locking phenomena, optical cavity, experimental results 2−63319
shock tube, total temp. meas. using fine-wire thermocouple 2−49350
spark, decaying, plasma fireball, subsonic radiation front, shock wave 2−67636
stimulated emission contributions to a cathodic cavity plasma 2−82477
TEA, passive mode-locking using Ge 2−79227
TEM_{00} mode HF chemical laser oscillator 2−49348
three-level, effect of polarization pulling, determ. of degree of anisotropy 2−66741
waveguide, as amplifiers and oscillators 2−41987
Zeeman, monomode anisotropic, freq.- locking region obs. 2−52414
Ar-Xe, energy transfer as excitation mechanism 2−41988
Ar-ion, frequency stabilization 2−41990
Ar, c.w., characteristics 2−49357
Ar, molecular-beam-stabilized, 5145 Å 2−79185
Ar, oscill. quenching model, collisional and deexcitation processes 2−59143
Ar, second harmonic generation, 5145 Å 2−49358
Ar, single frequency, with absorbing film, spectral characteristics 2−42036
Ar and Kr, attenuation charact. in water 2−76512
Ar c.w., metal tube plasma container 2−63321
Ar c.w. i.r. laser, characteristics, output enhancement effects of He, Cl gases 2−52417
Ar discharge, hollow cathode, excitation mechanisms, electron and ion temp. and density 2−77308
Ar high gain neutral laser lines in pulsed discharge 2−41979
Ar ion laser, electron temp., meas. using Al double probe system 2−74349
Ar ion laser, stabilization rel. to I_2 resonance locking 2−67486
Ar ion ring laser, meas. of mode-competition discriminant 2−59141
Ar multiply ionized ions, laser oscill. in Z-pinch discharge 2−49352
Ar^+, population inversion, collisional radiative calc. 2−79197
Ar^+ ion laser, properties of emission spectrum 2−41989
C, pulsed stimulated emission 2−79194
CO_2:N_2:H_2O c.w. gas dynamic laser, unstable resonator calculations 2−82483
CO-CO_2, sealed room. temp. laser operating at 5 or 10μ 2−49364
CO_2-N_2-H_2O arc-driven supersonic laser operating in gas-dynamic mode, numerical analysis 2−49359
CO_2-N_2-He deexcited plasma, quantitative emission spectroscopy 2−79206
CO_2-N_2-He discharges, high-pressure, uniform glow, afterglow gain meas. 2−42003
CO_2-N_2 mixing laser, CW gasdynamic thermally excited and selectively pumped 2−63322
CO_2-N_2-^{3}He, high press., preionized in a reactor, performance 2−69916
CO, c.w. chemical type, R-branch emission, vibr. levels inversion ratios increase 2−73560
CO, chemical, arc excited flowing, performance 2−41993
CO, chemical, flowing, arc excited 2−73559
CO, chemical, transverse-flow transverse-pulsed 2−45727
CO, efficiency improvement, patent 2−42010
CO, electric-discharge gas-dynamic, operating parameters 2−45720
CO, forced convective flow laser 2−69920

Lasers continued
gaseous continued
CO, frequency gain profile obs. using tunable semiconductor laser 2−45718
CO, gain line shape measurement using tunable semicond. laser 2−45728
CO, high-gain double-discharge, pulsed and spectral output characts. 2−69913
CO, high pressure, electrically excited 2−45743
CO, intracavity water vapour cell to meas. absorptive losses, applic. to atmospheric transmission 2−82518
CO, laser line selection for high atmospheric transmission by intracavity water vapour cell 2−42001
CO, pulsed, potential scaling to large scale high power operation 2−82480
CO, quenching of lines by self absorpt. 2−69912
CO, sealed-off, Lamb dip evolution obs. 2−45719
CO, totally inverted vibr. population and i.r. chemilum. from O + acetylene reaction 2−61777
CO, water vapour absorption meas. 2−82519
CO TEA laser, laser action at 4.96-5.61 μm at 77K 2−79187
CO_2, 10.6 μ radar, parametric obs. 2−55681
CO_2, as industrial tool 2−55687
CO_2, atmospheric pressure, optically pumped 2−55689
CO_2, beam focusing characteristics 2−52420
CO_2, CO, transverse excitation pulsed laser in gas dynamically cooled mixtures 2−49362
CO_2, cathode glow discharge in transverse hollow cathode structure 2−79205
CO_2, closed cycle d.c. elec. discharge convection, r.f. augmentation 2−55690
CO_2, commercial air cooled, LG-17 type, construction and characteristics 2−41998
CO_2, competition effects on spatial coherence 2−55688
CO_2, continuous operation at atmospheric pressure 2−42002
CO_2, electric discharge convection, flow conditioning 2−59152
CO_2, electrical excitation of lasing levels 2−41997
CO_2, employing dielec. waveguide discharge tube 2−45729
CO_2, for power transmission 2−73620
CO_2, gas-dynamic, by detonation of solid explosive 2−45722
CO_2, harmonic generator 2−82505
CO_2, high-pressure, gas-dynamic, performance 2−45723
CO_2, high power, gas circulation regime at optimized partial pressure for CO_2-N_2-He mixture 2−45731
CO_2, high power, hole burning 2−69910
CO_2, high power, review 2−52419
CO_2, high power, thermal effects and molecular dissociation 2−76473
CO_2, high power 2−69907
CO_2, high press., pulsed, gas breakdown, ionization by rad., operating press. limit 2−69919
CO_2, high pressure pulsed chemical transfer laser 2−59154
CO_2, initiated by cold cathode glow discharge electron gun 2−69915
CO_2, LG 1061, with 100 W 2−59153
CO_2, laser action, transverse, press. to 6 'atm', peak power, optimum press 2−66745
CO_2, long pulse laser, excitation by short pulse longit. electron beam 2−55682
CO_2, matrix type, TEA, gain characts. 2−63323
CO_2, method for single frequency laser action from vibrational- rotational transition 2−66743
CO_2, mode-locked, pulse duration meas. using optical bridge 2−73563
CO_2, mode-locked TEA, single pulse selection 2−73562
CO_2, mode selective output-coupling apertures 2−73564
CO_2, monochromatic TEA, 10μ operation 2−52418
CO_2, optical investigation plasma composition and mechanism of laser action for various systems 2−49361
CO_2, parametric studies of electron beam controlled discharge 2−41996
CO_2, passive Q-switching near 9.2μ using difluorodichloromethane 2−45725
CO_2, photon-drag detector using p-Te 2−79170
CO_2, plasmatron excitation by plasma jet injection 2−69917
CO_2, pulse discharge development and generation process 2−45717
CO_2, pulse time modulation Q-switch, patent 2−69931
CO_2, pulsed, fast response thin film wattmeter for power obs. 2−63325
CO_2, pulsed, gasdynamic eqn. and vibr. relax. rate eqns. 2−69911
CO_2, pulsed transversly excited, gain, spatial and temporal depend. 2−49363
CO_2, Q-switched, spin-flip Raman scattering, obs. 2−45730
CO_2, Q-switched, vibr.-rot. line content 2−59144
CO_2, Q-switched, with variable pulse delay 2−66746
CO_2, Q-switched by rotating mirror, Doppler effect mechanism 2−59150
CO_2, Q-switching using active gas cell for Q-modulation 2−76481
CO_2, ring, high power, hybrid injection locking, frequency stabilization 2−45724
CO_2, Rogowski-type TEA, design, construction and operational parameters 2−63324
CO_2, single-mode, Doppler Q-switching by rot. mirror 2−69914
CO_2, single frequency and mode, frequency stabilization by phase control 2−76475
CO_2, spectrum generated at reduced pressure of working mixture 2−73566
CO_2, TEA, high power, high energy 2−42005
CO_2, TEA, pulsed volume, single transverse mode operation using unstable resonator 2−69918
CO_2, TEA, uniform discharge excitation method 2−66744
CO_2, TEA laser, medium diagnostics, interferometric obs. 2−49365
CO_2, transversely excited, cavity dumping 2−59149
CO_2, transversely excited atmospheric pressure, comparison of excitation methods 2−52412
CO_2, unit for cutting glass beam 2−41999
CO_2, unstable ring laser 2−41992
CO_2, wavelength and freq. meas., speed of light 2−78758
CO_2, with N_2 and He mixtures, temp. meas. from R-branch bands of N_2 2−46769

Lasers continued
gaseous continued
CO_2 cutting of various materials, techniques, advantages and disadvantages 2−82497
CO_2 diffusion, interaction kinetics of diffusion mixing of CO_2 and N_2 2−73565
CO_2 discharges, afterglow, power decay meas. 2−42004
CO_2 electric discharge convection lasers, model and experiment 2−45716
CO_2 electrically excited, electron energy conversion to optical energy 2−59151
CO_2 gas-dynamic laser system, gain and power output calculations 2−59145
CO_2 gas dynamic, importance of nozzle geometry 2−66748
CO_2 gas dynamic RASTA high power laser, design and performance 2−76480
CO_2 helical TEA, line structure 2−42000
CO_2 in MHD, ionization instabilities and discharge characteristics 2−79207
CO_2 inverted Lamb dip in spectroscopy and laser stabilisation 2−63326
CO_2 laser, transversely excited, simple longitudinal mode operation 2−59148
CO_2 lower laser level relax. saturation 2−59992
CO_2 optically pumped using transverse-discharge HBr laser 2−42006
CO_2 performance in presence of alpha-particle source 2−52415
CO_2 self-mode-locked atmospheric pressure laser, construction and operation 2−59147
CO_2 TEA-laser with high output pulses 2−42009
CO_2 TEA, cavity-dumped, short pulses 2−42008
CO_2 TEA, GW range in 50 nS pulses, modular construction 2−76476
CO_2 TEA, high-brightness volume excited using unstable resonator configuration for mode selectivity 2−41991
CO_2 TEA, high voltage high pressure 2−41984
CO_2 TEA, output energy depend. on excitation current pulse width 2−42007
CO_2 TEA amplifier, fluorescence and gain measurement 2−41995
CO_2 TEA as pump for methyl fluoride laser 2−42028
CO_2 TEA laser, input power, gain and output 2−66747
CO_2 TEA oscill., mode-locked, single 1 ns pulse generation at 10.6 μ 2−79195
CO_2 TEA oscillator amplifier, 2 GW peak power generation 2−41994
CO_2 transversely pulsed discharge, effect of discharge driving capacitance on small signal gain 2−79190
CO_2 waveguide laser, characts. 2−59136
CS_2/O_2 cw chemical., analysis in transverse flow system 2−72552
CS_2-O_2, chem., c.w. overtone bands 2−49360
CS_2-O_2 CW chem. laser, reactions producing vibrationally excited CO 2−79202
Cd ion, charge transfer excited, cathode glow discharge in transverse hollow cathode structure 2−79205
Cl, pulsed stimulated emission 2−79194
Co, high pressure, electrically excited, transient oscillator analysis 2−69921
Cu vapour, effective generation of visible band, with high ave. power 2−82475
DF-CO_2, chemical laser, vibrational energy transfer and de-excitation 2−49366
DF, chemical, pulsed, performance 2−73567
DF and DF-CO_2 chemical lasers, vibrational energy transfer processes 2−66751
DF chemical laser, vibrational energy transfer and de-excitation 2−49366
F, pulsed stimulated emission 2−79194
$F+H_2$ oscillator, closed-form solution for rate equations 2−69922
F_2+H_2 mixture excited by short electrical discharge, population of HF vibration-rotation levels, pulse laser investigation 2−66750
$GaAs_{1-x}P_x$, electrolum. diode, Zn diffusion in open-tube system 2−75126
$GaInS_3$, thermally stimulated cond., dark current, capture levels 2−75162
H_2:SF_6, chemical efficiency of HF production 2−79191
H_2, stimulated Werner band emission, v.u.v. radiation 2−42012
H_2, t.w. excitation in vacuum u.v. region, applications 2−82484
H_2, Werner band stimulated v.u.v. emission 2−42013
H_2 field emission electron beam excitation 2−42024
H_2 Lyman and Werner band v.u.v. emission 2−42014
HBr, TEA, chemical, performance, effect of gas additives 2−42015
HCN, high power, pulsed, optimization of discharge parameters 2−66749
HCN, modes obs. using liq. cryst. image convertor 2−42011
HCN, stabilization of output, automatic power control system and automatic frequency control system 2−45733
HCN, thermally stabilized, mode gain and visualiz. 2−52421
HCN meas. of resonant wavelengths at 311 and 337 μm using resonator interferometry 2−41985
HCl chem. lasers with $SOCl_2$, SO_2Cl_2, Cl_2CNCl and ClCN, pumping mechanisms 2−79192
HF-CO_2, chemical laser, vibrational energy transfer and de-excitation 2−49366
HF, rate eqns., closed-form soln. 2−82479
HF, transversely excited, gain and relaxation obs. 2−45732
HF and HF-CO_2 chemical lasers, vibrational energy transfer processes 2−66751
HF chemical, 1J, pulse discharge initiated 2−42020
HF chemical laser, vibrational energy transfer and de-excitation 2−49366
HF pulsed chemical laser, spectroscopy using i.r. vidicon camera tube 2−59140
H_2O FIR pulse excited, microwave power effects on output 2−59155
^2HF-CO_2 chemical transfer, model predictions and exptal. results 2−42016
H_2+F_2, pulsed, computer modelling and parametric study 2−41978
He-CO_2 chemical, pulsed, output pulse obs., pumping mechanism 2−73561
He-Cd, 4416 Å, excitation mechanism, and operation parameters 2−79181
He-Cd, determ. of wavelength for centre of Lamb dip 2−66754

Lasers continued
gaseous continued
He-Cd, gas mixture, glow discharge, laser action in Crookes region 2−79196
He-Cd, generating at 4416 Å 2−45749
He-Cd, pumping mechanism and plasma parameters 2−76474
He-Cd lasers using recirculation geometry 2−59157
He-Cd vapour-ion laser, CW, developments, review 2−42021
He-Cd vapour, role of thermal energy-charge exchange 2−42019
He-I_2, cw laser oscillation of singly ionized I_2 2−69923
He-Kr^+, ring shaped beam form., mechanism 2−63327
He-Mg vapour, role of thermal energy-charge exchange 2−42019
He-N_2-CO_2, TEA, double discharge trigger circuit 2−79199
He-N_2-O_2-CO, CW operation in some CO lines below 5.0 μ 2−45726
He-Ne, 0.63 μ, radiation fluctuations, parasitic generation influence 2−45736
He-Ne, atm. influence on wavelength, correction to laser interferometer 2−69957
He-Ne, automatic optical bias control, p.c.m. communication 2−66797
He-Ne, cathode glow discharge in transverse hollow cathode structure 2−79205
He-Ne, coupling modulation charact. 2−49368
He-Ne, effects of axial magnetic fields on mode intensity spectrum and output power 2−79208
He-Ne, elimination of unwanted lasing at 640.1 nm 2−79183
He-Ne, freq. stabilization using inverted Lamb dip and mode interaction effects 2−66753
He-Ne, frequency stabilization by saturated absorption in I_2 vapour 2−66752
He-Ne, gradual transition from single frequency to multifrequency 2−63328
He-Ne, hysteresis, production by conversion from single to double frequency 2−73558
He-Ne, impulse linear mag. field effect on generating power at $\lambda_{gen}=1.15$ μm 2−63329
He-Ne, in magnetic field, use for Zeeman spectroscopy 2−63428
He-Ne, incorporating light modulator, for distance meas. 2−82533
He-Ne, intensity correlation function, interferometry determ. 2−79200
He-Ne, LG 68, for building industry 2−66755
He-Ne, methane stabilized, frequency and wavelength det. at 3.39 microns, speed of light det. 2−42018
He-Ne, mode selection and polarization control using dielectric plate 2−82474
He-Ne, open cavity, aerosol particle detection and size obs. 2−56528
He-Ne, output power intensity dips, use in Zeeman spectroscopy 2−66857
He-Ne, output power rel. to electron temp. and density 2−45737
He-Ne, permeation of old laser with He to improve performance 2−42017
He-Ne, single frequency operation and change to multifrequency 2−69909
He-Ne, transverse mag. field effect on radiated power 2−59161
He-Ne, variation of longit. elec. field by internally modulated beam 2−49367
He-Ne, with active element using external mirrors 2−49356
He-Ne, with dispersive cavity 2−49353
He-Ne, with internal nonlinearly absorbing methane cell, 3.39μ freq. standard 2−59158
He-Ne 250 mW laser with Hg cathode 2−76482
He-Ne frequency stabilization by Ne absorption tube in laser cavity in alternating magnetic field 2−78757
He-Ne laser frequency measurement rel. to speed of light determination 2−48974
He-Ne output power, optimum tube diameter 2−59159
He-Ne output powers, experimental values 2−59160
He-Ne radiation coupling into out of rhodamine B doped polyurethane film ring laser 2−42055
He-Ne wavelength and freq. meas., speed of light 2−78758
He-Se vapour, role of thermal energy-charge exchange 2−42019
He-Xe 3.508 μ transition, freq. stabilization methods 2−63330
He-Zn, gas mixture, glow discharge, laser action in Crookes region 2−79196
He-Zn vapour, role of thermal energy-charge exchange 2−42019
^3He-^{20}Ne, magnetic field effect at 3.39 μ on ring lasers 2−45734
He + Ne, automatic frequency control and frequency fluctuations of difference wave 2−55691
He + Ne, output-power fluctuations reduction 2−55692
Hf, optically pumped, laser emission in rotational transition 2−50047
Hg vapour, performance, review 2−42021
I, photochem., energy transfer obs. 2−55693
I, photochem., kinetic processes 2−52440
I II, in He-CdI_2 discharge, oscillation at 6127 Å 2−45738
I_2 molecular vapour, optically pumped 2−49369
I_2 vapour, optically pumped, performance 2−42022
Kr, mode-locking of coupled transitions 2−82478
Kr, mode locked, fibre dispersion meas. 2−79235
Kr high gain neutral laser lines in pulsed discharge 2−41979
Kr II, cross modulation effects 2−66756
Kr singly ionized laser, optimum conditions for emission of 5208.3 Å, 5681.9 Å and 6470.9 Å lines 2−42023
Mg vapour, new i.r. laser lines 2−41980
N_2-CO transfer, low temp., energy exchange processes 2−69924
N, pulsed stimulated emission 2−79194
N multiply ionized ions, laser oscill. in Z-pinch discharge 2−49352
N_2, 3371 Å, with modified Blumlein excitation method 2−63331
N_2, coherence props. and saturation broadening of 337 nm pulses 2−73570
N_2, field emission electron beam excitation 2−42024
N_2, molecular, pulsed, wavelength meas. at low temp. 2−49370
N_2, pumped by intense electron beam 2−73569
N_2, TEA, u.v., applic. to pulsed Raman spectroscopy of atmos. pollutants 2−42025
N_2, transversely excited, spontaneous self-mode locking at 1.048 μm 2−73568
N_2 coaxial superradiant light source, emission props. at low repetition freq. 2−79203

Lasers continued
gaseous continued
N_2 high power laser 2-59163
N_2 pulsed laser with high repetition rate 2-59162
NH_3-N_2O, population inversion in exothermal decomposition reactions on shock 2-73553
N_2O, cw operation and assignment of laser lines using $^{14}NH_3$ absorption line 2-42026
Na, optically pumped, action between $3^2P_{1/2}$ and $3^2S_{1/2}$ levels 2-73555
Nd^{3+}:glass laser, set-up for obtaining a giant pulse by Q-factor modulation 2-76485
Nd^{3+}, giant light pulse generation for study of nonlinear optical effects 2-55685
Ne, fundamental characteristics and frequency stabilization 2-73571
Ne field emission electron beam excitation 2-42024
Ne levels, population changes by 0.61 μm and 3.39 μm laser action 2-76483
Ne multiply ionized ions, laser oscill. in Z-pinch discharge 2-49352
^{20}Ne, frequency stabilization 2-73552
^{87}Rb, frequency temperature coefficient, physical processes effecting 2-45739
Te in He or Ne buffer gas, cw laser action 2-56098
Xe, 3.5 μm superradiant radiation, saturation effect 2-82482
Xe, laser action on unclassified transitions in highly ionized plasma 2-59142
Xe, pulsed, effect of axial mag. field on output powder 2-73572
liquid
2-amino-7-nitrofluorene/1,2- dichlorobenzene, dye laser action 2-45742
2-amino-7-nitrofluorene/1,2-dichlorobenzene, special dye laser, solvent orientational relaxation 2-42040
anthracene, meso-substituted, obs. of laser emission in 4100-4400 Å range at low temp. 2-45745
cresyl violet, high efficiency, characteristics 2-73578
cresyl violet and rhodamine B pulsed dye laser, spectral properties 2-42041
c.w. dye, locking to inverted atomic transitions 2-55695
c.w. dye lasers, improved astigmatically compensated resonator 2-59133
c.w. pumped dye lasers, review 2-63333
c.w. rhodamine 6G dye laser, passive mode locking 2-42043
7-diethlyamine-4-methylcomarin, coaxial 11MW, 6.8J flashlamp pumped, performance 2-82476
dye, coaxial flashlamp, spectral characteristics 2-59272
dye, continuous tunable source of u.v. by frequency doubling 2-42030
dye, CW, rotational relax. and triplet state effects 2-79188
dye, CW, tunable, use in atomic beam deflection 2-73624
dye, CW, ultrasensitive response to selective extinction 2-73573
dye, c.w. and pulsed, review 2-55694
dye, CW mode-locked, intracavity pumped, wavelength tuning 2-73576
dye, cw operation, output coupling scheme 2-55698
dye, efficiency, pump parameter and triplet lifetime depend., calcs. 2-69927
dye, electronically tunable using acousto-optic filter 2-82481
dye, flashlamp pumped, spectral narrowing and freq. tuning 2-76486
dye, for wideband parametric upconversion of i.r. waves to visible region 2-82511
dye, frequency doubling for efficient generation of 2500-3250Å tunable radiation 2-79198
dye, high efficiency, tunable from u.v. to i.r. 2-73575
dye, linear water cooled ablating-wall flashlamp pumped for study of upper atmospheric composition 2-73580
dye, N_2-laser pumped, simultaneous two-wavelength selection technique 2-79186
dye, paraterphenyl, laser-pumped, u.v. output characts. 2-52426
dye, performance enhancement by chem. quenching of triplet state 2-63334
dye, prism, laser pumped, continuously tunable 2-69926
dye, recent developments and future applications in fundamental research and technology 2-76487
dye, saturated freq. chirping effect on mode-locked pulses 2-49372
dye, thermal resonator effects 2-79204
dye, tunable, atomic and molecular spectroscopy 2-79941
dye, vortex confined pumping discharge in laser soln. 2-49371
dye, wavelength tuning by rotatory dispersive elements 2-55696
dye fluorescence, quenching by absorption from excited singlet state 2-79970
dye laser, tuning range extension using tunable i.r. difference-frequency generation in $LiIO_3$ 2-63369
dye laser amplifier properties 2-52423
dye laser forced oscillator 2-45741
dye lasers, meas. of small relative concentrations of OH in atmosphere 2-42109
dye on surface of waveguide, gain by evanescent field coupling 2-42056
dyes, polarization of stimulated emission 2-49375
dyes, polymethine cyanine, bleaching kinetics 2-42039
ethanol solution, addition of anthracene, effect of triplet-triplet transfer on lasing threshold 2-76488
evanescent-field-pumped dye laser, pumping scheme using waveguide mode 2-79184
linear flaslamp pumped dye laser analysis & experiments 2-49374
4-methylumbelliferone, acidified solutions, influence of excitation intensity on laser spectra 2-77433
organic compounds as laser dyes, design criteria 2-42031
organic dye laser, construction, operation 2-49373
organic dye lasers, locking to atomic resonance lines 2-42032
organic dyes, flashlamp for pumping 2-76466
organic dyes, photobleaching 2-69928
picosecond dye laser pulses, frequency tunable, rhodamine 6G and B, and cresyl-violet 2-42045
polymethine, saturably absorbing dye solns., photostability 2-61809
polymethylene dyes, resonant combination laser pulse dispersion 2-49377
rhodamine, use of organic dye light converters 2-69929
rhodamine 6G, 12 joule output 2-55697

Lasers continued
liquid continued
rhodamine 6G, coaxial 11MW, 6.8J flashlamp pumped, performance 2-82476
rhodamine 6G, pumped by pinched discharge, energy characteristics 2-42046
rhodamine 6G, using impulse lamp for pumping, structure of emission field, thermo-optical distortion 2-52424
rhodamine 6G CW dye laser, passive mode locking, stable output, 5900-6100Å 2-79189
rhodamine 6G dye, flashlamp pumped, second harmonic and sum frequency generation 2-73577
rhodamine 6G dye laser, transistory absorption meas. and stimulated emission 2-42044
rhodamine 6G dye laser as tunable source of coherent u.v. radiation 2-79444
rhodamine 6G fluorescent dye laser, principle and design 2-59165
rhodamine 6J, dynamic compensation of thermooptical distortion 2-73579
rhodamine 6J, effect of transverse pumping distribution, on thermal-optical distortion 2-49376
rhodamine 6J, energy parameters of generation, effect of excitation 2-42034
rhodamine 6J, excitation by pulsed lamps of different types 2-69930
rhodamine B-rhodamine 6J mixed solution, generation characteristics 2-52425
Runge mode-locked dye laser, dispersive explanation of spectral behaviour 2-66758
short cavity tunable dye laser, longitudinal excitation by N_2 laser 2-66757
thin film organic dye, expts. 2-42035
xanthene dye, effect of triplet levels on energy characteristics when pumped with mode-locked laser 2-66759
N_2, effective stimulated scatt. in u.v. and gain dispersion in 1.06-0.26 band 2-46956
Nd:$POCl_3$-$ZrCl_4$, Q-switched, progress report 2-59166
Nd^{3+}:$POCl_3$-$ZrCl_4$ laser, line broadening of spectrum of Nd^{3+} ion in solution, stimulated emission cross section 2-42037
Nd, mode locked, obs. of transverse modes 2-42033
$POCl_3$:$ZrCl_4$:Nd^{3+}, amplification of mode-locked trains 2-59167
$POCl_3$-D_2O-Nd_2O_3 soln., lasing effect and prep. technique 2-45744
semiconductor
absorption saturation with optical pumping 2-49383
array, high power using fibre-optic coupling 2-42089
cloud height lidar system 2-44684
Coulomb interaction, calculation of optical gain rel. to plasma effects 2-42101
Coulomb interaction, stimulated emission process 2-61681
direct gap, highly excited III-V, II-VI, review of recent results 2-79217
double heterostructure, mesa stripe, fabrication and performance 2-42084
double heterostructure, spontaneous emission rate of increase reduction at threshold 2-66767
double heterostructure, transient theory of self-focusing behaviour of filaments 2-42087
double heterostructure injection lasers, reflectivity of cleaved facet and single mode operation 2-42076
dynamic behaviour by using equations of balance 2-79214
electron beam pumped, spatial modes far- field diffr. patterns time variations 2-79211
electron beam pumped scanning type 2-73590
emitted radiation, influence of refractive index nonlinearity on dynamics 2-42079
heterostructure, emission control by varying parameters of junction waveguide structure 2-42083
indirect gap, highly excited III-V, II-VI, isoelectronic traps, review 2-79217
injection, heterostructure, applics. conference (Cardiff, March 1972) 2-42082
injection, increased radiance method 2-69942
injection, large optical cavity heterojunction, transverse mode selection 2-59178
injection and reading of holograms 2-42142
injection laser diodes, future developments and applics., review 2-69947
junction, industrial and military applications 2-55705
junction, time delays and Q-switching, effect of impurity gradient 2-59180
laser canes for blind persons, design improvements 2-51893
magnetic field tuned, use in high resolution spectroscopy 2-70082
inoptical fibre bundle communication systems, rel. to lamps 2-42088
polarization junction laser 2-69944
pumped to induce pulsing at same frequency as applied microwave signal, patent 2-63344
pumping source for Nd YAG lasers with integrated focusing optics 2-69943
Q-switched junction diode, fabrication, patent 2-82487
quantum noise, 80K and room temp. 2-45753
resonance effects in dynamic behaviour rate equation approach for single mode operation 2-42085
room temperature laser diodes, recent trends 2-42078
self Q-switching with nonuniform pumping 2-42080
self-focusing mechanism, by energy depend. carrier scatt. 2-59179
self-Q-switching, when coupled to photovoltaic nonlinear absorber 2-63340
solid state light sources, review in book 2-55700
spontaneous pulsing, modulation, patent 2-59187
spontaneous pulsing, patent 2-59188
stripe-geometry heterostructure, proton bombardment formation 2-42081
thermal properties 2-49382
tunable, atmospheric pollution studies 2-65675
tunable, spectroscopic light source 2-42283
tunable monochromatic injection, fabrication 2-73593
waveguide resonator struct., props. in semicond. laser with electron beam pumping 2-52335
Al-Ga-In-P system, injection, properties 2-42096

- **Lasers** continued
  - **semiconductor** continued
    - $Al_xGa_{1-x}As$-GaAs-$Al_xGa_{1-x}As$ heterojunction laser, radiation spectral distrib. and polarization 2−63342
    - $Al_xGa_{1-x}As$-GaAs-$Al_yGa_{1-y}As$, double heterostruct., differential I/V correlating with laser threshold 2−66769
    - $Al_xGa_{1-x}As$-GaAs heterojunctions, elec. props., photoresponse, graded gap model, laser operation 2−81117
    - $Al_xGa_{1-x}As$ solid solns., in heterostructs., optical and electronic channelling rel. to comp. 2−63341
    - AlGaAsP solid soln., use in two-heterojunction injection lasers 2−63343
    - CdS, electron beam pumped, photon loss and gain 2−42077
    - CdS, optical cavity, total internal refl. and Fabry-Perot configs., electrolum., spectra, laser action 2−81413
    - CdS_xSe_{1-x}, graded band gap crysts., tunable laser emission by two photon excitation 2−69948
    - Cds super radiant light source, produced by electron beam pumping 2−79215
    - Ga-In-As-Sb system, injection properties 2−42096
    - GaAlAs laser diode array light sources, moderate power, near i.r., fabrication, applications 2−82491
    - GaAlAs laser diodes, structure, performance, applications 2−82490
    - $Ga_{1-x}Al_xAs$, superlattice surface laser applics. 2−69945
    - $Ga_xAl_{1-x}As$ heterostructure, injection type, construction and performance 2−42094
    - GaAs:Si, double heterostruct. diode, laser action 9100-9500 Å, threshold current conversion efficiencies 2−73591
    - GaAs/GaAlAs, mesa stripe geometry double heterostruct. injection laser, very low current operation 2−42093
    - GaAs-AlAs solid solution heterojunction, 7400-9000 Å range 2−73596
    - GaAs-$Al_xGa_{1-x}As$ double heterostruct. diodes, reproducible liq. phase epitaxial growth 2−49385
    - GaAs-$Al_xGa_{1-x}As$ double heterostruct., doping effect on GaAs lasing props. 2−49384
    - GaAs-$Ga_{1-x}Al_x$ single heterostructure, interferometric obs. of thermal elongation 2−42095
    - GaAs-$Ga_{1-x}Al_xAs$, single heterostructure laser diode, interferometric obs. of evaluation of thermal mirror deformation 2−73592
    - GaAs-$Ga_{1-x}Al_xAs$ double hetero structure optical guides, lasing characteristics 2−42092
    - GaAs-$Ga_xAl_{1-x}As$ heterojunction, time characteristics 2−42091
    - GaAs, applic. in optical communications using glass fibre waveguide 2−42102
    - GaAs, double heterostruct., threshold current rel. to press., light polarization flip 2−69949
    - GaAs, electron beam pumped, generation of controllable light pulses by spatial scanning of beam 2−42090
    - GaAs, freq. time shift for short current pulses 2−82485
    - GaAs, high radiance, room temp. with controlled radiation in single transverse mode 2−45754
    - GaAs, injection future prospects 2−42099
    - GaAs, injection spontaneous spectrum at 300K 2−79212
    - GaAs, optical filament formation, theory 2−42098
    - GaAs, self-pulsing, fibre dispersion meas. 2−79233
    - GaAs, single heterojunction, injection dependence of spectral mode frequencies on currents 2−42097
    - GaAs, solution-grown junction lasers, dependence of power efficiency on driving current and laser length 2−59182
    - GaAs, spontaneous emission behaviour across threshold 2−66766
    - GaAs, tunable, external dispersive cavity 2−59181
    - GaAs double heterostructure, injection, gradual degradation 2−42086
    - GaAs junction, coefficient of superlinear dependence of gain on current density 2−59183
    - GaAs narrow junction, fabrication techniques 2−73595
    - GaAs single mode, in external cavity 2−73594
    - $GaAs_xSb_{1-x}$-$Al_yGa_{1-y}As_xSb_{1-x}$ double heterojunction, prep. and emission spectra 2−59184
    - In:CdS, spin flip, visible, operation at liq. He temps. 2−66768
    - $InAs_xP_{1-x}$:Zn, growth, laser diode fabrication, lasing action 2−59185
    - InAsP thin platelet, mode coupling in edge to edge cavity config. 2−69946
    - $In_xGa_{1-x}As$:Zn, growth, laser diode fabrication, lasing action 2−59185
    - $In_xGa_{1-x}As$ with threshold current densities 2000 to 3000 A/cm^2 2−61726
    - $In_{1-x}Ga_xP$ diode, vapor grown, orange emission 2−49386
    - InP, injection photoluminescent and electroluminescent props. 2−42096
    - InSb, spin-flip Raman laser cavity, modes, transition schemes, gain, loss mechanisms 2−66770
    - n-InSb, stimulated spin-flip Raman scattering rel. to homogeneously broadened travelling-wave electronic Raman laser 2−42100
    - n-InSb, uniaxial stress, obs. of tunable component in spectrum 2−82488
    - PbTe epitaxial thin film diode, evaporated, injection luminesc. and laser action 2−57382
    - $TePb_{1-x}Sn_x$ diode, current tunable, detection of SO_2 pollution 2−57940
    - ZnS:Mn, gain calcs. 2−79213
  - **solid**
    - array control, by application of acoustic, electroacoustic pressure waves 2−66760
    - cylindrical ruby rods in elliptical condenser, energy distribution of pumping 2−42059
    - disc, developments and applics., review 2−69933
    - dye on surface of waveguide, gain by evanescent field coupling 2−42056
    - emission and propagation obs. using 128 × 128 channel computer controlled, dual parameter analyzers 2−73584
    - face-pumped laser, concept and implementation 2−42047
    - film optical waveguides, distributed feedback laser prod. 2−79210
    - generation of high-energy subnanosecond pulses, techniques and limitations 2−42049
    - glass: Nd, investigation of two-photon amplification using organic dyes 2−61808
    - glass:Nd^{3+}, struct. of radiation 2−59170

- **Lasers** continued
  - **solid** continued
    - glass:Nd, meas. of start photon number 2−52428
    - glass:Nd, set-up for plasma production 2−80294
    - glass, advances 2−55701
    - glass, material technology 2−82563
    - glass, with zig-zag beam, power improvement 2−69932
    - glass rod doped with Er or Er-Yb, luminescence sensitizing with Mo, patent 2−82486
    - glass-ceramic, Nd^{3+} doped, threshold and efficiency 2−73589
    - high power, giant pulse with unstable cavity 2−69934
    - Lamb-type, ideal, harmonic-oscillator vel. distrib. effect 2−66763
    - mode-locked, application to holography 2−63365
    - modes, weakly interacting, periodic motion 2−76489
    - noninstantaneous Q-switching for single pulse lasing 2−69902
    - optical coating problems 2−55699
    - organic dye in rigid host medium, triplet state population control and utilization 2−69941
    - organic dyes in solid matrices photobleaching 2−55704
    - periodic layered waveguide structure for distributed lasers 2−42051
    - picosecond pulse, applic. to nonlinear optics studies, review 2−63348
    - picosecond pulse transient behaviour, obs. on Q-switched ruby laser 2−69936
    - Pockel cell Q-switched Nd:glass oscillator, amplified output, picosecond structure 2−42070
    - Raman oscillators, stationary, molecular crystals, polariton theory 2−65273
    - rare earth:YLF, energy transfer and phonon interactions 2−42058
    - rhodamine B doped polyurethane film, light amplification and coupling 2−42055
    - ruby, characterization of generation region with darkened solns. of phthalocyanines 2−49379
    - ruby, cryptocyanine Q-switches, photochemical decomposition due to light source 2−49378
    - ruby, high-repetition-rate continuously pumped 2−45748
    - ruby, interferometric technique for obs. of coherence of single pulse 2−79348
    - ruby, intracavity modulation with frequency close to difference frequency of neighbouring axial modes 2−59171
    - ruby, light source, holographic interferogram of laser wavefront, det. of degree of spatial coherence 2−42125
    - ruby, mode-locked, applic. to holography 2−66781
    - ruby, output energy, effect of Cr^{2+} conc. 2−59169
    - ruby, pulsed, beam parameter obs. using holographic interferometry 2−79218
    - ruby, Q-switched, fracture of nonlinear crystals 2−79254
    - ruby, scatt. in plane-parallel resonator 2−79179
    - ruby, stimulated emission when exposed to ^{60}Co gamma rays 2−69935
    - ruby, stimulated radiation props., γ-ray effects 2−73585
    - ruby, TE and TM modes generation and self- focusing 2−42074
    - ruby disk, optical distortion and depolarization effects 2−82489
    - ruby TW ring laser, passive non-reciprocal element 2−66764
    - self focusing and self phase modulation in psec pulse oscillators 2−42054
    - self-destruction, more resistant materials and components 2−55702
    - side-coupled, distributed feedback 2−73583
    - solid state light sources, review in book 2−55700
    - spin-flip Raman, conversion efficiency 2−57358
    - spin-flip Raman, tunable, spectroscopic light source 2−42283
    - spin-flip Raman scatt., theory 2−57359
    - ultrashort pulse generation by optical coupling of two cavities 2−79176
    - ultraviolet, stabilized, operating at wavelengths 0.3 and 0.265 microns 2−59168
    - wave guiding of e.m. waves by double heterostruct. injection laser 2−59003
    - X-ray, soft, rel. to ionization, inversion, stimulated emission and Auger effect 2−79209
    - YAG, Ge photodiode detecting head 2−66761
    - γ-ray, based on crysts. of long lived nuclear isomers 2−66762
    - AlGaAsP, solution growth, luminescence, stimulated emission 2−45747
    - $Ba_2ZnGe_2O_7:Nd^{3+}$, absorpt. and fluorescence spectra, Nd^{3+} stimulated emission and laser action 2−61705
    - CaF_3-$YF_3:Er^{3+}$, spectroscopic study of stimulated radiation 2−61689
    - CdSe i.r. parametric oscillator, pumped by Q-switched Nd:YAG laser 2−42061
    - CdSe parametric oscillator, pumped with tunable dye laser 2−42053
    - $Er^{3+}:LiYF_4$ operation at 0.85 μm at room temperature 2−42062
    - Er, Ho, Yb, Tm:YAG, recirculating liquid N_2 system for cooling 2−63339
    - Er, propagation in CO_2 atmos. in near i.r. 2−42131
    - Ho^{3+}: apatites, properties and performance 2−42063
    - Ho versus Er as laser material rel. to visual safety 2−45750
    - $In_{1-x}Ga_xP$, solution growth, luminescence, stimulated emission 2−45747
    - KH_2PO_4, parametric light amplification and oscillation, with mode locked pump 2−42052
    - $LiGd(MoO_4)_2:Nd^{3+}$, stimulated emission 2−69938
    - $LiIO_3$ internal parametric oscillator, pumped by Nd:YAG laser 2−45746
    - $LiIO_3$ pulsed doubly resonant parametric oscillator, spectral and other props. 2−73586
    - $LiNbO_3$ parametric oscillator, pumped with tunable dye laser 2−42053
    - $NH_4H_2PO_4$ parametric oscillator, pumped with tunable dye laser 2−42053
    - Nd: glass, thermal distortion of laser resonance, study using pneumatic films 2−52429
    - Nd^{3+}: apatites, properties and performance 2−42063
    - Nd^{3+}: phosphate glasses, time development of wide- band generation spectra in resonator with diffusion 2−42073
    - Nd:CaLa silicate oxyapatite crystalline laser materials, pulsed and Q-swithced characteristics 2−42060
    - $Nd:CaLaSi(PO_4)_2CaF_2$, temp. dependence of refractive index 2−49380
    - $Nd:CaNb_2O_6$, CW operation 2−50592

Lasers continued
solid continued
Nd:glass, aqueous Cu(II) sulphate gel target to produce coherent X-rays 2−66765
Nd:glass, bis-(4-dimethylaminodithiobenzil)- Ni for Q-switching of i.r. laser 2−59175
Nd:glass, cylindrical rod plano-convex cavity, mirror transmission 2−76492
Nd:glass, mini face-pumped, free from thermal distortion 2−73582
Nd:glass, mode-locked, evolution of high power picosecond pulses 2−42069
Nd:glass, picosec. electrical pulse generation by rectification in LiTaO$_3$:Cu^{++} 2−79268
Nd:glass, pulsed, beam parameter obs. using holographic interferometry 2−79218
Nd:glass, Q-switching a convex optical cavity 2−76467
Nd:glass, second harmonic generation in laser created plasma 2−43146
Nd:glass, single mode, with continuously variable pulse duration 2−42071
Nd:glass, thermal lensing effects 2−63336
Nd:glass laser, damage mechanism and improvement of damage thresholds 2−42050
Nd:glass laser frequency conversion to u.v. in range 216 to 234 nm 2−73604
Nd^{3+}:YAG-YALO, hybrid operation at 1.064μ 2−69939
Nd:YAG, bibliography 2−42065
Nd:YAG, CW pumped, output fluctuations 2−45751
Nd:YAG, diode-pump-modulated, response to pump intensity sinusoidal modulation 2−52427
Nd:YAG, harmonic mode locking 2−59172
Nd:YAG, props. rel. to Nd:YALO, Nd:Yttralox, Nd:apatites 2−63338
Nd:YAG, pulsed, organic dyes as filters 2−73588
Nd:YAG, Q-switched, pumping CdSe i.r. parametric oscillator 2−42061
Nd:YAG, repetitive Q-switched, coherent ultraviolet radiation generation at 0.266, 0.355 μm, nonlinear optical technique 2−69956
Nd:YAG, single freq. travelling wave, output 2−73581
Nd:YAG, space qualified, design 2−69940
Nd:YAG electro-optically Q-switched laser, multipulsing behaviour 2−59173
Nd:YAG garnet, continuous wave, pumping from high-current arc discharge 2−55703
Nd:YAG laser material, holographic interferometry meas. of thermal refractive index and expansion coefficients 2−59174
Nd:YAG new laser transitions $^4F_{3/2}$ to $^4I_{9/2}$ 2−42066
Nd:YAG system for generation of controllable reproducible giant pulses 2−69925
Nd^{3+}:YAG, effect of pressure in Xe and Kr arc lamps on pumping efficiency 2−42072
Nd^{3+}:YAG, generation of subnanosecond 10 μ pulses 2−42068
Nd^{3+}:YAG, recirculating liquid N$_2$ system for cooling 2−63339
Nd^{3+}:YAG, target designators and range finders 2−42064
Nd^{3+}:YAG intracavity phase modulated, separation of mode locked states 2−42048
Nd:YALO laser material, holographic interferometry meas. of thermal refractive index and expansion coefficients 2−59174
Nd:YAP, polarization and crystal direction effects 2−42067
Nd:YAlO$_3$, design, device parameter obs. 2−45752
Nd:Yttralox, ceramic, lasing threshold, loss coeff. 2−49381
Nd-CaWO$_4$, active Q switching technique for high power in single longitudinal mode 2−63337
Nd-glass, production and meas. of pulses of several hundred picoseconds 2−59176
Nd-glass thin film waveguide for amplification at 1.06 microns 2−42057
Nd frequency depend. of spatial synchronism of emission harmonics 2−76491
Nd with molecular crystals, second harmonic generation 2−82515
NdP$_5$O$_{14}$, line widths/cross-sections and props. 2−73587
Nd^{3+}; yttrofluorite crystals, time development of wide-band generation spectra in resonator with diffusion 2−42073
Ne, single-pulse, with cascaded multipliers and tunable frequency converter 2−59177
Pm:YAG laser, radiative transition probabilities rel. to Nd:YAG 2−59186
Tm:Cr:YAlO$_3$ four-level operation at 2.35 microns 2−42075
YAG:Nd meas. of start photon number 2−52428
YAG:Nd^{3+}, quasicontinuous, spectral characts., and oscill. dynamics 2−79216
YAG, Q-switched, focused beam for thin film micromachining 2−73605

Latent heat
see also Heat of adsorption, etc.; Thermodynamic properties
atmosphere, release, vertical distrib. and mechanism of conditional instability of second kind 2−48446

Latent image *see Photographic process*

Lattice constants *see Crystal structure, atomic*

Lattice dynamics *see Crystals/lattice mechanics*

Lattice energy
− 2−67970
alkali metals, bulk density rel. to surface energy 2−77493
aromatic ion radical crystals, electrostatic energy calc. 2−51073
compressed matter, electron-lattice interaction energy, cryst. struct. depend. term 2−71788
cubic crystal, several different kinds of ions per unit cell, calc. 2−60700
cubic system, mag. anisotropy represented by lines of const. cryst. energy 2−78000
deformed crystal, point lattice half-space, total energy 2−50659
electrostatic energy calc. using modified Hubbard model for charge-transfer crystals 2−51073
f.c.c. microcrystallites, spherical, geometry and stability 2−53598
hydroxyapatites, OH ions i.r. spectra, stretching and librational modes, H-bonding 2−61650
ionic crystals, electrostatic contrib. to Brugger-type elastic consts. 2−84057

Lattice energy continued
kenotetrahedral spinel and rutile types, Madelung number rel. to anion parameter 2−67926
metal, bulk moduli calc. from methods of homogeneous deofrm. and long waves 2−47177
metal, cohesive force conjugate to uniform expansion 2−67929
metal, electron field emission, effect of lattice potential 2−61457
metal, electrostatic contrib. to Brugger-type elastic consts. 2−84057
metal halides, overlap repulsion, modified logarithmic form 2−43502
minimization, rel. to molecular packing anal. 2−83880
N-methylphenazinium 7,7,8,8-tetracyanoquinodimethanide, Ewald's method calc. 2−67931
organic donor-acceptor crystals, electrostatic binding energy by Ewald's method and charge transfer in lattices 2−67928
TCNQ cpds., low temp. sp. ht., ionic binding contrib. 2−54052
transition metals, 3d, from L-shell X-ray appearance pot. spectra 2−61677
Wurster's blue perchlorate, electrostatic, using Ewald's method 2−67927
CaCO$_3$, Madelung parameters and electrostatic energies for calcite, aragonite and vaterite and charge distrib. on CO$_3^{2-}$ ion 2−43500
Cu alloys, influence on bonding contrib. to partial free enthalpy of formation of solid solns. 2−80811
H, solid, ground-state energy at high density 2−43501
H metallic phase, influence of expression for dielectric function in structure calcs. 2−77521
K$_2$SO$_4$(c)→2K$^+$(g) + SO$_4^{2-}$(g), Madelung parameter and electrostatic energy charge, calc. based on Evald Bertaut method 2−47179
MgIn intermetallic compound, pseudopot. and perturbation theory calc. 2−50623
N$_2$O, parameter detn. of nonvalence interaction curve at 0°K 2−71440
V$_3$Si, stabilization in high magnetic fields 2−77869

Lattice gas *see Statistical mechanics*

Lattices, theory and statistics
activity expansions for lattice gases, radius of convergence 2−69612
alloy, binary one-dimens., phase transitions 2−50980
antiferromagnetic chain, uniform, thermodynamic props. and magnetostriction 2−84439
Ashkin-Teller and eight-vertex model, duality relation 2−45288
Ashkin-Teller and eight-vertex models, symmetry props. 2−52092
Ashkin-Teller and eight-vertex models 2−58775
Ashkin-Teller model, susceptibility, high temp. series 2−69604
Baxter model, spin $^{1}._{2}$ lattice system, duality relation 2−78845
b.c.c., Green's functions, exact calcs. 2−55428
b.c.c. lattice sums applic. to ferromag. 2−48051
boundary free energy in lattice model, solution of paradox 2−52087
boundary structure between two phases, boundary free energy in lattice model, general formulation 2−52085
close-packed, density of states of simple excitations 2−57094
cluster series expansion for arbitrary model 2−58768
cooperative assemblies, with many body interactions, first order and critical point phase transitions 2−69605
critical phenomena, conf., New York, USA (June 1970) 2−52102
critical point exponents, inequalities for spin- spin and energy-energy correlation functions 2−63030
crystal frequency distribution functions, evaluation of exact moments 2−58770
cubic lattice, Watson sum 2−58772
damped Debye lattice, three-dimensional model for polystyrene 2−60104
density matrices for 4×4 square plasma net 2−52099
diatomic alternating lattices, Green's function 2−61051
dynamical spherical model, phase transitions 2−52104
eight-vertex and Ashkin-Teller models 2−58775
eight-vertex model, crit. index of vertical-arrow correl. length 2−66463
free fermion model, combinatorial soln. counting random walks on lattice 2−78844
Green's function of square lattice in diagonal direction, asymptotic form 2−69608
hard particle systems, one and two dimensional 2−45287
hard square lattice gas, surface tension calcs. 2−55426
harmonic chains, isotopically disordered, spectral theory of difference eqns. 2−66470
harmonic oscillator chain, dynamic and ergodic props. of impurity 2−66469
harmonics analysis of surface energy anisotropy data 2−43460
ice, three dimensional eight vertex model and proton-proton correlation function 2−47726
incoherent exciton quenching, time dependent excitation function 2−45290
Ising and Heisenberg models, cooperative phenomena 2−45295
Langevin eqn. for particle in general harmonic lattice 2−69610
lattice gases, of Fisher and Temperley, partition function, distrib. of zeros 2−66460
linear chain, semi-infinite, propagation of general disturbance 2−49027
magnetic lattice, 1 dimensional, field theory 2−52094
models for H-bonded solvents 2−41526
one-dimensional crystal, velocity autocorrelation function determ. 2−49029
one-dimensional spaces, exact nearest neighbour statistics 2−63026
ordered phase, point and planar singularities 2−78831
orthomodular lattice, near centre 2−82263
percolation processes rel. to cooperative phenomena 2−55425
phase transitions, model studies 2−58798
phase transitions, models 2−58799
plasma transitions in random cluster model 2−49030
quantum-anharmonic oscillator, thermodynamic perturbation theory 2−66471
random system, coherent and mean wave propag. 2−63027
random system, critical conc. against interaction range 2−52089
random variables, local theorems for nonidentical distributions 2−45294
rectilinear diameter law, coexistence curve diameter calc. 2−58769
second-order phase transitions, universality, scale factor for correl. length 2−63029

Lattices, theory and statistics continued
self-avoiding walks, distribution function, triangular and f.c.c. lattices 2−55427
self-avoiding walks, new approach to mean-square end-to-end length 2−52088
series expansions, new recurrence relation method for analysing singular behaviour 2−66458
simple cubic lattice Green function 2−61050
structural phase transition, two-fluid model, heat diffusion mode 2−84185
structure semilattice preserving congruences on normal band, chain condition 2−82265
subspaces of Hilbert space, interpretation as proportional calculus 2−76229
Toda lattice, relation to Hamiltonian oscillator system in stochastic regions of phase space 2−41525
topological spaces, quasi-homeomorphisms and lattice equivalences 2−82264
triangular and honeycomb lattice, Green's functions 2−61052
two-dimensional, generalized special freq. 2−45293
two-dimensional nets, classification 2−71299
two-dimensional systems, long range order and metastability 2−50407
valence bond wavefunctions, reduced density matrices 2−49028
vector model, critical behaviour, term struct. of series expansions 2−52090
vector model, high temp. expansions, weighting of graphs 2−52091
wind-tree models, absence of diffusion 2−45289
wind-tree models, analytic functions 2−63025
X-Y model, critical exponents calc., recursion relation 2−76226

Laves phases *see Alloys; Phase transformations/solid-state*

Lawrencium
No entries

Lawrencium compounds
No entries

LCAO calculations
ab initio LCAO-MO-SCF calcs. of cyanamide dipole moment in semi-rigid model 2−64176
adenine, electrostatic potentials, MO LCAO GTO SCF calculation 2−60041
auto-coherent LCAO field method, critical study 2−52977
benzoylacetonate anions, fragment calc. 2−83325
conjugated molecules, comparison of various expansions in perturbation theory calculations 2−42855
cubic lattices, electronic surface states calc. 2−47815
cyclopropylamine, SCF-LCAO-MO calculations of conformation 2−70786
cytosine, electrostatic potentials, MO LCAO GTO SCF calculation 2−60041
decacyclene SCF MO calc. of electronic spectrum in Pariser-Parr-Popl approx., comparison with exptl. data 2−42976
dipole transition moment determ. of isoelectronic tetroxy anions 2−77063
dipole transition moments of tetroxy anions of third transition metal series, calc. in terms of ligand mixing coeff. 2−42928
electric field gradient at nuclear sites in crysts. 2−68615
ethylbenzene, conformational structure correlation with semi-empirical LCAO calculations 2−60068
ferrocenoylacetonate anions, fragment calc. 2−83325
formaldehyde, semi-empirical SCF-LCAO calculations 2−42986
glyoxal, LCAO-MO-SCF calc. determ of energy for cis-trans isomerization 2−53065
hydrates of ions Li^+, Na^+, Be^{2+}, F^-, Cl^-, calc. by CNDO/2 method, determ. of H bond strength 2−50053
hydrogen bond stability, charge transfer influence 2−70671
LCAO-SCF-MO-CI ab initio calc. of hyperfine coupling in methyl and fluoromethyl radicals 2−77148
LCGO, minimal basis set, of large mols. 2−79989
maximal overlap method subject to additional condition 2−77033
Me-Oh (Me=Cr, Mn, Fe, Co, Ni, Cu, Zn) molecule calc. using semi-empirical LCAO-MO method 2−42867
methyl radical, LCAO-MO-SCF Gaussian wavefunctions 2−42994
methylenephosphorane, ab initio LCAO-MO-SCF study of bonding 2−56240
MO SCF calcs. on CS, new symmetry assignment to k state 2−70688
nitrosomethane, SCF-LCAO-MO calculations of barrier to internal rotation 2−70786
norbornadiene, electronic struct., LCGO minimal basis calc. 2−70785
SCF field molecular wave functions, approximations 2−42851
SCF perturbation theory and intermolecular interactions 2−42849
SCF-LCAO-MO constrained eqns. methods for solution, application to N_2 2−64099
SCF-LCAO-MO parameterized theory for transition metal compounds 2−46525
SCF-MO-LCAO method, quasi-relativistic approx. 2−67454
semi-empirical methods for optimization of mol. geometry 2−52987
semiconductor, amorphous, of electronic struct. 2−68414
semiempirical methods, comparison 2−77037
thiazyl fluoride, comparison with photoelectron spectra, vibr. analysis 2−53083
thymine, electrostatic potentials, MO LCAO GTO SCF calculation 2−60041
transition metal coordination cpds., electronic struct., SSP MO LCAO method in p.p.d.p approx. 2−50020
two-electron integrals in LCAO-MO calculations, economic storage and processing method 2−52979
CO_2, semi-empirical SCF-LCAO calculations 2−42891
$CaF_2:Tu^{2+}$ crystal, crystal field parameters by MO LCAO method 2−61611
Co complex, acetylacetonate, u.v. and visible spectra calc. 2−83326
H_2, H_6 ring system, electron density and correlation in ground states, simple LCAO approx. 2−67476
HCN, semi-empirical SCF-LCAO calculations 2−42891
HOF-H_2O mixed dimer, LCAO-MO-SCF calcs. of equilibrium structures and energies 2−67491
$(HOF)_2$ dimer, LCAO-MO-SCF calcs. of equilibrium structures and energies 2−67491

LCAO calculations continued
HOO, nonempirical LCAO MO SCF and CI studies of low lying electronic state 2−50040
I_2^+, MO LCAO model, spin-orbit coupling 2−70709
LCGO-SCF-MO method, mixed Gaussian basis, for ab initio calcs. 2−59978
NH_3^+, LCAO-MO-SCF Gaussian wavefunctions 2−42994
NH_2OH-H_2O mixed dimer, LCAO-MO-SCF calcs. of equilibrium structures and energies 2−67491
$(NH_2OH)_2$ dimer, LCAO-MO-SCF calcs. of equilibrium structures and energies 2−67491
NO bonds in X_3NO compounds, LCAO CNDO/2 calculations 2−42866
PO bonds in X_3PO compounds, LCAO CNDO/2 calculations 2−42866
SF_6, X-ray absorption spectra, MO LCAO interpretation 2−56196

Lead
see also Superconducting materials/lead
γ-irradiated temperature dependence of positron annihilation spectrum 2−71767
abundance in seawater in-situ analysis using synthetic fibres 2−75469
adsorbed layer, on Ni, low index surfaces, LEED obs. 2−60682
aerosol, ageing, numerical model simulating coagulation and sedimentation 2−64487
amorphous state, Hall effect 2−75048
anodic dissolution, in H_2SO_4 2−84658
atom, determ. of shell-wise photoelectric cross-sections at 100 and 279 keV by indirect method 2−49925
atom (6^1D_2), electronically excited, atomic absorption spectroscopy using attenuation of resonance radiation 2−79859
atoms, metastable and excited states, cross section for collisional quenching depolarization of alignment by inert gases 2−42785
auditory impairment and VDL and AP charges in chronically poisoned guinea pigs 2−45164
clusters, electronic props., mol. orbital calc. 2−81026
crystalline prisms, space dependent neutron spectra 2−70506
cyclic straining, subgrain formation 2−80763
dendrite growth, in gels, kinetics 2−47137
density changes of solid and molten state at elevated temps. 2−64699
density of Ag-doped specimens, annealing effects 2−71665
density of states, relativistic effects, mass velocity and Darwin terms 2−84242
diffusion of ^{124}Sb, temp. depend., 188-315°C 2−77617
diffusion of ^{22}Na, meas. by sectioning diffusion couples, 249-313°C, vacancy mechanism 2−77600
diffusion of Ag, isotope effect in dissociative mechanism 2−68044
diffusion of Cu, 0 to 56 kbars 2−47470
diffusion of Cu, evidence for two simultaneous mechanisms 2−84001
dislocation motion resistance, u.s. measurement 2−68030
elastic constants, 2nd and 3rd order, calc. using pseudopotential methods 2−60836
electrical resistance, as fn. of molar heat content, meas. by pulse method 2−64914
electron backscattering, spectral ang. distrib. meas. 2−84218
electron-ion interaction pseudopot. model, form factor, binding energy, resist., thermoelec. power 2−77812
exo-emission, threshold illumination intensity 2−44189
Fermi surface press. depend. 2−44034
film, epitaxial on Ni substrate, azimuthal disorientation of elementary nuclei 2−47122
film, on SiO, sticking coeff. effect of water vapour 2−64572
film, on W(100) surface, struct., LEED obs. 2−77511
film growth kinetics near melting point 2−60652
Hall effect, magnetoresist., $T \leqslant 4.2K$ 2−47836
hardness, scratch and indentation meas. 2−53841
isotope ratios in conformable ores and oceanic rocks, evolutionary model 2−61991
Kikuchi patterns, influence of thermal diffuse scattering 2−83935
liquid, diffusion of Tl 2−46945
liquid, elec. resist. and thermoelec. power temp. depend., models 2−60501
liquid, elec. resist. temp. depend., freezing point to 800°C 2−43388
liquid, optical consts. 2−43359
liquid, specific elec. resist., temp. depend., pseudopotential calc. 2−80478
liquid, struct. factor, X-ray diffr. apparatus 2−74516
liquid, struct. factor rel. to entropy of melting 2−64434
liquid, thermal cond., Lorenz no. 2−43347
liquid, u.s. velocity, theory and expt. 2−80469
lunar rocks, concentration obs. 2−44907
melting of small particles, size effect 2−43439
muonic atom, energies and relative intensities of transitions to and from 2s level 2−42823
optical constants ε_1 and ε_2, absolute values 2−48134
oxidation of evaporated layers, by low energy O_2^+ bombardment 2−61791
p-type, vacancy obs. using hydrostatic weighing 2−58691
in paint, chem. analysis, instrument 2−65418
prism, neutron wave propag. effect of cold neutrons 2−83044
reactor shielding, meas. of dose albedos of intermediate energy bremsstrahlung 2−76958
silicate glass emitters for magnetic electron multipliers 2−59104
sound excitation by electrons, positrons and photons 2−61089
specific heat, 0-300°C, determ. by monotonic heating method 2−51046
surface tension, 309°C 2−56577
thick target, energy loss of scatt. protons 2−80928
$2AgCl(g) + Pb(g) \rightarrow 2Ag(g) + PbCl_2(g)$ substitution reaction in hot hollow cathode 2−84641
Bi_2S_3:Pb, capture level parameters, thermo-stimulated cond. study 2−71923
n-GaSb-Pb contact, tunnelling spectroscopy and band struct. press. effects 2−84351
heat capacity, C_p to C_v conversion, using dilation correction 2−54050
KCl:Pb, rapidly grown from melt, thermal stress defect model 2−50649
$KCl:Pb^{2+}$, electrolytically coloured, T-centre struct. 2−64679

Lead continued
KCl:Pb^{2+}, grown from soln., inhomogeneous impurity distrib., spectrophotometric obs. 2−74796
LiH:Pb, X-ray luminesc. and thermoluminesc. 2−72422
Pb:Au, relax. effects, internal friction obs. 2−68069
Pb/NaCl-UCl_3 molten metal/fused salt system, surface and interfacial energy 2−52874
Pb-Al_2O_3-Al junction, impurity assisted tunnelling, 4.2-148 K 2−44140
Pb-Bi-Hg liquid metal systems, effectiveness of boiling separation 2−74594
Pb-Cd amalgam electrode, standard cell, reduced temp. coeff. 2−82118
Pb-GaAs Schottky barrier tunnel junction, zero bias anomaly, irrad. effects 2−71960
Pb-Si solid structure, etching technique for macrostructure obs. 2−56607
Pb-glass with semiconducting surface layer, delayed electron emission after electron bombardment 2−84384
Pb^+ ion gas-phase hydration, mass spectrometric obs. 2−80493
Pb_2, new molecular constants for ground electronic state determ. from laser excited resonance fluorescence 2−42929
Pb^{2+}, in KBr soln., nucleation and crystn., evolution of heat 2−47236
Pb^{2+}, in KCl aqueous soln., rel. to cryst. growth 2−47237
Pb^{2+}, in NaCl and KCl, polarized luminesc. and dipolar relax. of Pb-vacancy complexes 2−72424
^{203}Pb, carrier-free, for tracer obs. 2−69268
^{206}Pb muonic atom, analysis of muonic X-rays in terms of equivalent radius 2−59963
ZnS:Cu, Pb, Cl film, temp. depend. of electrolum. and thermal quenching 2−84533

Lead compounds
dicalcium lead propionate, spin-lattice relax. near crit. point 2−65196
halides, energy level splitting, effective hamiltonian theory 2−44319
$Pb_xLa_{1-x}(Zr, Ti)O_3$ ceramics for selectively erasable image storage and display 2−79454
Pb-In alloys, surface resistance variations with applied field 2−64942
pyrochlores, $Pb_2M_2O_7$, (M=Ru,Ir,Os), struct. and props. 2−60987
Sn-Pb alloy stainless steel fibre reinforced, fracture behaviour 2−50921
solder, k-shell differential cross sections, effective atomic numbers 2−54439
Au-Pb system, interstitial dissolution and compound formation 2−43826
(b,La)(Zr,Ti)O_3, cold pressing and low temp. sintering 2−50892
(Ba, Pb)TiO_3 ceramic, light emission by surface microplasma new Curie temp. 2−65303
Bi-Pb-Zn system, activity coeffs., calc. 2−43827
Bi-Pb alloy, thermal expansion meas. in room temp.-100°C range, applicability of rule of mixtures 2−60975
$CdBr_2$-Pb crystals, temp. depend. of recombinat. luminesc. and photocond. 2−72049
In-Hg-Pb alloy, supercond., thermodynamics, role of electron scatt. 2−81038
In-Pb alloy, Seebeck coeff., comp. depend., 120°C 2−81162
In-Pb alloys, liq., longit spin relax. of ^{115}In 2−50370
$K_2CO_3 + 2PbSiO_3$ subsolidus reaction, kinetics and mechanism 2−60996
$K_2CO_3 + 2(4PbO.SiO_2)$ reaction, kinetics and mechanism 2−50884
Na-Pb dilute alloy, liq., compressibility determ. 2−77415
Pb/P bronze, fibre composite, steady state creep meas. 2−47515
Pb-Ag alloys, ageing, softening mechanism and kinetics 2−43860
Pb-Bi-Sn eutectic, superplasticity 2−80839
Pb-Bi, liquid binary alloys, absolute thermoelectromotive force 2−56518
Pb-Bi alloy, neutron scattering law determ. 2−80931
Pb-Bi alloy, thermodynamic props., calorimetric obs. 2−57056
Pb-Bi alloys, nonequilib. freezing, quantitative predic. by classical eqn. 2−47032
Pb-Bi peritectic alloy, heat of solidification, calc. 2−43444
Pb-Cd-Sn alloy, eutectic morphology, unidirectional solidification microstruct. 2−74895
Pb-Ge-As-Se glass, microstruct. and immiscibility temp. 2−56561
Pb-In-Sn ternary alloy superconducting wire, magnetic properties, flux flow voltages 2−81037
Pb-In, superconducting alloys, strong coupling, mag. meas. 2−64950
Pb-In alloy, supercond., electronic thermal conductivity, temp. and mag. field depend. 2−47867
Pb-In alloy, superconductor, microwave surface resist. 2−54133
Pb-In alloy film, supercond., electronic thermal cond. 2−81042
Pb-In alloys, superconducting, thermal conductivity, temp. and mag. field depend. 2−71872
Pb-In alloys, thermal Hall effect and the Righi-Leduc angle, observations 2−68370
Pb-In dilute alloy, supercond., phonon spectra detn., elec. tunnelling obs. 2−54142
Pb-In superconducting alloy, phonon spectrum, hydrostatic pressure effects, tunnelling obs. 2−64936
Pb-Mn alloy, sp. ht., 0-300°C, determ. by monotonic heating method 2−51046
Pb-Mn superconducting films, tunnelling conductance curves 2−71851
Pb-Na alloy, superconducting, heterogeneous, anisotropic crit. currents 2−77864
Pb-Na liquid solution, thermodynamic props., e.m.f. cell obs. 2−71183
Pb-Sb-S system, amorphous like crystalline semicond., mag. suscept., comparison with B 2−77987
Pb-Sb alloy, precip. mechanism, hardness, resist. and microscopy studies 2−80858
Pb-Sb(8 to 17%) alloy, influence of annealing temp. on thermal expansion 2−43995
Pb-Sn alloy, dependence of γ ang. correlation of positron annihilation on composition 2−71766
Pb-Sn alloy, diffusion of Ag 2−56763

Lead compounds continued
Pb-Sn alloy, solder, interaction with NO_2, corrosion, humidity effects 2−65382
Pb-Sn alloy, superplastically deformed, const. stress creep and strain rate tensile tests 2−47504
Pb-Sn alloy, thermodynamics of melting, determ. of thermodynamics of Sn phase transform. 2−50950
Pb-Sn eutectic alloy reinforced by stainless steel fibres, tensile strength 2−77742
Pb-Sn liquid alloy, surface tension, max. bubble pressure method 2−53409
Pb-(40 at.%)Tl alloy, force free mag. fields, solns., for cylindrical geometry 2−44066
Pb-(40 at.%)Tl alloy, force free mag. fields, solns. for spherical geometry 2−44067
Pb-Tl alloy, Ginzburg-Landau parameters, temp. depend. 2−64921
Pb-Zn alloy, liq., elec. resist. at 500°C 2−60507
(Pb,La)(Hf,Ti)O_3, hot-pressed, material and electrooptic props. 2−56966
(Pb,La)(Zr,Ti)O_3, electrooptic ceramic, fabrication by atm. sintering 2−56967
(Pb,La)(Zr,Ti)O_3, phase boundary and defect struct. 2−56968
Pb Mo acousto-optic deflector 2−79419
$Pb_2B_5O_9Br(Cl)$, cryst. struct. 2−53657
PbBi film, thermal cond. 2−68344
$Pb_{0.9}Bi_{0.1}$ alloy, strong coupling superconductor, crit. mag. field temp. variation 2−68356
$Pb_{1-2x}Bi_xTl_x$, superconducting alloys, strong coupling, mag. meas. 2−64950
$PbBr_2$-$PbCl_2$ phase diagram and ideal soln. behaviour 2−50852
$PbBr_2$, elec. cond. in cell arrangement, space charge effects, elec. polarization 2−61420
$PbBr_2$, electronic cond., hole cond., elec. polarization 2−61419
$PbBr_2$, pure and Cu^+-doped, defects, ionic cond. and dielec. loss study 2−47402
$PbBr_2$, pure and doped, hole cond., defect chem. 2−61322
$PbBr_2$, pure and Tl^+-doped, vacancies, ionic cond. study 2−47401
$PbBr_2$, u.v. irrad., e.p.r. and luminesc. obs. of centres 2−44448
$PbBr_2$ pressed discs, u.v. irrad., photodecomposition 2−44491
$PbBr_2$ thin film, optical constants and exciton states for 2-10 eV absorption spectra 2−57321
$PbCl_2$:Eu^{2+}(Sm^{2+}), luminesc. 2−54447
$PbCl_2$, obs. of Fano effect in exciton spectrum 2−68647
$PbCl_2$, optical consts. and exciton states 2−68625
$PbCl_2$, pure and K^+-doped, defects, ionic cond. and dielec. loss study 2−47402
$PbCl_2$, u.v. irrad., e.p.r. and luminesc. obs. of centres 2−44448
$PbCrO_3$, perovskite, struct., elec. resist., mag. susceptibility 77-550K 2−61321
PbF_2-BaF_2, solid solution, theoretical study 2−64772
PbF_2-SrF_2, solid solution, theoretical study 2−64772
PbF, rotational analysis of (1,0), (0,0) and (0,1) bands of $B-X_2$ system 2−79994
PbF_2, Raman spectra, lattice dynamics 2−57040
PbF_2, thermal expansion, shell model calcs. rel. to phase transition 2−84216
$PbFe_{12}O_{19}$, saturation magnetization, reduced temp. depend. by As or P substitution 2−78019
$PbFe_{2/3}W_{1/3}O_3-PbTiO_3$ solid solution, phase diagram, ferromag. and ferroelec. props. 2−81229
$Pb_5Ge_3O_{11}$, ferroelec., soft optic phonon mode 2−43961
$Pb_5Ge_3O_{11}$, pyroelectric properties 2−57246
$Pb_5Ge_3O_{11}$ single crystal, ferroelec. optical rotation domains 2−44164
$Pb_{1-x}Ge_xTe$, lattice const., and phase transform. 2−84108
$Pb^{181}HfO_3$, perovskite-type, nucl. quadrupole interactions, perturbed-angular-correlation meas. 2−72244
PbI_2, band edge excitons, refl. study 2−68626
PbI_2, band struct. computation and optical absorp. spectra 2−68418
PbI_2, exciton spectrum, anomaly due to cationic nature of exciton 2−51324
PbI_2, for nuclear particle detection crystal growth and detection props. 2−46037
PbI_2, lattice parameters meas. by X-ray method in temp. range 25-114°C, evaluation of coeffs. of thermal expansion 2−61110
PbI_2, Mossbauer effect, isomer shift and quadrupole coupling 2−68614
PbI_2, O_2 chemisorption induced conductivity changes 2−47886
PbI_2 thin film, influence of nature of substrate and preparation conditions on exciton spectrum 2−48188
$Pb_{1-3x/2}La_x(Zr_{0.65}Ti_{0.35})O_3$ ceramic, acoustic detection of ferroelectric phase changes 2−51196
$Pb_{1-3x/2}La_xZr_{0.65}Ti_{0.35}O_3$, phase transitions 2−57245
$Pb_{1-x}La_x(Zr_yTi_z)_{1-x/4}O_3$ ceramic, radial mode coupling factors det. with large Poissons ratio variations 2−51195
$PbMg_{1/3}Nb_{2/3}O_3$-$PbTiO_3$-$PbZrO_3$ solid solution, hot-pressed, electrooptic props. 2−57328
$PbMg_{1/3}Nb_{2/3}O_3$ crystals, change in refractive index as function of electric field strength, use of prisms as light beam deflectors 2−42215
$Pb(Mg_{1/3}Nd_{2/3})O_3$ formation processes in the solid state reaction 2−77560
$Pb(Mn_xNb_{1-x})O_3$ perovskites, synthesis and characteriz. 2−50893
PbMnO$_2$OH, quenselite, cryst. struct. 2−53677
$PbMoO_4$:Cu, Gd site occupancies of dopant and trace impurity 2−68739
$PbMoO_4$, sign of Z-axis detn., etch config. and Schaefer-Bergmann diffr. obs. 2−43568
$PbMo_6S_7$, superconducting properties, heat capacity, Debye temp. 2−81051
α-$Pb(N_3)_2$:Mn^{2+}, e.s.r. spectrum, spin Hamiltonian parameters and linewidth temp. dependence 2−44447
$Pb(N_3)_2$, growth from solution 2−83900
$PbNb_4O_{11}$, absolute signs of second harmonic generation coeffs. 2−44332
PbO-Al_2O_3-SiO_2-B_2O_3 glass, between metal electrodes, memory effect 2−71915
PbO-GeO_2 system single crystal growth 2−74666
PbO-P(As)(V)$_2O_5$ systems, synthesis and crystallography 2−74741

Lead compounds continued
- PbO-RO-GeO_2, R=Mg, Ca, Sr, Ba, glass, struct. and props. 2−53540
- PbO-SiO_2 glass, hopping cond., photoemission obs. 2−44206
- PbO-V_2O_5 flux system, for oxide crystal growth 2−50589
- PbO-YF_3-Al_2O_3 melts, crystallization of YAG and det. of stability range 2−74692
- PbO, autocompensated photoconductor, inversion of the sign of conductivity 2−44175
- PbO, for nuclear particle detection, crystal growth and detection props. 2−46037
- PbO, formation by low energy O_2^+ bombardment of Pb layers 2−61791
- PbO film, optical absorption 2−57352
- Pb_3O_4, quadratic-orthorhombic transition, low temp. 2−74939
- $5PbO.3GeO_2$, ferroelec. material, acousto-optical figure of merit, acoustic attenuation 2−64849
- $5PbO.3GeO_2$, Raman scatt. by ferroelec. modes 2−61669
- $PbO.6Fe_2O_3$, unsaturated crystals, ferromagnetic resonance, 36-52 GHz 2−72455
- PbS, refl. spectra, X-ray photoemission, spin-orbit splitting 2−78092
- PbS film, epitaxial, struct. rel. to substrate surface struct. 2−64571
- PbS film, prep. by chem. precip., transmission spectra, optimum prep. conditions 2−75304
- PbS film on semiconductor substrate, crystallization from aqueous solution 2−80562
- PbS layers, photocond. mechanism, elec. cond. and Hall effect obs. 2−81166
- PbS photosensitive layers, prepared by different methods, adsorption properties 2−61652
- PbS quantum yield of internal photoelec. effect and impact ioniz. 2−72065
- $PbSO_4$-$BaSO_4$, solid solution, theoretical study 2−64772
- $PbSO_4$-$SrSO_4$, solid solution, theoretical study 2−64772
- $PbSO_4$, coherent neutron scatt. amplitudes from powders 2−53654
- PbS(Se)(Te), mech. props., carrier conc. effect 2−50784
- $XPbSe$-$Ge_{1.5}As_{0.5}Se_3$, pseudobinary system, glass formation 2−80531
- PbSe, band struct., absorp. edge and intraband transition region obs. 2−81402
- PbSe, defect obs. using hydrostatic weighing 2−58691
- PbSe, Faraday effect, free carrier dependence 2−84469
- PbSe, refl. spectra, X-ray photoemission, spin-orbit splitting 2−78092
- n-PbSe, reflectivity and magnetoreflectivity 2−61651
- PbSe, solid and liq., thermal cond. up to 1500K 2−68259
- PbSe epitaxial films on NaCl substrate, effect of ambient gases on electrical properties 2−65008
- PbSe film, epitaxial, struct. rel. to substrate surface struct. 2−64571
- PbSe film on semiconductor substrate, crystallization from aqueous solution 2−80562
- PbSe monocryst., heat treated, mag. suscept. meas., bonds 2−48035
- PbSe n and p type anisotropy of cyclotron and spin mass 2−80984
- n-PbSe(Te), hot-electron cond., velocity-field characts., 77 and 4.2K 2−68407
- $PbSnS_3$, cryst. struct. 2−77556
- $Pb_{0.8}Sn_{0.2}Te$, epitaxial film, photocond. 2−65085
- $Pb_{1-x}Sn_xTe$, epitaxial growth from soln., surface quality improvement 2−60656
- n-$Pb_{1-x}Sn_xTe$, hot-electron cond., velocity-field characts., 77 and 4.2K 2−68407
- $Pb_{1-x}Sn_xTe$, i.r. plasma refl. study 2−84504
- $Pb_{1-x}Sn_xTe$, optical props., refl. meas., Kramers-Kronig analysis 2−48165
- $Pb_{1-x}Sn_xTe$, reflectivity, optical consts., energy band struct. 2−48164
- $Pb_{1-x}Sn_xTe$ alloy, crystal growth and isothermal annealing 2−53618
- PbTe:In, donor level above the bottom of the cond. band 2−84281
- PbTe/PbS interface, misfit dislocations, image contrast 2−71483
- p-PbTe-PbSe alloys, thermoelec. props., temp. depend. 2−75164
- PbTe-PbSe system, phase diagram, rel. to cryst. growth technique selection 2−47702
- PbTe-UTe system, phase diagram 2−47717
- PbTe, efficiency criterion for thermogenerators 2−75158
- PbTe, electronic charge density 2−44121
- PbTe, epitaxial film, photocond. 2−65085
- p-PbTe, high field transport, current-field curves, mixed scatt. by phonons 2−81068
- PbTe, mag. susceptibility calc. 2−68519
- PbTe, optical props., refl. meas., Kramers-Kronig analysis 2−48165
- PbTe, performance as solar thermoelectric generator material 2−59058
- PbTe, refl. spectra, X-ray photoemission, spin-orbit splitting 2−78092
- PbTe, solid and liq., thermal cond. up to 1350K 2−68259
- PbTe, surface free energies, calc., reply to comments 2−77491
- PbTe, surface free energies, calc., comments 2−77490
- PbTe, TO lattice mode, low temp. far i.r. detn. 2−65265
- PbTe, thermoelec. props. rel. to partial substitution of Pb by Ga, In, Th 2−72053
- PbTe, transverse optic mode softening, Curie law temp. depend. 2−68230
- PbTe epitaxial thin film diode, evaporated, injection luminesc. and laser action 2−57382
- PbTe film, epitaxial, struct. rel. to substrate surface struct. 2−64571
- PbTe film, O_2 and N_2 effects on Hall and field effect mobilities 2−57191
- PbTe film, optical and elec. props. 2−57172
- PbTe film, sputtered and evap., optical props. as function of deposition conditions 2−48131
- PbTe meas. of complex structure potentials by convergent electron diffraction 2−83932
- p-PbTe room temp. transport props., scattering mechanisms, relative importance 2−54161
- $Pb(Ti, Zr)O_3$ plate, dispersion curves of flexural modes 2−84205
- $Pb(Ti,Zr)O_3$, cold pressing and low pressing and low temp. sintering 2−50892
- $Pb(Ti,Zr)O_3$ system, intrinsic nonstoichiometry 2−50894
- $PbTiO_3$-$Pb(Cd_{0.5}W_{0.5})O_3$ ceramic, electromechanical props. 2−64788
- $PbTiO_3$, absolute signs of second harmonic generation coeffs. 2−44332
- $PbTiO_3$, conversion to semicond. state by doping resist. positive temp. coeff. 2−81098
- $PbTiO_3$, dielectric const. changes after electron or gamma irrad., X-ray study 2−65047
- $PbTiO_3$, plate-like growth and exam. of domain struct. 2−71398
- $PbTiO_3$, pyroelectric i.r. detector 2−55572
- $PbTiO_3$ in m-i-m structure Seebeck effect 2−44169
- $PbTiO_3$ plate, dispersion curves of flexural modes 2−84205
- $PbTiO_3-PbF_{2/3}W_{1/3}O_3$ solid solution, phase diagram, ferromag. and ferroelec. props. 2−81229
- $PbTiP_2O_6$, flux growth and single cryst. X-ray diffr. 2−60717
- $Pb_{0.5}Tl_{0.5}$ films, supercond., phonon generation 2−47735
- $Pb(Zn_{0.33}Nb_{0.67})O_3$ ceramic, electrooptical props. rel. to sintering conditions 2−65223
- $PbZnO_3$, internal electric field gradient by perturbed angular correlations 2−81156
- $Pb(Zr, Ti)O_3$, pyroelectric, heat diffusion and heat sink problems for pyroelec. detectors 2−77960
- $Pb(Zr, Ti)O_3$, shock induced electromech. conversion, additives influence 2−84359
- $Pb(Zr,Ti)O_3$-Si-$LiNbO_3$, convolution and correlation by nonlinear interactions between sonic induced space charge and field waves 2−51015
- $Pb(Zr,Ti)O_3$, thermodynamic theory of morphotropic phase transition 2−75153
- $Pb(Zr,Ti)O_3$ ceramic, microstruct., role of Fe_2O_3 2−50895
- $Pb(Zr,Ti)O_3$ type, static dielec. const. and dissipation factor, nonlinear field depend. 2−72035
- $PbZrO_3$, dielectric const. changes after electron or gamma irrad., X-ray study 2−65047
- $PbZrO_3$, growth and obs. of intermed. ferroelec. phase 2−81140
- $PbZrTiO_4$ electrostrictive transducer material, fatigue testing 2−71625
- $PbZr_{0.5}Ti_{0.5}O_3$, single-phase, intrinsic nonstoichiometry 2−50896
- Pd_2MnSb, ferromagnet, hyperfine fields, n.m.r. study 2−61750
- Sn-Pb alloy, rapid detn. of Sb, Pb, Sn and Cu by atomic absorp. spectroscopy 2−78218
- Sn-Pb alloy, unidirectional solidification, uniaxed crystal origin 2−74882

Leak detection
- cyclotron leak monitoring 2−70328
- failure, possible causes in tests for vacuum tightness 2−58660
- space simulation chambers using rotatable gas analyzer 2−78706
- vacuum system, modulation of gas flow 2−78710
- ^3H-fuelled batteries, leak testing 2−49254

Leather *see Materials*

Lee model
- eigenvalue problem in NΘΘ-sector, algebraic soln. 2−76562
- with Fermi coupling, explicit solution in low sectors 2−52524
- infinite mass renormalization and Z=0 condition 2−79456
- infinity suppression due to nonlinearity 2−59349

LEED
- adatoms, thermal disorder, 1-dimens. model, diffr. pattern calc. 2−60672
- apparatus, low temp., 20-150K 2−71296
- averaged spectra data, quasi-kinematic parameter relations 2−74611
- camera, specimen manipulator 2−60739
- chemisorption, struct. types 2−56600
- crystal surface, inelastic scatt. by one phonon processes, theory 2−50986
- data processor, u.s. light diffractors, high speed printer 2−76116
- Debye temp., effective, energy depend. 2−61062
- diffraction intensities for perfect cryst., numerical evaluation 2−64619
- electrodes and circuits for LEED-AES system 2−74612
- film nucleation and growth obs. with LEED-Auger instrument 2−74624
- inelastic, dynamical theory, constructed using quantum field theory 2−74711
- insulator, charging effects 2−64547
- intensities, effects of deviation from Bethe model, investigation for exactly soluble one-dimensional model 2−50419
- intensity profiles rel. to spin-polarization, atomic core scatt., surface barrier struct. 2−77483
- limitations and present state-of-art 2−71409
- metal, f.c.c., {001} surface, expt. and theory 2−50428
- metal surface, kinematic intensities extraction from averaged data 2−43462
- microscopy combined with u.h.v. electron emission microscopy 2−79048
- reduction of intensities from rot. diags. for surface crystallography 2−53546
- review, crystal surface struct. techniques 2−80555
- selected area, in emission electron microscope 2−79080
- spectro-goniometer realization 2−60738
- state-of-the-art 2−50420
- substrate design incorporating single crystal disc for use in ultra high vacuum 2−60617
- surface struct. analysis, electron dynamical scatt. problem soln. 2−56624
- surface struct. determ., intensities, Fourier analysis 2−47073
- surface vibrational spectra, inelastic law energy electron scatt., theory 2−71706
- two-dimensional nets, classification 2−71299
- ultrahigh vacuum electron emission microscope, LEED and RHEED 2−79096
- vacuum chamber of stainless steel and molec. beam assembly, H and N desorption phenomena 2−67922
- Ag, adsorption of oxygen studies 2−60675
- Ag, chemisorption of O_2, rel. to surface struct. LEED and secondary electron spectroscopy 2−51442
- Al, (100) and (111) faces, intensities, quantum field theory calc. 2−74712
- Al, (100) face, rotation diagram, calc. 2−74618

LEED continued
Al, {111} and {110} surfaces, spectra, calc. 2−83857
Al, expt. and theoretical rotation diagrams 2−50433
Al, intensity temp. depend., Debye temp. calc. 2−60624
Al, on (001) surface 2−64549
Al, surface characterization, 40-80 eV 2−50437
Al, surface plasmon dispersion, inelastic scatt. obs. 2−51090
Al (100) surface, elastic and inelastic scatt., bulk and surface plasmon excitation 2−50434
Al (100) surface, intensity profiles 2−50436
Al film, oxidation 2−51445
Al surface, kinematic intensities extraction from averaged data 2−43462
Al_2O_3, (0001) surface structure detn. 2−67897
α-Al_2O_d, alumina, (0001) surface, structure obs. 2−50435
Au film, surface struct., LEED, RHEED 2−77500
Au surface, kinematic intensities extraction from averaged data 2−43462
Be (0001) surface, beam intensities 2−50438
Be cleaved surface, intensity-energy curves 2−60625
Be cleaved surface, intensity energy curves 2−60625
C fibres, thinned 2−64634
CdS (0001), (00) beam intensity at normal incidence 2−71308
Cr (100) surface, Debye-Waller factor and thermal exp. coeff. detn. 2−50992
Cu-Ni alloy, adsorption of CO and O_2, LEED obs. 2−50536
Cu, (001) and (111), (00) beam intensity at normal incidence 2−71308
Cu, weak adsorp. of CO and H_2 obs. 2−50537
Cu (100) surface, structure rel. to CO weak adsorp. 2−50538
Cu surface, phase transitions in two dimensional adsorbed layer of S ions obs. 2−50535
Fe-2.89%Si (100) face, surface composition rel. to photoelec. work function 2−61463
Fe single and polycrystals, secondary electron obs. rel. to rocking curves 2−54281
Ga, surface struct. rel. to plastic deform. by unidirectional abrasion and rolling 2−83856
GaAs, surface stoichiometry and struct. obs., surface vacancy model 2−50445
GaP, surface stoichiometry and struct. obs., surface vacancy model 2−50445
GaSe, surface struct., surface states 2−48024
Ge, surface reaction with O_2 obs. 2−50448
InAs, surface struct. obs. 2−50449
Ir, coated with Xe film, determ. of Ir surface struct. 2−47077
LiH, surface struct., contamination 2−47078
MgO cleavage faces, beam splitting, model 2−60627
Mo, adsorption of alkali metals, LEED obs 2−50540
Mo (100) surface, Debye-Waller factor and thermal exp. coeff. detn. 2−50992
Nb, deposition of Al, LEED and Auger spectroscopy obs., 22-1200°C 2−50484
Nb surface condition, superconducting r.f. cavities in accelerators 2−70337
Ni, (001) surfaces, absolute intensity energy LEED spectra 2−50459
Ni, (111) surface, averaged LEED intensities 2−50460
Ni, chemisorption of S, Se, O, obs. of bonding 2−48328
Ni, low index surface, adsorbed Pb layer obs. 2−60682
Ni, obs. of reactions of O_2 and S on surface 2−78184
Ni, surface interplanar spacings, Bragg peak widths 2−77486
Ni (100) surface, plasmon angular profiles 2−51093
Ni (111), (00) beam intensity at normal incidence 2−71308
Ni crystal face, benzene and cyclohexane adsorp. obs. 2−50545
Pb film, on W(100) surface, struct., 2−77511
Rh, averaging method for extraction of M-S data due to intralayer structure 2−71315
Si, intrinsic, photoemission processes analysis and band bending profiles as a function of caesium coverage 2−72082
Si, surface struct., rel. to surface states 2−77800
n-Si (111) surface, structure obs. 2−50464
W, adsorption of CO obs. 2−60692
W, adsorption of Cs and O, double layer form. 2−47169
W, adsorption of N_2O, binding states, LEED obs. 2−64581
W, obs. of oxide form. at 1000 K 2−78196
W, surface interplanar spacings, Bragg peak widths 2−77486
W (110) surface, plasmon angular profiles 2−51093
W surface, alkalis, rare gases and H_2 adsorbate structure 2−50554
Xe (111), one phonon thermal diffuse scattering calc. 2−60632
Xe (111) surface, thermal scatt. obs. 2−50470
Zn cleaved surface, intensity-energy curves 2−60625
Zn cleaved surface, intensity-energy curves 2−60625

Length measurement
see also Micrometry; Strain gauges; Thickness measurement
amplitude frequency characteristics of discrete transducers, det. by subtraction circuit 2−69537
Apollo 15 altimeter measurements, lunar laser altimetry 2−62682
creep, irradiated specimens, measurement by neutron radiography 2−82593
dilatometer fast-acting, two-coordinate recording system 2−76150
dilatometer for phase transformation obs. in structural steels 2−57008
dilatometer using photoelectric recording of elongation 2−71749
displacement, by holographic interferometry 2−41446
displacement, holographic interferometry applic. rel. to geophysical studies 2−61845
displacements, elastic sensing elements, optical projection microscopes for det. 2−45805
displacements of metal during mag. pulse treatment 2−76360
Earth-Moon distance measurements using lasers 2−44932
electronic, using analogue and digital techniques 2−76154
electrooptical distance measuring instrument for surveying 2−82533
in-plane displacement, moire gauging using double aperture imaging 2−66403
inductive transformer transducers of linear displacements 2−69536
laser interference fringe counting in high accuracy length measurement 2−55358
laser interferometer, linear displacements in wavelengths of light 2−59229

Length measurement continued
laser interferometer for strain amplitude meas. in internal friction exprts. 2−73395
lidar location of light reflector on Lunokhod-1 vehicle on Moon's surface, distance measurements 2−69953
line standards subdivisions length meas., temp. errors of comparator method 2−76153
linear capacitance micrometer, output voltage proportional to displacement 2−62959
linear dimensions, pneumatic gauging at low temps. 2−76156
manometer column height, using ultrasonics 2−45226
methods of counting and interpolating interference fringes rel. to length and angle measurement 2−76155
microdisplacement transducers 2−62957
multi-pass Michelson interferometer 2−76518
optical probe for displacement meas. 2−79394
Phocosin photoelectric digitization system with digital increments of 0.1 micron 2−52033
plane circular displacement transducers with variable area 2−69535
radar echoes, seeded convective cloud height temperature, NaCl, AgI 2−84829
reflecting objects displacement meas. using two beam interferometer 2−79354
rulers, linearity testing, using two-areas method 2−82133
scales reading process using interferometry 2−41448
semi-automatic, displacement transducer, void swelling in irradiated metals 2−83092
small displacements, photoelectric intensity microscope 2−55360
standard 2−48972
standard unit, reproduction and assignment of its value to secondary standards 2−58689
thermal expansion, laser interferometer dilatometer 2−49183
thermal expansion meas. at high-temps. by dilatometer reference materials 2−57071
thermally stabilized 10 m, measuring base 2−44517
three dimensional location, using planar X-ray system 2−62960
unified time-frequency-length standard using constancy of speed of light and optical frequencies 2−63370
u.s. welding equipment, microinch displacement monitoring, optical, accoustical techniques 2−69755
Fe, α-γ-α transform, dilatometric behaviour 2−53987

Length standards *see Standards*

Lennard-Jones and Devonshire theory *see Liquids/theory*

Lennard-Jones potential *see Kinetic theory; Molecules/intermolecular mechanics*

Lenses
see also Electron lenses
— 2−70051
— 2−70054
— 2−73161
air jet as acoustic lens or waveguide 2−45508
Andeyev's eyepieces, study of demerit values 2−70000
assembly system, mini computer controlled 2−79399
automatic design, desensitizing model 2−79406
contact microscope epiobjective 2−70004
corrected, wave aberration as function of defocussing and pupil position 2−45777
design, computer applications 2−70001
design for optical Fourier transform systems 2−49409
design system, LASL, improved speed 2−79405
evaluation using optical transfer function data 2−42175
extremely wide angle, design and aberrations 2−59216
Fabry, application to astronomy 2−66237
finite conjugate zoom lens system comprising single unit lens system with movable elements 2−79430
focusing, sensitivity of shadow test 2−59213
Fourier analysis of square wave targets used in lens MTF meas. 2−59221
gas lens, effect of initial section, constant heat flow 2−79333
geodesic, thin film, for laser beam focusing in integrated optics 2−49393
glare characteristics in visible region 2−66824
glass, drop-ball testing 2−42228
glass, optical surface layer, purification and preparation of melt surfaces, two-strength spectacle glass 2−82564
glass of high refractive index with low dispersion for correction of medium and high ametropia 2−66329
gravitational lens, uniform, transparent 2−58729
holographic two element off axis lens system design 2−79272
interferometric fan trace plotter for evaluation of lens systems 2−79420
interferometric testing, computer generated holograms 2−82572
Kirchhoff diffraction theory of thermal lensing in solids 2−55727
long focal length measurement using laser beam in optical resonator 2−76537
many conjugate zoom systems 2−59212
microreproduction for manufacture of photoresist phototemplates 2−70045
modulation transfer function, fast calc. in presence of diffraction 2−42176
optical design, application of Delano diagram 2−79402
optical transfer function, signal dependent noise 2−79294
phase acceptance of alternating gradient quadrupole doublet with quadrupoles of different apertures 2−45679
phase holograms as optical elements 2−42143
plane symmetric, aberration coeffs. determ. 2−73627
protective, ballistic testing of materials 2−48926
protective, ballistic testing of materials 2−48926
pump induced in lasers, meas. of focal length 2−41959
real time wave front meas. system for display of surface quality and lens performance 2−79398
safety, simulated, effect of thermal toughening on impact resistance 2−48927
safety, simulated, effect of thermal toughening on impact resistance 2−48927
scattering from inhomogeneous cylindrically symmetric lens with line infinity in refractive index 2−63374
sessile lenticular configs., translationally and rotationally symmetric lenses 2−74510

Lenses continued
spectacle, comparison of reliability and durability for glass and plastic lenses 2—58647
spherical aberration of two surfaces with object at infinity 2—59214
stigmatic, structure of e.m. field near focus 2—69826
striae solubility in glass melt 2—59260
telecentric, portable, applic. to moire strain obs. 2—45784
testing technique using optical autocorrelator for optical transfer function determ. 2—73628
testing using optical autocorrelator based on Aagnac interferometer 2—76532
thin film, photolithographic fabrication 2—73629
thin film geodesic lenses for integrated optics 2—79401
tinted ophthalmic lenses, function, evaluation and evaluation 2—62881
two-lens systems of reversed Ramsden and reversed Huygenian types, primary aberration 2—63373
zoom autocollimator for centring optical surfaces 2—79397
zoom objective for spatial frequency range scanning 2—63346
aspherical
convex elliptical, parabolic and hyperbolic surfaces, quality control technique 2—63375
design by computer, curvilinear bicubic spline fit interpolation scheme 2—79404
inspection parameters, computation for second order surfaces 2—70043
Selfoc lens, imaging and resolution 2—70003
surface control by holography and moire fringes 2—52433
surface inspection using correction plates made by vacuum deposition of aspherizing layers 2—59262
unusual image distortion, use of spline aspheric surfaces 2—79403
photographic
condenser systems, dispositive plane, light intensity distribution calc. 2—59217
flare meas. by three colours 2—63449
resolving power, meas. from radial and line targets 2—59328
selection suggestions 2—73689
slit shutter effect on modulation transfer function 2—59329
telescopic system of two conical reflecting mirrors for panoramic photography 2—70098
zoom lens, depth-of-focus calculator 2—52449
zoom lenses, optical design and aberrations, tutorial series 2—52448
Leptons
see also Electrons; Mesons; Muons; Neutrinos and antineutrinos
Adler sum, rule for inelastic lepton-hadron processes 2—82642
colliding-beam inclusive reactions, parton dual-resonance model 2—66931
conjugation symmetry of lepton number 2—76701
conservation of lepton number, test proposal 2—73749
currents relation with spin - $^{1}._{2}$ quarks in $O_{4,2}$ current algebra 2—42330
exclusive processes, study of form factors, dimensionalities of operators, fixed singularities and Bjorken limit 2—66932
gauge model applic. to hadron interactions 2—76629
heavy, existence models 2—52554
heavy particle concept., model of weak interactions 2—52556
higher-order corrections to leptonic processes, renormalization of Weinberg's theory of weak interactions in unitary gauge 2—79497
highly inelastic processes, comparison of parton and light cone analyses 2—55816
inelastic lepton-hadron scattering, parton model, coherent contrib. to breaking of Bjorken's scaling law for small Q^2 2—82727
inelastic scattering, parton models 2—59414
interaction, renormalizable gauge model 2—76599
interactions, model, $SU(2)_l \times Y_l$ gauge theory 2—66934
lepton-hadron interactions, theory 2—82679
lepton-hadron scatt., duality, scaling and fixed poles in virtual Compton scatt. 2—63506
lepton-hadron scatt., high energy, review 2—82678
lepton-hadronic inclusive reactions, parton dual-resonance model 2—66931
lepton-lepton scattering formulas 2—73760
lepton-nucleon deep inelastic scattering, form factors of nucleon 2—67043
lepton-nucleon inelastic structure functions, scaling, Greens functions of currents 2—70150
lepton-nucleon scatt. linked by sum rule to baryon mass splitting D/F ratio 2—70153
lepton-nucleon scattering, parton model predictions in Weinberg theory 2—45886
magnetic moment, second-order weak corrections in Weinberg model 2—59408
massive lepton pair production, parton model 2—42333
massive pair production in hadron collisions, parton model 2—70178
nonconservation in nuclear physics review 2—46066
pair photoproduction, improved Weizsacker Williams method for calc. of energy-angle distrib. 2—66930
pair production by neutrinos 2—46239
pair production in hadronic interactions, scaling model 2—82688
photon-lepton scatt., fourth-order Compton amplitude in Weinberg model, Drell-Hearn sum rule 2—59408
polarized, inelastic scattering from polarized nucleons, determ. of threshold relations 2—63507
production of pairs at CERN ISR, predictions 2—63505
resonances, fine structure in K_{l3}^0 decay 2—49543
S-matrix theory, unified weak and e.m. interactions 2—82641
scattering, deep inelastic, on nucleons, recent developments 2—76583
scattering, deep-inelastic, parton models 2—63528
scattering on hadrons deep inelastic, weak interaction processes 2—59392
self-mass, logarithmically divergent 2—73760
stigma equation, Poincare noninvariance proved 2—42331
structure, relation to origins of electron and muon masses, weak interactions, neutrino-flip expts. 2—49502
structure functions of inelastic lepton-nucleon scattering, light-cone approach to scaling-limit inequalities 2—66935
symmetry models for gauge theory of weak and electromagnetic interactions of leptons and hadrons 2—42332
trident prod., differential cross section 2—70151

Leptons continued
triplets, neutrino prod. in Coulomb field 2—79500
two-component spin-1/2 wave equations 2—78824
unified theory for muon, electron and two neutrinos 2—59413
weak and electromagnetic interactions, three-quark model 2—73750
weak and e.m. interaction symmetry 2—66933
weak interaction, universal, theory 2—70152
weak interactions, leptonic and semileptonic, lowest order V-A perturbation theoretic predictions 2—52555
weak interactions test 2—79500
weak processes, leptonic and semileptonic, lepton-number and chirality nonconservation 2—45865
Weinberg's theory of weak and e.m. interactions, exptl. tests 2—45875
Weinberg model, calc. of weak interaction contribution to muon magnetic moment 2—66944
$l^-l^+ \to \nu\nu\gamma$, electromag. and weak interactions, differential cross section 2—76600
ν-lepton interaction, and intermediate vector boson 2—55819
Lie groups *see Group theory. For applications see Elementary particles; Field theory, quantum*
Ligands *see Bonds; Molecules*
Light
see also Diffraction; Interference, etc.; Doppler effect; Radiation
amplitude fluctuation correlation in angle spaced beams 2—79318
beam gravity centre floating in turbulent atmosphere, correlation meas. 2—48435
coupling between optical waveguides 2—79400
Einstein effect, fourth, bending and retardation of light in a gravitational field 2—66426
focused beam intensity meas. in gravity centre 2—55723
frequency division in case of demultiplication resonance 2—63379
gravitational field, interacting with light, Newtonian 2—55383
i.r. to visible parametric upconversion in proustite 2—49388
Markov random process rel. to light beam displacement in turbulent medium 2—79317
medical significance and effects 2—82067
optically thin anisotropic media, propag., theory 2—79332
plane wave propagation in randomly inhomogeneous medium, geometrical optics and Markov's process approximation 2—55726
pressure, force moments det., photoelectric instrument 2—55725
self-defocusing of laser light by adiabatic following in Rb vapour 2—70608
Stokes parameters, significance and transformation equations 2—45780
in turbulent atmosphere, meas. illumination and intensity fluctuations 2—49413
visible flux effect on D-region electron density 2—48577
wavelength converter, i.r. region, antiStokes mechanism, heterojunction structure 2—66848
white light colour rendering capability and luminosity obs. 2—73652
coherence
see also Lasers
aeroscopic wave function, coherence 2—41941
apodisation for coherent imagery of extended objects, application to semi-transparent phase edges 2—76526
atmospheric coherence meas. of laser beams at 10.6 and 0.63μ 2—81674
atom, macroscopic optical coherence phenomena rel. to n.m.r. studies 2—59907
beam, det. by obs. of time between consecutive photons 2—49337
bleachable absorber-laser amplifier-detector combination, wide-angle low-noise laser receiver 2—45755
Bloch equations, solution method 2—69841
coherence area on basis of photoelectron distrib. anal. 2—73540
correlation tensors, light-ray approximation 2—73625
counting statistics of mixed modulated coherent light 2—69993
crystal, harmonic generator, patent 2—42171
diffraction by defocused circular aperture illuminated by partially coherent light 2—52458
diffraction images of partially coherent phase discs with variable phase plates 2—76519
diffusing surfaces, coherent light diffraction 2—59235
duration and coherence time in pulsed fields 2—45697
far-field diffraction by apodized slit apertures 2—59234
frequency modulation and transient effects in resonant propagation of pulses 2—42156
Gaussian beam, propagation and focusing effects 2—79342
harmonic generation 2—82505
high power steady state propagation in resonant media 2—76513
holographic process, patent 2—66792
imaging, noise suppression 2—79307
information transfer by light, characteristica 2—82547
information transfer by light, characteristics 2—82547
interferometric method determ. 2—76517
Jamin interferometer, use in investigating transverse and longitudinal spatial coherence of radiation field 2—66813
laser, injection, large optical cavity heterojunction, transverse mode selection 2—59178
laser beams, complex coherence factor eval. by superposition of two systems of stationary waves 2—73603
laser pulse, interferometric technique for obs. 2—79348
laser pumping, effect on freq. conversion and parametric amplification 2—59125
laser wavefront, det. using holography 2—42125
linear optical data processors used with coherent or incoherent light 2—79293
measurement and computation by light rays 2—63409
mutual coherence function of finite cross section optical beam propagating in turbulent medium 2—49390
mutual coherence function propagation, angular spectrum approach 2—42187
optical field, coherence and fluctuation props. 2—82463
optical fields fluctuation props. 2—82464
partial, two point resolution, microscopy 2—52457
partially coherent, comparisons of modulations of periodic targets 2—55724
phase modulation, by liq. crysts. 2—42160

Light continued
coherence continued
photoelectron count distrib. in partially coherent Gaussian light 2−55674
polarization junction laser 2−69944
polarizing microscope, partially coherent image of opaque edge 2−42233
propagation in inhomogeneously broadened medium 2−41942
propagation in optically inhomogeneous medium scattering 2−79253
pulse propagation, superradiance, nonlinear reactions 2−41940
pulsed discharge production in visible range, use for laser pumping 2−69890
radiative transfer eqn. rel. to coherence theory 2−78834
rectangular waveguide, coherent light, intensity distrib. 2−63413
resonant medium, coherent radiation damping 2−59122
solid state light sources, review in book 2−55700
spatial, meas. using speckle patterns 2−52442
spatial and temporal, definitions 2−69893
speckle reduction using multicolour illumination 2−79267
stimulated elastic scattering, effect of coherence 2−42205
superposed chaotic and coherent fields, simulation using h.f. signal processor 2−49406
techniques for engineering meas. 2−49392
two proton propagation and self induced transparency of optical pulses in K three level system 2−44330
two-photon propagation in three-level system 2−82510
u.v. radiation generation, nonlinear optical technique using Q-switched Nd:YAG laser 2−69956
Van Cittert theory, joint probability density of partially coherent wave amplitudes 2−79289
CO$_2$ laser, competition effects on spatial coherence 2−55688
He-Ne laser, freq. stabilization using inverted Lamb dip and mode interaction effects 2−66753
N$_2$ laser, 337 nm pulses, coherence props. and saturation broadening 2−73570

electromagnetic theory
beam shape effects on phase fluctuations of e.m. propagation in turbulent medium, atmospheric application 2−44728
coherent optical pulse propagation, superradiance, nonlinear reactions 2−41940
correlation tensors, light-ray approximation 2−73625
fourth statistical moment of scalar wave propagating in random medium 2−59219
guidance and control in semiconductor epitaxial films 2−42236
modular ray trace program, Fortran program 2−79345
monochromatic Gaussian beam, field anomalies 2−79341
mutual coherence function propag. in random medium 2−78968
propagation along complex dielectric constant lens like medium 2−49412
propagation along lenslike medium 2−76510
propagation in random media, equivalence of Dyson and Bethe-Salpeter eqn. and Huygens-Fresnel principle 2−49414
propagation in space time modulated media using many space scale perturbation theory 2−63378

modulation
acoustic, by nematic liquid crystal 2−59241
acousto-optic and electro-optic modulators, developments 2−73657
acousto-optical laser beam modulation 2−59128
acoustooptic diffraction grating modulators, design theory 2−79221
aerial cameras, aerial, focussing, using modulation measurement 2−63447
by anisotropic waveguides, electrooptic effects 2−63410
area modulated signal recordings for coherent optical correlators 2−49407
beam, modulated by circular aperture, Fourier spectra 2−79315
binary signal demodulation photon count statistics 2−41947
camera lens, slit shutter effect on modulation transfer function 2−59329
chaotic and coherent radiation, superposed, simulation using h.f. signal processor 2−49406
circular aperture diffraction limited MTF 2−63385
coherent, by liq. crysts. 2−42160
coherent pulse chirping in self-induced transparency 2−59205
counting statistics of mixed modulated coherent light 2−69993
electro-optical light modulator, use with nonlaser light sources 2−76528
electro-optical spatial light modulator for optical data processing, two dimensional, adaptive, online 2−79418
electron-optical image convertor, with microchannel intensification stage, modulation transfer function 2−70069
extinction ratio of light modulators, thermally self-induced decline 2−59208
fibre optic devices, modulation transfer functions 2−59269
Fourier analysis of square wave targets used in lens MTF meas. 2−59221
frequency modulation and transient effects in resonant propagation of coherent light pulses 2−42156
gas laser, multifrequency, variation of emission spectrum due to small harmonic signal 2−69908
guided wave structures for electrooptical modulation at 10.6 μm 2−42157
heterodyning with noncritical angular alignment using pair of u.s. light modulators 2−79240
h.f., resonator 2−49347
holography for large volume scenes using coherent microwave oscillation 2−59202
infrared circular dichroism meas. instrument 2−67521
interdigital electro-optic thin film modulator using nitrobenzene 2−79376
laser beams r.f. modulation and demodulation for communication 2−52444
laser pulse, returning auxiliary passive resonator by u.s. 2−69900
lasers, automatic optical bias control, p.c.m. communication 2−66797
lasers, high-power, simultaneous passive mode locking and Q-switching using optical Kerr effect 2−66737
masers, 1.5 GHz toroidal-type cavity modulator for 2−69892
metal clad dielec. waveguide, mode selective props., attenuation, phase consts. 2−78964

Light continued
modulation continued
metal-to-metal point contact diode, i.r. generation by laser and microwave freq. mixing 2−69839
mode locked laser, short light pulse generation, operation, applications 2−41975
periodic targets in partially coherent light 2−55724
phase modulation noise in reconstructed image of Fourier transform plane phase hologram 2−79246
piezosemiconductor, transmission modulation on passage of acoustoelec. domain 2−54033
polarization modulations, mechano-optic using reflection attraction grating 2−70036
ruby laser, intracavity modulation with frequency close to difference frequency of neighbouring axial modes 2−59171
scalar wave, by caustic surfaces, statistical moments of wave field 2−42200
screens, ground-glass, modulation transfer functions 2−70032
self-phase, electronic mechanism for production in liquids and solids 2−45770
sensitometer with high range of non-selective modulation 2−70040
short pulse falling on linear dielectric medium, calc. of reflected wave 2−66809
signal carrying, information transmission, wave guides, optical circuits, design 2−82546
spatial, study of transparent objects 2−45806
spectral intensity second harmonic growth with exciting radiation freq. half width growth 2−69994
transfer functions meas. for focusing screens 2−70039
transversal, optimum cut of KH$_2$PO$_4$-type crystal 2−61592
travelling wave light intensity modulator using polarization rotated reflection 2−42158
t.w. electro-optic modulators, performance 2−73661
t.w. modulator, asymmetrical sidebands generation 2−49408
u.s. in flint 2−70025
wide band, by u.s. waves, real-time u.s. kinoform 2−73623
Bi$_{12}$SiO$_{20}$ electro-optic image modulator, sensitivity and resolution 2−79417
Bi$_{12}$SiO$_{20}$ electro-optic image modulator for optical processing 2−79416
CdS, by acoustic phonon flux 2−61088
Fe, garnet film magneto-optic film waveguide, light modulation and switching 2−81323
GaAs, i.r. radiation at piezoresonance 2−57329
GaAs crystal modulator, phase characteristics 2−63362
GaAs film, epitaxial, guiding and electrooptic modulation of light 2−68608
n-Ge, in strong elec. fields by non-equilib. optical phonons 2−78069
He-Ne laser, coupling modulation charact. 2−49368
LiNbO$_3$ crystals, electrooptical effects 2−69988
LiNbO$_4$ crystal cuts with low half wave voltage for phase and polarization modulation 2−42170

quantum theory *see Photons; Quantum electrodynamics; Quantum theory*

velocity *see Velocity/light*

Light guides *see Optical instruments*

Light modulation *see Light/modulation*

Light sources
see also Lasers; Monochromators; Photometry/light sources; Spectroscopy/ light sources
basis functions of tristimulus coordinate spaces 2−42253
coaxial flashlamp for liquid dye lasers, spectral characteristics 2−59272
coffered and surface luminaires, equivalent luminances 2−52476
coherent, radiometry 2−79172
coherent, tunable monochromatic injection lasers, fabrication 2−73593
colour rendering investigation 2−45802
commercial lamps, colour rendering capability 2−42248
contrast enhancement, selectively absorbing filters 2−55763
control circuit for laser pump lamp power supply 2−45648
diodes for photoelectric indicating instruments 2−61900
discharge, multiple spark system 2−56397
electrical, principle of energy conversion 2−68439
electroluminescent cell, obs. of non-linear effects using computer 2−63420
electroluminescent devices, apparatus for obs. of quantum efficiency 2−55759
for electron emission microscope 2−79004
flash tubes, time, peak power and spectral advantages 2−76539
flashlamp for pumping stations of organic dyes 2−76466
flashlamp of rectangular cross-section, gas-discharge 2−77311
flashlamps, microwave technique to extend lifetime and increase efficiency 2−63419
flattery and colour rendition indices 2−52475
fluorescent lamps, colour and luminous efficiency 2−42250
fluorescent lamps, effect of temp. on colour rendering props. 2−49444
fluorescent lamps, performance improvement through additives to glass 2−52474
gas discharge lamps, electrode material losses 2−70999
gas plasmas as radiation sources 2−60307
geometrically total flux det. with goniophotometer 2−79365
halogen-metal vapour lamps for colour TV conditioned floodlighting of sports fields 2−45811
high intensity, selection for particular application and construction 2−76538
holographic, book 2−42154
ignition of halogen metal vapour lamps 2−73671
illuminating systems, semiautomatic design 2−42249
incandescent lamps for film printing, luminous flux variation 2−66874
incoherent, ruby laser, det. of degree of spatial coherence of emitted wave, holographic obs. 2−42125
i.r. laser sources, tuning methods, review 2−76469
lamp, straight tubular gas-discharge, effect of bulb on brightness distrib. 2−43208
lamps and lighting, book 2−79387

Light sources continued
  laser illumination system, frequency-doubled four- level, for stopaction photos 2−55781
  luminaires, for large rooms, visual comfort probability 2−49446
  matching flashlamps for pulsed lasers 2−63312
  metal halide lamp, high wattage, high-density line spectra, design 2−52477
  metal halide lamps, selective getter 2−52478
  for microscope, design 2−42252
  near i.r., GaAlAs laser diode array 2−82491
  P-15 phosphor, meas. of decay time by delayed coincidence technique 2−48260
  photographic, colour rendering index 2−82596
  photographic, developments 2−49432
  pulsed, high power, tubular lamps, pulse efficiency 2−45814
  pulsed, light output control for use in stabilizing scintillation detectors 2−82575
  pulsed lamps for excitation of rhodamine 6J lasers 2−69930
  pulsed plasma arc lamps, transmittance measurements 2−83643
  quartz Hg arc, far i.r. emission 2−55766
  radioactive reference lights, transient temperature dependence 2−49443
  red highway flares, luminous power spectrum 2−59270
  review 2−70067
  rhodamine 6G dye laser as tunable source of coherent u.v. radiation 2−79444
  ruby lasers, cryptocyanine Q-switches, photochemical decomposition due to light source 2−49378
  short duration, photometry and calibration 2−76523
  tubular lamp, pulse efficiency, from obs. of luminesc. of Nd glass 2−45814
  u.v., tunable, by frequency doubling of emission of rhodamine 6G dye laser 2−73577
  u.v., visible emission obtained by using fluorescent plastics 2−63421
  Westinghouse Electric Corporation products, review 2−42222
  white light, colour luminosity and colour rendering capability 2−59271
  Xe 50 KW short arc lamp in elliptical collector 2−76540
  Ar arc lamp 400 KW for solar simulation 2−78414
  Cd vapour arc, for deep ocean waters 2−49442
  H_2 t.w. vacuum u.v. laser, applications 2−82484
  Hg lamp, for illuminating people 2−42251
  Hg vapour fluorescent lamps, colour and luminous efficiency 2−42250
  Kr lamp use in light freq. and vel. determ. 2−69997
  Mg isotopes beam, theory and experimental verification 2−64057
  Nd:YAG laser, coherent radiation generation using nonlinear optical techniques 2−69956
  ^{87}Rb, optical pumping, hyperfine structure of D_1 line 2−73670
  Si:GaAs light emitting diode MV-50, fast luminescent decay meas. and electronic module for driving 2−45812
  Xe arc lamp, stability tests 2−45813
  Xe follow spotlight 2−49445
  Xe radiation source, short arc, high reliability and power for solar simulation 2−76535
  Zn vapour arc, for deep ocean waters 2−49442
Lighting *see Illumination*
Lightning
  atmospheric radio noise, l.f. and v.h.f. obs. (1969-71) 2−75613
  atmospheric radio noise meas. rel. to lightning flashes in India 2−84790
  ball, discussion of hypotheses 2−68921
  ball, mechanism of formation, laser analogue 2−81665
  ball, new theory, seed for linear lightning 2−65802
  ball, rel. to antimatter 2−81666
  building protection, verticle lightning conductors, protective angles 2−65790
  causes in deep cloud cover 2−68875
  cloud and air discharges, stepped leaders, theory and observation 2−65791
  cloud-to-ground discharges in tropical area 2−58007
  cylindrical cloud charge model 2−72807
  discharges, causing forest fires 2−65795
  discharges which do not reach ground, tropical area 2−58008
  electric breakdown, gaseous ionization 2−46802
  electric field recovery, response of conducting atmosphere to field charge 2−68919
  electron whistler coupling to ion whistler at crossover level 2−72849
  electron-water vapour interaction effects 2−53019
  frequency and topography in Slovak Tatra, oriental part 2−51626
  frequency of lightning strikes rel. to topography in Tatra mountains 2−72808
  international lightning counter, construction, aims and results 2−62280
  optical absorption in lightning-stroke channel 2−65796
  OSO-5 dim light monitor 2−72943
  photographic studies in northern Poland using rotating camera 2−65788
  photographic studies near east coast of South America, air discharges 2−65787
  photographic studies using stationary camera, upward flashes 2−65789
  recovery curves of electric field following lightning 2−72810
  return strokes, electric field risetimes 2−68917
  station for automatic observations of properties 2−68920
  stroke counter, transistorized battery powered, 100-2500 Hz 2−62279
  thermonuclear detonation generation 2−65794
  triggered, unsuspected hazards 2−65800
  triggered artificially by small rockets 2−65792
  triggering by Apollo rocket 2−62278
  u.h.f. lightning receiver, direction finding apparatus 2−65799
  v.h.f. emissions, bremsstrahlung as source 2−65801
  water droplets, interactions with positive corona streamers, atmospheric significance 2−64489
Linear accelerators *see Particle accelerators/linear*
Linewidths *see Spectral line breadth*
Liouville equation *see Statistical mechanics*
Liquefaction, gases
  see also Low-temperature production
  binary mixture, transient heat and mass transfer controlled 2−77466
Liquid crystals
  acetylene derivatives, synthesis and props. 2−46929
  alkali, electron spectrum calc. by cell method 2−83797
  alkane monoiodide solutions, X-ray diffraction study, quasiliquid crystal form 2−50318
  p- alkoxy-p′-acyloxyazoxybenzenes, homologous, nematic mesomorphic behaviour 2−80453
  alkoxyazoxybenzenes, conform. changes, Raman spectra 2−81386
  p-n-alkoxybenzoic acid, periodic oriented oscillations of domain struct. in alt. elec. fields 2−71159
  4-n-alkoxybenzylidene-4′-phenylazoanilene, nematic-spectra A phase transition, n.m.r. meas. on molecular orientation 2−53402
  anils, thermotropic, transition temps. and mesophase identification 2−50326
  anisaldazine, Raman scattering by Ar laser 2−60476
  azobenzene, azoxybenzene, Schiff base, liquid crystalline behaviour rel. to molecular struct. 2−60428
  p-azoxyanisole, dielectric anisotropy produced by magnetic field 2−50336
  p-azoxyanisole, mol. conformations in nematic and isotropic states, Raman spectra 2−81382
  p-azoxyanisole, nematic, elastic constants, calc. based on lattice model 2−50325
  p-azoxyanisole, nematic, thermal cond., interfacial effect 2−50323
  p-azoxyanisole, nematic phase, temp. dependence of intermolec. interaction 2−50335
  p-azoxyanisole, n.m.r., strong collision relaxation in rotating frame 2−61747
  n-azoxyanisole, polarization of i.r. spectra 2−82588
  4,4′-azoxyanisole, Raman scattering by Ar laser 2−60476
  p,p′-azoxyanisole, thermal conductivity in magnetic fields 2−67828
  p-azoxyanisole, ultrasonic absorption and viscosity anisotropy in oriented crystals 2−50334
  p-azoxyanisole in Poiseuille flow, apparent viscosity calc. by continuum theory 2−50337
  p-azoxyphenetole, oriented nematic phase, cylindrical atom distrib., X-ray scatt. 2−80441
  p-azoxyphenetole ultrasonic absorption and viscosity anisotropy in oriented crystals 2−50334
  benzylidene anilines, terminally substituted, synthesis, properties 2−83767
  biaxial phase, molecular field lattice model for repulsive interaction between platelike molecules 2−80445
  bilayers, mol. ordering 2−83769
  biological materials, viscoelastic props. in vicinity of isotropic-cholesteric phase transition 2−51881
  camera design for visual obs. of laser modes 2−52421
  cathodochromic sodalite, storage and display applications 2−63423
  cholesteric, applic. to nondestructive crack detection in alloys 2−43760
  cholesteric, Brillouin scattering study of propag. of hypersonic waves near cholesteric-isotropic transition 2−80454
  cholesteric, dielec. loss and const., function of temp. and freq. 2−71229
  cholesteric, effect of a magnetic field on the optical transmission 2−84468
  cholesteric, governing hydrodynamic equations 2−50332
  cholesteric, in isotropic phase, pretransitional increase in optical rotation 2−80434
  cholesteric, material coeff. in continuum theory 2−80455
  cholesteric, rapid conical-helical perturb., a.c.-d.c. technique obs. 2−71217
  cholesteric, thermomechanical coupling 2−60431
  cholesteric, u.s. impedence studies 2−43350
  cholesteric mesophase, induced circular dichroism method for determ. of existence and chirality 2−80460
  cholesteric mesophases, normal stress effects 2−83770
  cholesteric mixtures, shear-induced struct. changes 2−64438
  cholesteric nematic transition, ultrasonic investigation 2−80456
  cholesteric solns. with helically arranged mols., circular dichroism 2−53394
  cholesteric struct., Grandjean discontinuities 2−46925
  cholesteric struct., planar, mag. field induced distortions 2−46927
  cholesterics, infinite, low-temp. phase phenomena 2−60429
  cholesterol, form. of both cholesteric and smectic mesophases 2−80457
  cholesteryl derivatives, crystal nucleation in supercooled mesomorphic phases 2−77414
  cholesteryl esters, effect of substituent groups on mesophase transition temp. and range 2−80452
  cholesteryl nonanoate and myristate in smectic-A, cholesteric and isotropic phases, X-ray scatt. 2−67807
  condensed matter theory, phase transitions 2−47822
  p,p′-di-n-butyl azoxybenzene, instabilities in elec. fields, domains and reorientation 2−56477
  4,4′-di-n-heptyloxyazoxybenzene, nematic phase, anomalous alignment due to elec. fields 2−77412
  4,4′-dibutoxyazoxybenzene, p.m.r. obs. 2−50338
  diethyl 4,4′-azoxydibenzoate, p.m.r. obs. 2−50338
  4,4′-dipropoxyazoxybenzene, p.m.r. obs. 2−50338
  display, matrix-addressed, discrimination problems 2−52480
  EHD instability phenomena and dielec. const. relax. 2−53395
  e.m. hydrodynamics 2−50330
  4-ethoxy-4′-n-alkanoyloxyazobenzenes, anomalous melting behaviour at solid-nematic transition 2−56483
  ethoxybenzylidene-p′-n-butylaniline: 1-menthol (racemic menthol), optical storage effects 2−43365
  p-ethoxybenzylidene-p-n-butylaniline, proton spin-lattice relaxation in nematic phase 2−56524
  p-ethoxyphenylazo phenylheptanoate, proton spin-lattice relaxation in nematic phase 2−56524
  film, nematic, size effects near second order phase transition 2−83869
  film, vacuum deposited, surface orientation 2−71157
  furan-2, 5-dialdehyde partially oriented in nematic phase, n.m.r., conform. obs. 2−70769

Liquid crystals continued
- p-n-hexyloxybenzylidene-p′-aminobenzonitrile, temp. depend of flow alignment 2–50339
- holographic medium instantaneous 2–79243
- hydrodynamics of nematic phase applic. of unified formulation for normal liquids, liquid crystals and solids 2–43325
- image convertor, plasma diagnostics applic. 2–53208
- image convertor obs. of HCN laser modes 2–42011
- in i.r. photomicrography and thermal imaging 2–52501
- isotropic-nematic transition temp., alkyl chain length depend. for homologous series 2–74518
- Kerr effect, isotropic phase of some nematogenic compounds, investigation, temperature dependence and relaxation times 2–53430
- kinematics of nematic crystals 2–43279
- light propag., evolution of ellipse of polarization 2–79322
- lophenol, fatty acid esters, form. of smectic mesophase 2–80457
- MBBA, Kerr const. temp. depend. near isotropic-liq. cryst. transition 2–77430
- MBBA, nematic liquid crystals, proton spin-lattice relaxation mechanisms 2–84596
- MBBA, small angle X-ray scatt. near nematic-isotropic transition temp. 2–43328
- MBBA dynamic scatt. in hydrodynamic regime, relax. time 2–77438
- MBBA nematic liquid films with free surfaces, electro-optic and hydrodynamic props. 2–67804
- MBBA ultrasonic absorption and viscosity anisotropy in oriented crystals 2–50334
- l-menthol in nematic solvent, optical activity and circular dichroism 2–80442
- methoxy benzylidene butyl aniline, nematic, bend oscillations in dielectric electrohydrodynamical instability 2–46931
- p-methoxy benzylidene p-n butylaniline, nematic-isotropic liq. phase transition, sp. ht. obs. 2–74523
- p-methoxybenzilidene p-n-butylaniline, nematic phase, anomalous alignment and domains 2–71161
- p-methoxybenzylidene p-n butylaniline, dynamical behaviour above nematic-isotropic transition from spin-lattice relaxation 2–71160
- p-methoxybenzylidene-p-butylaniline, electrical conductivity variation in electric and magnetic fields 2–46985
- p′-methoxybenzylidene-p-n-butylanilene, temp. depend of flow alignment 2–50339
- p-methoxybenzylidene-p-n-butylaniline, nematic phase electric const. 2–60427
- N-P-methoxybenzylidine-p-butylaniline, temp. dependence of anisotropic u.s. propagation 2–46953
- microwave hologram display for concealed weapon detection 2–69975
- microwaves visualisation 2–46977
- nematic, acoustic modulation of light 2–59241
- nematic, alignment in solid surface 2–53397
- nematic, alignment kinetics in mag. fields, viscosity coeff. 2–53400
- nematic, angular depend. studies of permeab. and dielec. anisotropies 2–80459
- nematic, application as phase grating of electrically tunable spatial frequency 2–64443
- nematic, applied a.c. voltage effects on birefringence 2–53431
- nematic, at const. molar vol., temp. depend. of orientational order 2–56481
- nematic, dynamic scatt., effect of charge transfer acceptors, voltage transmission characts. 2–71201
- nematic, elastic constants, calc. based on lattice model 2–50325
- nematic, elastic constants 2–46926
- nematic, elastic consts., normal deform. in elec. and mag. fields 2–53399
- nematic, elec. field induced light scatt., appl. to p-n junction and insulating layer investigation 2–77918
- nematic, elec. field quenching of thermal fluctuations of orientation 2–43332
- nematic, electrical and optical props. 2–53398
- nematic, electrohydrodynamic instabilities in low-freq. fields 2–43326
- nematic, estimation of nematic-isotropic points 2–50328
- nematic, flow alignment 2–60426
- nematic, free surface thermal fluctuation spectra 2–56479
- nematic, homeotropic geometry, electrohydrodynamic solns. 2–71150
- nematic, instabilities under a.c. fields, special effects near cut-off freq. 2–56478
- nematic, mechanochromatic effects 2–83363
- nematic, mol. theory, stability, thermodynamic conditions 2–46930
- nematic, nonsingular model for screw disclinations 2–56482
- nematic, obs. of n.m.r. spectra of dissolved deuterated methanes and 2,2-dimethylpropane 2–71238
- nematic, optical method of obs. of viscoelastic props. 2–71141
- nematic, orientation behaviour, elec. and optical behaviour 2–80444
- nematic, orientation correlations and the mean-field approximation 2–67808
- nematic, oscillation modes 2–50321
- nematic, photovoltaic effect obs. 2–71223
- nematic, piezoelectric properties, molecular statistical approach in one-dimensional model 2–46972
- nematic, rise and decay times for dynamic light scattering for hometropic, homogeneous boundary conditions 2–64442
- nematic, screw disclinations of strength $S = +1$, theory 2–74520
- nematic, surface tension and viscosity coeffs., scattered light obs. 2–56480
- nematic, transition between cond. and dielec. regimes of e.h.d. instabilities 2–43330
- nematic, two-dimens., nonlinear response to applied field 2–46928
- nematic, Williams domain and variable grating mode boundary value soln. 2–50319
- nematic, with negative dielec. anisotropy, cond. regime 2–60494
- nematic, with positive dielec. anisotropy, instabilities in elec. fields, domains and reorientation 2–56477
- nematic, with surfactant-produced homogeneous alignment, performance advantages 2–64441
- nematic and cholesteric, irregularities on dislocation lines 2–64430
- nematic film, domain wall motion 2–74521

Liquid crystals continued
- nematic film, polarimetry and interferometry studies 2–43329
- nematic film in variable field, transient distortions 2–53396
- nematic order, Monte Carlo calculation 2–50331
- nematic phase, degree of order, e.s.r. obs. 2–50333
- nematic phase n.m.r. spectroscopy of partially oriented monosubstituted benzenes 2–77104
- nematic thread formation during light scatt. 2–67805
- nematic-isotropic transition, comparison with crit. behaviour of ferromagnets 2–53401
- nematic-phase n.m.r. spectroscopy of 2-furanaldehyde for conform. analysis 2–77147
- nematic-smectic A phase transition, n.m.r. meas. on molecular orientation 2–53402
- nematic-smectic C phase transition, periodic free surface disclination obs. 2–60432
- nematics, method for meas. twist elastic constant and shear viscosity 2–50329
- nematics, noise meas. rel. to generation recombination and diffusion processes 2–83802
- nematogenic azobenzene derivatives, anomalous melting behaviour at solid-nematic transition 2–56483
- neutron quasielastic scattering, incoherent cross-section 2–46924
- n.m.r. and e.p.r. applic. to struct. and dynamical processes determ. 2–83805
- 31-norcycloartanol, fatty acid ester, prep. from a triterpene 2–46936
- optical devices, non-destructive testing appl., useful life lengthening 2–60430
- ordered phase, point and planar singularities 2–78831
- organic ionic salt mesophases, struct. behaviour 2–71158
- p-anisylidene p-aminophenylacetate, nematic, influence of interface on thermal conduction 2–80467
- p-methoxybenzylidene-p′-amino phenyl acetate, nematic, dynamic scatt. life, current density effects 2–71203
- phase modulation of coherent light 2–42160
- phase transformations, theory 2–50322
- phospholipid-water mixtures, i.r. and Raman spectra 2–43374
- phthalazine, nematic phase, n.m.r. spectra 2–50324
- positron annihilation, appl. to struct. and props. determ. 2–47771
- positron annihilation, phase and temp. dependence 2–64439
- PPA, nematic, order characterization 2–83777
- properties, nematic displays, advances and technologies 2–83768
- properties in ultrasonic, electric and optical fields 2–50320
- proton spin-lattice relax., intermol. and intramol. contribs. 2–64440
- quenched nematic, alignment obs. using Mossbauer effect 2–60425
- quick clays, Rosenqvist theory, liquid crystal dispersant 2–60517
- review, role in inanimate and animate systems 2–53392
- smectic, A-type, X-ray scatt. intensity 2–43327
- smectic, C-type phase obs., twisting 2–53393
- smectic, nematic and cholesteric mesophases, characteristic structural features and uses in testing materials 2–60931
- smectic, type A, elec. induced hydrodynamic instabilities 2–80462
- smectic, X-ray diffr. and polymorphism, D and E modifications 2–50327
- smectic A, struct. of interior of conical focals 2–83766
- smectic A conform. analogy with supercond. 2–43331
- smectic mesophase, texture 2–74519
- smectic-C, quasielec. Rayleigh, scatt., twist mode obs. 2–67833
- steroids, influence of ring unsaturation position and delta eight double bond on mesophase 2–80458
- stratified media, parallel, anisotropic and homogeneous, equivalent permittivity tensor calc. 2–80483
- temperature sensitive elements for semiconductor investig. 2–69804
- thermography in medicine and physiology 2–76071
- thermotropic, review 2–67806
- thermotropic nematic, p.m.r. study of ethylene carbonate and ethylene monothiocarbonate solutes 2–83800
- triterpenes, influence of ring unsaturated position and delta eight double bond on mesophase 2–80458
- viscosity, temp. depend., equations 2–80464
- viscosity and thermal conductivity in mag. field 2–80463
- X-ray studies, by cylindrical distrib. 2–83765
- o-xylene partially oriented in nematic phase, indirect spin-spin coupling consts. 2–77157
- Zwanzig model 2–83772
- C, smectic, magnetic instabilities 2–60433

Liquid-drop model *see Nucleus/models*

Liquid flow *see Flow/liquids*

Liquid helium *see Helium/liquid*

Liquid lasers *see Lasers/liquid*

Liquid metals
- — 2–60191
- alkali, determ. of pseudo-Gruneisen parameters 2–74540
- alkali, self-diffusion, temp. depend. 2–67817
- alkali, significant liquid-structure theory of viscosity and self-diffusion 2–56489
- alkali metal alloys, Knight shift and Pauli susceptibilities 2–72515
- alkali metals, significant structure theory of surface tension 2–50346
- alkalis, interionic interaction and thermodynamic potl., analysis 2–84650
- alloy, binary, heat of soln. at infinite dilution, pseudopotential perturbation method 2–56495
- alloy, binary, surface electric charge rel. to thermodynamic props. 2–56515
- alloy, binary microsegregation, X-ray diffr. 2–60570
- alloy, diffuse Laue-scatt. and prepeaks in partial struct. factors 2–53391
- alloy, dil., mag. susceptibility, quasi-atomic model 2–53454
- binary alloys, absolute thermoelectromotive force 2–56518
- binary systems, cluster model 2–46917
- contact interaction with refractory carbides 2–68190
- critical surface energy of spreading in liq. metal- ceramic systems 2–50425
- diffusion of Tl, phonon scatt. 2–46945
- dilute alloys, 3d transition metals in Cu, CuZn, Zn, ZnGa, Ga, GaGe, GeAs, As, mag. susceptibility 2–80485
- electrical conductivity meas. at critical temp. and pressures 2–83804
- electrical resist. expression 2–60492

Liquid metals continued
- electrical resistance, specific, detn. by pseudopotential method, accuracy of integral 2−80477
- electrical resistivity, near crit. point, calc. 2−67838
- electrodynamic forces in e.m. stirrer 2−50183
- electron transport rel. to hard-sphere interference functions, temp. dependence 2−67796
- electronic density of states, tight-binding model 2−46920
- electronic struct. and n.m.r. prop. 2−67842
- embrittlement of Al 2−43721
- enthalpy, press., vol., resist. meas. technique at high temps. and press. 2−46949
- flow in magnetic field through dendritic conducting filter 2−64576
- flow rate obs. using e.m. flowmeters 2−83763
- forming process, upper bound approach for conical flows 2−46882
- Hall effect, method of determ. 2−64469
- Hall resistivity, formal expression using nonequilib. statistical operator 2−71776
- hard-sphere interference functions, temp. dependence 2−67796
- heat pipes, vapour transport limits, for nucl. plants 2−83128
- induction convertor, energy loss due to discrete tooth-slot arrangements 2−63219
- ion-ion potentials, effective interaction, hard sphere dias., sp. ht., entropies 2−60415
- iron, diffusivity, of oxygen, potentiostatic electrochemical measurements 2−60456
- MHD generator, piston-type, characts.· 2−41906
- MHD machines with liquid metal and plasma secondary, design and operation 2−52359
- MHD power generator, effect of heterogeneity and Hall current 2−69849
- molten, calc. of interference function 2−50310
- muffin tin potentials, canonical density matrix 2−51071
- n.m.r. properties rel. to hard-sphere interference functions, temp. dependence 2−67796
- noble, nearby-free-electron susceptibility 2−48034
- nuclear quadrupole relaxation, ionic motion contrib., 2−43316
- optical consts. 2−43359
- optical props. and electronic transitions, review 2−72292
- pair potential, effects of pressure 2−60419
- pseudopotential applic., review 2−50311
- self diffusion model 2−46944
- solid electrolyte cells in liquid metals, e.m.f. meas. 2−66681
- sound speed calc. using perturbation and pseudopotential theories 2−46952
- specific electrical resistance, temp. depend., pseudopotential calc. 2−80478
- statistical mechanical perturbation theory 2−80461
- structure, problems of investigation, short range order models 2−46923
- structure, radial distrib. function anal. 2−83764
- structure factor, rel. to entropy of melting, Percus-Yevick formulation 2−64434
- supercooling, homogeneous nucleation study 2−71275
- surface tension meas. using drop-weight (volume) technique 2−74531
- theory of single-atomic metals 2−71152
- thermal diffusivity, laser flash determ. method 2−53423
- thermodynamic properties, temp. depend. hard sphere model 2−67824
- transition and noble elec. resist., nearly free electron model, muffin tin potential 2−56514
- u.s. velocity, calc. 2−80469
- wetting of carbides, relative surface energies 2−50427
- X-ray diffr. apparatus 2−74516
- Ag-Ga alloy, free enthalpy of mixing 2−53422
- Ag-Ge alloy, free enthalpy of mixing 2−53422
- Ag-In alloy, free enthalpy of mixing 2−53422
- Ag-In molten alloy, Ag diffusion, capillary reservoir technique 2−56491
- Ag-Sn melt, electrotransport, current density effects 2−50348
- Al-Fe(Co)(G) alloy, resist., conc. depend., 1650°C 2−46980
- Al, ion-ion pot. calc. from diffr. data 2−50315
- Al, n.m.r. obs., 600-1100°C 2−54503
- Al, structure factor meas. using neutron diffraction techniques 2−64435
- Al based alloy, Cr or Mn impurity, susceptibility near nonmag.-mag. transition 2−80486
- Au-Ga alloy, free enthalpy of mixing 2−53422
- Au-Ge alloy, free enthalpy of mixing 2−53422
- Au-In alloy, free enthalpy of mixing 2−53422
- Bi-Zn alloys, density obs. between m.p. and 600°C 2−43339
- Bi, density obs. between m.p. and 600°C 2−43339
- Bi, effective interionic pair potentials, calc. from structural diffraction data 2−50312
- Cd-Cu(In)(Zn) systems, elec. resist., nearly free electron theory 2−46981
- Cd-In, binary systems, electrotransport and elec. resist. detn. for density of states at Fermi level 2−80476
- Cd-Tl, binary systems, electrotransport and elec. resist. detn. for density of states at Fermi level 2−80476
- Co-Al melt, interatomic interaction energy, viscosity study 2−71155
- Cs, elec. resist. and electron collapse 2−46982
- Cu-Al alloys, with Mn and Fe impurities, cond.-electron spin polarization obs. 2−53455
- Cu_x-Sn_{1-x} alloy, resistivity and thermopower computation, comparison with exptl. data 2−43387
- Cu, positron annihilation 2−75004
- Cu, with Mn and Fe impurities, cond.-electron spin polarization obs. 2−53455
- Fe-(B-metal) alloy, paramag. props. 2−80488
- Fe, contact interaction with Mo_2C 2−77728
- Fe, diffusion of C, O, H, N and S, temp. depend. 2−43661
- Fe and Ni alloy, thermodynamic study by electromagnetic levitation melting in inert atmosphere 2−67871
- Ga-Hg alloy, sp. ht. anomaly near phase separation critical pt. 2−50354
- Ga, Hall mobility meas. apparatus using Corbino method 2−71224
- Ga, multiple neutron scatt., effective scatt. factors 2−60422

Liquid metals continued
- Hg-Bi-Pb systems, effectiveness of boiling separation 2−74594
- Hg-Cd(Ga)(In)(Tl)(Sn)(Sb)(Bi) amalgams, dil., viscosity, comp. depend., 0-100°C 2−64451
- Hg-In alloy, reflectivity meas. from 0.31 to 9 eV 2−64467
- Hg-K alloy, electrotransfer and elect. resist. 2−56517
- Hg, absolute thermopower, density depend., metal-nonmetal transition 2−60499
- Hg, Hall mobility meas. apparatus using Corbino method 2−71224
- Hg, thermal diffusivity det. by laser flash technique at elevated temps. 2−46946
- In-Bi(Pb)(Tl) alloys, longit. spin relax. of ^{115}In 2−50370
- In-Ga(Sn) alloy, surface tension and density, comp. depend., 700K 2−67815
- In-Hg amalgam, diluted, cond. near metal-nonmetal transition of pure Hg 2−53451
- In-Te system, elec. cond. and thermoelec. power 2−77446
- In, thermal cond., Lorenz no. 2−43347
- K-Cs alloys, elec. resist., temp. depend. 2−64471
- K-Hg alloys, zero wave vector partial struct. factors 2−43318
- K, effective pair pots. 2−50317
- Li-Bi alloy, solubility of Nd and Th 2−43334
- Li-Na alloys, immiscibility 2−53404
- Na-Cs alloys, elec. resist., temp. depend. 2−64471
- Na-Hg alloy, electrotransfer and elec. resist. 2−56517
- Na-K alloys, zero wave vector partial struct. factors 2−43318
- Na, coherent X-ray diffraction patterns at very high pressures, along melting curve 2−67803
- Na, density response function from Mori's generalized Langevin eqn. 2−83776
- Na, effective pair pots. 2−50317
- Na, structure factors, expt. and theoret. 2−50314
- Na, with small O content, oxidation of UC 2−51452
- Na alloy, compressibility determ. 2−77415
- Na bond disruption by gas bubbles in fast breeder reactor 2−49888
- Na liquid cooling problems of fast breeder reactor 2−52843
- Pb/NaCl-UCl_3 molten metal/fused salt system, surface and interfacial energy 2−52874
- Pb, heat capacity, 300-850K 2−54050
- Pb, specific elec. resist., temp. depend., pseudopotential calc. 2−80478
- Pb, thermal cond., Lorenz no. 2−43347
- Pb electron-ion interaction pseudopot. model 2−77812
- Rb, sound velocity meas., 40-200°C, 0-20000 p.s.i. 2−71195
- Sb-Sn-Zn system, heats of mixing, 650°C 2−43336
- Sb, effective interionic pair potentials, calc. from structural diffraction data 2−50312
- Sn-Ag alloy, determ. of interdiffusion coeffs. 2−53415
- Sn-Ag(Sb) alloys, interdiffusion coeffs. 2−50349
- Sn-Sb alloy, determ. of interdiffusion coeffs. 2−53415
- Te, n.m.r. obs. rel. to electronic transport behaviour 2−71237
- Zn-Bi alloy, surface tension, 860-920K 2−43341
- Zn, next-neighbour distribs. 2−64432

Liquid oscillations
- double-layer in circular cylindrical vessel rotating about axis 2−83727
- elastic damping barriers effect in rectangular vessel 2−43293
- films, supersonic streams interactions, nonlinear stability 2−78934
- free, in solid vessels 2−53368
- inertial, in Mediterranean, vertical structure of motion determined 2−44628
- Jervis Bay, N.S.W. calc. of longitudinal free oscillations by Galerkin method 2−75480
- liquid layer placed in time-periodic external forces 2−67822
- quasihomogeneous marine media, kinetic energy distrib., in vertical oscillations 2−81591
- supercritical flow in curved channels, hydraulic model obs. 2−83747
- two-dimensional free, of natural basins, reson. iteration method 2−65620
- underwater bubbles, planar, cylindrical and spherical, expansion and contraction 2−77405
- water drops disruption by electric forces 2−64426
- He superfluid baths coupled through a small hole, oscillations 2−47014

Liquid waves
- *see also Acoustic waves*
- aerodynamic pressure measurement below crests, submersible pressure probe 2−67780
- Arctic Ocean, internal wave spectra, temp. profile study 2−62039
- barotropic long, in Florida Straits 2−54793
- capillary, interac. with gravity waves, Fokker-Planck type eqn. 2−50304
- cross waves, formation and growth 2−80428
- cross waves, theory of instability mechanism 2−80427
- damped internal, forced resonant second-order interaction 2−83738
- deep-sea internal wave energy distrib., model 2−57905
- dissipative two-layer model, anomalous baroclinic response 2−54781
- edge and geostrophic, current shear effect 2−54791
- energy exchange between internal waves of finite amplitude and simple steady shear flow 2−43292
- energy spectra of random field of internal waves in deep ocean 2−54773
- glycerine solutions, inception in falling films 2−50287
- gravity, nonlinear, phase and group vel. 2−54786
- gravity, weakly nonlinear surface and internal, interaction 2−54789
- gravity on water of uniform depth, nonlinear modulation 2−77372
- gravity-capillary wave spectra, nonlinear energy transfer 2−67778
- inertia-gravity, propag. during geostrophic adjustment, variable Coriolis parameter 2−54790
- internal, sheeted thermocline 2−46897
- internal gravity waves, refl. by small density variations 2−60397
- internal surge in Loch Ness 2−44607
- Kelvin, large amplitude, generation and propag. in shallow layer 2−54792
- Kelvin-Helmholtz instability, nonlinear development 2−56468
- large stratified lakes, response to wind stress 2−62031
- lee waves caused by slender body and cylinder towed through density stratified fluid 2−46874

Liquid waves continued
linear, generalized dispersion relation 2–54785
long nonlinear internal and quasi-steady lee, generation mechanism 2–57911
in longshore current generation, wave height relationship 2–54795
non-linear, slowly varying, and their instabilities 2–50301
nonlinear, in dispersive media, stationary solutions and stability 2–82153
North Atlantic Ocean, internal waves and turbulence 2–62040
ocean, internal, caused by periodic fluctuations of atmospheric pressure 2–51558
ocean, internal, caused by periodic wind fluctuations 2–51559
ocean, internal, effect of travelling atmospheric disturbances 2–51554
ocean, internal, generation under action of atmospheric disturbances 2–51556
ocean, propagation across continental shelf 2–57842
oceanic, radar meas. 2–48430
oceanography, circular islands as resonators of long-wave energy 2–48424
oceans, ihomogeneous and variable depth, analysis by ray method 2–81636
oscillatory flow, viscous damping 2–53349
in parabolic container, vibrating behaviour 2–60396
propagation and stability of electro-fluid- mechanical space charge and polarization waves 2–46872
Rossby, behaviour in mean current, model 2–54780
Rossby, forced l.f., model 2–54779
Rossby waves, scatt. by semiinfinite barrier 2–62041
ship resistance, Havelock-Oseen theory 2–77375
shoaling, momentum transfer and nearshore current development 2–54794
solid interface, Stoneley wave equn. 2–41676
solitary, stability, anal. by Korteweg-de Vries eqn. 2–46898
spherical shell, translatory motion under the effect of spherical wave in compressible liquid 2–71122
Stokes, nonlinear, phase and group vel. 2–54786
stratified ocean, coastal upwelling 2–57907
stratified ocean, vertical structure of planetary waves 2–51560
suddenly falling stream, self-excited oscillations, stabilization 2–80423
topographic Rossby waves, exptl. models of double Kelvin and continental shelf waves 2–44626
velocity in proximal aorta 2–66249
viscous fluid, perturbation similarity solution 2–67744
water, due to plane shock wave refl. at free surface 2–83746
water, fairly-long, review 2–46896
water, gravity waves, nonlinear modulation, singular perturbation methods 2–71144
water, inception in falling films 2–50287
wavy flow, of thin film 2–53381
N_2-Hg two-phase system, propagation of pressure wave 2–71148

surface
see also Oceanography
— 2–62060
— 2–62061
— 2–62059
— 2–61911
aerodynamic growth of sinuous waves on sheets 2–67779
air-water cocurrent flow on flat plate, enhancement of heat transfer by waves 2–56494
asymptotic motion, short-wave, due to cylinder heaving on water 2–50300
Black Sea tsunami energy, and wave field charts 2–48421
breakers, air entrainment 2–57924
breaking, wave generation by wind and momentum conversion to steady currents 2–78335
Cannikin nuclear explosion, long period water wave meas. 2–62068
capillary-gravity, decay due to underwater turbulence 2–53367
capillary-gravity waves, flow over wavy bottom 2–77374
damping equation, Dorrestein, physical interpretation for surface active materials 2–56466
deep water, effect of fixed vertical barrier on obliquely incident waves 2–50299
fetches, short, distribution of wave heights in sea 2–62053
films, supersonic streams interactions, nonlinear stability 2–78934
flow, wave motion, generated by submerged periodic point source 2–53369
generation by oscillations of bottom of basin with dock 2–83742
generation theories, invalidity 2–54796
Gerstner's trochoidal waves, first-order irrotationality, gravity wave motion 2–50284
gravity wavefield, random, nonlinear dispersion relation 2–54784
height variation around vertical cylinders 2–57880
incident on 2 vertical parallel barriers, approx. soln. 2–83737
Kelvin ship-wave pattern, nonlinear distortion 2–80433
Kelvin wave attenuation along nearly straight coastlines 2–44624
Langmuir streaks, smooth water-floating debris interaction 2–62085
long dispersive waves, on a rotating ocean, generation by wind stress distributions 2–84716
Mediterranean Sea, thermistor buoy obs. of surface response to wind and sea state 2–57922
moving oscillatory surface pressure, viscosity effects 2–60398
nonlinear transient motion, free-surface, initial value techniques 2–56467
nonlinear wave radiation in surf zone, qualitative aspects 2–68865
ocean, effect of travelling atmospheric disturbances 2–51554
ocean, energy transfer from wind 2–78315
ocean, height measurement with nanosecond radar 2–44647
ocean, irregular wind induced review, prediction methods 2–44641
ocean, Rayleigh, resonant coupling to Apollo rocket shock cones 2–57621
ocean, variable mag. field obs. 2–48596
ocean wave breaking on submarine bar 2–57874
ocean waves, deep, spectra, meas., review 2–64416
ocean wind wave spectra, underwater acoustic remote sensing 2–57886
oceanic, periodicity in whitecaps 2–81620
oceanographic, land-sea breeze effects 2–57866

Liquid waves continued
surface continued
oceanographic diurnal variation in visually -observed breaking waves 2–57867
oceans, inhomogeneous and variable depth, analysis by ray method 2–81636
periodicities at surface of cohesionless medium and fluid, time-dimensional parameter 2–54766
ripples in core annular flow 2–80439
sea, characteristics in coastal area 2–44643
sea, wind driven, exptal det. of phase velocities of spectral components 2–44619
sea level oscillations, shelf seiches at La Parguera, Puerto Rico, semi-monthly periodicity 2–57878
sea surface, wave height rel. to temperature fluctuations 2–57890
sea wave generation, energy balance, relation to wind flow 2–78336
sea wave generation by turbulent wind 2–44608
seawater atm. turbulent boundary layer flow 2–84717
seawater surge, crest and hollow distrib. 2–54743
sediment entrainment by periodic waves breaking on sand beaches, computer based electrooptical measurement system 2–68874
set-up on coral reefs 2–65606
solitary, ninth order soln. 2–43291
supercritical flow in curved channels, hydraulic model obs. 2–83747
surface profile above fully developed Poiseuille channel flow-undular bore 2–71145
temperature fluctuations at air-water interface caused by surface waves 2–65616
transmission of water waves through small apertures 2–77393
transport phenomena, evaporation at air water interface 2–77395
transport phenomena, isothermal conditions, shear prediction methods 2–77394
tsunami, nonlinear effects in propagation 2–51555
tsunamis, amplitude patterns from submarine earthquakes 2–65611
vertical velocity of water surface, registration using e.m. induction method 2–72717
viscous liquid of finite depth, eigen oscillations 2–71143
water, interaction with acoustic fields, spatial resonance phenomena 2–43295
water, linear theory, asymptotic expansion of integrals 2–82154
water, permanent form, conformal transformation 2–64417
water, spatial resonance, vibrating in bell mode 2–43296
water of varying depth, interaction between surface waves and currents 2–83726
water waves, small amplitude shallow effect of bottom irregularities 2–83735
water with depths less than boundary layer thickness 2–74503
wave propagation in uniformly rotating fluid, surface and inertial waves 2–50164
whitecap, spray and capillary wave obs. 2–62084
wind driven, waveheight probability structure 2–77392
wind induced, rel. to microscale pressure fluctuations 2–68871
wind stress fluctuations in continuously stratified ocean, quasi-geostrophic response 2–57906
wind-disturbed water, curvature distrib. 2–57925
Li_2MoO_4-$Pu(MoO_4)_2$ system, existence of scheelite phases 2–71694
$LiNbO_3$, nonlinear interac. of hypersonic waves along [001] axis in an acoustic resonator 2–71734
$LiNbO_3$ single crystal longitudinal and shear hypersonic waves excitation 2–71741
ZnO, electron concentration determ. using T activity 2–71934
p-ZnTe, high photosensitivity 2–72071

Liquids
see also Association/liquids; Diffusion in liquids; Solutions
adsorption, of mixtures on solids, excess props. and temp. coeffs. using Gibbsian thermodynamics 2–53583
atomization and mixing of gas/liquid coaxial injector elements 2–62415
atomization by u.s. waves 2–60379
binary mixture, Rayleigh scatt., Kawasaki mode-mode coupling theory nonlocal shear viscosity correction 2–67829
Brillouin scattering from low temp. liquids 2–64459
bubble-liquid mixtures, shock wave propagation and relaxation effects 2–77453
condensed matter physics, conf., Fribourg, Switzerland [Sept. 1972] 2–60563
convection formation in horizontal layer placed in time-periodic external forces 2–67822
dielectric constants, method for precise obs. in wide frequency range 2–46973
dielectric discharge, investigation using X-ray flash tube 2–85181
heat transfer of Newtonian fluids in agitated vessels 2–67818
hydraulic shock in closed reservoirs 2–43294
insulating, in elec. field, hydrodynamic stability conditions 2–83527
intermolecular interactions using oscillation spectra 2–77431
ion mobility, hydrodynamic determ. 2–71163
Kerr, optical filaments, pulse distortion, optical shock, dispersion effects 2–79234
level detection using ultrasonic flexural wave attenuation in tube 2–49168
level signalling device, using transformer transducer 2–56460
low dispersive, enhanced optical four photon parametric interaction 2–79237
molecular rotational relaxation, inclusion of arbitrary reorientation angles 2–80138
nonlinear optical effects, excitation by psec. and nsec. u.v. pulses 2–43356
optical scatter loss formulated in terms of fundamental material properties 2–50357
particle retention in filters 2–66361
polar, microwave radiation absorption 2–55604
relaxation time determ. by laser probing 2–46958
semiconductor, conference review 2–61259
solutes, diffusion in dilute polymeric solns. 2–53411
supercooled, organic, mol. motion, Mossbauer scatt. obs. 2–61609
temperature fluctuations of liquid heated in container 2–71181

Liquids continued
- temperature oscillations undergoing free correction, effect on solidification 2−47028
- thermodynamic equilib. props. from interactions of walks 2−46948
- transparent, dielec., superbroadening of ultrashort pulse spectrum 2−43368
- transport processes of liquids under high shearing forces, computer simulation 2−60442
- turbulent heat transfer to non-Newtonian liquids 2−50297
- u.s. atomization 2−80495
- u.s. meas. using thermocouple 2−69719
- u.s. methods of investigation, short review 2−60374
- u.s. velocity, velocimeter design 2−60470
- volume as function of temp., dilatometer 2−46935

structure
- acetic acid/acetone mixtures, H bond formation causing ultrasonic relaxation, two state model 2−43322
- alcohols, compressional study through pseudo-Gruneisen parameters 2−83789
- alkali halides, interionic distance estimation 2−43320
- alkali metals, significant structure theory of surface tension 2−50346
- alkane monoiodide solutions, X-ray diffraction study, quasiliquid crystal form 2−50318
- alloy, diffuse Laue-scatt. and prepeaks in partial struct. factors 2−53391
- anomalous water, fabrication environment and impurities 2−53385
- asymmetric top molecules, Mori's method of calc. collective orientation correlation functions 2−50313
- Atomix teaching model, atomic structs. of liqs. and solids 2−45205
- binary alloys, cluster model 2−46917
- carbon tetrachloride, comparison of neutron diffraction data wtih perturbed crystal model of short-range order 2−64431
- carbon tetrachloride, Kerr effect induced by fluctuational statistical processes 2−46955
- chloroform, ang. autocorrel. function determ. from Raman spectra 2−71213
- chloroform, molecular motion from ^{13}C magnetic relaxation rates 2−56525
- cyclohexane, cyclohexanol, cyclohexanone, rot. correl. times 2−80446
- deuterochlorofrom, comparison of neutron diffraction data with perturbed crystal model of short-range order 2−64431
- dioxan-water mixtures, effects on o-positronium pick-off quenching rate 2−64448
- gas flame heating equipment producing temps. up to 2300C for X-ray diffractometer 2−67800
- glass, chalcogenide, solid and liq., struct., n.m.r. and i.r. vibr. spectra obs. 2−60595
- halobenzenes, significant struct. theory applic. 2−83778
- hydrocarbons, mobility of localized electrons 2−67840
- hydrogen bonded, review of i.r. and Raman spectroscopy relating to structure properties 2−43315
- memory functions, effective-field approxs. 2−80443
- metal, effect of pressure on pair potential 2−60419
- metal, electronic density of states, tight-binding model 2−46920
- metal, electronic struct. and n.m.r. prop. 2−67842
- metal, problems of investigation, short range order models 2−46923
- metal, statistical mechanical perturbation theory 2−80461
- metal, struct. factor, rel. to entropy of melting, Percus-Yevick formulation 2−64434
- methane, mol. motion, neutron scatt. cross section 2−43324
- methanol-water mixtures, effects on o-positronium pick-off quenching rate 2−64448
- microsegregation in binary melts, X-ray diffr. 2−60570
- optimized cluster expansion calc. for ionic solutions and atomic liquids 2−74513
- pair potential from exact Born-Green eqn. 2−83773
- polar, solvated electron states 2−50308
- polar molecules in non-polar solvents, dilute solution, dependence of dielectric const. on geometry 2−74551
- polywater, obs. on hydrogen bonded HBr 2−43314
- polywater 2−53386
- radial distribution function analysis 2−83764
- relaxation time, evaluation from equation of state 2−46919
- self-consistent theory 2−60366
- short-range order in molecular liquids, 'perturbed crystal' model 2−64431
- significant, numerical methods 2−56475
- significant structure theory, acoustic props. calc. 2−46918
- simple, next-neighbour distribs. 2−64432
- sodium borosilicate melt, critical-composition fluctuation in real space 2−67812
- velocity autocorrel., memory function 2−64433
- very high pressures, X-ray diffraction studies along melting curves 2−67799
- vibrational properties, frequency spectrum moment method 2−50981
- viscoelastic relaxation, defect-diffusion model 2−64449
- water, and magnetic treatment for purification 2−54521
- water, complications from solubility relationships for non-polar gases 2−56485
- water, direct correl. function near triple pt. 2−74514
- water, molec. dynamics study of temp. effects on structure and kinetics 2−60417
- water, molecular model, props. deduced 2−43317
- water, near i.r. studies in mixed solvent systems 2−50316
- water, second order fluctuations in particle no., integration over X-ray scattering interactions 2−74517
- water, theory of structure 2−77413
- water boundary layers, rel. to temp. depend. of mech. and thermal props. 2−67739
- X-ray diffr. apparatus 2−74516
- Al, ion-ion pot. calc. from diffr. data 2−50315
- Al, structure factor meas. using neutron diffraction techniques 2−64435
- Ar, dynamics from first moments of coherent neutron scattering function 2−46922
- Ar, Kerr effect induced by fluctuational statistical processes 2−46955
- Ar, neutron scatt., coherent- and incoherent-scatt. laws 2−67798

Liquids continued
structure continued
- Ar, next-neighbour distribs. 2−64432
- BeF$_2$, determ. from molecular dynamics calcs. 2−74515
- Cl$^-$, hydrated binding energy calc. by ab initio, semi-empirical MO and classical methods 2−50030
- Co-Al alloy, interatomic interaction energy, viscosity study 2−71155
- Cs-NH$_3$ solutions, velocity of 10 MHz waves on function of temp. and metal concentration, structural changes 2−43352
- Cu-Ge alloy, X-ray diffr. interference functions 2−83774
- Cu-In alloy, X-ray diffr. interference functions, 700°C 2−83775
- CuH$_2$SO$_4$.5H$_2$O isotope effects in structure, fractionation of O 2−47324
- Cu$_2$S-CuCl melt, from phase diagram calc. and density 2−46983
- CuTe, total neutron scatt. patterns obs. 2−60421
- D$_2$O, atom pair correlation functions from neutron and X-ray diffraction 2−43323
- F$^-$, hydrated, binding energy calc. by ab initio semi-empirical MO and classical methods 2−50030
- FeS-FeCl$_2$ melt, from phase diagram calc. and density 2−46983
- Ga, multiple neutron scatt., effective scatt. factors 2−60422
- Ge, X-ray diffr. obs. 2−60424
- HBr.4H$_2$O, H-bonds, Raman and i.r. spectra 2−43314
- HClO$_4$, time differential perturbed ang. correlation studies using ^{154}Gd 2−60511
- H$_2$O, effects of silica surface from adsorbed layer studies 2−60686
- H$_2$O, in relatively nonpolar organic solvents and in NAClO$_4$, meas. of i.r. absorption spectra 2−46932
- H$_2$SO$_4$ 100%, X-ray determ. of molecular density correlation function and mean amplitude variation, geometric model 2−67801
- Hg-In alloy, partial struct. factors and atomic distribs. 2−64437
- Hg-Tl alloy, partial struct. factors and atomic distribs. 2−64437
- Hg, interference functions temp. range 50-150C, X-ray obs. 2−67802
- In-Ga(Sn) alloy, surface tension and density study 2−67815
- K-Hg alloys, zero wave vector partial struct. factors 2−43318
- K, effective pair pots. 2−50317
- K, expt. and theoretical structure factors 2−50314
- KCl ionic melt, microstructure, computer generated configurations 2−43319
- KClO$_3$, ClO$_3$$^-$ struct., Raman spectra study 2−74545
- K$_2$MgCl$_4$, ion clusters, Raman spectrum interpret. 2−67797
- Kr, longitudinal phonons and the law of corresponding states 2−71156
- Li$^+$, hydrated binding energy calc. by ab initio, semiempirical MO and classical methods 2−50030
- LiBeF$_3$, determ. from molecular dynamics calcs. 2−74515
- LiF, determ. from molecular dynamics calcs. 2−74515
- ^{15}NH$_3$, ^{15}ND$_3$, ^{15}N spin-lattice relaxation meas., spin-rotational and intramolecular dipolar interactions 2−50371
- Na-K alloys, zero wave vector partial struct. factors 2−43318
- Na, coherent X-ray diffraction patterns at very high pressures, along melting curve 2−67803
- Na, density response function from Mori's generalized Langevin eqn. 2−83776
- Na, effective pair pots. 2−50317
- Na, expt. and theoretical structure factors 2−50314
- Na, X-ray scattering, static structure function and atomic density distribution 2−47301
- Na$^+$, hydrated binding energy calc. by ab initio, semi-empirical MO and classical methods 2−50030
- NaClO$_3$, ClO$_3$$^-$ struct., Raman spectra study 2−74545
- Ne, electronic bubble states 2−43321
- Ne, three atom correlations 2−80447
- Pb-Sn alloy, changes rel. toanomalous behaviour of surface tension 2−53409
- Rb, structure factors determ. from hard sphere diameter 2−71195
- Te, neutron scatt. obs., review 2−60423
- Tl$_2$SeAs$_2$Te$_3$ chalcogenide semiconductor, n.m.r. and i.r. absorp. obs. 2−60420
- Xe, longitudinal phonons and the law of corresponding states 2−71156
- Zn, next-neighbour distribs. 2−64432

theory
- *see also Dielectric phenomena; Equations of state/liquids*
- alkali halides, interionic distance estimation 2−43320
- binary alloys, cluster model 2−46917
- binary mixtures, variational approach to prediction of excess thermodynamic props. 2−43312
- binary mixtures of Lennard-Jones (12-6) liquids, Monte Carlo calc. of thermodynamic properties 2−71182
- binary mixtures of Lennard-Jones liquids, Monte Carlo calcs. of excess thermodynamic properties 2−74539
- binary mixtures of molecules interacting via Kihara potential, Percus-Yevick theory 2−67552
- Brownian particle, autocorrelation functions 2−58778
- classical, thermal motion of liq., particles, microscopic theory 2−50309
- collision frequency, computation using cell model and exact formula 2−53389
- diethyl ether, correl. factor determ. 2−53387
- disordered systems, correlation phenomena 2−64815
- equations of state, from Ursell-Mayer density expansion compressibility factors 2−53108
- Kawasaki mode-mode coupling theory applied to 2,6-lutidine-water 2−46941
- kinetic energy density fluctuations, in classical liquid 2−46915
- liquid-liquid transition, solution model 2−71154
- localized states density in dense fluid 2−51070
- 2,6-lutidine-water, crit. binary mixture, rel. to light scatt. and shear viscosity 2−50344
- 2,6-lutidine-water, crit. binary mixture, rel. to transport props. 2−46941
- memory functions, effective-field approxs. 2−80443
- metal, applic. of pseudopotentials, review 2−50311
- metal, electronic density of states, tight-binding model 2−46920
- metal, molten, calc. of interference function 2−50310
- metal, short range order models 2−46923
- metal, single-atomic 2−71152

Liquids continued
theory continued
metals, temp. dependence of hard-sphere interference functions 2−67796
Metropolis Monte Carlo method in isobaric and canonical ensemble formalisms 2−64428
mixed solvent systems, solubility parameter theory 2−43333
molecular, application of optimized cluster expansions for clasical fluids 2−67554
molecular rotation, conditional fast rotational diffusion 2−60414
molecule, dipole, matrix description of rotational motion 2−74307
muffin tin potentials, canonical density matrix 2−51071
non-electrolyte liquids and solutions, thermodynamic properties 2−46913
non-Newtonian, heat transfer in agitated vessels 2−74538
normal, internal energy and mechanical properties 2−56450
pair potential from exact Born-Green eqn. 2−83773
pair-correlation function, criticism of asymptotic form 2−43313
Percus Yevick liquids, c.f. with density fluctuations in water 2−74517
phase transitions, decoupled-mode dynamic scaling theory 2−52103
polar, simple, thermodynamics using Prigogine's cell theory 2−53421
polar, solvated electron states 2−50308
polymer solution, having draining effect, normal stress effect 2−71164
rotational diffusion of spherical-top molecules, comment on paper by McClung (1969 2−71178
significant structure theory, acoustic props. calc. 2−46918
solvated electron, polarization energy 2−46914
stability limits, and hyper-chain approx. convergence 2−74512
Van der Waals model correction 2−64429
van der Walls interactions between rare gas atoms in a dense classical fluid 2−74234
velocity autocorrel., memory function 2−64433
vibrational relaxation, binary collision model 2−53388
water, mixture-model approach 2−83771
water, molec. dynamics study of temp. effects on structure and kinetics 2−60417
water, theory of liquid structure 2−77413
water, two-state theory calc. of refractive index temp. dependence 2−60473
water-like particles in two dimensions, statistical mechanics of one-component systems 2−80449
water-like particles in two dimensions, statistical mechanics of two-component system, hydrophobic interaction 2−80450
weakly polar system, correl. factor determ. 2−53387
Ar, memory effects and dynamical correlations 2−60416
Bi, effective interionic pair potentials, calc. from structural diffraction data 2−50312
Ne, liquid, negative carrier mobility rel. to localized electrons 2−46916
Ne, three atom correlations 2−80447
Sb, effective interionic pair potentials, calc. from structural diffraction data 2−50312
Te, effective interionic pair potentials, calc. from structural diffraction data 2−50312

Lithium
anode, in organic electrolyte batteries with high energy densities 2−66688
atom, 2^2P state, electron correlations and quadrupole hyperfine structure 2−70587
atom, accurate perturbative calc. based on Hartree H_0 2−46432
atom, beam-foil excited, 40 keV, meas. of relative level populations 2−52955
atom, elastic electron scatt., differential cross section calc. 2−79883
atom, electron-impact double excitation cross sections calc. in Born Oppenheimer approx. 2−70607
atom, intermediate Hamiltonians 2−52923
atom, radial, lower bounds for energies 2−56099
atom, three-electron excited S states, Hylleraas-type wave functions 2−76991
atom and Li^-, approximate natural orbitals calc., electron affinity 2−46433
atomic, photodetachment cross section of Li- 2−49984
atomic transitions, model pot. calcs. 2−76976
atoms, photoionization, pseudopotential calculation of cross-section 2−46448
Auger spectra, relative intensities determ. and interpret. 2−65111
band structure, rapidly convergent pseudopotentials 2−75030
b.c.c., lattice dynamics, phonon freqs., sp.ht., Debye temp., from Krasko-Gurskii model 2−68227
chemical reactions in upper atmosphere 2−58030
compensated Ge γ spectrometer 2−52678
diffusion and solubility in Ge, hydrostatic press. effect 2−47443
dispersion in vaseline, r.f. Faraday effect 2−43410
drift and precipitation in Si crystals 2−50692
electrical resistivity, contribution of Umklapp processes 2−84293
electron-electron interaction and spin diffusion length, conduction e.s.r. study 2−48288
film, 2-3.8 eV, meas. by excitation of nonradiative surface plasmons 2−75256
film, cond. e.p.r. line shapes, theory and expt. 2−81450
films, optical absorption and structure 2−65260
Hartree-Fock calculation, of electron states 2−80978
interstellar, production by cosmic rays 2−84970
interstellar possible production by low energy cosmic rays 2−62593
interstitial diffusion in Ge, press. depend. 2−47442
ionic motion in alkali borate and silicate glasses, n.m.r. obs. 2−64690
ions, scattering, multiple, by C and Ge foils 2−47781
isoelectronic sequence, electron impact excitation of ions, interpolation formulae 2−74244
K-shell fluorescence yields by synchrotron radiation 2−77012
liquid, as coolant in toroidal fusion reactor, calc. of pumping power 2−46748
liquid, electron spectrum, calc. by cell method 2−83797
liquid, self-diffusion, 195 to 440°C 2−67817
liquid, use of coolant in toroidal fusion reactor, stress limitations 2−46749

Lithium continued
metallic, rigid neutral atom density, selfconsistent calc., auxiliary neutral atom model 2−71787
neutron activation analysis using (n, α) reaction 2−84686
optical constants ε_1 and ε_2, absolute values 2−48134
particles, electron microscope examination, technique 2−43555
plasma, laser produced, ion energy, retarding potential probe obs. 2−43168
plasma, stability and spectroscopic discharge properties 2−53197
quantitive det. in various matrices using nuclear track technique 2−48364
in rocket vapour trail, neutral wind meas., daytime thermosphere 2−84886
scintillation counter, detection sensitivity 2−55909
spin echo on cond. electrons 2−44314
thermal expansion coefficient and Gruneisen parameter, lattice dynamical calculation 2−84179
trace metal in rainwater following injection into cloud base during storm 2−57986
X-ray Compton profiles, theory and expt. 2−84255
X-ray K emission band, short-wave satellites 2−51361
CdF_2:Er^{3+}, Li^+, correlated e.p.r. and optical study 2−78164
CdF_2:Li^+, ionic thermocurrents, temp. depend. 2−81089
CdTe:Li, self-compensation and interaction of Li with defects 2−75107
Ge:Li, electron irrad., Hall effect and minority carrier diffusion length obs. 2−47927
Ge(Li) γ-ray detectors, evaluation procedures 2−55919
KCl:Li, generation and detection of 55 GHz phonons, paraelec. reson. study 2−84191
KCl:Li^+, ENDOR of A-centre electrons rel. to external elec. field 2−78176
KCl:Li^+,Br-(I-), H_a(Li^+)-type centres, e.p.r. obs. 2−60825
Li/Cl secondary cell with inorganic electrolyte 2−66689
Li/CuF_2 secondary cell with inorganic electrolyte 2−66689
Li/S secondary cell with inorganic electrolyte 2−66689
Li/S secondary cells 2−66687
Li^+-He, oscillation of charge exchange cross section 2−64053
Li-ammonia solution relaxation times and Overhauser enhancements for protons obs. 2−46988
Li-glass scintillator tip for detection of secondary electrons in electron microscopes, long life 2−82430
Li, electron dispersion law, spectrum and related charact. near Fermi surface 2−80945
Li, model potential calc. of electron affinity 2−42752
Li I, doubly excited states, energies and lifetimes 2−42735
Li II, obs. of transition between doubly excited state using beam-foil technique 2−52954
Li^-, continuous absorption coeff. contribs. from bound-free and free-free transitions 2−70586
Li^- ion, continuous absorpt. coeff. rel. to temp. and wavelength 2−70583
Li^+, collision with H_2, model potential for vibrational excitation of H_2 2−43038
Li^+, exp. investigation of ion source 2−59116
Li^+, hydrated binding energy calc. by ab initio, semiempirical MO and classical methods 2−50030
Li^+, influence of electron correlation on one-particle electron density and radial expectation values 2−52950
Li^+, intensity decay curves, cascade-induced alignment changes 2−42753
Li^+, Li^{2+} ions, beam foil excited, u.v. spectra, radiative mean lives 2−67420
Li^+, oscillator orbitals in CI calculations 2−59883
Li^+, vibrational excitation of H_2, quantum mechanical studies 2−77171
Li_2, computation of force constants and dipole moment derivatives using Hartree-Fock 2−50052
Li_2 mol., vibr. force const. and electron relax. 2−60002
Li_2 molecule, improved alternant molecular orbital function 2−56183
^6Li semiconductor sandwich neutron spectrometer 2−42448
$^7Li + Ar$ collisions, absolute total scattering cross sections, derivation of interatomic potential 2−49968
$Li^+ + He$, elastic and inelastic scattering, rotational coupling 2−42816
$Li^+ + He$, elastic and inelastic scattering 2−42815
$Li^+ + He$, elastic and inelastic scattering, charge exchange channels 2−42790
$Li^+ + He$, elastic scattering cross sections, repulsive potential derivation 2−59934
$Li + Na^+$ asymmetric nonresonant charge transfer, theoretical description by two-state approx. 2−70626
$Li + Na^+ \rightarrow Li^+ + Na$, nonresonant charge-transfer, multistate mol. wave-function approach 2−76980
$Li^+ + Na$ asymmetric nonresonant charge transfer, theoretical description by two-state approx. 2−70626
in NH_3 liquid, magnetic susceptibility in 1.5-296 K range 2−43389
RbCl, F_a(Li) centre, a.c. photocond. study 2−71530
in p-Si:B, compensation influence on irrad. defect form. 2−47390
Si:Li, electron irrad., luminesc., annealing and Li impurity effects 2−48229
n-Si:Li, irrad., Li-defect interactions, e.p.r. obs. 2−48293
n-Si:Li, role in irrad. defect prod. 2−47385
in Si, effect on recomb. luminesc. of electron irrad. crysts. 2−48231
Si X-ray spectrometer 2−49650
Si(Li) nuclear radiation detector, damage by thermal neutrons 2−76732
ZnO:Li, light scatt., and photoconductivity, anisotropic 2−75317

Lithium compounds
acetate, elastic consts. meas. by Brillouin effect 2−50732
alloy, dil. nucl. spin relax. of ^7Li and translational diffusion 2−44317
alloy, liq., semicond., e.s.r., spin flip processes 2−60510
ferrites, magnetostriction, effect of Co ions 2−65158
formate monohydrate, n.m.r. of ^7Li 2−54512
silicate glass, γ-irrad., thermolum. 2−81410
silicate glass ceramic, fracture energy as function of struct. 2−50886
Al-Li alloys, behaviour of neutron irradiation produced gas atoms observed by ^3H autoradiography 2−44009

Lithium compounds continued
Al-Li alloys, neutron irrad., inert gas bubble effects on mech. props. 2−43688
B_2O_3-Li_2O-H_2O system borate hydrates, cryst. chem., equil. 2−47181
$Ba_2LiNb_5O_{15}$, cryst. growth, Czochralski method 2−60721
Li-Al-Mg alloy, 01420, ageing, phase comp. changes 2−47594
Li-B-N system, phase equilib., rel. to cubic BN growth 2−50970
Li-Bi liquid alloy, solubility of Nd and Th 2−43334
Li-Mg(Al) solid solution, electronic props., Green function calc. 2−75029
Li-NH_3 solution, Hall coeff. and elec. cond., 203-243K 2−46984
Li-Na alloys, liq., immiscibility 2−53404
Li complex, Li^+-H_2O, config. determination from H_2O energy surface data 2−60010
Li He, interaction potential, group function method 2−67487
$LiAlF_6$, mag susceptibility, temp. depend., 300-700K 2−72110
$LiAl_5O_8:Fe^{3+}$, ordered and disordered, phosphorescence and excitation spectra, zero-phonon transition, fine structure 2−48253
$LiAl_5O_8$, ceramic, transparent, prod. by hot-pressing 2−43873
$LiAlSiO_4$-SiO_2, partial volume determination, influence of composition for solid solution glass ceramics 2−56562
$LiAlSiO_4$, beta eucryptite, high temp. form structural relation to high quartz 2−56659
($LiAlSiO_4$), β-eucryptite, structural relationship between low temp. form and low quartz 2−56658
β-$LiAlSiO_4$, eurocryptite, thermal expansion of lattice consts., 20-1100°C 2−54060
$Li_2B_4O_7$:Mn, optimum thermoluminescent properties for dosimetry applic. 2−49913
$Li_2B_4O_7$:Mn thermoluminescent dosimeter, energy response 2−58623
$LiBO_2$, evaporation, mass spectrometric obs. 2−64512
$Li_2B_4O_7$, crystallization from melt 2−53617
$Li_2B_4O_7$, mass attenuation and energy absorption coeffs. for 1 to 150 keV photons 2−64871
$Li_2B_4O_7$, preparation of U minerals for X-ray fluorescence measurements, pressed fused disc method 2−65586
$LiBaF_3$, elastic and thermoelastic consts. 2−53781
$LiBeF_3$ melt, structure and motion, molecular dynamics calc. 2−74515
Li_2BeF_4, crystal structure, interpretation in terms of Born-Mayer-Huggins model 2−77564
LiBr:Tl, aqueous soln., excitation luminesc. spectra, effect of tl ion conc. 2−53441
LiBr, aqueous, equilibrium phases, entropy-temp. diagram 2−58942
LiBr absorption machine, thermodynamic cycle 2−62892
LiBr absorption refrigerator, with sprinkler generator 2−62891
LiCl:Tl, aqueous solution, excitation luminescence spectra, effect of concentration of Tl ions 2−53441
LiCl-$UCl_{3(4)}$ systems, binary and ternary, melting point diags. 2−67873
LiCl, elastic consts. 2−50726
LiCl, F-centre hyperfine interactions, press. depend., ENDOR study 2−83986
LiCl, gradient-elastic consts. determ. by n.m.r. 2−77637
LiCl, Hartree-Fock band structure 2−61172
LiCl, heat capacity, size-disparity anharmonicity 2−71748
LiCl, hyperfine spectra in zero magnetic and low electric fields using new electric resonance molecular beam apparatus 2−46557
LiCl, in sulfolane-water mixtures, conductance at 35°C 2−78199
LiCl heated hygrometer, phase transition between solid hydrate and saturated soln. 2−56486
LiCl solutions, Brillouin scatt. 2−67835
LiCl wave function regeneration, possibility for localized electrons for F-centres 2−68041
$LiClO_4$ electrolyte soln. in dimethylformamide, thinning of Mg-Li alloy foils 2−80548
$LiClO_3.3H_2O/LiMnO_4.3H_2O$ mixed crystal, effect of uniaxial pressure on absorption spectra, confirmation of red band system of MnO_4^- as $^1T_1 \leftarrow {}^1A_1$ 2−81372
$LiCo_3$ molten, production of C-H-O fuels for high temp. fuel cells 2−59042
$Li_{0.5}Cr_{1.25}Fe_{1.25}O_4$, thermal reversal of residual magnetisation, demonstration expt. 2−61476
$LiCuCl_3.2H_2O$, antiferromag. resonance, crit. paramag. linewidth obs. 2−68727
$LiCuCl_3.2H_2O$, antiferromag., mag. phase boundaries, anisotropy, exchange fields 2−68574
$LiCuVO_4$, n.m.r. and long-range superexchange interactions via Cu-O-V-O-Cu linkages 2−72511
LiD:H crystal, Raman scattering due to localized lattice vibrations 2−61668
LiD, phonon dispersion, three body force shell model 2−68217
LiF_4, disloc. displacement mechanism during formation of small disloc. layer at cryst. surface 2−71492
$Li_{0.5}Fe_{2.5-x}Al_xO_4$, lattice const., comp. depend. 2−47334
$Li_{0.5}Fe_{2.5-x}Al_xO_4$, magnetization process, domain wall reson. study 2−72198
$Li_{0.5}Fe_{2.5-x}Al_xO_4$ $(0\leqslant x\leqslant 1)$ and $Li_{0.5}Fe_{2.5-x}Ga_xO_4$ $(0\leqslant x\leqslant 1.63)$, electric fields at lattice points and magnetic anisotropy 2−72194
$LiFe_2F_6$, electron hopping obs. by Mossbauer effect, 350-700K 2−71913
$LiFe_2F_6$, mag. struct. 2−44302
$LiFe_2F_6$, trirutile, mag. struct. 2−72220
$LiFe_2F_6$, trirutile, mag. structure, neutron diffr. obs. 2−65183
$Li_{0.5}Fe_{2.5-x}Ga_xO_4$, supertransferred hyperfine fields at ^{69}Ga and ^{71}Ga 2−54511
$Li_{0.5}Fe_{0.5}O$-Fe_2O_3-FeO, coexisting phases equilibrium and thermodynamics, 900-1200°C 2−74931
$Li_{0.5}Fe_{2.5}O_4$, ferromag. relax. of parametric spin waves 2−72228
$Li_{0.5}Fe_{2.5}O_4$, mag. props., synthesis conditions influence 2−44277
$Li_{0.5}Fe_{2.5}O_4$, reson. phenomena at moving domain boundaries 2−72456
$Li_{0.5}Fe_{2.5}O_4$, supertransferred hyperfine field at ^{57}Fe, n.m.r. study 2−78169
$LiGaO_2$, piezoelec., elastic and dielec. props. 2−51206
$LiGd(MoO_4)_2:Nd^{3+}$, laser, stimulated emission 2−69938
LiH:Pb, X-ray luminesc. and thermoluminesc. 2−72422
Li(H,D) system, lattice consts., isotopic comp. depend. 2−43582

Lithium compounds continued
LiH, calc. of force constants by Hellmann-Feynman theory 2−80055
LiH, calc. of magnetic shielding and spin-rotation constants associated with nuclei using molecular orbital theory 2−42850
LiH, computation of force constants and dipole moment derivatives using Hartree-Fock 2−50052
LiH, enthalpy and heat of fusion meas. 2−64507
LiH, extended Hartree-Fock calculations using corresponding orbitals 2−53021
LiH, forbidden band width, contact pot. difference meas. 2−57127
LiH, molecular vibration effect on apparent bond lengths 2−56136
LiH, self-consistent local orbitals 2−75031
LiH, self-consistent procedures for generalized valence bond wavefunctions 2−53012
LiH, surface struct., contamination, LEED and Auger spectroscopy obs. 2−47078
LiH activated by Hg-like elements, luminescence and excitation spectra 2−78137
LiH crystal, Mg-activated, photocond. excitation spectra meas. 2−77799
LiH mol., polarisability using max. overlap method with additional conditions 2−83273
$LiHC_2O_4.H_2O$, X-ray diffraction study of isotope effect and structure 2−56657
$LiH_3(SeO_3)_2$, ferroelec., thermal expansion rel to band arrangement, -150 to +25°C 2−68253
LiI, lines profiles rel. to plasma parameters determ. 2−60247
LiI(Eu) crystal detector, meas. of fast- and thermal neutron fluxes 2−42461
$LiIO_3$, α and β forms, optical properties compared 2−81326
$LiIO_3$, elastic surface wave props. and device applics. 2−77778
$LiIO_3$, near and far i.r. investigations for α and β crystals 2−84511
$LiIO_3$, noncollinearly phase matched second harmonic generation using Nd:YAG laser 2−79230
$LiIO_3$, polariton dispersion, light scatt. associated with photons 2−68617
$LiIO_3$, solubility in water, rel. to cryst. growth process 2−50584
$LiIO_3$, tunable i.r. difference-frequency generation 2−63369
$LiIO_3$ internal parametric oscillator, pumped by Nd:YAG laser 2−45746
$LiIO_3$ pulsed doubly resonant parametric oscillator, spectral and other props. 2−73586
$Li_{0.45}Mn_xFe_{2.55-x}O_4$, anisotropy contrib. of Mn^{3+} and related directional orders 2−65170
$LiMn(PO_3)_3$, crystallographic data 2−64641
$Li_2Mn(PO_3)_4$, crystallographic data 2−64641
Li_2MoO_4-$Cr_2(MoO_4)_3$ solid soln., phase diagram 2−57033
$Li(NH_3)_4$, Hall effect, magnetoresist., thermoelec. power, carrier mobility 2−47894
$Li(NH_3)_4$, magnetic susceptibility obs. in 1.5-194 K range 2−43389
$LiN_2H_5SO_4$, anomalous neutron scatt. and absence of ferroelectricity 2−84357
$LiN_2H_5SO_4$, n.q.r. of ^{14}N, transition freqs. 2−68755
$Li(N_2H_5)SO_4$ dielectric const., 6 to 5.10^6 Hz, 20 to 200°C 2−77931
$LiNO_3$-KNO_3, molten mixtures, electrical conductivity, temp. dependence 2−53452
$LiNO_3$, molten, interdiffusion coeff. of Ag^+ 2−65383
$(LiNa)^+$, charged transfer, transition, dipole moment, cross sections of vibr. levels 2−60009
$Li_{0.93}Na_{0.07}Fe_5O_8$, sintering, effect of conditions on density and particle size 2−64790
$LiNbO_3:Cr^{3+}$, optical excitation, dipole moments and macroscopic polarization 2−48138
$LiNbO_3:Fe^{3+}$, e.p.r. 2−65324
$LiNbO_3:Mn^{2+}$ ferroelectric, e.s.r. studies of crystal field parameters 2−81451
$LiNbO_3$:Rh, reversible holographic storage 2−69984
$LiNbO_3$-Si, $LiNbO_3$-CdS, $LiNbO_3$-Si-Pb(Zr,Ti)O_3, convolution and correlation between sonic induced space charge and field waves 2−51015
$LiNbO_3$-Si layered structure, transverse acoustoelectric effect obs. using capacity probes 2−51038
$LiNbO_3$, acoustic convolution and correl., nonlinearity parameters 2−51014
$LiNbO_3$, directional dispersion and assignment of optical phonons 2−77764
$LiNbO_3$, dispersion of elastic waves and permittivity along trigonal axis 2−72033
$LiNbO_3$, doped, as erasable optical recording medium 2−73612
$LiNbO_3$, electro-optical effects light modulation applications 2−69988
$LiNbO_3$, electro-optical effect, calc. from light wave intensity reduction 2−65222
$LiNbO_3$, ferroelec. domain struct., growth 2−65063
$LiNbO_3$, hypersonic attenuation, 2620 MHz, temp. depend., 77-300 K 2−57050
$LiNbO_3$, laser irrad., surface damage, ferroelec. props. effects 2−79252
$LiNbO_3$, light scatt. by elastic waves and rot. of polarisation plane 2−72358
$LiNbO_3$, nonlinear surface wave generation 2−51007
$LiNbO_3$, obs. of triply phase matched five wave acoustooptic interaction 2−44349
$LiNbO_3$, parametric, rapidly tunable dye-laser pumped 2−73547
YZ$LiNbO_3$, periodic arrays, reflection of elastic surface waves 2−51022
$LiNbO_3$, propagation of Rayleigh-mode piezoelectric surface wave 2−61095
$LiNbO_3$, Raman scattering and obs. of polaritons by photographic method 2−81374
$LiNbO_3$, Rayleigh wave electromech. coupling const., acoustic wave vel. obs. 2−43969
$LiNbO_3$, rotated Y cuts, leaky wave attenuation 2−51025
$LiNbO_3$, shear wave excitation by interdigital transducer operated at surface-wave centre freq. 2−51008
$LiNbO_3$, spin-lattice relaxation times determ. by tone- bursting technique in quadrupolar nuclei 2−48312
$LiNbO_3$, substrate for n-InSb, surface wave amplification 2−77774
$LiNbO_3$, surface acoustic wave correlation echo, generation from coupling to charge carriers 2−57045

Lithium compounds continued
- $LiNbO_3$, surface acoustic wave velocity change caused by thin conducting film 2−51017
- $LiNbO_3$, surface wave device, acoustic shear wave probing using laser beam 2−68232
- $LiNbO_3$, thinning by ion etching for acousto-optic deflectors 2−63417
- $LiNbO_3$, third-order nonlinear optical susceptibility, using tunable dye lasers 2−72252
- $LiNbO_3$, transition metal doped, optical and holographic storage properties 2−63356
- $LiNbO_3$, triply phase-matched 5 wave acousto-optic interaction 2−48139
- $LiNbO_3$, undoped, holographic recording applications, physical model, transport theory 2−63355
- $LiNbO_3$, X-cut, microwave phonon attenuation, hypersonic attenuation obs., temp. effects 2−68225
- $LiNbO_3$, Y cut, parameter periodic coupling of volume acoustic modes 2−51003
- $LiNbO_3$, YZ, Rayleigh wave reflection from electrically loaded interdigital transducers 2−51021
- $LiNbO_3$ crystal, harmonic generator, patent 2−42171
- $LiNbO_3$ crystal cuts with low halfwave voltage for optical phase and polarization modulation 2−42170
- $LiNbO_3$ for multiple storage of thick phase holograms 2−45762
- $LiNbO_3$ luminescence irradiated by ruby laser 2−44426
- $LiNbO_3$ nonlinear crystal, fracture by ruby laser radiation 2−79254
- $LiNbO_3$ parametric oscillator, pumped with tunable dye laser 2−42053
- $LiNbO_3$ polariton eigenfreqs. and eigenvectors, small wave vector case 2−64833
- $LiNbO_3$ single domain crystals growth by pulling method in h.f. induction furnace, electro-optical properties, applications 2−77528
- $LiNbO_3$ spontaneous parameteric scattering, idler absorption and dispersion 2−44337
- $LiNbO_3$ switching and steering of surface waves by nonlinear mixing in anisotropic media 2−51005
- $LiNbO_3$ temp. of phase synchronization for two wave freq. addition 2−48128
- $LiNbO_3$ with CdSe film, surface state effect on surface wave amplification 2−84201
- $LiNbO_3$ with semiconductor layer, surface wave convolution 2−47741
- $Li_{0.5}Nd_{0.5}TiO_3$, perovskite, prep., mag. susceptibility cryst. field effects, 2-600K 2−54294
- Li_2O-Al_2O_3-SiO_2 glass-ceramic, strength and microstruct. 2−53931
- Li_2O-B_2O_3-GeO_2 glass, struct. and props. 2−47059
- Li_2O-Fe_2O_3-SiO_2 system, dielec. and magnetic props. 2−54333
- Li_2O-MgO-Al_2O_3-SiO_2-TiO_2, glass-ceramic, crystn., microstruct., indentation hardness 2−80535
- Li_2O-MgO-Al_2O_3-SiO_2 glass, crystallization, F addition effects 2−47058
- LiO_2-Sc_2O_3-SiO_2-H_2O, hydrothermal crystallization 2−71383
- Li_2O-2SiO_2 and Li_2O-K_2O-4SiO_2 glass, static longitudinal modulus, u.s. determ. 2−56773
- Li_2O-SiO_2 glass, phase separation and crystn., X-ray obs. 2−56560
- Li_2O-Tb_2O_3-SiO_2, glass, fluorescence rel. to crystalline phases 2−51376
- LiO $X^2\pi$ and $A^2\Sigma^+$ states, pot. curves and mol. props. 2−60011
- $LiO_2(5-2t)Fe_2O_3tCr_2O_3$ ferrite, cryst. struct., influence of heat treatment 2−57021
- $Li_2O.Al_2O_3.2SiO_2$, glass, fibres, ion exchanged, internal friction, Li and Na conc. profiles 2−80754
- Li_2SO_4, liq., u.s. vel. 2−53426
- Li_2SO_4, polycryst. pellet, dielec. props. at radio and microwave freqs. 2−61413
- Li_2SO_4, pyroelectric coeff. determ. 2−65072
- $Li_2SO_4-Cs_2SO_4(Na_2SO_4)(Rb_2SO_4)$ systems, phase diagrams 2−80527
- $LiScF_4$, relative ionization cross-section determ. 2−46556
- Li_4SiO_4-Zn_2SiO_4-Mg_2SiO_4-SiO_2 glass, phase equilibria and crystallization 2−64520
- $LiTaO_3$:Cr^{3+}. optical excitation, dipole moments and macroscopic polarization 2−48138
- $LiTaO_3$:Cu^{++}, rectification of Nd:glass laser beam for psec. electrical pulse generation 2−79268
- $LiTaO_3$:Cu^{2+}, optical generation of intense picosec. electrical pulses 2−45768
- $LiTaO_3$:Cu^{2+}, optical generation of picosecond electrical pulses 2−44336
- $LiTaO_3$, ferroelec.-paralec. phase transition 2−44162
- $LiTaO_3$, laser irrad., breakdown threshold at Curie temp. 2−79252
- $LiTaO_3$, Rayleigh wave electromech. coupling const., acoustic wave vel. obs. 2−43969
- $LiTaO_3$, self-induced thermal effects on light extinction 2−72254
- $LiTaO_3$, spin-lattice relaxation times determ. by tone-bursting technique in quadrupolar nuclei 2−48312
- $LiTaO_3$, subnanosecond pyroelectric detector, for use with pulsed lasers 2−82466
- $LiTaO_3$, surface acoustic wave velocity change caused by thin conducting film 2−51017
- $LiTaO_3$, surface acoustic wave velocity temp. depend. 2−51019
- $LiTaO_3$ single crystal, pulling, dielec., thermal and optical props. 2−72008
- Li_2TiO_3, structure det. from X-ray data 2−71425
- $Li_xTi_{1.1}S_2$, $0.1<x\leqslant0.3$, superconductivity, noncubic compounds of high transition temp. 2−47858
- $LiTmF_4$:Ho^{3+}, optical absorpt., emission and excitation spectra 2−81418
- $LiVO_3$:Mn^{2+}, e.p.r. at 9.3 and 36.9 GHz 2−72493
- $LiVO_3$, cryst. growth and characteriz. 2−47261
- Li_2WO_4, anhydrous, ^{183}W Mossbauer effect, effective Debye temp. detn. 2−71720
- $Li_6W_2O_9$ phase existence, cryst. struct., peritectoid decomp. 2−54007
- $LiYF_4$:Er^{3+}, crystal parameters verified 2−51240
- $LiYF_4$:Er^{3+} pulsed laser operation at 0.85 μm at room temperature 2−42062
- $Li_7Y_3(MoO_4)_8$, prep., decomp. at 735°C to solid and liq. phase 2−74904

Lithium compounds continued
- $Li_{1-x}Zn_{2x}Fe_{5-x}O_8$, high temp. enthalpy and specific heat 2−54049
- $Li_2Zn_2Mo_3O_{12}$, orthorhombic, cryst. struct. 2−77555
- $LiZnNbO_4$, i.r. absorpt. spectra, ionic ordering 2−72342
- $LiIO_3$ oblique polaritons, freq. dispersion 2−77770
- $Na_2LiBe_2F_7$, cryst. struct. 2−71438

lithium fluoride
- (TLD-100), thermoluminescence, emission spectrum at low and high exposures 2−44414
- bicrystal, interaction of stress waves with a boundary 2−84061
- colour centres, 340 nm centres and thermoluminesc. 2−43650
- colour centres, electron microscope obs. in cathode luminescence mode 2−80708
- deformable shell model studies 2−50995
- detector, thermoluminescent, for meas. of steep dose gradients at interfaces 2−82822
- detector, thermoluminescent, for neutron and gamma radiation 2−52691
- dielectric consts., l.f., press. and temp. derivatives 2−51188
- dislocation etch pit, morphology, effect of anions in etchant 2−56609
- dislocation etch pit. morphology rel. to Cu(II) complex in etchant 2−56608
- dislocation loops and radiation colloids, elec. microscope obs. 2−74760
- dislocation mobility obs. on (001) face, effects of H_2O adsorption 2−43627
- dislocations, dynamic scattering of slow transverse phonons, 0.04 to 0.8°K 2−68218
- dose rate dependence for exposures above 15000 R per pulse 2−59634
- dosimeter, changes in gamma sensitivity of ^{7}LiF 2−85084
- dosimeter, mixed γ-n, responses to both 2−83161
- dosimeter, thermoluminescent, response to 1.7-3.7 MeV α and 2.4-13.3 MeV p 2−85135
- dosimeters, clinical radiation dose measurements 2−69431
- dosimetric grade powders, influence of thermal and chemical treatment on TSEE and TSL phenomena 2−67090
- dosimetry based on radiophoto luminescence 2−55926
- dosimetry grade, thermolum. mechanism 2−61720
- dosimetry of mixed field of gamma-rays and thermal neutrons 2−73948
- elastic wave damping, effective anharmonicity consts. 2−80913
- energy level structure, excited particle velocity spectrum on Ar-ion bombardment 2−48030
- F-centre hyperfine interactions, press. depend., ENDOR study 2−83986
- film on Al, thickness monitoring by reflectance meas. using 1216 ÅÅ line of H 2−55733
- film overcoat on Al, effect on u.v. refl. 2−79370
- foil sample thickness obs. in X-ray transmission texture photography 2−41447
- friction and wear, fund. review 2−47554
- Hartree-Fock band structure 2−61172
- high-level dosimetry, radiation induced optical absorption and photoluminescence 2−67096
- hydrostatic pressure influence on microstructure of single crystals containing cavities 2−83973
- i.r. absorpt. and refl., breathing shell model 2−78102
- i.r. absorption, assignments of two-phonon spectrum 2−61645
- i.r. absorption, isotope-induced one-phonon 2−78103
- limiting optical frequency, temp. variation calc. 2−72311
- mass attenuation and energy absorption coeffs. for 1 to 150 keV photons 2−64871
- melt, structure and motion, molecular dynamics calc. 2−74515
- multiphonon i.r. absorption spectra, effects of melting 2−68220
- neutron irradiated, defects, X-ray obs. 2−80660
- n.m.r. detection using Josephson junction magnetometer 2−66674
- phonons, thermal cond. and Poiseuille flow in thin layers and plates 2−61058
- powder phosphor, characteristics for thermally stimulated exoelectron emission dosimetry 2−67091
- proton irrad., surface damage monitoring using (p,α) reaction 2−43610
- R_2 centre, analysis of absorp. struct. 2−51342
- R-centre states, in F and M band regions 2−47445
- radiation-induced thermally activated depolarization 2−72007
- shock wave compression, X-ray diffr. obs. in single crystals 2−56646
- spark discharge induced damage 2−68013
- sputtering, positive ion ejection patterns 2−44008
- Stark effect of M-centres 2−61624
- substrate for deposited Hg film, thermal He atom scattering 2−56573
- surface, (001), gas atom-surface potentials 2−50450
- surface, scatt. of He atoms, one-phonon transitions 2−50451
- surface phonons on (001) face, calc. using shell model 2−68226
- surface polarons, binding energy and ground state wave function 2−84267
- surface thermoluminescence of compressed plate, after immersion in boiling water 2−48256
- teflon rod dosemeters, calibration for internal β-ray dosimetry 2−45050
- thermoluminescence dosimeter characts. as personnel monitor 2−70552
- thermoluminescence dosimeters, response to fast neutrons 2−79671
- thermoluminescence following plastic deformation 2−61721
- thermoluminescence of single crystal prod. by edge-defined film-fed growth technique 2−67943
- thermoluminescence phosphor, study of sensitivity factor mechanism 2−68698
- thermoluminescent, in teflon discs, consistency of dosimetric properties over repeated cycles of use 2−67087
- thermoluminescent dosimeter, for obs. during radiotherapy 2−69400
- thermoluminescent dosimeters, response to fast neutrons 2−85082
- thermoluminescent dosimeters, TLD-700, response to protons and α-particles 2−81979
- thermoluminescent dosimetry grade 100 powder incorporated in silicone rubber, dependence of energy response on grain size 2−68702
- thermoluminescent personal dosimeter system 2−69432

Lithium compounds continued
lithium fluoride continued
wave function regeneration, possibility for localized electrons for F-centres 2−68041
X-irradiated, thermolum., temp. depend. 2−65313
X-ray diffraction, extinction obs. in spherical crystal, Zachariasen's theory 2−67994
X-ray diffraction extinction obs. in large crystals 2−67993
X-ray Raman spectrum, peaks superimposed on Compton distrib. 2−72386
He atom elastic scatt. from LiF solid surface, Yukawa-type interaction 2−74239
layer between Fe-Co layers, interacting interdomain boundaries, electron microscope obs. 2−61534
LiF:Mg, high temp. plasticity, range 300−800K 2−74840
LiF:Mg, impurity associations decomp., light scatt. obs. 2−83983
LiF:Mg, thermoluminesc. sensitivity enhancement by Mn 2−44415
LiF:Mg, thermoluminescence variation with impurity distribution 2−84552
LiF:Mg thermal-activation analysis study of impurity hardening 2−71491
LiF:Mg^{2+}, thermoluminesc. depend. on state of aggregation of Mg^{2+} vacancy pairs 2−44416
LiF:Mn^{2+}, low-field X-band e.p.r. transitions 2−72492
LiF:Ti thermoluminescence variation with impurity distribution 2−84552
LiF-100, (-7) thermoluminescence, dose relationship, energy response and rate dependence from 8 keV-30 MeV 2−68701
LiF phosphor, study of sensitivity factor mechanism 2−68698
Mg_2SiO_4(Tb) thermoluminescence phosphor, study of sensitivity factor mechanism 2−68698
Ne atomic beam scatt. from (001) LiF surface, systematic trials study 2−74241
Ne atomic beam scatt. from surface, Lennard-Jones potential calc. 2−74240
Lithosphere *see Earth*
Localized states *see Crystal electron states*
Loges (molecular bonds) *see Bonds; Molecules/electronic structure*
Lorentz-Lorenz relation *see Dielectric phenomena*
Lorentz transformation *see Relativity/special*
Lorenz number *see Conductivity, electrical/solids; Conductivity, thermal/solids*
Loschmidt number (= Avogadro number) *see Constants*
Loudness *see Hearing; Intensity measurement, acoustics*
Loudspeakers *see Acoustic radiators*
Love waves *see Elastic waves; Seismic waves*
Low energy electron diffraction *see LEED*
Low-temperature phenomena
see also Helium/liquid; Helium/solid; Joule-Thomson effect; Superconducting materials; Superconductivity; Superfluidity
^{3}He-^{4}He solns., osmotic press. along phase separation curve near absolute zero 2−80500
binary intermetallics with large nucl. moments for thermometry 2−48939
binary intermetallics with large nucl. moments for thermometry 2−48939
cerium ethyl sulphate, heat capacity, demagnetiz. and susceptibility meas. below 1K 2−68551
conference, Freudenstadt, Germany (Apr. 1972) 2−45183
conference, Jerusalem, Israel (May 1972) 2−70340
European Phys. Soc. conf., Wiesbaden, Germany (Oct. 1972) 2−76139
fluids in saturated liquid state, calc. of kinematic viscosity 2−83732
glasses, thermal expansion and props. around 1K 2−61107
magnetic systems, concepts of negative and rotating temperatures 2−61472
steel, stainless 18-8, fatigue props. at cryogenic temps. 2−56939
$Ce_2Mg_3(NO_3).24H_2O$, temp. scale to 1.6 mK 2−45187
Cu-constantan thermocouple, magnetic field effects on Seebeck effect 2−63162
He, plasma, cryogenic, electron-ion recomb. coeff. 2−77264
He, superfluid, dissipative flow theory 2−71257
^{3}He-^{4}He dil. mixtures, osmotic press. 2−47005
^{3}He-^{4}He dil. solns., equil. theory 2−43416
^{3}He-^{4}He dilute mixtures, osmotic press., 20-400 mK 2−73242
^{3}He-^{4}He saturated mixtures, osmotic press. below 300 mK 2−43423
^{3}He melting press. thermometry, review 2−80515
Ta-H alloy, quenching at liq. He temps. 2−56907
YIG:Si^{4+},Ca^{2+}, rel. to mag. field inclination to crystallographic axes at 4.2K, 77K and room temp., obs. 2−84437
Low-temperature production
see also Joule-Thomson effect; Liquefaction/gases; Magnetic cooling
desorption cooling below 12 K using ^{4}He desorbed from synthetic zeolite 2−52009
desorption refrigeration systems performance 2−73247
difluorochloromethane, bubble evaporation, influence of pressure 2−73244
dilution refrigerator, temp. stabilization 2−82076
freons, boiling heat transfer, smooth tubes, finned tubes 2−82249
heat exchanger props. in dilution refrigerator 2−73243
mechanical refrigeration system, mixed fluorocarbon refrigerant, thermal capacity 300 watts at −130°C 2−73246
refrigerator, dilution, heat exchanger construct. 2−45192
refrigerator, dilution, using Pomeranchuk cell 2−45191
Cu, nuclear refrigeration, by adiabatic demagnetization 2−66364
He I refrigerant, heat transfer modes 2−64491
He II bath, thermal exchange props. 2−64498
^{3}He refrigerator, 200 mW recirculating 2−52008
LiBr absorption machine, thermodynamic cycle 2−62892
LiBr absorption refrigerator, with sprinkler generator 2−62891
Low-temperature technique
all glass liquid He Dewar using no auxiliary cryogens 2−58653
apparatus for heat capacity obs. 2−58652
apparatus for superhigh freqs. studies up to 1°K 2−58656
baffle, for single crystal X-ray diffraction 2−58654
bellows seal superfluid value 2−85166
calibration of resistance thermometers in 4-90 K range 2−85163
conference, Freudenstadt, Germany (Apr. 1972) 2−45183
Low-temperature technique continued
cryogenic emission electron microscope, design and specimen prep. 2−79049
cryogenic equipment, minimum refrigerant requirements for pre-cooling 2−66366
cryogenic systems, compressor and drive considerations 2−62890
cryogenics development and prospect 2−82077
cryomagnetic assembly for neutron diffraction studies 2−66372
cryopumping with liquid H_2, advantages over He refrigerator 2−78705
d.c. ratio transformer, standardisation and current detection 2−82421
dielectric cell for permittivity meas. 2−82414
FEP teflon seals, design 2−69486
film, heat capacity measurement at ^{3}He temp., d.c. temp. technique 2−81041
forced cooled superconducting systems, cryogenic problems 2−66365
freeze drying and low temp. stage for electron microscope 2−79110
freeze-etching technique, temperature, vacuum and fracturing considerations in electron microscopy 2−79100
freeze-fracture of biological samples for scanning electron microscopy 2−82080
gas cooled current leads with varying cross section 2−52007
glass dewar for microscopic obs. of magneto optical phenomena 2−69490
glass-ceramic capacitance thermometer, performance in 0.007 to 0.040 K range 2−66371
glass-ceramic capacitance thermometer for obs. in 1.7 to 300K range 2−76404
hydraulically actuated valve 2−58665
liquid N_2 level indicator, semiconductor detectors, thermistors 2−85164
low density aerodynamic tube, cryogenic pump calc. 2−82078
magnetometer, cryogenic, for rock magnetization meas. 2−54959
meas. of low temp. using thermal noise in Ge sensor 2−62889
metallized ceramic heat sink, thermal cond. obs. 2−76118
MHD convertor cooling 2−69848
microwave X-band spectrometer, dewar insert for Gigahertz-ultrasonics and ultrasonic paramagnetic resonance obs. 2−63203
multiconductor electrical feedthrough 2−48937
multiconductor electrical feedthrough 2−48937
mylar, thermal conductivity between 0.05 and 0.5K 2−47759
n.m.r. probe, crossed-coil, high sensitivity low-temp. meas. 2−82410
n.m.r. spectrometer probe 2−55635
nuclear target orientation using cryogenic apparatus of ^{3}He refrigerator and solenoid superconducting magnet 2−76736
optimal parameters of high pressure cryogenic fluid storage systems 2−76120
osmotic press. thermometry with dil. ^{3}He-^{4}He mixtures 2−45184
pressure regulator with pneumatic electric control 2−69487
pressure transmitting media, behavour of talc and teflon, down to 2K 2−73248
radiation damage studies of crystals in 8-300 K range using h.v. electron microscopy 2−79141
shock tube, operating at 30K min. 2−46550
specific heat meas. 2−41868
specimen preparation with freeze-drying technique for electron microscopy 2−79098
spectrograph, vacuum u.v., for crystal study 2−49454
SQUID, applic. to magnetic susceptibility obs. 2−52384
stabilization of temp. of dilution refrigerator 2−82076
Teflon cementing using ordinary rubber cement 2−85168
temp. controller for dilution refrigerator for temp. range 0.1-0.4K 2−85167
temperature control device for e.p.r. samples, 4.2-100K 2−76425
temperature scales defined by noise thermometry and ^{60}Co γ-ray anisotropy 2−45186
thermal switch using sorption pump 2−69485
thermometer, $Na_3[Ce(C_7H_3NO_4)_3].15H_2O$, for 2.20 mK range 2−82079
turbines and other machines, design, computer for obs. of gas state 2−52006
Ag solder alloy, superconducting transition at 64.4 mK 2−75058
Au-Fe thermocouples, calibration rel. to KP, Ag, Cu, temp. range 4K-280K 2−81158
C resistor thermometer, method of reducing effective magnetoresistance 2−52295
Cu n.m.r. thermometer, pulsed, for use below 0.5 K, construction and use 2−49185
EuS-EuF_2 films, prep. for magneto-optical obs. at low temps. 2−64567
H_2 liquefier 2−45188
^{1}H liquid target system development, use of closed cycle refrigerator 2−46034
^{2}H liquid target system development, use of closed cycle refrigerator 2−46034
He, liquid, level indicator for dewars 2−55327
He, liquid, level indicator for small metal Dewar vessels 2−58651
He liquid cooled stage for scanning electron microscope 2−82439
He liquid stage for scanning electron microscope 2−79119
^{3}He-^{4}He dilution refrigerator, acoustic device of ^{3}He concentration monitoring 2−85165
^{3}He-^{4}He dilution refrigerator, acoustic device of ^{3}He concentration monitoring 2−82574
N_2, liquid, level regulator 2−55328
Si:P thermometers, implanted, for 10 mK to 20 K 2−48938
Si:P thermometers, implanted, for 10 mK to 20 K 2−48938
LS coupling *see Atoms; Spectra/atoms*
Lubrication
see also Friction
ball and peg testing machine 2−68123
calcium stearate monolayers, shear strength 2−53383
centripetal pressure method, physical processes 2−77658
cylinders, glass and plastic, contact stresses, elastohydrodynamic lubrication 2−47559
elastohydrodynamic problem, finite element numerical solution 2−68114
flow stability between rotating cylinders liquid 2−67741
glass, hot viscous, sliding on metal surfaces, mechanics 2−56553

Lubrication continued
- lubricated sliding point contacts, load, traction, film thickness meas. device 2−53864
- non-Newtonian media, deformation velocity, relationship with strain, applications in lubrication 2−50162
- oils, viscosity index, repeatability and reproducibility 2−60448
- polymer with inorg. chain mols., self-lubricating heat-resisting antifriction props. 2−43745
- slip ring contacts, use of MoS_2 sputtered films 2−56596
- steel, lubricated friction against Al, oxidation influence 2−53844
- weight bearing joints in body, prostheses design applics. 2−69219
- MoS_2 coating, applied to steel by detonation, friction resist. 2−43744

Luder's bands *see Plastic deformation*

Ludwig-Soret effect *see Diffusion in solids*

Luminescence
- *see also Cathodoluminescence; Chemiluminescence; Electroluminescence; Fluorescence; Luminescent devices; Phosphorescence; Stimulated emission; Thermoluminescence; X-ray fluorescence*
- alternation effect in electronic spectra of organic compounds containing methylene chains 2−53040
- 3-amino-N-methylphthalimide exiplexes with acetone, pyridine and dimethyl formamide 2−64169
- atom, X-ray fluorescence, intermediate state proximity effects 2−70563
- aurora, rel. to space-time regularities and electron fluxes 2−68944
- bioluminescence, in marine teleost Porichthys notatus 2−55202
- bioluminescence obs., data acquisition system 2−52005
- bioluminescence phenomena, new biotelemetric method 2−85112
- charge transfer systems, excitation by coherent light, effect of nonuniform broadening on energy migration processes 2−54443
- colchicine, excited states multiplicity of absorpt. and emission 2−65392
- complex molecules, effect of solvent on electronic vibrational spectra 2−74253
- complex molecules in solid solutions, with two-photon excitation, determ. of polarization 2−42837
- cross-relaxation due to resonance transmission of excitations in spectral-inhomogeneous medium of impurity centres 2−84525
- crystal, excitonic region, review 2−72317
- decay measurements, multichannel photon counter 2−78127
- 1,1′- diethyl-2,2′-cyanine, adsorbed on Ag halide emulsion grains, J-aggregates props. 2−81027
- donor-acceptor pair recomb. emission, random distrib. effects, unified treatment 2−78124
- dosimetry, conference part II, Denmark, 1971 2−68675
- dosimetry, third international conference, 1971 2−82819
- dyes, selective light quenching 2−53074
- excitation transfer between electronic levels of impurity centres 2−78126
- eximeric bands 2−72389
- flavins, molecular luminescence, excited states 2−46605
- Forster-Dexter-Galanin theory of inductive resonance energy transfer, applicability criteria 2−78125
- gamma-ray excited, for visual control of γ-ray sources 2−85177
- impurity centres, polarization, rel. to nuclear spin 2−44405
- interplanetary scintillation of radiosources rel. to enhanced density irregularities of solar wind 2−85058
- kinetics, statistical method of determ., analysis of main errors 2−83238
- liquid solutions, quenching by electrostatic interaction of particles 2−60479
- luminophore grains, in dielec. medium, equiluminesc. curve 2−48213
- micelle solns., electron excitation energy transfer and conc. phenomena 2−60523
- molecular crystal, in contact with ferromagnet, emission due to exchange interaction 2−77838
- orthooxyazomethynes molecules, and radiationless transitions 2−53047
- pair photoluminescence, peak energy, excitation intensity depend. 2−75318
- personnel monitoring, application of luminescence methods 2−69428
- phenanthrene, excited dimer luminescence of pairs of molecules 2−56253
- phosphors oxychloride, for i.r. to visible conversion 2−84531
- phosphors quantum yield for u.v. 2−44413
- photoluminescence, comments on theory of concentrational depolarization 2−78146
- photoluminescence, laminar specimen, obs. technique 2−57343
- phthalimide derivatives, selective light quenching 2−53074
- phthalimides and other dyes, bathochromic luminescence in alcoholic solutions and polymer matrices 2−77440
- polyatomic mols., absorpt. and luminesc. relationship in four-level system of electronic states 2−64087
- porphyrins, intramolecular spin-orbital perturbations 2−53077
- powder luminophore, elec. field influence 2−48214
- primary reconstruction, Becquerel formula 2−72390
- radiant, statistical method for recording regularities 2−63310
- Renner systems, absorpt. and luminesc. bands due to crystal imperfections, semiclassical approximation 2−81393
- scintillated crystals, dependence of yield on radiation energy 2−59604
- semiconductor, trapping centres, defect related luminesc., two centre model 2−61680
- solid, slow vibrational relax. effect on Stokes shifted luminescence 2−51374
- solids, concentration quenching, theory 2−54445
- sugar, intensity obs. rel. to elastic const. detn. 2−51396
- tartaric acid, intensity obs. rel. to elastic const. detn. 2−51396
- trifluorochloroethylene, absorption saturation and optical strength for CO_2 laser pulses 2−67523
- Ag halides, physics and chem., conf., Montreal, Canada, Aug. (1972) 2−81541
- Co, energy dependence of collisional deactivation cross section 2−46646
- $DyNi_2$, magnetization mechanisms 2−72107
- GaAs photodiode with anti-Stokes luminors 2−77967
- Li transitions, model pot. calcs. 2−76976

Luminescence continued
- N_2, decay time obs. α-particle excited 2−50057
- N_2, energy dependence of collisional deactivation cross section 2−46646
- Nb, obs. in Ar matrix at 14 K 2−83178
- Ne, polarization of light emitted on de-excitation under H ion impact 2−42736
- O_2, energy dependence of collisional deactivation cross section 2−46646
- $O(^1S)$ deactivation by CO_2, O_2, N_2, Ar, temp. depend. 2−79871
- $(UO_2F_5)^{3-}$, frequencies and form of normal vibrations, interpretation of luminescence spectra 2−64159
- YF_3:Yb^{3+}-Ho^{3+}, anti-Stokes luminescence, spectrum and excitation energy dependence 2−61688

gases
- air, decay time obs. α-particle excited 2−50057
- anthracene and derivatives, sensitized anti- Stokes delayed annihilation fluoresc. 2−74284
- ethylene, laser induced combination band luminescence, vibration-rotation energy transfer 2−60066
- Cm, L_2 subshell, fluoresc. yield 2−79924
- HF vib. fluorescence, vib.-vib. energy transfer time detn. 2−60005
- O_2 emission in night glow of Martian atmosphere, height of emitting layer 2−55145

liquids and solutions
- alkali halides, γ-irrad., aquoluminescence on dissolution, isothermal annealing effect 2−43376
- 3-aminobenzaldehyde, in aprotic solvent, chemilum. on ozonization 2−54538
- anthracene dyes in alcohol soln., fluoresc. correl. with photochem. activity 2−77432
- anthracene solns., quenching under intense excitation 2−54471
- aromatic alcohols, quantum yields of free radicals, effect of transannular interaction 2−71212
- 2-(N-arylamino)-6-naphthalene sulphonates, fluoresc. emission and quenching analysis 2−80077
- azomethines with fluorine- containing substituents, in solutions 2−75326
- benzene, quantum yields of free radicals, effect of transannular interaction 2−71212
- benzene solutions of aromatic hydrocarbons, radiation-induced fluorescence 2−53447
- benzene solutions of aromatic hydrocarbons, radiation-induced fluorescence 2−53448
- benzoquinoline, 7,8- and 5,6-, dipole moments in fluorescent states 2−74281
- complex molecule solutions, dependence of fluorescence spectra on exciting light 2−60480
- concentration depolarization and quenching in photoluminesc. in solutions 2−83791
- concentration quenching, theory 2−54445
- concentration quenching of fluorescence polarization in two and three dimensional solution 2−64462
- cryptocyanine, fluoresc. quantum yield, 140−300K 2−77441
- cyclohexane solutions of aromatic hydrocarbons, radiation induced fluorescence 2−53446
- cyclohexane solutions of aromatic hydrocarbons, radiation- induced fluorescence 2−53449
- cyclohexane solutions of aromatic hydrocarbons, radiation-induced fluorescence 2−53448
- cyclohexane solutions of aromatic hydrocarbons, radiation-induced fluorescence 2−53447
- decay law, multipolar delayed interaction in transfer of excitation energy 2−53439
- dibenzofuran excimer emission 2−46967
- dimer conc. and equilib. const. determ. from photolum. 2−81503
- diphenylamine, two-photon fluorescence patterns, absorption cross sections and picosecond relaxation times 2−43379
- 2,5-diphenyloxazol, anthryl derivatives, dependence of threshold of generation on pumping polarization 2−53450
- dye, triplet lifetime effects on laser efficiency 2−69927
- electron transfer photoprocesses, fluorescence extinction and exiplex formation 2−48346
- erythrosin molecule in alcohol and isopropanol solvents, dynamics of ultrafast decay processes 2−43367
- ethanol-dye soln., fluoresc. depolarization, vitreous transition obs. 2−60602
- excitation energy transfer between ions and electrostatic interaction 2−60478
- excitation transfer between identical luminescent molecules in solutions, effect produced by initial shock 2−50368
- fluorescein solns. luminance, rel. to contact lens practice 2−55318
- indole, interaction with methanol, kinetics 2−53069
- indole and derivatives in aqueous salt solns., effect of adding salt on deactivation of excited state 2−77442
- ketone energy transfer to rare earth ions, mechanism 2−60482
- luminol-alkali-^{32}P system, internal irrad. induced chemiluminesc. 2−48325
- macromolecules in soln., polarized luminescence for investigation of intramolecular mobility 2−60090
- 1-methylnaphthalene, excimer-monomer equil., deactivation processes, temp. effects 2−71214
- organic dye solutions in far anti-Stokes region, correspondence with absorption spectra 2−74546
- organic dyes: Eu^{3+}, Tb^{3+}, quenching due to dipole-dipole transfer of energy from ions 2−54460
- organic solns., temp. depend. of non-radiative, deactivation processes 2−80070
- organoluminophores in solvents of different polarities, activation energies of radiationless transitions 2−53443
- organoluminor solution, obs. of stimulated emission by exciplexes 2−67836
- phthalimide solution, double-band generation, fluorescence spectra 2−43377
- polymer solutions dependence of threshold of generation on pumping polarization 2−53450
- polymers of phenyl containing anthracene, conformal depolarization of luminescence, dependence on polymer chemical structure 2−53444
- polymethine dyes, stimulated fluorescence depend. on exciting illumination 2−77443

Luminescence continued
liquids and solutions continued
polyphenylene, fluorescence spectra, energy transfer mechanism 2−71209
polystyrene with paraterphenyl, energy transfer of electronic excitation 2−71216
pyrene solns., quenching under intense excitation 2−54471
rare earth elements in solution, transfer of electron excitation energy between ions, dependence on solvent nature 2−53442
rare earth ion aqueous solns., fluoresc. quenching by vibrs. of solvent mols. 2−60481
reserpine solution, fluoresc. detection reaction, sensitivity increase by Th ion addition 2−71215
rhodamine 6G, two-photon fluorescence patterns, absorption cross sections and picosecond relaxation times 2−43379
Rhodamine 6G excited mols., second electron state studies 2−60484
Rhodamine 6G monomers and associates, intramol. degradation processes of electron excitation energy 2−60485
rhodamine B, in aqueous soln., fluoresc. excitation spectra 2−64465
rhodamine B solution in methanol, anti-Stokes fluorescence in organic dye solutions 2−43378
rhodamine solutions, quenching by anthracene compounds 2−43380
self-depolarization theory 2−53438
sonoluminescence of liquids, effect of dissolved salts and reducing agents 2−71210
squalane containing biphenyl, variation of thermoluminescence with concentration 2−46969
tetraphenylbutadene dependence of threshold of generation on pumping polarization 2−53450
thiacarbocyanine dyes with different substituents in meso position 2−61701
thianthrene complexes in solution, fluorescence study, enthalpies 2−84637
toluene, quantum yields of free radicals, effect of transannular interaction 2−71212
toluene and polymeric solutions of derivatives of oxazoles and oxadiazoles, stimulated emission 2−59164
triphenylamine in alkane, ion recombination fluorescence, viscosity dependent rate 2−46968
uranyl compounds in solution, transfer of electron excitation energy between ions, dependence on solvent nature 2−53442
vacuum chamber for obs. 2−58670
vinylparaterphenyl with styrene, energy transfer of electronic excitation 2−71216
Eu in complexes with β- diketones, Tb sensitized luminescence 2−74549
Gd^{3+} ions in solutions of complex compounds 2−71211
H_2O:Tl, effect of concentration of Tl ions 2−53441
KCl soln., aquoluminesc. after γ-irradiation 2−84662
LiBr:Tl, aqueous solution, effect of concentration of Tl ions 2−53441
LiCl:Tl, aqueous solution, effect of concentration of Tl ions 2−53441
$POCl_3$ solns., electrolum. of trivalent rare earth ions, emission mechanism 2−46966
Sm complexes with β-diketones, Tb sensitized luminescence 2−74549
$TbNi_2$, magnetization mechanisms 2−72107
solids, inorganic
alkali halides, Cu doped, fluorescence spectra obs., Mollow-Ivey relations 2−61712
alkali halides, excited F-centres, emission mechanisms 2−80709
alkali halides, fast recomb. transition lifetimes 2−54450
bulk effects in photoluminescence meas. 2−72391
$CaF_2.3Ca_3(PO_4)_2:Nd^{3+}$, local compensation of Nd^{3+} ionic charge 2−64681
CaF_2, thermoluminesc., due to low temp. plasma produced radiational defects 2−71452
chalcogenide, amorphous, photoluminesc., review 2−61445
colour centre behaviour and band modes in semiconductors and insulators 2−54448
donor-acceptor emission energy shift on varying the excitation intensity 2−72388
electroluminescent film, electrode current rel. to applied stress 2−81435
energy degradation mechanism of rare earth and transition metal ions 2−61678
energy transfer from hot donor to acceptor 2−51363
exciton emission lines, at high exciton conc., theory 2−71807
fluctuations, MHD waves and mag. variations 2−72912
fluoranthene, quenching due to exciton- exciton interaction, determ. of rate const. and exciton migration rate 2−81426
fluorite, relative thermoluminesc. effects of α- and β-radiation 2−51379
glass:Eu^{3+}, comp. and temp. depend., effective cryst. field props. 2−78130
glass:Nd, fluoresc., effect of phase separation 2−57372
glass:Nd, ion-ion energy transfer temp. depend. laser induced line narrowing obs. 2−65307
glass, Ag activated phosphate, dosimetry props. rel. to melting and heat treatment 2−51381
glass, due to 5.6 keV inert gas ions 2−61123
glass, Nd-activated, excitation of luminescence 2−78135
glass, rare earth doped, fluoresc., quenching by OH^- ions 2−54467
glasses, low temp., vacuum chamber for obs. 2−58670
graphitic diamonds, electroluminescence at 480-780 nm, determ. of voltage and frequency dependence of intensity 2−84546
groups III-V luminescent materials 2−44417
KI:Tl, total emission spectra and energy transfer from excitons to activator 2−61710
luminophores activated with Eu^{2+}, oxidation effects 2−54483
Me^{II}, $Me^{VI}O_4$:U single crystals with scheelite structure, Me^{II}=Ca, Sr, Ba, Me^{VI}=Mo, W, obs. between 300K and 4.2K 2−68676
metals, theory of photoluminescence in two-band model 2−72439
metaphosphate glasses, silver-activated, influence of base glass on radiophotoluminescence 2−57383
p-n junctions, photoluminesc., quenching by elec. field in space charge region 2−65290

Luminescence continued
solids, inorganic continued
phenylcyclopropanes and phenylethanes, emission spectra, 77K 2−84663
phosphate glass, energy transfer between Sm^{3+} and Eu^{3+} 2−48238
phosphor, cathodoluminescent, absolute radiative efficiency 2−72432
phosphors with two capture levels, thermolum., model 2−65313
quartz, relative thermoluminesc. effects of α- β-radiation 2−51379
rare earth complexes, luminescence relaxation time, probabilities of inter- and intra-molecular energy transfer 2−54449
rare earth lithium mixed oxides, of Eu^{3+}, energy levels 2−48226
rare earth oxides, Eu^{3+} and Tb^{3+} doped, flame excited luminesc., temp. depend. 2−48270
rare earth oxysulphide multilayer films, efficiency 2−48224
rare earth phosphors, quenching, energy transfer between unlike ions 2−54457
rochelle salt, intensity obs. rel. to elastic const. detn. 2−51396
rochelle salt, triboluminesc. intensity obs. rel. to elastic const. detn. 2−51396
ruby, quantum yield with u.v. excitation 2−61684
ruby, sharp-line, for measurement of pressure in diamond-anvil high-pressure cell 2−58658
semiconductor, exciton luminesc., effect of absorpt., surface annihilation of excitons 2−78129
semiconductor, group II-VI cpds., radiation induced and growth defect obs. 2−47372
semiconductor, impure, multiphoton luminesc. satellites in strong e.m. field 2−61679
semiconductor, non-equilib. charge carrier condensation and recomb. radiation 2−54184
semiconductor, nonparabolic energy bands, mag. susceptibility calc. 2−71928
semiconductor, optical detection of dynamic polarization of nuclei 2−44323
semiconductor, p-type, recomb. of excitons bound to deep neutral donors and acceptors 2−68682
semiconductor, recombination luminesc. rel. to absorption, recomb. and field mechanisms 2−78128
semiconductor, recombination radiation, recording 2−51364
semiconductor, stimulated effects in radiative recomb. from electron-hole liq. 2−65289
semiconductor, with nipi superstruct., critical and electrical props. 2−65237
semiconductor II-VI cpds., donor and acceptor identification 2−50573
semiconductors, II-VI, deep Cu impurity, dynamical Jahn-Teller interaction 2−80954
silicates, of Eu^{3+}, spectral characts. and quantum efficiencies 2−48233
soda glass:Tb^{3+}, excitation and decay times 2−57374
1,2,4,5-tetracyanobenzene-durene complex, quenching due to exciton-exciton interaction, determ. of rate const. and exciton migration rate 2−81426
uranyl compounds, electron-vibrational spectra 2−54458
vitreous solutions doped with molecular anions, low temp. study 2−54444
wavelength converter, i.r. region, antiStokes mechanism, heterojunction structure 2−66848
$[Al(ha)_6]Br:Ti^{3+}$, $^2E \rightarrow {}^2T_2$ transition mechanism 2−65302
Ag activated phosphate glasses, radiation induced photoluminescence, laser pulse excitation 2−68713
AgBr, chemical sensitization by doping, obs. of electronic mechanisms 2−81545
AgBr, emulsions and crysts., red luminesc. at 77K, electron-hole recomb. 2−81438
AgBrI, photographic emulsion coatings, at 77K 2−81437
AgCl:I-, 4.2-80K, decay mechanism of bound exciton 2−72392
Al:Dy, Tb, galvanoluminesc. 2−57380
Al radiation generated during rapid deform. and rupture, tribolum. 2−54482
$Al_xGa_{1-x}As$, $0.16 \leqslant x \leqslant 0.58$, photolum. spectra, 1.6-300K 2−61683
$Al_xGa_{1-x}As$ grown- diffused electroluminescent planar monolithic diodes 2−51386
AlGaAsP, solution growth, stimulated emission, laser operation 2−45747
AlGaAsP, solution growth, stimulated emission, laser operation 2−45747
AlN:Eu,Mn, radical recomb. luminesc. and photoluminesc. 2−57371
AlN:Mn, spectrum of luminescence centres 2−75319
$Ar:O_2$, mol. oxygen luminesc. and excitation spectra at 4.2K 2−48215
$Ar-O_2$ system, luminesc. sidebands obs. 2−75310
As_2Se_3, vitreous, recombination centre nature 2−61686
As_2Se_3, vitreous and monocryst., recomb. radiation 2−54451
As_2Te_2Se, amorphous semicond., thermalization in energy band tails 2−61685
Au discontinuous film, photon emission on applic. of strong electric field 2−48266
BN, hexagonal, blue thermolum. emission, paramag. centre identification 2−72430
B_2O_3 glasses, photo- and X-ray luminescence, obs. of luminescent centres 2−84547
B_2O_3 glasses, photo- and X-ray luminescence, obs. of luminescent centres 2−84547
$(Ba, Pb)TiO_3$ ceramic, light emission by surface microplasma new Curie temp. 2−65303
$BaCaAlF_7:Eu^{2+}$, three polymorphs 2−72420
$BaF_2:Yb^{3+}-Ho^{3+}$, anti-Stokes luminescence, spectrum and excitation energy dependence 2−61688
BaF_2, thermoluminesc., due to low temp. plasma produced radiational defects 2−71452
$Ba_2MgGe_2O_7:Eu^{3+}$, Tb^{3+}, Nd^{3+}, crystal and glass matrices 2−72423
$Ba_{2.96}MgSi_2O_8:Eu^{2+}$, prep. depend. 2−84550
$BaO-ZrO_2-SiO_2$, excitation and emission spectra 2−75320
BaO powder, recomb. luminesc., 103-423 K 2−61687
$BaTiO_3$, light emission due to uniaxial stress pulses 2−72440

Luminescence continued
solids, inorganic continued
$Ba_2ZnGe_2O_7:Nd^{3+}$, absorpt. and fluorescence spectra, Nd^{3+} stimulated emission and laser action 2−61705
Bi, radiation generated during rapid deform. and rupture, tribolum. 2−54482
BiI_3, localized states and electron-hole processes obs. 2−61706
$BuF_2:Sm^{2+}$, fluoresc., one phonon sidebands, theory 2−65304
Ca radiation generated during rapid deform. and rupture, tribolum. 2−54482
$CaCO_3$, rare earth doped, X-ray excited optical fluorescence 2−61707
$CaF_2:Er^{3+}$, two photon excitation by Nd laser wavelength depend. 2−48216
$CaF_2:Gd^{3+}$, thermolum. glow curves, hole activation energies, 4.2 to 600K 2−57377
$CaF_2:Ho^{3+}$, two photon excitation by Nd laser wavelength depend. 2−48216
$CaF_2:Mn$, $CaF_2:Tb$, relative thermoluminesc. effects of α- and β-radiation 2−51379
$CaF_2:Mn$, thermoluminescence, trapping centres 2−68699
$CaF_2:Mn$ thermoluminescence dosimeters, influence of size on ^{60}Co γ-ray dosimetry in extended media 2−67088
$CaF_2:Nd_2O_3$ (NdOF), optical spectra of Nd^{3+}, Stark effect obs. 2−61702
$CaF_2:Tb^{3+}$, photo- and X-ray luminescence, obs. of luminescent centres 2−84547
$CaF_2:Tb^{3+}$, photo- and X-ray luminescence, obs. of luminescent centres 2−84547
CaF_3-$YF_3:Er^{3+}$, spectroscopic study of stimulated radiation 2−61689
CaF_2, $\langle 100\rangle$ and $\langle 110\rangle$ oriented F_2-centre obs. 2−53751
CaF_2, thermoluminescence under exposure to u.v. light 2−68700
$CaI_2:K$, Pb, Mn, investigation using 365 nm u.v. irradiation 2−51387
$CaMoO_4$, photoluminescent props. 2−72441
CaO-ZrO_2-SiO_2, excitation and emission spectra 2−75320
CaO, F^+ and F-centres, temp. depend. 2−84537
CaO, Jahn-Teller coupling in excited level of F^+ centre, uniaxial stress effects 2−68635
CaO, neutron irrad., $F_a{}^+$ centre, emission band obs. 2−71522
CaO, rare earth doped, X-ray excited optical fluorescence 2−61707
CaS:Bi:Fe phosphors, emission characteristics, role of S^{2-} and Cl^- determ. by Fe^{3+} impurity 2−65311
CaS:Bi, Pd phosphors, thermally stimulated, kinetics 2−54475
CaS phosphor, activator and co-activator emission characts. 2−48239
CaS phosphors, self activated emission, study of trap depths and nature of trapping centres 2−54473
$CaSO_4:Mn$ thermoluminescence, dose relationship, energy response and rate dependence from 8 keV-30 MeV 2−68701
$CaSO_4:Sm$, Mn activators, thermoluminesc. spectra 2−48255
$CaSo_4:Mn$, relative thermoluminesc. effects of α- and β-radiation 2−51379
$Ca_3(VO_4)_2$, spectra, wavelength range 300-700 nm 2−84534
$CdBr_2$-Pb crystals, temp. depend. of recombinat. luminesc. and photocond. 2−72049
$CdBr_2(Pb,Mn)$, recombination interact. of luminescence centres, 90-400 K 2−84544
$CdCl_2(Pb,Mn)$, recombination interact. of luminescence centres, 90-400 K 2−84544
$CdF_2:Er^{3+}$, i.r. transitions, Stark dissoc. by cryst. field 2−65305
$CdF_2:Er^{3+}$, M^+, (M=Li, Na, Ag or K), C_{2v} local-site symmetry 2−78164
CdF_2, fluoresc. of Er^{3+}, ion site obs. 2−54416
CdP_2, cathodolum. and photolum., recomb. mechanisms 2−72394
CdS:Ag, radiative recomb. mechanisms 2−61690
CdS:Cu, optoelectronic effects, i.r. quenching 2−65000
CdS:Cu powder phosphors, a.c. electroluminesc. characts. 2−44420
CdS:Cu powder phosphors, d.c. electroluminesc. characts. 2−44419
CdS, bound-to-bound emission at 510 nm 2−61691
CdS, donor-acceptor luminesc., temp. depend. 2−48261
CdS, donor-acceptor pair emission, electron irrad. damage effects 2−54478
CdS, doped, 2.0 eV luminesc. band, donor-acceptor recomb. model 2−84539
CdS, exciton-exciton emission line shift 2−44407
CdS, exciton-impurity complex, radiative recomb. 2−72324
CdS, exciton photoluminesc., picosec. and nanosec. spectroscopy obs. 2−72421
CdS, fast electron excitation, phonon assisted exciton recombination 2−48240
CdS, photosensitivity, luminesc. intensity, rel. to donor-acceptor photothermal dissociation 2−72393
CdS, piezoemission from free excitons 2−78143
CdS, production of super radient light sources by electron beam pumping 2−79215
CdS, pulsed region cathodolum., thermal cond. obs. 2−54077
CdS, radiation from donor- acceptor pairs and phonic recurrence 2−72395
CdS, retaining metastable phases by quenching under pressure 2−84152
CdS, spectra fine struct., localized exciton struct., at 4.2K 2−51366
CdS, strain splitting of bound excitons 2−68678
CdS cathodoluminescence, electron beam microprobe exam. of crystal structure defects 2−53745
CdS phosphor, Schon-Klasens model interpret. 2−51213
CdS platelets, electron irradiated, radiation damage effects on luminescence at low temperatures 2−68703
CdS polariton emission 2−48218
CdS powder, electroluminesc. brightness, effect of nonstoichiometric deviations 2−61716
CdS(Se), 2-100K, exciton interactions 2−68677
CdS(Te), photolum. and thermal neutron damage 2−48219
CdSe, exciton bound to ionized centre, magneto- optical obs. 2−68636
CdSe, exciton photoluminesc., picosec. and nanosec. spectroscopy obs. 2−72421
CdSe, spontaneous and stimulated luminescence by high-density excitations in 77 to 300 K range 2−44406
CdSe laser crystal, electron beam excited 2−77965

Luminescence continued
solids, inorganic continued
$CdSnP_2:Ag(Cu)$, spontaneous- and stimulated- emission spectra 2−51365
CdTe, electron radiation damage and cathodolum. edge emission 2−48254
CdTe, photoluminescence obs. of ion implanted impurity states 2−74790
CdTe, spontaneous luminescence and lum. spectra detn. 2−72417
p-CdTe film, photolum. spectrum 2−48217
$Ce_2Si_2O_7$, photoluminesc., Tb-activator prop., energy transfer mechanism 2−48220
Cr complexes, Cr(III) dimethylsulfoxide compounds, low temp. luminescence and vibrational spectra 2−51375
Cr complexes, tris sulphur chelates chromium (III) 2−65306
$Cr(ur)_6I3$, and deuterated complex, low temp. spectra, obs. of ^2E level splitting, zero-phonon transitions 2−51290
CsBr, CsBr:Tl, CsBr:In, luminesc. crystals, exciton and hole migration 2−48242
CsI:Na, mechanism of thermally stimulated afterglow in 60-90 K range 2−72431
CsI:Tl, α and γ scintillation, growth times 2−73938
CsI:Tl single crystal, influence of channelling on scintillation efficiency 2−72396
CsI, relaxed state of self-trapped exciton 2−65291
CsI(Na), nature of luminescence centres, hypothesis based on properties of CsI crystals 2−68679
$Cs_2ZrB_6:Re^{47}$, sharp- line luminesc., vibr. mode energies 2−57370
CuCl, two-photon, and second harmonic generation in exciton region 2−54453
CuI, emission under high density excitation 2−72397
Cu_2O, exciton luminesc. spectra, ortho- and para-exciton interactions, optical phonon freq. 2−57133
$CuSO_4$, intensity obs. rel. to elastic constant detn. 2−51396
$CuSO_4$, triboluminesc. intensity obs. rel. to elastic const. detn. 2−51396
Er with Mo for glass laser, patent 2−82486
Er^{3+}, spectra in phosphate and borate glasses, emission and absorpt. cryst. field effects, luminesc. efficiency 2−75307
Er^{3+} doped oxides, visible, i.r. excited, effect of host lattice 2−78140
Er^{3+} glass, stimulated emission cross section, relative gain coeff., absorpt. and fluorescence spectra obs. 2−75323
$Er_2O_2S:Er^{3+}$, fluorescence spectra, energy levels and crystal field splittings detn. 2−51339
Eu compounds with aromatic acids 2−75324
$EuAlO_3:Mn^{4+}$, Raman luminescence 2−44428
Eu_3SiO_5, photoluminesc., single emission band 2−48173
$FeCl_4{}^-$ containing compounds, investigation at 85K 2−51367
(Ga, Al)As/GaAs, epitaxial luminesc. diodes, emission delay time between elec. and optical signals 2−72401
$Ga_{1-x}Al_xAs:Si$ diodes, substrate orientation depend. 2−51153
$Ga_{1-x}Al_xAs$, indirect gap semicond., direct band recombination 2−75337
n-$Ga_{1-x}Al_xAs$ epitaxial film, edge photoluminesce, free exciton annihilation contrib. 2−81432
$Ga_xAl_{1-x}As$, polarization in applied r.f. field, freq. depend. 2−61695
GaAs:Cr, deep levels and radiative recomb., photolum. study 2−71927
GaAs:Cr, instability of recomb. radiation and photocurrent 2−84540
GaAs:Ge p-n junction, Zn- diffused, photolum., 8100-8500 Å 2−72404
GaAs:Sn, photoluminescence props. 2−44427
GaAs:Te, heavily-doped, defect studies 2−71926
GaAs-$Al_xGa_{1-x}As$ p-n heterojunction, current flow during electrolum. 2−72438
GaAs-$Ga_xAl_{1-x}As$ n-p heterojunction, field effect of GaAs photolum. 2−72399
GaAs-GaP n-p heterojunction, field effect of GaAs photolum. 2−72399
GaAs, bound exciton photoluminesc. 2−57373
GaAs, electrolum. diode, sinusoidal modulated, recomb. emission phase shifts rel. to injection levels 2−72400
p-GaAs, electron beam excited, internal quantum efficiency, effect of beam voltage increase 2−72433
n-GaAs, electron irrad., annealing behaviour 2−47918
GaAs, epitaxial, photolum., 8250-8450Å 2−61694
GaAs, exciton-exciton and electron-exciton interactions in highly excited material 2−78132
n-GaAs, from implanted Zn ions 2−48222
GaAs, generated by acoustoelec. domains 2−80912
GaAs, heat treated, photoluminesc. obs. of acceptor centres 2−61343
n-GaAs, heavily doped, band-to-band recomb., quantum efficiency, lifetime, rel. to impurity conc. 2−61697
GaAs, LPE-grown shallow acceptor identification 2−54454
GaAs, photoluminesc., nonequilib. carriers strong interaction, 77K 2−68680
GaAs, radiative recomb. of screened excitons 2−72408
GaAs epitaxial film, cathodolum., carrier mobility effects 2−72434
GaAs epitaxial film, substrate orientation effects 2−47436
GaAs epitaxial layer 2−72442
GaAs junction laser, spontaneous emission behaviour across threshold 2−66766
GaAs targets, luminescence obs. 2−54479
$GaAs_{1-x}P_x:N$, photoluminescence, spontaneous and stimulated, from N A-line and NN pair, transitions 2−81414
GaAsP wafers, obs. using scanned-laser microscope 2−55706
$GaAs_{1-x}P_x$, p- and n-type, direct and indirect gap, photoluminesc. spectra 2−84538
GaN:Zn(Cd), acceptor site location and new emission band obs. 2−72398
GaN, bands, positions, half-widths, intensities, rel. to temp. 2−65299
GaP: Zn, Al, photolum. and electrolum., 1.7 to 2.3eV 2−75321
GaP:Bi, kinetics due to bound excitons, 77.3K 2−65292
p-GaP:Cu,O, bound exciton luminesc., emission and excitation spectra 2−78131

Luminescence continued
solids, inorganic continued
GaP:Mn, i.r. luminesc. due to $^4T_1 \rightarrow {}^6A_1$ internal transition, dynamic Jahn-Teller effect 2−81424
GaP:N, null field splitting of B-line 2−61692
GaP:N, Zeeman effect on bound exciton-complex 2−61693
GaP:N(Bi), exciton binding to impurities, uniaxial stress effects 2−75108
GaP:Sb, recomb. radiation involving isoelectronic centres 2−72407
p-GaP:Zn,O, photolum. efficiency and kinetics of Zn-O complex formation 2−51368
p-GaP:Zn,O, red-emitting, quantum efficiency limits 2−68681
GaP:Zn,O, time response rel. to multiple trapping at Zn-O impurity centres, 4-120K 2−61696
GaP, green electrolum. efficiency, weak photolum. band 2−84548
GaP, melt-grown, S-pit correl. with reduced efficiencies 2−50595
GaP, pair photolum., peak energy, excitation intensity depend. 2−75318
GaP, physics of radiative centres 2−61724
GaP, red photolum. quantum efficiency 2−47268
GaP green emitting diode fabrication by double- bin liquid-phase epitaxy 2−72437
GaP p-n-p-n green light emitting diode 2−72436
GaP photoluminescence, laminar specimen, obs. technique 2−57343
GaP red-emitting diodes, scanning electron microscope characteriz. 2−51389
p-GaP(Zn,O), p-GaP(N), minority carrier lifetime, decay time obs. 2−48221
β-Ga_2S_3, excitation and emission spectra 2−84532
GaSb:Te, lightly doped, photolum. at high excitation levels 2−72402
GaSb:Te(Zn)(Te + Zn), heavily doped, photolum. at high excitation levels 2−72403
p-GaSb, undoped, photoluminesc., acceptor states and excitons 2−61708
GaSe, of free and bound excitons, 4.2 and 1.8K 2−72406
$GdLiO_2$, of Eu^{3+}, energy levels 2−48226
Gd_2O_3:Eu^{3+}, transparent ceramic phosphor 2−72409
Gd_2O_3:$Eu^{2+}(Tb^{3+})$, flame excited luminesc., temp. depend. 2−48270
$GdVO_4$, dependence on electronic transitions in $VO_4{}^{3-}$ 2−65300
Ge, condensed electron-hole state, temp. depend. props. 2−68683
Ge, electron-hole drops 2−68432
Ge, electron and γ-irrad., Mossbauer type photoluminesc. spectra obs. 2−48243
Ge, emission band, two electron band-to-band transitions, excitation intensity 2−61699
Ge, pure and doped, radiative recomb. during electron-hole condensation 2−78133
Ge, radiative recomb., 2-77K, effect of electron-phonon interaction 2−68684
Ge, radiative recomb. of biexcitons 2−78134
Ge single crystal, bound exciton luminesc. 2−68692
p-$Hg_{1-x}Cd_xTe$, carrier freeze-out and acceptor energies determ. 2−57194
HgI_2 single crystal, tetragonal, exciton luminesc., temp. depend. 2−84541
n-InAs, photolum., 77-200K, temp. effects 2−72412
InP, bound exciton photoluminesc. 2−57373
InP, free and bound electron transitions to acceptors, 1.3776 eV emission 2−72411
InP, free and bound exciton decay 2−72410
InP, group IV doped, charact. photolum., spectral peak assignment 2−47272
InP, photoluminesc. of bound excitons 2−68685
InP, photoluminesc. of excitons bound to neutral acceptors, strain effects 2−48223
InP, photoluminescence spectra of excitons bound to group II acceptors 2−84279
n-InP, photon replicas in the induced luminescence spectra under the conditions of two photon excitation 2−81429
p-InSb, lightly doped, radiative recomb. parameters temp. depend., 10-400K 2−65293
n-InSb, recomb. radiation from impact-ionized shallow donors 2−68707
InSb, recomb. rate rel. to elec. field, drifted Maxwellians approx. 2−81077
KBr:Na, F_b centres 2−64682
KBr:PO_2, recombination luminescence, F-centre accumulation during β-irradiation 2−78136
KBr, crystals, vibrational transitions of OH^- molecular ion 2−57369
KBr crystals, u.v. irrad. and colour centre prod. from exciton decay 2−71527
KBr(I) fast recomb. transition lifetimes 2−54450
KCl:In detection of In^+ centres by characteristic emission 2−81001
KCl:KI, films, slow electron impact, luminescence excitation and characteristic energy losses 2−81417
KCl:Na, F_b centres 2−64682
KCl:Pb, polarized luminesc. and dipolar relax. of Pb-vacancy complexes 2−72424
KCl:Sn, M^{2+} (M = Mg,Ca,Ba,Zn,Cd), exptl. investigation 2−65294
KCl:Sr, X-ray induced defects, thermal annealing effects 2−64684
KCl:Tl, excitation spectra in the region of fundamental absorpt. 2−48244
KCl:Tl, KBr:Tl detection of Tl^+ centres by recombination radiation from F centers 2−81001
KCl:Tl, thermal glow traps responsible single negative ion vacancies 2−75333
KCl-KI:Tl, intracentre luminesc. 2−81425
$2KCl$-$SnCl_2.2H_2O$, also absorption and excitation spectra 2−54456
KCl crystals, vibrational transitions of OH^- molecular ion 2−57369
KCl(Br)(I), Ag^- centres, polarization and decay time of luminesc. 2−80710
$KCl.SnCl_2.H_2O$, also absorption and excitation spectra 2−54456
KI:Tl, host-sensitized luminesc., elec. field effects 2−81419
KI films, slow electron impact, luminescence excitation and characteristic energy losses 2−81417
$KIPbI_2.2H_2O$, also absorption and excitation spectra 2−54456
KX:$PO_2{}^-$, X = halide, photoluminescence, singlet-triplet transitions in $PO_2{}^-$, low temp. study 2−54455

Luminescence continued
solids, inorganic continued
$LaAlO_3$:Nd^{3+} laser crystal, spectroscopic obs. 2−75302
$La_{1-x-y}Ce_xTb_yPO_4$, fluoresc. quantum efficiency 2−48246
LaF_3:Ho^{3+}, optical transition probabilities for Ho^{3+} 2−54468
LaF_3, X-ray luminesc. excitation efficiency of lanthanide ions 2−84549
$LaGaO_3$:Bi^{3+}, u.v. fluoresc. 2−48245
La_2O_2S:Eu, correlation with photocond. 2−72064
$LaTaO_4$, fergusonite crystal struct. 2−61711
$LiAl_5O_8$:Fe^{3+}, ordered and disordered, phosphorescence and excitation spectra, zero-phonon transition, fine structure 2−48253
$Li_2B_4O_7$:Mn, optimum thermoluminescent properties for dosimetry applic. 2−49913
$Li_2B_4O_7$:Sm, Mn activators, thermoluminesc. spectra 2−48255
LiF:Mg, thermoluminesc. sensitivity enhancement by Mn 2−44415
LiF:Mg^{2+}, thermoluminesc. depend. on state of aggregation of Mg^{2+} vacancy pairs 2−44416
LiF-100, (-7) thermoluminescence, dose relationship, energy response and rate dependence from 8 keV-30 MeV 2−68701
LiF, compressed, surface thermolum. after immersion in boiling water 2−48256
LiF, dosimetry grade, thermolum. mechanism 2−61720
LiF, thermoluminesc. dependence on 340 nm colour-centres 2−43650
LiF, X-irrad., thermolum., temp. depend. 2−65313
LiF (Tld-100) thermoluminescent emission spectrum at low and high exposures 2−44414
LiF dosimetry based on radiophoto luminescence 2−55926
LiF in teflon discs, consistency of dosimetric properties over repeated cycles of use 2−67087
LiF personal thermoluminescent dosimeter system 2−69432
LiF phsophor, study of sensitivity factor mechanism 2−68698
LiF thermoluminescence of single crystal prod. by edge-defined film-fed growth technique 2−67943
LiF thermoluminescent dosimetric grade powders, influence of thermal and chemical treatment on properties 2−67090
LiF thermoluminescent dosimetry grade 100 powder incorporated in silicone rubber, dependence of energy response on grain size 2−68702
LiF undoped power, high-level dosimetry, radiation induced optical absorption and photoluminescence 2−67096
LiH:Pb, X-ray luminesc. and thermoluminesc. 2−72422
LiH activated by Hg-like elements, luminescence and excitation spectra 2−78137
$LiNbO_3$ irradiated by ruby laser 2−44426
Li_2O-Tb_2O_3-SiO_2 glass, fluorescence rel. to crystalline phases 2−51376
$LiTmF_4$:Ho^{3+}, optical absorpt., emission and excitation spectra 2−81418
$LuLiO_2$, of Eu^{3+}, energy levels 2−48226
Lu_2O_3:$Eu^{2+}(Tb^{3+})$, flame excited luminesc., temp. depend. 2−48270
$LuVO_4$, dependence on electronic transitions in $VO_4{}^{3-}$ 2−65300
$(M,Cr)(ur)_6(ClO_4)_3$, M = Al, Ga, low temp. spectra, obs. of ^2E level splitting, zero-phonon transitions 2−51290
$(M,Cr)(ur)_6I_3$, M = Al, Ga, low temp. spectra, obs. of ^2E level splitting, zero-phonon transitions 2−51290
MgO, rare earth doped, X-ray excited optical fluorescence 2−61707
MgO, thermally stimulated, u.v. excitation, glow peak assignment 2−57378
$6MgO.As_2O_5$, Mn activated phosphor, flux growth method 2−43525
Mg_2SiO_4(Tb) thermoluminescence phosphor, study of sensitivity factor mechanism 2−68698
Mg_2Sn, retaining metastable phases by quenching under pressure 2−84152
Mo, radiation generated during rapid deform. and rupture, tribolum. 2−54482
NaCl:Pb, polarized luminesc. and dipolar relax. of Pb-vacancy complexes 2−72424
NaCl:Tl, X-irrad., traps responsible for 360 and 390 K glow peaks 2−54476
NaCl fast recomb. transition lifetimes 2−54450
NaF: $Eu^{3+}(Sm^{3+})$, Ce^{3+} impurity effect on $Eu^{3+}(Sm^{3+})$ luminescence 2−65295
NaF:Eu crystals grown by Czochralski method, luminescence, absorption and excitation spectra 2−68686
NaF, M centre, optical props. and reorientation 2−51343
NaI:Tl, fluorescence intensity changes during X-ray dynamical diffr. 2−65301
NaI:Tl, recomb. luminesc. of crysts. excited in A-band by activator absorpt. 2−75334
NaI, adsorbed O effects 2−81399
$NaIPbI_2.4H_2O$ also absorption and excitation spectra 2−54456
$NaNO_3$, thermoluminesc. glow curves, capture cross-sections and trap. parameters detn. 2−48257
$NaYF_4$:Yb, Er, phosphor, upconversion, i.r.-pumped visible luminesc. 2−72413
Na_2ZrSiO_5:Eu^{3+}, Stark splitting and spectral intensities 2−72414
NbN film, photolum. spectra, freq. shift gap struct. 2−68687
Nb_3Sn, photolum. spectra, freq. shift gap struct. 2−68687
$O_2{}^-$ ion, in synthetic sodalite, photolum. spectra, 4.2- 300 K, fine struct., multiband spectra 2−81422
$PbBr_2(Cl_2)$, u.v. irrad., pairs and colloidal centres obs. 2−44448
$PbCl_2$:Eu^{2+}, 15K 2−54447
$PbCl_2$:Sm^{3+}, 150 K 2−54447
RbCl:Na, F_b centres 2−64682
$S_2{}^-$ ion, in synthetic sodalite, photolum. spectra, 4.2-300 K, fine struct., multiband spectra 2−81422
SbSI, ferroelec. semicond., photoluminescence of single crystals 2−72443
$ScLiO_2$, of Eu^{3+} energy levels 2−48226
Si:GaAs light emitting diode MV-50 fast decay meas. 2−45812
Si:Li, electron irrad., annealing and Li impurity effects 2−48229
Si, emission band, two electron band- to-band transitions, excitation intensity 2−61699
Si, exciton recomb. luminesc., 20-77K 2−78138
Si, irrad., recomb. luminesc., annealing and impurity effects 2−48231

Luminescence continued
- **solids, inorganic** continued
  - Si, irrad., recomb. luminesc., uniaxial stress effects and temp. depend. 2—48230
  - Si, γ-irrad., vibronic spectra, temp. depend. 2—48262
  - Si, photon emission line from condensed phase of nonequilibrium carriers 2—51370
  - Si, pure and doped, radiative recomb. during electron-hole condensation 2—78133
  - Si, radiative recomb. rate, 300K, carrier conc. depend. 2—81430
  - Si, radiative two-electron transitions in the electron-hole plasma 2—78139
  - Si, strongly excited, spectrum and decay of recombination radiation 2—61700
  - SiC:H(D), implanted, recomb. radiation of excitons and vibr. spectrum 2—68688
  - β-SiC, electron irrad. effects 2—48232
  - SiC, H- and D-implanted, CH and Cd bond-stretching mode 2—65296
  - α-SiC, influence of struct. defects 2—71774
  - SiC, Zeeman splittings, bound excitons 2—48227
  - SiO_2-CaO-MgO-Na_2O-AlF_3:Dy^{3+} glass syst., intensity distr., effect of heat treatment 2—48228
  - SiO_2 films, with aminophthalimide or fluorescein added, transparency measurement 2—44340
  - SnTe-GeTe alloys, retaining metastable phases by quenching under pressure 2—84152
  - SnTe, retaining metastable phases by quenching under pressure 2—84152
  - Sr fluorophosphate, Mn^{2+} doped, optical excitation and fluoresc. spectra of Mn^{2+} 2—81421
  - $SrAlF_5$:Eu^{2+}, characterization 2—60726
  - $SrB_2Si_2O_8$:Eu^{2+}, meas. of diffuse reflection, excitation and emission spectrum 2—81420
  - $SrCaAlF_7$:Eu^{2+}, three polymorphs 2—72420
  - SrF_2, ⟨100⟩ and ⟨110⟩ oriented F_2-centre obs. 2—53751
  - SrF_2, thermoluminesc., due to low temp. plasma produced radiational defects 2—71452
  - $Sr_{2.96}MgSi_2O_8$:Eu^{2+}, prep. depend. 2—84550
  - SrO-ZrO_2-SiO_2, excitation and emission spectra 2—75320
  - SrS:Mn, Zr phosphors decay study 2—75330
  - SrS phosphors, activated by Zr, Sn, Pb and Th 2—61713
  - SrS phosphors activated by Zr, Sn, Pb and Th, thermoluminescence and phosphorescence decay 2—65314
  - $Tb_3Al_5O_{12}$, time depend., dipolar transfer 2—54459
  - $Tb_{1-x}Y_xPO_4$, strong selective excitation of $^5D_4$ of Tb^{3+} ion 2—54469
  - TiO_2 amorphous film, photolum. 2—72068
  - Tl^+-Gd^{3+} energy transfer, in inorganic glasses, fluorescence obs. 2—61709
  - TlCl(I,Be) scintillation crystals, response to energetic ionizing radiation 2—49649
  - Tm^{3+}, spectra in phosphate and borate glasses, emission and absorpt., cryst. field effects, luminesc. efficiency 2—75307
  - (Y,Yb,Er)F_3 phosphor., i.r. convertor, prep. by coprecipitation 2—48248
  - YAG, of Tb^{3+}, quenching by direct transfer and migration 2—54459
  - $YAlO_3$:Ho^{3+}, optical transition probabilities for Ho^{3+} 2—54468
  - $YAlO_3$, exchange coupled Cr^{3+} pair obs. 2—72415
  - YBO_3:Ce, thermoluminescence during cathodic excitation, also dependence on Ni, Co and Fe impurities 2—54477
  - YF_3: Yb, Ho, diffusion and transfer of optical excitation 2—61714
  - YF_3:Er^{3+},Yb^{3+}, mechanisms and controlling factors of i.r. to visible conversion 2—54470
  - $YLiO_2$, of Eu^{3+}, energy levels 2—48226
  - Y_2O_3:Eu^{3+}(Tb^{3+}), flame excited luminesc., temp. depend. 2—48270
  - Y_2O_3, phonon-assisted energy transfer between Ln^{3+} ions 2—48234
  - Y_2O_3 phosphor, effect of Eu^{3+} and Tb^{3+} concentration 2—48235
  - YOCl:Er^{3+}, Yb^{3+}, mechanisms and controlling factors of i.r. to visible conversion 2—54470
  - Y_3OCl_7:Er^{3+},Yb^{3+}, mechanisms and controlling factors of i.r. to visible conversion 2—54470
  - Y_2O_2S:Er^{3+}, fluorescence spectra, energy levels and crystal field splittings detn. 2—51339
  - Y_2O_2S:Eu^{3+}, sensitization by Pr^{3+} and Tb^{3+} 2—51371
  - Y_2O_2S phosphor, effect of Eu^{3+} and Tb^{3+} concentration 2—48235
  - Y_2SiO_5:Nd^{3+}, 4.2, 77 and 290K 2—78123
  - YVO_4, dependence on electronic transitions in VO_4^{3-} 2—65300
  - Yb^{3+} doped oxides, visible, i.r. excited, effect of host lattice 2—78140
  - (Zn, Cd)S:Ag, Ni, fluorescence, efficiency curves, investigation of Klasens' simple thermal quenching theory 2—48250
  - (Zn,Cd)S phosphors, diffuse reflection spectra for studying and controlling properties 2—75332
  - (ZnCd)S:Cu,Cl phosphors, emission spectra and decay characteristics as a function of temperature 2—78120
  - $Zn_xCd_{1-x}S$:Cu, Cl temp. and i.r. quencging of luminescence and photocond. 2—84543
  - $ZnCd_{1-}S$, steeply graded, photoluminescence and growth 2—72444
  - $Zn_xCd_{1-x}Te$, luminesc. reson. Raman scatt., exciton transition 2—54437
  - $Zn_xCd_{1-x}Te$ crystals, spontaneous luminescence and lum. spectra detn. 2—72417
  - ZnO, electrode potential control, possible use as probe for electrochemical reactions 2—61717
  - ZnO depend. on adsorbed gases 2—78121
  - ZnS:Ag,Mn,Cl phosphors, mechanism of activator interactions 2—84551
  - ZnS:Ag phosphors, stimulated emission characteristics 2—65297
  - ZnS:Cl, quenching of photolum. by elec. field 2—72416
  - ZnS:Cu, recombination of green luminesc., tunnelling effects 2—48236
  - ZnS:Cu phosphor particles with nonluminescent coatings, cathode-ray efficiency, voltage depend. 2—51383
  - ZnS:Cu phosphors, extralinear effects in thermostimulated luminescence 2—75335
  - ZnS-CdS:Er^{3+} mixed fluorescent compounds, spectroscopic investigation 2—84545
  - ZnS-Cu,Co,Cl, differences between optical and thermal depths of electron traps 2—51395

Luminescence continued
- **solids, inorganic** continued
  - ZnS-Cu crystallites, electroluminesc., influence of milling 2—51390
  - ZnS, Cu, Pb, Cl film, temp. depend. of electrolum. and thermal quenching 2—84533
  - ZnS, disappearance of electron traps under influence of pressure 2—61722
  - ZnS, extinction of luminescence by electric field 2—75331
  - ZnS, luminophors, prep., 36-180°C 2—78141
  - ZnS, photolum. and electrolum., temp. depend. 2—48267
  - ZnS, self-activated, excitation spectra of blue emission bands 2—61682
  - ZnS luminophor, Gudden-Pohl effect, optical quenching 2—51393
  - ZnS phosphor, Schon-Klasens model interpret. 2—51213
  - ZnS photoelectroluminescence following u.v. irradiation, confliction with Fischer model 2—51391
  - ZnS with Cu and Cl impurities, photo- and electroluminescent props. 2—51394
  - $ZnS_{1-x}Se_x$, thermoluminesc. rel. to stimulated cond. with persistent memory 2—75104
  - ZnSe:Mn, enhancement by electric fields in polycryst. and crystalline samples 2—48249
  - ZnSe, pair photolum., peak energy, excitation intensity depend. 2—75318
  - ZnSe, substitutional donor props. 2—51372
  - ZnSe (Cu, Ga), epitaxial thin films, photoluminescent, oscillations of photocurrent 2—78147
  - n-ZnSe(Cu,Ga) film, photolum., photocurrent oscills., 80-220K, luminesc. field quenching 2—81168
  - Zn_2SiO_4:Mn, thermoluminesc., glow curves, impurity depend. 2—48258
  - Zn_2SiO_4:Mn^{2+}, willemite, cathodoluminesc., electron microprobe obs. 2—51382
  - ZnTe, double-acceptor cathodolum. 2—54480
  - ZnTe, spontaneous luminescence and lum. spectra detn. 2—72417
  - ZnTe, threshold energy for Te displacement, cathodoluminesc. obs. 2—68018
  - $ZnWO_4$:Cr^{3+}, impurity conc. determ. 2—78157
- **solids, organic**
  - ammonium oxalate, intensity obs. rel. to elastic const. detn. 2—51396
  - ammonium oxalate, triboluminesc. intensity obs. rel. to elastic const. detn. 2—51396
  - anthracene, blue fluorescence spectra, two-photon absorption 2—44410
  - anthracene, carrier-exciton interactions, delayed fluoresc. quenching 2—65308
  - anthracene, dye-sensitized, delayed fluorescence, magnetic hyperfine modulation 2—65309
  - anthracene, fluoresc. quenching by CCl_4 wavelength effects 2—68694
  - anthracene, mag. field effect on prompt fluoresc., singlet exciton fission obs. 2—81521
  - anthracene, quenching of triplet excitons by trapped carriers used to determ. charge density gradient 2—47907
  - anthracene, quenching under intense excitation 2—54471
  - anthracene, singlet exciton collision fluorescence decay following laser stimulation 2—78144
  - anthracene, surface exciton states 2—54461
  - anthracene, tetracene-doped, singlet-exciton energy transfer, generalized random walk model 2—84270
  - anthracene, triplet exciton annihilation fluorescence changes induced by neutron radiation damage 2—84553
  - anthracene crystal, reflection and luminescence spectra, evidence for surface states 2—44408
  - anthracene crystal, rel. to photoconduction and depend. on surface quenching of triplet excitons 2—81169
  - anthracene crystals, calculation of light reabsorption 2—61715
  - anthracene diode, double injection electrolum., and carrier injection props. of C fibres 2—75338
  - anthracene monocrystals, eximeric emission from mechanically worked surfaces 2—65298
  - anthracene single crystal, intensity of fluorescence depend. on triplet exciton generation, decay and surface quenching 2—81427
  - aromatic molecules in complexes with hydrogen bonds, quenching of triplet state, study at 77K 2—54462
  - azomethines with fluorine-containing substituents 2—75326
  - benzene and n-paraffin mixture, luminescence at 77 K 2—51378
  - benzol crystal with impurities, low-temperature spectral investigations of formation of local exciton states 2—54464
  - benzophenone, kinetics of quenching and quantum emission in relation to energy of exciting laser pulse 2—54463
  - benzophenone, triplet exciton and phosphoresc., low temp. 2—61718
  - benzophenone crysts., phosphorescence, temp. depend., T→S emission 2—65312
  - 5,6- and 7,8- benzoquinoline trapped in n-paraffins at 77K, vibrational analysis of quasilinear spectra 2—50080
  - benzyl, kinetics of quenching and quantum emission in relation to energy of exciting laser pulse 2—54463
  - coronene (III) in crystalline solutions of isooctane and CCl_4, 77K-melting point 2—51377
  - cyanine dyes, luminescence of solid films 2—75327
  - cyclopentanone, transient effects in microwave optical double resonance 2—81524
  - dibromobenzene:naphthalene in T_1 state, phosphorescence spectra, study of external spin-orbit coupling mechanism 2—72427
  - 1,4-dibromonaphthalene, phosphorescence study of triplet exciton state band structure 2—47820
  - diethylamine phosphor activated by TiCl 2—54484
  - diphenyl, phosphorescence sensitization by triplet excitons, nonlinear dependence on exciting illumination 2—54474
  - diphenyl crystal, fluoresc. and electron excitation energy migration 2—72425
  - diphenylene sulphide (V) in crystalline solutions of isooctane and CCl_4, 77K-melting point 2—51377
  - 2,5-diphenyloxazol, anthryl derivatives, dependence of threshold of generation on pumping polarization 2—53450
  - distyryldurene derivatives synthesis as wavelength shifters in plastic scintillators 2—61703
  - doped crystal, diffusion theory applic. 2—75325

Luminescence continued
  solids, organic continued
    dyes: Eu^{3+}, Tb^{3+}, solid solution quenching due to dipole- dipole transfer of energy from ions 2—54460
    ethanol glass, trapped electrons produced by biphotonic photoioniz. rel. to delayed emission of indole ring 2—54559
    ethylamine phosphor activated by TlCl 2—54484
    europium dibenzoylmethide chelate with ethanolamine 2—65310
    fine structure obs. in fluorescence spectra of laser-excited complex molecules, solid solvent selection 2—68693
    fluoranthene crystal, spectral response of lifetime to determine purity 2—84536
    hexachloroethane, γ-irrad., thermolum. and e.s.r. 2—48259
    hexahydrotriphenylene (II) in crystalline solutons of isooctane and CCl_4, 77K-melting point 2—51377
    intermolecular complexes, mol. crysts., bibliography 2—48159
    l-methylnaphthalene, activated by oxazoles and oxadiazoles, concentr. depend., role of triplet mols. 2—48237
    naphthalene, anthracene- and tetracene-doped, singlet-exciton energy transfer, generalized random walk model 2—84270
    naphthalene, impurity centre conc. and distrib., exciton scatt. theory calc. 2—81436
    naphthalene, migration of excitation energy between impurity molecules studied by polarization method 2—54465
    naphthalene, spherical single cryst., polarization luminesc. rel. to impurity molecule orientation 2—75328
    naphthalene with indol impurity, spectra 2—54466
    naphthalene-d_8 phosphorescence, comparison of matrix emission spectra with frozen solution spectra in cyclohexene hosts 2—72428
    n-nonane:coronene, fluoresc., 77K, complex struct. of doublets 2—78145
    ovalene in condensed media at room and liquid N temp. obs. of two-level emission as function of pressure 2—50105
    n-paraffin-aromatic hydrocarbon system, radiative and non-radiative processes 2—61719
    phenanthrene, blue fluorescence spectra, two-photon absorption 2—44410
    phenanthrene-naphthacene thin layer, u.v excited sensitized luminesc. 2—48251
    phthalocyanine and derivatives, fluoresc. and photocond. 2—72426
    pyrene, character of nonlinear quenching in temperature range 77-373 K 2—54442
    pyrene, temp. depend. of nonlinear luminesc. quenching 2—44409
    pyrimidine-benzene mixed crystals, fluorescence at 4.2K 2—44412
    rubin, electron irrad., phosphoresc. 2—72429
    sodium tartrate, intensity obs. rel. to elastic const. detn. 2—51396
    sodium tartrate, triboluminesc. intensity obs. rel. to elastic const. detn. 2—51396
    sugar, triboluminesc. intensity obs. rel. to elastic const. detn. 2—51396
    tartaric acid, triboluminesc. intensity obs. rel. to elastic const. detn. 2—51396
    tetracene, fluoresc., exponential decay time, singlet fission 2—54472
    tetraphenylbutadene solid solutions, dependence of threshold of generation on pumping polarization 2—53450
    thiarcarbocyanine dyes with different substituents in meso position 2—61701
    toluene and polymeric solutions of derivatives of oxazoles and oxadiazoles, stimulated emission 2—59164
    triethylamine phosphor activated by TlCl 2—54484
    triphenylene (I) in crystalline solutions of isooctane and CCl_4, 77K-melting point 2—51377
    vanadium$(urea)_6$ $(ClO_4)_3$ and $(urea)_6I_3$, near i.r. sharp line luminesc. 2—81409
    vibronic spectra of absorption and luminescence, distortion of mirror symmetry 2—78108
    vinylnaphthalene polymers and copolymers with styrene and methyl methacrylate, triplet depletion 2—68805
    2,2′-bipyridinetetracarbonylchromium -molybdenum and -wolfram, charge-transfer triplet excited state 2—68689
Luminescence chambers
  scintillation efficiency for random and heavy channelled ions at intermed. vels., track-account theory 2—70316
Luminescent devices
  see also Counters/ scintillation
  anthracene diode, double injection electrolum., and carrier injection props. of C fibres 2—75338
  diodes, light emitting, response time 2—51385
  electroluminescent capacitor, brightness, temp. depend. 2—72435
  image storage panel, electroluminesc. characts. 2—70068
  multicolour CRT phosphors, voltage-controlled, prep. and charact. 2—75329
  radioactive phosphors, detection of breast tumour 2—62867
  scintillating phosphors in radiative reference lights, transient temperature dependence 2—49443
  semiconductor, review 2—51178
  solid state light sources, review in book 2—55700
  $Al_xGa_{1-x}As$ grown- diffused electroluminescent planar monolithic diodes 2—51386
  $Al_xGa_{1-x}As$ heterojunction, electroluminescence characs. 2—81431
  CaF_2:Dy, scintillating phosphors in radioactive reference lights, transient temperature dependence 2—49443
  CaF_2:Mn, scintillating phosphors in radioactive reference lights, transient temperature dependence 2—49443
  $CaSO_4$:Tm phosphor powder use for fast neutron dosimetry 2—78666
  $Ga_{1-x}Al_xAs$:Si diodes, substrate orientation depend. 2—51153
  $Ga_{1-x}Al_xAs$ epitaxial layer growth 2—47288
  $Ga_{1-x}Al_xAs$ light emitting diode, epitaxial growth on GaP substrates 2—51388
  GaAs:Ge p-n junction, Zn- diffused, photolum., 8100-8500 Å 2—72404
  GaAs-$Al_xGa_{1-x}As$ p-n heterojunction, current flow during electrolum. 2—72438
  GaAs, electrolum. diode, electron diffusion length, internal quantum efficiency, temp. depend. 2—61725
  GaAs diodes, power and radiation pattern meas. 2—51369
  $GaAs_{1-x}P_x$, light emitting diodes 2—44421
  $GaAs_{1-x}P_x$, light emitting diodes characteristics, applications 2—44422

Luminescent devices continued
  $GaAs_{1-x}P_x$ light emitting diodes, reliability 2—44423
  GaP, melt-grown, S-pit correl. with reduced efficiencies 2—50595
  GaP diode, etching phenomena, scanning elec. microscope obs. 2—71972
  GaP diodes, physics of radiative centres 2—61724
  GaP green emitting diode fabrication by double- bin liquid-phase epitaxy 2—72437
  GaP p-n-p-n diode, green emission, quantum efficiency 2—72436
  GaP p-n junction diode with nonuniform distribution of isoelectronic N_2 traps, patent 2—54485
  GaP p-n junction growth by liq. phase epitaxy 2—47287
  GaP red-emitting diode manufacture, cryst. growth technique 2—60711
  GaP red-emitting diodes, scanning electron microscope characteriz. 2—51389
  Gd_2O_2S:Tb as phosphor for X-ray image intensifier screen 2—73251
  $In_xGa_{1-x}As$ prep. and props. rel. to electroluminescent diodes 2—68708
  $In_{1-x}Ga_xP$ diode, vapour grown, bright electroluminesc. 2—49386
  $In_{1-x}Ga_xP$ p-n junction, bright yellow emission 2—44425
  LiF thermoluminescent dose meter 2—67068
  NaI(Tl), scintillating phosphors in radioactive reference lights, transient temperature dependence 2—49443
  PbTe epitaxial thin film diode, evaporated, injection luminesc. and laser action 2—57382
  ZnS, scintillating phosphors in radioactive reference lights, transient temperature dependence 2—49443
Lumino(pho)rs *see Luminescencs/ solids, inorganic; Luminescence/ solids, organic; Luminescent devices*
Lutetium
  solar photospheric abundance det. from spectrum synthesis 2—58554
  Lu-C system, vaporization investigations in temp. range 2100 to 2600K 2—64518
  Lu I, absorp. line series, u.v. region 2—56100
  Lu I, theoretical study of odd configurations $5d6s6p + 6s^27p + 5f6s^2 + 5d^26p$ 2—64018
  Lu IV $4f^{13}6s$, $4f^{13}6p$, $4f^{13}5d$ configurations and effective magnetic operations for inequivalent electrons 2—79936
  ^{176}Lu and s-process nucleosynthesis 2—58158
Lutetium compounds
  Lu-H(D) system, α-phase characts. 2—77749
  Lu-Zr alloys, form. of low temp. metastable allotropic solid solns. 2—47646
  LuB_{12}, electronic spectra and phys. props. 2—47838
  $LuCrO_3$, n.m.r. of ^{53}Cr, h.f.s., mag. props. 2—48307
  LuD, obs. of new electronic system in 4000-8000 Å region, determ. of molecular consts. 2—70711
  LuF, new electronic spectrum obs. in 3000-8000 Å region, determ. of molecular constants 2—70712
  $LuFe_{9,5}$, ferromag.-helimag. transition 2—54325
  $Lu_3Fe_5O_{12}$, garnet, cell parameters, X-ray powder data 2—74745
  LuH, electronic band systems analysis, 4200 and 5000 Å 2—74268
  LuH, obs. of new electronic system in 4000-8000 Å region, determ. of molecular consts. 2—70711
  $LuLiO_2$, luminesc. of Eu^{3+}, energy levels 2—48226
  Lu_2O_3:Eu^{3+}(Tb^{3+}), flame excited luminesc., temp. depend. 2—48270
  $LuTe_{3-x}S_x$ solid solns., high temp. homogeneity regions 2—53905
  $LuVO_4$, luminescence dependence on electronic transitions in VO_4^{3-} 2—65300
Luxemburg effect *see Electromagnetic wave propagation/ ionosphere*
M-centres *see Colour centres*
M-regions *see Sun*
Mach's principal *see Relativity*
Mach number *see Aerodynamics; Shock waves; Supersonic flow*
Machines, electrical *see Electrical machines*
Macromolecules
  see also Molecules/ configuration and dimensions, macromolecules; Polymers; Proteins
  adiabatic rapid passage spectra from slowly tumbling spin labels 2—83339
  asymmetric-top molecule in soln. effect of molecular shape and flexibility on γ-ray directional correlation for bound nucleus 2—51474
  biological, electron diffraction reconstruction of spatial structure 2—81980
  biological, quasielastic light scattering 2—81991
  biological complexes by dark field electron microscopy 2—82001
  chain molecules, computing methods for determ. of possible conformations and electronic band structure 2—42860
  chromosomes, X-ray irrad. electron microscope obs. 2—62853
  DNA, λ phage, conformation changes rel. to u.v. irrad. 2—60093
  DNA, electron correl. influence on struct. and props. 2—77159
  DNA, electron excitation energy long range migration 2—56265
  DNA, helix-coil transition 2—67526
  DNA, in mice leukemic cells, replication, radiation effects 2—62852
  DNA, phosphoresc. decay rate, 4.2 to 160K 2—65393
  DNA, radical transfer with protein in DPA, e.s.r. obs. 2—60094
  DNA, simultaneous motion of protons in hydrogen bonds, Schrodinger eqn. soln. 2—70799
  DNA base pairs, proton transitions in H bonds 2—80115
  DNA bases, chem, shifts of inner-shell electrons, CNDO/2 calcs. charge redistrib. effect 2—83345
  DNA hypochromism, sequence depend. using Hartree calcs. 2—80118
  DNA natural and synthetic, denaturation 2—60097
  DNA single-strand breaks produced by γ-ray after treatment with 2, 4-dinitrophenol 2—66272
  fatty acid molecules, monomolecular layers, improved resolution technique 2—55765
  fluorescence polarization dynamics 2—56266
  intramolecular mobility in solutions, solvent effects 2—43337
  intramolecular mobility study using polarized luminescence in solution 2—60090
  isolated, memory effect 2—53087
  linear chain of r elements, transport properties and theorem of corresponding states 2—83340

Macromolecules continued
micelle solns., electron excitation energy transfer and conc. phenomena 2−60523
n.m.r. lineshape, alternate linear chains of inequivalent nuclei coupled by indirect exchange interaction 2−43019
normal vibration analysis by digital computer, method for calc. helix parameters, coords. of atoms 2−43017
nucleic acids, struct., review 2−83383
polarized fluorescence and rot. Brownian motion 2−60091
polyelectrolyte, adsorption on flat interface, approx. theory for low potentials 2−61793
polyethyleneoxalate, polyethylenesuccinate, intramolec. contributions to entropy and energy of fusion 2−46637
polypeptide monolayer raft, non-Newtonian surface viscosity, flow equation derivation 2−74528
polypeptide raft, non-Newtonian surface viscosity 2−74529
polysaccharides, struct., review 2−83383
polystyrene in cyclohexane soln., conc. fluctuation dynamics near critical pt. 2−46996
pyrimidine nucleosides, electronic spectra from circular dichroism data 2−74299
Salmonella flagella, polymorphism, phenomenological theory 2−53088
solution, electric birefringence, relaxation spectrum, decay curve, numerical method 2−74543
sound absorption, interaction in erythrocytes 2−48878
spectral analysis by analogue time correlation of light scattered from macromolecule solutions 2−82585
stearate multilayer struct. 2−46633
tobacco mosaic virus, molecular dimensions from light scattering in absorbing solutions 2−50378
transient light scattering from absorbing solutions in pulsed elec. fields 2−50378
translational diffusion study by photon correlation spectroscopy using digital PDP-9 computer 2−79443
vegetable pigments in soln. and chloroplastic media, reson. Raman spectra 2−81977

Madelung constant *see Solids/structure*

Maggi-Righi-Leduc effect *see Magnetothermal effects*

Magnesium
— 2−67388
— 2−60012
inAl-6.8% Zn alloy, effect on diffusion 2−56753
in 56 Arietis spectrum, variations 44860 2−44860
atom, 1s-2p transitions during bombardment with 21 MeV O ions 2−46469
atom, electron-impact double excitation cross sections calc. in Born Oppenheimer approx. 2−70607
atom adsorbed on W surface, backscattering cross sections for K-shell ionization by electron impact 2−79919
atomic beam as light source, theory and experiment 2−64057
atomic spectrum, broadening and shift of lines by van der Waals interaction with Ar atoms 2−70588
Auger spectra 2−71313
chemical reaction with bismuth oxide ceramics rel. to use in nuclear fuels 2−83064
decarburizing of cast Fe with graphite, struct. effects 2−43837
diffusion in Al, interpreted using oscill. form of inter-ion potential 2−64691
electron emission, secondary, Auger satellite rel. to plasmon absorpt. and double ionization processes 2−77971
electron momentum distribution, from Doppler-broadened annihilation lineshapes 2−71782
electron transmission, det. of lattice potentials 2−83942
engineering properties and applications, book 2−60936
exo-emission, threshold illumination intensity 2−44189
Fermi surface, hydrostatic press. effects 2−84250
film, evap., optical constants in e.u.v. 2−48133
K-shell ionization cross sections by ^{20}Ne and ^{22}Ne bombardment, isotope effect 2−74216
laser lines obs. in near i.r. 2−41980
liquid, struct. factor rel. to entropy of melting 2−64434
neutron irrad., distortion and swelling, effects of alloying additions 2−60778
neutron irrad., pt. defect clustering, low temp. electron microscope obs. 2−60783
neutron irradiated, struct. damage and annealing 2−80683
phonon freqs. from Krasko and Gurshii model potential 2−74976
photoelectric determination of electron attenuation length 2−44201
photoionization cross-sections, excited by tunable u.v. lasers 2−43200
plane strain extrusions, yield anisotropy and texture control 2−80848
slip, pyramidal, dislocation configs. 2−47420
solar overabundance, accelerated by solar flares 2−76001
solar X-ray spectrum, satellite lines of He like Mg 2−55171
stellar resonance doublet, balloon borne spectrophotometry 2−58282
stellar spectra, u.v. 2−62533
substitutional soln. hardening 2−43855
surface, cleaned and oxidized, secondary ion yield 2−61471
tropical Atlantic, distribution 2−54763
X-ray emission spectra, satellites, rel. to double ionization theory 2−72381
X-ray L emission band, short-wave satellites 2−51361
X-ray spectra, K-series X-ray valence band line, many body effects 2−68673
Al-Mg, interdiffusion, 325-425°C 2−64692
He-Mg vapour laser, role of thermal energy-charge exchange 2−42019
LiF:Mg, high temp. plasticity, range 300−800K 2−74840
LiF:Mg, impurity associations decomp., light scatt. obs. 2−83983
Mg/Fe cosmic abundance ratio rel. to Type I carbonaceous meteorites 2−69175
Mg/MoS_2 film/substrate system, curvilinear dislocations 2−80554
Mg-Al-Cu alloy, oversaturated solid soln. state, mech. props. rel. to strain rate and temp. 2−56547
Mg-He gas mixture, double ionization of Mg by thermal collisions with He 2−70980
Mg I 4571 Å, solar spectrum, determ. of minimum temp. of atmos. 2−76011
Mg II, elec. quadrupole transitions, multiplet strengths 2−56102

Magnesium continued
Mg II in Vega spectra, u.v. absorption lines 2−81831
Mg II solar u.v. line anal., statistical equilibrium and radiative transfer equations 2−51847
Mg IV spectrum, radial integrals and level assignments, 90-2100 Å 2−59899
Mg in LiF, impurity distribution effect on thermoluminescence 2−84552
Mg X solar spectral line, x.u.v., rocket measurements 2−55167
Mg^+, measurement and calculation of Stark broadening parameters for resonance lines 2−42727
Mg^+, reson. lines, electron impact broadening 2−59914
Mg_2, Franck-Condon factors in A-X system, rot. depend. 2−64141
Mg_2, matrix-isolated, absorpt. peaks 3540-3700, absence of optical pumping 2−80041
Mg^{2+}, meas. of termolecular association rate constants with Ar, O_2, N_2, CO, CO_2, N_2O, H_2O in flowing afterglow 2−48316
Mg^{2+} in LiF, thermoluminesc. depend. on state of aggregation of vacancy pairs 2−44416
MgI, λ4571 forbidden spectral line in Sun, measurements of limb darkening 2−45000
MgI and MgII dayglow, near u.v. 2−65884
MgI b_1, solar photosphere λ5183.6 line, residual intensity fluctuation measurements in wings 2−48793
MgII line profiles in β Aur, meas. by u.v. orbiting stellar spectrophotometer S59 2−55044
MgII solar resonance lines, observations using a compact grating spectroheliograph 2−45014
MgII vapour ion laser, exptl. and theoretical studies including spectroscopic data 2−52422
^{24}Mg, ^{25}Mg, ^{26}Mg isotopes, coherent neutron-scatt. amplitudes 2−67995
NgII resonance line, model chromosphere of Procyon 2−75712
Si:Mg, cond. band. deform. potential const. from piezospectroscopy of donors 2−68438
Si:Mg, donor levels, excitation spectra 2−72351

Magnesium compounds
— 2−72495
— 2−66840
— 2−67995
aalloy, internal hydride form., kinetics and equilibria 2−47639
alloy, engineering properties and applications, book 2−60936
alloy, fatigue failure at elevated temps., effect of material properties 2−60893
alloy, h.c.p., supercond. transition temp., electronic sp. ht., Debye temp. 2−47859
alloy, stress corrosion crack propagation, film rupture mechanism 2−43727
alloy, superplastic, internal stresses 2−74841
alloy cladding for fuel elements, composition, fabrication, properties, structure, development and use 2−83089
alloys, soln. hardening, stress equivalence 2−80834
composite, fuel cladding, corrosion in CO_2 2−57424
crystalline ceramics, precipitation 2−84063
dislocation loops, self climb 2−80672
enstatite, Rayleigh approximation, and emission cross sections of non-spherical particles 2−64477
ferrites, magnetostriction, effect of Co ions 2−65158
ferroaluminate, Co-doped, formation from metal hydroxides 2−47239
ferrous formate-magnesium formate system, mixed crystn., Mossbauer obs. 2−56673
glass, highpolyphosphate, thermal properties and crystallization 2−83851
magnesia, polycrystalline, deformation in compression, 1100-1750°C 2−68167
marine deposits, Mg content and crystal habits in ancient carbonates 2−54754
Mg_2SiO_4-Fe_2SiO_4 olivine transformed spinel system, equations of state det. using Birch's law 2−43504
neutron irrad., distortion and swelling, effects of alloying additions 2−60778
phthalocyanine films, impurity level energies from photoemission and cond. obs. 2−81028
steatite, mech. props., effect of firing temp. 2−50890
Al-Cu-Mg-Mn alloy, mosaic angle and dislocation density, tensile deform. depend. 2−80772
Al-Cu-Mg-Ni, forged after quencing, forged treatment, creep strain mechanisms 2−43804
Al-Mg-Si alloy, structure of metastable precipitates formed during ageing 2−56909
Al-Mg-Si alloys, quenched-in defect elimination mechanism 2−84149
97.4%Al-Mg alloy, fatigue crack dependence, temperature dependence 2−56866
Al-Mg alloy, high temp. creep mechanism 2−68089
Al-Mg alloy, intergranular corrosion susceptibility 2−71646
Al-Mg alloy, kinetics of isothermal coalescence of dispersed phase 2−47611
Al-Mg alloy, Portevin-Le Chatelier effect, role of vacancies 2−47490
Al-Mg alloy, slip struct. and crack growth during fatigue 2−47519
Al-Mg alloy, solute-vacancy binding energy, determ. from quenched-in defect conc. 2−74762
Al-Mg alloy, stress corrosion cracking, effect of Cu and Zr addition 2−50775
Al-Mg alloys, viscous glide in solid solution, dislocation climb and Newtonian viscous deformation mechanisms 2−64718
Al-Mg and Al-Mg-Zn alloys, preprecip. zone obs. 2−53885
Al-Mg single crystals, infl. of strain rate and temp. on Portevin-Le Chatelier effect 2−71560
Al-9%Mg alloy, effects of additional elements on clustering and precip. during ageing 2−50801
Al-(3 at.%)Mg alloy, high temp. deformation, lattice rotation, dislocation dragging 2−74835
Al-Zn-Mg-Cu-Mn forging alloy, fracture toughness rel. to microstructure 2−53826
Al-Zn-Mg-Cu alloy, fatigue behaviour of bolted joints 2−71622
Al-Zn-Mg alloy, ageing process after quenching and cold work, resistometric obs. 2−71632

Magnesium compounds continued

Al-Zn-Mg alloy, precipitate free zone, elec. microscope obs. 2−56902
Al-Zn-Mg alloy, solute distrib. using electron probe analyzer EMMA-4 2−56924
Al-Zn-Mg alloy, stress corrosion crack paths 2−43732
Al-1% Mg alloy, creep deformation, electron microscopic obs. 2−80753
Al-1.2 wt%Mg_2Si alloy, two-step ageing behaviour 2−64765
Al1-5% Mg alloy, serrated flow study −50 to 150°C 2−43706
$CaMg(CO_3)_2$, monocryst., elastic consts., u.s. obs. 2−80727
$Ce_2Mg_3(NO_3)_{12}.24H_2O$, caloric and mag. obs. 2−68523
$Ce_2Mg_3(NO_3)_{12}.24H_2O$, diluted, adiabatic demagnetiz. 2−45185
$Ce_2Mg_3(NO_3).24H_2O$, temp. scale to 1.6 mK 2−45187
CoO-MgO solid solns., porosity effect on elastic moduli 2−50729
Cu-Mg solid solns., binding energy of dislocations to impurities, internal friction obs. 2−43630
Cu-Ni-Mg alloys eutectic mixtures constitution 2−84103
Fe-Mg-Ni alloy, austenite transform. 2−53991
Fe-Mg-O system, activities, calc. by Darken's method 2−43815
$(Fe,Mg)_2Mo_3O_8$, Mossbauer effect 2−75270
GaN:Mg, diode, electrolum., fabrication, props. 2−72387
$La_2Mg_3(NO_3)_{12}.24H_2O$:Nd, spin diffusion props. from spin heat bath relax. time 2−78049
$La_2Mg_3(NO_3)_{12}.24H_2O$, spin system dynamics obs. 2−84445
Li-Mg solid solution, electronic props., Green function calc. 2−75029
Li-alloys, thin foil prep. using a non aqueous electrolyte 2−80548
$LiAlO_2$, partial volume determination, influence of composition for solid solution glass ceramics 2−56562
Li_4SiO_4-Zn_2SiO_4-Mg_2SiO_4-SiO_2 glass, phase equilibria and crystallization 2−64520
Mg:Gd, dil. mag. alloy, exchange narrowing of fine structure 2−72496
Mg-Ag alloy, application of Lindemann's rule for melting 2−74582
9.5 wt.%Mg-Al:Ti,Zr,Mo,B alloy, mech. props., fracture toughness, cracking effect of alloy in additions 2−47546
Mg-Al-Cu-Mn-Fe-Si-Ni-Zr-Ti, alloy, D16T, cryst. and uncryst. struct., fracture under static and cyclic conditions 2−47527
Mg-Al-Cu-Zn alloy, tensile deform. and high-temp. creep rel. to microstruct. 2−56800
Mg-Al-Cu alloy, eutectic, microstruct., orientation relationships 2−74893
Mg-Al-Li alloys, 01420, ageing, phase comp. changes 2−47594
Mg-Al-Mn-Fe-Cu-Si alloy, AK6, ageing temp.- time ranges 2−50802
Mg-Al-Si alloy, strength rel. to dislocation motion and GP zones 2−56717
Mg-Al-Zn alloy, decomposition, phase transform., influence of Zn 2−43911
Mg-Al-Zn alloy, soln. softening effect of Zn additions at high temps. 2−47613
Mg-Al alloy, band struct., Fermi surface, energy gaps 2−77826
Mg-Al alloy, dislocation network form. during hot deform. 2−56712
2.5 wt.%Mg-Al alloy, neutron irrad., transmutation produced Mg_2Si precip. 2−56922
Mg-Al alloys, β, γ phases, atomic structure 2−71642
5 at.%Mg-Al solid soln., steady state creep, dislocation mechanism, 570-800K56801 2−56801
Mg-Bi amorphous alloy, exciton screening 2−78115
Mg-Cd alloy, poison rod, burn-up, expt. and theory 2−49879
Mg-Cd alloys, diamagnetism, susceptibility curves 2−81203
Mg-Cd alloys, supercond. transition temp., electronic sp. ht., Debye temp. 2−47859
Mg-Cu-Ni alloy, Laves phases, enthalpies of soln. and formation detn. 2−47692
Mg-Cu alloy, weakening resist. rel. to deform., heating time and temp. 2−50764
Mg-Er alloy, dilute, exchange interact. with cond. electrons, e.p.r. obs. 2−72467
Mg-Mn-Al-Zn alloy, strength rel. to rest between quenching and ageing, effect of additions 2−50803
Mg-Mn alloy, derivation of Kikuchi map for c.p.h. structure 2−67956
Mg-Mn alloy, e.p.r., relaxation bottleneck theory applied 2−44438
Mg-Mn ferrite film, transparent, light diffr. by mag. stripe domains 2−65220
Mg-Mn ferrites, electronic struct. of Mn and Fe ions 2−47182
Mg-Sb amorphous alloy, exciton screening 2−78115
Mg-Sn alloy, liquid, elec. resist., Faber-Ziman theory, partial interference functions 2−83799
Mg-Th, Mg-Th-Mn, Mg-Mn, Mg-Zr alloys, precipitation processes elec. microscope obs. 2−53993
Mg-Th and Mg-Th-Zr systems, e. microscopy exam. of precipitation 2−71690
Mg-(10.8 at.%)Y alloy, thermomech. treatment for increased ductility and high strength 2−47588
Mg-Zn-Ni alloy, Laves phases, enthalpies of soln. and formation detn. 2−47692
Mg-Zn alloys, Ostwald ripening during solidification of nondendritic spherical structures, model 2−64508
Mg-Zn and Mg-Zn-Zr dendritic and nondendritic structs., soln. kinetics of secondary phases 2−47640
Mg-Zr alloy, Ni diffusion and precip. formation 2−47467
Mg-ferrite, spin-wave instability, obs. 2−78151
$MgAl_2O_4$-Al_2O_3 system, liquidus- solidus determ. 2−50971
$MgAl_2O_4$, cryst. growth, modified Verneuil technique 2−47274
$MgAl_2O_4$ polycryst. ceramic prep. and characteriz. 2−50887
$MgAl_2O_4$ spinel, cation disorder, e.s.r.obs. 2−65325
$MgAl_2O_4$ spinel, densification kinetics 2−50889
MgB_4, cryst. struct. 2−60762
$MgCO_3$, monocryst., elastic consts., u.s. obs. 2−80727
$MgCO_3$, polycrystalline, elastic props. to 10 kbars 2−65573
$MgCl_2$, adiabatc compressibility and sound propag. speed, reln. to molec. struct. 2−72564
$MgCl_2$, MgF_2, electronic structure and conformation, CNDO approx. 2−46529
$Mg_{1-y}Co_yFe_2O_4$, mag. anisotropy, ferromag. reson. study 2−81283
MgCuGa, Laves phases, enthalpies of soln. and formation detn. 2−47692

Magnesium compounds continued

MgF_2:CO(Mn)(Ni), impurity-ion spin-forbidden absorpt. enhancement by colour centres 2−78104
MgF_2-P_2O_5-LaF_3, R=Ba, Mg, triangular diagrams, crystn. and vitrification regions 2−57035
MgF_2, a priori and semiempirical calculations of molecular conformation 2−42908
MgF_2, hot pressed, temp. depend. of elec. cond. 2−47898
MgF_2, multilayer, quarter wave, generalized Brewster angle condits. at non-normal incidence 2−79410
MgF_2, refl. and emission spectra, transmittance 2−72381
MgF_2, static electric quadrupole interaction of beta emitter ^{20}F produced by capture of polarized neutrons, n.m.r. obs. 2−75356
MgF_2, valence band energies 2−54109
MgF_2, valence band struct. by tight-binding method, computation 2−61186
MgF_2, X-ray structural study of texture of KO-1 optical ceramic 2−70042
MgF_2 as low temp. photometer filter in 20 μ atmospheric window 2−63399
MgF_2 film, elec. props., thermally assisted hopping mechanism, Poole-Frenkel cond. 2−68279
MgF_2 film, evap., optical constants in e.u.v. 2−48133
MgF_2 film, thickness det., comparison of multiple beam Fizeau interferometry, photoelectric shearing interferometry and stylus instrument methods 2−47118
MgF_2 film overcoat on Al, effect on u.v. refl. 2−79370
MgF_2 films on Al, thickness monitoring by reflectance meas. using 1216 Å line of H 2−55733
MgF_2 ring, laser generated stress waves 2−45436
$MgFe_2O_4$, exchange anisotropy and relax., degree of treatment depend. 2−72156
$MgFe_2O_4$, ferromag. relax. of parametric spin waves 2−72228
$MgFe_2O_4$, temp. depend. of permeability, anomaly at Curie temp. 2−72167
$MgFe_2O_4$ films, mag. polarity reversal, temp. effect 2−61537
$Mg_xFe_{1-x}SiO_4$ olivine, lunar sample, temp. dependent Mg, Fe distribution 2−44908
$Mg_{0.5}Fe_{0.5}Ti_2O_5$, armalcolite, crystal structure, X-ray study, comparison with lunar rock sample 2−44928
$MgGa_2O_4$, growth by Czochralski method, substrate for direct liq. phase epitaxy 2−71380
n-Mg_2Ge, Hall mobility, magnetoresist., transport mechanisms 2−51143
MgH in solar sunspot spectrum, 4900- 6441 Angstrom range 2−62743
$MgHPO_4.3H_2O$, newberyite, thermal transform 20-900°C 2−57022
MgIn, structural energy, pseudopot. and perturbation theory calc. 2−50623
$MgMn_xAl_{2-x}O_4$, $0.3 \leqslant x \leqslant 1.2$, spinel compounds, paramag. suscept. detn. 2−48039
$MgMoO_4$, i.r. reflection bands, shifts of polar phonon frequencies 2−81352
$MgMoO_4$, optical phonon spectra of single crystals 2−68656
$Mg(NH_3)_6Cl_2$ and $Mg(ND_3)_6Cl_2$, i.r. active vibr. freqs. assignment 2−77058
$Mg(NO_3)_2$, precip. in KNO_3, solid soln. form. 2−56942
MgO:Co^{2+}, i.r. magnetic circular dichroism, study of first ^2E_g excited state 2−81365
MgO:Cr^+, g-factor, cubic field splitting and hyperfine const., e.p.r. obs. 2−75346
MgO:Cr^{3+}, phonon sideband of R line 2−48187
MgO:Fe^{2+}, crystal field splitting, effect of configuration interaction 2−51293
MgO:Fe^{2+}, higher order acoustic paramagnetic resonance transitions 2−51406
MgO:Fe^{2+}, phonon conductivity 2−64864
MgO:Fe^{3+}, charge transfer bands, magneto-opt. struct. 2−72339
MgO:$Mn^{2+}(Fe^{3+})$, spin-lattice coeffs., relativistic cryst. field contrib. 2−65203
MgO:Ni^{2+}, Brillouin spectra from microwave phonon bottleneck 2−65283
MgO:V optical absorption and magnetic circular dichroism of impurity 2−68646
MgO-Al_2O_3-ZrO_2-SiO_2 glass, complex particle growth, small-angle X-ray scatt. obs. 2−67887
MgO-$Al_2O_3(Y_2O_3)$ system, noncrystalline film prep. by sputtering 2−47114
MgO-B_2O_3, phase relations determined by quenching 2−74936
MgO-B_2O_3, system, phase relations, quenching method 2−57031
MgO-B_2O_3 system, phase relation obs. using thermobalance 2−73283
MgO-CoO neutron dosimeter, high temperature 2−49684
MgO-Cr_2O_3-CuO(Cu_2O) system, phase diagram 2−43931
MgO-FeO-SiO_2 system in mantle minerals, phase equilibria and elastic properties 2−57711
MgO-Li_2O-Al_2O_3-SiO_2-TiO_2, glass-ceramic, crystn., microstruct., indentation hardness 2−80535
MgO-$MgAl_2O_4$ system, eutectic solidification, microstruct., mech. prop. 2−47658
MgO-Na_2O-CaO-SiO_2 glass, phase equilib. in glass forming region 2−57023
MgO-Sc_2O_3 solid soln., phase diagram, defects, disintegration, decomp., precip. 2−74906
MgO-SiO_2-Al_2O_3, pressure sintered specimens, phase composition and dielectric constants 2−57226
MgO-TiN solid soln., solid phase interaction, diffusion of Ti, 1700-2000 K 2−53907
MgO-1% CoO as neutron dosimerer at high temps., prep. 2−73949
MgO-c inclusions, polycryst., creep, four point bending obs. 2−56805
MgO, adsorption of aromatic gaseous molecules, photoactivation by u.v. radiation 2−78206
MgO, adsorption of chlorine and oxygen obs. of ESR signal, charge transfer effects 2−47139
MgO, anion doped, grain boundary diffusion of Ni^{2+} 2−50710
MgO, Auger spectra using spectrometer with concentric hemispheres 2−74610
MgO, C or ZrO_2 discontinuous fibre-reinforced, fabrication and mech. props. 2−50918

Magnesium compounds continued
- MgO, cation self-diffusion up to 2350C 2−56761
- MgO, coincidence twist boundaries energies, Born-Mayer pot. and rigid lattice approx. 2−56735
- MgO, compression creep at high temps. 2−74845
- MgO, cryst. growth, elec. and optical props. 2−47223
- MgO, crystal dynamics, three body interactions in shell model 2−61077
- MgO, e.p.r. linewidth of iron group ions, temp. depend. 2−48289
- MgO, e.p.r. of adsorbed COS- and CS_2-, g-tensor shifts 2−72494
- MgO, elastic wave damping, effective anharmonicity consts. 2−80913
- MgO, elec. cond. and migrational polarization, 800-1300°C 2−81065
- MgO, $F^+ \rightleftharpoons F$ centre conversion obs. 2−68043
- MgO, ground state of Cr^{2+} from thermal cond. meas. 2−72238
- MgO, heat of adsorption of sulphur dioxide, 423K, adiabatic calorimetric obs. 2−83871
- MgO, heat radiation, influence of surface roughness 2−55574
- MgO, high resolution Auger electron spectra meas. with new Auger spectrometer 2−77972
- MgO, hot-pressed, annealing effect on elastic props. 2−50888
- MgO, hot-pressed, strength and fracture reln. to annealing rates 2−71589
- MgO, ionicity, dispersion, and optical spectra 2−44374
- MgO, lattice dynamics, elastic properties, seismic velocity and density profiles 2−72636
- MgO, luminescence, thermally stimulated, u.v. excitation, glow peak assignment 2−57378
- MgO, MeV Ne^+ irrad., F-type centre prod., absorpt. band obs. 2−68042
- MgO, microcavities, volume determ. by tracer method 2−43623
- MgO, periclase, electron diffr., energy distrib. in Kikuchi band 2−60761
- MgO, plastic deform. during cleavage fracture 2−71570
- MgO, plastic yielding, high pressure effects 2−68081
- MgO, plastically deformed, pipe diffusion prod. of prismatic dislocation loops after annealing 2−64689
- MgO, radiation-induced $[Na]^0$ centres 2−43651
- MgO, Raman relax. of Ni^{2+}, Cr^{3+} and V^{2+} ions, substitutional effects 2−48114
- MgO, rare earth doped, X-ray excited optical fluorescence 2−61707
- MgO, refl. and emission spectra, transmittance 2−72381
- MgO, Schottky defect, energy of formation 2−64660
- MgO, second-order Raman scatt. tensor calc. 2−71713
- MgO, shock waves and temp. derivation along Hugoniot curves 2−84188
- MgO, shocked, elastic wave vel. meas. 2−60853
- MgO, sintering, surface area and pore-size distrib. obs. 2−50866
- MgO, spin-lattice relax., effect of anharmonic interactions of Cr^{3+} and Ni^{2+} ions 2−65195
- MgO, thermal grooving and growth kinetics 2−80545
- MgO, V_{oh} centre obs. from absorpt. at 2.21 eV 2−54426
- MgO, V_1 paramag. colour centre 2−64685
- MgO (001) single crystal with Fe deposit, LEED-AES system analysis 2−74612
- MgO and TiO_2 coupled solute solid soln. softening of alumina 2−47653
- MgO cleavage faces, LEED beam splitting, model 2−60627
- MgO film, evaporated, refr. index and absorpt., 0.22-8μ . 2−79369
- MgO film, spectral emission by polaritons, 400-1300 cm^{-1} 2−65252
- MgO in solar sunspot spectrum, 4900- 6441 Angstrom range 2−62743
- MgO influence of inclusions on high temp. phenomena 2−56964
- MgO powders, thermally activated, O_2^- ion e.s.r. obs. 2−56602
- MgO refractories, effect of stress on grain growth 2−74915
- MgO single crystal, ionic conduction 2−65052
- MgO surface, V_{oh}^* trapped hole centre obs. by e.p.r. 2−81447
- $Mg_5(O)(OH)_5[BO_3].nH_2O$, Wightmanite, octahedral 3 Å framework structure with pipe feature 2−72695
- MgO(54 wt%)Fe_2O_3(12 wt%)CaO(10 wt%) Al_2O_3(12 wt%)SiO_2(12 wt%) mixture, phase transformations during heating 2−83839
- $MgO.Al_2O_3$ spinel, oxygen self-diffusion 2−50711
- $MgO.Al_2O_3$ spinel, substrate for epitaxial Si, optical characts. 2−77910
- $MgO.Al_2O_3.SiO_2$ glass-ceramic, ZrO_2-nucleated, phase transitions 2−47691
- $6MgO.As_2O_5$, Mn activated phosphor, crystal growth 2−43525
- 2 $MgO.5SiO_2.2Al_2O_3.nCr_2O_3$ glass due to Cr_2O_3 additions, e.s.r. obs. 2−83850
- $Mg_2P_2O_7$, i.r. spectra and normal coordinate analysis 2−77079
- $Mg_xPb_{1-x}Se$ alloy, Hall coeff., Hall mobility, thermoelec. power, optical energy gap, 77-450 K 2−64977
- MgS, self-consistent local orbitals 2−75031
- $MgSO_4.7H_2O$, crystal formation in presence of seed 2−74681
- $MgSO_4.7H_2O$ crystal, growth rate and stepped relief of artificial vicinal faces 2−74680
- Mg_2Si-Al alloy, supersaturated solid soln., precip. clustering mechanism 2−50822
- $MgSi_{1.72}$-$CrSi_2$ solid soln., prep., thermal e.m.f., elec. and thermal cond. 2−74905
- $MgSi_{1.72}$-Ge solid soln., prep., thermal e.m.f., elec. and thermal cond. 2−74905
- Mg_2Si, powdered and doped, e.p.r., 2-300K 2−65337
- $MgSiF_6.6H_2O$, phase transition at 25°C, cryst. struct. of low temp. form 2−67996
- Mg_2SiO_4:Tb, thermolum. dosimeter characts. as personnel monitor 2−70552
- Mg_2SiO_4, forsterite, piezo-optic behaviour 2−44350
- Mg_2SiO_4, localization of Mn^{2+} 2−84288
- Mg_2SiO_4 polymorphs, observed and hypothetical, crystal structure simulation 2−47335
- Mg_2SiO_4 spinel, lattice dynamics, elastic properties, seismic velocity and density profiles 2−72636
- Mg_2SiO_4 with Mn impurity as e.p.r. field marker and intensity reference 2−66664
- Mg_2SiO_4(Tb) thermoluminescence phosphor, study of sensitivity factor mechanism 2−68698

Magnesium compounds continued
- Mg_2Sn, retaining metastable phases by quenching under pressure 2−84152
- Mg_2Sn pressure dependence of electrical resistance 2−84326
- MgTe-CdTe mixed crystals, lattice vibrs., Raman spectra study 2−71714
- Mg_2TiO_4, i.r. absorpt. spectra, ionic ordering 2−72342
- $Mg_yU_{1-y}O_{2-x}$, structural analysis by X-ray and electron microscope meas. 2−47336
- $MgWO_4$:Fe^{3+}, e.p.r., elec. field effect 2−48286
- $MgZn_2$, deformed by u.s. vibrs., dislocation behaviour 2−64666
- $^{24}MgH^+$, $^{25}MgH^+$, $^{26}MgH^+$, rot. analysis of $A^1\Sigma^+ \to X^1\Sigma^+$ and $B^1\Pi \to X^1\Sigma^+$ systems 2−56184
- mischmetal-Mg alloys, dilute, metallographic study of phase transformations 2−80794
- Mn-Mg-Fe ferrite film, flash evaporated, chem. comp., X-ray fluoresc. obs. 2−71331
- $Mn_xMg_{1-x}Al_2O_4$ spinel, e.s.r. parameters 2−48290
- MnO-MgO, dense solid soln., preparation for testing 2−74907
- Mn_xO-MgO system, interdiffusion 2−50714
- $PbMg_{1/3}Nb_{2/3}O_3$-$PbTiO_3$-$PbZrO_3$ solid solution, hot-pressed, electrooptic props. 2−57328
- PbO-MgO-GeO_2 glass, structure and properties 2−53540
- SiO_2-Al_2O_3-Na_2O-K_2O-CaO-MgO glass, viscosity-temp. relations 2−67883
- SiO_2-CaO-MgO-Na_2O-AlF_3:Dy^{3+} glass system, luminesc., effect of heat treatment 2−48228

Magnetic amplifiers *see Amplifiers; Magnetic devices*

Magnetic anisotropy
- antiferromagnets, spin waves and correlation function 2−81305
- chloroacetylene, Zeeman effect obs. 2−70758
- cubic system, represented by lines of const. cryst. energy 2−78000
- ferrite, Fe rich, induced anisotropy and disaccommodation, mag. relax. obs. 2−48112
- ferromagnet, change during phase transform., mag. dipole radiation 2−78007
- ferromagnet, domain struct., calc. for various types of anisotropy 2−81270
- ferromagnet, due to anisotropic impurity spin, theory 2−81237
- ferromagnet, Heisenberg, energy spectrum and magnetization, monoionic anisotropy effects 2−51243
- ferromagnetic film, rel. to realization of trigger effect 2−75228
- ferromagnetic film with anomalous surface anisotropy, static magnetic susceptibility 2−72178
- ferromagnetic-antiferromag. coupled film systems, interfacial exchange coupling, thermal fluctuation aftereffect model 2−81231
- film, effect on ferromagnetic resonance 2−68717
- film, uniaxial, ang. dispersion of anisotropy effect on hysteresis loop 2−61521
- film magnetostrictive, anisotropy skew patterns, temperature gradient effects 2−72177
- garnets, modification by ion implantation, hard bubble elimination 2−65164
- helical magnetic structure, rel. to spin wave spectrum 2−57278
- measurement using rotating sample magnetometer 2−41911
- Ni(100) single crystal films, room temp. 2−44264
- Permalloy film, oxidized antiferromag. surface layer, mag. after effect 2−44267
- permalloy film −180 to +120°C, influence of substrate 2−84411
- Permalloy films, annealing depend. 2−61525
- Permalloy films, electrodeposited, comp. and depositing current effects 2−57302
- polycrystalline materials, determ. from magnetization curve singularities 2−51232
- rare earth, paramag., exchange anisotropy, variation with lattice parameters 2−51236
- rare earth cobalt intermetallics, 2-17 type, characteriz. for permanent magnets 2−61510
- rare earth metals, rel. to spin wave gap calc. 2−75226
- spin wave theory interpret. of anisotropy consts. temp. depend. 2−54321
- ytterbium ethylsulphate, mag. and thermal props. 2−51241
- $Ba_5Co_2(Cu_2)Ti_3Fe_{12}O_{31}$, props. rel. to microwave applic. 2−44273
- $Ba_3Zn_2Fe_{24}O_{41}$, hexagonal, comparison with $BaMg_2Fe_{12}O_{22}$ 2−72451
- C fibre, susceptibility and anisotropy ratio, tensile modulus and structure depend. 2−57270
- $CdCr_2S_4$:Fe^{2+}, of tetrahedral Fe^{2+} ions 2−72161
- Co-Fe (8 at.% Fe) alloys, anisotropic magnetization and magnetic anis. 2−81255
- Co, h.c.p., determ. from band struct. calc. 2−61181
- Co film, evaporated at oblique incidence, mag. contrib. of columnar grains 2−72184
- Co film, rel. to n.m.r. 2−81471
- $Cr_{1-x}Te$, magnetic anisotropy with X=0.077 2−84415
- $CsMnCl_3.2H_2O$, short range order effect 2−44295
- Cu(II) complexes meas. of mean susceptibilities and anisotropies in temperature range 300K to 68K 2−54285
- Dy single cryst., mag. struct. from neutron depolariz. meas. near Curie point 2−51251
- Fe-Al alloy, disordered matrix with Fe_3Al phase precipitates 2−54319
- Fe-Co equiatomic alloys, energetics, determ. of order 2−61507
- Fe-Ni alloy film, rotating anisotropy, temp. depend. 2−57300
- Fe-Ni films, perpendicular anisotropy from galvanomag. meas. 2−61529
- Fe_3Al, compression induced, and superlattice dislocations 2−61516
- GdFe garnet polished platelets, uniaxial anisotropy 2−44276
- K, non-saturating anisotropy of induced torque 2−48036
- $KMnCl_3.2H_2O$, from mag. phase boundaries meas. 2−68574
- $LiCuCl_3.2H_2O$, from mag. phase boundaries meas. 2−68574
- $Li_{0.5}Fe_{2.5-x}Al_xO_4$ $(0 \leqslant x \leqslant 1)$ and $Li_{0.5}Fe_{2.5-x}Ga_xO_4$ $(0 \leqslant x \leqslant 1.63)$, spinel ferrites, electric fields at lattice points and magnetic anisotropy 2−72194
- $Li_{0.45}Mn_xFe_{2.55-x}O_4$, anisotropy contrib. of Mn^{3+} and related directional orders 2−65170
- $Mg_{1-y}Co_yFe_2O_4$, ferromag. reson. study 2−81283
- $MgFe_2O_4$, exchange anisotropy and relax., degree of treatment depend. 2−72156
- MnF_2, rel. to crit. point anomaly in e.p.r. linewidth 2−78165

Magnetic anisotropy continued
- MnGaGe, ferromagnet, temp. depend. 2−72168
- MnZn ferrites, influence of Ti ions on magnetic properties 2−84405
- $NaMnF_3$, powder, magnetization, susceptibility, canting, effective exchange, anisotropy fields 2−48098
- Ni-Fe alloy films, transverse anisotropy consts. 2−61538
- Ni-Fe film, uniaxial anisotropy, effect on ripple spectrum 2−81279
- Ni-Fe films, polycryst., edge anisotropy 2−61527
- Ni-Fe(18 wt%) electrodeposited film, hyper-crit. thickness, fluctuations 2−84409
- Ni-Fe(50-50) alloy, mag. annealing effects 2−81241
- Ni-Zn-Co ferrite film, anisotropy induced by thermomagnetic treatment 2−81228
- Ni, anisotropy of depolarization of neutron beams 2−61509
- Ni film, mag. props., internal stresses induced 2−48095
- Ni powder, rel. to temp. depend. of mag. props. 2−51260
- NiFe permalloy, film, oxidized, exchange anisotropy effects, hysteresis loop, 5-300 K 2−81230
- $NiFe_2O_4$, iodine additive effects 2−44279
- $RbNiF_3$, crystal field theory 2−61546
- $TbPO_4$, low temp. 2−78046
- UAsS(Se, Te), magnetization rel. to temp. and mag. field, 3 K to Curie point, hysteresis loop, anisotropy 2−72172
- $Y_3Fe_{5-x}Al_xO_{12}$, garnet, obs. by natural ferromag. reson. 2−78148
- $Y_3Fe_5O_{12}$:Co^{2+}, Mn^{3+}, anisotropy and magnetostriction consts. rel. to Co^{2+} and Mn^{3+} ion substitutions 2−75233
- $Y_{2.5}Gd_{0.5}Fe_4Ga_1O_{12}$ garnet, film, magnetization orient. depend., induced anisotropies, magnetooptic Faraday effect obs. 2−72188
- YIG, Al^{3+}-substituted, Ru^{3+} -doped, ferromag. reson. study 2−81444
- YIG, iodine additive effects 2−44279
- YIG, nucl. gamma reson. study 2−81266
- YIG discs, epitaxial, effects on magnetostatic modes 2−44432

Magnetic bays *see Earth/magnetic field, variations; Magnetic storms*

Magnetic bottles *see Magnetic fields; Plasma/confinement*

Magnetic cooling
- cerium ethyl sulphate, adiabatic demagnetiz. 2−44229
- erbium ethyl sulphate, adiabatic demagnetiz. 2−44229
- yttrium ethyl sulphate; Yb^{3+}, Dy^{3+}, proton polarization and relaxation by rotational cooling 2−48122
- $Ce_2Mg_3(NO_3)_{12}.24H_2O$, diluted, adiabatic demagnetiz. 2−45185
- $Ce_2Mg_3(NO_3).24H_2O$, temp. scale to 1.6 mK 2−45187
- Cu nucl. spin-lattice relax. of Zeeman and spin-spin systems, 1 to 17 mK 2−68581
- ^3He, solid, Pomeranchuk cooling 2−80515
- $Na_3[Ce(C_7H_3NO_4)_3].15H_2O$, mag. and thermometric props. in 2-20 mK range 2−82079
- Pr, nuclear cooling, hyperfine enhancement 2−65121

Magnetic devices
- bubbles and their appl. 2−81262
- coils, axially symmetric air-core with homogeneous and strong mag. field 2−69854
- coils, high field, uniform current density, stress calcs., computer program 2−73519
- cylindrical magnetron diode, pulse discharge, spectroscopic investigation 2−60299
- direction controllable magnet variometer 2−82425
- ferrite cores, internal effective field during nonuniform rotation 2−69857
- ferrite memory cores, strength rel. to water environment, comments 2−80756
- ferrite memory cores, strength rel. to water environment 2−77652
- garnet mag. films, domain interaction with laser beam, domain writing 2−75230
- garnets bubble films, elimination of hard bubbles by second magnetic layer 2−65164
- magnetic bubbles, multilayer epitaxial garnet films for hard bubble suppression 2−65162
- memory, using micron size bubbles 2−69856
- memory materials and devices, conference (Princeton, 1 May, 1972) 2−69478
- Permalloy field access bubble domain drive ccts., magnetostatic pot. wells, drive fields, meas. technique 2−73507
- Permalloy plated-wire memory, domain struct., electron microscope obs. 2−75231
- rod, magnetization characteristics using numerical analysis 2−76438
- solenoid with water cooling 2−59071
- superconducting magnetic flux exclusion tube for particle physics expts. 2−76446
- ultrasonic generator, tunable by magnetically biased laminated Fe core 2−49132

Magnetic domains *see Domains*

Magnetic field measurement
- a.c. fields 2−45663
- aeromagnetometer reliability rel. to intermittent failures 2−45662
- alkali vapour magnetometer, optically pumped, effect of nonresonant r.f. field 2−59066
- astatic magnetometer for measuring remanent rock magnetization 2−66695
- astatic magnetometer with feedback for magnetized rock specimens 2−63259
- circular coils, arbitrary array 2−59068
- current balance, classroom expt. 2−48962
- cyclotron 107 model magnet, design of full scale magnet 2−79705
- detection coil systems for vibrating sample magnetometers 2−82428
- Earth's field, horizontal component meas. using direction controllable magnet variometer 2−82425
- electron lenses, using cylindrical search coil 2−79065
- e.p.r. magnetometer, sensitivity improvement 2−69852
- e.p.r. magnetometer 2−76441
- Faraday rotation probe for plasma magnetic flux density meas. 2−77279
- ferromagnetic high coercivity single domain particles, sensitive vibrating sample magnetometer 2−55644
- flux, primary state standard in USSR system 2−76440
- fluxgate magnetometer for geomagnetic variations in shallow seas 2−69851
- geomagnetic induction, wide frequency band measurements 2−58111

Magnetic field measurement continued
- Hall effect magnetometer, elimination of temp. on flux density meas. accuracy 2−49309
- harmonic field contents of pulsed quadrupole magnets using stepping search coil 2−76444
- hysteresigraph, l.f., Preisach's theory verification 2−66694
- intensity in strip line 2−55651
- Josephson junction magnetometer detection of n.m.r. 2−66674
- lines-of-force of anomalous magnetic field used for locating and delineating magnetized bodies 2−54927
- lunar surface magnetometer experiments, transient and steady meas. 2−55130
- lunar surface meas. and interior properties 2−55128
- magnetometer, alternating force, for mag. moment obs. 2−66698
- magnetometer, automatic recording, for use at high temps. 2−73513
- magnetometer, self-compensating, with superconducting solenoid 2−59063
- magnetometer for weak field with resolution of 10 ppm 2−55648
- magnetometer rotating sample for ferromagnetic anisotropy meas. 2−41911
- magnetometers, bibliography 2−66696
- model beam analyzing magnet, field inhomogeneities measurement 2−63722
- moon, remnant magnetization mapping by Apollo 15 subsatellite 2−55129
- multimagnetometer system, use in determining spacecraft fields 2−66024
- n.m.r. applies to flux density obs. of varying field 2−76443
- n.m.r. signal detectors, uniform magnetic field of Helmholtz coil pair, for living bodies 2−59013
- n.m.r. spectrometer, low level, for in situ obs. at low temps. 2−63209
- nuclear magnetometer using stable oscillator 2−55649
- ore exploration using 3-component drill hole magnetometers 2−58122
- peak fields of pulsed quadrupole magnets, peak to d.c. comparison method 2−55647
- permeameters for industrial inspection of permanent magnets 2−76442
- plasma, magnetic field direction, spatial meas. by microwave method 2−64302
- plasma, using light scatt. 2−64301
- powder, magnetic testing, comparison of use of a.c. and d.c. produced magnetic fields 2−59067
- pulsed discharges in rarefied gases, by Faraday effect 2−78992
- remanent magnetization of long cores of sediment, rapid measurement 2−54944
- semiautomatic analyser, with magnetic probes 2−49308
- space, optimization of multimagnetometer system positioning on spacecraft 2−62418
- SQUID, applic. to magnetic susceptibility obs. 2−52384
- stray fields in cylindrical coils determ. with desk calculator 2−76407
- superconducting solenoid monitoring using ^{133}Cs n.m.r. 2−66700
- synthetic magnetic anomaly curves, paleomagnetic applications 2−44779
- three Josephson junction interferometer, mag. field sensitivity and amplitude deviation 2−51118
- transistorized gaussmeter using Ge diode as sensitive mag. probe 2−55643
- varying, frequency dependence of Hall e.m.f. 2−52383
- vibrating sample magnetometer for protein research 2−45669
- vibration magnetometer, optimal configuration of receiving coils 2−55646
- He laser magnetometers, directional sensor errors 2−52382
- Ni-Fe strip of sensor for two-dimensional magnetic field distributions 2−73508
- Rb magnetometer, vector, operation and performance 2−73511

Magnetic fields
- *see also Earth/magnetic field; Electromagnetic fields; Interplanetary magnetic fields; Sun/magnetism*
- alternating, production in belt apparatus 2−57267
- annihilation in plasma 2−43129
- apparatus for superhigh freqs. studies up to 1°K 2−58656
- chamber for Rontgen unit determ. 2−58675
- charged rotating sphere, investigation of field at arbitrary point on surface 2−73514
- coils, axially symmetric air-core with homogeneous and strong mag. field 2−69854
- computation, derivatives of elliptic integrals of the third kind 2−45232
- conducting ferromagnetic plates, analogue computer study 2−73509
- control, proton magnetic resonance method 2−82413
- current sheet confined to surface of sphere, field expressions 2−55645
- in electric machines, calc. 2−63217
- excited at Earth's surface by ionospheric currents and Hall current 2−48572
- faint, formation of absorption lines, theory of transfer radiation 2−49307
- field distribution along channel axis in magnet system of conduction pump 2−49261
- fluids, potential equations 2−50166
- Galactic, origin and form, primordial-field model 2−69018
- generation in astrophysical bodies, solar dynamo 2−58542
- intergalactic, upper strength limits, role in hot model of Universe and galaxy formation 2−66049
- inversely proportional to r, with periodic azimuthal inhomogeneity 2−63254
- linkage, teaching 2−48970
- loop buried in earth, step-function excited 2−45665
- lunar, origin theories, review 2−51807
- lunar, satellite obs., remanent magnetization 2−62658
- lunar, transient and steady, interior electrical conductivity det. 2−51810
- β Lyrae, rel. to underluminosity 2−58349
- magnetic bubble in uniaxial mag. sheet, stray fields calc. 2−45668
- magnetic implosion system, energy transfer efficiency 2−69853
- magnetopause, structure in dawn to noon quadrant from Explorer 43 meas. 2−62316

Magnetic fields continued
multipole components in quadrupole end fields caused by longitudinal field components and sag of probe arm, distortions in analysis 2−55656
neutral-sheet type, Hamiltonian formulation of charged particle motion 2−59077
nonuniformity of superconducting solenoid, compensators 2−61250
particle accelerator low phase velocity supercon. resonant cavities 2−49700
permanent magnet system, using digital computer 2−73516
permanent magnet with plane and cylindrical symmetry, calc. 2−78952
pitch angle distrib. of particle fluxes, calc. method based on rocket and satellite data 2−72825
plasma, det. in vacuum for two dimensional MHD equilibria 2−64264
pulsar, rotating, Hamiltonian anal. of charged particle motion 2−62613
Schrodinger-Pauli-type eqn. for constant homogeneous electric and magnetic fields, Green's function 2−69589
solar, derived from $H\alpha$ filtergrams 2−75938
solar, diffusion in weak plage regions 2−78605
solar, meridional circulation 2−58543
solar, microwave burst generating region, decay 2−48796
solar, rel. to interplanetary field (1969) 2−75937
solar corona, atlas 2−73151
solar photosphere, flare associated, real-time anal. 2−75980
solar photospheric, latitude distrib. rel. to temp. distrib. 2−75976
solenoidal vector field represent. by poloidal and toroidal scalars 2−76408
solutions representing dipole field immersed in plasma 2−43130
steady-state galactic magnetic field, azimuthal component 2−81814
stellar toroidal fields, effects of additional poloidal field on stability 2−62496
strong pulsed field, solenoid wound with bimetallic wire 2−63255
Sun, polar, variations (1960-1971) 2−75941
sunspot, measurement methods 2−78602
Tokamak type apparatus, field distrib. near gap formed by sectionalized shells 2−64288
toroidal conductor, uniformity optimization 2−59070
universe and galaxies, structure 2−51690
very homogeneous, cylindrical coil with graduated current density 2−66699

effects
air 20 kW plasma torch induction and applications 2−46757
anisotropic elastic cylinder, torsional oscillations 2−52206
anisotropic harmonic oscillator in magnetic field, calc. of energy spectrum and wave functions 2−76206
antiferromagnets, biaxial domain structure in tilted mag. field 2−81306
arcs, deformation and cut-off model 2−60321
atom, ground state spin rearrangement in strong mag. field 2−67383
atomic spin system under alternating field, quantum structure of resonance effects 2−76966
axial and convergent guide field interaction with relativistic accelerator electron beam 2−70320
p,p'-azoxyanisole liquid crystals, thermal conductivity 2−67828
biological systems, effects of const. field 2−69229
Boltzmann temperature of oxide cathodes 2−59103
capillary wicking of distilled water in quartz sand and cylindrical glass capillaries in magnetic fields 2−60402
charge moving in field of arbitrary config., classical eval. 2−49315
charged Bose gas, properties in a magnetic field 2−73338
charged particle drift velocity, effect of small magnetic field 2−55653
composite cylindrical shell, radial vibration in magnetic field 2−66581
compression of high current relativistic electron beams by converging magnetic fields 2−73530
conductivity, microwave-induced anisotropy, for semiconductors in quantizing magnetic field 2−71893
convection, finite amplitude, effect of magnetic field, application to solar convective layer 2−58961
correlation function of conduction electrons in metals 2−77798
cosmic noise absorption at 24.6 MHz, effect of magnetic activity at low latitudes 2−54935
crystals, effects of external force gradients on i.r. and Raman activity of long wavelength optical phonons 2−84513
discharge development in homogeneous and heterogeneous fields 2−70993
elastic solids, perfectly conducting, plane dynamic deformation discontinuity expansion solution 2−66603
electrodynamic effect on non-magnetic conducting monolithic and laminar bodies 2−59027
electrodynamic force acting on sphere in travelling magnetic field 2−49195
electrodynamic force moment, effect of a non-magnetic conducting cylindrical case 2−59026
electrodynamics in strong magnetic field, phenomena studied by perturbation formalism 2−63265
electrolysis, effect of uniform field on mass transfer 2−54550
electron beam defocusing due to filament fields in gun 2−49691
electron beam injection into plasma and subsequent motion 2−74358
electron beams, high current, quasi-onedimensional solutions of equations 2−76455
electron gas at absolute zero, orbital magnetisation 2−45333
electron-hole-phonon quasiparticle bound states in strong mag. fields 2−68302
electrostatic instability excited by electron beam trapped in magnetic mirror of magnetosphere 2−48537
equilibrium configuration of slowly rotating liquid mass in poloidal magnetic field 2−77255
excitation of ionized laser with external magnetic field 2−49349
ferrite core, fast magnetization reversal by external magnetostatic field 2−61542
ferromagnet, uniaxial, with plate-like domain structure 2−72118
ferromagnetic plate, in mag.field, ground state and phase transition 2−72159
film, cross-tie-Neel domain wall transition, hysteresis change, in mag. field 2−48090

Magnetic fields continued
effects continued
fluid, flow over porous flat plate in transverse mag. field, Hall current effects 2−46704
gas discharge reactive oscillations, longitudinal field effect 2−80363
gases of linear molecules, time correlation functions 2−46853
geophysical exploration, non-stationary mag. fields probing, curves transformation 2−44589
graphite, neutron irrad., mag. energy, anomalous Schottky anomaly, sp. ht. obs. 2−57063
hydrogenlike atoms, calc. of energy levels in magnetic field by new method 2−70634
infinite cylinder, magneto-thermoelastic interactions on temp. due to line heat source 2−52197
insulation, conditions for feasibility 2−45672
ion-acoustic waves in magnetized plasma 2−67674
irreversible displacement phenomena in cylindrical ferromagnetic, Barkhausen effect meas. 2−81227
isentropic materials compression technique and apparatus 2−52010
Ising finite antiferromagnetic chain, order and correlation 2−75235
Josephson junction interferometers, critical current periodicity, interf. patterns 2−61254
liquid crystal, nematic, field induced distortions 2−53399
liquid crystals, influence on viscosity and thermal conductivity 2−80463
magnetically suspended rotating spheres, residual drag torque 2−73350
magnetoelastic buckling of beams and thin plates of magnetically soft material 2−66554
magnetoelastic waves, dispersion and polarisation for propagation along acoustic axes 2−68071
main-sequence stars, effects of uniform rotation and strong dipolar magnetic fields on structure and properties 2−84986
microwave frequency spectrum emitted by relativistic electron moving in spatially modulated magnetic field 2−66703
moments of forces, space vehicles 2−75646
muonium two-particle procession in strong mag. fields, polarization changes 2−70649
neutron diffusion, anal. of kinetic transport eqns. 2−76895
nuclear magnetic resonance, multiple, perturbing fields and audio frequency modulation, density matrix analysis 2−55636
optical orientation of excitons in crystals with wurtzite struct. 2−71804
optically inactive crystals, opt. rotat. induced by crossed elec. and mag. fields 2−78066
Penning source, formation position of ions 2−53262
n-pentane magnetic quenching of positronium due to 10.25 kG magnetic field 2−53384
perspex magnetoelectrets, effect of forming magnetic field on dielectric behaviour 2−65074
physical props. of matter in superstrong mag. field 2−81858
piperylenes, photosensitized reactions 2−65397
plasma, laser produced, breakdown thresholds and heating 2−43134
plasma, striations in transverse mag. field 2−64326
plasma heating, in CO_2 laser produced plasma 2−70929
plasma microwave discharge, mag. field stabilized 2−64271
plasma resonances in collisionless heating by transit time magnetic pumping 2−64314
plasma r.f. torch, effects of pulsed magnetic field 2−70923
polyatomic gas, meas. of thermomagnetic force on thin disc in 30-35°C range 2−43264
polynuclear hydrocarbons, quenching of triplet excited states by O_2, possible effects of magnetic fields 2−50124
Reiss type viscoelastic rod disturbances 2−66580
remanent demagnetization change under influence of mag. fields 2−54939
retrograde motion of low pressure discharge in transverse fields 2−70996
rock demagnetization apparatus using alternating magnetic field 2−51662
on ruby fluorescence, intensity, decay time changes 2−72419
semiconductor, ambipolar diffusion noise spectrum 2−61269
semiconductor, supercond., rel. to state mixing between bands due to e.m. field 2−77872
semiconductor cyclotron resonance linewidth in quantum limit 2−51148
semiconductor p-n junction photographic system, resolving power enhancement 2−75123
semiconductor plate, elec. cond. anisotropy 2−75087
semiconductor with contacting bands, transversal dielec. function in mag. field, RPA approx. 2−77942
semiconductors with nonparabolic bands, transport props. 2−81101
semimetal, influence on the intraband and interband scattering of excitonic insulator 2−81003
SH reflection from core-mantle boundary 2−72639
spectrochemical trace analysis in arc plasmas, use of external magnetic fields 2−51477
stellar and solar atmospheres, effect on absorption lines 2−48684
stilbenes, photosensitized reactions 2−65397
superconductor, gap, equilib. value, rel. to weak alternating fields 2−57157
suspension of a permanent magnet over a superconductor, expt. 2−59069
terrestrial magnetic field effect on satellite motion about its centre of gravity 2−72938
thermocouples, temperature measurement errors due to improper grounding 2−66652
thyratron employing orthogonal electric and magnetic fields 2−70994
trace element analysis in arc plasma, spectral line intensity depend. on magnetic field 2−48356
transverse, effects in Tuman-2 plasma device 2−80295
transversely isotropic finite cylindrical magnetic field 2−66582
turbulence suppression 2−50184
type II superconductor in crossed electric and magnetic fields, coherent quasiparticle excitation 2−84307
video-tape recording, influence on ponderomotive forces causing surface deformation of carrier 2−73237

Magnetic fields continued
- **effects** continued
  - viscoelastic composite layer, disturbance propag. in mag. field 2−55462
  - viscoelastic fluid layer, thermal instability 2−80224
  - water purification and structure 2−54521
  - Bi liquid-solid interface, oscillation damping 2−71303
  - C, line spectra intensity, d.c. arc, effect of field, 230-790 Oe 2−49943
  - $CaWO_4:Nd^{3+}$, photon echoes, generation, detection, mag. field and temp. depend. 2−72251
  - Cu-constantan thermocouple, Seebeck effect at low temps. 2−63162
  - Cu, line spectra intensity, d.c. arc, effect of field, 230-790 Oe 2−49943
  - Cu electrowinning in coupled electric and magnetic field 2−68796
  - $Cu_{0.5}Fe_{2.5}O_{4\|x}$, spinel ferrite, neutron-diffraction study, with and without mag. field 2−61543
  - Fe-Ni-Mn alloy, isothermal martensitic transform. rel. to mag. field 2−50937
  - Fe loss, of Si steel plates due to rotating magnetic field 2−84422
  - GaAs, compensated, negative magnetoresist. temp. depend., influence of mag. field 2−71900
  - GaAs, current instability rel. to mag. field, negative resist 2−64984
  - GaAs, high purity, optically pumped stimulated emission shift 2−61698
  - Ge:Cu $P^+-\pi-N^+$ structures, effect of magnetic field on forward current 2−75130
  - Ge, galvanomagneto-recombination effect kinetics rel. to elec. and mag. fields 2−65015
  - Ge, plasma, screw instability in strong mag. fields 2−77844
  - H atom, binding energy, lowest excitation energy, in mag. field 10^8-10^{11} gauss 2−67419
  - He-Ne laser, impulse linear field effect on generating power at $\lambda_{gen}=1.15\ \mu m$ 2−63329
  - He-Ne laser, mode intensity spectrum and output power 2−79208
  - He-Ne laser, transverse field effect on radiated power 2−59161
  - He hollow cathode discharge, V-I characteristics 2−64347
  - ^{3}He-^{20}Ne ring laser at 3.39 μ 2−45734
  - Hg filaments in chrysotile asbestos, supercond. rel. to external mag. field 2−84313
  - InSb, electron-hole plasma in mag. field, carrier wave growth 2−61316
  - n-InSb, Gunn effect threshold in transverse mag. field, travelling domain form. 2−71908
  - n-InSb, transverse, elec. fields, current, charge densities, impact ionization phenomena 2−61317
  - $Nd_2Mg_3(NO_3)_{12}.24H_2O$, spin-lattice relax., external mag. field depend., 1.5-2.0K 2−48115
  - Ni-Cr alloy, hydrogenated, elec. resist. rel. to mag. field, localized moments 2−81034
  - Ni-Zn-Co ferrite film, anisotropy induced by thermomagnetic treatment 2−81228
  - NiO, f.c.c. cryst., antiferromag., magnons, light scatt., dispersion and absorpt. 2−61550
  - Pt, line spectra, effect of ext mag. field on intensity 2−49954
  - p^+-n Si:Au diode, current filament behaviour in mag. field 2−71975
  - Ti sputter ion pumps, influence of asymmetry 2−62899
  - $TmFeO_3$, orthoferrite, domain struct., effect on mag. field 2−57306
  - Xe laser output power 2−73572
  - Y_2O_3, low loss dielec. film, use of mag. fields in electron beam evaporation 2−77947

Magnetic films *see Films, solid/magnetic properties*

Magnetic flux *see Magnetic field measurement; Magnetic fields*

Magnetic hysteresis *see Magnetization process*

Magnetic lenses *see Electron lenses/magnetic; Ion optics*

Magnetic measurement
- *see also Magnetic field measurement. Entries describing measurement methods for specific magnetic quantities and effects may also be found listed under the various headings for the subjects concerned*
- a.c. susceptibility at r.f., using tunnel diode oscillators 2−68513
- anisotropy meas. in polycrystalline samples using magnetization curve 2−51232
- apparatus for obs. of magnetostriction in pulsed magnetic field 2−45667
- balance, for determ. of ferrite phase in austenitic stainless steel 2−44245
- bridge silicon mag. diode, volt-tesla charact., 01-3 T 2−82416
- demagnetization, shock induced, investig. method 2−48081
- dynamic characteristics, hysteresis curves, apparatus, closed ferromagnetic cores 2−82426
- ferromagnet, spontaneous magnetiz., Hall effect obs. 2−75219
- ferromagnetic materials, dynamic hysteresis cycles, apparatus for direct recording using sampling techniques 2−45664
- Gouy magnetometer, lateral instability 2−73510
- at high temperatures, changes of magnetisation of weakly magnetic substances 2−59062
- hysteresis loop tracer, for nonconductive ferromagnets 2−66697
- internal field, magnetoelastic reson. method, appl. to YIG 2−57285
- magnetometer, cryogenic, for rock magnetization meas. 2−54959
- magnetometer, for remanent magnetism of rock and mud samples 2−54958
- magnetostriction constants, meas. by ferromag. reson., appl. to YIG 2−72176
- microprobe analyzer for thin films 2−66702
- nuclear reactors, in pile measurements, maximum temp. in irradiated samples 2−67363
- Permalloy field access bubble domain drive ccts., magnetostatic pot. wells, drive fields, meas. technique 2−73507
- pitch of solenoid det. by noncontacting magnetic pick up probes 2−78994
- pole profile determination for magnets with weak focusing fields 2−55650
- south east Australian coast, magnetic variometer array 2−72908
- susceptibility, static, Faraday balance for low temp. obs. 2−73512
- susceptibility, using iron-less coil devices with intense uniform forces 2−41910
- susceptibility balance, sapphire filaments as hang down supports 2−45673

Magnetic measurement continued
- torsion, calibration with conducting loop 2−66018
- torsional balance, improved feedback circuit 2−76439
- uniaxial film, hysteresis loop meas., magnetization and thickness estimation method 2−68559
- vibrating reed magnetometer, for magnetization process investigation in small ferromag. specimens 2−55543

Magnetic memories *see Calculating apparatus; Magnetic devices*

Magnetic mirrors *see Magnetic fields; Plasma/confinement*

Magnetic monopoles
- Dirac, slowing down in metals and ferromagnets, calc. 2−79490
- geomagnetic data, monopole term in spherical harmonic reduction 2−65996
- historical outline 2−49476
- relativistic Kepler problem, quaternionic solutions 2−52060
- tachyon monopoles, searches in photoproduction reactions at 1 MeV, detection by emitted Cherenkov radiation 2−82638

Magnetic permeability
- circular coils, arbitrary array, magnetic field meas. 2−59068
- ferrites for inductance cores, automatic apparatus for measurement of long term losses 2−45661
- ferrites of nickel/zinc, hot-pressed, flame-sprayed, permeability; temperature coefficient changes 2−84430
- liquid crystals, nematic, angular depend. studies of anisotropy 2−80459
- metallic cores, freq. depend., Jordan's relations 2−61511
- reversible, apparatus for obs. 2−59065
- soft magnetic material, SIFERRIT N32, broad temp. range 2−61501
- $BaCo_xTi_xFe_{12-2x}O_{19}$, temp. depend. 2−48102
- Co, calc. from optical spectra 2−65155
- Fe, calc. from optical spectra 2−65155
- $MgFe_2O_4$, anomalous temp. depend. at Curie point 2−72167
- Ni, after demagnetization by longitudinal alternating field 2−48074
- Ni, calc. from optical spectra 2−65155

Magnetic properties of dilute systems
- alloy, dilute, infinite U Anderson model, mag. susceptibility 2−61494
- alloy, liq., susceptibility, quasi-atomic model 2−53454
- alloy, liq., susceptibility, quasi-atomic model 2−53454
- alloy, spin reson. theory 2−78160
- Anderson model, t-matrix approach 2−48033
- ferromagnet, anisotropy due to anisotropic impurity spin, theory 2−81237
- ferromagnet with four-spin interaction, critical behaviour 2−72128
- finite impurity spin lifetime concept. and resist. calc. 2−54287
- Heisenberg spins, spatially random, very low temp., antiferromagnet 2−72136
- Heisenberg spins, spatially random, very low temp., ferromagnet 2−72135
- Heisenberg system, transition temp. depend. 2−48046
- ion, with orbital ang. momentum, interactions in insulators, review 2−65112
- Kondo temperature of strongly coupled pair of magnetic impurities 2−72103
- magnetic centres in effective energy band, Hubbard model, functional integral approach 2−77983
- magnetic impurity in quantum chain, reson. behaviour 2−81201
- magnetization of nearly mag. alloys, linear response region 2−44218
- metal alloys, local spin fluctuations, renormalized theory 2−61492
- metals, mag. impurities, mag. hyperfine interaction studies, review 2−84397
- nonmetallic diamag. cryst. with mag. impurity, spin diffusion and nucl. relax. 2−81313
- paramagnetic metal with Sm impurity giant, dwarf and negative moments 2−44222
- random impurity potential, high temp. Kondo effect 2−72102
- rare earths in metals, indirect exchange 2−44217
- s-d exchange interaction, electron energy renormalization and resist. 2−51274
- Schrieffer-Wolff transform., Kondo model rel. to Anderson model, diagrammatic eqns. 2−48042
- specific heat anomalies due to simultaneous effects of exchange and mag. fields, low temp. 2−57308
- superconductivity in s-d exchange model, effect of localized magnetic moment 2−47840
- superconductor, local spin excitations and moments 2−57162
- surface-gas-solid interactions 2−84395
- thermoelectric power of magnetic alloys 2−54242
- 3d transition metal alloys, localized moments, detection from lattice const. obs. 2−53660
- transition metals and alloys, localized moments, generalization of Anderson model 2−68515
- transition metals with actinide impurities, hyperfine field data 2−68588
- Ag-Mn alloys, s-d exchange interaction constant from electrical resistivity measurements 2−44214
- Al-Mn, neutron scatt. by spin fluctuations 2−61473
- Al, mag. scatt. of neutrons from dissolved Mn atoms 2−61474
- Al with transition metal impurities, temp. depend. of charge perturbation 2−48304
- As-V(Cr)(Mn)(Fe)(Co)(Ni) liquid alloy, susceptibility 2−80485
- Au-V alloy, susceptibility, field depend. 2−61475
- Au-V alloys, susceptibility, 2-293K, local behaviour 2−68517
- Au-Yb, localized moments, Mossbauer obs. 2−81210
- $CeRh_xPd_x$ alloys electronic state, magnetic susceptibility and lattice spacings 2−81317
- $Ce_{0.25}(Y,La)_{9.75}Al_2$, susceptibility calc. from cryst. field levels of Ce^{3+} 2−72105
- $Ce_xY_{1-x}Sb$, $Ce_xLa_{1-x}Sb$ solid solutions, antiferromagnetically ordered, Neel temp. dependence on lattice constants 2−72212
- Co-As internal hyperfine mag. field determ. 2−44321
- $Co_{0.91}Fe_{0.09}$, f.c.c., temp. dependence of moment distrib. 2−65165
- Cr-Re dil. alloys, single cryst., mag. struct., neutron diffr. exam. 2−61553
- Cr alloy, ordering wave-vector, model 2−84441
- (Cu-Au)-Fe alloy, susceptibility 2−61483
- Cu-Co, n.m.r. and double resonance studies of electron spin density near Co atoms, obs. of satellite lines 2−75204
- Cu-Fe alloy, paramag. susceptibility, 1.7-300K 2−61483

Magnetic properties of dilute systems continued
- Cu-Mn dilute alloy, thin film, e.s.r. study 2−44446
- Cu-V(Cr)(Mn)(Fe)(Co)(Ni) liquid alloy, susceptibility 2−80485
- Cu and Cu-Al alloys, liq. with Mn and Fe impurities, cond.-electron spin polarization obs. 2−53455
- CuZn-V(Cr)(Mn)(Fe)(Co)(Ni) liquid alloy, susceptibility 2−80485
- EuO, doped, susceptibility, metal-semiconductor transitor 2−77842
- Fe-Al alloy, ave.-moment-internal field variations 2−78008
- Fe-Cr alloy, spin disturbance produced by solute 2−44354
- Fe-Si alloy, ave.-moment- internal field variations 2−78008
- Fe alloys, Curie temp., effect of indirect exchange interactions 2−44248
- Ga-V(Cr)(Mn)(Fe)(Co)(Ni) liquid alloy, susceptibility 2−80485
- GaGe-V(Cr)(Mn)(Fe)(Co)(Ni) liquid alloy, susceptibility 2−80485
- Ge-V(Cr)(Mn)(Fe)(Co)(Ni) liquid alloy, susceptibility 2−80485
- GeAs-V(Cr)(Mn)(Fe)(Co)(Ni) liquid alloy, susceptibility 2−80485
- La-Ce(Gd) alloys, temp.-depend. pair breaking, spin-flip scatt. obs. using supercond. 2−54144
- $(La,Gd)Al_2$, n.q.r. and relax. obs., ordering onset 2−68754
- $La_{3-x}Ce_xIn$ alloys, supercond. and mag. props. 2−64946
- Mg:Gd, exchange narrowing of fine structure 2−72496
- Nb-Mo:Fe alloy, localized moments on Fe, Mossbauer obs. 2−48149
- Nb-Mo-Fe, discontinuous formation of localized moments, Mossbauer study 2−78076
- Ni-As internal hyperfine mag. field determ. 2−44321
- Ni-W alloy, impurity moment orientation, ^{182}W Mossbauer study 2−75273
- Pd-Co(Fe)(Mn) alloys, ordering, sp. ht. and resist. meas. 2−81246
- Pd-Mn alloys, giant moment of Mn 2−44257
- Pd-rare earth alloys, magnetiz., susceptibility, moments 2−44224
- Pt-Co alloy, disappearance of giant mag. moments 2−81211
- Pt-Co alloys, nucl. sp. ht., low temp. 2−43986
- Sn-Mn film, mag. state of Mn rel. to supercond. 2−68512
- $V_xCr_{1-x}B_2$, nuclear magnetic resonance study of antiferromagnetic transition 2−72521
- Zn-V(Cr)(Mn)(Fe)(Co)(Ni) liquid alloy, susceptibility 2−80485
- ZnGa-V(Cr)(Mn)(Fe)(Co)(Ni) liquid alloy, susceptibility 2−80485

Magnetic properties of substances
- *see also Films, solid/magnetic properties Magnetic anisotropy; Magnetic permeability; Magnetic structure*
- actinide Halide compounds 2−68505
- actinide metals, hybridization 6d and 5f virtual-bound-states model 2−68516
- Al-Ni alloy, influence of short-range order on elec. and mag. resist. 2−71423
- alkali halide, moments and susceptibility rel. to electrons trapped in edge dislocations 2−81200
- alloy, mictomagnetic, struct. model 2−65166
- basalt, submarine pillow, induced and saturation magnetization in relation to titanomagnetic grains 2−68990
- brass, magnetic susceptibility obs. using SQUID 2−52384
- C16-type pseudobinary alloys, susceptibility, valence electron conc. depend. 2−51104
- carbons irradiated by neutrons and annealed, props. changes of magnetic susceptibility 2−68137
- chondrites, carbonaceous, magnetic memory 2−58532
- conference, Freudenstadt, Germany, (12-14 April, 1972) 2−77982
- deuteromethane, solid, proton mag. susceptibility 2−65351
- dust particles, microscopic determination of magnetic moments 2−53456
- glass, containing metal ions, mag. props. rel. to struct. 2−64526
- glass, structure, contrib. of classical magnetic measurements 2−60581
- ilmenite-haematite solid solution, self-reversal and X-phase rel. to palaeomagnetic investigations 2−54960
- linear conducting chains, review 2−61140
- magnesium ferroaluminate: Co, formed from metal hydroxides 2−47239
- magnetite dispersion, magnetic characteristics rel. to palaeomagnetism 2−58139
- metabasic rocks, susceptibility and natural remanent magnetization 2−75639
- metal film, fluctuation enhancement of mag. moment 2−81209
- metal oxides, rel. to elec. cond. characts. 2−57106
- metal systems, data compilation, NBS Permuted Materials Index 2−68155
- metal/hydrogen systems, conf., Julich, Germany (Mar 1972) 2−77713
- metallic fine particles, effect of discrete energy levels 2−81215
- meteorite, Allende, individual chondrules examined 2−58537
- meteorite, Bjurbole, individual chondrules examined 2−58537
- meteorite, Chainpur, individual chondrules examined 2−58537
- multilevel systems, susceptibility elec. simulat. 2−84572
- multiphase mixtures, composition dependence of flux propagations 2−75252
- nematic film in variable field, transient distortions 2−53396
- neutron scattering on fluctations 2−71151
- octahedral d^1 complexes, susceptibility calcs. 2−59987
- permalloy films epitaxially grown on fcc metals, structural and standing spin wave resonance props. 2−78149
- polymers, semiconducting, Co chelate, of dihydroxyquinones, meas. of mag. moment and susceptibility 2−80815
- rare earth hydrides, ordering, sensitivity to hydrogen conc. 2−77986
- rare earth metals, orbital contribs. effects review 2−84392
- reversible magnetic permeability, apparatus for obs. 2−59065
- rocks from Giles Complex, central Australia, stability tests 2−75638
- sediments, role of Brownian motion in control of detrital remanent magnetization 2−74564
- semiconductor, III-V, transition metal doped, anomalous props. 2−68405
- semiconductor, strongly doped, model interpret. of susceptibility 2−77880
- semimetal, indirect exchange interactions, interband susceptibility calc. 2−75022
- singlet ground state system, excitations pseudospin formalism 2−72233
- solid state and quantum electronics, book 2−57092
- solids without resonant nuclei, with sorbed gases, susceptibility, n.m.r. determ. 2−60671

Magnetic properties of substances continued
- superconductors, relevant theories 2−84300
- susceptibility, instrumentation and applics., review 2−52381
- susceptibility, molecular orbital theory 2−42850
- susceptibility effective magnetic moment, units 2−82132
- TCNQ complexes, quasi-one-dimensional disordered systems, Mott transition, susceptibility obs. 2−84238
- TCNQ salts, susceptibility, role of disorder 2−64920
- thioformaldehyde, obs. of high-field rotational Zeeman effect, determ. of magnetic susceptibilities 2−43010
- titanomagnetite dispersion, magnetic characteristics rel. to palaeomagnetism 2−58139
- transition metal ion, in liq. state, by e.s.r., review 2−54569
- transition metal-actinide alloys, susceptibility interpret., narrow band reson. model 2−54286
- transition metals, direct exchange interact. calc., generalized Heitler-London model 2−68529
- two-level magnetic system damped by interaction with bosons, transverse susceptibility 2−49022
- zeolite, with sorbed methane, static susceptibility, n.m.r. determ. 2−60671
- AmI_2, meas. of magnetic susceptibility and effective magnetic moment 2−80643
- AsSI and AsSeI, vitreous and molten, temperature dependence of susceptibility 2−84393
- B_2O_3-BaO-Fe_2O_3 glass, superparamag. props. rel. to microstruct. 2−56558
- $Ba(Ce_{1-x}Ta_x)O_3$, ion pair valency at high and low temps. det. from magnetic moments 2−75203
- BaO-B_2O_3-Fe_2O_3 glass, magnetiz., microstruct. effects 2−65113
- $BaTi_{1-x}{}^{4+}Ti_x{}^{3+}O_{3-x}F_x$ solid solution 2−47705
- Bi:Te, effect of high hydrostatic pressures on mag. susceptibility 2−81102
- C, smectic liquid crystal, mag. instabilities 2−60433
- CdSb:Te, with low Te content, reluctance, 78-293K 2−61307
- $CeMg_2(NO_3)_6$, powder, Johnson noise temp. rel. to 16Hz mag. temp., 2-20 mK 2−71897
- $CeSn_3$, absence of magnetic ordering from n.m.r. obs. 2−84588
- $Ce_xY_{1-x}Al_2$, susceptibility, 4.2-300K 2−64912
- $CoFe_2O_4$-Co_3O_4 alloy, quenched, aged, saturation magnetization, intrinsic coercive force, rel. to microstruct. 2−81233
- Cr ternary alloy, nonferromagnetic Invar alloy, Elinvar characs. 2−77981
- Cu complexes in solutions, study of metal-ligand bonding, magnetic susceptibility and moment of Cu(II) ion 2−64473
- Cu(II) complexes, tetrameric, $Cu_4OX_6L_4$, $X=Cl$, $L=(C_6H_5)_3PO$ and $X=Br$, $L=(C_6H_5)_3PO$ or C_5H_5N, susceptibility 2−51233
- Cu(II) complexes meas. of mean susceptibilities and anisotropies in temperature range 300K to 68K 2−54285
- CuO-SeO_2 system phases, anomalous behaviour 2−84573
- Er-B system phases, susceptibility 2−50964
- Fe-B-metal melts, behaviour 2−72138
- Fe atoms in YuNDK24 alloy, exam. by nuclear γ reson. after thermomagnetic treatment 2−84471
- $Fe_{1-x}Mn_xSi$ solid solution, thermomag. meas. 2−48068
- $Fe_xPd_{80-x}P_{20}$ $(13 \leqslant x \leqslant 44)$, amorphous alloy, magnetic properties study from Mossbauer effect of ^{57}Fe 2−65114
- $FeSb_2$, and elec. props. 2−61340
- GaAs, mag. susceptibility, calc. and expt. 2−71928
- Gd, interactions, e.p.r. obs. 2−75352
- $GdCo_5$, powder, coercive force rel. to sintering temp., decomp. stability 2−68511
- $Gd(OH)_2$, magnetic specific heat, and ac susceptibility measurements using a r.f. tunnel diode oscillator 2−68513
- ^3He, Neel temp., triple exchange effects 2−83830
- HfV_2, susceptibility anomaly 120 K 2−54507
- $LaCoO_3$, high-spin-low spin equil. and localized-collective electron transition 2−54288
- Mn-Zn system, phase diagram from mag. obs. 2−57032
- Mn, α and γ phases, Invar effect 2−57269
- $MnBr_2.4H_2O$, adiabatic magnetiz., mag. phase diagram detn. 2−65115
- $NbSe_2$, susceptibility, 5-298 K 2−47339
- Ni-Pd disordered alloy, spin susceptibility calc. 2−65117
- Ni-Rh disordered alloy, spin susceptibility calc. 2−65117
- Ni complexes, trimethylphosphines Ni(II), magnetic moments 2−77091
- NiB, susceptibility, room temp. 2−51099
- Np compounds, hybridized band model 2−84396
- Pr, mag. exciton excitation spectra, crystal field effects 2−75205
- $PrCl_3$, low temp. cooperative behaviour, n.m.r. obs. 2−72166
- Pt-Co alloy, electrodeposited 2−44268
- Pt-Pd disordered alloy, spin susceptibility calc. 2−65117
- Pu compounds, hybridized band model 2−84396
- Rh-Pd disordered alloy, spin susceptibility calc. 2−65117
- S, crystalline and glassy, low temp. susceptibility 2−61477
- Se, crystalline and glassy, low temp. susceptibility 2−61477
- Sm-Sn system intermetallics, correl. with electronic struct. 2−47573
- $SmCo_5$, powder, coercive force rel. to sintering temp., decomposition stability 2−68511
- $(Sm_{1-x}Pr_x)Co_5$, $0<x<1$, alloys, saturation magnetization, anisotropy field, coercive force 2−68510
- $Tb(OH)_2$, magnetic specific heat, and ac susceptibility measurements using a r.f. tunnel diode oscillator 2−68513
- TiO-MnO alloy, mag. susceptibility 2−74908
- $Tm_2(SO_4)_3.8H_2O$, exchange induced magnetiz., heat capacity obs. 2−64857
- U compounds, hybridized band model 2−84396
- $U(C_{1-x}N_x)$, mag. suscept. rel. to electronic props. 2−57268
- α-USe_2, mag. props., magnetization, 4.2-1000K 2−72108
- V^{3+} complexes, trigonally distorted octahedral, lattice-ion interactions in the ligand field theory 2−81205
- $(V_{1-x}Cr_x)_3Si$, ternary alloys, physical props. and electron struct. and susceptibility 2−68514
- VO_x, susceptibility, 300K 2−64991
- V_nO_{2n-1} $(n=3,4,\ldots,8)$ single cryst., temp. depend. of susceptibility, meas. 2−43509
- Yb-Sn system intermetallics, correl. with electronic struct. 2−47573
- $YbCu_{6.5}$, susceptibility 2−43594

Magnetic properties of substances continued
$YbMnO_3$-$YbCrO_3$, $YbMnO_3$-$YbFeO_3$, solid solns., suscept. and elec. cond. 2−51235
$YbPd_3$, cryst. field and Mossbauer obs. 2−54393
Zn, steady susceptibility, uniaxial stress depend. 2−81204
antiferromagnetic
see also Antiferromagnetism
− 2−72511
alloy, b.c.c., spontaneous magnetiz., interstitials influence 2−43818
alloy, binary, spin-orbit interaction effects on kinetic properties 2−57295
cerium ethyl sulphate, heat capacity, demagnetiz. and susceptibility meas. below 1K 2−68551
cerium ethyl sulphate, ordering and low temp. calorimetry 2−44229
copper formate, thermal conductivity meas. 2−51062
copper formate tetrahydrate, thermal cond., magnon contrib. 2−72226
dilute system, spatially random Heisenberg spins at very low temps. 2−72136
domain structure in tilted mag. field 2−81306
domain structure in uniaxial antiferromagnets 2−68536
erbium ethyl sulphate, ordering and low temp. calorimetry 2−44229
exchange coupled ferromag.-antiferromag. pair, transverse susceptibility rel. to field 2−72155
exchange coupled films, ferro-antiferromag., microscopic mag. switching 2−78030
excitation spectrum of antiferromagnetic hamiltonian 2−81295
insulator, magnon induced sidebands in optical transitions 2−54408
magnetoordered crystals with small exchange constant, spin waves and scatt. proc. of neutrons and light 2−72209
manganese formate, phase diagram studies 2−44293
manganese formate dihydrate, mag. diagram of state, spin-flop transition 2−68577
metals, particle scattering by coupled electromagnetic-magnon waves 2−84443
neutron and light scattering, in ferromagnet with weak antiferromagnetism 2−78012
nickel acetate tetrahydrate, rel. to sp. ht., 0.43-10.73 K 2−78040
order-disorder transitions, sound propag. phenomena 2−54026
Permalloy film, oxidized antiferromag. surface layer, mag. after effect 2−44267
rare earth chalcogenides, exchange interaction problems 2−54373
rare earth cobalt intermetallics, 2-17 type, characteriz. for permanent magnets 2−61510
rare earth gold intermetallics, struct., s-f interaction 2−44308
rare earth metals, crit. scatt. role in elec. resist. 2−57271
rare earth metals, light, struct. 2−61517
rare earth metals, spin correls. and elec. resist. 2−57272
rare earth metals, thermal cond. and Lorenz function abnormalities at Neel pt. 2−57311
rare earth orthochromites, n.m.r. of ^{53}Cr, sublattice magnetiz. 2−48307
rare earth orthoferrites, possibility of intermediate state existence for first order phase transformation 2−81291
rare earth orthoferrites and orthochromites, ang. depend. of superexchange interactions 2−68569
rare earth tetraborides, 2-600K meas. 2−81293
rare earth-nickel intermetallics, mag. struct. 2−48080
rare earth-transition metal intermetallics, pulsed field magnetiz., critical phenomena 2−51261
spin waves in anisotropic antiferromagnets 2−81305
spin-electromagnetic waves in antiferromagnetic with small exchange constants 2−81290
substitutionally disordered antiferromagnets, localized excitations 2−44285
TCNQ anion radical salts, mag. susceptibility Schottky type behaviour 2−68575
tetramethylammonium manganese chloride, low-temp. transitions 2−72530
tetramethylammonium manganese chloride, susceptibility in fields of 250Oe, 10kOe and 50kOe 2−72227
transition metal alloys, itinerant model 2−44286
tricritical susceptibility exponent in Ising-model metamagnet 2−54302
$Al_2Fe_3(SiO_4)_3$, almandite, garnet, mag. struct. 2−54349
Al_2O_3-Fe_2O_3 solid solution, mag. interactions, e.p.r. study 2−75351
$BaCoF_4$, two-dimens. antiferromagnet, mag. ordering 2−72211
$Ba(Fe_{0.35}Al_{0.65})_2O_4$, disordered solid solution, blocking temps. of mag. random clusters from Mossbauer spectra 2−57309
Ba_2FeUO_6, susceptibility and magnetization saturation 2−68570
Ba_2MReO_6, (M=Mn,Re,Co,Ni), perovskites, characteriz. 2−50876
CeB_2, exchange interactoon and fluctuation effects 2−54339
CeBi, struct., ordering 2−44291
CeSb, ordering, struct. 2−44292
$Ce_xY_{1-x}Sb$, $Ce_xLa_{1-x}Sb$ solid solutions, Neel temp. dependence on lattice constants 2−72212
Co complex, $[Co(NH_3)_6][CuBr_3Cl_2]$, susceptibility, 4.2-292K 2−81296
$CoBr_2.6H_2O$, phase diagram studies 2−44293
$CoCO_3$, spontaneous mag. moment along trigonal axis 2−68572
$CoCl_2[(NH_2)CS]_4$, paramag.-antiferromag. and antiferromag.-spin flop phase boundaries, thermal cond. study 2−81302
$CoCl_2.2H_2O$, relax. phenomena of metamagnetic transition, a.c. suscept. obs. 2−57310
$CoCl_2.6H_2O$, 2- and 3-phonon processes, rel. to proton spin-lattice relax. 2−7[illegible]050
$CoCl_2.6H_2O$, oriented ^{54}Mn, γ radiation pattern change, obs. by spin flop transition 2−61552
$CoCl_2.6H_2O$, partially deuterated, sublattice coupling 2−54350
$CoCl_2.6H_2O$, phase diagram studies 2−44293
$CoCl_2.6H_2O$, spin wave theory 2−54351
$Co_4Nb(Ta)_2O_9$, Neel temp. determ. from magnetoelectric susceptibility obs. 2−54359
CoO-Al_2O_3-SiO_2 glass system, low field suscept. 2−65178
$(CoO)_{1.4}.P_2O_5$, glasses, antiferromag. interactions 2−75237
Cr:Fe, high temp. Neel points at different field intensities 2−68567
Cr-Re dil. alloys, single cryst., mag. struct., neutron diffr. exam. 2−61553
Cr, antiferromag.- paramag. transition, sp. ht., 280-330K 2−75238

Magnetic properties of substances continued
antiferromagnetic continued
Cr, cold-worked, Neel point, rel. to recovery 2−53805
Cr, first-order transition 2−57119
Cr, Invar effect 2−57269
Cr, itinerant, 2 band model 2−44289
Cr, magnetic generalized spin susceptibility, interband contribs., Lindhard expression 2−61554
Cr, magnetic struct. intensity, temp. hysteresis, sign change 2−54328
Cr, magnon-phonon interaction 2−48109
Cr, Q-switch and polarization domains, obs. with neutron diffraction topography 2−65179
Cr and alloys, thermal cond. and Lorenz function abnormalities at Neel pt. 2−57311
Cr complex, $[Cr_3O(CH_2COO)_6(H_2O)_3]^+$, insufficiency of Heisenberg model 2−44294
Cr complex, di-μ-hydroxotetraglycinatodichromium (III), susceptibility, 4.2 to 100K 2−80645
Cr dilute alloy, ordering wave-vector, model 2−84441
Cr_2O_3-Ti_2O_3 solid solution, ordering, diffr. and e.s.r. obs. 2−48104
Cr_2O_3-V_2O_3 solid solution, ordering, diffr. and e.s.r. obs. 2−48104
Cr_2O_3, e.p.r. spectra below Neel temp., paramagnetic transition 2−54492
$Cr_2(SO_4)_3$, $(CH_3NH_3)_2SO_4$, $24H_2O$, sp. ht. and susceptibility and above crit. temp. 2−48105
$CsCoCl_3$, neutron diffr. obs. of struct. 2−72213
$CsCoCl_3$, one-dimens. mag., Mossbauer obs. 2−72160
$CsCoCl_3.2H_2O$, Ising linear-chain antiferromagnet, mag. struct., magnetization, shor-range spin correls. 2−72214
$CsCrCl_3$, ligand field, magnetic coupling between Cr ions 2−81363
$CsFeF_4$, planar atniferromagnet, X-ray diffr., suscept., and Mossbauer obs. 2−65180
$CsMnF_3$, antiferromag. and paramag. reson. linewidths near Neel temp. 2−68726
$CsNiCl_3$, n.m.r. of ^{35}Cl and ^{133}Cs, determ. of mag. props. and struct. 2−72215
$CsNiCl_3$, one-dimens., spin-wave approach 2−54352
$CsNiCl_3$, one-dimens. mag., Mossbauer obs. 2−72160
$CsNiF_3$, one-dimens. behaviour 2−44241
$CsNiF_3$, three dimensional mag. struct., neutron diffr. obs. 2−61556
$CuCl_2.2H_2O$, 2- and 3-magnon processes, rel. to proton spin- lattice relax. 2−78050
Cu_2FeSnS_4, ordering, Mossbauer obs. 2−75239
$CuLiCl_3.2H_2O$, phase diagram studies 2−44293
$Cu_4Mn_2Te_4$, transitions 2−84442
$Cu(NH_4)_2Cl_4$, susceptibility and transition, 1.1 to 300K 2−65152
$Cu(NH_3)_4SO_4.NH_3$, exchange integral variation with lattice spacing, sp. ht. obs. 2−54353
$Cu(NO_3)_2.2^1/_2H_2O$, differential susceptibility, energy levels and relaxation effects 2−48106
Dy-Nd alloys, ordering, Neel pt. phenomena, spin disorder 2−51237
$DyIn_3$ theoretical and experimental study 2−72223
DySb, ordering, struct. 2−44292
$Er_{0.6}$-$Ho_{0.2}$-$Dy_{0.2}$ alloy, magnetization curves, study at 4.2 K 2−65174
Er, phase transitions, microwave absorpt. obs. 2−51257
$ErAg_2$, magnetic structure, 297-1.5K, neutron powder diffraction study 2−61551
$ErAl_3$, mag. struct., neutron diffr. obs. 2−81275
$ErAu_2$, struct., neutron diffr. obs. 2−72216
ErC_2, struct., 297-2K, neutron diffr. obs. 2−72217
Er_2O_3, spectral line shift and splitting at onset of antiferromag. ordering 2−81369
ErOOH, monoclinic, struct. 2−44296
EuTe, e.p.r. linewidth near crit. point 2−75341
EuTe, para- and antiferromag. resonances, critical phenomena near Neel temp. 2−61728
Fe-Ge system, $FeGe_2$ phase, susceptibility 2−64821
Fe-Mn alloy, austenitic, antiferromag. transform., rel. to mech. props. 2−50783
Fe-Pd alloys, f.c.c., mixed exchange interactions, neutron scatt. obs. 2−84421
Fe-Rh, Fe-Rh-Ir alloys, magnetic contrib. to electronic sp. ht. 2−64856
Fe-Rh alloy, f.c.c., Neel temp., Mossbauer study 2−78072
Fe-Rh alloy, magnetoresist., temp. depend. 2−54330
$FeBO_3$, n.m.r. and weak ferromag. temp depend. 2−72523
$FeBO_3$, sublattice struct. recreation by mag. field 2−54355
$FeBO_3$, weak ferromagnetic moment and Dzyaloshinskii field temp. depend. 2−72523
$FeBr_2$, antiferromag.-ferromag. transition, mag. rot. power 2−65218
$FeCO_3$, Ising behaviour, magnon-phonon coupling 2−44297
$FeCO_3$, magnetic structure, nonuniformities at metamagnetic transformation 2−65219
$FeClO_4$, frozen solns., Fe^{3+} ion behaviour, Mossbauer effect 2−78070
$FeCl_3.6H_2O$, spontaneous magnetization, mag. ordering, mag. hyperfine fields, Mossbauer reson., $T<4.2$ K 2−75272
FeF_2, mag. hyperfine interactions of Fe^{2+} interpret. 2−61604
FeF_2, magnon-phonon interactions, coupling, spin Hamiltonian 2−80886
FeF_2, magnon-phonon interaction 2−44298
FeF_2, neutron scatt. struct. factor, nonlinearity effect 2−48107
FeF_2, two-magnon Raman scatt., temp. depend., calc. 2−81304
Fe(II) complex, $Fe(phen)_2(NCS)_2$, mag. heat capacity due to low spin $^1A_1 \rightleftharpoons$ high spin $^5T_2$ transition 2−75240
$(Fe_xMg_{1-x})_2SiO_4$, mag. transitions, comp. depend., 4-300K 2−68987
$Fe_{0.9}Nb_{1.1}O_4$ magnetic structure, neutron diffr. obs. 2−65181
Fe_2O_3- P_2O_5 glass, forming range and mag. suscept. 2−54354
α-Fe_2O_3, *c*-axis moment obs. 2−44299
α-Fe_2O_3, haematite, magnon energy of optic mode, Morin transition 2−51278
α-Fe_2O_3, haematite, Mossbauer effect of ^{119}Sn and ^{57}Fe, Morin transition obs. 2−65234
Fe_2O_3, produced from α-, β-, γ- and δ-FeOOH, Morin point, neutron diffr. obs. 2−81292
α-Fe_2O_3 and natural haematite, true heat capacity, mag. component 2−43984
Fe_3O_4, magnetite, metal-insulator transition, Verwey temp. 2−57125

Magnetic properties of substances continued
antiferromagnetic continued
$(Fe_2O_3)_{0.79}.P_2O_5$, glasses, antiferromag. interactions 2−75237
$Fe(Pd_xPt_{1-x})_3$, magnetic phase changes, Mossbauer obs. 2−48108
FeRh, first-order antiferromag.-ferromag. transition, electronic struct. changes 2−84438
FeRh, mag. field depend. of antiferromag.-ferromag. transition temp. 2−81288
FeS, Mossbauer effect determ. of spin arrangements, quadrupole interaction, internal magnetic field, chemical shift 2−81344
Fe_3S_4, synthetic samples, Mossbauer spectra study 2−81338
$Fe_{1\|\delta}Sb$, antiferromagnetism, Mossbauer effect meas. 2−84440
$GdAlO_3$, magnetoeleastic coupling and antiferroacoustic resonances 2−72462
$GdAlO_3$, obs. of u.s. attenuation in high magnetic field, spin wave interactions 2−54348
GdAs, exchange consts. calc. 2−61549
$GdGa_xCu_{1-x}$, mag. order and cond. electron conc. 2−78020
$GdIn_3$ theoretical and experimental study 2−72223
$GdIn_xAg_{1-x}$, mag. order and cond. electron conc. 2−78020
β-Gd_2MoO_4, electrically polarized, magnetic moment from 0.4 to 4.2K along b crystal axis 2−51277
β-$Gd_2(MoO_4)_3$, electrically polarized, 0.4 to 4.2K, up to 90 kG along a crystal axis, magnetic moment 2−44290
Gd_3NF_6, susceptibility, weak moments 2−48110
GdP exchange consts. calc. 2−61549
GdSi, magnetic structure, susceptibility 2−68568
Gd_5Si_3, magnetic structure, magnetic susceptibility 2−68568
$GdZn_xAg_{1-x}$, mag. order and cond. electron conc. 2−78020
$GeMnO_3$, magnetoelec. susceptibilities and sp. ht. 2−44300
Ho-50%Tb, spiral spin state, anomalous behaviour of u.s. propagation 2−64843
Ho single crystals, 4.2-300K, extremum values of magnetoresistance and Hall field at magnetic transition temps. 2−68548
$HoAu_2$, struct., neutron diffr. obs. 2−72218
$HoCrO_3$, spontaneous magnetization, susceptibility, exchange interaction, 4.2-300 K 2−48070
$HoZn_2$, struct., ordering 2−68573
$KCuF_2$, thermal conductivity meas. 2−51062
$KCuF_3$, one dimensional antiferromagnet, anomalous thermal cond. 2−71760
$KFeF_4$, critical behaviour, neutron and Mossbauer obs. 2−44301
$KFeF_4$, planar antiferromagnet, neutron scatt. and Mossbauer obs. 2−78043
$KMnCl_3.2H_2O$, mag. phase boundaries, anisotropy exchange fields, mol. field theory 2−68574
$K(Mn_{1-c}Co_c)F_3$, critical condition for magnon localization found for all impurity concentrations 2−44284
$KMn_{1-x}Co_xF_3$, spin waves theory and coherent potl. approx. applic. to mag. excitations 2−78044
$KMnF_3$, anomalous thermal cond. 2−71761
$KMnF_3$, doped, impurity effects on excitation spectra 2−44282
$KMnF_3$, $KMnF_3$:Mg, temperature dependence of e.p.r. line width, room to liquid nitrogen temp., effect near Neel temp. 2−44440
$KMnF_3$, susceptibility anomalies interpret., magnetoelastic effects 2−54356
K_2MnF_4, e.p.r. linewidth temp. depend. 2−75345
K_2MnF_4, e.p.r. linewidth temp. depend. 2−75345
K_2MnF_4, hyperfine contribs. to ^{19}F n.m.r. lineshift 2−54510
K_2MnF_4, mag. struct. near crit. point, neutron scatt. study 2−65182
$KNiF_3$, mag. linear dichroism 2−81329
$KNiF_3$, Neel point determ., elastic, magneto-optical and heat capacity meas. 2−72219
$La_{3-x}Ce_xIn$ alloys, susceptibility, conc. depend., ordering 2−64946
$La_{3-x}InCe_x$, supercond. and magnetic props., conc. depend. 2−47854
$LiCuCl_3.2H_2O$, mag. phase boundaries, anisotropy exchange fields, mol. field theory 2−68574
$LiFe_2F_6$, trirutile, mag. structure, neutron diffr. obs. 2−65183
$LiFe_2F_6$, trirutile, neutron diffr. obs. of struct. 2−72220
$Li_{0.5}Fe_{2.5}O_4$, superexchange bond, ^{57}Fe n.m.r. study 2−78169
$Li(NH_3)_4$, susceptibility obs. in 1.5-10 K range, antiferromagnetic metal and electron gas models for behaviour 2−43389
$MdPd_3$, mag. struct. from neutron diffr. obs. 2−54360
Mn-Ga alloys, antiferromag. transform., rel. to internal friction 2−50735
Mn-Permalloy bimetal film, mag. after-effect 2−81224
Mn-permalloy film, exchange anisotropy, ferromag. to anitoferromag., thermomag. recording 2−57286
α-Mn, ^{55}Mn n.m.r. study 2−61748
α-Mn, Neel temp. press. depend. 2−54357
Mn complex, $(CH_3)_4NMnCl_3$, direct process n.m.r. relaxation by spin waves 2−51414
Mn complex, di-μ-oxo-tetrakis(2,2′-bipyridine)dimanganese(III,IV) perchlorate trihydrate, superexchange coupling 2−44303
Mn_2As, high press. form., and cryst. struct. 2−53670
$MnAu_2$, spiral phase, reson. of disordered spin component 2−44429
MnB_2, struct., neutron diffr. obs. 2−44306
MnB_2, weak ferromagnetism, s-d exchange model 2−81257
$MnBr_2.4H_2O$, 2- and 3-magnon processes, rel. to proton spin-lattice relax. 2−78050
$MnBr_2.4H_2O$ meas. of Br n.m.r. spectra down to 0.4K, determ. of magnitude and orientation of internal mag. field 2−65175
$Mn_{1-x}Co_xF_2$, spin waves theory and coherent potl. approx. applic. to mag. excitations 2−78044
$MnCoP_4$, high-press. synthesis and props. 2−83899
$MnCr_2S_4$ spinel, sublattice magnetiz. and magnetostrictive effects 2−48073
$MnF_2:Fe^{2+}$, exchange field obs. under press. 2−44304
MnF_2, critical neutron scatt., spin fluctuations 2−54361
MnF_2, doped, impurity effects on excitation spectra 2−44282
MnF_2, e.p.r. linewidth, crit. point anomaly, role of anisotropy 2−78165
MnF_2, e.p.r. linewidth, crit. point anomalies 2−78159
MnF_2, longit. neutron scatt. behaviour below crit. temp. 2−54362
MnF_2, mag. hyperfine interactions of Fe^{2+} interpret. 2−61604
MnF_2, principal susceptibilities, calc. using Heisenberg model 2−65172
MnF_2, two-magnon absorpt., spin-flop transition effects 2−54358
MnF_2, two-magnon Raman scatt., temp. depend., calc. 2−81304

Magnetic properties of substances continued
antiferromagnetic continued
MnF_2, zero field circular dichroism in magnon sideband region 2−44376
$MnGeO_3$, magnetoelec. signal near critical field for spin flop 2−44305
MnN_x, hexagonal, mag. and Mossbauer obs. 2−54331
$MnNb_2O_6$, ordering, magnetoelectric and susceptibility obs. 2−65184
$Mn_4Nb(Ta)_2O_9$, Neel temp. determ. from magnetoelectric susceptibility obs. 2−54359
MnO, exchange consts. calc. 2−61549
MnO, spin waves, inelastic neutron scatt. obs. 2−61558
MnO(S), e.p.r. linewidth, crit. point anomalies 2−78159
MnP, effect of press. on susceptibility and transitions 2−48072
α- MnS exchange consts. calc. 2−61549
Mn_5Si_3, noncollinear antiferromag.-collinear antiferromag.-paramag. transition 2−78042
α′-$NaV_2O_{5-x}F_x$, $0 \leqslant x \leqslant 1$, d electron distrib. on V atoms, from elec. and mag. props. 2−75080
Nd, phase transitions, phenomenological theory 2−51279
$NdCrO_3$, anomalies in temp. depend. of spontaneous magnetiz. 2−72222
$NdFeO_3$, spontaneous magntiz., moment temp. depend., effective field 2−72221
$NdIn_3$ theoretical and experimental study 2−72223
NdS, domain struct., and temp. depend. of susceptibility 2−81307
NdSb, ordering, struct. 2−44292
Ni-Cu-Mn alloy, magnetization, temp. depend. 2−78025
$NiCl_2.6H_2O$, 2- and 3-phonon processes, rel. to proton spin- lattice relax. 2−78050
$Ni(NH_3)_2.Ni(CN)_4.2C_6H_6$, mag. susceptibility, rel. to sp. ht., 1.2-4.2K 2−75241
$Ni(NO_3)_26NH_3$, susceptibility and specific heat obs. 2−65185
NiO, exchange interactions, crystal field theory 2−68564
NiO, mag. superlattice X-ray diffr. peaks 2−44307
NiO, spin wave dispersion, inelastic neutron scatt. study 2−81303
NiO exchange consts. calc. 2−61549
$NiSnCl_6.6H_2O$, susceptibility, magnetization and heat capacity, 0.35-4.2 K 2−78039
$PbCrO_3$, perovskite, struct., elec. resist., mag. susceptibility 77-550K 2−61321
$PbFe_{2/3}W_{1/3}O_3-PbTiO_3$ system, phase diagram, antiferromag., ferromag., and paramag. regions 2−81229
Pr:Fe, high temp. Neel points at different field intensities 2−68567
Pr, Neel temp., elec. resist. anomaly 2−51281
$PrCu_2$, cooperative nuclear magnetic order below 54 mK 2−51282
$PrIn_3$, negative paramagnetic Curie temperature indicating antiferromagnetism 2−72223
Pr_3X-La_3X system, (X=Al, Ga, In, Tl, Sn, Pb), rel. to supercond. behaviour 2−61244
$RbCoF_3$, one- and two-magnon scatt. below Neel pt. 2−54435
Rb_2CoF_4, critical behaviour, n.m.r. obs. 2−44458
$RbFeF_4$, two-dimens. antiferromag. ordering, susceptibility and neutron diffr. obs. 2−54363
$RbMnF_3$, critical neutron scatt., spin fluctuations 2−54361
$RbMnF_3$, e.p.r. linewidth, crit. point anomalies 2−78159
$RbMnF_3$, magnon struct. of absorp. spectra in 3900 Å region 2−65266
$RbMnF_3$, temperature dependence of e.p.r. line width, room to liquid nitrogen temp., effect near Neel temp. 2−44440
$RbNiCl_3$, one-dimens., spin-wave approach 2−54352
$RbNiCl_3$, one-dimens. mag., Mossbauer obs. 2−72160
$RbNiCl_3$, struct., ordering 2−48111
$SmIn_3$, theoretical and experimental study 2−72223
$SrCoO_{2.5}$, mag. struct., neutron diffr. obs. 2−81294
Tb-Sc alloys, T_n vs G, and magnetostrictive behaviour 2−68576
$TbAsO_4$, magnetically controllable phase transition 2−78045
$TbAsO_4$, paramag. to antiferromag. transition, susceptibility study 2−65187
$TbCu_2$, struct., zero field, moments, hysteresis, critical phenomena 2−44309
$TbFeO_3$, mag. struct., shape effects 2−61559
$Tb_xHO_{1-x}FeO_3$, magnetic properties, rare-earth grids, Neel temps. of sublattices, easy magnetization axis, rare earth ion interactions 2−65033
TbO_2, mag. struct. 2−72224
$TbPO_4$, low temp. mag. moment and sp. ht. anomalies 2−78046
TbSB, singlet ground state system, excitations; pseudospin formalism 2−72233
$TmFeO_3$, spin reorientation, n.m.r. study 2−44460
$Tn_xMn_{1-x}O$, $0.07 \leqslant x \leqslant 0.9$, mag. props., mag. susceptibility, struct., 100-1000 K 2−54364
UAs-US system, magnetic phase diagram, neutron diffr. obs. 2−65188
$UAs_{1-x}S_x$ system, mag. phase diagram 2−44258
$UC_{1-x}N_x$ x=0.6 to 1, derivation of Neel temperature from resistivity-temperature relation 2−44105
UPb_3, mag. struct., neutron diffr. obs. 2−78041
$V_xCr_{1-x}B_2$ transition in nuclear magnetic resonance study 2−72521
$V_{2-x}Cr_xO_3$, domain form. during Mott metal-insulator transition, geometry and crystallography 2−71785
V_2O_5-P_2O_5 glass, microstruct., mag. ordering mag. props., e.s.r. 2−44310
V_2O_3, model for metal-insulator transiton 2−72225
V_nO_{2n-1}, ordering, ^{57}Fe Mossbauer study 2−72286
Y orthoferrites and orthochromites, ang. depend. of superexchange interactions 2−68569
$YFeO_3$, intrinsic domain-wall damping 2−65176
$YFeO_3$, melt-grown cryst. characteriz. 2−50605
$Zn_{1-x}Cu_xCr_2Se_4$, magnetization and susceptibility, 4.2-900 K 2−44311
ZnF_2, mag. hyperfine interactions of Fe^{2+} interpret. 2−61604
diamagnetic
see also de Haas-van Alphen effect; Diamagnetism
aromatic molecules, magnetic anisotropy, comparison of theory and expt. 2−60049
chalcogenide glass, evidence for states in band gap 2−61334
diamagnetic susceptibility enhancement of disordered or highly compensated crystalline semiconductors 2−81206

Magnetic properties of substances continued
diamagnetic continued
heavy atoms and positive ions, calc. of diamagnetic susceptibility using semiempirical model for electrons 2−70570
heterocyclic compound, saturated five membered, susceptibility temp. variation 2−71232
noble metals, nearly-free-electron susceptibility 2−48034
semiconductor, amorphous, diamag. enhancement of susceptibility, mechanisms 2−44219
semiconductor glass, susceptibility, temp. and comp. depend. 2−61480
Al based liquid alloy, Cr or Mn impurity, susceptibility near nonmag.-mag. transition 2−80486
B, crystalline, comparison with amorphous like crystalline semicond. 2−77987
$B_{10}H_{14}$, susceptibility and shielding const., SCF study 2−64115
B_2H_6, susceptibility and shielding const. from minimum basis set and extended Slater orbital wave functions 2−64114
$Bi_{88}Sb_{12}$, mag. susceptibility, effects of SN and Te impurities 2−72109
C fibre, neutron irrad. effects 2−56998
C fibre, susceptibility and anisotropy ratio, tensile modulus and structure depend. 2−57270
C fibres, diamag. susceptibility, 77-300 K, meas. 2−68331
Cd-Hg, susceptibility curves 2−81203
Cd-Mg, susceptibility curves 2−81203
CdTe, susceptibility, 4.2-290K 2−77980
CoP_2, high-press. synthesis and props. 2−83899
$CsAlF_6$, susceptibility, temp. depend., 300-700K 2−72110
$(Fe, Zn)_2Mo_3O_8$, mag. struct., Mossbauer obs. 2−75270
$FeAs_2$, diamag. semicond. 2−61340
$Fe(CN)_5(OH_2)^{2-}$-$Fe_2(CN)_{10}^{4-}$ equilibrium mixture in aqueous solution, study by magnetic circular dichroism 2−71231
Ga-Sb system, susceptibility, 30-1200°C 2−64820
H_2^+, variation-perturbation calculation 2−53008
H_2^+, variation-perturbation calculation, effect of varying internuclear separation 2−53009
I-, susceptibility, accurate analytical wave functions 2−42733
$K_{1-x}Rb_xI$, susceptibility, comp. depend. 2−54289
Li_3AlF_6, susceptibility, temp. depend., 300-700K 2−72110
Pb-Sb-S system, amorphous like crystalline semicond., comparison with B 2−77987
PbSe monocryst., heat treated, suscept. meas. 2−48035
PbTe, mag. susceptibility calc. 2−68519
Pd complexes, meas. of mag. susceptibility 2−77979
PtSi, susceptibility obs. 2−65348
Rb_3AlF_6, susceptibility, temp. depend., 300-700K 2−72110
Se, amorphous and cryst., mag. susceptibility, 40-300K 2−77988
Sn superconducting fine particles, susceptibility, temp. depend. 2−71852
TaS_2, 1S and 2S polymorphs, susceptibility 2−47226
Te, susceptibility anisotropy of holes, calc. 2−81214
Th-H, Th-D systems, mag. suscept. rel. to superconductivity 2−54143
Th_4H_{15} mag. suscept. rel. to superconductivity 2−54143
$Ti_xTa_{1-x}S_2$ $(0.1 \leqslant x \leqslant 0.9)$ solid solutions, change to paramagnetic behaviour 2−61266

ferrimagnetic
see also Ferrimagnetism
$Cr_2S_2Te_x$, $0<x \leqslant 1$, magnetization, susceptibility, ordering of vacancies, 80-800K 2−54343
excitations, ordering, spin interactions, spin one ion Hamiltonian 2−48101
hexaferrites, Y-structures and more complex structures anti-symmetric exchanges between spins of cations 2−84436
insulators, magnetic modes coupling to e.m. waves 2−72191
oscillations and waves in ferrimagnetic solids 2−44272
rare earbh cobalt intermetallics, RCo_2 type, first order transition 2−44280
rare earth iron garnets, props. near compensation temp. 2−81286
rare earth metals, light, struct. 2−61517
rare earth-Co Laves phases, $LnCo_2$, temp. depend. of magnetization 2−81276
spinal ferrite, temp. and composition depend. 2−48100
susceptibility meas., analysis using Neel's graphical techniques 2−84433
susceptibility meas. on ferrimagnets, graphical analysis 2−81280
titanomagnetites, effect of annealing on exchange anisotropy 2−72927
$Ba_5Co_2(Cu_2)Ti_3Fe_{12}O_{31}$, magnetiz. and anisotropic props., rel. to microwave applic. 2−44273
$BaCo_xTi_xFe_{12-2x}O_{19}$, permeability, temp. depend. 2−48102
$BaFe_{12-x}Ti_xZn_xO_{19}$, Ti-Zn cation distrib. effects, mag. saturation and neutron diffr. obs. 2−72195
$Ba_3Zn_2Fe_{24}O_{41}$, hexagonal, anisotropy, comparison with $BaMg_2Fe_{12}O_{22}$ 2−72451
$CdEr_2Se_4$, susceptibility, temp. depend. 2−72113
$CdHo_2Se_4$, susceptibility, temp. depend. 2−72113
$Co_xNi_{1-x}Fe_2O_4$, temp. variation 0-500C 2−72196
$CsCoCl_3$, neutron diffr. obs. of struct. 2−72213
DyAl garnet, mag. sp. ht. 2−43983
$Dy(Co,Ni)_2$, intrinsic mag. aftereffect 2−44274
$ErFeO_3$, with high coercivity surface layer, domain struct., magnetooptical study 2−81284
$FeCr_2S_4$ spinel, mag. split Mossbauer spectra obs. 2−57331
Fe_xGd_y alloy films, amorphous, conc. depend. 2−44275
$Gd(Co_{1-x}Ni_x)_3$ and $Gd(Fe_{1-x}Ni_x)_3$, transition metal moment obs. 2−51271
GdFe garnet polished platelets, uniaxial anisotropy 2−44276
GdIG, high temp. high press. phase 2−57024
GdIG, substituted, compensation temp., applic. to beam- addressable magneto-optic memory 2−72193
$Ho_xEr_{1-x}Fe_2$ system, spin orientation diagram 2−72197
$HoFe_3$, struct., neutron diffr. and thermal magnetiz. obs. 2−51272
$Li_{0.5}Fe_{2.5-x}Al_xO_4$, magnetization process, domain wall reson. study 2−72198
$Li_{0.5}Fe_{2.5}O_4$, reson. phenomena at moving domain boundaries 2−72456
$Li_{0.5}Fe_{2.5}O_4$, superexchange bond, ^{57}Fe n.m.r. study 2−78169
$Li_{0.5}Fe_{2.5}O_4$, synthesis conditions influence 2−44277

Magnetic properties of substances continued
ferrimagnetic continued
$Li_{0.45}Mn_xFe_{2.55-x}O_4$, anisotropy contrib. of Mn^{3+} and related directional orders 2−65170
Mg-Mn ferrite film, transparent, light diffr. by mag. stripe domains 2−65220
$Mg_{1-y}Co_yFe_2O_4$, mag. anisotropy, ferromag. reson. study 2−81283
Mn-Zn-Fe ferrite, permeability, thermal change, resonance type profiles 2−61545
$MnFe_2O_4$, acoustic magnon dispersion, neutron diffr. obs. 2−61544
$MnFe_2O_4$, reson. phenomena at moving domain boundaries 2−72456
MnO-Fe_2O_3 single-crystal films, static and dynamic domain structure 2−68561
Mn_3Pd_5 phase, crystal and magnetic struct. 2−83960
MnZn ferrites, influence of Ti ions 2−84405
$Mn_{1-x}Zn_xFe_2O_4$, neutron diffr., Mossbauer and mag. obs. 2−65168
$Na_5Co_3F_{14}$, chiolite-type phase 2−72199
$Na_5Fe_3F_{14}$ and $Na_5Fe_2CoF_{14}$, chiolite-type phase 2−72199
$Na_5V_3F_{14}$, chiolite-type phase 2−72199
Ni-Zn ferrite powder, quality characterization 2−57312
Ni-Zn ferrites, mag. losses in h.f. fields 2−84435
$NiCr_2O_4$ mag. struct. determ. by representation anal. 2−84429
NiFe ferrites, freq. effect, torque obs. 2−44278
$NiFe_{0.8}Cr_{1.2}O_4$, statistical angular spin configurations 2−72200
$NiFe_{0.8}Cr_{1.2}O_4$, structural transition at mag. transformation, Mossbauer and X-ray obs. 2−72201
$NiFe_2O_4$, magnetocryst. anisotropy, reson. fields, iodine additive effects 2−44279
$NiFe_2O_4$, reson. phenomena at moving domain boundaries 2−72456
$Ni_{1.2}Fe_{1.7}Sb_{0.1}O_4$, supertransferre d hyperfine fields and covalency at diamag. cations 2−48150
$Ni_xZn_{1-x}Fe_2O_4$, thermal expansion coeffs. at Curie pt., conc. depend. 2−81281
$RbNiF_3$, crystal field theory of mag. anisotropy 2−61546
$RbNiF_3$, spin waves, neutron scatt. obs. 2−65171
$SrFeO_3$, mag. struct., neutron diffr. obs. 2−81282
$SrFe_{12}O_{19}$, crystallized from B_2O_3-SrO-Fe_2O_3 glasses 2−54345
TbIG, high temp. high press. phase 2−57024
Y-Fe garnet, effect of magnetic ordering on optical absorption spectrum 2−81392
$Y_3Fe_{5-(x\|y)}Al_xGa_yO_{12}$ garnet, magnetiz. and ferromag. resonance 2−72204
$Y_3Fe_5O_{12}$:Co^{2+}, Mn^{3+}, anisotropy and magnetostriction consts. rel. to Co^{2+} and Mn^{3+} ion substitutions 2−75233
$YFeO_3$, with high coercivity surface layer, domain struct., magnetooptical study 2−81284
YIG:Ru, magnetostriction consts. 2−44281
YIG, Ca-Si substituted, flux grown crystals 2−47278
YIG, d.c. magnetization produced by parallel optical pumping 2−72203
YIG, diamagnetically substituted, rel. to Mossbauer spectra in crit. region 2−78077
YIG, high temp. high press. phase 2−57024
YIG, hysteresis loop, magnetization mechanism, role of wall displacement and bulging 2−65167
YIG, magnetocryst. anisotropy, reson. fields, iodine additive effects 2−44279
YIG, nonmag. ion substituted, polycryst., ferrimag. resonance obs. 2−61547
YIG, reson. phenomena at moving domain boundaries 2−72456
YIG, spin relaxation near Curie temp. studied by high frequency magnetic susceptibility 2−84417
YIG, substituted, ultra-low bandwidth, microwave loss 2−44435
YIG, surface spin wave propagation in inhomogeneous fields 2−78037
YIG cylindrical rod, mode separation of magnetostatic waves 2−59005
YIG film, Fe-deficient, magnetization 2−72202
YIG single cryst./polycryst. composites, amplified Hahn-type echoes 2−44270
YIG single crystal film, domain wall mobility meas. by light diffraction 2−84434
YbFe, garnet, stat. mol. field interpret. 2−72205
YbFe garnet, Ca-Si substituted, flux grown crystals 2−47278
$Zn_xMFe_{2-x}O_{4-x}F_x$, M=Ni, Co, ferrite, synthesis, magnetization, hopping cond. 2−75234

ferromagnetic
see also Ferromagnetic relaxation; Ferromagnetic resonance; Ferromagnetism; Magnetization process; Magnetization state
alloy, anomalous Hall effect, phonon scatt. effects 2−81223
alloy, b.c.c., spontaneous magnetiz., interstitials influence 2−43818
alloy, binary, spin-orbit interaction effects on kinetic properties 2−57295
alloy, f.c.c., spontaneous magnetiz., interstitials influence 2−43817
alloy, multicomponent, spatially random Heisenberg spins at very low temps. 2−72137
alloy weakly magnetic, influence of heterogeneities on magnetic isotherms 2−65150
alloys, coherent potential approximation, application 2−61500
amorphous, susceptibility and Curie temp. rel. to spin fluctuations 2−57277
anisotropy meas., rotating sample magnetometer 2−41911
Bloch walls, cold neutron diffr., nonelastic scatt., macroscopic anal. 2−51248
bubble garnets, magnetiz. reversal due to annealing 2−51253
bubbles and their appl. 2−81262
catalyst for ortho-para H_2 conversion, surface magnetization orientation effects 2−71342
cerium ethyl sulphate, heat capacity, demagnetiz. and susceptibility meas. below 1K 2−68551
closed cores, dynamic characteristics, apparatus for plotting hysteresis curves 2−82426
near compensation temperature T_k, galvanomagnetic phenomena and Hall effect 2−72158
conductivity of ferromagnets, infl. of domains 2−72147
conference, Freudenstadt, Germany, (12-14 April, 1972) 2−77982
cubic lattices, determ. of Curie temperature and critical index using exchange interaction model 2−44233

Magnetic properties of substances continued
  ferromagnetic continued
    degenerate electron gas, implications for metals, white dwarfs and neutron stars 2−47823
    dielectric- ferromagnet boundary, triplet excitons 2−77838
    dilute system, spatially random Heisenberg spins at very low temps. 2−72135
    disordered alloy, magnetiz.-temp. curves, influence statistical fluctuations of conc. 2−61512
    domain structure, effect on thermodynamic parameters near Curie point 2−72146
    domain structure in weak ferromagnets 2−68536
    domains, symmetry props. 2−77522
    EuO, ferromag. semicond., Redfield technique detn. of Hall mobility of photoelectrons 2−81060
    exchange coupled ferromag.-antiferromag. pair, transverse susceptibility rel. to field 2−72155
    exchange coupled films, ferro-antiferromag., microscopic mag. switching 2−78030
    Faraday effect and anisotropy of g-factor of rare-earth ion, low temp. study 2−65217
    ferromagnets, hypersound parametric excitation, mag. moment amplitude oscills. 2−81264
    film, coupled two-layer system, hysteresis loops, calc. 2−48087
    film, domain boundary creep, thickness and props. influence 2−72179
    film, factors influencing realization of trigger effect 2−75228
    film, Lorentz microscopy and spatial filtering 2−48088
    film, magnetoresist., effect of angular dispersion of magnetization 2−48086
    film, spin waves and resonance, stability 2−48089
    film, stripe-domain width, longitudinal field intensity depend. 2−57296
    film, supercrit. props. of stripe structs. 2−61520
    film, surface free-energy for spin-wave and molecular field models 2−75229
    film, surface spin-wave excitation 2−68716
    film, uniaxial, ang. dispersion of anisotropy effect on hysteresis loop 2−61521
    film. with periodic banded domain structure, spin wave spectrum 2−68553
    film with anomalous surface anisotropy, static magnetic susceptibility 2−72178
    films, electron microscopy of magnetic structure, review 2−84428
    grain-oriented polycrystals, saturation approach law of longitudinal magnetostriction 2−54335
    Hall effect, anomalous, in ferromagnetic semiconductors with strong s-d coupling 2−71879
    Hall effect, anomalous in metals and alloys, spin-orbital interaction effects on electron scatt. 2−72157
    high anisotropy multi-domain particles, magnetization reversal 2−44243
    high-coherence alloys, magnetic after effect 2−68552
    hysteresis loop tracer, for nonconductive ferromagnets 2−66697
    insulators, acoustic attenuation and frequency shift for 2 magnon-one phonon processes 2−80907
    Invar, elastic consts. anomalous temp. depend. in ferromag. state 2−84053
    Invar, mag. moment temp. depend., $T/T_c<0.5$ 2−65154
    Invar, spontaneous magnetostriction, itinerant electron model interpret. 2−48085
    irreversible displacement phenomena in cylindrical ferromagnetic, Barkhausen effect meas. 2−81227
    irreversible processes during reversal 2−54322
    Ising model spin-phonon interaction, effect of lattice vibrations on phase transitions 2−68524
    magnetic, crystalliz. from high Fe glasses, magnetiz. obs. 2−54329
    magnetic oxide powders, sub-micron range, particle size distribution measurement, electron microscopy 2−71654
    magnetization process, vibrating reed magnetometer for investigation of small specimens 2−55543
    magnetoacoustic instability during biharmonic pumping 2−84559
    metal, magnetiz. and hyperfine field temp. depend. comparison 2−54323
    metal films, meas. of longitudinal Faraday effect 2−54379
    metallic systems, elec. resist. in crit. region 2−57279
    mischmetal-Co permanent magnets, development 2−84406
    Mossbauer diffraction in magnetically ordered crystals, kinematic theory including Rayleigh dispersion 2−68610
    mushketovite, mag. props. rel. to ion content 2−51246
    neutron and light scattering, in ferromagnet with weak antiferromagnetism 2−78012
    order-disorder transitions, sound propag. phenomena 2−54026
    permalloy, magnetic hyperfine field at ^{57}Fe, Mossbauer spectra 2−54386
    permalloy film, changes in domain structure during pulsed a.c. magnetization, thermofluctuational character 2−68556
    permalloy film, coercive force and anisotropy, influence of substrate 2−84411
    Permalloy film, cross-tie walls, motion threshold field and behaviour at inhomogeneities 2−77994
    Permalloy film, oxidized, slow domain wall motion 2−54340
    Permalloy films, anisotropy, annealing depend. 2−61525
    Permalloy films, domain boundary motion, effect of struct. factors 2−61526
    Permalloy films, electrodeposited, comp. and depositing current effects 2−57302
    Permalloy films, l.f. slip of domain boundaries 2−61528
    Permalloy films and perfect monocryst. laminae, stripe struct., magneto-optical obs. 2−61531
    Permalloy films with supercrit. hysteresis loop, domain struct. 2−61532
    permalloy supercritical films, static and dynamic properties, domain structure 2−68557
    Permalloy thin wires, Bitter pattern obs. 2−61535
    Permalloy-Mn bimetal film, mag. after-effect 2−81224
    Permalloy-SiO- Permalloy multilayer systems, stripe domain struct. 2−61530
    phonon polarization operator in Ising model, calc. using spin-phonon interaction Hamiltonian 2−81265

Magnetic properties of substances continued
  ferromagnetic continued
    polydomain ferromagnets, singularities of elastic and inelastic scattering of neutrons 2−81226
    rare earth chalcogenides, exchange interaction problems 2−54373
    rare earth cobalt intermetallics, 2-17 type, characteriz. for permanent magnets 2−61510
    rare earth gallium intermetallics, LnGa, magnetization and susceptibility, temp. depend. 2−72170
    rare earth ionic cpds. with mag. dipole-dipole interaction, caloric and mag. obs. 2−68523
    rare earth iron garnet, damping of domain wall motion 2−57304
    rare earth metals, crit. scatt. role in elec. resist. 2−57271
    rare earth metals, effective f-f exchange interaction, temp. depend. 2−54317
    rare earth metals, light, struct. 2−61517
    rare earth metals, review 2−51239
    rare earth metals, spin correls. and elec. resist. 2−57272
    rare earth metals, spin wave gap calc. 2−75226
    rare earth metals, with helical spin struct., magnon- phonon interaction 2−75225
    rare earth- gallium intermetallics, equiatomic 2−48079
    rare earth-Co Laves phases, $LnCo_2$, temp. depend. of magnetization 2−81276
    rare earth-Ni Laves phase, $LnNi_2$, 4.2-700K 2−81277
    rare earth-nickel intermetallics, mag. struct. 2−48080
    rare earth-transition metal intermetallics, pulsed field magnetiz., critical phenomena 2−51261
    rare earths, spin wave energy rel. to interatomic exchange Heisenberg parameters, exchange coupling 2−61505
    soft magnetic material, SIFERRIT N32, broad temp. range 2−61501
    solid state physics, an overview 2−57093
    spin-electromagnetic waves in ferromag. semicond. and metals, theory 2−81225
    steel, ε-carbide, Curie temp. determ. 2−72165
    superconducting pairing tendency in nearly-ferromag. systems 2−57163
    surface dynamics and waves in mag. mats. 2−68527
    titanomagnetites, effect of annealing on exchange anisotropy 2−72927
    transformer steel, effect of induced magnetic anisotropy on magnetic properties and domain structure 2−68539
    transition metal, ferromag. transition phenomena 2−77989
    transition metal, magnetostriction, band model using spin-orbit term 2−48082
    transition metal alloys, 3d, crit. point phenomena 2−54332
    transverse mag. field, effect on ferromagnet, uniaxial, with plate-like domain structure 2−72118
    tricritical susceptibility exponent in Ising-model metamagnet 2−54302
    uniaxial, mag. field induced phase transitions 2−65149
    visco-plastic fluid, mag. field influence on heat exchange 2−80466
    Al based liquid alloy, Cr or Mn impurity, susceptibility near nonmag.-mag. transition 2−80486
    Al_2O_3-Fe_2O_3 solid solution, mag. interactions, e.p.r. study 2−75351
    $BaFe_{12}O_{19}$, props, during sintering 2−77738
    $BaFe_{12}O_{19}$, saturation magnetization, reduced temp. depend. by As or P substitution 2−78019
    Ba_2MReO_6, (M=Mn,Re,Co,Ni), perovskites, characteriz. 2−50876
    $Ba_3Zn_2Fe_{24}O_{41}$, hexagonal, anisotropy, comparison with $BaMg_2Fe_{12}O_{22}$ 2−72451
    $Ca_3Cr(GeO_4)_3$, mag. struct. and space group determ. 2−72145
    $CdCr_2S_4$:Fe^{2+}, anisotropy of tetrahedral Fe^{2+} ions 2−72161
    $CdCr_2S_4$, red shift peak in absorpt. band, mag. F′ centre model 2−80712
    n-$CdCr_2Se_4$:Ga, ordering effect on h.f. elec. cond. 2−44095
    $CdCr_2Se_4$, mag. permeability rel. to illum., photoferromag. effect 2−54324
    $CdCr_2Se_4$ film, vacuum deposited, saturation magnetization 2−60649
    CeBi, struct., ordering 2−44291
    $CeCo_5$, permanent mag. 2−52385
    Ce_2Fe_{17}, ferromag.-helimag. transition 2−54325
    $Ce_{1-x}Gd_x(Tb_x)Ru_2$, mag. ordering and supercond. coexistence 2−43981
    CeSb, ordering, struct. 2−44292
    Co-C interstitial solid solution, sat. magnetiz. and high field suscept. 2−81249
    Co-C system, Curie temp. depend. on C conc., thermodynamic evaluation 2−44246
    Co-Cu-Fe-Ce permanent magnet, sintered 2−50910
    Co-P film, hysteresis characts. rel. to heat treatment conditions 2−48091
    Co-Pr-Sm alloys, 10000 Oe B-coercive force magnet, props. optimization 2−44247
    Co-Sm permanent magnet alloy, sintering mechanisms 2−57289
    Co, anisotropy consts. temp. depend. 2−54321
    Co, domain width thickness depend., theory 2−65145
    Co, electrodeposited with [0001] axis of preferred orientation, dependence on texture perfection 2−54327
    Co, h.c.p., determ. from band struct. calc. 2−61181
    Co, mag. after-effect of hydrogen 2−78029
    Co, mag. domains, electron microscope obs. 2−44262
    Co, magnetic saturation determination using Stern-Gerlach experiment with neutrons 2−54326
    Co domain wall movement retardation, due to interaction with dislocations 2−68540
    Co effective mag. field on ^{67}Zn 2−84404
    Co film, anisotropy, rel. to n.m.r. 2−81471
    Co film, epitaxial growth and domain config. 2−61524
    Co film, evaporated at oblique incidence, mag. contrib. of columnar grains 2−72184
    Co film, in Al-Al_2O_3-Co supercond. junc., electron spin polariz. detn. 2−64958
    Co magnetization process, h.v. electron microscopy 2−84402
    Co particles, saturation, coercive force and squareness ratio, and preparation 2−75218
    $Co_{0.91}Fe_{0.09}$, f.c.c., temp. dependence of moment distrib. 2−65165

Magnetic properties of substances continued
ferromagnetic continued
$CoFe_2O_4$ films, monocryst., domain struct. and mag. polarity reversal 2−61523
$Co_{1-x}Fe_xSi$ solid solution, thermomag. meas. 2−48068
Co_2MnSn, Heusler alloy, atomic and mag. struct. 2−48075
Co_5Sm, mag. moment and hysteresis props. 2−51254
Co_2TiSn, Heusler alloy, Curie temp. and mag. moment 2−51255
Co_2VSn, Heusler alloy, Curie temp. and mag. moment 2−51255
$CrBr_3$, three-dimens. magnetization struct., Faraday effect obs. 2−78013
Cr_2O_3 magnetic tape, pulse recording and FM applications, thermoremanent duplication 2−66701
$Cr_{1-x}Te$, magnetic anisotropy with $X=0.077$ 2−84415
$Ct_3{\sim}Te_4$, Curie temp., press. effect 2−54336
$Cr_7\square Te_8$, Curie temp., press. effect 2−54336
$CsCuCl_3$, one-dimens. mag., Mossbauer obs. 2−72160
$CsMnCl_3.2H_2O$, anisotropy, short range order effect 2−44295
$CsNiF_3$, one-dimens. behaviour 2−44241
Cu-Ni alloys, susceptibility in high intensity fields 2−65151
Cu complex, Cu(II) croconate trihydrate, mag. susceptibility, 3-292 K 2−72106
$CuCr_2Se_4$, galvanomag. props., 100-650K 2−81091
$CuK_2(Rb_2)Cl_4.2H_2O$, critical dynamics of thermal cond. 2−57288
$Cu(NH_4)_2Br_4.2H_2O$, low temp. magnetization 2−61514
$Cu(NH_4)_2Cl_4$, susceptibility and transition, 1.1 to 300K 2−65152
$CuRb_2Br_4.2H_2O$, low temp. magnetization 2−61514
Dy single cryst., mag. microstruct. near Curie point 2−51251
Dy_xCo_y, critical fields, ordering temps., magnetization curves at 4.2K 2−68544
$DyCo_{3-x}Ni_x$ and $DyFe_{3-x}Ni_x$, varying electron conc. effect on ordering 2−51256
$Dy(OH)_3$, relax. meas. 2−54334
DySb, ordering, struct. 2−44292
$Er_{0.6}$-$Ho_{0.2}$-$Dy_{0.2}$ alloy, magnetization curves, study at 4.2 K 2−65174
Er, phase transitions, microwave absorpt. obs. 2−51257
$ErAl_2$ and $Er_xY_{1-x}Al_2$, mag. struct., neutron diffr. obs. 2−81275
ErC_2, struct., 297-2K, neutron diffr. obs. 2−72217
EuH_2, ordering, sensitivity to hydrogen conc. 2−77986
EuO:Gd, exchange-induced imperfection ionization, investigation using optical absorption and Faraday rotation 2−68598
EuO, effect of hydrostatic press. on exchange interactions 2−48057
EuO, $Eu_{0.97}Gd_{0.03}O$, and $Eu_{1-x}Ca_xO$, magnetic props. exchange interactions, temp. depend. of magnetization 2−68545
EuO, insulator-metal transition and bound mag. polarons 2−80975
EuS-Sn, nonmag. impurity effects, first and second neighbour exchange 2−65138
EuS, effect of hydrostatic press. on exchange interactions 2−48057
n-EuS, elec. resist. and Hall effect, 140 kOe, Curie pt. phenomena 2−47895
EuS film, effective exchange parameters and surface anisotropy 2−68532
EuSe, effect of hydrostatic press. on exchange interactions 2−48057
Eu_3SiO_5, absorpt. edge shifts rel. to Curie temp. 2−48173
EuTe, effect of hydrostatic press. on exchange interactions 2−48057
Eu_2TiO_4, rel. to cryst. chem. 2−51249
$Eu_3Ti_2O_7$, rel. to cryst. chem. 2−51249
Fe/LiF/Fe-Co film system, quasistatic mag. reversals 2−84408
Fe-Co-Ni-Ti-Al-Cu alloy, YuNDK42T8, homogenizing effects 2−47688
Fe-Co-Ni alloy powder, highly disperse, effect of electrolytic prep. variables 2−68543
Fe-Co alloy, equiatomic, ordering effects on electronic struct. 2−44249
Fe-Co alloy, temp. depend. 2−51258
Fe-Cr σ-phase, Mossbauer obs. 2−44253
Fe-Ga alloys, magnetic props. and Mossbauer investigations 2−84416
Fe-Mn-Ni system using semihard magnetic alloys 2−84407
Fe-Ni-Al-Cu alloys, coercive force, remanence, energy, alloying additive effects 2−43845
Fe-Ni-Co alloys, influence of austenite ferromag. on vol. change at M_s 2−65146
Fe-Ni-Mo, rel. to powder metallurgy, carbonyl prod. method 2−68159
Fe-Ni alloy, Invar, Hall and Nernst-Ettinghausen study 2−72164
Fe-Ni alloy film, crit. fields, effect of elastic stresses 2−51264
Fe-Ni alloy film, rotating anisotropy, temp. depend. 2−57300
Fe-Ni doped invar alloys, f.c.c. lattice, mean magnetic moment and effective magnetic field of ^{57}Fe 2−68533
Fe-Ni film, domain struct., influence of temp., elec. microscope obs. 2−72185
Fe-Ni films, perpendicular anisotropy from galvanomag. meas. 2−61529
Fe-Ni Invar alloy, magnetostriction, rel. to temp. depend. of elastic consts. 2−80751
Fe-Ni single crystals, domain struct., Kerr effect obs. 2−78017
Fe-Pd alloy, powder, remag. mechanism, hysteresis characts. 2−48097
Fe-Pd alloys, f.c.c., mixed exchange interactions, neutron scatt. obs. 2−84421
Fe-Rh alloy, magnetoresist., temp. depend. 2−54330
Fe-Sb system, $FeSb_2$, phase susceptibility 2−64821
Fe-Si, domain width, sample thickness and cryst. orientation depend. 2−48061
Fe-Si, magnetization and mag. reversals, mag. texture effect 2−51252
Fe-Si, Neel lines, magnetooptic Kerr effect obs. 2−78014
Fe-Si, obs. of domain changes under cyclic tensile loading for specimens in remanent cond. 2−65147
Fe-Si, temp. depend. of specific energy loss during remagnetization 2−48069
Fe-Si sheet, grain oriented, magnetostriction meas. by optical lever method 2−65160
Fe-Si sheet Goss-oriented, elastic properties rel. to magnetostriction 2−53778
Fe-(3 wt.%)Si alloy, surface films influence on effectiveness of thermomag. treatment44261 2−44261

Magnetic properties of substances continued
ferromagnetic continued
Fe-V alloys, meas. of longitudinal and transverse magnetoresistance at 4.2K, 77K, 273K 2−48063
Fe-V σ-phase, Mossbauer obs. 2−44253
Fe-rich solid solutions, summary 2−81243
Fe, anisotropy, represented by lines of const. cryst. energy 2−78000
Fe, annealed in dry H_2 atmosphere, effects of annealing temperature, holding time, cooling rate 2−81271
Fe, atomic magnetic moment dependence on the lattice parameter 2−81256
Fe, critical and spin wave fluctuations by neutron scatt. 2−54309
Fe, domain wall movement retardation due to interaction with dislocations 2−68540
Fe, effective mag. field on ^{67}Zn 2−84404
Fe, finely divided, suspension in toluene, magnetization, temp. depend. 2−77450
Fe, freq. spectrum of Barkhausen noise 2−61515
Fe, mag. moment temp. depend., $T/T_c<0.5$ 2−65154
Fe, model for origin and ave.-moment-internal field variations in dil. Fe-Si(Al) alloys 2−78008
Fe, Mossbauer examination of internal mag. field variation with temp. and pressure 2−68330
Fe, multidomain, neutron irradiation effects on remanent magnetism rel. to magnetization of lunar samples 2−58458
Fe, sign of hyperfine fields for rare earth impurities 2−44322
Fe, small-angle magnon scatt. collapse 2−44242
Fe, soft X-ray emission spectrum, structural features within d bands 2−61672
Fe, spin-density asphericity, temp. depend. 2−44250
Fe and Fe-Cr alloys, sp. ht. and thermopower near crit. pts. 2−57290
Fe film, asymmetric 180° domain walls, Lorentz microscopy obs. 2−48092
Fe film, in Al-Al_2O_3-Fe supercond. junc., electron spin polariz. detn. 2−64958
Fe polycrystalline, meas. of longitudinal and transverse magnetoresistance at 4.2K, 77K, 273K 2−48063
Fe whiskers, mag. stray fields of 180° Bloch walls, Permalloy probe study 2−78015
Fe_3Al, compression induced mag. anisotropy and superlattice dislocations 2−61516
$FeBO_3$, weak ferromag. moment and Dzyaloshinskii field, temp. depend. 2−72523
$FeBO_3$ single crystals, in mag. field, 77-300°K, magnetic and magnetoelastic properties 2−72175
$FeBO_4$, ferromagnetic moment rotation, high n.m.r. amplification inside domains 2−68745
$FeBr_2$, antiferromag.-ferromag. transition, mag. rot. power 2−65218
Fe_3C, mag. domains, electron microscope obs. 2−44262
$(Fe_{1-x}Co_x)Si$ solid solns., moment form., n.m.r. obs. 2−44223
$(Fe_xMg_{1-x})_2SiO_4$, mag. transitions, comp. depend., 4-300K 2−68987
Fe_2MoO_4, spinel, X-ray and neutron diffraction studies 2−84414
FeN_x, hexagonal, mag. and Mossbauer obs. 2−54331
$Fe_{16}N_2$ film, deposited in N_2 atmosphere, ultrahigh mag. moment 2−57299
$0.35Fe_3O_4$-Fe_2TiO_4, self-reversal of thermoremanent magnetization 2−48609
α-Fe_2O_3, c-axis moment obs. 2−44299
α-Fe_2O_3, haematite, Mossbauer effect of ^{119}Sn and ^{57}Fe, Morin transition obs. 2−65234
α-Fe_2O_3, hematite, from conversion of γ-FeOOH, lepidocrocite 2−57287
Fe_2O_3, piezomagnetic properties, effect of annealing 2−48083
Fe_3O_4 micropowders, grain-size dependence of anhysteresis susceptibility 2−54341
Fe_3P, struct., anomalous n.m.r. spectrum 2−44251
FeRh, first-order antiferromag.-ferromag. transition, electronic struct. changes 2−84438
FeRh, mag. field depend. of antiferromag.-ferromag. transition temp. 2−81288
$F\grave{e}_3S_4$, synthetic samples, Mossbauer spectra study 2−81338
FeSi-CoSi system, itinerant ferromag., ^{59}Co n.m.r. obs. 2−61745
$Fe_{1-x}Ti_{1\|x}$, rel. to resist. minimum 2−44252
Gd, anisotropy consts. temp. depend. 2−54321
Gd, elec. resist. anomaly near Curie pt. 2−57291
Gd, mag. permeability rel. to plastic deform. and recrystn. 2−81234
Gd, spin correlation function field depend rel. to elastic const. behaviour, 270-320 K 2−44260
Gd, transient magnetic precession of Gd 2−65143
Gd film, in Al-Al_2O_3-Gd supercond. junc., electron spin polariz. detn. 2−64958
Gd film, superferromagnetism 2−48093
$GdAl_2$, mag. induced elec. field gradient, spin echo obs. 2−72509
$GdCl_3$, dipole-dipole interact. theory 2−68534
GdFe garnet, bubble domains, flux switching 2−57305
$GdGa_xCu_{1-x}$, mag. order and cond. electron conc. 2−78020
GdIG, sublattice rotation near mag. compensation point, sp. ht. study 2−61508
$GdIn_xAg_{1-x}$, mag. order and cond. electron conc. 2−78020
GdS, magnetic coupling and band structure, electron photoemission studies 2−72139
$GdZn_xAg_{1-x}$, mag. order and cond. electron conc. 2−78020
Ho single crystals, 4.2-300K extremum values of magnetoresistance and Hall field at magnetic transition temperatures 2−68548
$HoAl_2$, ordering, neutron diffr. obs. 2−75217
$HoCo_{3-x}Ni_x$ and $HoFe_{3-x}Ni_x$, varying electron conc. effect on ordering 2−51256
$HoCrO_3$, spontaneous magnetization, susceptibility, exchange interaction, 4.2-300 K 2−48070
$Ho(OH)_3$, relax. meas. 2−54334
K_2CuF_4, two-dimes. ferromagnet 2−81239
K_2CuF_4, two dimensional ferromagnet temp. and frequency dependence of the e.s.r. line width 2−84563
K_xFeF_3, Curie temp. 2−48071
$K_{0.2}FeF_{2.8}O_{0.2}$, Curie temp. 2−48071
$LaCo_5$, permanent mag. 2−52385
$La_{1-x}Gd_xRu_2$, mixed cryst., supercond. and mag. props., T_c depression 2−68549
$LaMnO_3$, doped, quantum theory of double exchange 2−54295

- **Magnetic properties of substances** continued
  - **ferromagnetic** continued
    - $La_{1-x}Pr_xRu_2$, mixed cryst., supercond. and mag. props., T_c depression 2−68549
    - La_3Tl-Pr_3Tl, induced moment system, onset of ferromagnetism 2−72115
    - $LiFe_2F_6$, trirutile, neutron diffr. obs. of struct. 2−72220
    - Li_2O-Fe_2O_3-SiO_2 system, magnetiz., hysteresis, composition depend. 2−54333
    - $LuFe_{9.5}$, ferromag.-helimag. transition 2−54325
    - $MgFe_2O_4$, exchange anisotropy and relax., degree of treatment depend. 2−72156
    - $MgFe_2O_4$, temp. depend. of permeability, anomaly at Curie temp. 2−72167
    - $MgFe_2O_4$ films, mag. polarity reversal, temp. effect 2−61537
    - Mn-Al-Ge alloy, domain structure and nucleation centres 2−68550
    - Mn-Al alloy, effect of $\varepsilon \rightarrow \tau$ transform 2−57280
    - Mn-Bi alloy, hysteresis, domain structure and nucleation centres 2−68550
    - Mn-Bi film, intermediate cpds., domain patterns 2−57301
    - Mn-Fe-Ti-O system ferrites, saturation moments, Curie temp. 2−44254
    - Mn-Permalloy film, coercivity, influence of driving field 2−81278
    - Mn-permalloy film, exchange anisotropy, ferromag. to anitoferromag., thermomag. recording 2−57286
    - Mn phosphate glass, variable temp. mag. suscept. obs. 2−57292
    - MnAlGe, n.m.r. studies 2−84586
    - MnAs whiskers, phase boundary motion at coupled lattice- and spin-disorder transition, resist study 2−78021
    - Mn_3As_2, MnAs, Mn_2Sb, e.s.r. and thermomagnetic meas. rel. to determination of Lande factor 2−51411
    - MnB_2, struct., neutron diffr. obs. 2−44306
    - MnBi films, Ti-substitution effect 2−51265
    - MnBi thin films, prepared by Williams method effects of residual gas pressure, evaporation rate on magnetization 2−68560
    - $MnBi_{(1-x)}Te$ thin films magneto-optical props. 2−72264
    - $MnCr_2S_4$ spinel, sublattice magnetiz. and magnetostrictive effects 2−48073
    - MnGaGe, magnetization, susceptibility and anisotropy 2−72168
    - MnP, effect of press. on susceptibility and transitions 2−48072
    - $Mn_{0.8}Ti_{0.2}Bi$ film, Curie-temp. writing 2−78032
    - $Mn_{1-x}Zn_xFe_2O_4$, Curie temp., saturation and sublattice magnetization 2−78022
    - $(NH_4,Rb)_2CuBr_4.2H_2O$, superexchange interactions 2−65144
    - NH_4Cl, ferromagnetic ordering mechanism 2−75215
    - $NaMnF_3$, powder, magnetization, susceptibility, canting, effective exchange, anisotropy fields 2−48098
    - $NdFeO_3$, spontaneous magntiz., moment temp. depend., effective field 2−72221
    - $Nd_{1-x}Ho_xCo_3$, mag. moments, Curie temps., spin polarization effects 2−68535
    - $Nd_{1-x}Ho_xCo_3$, mag. moments, Curie temps., spin polarization effects 2−68535
    - NdSb, ordering, struct. 2−44292
    - Ni-C interstitial solid solution, sat. magnetiz. and high field suscept. 2−81249
    - Ni-Co alloys, exchange consts. and saturation magnetiz. 2−44265
    - Ni-Co alloys, magnetic structure during electrodeposition in presence of magnetic field 2−77995
    - Ni-Cr alloy, hydrogenated, elec. resist. rel. to mag. field, localized moments 2−81034
    - Ni-Cr alloys, temp. depend., deform. and annealing influence 2−44256
    - Ni-Cu-Mn alloy, magnetization, temp. depend. 2−78025
    - Ni-Cu alloys single crystals, magnetostriction constants by optical lever method 2−65159
    - Ni-Fe/Fe-Co alloy layers, permeability, intrinsic magnetization, coercivity, remance 2−61536
    - Ni-Fe-Mo alloys, thin strips, magnetic properties and texture 2−68509
    - Ni-Fe-Nb alloy, and resistivity and hardness 2−57293
    - Ni-Fe-W high permeability alloy 2−48076
    - 81%Ni-Fe, Barkhausen effect, after heat treatment 2−78023
    - Ni-Fe (18 wt%) electrodeposited film, hyper-crit. thickness, anisotropy fluctuations 2−84409
    - Ni-Fe alloy, spinwave dispersion coeff. in the Invar region, compositional depend. 2−48077
    - Ni-Fe alloy films, temp. depend. and transverse anisotropy 2−61538
    - Ni-Fe alloys with f.c.c. structure, Curie temp. conc. depend. 2−68541
    - Ni-Fe film, coercive force, field and freq. depend. 2−78033
    - Ni-Fe film, electrodeposition, mag. props. optimization 2−61540
    - Ni-Fe film, ripple spectrum, depend. on anisotropy, crystallite size, thickness and field 2−81279
    - Ni-Fe films, polycryst., edge anisotropy 2−61527
    - Ni-Fe(Pd) films, magnetoresist. anisotropy 2−44266
    - Ni-Pd alloys, Mossbauer effect of ^{61}Ni, conc. depend., hyperfine field interactions 2−72285
    - Ni-Pd(Pt) alloys, matrix and impurity cluster polarization 2−44358
    - Ni-W alloy, impurity moment orientation, ^{182}W Mossbauer study 2−75273
    - Ni-Zn-Co ferrite film, anisotropy induced by thermomagnetic treatment 2−81228
    - Ni, anisotropy, represented by lines of const. cryst. energy 2−78000
    - Ni, band model and photoelectron energy distrib. above and below Curie temp. 2−65108
    - Ni, critical and spin wave fluctuations by neutron scatt. 2−54309
    - Ni, critical region, susceptibility, 0.6 to 6.0 kc 2−78024
    - Ni, dislocation-induced spin disorder rel. to elec. resist. 2−81033
    - Ni, electrolytic Matteucci effect, influence of cathodic H 2−48084
    - Ni, electron irrad., low temp. recovery of mag. after-effect 2−64655
    - Ni, electron irradiated, ferromag. after effect at 55K 2−78026
    - Ni, ferromag. domains, anisotropy of depolarization of neutron beams 2−61509
    - Ni, internal demangetizing factor, temp. and alternating field direction depend. 2−48074
    - Ni, itinerant ferromagnetism, intermediate-coupling theory 2−54301
    - Ni, mag. after-effect of hydrogen 2−78029

- **Magnetic properties of substances** continued
  - **ferromagnetic** continued
    - Ni, mag. moment temp. depend., $T/T_c<0.5$ 2−65154
    - Ni, magnetic saturation determination using Stern-Gerlach experiment with neutrons 2−54326
    - Ni, magnetoelastic effects as function of elastic distortion 2−78028
    - Ni, near Curie temp., crit. depolarization of neutrons 2−81268
    - Ni, paramag.- ferromag. transition, rel. to inhomogeneous states 2−57283
    - Ni, plastically deformed, susceptibility and magnetization in strong fields 2−51259
    - Ni, u.s. attenuation, 5-135MHz, u.s. attenuation, 5-134MHz, mag. contribution 2−77782
    - Ni $\langle 110 \rangle$ single cryst., domain struct., rel. to n.m.r. 2−78173
    - Ni domain wall movement retardation, due to interaction with dislocations 2−68540
    - Ni film, adsorption of H_2, effect on saturation magnetization 2−48094
    - Ni film, in Al-$Al_{-2}O_3$-Ni supercond. junc., electron spin polariz. detn. 2−64958
    - Ni film, magnetoresist., thickness depend. 2−51266
    - Ni film, porous, magnetostriction, field depend. 2−72187
    - Ni film, residual magnetization, susceptibility, anisotropy, Hall effect 2−48095
    - Ni film, spontaneous magnetization rel. to Hall effect 2−48096
    - Ni powder, temp. depend. 2−51260
    - $Ni_3Al(Ga)$, band model approach to weak itinerant ferromag. 2−81245
    - Ni_3Cr alloy, oxidation effects on suscept. 2−54338
    - NiFe permalloy, film, oxidized, exchange anisotropy effects, hysteresis loop, 5-300 K 2−81230
    - Ni_2MnSb, Ni_2MnSn, Heusler alloys, atomic and mag. struct. 2−48075
    - $Ni_{1-x}S:O(Se)$, susceptibility conc. depend. rel. to cryst. chemistry 2−44255
    - Ni(100) single crystal films, magnetoelastic coefficients at room temp. 2−44264
    - Ni. domain struct. after plastic deform. 2−44244
    - $PbFe_{12}O_{19}$, saturation magnetization, reduced temp. depend. by As or P substitution 2−78019
    - $PbFe_{2/3}W_{1/3}O_3-PbTiO_3$ solid solution, susceptibility, temp. and comp. depend. 2−81229
    - Pd-Mn dil. alloys, giant moment of Mn 2−44257
    - Pd-Ni alloy, spin susceptibility, calc. 2−65125
    - Pr, f.c.c., singlet-ground-state system, magnetic excitons 2−72153
    - Pr, f.c.c., singlet-ground-state system, neutron scatt. obs. 2−72152
    - Pr, mag.-ground-state props. of single crysts. 2−48078
    - PrB_4, ordering, 2-300K 2−81293
    - $PrCl_3$, low temp. cooperative behaviour, n.m.r. obs. 2−72166
    - $PrCo_5$, effect of sintering with Sm-Co additive 2−50797
    - $PrCo_5$, permanent mag. 2−52385
    - Pr_3Tl, singlet-ground-state system, neutron scatt. obs. 2−72152
    - Pr_3Tl, singlet-ground-state system, magnetic excitons 2−72153
    - Pr_3Tl and $(Pr_{1-x}La_x)_3Tl$, induced-moment system 2−72154
    - Pr_3X-La_3X system, (X=Al, Ga, In, Tl, Sn, Pb), rel. to supercond. behaviour 2−61244
    - Pt-Ni alloy, spin susceptibility, calc. 2−65125
    - $RbFeCl_3$, one-dimens. mag., Mossbauer obs. 2−72160
    - Rh-Mn-Sb system, Cl_b type alloy, mag. props. and cryst. struct. 2−65156
    - Sc_3In, itinerant ferromagnet, theory of magnetic fluctuations 2−65157
    - Sc_3In, magnetization, sound velocity and sp.ht. 2−81258
    - Si-Fe laminations, dynamic domain wall response to a.f. field, rel. to eddy current losses 2−48062
    - Sm-Co alloys, comp. effect 2−51262
    - Sm metallic material, ordered moment estimated 2−61518
    - $SmCo_5$, domain spacing at low temperatures 2−51250
    - $SmCo_5$, permanent mag. 2−52385
    - $SrCo_{1-x}Fe_xO_{3-y}$, Curie temp. and magnetization 2−81238
    - $SrFe_{12}O_{19}$, saturation magnetization, reduced temp. depend. of As or P substitution 2−78019
    - Tb films, phonon emission at 15 GHz, dynamic magnetoelastic coupling obs. 2−68562
    - $TbAl_2$, ordering, neutron diffr. obs. 2−75217
    - $TbFeO_3$, mag. struct., shape effects 2−61559
    - $Tb(OH)_3$, relax. meas. 2−54334
    - Ti_xO_g, molar mag. susceptibility rel. to temp., effective mag. moment, mag. parameters 2−75221
    - $TmFeO_3$, weak ferromagnetism, temp. depend., n.m.r. study 2−44460
    - $Tn_xMn_{1-x}O$, $0.07 \leqslant x \leqslant 0.9$, mag. props., mag. susceptibility, struct., 100-1000 K 2−54364
    - $UAs_{1-x}S_x$ system, mag. phase diagram 2−44258
    - UAsS(Se, Te), magnetization rel. to temp. and mag. field, 3 K to Curie point, hysteresis loop, anisotropy 2−72172
    - US, mag ordering, ordered mag. moments, neutron diffr. obs. 2−84418
    - US, mag. moment distrib., polarized neutron diffr. obs. 2−72171
    - α-US_2, mag. props., magnetization, 4.2-1000K 2−72108
    - USe, mag. ordering, ordered mag. moments, neutron diffr. obs. 2−84418
    - UTe, mag. ordering, ordered mag. moments, neutron diffr. obs. 2−84418
    - U_3X_4 compounds, theory of noncollinear ferromagnetism 2−75222
    - V_2O_3, model for metal-insulator transiton 2−72225
    - Y-Co-Ni pseudobinary compounds, magnetization minima 2−75223
    - YCo_5, permanent mag. 2−52385
    - $YFe_xCr_{1-x}O_3$, mixed orthoferrite, x=0, 0.3, 0.5, 0.7, 1, 78K to Neel point 2−77996
    - YIG/dielectric/conductive plane, magnetostatic propag. 2−51268
    - YIG, light-induced Bloch wall pinning 2−48060
    - YIG, magnetostriction consts., meas. by ferromag. reson. 2−72176
    - YIG rod, internal field distrib., magnetoelastic reson, determ. 2−57285
    - $Zn_{1-x}Cu_xCr_2Se_4$, magnetization and susceptibility, 4.2-900 K 2−44311
    - $Zr_{1-x}Ti_x(Hf_x)Zn_2$, itinerant ferromag., e.p.r. obs. 2−72173

Magnetic properties of substances continued
paramagnetic
see also Paramagnetic resonance and relaxation; Paramagnetism
acoustic attenuation due to spin-phonon interactions in a conc. paramag. crystal, $S={}^{1}._{2}$ 2—64846
alkali borate glass containing Fe 2—65230
cerium ethyl sulphate, low temp. calorimetry 2—44229
cobaltocene, magnetic susceptibility meas., determ. of electronic structure 2—56226
CoSi, near-stoichiometric, susceptibility, Curie-Weiss behaviour 2—68521
erbium ethyl sulphate, low temp. calorimetry 2—44229
excitation spectrum calc. of van Vleck paramagnets 2—61479
Faraday effect and anisotropy of g-factor of rare-earth ion, low temp. study 2—65217
formaldehyde with Slater basis sets, susceptibility and ^{13}C and ^{17}O n.m.r. shielding constants, perturbed Hartree-Fock study 2—50094
GdB_6, polycrystalline, observation of Curie-Weiss behaviour above Neel temperature (16.4K) 2—72486
metal, spin susceptibility calc. for interacting electron gas 2—75207
nickel (II) oxalate complexes, magnetic susceptibility meas., resolution of structure 2—61659
nickel sodium triacetylacetonate-dioxane-benzene, cross relaxation study by meas. of dynamic susceptibility 2—65122
perturbed γ-γ angular correl., effect of spin-lattice relax. and ultrasound 2—72241
precious metal pyrochlores, semicond. and metallic 2—60987
rare earbh cobalt intermetallics, RCo_2 type, first order transition 2—44280
rare earth, exchange anisotropy, variation with lattice parameters 2—51236
rare earth cobaltides, Co atom moments 2—72116
rare earth ethyl sulphates, interactions contrib. to sp. ht. 2—57314
rare earth gallium intermetallics, LnGa, magnetization and susceptibility, temp. depend. 2—72170
rare earth garnets with ions on dodecahedral and octahedral sites, ordering 2—44226
rare earth ionic cpds. with mag. dipole-dipole interaction, caloric and mag. obs. 2—68523
rare earth metals, crit. scatt. role in elec. resist. 2—57271
rare earth metals, light, struct. 2—61517
rare earth metals, review 2—51239
rare earth metals, spin correls. and elec. resist. 2—57272
rare earth metals, susceptibility anisotropy, 5 to 750°C 2—44227
rare earth oxyselenides, susceptibility, anisotropy 2—44228
rare earth-Ni Laves phase, $LnNi_2$, 4.2-700K 2—81277
semiconductor, spin susceptibility of impurity band electrons, correl. effects 2—68520
semiconductor glass, susceptibility, temp. and comp. depend. 2—61480
solid state physics, an overview 2—57093
spin waves in paramagnetic region of anisotropic antiferromagnets 2—81305
superconducting pairing tendency in nearly-ferromag. systems 2—57163
susceptibilities of $s=1$ systems, temp. dependence, application of theory to dipolar systems 2—65119
TCNQ quaternary ammonium salts, triplet state behaviour 2—84399
transition metal alloys, 3d, crit. point phenomena 2—54332
ytterbium ethylsulphate, mag. and thermal props. 2—51241
Al-Mn dilute alloy, neutron scatt., by spin fluctuations 2—61473
As_2Se_3, vitreous, low temp. susceptibility 2—54293
Ba_2LnMoO_6, susceptibility, rel. to Mo valence state determ. 2—72112
$BaPrO_3$, neutron diffr. and mag. susceptibility meas. 2—81217
Ba_2TaCoO_6, susceptibility, temp. depend. 2—47316
C, non-crystalline, susceptibility rel. to specific heat 2—65123
$CdEr_2S_4(Se_4)$, susceptibility, temp. depend. 2—72113
$CdHo_2S_4(Se_4)$, susceptibility, temp. depend. 2—72113
$CdLu_2S_4$, susceptibility, temp. depend. 2—72113
CdTe, susceptibility meas., determination of covalence character of chemical bonds 2—61482
CdTe, susceptibility of defects, 4.2-290K 2—77980
α-Ce, exchange-enhanced, resist. temp. and press. depend., spin-fluctuation resist. 2—81219
$CeAl_x$, n.m.r. and magnetic susceptibilities 2—84594
$CeRh_xPd_x$ alloys electronic state, magnetic susceptibility and lattice spacings 2—81317
Cm metal, susceptibility 2—48037
CmF_3, susceptibility 2—48037
CmOCl, susceptibility 2—48037
$CoCl_2[(NH_2)CS]_4$, paramag.-antiferromag. and antiferromag.-spin flop phase boundaries, thermal cond. study 2—81302
$Co_{1-x}Mn_xSi$ solid solution, thermomag. meas. 2—48068
CoO-Al_2O_3-SiO_2 glass system, low field suscept. 2—65178
Cr, antiferromag.- paramag. transition, sp. ht., 280-330K 2—75238
Cr, cold-worked, Neel point, rel. to recovery 2—53805
CrN_x, hexagonal, mag. and Mossbauer obs. 2—54331
Cr_2O_3, e.p.r. spectra below Neel temp., transition to antiferromagnetic 2—54492
$CsCoCl_3$, neutron diffr. obs. of struct. 2—72213
$CsMnCl_3.2H_2O$, anisotropy, short range order effect 2—44295
Cu-Fe dilute alloy, susceptibility, 1.7-300K 2—61483
$Cu_4Mn_2Te_4$, susceptibility 2—84442
Dy-Nd alloys, ordering, Neel pt. phenomena, spin disorder 2—51237
Dy, susceptibility anisotropy, 5 to 750°C 2—44227
$DyCo_2$, Co atom moments 2—72116
Er, phase transitions, microwave absorpt. obs. 2—51257
Er, susceptibility anisotropy, 5 to 750°C 2—44227
$ErAsO_4$, a.c. susceptibility, absence of phase transition down to 0.6K 2—65187
$ErCo_2$, Co atom moments 2—72116
$ErPO_4$, a.c. susceptibility, absence of phase transition down to 0.6K 2—65187
$ErVO_4$, a.c. susceptibility, absence of phase transition down to 0.6K 2—65187
Eu complex, tris(2,2,6,6-tetramethyl-3,5-heptadionato-) europium dimer, susceptibility down to 4.2 K 2—61481
EuB_6, exchange interactions, e.p.r. obs. 2—81468
EuO, insulator-metal transition and bound mag. polarons 2—80975

Magnetic properties of substances continued
paramagnetic continued
Fe-Ge system, $FeGe_2$ phase, susceptibility 2—64821
Fe-Ni alloy, high field susceptibility, conc. depend. 2—72114
Fe-Ni alloy, Invar, Hall and Nernst-Ettinghausen study 2—72164
Fe-Sb system, $FeSb_2$, phase susceptibility 2—64821
Fe-(B-metal) alloy, molten, susceptibility, temp. depend 2—80488
Fe, soft X-ray emission spectrum, structural features within d band 2—61672
Fe film, Mossbauer spectra, 15-350 K, superparamagnetic fluctuations 2—68611
$Fe(CN)_5(OH_2)^{2-}$-$Fe_2(CN)_{10}{}^{4-}$ equilibrium mixture in aqueous solution, study by magnetic circular dichroism 2—71231
$FeClO_4$, frozen solns., Fe^{3+} ion behaviour, Mossbauer effect 2—78070
$(Fe_{1-x}Co_x)Si$ solid solns., moment form., n.m.r. obs. 2—44223
$Fe(KSO_4)_2.6H_2O$, susceptibility, anisotropy and ligand fields 2—54292
$(Fe_xMg_{1-x})_2SiO_4$, mag. transitions, comp. depend., 4-300K 2—68987
$Fe(NH_4SO_4)_2.6H_2O$, susceptibility, anisotropy and ligand fields 2—54292
γ-Fe_2O_3, superparamag., magnetiz. and Mossbauer obs. 2—48038
γ-FeOOH, lepidocrocite, at temp. of conversion to α-Fe_2O_3, hematite 2—57287
Fe_2TiSn, Heusler alloy, suscept. 2—51255
Gd-Th alloys, disorder resist. 2—84294
Gd, susceptibility anisotropy, 5 to 750°C 2—44227
GdAg, mag. susceptibility and e.p.r. 2—51404
GdB_6, exchange interactions, e.p.r. obs. 2—81468
$GdCl_3$, low temp. behaviour, n.m.r. study 2—72166
$GdCo_2$, Co atom moments 2—72116
GdCu, mag. susceptibility and e.p.r. 2—51404
H_2, susceptibility of ground state, calc. upper and lower bounds 2—46524
H_2O molecule, susceptibility, perturbation theory calc. 2—46541
Ho, quadratic field depend. of attenuation coeff. of u.s. waves 2—68522
Ho, susceptibility anisotropy, 5 to 750°C 2—44227
Ho single crystals, 4.2-300K, extremum values of magnetoresistance and Hall field at magnetic transition temps. 2—68548
$HoCo_2$, Co atom moments 2—72116
K_xFeF_3, Curie temp. 2—48071
$K_{0.2}FeF_{2.8}O_{0.2}$, Curie temp. 2—48071
$KMnF_3$, $KMnF_3$:Mg, temperature dependence of e.p.r. line width, room to liquid nitrogen temp., effect near Neel temp. 2—44440
K_2MnF_4, mag. struct. near crit. point, neutron scatt. study 2—65182
$K_{0.5}Nd_{0.5}TiO_3$, perovskite, prep., mag. susceptibility, cryst. field effects, 2-600K 2—54294
$K_2Pt(CN)_4Br_{0.3}\times 3H_2O$, magnetic susceptibility 2—84401
La_3Tl-Pr_3Tl, induced moment system, comp. depend. 2—72115
Li, susceptibility obs. in 1.5-296 K range 2—43389
$LiCuVO_4$, n.m.r. and long-range superexchange interactions 2—72511
$LiFe_2F_6$, trirutile, neutron diffr. obs. of struct. 2—72220
$Li(NH_3)_4$, susceptibility obs. in 1.5-194 K range 2—43389
$Li_{0.5}Nd_{0.5}TiO_3$, perovskite, prep., mag. susceptibility cryst. field effects, 2-600K 2—54294
$LiYF_4:Er^{3+}$, susceptibility calc. 2—51240
$MgMn_xAl_{2-x}O_4$, $0.3 \leqslant x \leqslant 1.2$, spinel compounds, mag. suscept. detn. 2—48039
Mn complex, Mn-amine, exchange interactions, susceptibility 2—65124
Mn^{3+} complexes, octahedral, susceptibilities, for all crystal field strengths 2—61484
MnAs whiskers, phase boundary motion at coupled lattice- and spin-disorder transition, resist study 2—78021
Mn_5Si_3, noncollinear antiferromag.-collinear antiferromag.-paramag. transition 2—78042
NH_3, susceptibility obs. in 1.5-296 K range 2—43389
$Na_{0.5}Nd_{0.5}TiO_3$, perovskite, prep., mag. susceptibility, cryst. field effects, 2-600K 2—54294
Nb, susceptibility, 78-400 K 2—51238
Nb single crystals, paramagnetic susceptibility, infl. of plastic deform. 2—81216
$NdCo_2$, dissolved hydrogen effect on Curie temp. 2—48040
$NdNi_2$, $NdAl_2$, $NdCo_2$, Laves phases, rel. to low temp. specific heat, cryst. field and exchange effect model 2—57067
$Nd_{3-y}R_yR_xGa_{2-x}Ga_3O_{12}$, garnet, R=Yb, Tm, Er, Ho, Dy, mag. props., 1.6-300K 2—61485
NdS, susceptibility, temp. depend. 2—81307
Ni-Cr alloys, susceptibility temp. depend., deform. and annealing influence 2—44256
Ni-Cu-Mn alloy, comp. effects 2—78025
Ni, critical region, susceptibility, 0.6 to 6.0 kc 2—78024
Ni, paramag.- ferromag. transition, rel. to inhomogeneous states 2—57283
Ni, plastically deformed, susceptibility and magnetization in strong fields 2—51259
$Ni(NH_3)_2.Ni(CN)_4.2C_6H_6$, mag. susceptibility, rel. to sp. ht., 1.2-4.2K 2—75241
Ni_2TiSn, Heusler alloy, suscept. 2—51255
Ni_2VSn, Heusler alloy, suscept. 2—51255
$PbFe_{2/3}W_{1/3}O_3-PbTiO_3$ system, phase diagram, antiferromag., ferromag., and paramag. regions 2—81229
Pd-Ni alloy, spin susceptibility, calc. 2—65125
Pd-Pt alloy, spin susceptibility, calc. 2—65125
Pd-rare earth dil. alloys, magnetiz., susceptibility, moments 2—44224
Pd, thermal expansion and elec. cond., 77-300K, effect of paramagnons 2—61226
Pr, in magnetic fields, determination from nuclear heat capacity and application to nuclear cooling 2—65121
Pr, Neel temp., elec. resist. anomaly 2—51281
Pr complex, tris(2,2,6,6-tetramethyl-3,5-heptadionato-) praeseodymium dimer, susceptibility down to 4.2 K 2—61481
$PrCl_3$, low temp. behaviour, n.m.r. study 2—72166
$PrCo_2$, dissolved hydrogen effect on Curie temp. 2—48040
$PrCu_2$, spontaneous mag. order, 54 mK 2—44225
PrH_2, sensitivity to hydrogen conc. 2—77986
Pt-Ni alloy, spin susceptibility, calc. 2—65125

Magnetic properties of substances continued

- **paramagnetic** continued
  - Rb_2CoF_4, critical behaviour, n.m.r. obs. 2−44458
  - $RbMnF_3$, impure exchange-coupled, substitutions effect on e.p.r. linewidth and g-values 2−48292
  - $RbMnF_3$, temperature dependence of e.p.r. line width, room to liquid nitrogen temp., effect near Neel temp. 2−44440
  - ReO_3, mag. susceptibility, 77-300K 2−75208
  - Sc_2O_3-V_2O_3 solid solution, susceptibility, comp. depend. 2−48041
  - Si:P, heavily doped, susceptibility, e.s.r. linewidth study 2−72500
  - Sm metallic compounds, susceptibility theory 2−65126
  - $SrMoO_4$: Er^{3+}, susceptibility calc. 2−51240
  - Tb, susceptibility anisotropy, 5 to 750°C 2−44227
  - $TbAsO_4$, magnetically controllable phase transition 2−78045
  - $TbAsO_4$, paramag. to antiferromag. transition, susceptibility study 2−65187
  - $TbCo_2$, Co atom moments 2−72116
  - $TbFeO_3$, mag. struct., shape effects 2−61559
  - $Ti_xTa_{1-x}S_2$ $(0.1 \leqslant x \leqslant 0.9)$ solid solutions, diamagnetic to paramagnetic behaviour 2−61266
  - Tm_3Al_2, indirect s-f exchange interaction 2−48155
  - TmSb, anisotropic magnetiz. and ideal crystal field only behaviour 2−65127
  - UC, UC_2, U_2C_3 mag. susceptibility, after neutron irradiation, anomalous behaviour 2−84398
  - $V_{1-x}Cr_xBe_2$, susceptibility 2−72520
  - VN_x, hexagonal, mag. and Mossbauer obs. 2−54331
  - $V_{1-x}Nb_xO_2$, metal-insulator transition obs. 2−75102
  - $V_{1-x}Nb_xO_2$, metal-insulator transition, theory 2−75103
  - YNi_2, Laves phase, 4.2-700K 2−81277
  - $YbAl_2$, $YbAl_3$ magnetic susceptibility and expansion coefficient 2−81218
  - $YbAsO_4$, a.c. susceptibility, absence of phase transition down to 0.6K 2−65187
  - $Zn_{1-x}Cu_xCr_2Se_4$, magnetization and susceptibility, 4.2-900 K 2−44311
  - $ZnSiF_6.6H_2O$ mag. states lifetimes from Cu^{2+} spin-lattice relax. linewidth temp- depend. 2−84456
  - Zr-Co alloy system, paramagnetic behaviour in non stoichiometric composition of the Laves phase compound 2−81220
  - $Zr_xTa_{1-x}Co_2$, Laves-phase compound, mag. susceptibility, temp. depend. 2−65128
- **transitions**
  - — 2−58776
  - antiferromagnet, e.p.r. linewidth and zero field relaxation time, crit. point anomalies 2−78159
  - antiferromagnet, two-dimens., with nearest-neighbour exchange interaction 2−68566
  - antiferromagnet, uniaxial, of finite dimensions 2−72208
  - antiferromagnetic- ferromagnetic transition point, fluctuations and scatt. of slow neutrons and e.m. waves 2−72207
  - bandwidth requirements for recording of transitions under pulsed field conditions 2−75202
  - critical superparamagnetism 2−61513
  - diamonds, Ni inclusions, determ. of Curie points for different coloured diamonds 2−81213
  - elastic constants and the ΔE effect 2−77664
  - $Fe_xPd_{80-x}P_{20}$ $(13 \leqslant x \leqslant 44)$, amorphous transition temperature from Mossbauer effect and magnetic measurements 2−65114
  - ferromagnet, itinerant, electron model, behaviour thermodynamic quantities near critical point 2−84427
  - ferromagnet, uniaxial, mag. field induced phase transitions 2−65149
  - ferromagnetic phase transformation, effect of lattice vibrations 2−68524
  - ferromagnets near compensation temp. T_k, thermodynamic and magnetoelectric props. 2−72158
  - Heisenberg ferromagnet, partially finite, phase transition 2−75212
  - manganese formate, phase diagram studies 2−44293
  - manganese formate dihydrate, mag. diagram of state, spin-flop transition 2−68577
  - metal-nonmetal transition, two-band model in Hartree-Fock approx. 2−57307
  - metallic systems, elec. resist. in crit. region 2−57279
  - MO_2 (M = Na, K, Rb, Cs), susceptibility meas., obs. of structural and magnetic transformations 2−65116
  - n.m.r. and spin-lattice relax. applicability 2−84599
  - non-Heisenberg magnet, exchange interaction effects 2−72133
  - one-dimensional model soln. using transfer-matrix approach 2−61489
  - order-disorder, sound propag. phenomena 2−54026
  - paramagnetic-ferromagnetic phase transition, spontaneous symmetry breaking and propagating hydrodynamic wave in the initial region 2−84413
  - Pippard's relations applied to λ transitions 2−61490
  - rare earbh cobalt intermetallics, RCo_2 type, first order transition 2−44280
  - rare earth intermetallics, $R_2(Co_{1-x}Fe_x)_{17}$ type, Curie temps. 2−50626
  - rare earth iron garnets, props. near compensation temp. 2−81286
  - rare earth metals, crit. scatt. role in elec. resist. 2−57271
  - rare earth metals, ferromag. transition, theory 2−54317
  - rare earth metals, thermal cond. and Lorenz function abnormalities at Neel pt. 2−57311
  - rare earth tetraborides, 2-600K meas. 2−81293
  - rare earth-transition metal compounds, Fe_3C struct. type, mag. props. 2−61504
  - rare earth-transition metal intermetallics, pulsed field magnetiz., critical phenomena 2−51261
  - scaling laws and crit. phenomena, geometrical interpret. 2−72119
  - spin systems with mixed ferro- and antiferromag. coupling, crit. temps. 2−65131
  - steel, ε-carbide, Curie temp. determ. 2−72165
  - tetramethylammonium manganese chloride, low-temp. transitions 2−72530
  - titanomagnetites, effect of annealing on exchange anisotropy 2−72927
  - transition metal, ferromag. transition phenomena 2−77989
  - transition metal alloys, 3d rel. to sp. ht. anomaly 2−54332
  - Al based liquid alloy, Cr or Mn impurity, susceptibility near nonmag.-mag. transition 2−80486

Magnetic properties of substances continued

- **transitions** continued
  - $BaTbO_3$, neutron diffr. and mag. susceptibility meas. 2−81217
  - $2CaO.Mn_xFe_{2-x}O_3$ $(O \leqslant x \leqslant 0.5)$, Neel temp. comp. depend. 2−43644
  - Ce alloy, γ phase stability rel. to mag. ordering 2−68571
  - β-Ce and Ce-Y alloys, low temp. heat capacity and mag. ordering 2−47748
  - Ce_2Fe_{17}, ferromag.-helimag. transition 2−54325
  - $CoBr_2.6H_2O$, phase diagram studies 2−44293
  - $CoCl_2[(NH_2)CS]_4$, paramag.-antiferromag. and antiferromag.-spin flop phase boundaries, thermal cond. study 2−81302
  - $CoCl_2.2H_2O$, relax. phenomena of metamagnetic transition, a.c. suscept. obs. 2−57310
  - $CoCl_2.6H_2O$, phase diagram studies 2−44293
  - $Co_4Nb(Ta)_2O_9$, Neel temp. determ. from magnetoelectric susceptibility obs. 2−54359
  - CoO-Al_2O_3-SiO_2 glass system, low field suscept., antiferromag. transition 2−65178
  - Cr-Re dil. alloys, first-order at Neel pt., neutron diffr. obs. 2−61553
  - Cr, antiferromag.- paramag., sp. ht., 280-330K 2−75238
  - Cr, cold-worked, Neel point, rel. to recovery 2−53805
  - Cr, first-order antiferromag. transition 2−57119
  - Cr and alloys, thermal cond. and Lorenz function abnormalities at Neel pt. 2−57311
  - Cr dilute alloy, ordering wave-vector, model 2−84441
  - Cr_2O_3, Neel pt. rel. to supermagnetism, e.p.r. obs. 2−54492
  - CrTe, mag. props. and lattice parameters detn., 67-400K 2−72148
  - $Cr_3\sim Te_4$, Curie temp., press. effect 2−54336
  - $Cr_7\square Te_8$, Curie temp., press. effect 2−54336
  - $CsCoCl_3$, second order transition theory interpret. of struct. 2−72213
  - $CsMnF_3$, antiferromag. and paramag. reson. linewidths near Neel temp. 2−68726
  - $CsNiCl_3$, n.m.r. of ^{35}Cl and ^{133}Cs, determ. of mag. props. and struct. 2−72215
  - CsO_2, antiferromagnetic transition at 28K, obs. from susceptibility meas. 2−65116
  - $CuLiCl_3.2H_2O$, phase diagram studies 2−44293
  - $Cu_4Mn_2Te_4$, susceptibility 2−84442
  - $Cu(NH_4)_2Cl_4$, ordered state props., 11.2K obs. 2−65152
  - Dy single cryst., mag. microstruct. near Curie point 2−51251
  - Er, microwave absorpt. obs. 2−51257
  - Er_2O_3, spectral line shift and splitting at onset of antiferromag. ordering 2−81369
  - n-EuS, elec. resist. and Hall effect, 140 kOe, Curie pt. phenomena 2−47895
  - Fe-Cr σ-phase, conc. depend. of Curie temp., Mossbauer obs. 2−44253
  - Fe-Ge system, Neel point of FeGe phase 2−64821
  - Fe-Mn alloy, austenitic, antiferromag. transform., rel. to mech. props. 2−50783
  - Fe-Rh alloy, antiferromag.-ferromag., rel. to temp. depend of magnetoresist. 2−54330
  - Fe-Rh alloy, f.c.c., Neel temp., Mossbauer study 2−78072
  - Fe-Sb system, Curie temp. 2−64821
  - Fe-V σ-phase, conc. depend. of Curie temp., Mossbauer obs. 2−44253
  - Fe and Fe-Cr alloys, sp. ht. and thermopower near crit. pts. 2−57290
  - Fe dil. alloys, Curie temp., effect of indirect exchange interactions 2−44248
  - $FeBr_2$, antiferromag.-ferromag. transition, mag. rot. power 2−65218
  - $FeBr_2$, mag. transition energy variation and Neel temperature 2−64852
  - $FeCl_2$, mag. transition energy variation and Neel temperature 2−64852
  - Fe(II) complex, $Fe(phen)_2(NCS)_2$, mag. heat capacity due to low spin $^1A_1 \rightleftharpoons$ high spin $^5T_2$ transition 2−75240
  - $(Fe_xMg_{1-x})_2SiO_4$, 4-300K, comp. depend. 2−68987
  - α-Fe_2O_3, haematite, Mossbauer effect of ^{119}Sn and ^{57}Fe, Morin transition obs. 2−65234
  - Fe_2O_3, produced from α-, β-, γ- and δ-FeOOH, Morin point, neutron diffr. obs. 2−81292
  - α-Fe_2O_3 and natural haematite, true heat capacity, mag. component 2−43984
  - Fe_3O_4, magnetite, metal-insulator transition, Verwey temp. 2−57125
  - γ-FeOOH, lepidocrocite, at temp. of conversion to α-Fe_2O_3, hematite, para-ferromag. transition 2−57287
  - $Fe(Pd_xPt_{1-x})_3$, magnetic phase changes, Mossbauer obs. 2−48108
  - $Fe(Pd_xPt_{1-x})_3$, phase diagram model showing quadrupole point 2−51234
  - FeRh, first-order antiferromag.-ferromag. transition, electronic struct. changes 2−84438
  - FeRh, mag. field depend. of antiferromag.-ferromag. transition temp. 2−81288
  - Gd, Curie pt. obs. of elastic const. and sound attenuation 2−44260
  - Gd, elec. resist. anomaly near Curie pt. 2−57291
  - ^3He, solid, λ transition to ordered antiferromag. phase 2−56537
  - Ho single crystals, 4.2-300K extremum values of magnetoresistance and Hall field at magnetic transition temperatures 2−68548
  - $KFeF_4$, critical behaviour, neutron and Mossbauer obs. 2−44301
  - K_xFeF_3, Curie temp. 2−48071
  - $K_{0.2}FeF_{2.8}O_{0.2}$, Curie temp. 2−48071
  - $KMnF_3$, resonance behaviour 2−84556
  - K_2MnF_4, mag. struct. near crit. point, neutron scatt. study 2−65182
  - $LiFe_2F_6$, paramag.-antiferromag. transition 2−72220
  - $LuFe_{9.5}$, ferromag.-helimag. transition 2−54325
  - Mn-Ga alloys, antiferromag. transform., rel. to internal friction 2−50735
  - MnAs whiskers, phase boundary motion at coupled lattice- and spin-disorder transition, resist study 2−78021
  - MnF_2, critical neutron scatt., spin fluctuations 2−54361
  - MnF_2, two-magnon absorpt., spin-flop transition effects 2−54358
  - $MnGeO_3$, magnetoelec. signal near critical field for spin flop 2−44305
  - $Mn_4Nb(Ta)_2O_9$, Neel temp. determ. from magnetoelectric susceptibility obs. 2−54359
  - MnP, ferromag. ordering temp., and ferromag.-antiferromag. transition, press. effects 2−48072
  - Nd, phenomenological theory 2−51279

Magnetic properties of substances continued
transitions continued
$NdCo_2$, dissolved hydrogen effect on Curie temp. 2−48040
$NdCrO_3$, spin reorientation obs. from opt. spectroscopy 2−84512
Ni/SiO_2 cermet films, granular, Curie temp. depression 2−50498
Ni-Fe alloys with f.c.c. structure, Curie temp. conc. depend. 2−68541
Ni-Ti-Fe-O system, spinel solid solution, effect of saturation mag. moment and Curie temp. on solubility 2−83840
Ni, critical region, susceptibility, 0.6 to 6.0 kc 2−78024
Ni, near Curie temp., crit. depolarization of neutrons 2−81268
Ni, paramag.- ferromag. transition, rel. to inhomogeneous states 2−57283
$NiCl_2$, in graphite, two dimens. paramag. transition to mag. ordered state 2−54320
$NiFe_{0.8}Cr_{1.2}O_4$, ferrite, structural transition at mag. transformation, Mossbauer and X-ray obs. 2−72201
$Ni(NO_3)_26NH_3$, antiferromag. transition, susceptibility and specific heat obs. 2−65185
NiO, magnetocatalytic effects at Neel pt. 2−44480
NiS, metal- to-semimetal transition, stoichiometry and impurity effects 2−51280
$Ni_xZn_{1-x}Fe_2O_4$, thermal expansion coeffs. at Curie pt., conc. depend. 2−81281
$PbFe_{2/3}W_{1/3}O_3-PbTiO_3$ system, phase diagram, antiferromag., ferromag., and paramag. regions 2−81229
Pd-Ni alloy, critical conc. for ferromag. behaviour, calc. 2−65125
Pr, f.c.c., singlet-ground-state ferromagnet, neutron scatt. obs. 2−72152
Pr, Neel temp., elec. resist. anomaly 2−51281
$PrCo_2$, dissolved hydrogen effect on Curie temp. 2−48040
$PrCu_2$, cooperative nuclear magnetic order below 54 mK 2−51282
Pr_3Tl, singlet-ground-state ferromagnet., neutron scatt. obs. 2−72152
Pr_3Tl and $(Pr_{1-x}La)_x)_3Tl$, induced-moment system, La substition effects on Curie temp. 2−72154
Pt-Ni alloy, critical conc. for ferromag. behaviour, calc. 2−65125
Rb_2CoF_4, critical behaviour, n.m.r. obs. 2−44458
$RbMnF_3$, critical neutron scatt., spin fluctuations 2−54361
RbO_2, antiferromagnetic transition at 15.3K, obs. from susceptibility meas. 2−65116
Sc_2O_3-V_2O_3 solid solutions 2−48041
$SrCo_{1-x}Fe_xO_{3-y}$, Curie temp. 2−81238
Tb-Sc alloys, T_n and O_p depend. on G (de Gennes function 2−68576
$TbAsO_4$, paramag. to antiferromag., susceptibility study 2 −65187
$TbFeO_3$, phase diagram calc. 2−61559
$TbPO_4$, low temp. mag. moment and sp. ht. anomalies 2−78046
ThN, mag. sp. ht., 7 to 300K 2−43988
UAs-US system, magnetic phase diagram, neutron diffr. obs. 2−65188
$V_xCr_{1-x}B_2$, antiferromagnetic transition, n.m.r. obs. 2−72521
$Y_3Fe_5O_{12}$ garnet, mag. phase transition, polarized neutrons, and RF susceptibility obs. 2−57284
$Y_3Fe_5O_{12}$ garnet, ultrasound absorpt. in vicinity of mag. phase transition 2−71735
YIG, spin relaxation near Curie temp. studied by high frequency magnetic susceptibility 2−84417

Magnetic resonance and relaxation
see also Antiferromagnetic resonance; Ferrimagnetic resonance; Ferromagnetic relaxation; Ferromagnetic resonance; Nuclear magnetic resonance and relaxation; Paramagnetic resonance and relaxation Spin-lattice relaxation; Spin-spin relaxation
adiabatic rapid passage, radiation damping, Bloch eqns. 2−81318
aligned spin-assembly 2−76977
alkali borate glass containing Fe 2−65230
alkali metal vapours, optical detection using D_1 and D_2 radiation simultaneously 2−56443
atomic spin system under alternating field, quantum structure of resonance effects 2−76966
Bloch equations, solution method 2−69841
ellipsoid of alignment and its precessional motion 2−76978
ferrite discs, resonance phenomena in presence of domain structure 2−68714
ferromagnet, thermally activated relax. and Jordan aftereffect 2−54307
focusing atomic beam magnetic resonance apparatus, construction 2−69842
focusing atomic beam magnetic resonance apparatus optimum design 2−69843
Fresnel evanescent wave, TEM case 2−73476
Fresnel evanescent wave, transverse mag. mode case 2−63306
liquids, effect of diffusion on intermolecular dipolar relaxation 2−74536
magnetic impurity in quantum chain, reson. behaviour 2−81201
metal, conduction electron spin resonance, Azbel-Kaner cyclotron resonance radio frequency size effects 2−57384
methyl group rotation and proton spin symmetry in crystals 2−68715
negative and rotating temperatures in magnetic systems 2−61472
polarimetry applic. to reson. problems 2−78984
Provotorov eqns. with field modulation 2−81441
pulsed, and optical resonance, Ampere Inst. Summer School, Ljubljana, Yugoslavia (1971) 2−59008
quasithermodynamics theory of relaxation 2−51283
quinoline in durene, triplet absorption detection of magnetic resonance 2−50114
spin-flip probability calc., use of Sylvester's formula 2−41439
superconducting resonators, harmonic generation 2−73485
1,2,4,5-tetrabromobenzene, o.d.m.r. and p.m.d.r. studies of $^3\pi\pi^*$ state 2−60086
1, 2, 4, 5-tetrabromobenzene, ODMR obs. of phosphorescent state props. 2−56260
1,2,4,5-tetrachlorobenzene, o.d.m.r. and p.m.d.r. studies of $^3\pi\pi^*$ state 2−60086
theory of magnetic resonance, book 2−84560
, B, h.f.s. in ground multiplets, mag. dipole radial parameters 2−70576
Al, h.f.s. in ground multiplets, mag. dipole radial parameters 2−70576
$CaF_2:Dy^{3+}$, giant spin relaxation times, detection using magnetic circular dichroism 2−44313

Magnetic resonance and relaxation continued
$CoCl_2.2H_2O$, relax. phenomena of metamagnetic transition, a.c. suscept. obs. 2−57310
Cs atom, optically pumped, influence of modulation of crossbeam on amplitude of r.f. field 2−52934
Cs atom, two level spin system 2−56110
Cu, magnetic surface levels and electron-phonon scatt. rate determ. 2−68290
Er, microwave absorpt. obs., 24 GHz and 100 GHz 2−65318
He, Stark splitting between Zeeman sublevels 2−83215
InSb, magnetophonon mass change in drifting hot carriers 2−68389
$MnAu_2$, microwave absorpt. obs. 2−65318
$MnAu_2$, spiral phase, microwave absorpt. peaks interpret. 2−44429
NO_2, laser resonance at 311 and 337 μm 2−42912
$Nd(C_2H_5SO_4)_3.9H_2O$, relaxation processes measurement using a r.f. tunnel diode oscillator 2−68513
Ne, press. shift of lines in He-Ne laser 2−64024
Ni-Co-Zn ferrite, H.F. mag. spectra, temp. depend. 2−68723
O_2, laser magnetic resonance lines obs. 2−74274
YIG rod, internal field distrib., magnetoelastic reson. determ. 2−57285

Magnetic storms
see also Micropulsations
1965, April 17, changes in distrib. of low energy trapped protons 2−65924
1967, May 25, non-adiabatic processes rel. to geomagnetically trapped electrons 2−78406
1967, May 25-27, topside electron density during storm 2−72867
1967, October 28, effect of rotational discontinuity in solar wind 2−72922
1969, February 11, incoherent diffusion obs. 2−44772
1970, March 8, development peculiarities rel. to solar wind, magnetosphere and aurora 2−84917
1970, March 8, trapped and precipitated protons 2−48556
1970, May 28, obs. of F-region electron density variation 2−65986
activity rel. to interconnection of interplanetary mag. force lines and magnetosphere 2−51659
auroral latitudes, precipitating energetic heavy ion obs. 2−65911
auroral substorm activity on v.h.f. radar records 2−62346
bay, accompanying aurora, keV electron spectra 2−58064
Birkeland currents intensification due to elec. fields 2−65904
control factors for evolution of F_2-layer at sunrise 2−84909
correlated storm associated u.l.f. magnetic oscillations, simultaneous ground and satellite obs. 2−62392
and cosmic rays 2−55888
DR-currents and middle lattitude red arcs, dynamics during magnetic storm 2−48558
effects of solar flares 2−81955
F_2 region, electron density disturbances 2−75631
field structure, determination by spherical harmonic analysis 2−54926
flare induced shocks and corotating streams in interplanetary medium as agents in onset of geomagnetic storms 2−62723
ion and electron densities and temps., meas. in height range 1000km-2500km from spherical electrostatic analysers 2−62309
ionospheric D-layer absorpt. depend. 2−81730
ionospheric response to v.l.f. ion-acoustic waves rel. to sudden geomagnetic storms 2−83614
rel. to ionospheric storm 2−62363
Jicamarca, March 8, 1970, data synthesis 2−72916
loss cone electron fluxes during strong precip. events in 1969 storm period 2−65835
low latitude asymmetric disturbance, high time resolution 2−66000
magneto-ionospheric effects 2−48601
magnetosphere, conference (Moscow, Aug. 1971) 2−81708
magnetosphere, substorm depression and expansion phases 2−62334
magnetospheric, daytime irregular geomagnetic pulsation 2−72914
magnetospheric, model 2−48532
magnetospheric substorm, shock wave in tail of magnetosphere as reson for active phase 2−72824
magnetospheric substorm adiabatic processes 2−65871
magnetospheric substorm development model 2−75635
magnetospheric substorm expansive phase triggering 2−65870
magnetospheric substorm Pi 1 micropulsations, ground-satellite correlations 2−62332
magnetospheric substorms, behaviour of low-energy particles 2−81711
magnetospheric substorms, outer radiation zone behaviour and model 2−81709
magnetospheric substorms, plasma sheet variations 2−81710
magnetospheric substorms, rel. to changes in geomag. tail, growth phase 2−81746
midday auroras at South Pole during magnetospheric substorms 2−65900
modulation of magnetic records 2−54915
pc 1 micropulsation event after 3 May 1967 storm, periodicity and formation mechanism 2−84924
plasma sheet obs. in geomag. tail during substorm 2−65872
plasmapause behaviour, longit. and temporal characts. 2−65883
plasmapause whistlers, e.l.f. hiss and discrete emissions obs. 2−65850
Polar, meas. of MeV electrons during recovery phase 2−68981
polar magnetic substorms, ring current and field aligned current rel. to ionospheric electric current 2−81712
polar substorm, Mar. 1970, particle acceleration and loss obs. 2−65873
polar substorms, correlation with interplanetary magnetic field structure 2−66006
polar substorms, post breakup phase, VLF emissions 2−72915
polar substorms, signatures of growth and expansion phases 2−66007
polar substorms 03 to 06 U.T., magnetic effects associated with westward travelling surge 2−68888
positive geomagnetic bays and connection with partial ring current 2−78405
ring current growth rel. to growth rate of main phase field 2−72845
soft electron zone depend. on substorm activity 2−65903
solar cosmic-rays cutoff rigidity increase during polar cap absorption event at commencement of geomagnetic disturbance 2−48802

Magnetic storms continued
solar flare producing regions statistical analysis of relationship to geomagnetic storms, Forbush decreases and SC + Si events 2−54925
solar flares of September and June 1963, correlation 2−51658
spectral analysis of geomagnetic variation rel. to tide and storm modulation effects 2−84920
substorm, formation of auroral patches in midday sector 2−66008
substorm activity and interplanetary magnetic field variations 2−66012
substorms, local time dependence of electron flux and magnetic field at ATS-1 2−62310
substorms in magnetosphere, DP-2 manifestation 2−72910
trapped alpha particle intensity and $j\alpha/jp$ ratio meas. 2−65936
trapping boundary and field-line motion during 2−65932
W. Atlantic 'quiet zone', obs. 2−54922
O airglow emission at 6300 Å 2−48540

Magnetic structure
see also Domains
alkali borate glass containing Fe 2−65230
alloy, mictomagnetic, model 2−65166
crystals, optical gyrotropy or symmetry property 2−60729
cubic and uniaxial compounds, ambiguity in powder neutron diffr. lattice dimensions 2−54283
exchange interaction of electric and magnetic polarizations 2−81212
f.c.c. spin lattice system, exchange and dipolar interactions, mean field approx. 2−84426
ferroceramics, microstruct., domain struct. 2−53925
ferromagnet, multiaxial, effect on magnetization and mag. reversals 2−51252
ferromagnetic films, electron microscopy of magnetic structure, review 2−84428
film, domain wall parameters from Lorentz electron microscopy 2−72182
film, magnetic ordering, Hubbard model, Stoner mol. field approx. 2−72180
group report on work at Grenoble Nuclear Centre 2−44216
Heesch magnetic groups, morphology and associated mag. aspect groups 2−51231
helicoidal, Mossbauer diffraction, kinematic theory 2−68610
Jahn-Teller ion containing crysts., from superexchange ordering of degenerate orbitals 2−68565
minimum-energy spin configs. in mag. field, calc. method 2−48049
Mossbauer spectroscopy using polarized recoil-free γ-rays 2−44351
ordering significance of multiplicity indeterminacy 2−68504
Permalloy plated-wire memory, domain struct., electron microscope obs. 2−75231
rare earth gold intermetallics, s-f interaction 2−44308
rare earth ionic cpds. with mag. dipole-dipole interaction, caloric and mag. obs. 2−68523
rare earth metals, helicoidal magnetic structure, pressure effects, temp. depend. 2−68542
rare earth metals, light neutron diffr. obs. 2−61517
rare earth-nickel intermetallics 2−48080
$[YCa_2][Zr_2](Fe_{2.75}Ge_{0.25})O_{12}$ garnet, mag. struct., neutron diffr. obs. 2−78038
$Al_2Fe_3(SiO_4)_3$, almandite, garnet, antiferromag. ordering 2−54349
$BaCoF_4$, two-dimens. antiferromagnet 2−72211
$BaCo_xTi_xFe_{12-x}O_{19}$, permeability study 2−48102
$Ca_3Cr_2(GeO_4)_3$, neutron diffr. obs. 2−72145
Cd alloys, diamagnetism 2−81203
CeSb, neutron diffr. obs. 2−44292
Co, electron microscope study of magnetic domains 2−44262
$CoCl_2.6H_2O$, partially deuterated, sublattice coupling 2−54350
Co_2MnSn, Heusler ferromag. alloy 2−48075
Cr-Re dil. alloys, single cryst., neutron diffr. exam. 2−61553
Cr, magnetic struct. intensity, temp. hysteresis, sign change 2−54328
$CrBr_3$, three-dimens. magnetization struct., Faraday effect obs. 2−78013
Cr_2O_3-Ti_2O_3, neutron and X-ray diffr. and e.s.r. obs. 2−48104
Cr_2O_3-V_2O_3, neutron and X-ray diffr. and e.s.r. obs. 2−48104
$Cr_{1-x}Te$, magnetic anisotropy with $X = 0.077$ 2−84415
$CsCoCl_3$, neutron diffr. obs. 2−72213
$CsCoCl_3.2H_2O$, Ising linear-chain antiferromagnet, and magnetization and short-range spin correlations 2−72214
$CsNiF_3$, three dimensional, neutron diffr. obs. 2−61556
$Cu_{0.5}Fe_{2.5}O_{4\|x}$, spinel ferrite, sublattice structure from neutron diffr. obs. 2−61543
Cu_2FeSnS_4, antiferromag. ordering, Mossbauer obs. 2−75239
Dy single cryst., mag. microstruct. near Curie point 2−51251
DySb, neutron diffr. obs. 2−44292
$ErAg_2$, 297-1.5K, neutron powder diffraction study 2−61551
$ErAl_2$ and $Er_xY_{1-x}Al_2$, neutron diffr. study 2−81275
$ErAl_3$, neutron diffr. study 2−81275
$ErAu_2$, neutron diffr. obs. 2−72216
ErC_2, 297-2K, neutron diffr. obs. 2−72217
$ErFeO_3$, Mossbauer obs. 2−44351
ErOOH, monoclinic, neutron diffr. obs. 2−44296
EuSe:Gd(La), Mossbauer effect, ^{151}Eu hyperfine interactions 2−48145
Fe-Al-Ni-Co-Ti alloy, columnar struct., prod. by Magnicol process, reaction mechanisms 2−43834
Fe-Co alloy equiatomic mag. scatt. form factors 2−44249
Fe-Co equiatomic alloys, order from magnetic anisotropy energy considerations 2−61507
Fe-Ni single crystals, domain struct., Kerr effect obs. 2−78017
Fe-Si, effect of magnetization and mag. reversals 2−51252
Fe-Si, Neel lines, magnetooptic Kerr effect obs. 2−78014
$(Fe, Zn)_2Mo_3O_8$, Mossbauer obs. 2−75270
Fe, soft X-ray emission spectrum study 2−61672
Fe, spin-density asphericity, temp. depend. 2−44250
α-Fe, spin order rel. to elastic consts., 25-900°C 2−60842
Fe domain wall movement retardation, due to interaction with dislocations 2−68540
$FeBO_3$, sublattice struct. recreation by mag. field 2−54355
Fe_3C, electron microscope study of magnetic domains 2−44262
$FeCO_3$, non-uniformities at metamagnetic transformation 2−65219
$FeCl_3.6H_2O$, spontaneous magnetization, mag. ordering, mag. hyperfine fields, Mossbauer reson., $T < 4.2$ K 2−75272

Magnetic structure continued
FeF_2, neutron scatt. struct. factor, nonlinearity effect 2−48107
Fe_2MoO_4, spinel, X-ray and neutron diffraction studies 2−84414
$Fe_{0.9}Nb_{1.1}O_4$ neutron diffr. obs. 2−65181
FeOCl, Mossbauer obs. 2−44351
Fe_3P, anomalous n.m.r. spectrum 2−44251
FeV_2Te_4, mag. susceptibility, mag. ordering at 5K 2−60757
GdIG, sublattice rotation near mag. compensation point, sp. ht. study 2−61508
GdSi 2−68568
Gd_5Si_3 2−68568
$HoAl_2$, neutron diffr. study 2−75217
$HoAu_2$, neutron diffr. obs. 2−72218
$Ho_xEr_{1-x}Fe_2$ system, spin orientation diagram 2−72197
$HoFe_3$, neutron diffr. and thermal magnetiz. obs. 2−51272
Ho_2O_2Se, comparison with the oxysulphide 2−44228
$KFeF_4$, planar antiferromagnet, neutron scatt. and Mossbauer obs. 2−78043
$KMnCl_3.2H_2O$, mag. phase boundaries, anisotropy exchange fields, mol. field theory 2−68574
K_2MnF_4, near crit. point, neutron scatt. study 2−65182
$(La,Gd)Al_2$, dilute system, n.q.r. and relax. obs., ordering onset 2−68754
$LiCuCl_3.2H_2O$, mag. phase boundaries, anisotropy exchange fields, mol. field theory 2−68574
$LiFe_2F_6$, neutron diffr. obs. 2−44302
$LiFe_2F_6$, trirutile, collinear struct. 2−72220
$LiFe_2F_6$, trirutile, neutron diffr. obs. 2−65183
α-Mn, antiferromagnet, ^{55}Mn n.m.r. study 2−61748
MnB_2, neutron diffr. obs. 2−44306
MnBi film, domain struct. 2−44263
$MnPd_3$, neutron diffr. obs. 2−54360
Mn_3Pd_5 phase, crystal and magnetic struct. 2−83960
NdSb, neutron diffr. obs. 2−44292
Ni-Fe, f.c.c., domain struct. after different annealing treatments, Kerr effect obs. 2−78016
Ni ⟨110⟩ single cryst., domain struct., rel. to n.m.r. 2−78173
Ni magnetic domain walls, 180°, tilted, struct. from Lorentz electron images 2−72151
$NiCl_2$, in graphite, two dimens. paramag. transition to mag. ordered state 2−54320
$NiCr_2O_4$ determ. by representation anal. 2−84429
Ni_2MnSb, Ni_2MnSn, Heusler ferromag. alloys 2−48075
NiO, mag. superlattice X-ray diffr. peaks 2−44307
Pb, intermediate state, path-depend. mag. struct. 2−47864
Pb, superconducting thin film, current- induced intermediate state, magneto-opt. obs. 2−54151
$RbFeF_4$, two-dimens. antiferromag. ordering, susceptibility and neutron diffr. obs. 2−54363
$RbNiCl_3$, neutron diffr. obs. 2−48111
$RbNiF_3$, ferrimagnet, spin waves, neutron scatt. obs. 2−65171
$SrCoO_{2.5}$, neutron diffr. study 2−81294
$SrFeO_3$, neutron diffr. obs. 2−81282
$SrO(6-x)Fe_2O_3xAl_2O_3$, influence of thermal history on Mossbauer spectra 2−48144
$TbAl_2$, neutron diffr. study 2−75217
$TbCu_2$, neutron diffr. obs. 2−44309
$TbFeO_3$, shape effects 2−61559
$TbNi_{1-x}Cu_x$, sinusoidal wave mag. structs., stability, at 1.3 K 2−75216
TbO_2, antiferromagnet 2−72224
Tb_2O_3, effect of crystal field on direction of magnetic moments of ions in low site symmetry 2−65186
TmSb, cryst. field effects in mag. form factor 2−81254
UAs-US system, magnetic phase diagram, neutron diffr. obs. 2−65188
UPb_3, neutron diffr. obs. 2−78041
US, mag. ordering, ordered mag. moments 2−84418
USe, mag. ordering, ordered mag. moments neutron diffr. obs. 2−84418
UTe, mag. ordering, ordered mag. moments neutron diffr. obs. 2−84418
V_2O_5-P_2O_5 glass, microstruct., mag. ordering mag. props., e.s.r. 2−44310
$Y_3Fe_5O_{12}$ garnet, mag. phase transition, polarized neutrons, and RF susceptibility obs. 2−57284
Yb_2O_2Se, comparison with the oxysulphide 2−44228

Magnetic traps *see Plasma/confinement*

Magnetic wells *see Plasma/confinement*

Magnetism
see also Antiferromagnetism; Diamagnetism; Earth/magnetic field; Exchange interactions; Ferrimagnetism; Ferromagnetism; Gyromagnetic effect; Magnetohydrodynamics; Paramagnetism; Rock magnetism; Stars/magnetism; Sun/magnetism
atom, oscillator strengths for resonance transitions 2−79875
autistic magnets, flux quantization, evanescent electronic wave nondestructive interference 2−81202
conference, Jerusalem, Israel (May 1972) 2−70340
critical point exponents, inequalities for spin- spin and energy-energy correlation functions 2−63030
film, Heisenberg ferromagnet 2−51263
filtration, high intensity, for selective separation of micron-size particles 2−41912
Heisenberg model, spin diffusion at infinite temp. 2−81207
helical magnetic structure, rel. to spin wave spectrum 2−57278
linear spin chain, energy diffusion 2−81242
magnetic centres in effective energy band, Hubbard model, functional integral approach 2−77983
moon, rock and subsatellite evidence 2−58466
non-Heisenberg exchange interaction and effects 2−72133
nuclei plus electrons system, numerical analyses 2−54284
ordered sample, Mossbauer hyperfine spectra, temp. depend. line shape 2−75263
organic moleucles, ring shaped, having permanent magnetization, required conditions 2−77131
Potts model at critical point, equiv. to linear Heisenberg chain 2−81253
spin polarized case, local exchange-correlation potential 2−57266
susceptibility, random one-dimensional transverse Ising model 2−52093

Magnetism continued
suspension of a permanent magnet over a superconductor, expt. 2−59069
temperature concepts in magnetic systems 2−61472
vitreous state, structure contrib. of classical magnetic measurements 2−60581

Magnetization process
see also Demagnetization; Ferromagnetic relaxation
bubble garnets, reversal due to annealing 2−51253
curve, magnetization, singular point in second derivative 2−51232
ferrimagnet, hysteresis loop, role of wall displacement and bulging 2−65167
ferrite rod, teaching expt. to determ. relative permeability 2−41433
ferromagnet, amorphous susceptibility and Curie temp. rel. to spin-fluctuations 2−57277
ferromagnet, irreversible processes during reversal 2−54332
ferromagnetic, vibrating reed magnetometer for investigation of small specimens 2−55543
ferromagnetic film with anomalous surface anisotropy, static magnetic susceptibility 2−72178
ferromagnetic material, loss measurement error, pulsed magnetiz. 2−75220
ferromagnetic metal, hyperfine field, temp. depend. 2−48066
film, SHF susceptibility, influence of domain structure 2−68554
high anisotropy multi-domain particles, magnetization reversal 2−44243
irreversible displacement phenomena in cylindrical ferromagnetic, Barkhausen effect meas. 2−81227
meteorites, natural remanent magnetization, possibility of external mechanisms 2−48787
Northern Irish basalts, magnetization history 2−54936
permalloy film, changes in domain structure during pulsed a.c. magnetization, thermofluctuational character 2−68556
polycrystalline materials with uniaxial symmetry, singular point in second derivative 2−51232
semiconductor, canted antiferromag., s-d model, magnetization curve 2−81309
spin and orbital susceptibilities of nearly free electrons in spatially varying field 2−61493
superconductor, hard, hysteretic model 2−68364
superconductor, type II, magnetic hysteresis 2−68363
$CdCr_2Se_4$, mag. permeability rel. to illum., photoferromag. effect 2−54324
$CdFe_2O_4$, saturation depend. on pH of soln., time of boiling and Si 2−84432
Co-Fe (8 at.% Fe) alloys, anisotropic magnetization and magnetic anis. 2−81255
Co, domain nucleation, h.v electron microscopy 2−84402
Co, magnetic saturation determination using Stern-Gerlach experiment with neutrons 2−54326
Dy_xCo_y, critical fields, ordering temps., magnetization curves at 4.2K 2−68544
$DyNi_2$, magnetization mechanisms 2−72107
Fe-Ni alloys, elimination of Barkhausen effect in electrodeposited films 2−72169
Fe-Pd alloy, powder, remag. mechanism 2−48097
Fe-Si, temp. depend. of specific energy loss during remagnetization 2−48069
armco Fe, 20-900°C magnetization and magnetic susceptibility 2−68546
Fe, freq. spectrum of Barkhausen noise 2−61515
Fe, Mossbauer examination of internal mag. field variation with temp. and pressure 2−68330
Fe_2MoO_4, spinel, X-ray and neutron diffraction studies 2−84414
Fe_3O_4 micropowders, grain-size dependence of anhysteresis susceptibility 2−54341
FeRh, first-order transition expt. demonstration 2−61476
GdFe garnet, bubble domains, flux switching 2−57305
$Li_{0.5}Cr_{1.25}O_4$, thermal reversal, demonstration expt. 2−61476
$Li_{0.5}Fe_{2.5-x}Al_xO_4$, domain wall reson. study 2−72198
MnAs, first-order transition expt. demonstration 2−61476
$MnBr_2.4H_2O$, adiabatic, mag. phase diagram detn. 2−65115
MnZn ferrites, influence of Ti ions 2−84405
Ni-Fe/Fe-Co alloy, layers, permeability, intrinsic magnetization, coercivity, remanence 2−61536
81%Ni-Fe, Barkhausen effect, after heat treatment 2−78023
Ni-Re alloys, elimination of Barkhausen effect in electrodeposited films 2−72169
Ni-Zn ferrites, mag. losses in h.f. fields 2−84435
Ni, magnetic saturation determination using Stern-Gerlach experiment with neutrons 2−54326
Ni, magnetization and magnetic susceptibility, 20-600°C 2−68546
Si-Fe textured sheet, permeability, eddy current loss, angle and field depend. rel. to domains 2−65153
$TbNi_2$, magnetization mechanisms 2−72107
$Tm_2(SO_4)_3.8H_2O$, exchange induced, heat capacity obs. 2−64857
YIG, d.c. magnetization produced by parallel optical pumping 2−72203
YIG, hysteresis loop, role of wall displacement and bulging 2−65167

Magnetization state
see also Domains; Magnetic anisotropy; Magnetic permeability; Magnetic structure
alloy, b.c.c., spontaneous magnetiz., interstitials influence 2−43818
alloy, dilute, infinite U Anderson model, mag. susceptibility 2−61494
alloy, f.c.c., spontaneous magnetiz., interstitials influence 2−43817
alloy, mictomagnetic, struct. model 2−65166
alloy 79 NM, influence of thermomagnetic treatment on mag. props. 2−72048
alloy weakly magnetic, influence of heterogeneities on magnetic isotherms 2−65150
basalt, submarine pillow, induced and saturation magnetization in relation to titanomagnetic grains 2−68990
basalts, from JOIDES programme in Atlantic Ocean 2−58135
Blume-Capel Ising ferromagnet, tricritical point, droplet model 2−65135

Magnetization state continued
boracite, reln. between elec. and mag. polarization, T<64K 2−72104
canted ferrimagnet, intrinsic biquadratic exchange and sublattice magnetizations 2−54346
curve singularities, determ. of anisotropy in polycryst. mats. 2−51232
double exchange ferromagnet, quantum theory 2−54295
exchange coupled ferromag.-antiferromag. pair, transverse susceptibility rel. to field 2−72155
ferrite core, fast reversal by external magnetostatic field 2−61542
ferrite cores, internal effective field during nonuniform rotation 2−69857
ferro-antiferromagnetic exchange coupled films, microscopic mag. switching 2−78030
ferromagnet, amorphous, one dimensional Ising model 2−57273
ferromagnet, Heisenberg model, computer simulation 2−81272
ferromagnet, Heisenberg model, monoionic anisotropy effect 2−51243
ferromagnet, model with narrow s-band, temp. depend. 2−65140
ferromagnet, multiaxial, influence of mag. texture 2−51252
ferromagnet, periodic distrib., theory 2−81222
ferromagnet, spontaneous magnetiz. measurement using Hall effect 2−75219
ferromagnet, temp. depend. of local magnetiz. at domain boundary 2−61488
ferromagnet, thermally activated relax. and Jordan aftereffect 2−54307
ferromagnetic catalyst for ortho-para H_2 conversion, surface magnetization orientation effect 2−71342
ferromagnetic disordered alloy, magnetiz.- temp. curves, influence statistical fluctuations of conc. 2−61512
ferromagnetic film, angular dispersion, effect on magnetoresist. 2−48086
ferromagnetic film, rel. to realization of trigger effect 2−75228
ferromagnetic high coercivity single domain particles, sensitive vibrating sample magnetometer 2−55644
ferromagnetic plate, in mag.field, ground state and phase transition 2−72159
ferromagnetic small particles, remanence, influence of curling 2−77999
ferromanganese nodules, strong field magnetization 2−58142
film, cross-tie-Neel domain wall transition, hysteresis change, in mag. field 2−48090
film, uniaxial, ang. dispersion of anisotropy effect on hysteresis loop 2−61521
glass, lunar, terrestrial tektites, mag. susceptibility, 1050-4.2K 2−73073
granite, precambrian, remanent magnetiz. obs. 2−62403
granitic rock, magnetite bearing, complex magnetization 2−58140
harmonic oscillator assemblies, ergodic properties 2−49023
Heisenberg ferromagnet, nonmag. impurity effects, first and second neighbour exchange 2−65138
ilmenite-haematite solid solution, self- reversal and X-phase rel. to palaeomagnetic investigations 2−54960
impact glasses, remanence meas. 2−54967
Ising ferromag., with nonmag. impurities, susceptibility, high temp. expansion techniques 2−61491
Ising ferromagnet, mag. susceptibility rel. to nonmag. impurities, series expansion 2−77992
magnetoelasticity, dislocation theory applic. 2−61519
metal, ferromag., magnetiz. and hyperfine field temp. depend. comparison 2−54323
one dimensional antiferromagnetic spin chain, rel. to stability in mag. field 2−65173
Permalloy film, effective demag. field rel. to thickness and mag. moment 2−61539
Permalloy films, magnetiz. 'ripple', rel. to domain boundary motion 2−61526
Permalloy-SiO-Permalloy multilayer systems, relative residual magnetiz. 2−61530
rare earth cobalt intermetallics, 2-17 type, characteriz. for permanent magnets 2−61510
rare earth gallium intermetallics, LnGa, temp. depend. 2−72170
rare earth iron garnets, mixed, easy magnetiz. direction 2−51314
rare earth orthochromites, n.m.r. of ^{53}Cr, sublattice magnetiz. 2−48307
rare earth orthoferrites, possibility of intermediate state existence for first order phase transformation 2−81291
rare earth-Co Laves phase, $LnCo_2$, temp. depend. 2−81276
rare earth-transition metal intermetallics, pulsed field magnetiz., critical phenomena 2−51261
red beds, Mossbauer studies of magnetization affecting components 2−58141
rock susceptibility anisotropy, significance in geophysics and geology 2−72924
ruby, crossrelaxation, two step, freq. depend. susceptibility meas., generalized thermodynamics 2−61561
sedimentary cores from lakes in N.W. Europe 2−54954
spin and orbital susceptibilities of nearly free electrons in spatially varying field 2−61493
spinel ferrite, rel. to time variation of electrical conductivity 2−47882
steel, transform. of austenite, obs. of coercive force 2−47690
steel, transformer, precip. at grain boundaries, rel. to coercive force 2−47632
TCNQ anion radical salts, mag. susceptibility Schottky type behaviour 2−68575
tektites, remanence meas. 2−54967
3d transition metal alloys, effect on lattice constants 2−53660
uniaxial film, and thickness estimation method 2−68559
wurstite, increase in remanent magnetization during heating 2−62407
XY chain, excitations of single spin 2−77997
Au-V alloy, dil., rel. to field depend. of susceptibility 2−61475
$Ba_5Co_2(Cu_2)Ti_3Fe_{12}O_{31}$, props. rel. to microwave applic. 2−44273
$BaFe_{12}O_{19}$, saturation magnetization, reduced temp. depend. by As or P substitution 2−78019
$BaFe_{12-x}Ti_xZn_xO_{19}$ ferrite, mag. saturation, Ti-Zn cation distrib. effects 2−72195

Magnetization state continued
Ba_2FeUO_6, magnetization saturation below Neel point 2−68570
BaO-B_2O_3-Fe_2O_3 glass, microstruct. effects 2−65113
Be, $\partial M/\partial H$ oscillations rel. to transport prop. quantum oscill. waveforms 2−80963
$CdCr_2Se_4$ film, vacuum deposited, saturation magnetization 2−60649
$Ce_xY_{1-x}Sb$, $Ce_xLa_{1-x}Sb$, high field anisotropic meas. rel. to cryst. field splitting 2−61570
Ce_xLa_{1-x} Sb, crystal field splitting of Ce^{3+} obs. 2−61570
Co-C interstitial solid solution, sat. magnetiz. and high field suscept. 2−81249
2 at.%Co-Cu alloy, superparamag. relax. time rel. to Co precip. particle size 2−48067
Co-Pr-Sm alloys, 10000 Oe B-coercive force magnet, props. optimization 2−44247
Co film, two-layer, rel. to bonding energy determ. 2−57298
$CoCO_3$, antiferromag., rhombohedral, spontaneous mag. moment along trigonal axis 2−68572
$CoCl_2.6H_2O$, sublattice, antiferromag. spin wave theory calc. 2−54351
$CoFe_2O_4$-Co_3O_4 alloy, quenched, aged, saturation magnetization, intrinsic coercive force, rel. to microstruct. 2−81233
$CoFe_2O_4$ films, monocryst., domain struct. and mag. polarity reversal 2−61523
$Co_xNi_{1-x}Fe_2O_4$ ferrite, mag. parameters, temp. variation 2−72196
Cr, magnetic generalized spin susceptibility, interband contribs., Lindhard expression 2−61554
Cr, magnetic struct. intensity, temp. hysteresis, sign change 2−54328
$CrBr_3$, three-dimens. magnetization struct., Faraday effect obs. 2−78013
$Cr_2S_2Te_x$, $0<x\leqslant 1$, ferrimag. props., 80-800K 2−54343
$CsNiF_3$, sublattice magnetiz. temp. depend. rel. to three dimensional mag. struct. 2−61556
$Cu(NH_4)_2\ Br_4.2H_2O$, uniaxial ferromag., low temp. 2−61514
$CuRb_2Br_4.2H_2O$, uniaxial ferromag., low temp. 2−61514
Dy_3Al_2, DyCoNi, magnetic after effect associated with narrow domain walls 2−54318
$Dy(Co,Ni)_2$, intrinsic mag. aftereffect 2−44274
Dy_xCo_y, critical fields, ordering temps., magnetization curves at 4.2K 2−68544
$Dy(OH)_3$, ferromag. relax. 2−54334
ErGa garnet, metamagnetism, Ising model 2−61557
(Eu,Sm)Fe, and (Eu, Ho)Fe garnets, mixed, easy magnetiz. direction 2−51314
EuO, $Eu_{0.97}Gd_{0.03}O$, and $Eu_{1-x}Ca_xO$, magnetic props. exchange interactions, temp. depend. of magnetization 2−68545
Fe-Ni-Al-Cu alloys, coercive force, remanence, energy, alloying additive effects 2−43845
Fe-Ni alloys, magnetisation and magnetostriction in strong magnetic fields 2−68507
Fe-Ni film, magnetiz. ripples, influence of temp., elec. microscope obs. 2−72185
Fe-Ni film, saturation magnetization, temp. depend. 2−57300
Fe-Si, influence of mag. texture 2−51252
Fe-Si, obs. of domain changes under cyclic tensile loading for specimens in remanent cond. 2−65147
Fe-Si alloys, remagnetization specific energy losses rel. to specimen thickness and mag. induction amplitude 2−72163
Fe, finely divided, suspension in toluene, temp. depend. 2−77450
Fe, multidomain, neutron irradiation effects on remanent magnetism rel. to magnetization of lunar samples 2−58458
$FeCl_3.6H_2O$, spontaneous magnetization, mag. ordering, Mossbauer reson. obs., $T<4.2$ K 2−75272
$Fe_{16}N_2$ film, deposited in N_2 atmosphere, ultrahigh mag. moment 2−57299
γ-Fe_2O_3, superparamagnetism 2−48038
$Fe(Pd_xPt_{1-x})_3$, phase diagram model showing quadrupole point 2−51234
$Fe_{1-x}Ti_{1+x}$, temp. depend., rel. to resist. minimum 2−44252
FeV_2Te_4, mag. susceptibility, mag. ordering at 5K 2−60757
GGG, epitaxial magnetic film, prep. by chem. vapour deposition 2−77527
Gd, mag. permeability rel. to plastic deform. and recrystn. 2−81234
Gd film, superferromagnetism 2−48093
$GdCl_3$, ferromag., dipole-dipole interact. theory 2−68534
$GdCo_5$, powder, coercive force rel. to sintering temp., decomp. stability 2−68511
$HoCrO_3$, spontaneous magnetization, susceptibility, exchange interactions, 4.2-300 K 2−48070
$Ho(OH)_3$, ferromag. relax. 2−54334
In fine particles, rel. to supercond. props. 2−71847
$K_{0.5}Nd_{0.5}TiO_3$, perovskite, prep., mag. susceptibility, cryst. field effects, 2-600K 2−54294
$Li_{0.5}Nd_{0.5}TiO_3$, perovskite, prep., mag. susceptibility cryst. field effects, 2-600K 2−54294
Li_2O-Fe_2O_3-SiO_2 system, composition depend. 2−54333
$MgFe_2O_4$ films, mag. polarity reversal, temp. effect 2−61537
Mn-Zn-Fe ferrite, permeability, thermal change, resonance type profiles 2−61545
$MnCr_2S_4$ spinel, sublattice magnetiz. 2−48073
MnGaGe, ferromagnet, temp. depend. 2−72168
$Mn_{1-x}Zn_xFe_2O_4$, saturation and sublattice magnetization 2−78022
$NaMnF_3$, powder, magnetization, susceptibility, canting, effective exchange, anisotropy fields 2−48098
$Na_{0.5}Nd_{0.5}TiO_3$, perovskite, prep., mag. susceptibility, cryst. field effects, 2-600K 2−54294
Nb-Mo:Fe alloy, local moments on Fe, Mossbauer obs. 2−48149
$NdCrO_3$, anomalies in temp. depend. of spontaneous magnetiz. 2−72222
$NdFeO_3$, spontaneous magntiz., moment temp. depend., effective field 2−72221
Ni-C interstitial solid solution, sat. magnetiz. and high field suscept. 2−81249
Ni-Co alloys, exchange consts. and saturation magnetiz. 2−44265
Ni-Cu-Mn alloy, temp. depend. 2−78025
Ni-Fe/Fe-Co alloy, layers, permeability, intrinsic magnetization, coercivity, remanence 2−61536

Magnetization state continued
Ni-Fe alloy films, saturation and relative residual magnetiz. 2−61538
Ni-W alloy, saturation magnetization, rel. to ^{182}W Mossbauer effect 2−75273
Ni-Zn ferrite powder, quality characterization 2−57312
Ni, paramag.- ferromag. transition, rel. to inhomogeneous states 2−57283
Ni, plastically deformed, in strong mag. field 2−51259
Ni film, adsorption of H_2, effect on saturation magnetization 2−48094
Ni film, residual magnetization, susceptibility, anisotropy, Hall effect 2−48095
Ni film, spontaneous magnetization rel. to Hall effect 2−48096
Ni single crystal film, ripple magnetiz. effects in ferromag. resonance 2−65317
$NiSnCl_6.6H_2O$, isothermal magnetization, 0.35- 4.2 K 2−78039
$PbCrO_3$, perovskite, struct., elec. resist., mag. susceptibility 77-550K 2−61321
$PbFe_{12}O_{19}$, saturation magnetization, reduced temp. depend. by As or P substitution 2−78019
PbTe, mag. susceptibility calc. 2−68519
$PrCl_3$, low temp. cooperative behaviour, n.m.r. obs. 2−72166
$PrCo_5$, effect of sintering with Sm-Co additive 2−50797
Rh-Mn-Sb system, Cl_b type alloy, mag. props. and cryst. struct. 2−65156
Sc_3In, 1.5 and 4.2K 2−81258
$SmCo_5$, powder, coercive force rel. to sintering temp., decomposition stability 2−68511
$SrCo_{1-x}Fe_xO_{3-y}$, comp. depend. 2−81238
$SrFe_{12}O_{19}$, saturation magnetization, reduced temp. depend. by As or P substitution 2−78019
$Tb(OH)_3$, ferromag. relax. 2−54334
$TbPO_4$, low temp. 2−78046
Ti_xO_g, molar mag. susceptibility rel. to temp., effective mag. moment, mag. parameters 2−75221
TmSb, anisotropic, and ideal crystal field only behaviour 2−65127
$Tn_xMn_{1-x}O$, $0.07\leqslant x\leqslant 0.9$, mag. props., mag. susceptibility, struct., 100-1000 K 2−54364
UAsS(Se, Te), magnetization rel. to temp. and mag. field, 3 K to Curie point, hysteresis loop, anisotropy 2−72172
US, mag. ordering, ordered mag. moment, neutron diffr. obs. 2−84418
α-US_2, mag. props., magnetization, 4.2-1000K 2−72108
USe, mag. ordering, ordered mag. moment, neutron diffr. obs. 2−84418
α-USe_2, mag. props., magnetization, 4.2-1000K 2−72108
UTe, mag. ordering, ordered mag. moment, neutron diffr. obs. 2−84418
U_3X_4 compounds, theory of noncollinear ferromagnetism 2−75222
V, magnetization curve, 0K, calc. 2−61233
Y-Co-Ni pseudobinary compounds, magnetization minima 2−75223
Y-Fe garnet, l.f. magnetization oscillations where absorption maximum coincides with ferromagnetic resonance 2−75340
YCo_2, Laves phase, temp. depend. 2−81276
$Y_3Fe_{5-(x+y)}Al_xGa_yO_{12}$ ferrite garnet 2−72204
$Y_{2.5}Gd_{0.5}Fe_4Ga_1O_{12}$ garnet, film, magnetization orient. depend., induced anisotropies, magnetooptic Faraday effect obs. 2−72188
YIG:Si, magnetiz. switching by i.r. irrad., linear dichroism obs. 2−68599
YIG, epitaxial magnetic film, prep. by chem. vapour deposition 2−77527
YIG, nonmag. ion substituted, polycryst., ferrimag. resonance obs. 2−61547
YIG film, Fe-deficient 2−72202
$Zn_{1-x}Cu_xCr_2Se_4$, temp. depend., 4.2-900 K 2−44311
$Zn_xMFe_{2-x}O_{4-x}F_x$, M=Ni, Co, ferrite, synthesis, magnetization, hopping cond. 2−75234

Magneto-optical effects
see also Faraday effect; Magneto-reflectance; Optical constants; Zeeman effect
alkali halides, mag. circular dichroism of F-centre absorpt. band 2−53750
benzene, absolute delay in Cotton-Mouton effect 2−43364
chlorobenzene, absolute delay in Cotton-Mouton effect 2−43364
chloroform, absolute delay in Cotton-Mouton effect 2−43364
coronene ions, magnetic circular dichroism meas. 2−80089
cyclohexanol, polar liquid, microwave Kerr effect, Kerr const. 2−80470
diffraction at periodic mag. structs. 2−61590
electronic transitions and collective plasmic excitations, review 2−72294
ferrite garnets, distribution of electromagnetic waves near compensation temp. 2−65211
ferrite-garnets, birefringence 2−65216
furan, normal magneto-optical rot. dispersions, mag. moments 2−70770
garnet film, epitaxial single cryst., optical waveguides 2−70059
gas-discharge plasma, e.m. radiation modulation 2−77266
glass, self-focusing rel. to electrostriction and Kerr effect, damage threshold 2−75249
Kerr effect, isotropic phase of some nematogenic compounds, investigation, temperature dependence and relaxation times 2−53430
longitudinal Kerr effect in 4 layer system of ZnS, Fe, MgF_2 in Ag base, calculation 2−42216
materials, review in book 2−57282
metal film, monocryst., orientational effect 2−61589
optical images recording on magnetic plate 2−52469
optomagnetic waves in the case of polarized light flux 2−75261
Permalloy film, oxidized, slow domain wall motion, Kerr effect obs. 2−54340
Permalloy film, oxidized antiferromag. surface layer, mag. after effect 2−44267
Permalloy films and perfect monocryst. laminae, stripe domain struct. obs. 2−61531
polystyrene solutions, atactic and isotactic, configurational and conformational effects on magnetic circular dichroism 2−43366
pyridine, normal magneto-optical rot. dispersions, mag. moments 2−70770
rare earth monochalcogenide film characteriz. 2−50502

Magneto-optical effects continued

- semiconductor, conf., Warsaw, Poland, July (1972) 2−68384
- semiconductor, cubic, anisotropic magneto- microwave Kerr effect in Voigt config. 2−68603
- semiconductor, electron-phonon resonance, many-body theory 2−68604
- semiconductor, magnetooptical transitions, plasmon assisted, cyclotron reson., lineshape calcs. 2−68320
- semiconductor, microwave Voigt-type effect 2−65215
- semimetal, group V, magneto-optical transitions, energy band struct. model 2−68285
- toluene, absolute delay in Cotton-Mouton effect 2−43364
- tri-o-cresylphosphate, polar liquid, microwave Kerr effect, Kerr const. 2−80470
- CaF$_2$:Ce^{3+}, paramag. relax., obs. by magnetooptic Faraday effect 2−72231
- CaF$_2$:Dy^{3+}, magnetic circular dichroism rel. to detection of giant spin relaxation times 2−44313
- CaF$_2$:Eu, spectra and g-values rel. to electronic coupling in 4f^6 5d config. 2−72237
- CdCr$_2$S$_4$, red shift peak in absorpt. band, mag. F′ centre model 2−80712
- Co, Kerr effect meas. for increasing accuracy of magneto-opt. parameters 2−84461
- Cr(III)S$_6$ trigonal systems, electronic structures and MCD spectra 2−59997
- Cs$_2$ZrCl$_6$:Ir^{4+}, high resolution magnetic circular dichroism spectra 2−57342
- Cs$_2$ZrCl$_6$, mag. circular dichroism spectra analysis 2−75289
- ErFeO$_3$, with high coercivity surface layer, domain struct. obs. 2−81284
- Eu$_3$SiO$_5$, absorpt. edge shifts rel. to Curie temp. 2−48173
- Fe-Ni single crystals, domain struct., Kerr effect obs. 2−78017
- Fe-Si, Kerr effect obs. of Neel lines 2−78014
- Fe, garnet film magneto-optic film waveguide, light modulation and switching 2−81323
- Fe, Kerr effect meas. for increasing accuracy of magneto-opt. parameters 2−84461
- FeBr$_2$, temp. and field depend., of mag. rot. power 2−65218
- FeCO$_3$, magnetic structure, non-uniformities at metamagnetic transformation 2−65219
- Fe(III) complexes, magnetic circular dichroism of d-d transition, ligand field theory analysis 2−48176
- GaAs, exciton struct. of fundamental absorpt. edge and oscillatory magnetoabsorpt. 2−72331
- GdFe garnet with Co^{2+} substituted 2−84460
- GdIG, substituted, compensation temp., applic. to beam- addressable magneto-optic memory 2−72193
- Ge, electromodulation study of forbidden indirect transitions 2−72333
- Ge, i.r. Faraday effect, hot electron transfer between equivalent valleys obs. 2−78067
- HgTe, magnetoabsorpt. of i.r. and submillimetric waves rel. to mag. field, band struct. 2−68294
- n-HgTe, pure, magnetoopical absorp., transport props. detn. 2−78101
- n-InSb, Faraday and Kerr effects of hot electrons in i.r. 2−57326
- n-InSb, uniaxial stress, obs. of tunable component in spectrum 2−82488
- KBr:Tl$^+$, circular dichroism and Jahn Teller effect 2−68606
- KCl, F-centre g_{orb} factor determ. by mag. circular dichroism 2−77596
- KNiF$_3$, antiferromag. phase, linear dichroism 2−81329
- KNiF$_3$, Neel point determ., elastic, magneto-optical and heat capacity meas. 2−72219
- MgO:Fe^{3+}, charge transfer bands, magneto-opt. struct. 2−72339
- MgO:V optical absorption and magnetic circular dichroism of impurity 2−68646
- n-MgTe, interband magnetoabsorpt., $\Gamma_6 \rightarrow \Gamma_8$, transmission obs. at 4.4K 2−68644
- Mh-Zn ferrites single crystal, signal processing technique to obtain Kerr effect M-H loops 2−48064
- Mn ferrite, Kerr effect and optical consts., magnetooptical reson. in visible 2−81337
- MnBi films, Ti-substitution effect 2−51265
- MnF$_2$, zero field circular dichroism, uniaxial stress depend. 2−44376
- Mn$_{0.8}$Ti$_{0.2}$Bi film, Curie-temp. writing 2−78032
- MoS$_2$, layer semicond., interband absorp., energy band model 2−81333
- Ni-Fe, f.c.c., domain struct. after different annealing treatments, Kerr effect obs. 2−78016
- Ni-Mo alloy, Kerr and magneto-optical effect meas., electronic structure 2−72265
- Ni, absorption, i.r. resonance, exchange energy detn. 2−65264
- Ni, ferromagnetic, theory 2−54380
- Ni, Kerr effect meas. for increasing accuracy of magneto-opt. parameters 2−84461
- Ni$_3$Fe, Kerr and magneto-optical effect meas., electronic structure 2−72265
- Pb, supercond., Landau domain struct., motion induced by electric transport current, magneto-optic obs. 2−75074
- Pb, superconducting thin film, current- induced intermediate state obs. 2−54151
- SmSe film, magneto-optical props. 2−81324
- SmTe film, magneto-optical props. 2−81324
- SrCl$_2$, mag. circular dichroism on F-centre absorpt. band, $g_{orbital}$ factor 2−74805
- TlCl, X-point direct exciton, magnetoabsorp. obs. 2−72352
- YFeO$_3$, with high coercivity surface layer, domain struct. obs. 2−81284
- Y$_{2.5}$Gd$_{0.5}$Fe$_4$Ga$_1$O$_{12}$ garnet, film, magnetization orient. depend., induced anisotropies, magnetooptic Faraday effect obs. 2−72188
- YIG, laser beams diffraction by domains 2−44348
- YIG, temp. depend. 2−72266

Magnetoacoustic effects

- attenuation, deformation potential theory 2−71737
- cylindrical layered ferrite-metal medium, independent propagation of magnetostatic surface waves 2−81285
- electron relaxation time determination 2−77819

Magnetoacoustic effects continued

- electron relaxation time determination 2−77818
- extrinsic, nondegenerate, magnetoacoustic amplification 2−80906
- ferromagnet, acoustic wave freq. shift at low temps. in mag. field 2−74985
- ferromagnet, magnetoacoustic instability during biharmonic pumping 2−84559
- ferromagnet, magnetoelastic phenomena in parametric mode magnetiz. oscillation 2−68719
- ferromagnet, Mossbauer sidebands due to r.f. acoustic vibrs. 2−48141
- ferromagnets, hypersound parametric excitation, mag. moment amplitude oscills. 2−81264
- metal, shear acoustic waves, electromagnetic excitation, influence of magnetoacoustic oscillations 2−71736
- metal, transverse acoustic waves in strong mag. field, dispersion law 2−81008
- nonlinear magnetic sound in gravitational field, shock wave formation 2−80302
- piezoelectric semiconductor, u.s. second harmonic generation in mag. field 2−68239
- semiconductor, elastomagnetic waves, coupled e.m. and lattice oscills. 2−64848
- semimetal, e.m. excitation of sound, quantum effects 2−81010
- semimetal, transverse acoustic waves in strong mag. field, dispersion law 2−81008
- spin-electromagnetic waves in ferromag. semicond. and metals, theory 2−81225
- Au, quantum oscill. of u.s. attenuation 2−51037
- Bi:Sn, oscillations with mag. field orthogonal to sound propagation 2−71738
- Bi:Sn, oscills., field orthogonal to sound propag. 2−54032
- Bi:Sn oscills. with mag. field orthogonal to sound propag. direct., fields to 100 kG 2−84203
- Bi, anisotropic deformation potential for electrons, holes, ultrasonic determination 2−61096
- Ca-Bi-V ferrite rods, excitation of longit. acoustic waves 2−43968
- Cd, Fermi surface topology rel. to hydrostatic press., magnetoacoustic meas. 2−77806
- Cu, electron relax. time determ. 2−77818
- Cu, electron relax. time determ. 2−77819
- GaAs magnetic enhancement of acoustoelectric gain, obs. by Brillouin scattering 2−51034
- Gd, sound attenuation, 13 kOe max., 270-320 K 2−44260
- n-InSb, magnetoacoustoelectric effect, acoustoelec. domain form. and instabilities 2−64850
- n-InSb, magnetophonon osc., uniaxial stress apparatus 2−47571
- InSb, n-type, effective mass of conduction electrons det. from magnetophonon effect, undergad. expt. 2−65009
- n-InSb, uniaxial stress effect on magnetophonon effect 2−44115
- Ni, u.s. attenuation, 5-135MHz, u.s. attenuation, 5-134MHz, mag. contribution 2−77782
- PbSe n and p type anisotropy of cyclotron and spin mass 2−80984
- Tb, u.s. wave vel. near mag. phase transitions 2−60846
- Tb, ultrasonic propagation, magnetic fields effects and temperature dependence 2−51036
- Te, acoustomagnetoelectric effect 2−74986
- YIG, ferroacoustic surface wave resonance 2−51035
- YIG garnet, sound wave absorpt. effects, magnetoelasticity, domain wall motion 2−61097

Magnetocaloric effects *see Magnetothermal effects*

Magnetocrystalline anisotropy
see also Magnetic anisotropy
No entries

Magnetoelastic effects *see Magnetoelastic waves*

Magnetoelastic waves

- — 2−60178
- cylindrical layered ferrite-metal medium, independent propagation of magnetostatic surface waves 2−81285
- dispersion and polarization for propagation along acoustic axes 2−68071
- elastic solids, perfectly conducting, plane dynamic deformation, discontinuity expansion solution 2−66603
- ferrite-dielectric interface, gyromag. surface waves 2−44271
- ferromagnet, associated magnetoelastic waves, dispersion laws and polarization 2−57294
- ferromagnetic crystal, interaction between elastic oscillations and precessing mag. moment 2−81208
- interaction, relativistic theory 2−41616
- magneto-thermo-elasto-statics, solution of plane problems 2−45432
- moving loads in initially stressed conducting medium 2−41622
- nonlinear magnetoelastic phenomena in ferromag. resonance 2−72447
- Rayleigh, axial, in visco-elastic cylinder in mag. field 2−73417
- Rayleigh, axial, on cylindrical surfaces of transversely isotropic material and varying density in mag. fields 2−73418
- Dy, lattice excitation and magnon spectra, magnetoelastic effects 2−65141
- Gd, elastic const., C$_{33}$, meas., 13 kOe max., 270-320 K 2−44260
- GdAlO$_3$, antiferroacoustic resonances and magnetoelastic coupling 2−72462
- KMnF$_3$, u.s. attenuation decrease below canting transition due to magnetoelastic propag. 2−54356
- Ni(100) single crystal film, magnetoelastic coefficients at room temp. 2−44264
- Tb, lattice excitation and magnon spectra, magnetoelastic effects 2−65141
- Tb, meachnism for mixing of acoustic magnons and optic phonons propagating along c axis 2−75227
- YIG, tangentially magnetized substrate, Rayleigh type surface wave 2−43976
- YIG garnet, sound wave absorpt. effects, magnetoelasticity, domain wall motion 2−61097

Magnetoelectric effects
see also Galvanothermomagnetic effects; Hall effect; Magnetoresistance

- alkaline solns., nonlinear effects and transient phenomena, pot. barrier height 2−61795

Magnetoelectric effects continued
composite magnetostrictive phase, piezolec. phase, magnetoelec. prod. prop. 2—47664
crystals, antiferromagnetic state, symmetry properties 2—44331
ferrite/semiconductor interface, interaction of surface magnetostatic waves with carriers 2—84420
ferromagnetics, near compensation temp. T_k 2—72158
film, semicond., transverse quantum galvanomag. effects rel. to elastic scatt. by optical phonons 2—64973
galvanomagnetic phenomena, longitudinal, in thin wires, oscillations of resistances 2—68328
graphite, I-V characts., in transverse mag. field, multiple kink effect 2—44093
graphite, pressure effects, energy level and carrier scattering models 2—57110
p-InSb, galvanomagnetic effects and magnetothermoelectric power 2—72050
magnetic crystal classes, invariant magnetoelec. coeff. 2—84390
metals, meas. method for rectangular plates 2—59029
semiconductor, $A^IB^{III}C^{VI}_2$, rel. to band struct. 2—71886
semiconductor, diffusivity-mobility ratio, in high mag. field, doping depend. 2—57181
semiconductor, electron-hole plasma, eddy currents in oscill. mag. field 2—80995
semiconductor, hot carrier instabilities, in strong mag. field 2—75106
semiconductor, magnetosensitive injection- field effect 2—44090
semiconductor, surface magnetovoltaic effect in Hall effect measurements 2—68424
semiconductors, negative photoconductivity 2—81174
semiconductors, surface magnetoplasmons, theory 2—47920
Bi:Te, effect of high hydrostatic pressures on props. 2—81102
Bi, magnetoresistivity coeffs, electron and hole transport, low field galvanomag. tensors, 77-300K 2—84233
p-Bi_2Se_3, Hall and cond. mobilities, carrier compensation, galvanomag. effects, 4.2-300K 2—81076
$Co_4Nb(Ta)_2O_9$, obs. and Neel temp. determ. 2—54359
Cu_2Te-Ag_2Te system, comp. and temp. dependence of Hall mobility 2—84323
n-GaAs, low field galvanomag. transport, Boltzmann eqn. soln. in mag. field, 77-300K 2—71902
n-GaSb(Te), galvanomag. props. rel. to hydrostatic press. at 4.2K 2—68400
Gd, galvanomag. effect rel. to press., 77-400K 2—77858
Ge, electromodulation study of forbidden indirect transitions 2—72333
Ge, galvanomagneto-recombination effect kinetics rel. to elec. and mag. fields 2—65015
$GeMnO_3$, powder susceptibilities 2—44300
HgTe, in high mag. field, 4.2, 77 and 300 K 2—64988
Ho single crystals, 4.2-300K extremum values of magnetoresistance and Hall field at magnetic transition temperatures 2—68548
n-InSb, nonlinear transport props. of hot electrons in strong mag. field 2—47896
$MnGeO_3$, magnetoelec. signal near critical field for spin flop 2—44305
$MnNb_2O_6$, antiferromag. ordering obs. 2—65184
$Mn_4Nb(Ta)_2O_9$, obs. and Neel temp. determ. 2—54359
Ni, electrolytic Matteucci effect, influence of cathodic H 2—48084
Ru, 4.2 K, interpreted rel. to Fermi surface 2—51103
n-Si, weak cond. anisotropy in static mag. field, e.m. propag. obs. 2—84343
Tb, galvanomag. effect rel. to press., 77-400K 2—77858

Magnetogasdynamics *see Magnetohydrodynamics*

Magnetohydrodynamic generators *see Electricity, direct conversion/magnetohydrodynamic*

Magnetohydrodynamic waves
Alfven in plasma heated by transit time magnetic pumping 2—64314
Alfven waves, effect on struct. of turbulence 2—50181
Alfven waves, excitation in high β-plasma 2—64324
Alfven waves, $m=1$, propagation in high beta plasma 2—83630
Alfven waves, nonlinear dissipation in cosmic plasmas 2—75784
Alfven waves in incompressible beam-plasma system 2—67633
Alfven waves in inhomogeneous mag. fields 2—64252
Alfven-gravitational, momentum transport in perfectly conducting shear flow 2—60196
Alfven-gravitational, propagation in stratified perfectly conducting flow with mag. field 2—60195
atmospheric, launched by expanding metallic sphere 2—65686
Cherenkov waves in cylindrical waveguide due to moving source 2—83525
conditions for emergence within F_2-layer at sunrise 2—84909
critical level in rotating fluid 2—46705
detonation waves, props. 2—80220
generation and propagation during spin-up of electrically conducting viscous fluid 2—46706
generation by mechanical radiators, theory 2—77257
during geomagnetic atoms 2—72912
h.f., in plasma, nonlinear interaction 2—46772
incompressible, transmission of energy to conducting solid 2—43105
ionosphere, F-region motion interpret. 2—62377
ionospheric propagation of oblique hydromagnetic plane waves at micropulsation frequencies 2—65959
magneto-optical obs., review 2—72294
magnetosphere, shock normal expressions, determ. using mag. field and plasma flow parameters 2—65843
magnetospheric Pc 1 hydromagnetic wave propagation across North America 2—68936
nonlinear, in dispersive media, stationary solutions and stability 2—82153
paramagnetic-ferromagnetic phase transition, spontaneous symmetry breaking and propagating hydrodynamic wave in the initial region 2—84413
pc 1 hydromagnetic whistler diurnal effects rel. to early afternoon source model 2—84922
plasma, ergodic behaviour in cold collisionless system 2—80304
reflection and refraction laws at fluid-solid interface 2—43104
resistance free magnetosonic shocks, upper critical conditions 2—80324
shock, reflection from boundary shock 2—71067

Magnetohydrodynamic waves continued
slow shock wave propag. 2—80223
unsteady, and currents as approx. of theory of long waves 2—43103
weak nonlinear, propagation 2—50168
Ar plasma, propagation of non-axisymmetric Alfven waves 2—53231
Bi, Alfven-waves damping 2—68316
H, ionized, longitudinal waves, upper bound of frequency 2—74347

Magnetohydrodynamics
see also Electrohydrodynamics; Magnetohydrodynamic waves; Plasma/magnetohydrodynamics
arc in transverse magnetic field, deformation and cut-off model 2—60321
boundary layer flow around oscillating axisymmetric body 2—60192
boundary layer flow past magnetized plate, mag. field oscillations effects 2—83530
boundary layers, interaction with weak shock waves 2—50174
Chandrasekhar's equation and correlation functions for isotropic turbulence, resolution of equation 2—70871
channel entrance flow, linearized analysis 2—70869
channel flow, nonlinear stability 2—50172
channel flow between conducting walls, heat transfer 2—43108
channel flow with arbitrary inlet vel. profile 2—56323
channel load characteristics for optimum resistivity distribution in working body 2—60184
combined current and vortex sheet stability in compressible, perfectly conducting fluid 2—64254
combustion front, velocity and existence 2—60179
compensating current in winding or single phase MHD machine with parallel branches in phase 2—49260
conducting fluid, secondary flow in rotating straight annular pipe 2—56321
conducting fluid in magnetic field, approx. for double-time Green's functions 2—74346
conducting media, taking into account kinematic viscosity 2—50171
conducting source flow in inhomogeneous magnetic field, nonlinear boundary value problem 2—80222
conduction pump, single phase single section, model in electrodynamic approximation 2—52361
conduction pumps, optimum efficiency 2—60188
conduction rotation of conducting liquid in cylindrical vessel with uniform axial magnetic field and radial electric field 2—50177
convective heat transfer from vertical plates to conducting fluid in magnetic field 2—60181
convertors, influence of blow-in on characteristics 2—52360
Couette flow, nonsteady-state, zero net fluid flow 2—70870
Couette flow between cond. walls with heat transfer, effects of ext. circuit 2—46703
critical points meas. of liquid metals 2—83804
crossed electric and magnetic field effects on two phase flow motion in MHD separator 2—60190
cylinder rolling down a plane covered with conducting liquid in magnetic field 2—53166
deflagration front stability 2—53149
deformation of perturbations in uniform magnetic field for plane flow in circular region 2—60198
diffusive toroidal hydromagnetic equilibria without PS enhancement 2—46730
disturbances due to sudden introduction of an oscillating dipole in a fluid of finite conductivity 2—67618
duct flow, corner regions in asymptotic solution of $\varepsilon \mathrm{grad}^2u=\partial u/\partial y$ 2—50180
dynamo action, large mag. Reynolds no., kinematic theory 2—60202
dynamo action in rotating conducting fluid 2—43107
dynamo theory of terrestrial magnetism, numerical soln. to MHD eqn. of Earths core 2—48594
Earth's core, hydromagnetic oscillations rel. to geomagnetic secular variation 2—62378
Earth's core, model 2—81640
effects in compressible conducting media 2—50179
Ekman layer, uniform angular velocity in vertical magnetic field 2—43106
electric field of fluid in transverse non-uniform magnetic field 2—60182
electrically cond. fluid, aligned flows 2—56318
electroconvection of dielectric fluids under alternating electric field 2—53151
electrodynamic forces in e.m. stirrer for molten metals 2—50183
e.m. coupling in fixed oscillatory mode between two unidimensional laminar streams of viscous electroconductive liquid 2—56317
e.m. force on moving liquid in cylinder in travelling magnetic field 2—50178
entrance flow in channel, in Prandtl approx. 2—60205
equilibrium and stability of rotating gaseous systems 2—48641
equilibrium configuration of slowly rotating liquid mass in poloidal magnetic field 2—77255
ferromagnetic liquids, self propagating thermal convection 2—53160
field distribution along channel axis in magnet system of conduction pump 2—49261
flow, about curved neutral sheet 2—80225
flow, development in entrance region of channel 2—64253
flow, in region of discontinuity in conductivity of wall 2—53165
flow, of perfectly conducting fluid, multiplicity theorem 2—50173
flow, stabilization by distributed feedback system 2—53163
flow, with shear, effect of mag. field on turbulence 2—70873
flow at low and moderate Hartmann numbers, application of Gringberg's soln. to design of duct 2—67613
flow between 2 rotating discs with noncoincident parallel axes of rotation 2—56322
flow between concentric rotating cylinders, solution of equations 2—56320
flow in conducting fluid, induced by elec. current discharge 2—56305
flow meas., laser Doppler velocimeter, obs. 2—80217
flow near time-varying accelerated plate 2—67611
flow past a hollow sphere on mag. field 2—80219
flow past flat plate with nonaligned mag. field 2—53155
flow round profile perpendicular to plane of flow 2—53167
fluctuating flow along infinite flat wall with variable suction 2—53168

Magnetohydrodynamics continued
fluid, flow over porous flat plate in transverse mag. field, Hall current effects 2—46704
fluids, potential equations 2—50166
free convection in electrically conducting nonmagnetic fluid flowing past flat plate 2—53150
gas, transverse field effects on high temp. flow in channel with high thermal insulations 2—77258
general MHD duct flow problems, numerical method of solution 2—46707
general relativistic, action principle 2—56316
Hall effect in turbulent moving medium, effect of conductivity 2—43110
Hartman flow, hydrodynamic stability in two dimensional perturbations 2—50182
hydromagnetic couette flow with time dependent suction or injection, analysis for transverse magnetic field 2—56319
incompressible, validity of Batchelor's invariant of turbulence 2—83529
induction pumps and bearings, efficiency 2—50169
interplanetary, oblique nonlinear waves, correlation with local solar wind plasma density fluctuations 2—62784
interplanetary mag. field, statistical properties of MHD discontinuities 2—62738
interstellar self gravitating gas cloud, effect of tangential shippage on hydromagnetic stability 2—55077
inviscid fluid flow between rotating cylinders stability of nonrotationally symmetric disturbances with axial magnetic field 2—43109
inviscid fluid flow between rotating cylinders under circular magnetic field, stability of non-rotationally symmetric disturbances 2—43111
ionospheric waveguide, hydromagnetic pulse propagation 2—84897
jet, inviscid cylindrical, electric current effect on capillary instability 2—60401
jet flow near wall, convective heat transfer 2—60200
jet propagation in transverse magnetic field, degeneration to elliptical shape 2—60183
kinematic dynamo equations, Lagrangians and variational principles 2—56315
kinematic dynamo models 2—64251
laminar boundary layer, self-modelling flow during blowing and suction 2—67614
laminar boundary layer stability on concave walls 2—80221
laminar boundary layers along infinite porous plate 2—60204
laminar flow of liquid in conducting pipes, extremum principles 2—60203
linear inductors, single phase rotor with variable phase velocity 2—53152
linear stability of flow in circular pipe in transverse mag. field 2—67616
liquid metal flow through dendritic conducting filler 2—64576
magnetic weight function for conduction channel in static system 2—60187
magneto- and electro-rheology in dispersive systems 2—58854
magneto-thermo-elastic stresses in long cylindrical conductor carrying axial current 2—60178
magnetogasdynamic flows of radiated gas caused by piston motion 2—67615
main-sequence stars, effects of uniform rotation and strong dipolar magnetic fields on structure and properties 2—84986
non stationary flow of real conducting gas in MHD channel with continuous electrodes 2—60201
nonequilibrium flow of weakly conducting liquid, near critical point in magnetic field 2—53164
nonlinear dynamo waves for solar cycles 2—73134
nonstationary gas flow in conduction channel, numerical computation 2—60189
Nyquist criterion for kinematic dynamo action 2—56324
oblique field, quasi one-dimensional, non-steady non-uniform shock waves 2—43101
oscillatory flow of electrically conducting gas, numerical solution 2—46708
peristaltic flow in slotted channel 2—60180
perturbation produced by momentary current in semi-infinite fluid of finite conductivity 2—53171
Petschek's mechanism, modification and criticism 2—81762
plane and laminar motions, asymptotic exponential stability 2—43102
plane linear induction pumps with side bars, e.m. field distrib. 2—50170
plasma equilibria, computational problems 2—80267
Poisson equation solution 2—48977
polarizable and magnetizable media, arbitrary law connecting induction and poles 2—53159
prominences, quiescent, formation by condensation 2—78615
propagation of cylindrical magnetogasdynamic shock in nongravitating system 2—53185
pulsating flow in pipes 2—64250
rectangular channel with segmented side walls, transverse edge effect 2—53161
relativistic, infinite conductivity 2—74345
retrograde motion of low pressure discharge in transverse fields 2—70996
shear flow heterogeneous, hydromagnetic stability in variable magnetic field 2—77251
single phase transformation pump with disc shaped channel 2—60185
slider bearing between two elec. cond. plates, external cct. effects 2—67617
solar flare production by dynamo action 2—78618
spherical bearing 2—60186
stability, rotating fluid with finite resistivity, self-gravitation 2—50167
stability of flow with power function rheological law in transverse field 2—60199
stability of fluid with radial gravitational force, influence of geostrophic force 2—60177
stability of magnetic baroclinic flow of unbounded fluid with linear velocity profile 2—78585
stationary dynamo model 2—77253

Magnetohydrodynamics continued
subsonic flow of real gases, in annular channels with curvilinear walls 2—50176
surface waves, anisotropic motions, electrically conducting fluid under uniform magnetic and current fields 2—60193
Sweet's mechanism for mag. flux destruction 2—67612
thin film of conducting liquid in transverse magnetic field, wave flow regime 2—53162
time evolution and functional form of magnetostatic equilibria in axisymmetry 2—80226
toroidal hydromagnetic waves, in dipole field, asymmetry 2—65863
transformations in gas- and magnetogas-dynamics 2—77259
transient free convection flow $P_m=1$ near flat plate 2—53157
transition processes in liquid metal loop due to voltage changes in MHD pump 2—60191
turbulence and flow stability in M shaped velocity profiles 2—60206
turbulence suppression by magnetic field 2—50184
turbulent flow, complex and non-self-similar 2—77321
turbulent streams of conducting fluid, generation of sound 2—53170
uniform flow, finite magnetic Reynolds number, electromagnetic characteristics 2—50175
universes of Godel type 2—51684
unsteady flow due to porous rotating disc 2—46702
unsteady flow over yawed infinite cylinder 2—70872
unsteady free convection flow past infinite vertical plate, variable suction 2—83526
unsteady laminar motion of electroconducting liquid under transverse magnetic field 2—60194
unsteady slip flow past infinite flat plate 2—53169
visco-plastic ferromagnetic hydrodynamics, laminar flow equation of motion soln. 2—60197
viscous compress. flow, electrically and thermally conducting, weak fluctuation modes in homogeneous mag. field 2—53153
viscous entrainment of conducting liquid 2—53156
viscous incompressible fluid with finite resistivity, Rayleigh-Taylor instability under inhomogeneous horizontal magnetic field 2—70868
vortex sheet, hydromag. stability, effect of discontinuity in density or cond. 2—53158
vorticity jump across stationary MGD discontinuity 2—53154
water, magnetic treatment and structure 2—54521
wave generation in magnetically confined and field-permeated axisymmetric jet 2—77256
Ar, partially ionized, heat transfer in laminar flow in pressure of transverse mag. field 2—53298
UF_6 MHD units, thermal efficiency 2—63964

Magnetomechanical effects
see also Gyromagnetic effect; Magnetoelastic waves; Magnetostriction
— 2—72462
deformable saturated media, constitutive theory 2—63077
domain boundary displacement due to magnetoelastic interaction force of moving dislocations 2—72143
domain wall movement retardation due to interaction with dislocations 2—68540
ferromagnet, magnetoelastic phenomena in parametric mode magnetiz. oscillation 2—68719
ferromagnetic materials, stress depend. damping at stresses to fatigue limit 2—74826
magneto-elastic boundary-value problems, minimum principle presented 2—58835
magnetoelasticity, dislocation theory applic. 2—61519
magnetoelasticity of thin solids 2—76283
micromagnets, continuum theory, dissipative processes 2—84394
oriented elastic continuum as model of magnetoelastic body 2—69668
permalloy film electrodeposited on Cu wire, and e.m. props. 2—77990
postbuckling anal. of magnetoelastic beam 2—45381
rare earth metals, magnetoelastic effects, theory 2—75226
rare earth metals, with helical spin struct., magnon-phonon interaction 2—75225
Co, domain wall movement retardation due to interaction with dislocations 2—68540
Co, mag. after-effect of hydrogen 2—78029
Fe-Ni alloy, thermal stability of elastic modulus, contrib. of Invar anomaly and ΔE effect 2—50724
Fe-Ni alloy film, crit. fields, effect of elastic stresses 2—51264
Fe domain wall movement retardation due to interaction with dislocations 2—68540
Fe_2O_3, piezomagnetic properties, effect of annealing 2—48083
$Li_{0.45}Mn_xFe_{2.55-x}O_4$, anisotropy contrib. of Mn^{3+} and related directional orders 2—65170
Ni, electrolytic, anisotropic effects in magnetoelastic damping 2—54337
Ni, electrolytic Matteucci effect, influence of cathodic H 2—48084
Ni, electron irrad., low temp. recovery of mag. after-effect 2—64655
Ni, mag. after-effect of hydrogen 2—78029
Ni, magnetoelastic effects as function of elastic distortion 2—78028
Ni domain wall movement retardation due to interaction with dislocations 2—68540
NiFe ferrites, freq. effect, torque obs. 2—44278
Ni(100) single crystal film, magnetoelastic coefficients at room temp. 2—44264
$RbMnF_3$ antiferromagnet, magnetoelastic theory of ^{19}F nuclear acoustic resonance and lattice imperfection 2—51412
Tb films, phonon emission at 15 GHz, dynamic magnetoelastic coupling obs. 2—68562
Y garnets, magneto-elastic bonding of Fe^{3+} and Cr^{3+} ions 2—65321

Magnetometers *see Magnetic field measurement*

Magnetoreflectance
No entries

Magnetoreflection *see Magneto-optical effects*

Magnetoresistance
see also Magnetoelectric effects
alkali metals, duality theorem and high-field linear magnetoresistance, geometrical effects 2—81031
alkali silicate glass, γ-irrad., rel. to thermolum. 2—81410

- **Magnetoresistance** continued
  - band struct. analysis, review 2−72298
  - carbons irradiated by neutrons and annealed, props. changes 2−68137
  - double exchange ferromagnet, quantum theory 2−54295
  - electron gas, free, const. m.f.p. 2−80971
  - ferromagnetic film, effect of angular dispersion of magnetization 2−48086
  - galvanomagnetic size effects in thin films 2−54126
  - graphite, extremal mag. field positions 2−57121
  - graphite, pyrolytic, 1.2-300 K, c-axis conduction mechanism 2−57109
  - graphite, rel. to struct. imperfections 2−57190
  - graphite, spectrum at high fields 2−57340
  - graphite very thin crysts., total carrier density behaviour 2−54102
  - i.r. reflectivity meas. at low temps. and high magnetic field 2−82569
  - metal, linear magnetoresist. and anisotropic quantum fluctuations 2−57141
  - metal, size effect of transverse magnetoresist. 2−51095
  - metals, meas. method for rectangular plates 2−59029
  - semiconductor, doped with nonmag. impurities, negative magnetoresist., model 2−68323
  - semiconductor, heavily doped, calc. at low temps. and weak mag. field 2−51132
  - semiconductor, heavily doped, temp. effects on two-band model for neg. magnetoresistance 2−64970
  - semiconductor, III-V, hot electron magnetophonon reson., theory 2−68386
  - semiconductor, in strong electric fields 2−75086
  - semiconductor, low temp. longit., intense mag. fields 2−68388
  - semiconductor, nonparabolicity contrib. to longit. magnetoresistance at quantum mag. fields 2−64966
  - semiconductor, nonpolar, longitudinal magnetoresist., magnetophonon struct. 2−84327
  - semiconductor, obs. of Shubnikov-de Haas effect at relatively high temps. after strong light illumination 2−81004
  - semiconductor, polar, oscill. struct. of magnetophonon effect transverse config. 2−57179
  - semiconductor, transport processes, magnetophonon spectroscopy study 2−68385
  - semiconductor film, calc. 2−71892
  - semiconductor inversion layer, theory 2−68387
  - semiconductors, amorphous, bridge method of measurement, applic. to Ge 2−44122
  - semiconductors, anomalies due to surface effect, freq. response and carrier lifetime 2−65005
  - semiconductors with nonparabolic bands, calc. from transport props. 2−81101
  - semicondutcor with non-standard zone, in alternation mag. field, theory 2−84318
  - s.h.f. transmitting power meas. by magneto-resistance sensors 2−78993
  - size effect theory in thin metallic films 2−77984
  - size-limited conductor, negative longit. magnetoresist., kinetic theory 2−54125
  - spinal ferrite, temp. and composition depend. 2−48100
  - sum frequency method of obs. in belt apparatus 2−57267
  - transverse, sensitive method of obs. 2−64963
  - VB$_2$, one and two-zone model and measurements, comparison 2−77881
  - Al, magnetoresistivity from audio freq. helicon resons. 2−57136
  - Al, quenched, annealing kinetics of point defects 2−80680
  - Au island films on insulators 2−84298
  - AuFe dilute polycrystalline alloy, negative transverse magnetoresistance 2−64911
  - Be, quantum oscillation waveforms rel. to $\partial M/\partial H$ oscillations 2−80963
  - Bi-Sb alloy, effects of Ag, In and Pt addition 2−71896
  - Bi, magnetoresistivity coeffs, electron and hole transport, low field galvanomag. tensors, 77-300K 2−84233
  - Bi, polycrystalline, obs. by sum frequency method in belt apparatus 2−57267
  - Bi, quenched in liquid N$_2$, resistivity and thermoelectric power 2−68336
  - Bi, tensor components, at intermediate mag. fields, 77 K 2−75053
  - Bi film, as function of thickness 2−84332
  - Bi whiskers, new oscills., obs. at 4.2 K 2−68338
  - p-Bi$_2$Te$_3$, low- and high-field props. 2−51135
  - p-Bi$_2$Te$_3$, valence band struct., Shubnikov-de Haas oscills. of magnetoresist. 2−77805
  - C, multiphase system, mag. field depend. 2−57112
  - C, pyrolytic, anisotropic neg. and posit. magnetoresistance 2−57111
  - C resistor thermometer, method of reduction 2−52295
  - Cd$_{2.8}$Zn$_{0.2}$As, high mobility, rel. to scattering parameter determ. 2−81090
  - Cu-Ni-Mn, dil. alloy, resist., Z-100K, Kondo effect 2−47835
  - Cu-Ni(Cr) alloy, Kondo effect 2−64913
  - Fe-Co alloy, temp. $\leqslant$4.2K 2−47836
  - Fe-Cr alloy, temp. $\leqslant$4.2K 2−47836
  - Fe-Rh alloy, temp. depend., rel. to mag. transition 2−54330
  - Fe-V alloys, meas. of longitudinal and transverse magnetoresistance at 4.2K, 77K, 273K 2−48063
  - Fe, polycrystalline, meas. of longitudinal and transverse magnetroresistance at 4.2K, 77K, 273K 2−48063
  - Fe, temp. $\leqslant$4.2K 2−47836
  - Ga, Gantmakher-Kaner effect 2−47797
  - GaAs, compensated, negative magnetoresist. temp. depend., influence of mag. field 2−71900
  - n-GaAs, low field galvanomag. transport, Hall mobility, magnetoresist. coeff., 77-300K 2−71902
  - n-GaAs, rel. to impurity distrib. coeff. anisotropy 2−47437
  - GaAs, rel. to mag. field effect on electron transfer and velocity-field characts. 2−44100
  - GaSb, Landau levels obs. 2−71795
  - Gd, in strong effective fields at 4.2K 2−77859
  - Ge, microwave field depend. 2−77909
  - p-Ge, theory extended to include optical phonon scatt. 2−65011
  - n-Ge, transverse and longit., of hot electrons 2−65012
- **Magnetoresistance** continued
  - n-Ge, transverse magnetoresist. in quantizing mag. fields, calc. 2−71939
  - HgSe, Shubnikov-de Haas effect, effect of uniaxial stress 2−68402
  - Ho, in strong effective fields at 4.2K 2−77859
  - Ho single crystals, 4.2-300K extremum values of magnetoresistance and Hall field at magnetic transition temperatures 2−68548
  - n-InAs, rel. to thermoelec. power in quantizing mag. fields 2−84372
  - InSb, deformation potentials, from Shubnikov-de Haas measurements 2−68416
  - InSb, Landau levels obs. 2−71795
  - n-InSb magnetoresistance meas. 2−46729
  - In$_2$Te$_3$-Hg$_3$Te$_3$ alloy, negative magnetoresist., 77-400K 2−44102
  - IrO$_2$, high-field obs., monotonic and oscillatory components, Fermi surface model 2−68295
  - K, duality theorem and high-field linear magnetoresistance, geometrical effects 2−81031
  - K, non-saturating anisotropy of induced torque 2−48036
  - KI, first exciton obs. 2−51322
  - Li(NH$_3$)$_4$, carrier mobility determ., 1.5-77.5K 2−47894
  - n-Mg$_2$Ge, weak-field obs. 2−51143
  - Nd, transverse and longit., at 1.38K, 4.2K, 13.96K and 20.4K 2−71836
  - Ni-Cr alloy, hydrogenated, elec. resist. rel. to mag. field, localized moments 2−81034
  - Ni-Fe(Pd) films, magnetoresist. anisotropy 2−44266
  - Ni, electrical resistivity due to dislocations, at low temps. 2−81033
  - Ni film, thickness depend. 2−51266
  - Pb, temp. $\leqslant$4.2K 2−47836
  - PbO-Al$_2$O$_3$-SiO$_2$-B$_2$O$_3$ glass, between metal electrodes, rel. to memory effect 2−71915
  - n-PbSe, elec effective mass and relaxation time detn. 2−61651
  - PbSe epitaxial films on NaCl substrate, effects of ambient gas uptake 2−65008
  - PbTe, low temp. far i.r., TO lattice mode obs. 2−65265
  - Pd-Ni alloy, due to scatt. by spin fluctuations 2−48058
  - Pd alloyed with nonmag. impurities, negative contrib. 2−61152
  - Pt-W strain gauge, temp. dependence 2−68121
  - Pt island films on insulators 2−84298
  - RbI, first exciton obs. 2−51322
  - Sb-Bi alloys, band struct. obs. 2−54405
  - Se-Te alloy, liquid, switching phenomena 2−60504
  - Se, liquid, anomalous 2−60505
  - Se, liquid, rel. to switching phenomena 2−60504
  - n-Si, degenerate, transverse magnetoresist., low temp. 2−84344
  - n-Si, doped, rel. to microwave propag. 2−54197
  - n-Si, transverse magnetoresist., mag. field strength depend. 2−65018
  - Sn-Ge alloy, Shubnikov-de Haas oscills. rel. to carrier heating in cond. band 2−81080
  - SnTe, Shubnikov-de Haas effect, Fermi surface determ. 2−68420
  - Te valence band structure from Shubnikov-de Haas expts. 2−84245
  - Tl$_2$Se.As$_2$Te$_3$, amorphous 2−61331
  - Zr, Fermi surface determ. 2−84248
- **Magnetosphere**
  - ambient plasma velocity, nucleation of artificially deposited Ba ion cloud striations 2−62301
  - amplitude variations in artificially stimulated v.l.f. emissions 2−54881
  - auroal particles, origin, props. 2−68943
  - average plasma-sheet configuration near 60 Earth radii 2−65848
  - barium cloud release, balloon meas. of ionospheric electric fields and precipitating particles 2−62365
  - barium ion cloud, initial expansion phase investigated using computer model 2−62305
  - barium ion cloud expt., analysis of optical data obtained by NASA 2−62299
  - Birkeland currents intensification due to elec. fields 2−65904
  - boundary with solar wind, wave coupling at collisionless plasma discontinuity 2−83615
  - bow shock, determ. of perturbation vectors of waves up and downstream from region of maximum compression 2−62320
  - bow shock, electron plasma oscillations 2−65846
  - bow shock, interaction with interplanetary shocks 2−62294
  - bow shock, large-scale coherence and high velocities meas. from three satellites 2−68932
  - bow shock, nonuniform structure rel. to interplanetary field orientation 2−65847
  - bow shock, Ogo 5 magnetic-field data rel. to low-frequency magnetic wave theory 2−65840
  - bow shock, reinterpretation of Pioneer 6 crossing 2−62336
  - bow shock, wave structure during steady solar-wind conditions 2−65852
  - bow shock obs. from lunar orbit, meas. of electron plasma properties across shock and in magnetotail 2−62313
  - charged particle motion in neutral-sheet type magnetic field, Hamiltonian formulation 2−59077
  - charged particle motion near neutral plane, Hamiltonian analysis 2−69862
  - charged particles influence on scintillation detectors 2−51634
  - colliding plasmas, e.m. instability 2−60213
  - compressional wave propagation to the ground 2−68935
  - computer simulation of whistler turbulence, particle pitch angle and energy diffusion 2−65867
  - convection, effect of polar cap elec. fields 2−65962
  - convection electric fields in high latitudes, satellite measurements 2−75626
  - convection obs. from Ba cloud motions 2−62298
  - convective currents, generation of long-period pulsations at boundaries 2−48534
  - cosmic ray meas. by Intercosmos 3, PG-1 apparatus 2−81650
  - cusp region, electron temp. and soft particle precip., Te enhancement meas. 2−62357
  - day-side, high latitude boundary of stably trapped radiation zone 2−44746
  - dayside auroral particle precipitation mechanism, mid-latitude v.l.f. emissions 2−48538
  - dayside limit of closed field lines rel. to solar particles 2−68982

Magnetosphere continued
dayside polar cusp boundaries, magnetospheric observations of plasma waves 2−65853
deformations, discontinuities and models, geomagnetic effects 2−48603
distant bow shock, meas. of locations and orientations, effect of geomagnetic disturbance 2−62318
disturbance environment during NASA-MPE Ba ion cloud experiment 2−62304
disturbances in polar cap S_q^p and DP-2 2−72910
drift-shell splitting at arbitrary pitch angle 2−65841
ducts, propagation of u.l.f. waves, theoretical investigation of leakage 2−65861
dynamics, radial diffusion of He^+ and protons 2−65849
effective height integrated conductivity current flow 2−65949
electric field, induced by radial penetration of hot plasma 2−65862
electric fields, computer model 2−65879
electric fields, decaying ring current as origin 2−78386
electric fields, meas. techniques and props. 2−72878
electric fields deduced from drifting whistler paths 2−65859
electrical charging of synchronous satellite 2−66025
electrodynamic coupling with ionosphere, rel. to quiet auroral arcs 2−65905
electrojet, nonlinear theory of cross field instability 2−65920
electron auroral morphology, substorms and magnetospheric processes 2−84875
electron cyclotron and Langmuir frequency ratio, satellite measurements 2−72841
electron density trough, magnetic shell alignment, Ariel 3 data 2−72863
electron dynamics, conjugate features obs. at balloon altitudes 2−72828
electron echo expt., particle data analysis 2−65882
electron echo expt., returning beam profile analysis 2−65881
electron energy spectra in the magnetopause and magnetotail, meas. using electrostatic analysers on satellite 2−62323
electron flux and magnetic field at ATS-1 during substorms, local time dependence 2−62310
electron precipitation to lower ionosphere at time of sudden commencement, theory 2−65837
electron-density profiles deduced from plasmapause whistlers 2−68939
electrostatic instability excited by electron beam trapped in magnetic mirror of magnetosphere 2−48537
e.l.f. hiss between 1 and 1000 Hz, detection by triaxial search coil magnetometers 2−62331
energetic particle obs. at very low altitudes near geomag. equator 2−65880
energetic particle population, solar particle event effects 2−68941
energetic particles, motion and diffusion 2−65864
equilibrium potential of magnetospheric satellite in eclipse situation 2−72933
external mag. field, theories and obs., review 2−78387
field distortions at high latitudes 2−65876
flow of ionospheric dynamo currents and interaction with ocean effects on daily geomag. variations 2−84926
fluctuating magnetic fields, u.l.f. waves 2−75622
fluctuations, MHD waves and mag. variations during mag. storms 2−72912
frequency-time analysis of e.m. waves in magnetosphere 2−84703
geomagnetic storm of 1970, March 8, development peculiarities rel. to solar wind, magnetosphere and aurora 2−84917
geomagnetic tail, electrical noise, v.l.f. emission 2−81715
geomagnetic tail, internal structure of neutral sheet 2−65836
geomagnetic tail model, consequences of isotropic static plasma sheet 2−54887
geomagnetic trail, possible crossing at 3000 earth radii by automatic interplanetary station, Mars-3 2−75623
hot magnetoplasma, electrostatic resonance assoc. with maximum frequencies of cyclotron harmonic waves 2−65851
interplanetary mag. force lines interconnection, rel. to geomagnetic activity 2−51659
ion and electron densities and temps. during magnetic storm, meas. from spherical electrostatic analysers 2−62309
ionosphere interactions, conference review 2−48568
Kosmos-219 satellite, combined meas. of components of mag. field and proton flux and energy spectra 2−72829
LHR hiss rel. to magnetospheric and auroral activity 2−68953
light ion trough rel. to concentrations of H^+ ahd He^+ satellite meas. 2−84889
local bow shock, binary index for assessing oblique structure 2−62319
low energy electron flux in midnight-dawn sector, meas. in equatorial region and intermediate latitudes 2−62321
lower hybrid resonance meas. of low electron densities 2−62330
magnetic field variation of the SI, analysis using Explorer 26 data 2−62308
magnetic-field measurements in high-geomagnetic latitude outer magnetosphere 2−68931
magnetopause, electric and magnetic field structure in dawn to noon quadrant from Explorer 43 meas. 2−62316
magnetopause, mapping of proton and alpha particle distribs. 2−65909
magnetoplasma containing negative ions, right-hand circularly polarized wave propagation, thermal effects 2−80229
magnetosheath electron precipitation rel. to dayside auroral-oval plasma density and conductivity 2−65854
magnetosheath particle precipitation, effects on dayside ionosphere 2−58073
magnetosheath structure obs. by 3 ALSEP/SIDE plasma detectors on lunar surface 2−62315
magnetotail, solar electron and proton content during solar particle event 2−65842
MHD, Petschek's mechanism, modification and criticism 2−81762
MHD magnetosphere, shock normal expressions, determ. using mag. field and plasma flow parameters 2−65843
midday auroras at South Pole during magnetospheric substorms 2−65900
mirror-confined plasma trapped near equator in geomagnetic field, electrostatic instabilities 2−62333

Magnetosphere continued
models, exptl. test based on triangulation data on Ba ion traced field lines 2−62306
momentum transfer from ambient magnetospheric to seeded Ba plasma, NASA/MPE cloud expt. 2−62300
morphology of Ba cloud released at 6.1 Re geocentric distance 2−62302
neutral sheet, magnetic effects 2−68975
outer, butterfly pitch angle distrib. of electrons in postnoon to midnight region 2−62311
outer, energetic particle obs., role of plasmapause 2−58050
outer geocorona, H_2 Lyman α obs. 2−65856
partial ring current rel. to positive geomagnetic bays 2−78405
particle flux gradients determ. using energetic protons as probes, structure of magnetopause studied 2−62312
pi 1 micropulsations sub-class rel. to diurnal transit of neutral sheet 2−84921
pitch angle distrib. of particle fluxes, calc. method based on rocket and satellite data 2−72825
plasma, finite conductivity 2−51636
plasma, l.f. impedance obs. 2−48533
plasma, mirror-confined, with anisotrpic vel. distrib., electrostatic instabilities 2−65866
plasma, warm, v.l.f. electric dipole radiation characts. 2−74364
plasma arcs and loops, trapping 2−78577
plasma circulation speed meas. using quadripole probe on spacecraft 2−84871
plasma diagnostic phenomena 2−78397
plasma flow in Earth's magnetotail meas. by spin-modulation in flux of plasma protons 2−62324
plasma motion during sudden commencement on February 15th, 1967, analysis of ground magnetograms 2−62307
plasma sheet, magnetic noise as meas. by Explorer 34 satellite 2−62325
plasma sheet obs. in geomag. tail during substorm 2−65872
plasmapause, light ion trough characts. 2−58047
plasmapause, lower-hybrid-resonance noise bursts, whistlers, e.l.f. hiss and discrete emissions obs. during large magnetic storm 2−65850
plasmapause, obs. of optical emissions 2−62326
plasmapause, thermalization of colliding ion streams 2−65946
plasmapause, wave-particle interactions, instabilities 2−62329
plasmapause behaviour, longit. and temporal characts. 2−65883
plasmapause obs. in pre-dawn region 2−62335
plasmasphere, convection penetration 2−58048
plasmasphere bulge interpret. as due to short- duration gusts 2−58051
plasmasphere pitch angle diffusion of radiation belt electrons 2−72830
plasmasphere struct. and dynamics 2−58045
plasmasphere-ionosphere diffusive coupling 2−58049
plasmasphere-plasmapause dynamics 2−58046
polar, v.l.f. hiss and plasma obs. 2−65839
polar cap illumination by solar protons 2−65877
polar cap mag. field disturbances 2−65875
polar cap particle flux variations, two-satellite observations 2−68937
polar cap structures of solar protons, obs. during passage of interplanetary discontinuities 2−65857
polar caps, solar proton flux propag., uneven illumination analysis 2−65878
polar cusp depend. on N-S component of interplanetary field 2−65874
polar magnetic substorms, ring current and field aligned current rel. to ionospheric electric current 2−81712
polar substorm, Mar. 1970, particle acceleration and loss obs. 2−65873
polar wind model, O^+, H^+ and He^+ distributions 2−81698
projection of midday magnetospheric boundary with diverse geomagnetic dipole orientation 2−54879
proton diffusion by turbulent electrostatic oscillations 2−68940
proton fluxes $\gtrsim 30$ keV obs. upstream from bow shock and in magnetosheath 2−62314
proton motion due to electric field as explanation of frequency drift of PDP type geomagnetic pulsations 2−48599
quasimonochromatic whistler mode wave packets, shape evolution and interactions 2−84891
red arc, satellite and ground based observations, formation and likely source of energy 2−62328
resonance scattering of solar radiation from Ba ion cloud at 31000 km 2−62303
resonant interaction of electrostatic wave with electrons in current sheet 2−72826
ring current effect, from plasmapause whistlers 2−54880
ring current particle injection investigated using dynamical model of radiation belt in self-consistent magnetic field 2−62349
seasonal changes in flux at synchronous altitudes 2−48531
shape, det. from ESRO satellite obs. in polar regions 2−48539
soft electron zone, effects of dipole tilt, interplanetary field and substorms 2−65903
solar particle entry anomalies, magnetospheric models 2−65865
solar wind discontinuities, effect on magnetosphere, space-time correlations 2−72823
south magnetic pole region, automatic measuring station using isotopic generator 2−51637
Speiser model of current sheet, field consistency and particle motion 2−84887
Sq currents, north south asymmetry, study using ionospheric dynamo model 2−58114
stress balance in plasma sheet on closed field lines 2−62322
structure, variation with direction of interplanetary mag. field and geomagnetic activity 2−65858
sub-auroral plasma trough morphology 2−58056
substorm, model 2−48532
substorm adiabatic processes 2−65871
substorm depression and expansion phases, Fourier analysis 2−62334
substorm expansive phase triggering 2−65870
substorm Pi 1 micropulsations, ground-satellite correlations 2−62332

- **Magnetosphere** continued
  - substorms, behaviour of low-energy particles 2–81711
  - substorms, conference (Moscow, Aug. 1971) 2–81708
  - substorms, daytime irregular geomagnetic pulsation 2–72914
  - substorms, electric field variations, OGO 6 obs. 2–81714
  - substorms, equatorward motion of midday auroras 2–65893
  - substorms, mag. field fluctuations 2–81713
  - substorms, outer radiation zone behaviour and model 2–81709
  - substorms, plasma sheet variations 2–81710
  - substorms, rel. to changes in geomag. tail, growth phase 2–81746
  - sudden impulses in geomagnetic tail and magnetosheath, propagation 2–72913
  - tail, characteristic oscillations, plasma sheet effect 2–51635
  - tail, shock wave as reason for active phase of substorm 2–72824
  - thermal anisotropy influence on best fit estimates of shock normals 2–65860
  - thermal plasma densities in magnetosphere, digital sonograms of hydromagnetic whistlers 2–48535
  - thermal positive ions in outer ionosphere and magnetosphere 2–65844
  - thundercloud, calc. of electric field in ionosphere and magnetosphere 2–62347
  - toroidal hydromagnetic waves, in dipole field, asymmetry 2–65863
  - two-dimensional model with neutral layer 2–51633
  - upper-hybrid reson. noise obs. by IMP-6 AC-elec. fields expt. 2–65869
  - v.l.f and u.l.f. waves, monochromatic, circularly polarized, nonlinear theory 2–68930
  - v.l.f. emission and propag., sources 2–68960
  - v.l.f. emissions, naturally occurring and triggered 2–81706
  - v.l.f. emissions, summary 2–81707
  - v.l.f. waves in whistler mode propagation 2–78384
  - v.l.f./e.l.f. radiation patterns rel. to satellite transmitting sytem design 2–68933
  - whistler dispersion and electron density variation during one solar cycle 2–44744
  - Whistler mode waves, quasi-linear interaction with nonthermal electrons 2–58043
  - whistler propag. at low latitudes 2–84884
  - whistler propagation, effect of the ring current 2–48536
  - whistler wave amplification, pitch angle and energy diffusion coefficients 2–48516
  - whistler- mode signals in conjugate region, 200 kHz satellite observations 2–65943
  - Ba cloud, mag. field meas. 2–62297
  - Ba cloud experiments rel. to mechanism of photoionization and radiative transfer problem in freely expanding gaseous clouds 2–46791
  - Ba cloud release at five earth radii 2–62296
  - Ba release experiment, Portuguese obs. of related luminous phenomena 2–72831
  - H densities at exobase 2–65832
  - He and He^+ emission from magnetosphere, e.u.v. resonance radiation 2–68934
- **Magnetostatic waves** *see Spin waves*
- **Magnetostriction**
  - ΔE effect, elastic consts. and crit. pt. obs. 2–77664
  - antiferromagnetic chain, uniform, thermodynamic props. and magnetostriction 2–84439
  - cavitation erosion, determination of resistance of materials by magnetostrictive vibratory method 2–76115
  - composite magnetostrictive phase, piezolec. phase, magnetoelec. prod. prop. 2–47664
  - curves determ. by EDP 2–81244
  - ferrite, spinel struct., mag. dipolar interact. contrib. 2–78036
  - ferrite magnetostrictive transducer material, fatigue testing 2–71625
  - ferromagnet, Mossbauer sidebands due to r.f. acoustic vibrs. 2–48141
  - ferromagnetic crystal, rel. to interaction between elastic oscillations and precessing mag. moment 2–81208
  - ferromagnetic cubic materials, rel. to grain orientation 2–63078
  - ferromagnetic insulators, acoustic attenuation and frequency shift for 2 magnon-one phonon processes 2–80907
  - ferromagnetic single crystals, spherical samples, form efffect 2–78027
  - film, anisotropy skew patterns, temperature gradient effects 2–72177
  - grain-oriented ferromagnetic polycrystals, saturation approach law of longitudinal magnetostriction 2–54335
  - Invar, spontaneous magnetostriction, itinerant electron model interpret. 2–48085
  - magnetic crystal classes, invariant piezomag. coeff. 2–84390
  - Permalloy films, electrodeposited, comp. and depositing current effects 2–57302
  - phenomena in thin wires and spark chamber design 2–73954
  - polycrystalline cylindrical samples, measuring method 2–75224
  - in pulsed mag. fields, apparatus for obs. 2–45667
  - rare earth, paramag., rel. to exchange anisotropy, variation with lattice parameters 2–51236
  - rare earth metals, rel. to spin wave gap calc. 2–75226
  - rare earth metals, study of pressure effect and temp. depend. of helicoidal magnetic structure 2–68542
  - second order elasticity effects 2–44259
  - thin films, prep. by tetrode plasma sputtering 2–43473
  - transition metal, ferromag., band model using spin-orbit term 2–48082
  - transition metal, paramagnetostriction, oscillatory magnetostriction, rel. to Fermi surface 2–54290
  - Al, Fermi surface press. depend. 2–61180
  - Al, rel. to Fermi surface 2–68286
  - $Co_xNi_{1-x}Fe_2O_4$ ferrite, temp. variation 0-500c 2–72196
  - Dy, rel. to magnon spectra free lattice to frozen lattice transition 2–65141
  - Fe-Ni alloys, magnetisation and magnetostriction in strong magnetic fields 2–68507
  - Fe-Ni Invar alloy, rel. to temp. depend. of elastic consts. 2–80751
  - Fe-Si sheet 'grain-oriented', meas. by optical lever method 2–65160
  - Fe-Si sheet Goss oriented rel. to elastic props. 2–53778
  - Fe-(3 wt.%)Si alloy, surface films influence on effectiveness of thermomag. treatment 2–44261
  - $FeBO_3$ single crystals, in mag. field, 77-300°K 2–72175
- **Magnetostriction** continued
  - Li ferrites, effect of Co ions 2–65158
  - Mg ferrites, effect of Co ions 2–65158
  - $MnCr_2S_4$ spinel, rel. to sublattice magnetiz. 2–48073
  - Ni-Cu alloys single crystals, by optical lever method 2–65159
  - Ni-Fe-W high permeability alloy 2–48076
  - Ni film, porous, field depend. 2–72187
  - Ni(100) film, five-const. representation, extended theory of ferromagnetic resonance 2–44264
  - Sn, white, Fermi surface cross sections stress derivatives, oscill. magnetostriction 2–75033
  - Tb-Sc alloys, and magnetostructure energy contribs. 2–68576
  - Tb, rel. to magnon spectra free lattice to frozen lattice transition 2–65141
  - Y garnets, diamagnetically displaced, magneto-elastic bond 2–65161
  - Y garnets, magneto-elastic bonding of Fe^{3+} and Cr^{3+} ions 2–65321
  - $Y_3Fe_5O_{12}$:Co^{2+}, Mn^{3+}, anisotropy and magnetostriction consts. rel. to Co^{2+} and Mn^{3+} ion substitutions 2–75233
  - YIG:Ru, ferrimag. reson. obs. 2–44281
  - YIG:Si^{4+},Ca^{2+}, rel. to mag. field inclination to crystallographic axes at 4.2K, 77K and room temp. obs. 2–84437
  - YIG, meas. by ferromag. reson. 2–72176
  - Zn, Fermi surface stress depend. obs. 2–61194
  - Zn, steady magnetostriction, uniaxial stress depend. 2–81204
- **Magnetothermal effects**
  - *see also Galvanothermomagnetic effects*
  - alloy 79 NM, influence of thermomagnetic treatment on mag. props. 2–72048
  - ferromagnetic visco-plastic fluid, mag. field influence on heat exchange 2–80466
  - ferromagnetics near T_k, heat capacity and magnetocaloric effect 2–72158
  - graphite, Nernst-Ettingshausen effect, coupled Boltzmann equation 2–54243
  - graphite, Nernst-Ettingshausen effect 2–57249
  - group IV-VI chalcogenide, transverse Nernst-Ettingshausen effect, hydrostatic compression effects 2–75159
  - p-InSb, thermomagnetic effects and magnetothermoelectric power detn. 2–72050
  - methane, temp. dependence of Scott thermomagnetic torque 2–46861
  - Nernst thermomagnetic effects, sensitive method of obs. 2–64963
  - polyatomic gas, meas. of thermomagnetic force on thin disc in 30-35°C range 2–43264
  - semiconductor, $A^IB^{III}C^{VI}_2$, rel. to band struct. 2–71886
  - semiconductor, Nernst-Ettingshausen coeff. rel. to nondegeneracy transition at low temps. in strong mag. field 2–71890
  - siderite, thermal decomposition from mag. props. 2–72666
  - Ag-Au(Cd)(In) dilute alloy, Righi-Leduc coeff., 2.5-120 K 2–75050
  - Ag Hall and Righi-Leduc coeffs., 4-125 K, Weidemann-Franz law 2–61224
  - n-Ag_2Te, Maggi-Righi-Leduc effect, rel. to Lorenz number and electron scatt. inelasticity obs. 2–84337
  - Au Hall and Righi-Leduc coeffs., 4-125 K, Weidemann-Franz law 2–61224
  - Bi-Sb alloy, temp., mag. field and cryst. direction depend. 2–75161
  - Bi, phonon drag thermomag. at low temps. 2–54244
  - Bi and Bi-Sb (Ag) alloys, characterization for device appl. 2–59064
  - Cd_3As_2-NiAs eutectic, characterization for device appl. 2–59064
  - Cd_3As_2-NiAs eutectic, Nernst effect and thermal radiation detector fig. of merit 2–54246
  - $CoCl_2[(NH_2)CS]_4$, thermal cond., 0.35-20K, in mag. fields up to 20 kG 2–81302
  - Cu Hall and Righi-Leduc coeffs., 4-125 K, Weidemann-Franz law 2–61224
  - Fe-Ni alloy, Invar, Nernst-Ettingausen effect, 100-300°C 2–72164
  - armco Fe, Nernst-Ettinghausen effect 2–68546
  - HD, temp. dependence of Scott thermomagnetic torque 2–46861
  - In, Righi-Leduc effect, 3.5-8K 2–75163
  - InSb-NiSb eutectic, characterization for device appl. 2–59064
  - Mn-permalloy film, exchange anisotropy, ferromag. to anitoferromag., thermomag. recording 2–57286
  - MnF_2, longit. neutron scatt. behaviour below crit. temp. 2–54362
  - N_2, temp. dependence of Scott thermomagnetic torque 2–46861
  - N_2 gas, kinetic theory of thermomagnetic torque 2–50271
  - NO gas, meas of thermomagnetic force on thin disc in 30-35°C range 2–43264
  - Ni-Co alloy, Nernst-Ettinghausen effect, temp. depend. 2–72051
  - Ni, Nernst-Ettinghausen effect 2–68546
  - O_2 gas, meas. of thermomagnetic force on thin disc in 30-35°C range 2–43264
  - p-PbTe, Nernst-Ettingshausen coeff., rel. to room temp. transport props. 2–54161
  - $Y_3Ga_{1.1}Fe_{3.9}O_{12}$ layer, laser beam thermomagnetic recording 2–51273
- **Magnetrons** *see Electron tubes; Microwave techniques and devices*
- **Magnets**
  - *see also Superconducting magnets*
  - bar, couple depend. on mag. field strength 2–41913
  - complex solenoid with external superconductor 250 kG 2–73517
  - conducting winding, optimization of field uniformity 2–59070
  - cyclotron, model and mag. field obs. 2–79705
  - drag force when moving near a thin conductor 2–78953
  - electromagnet, ANU 30T, testing and performance 2–59075
  - electromagnet, inner solenoid design and construction 2–59074
  - electromagnet, outer solenoid, design and construction 2–59073
  - electromagnets, design principles relating to strength and structure 2–59072
  - hysteresis curve automatic recording apparatus 2–82427
  - impulse, 300 kilograms 2–69855
  - mischmetal-Co permanent magnets, development 2–84406
  - model beam analyzing magnet, field inhomogeneities measurement 2–63722
  - n.m.r. spectrometer electromagnet current stabilizer 2–76424
  - organic, molecular requirements 2–77131
  - particle accelerator, for radiation resistant system 2–82832
  - permanent, computer-aided design 2–73516
  - permanent, permeameters for industrial inspection 2–76442

Magnets continued
- permanent, Recoma, features and applications 2−73515
- permanent, temperature coeff. meas. 2−59061
- permanent, with plane and cylindrical symmetry, field calc. 2−78952
- pole profile determination for weak focusing fields 2−55650
- septum, for beam extraction, construction of hollow current conducting plate 2−70335
- solenoid apparatus for reconstruction 2−63256
- solenoids, equally loaded forceless configuration, comparison of parameters 2−63258
- surface replication, polymeric, modulation by surface mag. and elec. fields 2−64539
- synchrotron, very high field, Fe yokes, saturation and error fields 2−73518
- $CeCo_5$, permanent mag. field 2−52385
- Co-Cu-Fe-Ce, prep. by directional solidification 2−43787
- Co-Cu-Fe-Ce alloy, sintered, prep. and props. 2−50910
- Co-Pr-Sm alloys, 10000 Oe B-coercive force magnet, props. optimization 2−44247
- Fe-Al-Ni-Co-Ti alloy, prod. by Magnicol process 2−43834
- $LaCo_5$, permanent mag. field 2−52385
- $PrCo_5$, permanent mag. field 2−52385
- $PrCo_5$, sintering with Sm-Co additive 2−50797
- $SmCo_5$, permanent mag. field 2−52385
- $SmCo_5$, prod. using single phase sintering aid 2−43795
- YCo_5, permanent mag. field 2−52385

Magnons *see Spin waves*

Magnus effect *see Aerodynamics*

Majorana effect *see Magneto-optical effects*

Majorana forces *see Nuclear forces*

Malter effect *see Electron emission/secondary; Photomultipliers*

Mandelstam representation *see Elementary particles/scattering*

Manganese
- a.c. polarographic det. in $CaCO_3$ 2−48353
- adsorption of CO, change in work function 2−71348
- atom, dissolved in Al, magnetic scatt. of neutrons 2−61474
- atomic, Mn VIII to XV, classification of transitions 2−49948
- cosmic spherules concentration in deep-sea Mn nodules from cores 2−75931
- in Cu and Cu-Al alloys, liq., cond.-electron spin polarization obs. 2−53455
- diffusion in α-Fe, pure and alloyed, 778.3-901°C 2−83994
- diffusion in ZnS single cryst. 2−56764
- film, amorphous, deposition and annealing, resist. study 2−77499
- foils, ultra-cold neutron detection by activation 2−67084
- Invar effect, in α and γ phases 2−57269
- marine nodules, neutron capture gamma ray studies 2−61846
- in marine suspension, microquantities det. 2−54768
- solar abundance determinations 2−55158
- solar overabundance, accelerated by solar flares 2−76001
- AlN:Eu,Mn, radical recomb. luminesc. and photoluminesc. 2−57371
- AlN:Mn, spectrum of luminescence centres 2−75319
- $Ca(OH)_2:Mn^{2+}$, e.p.r., 4.2−800 K, vibronic effects 2−78163
- $CdS_{1-x}Se_x:Mn^{2\cdot}$ hyperfine interaction const., temp. and comp. depend., e.p.r. study 2−81456
- in $CdS_{1-x}Se_x$, Mn^{2+} conc., e.p.r. determ. 2−72481
- in $Cd_{1-x}Zn_xS$, e.p.r. determ. 2−72481
- GaP:Mn, i.r. luminesc. due to $^4T_1 \rightarrow {}^6A_1$ internal transition, dynamic Jahn-Teller effect 2−81424
- GaP:Mn,S, Mn-S nearest neighbour complex, e.s.r. obs. 2−75344
- Ge:Mn, nonlinear IV characts., exclusion and charge exchange between impurity levels 2−75115
- β-$KNO_3:Mn^{2+}$, e.p.r., phonon sidebands 2−72490
- $6MgO.As_2O_5$, Mn activated phosphor, crystal growth 2−43525
- Mn-Permalloy bimetal film, mag. after-effect 2−81224
- α-Mn, antiferromagnet, n.m.r. study 2−61748
- α-Mn, Neel temp. and residual resist., press. depend. 2−54357
- Mn I, e^6D-y^6P multiplet lines, hyperfine structure, solar spectrum 2−48790
- Mn I, relative oscillator strengths, precision obs. 2−55040
- Mn^{2+}, diffusion in NaCl, coeff. meas. using e.p.r. 2−50700
- Mn^{2+}, in CaO or MgO, spin-lattice coeffs., relativistic cryst. field contrib. 2−65203
- Mn^{2+}, in chalcogenide glass, e.p.r., fine struct. 2−72476
- Mn^{2+}, in cubic antiferrodielectric, admixture of $^4T_{1g}$ state to $^6A_{1g}(^6S)$ state 2−65202
- Mn^{2+}, in K_2ZnF_4, e.s.r., spin Hamiltonian parameters detn. 2−65323
- Mn^{2+}, in MgF_2, impurity-ion spin-forbidden absorpt. enhancement by colour centres 2−78104
- Mn^{2+}, Jahn-Teller effect in $RbMnF_3$, spectrum uniaxial stress effects, obs. 2−65267
- Mn^{2+}, Jahn-Teller effect in $RbMnF_3$, spectrum uniaxial stress effects, obs. 2−65268
- Mn^{2+} e.p.r. linewidth in MgO, temp. depend. 2−48289
- Mn^{2+} e.s.r. in TlN_3, spin Hamiltonian parameters, temp. depend. 2−72502
- Mn^{2+} in $Ca_5(PO_4)_3Cl$, e.p.r. obs., site substitution by Mn, field parameters 2−72479
- Mn^{2+} in LiF, low-field X-band e.p.r. transitions 2−72492
- Mn^{2+} in lunar plagioclases, e.p.r. obs. 2−62686
- Mn^{2+} in Sr fluorophosphate, optical excitation and fluoresc. spectra 2−81421
- Mn^{2+} localization in low symmetry crysts. 2−84288
- Mn^{3+} complexes, octahedral, paramagnetic susceptibilities for all crystal field strengths 2−61484
- Mn^{4+}, in $CaO:Li^+,Na^+$, e.p.r., spin Hamiltonian parameters detn. 2−51402
- MnI, mag. dipolar h.f.s. of e^6D-y^6P multiplet 2−79894
- inNaCl, vacancy-impurity complex, slow motion press. effects, n.m.r. study 2−72514
- SrS:Mn, Zr phosphors decay study 2−75330
- TiO_2:Li,V,Cr,Mn,Fe, transition metal impurity levels, esr determ. 2−44117
- $Y_3Fe_5O_{12}:Co^{2+}$, Mn^{3+}, anisotropy and magnetostriction consts. rel. to Co^{2+} and Mn^{3+} ion substitutions 2−75233

Manganese continued
- ZnS:Ag,Mn,Cl phosphors, mechanism of activator interactions 2−84551
- $ZnS:Mn^{2+}$, ^4E level, uniaxial stress effects, absorpt. study 2−84506
- ZnSe:Mn, luminesc. enhancement by electric fields in polycryst. and crystalline samples 2−48249
- Zn_2SiO_4:Mn, thermoluminesc., glow curves, impurity depend. 2−48258
- $Zn_2SiO_4:Mn^{2+}$, willemite, cathodoluminesc., electron microprobe obs. 2−51382

Manganese compounds
- — 2−67956
- chemical bonding study using X-ray photoelectron spectroscopy 2−53002
- dilute liquid alloy, Mn in Cu, CuZn, Zn, ZnGa, Ga, GaGe, GeAs, As, mag. susceptibility 2−80485
- ferrite, Kerr effect and optical consts., magnetooptical reson. in visible 2−81337
- ferromanganese nodules, thermomagnetic behaviour 2−58142
- formate, mag. phase transitions 2−44293
- formate dihydrate, mag. diagram of state, spin-flop transition 2−68577
- oxides, adsorption of chemically nonrequirement O atoms (ions) 2−47167
- spinel, domain structure formation due to atomic displacements 2−68021
- $[Mn(H_2O)_6]^{2+}$ complex, approx. SCF calc. with minimal basis set 2−56185
- Ag-Mn-Al alloy, high coercivity, struct. of ferromag. precip. 2−43821
- Ag-Mn dilute alloys, s-d exchange interaction constant from electrical resistivity measurements 2−44214
- Al-Cr solid solution, high supersaturated, range extension in equilibrium diagram when cooled 2−43824
- Al-Cu-Mg-Mn alloy, mosaic angle and dislocation density, tensile deform. depend. 2−80772
- Al-(N at.%) Mg, N=10, 8, age hardening and related properties 2−47612
- Al-Mn alloy, dil., neutron scatt. by spin fluctuations 2−61473
- Al-Mn alloy, structural features of a plane strip obtained directly from melt by Stepanov method 2−50821
- Al-Mn dil. alloys, high temp. impurity resist. 2−44050
- Al-Mn dilute alloys impurity resistivity, temp. dependence 2−84278
- Al-(1.8 wt.%)Mn, decomp. products47615 2−47615
- Al-(1.8 wt.%)Mn alloy, decomp. products 2−47615
- Al-Zn-Mg-Cu-Mn forging alloy, fracture toughness rel. to microstructure 2−53826
- AlMn, impurity resistivity, 4-200K 2−68337
- AlMn, supercond transition temp., 0-20 kbar press. 2−47870
- Au-Mn dilute alloys, deviation from Matthiessen's rule, 0.5-60 K 2−77854
- Co-Mn-Al system, decomp. studies 2−64816
- Co-Mn dilute alloy, n.m.r. and nuclear relaxation study of satellite lines 2−44454
- Cu-Al-Mn alloys, martensitic transform., interphase boundary shifting 2−43910
- Cu-Mn alloy, thermo-e.m.f., 4.2-250K 2−57250
- Cu-Mn dil. alloys, neck effect in ang. correl. of positron annihilation 2−44046
- Cu-Mn dilute alloy, thin film, e.s.r. study 2−44446
- Cu-Ni-Mn, dilute soln., resist., magnetoresist., Z-100K, Kondo effect 2−47835
- Cu-Ni-Mn alloy, order-disorder transform., resist. and thermopower study 2−54001
- Cu-Zn-Mn system, phase diagram 2−50963
- Fe-Cr-Mn system, phase boundary $\alpha+\gamma/\gamma$ determ. 2−84164
- Fe-Mn-C alloy, long period stacking order structure formed by thermal cycling 2−67990
- Fe-Mn-C alloy, orientation relationship of the (225) martensitic transform. 2−74928
- Fe-Mn-Ni system using semihard magnetic alloys 2−84407
- Fe-Mn-O system, activities, calc. by Darken's method 2−43815
- Fe-Mn-Ti alloys, ferritic and martensitic, hardening 2−47592
- Fe-Mn-(B)-C, struct. and strength 2−56941
- Fe-(30 wt.%)Mn alloy, austenitic, strengthening by shock loading 43841 2−43841
- Fe-Mn alloy, austenitic, singularities of hardening 2−50783
- Fe-Mn alloy, b.c.c., shock deformed, recovery 2−56912
- Fe-Mn alloy, field ion microscopy exam. comparing orientation to ferrite α and iron nitride 2−64777
- Fe-Mn alloy, kinetics of manganese-wustite scale formation 2−48333
- Fe-Mn alloys, $\gamma \rightleftharpoons \varepsilon$ transformations, austenite stabilisation, effect of interstitials and substitutional atoms 2−71682
- Fe-Mn and Fe-Mn-C alloys, martensitic transformations and temp. conc. boundaries 2−71683
- Fe-Mn system, b.c.c. martensite growth 2−64591
- Fe-Ni-Mn martensitic alloys, reversion behaviour 2−77747
- $(Fe,Mn)_2Mo_3O_8$, Mossbauer effect 2−75270
- Fe_xO-MnO solid solns., optical props. 2−48174
- Fe_2SiO_4-Mn_2SiO_4 phase diagram and ideal soln. behaviour 2−50852
- Ge-Mn-Te alloy, degenerate semicond., e.s.r. obs. 2−48273
- $Li_{0.45}Mn_xFe_{2.55-x}O_4$, anisotropy contrib. of Mn^{3+} and related directional orders 2−65170
- $M_2K_2(SO_4)_22H_2O$ crystal struct. determ. 2−77545
- $MdPd_3$, mag. struct. from neutron diffr. obs. 2−54360
- Mg-Mn, Mg-Th-Mn alloys, precipitation processes, elec. microscope obs. 2−53993
- Mg-Mn alloy, e.p.r., relaxation bottleneck theory applied 2−44438
- Mg-Mn ferrite film, transparent, light diffr. by mag. stripe domains 2−65220
- Mg-Mn ferrites, electronic struct. of Mn and Fe ions 2−47182
- Mg-Zn-misch metal alloy, struct. 2−50624
- Mn-Zn ferrites single crystal, signal processing technique to obtain Kerr effect M-H loops 2−48064
- Mn-Al-Cu-Mg-Fe-Si-Ni-Zr-Ti, alloy, D16T, recryst. and uncryst. struct., fracture under static and cyclic conditions 2−47527
- Mn-Al-Cu alloy, heat treatment, homogenization, precip. 2−43786
- Mn-Al-Ge alloy, domain structure and nucleation centres 2−68550

Manganese compounds continued
- Mn-Al-Mg-Fe-Cu-Si alloy, AK6, ageing, temp.- time ranges 2–50802
- Mn-Al-Zn-Mg alloy, strength rel. to rest between quenching and ageing, effect of additions 2–50803
- Mn-Al alloy, mag. props., effect of $\varepsilon \rightarrow \tau$ transform. 2–57280
- Mn-Al alloy, τ phase, microstruct. 2–50838
- Mn-Bi alloy, hysteresis, domain structure and nucleation centres 2–68550
- Mn-Bi films, intermediate cpds., polarization microscope images 2–57301
- Mn-Cr-Fe alloy, α-γ phase equilib., effect of transition metal-additions 2–47687
- Mn-Cu-Al alloy, spinodal, interphase interfaces, interfacial dislocations 2–56719
- Mn-Cu-Mo alloy, cold worked, heat treated, Young's modulus, rigidity, hardness, thermal expansion 2–47476
- Mn-Cu-W alloy, cold worked, heat treated, Young's modulus, rigidity, hardness, thermal expansion 2–47477
- Mn-Cu alloys, short range ordering, neutron diffraction observations 2–71644
- Mn-Fe-Ni alloy, isothermal martensitic transform. rel. to mag. field 2–50937
- Mn-Fe-Ti-O system ferrites, mag. props. and crystallochem. 2–44254
- Mn-Ga alloys, internal friction 2–50735
- Mn-Mg-Fe ferrite film, flash evaporated, chem. comp., X-ray fluoresc. obs. 2–71331
- Mn-Permalloy film, coercivity, influence of driving field 2–81278
- Mn-Zn-Fe ferrite, permeability, thermal change, resonance type profiles 2–61545
- Mn-Zn ferrite powders, comp. effects on technological props. 2–68163
- Mn-Zn system, phase diagram, X-ray and magnetic obs. 2–57032
- Mn-permalloy film, exchange anisotropy, thermomag. recording 2–57286
- $(Mn, Fe)_3O_4$, i.r. absorp. and cation distrib. 2–61648
- Mn (II), complex, tris(octamethylpyrophosphoramide) manganese (II) perchlorate, h.f. splitting parameter 2–81513
- Mn $(NH_4)_2(SO_4)_2.6H_2O$ paramagnetic salt temperature scale for 0.9 to 18 K range 2–55586
- Mn complex, $(CH_3)_4NMnCl_3$, direct process n.m.r. relaxation by spin waves in one dimensional antiferromagnet 2–51414
- Mn complex, di-μ-oxo-tetrakis(2,2′-bipyridine)dimanganese(III,IV) perchlorate trihydrate, antiferromagnet, superexchange coupling 2–44303
- Mn complex, Mn-amine, exchange interactions, mag. susceptibility 2–65124
- Mn phosphate glass, mag. props. and structure 2–57292
- MnAl, supercond. transition temp., 0-20 kbar press. 2–47870
- MnAlGe, ferromagnetic, n.m.r. studies 2–84586
- MnAs, first-order transition, demonstration experiment 2–61476
- MnAs whiskers, phase boundary motion at coupled lattice- and spin-disorder transition, resist study 2–78021
- Mn_2As, high press. form., struct., antiferromag. props. 2–53670
- Mn_3As_2, MnAs, Mn_2Sb, e.s.r. and thermomagnetic meas. rel. to determination of Lande factor 2–51411
- $MnAu_2$, mag. reson., microwave absorpt. obs. 2–65318
- $MnAu_2$, spiral phase, mag. reson., 20-26 GHz 2–44429
- MnB_2, mag. struct. 2–44306
- MnB_2, weak ferromagnetism, s-d exchange model 2–81257
- MnBi film, prep., props., domain struct. 2–44263
- MnBi film, struct. and orientation, electron microscope and diffr. obs. 2–47119
- MnBi films, Ti-substitution effect on struct., mag. and magneto-optic props. 2–51265
- MnBi thin films, preparation by Williams method effects of residual gas pressure, evaporation rate on magnetization 2–68560
- $MnBi_{(1-x)}Te$ thin films magneto-optical props. 2–72264
- $MnBr_2.4H_2O$, adiabatic magnetiz., mag. phase diagram detn. 2–65115
- $MnBr_2.4H_2O$, proton spin-lattice relax. time, 1.12–4.18 K 2–78050
- Mn_6C mixture with VC, X-ray analysis 2–44506
- $Mn(CO)_5$-X_3M adducts, single crystals, ^{55}Mn broad-line n.m.r. at room temp. 2–68747
- $MnCO_3$, polycrystalline, elastic props. to 10 kbars 2–65573
- $Mn_2(CO)_{10}$ single crystal, broadline n.m.r., quadrupole coupling and anisotropic chemical shift 2–57397
- $Mn(CO)_5H$ and $Mn(CO)_5CH_3$ photoelectron spectra, ab initio SCF MO calcs. of electronic structure 2–70713
- $Mn(CO)_4NO$ complex, i.r. spectra meas. in vapour phase and in solution, assignment of structure and fundamental modes 2–42909
- $MnCl_2$-ACl, where A = Li, Na, K and Cs, e.m.f. meas. and detn. of thermodynamic props. 2–77787
- $MnCl_2$, X-ray Kβ emission and K absorpt. spectra 2–65287
- $MnCl_2$ molecular beam, effect on vaporization rate of KCl 2–71281
- $MnCo_3$, antiferromag. and nucl. mag. reson. freq. shift phenomena 2–81482
- $Mn_{1-x}Co_xF_2$, spin waves theory and coherent potl. approx. applic. to mag. excitations 2–78044
- $MnCoP_4$, high-press. synthesis and props. 2–83899
- $MnCr_2S_4$ spinel, sublattice magnetiz. and magnetostrictive effects 2–48073
- $Mn_{1-x}Cr_xSb$, hyperfine fields, ^{55}Mn n.m.r. and ^{121}Sb mossbauer obs. 2–54514
- $Mn_{1-x}Cr_xSb$ films, ferromag. reson. 2–72450
- $Mn_{1.92}Cr_{0.08}Sb$, mag. domain patterns, Bitter pattern technique obs. 2–65148
- MnF_2:Fe^{2+}, exchange field obs. under press. 2–44304
- MnF_2:Fe^{2+}, exchange polariz. in superexchange interactions, far i.r. obs. 2–81297
- MnF_2, antiferromag. reson. linewidth 2–81443
- MnF_2, antiferromag. resonance, fundamental relax. mechanisms, linewidth obs. 2–51398
- MnF_2, covalency parameters 2–77057
- MnF_2, critical neutron scatt., spin fluctuations 2–54361
- MnF_2, e.p.r. linewidth, crit. point anomalies 2–78159

Manganese compounds continued
- MnF_2, e.p.r. linewidth, crit. point anomaly, role of anisotropy 2–78165
- MnF_2, exchange polariz. in superexchange interactions, far i.r. obs. 2–81297
- MnF_2, longit. neutron scatt. behaviour below crit. temp. 2–54362
- MnF_2, mag. hyperfine interactions of Fe^{2+} interpret. 2–61604
- MnF_2, magnon sideband intensity 2–61647
- MnF_2, principal susceptibilities, calc. using Heisenberg model 2–65172
- MnF_2, temp. depend. oscill. strengths of optical absorp. 2–54428
- MnF_2, two-magnon absorpt., spin-flop transition effects 2–54358
- MnF_2, two-magnon Raman scatt., temp. depend., calc. 2–81304
- MnF_2, two exciton transition, temp. depend. intensity calc. 2–61654
- MnF_2, zero field circular dichroism, uniaxial stress depend. 2–44376
- MnF_6^{-2}, molecular constants calc. 2–46559
- MnF_6^{2-}, force constants and generalised mean amplitude of vibration calc. using seven parameter Urey-Bradley force 2–60013
- $MnFe_2O_4$, acoustic magnon dispersion, neutron diffr. obs. 2–61544
- $MnFe_2O_4$, ferrite, single cryst. film, spin wave resonance 2–72454
- $MnFe_2O_4$, reson. phenomena at moving domain boundaries 2–72456
- $Mn_xFe_{3-x}O_4$, ferromag. reson., 77-350K, 9.3 GHz 2–44430
- $Mn_xFe_{3-x}O_4$ Jahn-Teller domains, electron microscope obs. 2–43922
- MnGaGe, ferromag. props. 2–72168
- $MnGeO_3$, magnetoelec. signal near critical field for spin flop 2–44305
- $Mn_xHg_{1-x}Te$ films, Hall coeff., Hall mobility and electrical condutivity 2–71885
- Mn(I) complex, $K_5[Mn(CN)_6]$, vibr. spectra and force consts. 2–77074
- Mn(II) complex, tetrahalogenomangonates, structure obs. in diffuse reflectance and phosphorescence excitation spectra at 77K 2–67488
- Mn(II) complexes, octahedral, halogen-bridged, Raman and far i.r. spectra 2–46558
- Mn(III) dithiocarbamates diluted in Co(III) analogues, e.s.r. studies 2–48281
- $MnKH(SO_4)_2.2H_2O$, Zeeman decomp. of visible absorpt. lines 2–54427
- $Mn_xMg_{1-x}Al_2O_4$ spinel, e.s.r. parameters 2–48290
- MnN_x, hexagonal, magnetic and Mossbauer obs. 2–54331
- $Mn(NH_4)_2(SO_4)_2.6H_2O$ paramag. relax. times meas. 2–84455
- $Mn(NO_3)_2$ aqueous solutions, e.s.r. 2–71233
- $MnNb_2O_6$, antiferromag. ordering., magnetoelectric and susceptibility obs. 2–65184
- $Mn_4Nb(Ta)_2O_9$, magnetoelectric effect and Neel temp. determ. 2–54359
- MnO:Li, electro-transmission in visible and near i.r. charge carrier obs. 2–51323
- MnO-MgO, dense solid soln., preparation for testing 2–74907
- Mn_xO-MgO system, interdiffusion 2–50714
- MnO-TiO alloy, synthesis, struct., density, elec. cond., mag. susceptibility, thermal e.m.f. 2–74908
- MnO, antiferromag. ordering, exchange consts. calc. 2–61549
- MnO, antiferromag. reson 2–72463
- MnO, band struct., refl. and thermorefl. study 2–84505
- MnO, Compton profiles, electron momentum distrib. 2–78116
- MnO, dispersion props., three body force shell model 2–61078
- MnO, elastic constants and acoustic absorption coefficients 2–43971
- MnO, exchange polariz. in superexchange interactions, far i.r. obs. 2–81297
- MnO, point defects, thermodynamic analysis, migration processes 2–56684
- MnO, positron lifetime spectra, rel. to cond. and nonstoichiometry 2–71825
- MnO, spin waves, inelastic neutron scatt. obs. 2–61558
- MnO_2 deposition in marine environment, pressure effects 2–54620
- MnO_{4}-, resonance Raman spectra, analysis of ν_1 breathing mode 2–50054
- MnO_4^-, ground states, SCF-MO calcs. and X-ray spectroscopy 2–77095
- MnO_4^-, valence region X-ray photoelectron spectra, energy spread of ioniz. pots. 2–80004
- Mn_3O_4, flux growth 2–60717
- MnO(S), e.p.r. linewidth, crit. point anomalies 2–78159
- MnP, mag. susceptibility and transitions, press. effects 2–48072
- $Mn_2(PO_4)Cl$, cryst. struct. 2–67997
- $Mn_2(PO_4)F$, cryst. struct. 2–67998
- Mn_3Pd_5 phase, crystal and magnetic struct. 2–83960
- α- MnS, antiferromag. ordering, exchange consts. calc. 2–61549
- MnS, α-, β- and δ-forms, Kβ emission and K absorpt. spectra 2–51358
- MnS, photocond. spectrum, room temp. 2–68480
- α-MnS from sulphurization of Mn in H_2S-H_2 gas mixtures at 550° to 711°C, elec. cond. and thermoelec. power, obs. 2–75079
- MnS inclusion size, in steel, effect of solidification rate and S content 2–43852
- MnSb-(Sb,Bi) and MnSb-(Sb,Sn) eutectics, morphology, growth rate effects 2–47641
- MnSb, internal mag. fields, n.m.r. obs. 2–54513
- MnSi, elec. cond., thermal e.m.f.. and Hall coeff. detn. 2–77797
- Mn_5Si_3, noncollinear antiferromag.-collinear antiferromag.-paramag. transition 2–78042
- MnTe, cryst. growth from nonstoichiometric melts by liq. encapsulation 2–50598
- MnTe, mag. semicond., thermopower, magnon drag effect 2–54165
- $Mn_{0.8}Ti_{0.2}Bi$ film, Curie-temp. writing 2–78032
- $MnWO_4$, flux growth 2–60717
- $(Mn_{1-c}Zn_c)F_2$, i.r. absorption meas. 2–65261
- $(Mn_{1-c}Zn_c)F_2$, two-magnon Raman scattering meas. 2–65261
- $Mn_{1-x}Zn_xFe_2O_4$, mag. order obs. 2–65168
- $Mn_{1-x}Zn_xFe_2O_4$, mag. order 2–78022
- Ni-Cu-Mn alloy, mag. props. 2–78025
- Ni-Mn system, Ni_3Mn ordered alloy, 4-s band struct. perturbation calc. 2–71801
- $Ni_3(Mn,Co)$ and $Ni_3(Mn,Fe)$ alloys, electron and hole mobility obs. 2–47837

Manganese compounds continued
  $Ni_{0.6}Mn_{2.4}O_4$, elec.-field-depend. cond. for hopping-type charge transport 2−81082
  Pb-Mn alloy, sp. ht., 0-300°C, determ. by monotonic heating method 2−51046
  Pb-Mn superconducting films, tunnelling conductance curves 2−71851
  Pd-Mn, dil. alloys, mag. ordering obs. 2−81246
  Pd-Mn dil. alloys, giant moment of Mn 2−44257
  Rh-Mn-Sb system, Cl_b type alloy, mag. props. and cryst. struct. 2−65156
  Sn-Mn alloy film, mag. state of Mn rel. to supercond. 2−68512
  Zn-Mn alloy, dilute, elec. resist., $T<0.1K$ 2−68342
  Zn-Mn dilute alloy, Kondo effect and localized spin fluctuations 2−64918
  Zn-Mn Kondo alloys, supercond. below 0.1K 2−44082
  $(Zn, Mn, Fe)Ti_3O_7$, landauite, Baumhauer type twins 2−71499
Manometers
  see also Vacuum gauges
  catheter manometer systems, compensation amplifier 2−51896
  column height, sonic obs. 2−45226
  compression, error due to nature of scale 2−45223
  differential, using tensometer, 100-300 bar, accuracy of 50-2000 mbar 2−55372
  differential manometer gas flowmeter with automatic pressure and temp. correction 2−71079
  Knudsen absolute manometer, modified, kinetic theory 2−76127
  for liquids and gases pressure meas. 2−66410
  volume change of springs, calc. 2−55371
Many-body problems
  − 2−72966
  − 2−72964
  area-preserving mapping, stability 2−62455
  atomic response, statistical formulation 2−70600
  book, applic. to nuclear physics, liquid helium, neutron matter and superconductors 2−82240
  in celestial mechanics, collision singularitiy in perturbed N-body problem 2−62454
  charged particle interactions 2−79462
  classical action-at-a-distance electrodynamics, straight-line motion 2−55655
  classical gas, dynamical correlation function, first order perturbation calculation 2−43258
  classical systems, decay of order 2−52096
  classical systems, decay of order 2−52095
  classical three-body problem, symmetries, Lagrangian and Euler eqns. 2−82285
  clusters of galaxies, qualitative behaviour 2−58233
  correlation decay, necessary and sufficient conditions 2−41544
  critical inclinations and eccentricities in N-planet problems 2−85033
  depolarization of light by simple gases, contrib. of many-body effects 2−53338
  entropy density of large system at low temperatures, lower limits 2−55429
  equinoctial orbit elements for two-body problem 2−62452
  four and five body systems, dynamics, equations of motion, stability 2−58260
  gas of hard spheres, three-particle collision integrals 2−46851
  Gaussian unitary and orthogonal ensembles, probabilities for eigenvalues of random matrix 2−58801
  hadron interactions, review 2−82719
  hard particle system, Percus-Yevick equation rel. to functional equations in fluid theory 2−43046
  hyperbolic two-body problem, (E, r, α, β) summability 2−84934
  large-scale cosmic systems with variable gravitational constant, dynamical consequences 2−81769
  mass effects in three-body problem, orbital parameters 2−84937
  momentum autocorrelation functions of noninteracting particles in box 2−49038
  N-body, applic. of orthogonal and unitary group methods, review 2−58804
  N-body systems, continuum bound states and quantum mechanical virial theorem 2−41542
  non-relativistic N-body problem, group theoretic approach 2−52070
  non-rigid bodies system, translational dynamical equations for relative motion 2−69632
  nonuniform system under external pot., canonical enemble limit 2−58786
  nuclear, collective motions and single particle models 2−52719
  nucleus, c.m. spuriosity effects on charge form factor 2−67145
  one-dimensional system of three particles with pairwise interaction, solution of Faddeev equations 2−41543
  parallel hard squares, comparison of two simple theories with molecular dynamics 2−52105
  planar three-body problem, regularization of binary collisions 2−81758
  quantum, time-delayed correlation functions of X-Y model 2−81269
  quantum electrodynamics, mass spectrum in pure Coulomb field 2−49471
  quantum-mechanical description of many-particle reactions 2−82273
  relativistic interacting particle system, asymptotic limit for speed of sound 2−66429
  relativistic quantum theory, Riemannian space-time, applic. to superdense matter 2−66447
  restricted four body problem, revolution around smallest primary 2−41556
  restricted four body problem, sphere of interaction 2−68996
  restricted three body, periodic perturbation of libration points 2−78427
  restricted three body problem, periodic librations 2−58168
  restricted three-body problem, computational aspects of asymptotic matching 2−48655
  retarded van der Waals forces between macroscopic particles, theory and exptl. evidence 2−58803
  Schrodinger algebra realization rel. to canonical variables of N-particles 2−63006
  Schrodinger Hamiltonians with weak pots., asymptotic completeness 2−58749
  Schrodinger operators with permutation and rotation symmetries, spectral theory 2−73318
Many-body problems continued
  single close encounters in three-body problem rel. to planetary problem 2−81759
  soft sphere fluid, inverse-12 potential, radial distribution functions 2−49039
  stability of systems with singular potentials 2−49013
  star-Sun-comet system using restricted hyperbolic three-body problem 2−85032
  stellar encounters, new treatment in computation of N-body systems 2−58170
  thermodynamics, exact dynamical basis for fluctuating cell model 2−63038
  three, collision and regularisation 2−81775
  three, general problem, stability of solns. 2−55432
  three, hyperbolic-elliptic motion 2−81776
  three, joined by elastic cables, rotation stability 2−73337
  three, numerical integration 2−81777
  three, numerical solns., low thrust outer planet orbiter 2−54992
  three, potential harmonics 2−67119
  three bodies, three dimensional restricted problem, periodic solutions 2−51696
  three body break-up processes, Kohn variational principle 2−41516
  three body problem, improved criteria for hyperbolic elliptic motion 2−66046
  three body problem treated by path integral approach of Feynman 2−41509
  three body quantum mechanical problem, approximate solutions 2−52081
  three body restricted problem, periodic orbits of collision 2−49054
  three-body, path integration 2−52109
  three-body cluster energy in nuclear matter 2−82858
  three-body D-function, new parameterization 2−49012
  three-body problem, class of high energy close approach trajectories 2−48659
  three-body problem, new form of differential equations of relative motion of planets 2−81756
  three-body problem in 1-d, with interacting, impenetrable particles 2−82228
  three-nucleon problem, two-term nonlocal separable potentials 2−82845
  triple gravitational systems, evolution, termination of binary 2−58175
  triple star systems, stability criteria 2−58169
  triple systems, binary formation 2−51775
  two, finite, common and individual rotation 2−81780
  two-body systems in fast motion, wave functions 2−82215
Many-particle systems *see Statistical mechanics/quantum*
Markov processes *see Statistical analysis*
Mars
  1971 opposition, photographic observations at six wavelengths 2−75889
  − 2−73090
  activity, reappraisal from Mariner 4 data 2−62700
  aeolian deposition of dust, Mariner 9 photographs 2−66176
  aeronomy of CO_2 atmospheres rel. to Mars and Venus 2−73075
  atmosphere, chem. dynamic model 2−85046
  atmosphere, CO_2 emission behaviour 2−77303
  atmosphere, determ. of water vapour and minor constituents using i.r. spectral data 2−78541
  atmosphere, effect of dust on temperature 2−48775
  atmosphere, Mariner 9 radio occultation meas. 2−58504
  atmosphere, minor constituents, Mariner borne i.r. spectrometer 2−69156
  atmosphere, minor constituents, u.v. spectroscopy from Orbiting Astronomical Observatory 2−69140
  atmosphere, OI 1304 Å emission, Mariner 9 obs. 2−58505
  atmosphere, sterilization probability for small particles 2−62701
  atmosphere, thermal probing by spectral dependence of thermal radiation 2−75906
  atmosphere, thermal structure from Mariner 9 i.r. spectroscopy expt. 2−75898
  atmosphere, upper, implications of $CO(A^1\Pi)$ 2−56164
  atmosphere radiative transfer, use of dimensionless parameter 2−44946
  atmosphere radiative transfer by CO_2 2−65770
  atmosphere-polar cap, numerical simulation of radiative-conductive heating 2−69150
  atmospheric structure meas. during Viking lander entry phase 2−75891
  bistatic radar measurements of surface, oblique reflection from Mariner 2−69151
  bistatic radar occultation experiment rel. to spherical symmetry of model atmosphere 2−48776
  chaotic terrain, tectonic interpret. from Mariner 6 imagery 2−58500
  circular polarization spectrum 2−81910
  colouring of Martian surface rel. to laboratory studies $(C_3O_2)n$ polymer 2−78542
  control net from Mariner 6 and 7 pictures, coordinates of features 2−75887
  crater circularity, radius deviation 2−85039
  craters, origin studies using Mount Etna and Stromboli geologic and photoballistic obs. 2−81567
  craters, regional variations in degradation and density 2−66181
  crust rel. to Earth and lunar crusts, three-dimensional model 2−81917
  crustal evolution from spacecraft investigations of geomorphology and composition 2−78507
  Deimos, dynamical characteristics, review 2−62703
  Deimos, orbit determ. from Mariner IX data 2−78489
  Deimos, polarization obs. in blue light 2−58493
  Deimos satellite, ground-based studies about surface properties 2−58501
  discrete white clouds, diurnal and seasonal behaviour 2−69152
  doublet crater simulation studies 2−69159
  doublet craters, Monte Carlo simulation model, origins 2−66180
  dust areas, estimate of their position when Viking landers arrive 2−81920
  dust storm of 1971, photographs 2−55149
  dust storms, CO_2 absorption obs. at 10500 Å 2−81918
  electron temp. in ionosphere 2−55146

Mars continued
evolution of atmosphere and surface temperature 2−73083
exosphere, H_2O and CO_2 outgassing role in evolution 2−58507
exosphere, He loss, thermal and non-thermal loss mechanisms 2−58509
exploration beyond Viking 1975 project 2−78543
exploring observatories 2−58495
far u.v. emission spectra and features of Venus rel. to Mars 2−78566
geological features survey 2−62699
gravity field, from Mariner 9 tracking data 2−75904
gravity field from Mariner 9 tracking data 2−58499
gravity simulator for Viking landing tests 2−78420
ground-atmosphere thermal boundary layer structure, transient variation 2−66175
Hellas and cratered terrain, transition zone, relative age 2−48773
integral radiation during opposition of 1971, radio temperature of soil 2−44949
internal constitution, models 2−66179
ionosphere, effective collision freq., h.f. cond. and complex refr. index calc. 2−51828
ionosphere, model, two-freq. bistatic-radar occultation expt., spherical symmetry departures influence 2−58510
i.r. emission spectra, 5-50 μ range 2−75897
i.r. spectroscopy from Mariner 9, temp. profiles of Southern Hemisphere 2−75905
landing sites, photogrammetric mapping 2−55144
life forms research, Viking project, space craft instrumentation 2−75647
lineament systems, analysis of photographs of Mariners 4, 6, and 7 2−55148
lineament systems from Mariner 4,6,and 7 photographs 2−81915
map, by Mariner 9 2−69158
Mariner 1969 mission, tracking and data system support 2−72941
Mariner 1969 mission, tracking and data systems support 2−72942
Mariner 1969 obs., review 2−44954
Mariner 7 u.v. spectrometer expt., topographic slopes of south polar region 2−69155
Mariner 9 encounter 2−58494
Mariner 9 Mars TV experiment, observations and results 2−75892
Mariner 9 mission, scientific objectives rel. to Mariner Mars 1971 Project 2−75645
Mariner 9 obs. 2−48777
Mariner 9 obs. 2−55143
Mariner 9 photographs 2−66177
Mariner 9 photographs results 2−48772
Mariner IX, electronic 'Brownie' 2−58476
Mariner Mars, 1971, preliminary geologic results 2−81940
Mariner orbiter mission (1971), i.r. radiometer experiment 2−85076
micrometer thermal emission, Mariner 9 i.r. radiometer obs. 2−75900
Mountains of Mitchel, location and nature from Mariner 7 pictures 2−69154
north polar cap, annual heat balance 2−73084
north polar region, O_3 absorption 2−75896
Phobos, dynamical characteristics, review 2−62703
Phobos, orbit determ. from Mariner IX data 2−78489
Phobos and Deimos, space missions for exploration 2−78528
photographic positional observations with Pulkovo short focus double astrograph 2−48774
photometric props., effect of surface roughness 2−44951
photometry and topography, u.v. spectral obs. 2−44950
planetology congress (Montreal, September, 1972) 2−78499
plasma exprts. of Mars 2 and 3 probes 2−78554
polar cap formation rel. to CO_2 and H_2O ice layers 2−81931
polar cap seasonal change during early period of 1971 apparition 2−78505
radar observations during 1971 opposition, elevation profiles and crater depths 2−78506
radiative-dynamical model for static stability of rotating atmospheres 2−58480
radio occultation meas. with Mariners 6 and 7 2−48767
regional contrasts in 1971 rel. ~~to~~ 1969, visibility of albedo features 2−81916
remote exploration, Viking lander spacecraft camera system, design 2−85077
rough surface, circular polarization of scattered light 2−63395
satellite debris, dust belt formation 2−78490
simulation samples, size classification 2−69160
Sinus Meridiani and South Polar charts from Mariner 6 and 7 wide-angle pictures 2−44953
soil analytical instrumentation of Viking spacecraft for life detection 2−54977
soil gas chromatography/mass spectrometry for life detection by Viking spacecraft 2−55147
solar wind flow past planet, ionospheric interaction 2−78574
solid surface and atm. shape obs. from occultation expts. 2−75903
south polar cap, u.v. reflectance and 1971 dust cloud 2−75895
south polar region, Mariner 9 pictures analysis 2−62704
south pole, orthographic photomap from Mariner 7 2−69153
spacecraft observations, Mariner 9, Mars 2 and Mars 3 2−44947
spectrum between 8 and 13 microns 2−62702
spin axis direction rel. to Earth equator of 1950 from Mariner IX data 2−81921
surface, eolian processes as crater degradation mechanism 2−81913
surface and atmosphere study by Soviet probes 2−73082
surface brightness temp., Marinery 9 i.r. radiometer obs. 2−75901
surface colour rel. to basaltic magnetite oxidation to red haematite 2−78546
surface comp., atmospheric thermal struct. and topography 2−58503
surface emission and aerosol emission and transmission effects in i.r. spectra 2−78547
surface features during 1971 opposition, photometric observations 2−78545
surface features from local colour var. using Mariner Mars '69 multispectral TV pictures 2−81941
surface materials, mid i.r. remote sensing of composition 2−58492
surface materials, spectrophotometric obs. of photometric function, composition and distribution 2−66182
surface materials rel. to i.r. spectrophotometric mapping 2−78544

Mars continued
surface pressure and topographic mapping from i.r. spectral obs. 2−75899
surface variable features, Mariner 9 obs. 2−58496
Syrtis Major, 1971 variation in contrast 2−75886
Syrtis Major blue clearing phenomenon 2−44952
teaching paper, features explained in terms of elementary physics 2−78714
telescopic observations, August to September 1971 2−44948
temperature conditions in top surface layer during 1971 opposition 2−73081
thermal emission, Mariner 9 i.r. radiometer obs. 2−58498
thermosphere, emission spectrum and altitude depend., response to solar activity 2−58502
thermosphere comp. maintenance by large-scale circulation 2−58508
topographical variations, data preparations from direct radar ranging and CO_2 spectroscopy 2−51827
topography, contour map 2−81911
topography, effect on baroclinic instability 2−85037
topography and atm. obs. using Mariner 9 radio occultation data. 2−75902
topography and photometry, Mariner 9 u.v. spectrometer expt. 2−58497
upper atm. structure, temp. and composition 2−75894
upper atmosphere, CO Cameron band emission, electron impact dissociation of CO_2 2−64117
u.v. observations from the OAO, albedo curves from 2000-3700 Angstroms 2−78555
u.v. spectroscopy from Mariner 9 in 1100-3500 Angstroms region 2−75893
Viking entry mass spectrometer rel. to obs. of martian upper atmosphere 2−75653
Viking ionospheric meas. during atmospheric entry phase 2−75890
volcanic landform possibilities from Mariner 6 and 7 data 2−81914
water of hydration, high altitude aircraft i.r. spectrometric observations 2−78553
white clouds possible composition as H_2O 2−66183
wind generation mechanisms 2−58506
yellow storm survey 2−81919
CO_2 distrib., ground-based obs. 2−62705
CO_2 distrib. on surface for 1971 opposition 2−81912
CO_2^+, CO and O airglow, u.v. spectral obs. 2−66178
H_2O 8200 Angstroms band, ground based photoelectric observations during Mariner 9 mission 2−78551
H_2O 8200 Angstroms band studies with ground-based Varo image tube 2−78552
K-Ar age determination planned for soft landing 2−62706
O_2, mol., detect. 2−85047
O_2 7620 Angstroms A-band observations during and after 1971 dust storm 2−78549
O_2 7635 Angstroms band observations rel. to atmospheric composition 2−78548
O_2 A-band at 7620 Å, detection in Martian atmosphere 2−69157
O_2 abundance upper limits and mixing ratio with CO_2 from photoelectric spectra 2−78550
O_2 emission in night glow of atmosphere, height of layers 2−55145

Masers
see also Stimulated emission
astronomical, search for departure of radiation from Gaussian statistics 2−73048
astronomical interstellar scattering effects on apparent size 2−75787
cavity pulling in passive frequency standards 2−63304
electric field of ring electrets, application to state selection of masers 2−78955
H pulsed double-mode, determ. effect of number mass on bound electron g factor 2−42796
microwave resonator grating fabrication technology 2−41956
paramagnetic push-pull, inversion ratios, comparison with three-level devices, magnetic field intensities 2−82467
steady state emission, spectral power distrib. for multisublevel system 2−45706
toroidal-type cavity modulator for, 1.5 GHz, low control power 2−69892
t.w., three level, frequency conversion coefficient 2−69891
$Bi_{92}Sb_{08}$, dc-pumped, line narrowing of microwave radiation caused by nuclear electric quadrupole transition in ^{209}Bi 2−44403
Cs, possible construction, rel. to optical pumping studies of ^{133}Cs 2−70599
H physical processes, review 2−49342
HCN beam type, operation, frequency stability measurements at 88.6 GHz 2−52408
H_2O, at HII regions boundaries, gain parameters 2−69047
Na optically pumped, obs. of maser transitions between Paschen-Back levels of ground state 2−52935
OH, at HII regions boundaries, gain parameters 2−69047
OH, excited potential states, thermal and maser emission obs. 2−75790
OH interstellar molecule, pumping by polarized i.r. radiation, maser emission 2−81851
OH sources, astronomical, statistics of radiation 2−58368
OH stars, emission spectra rel. to laser and maser mechanisms 2−51754
Oh astrophysical, parametric down conversion 2−62590
Rb, isotopic filter 2−59126
Rb atomic oscillator, fundamental characteristics and frequency stability 2−73544
optical *see Lasers; Optical pumping*

Mass differences
baryon, e.m., deep-inelastic contribution 2−76705
electromagnetic, of hadrons, partial differential equations w.r.t. coupling constants 2−82698
electron, intense-field mass shift determ. from vacuum polarization on mass shell 2−66904
electron-muon, Machian theory of inertia 2−76606
e.m., in deep inelastic electron scattering 2−49506
hadrons, e.m. mass difference, deep inelastic contrib. 2−66955
isotopic $\Delta T=2$, divergence compensation rel. to current algebra calc. in weak and e.m. interactions 2−45844
neutron rich light nuclei, calc. of stable isotopes 2−82841
parton model, e.m. mass shifts and approach to scaling 2−55827

Mass differences continued
proton-neutron, divergent contribution in Weinberg model 2−67048
proton-neutron, finite contribution 2−49589
proton-neutron, investigation in configuration space 2−55875
proton-neutron, rel. to axial-vector massive photons 2−70253
proton-neutron mass difference and related topics, report 2−49590
virtual processes, mechanisms for finite mass differences from light-cone analysis 2−49469
A_1 isomultiplet, cancellation of divergences, dynamic chiral symmetry 2−52628
K^0_l-K^0_s connection to pole-approximation calcs. 2−67009
K_l-K_s chiral approach, two-pion contribution 2−70219
π isomultiplet, cancellation of divergences, dynamic chiral symmetry 2−52628
ρ isomultiplet, cancellation of divergences, dynamic chiral symmetry 2−52628
$H_2^+ - D^+$, meas. using ion cyclotron resonance technique 2−70254
$MnBi_{(1-x)}Te_x$ film, prep. and props. 2−72264
Mass formulae
alpha-particle nuclear model, calc. of interaction energy among last 2 neutrons and last 2 protons in nucleus 2−63742
baryon excited states, mass splittings within SU(3) and SU(2) multiplets 2−52630
baryons, ladder U(6,6) symmetry, classification and mass formulae 2−45990
elementary particles, empirical relation 2−73740
empirical, for masses of mesons and baryons 2−67041
Garvey-Kelson, applic. to light hypernuclei binding energies 2−46115
meson, dynamic interpretation 2−63649
mesons, empirical formula 2−70203
Nambu's and the cohesive force of the electron 2−70157
pion-muon model, discrepancy for π°, μ° 2−79555
resonances with identical strangeness, parity, ordinary and isotopic spin 2−73741
SU(3) × SU(3) spontaneous breaking, mass relations and particle mixings 2−66910
π-μ model, linear mass relationships 2−59526
Mass spectra
see also Chemical analysis/by mass spectrometry
alkali metal metaborates, interpretation 2−59889
of baryon radial mode 2−76616
computer pattern recognition, low resolution spectra 2−81559
correction for type of scan of instrument 2−56087
n-decane, metastable ions 2−59884
1,1-dimethylhydrazine-monoborane, determ. of molecular structure, vibrational assignments 2−53057
inert gas ions, collision-induced ioniz., ion kinetic energy spectra 2−83175
ion-molecule collisions, inelastic, time-of-flight analysis of neutral products 2−70807
ions emitted from solid area under electron bombardment 2−59888
methane, isotope effects 2−83321
negative ions produced by surface ionization 2−79851
nitrobenzene, negative ion spectra, electron energy and press. range 2−84680
perfluoropropane, negative ion formation 2−60079
perfluoropropylene, negative ion formation 2−60079
quantum electrodynamics, in pure Coulomb field 2−49471
small ion current detection, using photomultipliers 2−45689
thiazole and derivatives, ioniz. pots. obs. 2−83305
time-of-flight, method for calc. m/e's of peaks 2−56083
toluene, photo fragmentation, obs. 2−70794
trinitrotoluene, negative ion spectra, electron energy range 2−84680
water jet, mass and phase spectrometry 2−49986
Ar^+ beam interacting with surface, obs. of intense peaks at masses 26 and 28 2−79849
CO_2, mass spectrometric study of dissociative electron attachment 2−42883
$CS_2 + S = CS + S_2$ gaseous equil., heat of form. of CS 2−72544
CuCl, gaseous mols., dissociation energy 2−83255
Cu_2Cl_2 gaseous mols., dissociation energy 2−83255
GaBi, mass spectrometric determ. of dissociation energy 2−64126
Hg_2^+ form. in positive column of l.p. Hg-Ar discharge 2−83640
K-Ar dating, orifice correction 2−59959
KBr, ion bombardment, mass spectrometer obs. of sputtering and ion emission 2−71765
O^+ beam interacting with surface, obs. of intense peaks at masses 26 and 28 2−79849
Pb^+ ion gas-phase hydration 2−80493
$RhC_{(2)}$, heats of atomization determ. by high temp. spectrometry 2−84623
TiC_2, heats of atomization determ. by high temp. spectrometry 2−84623
Mass spectrometers
see also Ion optics
— 2−67417
chamber, field ionization of atoms and mols., ion current and ion distrib. 2−49921
computer applications 2−59887
control and output system 2−67375
development and applications, review 2−59885
double focusing high resolution, modification for negative ionisation 2−84680
double-focusing, modifications and use of data acquisition interface 2−49985
field distortion effect on transverse displacement of ions 2−74198
gas chromatography, RM-50 GC model 2−42704
ion cyclotron resonance spectroscopy, equations of motion for ion 2−70558
ion emission from electron bombarded solids, application 2−75201
ion microanalyzer, analytical technique for insulating materials 2−84687
ion microprobe mass analyzer, description of instrument 2−63298
ion microprobe mass analyzer 2−42706
ion source, for studying low energy ion mol. reactions 2−82458
ion source design, analysis of corrosive gases 2−81555
ion source including, patent 2−63991
ion sources, optimal adjustment for isotope geology applic. 2−46398
low energy ion-molecule scattering apparatus 2−63302
Mass spectrometers continued
M/e stability, ion source adapted to analyser 2−56084
magnetic, multipassage, resolving power and props. 2−63989
magnetic dispersion field, patent 2−83167
magnetic scan improvements 2−63988
mass peak-locking rel. to stabilization of high-resolution spectrometers 2−67377
with mass spectrometer, patent 2−59890
modification for metastable data collection 2−59884
molecular beam spectrometry, i.r. laser modulated 2−81490
multiple-focusing time-of-flight, with equal energy acceleration 2−67374
Nier type, with pressure, variation of resolving power 2−52900
omegatron, measurement and supply system 2−78687
Planetary Atmosphere Experiments Test, terrestrial mass spectrometer experiment 2−75533
prism, with wedge-shaped poles 2−70559
quadrupole, assembly with accurate electrode alignment 2−74199
quadrupole, maximum resolution 2−42705
quadrupole, shape of mass peak 2−63990
quadrupole ion entrance masking, computer analysis 2−42707
receiving device, short lived isotopes, semiconductor defectors 2−83164
repeller voltage and shield voltage; effect on ionization potentials 2−79850
residual gas analysis, comparison with quartz crystal microbalance 2−78707
response in upper atmos., O beam system for determ. 2−64058
scan function regulation, preset timer 2−67376
spark-source, semi-automatic system for operation of electric detection 2−84700
spurious F^+ signals, source and behaviour 2−74200
thermal ionization, computer controlled 2−63987
time-of-flight, radial ion paths, theoretical anal. 2−83162
time-of-flight, with shock tube coupled through molecular beams 2−71107
TOHOKU charge spectrometer, modified as cascade type mass spectrometer 2−83165
Cs^+ ion sputtering source 2−69885
accessories
see also Ion sources
bakable changeover valve, comparison of isotopic composition of gases 2−74201
diffusion pumps, two in tandem, bounded of a high resolution mass spectrometer 2−83166
digital recording mass spectra in geologic studies, digital recording using magnetic tape 2−72600
electrohydrodynamic ion source 2−74203
electrostatic hexapole lens, third-order transfer matrix 2−59078
gas inlet system, adjustable 2−74202
ion source tapes, stabilizer of current which heats 2−56085
laser ion source for mass spectrographic laser microanalysis of solids 2−82456
oil-vapour evacuation system in MKh1307 chromato, high vacuum trap 2−56086
pulse counting apparatus for particle beam 2−82811
pulsed-field ion source 2−59886
applications
see also Chemical analysis/by mass spectrometry
adsorption and desorption of O_2 on W as function of coverage 2−47171
blood and gas tissue meas., membrane 2−51892
burnup estimation for thermal reactor 2−42652
charge transfer observation 2−46400
high-pressure system, for retardent action 2−49920
implantation profiles determ. by secondary ion mass spectrometry 2−74794
ion cyclotron resonance mass spectrometer, electron impact excitation spectra 2−80135
ion-molecule reaction rate constants by ion cyclotron resonance 2−61768
ion-sensitive plate response, depend. on ion struct. and comp. 2−83163
ionization onset potentials, determination method 2−46399
ionization potentials, third derivative method of determination 2−60286
isotope abundance determ., systematics of double spiking 2−64081
isotope geology, optimal adjustment of ion source 2−46398
mass spectrometer control 2−73233
metastable ions, determ. of lifetimes by field ionization mass spectrometry 2−46789
oil-paper insulation systems, chemical analysis of gaseous decomposition products 2−68824
outer planet atmospheres analysis using ionization threshold spectrometer 2−76962
plasma parameter det. for laser microplasmas 2−83551
plasma sampling diagnostics using ion kinetic energy distributions 2−60258
surface analysis, by mass spectrometry of sputtered neutrals 2−64541
surface and bulk properties of solids, ion-ion emission technique 2−61469
Viking entry mass spectrometer rel. to obs. of martian upper atmosphere 2−75653
Ar cluster fragmentation, detection 2−42870
B_2O_3 glasses, diffusion obs. of Ar and Ne 2−53758
CO_2, on W(100), flash desorp. obs. rel. to decomposition 2−50551
CdSe, homogeneity regions, solubility of Cd and Se 2−83837
^{109}Cd, charge states of ions prod. by electron decay capture 2−79884
GaN, crystal growth, vapour phase processes obs. 2−53606
H atomic beam detection 2−67427
In film, on Si substrate, condensation and nucleation obs. 2−47117
$LiScF_4$, relative ionization cross-section determ. 2−46556
Ni crystal face, benzene and cyclohexane adsorp. obs. 2−50545
O density in thermosphere, meas. with rocket-borne open-source mass spectrometers 2−68929
O_2, chemisorption on W, obs. of desorption 2−48327
O_2 partial pressure meas., W cathode pumping effect 2−48943
O_2 partial pressure meas., W cathode pumping effect 2−48943
Ta getter, in evacuated valve, residual gas sorption obs. 2−76130

Mass spectrometers continued
  applications continued
    ^{235}U/^{238}U isotope ratio meas. 2−83216
    VO, determination of heat of formation 2−44476
    VO$_2$, determination of heat of formation 2−44476
    V$_4$O$_{10}$, determination of heat of formation 2−44476
    V$_4$O$_8$, determination of heat of formation 2−44476
Mass standards *see Standards*
Mass transfer
    absorption and rectification in rotary film columns 2−83494
    absorption of single gas in liquid film, stable laminar flow 2−67749
    aerosols, laminar flow in narrow rectangular channel with axial radial diffusion 2−53269
    air with injected species, two-dimensional stagnation point flows 2−45576
    atmospheric geostrophic drag, heat and mass transfer coefficients for the diabatic Ekman layer 2−57957
    benzoic acid/water, mass transfer coeffs. on flat plate by parallel channel flow and turbulence promoter 2−67601
    bibliography, Russian publications 2−45583
    bibliography of Polish works (1969-1970) 2−58951
    bibliography of Soviet work in 1970 2−55579
    bubble, in non-Newtonian fluid, thin boundary layer approx. 2−53376
    bubble, vapour, growing 2−53377
    bubbles, non-Newtonian liqs., with chem. reacts., power law model 2−53374
    to bubbles following entrance into liquid 2−43299
    capillary, analytical problems 2−83720
    chemical reaction coupled with absorption in agitated thin-film reactor 2−83495
    cocurrent oblique crossflow transfer, angle between flow directions between 0 and 90 degrees 2−50146
    control of binary gas mixture condensation 2−77466
    corneal thickness control, unsteady state description of corneal mass transport 2−78670
    Danckwerts surface renewal theory, relation with Reynolds flux 2−45595
    diffusion coefficient determination, for Ni on W surface 2−50466
    droplet, from vapour during nucleation, kinetic theory 2−60551
    electro-winning cell, decrease in mass-transfer rate obs. due to opposing convective flows 2−46868
    electrochemical, rate meas. at rough surfaces 2−54552
    electrolytes in porous systems, subject to MHD pressure, kinetic steady-state and transient phenomena 2−71133
    estuaries, partially stratified, mass transport mechanisms 2−51535
    flow, laminar, through circular tubes, low Peclet number entrance-region mass transfer of diffusing matters 2−77226
    flow in entrance section of circular tube 2−64236
    flow of gases in shallow fluidized beds, meas. of concentration profiles and mass transfer coeffs. 2−60330
    flow reactor for chem. vapour deposition, props. rel. to gas flow pattern and mass transfer 2−83896
    in flowing electrolyte with quasi porous electrode 2−68794
    fluid containing high molecular weight polymer, non-Newtonian flow 2−50289
    fluidized beds of wetted sperical particles 2−83497
    forced convection, elec. field influence 2−52282
    gas absorption into turbulent liquid 2−50298
    gas transfer from bubbles in fluidized bed to dense phase 2−80163
    gas-liquid flow, concurrent, sampling error calc. 2−53121
    gas-liquid flow in channel, partial transfer coefficients for each phase 2−50290
    HeI, ^{3}He mass transport, obs. by thermal-neutron method 2−67855
    interfacial, between finite vol. of homogenized fluid and sphere with finite transport coefficients 2−46990
    interferometer long path difference, 30 cm diameter for mass and heat transfer aerodynamics 2−59231
    ionic, in parallel plate electrochemical cells 2−59040
    laminar, from stepwise discontinuous naphthalene disc rotating in uniform forced stream 2−73465
    laminar flow, in rotating cylinder cell 2−53346
    lava pond surface heat and mass transfer, obs. 2−78249
    liquid, local natural convection mass transfer, electrochemical technique obs. 2−50288
    liquid film for protecting solid surface in hot gas streams cooling and mass transfer, correlation 2−67795
    liquid-gas, Marangoni instability 2−60550
    liquid-liquid interface, unsteady state transfer of solute, effect of heat of solution on Marangoni convection 2−77381
    moisture transfer in porous elastic solids, stress development 2−46889
    momentum transfer between rotating cylinders, narrow fluid gap problem 2−46692
    multistage vibrating disk gas absorption column, backmixing effect 2−67564
    naphthalene/air, mass transfer coeffs. on flat plate by parallel channel flow and turbulence promoter 2−67601
    2- naphthol particles to flowing water 2−71129
    nuclear fuel, oxide, redistrib. during irrad. 2−52852
    nuclear reactor cooling systems, effect of Na corrosion deposits on heat transfer coeffs. 2−83117
    paradichlor benzene/air and ammonia/air, mass transfer coeffs. on flat plate by parallel channel flow and turbulence promoter 2−67601
    plate, porous, in fluid flow, using Laplace transform. 2−49176
    plate in incident longitudinal flow 2−46663
    porous medium, fluid-filled, nonequilib. thermodynamics 2−50137
    problem solving using vector maths. 2−82276
    Rayleigh-Taylor instability, effects 2−46687
    reaction, coupling with membrane transport processes 2−56493
    rear of cylinder in crossflow 2−43097
    obs. using refractometer, one-dimensional focusing critical angle 2−55760
    regenerators, prediction of coupled heat and mass transfer 2−45581
    rotating bubble bed 2−83498
    rotating bubble bed 2−83498
    semi-batch packed bubble column 2−74508
Mass transfer continued
    single gas bubble rising in water 2−46907
    small diameter packed beds in nuclear reactor 2−42656
    spatial variation, over a flat plate with laminar air jet impinging normally 2−53267
    sphere with blow, effects on temp. field 2−77345
    steel, melting in Fe-C melts, with natural convection, rates for various C concentrations 2−43438
    three dimensional parabolic flow, calc. procedure for heat mass and momentum transfer 2−67571
    three-body problems, effect of mass changes on orbital parameters 2−84937
    three-dimensional stagnation point flows, transfer from foreign gas injection 2−64370
    turbulent, from large body of water 2−57891
    turbulent boundary layer, discontinuity in wall temp. and concentration 2−53274
    in turbulent boundary layers, data survey 2−43055
    turbulent flow, in rotating cylinder shell 2−53347
    turbulent flow in plain tube, radial and tangential eddy diffusivities 2−76397
    variational analysis of rates from spherical particle boundary-layer injection suction considerations 2−77397
    wall, during flow in tubes and ducts, determ. of heat transfer 2−83443
    wall to fluid stream in small dia. packed beds 2−83436
    in water cooled column, efficiency, effect of axial dispersions in gas, liquid phases 2−67875
    wave roughened gas-liquid interface in annular two-phase two-component flow 2−77409
    through wavy air-water interface over which turbulent wind is passing 2−72748
    wet vapour flow in relaxation zone behind front of shock wave 2−60407
    Mo powder, sintering mechanism, mass transfer by diffusion- viscous flow 2−53941
    N$_2$ + C$^+$ reactive collisions, 3 to 100 eV, mass transfer reaction cross section 2−48322
    Na reactor coolant corrosion and mass transfer analysis using ion probe mass spectrometer 2−83118
    O across gas-liquid fluidized beds 2−67547
    O$_2$ + C$^+$ reactive collisions, 3 to 100 eV, mass transfer reaction cross section 2−48322
    Zn/air battery, effect in flowing electrolyte 2−59039
Master equation *see Transport processes*
Materials
    see also Individual materials (if separately named) e.g. Ruby
    acoustic bonding, for u.s. delay line, high temp. characs. 2−77777
    billets, surface inspection, Billetscan eddy current device 2−43764
    bone, low temp., thermal cond., phonon mean free path, hydroxyapatite crystallite struct. 2−61115
    bone, separated animal tibias, acoustic resonance frequency 2−81998
    brittle, dependence of test results on nature of stress state 2−56841
    for cardiovascular implants, electrochemical method for selection and eval. 2−69226
    cement, hardened paste, short time creep recovery 2−80755
    coatings, high-temp., nondestructive testing technique 2−43763
    coral, Pu content in biological samples, separation and anal. 2−62045
    engineering, thermal expansion, tabulation of quadratic function coefficients 2−71639
    erosion resistant, for combustion chambers and nozzles of rocket engines with F$_2$ and metal combustion 2−48619
    fatigue failure, under narrow band random vibrations 2−48623
    granular, specific heat meas. by continuous flow Callendar and Barnes method 2−57057
    insulating, analytical technique using ion microanalyzer 2−84687
    insulators and structural materials, thermal conductivity and diffusivity and specific heat 2−57080
    for intravascular pressure transducer 2−69225
    joints, diffusion bonded, tensile strength rel. to pulse echo, testing technique 2−43766
    microplasticity, strain release method of obs. 2−50789
    mixer for free flowing materials in spectral analysis 2−84681
    negative electron affinity, in photomultipliers, review 2−49676
    neutron radiography, nondestructive testing technique, review 2−43765
    non-destructive testing, electrothermal method, metal structures 2−43769
    non-destructive testing, holographic, with mech. impact excitation 2−56676
    non-destructive testing, i.r. thermography of laminated materials, subsurface defect obs. 2−43767
    non-destructive testing by holography 2−71608
    nondestructive testing, application of resistivity meas. in massive conductors 2−45643
    nondestructive testing, metrological techniques, laser holography and speckle patterns 2−45763
    nondestructive testing by ultrasonics 2−69757
    nondestructive testing of filament wound pressure vessels and composites 2−64791
    nondestructive testing of plastics ageing, colorimetric aspects 2−47671
    nuclear, preservice and inservice inspections, design and metallurgical problems 2−52887
    nuclear research, conference (Galtinburg USA, Oct 1971) 2−49617
    nuclear research, preparation in e.m. isotope separator 2−49614
    nylon-epoxide adhesive, creep and tensile microstrain 2−47673
    Pc 1 hydromagnetic wave propagation across North America 2−68936
    poroelastic, two phase, bone model, stress analysis 2−41571
    Portland cement, use in cloud seeding expt. 2−62208
    portland cement paste, microstruct. effects on deform. and fracture 2−60995
    refractory bricks, thermal conductivity, hot wire method 2−51055
    response meas. holographic interferometric techniques 2−49402
    teaching and research at McMaster University 2−43761
    tertilium explosive, electrical conductivity during detonations induced by shock waves 2−63139

Materials continued
tester, cast iron abrasive wear, obs. 2−50792
testing automation, review 2−77687
testing machines, development 2−43770
thermorheologically simple, identification problem 2−41567
trotilium explosive, electrical conductivity during detonations induced by shock waves 2−63139
vibration isolating, meas. system for dynamic stiffness and transmissibility 2−49086
X-ray diffraction, appl. to materials science, review 2−64744

Materials testing *see Mechanical strength*

Mathematical methods *see Calculation; Statistical analysis*

Mathematics
applied, conf., Providence, USA (1971) 2−52038
automatic correction methods, application to design of optical systems 2−45803
book, mathematical analysis of physical problems 2−82181
boundary-initial-value problems, semidiscrete approx. 2−63053
dynamical system, monotonic nature of phase trajectories, bifurcation curves 2−66414
education, integrated course in physics and mathematics for A level biology and arts students 2−41430
eigenvalue theory, application to nuclear atomic and molecular spectra 2−69550
Euler Lagrange operators of quantum field theory 2−70101
extrapolation, analytic from boundary and interior points 2−58703
Fourier series, absolute Norlund summability 2−69542
functional analysis, text book for first year graduate student 2−82182
Hopf bifurcation theorem generalization 2−76170
initial conditions of exterior case, world conditions 2−58699
invariant embedding and nonlinear scattering 2−52048
Kampe de Feriet expansion formulae evaluation of integrals 2−55373
linear systems, variational estimates and generalized perturbation theory for ratios of linear and bilinear functionals 2−58702
manifolds, even-dimensioned differentiable, derivations, forms and usual operators of spinor fields 2−58698
modelling in theory of structures 2−52134
nonlinear σ-model, determ. of renormalization constants 2−73732
physical theories, construction of model 2−76136
solid state, neutron, theoretical, nuclear, maths. and computation, progress report of Atomic Energy of Canada 2−62910
thermodynamic systems, second order differential operator with eigenvalue degeneracy 2−52100
variational methods modification to approx. arbitrary functionals in transport theory 2−66480
variational principle based on spatial variation 2−52039

Matrices
acoustic wave propagation, high-order finite element analysis 2−69722
atomic structures, one- and two-electron operators 2−42712
atomic structures, one- and two-electron operators 2−42711
calculus, elementary formulas and their application in continuum mechanics 2−55375
density, linear inequalities 2−82262
density matrix values in configuration space, computation 2−52897
diagonalization techniques for computer programme for molecular rotation calculations 2−64095
electrodynamic representation theorems, elastic wave scattering 2−78898
electron density, cusp conditions as constraints 2−42858
ensemble density matrices, diagonal N-representability 2−66475
equicofactor and indefinite-admittance matrices 2−82167
force const. matrices, prop. satisfying vibr. eqns. of two isotopic species 2−83219
force constant calculation using generalized inverse matrix 2−59971
force constants, implication methods 2−67450
H-matrix relevant to two-group neutron transport problem, existence and uniqueness 2−83049
hydrodynamics $SO(3) \times SO(3)$ symmetry, closed system 2−77174
incidence eqn. $AA^t = PA$, theorem proof 2−82168
molecular orbitals, numerical integration techniques 2−52978
molecular vibrational force constant solutions with singular jacobian extremal nature 2−49996
molecular vibrations, normal coordinate analysis 2−70665
n-electron problem and matrices representing symmetric groups 2−52896
N-representable reduced 2-matrices, convex struct. 2−82229
nucleus, electric transitions, generation of matrix elements from vector potential 2−46102
optical polarization transfer matrices, consequences of non-commutability 2−79331
phonon inelastic surface scatt. transition matrix for bound state interactions 2−83854
real nearly-symmetric, convergence of lowest eigenvalue 2−63011
rectangular 2−69548
scattering, three-body problem in 1-D, with interacting, impenetrable particles 2−82228
singular matrix representations, reln. to group representations 2−78771
spacecraft attitude determ. matrix transformations 2−82171
transformation, Wigner basis, for reduced Poincare group 2−82649
transformations of monotonic product sequences 2−52043
transition density matrices, suggested calculations 2−59882
$U_{n,1}$ and IU_n representation matrix elements, props. 2−82164
Van Vleck expansions, operators in closed form 2−52042
variance, applications, significance criteria 2−63010
vibrating molecule or solid, mean square amplitude matrix, low-temperature limit 2−59970
vibrational analysis of framed structures 2−76355

Matrix-isolation methods *see Free radicals; Molecules*

Matteucci effect *see Magnetoelectric effects; Magnetomechanical effects*

Maxwell-Boltzmann distribution *see Kinetic theory; Statistical mechanics*

Maxwell effect *see Double refraction/flow*
Maxwell equations *see Electromagnetism*

Measurement
see also Instruments; Recording; Standards; Units; Acoustical measurement; Dielectric measurement; Electrical measurement; Magnetic measurement; Mechanical measurement; Radioactivity measurement; Thermal measurement; X-ray measurement. Some specific quantities are listed separately, e.g. Calorimetry; Density measurement. Where no separate heading exists, measurement methods and instruments are included among the other entries under the heading of the appropriate quantity or subject
adaptation of apparatus to variable working conditions, theoretical considerations 2−82134
coherent light techniques for engineering meas. 2−49392
engineering metrology laboratories, design and equipping 2−69530
geometrical theory, historical review 2−52030
geophysical data, simultaneous interpretation 2−57447
holography, measuring technology and metrology applications 2−58681
industrial in mechanical systems, lasers applic. 2−76493
laser beam, industrial applications for alignment, length, granularity, angle and velocity 2−82494
laser beams applics. to metrology, systems description and examples of applications 2−69950
light pulses, picosecond, techniques for detect and meas. 2−82512
quantum mechanics formalism 2−69534
sound power level of single noise source in closed space 2−82358
theory of meas. systems with periodic conversion function 2−76148

errors
see also Statistical analysis
— 2−69036
airborne sound insulation in buildings, standardization of measuring techniques 2−52251
anemometer, X-array hot wire, effect of wire length and seperation 2−64367
astronomical absolute flux meas., errors in standard star Vega 2−81974
astronomical obs. night errors, refraction anomalies or variable systematic instrumental errors 2−66240
Bayes estimation of observation error variance in linear systems 2−69533
combination of observations of unequal accuracy 2−66402
compression manometer, due to nature of scale 2−45223
counters, random events, Poisson distributed 2−49615
coupling effect of systematic errors in transmission ellipsometry 2−55743
design of experiments and estimation of errors for project work in schools 2−62951
dielectric layers with imposed spectral characts., control and preparation 2−63418
diffraction grating spacing errors reduction 2−73654
dosimetry, timer error in patient daily dose 2−69418
dynamic, instruments with limited stiffness of measuring base 2−45213
edge errors in size distribution measurements with linear scanning instruments, a new formula 2−55356
electron, microprobe, statistical calc. by Castaing's first approximation 2−82083
electron energy loss spectrum meas. by electron microscopy and energy analyser, statistical analysis 2−73524
ferromagnetic material, loss measurement error, pulsed magnetiz. 2−75220
flow in circular pipes, errors in velocity-area method of obs. 2−83522
galactic distance scale determinations, methods and accuracy 2−69019
gamma camera, anal. and correction of spatial distortions 2−48855
gas-liquid flow, concurrent, sampling error calc. 2−53121
intermittency in turbulent free shear flows, due to circuit calibration 2−46811
least squares method treatment of results 2−55355
line standards subdivisions length meas., temp. errors of comparator method 2−76153
linear analysis, methods for edge error correction 2−64519
lunar motions, numerical methods, lasers, Doppler effects 2−84939
machine noise, ISO recommendation 2−41815
magnetic component obs. at sea, corrections for deviations 2−72906
magnetometers, helium lasers, directional sensor errors 2−52382
mathematical expectation error estimate accuracy, effect of meas. ranges 2−76152
Meridian Circle graduation, Brun's method for error determ. 2−73164
musical sounds, almost periodic, approximation errors 2−82350
noise, community level distribs., sampling errors 2−82354
noise, obtaining signal information from intersection points of different apparatus 2−41445
optical electronic goniometers, modulation characteristics 2−55359
optoelectronic angle sensors, effects of atmospheric turbulence 2−58690
phase errors in interferometry, identification and removal 2−66241
photoelectric instruments, effects of nonuniform energy absorption in compensator plate on accuracy 2−70050
photometry, instrumental errors in meas. of quasiharmonic signals 2−45800
radar Doppler spectrum of meteorological echoes, uncertainties in coherent meas. of mean frequency and variance 2−75507
radar raingauge accuracy rel. to drop size distribution and rainstorm type 2−75593
radio meteor velocity, mean-square error determination 2−58526
rain drop size distribution determ. by radar, errors rel. to vertical air motion 2−75592
rulers, linearity testing, using two-areas method 2−82133
selsyn-type electric machines, error determinations 2−76437
slit diaphragm photometer 2−73648
soil stress during transitory loads 2−78277
spectrochemical analysis, concentration determination limits 2−84698
spectrochemical analysis, limit of concentration determination 2−84697
stellar distance determination, trigonometric parallaxes 2−69055
systematic and random, simple mathematical treatment for school students 2−62952

Measurement continued
- **errors** continued
  - teaching students statistics, a demonstrative experiment 2−63048
  - temperatures obs. and distribution in experiment performed in Tuttle hydrothermal pressure vessel 2−45597
  - thermal fluctuation method of integral temp. obs. over thickness of dielectric 2−76403
  - thermodynamic limits, accuracy of physical measurements 2−58685
  - thin specimen resistivity measurement using electrical-contact four-electrode transducer 2−45642
  - tuned gyroscope, multigimbal elastically supported, theory 2−82121
  - u.s. velocity meas., absolute accuracy of pulse-echo overlap and pulse-superposition methods 2−73431
  - vibration-frequency transducers, errors resulting from elastic imperfections in their materials 2−58696
  - ^{87m}Sr radiation dose calculation, evidence for calculation errors 2−76096

Mechanical measurement
- *Individual quantities and instruments are listed separately e.g. Length measurement*
- — 2−71617
- apparatus for testing materials for wear in liquid and vaporised alkali metals at temps. up to 700°C 2−82127
- apparatus for testing metal foils for creep 2−56852
- automatic static deformation recorder 2−56854
- automation using process control computer 2−58822
- bend endurance testing unit for thin flat samples 2−56853
- biaxial flexure test method for ceramic substrates 2−60919
- bibliography 2−66404
- brittle rupture tests, method of forming axially symmetric surface cracks 2−50785
- brittle surface layers, relative hardness det. using u.s. oscillations 2−56845
- bulk modulus loss factor determ. using ultrasound, of small specimens 2−71615
- cladding from irrad. fuel pins, burst testing 2−43776
- combined tension-torsion creep testing of polymers, apparatus 2−71619
- composite, unidirectional C-fibre reinforced plastic, shear strength and modulus 2−74921
- computational techniques, conf., Leeds, England, Jan. (1971) 2−58820
- crack depth, using u.s. surface waves 2−71614
- Cranz-Schardin camera for dynamic photomechanics 2−63448
- creep and strength testing method, effect of error on statistical spread 2−53847
- creep apparatus, high vacuum and rarefied atmos, 2−60918
- creep machine for testing neutron effects in nuclear reactor 2−46391
- creep testing method for metal in thin wall 2−68120
- damping capacity testing apparatus for use under direct cyclic stresses 2−53861
- defects in fusion welds rel. to basic metallurgy for non-destructive testing 2−53845
- device for obs. of action of first impact impulse in dynamic destruction 2−56851
- displacement and deformation, holographic interferometry 2−82150
- dynamic biaxial loading in plate testing 2−64750
- dynamic fracture toughness meas. technique 2−82124
- dynamic puncture resistance, determ. for polymer thin films and sheeting 2−60920
- elastic and plastic strains, using symmetrical telecentric lens 2−45784
- environmental chamber for hertzian fracture testing 2−56855
- equipment for stress relaxation tests at nonstationary temps. 2−68119
- fatigue, two-axial stress state specimens, machine for testing 2−43755
- fatigue crack damage in composites, vibr. testing 2−60921
- fatigue resistance, effect of loading frequency at high temps. 2−56839
- fatigue strength, alternating tension and compression, plain and notched high strength mats., 500-700°C 2−74870
- fatigue testing apparatus for simultaneous handling of four flat specimens 2−53854
- fatigue testing apparatus for use in controlled atmospheres 2−47566
- fatigue testing apparatus for use in controlled atmospheres 2−47565
- fatigue testing at high temp. in liquid corrosive medium 2−53848
- fatigue testing machine with programmed amplitude and frequency variation, temp. range 4.2 to 1000K 2−53853
- fatigue testing under bending and rotation, gripping collet design 2−53855
- fibre/fibre friction meas. with scanning electron microscope 2−82441
- film, Vickers type ultra-microhardness tester 2−43471
- fine wire with small remanent strain, elastic limit det. 2−43676
- force displacement meas. apparatus contained entirely within pressure vessel 2−68080
- fracture characteristics, electron- fractographic obs. 2−43751
- fracture speed meas. using u.s. fractography applic. to Si and Ge 2−82123
- fragility testing, simple economical method 2−56856
- hardness measurement, British Standard methods 2−58684
- holographic interferometric appls. 2−84168
- holographic strain anal. using spline functions 2−82142
- hot hardness testing 2−77680
- impact fatigue testing machine, rotating disc type and applic. 2−80809
- inertial mass variation, exp. test 2−52118
- instrument for recording time of initiation of fatigue crack and rupture of specimen 2−71610
- internal friction and elastic modulus, high temp. system for continuous recording 2−53852
- Knoop indentation testing, resolved shear stress distrib. calcs., computer program 2−60941
- load cells, design, manufacture and use 2−41452
- lubricated sliding point contacts, load, traction, film thickness meas. device 2−53864
- machine for low cycle fatigue bending, torsion, and tension compression testing 2−64740
- machine for testing antifriction materials up to 700°C 2−56848

Mechanical measurement continued
- machine for testing microsamples of fragile materials 2−56846
- machine for testing vibration creep and vibration strength 2−56847
- machine for wear testing 2−56849
- mass measurement by measuring frequencies of natural oscillations of body 2−66406
- materials, testing machines, development 2−43770
- materials testing, electrical and electronics industry 2−80790
- metals, normal wear, methods of obs. and diagnostics 2−43754
- microcreep and dimensional stability measuring system 2−71620
- microhardness meas. by method of small penetration of indentor 2−47549
- neutron radiography in non-destructive testing of plate assemblies 2−53846
- non-destructive testing conference, London (1971) 2−43782
- nondestructive testing, application of resistivity meas. in massive conductors 2−45643
- notch toughness characterization of metals, criteria and design of expts. 2−60922
- notched beam test for fracture energy meas. of ceramics 2−50858
- nuclear reactor component, nondestructive testing 2−84065
- physics laboratory demonstration for students 2−62961
- plastic, fixture for testing rings by pulsed external pressure 2−53858
- plastic deformation, transmission electron microscopy obs. straining holder using piezoelectric effect 2−79107
- plastics, structural, strength and deformational characteristics 2−43756
- plastics test methods handbook 2−53865
- polyethylene terephthalate, non-linear viscoelastic behaviour 2−56777
- polymer testing machine for simultaneous study of structure and mechanical properties 2−53857
- polymers, relaxation stresses, rigid dynamometer for obs. 2−43757
- radiation defect accumulation and annealing kinetics, testing apparatus 2−84062
- reactor fuel particle coatings, tensile strength determ. 2−50790
- reactor fuel post-irrad. test methods and apparatus 2−43775
- reduction in area of metallic materials on basis of hardness 2−43753
- refractory metal, strength behaviour at elevated temps., vacuum technique 2−77683
- residual stress det. for 2-10 mm zone, application to weld joints in steam pipes 2−53850
- rock samples, slake-durability test 2−54734
- roller machine, three section single- contact, friction obs. of polymers 2−56850
- roundness, center and direction of axis, use of cyclogram 2−55361
- rubbers, apparatus for testing for wear in liquids 2−82128
- scanning electron microscope, high temp. straining stage 2−79121
- sensitivity estimates for asymmetrical loading cycles from strain diagrams 2−56840
- service automatically plotting torsion diagrams for wire testing 2−71612
- sheet steel inspection, acoustic anisotropy obs. by pulse resonance method 2−64773
- small pressure change rates, variometers 2−55370
- stand for testing polymers for creep and long term strength 2−71611
- steel, fatigue life testing, simulation of infrequent cycling 2−71593
- strain, using optical correlation methods 2−82141
- strain-rate meter based on Doppler shift of laser light 2−84148
- strength testing methods comparison 2−47563
- strength testing of metals saturated with gases in glow discharge 2−47564
- tensile creep testing apparatus using simple knife edge universal joints for ceramics 2−47568
- tensile stage for adhesion meas. during scanning electron microscope obs. 2−82440
- tensile testing apparatus and grid production device for fracture obs. 2−84014
- tensile testing device, usable from room temp. to −150°C in electron microscope 2−71613
- tensile testing machine, for filamentary specimens 2−43759
- tension/compression stage for scanning electron microscope 2−79120
- test data analysis methods 2−58821
- testing automation, review 2−77687
- testing machine, THASh-5s-65, high temp., special fixturing 2−53856
- thick tube fatigue test apparatus using external and internal pressures 2−69500
- thick walled cylinder failure test-machine using fracture mechanics on pressure cycling 2−69501
- torsional split Hopkinson bar development for materials testing 2−68124
- uniaxial stress apparatus, design and construction 2−47571
- u.s. transducer material, fatigue testing of magneto- and electrostrictive materials 2−71625
- vibration and deflection meas., projected ruling Moire method, holographic interferometry 2−82149
- weighing solids in 2 phase flow of hydrotransportline 2−46700
- weight meas., balances, chemical analyses 2−57441
- wide range strain gauge device for static strain obs. 2−60929
- Al alloys, crack growth rate obs. in fatigue, special gauges for det. 2−60934

Mechanical properties of substances
- *see also Individual properties, e.g., Abrasion; Elastic deformation; Mechanical strength; Plastic deformation; Slip; Wear; etc.*
- alloy, and coherent phase formation, review 2−57007
- asbestos filled PVC, anisotropy 2−77668
- bone, considered as solid-liquid composite 2−69220
- carbon phenolic, two dimensionally reinforced, re-entry material, characterization 2−56980
- ceramic tile bodies, effect of polymer impregnation on physical and mech. props. 2−80759
- ceramics, texture with ref. to mech. props. 2−67949
- cermet, Fe-based, effects of protective sintering atmos. on physiomech. props. 2−68166
- composite materials, fibrous and laminates review 2−43901
- deformable solids, shear props., layered waveguide technique for determ. 2−64751
- engineering materials, hot hardness testing 2−77680

Mechanical properties of substances continued
epoxide resin Epidian 2, short-term props. 2−47672
α-Fe and low C steels, effect of deformation temp. on changes of the mech. props. 2−84159
fragile material microsamples, machine for det. 2−56846
furfuryl methacrylate, thermomechanical props. polymer and copolymer 2−50751
gelatine in photographic layers and means of modification 2−52508
glass ceramics, workability 2−43868
graphite, nuclear, production by mixing different cokes 2−68174
graphite, nuclear, production by mixing different cokes 2−68174
graphite, X-irrad., dynamical mech. props. 2−53777
graphite polycrystalline, environment effect on mech. anisotropy 2−68173
at high shear-strain rates, meas. using torsional split Hopkinson pressure bar 2−53821
high temperature measurement techniques 2−71616
ice I_h crystals, mechanical response 2−72013
liquid crystal, nematic mechanochromatic effects 2−84463
liquids, shear props., layered wqveguide technique for determ. 2−64751
lunar soil samples, Luna-16 automatic spacecraft 2−55117
metal, pressurization, structural changes and effect on mech. characts. 2−68079
methyl methacrylate polymer and copolymer, thermomechanical props. 2−50751
mullite, stoichiometric ceramic compact 2−50873
muscle during development of rigor mortis, dynamic Young's modulus det. 2−66252
nylon 6, effect of anisotropy, orientation and water on relaxation behaviour from 4.2 to 300 K 2−71559
poly(2,6-diphenyl-p-phenylene-oxide), molecular motion study by meas. of Young's modulus and mechanical damping 2−74819
poly(ethyl methacrylate)/poly(n-butyl acrylate) 2−64490
cis-1,4-polybutadiene rubber vulcanizates, mechanical props., dynamic loading 2−60855
polybutadiene/polystyrene latex IPN's, synthesis and dynamic mech. props. 2−64490
poly(n-butyl acrylate) lightly crosslinked network, dynamic mechanical behaviour in rubberlike region 2−71544
poly(n-butyl methacrylate) lightly crosslinked network, dynamic mechanical behaviour in rubberlike region 2−71544
polycaprolactum polyethyleneimine graft copolymers, mech. props. as a function of av. mol. wt. 2−64799
polyethylene oxide, mechanical damping index obs. with torsional braid analyser 2−71547
polyethylene terephthalate, structural characterization 2−50721
polyethylene terephthalate films, influence of liq. media 2−50750
polyimide, hydrostatic press. effect on mech. behaviour 2−83347
polymer, testing machine, broad temp. range 2−53857
polymer films, rel. to mol. orientation, sound vel. obs. 2−47536
polymer films, v. thin, tensile and elongation props. 2−60887
polymeric mats., rel. to spatial gradients and applics. 2−61026
polymers, low-temperature mechanical relaxation, assignment of molecular mechanisms 2−71557
polymers, strain effect rel. to conductivity and diffusion 2−57232
polypropylene, T-die film, rel. to mol. orientation 2−47537
polystyrene, effect of solvents on cryogenic dynamic mechanical properties 2−74820
polystyrene, foamed, rel. to struct. 2−43412
polyurethane, porous, shock response, Hugoniot elastic limits, model 2−61024
pressed parts, produced by dynamic pressing 2−53879
PVC-filler composites, influence of fillers 2−64792
rubber like materials, thermomech. behaviour, Valanis- Landel strain energy function 2−82312
skin, specific mechanical impedance, probe effects 2−66245
solid, effect on pressure pulse propagation 2−68074
stainless, managing, high-strength, struct., props., optimum comp. 2−60881
stainless steel cladding for fast reactor fuel elements, tensile and creep properties 2−59846
stainless steel type 304, effect of irradiation on strain rate dependence of mechanical properties 2−83122
steatite materials, effect of modifying agents on electromechanical behaviour 2−53933
steel, ausformed by extrusion 2−47327
steel, austenitic, rel. to V content 2−47636
steel, austenitic, stainless, rel. to Co content 2−47474
steel, eutectoid, rel. to directional growth of pearlite and rolling 2−47529
steel, quenched, effect of cooling rate 2−47587
steel, rel. to stress fields around inclusions 2−47491
steel, short term fracture at elevated temps. and pressures 2−60917
steel, sintered, model to explain behaviour of elastic moduli 2−84128
steel, structural, rel. to inclusion shape and orientation 2−43713
steel, untempered, low-alloy, segregation effects and toughness 2−80822
styrene polymer and copolymer, thermomechanical props. 2−50751
styrene-diene-styrene block copolymers 2−71584
viscoelastic materials, dynamic properties, mechanical impedance technique 2−74874
water boundary layer, temp. depend. 2−67739
wood, vibration method of det. 2−56844
X-ray flash tube applic. for study of fast processes 2−85181
zircaloy-2, -4, tensile props. rel. to neutron irrad. 2−80664
Al-9.5 wt.%Mg:Ti,Zr,Mo,B alloy, rel. to alloy additions 2−47546
Al-Cu-Mg alloy, oversaturated solid soln. state rel. to strain rate and temp. 2−56547
Al-Fe alloy, rapidly solidified 2−50827
Al-Mg-Zn alloy, soln. softening effect of Zn additions at high temps. 2−47613
Al, polycrystalline, recovery after severe rolling 2−71633
C-C composites and nondestructive testing 2−61016
C-C composites unidirectionally reinforced with carbon and graphite fibres, exam. of props. 2−68176
C fibre reinforced chem. vap. deposited C composites, micromechanics 2−53955
C fibres, radiation effects on mech. props. based on 'sheath' and 'core' model of fibre structure 2−64702
C glassy monofilament, prep. and props. 2−56982
$CaO-ZrO_2$ ceramic, thermomech. props. 2−43876
Co alloy, dispersion hardened 2−50831
Cu-Al-alloys, microstructures and mechanical props. of phases after quenching and isothermal treatment 2−60932
Cu-Al alloy, rel. to superplasticity 2−50745
Cu-Al alloys, mechanical properties and ductility as a function of temperatures 2−64776
Cu-Pd alloys, influence of domain size and ordering on mech. props. and elec. resist. 2−68506
Cu-Zn alloy, rel. to superplasticity 2−50745
Cu-Zn(40%) microduplex, metallographic study of superplasticity and cavitation 2−80738
Cu, polycrystalline, recovery after severe rolling 2−71633
Cu films in storage, ageing effects on substruct. and mech. props. 2−83863
Cu porous, shock response, Hugoniot elastic limits, model 2−61024
Fe-Al-Cr alloys, effect of zirconium 2−60935
Fe-Co-Ni-Ti-Al-Cu alloy, YuNDK42T8, homogenizing effects 2−47688
Fe alloy, in martensitic transform. 2−50943
Fe porous, shock response, Hugoniot elastic limits, model 2−61024
p-H_2, polycrystalline parahydrogen and n-D_2, comparison and influence of zero energy 2−71569
Mg, props. and applications, book 2−60936
Mg alloy, props. and applications, book 2−60936
Mg alloys, and radiation damage resistance 2−60778
Mo-Ti alloy, effect of deform. rate and temp. 2−47503
NaCl, mech. props. and disloc. struct. in single slip 2−71579
NaF, mech props. and disloc. struct. in single slip 2−71579
Nb-N, interstitial soln., mech. props. depend. on conc. and temp. 2−84009
Nb-O, interstitial soln., mech. props. depend. on conc. and temp. 2−84009
Ni-Cr-Mo alloy, porous material 2−53977
Ni-Mo alloy, porous material 2−53977
$PbTiO_3-Pb(Cd_{0.5}W_{0.5})O_3$ ceramic, electromechanical props. 2−64788
TZM alloy, arc casted, props. and applications 2−53825
TaC_x, lattice instability effects 2−68349
Ti alloy, rel. to superplasticity 2−50745
TiNi, unique property changes related to martensitic transformation 2−68200
V, neutron irrad., anneal and radiation hardening, tensile props. 2−80665
W-Mo-Ti alloy, and technological props. 2−47535
W-Ti-Zr alloy, and technological props. 2−47535
W-Ti alloy, and technological props. 2−47535
W alloy, T15K6, effect of tungsten prep. 2−56916
W porous, shock response, Hugoniot elastic limits, model 2−61024
YIG, photomechanical effect 2−81332
Zn-Al alloys, strain-rate depend. of deform. mechanism and slip system changes 2−84011
ZnS(Se), vapour deposited transparent polycryst. characteriz. 2−50578
Zr-Cr-Fe alloy, correlation with microstruct. 2−53922

Mechanical strength
see also Elasticity; Hardness
AK-4 alloy, strengthening and roughness of rubbing surfaces, effect on wear and bearing capacity 2−60916
alloys, fracture resist., physical and technological significance 2−71580
anisotropic materials under combined loading 2−45358
b.c.c. metals, disloc. distrib. rel. to strengthening 2−60799
BORSIC aluminium fibre-matrix interfacial region, exam. 2−64546
Boussinesq problem for thick elastic layer under a punch of arbitrary profile 2−58862
brazed joints to graphite 2−71627
brittle material, testing methods comparison 2−47563
brittle surface layers, relative hardness det. using u.s. oscillations 2−56845
bronze powder, spherical particles, rel. to sintering kinetics determ. 2−43890
ceramic, brittle, review 2−47520
ceramic, microstruct. influence, review 2−47521
ceramic, porous, polymer impregnated, rel. to temp. 2−43899
ceramic alloy B2Zh, prep. and mech. characterization 2−77720
ceramic composites with alumina matrix, impact strength and dynamic loading 2−80758
ceramic matrix, chemically reacted, for fibre reinforced composites 2−56972
ceramic substrate, biaxial flexure test method 2−60919
ceramics, strength/grain size effects 2−68092
cermet steel, dynamic hot pressing, thermal treatment effects 2−84146
cermet. ZHGp1.5D2.5, effects of cooling after sintering on struct. and mech. properties 2−77722
Charpy impact specimens, irradiated, testing 2−60926
codes of practice, asset or liability 2−56891
composite, fibre reinforced, review 2−61009
composite, glass-crystal two-phase, theory 2−74860
composite, Ni-Cr base alloy, Mo alloy or W filament reinforced 2−56988
continuous testing apparatus for crack detection using water-washable penetrants 2−56857
conversion of hot strength parameters to different temperatures 2−64742
cracks, radial, in a circular ring, elastic anal. and comparison to internally pressurized cylinders 2−69647
creep rupture, applic. of wedge-crack growth theory for hot torsion 2−68095
dynamic biaxial loading in plate testing 2−64750
dynamic errors, instruments with limited stiffness of measuring base 2−45213
elastomers, strength and toughness at low temperatures 2−60886
embrittled specimens, stress-intensity factors 2−60857
fatigue strength of nodular cast iron, testing temp. effects 2−60923

Mechanical strength continued
ferrite memory cores, firing time depend. 2 — 84431
fibre composite, brittle matrix, reinforced 2 — 53968
fibre composite, fracture toughness 2 — 77667
filaments, high temp. testing of strength 2 — 60956
fuel capsule of radioisotopic cardiac pacemakers against fire-arms 2 — 49250
fuel pin burst properties, evaluation of effect of intergranular attack 2 — 76942
glass, $Na^+ \rightarrow K^+$ ion exchanged 2 — 64787
glass, tempered, plate, residual surface stress measurement using birefringence 2 — 60989
glass ceramic, fluor-richterite composition of high mechanical strength, microstructure determ. 2 — 77704
glass safety lenses, drop-ball testing 2 — 42228
graphite, fracture strength and fatigue failure 2 — 53827
graphite, fracture toughness 2 — 56828
graphite, HTGR fuel block, due to irradiation 2 — 56045
graphite composite, Pyrostrand, rel. to fabrication and struct. 2 — 53960
graphite electrode, at high temp., integrated evaluation 2 — 56813
graphite-epoxy composites, radiation effects on mech. props. 2 — 64795
illite, microstructure and chemical comp. 2 — 84710
jade, toughness 2 — 50856
low alloy steel, creep rupture strength, microstruct. depend. 2 — 77685
Lower Devonian sandstone, strain rate effects 2 — 54735
material integrity of mechanical structures by computer interpretation of vibration analysis 2 — 60925
materials testing automation, review 2 — 77687
metal, needle-like microcrysts., adsorption effects, ion emission microscope obs. 2 — 80729
metal, notch toughness characterization, criteria and design of expts. 2 — 60922
metal-ceramic materials, technique for determ. 2 — 68161
metal-matrix composite materials, development 2 — 43900
metals, review of dislocation substructure strengthening and mechanical-thermal treatment 2 — 84099
mica glass-ceramics, rel. to microstruct. 2 — 60999
9Ni-4Co-0.30C, fracture mechanics of crack growth at elevated temperatures 2 — 56867
non-destructive testing of stressed materials, meas. of internal noise 2 — 60927
nondestructive testing, a 1972 up-date 2 — 56892
polymer films, filled with fragmented glass fibres, mechanical anisotropy 2 — 84131
polymer films, rel. to mol. orientation, sound vel. obs. 2 — 47536
polypropylene, effects of cooling rate from melt 2 — 56908
Rebinder effect, applications 2 — 53869
refractory carbides, nitrides and borides, NASA research 2 — 64801
refractory metal, at elevated temps., vacuum technique obs. 2 — 77683
refractory oxide, oxide filament reinforced 2 — 56973
resistance to fracture of materials, particularly metal alloys, physical and technological significance 2 — 71580
rheological approach to cumulative damage and strength 2 — 52136
rocks, fracture and flow 2 — 57822
rupture, instrument for recording time of initiation 2 — 71610
SAP-1 plate, effect of recrystn. 2 — 53870
solid, effect on pressure pulse propagation 2 — 68074
spring material under atmospheric ambient 2 — 43748
steel, 18-8 stainless, carbide precip. rel. to creep rupture strength 2 — 77684
steel, 38KRM Yu A, strengthening and roughness of rubbing surfaces, effect on wear and bearing capacity 2 — 60916
steel, austenitic, after strengthening by ageing 2 — 53876
steel, deformed by reverse bending, fatigue behaviour 2 — 50769
steel, fracture toughness, effect of heat treatment temp. 2 — 53842
steel, high-speed W-Mo, effects of Co 2 — 53992
steel, hot-worked austenitic and ferritic, rel. to recrystn. during continuous cooling 2 — 53873
steel, impact props, rel. to FeO type inclusions 2 — 47530
steel, impact strength, effect of grain boundary form 2 — 80765
steel, impact strength, influence of cold rolling and heat treatment 2 — 80777
steel, low alloy, microduplex processing effects 2 — 43835
steel, low carbon, inelastic phenomena and kinetics of damage for cyclic loading 2 — 60915
steel, low-alloy, effect of Ce addition 2 — 53831
steel, low-alloy, structural behaviour during controlled rolling 2 — 64778
steel, low-C, low-alloy, effect of AlN precip. 2 — 50833
steel, martensitic, effect of lath boundary precip. on fracture toughness 2 — 57018
steel, martensitic stainless, ageing effects 2 — 53989
steel, medium carbon, effects of forge quenching treatment 2 — 80806
steel, multilayer, effect of soft layer percentage 2 — 53824
steel, quenched, tempered, resist. to plastic deform. and cold brittle failure 2 — 47502
steel, stainless, melted by different methods, O impurity effects 2 — 53899
steel, ultrahigh strength, untempered, high fracture toughness 2 — 53872
steel, untempered, low-alloy, segregation effects and toughness 2 — 80822
steel, u.s. vibr. effects 2 — 53877
steel alloys, high strain rate effect 2 — 60877
steel targets, effect on ballistic behaviour 2 — 60980
strong materials, book 2 — 60878
testing method, effect of error on statistical spread 2 — 53847
testing of materials using liquid crystals 2 — 60931
thermoplastics, long term strength, ductile failure, brittle failure 2 — 43718
titania, room-temp. strengths for various biaxial stress states 2 — 77677
untempered ultrahigh strength steels of high fracture toughness 2 — 53872
u.s. nondestructive material testing, h.v. magnetic pulser cct., patent 2 — 84166

Mechanical strength continued
vibration, machine for testing, constructional foam plastics 2 — 56847
weld metal, toughness below 0°C, effect of metallurgically conditioned inhomogeneities 2 — 74890
welded joints, finite element method of strength assessment 2 — 63065
Zircaloy-2, containing ZrH_x, fracture toughness 2 — 47649
Ag, films, indentation and impact studies of loading 2 — 77708
$Al-Al_2O_3$ alloy, ball-milled 2 — 53887
Al-B composite, deform. and failure under transverse loading 2 — 84110
Al-Mg-Si alloy, strength rel. to dislocation motion and GP zones 2 — 56717
Al-Mg-Si alloy, toughness, effect of extrusion temp. 2 — 60974
Al-Zn-Mg-Cu-Mn forging alloy, fracture toughness rel. to microstructure 2 — 53826
Al-Zn-Mg-Mn alloy, rel. to rest between quenching and ageing, effect of additions 2 — 50803
Al-Zn-Mg alloy, toughness, effect of extrusion temp. 2 — 60974
Al, effect of dislocations on substruct. strengthening 2 — 50763
Al alloy, superstrength, by continuous cyclic thermomech. treatment 2 — 47614
Al alloy hand forgings, fracture toughness and stress corrosion cracking 2 — 60905
Al alloy hand forgings, fracture toughness and stress corrosion cracking 2 — 60906
Al alloys, multiphase, strengthening by dislocation substructures 2 — 56706
Al pressure-vessel alloys, tensile, creep and stress-rupture tests 2 — 77671
Al_2O_3, alumina, characteriz. 2 — 50863
β-Al_2O_3, alumina, hot-pressed, characteriz. 2 — 50875
Al_2O_3, alumina, phosphate bonded, elec. microscope obs. 2 — 77662
Al_2O_3, biaxial flexure tests 2 — 60919
Al_2O_3, high temp. strength improvement by surface prestressing 2 — 50870
Al_2O_3, sapphire filaments, strength enhancement due to continuous flame polishing 2 — 80867
Al_2O_3 ceramic, fine grain, Cr_2O_3 additions effect 2 — 50867
Al_2O_3 ceramics, high temp. characteriz. 2 — 50868
$Al_2(SiO_3)_3$, room-temp. strengths for various biaxial stress states 2 — 77677
B epoxy composites, irrad. in nuclear reactor, strength 2 — 80801
Ba-mica/Al_2O_3 composite 2 — 56977
$3BaO.5SiO_2$ glass-ceramic, mechanical props. 2 — 53930
C-C composite, fluted core, 3D reinforced, effects of processing 2 — 53961
C-graphite matrix composites, effects of microstruct. 2 — 61015
C composite, filament wound cylinders, CVD C infiltrated, mech. props. 2 — 56985
C fibre, and Griffith equation 2 — 53944
C fibre monofilament substrate/chem. vap. deposited B composite 2 — 53956
Co-Cr-C alloy, effect of $Cr_{23}C_6$ precip. on strengthening 2 — 57011
Co-base composite materials, superalloys with fibres obtained by directed solidification, properties 2 — 64793
Co alloy, hot strength, mech. props., microstruct. 2 — 50831
2-$^1/_4$ Cr-1 Mo steel, effect of carbon content on high temperature properties 2 — 60880
Cu-Bi alloy, grain boundary fragility and segregation 2 — 53830
Cu-X alloy, X = Mg,Cd,Zr,Cr,Ag, weakening resist. rel. to deform., heating time and temp. 2 — 50764
Cu, inelastic phenomena and kinetics of damage for cyclic loading 2 — 60915
Cu, influence of air, oxygen or vacuum on durability 2 — 60912
Cu base solid solution, grain boundary strengthening 2 — 53891
Fe-Cu alloy, dispersion strengthening model, yield strength 2 — 50744
Fe-Mn alloy, austenitic, strengthening coeffs. 2 — 50783
Fe-Ni alloy, quenched, aged, toughness, ductility, inverse temp. depend 2 — 47501
Fe, strengthening mech., dynamic strain ageing, dislocation struct. 2 — 56911
$HfN-ZrB_2$ cutting tool materials characteriz. 2 — 50883
HfN, hot pressing for high temp. bearing applications, NASA research 2 — 64801
$Li_2O-Al_2O_2-SiO_2$ glass-ceramic, effect of microstruct. and heat treatment 2 — 53931
MgO, hot-pressed, strength and fracture reln. to annealing rates 2 — 71589
Mo-Hf, internal nitriding, high-temp. props. 2 — 60968
Mo, effect of B addition 2 — 56943
Mo alloy, strengthening by precip. of Ti and Zr carbides during ageing 2 — 47643
Mo base alloys, properties under He high temperature conditions 2 — 42674
Nb, multi-mechanical-thermal- treatments, role of oxygen and nitrogen solutes 2 — 64722
Nd, technological props. 2 — 47532
$Ni-HfO_2$ powders, effect of dispersion strengthening phase on thermal stability 2 — 77739
$Ni-ThO_2$, dispersion-strengthening effects on hydrogen susceptibility 2 — 74862
Ni-base composite materials, superalloys with fibres obtained by directed solidification, properties 2 — 64793
Pt-Nb alloy, strength characts. 2 — 47533
Pt-Re alloy, strength characts. 2 — 47533
Pt-Ta alloy, strength characts. 2 — 47533
Pt-Ti alloy, strength characts. 2 — 47533
Pt-W alloy, strength characts. 2 — 47533
SiC, and base composites, impact strengths, 72-2400°F 2 — 60885
SiC, and strength oxidation resist., thermal shock resist. 2 — 60882
SiC, polycryst., effects of crystallite size 2 — 56774
$Si_3N_4-Cr_2O_3$ refractories impact strength and porosity depend. 2 — 68162
Si_3N_4, and base composition, impact strengths, 72-2400°F 2 — 60885
Si_3N_4, ceramic, hot pressed, strength fracture energy, microstruct. relationships 2 — 60883
Si_3N_4 ceramic, hot-pressed, at high temps. 2 — 60884
Ti-(13 wt.%)V-(11 wt.%)Cr-(3 wt.%)Al, deformation substructures rel. to strengthening56950 2 — 56950

Mechanical strength continued
  Ti, dislocation structure effects 2−56714
  Ti martensite, effect of Si, Zr, Al and Mo on struct. and strength 2−64723
  UO$_2$, rel. to porosity 2−43699
  V-Ti(Cr)(Sn)(Al) alloys 2−53912
  Zr containing refractories, influence of Cr$_2$O$_3$ content, increase on addition of CeO$_2$ 2−84095
  ZrC$_x$ fibres, physical and mech. props. detn. 2−68178
 compressive
  — 2−66536
  aluminas, polycrystalline, influence of texture on mechanical props. 2−68093
  bismuth oxide ceramics, rel. to use in nuclear reactors 2−83064
  brittle materials under compressive forces, limiting strength problem 2−80736
  clay, fusible, change on calcining 2−64784
  Coconino sandstone, fracture under confining pressure, effects of pore-fluid chemistry, temperature 2−68858
  compliance K-calibration for a pressurized thick wall cylinder with radial crack 2−69644
  composite, fibre reinforced resin, effect of metal incorporation 2−50923
  elasto-plastic plates, nonlinear analysis 2−73389
  fatigue, alternating tension and compression, plain and notched high strength mats., 500-700°C 2−74870
  ferrous alloys, strength-differential effect, effective modulus interpretation 2−74853
  glasses, elastic deformations in hardness testing 2−64739
  norite, post-failure stress strain path dependence 2−62009
  oval cylindrical shell, buckling and initial postbuckling 2−76290
  polymeric rod, influence of cold extrusion and cold drawing, directional effects 2−80810
  polypropylene, hydrostatically extruded, yield strength 2−43709
  pyrocarbon coating, neutron irrad. effects on crushing stress 2−56771
  pyrofoil tape, production and characterisation for reactor use 2−56050
  pyrophyllite, firing temp. depend. 2−50890
  rock, brittle, complete stress-volumetric strain equation, up to strength failure 2−75455
  rocks, effect of triaxial stress system 2−72679
  rocks, statistical theory of polyaxial strength 2−72670
  Solenhofen limestone, effect of strain rate changes 2−62007
  steatite, firing temp. depend. 2−50890
  steel vessel, welded, internal pressure tests 2−68153
  steels, carbon, dynamic strengthening singularities under infl. of shock waves 2−84075
  thick walled cylinder failure test-machine using fracture mechanics on pressure cycling 2−69501
  ALN-Al$_2$O$_3$-MO cermet 2−43869
  Al bar, annealed, containing a circumferential semicircular notch 2−77689
  Cu, dynamic strengthening singularities under infl. of shock waves 2−84075
  Fe, dynamic strengthening singularities under infl. of shock waves 2−84075
  HfC, hot pressing for high temp. bearing applications, NASA research 2−64801
  MgO-SiO$_2$-Al$_2$O$_3$, compaction and contraction behaviour after pressure sintering 2−57226
  Ni, dynamic strengthening singularities under infl. of shock waves 2−84075
  Ti, dynamic strengthening singularities under infl. of shock waves 2−84075
  ZrC-NbC, solid solution, creep over temp. range 2600-3150 K 2−84033
 shear
  calcium stearate lubricant monolayers 2−53383
  composite, C continuous fibre reinforced ceramics and glass 2−50919
  composite, unidirectional C-fibre reinforced plastic 2−74921
  cracks, circular, propagation for tension and torsion 2−60900
  cyclic straining, subgrain formation 2−80763
  Georgia marbles, pressure dependence to 80 kbar 2−54741
  interfacial, Auger electron spectroscopy 2−56571
  mild steel and plexiglass, detonative loading, breakage and stress waves 2−84048
  nematics, method for meas. shear viscosity 2−50329
  oil-extended vulcanizates, SBR, dynamic props., principle of superposition of time, temp. and conc. 2−83367
  pastes and polymers, shear strength limit, deform. processes 2−68085
  plastic, C-fibre reinforced, interlaminar-shear fatigue props. 2−71656
  polymer systems, conc., constitutive equations for nonlinear viscoelasticity 2−82316
  polymers, solutions and melts, review of recent non-linear viscoelasticity expts. 2−83364
  polystyrene solution and latex, nonlinear viscoelasticity 2−83368
  rubber, relationships between viscosity meas. at variable rates of shear and processing behaviour 2−53788
  Solnhofen limestone, pressure dependence to 80 kbar 2−54741
  steel, shear behaviour in heavy forming apparatus 2−53823
  torsional split Hopkinson pressure bar for meas. of materials at high shear-strain rates 2−53821
  Ar, ideal strengths, computer calc. 2−77630
  C, glassy and pyrolytic, activation energies for creep 2−53815
  C fibre reinforced glass, fracture energy 2−84104
  C fibres, adhesion to organic matrices 2−84101
  Cu, deformation potentials for shear strain, determ. of strain-induced shifts of energy levels 2−80976
  KCl crystals, effect of γ-irradiation on critical resolved shear stress 2−47492
  NaCl ideal strengths, computer calc. 2−77630
  Ti, meas. using torsional split Hopkinson pressure-far and pneumatic-mechanical torsion testing machine 2−53797
 tensile
  — 2−71617
  — 2−56919

Mechanical strength continued
 tensile continued
  — 2−56920
  acrylonitrile butadiene styrene, temp. dependence. 2−53784
  alloy 800, low-cycle fatigue and stress relaxation at elevated temps. 2−60947
  alloys, commercial, method for correlating creep and rupture strengths 2−47607
  bismuth oxide ceramics, rel. to use in nuclear reactors 2−83064
  brittle material, tensile testing, application of point loaded discs and blocks 2−66526
  ceramic tile bodies, effect of polymer impregnation on physical and mech. props. 2−80759
  composite, Auger electron spectroscopy 2−56571
  composite, C continuous fibre reinforced ceramics and glass 2−50919
  composite, C discontinuous fibre reinforced ceramics and glass, fracture strength 2−50918
  composite, fibre reinforced resin, effect of metal incorporation 2−50923
  composite, metal strengthened by explosive incorp. of strong wires 2−61011
  composite, steel wire reinforced polyester resin, fracture toughness 2−47528
  composite fuel annular bodies, fracture and elastic props. 2−71588
  composite materials, glass fibre reinforced, laminated 2−84123
  composite porous fibre material, rel. to porosity 2−43707
  $^1/_2$Cr-Mo-V steels, high-strain fatigue properties 2−60948
  cracks, circular, propagation for tension and torsion 2−60900
  deformation behaviour of high temperature materials, model 2−56887
  deformation studies using a combination (synenergy) method of X-ray line profile topography and trans. e. microsc. 2−82432
  earth mantle materials, yield strength meas. method under high pressure 2−60879
  epoxide resin Epidian 2, short-term props. 2−47672
  fatigue, alternating tension and compression, plain and notched high strength mats., 500-700°C 2−74870
  ferrite memory cores, strength rel. to water environment, comments 2−80756
  ferrite memory cores, strength rel. to water environment 2−77652
  ferrous alloys, strength-differential effect, effective modulus interpretation 2−74853
  fibre composites, longitudinal failure 2−64745
  filament reinforced materials, plastic limit behaviour and failure 2−84086
  filamentary specimens, tensile testing machine 2−43759
  galena, as function of shallow tectonic temp. and pressure 2−61969
  glass, effect of high pressure organic impregnation 2−53520
  glass, fluor-richterite comp., treatment for obtaining high strength polycryst. material 2−47651
  glass plastics, porosity influence 2−47522
  glass reinforced plastics, debonding and cracking under tensile and fatigue loading 2−64725
  glass reinforced plastics, stress distribs., debonding, stress concentrators effects, microdamage effects 2−64724
  graphite, nuclear, strength distrib. functions, effect of high temp. fast neutron irrad. 2−53822
  graphite, oriented, rigidity and limiting strength, comparative estimates 2−47475
  graphite, pyrolytic, ribbon for reinforcement 2−56999
  graphite−ZrC$_x$(−Zr) composite materials, rel. to comp. and structure 2−77741
  graphite fibre, fast neutron irrad. effects 2−56992
  graphite from isotruxene carbons 2−61023
  graphite joints, high temperature strength 2−71627
  Inco 713C alloy, low cycle fatigue tests and crack propagation rate at 1400F 2−56885
  Inconel 718, surface integrity effect on fatigue at elevated temps. 2−60944
  joints, diffusion bonded, rel. to pulse echo, testing technique 2−43766
  liquid bridges, effects of reduced pressures 2−71176
  low-cycle, machine for testing 2−64740
  low-cycle creep fatigue testing, method and equipment 2−56874
  low-cycle fatigue cracking, prediction method including biaxial stress and notch effects 2−56888
  metal, cold worked, press. induced thermal activation 2−43781
  metals, polycrystalline and monocrystalline sheet specimens, changes in misorientation during plastic deformation, X-ray study 2−84046
  microhardness tester attachment for meas. of deformation of wire in coiling 2−82129
  mild steel and plexiglass, detonative loading, breakage and stress waves 2−84048
  mullite, press.-sintered, porosity depend. 2−50722
  notched specimens, fatigue strength estimation method 2−73390
  polyethylene, rigidity and limiting strength, comparative estimates 2−47475
  polymer, yield strength, press. effects 2−68094
  polymer films, v. thin 2−60887
  polymeric rod, influence of cold extrusion and cold drawing 2−80810
  polymers, stand for testing 2−71611
  polypropylene, hydrostatically extruded, yield strength 2−43709
  PVA, uniaxially stretched film, mechanical anisotropy 2−83365
  pyrofoil tape, production and characterisation for reactor use 2−56050
  pyrophyllite, firing temp. depend. 2−50890
  pyrrhotite, as function of shallow tectonic temp. and pressure 2−61969
  ratcheting under cyclic axial strain with torsional stress 2−56876
  ratchetting, parametric study for design curves and design rules 2−56895
  reactor fuel particle coatings, meas. technique 2−50790
  reactor fuel particles, irrad., rupture stress, meas. device 2−43772
  reactor fuel post-irrad. test methods and apparatus 2−43775
  Rene 80, Inconel 718, surface integrity effect on fatigue at elevated temps. 2−60944
  Rene 95, Inconel 718, surface integrity effect on fatigue at elevated temps. 2−60944

Mechanical strength continued
  tensile continued
    rock discs and rings loaded in diametral compression, controlled failure 2−62011
    rocks, effect of stress gradient on brittle fracture initiation 2−72667
    rubber, fracture at low temp. 2−43710
    rubber elasticity on chemical relaxation 2−83378
    rupture machine for plastics testing 2−43756
    rupture of perfectly elastic mats., path-independent integral 2−58874
    sapphire filament, void-free, rel. to edge-defined film-fed growth 2−60720
    sphalerite, as function of shallow tectonic temp. and pressure 2−61969
    stainless, type 403, influence of NaCl in steam on v.h.f. high- cycle fatigue 2−60955
    steatite, firing temp. depend. 2−50890
    steatite materials, effect of modifying agents 2−53933
    steel, austenitic, type 316, creep-rupture behaviour relative to boron content 2−60872
    steel, C, effect of structures on mech. props. at dynamic loading 2−84161
    steel, effect of cyclic bending, at 20 and −60°C 2−84080
    steel, effect of isothermal treatment 2−53874
    steel, effect of rare earth alloying 2−53900
    steel, hot impact tension testing 2−60978
    steel, impact strength variation during heat treatment 2−43792
    steel, low-C, effect of grain size, strain rate, and temp. 2−43695
    steel, low-C, hot-rolled, quenched, transformation effects 2−57017
    steel, low-C martensitic, alloying element effects 2−50834
    steel, maraging, plane strain fracture toughness tests 2−60979
    steel, martensitic, low-C Mn, effect of Sb on high temp. tempering, tensile testing 2−56905
    steel, mild, dissolved oxygen influence 2−47628
    steel, Mn-Cr-B spring, tempering behaviour 2−77688
    steel, pearlite, yield strength, struct. effects 2−43724
    steel, sintered, for fuel element jackets, processing and mech. characterization 2−76951
    steel, stainless, AISI 304, low-cycle fatigue, effect of strain rate and hold periods 2−60954
    steel, stainless, characteriz. for fast breeder reactors 2−50648
    steel, stainless, low-cycle fatigue and stress relaxation at elevated temps. 2−60947
    steel, thick-walled cylinders, fatigue strength 2−64781
    steel, true hardening curve between −196 and +25°C 2−56843
    steels, stainless, types 301 and 304, different strain rates 2−64746
    styrene-diene-styrene block copolymers 2−71584
    test data analysis methods 2−58821
    testing device, usable from room temp. to −150°C in electron microscope 2−71613
    testing of metals saturated with gases in glow discharge 2−47564
    thermal ratcheting, review 2−56875
    thermo-plastics, long-period rupture strength and time welding factors 2−53880
    thermoacoustic fatigue testing of space shuttle thermal protection panels 2−56873
    thin section material, low cycle fatigue bend test method 2−47570
    Waspaloy sheet, sensitivity of creep-rupture properties to sharp-edged notches in temp. range 1000-1400°F 2−47609
    whiskers, apparatus for testing 2−80789
    Zircaloy tubing, effect of oxygen and fabrication variables 2−53915
    Zircaloy-2, dispersion strengthened with yttria 2−53917
    Al/α-Al_2O_3 composite 2−53947
    Al-Li alloys, neutron irrad., inert gas bubble effects 2−43688
    Al, 7075, laser shock-induced yield strength change 2−68075
    Al, high purity, and dil. alloys, review 2−68076
    Al alloy strip with steel rod inserts, transverse tensile properties 2−64701
    Al bar, annealed, containing a circumferential semicircular notch 2−77689
    Al pressure-vessel alloys, tensile, creep and stress-rupture tests 2−77671
    Al single crystal, programme toughened, crit. sliding stress temp. depend. 2−71582
    Al tube, steel wire reinforced, bursting under biaxial tension stresses 2−71661
    Al tube, wound with steel wire, bursting strength and toughness 2−71660
    Al1-5% Mg alloy, tensile tests −50 to 150°C, obs. of serrated flow43706 2−43706
    AlN-Al_2O_3-Mo cermet, bending and compressive 2−43869
    $Al_2O_3/ZrO_2/Y_2O_3$ eutectic, directionally solidified 2−47526
    $Al_2O_3/ZrO_2/Y_2O_3$ system eutectics 2−47525
    Al_2O_3, sapphire, rel. to fracture surface analysis 2−50774
    Al_2O_3, sapphire, temp. depend 2−50762
    Al_2O_3, sapphire filament, fracture strength in tension 2−50917
    Al_2O_3, static and cyclic fatigue behaviour 2−50766
    Ar, ideal strengths, computer calc. 2−77630
    Ar, ideal tensile strength, relationship to surf. energy, expt. 2−64721
    BN, hexagonal, rigidity and limiting strength, comparative estimates 2−47475
    BeO high pressure effects on single crysts. and polycrystalline mat. 2−68082
    C-C composite, rel. to ‘moulded carbon’ process 2−53962
    C-metal composite, high strength, evaluation as sliding material 2−61019
    C, glassy fibres, derived from phenolic resin, mech. props. 2−84100
    C composite, chem. vap. deposited felt and filament wound, flight-tested, phys. props. 2−61017
    C composite, chem. vap. deposited felts, compressed 2−61018
    C fibre-reinforced composite, oxidation effect 2−53951
    C fibre, fast neutron irrad. effects 2−56992
    C fibre, fast neutron irrad. effects 2−80830
    C fibre, neutron irrad. effect 2−43708
    C fibre, S impurity effects 2−50913
    C fibre, thermal expansion anisotropy effects 2−54054
    C fibres, effect of fast neutron irradiation 2−71662
    C PHS composite, PHS, effect of variation in precursor resin on struct. and mech. props. 2−53958
    Co alloys, metallurgical structure and properties 2−71667

Mechanical strength continued
  tensile continued
    Cr-Ni alloy, stress rupture test, hardness, alloying additions effect 2−74856
    2-$^{1}/_{4}$ Cr-1 Mo steel, effect of carbon content on high temperature properties 2−60880
    Cr, coarse-grain melted, failure by rupture 2−68098
    Cr, high-purity phase obs. 2−47531
    Cu-Ni alloy plates for relay thin leaf springs 2−80862
    Cu, deformed at 77K, neutron irrad. effects 2−83968
    Cu, intermetallic compounds, obs. 2−50782
    Cu alloy, containing secondary phases, hot strength 2−84135
    Cu single crystal, programme toughened, crit. sliding stress temp. depend. 2−71582
    Fe-Al-Cr alloys, effect of zirconium 2−60935
    Fe-Co-C, microstruct. effects 2−56941
    Fe-Mg-Ni alloy, austenite transform., cooling rate effect on fracture toughness 2−53991
    Fe-Mn-(B)-C, microstruct. effects 2−56941
    Fe-Ni-C alloy, effect of deform. martensite formation 2−71684
    Fe-Ni alloys, deform. martensite obs. 2−43838
    Fe-Si, influence of microstruct. 2−80778
    Fe-Ta alloy, ductility enhancement using allotropic phase change 2−57020
    Fe-3%Si foil specimens, at low temp., h.v. electron microscope obs. 2−80872
    Fe, Armco, grain size depend. 2−43846
    Fe, grain size and temperature effects on cyclic strength and fracture 2−56896
    Fe, high parity and Swedish pure, creep testing during thermal cycling 2−56881
    Fe single crystal plates, surface orientation depend. 2−71583
    KBr, pure and doped, yield strength 2−56835
    KCl, pure and doped, yield strength 2−56835
    Li_2O-MgO-Al_2O_3-SiO_2, F addition effects rel. to crystallization 2−47058
    Mg-(10.8 at.%)Y alloy, thermomech. treatment for increased ductility and high strength 2−47588
    MgO-$MgAl_2O_4$ system eutectic struct. 2−47658
    NaBr, pure and doped, yield strength 2−56835
    NaCl, ideal tensile strength, relationship to surf. energy, expt. 2−64721
    NaCl, pure and doped, yield strength 2−56835
    NaCl ideal strengths, computer calc. 2−77630
    Nb, yield strength, meas. under high pressure 2−60879
    Ni-Cr-Ti alloys, strengthening by precip. of intermetallic phases 2−43859
    Ni-base superalloy, dispersion strengthened, rotating bending fatigue tests 2−56883
    Ni-base superalloy, low-cycle fatigue with thermal and strain cycling 2−56880
    Ni alloy, microstruct. effects, transmission electron microscope obs. 2−56945
    Ni alloy, relative abilities of time-temperature parameters to correlate and extrapolate stress- rupture data 2−47608
    Ni alloys, dispersion hardened, role of grain size and shape in strengthening 2−71648
    PbS(Se)(Te), carrier conc. effect 2−50784
    SiC, rigidity and limiting strength, comparative estimates 2−47475
    Sn-Pb eutectic alloy reinforced by stainless steel fibres 2−77742
    Ta-W-Hf alloy, effects of O contamination, 1204°C 2−43862
    Ti-Mo base β-alloy, ageing characteristics 2−50807
    TiC-Mo_2C-Ni alloy, rupture strength rel. to microstruct. 2−47538
    TiC-Ni-Mo alloy, cermet, bending strength, Mo alloying effects 2−47534
    W-Re-ThO_2 alloy, creep, strength to rupture, 1800-2200°C 2−64719
    W, at high temperatures, increase due to submicroscopic bubbles 2−71581
    W, coarse-grain melted, failure by rupture 2−68098
    W filament, rel. to appl. to composite reinforcement 2−53970
    W film, chem. vapour deposited, effect of deposition conditions 2−47131
    Zr-(1.5wt.%)Cr-(0.1wt.%)Fe tubing, heat-treated and hydrided 2−53918
    Zr-(2.5wt.%)Nb press. tubes, irrad. effects 2−53913
    Zr-(2.5 wt.%)Nb press. tubing, hydride orientation effect50849 2−50849
    Zr-Sn alloys, solute strengthening at high temps. 2−50846
    Zr alloys, high-strength, characteriz. for press. tubes 2−53921
    Zr alloys, high-strength, development 2−53920
    ZrO_2, calcia-stabilized, fracture toughness 2−50777
Mechanics
    see also Dynamics
    air track photodiode timing gate 2−55347
    autonomous mechanical system, stability theory 2−76242
    Babuska’s paradox of simply supported Kirchhoff plate and finite element method 2−78894
    body filled with liquid, rotating motion 2−66486
    book, 3rd edition 2−41557
    Carter Hall circle, formula for diameter 2−45338
    chain collisions, velocity, momentum and energy transmission 2−55444
    classical, rel. to quantum mechanics, book 2−78830
    classical, use of air table for demonstrating fundamental laws 2−62932
    classical motion of two particles, ASA FORTRAN program 2−52127
    classical relative motion of two particles, ASA FORTRAN program 2−52126
    coin spinning on table 2−73280
    continuous media, finite powers principle application, systemization of forces 2−49049
    continuous media, integral eqn. problems, Hankel and Miller-Fok transforms. 2−63056
    continuum, application of elementary formulas of matrix calculus 2−55375
    continuum, with random loads, method for linear dynamical problems 2−76244
    continuum model of dynamical systems 2−76246

Mechanics continued
cylindrical shell stressed by internal pressure optimal thickness 2−82324
elastic bodies, physico-mathematical foundation 2−52122
elastic half-space, pressure of strip block 2−63057
elastomechanics, bounds on field quantities in natural vibration problems 2−41609
finite element analysis in mechanics of deformable bodies 2−76248
forces at pivot bearing of compound pendulum 2−45345
impact of spherical tool against sonic transmission line 2−55446
instability of equilibrium of nonlinearity damped holonomic mechanical systems 2−76240
Lagrange's equations, derivation from Newtons second by projection onto moving tangent 2−78724
Lagrangian, rapid determ using complex numbers 2−78725
Lagrangian, with constraints, applic. of differential geometry 2−58827
local equivalence and frame indifference generalizations 2−52056
macroscopic linear laws, conditions for derivation from microscopic law 2−49025
magnetoelastic interaction, relativistic theory 2−41616
Martini perpetual motion machine 2−49051
micromechanics of continuous media, applications to engineering problems 2−58877
Mossbauer spectrometer application to structural mechanics 2−55901
non-holonomic, reduction of differential equations to Lagrangian form 2−52124
non-selfadjoint mechanical systems, stability theory 2−73353
nonlinear solid, thermodynamic foundations 2−56766
nonlinear stochastic problems 2−69629
nonuniform anisotropic media, criteria for optimal design 2−82295
plane mechanisms, structure and classification 2−58824
postcritical behaviour of discrete conservative systems 2−76243
potential energies for which particle motion is same in classical and quantum mechanics 2−78806
reinforced axially symmetric shells, momentless stressed state 2−66487
rock burst mechanics study 2−72696
school physics, concepts 2−55343
simple harmonic motion, a teaching example 2−55445
solid deformable bodies, mechanics rel. to solution of tectonophysics problems 2−81614
stability of rectangular thin elastic plate acted on by 3 concentrated forces 2−69631
structural, integral equation method for boundary value problems solution 2−58826
structural, integral equation method for solution of boundary value problems 2−58825
structural optimization by geometric programming 2−41558
symmetric plane motion, characteristic properties 2−45349
teaching, new approach 2−73271
theoretical and applied, conference (Moscow, Aug. 1972) 2−76247
three-dimensional elastic media, causality in relativistic theory 2−78873
time reversal in classical mechanics, a paradox 2−63055
virial theorem rel. to invariance prop. of Lagrange function 2−82298
C fibre reinforced chem. vap. deposited C composites, micromechanics 2−53955
Mechanics of gases *see Aerodynamics*
Mechanics of liquids *see Hydrodynamics*
Medical science
see also Physiology; Radiation protection
abnormal pulmonary circulatory dynamics, simulation 2−48862
acoustical holographic imaging for diagnosis 2−76089
alpha activity, change in freq. following eye opening and closure 2−78672
alveolar deposition of aerosols, algebraical model 2−69234
aorta, in vivo meas. of press./vol. characts., balloon pulsation system 2−62830
aortic diameter pulsatile variations, u.s. meas. 2−51944
arterial stenoses models, flow, geometry influence 2−51904
arterial volume determ. using aortic characteristics 2−73172
automated radiation therapy, synchrocyclotron sterotaxis 2−69315
biology and health physics division Atomic Energy Canada, progress 2−85132
bioluminescence phenomena, new biotelemetric method 2−85112
biotelemetry, conference (Nijmegen, Netherlands, May 1971) 2−82003
biotelemetry system, operating in 1 to 7 channels 2−82006
biotelemetry systems and techniques, conference (Pretoria, S. Africa Dec. 1972) 2−73179
blood bank computerized management information system 2−82031
body composition, dual photon radionuclide absorptiometry 2−69294
bone Ca content from neutron activation analysis 2−69364
bone scanning, internal dosimetry of ^{85}Sr, ^{18}F, ^{99m}Tc polyphosphates 2−55274
bore mineral content of the radius, femoral neck and thoracic vertebrae 2−69356
calcipenic osteopathy, X-ray densitometry, computer evaluation 2−69374
celebral scanning, comparison with neuroradiology 2−48887
cellular response to radiation, computer generated model 2−69326
chronic respiratory monitoring using ultrasonic spirometer 2−55247
ciliated organisms, model for micro-structure and fluid movement 2−78651
clinical diagnosis, u.s. pulse echo visualization 2−51942
clinical laboratory, on-line data acquisition effectiveness 2−62862
conference, Gothenburg, Sweden (1972) 2−69231
contaminant retention by organism, random sequence treatment 2−48877
data retrieval system for recalling interesting scans 2−66262
dental radiography processing system 2−66274
devices displayed at 1972 Physics Exhibition 2−58581
diagnostic clinical indices for human left ventricular chamber 2−69358
diagnostic photography, review 2−76075
diagnostic problem solving methods used by neurologists, investigation 2−76067

Medical science continued
diagnostic ultrasonic moving target indicator systems 2−51931
display systems, reliability 2−85079
distributed sources in human phantom, whole body efficiency calcs. 2−58614
echoencephalography, u.s. tomogram 2−69366
e.e.g. findings in hyperthyroidism 2−45019
future technology, conference (Minneapolis USA Sept. 1972) 2−76055
gamma-ray imaging for diagnosis, imaging cosmetics 2−76077
gammatomography, transversal transmission procedure 2−69232
heredo-familial optic atrophies, diagnostic criteria 2−55317
holography, biomedical applications 2−78662
hormone effects on retention of ^{46}Sc, ^{60}Co, ^{65}Zn, ^{85}Sr, ^{89}Sr, ^{144}Ce in rats 2−55260
hyperbaric oxygen toxicity in central nervous system, changes in electrical activity of brain as criterion 2−62866
in vivo tissue transfer fns., crosscorrelation techniques 2−69214
inspiration- expiration scintiphotographs, det. of intrinsic or extrinsic nature of liver defects 2−66259
integrated human thermal system, optimal control at unsteady state condition 2−69216
i.r. system application 2−84764
i.r. thermography, appls. 2−76076
laser beam applications and fundamentals 2−69961
laser canes for blind persons, design improvements 2−51893
light ions effect on human being 2−58585
line spread function sampling distance choice for MTF computation of radiographic screen film systems 2−78654
living organisms, pathological effects of electric current 2−55207
materials for body replacement devices 2−73176
medical heavy ion beams, composition 2−69321
metabolic processes induced by new radiopharmaceuticals on small animals 2−55223
mobile telemetric equipment for e.c.g. and respiratory frequency data transmission 2−82010
multichannel e.m. flowmeter telemetry system 2−82008
multichannel miniaturized f.m./a.m. telemetering system 2−82009
multichannel telemetry system for physiological data collection during exercise 2−82004
multivariate statistical analysis applications 2−78650
nuclear, gamma camera, applic. 2−73192
nuclear medicine, application of multi-wire proportional chamber 2−49639
nuclear medicine, computer analysis 2−69323
nuclear medicine, diagnostic image quality using scintillation and semiconductor detectors 2−49645
nuclear medicine, nomenclature for Fourier transforms of spread functions of imaging systems 2−76065
occipital spikes rel. to visual evoked responses in photosensitive epilepsy 2−45027
on-line biomedical computing, AAMI Conf., Los Angeles, March (1971) 2−62861
oral mucosa, u.s. echo ranging applic. 2−51945
orthostatic tolerance modification with periodic lower body negative pressure 2−62829
pancreas scanning after ten years' experience 2−76086
patient identification and disease categorization using discriminant and cluster analyses 2−69361
photography, capabilities in terms of human-performance 2−76070
photoscanning, daignosis of splenic infarction 2−66280
physics, course based on hospital field experience 2−55346
pituitary adrenal system, cybernetic aspects 2−69217
plethysmography, venous occlusion, temp. dependence of pressure change 2−45034
polythene catheters, heparinization method 2−69291
programmable four channel radio telemetry system 2−82005
rabbits, phrenic neurons activity, effect of increased respiratory resistances 2−81996
radiation therapy facility at NAL 2−69320
radiobiology, modification of radiation response 2−69325
radioisotope angiography of spinal cord for diagnosis 2−66282
radioisotope metabolism of Na, Cs, Ca, Sr, I, procedures for calc. of metabolic constants in compartment models 2−55222
review paper given to practising doctors 2−85091
secondary standard, therapy- level X-ray exposure meter 2−76149
skeletal muscle dynamics, fatigue, stochastic model 2−69215
skin contamination, rel. to contaminative behaviour of $PuCl_4$ on protein film 2−78648
skull bone, specific acoustic impedance, broad band ultrasonic technique 2−48890
speech analysis for laryngeal disorder detection 2−45072
standardization in health care 2−66255
sterilisation, throw-away medical articles using Van de Graaff generator 2−85119
three dimensional density reconstruction from series of two dimensional projections 2−49047
three-channel telemetry system for e.e.g. and e.c.g. 2−85097
total body Ca from meas. of ^{37}Ar in expired air after low level neutron irradiation 2−69365
tracer kinetic data, optimization procedures 2−48885
transcutaneous aortovelography and cardiovascular information 2−69357
transmission-emission scanning in diagnosis of pericardial effusion 2−58606
tumor sensitivity, synergistic effect, hyperthermia 2−69329
ultrasonic arteriography using phase locked echo tracking for meas. of arterial diameter changes 2−51932
ultrasonic Doppler probe for studying foetal cardiac activity 2−51939
ultrasonic imaging, with good lateral resolution, for medical diagnosis 2−51935
ultrasonic pulsed Doppler velocity detector, evaluation 2−51933
urinary tract flow dynamics 2−51902
u.s. B-scanning in differentiation of Baker's cyst and thrombophlebitis 2−78636
u.s. rotational fast scanner applic. to diagnosis 2−51943
Wiener filters, digital image processing, nucl. medicine 2−82810
wound contamination with insoluble ^{239}Pu and ^{241}Am, treatment and control 2−58592

Medical science continued
  X-ray visualization and memorization device 2—76744
  π^- beams, radiotherapy, biomedical facilities 2—69341
  ^{141}Ce, mechanism of uptake in isolated perfused rat liver 2—55225
  ^{144}Ce, biological half-life in human chest determ. from in vivo meas. following accidental inhalation 2—55233
  ^{60}Co, absorption and retention in man, det. by whole body counting 2—62841
  ^{60}Co teletherapy apparatus, rotational type 2—69349
  ^{137}Cs, ^{133}Cs, distrib. of radioactive and stable isotropes to human body 2—55224
  ^{152}Eu, mechanism of uptake in isolated perfused rat liver 2—55225
  ^{67}Ga scintillography, detection of metastatic lung tumours 2—48886
  pO_2 telemetry system for obs. during exercise 2—82011
  ^{239}Pu, determ. of quantity in living human organism from rate of elimination 2—55301
  ^{239}Pu, in lungs, determ. of effective tissue thickness 2—85124
  ^{224}Ra, ^{226}Ra, analysis of γ spectra in non-equilibrium with decay products, application to retention in mice 2—58615
  ^{90}Sr concentration in human bones, ratio of spongious/compact bone in relation to age and time 2—58594
  wound contaminated with Pu, assessment and treatment 2—58593
  ^{175}Yb, mechanism of uptake in isolated perfused rat liver 2—55225
Meissner effect *see Superconductivity*
Melting
  see also Zone melting and refining
  alloys production by ultrasonics that are otherwise difficult to make 2—50820
  covalent crystals IV-IV III-V and II-VI scaling theory of melting temperatures 2—74583
  crystals, monatomic, entropy and free energy 2—53488
  4-ethoxy-4′-n-alkanoyloxyazobenzenes, anomalous melting behaviour at solid-nematic transition 2—56483
  glaciers, eustatic sea level change and deformation of Earth 2—75448
  glass, Ag activated phosphate, dosimetry props. rel. to heat treatment 2—51381
  glass, nontransparent quartz, colour centre formation, importance of melting temp. and atmosphere 2—84482
  Green's functions for solving problems in cylindrical coordinate system 2—47030
  h.p., pair pots. rel. to melting curves 2—56541
  ice, classical wire expt., heat conduction mechanism 2—45587
  ice, permittivity evolution in premelting stage 2—53497
  large earthquakes, melting on fault planes 2—72637
  lattice theory, Lennard-Jones and $1/r^{12}$ system 2—77468
  liquid structure at very high pressures, X-ray diffraction studies along melting curves 2—67799
  lunar rocks and minerals, impact induced rel. to normal 2—51821
  melting-curve maximum criterion for systems with exponential type repulsive pair potentials 2—71272
  metal, shear modulus near the melting point and internal pressure 2—80746
  metallic conductors under action of large current impulses 2—77469
  metallurgical vacuum melting and degassing, activated reactive evaporation 2—55336
  naphthalene crystal faces, appearance of nonsingular surfaces on equilibrium form. 2—50561
  nematogenic azobenzene derivatives, anomalous melting behaviour at solid-nematic transition 2—56483
  nuclear fuel, peak burnups optimization 2—49882
  phlogopite + enstatite, stability at high pressures, model of micas in upper mantle 2—78221
  poly(ethylene oxide), cryst. from soln. 2—83361
  poly(ethylene terephthalate) superheating and reorganization 2—71271
  poly(ethyleneterephthalate) multiple endotherm melting behaviour due to recrystallization, relation to morphology 2—71291
  poly(hexamethylene sebacamide) (nylon 610), effects on dielectric relaxation 2—44151
  polychloroprene-rubber, rel. to recrystalliz. and reorganization processes, calorimetric obs. 2—71289
  polyethylene, behaviour of sample crystallized in pressure capillary viscometer 2—60546
  polyethylene, high pressure 2—50414
  polyethylene oxide, data used to compute end interfacial free energy 2—71274
  polyethyleneoxalate, polyethylenesuccinate, intramolec. contributions to entropy and energy of fusion 2—46637
  trans-1,4-polyisoprene, equilib. melting temp. of two crystalline modifications 2—71292
  polystyrene, isotactic, melting behaviour 2—47034
  rocks, partial melting under low stresses 2—57764
  rubber, multiple melting transitions 2—60545
  sludges and slurries, aqueous, effect of freeze/thaw treatment on precip. 2—83807
  snow, runoff and heat balance in small drainage area 2—75444
  solid solns., metallic, application of Lindemann's rule for melting 2—74582
  solids with U_s-u_p linear relationship, melting line determ. 2—80518
  steel, in Fe-C melts, heat and mass transfer obs. 2—43438
  steel plates in Fe-C melts, melting problem, numerical solution 2—60543
  system, plastic deformation, microhardness, emission electron microscopy 2—74843
  water, porous rocks, periglacial zone, freezing-thawing process 2—75446
  Al_2O_3, vol. change 2—80465
  BP-P system, h.p. phase equil. 2—50956
  Be, melting enthalpy 2—53491
  Bi, phenomenological relationship between solid and liquid phases 2—74581
  Co, density at elevated temps., exptl. results for liquid and solid phases 2—64505
  Cr-V alloy system, melting equil. diagram 2—47709
  Cr_2O_3, vol. change 2—80465
  Cu-Au alloy, strain energy effects 2—53492
  Er-B system, temp.-comp. phase diagram 2—50964
  Fe, density at elevated temps., exptl. results for liquid and solid phases 2—64505
  Fe, thermodynamic properties, significant structure theory 2—56542
Melting continued
  Fe liquid and Ni alloy, thermodynamic study by electromagnetic levitation melting in inert atmosphere 2—67871
  Gd-B system, temp.-comp. phase diagram 2—50969
  H_2S, solid, lower phase transition temp. 2—50398
  ^{3}He, solid, review 2—80515
  In, polycryst. thin film, e. diffr. study 2—83845
  In small particles, size effect 2—43439
  $KAlSi_3O_8$-Al_2O_3-SiO_2-H_2O system, muscovite melting to 30 kbars 2—61851
  KBr, effect on multiphonon i.r. absorpt. spectra 2—68220
  LiF, effect on multiphonon i.r. absorp. spectra 2—68220
  Na, coherent X-ray diffraction patterns at very high pressures, along melting curve 2—67803
  NaCl, effect on multiphonon i.r. absorp. spectra 2—68220
  Ni, density at elevated temps., exptl. results for liquid and solid phases 2—64505
  Pb small particles, size effect 2—43439
  SiO_2CaO-Al_2O_3 glass, stratification, liquation, opalescence 2—56564
  Sm_2O_3, vol. change 2—80465
  U, melting enthalpy 2—53491
  UF_4, induction levitation melting 2—50810
  UF_4 h.f. levitation melting, prep. of targets 2—73906
  Zn energy of melting from nonlocal pseudopotential theory 2—60544
  ZnTe, entropy of melting, DTA determ. 2—47033
Melting point
  σ phases melting points and compositions 2—80799
  p,p′-di-n-alkylazobenzenes, melting point and dielectric constants, determination and explanation 2—56484
  p,p′-di-n-alkylazoxybenzenes, melting point and dielectric constants, determination and explanation 2—56484
  eutectics, as secondary temp. standards above 2327 K 2—53489
  melting pt./volume relation and Gruneisen const. functional 2—47031
  metal, single-atomic activation energy at temp. of fusion 2—71152
  minerals in Earth's mantle, olivine, spinel and periclase melting curves 2—57481
  molecular crysts., rel. to intensity of incident u.v. radiation 2—50399
  molecular dynamics simulation 2—56540
  Ag-Cu alloy, eutectic, freezing and melting point determ. 2—53486
  α-Al_2O_3, corundum, high temp. calorimeter obs. 2—53490
  Bi, superheated, anomaly between small particles and bulk 2—77467
  $CaSiO_3$-$NdSiO_5$ system, homogeneous phase 2—47707
  $CdGeP_{2x}As_{2-2x}$, comp. depend. 2—47616
  $CdGe_xSi_{1-x}P_x$, comp. depend. 2—47616
  CsCl, effects of KCl and NaCl additions 2—43932
  Cu film, growth kinetics near melting point 2—60652
  Dy_2O_3-WO_3 solid soln., of phases 2—57013
  EuO, determ. by sealed crucible technique 2—67872
  EuS, determ. by sealed crucible technique 2—67872
  EuSe, determ. by sealed crucible technique 2—67872
  EuTe, determ. by sealed crucible technique 2—67872
  Ga, lowering by presence of Cr 2—64817
  $Gd_2O_3.GaO_2,Ge_2O_3.2GeO_2$, from phase diagram of Gd_2O_3-GeO_2 system 2—84097
  Hg-Tl system, press. depend. of m.p. of Hg_5Tl_2 2—71273
  $IrB_{1.1}$ characterization 2—47657
  $LiCl$-$UCl_{3(4)}$ systems, binary and ternary, melting point diags. 2—67873
  Mo, temp. secondary fixed point 2—53493
  Nb, pulse heating method 2—53487
  Pb film, growth kinetics near melting point 2—60652
  W, determ. by pulse heating method 2—74584
  ZnTe, DTA determ. 2—47033
Membranes
  biological, plasticity, nonstatic model 2—81989
  capacitance microphone, dynamic deflections 2—41767
  cellulose acetate, porosity rel. to intrusion cell formation 2—53420
  charge-mosaic, piezodialytic salt flux reduction, geometric effects 2—53419
  charged, determination of semi-permeable characteristics, diaphragm cell for 2—68758
  charged, ion separation by hyperfiltration through, calculation based on Teorell-Meyer and Sievers model 2—50351
  collodion-polybase, charged, ion separation by hyperfiltration through, separation performance 2—50352
  cylindrical film equil. under hydrostatic press., axisymmetric problem 2—78903
  deformation of nonlinear membranes subjected to internal pressure 2—76312
  elastic, curved, geometry induced equil. hysteresis 2—43668
  elastic, homogeneous, incompressible, isotropic, deform. 2—78880
  elastic, stability of finite deformation 2—58872
  elastic, stability under finite deformation 2—52181
  elastically supported vibrating, bounds for lowest eigenvalue 2—82346
  excitable, dipole model and cooperative behaviour 2—60459
  insoluble monolayer leakage across movable barriers, radiotracer detection method 2—53416
  ion exchange and electrolyte solution, Hall mobility 2—43386
  ion-exchange, multicomponent solution hyperfiltration, integration method for extended Nernst-Planck eqns. 2—53418
  kettledrum, vibration 2—41647
  phospholipid, $^{22}Na^+$ effects 2—58587
  polymer, self-diffusion through of organic vapours, obs. using radio tracer technique 2—71180
  preselective, ion and water movements, equilib. props. 2—60460
  pressure membrane cell for use in pressure filtering 2—68757
  rubber fluid storage bags, mech. behaviour, contact problem 2—66497
  spinning disc with central hub, coupled transverse vibrations 2—78904
  thermodynamics of electrocapillary phenomena and thin films 2—43344
  thick, behaviour under small deflections, singular perturbation methods 2—45441
  thin membrane shells, generalised theory of elastic plastic deformation 2—45414
  α-tocopherol, photovoltaic e.m.f. 2—85089

Membranes continued
- transport, against external driving force due to mass transfer reaction coupling 2−56493
- ultrathin, pore size distrib., N_2 gas adsorption isotherms, -195°C, BET equation 2−74537
- vibrating, in stream of ideal liquid, determ. of lifting force and longitudinal momentum 2−83744
- vibrating, natural freqs., estimation method 2−49093
- vibrating clamped, isoperimetric inequality for first eigenfunction 2−58898
- vibration freqs., stability of finite difference methods 2−63102
- water transport across, study technique 2−69207

Memory devices *see Calculating apparatus; Magnetic devices; Storage devices; Superconducting devices*

Mendelevium
- No entries

Mendelevium compounds
- No entries

Mercury
- adsorbed on ZnO, interaction between molecules and adsorbed atoms 2−47175
- adsorption on Ni, alloy formation 2−77489
- atom, differential and total cross sections for elastic and inelastic electron scattering at 6.703 eV 2−79881
- atom, electron-impact excitation of 6^1P_1 and $6p'\,^3P_1$ states 2−42732
- atom, interatomic pots. with light projectiles 2−77015
- atom, self broadening of Hanle signals, backscattered light obs. 2−59932
- atomic absorption spectrophotometry, relative sensitivities of 184.9 and 253.7 n.m. lines 2−52489
- atoms, study of electron spin polarization caused by inelastic electron scattering 2−42763
- band struct. and Fermi surface, pseudopot. calcs. 2−64890
- capillary depression, development of equation 2−60403
- contact angle on polymer films, meas. using scanning electron microscope 2−46942
- contamination associated with McLeod gauge vacuum pumps 2−69508
- counter-current flow with N or He in packed bed system, criteria for flooding 2−50294
- critical fluid, thermoelec. power, influence of metal-nonmetal transition 2−60377
- detection by cold vapour fluorescence 2−75405
- diffusion in Sn, obs. and mechanism 2−68054
- discharge, high pressure, incremental impedance 2−71015
- discharge, properties of long capillary positive column 2−60303
- discharge lamp, for illuminating people 2−42251
- discharge lamp, recalibration of spectral radiance in near u.v. 2−79450
- discharge tube, ionization in nuclear reactor 2−53252
- discharge with axially uniform column, arc chopping 2−70995
- droplets, crystallization and nucleation 2−71382
- drops on glass, determ. of smallest non-collapsing drop 2−77492
- dropwise condensation, modified theory 2−52899
- electrical props., evidence for pseudogap 2−77445
- electrodes, metal dendrite formation at limiting current 2−68795
- electron scattering, spin polarization and ang. distrib. 2−42789
- filling of ultrafine channels in zeolites 2−84153
- film, deposited on LiF substrate, thermal He atom scattering 2−56573
- gas discharge tubes, anode glow oscillations, optical studies 2−71020
- Hall mobility meas. apparatus using Corbino method 2−71224
- Hg, vapour pressure, ebulliometric meas. and variations with temp. 2−67877
- HR 4072 and chi Lupi Hg syndrome stars, equivalent width meas. 2−69108
- ideal resistivity, at low temps. 2−57153
- illuminator, with mixtures of K, Na and Rb, at ultra-high pressure, working model 2−45828
- ion sound wave, parametrically excited in Tonks-Dattner resonance, radial pattern obs. 2−70932
- liquid, compressibility, statistical mechanical perturbation theory calc. 2−80461
- liquid, interference functions temp. range 50-150C, X-ray obs. 2−67802
- liquid flow in tube, temp. fluctuation spectra 2−64413
- MHD unsteady free convection flow past infinite vertical plate, variable suction 2−83526
- monomolecular films on Hg, review 2−74645
- muonic atom, energies of 5g to 4f X-rays, higher order vacuum polarization corrections 2−59962
- optical consts. 2−43359
- plasma, afterglow, transition from free-fall to ambipolar diffusion 2−60212
- plasma, parametric excitation of lower hybrid modes 2−70935
- plasma, radially propagating ion-acoustic wave in positive column, microwave scatt. obs. 2−74387
- plasma, s.h.f. emission 2−67641
- polymers contact, electric field effect 2−57236
- pulsed discharge, vapour density decay 2−70991
- rapid mean flow in annular channel produced by moving heat source 2−53355
- shock tube flow of partially ionized gas, boundary layer growth 2−64389
- solid, de Haas-van Alphen amplitude meas. between 1 and 17K 2−57140
- solid and liq., Lorenz number, thermal cond., meas. by modified Kohlrausch method 2−71189
- spectral lamp in u.h.p. cavity resonator, optical pumping 2−73550
- superconducting, aligned mag. inclusion effects 2−64945
- supercritical, conductivity, density depend. 2−54101
- supercritical state, cond. nature 2−60500
- surface active-melt, in contact with Zn, effect on deform. characts. 2−74830
- surface tension, effect of base-metal impurities 2−74534
- surface waves, nonlinear effects when resonantly driven 2−80161
- surface-induced vectorial optical props. 2−77436
- thermal diffusivity, laser flash determ. method 2−53423

Mercury continued
- thermal diffusivity det. by laser flash technique at elevated temps. 2−46946
- thermopower in liq. and supercrit. states, density depend., metal-nonmetal transition 2−60499
- turbulence, small-scale structure, temp. obs. 2−77323
- vapour, absorpt. coeff. meas. in reson. region 2−46428
- vapour, breakdown, effect of changing electrodes at low density 2−74436
- vapour, cond. mechanism in metal-insulator transition range of densities 2−60378
- vapour, electric breakdown potential, Hg vapour, between hemispherical electrodes 2−71030
- vapour, l.p. discharge, secondary ioniz. coeffs. 2−53253
- vapour, nucl. spin relax., solid surface influences 2−42731
- vapour, selective refl., crossing effect between Zeeman sublevels of isotopes 2−79900
- vapour, spectral line intensity in glow discharge in transverse mag. field 2−52919
- vapour discharge, low pressure type, properties 2−71011
- vapour fluorescent lamps, colour and luminous efficiency 2−42250
- vapour laser, performance, review 2−42021
- Venusian cloud size 2−75915
- CO laser, efficiency improvement, patent 2−42010
- Cd-Pb amalgam electrode, standard cell, reduced temp. coeff. 2−82118
- H-Hg elastic scatt., orbiting resons., rel. to vibr.-rot. levels obs. of diatomic mol. 2−77018
- Hg-Ar-Ne discharge, probe measurements in positive column 2−74425
- Hg-Ar and Hg-Ar-N_2 discharges, electrodeless, r.f., electrical characteristics 2−71014
- Hg-Ar arc discharge, cathode spaces, influence of cathode qualities 2−60324
- Hg-Ar discharge, l.p., mass spectrometric analysis of Hg_2^+ form. in positive column 2−83640
- Hg-Ar discharge, voltage frequency influence on instantaneous densities of excited Hg atoms and electronic energies 2−74424
- Hg-Bi-Pb liquid metal systems, effectiveness of boiling separation 2−74594
- Hg-Cd sensitized fluoresc., amplitude modulation 2−64014
- Hg-Xe layer, insulator-metal transition, Wannier exciton disappearance, u.v. spectra obs. 2−51079
- Hg 2537 Angstroms fluorescence rel. to remote sensing of oil pollution on water 2−84771
- Hg quartz arc lamp, far i.r. emission 2−55766
- Hg_2 mol., fluoresc., transitions between vibr. levels and ground state 2−53020
- ^{193}Hg 3.5h, h.f.s. and isotope shift, by new Zeeman-scanned optical pumping method 2−46429
- ^{199}Hg isotope, hyperfine struct. for (6s, 6d) configuration 2−56095
- $^{202}Hg^+$ ion source, collimating system for mass spectrometer, with distributed ionization region 2−69883
- Hg*-CO collisions, electronic-vibrational energy transfer 2−80144
- Hg(6^3P_1), spin-orbit relaxation in presence of various gases 2−46461
- N_2-Hg two-phase system, propagation of pressure wave 2−71148
- inNaCl, vacancy-impurity complex, slow motion press. effects, n.m.r. study 2−72514

Mercury, planet
- daylight observations when close to inferior and superior conjunction 2−48781
- diameter obs. using photoelectric Hertzsprung's method 2−44957
- exospheric and thick and thin atmospheric models 2−78433
- interior, determination of related parameters 2−75888
- Mariner 1973 rel. to exploration of Mercury, mission objectives 2−78503
- null phase obs. using Lyot coronograph 2−44956
- perihelion, Brans-Dicke theory, gravitation 2−78430
- perihelion advance, radar determ., general relativity confirmed 2−51824
- planetology congress (Montreal, September, 1972) 2−78499
- rotational resonances and Cassini's laws 2−78498
- rough surface, circular polarization of scattered light 2−63395
- structure and cartography, review 2−78502
- surface composition from reflection spectrum, 0.32−1.05 microns 2−78556
- unipolar interaction with solar wind, steady state bow shock problem 2−69145
- unipolar interaction with solar wind, steady state bow shock problem 2−44955

Mercury compounds
- halides, molec. bending in dioxane and benzene solutions, determination from i.r. and Raman spectra 2−64463
- mercuric cyanide.tetrahydrofuran addition compound, development of {111} habit 2−60706
- picramate, cryst. data, orthorhombic cell dimens. 2−74754
- Ag-Hg amalgam whisker, growth on Hg surface from aqueous solns. 2−60669
- Cd-Hg alloy, 0-14 at.% Hg, room temp. Hall effect 2−77855
- $Cd_xHg_{1-x}Te$ mixed crysts., reststrahlen spectra, transverse optical modes 2−44366
- Ga-Hg alloy, liq., sp. ht. anomaly near phase separation critical pt. 2−50354
- Hg-Cd alloy, thermodynamic props., calorimetric obs. 2−57056
- Hg-Cd alloys, diamagnetism, susceptibility curves 2−81203
- Hg-Cd(Ga)(In)(Tl)(Sn)(Sb)(Bi) amalgams, dil., viscosity, comp. depend., 0-100°C 2−64451
- Hg-Ga discharge, use of GdI_3 2−53251
- Hg-In alloy, thermodynamic props., calorimetric obs. 2−57056
- Hg-In liquid alloy, partial struct. factors and atomic distribs. 2−64437
- Hg-In liquid alloy, reflectivity meas. from 0.31 to 9 eV 2−64467
- Hg-K melt, electrotransfer and elec. resist. 2−56517
- Hg-Tl liquid alloy, partial struct. factors and atomic distribs. 2−64437
- Hg-Tl system, m.p. of Hg_5Tl_2, press. effects 2−71273
- Hg-chalcogenides, solid-liquid phase equilibrium and physico-chemical properties 2−68759
- $HgAr^+$, rotational analysis of u.v. emission spectrum 2−46553

Mercury compounds continued
$HgAr^+$, rotational energy levels, example of Hund's coupling case (c) 2−50048
HgCN, e.p.r. and chemical bonding 2−50072
$Hg(CN)_2$, crystal growth, through slow decomp. of tetrahydrofuran solvate crystal to the air 2−47208
$Hg_{1-x}Cd_xTe$ and InSb i.r. detectors, comparison for low contrast target detection 2−63142
p-$Hg_{1-x}Cd_xTe$, carrier freeze-out and acceptor energies determ. 2−57194
$Hg_{1-x}Cd_xTe$, sweep out of minority carrier holes 2−54255
$Hg_{1-x}Cd_xTe$ alloy, cryst. growth using Te as solvent 2−47271
$HgCr_2Se_4$, spinel structure formation, X-ray diffract. study 2−77563
HgFOH, ^{19}F and ^1H n.m.r. 2−84591
HgH, quasibound vibr.-rot. levels obs. from orbiting resons. in Hg + Hg scatt. 2−77018
HgI_2, for nuclear particle detection crystal growth and detection props. 2−46037
HgI_2, red tetragonal phase, sublimation growth in vacuum 2−74671
HgI_2 gamma ray spectrometer 2−49627
HgI_2 room-temperature radiation possibilities 2−52692
HgI_2 single crystal, tetragonal, exciton luminesc., temp. depend. 2−84541
HgO, i.r. absorption, reln. to colour and structure changes 2−68643
$Hg(OH)NO_3$, cryst. struct. 2−47331
α-HgS, cinnabar, hydrothermal growth 2−47235
HgS, Cinnabar, refl. spectra and optical constants 2−61615
HgS, hole photoemission into S, 2.11 to 3.54 eV 2−84265
HgS, polytypic growth of single crystals 2−60769
α-HgS, synthetic, rotatory power and Faraday effect 2−75258
HgS, X-ray induced electron emission, core electron energy levels detn. 2−48019
$Hg(SCN)_2$, crystal and molecular structure 2−50620
$HgS_{0.2}Se_{0.8}$ solid soln., plasma i.r. reflection at 100 and 300K 2−54404
HgSe, HgSe-HgS solid solution, optical absorption, energy band struct. obs. 2−84522
HgSe, $\Lambda_3-\Lambda_1$ transition, electrorefl. 2−68624
HgSe, Shubnikov-de Haas effect, effect of uniaxial stress 2−68402
HgSe, sublimation, partial press. of Hg and Se, equilib. total dissociation press. 2−74596
HgSe, X-ray induced electron emission, core electron energy levels detn. 2−48019
Hg_3Te_3-Ge_2Te_3 alloy, transport processes, Hall mobilities, near semimetal-semicond. transition at high press. 2−68406
Hg_3Te_3-In_2Te_3 alloys, h.p. phases, cond. types, band struct. 2−54175
HgTe, electrochem. preparation 2−75384
HgTe, galvanomag. props. in high mag. field, 4.2, 77 and 300 K 2−64988
HgTe, Hall coeff. and self-conc. of carriers 2−61314
HgTe, magnetoabsorpt. of i.r. and submillimetric waves rel. to mag. field, band struct. 2−68294
HgTe, pure, i.r. and magnetooptical absorp. 2−78101
HgTe, reststrahlen spectra, transverse optical modes 2−44366
HgTe films, temp. dependence of Hall coeff. and electrical conductivity 2−54174
$Hg_3Te_2Cl_2$, cryst. growth and optical props. 2−71374
$Hg_3Tl_4As_8Sb_2S_{20}$, vrbaite, cryst. struct. 2−53664
$Hg_2V_2O_7$, high press. prep. 2−71367
HgX_2, (X = halogen), u.v. absorption spectra in aromatic solvents 2−43370
HtTe, X-ray induced electron emission, core electron energy levels detn. 2−48019
In-Hg-Pb alloy, supercond., thermodynamics, role of electron scatt. 2−81038
In-Hg alloy, supercond., thermodynamics, role of electron scatt. 2−81038
In-Hg amalgam, liq. diluted, cond. near metal-nonmetal transition of pure Hg 2−53451
In_2Te_3-Hg_3Te_3 alloy, negative magnetoresist., 77-400K 2−44102
K-Hg alloys, liq., zero wave vector partial struct. factors 2−43318
n-MgTe, interband magnetoabsorpt., $\Gamma_6 \rightarrow \Gamma_8$, transmission obs. at 4.4K 2−68644
Na-Hg alloy, liq., compressibility determ. 2−77415
Na-Hg melt, electrotransfer and elec. resist. 2−56517
Mesic atoms *see Atoms, mesic and muonic*
Mesic molecules *see Molecules, mesic and muonic*
Mesomorphic state *see Liquid crystals*
Meson field theory *see Field theory, quantum/meson field*
Mesons
see also Atoms, mesic and muonic; Cosmic rays/mesons; Hyperons; Kaons; Molecules, mesic and muonic; Pions
baryon non-local field, construction of mesons 2−79463
current algebra sum rules, by hard-meson technique 2−70123
current-stress-tensor commutators and Ward identities 2−73718
meson nucleon sigma terms, theoretical estimate 2−63571
Neveu-Schwarz transition from Ramond fermion, general dual vertex 2−76617
scalar, exchange in μp scattering, cause of anomalies interaction at low energies 2−63526
scalar, in one-boson exchange model for low energy NN scattering using relativistic Blankenbecler-Sugar eqn. 2−67047
spectroscopy, conf., Philadelphia, USA (Apr. 1972) 2−73796
spectroscopy, current problems and future directions, theory 2−73797
weak currents of second class, existence in weak interactions 2−66993
X-particle intepret. rel. to O(4) symmetry 2−55844
absorption
No entries
capture
see also Nuclear reactions and scattering due to/mesons
No entries
decay
3^- nonet of states $\rho(1670)$, $\omega(1680)$, $K^*(1760)$, $\varphi(1820)$ into 0^- and 1^- mesons 2−67038
$\rho(1.71)$, resonance, produced in $\pi^- p \rightarrow p\pi^+\pi^-\pi^-\pi^0$ reaction 2−49582

Mesons continued
decay continued
charmed mesons, leptonic decay in new hadron quartet model 2−70201
e.m., π-p obs. 2−70202
inclusive expts. with unstable particles, kinematics 2−79554
lepton decay, of neutral vector meson, polariz. effects 2−49578
leptonic decay of neutral vector mesons, e.m. corrections 2−70247
nonstrange, produced in K^-p interactions at 3.9 and 4.6 GeV/c, comparison with SU(3) and quark-model predictions 2−66994
quark-loop dynamics, determ. of SU(3) mass splitting of 0^- octet and 1^- nonet 2−73770
radiative lepton decay, of neutral vector meson, polariz. effects 2−49578
resonance decays involving two partial waves, test for basic violation of $SU(6)_w$ 2−63642
resonance decays involving two partial waves, test for basic violation of $SU(6)_w$ 2−63642
vector and tensor, current algebra and the triangle approx. 2−63637
vector meson, $\rho\omega$ mixing phenomena 2−59552
$0^-(J^p) \rightarrow 2$ vector mesons, Einstein Podolsky Rosen paradox investigation 2−73315
$(\eta \rightarrow \gamma\gamma)/(\pi^0 \rightarrow \gamma\gamma)$ decay width ratio, SU(3) prediction 2−79553
$A_{-2} \rightarrow K^0{}_s K^-$, produced in π-p reaction at 20.3 GeV/c, meas. of A2 mass spectrum shape and decay angular distrib. 2−63641
$D^0 \rightarrow \delta^\pm \pi^\pm$, obs. in pp annihilation at 700 MeV/c 2−63640
$E^0 \rightarrow \delta^\pm \pi^\pm$, obs. in pp annihilation at 700 MeV/c 2−63640
E(1420), radiative decay studies 2−52626
η four-body decay rates and branching ratios calc. using vector meson dominance and SU(3) symmetry 2−52590
η in pseudoscalar nonet, review 2−63574
$\eta^0 \rightarrow \gamma$ + positronium, $\eta^0 \rightarrow \gamma$ + muonium, probability calculation 2−45948
$\eta \rightarrow 2\gamma$, approach using scheme of chiral u(4)xu(4) symmetry 2−66996
$\eta \rightarrow 3\pi$, Moffat's model applic. 2−55843
$\eta \rightarrow \gamma e^+e^-$, invariant mass spectrum of Dalitz pair, radiative corrections 2−55807
$\eta \rightarrow \mu^+\mu^-$, $\eta \rightarrow \gamma\mu^+\mu^-$, rate evaluation in baryon loop model 2−45930
$\eta \rightarrow \pi^0\pi^0\pi^0$, SU(3) × SU(3) broken symmetry model 2−70206
$\eta \rightarrow \pi^+\pi^-\gamma$, charge asymmetry, C-invariance 2−59506
$\eta \rightarrow \pi^+\pi^-\gamma$, coupling strengths, interfering meson models, finite dispersion relation restrictions 2−45988
$\eta \rightarrow \pi^+\pi^-\pi^0$, charge asymmetry, C-invariance 2−59507
$\eta \rightarrow \pi^+\pi^-\pi^0$, meson-pole-dominance model calc. and octet scalar mesons 2−66995
$\eta \rightarrow \pi\pi\gamma/\eta \rightarrow \gamma\gamma$ branching ratio calc. 2−63576
$\eta \rightarrow \pi\pi\gamma\gamma$, partial width determ. 2−63576
$\eta \rightarrow \pi\pi\pi$, model satisfying analyticity, crossing symmetry and approximate unitarity 2−76649
η′ in pseudoscalar nonet, review 2−63574
$\eta' \rightarrow \eta\pi\pi$, calc. of decay rate with chiral and dilatational symmetry breaking 2−52591
$\eta' \rightarrow \eta\pi\pi$, decay rate, breaking of chiral and scale symmetries 2−55866
$f^0 \rightarrow KK$ branching ratio, $f^0A_2{}^0$ interference 2−45985
g(1660), with $J^{pc} = 3^{--}$, decay modes 2−63635
K_n(1760, with $J^{pc} = 3^{--}$, decay modes 2−63635
$\omega^0 \rightarrow e^+e^-(\mu^+\mu^-)$,, partial decay widths, e.m. corrections 2−70247
$\omega \rightarrow \pi^-\pi^+\pi^0$, ang. decay spectra 2−63591
$\varphi^0 \rightarrow e^+e^-(\mu^+\mu^-)$, partial decay widths, e.m. corrections 2−70247
$\varphi \rightarrow K^-K^+$, ang. decay spectra 2−63591
$\varphi \rightarrow \eta\gamma$ e.m. decay mode, branching ratio, π-$p \rightarrow \eta\varphi$ reaction obs. 2−63643
$\varphi_n(1650)$, with $J^{pc} = 3^{--}$, decay modes 2−63635
$\varphi_n(1830)$, with $J^{pc} = 3^{--}$, decay modes 2−63635
ρ electroproduction and decay to 2π 2−79601
$\rho^0 \rightarrow e^+e^-(\mu^+\mu^-)$, partial decay widths, e.m. corrections 2−70247
$X^0 \rightarrow \gamma\gamma$, from $\pi^-p \rightarrow$ neutral meson + neutron at 3.8 GeV/c, meas. of branching-ratio 2−67037
$X^+ \rightarrow \pi^+\pi^-$ interpret. rel. to O(4) symmetry 2−55844
X° (960), radiative decay studies 2−52626
detection, measurement
pp annihilation spectrometer for investigation of heavy meson spectra 2−73926
effects
No entries
interactions
see also Nuclear reactions and scattering due to/mesons
broken scale invariance in tree and seagull approx., current algebra, massive gravitation 2−79482
coupling const. with quarks, calc. by four fermion model 2−49538
effective-Lagrangian model of strong interactions of spin-one and spin-zero mesons with $1/2^+$ baryons 2−76703
helicity conservation in vector meson interactions, s-channel Pomeron coupling 2−70142
helicity conservation in vector meson interactions, s-channel, Pomeron coupling 2−70141
longitudinally polarized V^0 mesons, interaction with nucleons in $\pi^-A \rightarrow V^0A'$ 2−70233
meson-baryon hypercharge exchange reactions, differential cross-sections by new interference model 2−55868
meson-nucleon cross sections, determ. from elon-nucleus collisions 2−76648
meson-nucleon dynamics, Ward identity for axial current, Wilson expansions and commutators 2−49461
scalar currents, analogue model extension 2−79532
scalar mesons and symmetry breaking in SU(3) × SU(3) nonlinear models 2−79479
weak interaction Hamiltonian and parity violating meson-nucleon coupling, meson-dominance model 2−73833
$\omega\rho\pi$ nonrenormalizable, ladder approximation for vertex function 2−52627
ρ, interaction of I-spin triplet with N and π, low-energy theorems 2−76697
magnetic moment
dipole, tensor approach to spin-one mesons 2−82626
hadronic contribution, lower bound 2−49509

Mesons continued
mass
empirical formula relating baryon and meson masses 2-67041
empirical mass formula 2-70203
four fermion model with indefinite metric 2-49538
mass formulae, dynamic interpretation 2-63649
pseudoscalar and vector, medium strong mass splittings in fifth interaction 2-70204
quantization and duality 2-73798
resonances in 1 to 3 GeV region predicted by diatomic-molecule type $SU(6)\times O(3)$ quark model 2-76690
singlet, calculation of masses from beta decay of neutron using Heisenberg uncertainty principle 2-67042
splitting, coefficient of symmetry break current 2-63533
η', parameters determ. from $K^-p\rightarrow\Lambda\eta'$ at 2.2 GeV/c 2-76692
G(1660), with $J^{pc}=3^{--}$ 2-63635
$K_n(1760)$, with $J^{pc}=3^{--}$ 2-63635
φ, determination using $e^+e^-\rightarrow\varphi\rightarrow K^0{}_lK^0{}_s\rightarrow\pi^+\pi^-$ 2-59553
$\varphi_n(1650)$, with $J^{pc}=3^{--}$ 2-63635
$\varphi_n(1830)$, with $J^{pc}=3^{--}$ 2-63635
S-wave resonance, $M_0=0.74$ GeV 2-82764

production
— 2-59545
boson resonance with spin J in e^+e^- annihilation 2-70230
electroproduction, survey of exptl. information 2-82694
neutral meson, evidence at 1150 MeV in 2.4 GeV/c $\pi^-p\rightarrow M^0n$ reaction 2-70207
nonstrange, in K^-p interactions at 3.9 and 4.6 GeV/c, comparison with SU(3) and quark-model predictions 2-66994
particle interaction with nuclei, multiplicity depend. on energy of primary 2-74057
ps. meson, photoproduction, scale dimension of chiral symmetry breaking Hamiltonian 2-49540
pseudoscalar, high energy photoproduction models, review 2-59504
pseudoscalar, in νN collisions, generalized similarity relation and trilinear matrix elements 2-76724
resonance electroproduction, longit./transverse cross sections ratio, quark model 2-59546
resonance photoproduction in backward direction, cross sections prediction 2-63644
resonances, peripheral production, not by π-exchange, four nonets of mesons in $L=1$ quark classification 2-76691
vector, photo and electroprod., triple-Regge formulae 2-79494
vector and axial vector resonances, photoproduction in broken non-linear chiral $SU_3\times SU_3$ dynamics 2-59547
vector meson, photoprod. differential cross-sections, quark model 2-55864
vector meson, photoproduction on protons, review of diffraction dissociation models 2-59551
vector meson electroproduction, simple diffraction considerations and relations between σ_t and slope 2-59548
vector meson $J^p=1^-$ photoproduction using linearly polarized 9.3 GeV γ rays 2-76695
vector meson photoproduction, $\rho\omega$ mixing phenomena 2-59552
vector meson photoproduction, and nucleon Compton scatt. amplitude, quark model 2-55865
vector meson photoproduction in Pomeron exchange reactions 2-76694
vector-meson, with hypercharge exchange, study of $K^-p\rightarrow(\omega,\varphi)\Lambda$ and $\pi^-p\rightarrow K^{*0}\Lambda$ reactions 2-82743
A_1, in π^-p at 40 GeV/c 2-76699
A_1 and A_2 prod. in $\pi^-p\rightarrow\pi^-\pi^-\pi^+p$ and $\pi^-p\rightarrow\pi^-\pi^0\pi^0p$, 7 GeV/c 2-55867
A_1 diffraction production 2-82768
A_1 production in $\pi^+p\rightarrow\pi^+\rho^0p$ and $\pi\text{-}n\rightarrow\pi\text{-}\rho\text{-}p$ at 7 GeV/c, dual model interpretation 2-49584
A_1^+ properties in π^+p interactions at 5.45 GeV/c 2-73838
A_2, coherent production in π^+d reaction 2-59555
A_2, in π^-p at 40 GeV/c 2-76699
$e^\pm e^-\rightarrow e^\pm e^-W^+W^-$, total cross section determ. 2-79508
η, in π^-p reactions, intrinsic props. 2-73835
η, intermediate production in $K_l\rightarrow3\pi$ and $K_l\rightarrow2\gamma$ 2-45937
η in K^-p interactions at 3.95 GeV/c, study of $\eta\Lambda$ and $\eta'\Lambda$ final states 2-59518
η in pseudoscalar nonet, review 2-63574
η photoproduction, Virasoro model 2-70205
η^0, analysis of $p+d\rightarrow{}^3He3+X^0$ reaction 2-42411
η^0, in K^+p interactions 2-73809
η^0, in π^-p interactions of 3.67 and 4.38 GeV/c at large momentum transfers 2-63575
η^0 in pp annihilation at 700 MeV/c, evidence for decays of D- and E-mesons into $\delta\pi$ 2-63640
η' in pseudoscalar nonet, review 2-63574
$\eta\gamma\gamma$, $\eta'\gamma\gamma$ vertices, investigation using electron-positron storage rings 2-49497
$\eta\gamma\gamma$, $\eta'\gamma\gamma$ vertices, investigation using electron-positron storage rings 2-49496
$\eta\pi$ mass spectrum in $\pi^-p\rightarrow\eta\pi^-p$ at 6 GeV/c 2-76670
K^* (890) production in final state with K° in 3.4 GeV/c interactions 2-67011
$KK\pi$, in pp annihilation at 1.2 GeV/c 2-73839
$KK\pi$, in pp annihilations at 1.2 GeV/c 2-73839
$K^{*-}(890)$, $K^{*-}(1400)$ in $K^-p\rightarrow K^0\pi^-p$ reaction at 3.95 GeV/c, meas. of differential cross sections and density matrix elements 2-70221
$K^*(892)$, in K^+p interactions 2-73809
$K^*(892)$ and $K^*(1420)$ prod. in $K^+d\rightarrow K\pi N(N_s)$, 4.6 GeV/c 2-67040
ω, in K^-p interactions, 3.95 GeV/c 2-63592
ω (785) production in final state with Λ in 3.4 GeV/c interactions 2-67011
ω^0, analysis of $p+d\rightarrow{}^3He+X^0$ reaction 2-42411
ω^0, in K^+p interactions 2-73809
pi^{0}p$\rightarrow\rho^0$p Regge-pole theory with nonsense wrong signature zeros 2-59529
$pp\rightarrow\pi^-\pi^+$, 2.3 GeV/c, comparison of data with other two meson states 2-63657
φ, in K^-p interactions, 3.95 GeV/c 2-63592
φ^0, 'elastic' photoproduction from hydrogen at 8.5 GeV 2-49580
$\pi^-p\rightarrow B^-p$, cross-section, OMEA model, rel. to B-meson spin parity 2-76698

Mesons continued
production continued
$\pi^0p\rightarrow\rho^0p$, Regge-pole theory with nonsense- wrong signature zeros 2-59529
Q, backward produced in K^+p interactions 2-79562
Q^0 and Q^0 prod. in K^0p interactions from 4 to 12 GeV/c 2-67034
ρ, by pions at 15 GeV/c, vector dominance and ρ-ω interference 2-82765
ρ, coherent photoprod. from deuterons 2-82676
ρ, in K^-p interactions, 3.95 GeV/c 2-63592
ρ, in K^+p interactions 2-73809
ρ, in reactions $\pi^\pm p\rightarrow\rho N$ at 16 GeV/c, study of exchange mechanisms 2-70236
ρ, photoproduction on deuterons, Glauber-model formalism 2-63638
ρ (765) production in final state with Λ in 3.4 GeV/c interactions 2-67011
ρ electroproduction and decay to 2π 2-79601
ρ^0, forward slope in photoproduction and electroproduction, application of dual-absorptive model 2-73837
ρ^0 photoprod. on protons, 4-6 GeV 2-79492
ρ°, 'elastic' photoproduction from hydrogen at 8.5 GeV 2-49580
T direct channel formation in pp interactions 2-76700
U direct channel formation in pp interactions 2-76700
$W^\pm$, possible bounds on production in super-high-energy hadron-hadron collisions 2-63537

resonances
3^- nonet of states $\rho(1670)$, $\omega(1680)$, $K^*(1670)$, $\varphi(1820)$, Regge recurrences of 1- nonet 2-67038
boson missing-mass spectrum of $\pi^-p\rightarrow X^-p$ process 2-76679
boson production, high-spin, s-channel vertices. 2-59545
boson with spin J, production in e^+e^- annihilation 2-70230
broad resons., produced in pp annihilation, methods of analysis 2-59583
charged vector meson, high-energy scattering in static field, exponentiation and s-channel helicity conservation 2-67036
charged vector meson with elec. dipole moment, Coulomb scattering 2-59550
damped pseudoscalar- and vector-meson model for elastic NN scattering 2-76709
DD $K^*(892)$, prod. in K^+p interactions 2-73809
decay, inclusive expts. with unstable particles, kinematics 2-79554
decays, $\rho\omega$ mixing phenomena 2-59552
decays, effective lagrangian techniques 2-63634
decays involving two partial waves, test for basic violation of $SU(6)_w$ 2-63642
electroproduction, longit./transverse cross sections ratio, quark model 2-59546
final state analysis of pp annihilations 2-59585
heavy vector meson, obs. in study of pion form factor 2-70226
helicity conservation in vector meson interactions, s-channel Pomeron coupling 2-70142
helicity conservation in vector meson interactions, s-channel, Pomeron coupling 2-70141
iso-vector 0^+ meson, 'near universality' of functions in dual reson. model 2-66970
Lee-Wick massive e.m. bosons, production cross section for $1^\pm+Z$ resonant process at high energies 2-45980
leptonic decay of neutral vector mesons, e.m. corrections 2-70247
longitudinally polarized V^0 mesons, interaction with nucleons in $\pi^-A\rightarrow V^0A'$ 2-70233
mass values in 1 to 3 GeV region predicted by diatomic- molecule type $SU(6)\times O(3)$ quark model 2-76690
massive non-Abelian vector, renormalizable models 2-73768
meson-baryon resonances, high energy forward scattering, duality and SU(3) 2-42404
meson-dominance model for weak interaction Hamiltonian and parity violating meson-nucleon coupling 2-73833
multipion resonances having two units of electric charge, search for in 7 GeV/c π^-d interactions 2-67019
narrow effects in pp annihilations 2-59584
neutral, spin determ. from coherent photoprod. on spin-O nuclei obs. 2-82767
neutral meson, lepton and radiative lepton decays, polariz. effects 2-49578
nonstrange, produced in K^-p interactions at 3.9 and 4.6 GeV/c, comparison with SU(3) and quark-model predictions 2-66994
octet dominance of baryon matrix elements, explanation for vanishing of neutron charge radius 2-67059
one-boson exchange model for low energy NN scattering using relativistic Blankenbecler-Sugar eqn. 2-67047
overlapping resonance scattering, exact formalism 2-70249
parameters from partial-wave amplitudes 2-63636
peripheral production, not by π-exchange, four nonets of mesons in $L=1$ quark classification 2-76691
photoproduction, $\rho\omega$ mixing phenomena 2-59552
photoproduction, comparison of angular decay distribs. in three quark models 2-55813
photoproduction in backward direction, cross sections prediction 2-63644
photoproduction in resonance region, multichannel analysis 2-66927
photoproduction of vector mesons on complex nuclei, determ. of strong interaction nuclear radii 2-70433
photoproduction on protons, review of diffraction dissociation models 2-59551
pion-pole dominance of divergence of weak parity-nonconserving NNP amplitude 2-82662
production in K^-d interactions at 5.5 GeV/c 2-63594
production of 2^+ and 1^+ mesons in πN and kN collisions, $U(6,6)\otimes O(3,1)$ peripheral absorption model 2-55863
$S=+2$ exotic meson, weakly decaying, search in K^+p reactions 2-59549
spectroscopy, conf., Philadelphia, USA (Apr. 1972) 2-73796
spectroscopy, vector mesons, quark model predictions 2-59431
spin distribution function in dual resonance model 2-42358
states with mass $>2M_n$, existence from cross section data 2-73830
three-meson, in relativistic Faddeev approach 2-76696
two-pion final states in π^+d interac. at 7 GeV/c 2-45957
vector, e.m. decay 2-76647

Mesons continued
resonances continued
vector, e.m. decay 2−70202
vector, light hypothesis for existence as cause of negative exptl. result for $K_l \to 2\mu$ 2−67007
vector, photo and electroprod., triple-Regge formulae 2−79494
vector, prod. in e^+e^- annihilation processes 2−63518
vector, rel. to e.m. form factors and meromorphic function interpret. 2−52579
vector and axial vector photoproduction in broken nonlinear chiral $SU_3 \times SU_3$ dynamics 2−59547
vector and tensor meson decays, current algebra and the triangle approx. 2−63637
vector dominance and ρ-ω interference in ρ prod. by pions 2−82765
vector dominance relations in photon processes, phenomenological consequences of parton models 2−66923
vector meson, medium strong mass splittings in fifth interaction 2−70204
vector meson, neutral, search for existence in K_l decay 2−52596
vector meson, photoprod. on nucleons, differential cross-sections, quark model 2−55864
vector meson, photoprod. on nucleons and nucleon Compton scatt. amplitude, quark model 2−55865
vector meson dominance in $\gamma p \to \pi^- X$ inclusive reaction in photon fragmentation region 2−79613
vector meson dominance in Compton scattering, estimation of corrections using light cone expansion 2−42326
vector meson dominance model, applications 2−66916
vector meson dominance rel. to coupling of Reggeized ρ to 'charged' photons 2−79539
vector meson electroproduction, simple diffraction considerations and relations between σ_t and slope 2−59548
vector meson exchange in pp scattering, coherent droplet model including Yukawa interaction term 2−70258
vector meson intermediate state, search for in K^0_l decay 2−82769
vector meson $J^p=1^-$ photoproduction using linearly polarized 9.3 GeV γ rays 2−76695
vector meson photoproduction, Regge model 2−67035
vector meson photoproduction in Pomeron exchange reactions 2−76694
vector meson production from γ-rays, quark model coupling constants 2−73834
vector meson production in πN reactions studied in model of higher baryon coupling 2−45983
vector mesons photoproduction, quark model predictions for angular decay distributions in inclusive processes 2−52624
vector particle scattering, current conservation 2−49490
vector-meson dominance hypothesis in pion production processes 2−70230
vector-meson production with hypercharge exchange, study of $K^-p \to (\omega,\varphi)\Lambda$ and $\pi^-p \to K^{*0}\Lambda$ reactions 2−82743
vector-meson scattering, application of quark-model like results from duality 2−45984
, G_{39}, evidence for in πN scattering 2−70239
A_{-1} production in π-K^+ and π-p, at 2.45 GeV/c 2−42403
$A_{-2} \to K^0{}_s K^-$, produced in π-p reaction at 20.3 GeV/c, meas. of A2 mass spectrum shape and decay angular distrib. 2−63641
A, production in π-P scattering, Regge pole analysis 2−63630
A enhancement and A3 peak observed in 3π mass spectrum in π-p reaction at 20 GeV/c 2−45963
$A^-{}_2$ production in π-K^+ and π-p, at 2.45 GeV/c 2−42403
A_1 and A_2 prod. in $\pi^-p \to \pi^-\pi^-\pi^+p$ and $\pi^-p \to \pi^-\pi^0\pi^0p$, 7 GeV/c 2−55867
A_1 diffraction production 2−82768
A_1 isomultiplet, dynamic chiral symmetry and cancellation of divergences in mass differences 2−52628
A_1 prod. in π^-p at 40 GeV/c 2−76699
A_1 production in $\pi^+p \to \pi^+\rho^0 p$ and π-n$\to\pi$-ρ-p at 7 GeV/c, dual model interpretation 2−49584
A_1 production in $\pi N \to \rho\pi N$, dual model 2−63613
$A_1{}^+$ production properties in π^+p interactions at 5.45 GeV/c 2−73838
$A_1 \to \pi\gamma$, presence of fixed pole in angular momentum phase determ. from pion Compton scattering 2−76671
A_2, coherent production in π^+d reaction 2−59555
A_2, interfering meson models, finite dispersion relation restrictions on coupling strengths 2−45988
A_2, spin-parity determ., production in 7 GeV/c π^-p interactions 2−67026
A_2 prod. in π^-p at 40 GeV/c 2−76699
A_2 production in π-p scattering, Regge pole analysis 2−63630
$A_2{}^0$, produced in π^-p reactions, intrinsic props. 2−73835
$A_2 \to \pi\gamma$, presence of fixed pole in angular momentum phase determ. from pion Compton scattering 2−76671
A_2A_2 Regge cuts in forward nucleon-nucleon scattering 2−67045
ABC effect in missing mass spectra from $dp \to {}^3He\,(mm)^0$ and $dp \to {}^3H(mm)^+$ reactions 2−76727
$A_1(1^+)$ density-matrix elements deduced from eikonal Regge model for $\pi^\pm p \to A_1{}^\pm p$ 2−45966
$A_3(f\pi)$, produced in $\pi^-p \to p\pi^+\pi^-\pi^-$ reaction, spin-parity analysis 2−49581
$A_1\pi \to \pi\pi$, applic. of crossing symmetric dual amplitude with geometrical structure 2−59474
$A_1\rho\pi$ coupling constants, determination using collinear dispersion relations 2−63639
$A_1\rho\pi$ couplings and t-channel helicity conservation 2−59554
B meson exchange contribution to $\pi^+n \to \omega p$ 2−42387
B^-, absorption model and spin parity 2−76698
B^- production in π-K^+ and π-p, at 2.45 GeV/c 2−42403
compositeness rel. to t-depend. of N form factor 2−59557
D^0 decay into $\delta\pi$, obs. in pp annihilation at 700 MeV/c 2−63640
$\Delta(1236)$, effects in nuclear matter and tri- nucleon system 2−49712
$\delta^0(963)$ obs. in $\pi^-p \to M^0n$ at 2.4 GeV/c 2−76693
E^0 decay into $\delta\pi$, obs. in pp annihilation at 700 MeV/c 2−63640
E(1420), radiative decay studies 2−52626
eN, vector meson dominance model 2−59406
ε, in $I=0$ $\pi\pi$ s wave, low-energy theorems of broken scale invariance 2−76689
ε, rel. to Veneziano model interpret. of low energy π-π final state interaction 2−55855

Mesons continued
resonances continued
ε exchange, role in K^+p scatt. 2−63597
$\varepsilon(700)$ meson, rel. to Goldstone boson of broken scale invariance 2−45982
η^0, prod. in K^+p interactions 2−73809
η', in pseudoscalar nonet, review 2−63574
η', parameters determ. from $K^-p \to \Lambda\eta'$ at 2.2 GeV/c 2−76692
$\eta' \to \eta\pi\pi$, decay rate, breaking of chiral and scale symmetries 2−55866
f^0-$A_2{}^0$ interference, rel. to $f^0 \to KK$ branching ratio 2−45985
f and f′ production in K^-p interactions at 3.95 GeV/c 2−79604
f^0, production and decay angular distribs. in π-p$\to\pi$-π^+n at 8 GeV/c 2−79600
f^0 production in π-p$\to$p$\pi^+\pi$-π- at 20 GeV/c 2−45963
F_1 (1540) obs. in $pp \to K^*K\pi$ and in $\pi p \to K^*Kp$ as kinematic enhancement 2−63633
f^o exchange effects about 200 GeV in pp elastic scatt. 2−79614
f° in π^+d interac. at 7 GeV/c 2−45957
F′(1519), produced in K^-p interactions, meas. of mass, width and branching ratios 2−66994
g^- (1675), spin-parity determ., production in 7 GeV/c π^-p interactions 2−67026
g° in π^+d interac. at 7 GeV/c 2−45957
g(1660), nonet struct., $J^{pc}=3^{--}$ 2−63635
γN, vector meson dominance model 2−59406
γp, production of $A_1{}^0$, axial vector meson 2−66925
$\gamma p \to K^+\Lambda$, K^*-K^{**} absorbed exchanges 2−70210
$\gamma p \to K^+\Sigma$, K^*-K^{**} absorbed exchanges 2−70210
K* (890) production in final state with K° in 3.4 GeV/c interactions 2−67011
K* exchange in $K^-p \to K^-\pi^-\Delta^{++}(1236)$ at 8.25 GeV/c 2−55847
KK, production in pp annihilations at 1.2 GeV/c 2−73839
$KK\pi$, production in pp annihilations at 1.2 GeV/c 2−73839
K*, bootstrap calculation using effective-potential method 2−45989
K*, K^+p interactions in bubble chamber 2−45941
K* in $KN \to K^*(890)N$, Regge pole ρ_{10} production, unnatural parity exchange 2−49586
K^{*-} production in $K^-p \to pK^0\pi^+\pi^-\pi^-(\pi^0)$ reaction at 10 GeV/c 2−73808
K^{*-} spectrum in $K^-p \to K^{*-}p$ at 10.9, 13.4, 15.9 GeV/c meas. using missing mass technique 2−49585
K^{*o} produced in π-p$\to K^{*o}\Lambda$ 3.9 GeV/c, amplitude structure determ. from decay correlations 2−42391
K*(1420), study of interference effects with background as obs. in $K^-p \to K^-\pi^+n$ reaction 2−63647
K^{*0}(1890), (1420) production in K^-d interactions at 5.5 GeV/c 2−59515
K*-(890), prod. in K-n interac., 4.91 GeV/c 2−42372
K*(890), in three-meson systems, relativistic Faddeev approach 2−76696
K*(890), study of interference effects with background as obs. in $K^-p \to K^-\pi^+n$ reaction 2−63647
K*(890) coherent production in elon-nucleus collisions 2−76648
K^{*-}(890), K^{*-}(1400) production in $K^-p \to K^0\pi^-p$ reaction at 3.95 GeV/c, meas. of differential cross sections and density matrix elements 2−70221
K*(892) and K*(1420) prod. in $K^+d \to K\pi N(N_s)$, 4.6 GeV/c 2−67040
$k_1{}^0k_1{}^0\omega^0$ final state in region of T-meson, direct s-channel effects 2−67039
K_n(1760), nonet struct., $J^{pc}=3^{--}$ 2−63635
$K\pi\pi$ coherent production in 3.8 GeV/c K^+d interactions 2−66999
$K\pi\pi$ enhancement in Q region, in K-d$\to$K-π-π^+np, at 7.3 GeV/c 2−42370
$K\pi\pi$ enhancement in Q region (1200-1450 MeV) in K^-d reactions at 7.3 GeV/c, structure and decay properties of Q 2−82770
$K\pi\pi$ low mass systems, in 12 GeV/c K^+p interactions 2−59519
κ-dominance model, weak, for K_{l3} decays 2−76656
κ, rel. to K_{l3} form factors 2−70209
$M^0(940)$ obs. in $\pi^-p \to M^0n$ at 2.4 GeV/c 2−76693
M(953), existence from K^-p reactions 2−73831
$N\rho \to N^*\pi$, pion-gauge conditions 2−52632
ω-φ mixing angle predictions from extension of Odorico's bootstrap 2−73836
ω, produced in π^-p reactions, intrinsic props. 2−73835
ω (785) production in final state with Λ in 3.4 GeV/c interactions 2−67011
ω photoproduction in γd interactions at 4.3 GeV, determ. of direct vector meson photon coupling 2−49579
ω prod. in K^-p interactions, 3.95 GeV/c 2−63592
ω production in π^+p interactions at 2.67 and 2.30 BeV/c, differential cross sections, decay density matrix elements 2−45987
ω^0, prod. in K^+p interactions 2−73809
ω^0 production in $K^-p \to pK^0\pi^-\pi^-\pi^-\pi^0$ reaction at 10 GeV/c 2−73808
ω^0 spin-density matrix studied in π-p$\to\omega^o$n in 3.65, 4.5, 5.5 GeV/c 2−52625
$\omega^0 \to e^+e^-(\mu^+\mu^-)$, partial decay widths, e.m. corrections 2−70247
$\omega \to \eta\gamma$, search for decay mode in $\pi^-p \to n$ + neutral boson 2−79603
$\omega \to \pi^-\pi^+\pi^0$, ang. decay spectra 2−63591
$\omega\pi$ produced in $pp \to \omega\pi^+\pi^-$ annihilation 2−59580
$\omega\pi^\pm$, m∼1250 MeV, spin 1, in pp annihilation 2−79602
$\omega\rho\pi$ nonrenormalizable, ladder approximation for vertex function 2−52627
$pp \to 6\pi$, 2.5 GeV/c, ω, ρ production resonance production 2−79615
φ, mass determination using $e^+e^- \to \varphi \to K^0{}_l K^0{}_s \to \pi^+\pi^-$ 2−59553
φ, produced in π^-p reactions, intrinsic props. 2−73835
φ prod. in k^-p interactions, 3.95 GeV/c 2−63592
$\varphi^0 \to e^+e^-(\mu^+\mu^-)$, partial decay widths, e.m. corrections 2−70247
$\varphi \to K^-K^+$, ang. decay spectra 2−63591
$\varphi \to \eta\gamma$ e.m. decay mode, branching ratio, π-p$\to\eta\varphi$ reaction obs. 2−63643
φ°, 'elastic' photoproduction from hydrogen at 8.5 GeV 2−49580
φ(1019), produced in K p interactions, meas. of mass, width and branching ratios 2−66994
φ_n(1830), nonet struct., $J^{pc}=3^{--}$ 2−63635
φ_n(1850), nonet struct., $J^{pc}=3^{--}$ 2−63635
πA_1-πA_1, analysis using hard-pion constraints of current algebra and current conservation in the Veneziano model 2−63632

- **Mesons** continued
  - **resonances** continued
    - $\pi N \rightarrow \rho N$, dynamical model for $P_{13}(1860)$ $Pp_{31}(1910)$ and $F_{35}(1890)$ resonances 2−49583
    - $\pi^{\pm}p$, elastic scatt., f exchange amplitudes 2−59540
    - $\pi\pi$, I=o, s-wave predicted s and p wave inverse scatt. amplitudes 2−73829
    - $\pi^{+}\pi^{+}$, produced in pp annihilation, multi-peripheral model analysis 2−59578
    - $\pi^{-}\pi^{+}n$ prod. in $\pi^{-}p$ interaction at 25 GeV/c 2−45969
    - $\pi^{-}\pi^{-}\pi^{+}p$ prod. in $\pi^{-}p$ interaction at 25 GeV/c 2−45969
    - Q, backward produced in $K^{+}p$ interactions 2−79562
    - Q^{0} and Q^{0} prod. in $K^{0}p$ interactions from 4 to 12 GeV/c 2−67034
    - ρ-ω decay, overlapping resonance scattering, exact formalism 2−70249
    - ρ-ω mixing phase and strength, conditions imposed by time-reversal invariance 2−45986
    - ρ^{0}-ω interference in $\gamma N \rightarrow \pi^{+}\pi$-$\Delta$ reactions 2−59402
    - ρ^{0}-ω mixing producing a violation of isotopic symmetry in $\pi N \rightarrow \omega(N,\Delta)$ 2−63615
    - ρ- production in π-K^{+} and π-p, 2.45 GeV/c 2−42403
    - ρ, coherent photoprod. from deuterons 2−82676
    - ρ, implications in $\pi\pi$ scattering 2−76688
    - ρ, interaction of I-spin triplet with N and π, low-energy theorems 2−76697
    - ρ, photoproduction on deuterons, Glauber-model formalism 2−63638
    - ρ, prod. in $K^{+}p$ interactions 2−73809
    - ρ, produced in $\pi^{-}p$ reactions, intrinsic props. 2−73835
    - ρ, rel. to Veneziano model interpret. of low energy π-π final state interaction 2−55855
    - ρ, slope of trajectory in interactions at high energy 2−63603
    - ρ,f Regge trajectories representation by mass^{2} operator 2−45924
    - ρ (765) production in final state with Λ in 3.4 GeV/c interactions 2−67011
    - ρ electroproduction and decay to 2π 2−79601
    - ρ exchange in πN scattering, hypothesis of flip dominance studied in ABFST multiperipheral model 2−42398
    - ρ exchange invariant amplitudes, estimates for various reactions 2−63544
    - ρ isomultiplet, dynamic chiral symmetry and cancellation of divergences in mass differences 2−52628
    - ρ meson exchange in hadron-hadron scattering, calc. of t-channel discontinuity in resonance approx., eikonal form 2−42365
    - ρ photoproduction, vector-meson dominance model 2−76632
    - ρ polarization analyses in π-$p \rightarrow \rho^{0}n$ and π-$p \rightarrow \rho$-p 2−63646
    - ρ prod. by pions at 15 GeV/c vector dominance and ρ-ω interference 2−82765
    - ρ prod. in $K^{-}p$ interactions, 3.95 GeV/c 2−63592
    - ρ production in π- scattering, Regge pole analysis 2−63630
    - ρ production in $\pi N \rightarrow \rho N$, baryon Regge pole exchange model 2−52623
    - ρ production in $\pi N \rightarrow \rho\pi N$, dual model 2−63613
    - ρ production reactions $\pi^{\pm}p \rightarrow \rho N$ at 16 GeV/c, study of exchange mechanisms 2−70236
    - ρ Regge exchange amplitude nature 2−59496
    - ρ trajectory, arbitrary intersection, inclusion in Neveu-Schwarz model 2−59438
    - ρ^{0}, forward slope in photoproduction and electroproduction, application of dual-absorptive model 2−73837
    - ρ^{0}, production and decay angular distribs. in π-$p \rightarrow \pi$-$\pi^{+}n$ at 8 GeV/c 2−79600
    - ρ^{0} photoprod. on protons, 4-6 GeV 2−79492
    - ρ^{0} photoproduction in γd interactions at 4.3 GeV, determ. of direct vector meson photon coupling 2−49579
    - ρ^{0} production in $K^{-}p \rightarrow pK^{0}\pi^{+}\pi^{-}\pi^{-}$ reaction at 10 GeV/c 2−73808
    - ρ^{0} production in π-$p \rightarrow p\pi^{+}\pi$-$\pi$- at 20 GeV/c 2−45963
    - ρ^{0} produnction in p-$p \rightarrow p\pi^{+}\pi$-$\pi$- at 20 GeV/c 2−45963
    - $\rho^{0} \rightarrow e^{+}e^{-}(\mu^{+}\mu^{-})$, partial decay widths, e.m. corrections 2−70247
    - ρ°, 'elastic' photoproduction from hydrogen at 8.5 GeV 2−49580
    - ρ° prod. in $\pi^{+}d$ interac. at 7 GeV/c 2−45957
    - ρ', ρ contribution to π charge radius 2−76663
    - $\rho(1.71)$, produced in $\pi^{-}p \rightarrow p\pi^{+}\pi^{-}\pi^{-}\pi^{0}$ reaction, decay properties 2−49582
    - $\rho(765)$ in three-meson systems, relativistic Faddeev approach 2−76696
    - $\rho\omega$ interference, obs. in pp annihilation at 2.32 GeV/c 2−70261
    - $\rho\omega$ mixing, review 2−59552
    - $\rho\pi\pi$ coupling constants, determination using collinear dispersion relations 2−63639
    - $\rho\rho$ P triple-Regge vertex calc. from two-body scattering data assuming duality and f-coupled Pomeron 2−55842
    - $\rho\rho$ Regge cuts in forward nucleon-nucleon scattering 2−67045
    - $\rho\rho \rightarrow \rho\sigma$, derivation of finite energy sum rules, and intermediate ρ Born contrib. to parity conserving helicity amplitudes 2−63552
    - S-meson region structures 2−59544
    - S-wave resonance parameters from $\pi^{-}p \rightarrow \pi^{0}\pi^{0}n$ and $\pi^{+}n \rightarrow \pi^{0}\pi^{0}p$ 2−82764
    - S^{0}, produced in $\pi^{-}p$ reactions, intrinsic props. 2−73835
    - S*(980), in I=0 $\pi\pi$ s wave, low-energy theorems of broken scale invariance 2−76689
    - S(1929), determ. upper limit to pp coupling 2−63664
    - T-region of $pp \rightarrow K_{1}^{0}K_{1}^{0}\omega^{0}$ reaction, direct S-channel effects 2−59575
    - T-region reson. studies in proton annihilation expts. 2−59571
    - T direct channel formation in pp interactions 2−76700
    - U-mesons, existence search in pp interactions 2−59567
    - U direct channel formation in pp interactions 2−76700
    - V^{0} photoproduction on protons studied in Regge pole model with cuts 2−49577
    - w exchange effects about 200 GeV in pp elastic scatt. 2−79614
    - $W_{0,1}$ intermediate bosons, production cross sections for $\nu_{e}(\nu_{e})+Z$ resonant process at high energies 2−45980
    - W_{0} production by colliding $e^{+}e$- beams 2−45979
    - $W^{\pm}$, possible bounds on production in super-high-energy hadron-hadron collisions 2−63537
    - W_{1} production by colliding $e^{+}e$- beams 2−45979
    - X^{0}, produced in $\pi^{-}p$ reactions, intrinsic props. 2−73835
    - X^{0} prod. in $pp \rightarrow pp\pi^{+}\pi^{-}X^{0}$, effective mass enhancement in $p\pi^{-}X^{0}$ system 2−63654
    - X^{0} production in π-$p \rightarrow \pi$-pX^{0}, 13.4 GeV/c. 2−52616
    - $X^{0} \rightarrow \gamma\gamma$, from $\pi^{-}p \rightarrow$ neutral meson + neutron at 3.8 GeV/c, meas. of branching-ratio 2−67037
    - $X^{\circ}(960)$, radiative decay studies 2−52626
    - $X^{0}(958)$, study of meson mass spectrum in $\pi^{-} + p \rightarrow$ mssing mass + n near threshold 2−42402
    - $X^{0}(958)$ region in $\pi^{-}p \rightarrow nX^{0}$ reaction, missing mass obs. 2−76676
    - $X^{0}(960)$, spin and parity determination in proton antiproton annihilation at rest 2−45981
    - K* decays, effective lagrangian techniques 2−63634
    - $pp \rightarrow \pi^{+}\pi^{+}\pi^{-}\pi^{-}$, 3.6 GeV/c, analysis in terms of multiperipheral model including resonances 2−73845
  - **scattering**
    - − 2−67036
    - charged vector meson with elec. dipole moment, Coulomb scattering 2−59550
    - effective Lagrangian model, SU(3) × SU(3) symmetry, model of spontaneous breakdown 2−66953
    - iso-vector 0^{+} meson, 'near universality' of functions in dual reson. model 2−66970
    - meson baryon, elastic, σ-term in any (8,8) model of chiral symmetry 2−45928
    - meson-baryon, backward amplitudes and average radius of interaction on duality basis 2−66997
    - meson-baryon, multiple scatt. model, duality breaking effects 2−63572
    - meson-baryon, partial wave relations from fixed-u dispersion relations 2−59505
    - meson-baryon, problem of sigma terms 2−45929
    - meson-baryon, pseudoscalar, exchange degeneracy rel. to baryon state mixing model 2−63648
    - meson-baryon, strangeness-exchange interactions at high energy 2−76650
    - meson-baryon, SU(3) × SU(3) model with broken chiral symmetry 2−73774
    - meson-baryon resonances, duality and SU(3) 2−42404
    - meson-hadron scattering, finite energy sum rule 2−70188
    - meson-meson, meson-baryon and baryon-baryon scattering, unified treatment in Veneziano model 2−70190
    - meson-meson, partial wave relations from fixed-u dispersion relations 2−59505
    - meson-nucleon backward scattering extrapolations to baryon pole, rel. to coupling constant 2−76702
    - meson-nucleon in Eckmann model 2−76570
    - pseudoscalar-pseudoscalar and pseudoscalar-baryon, calc. of s- and p-wave lengths 2−63573
    - scalar bosons, complex Pomeranchukon singularities and asymptotic behaviour 2−49539
    - $A_{1}\pi \rightarrow \pi\pi$, applic. of crossing symmetric dual amplitude with geometrical structure 2−59474
    - $\pi\eta \rightarrow \pi\eta,\pi\rho$, t-channel Regge amplitudes for local duality 2−63552
  - **spin and parity**
    - d $X^{0}(960)$, determination in proton antiproton annihilation at rest 2−45981
    - $A_{3}(f\pi)$, produced in $\pi^{-}p \rightarrow p\pi^{+}\pi^{-}\pi^{-}$ reaction, spin-parity analysis 2−49581
    - E(1420), possible determination from radiative decay data 2−52626
    - $\pi N \rightarrow \rho\pi N$, dual resonance model accounting for ρ spin 2−63613
    - $\pi^{-}p \rightarrow B^{-}p$, cross-section, OMEA model, rel. to B-meson spin parity 2−76698
    - X° (960), possible determination from radiative decay data 2−52626
- **Mesosphere** *see Atmosphere*
- **Metal-insulator-metal structures and devices**
  - *see also Tunnelling*
  - Al electrode- $V_{2}O_{5}$-$P_{2}O_{5}$ glass system, electrical pulse regime and switching study 2−77917
  - cathode surface roughness, influence on emitted electron distributions 2−47948
  - current density, emitter boundary electron density depend. 2−84354
  - d.c. conduction mechanisms, thermally stimulated current analysis 2−61394
  - dielectric loss model, based on interfacial electron tunnelling 2−47964
  - discrete lattices, non-steady-state diffusion currents in large elec. fields 2−51066
  - electroluminescence characteristics 2−68448
  - frequency response of m.o.m. diodes at 1.15 μm radiation with a d.c. bias 2−45769
  - junction, nonequil. phenomena in electron tunnelling 2−68373
  - magnetically doped tunnel junctions, mag. interactions 2−68449
  - metal-insulator boundary, surface exciton spectra, image forces 2−77921
  - metal-ZnTe-metal device, switching and memory props. 2−44142
  - polymer film, electrical conductivity, use as dielectric layers in m.i.m. structures 2−83859
  - Poole-Frenkel pre-exponential factor 2−57217
  - quartz crystal insulator, uniaxial plane-parallel, e.m. wave amplifier 2−63177
  - space charge limited to electrode limited current transition, theory 2−47949
  - switching, of thin film memory elements in low conductivity condition 2−71986
  - tunnel junction, band struct. effect on VI characs. 2−51184
  - tunnel junction, paramagnetic impurity effects 2−47789
  - two laser mixing and direct frequency meas. using m.i.m. point-contact diodes 2−45757
  - Zircaloy-2 anodic oxide, pre-breakdown electrical switching 2−47951
  - Ag-Se-Al thin film structure, electro-physical characteristics 2−71987
  - Ag-SiO, Se-Al structure, electrophysical characteristics 2−71988
  - Al-$Al_{2}O_{3}$- Au(Ag)(Al), transients, capacitance variation with temp. 2−57219
  - Al-$Al_{2}O_{3}$-Al, current density in thermionic and thermionic field emission regions 2−61395
  - Al-$Al_{2}O_{3}$-Al, photosensitive tunnelling conductance 2−54222

Metal-insulator-metal structures and devices continued

- Al-Al_2O_3-Al, space charge dependence of barrier height on insulator thickness 2−51185
- Al-Al_2O_3-Al and Al-SiO_x-Al, eff. of reactor radiation on elec. and dielec. props. 2−81114
- Al-Al_2O_3-Al thin film, cold emission, distribution 2−81125
- Al-Al_2O_3-Au, thermally stimulated currents measurement 2−77928
- Al-Al_2O_3-Pb junction, impurity assisted tunnelling, 4.2-148 K 2−44140
- Al-CdS-In thin film struct., memory effect, switching characts. 2−44139
- Al-MgF_2-Al interference filters, automatic apparatus for preparation 2−70029
- Al-MoO_3-Al, donor band and Schottky barrier obs. using dielectric relax. currents 2−68453
- Al-SiO_x/B_2O_3-Al, current-voltage characts. 2−47950
- Al-(Al-oxide)-Al tunnelling structs., transient phenomena rel. to insulator barrier, 100 K 2−68452
- Al-(Al-oxide)-metal sandwiches, aqueously anodized, current-voltage characts., 77 K 2−68451
- Al-borosilicate glass-Al thin film sandwich, elec. cond. props., negative resist., electroforming and electron emission 2−71989
- Al_2O_3, anodic, breakdown by impact ionization 2−57235
- Au-MoO_3-Au, a.c. elec. props. and I-V characts. under d.c. bias 2−68454
- Au-TiO_2-Pt, bistable and threshold switching after forming process 2−44141
- CdS, in m.i.s.m. and m.s.i.m. structures, electron emission 2−57218
- M-CdS-I-M, thin film device, electron emission 2−68450
- Nb-Nb_2O_5- metal diodes, switching obs. 2−54223
- Nb-NbO_x-Al, VI characs., varying surface barrier at NbO_x-Al interface obs. 2−68455
- Nb_2O_5, amorphous, conductivity and switching time obs. 2−61320
- Sn-SnO-Sn Josephson tunnel junction, Josephson and quasiparticle currents, microwave radiation effects 2−68375
- Ta-Ta_2O_5-Au, electron energy distrib. for Schottky/Poole-Frenkel conduction 2−68456
- Ta-Ta_2O_5-Au(Ag)(Al), transients, capacitance variation with temp. 2−57219
- Ti-TiO_2-Au film diode, I-V characts., negative resist. 2−61390
- Ti-TiO_2-Au(Ag)(Al), transients, capacitance variation with temp. 2−57219
- W-SiO_2:C-Au tunnel cathode, using amorphous dielectric, threshold emission and elec. switching 2−81122
- Zr-ZrO_2-Au, thermally stimulated currents measurement 2−77928

Metal-insulator-semiconductor structures and devices

see also Tunnelling

- automatic meas. and recording of electrical characteristics 2−63214
- C-V characteristics of MIS structures, influence of defects 2−61396
- charge coupled device shift register, two phase stepped oxide using undercut isolation 2−51186
- DSA-MOS transistor, fabrication, using preferential etching of Si 2−71316
- electroluminescence characteristics 2−68448
- f.e.t., noise at long time constants 2−44136
- field effect in semiconducting glass 2−65042
- m.a.o.s., instability, EV characs. obs. 2−65044
- m.a.o.s. diode, cond.-voltage characts. 2−61400
- m.a.o.s. structure, C-V curve broadening 2−61401
- m.a.s. diode, shifting characts. of flat band voltage, X-ray effects 2−57220
- metal-polymer- Si structures, carrier injection and trapping phenomena 2−71991
- metal-SiO_2(TiO_2)- Si-SiO_2(TiO_2)-metal, for light signal amplification 2−45694
- MI_1I_2S structures, storage charges reduction 2−81121
- m.i.s.i.m., pre-breakdown region operation, light pulse memory action 2−75137
- m.i.s.i.m. structs., light detect. by charge accumulation obs. 2−65095
- m.i.s.i.m. structs., props. rel. to electron capture and liberation by surface traps 2−65037
- m.n.o.s., elec. instability, suppression of ionic combination during Si_3N_4 deposition 2−71336
- M.N.O.S., max. tunnelling distance, theory 2−47953
- m.o.s., C-V characts., rel. to Na^+ ion transport in SiO_2 layer 2−77936
- m.o.s., surface state density at Si/SiO_2 interface 2−61403
- m.o.s. capacitance meas. of Si:Au levels 2−61362
- m.o.s. capacitor detectors, time resolved X-ray detection 2−49669
- m.o.s. device, interface charge inhomogeneities, admittance rel. to interface state admittance 2−61399
- m.o.s. diode capacitance rel. to SiO_2 film fabrication conditions 2−71999
- m.o.s. Hall technique for elec. prop. determ. of Si on sapphire 2−51169
- m.o.s. junctions, temp. depend. tunnelling into amorphous Si 2−47952
- m.o.s. transistors, differential charge pumping effect 2−44145
- m.o.s.t. structure, positive charge distribution meas. in SiO_2 by channel conductance and step etching methods 2−71998
- multilayer insulating films 2−75136
- photodetecting devices 2−77929
- sapphire, substrate, transport props., electron injection by internal photoemission 2−81110
- surface-state density determ. by photovoltage meas. 2−44144
- surface-state density determ. by photovoltage meas. 2−44143
- transistor, meas. of drain-source conductance in saturated current region 2−63211
- transistor, transconductance meas. using differential amplifier 2−63210
- Al-AlN-Si structure, prep. and elec. props. 2−54225
- Al-Si_3N_4-Si, tunnelling with insulator valence band as barrier 2−71993
- Al-SiO_2-Si, IV characs., breakdown, and switching 2−71996
- Al-SiO_2-Si, transport props. in inversion region, 123-573K 2−47954
- Al-SiO_2-Si system, effect of bias-temp. treatments 2−84345
- Al-pyrolytic SiO_2-Si system, effect of heat treatment on density of fast surface states 2−77915

Metal-insulator-semiconductor structures and devices continued

- Au/W-SiO_2-Si system, effect of bias-temp. treatments 2−84345
- Au-lacquer-Se structure current passage mechanism 2−84348
- CdS m.o.s. system, amplification of pulse photoelectric current 2−44146
- GaAs interface, n-type, small-signal admittance meas. 2−65039
- GaN diodes, luminescence due to electric field polarity reversal 2−71990
- Ge-SiO_2, low temp. C-U characts. 2−61402
- Ge_3N_4-Ge, CV hysteresis, depend. on Ge_3N_4 film deposition temp. 2−54224
- Nb_2O_5 film, r.f. sputtered, ionic instability, m.o.s. capacitance obs. 2−71995
- Pt-SiO_2-Si, electron tunnelling through oxide barrier 2−61359
- Si-Ge alloy oxide layer etched away, reoxidation, production of MOS transistors 2−75132
- Si-SiO_2-metal, m.o.s., potentials and d.c. rel. to oxide thickness and interface states 2−61406
- Si-SiO_2, cation transport in steam grown SiO_2 2−61405
- Si-SiO_2 capacitor, frequency response of interface states 2−61404
- Si-SiO_2 interface, effects of illumination on electrical properties 2−44147
- Si-SiO_2 interface, fixed charge behaviour, rel. to growth conditions 2−54227
- Si-SiO_2 interface, ion implanted, deep energy level detn. by m.o.s. technique 2−80938
- Si-SiO_2 interface, photoemission from Si to SiO_2 during laser irrad., photocurrents 2−81119
- Si-SiO_2 interface, scatt. of conduction electrons by surface oxide charge 2−72000
- Si-SiO_2 interface, surface state distrib. 2−47956
- Si-SiO_2 system, tunnelling rel. to interface states 2−68459
- Si, current and capacitance transients, theory and applic. to initially depleted surface 2−47957
- Si, inversion layer, hole field effect mobility rel. to dielec. charge 2−71992
- Si, neutralization of Na^+ ions in the HCl grown SiO_2 2−51187
- Si, surface, orientation effects on electron and hole transport props. 2−51173
- Si, surface barrier electroreflectance obs. 2−65241
- Si m.i.s., using vapour-grown Al_2O_3 films, structure charact. 2−71997
- Si m.o.s. structure, flat band voltage measurement by i.r. excitation 2−71994
- Si minority carrier lifetime and surface reconstruction velocity, m.o.s. transient response obs. 2−65017
- Si n-channel junction f.e.t., neutron damage annealing 2−51181
- Si n-channel m.o.s.f.e.t., electron mobility, electron surfon interact. calc. 2−51172
- Si p-channel charge coupled devices with resistive gate structure 2−61398
- Si_3N_4-GaAs interface, deposition and surface state density obs. 2−65040
- Si_3N_4-GaAs m.i.s. capacitor, surface states and insulator traps 2−77919
- Si_3N_4 dielectric film on Si, interface states, effect of ambient annealing 2−61397
- Si_3N_4 gate dielectric, high prod. system for deposition 2−71952
- SiO_2:Au ion implanted, charge storage rel. to floating gate devices 2−68458
- SiO_2/Si, induced surface charge on oxidized surfaces 2−77916
- SiO_2/Si interface, surface-state density, obs. 2−65041
- SiO_2-GaAs interface, deposition and surface state density obs. 2−65040
- SiO_2, Fowler-Nordheim tunnelling and dielec. breakdown 2−47955
- SiO_2, interface states and potential barriers 2−65043
- SiO_2, photoinjection over interface barrier, exponential charging profiles effect on photocurrent 2−54226
- SiO_2 dielectric film on Si, interface states, effect of ambient annealing 2−61397
- SiO_x, r.f. sputtered in Ar-O_2, elec. props., O_2 conc. effects 2−60667
- Te-SiO, interface states, flat band voltage temp. depend. obs. 2−77930

Metal-semiconductor boundaries *see Semiconductor-metal boundaries*

Metallo-organic compounds *see Organic compounds*

Metallography

- anodic sectioning technique 2−60817
- computational techniques, conf., Leeds, England, Jan. (1971) 2−58820
- diffusion coeff. determ. method using soln. treatments and metallography 2−56748
- electron emission microscope examination of deformation and recrystallization 2−43779
- electron microscope application, developments in UK, (1948-1960) 2−67958
- fractography by crack replication 2−47545
- fracture characteristics, electron- fractographic obs. 2−43751
- high voltage microscopy, and applics. 2−56632
- holographic interferometry, examination of impact loaded objects 2−45765
- inclusion identification by vapour phase deposited interference layers 2−56737
- instrumentation for quantitative image analysis 2−43557
- magnox fuel element components prep. 2−43773
- materials testing, electrical and electronics industry 2−80790
- metals, hard, phase picture production using ZnSe coatings 2−56918
- orientation sections in single crysts., prep. method 2−43547
- oriented microsections of single crysts., prep. method 2−43534
- preparation techniques effects on statistical analysis of metallographic electron micrographs 2−43550
- quantitative analysis of dislocation distribution, correspondence 2−68025
- quantitative analysis of dislocation distributions, comments 2−68024
- quantitative defectoscopy, and computer-simulation of images 2−60745
- reactor absorber materials performance in HFIR control cylinders 2−83129
- reactor fuel element specimen prep. 2−42685
- reactor fuel pins, irrad., microsegregation of Cs, obs. technique 2−43774

ABSTRACTS AND CURRENT PAPERS JOURNALS

Three main subject areas are covered by INSPEC abstracts and current papers journals: physics, electrical and electronics engineering, and computer and control engineering. For each field an abstracts journal and a companion titles journal are published. The abstracts journals are intended as library tools for retrospective information retrieval, whereas the companion titles journals, which omit the abstracts and associated indexes, are intended as low-cost current-awareness tools for the individual.

SUBSCRIPTION PRICES

ABSTRACTS JOURNALS	Annual subscription Paper or microfiche	Annual subscription Combined paper and microfiche
Physics Abstracts (PA) Published every two weeks in conjunction with the American Institute of Physics, New York, and the Institute of Physics, London	£130	£195
Electrical & Electronics Abstracts (EEA) Published monthly jointly with the Institute of Electrical & Electronics Engineers Inc., New York	£105	£157
Computer & Control Abstracts (CCA) Published monthly jointly with the Institute of Electrical & Electronics Engineers Inc., New York	£55	£82
Combined Subscription to Electrical & Electronics Abstracts and Computer & Control Abstracts (EEA/CCA)	£135	£202

CURRENT PAPERS JOURNALS	Annual subscription IEE, AIP, IEEE, IOP, IERE members	Annual subscription Non-members
Current Papers in Physics (CPP) Published every two weeks in conjunction with the American Institute of Physics, New York, and the Institute of Physics, London	£7	£14
Current Papers in Electrical & Electronics Engineering (CPE) Published monthly jointly with the Institute of Electrical & Electronics Engineers Inc., New York	£7	£14
Current Papers on Computers & Control (CPC) Published monthly jointly with the Institute of Electrical & Electronics Engineers Inc., New York	£6	£12

CUMULATIVE INDEXES

Cumulative indexes are available for *Physics Abstracts*, *Electrical & Electronics Abstracts*, and *Computer & Control Abstracts*, for both authors and subjects. These cumulations generally cover a period of four years, with the exception of *Computer & Control Abstracts* where the initial volume covered the period 1966–68. The table below shows the prices and periods for the two types of cumulative index.

	Physics Abstracts		Electrical & Electronics Abstracts		Computer & Control Abstracts	
	Subject	Author	Subject	Author	Subject	Author
1955–59	£20	£20	£15	£20	—	—
1960–64	£40	£17	£20	£12	—	—
1965–68	£60	—	£35	£20	—	—
1966–68	—	—	—	—	£15 (combined)	

ORDERING PROCEDURE

AMERICAN SUBSCRIPTIONS

Physics Abstracts
Current Papers in Physics

For AIP members, wherever they reside, and from the public in the Americas, to the Subscription Department, American Institute of Physics, 335 East 45th Street, New York, NY 10017, USA. Please allow six weeks' notice for change of address, send both old and new addresses and include an address label from a recent issue.

Electrical & Electronics Abstracts
Computer & Control Abstracts and associated current papers journals in these fields

For IEEE members wherever they reside, and from the public in the Americas, to the Fulfillment Manager, Institute of Electrical & Electronics Engineers Inc., 345 East 47th Street, New York, NY 10017, USA.

REMAINDER OF THE WORLD

Abstracts Journals
Current Papers
Cumulative Indexes

For all remaining subscriptions, and for all cumulative indexes, to IEE, Savoy Place, London WC2R 0BL, England. Telephone 01-240 1871, Telex 261176, Telegrams Voltampere London WC2.

OTHER INSPEC SERVICES

SDI

(Selective Dissemination of Information.) This is a service individually tailored to the requirements and interests of the engineer or research worker. Details of information relevant to the interest profile of the individual subscriber are selected from the data being processed for the INSPEC database. Information is dispatched weekly on 150 mm × 100 mm (6″ × 4″) cards.

TOPICS

This is an SDI service based on standard profiles. There are 72 subjects covering high-activity areas of research and development. This is an inexpensive card service designed to alert engineers and researchers to the availability of literature within their subject area.

MAGNETIC TAPES

These are produced, containing all the information included in the INSPEC publications. They enable the larger research and development organisations to produce their own internal information and current-awareness services.

For more details of any of these services please write to:
INSPEC Marketing Department, The Institution of Electrical Engineers, Savoy Place, London WC2R 0BL, England

Cables Voltampere London WC2
Grams Voltampere London Telex

Telephone 01-240 1871
Telex 261176

inspec
The Institution of Electrical Engineers

All things being relative...

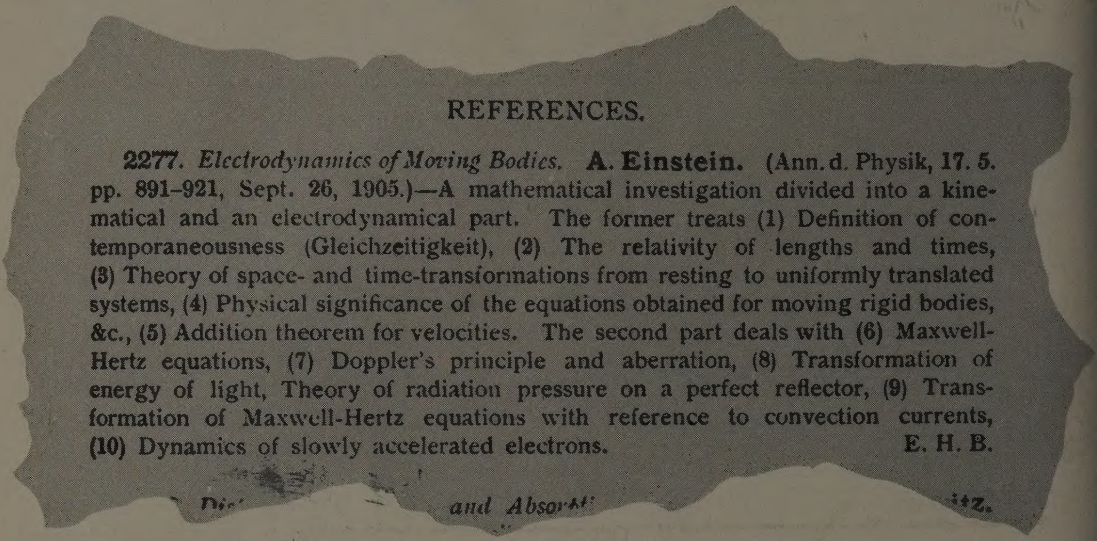

REFERENCES.

2277. *Electrodynamics of Moving Bodies.* **A. Einstein.** (Ann. d. Physik, 17. 5. pp. 891–921, Sept. 26, 1905.)—A mathematical investigation divided into a kinematical and an electrodynamical part. The former treats (1) Definition of contemporaneousness (Gleichzeitigkeit), (2) The relativity of lengths and times, (3) Theory of space- and time-transformations from resting to uniformly translated systems, (4) Physical significance of the equations obtained for moving rigid bodies, &c., (5) Addition theorem for velocities. The second part deals with (6) Maxwell-Hertz equations, (7) Doppler's principle and aberration, (8) Transformation of energy of light, Theory of radiation pressure on a perfect reflector, (9) Transformation of Maxwell-Hertz equations with reference to convection currents, (10) Dynamics of slowly accelerated electrons. E. H. B.

and Absor

...you probably missed this Science Abstract

Einstein's paper on the special theory of relativity, published in September 1905, is only one of the many vital papers which have appeared in Science Abstracts since they began publication in 1898.

You can forgive yourself for missing that one, but are you sure there are no other knowledge gaps in your literature searches?

If there are, back issues of Science Abstracts will fill those gaps.

Abstracts journals, containing titles, authors, abstracts, together with information necessary to locate the source of the original document, are produced in three separate publications: Physics, Electrical & Electronics and Computer & Control Abstracts. They are also published in concurrent microfiche form.

Back issues of Science Abstracts can do for you what the apple did for Newton!

To obtain a quotation for supplying your missing issues, please write to:

INSPEC Marketing Department The Institution of Electrical Engineers
Savoy Place London WC2R 0BL England
Telephone 01-240 1871

inspec
The Institution of Electrical Engineers